Cover Picture



Franciscus M. H. de Groot,* Carsten Albrecht, Ralph Koekkoek, Patrick H. Beusker, and Hans W. Scheeren,

Roey J. Amir, Neta Pessah, Marina Shamis, and Doron Shabat*

Cascade-release dendrimers or self-immolative dendrimers, as shown in the cover picture, spontaneously release all the end-group molecules following a single activation event. This triggering event induces a cascade of self-eliminations which leads to complete dissociation of the dendrimer into its separate building blocks. As the research groups of both F. M. H. de Groot (on page 4490 ff) and D. Shabat (on page 4494 ff) describe, such functionally novel dendrimers open up new modes of application of dendrimers, for example, for drug delivery.

Contents

Angewandte EarlyView

The following articles are available online (in Wiley InterScience). You can find them at www.angewandte.org, under Full Text, Early View.

D. F. Perepichka, M. R. Bryce, C. Pearson, M. C. Petty, E. J. L. McInnes, J. P. Zhao:*
A Covalent Tetrathiafulvalene–Tetracyanoquinodimethane Diad: Extremely Low HOMO–LUMO Gap, Thermoexcited Electron Transfer, and High-Quality Langmuir–Blodgett Films
DOI: 10.1002/anie.200351876
Published online: September 11, 2003

T. Kinoshita, S. Okada, S.-R. Park, S. Matsunaga, M. Shibasaki:*
Sequential Wittig Olefination–Catalytic Asymmetric Epoxidation with Reuse of Waste $Ph_3P(O)$: Application of α,β-Unsaturated N-Acyl Pyrroles as Ester Surrogates
DOI: 10.1002/anie.200352509
Published online: September 11, 2003

T.-C. Chou, H. Dong, A. Rivkin, F. Yoshimura, A. E. Gabarda, Y. S. Cho, W. P. Tong, S. J. Danishefsky:*
Design and Total Synthesis of a Superior Family of Epothilone Analogues, which Eliminate Xenograft Tumors to a Non-Relapsable State
DOI: 10.1002/anie.200352361
Published online: September 11, 2003

Articles judged by the referees or the editor as being either very important or very urgent are immediately edited, proof-read, and electronically published once the manuscript has arrived in the editorial office in final form. As long as there is no page number available these articles should be cited in the following manner:

Author(s) *Angew. Chem. Int. Ed.*, online publication date, DOI.

News

Awards for Vögtle (Organic Chemistry), Snieckus (Organometallic Chemistry), Hillenkamp and Karas (mass spectrometry) ____ **4424**

Web Sites

http://www.chemcases.com/ ____ **4425** Chemical Case Studies *J. Emsley*

Books

Organolithiums: Selectivity for Synthesis ____ **4426** Jonathan Clayden *reviewed by R. W. Hoffmann*

Multilayer Thin Films ____ **4426** Gero Decher, Joseph B. Schlenoff *reviewed by L. Dähne*

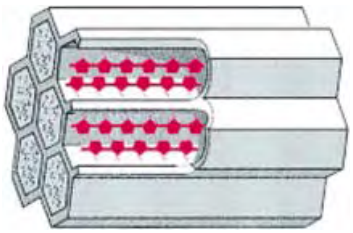
Thermodynamics of Biochemical Reactions ____ **4428** Robert A. Alberty *reviewed by A. J. Kirby*

Highlights

Host/Guest Polymerization

S. Spange* ____ **4430 – 4432**

Insulated Nanowire Bundles through Consecutive Template Synthesis



Conducting research and wiring zeolites: By a sol–gel process MCM-41 zeolite scaffolds are prepared, the channels of which are evenly loaded with pyrrole or thiophene template monomers. Redox-initiated polymerization leads to linking of the monomer units in the channels to form insulated potentially conducting molecular wires. These strategies increase the synthetic palette available for the targeted preparation of organic–inorganic hybrid materials.

Essays

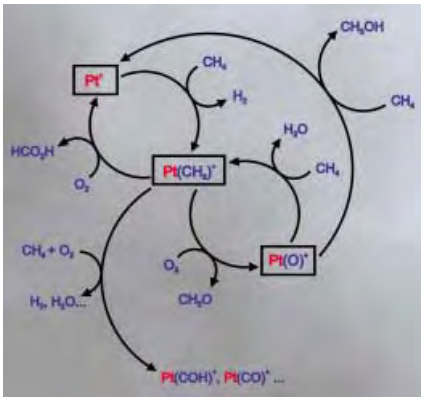
Responsibility in Science

R. R. Ernst* ——— **4434 – 4439**

The Responsibility of Scientists, a European View

The necessity to take on more responsibility for societal matters is something scientists can no longer avoid. This essay is an appeal to researchers and teachers in academia to extend their activities to transgress their own specialist fields and to face up to the important questions of our times.

Reviews



Ions in the Gas Phase

H. Schwarz* ——— **4442 – 4454**

Relativistic Effects in Gas-Phase Ion Chemistry: An Experimentalist's View

Relatively speaking: Bond energies, structural properties, and reactivity patterns of 5d transition metals are heavily affected by relativistic effects. Typical examples concern the unique ability of 5d metal cations in the electronic ground state to spontaneously dehydrogenate methane at room temperature (see scheme), and the dramatic effect of ligands on the ionization energy of gold.

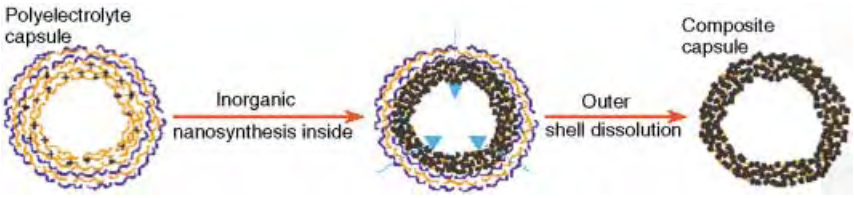
Chemical Safety

S. Gärtner, J. Küllmer, U. Schlottmann* ——— **4456 – 4469**

Chemical Safety in a Vulnerable World

The risks connected with chemical substances have been assessed in a number of conventions that have aimed to apply restrictions on the use of dangerous chemicals, and control of their worldwide trade. The developments in chemicals policy at the European and world level are discussed, with an insight into the interlaced structure of international cooperation that exists at both the political and the technical level.

Communications



Inorganic/Organic Microcapsules VIP

D. G. Shchukin, G. B. Sukhorukov,* H. Möhwald ——— **4472 – 4475**

Smart Inorganic/Organic Nanocomposite Hollow Microcapsules

Inorganic/organic polyelectrolyte microcapsules (see diagram for synthetic approach) possess the advantages of inorganic materials (i.e., high mechanical stability) and of conventional polyelectrolyte microcapsules (i.e., the ability to control the release/uptake properties of the capsule shell by changing pH value and ionic strength). Their initial spherical shape and controlled release properties remain after drying.

For the USA and Canada:
ANGEWANDTE CHEMIE International Edition (ISSN 1433-7851) is published weekly by Wiley-VCH PO Box 191161, D 69451 Weinheim, Germany. Air freight and mailing in the USA by Publications Expediting Inc. 200 Meacham Ave., Elmont, NY 11003. Periodicals postage paid at Jamaica NY 11431. US POSTMASTER: send address changes to *Angewandte Chemie*, Wiley-VCH, 111 River Street, Hoboken, NJ 07030. Annual institutional subscription price for institutions: Europe € 3430.00/3118.00. Outside Europe US$ 4499.00/4090.00 (valid for print and electronic/print or electronic delivery); for individuals who are personal members of a national chemical society, or whose institution already subscribes, or who are retired or self-employed consultants, print only. Europe € 248.00/Outside Europe US$ 378.00. Postage and handling charges included. All Wiley-VCH prices are exclusive VAT.

 © 2003 Wiley-VCH Verlag GmbH & Co. KGaA, Weinheim

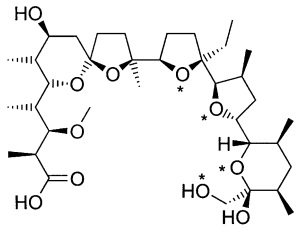
Contents

Polyether Biosynthesis

Z. A. Hughes-Thomas, C. B. W. Stark, I. U. Böhm, J. Staunton, P. F. Leadlay* ——— **4475 – 4478**

Intermediates Released from a Polyether-Producing Polyketide Synthase Provide Insight into the Mechanism of Oxidative Cyclization

Stereochemistry resolved: The introduction of hybrid polyketide synthases in *Streptomyces cinnamonensis* has shown that the *E* forms of a tetraketide and pentaketide are intermediates in the biosynthesis of the antibiotic ionophore monensin A (see structure). Furthermore, the *trans* double bond present in these intermediates has been identified as one of the targets for the epoxidase that initiates oxidative cyclization.

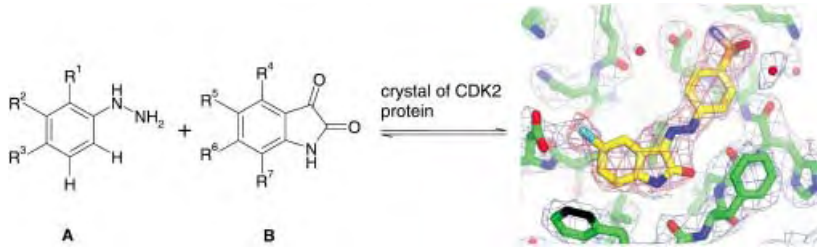


1

Dynamic Combinatorial Chemistry

M. S. Congreve,* D. J. Davis, L. Devine, C. Granata, M. O'Reilly, P. G. Wyatt, H. Jhoti ——— **4479 – 4482**

Detection of Ligands from a Dynamic Combinatorial Library by X-ray Crystallography



A B

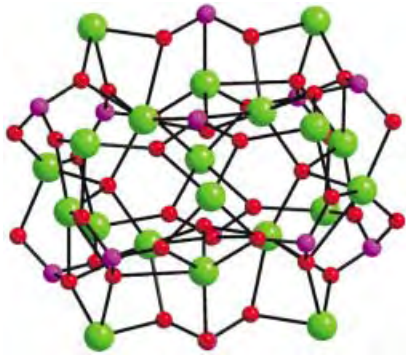
A dynamic combinatorial library of ligands derived from hydrazines **A** and isatins **B** was assembled in the presence of crystals of the target protein, cyclin-dependent kinase 2 (CDK2). Unambiguous detection of potent ligands, formed as part of the library, was successfully achieved by X-ray crystallographic analysis.

Cadmium Phosphonate Aggregates

G. Anantharaman, M. G. Walawalkar, R. Murugavel, B. Gábor, R. Herbst–Irmer, M. Baldus, B. Angerstein, H. W. Roesky* ——— **4482 – 4485**

A Nanoscopic Molecular Cadmium Phosphonate Wrapped in a Hydrocarbon Sheath

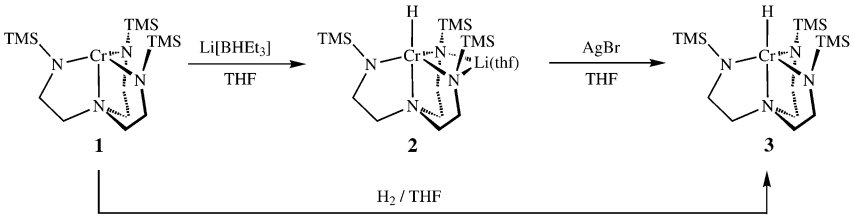
The molecular cadmium phosphonate $[(MeCd)_{10}\{(thf)Cd\}_4Cd_6(\mu_4\text{-}O)_2(\mu_3\text{-}OH)_2(t\text{BuPO}_3)_{12}]$ (see picture) is unlike all other such Cd compounds, which are polymeric or layered structures. It contains a 68-atom inorganic hollow skeleton made up of twenty cadmium (green), twelve phosphorus (purple), and thirty-six oxygen atoms (red), held together internally by pairs of oxo and hydroxo groups.



Mononuclear Chromium Hydrides

A. C. Filippou,* S. Schneider, G. Schnakenburg ——— **4486 – 4489**

A Pair of Remarkably Stable Mononuclear Chromium(III) and Chromium(IV) Hydrides



1 2 3

Often regarded as rare and unstable species, mononuclear Cr^{III} and Cr^{IV} hydrides (**2** and **3**, respectively; see scheme) have been prepared by various methods, and their interplay is illustrated by various reactions. The electronic structures of the hydrides were elucidated by utilizing several theoretical methods.

 © 2003 Wiley-VCH Verlag GmbH & Co. KGaA, Weinheim

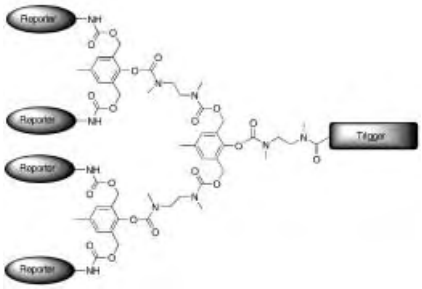


A single triggering event in the core of a dendrimer composed of two or more generations of multiple-release monomeric building blocks can induce the release of all end groups at the termini of the dendrimer (see schematic representation). Such multiple-release systems could find application, for example, in the field of (targeted) drug delivery, where a disease- or organ-specific activation event could trigger simultaneous release of multiple biologically active molecules.

Cascade-Release Dendrimers

F. M. H. de Groot,* C. Albrecht, R. Koekkoek, P. H. Beusker, H. W. Scheeren ——— **4490 – 4494**

"Cascade-Release Dendrimers" Liberate All End Groups upon a Single Triggering Event in the Dendritic Core

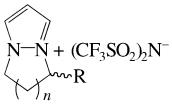


Docking the tails: The triggering of a single cleavage at the core of a new class of dendrimers (see, for example, the second generation dendron) results in a spontaneous chain fragmentation and the release all of the tail (reporter) units. Such dendrimers may be applied as a general platform for prodrugs or sensor molecules for enzymatic activity.

Dendritic Delivery Systems

R. J. Amir, N. Pessah, M. Shamis, D. Shabat* ——— **4494 – 4499**

Self-Immolative Dendrimers



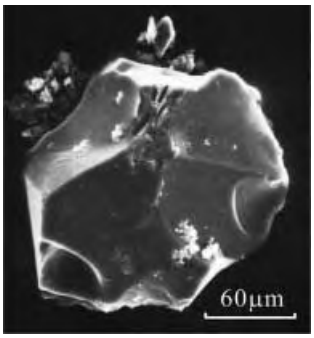
1 : $n = 2$; R = CH_3

Plastic batteries: Pyrazolium trifluoromethanesulfonimide **1** displays a single plastic crystalline phase (20–65 °C). When doped with a lithium salt (2 mol %), solid-state conductivity values above 10^{-4} S cm^{-1} at 55 °C are measured. The superior properties of these materials make them candidates for a new generation of lithium batteries.

Conductive Plastic Crystals

Y. Abu-Lebdeh,* P.-J. Alarco, M. Armand ——— **4499 – 4501**

Conductive Organic Plastic Crystals Based on Pyrazolium Imides



Diamonds in the rough: Crystals as large as 510 μm in diameter were formed at a temperature as low as 500 °C by the reduction of magnesium carbonate with metallic sodium (see picture). The product mixture was found to contain cubic diamonds by X-ray diffraction and micro-Raman spectrum analysis. The yield of diamond is about 6.6 % with respect to carbonate carbon. Magnesium carbonate is nontoxic, cheap, and abundant, and the temperature of this process is much lower than that of traditional methods. Therefore, the results of these studies could be applied in the production of industrial low-cost diamonds.

Low-Temperature Diamond Synthesis

Z. Lou, Q. Chen,* W. Wang, Y. Qian, Y. Zhang ——— **4501 – 4503**

Growth of Large Diamond Crystals by Reduction of Magnesium Carbonate with Metallic Sodium

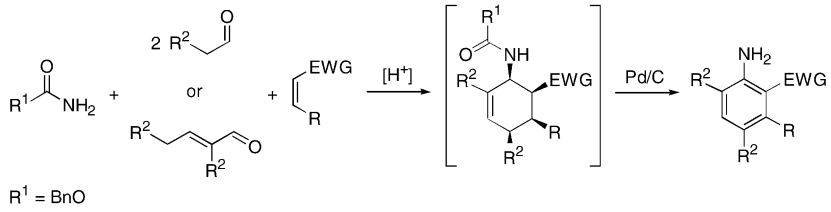
 © 2003 Wiley-VCH Verlag GmbH & Co. KGaA, Weinheim

Contents

Aniline Synthesis

H. Neumann, A. Jacobi von Wangelin, S. Klaus, D. Strübing, D. Gördes, M. Beller* ——— **4503 – 4507**

Anilines Made Easily: From Aldehydes to Tri-, Tetra-, and Pentasubstituted Anilines in Two Steps



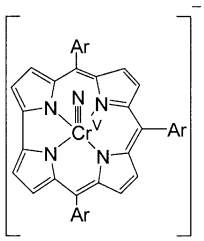
Easy as one, two, three. Highly substituted anilines are accessible with unprecedented efficiency from the three-component-coupling reaction of *O*-benzyl carbamate, aldehydes, and dienophiles followed by a new domino aromatization/deprotection reaction involving transfer hydrogenation (see scheme). EWG: electron-withdrawing group.

High-Oxidation-State Cr Complexes

G. Golubkov, Z. Gross* ——— **4507 – 4510**

Chromium(v) and Chromium(vi) Nitrido Complexes of Tris(pentafluorophenyl)-corrole

Nitrogen-atom transfer from a (nitrido)-manganese(v) complex to a Cr^{III} complex of the 5,10,15-tris(pentafluorophenyl)corrole trianion gave the stable Cr^{V} nitrido complex **1** (Ar = C_6F_5). In contrast, treatment of the same Cr^{III} starting material with ammonia/sodium hypochlorite gave the Cr^{VI} analogue of **1**.

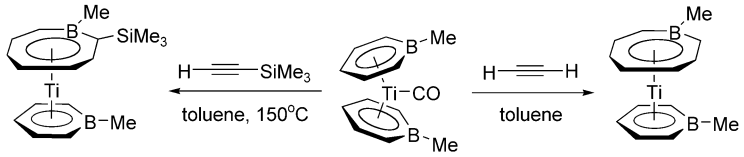


1

Boratacyclooctatetraene Ligand

X. Fang, D. Woodmansee, X. Bu, G. C. Bazan* ——— **4510 – 4514**

The Boratacyclooctatetraene Ligand: An Isoelectronic Trianionic Analogue of the Cyclooctatetraene Dianion



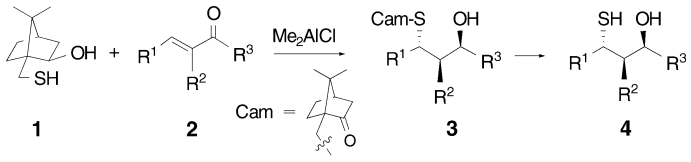
2 **1**

Expanding the ring: Acetylene inserts into one of the intracyclic B–C bonds of $[(C_5H_5B–Me)_2Ti(CO)]$ (**1**) to yield $[(C_7H_7B–Me)(C_5H_5B–Me)Ti]$, which contains the formally trianionic methylboratacyclooctatetraene ligand and a boratabenzene ligand. Similarly, the reaction of **1** with trimethylsilylacetylene produces $[(2\text{-}SiMe_3–C_7H_6B–Me)(C_5H_5B–Me)Ti]$ (**2**), in which the trimethylsilyl group occupies the sterically more encumbering site adjacent to boron (C_α; see picture). The regiochemistry of **2** indicates that the transmetallation step may be viewed as an electrophilic attack of boron on the metal coordinated acetylene ligand.

Tandem Asymmetric Reactions

K. Nishide, M. Ozeki, H. Kunishige, Y. Shigeta, P. K. Patra, Y. Hagimoto, M. Node* ——— **4515 – 4517**

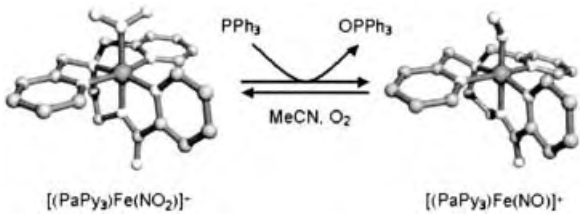
One-Step Stereocontrol of Three Contiguous Stereogenic Centers in Acyclic Systems: The Tuning Effect of an Additive in a Tandem Asymmetric Michael Addition and Meerwein–Ponndorf–Verley Reduction



1 **2** **3** **4**

A domino addition–reduction sequence to construct three contiguous stereogenic centers with a high level of diastereoselectivity makes use of the chiral camphor-derived thiol **1** in a Michael addition to acyclic α,β-disubstituted α,β-unsaturated ketones **2** (see scheme). The effect of additives was investigated, and it was also shown that compounds **3** are suitable precursors to 1,3-hydroxythiols of type **4**. R^1 = aryl, R^2 = alkyl, R^3 = alkyl or phenyl.

 © 2003 Wiley-VCH Verlag GmbH & Co. KGaA, Weinheim

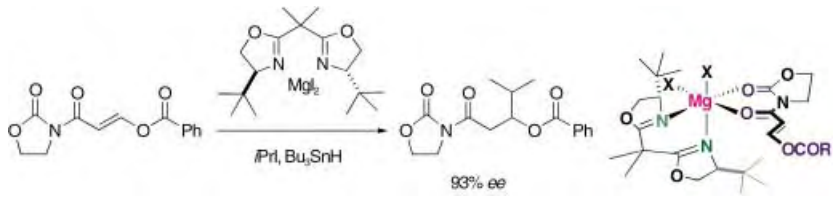


The non-heme iron(III) complex $[(PaPy_3)Fe(NO_2)](ClO_4)$ (**1**) transfers oxygen in the temperature range 45–65 °C to PPh_3 to afford $OPPh_3$ in MeCN. The product, $[(PaPy_3)Fe(NO)](ClO_4)$, a $\{Fe\text{-}NO\}^7$ species, reverts rapidly back to **1** in the presence of dioxygen, thus making the system catalytic (see scheme). Formation of an oxo-bridged species terminates the oxo-transfer process ($PaPy_3H$ = *N*-[*N*,*N*-bis(2-pyridylmethyl)-aminoethyl]-2-pyridinecarboxamide).

O-Atom Transfer in Fe Complexes

A. K. Patra, R. K. Afshar, J. M. Rowland, M. M. Olmstead, P. K. Mascharak* ——— **4517 – 4521**

Thermally Induced Stoichiometric and Catalytic O-Atom Transfer by a Non-Heme Iron(III)–Nitro Complex: First Example of Reversible $\{Fe\text{–}NO\}^7 \leftrightarrow Fe^{III}\text{-}NO_2$ Transformation in the Presence of Dioxygen

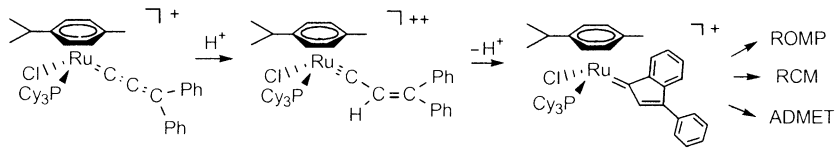


An unusual bond-construction strategy based on conjugate radical additions leads to acetate aldol-like products with high enantioselectivity (see scheme). Unlike their ionic counterparts, the enantioselective nucleophilic radical addition to β-acyloxyenoates proceeds without elimination and occurs by an *Si*-face radical addition to an s-*cis* conformer of the substrate (as shown).

Conjugate Radical Addition

M. P. Sibi,* J. Zimmerman, T. Rheault ——— **4521 – 4523**

Enantioselective Conjugate Radical Addition to β-Acyloxy Acrylate Acceptors: An Approach to Acetate Aldol-Type Products



A cat. for all seasons: The transformation of the allenylidene-ruthenium complexes $[RuCl(\eta^6\text{-arene})(=C=C=CR_2)(PR'_3)][CF_3SO_3]$ into indenylidene species $[RuCl(\eta^6\text{-arene})(indenylidene)(PR'_3)][CF_3SO_3]_2$ by the simple protonation with CF_3SO_3H and formation of an alkenylcarbyne intermediate (see picture; arene = *p*-cymene) is observed by low temperature NMR experiments. The new in situ generated 18 electron ionic indenylidene species are highly active in the polymerization of cyclooctene and cyclopentene, ring-closing metathesis of dienes and enynes, and the acyclic diene metathesis of decadiene, thus making it a catalyst for all seasons.

Active Catalysts in Alkene Metathesis

R. Castarlenas, P. H. Dixneuf* ——— **4524 – 4527**

Highly Active Catalysts in Alkene Metathesis: First Observed Transformation of Allenylidene into Indenylidene via Alkenylcarbyne–Ruthenium Species

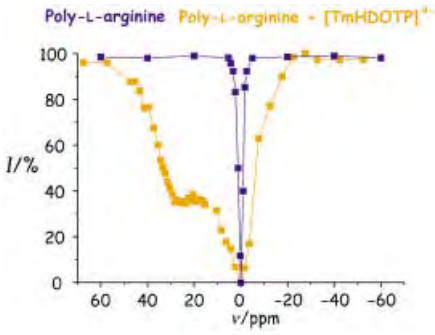
 © 2003 Wiley-VCH Verlag GmbH & Co. KGaA, Weinheim

Contents

Polypeptide Imaging Agents

S. Aime,* D. Delli Castelli, E. Terreno ——— **4527 – 4529**

Supramolecular Adducts between Poly-L-arginine and [Tm^{III}dotp]: A Route to Sensitivity-Enhanced Magnetic Resonance Imaging–Chemical Exchange Saturation Transfer Agents

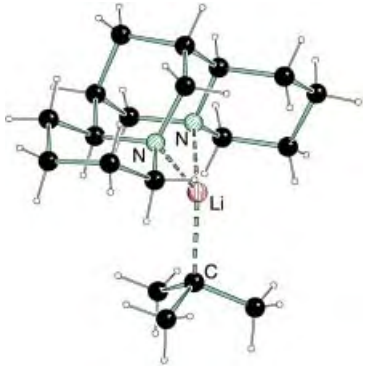


Markedly improved sensitivity is achieved in a contrast agent through formation of a supramolecular adduct between a diamagnetic system endowed with a high number of exchangeable protons (poly-L-arginine) and a paramagnetic shift reagent ($[Tm(Hdotp)]^{4-}$). The increase in the chemical shift separation between the two exchanging proton pools, induced by the shift reagent, allows irradiation of the mobile guanidine protons of the polymer, thus resulting in a very efficient saturation transfer (see graph).

Monomeric Butyllithium Compound

C. Strohmann,* T. Seibel, K. Strohfeldt ——— **4531 – 4533**

[*t*BuLi·(−)-Sparteine]: Molecular Structure of the First Monomeric Butyllithium Compound

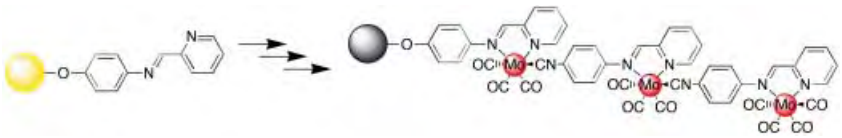


A chiral butyllithium reagent: Monomeric [*t*BuLi·(−)-sparteine] crystallizes from a solution in *n*-pentane on cooling. At the lithium center of the compound a formally free coordination site with a chiral environment is formed through angular distortion of the *tert*-butyl group (see structure).

Polymer-Bound Mo Complexes

K. Heinze,* J. D. B. Toro ——— **4533 – 4536**

Stepwise Solid-Phase Synthesis of Di- and Trinuclear Metal Complexes

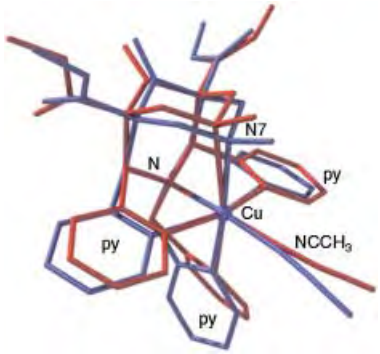


Step by step: Oligonuclear organometallic complexes are constructed in a stepwise manner on insoluble polymeric matrices and directly characterized on the support (see scheme). Liberation under mild conditions yields the corresponding soluble oligonuclear complexes.

Jahn-Teller Effects

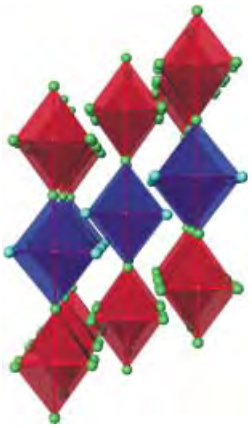
P. Comba,* A. Hauser, M. Kerscher, H. Pritzkow ——— **4536 – 4540**

Bond-Stretch Isomerism: Trapped Isomeric Structures of Hexacoordinate Copper(II) Bispidine Chromophores along a Jahn–Teller Active Vibrational Coordinate



The long and the short of it: Copper(II) complexes of the pentadentate bispidine ligands exist in two isomeric forms (see structure) with bond-length differences up to 0.5 Å. The stabilization of either isomer may be achieved by a variation of the substituent at N7.

 © 2003 Wiley-VCH Verlag GmbH & Co. KGaA, Weinheim



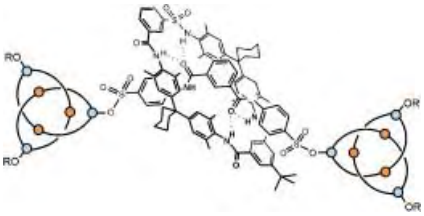
Wetting the appetite for Ti^{II} chemistry: Titanium metal is dissolved by aqueous acids in the presence of fluoride ions. The resulting green solution does not contain Ti^{III} but a mixture of Ti^{II} and Ti^{IV} complexes. The presence of a d^2 Ti^{II} species is confirmed by UV/Vis spectroscopy. A mixed-valent solid, $Ti^{II}(Ti^{IV}F_6)(H_2O)_4$, can be isolated from the solution and its structure parameters determined by powder diffraction (see picture, Ti^{IV} red, Ti^{II} blue).

Mixed-Valent Titanium Complex

U. Kölle,* P. Kölle ——— **4540 – 4542**

Aqueous Chemistry of Titanium(II) Species

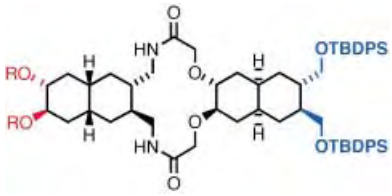
Get knotted: Molecular knots have been used as stoppers in the assembly of "knotaxanes", a new family of topologically chiral rotaxanes (see picture). Two knotaxanes were separated into enantiomers using HPLC with a chiral stationary phase and characterized by measuring their CD spectra. The chirality designation of these topological species is reminiscent of the Fischer projections of open-chain sugar acids.



Knotaxanes

O. Lukin, T. Kubota, Y. Okamoto, F. Schelhase, A. Yoneva, W. M. Müller, U. Müller, F. Vögtle* ——— **4542 – 4545**

Knotaxanes—Rotaxanes with Knots as Stoppers



Passing on information. Two conformational switches, decalin units, were coupled to a 14-membered bislactam ring (see formula, TBDPS = *tert*-butyldiphenylsilyl). Removal of a bisacetal clamp on the left side of the molecule resulted in a double ring-flip of the left decalin unit. Conformational coupling through the bislactam unit led to a double ring-flip in the right decalin unit.

Biconformational Bisdecalin Switch

M. Karle, D. Bockelmann, D. Schumann, C. Griesinger,* U. Koert* — **4546 – 4549**

Conformative Coupling of Two Conformational Molecular Switches

---

VIP Communications labeled with this symbol have been judged by two referees as being "very important papers".

The publication of Communications labeled with this symbol has been accelerated because of their topical or highly competitive nature.

The issues for September 2003 appeared online on the following dates
Issue 33: August 22. · Issue 34: September 5. · Issue 35: September 15. · Issue 36: September 17

 © 2003 Wiley-VCH Verlag GmbH & Co. KGaA, Weinheim

Sources

Product and Company Directory

You can start the entry for your company in "Sources" in any issue of *Angewandte Chemie*.

If you would like more information, please do not hesitate to contact us.

Wiley-VCH Verlag – Advertising Department
Tel.: 0 62 01 - 60 65 65
Fax: 0 62 01 - 60 65 50
E-Mail: MSchulz@wiley-vch.de

Service

Keywords ____ 4550

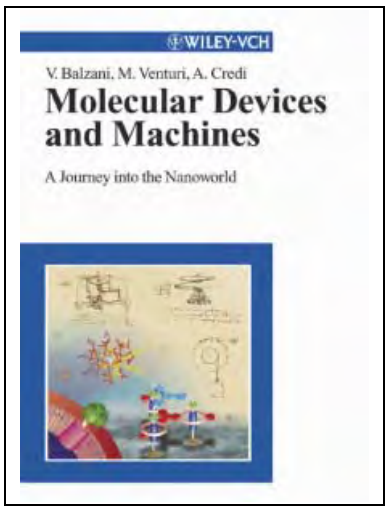
Authors ____ 4551

Sources ____ A51

Vacancies ____ A53

Preview ____ 4553

Key-Technologies of the Future



ISBN 3-527-30506-8
€ 99,- / sFr 146,-*

**The Euro price is only valid for Germany.*

VINCENZO BALZANI, Italy, ALBERTO CREDI, and MARGHERITA VENTURI, all of University of Bologna, Italy

Molecular Devices and Machines
A Journey into the Nanoworld
2003. XVII, 494 pp Hbk

The miniaturization of bulky devices and machines is a process that confronts us on a daily basis. However, nanoscale machines with varied and novel characteristics may also result from the enlargement of extremely small building blocks, namely individual molecules. This bottom-up approach to nanotechnology is already being pursued in information technology, with many other branches about to follow.
Written by Vincenzo Balzani and his team of co-authors, this book provides a comprehensive overview of this fascinating and multifarious topic, offering newcomers and experts alike a wealth of information.

- Most important new technologies for a broad audience
- Unifying, critical, and stimulating overview of red-hot topics

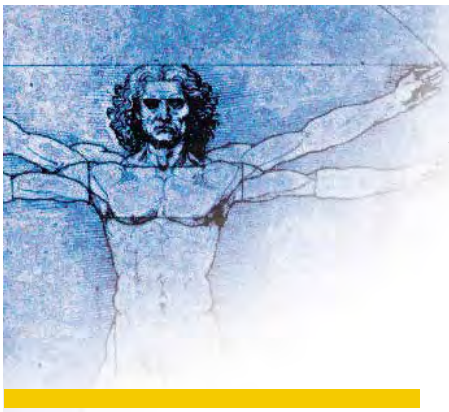
Wiley-VCH Verlag
Fax: +49 (0)6201 606 184
e-Mail: service@wiley-vch.de
www.wiley-vch.de

Register now for the free
WILEY-VCH Newsletter!
www.wiley-vch.de/home/pas

WILEY-VCH

50303032_kn

 © 2003 Wiley-VCH Verlag GmbH & Co. KGaA, Weinheim



GDCh Awards

At the annual general meeting of the Gesellschaft Deutscher Chemiker (GDCh) in Munich from October 6 to 11, 2003, numerous awards will be presented to outstanding researchers. We have already reported on Helmut Schwarz (Technische Universität Berlin, Germany; see his Review in this issue) and Jan-E. Bäckvall (University of Stockholm, Sweden), recipients of the Otto Hahn Award and of the August Wilhelm von Hofmann Lecture, respectively. Below we report on some of the other GDCh awards for 2003.

F. Vögtle receives the Adolf von Baeyer Medal

Fritz Vögtle, Professor of Organic Chemistry at the Universität Bonn (Germany), has been awarded the Adolf von Baeyer Medal for his outstanding work on esthetic, original, and unusual molecular structures. Vögtle studied in Freiburg and carried out his PhD under the guidance of H. A. Staab in Heidelberg, where he completed his habilitation in 1969 on steric effects inside large ring compounds. After a period at the Universität Würzburg, he moved in 1975 to take up a position in Bonn. His research is focused on molecular receptors, molecular recognition, and selective host–guest chemistry, although phanes, dendrimers,[1a] catenanes, and knotanes are also studied by his research group.[2] Vögtle coedited "Stimulating Concepts in Chemistry" with J. F. Stoddart and M. Shibasaki.[1b]



F. Vögtle

Arfvedson–Schlenk Award to V. Snieckus

The Arfvedson–Schlenk Award is presented for outstanding work in lithium chemistry. The most recent recipient, Victor Snieckus, was born in Lithuania and studied in Alberta (Canada) and Berkeley (California, USA). He completed his PhD in Oregon (USA) under the supervision of V. Boekelheide. From 1966 to 1998 he worked at the University of Waterloo (Ontario, Canada), and he is currently a professor at Queen's University in Kingston (Ontario). His research is focused on new methods and strategies for organic synthesis, with biomolecules playing an increasingly important role. The Award recognizes his fundamental contributions to the synthesis of organolithium compounds, for example, the *ortho*-metalation of arenes and heterocycles. A Communication from his research group recently appeared in *Angewandte Chemie*, entitled "Di(isopropylprenyl)-borane: A New Hydroboration Reagent for the Synthesis of Alkyl and Alkenyl Boronic Acids".[3] A Review on deprotonation reactions beyond thermodynamic acidity will appear at the beginning of 2004.



V. Snieckus

Fresenius Prize Awarded to F. Hillenkamp and M. Karas

The GDCh awards the Fresenius Prize in memory of Remigius Fresenius (1818–1897) for services to scientific development and the advancement of analytical chemistry. The recipients Franz Hillenkamp (Universität Münster, Germany) and Michael Karas (Universität Frankfurt am Main, Germany) have made significant advances in mass spectrometry. Their lecture for the presentation ceremony is entitled "Everything we do not know about MALDI or In Praise of Controversy". The MALDI technique was developed in the research group of Hillenkamp between 1985 and 1988. In this technique, macromolecules, such as proteins, nucleic acids, or carbohydrates, are transferred intact into the gas phase through laser impulses and then studied by mass spectrometry. Pioneering studies in this area were published in *Angewandte Chemie*.[4]



F. Hillenkamp

Hillenkamp studied physics at the Technische Universität München (Germany) and Purdue University in West-Lafayette, Indiana (USA). His career took him via the University of Maryland (USA) and the Universität Frankfurt to the Institut für Medizinische Physik und Biophysik in Münster in 1986. He retired in 2001.



M. Karas

Karas completed undergraduate studies and his PhD in physical chemistry in Bonn and was an assistant in Hillenkamp's research group in Frankfurt and Münster. He became Professor of Instrumental Analytical Chemistry at Frankfurt am Main in 1995. His research interests include the study of the physical-chemical principles and methodology of ion generation in MALDI and ESI MS.

[1] a) G. R. Newkome, C. N. Moorefield, F. Vögtle, *Dendrimers and Dendrons*, Wiley-VCH, Weinheim, **2001**; b) *Stimulating Concepts in Chemistry* (Eds.: F. Vögtle, J. F. Stoddart, M. Shibasaki), Wiley-VCH, Weinheim, **2000**.

[2] O. Lukin, J. Recker, A. Böhmer, W. M. Müller, T. Kubota, Y. Okamoto, M. Nieger, R. Fröhlich, F. Vögtle, *Angew. Chem.* **2003**, *115*, 458; *Angew. Chem. Int. Ed.* **2003**, *42*, 442.

[3] A. V. Kalinin, S. Scherer, V. Snieckus, *Angew. Chem.* **2003**, *115*, 3521; *Angew. Chem. Int. Ed.* **2003**, *42*, 3399.

[4] M. Karas, U. Bahr, A. Ingendoh, F. Hillenkamp, *Angew. Chem.* **1989**, *101*, 805; *Angew. Chem. Int. Ed. Engl.* **1989**, *28*, 760.

 © 2003 Wiley-VCH Verlag GmbH & Co. KGaA, Weinheim

Host/Guest Polymerization

Insulated Nanowire Bundles through Consecutive Template Synthesis

*Stefan Spange**

Keywords:
host–guest systems · polymerization · sol–gel processes · template synthesis · zeolites

Since the discovery of hexagonal MCM-41[1] and related silicate materials with a defined pore radius,[2] hardly a week goes by when a new application or specification of these materials is not reported. The search engine Google currently finds more than 4000 entries on MCM-41 on the Internet.

It is extraordinary how the scientific fantasy and experimental art of chemists is pointing to new targets and directions for materials science in the area of organic–inorganic hybrid materials. An example is the targeted introduction of organic functional groups into the interior of the MCM-41 channels.[3] The palette currently extends from photoswitchable morphology control, through *cis–trans* isomerization of stilbene units covalently incorporated into the wall of MCM-41,[4] and the directed energy transfer between internally immobilized porphyrin units,[5] to photoinduced reversible liberation of guest molecules from coumarin-modified MCM-41.[6] The development of new generations of solid catalysts immobilized in MCM-41 channels has expanded into a research area of its own as shown by the exponential growth in the number of original scientific publications and patents.[7–10]

A particularly important challenge is the formation of molecular wires of electrically and photochemically active compounds.[11a] To be able to generate molecular wires as desired and with defined lengths to be placed between two molecular or supramolecular poles, they must be completely insulated externally to avoid short circuits owing to faulty contacts or electrical interference.[11b] The materials from which these wires are made, doped polypyrrole, polythiophene, and polyacetylene, are extremely sensitive to oxidation so insulation is also necessary for chemical reasons.[12,13] The encapsulation of conducting polymers can be carried out using various strategies.[11]

A possible solution to this insulation problem is given by a new and amazingly simple but elegant method. A procedure was recently published in two papers which appeared almost simultaneously.[14,15] To better understand these concepts, the three basic procedures for encapsulating conducting polymers in mesoporous materials are presented briefly here.

A) The already synthesized polymer is encapsulated using organic vinyl monomers in a sol–gel process or by cross-linking copolymerization. Such procedures, which were developed for various types of organic templates,[16,17] are however, not applicable or only have limited applicability for mesoporous materials, as conducting polymers are usually very poorly soluble and are chemically extremely sensitive when doped, that is, they react readily with oxygen and water. To what extent such wires can be moved over insulator surfaces, arranged between poles and then insulated through chemical processes and fixed is still a challenge. For semiconducting polymers, however, template procedures could be used.[18]

B) The guest polymer is produced by polymerization in the insulating host.[19–26] There has been much research activity in recent years in the area of host–guest polymerization, which has included more than just the synthesis of molecular wires of polypyrrole or polythiophene in inorganic hosts. In particular the pioneering work of Bein and co-workers should be mentioned in this context.[20] Inspired by this work, various synthesis procedures have been developed to generate polymers directly in inorganic hosts, such as HY-zeolites or MCM-41, by using various polymerization techniques. Vinyl monomers can be polymerized using radicals,[20] with immobilized transition-metal complexes,[21–23] or cationically as the organic guest in an inorganic host.[24] The polymerization of aniline, pyrrole, or thiophene is initiated in the inorganic host using redox catalysts, preferably $FeCl_3$ or immobilized Cu^{2+} ions.[20,25,26]

C) The inorganic insulating layer and the potentially electrically conducting polymer are constructed simultaneously. A first very promising experiment was carried out by Aida et al. two years ago.[27] Substituted diacetylenes were incorporated covalently into MCM-41 and converted into polyenynes by thermally induced polymerization. Polyenynes are often insoluble and difficult to characterize.[27] Furthermore polyenynes are only suitable as nanowires under certain conditions because of energetically unfavorable band gaps. However, important pioneering conceptual work was possible with these inorganic–organic hybrid materials.

Route C is particularly promising, as the solubility problems of electrically conducting polymers and the slow ad-

[*] Prof. Dr. S. Spange
Institut für Chemie
Technische Universität Chemnitz
Strasse der Nationen 62
09111 Chemnitz (Germany)
Fax: (+49) 371-531-1642
E-mail: stefan.spange@chemie.tu-chemnitz.de

 © 2003 Wiley-VCH Verlag GmbH & Co. KGaA, Weinheim DOI: 10.1002/anie.200301654

sorption of the guest monomer into the inorganic host are circumvented. The latter effect often leads to a broad molecular-mass distribution of the encapsulated polymer or to blockage of the nanopore entries of the host,[24,25] as polymer fractions are formed initially in the entry area of the nanopores as a result of catalyst diffusion.

A prerequisite for the synthesis of defect-free polymer chains, that is, molecular wires with no breaks, is the regular and synergistic formation of the channel with monofunctional monomer building blocks in the hybrid material. The simultaneous formation of the MCM-41 framework and the linear, immobilized, guest-monomer components in a balanced stoichiometric ratio has been realized and verified by two research groups almost simultaneously.

Aida's group used a template with a terminal N-functionalized pyrrole group as the polymerizable monomer along with a non-polymerizable cotemplate (usually dodecyltrimethylammonium bromide) for the known MCM-41 framework synthesis using tetramethoxylsilane (TMOS) in the sol–gel process.[14] After MCM-41 formation the post-functionalization of the immobilized pyrrole unit to a one-dimensional (1D) polypyrrole wire is effected by $FeCl_3$ (Figure 1). A slight modification of the procedure allows the construction of two-dimensional (2D) polypyrrole structures. For example, if di(dodecyl)-dimethylammonium bromide is used as a cotemplate then morphology control and formation of lamellar silicate films are achieved.

Li, Fuhrhop et al. had almost the same idea for the 1D polymer structure.[15] They used terminal thiophen-3-yl-substituted trimethylammonium salts as the monomer template (Figure 2). As in the previous example, the redox catalyst $FeCl_3$ was used to initiate the polymerization of the immobilized thiophene units giving a polythiophene guest polymer. The channel diameter is exactly 3 nm. After the inorganic matrix has been dissolved in HF the encapsulated polymers can be readily investigated because of the solubilizing properties of the side chains (see also ref. [18]. For the characterization of polymers in MCM-41 see ref. [24c]). The defect-free polythiophene chains with lengths of

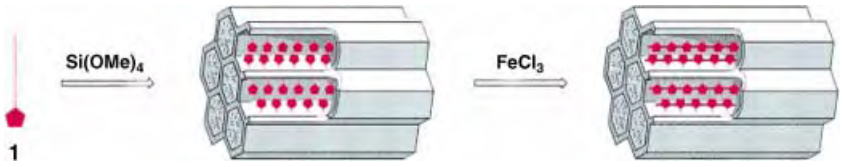


Figure 1. Template synthesis of a polypyrrole/MCM-41 nanocomposite using 1-[12-(pyrrol-1-yl)-dodecyl]trimethylammonium or 1-[10-(pyrrol-1-yl)decyltrimethylammonium bromide (**1**) with tetramethoxysilane in a sol–gel process and subsequent polymerization with $FeCl_3$.[14]

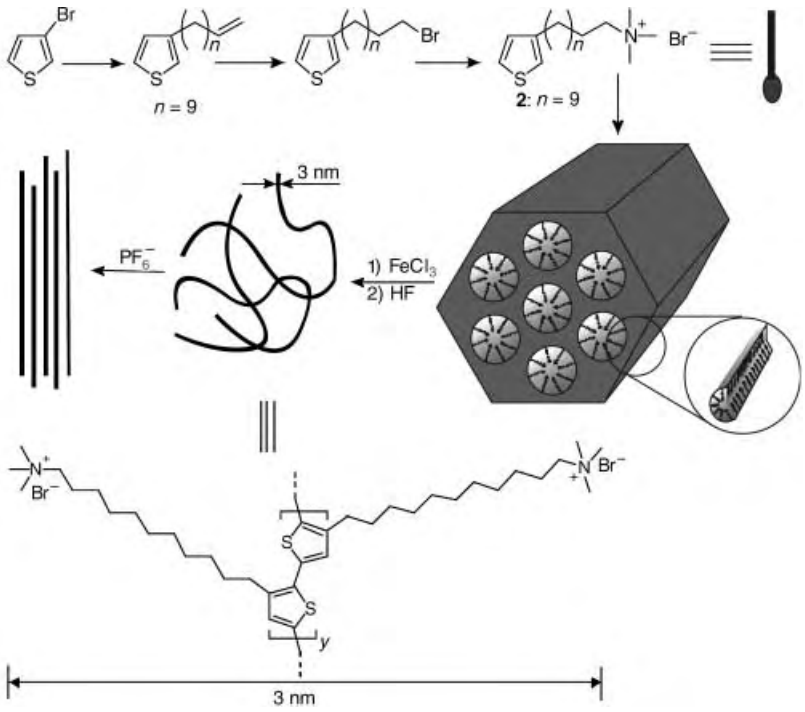


Figure 2. Scheme showing the production of polythiophene chains in mesoporous MCM-41. The template monomer trimethyl[11-thiophen-3-yl-undecyl)ammonium bromide (**2**) is first synthesized, then inserted into the MCM-41 (Figure 1), and finally the polymerization is initiated by $FeCl_3$. The polymer chains are liberated by dissolving the inorganic host in HF. Replacing Br^- by PF_6^- ions leads to extension and association of the polymer chains.[15]

100 nm (corresponding to ca. 330 thiophene units) were thus prepared.

It is particularly pleasing to see how the nature of the counterion controls the conformation of the C_{11}-chains with terminal trimethylammonium groups bonded to 2,2′-linked thiophene units. Replacing the solvating bromide by the non-nucleophilic PF_6^- ion leads to alignment of the chains (see Figure 2). Thus the method of Li and Fuhrhop[15] also offers the possibility, by using the MCM-41 template effect, of obtaining water-soluble polymers which are potentially electrically conducting, with defined molecular masses on a gram scale. As a result, by use of template co-monomers and the current synthesis routes employing MCM-41, materials scientists have a very promising tool available for immobilizing membranes or porous films with enclosed bundles of wires on conducting catalysts.[28] These examples will be able to be used for preliminary experiments on linking nano building blocks and molecular wires. A further possibility is the use of templates functionalized at both ends which contain both the organic monomer unit and a trialkoxysilane group as the potential inorganic component. Although the problem of precisely adjusting the reaction conditions still exists, with this method it may be possible to produce a conducting molecular wire with an insulating silicate layer.[28] These ideas and the possibilities offered by the synthetic procedures certainly bring the possibility of

 © 2003 Wiley-VCH Verlag GmbH & Co. KGaA, Weinheim

formation of molecular wires made up of linearly arranged monomers nearer.

[1] C. T. Kresge, M. E. Leonowicz, W. J. Roth, J. C. Vartuli, J. S. Beck, *Nature* **1992**, *359*, 710.

[2] P. Behrens, G. D. Stucky, *Angew. Chem.* **1993**, *105*, 729 – 732; *Angew. Chem. Int. Ed. Engl.* **1993**, *32*, 696 – 772.

[3] T. Asefa, M. J. MacLachan, N. Coombs, G. A. Ozin, *Nature* **1999**, *402*, 867 – 871.

[4] M. Alvaroa, B. Ferrer, H. Garcìa, *Chem. Commun.* **2003**, 2012 – 2013.

[5] N. K. Mal, M. Fujiwara, Y. Tanaka, *Nature* **2003**, *421*, 350 – 353.

[6] H. Furukawa, T. Watanabe, K. Kuroda, *Chem. Commun.* **2001**, 2002 – 2003.

[7] a) A. Corma, *Top. Catal.* **1997**, *4*, 249 – 260; b) A. Corma, *Chem. Rev.* **1997**, *97*, 2373 – 2419.

[8] G. Gerstberger, C. Palm, R. Anwander, *Chem. Eur. J.* **1999**, *5*, 997 – 1005.

[9] A. Stein, B. J. Melde, R. C. Schroden, *Adv. Mater.* **2000**, *12*, 1403 – 1419.

[10] P. M. Price, J. H. Clark, D. J. Macquarie, *J. Chem. Soc. Dalton Trans.* **2000**, 101 – 110.

[11] a) R. L. Carroll, C. B. Gorman, *Angew. Chem.* **2002**, *114*, 4556 – 4579; *Angew. Chem. Int. Ed.* **2002**, *41*, 4378 – 4400; b) D. J. Cardin, *Adv. Mater.* **2002**, *14*, 553 – 563, and references therein.

[12] G. Wegner, *Angew. Chem.* **1981**, *93*, 352 – 371; *Angew. Chem. Int. Ed. Engl.* **1981**, *20*, 361 – 381.

[13] a) H. Shirakawa, *Angew. Chem.* **2001**, *113*, 2642 – 2648; *Angew. Chem. Int. Ed.* **2001**, *40*, 2574 – 2580; b) A. G. MacDiarmid, *Angew. Chem.* **2001**, *113*, 2649 – 2659; *Angew. Chem. Int. Ed.* **2001**, *40*, 2581 – 2590; c) A. J. Heeger, *Angew. Chem.* **2001**, *113*, 2660 – 2682; *Angew. Chem. Int. Ed.* **2001**, *40*, 2591 – 2611; d) A. J. Heeger, *J. Phys. Chem. B* **2001**, *105*, 8475 – 8491.

[14] M. Ikegame, K. Tajima, T. Aida, *Angew. Chem.* **2003**, *115*, 2204 – 2207; *Angew. Chem. Int. Ed.* **2003**, *42*, 2154 – 2157.

[15] G. Li, S. Bhosale, T. Wang, Y. Zhang, H. Zhu, J.-H. Fuhrhop *Angew. Chem.* **2003**, *115,* 3948 – 3951; *Angew. Chem. Int. Ed.* **2003**, *42*, 3818 – 3821.

[16] N. R. B. Coleman, N. O'Sullivan, K. M. Ryan, T. A. Crowley, M. A. Morris, T. R. Spalding, D. C. Steytler, J. D. Holmes, *J. Am. Chem. Soc.* **2001**, *123*, 7010 – 7016.

[17] K. J. C. van Bommel, A. Friggeri, S. Shinkai, *Angew. Chem.* **2003**, *115*, 1010 – 1030; *Angew. Chem. Int. Ed.* **2003**, *42*, 980 – 999.

[18] K. Kuroda, T. M. Swager, *Chem. Commun.* **2003**, 26 – 27.

[19] K. Tajima, T. Aida, *Chem. Commun.* **2000**, 2399 – 2412, and references therein.

[20] a) C.-G. Wu, T. Bein, *Science* **1994**, *264*, 1757; b) C.-G. Wu, T. Bein, *Chem. Mater.* **1994**, *6*, 1109 – 1112; c) T. Bein, P. Enzel, *Angew. Chem.* **1989**, *101*, 1737 – 1738; *Angew. Chem. Int. Ed. Engl.* **1989**, *28*, 1692 – 1694; d) P. Enzel, T. Bein, *J. Phys. Chem.* **1989**, *93*, 6270 – 6272; e) K. Moller, T. Bein, R. X. Fischer, *Chem. Mater.* **1998**, *10*, 1841 – 1852; f) K. Moller, T. Bein, *Chem. Mater.* **1998**, *10*, 2950 – 2963.

[21] a) S. M. Ng, S. Ogino, T. Aida, K. A. Koyano, T. Tatsumi, *Macromol. Rapid Commun.* **1997**, *18*, 991 – 996; b) S. M. Ng, S. Ogino, T. Aida, K. A. Koyano, T. Tatsumi, *Macromol. Rapid Commun.* **1997**, *18*, 991 – 996; c) K. Kageyama, J. i. Tamazawa, T. Aida, *Science* **1999**, *285*, 2113 – 2115.

[22] P. Lehmus, B. Rieger, *Science* **1999**, *285*, 2081 – 2082.

[23] a) R. Ramachandra Rao, B. M. Weckhuysen, R. A. Schoonheydt, *Chem. Commun.* **1999**, 445; b) M. Weckhuysen, R. Ramachandra Rao, J. Pelgrims, R. A. Schoonheydt, P. Bodart, G. Debras, O. Collart, P. Van Der Voort, E. F. Vansant, *Chem. Eur. J.* **2000**, *6*, 2960 – 2970.

[24] a) A. Gräser, S. Spange, *Chem. Mater.* **1998**, *10*, 1814 – 1819; b) S. Spange, A. Gräser, P. Rehak, C. Jäger, M. Schulz, *Macromol. Rapid Commun.* **2000**, *21*, 146 – 150; c) S. Spange, A. Gräser, H. Müller, Y. Zimmermann, P. Rehak, C. Jäger, H. Fuess, C. Baehtz, *Chem. Mater.* **2001**, *13*, 3698 – 3708; d) S. Spange, A. Gräser, A. Huwe, F. Kremer, C. Tintemann, P. Behrens, *Chem. Eur. J.* **2001**, *7*, 3722 – 3728.

[25] A. Matsumoto, T. Kitajima, K. Tsutsumi, *Langmuir* **1999**, *15*, 7626 – 7631.

[26] J. R. Choi, Y. Kim, M. Yoon, *Bull. Korean. Chem. Soc.* **2001**, *22*, 1045 – 1048.

[27] T. Aida, K. Tajima, *Angew. Chem.* **2001**, *113*, 3919 – 3922; *Angew. Chem. Int. Ed.* **2001**, *40*, 3803 – 3806.

[28] T. Bein und Mitarbeiter, unpublished results, presented to the DFG final colloquium "Nanostrukturierte Wirt-GAste-Systeme", Berlin, October 2002; see also *Host/Guest Systems on Nanoporous Crystals* (Ed.: F. Schüth), Wiley-VCH, Weinheim, **2003**.

 © 2003 Wiley-VCH Verlag GmbH & Co. KGaA, Weinheim

Responsibility in Science

The Responsibility of Scientists, a European View**

*Richard R. Ernst**

Keywords:
science ethics · science philosophy · university politics

Why should we researchers and university teachers carry particular societal responsibility?—The answer follows from the function of universities within our society, to educate future generations and to act as "truth-seeking" centers. Given the increasing public costs of universities, there has also been a rise in the expectations in their beneficial output for society. The current global political and economic situation places even more responsibility on the universities to be far-sighted.

And why is there a relevant European context?—Fundamentally, science has no national or continental borders. On the contrary, science helps to bridge gaps that originate from political or economic developments or from ethnical traditions. Scientific results have truly universal validity. Nevertheless, scientists are citizens who are rooted in a national, continental, and cultural context. Science is supported by national authorities, and is expected to foster regional prosperity and to help solve national problems. Perhaps most importantly, an active science community is indispensable in any flourishing society that desires to remain competitive on an international scale. Whenever economic or political unbalance starts to develop between nations or continents, national or continental concerns may become relevant also in science. In such a situation, science is expected to contribute its share to strengthening the national impact on a global scale to re-establish balanced competitiveness. Today, where hegemony of the USA on the political, but also economic platform, is becoming more and more of a serious challenge, the positioning of European science and technology needs to be reconsidered. In this respect, it seems appropriate to me for European scientists to develop a specifically European opinion, keeping in mind that the major obligation of science is to remain far-sighted in all respects, also in the geographical ones, and to strengthen international and intercontinental ties rather than questioning them.

[*] Prof. Dr. R. R. Ernst
Laboratorium für Physikalische Chemie
ETH Hönggerberg HCI
8093 Zürich (Switzerland)
Fax: (+41) 1-632-1257
E-mail: richard.ernst@nmr.phys.chem.ethz.ch

[**] The thoughts expressed in this essay have been presented in numerous lectures, such as in Pune (January 2000), Munich (April 2000), Fribourg (June 2000), Santander (September 2000), Glion (May 2001), Fribourg (August 2001), Istanbul (September 2001), Cornell University (September 2001), Lulea (December 2001), Prague (June 2002), St. Gallen (June 2002), Qingdao (July 2002), Madrid (August 2002), Fontainbleau (September 2002), Sevilla (November 2002), Göttingen (November 2002), Leipzig (December 2002), Munich (December 2002), Madrid (December 2002), New Delhi (January 2003), Bangalore (January 2003), Zurich (March 2003, April 2003), Bern (March 2003), London (May 2003), Helsinki (June 2003), St. Petersburg (June 2003).

It seems appropriate to me for European scientists to develop a specifically European opinion, keeping in mind that the major obligation of science is to remain far-sighted in all respects, also in the geographical ones.

Thoughts on the State of the World

The current state of the world concerns me, and in particular the following:

- *Many citizens are still convinced that all our visions, even our most daring ones, can be implemented by technological means*: Energy and food problems are solvable without significantly restricting our consumption. With detailed knowledge of the human genome, we have a key at hand for preventing and healing most diseases. Interplanetary travel will cause no insurmountable difficulties. And global peace in democratic harmony is achievable, if necessary by force.
- *Many of us still trust, unconditionally, the principles of global free market economy.* The fewer national or international regulatory restrictions, the better is the functioning of a self-regulating market, and the higher will be the added value, provided it is measured in proper terms.
- *Sometimes, we realize, nevertheless, that our natural resources are indeed finite.* This applies to air quality, water, fertile soil, and particularly to fossil fuels.
- *The gap between poor and rich is growing frightfully*, both within individual countries and between industrial and developing nations. It appears as if the functioning of our global system relies on the existence of a gradient of wealth. It offers incentives for the ascent on the societal ladder, and allows those who have already reached the top of the ladder to gain profits.
- *Ethics and moral principles are often mentioned by decision-makers* but

 © 2003 Wiley-VCH Verlag GmbH & Co. KGaA, Weinheim DOI: 10.1002/anie.200330065

hardly applied in reality. Success seems to justify all deeds as long as they do not severely violate the state laws.

- *Today, only one single superpower is left* with its unlimited claim for political, economic, and ideological hegemony. In my opinion the world today is far from a multipolar democratic situation in which each nation has its appropriate say.

Tasks of Universities

But what is the relevance of these facts for science and for chemistry and for the tasks of universities?—Indeed, at first sight, its relevance seems minute, except that scientists and chemists are also members of the global society and carry co-responsibility or, possibly, co-complicity for mistakes. But this kind of responsibility is easy to bear as it is distributed on not less than 6.4 billion global citizens.

In comparison, our traditional academic obligations appear to be of higher relevance: What could be more valuable than exploring the natural laws and their consequences for gaining insight and enabling technological applications. We are supporting industrial prosperity to the advantage of society and of the consumers, whose consumption, in turn, is indispensable for a prosperous economy.—But sometimes, doubts arise in my mind whether fundamental research is truly our single obligation. Indeed, the generous public support that we receive is justified not only by our specialized knowledge and our scientific excellence, but it is motivated by the expectation of conscientious contributions for shaping a beneficial future for the entire society.

We scientists often like to stress our indispensable academic independence, which gives us the jester's license to do whatever we want. Although our employment contracts are often fixed-term, it is hardly possible to find anywhere in society more job security than on a professorial chair. The envy of industrial employees is well justified; they never know from one week to the next whether they will still be employed or whether they will meet some of their equally frustrated colleagues, on a rainy street in front of the nearby job center. Politicians do not fare far better, facing the mood swings of the voters and re-election on a regular basis. Who can expect from industrial managers or politicians, in their unsafe positions, to articulate unpopular but honest opinions or even to take courageous measures that could endanger their own position?

In this situation, researchers and university teachers are not only predestined but obliged to frankly articulate their opinions and convictions for the sake of society, even to questions that lie far outside of their official teaching obligations. The excuse that we, as classical scholars, as quantum-field theoreticians, or as peptide chemists, cannot possibly possess well-founded knowledge in all conceivable public domains is hardly acceptable. It merely underlines our lack of interest for societal questions and our preset priorities in view of prolonging our already quite respectable list of publications. Karl Popper said in 1958 that: *"I am thinking of the obligation of each intellectual to help others for liberating themselves and for developing a critical mind, a duty which most intellectuals have forgotten since Fichte, Schelling, and Hegel. Unfortunately, the desire to impress and, as Schopenhauer said, to infatuate instead of instructing is widespread among intellectuals."*[1] In a similar context Sigmund Freud wrote in a famous letter to Albert Einstein in 1932: *"We should be at greater pains than heretofore to educate a superior class of independent thinkers, unamenable to intimidation and fervent in the quest of truth, whose obligation it would be to guide the dependent masses."*[2] Even if we use slightly different words today, the two requests harmonize well with the goals of this essay.

> ***I am thinking of the obligation of each intellectual to help others for liberating themselves and for developing a critical mind.***
>
> **Karl Popper**

After all, we are bound by a contractual obligation to educate a future generation of academics. Hopefully, we prepare them in a way to do a better job in the future than our generation has done so far, preventing a perpetuation of our errors. Education is not limited to acquiring scientific knowledge, which is being taught, hour by hour, at our universities. The real goal of university education is the development of personalities who will courageously address future challenges and who will not succumb to the monetary temptations of our "bluff society", often to the disadvantage of its weakest members. At nearly all universities, additional, separate courses are offered for widening the horizons of the students. But time restraints are severe, and often these courses are the first victims of low attendance. Most likely, it is best to integrate much of the more general reasoning into the major courses themselves, if only as side remarks, motivating the students for self-studies. It is important to note that the majority of future industrial and political leaders pass once through our universities! Here we have a unique chance to influence them during their development by our, hopefully, positive example.

The German philosopher Hans Jonas has defined "responsibility" in his important treatise "The Principle Responsibility": *"Act so that the effects of your action are compatible with the permanence of genuine human life."* He writes further: "*Prometheus, liberated at last, who received from science inconceivable power and from economics the restless impetus, calls for an ethics which, by free restraint, limits its potency from becoming fatal to human beings… What can serve as a compass? The envisioned danger itself!*"[3] Sustainability and foresight are thus required.

In order to reach the goal of academic accountability, we do not necessarily have to revise all our current curricula. More important are changes in the personal attitude of the teachers and of the focus in their courses. Often, a few brief comments in a lecture course are sufficient to illuminate the societal context and to relate to questions of general relevance.—By the way, hardly anybody doubts that our spectacular performances in large lecture halls serve more the convenience and the ego of the

 © 2003 Wiley-VCH Verlag GmbH & Co. KGaA, Weinheim

teacher than the efficiency of learning, and that active learning in small discussion groups or in the laboratory can be significantly more effective. Interim placements in industrial enterprises as part of the coursework could also be quite revealing.

Universities should consider themselves as cultural centers with far-reaching radiance rather than merely serving as training grounds for academic specialists. The integration of knowledge, perception, and comprehension, as well as compassion, is at least as relevant as extreme specialization. Obviously, scientific excellence is indispensable, but insufficient in isolation. Or as Georg Christoph Lichtenberg put it "*He who understands nothing but chemistry does not truly understand chemistry either.*"

Naturally, the student population will always show a wide spectrum in terms of receptivity. Some students will rapidly acquire rather comprehensive knowledge and understanding, whereas others will remain relatively narrow and focused on specific technical skills. But in general, a broad education should be encouraged, at least as an option, for all students. Motivation for voluntary involvement in other subjects is far more efficient than reglementary enforcement.

I am convinced that science departments with a broad scope, integrating also societal concerns and questions of global relevance in their courses and daily discussions, will succeed in overcoming the present difficulties of recruiting students. Today, potential university students often regard science departments as too one-sided and too specialized for motivating them to invest their precious time and energy. They rather chose subjects that lie near to their societal inclinations. I have to admit that I myself would prefer, if I had to start again, a study that combines top science with societal concerns and global vision, rather than detached, stand-alone science, even if the latter would be taught by the most knowledgeable international specialists.

With these goals in mind, I think that an extension of the appointment contracts of university teachers is desirable covering not only research and teaching tasks but also societal obligations. Providing comprehensive opportunities for life-long-learning for professionals and for citizens is part of this obligation. Teaching assignments in favor of the broader society have much in common with planning a safe long-term future for all. It is obvious that the importance of education will have to rise in the future if we want to provide job opportunities for a majority of citizens. The planning of the future cannot successfully be undertaken in splendid isolation within our ivory towers but requires active interaction with society in the form of seminars, consensus conferences, public lectures, and discussions. Obviously, without additional funding and additional personnel, it will be impossible to satisfy these demanding tasks. But first of all, they require a new prioritization within our universities, perhaps followed by painful cuts of some beloved but antiquated academic pigtails, such as the desire of each professor to preferentially discuss his own specialty within compulsory courses.

University teachers should cover not only research and teaching tasks but also societal obligations.

The European Context

The preceding remarks apply to all universities and the entire academic community worldwide. But where is the specifically "European" element that has been mentioned at the beginning?—The following lines contain proposals that I feel would help to remedy the present global situation. The primary aim is to strengthen the European position rather than to weaken any other one. After all, we can change only our own mind and not the one of our neighbor, or in the words of Mahatma Gandhi: "*We must be the change we want to see.*" Becoming strong, co-equal players, ready for fruitful collaboration, would be of advantage for all nations and continents.

We must be the change we want to see.
Mahatma Ghandi

My admiration for US science, for the American confidence in technological progress, and for the willingness to undergo risks, I share with many, perhaps most scientists in Europe. Europeans, on the other hand, often act rather guided by tradition within a well-developed network of regulations and social security.

The positive and negative consequences of American motivation and initiative are obvious in politics, economics, and science. Although Europe, as a continent, exceeds the USA in terms of population numbers, the USA appears to dominate in all these three essential domains. Without a flourishing economy, top science could no longer be financed, and without advanced science, the American economy would cease to stay ahead.

It is often claimed, not incorrectly, that a strong American economy will also support the economy in the rest of the world, in the same manner as the wealth of the rich creates jobs for the poor, for those who still believe in Adam Smith's "invisible hand".[4] But it leads to a situation that is hardly compatible with the national pride of other countries. At this point, novel long-term concepts are required to heal the international relations. Surely, the solution cannot be found in perpetuating and cementing the present situation in which a single nation dominates world affairs.

But who can develop such novel, farsighted concepts?—We can not expect much radical change and idealistic development from the side of economics. Too dominant are company's interests in the fight for survival and profits. Also in politics, there are few free valences; the short-term monetary and hegemonic problems are of sufficiently high priority to forget the lurking dangers of our long-term global future.—No doubt, the academic community has to accept the challenging obligation for conceiving avenues towards a future global equality in politics, economics, and in science. This task deserves a high priority among academic obligations, more important, perhaps,

 © 2003 Wiley-VCH Verlag GmbH & Co. KGaA, Weinheim

than any single, specific exploration at the forefront of science.

It would be unreasonable to expect a ready-made concept from me. Its development requires the cooperation of all academics from all disciplines and all countries, including the USA, and it needs time to ripen. But it is essential that this concern remains constantly in our consciousness, that it moves our thoughts, and influences our decisions. It will become necessary to organize conferences and symposia to discuss the global development. It is advisable to form discussion panels for treating this issue. At the ETH Zürich, for example, successful interdisciplinary lecture series have been organized for many years, and for the last six years, the Collegium Helveticum has functioned well as a platform for in-depth interdisciplinary discussion.

Europe is still weak in terms of transnational academic institutions. They need to be strengthened to achieve sufficient influential power. The European academy, Academia Europaea, is still weak and exerts very little, if any, political influence yet.[5] Strong support by national academies would be necessary. Unfortunately, national academies are still lacking in many European countries, and, when they do exist, they are hardly representative for the entire academic community. Academies need to be more than, what many of them are today, just scientific pigtails. Numerous European journals have gained international profile, and they deserve to be further promoted and supported by international authors. Another issue is international conferences in Europe that also need additional support to strengthen the European science position.

Influencing the long-term development is intimately connected with educational issues. We are supposed to be educating a future generation that is capable of promoting, at the same time, global responsibility and European self-esteem, without neglecting the interaction with the USA, but without overrating its importance. In this context, it is certainly indispensable to further unify the European educational system with a well-conceived European educational model. Not stream-lining is required but liberal, open-minded coordination that will satisfy a broad range of requests and that will lead to an error-tolerant system that allows for more than one chance. The general usage of a single teaching language, English, in all higher education would help to convert Europe into a freely permeable educational area. The *Bologna declaration on the European space for higher education: "searching for a common European answer to common European problems"*[6] is a positive beginning of a unifying process, but certainly not yet the envisioned final goal. It is advisable, for example, that all students attend part of their studies in a foreign country, to help break down the barriers between nations and to develop a European identity. And university teachers should satisfy part of their teaching obligations in another country, as well. In spite of European coordination, traditional cultures deserve to be preserved; they are valuable and form our safe living grounds.

Independent universities are a prerequisite for educating courageous, independent thinkers.

Necessary Prerequisites

The leading role in conceiving a long-term future, that the academic community shall assume, presupposes that the universities receive also the required autonomy. In many countries, the bureaucratic control of universities is still excessive and impedes the acceptance of full academic accountability. Independent universities are a prerequisite for educating courageous, independent thinkers. More important than excessive dependencies on the local magistrates are transnational academic connections to universities with similar goals, leading to cooperation and mutual stimulation.

I am convinced that even the most abstract theoretical work can be explained and justified in simple terms provided it makes sense.

But autonomy alone is insufficient. Without adequate monetary means, it is impossible to improve quality and impact of universities. For financing the societal tasks emphasized in this essay, support by private, idealistic foundations is highly desirable, but a significant part of the funding will have to come from governmental sources. In general, the funding of European science has to be put on a significantly stronger basis, if Europe is to continue to succeed as a global player. It goes without saying that additional funds should be distributed according to thoroughly evaluated quality measures. It is often suggested that also in Europe, similarly as in the USA, research (and teaching) is financed much more by private donations than today. This desire has its good justification, but for its implementation numerous obstacles have first to be removed. They concern a tax system that does not encourage donations, a regionally too fragmented educational system, and particularly the missing tradition of generous donations. In spite of increasing efforts in this direction, no miracles should be expected in the short run.

The European Framework Program will have to assume special responsibility in promoting the European idea by the support of interdisciplinary initiatives for planning our future. A separate, well-funded program is needed for this purpose with an open-minded scope that allows interaction also with the human and social sciences. Many voices have been raised deploring the excessive inefficiency of the European Framework Program. It is hoped that the planned European Research Council, *"focusing on excellence as the basis for its funding decisions"*,[7] will introduce more flexibility and more scientific professionalism into the organization. Bringing more competition into the funding of European science may be to the disadvantage of less-than-top scientists. But is less-than-top science really worth support?

Generous autonomy and adequate financing are still not sufficient for

 © 2003 Wiley-VCH Verlag GmbH & Co. KGaA, Weinheim

reaching the proposed goals. Most important is the proper mind set of researchers and teachers who adjust their priorities to the long-term requirements of a global society. Some of the presently treated scientific questions may superficially appear to have limited relevance in view of the existential questions. It remains one of our obligations to put the daily work into a relevant larger context. Scientific research necessarily deals with meticulous details, but it must remain explainable in terms of its general significance, also to non-specialists. I am convinced that even the most abstract theoretical work can be explained and justified in simple terms, provided it makes sense.

Scientists who acknowledge their societal function will more easily gain respect and admiration by students and by society, and the financing of their endeavors will be facilitated. My experience is that young, highly motivated students have a particularly clear sensory for relevance. They still retain their inborn idealism that the elder researchers often have lost in their daily routine.

Specific Questions Concerning our Future

The questions of long-term relevance and development to be addressed in university discussion groups are obviously not restricted to academic concerns. On the contrary, political, social, and economic questions are most relevant for our future. Clearly, they cannot even comprehensively be listed within this brief essay. Just two questions shall be mentioned as examples.

In the political realm, perhaps the most relevant questions concern international collaboration and establishing strong supernational organizations. These institutions form our best hope for a peaceful and globally just future. The democratic postulate deserves to be implemented not only within but also between States. In this regard, the academic community could make a significant contribution. Within science, transnational collaboration is a daily reality. Why not try to transfer some of the beneficial scientific experiences into politics? The concept of the UN, where also smaller nations have a say, corresponds well to the fundamental principles of democracy.

Not only has the US government followed almost exclusively its own interests, also European States act primarily to their own advantage. But the case USA is truly remarkable. Its government systematically boycotts supernational organizations whenever they seem to serve not directly American interests; there are more examples than fingers on two hands, from banishing the Kyoto protocol to rejecting the International Criminal Court (ICC). The present tragic play for achieving immunity for US offenders abroad defies all our legal understanding. It is well known that also within the European Union, the diverging nationalistic tendencies are often stronger than foresighted cohesion. The conception of strong and lasting international organizations is a problem that requires the close attention by the scientific community. Let me cite once more from the exchange of letters between Albert Einstein and Sigmund Freud, this time with the words of Einstein: *" The quest for international security requires that each Nation unconditionally surrenders some fraction of its liberty of action, of its sovereignty, and it is obvious that there is no other way towards this security."* [2]

The quest for international security requires that each Nation unconditionally surrenders some fraction of its liberty of action.
Albert Einstein

Numerous open questions remain also in international economics that are strongly interlinked with politics. Even if we will be unable to conceive a better alternative to the present free market system, we are nevertheless encouraged to question some of its principles: How free shall be the "free" market economy? What is a proper balance between the entrepreneur's profit taking and societal concerns? How can an economic domain survive in a fully saturated market without creating unnecessary desires by dubious sales promotion? How can international trade laws be effectively implemented? How can poor nations be developed and traditional cultures efficiently preserved?

Science is an intellectual activity, relying on rationality, intuition, and idealistic concepts. Correspondingly, scientists might also expect from economics a more idealistic motivation than appears to be compatible with reality. Instead of letting a self-regulating feedback system, with profit and shareholder value as optimizing targets, operate freely by itself, it is tempting to define beforehand idealistic goals which should be shared by all partners. An economic operator would then act out of idealistic conviction rather than to optimize his own personal profits, in opposition to the principles put forward by Adam Smith in 1776,[4] proposing the action of an "*invisible hand*" that will turn even very selfish actions to the benefit of society. It is easy to show that the Smith's "invisible hand" often turns into a cloven foot, rather than fostering beneficial providence. Long-term damage is, for example, unavoidable when the feedback mechanism acts too slowly, particularly when detrimental effects in nature remain invisible for a long time or when, by market forces, invaluable human cultures and traditions are destroyed irreversibly. No corrective reaction can be expected in such cases. Frequently, the monetary gains will be spent long before the damage becomes manifest. Besides the strengthening of the idealistic motivation of future managers—one of the abovementioned tasks of today's universities—the introduction of corrective taxes could serve as an appropriate method to establish a more accountable lasting economy.

I am left with the feeling that our economic system is in the midst of an identity crisis. Overproduction, saturation of the market, and senseless consumption are a few keywords that come to mind about our—and by the way that also includes the Swiss—economic system; a small but insatiable minority remains unhappy despite of its material surplus, while the majority suffers. A self-regulating feedback mechanism, maximizing material wealth, can never lead to a deeper justification and to a gratifying meaning of our existence. To support personal attempts in finding a

 © 2003 Wiley-VCH Verlag GmbH & Co. KGaA, Weinheim

meaning in one's own life is an everlasting obligation of the academic community.

It is worth mentioning that the application of free market principles to the educational domain, as it is intended by the GATS agreement (General Agreement on Trade in Services; is an initiative from over 140 members of the World Trade Organization),[8] could have frightening consequences. A complete liberalization and partial privatization of the educational market could torpedo much of the previous achievements towards equal educational chances in Europe and even more so in poor nations. Here, greatest restraint is in place to maintain the previous accountability of our States for education, in general, and to preserve their willingness of making major investments into the future of our children without restricting in an undue manner contents and form of teaching.

Numerous further domains of societal relevance are even nearer to our scientific interests. They also deserve intensified attention from our side: the vast environmental domain, sustainability, recycling of waste, economics of energy usage based on sustainable sources, sociological studies on competition and collaboration, on consumption and superfluous luxury, on progress and cultural tradition, and on fairness and social peace.

Concluding Words

Two main aspects have been addressed in this essay: The long-term responsibility of universities, which goes far beyond our common understanding of academic obligations, restricted to teaching and research, and our specifically European contribution to a future global equilibrium. It was not my intention to give answers to specific questions but rather to appeal to the academic community to discuss, more than in the past and on all conceivable occasions, questions that relate to society and its future, in the hope of stimulating a lively discussion culture at universities. It may well be that I have misjudged numerous facts, causes, and effects that determine the societal and scientific developments—but my main goal was to raise the awareness for societal questions in the academic community.

The appeal to accept more societal responsibility is compatible with our future-oriented scientific endeavors. When we set out, by our research activities in the laboratory, to incrementally influence the course of history, we are also requested to contemplate the desired long-term global development. Who else, if not the scientists, is responsible for setting guidelines for defining progress and for protecting the interests of future generations? Even we rational researchers are human beings with ethical principles and with compassion towards the less favored members of society. Only when we act as full personalities, taking serious also our emotions and our anxieties, our hope, and our despair, will we be able to make valuable cultural contributions with a lasting effect.

Optimism is our duty. We all are co-responsible for what is coming.
Karl Popper

The second appeal to strengthen European science and the European identity in general is a consequence of the fact that regional boundaries contradict our universal understanding of a limitless science. To achieve a global equilibrium, a specific strengthening of the scientific aspirations in Europe is necessary. The goal is not to disfavor others but to increase the impact of our own European contributions, allowing for true partnership of equivalent players. A unipolar world will surely lead to a disaster in politics, economics, and science. Only a multipolar dynamic interplay between equal partners can lead to long-term stability. To strengthen the European position, we need more European collaboration in science and an improved funding situation. Only then, will we be able to play a significant role in the international science community.

The appeal to researchers and teachers to widen their scope beyond their fascinating specialties is close to my heart. I am convinced that we academics have to search actively for valid answers to the great existential questions of our time. Nobody else, for practical reasons, is in a better position to provide long-term guidance into a prosperous future for the entire globe. In conclusion, we perhaps should take to heart the two brief sentences that Karl Popper expressed on December 17, 1993, in Berlin: "*Optimism is our duty. We all are co-responsible for what is coming.*"[1]

[1] K. R. Popper, *Alles Leben ist Problemlösen. Über Erkenntnis, Geschichte und Politik*, Piper, München, **1996**.
[2] A. Einstein, S. Freud, *Warum Krieg? Ein Briefwechsel*, Diogenes, Zürich, **1966**.
[3] H. Jonas, *Das Prinzip Verantwortung. Versuch einer Ethik für die Technologische Zivilisation*, Suhrkamp, Frankfurt am Main, **1979**.
[4] A. Smith, *An Inquiry into the Nature and Causes of the Wealth of Nations*, Random House, New York, **1937**.
[5] http://www.acadeuro.org.
[6] http://europa.eu.int/comm/education/programmes/socrates/erasmus/guide/bologna.pdf.
[7] *New Structures for the Support of High-quality Research in Europe*, European Science Foundation, **2003**.
[8] http://www.wto.org/english/tratop_e/serv_e/gats_factfiction_e.htm.

 © 2003 Wiley-VCH Verlag GmbH & Co. KGaA, Weinheim

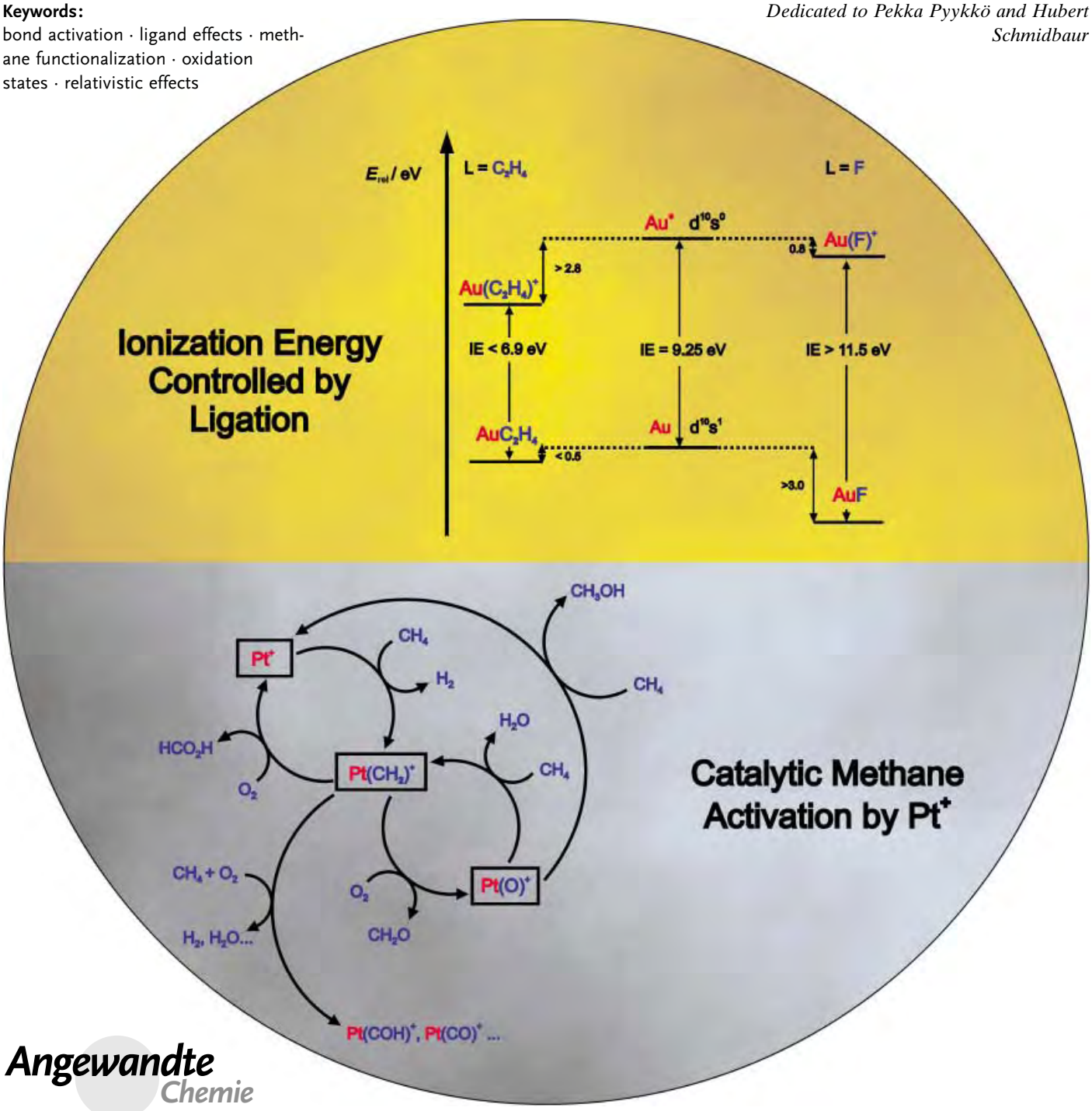
Ions in the Gas Phase

Relativistic Effects in Gas-Phase Ion Chemistry: An Experimentalist's View

*Helmut Schwarz**

Keywords:
bond activation · ligand effects · methane functionalization · oxidation states · relativistic effects

Dedicated to Pekka Pyykkö and Hubert Schmidbaur



© 2003 Wiley-VCH Verlag GmbH & Co. KGaA, Weinheim
DOI: 10.1002/anie.200300572

Gas-phase experiments provide information which, in conjunction with results from electronic structure calculations, help to unravel the critical role relativistic effects play in many areas of transition-metal chemistry. Examples include the thermochemical data of gold halides in different oxidation states, the fascinating structural properties of gold(I) complexes, the dramatic effects of ligands on the ionization energy of gold, or the binding in cationic metal–carbene complexes. Furthermore, in the context of methane functionalization, special emphasis is paid to the chemistry of cationic metal–carbene complexes, and at uncovering the mechanistic details of important carbon–heteroatom coupling reactions. It is the interplay of conducting experiments of "isolated" molecules under well-defined conditions with reliable electronic structure calculations that has considerably improved our understanding of the role relativistic effects play in the context of transition-metal chemistry, catalysis, and beyond.

From the Contents

1. Introduction 4443

2. Unusual Thermochemistry and Atypical Geometric Features 4443

3. Reactivity Patterns Controlled by Relativistic Effects 4448

4. Miscellaneous Systems 4452

5. Conclusions 4452

> "*[Relativistic effects] are therefore of no importance in the consideration of atomic and molecular structure and ordinary chemical reactions.*"
> Paul A. M. Dirac[1]

1. Introduction

The theories of relativity and quantum mechanics constitute two of the pillars of the scientific development of the last century. The concept of non-relativistic quantum mechanics was, by and large, formulated around 1926, and a major contribution followed less than two years later with Dirac's incorporation of special relativity.[1,2] While, in a sense, it is ironic that Dirac himself was convinced about the limited role of relativistic effects in everyday chemistry,[1] it took nearly half a century to revise his dictum and to fully appreciate the consequences of relativity in chemistry.[3]

Nowadays, it is generally agreed that many atomic and molecular properties are caused by relativistic effects. Prominent examples include the increase of ionization energies (IEs), electron affinities (EAs), heats of atomization, and melting points of gold in comparison with its light congener silver; further, the yellow color of gold[4] or the smaller size of Au^I versus Ag^I compounds[5] result from a relativistic contraction of the 6s orbital and a destabilization of the 5d orbital of gold. In addition, the unusual attraction between Au^I cations that led Schmidbaur to coin the term "aurophilicity",[6] was also suggested to be due to a relativistic effect,[7] although there exists different interpretations according to which dispersion effects are most important.[8] However, there is consensus for a local maximum of relativistic effects with gold, which is viewed as *the* "relativistic element".[3c] Naturally, quite a few atomic, spectroscopic, and molecular properties of other heavy elements are also affected by relativistic effects, and an excellent, timely book on the subject was published recently.[9a]

This Review will focus on discussing selected thermochemical, structural, and reactivity aspects of "bare" atoms and molecules—in various charge states—which are generated and probed in the highly diluted gas phase. Because of the very nature of the experiments, obscuring effects, such as aggregation, solvation, or the role of counterions can be excluded, thus permitting the study of the intrinsic features of the objects of interest. Most of the experiments employ advanced, if not state-of-the-art, mass-spectrometric methods that allow the generation of mass-selected, electronic ground-state species and to explore their chemistry under well-defined (mostly) single-collision conditions. Rather than giving a description of the various experimental techniques, the interested reader is referred to the original references.

2. Unusual Thermochemistry and Atypical Geometric Features

2.1. Elusive Gold Halides

The starting point for my research group in the topic of relativistic effects was the experimental detection of solitary AuF in the gas phase, historically one of the most elusive of all the metal halides.[10] While the statement that "there is still no evidence for the existence of a definitively characterized gold(I) fluoride"[11] is still true in that the compound does not exist in bulk and, based on advanced electronic structure calculations, was predicted to undergo exothermic disproportionation to $Au_{(s)}$ and $AuF_{3(s)}$,[12a] the situation for an "isolated" AuF molecule may well differ. In fact, the dissociative ionization of AuF_3 in the gas phase [Eq. (1)],

$$AuF_3 \xrightarrow{70\,eV} AuF^+ \xrightarrow{N} AuF \xrightarrow{R} AuF^+ \qquad (1)$$

[*] Prof. Dr. H. Schwarz
Institut für Chemie, Sekr. C.4
Technische Universität Berlin
Straße des 17. Juni 135, 10623 Berlin (Germany)
Fax: (+49) 30-314-21102
E-mail: helmut.schwarz@www.chem.tu-berlin.de

 DOI: 10.1002/anie.200300572 © 2003 Wiley-VCH Verlag GmbH & Co. KGaA, Weinheim

followed by electron-transfer experiments with mass-selected AuF^+ using the powerful technique of neutralization–reionization (NR) mass spectrometry,[13] provided unambiguous evidence for the existence of this long-sought molecule in line with predictions based on earlier electronic structure calculations.[12b,c] This spectacular finding was later confirmed by recording both the emission[14] and the microwave[15] spectra of AuF. The latter method provided molecular constants including an equilibrium bond length of $r = 1.9184$ Å for solitary AuF, which is in reasonable agreement with the data of several ab initio predictions.[12a,16] Based on ion–molecule reactions, the bond dissociation energy (BDE) of neutral AuF was determined to 73 ± 5 kcal mol^{-1};[10] this value is in reasonable agreement with data obtained from various high-level electronic structure calculations (ranging from 67 to 77 kcal mol^{-1} for D_0).[12a,16b,17] A comparison of non-relativistic versus relativistic calculations reveals that the contribution of relativistic stabilization to the bond energy of AuF is the largest so far known for any existing diatomic molecule.

For the heavier diatomic gold halides AuX (X = Cl, Br, I) and their cationic analogues AuX^+, thermochemical data were recently derived in a combined experimental/computational approach based on Fourier-transform ion cyclotron resonance mass spectrometry and ab initio calculations at a quasi-relativistic CCSD(T) level of theory.[18] After conversion to 0 K, the following data (in kcal mol^{-1}) were obtained: $D_0(\text{Au-Cl}) = 66 \pm 3$, $D_0(\text{Au-Br}) = 50 \pm 5$, as well as the limiting values $52 < D_0(\text{Au-I}) < 64$, and $54 < D_0(\text{Au}^+\text{-I}) < 66$. Of particular interest is a comparison of the bond dissociation energies for the light and heavy gold halides, that is, Au-F/Au^+-F versus Au-I/Au^+-I, for this will shed some light on the bonding situation prevailing in gold(I) and gold(II) compounds. For example, $D(\text{Au}^+\text{-F}) = 18$ kcal mol^{-1}[10,12a,19] probably represents one of the weakest metal–fluorine bonds known; its magnitude is comparable to those of the ionized alkali halides. Clearly, any covalent binding of an Au^+ ion to an open-shell ligand X$^\bullet$ would involve excitation of the $6s^0 5d^{10}$ ground state to a $6s^1 5d^9$ state, formally resulting in an unfavorable Au^{II} compound. Rather, the Au^+–X bond is better described in terms of an ion–dipole complex of the gold(I) cation with an X$^\bullet$ radical. Hence, the counterintuitive fact that the value of $D(\text{Au}^+\text{-X})$ increases significantly from X = F to X = I is self-explanatory for both the polarizability and charge-transfer stabilization increase with the size of X. Precisely the opposite applies for the binding of neutral gold to X$^\bullet$ radicals, in that the neutral species involve coupling of the $6s^1 5d^{10}$ configuration of Au with the unpaired electron of X$^\bullet$, which leads to a chemical bond with an appreciable binding energy. Upon ionization of AuX, however, one of the binding electrons is essentially removed. As an interesting consequence, open-shell X$^\bullet$ ligands lead to a drastic increase of IE(AuX), as compared to IE(Au) = 9.25 eV; for example, IE(AuF) $\approx$ 11.5 eV.[12a,20]

Despite several claims,[21] genuine gold(II) dichloride $AuCl_2$ is not known in the condensed phase. However, recent mass spectrometry experiments, employing no less than three different techniques, provide unambiguous evidence not only for the existence of neutral AuX_2 (X = Cl, Br),[22] but also the exciting finding that in these gold dihalides, at least as isolated molecules, gold can exist in three different oxidation states, namely: AuX_2^- (formally Au^I), AuX_2 (formally Au^{II}), and AuX_2^+ (formally Au^{III}). The dihalide X-Au-X connectivity is strongly preferred for anionic and neutral gold, whereas experimental and extensive computational studies suggest X–X bond formation to occur in the oxidation of neutral AuX_2 to $Au(X_2)^+$. Figure 1 shows the redox profile of $AuCl_2^-$, $AuCl_2$, and $AuCl_2^+$ according to scalar relativistic coupled cluster approach (CCSD(T)) calculations; the agreement between experiment and theory is good, if not excellent.[22]

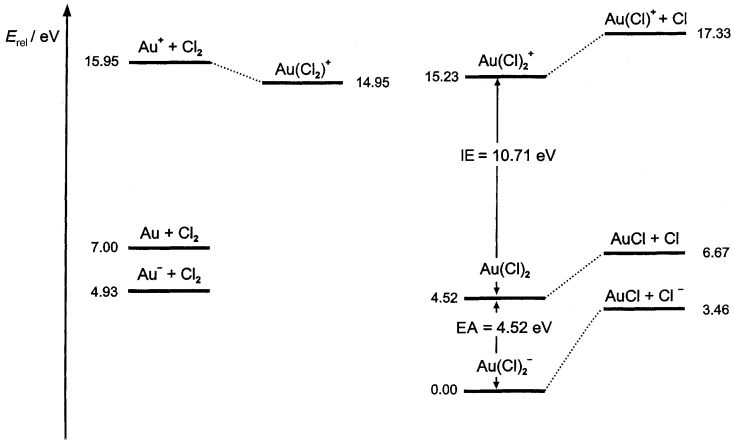


Figure 1. Redox profile of $AuCl_2^-$, $AuCl_2$, and $AuCl_2^+$ (adapted from ref. [22]).

With respect to the stability of $AuCl_2$ in the condensed phase, Born–Haber cycle considerations suggest that disproportionation of neutral gold(II) dichloride according to Equation (2) is endothermic by 38 kcal mol^{-1}.

$$2\,AuCl_2 \rightarrow AuCl + AuCl_3 \qquad (2)$$

Thus, whereas gaseous $AuCl_2$ is stable against disproportionation, the molecule is likely to exist as $Au^+[AuCl_4]^-$ in the condensed phase, due to the preferred Au^I and Au^{III} oxidation



Helmut Schwarz read chemistry at the Technische Universität Berlin TUB, where he obtained his PhD under the supervision of F. Bohlmann in 1972 and completed his Habilitation in 1974. Postdoctoral and related work followed at MIT Cambridge, ETH Zürich, and Cambridge University. Then in 1978 he accepted a professorial position at TU Berlin, where he remains today. His scientific achievements have been rewarded with, amongst others, the Otto Bayer Prize (1989), the Liebniz Research Award, the Lise Meitner Award (1997), the Liebig Medal (1998), the Field and Franklin Award (2001), and the Otto Hahn Prize for Chemistry and Physics (2003). He is currently serving as vice president of the German Research Foundation.

 © 2003 Wiley-VCH Verlag GmbH & Co. KGaA, Weinheim

states. The preparation of bulk gold(II) dichloride therefore requires the prevention of disproportionation by an appropriate ligand environment. An excellent example for such a stabilization of a gold(II) compound by ligation is the $[AuXe_4^{2+}]([Sb_2F_{11}]^-)_2$ salt, recently characterized by Seppelt and co-workers.[23]

2.2. Cationic Au^I Complexes: What Makes Them So Unique?

Complexation of the gold(I) cation by various inorganic and organic ligands containing heteroatoms has been examined comprehensively by experimental and theoretical means. For the celebrated $Au(Xe)^+$ complex, CCSD(T) calculations using large basis sets have estimated a binding energy of $D_0(Au^+\text{-}Xe) = 30.1\ kcal\,mol^{-1}$,[20] and this benchmark value has been used as an absolute reference to relate calculated and experimentally bracketed binding energies of $Au(L)^+$ complexes with a relative gold(I) cation affinity scale for heteroatomic ligands L, for instance: $Xe < C_6F_6 < H_2O < CO < H_2S < CH_3CN \approx C_2H_4 \approx NH_3 \approx CH_3NC < CH_3SCH_3 < PH_3$. The binding energies of these closed-shell ligands cover an exceptionally large range (30–96 $kcal\,mol^{-1}$), thus making Au^I ions unique in comparison to other singly-charged transition-metal cations. In addition, some of the structural details of these complexes are quite remarkable.

A versatile route for the gas-phase synthesis of $Au(L)^+$ has been provided by the reaction of mass-selected Au^+ ions with hexafluorobenzene, C_6F_6. At 9.91 eV, the $IE(C_6F_6)$ value is large enough to prevent electron transfer, and the ligand has a sufficient number of rovibronic states to allow for efficient formation of the $Au(C_6F_6)^+$ complex via radiative stabilization in the low-pressure regime according to Equation (3).[24]

$$Au^+ + C_6F_6 \rightarrow Au(C_6F_6)^+ + h\nu \quad (3)$$

In an excess of C_6F_6, the monoadduct continues to react, which yields the dicoordinated ion [Eq. (4)].

$$Au(C_6F_6)^+ + C_6F_6 \rightarrow Au(C_6F_6)_2^+ \quad (4)$$

Yields of $Au(C_6F_6)^+$ of up to 70% (based on Au^+) can be achieved in a rapid and reproducible manner, and in consecutive reactions C_6F_6 can be exchanged by other equally well or more strongly bound ligands L or L′ according to Equations (5) and (6), thus providing a convenient means to

$$Au(C_6F_6)^+ + L \rightarrow Au(L)^+ + C_6F_6 \quad (5)$$

$$Au(L)^+ + L' \rightarrow Au(L')^+ + L \quad (6)$$

generate nearly all kinds of bare Au^I complexes.

While ligand exchange of $Au(C_6F_6)^+$ was not observed for H_2, N_2, CO_2, and O_2, nor for the rare gases Kr and Ar, thus pointing to a much smaller binding energy of these ligands relative to $D(Au^+\text{-}C_6F_6)^+$, efficient ligand exchange with water or with Xe takes place at room temperature (Figure 2).

A detailed analysis of the experimental findings,[20] in conjunction with reliable computational studies, revealed some remarkable trends of the binding energies $D(Au^+\text{-}L)$ relative to $D_0(Au^+\text{-}Xe) = 30.1\ kcal\,mol^{-1}$. Selected examples include: $D(Au^+\text{-}C_6F_6) \approx 34$,[20] $D(Au^+\text{-}OH_2) \approx 38$,[20,24–26] $D_0(Au^+\text{-}CO) = 48$,[20,27] $D(Au^+\text{-}SH_2) \approx 55$,[20] $D(Au^+\text{-}C_2H_4) \geq 65$,[20,26,28] $D(Au^+\text{-}NH_3) \geq 68$,[20] and $D(Au^+\text{-}PH_3) \geq 80$–$95\ kcal\,mol^{-1}$.[20,29] Clearly, some of the binding energies are outstandingly large. For example, the $Au^+\text{-}C_2H_4$ interaction is almost twice that of the lower congeners copper and silver.[28,30] The bond strength in $Au^+\text{-}C_2H_4$ is even sufficient for ethene to replace the formally covalent iodine ligand associated with the Au^I cation in Equation (7).[24]

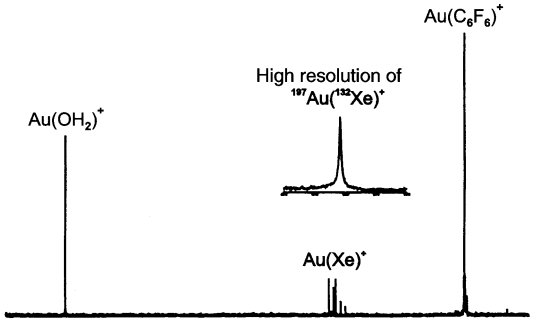


Figure 2. Generation of $Au(Xe)^+$ and $Au(H_2O)^+$ upon reacting mass-selected $Au(C_6F_6)^+$ with xenon and background water (adapted from ref. [9b]).

$$Au(I)^+ + C_2H_4 \rightarrow Au(C_2H_4)^+ + I \quad (7)$$

An analysis of the origin of these anomalously large effects will be attempted below after briefly describing some unusual structural features of a few selected $Au(L)^+$ complexes.

For the $Au(C_2H_4)^+$ system, an atoms-in-molecules (AIM) analysis[31] reveals a bonding scheme that is best described as being of a tightly bound cationic metallacyclopropane, rather than a simple archetypical Dewar–Chatt–Duncanson metal–olefin complex.[30] In contrast, for Cu^+ and Ag^+, this analysis reveals primarily T-shaped electrostatic bonding for $Cu(C_2H_4)^+$ and $Ag(C_2H_4)^+$. These structural differences are also reflected in the extent of pyramidalization of the methylene groups of C_2H_4 upon complexation to M^+ (M = Cu, Ag, Au).[30] CCSD(T)-optimized structures revealed the following H_2CC dihedral angles: 180° in free ethene, 167.9° in $Cu(C_2H_4)^+$, 169.8° in $Ag(C_2H_4)^+$, and 163.2° in $Au(C_2H_4)^+$.

As equilibrium isotope effects (EIEs) have often provided detailed insight into bonding mechanisms of transition-metal complexes,[32] and as the study of "naked" $M(olefin)^+$ complexes in the gas phase is not obscured by any disturbing effects that exist in the condensed phase, a detailed mass spectrometric investigation, complemented by a thorough theoretical analysis, has been conducted for the exchange reaction described in Equation (8) (M = Cu, Ag, Au):

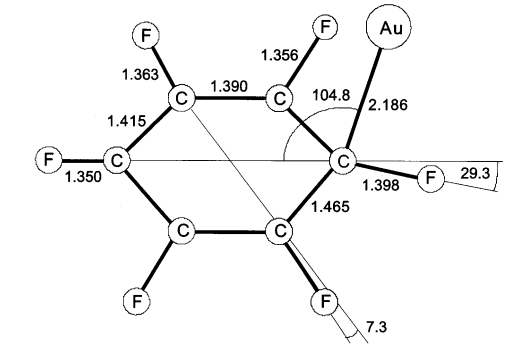
$$M(C_2D_4)^+ + C_2H_4 \rightleftharpoons M(C_2H_4)^+ + C_2D_4 \quad (8)$$

The measured inverse secondary EIEs of 0.86 ± 0.02 for $Cu(C_2H_4)^+/Cu(C_2D_4)^+$, 0.83 ± 0.02 for $Ag(C_2H_4)^+/Ag(C_2D_4)^+$, and 0.74 ± 0.02 for $Au(C_2H_4)^+/Au(C_2D_4)^+$, in

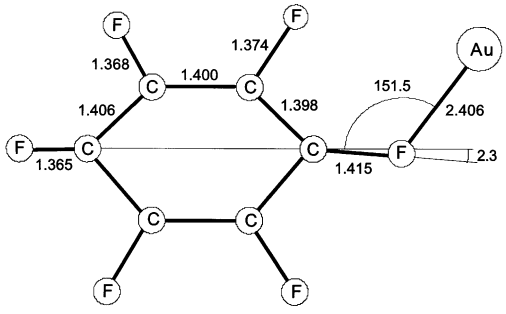
 © 2003 Wiley-VCH Verlag GmbH & Co. KGaA, Weinheim

favor of the respective deuterated metal complexes, are fully consistent with computed values of 0.86, 0.83, and 0.74, respectively. However, the major conclusion from this benchmark study is that EIEs do not provide generally valid probes for binding mechanisms of olefins, structural reorganizations, the distinction between sp^2 and sp^3 carbon atoms, and the associated degree of pyramidalization. Thus, while the bonding schemes and the extent of pyramidalization in $M(C_2H_4)^+$ behaves *discontinuously* from copper to gold, the EIEs are found to decrease *monotonically* from Cu^+ to Au^+.

The tendency of Au^+ ions to prefer covalent rather than predominantly electrostatic bonding[28] is also observed in the $Au(C_6H_6)^+$ and $Au(C_6F_6)^+$ complexes. Theoretical studies of the $Au(C_6H_6)^+$ complex reveal that, unlike most other monocationic metal–benzene complexes, cationic Au^+ takes advantage of C_{6v} symmetry, in that η^1- and η^2-type coordination modes are strongly preferred.[34] The behavior of Au^+ ions resemble that of a "big" proton[35] interacting with benzene,[36a,b] and the facile interconversion of the η^1 and η^2 structures of $Au(C_6H_6)^+$ finds its equivalent in the hydrogen ring-walk of protonated arenes.[36c,d] For the $Au(C_6F_6)^+$ complex, calculations also predict two structural isomers.[20] The most stable form (isomer **I**; Figure 3) exhibits C_s symmetry with the gold(I) cation η^3-coordinated to hexafluorobenzene above the ring plane. In analogy to protonated fluoroarenes,[37] however, the η^1 end-on coordination of Au^+ to a fluorine atom is only 4.6 kcal mol^{-1} less stable (isomer **II**; Figure 3); a hypothetical C_{6v} symmetrical structure is 18.1 kcal mol^{-1} more energetic and bears two imaginary frequencies.



I



II

Figure 3. Calculated structures of η^3- and η^1-coordinated $Au(C_6F_6)^+$ isomers **I** and **II**; selected bond lengths [Å] and angles [°] (adapted from ref. [20]).

The coordination geometries of the $Au(H_2O)^+$ and $Au(H_2S)^+$ complexes are also noteworthy. While all other monocationic complexes $M(H_2O)^+$ and $M(H_2S)^+$ (M = main-group or transition metal) prefer planar geometries, both $Au(H_2O)^+$ and $Au(H_2S)^+$ are nonplanar molecules.[20,25] This deviation from planarity for $Au(H_2O)^+$ (Figure 4) is basically due to the fact that Au^+, also in these two complexes, behaves like a "big" proton[35,38,39] in H_3O^+ and H_3S^+. Thus, Au^+ prefers covalent rather than predominantly electrostatic bonding.[28] The latter interaction would result in a planar C_{2v} symmetry, because of the perfect alignment of the H_2O and H_2S dipoles with the Au^+ center.

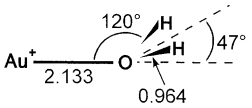


Figure 4. Calculated structure of $Au(H_2O)^+$; selected bond lengths [Å] and angles [°] (adapted from refs. [9, 20]).

The origin of the exceptional behavior of gold is due to relativity; the following is a simple chemical mnemonic for the "coinage metals". Cu, Ag, and Au have $d^{10}s^1$ ground states for the neutral atoms and $d^{10}s^0$ ground states in their monovalent cationic states. Relativistic effects significantly stabilize the 6s orbital of the gold atom by about 2 eV, while these effects are almost negligible for copper and silver, being roughly proportional to the square of nuclear charge.[3,42] As a consequence, the 6s orbital of Au becomes much more electrophilic, as compared to the 4s and 5s orbitals of Cu and Ag, respectively. Purely electrostatic interactions would suggest that the binding energies to a ligand decreases from copper to gold. However, because of the electrophilicity of the 6s orbital of Au^+, dative interactions involving partial electron transfer from the ligand to gold become significant, and result in an increase of covalent binding in gold(I) complexes, dependent on how low the IE of the ligand is.[24,43] With regard to the examples mentioned above, the binding situations can be explained as follows: 1) Similar to the oxonium and sulfonium ions H_3O^+ and H_3S^+, the $Au(H_2O)^+$ and $Au(H_2S)^+$ ions trade-off planarity because the ligands can act as σ donors.[25] As already stated (and outlined in detail in ref. [35]), the binding features of gold(I) species show some distinct similarities to those of a proton. 2) The exceptionally large gold(I)–ethene binding energy ($D(Au^+\text{-}C_2H_4)$ > 65 kcal mol^{-1}) can be traced back to the fact that ethene is a good π donor, and the difference of $IE(C_2H_4) = 10.5$ eV and $IE(Au) = 9.35$ eV is not so large to disallow partial electron transfer. Similarly, $D(Au^+\text{-}PH_3)$ is even larger than $D(Au^+\text{-}C_2H_4)$ because phosphane has better donor properties, as well as a lower ionization energy (9.87 eV) than C_2H_4. 3) The dramatic effects of ligation on the ionization energy of Au(L) (Figure 5) can also be rationalized by considering the electronic situation. Due to the singly occupied 6s orbital in the neutral gold atom, the Au–L interactions are weak in the neutral complexes with *closed*-shell ligands L (e.g.,

 © 2003 Wiley-VCH Verlag GmbH & Co. KGaA, Weinheim

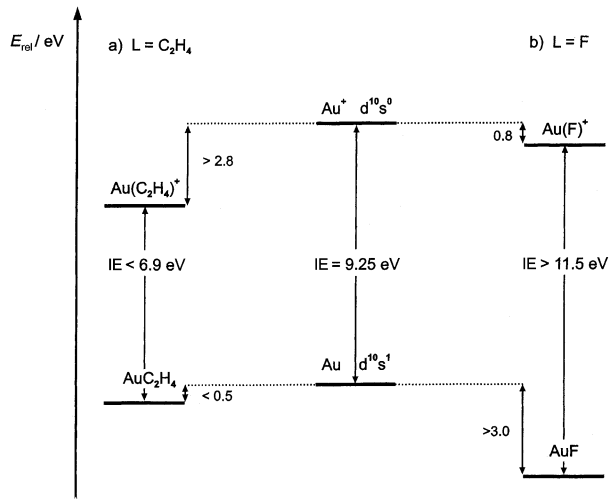


Figure 5. Schematic presentation of the effect of complexation on the ionization energy of gold: a) closed-shell ligand, L = C_2H_4; b) open-shell ligand, X = F.

< 12 kcal mol^{-1} for L = C_2H_4).[44] In contrast, strong electrostatic and covalent interactions, along with charge transfer, arise for Au^+, and a combination of the respective binding energies of D(Au-L) and D(Au^+-L) implies that for the case where L = C_2H_4, a *lowering* of the IE of gold occurs upon ligation with ethene by almost 2.3 eV. Results reported by Häberlen and Rösch[29] suggest that the value for IE(Au(PH_3)) is 2.9 eV lower than IE(Au). As stated above in the discussion of the bond energies of the gold(I) halides, precisely the opposite applies for the binding of gold to X$^\bullet$ radicals, in that the coupling of the $5d^{10}6s^1$ electronic configuration of the gold neutral species with the unpaired electron of X$^\bullet$ leads to a strong AuX bond (> 70 kcal mol^{-1} for X = F). Upon formation of the cation, however, one of the binding electrons is essentially removed, thus weakening the bond appreciably. As a consequence, open-shell ligands X$^\bullet$ lead to a drastic *increase* in the value of IE(AuX).[12a,20]

2.3. Metal–Carbene Complexes

Methane activation by bare transition-metal ions M^+ has been at the focus of a number of fundamental gas-phase ion studies.[45] While several electronically excited ions were reported to dehydrogenate methane at ambient temperature [Eq. (9)] and to form metal–carbene complexes $M(CH_2)^+$,[46]

$$CH_4 + M^+ \rightarrow M(CH_2)^+ + H_2 \quad (9)$$

thermalized ground-state monoatomic 3d- and 4d-transition-metal cations do not react with methane.[45b,47]

To make the dehydrogenation of methane thermochemically feasible, the metal–methylidene bond strength D_0(M^+-CH_2) has to exceed 111 kcal mol^{-1}. Irikura and Beauchamp were the first to discover that bare third-row transition-metal cations M^+ (M = Ta, W, Os, Ir, Pt) spontaneously dehydrogenate methane in a stoichiometric manner to yield $M(CH_2)^+$.[48,49] This dramatic difference in reactivity can be attributed to the significantly stronger M^+–CH_2 bonds of the 5d metals.[50] For example, the dissociation energies D(Ni^+-CH_2) = 76 kcal mol^{-1} and D(Pd^+-CH_2) = 68 kcal mol^{-1} are much lower than for the 5d congener, D(Pt^+-CH_2) = 112 kcal mol^{-1}.[51] This remarkable increase in bond strength can be attributed to relativistic stabilization of the cationic complexes $M(CH_2)^+$[50] as demonstrated for M = Pt by fully relativistic four-component Dirac–Fock–Coulomb benchmark calculations including correlation effects.[52] This stabilization of the 6s orbitals of the 5d metal cations is complemented by a significantly better overlap between the π orbitals of the carbene fragments with the $5d_\pi$ orbitals of Pt, when compared to the $3d_\pi$ and $4d_\pi$ counterparts of Ni and Pd. The reactions of Ir^+,[47d,53] Pt^+,[54] and other transition-metal cations with methane have also formed the subject of detailed theoretical investigations using different levels of theory.[55]

2.4. Miscellaneous Examples for Relativistically Stabilized Systems

One of the reasons for the rather low IEs of actinide atoms is the relativistic destabilization of their 6d orbitals. In some cases, the values are close to the IEs of alkali metals (e.g., IE(Ac) = 5.17 and IE(Na) = 5.12 eV, respectively). This decrease of ionization energies in the actinides permits the generation of several multiply-charged cations in oxidation and charge states which are difficult, if not impossible, to reach with other elements. For example, the diatomic cations UF^{n+} (n = 1–3) can be generated by dissociative electron ionization of UF_6. Moreover, not only the mono- and dications, but even diatomic UF^{3+} is thermochemically stable, in that the Coulomb explosion according to Equation (10) is endothermic by 1.9 eV (Figure 6).[56,57] In comparison, while the diatomic trication TiF^{3+} exists in a local minimum, it is unstable with respect to charge separation by more than 5 eV [Eq. (11)].[58]

$$UF^{3+} \rightarrow U^{2+} + F^+ \quad (10)$$

$$TiF^{3+} \rightarrow Ti^{2+} + F^+ \quad (11)$$

Finally, a particularly intriguing case deserves brief mention, namely, the case of the Mo–O bond strengths in MoO^+ and MoO_2^+. The non-relativistically computed value D(Mo^+-O) = 88 kcal mol^{-1} increases to 107 kcal mol^{-1} when relativity is included, whereas for the corresponding dioxide the non-relativistic and relativistic values of D(OMo^+-O) = 122 kcal mol^{-1} are practically identical within the accuracy of the calculations. Hence, relativity is of prime importance for MoO^+, but negligible for MoO_2^+. The origin of this unusually large difference is associated with the significant occupation of the 5s orbital in the bonding of MoO^+, while this is small in Mo^+(^{6}S) and MoO_2^+($^2A_1$). The lowering of the 5s orbital due to relativity therefore results in a differential stabilization which is most pronounced for MoO^+. This significant relativistic effect is notable as molybdenum is a 4d element for which relativistic effects are often assumed negligible.[60]

© 2003 Wiley-VCH Verlag GmbH & Co. KGaA, Weinheim

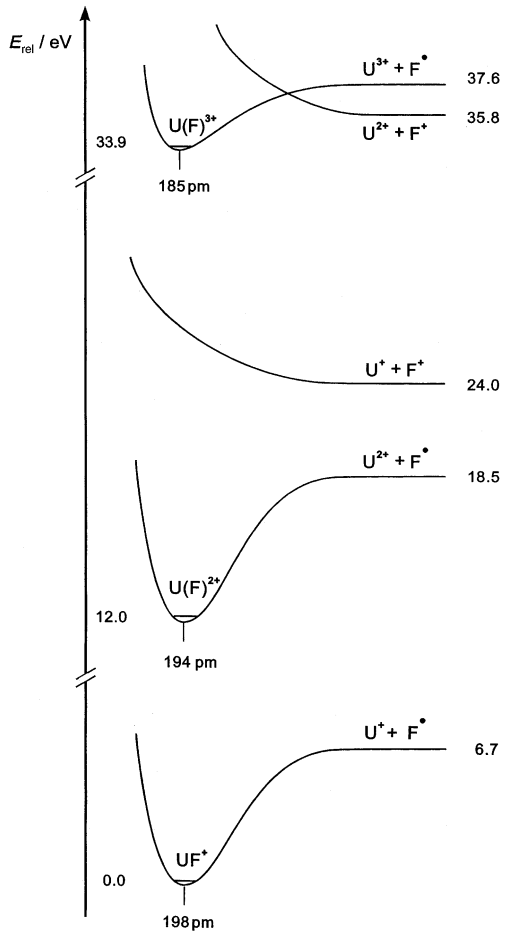


Figure 6. Stability diagram of the diatomic UF^{n+} ions ($n = 1$–3) and the associated dissociation asymptotes. Note that the energy axis is not proportional (adapted from ref. [56]).

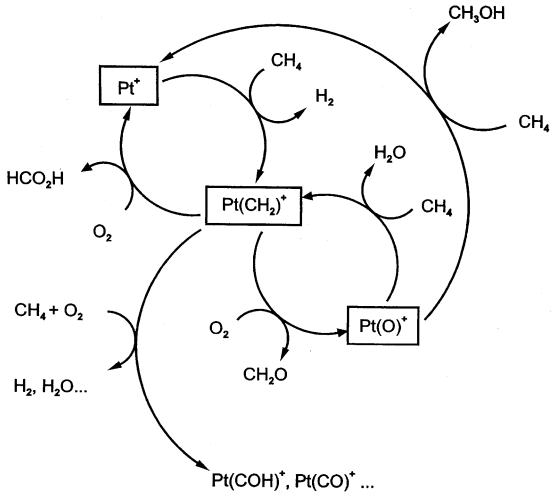
3. Reactivity Patterns Controlled by Relativistic Effects

3.1. Gas-phase Reactions of $M(CH_2)^+$

In this section, an overview will be given on the gas-phase reactions of several $M(CH_2)^+$ complexes with molecular oxygen, various nucleophiles (e.g., NH_3, PH_3, H_2O, H_2S), and carbon dioxide, which is aimed at uncovering the intrinsic mechanistic details of these important coupling reactions by which, amongst other things, methane is converted to CH_3OH, CH_2O, CH_3CO_2H, HCN, and other carbon–heteroatom coupling products. Experimental and computational details are not discussed; these can be found in the references, as well as in several review articles on gas-phase metal-ion chemistry.[45,47b,61] Further, relativity is not explicitly addressed because reactivity is determined by thermochemical and kinetic aspects, and non-relativistic considerations of reactivity patterns exhibited by "heavy" elements are almost meaningless (see above). Finally, while for lighter metals (and their derivatives) spin constraints can affect chemical reactivity and may even become a decisive factor,[62] in the reactions of heavy elements, spin selection rules have little impact on reactivity patterns, because of strong spin–orbit coupling effects.

3.1.1. Oxidation of $Pt(CH_2)^+$ with Molecular Oxygen

The discovery[63] that bare Pt^+ ions uniquely catalyze the partial oxidation of methane by molecular oxygen to methanol, formaldehyde, and higher oxidation products



Scheme 1. Catalytic oxidation of methane by Pt^+ ions and molecular oxygen (adapted from ref. [63]).

(Scheme 1) has generated considerable interest. A key intermediate in the catalytic cycle is the carbene $Pt(CH_2)^+$, which is formed according to Equation (9) with an efficiency $\phi = 0.8$.[64] This carbene subsequently reacts with O_2 to give Pt^+ ions (70%) via the liberation of neutral HCO_2H. In a parallel channel, PtO^+ and CH_2O are formed (30%), and PtO^+ then serves as an efficient oxidant[66] of CH_4 to produce the complexes $Pt(CH_2)^+/H_2O$ (75%) and Pt^+/CH_3OH (25%) in competition. Regeneration of Pt^+ closes the catalytic cycle. Insight into the mechanistic details of this complicated reaction sequence was provided by electronic structure calculations, which included scalar relativistic and spin–orbit effects.[54c] While some of the steps depicted in Scheme 1 correspond to well-known organometallic mechanisms (e.g., oxidative addition, reductive elimination, or hydrogen-atom transfer), some less common types of reactions are also involved. For example, one of the key steps in the cycle [Eq. (12)] must not be confused with a formal metathesis

$$Pt(CH_2)^+ + O_2 \rightarrow PtO^+ + CH_2O \qquad (12)$$

process; rather the computations reveal an extraordinarily rich and complex potential energy surface, and at least four discrete minima are involved.

 © 2003 Wiley-VCH Verlag GmbH & Co. KGaA, Weinheim

3.1.2. Platinum-Mediated Coupling of Methane and Small Nucleophiles[68d]

The focus of this section will be on the $Pt^+/CH_4/NH_3$ and $Pt^+/CH_4/H_2O$ systems, while reactions of $Pt(CH_2)^+$ with PH_3 and H_2S are mentioned only briefly. The common intermediate in all of the processes is the cationic platinum carbene $Pt(CH_2)^+$. $Pt(CH_2)^+$ reacts rapidly ($\phi = 0.3$) with NH_3 under the formation of $CH_2NH_2^+$, $Pt(C(H)NH_2)^+$, and NH_4^+ [Eq. (13)].[67]

Whereas the formation of NH_4^+ is a simple acid–base reaction, C-N coupling is achieved through the two other channels. The major pathway, to produce $CH_2NH_2^+$, is found to be exothermic by 23 kcal mol^{-1} (relative to the separate reactants $Pt(CH_2)^+/NH_3$), and all stationary points are located below the entrance channel.[67b] The second pathway involves

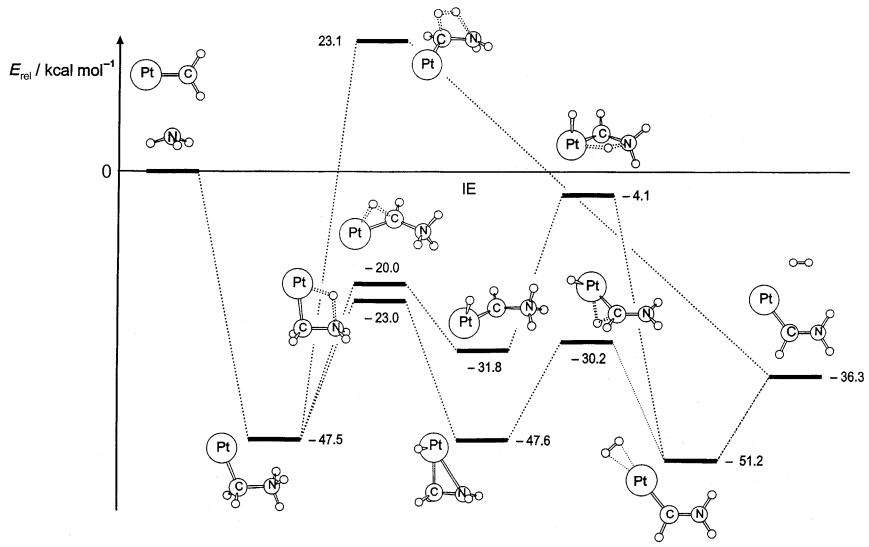


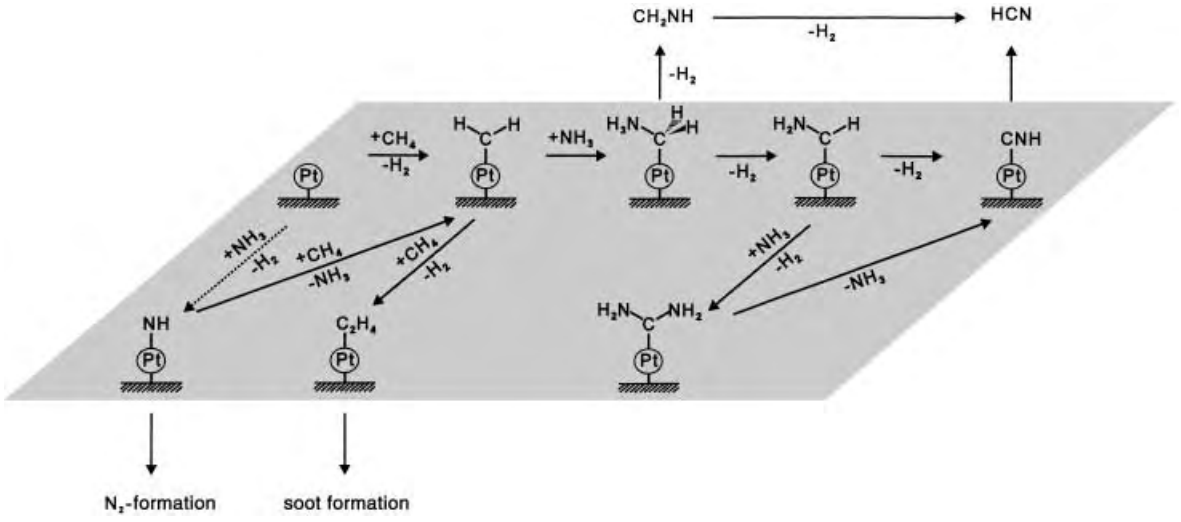
Figure 7. Potential energy surface for the dehydrogenation of $Pt(CH_2)^+/NH_3$ to yield $Pt(C(H)NH_2)^+$ at the B3LYPTZP//B3LYPDZP level including corrections for zero-point vibrational energies; charges in the structures are omitted (adapted from ref. [67b]).

$$Pt(CH_2)^+ + NH_3 \xrightarrow{70\,\%} CH_2NH_2^+ + PtH \quad (13a)$$
$$\xrightarrow{25\,\%} PtC(H)NH_2^+ + H_2 \quad (13b)$$
$$\xrightarrow{5\,\%} NH_4^+ + PtCH \quad (13c)$$

dehydrogenation to yield the aminocarbene complex $Pt(C(H)NH_2)^+$. There are three mechanistic options in the generation of the aminocarbene complex (Figure 7). The most energetically favored route is a reaction commencing with a Pt^+-mediated N–H bond activation of the organometallic ion $Pt(CH_2NH_3)^+$, followed by activation of a C–H bond of the methylene group, and the eventual liberation of H_2. Much less favored is a reversed sequence in which a 1,2-hydrogen shift from the carbon to the platinum center precedes the 1,3-hydrogen migration from N to Pt. While in these two routes platinum is involved directly and exploited as a catalyst, the direct 1,2-elimination of molecular hydrogen across the C–N unit, a process in which the metal center only serves as a spectator, is 23 kcal mol^{-1} above the energy of the reactants, and can thus be discarded.[67b] Additional experimental studies (including labeling experiments and the characterization of products and intermediates) as well as electronic structure calculations led to the suggestion of a mechanistic scenario (Scheme 2) similar to the DEGUSSA process that generates HCN from CH_4 and NH_3 [Eq. (14)].

$$CH_4 + NH_3 \xrightarrow{[Pt]} HCN + 3\,H_2 \quad (14)$$

Thus, HCN is proposed to be formed along two competing routes; a surface-bound pathway via platinum aminocarbenes and a gas-phase channel involving the successive dehydrogenation of methanimine. The Pt^+-mediated activation of methane is common to both steps. A crucial aspect is the

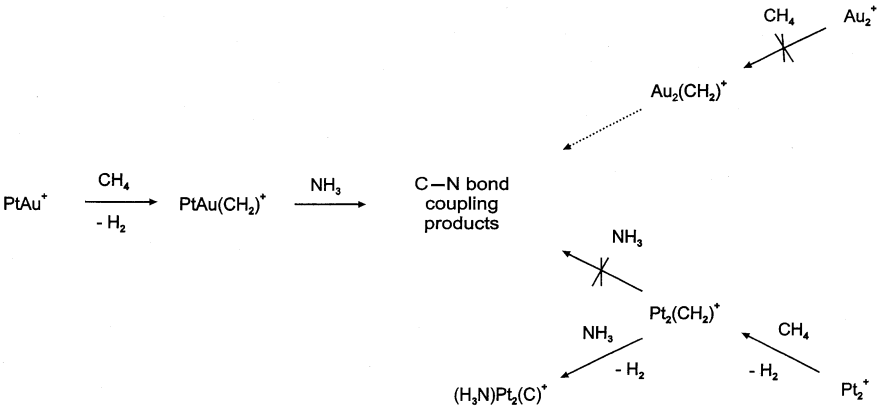


Scheme 2. The elementary steps of the DEGUSSA process (adapted from ref. [67b]).

 © 2003 Wiley-VCH Verlag GmbH & Co. KGaA, Weinheim

remarkable selectivity observed, that is, Pt^+ ions only react with methane (and not with NH_3), while the resulting complex $Pt(CH_2)^+$ preferentially reacts with NH_3. Oligomerization with CH_4 occurs at a much reduced rate.[48,68a]

A pivotal question is whether the gas-phase process of metal-mediated carbon–nitrogen coupling [Eq. (13)] in the functionalization of methane is confined to platinum, or if other metal cations can also mediate C–N bond formation [Eq. (15)]. Therefore, explorative studies with selected 3d, 4d, and 5d elemental ions M^+ were conducted (M = Fe, Co, Rh, W, Os, Ir, Pt, Au).[67b]



Scheme 3. Reactivity tuning of bond activation and fragment coupling by cooperative effects in the bimetallic clusters $PtAu^+$, Pt_2^+, and Au_2^+ (adapted from ref. [68b]).

$$M^+ \xrightarrow{CH_4} M(CH_2)_2^+ \xrightarrow{NH_3} \text{C–N coupling product} \qquad (15)$$

The carbenes of the 3d metals Fe^+ and Co^+ are unreactive toward ammonia, and an analysis of thermochemical data does not seem to reflect trends of $D(M^+\text{-}CH_2)$ as a possible origin; rather, orbital-controlled factors were made responsible for the lack of reactivity in the nucleophilic attack of $M(CH_2)^+$ by NH_3 (M = Fe, Co). The carbenes of the 4d and 5d metals Rh, W, Os, and Ir show moderate efficiencies in their reactions with NH_3. The major pathway in the reaction of $Rh(CH_2)_2^+$ and NH_3 yields Rh^+ and CH_3NH_2, a product channel that is not observed for platinum and the other 5d metals. Only two reaction pathways are observed for the 5d-metal carbenes $W(CH_2)^+$, $Os(CH_2)^+$, and $Ir(CH_2)^+$, namely, dehydrogenation and an acid–base reaction to yield NH_4^+ concomitant with neutral MCH. Conceptually, these carbyne species can be considered as precursors for soot formation. The reaction of $Au(CH_2)^+$ and NH_3 exclusively yields $CH_2NH_2^+$ and neutral AuH with high efficiency (ϕ = 0.60), and the high exothermicity of this reaction [Eq. (16)]

$$Au(CH_2)^+ + NH_3 \rightarrow CH_2NH_2^+ + AuH \qquad (16)$$

with $\Delta_r H = -43\ \text{kcal mol}^{-1}$ is due to comparatively weak $Au^+\text{–}CH_2$ and strong Au–H bonds, as compared to the $Pt(CH_2)^+/NH_3$ system. Relevant bond energies are, as follows: $D_0(Au^+\text{-}CH_2) = 88.9$, $D_0(Pt^+\text{-}CH_2) = 112.5$, $D_0(Au\text{-}H) = 77.5$, and $D_0(Pt\text{-}H) = 78.1\ \text{kcal mol}^{-1}$.[67b] However, as Au^+ ions are incapable of activating methane, the Pt^+ system is most efficient among all elements studied, for it combines two essential properties in a most favorable manner: 1) the ability to activate methane but not ammonia, and 2) preferential attack of the metal carbene by ammonia rather than methane. Experiments with heteronuclear Pt_x/Au_y^+ clusters are indicated, and preliminary studies with the mixed diatomic cluster $PtAu^+$ look extremely promising.[68b] For example, while Pt_2^+ brings about efficient methane activation, the resulting $Pt_2(CH_2)^+$ complex does not react further with NH_3 to yield C–N coupling products. Similarly, the homonuclear cluster Au_2^+ fails to activate methane. In distinct contrast, the heteronuclear cluster $PtAu^+$ dehydrogenates methane and the resulting complex $PtAu(CH_2)^+$ efficiently couples with NH_3 (Scheme 3).[68b] This example demonstrates how bond activation in the gas phase can be tuned by cooperative effects in bimetallic clusters, and future work is likely to exploit this concept.

In the reaction of $Pt(CH_2)^+$ with PH_3 (ϕ = 0.62), the third-row congener of ammonia, the major products correspond to $Pt(PH)^+$ and CH_4.[69] Compared with NH_3, the differences in product distributions (compare Eqs. (13) and (17)) can be

$$Pt(CH_2)^+ + PH_3 \xrightarrow{65\ \%} Pt(PH)^+ + CH_4 \qquad (17a)$$

$$Pt(CH_2)^+ + PH_3 \xrightarrow{25\ \%} [Pt,C,H,P]^+ + 2H_2 \qquad (17b)$$

$$Pt(CH_2)^+ + PH_3 \xrightarrow{10\ \%} [Pt,C,H_3,P]^+ + H_2 \qquad (17c)$$

ascribed to two major factors: 1) the lower basicity of PH_3 (compared to NH_3), and 2) the less favorable π bonding of phosphorus. Thus, the formation of PH_4^+ and $CH_2PH_2^+$ is not observed. Interestingly, the main primary ionic product $Pt(PH)^+$ reacts consecutively with excess PH_3 to yield $[PtP_mH_n]^+$ (m = 1–6; n = 0–3). Saturation is achieved after the addition of six phosphorus atoms and, based on circumstantial evidence, these platinum clusters are suggested to contain P_2 building blocks, rather than intact P_4 or P_6 units.[70]

Despite some similarities, there are distinct differences in the reaction of $Pt(CH_2)^+$ with H_2O when compared with the $Pt(CH_2)^+/NH_3$ system. For example, the efficiency of the reaction [Eq. (18)] is extremely low (ϕ = 0.002). The initially formed platinum hydroxycarbene complex $Pt(C(H)OH)^+$ is generated in only small concentration due to a fast consec-

$$Pt(CH_2)^+ + H_2O \xrightarrow{5\ \%} Pt(CO)^+ + 2H_2 \qquad (18a)$$

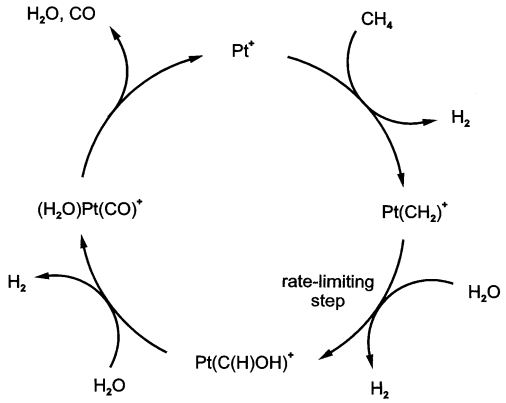
$$Pt(CH_2)^+ + H_2O \xrightarrow{95\ \%} Pt(C(H)OH)^+ + H_2 \qquad (18b)$$

 © 2003 Wiley-VCH Verlag GmbH & Co. KGaA, Weinheim

utive process with H_2O that yields H_2 and the dicoordinate $Pt(H_2O)(CO)^+$ complex [Eq. (19)]. Interestingly, the com-

$$Pt(C(H)OH)^+ + H_2O \rightarrow Pt(H_2O)(CO)^+ + H_2 \quad (19)$$

bined reactions of $Pt(CH_2)^+$, formed from Pt^+ and CH_4, with two molecules of water to yield $Pt(H_2O)(CO)^+$ constitutes a conceptual gas-phase model for the platinum-mediated generation of water gas (Scheme 4).



Scheme 4. Gas-phase model for a Pt^+-mediated water gas reaction: $CH_4 + 2\,H_2O \rightarrow CO + 2\,H_2$ (adapted from ref. [69]).

As previously mentioned, it is not the activation of methane but the addition of H_2O to $Pt(CH_2)^+$ that constitutes the rate-determining step in the sequence to produce $Pt(H_2O)(CO)^+$ (Scheme 4). Furthermore, as thermalized ions undergo only exothermic or thermoneutral reactions in gas-phase ion–molecule experiments of the type described here, the reaction stops after exothermic formation of the $Pt(H_2O)(CO)^+$ complex. According to thermochemical estimates, the final ligand detachment of H_2O and CO has to be introduced by an external input of about 102 kcal mol^{-1} to regenerate the bare Pt^+ "catalyst".[54c] Clearly, this situation is analogous to many systems in heterogeneous catalysis, where product liberation from the catalytic center is achieved by heating.

In the reasonably efficient ($\phi = 0.32$) reaction of $Pt(CH_2)^+$ with H_2S [Eq. (20)], $Pt(CS)^+$ and $Pt(CH_2S)^+$ are both formed in 15% yield. Consecutive dehydrogenative reactions of PtS^+

$$Pt(CH_2)^+ + H_2S \xrightarrow{70\,\%} PtS^+ + CH_4 \quad (20a)$$

$$Pt(CH_2)^+ + H_2S \xrightarrow{15\,\%} Pt(CS)^+ + 2H_2 \quad (20b)$$

$$Pt(CH_2)^+ + H_2S \xrightarrow{15\,\%} Pt(CH_2S)^+ + H_2 \quad (20c)$$

with H_2S also take place to achieve sulfur saturation for $Pt(S_4)^+$.[69]

In conclusion, in the ion–molecule processes of $Pt(CH_2)^+$ with the nucleophiles NH_3, PH_3, H_2O, and H_2S four general types of reactions can be distinguished:

- Carbon–heteroatom coupling by nucleophilic attack at the carbene is found for both NH_3 and H_2O.
- For PH_3 and H_2S, carbon–heteroatom bond formation is feasible but, based on labeling experiments, the dehydrogenation probably proceeds via initial activation of the heteroatom–hydrogen bond at the platinum center, rather than nucleophilic attack at the carbene carbon atom.
- The activation of element–hydrogen bonds at platinum is followed by loss of methane instead of the elimination of H_2 as mentioned above.
- For H_2S and PH_3, this formal metathesis process and subsequent dehydrogenation of H_2S and PH_3 yield, amongst other things, the novel platinum complexes $Pt(S_2)_2^+$ and $Pt(P_2)_3^+$.

3.1.3. Coupling of Methane and Carbon Dioxide using $Ta(CH_2)^+$

While selectivity in the C–H bond activation of alkanes was referred by Sir Derek Barton to be "the chemists' Holy Grail",[71] an even greater challenge, maybe falling into the category of "dream chemistry", concerns the simultaneous coupling of alkanes with CO_2 to yield the corresponding carboxylic acids [Eq. (21)], the difficulty of which arises from inherent thermochemical and kinetic obstacles.

$$RH + CO_2 \xrightarrow{[M]} RCO_2H \quad (21)$$

The formation of acetic acid ($R = CH_3$) from CH_4 and CO_2 is, for example, of particular economic importance, and with regard to a metal-mediated realization of this reaction there are some prerequisites to be fulfilled by the metal center: 1) It has to be capable of activating both CH_4 and CO_2, and 2) coupling of the fragments to the metal center has to be brought about and followed by product release to regenerate the metal catalyst. So far, the achievements obtained are disappointingly limited. However, with regard to the realization of at least some elementary steps in the coupling of CH_4 and CO_2, a *stoichiometric* variant was found when Ta^+ ions were used.[72] While Ta^+ ions efficiently reduce CO_2 to generate TaO_n^+ ($n = 1, 2$), in contrast to many late-transition-metal oxides,[61b] neither TaO^+ nor TaO_2^+ activate CH_4 in the gas phase. However, the carbene $Ta(CH_2)^+$, which forms efficiently from CH_4 and Ta^+ at ambient temperature [Eq. (22)][47c,48a–c,54a,63] is able to deoxygenate CO_2 rapidly ($\phi > 0.95$) to yield CO and $OTa(CH_2)^+$ [Eq. (23)]. The latter ion reacts slowly ($\phi = 0.20$) with a further equivalent of CO_2 to yield the dioxocation TaO_2^+ as the only product. The driving force for this process is the high oxophilicity of tantalum. Based on thermochemical data and mechanistic considerations, the neutral product C_2H_2O formed in Equation (24) corresponds to ketene, which serves as an acetic acid equivalent. While the overall reactions remain stoichiometric with respect to Ta^+, the sequence of Equations (22)–(25)

$$CH_4 + Ta^+ \rightarrow Ta(CH_2)^+ + H_2 \quad (22)$$

$$CO_2 + Ta(CH_2)^+ \rightarrow OTa(CH_2)^+ + CO \quad (23)$$

$$CO_2 + OTa(CH_2)^+ \rightarrow TaO_2^+ + C_2H_2O \quad (24)$$

$$C_2H_2O + H_2O \rightarrow CH_3CO_2H \quad (25)$$

$$CH_4 + 2CO_2 + H_2O + Ta^+ \rightarrow TaO_2^+ + H_2 + CO + CH_3CO_2H \quad (26)$$

© 2003 Wiley-VCH Verlag GmbH & Co. KGaA, Weinheim

demonstrates that, at a molecular level, the coupling of CH_4 and CO_2 to CH_3CO_2H can be achieved [Eq. (26)]. With regard to the elementary steps and the mechanisms operative in this system, computational work by Sändig and Koch has proved extremely insightful.[73] For example, in contrast to the Pt^+/CH_4 couple,[50,52a,54c,d] the dehydrogenation of CH_4 by Ta^+ does not proceed adiabatically on one potential energy surface; rather, along the reaction coordinate there are several changes in spin multiplicity. Further, in contrast to the oxidation of $Pt(CH_2)^+$ with O_2, which generates PtO^+ and CH_2O in a non-metathesis fashion (see above),[54c] a genuine metathesis process is operative in the actual coupling step to generate ketene [Eq. (24)], as was originally suggested.[72]

4. Miscellaneous Systems

The examples described so far referred mostly to the chemistry of the d-block elements. As space limitation does not permit the detailed discussion of several remarkable transformations promoted by lanthanides,[74] actinides,[75] as well as their oxides,[76] it may suffice to mention briefly only the following systems: Due to relativistic effects, reactions as diverse as C–C couplings,[77] selective multiple C–F bond activations,[78] alkene oxidations,[79] and alkadiene oligomerizations[76c] take place, and have been studied in great detail. In this context, an elegant technology developed by Gibson is noteworthy as it permits the investigation of the gas-phase ion chemistry of "hot" elements such as plutonium,[80] the properties of which are clearly affected by relativistic effects.

5. Conclusions

This Review has attempted to demonstrate that the gas-phase chemistry of transition metals, lanthanides, and actinides is significantly influenced by relativistic effects. Qualitatively, these effects become apparent in the comparison of certain structural properties, thermochemical data, or reactivity patterns for a group of metals, for example, trends in the chemistry of the coinage metals Cu, Ag, and Au, or the role of oxidation states for a given metal. Similarly, the analysis of thermochemical data, for example, changes in ionization energies for gold upon coordination with closed- or open-shell ligands helps to unravel the operation of relativistic effects. Not surprisingly, much of the fascinating chemistry of the 5d metals with regard to C–H bond activation and carbon–heteroatom coupling processes is a direct consequence of relativity. For a quantification of relativistic effects, however, the experimental findings need to be related with the results of adequate electronic structure calculations, and it is the combined experimental/computational approach that provides the required insight. Clearly, looking at and learning from the chemistry and physics of isolated (mostly simple) molecules has improved our understanding of relativistic effects in ordinary chemical systems.[81] In fact, depending on the property to be studied and the definition of the term "important", in the words of Pekka Pyykkö[3c] "relativistic energy contributions are already needed for H_2^+ and H_2…". What a fundamental change of views since Paul Dirac's 1929 verdict about the limited role of relativistic effects in ordinary chemical reactions!

This research was financially supported by generous grants from the Deutsche Forschungsgemeinschaft, the Fonds der Chemischen Industrie, the BASF AG, the BAYER AG, and the DEGUSSA AG; allocation of computer time by the Konrad Zuse Zentrum für Informationstechnik, Berlin, is appreciated. However, I myself would have achieved nothing without the practical, conceptual, and intellectual contributions of my research group at TU Berlin and the cooperation of colleagues from all over the world. Technical assistance in the preparation of the article by Andrea Beck and Maria Schlangen is gratefully acknowledged, and helpful comments by Professor Christoph van Wüllen are appreciated.

Received: January 20, 2003 [A572]

[1] P. A. M. Dirac, *Proc. R. Soc. London Ser. A* **1929**, *123*, 714.
[2] a) P. A. M. Dirac, *Proc. R. Soc. London Ser. A* **1928**, *117*, 610; b) P. A. M. Dirac, *Proc. R. Soc. London Ser. A.* **1928**, *118*, 351.
[3] a) K. S. Pitzer, *Acc. Chem. Res.* **1979**, *12*, 271; b) P. Pyykkö, J. P. Desclaux, *Acc. Chem. Res.* **1979**, *12*, 276; c) P. Pyykkö, *Chem. Rev.* **1988**, *88*, 563; d) B. A. Hess, *Ber. Bunsen-Ges.* **1997**, *101*, 1; e) N. Kaltsoyannis, *J. Chem. Soc. Dalton Trans.* **1997**, 1; f) P. Pyykkö, *Angew. Chem.* **2002**, *114*, 3723; *Angew. Chem. Int. Ed.* **2002**, *41*, 3573.
[4] N. Bartlett, *Gold Bull.* **1998**, *31*, 22.
[5] A. Bayler, A. Schier, G. A. Bowmaker, H. Schmidbaur, *J. Am. Chem. Soc.* **1996**, *118*, 7006.
[6] a) H. Schmidbaur, F. Scherbaum, B. Huber, G. Müller, *Angew. Chem.* **1988**, *100*, 439; *Angew. Chem. Int. Ed. Engl.* **1988**, *27*, 419; b) H. Schmidbaur, *Gold Bull.* **1990**, *23*, 1; c) H. Schmidbaur, *Gold Bull.* **2000**, *33*, 3; d) H. Schmidbaur, A. Hamel, N. W. Mitzel, A. Schier, S. Nogai, *Proc. Natl. Acad. Sci. USA* **2002**, *99*, 4916.
[7] a) A. Görling, N. Rösch, D. E. Ellis, H. Schmidbaur, *Inorg. Chem.* **1991**, *30*, 3986; b) O. D. Häberlen, H. Schmidbaur, N. Rösch, *J. Am. Chem. Soc.* **1994**, *116*, 8241.
[8] a) J. Li, P. Pyykkö, *Chem. Phys. Lett.* **1992**, *197*, 586; b) P. Pyykkö, J. Li, N. Runeberg, *Chem. Phys. Lett.* **1994**, *218*, 133; c) L. Magnko, M. Schweizer, G. Ranhut, M. Schütz, H. Stoll, H.-J. Werner, *Phys. Chem. Chem. Phys.* **2002**, *4*, 1006.
[9] a) *Relativistic Effects in Heavy-Element Chemistry and Physics* (Ed.: B. A. Hess), Wiley-VCH, Weinheim, **2003**; b) D. Schröder, M. Diefenbach, H. Schwarz, A. Schier, H. Schmidbaur, *Relativistic Effects in Heavy-Element Chemistry and Physics* (Ed.: B. A. Hess), Wiley-VCH, Weinheim, **2003**, chap. 7.
[10] D. Schröder, J. Hrušák, I. C. Tornieporth-Oetting, T. M. Klapötke, H. Schwarz, *Angew. Chem.* **1994**, *106*, 223; *Angew. Chem. Int. Ed. Engl.* **1994**, *33*, 212.
[11] *Gmelin Handbook, Au Suppl. Vol. B1*, Springer, Berlin, **1992**, p. 113.
[12] a) P. Schwerdtfeger, J. S. McFeaters, M. J. Liddell, J. Hrušák, H. Schwarz, *J. Chem. Phys.* **1995**, *103*, 245; b) P. Schwerdtfeger, *J. Am. Chem. Soc.* **1989**, *111*, 7261; c) P. Schwerdtfeger, M. Dolg, W. H. E. Schwarz, G. A. Bowmaker, P. D. W. Boyd, *J. Chem. Phys.* **1989**, *91*, 1762.
[13] a) C. A. Schalley, G. Hornung, D. Schröder, H. Schwarz, *Int. J. Mass Spectrom. Ion Processes* **1998**, *172*, 181; b) C. A. Schalley, G. Hornung, D. Schröder, H. Schwarz, *Chem. Soc. Rev.* **1998**, *27*, 91; c) F. Cacace, *Chem. Eur. J.* **2002**, *8*, 3839.
[14] S. Andreev, J. J. BelBruno, *Chem. Phys. Lett.* **2000**, *329*, 490.

[15] C. J. Evans, M. C. L. Gerry, *J. Am. Chem. Soc.* **2000**, *122*, 1560.
[16] a) J. K. Laerdahl, T. Saue, K. Faegri, Jr., *Theor. Chim. Acta* **1997**, *97*, 177; b) M. Iliaš, P. Fardik, M. Urban, *J. Phys. Chem. A* **1998**, *102*, 5263.
[17] C. van Wüllen, *J. Chem. Phys.* **1998**, *109*, 392.
[18] J. R. Brown, P. Schwerdtfeger, D. Schröder, H. Schwarz, *J. Am. Soc. Mass Spectrom.* **2002**, *13*, 485.
[19] P. Schwerdtfeger, J. S. McFeaters, R. L. Stephens, M. J. Liddell, M. Dolg, B. A. Hess, *Chem. Phys. Lett.* **1994**, *218*, 362.
[20] D. Schröder, H. Schwarz, J. Hrušák, P. Pyykkö, *Inorg. Chem.* **1998**, *37*, 624.
[21] *Gmelin Handbook, Au Suppl. Vol. B1*, Springer, Berlin, **1992**, p. 189.
[22] D. Schröder, R. Brown, P. Schwerdtfeger, X.-B. Wang, X. Yang, L.-S. Wang, H. Schwarz, *Angew. Chem.* **2003**, *115*, 323; *Angew. Chem. Int. Ed.* **2003**, *42*, 311.
[23] a) S. Seidel, K. Seppelt, *Science* **2000**, *290*, 117; b) T. Drews, S. Seidel, K. Seppelt, *Angew. Chem.* **2002**, *114*, 470; *Angew. Chem. Int. Ed.* **2002**, *41*, 454.
[24] D. Schröder, J. Hrušák, R. H. Hertwig, W. Koch, P. Schwerdtfeger, H. Schwarz, *Organometallics* **1995**, *14*, 312.
[25] J. Hrušák, D. Schröder, H. Schwarz, *Chem. Phys. Lett.* **1994**, *225*, 416.
[26] R. H. Hertwig, J. Hrušák, D. Schröder, W. Koch, H. Schwarz, *Chem. Phys. Lett.* **1995**, *236*, 194.
[27] T. K. Dargel, R. H. Hertwig, W. Koch, H. Horn, *J. Chem. Phys.* **1998**, *108*, 3876.
[28] J. Hrušák, D. Schröder, R. H. Hertwig, W. Koch, P. Schwerdtfeger, H. Schwarz, *Organometallics* **1995**, *14*, 1284.
[29] O. D. Häberlen, N. Rösch, *J. Phys. Chem.* **1993**, *97*, 4970.
[30] R. H. Hertig, W. Koch, D. Schröder, H. Schwarz, J. Hrušák, P. Schwerdtfeger, *J. Phys. Chem.* **1996**, *100*, 12253.
[31] R. F. Bader, *Atoms in Molecules*, Clarendon, Oxford, **1994**.
[32] For an example and leading references, see: B. R. Bender, G. J. Kubas, L. H. Jones, B. I. Swanson, J. Eckert, K. B. Capps, C. D. Hoff, *J. Am. Chem. Soc.* **1997**, *119*, 9179.
[33] D. Schröder, R. Wesendrup, R. H. Hertwig, T. K. Dargel, H. Grauel, W. Koch, B. R. Bender, H. Schwarz, *Organometallics* **2000**, *19*, 2608.
[34] a) R. H. Hertwig, J. Hrušák, D. Schröder, W. Koch, H. Schwarz, *Chem. Phys. Lett.* **1995**, *236*, 194; b) T. K. Dargel, R. H. Hertwig, W. Koch, *Mol. Phys.* **1999**, *96*, 583; c) D. Schröder, P. Brown, P. Schwerdtfeger, H. Schwarz, *Int. J. Mass Spectrom.* **2000**, *203*, 155.
[35] H. Schmidbaur, S. Hofreiter, M. Paul, *Nature* **1995**, *377*, 503.
[36] a) M. N. Glukhovtsev, A. Pross, A. Nicolaides, L. Radom, *J. Chem. Soc. Chem. Commun.* **1995**, 2347; b) G. Bouchoux, M. Yañez, O. Mo, *Int. J. Mass Spectrom.* **1999**, *185–187*, 241; c) D. Kuck, *Mass Spectrom. Rev.* **1990**, *9*, 583; d) D. Kuck, *Int. J. Mass Spectrom.* **2002**, *213*, 101.
[37] a) J. Hrušák, *Theor. Chim. Acta* **1990**, *78*, 203; b) J. Hrušák, D. Schröder, T. Weiske, H. Schwarz, *J. Am. Chem. Soc.* **1993**, *115*, 2015; c) M. Tkaczyk, A. G. Harrison, *Int. J. Mass Spectrom. Ion Processes* **1994**, *132*, 73.
[38] For aspects of the fascinating molecular architecture of multiply aurated oxygen, nitrogen, and carbon dications, i.e., $O(AuL)_4^{2+}$, $N(AuL)_5^{2+}$, and $C(AuL)_6^{2+}$, see refs. [35] and [39]. We note that these multiply charged cations can be regarded as analogues of the elusive dications OH_4^{2+}, NH_5^{2+}, and CH_6^{2+}, which are suggested to exist in the gas phase (ref. [40]) as well as condensed media (ref. [41]). Once more, the striking similarities between Au^+ and H^+ are quite obvious.
[39] a) H. Schmidbaur, *Chem. Soc. Rev.* **1995**, *24*, 391; b) A. Schier, A. Grolmann, J. M. López de Luzuriaga, H. Schmidbaur, *Inorg. Chem.* **2000**, *39*, 547.
[40] K. Lammertsma, P. von R. Schleyer, H. Schwarz, *Angew. Chem.* **1989**, *101*, 1313; *Angew. Chem. Int. Ed. Engl.* **1989**, *28*, 1321.
[41] a) G. A. Olah, *Angew. Chem.* **1993**, *105*, 805; *Angew. Chem. Int. Ed. Engl.* **1993**, *32*, 767; b) G. A. Olah, *Angew. Chem.* **1995**, *107*, 1519; *Angew. Chem. Int. Ed. Engl.* **1995**, *34*, 1393.
[42] a) H. Basch, T. Hoz, *The Chemistry of Triple-Bonded Functional Groups, Vol. 2, Suppl. C* (Ed.: S. Patai), Wiley, London, **1994**, p. 1; b) I. Antes, S. Dapprich, G. Frenking, P. Schwerdtfeger, *Inorg. Chem.* **1996**, *35*, 2089.
[43] In this respect, the nature of the bond in $Au(C_6H_6)^+$ is particularly intriguing, because the IEs of gold and benzene are virtually identical. For an elaborate discussion, see ref. [34b].
[44] G. Nicholas, F. Spiegelman, *J. Am. Chem. Soc.* **1990**, *112*, 5410.
[45] a) D. Schröder, H. Schwarz, *Angew. Chem.* **1990**, *102*, 1468; *Angew. Chem. Int. Ed. Engl.* **1990**, *29*, 1433; b) J. C. Weisshaar, *Acc. Chem. Res.* **1993**, *26*, 213.
[46] a) L. F. Halle, P. B. Armentrout, J. L. Beauchamp, *J. Am. Chem. Soc.* **1981**, *103*, 962; b) R. Georgiadis, P. B. Armentrout, *J. Phys. Chem.* **1988**, *92*, 7067.
[47] a) M. P. Irion, A. Selinger, *Ber. Bunsen-Ges.* **1989**, *93*, 1408; b) P. B. Armentrout, J. L. Beauchamp, *Acc. Chem. Res.* **1989**, *22*, 315; c) S. W. Buckner, T. J. McMahon, G. D. Byrd, B. S. Freiser, *Inorg. Chem.* **1989**, *28*, 3511; d) J. K. Perry, G. Ohanessian, W. A. Goddard III, *Organometallics* **1994**, *13*, 1870.
[48] a) K. K. Irikura, J. L. Beauchamp, *J. Am. Chem. Soc.* **1989**, *111*, 75; b) K. K. Irikura, J. L. Beauchamp, *J. Am. Chem. Soc.* **1991**, *113*, 2769; c) K. K. Irikura, J. L. Beauchamp, *J. Phys. Chem.* **1991**, *95*, 8344.
[49] For a review, see: H. Schwarz, D. Schröder, *Pure Appl. Chem.* **2000**, *72*, 2319.
[50] C. Heinemann, R. H. Hertwig, R. Wesendrup, W. Koch, H. Schwarz, *J. Am. Chem. Soc.* **1995**, *117*, 495.
[51] X.-G. Zhang, R. Liyanage, P. B. Armentrout, *J. Am. Chem. Soc.* **2001**, *123*, 5563.
[52] a) C. Heinemann, H. Schwarz, W. Koch, K. G. Dyall, *J. Chem. Phys.* **1996**, *104*, 4642; b) F. Rakowitz, C. M. Marian, B. Schimmelpfennig, *Phys. Chem. Chem. Phys.* **2000**, *2*, 2481.
[53] D. G. Musaev, K. Morokuma, *Isr. J. Chem.* **1993**, *33*, 307.
[54] a) C. Heinemann, R. Wesendrup, H. Schwarz, *Chem. Phys. Lett.* **1995**, *239*, 75; b) J. J. Caroll, J. C. Weisshaar, P. E. M. Siegbahn, C. A. M. Wittborn, M. R. A. Blomberg, *J. Phys. Chem.* **1995**, *99*, 14388; c) M. Pavlov, M. R. A. Blomberg, P. E. M. Siegbahn, R. Wesendrup, C. Heinemann, H. Schwarz, *J. Phys. Chem. A* **1997**, *101*, 1567; d) U. Achatz, M. Beyer, S. Joos, B. S. Fox, G. Niedner-Schatteburg, V. E. Bondybey, *J. Phys. Chem. A* **1999**, *103*, 8200.
[55] a) M. R. A. Blomberg, P. E. M. Siegbahn, M. Svensson, *J. Phys. Chem.* **1994**, *98*, 2062; b) D. G. Musaev, K. Morokuma, *J. Phys. Chem.* **1996**, *100*, 11600; c) M. Hendrickx, M. Ceulemans, L. Vanquickenborne, *Chem. Phys. Lett.* **1996**, *257*, 8.
[56] D. Schröder, M. Diefenbach, T. M. Klapötke, H. Schwarz, *Angew. Chem.* **1999**, *111*, 206; *Angew. Chem. Int. Ed.* **1999**, *38*, 137.
[57] For a review on small, thermochemically stable polycations, see: D. Schröder, H. Schwarz, *J. Phys. Chem. A* **1999**, *103*, 7385.
[58] D. Schröder, J. N. Harvey, H. Schwarz, *J. Phys. Chem. A* **1998**, *102*, 3639.
[59] I. Kretzschmar, A. Fiedler, J. N. Harvey, D. Schröder, H. Schwarz, *J. Phys. Chem. A* **1997**, *101*, 6252.
[60] The thermochemistry and the mechanism of the gas-phase formation of $Pd(CH_2I)^+$ may serve as a good example as well as a convincing case for the crucial role adequate theoretical methods occasionally play in the interpretation of experimental findings; for details, see: a) J. Schwarz, C. Heinemann, D. Schröder, H. Schwarz, J. Hrušák, *Helv. Chim. Acta* **1996**, *79*, 1; b) J. Schwarz, D. Schröder, H. Schwarz, C. Heinemann, J. Hrušák, *Helv. Chim. Acta* **1996**, *79*, 1110.
[61] a) K. Eller, H. Schwarz, *Chem. Rev.* **1991**, *91*, 1121; b) D. Schröder, H. Schwarz, *Angew. Chem.* **1995**, *107*, 2126; *Angew. Chem. Int. Ed. Engl.* **1995**, *34*, 1973.

 © 2003 Wiley-VCH Verlag GmbH & Co. KGaA, Weinheim

[62] See for example, the formally spin-forbidden reactions of some 3d-metal-oxide cations with hydrocarbons which occur at ambient temperature via surface crossings mediated by spin–orbit coupling ("two-state reactivity concept"): a) A. Fiedler, D. Schröder, S. Shaik, H. Schwarz, *J. Am. Chem. Soc.* **1994**, *116*, 10734; b) S. Shaik, D. Danovich, A. Fiedler, D. Schröder, H. Schwarz, *Helv. Chim. Acta* **1995**, *78*, 1393; c) S. Shaik, M. Filatov, D. Schröder, H. Schwarz, *Chem. Eur. J.* ***1998****,* *4*, 193; d) D. Schröder, S. Shaik, H. Schwarz, *Acc. Chem. Res.* **2000**, *33*, 139; e) Y. Shiota, K. Yoshizawa, *J. Am. Chem. Soc.* **2000**, *122*, 12317; f) D. R. Yarkony, *J. Phys. Chem. A* **2001**, *105*, 6277; g) S. Shaik, S. P. de Visser, F. Ogliaro, H. Schwarz, D. Schröder, *Curr. Opin. Chem. Biol.* **2002**, *6*, 556; h) R. Poli, J. N. Harvey, *Chem. Soc. Rev.* **2003**, *32*, 1.

[63] R. Wesendrup, D. Schröder, H. Schwarz, *Angew. Chem.* **1994**, *106*, 1232; *Angew. Chem. Int. Ed. Engl.* **1994**, *33*, 1174.

[64] Given as $\phi = k_r/k_c$ where k_r is the experimentally observed rate constant and k_c is the collision rate constant derived from capture theory.[65]

[65] T. Su, *J. Chem. Phys.* **1994**, *100*, 4703, and references therein.

[66] An even more powerful oxidant than PtO^+ is the dioxide PtO_2^+; this formally Pt^V compound is capable of activating inert substrates such as H_2, CO, and CH_4 with a turnover number > 100 for the conversion $CO + N_2O \rightarrow CO_2 + N_2$ for the catalytically active species PtO_n^+ ($n = 0$–2): a) M. Brönstrup, D. Schröder, I. Kretzschmar, H. Schwarz, J. N. Harvey, *J. Am. Chem. Soc.* **2001**, *123*, 142; b) D. K. Bohme, personal communication, **2002**.

[67] a) M. Aschi, M. Brönstrup, M. Diefenbach, J. N. Harvey, D. Schröder, H. Schwarz, *Angew. Chem.* **1998**, *110*, 858; *Angew. Chem. Int. Ed.* **1998**, *37*, 829; b) M. Diefenbach, M. Brönstrup, M. Aschi, D. Schröder, H. Schwarz, *J. Am. Chem. Soc.* **1999**, *121*, 10614; for theoretical and experimantal work on $D_0(Au^+\text{-}CH_2)$ in particular, see: c) ref. [50]; d) J. Hrušák, *S. Afr. J. Chem.* **1997**, *50*, 93; e) K. K. Irikura, W. A. Goddard III, *J. Am. Chem. Soc.* **1994**, *116*, 8733; f) F. Aguirre, J. Husband, C. J. Thompson, R. B. Metz, *Chem. Phys. Lett.* **2000**, *318*, 466.

[68] a) For the reaction of Pt_n^+ clusters ($n = 1$–5) with CH_4, NH_3, and other simple substrates, see: K. Koszinowski, D. Schröder, H. Schwarz, *J. Phys. Chem. A*, submitted; b) K. Koszinowski, D. Schröder, H. Schwarz, *J. Am. Chem. Soc.* **2003**, *125*, 3676; c) K. Koszinowski, D. Schröder, H. Schwarz, *ChemPhysChem*, in press; d) an overview of the reactions of $Pt_n(CH_2)^+$ clusters ($n = 1$–5) with O_2, CH_4, NH_3, and H_2O is given in: K. Koszinowski, D. Schröder, H. Schwarz, *Organometallics*, submitted.

[69] M. Brönstrup, D. Schröder, H. Schwarz, *Organometallics* **1999**, *18*, 1939.

[70] For the gas-phase generation of P_6, a new phosphorus allotrope, see: a) D. Schröder, H. Schwarz, M. Wulf, H. Sievers, P. Jutzi, M. Reiher, *Angew. Chem.* **1999**, *111*, 3723; *Angew. Chem. Int. Ed.* **1999**, *38*, 3513; b) M. Reiher, D. Schröder, *Chem. Eur. J.* **2002**, *8*, 5501.

[71] D. H. R. Barton, *Aldrichimica Acta* **1990**, *23*, 3.

[72] R. Wesendrup, H. Schwarz, *Angew. Chem.* **1995**, *107*, 2176; *Angew. Chem. Int. Ed. Engl.* **1995**, *34*, 2033, and references therein.

[73] a) N. Sändig, W. Koch, *Organometallics* **1997**, *16*, 5244; b) N. Sändig, W. Koch, *Organometallics* **1998**, *17*, 2344.

[74] H. H. Cornehl, C. Heinemann, D. Schröder, H. Schwarz, *Organometallics* **1995**, *14*, 992.

[75] C. Heinemann, H. H. Cornehl, H. Schwarz, *J. Organomet. Chem.* **1995**, *501*, 201.

[76] a) C. Heinemann, H. Schwarz, *Chem. Eur. J.* **1995**, *1*, 7; b) H. H. Cornehl, C. Heinemann, J. Marçalo, A. Pires de Matos, H. Schwarz, *Angew. Chem.* **1996**, *108*, 950; *Angew. Chem. Int. Ed. Engl.* **1996**, *35*, 891; c) H. H. Cornehl, R. Wesendrup, J. N. Harvey, H. Schwarz, *J. Chem. Soc. Perkin Trans. 2* **1997**, 2283.

[77] C. Heinemann, D. Schröder, H. Schwarz, *Chem. Ber.* **1994**, *127*, 1807.

[78] a) C. Heinemann, N. Goldberg, I. C. Tornieporth-Oetting, T. M. Klapötke, H. Schwarz, *Angew. Chem.* **1995**, *107*, 225; *Angew. Chem. Int. Ed. Engl.* **1995**, *34*, 213; b) H. H. Cornehl, G. Hornung, H. Schwarz, *J. Am. Chem. Soc.* **1996**, *118*, 9960; c) R. H. Hertwig, W. Koch, *Chem. Eur. J.* **1999**, *5*, 312; d) D. Zhang, C. Zhang, C. Liu, *J. Organomet. Chem.* **2001**, *640*, 121; e) D. Zhang, C. Liu, S. Bi, *J. Phys. Chem. A* **2002**, *106*, 4153; f) D. Caraiman, G. K. Koyanagi, A. Cunje, A. C. Hopkinson, D. K. Bohme, *Organometallics* **2002**, *21*, 4293; g) for a feature article on this topic, see: U. Mazurek, H. Schwarz, *J. Chem. Soc. Chem. Commun.* **2003**, 1321.

[79] a) C. Heinemann, H. H. Cornehl, D. Schröder, M. Dolg, H. Schwarz, *Inorg. Chem.* **1996**, *35*, 2463; b) H. H. Cornehl, R. Wesendrup, M. Diefenbach, H. Schwarz, *Chem. Eur. J.* **1997**, *3*, 1083.

[80] For reviews, see: a) J. K. Gibson, *J. Mass Spectrom.* **2001**, *36*, 284; b) J. K. Gibson, *Int. J. Mass Spectrom.* **2002**, *214*, 1.

[81] a) K. Stark, H.-J. Werner, *J. Chem. Phys.* **1996**, *104*, 6515; b) W. Kutzelnigg, *Theor. Chem. Acc.* **2000**, *103*, 182.

 © 2003 Wiley-VCH Verlag GmbH & Co. KGaA, Weinheim

Chemical Safety

Chemical Safety in a Vulnerable World**

*Sabine Gärtner, Jens Küllmer, and Ulrich Schlottmann**

Keywords:
chemical policy · conservation · environmental chemistry · international cooperation



© 2003 Wiley-VCH Verlag GmbH & Co. KGaA, Weinheim
DOI: 10.1002/anie.200300584

The title of this article is the motto of the fourth meeting of the Intergovernmental Forum on Chemical Safety (Forum IV), which is to be held in Bangkok in November 2003. The IFCS has been in existence for 10 years. During this period politicians, scientists, and the general public have become increasingly aware of the risks associated with chemicals. International conventions providing for prohibitions and restrictions of dangerous chemicals, and for better control of trade have been set up. These conventions will soon be binding under international law. In developing countries many people who handle or use hazardous chemicals are illiterate or poorly educated; they may not fully understand what they are handling. The industrialized countries therefore have a special duty to incorporate chemical safety in development cooperation measures. Through their presence at this year's forum, prominent chemists such as Carl Djerassi will seek to underline the fact that a long term preventive approach to healthcare and the environment is only possible through international cooperation. This overview describes current developments in the field of chemical safety policy and presents a selection of the legislation currently in force for chemicals in the European Union. It also provides an insight into the interwoven structure of international cooperation that takes place at both the political and the technical level.

From the Contents

1. Introduction 4457

2. National and EC Regulations 4457

3. International Activities 4462

4. Outlook 4468

1. Introduction

The industrialization that the world has achieved in the past two hundred years is inextricably connected with the production and use of chemicals. Chemical production accounts for a substantial proportion of German economic output. In 2000, sales resulting from the production of and trade in chemicals came to more than € 1700 billion worldwide, of which Germany accounted for € 100 billion, making it the third-largest producer after the USA and Japan. According to OECD estimates, sales are twice as high as in the telecommunications sector.[1] Chemical products have undoubtedly contributed to a substantial improvement in the quality of life. Plastics, surfactants, and a large number of basic chemicals are improving the medical and hygienic situation worldwide. However, numerous toxic substances present risks and hazards that occur during the entire life cycle of a substance: during production, during transport and trade, and during storage, use, and disposal. Awareness of environmental and health risks has grown over the last 20 years. Today this is making itself felt in an increasingly complex set of international regulations on chemical safety. The focus is increasingly shifting towards the developing countries and their populations, as people there are less aware of the risks and hazards than those in the industrialized countries. Today the worldwide spread of persistent, bioaccumulating, and toxic chemicals by air or water, their occurrence in places where they are not used, and the destruction of the ozone layer are making it clear to everyone that "Chemical Safety—An International Challenge"[2] is not just an empty phrase.

But it should not be necessary for risks arising from chemicals to assume international dimensions before action is taken. That is why national or European regulations provide an appropriate framework for a large number of chemicals. Moreover, national laws and European Community (EC) legislation are enforceable law. Compliance with this law is monitored, while noncompliance is prosecuted and punished.

2. National and EC Regulations

2.1. Main Features of Chemicals Legislation

In the European Union (EU) the legal provisions on the trade in chemical products are largely well harmonized. One particular reason for this harmonization is the great relevance for the single market that arises from the lively trade in chemical products. National regulations have been largely confined to the requirements laid down by the EU, which in turn determines their content. It is nevertheless worth quoting at this point the purpose of the German Chemicals Act, which in particular transposes into national law the general chemicals directive of the EC, as set out in the Seventh Amendment to the directive:

The purpose of the Act is to protect people and the environment from harmful impacts of dangerous substances

[*] Prof. Dr. U. Schlottmann, Dr. S. Gärtner, J. Küllmer
Federal Ministry for the Environment, Nature Conservation and Nuclear Safety (BMU)
Postfach 120629, 53048 Bonn (Germany)
Fax: (+49) 228-305-3524
E-mail: ulrich.schlottmann@bmu.bund.de

[**] This article is an update of "Chemical Safety—An International Challenge" by Bernd-Ulrich Hildebrand and Ulrich Schlottmann.[2]

 DOI: 10.1002/anie.200300584 © 2003 Wiley-VCH Verlag GmbH & Co. KGaA, Weinheim

and preparations, and in particular to make such impacts identifiable, avert them and prevent their occurrence.[3]

This definition alone is sufficient to identify certain fundamental features of chemicals legislation:

1. Chemicals legislation is committed to the precautionary principle.
2. Chemicals legislation transcends the various protection objectives, that is, the same weight is given to general health or consumer protection, occupational safety, and environmental protection.
3. Chemicals legislation works with the elements of hazard identification, risk assessment, and risk containment.

Hazard identification gathers information about the intrinsic characteristics of a chemical; data on safety-relevant properties, such as explosion risks or flammability, toxicological properties, and on the whereabouts and behavior of a substance in the environment are obtained by means of testing. Risk assessment assesses the potential frequency and severity of the negative effects on man and the environment that may be caused by a chemical. Risk management is the process of identifying, assessing, selecting, and implementing measures designed to reduce the risk to man and the environment. Such measures may range from safety advice on handling a chemical, through restrictions on trade and use, to prohibition.

2.2. Some Selected EC Legal Acts

Community legal acts continue to be legal acts of the European Community and not of the European Union, since only the EC possesses law-making powers. The sole right to take initiatives for Community legal acts rests with the European Commission. Before a proposal for a Community measure is submitted, detailed analyses of the costs and benefits of the planned measure are performed and assessed. The results of an enacted measure, especially the implementation of the measure in the Member States, including the benefits and burdens for those concerned, are usually documented by a Commission experience report. Such an experience report may become the starting point for practical clarifications, amendments, or additions to the legal act under consideration (http://europa.eu.int/eur-lex/de/treaties/). The organization within the EU Commission, especially the Directorates General for the Environment and for Enterprises (Figure 1) and the various EC legal acts in the field of chemical safety (Figure 2) are set out in tabular form.

2.2.1. Basic Directives on Dangerous Substances

The EC's fundamental set of regulations for chemicals is Directive 67/548/EEC, concerning the Harmonization of Legal and Administrative Provisions for the Classification, Packaging, and Labeling of Dangerous Goods, which dates from 1967. This directive, which has undergone numerous substantive amendments and technical adaptations over the years, contains, amongst other things, the provisions on

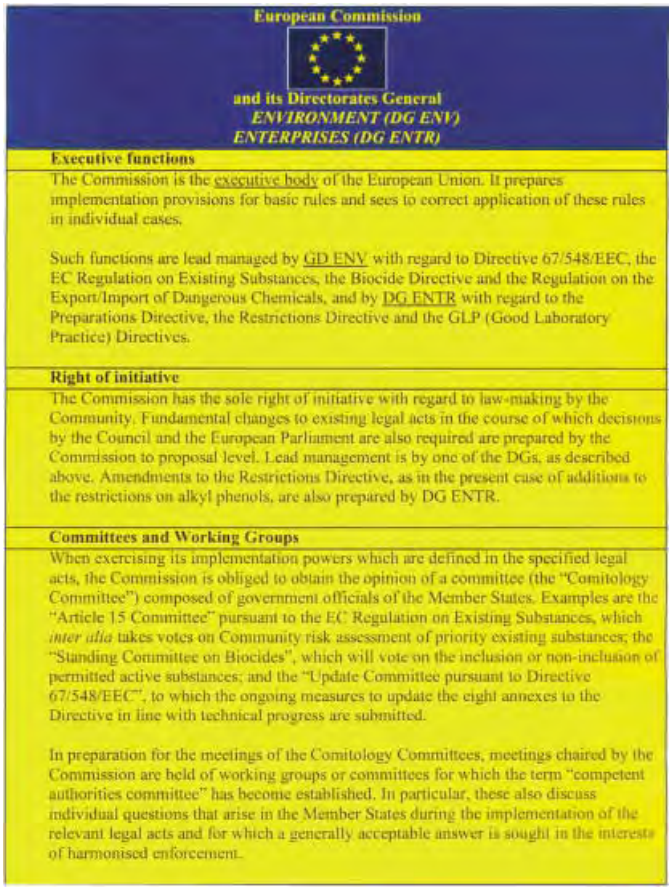


Figure 1. The EU Commission and its Directorates General "Environment" and "Enterprises".



Sabine Gärtner studied biology (Diplom-Biologin), then gained her doctorate in Biochemistry under Konrad Sandhoff. From 1988 to 1990, with a grant from the Fritz Thyssen Foundation, she worked at the University of Bonn on the project "Molecular Biology Analyses of Human Hereditary Diseases". Since 1990 she has been an assistant Head of Division at the Federal Ministry for the Environment, Nature Conservation, and Nuclear Safety in Bonn, with a special focus on issues in the field of the EC legislation of substances.



Jens Küllmer, born in 1972, has degrees in Forestry and Environmental Studies (Diplom-Forstwirt, Diplom-Umweltwissenschaftler), and an MBA in International Business Management. In 1998 he was scientific assistant at the Great Lakes Forestry Center (Marie, Canada), and between 1999–2002 was scientific assistant at the Rhineland-Palatinate regional parliament, Mainz. He is now assistant head of division responsible for International Chemicals Policy at the Federal Ministry for the Environment, Nature Conservation, and Nuclear Safety in Bonn.

 © 2003 Wiley-VCH Verlag GmbH & Co. KGaA, Weinheim

classification and labeling, on information about special risks and safety advice (known for short as R and S phrases), listed in Annex I, and continuously updates the dangerous substances for which EC-wide classifications exist. In addition, Annex V describes the methods that are used for conducting the prescribed tests. The Sixth Amending Directive, dating from 1979 (Directive 79/831/EEC), was the first to introduce a registration procedure for the marketing control of chemicals, while the Seventh Amending Directive, dating from 1992 (Directive 92/32/EEC), developed the registration procedure further, in particular by defining the data to be submitted for a substance on a graduated basis that depends on the volume traded; the hazard symbol "dangerous to the environment" was introduced, and the Directive laid down that public authorities were to undertake a risk assessment for a registered substance on the basis of the data available. It is very important to note that the question of whether or not a registered substance may be traded depends not on compliance with substantive requirements, but merely on whether the registrant has submitted the full data required, which the competent national authority has to determine within a short period (for instance, 60 days). A considerably more stringent kind of control would be an authorization procedure, but this was not chosen for general chemicals. In an authorization procedure, the question of marketability is linked to compliance with substantive requirements; furthermore, the substance may not be marketed until the competent authority has expressly given permission (see also Section 2.2.4.). The registration procedure is nevertheless considered to have a considerable controlling effect. According to the industry, where internal investigations reveal that substances are too unfavorable from the point of view of chemical legislation, these substances are not registered and hence not placed on the market. Even so, it must be said that nearly every substance registered has to be assigned at least one hazardous property, and roughly half of the substances are classed as "dangerous to the environment".

In addition to a number of special exemptions from the registration procedure that are allowed under chemical legislation (for example, for research and development substances and petty quantities), there is one very fundamental exemption: The registration procedure does not apply to "existing substances", in other words, those substances which were already in existence on the European market before September 18, 1981, and which are listed in the European



Ulrich Schlottmann, born in 1941, gained his doctorate under Horst Böhme. After working in the Federal Ministry for Youth, Family, and Health he was made head of the "Chemicals" department in 1982, and in 1986 he moved to the newly established Environment Ministry. He specializes in international chemical safety, test methods, good laboratory practice, and alternatives to animal experiments. Since 1979 he has been visiting lecturer at the University of Bonn; chairman of the GDCh expert group on "Environmental Chemistry and Ecotoxicology and a member of the GDCh board.

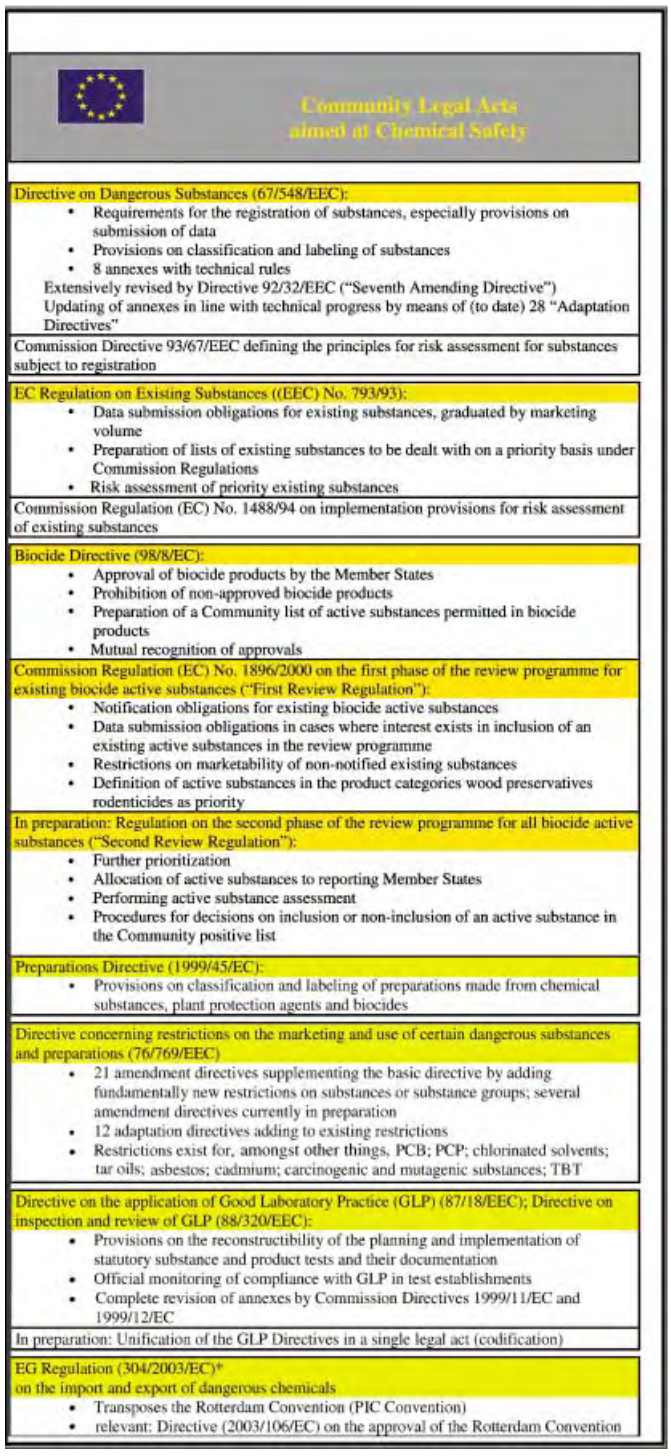


Figure 2. Except as otherwise stated ("Commission Directive"), the legal acts listed above were passed by the Council (before being introduced in the Maastricht Agreement) or by the Council and the European Parliament (after coming into effect in the Maastricht Agreement). The relationship between a legal act passed by the Council, or by the Council and the EP, and one passed by the Commission is roughly the same as the relationship between an act and a government ordinance. EC directives have to be transposed, that is, they do not take effect in the Member States until they have been transposed into national law. EC regulations, by contrast, are directly applicable law. The legal acts listed are (with the exception of *) based on Article 95, formerly Article 100a, of the EC Treaty. They are thus measures which are intended to contribute to the functioning of the single European market.

 © 2003 Wiley-VCH Verlag GmbH & Co. KGaA, Weinheim

Inventory of Existing Commercial Chemical Substances (EINECS). Thus those substances which, because of their large production and marketing volumes, their multifarious uses of which the public are generally unaware, and their resulting input into the environment, give rise to the real risks to man and the environment, initially remained unregulated.

2.2.2. Regulations on Existing Substances

Since the enactment of the EC regulation on existing substances, the Council Regulation (EEC) No. 793/93 of March 23, 1993 on the evaluation and control of the environmental risks of existing chemical substances, there has been a range of instruments for testing and assessing existing substances.

EINECS lists some 100000 existing substances, of which approximately 30000 are thought to be actually in use. For these substances the EC Regulation on existing substances lays down two complementary systems: a general system based on the volume marketed, and a special system based on the individual substance. Until 1995 producers of existing substances with a marketing volume of more than 1000 tonnes had to supply certain data to the EU Commission, and until 1998 this also applied to the producers of existing substances with a marketing volume of 10 to 1000 tonnes. However, substantive data on safety-relevant aspects, toxicology, and ecotoxicology only had to be supplied for the 1000-tonne substances, and then only where available. On the basis of these data the Commission lays down the order in which the existing substances must be dealt with. Since 1994 the EU Commission has issued lists of existing substances to be dealt with on a priority basis and allocated them to specific Member States, which assume reporting duties in accordance with the EC Regulation on existing substances. The aim is to adopt, for each of these priority substances, a coordinated Community risk assessment combined with a recommendation on measures to minimize risks. As the scope of the EC Regulation on existing substances does not include risk management, any risk mitigation measure suggested, whether it be an occupational safety measure or a restriction on use or trade, must in any case be implemented within the context of other sets of regulations. Nine years after the EC Regulation on existing substances was enforced, the results are sobering:

- 139 existing substances are to be found on four priority lists currently in use,
- for 16 existing substances the Commission has adopted recommendations on Community risk assessments,
- not a single existing substance has so far been made the subject of restriction on use or trade.

2.2.3. Directives Relating to Restrictions on Dangerous Substances and Preparations

As already mentioned, any risk mitigation measures that prove necessary on the basis of the risk assessment are implemented under other Community legal acts. The most important set of rules for restrictions on the use and marketing of substances and preparations is Directive 76/769/EEC, known for short as the Restrictions Directive.[4] Every introduction of additional restrictions supplementary to this Directive requires a relatively complex procedure, since both the Council of Ministers and the European Parliament (EP) are involved in making decisions. A number of important measures have nevertheless been introduced in the context of the Restrictions Directive, such as restrictions on PCBs, PCP. tar oils, tributyltin; no restrictions have yet been imposed on any substance for which a risk assessment has been undertaken under the EC Regulation on existing substances.

This result must be regarded as a virtual failure for the EC policy on existing substances. Even though more knowledge is now available on a number of important substances, the real objective has not been achieved, namely to reduce the risks to man and the environment arising from chemicals and to ensure that chemicals exhibiting unreasonable risks for man and the environment are rapidly removed from the substance cycle. There are undoubtedly a number of reasons for this failure:

- The principal player in the task of dealing with existing substances in the EC, namely the Commission, does not possess a separate administrative unit with good personnel resources for rapid performance of its tasks under the Regulation on existing substances.
- The rapporteurs do not have any enforcement rights in relation to industry and have to go through a tedious process of obtaining Community decisions to complete dossiers.
- The completion of an assessment procedure is not tied to any specific deadlines, which means that continual submission of new and supplementary data can turn into a never-ending story.
- The failure to involve downstream users and a consequent lack of knowledge about such users means there is a great deal of uncertainty about exposure to the substance, the risk arising from the substance, and the choice of appropriate risk-mitigation measures.
- The onus of proof is on the authorities.

2.2.4. Biocide Directive

A fundamentally different approach was taken for a group of special products known collectively as "biocide products". Designed to control these products, the Directive 98/8/EC on the Marketing of Biocide Products (February 16, 1998) is still relatively young. The area of application of the EC Biocide Directive covers a large number of products ranging from disinfectants to mothballs, from large-volume industrially used material preservatives to niche products, from enclosed use in cooling circuits to open use as rat poisons. The only thing these products have in common is that they are used against living organisms that are regarded by humans as harmful. Thus biocides have by definition the effect of impairing or killing living organisms. In view of this property, which they share with plant protection agents, the model used for the EC Biocide Directive was not general chemical legislation, but the EC Plant Protectives Directive.

Although it has been in force since May 2000 and was eventually transposed into national law in Germany in June 2002 (announcement of revised version of the Chemicals Act

of June 20, 2002, Federal Law Gazette I. page 2090, see http://www.bmu.de), no practical experience exists to date regarding the application of the regulations. In particular, the abovementioned heterogeneity of the products concerned is probably a major challenge for the competent authorities, which renders it difficult to arrive at correct assessments. For this reason, critics of the directive are already prophesying its failure. Compared with the aforementioned sets of rules, however, the EC Biocide Directive has a major advantage, which gives the authorities more enforcement power and probably exerts more pressure on the relevant industries to contribute to timely completion of the individual testing and decision procedures. What the EC Biocide Directive prescribes is an authorization, rather than a registration procedure. In other words, the marketing of a biocide product remains prohibited until the approval authority grants approval on the basis of comprehensive documents to be submitted by the applicant and the evaluation thereof; the onus of proof regarding the acceptability of the product rests with the applicant. This also has an impact on the testing program for old biocide-active substances, that is, for those active substances that were already on the European market when the implementation deadline expired in May 2000. Admittedly existing biocide-active substances and biocide products containing such active substances are subject to transitional rules. These however include an arrangement in which the existing active substances are fed into a multiphase review program. Existing active substances that have not cleared the first hurdle of this review program, in accordance with the First Review Regulation (EC) No. 1896/2000, will shortly cease to be marketable, as will the biocide products containing such active substances. The Biocide Directive is not affected by the amendments to EC chemicals legislation described below.

2.3. Revision of European Chemicals Policy[*]

The sobering balance after several years of the Regulation on existing substances, and the manifestly poor interaction of this regulation with the Restrictions Directive, set in motion in 1998 a process of discussion about the European policy on chemicals, which led from the informal council of environment ministers under the British presidency of the Council (Chester, 1998), via the EU Commission's report of 1998 about the functioning of EC chemicals legislation, to the decision by the council of environment ministers on the cornerstones of a new chemical policy in June 1999. In February 2001 the Commission submitted its White Paper on future chemicals policy in the European Union.

The implementation of the White Paper requires a fundamental reform of EC chemical legislation aimed at the total replacement of the existing regulations. The Council and the EP have basically welcomed the goals and content of the White Paper and made numerous proposals for its implementation. At present this process is at a standstill, because the continuation of a substantive discussion about future chemicals policy is tied to the submission of concrete law-making proposals by the Commission, which are currently lacking. This is probably also an indication of the enormous economic pressure that the Commission has been exposed to since the beginning of the White Paper process. The process nevertheless appears to be irreversible, since there is a general consensus that the EC work on existing substances cannot be continued along old lines.

The core of the White Paper is the REACH-System (Registration, Evaluation and Authorization of Chemicals).[5]

- The distinction between existing and new substances is to be abolished. All chemicals (above a certain threshold quantity) are to be registered with their respective uses. The timing of the registration and the necessary documents are to be geared to the production and marketing volumes.
- The manufacturers and users must perform an initial risk assessment. Subsequent users, that is, downstream users, are also to be included. The onus of proof regarding the safety of the use of a substance will rest with industry. An official review of this assessment or a separate assessment by the authority itself will only be undertaken in the case of high-volume substances and especially problematic substances.
- The use of substances with especially harmful properties is to be made subject to an authorization procedure; this will include not only carcinogenic, mutagenic, and teratogenic substances, but probably also persistent and bioaccumulating substances. Risk assessment and risk management are to be dovetailed more effectively. Restrictive measures are no longer to be decided by the Council and the EP, but by the Commission and the Member States in a committee procedure.
- To ensure the smooth performance of the necessary tasks, an agency of the Commission is to be set up with the necessary competencies and appropriate resources (working title: Chemicals Agency).

The chemicals policy proposed in the White Paper opens up a realistic perspective that might put an end to the enormous gaps in the data, the backlog of assessments, and the management deficits relating to existing substances within a finite period of time.

The Federal Ministry for the Environment considers the reform necessary. If properly designed, it will:

- increase confidence in the products of the chemical industry,
- open up opportunities for innovation and competition by means of providing more reliable information on substances and better communication between producers and downstream users,
- and above all it will bring about necessary improvements in environmental protection, consumer protection, and occupational safety.

Central to the acceptance and success of the new system is the practical orientation of its concrete design. In the

[*] The selection describes the situation in spring 2003. Since then, the European Community has presented a draft regulation for future chemicals policy (REACH regulation). This draft was published on the Internet, especially to allow nongovernmental organizations to comment on the proposed regulations. By the deadline (July 10, 2003) 7000 statements had been received.

 © 2003 Wiley-VCH Verlag GmbH & Co. KGaA, Weinheim

forthcoming discussions at EU level it is therefore necessary to make proposals for realistic and practicable solutions for the numerous individual issues, in order to contribute to the success of the reform. The joint position of the Federal Government, the Chemical Industry Association (VCI) and the Mining, Chemical, and Energy Trade Union (IG BCE) of March 2002 contains a number of concrete proposals to this end. (http://www.bundesregierung.de/artikel,-72155/Gemeinsame-Position-der-Bundes.htm)

3. International Activities

3.1. Protocols and Conventions

3.1.1. The Montreal Protocol

The gaps in the ozone layer over the polar regions present a threat to humans, animals, and plants, because of the increase in UV-B radiation reaching the surface of the earth. This natural protective shield has been damaged by the worldwide use of ozone-damaging substances, such as chlorofluorocarbons (CFCs) and halons, which are used for fire protection materials.

The Montreal Protocol (MP) is the international contractual basis for the United Nations worldwide program for discontinuing the use of ozone-damaging substances. 16 years ago, 46 countries undertook to stop producing and using substances that were damaging to the ozone layer. In the meantime more than 180 countries have signed this protocol. The signatory states are responsible for a total of over 90% of the consumption of these substances. The original target (from 1987) of halving the consumption of CFCs by the year 2000 has since been raised considerably on a number of occasions in light of the alarming reports on the status of the ozone layer. For example, the production of CFCs in the industrialized countries was discontinued at the beginning of 1996.

The amendment to the MP which, was passed in Peking in 1999, states that from 2002 onwards the production and use of the substance bromochloromethane, which can be used as a solvent and fire extinguisher, is to be totally banned in the signatory states. This amendment and the treaty modifications adopted at the same meeting were transposed into Community law by decree of the EC Council (2002/215/EC). It follows from the reasons given for this decision that additional steps must be taken to monitor trade in ozone-depleting substances, especially partially halogenated CFCs and new substances. Methyl bromide remained unnoticed by the public for a very long time; this is despite the fact that one atom of bromine destroys 80 times more ozone than a chlorine atom.[6] Thus the bromine content of a compound such as methyl bromide is more reactive and has a greater impact on stratospheric ozone than the chlorine content of CFCs. This pesticide has nevertheless been in use for decades as a preferred means of treating arable land. In Germany its use in the agricultural sector was banned in 1982 owing to its harmful effects on the groundwater. Since then, most of the industrialized countries have banned the use of methyl bromide. However, the USA, Italy, and South Africa continue to oppose a ban on methyl bromide. Under the MP, the USA is to stop using it by 2005 and the developing countries by 2015.

The Montreal Protocol is closely linked to the Convention on Climate Change (Kyoto Protocol). At the most recent conference of the parties in Rome in November 2002, the Multilateral Fund (MLF) for the Montreal Protocol was increased to a figure of US$ 573 million for a period of three years (2003–2005). With this sum the industrialized countries are fulfilling their contractual obligation to ensure that compliance with the discontinuation is not impeded by a lack of financial resources, in particular regarding the G77 states (in the UN sector originally 77 developing countries, today about 135 nations) and China.

The current contribution formula for the MP shows a figure of around 12% for Germany, equating to some US$ 57 million. At the same time, however, Germany will again exercise its option to supply 20% of its contributions to the MLF in the form of creditable bilateral development cooperation projects, which account for a sum of around US$ 4 million per annum. The design and execution of the projects is handled for the Federal Government largely by the development aid agency GTZ (Deutsche Gesellschaft für Technische Zusammenarbeit). The ProKlima project is an example of implementation of the MP. (http://www.gtz.de/climate/deutsch/activities.htm)

3.1.2. The POPs Convention

In May 2001 the signatory conference for the POPs Convention took place in Stockholm. The POPs Convention (Figure 3)[7] implements international prohibition and restriction measures with regard to certain persistent organic pollutants (POPs). The core of the Convention is that twelve particularly dangerous POPs for the environment are to be prohibited or reduced until they are totally eliminated. The dynamic design of the rules of the Convention allows the original POP substances to be joined by further substances that meet the four criteria of persistency, bioaccumulation, long-range transport potential, and harmful properties. The POPs Convention prohibits the following chemicals: aldrin,

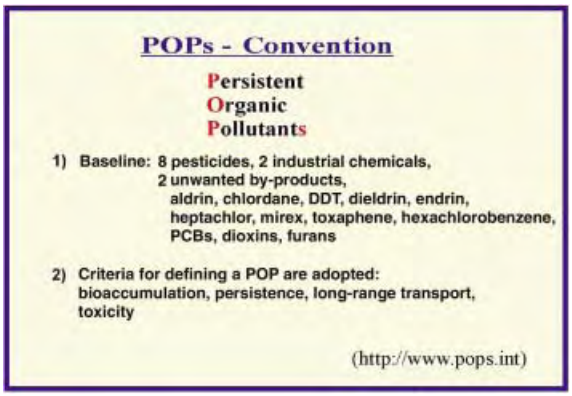


Figure 3. The POPs Convention.

 © 2003 Wiley-VCH Verlag GmbH & Co. KGaA, Weinheim

dieldrin, endrin, chlordane, mirex, toxaphene, heptachlor, hexachlorobenzene, di(*para*-chlorophenyl)trichloroethane (DDT), polychlorinated biphenyls (PCBs), polychlorinated dibenzodioxins (PCDDs) and polychlorinated dibenzofurans (PCDFs). With the exception of DDT, which may still be produced and used on a country-specific basis for combating malaria, and of unwanted by-products, all other substances are listed in the Appendix (Appendix A) to the Convention, which regulates the phasing out of the production and use of these substances. The production and use of DDT for vector control will remain necessary until inexpensive alternatives become available. The relevant countries must inform the United Nations Environment Program (UNEP) on Chemicals and the World Health Organization (WHO) about the use of DDT. The use of DDT as a pesticide in the agricultural sector is however prohibited.

3.1.3. The PIC Convention

According to estimates by the WHO, about one million accidents each year are caused worldwide through poisoning from pesticides. The worldwide trade in dangerous chemicals is merely the beginning of the life cycle of a chemical; it is followed by storage, use, and the disposal of residual stocks. That is why steps should be taken as early as the trade stage to ensure that dangerous chemicals do not adversely affect man and the environment. This applies particularly to developing countries, most of which are today suffering from the effects of incorrect usage.

For this reason, a meeting of the International Community of States (Rotterdam, 1998) decided to adopt a convention defining binding rules for the trade in dangerous chemicals (PIC Convention). In accordance with the precautionary principle, this convention allows states to impose a ban on imports before a chemical is imported. This does not prohibit trade in chemicals, but makes it subject to very stringent rules, namely the "PIC procedure", where PIC stands for "prior informed consent". In the context of imports, this means that the potential importing country must be informed about the chemical and take a decision before the chemical is actually imported. To date this has applied to 26 agricultural and five industrial chemicals, including DDT, aldrin and heptachlor. The substances agreed in the convention may only be imported by one country into another if the receiving country has first consented to the import. The convention requires that the dangerous properties of the chemicals must be made known so that a potential receiving country can reach an informed decision on an import application. This information enables the receiving country to take appropriate risk mitigation measures, which may range from protective and qualification measures for users to a ban on importation. Taking appropriate risk management measures is regular practice within the European community of states. The PIC Convention was developed primarily to protect the poorer regions of the world, which currently have a less than adequate monitoring system for chemical management, and for which the PIC procedure aims to provide better protection for the environment and human health, hence saving lives.

Spring 2003 saw the introduction of Regulation (EC) No. 304/2003 of the European Parliament and the Council on the Export and Import of Dangerous Chemicals. This superseded the existing Council Regulation (EEC) No. 2455/92 (July 1992) concerning the Export and Import of Certain Dangerous Chemicals. No reductions were to be made in the level of environmental and health protection in the importing countries. In order to achieve this goal, some of the provisions go beyond those of the PIC Convention. This conforms with Article 15, Paragraph 4 of the PIC Convention, which states that the contracting parties may take measures that provide more stringent protection for human health and the environment than laid down in the Convention, provided these measures are compatible with the Convention and with international law. The Community also considered it advantageous in terms of practicability that there should be a single agency responsible for contact between the Community, the PIC Secretariat, other contracting parties, and other countries. The Commission has assumed the function of the point of contact for this purpose. Exports of dangerous chemicals that are prohibited in the Community or subject to strict restrictions continue to be subject to a joint export notification procedure. In the case of imports, the Community must take decisions before the importation of chemicals that are subject to the international PIC procedure is allowed. The fact that exporters and importers are obliged to furnish information on the quantities of chemicals in international trade that are covered by this Regulation makes for better monitoring and assessment of the impacts and effectiveness of this new Regulation.

In autumn 2002, the 9th Intergovernmental Conference (9^{th} INC PIC) on trade in dangerous chemicals was held in Bonn. The conference was attended by more than 200 delegates from about 100 nations, and numerous representatives of nongovernmental organizations (NGOs). The meeting proposed the inclusion of the toxic insecticide monocrotophos in the PIC list of substances. This insecticide is used as a pesticide, particularly in cotton production. In Europe a recent Community decision (2002/371/EC) already states that textile fibers made of cotton may no longer contain any monocrotophos. In addition the conference paved the way for the inclusion of three more pesticides (DNOC, GRANOX TBC, and SPINOX T) and all carcinogenic forms of asbestos. To this end the mandate of the Interim Review Committee, an expert body which prepares the inclusion of new substances, was extended. It is to continue its work with virtually unchanged membership until the first Conference of the Parties; this ensures the continuity of its work (http://www.pic.int).

The Federal Government is seeking to ensure that the permanent secretariat of the Rotterdam Convention (PIC) and of the Stockholm Convention on the Prohibition of Persistent Organic Chemicals (POPs) will in future be located in Bonn. The relevant decision will be taken at the First Conference of the Parties (COP-1), which has to be held within one year of coming into effect (90 days after the 50th ratification), probably in the second half of 2004. In August 2003 the PIC Convention had been ratified by 46 countries and the POPs Convention by 35 countries.

 © 2003 Wiley-VCH Verlag GmbH & Co. KGaA, Weinheim

3.2. Intergovernmental Forums and Activities

3.2.1. Intergovernmental Forum for Chemical Safety (IFCS)

The first Conference on Environment and Development (UNCED) was held in Rio de Janeiro in 1992, in which the positive experiences of the Montreal Protocol were maintained. Numerous heads of state and heads of government approved Chapter 19 of Agenda 21, which sets out details of the principles for internationally effective chemical safety. This chapter contains objectives for environmentally sound handling and use of chemicals, including measures to prevent illegal international trade in toxic and dangerous products (Figure 4).

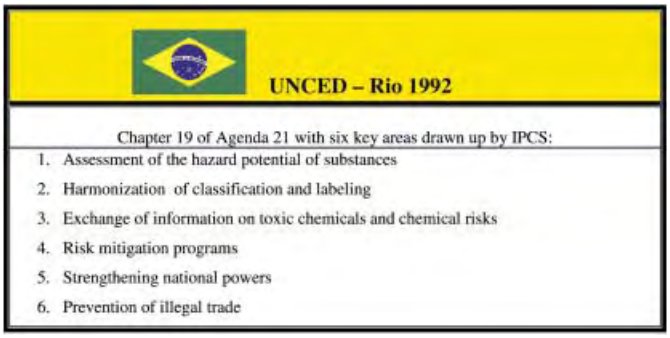


Figure 4. Key areas of Chapter 19 of the UNCED Agenda 21.

An important point is the intensification of international cooperation and the coordination of ongoing international and regional activities. As part of the implementation of this program, the International Conference on Chemical Safety was held in Stockholm in April 1994, which was organized by the United Nations Environment Program (UNEP), the International Labor Organization (ILO) and the World Health Organization (WHO). The conference established the Intergovernmental Forum on Chemical Safety (IFCS), the central task of which is to promote, monitor, and harmonize the implementation of Chapter 19. The Forum is to draw up recommendations for governments and for international and intergovernmental organizations. Moreover, Forum I in 1994 laid down a concrete plan of action on the six key areas of Chapter 19 with a time scale extending until 2000. In 1995, to coordinate the work of the international organizations, the Inter-Organization Program for the Sound Management of Chemicals (IOMC) was set up, comprising UNEP, WHO, ILO, FAO, UNIDO, UNITAR (1998) and OECD.

In 2000 the participants in the IFCS Forum III approved the Bahia Declaration and a concrete plan of action.[8] This declaration makes recommendations on measures in the field of chemical safety after the year 2000. At Forum IV in Bangkok in November 2003, which will be held under the motto "Chemical Safety in a Vulnerable World", the measures implementing the Bahia Declaration are to be evaluated (see the historical development of the IFCS in Figure 5). A further main focus is the systematic improvement and continuation of assistance for the threshold and developing countries. In the interests of better worldwide sharing of



Figure 5. The historical development of the IFCS.

information, work is already in progress on developing a computer-based information system accessible to the general public (Information Exchange Network on Capacity Building for the Sound Management of Chemicals, INFOCAP, http://www.infocap.info).

3.2.2. The Classification and Labeling of Chemicals (Globally Harmonized System, GHS)

The above-mentioned conference in Rio de Janeiro made the first move towards developing a globally harmonized system for the classification and labeling of dangerous chemicals (Figure 6). This goal was achieved at the follow-up conference, the World Summit in Johannesburg in 2002. Since December 2002 a draft GHS for implementation has been on the table, the content of which was passed by the United Nations body ECOSOC (Economic and Social Council) after years of negotiation. In July 2003 this draft was approved and published as a United Nations recommendation. As soon as the GHS is implemented, trade barriers will be abolished and costs will be reduced. Animal experiments, many of which are unnecessary because of widespread repetition and duplication of tests, will be eliminated. Moreover, greater transparency will be achieved in the use of chemicals.

The GHS is to address the fields of transport, workplace, consumers, and environment. The harmonization approach encompasses the classification criteria and labeling provisions on physicochemical, health-endangering, and environmentally harmful properties. On the one hand the new system is to be based on successful existing precursor models. At the same time, however, it is to introduce standardized safety data sheets worldwide and easily understood hazard symbols

 © 2003 Wiley-VCH Verlag GmbH & Co. KGaA, Weinheim

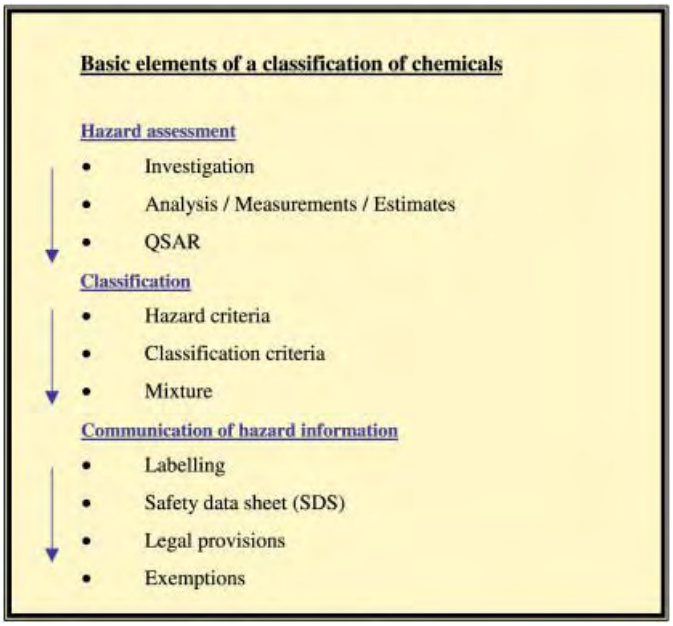


Figure 6. GHS Classification and Labeling Criteria.

which make clear the risks to humans and the environment that arise when using chemicals. The labeling and information sheets would be used for the carriage of dangerous goods and the use of chemicals in industry and agriculture. This will unify the existing classification and labeling systems and supersede the separate systems for dangerous goods and hazardous substances (http://www.unece.org/trans/danger/danger.html).

The principal technical work on this harmonization will be undertaken by the expert bodies of the OECD, UNCETDG, and ILO. Their ambitious and demanding work programs are extensive. In December 2002 the EU member states instructed the Commission to submit a proposal for EU-wide implementation of the GHS by 2005. The action plans of Bahia and Johannesburg envisage worldwide introduction of the GHS by 2008. Furthermore, the GHS will make a major contribution toward the objective of worldwide sustainability in the safe use of chemicals by the year 2020 (http://www.unece.org/trans/danger/publi/ghs/ghs.html) .

3.2.3. Development Assistance for Chemical Management (Capacity Building)

In the last 15 years Germany has made financial resources of as much as € 280 million available for improving chemical safety in developing countries. At the 9th INC PIC in Bonn, states from South and Central America announced further workshops on chemical safety. The "Convention Project Chemical Safety" run by the GTZ, in cooperation with the Federal Ministry for the Environment, has already brought about improvements in chemicals management in model projects of the kind implemented in Argentina. For example, poison information centers have been set up on German lines. Moreover in the interests of improving the use of chemicals in developing countries, the new EC Regulation on Export and Import of Dangerous Chemicals provides that all chemicals exported must have a sufficient storage life to permit effective and safe use. With the help of European assistance, Argentina and Thailand, for example, are now able to integrate further chemicals into the PIC procedure that are classified as dangerous. Particularly in the case of pesticides and, above all, their export to developing countries, it is essential that information on proper storage conditions be disseminated and that storage containers be appropriately sized to prevent residual stocks of expired chemicals. In cooperation with relevant international organizations, such as the FAO, UNEP, and ILO, development assistance is promoting, amongst other things, the implementation of the GHS system and the control of exports/imports of chemicals in southern Africa, the documentation and disposal of obsolete pesticides and PCBs in African and Asia countries, and the introduction of management systems for safe and economic use of chemicals in small and medium enterprises in developing countries.

3.2.4. Sustainable Chemistry

The term "sustainable chemistry" describes a fundamental strategy that aims not only to reduce the environmental impact of chemicals, but also to minimize all burdens on the environment and to conserve resources;[9] it includes legal regulations. Its broadly based objective is a networked and closely coordinated design of chemical and product policy, environmental and health policy which takes account of social, economic, and ecological aspects.

A sustainable chemicals policy can only be implemented jointly with industry and should not restrict its competitiveness. In the long term, ecological benefits go hand-in-hand with economic benefits. The chemical industry has been demonstrating this for years in cases where process innovations that make ecological sense have been systematically implemented, thus giving rise to profitable energy-saving effects. A global sustainability policy in the chemicals sector lends special significance to the responsibility of industry and the industrialized countries for the developing countries. For this reason the systematic implementation of modern knowledge management (e.g., through a GHS) and an approach based on substance flows should be an essential component of the future sustainability strategy in chemicals policy, since more transparency leads to greater safety. The approach of an integrated product policy (IPP) also makes a contribution to the sustainable use of chemicals. IPP can be developed and improved. The EU Commission therefore proposes to present new proposals for the development of IPP in 2003. At the same time it is necessary to consider how IPP and substance-flow management can best be kept compatible.

3.3. International Program on Chemical Safety, IPCS

The IPCS was founded in 1980 as a joint venture by the UNEP, WHO, and ILO (Figure 7). The aim of the IPCS is to produce a fundamental scientific base for reducing the risks to

 © 2003 Wiley-VCH Verlag GmbH & Co. KGaA, Weinheim

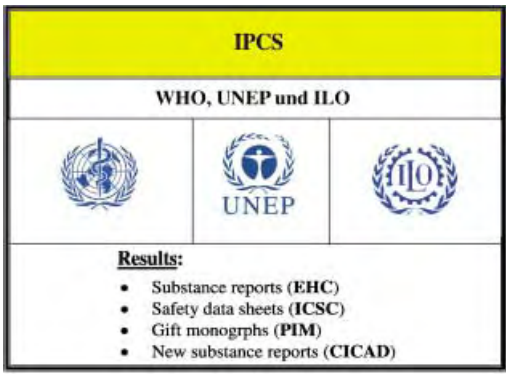


Figure 7. The IPCS.

human health and the environment that are caused by chemicals. It seeks to strengthen national and international efforts in the field of chemical safety. This benefits not only the participating states, but also, in particular, those states where the structures for chemical safety and the knowledge needed for building up such structures are not yet very well developed. One key area of the work of the IPCS is to compile and disseminate findings regarding risks to man and the environment arising from chemicals which may be of both industrial and natural origin. To this end numerous monographs on substances and assessment methods have been produced. States which are active in the IPCS work with internationally recognized experts from all over the world. The following items have been published:

- Substance reports (Environmental Health Criteria, EHC)
  These reports prepared for scientific experts contain up-to-date information on health hazards and risks for a specific substance or group of substances. Recent EHCs also contain information on environmental impacts. There are currently 228 EHC reports, with more than 1000 CAS entries.
- Safety data sheets (International Chemical Safety Cards, ICSC)
  These summarize the principal data on a product and information on health protection and safe handling tailored to the use of the product; for example, in factories or the agricultural sector. There are currently 1305 ICSCs for 1315 compounds at the UN level.
- Poisons Information Monographs (PIMs)
  These contain a brief description of the main chemical, physical, and toxicological properties of individual substances and provides information on diagnosis and the treatment of poisoning. PIMs are intended for poison emergency centers and other advisory units. There are currently 230 PIMs covering 462 substances.
- New substance reports (Concise International Chemical Assessment Documents, CICAD)
  These contain information of the hazard potential of a substance, dose-response relationships and, on the basis of sample exposure data, risk characterizations. As a rule, CICADs are based on existing substance reports. The intention is that national substance reports prepared in accordance with the CICAD procedure should be capable of easy transformation into internationally usable and recognized substance reports with a minimum of financial input. There are 47 CICADs, covering 147 chemicals. They are published by the Wissenschaftliche Verlagsgesellschaft in Stuttgart.

The steering group (PAC) of the IPCS last met in Peking in 2002, where it was decided to reorganize the IPCS into the following activity areas:

1. Risk assessment, including harmonization of methods and rule-making functions with a view to defining target parameters (e.g., the WHO Drinking Water and Air Quality Guidelines)
2. Poisons information, precautions, and management, including epidemiology, continuation of case collections, and the use of aggregated sources on toxicological data of relevance to humans
3. Chemical accidents and emergencies, including preparedness for public health precautions and monitoring
4. Assistance with establishing appropriate structures (Capacity Building).

The new structure of the IPCS is to be published in the course of 2003.

3.4. The OECD

The OECD must continue to be regarded as a very important body for the development of international chemical safety; some 80% of worldwide production of chemicals takes place in the member countries of the OECD. This percentage will increase sharply with the accession of states planned to be involved in EU enlargement in 2004, and the possible inclusion of Russia, Brazil, and China, which are also expected to apply for membership. The growing number of members (currently 29) combined with the shrinking budget has given rise to a substantive debate about the original work of the OECD. In the Environment Health and Safety Program (EHS), which has been in existence since 1971, the OECD has maintained its proven long-term key activities for the year 2003/4. Notable examples include good laboratory practice (GLP) in the testing of pharmaceuticals, chemicals, and pesticides, the chemical test methods, the harmonization of classification and labeling (GHS), and risk assessment. The OECD can be expected to emerge strengthened from the initiated reform process if it plays an active part in shaping this process itself.

A significant decision at the last plenary session (34th Joint Meeting on Chemicals in November 2002) was to continue the ICCA program until 2005, now that the pilot phase has been completed. ICCA stands for International Council of Chemical Associations, a voluntary worldwide chemical industry program that seeks to close the data gaps for the most important industrial chemicals (HPV chemicals). The advisory body on existing substances (BUA) of the German Chemical Society (GDCh, http://www.gdch.de) has so far dealt with 23 substances in the ICCA program, which have already been approved by the OECD. At the end of 2002 another 33 of the substance dossiers prepared by the OECD member states were discussed. By the end of 2002, a total of 89 substances in this program had been dealt with.[10]

 © 2003 Wiley-VCH Verlag GmbH & Co. KGaA, Weinheim

Furthermore, the pilot phase of monitoring national compliance with the OECD principles for GLP by means of inspections (mutual joint visits, MJV) has been completed. The GLP principles require compliance with the provisions on the reconstructibility of the planning and implementation of legally prescribed substance and product tests and their documentation. The OECD has also developed and laid down guidelines for ensuring official monitoring of compliance with the GLP principles in test establishments. If a test establishment uses an OECD-recognized test method in an officially prescribed test, complies with the GLP principles, and is officially monitored, then the test results obtained are to be recognized throughout the OECD. Mutual recognition of data is one of the major goals of the chemical program.

This program is open to countries outside the OECD if they satisfy the requirements. The test methods[11] and the GLP principles[12] are the basic building blocks for the mutual acceptance of data (MAD). In the next few years the OECD will be devoting increasing attention to structure–activity relationships (SARs), aspects of toxicogenomics, and sustainability in the chemicals sector (http://www1.oecd.org/ehs/chem2.htm).

3.5. World Summit, Johannesburg 2002

Ten years after the conference in Rio de Janeiro, the World Summit for Sustainable Development (WSSD) in Johannesburg ended with the approval of the declaration tabled by South Africa of the action plan that had been negotiated over a period of several months ("Johannesburg Plan of Implementation"). In the period leading up to the conference, the EU had urged that decisions be passed in Johannesburg on concrete targets, timetables, and implementation programs for chemical safety (Figure 8). Item 23 of the plan of implementation contains a renewal of the commitments in Agenda 21. Throughout their entire life cycle, chemicals are to be properly handled in the interests of sustainable development and the protection of human health and the environment, with the aim of ensuring by the year 2020 that chemicals are used and produced in such a way that significant negative impacts on human health and the environment are minimized. Transparent procedures for risk assessment and risk management that are based on scientific findings are to be used, and the precautionary principle in Principle 15 of the Rio Declaration for Environment and Development is to be taken into account. Developing countries are to be given technical and financial assistance with building up their capacities for the proper handling of chemicals and hazardous wastes (capacity building).



Figure 8. An overview of the principal statements on chemicals policy in the Johannesburg Plan of Implementation, 2002.

3.6. Governing Council of the United Nations Environment Program

The United Nations Environmental Program (UNEP) was founded as a UN institution in Stockholm in 1972 to address global problems of environment policy that can only be dealt with meaningfully by adopting a multilateral approach. The UNEP Governing Council (UNEP GC) meets every two years to decide the UNEP work program, in line with the political objectives.

For this reason delegates from 148 countries met in Nairobi for the 22nd UNEP GC in February 2003 to take the first steps towards the implementation of an action plan whose objective is to minimize the health and environmental impacts of chemicals by 2020. The agenda included the following decisions in the chemicals sector: the PIC and POPs Conventions, worldwide discontinuation of the use of lead, a global reduction in mercury levels, and a Strategic Approach to International Chemicals Management (SAICM, http://www.chem.unep.ch/irptc/strategy/default.htm).

The resolutions passed on the PIC and POPs Conventions are primarily intended to bring an earlier introduction of these conventions and to bring their practical implementation forward on a voluntary basis.

In the case of lead, the UNEP was particularly requested to assist the developing countries in their efforts to stop using lead in fuels, dyes, and other areas particularly dangerous to humans through capacity building.

Following the UNEP's submission of a worldwide mercury evaluation in 2002, concrete steps to reduce the use of Hg worldwide are to follow. The UNEP GC kept open the option of using legal or other methods to achieve this objective. The UNEP GC also decided to include in the reduction drive other heavy metals that are dangerous to humans and the environment (http://www.chem.unep.ch/mercury/default.htm).

The UNEP GC also decided that, in conjunction with the other UN organizations, it would analyze worldwide activities in the field of chemicals management, identify deficits, and draw up first proposals for a strategic approach (SAICM). The decision to develop an SAICM is based on the resolutions passed by the UNEP Global Ministerial Environment Forum (GMEF) in Cartagena in February 2002 and by the WSSD. A strategic approach allows for a clear and meaningful statement of priorities that groups a number of different of activities and brings together the existing chemicals management organizations. The main goal of this strategic approach is thus to implement the sustainable use of chemicals as

 © 2003 Wiley-VCH Verlag GmbH & Co. KGaA, Weinheim

speedily and efficiently as possible. The global strategic approach for international chemicals management is to be approved by the GMEF in 2006. Organizing the necessary conferences and developing the SAICM calls for financial assistance, which UNEP puts at between US$ 4–5 million.

4. Outlook

The Montreal Protocol and the PIC and POPs Conventions are successful examples of the international efforts that are being made to achieve greater chemical safety. International negotiations are usually lengthy and difficult, because the interests of the individual countries often differ widely. International conventions will undoubtedly become increasingly important with the internationalization of the markets, since the protection of humans and the environment from dangerous chemicals can only be achieved on a worldwide basis. This realization is increasingly being accepted by the chemical industry worldwide, which in the past has tended to be guided by a purely commercial business philosophy.

In view of declining financial and human resources, it is essential to set meaningful priorities so that activities do not stop at declarations of intent, but are followed by practical action. In particular, international negotiations should not be misused as an excuse for delaying or preventing the adoption of measures for which a European framework is appropriate. The European framework, which is admittedly large but still manageable, provides an opportunity to document the feasibility of measures. This can be used to further the development of management institutions and processes. In the past, Europe has frequently shown itself to be a driving force behind progressive environmental protection: Prevention is better than cure.

List of Important Abbreviations

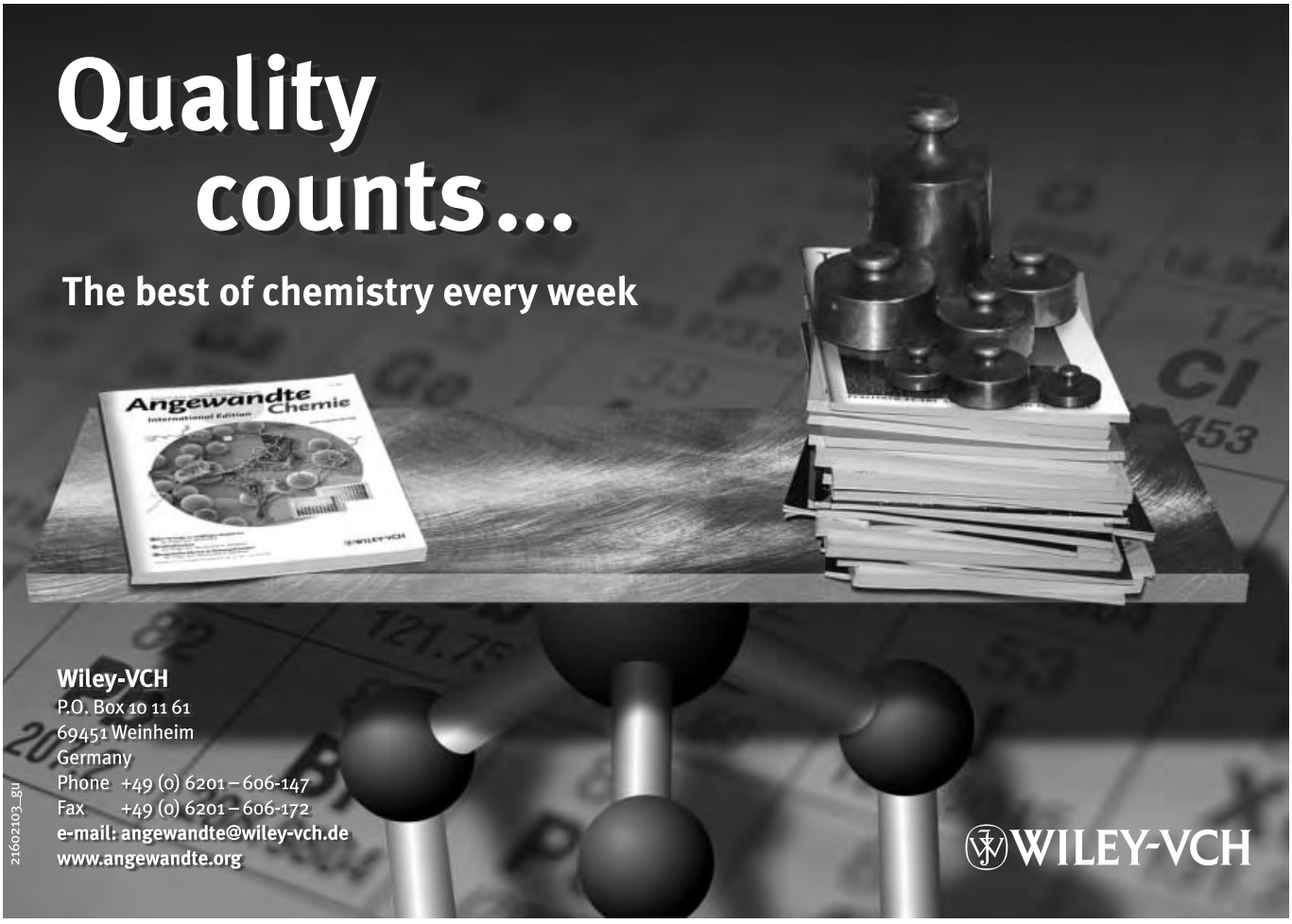
BMU	Federal Ministry for the Environment, Nature Conservation and Nuclear Safety (*Bundesministerium für Umwelt, Naturschutz und Reaktorsicherheit*)
BUA	Advisory Council on Existing Substances *(Beratergremium für Altstoffe)*
CAS	Chemical Abstracts Service
CICAD	Concise International Chemical Assessment Documents (WHO)
COP	Conference of the Parties
EC	European Community
EHC	Environmental Health Criteria Documents (WHO)
EINECS	European Inventory of Existing Commercial Chemical Substances
EU	European Union
FAO	Food and Agriculture Organization (of the United Nations, Rome)
GC	Governing Council
GDCh	German Chemical Society *(Gesellschaft Deutscher Chemiker)*
GLP	Good Laboratory Practice
GMEF	Global Ministerial Environment Forum
GTZ	*Deutsche Gesellschaft für Technische Zusammenarbeit mbH* (German development assistance agency)
G77	Third World interest group founded in 1964 by 77 developing countries
HPV Chemicals	High Production Volume Chemicals
ICCA	International Council of Chemical Associations
IFCS	Intergovernmental Forum on Chemical Safety
ILO	International Labor Organization (Geneva)
INC	Intergovernmental Negotiating Committee
IPCS	International Program on Chemical Safety
IPP	Integrated Product Policy
MLF	Multilateral Fund of Montreal Protocol
MP	Montreal Protocol
OECD	Organization for Economic Cooperation and Development (Paris)
PAC	Program Advisory Committee of IPCS
PCB	Polychlorinated biphenyls
PCP	Pentachlorophenol
PIC	Prior Informed Consent (Procedure)
PIM	Poisons Information Monographs (of the WHO)
POPs	Persistent Organic Pollutants
QSAR	Quality-Structure–Activity Relationship
SAICM	Strategic Approach on International Chemicals Management
UN	United Nations
UNCED	United Nations Conference on Environment and Development (Rio 1992)
UNCETDG	United Nations Committee of Experts on the Transport of Dangerous Goods
UNEP	United Nations Environment Program (Nairobi)
UNEP GC	UNEP Governing Council
UNIDO	United Nations Industrial Development Organization
UNITAR	United Nations Institute for Training and Development
WHO	World Health Organization
WSSD	World Summit for Sustainable Development (Johannesburg 2002)

We wish to thank Peter Reichling, BMU, for preparing the graphics in this article.

Received: February 14, 2003 [A584]

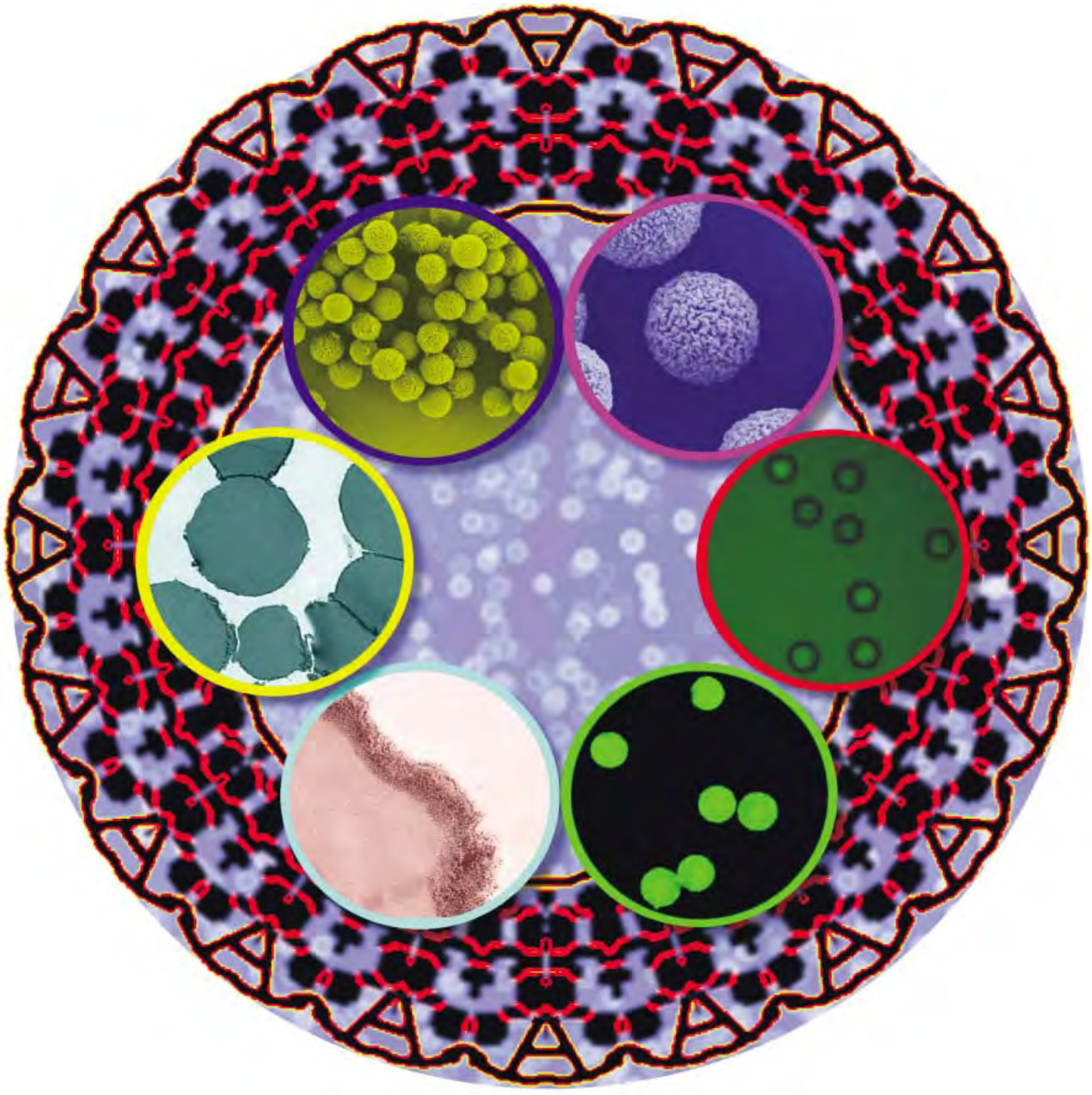
[1] BMZ Division 412, Environment, Poverty, and Sustainable Development, 11. Chemical Safety, self published. (BMZ = Bundesministerium für wirtschaftliche Zusammenarbeit und Entwicklung (Federal Ministry for Economic Cooperation and Development).

[2] a) B.-U. Hildebrand, U. Schlottmann, *Angew. Chem.* **1998**, *110*, 1382 – 1393; *Angew. Chem. Int. Ed.* **1998**, *37*, 1316 – 1326.
[3] W. Mahlmann, *Chemikalienrecht, Einführung und Erläuterung*, Wissenschaftliche Verlagsgesellschaft, Stuttgart, **2000**, p. 355.
[4] a) S. Gärtner, *Nachr. Chem. Tech. Lab.* **1997**, *45*, 607 – 608; b) S. Gärtner, *Nachr. Chem. Tech. Lab.* **1996**, *44*, 978 – 980.
[5] J. Ahlers, B. Schwarz-Schulz, H.-C. Stolzenberg, *Umweltwiss. Schadst.-Forsch.* **2001**, *13*, 75 – 78.
[6] Scientific Assessment of Ozone Depletion, WMO Global Ozone Research and Monitoring Project, no. 37, Genf, 1999 (WMO = World Meteorological Organization); *Global Aspects of Atmospheric Chemistry* (Ed.: R. Zellner), Steinkopf, Springer, Darmstadt, **1999**.
[7] U. Schlottmann, M. Kreibich, *Nachr. Chem.* **2001**, *49*, 605 – 614.
[8] H. Behret, *Nachr. Chem.* **2001**, *49*, 141 – 144.
[9] a) M. Eissen, J. O. Metzger, E. Schmidt, U. Schneidewind, *Angew. Chem.* **2002**, *114*, 402 – 425; *Angew. Chem. Int. Ed.* **2002**, *41*, 414 – 436; b) C. Brandt, *Chemie* **2002**, *36*, 214 – 224; c) V. Hauff, *Chemie* **2002**, *36*, 207.
[10] H. Greim, *Mitteilungen der Fachgruppe für Umweltchemie und Ökotoxikologie* **2003**, *1*, 9 – 11.
[11] U. Schlottmann, *Prüfmethoden für Chemikalien*, Hirzel, Stuttgart, **2002**, loose-leaf.
[12] U. Schlottmann, D. Kayser, *Gute Laborpraxis*, 3rd Ed., Behr's, Hamburg, **1997**, loose-leaf; http://www.wissenschaftliche-verlagsgesellschaft.de.



 © 2003 Wiley-VCH Verlag GmbH & Co. KGaA, Weinheim

Communications



The formation of composite microcapsules consisting of inorganic nanoparticles within polyelectrolyte shells is presented by G. B. Sukhorukov and co-workers on the following pages. The interior serves to prevent collapse on drying, while the release properties of the exterior are controlled through pH changes.

DOI: 10.1002/anie.200352068
© 2003 Wiley-VCH Verlag GmbH & Co. KGaA, Weinheim

Inorganic/Organic Microcapsules

Smart Inorganic/Organic Nanocomposite Hollow Microcapsules**

Dmitry G. Shchukin, Gleb B. Sukhorukov, and Helmuth Möhwald*

Polymeric capsules with shells made of polyelectrolyte multilayers[1] have recently attained widespread interest as novel types of carriers and microreactors with designed properties because they exhibit controllable permeability and surface functionality.[2,3] This should enable many applications in drug delivery, the food and cosmetic industries, or biotechnology. Another most important attribute of the capsules is the variety of mechanical properties that are available, since they can be made either of very flexible organic materials or of organic/inorganic composites, as well as exclusively inorganic materials (e.g., SiO_2, TiO_2, Fe_2O_3). For the latter case, an organic/inorganic composite has been calcined, thus removing the organic component.[4,5] Sintering of the inorganic particles leads to hollow but porous inorganic capsules. However, the permeability of these inorganic capsules is not controllable, which strongly limits their application. Hence, what is needed is a composite material where the inorganic fraction yields mechanical strength to withstand, for example, drying and osmotic pressure, and the organic fraction allows for controllable permeability. Beyond that, the inorganic component may also contribute specific optical,[6] magnetic,[7,8] and sorption properties.

In this work we report an elegant and direct way to prepare capsules under ambient conditions with inorganic particles as building blocks glued together by a pH-sensitive polyelectrolyte. By means of three examples we demonstrate controllable permeability in combination with mechanical strength. Alternatively YF_3, magnetic Fe_3O_4, and calcium hydroxyapatite $Ca_{10}(PO_4)_6(OH)_2$ inorganic/organic shells were used as examples of this new type of microcontainer, to demonstrate the general fabrication approach, mechanical properties, and the release activity of the inorganic composite capsules after redispersion. YF_3 shells can find application as adsorbents for rare earth ions, Fe_3O_4 shells are of practical importance in delivery systems due to their magnetic activity, while calcium hydroxyapatite shells can also be interesting in bioceramics, as an adsorbent for biomaterials, and as a chemical sensor, catalyst, and bone-repairing agent.

To synthesize composite inorganic/organic capsules, poly(styrene sulfonate) (PSS)/poly(allylamine hydrochloride) (PAH) polyelectrolyte capsules[2] containing PAH macromolecules were initially used as template microreactors. A suspension of $MnCO_3$ particles (1 mL, 3.6 μM, 5×10^8 particles per cm^3)[9] was mixed with a solution of citric acid (5 mL, 5 mM). Then an aqueous solution of PAH (0.7 mL, 1 mg mL^{-1}) was added while stirring, which formed a water-insoluble PAH/citrate complex on the surface of the template particles. The deposition of the first PAH/citrate layer was followed by layer-by-layer assembly of polyelectrolyte PAH/PSS multilayers using PAH (1 mg mL^{-1}) solution and PSS (2 mg mL^{-1}) solutions. After formation of the PAH/PSS shells, the $MnCO_3$ core was dissolved in 0.1 M HCl and hollow capsules composed of the inner thick PAH/citrate layer and outer PAH/PSS layer were formed. A more detailed description of the synthesis of hollow PAH/PSS capsules can be found elsewhere.[2,3,10]

The positive charge of the inner PAH layer, which is covered by the outer PAH/PSS shell, is compensated by negatively charged citrate ions; this results in a stable PAH/citrate complex.[3] The citrate ions can be replaced by other anions which can act as a precipitating agent to synthesize insoluble inorganic material exclusively inside the polyelectrolyte capsules. Exposing PAH/citrate–PAH/PSS capsules to a solution containing 0.01 M NaOH, 0.1 M H_3PO_4, or 0.1 M HF results in the rapid substitution of citrate ions to OH^-, PO_4^{3-} or F^- ions, and the formation of PAH/OH^-–PAH/PSS, PAH/PO_4^{3-}–PAH/PSS or PAH/F^-–PAH/PSS capsules. The presence of PO_4^{3-} and F^- ions in the capsule volume was confirmed by atomic absorbance spectroscopy; the absence of citrate ions after substitution was proved by FTIR spectroscopy. Thus, by such a simple procedure, PAH/PSS capsules containing the precipitating agent were obtained (Figure 1; stage a and b). These "initial" PAH/PSS capsules irreversibly collapse upon drying to form flat films (see scanning electron microscopy (SEM, Gemini Leo 1550) image in Figure 1).

After anion replacement the polyelectrolyte capsules were treated with 0.5 M $FeSO_4$ and 0.5 M $Fe_2(SO_4)_3$ (OH^--containing capsules), 1 M $CaCl_2$ adjusted to pH 9 by NaOH (PO_4^{3-}-containing capsules), or 0.1 M $Y(NO_3)_3$ (F^--containing capsules) solutions to deposit water-insoluble Fe_3O_4, hydroxyapatite or YF_3 particles, respectively, inside the capsules (Figure 1; stage c). The inorganic scaffold in the capsule interior prevents capsule collapse by forming micrometer-sized capsules with spherical morphology in the dry state, which are reminiscent of those of the original polyelectrolyte capsule in solution (see SEM image in Figure 1). Folds and creases spreading from one inorganic composite capsule to another are observed demonstrating partial shrinkage of the capsule shell. Wide-angle X-ray scattering analysis confirmed the presence of a weakly crystalline inorganic phase inside the polyelectrolyte capsules with traces of the corresponding metal oxides (Fe_2O_3, Y_2O_3); for $Ca_{10}(PO_4)_6(OH)_2$, a small amount of $CaPO_4$ was detected.

As has already been documented,[11] the PAH/PSS complex is unstable in strong alkaline (pH > 12) solution and can be dissolved. To remove the outer PAH/PSS shell, the resulting PAH/inorganic–PAH/PSS polyelectrolyte capsules loaded with inorganic material were added to 0.2 M NaOH solution for 24 h (Figure 1; stage d). SEM images of the capsules after PAH/PSS dissolution show individual spherical particles without polyelectrolyte material overlapping adja-

[*] Dr. G. B. Sukhorukov, Dr. D. G. Shchukin, Prof. Dr. H. Möhwald
Max Planck Institute of Colloids and Interfaces
14424 Potsdam (Germany)
Fax: (+49) 331-567-9202
E-mail: gleb@mpikg-golm.mpg.de

[**] This work was supported by the Sofja Kovalevskaja Program funded by the Alexander von Humboldt Foundation and the German Ministry of Education and Research.

 © 2003 Wiley-VCH Verlag GmbH & Co. KGaA, Weinheim DOI: 10.1002/anie.200352068

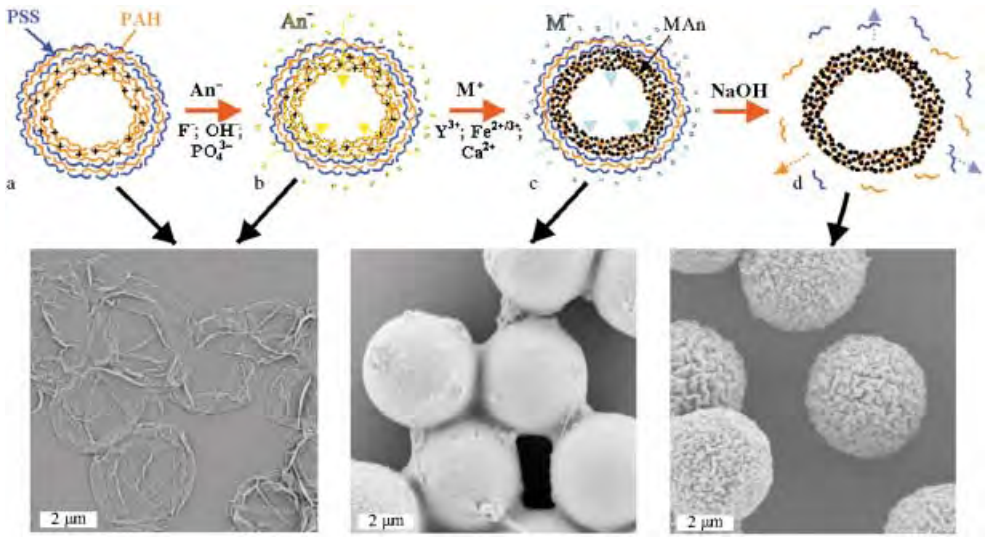


Figure 1. Schematic illustration of the preparation of inorganic/organic hollow capsules. $An^- = F^-$, OH^-, or PO_4^{3-}; $M^+ = Y^{3+}$, $Fe^{2+/3+}$, or Ca^{2+}; MAn = YF_3, Fe_3O_4, or hydroxyapatite; below: scanning electron microscopy images of the YF_3 capsules at different preparation stages (see text for details).

cent capsules (Figure 1, and Figure 2 a, b). Partial reduction of the capsule size and folding of the particle surface can be explained by minor shrinkage of the capsules after drying.

Raman microscopy and UV/Vis spectroscopy were employed to determine the extent of the dissolution of the outer PAH/PSS complex. 99% of the PSS used for shell assembly was recovered from the supernatant solution after washing out the capsules after NaOH treatment. Raman spectra from individual capsules recorded after PAH/PSS dissolution using a Raman microscope indicated the absence of PSS bands, however, signals from the inner PAH layer were found. Thus, it can be concluded that the resulting inorganic capsules consist of inorganic particles connected to each other by PAH from the inner PAH/anion layer.

To obtain information about the inner structure of the composite inorganic capsules, they were ultramicrotomed into thin slices (30–100 nm) and analyzed with a transmission electron microscope (Zeiss EM 912 Omega). As shown in Figure 2 d–f, the composite inorganic capsules are hollow and inorganic particles form a shell-like structure that prcipitates on the inner side of the initial polyelectrolyte shell where PAH, which acts as a source of precipitating anions, exhibits the highest concentration. A continuous 30–150 nm layer consisting of 7–10 nm particles was observed for all of the inorganic/polymer capsules that were fabricated.

Composite inorganic–polymer capsules have higher mechanical stability compared to the polyelectrolyte examples. Besides their shape persistence after drying, the capsules are stable to ultrasonic treatment; processing inorganic capsules in an ultrasonic bath for 1 h does not affect their surface morphology or permeability properties. A mechanical force applied to the composite capsule through a cantilever leads, at first, to their reversible elastic deformation; a further increase of the force results in irreversible plastic deformation of the inorganic capsules (deformed YF_3 composite capsules are represented in Figure 2 c). The strength of the force that must be applied to initiate plastic deformation of the

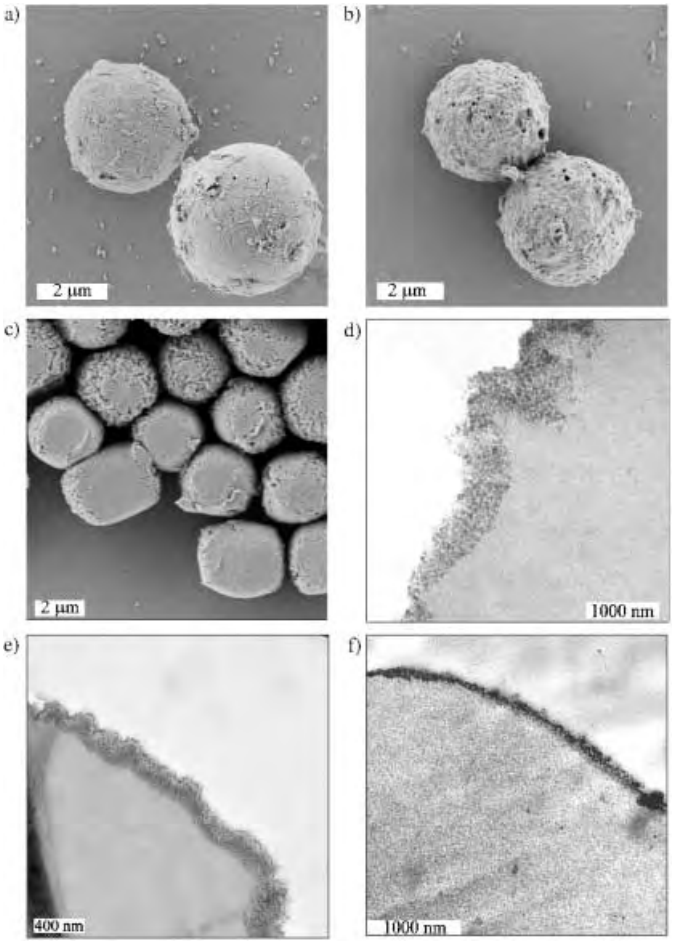


Figure 2. Scanning electron microscopy images of a) Fe_3O_4/PAH capsules; b) hydroxyapatite/PAH capsules; c) YF_3/PAH capsules that have undergone plastic deformation. Transmission electron microscopy images of d) ultramicrotomed Fe_3O_4/PAH capsules; e) hydroxyapatite/PAH capsules; f) YF_3/PAH capsules.

 © 2003 Wiley-VCH Verlag GmbH & Co. KGaA, Weinheim

inorganic composite capsule depends on the inorganic nanomaterial synthesized.

Composite inorganic/organic capsules can incorporate with various organic and bioorganic materials (e.g., drugs, polymers, and enzymes) in a controlled manner. For this purpose, permeability and release properties were studied employing dextran (molecular weight = 2000 kDa) labeled with fluorescein isothiocyanate, which acts as a probe for YF_3/PAH capsules. The experimental procedure was as follows: YF_3/PAH capsules were added to a buffer solution with an appropriate pH value (2 or 8) and, after 5 min, were mixed with the labeled dextran solution. Fluorescence images were acquired using a Leica TSC SP fluorescent confocal microscope (see Figure 3). The YF_3/PAH capsules with dextran were shown to have an open formation at pH 5, while at pH 10, all inorganic/organic capsules are closed and the dextran molecules are captured inside. Changing the pH value again to give a more acidic media results in opening the capsule shell and the release of dextran molecules into the surrounding solution. A similar permeability versus pH dependence was observed for "initial" PAH/PSS capsules with no inorganic material at their interior.[12] Thus, one can conclude that inorganic/PAH capsules possess the main advantage of polyelectrolyte capsules, that is, controlled permeability. Drying dextran-containing YF_3/PAH capsules does not influence the controlled release properties (Figure 3). In the dried state the fluorescence from captured dextran molecules was observed. Further redispersion of dried inorganic/organic composite capsules in acidic and alkali media showed the preservation of their controlled-permeability properties. Under acidic conditions (pH 2) YF_3/PAH capsules release dextran molecules into the surrounding solution, while at pH 8 dextran molecules remain within the capsules. The possibility of switching the open/closed state of the inorganic/organic capsules, together with their stability upon drying or mechanical deformation, combine to provide a powerful tool for controlling the release of the organic materials, which may find applications for the protection, delivery, and storage of substances with unstable formulations. The capsules are thus suitable for applications where purely inorganic capsules obtained by the complete removal of organic components (calcination)[5] can not be envisaged. All the encapsulation procedures developed previously for polyelectrolyte capsules[3,6,8,10,12] can be applied for the inorganic/organic capsules presented herein.

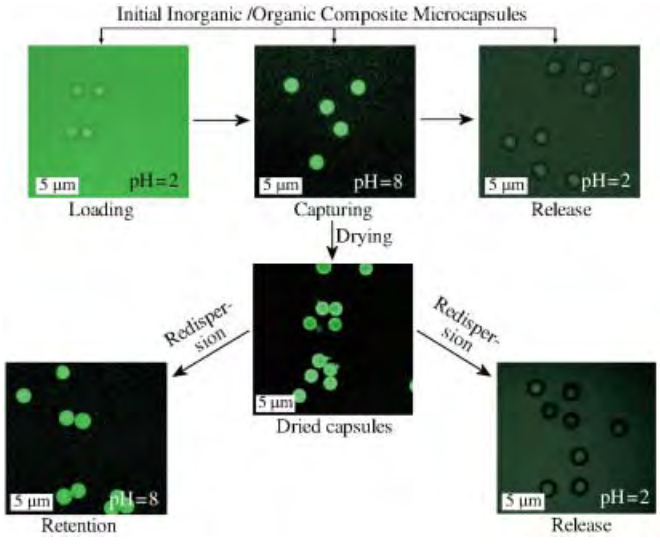


Figure 3. Permeability of YF_3/PAH capsules towards dextran molecules (molecular weight = 2000 kDa) labeled with fluorescein isothiocyanate. Measurements of the permeability of YF_3/PAH capsules before drying, in their dried state, and after redispersion in solutions with appropriate pH values were made using confocal fluorescent microscopy. The figure demonstrates that controlled permeability properties are retained in the composite inorganic/organic capsules after drying.

A versatile approach for the synthesis of new inorganic/organic composite capsules has been developed in this study. These inorganic capsules have both the advantages of inorganic materials (i.e., high mechanical stability) and conventional polyelectrolyte capsules (i.e., the controlled release/uptake properties of the capsule shell resulting from changes in, amongst others, pH value and ionic strength). Such possibilities have been demonstrated in this paper with the example of the controllable encapsulation and release of a polysaccharide (dextran). Defined characteristics (optical, magnetic, and mechanical) can be attributed to the composite capsules by varying the inorganic nanocomponent. Besides the common applications of polyelectrolyte capsules in controlled release, these composite inorganic/organic capsules can also be used as mechanically stable microreactors for enzymatic reactions and synthesis employing gas-phase reagents, in the form of hollow catalytically active microcontainers. The inorganic part can also find medical application that, together with encapsulated drug material, can provide synergetic curing effects (e.g., the application of hydroxyapatite-containing capsules in bone repair). Moreover, due to the preservation of the initial spherical shape and controlled-release properties upon drying, the inorganic/organic capsules can be employed as protective solid microcontainers for biochemical compounds that are unstable in solution or under UV/Vis irradiation, which can then be redispersed in solution to release the encapsulated compound in a controlled manner. In addition, the release properties of the inorganic/organic capsules can be adjusted mechanically by applying mechanical forces.

Received: June 5, 2003 [Z52068]
Published Online: September 1, 2003

Keywords: microcapsules · nanostructures · organic–inorganic hybrid composites · polyelectrolytes · template synthesis

[1] a) G. Decher, *Science* **1997**, *277*, 1232–1237; b) J. Hiller, J. D. Mendelsohn, M. F. Rubner, *Nat. Mater.* **2002**, *1*, 59–63.
[2] a) E. Donath, G. B. Sukhorukov, F. Caruso, S. Davis, H. Möhwald, *Angew. Chem.* **1998**, *110*, 2324–2327; *Angew. Chem. Int. Ed.* **1998**, *37*, 2202–2205; b) G. B. Sukhorukov, E. Donath, S. Davis, H. Lichtenfeld, F. Caruso, V. I. Popov, H. Möhwald, *Polym. Adv. Technol.* **1998**, *9*, 759–767.
[3] G. B. Sukhorukov in *Novel Methods to Study Interfacial Layers* (Eds.: D. Mobius, R Miller), Elsevier Science, **2001**, pp. 384–414.

 © 2003 Wiley-VCH Verlag GmbH & Co. KGaA, Weinheim

[4] L. M. Liz-Marzan, M. Giersig, P. Mulvaney, *Langmuir* **1996**, *12*, 4329 – 4335.
[5] a) R. A. Caruso, A. S. Susha, F. Caruso, *Chem. Mater.* **2001**, *13*, 400 – 407; b) F. Caruso, R. Caruso, H. Möhwald, *Science* **1998**, *282*, 1111 – 1114; c) F. Caruso, R. Caruso, H. Möhwald, *Chem. Mater.* **1999**, *11*, 3309 – 3314.
[6] I. L. Radtchenko, G. B. Sukhorukov, N. Gaponik, A. Kornowski, A. L. Rogach, H. Möhwald, *Adv. Mater.* **2001**, *13*, 1684 – 1687.
[7] E. L. Bizdoaca, M. Spasova, M. Farle, M. Hilgendorff, F. Caruso, *J. Magn. Magn. Mater.* **2002**, *240*, 44 – 46.
[8] G. Ibarz, L. Dahne, E. Donath, H. Möhwald, *Adv. Mater.* **2001**, *13*, 1324 – 1327.
[9] D. G. Shchukin, G. B. Sukhorukov, *Langmuir* **2003**, *19*, 4427 – 4431.
[10] G. B. Sukhorukov, E. Donath, S. Moya, A. S. Susha, A. Voigt, J. Hartmann, H. Möhwald, *J. Microencapsulation* **2000**, *17*, 177 – 185.
[11] I. L. Radtchenko, G. B. Sukhorukov, S. Leporatti, G. B. Khomutov, E. Donath, H. Möhwald, *J. Colloid Interface Sci.* **2000**, *230*, 272 – 280.
[12] G. B. Sukhorukov, A. A. Antipov, A. Voigt, E. Donath, H. Möhwald, *Macromol. Rapid Commun.* **2001**, *22*, 44 – 46.

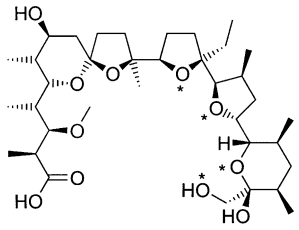
 © 2003 Wiley-VCH Verlag GmbH & Co. KGaA, Weinheim

Polyether Biosynthesis

Intermediates Released from a Polyether-Producing Polyketide Synthase Provide Insight into the Mechanism of Oxidative Cyclization**

*Zoë A. Hughes-Thomas, Christian B. W. Stark, Ines U. Böhm, James Staunton, and Peter F. Leadlay**

Monensin A (**1**) from *Streptomyces cinnamonensis* is an antibiotic ionophore[1] widely used in veterinary medicine and also as a food additive in animal husbandry. It is one of the most important and best-studied members of a very large family of structurally related polyketide secondary metabolites, the polyethers. As with all natural polyethers, the molecule contains a multiplicity of asymmetric centers, but only one stereoisomer (out of 2^{17}) is produced by *S. cinnamonensis*. The molecular basis for this exquisite stereocontrol is not understood, and even the nature of the intermediates in polyether biosynthesis has until recently been a matter for conjecture. The results of early feeding studies using carbon-14-labeled precursors showed that monensin A is derived by a polyketide pathway from five acetate, one butyrate, and seven propionate units,[2] and similar studies showed that oxygen atoms (O)1, (O)3, (O)4, (O)5, (O)6, and (O)10 arise from the carboxylate oxygen atoms of the corresponding carboxylic acid precursor units, while four other oxygen atoms, at C(13), C(17), C(21), and C(26), are derived from molecular oxygen (Scheme 1).[3] On this basis, several plausible mechanisms have been suggested for the key oxidative steps.[3b,4] These hypotheses all involve the intermediacy of open-chain precursors, but the key difference concerns the stereochemistry of the double bonds (compare, for example, structures **2** and **3** in Scheme 2a and b, respectively). However, the exact nature of the pathway has proved elusive because it has not been possible to detect any intermediates prior to oxidative ring formation.



1

Scheme 1. The polyether ionophore monensin A (**1**). Oxygen atoms arising from molecular oxygen are shown with asterisks.

An appropriately functionalized triketide precursor has been successfully incorporated intact into monensin A[5] in the presence of an inhibitor of fatty acid oxidation, thus supporting the view that the carbon backbone is assembled by processive operation of a modular polyketide synthase (PKS).[6] However, a synthetic sample of the full-length putative linear triene precursor **2** was found not to be incorporated into monensin A by *S. cinnamonensis*.[7] Therefore, the configuration of the double bonds in a putative linear pre-monensin, as well as the mode of oxidative cyclization, have remained undefined. Indeed, if oxidative cyclization can be initiated on the growing polyketide chain while it is attached to the PKS, then such full-length linear polyketides as, for example, **2** and **3** may not even be true intermediates.

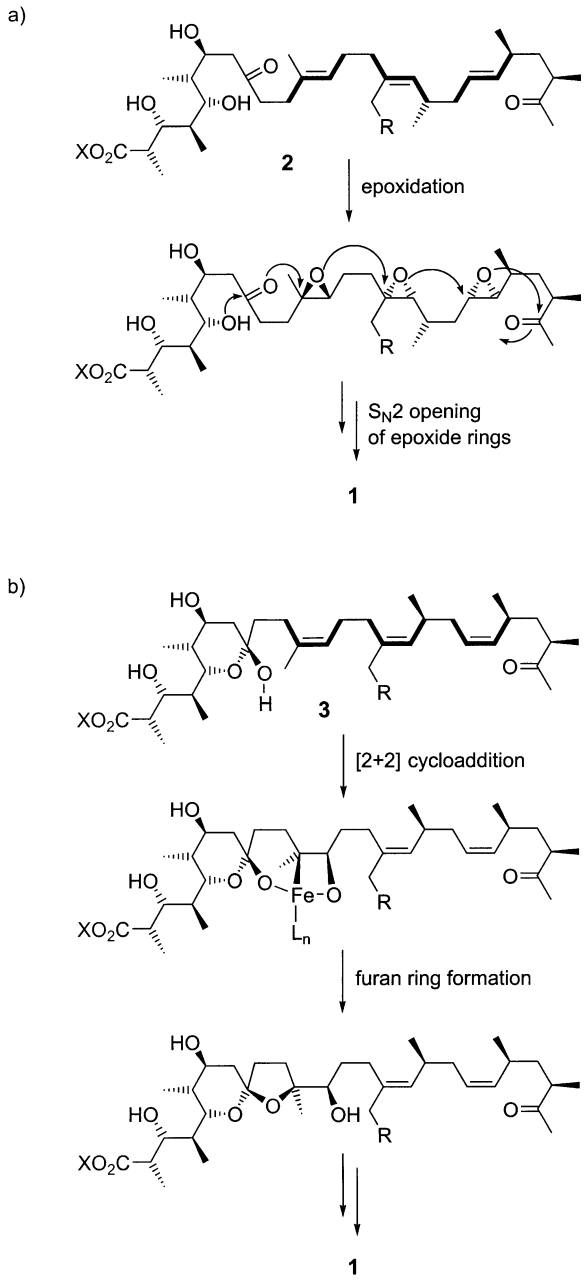
The entire monensin biosynthetic gene cluster has recently been sequenced[8] and it has been found to contain eight contiguous open reading frames (ORFs) housing a modular PKS with 12 extension modules, which is consistent

[*] Prof. Dr. P. F. Leadlay, Z. A. Hughes-Thomas, Dr. I. U. Böhm
Department of Biochemistry
University of Cambridge
80 Tennis Court Road, Cambridge CB2 1GA (UK)
Fax: (+44) 1223-76-6091
E-mail: pfl10@mole.bio.cam.ac.uk
Dr. C. B. W. Stark,[+] Prof. Dr. J. Staunton
University Chemical Laboratory
University of Cambridge
Lensfield Road, Cambridge CB2 1EW (UK)
[+] current address:
Freie Universität Berlin
Institut für Chemie—Organische Chemie
Takustrasse 3, 14195 Berlin (Germany)

[**] This research was supported by the Biotechnology and Biological Sciences Research Council (BBSRC). We gratefully acknowledge the support of a studentship from the BBSRC (to Z.A.H.-T.), the support of I.U.B. through a grant from Glaxo Group Research, Stevenage, UK (to P.F.L. and J.S.), and a grant from Roche Pharmaceuticals (Basel) and an EU Marie Curie Postdoctoral Training Fellowship (to C.B.W.S.).

Supporting information for this article is available on the WWW under http://www.angewandte.org or from the author.

 DOI: 10.1002/anie.200351375 © 2003 Wiley-VCH Verlag GmbH & Co. KGaA, Weinheim



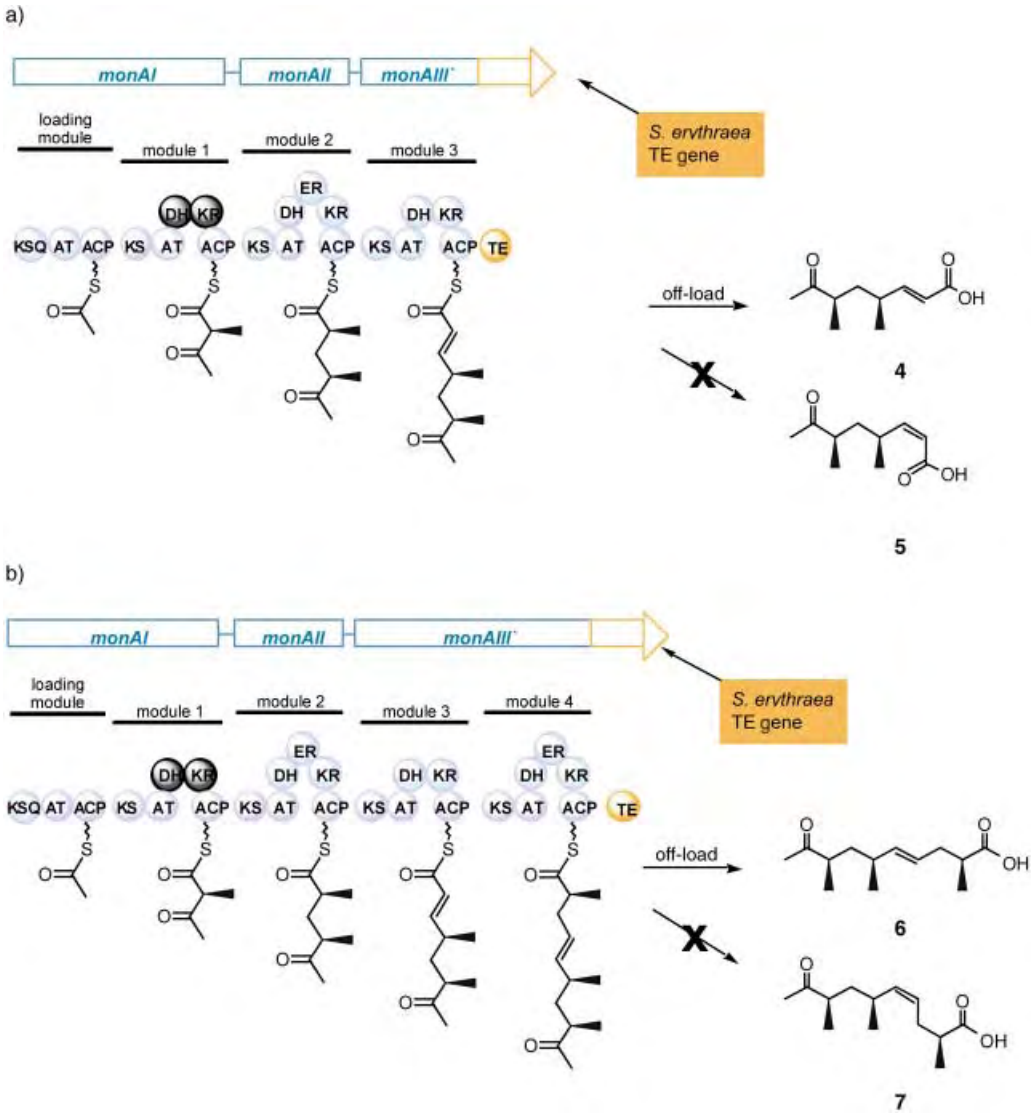
Scheme 2. Examples of alternative mechanisms for oxidative cyclization to produce monensin. a) Cane–Westley proposal of a polyepoxide cyclization cascade starting from *E*,*E*,*E* triene **2**; b) Townsend–Basak proposal involving [2+2] cycloadditions starting from the *Z*,*Z*,*Z* triene **3**. Monensin A: R = CH_3; monensin B: R = H.

with the production of a premonensin polyketide chain, together with numerous other genes likely to be involved, for example, in antibiotic regulation and export. Analysis of the DNA sequence revealed in particular a set of four unusual ORFs which, on the basis of database comparisons, appear to relate to the unusual oxidative cyclizations that are required to produce the polycyclic product.[4f] Here we describe an experimental approach to isolate and identify crucial open-chain intermediates from the monensin-producing PKS, and to gain the first insight into the stereochemistry and timing of the oxidative steps.

The study of DEBS, the modular PKS governing the biosynthesis of the macrolide erythromycin A in *Saccharopolyspora erythraea*, was greatly advanced when it was found that the chain-terminating thioesterase (TE) domain could release truncated polyketide chains when it was relocated from the C-terminal end of DEBS extension module 6 to the C-termini of extension modules 2, 3, or 5.[9] It was hoped that the introduction of the DEBS TE domain at the end of certain extension modules in the monensin PKS in *S. cinnamonensis* would provoke the release of specific linear intermediates, even though the normal action of the TE involves cyclization. It should be noted that in erythromycin A biosynthesis, the C-2 and C-3 positions in the polyketide intermediates normally bear methyl and hydroxy groups, respectively, while, in contrast, a number of the monensin PKS-bound intermediates would contain C-2 methyl and C-2,3 olefinic groups. However, the *N*-acetylcysteamine thioesters of structural analogues of such intermediates are hydrolyzed by the purified DEBS TE in vitro and previous studies both in vivo and in vitro have shown that in general the TE has a relaxed specificity.[10a] Thus, the 3′-portion of the *eryAIII* gene which encodes the TE domain was positioned downstream of either module 3 or module 4 of the monensin PKS to create a tetra- and a pentaketide synthase, respectively (Scheme 3). We hoped in this way to isolate the specific products from these hybrid enzymes, and thus to deduce the stereochemistry and structure of both the tetraketide and pentaketide intermediates.

Introduction of the TE domain from the DEBS cluster was accomplished by homologous recombination into wild-type *S. cinnamonensis* by a single crossover event. Correct integration into the chromosome was proved for both mutant strains ZAHT-2 (tetraketide synthase) and ZAHT-1 (pentaketide synthase) by Southern hybridization. No monensin was produced by either of these mutants, as judged by HPLC analysis. The truncated monensin PKSs were expected to produce either the *E* tetraketide acid **4** and the *E* pentaketide acid **6**, respectively, or their corresponding *Z* isomers, **5** and **7** (Scheme 3), or conceivably both isomers as a mixture. Analysis was carried out by GC-MS after methylation of the crude extracts using (trimethylsilyl)diazomethane (TMS-diazomethane).[11] Both analytes showed a major peak corresponding to the predicted mass of the tetra- and pentaketide derivatives, respectively (Figure 1). The structure of the tetraketide was determined by comparison with an authentic sample derived by chemical synthesis.[12] GC-MS analysis clearly indicated that the *trans* isomer of the tetraketide was formed (corresponding to **4**). However, it is possible that isomerization of the double bond (which is conjugated to the carbonyl group) might have occurred during extraction under the acidic conditions used (pH 3.5). To enable the stereochemistry of the pentaketide to be determined, a 500 mL culture of mutant ZAHT-1 was grown under standard conditions[4e] and the crude extract of the supernatant was then sequentially purified by column chromatography to yield 22 mg of pure pentaketide acid.[13] Detailed NMR analysis of this acid unequivocally showed the configuration of the disubstituted double bond to be *trans*; the intermediate giving rise to this would be **6**. No evidence of the presence of an

 © 2003 Wiley-VCH Verlag GmbH & Co. KGaA, Weinheim



Scheme 3. Truncated polyketide synthases generated from the monensin PKS by integration into *S. cinnamonensis* of the DNA encoding the C-terminal thioesterase domain of the erythromycin-producing PKS C-terminal of a) extension module 3 (in strain ZAHT-2) and b) extension module 4 (in strain ZAHT-1). ACP, acylcarrier protein; KS, ketoacyl-ACP synthase; AT, acyltransferase; KR, ketoacyl-ACP ketoreductase; DH, dehydratase; ER, enoyl-ACP reductase; KSQ, malonyl-ACP decarboxylase; TE, thioesterase. The tetraketide and pentaketide products released from these synthases are also shown as **4** and **6**, respectively. Products **5** and **7** were not detected.

oxidized derivative of either tetraketide or pentaketide was obtained in either of these analyses of the presence of an oxidized derivative, which suggests (though it does not prove) that further elongation of the polyketide chain is required before epoxidation of the double bond in these intermediates can take place.

Taken together, these results directly implicate the *E* forms of the tetraketide and pentaketide as intermediates in monensin biosynthesis and the *trans* double bond that they contain as one of the targets for the epoxidase MonC1 which initiates oxidative cyclization.[4f] This is consistent with mechanisms which invoke triepoxide intermediates, as proposed by Cane and Westley[4a] (Scheme 2a) and by us,[4e] but not with the mechanistic proposal of Townsend and Basak.[4c] Furthermore, our results underscore the utility of the DEBS TE domain for the specific release of truncated intermediates from a heterologous PKS and suggest that the same experimental approach may permit structural characterization of more elaborate open-chain precursors of monensin A. In particular, the stage is set for dissection of the respective contributions of the PKS and of the "post-PKS" enzymes MonCI (epoxidase), MonCII (cyclase), MonBI, and MonBII (putative isomerases) to the stereocontrol of polyether biosynthesis.

Received: March 12, 2003 [Z51375]

Keywords: antibiotics · configuration determination · natural products · oxidation · polyethers

 © 2003 Wiley-VCH Verlag GmbH & Co. KGaA, Weinheim

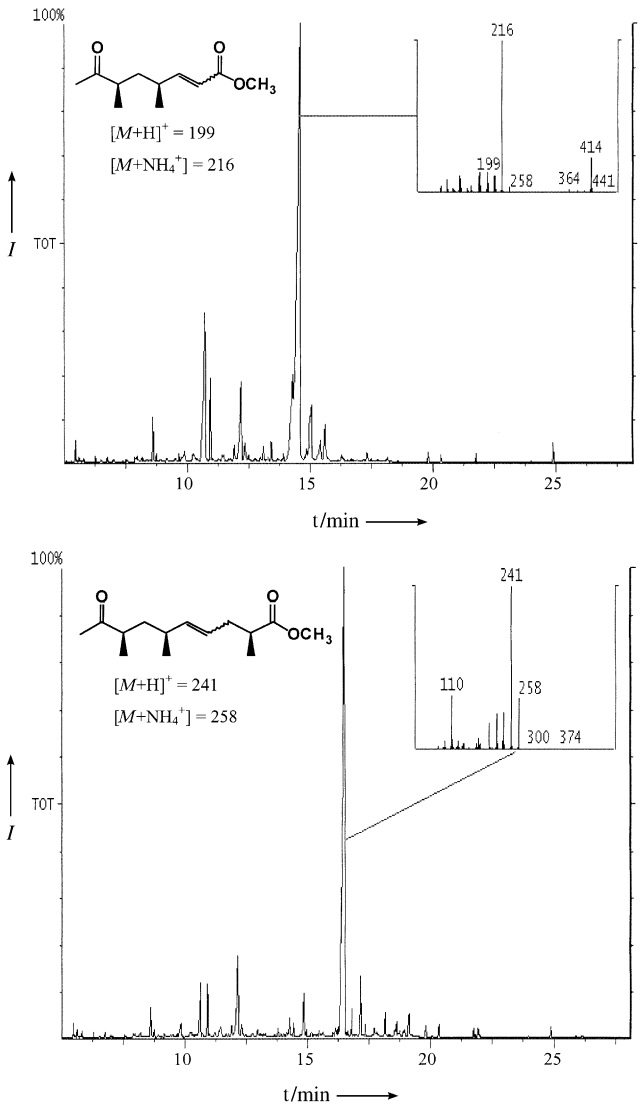


Figure 1. GC-MS analysis of a crude extract of a) the tetraketide-producing strain ZAHT-2 and b) the pentaketide-producing strain ZAHT-1 after methylation of the samples indicating the presence of **4** and **6**, respectively.

[1] A. Agatrap, J. W. Chamberlin, M. Pinkerton, L. Steinrauf, *J. Am. Chem. Soc.* **1967**, *89*, 5737–5748.

[2] L. E. Day, J. W. Chamberlin, E. Z. Gordee, S. Chen, M. Gorman, R. L. Hamill, T. Ness, R. E. Weeks, R. Stroshane, *Antimicrob. Agents Chemother.* **1973**, *4*, 410–414.

[3] a) D. E. Cane, T. C. Liang, H. Hasler, *J. Am. Chem. Soc.* **1981**, *103*, 5962–5965; b) D. E. Cane, T. C. Liaqng, H. Hasler, *J. Am. Chem. Soc.* **1982**, *104*, 7274–7281; c) A. A. Ajaz, J. A. Robinson, *J. Chem. Soc. Chem. Commun.* **1983**, 679–680.

[4] a) D. E. Cane, W. D. Celmer, J. W. Westley *J. Am. Chem. Soc.* **1983**, *105*, 3594–3600; b) A. A. Ajaz, J. A. Robinson, D. L. Turner, *J. Chem. Soc. Perkin Trans. 1* **1987**, 27–36; c) C. A. Townsend, A. Basak, *Tetrahedron* **1991**, *47*, 2591–2602; d) F. E. McDonald, T. B. Towne, *J. Am. Chem. Soc.* **1994**, *116*, 7921–7922; e) P. F. Leadlay, J. Staunton, M. Oliynyk, C. Bisang, J. Cortés, E. Frost, Z. A. Hughes-Thomas, M. A. Jones, S. G. Kendrew, J. B. Lester, P. F. Long, H. A. I. McArthur, E. L. McCormick, Z. Oliynyk, C. B. W. Stark, C. J. Wilkinson, *J. Ind. Microbiol. Biotechnol.* **2001**, *27*, 360–367; for a review, see f) U. Koert, *Angew. Chem.* **1995**, *107*, 326–328; *Angew. Chem. Int. Ed. Engl.* **1995**, *34*, 298–300.

[5] H. Patzelt, J. A. Robinson, *J. Chem. Soc. Chem. Commun.* **1993**, 1258–1260; H. Patzelt, Ph.D. thesis, University of Zürich, **1996**.

[6] a) J. Cortés, S. F. Haydock, G. A. Roberts, D. J. Bevitt, P. F. Leadlay, *Nature* **1990**, *348*, 176–178; b) S. Donadio, M. J. Staver, J. B. McAlpine, S. J. Swanson, L. Katz, *Science* **1991**, *252*, 675–679; c) J. Staunton, K. J. Weissman, *Nat. Prod. Rep.* **2001**, *18*, 380–416.

[7] D. S. Holmes, J. A. Sherringham, U. C. Dyer, S. T. Russell, J. A. Robinson, *Helv. Chim. Acta* **1990**, *73*, 239–259.

[8] M. Oliynyk, C. B. W. Stark, A. Bhatt, M. A. Jones, Z. A. Hughes-Thomas, Z. Oliynyk, Y. Demydchuk, J. Staunton, P. F. Leadlay, *Mol. Microbiol.* **2003**, *48*, in press; see also M. Oliynyk, Ph.D. thesis, University of Cambridge, **1998** and reference [4e].

[9] a) J. Cortés, K. E. H. Wiesmann, G. A. Roberts, M. J. B. Brown, J. Staunton, P. F. Leadlay, *Science* **1995**, *268*, 1487–1489; b) C. M. Kao, G. L. Luo, L. Katz, D. E. Cane, C. Khosla, *J. Am. Chem. Soc.* **1995**, *117*, 9105–9106; c) C. M. Kao, G. L. Luo, L. Katz, D. E. Cane, C. Khosla, *J. Am. Chem. Soc.* **1996**, *118*, 9184–9185.

[10] a) M. L. Heathcote, unpublished results; for previous in vivo and in vitro studies showing that the TE has a relaxed specificity, see b) R. Aggarwal, P. Caffrey, P. F. Leadlay, C. J. Smith, J. Staunton, *J. Chem. Soc. Chem. Commun.* **1995**, 1519–1520; c) K. J. Weissman, C. J. Smith, U. Hanefeld, R. Aggarwal, M. Bycroft, J. Staunton, P. F. Leadlay, *Angew. Chem.* **1998**, *110*, 1503–1506; *Angew. Chem. Int. Ed.* **1998**, *37*, 1437–1440; d) R. S. Gokhale, D. Hunziker, D. E. Cane, C. Khosla, *Chem. Biol.* **1999**, *6*, 117–125; e) M. L. Heathcote, J. Staunton, P. F. Leadlay, *Chem. Biol.* **2001**, *8*, 207–220.

[11] a) The construction and fermentation of the mutant strains of *Streptomyces cinnamonensis* containing the plasmids pZAHT-1 (pentaketide synthase) and pZAHT-2 (tetraketide synthase), respectively, is described in the Supporting Information. The experimental design led to the introduction of an additional *Mfe*I restriction site at the 3′-end of the ACP domain in each case. For the tetraketide synthase, this altered the C-terminal residue of the ACP domain from module 3 of the *mon* PKS from a histidine to a glutamine residue. The counterpart residue in the ACP domain of module 4 of the pentaketide synthase was altered from arginine to glutamine. Both substitutions at this position are known in natural PKS ACP domains. b) N. Hashimoto, T. Aoyama, T. Shiori, *Chem. Pharm. Bull.* **1981**, *29*, 1475.

[12] Spectral data for **4** were in accord with published data, see a) M. H. Block, D. E. Cane, *J. Org. Chem.* **1988**, *53*, 4923–4928; b) U. C. Dyer, J. A. Robinson, *J. Chem. Soc. Perkin Trans. 1* **1988**, 53–60; c) D. V. Patel, F. Van Middlesworth, J. Donaubauer, P. Gannett, C. J. Sih, *J. Am. Chem. Soc.* **1986**, *108*, 4603–4614; see also references [5] and [7].

[13] Spectral data for the pentaketide acid **6**: ^{1}H NMR (500 MHz, $CDCl_3$, 25 °C): $\delta = 0.98$ (d, $J = 6.7$ Hz, 3H), 1.03 (d, $J = 6.9$ Hz, 3H), 1.16 (d, $J = 7.0$ Hz, 3H), 1.23 (m, 1H), 1.58 (ddd, $J = 9.8$, $J = 5.3$, $J = 5.3$ Hz, 1H), 2.09 (s, 3H), 2.13 (m, 2H), 2.34 (ddq, $J = 7.1$, $J = 6.9$, $J = 1.0$ Hz, 1H), 2.49 (m, 2H), 5.24 (dd, $J = 15.2$, $J = 8.4$ Hz, 1H), 5.34 ppm (dt, $J = 15.2$, $J = 6.9$ Hz, 1H); the coupling constant of $J = 15.2$ Hz between the hydrogen atoms located on the C=C bond is indicative of a *trans* configuration (typical range 14–16 Hz);^{13}C NMR (125.8 MHz), $CDCl_3$, 25 °C): $\delta = 13.9$, 15.6, 16.1, 27.2, 34.8, 36.2, 39.2, 39.4, 45.0, 125.9, 138.1, 180.8, 213.1 ppm; IR ($CHCl_3$): $\tilde{\nu} = 3683$, 3029, 2433, 2399, 2242, 1748, 1706, 1601, 1521, 1476, 1423, 1334, 1214, 1016, 928, 849 cm^{-1}; HRMS (ES) calcd for $C_{14}H_{24}O_3Na^+$ $[M+Na]^+$: 263.1627, found: 263.1618.

 © 2003 Wiley-VCH Verlag GmbH & Co. KGaA, Weinheim

Dynamic Combinatorial Chemistry

Detection of Ligands from a Dynamic Combinatorial Library by X-ray Crystallography**

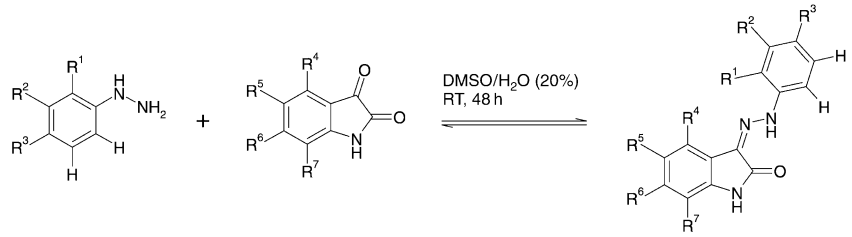
Miles S. Congreve, Deborah J. Davis, Lindsay Devine, Cesare Granata, Marc O'Reilly, Paul G. Wyatt, and Harren Jhoti*

Dynamic combinatorial chemistry (DCC) is an approach to molecular recognition in which specific members of a combinatorial library are selected and amplified with the use of a template.[1–6] The principle difference between DCC and traditional combinatorial chemistry is that the reaction linking the building blocks together in DCC is reversible and there is an ongoing interchange between the different members of the dynamic combinatorial library (DCL) under thermodynamic control.[7] A DCL is therefore able to respond to molecular recognition events owing to the presence of a template, such as a protein, which can stabilize a particular member of the library and induce a shift in the equilibrium, favoring the formation of the selected species. A drawback of the method is that it usually requires excess quantities of protein for an effect on the equilibrium to be observed. Also, the effect can only be detected by comparison of identical libraries, generated with and without the protein component present, using either mass spectrometric analysis or HPLC chromatograms as a fingerprint. We now report a complimentary approach in which ligands are observed directly by X-ray crystallography by interpretation of electron-density maps from crystals exposed to a dynamic combinatorial library mixture. We call this technology dynamic combinatorial X-ray crystallography or DCX. This approach was used to detect rapidly potent inhibitors of the cyclin-dependent kinase 2 protein. DCX has key advantages over previously reported DCC technologies[8,9] in that direct identification of the ligand is possible from the mixture of components in the DCL, and its detailed binding mode is defined from the electron-density maps. Furthermore, only very small amounts of protein are required for each individual DCX experiment compared with previously reported DCC protocols.

It has been established with both X-ray crystallography and NMR spectroscopic techniques that very small molecules or "fragments" ($M_W = 100$–200) are capable of binding to proteins in a reproducible and specific manner, even though their intrinsic potency, as determined with an in vitro biological assay, is very weak (IC_{50} μM–mM).[10–14] We postulated that fragments bound to adjacent pockets within the active site of a protein could, in principle, self-assemble to generate larger, more potent ligands if they had complimentary chemical reactivities.[15] Such a method would have key advantages, as the time-consuming and expensive practice of conventional synthesis, purification, and testing of combinatorial libraries designed to discover potent inhibitors might be obviated.

To explore the potential of DCX, we used cyclin-dependent kinase 2 (CDK2) for an initial proof-of-principle study. This target has been the subject of intense investigation by many groups, with the aim of developing inhibitors for the treatment of a number of human cancers.[16–17] We chose an inhibitor series developed for CDK2 based on an oxindole template.[18] These inhibitors (Table 1) present substituents in adjacent lipophilic binding pockets within the ATP-binding site of the kinase and can be disconnected to reactive fragments (termed monomers) of approximately equal size and complexity (hydrazines **A** and isatins **B**; Table 1). Before attempting to perform DCX with crystals of CDK2, we first established the suitability of the chemistry for synthesizing a

Table 1: Combinatorial array of oxindole compounds synthesized by reaction of hydrazines **A** and isatins **B**.[a]



A **B** **A1–6 B1–5**

A×B		A1 –[b]	A2 R^1 = Cl	A3 R^2 = Cl	A4 R^3 = Cl	A5 $R^3 = SO_2NH_2$	A6 R^1 = Cl; $R^3 = SO_2Me$
B1	$R^5 = NO_2$	10–25	60–95	60–95	30–50	60–95	30–50
B2	R^5 = Cl	60–95	60–95	60–95	60–95	60–95	30–50
B3	$R^5 = SO_3H$	10–25	60–95	30–50	10–25	60–95	30–50
B4	$R^7 = CF_3$	30–50	60–95	60–95	60–95	60–95	30–50
B5	$R^5 = OCF_3$	30–50	60–95	60–95	60–95	60–95	10–25

[a] Values indicate the extent to which the reaction occurred in aqueous DMSO after 48 h at room temperature as assessed by percentage purity by peak area of the product by LC/MS (10–25%, 30–50%, or 60–95% of total peaks excluding solvent front). [b] R groups = H unless indicated otherwise. DMSO = dimethyl sulfoxide.

[*] Dr. M. S. Congreve, Dr. D. J. Davis, L. Devine, C. Granata, Dr. M. O'Reilly, Dr. P. G. Wyatt, Dr. H. Jhoti
Astex Technology
436 Cambridge Science Park
Milton Road, Cambridge CB4 0QA (UK)
Fax: (+44) 1223-226-201
E-mail: m.congreve@astex-technology.com

[**] The authors thank Professor Chris Abell, Dr. Robin Carr, Dr. David Rees, and Dr. Chris Murray for useful suggestions and discussions. DCX is a Trade Mark of Astex Technology, Ltd.

Supporting information for this article is available on the WWW under http://www.angewandte.org or from the author.

 DOI: 10.1002/anie.200351951 © 2003 Wiley-VCH Verlag GmbH & Co. KGaA, Weinheim

DCL based on these oxindole inhibitors. Hydrazone chemistry, used for assembly of the library products, has previously been shown to be highly suitable for dynamic combinatorial library syntheses.[19–20] A range of hydrazines (**A1–6**) and isatins (**B1–5**) were selected that would present a variety of functional groups to the lipophilic pockets in the ATP-binding site. The selection of these monomers was aided by knowledge of the features of the active site. A trial of each of the 30 possible reactions was then carried out under aqueous conditions in the presence of 20% of the cosolvent dimethylsulfoxide (DMSO) over a 48-hour period, and the results showed that each product was successfully synthesized (Table 1). Further monomer competition studies were then carried out and these indicated that all the possible products could be formed as part of the DCL.[21]

Once the suitability of the chemistry was established, the reactions were then carried out in the presence of protein crystals. A summary of these experiments is given in Table 2.

Table 2: Summary of X-ray crystallography experiments and biological assay results.[a]

Mixture composition	Product	IC_{50} [nM]
A5 + B1	YES	30
A5 + B2	YES	30
A5 + B3	YES	30
A5 + B4	NO	inactive
A5 + B5	YES	30
B2 + (A1,A2,A3,A4)	NO	N/A
B2 + (A1,A2,A3,A4,A5,A6)	YES (**A5B2**)	N/A
(B1,B2,B3,B4,B5) + (A1,A2,A3,A4,A5,A6)	YES (**A5B2**)	N/A

[a] Table indicates if electron density consistent with a reaction product from mixtures of isatins and hydrazines was detected upon exposure to CDK2 protein crystals. The biological activity subsequently measured of the corresponding purified product of the reaction is also given when synthesized. Full details of the X-ray data collected and biological assay conditions are described in the Supporting Information.

The first studies were performed with individual crystals of CDK2[22–24] soaked in reaction solutions containing monomer **A5** and each of the isatin monomers (**B1–5**) in turn. In all but one case (**A5 + B4**) the resulting electron density in the ATP pocket indicated that the corresponding ligand had bound (Table 2, Figures 1a–d). To correlate these findings with the biological activity, each of these ligands was then synthesized as purified single compounds, and the activity determined in an assay for CDK2. Each of the ligands that had bound in the protein crystal was shown to be a potent enzyme inhibitor. Analogue **A5B4**, which did not bind in X-ray studies, was biologically inactive (Table 2).[25] These data are broadly consistent with the published structure–activity relationships for this series of inhibitors.[18]

Studies were then carried out to investigate the use of our approach to detect ligands from a dynamic combinatorial library mixture. Firstly, two "cocktails" of reaction solutions were added to CDK2 crystals to explore the potential of the method to discover potent inhibitors from a mixture of nonbinders. Comparison of the cocktail containing (**A1–4**) + **B2** with the cocktail that contained (**A1–6**) + **B2** revealed electron density that was consistent with ligand binding only in the latter case (Table 2). Furthermore, the electron density was consistent with the expected potent ligand **A5B2** (Figure 1e). Next, the degeneracy of the DCL was increased to 30 possible ligands using a reaction cocktail that contained hydrazines (**A1–6**) and isatins (**B1–5**). Difference electron density consistent with the reaction product **A5B2** was again observed, clearly demonstrating that the method is useful for the identification of ligands from a DCL mixture (Figure 1f).

The detection of ligands formed in this study does not rely on an observed perturbation of the reaction equilibrium in the way that is conventionally used in the screening of dynamic combinatorial libraries. Indeed, since the total amount of protein in the crystals is very small compared to the total amount of the monomers present in solution, one would not expect to be able to measure any gross changes in the outcome of the reaction caused by binding of product ligands to the crystals. However, it is still possible that the protein influences the outcome of the chemical reactions occurring directly in the crystals. In this study the reaction products are formed reversibly, and each product might be formed in situ within the protein crystal, under thermodynamic control. A consideration of the environment within the protein crystal would lead one to suggest that the monomers may tend to compete for occupancy of the ATP-binding groove, allowing "templating" to occur and helping to drive selection of the most potent ligands in the active site. Indeed, this effect has been previously shown in studies of reactions that occur in the active site of a protein, but under kinetic control.[26] However, it cannot be discounted that the effect observed in this case might be driven by equilibration of the ligands themselves into the CDK2 crystals, preformed by reaction of monomers present in the aqueous solution. Experiments designed to distinguish between these two possible situations are underway in our laboratories.

In conclusion, we have demonstrated that X-ray crystallography can be used to detect small-molecule ligands generated in situ and bound to a target protein. These findings provide the basis for a new drug discovery technology in which dynamic combinatorial libraries can be used to identify novel, potent ligands. We believe this approach could be broadly applicable to the discovery of inhibitors of therapeutically useful proteins within drug discovery programs.

Received: May 22, 2003 [Z51951]

Keywords: analytical methods · combinatorial chemistry · medicinal chemistry · proteins · X-ray diffraction

[1] S. Otto, R. L. E. Furlan, J. K. M. Sanders, *Drug Discovery Today* **2002**, 117 (*Combinatorial Chemistry*: A Supplement).
[2] J.-M Lehn, A. V. Eliseev, *Science* **2001**, *291*, 2331.
[3] C. Karan, B. L. Miller, *Drug Discovery Today* **2000**, *5*, 67.
[4] O. Ramström, J.-M. Lehn, *Nat. Rev. Drug Discovery* **2002**, *1*, 26.
[5] D. A. Erlanson, J. W. Lam, C. Wiesmann, T. N. Luong, R. L. Simmons, W. L. DeLano, I. C. Choong, M. T. Burdett, W. M. Flanagan, D. Lee, E. M. Gordon, T. O'Brien, *Nat. Biotechnol.* **2003**, *21*, 308.

 © 2003 Wiley-VCH Verlag GmbH & Co. KGaA, Weinheim

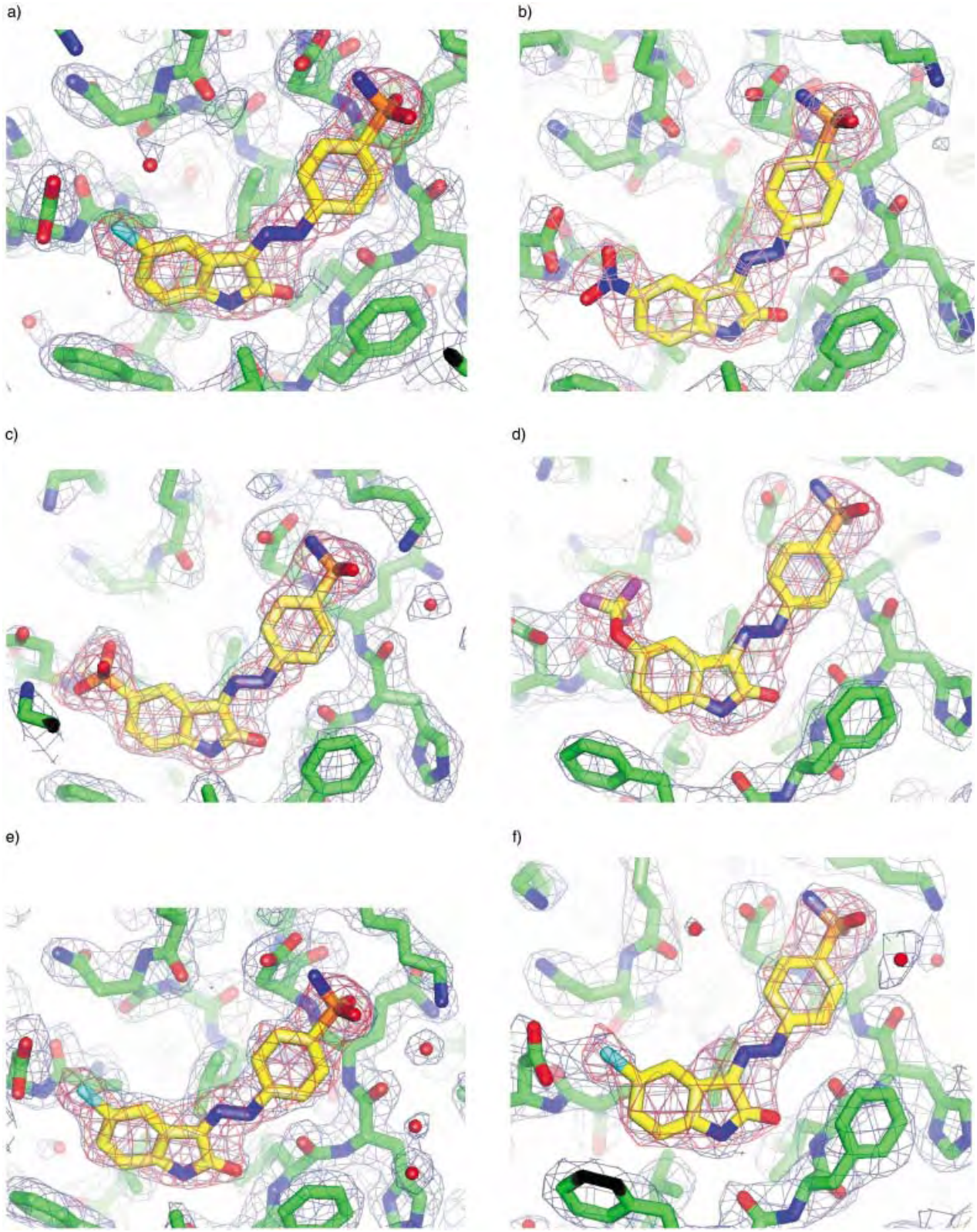


Figure 1. (F_o–F_c) and ($2F_o$–F_c) maps for the singlet and cocktail reactions. All (F_o–F_c) maps are colored red and trimmed to within 2.5 Å of the ligand. The difference maps were generated after segmented rigid body, positional, and isotropic B-factor refinements of the protein, in the absence of any ligand. The final refined protein–ligand structures and corresponding final ($2F_o$–F_c) maps (contoured at 1.0σ and colored gray) are shown in all six figures for reference. Elements in the ligands are colored as follows: yellow (C), blue (N), red (O), cyan (Cl), pink (F), and orange (S). Atoms in the protein are colored similarly, except that carbon atoms are green. a) 2.5σ (F_o–F_c) map for the reaction (**A5** + **B2**); b) 2.0σ (F_o–F_c) map for the reaction (**A5** + **B1**); c) 2.5σ (F_o–F_c) map for the reaction (**A5** + **B3**). d) 2.0σ (F_o–F_c) map for the reaction (**A5** + **B5**). e) 2.5σ (F_o–F_c) map for the reaction **B2** + (**A1**–**6**). f) 2.5σ (F_o–F_c) map for reaction (**A1**–**6**) + (**B1**–**5**). Maps for the reaction (**A5** + **B4**) are provided in the supplementary data. All figures were generated with AESOP (M.E.M. Noble, Oxford, unpublished results).

 © 2003 Wiley-VCH Verlag GmbH & Co. KGaA, Weinheim

[6] P. A. Brady, R. P. Bonar-Law, S. J. Rowan, C. J. Suckling, J. K. M. Sanders, *Chem. Commun.* **1996**, *3*, 319.
[7] P. Seneci, *Solid-Phase Synthesis and Combinatorial Technologies*, Wiley-Interscience, New York, **2000**.
[8] M. Hochgürtel, H. Kroth, D. Piecha, M. W. Hofmann, C. Nicolau, S. Krause, O. Schaaf, G. Sonnenmoser, A. V. M. Eliseev, *Proc. Natl. Acad. Sci. USA* **2002**, *99*, 3382.
[9] W. G. Lewis, L. G. Green, F. Grynszpan, Z. Radic, P. R. Carlier, P. Taylor, M. G. Finn, K. B. Sharpless, *Angew. Chem.* **2002**, *114*, 1095; *Angew. Chem. Int. Ed.* **2002**, *41*, 1053.
[10] T. L. Blundell, C. Abell, A. Cleasby, M. J. Hartshorn, I. J. Tickle, E. Parasini, H. Jhoti, *Drug Des. Discovery* **2002**, *279, 53* (Special Publication: Proceedings of the Royal Society of Chemistry Meeting—Cutting Edge Approaches to Drug Design, March 2001, Ed.: D. Flower, Royal Society of Chemistry, London).
[11] R. Carr, H. Jhoti, *Drug Discovery Today* **2002**, *7*, 522.
[12] T. L. Blundell, H. Jhoti, C. Abell, *Nat. Rev. Drug Discovery* **2002**, *1*, 45.
[13] V. L. Nienaber, P. L. Richardson, V. Klighofer, J. J. Bouska, V. L. Giranda, J. Greer, *Nat. Biotechnol.* **2000**, *18*, 1105.
[14] P. J. Hajduk, R. P. Meadows, S. W. Fesik, *Q. Rev. Biophys.* **1999**, *32*, 211.
[15] B. A. Katz, J. Finer-Moore, R. Mortezaei, D. H. Rich, R. M. Stroud, *Biochemistry* **1995**, *34*, 8264.
[16] M. Knockaert, P. Greengard, L. Meijer, *Trends Pharmacol. Sci.* **2002**, *23*, 417.
[17] P. M. Fischer, D. P. Lane, *Curr. Med. Chem.* **2000**, *7*, 1213.
[18] H. N. Bramson, J. Corona, S. T. Davis, S. H. Dickerson, M. Edelstein, S. V. Frye, R. T. Gampe, P. A. Harris, A. Hassell, W. D. Holmes, R. N. Hunter, K. E. Lackey, B. Lovejoy, M. J. Luzzio, V. Montana, W. J. Rocque, D. Rusnak, L. Shewchuk, J. M. Veal, D. H. Walker, L. F. Kuyper, *J. Med. Chem.* **2001**, *44*, 4339.
[19] J. K. M. Sanders, *Pure Appl. Chem.* **2000**, *72*, 2265.
[20] V. Berl, I. Huc, J.-M. Lehn, A. DeCian, J. Fischer, *Eur. J. Org. Chem.* **1999**, *11*, 3089.
[21] Further details of the experiments carried out to confirm the suitability of the chemical process used are described in the Supporting Information.
[22] J. Rosenblatt, H. De Bondt, J. Jancarik, D. O. Morgan, S. H. Kim, *J. Mol. Biol.* **1993**, *230*, 1317.
[23] A. M. Lawrie, M. E. M. Noble, P. Tunnah, N. R. Brown, L. N. Johnson, J. A. Endicott, *Nat. Struct. Biol.* **1997**, *4*, 796.
[24] H. L. De Bondt, J. Rosenblatt, J. Jancarik, H. D. Jones, D. O. Morgan, S. H. Kim, *Nature* **1993**, *363*, 595.
[25] Details of the biological assay used and further biological results on additional library members are described in the Supporting Information.
[26] R. Nguyen, I. Huc, *Angew. Chem.* **2001**, *113*, 1824; *Angew. Chem. Int. Ed.* **2001**, *40*, 1774.

Cadmium Phosphonate Aggregates

A Nanoscopic Molecular Cadmium Phosphonate Wrapped in a Hydrocarbon Sheath**

*Ganapathi Anantharaman, Mrinalini G. Walawalkar, Ramaswamy Murugavel, Bunkóczi Gábor, Regine Herbst–Irmer, Marc Baldus, Brigitta Angerstein, and Herbert W. Roesky**

Dedicated to Dr. Manfred Flad on the occasion of his 90th birthday

Preparing a material that has particles of uniform dimension has been one of the biggest challenges for chemists as well as material scientists. The traditional ways of imparting order at the nanoscopic level have changed since the synthesis of fullerene clusters.[1] The use of techniques such as epitaxy and metal–organic chemical vapor deposition (MOCVD) have been used extensively in this regard. The synthesis of giant inorganic molecules, such as polyoxoanions,[2] Al_{77},[3] and Ga_{84}[4] clusters are examples of inorganic counterparts of fullerenes. The synthesis of metal phosphonates using organometallic routes in recent years has led to the realization of a series of oligomeric transition-metal and main-group-metal phosphonates.[5,6] In all these reports, the size of the oligomeric structure is highly dependent on the substituent on the metal center as well as at the phosphorus center. The metal phosphonates can be synthesized either using metal precursor–phosphonic acid interactions via an acid exchange or by starting from metal alkyls/amides/alcoholates by elimination of alkanes/amines/alcohols.[5–7] It has been demonstrated that metals belonging to the same group of the periodic table yield molecular phosphonates of the same topology if the substituents on the metal and phosphorus centers are kept the same. Although examples of zinc phosphonates following both the synthetic methodologies have been reported, there have been no examples of molecular cadmium phospho-

[*] Prof. H. W. Roesky, Dr. G. Anantharaman, Dr. M. G. Walawalkar, Prof. R. Murugavel, B. Gábor, Dr. R. Herbst–Irmer
Institut für Anorganische Chemie
Universität Göttingen
Tammannstrasse 4, 37077 Göttingen (Germany)
Fax: (+49) 551-393-373
E-mail: hroesky@gwdg.de
Dr. M. Baldus, B. Angerstein
Max Planck Institute of Biophysical Chemistry
Department of NMR based Structural Biology
Fassberg 11, 37077 Göttingen (Germany)
Dr. M. G. Walawalkar, Prof. R. Murugavel
Department of Chemistry
IIT-Bombay
Powai, Mumbai (India)

[**] This work was supported by the Deutsche Forschungsgemeinschaft (Graduiertenkolleg: Spektroskopie und Dynamik Molekularer Aggregate, Ketten, Knäuel und Netzwerke) and the Göttinger Akademie der Wissenschaften. M.G.W. and R.M. thank the Alexander von Humboldt Foundation, Bonn (Germany), for a research fellowship and IIT-Bombay for leave.

 © 2003 Wiley-VCH Verlag GmbH & Co. KGaA, Weinheim DOI: 10.1002/anie.200352133

nates.[8] The known examples of cadmium phosphonates are either polymeric or layer-type structures.[9]

Molecular cadmium clusters, analogous to those of zinc, should in principle be realizable by the use of a cadmium alkyl precursor, such as CdR_2, and phosphonic acid, such as *tert*-butylphosphonic acid. Our recent synthesis of a dodecanuclear zincophosphonate containing a $\{Zn_4(\mu_4\text{-}O)\}$ core has been an extension of a cluster-building strategy via organometallic routes.[8a] Surprisingly, the application of a similar strategy for the reaction of dimethylcadmium with *tert*-butylphosphonic acid in a THF solution afforded a still larger aggregate as colorless crystals, which contains 68 heteroatoms arranged in the form of a hollow sphere (see below). Although the initial yield of this reaction was poor, the addition of a stoichiometric amount of water during the reaction significantly enhanced the yield (20%). The ^{1}H NMR intensities of the solid-state CP-MAS NMR spectrum reveal that the methyl protons on each cadmium atom resonate at $\delta = 0.6$ ppm while the methyl protons of *tert*-butyl groups attached to phosphorus appear at $\delta = 1.7$ ppm. However, the ^{31}P NMR spectrum of **1** in the solid state (Figure 1) displays at least four well-resolved signals in the range $\delta = 30$–50 ppm, which can be assigned to phosphorus atoms having four different environments.

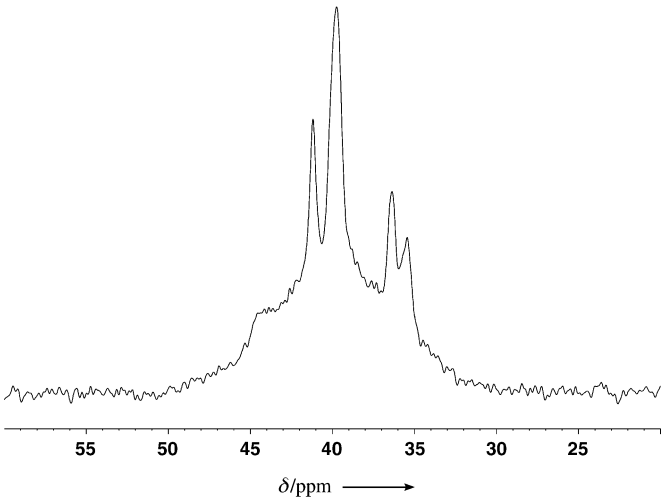


Figure 1. ^{31}P CP-MAS NMR spectrum of $[(MeCd)_{10}\{(thf)Cd\}_4Cd_6(\mu_4\text{-}O)_2(\mu_3\text{-}OH)_2(t\text{BuPO}_3)_{12}]$.

The single-crystal X-ray diffraction study[10] reveals that compound **1** is the largest cadmium phosphonate aggregate known, $[(MeCd)_{10}\{(thf)Cd\}_4Cd_6(\mu_4\text{-}O)_2(\mu_3\text{-}OH)_2(t\text{BuPO}_3)_{12}]$ (**1**), which contains a skeleton made up of 20 cadmium atoms and 12 phosphorus atoms that are held together by 36 surface oxygen atoms along with a pair of oxo and hydroxo groups in the interior of the sphere (Figure 2). The packing diagram of **1** (Figure 3) shows the arrangement of $Cd_{20}P_{12}$ polyhedra in the solid state. Compound **1** appears to have an inversion center, which however is absent in the final structure due to the small variations observed in the coordination geometry of the cadmium centers. The inorganic core of this molecule is embedded in the organic sheath made

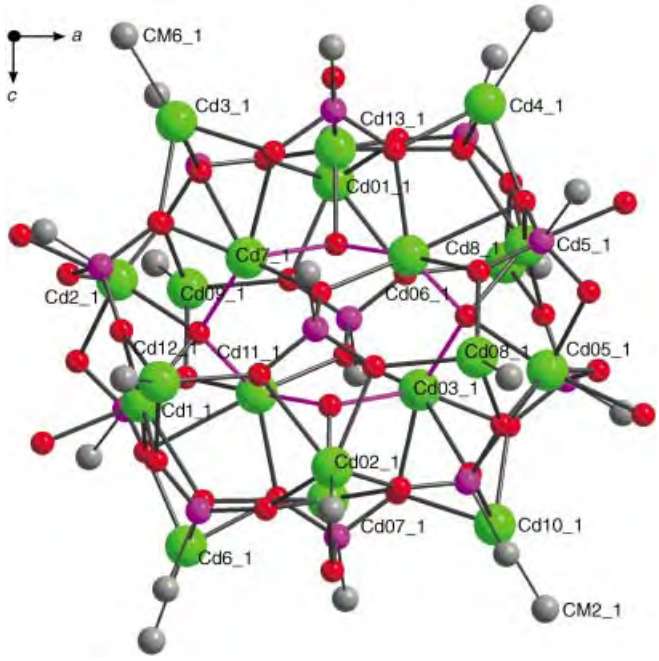


Figure 2. Molecular structure of **1** showing the $Cd_{20}P_{12}$ polyhedra (the solvent THF molecules, hydrogen atoms, and the methyl groups of the *tert*-butylphosphonate group are omitted for the sake of clarity).

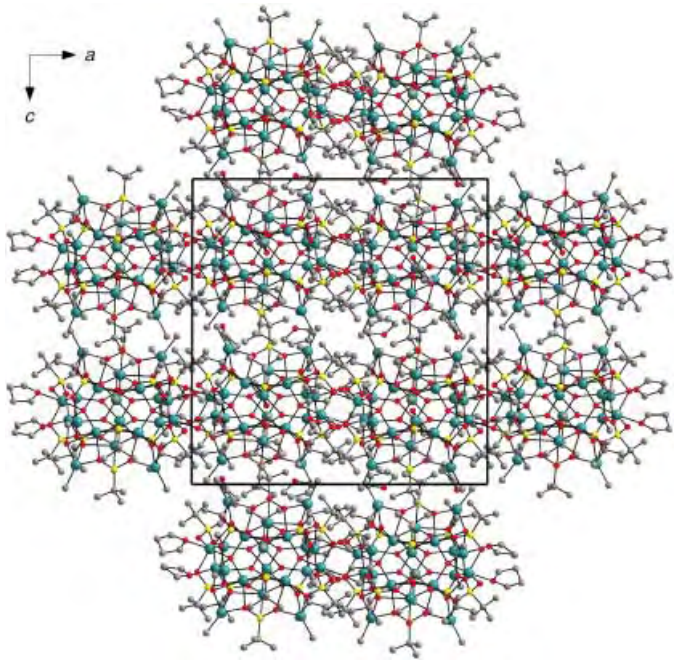


Figure 3. Packing diagram of **1** showing the arrangement of the $Cd_{20}P_{12}$ polyhedra in the solid state.

up of ten methyl groups (attached to ten cadmium atoms), four THF molecules (attached to four cadmium atoms) and twelve *tert*-butyl groups (attached to the twelve phosphorus atoms). The twenty cadmium atoms can be categorized into six classes (1–6) depending on the coordination geometry and the environment around them (Table 1). In the molecule, there are 32 polyhedra in total: 20 tetrahedra (12 from

 © 2003 Wiley-VCH Verlag GmbH & Co. KGaA, Weinheim

Table 1: Arrangement of cadmium atoms within the molecule **1**.

Class	Cd atoms	Geometry	Environment around cadmium
1	Cd3_1, Cd4_1, Cd6_1, Cd8_1, Cd08_1, Cd09_1, Cd10_1, Cd12_1	tetrahedral	3 phosphonate oxygen atoms, 1 methyl group
2	Cd01_1, Cd02_1	square pyramidal	4 phosphonate oxygen atoms, 1 methyl group
3	Cd07_1, Cd13_1	trigonal bipyramidal	1 μ_3-O atom, 4 phosphonate oxygen atoms
4	Cd2_1	trigonal bipyramidal	1 μ_4-O atom , 3 phosphonate oxygen atoms, one THF group
5	Cd1_1, Cd5_1, Cd05_1	octahedral	1 μ_4-O atom, 4 phosphonate oxygen atoms, 1 THF group
6	Cd03_1, Cd06_1, Cd7_1, Cd11_1	octahedral	1 μ_4-O atom, 1 μ_3-O atom, 4 phosphonate oxygen atoms

phosphonate groups and eight from cadmium atoms), seven cadmium octahedra, two cadmium square-based pyramids, and three cadmium trigonal bipyramids. The phosphonate tetrahedra are linked to the cadmium polyhedra either by corner sharing via an oxygen atom or by edge sharing through two oxygen atoms (Figure 4). Depending on the coordination

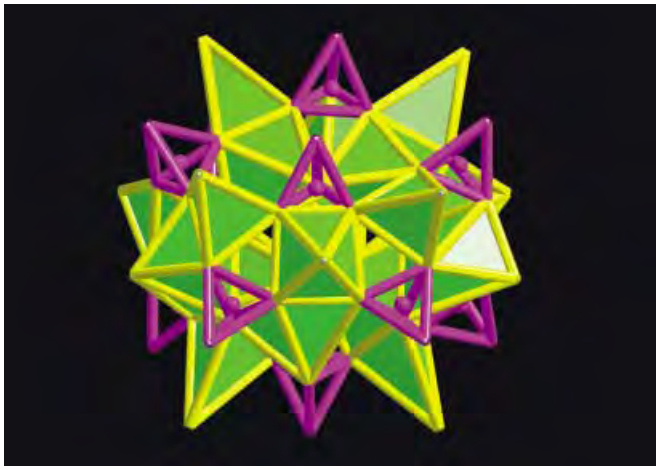
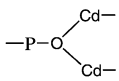
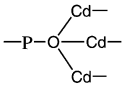


Figure 4. Polyhedral arrangement showing cadmium (as closed polyhedra with green interior and yellow edges) and phosphorus (open polyhedra in pink) atoms.

modes the twelve phosphonate groups can be classified into four different types (A—D; Table 2). This coordination mode of phosphonates in the cluster results in the formation of nine CdO_2P four-membered rings. The two μ_3-OH and two μ_4-O groups present in the molecule are located in the space available inside the spherical hollow ball. It appears that the entire cluster is built around these two oxo (OQ1_1 and OQ2_1) and two hydroxo groups (OT1_1 and OT2_1), since

Table 2: Different coordination modes of phosphonate groups in **1**.

No. of	No. of 	No. of 	Type	No. of P atoms
1	2	–	A	4
1	1	1	B	2
–	3	–	C	3
–	2	1	D	3

these four oxygen centers hold as many as 12 cadmium ions together (Figure 5). Another way of understanding the structure of this molecule is by considering an inner eight-membered $\{Cd_4O_4\}$ core, which is surrounded by remaining cadmium and phosphonate moieties (Figure 5). The $\{Cd_4O_4\}$ core contains two $\{Cd(\mu_3\text{-OH})\}$ and two $\{Cd(\mu_4\text{-O})\}$ moieties and adopts a crown conformation.

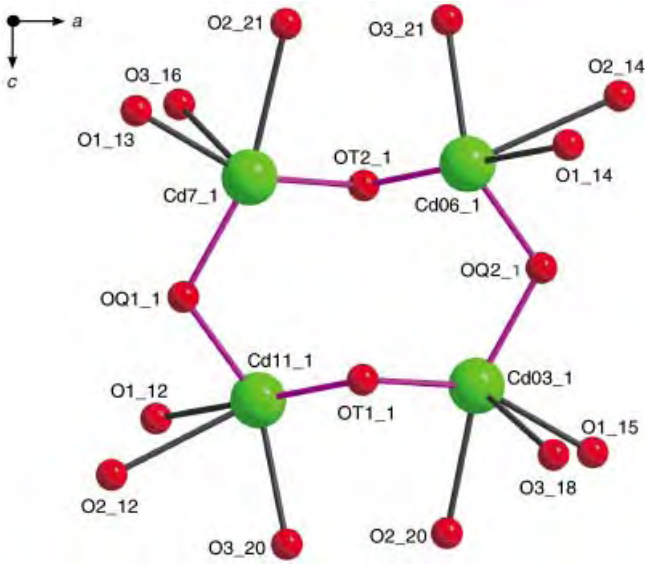


Figure 5. Central Cd_4O_4 moiety containing the μ_3-O (OT1_1 and OT2_1) and μ_4-O (OQ1_1 and OQ2_1) atoms in **1**, around which the phosphonate groups are arranged.

Among the reported cadmium phosphinates, phosphonates, phosphates, and oxides, there is no report on the presence of a $\{Cd(\mu_4\text{-O})\}$ central unit, whereas $\{Cd(\mu_3\text{-OH})\}$ is a quite well known structural motif in these systems.[11] The average bond lengths in $\{Cd\text{-}\mu_4\text{-O}\}$ (2.208(7) Å) and $\{Cd\text{-}\mu_3\text{-OH}\}$ (2.256(7) Å) are comparable to those in the reported cadmium complexes containing oxo and hydroxo bridges.[11] The average distance between the methyl substituents on the diagonally opposite cadmium atoms (CM6_1 to CM2_1; Figure 2) is ≈15.4 Å, while the average distance between the opposite carbon atoms of the *tert*-butyl groups is 14.9 Å, and the average distance between the hydrogen atoms of the opposite THF atoms is 20.03 Å. Within the inorganic core, the diagonally opposite Cd···Cd and P···P distances are 10.9 and 9.8 Å, respectively. Hence, this molecule falls truly into the

 © 2003 Wiley-VCH Verlag GmbH & Co. KGaA, Weinheim

nanomolecular regime, as the molecular diagonal distances measured fall in the range of 10 to 20 Å. Thus, this giant molecule can easily encapsulate three C_{60} molecules at one time.[1]

Experimental Section

1: Dimethylcadmium (0.65 g, 4.6 mmol) was added dropwise to a solution of *tert*-butylphosphonic acid (0.32 g, 2.3 mmol) in THF (50 mL) at room temperature. After the evolution of methane gas ceased, the resulting solution was stirred for 6 h. The solution was then concentrated to 5 mL and toluene (5 mL) was added. Colorless crystals of **1**, insoluble in common organic solvents, were obtained over the period of a month at room temperature (0.12 g, 14%); m.p. $>300\,^{\circ}C$; solid-state NMR of **1**: ^{1}H NMR (399.92 MHz, TMS): $\delta = 0.6$ (s, $CdCH_3$), 1.7 ppm (br, $C(CH_3)_3$); ^{31}P NMR (161.90 MHz, 85% H_3PO_4): $\delta = 35.4$, 36.3, 39.7, 41.2 ppm; IR (nujol): $\tilde{\nu} = 3181$ vw, 2232 vw, 1615 vw, 1478 s, 1461 s, 1393 m, 1365 s, 1261 w, 1231 w, 1202 w, 1127 m, 1051 vs, 1027 vs, 969 vs, 884 w, 832 m, 804 w, 727 w, 680 vs, 660 vs, 557 s, 520 vs, 508 s, 487 m, 435 cm^{-1} m; elemental analysis (THF molecules were removed by drying under vacuum) calcd (%) for $C_{58}H_{140}Cd_{20}O_{40}P_{12}$ (4097.61): C 17.00, H 3.44; found: C 16.25, H 3.48.

Received: June 13, 2003 [Z52133]

Keywords: aggregates · cadmium · cage compounds · nanomaterials · P ligands

[1] a) *Fullerenes*: *Chemistry, Physics, and Technology*, (Eds.: K. M. Kadish, R. S. Ruoff), Wiley, New York, **2000**; b) *Buckminsterfullerenes* (Eds.: W. E. Billups, M. A. Ciufolini), VCH, Weinheim, **1993**.

[2] a) A. Müller, E. Krickemeyer, H. Bögge, M. Schmidtmann, F. Peters, *Angew. Chem.* **1998**, *110*, 3567–3571; *Angew. Chem. Int. Ed.* **1998**, *37*, 3360–3363; b) M. I. Khan, J. Zubieta, R. C. Haushalter, *Prog. Inorg. Chem.* **1995**, *43*, 1–149; c) J. Salta, Q. Chen, Y.-D. Chang, J. Zubieta, *Angew. Chem.* **1994**, *106*, 781–783; *Angew. Chem. Int. Ed. Engl.* **1994**, *33*, 757–760.

[3] a) A. Ecker, E. Weckert, H. Schnöckel, *Nature* **1997**, *387*, 379–381; b) H. Schnöckel, A. Schnepf, *Adv. Organomet. Chem.* **2001**, *47*, 235–281.

[4] a) A. Schnepf, H. Schnöckel, *Angew. Chem.* **2001**, *113*, 734–737; *Angew. Chem. Int. Ed.* **2001**, *40*, 712–715; b) A. Schnepf, H. Schnöckel, *Angew. Chem.* **2002**, *114*, 3682–3704; *Angew. Chem. Int. Ed.* **2002**, *41*, 3532–3552.

[5] M. G. Walawalkar, H. W. Roesky, R. Murugavel, *Acc. Chem. Res.* **1999**, *32*, 117–126.

[6] a) M. R. Mason, *J. Cluster Sci.* **1998**, *9*, 1–23; b) M. R. Mason, A. M. Perkins, R. M. Matthews, J. D. Fisher, M. S. Mashuta, A. Vij, *Inorg. Chem.* **1998**, *37*, 3734–3746; c) M. R. Mason, A. M. Perkins, V. V. Ponomarova, A. Vij, *Organometallics* **2001**, *20*, 4833–4839.

[7] a) E. K. Brechin, R. A. Coxall, A. Parkin, S. Parsons, P. A. Tasker, R. E. Winpenny, *Angew. Chem.* **2001**, *113*, 2772–2775; *Angew. Chem. Int. Ed.* **2001**, *40*, 2700–2703; b) M. Mehring, M. Schürmann, *Chem. Commun.* **2001**, 2354–2355; c) M. Mehring, G. Guerrero, F. Dahan, P. H. Mutin, A. Vioux, *Inorg. Chem.* **2000**, *39*, 3325–3332; d) V. Chandrasekhar, S. Kingsley, *Angew. Chem.* **2000**, *112*, 2410–2412; *Angew. Chem. Int. Ed.* **2000**, *39*, 2320–2322.

[8] a) Y. Yang, J. Pinkas, M. Noltemeyer, H.-G. Schmidt, H. W. Roesky, *Angew. Chem.* **1999**, *111*, 706–708; *Angew. Chem. Int. Ed.* **1999**, *38*, 664–666; b) V. Chandrasekhar, S. Kingsley, B. Rhatigan, M. K. Lam, A. L. Rheingold, *Inorg. Chem.* **2002**, *41*, 1030–1032.

[9] a) C. V. K. Sharma, A. Clearfield, *J. Am. Chem. Soc.* **2000**, *122*, 1558–1559; b) F. Fredoueil, M. Evain, D. Massiot, M. Bujoli-Doeuff, P. Janvier, A. Clearfield, B. Bujoli, *J. Chem. Soc. Dalton Trans.* **2002**, 1508–1512; c) P. Ayyappan, O. R. Evans, Y. Cui, K. A. Wheeler, W. Lin, *Inorg. Chem.* **2002**, *41*, 4978–4980; d) P. Ayyappan, O. R. Evans, B. M. Foxman, K. A. Wheeler, T. H. Warren, W. Lin, *Inorg. Chem.* **2001**, *40*, 5954–5961; e) C. V. K. Sharma, A. Clearfield, A. Cabeza, M. A. G. Aranda, S. Burque, *J. Am. Chem. Soc.* **2001**, *123*, 2885–2886; f) N. Choi, I. Khan, R. W. Matthews, M. McPartlin, B. P. Murphy, *Polyhedron* **1994**, *13*, 847–850; g) N. El Messbahi, J.-P. Silvestre, N. Q. Dao, M.-R. Lee, Y. Leroux, A. Neuman, H. Gillier-Pandraud, *Phosphorus Sulfur Silicon Relat. Elem.* **2000**, *164*, 45–59.

[10] Crystal data for **1**: $C_{74}H_{172}Cd_{20}O_{44}P_{12}$ (**1**·4 C_4H_8O), $M_r = 4385.56$, monoclinic, space group $P2_1/c$, $a = 24.303(5)$, $b = 25.294(5)$, $c = 25.107(5)$ Å, $\beta = 90.14(3)^{\circ}$, $V = 15434(5)$ Å^3, $Z = 4$, $\rho_{calcd} = 1.938$ g cm^{-3}, $F(000) = 8694$, $\lambda = 0.71073$ Å, $T = 133$ K, $\mu(Mo_{K\alpha}) = 28.78$ cm^{-1}, min./max. transmission 0.3271/0.5968, crystal dimensions $0.5 \times 0.4 \times 0.2$ mm^3, $3.32^{\circ} < \theta < 25.19^{\circ}$; 158685 reflections were collected, of which 28040 were independent ($R_{int} = 0.1052$) and 27363 were used for refinement. For the final refinement of 1550 parameters, 713 restraints were used. The R values were: $R_1 = \Sigma | F_o - F_c | / \Sigma F_o = 0.0587$ for $I > 2\sigma(I)$, and $wR_2 = [\Sigma w(F_o^2 - F_c^2)^2 / \Sigma w F_o^4]^{1/2} = 0.1483$ for all data; max/min. residual electron density: 2.429/−1.956 e Å^{-3}. The unit cell contains four molecules of **1** and 16 molecules of THF. The crystal was covered with a drop of inert perfluorinated polyether oil and flash-cooled in a nitrogen stream. Intensity data were collected on a Huber four-circle instrument and a Siemens 1 K-CCD area detector. A semi-empirical absorption correction was employed using the Bruker AXS program SADABS. The observed systematic absences did not correspond to any space group in the apparent orthorhombic crystal system, which suggested the presence of pseudo-merohedral twinning with a twofold rotation about the *c* axis. The structure was solved with direct methods (SHELXS-97)[12] and refined against F^2.[13] Non-hydrogen atoms in **1** were refined anisotropically except for atoms with very low (<0.1) occupancy. Eight out of twenty cadmium atoms (Cd1_1, Cd2_1, Cd3_1, Cd4_1, Cd5_1, Cd6_1, Cd7_1, and Cd8_1) were found to adopt a minor second position and the occupancy of these alternative positions varies by <0.1. Solvent molecules were refined isotropically. The riding model was used for the hydrogen atoms. The fractional contribution from the second twin domain was determined as 44%. CCDC-210527 contains the supplementary crystallographic data for this paper. These data can be obtained free of charge via www.ccdc.cam.ac.uk/conts/retrieving.html (or from the Cambridge Crystallographic Data Centre, 12, Union Road, Cambridge CB2 1EZ, UK; fax: (+44) 1223-336-033; or deposit@ccdc.cam.ac.uk).

[11] a) A. K. Duhme, H. Strasdeit, *Eur. J. Inorg. Chem.* **1998**, 657–662; b) J. Fornies, J. Gomez, E. Lalinde, M. T. Moreno, *Inorg. Chem.* **2001**, *40*, 5415–5419; c) M. Weidenbruch, M. Herrndorf, A. Schäfer, S. Pohl, W. Saak, *J. Organomet. Chem.* **1989**, *361*, 139–145.

[12] "SHELXS-97, *Program for Structure Solution*": G. M. Sheldrick, *Acta Crystallogr. Sect. A* **1990**, *46*, 467–473.

[13] G. M. Sheldrick, SHELXL-97, *Program for Structure Refinement*, Universität Göttingen, **1997**.

 © 2003 Wiley-VCH Verlag GmbH & Co. KGaA, Weinheim

Mononuclear Chromium Hydrides

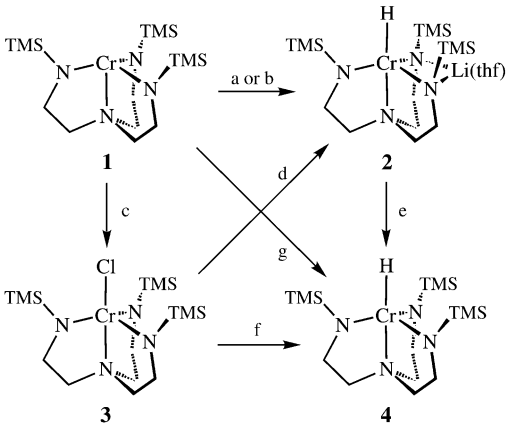
A Pair of Remarkably Stable Mononuclear Chromium(III) and Chromium(IV) Hydrides**

Alexander C. Filippou, Sven Schneider, and Gregor Schnakenburg*

Dedicated to Prof. E. O. Fischer on the occasion of his 85th birthday

The coordination and organometallic chemistry of chromium(IV) is much less developed than that of chromium in the oxidation states +II, +III, and +VI.[1] This can be traced back to the high oxidation potential of chromium(IV) complexes and their pronounced tendency to undergo valence disproportionation and reductive elimination reactions.[2] Therefore, it is not surprising that only very few reports have appeared on chromium(IV) and chromium(III) hydrides, which are suggested to be thermodynamically unstable and quite reactive compounds. In fact, CrH_4 remains elusive and its tetrahedral $^3A_2$ ground-state structure was calculated to lie 38.5 kcal mol^{-1} higher in energy than that of the dihydrogen complex isomer $[CrH_2(\eta^2\text{-}H_2)]$ ($^5A_1$) at the CCSD/TZP level of theory.[3,4] Similarly, $[Cr^{IV}H(O)(OH)]$, which was generated upon photolysis of matrix-isolated $[CrO_2(\eta^2\text{-}H_2)]$, was calculated to rearrange exothermally to its tautomer $[Cr^{II}(OH)_2]$ ($\Delta E = -22.4$ kcal mol^{-1}, B3LYP/6-311++G(d,p)),[5] and pyramidal CrH_3 ($^4A_1$) is 20.5 kcal mol^{-1} less stable than $[CrH(\eta^2\text{-}H_2)]$($^6A_1$) at the B3PW91/6-311++G(d,p)/SDD level of theory.[4c,6] To date, mononuclear chromium(III) hydrides are unknown[7] and only two chromium(IV) hydrides, $[CrH_4(dmpe)_2]$ (dmpe = $Me_2PCH_2CH_2PMe_2$)[8] and the *ansa*-chromocene derivative $[CrH\{C_2Me_4(\eta^5\text{-}C_5H_4)(\eta^5\text{-}C_5H_3B(C_6F_5)_3)\}(CO)]$[9] have been isolated and structurally characterized. We report herein the synthesis, characterization, and theoretical calculations of mononuclear chromium(III) and chromium(IV) hydrides stabilized by a triamidoamine ligand.

Treatment of $[Cr(N_3N)]$ ($(N_3N)^{3-}$ = $\{(Me_3SiNCH_2CH_2)_3N\}^{3-}$) (**1**)[10] with $Li[BEt_3H]$ or *s*BuLi in THF affords the hydridochromate(III) $[Li(thf)Cr(N_3N)H]$ (**2**) in 70 and 72% yields, respectively (Scheme 1).[11] Previous attempts to prepare chromium(III) hydrides by means of hydride-transfer reagents were unsuccessful due to reduction.[12] Addition of *s*BuLi to **1** is suggested to give the alkylchromate "$[Li(thf)Cr(N_3N)sBu]$", which rapidly undergoes β-hydride elimination of butene to afford **2**. Indirect evidence for the intervention of "$[Li(thf)Cr(N_3N)sBu]$" is given by the selective formation of stable alkylchromate(III) complexes $[Li(thf)Cr(N_3N)R]$ (R = Me, CH_2SiMe_3) from **1** and LiR, when the R group lacks β-hydrogen atoms.[13] The hydridochromate **2** can be also prepared in 46% yield by the reaction of $[Cr(N_3N)Cl]$ (**3**) with 2.1 equiv of *s*BuLi in THF (Scheme 1). Complex **2** was isolated after crystallization from pentane as green-black, highly air-sensitive needles, which melt without decomposition at 114–115 °C. In solution, it is instantaneously oxidized by air to give the chromium(IV) hydride $[Cr(N_3N)H]$ (**4**). Two efficient methods were employed for the synthesis of **4**; these are the metathetical exchange of $[Cr(N_3N)Cl]$ (**3**) with $Na[BEt_3H]$ in toluene and the oxidation of **2** with AgBr in THF to afford **4** in 64 and 78% yield, respectively (Scheme 1). Taking advantage of the latter reaction, a one-pot synthesis of **4** from $[Cr(N_3N)]$ (**1**) was developed, which involves addition of $Na[BEt_3H]$ in THF followed by oxidation with AgBr (49% yield). Complex **4** can be also directly obtained from **1** upon hydrogenation with H_2 (2.5 bar) in THF at 65 °C. This reaction provides the first example for an oxidative addition of H_2 to a chromium(III) center.[14] The chromium(IV) hydride **4** is a brick-red, water-sensitive solid of remarkable thermal stability, which melts at 95–98 °C and can be sublimed without decomposition under vacuum ($\approx 10^{-1}$ mbar) at 80–90 °C.[15] It does not react with ethylene (1 bar) in toluene at 60 °C and is quite resistant to oxidation by pure oxygen in pentane solution at ambient temperature.



Scheme 1. Syntheses of the chromium hydrides **2** and **4** (TMS = $SiMe_3$; all reactions were started at low temperature and then warmed slowly to ambient temperature unless otherwise noted). a) $Li[BEt_3H]$ in THF; b) *s*BuLi in THF; c) AgCl in THF; d) *s*BuLi (2.1 equiv) in THF; e) AgBr in THF; f) $Na[BEt_3H]$ in toluene; g) H_2 in THF at 65 °C.

Complexes **2** and **4** have been fully characterized.[11] The IR spectra of **2** and **4** (in nujol) display a characteristic absorption band for the Cr–H stretching vibration at 1657 and 1712 cm^{-1}, respectively.[16] The effective magnetic moments of **2** (3.9 μ_B) and of **4** (2.9 μ_B) in benzene solution at room temperature compare well with the spin-only μ_{eff} values

[*] Prof. Dr. A. C. Filippou, Dr. S. Schneider, Dipl.-Chem. G. Schnakenburg
Institut für Chemie
Humboldt-Universität zu Berlin
Brook-Taylor-Straße 2, 12489 Berlin (Germany)
Fax: (+49) 30-2093-6939
E-mail: filippou@chemie.hu-berlin.de

[**] We thank the Humboldt-Universität zu Berlin and the Graduiertenkolleg GRK-352/3 "Synthetische, mechanistische und reaktionstechnische Aspekte von Metallkatalysatoren" for financial support and Dr. B. Ziemer and P. Neubauer for the single-crystal X-ray diffraction study of **4**.

Supporting information for this article is available on the WWW under http://www.angewandte.org or from the author.

 © 2003 Wiley-VCH Verlag GmbH & Co. KGaA, Weinheim DOI: 10.1002/anie.200352177

expected for high-spin d^3 (3.87 μ_B) and d^2 (2.83 μ_B) metal complexes, respectively. Consequently, the ^1H and $^{13}C\{^1H\}$ NMR spectra of **2** and **4** display at room temperature very broadened and shifted signals for the trimethylsilyl and backbone methylene protons of the triamidoamine ligand.[17] The number and relative intensities of the signals indicate threefold symmetry of complex **4** in solution. The NMR spectra of **2** in C_6D_6 and $[D_8]$THF are consistent with the presence of intact pseudo C_s symmetric ion-pairs in solution, as found in the solid state by X-ray diffraction. The molecular structures of **2** and **4** were determined by single-crystal X-ray diffraction (Figures 1 and 2).[18] Both five-coordinate complexes exhibit distorted trigonal-bipyramidal geometry, with the bridgehead amine nitrogen atom N4 of the tetradentate N_3N ligand and the hydrido ligand occupying the axial positions (**2**: N4-Cr-H 177.3(8)°; **4**: N4-Cr-H 175.8(9)°). The observed coordination geometry is uncommon for Cr^{III} and Cr^{IV} complexes.[19] The chromium atom is displaced from the equatorial plane of the three amide nitrogen atoms N1–N3 by 0.22 (**2**) and 0.183 Å (**4**) towards the hydrido ligand, which could be located on the difference Fourier map at a distance of 1.58(2) Å (**2**) and 1.56(3) Å (**4**) from the chromium center. The Cr–H bond lengths of **2** and **4** compare well with those of $[CrH_4(dmpe)_2]$ (1.53(3)–1.60(3) Å).[8] In complex **2**, two amide nitrogen atoms are bonded to the lithium center to form a puckered Cr-N2-Li-N3 ring with a hinge angle of 28.3°. The almost trigonal-planar coordination sphere of the lithium center (sum of bond angles at Li = 357.3°) is completed by one THF molecule. The Li–N_{amido} (1.999(4) and 2.006(3) Å) and Li–O bond lengths (1.905(4) Å) of **2** are close to those found in $[Li_3(N_3N)(thf)_2]$ ($(Li–N)_{av}$ 1.964(6) Å; $(Li–O)_{av}$ 1.938(5) Å).[20] Coordination of the nitrogen atoms N2 and N3 to Li reduces the local symmetry of the CrN_3N core in **2** from C_3 to roughly C_s, thus lifting the degeneracy of the metal d_{xy} and $d_{x^2-y^2}$ orbitals (see below). This is accompanied by a pyramidalization of the bridging amido groups, a reduction of the N2-Cr-N3 angle to 94.10(7)° (compared with N1-Cr-N2 125.62(8)°, N1-Cr-N3 136.33(7)°), and an elongation of the bridging Cr–N_{amido} bonds (Cr–N2 2.039(2) Å, Cr–N3 2.069(2) Å) relative to the terminal Cr–N_{amido} bond (Cr–N1 1.933(2) Å; sum of angles at N1 = 359.8°). In comparison, complex **4** features roughly C_3 symmetry, reminiscent of the structures of $[Cr(N_3N)X]$ (X = Cl, Br, CN).[2,10] The amido groups are planar, all N_{amido}-Cr-N_{amido} angles are close to 120°, and the Cr–N_{amido} bonds ($(Cr–N)_{av}$ 1.864 Å) of **4** are shorter than that of **2** suggesting, in agreement with the theoretical studies, a stronger $(N_{amido})_{terminal} \rightarrow Cr$ π-electron donation in **4** than in **2**. The Cr–N_{amine} bond lengths of **2** (2.138(2) Å) and **4** (2.140(2) Å) are considerably longer than that of $[Cr(N_3N)Cl]$ (2.043(3) Å),[2,10] which indicates the strong *trans* influence of the hydrido ligand.

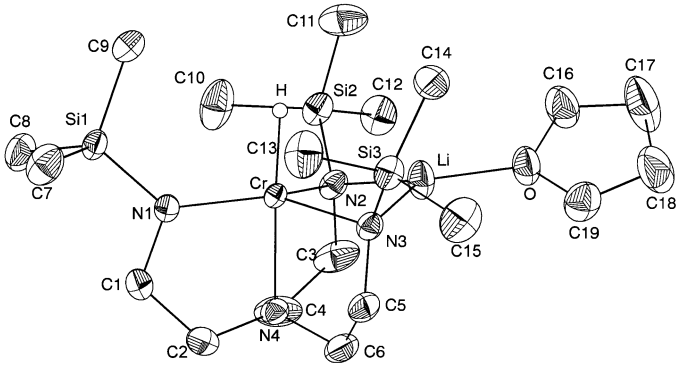


Figure 1. Diamond plot of the molecular structure of **2** with thermal ellipsoids set at the 50% probability level. Hydrogen atoms are omitted for clarity except that bonded to the chromium atom. Selected bond lengths [Å] and bond angles [°]: Cr-H 1.58(2), Cr-N1 1.933(2), Cr-N2 2.039(2), Cr-N3 2.069(2), Cr-N4 2.138(2), Li-N2 1.999(4), Li-N3 2.006(4), Li-O 1.905(4); H-Cr-N4 177.3(8), N1-Cr-N4 84.20(7), N2-Cr-N4 84.15(7), N3-Cr-N4 82.56(6), N1-Cr-N2 125.62(8), N1-Cr-N3 136.33(7), N2-Cr-N3 94.10(7), Cr-N2-Li 81.6(1), Cr-N3-Li 80.7(1), N2-Li-N3 97.3(2), O-Li-N2 129.6(2), O-Li-N3 130.4(2).

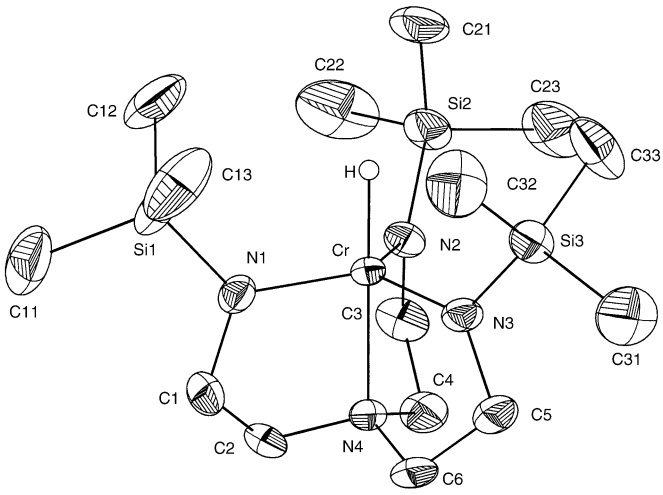


Figure 2. Diamond plot of the molecular structure of **4** with thermal ellipsoids set at the 50% probability level. Hydrogen atoms are omitted for clarity except that bonded to the chromium atom. Selected bond lengths [Å] and bond angles [°]: Cr-H 1.56(3), Cr-N1 1.875(2), Cr-N2 1.858(2), Cr-N3 1.860(2), Cr-N4 2.140(2); H-Cr-N4 175.8(9), N1-Cr-N4 83.70(8), N2-Cr-N4 84.87(8), N3-Cr-N4 84.54(8), N1-Cr-N2 117.53(8), N1-Cr-N3 121.08(8), N2-Cr-N3 118.53(8).

Complexes **2** and **4** were calculated at different levels of theory ((RI)-BP86, B3LYP) with different basis sets (TZVPP, TZVP, LANL2DZ, 6-311G(d,p)).[11] The geometrical parameters of the optimized structures are in good agreement with the experimental values. Both molecules adopt a high-spin ground-state configuration ($\Delta E_{HS/LS}(\mathbf{2}) = -63.6$ kJ mol^{-1}; $\Delta E_{HS/LS}(\mathbf{4}) = -145.7$ kJ mol^{-1}; RI-BP86/TZVP) as found by the magnetic measurements.[11] The frontier orbitals of **4** form a pair of almost degenerate metal-based (d_{xz} and d_{yz}) singly occupied molecular orbitals (SOMO and SOMO + 1) and a pair of nearly degenerate LUMOs resulting from the antibonding interaction of the metal d_{xy} and $d_{x^2-y^2}$ orbitals with the p-type lone-pair orbitals of the amide ligands (Figure 3). Addition of one electron to **4** to give the anion $[Cr(N_3N)H]^-$ is accompanied by a Jahn–Teller distortion, which causes a decrease of the N2-Cr-N3 angle from 119.0 to 103.3° (BP86/6-311(d,p)), lifts the degeneracy of the d_{xy} and $d_{x^2-y^2}$-based orbitals, and lowers the energy of the $d_{x^2-y^2}$-based orbital (SOMO + 2). Coordination of $Li(thf)^+$ to the anion $[Cr(N_3N)H]^-$ to give **2** further reduces the calculated N2-Cr-

 © 2003 Wiley-VCH Verlag GmbH & Co. KGaA, Weinheim

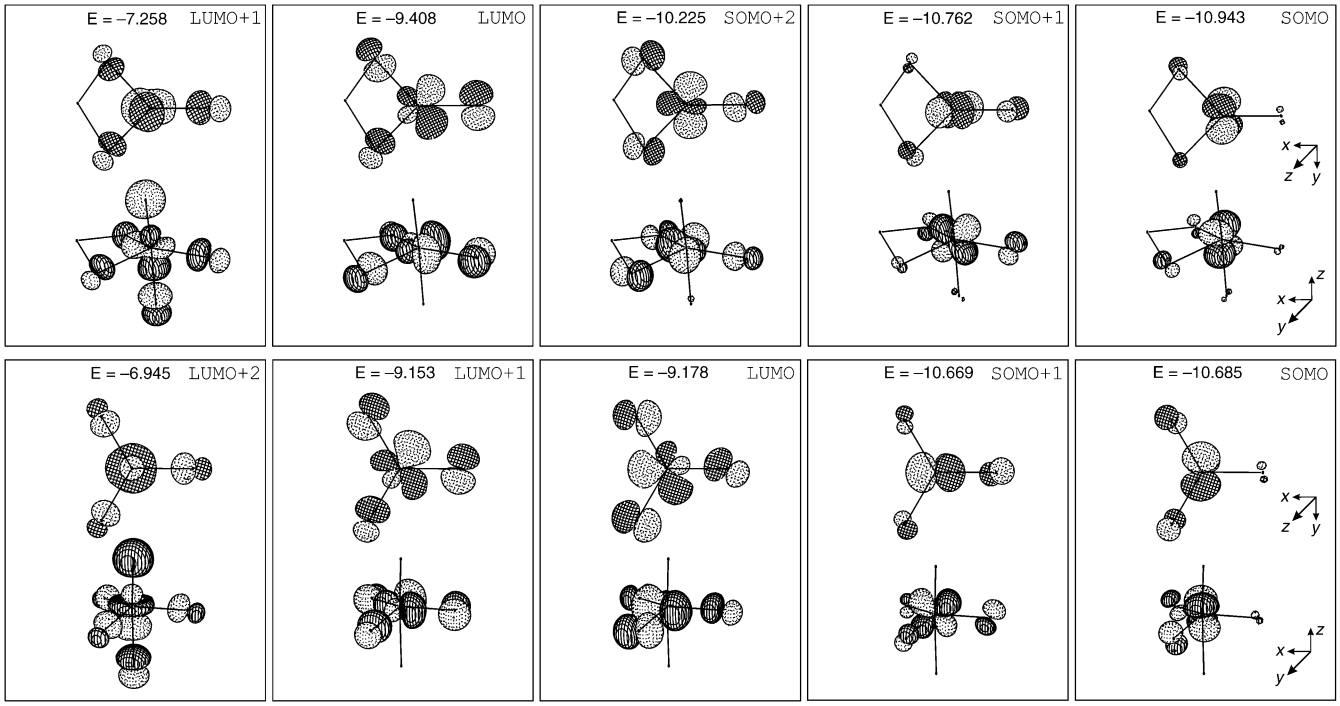


Figure 3. Frontier orbitals of **2** (top) and **4** (bottom) from extended Hückel calculations on the BP86/6-311G(d,p) optimized structures. Si, C, and H atoms (except the hydride ligand) are omitted for clarity. The N4 atom and the hydride ligand are omitted in the top views.

N3 angle to 93.9°. The $Cr-N_{amide}$ antibonding character of the SOMO + 2 orbital of **2** (Figure 3) provides an interpretation for the lower Wiberg Bond Index (WBI) values of the $Cr-N_{amide}$ bonds of **2** (Table 1). A comparison of the natural population analysis (NPA) charges reveals that oxidation of **2** to give **4** does not change the electron density at chromium (**2**: +1.34; **4**: +1.33), but is accompanied by a charge drift from the N_{amide} atoms to the chromium center (Table 1). The Gibbs free bond dissociation energies (BDEs) of the Cr–H bonds (**2**: 297.1 kJ mol^{-1}, **4**: 195.9 kJ mol^{-1}; BP86/LANL2DZ) can be compared with those of the Cr^{II} hydrides $[CpCr(CO)_2(L)H]$ (L = CO, $P(OMe)_3$, PPh_3, PEt_3) (BDE = 250.2–262.3 kJ mol^{-1}) providing a rationale for the high thermodynamic stability of **2**.[21]

The present results not only illustrate the marked differences between chromium and its heavier congeners molybdenum and tungsten,[15,22] but also provide the impetus for tackling the synthetic challenge of assembling other hydrido complexes of the 3d metals in unusual oxidation states and coordination geometries.

Table 1: Atomic charges, natural electron configuration, results of the topological analyses of the electron density distribution (AIM), and Wiberg Bond Indices (WBI) of **2** and **4** (BP86/6-311G(d,p)).

	NPA charges[a]							
	Cr	H	N1	N2	N3	N4	Li	O
2	+1.34	−0.42	−1.19	−1.31	−1.31	−0.58	+0.87	−0.65
Natural electron configuration (Cr)	$4s^{0.29}$	$3d^{4.38}$	$4d^{0.01}$					
4	+1.33	−0.33	−1.05	−1.05	−1.05	−0.57		
Natural electron configuration (Cr)	$4s^{0.30}$	$3d^{4.35}$	$4d^{0.01}$					

AIM analyses and Wiberg Bond Indices

	2				**4**			
A–B	% A[b]	$\nabla^2\rho$[c]	ε_c[d]	WBI	A–B	% A[b]	$\nabla^2\rho$[c]	ε_c[d]	WBI
Cr–N1	48.8	9.47	0.02	0.57	Cr–N1	50.3	9.13	0.08	0.76
Cr–N2	48.7	6.86	0.17	0.38	Cr–N2	50.3	9.11	0.08	0.76
Cr–N3	50.3	6.65	0.17	0.39	Cr–N3	50.3	9.23	0.08	0.76
Cr–N4	48.0	6.34	0.02	0.16	Cr–N4	48.1	5.62	0.00	0.15
Cr–H	61.9	2.04	0.01	0.64	Cr–H	62.9	1.11	0.00	0.69
N2–Li	63.6	4.58	0.19	0.03					
N3–Li	63.6	4.49	0.18	0.04					

[a] NPA: natural population analysis. [b] Position of the bond critical point (r_c) given by $d(r_c\text{–A})/d(\text{A-B}) \times 100$. [c] Laplacian of electron density at the bond critical point in e Å^{-5}. [d] Ellipticity $\varepsilon_c = \lambda_1/\lambda_2 - 1$, where λ_1 and λ_2 are negative eigenvalues of the electron density Hessian.

Received: June 23, 2003 [Z52177]

Keywords: chromium · density functional calculations · hydrides · N ligands · tripodal ligands

[1] a) L. F. Larkworthy, K. B. Nolan, P. O'Brien in *Comprehensive Coordination Chemistry, Vol. 3*, 1st ed. (Eds.: G. Wilkinson, R. D. Gillard, J. A. McCleverty), Pergamon, Oxford, **1987**, pp. 699–969; b) M. J. Winter, S. Woodward in *Comprehensive Organometallic Chemistry II, Vol. 5*, 1st ed. (Eds.: E. W. Abel,

F. G. A. Stone, G. Wilkinson), Pergamon, Oxford, **1995**, pp. 281–329.
[2] A. C. Filippou, S. Schneider, B. Ziemer, *Eur. J. Inorg. Chem.* **2002**, 2928–2935, and references therein.
[3] a) D. M. Hood, R. M. Pitzer, H. F. Schaefer III, *J. Chem. Phys.* **1979**, *71*, 705–712; b) B. Ma, C. L. Collins, H. F. Schaefer III, *J. Am. Chem. Soc.* **1996**, *118*, 870–879.
[4] For reactions of matrix-trapped chromium atoms with hydrogen atoms or H_2 to give $[CrH(\eta^2\text{-}H_2)_n]$ ($n=0,1$) and $[CrH_2(\eta^2\text{-}H_2)_n]$ ($n=0,1,2$) see: a) R. J. Van Zee, T. C. DeVore, W. Weltner, Jr., *J. Chem. Phys.* **1979**, *71*, 2051–2056; b) Z. L. Xiao, R. H. Hauge, J. L. Margrave, *J. Phys. Chem.* **1992**, *96*, 636–644; c) X. Wang, L. Andrews, *J. Phys. Chem. A* **2003**, *107*, 570–578.
[5] M. Zhou, L. Zhang, L. Shao, W. Wang, K. Fan, Q. Qin, *J. Phys. Chem. A* **2001**, *105*, 10747–10752.
[6] N. B. Balabanov, J. E. Boggs, *J. Phys. Chem. A* **2000**, *104*, 7370–7374.
[7] Only the mixed-valent tetranuclear chromium(II/III) hydride cluster $[(\eta^5\text{-}Cp^{**})_4Cr_4H_7]$ ($Cp^{**}=C_5Me_4Et$) has been reported so far: R. A. Heintz, T. F. Koetzle, R. L. Ostrander, A. L. Rheingold, K. H. Theopold, P. Wu, *Nature* **1995**, *378*, 359–362.
[8] a) G. S. Girolami, J. E. Salt, G. Wilkinson, M. Thornton-Pett, M. B. Hursthouse, *J. Am. Chem. Soc.* **1983**, *105*, 5954–5956; b) J. E. Salt, G. S. Girolami, G. Wilkinson, M. Motevalli, M. Thornton-Pett, M. B. Hursthouse, *J. Chem. Soc. Dalton Trans.* **1985**, 685–692.
[9] P.-J. Sinnema, P. J. Shapiro, D. M. J. Foo, B. Twamley, *J. Am. Chem. Soc.* **2002**, *124*, 10996–10997.
[10] S. Schneider, A. C. Filippou, *Inorg. Chem.* **2001**, *40*, 4674–4677.
[11] Experimental and computational details of **2** and **4** can be found in the Supporting Information.
[12] a) R. A. Heintz, B. S. Haggerty, H. Wan, A. L. Rheingold, K. H. Theopold, *Angew. Chem.* **1992**, *104*, 1100–1102; *Angew. Chem. Int. Ed. Engl.* **1992**, *31*, 1077–1079; b) R. A. Heintz, R. L. Ostrander, A. L. Rheingold, K. H. Theopold, *J. Am. Chem. Soc.* **1994**, *116*, 11387–11396.
[13] The complexes $[Li(thf)Cr(N_3N)R]$ ($R=Me$, CH_2SiMe_3) were characterized by X-ray crystallography and display similar structural features with **2**: S. Schneider, dissertation, Humboldt-Universität zu Berlin, Cuvillier Verlag, Göttingen, **2003**.
[14] An appreciable amount of $(Me_3SiN(H)CH_2CH_2)_3N$ is also formed in this reaction, which is difficult to separate from **4** by repeated recrystallizations from pentane without considerable loss in yield.
[15] The isosterous molybdenum(IV) hydride $[Mo(N_3N)H]$ eliminates H_2 at 100 °C to give the cyclometallation product $[Mo(CH_2SiMe_2NCH_2CH_2)N(CH_2CH_2NSiMe_3)_2]$: R. R. Schrock, S. W. Seidel, N. C. Mösch-Zanetti, K.-Y. Shih, M. B. O'Donoghue, W. M. Davis, W. M. Reiff, *J. Am. Chem. Soc.* **1997**, *119*, 11876–11893.
[16] The broad ν(Cr–H) absorption band of **4** at 1712 cm^{-1} carries a shoulder at 1754 cm^{-1}.
[17] The ^1H NMR signal of the hydrido ligand in **2** and **4** could not be detected. The ^{13}C NMR spectra of **2** and **4** displayed between ± 1000 ppm signals that were tentatively assigned to the $SiMe_3$ groups and coordinated THF (**2**).
[18] Crystal structure determination of **2**: $C_{19}H_{48}CrLiN_4OSi_3$, $M_r=491.82$; black crystals ($0.60\times0.48\times0.20$ mm), which appear olive green in transmitted light, from a saturated pentane solution upon cooling from 20 to −25 °C, $T=180(2)$ K, $\lambda(Mo_{K\alpha})=0.71073$ Å, monoclinic, space group $P2_1/c$, $a=9.878(2)$, $b=11.470(2)$, $c=25.242(8)$ Å, $\alpha=\gamma=90$, $\beta=90.86(3)°$, $V=2859.9(12)$ Å^3, $Z=4$, $\rho_{calcd}=1.142$ g cm^{-3}, $2\theta_{max}=50.5°$, $\mu=0.542$ mm^{-1}, $F(000)=1068$, 17661 reflections, 4862 unique reflections, 275 parameters, GOF = 1.019, $R_1=0.0330$ [$I>2\sigma(I)$], w$R_2=0.0918$, min./max. residual electron density −0.400/0.509 e Å^{-3}. Crystal structure determination of **4**: $C_{15}H_{40}CrN_4Si_3$, $M_r=412.78$; brick-red rectangular parallelepipeds ($0.40\times0.24\times0.12$ mm) from a saturated pentane solution upon cooling from 20 to −78 °C, $T=180(2)$ K, $\lambda(Mo_{K\alpha})=0.71073$ Å, monoclinic, space group $P2_1/n$, $a=9.618(2)$, $b=16.662(2)$, $c=15.316(3)$ Å, $\alpha=\gamma=90$, $\beta=101.78(2)°$, $V=2402.8(8)$ Å^3, $Z=4$, $\rho_{calcd}=1.141$ g cm^{-3}, $2\theta_{max}=50.5°$, $\mu=0.630$ mm^{-1}, $F(000)=896$, 14862 reflections, 4286 unique reflections, 221 parameters, GOF = 0.907, $R_1=0.0337$ [$I>2\sigma(I)$], w$R_2=0.0776$, min./max. residual electron density −0.214/0.368 e Å^{-3}. CCDC-200256 and CCDC-200257 contain the supplementary crystallographic data for this paper. These data can be obtained free of charge via www.ccdc.cam.ac.uk/conts/retrieving.html (or from the Cambridge Crystallographic Data Centre, 12, Union Road, Cambridge CB21EZ, UK; fax: (+44) 1223-336-033; or deposit@ccdc.cam.ac.uk).
[19] Chromium(III) complexes usually display an octahedral and rarely a square-pyramidal, trigonal-bipyramidal, or trigonal-planar coordination sphere, and chromium(IV) complexes are in general tetrahedral: a) references [1] and [2]; b) V. C. Gibson, C. Newton, C. Redshaw, G. A. Solan, A. J. P. White, D. J. Williams, *Eur. J. Inorg. Chem.* **2001**, 1895–1903; c) L. A. MacAdams, W.-K. Kim, L. M. Liable-Sands, I. A. Guzei, A. L. Rheingold, K. H. Theopold, *Organometallics* **2002**, *21*, 952–960; d) V. C. Gibson, C. Newton, C. Redshaw, G. A. Solan, A. J. P. White, D. J. Williams, *J. Chem. Soc. Dalton Trans.* **2002**, 4017–4023.
[20] Z. Duan, V. G. Young, Jr., J. G. Verkade, *Inorg. Chem.* **1995**, *34*, 2179–2185.
[21] a) G. Kiss, K. Zhang, S. L. Mukerjee, C. D. Hoff, G. C. Roper, *J. Am. Chem. Soc.* **1990**, *112*, 5657–5658.
[22] a) R. R. Schrock, K.-Y. Shih, D. A. Dobbs, W. M. Davis, *J. Am. Chem. Soc.* **1995**, *117*, 6609–6610; b) D. A. Dobbs, R. R. Schrock, W. M. Davis, *Inorg. Chim. Acta* **1997**, *263*, 171–180.

 © 2003 Wiley-VCH Verlag GmbH & Co. KGaA, Weinheim

Cascade-Release Dendrimers

"Cascade-Release Dendrimers" Liberate All End Groups upon a Single Triggering Event in the Dendritic Core**

Franciscus M. H. de Groot, Carsten Albrecht, Ralph Koekkoek, Patrick H. Beusker, and Hans W. Scheeren*

Dendrimers are well-defined, branched treelike molecules with multiple end groups.[1,2] Numerous applications of these starlike structures have been explored.[3,4] They can be utilized in areas such as magnetic resonance imaging (MRI), gene therapy,[5] liquid crystals, sensors, and catalysis. The application of dendrimers in drug delivery is currently receiving much scientific attention.[6–9] Most dendrimers reported so far have been constructed as a branched skeleton that incorporates functional molecules either covalently or noncovalently. Biologically active substances that are attached to the termini of dendritic structures[10] can be liberated by chemical or biological methods.[11] Several branched constructs have been reported which contain covalently linked doxorubicin molecules as end groups.[12–14] However, in all the branched structures or dendrimers reported so far, each single drug has to be independently cleaved to be released. Here, we report dendrimers that have been built to completely and rapidly dissociate into separate building blocks upon a single triggering event in the dendritic core. This process induces simultaneous release of all end-group molecules connected to the dendritic termini. We term these multiple-release dendritic systems "cascade-release dendrimers". Such dendrimers collapse into their separate monomeric building blocks after a single (chemical or biological) activation step that triggers a cascade of self-elimination reactions, thereby releasing all the end groups from the periphery of the "exploding" cascade-release dendrimer (see Supporting Information).

Functional dendrimers of this kind may find application in several fields. One particular area is (targeted) drug delivery, where cascade-release dendrimers possess two major advantages over conventional dendrimers: 1) multiple covalently bound drug molecules can be site-specifically released from the targeting moiety by a single cleaving step; and 2) they are selectively as well as completely degraded. Thus, in contrast to conventional dendrimers, they can be easily drained from the body. Clearance of macromolecules from the body may be a limiting factor in current macromolecular drug-delivery systems,[15] as the long-term effects of some synthetic macromolecules in parenteral medicine are not completely known.[16]

To facilitate drug release, linkers are frequently incorporated between the drug molecule and a cleavable carrier, which is termed the "specifier" (Figure 1).

Cascade-release dendrimers are constructed from two or more generations of branched self-elimination linkers, each of which releases multiple leaving groups after a single activation (Figure 2). We present here two such structurally distinct monomeric multiple-release building blocks. Both linkers are based on a general type of single-release linker that is eliminated as a consequence of shifting conjugated electron

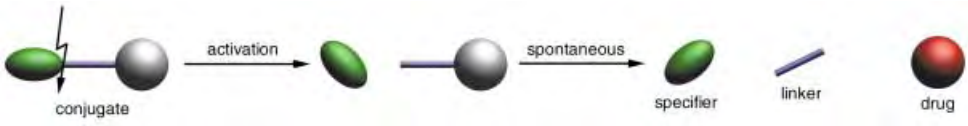


Figure 1. A conjugated drug (gray) is released from an inactive conjugate. Cleavage between the specifier (green) and the linker (blue) induces spontaneous self-elimination of the linker, thus releasing the drug molecule (red) with regained activity.

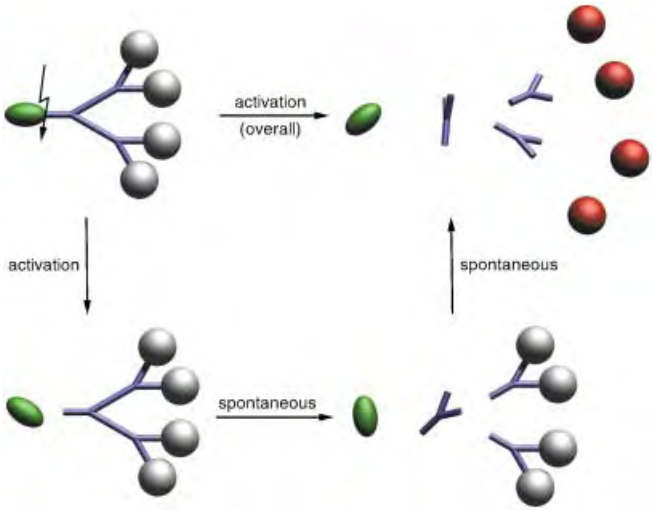


Figure 2. A single activation of a second generation cascade-release dendrimer triggers a cascade of self-eliminations and induces release of all end groups. Covalently bound end groups are depicted in gray, branched self-elimination linkers in blue, and the specifier in green. The released end groups are depicted in red.

[*] Dr. F. M. H. de Groot, Dr. P. H. Beusker
Syntarga B.V.
Toernooiveld, 6525 ED Nijmegen (The Netherlands)
Fax: (+31) 24-365-2929
E-mail: fmhdegroot@syntarga.com
C. Albrecht, R. Koekkoek, Dr. H. W. Scheeren
Department of Organic Chemistry
University of Nijmegen
Toernooiveld 1, 6525 ED Nijmegen (The Netherlands)

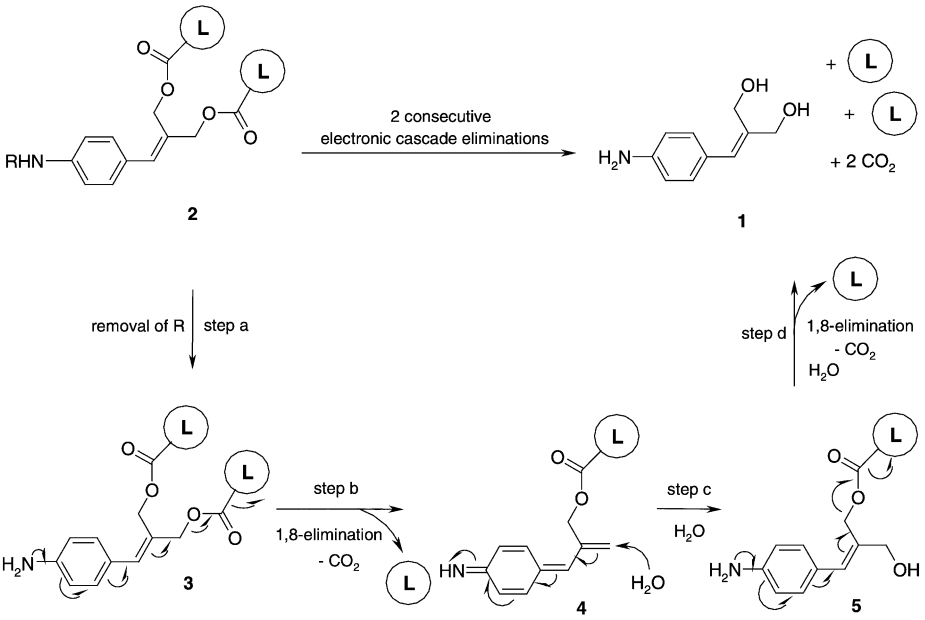
[**] We thank NWO-ZonMw for a STIGON grant. Prof. J. C. M. van Hest, Dr. F. L. van Delft, and Prof. R. J. M. Nolte are thanked for their helpful comments. Dr. D. de Vos (Pharmachemie B.V., Haarlem, The Netherlands) is acknowledged for a gift of paclitaxel. We are grateful to Dr. H. Engelkamp for assistance in preparing Figures 1 and 2.

Supporting information for this article is available on the WWW under http://www.angewandte.org or from the author.

 © 2003 Wiley-VCH Verlag GmbH & Co. KGaA, Weinheim DOI: 10.1002/anie.200351942

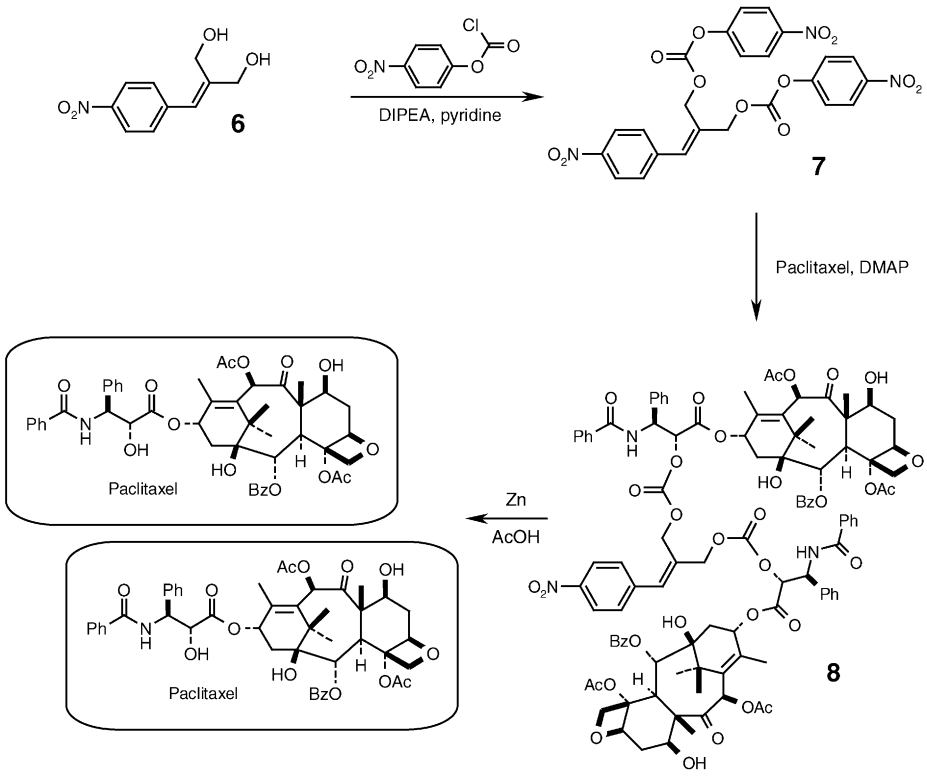
pairs, which leads to expulsion of the leaving group (for example, a drug). The most prominent example of this self-elimination linker type is the highly versatile and well-known 4-aminobenzyl alcohol linker.[17] We recently reported that the elongation of this conventional 1,6-elimination linker results in enhanced rates of drug release.[18] It was shown that the elongated 4-aminocinnamyl alcohol linker released paclitaxel (taxol) following 1,8-elimination.[19] Herein, proof of principle is reported for both the release of two leaving groups from a branched double-release linker, which can be obtained by introduction of branching into the 4-aminocinnamyl alcohol linker, and for the release of three leaving groups from a branched triple-release linker, which is based on the 1,6-elimination linker. Furthermore, we demonstrate that a cascade-release dendrimer which contains two generations of double-release linkers completely falls apart into its free monomers and releases all end groups upon a single activating event.

The double-release self-elimination AB_2-type monomer 2-(4-aminobenzylidene)propane-1,3-diol (**1**) and the proposed mechanism of the release of two leaving groups upon activation are depicted in Scheme 1. The multiple-release system is stable as long as the amine function in **2** is capped by a protecting group. Unmasking (step a) the protected amine **2** triggers two 1,8-elimination reactions from amine **3**, in which two molecules of CO_2 and two leaving groups L are liberated. The intermediate non-aromatic species **4** that is formed after the first self-elimination (step b) is trapped by a nucleophile, such as water, in step c to regenerate an aromatic species **5** that can undergo the second self-elimination (step d). Quenching of the intermediate with water (for example, under physiological conditions) will generate aminodiol building block **1**.



Scheme 1. Structure of double-release linker **1** and the proposed mechanism of elimination of both leaving groups L upon activation of **2**.

Proof of concept for complete release of both end groups from the double-release linker was firmly established in a branched system in which nitrodiol **6**[20] formed the core (Scheme 2). The nitro function can be considered as a masked amine. Chemical reduction of the nitro group to the amine should trigger the cascade of self-eliminations. Nitrodiol **6** was activated using 4-nitrophenyl chloroformate to give the corresponding bis(4-nitrophenyl carbonate) **7**, which was subsequently coupled with two equivalents of paclitaxel to yield dendron **8**. To demonstrate the generality of the concept, the chemotherapeutic drug paclitaxel was chosen as a model compound because of its complex structure and bulkiness. At 0°C paclitaxel reacted specifically with the activated carbonates through its most reactive 2′-hydroxy function. The nitro function was then

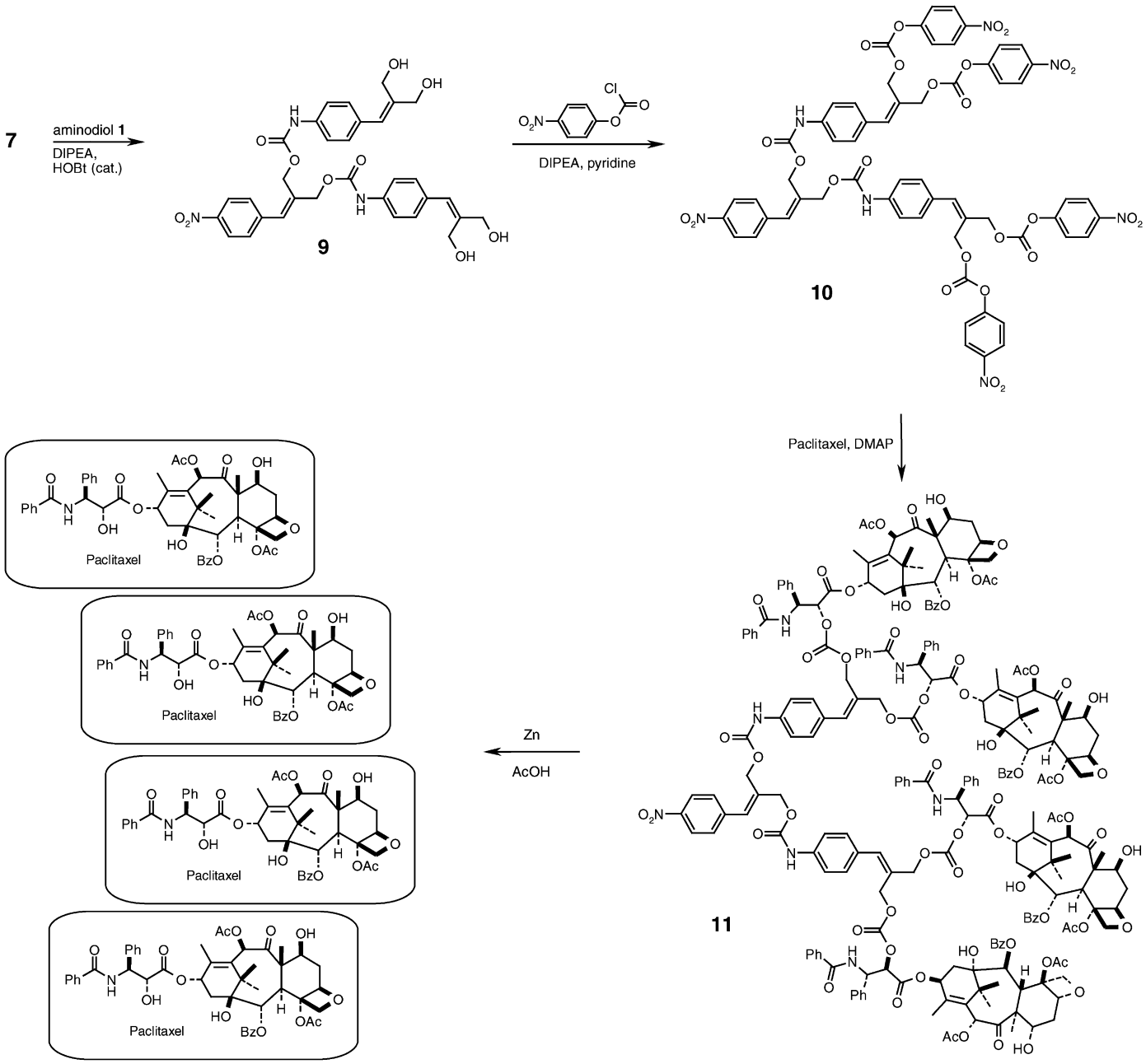


Scheme 2. Synthesis of branched construct **8** and elimination of two paclitaxel (taxol) molecules upon a single triggering reaction (reduction of the nitro function). DIPEA = *N*,*N*,-diisopropylethylamine, DMAP = 4-dimethylaminopyridine, Bz = benzoyl.

 © 2003 Wiley-VCH Verlag GmbH & Co. KGaA, Weinheim

reduced under mild conditions (Zn, acetic acid; Scheme 2). Analysis by thin-layer chromatography indicated complete disappearance of the starting material and formation of unconjugated paclitaxel within 30 minutes. ^{1}H NMR spectroscopic studies unambiguously confirmed the complete release of both paclitaxel molecules (see Supporting Information). Although the NMR spectra of large paclitaxel derivatives are generally complicated, the 2′-H signal of **8** can be identified as a clearly distinguishable signal at $\delta = 5.46$ ppm, which is indicative of a 2′-hydroxy group functionalized with an alkyloxycarbonyl group. This signal completely vanished following the multiple-release cascade, thus indicating that no conjugated paclitaxel was present, whereas the characteristic paclitaxel 2′-H signal at $\delta = 4.74$ ppm was clearly present. Mass spectrometric studies showed that compound **8**, its reduced congener, or any of the intermediates similar to the ones in Scheme 1 were no longer present, and clearly showed a major peak corresponding to free paclitaxel. No degradation or formation of side products had taken place (TLC, NMR), thus showing the validity of the concept. The kinetics for electronic cascade self-eliminations are generally fast.[17] Paclitaxel was immediately formed, which left the triggering reaction as the rate-limiting step for complete dissociation.

With the double-release linker in hand, we now focused on the construction of a dendritic structure to unequivocally establish that multiple release occurred from a cascade-release dendrimer. A divergent route, starting with the dendrimer core (Scheme 3), was used to synthesize cascade-

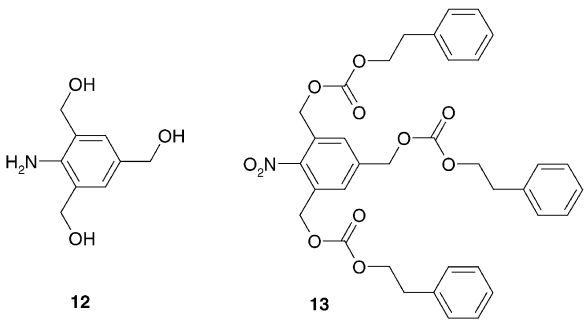


Scheme 3. Synthesis of second-generation cascade-release dendrimer **11** and release of four paclitaxel leaving groups upon reduction. HOBt = 1-hydroxy-1*H*-benzotriazole.

 © 2003 Wiley-VCH Verlag GmbH & Co. KGaA, Weinheim

release dendrimer **11**. Two generations of double-release linkers were connected through carbamate linkages by coupling two molecules of aminodiol **1** to the bis(4-nitrophenyl carbonate) **7** to yield **9**. The four terminal alcohol groups were then activated to give tetracarbonate **10**, which was coupled to four equivalents of paclitaxel to yield the second-generation cascade-release dendrimer **11** loaded with four paclitaxel molecules at the dendritic termini. To prove the validity of the dendritic cascade-release concept, second generation dendrimer **11** was subjected to reduction using Zn and acetic acid (Scheme 3). Chromatographic analysis once again indicated rapid and complete disappearance of the starting compound and formation of paclitaxel. ^{1}H NMR spectroscopic analysis demonstrated complete formation of liberated paclitaxel and no degradation products. No conjugated paclitaxel was present, thus demonstrating that **11** behaves as a cascade-release dendrimer that releases all end groups according to the sequence depicted in Figure 2.

We have also designed and synthesized a second multiple-release linker, (2-amino-3,5-di(hydroxymethyl)phenyl)methanol (**12**, Scheme 4). This triple-release linker is an aniline



Scheme 4. Structures of triple-release linker **12** and its functionalized nitroaromatic derivative **13**.

derivative with a hydroxymethyl group at the 2-, 4-, and 6-positions, and it combines one 1,6- with two 1,4-elimination systems in a single linker.[17] We synthesized a nitrotriol derivative of this AB_3-type monomeric building block[21] (**13**) containing three phenethyl alcohol molecules as leaving groups connected by carbonate linkages. All the starting material was, again, completely converted into free phenethyl alcohol (MS, NMR) upon reduction of the nitro function, thus validating aminotriol **12** as a triple-release monomeric linker.

To prove that the conditions used for the reduction of the nitro function in the synthesized compounds did not directly effect cleavage of the paclitaxel carbonate or phenethyl carbonate linkages, we treated reference compounds dibenzyl carbonate and 2′-*O*-(cinnamyloxycarbonyl)paclitaxel with Zn/acetic acid. Both compounds remained fully intact under these conditions (as observed by ^{1}H NMR spectroscopy), thus indicating that the nitro-containing multiple-release compounds are only degraded on reduction of the nitro group.

Since the reported cascade-release dendrimers may be useful for drug delivery, we have evaluated both multiple-release monomers aminodiol **1** and aminotriol **12**, which are expected to be regenerated under physiological conditions upon dendritic disintegration, for their cytotoxicity in a panel of seven well-characterized human tumor cell lines. Neither compound displayed any toxicity. Details concerning the experimental procedures and in vitro cytotoxicity are enclosed as Supporting Information.

Cascade-release dendrimers, as well as the multiple-release monomers, may show utility in fields such as (targeted) drug delivery, biodegradable materials, controlled release, and diagnostics. Much room is left for the variation of individual components for the design of a cascade-release dendrimer with desired properties. The characteristics of the activation can be modified by the choice of specifier. An appropriate specifier can, for example, be a specific peptide substrate for a disease-associated enzyme, or it may contain an additional targeting moiety, such as, for example, an antibody. Two or more different parent compounds can be attached as end groups. Linear self-elimination linkers can be incorporated between the specifier and the first branched linker to improve the efficiency of drug release.[18] Linear self-elimination linkers can be incorporated between generations of branched monomers to increase the outer sphere surface and the number of end groups that can be accommodated.

Cascade-release dendrimers can be used for drug delivery, particularly for tumor-targeted drug delivery,[22,23] where they may potentially induce a substantial therapeutic advantage over single-release unbranched conjugates.[24–26] The cascade-release dendrimer amplifies the effect of one tumor-specific activating reaction, by triggering a "cytotoxic explosion". Cascade-release dendrimers of sufficient size will also passively target by the enhanced permeability and retention (EPR) effect,[27] and, as for conventional dendrimers, they can be manufactured as monodisperse and homogeneous compounds. The monomers presented here are appropriate for tumor targeting, because self-elimination of the double- and triple-release monomers proceeds with a short half-life,[17,18] and because the monomers can be connected through carbamate linkages that are generally stable under physiological conditions.[28] We have reported chemical proof of the concept of cascade-release dendrimers. Their potential in tumor targeting should be exploited, for example, by choosing a specifier that is a substrate for tumor-associated or tumor-targeted enzymes and a highly toxic anticancer agent for attachment at the dendritic termini.

Received: May 21, 2003
Revised: July 10, 2003 [Z51942]

Keywords: dendrimers · drug delivery · fragmentation · multiple release · prodrugs

[1] D. A. Tomalia, A. M. Naylor, W. A. Goddard III, *Angew. Chem.* **1990**, *102*, 119–157; *Angew. Chem. Int. Ed. Engl.* **1990**, *29*, 138–175.
[2] G. R. Newkome, A. Nyak, R. K. Behera, C. N. Moorefield, G. R. Baker, *J. Org. Chem.* **1992**, *57*, 358–362.
[3] M. Fischer, F. Vögtle, *Angew. Chem.* **1999**, *111*, 934–956; *Angew. Chem. Int. Ed.* **1999**, *38*, 884–905.
[4] A. W. Bosman, H. M. Janssen, E. W. Meijer, *Chem. Rev.* **1999**, *99*, 1665–1688.

 © 2003 Wiley-VCH Verlag GmbH & Co. KGaA, Weinheim

[5] R. F. Service, *Science* **1995**, *267*, 458 – 459.
[6] M. Liu, J. M. J. Fréchet, *Pharm. Sci. Technol. Today* **1999**, *2*, 393 – 401.
[7] N. Malik, R. Wiwattanapatapee, R. Klopsch, K. Lorenz, H. Frey, J. W. Weener, E. W. Meijer, W. Paulus, R. Duncan, *J. Controlled Release* **2000**, *65*, 133 – 148.
[8] O. L. Padilla De Jesús, H. R. Ihre, L. Gagne, J. M. J. Fréchet, F. C. Szoka, Jr., *Bioconjugate Chem.* **2002**, *13*, 453 – 461.
[9] A. K. Patri, I. J. Majoros, J. R. Baker, Jr., *Curr. Opin. Chem. Biol.* **2002**, *6*, 466 – 471, and references therein.
[10] M. J. Cloninger, *Curr. Opin. Chem. Biol.* **2002**, *6*, 742 – 748.
[11] D. Seebach, G. F. Herrmann, U. D. Lengweiler, B. M. Bachmann, W. Amrein, *Angew. Chem.* **1996**, *108*, 2969 – 2971; *Angew. Chem. Int. Ed. Engl.* **1996**, *35*, 2795 – 2797.
[12] H. D. King, D. Yurgaitis, D. Willner, R. A. Firestone, M. B. Yang, S. J. Lasch, K. E. Hellstrom, P. A. Trail, *Bioconjugate Chem.* **1999**, *10*, 279 – 288.
[13] D. Wang, P. Kopeckova, T. Minko, V. Nanayakkara, J. Kopecek, *Biomacromolecules* **2000**, *1*, 313 – 319.
[14] M. Kovář, J. Strohalm, T. Etrych, K. Ulbrich, B. Říhová, *Bioconjugate Chem.* **2002**, *13*, 206 – 215.
[15] L. W. Seymour, *Crit. Rev. Ther. Drug Carrier Syst.* **1992**, *9*, 135 – 187.
[16] A. C. Hunter, S. M. Moghimi, *Drug Discovery Today* **2002**, *7*, 998 – 1001.
[17] P. L. Carl, P. K. Chakravarty, J. A. Katzenellenbogen, *J. Med. Chem.* **1981**, *24*, 479 – 480.
[18] F. M. H. de Groot, W. J. Loos, R. Koekkoek, L. W. A. van Berkom, G. F. Busscher, A. E. Seelen, C. Albrecht, P. de Bruijn, H. W. Scheeren, *J. Org. Chem.* **2001**, *66*, 8815 – 8830.
[19] E. W. P. Damen, T. J. Nevalainen, T. J. M. Van den Bergh, F. M. H. de Groot, H. W. Scheeren, *Bioorg. Med. Chem.* **2002**, *10*, 71 – 77.
[20] P. Vanelle, J. Maldonado, M. P. Crozet, K. Senouki, F. Delmas, M. Gasquet, P. Timon-David, *Eur. J. Med. Chem.* **1991**, *26*, 709 – 714.
[21] F. Piozzi, *Gazz. Chim. Ital.* **1953**, *83*, 673 – 676.
[22] G. M. Dubowchik, M. A. Walker, *Pharmacol. Ther.* **1999**, *83*, 67 – 123.
[23] F. M. H. de Groot, E. W. P. Damen, H. W. Scheeren, *Curr. Med. Chem.* **2001**, *8*, 1093 – 1122.
[24] D. DeFeo-Jones, V. M. Garsky, B. K. Wong, D. M. Feng, T. Bolyar, K. Haskell, D. M. Kiefer, K. Leander, E. McAvoy, P. Lumma, J. Wai, E. T. Senderak, S. L. Motzel, K. Keenan, M. van Zwieten, J. H. Lin, R. Freidinger, J. Huff, A. Oliff, R. E. Jones, *Nat. Med.* **2000**, *6*, 1248 – 1252.
[25] P. H. J. Houba, E. Boven, I. H. van der Meulen-Muileman, R. G. G. Leenders, J. W. Scheeren, H. M. Pinedo, H. J. Haisma, *Int. J. Cancer* **2001**, *91*, 550 – 554.
[26] F. M. H. de Groot, L. W. A. van Berkom, H. W. Scheeren, *J. Med. Chem.* **1999**, *42*, 5277 – 5283.
[27] H. Maeda, Y. Matsumura, *Crit. Rev. Ther. Drug Carrier Syst.* **1989**, *6*, 193 – 210.
[28] F. M. H. de Groot, L. W. A. van Berkom, H. W. Scheeren, *J. Med. Chem.* **2000**, *43*, 3093 – 3102.

 © 2003 Wiley-VCH Verlag GmbH & Co. KGaA, Weinheim

Dendritic Delivery Systems

Self-Immolative Dendrimers**

*Roey J. Amir, Neta Pessah, Marina Shamis, and Doron Shabat**

Dendrimers are perfectly cascade-branched, highly defined, synthetic macromolecules, which are characterized by a combination of high number of functional groups and a compact molecular structure.[1] The concept of repetitive growth with branching creates a unique spherical monodisperse dendrimer formation, which is defined by a precise generation number.[2] For example, first-generation dendrimer (G1) will have one branching unit, and the second-generation dendrimer (G2) will have an additional two branching units, etc. The structural precision of dendrimers has motivated numerous studies aimed at developing biological applications,[3–6] such as, the amplification of molecular effects or the creation of high concentrations of drugs,[7] molecular labels, or probe moieties.[8]

Most of the applications of dendrimers rely mainly on the high number of functional groups and not on their unique structures.[9,10] An appropriate dendrimer could be structurally designed to release all of its tail molecules with a single cleavage event at the dendrimer's core. Here we propose the design and synthesis of a novel dendritic structure with a trigger that can initiate the fragmentation of the dendrimer molecule to its building blocks in a self-immolative manner[11,12] with consequent release of the tail-group units.[13]

The design of the first-generation self-immolative dendron (SID) is based on an adaptor molecule that has three functional groups. Two identical functionalities are linked to reporter molecules and the third is attached to a trigger (Figure 1, **I**). Cleavage of the trigger initiates a sequence of self-immolative reactions that leads to a spontaneous release of the two reporter molecules. The adaptor molecule can be linked to two additional identical units, which are each attached to two reporter molecules (Figure 1, **II**). The head position of the first adaptor unit is linked to a trigger. The G2 dendron can be prepared by this approach, and, similarly, the design can be extended to higher generations of dendrons

[*] Dr. D. Shabat, R. J. Amir, N. Pessah, M. Shamis
Department of Organic Chemistry
School of chemistry, Faculty of Exact Sciences
Tel Aviv University, Tel Aviv 69978 (Israel)
Fax: (+972) 3-640-9293
E-mail: chdoron@post.tau.ac.il

[**] We wish to thank Dr. Benjamin List, The Scripps Research Institute, for early contribution to this research, and Mr. Ophir Flomenbom, School of Chemistry at the Tel-Aviv University, for technical assistance with the kinetic analysis. Special thanks go to Dr. Michael Lital and Dr. Daniel Meijler for their helpful comments. We would also like to thank Mrs. Osnat Pass and Mr. Ofer Shkedi for their help with the graphical figures. Mr. Michael Shafir is acknowledged for financial support for the graphics.

Supporting information for this article is available on the WWW under http://www.angewandte.org or from the author.

 © 2003 Wiley-VCH Verlag GmbH & Co. KGaA, Weinheim DOI: 10.1002/anie.200351962

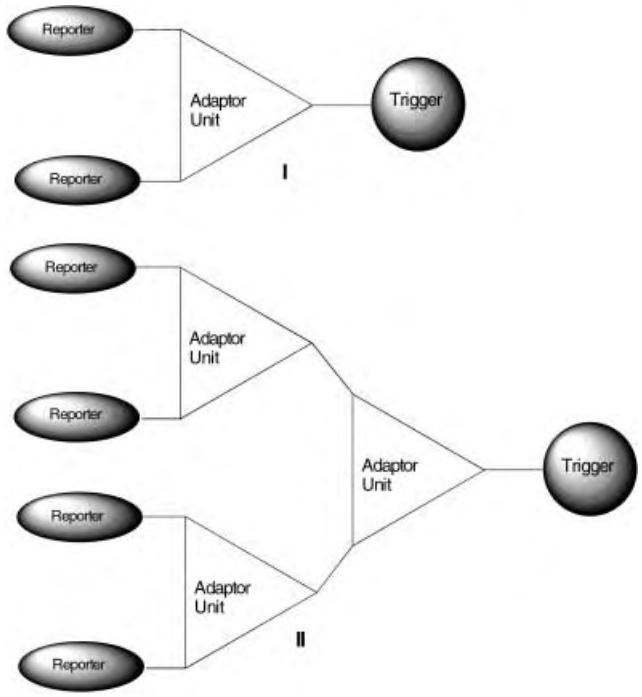
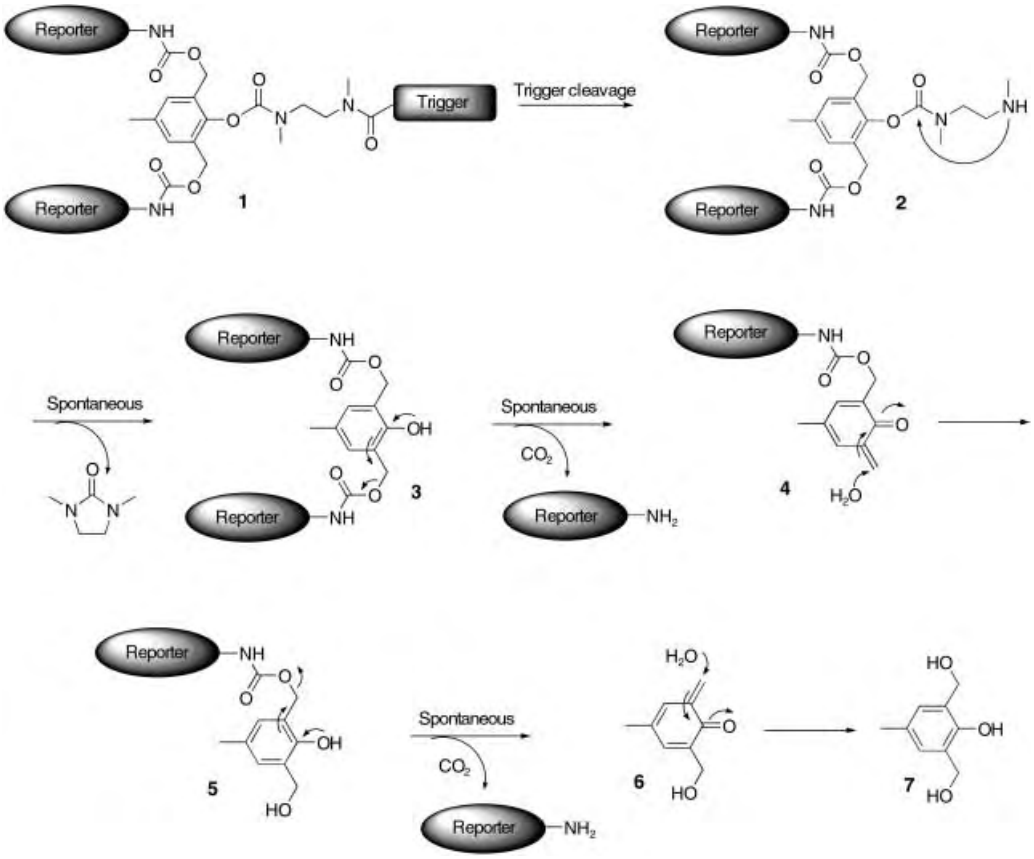


Figure 1. Graphical representation of a first generation (G1) self-immolative dendron with a trigger and two tail units (**I**). Graphical representation of a second generation (G2) self-immolative dendron with a trigger and four tail units (**II**).

and dendrimers. The cleavage of the trigger will initiate self-immolative chain reactions that will consequently fragment the dendrimer and release all of the tail molecules.

The adaptor unit of our dendrimer is based on 2,6-bis(hydroxymethyl)-*p*-cresol (**7**), a commercially available compound, which has three functional groups (Scheme 1). The two hydroxybenzyl groups are attached through a carbamate linkage to reporter molecules and the phenol functionality is linked to a trigger through a short spacer (*N*,*N*′-dimethylethylenediamine) to form **1**. Cleavage of the trigger initiates a sequence of self-immolative reactions of the amine intermediate **2**, starting with spontaneous cyclization to form an *N*,*N*′-dimethylurea derivative. The generated phenol **3** undergoes a 1,4-quinone methide rearrangement, followed by spontaneous decarboxylation to liberate one of the reporter molecules. The quinone methide species **4** is rapidly trapped by a water molecule (from the reaction solvent) to form a phenol **5**, which again undergoes a 1,4-quinone methide rearrangement to liberate the second reporter molecule. The generated quinone methide species **6** is then trapped by another water molecule to form **7**. As far as we know, this is the first reported example of a double 1,4-quinone methide rearrangement for this type of aromatic system.

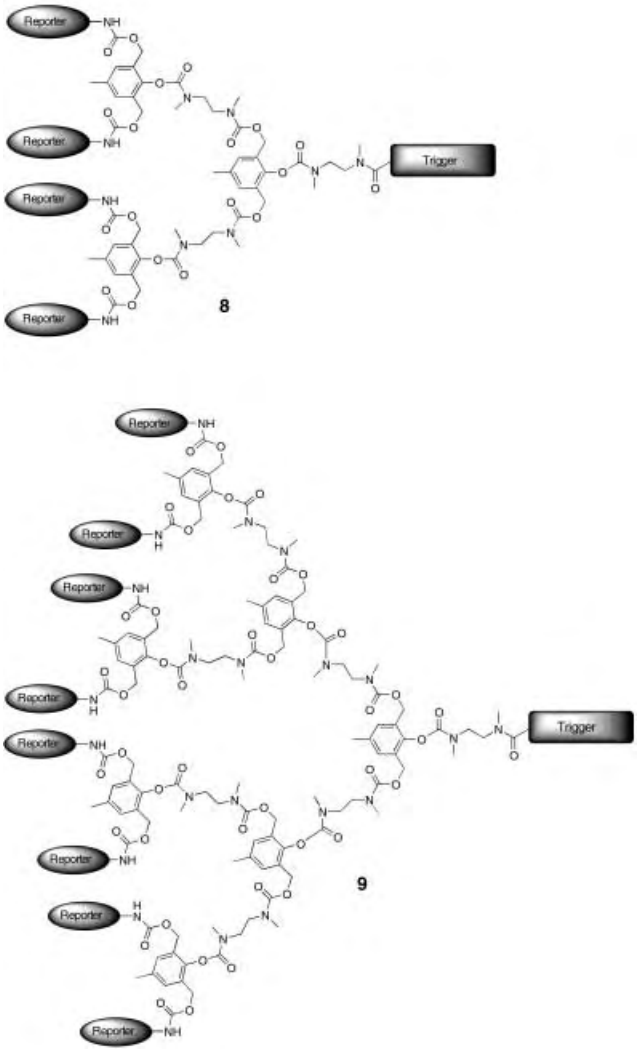
To extend the synthesis to higher generations of dendrons, two identical units of G1 dendrons can be attached to the hydroxybenzyl functionalities of the first unit to give a



Scheme 1. Schematic representation of the activation of a G1 self-immolative dendron through a spontaneous chain reaction that is based on a cyclization and 1,4-quinone methide rearrangement.

 © 2003 Wiley-VCH Verlag GmbH & Co. KGaA, Weinheim

G2 dendron **8** (Scheme 2). The attachment is performed through a double carbamate linkage using *N*,*N*-dimethylethylenediamine as a spacer. The G3 dendrimer can similarly be obtained by linking two G2 units to the hydroxybenzyl groups of the first unit to give **9**. The carbamate linkage between the units is highly stable until the trigger is cleaved and the self-immolative reaction sequence is initiated.



Scheme 2. General chemical structure of G2 and G3 self-immolative dendrons.

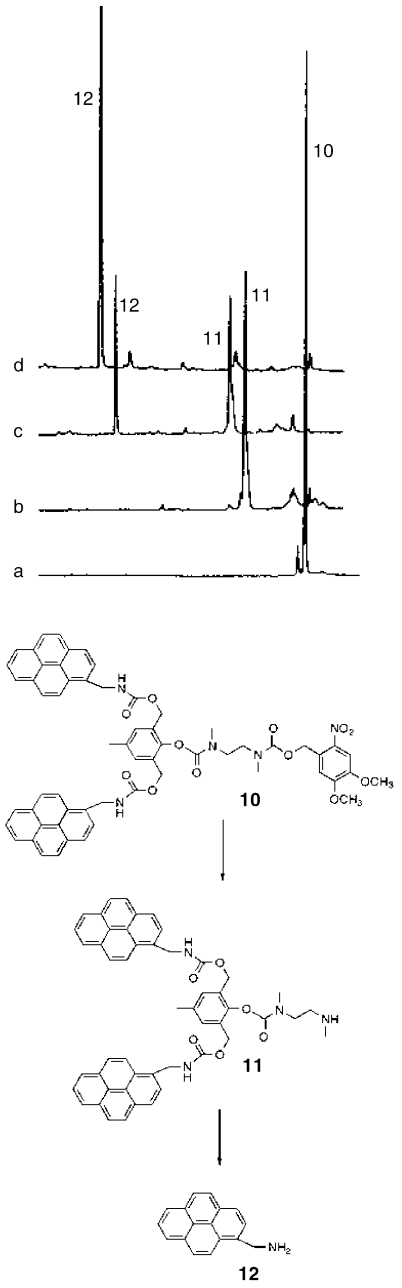


Figure 2. HPLC chromatograms showing the self-immolative dendron activation of G1 to release aminomethylpyrene (50 μM **10** in methanol with 10% triethylamine): a) before radiation; b) after radiation, $t=0$; c) $t=4$ h; d) $t=11$ h.

To prove our concept we initially synthesized a G1 SID **10** with aminomethylpyrene as the tail unit and a photolabile trigger (see the Supporting Information). The dendrimer was dissolved in methanol, the solution was irradiated with UV light ($\lambda=360$ nm) to cleave the trigger, and 10% triethylamine was added to initiate the self-immolative reactions (the triethylamine is needed to generate the mildly basic media which is required for the quinone methide rearrangement). The release of aminomethylpyrene (**12**) was monitored by HPLC and the results are shown in Figure 2. Cleavage of the photolabile trigger generated amine **11**, which gradually degraded to the tail units through the previously explained self-immolative process. The release of aminomethylpyrene was completed after 11 h. Since no intermediates other than amine **11** were observed we concluded that the rate-limiting step of the self-immolative sequence is the cyclization of amine **11** to form an *N*,*N*′-dimethylurea derivative and a phenol which rapidly rearranges to release the tail units. We have characterized amine **11** by HRMS and by comparison with the HPLC spectrum of a reference compound.

Next, we synthesized a G2 SID **13** with a similar tail unit and a photolabile trigger. We repeated the previous experi-

 © 2003 Wiley-VCH Verlag GmbH & Co. KGaA, Weinheim

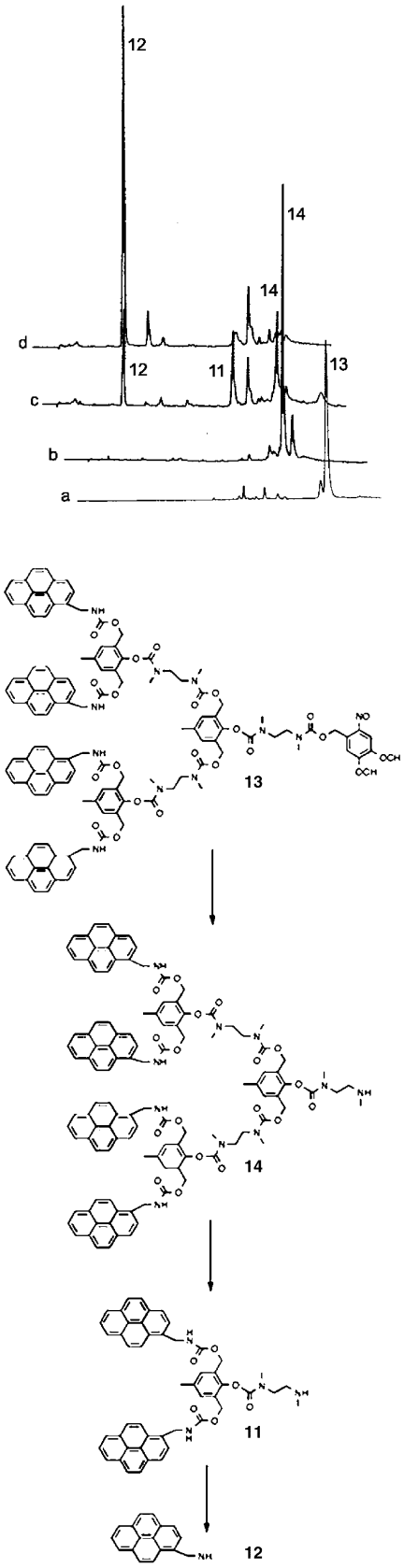


Figure 3. HPLC chromatograms showing the self-immolative dendron activation of G2 to release aminomethylpyrene (50 μM **13** in methanol with 10% triethylamine): a) before radiation; b) after radiation, $t=0$; c) $t=6$ h; d) $t=20$ h.

ment and monitored the release of the tail molecules. It was clearly shown (Figure 3) that upon cleavage of the trigger, to form amine **14**, the self-immolative release of aminomethylpyrene **12** is initiated and completed after 21 h.

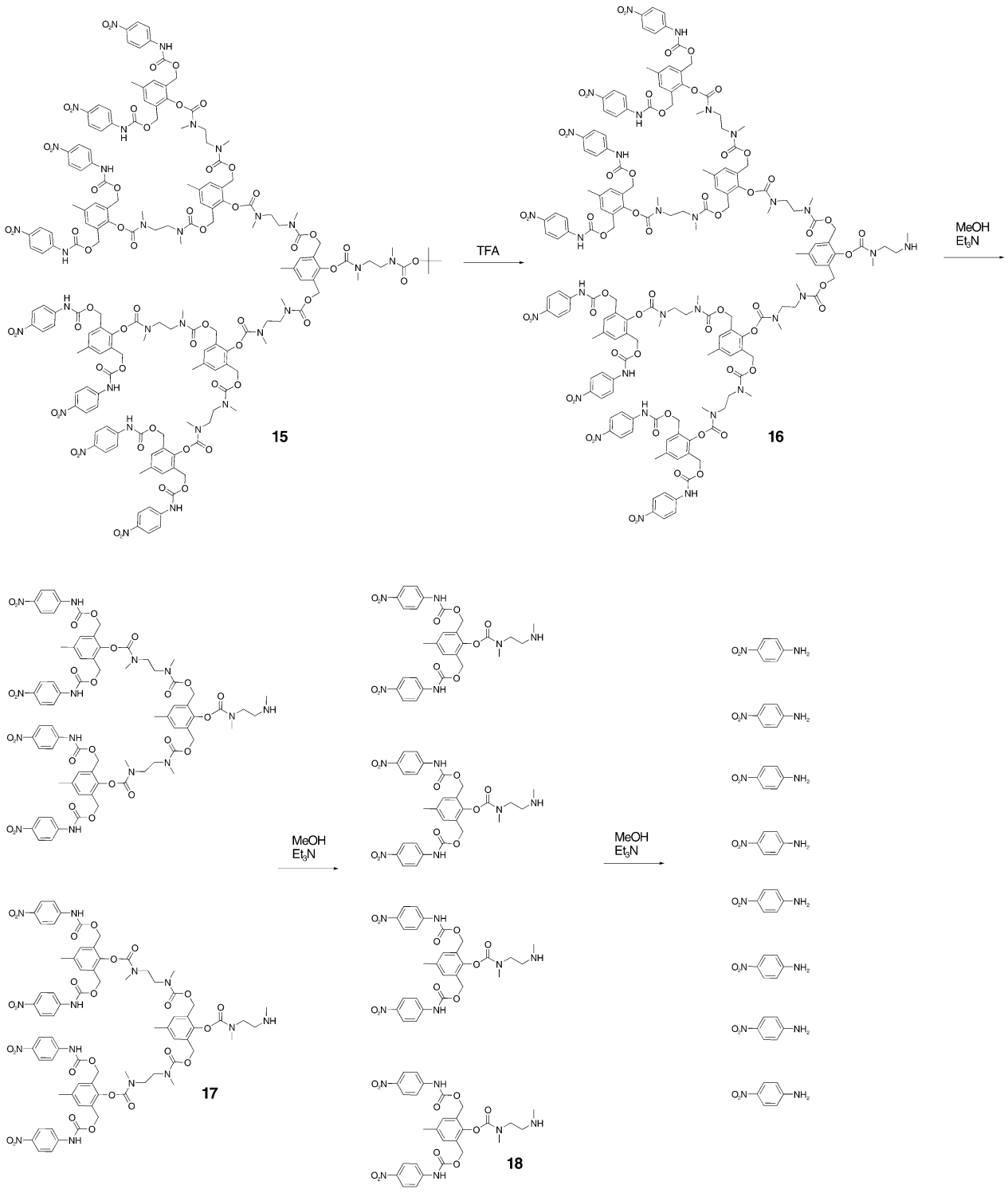
Our attempts to synthesize a G3 SID with an aminomethylpyrene as the tail unit have not succeeded so far. A possible obstacle could be that eight molecules of pyrene do not fit into the limited space of the dendrimer's partial sphere because of possible steric problems. To test this hypothesis, we tried to synthesize a G3 SID with 4-nitroaniline instead of pyrene. 4-Nitroaniline is a significantly smaller molecule than pyrene and has a yellow color that is easy to observe when it is in a free state. To our delight, we successfully accomplished the synthesis, thus possibly confirming our previous hypothesis. The G3 SID **15** was synthesized with a trigger group (*tert*-butoxycarbonyl, Boc) that can be chemically removed by trifluoroacetic acid to form amine **16**. The deprotected dendrimer **16** was dissolved in methanol containing 10% triethylamine and the release of 4-nitroaniline was monitored by HPLC and UV analysis. The expected pattern of the self-immolative process was observed (Scheme 3). The intermediates **17** and **18** were gradually generated and then disappeared to finally release eight molecules of 4-nitroaniline. The dendrimers were found to be highly stable in control experiments as long as the trigger was not removed, and no decomposition was observed for at least 72 h.

The dendrimers' platform is constructed of building blocks which, upon triggering, have the capability to fragment through a process of self-immolative chain reactions, based on cyclization (*N*,*N*′-dimethylethylenediamine) and elimination (1,4-quinone methide rearrangement) reactions. To establish additional support for the suggested release mechanism, we carried out first-order kinetic calculations and found an excellent correlation with the experimental results. The calculated first-order rate constant of $2.2\times10^{-3}\,\mathrm{min}^{-1}$ was observed for the G1, G2, and G3 SIDs (see Supporting Information).

The structural unit of the SIDs, 2,6-bis(hydroxymethyl)-*p*-cresol, can be viewed as an amplifier of a chemical signal. The input of the process is the cleavage of a single chemical bond, which is amplified to an output of two signals in the form of a double cleavage. The linking of an additional two structural units to the output of the first, will consequently amplify one signal into four, etc. We also determined that the self-immolative fragmentation can readily take place in aqueous medium. Therefore, SIDs can potentially be used to amplify chemical or biological signals, depending on the applied trigger and reporter units. For example, the trigger could be an enzyme substrate and the reporter could be a drug. This type of SID will release all of its tail drug molecules by a single catalytic cleavage of the enzyme substrate.

In conclusion, we have designed and synthesized a new class of dendritic molecules that we have termed self-immolative dendrimers. This structurally unique dendrimer can release all of its tail units through a self-immolative chain fragmentation, which is initiated by a single cleavage at the dendrimer's core. SIDs may be applied as a general platform for prodrugs or sensor molecules for enzymatic activity. We

 © 2003 Wiley-VCH Verlag GmbH & Co. KGaA, Weinheim



Scheme 3. G3 self-immolative dendron triggered with trifluoroacetic acid (TFA) to release the 4-nitroaniline tail units.

have recently accomplished the bioactivation of dendritic prodrugs with catalytic antibodies.[14]

Received: May 23, 2003 [Z51962]

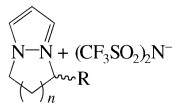
Keywords: amides · dendrimers · dyes · fragmentation · rearrangement

[1] D. A. Tomalia, J. M. J. Frechet, *J. Polym. Sci. Part A* **2002**, *40*, 2719.
[2] D. A. Tomalia, A. M. Naylor, W. A. Goddard III, *Angew. Chem.* **1990**, *102*, 119; *Angew. Chem. Int. Ed. Engl.* **1990**, *29*, 138.
[3] M. W. Grinstaff, *Chem. Eur. J.* **2002**, *8*, 2839.
[4] D. Seebach, G. F. Herrmann, U. D. Lengweiler, B. M. Bachmann, W. Amrein, *Angew. Chem.* **1996**, *108*, 2969; *Angew. Chem. Int. Ed. Engl.* **1996**, *35*, 2795.

 © 2003 Wiley-VCH Verlag GmbH & Co. KGaA, Weinheim

[5] Y. Kim, S. C. Zimmerman, *Curr. Opin. Chem. Biol.* **1998**, *2*, 733.
[6] O. L. Padilla De Jesus, H. R. Ihre, L. Gagne, J. M. J. Frechet, F. C. Szoka, Jr., *Bioconjugate Chem.* **2002**, *13*, 453.
[7] A. K. Patri, I. J. Majoros, J. R. Baker, *Curr. Opin. Chem. Biol.* **2002**, *6*, 466.
[8] S.-E. Stiriba, H. Frey, R. Haag, *Angew. Chem.* **2002**, *114*, 1385; *Angew. Chem. Int. Ed.* **2002**, *41*, 1329.
[9] C. Kojima, K. Kono, K. Maruyama, T. Takagishi, *Bioconjugate Chem.* **2000**, *11*, 910.
[10] H. R. Ihre, O. L. Padilla De Jesus, F. C. Szoka, Jr., J. M. J. Frechet, *Bioconjugate Chem.* **2002**, *13*, 443.
[11] R. Madec-Lougerstay, J.-C. Florent, C. Monneret, *J. Chem. Soc. Perkin Trans. 1* **1999**, 1369.
[12] R. Lougerstay-Madec, J.-C. Florent, C. Monneret, F. Nemati, M. F. Poupon, *Anti-Cancer Drug Des.* **1998**, *13*, 995.
[13] D. Shabat, , U.S. provisional patent AN 60/406,958, **2002**
[14] M. Shamis, D. Shabat, unpublished results.

 © 2003 Wiley-VCH Verlag GmbH & Co. KGaA, Weinheim



$n = 1,2,3$; R = H, CH_3

1 : $n = 2$; R = CH_3

Figure 1. N,N′-cyclized pyrazolium trifluoromethanesulfonimide salts.

Conductive Plastic Crystals

Conductive Organic Plastic Crystals Based on Pyrazolium Imides

Yaser Abu-Lebdeh, Pierre-Jean Alarco, and Michel Armand*

Interest in conductive organic plastic crystals was recently increased when significant conductivity at room temperature was reported and a new type of solid-state ionic conductor was identified.[1,2] Most of the work in the past was focused on salts of either tetraalkylammonium[3] or certain heterocyclic cations.[4] It was suggested that the plastic crystalline phases of *N*-substituted pyrrolidinium[5] or pyrrolinium imides[6] can be doped with a lithium imide salt to be utilized as solid electrolytes for lithium batteries. Although high conductivity is still to be obtained at room temperature, the high plasticity and diffusivities of the plastic phases relative to conventional solid electrolytes[7] enables the use of these materials in lithium batteries and other electrochemical devices.

The disadvantage of the pyrrolidinium-based salts is that they show multiple plastic phases before melting.[8] One may then question the exact nature of the conductivity mechanism; the possibility of the formation of a liquid phase from eutectics at the grain boundaries cannot be totally excluded, especially at high doping levels.

In work presented herein, we synthesized a series of salts based on *N,N′*-cyclized pyrazolium cations (Figure 1). The cations adopt a disklike shape, which is favorable for plastic crystal behavior. Indeed, all the compounds exhibited behavior typical of plastic crystals. Amongst these, 5-methyl-5,6,7,8-tetrahydropyrazolo[1,2-*a*]pyridazin-4-ium trifluoromethanesulfonimide (TFSI, **1**), showed a single plastic crystalline phase with a wide temperature range. Furthermore, the plastic crystal region began at room temperature (precisely at 20 °C), extending up to the melting point at 65 °C. Most interestingly, when we doped this plastic crystalline phase with a lithium trifluoromethanesulfonimide salt (LiTFSI) to increase and possibly add a Li^+ ion contribution to the total conductivity. To our knowledge, this is the first reported single-phase ion-conducting organic plastic crystal.

DSC curves of the neat and LiTFSI-doped (1 and 2 mol %) salts showed two transitions (Figure 2). The first, at 20 °C (for the neat salt and that doped with 1 mol % LiTFSI), can be assigned to the conventional crystal-to-plastic crystal transition followed by a second peak corresponding to their melting at around 65 °C. In the case of the doped imide (2 mol %), the first transition temperature is shifted upwards to only 25 °C.

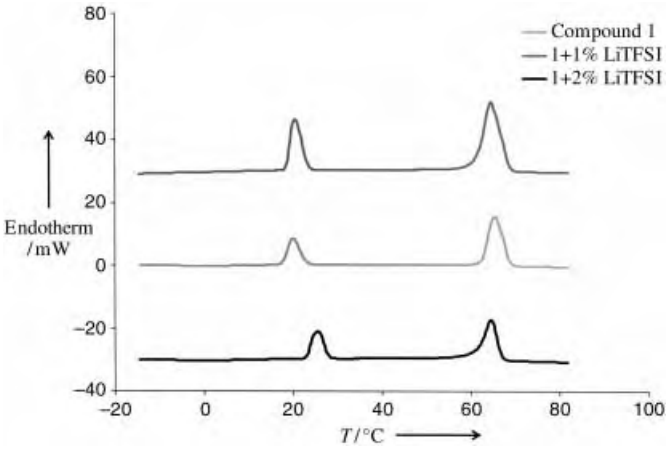


Figure 2. DSC scans of **1** and of **1** doped with 1 and 2 mol % LiTFSI.

The melting entropies (ΔS°_m) of the salts are 48.7 (neat), 45.6 (1 mol %), and 38.4 $J K^{-1} mol^{-1}$ (2 mol %). These values are higher than the criterion set by Timmermans:[9] $\Delta S^{\circ}_m \leq 20 J K^{-1} mol^{-1}$ for plastic crystals. However, McFarlane et al. have also reported higher ΔS°_m values.[10] They attributed this residual entropy of melting to the flexibility of the imide anion, which according to them, contributes largely to the entropy of melting.[11] The nature of this increase is still not clear and remains open to further study. In fact, there is a strong case to consider higher values than the limit of $20 J K^{-1} mol^{-1}$, which appears to work only for weakly

[*] Dr. Y. Abu-Lebdeh, Dr. P.-J. Alarco, Prof. M. Armand
International Laboratory for Electroactive Materials (UMR 2289)
Department of Chemistry, University of Montreal
Montreal H3C 3J7 (Canada)
Fax: (+1) 514-343-2468
E-mail: y.abu-lebdeh@umontreal.ca

 DOI: 10.1002/anie.200250706 © 2003 Wiley-VCH Verlag GmbH & Co. KGaA, Weinheim

interacting, nonionic, organic compounds. The argument for the use of ΔS°_{m} as a criterion to define ionic organic plastic crystals is beyond the scope of this Communication and can be found elsewhere.[1]

The conductivity of the neat and the doped salts was measured over a temperature range of −10 to 80 °C (Figure 3). From the DSC of **1**, we found that the conventional crystal-to-plastic transition and melting occur at 20 °C and 65 °C, respectively. This observation clearly correlates to the observed conductivity behavior by a small but significant jump in conductivity at 20 °C and the expected change of regime after melting at 65 °C (the lines are provided as a visual guide). Therefore, the temperature dependence of the conductivity behavior can be divided into three distinctive zones:

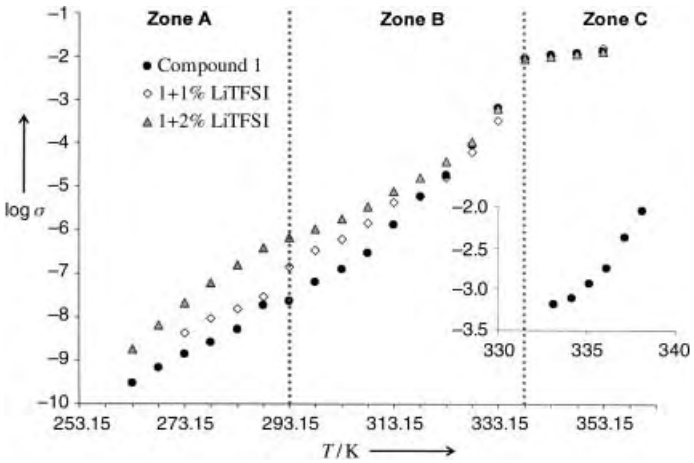


Figure 3. Conductivity of **1** and of **1** doped with 1 and 2 mol% LiTFSI as a function of temperature.

1) Zone A (−10–20 °C): This is the conventional crystal region in which we observe a monotonic increase in conductivity with temperature; such a significant increase in conductivity was observed (up to 30-fold in the presence of 2 mol% Li ions).
2) Zone B (20–65 °C): This is the plastic crystal zone in which the conductivity dependence changes from a linear to a polynomial function. For the 2-mol%-doped material, the conductivity increases from $1.0\times10^{-6}\,S\,cm^{-1}$ at the lower limit of the range (25 °C) to $6.2\times10^{-4}\,S\,cm^{-1}$ at 60 °C. High conductivities (above $10^{-4}\,S\,cm^{-1}$) are observed starting at temperatures as low as 55 °C. We believe that the high conductivity is due to the existence of long dislocated defects, which form interconnected channels (or pipes) that provide an efficient pathway for ions and defects to move rapidly. This is perfectly reasonable as it is well-established that, besides lattice diffusion, a pipe-diffusion mechanism is involved in nonionic plastic crystals.[12] When 1 mol% of LiTFSI was added to the neat salt, the conductivity was increased fivefold at the lower limit of the plastic domain. This increased further (to 17-fold) when 2 mol% of the lithium salt was added. Preliminary investigation of the least-squares fit of the temperature–conductivity curves showed a second-order polynomial variation.
3) Zone C (65–80 °C): This is the ionic-liquid zone. The conductivity in this temperature range shows a linear dependence with low activation energy typical of ionic liquids, and values in the order of $10^{-2}\,S\,cm^{-1}$ were obtained. The conductivity decreased with increased doping levels of the lithium imide salt. This could be due to an increase either in the viscosity or in the ionic interactions, thus leading to less-mobile species.

At this stage, the doping-induced increase in conductivity cannot be attributed only to the participation of lithium ions as opposed to the pyrazolium cations. We are presently addressing this aspect by performing measurements of the Li^+ transport number, t_{Li+}.

The simplicity of having a single-phase plastic-crystal system allowed us to shed light on the temperature–conductivity pattern of such new solid electrolytes. In multiphase systems, the uniqueness of this behavior to plastic crystal electrolytes has either been overlooked or oversimplified to multilinear fittings.[13] This dependence of σ on T cannot be adequately interpreted by the known methods of analysis, such as Arrhenius or VTF (Vogel–Tammann–Fulcher). As we pointed out earlier, it displays a binomial dependence, the details of which will be discussed in the near future.

In conclusion, a single-phase organic plastic crystal based on a cyclic pyrazolium cation was synthesized. Its plastic-crystalline range extends from 20 to 65 °C. Within the plastic-crystal phase, conductivities reached $1.0\times10^{-4}\,S\,cm^{-1}$ at 55 °C and $6.2\times10^{-3}\,S\,cm^{-1}$ at 60 °C. The conductivity at room temperature increased tenfold (reaching $\sim10^{-6}\,S\,cm^{-1}$) by doping with small amounts of LiTFSI.

Experimental Section

All reagents and solvents were commercially available and used without further purification. NMR spectra were run on a 400 MHz Bruker spectrometer.

Doping of **1** was achieved by adding the required amount of lithium imide salt to **1**. The mixture was then melted and stirred in a He-flushed glovebox (dew point −95 °C, $O_2 < 1$ vpm).

Conductivities of the samples were measured on a Radiometer conductivity cell with a cell constant of $0.92\,cm^{-1}$. All samples and measurements were carried out in the glovebox. Values for the resistance were obtained on an HP frequency analyzer by sweeping the frequency from 10 μ to 13 MHz with an amplitude of 10 mV.

Temperature–conductivity curves were obtained between −10 and 80 °C with 5 °C increments, allowing 30 minutes for thermal equilibration at each temperature.

Differential-scanning-calorimetric analysis (DSC) was performed on a Perkin-Elmer Pyris 1. Samples were sealed in aluminum pans in the dry box and then scanned at $20\,°C\,min^{-1}$ from −150 to 160 °C.

1: Pyrazole (3.404 g, 50 mmoles) was dissolved in dry dioxane (100 mL) in a 250-mL round-bottomed flask under argon. Dry sodium hydride (95%; 1.263 g, 50 mmoles) was added, in small portions, to the rapidly stirred solution, at such a rate that the dioxane was barely boiling. The solution was left to cool with stirring, and the reaction flask was fitted with an addition funnel filled with (±)-1,4-dibromopentane (11.498 g, 50 mmoles). The dibromide was added drop wise over a period of 5 min. The reaction mixture was stirred for 20 min at room temperature and then heated at reflux for 16 h. The resulting suspension was allowed to cool, and the precipitate was filtered and

 © 2003 Wiley-VCH Verlag GmbH & Co. KGaA, Weinheim

rinsed with diethyl ether. The solid was then dissolved in acetone and filtered to remove sodium bromide, and the solvent was removed in vacuo to afford (±)-5-methyl-5*H*,6*H*,7*H*,8*H*-pyrazolo[1,2-*a*]pyridazin-4-ium bromide (9.98 g, 92%). The bromide salt (2.171 g, 10 mmoles) was dissolved in water (50 mL) and the solution was added to a solution of potassium trifluoromethanesulfonimide (3.192 g, 10 mmoles) in water (50 mL). The plastic salt precipitated out of solution as a fine white powder. The solid was collected by filtration and dried under vacuum to yield (±)-5-methyl-5*H*,6*H*,7*H*,8*H*-pyrazolo[1,2-*a*]pyridazin-4-ium trifluoromethanesulfonimide (**1**; 4.055 g, 97%). ^{1}H NMR (300 MHz, [D$_6$]DMSO, 25°C): $\delta = 1.61$ (d, $^3J = 6.5$ Hz, 3H, CH_3), 1.85 (m, 1H, CH_2), 1.98–2.28 (m, 2H, CH_2); 3.37 (d, $^3J = 0.7$ Hz, 1H, CH_2), 4.37 (m, 1H, CH), 4.50–4.69 (m, 2H, CH_2), 6.95 (t, $^3J = 2.9$ Hz, 1H, CH), 8.47 (d, $^3J = 2.6$ Hz, 1H, CH), 8.64 ppm (d, $^3J = 2.9$ Hz, 1H, CH); ^{13}C NMR (75 MHz, [D$_6$]DMSO, 25°C): $\delta = 17.58$, 19.66, 26.32, 48.37, 55.89, 106.99, 119.00 (q, $J = 322.3$ Hz, CF_3), 134.84, 136.17 ppm.

Received: December 5, 2002
Revised: April 10, 2003 [Z50706]

Keywords: batteries · conducting materials · lithium · nitrogen heterocycles · plastic crystals

[1] D. MacFarlane, M. Forsyth, *Adv. Mater.* **2001**, *13*, 957–966.
[2] E. Cooper, C. Angell, *Solid State Ionics* **1986**, *18–19*, 570–576.
[3] S. Fukada, H. Yamamoto, R. Ikeda, D. Nakamura, *J. Chem. Soc. Faraday Trans. 1* **1987**, 3207.
[4] D. MacFarlane, P. Meakin, N. Amini, M. Forsyth, *J. Phys. Condens. Matter* **2001**, *13*, 8257–8267.
[5] D. MacFarlane, J. Huang, M. Forsyth, *Nature* **1999**, *402*, 792–794.
[6] J. Sun, D. MacFarlane, M. Forsyth, *Solid State Ionics* ***2002****, 148, 145–151*.
[7] M. Forsyth, J. Huang, D. MacFarlane, *J. Mater. Chem.* **2000**, *10*, 2259–2265.
[8] D. MacFarlane, J. Sun, J. Golging, P. Meakin, M. Forsyth, *Electrochim. Acta* **2000**, *45*, 1271.
[9] J. Timmermans, *J. Phys. Chem. Solids* **1961**, *18*, 1.
[10] D. MacFarlane, P. Meakin, J. Sun, N. Amini, M. Forsyth, *J. Phys. Chem. B* **1999**, *103*, 4164–4170.
[11] J. Huang, M. Forsyth, D. MacFarlane, *Solid State Ionics* **2000**, *136–137*, 447–452.
[12] J. Sherwood, *The Plastically Crystalline State: Orientationally Disordered Crystals*, Wiley, Chichester, UK, **1979**, p. 51.
[13] A. Hill, J. Huang, J. Efthimiadis, P. Meakin, M. Forsyth, D. MacFarlane, *Solid State Ionics* **2002**, *154–155*, 119–124.

 © 2003 Wiley-VCH Verlag GmbH & Co. KGaA, Weinheim

Low-Temperature Diamond Synthesis

Growth of Large Diamond Crystals by Reduction of Magnesium Carbonate with Metallic Sodium**

Zhengsong Lou, Qianwang Chen, Wei Wang, Yitai Qian, and Yufeng Zhang*

Diamond is a material with uniquely attractive physical, thermal, and optical properties, and is used in applications ranging from abrasives, tool coating, bearing surfaces, microelectronics, and optics to corrosion protection.[1–4] The diamond is grown commercially by using high-pressure and high-temperature,[5] chemical vapor deposition for thin films[6] and shock-wave processes.[7] Alternative routes to diamond preparation include the reduction of CCl_4 by metallic sodium,[8] and hydrothermal process with carbon, water, and metal near 800 °C and at 1.4 Kbar pressure.[9] Recently, the synthesis of diamond-structured carbon from silicon carbide in chlorine-containing gases at temperatures not exceeding 1000 °C was also achieved.[10] Herein we report the synthesis of high-purity cubic diamond particles by the reduction of magnesium carbonate with metallic sodium at a temperature as low as 500 °C.

The X-ray diffraction (XRD) pattern of a powder sample after washing with $HClO_4$ was shown in Figure 1. The

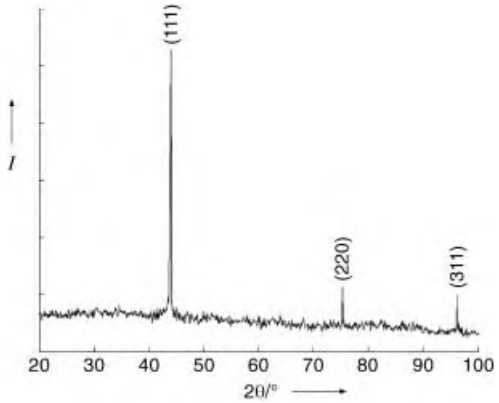


Figure 1. X-ray diffraction (performed on a Rigaku D/max-rA X-ray diffractometer) pattern for the as-prepared diamond. The reflection peaks, indexed with 111, 220, and 311, correspond unambiguously to cubic diamond with a lattice constant $a = 3.568$ Å. The peak splitting is due to the polychromatic nature of the incident $Cu_{K\alpha}$ radiation ($K_{\alpha1}$ and $K_{\alpha2}$). I = intensity (arbitrary units).

[*] Prof. Q. Chen, Z. Lou, W. Wang, Prof. Y. Qian, Y. Zhang
Structure Research Laboratory
University of Science & Technology of China
Hefei 230026 (China)
Department of Materials Science & Engineering
University of Science & Technology of China
Hefei 230026 (China)
Fax: (+86) 551-3607292
E-mail: cqw@ustc.edu.cn

[**] This work was supported by the National Natural Science Foundation under the contract No. 20125103 and 90206034.

 DOI: 10.1002/anie.200351478 © 2003 Wiley-VCH Verlag GmbH & Co. KGaA, Weinheim

reflection peaks, indexed with 111, 220 and 311, correspond to cubic diamond with a lattice constant $a = 3.566$ Å (JCPDS cards, 75-0623). Graphite was also formed during the reaction. In the XRD pattern of an unwashed sample there is a weak peak at 26.2°, thus indicating the presence of graphite. Micro Raman spectroscopy was also used to confirm the presence of diamond. The Raman spectrum of the sample exhibits an intense first-order peak at 1331.8 cm^{-1} [Figure 2], which is the

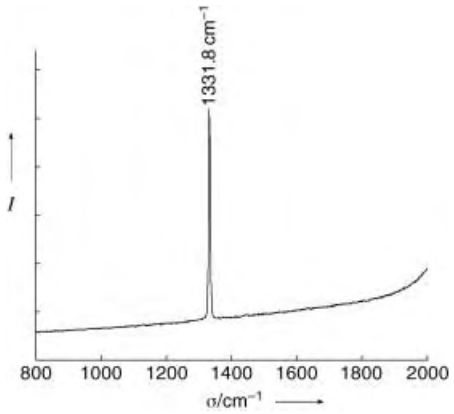


Figure 2. Raman spectrum of diamond microcrystals, an excitation wavelength of 514.3 nm was used. The strong Raman peak at 1331.8 cm^{-1} is characteristic signature of the cubic diamond. The measurements were performed on a LABRAM-HR Confocal Laser MicroRaman Spectrometer. I = intensity (arbitrary units).

characteristic signature of cubic diamond, thus indicating the formation of well-crystallized diamond. Figure 3 shows the Scanning electron-microscope (SEM) images of diamond grains selected from the sample. These diamond grains were about 120 μm long, with a larger particle up to 510 μm in length. Diamond grains were octahedral when their sizes were around 10 μm (not shown), whereas this shape disappeared with an increase in size. However, particles with polyhedral shapes can be seen (inset in Figure 3). At 500 °C and 860 atm the maximum transformation ratio for magnesium carbonate to diamond was found to be as high as 6.6 % (mole ratio, with reference to carbonate carbon).

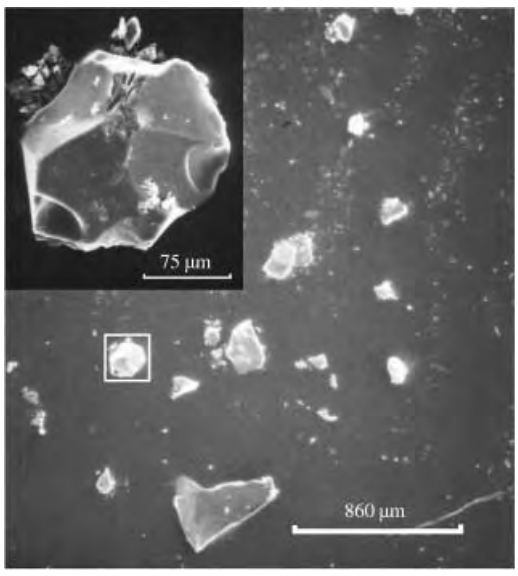


Figure 3. Photograph of diamonds, taken from a Scanning electron microscope. Most of the diamond particles are around 120 μm, a large particle can reach up to 510 μm in length. Inset is the enlarged image of the area of rectangle.

The yield of graphite increases as the reaction temperature decreases, while the amount of diamond decreases. No diamond could be detected by XRD analysis when the reactions were conducted at temperatures lower than 500 °C. When the temperature was kept at 500 °C the initial amount of magnesium carbonate was decreased from 0.061 to 0.052 mol the reaction only yielded graphite, which reveals the reduction of magnesium carbonate to diamond is sensitive to the temperature and pressure of the system. Interestingly, an increase in the amount of sodium is favorable for the reduction of magnesium carbonate to graphite, more graphite was detected by XRD analysis as the initial amount of metallic sodium was increased to 0.131 mol. At the beginning of the reaction, the pressure in the autoclave is relatively high. As magnesium carbonate and carbon dioxide is partially reduced by metallic sodium, the pressure decreases. Thus, more amounts of graphite would be formed because of long-term reactions occurring in a relatively low-pressure environment.

At the reaction temperatures, $MgCO_3$ pyrolyzes to give off carbon dioxide, and the carbon dioxide is in a supercritical state ($MgCO_3$ pyrolyzes at 350 °C, 1 atm). Under supercritical conditions, the polarity of carbon dioxide can be increased by controlling its density, with the dielectric constant of carbon dioxide ranging from 1 to 1.6,[11] which will enhance the absorption of carbon dioxide on the surface of the reductant, and may accelerate the electron transfer from the reductant to carbon dioxide. Further work will be done to understand the mechanism of carbonate reduction and the metastable growth of diamond.

In conclusion, the above studies illustrate a low-temperature diamond synthesis, in which diamond as large as 510 μm can form at 500 °C by the reduction of magnesium carbonate with metallic sodium. The yield of diamond is about 6.6 % with respect to carbonate carbon. The technique involves the reduction of magnesium carbonate to diamond in a simple autoclave reaction. Magnesium carbonate is cheap and abundant; therefore, this approach could be exploited for practical industrial diamond production.

Experimental Section

The synthesis was carried out in an autoclave (10 mL), in which magnesium carbonate and metallic sodium were added. The pressure was autogenetic, depending on reaction temperature and the amount of carbonate used. $MgCO_3$ was pyrolyzed at the reaction temperatures to give off carbon dioxide to ensure that the carbon dioxide was in a supercritical state. A typical reaction used 0.061 mol magnesium carbonate and 0.022–0.109 mol metallic sodium. In addition to the cases specifically mentioned, most of the reactions were conducted at 500 °C and 860 atm, for 12 h. The resulting black product was washed with ethanol, HCl (2.0 mol L^{-1}), and finally with distilled water several times then dried in an oven at 100 °C for 2 hrs. Under the most

 © 2003 Wiley-VCH Verlag GmbH & Co. KGaA, Weinheim

reducing conditions, the main products identified were diamond, graphite, Na_2CO_3, MgO, and carbon dioxide. In light of the detection of Na_2CO_3 and MgO in the product mixture by XRD analysis, the chemical reactions occurred at the operating temperature of 500 °C can be expressed by following chemical equations [Eqs. (1)–(3)]:

$$MgCO_{3(s)} \rightarrow MgO_{(s)} + CO_{2(g)} \quad (1)$$

$$CO_{2(g)} + 4\,Na_{(L)} \rightarrow C_{(diamond+graphite)} + 2\,Na_2O_{(s)} \quad (2)$$

$$CO_{2(g)} + Na_2O_{(s)} \rightarrow Na_2CO_{3(s)} \quad (3)$$

Pure diamond products can be obtained by treatment of the sample with $HClO_4$ to dissolve graphite.

Received: March 25, 2003 [Z51478]

Keywords: high-pressure chemistry · raman spectroscopy · reduction · synthetic methods · X-ray diffraction

[1] J. C. Angus, C. C. Hayman, *Science* **1988**, *241*, 913 – 921.
[2] J. E Graebner, S. Jin, G. W. Kammlott, J. A. Herb, C. F. Gardinier, *Nature* **1992**, *359*, 401 – 403.
[3] D. M. Gruen, I. Buckley-Golder, *MRS Bull.* **1998**, 23, 16 – 17.
[4] A. V. Palnichenko, A. M. Jonas, J. C. Chaarlier, A. S. Aronin, J. P. Issi, *Nature* **1999**, *402*, 162 – 164.
[5] F. P. Bundy, H. T. Hall, H. M. Strong, R. H. Wentorf, *Nature* **1955**, *176*, 51 – 55.
[6] G. Burkhard, K. Dan, Y. Tanabe, A. B. Sawaoka, K. Yamada, *Jpn. J. Appl. Phys.* **1994**, 33, 5875 – 5885.
[7] R. Roy, K. A. Cherian, J. P. Cheng, A. Badzian, *Innovations Mater. Res.* **1996**, 1, 65 – 87.
[8] X. Z. Zhao, R. Roy, K. A. Cherian, A. Badzian, *Nature* **1997**, *385*, 513 – 515.
[9] Y. Li, Y. Qian, H. Liao, Y. Ding, L. Yang, C. Xu, F. Li, G. Zhou, *Science* **1998**, *281*, 246 – 247.
[10] Y. Gogotsi, S. Welz, D. A. Ersoy, M. J. McNallan, *Nature* **2001**, *411*, 283 – 287.
[11] Q. Chen, Y. Qian, *Chem. Commun.* **2001**, 1402 – 1403.

 © 2003 Wiley-VCH Verlag GmbH & Co. KGaA, Weinheim

Aniline Synthesis

Anilines Made Easily: From Aldehydes to Tri-, Tetra-, and Pentasubstituted Anilines in Two Steps**

*Helfried Neumann, Axel Jacobi von Wangelin, Stefan Klaus, Dirk Strübing, Dirk Gördes, and Matthias Beller**

Dedicated to Professor Boy Cornils on the occasion of his 65th birthday

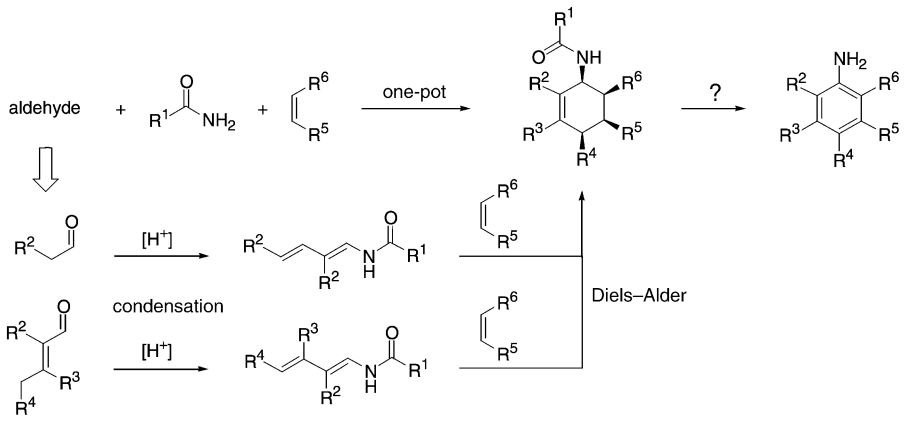
Polysubstituted anilines play a central role as building blocks in synthetic chemistry. Major technical applications include their use as intermediates in the manufacture of agrochemicals, pharmaceuticals, dyes, pigments, and rubber chemicals.[1] Although anilines have become accessible by new methods—in particular catalyzed by transition metals—in recent years, most technically feasible syntheses still rely on classical approaches. While sequential electrophilic nitration and reduction suffers from the relatively harsh reaction conditions,[2] nucleophilic aromatic amination requires the presence of special substituents.[3] The recently developed palladium-catalyzed[4] (Buchwald–Hartwig amination) and copper-catalyzed[5] aminations of aryl halides provide a general entry to this class of compounds. However, for these reactions as well as for other known syntheses of polysubstituted anilines, aromatic reactants with a defined substitution pattern are needed. In most cases, these starting materials are synthesized in numerous steps generating several equivalents of waste and salt as by-products.

Over the last years we have been involved in the development of new syntheses of amino compounds with special regard to transition-metal-catalyzed hydroaminations,[6] hydroaminomethylations,[7] and amidocarbonylations.[8] Recently, we reported on novel multicomponent reactions (MCRs)[9] of amides and aldehydes with dienophiles for the straightforward synthesis of a large variety of carbo- and heterocyclic amides.[10] As shown in Scheme 1, the underlying mechanism involves the intermediacy of an Oppolzer–Overman-type 1-(*N*-acylamino)-1,3-butadiene, which easily undergoes Diels–Alder addition with an electron-deficient dienophile.[11] The synthesized three-component adducts exhibit a high degree of diversity, which is based

[*] Prof. Dr. M. Beller, Dr. H. Neumann, Dr. A. Jacobi von Wangelin, S. Klaus, D. Strübing, Dr. D. Gördes
Leibniz-Institut für Organische Katalyse
Universität Rostock e.V. (IfOK)
Buchbinderstrasse 5–6, 18055 Rostock (Germany)
Fax: (+49) 381-466-9324
E-mail: matthias.beller@ifok.uni-rostock.de

[**] The authors thank S. Giertz and S. Buchholz for excellent technical and analytical assistence. Generous financial support from the state Mecklenburg-Western Pomerania (Landesforschungsschwerpunkt), the Fonds der Chemischen Industrie, and the Bundesministerium für Bildung und Forschung (BMBF) is gratefully acknowledged.

 DOI: 10.1002/anie.200351484 © 2003 Wiley-VCH Verlag GmbH & Co. KGaA, Weinheim



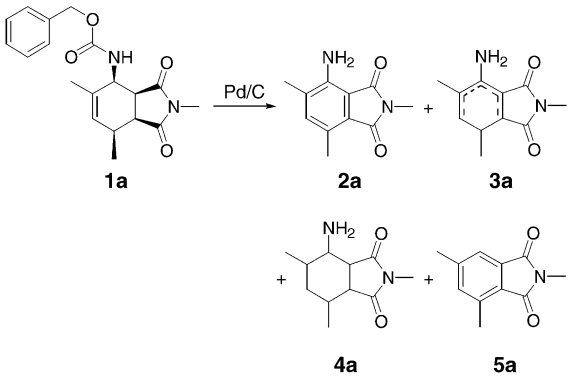
Scheme 1. Three-component-coupling reaction of amides, aldehydes, and dienophiles and the envisioned aromatization to give anilines.

upon structural variations of the simple, ubiquitous components—carboxamides, aldehydes, and olefins.

We considered the new three-component coupling products useful intermediates for the synthesis of anilines. Obviously, such a strategy constitutes a short and highly convergent synthetic approach. Although syntheses of arenes based on transition-metal-catalyzed cyclization reactions with alkynes[12] and Diels–Alder reactions with heterodienes[13] have been reported in the past, the operational difficulty and the laborious synthesis of the precursors diminish their general use. Here, we wish to report a novel reaction sequence for the synthesis of substituted anilines by the combination of a three-component-coupling reaction and a new transition-metal-catalyzed aromatization step (Scheme 1). To the best of our knowledge, such a strategy has not been used previously for the synthesis of anilines.

Initial studies on the aromatization of three-component coupling products of different aliphatic and aromatic amides in the presence of stoichiometric quantities of sulfur or catalytic amounts of Pd/C and various other oxidants gave low conversion or complex product mixtures (yield of anilines $< 5\%$). Therefore, we considered facilitation of the aromatization process by using a quasi-intramolecular[14] hydrogen transfer onto a powerful hydrogen acceptor within the molecule. The use of *O*-benzyl carbamate as the amide component could yield a coupling product that would fulfill this requirement. Reaction of propionaldehyde, *O*-benzyl carbamate ($CbzNH_2$, $R^1 = BnO$), and maleimide furnished 4-*N*-(benzyloxycarbonyl)aminohexahydro-1*H*-isoindole (**1a**) in 79% yield. Next, imide **1a** was subjected to different cleavage procedures [Eq. (1)]. When **1a** was heated at reflux in the presence of Pd/C and cyclohexene (as a hydrogen donor) in ethanol,[15] a mixture of products was afforded (Table 1). Three isomeric amino-substituted cyclohexenes (formed in 26% overall yield (6:7:13)) and the targeted oxidized species, aniline **2a** (28%), were identified as major products. When the reaction conditions were optimized, **2a** was obtained in excellent yield (91%).

In the presence of stronger hydrogen donors (H_2,[16] HCO_2H[17]), saturated cyclohexane **4a** was formed in moderate yield. A significant increase in the yield of aniline **2a** was observed when triglyme was employed as the solvent and the reaction was conducted at higher temperatures. The cyclohexene moiety in **1a** itself can act as an efficient hydrogen donor for the debenzylation of the carbamate (Table 1, entries 8–10),



(1)

Table 1: Palladium-catalyzed aromatization of 4-*N*-(benzyloxycarbonyl)aminohexahydro-1*H*-isoindole **1a** (GC yields).

Entry	Pd [mol%]	Solvent	H_2 donor	*t* [h]	*T* [°C]	Yield [%] **2a**	Yield [%] **3a/4a/5a**
1	32	EtOH	C_6H_{10}[a]	0.16	80	28	26/–/–
2	32	EtOH	C_6H_{10}[a]	16	80	37	13/–/7
3	32	MeOH	H_2[b]	24	25	–	–/35/–
4	32	MeOH	HCO_2H[c]	0.16	25	–	–/25/–
5	16	EtOH	C_6H_{10}[a]	24	80	40	
6	8	EtOH	C_6H_{10}[a]	24	120	36	
7	8	EtOH	–	24	120	30	
8	8	triglyme	–	24	120	50	
9	8	triglyme	–	24	140	71	
10	8	triglyme	–	24	140	95[d]	
11	4	triglyme	–	24	140	65[d]	

Conditions: **1a** (0.5 mmol), 10% Pd/C, solvent (10 mL), ACE pressure tube; [a] 200 mmol; [b] 15 bar; [c] 10 equiv; [d] Large scale: **1a** (3 mmol).

which supersedes the use of an extra hydrogen donor. This unprecedented reaction pattern involves H_2 elimination and Cbz cleavage. As Cbz cleavage cannot be effected without concomitant supply of hydrogen atoms from the ring aromatization, we propose the operation of a domino dehydrogenation/Cbz-cleavage process.[18] While both the palladium-catalyzed dehydrogenation[19] and the palladium-catalyzed Cbz-cleavage from amines[15–20] have been investigated as

 © 2003 Wiley-VCH Verlag GmbH & Co. KGaA, Weinheim

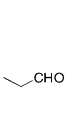
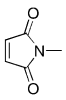
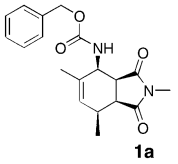
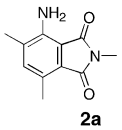
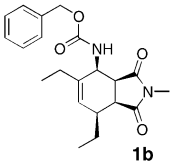
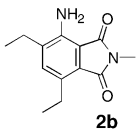
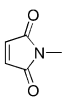
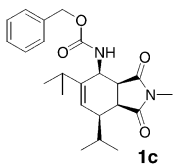
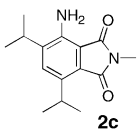
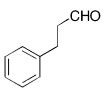
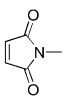
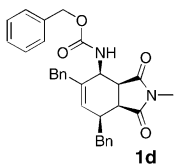
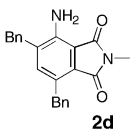
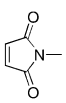
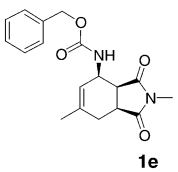
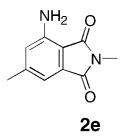
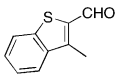
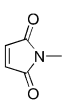
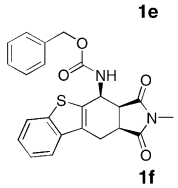
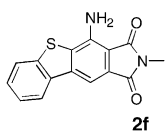
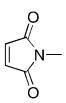
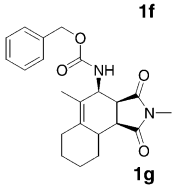
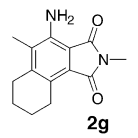
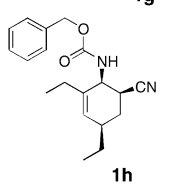
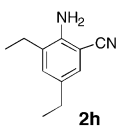
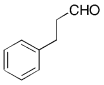
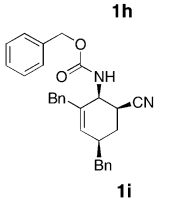
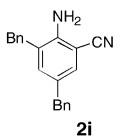
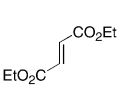
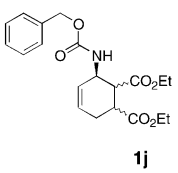
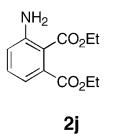
separate processes, no procedure involving the concurrent operation of both transformations has been reported so far.

We set out to extend the methodology to other *N*-(Cbz)aminocyclohexenes. Therefore, a variety of three-component adducts of *O*-benzyl carbamate, aldehydes, and dienophiles were prepared. Table 2 (middle) shows a selection of 10 adducts with diverse substituents. Regarding the aldehyde component, simple aliphatic (with an α-CH_2 moiety) and α,β-unsaturated (with a γ-hydrogen) aldehydes bearing linear or branched alkyl, aryl, or heteroaryl substituents were employed. While simple aldehydes lead to adducts with equivalent substituents on C4 and C6, reactions with α,β-unsaturated aldehydes are not subject to this restriction. Compounds **1f** and **1g** (Table 2, entries 6 and 7) illustrate the potential for the construction of anellated ring systems. Further diversity of the three-component adducts was attained by employing different dienophiles such as *N*-methyl maleimide, acrylonitrile, and diethyl fumarate. Apart from benzothiazole **1f** (44%), the three-component adducts were isolated in good yields (65–89%) without further optimization. NMR spectra established the *syn* configuration of the cycloadducts, as expected from a selective *endo* Diels–Alder reaction of the all-*trans* aminodiene.[21] However, reactions with diethyl fumarate gave an equimolar mixture of two isomers with an overall yield of 67% (Table 2, entry 10).

The domino dehydrogenation/Cbz-cleavage reaction of **1a–j** cleanly afforded the desired anilines (Table 2). Aromatization of imides **1a–f** yielded substituted 4-amino-1,3-dioxo-2,3-dihydro-1*H*-isoindoles **2a–g** (entries 1–7). The employment of 2-cyclohexylidenepropionaldehyde[22] proves the possibility to access hexasubstituted aminobenzenes in only two (!) reaction steps (entry 7). With dienophilic acrylonitrile, substituted 2-aminobenzonitriles (**2h**, **2i**) were accessed in a straightforward manner (entries 8, 9). These compounds constitute important intermediates for the synthesis of pharmaceuticals; for example, simple reaction with α-halocarboxylic acids and subsequent reduction affords 1,4-benzodiazepines.[23] Both isomers of diester **1j** gave the desired aniline in equivalent yields (entry 10).

In conclusion, we have developed a new, highly efficient strategy for the synthesis of substituted anilines. A palladium-catalyzed

Table 2: Pd/C-catalyzed synthesis of polysubstituted anilines.

Entry	Aldehyde	Dienophile	Coupling product	Yield [%]	Aniline	Yield [%]
1			 **1a**	79	 **2a**	91
2			 **1b**	88	 **2b**	79
3			 **1c**	74	 **2c**	80
4			 **1d**	73	 **2d**	91
5			 **1e**	87	 **2e**	64
6			 **1f**	44	 **2f**	78
7			 **1g**	45	 **2g**	40
8			 **1h**	68	 **2h**	63
9			 **1i**	66	 **2i**	62
10			 **1j**	67	 **2j**	78

 © 2003 Wiley-VCH Verlag GmbH & Co. KGaA, Weinheim

aromatization of three-component-coupling products, which is based on a new transfer hydrogenation reaction, is the key step of the described method. The sequential combination of a three-component-coupling reaction and a domino deprotection/aromatization reaction leads to the straightforward synthesis of polysubstituted anilines with diverse substitution patterns.[24] The overall procedure utilizes simple, readily available starting materials and is unique in that it allows the (regio)selective introduction of substituents in one *ortho*, one *meta*, and *para* position, as well as electron-deficient substituents in the other *ortho* and *meta* positions. To the best of our knowledge, this type of tri-, tetra-, and pentasubstituted anilines cannot be accessed by any other methods with similar efficiency.

Experimental Section

General procedure for the preparation of **1**: A mixture of *O*-benzyl carbamate (15 mmol), *p*-toluenesulfonic acid·H_2O (2 mol%), aldehyde (15 mmol), Ac_2O (15 mmol), maleimide (11 mmol), and *N*-methylpyrrolidone (10 mL) was sealed in an ACE pressure tube and stirred at 120°C. After 24 h the solvent and other volatile compounds were removed by high-vacuum distillation. Silica gel flash chromatography (heptane/ethyl acetate) of the residue afforded the three-component-reaction adducts as air-stable solids.

With α,β-unsaturated aldehydes, reactions were run in the presence of 7.5 mmol aldehyde and without Ac_2O. Reactions with acrylonitrile used a fourfold excess of the dienophile and required 4 d for completion.

General procedure for the synthesis of **2**: A 100-mL flask was charged with a mixture of carbamate **1** (2.9 mmol), Pd/C (10% Pd on C, 8 mol%), and triglyme (20 mL), equipped with a reflux condenser, and heated to 140°C. After 6–64 h the solution was filtered through a Celite pad, and solvent and other volatile compounds were removed by high-vacuum distillation. The residue was subjected to silica gel flash chromatography (heptane/ethyl acetate).

1a: According to the general procedure for **1**, *O*-benzyl carbamate (2.27 g, 15 mmol), propionaldehyde (0.87 g, 15 mmol), acetic anhydride (1.4 mL, 15 mmol), and *N*-methylmaleimide (1.28 g, 11.25 mmol) were employed. SiO_2 chromatography (hept/EtOAc 3:1): $R_f = 0.15$. 79% yield of isolated product (white solid). M.p. 62–66°C. IR (KBr): $\tilde{\nu} = 3395$ br vs, 3064 w, 3033 w, 2937 m, 1769 m, 1705 br vs, 1514 vs, 1437 s, 1384 s, 1336 s, 1287 s, 1232 s, 1045 s, 912 w, 836 m, 781 m, 749 m, 699 s, 662 w, 594 m, 531 cm^{-1}; MS (EI): 342 ([*M*]$^+$, 1%), 251 ([*M*−Bn]$^+$, 5%), 233 ([*M*−BnO]$^+$, 4%), 207 (93%), 122 (23%), 107 ([BnO]$^+$, 17%), 91 ([Bn]$^+$, 100%, no other peaks of >5%; HRMS: calcd for $C_{19}H_{22}N_2O_4$: 342.15796; found: 342.15788; NMR ([D$_6$]DMSO): ^{1}H $\delta = 7.44$–7.34 (m, 5H, Ph), 6.96 (d, 9.3 Hz, 1H, N*H*), 5.36 (s, 1H, C=), 5.15 (s, 2H, CH_2), 4.36 (m, 1H, NHC*H*), 3.33 (dd, 6.2/8.4 Hz, 1H, NHCHC*H*), 3.11 (t*, 7.7 Hz, 1H, CH_3CHC*H*CO), 2.78 (s, 3H, N*Me*), 2.49–2.43 (m, 1H, MeC*H*), 1.62 (s, 3H, *Me*C=), 1.28 ppm (d, 7.4 Hz, 3H, *Me*CH); ^{13}C{^{1}H} $\delta = 178.9$ and 177.1 (2 *C*O); 155.6 (*C*O_2), 137.3 (Me*C*=), 136.9, 128.4, 127.9, 127.7, and 127.1 (*C*H= and Ph), 65.8 (*C*H_2O), 49.7 (NH*C*H), 44.1 and 43.9 (NHCH*C*H*C*H), 29.6 (Me*C*H), 24.3 (N*Me*), 18.0 and 16.8 ppm (*Me*C= and *Me*CH).

2a: According to the general procedure for **2**, carbamate **1a** (1.0 g, 2.9 mmol) and Pd/C (0.25 g, 10% Pd on C) were employed. SiO_2 chromatography (hept/EtOAc 3:1): $R_f = 0.15$. 91% yield of isolated product (yellowish solid). M.p. 185–187°C. IR (KBr): $\tilde{\nu} =$ 3475, 3370 vs, 3200, 2924 w, 1740 s, 1690 s, 1642 s, 1614 m, 1596 m, 1492 s, 1441 s, 1382 m, 1370 m, 1313 w, 1268 s, 1235 m, 1159 w, 1125 w, 1024 s, 996 s, 761 s, 615 m, 560 cm^{-1}; MS (EI): 204 ([*M*]$^+$, 100%), 189 ([*M*−NH]$^+$, 18%), 147 ([*M*−CO−NMe]$^+$, 19%), 119 ([*M*−2CO−NMe]$^+$, 42%), no other peaks of >5%. HRMS: calcd for $C_{11}H_{12}N_2O_2$: 204.08890; found: 204.08987; NMR ([D$_6$]DMSO): ^{1}H $\delta = 7.07$ (s, 1H, Ph), 6.01 (s, 2H, NH_2), 2.91 (s, 3H, N*Me*), 2.35 (s, 3H, *Me*), 2.13 ppm (s, 3H, *Me*); ^{13}C{^{1}H} $\delta = 169.6$ and 169.5 (2 *C*O), 143.2, 130.2, 125.8, 124.3, and 109.2 (5*C* of Ph), 137.7 (*C*H of Ph), 23.0, 17.0, and 15.9 ppm (3 M*e*).

Received: March 25, 2003 [Z51484]

Keywords: anilines · multicomponent reactions · palladium · transfer hydrogenation

[1] a) K. Weissermel, H. J. Arpe, *Industrial Organic Chemistry*, Wiley-VCH, Weinheim, **1997**, pp. 374–377; b) R. J. Lindsay in *Comprehensive Organic Chemistry* (Ed.: I. O. Sutherland), Pergamon, Oxford, **1979**, part 6.3; c) T. Sugasawa, T. Toyoda, M. Adachi, K. Sasakura, *J. Am. Chem. Soc.* **1978**, *100*, 4842–4852; d) M. Adachi, T. Sugasawa, *Synth. Commun.* **1990**, *20*, 71–84; e) G. S. Zenchoff, A. Walser, R. I. Fryer, *J. Heterocycl. Chem.* **1976**, *13*, 33–39.

[2] a) W. Flitsch, *Chem. Ber.* **1961**, *94*, 2494–2501; b) R. Dabard, J. Tirouflet, *Bull. Soc. Chim. Fr.* **1957**, 565–570; c) C. H. Wang, T. C. Feng, B. E. Christensen, *J. Am. Chem. Soc.* **1950**, *72*, 4887–4890.

[3] J. March, *Advanced Organic Chemistry*, Wiley, New York, **1992**, pp. 668–669.

[4] a) B. H. Yang, S. L. Buchwald, *J. Organomet. Chem.* **1999**, *576*, 125–146; b) J. F. Hartwig, *Angew. Chem.* **1998**, *110*, 2154–2177; *Angew. Chem. Int. Ed.* **1998**, *37*, 2047–2067; c) J. P. Wolfe, S. Wagaw, J.-F. Marcoux, S. L. Buchwald, *Acc. Chem. Res.* **1998**, *31*, 805–818; d) J. F. Hartwig, *Synlett* **1997**, *5*, 329–340; e) M. Beller, *Angew. Chem.* **1995**, *107*, 1436–1437; *Angew. Chem. Int. Ed. Engl.* **1995**, *34*, 1316–1317.

[5] a) F. Y. Kwong, S. L. Buchwald, *Org. Lett.* **2003**, *5*, 793–796; b) F. Y. Kwong, A. Klapars, S. L. Buchwald, *Org. Lett.* **2002**, *4*, 581–584; c) A. A. Kelkar, N. M. Patil, R. V. Chaudhari, *Tetrahedron Lett.* **2002**, *43*, 7143–7146.

[6] a) M. Beller, C. Breindl, M. Eichberger, C. G. Hartung, J. Seayad, O. R. Thiel, A. Tillack, H. Trauthwein, *Synlett* **2002**, *10*, 1579–1594; b) A. Tillack, I. G. Castro, C. G. Hartung, M. Beller, *Angew. Chem.* **2002**, *114*, 2646–2648; *Angew. Chem. Int. Ed.* **2002**, *41*, 2541–2543; c) C. G. Hartung, A. Tillack, H. Trauthwein, M. Beller, *J. Org. Chem.* **2001**, *66*, 6339–6343; d) M. Beller, C. Breindl, T. H. Riermeier, A. Tillack, *J. Org. Chem.* **2001**, *66*, 1403–1412.

[7] a) A. Seayad, M. Ahmed, H. Klein, R. Jackstell, T. Gross, M. Beller, *Science* **2002**, *297*, 1676–1678; b) T. Gross, A. M. Seayad, M. Ahmed, M. Beller, *Org. Lett.* **2002**, *4*, 2055–2058.

[8] For a review on amidocarbonylations, see: M. Beller, M. Eckert, *Angew. Chem.* **2000**, *112*, 1026–1044; *Angew. Chem. Int. Ed.* **2000**, *39*, 1010–1027.

[9] a) I. Ugi, *Pure Appl. Chem.* **2001**, *73*, 187–191; b) H. Bienaymé, C. Hulme, G. Oddon, R. Schmitt, *Chem. Eur. J.* **2000**, *6*, 3321–3329; c) A. Dömling, I. Ugi, *Angew. Chem.* **2000**, *112*, 3300–3344; *Angew. Chem. Int. Ed.* **2000**, *39*, 3169–3210; d) L. F. Tietze, *Chem. Rev.* **1996**, *96*, 115–136; e) G. H. Posner, *Chem. Rev.* **1986**, *86*, 831–844.

[10] a) H. Neumann, A. Jacobi von Wangelin, D. Gördes, A. Spannenberg, M. Beller, *J. Am. Chem. Soc.* **2001**, *123*, 8398–8399; b) A. Jacobi von Wangelin, H. Neumann, D. Gördes, A. Spannenberg, M. Beller, *Org. Lett.* **2001**, *3*, 2895–2898; c) H. Neumann, A. Jacobi von Wangelin, D. Gördes, A. Spannenberg, W. Baumann, M. Beller, *Tetrahedron* **2002**, *58*, 2381–2387; d) A. Jacobi von Wangelin, H. Neumann, D. Gördes, S. Klaus, H. Jiao, A. Spannenberg, M. Beller, T. Krüger, C. Wendler, K. Thurow, N. Stoll, *Chem. Eur. J.* **2003**, *9*, 2273–2281 .

[11] a) J. M. Janey, T. Iwama, S. A. Kozmin, V. H. Rawal, *J. Org. Chem.* **2000**, *65*, 9059–9068; b) M. B. Smith, *Org. Prep. Proced.*

 © 2003 Wiley-VCH Verlag GmbH & Co. KGaA, Weinheim

Int. **1990**, *22*, 315 – 397; c) L. E. Overman, R. L. Freerks, C. B. Petty, L. A. Clizbe, R. K. Ono, G. F. Taylor, P. J. Jessup, *J. Am. Chem. Soc.* **1981**, *103*, 2816 – 2822; d) W. Oppolzer, L. Bieber, E. Francotte, *Tetrahedron Lett.* **1979**, 4537 – 4540.

[12] a) S. Saito, Y. Yamamoto, *Chem. Rev.* **2000**, *100*, 2901 – 2915; b) S. Saito, N. Uchiyama, V. Gevorgyan, Y. Yamamoto, *J. Org. Chem.* **2000**, *65*, 4338 – 4341.

[13] See for example: a) D. L. Boger, *Chem. Rev.* **1986**, *86*, 781 – 793; b) A. G. Elagamey, *Indian J. Chem. Sect. B* **1988**, *27*, 766 – 768; c) J. E. Cochran, T. Wu, A. Padwa, *Tetrahedron Lett.* **1996**, *37*, 2903 – 2906; d) A. Padwa, M. Dimitroff, A. G. Waterson, T. Wu, *J. Org. Chem.* **1997**, *62*, 4088 – 4096; e) A. Padwa, J. P. Snyder, E. A. Curtis, S. M. Sheehan, K. J. Worsencroft, C. O. Kappe, *J. Am. Chem. Soc.* **2000**, *122*, 8155 – 8167; f) P. Janvier, H. Bienaymé, J. Zhu, *Angew. Chem.* **2002**, *114*, 4467 – 4470; *Angew. Chem. Int. Ed.* **2002**, *41*, 4291 – 4294.

[14] The net balance constitutes an intramolecular consumption of two hydrogen atoms for the Cbz-cleavage and the release of two further hydrogen atoms. Although the hydrogen-transfer process is likely to proceed in intramolecular fashion, we cannot exclude the competitive operation of intermolecular pathways.

[15] A. E. Jackson, R. A. W. Johnstone, *Synthesis* **1976**, 685 – 687.

[16] M. Bergmann, L. Zervas, *Chem. Ber.* **1932**, *65*, 1192.

[17] B. El Amin, G. M. Anantharamaiah, G. P. Royer, G. E. Means, *J. Org. Chem.* **1979**, *44*, 3442 – 3444.

[18] The following reactions support this assumption: Subjection of **3a** to Pd/C-catalyzed aromatization afforded **2a** in 75% yield. Identical reaction conditions did not effect Cbz-cleavage from **1a**.

[19] a) C. A. Busacca, Y. Dong, *Synth. Commun.* **2000**, *30*, 501 – 509; b) J. Cossy, D. Belotti, *Org. Lett.* **2002**, *4*, 2557 – 2559.

[20] a) A. M. Felix, E. P. Heimer, T. J. Lambros, C. Tzougraki, J. Meienhofer, *J. Org. Chem.* **1978**, *43*, 4194 – 4196; b) M. Makowski, B. Rzeszotarska, L. Smelka, Z. Kubica, *Liebigs Ann. Chem.* **1985**, 1457 – 1464; c) R. S. Lott, V. S. Chauhan, C. H. Stammer, *Chem. Commun.* **1979**, 495 – 496; d) T. Tsuji, T. Kataoka, M. Yoshioka, Y. Sendo, Y. Nishitani, S. Hirai, T. Maeda, W. Nagata, *Tetrahedron Lett.* **1979**, 2793 – 2796.

[21] For details on equilibrating aminodienes, Diels–Alder selectivity, and crystal structure analyses, see refs. [10a–c].

[22] According to: E. J. Corey, D. Enders, M. G. Bock, *Tetrahedron Lett.* **1976**, 7 – 10.

[23] a) F. E. Ali, C. C. K. Yuan, S. T. Ross, L. B. Hall, *Mol. Diversity* **2000**, *5*, 1 – 5; b) T. W. Ku, F. E. Ali, W. E. Bondinell, K. F. Erhard, W. F. Huffman, J. W. Venslavsky, C. C. K. Yuan, *Tetrahedron Lett.* **1997**, *38*, 3131 – 3134; c) W. Müller, U. Stauss, *Helv. Chim. Acta* **1982**, *65*, 2118 – 2132.

[24] A. Fayol, J. Zhu, *Angew. Chem.* **2002**, *114*, 3785 – 3787; *Angew. Chem. Int. Ed.* **2002**, *41*, 3633 – 3635.

 © 2003 Wiley-VCH Verlag GmbH & Co. KGaA, Weinheim

High-Oxidation-State Cr Complexes

Chromium(V) and Chromium(VI) Nitrido Complexes of Tris(pentafluorophenyl)corrole**

*Galina Golubkov and Zeev Gross**

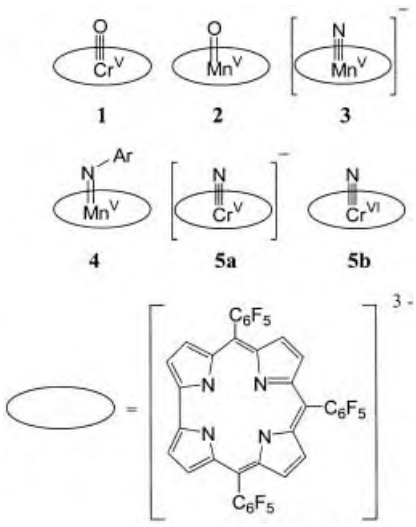
A unique feature of corroles relative to porphyrins and other related ligands is their ability to stabilize transition-metal ions in high oxidation states.[1,2] This phenomenon can not be related to the traditional means of obtaining high-valent metal complexes, which relies on π-donating and nonoxidizable ligands such as F^-, O^{2-}, and N^{3-}, since the corrole macrocycle in non-transition-metal complexes is easily oxidized.[3] Instead, recent theoretical and experimental evidence suggests that σ donation by corrole trianions raises the energy of metal d orbitals to a large extent. This leads to destabilization of low-valent oxidation states and is also manifested in the unique activation of molecular oxygen by chromium(III) and iron(III) corroles.[4,5] Taken together, the cooperation of both π and σ effects in oxo- and nitrido-metallocorroles could be an attractive methodology for obtaining novel complexes. The validity of this hypothesis is indicated by the stability of corrole complexes with pentavalent metal ions: [(tpfc)Cr^V(O)] (**1**),[4b] [(tpfc)Mn^V(O)] (**2**),[6] [(tpfc)Mn^V(N)]$^-$ (**3**),[7] and [(tpfc)Mn^V(NAr)] (**4**),[8] where tpfc stands for the trianion of 5,10,15-tris(pentafluorophenyl)corrole (Scheme 1).[9] However, complexes of the highly oxidizing Cr^{VI} ion were not reported for corroles or other related ligands.[10] A relevant result that explains why such complexes could not be obtained is that the one-electron oxidation of **1** is corrole- rather than metal-centered and leads to [(tpfc$^{\bullet}$)Cr^V(O)]$^+$ rather than [(tpfc)Cr^{VI}(O)]$^+$.[11] Since a comparison of nitrido and oxo complexes with identical ligands and metals reveals that the former are invariably more stable, we decided to explore the possibility of obtaining stable (nitrido)chromium corroles. These attempts were successful: both [(tpfc)Cr^V(N)]$^-$ (**5a**) and [(tpfc)Cr^{VI}(N)] (**5b**) were isolated and characterized by a combination of spectroscopic methods and electrochemistry.

The first approach was to treat [(tpfc)Cr^{III}(py)$_2$] (**6**) with an excess of NH_3 in the presence of a mild oxidant, under the assumption that ligand substitution and subsequent oxidation of the coordinated ammonia would lead to an imido or nitrido complex. Using Br_2 or *N*-bromosuccinimide (NBS), the reaction proceeded to the Cr^V(N) state, but partial bromination (up to four) of the β-pyrrolic C–H bonds of the corrole took place concurrently. On the other hand, the oxo complex

[*] Prof. Dr. Z. Gross, G. Golubkov
Department of Chemistry and
Institute of Catalysis Science and Technology
Technion—Israel Institute of Technology
Haifa 32000 (Israel)
Fax: (+972) 4-823-3735
E-mail: chr10zg@tx.technion.ac.il

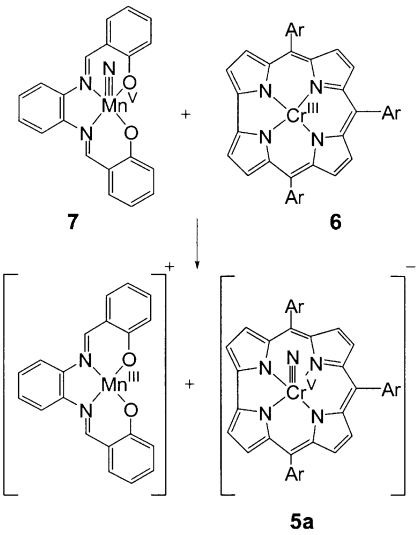
[**] This research (No. 368/00) was supported by the Israel Science Foundation, the Petroleum Research Fund (ACS), and the Fund for the Promotion of Research at the Technion.

 DOI: 10.1002/anie.200351793 © 2003 Wiley-VCH Verlag GmbH & Co. KGaA, Weinheim



Scheme 1. Formulas of recently reported oxo-, imido-, and nitrido-metallocorroles and of the new chromium complexes.

1 was formed when iodosylbenzene was utilized as oxidant. Because of these limitations, a very different route was adopted. It consists of preparing the stable (nitrido)manganese(v) complex of salophene,[12] [(saloph)Mn(N)] (**7**), and transferring its nitrogen atom to **6** (Scheme 2).[13]



Scheme 2. Synthesis of $[(tpfc)Cr^{V}(N)]^{-}$ (**5a**) by nitrogen-atom transfer from [(salop)Mn(N)] (**7**) to $[(tpfc)Cr^{III}(pyr)_2]$ (**6**).

Pronounced changes occur when the two reagents are mixed: Compund **6** is green and displays a very rich electronic spectrum, while **5a** is purple-green and shows a sharp Soret band at 427 nm and a characteristic Q band at 585 nm (Figure 1). Similar to the previously reported (nitrido)manganese(v) complex **3**, **5a** is particularly stable in acetonitrile, and accordingly the spectroscopic measurements were performed in this solvent. The strongest support for the assignment of **5a** as a (nitrido)chromium(v) complex resulting from a two-electron atom transfer from **7** is provided by EPR

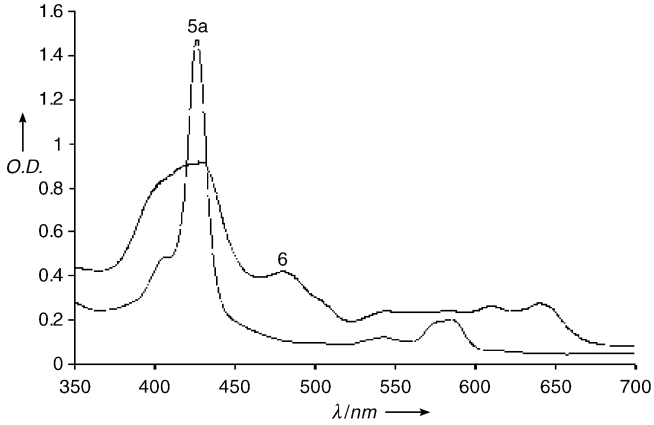


Figure 1. Spectral changes upon transformation of $[(tpfc)Cr^{III}(pyr)_2]$ (**6**) into $[(tpfc)Cr^{V}(N)]^{-}$ (**5a**) by addition of [(salop)Mn(N)] (**7**).

spectroscopy. The spectrum of **5a** (Figure 2b) is similar to that of the (oxo)chromium(v) complex **1** (Figure 2a): both display hyperfine coupling to ^{53}Cr ($A_{^{53}Cr}$) and superhyperfine coupling to nitrogen atoms ($A_{^{14}N}$) at room temperature. The presence of five ^{14}N atoms in **5a** as opposed to four in **1** is clearly evident from the 11 rather than nine lines, best seen in the inset of Figure 2b. In addition, the $A_{^{53}Cr}$ value of 2.67 mT in **5a** is within the range of 2.49–2.84 mT obtained for other (nitrido)chromium(v) complexes and, as expected, much larger than in **1** (1.96 in CH_3CN and 1.64 mT in CH_2Cl_2).

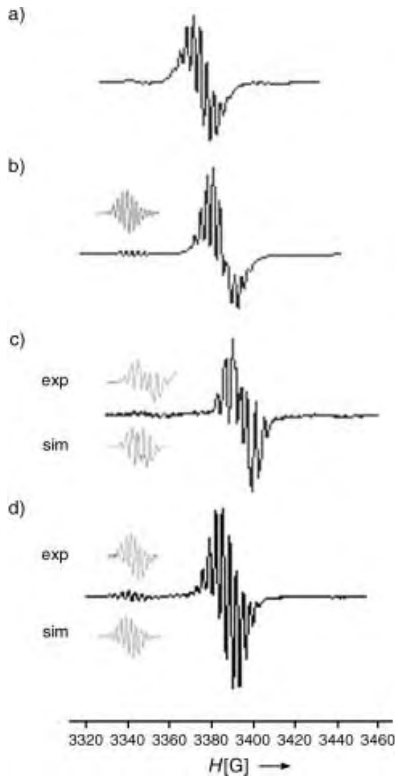


Figure 2. EPR spectra (in CH_3CN at RT) of a) $[(tpfc)Cr^{V}(O)]$ (**1**), b) $[(tpfc)Cr^{V}(N)]^{-}$ (**5a**), c) $[(^{15}N_4\text{-}tpfc)Cr^{V}(N)]^{-}$ (**$^{15}N_4$-5a**), and d) $[(tpfc)Cr^{V}(^{15}N)]^{-}$ (**5a-^{15}N**). Insets: experimental (exp) and simulated (sim) spectra of the low-field region.

 © 2003 Wiley-VCH Verlag GmbH & Co. KGaA, Weinheim

Examination of Figure 2b reveals one $A_{^{14}N}$ value of about 0.27 mT for all five nitrogen atoms. This is reminiscent of the recurring puzzle in the EPR spectra of all (nitrido)chromium(v) complexes with equatorial N donors (for example, salen, cyclam, and porphyrins),[14] in which the isotropic hyperfine couplings to the axial nitrido ligand and the other nitrogen atoms were found to be practically identical, with $A_{^{14}N} = 0.23$–0.28 mT. What is more, $A_{^{14}N}$(nitrido) = 0.29 mT in the pentacyano(nitrido)chromium(v) complex prepared by Jesper et al.,[15] the only example to date for which the superhyperfine coupling tensor to a nitrido ligand could be measured independently of couplings to other nitrogen atoms. In an attempt to solve the puzzle, analogues of **5a** in which either the four nitrogen atoms of the corrole or the unique nitrido ligand are ^{15}N-labeled ([($^{15}N_4$-tpfc)Cr^V(N)]$^-$ (**$^{15}N_4$-5a**) and [(tpfc)Cr^V(^{15}N)]$^-$ (**5a-^{15}N**), respectively) were prepared.[16] The spectra shown in Figure 2c and d reveal significantly different superhyperfine coupling constants, and the best simulations were achieved with $A_{^{14}N}$(nitrido) = 0.26 mT and $A_{^{14}N}$(corrole) = 0.36 mT for **$^{15}N_4$-5a** and $A_{^{14}N}$(nitrido) = 0.36 mT and $A_{^{14}N}$(corrole) = 0.27 mT for **5a-^{15}N**. Since the isotropic hyperfine coupling constant of ^{15}N is 40% larger than that of ^{14}N,[17] these measurements prove that the hyperfine couplings to the axial nitrido ligand and the other nitrogen atoms in complex **5a** are indeed identical.

Another major difference between **5a** and **1** is found in their cyclovoltammograms (Figure 3). As expected, nitrido complex **5a** is harder to reduce and easier to oxidize than oxo

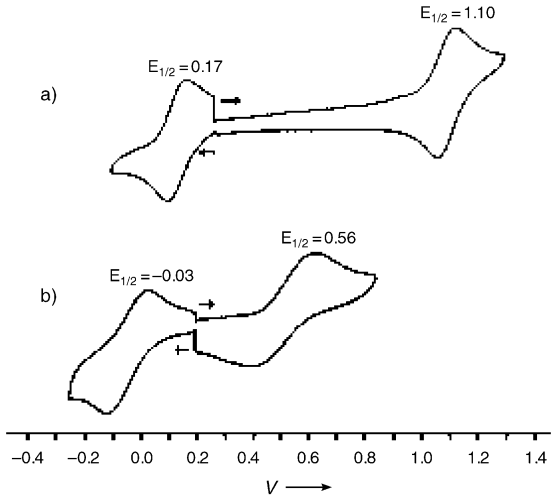


Figure 3. Cyclovoltammograms (in CH_3CN at RT) of a) [(tpfc)Cr^V(O)] (**1**) and b) [(tpfc)Cr^V(N)]$^-$ (**5a**).

complex **1**. Furthermore, the difference between the corresponding $E_{1/2}$ values in **5a** is only 0.59 V, and both its reduction and oxidation potentials (−0.03 and +0.56 V, respectively) are far from the values required for corrole-centered redox processes (< −1 and > +1 V, respectively).[3b] This is remarkably different from the (nitrido)chromium(v) porphyrin [(tpp)Cr(N)],[14a] whose redox potentials of −1.08 and +1.04 V are supportive of porphyrin- rather than chromium-centered processes.

Since the electrochemistry of **5a** suggested that the (nitrido)chromium(vi) complex **5b** should be quite stable, the chromium(iii) complex **6** was treated with sodium hypochlorite.[18] In contrast to porphyrin and salen complexes, for which this is the method of choice for preparation of the corresponding (nitrido)chromium(v) complexes,[12,14] the sole reaction product in the case of **6** was **5b** and not **5a**. This was proven by spectroscopy: **5b** is EPR-silent and displays well-resolved ^{19}F and ^{1}H NMR spectra (Figure 4). This is perfectly in line with expectations for a genuine chromium(vi) complex (d^0).[19]

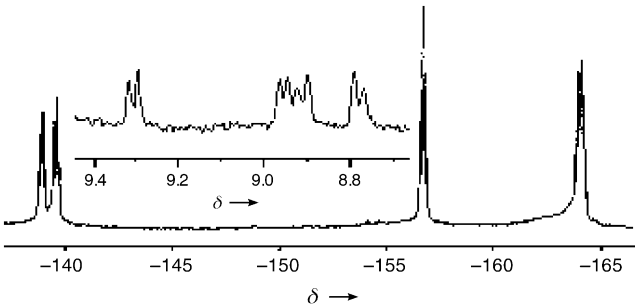


Figure 4. ^{1}H (inset) and ^{19}F NMR spectra of [(tpfc)Cr^{VI}(N)], **5b**, in CD_3CN at RT.

This study shows that the combination of σ donation by corrole trianions and π donation by N^{3-} is a fruitful approach for the preparation of metal complexes with unusually high oxidation states. The (nitrido)chromium(v) corrole was prepared by nitrogen-atom transfer from (nitrido)manganese(v) salophene, which also serves to demonstrate the large thermodynamic stability of the former complex. The ammonia/sodium hypochlorite method that is extensively used for the preparation of (nitrido)chromium(v) complexes of porphyrins and salens leads to (nitrido)chromium(vi) when applied to chromium(iii) corroles.

Received: May 2, 2003 [Z51793]

Keywords: chromium · cyclic voltammetry · EPR spectroscopy · N ligands · porphyrinoids

[1] a) S. Will, J. Lex, E. Vogel, H. Schmickler, J. P. Gisselbrecht, C. Haubtmann, M. Bernard, M. Gross, *Angew. Chem.* **1997**, *109*, 367; *Angew. Chem. Int. Ed. Engl.* **1997**, *36*, 357, and references therein; b) J. L. Sessler, S. J. Weghorn, *Expanded, Contracted & Isomeric Porphyrins*, Pergamon, Oxford, **1997**, Chap. 1 (Tetrahedron Organic Chemistry Series, Vol. 15); c) C. Erben, S. Will, K. M. Kadish in *The Porphyrin Handbook, Vol. 12* (Eds.: K. M. Kadish, K. M. Smith, R. Guilard), Academic Press, San Diego, **2000**, p. 235; d) Z. Gross, *J. Biol. Inorg. Chem.* **2001**, *6*, 733.

[2] For stabilization of high-valent metal ions by the triprotonic N_3C coordination core of carbaporphyrins, see a) M. A. Muckey, L. F. Szczepura, G. M. Ferrence, T. D. Lash, *Inorg. Chem.* **2002**, *41*, 4840; b) H. Furuta, T. Ogawa, Y. Uwatoko, K. Araki, *Inorg. Chem.* **1999**, *38*, 2676.

 © 2003 Wiley-VCH Verlag GmbH & Co. KGaA, Weinheim

[3] a) K. M. Kadish, Z. P. Ou, V. A. Adamian, R. Guilard, C. P. Gros, C. Erben, S. Will, E. Vogel, *Inorg. Chem.* **2000**, *39*, 5675; b) L. Simkhovich, A. Mahammed, I. Goldberg, Z. Gross, *Chem. Eur. J.* **2001**, *7*, 1041.
[4] a) S. P. de Visser, F. Ogliaro, Z. Gross, S. Shaik, *Chem. Eur. J.* **2001**, *7*, 4954; b) A. E. Meier-Callahan, H. B. Gray, Z. Gross, *Inorg. Chem.* **2000**, *39*, 3604.
[5] a) A. Mahammed, H. B. Gray, A. E. Meier-Callahan, Z. Gross, *J. Am. Chem. Soc.* **2003**, *125*, 1162; b) L. Simkhovich, I. Goldberg, Z. Gross, *Inorg. Chem.* **2002**, *41*, 5433.
[6] Z. Gross, G. Golubkov, L. Simkhovich, *Angew. Chem.* **2000**, *112*, 4211; *Angew. Chem. Int. Ed.* **2000**, *39*, 4045.
[7] G. Golubkov, J. Bendix, H. B. Gray, A. Mahammed, I. Goldberg, A. J. DiBilio, Z. Gross, *Angew. Chem.* **2001**, *113*, 2190; *Angew. Chem. Int. Ed.* **2001**, *40*, 2132.
[8] R. A. Eikey, S. I. Khan, M. M. Abu-Omar, *Angew. Chem.* **2002**, *114*, 3743; *Angew. Chem. Int. Ed.* **2002**, *41*, 3592.
[9] a) Z. Gross, N. Galili, I. Saltsman, *Angew. Chem.* **1999**, *111*, 1530; *Angew. Chem. Int. Ed.* **1999**, *38*, 1427; b) Z. Gross, N. Galili, L. Simkhovich, I. Saltsman, M. Botoshansky, D. Bläser, R. Boese, I. Goldberg, *Org. Lett.* **1999**, *1*, 599.
[10] A. L. Odom, C. C. Cummins, *Polyhedron* **1998**, *17*, 675.
[11] A. E. Meier-Callahan, A. J. Di Bilio, L. Simkhovich, A. Mahammed, I. Goldberg, H. B. Gray, Z. Gross, *Inorg. Chem.* **2001**, *40*, 6788.
[12] J. Du Bois, C. S. Tomooka, J. Hong, E. M. Carreira, *Acc. Chem. Res.* **1997**, *30*, 364.
[13] $[(tpfc)Cr^{V}(N)]^{-}$ (**5a**): Solid $[(saloph)Mn^{V}(N)]$ (22 mg, 57.4 μmol) was added to a solution of $[(tpfc)Cr^{III}(py)_2]$ (25 mg, 29.6 μmol) in acetonitrile (10 mL). After the color change from green to purple was complete (1 min, also monitored by UV/Vis), **5a** (16 mg, 18.6 μmol) was isolated by column chromatography (silica gel, CH_3CN). MS^{-}: *m*/*z* (%): 859 $[M^{-}]$ (100), 845 $[M^{-}-N]$, 80%; UV/Vis (CH_3CN) λ_{max} (relative ε): 427 (100), 585 nm (15); ^{19}F NMR (188 MHz, CD_3CN): $\delta = -139.0$ (br s, 6F), −156.6 (br s, 3F), −163.6 ppm (br d, 6F).
[14] a) J. T. Groves, T. Tadashi, B. M. William, *J. Am. Chem. Soc.* **1983**, *105*, 844; b) K. Meyer, J. Bendix, T. Weyhermueller, B. Eckhard, K. Wieghardt, *Inorg. Chem.* **1998**, *37*, 5180; c) A. Nagao, I. Yohko, Y. Hironobu, T. Kunihiko, L. Yong, Y. Jun, *Inorg. Chim. Acta* **1997**, *266*, 29.
[15] a) J. Bendix, R. J. Deeth, T. Weyhermuller, E. Bill, K. Wieghardt, *Inorg. Chem.* **2000**, *39*, 930; b) J. Bendix, K. Meyer, T. Weyhermueller, B. Eckhard, N. Metzler-Nolte, K. Wieghardt, *Inorg. Chem.* **1998**, *37*, 1767.
[16] **$^{15}N_4$-5a**: The labeled corrole was prepared by solvent-free condensation of [^{15}N]pyrrole (Aldrich) and pentafluorobenzaldehyde.[8] Insertion of chromium(III) ions and atom transfer from $[(saloph)Mn^{V}(N)]$ (13.5 mg, 35.3 μmol) to $[(^{15}N_4\text{-}tpfc)Cr^{III}(py)_2]$ (15 mg, 17.7 μmol) in acetonitrile (5 mL) provided **$^{15}N_4$-5a** (14 mg, 16.2μmol). MS^{-}: *m*/*z* (%): 863 $[M^{-}]$ (45), 849 $[M^{-}-{}^{14}N]$. **5a-^{15}N**: $[(saloph)Mn^{V}(^{15}N)]$ (27.7 mg, 72 μmol) was prepared by addition of $^{15}NH_4OH$ (3N, 0.68 mL, 2 mmol) and sodium hypochlorite (7 mL, 0.28 mmol) to $[(saloph)Mn^{III}Cl]$ (50 mg, 135 μmol) in methanol (5 mL). Atom transfer from $[(saloph)Mn(^{15}N)]$ (8.2 mg, 21.3 μmol) to $[(tpfc)Cr^{III}(py)_2]$ (15 mg, 17.8 μmol) in acetonitrile (5 mL) yielded **5a-^{15}N** (14 mg, 16.3 μmol). MS^{-}: *m*/*z* (%): 860 $[M^{-}]$ (50), 845 $[M\text{-}^{15}N]$ (100%).
[17] J. E. Wertz, J. R. Bolton, *Electron Spin Resonance: Elementary Theory and Practical Applications*, McGraw-Hill, New York, **1972**, Table C, inside cover.
[18] $[(tpfc)Cr^{VI}(N)]$, **5b**: Pyridine (1 drop), NH_4OH (0.014 mL, 0.36 mmol), and sodium hypochlorite (7.5 mL, 0.14 mmol) were added to a solution of $(tpfc)Cr^{III}(py)_2$ (25 mg, 24.9 μmol) in acetonitrile (10 mL) under argon. After the color change from green to purple was complete (1 min, also monitored by UV/Vis), sodium sulfate was added, and the solution was filtered and evaporated to dryness to afford **5b** (21.3 mg, 24.8 μmol). MS^{-}: *m*/*z* (%): 859 $[M^{-}]$ (10); UV/Vis (MeOH) λ_{max} (relative ε): 429 (100), 581 nm (25); ^{1}H NMR (200 MHz, CD_3CN): $\delta = 9.32$ (d, $J = 3.99$ Hz, 2H), 8.97 (d, $J = 3.81$ Hz, 2H), 8.93 (d, $J = 4.54$ Hz, 2H), 8.79 ppm (d, $J = 4.34$ Hz 2H); ^{19}F NMR (188 MHz, CD_3CN): $\delta = -138.8$ (d, $J = 23.9$ Hz, 2F), −138.9 (d, $J = 20.7$ Hz, 1F), −139.5 (d, $J = 24.05$ Hz, 2F), −139.6 (d, $J = 28.7$ Hz, 1F), −156.6 (t, $J = 20.4$ Hz, 2F), −156.8 (t, $J = 20.2$ Hz, 1F), −164.0 ppm (m, 6F).
[19] For a recent diamagnetic d^0 silver(III) corrole, see C. Brückner, C. A. Barta, R. P. Brinas, J. A. K. Bauer, *Inorg. Chem.* **2003**, *42*, 1673.

 © 2003 Wiley-VCH Verlag GmbH & Co. KGaA, Weinheim

Boratacyclooctatetraene Ligand

The Boratacyclooctatetraene Ligand: An Isoelectronic Trianionic Analogue of the Cyclooctatetraene Dianion**

*Xiangdong Fang, David Woodmansee, Xianhui Bu, and Guillermo C. Bazan**

Dedicated to Professor Gerhard E. Herberich and Professor Arthur J. Ashe III

The cyclooctatetraene dianion (COT^{2-}) and its derivatives are versatile ligands for transition metal atoms.[1] When bound to metal centers, they are formally considered as dianionic 10π electron donors. Their use in actinide and lanthanide chemistry, in particular, has been well documented.[1c] Representative examples from the literature include uranocene, $[(C_8H_8)_2U]$, and $[(C_8H_8)_2Ce]$.[2] Catalytic species can also be designed, for instance $[Ni_2(COT)_2]$ serves as an effective catalyst for acetylene tetramerization.[3]

Interest in the chemistry of boracycloalkenes, boraarenes and borataarenes stems from the concepts of π-electron aromaticity and conjugation across sp^2-hybridized boron.[1] Boratabenzene, the most representative example of this class of compound, is an anionic 6π electron main-group heterocycle, which was initially identified coordinated to transition-metal centers.[4] Recent applications of boratabenzene in transition-metal catalysis are of interest, because the electron density of the metal center can be modulated by the choice of the exocyclic boron substituent.[5] Changes in electron density

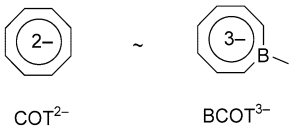
[*] Prof. Dr. G. C. Bazan, Dr. X. Fang, D. Woodmansee, Dr. X. Bu
Department of Chemistry and Materials
Center for Polymer and Organic Solids
The University of California
Santa Barbara, CA 93106 (USA)
Fax: (+1) 805-893-4120
E-mail: bazan@chem.ucsb.edu

[**] This work was generously supported by the US Department of Energy (Grant Number: DE-FG03098ER14910).

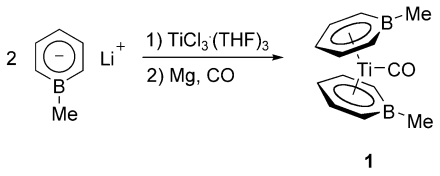
 © 2003 Wiley-VCH Verlag GmbH & Co. KGaA, Weinheim DOI: 10.1002/anie.200351911

result in modified catalytic activities and selectivities.[5e] Similar control of reactivity by exocyclic substituents in the cyclopentadienyl ligand is more difficult to achieve.[6]

Initial interest in applying the reactivity control by boracyclic ligands to other transition-metal-catalyzed processes prompted us to examine the synthesis and reactivities of low-valent titanium carbonyl complexes. Much of the motivation was provided by the alkyne hydroboration reactions catalyzed by $[Cp_2Ti(CO)_2]$ ($Cp = \eta^5$-C_5H_5).[7] Herein, we report on the synthesis of $[(C_5H_5B{-}Me)_2Ti(CO)]$ (**1**) and the conversion of boratabenzene into the formally trianionic boratacyclooctatetraene (BCOT) ligand upon insertion of acetylene into the intraring B–C bond. The BCOT ligand should facilitate the synthesis of novel transition-metal, lanthanide, and actinide complexes with reactivity that can be controlled by the electronic properties of the boron substituent.[5e]



The synthesis of $[(C_5H_5B{-}Me)_2Ti(CO)]$ (**1**) is shown in Scheme 1.[8] Reaction in THF of lithium 1-methyl boratabenzene[9] with $TiCl_3{\cdot}(THF)_3$,[10] followed by treatment with

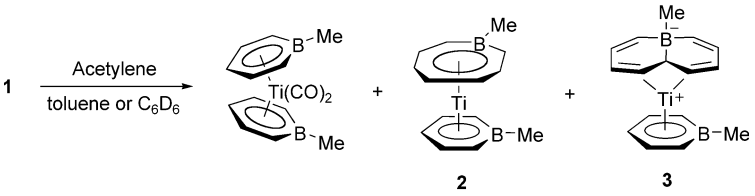


Scheme 1. Synthesis of $(C_5H_5B{-}Me)_2Ti(CO)$.

magnesium powder under one atmosphere of CO and extraction with hot toluene affords **1** in 47% yield as cubic dark-red crystals. The IR spectrum of **1** shows a single band in the carbonyl-stretching region, at $\tilde{\nu} = 1954\ cm^{-1}$. Single crystals suitable for X-ray diffraction experiments were obtained by crystallizing the product in hexane at room temperature and the result of these diffraction studies (see Supporting Information) is consistent with the structural assignment given in Scheme 1.[12b]

A study by ^{1}H NMR spectroscopy indicates that an addition of excess CO to a solution of **1** in C_6D_6 results in the formation of $[(C_5H_5B{-}Me)_2Ti(CO)_2]$, the spectrum of which shows broad signals at $\delta = 5.43$ (4H), 4.41 (4H) and 4.34 ppm (2H). As the resonance signals arising from $[(C_5H_5B\text{-}Me)_2Ti(CO)_2]$ increase, there is a concomitant decrease in the signals from **1**. Furthermore, two IR bands in the carbonyl region are observed at $\tilde{\nu} = 1996$ and $1949\ cm^{-1}$, which are consistent with the symmetric and antisymmetric CO-stretching combinations of a metal center with two carbonyl ligands. The removal of solvent regenerates **1**, thus indicating that the second carbonyl ligand is not strongly bound to titanium.

In the process of examining the reactivity of **1** with a variety of acetylinic substrates, we monitored the reaction of **1** with acetylene in C_6D_6 by using ^{1}H NMR spectroscopy (Scheme 2). Addition of one equivalent of acetylene yields



Scheme 2. Reaction of **1** with acetylene

three organometallic products. One was readily identified as $[(C_5H_5B{-}Me)_2Ti(CO)_2]$. A second product shows a resonance peak pattern reminiscent of the previously reported borate complex, [4a-phenyl-8a*H*-4a-boratanaphthalene][1-phenyl-boratabenzene]-zirconium(II).[11] Attempts to obtain single crystals of this species for X-ray structural determination were unsuccessful. We tentatively assign this product as compound **3** in Scheme 2. The third product shows resonance peaks at $\delta = 6.55$ (dd), 6.06 (t), 5.95 (d), and 5.68 ppm (dd). Such a pattern would be consistent with a 1-methyl-boratacyclooctatetraene (BCOT) ring structure. This structural assignment was also supported by high-resolution mass spectrometry.

We anticipated increased yields of **2**, relative to **3**, at low acetylene pressures by noting that the formation of **3** requires two equivalents of acetylene, whereas **2** is obtained by a single insertion. Indeed, when one monitors the reaction of **1** with acetylene at lower concentrations of C_2H_2, the ratio of **2** to **3** increases. As a preparatory method, we intentionally used an argon buffer layer on the top of a solution of **1** in toluene and then carefully layered 1.2 equivalents of acetylene on the top of the argon. The purpose of the argon layer is to decrease the diffusion rate of acetylene gas and reduce the effective acetylene concentration in toluene. The removal of solvent and recrystallization in hexane afford the desired BCOT complex **2** in 50% yield.

Dark-red single crystals of **2** were obtained by slow diffusion of pentane into a toluene solution at −35 °C. The results of X-ray diffraction studies show that there are four independent molecules of composition $[(C_7H_7B{-}Me)(C_5H_5B{-}Me)Ti]$ in the crystal lattice. Figure 1 shows a representative structure.[12] The overall molecular geometry is that of a parallel sandwich metallocene with an η^8-boratacyclooctatetraene ligand and an η^6-boratabenzene ligand. Average Ti–C and Ti–B distances are statistically shorter to the BCOT ligand (av. Ti–C = 2.269(6) Å, av. Ti–B = 2.416(6) Å) than to the boratabenzene ligand (av. Ti–C = 2.363(6) Å, av. Ti–B = 2.517(6) Å). These metrical data, together with the shorter Ti–(C_7B) centroid distance (1.313(6) Å), reflect the higher charge on the C_7B ring, relative to the C_5B ring (Ti–(C_5B) centroid distance:

 © 2003 Wiley-VCH Verlag GmbH & Co. KGaA, Weinheim

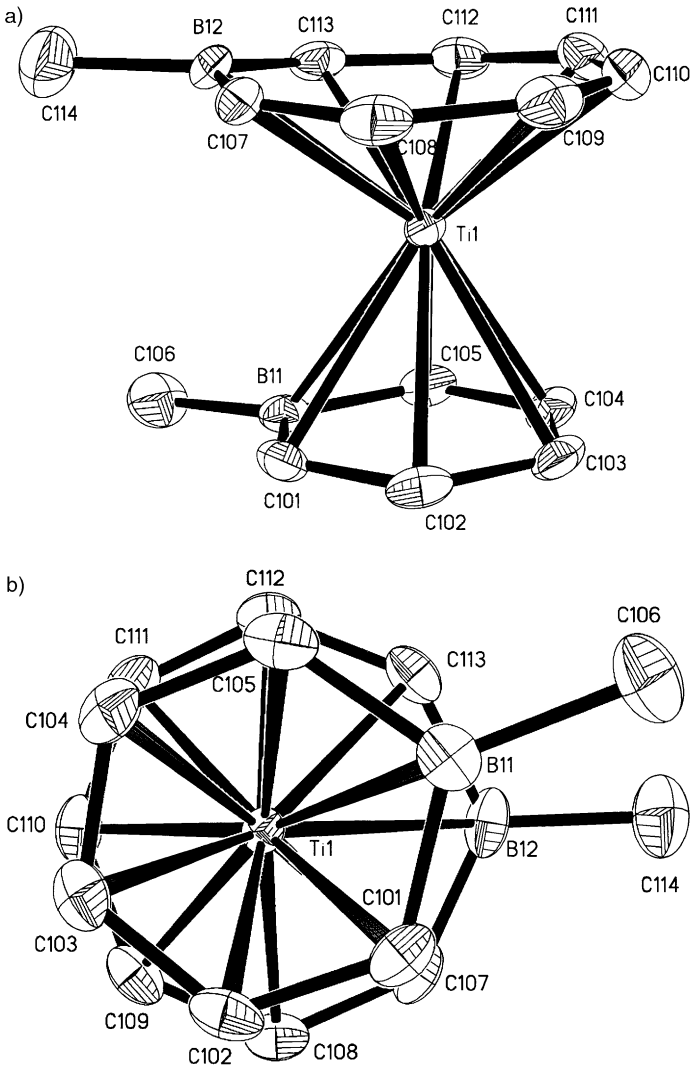
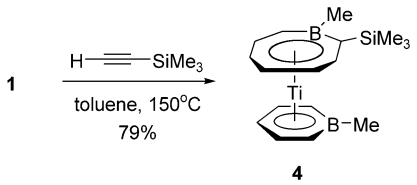


Figure 1. ORTEP diagrams of the molecular structure of compound **2**: a) side view; b) top view. Thermal ellipsoids set at the 30% probability level.

1.909(6) Å). The intraring C–C bond distances in the BCOT ring in **2** (**2**: 1.394(9)–1.426(9) Å) are within the range of coordinated aromatic boracycles.[4a] The intraring B–C bond lengths (**2**: 1.506(10)–1.508(10) Å) are considerably shorter than the exocyclic B–C bond lengths (**2**: 1.586(10) Å), which indicate an extensively delocalized structure within the BCOT ring. It is also significant that in **2** the resonance signals of the protons on the BCOT ring ($\delta = 5.68$–6.55 ppm in C_6D_6) are shifted to lower fields, relative to those of the boratabenzene ring ($\delta = 4.52$–5.57 ppm in C_6D_6), thus indicating strong ring current within the BCOT ligand.

Having determined that acetylene can insert into the boratabenzene fragment, we examined whether any regioselectivity was possible by using a monosubstituted substrate (Scheme 3). Thus, a solution of **1** in toluene was treated with 1.0 equivalent of trimethylsilylacetylene at 150 °C to afford [(2-$SiMe_3$–C_7H_6B–Me)(C_5H_5B–Me)Ti] (**4**) in 79% yield. A crystal of **4** suitable for X-ray diffraction studies was grown from hexane at 20 °C and the trimethylsilyl group was unambiguously found at the C_α site of the BCOT ring



Scheme 3. Study of the reaction selectivity by using a substituted alkyne.

(Figure 2).[12] The corresponding ^{1}H NMR spectrum shows a coupling pattern of the boratacyclooctatetraene ligand protons in the bulk product that is consistent with the solid-state structure.

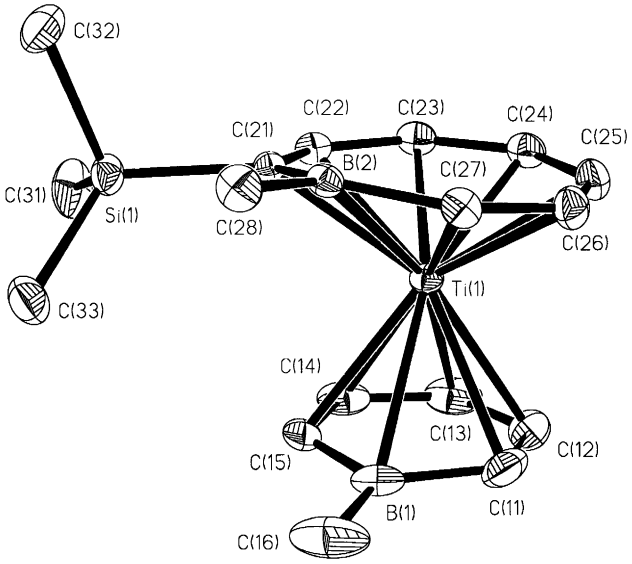
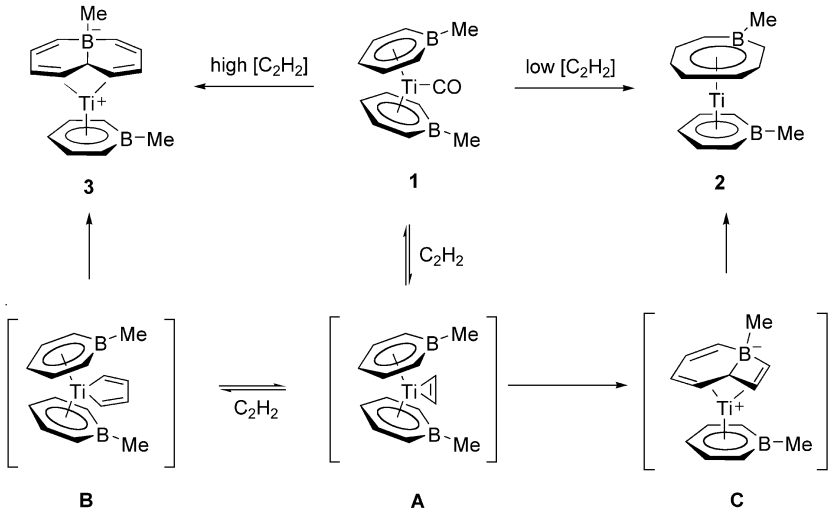


Figure 2. ORTEP diagram of the molecular structure of **4**. Thermal ellipsoids set at the 30% probability level.

A mechanism for the formation of **2** is proposed in Scheme 4. It is well-accepted that {Cp_2Ti^{II}}species can oxidatively coordinate one or two acetylene molecules to form titannacyclopropene or titannacyclopentadiene intermediates, respectively.[13] By analogy, a similar oxidative coupling process may be adopted by the {(C_5H_5B–Me)$_2Ti^{II}$} fragment.[11] In Scheme 4, the first intermediate is the titannacyclopropene species **A**, which forms upon coordination of acetylene to **1**. One equivalent of carbon monoxide is generated by this reaction, which is trapped by **1** to form [(C_5H_5B–Me)$_2$Ti(CO)$_2$] (not shown in Scheme 4, but observed in solution). Associative displacement reactions with [(C_5H_5B–Me)$_2$Ti(CO)$_2$] are not significant because of its inert 18 electron configuration. Compound **A** can undergo two types of reactions, depending on the acetylene concentration. At low concentrations of C_2H_2, direct transmetallation and subsequent reductive elimination affords the annulated bicyclic intermediate **C**. Next, the four-membered ring expands to yield the BCOT ligand. When the acetylene concentration is high, the intermediate **A** is trapped by a second equivalent of acetylene to give **B**, before the intra-

 © 2003 Wiley-VCH Verlag GmbH & Co. KGaA, Weinheim



Scheme 4. Proposed mechanism for the formation of **2**.

molecular ring expansion can take place. Compound **B** ultimately converts to **3**.[11]

The Lewis acidity of the boron atom plays an important role in facilitating the transmetallation step. We note that $[(C_5H_5B{-}NMe_2)_2Ti(CO)]$, in which B–N π bonding increases the electron density at boron, does not react with acetylenes under conditions similar to those in Scheme 2.[14] As electrophilic attack on vinylsilanes occurs selectively at the Si-C_α site,[15] we propose that the transmetallation step should be viewed as an electrophilic attack of boron on the coordinated acetylene ligand. The transition state of the regioselective insertion of trimethylsilylacetylene is depicted in Figure 3. The alignment between the electrophilic *p* orbital on boron and the nucleophilic *p* orbital on the C_α atom of the vinyl group prompts the concerted four-center four-electron transition state. These electronic requirements lead to placing the bulky trimethylsilyl group adjacent to the sterically more demanding methyl-substituted boron atom, instead of C_β substitution.

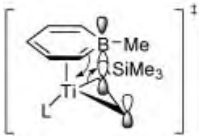


Figure 3. Transition state of the regioselective insertion of trimethylsilylacetylene.

In summary, we have demonstrated that the boratacyclooctatetraene (BCOT) ring system can be obtained from boratabenzene by a simple ring insertion step. A low concentration of acetylene in toluene favors the single insertion. The BCOT formation is most likely a result of an electrophilic attack of the boron atom on the coordinated acetylene fragment. The electronic requirements of this transmetallation step control the insertion regiochemistry. The existence of BCOT should facilitate the synthesis of transition-metal, lanthanide, and actinide complexes that are isoelectronic and isostructural to COT-containing compounds, but have an additional negative charge. We also foresee that the reactivity of BCOT complexes will be controlled by the choice of exocyclic boron substituents.

Experimental Section

Chemicals were obtained from Aldrich, Strem, Acros, and Fisher and, unless otherwise specified, were used without further purification. Alkynes were degassed, flushed with argon, dried over activated molecular sieves (4 Å) and distilled. Carbon monoxide and acetylene were purchased from PRAXAIR. All manipulations were carried out under an inert atmosphere by using standard glovebox and Schlenk techniques. Toluene and THF were distilled from sodium benzophenone ketyl. Hexane was distilled from sodium/potassium alloy. Methylene chloride was distilled from CaH_2. NMR spectra were recorded with a Varian Unity 400 or 500 spectrometer. ^1H and ^{13}C NMR spectra were calibrated by using signals from solvent and were reported downfield from $SiMe_4$. ^{11}B NMR spectra were calibrated and reported from external $BF_3{\cdot}EtO_2$. Mass spectrometric analyses were obtained by using a VG-70E double-focusing magnetic sector instrument operated with an OPUS-SIOS data system. Elemental analyses were performed at Desert Analytics, Inc., Tucson, AZ and Analytical Lab, Marine Science Institute, the University of California, Santa Barbara.

Lithium 1-methylboratabenzene[9] and $TiCl_3{\cdot}(THF)_3$[10] were synthesized according to the literature procedures.

1: THF (20 mL) was vacuum transferred to a 500 mL Schlenk tube containing a mixture of 1-methylboratabenzene lithium salt (1.00 g, 10.2 mmol) and $TiCl_3{\cdot}(THF)_3$ (1.90 g, 5.1 mmol) and a magnetic stirrer. The mixture was stirred at 20 °C for 10 h, after which time the volatile fractions were removed in vacuo. An excess of magnesium powder (147 mg, 6.1 mmol) was loaded, and THF (50 mL) were vacuum transferred to the Schlenk tube, which had been cooled to −196 °C. The resulting mixture was then stirred at 20 °C under one atmosphere of CO for 10 h. The volatile fractions were removed in vacuo and the black residue was extracted with toluene (2 × 25 mL). These extractions were filtered, and the solvent was removed in vacuo to give a dark residue, which was further extracted with hot toluene (30 mL). The solvent was again removed in vacuo, and the remaining solid was dissolved in hexane. Crystallization of the product at 25 °C afforded dark-red cubic crystals (630 mg, 47 % yield): m.p. 164–165 °C; IR (hexane): $\tilde{\nu} = 1955\ cm^{-1}$ (C≡O); ^1H NMR (400 MHz, C_6D_6, 25 °C, TMS): $\delta = 4.93$ (dd, $J = 9.6$, 2.0 Hz, 2H; H_α), 4.86 (tt, $J = 7.2$, 2.0 Hz, 1H; H_γ), 4.47 (dd, $J = 9.6$, 7.2 Hz, 2H; H_β), 1.17 ppm (s, 3H; B-Me); ^{13}C NMR (100 MHz, C_6D_6, 25 °C, TMS): $\delta = 121.4$ (C_β), 108.6 (b, C_α), 100.0 (C_γ), 5.72 ppm (b, B–Me); ^{11}B NMR (160 MHz, C_6D_6, 25 °C, $BF_3{\cdot}Et_2O$): $\delta = 31.7$ ppm; Elemental analysis calcd (%) for $C_{13}H_{16}B_2OTi$: C 60.57, H 6.26; found: C 59.99, H 6.33.

2: A bomb flask containing a solution of **1** (88 mg, 0.34 mmol) in toluene (20 mL) was attached through an adapter flask on the vacuum line. The bomb flask was evacuated and refilled with argon. The adapter flask (93.8 mL) was evacuated and recharged with acetylene gas ($\Delta p = 8$ mmHg, 1.2 equiv). Acetylene was allowed to slowly diffuse into the solution of **1** through the argon layer at 25 °C. The solution was stirred well at 25 °C for four days. The solvent was removed in vacuo, the product was extracted with hexane, and the crude product was obtained by crystallization at −35 °C. Recrystallization of the product by slow diffusion of pentane into the toluene solution at −35 °C afforded dark-red crystals of **2** (43 mg, yield 50 %): m.p. 88 °C; ^1H NMR (400 MHz, C_6D_6, 25 °C, TMS): $\delta = 6.55$ (dd, $J =$ 14.6, 12.4 Hz, 2H; BCOT), 6.06 (t, $^3J = 13.5$ Hz, 1H; BCOT), 5.95 (d, $^3J = 14.6$ Hz, 2H; BCOT), 5.68 (dd, $J = 13.5$, 12.4 Hz, 2H; BCOT), 5.57 (dd, $J = 10.2$, 7.2 Hz, 2H; Bb), 5.03 (dd, $J = 10.2$, 1.6 Hz, 2H; Bb), 4.52 (tt, $J = 7.2$, 1.6 Hz, 1H; Bb), 1.61 (s, 3H; B-CH_3(BCOT)), 0.72 ppm (s, 3H; B-CH_3(Bb)); ^{13}C NMR (100 MHz, C_6D_6, 25 °C,

 © 2003 Wiley-VCH Verlag GmbH & Co. KGaA, Weinheim

TMS): $\delta = 116.8$, 114.1 (b), 105.1, 101.3 (b), 100.8, 97.7, 96.4 ppm, Me not observed; ^{11}B (160 MHz, C_6D_6, 25 °C, $BF_3{\cdot}Et_2O$): $\delta = 31.1$, 26.6 ppm; HRMS: *m*/*z* calcd for $C_{14}H_{18}{}^{11}B_2{}^{48}Ti$, 256.1082; found, 256.1079; Elemental analysis calcd (%) for $C_{14}H_{18}B_2Ti$: C 65.74, H 7.09; found: C 65.41, H 6.81.

4: A solution of **1** (100 mg, 0.39 mmol) in 5 mL of toluene was treated with a solution of trimethylsilylacetylene (1.0 equiv) in 5 mL of toluene in a bomb reactor. The mixture was heated to 150 °C for 12 h. After removal of volatile fractions under reduced pressure, the residue was extracted with hot hexane (20 mL). The hexane extract was filtered and concentrated. The crystallization took place at 25 °C to afford dark-red parallelopiped crystals as the product (100 mg, yield 79 %): m.p. 114 °C; ^{1}H NMR(400 MHz, C_6D_6, 25 °C, TMS): $\delta =$ 6.97 (d, $^3J = 11.0$ Hz, 1H; BCOT), 6.54 (dd, $J = 14.3$, 11.0 Hz, 1H; BCOT), 6.09 (t, $^3J = 13.2$ Hz, 1H; BCOT), 5.92 (d, $^3J = 14.3$ Hz, 1H; BCOT), 5.79–5.71 (m, 3H; 2H(BCOT) and 1H(Bb)), 5.62 (ddd, $J =$ 10.0, 7.0, and 2.0 Hz, 1H; Bb), 5.12 (ddd, $J = 10.0$, 3.0, and 2.0 Hz, 1H; Bb), 4.90 (ddd, $J = 10.7$, 3.0, and 2.0 Hz, 1H; Bb), 4.72 (tt, $J = 7.0$, 2.0 Hz, 1H; Bb), 1.60 (s, 3H; B-Me(BCOT)), 0.67 (s, 3H; B-Me(Bb)), 0.55 ppm (s, 9H; $SiMe_3$); ^{13}C NMR (100 MHz, C_6D_6, 25 °C, TMS): $\delta =$ 121.4, 116.8, 116.2, 108.4, 104.5, 100.8, 98.5, 96.5, 3.6 ppm ($SiMe_3$), B-Me not observed; ^{11}B NMR (160 MHz, C_6D_6, 25 °C, $BF_3{\cdot}Et_2O$): $\delta =$ 31.8, 29.9 ppm; HRMS: *m*/*z* calcd for $C_{17}H_{26}{}^{11}B_2{}^{28}Si^{48}Ti$, 328.1479, found 328.1478; Elemental analysis calcd (%) for $C_{17}H_{26}B_2SiTi$: C 62.25, H 7.99; found: C 61.54, H 7.97.

Received: May 15, 2003 [Z51911]

Keywords: boratacycles · borates · heterocycles · ligand design · ring expansion · titanium

[1] a) C. Elschenbroich, A. Salzer, *Organometallics: A Concise Introduction*, 2nd revised ed., Wiley-VCH, Weinheim, **1992**, pp. 362–369; b) P. J. Garrett, *Aromaticity*, Wiley, New York, **1986**, and references therein; c) G. I. Fray, R. G. Saxton, *The Chemistry of Cyclooctatetraene and Its Derivatives*, Cambridge University Press, Cambridge, **1978**; d) F. T. Edelmann, *Angew. Chem.* **1995**, *107*, 2647–2669; *Angew. Chem. Int. Ed. Engl.* **1995**, *34*, 2466–2488.

[2] a) A. Streitwieser, Jr., U. Müller-Westerhoff, *J. Am. Chem. Soc.* **1968**, *90*, 7364; b) A. Streitwieser, Jr., U. Müller-Westerhoff, G. Sonnichsen, F. Mares, D. G. Morrell, K. O. Hodgson, C. A. Harmon, *J. Am. Chem. Soc.* **1973**, *95*, 8644–8649; c) T. R. Boussie, D. C. Eisenberg, J. Rigsbee, A. Streitweiser, A. Zalkin, *Organometallics* **1991**, *10*, 1922–1928.

[3] a) G. Wilke, *Angew. Chem.* **1988**, *100*, 189–210; *Angew. Chem. Int. Ed. Engl.* **1988**, *27*, 185–206; b) G. Wilke, *Pure Appl. Chem.* **1978**, *50*, 677–690.

[4] For reviews of boratabenzene chemistry see: a) G. E. Herberich, H. Ohst, *Adv. Organomet. Chem.* **1986**, *25*, 199–236; b) G. C. Fu, *Adv. Organomet. Chem.* **2001**, *47*, 101–119.

[5] a) G. C. Bazan, G. Rodriguez, A. J. Ashe III, S. Al-Ahmad, C. Müller, *J. Am. Chem. Soc.* **1996**, *118*, 2291–2292; b) G. C. Bazan, G. Rodriguez, A. J. Ashe III, S. Al-Ahmad, J. W. Kampf, *Organometallics* **1997**, *16*, 2492–2494; c) J. S. Rogers, G. C. Bazan, C. K. Sperry, *J. Am. Chem. Soc.* **1997**, *119*, 9305–9306; d) R. W. Barnhart, G. C. Bazan, T. Mourey, *J. Am. Chem. Soc.* **1998**, *120*, 1082–1083; e) G. C. Bazan, W. D. Cotter, Z. J. A. Komon, R. A. Lee, R. J. Lachicotte, *J. Am. Chem. Soc.* **2000**, *122*, 1371–1380.

[6] A. J. Ashe III, S. Al-Ahmad, X. D. Fang, J. W. Kampf, *Organometallics* **2001**, *20*, 468–473.

[7] a) X. M. He, J. F. Hartwig, *J. Am. Chem. Soc.* **1996**, *118*, 1696–1702; b) J. F. Hartwig, C. N. Muhoro, *Organometallics* **2000**, *19*, 30–38, and references therein.

[8] For the synthesis of Ti^{III} complexes, see: G. E. Herberich, U. Englert, A. Schmitz, *Organometallics* **1997**, *16*, 3751–3757.

[9] a) D. A. Hoic, J. R. Wolf, W. M. Davis, G. C. Fu, *Organometallics* **1996**, *15*, 1315–1318; b) S. Qiao, D. A. Hoic, G. C. Fu, *J. Am. Chem. Soc.* **1996**, *118*, 6329–6330; c) G. E. Herberich, B. Schmidt, U. Englert, *Organometallics* **1995**, *14*, 471–480.

[10] For the synthesis of $TiCl_3{\cdot}(THF)_3$, see: Inorganic Syntheses, *Vol. 21* (Ed.: J. P. Fackler, Jr.), Wiley, New York, **1982**, pp. 137–138.

[11] A. J. Ashe III, S. Al-Ahmad, J. W. Kampf, V. G. Young, Jr., *Angew. Chem.* **1997**, *109*, 2104–2106; *Angew. Chem. Int. Ed. Engl.* **1997**, *36*, 2014–2016.

[12] a) Crystal data for **2**: $C_{14}H_{18}B_2Ti$, $M_r = 255.80$, space group *C*2/*c*, $a = 25.024(7)$ Å, $b = 11.862(3)$ Å, $c = 39.738(10)$ Å, $\beta = 92.632(5)°$, $V = 11783(5)$ Å^3, $Z = 36$, dark red, crystal size $0.34 \times 0.26 \times 0.1^6$ mm^3, $Mo_{K\alpha}$, $\lambda = 0.71073$ Å, $T = 150$ K, $R =$ 7.59 %, $wR = 19.8$ % for 723 parameters and 6076 unique reflections with $I > 2\sigma(I)$. Crystal data for **4**: $C_{17}H_{26}B_2SiTi$, $M_r =$ 327.99, space group $P2_12_12_1$, $a = 10.3510(18)$ Å, $b =$ 10.8200(19) Å, $c = 15.739(3)$ Å, $V = 1762.7(5)$ Å^3, $Z = 4$, $T =$ 150 K, dark red, crystal size $0.24 \times 0.24 \times 0.2^4$ mm^3, $Mo_{K\alpha}$, $\lambda =$ 0.71073 Å, $R = 4.61$ %, $wR = 11.9$ % for 196 parameters and 3797 unique reflections with $I > 2\sigma(I)$. b) CCDC-210722 (**1**), 210544 (**2**), and 210545 (**4**) contains the supplementary crystallographic data for this paper. These data can be obtained free of charge via www.ccdc.cam.ac.uk/conts/retrieving.html (or from the Cambridge Crystallographic Data Centre, 12 Union Road, Cambridge CB2 1EZ, UK; fax: (+44) 1223-336-033; or deposit@ccdc.cam.ac.uk).

[13] a) E. Negishi, T. Takahashi, *Acc. Chem. Res.* **1994**, *27*, 124–130; b) "Synthesis and Reactivity of Zirconocene Derivatives": E. Negishi, S. Huo in *Titanium and Zirconium in Organic Synthesis* (Ed.: I. Marek), Wiley-VCH, Weinheim, **2002**, pp. 1–49.

[14] D. Woodmansee, G. C. Bazan, unpublished results.

[15] For reviews of electrophilic attack on vinylsilanes, see: a) J. S. Panek, Silicon Stabilization in *Comprehensive Organic Synthesis, Vol. 1* (Ed.: B. M. Trost, I. Fleming), Pergamon, Oxford, **1991**, pp. 579–627; b) T. A. Blumenkopf, L. E. Overman, *Chem. Rev.* **1986**, *86*, 857–873.

 © 2003 Wiley-VCH Verlag GmbH & Co. KGaA, Weinheim

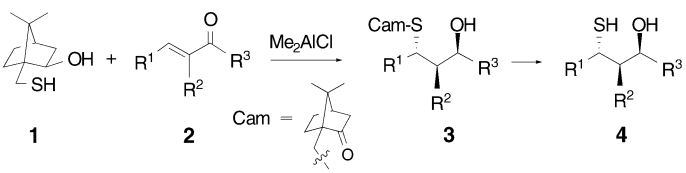
Tandem Asymmetric Reactions

One-Step Stereocontrol of Three Contiguous Stereogenic Centers in Acyclic Systems: The Tuning Effect of an Additive in a Tandem Asymmetric Michael Addition and Meerwein–Ponndorf–Verley Reduction**

*Kiyoharu Nishide, Minoru Ozeki, Hideaki Kunishige, Yukihiro Shigeta, Pranab K. Patra, Yuri Hagimoto, and Manabu Node**

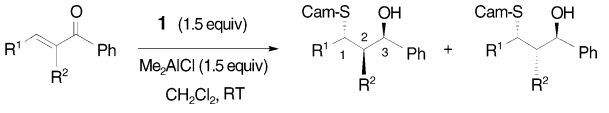
A significant amount of chemistry that involves chiral 1,3-oxathianes derived from optically active 1,3-hydroxythiols has been developed for asymmetric synthesis.[1] However, optically active 1,3-hydroxythiols are only available from natural sources,[1] for example, as 10-sulfanylisoborneol (**1**)[2] from camphor, and little attention has been focused on their synthesis.[3] The stereoselective construction of contiguous stereogenic centers in acyclic compounds is generally difficult compared to that in cyclic systems. For example, the asymmetric synthesis of cyclic systems with three contiguous stereogenic carbon centers by tandem conjugate addition to bis(α,β-unsaturated ester)s[4] and the tandem Michael–aldol cyclization of acyclic ω-oxo-α,β-unsaturated esters and ketones has been developed sufficiently.[5] Despite the sophisticated methodology of double aldol reactions[6] and of the catalytic hydrogenation of enamino ketones,[7] one-step stereocontrol of three contiguous stereogenic centers in acyclic compounds still remains a challenge for asymmetric synthesis, and the one-step asymmetric conversion of acyclic α,β-unsaturated ketones into acyclic compounds with three contiguous stereogenic carbon centers was previously unknown. We report herein the highly stereoselective construction of three contiguous stereogenic centers in a tandem Michael addition and Meerwein–Ponndorf–Verley (MPV) reduction of the α,β-unsaturated ketones **2** with (−)-**1** to give the alcohols **3**, thus allowing the asymmetric synthesis of 1,3-hydroxythiols **4** (Scheme 1).

We proposed that the tandem reaction[8] described above for the α,β-disubstituted α,β-unsaturated ketones **2** would involve asymmetric protonation[9] at the α-position in the Michael addition step and that the products **3** could be converted into the optically active 1,3-hydroxythiols **4** through a Wagner–Meerwein rearrangement followed by a thiol-exchange reaction.[9] The tandem reactions of the ketones **2** (R^1 = Ar, R^2 = alkyl, R^3 = Ph) are summarized in Table 1.



Scheme 1. Proposed tandem Michael addition–MPV reduction.

Table 1: Tandem Michael–MPV reaction of the α,β-unsaturated ketones **2**.



2 **3A** **3B**

Entry	**2**	R^1	R^2	*t* [days][a]	Yield [%][b]	**3A**/**3B**[c]
1	**a**	Ph (*E*)	Me	3	82	92:8
2	**a**	Ph (*Z*)	Me	3	79	93:7
3	**a**	Ph (*E*/*Z* 4.7:1)	Me	2	92	94:6
4	**b**	4-MePh	Me	2	86	93:7
5	**c**	4-(MeO)Ph	Me	2	67	94:6
6	**d**	4-ClPh	Me	2	87	94:6
7	**e**	Ph	Et	2	60	97:3
8	**f**	4-MePh	Et	2	68	93:7
9	**g**	4-MeOPh	Et	2	67	94:6
10	**h**	4-ClPh	Et	2	60	96:4
11	**i**	Ph	Pr	3	44	100:0
12	**j**	Ph	Bn	3	37	100:0

[a] Reaction time. [b] Yield of isolated product. [c] Ratio determined by ^{1}H NMR spectroscopy.

The reactions of both the *E*- and the *Z*-α-methylated chalcones **2a** with (−)-**1** and Me_2AlCl at room temperature for 3 days gave mixtures of **3A** and **3B** with high diastereoselectivity (≈93:7; Table 1, entries 1 and 2). These selectivities were almost identical to that observed in the reaction of an *E*/*Z* mixture of **2a** (Table 1, entry 3). When a sample of **2a** with homogeneous stereochemistry was used and the reaction was quenched after just 1 or 2 hours, an *E*/*Z* mixture of **2a** was recovered. This isomerization might result from reversible conjugate addition of the thiol **1**.[8] The substrates **2** in entries 4–12 of Table 1 were used as an *E*/*Z* mixture (major isomer: *E*). The electronic effects of the R^1 group on the selectivity were not significant (Table 1, entries 4–6 and 8–10). With increasing bulkiness of the R^2 group the diastereomeric ratios of the products **3** increased to 100:0 and the yields decreased (Table 1, entries 3, 7, 11, and 12).

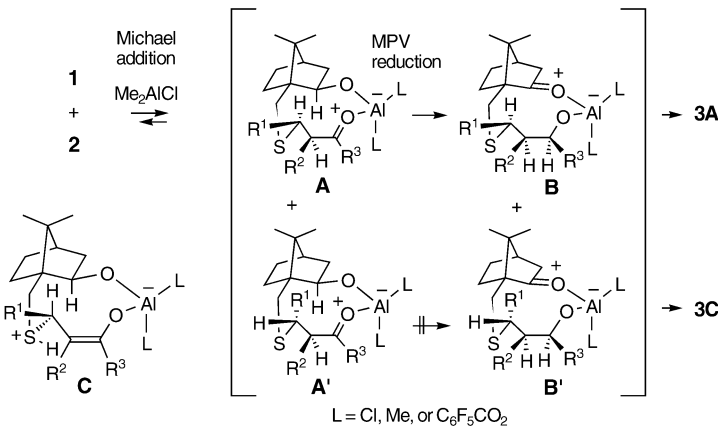
In each case the isomers **3A** and **3B** were the only products of the tandem reaction among the eight possible isomers, Table 1. It was suggested that this tandem reaction was controlled by dynamic kinetic resolution[8] involving the reversible Michael addition of the hydroxythiol **1** (Scheme 2). That is, the rate-determining step in the tandem reaction is the intramolecular MPV reduction of the Michael adducts **A** and

[*] Prof. Dr. M. Node, Prof. Dr. K. Nishide, M. Ozeki, H. Kunishige, Y. Shigeta, Dr. P. K. Patra, Dr. Y. Hagimoto
Department of Pharmaceutical Manufacturing Chemistry
Kyoto Pharmaceutical University
Misasagi, Yamashina, Kyoto 607-8414 (Japan)
Fax: (+81) 75-595-4775
E-mail: node@mb.kyoto-phu.ac.jp

[**] We are grateful to the Ministry of Education, Culture, Sports, Science, and Technology of Japan for partial support of this research [Grant-in-Aid for Scientific Research (B) (13470474)]. P.K.P. acknowledges the JSPS for a postdoctoral fellowship.

Supporting information for this article is available on the WWW under http://www.angewandte.org or from the author.

 DOI: 10.1002/anie.200351915 © 2003 Wiley-VCH Verlag GmbH & Co. KGaA, Weinheim

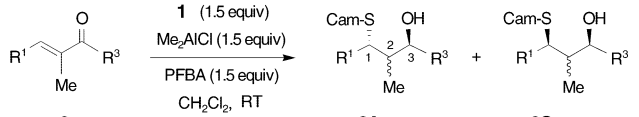


Scheme 2. A plausible mechanism.

A′. The steric congestion caused by the substituent R^1 on the chelated 10-membered ring in the adduct **A**′ results in the higher transition-state energy of **A**′ relative to that of the adduct **A** in which the R^1 group is in a more favorable orientation. Therefore, the stereoselectivity observed at C1 and C3 is based on the degree of kinetic control in the MPV reduction step, and the high stereoselectivity observed at C2 may be attributed to intramolecular protonation[9] in the aluminum enolate **C**, which bears a hydrosulfonium cation formed by the conjugate addition of the thiol **1** to the enone **2**.

Next, we examined the tandem reaction of other kinds of α,β-unsaturated ketones **2** (R^1 = Ar, R^2 = Me, R^3 = alkyl; Table 2). When the same reaction conditions were used as those for the reactions in Table 1, the products **3A** were formed with low to medium diastereomeric ratios (Table 2, entries 1, 3, and 5). To improve the diastereoselectivity, the effect of additives in the tandem reaction of **2m** was investigated. The addition of 1 equivalent of pyridine to the reaction medium improved the stereoselectivity **3m-A/3m-B** to 94:6, but the yield decreased to 6%. On the other hand, the addition[10] of trifluoroacetic acid (TFA; 1 equiv) led to an increase in both the yield (40%) and the stereoselectivity (**3m-A/3m-B** 94:6). However, in this case two additional diastereomers, **3m-C** (1.8%) and **3m-D** (2.2%), with the opposite configuration at C1, were also produced in the reaction. The relationship between the pK_a value of various acids used as additives and the yield of **3m** is plotted in Figure 1. Pentafluorobenzoic acid (PFBA; pK_a ≅2) was the most effective. From the results shown in Figure 2, the optimum amount of PFBA was determined to be 1.5 equivalents. The tandem reactions of (*E*)-**2k–q** in the presence of PFBA were investigated (Table 2, entries 2, 4, and 6–10). The reactions of the ketones **2l–q**, which have bulkier R^3 groups, exhibited higher diastereoselectivities in terms of the ratio **3A/3B** (d.r. ≥96:4) than the reaction of **2k**, which has an ethyl substituent.

Table 2: Effect of an additive in the tandem Michael–MPV reaction of the α,β-unsaturated ketones **2**.



2 **3A**: 2β-Me **3B**: 2α-Me **3C**: 2β-Me **3D**: 2α-Me

Entry	**2**	R^1	R^3	*t* [days][a]	Yield[b] (ratio)[c] **3A/3B**	**3C/3D**
1[d]	**k**	Ph	Et	2.5	78 (58:42)	–
2	**k**			2	71 (73:27)	14 (100:0)
3[d]	**l**	Ph	*i*Pr	3	46 (74:26)	–
4	**l**			2	55 (98:2)	10 (53:47)
5[d]	**m**	Ph	*c*-C_6H_{11}	3	31 (80:20)	–
6	**m**			3	50 (98:2)	5 (58:42)
7	**n**	Ph	*c*-C_7H_{13}	2	55 (100:0)	7 (66:34)
8	**o**	4-(MeO)Ph	*i*Pr	2	52 (97:3)[e]	6 (47:53)[e]
9	**p**	4-ClPh	*i*Pr	2	51 (96:4)	8 (58:42)
10	**q**	4-MePh	*i*Pr	2	55 (99:1)	8 (54:46)

[a] Reaction time. [b] Yield of the mixture of isolated products. [c] Determined by ^{1}H NMR spectroscopy. [d] PFBA was not added. [e] Each diastereomer was isolated by HPLC.

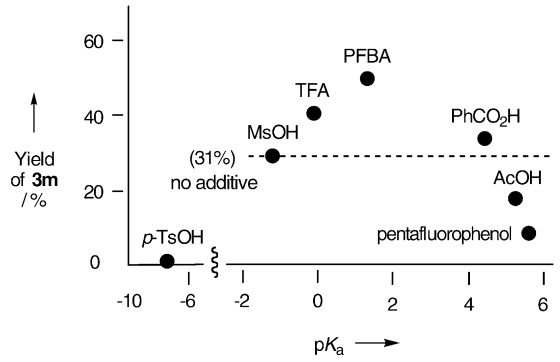


Figure 1. The relationship between pK_a of the additive and yield.

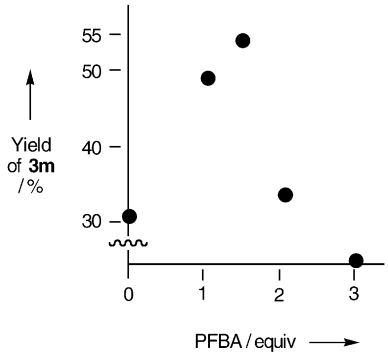


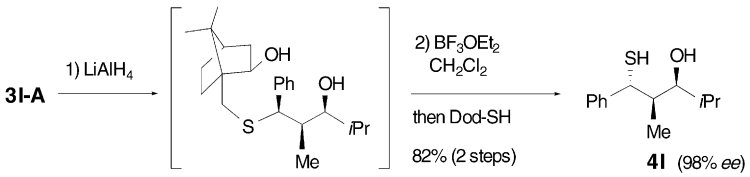
Figure 2. The relationship between yield and the amount of PFBA used.

We assume that PFBA replaces the remaining methyl group on the aluminum ate complex **A** (Scheme 2), which causes an increase in the reaction rate of the MPV reduction. Kinetic control becomes less strict at room temperature through this ligand exchange, such that the additional isomers **3C** and **3D** are produced, whereas the selectivity for **3A** over **3B** might be increased through a tighter MPV transition state favored by the resulting more reactive Al complex.

Transformation[9] of the major product **3l-A** into the 1,3-hydroxythiols **4l** could be carried out readily in good yield.

 © 2003 Wiley-VCH Verlag GmbH & Co. KGaA, Weinheim

Thus, the Wagner–Meerwein rearrangement of the boron trifluoride etherate of the isoborneol derivative obtained by reduction of **3l-A**, followed by a thiol-exchange reaction in the presence of odorless 1-dodecanethiol (Dod-SH),[11] gave **4l** with 98% *ee* (Scheme 3).



Scheme 3. Synthesis of an optically active 1,3-hydroxythiol.

Although the exact role of PFBA is unclear at this stage, the discovery of PFBA as an additive with an optimum pK_a value will be helpful for the fine tuning of reactions that involve an aluminum ate complex. In conclusion, we have reported the asymmetric transformation of the acyclic α,β-unsaturated ketones **2** into the 1,3-hydroxythiols **4** through the stereocontrol of three contiguous stereogenic centers.

Experimental Section

Typical procedure: Dimethylaluminum chloride (solution in hexane, 1.05 M, 0.51 mL, 0.54 mmol) was added dropwise to a solution of (−)-10-sulfanylisoborneol ((−)-**1**; 100 mg, 0.54 mmol) in dichloromethane (20 mL) at 0 °C. The reaction mixture was stirred for 0.5 h, then a solution of **2** (0.36 mmol) in dichloromethane (5 mL) was added dropwise (followed by a solution of an additive (0.54 mmol) in dichloromethane (7 mL), if used), and the mixture was stirred at room temperature under a nitrogen atmosphere for the time indicated. The reaction was then quenched with a saturated solution of ammonium chloride, and the aqueous layer was extracted with ethyl acetate. The combined organic layers were washed (if an additive was used: with a saturated solution of sodium hydrogen carbonate, then with brine; in the absence of an additive: with brine), and were dried over magnesium sulfate, filtered, and concentrated in vacuo. Purification of the residue by silica-gel column chromatography (hexane/ethyl acetate 10:1–20:1) gave **3** as a diastereomeric mixture in the yield indicated. The diastereomers of **3** were separated by recycling HPLC.

Received: May 16, 2003 [Z51915]

Keywords: asymmetric synthesis · domino reactions · Michael addition · reduction · synthetic methods

[1] a) E. L. Eliel, J. E. Lynch, W. R. Kenan, Jr., *Tetrahedron Lett.* **1981**, *22*, 2855–2858; b) J. E. Lynch, E. L. Eliel, *J. Am. Chem. Soc.* **1984**, *106*, 2943–2948; c) E. L. Eliel, J. E. Lynch, F. Kume, S. V. Frye, *Org. Synth.* **1987**, *65*, 215–223; d) K. Utimoto, A. Nakamura, S. Matsubara, *J. Am. Chem. Soc.* **1990**, *112*, 8189–8190; e) H. Nakano, Y. Okuyama, H. Hongo, *Tetrahedron Lett.* **2000**, *41*, 4615–4618; f) S, Matsubara, Y. Kasuga, T. Yasui, M. Yoshioka, B. Yamin, K. Utimoto, K. Oshima, *Chirality* **2003**, *15*, 38–40; g) V. K. Aggarwal, J. G. Ford, S. Fonquerna, H. Adams, R. V. H. Jones, R. Fieldhouse, *J. Am. Chem. Soc.* **1998**, *120*, 8328–8339; h) V. K. Aggarwal, A. Lattanzi, D. Fuentes, *Chem. Commun.* **2002**, 2534–2535, and references therein.

[2] E. L. Eliel, W. J. Frazee, *J. Org. Chem.* **1979**, *44*, 3598–3599.

[3] H. Shiraki, K. Nishide, M. Node, *Tetrahedron Lett.* **2000**, *41*, 3437–3441.

[4] a) S. Saito, Y. Hirohara, O. Narahara, T. Moriwake, *J. Am. Chem. Soc.* **1989**, *111*, 4533–4535; b) T. Uyehara, N. Shida, Y. Yamamoto, *J. Org. Chem.* **1992**, *57*, 3139–3145; c) N. Shida, T. Uyehara, Y. Yamamoto, *J. Org. Chem.* **1992**, *57*, 5049–5051.

[5] a) M. Ihara, K. Makita, Y. Tokunaga, K. Fukumoto, *J. Org. Chem.* **1994**, *59*, 6008–6013; b) K. Takasu, M. Ueno, M. Ihara, *J. Org. Chem.* **2001**, *66*, 4667–4672; c) C. Schneider, O. Reese, *Chem. Eur. J.* **2002**, *8*, 2585–2594; d) K. Yagi, T. Turitani, H. Shinokubo, K. Oshima, *Org. Lett.* **2002**, *4*, 3111–3114; e) D. F. Cauble, J. D. Gipson, M. J. Krische, *J. Am. Chem. Soc.* **2003**, *125*, 1110–1111; f) K. Nishimura, H. Tsubouchi, M. Ono, T. Hayama, Y. Nagaoka, K. Tomioka, *Tetrahedron Lett.* **2003**, *44*, 2323–2326.

[6] A. Abiko, T. Inoue, S. Masamune, *J. Am. Chem. Soc.* **2002**, *124*, 10759–10764, and references therein.

[7] D. G. Melillo, R. J. Cvetovich, K. M. Ryan, M. Sletzinger, *J. Org. Chem.* **1986**, *51*, 1498–1504.

[8] a) K. Nishide, Y. Shigeta, K. Obata, M. Node, *J. Am. Chem. Soc.* **1996**, *118*, 13103–13104; b) M. Node, K. Nishide, Y. Shigeta, H. Shiraki, K. Obata, *J. Am. Chem. Soc.* **2000**, *122*, 1927–1936.

[9] K. Nishide, S. Ohsugi, H. Shiraki, H. Tamakita, M. Node, *Org. Lett.* **2001**, *3*, 3121–3124.

[10] K. G. Akamanchi, N. R. Varalakshmy, *Tetrahedron Lett.* **1995**, *36*, 3571–3572.

[11] M. Node, K. Kumar, K. Nishide, S. Ohsugi, T. Miyamoto, *Tetrahedron Lett.* **2001**, *42*, 9207–9210.

 © 2003 Wiley-VCH Verlag GmbH & Co. KGaA, Weinheim

O-Atom Transfer in Fe Complexes

Thermally Induced Stoichiometric and Catalytic O-Atom Transfer by a Non-Heme Iron(III)–Nitro Complex: First Example of Reversible $\{Fe–NO\}^7 \leftrightarrow Fe^{III}\text{-}NO_2$ Transformation in the Presence of Dioxygen**

*Apurba K. Patra, Raman K. Afshar, John M. Rowland, Marilyn M. Olmstead, and Pradip K. Mascharak**

In recent years, a few Fe[1] and Co[2] porphyrin complexes with a bound nitro group have been employed to transfer an oxygen atom to substrates such as PPh_3, Me_2S, and styrene.

[*] Prof. Dr. P. K. Mascharak, Dr. A. K. Patra, R. K. Afshar, Dr. J. M. Rowland
Department of Chemistry and Biochemistry
University of California
Santa Cruz, CA 95064 (USA)
Fax: (+1) 831-459-2935
E-mail: pradip@chemistry.ucsc.edu
Dr. M. M. Olmstead
Department of Chemistry
University of California
Davis, CA 95616 (USA)

[**] Financial support from NIH (GM 61636) is gratefully acknowledged. The Bruker SMART 1000 diffractometer was funded in part by an NSF Instrumentation Grant CHE-9808259.

 DOI: 10.1002/anie.200352070 © 2003 Wiley-VCH Verlag GmbH & Co. KGaA, Weinheim

Other transition-metal nitro complexes[3] have also been successfully used in stoichiometric and catalytic O-atom transfer to CS_2, CO, alcohols, and alkenes. However, no non-heme iron complex with a bound nitrite group has been shown to perform O-atom transfer to any such substrate. In this paper we report the first non-heme Fe^{III} complex $[(PaPy_3)Fe(NO_2)](ClO_4)$ (**1**) derived from the *N*,*N*-bis-(2-pyridylmethyl)amine-*N*-ethyl-2-pyridine-2-carboxamide ligand ($PaPy_3H$ = *N*-[*N*,*N*-bis(2-pyridylmethyl)aminoethyl]-2-pyridinecarboxamide; H is the dissociable amide proton), which promotes stoichiometric and catalytic O-atom transfer to PPh_3 under mild conditions. We also report that the {Fe–NO}^{7}-type species $[(PaPy_3)Fe(NO)](ClO_4)$ (**2**) is the intermediate in the nitrite-to-nitrosyl conversion following O transfer to PPh_3. Since **2** is rapidly converted into **1** via electrophilic attack of dioxygen to the coordinated NO in **2**, the O-atom transfer reaction can be made catalytic in an atmosphere of dioxygen. We also report that in absence of dioxygen, the {Fe–NO}^{7} intermediate **2** is converted into the μ-oxo diiron(III) species $[(PaPy_3)FeOFe(PaPy_3)](ClO_4)_2$ (**3**) via a disproportionation reaction, as reported by Lippard and co-workers.[4] Complex **3** is the final product obtained from the O-atom transfer reaction.

Complex **1** has been synthesized by the addition of $[Fe(dmf)_6](ClO_4)_3$ to a mixture of $PaPy_3H$ and NEt_3 (1:1) in MeCN following the addition of $NaNO_2$. Coordination of the deprotonated carboxamido nitrogen atom to the Fe^{III} center is indicated by a red shift in the position of ν_{CO} (1634 compared to 1666 cm^{-1} for the free ligand). Complex **1** displays a rhombic EPR spectrum with *g* values at 2.347, 2.212, and 1.902. This large anisotropy is typical of the $(t_{2g})^5$ configuration for low-spin Fe^{III} ($S = 1/2$) centers, due to strong the spin–orbit interaction of the "hole" in the t_{2g} subshell.[5] The structure of the cation of **1** is shown in Figure 1;[6] the Fe^{III} center is in a distorted octahedral geometry. Three pyridine N atoms and the *tert*-amine N atom comprise the equatorial plane while the carboxamido N atom occupies one of the axial positions. The N-bound NO_2^- ligand is positioned *trans* to the carboxamido N atom; the length of the $Fe–N_{(amide)}$ bond is 1.8563(13) Å. This value is very close to the $Fe–N_{(amide)}$ distances noted in the $[(PaPy_3)Fe(X)]^+$ ($X = Cl^-$, CN^-) species.[7] The oxygen atoms of the nitro group are disordered and were refined with 0.752(5) occupancy for one set (O2A and O3A) and 0.248(5) occupancy for the other set (O2B and O3B) of oxygen atoms. The average Fe-N-O angles are 116.31(6)° and 120.90(6)°, while the average $Fe–N_{(py)}$ and $Fe–N_{(amine)}$ bond lengths are 1.9713(14) and 1.9847(14) Å, respectively.

The {Fe–NO}^{7} intermediate, complex **2**, has been independently synthesized by reacting one equivalent of NO(g) with a mixture of $PaPy_3H$, NEt_3, and $[Fe(MeCN)_4](ClO_4)_2$ (1:1:1) in thoroughly degassed MeCN. The IR spectrum of the dark brown-red solid displays ν_{NO} at ~1613 cm^{-1}, a value comparable to other {Fe–NO}^{7}-type complexes. The X-band EPR spectrum displays a strong signal at $g \approx 2.002$ indicating an $S = 1/2$ electronic ground state. The structure of $[(PaPy_3)Fe(NO)]^+$, the cation of complex **2**, is shown in Figure 2.[8] The distorted octahedral geometry around the iron center in this {Fe-NO}^{7} nitrosyl is similar to that observed in **1**. The Fe–N(O) bond length is 1.7515(16) Å and the Fe-N-O angle is 141.29(15)°. Both the Fe–N(O) distance and the smaller Fe-N-O angle of **2** are typical of the {Fe–NO}^{7} iron nitrosyl complexes.[9] The N–O bond length in **2** (1.190(2) Å) is close to that of free NO (1.15 Å) but far from that found in NO^- (1.26 Å).

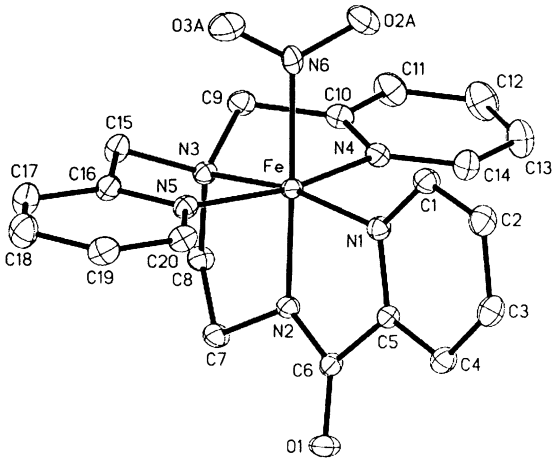


Figure 1. ORTEP diagram of $[(PaPy_3)Fe(NO_2)]^+$, the cation of **1**, showing the atom labeling scheme. All H atoms and the MeCN molecules present as solvent of crystallization have been omitted for clarity. Selected bond lengths [Å] and bond angles [°]: Fe-N1 1.9856(14), Fe-N2 1.8563(13), Fe-N3 1.9847(14), Fe-N4 1.9648(15), Fe-N5 1.9637(14), Fe-N6 2.0436(15), N6-O2(av) 1.240(5), N6-O3(av) 1.182(5); Fe-N6-O2(av) 116.31(6), Fe-N6-O3(av) 120.90(6), N6-Fe-N2 175.18(6), N1-Fe-N2 83.05(6), N1-Fe-N3 168.77(6), N1-Fe-N4 97.15(6), N1-Fe-N5 96.31(6), N2-Fe-N3 85.78(6), N2-Fe-N4 96.21(6), N2-Fe-N5 88.13(6), N3-Fe-N4 82.80(6), N3-Fe-N5 84.53(6), N3-Fe-N6 96.68(6), N4-Fe-N5 166.26(6), N4-Fe-N6 88.23(6), N5-Fe-N6 87.98(6).

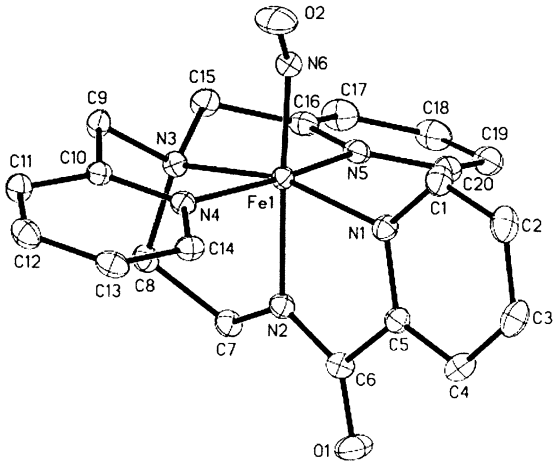


Figure 2. ORTEP diagram of $[(PaPy_3)Fe(NO)]^+$, the cation of **2**, showing the atom labeling scheme. All H atoms and the MeCN molecules present as solvent of crystallization have been omitted for clarity. Selected bond lengths [Å] and bond angles [°]: Fe-N1 1.9801(15), Fe-N2 1.9577(15), Fe-N3 1.9946(16), Fe-N4 1.9836(15), Fe-N5 1.9990(15), Fe-N6 1.7515(16), N6-O2 1.190(2); Fe-N6-O2 141.29(15), N6-Fe-N2 176.91(7), N1-Fe-N2 80.07(6), N1-Fe-N3 164.15(6), N1-Fe-N4 95.44(6), N1-Fe-N5 98.14(6), N2-Fe-N3 84.29(6), N2-Fe-N4 91.38(6), N2-Fe-N5 86.08(6), N3-Fe-N4 82.33(6), N3-Fe-N5 83.25(6), N3-Fe-N6 98.80(7), N4-Fe-N5 165.53(6), N4-Fe-N6 88.92(7), N5-Fe-N6 94.38(7).

 © 2003 Wiley-VCH Verlag GmbH & Co. KGaA, Weinheim

Complex **3**, the end product of the catalytic cycle, has been independently synthesized by allowing a stoichiometric amount of dioxygen to react with a mixture of $PaPy_3H$, NEt_3, and $[Fe(MeCN)_4](ClO_4)_2$ (1:1:1) in MeCN. The IR spectrum of **3** shows a strong band at 785 cm^{-1}, which corresponds to $\tilde{\nu}_{Fe\text{-}O\text{-}Fe}$. The structure of $[(PaPy_3)FeOFe(PaPy_3)]^{2+}$, the cation of **3**, is shown in Figure 3.[10] The high-spin ($S = 5/2$) nature of

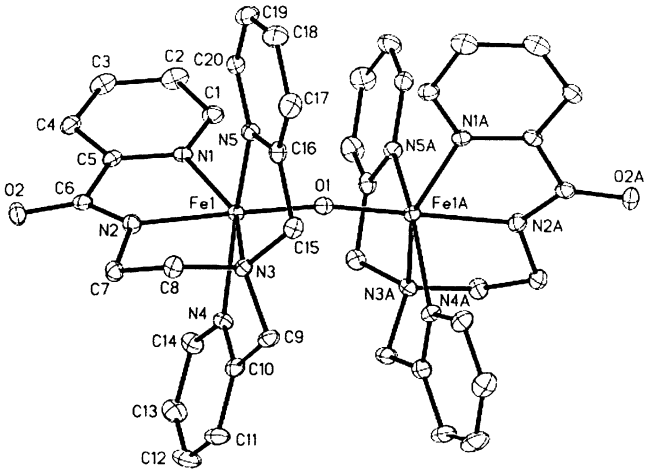
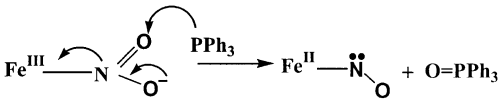


Figure 3. ORTEP diagram of $[(PaPy_3)FeOFe(PaPy_3)]^{2+}$, the cation of **3**, showing the atom labeling scheme. All H atoms and the EtOH molecules present as solvent of crystallization have been omitted for clarity. Selected bond lengths [Å] and bond angles [°]: Fe1-N1 2.144(3), Fe1-N2 2.064(4), Fe1-N3 2.200(3), Fe1-N4 2.181(3), Fe1-N5 2.169(3), Fe1-O1 1.8039(7); Fe1-O1-Fe1A 170.7(2), O1-Fe1-N2 172.19(10), N1-Fe1-N2 75.54(13), N1-Fe1-N3 154.04(13), N1-Fe1-N4 106.22(13), N1-Fe1-N5 98.54(13), N1-Fe1-O1 99.01(12), N2-Fe1-N3 79.51(13), N2-Fe1-N4 81.55(14), N2-Fe1-N5 92.53(14), N3-Fe1-N4 76.72(13), N3-Fe1-N5 75.37(13), N3-Fe1-O1 106.50(12), N4-Fe1-N5 152.07(13), N4-Fe1-O1 94.84(15), N5-Fe1-O1 93.83(13).

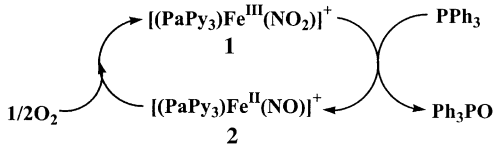
the two Fe^{III} centers in **3** is indicated by the longer Fe–N bond lengths compared to the structurally characterized low-spin Fe^{III} complexes of $PaPy_3H$ ligand. The average $Fe–N_{(py)}$ and $Fe–N_{(amine)}$ bond lengths are 2.164(3) and 2.200(3) Å, respectively, while the $Fe–N_{(amide)}$ bond is 2.064(4) Å. These bond lengths are similar to other μ-oxo diiron(III) complexes with high-spin Fe^{III} centers.[11] To the best of our knowledge, **3** is the first structurally characterized μ-oxo diiron(III) complex with amido nitrogen-atom coordination.

When a burgundy red solution of **1** in MeCN (λ_{max} = 510 nm) is warmed with PPh_3 at 45 °C under 1 atm of dioxygen, Ph_3PO is rapidly formed in the reaction mixture. Formation of Ph_3PO can be monitored by either ^{31}P NMR spectroscopy or by HPLC. The rates of O-atom transfer (K_{obs}) have been measured in MeCN in the presence of 100 equiv of PPh_3 under 1 atm of dioxygen. The psuedo-first-order rate constants are 1.12×10^{-4} and 2.65×10^{-4} s^{-1} at 45 °C and 65 °C, respectively. However, at temperatures above 65 °C, significant decomposition of **2** (leading to the formation of **3**) is observed. When **1** is heated with PPh_3 in MeCN without any added oxygen, the O-atom transfer reaction proceeds according to the equation $[(PaPy_3)Fe(NO_2)]^+ + PPh_3 \rightarrow [(PaPy_3)Fe(NO)]^+ + Ph_3PO$, and one obtains just one equivalent of Ph_3PO irrespective of the amount of PPh_3 in the reaction mixture. Under such strictly anaerobic conditions, the intermediate {Fe-NO}^{7} species **2** can be identified in the reaction mixture by UV/Vis spectroscopy by a strong band at ≈475 nm.



O-atom transfer from **1** results in an effective reduction of the metal center and generation of the {Fe–NO}^{7} species **2**. If heating is continued in absence of dioxygen, **2** eventually decomposes to the μ-oxo diiron(III) complex **3** (λ_{max} = 430 nm) presumably via a transient $\{FeNO\}_2$ species with an N–N bond, as suggested by Lippard and co-workers.[4] The **2**→**3** transformation can also be monitored by UV/Vis spectroscopy. One can isolate pure **3** from the reaction mixture after single turnover. This confirms that **3** does not promote O-atom transfer.

In MeCN, **2** reacts rapidly with dioxygen to form **1**. This nitrosyl-to-nitrite conversion in a non-heme system is unique[12] and can be easily monitored by UV/Vis spectroscopy. The reaction allows the O-atom transfer reaction to be catalytic under an atmosphere of pure dioxygen and in the presence of excess PPh_3. At 45 °C, the turnover number (TN)[13] is 37 after 1 h while at 65 °C, the TN increases to 84.[14] The overall catalytic efficiency of **1** becomes somewhat curtailed by the fact that during the **2**→**1** conversion, a small portion (< 1 %) of **2** is converted to **3** (as evidenced by UV/Vis spectroscopy) and thus the effective concentration of **1** in the reaction mixture decreases over time. Such damage can be minimized (easily monitored by the observation of the burgundy-red color of the solution) by running the O-atom transfer reaction at lower temperatures. The catalytic process can be schematically described as follows:



In summary, $[(PaPy_3)Fe(NO_2)](ClO_4)$ (**1**) is the first example of a non-heme iron–nitro species that promotes stoichiometric and catalytic O-atom transfer to PPh_3. We have also isolated and identified the intermediate $[(PaPy_3)Fe(NO)](ClO_4)$ (**2**), a {Fe–NO}^{7} species. This reversible nitrite-to-nitrosyl conversion is also the first example in non-heme iron chemistry. Formation of the μ-oxo diiron(III) complex $[(PaPy_3)FeOFe(PaPy_3)](ClO_4)_2$ (**3**) is the termination product of the catalytic cycle.

Experimental Section

1: A solution of $PaPy_3H$ (0.20 g, 0.58 mmol) in MeCN (15 mL) was added to a solution of $[Fe(DMF)_6](ClO_4)_3$ (0.46 g, 0.58 mmol) in MeCN (10 mL). Then a solution of NEt_3 (0.06 g, 0.58 mmol) in MeCN

 © 2003 Wiley-VCH Verlag GmbH & Co. KGaA, Weinheim

(7 mL) was slowly added with constant stirring. The deep-violet solution was stirred for 30 min and then solid $NaNO_2$ (0.125 g, 1.81 mmol) was added. The color of the reaction mixture changed slowly to red after 3 h, which was then filtered to remove excess $NaNO_2$ and concentrated to 15 mL. Et_2O (15 mL) was then added and the solution was stored at −20 °C for 24 h. The dark-red blocks were filtered and washed with Et_2O (0.32 g, 88 % yield). Crystals of $[(PaPy_3)Fe(NO_2)](ClO_4)\cdot 2\,MeCN$ (**4**·2 MeCN) were grown via diffusion of Et_2O into solution of the complex in MeCN at 4 °C. Elemental analysis calcd (%) for $C_{24}H_{26}ClFeN_8O_7$ (**4**·2 MeCN): C 45.77, H 4.13, N 17.78; found: C 45.71, H 4.09, N 17.71. FTIR (KBr): $\tilde{\nu} = 3065$ (w), 2958(w), 2852 (w), 2249 (m), 1636 (vs), 1607 (vs), 1470 (m), 1446 (m), 1364 (s), 1280 (m), 1090 (vs), 764 (m), 622 cm^{-1} (m). Electronic absorption spectrum in MeCN, λ_{max} (in nm) (ε in $M^{-1}cm^{-1}$): 512 (2730), 390 (sh, 2190), 360 (sh, 3900), 340 (sh, 4120).

2: A solution of $PaPy_3H$ (0.122 g, 0.35 mmol) and NEt_3 (0.05 g, 0.49 mmol) in MeCN (20 mL) was thoroughly degassed by freeze-pump-thaw cycles. Solid $[Fe(MeCN)_4](ClO_4)_2$ (0.148 g, 0.35 mmol) was added to the frozen MeCN solution, which was then allowed to warm to room temperature. The dark brown-red solution obtained was stirred for 30 min at room temperature and then cooled to 0 °C, where NO (11 mL, 0.49 mmol) was introduced to the reaction flask via a gas-tight syringe following evacuation. The resulting deep-brown reaction mixture was then stirred for 1 h. Et_2O (25 mL) was then added, and the reaction mixture was stored at −20 °C for 12 h. Dark brown-red blocks were filtered and washed with small portions of Et_2O and dried (0.135 g, 62 % yield). Elemental analysis calcd (%) for $C_{24}H_{26}ClFeN_8O_6$ (**2**·2 MeCN): C 46.96, H 4.23, N 18.25; found: C 46.86, H 4.19, N 18.24. FTIR (KBr): $\tilde{\nu} = 3072$ (w), 2942(w), 2860 (w), 2284 (w), 2249 (m), 1613 (vs), 1590 (vs), 1454 (m), 1401 (w), 1373 (w), 1284 (m), 1219 (w), 1085 (vs), 761 (m), 620 cm^{-1} (m). Electronic absorption spectrum in MeCN, λ_{max} (in nm) (ε in $M^{-1}cm^{-1}$): 830 (50), 476 (4300), 390 (sh, 3130), 370 (3170).

3: A solution of $PaPy_3H$ (0.1 g, 0.29 mmol) and NEt_3 (0.035 g, 0.35 mmol) in MeCN (10 mL) was thoroughly degassed using freeze-pump-thaw cycles. Solid $[Fe(MeCN)_4](ClO_4)_2$ (0.122 g, 0.29 mmol) was added to the frozen MeCN solution, which was then allowed to warm to room temperature. The dark brown-red solution obtained was stirred for 1 h and then pure dioxygen (6.5 mL measured with the aid of a gas-tight syringe) was added. Upon further stirring, the color of the reaction mixture changed to red-orange. Dry Et_2O (17 mL) was then added, and the mixture was stored at −20 °C for 12 h. Red-orange microcrystals of **3** were obtained by filtration and washed with Et_2O and dried (0.125 g, 85 % yield). Single crystals of $[(PaPy_3)FeO\text{-}Fe(PaPy_3)](ClO_4)_2\cdot 3\,EtOH$ (**3**·3 EtOH) suitable for diffraction studies were grown from a 1:1 (v/v) MeOH/EtOH solution by slow evaporation. Elemental analysis calcd (%) for $C_{46}H_{58}Cl_2Fe_2N_{10}O_{14}$ (**3**·3 EtOH): C 47.73, H 5.05, N 12.10; found: C 47.66, H 5.01, N 12.12. FTIR (KBr): $\tilde{\nu} = 3585$ (m), 3079(w), 2928(w), 2870 (w), 1622 (vs), 1594 (vs), 1567(s), 1486 (w), 1445 (m), 1399 (m), 1294 (m), 1094 (vs), 880(w), 784(vs), 624 cm^{-1} (m). Electronic absorption spectrum in MeCN, λ_{max} (in nm) (ε in $M^{-1}cm^{-1}$): 520 (sh, 2510), 430 (8790), 330 (11760), 248 (30660).

Conversion of **2** to **1** with dioxygen: Pure dioxygen (4 mL) was introduced into a solution of **2** (0.045 g, 0.073 mmol) in MeCN (5 mL). The initial brown-red color changed immediately to purple-red. The reaction mixture was stirred for 2 h and then stored at −20 °C following the addition of dry Et_2O (7 mL). Deep-red crystals of **1** were formed within 4 h. The crystals were filtered and washed with dry Et_2O (0.04 g, yield: 86 %).

O-atom transfer reactions: To determine the rate of the O-atom transfer reaction for **1**, a solid portion of **1** (30 mg, 0.048 mmol) was added to a solution of PPh_3 (1.26 g, 4.80 mmol) in MeCN (10 mL). The reaction mixture was kept at 45 °C (or 65 °C) under 1 atm of dioxygen. Aliquots (100 μL) were taken out every 5 min and diluted to 10 mL with MeCN:H_2O (65:35). These samples were analyzed on a Spectra-Physics UV 2000 HPLC apparatus (Grace VYDAC reverse-phase C18 column, 5 μm particle size, 250 × 4.6 mm, 20 μL loop volume, flow rate: 1 mL min^{-1}) using isocratic elution with MeCN/H_2O (65:35).[15] Retention times for Ph_3PO and Ph_3P were 3.60 and 11.05 min, respectively. The areas under the peaks were determined by running authentic samples of known concentration under identical conditions. The rate was calculated from the slope of the plot of $-\ln[PPh_3]_t/[PPh_3]_o$ versus time (t). Only a trace amount of Ph_3PO was detected when a solution of PPh_3 in MeCN (without **1**) was heated at 65 °C for 1 h under 1 atm of dioxygen.

The O-atom transfer reactions were also studied by ^{31}P NMR spectroscopy (Varian Unity Plus spectrometer). Following incubation at 65 °C for various time intervals, the reaction mixtures were evaporated to dryness and extracted with ethyl acetate. The extracts were filtered to remove the catalyst (and its decomposition products) and the filtrates were again evaporated to dryness. The residues were dissolved in $CDCl_3$ (or CD_3CN) and their ^{31}P NMR spectra were obtained using H_3PO_4 as the internal standard in coaxial tubes (δ for PPh_3: −5 ppm; for Ph_3PO: 30 ppm in $CDCl_3$).

Received: June 5, 2003 [Z52070]

Keywords: heterogeneous catalysis · iron · N ligands · nitrogen oxides · phosphanes

[1] a) L. Cheng, D. R. Powell, M. A. Khan, G. B. Richter-Addo, *Chem. Commun.* **2000**, 2301 – 2302; b) O. Q. Munro, W. R. Scheidt, *Inorg. Chem.* **1998**, *37*, 2308 – 2316; c) M. Frangione, J. Port, M. Baldiwala, A. Judd, J. Galley, M. DeVega, K. Linna, L. Caron, E. Anderson, J. A. Goodwin, *Inorg. Chem.* **1997**, *36*, 1904 – 1911; d) C. E. Castro, S. K. O'Shea, *J. Org. Chem.* **1995**, *60*, 1922 – 1923; e) M. G. Finnegan, A. G. Lappin, W. R. Scheidt, *Inorg. Chem.* **1990**, *29*, 181 – 185.

[2] a) H. Adachi, H. Suzuki, Y. Miyazaki, Y. Limura, M. Hoshino, *Inorg. Chem.* **2002**, *41*, 2518 – 2524; b) J. Goodwin, R. Bailey, W. Pennington, R. Rasberry, T. Green, S. Shasho, M. Yongsavanh, V. Echevarria, J. Tiedeken, C. Brown, G. Fromm, S. Lyerly, N. Watson, A. Long, N. D. Nitto, *Inorg. Chem.* **2001**, *40*, 4217 – 4225.

[3] a) M. A. Andrews, T. C.-T. Chang, C.-W. F. Cheng, *Organometallics* **1985**, *4*, 268 – 274; b) M. A. Andrews, T. C.-T. Chang, C.-W. F. Cheng, T. J. Emge, K. P. Kelly, T. F. Koetzle, *J. Am. Chem. Soc.* **1984**, *106*, 5913 – 5920; c) D. T. Doughty, R. P. Stewart, Jr., G. Gordon, *J. Am. Chem. Soc.* **1981**, *103*, 3388 – 3395; d) R. D. Feltham, J. C. Kriege, *J. Am. Chem. Soc.* **1979**, *101*, 5064 – 5065; e) B. S. Tovrog, S. E. Diamond, F. Mares, *J. Am. Chem. Soc.* **1979**, *101*, 270 – 272.

[4] A. L. Feig, M. T. Bautista, S. J. Lippard, *Inorg. Chem.* **1996**, *35*, 6892 – 6898.

[5] W. T. Oosterhuis, G. Lang, *Phys. Rev.* **1969**, *178*, 439 – 456.

[6] Crystal data for $[(PaPy_3)Fe(NO_2)](ClO_4)\cdot 2\,CH_3CN$ (**1**·2 CH_3CN): Red blocks, 0.22 × 0.21 × 0.12 mm^3, monoclinic, space group $P2_1/n$, $a = 13.1985(4)$, $b = 14.1008(5)$, $c = 15.3473(5)$ Å, $\beta = 103.422(8)°$, $V = 2752(16)$ Å^3, $Z = 4$, $\rho_{calcd} = 1.520$ Mg m^{-3}, $2\theta_{max} = 63°$, $\mu(Mo_{K\alpha}) = 0.704$ mm^{-1}, $\lambda = 0.71073$ Å; the data were collected at 90(2) K on a Bruker SMART 1000 diffractometer; a total of 27326 reflections were measured, of which 8816 were independent ($R_{int} = 0.054$) and included in the refinement; min/max transmission = 0.8605/0.9203; solution by direct methods (SHELXL-97, Sheldrick, **1990**); refinement by full-matrix least-squares based on F^2 (SHELXL-97, Sheldrick, **1997**); 381 parameters, $R1 = 0.0693$, $wR2 = 0.1009$ for all data; $R1 = 0.0391$ computed for 8816 observed data ($I > 2\sigma(I)$).

[7] J. M. Rowland, M. Olmstead, P. K. Mascharak, *Inorg. Chem.* **2001**, *40*, 2810 – 2817.

[8] Crystal data for $[(PaPy_3)Fe(NO)](ClO_4)\cdot 2\,CH_3CN$ (**2**·2 CH_3CN): Brown-red plates, 0.30 × 0.16 × 0.08 mm^3; monoclinic, space

 © 2003 Wiley-VCH Verlag GmbH & Co. KGaA, Weinheim

group $P2_1$, $a = 8.2530(4)$, $b = 13.9435(7)$, $c = 11.7823(6)$ Å, $\beta = 99.225(3)^{\circ}$, $V = 1338(12)$ Å^3, $Z = 2$, $\rho_{calcd} = 1.523$ Mg m^{-3}, $2\theta_{max} = 60°$, $\mu(Mo_{K\alpha}) = 0.719$ mm^{-1}, ω scans, $\lambda = 0.71073$ Å; the data were collected at 90(2) K on a Bruker SMART 1000 diffractometer; a total of 17556 reflections were measured, of which 7671 were independent ($R_{int} = 0.0305$) and included in the refinement; min/max transmission = 0.813/0.945; solution by direct methods; refinement by full-matrix least-squares based on F^2); 363 parameters, $R1 = 0.0376$, $wR2 = 0.0714$ for all data; $R1 = 0.0309$ computed for 6896 observed data ($I > 2\sigma(I)$).

[9] a) C. Hauser, T. Glaser, E. Bill, T. Weyhermuller, K. Wieghardt, *J. Am. Chem. Soc.* **2000**, *122*, 4352 – 4364; b) M. Ray, A. P. Golombek, M. P. Hendrich, G. P. A. Yap, L. M. Liable-Sands, A. L. Rheingold, A. S. Borovik, *Inorg. Chem.* **1999**, *38*, 3110 – 3115; c) D. Sellmann, N. Blum, F. W. Heinemann, B. A. Hess, *Chem. Eur. J.* **2001**, *7*, 1874 – 1880; d) D. Sellman, H. Kunstmann, M. Moll, F. Knoch, *Inorg. Chim. Acta* **1988**, *154*, 157 – 167; e) W. R. Scheidt, M. E. Frisse, *J. Am. Chem. Soc.* **1975**, *97*, 17 – 21; f) P. Berno, C. Floriani, A. Chiesi-Villa, C. Guastini, *J. Chem. Soc. Dalton Trans.* **1988**, 1409 – 1412.

[10] a) Crystal data for $[(PaPy_3)FeOFe(PaPy_3)](ClO_4)_2 \cdot 3\,EtOH$ (**3**·3 EtOH): Brown plate, $0.20 \times 0.06 \times 0.04$ mm^3; monoclinic, space group *C*2/*c*, $a = 17.649(3)$, $b = 13.383(2)$, $c = 22.371(4)$ Å, $\beta = 107.524(4)^{\circ}$, $V = 5038(15)$ Å^3, $Z = 4$, $\rho_{calcd} = 1.526$ Mg m^{-3}, $2\theta_{max} = 51°$, $\mu(Mo_{K\alpha}) = 0.758$ mm^{-1}, ω scans, $\lambda = 0.71073$ Å; the data were collected at 90(2) K on a Bruker SMART 1000 diffractometer; a total of 16306 reflections were measured, of which 4788 were independent ($R_{int} = 0.0772$) and included in the refinement; min/max transmission = 0.863/0.970; solution by direct methods; refinement by full-matrix least-squares based on F^2; 341 parameters, $R1 = 0.0940$, $wR2 = 0.1476$ for all data; $R1 = 0.0518$ computed for 3184 observed data ($I > 2\sigma(I)$); b) CCDC-211509 (**1**), -211510 (**2**), and -211511 (**3**) contains the supplementary crystallographic data for this paper. These data can be obtained free of charge via www.ccdc.cam.ac.uk/conts/retrieving.html (or from the Cambridge Crystallographic Data Centre, 12, Union Road, Cambridge CB21EZ, UK; fax: (+44) 1223-336-033; or deposit@ccdc.cam.ac.uk).

[11] A. K. Patra, M. M. Olmstead, P. K. Mascharak, *Inorg. Chem.* **2002**, *41*, 5403 – 5409.

[12] There is at least one example of such a nitrite-to-nitrosyl conversion in the case of a heme system. See reference [1a].

[13] Turnover numbers (TN) were obtained by dividing the total mass of Ph_3PO by the catalyst mass.

[14] The catalytic efficiency of the present system deserves attention since the only reported non-porphyrin system involving [Co(saloph)(py)(NO_2)] (saloph = *N*,*N*′-bisalicylidene-o-phenylenediamino) catalyzes the oxidation of PPh_3 with a TN of 8.7 after 16 h at 60 °C. See reference [3e].

[15] J. E. Haky, D. M. Baird, S. Falzone, *Anal. Lett.* **1989**, *22*, 2637 – 2651.

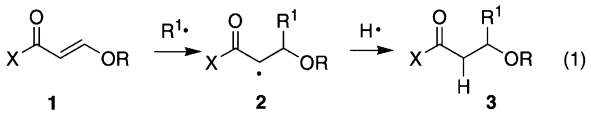
 © 2003 Wiley-VCH Verlag GmbH & Co. KGaA, Weinheim

Conjugate Radical Addition

Enantioselective Conjugate Radical Addition to β-Acyloxy Acrylate Acceptors: An Approach to Acetate Aldol-Type Products**

Mukund P. Sibi, Jake Zimmerman, and Tara Rheault*

The aldol reaction remains one of the most important reactions in synthetic organic chemistry. Many traditional ionic routes are currently available for diastereo- and enantioselective aldol reactions.[1] However, the development of radical methods for the preparation of aldols under neutral conditions is attractive.[2] With the exception of intramolecular cyclization reactions,[3] radical approaches towards aldol products remain largely unexplored.[4] We surmised that nucleophilic radical addition to β-acyloxyenoates using chiral Lewis acid catalysis could provide access to aldol products with high selectivity. A similar strategy using ionic nucleophiles is not possible because of elimination problems.[5] Herein we demonstrate for the first time an enantioselective intermolecular radical addition strategy for the synthesis of aldol acetates in high yields [Eq. (1)].



1 2 3 (1)

Our experiments began with the evaluation of the β-oxygen substituent in **4** with respect to the ease of radical addition (Table 1).[6] The addition of an isopropyl radical with and without any Lewis acid additive (100 mol% ytterbium triflate) was studied.[7] Radical addition to β-alkoxy substrates **4a** or **4b** were inefficient with or without the Lewis acid additive (entries 1 and 2). In contrast, reactions with **4c** containing an acetoxy substituent were moderately effective in the absence of the Lewis acid, and the addition of the Lewis acid resulted in a high yield of **5c** (80%, entry 3). The corresponding benzoate showed slightly higher efficiency (entry 4). In the absence of the Lewis acid, the electronic nature of the benzoyl substituent had an impact on the yield of the conjugate addition product: substrate **4e** with an electron-poor benzoyl group showed higher reactivity than **4f**

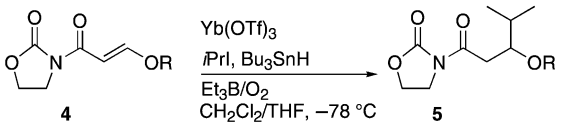
[*] Prof. M. P. Sibi, J. Zimmerman, Dr. T. Rheault
Department of Chemistry
North Dakota State University
Fargo, ND 58105–5516 (USA)
Fax: (+1) 701-231-1057
E-mail: mukund.sibi@ndsu.nodak.edu

[**] This work was supported by the National Institutes of Health (NIH-GM-54656). T.R. thanks the ACS Division of Organic Chemistry for a graduate fellowship.

Supporting information for this article is available on the WWW under http://www.angewandte.org or from the author.

 DOI: 10.1002/anie.200352096 © 2003 Wiley-VCH Verlag GmbH & Co. KGaA, Weinheim

Table 1: Effect of the acyl substituent on reactivity.[a]

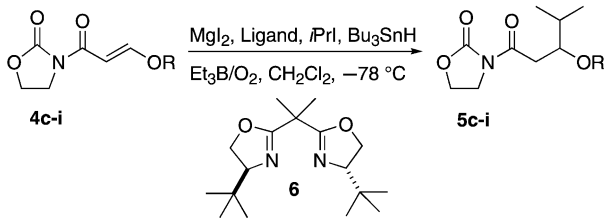


4 5

Entry	S.M.	R	Yield,[b] no Lewis acid [%]	Yield, $Yb(OTf)_3$ (1 equiv) [%]
1	**4a**	Me	0	< 2
2	**4b**	Bn	0	< 5
3	**4c**	$COCH_3$	35	80
4	**4d**	COPh	30	95
5	**4e**	4-FC_6H_4CO	40	88
6	**4f**	4-$OMeC_6H_4CO$	12	80
7	**4g**	2,6-$Me_2C_6H_3CO$	25	82
8	**4h**	1-naphthoyl	30	90
9	**4i**	2-naphthoyl	06	90

[a] For detailed reaction conditions see Supporting Information. [b] Yields are for isolated materials purified by column chromatography. S.M. = starting material, Bn = benzyl.

Table 2: Effect of the acyl group on the enantioselectivity.[a]



4c-i 5c-i 6

Entry	R	30 mol% Lewis acid[b] Yield [%]	*ee*[e] [%]	100 mol% Lewis acid[b] Yield [%]	*ee*[c] [%]
1	$COCH_3$	78	52	70	89
2	COPh	83	58(*R*)	90	93(*R*)
3	4-FC_6H_4CO	88	14	94	62
4	4-$OMeC_6H_4CO$	73	58	83	82
5	2,6-$Me_2C_6H_3CO$	88	31	82	73
6	1-naphthoyl	82	11	87	46
7	2-naphthoyl	83	12	79	80

[a] For details of the reaction conditions see the Supporting Information. [b] Yields are for isolated materials purified by column chromatography. [c] *ee* values were determined by HPLC on a chiral stationary phase.

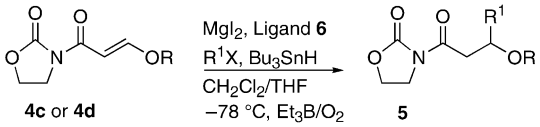
with an electron-rich substituent (compare entries 5 and 6). Other modifications did not lead to large improvements in the yield (entries 7–9). However, in reactions using the Lewis acid, the chemical yields varied only slightly with the nature of the acyloxy group.

Having found a competent acyloxy group for the radical addition, we then undertook a study to identify a chiral Lewis acid system that could provide high enantioselectivity. Magnesium Lewis acids in combination with bisoxazoline ligands were evaluated (Table 2) at two different catalytic loadings.[8] Although the reactions performed using a 30 mol% catalyst loading were chemically efficient, the enantioselection was low, regardless of the β-acyloxy substituent (Table 2). Of the different acyloxy groups examined, the acetate **4c** and the parent benzoate **4d** gave the most promising results (entries 1 and 2). Reactions using stoichiometric amounts of the chiral Lewis acids gave consistently higher levels of enantioselectivity (entries 1–7). These results demonstrate for the first time that acetate aldols can be obtained with *ee* values as high as 93% using radical chemistry.

A brief study of catalyst stoichiometry using **4d**, **6**, MgI_2, and *i*PrI showed a steady increase in the *ee* value with catalyst loading (50 mol% catalyst: 59% *ee*; 70 mol% catalyst: 80% *ee*; 90 mol% catalyst: 85% *ee*), and reached a maximum with one equivalent (93% *ee*). These results suggest that either the catalyst turnover is slow[9] or that a non-catalyzed reaction competes with the catalyzed process. It is interesting to note that increasing the catalyst loading to 150 mol% led to a small decrease in the selectivity (86% *ee*).

We have investigated the scope of the reaction with respect to the nature of the radical precursor (Table 3). The benzoate **4d** was the substrate of choice since it showed the best combination of yield and selectivity. Magnesium iodide in combination with ligand **6** was used as the chiral Lewis acid. In general, different types of radicals were chemically efficient, irrespective of their nature (primary, secondary, or tertiary) or size, with yields ranging from 70–90% (entries 1–10).[10] On the other hand, the enantioselectivity varied to some extent depending on the radical precursor. Addition of a primary ethyl radical gave **5j** with a moderate *ee* value at both 30 and 100 mol% catalyst loading (entry 1). Selectivity was

Table 3: Nucleophilic Radical Addition to **4c** or **4d**.[a]



4c or **4d** **5**

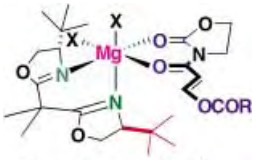
Entry	Product	R^1X	30 mol% Lewis acid Yield[b] [%]	*ee*[c] [%]	100 mol% Lewis acid Yield[b] [%]	*ee*[c] [%]
1	**5j**	CH_3CH_2I	82	33	90	50
2	**5k**	CH_3OCH_2Br	77	04	70	80
3	**5d**	*i*PrI	83	58(*R*)	90	93(*R*)
4	**5l**	CyI	75	52	70	84
5	**5m**	*t*BuI	91	46(*R*)	91	89(*R*)
6[d]	**5n**	*t*BuI	70	30	73	95
7	**5o**	1-AdI	73	02	76	60
8[d]	**5p**	1-AdI	92	02	92	57
9	**5q**	$ClCH_2CH_2CH_2(CH_3)_2CBr$	71	08	76	50
10[d]	**5r**	$ClCH_2CH_2CH_2(CH_3)_2CBr$	75	62	70	89

[a] For details of the reaction conditions see the Supporting Information. [b] Yields are for isolated materials purified by column chromatography. [c] *ee* values were determined by HPLC on a chiral stationary phase. [d] Acetate substrate **4c** was used for this reaction. Cy = cyclohexyl, Ad = adamantyl.

 © 2003 Wiley-VCH Verlag GmbH & Co. KGaA, Weinheim

higher in the reaction with the methoxymethyl radical using stoichiometric amounts of the chiral Lewis acid (80% *ee*, entry 2). Acyclic and cyclic secondary radicals gave high selectivity (93 and 84% *ee*, respectively) in the conjugate addition (entries 3 and 4). Bulky tertiary radicals (*tert*-butyl and adamantyl) were equally effective in the conjugate addition. Of these two, the addition of *tert*-butyl radicals gave higher selectivity (compare entries 5 and 7; 89 and 60% *ee*, respectively). The addition of a tertiary radical to the acetate **4c** was investigated to determine if the size of the acyloxy group had an impact on the selectivity. There was a significant improvement in the selectivity of *tert*-butyl radical addition (compare entries 5 and 6) but not of adamantyl radical addition (compare entries 7 and 8). A functionalized tertiary radical amenable for the formation of six-membered rings gave good yields in the conjugate addition (entries 9 and 10). More interestingly, the use of the acetate **4c** gave a dramatic increase in selectivity (compare entries 9 and 10; 50 and 89% *ee*, respectively). These results demonstrate that the acyloxy group can be tuned to provide improvements in reactivity as well as selectivity.

We have determined the absolute stereochemistry of **5d** and **5m** by hydrolysis and conversion into known compounds.[11] Assuming there is a tetrahedral or *cis*-octahedral geometry around the magnesium center,[12] the product stereochemistry is consistent with *si*-face radical addition to an s-*cis* conformer of the substrate. This is the same sense of



Stereochemical Model

selectivity as that obtained with oxazolidinone crotonates or cinnamates, which suggests that the rotamer geometry of the differentially substituted enoates is the same. The need for a stoichiometric amount of the chiral Lewis acid to obtain high selectivity with **4** is in contrast to the successful catalytic reactions with crotonates, and is most likely a reflection of the presence of an additional donor atom in the substrate.[9]

In conclusion we have described a novel radical-based methodology for the synthesis of aldol acetates with high enantioselectivity. Experiments are underway to investigate alternative protocols for carrying out the reactions using catalytic amounts of the Lewis acid and also to extend the methodology to more-complex substrates with α substituents.

Received: June 10, 2003 [Z52096]
Published Online: September 8, 2003

Keywords: acrylates · asymmetric catalysis · enantioselectivity · Lewis acids · radical reactions

[1] For general information on aldol reactions, see a) *Modern Carbonyl Chemistry* (Ed.: J. Otera), Wiley-VCH, Weinheim, **2000**, p. 539; for recent reviews, see b) B. Alcaide, P. Almendros, *Eur. J. Org. Chem.* **2002**, 1595; c) T. D. Machajewski, C.-H. Wong, *Angew. Chem. Int. Ed.* **2000**, *39*, 1352; *Angew. Chem.* **2000**, *112*, 1406; d) S. J. Nelson, *Tetrahedron: Asymmetry* **1998**, *9*, 357; e) J. S. Johnson, D. A. Evans, *Acc. Chem. Res.* **2000**, *33*, 325.

[2] For selected enantioselective methods for acetate aldol synthesis, see a) B. M. Trost, H. Ito, *J. Am. Chem. Soc.* **2000**, *122*, 12003; b) Y. M. A. Yamada, N. Yoshikawa, H. Sasai, M. Shibasaki, *Angew. Chem.* **1997**, *109*, 1942; *Angew. Chem. Int. Ed. Engl.* **1997**, *36*, 1871; c) B. List, R. A. Lerner, C. F. Barbas III, *J. Am. Chem. Soc.* **2000**, *122*, 2395; d) R. A. Singer, E. M. Carreira, *J. Am. Chem. Soc.* **1995**, *117*, 12360.

[3] a) M. P. Sibi, N. A. Porter, *Acc. Chem. Res.* **1999**, *32*, 163; b) M. P. Sibi, T. R. Rheault in *Radicals in Organic Synthesis* (Eds.: P. Renaud, M. P. Sibi), Wiley-VCH, Weinheim, **2001**, chap. 4.5; c) M. P. Sibi, S. Manyem, *Tetrahedron* **2000**, *56*, 8033.

[4] For chiral auxiliary mediated intermolecular radical reactions leading to aldol-like products, see a) P. Garner, R. Leslie, J. T. Anderson, *J. Org. Chem.* **1996**, *61*, 6754; b) P. Garner, J. T. Anderson, P. B. Cox, S. J. Klippenstein, R. Leslie, N. Scardovi, *J. Org. Chem.* **2002**, *67*, 6195; c) P. Garner, J. T. Anderson, *Org. Lett.* **1999**, *1*, 1057; for radical reactions leading to the formation of β-oxygenated acetate-like products, see d) Y. Guindon, R. C. Denis, *Tetrahedron Lett.* **1998**, *39*, 339; e) E. Lee, J. S. Tae, C. Lee, C. M. Park, *Tetrahedron Lett.* **1993**, *34*, 4831; f) E. Lee, S.-K. Yoo, H. Choo, H. Y. Song, *Tetrahedron Lett.* **1998**, *39*, 317; g) P. A. Evans, V. S. Murthy, J. D. Roseman, A. L. Rheingold, *Angew. Chem.* **1999**, *111*, 3370; *Angew. Chem. Int. Ed.* **1999**, *38*, 3175; h) E. Lee, S. J. Choi, *Org. Lett.* **1999**, *1*, 1127.

[5] For multiple examples of the stability of β-alkoxy groups to elimination, see a) C. P. Jasperse, D. P. Curran, T. L. Fevig, *Chem. Rev.* **1991**, *91*, 1237; b) E. Lee, C. M. Park, J. S. Yun, *J. Am. Chem. Soc.* **1995**, *117*, 8017, and references therein.

[6] For the synthesis of the starting materials and characterization data see the Supporting Information.

[7] For general information and reaction details for Lewis acid mediated conjugate radical addition, see M. P. Sibi, J. Ji, J. B. Sausker, C. P. Jasperse, *J. Am. Chem. Soc.* **1999**, *121*, 7517 see also P. Renaud, M. Gerster, *Angew. Chem.* **1998**, *110*, 2704; *Angew. Chem. Int. Ed.* **1998**, *37*, 2562.

[8] In addition to ligand **6**, we have evaluated bisoxazolines derived from amino indanol and phenyl glycinol and found them to be less efficient with respect to selectivity. Of the four magnesium Lewis acids tested (bromide, iodide, perchlorate, and triflimide), the iodide gave the best results in combination with **6**.

[9] The aldol product containing donor atoms may not readily dissociate from the chiral Lewis acid and thus compete for coordination with the substrate. This explanation is consistent with the need for stoichiometric amounts of the chiral Lewis acid to obtain high *ee* values. REACT IR studies provide additional support for our explanation. These results will be reported later.

[10] In reactions where radical addition is inefficient, triethylborane can participate and provide minor amounts of a product derived from ethyl radical addition.

[11] See Supporting Information.

[12] For a discussion on the geometry of the reactive complex, see a) M. P. Sibi, J. Ji, J. H. Wu, S. Gürtler, N. A. Porter, *J. Am. Chem. Soc.* **1996**, *118*, 9200; b) M. P. Sibi, J. Ji, *J. Org. Chem.* **1997**, *62*, 3800; c) M. P. Sibi, M. Liu, *Curr. Org. Chem.* **2001**, *5*, 719.

 © 2003 Wiley-VCH Verlag GmbH & Co. KGaA, Weinheim

Active Catalysts in Alkene Metathesis

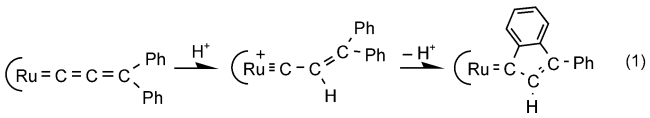
Highly Active Catalysts in Alkene Metathesis: First Observed Transformation of Allenylidene into Indenylidene via Alkenylcarbyne—Ruthenium Species**

*Ricardo Castarlenas and Pierre H. Dixneuf**

Dedicated to Professor Jean-Pierre Genet, on the occasion of his 60th Birthday

Alkene metathesis has recently led to remarkable applications in organic synthesis as well as in polymer science through ring-opening-metathesis polymerization (ROMP).[1] Since the advent of functional group tolerant ruthenium alkylidene catalysts,[2] this reaction has reached a tremendous level of development for the production of a variety of macromolecules with both C=C bonds and functional groups regularly placed.[3] Ruthenium catalysts for alkene metathesis are not restricted to alkylidene precursors of type $L_nRu{=}CHR$. The ionic 18 electron ruthenium allenylidene complexes $[RuCl(=C{=}C{=}CAr_2)(PR_3)(p\text{-cymene})][X]$[4] ($X = PF_6$, BPh_4, CF_3SO_3) promote ring-closing metathesis (RCM) of dienes and enynes[5] as well as ROMP.[6] Indenylidene derivatives of type $RuCl_2(PCy_3)(L)$(indenylidene) ($L = PCy_3$, imidazolylidene), expected to result from the corresponding allenylidene although this has not been fully demonstrated, have also shown good activity in RCM.[7] Werner and co-workers reported that coordinatively unsaturated ionic carbyne ruthenium precursors,[8] and especially hydridocarbyne ruthenium complexes,[9] are active in ROMP of cyclooctene and cross-metathesis.

Tremendous efforts are currently made to produce more efficient and stable catalysts to decrease the process cost and the level of metal traces in fine chemicals and polymers.[10] Herein we report the first observation that alkenylcarbyne ruthenium intermediates, easily obtained from allenylidene ruthenium arene complexes, are the key intermediates for metal–indenylidene complex formation [Eq. (1)] and that the latter show impressive turn-over frequencies (TOFs) for the polymerization of cyclooctene and cyclopentene under mild conditions as well as RCM reactions.



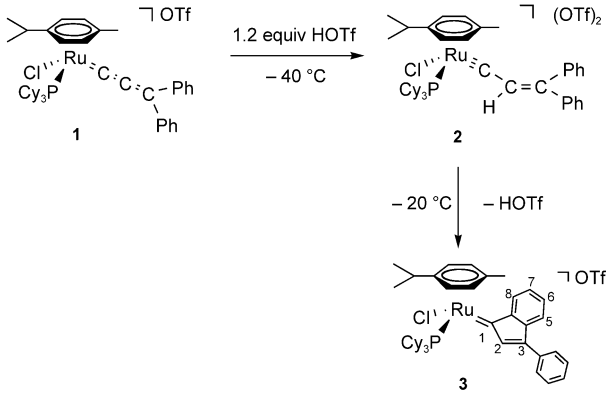
(1)

In the course of our study on cyclooctene polymerization promoted by allenylidene ruthenium(II) complexes, we have observed that the addition of a strong acid to the initiator $[RuCl(=C{=}C{=}CPh_2)(PCy_3)(\eta^6\text{-}p\text{-cymene})][CF_3SO_3]$ (**1**) largely increases the rates of polymerization. Thus, when five equivalents of HBF_4 or CF_3SO_3H are added to catalytic solutions of **1**, TOF values increase by three orders of magnitude (Table 1, entries 1–3). To understand the nature of the catalytic species and control their synthesis, low temperature NMR studies of protonated complex **1** have been undertaken. The addition of 1.2 equivalents of triflic acid to CD_2Cl_2 solutions of **1** at −40 °C led to a change from dark red to dark orange, while a new $^{31}P\{^1H\}$ NMR signal appeared at $\delta = 78.6$ ppm during the disappearance of that of **1** at $\delta = 57.6$ ppm. The conversion was completed in 20 min at −40 °C. The $^{13}C\{^1H\}$ and ^1H NMR data are consistent with the alkenylcarbyne derivative $[RuCl(\eta^6\text{-}p\text{-cymene})(\equiv C\text{-}CH{=}CPh_2)(PCy_3)][CF_3SO_3]_2$ (**2**) resulting from protonation at the C_β of the allenylidene ligand (Scheme 1). Indeed, the $^{13}C\{^1H\}$

Table 1: Cyclooctene polymerisation at room temperature.[a]

Entry	Cat.	Ratio[b]	Acid[c]	Time	Yield	$10^{-3} \times \bar{M}_n$[d]	PDI[e]	% cis[f]	TOF[g]
1	**1**	1.000	–	15 h	95%	143	1.9	27	63
2	**1**	1.000	HBF_4 (5 equiv)	1 min	92%	224	1.7	40	55200
3	**1**	1.000	HOTf (5 equiv)	1 min	95%	238	1.6	38	57200
4	**1**	10000	HOTf (5 equiv)	5 min	97%	387	1.5	28	116400
5	**1**	100000	HOTf (100 equiv)	5 min	88%	857	1.4	35	1096000
6	**4**	10000	HOTf (5 equiv)	10 min	73%	220	1.8	25	43800
7	**5**	10000	HOTf (5 equiv)	8 h	25%	107	1.9	22	312
8	**6**	10000	HOTf (5 equiv)	5 min	92%	286	1.6	26	110000

[a] 4.5×10^{-3} mol of cyclooctene in 2.5 mL of PhCl. [b] [cyclooctene]/[Ru]. [c] Related to complex. [d] determined by GPC in THF versus polystyrene standards. [e] Polydispersity index $\bar{M}_w/\bar{M}_n$. [f] determined by ^{13}C NMR. [g] Turnover frequency in moles per hour. Cat. = catalyst.



Scheme 1. The formation of indenylidene species at low temperature.

[*] Prof. Dr. P. H. Dixneuf, R. Castarlenas
Institut de chimie de Rennes, UMR 6509 CNRS
Université de Rennes
Organométalliques et Catalyse
Campus de Beaulieu, 35042, Rennes (France)
Fax: (+33) 2-2323-6939
E-mail: pierre.dixneuf@univ-rennes1.fr

[**] This work was supported by the CNRS, the Ministère de la recherche, the European Union within the EU network Polycat (UPRN-CT-2000-10) and a Marie Curie Fellowship to RC, and the Région Bretagne with the program PRIR (No.169 AOC).

 © 2003 Wiley-VCH Verlag GmbH & Co. KGaA, Weinheim DOI: 10.1002/anie.200352108

NMR spectrum displays a doublet at 328.1 ppm ($^2J_{P\text{-}C}$ = 11 Hz) for the Ru≡C carbon and C_β (δ = 130.5 ppm) and C_γ (δ = 193.2 ppm) correlate with the olefinic proton (δ_H = 7.05 ppm) in ^1H–^{13}C HMQC and HMBC experiments, respectively. The ^1H NMR spectrum of **2** also displays two doublets at δ = 6.75 and 6.61 ppm showing the retention of the coordinated *p*-cymene ligand.

When the temperature was raised to −20 °C a new signal appeared at δ = 48.3 ppm in the $^{31}P\{^1H\}$ spectrum. Complete conversion was achieved in 30 min with a color change to violet. The nature of this intermediate was consistent with the indenylidene ruthenium complex [RuCl(η^6-*p*-cymene){=C−CH=C(Ph)C_6H_4}(PCy_3)][CF_3SO_3] (**3**) containing both PCy_3 and *p*-cymene groups (Scheme 1). Complex **3** results from phenyl substitution by the electrophilic C_α carbon of **2**, thus a contribution of the canonical form **2B** favors this rearrangement.

[Ru^+≡C−CH=CPh_2 (**2A**)↔Ru=C^+−CH=CPh_2 (**2B**)].

The $^{13}C\{^1H\}$ NMR spectrum shows a doublet ($^2J_{P\text{-}C}$ = 10 Hz) at δ = 334.1 ppm corresponding to Ru=C carbon atom as well as signals for every carbon of indenylidene group (see experimental section). The ^1H spectrum displays a singlet at δ = 6.88 ppm that correlates with C_2 (δ = 143.1 ppm) in a HMQC experiment and with C_1 and C_3 (δ = 154.6 ppm) in a HMBC experiment. Indeed, the unambiguous presence of the indenylidene ligand arises from the correlation of C_1 and H_8 of the indenylidene ligand in the HMBC experiment, which is not observed for its alkenylcarbyne precursor **2**. Four doublets between δ = 6.36 and 6.15 ppm were observed for the four arene protons of the coordinated *p*-cymene ligand. Attempts to isolate complex **3** were unsuccessful because of slow decomposition of the complex at room temperature by loss of *p*-cymene ligand and formation of [$HPCy_3$][CF_3SO_3] as observed in ^1H and $^{31}P\{^1H\}$ NMR spectra.

Whereas alkenylcarbyne osmium[11] complexes have been fully described, only two types of unstable dicationic alkenylcarbyne ruthenium intermediates were recently reported on the protonation of the corresponding allenylidene ruthenium complexes, [RuCl(≡CCH=CPh_2)(κ^2-P,O-$Cy_2PCH_2CH_2OCH_3$)(κ-P-$Cy_2PCH_2CH_2OCH_3$)][BF_4,PF_6] by Werner et al.[12] and [Cp*Ru(dippe)(≡CCH=CPh_2)][$B(Ar_F)_4$]$_2$ by Valerga and co-workers.[13] No formation of related indenylidene complexes was observed in these examples. It is noteworthy that the formation of indenylidene ruthenium derivatives [$RuCl_2(PR_3)_2$(indenylidene)] was observed while attempting to produce the corresponding allenylidene ruthenium complex.[7c] However, the rearrangement of allenylidene into the indenylidene ligand was never directly observed.[7] Thus, the above results show for the first time the direct intramolecular transformation of an allenylidene ruthenium species into an indenylidene species on protonation via an alkenylcarbyne intermediate.

The activity in ROMP of the in situ prepared species **3** was thus evaluated. To quickly generate species **3**, complex **1** was first treated with CF_3SO_3H at room temperature. When 10000 equivalents of cyclooctene (1.46 M) in PhCl were added, complete gelatification was observed within 1 minute, but the reaction was stirred for a further 5 min before being quenched with ethyl vinyl ether (Table 1, entry 4). The isolation of low polydispersed polyoctenamer showed a conversion of 97 % corresponding to a calculated TOF value of 116000 mol per hour. Indeed, a tremendous increase in the TOF value to more than 1000000 mol per hour was reached when 100000 equivalents of monomer were loaded (entry 5). It was verified that polymerization does not take place with CF_3SO_3H in the absence of the ruthenium catalyst.

Slight modifications of the starting allenylidene complex were made by changing subtituents in the phenyl groups [RuCl(η^6-*p*-cymene){=C=C=C(***p*-OMe-Ph**)$_2$}(PCy_3)][CF_3SO_3] (**4**), in the phosphane [RuCl(η^6-*p*-cymene)(=C=C=CPh_2)(**PPh_3**)][CF_3SO_3] (**5**) or in the η^6-arene ligand [RuCl)(η^6-**1,2,4,5-tetramethylbenzene**)(=C=C=CPh_2)(PCy_3)][CF_3SO_3] (**6**). The addition of five equivalents of triflic acid to solutions of **4**–**6** also promoted the formation of cyclooctenamer (entries 6–8). Only precursor **6** led to similar results as those of **1**, thus showing that either the less electron-donating phosphane PPh_3 (**5**) or the introduction of electron releasing groups in the phenyl rings (**4**) reduces catalytic activity.

Due to the high activity of the indenylidene complex, **3**, for the ROMP of cyclooctene, the polymerization of the less reactive cyclopentene was evaluated. A Schlenk tube was charged with allenylidene complexes (**1, 4**, or **6**), 1000 equivalents of cyclopentene (2.33 M), PhCl, and 5 equivalents of triflic acid at 0 °C (Figure 1). To make a comparison of

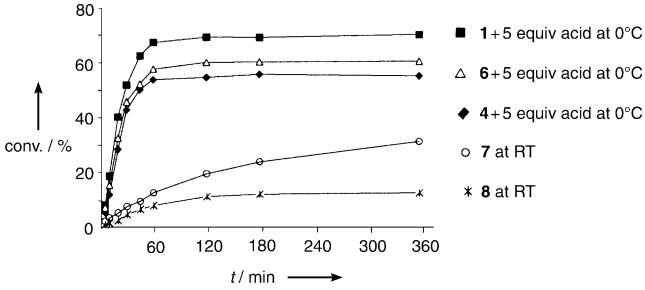


Figure 1. Cylopentene polymerization with different catalysts and monitored by ^1H NMR experiments. Conv. = conversion

the activity of these catalysts, experiments with the well-known stable ruthenium alkylidene catalysts $RuCl_2$(=CHPh)(PCy_3)$_2$ (**7**)[2c] and $RuCl_2$(=CHPh)-(PCy_3)$_2${=CN(Mes)CH_2CH_2N(Mes)} (**8**)[2a] were carried out at room temperature. The analysis of calculated TOF values clearly demonstrates the excellent catalytic performance of in situ generated indenylidene species from **1, 4**, or **6** with TOF values lying between 540 and 670, eight times more than those observed for the catalyst **8** (Table 2). In addition, when five equivalents of triflic acid were added to vessel containing **8**, even lower yields and lower TOF values were observed, which is in agreement with the previous observation that the addition of HCl does not increase activity of pure **8**.[14] It was described that with Schrock-type initiators of such as [W(=CH*t*Bu)($OtBu$)$_2$(NAr)], the polymerization of cyclopentene took place at temperatures below −40 °C ([cata-

 © 2003 Wiley-VCH Verlag GmbH & Co. KGaA, Weinheim

Table 2: Cyclopentene polymerization with the catalytic system RuCl(η⁶-*p*-cymene)(=C=C=CR₂)(PR′₃)][CF₃SO₃] + HOSO₂CF₃.[a]

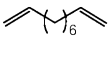
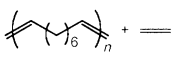
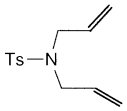
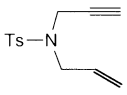
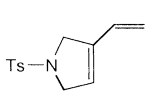
Entry	Complex	*T* [°C]	Acid[b]	Time	Yield	$10^{-3}\times\bar{M}_n$[c]	PDI[d]	% *cis*[e]	TOF[f]
1	**1**	0	5 equiv	1 h	67%	106	1.5	15	670
2	**4**	0	5 equiv	1 h	54%	90	1.8	18	540
3	**6**	0	5 equiv	1 h	60%	88	1.7	16	600
4	**7**	20	–	3 h	12%	31	1.5	21	40
5	**8**	20	–	3 h	24%	60	1.6	19	80
6[h]	**1**	−40	5 equiv	15 min	91%	–	–	–	44444

[a] 7.3×10^{-3} mol of cyclopentene in 2.5 mL of PhCl [cyclopentene]/[Ru] = 1000. [b] Related to Ru complex. [c] determined by GPC in THF versus polystyrene standards. [d] Polydispersity index $\bar{M}_w/\bar{M}_n$. [e] determined by ^{13}C NMR. [f] Turnover frequency in moles per hour. [g] bulk polymerization, [cyclopentene]/[Ru] = 10000.

lyst]:[monomer] = 1:200, 4 h, 95% conversion).[15] At this temperature, the in situ generated complex **3** was able to polymerize in fifteen minutes up to 90% of cyclopentene in bulk conditions with extremely low loading of the catalyst (1:10000) showing even better activity (Table 2, entry 6). The above experiments constitute the first evidence of an indenylidene–metal catalyst precursor for ROMP.

The indenylidene species **3** is also an active catalyst precursor in other typical alkene metathesis reactions. Monitoring the RCM of diallyltosylamide with the catalytic system made from **1** and five equivalents of CF_3SO_3H was carried out in an NMR tube. Initially, the mixture was cooled to −40 °C. The formation of **2** was observed by $^{31}P\{^1H\}$ NMR but no RCM product was formed after 1 hour at −40 °C. At 0 °C the formation of **3** was observed and the RCM reaction took place at 0 °C reaching 99% of conversion in 30 min. Other typical alkene metathesis reactions like acyclic diene metathesis (ADMET) of decadiene and ring closing metathesis of allylpropargyltosylamide were carried out, thus showing versatility of catalyst **3** (Table 3). Therefore, the

Table 3: Alkene metathesis with *in situ* prepared catalyst **3** from RuCl(η⁶-*p*-cymene)(=C=C=CPh₂)(PCy₃)][CF₃SO₃] (**1**) + HOSO₂CF₃ at 0 °C.[a]

	Substrate	Product	Time	Yield	TOF[b]
ADMET			12 h	94%	4
RCM			30 min	99%	98
Enyne metathesis			3 h	75%	12.5

[a] 4.5×10^{-6} mol of **1** + 22.5×10^{-6} mol of $HOSO_2CF_3$ in 0.5 mL of CD_2Cl_2 [substrate/[Ru] = 50. [b] Turnover frequency in moles per hour.

activity of 18 electron, ionic indenylidene-arene complex **3** seems higher than that of previously reported 16 electron, neutral diphosphane indenylidene or phosphane imidazolylidene indenylidene ruthenium complexes[7] probably because the *p*-cymene ligand is easily released, thus generating active initiators.

The above results show for the first time that the direct intramolecular transformation of an allenylidene ruthenium complex into an indenylidene ruthenium derivative, on protonation via an alkenylcarbyne compound. Moreover they show the birth of a new in situ generated 18 electron, ionic arene indenylidene ruthenium catalytic species, highly active for ROMP of cyclooctene and cyclopentene, RCM or ADMET reactions even operating at 0 °C and arising from easily made allenylidene complexes.

Experimental Section

Preparation of **2**: A dark-red solution of **1** (40 mg, 0.045 mmol) in CD_2Cl_2 (0.5 mL) in an NMR tube under argon atmosphere at 233 K was treated with triflic acid (5 μL 0.056 mmol). The solution immediately turned dark orange and after sealing the NMR tube under argon atmosphere measurements were made. ^{1}H NMR (300 MHz, CD_2Cl_2, 233 K): δ = 8.12 (vt, $J_{H\text{-}H}$ = 7.0 Hz, 2H, $H_{meta\text{-}Ph}$), 7.8–7.3 (m, 6H, H_{Ph}), 7.05 (s, 1H, Ru≡C−CH=), 6.92 (vt, $J_{H\text{-}H}$ = 7.5 Hz, 2H, $H_{meta\text{-}Ph}$), 6.75 and 6.61 (both d, $J_{H\text{-}H}$ = 6.0 Hz, 4H, η⁶-*p*-cymene), 2.9–2.6 (m, 4H, ^{i}Pr and PCH), 2.28 (s, 3H, CH_3), 2.1–0.9 ppm (m, 36H, Cy and *i*Pr). $^{13}C\{^1H\}$ NMR + DEPT, HMQC and HMBC (75.4 MHz, CD_2Cl_2, 233 K): δ = 328.1 (d, $J_{C\text{-}P}$ = 11 Hz, Ru≡C), 193.2 (s, CH=*C*Ph₂), 140.5 and 137.6 (both s, $C_{ipso\text{-}Ph}$), 136.0, 134.8, 134.2, 130.3, 129.4, and 127.8 (all s, C_{Ph}), 130.5 (s, Ru≡C−*C*H=), 128.2 and 125.8 (both s, $C_{ipso\text{-}p\text{-}cymene}$), 120.4 (c, $J_{C\text{-}F}$ = 320.0 Hz, CF_3), 111.8, 108.7 (both s, $C_{p\text{-}cymene}$), 33.3 (s, CH_{iPr}), 31–24 (br, Cy), 25.1, 22.2 (s, $CH_{3\text{-}iPr}$), 19.9 ppm (s, CH_3). $^{31}P\{^1H\}$ NMR (121.4 MHz, CD_2Cl_2, 233 K): δ = 78.6 ppm (s).

Preparation of **3**: A dark-red solution of **1** (40 mg, 0.045 mmol) in CD_2Cl_2 (0.5 mL) in an NMR tube under argon atmosphere at 253 K was treated with triflic acid (5 μL 0.056 mmol). The tube was sealed under argon and reaction was monitored by ^{31}P NMR. The formation of **2** was first observed and a new species, **3**, was progressively formed. The formation of **3** was completed in 20 min. ^{1}H NMR (300 MHz, CD_2Cl_2, 233 K): δ = 8.33 (m, 1H, $H_{8\text{-}ind}$), 7.84 (d, $J_{H\text{-}H}$ = 7.5 Hz, 2H, $H_{orto\text{-}Ph}$), 7.75 (t, $J_{H\text{-}H}$ = 7.5 Hz, 1H, $H_{para\text{-}Ph}$), 7.60 (vt, $J_{H\text{-}H}$ = 7.5 Hz, 2H, $H_{meta\text{-}Ph}$), 7.42 (m, 2H, $H_{7\text{-}ind}$ and $H_{6\text{-}ind}$), 7.13 (m, 1H, $H_{5\text{-}ind}$), 6.88 (s, 1H, Ru=C−CH=), 6.36, 6.31, 6.19, and 6.15 (all d, 4H, $J_{H\text{-}H}$ = 6.0 Hz, η⁶-*p*-cymene), 2.83 (m, 1H, ^{i}Pr), 2.78 (m, 3H, PCH), 2.31 (s, 3H, CH_3), 2.1–0.9 ppm (m, 36H, Cy and *i*Pr). $^{13}C\{^1H\}$ NMR + DEPT, HMQC and HMBC (75.4 MHz, CD_2Cl_2, 233 K): δ = 334.1 (d, $J_{C\text{-}P}$ = 10 Hz, Ru = C), 154.6 (s, $C_{3\text{-}ind}$), 146.8 (s, $C_{9\text{-}ind}$), 143.1 (d, $J_{C\text{-}P}$ = 2 Hz, $C_{2\text{-}ind}$), 136.5 (s, $C_{4\text{-}ind}$), 134.7 (s, $C_{7\text{-}ind}$), 133.4 (s, $C_{8\text{-}ind}$), 132.7 (s, $C_{6\text{-}ind}$), 132.5 (s, $C_{para\text{-}Ph}$), 131.7 (s, $C_{ipso\text{-}Ph}$), 130.0 (s, $C_{meta\text{-}Ph}$), 127.8 (s, $C_{orto\text{-}Ph}$), 126.3 and 125.3 (both s, $C_{ipso\text{-}p\text{-}cymene}$), 121.2 (s, $C_{5\text{-}ind}$), 120.4 (c, $J_{C\text{-}F}$ = 320.0 Hz, CF_3), 103.6 and 99.7 (both s, $C_{p\text{-}cymene}$), 33.8 (s, CH_{iPr}); 30–24 (br, Cy); 24.2 and 22.8 (both s, $CH_{3\text{-}iPr}$); 19.6 ppm (s, CH_3). $^{31}P\{^1H\}$ NMR (121.4 MHz, CD_2Cl_2, 233 K): δ = 48.3 ppm (s).

Polymerisation of cyclolefins: **1** (8 mg 9 μmol) was dissolved in PhCl (0.5 mL) at 253 K and 4 μL (45 μmol) of triflic acid was added. After 30 min at this temperature desired amount of freshly prepared catalyst was transferred to a vessel at chosen temperature containing PhCl (2.5 mL) and monomer (500 mg; 4.5 mmol of cyclooctene, 1.46 M; 7.3 mmol of cyclopentene 2.33 M). After the reaction had finished, the resulting viscous mixture was dissolved with $CHCl_3$ containing 0.1% of 2,6-di-*tert*-butyl-4-methylphenol (BHT; 20 mL) and vinyl ethyl ether (0.3 mL). This solution was poured into methanol (300 mL) to precipitate the polymer, which was collected by filtration, dried under vacuum, and characterized by ^{1}H and ^{13}C NMR. Average molecular weights were determined using gel-

 © 2003 Wiley-VCH Verlag GmbH & Co. KGaA, Weinheim

permeation chromatography GPC calibrated with polystyrene standards.

Received: June 10, 2003 [Z52108]

Keywords: carbenes · carbyens · heterogeneous catalysis · metathesis · ring-opening polymerization · ruthenium

[1] a) T. M. Trnka, R. H. Grubbs, *Acc. Chem. Res.* **2001**, *34*, 18 – 29; b) A. Fürstner, *Angew. Chem.* **2000**, *112*, 3140 – 3172; *Angew. Chem. Int. Ed.* **2000**, *39*, 3012 – 3043; c) M. R. Buchmeiser, *Chem. Rev.* **2000**, *100*, 1565 – 1604.

[2] a) C. W. Bielawski, R. H. Grubbs, *Angew. Chem.* **2000**, *112*, 3025 – 3028; *Angew. Chem. Int. Ed.* **2000**, *39*, 2903 – 2906; b) T. Weskamp, W. C. Schattenmann, M. Spiegler, W. A. Herrmann, *Angew. Chem.* **1998**, *110*, 2631 – 2633; *Angew. Chem. Int. Ed.* **1998**, *37*, 2490 – 2493; c) P. Schwab, R. H. Grubbs, J. W. Ziller, *J. Am. Chem. Soc.* **1996**, *118*, 100 – 110; d) S. T. Nguyen, R. H. Grubbs, J. W. Ziller, *J. Am. Chem. Soc.* **1993**, *115*, 9858 – 9859.

[3] a) R. Castarlenas, C. Fischmeister, P. H. Dixneuf, *New J. Chem.* **2003**, *27*, 215 – 217; b) H. Wakamatsu, S. Blechert, *Angew. Chem.* **2002**, *114*, 2509 – 2511; *Angew. Chem. Int. Ed.* **2002**, *41*, 2403 – 2405; c) L. Delaude, M. Szypa, A. Demonceau, A. F. Noels, *Adv. Synth. Catal.* **2002**, *344*, 749 – 756; d) M. B. Dinger, J. C. Mol, *Adv. Synth. Catal.* **2002**, *344*, 671 – 677; e) S. B. Garber, J. S. Kingsbury, B. L. Gray, A. H. Hoveyda, *J. Am. Chem. Soc.* **2000**, *122*, 8168 – 8179; f) D. Amoroso, D. E. Fogg, *Macromolecules* **2000**, *33*, 2815 – 2818; g) S. M. Hansen, M. A. O. Volland, F. Rominger, F. Eisenträger, P. Hofmann, *Angew. Chem.* **1999**, *111*, 1360 – 1364; *Angew. Chem. Int. Ed.* **1999**, *38*, 1273 – 1276.

[4] a) A. Fürstner, M. Picquet, C. Bruneau, P. H. Dixneuf, *Chem. Commun.* **1998**, 1315 – 1316; b) A. Fürstner, M. Liebl, C. W. Lehmann, M. Piquet, R. Kunz, C. Bruneau, D. Touchard, P. H. Dixneuf, *Chem. Eur. J.* **2000**, *6*, 1847 – 1857.

[5] a) D. Sémeril, J. Le Nôtre, C. Bruneau, P. H. Dixneuf, A. F. Kolomiets, S. N. Osipov, *New J. Chem.* **2001**, *25*, 16 – 18; b) M. Picquet, D. Touchard, C. Bruneau, P. H. Dixneuf, *New J. Chem.* **1999**, *23*, 141 – 143; c) M. Picquet, C. Bruneau, P. H. Dixneuf, *Chem. Commun.* **1998**, 2249 – 2250.

[6] a) S. Csihony, C. Fischmeister, C. Bruneau, I. T. Horvath, P. H. Dixneuf, *New J. Chem.* **2002**, *26*, 1667 – 16670; b) R. Castarlenas, D. Sémeril, A. F. Noels, A. Demonceau, P. H. Dixneuf, *J. Organomet. Chem.* **2002**, *663*, 235 – 238.

[7] a) A. Fürstner, A. Leitner, *Angew. Chem.* **2003**, *115*, 320 – 323; *Angew. Chem. Int. Ed.* **2003**, *42*, 308 – 311; b) A. Fürstner, F. Jeanjean, P. Razon, *Angew. Chem.* **2002**, *114*, 2203 – 2206; *Angew. Chem. Int. Ed.* **2002**, *41*, 2097 – 2101; c) A. Fürstner, O. Guth, A. Düffels, G. Seidel, M. Liebl, B. Gabor, R. Mynott, *Chem. Eur. J.* **2001**, *7*, 4811 – 4820; d) L. Jafarpour, H.-J. Schanz, E. D. Stevens, S. P. Nolan, *Organometallics* **1999**, *18*, 5416 – 5419; e) H.-J. Schanz, L. Jafarpour, E. D. Stevens, S. P. Nolan, *Organometallics* **1999**, *18*, 5187 – 5190; f) K. J. Harlow, A. F. Hill, J. D. E. T. Wilton-Ely, *J. Chem. Soc. Dalton Trans.* **1999**, 285 – 291.

[8] P. Gonzalez-herrero, B. Weberndörfer, K. Ilg, J. Wolf, H. Werner, *Organometallics* **2001**, *20*, 3672 – 3685.

[9] a) S. Jung, K Ilg, C. D. Brandt, J. Wolf, H. Werner, *J. Chem. Soc. Dalton Trans.* **2002**, 318 – 327; b) W. Stüer, J. Wolf, H. Werner, P. Schwab, M. Schulz, *Angew. Chem.* **1998**, *110*, 3603 – 3606; *Angew. Chem. Int. Ed.* **1998**, *37*, 3421 – 3423.

[10] a) S. J. Connon, A. M. Dunne, S. Blechert, *Angew. Chem.* **2002**, *114*, 3989 – 3993; *Angew. Chem. Int. Ed.* **2002**, *41*, 3835 – 3838; b) J. Kingsbury, S. B. Garber, J. M. Giftos, B. L. Gray, M. M. Okamoto, R. A. Farrer, J. T. Fourkas, A. H. Hoveyda, *Angew. Chem.* **2001**, *113*, 4381 – 4386; *Angew. Chem. Int. Ed.* **2001**, *40*, 4251 – 4256; c) J. Dowden, J. Savovi', *Chem. Commun.* **2001**, 37 – 38; d) K. Melis, D. De Vos, P. Jacobs, F. Verpoort, *J. Mol. Catal. A* **2001**, *169*, 47 – 56; e) M. Bartz, J. Küther, R. Seshadri, W. Tremel, *Angew. Chem.* **1998**, *110*, 2646 – 2649; *Angew. Chem. Int. Ed.* **1998**, *37*, 2466 – 2468.

[11] for examples see: a) R. Castarlenas, M. A. Esteruelas, Y. Jean, A. Lledós, J. Tomás, E. Oñate, *Eur. J. Inorg. Chem.* **2001**, 2871 – 2883; b) T. B. Wen, Y. K. Cheung, J. Yao, W.-T. Wong, Z. Y. Zhou, G. Jia, *Organometallics* **2000**, *19*, 3803 – 3809; c) M. Baya, P. Crochet, M. A. Esteruelas, E. Gutierrez-Puebla, A. M. Lopez, J. Modrego, E. Oñate, N. Vela, *Organometallics* **2000**, *19*, 2585 – 2596.

[12] S. Jung, C. D. Brandt, H. Werner, *New J. Chem.* **2001**, *25*, 1101 – 1103.

[13] E. Bustelo, M. Jimenez-Tenorio, K. Mereiter, M. C. Puerta, P. Valerga, *Organometallics* **2002**, *21*, 1903 – 1911.

[14] J. P. Morgan, R. H. Grubbs, *Org. Lett.* **2000**, *2*, 3153 – 3155.

[15] a) P. Dounis, W. J. Feast, A. M. Kenwright, *Polymer* **1995**, *36*, 2787 – 2796; b) R. R. Schrock, K. B. Yap, D. C. Yang, H. Sitzmann, L. R. Sita, G. C. Bazan, *Macromolecules* **1989**, *22*, 3191 – 3200.

 © 2003 Wiley-VCH Verlag GmbH & Co. KGaA, Weinheim

Polypeptide Imaging Agents

Supramolecular Adducts between Poly-L-arginine and [Tm^{III}dotp]: A Route to Sensitivity-Enhanced Magnetic Resonance Imaging–Chemical Exchange Saturation Transfer Agents**

Silvio Aime, Daniela Delli Castelli, and Enzo Terreno*

The last few years have witnessed a growth in interest in a novel class of contrast media for magnetic resonance imaging (MRI) applications, the so-called chemical exchange saturation transfer (CEST) agents,[1–4] primarily because of their ability to act as responsive agents for parameters of diagnostic relevance.[5–8]

Such agents possess mobile protons that, upon irradiation of their resonance frequency, transfer saturated magnetization to the bulk water resonance.[9] In an MR image this results in a loss of signal (negative agent). Several parameters control the extent of the saturation transfer (ST) effect. Some of them are strictly dependent upon the instrumental modality through which the selectivity and power of the irradiation rf field is applied. Others are related to the characteristics of

[*] Prof. S. Aime, Dr. D. Delli Castelli, Dr. E. Terreno
Dipartimento di Chimica I.F.M.
Via P. Giuria 7, 10125 Torino (Italy)
and
Molecular Imaging Center
Via P. Giuria 15, 10125 Torino (Italy)
Fax: (+39) 011-6707-855
E-mail: silvio.aime@unito.it

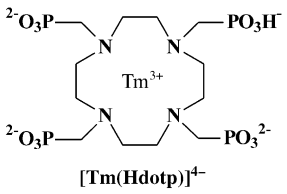
[**] Financial support from Bracco Imaging S.p.A. and MIUR are gratefully acknowledged. This work has been carried out under the framework of the EU-COST D 18 action. H_8dotp = 1,4,7,10-tetraazacyclododecanetetrakis(methylenephosphonic acid).

 DOI: 10.1002/anie.200352132 © 2003 Wiley-VCH Verlag GmbH & Co. KGaA, Weinheim

the CEST agent, namely the chemical shift separation $\Delta\omega$ (in rad Hz) between the resonance of the mobile protons and water, the exchange rate of the mobile protons k_{ex}, the number of exchangeable protons n, and the longitudinal relaxation time of the bulk water protons in the presence of the irradiating rf field T_1^{sat}. As long as the condition $\Delta\omega > k_{ex}$ holds, ST and k_{ex} are directly related. Therefore, paramagnetic systems displaying large $\Delta\omega$ values are candidates of choice because they allow the exploitation of large k_{ex} values.[2,4,6–8] Currently, the main limitation of the CEST agents is their relatively low sensitivity. The most sensitive systems so far reported yield ST effects of 5% (which ensures the detection of the contrast in the MR image) at a concentration of 0.5 mM.[6,8]

van Zjil and co-workers tackled the sensitivity problem by investigating the ST properties of several cationic diamagnetic macromolecular systems (polyaminoacids and dendrimers). They found an ST effect for the most sensitive system of almost 50% for a 100 μM solution of a poly-L-lysine of 488 kDa.[3] Clearly, the high sensitivity displayed by this system is a result of the huge number of irradiated mobile protons (about 2300 backbone amide protons per molecule versus 2 or 8 water or amide protons for the most sensitive of the paramagnetic agents). Although these findings represent an important step in the search for CEST agents with improved sensitivity, it is evident that a much greater improvement could be achieved if such an exchangeable proton pool were endowed with much larger $\Delta\omega$ values. On this basis, we deemed it of interest to explore a new route to enhance the sensitivity of CEST agents. Our approach is based on the formation of supramolecular adducts between a species containing a high number of exchanging protons and a paramagnetic shift reagent that is able to markedly increase its $\Delta\omega$ value in such a way that $|\Delta\omega| > k_{ex}$. A further advantage lies in the fact that the resonance frequency of the mobile protons is shifted away from its diamagnetic position upon interacting with the paramagnetic agent, thus the observed ST effect is not affected by the contribution from protons belonging to endogenous molecules.

As a model system to prove the efficacy of the proposed approach, we have considered the supramolecular adduct formed by the cationic polypeptide poly-L-arginine (53.5 kDa) and the negatively charged lanthanide complex $[Tm(Hdotp)]^{4-}$ (at pH 7.4), whose ability to act as an NMR shift reagent for cationic species is well documented.[10–12]



$[Tm(Hdotp)]^{4-}$

In the absence of the shift reagent, the exchange rate of the mobile guanidine protons of the polypeptide at pH 7.4 and 312 K is so fast that no ST can be measured (Figure 1, open squares). When $[Tm(Hdotp)]^{4-}$ is added to the poly-L-arginine solution, a remarkable transfer of saturated magnetization takes place when the rf irradiating field is set at 20–30 ppm downfield of the water resonance (Figure 1, filled squares). This is an unambiguous indication of the formation of a tightly associated ion pair. It is likely that a $[Tm(Hdotp)]^{4-}$ chelate sweeps along the polypeptide surface, thus causing an overall shift of all the guanidine protons whose saturation causes a strong decrease in the intensity of the water signal. An 18:1 ratio between the paramagnetic chelate and the polypeptide has been found to provide optimal ST effects. Higher ratios yielded extensive precipitation of the adduct as a consequence of the decrease in the effective residual electric charge.

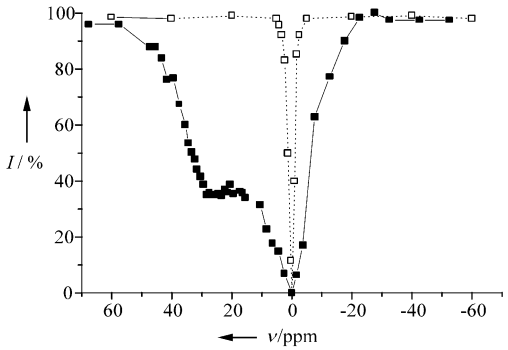


Figure 1. CEST spectra (7.05 T, pH 7.4 and 312 K) showing the intensity of the NMR signal of the bulk water protons (normalized to 100) as a function of the irradiation frequency (in ppm). Open squares: poly-L-arginine 0.11 mM. Filled squares: poly-L-arginine 0.11 mM in the presence of 2.0 mM $[Tm(Hdotp)]^{4-}$. Irradiation conditions: pulse: rectangular, duration: 2 s, power: 25.0 μT.

The noticeable improvement in the sensitivity brought about by such a supramolecular system is evident by measuring the ST effect of solutions containing a different absolute concentration of the interacting species (at the fixed $[Tm(Hdotp)]^{4-}$/[poly-L-Arg] ratio of 18:1; Figure 2). Inspection on the results reported in Figure 2 shows that a 5% ST effect can be observed at very low concentrations of polymer (1.7 μM) and metal complex (30 μM), thus demonstrating the great sensitivity enhancement that can be attained by this approach.

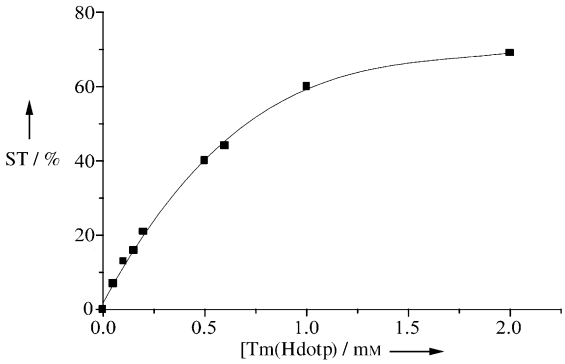


Figure 2. ST effect as a function of the absolute concentration of $[Tm(Hdotp)]^{4-}$ of solutions containing a fixed $[Tm(Hdotp)]^{4-}$/[poly-L-Arg] ratio of 18:1. Experimental conditions: 7.05 T, pH 7.4, 312 K, irradiation pulse: train of 2000 e-burp pulses (1 ms each), irradiation frequency: ±6000 Hz from the water protons, irradiation power: 86.7 μT.

 © 2003 Wiley-VCH Verlag GmbH & Co. KGaA, Weinheim

Finally, the CEST properties of the $[Tm(Hdotp)]^{4-}$/poly-L-Arg system have been assessed by means of an in vitro MRI experiment. Figure 3 shows an MR difference (on-off) CEST image (see the Experimental Section) of a phantom made of four specimens containing $[Tm(Hdotp)]^{4-}$ and poly-L-arginine (at a fixed concentration ratio of 18:1), where the concentration of the metal complex ranges from 50 to 500 μM. The acquisition of such a CEST image takes about 24 minutes (irradiation time of 2 s), whereas the same experiment with a typical diamagnetic CEST agent is much more time consuming. In fact, the long T_1^{sat} values displayed by the diamagnetic systems require much longer irradiation times (usually 10 s) to fully exploit the maximum ST effect.

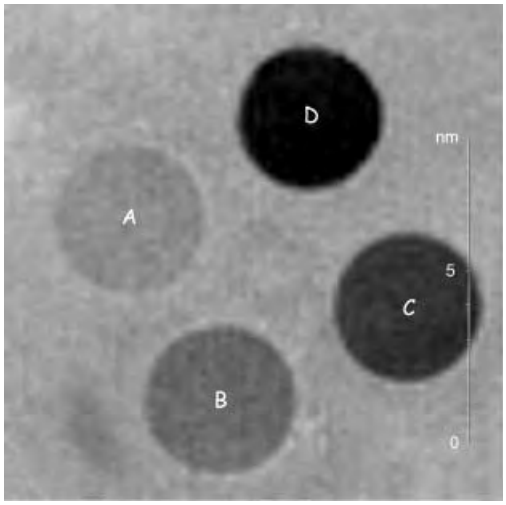


Figure 3. Difference spin-echo MR images (on-off) of a phantom consisting of four solutions of $[Tm(Hdotp)]^{4-}$/poly-L-arginine at the following concentrations: A: 50 μM/2.8 μM, B: 100 μM/5.5 μM, C: 200 μM/11.1 μM,D: 500 μM/27.8 μM. Experimental conditions: 7.05 T, pH 7.4, 312 K, echo sequence: TR/TE/NE = 6 s/5 ms/1, irradiation pulse: train of 2000 sinc pulses (1 ms each), irradiation frequency: ±6000 Hz from the water protons, irradiation power: 47.8 μT.

In summary, the results reported herein show that a new class of CEST agents can be envisaged. They are based on the formation of reversible adducts between a diamagnetic system, the pool of a high number of exchanging protons, and a paramagnetic shift reagent that enables them to combine a large chemical shift value with the shortening of the water T_1 value. Such a control of the determinants of the CEST effect provides extremely sensitive systems, in terms of the concentrations of both the metal complex and the polymer. The observed sensitivity enhancement markedly decreases the detection limit of an MRI-CEST experiment, and it now approaches the concentration limit achieved in conventional Gd^{III}-based contrast agents.

Experimental Section

$[Tm(Hdotp)]^{4-}$ has been prepared according to the literature.[11] Poly-L-arginine (DP 270, 53.3 kDa) was purchased from Sigma. ST measurements were carried on a Bruker Avance300 spectrometer. ST values (expressed as percentages) were calculated by using the following equation:

$$ST\,\% = \left(1 - \frac{I_s}{I_0}\right) 100$$

where I_S and I_0 refer to the intensity of the bulk water signal when the irradiation pulse is set on-resonance (frequency ν^{on}, signal intensity I_S) and off-resonance ($\nu^{off} = -\nu^{on}$, I_0) with respect to the frequency of the bulk water protons. The off-resonance measurement is necessary to take into account the direct saturation effect on the bulk water signal by the irradiation pulse.

The MR images were obtained on the same spectrometer equipped with a microimaging probe (inner diameter 30 mm). The image reported in Figure 3 is the difference between the image acquired by irradiating the resonance frequency of the guanidine protons (on-image, 6000 Hz from water protons) and that acquired off-resonance (off-image, −6000 Hz from the water protons). Both images were obtained using a conventional spin-echo sequence (TR/TE/NE = 6 s/5 ms/1) preceded by a train of sinc pulses (2000, 1 ms each, irradiation power 47.8 μT).

Received: June 13, 2003 [Z52132]

Keywords: imaging agents · polymers · supramolecular chemistry · thulium

[1] K. M. Ward, A. H. Aletras, R. S. Balaban, *J. Magn. Reson.* **2000**, *143*, 79–87.
[2] S. Zhang, P. Winter, K. Wu, A. D. Sherry, *J. Am. Chem. Soc.* **2001**, *123*, 1517–1518.
[3] N. Goffeney, J. W. M. Bulte, J. Duyn, L. H. Bryant, Jr., P. C. M. van Zjil, *J. Am. Chem. Soc.* **2001**, *123*, 8628–8629.
[4] S. Aime, A. Barge, D. Delli Castelli, F. Fedeli, A. Mortillaro, F. U. Nielsen, E. Terreno, *Magn. Reson. Med.* **2002**, *47*, 639–648.
[5] K. M. Ward, R. S. Balaban, *Magn. Reson. Med.* **2000**, *44*, 799–802.
[6] S. Zhang, L. Michaudet, S. Burgess, A. D. Sherry, *Angew. Chem.* **2002**, *114*, 1999–2001; *Angew. Chem. Int. Ed.* **2002**, *41*, 1919–1921.
[7] S. Aime, D. Delli Castelli, F. Fedeli, E. Terreno, *J. Am. Chem. Soc.* **2002**, *124*, 9364–9365.
[8] S. Aime, D. Delli Castelli, E. Terreno, *Angew. Chem.* **2002**, *114*, 4510–4512; *Angew. Chem. Int. Ed.* **2002**, *41*, 4334–4336.
[9] S. Forsén, A. Hoffmann, *J. Chem. Phys.* **1963**, *39*, 2892–2901.
[10] A. D. Sherry, J. Ren, J. Huskens, E. Brucher, E. Toth, C. F. G. C. Geraldes, M. M. C. A. Castro, W. P. Cacheris, *Inorg. Chem.* **1996**, *35*, 4604–4612.
[11] J. Ren, C. S. Springer, Jr., A. D. Sherry, *Inorg. Chem.* **1997**, *36*, 3493–3498.
[12] S. Aime, M. Botta, S. Geninatti Crich, E. Terreno, P. L. Anelli, F. Uggeri, *Chem. Eur. J.* **1999**, *5*, 1261–1266.

 © 2003 Wiley-VCH Verlag GmbH & Co. KGaA, Weinheim

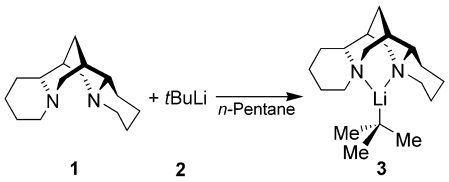
Monomeric Butyllithium Compound

[*t*BuLi·(−)-Sparteine]: Molecular Structure of the First Monomeric Butyllithium Compound**

Carsten Strohmann, Timo Seibel, and Katja Strohfeldt*

Without doubt *n*-butyllithium (*n*BuLi), *sec*-butyllithium (*s*BuLi), and *tert*-butyllithium (*t*BuLi) are amongst the most important organolithium compounds. However, the high tendency of these compounds towards aggregation, both in solution and in the solid state, hinders the identification of the reactive BuLi species in the reactions of these reagents. *n*BuLi crystallizes from *n*-pentane as the hexamer, *t*BuLi as the tetramer;[1] in the presence of coordinating compounds *n*BuLi and *t*BuLi crystallize as tetramers and dimers, respectively.[1,2] Mixed aggregates of BuLi isomers and lithium amides or alkoxides[3] as well as of BuLi isomers and other organolithium compounds[4] are also known. To simplify the interpretation of reactions with these lithium reagents—and possibly to increase their reactivity—attempts are usually made to suppress their aggregation by the addition of coordinating solvents or compounds. Although the presence of monomeric BuLi derivatives in solution is under discussion, to date no such compound has been characterized in the solid state.[5] Herein we report the preparation of monomeric [*t*BuLi·(−)-sparteine] (**3**) and its molecular structure in the solid state.

During the investigation of deprotonation reactions we noted that during slow warming of a mixture of *t*BuLi and (−)-sparteine in *n*-pentane from −78 to −50 °C colorless, needle-shaped crystals were formed which on further warming changed into a colorless, amorphous powder; this observation is typical for a temperature-dependent phase change. The colorless solid dissolved in *n*-pentane at room temperature to give a yellow solution. At −30 °C light brown platelets of **3** crystallized from this solution (Scheme 1). The lattice constants of both crystal forms were identical; however, the colorless needles decomposed within approximately 1 h in the cooling gas flow of the diffractometer,



1 2 3

Scheme 1. Preparation of [*t*BuLi·(−)-sparteine] (**3**).

[*] Dr. C. Strohmann, T. Seibel, K. Strohfeldt
Institut für Anorganische Chemie
Universität Würzburg
Am Hubland, 97074 Würzburg (Germany)
Fax: (+49) 931-888-4605
E-mail: mail@carsten-strohmann.de

[**] We thank the Deutsche Forschungsgemeinschaft, the Graduiertenkolleg 690, and the Fonds der Chemischen Industrie for financial support of this work.

whereas the light brown crystals were stable between −30 and −100 °C. Moreover, the title compound **3** proved to be significantly less sensitive than $(t\text{BuLi})_4$ or $(t\text{BuLi}\cdot\text{OEt}_2)_2$ during experimental manipulation.

Compound **3** crystallizes in the monoclinic crystal system in the chiral space group *C*2.[6] The asymmetric unit contains one molecule of [*t*BuLi·(−)-sparteine] (Figure 1). The Li–C1

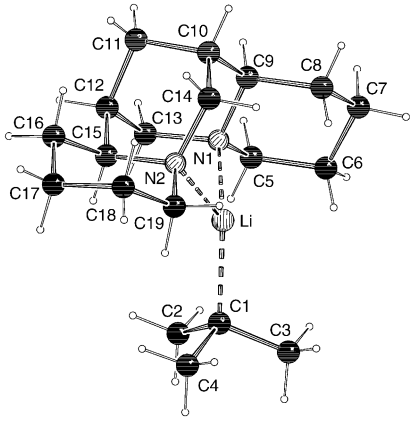


Figure 1. Crystal structure of **3** (SCHAKAL plot).[10] Selected bond lengths [pm] and angles [°]: Li-C1 211.4(4), Li-N1 206.2(3), Li-N2 206.2(3); N1-Li-N(2) 89.50(13), N1-Li-C1 126.87(16), N2-Li-C1 133.36(14), C4-C1-Li 112.30(15), C3-C1-Li 112.26(15), C2-C1-Li 110.35(15).

separation of 211.4(4) pm is smaller than the observed Li–C separation of 217.4–219.4(6) pm in $(t\text{BuLi}\cdot\text{OEt}_2)_2$,[1] 221.5(11)–222.7(9) pm in $[(n\text{BuLi}\cdot\text{tmeda})_2]$,[2a] and 214.5(11)–232.6(8) pm in $[\{(n\text{BuLi})_4\cdot\text{tmeda}\}_\infty]$ (tmeda = *N*,*N*,*N*′,*N*′-tetramethyl-1,2-ethanediamine).[2] Similarly small Li–C separations in alkyl lithium compounds have been observed in dilithiated systems, such as $[Li_2(thf)_2\{(Me_3Si)_2C\text{-}C(SiMe_3)_2\}]$[7] (209.6(29)–211.3(30) pm) and sterically crowded monomeric compounds, such as $[Li\{C(SiMe_2Ph)_3\}(thf)]$[8] (212(2) pm). The Li–N1 and Li–N2 separations of 206.2(3) and 206.2(3) pm are also somewhat smaller than in $[\{(n\text{BuLi})_4\cdot\text{tmeda}\}_\infty]$[2] (213.1(8) pm) and $[(n\text{BuLi}\cdot\text{tmeda})_2]$[2a] (220.9(12)–222.3(10) pm). Li–N separations of between 201.7 and 216.7 pm have been observed for (−)-sparteine-coordinated organolithium compounds; in each case in the solid state the sparteine ligand assumed the conformation also found in **3**.[9] The coordination number of 3 for the lithium center leads to short Li–C and Li–N bonds. The somewhat pyramidalized environment of the lithium center in **3** (angle sum at Li = 349.7°) arising from angular distortion of the *tert*-butyl group is unusual. Steric interactions between the *tert*-butyl group and the sparteine ligand—in particular with the sparteine methylene groups C19, C6, and C5—lead to this angular distortion (small H···H separations: H2c···H5b 235.0, H3c···H6b 244.4, H4c···H19b 252.4, and H4a···H19b 257.0 pm). The smallest intermolecular distance to the lithium center, Li···H3b′ = 279.0 pm, shows that no significant intermolecular interactions are present.

Energy minimization of **3** with DFT methods[B3LYP/6-31 + G(d)] supports the conformation determined by X-ray

 DOI: 10.1002/anie.200351308 © 2003 Wiley-VCH Verlag GmbH & Co. KGaA, Weinheim

structure analysis. Thus the solid-state structure is not imposed by packing effects.[11] The attempt to find a stationary point for a C_2 symmetrical dimer of **3** with a central Li_2C_2 four-membered ring gave merely a minimum with two separated monomers.

Compound **3** is not only the first BuLi compound which exists as the monomer in the solid state, but is also the first structurally characterized BuLi derivative with a (−)-sparteine ligand. This result is of interest since combinations of *n*BuLi, *s*BuLi, or *t*BuLi with (−)-sparteine are used as reagents in kinetically controlled, diastereoselective deprotonations,[12] where *s*BuLi·(−)-sparteine has proved to be the most successful to date. The decisive properties of these reagents are their aggregation and conformation, especially in regard of eductlike transition states involved in the deprotonation steps.[13]

The chiral (−)-sparteine ligand strongly shields the lithium center so that only one side of the molecule is available for coordination of further ligands. A potentially free coordination site is formed by the angular distortion of the *tert*-butyl group arising from steric interactions with the sparteine ligand. The space-filling model of the crystal structure of **3** shows clearly this free coordination site with its chiral environment (Figure 2).

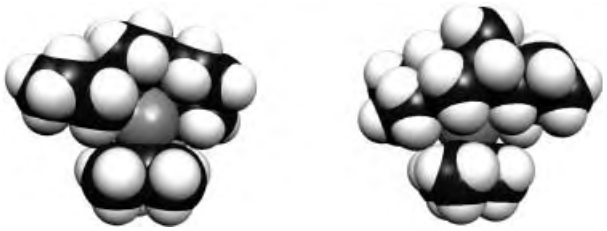


Figure 2. Space-filling model of the crystal structure of **3** (two views).[14]

The presence of monomeric **3** in the solid state also confirms the quantum mechanical studies of Wiberg and Bailey on the deprotonation of *N*-(*tert*-butoxycarbonyl)pyrrolidine with *t*BuLi in the presence of (−)-sparteine.[15] In this case a monomeric [*t*BuLi·(−)-sparteine] adduct with precoordinated *N*-(*tert*-butoxycarbonyl)pyrrolidine unit was also assumed as model compound. In these studies the energetically most favorable **3**-*N*-(*tert*-butoxycarbonyl)pyrrolidine adduct is formed through inversion of the lithium center of **3**. This mechanism would, however, require the establishment of a thermodynamic equilibrium on the reaction time scale at low temperatures. We are currently attempting to elucidate the solid-state structure of more −-sparteine alkyl lithium adducts. The results of initial DFT studies with [*s*BuLi·(−)-sparteine] and [*i*PrLi·(−)-sparteine] suggest that in these cases too, C_2 symmetrical dimers should be energetically unfavorable compared to the monomers because of steric interactions.

Experimental section

(−)Sparteine (50.0 mg, 2.13×10^{-4} mol) was dissolved in *n*-pentane (10 mL). The solution was cooled to −78 °C (formation of a (−)sparteine precipitate) and treated with a 1.7 M solution of *t*BuLi in *n*-pentane (13.0 μL, 2.21×10^{-4} mol). The reaction mixture was then warmed to −50 °C over 5 h when colorless, needle-shaped crystals of **3** were formed. The solid redissolved on warming to room temperature. Compound **3** crystallized from this yellow solution at −30 °C in the form of light brown platelets in a yield of 71 %. ^{1}H NMR (400 MHz, $C_6D_5CD_3$, 25 °C): $\delta = 0.82$ (s, 9H; CH_3), 0.85–2.80 ppm (m, 26H; (−)-sparteine); $^{13}C\{^1H\}$ NMR (100 MHz, $C_6D_5CD_3$, 25 °C): $\delta =$ 24.7 (CCH_3), 18.5, 24.8, 25.0, 25.3, 25.6, 28.3, 29.9 (CCH_2C), 35.2, 35.5 ($NCHCH(CH_2)_2$), 45.9, 53.2 (NCH_2CH_2), 57.3, 61.2 (NCH_2CH), 59.2, 67.1 ppm (NCH), $C(CH_3)_3$ of *t*BuLi not found. ^{7}Li NMR (117 MHz, $C_6D_5CD_3$, 25 °C): $\delta = 1.5$ ppm.

Received: March 3, 2003 [Z51308]

Keywords: carbanions · chirality · lithium · sparteine · structure elucidation

[1] T. Kottke, D. Stalke, *Angew. Chem.* **1993**, *105*, 619–621; *Angew. Chem. Int. Ed. Engl.* **1993**, *32*, 580–582.

[2] a) M. A. Nichols, P. G. Williard, *J. Am. Chem. Soc.* **1993**, *115*, 1568–1572; b) N. D. R. Barnett, R. E. Mulvey, *J. Am. Chem. Soc.* **1993**, *115*, 1573–1574.

[3] a) M. A. Beswick, B. R. Elvidge, N. Feeder, S. J. Kidd, D. S. Wright, *Chem. Commun.* **2001**, 379–380; b) J. K. Brask, T. Chivers, G. P. A. Yap, *Chem. Commun.* **1998**, 2543–2544; c) R. P. Davies, P. R. Raithby, R. Snaith, *Angew. Chem.* **1997**, *109*, 1261–1263; *Angew. Chem. Int. Ed. Engl.* **1997**, *36*, 1215–1217; d) G. B. Deacon, C. M. Forsyth, N. M. Scott, *J. Chem. Soc. Dalton Trans.* **2001**, 2494–2501; e) A. Feustel, G. Müller, *Chem. Commun.* **2001**, 1024–1025; f) B. Goldfuss, S. I. Khan, K. N. Houk, *Organometallics* **1999**, *18*, 2927–2929; g) B. Goldfuss, M. Steigelmann, F. Rominger, *Angew. Chem.* **2000**, *112*, 4299–4302; *Angew. Chem. Int. Ed.* **2000**, *39*, 4133–4136; h) B. Goldfuss, M. Steigelmann, F. Rominger, H. Urtel, *Chem. Eur. J.* **2001**, *7*, 4456–4464; i) J. Jubb, P. Berno, S. Hao, S. Gambarotta, *Inorg. Chem.* **1995**, *34*, 3563–3566; j) B.-T. Ko, C.-C. Lin, *J. Am. Chem. Soc.* **2001**, *123*, 7973–7977; k) M. Marsch, L. Lochmann, G. Boche, K. Harms, *Angew. Chem.* **1990**, *102*, 334–336; *Angew. Chem. Int. Ed. Engl.* **1990**, *29*, 308–310; l) J. Schneider, E. Popowski, H. Reinke, *Z. Anorg. Allg. Chem.* **2002**, *628*, 719–720; m) P. G. Williard, C. Sun, *J. Am. Chem. Soc.* **1997**, *119*, 11693–11694.

[4] a) J. Arnold, V. Knapp, J. A. R. Schmidt, A. Shafir, *J. Chem. Soc. Dalton Trans.* **2002**, 3273–3274; b) J. G. Donkervoort, J. L. Vicario, E. Rijnberg, J. T. B. H. Jastrzebski, H. Kooijman, A. L. Spek, G. van Koten, *J. Organomet. Chem.* **1998**, *550,* 463–467; c) K. Ruhlandt-Senge, J. J. Ellison, R. J. Wehmschulte, F. Pauer, P. P. Power, *J. Am. Chem. Soc.* **1993**, *115*, 11353–11357; d) C. Strohmann, B. C. Abele, *Organometallics* **2000**, *19*, 4173–4175; e) P. Wijkens, E. M. van Koten, M. D. Janssen, T. B. H. Jastrzebski, A. L. Spek, G. van Koten, *Angew. Chem.* **1995**, *107*, 239–242; *Angew. Chem. Int. Ed. Engl.* **1995**, *34*, 219–222; f) P. Wijkens, J. T. B. H. Jastrzebski, N. Veldman, A. L. Spek, G. van Koten, *Chem. Commun.* **1997**, 2143–2144.

[5] a) W. Bauer, W. R. Winchester, P. v. R. Schleyer, *Organometallics* **1987**, *6*, 2371–2379; b) H. Luitjes, M. Schakel, M. P. Aarnts, R. F. Schmitz, F. J. J. de Kanter, G. W. Klumpp, *Tetrahedron* **1997**, *53*, 9977–9988.

[6] Crystal structure analysis of **3**: $C_{19}H_{35}LiN_2$, $M_r = 298.43$, monoclinic, space group $C2$, $a = 18.169(9)$, $b = 9.418(4)$, $c = 12.328(7)$ Å, $\beta = 119.37(7)°$, $V = 1838.4(15)$ Å^3, $Z = 4$, $\rho_{calcd} = 1.078$ Mg m^{-3}, $Mo_{K\alpha}$ radiation ($\lambda = 0.71073$ Å), $T = 173$ K; a light brown platelet ($0.3\times0.3\times0.15$ mm^3) was mounted on a Stoe-IPDS diffractometer in an inert oil.[16] The intensities were measured in the range $2\theta = 5$–$52°$. From a total of 13347 reflections 3467 were independent ($R_{int} = 0.0593$). The structure

 © 2003 Wiley-VCH Verlag GmbH & Co. KGaA, Weinheim

was refined anisotropically on F^2 (G. M. Sheldrick, SHELXS-97, Universität Göttingen, **1997**): $R_1 = 0.0370$, $wR_2 = 0.0817$ (all data). CCDC-204440 (**3**) contains the supplementary crystallographic data for this paper. These data can be obtained free of charge via www.ccdc.cam.ac.uk/conts/retrieving.html (or from the Cambridge Crystallographic Data Centre, 12 Union Road, Cambridge CB2 1EZ, UK; fax: (+44) 1223-336-033; or deposit@ccdc.cam.ac.uk).

[7] A. Sekiguchi, T. Nakanishi, C. Kabuto, H. Sakurai, *J. Am. Chem. Soc.* **1989**, *111*, 3748 – 3750.

[8] C. Eaborn, P. B. Hitchcock, J. D. Smith, A. C. Sullivan, *J. Chem. Soc. Chem. Commun.* **1983**, 1390 – 1391.

[9] a) G. Boche, M. Marsch, J. Harbach, K. Harms, B. Ledig, F. Schubert, J. C. W. Lohrenz, H. Ahlbrecht, *Chem. Ber.* **1993**, *126*, 1887 – 1894; b) L. T. Byrne, L. M. Engelhardt, G. E. Jacobsen, W. P. Leung, R. I. Papasergio, C. L. Raston, B. W. Skelton, P. Twiss, A. H. White, *J. Chem. Soc. Dalton Trans.* **1989**, 105 – 113; c) I. Hoppe, M. Marsch, K. Harms, G. Boche, D. Hoppe, *Angew. Chem.* **1995**, *107*, 2328 – 2330; *Angew. Chem. Int. Ed. Engl.* **1995**, *34*, 2158 – 2160; d) B. Ledig, M. Marsch, K. Harms, G. Boche, *Angew. Chem.* **1992**, *104*, 80 – 81; *Angew. Chem. Int. Ed. Engl.* **1992**, *31*, 79 – 80; e) B. Ledig, M. Marsch, K. Harms, G. Boche, *Z. Kristallogr.* **1999**, *214*, 511 – 512; f) M. Marsch, K. Harms, O. Zschage, D. Hoppe, G. Boche, *Angew. Chem.* **1991**, *103*, 338 – 339; *Angew. Chem. Int. Ed. Engl.* **1991**, *30*, 321 – 323; g) R. I. Papasergio, B. W. Skelton, P. Twiss, A. H. White, C. L. Raston, *J. Chem. Soc. Dalton Trans.* **1990**, 1161 – 1172; h) D. J. Pippel, G. A. Weisenburger, S. R. Wilson, P. Beak, *Angew. Chem.* **1998**, *110*, 2600 – 2602; *Angew. Chem. Int. Ed.* **1998**, *37*, 2522 – 2524.

[10] E. Keller, SCHAKAL99, A Computer Program for the Graphic Representation of Molecular and Crystallographic Models, Universität Freiburg, Freiburg, **1999**.

[11] Gaussian 98 (Revision A.7), M. J. Frisch, G. W. Trucks, H. B. Schlegel, G. E. Scuseria, M. A. Robb, J. R. Cheeseman, V. G. Zakrzewski, J. A. Montgomery, R. E. Stratmann, J. C. Burant, S. Dapprich, J. M. Millam, A. D. Daniels, K. N. Kudin, M. C. Strain, O. Farkas, J. Tomasi, V. Barone, M. Cossi, R. Cammi, B. Mennucci, C. Pomelli, C. Adamo, S. Clifford, J. Ochterski, G. A. Petersson, P. Y. Ayala, Q. Cui, K. Morokuma, D. K. Malick, A. D. Rabuck, K. Raghavachari, J. B. Foresman, J. Cioslowski, J. V. Ortiz, B. B. Stefanov, G. Liu, A. Liashenko, P. Piskorz, I. Komaromi, R. Gomperts, R. L. Martin, D. J. Fox, T. Keith, M. A. Al-Laham, C. Y. Peng, A. Nanayakkara, C. Gonzalez, M. Challacombe, P. M. W. Gill, B. G. Johnson, W. Chen, M. W. Wong, J. L. Andres, M. Head-Gordon, E. S. Replogle, J. A. Pople, Gaussian, Inc., Pittsburgh, PA, **1998**; energy minimization of **3**: B3LYP/6-31 + G(d)//B3LYP/6-31 + G(d); sum of the electronic energies = −862.162624 Hartree; sum of the electronic and zero-point energies = −861.640739 Hartree.

[12] a) D. Hoppe, T. Hense, *Angew. Chem.* **1997**, *109*, 2376 – 2410; *Angew. Chem. Int. Ed. Engl.* **1997**, *36*, 2282 – 2316; b) A. Basu, S. Thayumanavan, *Angew. Chem.* **2002**, *114*, 740 – 763; *Angew. Chem. Int. Ed.* **2002**, *41*, 716 – 738; c) NMR spectroscopic studies of a dimeric *i*PrLi (−)sparteine diethyl ether complex : D. J. Gallagher, S. T. Kerrick, P. Beak, *J. Am. Chem. Soc.* **1992**, *114*, 5872 – 5873.

[13] K. B. Wiberg, W. F. Bailey, *Angew. Chem.* **2000**, *112*, 2211 – 2213; *Angew. Chem. Int. Ed.* **2000**, *39*, 2127 – 2129.

[14] P. Flükiger, H. P. Lüthi, S. Portmann, J. Weber, Swiss Center for Scientific Computing, MOLEKEL 4.0, Manno (Switzerland), **2000**.

[15] a) K. B. Wiberg, W. F. Bailey, *J. Mol. Struct.* **2000**, *556*, 239 – 244; b) K. B. Wiberg, W. F. Bailey, *J. Am. Chem. Soc.* **2001**, *123*, 8231 – 8238.

[16] D. Stalke, *Chem. Soc. Rev.* **1998**, *27*, 171 – 178; b) T. Kottke, R. J. Lagow, D. Stalke, *J. Appl. Crystallogr.* **1996**, *29*, 465 – 468; c) T. Kottke, D. Stalke, *J. Appl. Crystallogr.* **1993**, *26*, 615 – 619.

 © 2003 Wiley-VCH Verlag GmbH & Co. KGaA, Weinheim

Polymer-Bound Mo Complexes

Stepwise Solid-Phase Synthesis of Di- and Trinuclear Metal Complexes**

Katja Heinze and Juan D. Bueno Toro*

Monodisperse oligomers play a central role in understanding the chemistry and the physics of polymeric organic and inorganic materials.[1] The synthesis of monodisperse oligomers can be achieved by self-organization processes, random synthesis followed by separation processes, or by a step-by-step synthesis. All these strategies present their own advantages and disadvantages. Full control over chain length, end groups, and building-block sequence can be achieved using a stepwise approach. While this strategy is conceptually straightforward, it becomes increasingly tedious for higher oligomers owing to the purification steps needed. A particular elegant method for a repeated stepwise synthesis is the solid-phase synthesis methodology which allows the purification of all intermediates by simple filtration. This strategy has been successfully applied to the synthesis of organic oligomeric compounds[2] while organometallic oligonuclear complexes have not been prepared in a stepwise manner by solid-phase synthesis. Mononuclear metal complexes have been prepared by solid-phase synthesis[3–12] for example, for biolabeling purposes or oligonucleotide-DNA/RNA binding studies and a dinuclear complex[13] has been synthesized by simultaneous double metalation of a peptide bound to a solid phase.

We have already designed a system (polystyrene (PS)/divinyl benzene–silyl ether linker–bidentate Schiff base ligand; **1b** in Scheme 1) which allows standard reactions of coordination and organometallic chemistry to be performed under solid-phase reaction conditions and the release of the final products from the insoluble matrix by fluoridolysis of the silyl ether linker.[14,15] The first application of this solid-phase reaction system to the synthesis of di- and trimetallic complexes is reported herein.

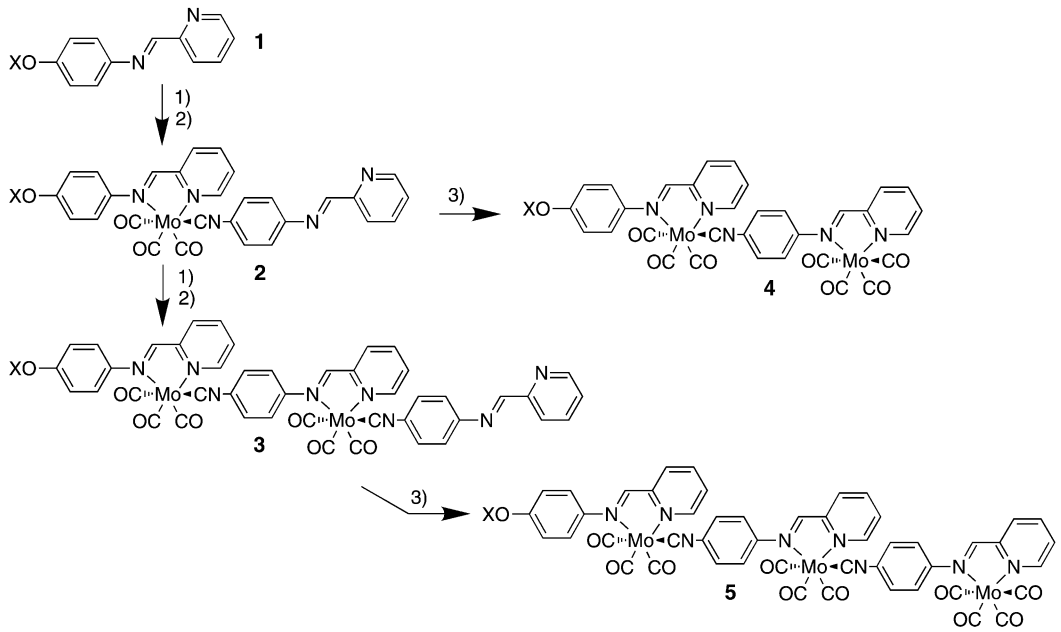
The molybdenum carbonyl complexes reported herein possess several properties which make them suitable for solid-phase synthesis approach, these are: 1) substitutionally inert metal–ligand bonds (molybdenum–carbonyl and molybdenum–isonitrile bonds), 2) carbonyl and isonitrile ligands which serve as sensitive analytical probes for IR spectroscopic analysis of the solid-phase system,[16,17] 3) highly colored complexes which permits UV/Vis spectroscopic analysis of

[*] Dr. K. Heinze, Dipl.-Chem. J. D. B. Toro
Anorganisch-Chemisches Institut
Universität Heidelberg
Im Neuenheimer Feld 270, 69120 Heidelberg (Germany)
Fax: (+49) 6221-545-707
E-mail: katja.heinze@urz.uni-heidelberg.de

[**] This work was supported by the Deutsche Forschungsgemeinschaft and the Fonds der Chemischen Industrie. The generous support of Prof. Dr. G. Huttner is gratefully acknowledged.

Supporting information for this article is available on the WWW under http://www.angewandte.org or from the author.

 DOI: 10.1002/anie.200351849 © 2003 Wiley-VCH Verlag GmbH & Co. KGaA, Weinheim



Scheme 1. Synthesis of oligonuclear molybdenum carbonyl complexes by solution phase (**1a**–**5a**; X = H) and solid-phase (**1b**–**5b**; X = PS-Si(*i*Pr)$_2$) methods. 1) $[(CH_3CN)_3Mo(CO)_3]$; 2) CN–(N∩N′); 3) $[(CH_3CN)_2Mo(CO)_4]$.

the solid-phase system), and 4) thermally releasable carbonyl ligands which can be detected by thermogravimetric (TG) analysis of the solid-phase system.

The reactions performed are summarized in Scheme 1. Stirring the functionalized resin **1b**[15] with an excess of $[(CH_3CN)_3Mo(CO)_3]$ yields a reactive, immobilized [(diimine)$Mo(CO)_3(CH_3CN)$] complex which, after filtration and washing, can then be treated with an excess of the bridging isonitrile Schiff base ligand CN–(N∩N′)[18] to give the green, immobilized tricarbonyl isonitrile complex **2b** (Scheme 1) (the replacement of the CO ligands by CN–(N∩N′) does not occur under these conditions[15]). This complex possesses a potential chelating diimine moiety. To this diimine unit a {$Mo(CO)_4$} end cap is attached by treating the resin with an excess of $[(CH_3CN)_2Mo(CO)_4]$ to give the black dinuclear complex **4b** (Scheme 1). Alternatively, the chain-growth steps can be repeated by adding $[(CH_3CN)_3Mo(CO)_3]$ and CN–(N∩N′) to form the green dinuclear complex **3b** (Scheme 1). End capping with $[(CH_3CN)_2Mo(CO)_4]$ furnishes the immobilized trinuclear complex **5b**.

Thermogravimetric analysis of the metal-complex-functionalized resins **2b**–**5b** shows that upon heating to 200 °C carbon monoxide is released. This result is confirmed by IR spectroscopic analysis of the gas phase and by thermogravimetric analysis of the free complex **2a** (see Supporting Information). The amount of CO released at 200 °C corresponds well to the expected CO loss.[19] This finding indicates the expected number of molybdenum–carbonyl units are present in the polymers **2b**–**5b**.

As IR and UV/Vis spectra of these oligonuclear complexes are superpositions of spectra of corresponding mononuclear complexes (see the Supporting Information and refs. [18,20,21]) the complex growth on the solid support can

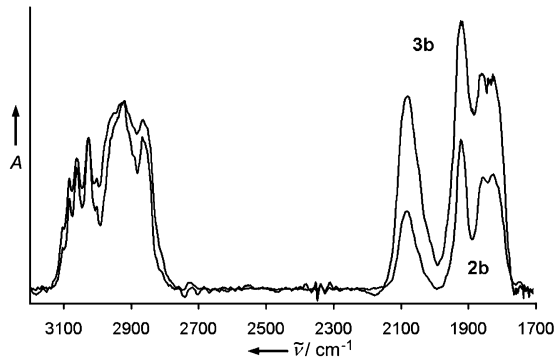


Figure 1. IR spectra of resins **2b** and **3b**.

conveniently be observed by these methods. Figure 1 shows the IR spectra of polymers **2b** and **3b**. The relative intensities of the ν_{CO} band ($\tilde{\nu}$ = 1923, 1856, 1828 cm^{-1}) and ν_{CN} band ($\tilde{\nu}$ = 2080 cm^{-1}) approximately double when a second {$Mo(CO)_3$CN–(N∩N′)} fragment is added to resin **2b** to give **3b** (compared to the ν_{CH} bands of the polystyrene backbone as internal standard). The same observation holds for resins **4b** and **5b** which additionally display the characteristic ν_{CO} absorption bands ($\tilde{\nu}$ = 2013 cm^{-1}) of the {$Mo(CO)_4$} fragments (Figure 2).

The colors of the complex-functionalized resins arise from several absorption bands in the visible region: π–π* absorptions of the diimine chromophore at around 400 nm, metal-to-ligand charge transfer (MLCT) bands of the [(diimine)$Mo(CO)_3$(CN-R)] chromophore at around 680 nm and MLCT bands of the [(diimine)$Mo(CO)_4$] chromophore at around 600 nm.[15,18,20,21] Consequently, the UV/Vis spectra of the immobilized di- and trinuclear complexes display absorption bands corresponding to the presence of the incorporated

 © 2003 Wiley-VCH Verlag GmbH & Co. KGaA, Weinheim

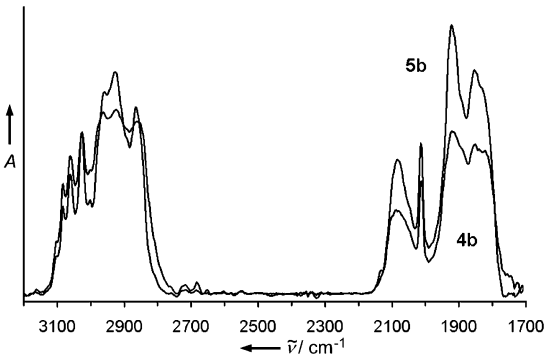
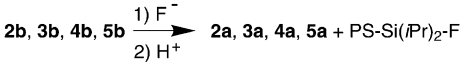


Figure 2. IR spectra of resins **4b** and **5b**.

chromophores: resins **2b** and **3b** exhibit absorption bands at 400 and 680 nm, while resins **4b** and **5b** additionally absorb at 600 nm. Thus resins **2b** and **3b** with only [(diimine)Mo(CO)$_3$(CN-R)] chromophores appear green and resins **4b** and **5b** with additional [(diimine)Mo(CO)$_4$] chromophores appear black.

Cleavage of the immobilized complexes **2b**, **3b**, **4b**, and **5b** with tetra-*n*-butylammonium fluoride and protonation of the soluble anionic complexes with acetic acid (Scheme 2) is



Scheme 2. Cleavage of the complexes **2a**–**5a** from the support.

easily monitored by IR spectroscopy of the solution. The appearance of ν_{CO} absorption bands in the IR spectra of the solutions indicates the release of the carbonyl complexes from the solid support into solution, protonation of the anionic complexes shifts all the ν_{CO} absorption bands to higher energy as expected (see Experimental Section). Removing the insoluble support by filtration gives complexes **2a**, **3a**, **4a**, and trinuclear complex **5a**, respectively (Scheme 2). The soluble complexes **2a**–**5a** were characterized by standard spectroscopic techniques. The ^{1}H NMR spectra of solutions of **2a**–**5a** display several resonance signals in the aromatic region. Significant shifts of signals arising from the protons of the dangling CN−(N∩N′) ligand in **2a** and **3a** are observed upon coordination of the {Mo(CO)$_4$} unit to give **4a** and **5a**, respectively: the signal of the α proton of the pyridine part of the dangling ligand is shifted downfield by 0.6 ppm, the signal of the δ proton is shifted to upfield by 0.3 ppm, and the signal of the imine proton is shifted to higher field by 0.1 ppm as a result of coordination to the metal and the transoid/cisoid rearrangement of the ligand (Scheme 1, see Supporting Information).

For comparison purposes all these complexes have also been prepared by standard solution synthesis (Scheme 1, X = H; see Supporting Information). In the solution-phase synthesis fewer synthetic steps are needed for the synthesis of oligonuclear complexes. However, purification of intermediates is much more difficult. Additionally, in solution, exact stoichiometric conditions have to be complied with to avoid tedious separations. In contrast the solid-phase approach enables the use of simple purification techniques that are identical for all intermediates and optimization of each step is not needed. Moreover, regents can be used in excess to drive the reactions to completion and thus avoiding premature chain truncation. These advantages outweigh the additional steps needed for solid-phase synthesis (functionalization of the polymer and cleavage) especially for higher oligomers.

Experimental Section

1a, **1b** and (4-isocyanophenyl)pyridine-2-ylmethylene amine CN−(N∩N′) were prepared by published procedures.[15,18] All the polystyrene resins used were cross-linked with 2% divinyl benzene. Ligand loading of resin **1b** was 0.50 mmol g^{-1}. All manipulations were carried out under argon. For the solid-phase reactions a flask with a nitrogen inlet and a coarse-porosity fritted glass filter that allows addition and removal of solvents and reagents without exposure to the atmosphere was used. Spectroscopic measurements were carried out as described elsewhere.[15]

2b: [(CH$_3$CN)$_3$Mo(CO)$_3$] (115 mg, 0.38 mmol) dissolved in CH$_3$CN (4 mL) was added to resin **1b** (500 mg, 0.25 mmol) swollen in toluene (5 mL). The suspension was stirred for 20 min and the resin turned from yellow to blue. The solvents were removed by filtration and the polymer was washed with toluene/CH$_3$CN (1:1) until IR spectroscopy indicated complete removal of the excess [(CH$_3$CN)$_3$Mo(CO)$_3$]. Owing to the sensitivity of the immobilized complex, the resin swollen in toluene was immediately treated with the ligand CN−(N∩N′) (79 mg, 0.38 mmol) dissolved in THF (5 mL). The polymer turned green immediately and after 30 min the resin was washed with THF until IR spectroscopy indicated complete removal of the excess CN−(N∩N′). The resin **2b** was dried in vacuo giving a green powder or used directly for further reactions. No soluble [(diimine)Mo(CO)$_x$] complexes were detected by IR spectroscopy at any stage of the reaction. IR (CsI): $\tilde{\nu}$ = 2084 (m, CN), 1921 (vs, CO), 1857 (s, CO), 1826 cm^{-1} (s, CO). UV/Vis: λ_{max} = 660 nm. TG: $\Delta m/m$ = 4.4% at 200 °C.

3b: prepared by the same procedure as **2b** but starting from **2b** IR (CsI): $\tilde{\nu}$ = 2083 (m, CN), 1923 (vs, CO), 1856 (s, CO), 1830 cm^{-1} (s, CO). UV/Vis: λ_{max} = 660 nm. TG: $\Delta m/m$ = 7.7% at 200 °C.

4b: [(CH$_3$CN)$_2$Mo(CO)$_4$] (110 mg, 0.38 mmol) dissolved in THF (4 mL) was added to resin **2b** (obtained from 500 mg **1b**) swollen in toluene (5 mL). After stirring for 2 h the resin was washed with THF until IR spectroscopy indicated complete removal of the excess [(CH$_3$CN)$_2$Mo(CO)$_4$]. The resin **4b** was dried in vacuo giving a black powder. No soluble [(diimine)Mo(CO)$_x$] complexes were observed by IR spectroscopy at any stage of the reaction. IR (CsI): $\tilde{\nu}$ = 2086 (m, CN), 2013 (m, CO), 1919 (vs, CO), 1851 (s, CO), 1826 cm^{-1} (s, CO). UV/Vis: λ_{max} = 710 nm. TG: $\Delta m/m$ = 8.7% at 200 °C.

5b: was obtained by the same procedure as for **3b** but by starting from **3b**. IR (CsI): $\tilde{\nu}$ = 2084 (m, CN), 2014 (m, CO), 1922 (vs, CO), 1853 (s, CO), 1833 cm^{-1} (s, CO). UV/Vis: λ_{max} = 720 nm. TG: $\Delta m/m$ = 11.2% at 200 °C.

Cleavage of the resin bound complexes: tetra-*n*-butylammonium fluoride (TBAF·3H$_2$O; 158 mg, 0.5 mmol) in THF (5 mL) was added to the appropriate resin **2b**–**5b** (starting from 500 mg of **1b**; 0.25 mmol) swollen in THF (3 mL). The suspension was stirred slowly for 6 h. The colored solution was collected by filtration and the resin was washed thoroughly with THF until the washings were colorless. The combined filtrates were carefully acidified with degassed acetic acid (0.05 mL) to give intensely colored solutions of the respective complexes. Characteristic IR absorption bands before acidification: **2a**$^-$: $\tilde{\nu}$ = 2093 (m, CN), 1914 (vs, CO), 1840 (s, CO), 1810 cm^{-1} (s, CO); **3a**$^-$: $\tilde{\nu}$ = 2091 (m, CN), 1914 (vs, CO), 1839 (s, CO), 1812 cm^{-1} (s, CO); **4a**$^-$: $\tilde{\nu}$ = 2094 (m, CN), 2009 (m, CO), 1912 (vs, CO), 1897 (vs, CO), 1835 (s, CO), 1808 cm^{-1} (s, CO); **5a**$^-$: $\tilde{\nu}$ = 2094 (m, CN), 2009

 © 2003 Wiley-VCH Verlag GmbH & Co. KGaA, Weinheim

(m, CO), 1911 (vs, CO), 1900 (vs, sh, CO), 1835 (s, CO), 1808 cm^{-1} (s, CO). The complexes were precipitated by adding diethyl ether/hexanes. Overall yields (solid-phase synthesis, cleavage, and acidification) based on the loading of **1b** were between 40 and 85% (depending on the solubility of the complex). After cleavage, mass spectrometry of the remaining silyl fluoride resins indicated the complete removal of the complexes.[14,15] The complexes were characterized by IR, UV/Vis, and ^{1}H NMR spectroscopy and the obtained data correspond to those obtained from the solution-phase synthesized complexes **2a**–**5a** (see Supporting information).

Received: May 9, 2003 [Z51849]

Keywords: bridging ligands · molybdenum · polymer-bound complexes · polynuclear complexes · solid-phase synthesis

[1] *Electronic Materials: The Oligomer Approach* (Eds.: K. Müllen, G. Wegner), Wiley-VCH, Weinheim, **1998**.
[2] F. Zaragoza Dörwald, *Organic Synthesis on Solid Phase*, Wiley-VCH, Weinheim, **2000**.
[3] M. S. Robillard, A. R. P. M. Valentijn, N. J. Meeuwenoord, G. A. van der Marel, J. H. van Boom, J. Reedijk, *Angew. Chem.* **2000**, *112*, 3226–3229; *Angew. Chem. Int. Ed.* **2000**, *39*, 3096–3099.
[4] K. S. Schmidt, M. Boudvillain, A. Schwartz, G. A. van der Marel, J. H. van Boom, J. Reedijk, B. Lippert, *Chem. Eur. J.* **2002**, *8*, 5566–5570.
[5] M. S. Robillard, J. S. Leith, G. A. van der Marel, J. H. van Boom, J. Reedijk, *Eur. J. Inorg. Chem.* **2003**, 1529–2532.
[6] D. R. van Staveren, N. Metzler-Nolte, *Chem. Commun.* **2002**, 1406–1407.
[7] K. S. Schmidt, D. V. Filippov, N. J. Meeuwenoord, G. A. van der Marel, J. H. van Boom, B. Lippert, J. Reedijk, *Angew. Chem.* **2000**, *112*, 383–385; *Angew. Chem. Int. Ed.* **2000**, *39*, 375–377.
[8] S. I. Khan, A. E. Beilstein, M. W. Grinstaff, *Inorg. Chem.* **1999**, *38*, 418–419.
[9] S. I. Khan, A. E. Beilstein, M. Sykora, G. D. Smith, X. Hu, M. W. Grinstaff, *Inorg. Chem.* **1999**, *38*, 3922–3925.
[10] A. E. Beilstein, M. W. Grinstaff, *Chem. Commun.* **2000**, 509–510.
[11] I. Vargas-Baca, D. Mitra, H. J. Zulyniak, J. Banerjee, H. F. Sleiman, *Angew. Chem.* **2001**, *113*, 4765–4768; *Angew. Chem. Int. Ed.* **2001**, *40*, 4629–4632.
[12] J. F. Valliant, R. W. Riddoch, D. W. Hughes, D. G. Roe, T. K. Fauconnier, J. R. Thornback, *Inorg. Chim. Acta* **2001**, *325*, 155–163.
[13] S. van Zutphen, M. S. Robillard, G. A. van der Marel, H. S. Overkleeft, H. den Dulk, J. Brouwer, J. Reedijk, *Chem. Commun.* **2003**, 634–635.
[14] K. Heinze, U. Winterhalter, T. Jannack, *Chem. Eur. J.* **2000**, *6*, 4203–4210.
[15] K. Heinze, *Chem. Eur. J.* **2001**, *7*, 2922–2932.
[16] B. Yan, *Acc. Chem. Res.* **1998**, *31*, 621–630.
[17] B. Yan, H.-U. Gremlich, S. Moss, G. M. Coppola, Q. Sun, L. Liu, *J. Comb. Chem.* **1999**, *1*, 46–54.
[18] K. Heinze, V. Jacob, *Eur. J. Inorg. Chem.*, accepted.
[19] The theoretical amount of CO loss is calculated according to the following formula: $\Delta m/m = 100\,(n_{CO} \times M_{CO})/(M_{resin} + M_{complex})$ with $n_{CO} = 3$, 6, 7, 10, $M_{CO} = 28\ g\,mol^{-1}$, $M_{resin} = 1500\ g\,mol^{-1}$ (resin loading 0.5 $mmol\,g^{-1}$) and $M_{complex} = 387$, 774, 595, 982 $g\,mol^{-1}$ for resins **2b, 3b, 4b**,and **5b**, respectively, giving $\Delta m/m =$ 4.45, 7.39, 9.36, 11.28% for resins **2b, 3b, 4b**, and **5b**, respectively.
[20] K. Heinze, *J. Chem. Soc. Dalton Trans.* **2002**, 540–547.
[21] K. Heinze, V. Jacob, *J. Chem. Soc. Dalton Trans.* **2002**, 2379–2385.

 © 2003 Wiley-VCH Verlag GmbH & Co. KGaA, Weinheim

Jahn-Teller Effects

Bond-Stretch Isomerism: Trapped Isomeric Structures of Hexacoordinate Copper(II) Bispidine Chromophores along a Jahn–Teller Active Vibrational Coordinate

Peter Comba, Andreas Hauser, Marion Kerscher, and Hans Pritzkow*

Hexacoordinate copper(II) complexes usually have a typical structure, derived from an elongated octahedron. This is due to vibronic coupling between the two components of the relevant vibrational mode of e_g symmetry (in O_h) and the ^2E_g electronic wave function (in O_h), which leads to tetragonal (Q_θ) or rhombic (Q_ε) distortions (Figure 1).[1–5] The rim of the "Mexican hat" potential (dotted line in Figure 1b) corresponds to linear combinations of Q_θ and Q_ε and is warped with minima at $\phi = 0°$, 120°, and 240° (Figure 1c). Each of these minima corresponds to a tetragonally elongated structure with a $d_{x^2-y^2}$ ground state. The maxima represent tetragonally compressed structures in the d_{z^2} ground state.[1–4]

Two features emerge from Figure 1c: 1) Fluxionality, if the three minima have similar energy and the barriers are low, and 2) isomerism, if asymmetric ligands (or asymmetry arising from the crystal lattice) lead to three energetically and structurally distinct minima. A multiple (at least double) minima potential energy surface, for the same spin multiplicity of an isolated molecule, is the basis for distortional or bond-stretch isomerism. This phenomenon has been discussed since its first theoretical prediction[6] and putative experimental confirmation.[7–9] "Jahn–Teller isomers" (Figure 1c) have not been discussed in this context, although they fulfil the conditions for bond-stretch isomerism. This situation is not surprising, since, to date, for copper(II) complexes of asymmetric ligands, there are no reported examples of isolated and structurally characterized conformations related to the minima of the potential-energy surface shown in Figure 1c. Herein we report a structural study of hexacoordinate copper(II) bispidine complexes (Scheme 1), in which two distinct conformations of the chromophore (the structure of the metal ion and donor atoms) have been trapped as well as structurally and spectroscopically characterized.

A large variety of bispidine-type ligands and the corresponding transition-metal complexes have been reported in the last few years.[10–14] The ligands are derived from the 3,7-

[*] Prof. Dr. P. Comba, Dr. M. Kerscher, Dr. H. Pritzkow
Anorganisch-Chemisches Institut
Universität Heidelberg
Im Neuenheimer Feld 270, 69120 Heidelberg (Germany)
Fax: (+49) 6221-546-617
E-mail: peter.comba@aci.uni-heidelberg.de
Prof. Dr. A. Hauser
Département de chimie physique
Université de Genève
30 quai Ernest-Ansermet, 1211 Genève 4 (Switzerland)

Supporting information for this article is available on the WWW under http://www.angewandte.org or from the author.

 © 2003 Wiley-VCH Verlag GmbH & Co. KGaA, Weinheim DOI: 10.1002/anie.200351900

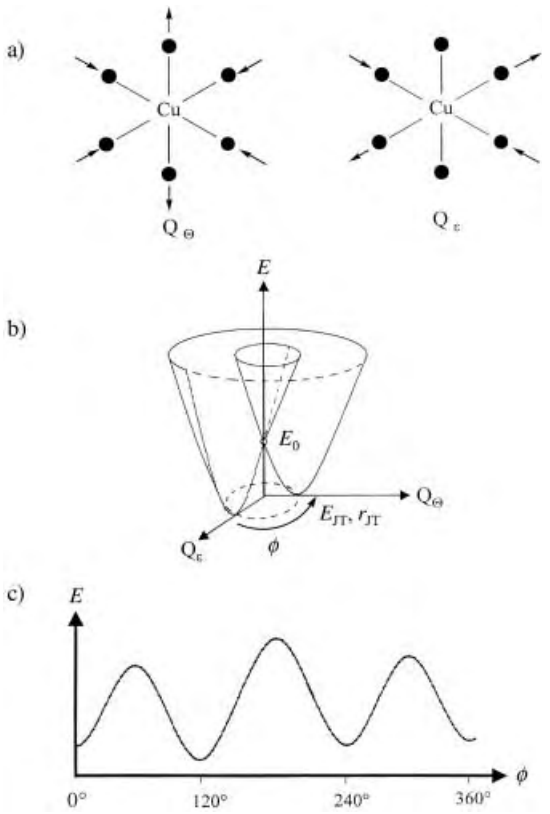
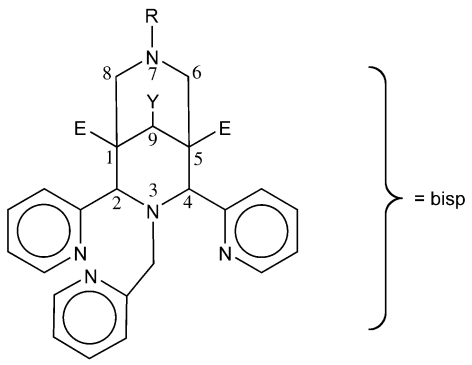


Figure 1. a) The Q_θ and Q_ε components of the e_g vibrational mode (in O_h symmetry), $Q_\theta = r_{JT}\cos\phi$, $Q_\varepsilon = r_{JT}\sin\phi$, $\Psi_{el} = d_{x^2-y^2}\cos(\phi/2) + d_{z^2}\sin(\phi/2)$. b) "Mexican hat" vibronic potential energy surface for a Cu^{II} center in an octahedral ligand field. c) Circular cross section of the warped rim in (b) as a function of ϕ with three nondegenerate minima, correspond to three distinct tetragonally elongated structures and the three nondegenerate saddle points, correspond to three distinct tetragonally compressed structures.



L^1 : R = CH_3, CY = C=O (mononuclear, ketone)
L^2 : R = CH_3, CY = $C(OH)_2$ (mononuclear, hydrate)
L^3 : R = $(CH_2)_2$bisp, CY = C=O (dinuclear, ketone)
L^4 : R = $(CH_2)_2$bisp, CY = $C(OH)_2$ (dinuclear, hydrate)

Scheme 1. Pentadentate bispidine ligands (E = $COOCH_3$).

diazabicyclo[3.3.1]nonan-9-one backbone, with various donors substituted at C2, C4, N3, N7 (Scheme 1). The bidentate 3,7-diazabicyclo[3.3.1]nonan-9-one fragment is highly preorganized, and the tetradentate 2,4-bis(2-pyridyl)-3,7-diazabicyclo[3.3.1]nonan-9-one has a high degree of complementarity for a range of first-row transition-metal ions,[15] which leads to high complex stabilities, reminiscent of those found with macrocyclic ligands.[16]

The coordination geometry enforced by the bispidine is of particular interest for copper(II) centers since the majority of resulting structures have a unique square-pyramidal (or *cis*-octahedral) geometry with a long Cu–N7 bond and a strong bond to substrates *trans* to N3.[14–18] Of note is that, while the bispidine-type ligands are rigid,[14] the coordination sphere is highly elastic,[15] and this leads to interesting structural variations.[14] The very flat potential-energy surface (elasticity of the coordination sphere) with shallow minima is also supported by computational studies,[14,15] as well as by the calculated small inner-sphere reorganization energy for the $Cu^{II/I}$ electron self-exchange process, which is in agreement with the experimental rate.[16]

Therefore, it is not surprising that, with the pentadentate ligands L^1–L^4, which have an additional pyridine donor *trans* to N7, the first distortional isomers of copper(II) chromophores along a Jahn–Teller active vibrational coordinate could be trapped. Figure 2 shows the single-crystal structures

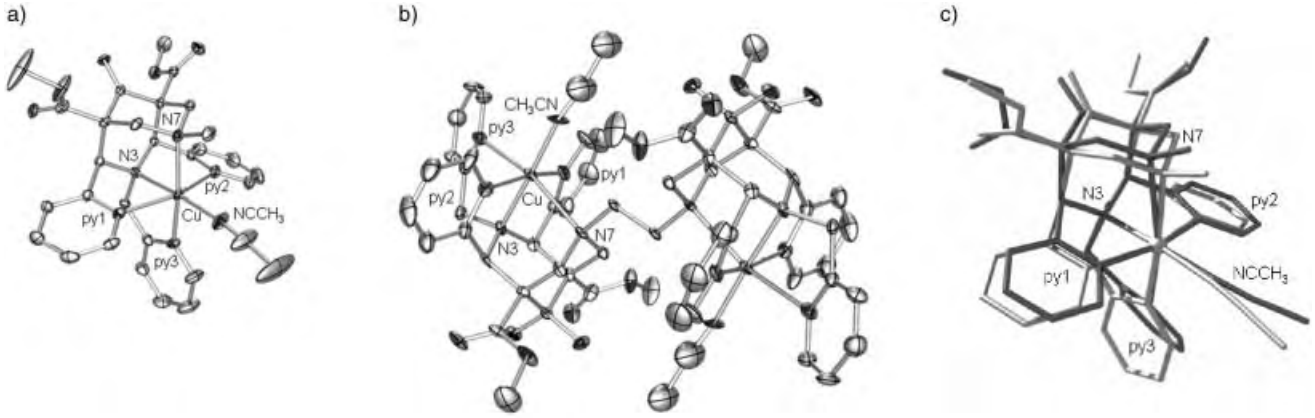


Figure 2. ORTEP[28] plots of the molecular cations of a) $[Cu(L^1)(NCCH_3)]OTf_2$ (**1**), b) $[Cu_2(L^4)(NCCH_3)_2]OTf_4$ (**4**). Plots of the other structures are available as Supporting Information. c) Overlay plot of the Cu^{II} chromophores of **1** and $[Cu_2(L^3)(NCCH_3)_2]OTf_4$ (**3**).

 © 2003 Wiley-VCH Verlag GmbH & Co. KGaA, Weinheim

of the mononuclear complex of copper(II) **1** with L^1 and of the dinuclear complex **4** with L^4, as trifluormethanesulfonate salts (OTf) with CH_3CN as coligand to complete hexacoordination. Selected structural parameters of complexes **1**–**4** are given in Table 1.[19] While the coordination geometry of the dinuclear complexes **3** and **4** (with L^3 and L^4) is similar to that of the published structure of $[Cu(L^2)(Cl)]Cl$,[12] with elongated Cu–N7 and Cu–py3 (*trans* to N7) bonds, the chromophores of the mononuclear complexes **1** and **2** (with L^1 and L^2) with coordinated CH_3CN or OH_2 are strikingly different, with short Cu–N7 and Cu–py3 bonds, and very long bonds to the two nitrogen atoms of the *trans*-disposed pyridine donors py1 and py2. That is, the two sets of structures are, with respect to the $CuN_2(py)_3(NCCH_3)$ chromophore, distortional isomers which correspond to different trapped molecular conformations along a Jahn–Teller active vibration. Of note is that the Cu–N7 and Cu–N3 bonds, specifically the extremely weak Cu–N7 bonds in structures **3** and **4** (Table 1) vary strongly as a function of the C9 substituents: the ligands with a ketone (L^1 and L^3), rather than a hydrate (L^2 and L^4) group, have a decreased nucleophilicity of the amine donors.[21,22] However, this is not the key driving force for the isomerization along the rim of the Mexican hat potential-energy surface.

Table 1: Selected structural parameters of $[Cu(L^1)(CH_3CN)](OTf)_2$ (**1**), $[Cu(L^2)(H_2O)](OTf)_2$ (**2a**), $[Cu(L^2)(Cl)]Cl$ (**2b**),[12] $[Cu_2(L^3)(CH_3CN)_2](OTf)_4$ (**3**), and $[Cu_2(L^4)(CH_3CN)_2](OTf)_4$ (**4**).[a,b]

	Cu–N3	Cu–N7	Cu–N_{py1}	Cu–N_{py2}	Cu–N_{py3}[c]	Cu–$NCCH_3$
1	2.105(2)	2.106(2)	2.353(2)	2.260(2)	2.027(2)	2.015(2)
2a (Cu 1)	2.058(3)	2.082(3)	2.330(3)	2.472(3)	2.038(3)	1.972(3)[d]
2a (Cu 2)	2.056(3)	2.072(3)	2.314(3)	2.519(3)	2.034(3)	1.983(3)[d]
2b	2.070(2)	2.478(2)	2.011(2)	1.987(2)	2.544(2)	2.255(1)[e]
3	2.029(2)	2.600(2)	2.021(2)	1.976(2)	2.372(2)	1.972(2)
4	2.052(3)	2.428(3)	2.027(3)	1.992(3)	2.331(3)	2.033(17)
4[f]	2.059(2)	2.456(2)	2.033(2)	2.001(2)	2.369(2)	2.035(8)

[a] All diffraction data at 100 K unless otherwise stated [b] in **4**, $NCCH_3$ is partially substituted by OH_2. [c] *trans* to N7. [d] Cu–OH_2. [e] Cu–Cl. [f] diffraction data at 298 K.

Molecular mechanics[14] and preliminary DFT calculations with the tetradentate bispyridine-substituted bispidine ligand indicate that the potential-energy surfaces of transition-metal bispidine chromophores are flat, in particular for Cu^{II}. Optimization of the two isomeric structures of the Cu^{II} complexes reported here with a model for the pentadentate ligands L^1–L^4,[23] using the same force field as before,[14] leads to nearly degenerate structures. Moreover, a continual change of the bond lengths along the two modes of elongation induces only a relatively small strain in the ligand skeleton, which indicates that the energy barrier between the two isomers is relatively small ($\leq$ 10–15 kJ mol^{-1}).[24] That is, the elasticity of the coordination sphere is not significantly perturbed by the additional pyridine donor py3. Based on the mononuclear chromophore and steric effects alone, one therefore would expect fluxionality between the two nearly degenerate structures. Owing to the rigidity of the bispidine backbone[25] the main structural change involved with the interconversion of the two conformations is a twist of the 3,7-diazabicyclo[3.3.1]nonan-9-one backbone, which leads to a compression of the Cu–N7 and an elongation of the Cu–py1,2 bonds (or vice versa), coupled to the adjustment of torsional angles involving the three pyridine donors (Figure 2c).

The electronic contribution to the energy differences between the minima of the warped rim of the Mexican hat potential is expected to be small,[26] specifically with donors which have similar electronic properties, such as tertiary amines and pyridines. It follows that steric effects arising from the substituents at N7 (L^1 and L^2 versus L^3 and L^4) are of major importance for the stabilization of either isomer, and this also emerges from force-field calculations. The difference between the structures **1** and **2** (Table 1) suggests that electronic effects might also be of importance for the stabilization of one of the isomers, but steric effects cannot be excluded either in this case.

For the Cu^{II} complexes of L^1–L^4 in CH_3CN solution (CH_3CN as coligand), there is a reversible temperature-dependent color change from blue (low temperature) to green. This is due to a shift to lower energy of the d–d and the ligand-to-metal charge transfer (LMCT) transitions with increasing temperature (Figure 3a).[27] There are three possible explanations for this temperature dependence: 1) An equilibrium involving a ligand exchange between py3 and a CH_3CN solvent molecule; 2) an equilibrium between the two Jahn–Teller isomers; 3) the

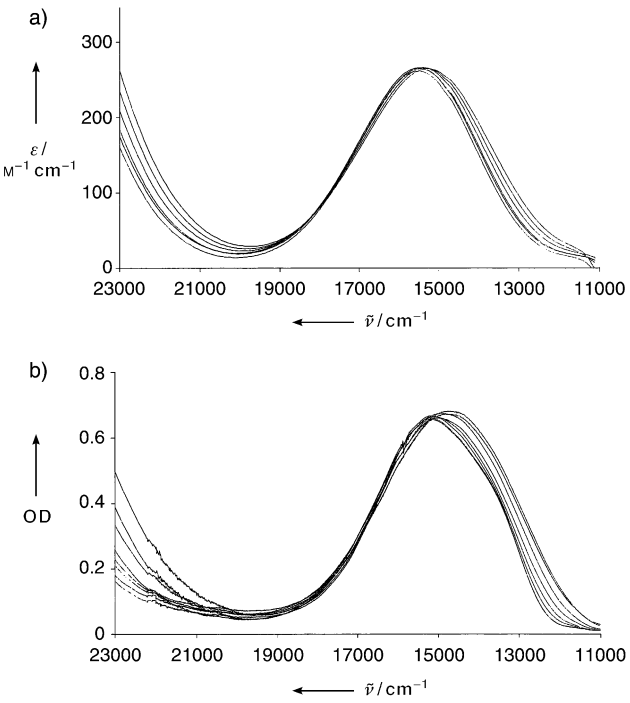


Figure 3. Temperature-dependent electronic spectra of Cu^{II}-bispidine complexes. a) solution spectra (CH_3CN, 273–353 K) of **4** b) Polarized solid-state (single crystal) absorption spectra (10–325 K); only one polarization direction is shown (crystal thickness $d = 60$ μm; see Supporting Information for further details.

 © 2003 Wiley-VCH Verlag GmbH & Co. KGaA, Weinheim

usual temperature dependence arising from vibronic coupling which leads to changes of the ligand-field strength. Ligand exchange can be excluded since the solid-state spectra of **4** (Figure 3) and the corresponding solution spectra are similar, and ligand exchange can be excluded in the solid. A temperature-dependent equilibrium between the two isomers, that is, a thermal population of the potential minimum corresponding to the Jahn–Teller distortion with a minimum at slightly higher energy is not compatible with the temperature dependence of the two X-ray structures of **4**, obtained at 100 K and 298 K (Table 1). Such an equilibrium would require the average Cu–N bond lengths along the Jahn–Teller axis, that is, Cu–N7 and Cu–py3, to decrease with increasing temperature. However, for all copper–donor bonds only the typical increase owing to anharmonicity is observed with increasing temperature. We therefore attribute the observed shift to an expansion of the chromophore resulting from the anharmonicity of the bonding potentials, and a population of the higher vibrational states at elevated temperature. In the solid a cooperative Jahn–Teller effect could stabilize one isomer, whereas in solution both isomers could still exist in a temperature-dependent dynamic equilibrium. In view of the similarity of solution and solid-state UV/Vis spectra this seems unlikely. The comparatively large shift in the d–d transitions is an indication for a flat energy surface, and this was anticipated based on various experimental and computational data. In agreement with this interpretation is the observation that the increase in total intensity of about 17% between 10 and 300 K. This variation indicates that a low-frequency odd parity vibrational mode is responsible for the temperature-dependent intensity borrowing from parity allowed transitions.

We have presented the first example of bond-stretch isomerism related to the chromophores of hexacoordinate Jahn–Teller-active Cu^{II} compounds with asymmetric ligands. The systems are not fluxional, and steric as well as electronic effects are assumed to be responsible for the stabilization of the isomer with an elongation along the py1-Cu-py2 axis for the unsubstituted (mononuclear; complexes **1** and **2**) chromophore. Steric effects (secondary interactions) are presumably responsible for the destabilization of this isomer with bulky substituents at N7 (dinuclear complexes **3** and **4**) and the selective population of the energy minimum with a chromophore elongated along N7-Cu-py3. The prerequisite for this isomerism is the combination of a rigid ligand backbone with an elastic coordination sphere. This combination leads to a flat potential-energy surface with various shallow minima (two in the present case) with strikingly different structures. In the present example the potential-energy surface is perturbed by steric interactions arising from substituents at the ligand backbone. The data indicate that a variation of the monodentate coligand may lead to drastic structural changes. We anticipate that fine-tuning of the system may lead to complexes where both isomers are thermally accessible. Recent studies indicate that subtle variations of the structures of transition-metal bispidine complexes lead to strikingly different reactivities.[11,12,16] The possibility to switch between active and inactive forms by a variation of external parameters, for example, a change of temperature, is an attractive possible extension of the present results.

Experimental Section

The piperidone precursor dimethyl-4-oxo-2,6-di-(2-pyridyl)-1-(2-pyridylmethyl)piperidine-3,5-dicarboxylate (pL)[10] and the ligand L^1[10] were prepared by published procedures. Variable-temperature solution UV/Vis spectra were measured in thermostated quartz cuvettes (1 cm). Single-crystal UV/Vis spectra were measured on a Bruker IFS66 FT-spectrophotometer connected with an Oxford-Instruments closed-cycle system for temperature control.

L^3: Aqueous formaldehyde (37%; 4.0 mL, 53.7 mmol) and 1,2-diaminoethane (0.90 mL, 13.4 mmol) were added to a hot solution of the precursor pL (10.0 g, 21.7 mmol) in THF (100 mL). The mixture was stirred under reflux for 2 h, then for 5 h at room temperature. The solvent was evaporated, the residue dissolved in hot ethanol (60 mL), stored for 2 days at 4°C, and the crude solid product collected by filtration. Water (150 mL) was added to the filtrate to precipitate a further crop. Recrystallization from CH_3CN (40 mL) yielded 2.6 g (2.53 mmol, 12%) of the bispidone L^3 as a fine white powder. Elemental analysis (%) calcd for $C_{56}H_{56}N_{10}O_{10}$ (1029.11): C 65.36, H 5.48, N 13.61; found: C 65.10, H 5.50, N 13.64. ^{1}H NMR (200.13 MHz,$CDCl_3$): $\delta = 2.36$ (s, 4H, N-CH_2-); 2.69 (d, $^2J = 11.8$ Hz, 4H, -CH_{ax}H$_{eq}$-); 3.12 (d, $^2J = 11.8$ Hz, 4H, -CH$_{ax}$$H_{eq}$-); 3.75 (s, 16H, O-$CH_3$, N-$CH_2$-); 5.42 (s, 4H, N-CH-); 6.76 (d, $^3J = 7.7$ Hz, 2H, H-aromat.); 6.95–7.01 (m, 2H, H-aromat.); 7.06–7.12 (m, 4H, H-aromat.); 7.38 (td, $^3J = 7.6$ Hz, $^4J = 1.7$ Hz, 2H, H-aromat.); 7.57 (td, $^3J = 7.7$ Hz, $^4J = 1.6$ Hz, 4H, H-aromat.); 7.94 (d, $^3J = 7.7$ Hz, 4H, H-aromat.); 8.41–8.47 (m, 6H, H-aromat.). ^{13}C NMR (50.32 MHz, $CDCl_3$): $\delta = 53.01$ (4C, O-CH_3); 55.06 (2C, N-CH_2-CH_2-N); 57.63 (2C, N-CH_2-); 59.61 (4C, N-CH_2-); 63.05 (4C, -C-CO); 70.63 (4C, N-CH-); 122.14, 123.18, 124.24, 124.88, 136.10, 136.35, 149.60, 157.18, 159.06 (30C, C-aromat.); 169.51 (4C, -COOCH$_3$); 203.95 ppm (2C, C=O).

The Cu^{II} complexes were obtained from CH_3CN solutions of the metal-free ligands and $Cu(OTf)_2$. Samples produced in strictly water-free solutions yielded the complexes **1** and **3** with the ketone-derivatives of the ligands (L^1 and L^3), otherwise the **2** and **4** with the hydrated ligands (L^2 and L^4) were obtained.

Structural plots of X-ray crystal structures **1**–**4**, the single crystal UV/Vis spectra of **4** and details of the molecular mechanics calculations are given as Supporting Information.

Received: May 14, 2003 [Z51900]
Published Online: September 8, 2003

Keywords: coordination chemistry · copper · Jahn–Teller effects · N ligands

[1] I. B. Bersuker, *Chem. Rev.* **2001**, *101*, 1067.
[2] M. A. Hitchman, *Comments Inorg. Chem.* **1994**, *15*, 197.
[3] B. N. Figgis, M. A. Hitchman, *Ligand Field Theory and its Applications*, Wiely-VCH, Weinheim, New York, **2000**.
[4] J. Bebendorf, H.-B. Buergi, E. Gamp, M. A. Hitchman, A. Murphy, D. Reinen, M. J. Riley, H. Stratemeier, *Inorg. Chem.* **1996**, *35*, 7419.
[5] A genuine Jahn–Teller effect is only present in hexacoordinate complexes with a degenerate ground state, that is, in octahedral or trigonal symmetries. Vibronic coupling similar to that described here for the general octahedral case also induces structural distortion and electronic stabilization with asymmetric ligand systems, which inherently lead to chromophores of lower than O_h symmetry and nondegenerate ground states.[2]
[6] W.-D. Stohrer, R. Hoffmann, *J. Am. Chem. Soc.* **1972**, *94*, 779.

 © 2003 Wiley-VCH Verlag GmbH & Co. KGaA, Weinheim

[7] An overview of the history, some early experimental studies (later disqualified as artifacts), and recent examples of bond-stretch isomerism are given in two review articles.[8,9]
[8] G. Parkin, *Chem. Rev.* **1993**, *93*, 887.
[9] M. M. Rohmer, M. Bénard, *Chem. Soc. Rev.* **2001**, *30*, 340.
[10] H. Börzel, P. Comba, K. S. Hagen, M. Merz, Y. D. Lampeka, A. Lienke, G. Linti, H. Pritzkow, L. V. Tsymbal, *Inorg. Chim. Acta* **2002**, *337*, 407.
[11] H. Börzel, P. Comba, K. S. Hagen, M. Kerscher, H. Pritzkow, M. Schatz, S. Schindler, O. Walter, *Inorg. Chem.* **2002**, *41*, 5440.
[12] P. Comba, M. Merz, H. Pritzkow, *Eur. J. Inorg. Chem.* **2003**, 1711.
[13] H. Börzel, P. Comba, K. S. Hagen, C. Katsichtis, H. Pritzkow, *Chem. Eur. J.* **2000**, *6*, 914.
[14] P. Comba, M. Kerscher, M. Merz, V. Müller, H. Pritzkow, R. Remenyi, W. Schiek, Y. Xiong, *Chem. Eur. J.* **2002**, *8*, 5750.
[15] P. Comba, W. Schiek, *Coord. Chem. Rev.* **2003**, *238–239*, 21.
[16] P. Comba, M. Kerscher, A. Roodt, unpublished results.
[17] P. Comba, A. Lienke, *Inorg. Chem.* **2001**, *40*, 5206.
[18] Subtle changes in the ligand structure may enforce a predictable change of the coordination geometry (Cu-N3 > Cu-N7 and the coligand *trans* to N7).[14,17]
[19] X-ray data were collected at −170 °C. As the OTf-anions were partly severely disordered, the SQEEZE option in PLATON[20] was used to eliminate these effects. For **4** OH_2 partially substitutes $NCCH_3$. CCDC 210369–210373 contain the supplementary crystallographic data for this paper. These data can be obtained free of charge via www.ccdc.cam.ac.uk/conts/retrieving.html (or from the Cambridge Crystallographic Data Centre, 12 Union Road, Cambridge CB2 1EZ, UK; fax: (+44) 1223-336-033; or deposit@ccdc.cam.ac.uk).
[20] A. L. Spek, *Acta Crystallogr. Sect. A* **2002**, *46*, C37.
[21] This has been observed before in other bispidine complexes, although with other metal ions the effect is less pronounced than with Cu^{II},[14] and, based on photoelectron spectra and molecular orbital calculations of diaazaadamantane derivatives,[22] it has been attributed to through-bond interactions and inductive effects.
[22] R. Gleiter, M. Kobayashi, J. Kuthan, *Tetrahedron* **1976**, *32*, 2775.
[23] L^1,L^2, substituents at C1, C5, and C9 omitted.
[24] This only includes the steric energy of the ligand; metal-centered electronic effects are excluded in this analysis. Two structures, with an elongation along the N7-Cu-py3 and the py1-Cu-py2 axis, were optimized. The ligand-induced strain (steric energies without terms including the metal ion) for the elongated py1-Cu-py2 axis structure is approximately 7 kJ mol^{-1} smaller than for the elongated N7-Cu-py3 axis structure. For details see the Supporting Information.
[25] Measured by the N3···N7 separation (2.92 ± 0.05 Å in the present structures, 2.93 ± 0.03 Å in 40 other structures with the tetradentate ligand).[14]
[26] M. A. Hitchman, Y. V. Yablokov, V. E. Petrashen, M. A. Augustyniak-Jablokov, H. Stratemeier, M. J. Riley, K. Lukaszewicz, P. E. Tomaszewski, A. Pietraszko, *Inorg. Chem.* **2002**, *41*, 229.
[27] The same effect is also observed for a dinuclear complex with a propylene bridge between the two bispidine chromophores (structure not yet available, no details reported here). The three sets of temperature-dependent spectra are significantly different but the temperature-dependent shifts are of similar magnitude. Preliminary experiments suggest that the aqua complexes have no significant temperature-dependent shifts of the d–d transitions.
[28] C. K. Johnson, ORTEP, A Thermal Ellipsoid Plotting Program, Oak National Laboratories, Oak Ridge, TN 1965.

 © 2003 Wiley-VCH Verlag GmbH & Co. KGaA, Weinheim

Mixed-Valent Titanium Complex

Aqueous Chemistry of Titanium(II) Species

Ulrich Kölle and Philipp Kölle*

Reports on titanium in the oxidation state +II are confined to solid-state compounds, such as the nonstoichiometric oxide TiO_x, the hydride TiH_2 as well as halides TiF_2 and $TiCl_2$ and a number of coordination compounds $[TiCl_2L_n]$. Although a calculated redox potential of $E°(Ti^{III}/Ti^{II}) = -0.37$ V versus the normal hydrogen electrode (NHE) appears in textbooks[1] and tables,[2] which suggests the existence of the Ti^{II}_{aq} ion, the aqueous chemistry of Ti^{II} is almost unknown.[1,3]

Titanium metal, though quite electropositive ($E°(Ti^{3+}/Ti° = -1.2$ V vs. NHE), does not dissolve in acids, except aqueous HF.[4] In the course of corrosion studies of titanium in HF Straumanis et al. observed a greenish-yellow complex which was assumed to contain the $[TiF_6]^{3-}$ ion.[5] The oxidation state +III of the Ti species formed was verified by redox titration and by monitoring the amount of hydrogen evolved on titanium metal dissolution.

We found that titanium metal (0.5 mm wire, >99%) dissolves readily with vigorous hydrogen evolution either in aqueous HF or in aqueous acids, such as HBF_4 (5%),[6] CF_3SO_3H, or H_2SO_4 (2 M) if these contained HF. Whereas the color of the resulting solution in HF resembles that described by Straumanis et al.,[7] a green solution is obtained in the stronger acids. The absorption spectrum in acid solution (Figure 1) which has two bands at 430 and 650 nm, is not in accord with a Ti^{III} complex.[8] Instead it is reminiscent of the spectrum of Ti^{II} doped into NaCl[9] and closely resembles that of the V^{3+}_{aq} ion ($\approx$400 and 600 nm assigned to $^3T_{1g} \rightarrow {}^3T_{2g}$ and $^3T_{1g} \rightarrow {}^3T_{2g}(P)$ transitions[10]), which, like the Ti^{II} species, has a

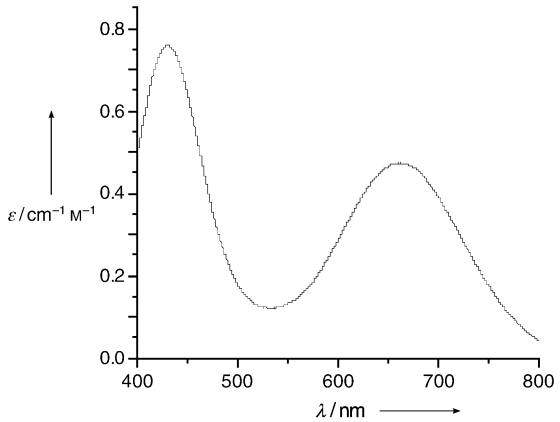


Figure 1. Absorption spectrum of Ti^{2+}_{aq} at pH 0.5.

[*] Prof. Dr. U. Kölle, Dipl. Chem. P. Kölle
Institute for Inorganic Chemistry
RWTH Aachen
52056 Aachen (Germany)
Fax: (+49) 241-80-92288
E-mail: u.koelle@ac.rwth-aachen.de

 © 2003 Wiley-VCH Verlag GmbH & Co. KGaA, Weinheim DOI: 10.1002/anie.200351280

d^2 configuration.[11] The green solution is moderately air sensitive and slowly turns brownish red (Ti^{III}) and finally to colorless (Ti^{IV}) on exposure to air.

Concentrating the solution to $\gtrsim 0.2$ M causes formation of a gray precipitate. The solid was collected and could be isolated after complete evaporation of water, followed by treatment with diethyl ether to remove excess HBF_4, and washing with acetone. Analysis of this material is in accord with the formula $TiF_3(H_2O)_2$.[12]

The structure of this compound was solved from X-ray powder data.[13] The Rietveld refinement converged with good to excellent R values, the observed and calculated profile plot is shown in Figure 2. However, standard deviations of positional parameters,[13] and therefore of bond lengths are unusually large. This effect might be due to crystallographic stacking faults of the chain structure, a problem that cannot be recognized nor resolved from powder data.

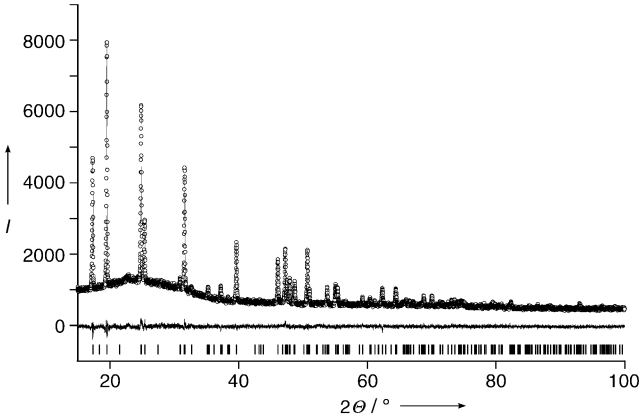


Figure 2. Upper trace: Observed verses calculated profile intensity of $Ti(TiF_6)(H_2O)_4$ as obtained from Rietveld refinement, lower trace: difference curve, position of the Bragg reflections.

The structure is built up from chains of corner-sharing, *trans*-bridged, TiX_6 octahedra of crystal chemical formulation $[TiF_4F_{2/2}][Ti(H_2O)_4F_{2/2}]$ stacked along the crystallographic c axis (Figure 3). The compound is isostructural with $Cu(H_2O)_4TiF_6$, described by Fischer et al.[14]. In accord with solution behavior (see below) the oxidation states are assigned as Ti^{IV} for $[TiF_4F_{2/2}]$ and Ti^{II} for $[Ti(H_2O)_4F_{2/2}]$. Since fluorine and oxygen are almost indistinguishable in terms of their X-ray scattering factors, labels have been assigned according to the two sets of Ti–X separations (X = F, O) found for the two Ti centers. The long distance of 2.07(2) Å was assigned to the Ti^{II}–OH_2 bond. This Ti^{II} center also has the longer bond to the bridging fluoride, 2.00(2) Å. The Ti^{IV} center has shorter bonds to terminal, 1.94(1) and bridging 1.97(2) Å fluorides. The chains are interconnected by hydrogen bonds, which is suggested by the shortest interchain contacts between water molecules of 2.65 Å. Adjacent chains are offset along the c axis by 2.62 Å, which results in an interlocked packing mode.

The X-band powder EPR spectrum of this material at room temperature shows two closely spaced lines with the same phase at $g = 1.9469$ and 1.9485 with linewidths 120 G and 24 G, respectively. The spectrum is indicative of a cubic $S = 1$ system with a very small value of the zero-field splitting parameter D ($D < 0.003$ cm^{-1}).

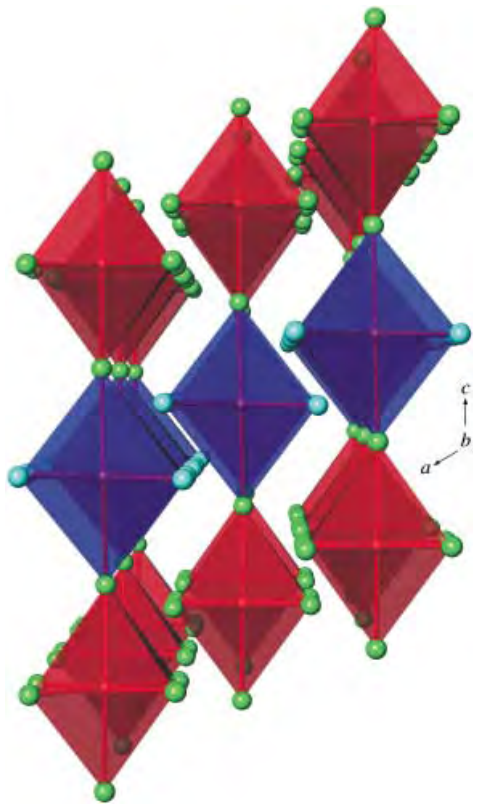


Figure 3. Structure of $Ti(TiF_6)(H_2O)_4$ viewed along the b axis. $Ti^{IV}F_6$ octahedra in red, $Ti^{II}F_2(H_2O)_4$ octahedra in blue.

The solid slowly dissolves in neutral water to give a clear yellow green solution which on acidification (with HBF_4, for example) turns into bright green and shows the same absorption spectrum as that obtained on dissolving titanium directly. We thus explain the dissolution of titanium metal in HF or acids containing HF according to Equation (1).

$$2\,Ti + 6\,HF \rightarrow [TiF_6]^{2-} + Ti^{2+} + 3\,H_2 \quad (1)$$

Owing to stoichiometric formation of Ti^{II} and Ti^{IV} the average oxidation state found for titanium in the ensuing solution, as well as the amount of hydrogen released, is the same as if Ti^{III} would have been formed, which explains the conclusions drawn by Straumanis et al.[7] Equation (1) further implies disproportionation of Ti^{III} in the presence of excess fluoride according to Equation (2).

$$2\,Ti^{3+} + 6\,F^- \rightarrow [TiF_6]^{2-} + Ti^{2+} \quad (2)$$

We verified that $TiCl_3$, dissolved in aqueous HF, directly gave the green yellow solution of Ti^{II}/Ti^{IV} which corresponds to Equation (2). A value of $E^O([TiF_6]^{2-}/Ti°) \approx -0.8$ V[4] from corrosion measurements of titanium in HF along with the calculated value of $E^O(Ti^{3+}/Ti°) = -1.2$ V leads to a very positive value for $E^O([TiF_6]^{2-}/Ti^{3+})$ and thus to a positive potential for the disproportionation in Equation (2).

 © 2003 Wiley-VCH Verlag GmbH & Co. KGaA, Weinheim

Excess F^- as well as $[TiF_6]^{2-}$ can be precipitated from the solution with Ba^{2+} or Ca^{2+} ions (as BF_4^- or $CF_3SO_3^-$ salts) whereby the absorption spectrum of the solution does not change. Since this spectrum is not influenced by the anion it must arise from the Ti^{2+} aqua ion, most probably $[Ti(H_2O)_6]^{2+}$. The formation of an insoluble hydroxide at $pH \approx 7$ is typical for a first-row +II transition-metal ion. Further characterization of the novel aqua ion and its complexing behavior is in progress in our laboratory.

Received: February 26, 2003
Revised: June 24, 2003 [Z51280]

Keywords: coordination chemistry · fluorides · structure elucidation · titanium · UV/Vis spectroscopy

[1] D. T. Richens, *The Chemistry of Aqua Ions*, Wiley, New York, **1997**, p. 208.
[2] M. Pourbaix, *Atlas d'Equlibres Electrochimiques*, Gauthier-Villars, Paris, **1963**, p. 214.
[3] F. A. Cotton, G. Wilkinson, *Advanced Inorganic Chemistry*, Wiley, New York, 5th ed, **1988**, p. 651.
[4] *Encyclopedia of Electrochemistry of the Elements, Vol. V* (Ed.: A. J. Bard), Marcel Dekker, New York, **1976**, p. 307, and references therein.
[5] M. E. Straumanis, C. H. Cheng, A. W. Schlechten, *J. Electrochem. Soc.* **1956**, *103*, 439; M. E. Straumanis, C. H. Cheng, A. W. Schlechten, *J. Electrochem. Soc.* **1956**, *103*, 440.
[6] The HF content of the HBF_4 is responsible for the dissolution of the titanium.
[7] Absorption spectra of solutions containing excess fluoride are very pH dependent, the $\lambda = 430$ nm band increases in intensity and shifts to slightly longer wavelengths at $pH > 3$. Since the spectrum of the aqua complex does not change up to pH 6.5, the yellowish species obtained at higher pH and observed by Straumanis must be a titanium(II) fluoro complex.
[8] A d^1 complex shows only one band in the visible region, the maximum Jahn–Teller splitting for this band in the case of Ti^{III} is ≈ 60 nm.
[9] Ti^{II}, 0.5 atom% in NaCl shows bands at $\lambda = 500$ and 800 nm in the UV/Vis spectra; a) W. E. Smith, *J. Chem. Soc. Chem. Commun.* **1972**, 1121; b) D. H. Brown, A. Hunter, W. E. Smith, *J. Chem. Soc. Dalton Trans.* **1979**, 79.
[10] a) ref. [1], p. 232; b) A. B. P. Lever, *Inorganic Electronic Spectroscopy*, Elsevier, Amsterdam, **1984**, pp. 399–401.
[11] From the bands at $\lambda = 430$ and 650 nm values of $B = 432\ cm^{-1}$ and $\Delta_{oct} = 11\,665\ cm^{-1}$ are calculated, compare V^{3+}_{aq} $B = 665\ cm^{-1}$ and $\Delta_{oct} = 18\,620\ cm^{-1}$.
[12] (%) Calcd: Ti 34.0, F 40.4; found Ti (photometrically H_2O_2) 35.7, F 40.0.
[13] STOE Debeye Scherrer diffractometer, 0.3 mm capillary, $Cu_{K\alpha}$ radiation, $15 \le 2\Theta \le 100°$. Structure solution with EXPO,[16] Rietveld refinement with FULLPROF[15] (pseudo-Voigt profile function, 5 profile parameters, 1 parameter for preferred orientation, 2 asymmetry parameters, 1 overall scale parameter, 4 parameters for lattice constants, 8 positional parameters, 5 isotropic displacement parameters). $R_p = 0.028$, $R_{wp} = 0.037$, $R_{Bragg} = 0.022$, GooF 0.97 for 226 Bragg reflections and 27 refined parameters. Space group: $C2/m$; lattice constants: $a = 5.7075(2)$, $b = 10.2193(3)$, $c = 7.8915(2)$ Å, $\beta = 117.421(1)°$; fractional coordinates and isotropic displacement parameters: Ti^{II} 0 0 0, B_{iso} 1.6(2) Å^2; Ti^{IV} 0 0 $^1/_2$, B_{iso} 1.1(2) Å^2; F(1) 0.998(5) 0 0.746(3), B_{iso} 2.4(1) Å^2; F(2) 0.732(2) 0.861(1) 0.411(1), B_{iso} 1.6(2) Å^2; O 0.708(2) 0.858(1) 0.900(2), B_{iso} 3.7(4) Å^2. Interatomic distances [Å]: Ti^{II}-F(1) 2.00(2), Ti^{II}-O 2.07(1), Ti^{IV}-F(1) 1.94(2), Ti^{IV}-F(2) 1.97(1).
[14] J. Fischer, G. Keib, R. Weiss, *Acta Crystallogr.* **1967**, *23*, 338.
[15] J. Rodriguez-Cavajal FULLPROF 2000, Version 1.9b Laboratoire Léon Brillouin **2000**.
[16] C. Giacovazzo, D. Siliqui, B. Carrozzini, A. Guagliardi, A. Moliterni, *J. Appl. Crystallogr.* **1999**, *32*, 115.

 © 2003 Wiley-VCH Verlag GmbH & Co. KGaA, Weinheim

Knotaxanes

Knotaxanes—Rotaxanes with Knots as Stoppers**

*Oleg Lukin, Takateru Kubota, Yoshio Okamoto, Frauke Schelhase, Albena Yoneva, Walter M. Müller, Ute Müller, and Fritz Vögtle**

Dedicated to Professor Karl Heinz Dötz on the occasion of his 60th birthday

In a recent report[1] we coined the name "knotaxane" for a challenging, yet hitherto unknown, hypothetical type of compound: a rotaxane in which the stoppers are molecular knots. Here we report the first successful synthesis of two members of this new topological family and their chiral resolution. Interest in this species comes on the one hand from their topological chirality,[2] since unlike having just a stereocenter, as in classical stereochemistry, the whole nano-sized molecular skeleton is chiral ("nanochiral"). Their chirality, therefore, should be quite pronounced,[3] and strong chiroptic effects and chiral inductions are expected. The use of the rotaxane platform,[2,4,5] on the other hand, makes such an assembly a particularly attractive architecture with an option to control the direction[6] of rotation or the shuttling[4c] of mechanically linked constituent parts.

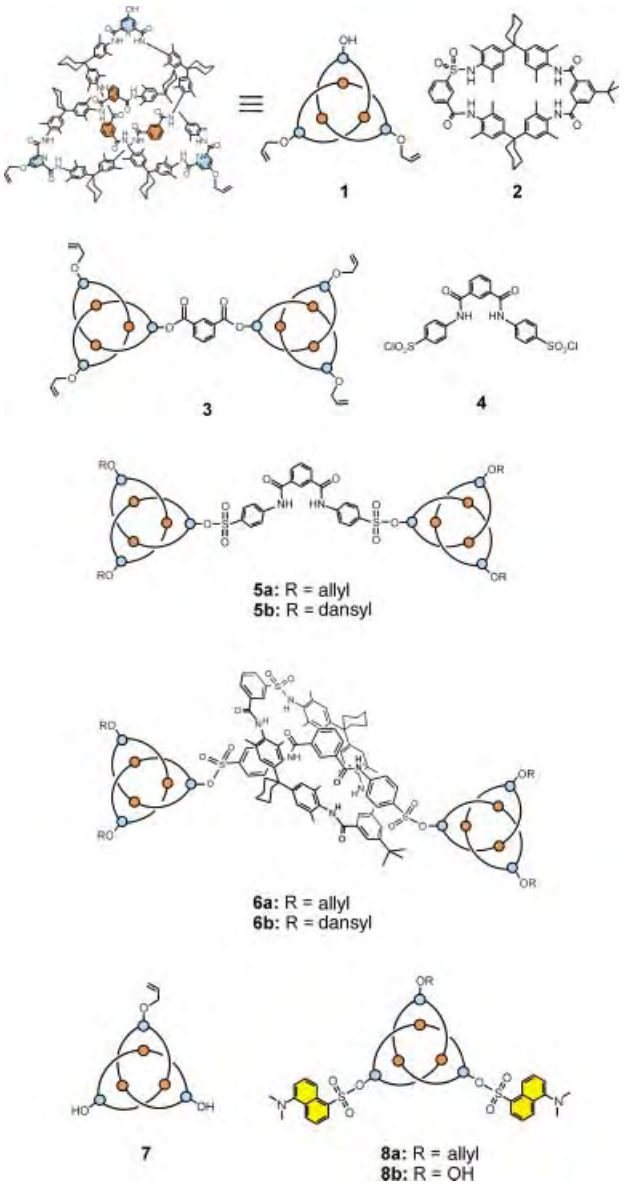
[*] Prof. Dr. F. Vögtle, Dr. O. Lukin, Dipl.-Chem. F. Schelhase, Dipl.-Chem. A. Yoneva, W. M. Müller, U. Müller
Kekulé-Institut für Organische Chemie und Biochemie
Rheinische Friedrich-Wilhelms-Universität Bonn
Gerhard-Domagk-Strasse 1, 53121 Bonn (Germany)
Fax: (+49) 228-735-662
E-mail: voegtle@uni-bonn.de
Dr. T. Kubota, Prof. Dr. Y. Okamoto
Department of Applied Chemistry
Graduate School of Engineering
Nagoya University
Chikusa-ku, Nagoya 464-8603 (Japan)

[**] Financial assistance by the Deutsche Forschungsgemeinschaft is gratefully acknowledged (Sonderforschungsbereich 624). O.L. thanks the Alexander von Humboldt Foundation for a fellowship. We would also like to thank Dipl.-Chem. S. Bitter, Dipl.-Chem. J. Brüggeman, and Dipl.-Chem. R. Henkel for recording MALDI-TOF mass spectra.

Supporting information for this article is available on the WWW under http://www.angewandte.org or from the author.

 © 2003 Wiley-VCH Verlag GmbH & Co. KGaA, Weinheim DOI: 10.1002/anie.200351981

Our previous efforts[1] showed that in spite of the significant achievements reached in the synthesis and derivatization of knotanes, the preparation of higher covalently linked knotanes meets severe difficulties, since such a synthesis implies the availability of selectively functionalized molecular knots, the preparation of which is once again difficult.[1,7,8] Our first attempt at the synthesis of a knotaxane[1] by the phenolate-trapping method[9] proved unsuccessful because of the partial decomposition of **1** in the basic solution.



An alternative method for the synthesis of amide-type rotaxanes,[10] which relies on the hydrogen-bond-templated threading of various dicarboxylic acid chlorides through cyclic tetraamides and offers mild reaction conditions, now turned out to be of advantage. The reaction of monohydroxy-knotane **1** with isophthaloyl chloride in the presence of the macrocycle **2**, however, yielded no rotaxane and only 17% of dumbbell **3**. The examination of molecular models and the low yield of **3** suggested that the lack of knotaxane formation are a consequence of the voluminous size of the knot stoppers and the shortness of the isophthaloyl linkage, which prohibits the threading of **2**.

Therefore, we designed an elongated axle **4** which, according to preliminary molecular modeling studies, could efficiently thread the macrocycle **2** and prevent noticeable overcrowding of the mechanically bound parts both in the transition state and the final assembly. Acylation of aniline with isophthaloyl chloride and sulfochlorination of the resulting isophthaloyldiphenyldiamide with chlorosulfonic acid accomplished the synthesis of **4**. The reaction of monohydroxy-knotane **1** with disulfonyl chloride **4** afforded the dumbbell **5a** and the desired knotaxane **6a** in yields of 55 and 19%, respectively. The structures of **5a** and **6a** were proved by means of MALDI-TOF mass spectrometry and ^{1}H NMR spectroscopy. The application of different ionization conditions in the former experiment enabled the observation of either signals corresponding to the molecular ion peaks only or characteristic fragmentation patterns brought about by the cleavage of the sulfonic esters. The appearance of a signal corresponding to the molecular ion of **2** ($M^+ = m/z$ 997) in the MALDI-TOF spectrum of **6a** at higher ionization potentials leaves no doubts about an efficient mechanical connection between the constituent parts of the knotaxane. The ^{1}H NMR spectra of **5a** and **6a** recorded in [D$_6$]DMSO show the amide signal pattern that is typical for mono-*O*-sulfonylated knotanes.[1] The other signals in the ^{1}H NMR spectra are also in line with the assignments that were recently reported by us.[11]

The expected D,L pairs of the knotaxane **6a** and the dumbbell **5a** were separated on noncommercial "Chiralpak AD" column material[12] containing tris(3,5-dimethylphenylcarbamoyl)amylose covalently linked to the silica gel support. Figure 1 shows that the enantiomers of **5a** and **6a** can be successfully separated. The chromatogram of **6a** reveals, however, a few peaks of impurities which reflects the difficulties in the preparative purification of **6a**. The MALDI-TOF mass spectra shown in Figure 2 confirm the successful purification and enantiomeric separation of knotaxane **6a**. The identification of the *meso* forms of both **5a** and **6a** is a major difficulty. In both cases the fractions of the

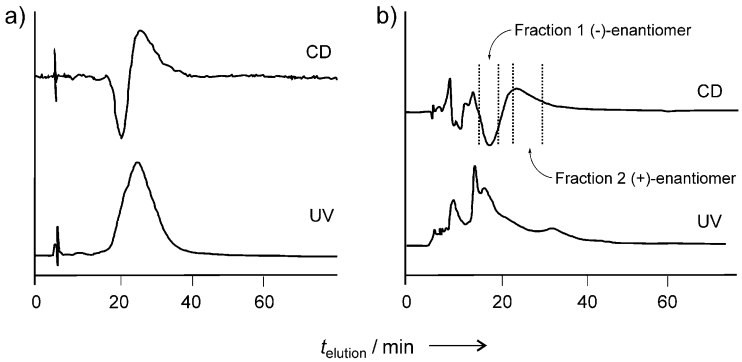


Figure 1. a) Separation of the enantiomers of **5a** (column: Chiralpak AD, eluent: hexane/chloroform (30/70), CD detection at 254 nm); b) separation of the enantiomers of **6a** (column: Chiralpak AD, eluent: hexane/chloroform/isopropanol (60/40/3), CD detection at 254 nm).

 © 2003 Wiley-VCH Verlag GmbH & Co. KGaA, Weinheim

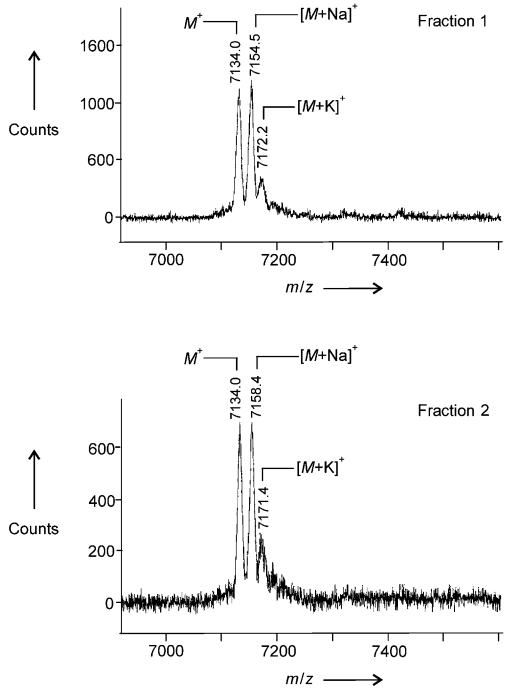


Figure 2. Sections of the MALDI-TOF spectra of fractions 1 and 2 of **6a** (matrix: 2,4,6-trihydroxyacetophenone).

meso forms show significant overlap with those of the enantiomers. The circular dichroism spectra of the enantiomers of **5a** and **6a**, recorded after preparative separation (Figure 3), reveals that the sulfonamide ring in the rotaxane only modifies the chiroptical properties of the dumbbell slightly.

The poor solubility and the ensuing purification and separation difficulties of the first member of the knotaxane family (**6a**) prompted us to develop new knotted stoppers. We recently showed that the solubility of knotanes can be efficiently tuned by introduction of specific substituents such as Frechét-type dendrons[9] and phosphoryl groups[11] at the outer edges of knotanes. The introduction of 5-(dimethylamino)naphthalenesulfonyl (dansyl) groups combining both lipophilicity and polarity seems attractive in this respect. The preparation of a new knotaxane with improved solubility properties necessitates, therefore, a knotane bearing two dansyl and one hydroxy group. For this purpose we have used dihydroxyallyloxy-knotane **7**, the isolation of which in the pure form is reported here for the first time. Sulfonylation of **7** with dansyl chloride followed by removal of the allyl group from the intermediate **8a** with Bu_3SnH readily gives the desired monohydroxy-knotane **8b**. The new knotaxane **6b**, which was synthesized from **8b** by a similar method as described for the preparation of **6a**, has been isolated in 20% yield. The purification of **6b** by chromatography on silica gel was indeed found to be easier than that of **6a**. HPLC analysis together with the ^{1}H NMR and MALDI-TOF spectra revealed the high purity of **6b**. Unlike its analogue **6a**, knotaxane **6b** was found to exhibit excellent solubility in alcohols. The latter property allowed us to achieve the separation of enantiomers of **6b** by HPLC using a commercial noncovalent Chiralcel OD material.[13] Figure 4 shows the circular dichrograms of the isolated enantiomers of **6b**. Similar to the case of **6a**, the fractions of the *meso* forms of **6b** showed overlap with those of the enantiomers.

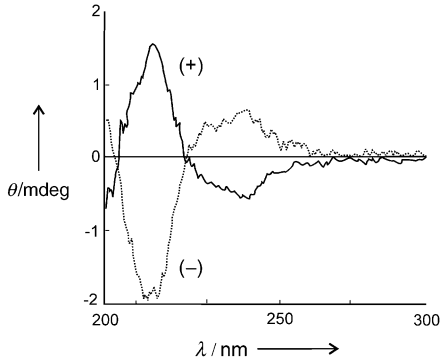


Figure 4. Circular dichroism spectra of enantiomers of knotaxane **6b** ($d = 0.1$ mm, CF_3CH_2OH).

The successful synthesis of the first knotaxanes demonstrates the advances made in synthetic chemistry in regard to such topological compounds. For the first time we have three topological stereogenic units held together both in an interlocked and covalent manner. Scheme 1 shows the analogy of the chirality designation of the topological dumbbell and knotaxane with the description of the stereochemistry of open-chain sugar acids developed by Emil Fischer in 1891.[14]

The topological chirality of the knotaxanes combined with their size, which exceeds 6 nm (Figure 5), makes such systems similar to natural macromolecular machines such as multi-enzyme complexes.[15] As a consequence of its C_s symmetry, sulfonamide macrocycle **2**[16] should exhibit a unidirectional rotation in the enantiomeric forms of the knotaxanes **6a**,**b** (Scheme 1). The detection of such a rotation would be an interesting challenge for AFM/STM techniques. Our next goal is to synthesize knotaxanes containing more than one wheel on the axle, to make the sugar-type skeleton (Scheme 1) longer, and to elucidate how the topological chirality is tuned.

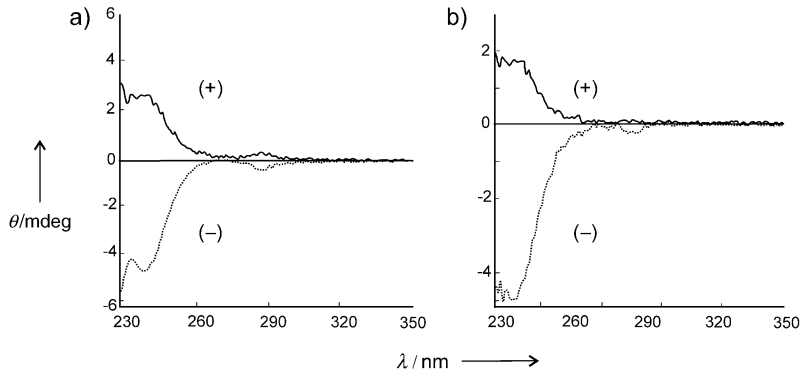
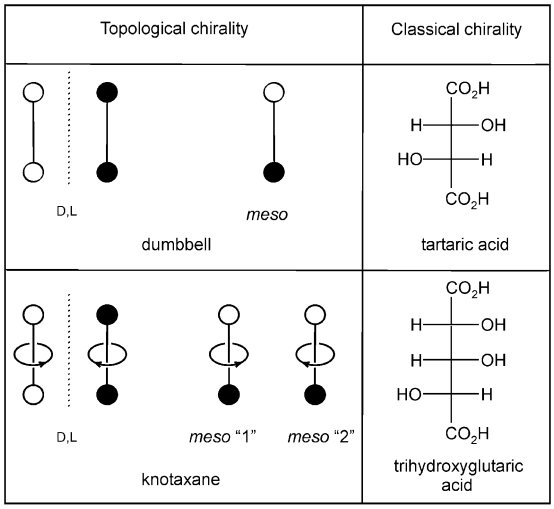


Figure 3. Circular dichroism spectra of a) dumbbell **5a** ($d = 0.1$ mm, $CHCl_3$), and b) knotaxane **6a** ($d = 0.1$ mm, $CHCl_3$).

 © 2003 Wiley-VCH Verlag GmbH & Co. KGaA, Weinheim



Scheme 1. Analogy of topological descriptors in chiral dumbbells (for example, **3, 5a**,**b**) and knotaxanes (**6a**,**b**) with the Fischer projections of chiral open-chain dicarboxylic acids. ○ = (+) knots, ● = (−) knots.

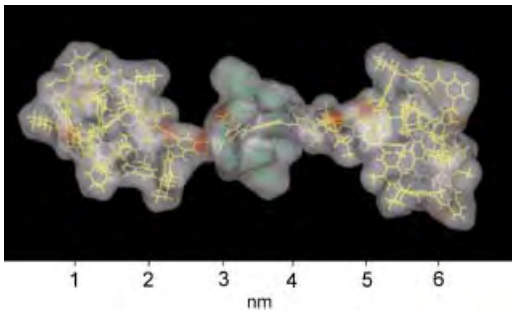


Figure 5. MMX energy-minimized model of knotaxane **6** (CPK surface is shown; allyl/dansyl substituents on the knot periphery are omitted).

Experimental Section

The preparation of compounds **3**–**8** can be found in the Supporting Information.

Received: May 26, 2003 [Z51981]

Keywords: chiral resolution · circular dichroism · molecular devices · rotaxanes

[1] O. Lukin, J. Recker. A. Böhmer, W. M. Müller, T. Kubota, Y. Okamoto, M. Nieger, F. Vögtle, *Angew. Chem.* **2003**, *115*, 458–461; *Angew. Chem. Int. Ed.* **2003**, *42*, 442–445.

[2] *Molecular Catenanes, Rotaxanes and Knots, A Journey Through the World of Molecular Topology* (Eds.: J.-P. Sauvage, C. Dietrich-Buchecker), Wiley-VCH, Weinheim, **1999**.

[3] F. Vögtle, S. Grimme, J. Hormes, K.-H. Dötz, N. Krause in *Interactions in Molecules—Electronic and Steric Effects. Sonderforschungsbereiche (DFG)* (Ed.: S. D. Peyerimhoff), Wiley-VCH, Weinheim, **2003**.

[4] The potential use of rotaxanes in molecular devices has been illustrated by numerous examples of "molecular shuttles" and electron-transfer systems. For the most recent examples, see a) N. Watanabe, N. Kihara, Y. Furusho, T. Takata, Y. Araki, O. Ito, *Angew. Chem.* **2003**, *115*, 705–707; *Angew. Chem. Int. Ed.* **2003**, *42*, 681–683; b) T. Da Ros, D. M. Gudi, A. F. Morales, D. A. Leigh, M. Prato, R. Turco, *Org. Lett.* **2003**, *5*, 689–691; c) M. Belohradsky, A. M. Elizarov, J. F. Stoddart, *Collect. Czech. Chem. Commun.* **2002**, *67*, 1719–1728; d) S. Chia, J. Cao, J. F. Stoddart, J. I. Zink, *Angew. Chem.* **2001**, *113*, 2513–2517; *Angew. Chem. Int. Ed.* **2001**, *40*, 2447–2451; e) A. M. Brouwer, C. Frochot, F. G. Gatti, D. A. Leigh, L. Mottier, F. Paolucci, S. Roffia, G. W. H. Wurpel, *Science* **2001**, *291*, 2124–2128; f) V. Bermudez, N. Capron, T. Gase, F. G. Gatti, F. Kajzar, D. A. Leigh, F. Zerbetto, S. W. Zhang, *Nature* **2000**, *406*, 608–611.

[5] The syntheses of rotaxanes equipped with stoppers possessing central chirality were also reported: a) A. Archut, W. M. Müller, S. Baumann, M. Habel, F. Vögtle, *Liebigs Ann.* **1997**, 495–499; b) T. Schmidt, R. Schmieder, W. M. Müller, B. Kiupel, F. Vögtle, *Eur. J. Org. Chem.* **1998**, 2003–2007; c) P. R. Ashton, J. A. Bravo, F. M. Raymo, J. F. Stoddart, A. J. P. White, D. J. Williams, *Eur. J. Org. Chem.* **1999**, 899–908.

[6] a) N. Koumura, R. W. J. Zijlstra, R. A. van Delden, N. Harada, B. L. Feringa, *Nature* **1999**, *401*, 6749; b) N. Koumura, E. M. Geertsema, A. Meetsma, B. L. Feringa, *J. Am. Chem. Soc.* **2000**, *122*, 12005–12006; c) N. Koumura, E. M. Geertsema, A. Meetsma, M. B. van Gelder, B. L. Feringa, *J. Am. Chem. Soc.* **2002**, *124*, 5037–5051; d) C. A. Stanier, S. J. Alderman, T. D. W. Claridge, H. L. Anderson, *Angew. Chem.* **2002**, *114*, 1847–1850; *Angew. Chem. Int. Ed.* **2002**, *41*, 1769–1772.

[7] The molecular knots published so far were mainly unfunctionalized or not intended to be reacted further: a) C. Dietrich-Buchecker, J.-P. Sauvage, *Angew. Chem.* **1989**, *101*, 192–194; *Angew. Chem. Int. Ed. Engl.* **1989**, *28*, 189–192; b) R. F. Carina, C. Dietrich-Buchecker, J.-P. Sauvage, *J. Am. Chem. Soc.* **1996**, *118*, 9110–9116; c) G. Rapenne, C. Dietrich-Buchecker, J.-P. Sauvage, *J. Am. Chem. Soc.* **1999**, *121*, 994–1001; d) S. C. J. Meskers, H. P. J. M. Dekkers, G. Rapenne, J.-P. Sauvage, *Chem. Eur. J.* **2000**, *6*, 2129–2134; e) H. Adams, E. Ashworth, G. A. Breault, J. Guo, C. A. Hunter, P. C. Mayers, *Nature* **2001**, *411*, 763; f) P. R. Ashton, O. A. Matthews, S. Menzer, F. M. Raymo, N. Spencer, J. F. Stoddart, D. J. Williams, *Liebigs Ann.* **1997**, 2485–2494; g) O. Safarowsky, M. Nieger, R. Fröhlich, F. Vögtle, *Angew. Chem.* **2000**, *112*, 1699–1701; *Angew. Chem. Int. Ed.* **2000**, *39*, 1616–1618.

[8] J. Recker, W. M. Müller, U. Müller, T. Kubota, Y. Okamoto, M. Nieger, F. Vögtle, *Chem. Eur. J.* **2002**, *8*, 4434–4442.

[9] a) G. M. Hübner, J. Gläser, C. Seel, F. Vögtle, *Angew. Chem.* **1999**, *111*, 395–398; *Angew. Chem. Int. Ed.* **1999**, *38*, 383–386; b) C. Seel, F. Vögtle, *Chem. Eur. J.* **2000**, *6*, 21–24.

[10] F. Vögtle, M. Händel, S. Meier, S. Ottens-Hildebrandt, F. Ott, T. Schmidt, *Liebigs Ann.* **1995**, 739–743.

[11] O. Lukin, W. M. Müller, U. Müller, A. Kaufmann, C. Schmidt, J. Leszczynski, F. Vögtle, *Chem. Eur. J.* **2003**, *9*, 3507–3517.

[12] N. Enomoto, S. Furukawa, Y. Ogasawara, H. Akano, Y. Kawamura, E. Yashima, Y. Okamoto, *Anal. Chem.* **1996**, *68*, 2798–2804.

[13] a) Y. Okamoto, M. Kawashima, K. Hatada, *J. Am. Chem. Soc.* **1984**, *106*, 5357–5359; b) Y. Okamoto, M. Kawashima, K. Hatada, *J. Chromatogr.* **1986**, *363*, 173–186.

[14] a) E. Fischer, *Ber. Dtsch. Chem. Ges.* **1891**, *24*, 1836; b) E. Fischer, *Ber. Dtsch. Chem. Ges.* **1891**, *24*, 2683; c) G. Helmchen, *Methods Org. Chem.* (Houben-Weyl), *4th ed. 1952–, Vol. E21*, **1995**; d) E. L. Eliel, S. H. Wilen, L. N. Mander, *Stereochemistry of Organic Compounds*, Wiley, New-York, **1994**; e) H. Kunz, *Angew. Chem.* **2002**, *114*, 4619–4632; *Angew. Chem. Int. Ed.* **2002**, *41*, 4439–4451.

[15] C. A. Schalley, K. Beizai, F. Vögtle, *Acc. Chem. Res.* **2001**, *34*, 465–476.

[16] C. Yamamoto, Y. Okamoto, T. Schmidt, R. Jäger, F. Vögtle, *J. Am. Chem. Soc.* **1997**, *119*, 10547–10548.

 © 2003 Wiley-VCH Verlag GmbH & Co. KGaA, Weinheim

Biconformational Bisdecalin Switch

Conformative Coupling of Two Conformational Molecular Switches**

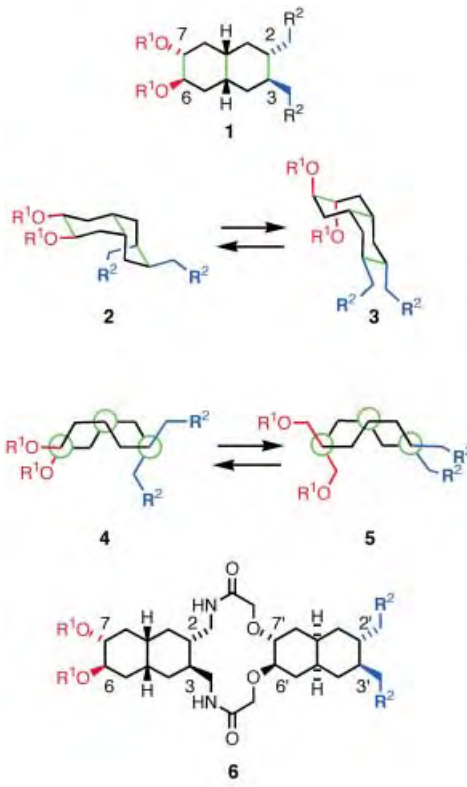
Michael Karle, Dirk Bockelmann, Dirk Schumann, Christian Griesinger, and Ulrich Koert**

A molecular switch consists of a molecule that can reversibly change states (on, off) upon an external stimulus.[1] There are photoswitches/chiroptical switches,[2] redox switches,[3] switchable rotaxanes and catenanes,[4] and switchable allosteric receptors.[5] Conformational switches have a biconformational basic framework. Biconformational *cis*-decalins[6] and *cis,anti,cis*-perhydroanthracenes[7] are suitable conformational switches for the transduction of molecular signals through conformational transmission.[8]

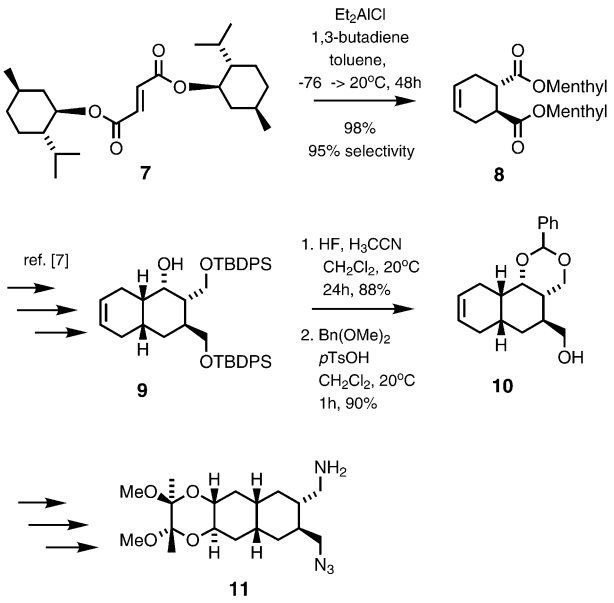
A 2,3,6,7-tetrasubstituted *cis*-decalin of type **1** has the two low-energy conformations **2** and **3** (Scheme 1).[6] A Newman projection along the three green C–C bonds in **1** illustrates the hinge function of these three bonds in the double ring-flip **4**→**5**.

In order to span greater distances with conformational switches (e.g. for signal transduction) or to use conformational switches in molecular circuits, one has to solve the problem of coupling two or more of these switches together.[9] Here we investigate whether a 14-membered macrobislactam of type **6** can be used for the conformational coupling of two *cis*-decalin switches.[10] Molecular modeling studies indicated that two low-energy conformations of the 14-membered ring should exist: one with an all-equatorial arrangement of the four junctions to the decalins (positions 2, 3, 6′, and 7′ in **6**) and one with an all-axial arrangement. Here we report on the synthesis of **6** and on studies with regard to the conformative coupling of the two decalins. We wondered whether a double ring-flip in the "left" decalin can induce, through the 14-membered bislactam ring, a double ring-flip of the "right" decalin.

The known synthesis of tetrasubstituted decalins of type **1** led to the racemic product only.[6a] However, to connect two decalins in a predictable and controlled way an enantioselective synthesis of the tetrasubstituted *cis*-decalins was required (Scheme 2). To this end we modified our previous synthesis by using a diastereoselective Diels–Alder reaction[11] of dimenthyl fumarate (**7**) with 1,3-butadiene to obtain



Scheme 1. The tetrasubstituted *cis*-decalin **1**, its double ring-flip **2**→**3** (as a Newman projection **4**→**5**), and the prototype of a coupled bisdecalin, **6**.



Scheme 2. Enantioselective synthesis of the tetrasubstituted azidoaminomethyldecalin **11**. TBDPS = *tert*-butyldiphenylsilyl.

[*] Prof. Dr. U. Koert, Dipl.-Chem. M. Karle, Dipl.-Chem. D. Schumann
Fachbereich Chemie
Philipps-Universität Marburg
Hans-Meerwein-Strasse, 35032 Marburg (Germany)
Fax: (+49) 6421-2825-677
E-mail: koert@chemie.uni-marburg.de
Prof. Dr. C. Griesinger, Dipl.-Chem. D. Bockelmann
Max-Plank-Institut für Biophysikalische Chemie
NMR-Based Structural Biology
Am Fassberg 11, 37077 Göttingen (Germany)
Fax: (+49) 551-201-2201
E-mail: cigr@mpibpc.mpg.de

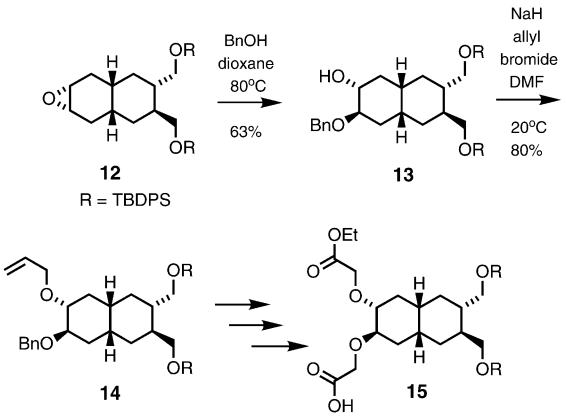
[**] This work was supported by the Volkswagen Foundation, the Deutsche Forschungsgemeinschaft, the Max-Planck-Gesellschaft, the Fonds der Chemischen Industrie, and the Pinguin Foundation.

Supporting information for this article is available on the WWW under http://www.angewandte.org or from the author.

 © 2003 Wiley-VCH Verlag GmbH & Co. KGaA, Weinheim DOI: 10.1002/anie.200352130

the cyclohexene **8**, which was transformed into alcohol **9** in a few steps. The two primary OH groups were differentiated by formation of the benzylidene acetal **10**, which could be converted into the azidoaminomethyldecalin **11** (see Supporting Information). Compound **11** represents the completely functionalized left decalin unit of **6**.

A key step in the synthesis of the right decalin unit was the regioselective opening of the enantiomerically pure epoxide **12** with benzyl alcohol to give the *trans*-diaxial β-benzyloxy alcohol **13**, which was converted via the allyl ether **14** into the carboxylic acid **15** (Scheme 3 and Supporting Information).



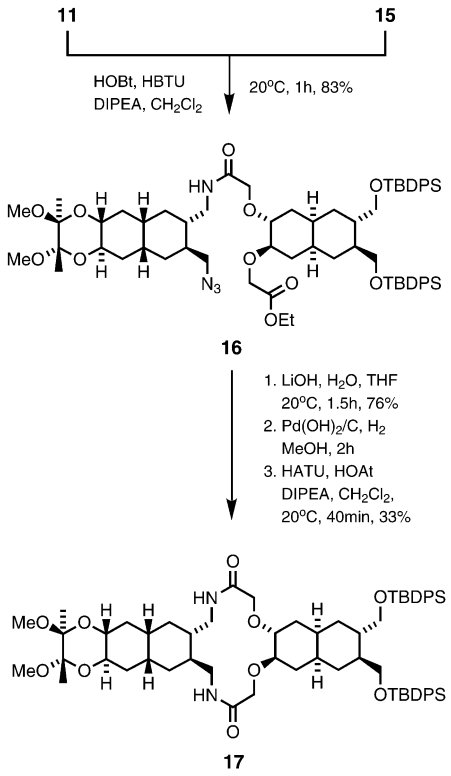
Scheme 3. Synthesis of the enantiomerically pure decalin **15**.

The formation of the 14-membered bislactam **17** started with the HBTU-mediated coupling of **11** and **15** to the amide **16** (Scheme 4). Hydrolysis of the ethyl ester and reduction of the azide provided an aminocarboxylic acid, which was cyclized to provide the target bislactam **17**.

The bisacetal group in **17** fixes the O substituents at C6 and C7 in equatorial positions. The overall structure of **17**, which is determined by this covalent clamp on the left decalin unit, and in specifically the pattern of axial/equatorial arrangements of the four substituents of each decalin unit, was determined unequivocally by DQF-COSY and ROESY experiments in $CDCl_3$. The resulting structural parameters (for ROE contacts and torsion angles, see the Supporting Information) were used as input for molecular modeling (InsightII/Discover, CVFF). Ten low-energy structures (e.g. **18** in (Scheme 5) were calculated in which the two decalins have the same double-chair conformation but the 14-membered bislactam has local differences .

The bisacetal group of the left decalin unit forces the substituents at C6 and C7 into equatorial positions, which fixes the substituents at C2 and C3 in axial positions. This in turn leads to an axial orientation of the C6′ and C7′ substituents on the right decalin unit, which brings the C2′ and C3′ substituents at the right end of the molecule into equatorial positions.

The covalent bisacetal clamp[12] of the left decalin unit was cleaved by reaction with HF, which remarkably did not affect the TBDPS groups. The resulting diol was protected as the diacetate **20** in order to facilitate the NMR analysis. The



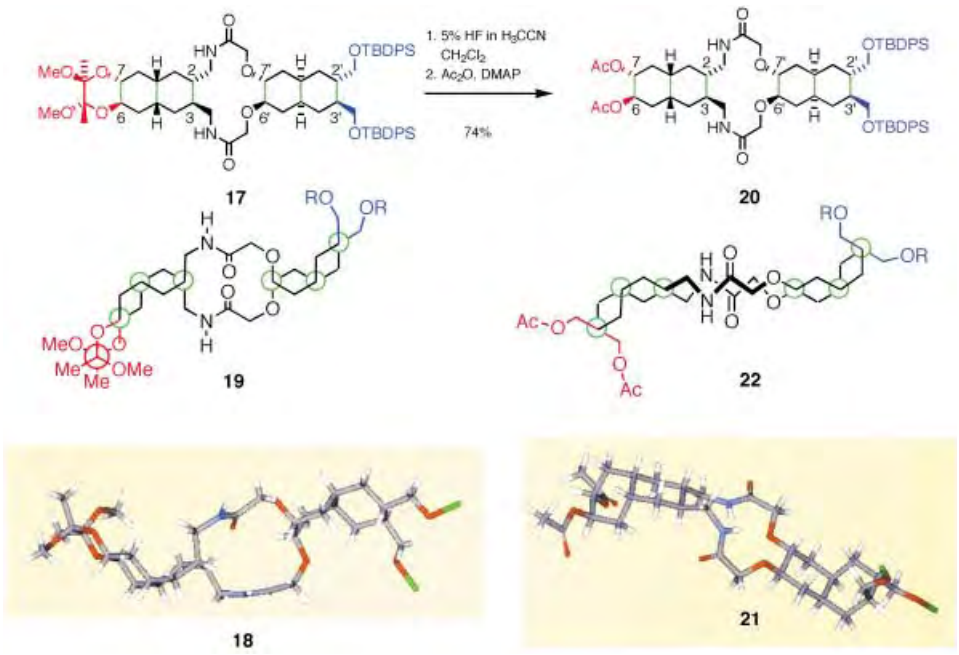
Scheme 4. Connection of both decalin units to the amide **16** and ring closure to the bislactam **17**. DIPEA = diisopropylethylamine, HATU = 2-(1-hydroxy-7-azabenzotriazol-1-yl)-1,1,3,3,-tetramethyluronium hexafluorophosphate, HBTU = 2-(1*H*-benzotriazol-1-yl)-1,1,3,3-tetramethyluronium hexafluorophosphate, HOAt = 1-hydroxy-7-azabenzotriazole, HOBt = 1-hydroxybenzotriazole.

resulting structural information (see Supporting Information) was again used in molecular modeling calculations, which led to several low-energy conformations. In these unequivocal, related structures (e.g. **21** in Scheme 5) the decalins assume a double-chair structure and the 14-membered bislactam ring has local variations. In the left decalin unit the substituents at C6 and C7 are now in axial positions.[13] This results in a double ring-flip of the left decalin, which leads to equatorial positions for the substituents at C2 and C3. This conformational change is transduced by the 14-membered ring to the right decalin unit, resulting in a double ring-flip. The substituents at C6′ and C7′ assume equatorial positions, and the substituents at C2′ and C3′ switch from equatorial to axial positions.

This is the first example of the conformative coupling of two decalin switches through a 14-membered bislactam ring. The switching distance from the left- (C6, C7) to the right-hand side (C2′, C3′) of the molecule is approximately 15 Å. It may be possible to couple more than two biconformational decalins in series. A functional chain of three decalin switches coupled by two 14-membered bislactam rings should be long enough to bridge the lipophilic part of a phospholipid bilayer and to transfer signals across membranes.

In conclusion, we have described the conformative coupling of two biconformational decalins though a 14-membered bislactam ring. This paves the way for the use of

 © 2003 Wiley-VCH Verlag GmbH & Co. KGaA, Weinheim



Scheme 5. The cleavage of the bisacetal clamp (**17**→**20**) leads to a double ring-flip in the left decalin unit, which induces a double ring-flip of the right decalin by conformative coupling of the 14-membered bislactam ring (**18**→**21**, **19**→**22**). Structures **19** and **22** are Newman projections along the C–C bonds in green in **17** and **20**, respectively.

conformational switches in molecular devices[14] (e.g. signal transduction, switchable ion channels, and molecular logic/circuits).

Received: June 12, 2003 [Z52130]

Keywords: conformational analysis · decalin · molecular devices · NMR spectroscopy · synthesis

[1] a) *Molecular Switches* (Ed.: B. L. Feringa), Wiley-VCH, Weinheim, **2001**; b) A. P. de Silva, H. Q. Gunaratne, T. Gunnlaugsson, A. J. M. Huxley, C. P. McCoy, J. T. Rademacher, T. E. Rice, *Chem. Rev.* **1997**, *97*, 1515–1566; c) J.-M. Lehn, *Supramolecular Chemistry*, VCH, Weinheim, **1995**.

[2] For a collection of excellent reviews: a) *Chem. Rev.* **2000**, *100*, 1683–1890 (special issue: Photochromism: Memories and Switches); b) B. L. Feringa, *Acc. Chem. Res.* **2001**, *34*, 504–513.

[3] a) L. Zelikovich, J. Libman, A. Shanzer *Nature* **1995**, *374*, 790–792; b) D. Kalny, M. Elhabiri, T. Moav, A. Vaskevich, I. Rubinstein, A. Shanzer, A.-M. Albrecht-Gary, *Chem. Commun.* **2002**, 1426–1427; c) H. Plenio, C. Aberle, *Chem. Eur. J.* **2001**, *7*, 4438–4446.

[4] a) R. A. Bissel, E. Córdova, A. E. Kaifer, J. F. Stoddart, *Nature* **1994**, *369*, 133–137; b) P. R. Ashton, V. Balzani, J. Becher, A. Credi, M. C. T. Fyfe, G. Mattersteig, S. Menzer, M. B. Nielsen, F. M. Raymo, J. F. Stoddart, M. Venturi, D. J. Williams, *J. Am. Chem. Soc.* **1999**, *121*, 3951–3957; c) M. Bauer, F. Vögtle, *Chem. Ber.* **1992**, *125*, 1675–1686.

[5] a) S. Shinkai in *Molecular Switches* (Ed.: B. Feringa), Wiley-VCH, Weinheim, **2001**, p. 281; b) S. Shinkai, M. Ikeda, A. Sugasaki, M. Takeuchi, *Acc. Chem. Res.* **2001**, *34*, 494–503.

[6] a) U. Koert, R. Krauss, H.-G. Weinig, C. Heumann, B. Ziemer, C. Mügge, M. Seydack, J. Bendig, *Eur. J. Org. Chem.* **2001**, 575–586; studies with substituted cyclohexanes: b) M. Raban, D. L. Burch, E. R. Hortelano, D. Durocher, D. Kost, *J. Org. Chem.* **1994**, *59*, 1283–1287; c) V. V. Samoshin, O. A. Zelenkina, I. V. Yartseva, N. S. Zefirov, *Zh. Org. Khim.* **1987**, *23*, 2244–2245; d) V. V. Samoshin, V. A. Chertkov, L. P. Vaatlina, E. K. Dobretsova, N. A. Simonov, L. P. Katorsky, D. E. Gremyachinsky, H.-J. Schneider, *Tetrahedron Lett.* **1996**, *37*, 3981–3984; e) G. W. Buchanan, K. Bourque, *Tetrahedron Lett.* **1984**, *25*, 3963–3966.

[7] a) H.-G. Weinig, R. Krauss, M. Seydack, J. Bendig, U. Koert, *Chem. Eur. J.* **2001**, *7*, 2075–2088; b) R. Krauss, H.-G. Weinig, M. Seydack, J. Bendig, U. Koert, *Angew. Chem.* **2000**, *112*, 1905–1908; *Angew. Chem. Int. Ed.* **2000**, *39*, 1835–1837; c) J. Berninger, R. Krauss, H.-G. Weinig, U. Koert, B. Ziemer, K. Harms, *Eur. J. Org. Chem.* **1999**, 875–884.

[8] a) R. Krauss, U. Koert, *Synlett* **2003**, 598–608; examples of other conformational switches: b) H. Yuasa, H. Hashimoto, *J. Am. Chem. Soc.* **1999**, *121*, 5089–5090; c) S. E. O'Connor, B. Imperiali, *J. Am. Chem. Soc.* **1997**, *119*, 2296; d) H. J. Schneider, F. Werner, *J. Chem. Soc. Chem. Commun.* **1992**, 490–491; e) V. A. Palyulin, S. V. Emets, V. A. Chertkov, C. Kasper, H.-J. Schneider, *Eur. J. Org. Chem.* **1999**, 3479–3482; f) J. N. H. Reek, H. Engelkamp, A. E. Rowan, J. A. A. W. Elemans, R. J. M. Nolte, *Chem. Eur. J.* **1998**, *4*, 716–722.

[9] Other examples for the (nonconformative) coupling of molecular switches: F. M. Raymo, S. Giordani, *Org. Lett.* **2001**, *3*, 3475–3478.

[10] The concept of macrocyclic stereocontrol was used before in the total synthesis of macrolide natural products: a) "Selectivity—A Goal for Synthetic Efficiency": W. C. Still, *Workshop Conferences Hoechst, Vol. 14* (Eds.: W. Bartmann, B. M. Trost), Verlag Chemie, Weinheim, **1983**; b) G. Quinkert, N. Heim, J. Glenneberg, U. M. Billhardt, V. Autze, J. W. Bats, G. Dürner, *Angew. Chem.* **1987**, *99*, 363–365; *Angew. Chem. Int. Ed. Engl.* **1987**, *26*, 362–364.

[11] K. Furuta, K. Iwanaga, H. Yamamoto, *Tetrahedron Lett.* **1986**, *27*, 4507–4510. The stereoselectivity was determined and the stereochemistry of the reaction product was assigned after the reductive cleavage of the menthyl ester. See the Supporting Information for details.

 © 2003 Wiley-VCH Verlag GmbH & Co. KGaA, Weinheim

[12] a) S. V. Ley, H. W. M. Priepke, S. L. Warriner, *Angew. Chem.* **1994**, *106*, 2410 – 2412; *Angew. Chem. Int. Ed. Engl.* **1994**, *106*, 2290 – 2292; b) J.-L. Montchamp, F. Tian, M. E. Hart, J. W. Frost, *J. Org. Chem.* **1996**, *61*, 3897 – 3899.

[13] The switch of the C6 and C7 substituents into axial positions was verified by inspection of the coupling pattern in the DQF-COSY spectrum; the small coupling constant for H6 and H7 is characteristic for bisequatorial protons.

[14] Review: a) V. Balzani, M. Gomez-Lopez, J.-F. Stoddart, *Acc. Chem. Res.* **1998**, *31*, 405 – 414; representative examples: b) T. R. Kelly, H. De Silva, R. A. Silva, *Nature* **1999**, *401*, 150 – 152; c) N. Koumura, R. W. J. Zijlstra, R. A. van Delde, N. Harada, B. L. Feringa, *Nature* **1999**, *401*, 152 – 154; d) A. P. de Silva, N. D. McClenaghan, *J. Am. Chem. Soc.* **2000**, *122*, 3965 – 3966.

 © 2003 Wiley-VCH Verlag GmbH & Co. KGaA, Weinheim

Cover Picture

Richard R. Schrock* and Amir H. Hoveyda*



Molybdenum imido alkylidenes along with the corresponding tungsten complexes have played a critical role in the emergence of catalytic olefin metathesis as one of the key transformations in chemical synthesis. R. R. Schrock and A. H. Hoveyda recount on page 4592 ff the journey that began with the discovery of tantalum alkylidenes and eventually led to the development of highly effective chiral catalysts, and even supported chiral catalysts (shown in the vials), for asymmetric metathesis.

Contents

Angewandte EarlyView

The following articles are available online (in Wiley InterScience). You can find them at www.angewandte.org, under Full Text, Early View.

R. T. Ruck, E. N. Jacobsen:*
Asymmetric Hetero-Ene Reactions of Trimethylsilyl Enol Ethers Catalyzed by Tridentate Schiff Base Chromium(III) Complexes
DOI: 10.1002/anie.200351591
Published online: September 23, 2003

T.-H. Kim, T. M. Swager:*
A Fluorescent Self-Amplifying Wavelength-Responsive Sensory Polymer for Fluoride Ions
DOI: 10.1002/anie.200352075
Published online: September 23, 2003

A. Glieder, R. Weis, W. Skranc, P. Poechlauer, I. Dreveny, S. Majer, M. Wubbolts, H. Schwab, K. Gruber:*
Comprehensive Step-by-Step Engineering of an (R)-Hydroxynitrile Lyase for Large-Scale Asymmetric Synthesis
DOI: 10.1002/anie.200352141
Published online: September 29, 2003

A. Alberola, R. J. Less, C. M. Pask, J. M. Rawson, F. Palacio, P. Oliete, C. Paulsen, A. Yamaguchi, R. D. Farley, D. M. Murphy:*
A Thiazyl-Based Organic Ferromagnet
DOI: 10.1002/anie.200352194
Published online: September 23, 2003

B. H. Lipshutz, J. M. Servesko:*
CuH-Catalyzed Asymmetric Conjugate Reductions of Acyclic Enones
DOI: 10.1002/anie.200352313
Published online: September 23, 2003

A. Suzuki, Y. Inada, A. Yamaguchi, T. Chihara, M. Yuasa, M. Nomura, Y. Iwasawa:*
Time Scale and Elementary Steps of CO-Induced Disintegration of Surface Rhodium Clusters
DOI: 10.1002/anie.200352318
Published online: September 25, 2003

N. Halland, T. Hansen, K. A. Jørgensen:*
Organocatalytic Asymmetric Michael Reaction of Cyclic 1,3-Dicarbonyl Compounds and α,β-Unsaturated Ketones—A Highly Atom-Economic Catalytic One-Step Formation of Optically Active Warfarin Anticoagulant
DOI: 10.1002/anie.200352136
Published online: September 29, 2003

K. Breuker, F. W. McLafferty:*
Native Electron Capture Dissociation for the Structural Characterization of Noncovalent Interactions in Native Cytochrome c
DOI: 10.1002/anie.200351705
Published online: September 23, 2003

I. Korobkov, S. Gambarotta, G. P. A. Yap:*
Amide from Dinitrogen by In Situ Cleavage and Partial Hydrogenation Promoted by a Transient Zero-Valent Thorium Synthon
DOI: 10.1002/anie.200352205
Published online: September 29, 2003

Articles judged by the referees or the editor as being either very important or very urgent are immediately edited, proof-read, and electronically published once the manuscript has arrived in the editorial office in final form. As long as there is no page number available these articles should be cited in the following manner:

Author(s) *Angew. Chem. Int. Ed.*, online publication date, DOI.

Web Sites

http://www.azom.com ——— **4568** The A to Z of Materials—for Chemists? *E. Kroke*

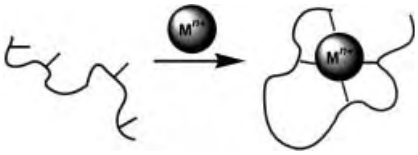
Books

Synthetic Applications of 1,3-Dipolar Cycloaddition Chemistry ——— **4569** Albert Padwa, William H. Pearson *reviewed by H. Suga*

Chemistry and Applications of Polyphosphazenes ——— **4570** Harry R. Allcock *reviewed by D. P. Gates*

© 2003 Wiley-VCH Verlag GmbH & Co. KGaA, Weinheim

Highlights



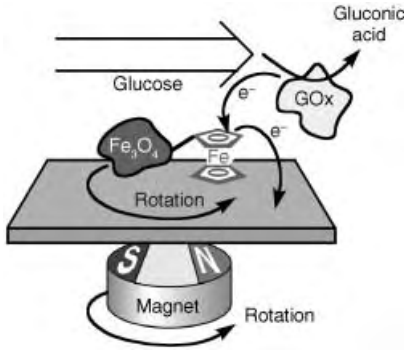
Natural selection: Peptide-based ligands for metal ions (see schematic representation) have a diverse range of applications that extends from stereoselective catalysis to the sensing of proteins. The possibility to screen large libraries of ligands for the selection of the best systems and their coexpression with proteins make peptide-based ligands powerful tools for bridging the gap between chemistry and biology.

Peptide-Based Ligands

G. Licini,* P. Scrimin* ____ **4572 – 4575**

Metal-Ion-Binding Peptides: From Catalysis to Protein Tagging

Minireviews



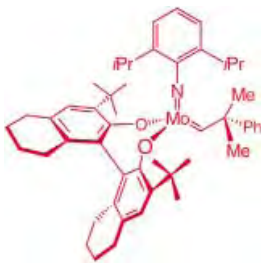
Going for a spin: Circular rotation of an external magnet enhances the bioelectrocatalytic oxidation of a substrate such as glucose when magnetic particles are functionalized with a redox-relay group such as ferrocene (see scheme). This example of a magneto-controlled electrocatalytic reaction may find application in sensor technology.

Bioelectrocatalysis and Magnets

I. Willner,* E. Katz ____ **4576 – 4588**

Magnetic Control of Electrocatalytic and Bioelectrocatalytic Processes

Reviews



25 years on: Molybdenum alkylidene complexes (see picture) have played a crucial role in the emergence of olefin metathesis as a powerful method in modern chemical synthesis. This review highlights the 25-year journey from the first high-oxidation-state tantalum alkylidene complex to chiral molybdenum catalysts for asymmetric olefin metathesis.

Olefin-Metathesis Catalysts

R. R. Schrock,*
A. H. Hoveyda* ____ **4592 – 4633**

Molybdenum and Tungsten Imido Alkylidene Complexes as Efficient Olefin-Metathesis Catalysts

For the USA and Canada:
ANGEWANDTE CHEMIE International Edition (ISSN 1433-7851) is published weekly by Wiley-VCH PO Box 191161, D 69451 Weinheim, Germany. Air freight and mailing in the USA by Publications Expediting Inc. 200 Meacham Ave., Elmont, NY 11003. Periodicals postage paid at Jamaica NY 11431. US POSTMASTER: send address changes to *Angewandte Chemie*, Wiley-VCH, 111 River Street, Hoboken, NJ 07030. Annual institutional subscription price for institutions: Europe € 3430.00/3118.00. Outside Europe US$ 4499.00/4090.00 (valid for print and electronic/print or electronic delivery); for individuals who are personal members of a national chemical society, or whose institution already subscribes, or who are retired or self-employed consultants, print only. Europe € 248.00/Outside Europe US$ 378.00. Postage and handling charges included. All Wiley-VCH prices are exclusive VAT.

 © 2003 Wiley-VCH Verlag GmbH & Co. KGaA, Weinheim

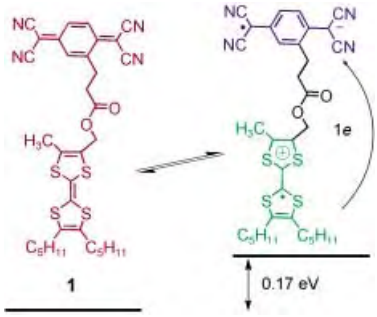
Contents

Communications

Covalent TTF–TCNQ Diad

D. F. Perepichka, M. R. Bryce,* C. Pearson, M. C. Petty, E. J. L. McInnes, J. P. Zhao ——— **4636 – 4639**

A Covalent Tetrathiafulvalene–Tetracyanoquinodimethane Diad: Extremely Low HOMO–LUMO Gap, Thermoexcited Electron Transfer, and High-Quality Langmuir–Blodgett Films



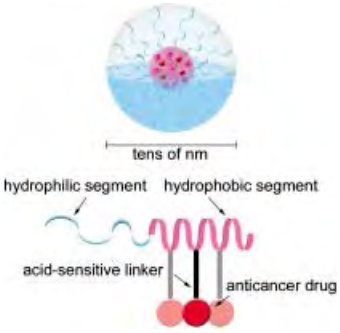
Nearly 30 years after theoretical prediction, a stable and well-characterized compound that covalently links tetrathiafulvalene and tetracyanoquinodimethane fragments has been synthesized (**1**, see scheme). The extremely low HOMO–LUMO gap of **1** (0.17 eV) allows the first observation of thermoexcited electron transfer in a donor–acceptor diad. Langmuir–Blodgett films of **1** are not electrically conducting.

Delivering Anticancer Agents

Y. Bae, S. Fukushima, A. Harada, K. Kataoka* ——— **4640 – 4643**

Design of Environment-Sensitive Supramolecular Assemblies for Intracellular Drug Delivery: Polymeric Micelles that are Responsive to Intracellular pH Change

Drug smuggling: Micelles made up of block copolymers and the anticancer drug adriamycin (ADR), which is linked to the polymer by a pH-sensitive linker, have been prepared (see picture). Treatment of cancer cells with the micelles shows that the micelles are transported into the cell by endocytosis, thus bypassing the cell-membrane transporters. In the cell, the decrease in pH value triggers the release of the ADR, which retains its cytotoxic effect. The released ADR fluoresces which allows its localization within the cells to be detected.



O_2 Insertion and Epoxidation

J. Lewiński,* Z. Ochal, E. Bojarski, E. Tratkiewicz, I. Justyniak, J. Lipkowski ——— **4643 – 4646**

First Structurally Authenticated Zinc Alkylperoxide: A Model System for the Epoxidation of Enones

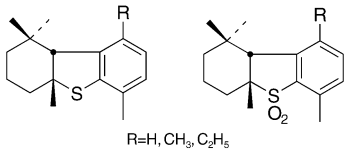


β-Ketoimine ligands stabilize zinc compounds: The dimeric zinc alkylperoxide $[\{(LL)ZnOOEt\}_2]$ (where $LL = HC\{(CMe)(2,6\text{-}iPr_2C_6H_3N)\}_2$) has been prepared and structurally characterized (see picture, Zn green, N blue, O red, C gray). This compound, which is formed by the insertion of dioxygen into the Zn–Et bond, is very active in the epoxidation of enones.

Organosulfur Compounds in Fuels

A. Charrié-Duhaut, C. Schaeffer, P. Adam,* P. Manuelli, P. Scherrer, P. Albrecht* ——— **4646 – 4649**

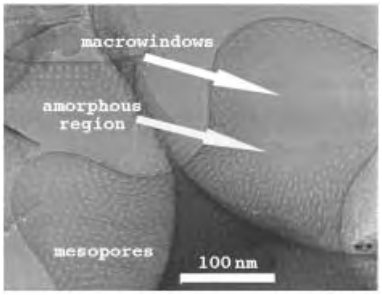
Terpenoid-Derived Sulfides as Ultimate Organic Sulfur Compounds in Extensively Desulfurized Fuels



Extremely hydrodesulfurization-resistant organosulfur compounds of biological origin are present in trace amounts in highly desulfurized fuels. A series of these compounds (see picture; left) was characterized by mass spectrometry and NMR spectroscopic structural elucidation of the corresponding sulfones (right), which were isolated after selective oxidation.

© 2003 Wiley-VCH Verlag GmbH & Co. KGaA, Weinheim

An entirely synthetic method is used to produce hierarchically ordered porous silica materials in a one-pot synthesis, with ordering on three different scales; that is, macropores (200–800 nm), interconnecting windows (70–130 nm), ordered mesoporous walls (80 nm) with narrow micropores (< 2 nm) in the presence of multiple templates (see picture). At the macro- and mesoscale both ordering and size is controlled whilst at the microscale the interconnectivity is controlled.

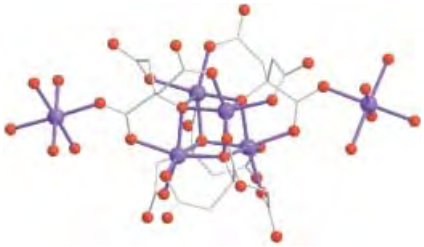


Hierarchically Ordered Porous Silica

T. Sen,* G. J. T. Tiddy, J. L. Casci, M. W. Anderson* ——— **4649 – 4653**

One-Pot Synthesis of Hierarchically Ordered Porous-Silica Materials with Three Orders of Length Scale

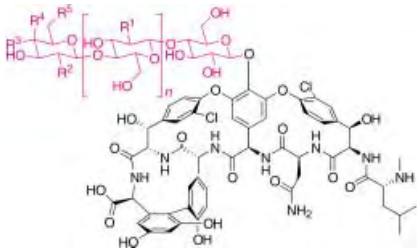
Small and attractive: The proligand citric acid has been used to assemble a new anionic hexanuclear cobalt(II) cluster (see picture). The complex displays single-molecule magnet (SMM) behavior, with an energy barrier to the reorientation of magnetization of 26 K, the highest value to have been recorded for a non-manganese based SMM.



Single-Molecule Magnets

M. Murrie,* S. J. Teat, H. Stœckli-Evans, H. U. Güdel* ——— **4653 – 4656**

Synthesis and Characterization of a Cobalt(II) Single-Molecule Magnet



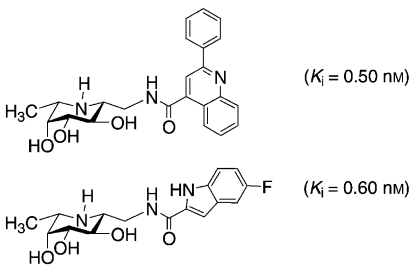
The notoriously difficult glycosylation of vancomycin was tackled in a one-pot procedure. A number of oligosaccharides were synthesized and attached to the vancomycin aglycon to create a library of derivatives (see formula) to probe the effect of glycosylation on the antibiotic activity.

Vancomycin–Oligosaccharide Library

T. K. Ritter, K.-K. T. Mong, H. Liu, T. Nakatani, C.-H. Wong* ——— **4657 – 4660**

A Programmable One-Pot Oligosaccharide Synthesis for Diversifying the Sugar Domains of Natural Products: A Case Study of Vancomycin

An efficient and simple method has been developed to identify potent and selective inhibitors against α-fucosidases based on the amide-forming reaction in a microtiter plate of a fuconojirimycin core with various carboxylic acids, followed by a direct inhibition assay without product isolation. The structures of the two most potent inhibitors are shown.



α-Fucosidase Inhibitors

C.-Y. Wu, C.-F. Chang, J. S.-Y. Chen, C.-H. Wong,* C.-H. Lin* ——— **4661 – 4664**

Rapid Diversity-Oriented Synthesis in Microtiter Plates for In Situ Screening: Discovery of Potent and Selective α-Fucosidase Inhibitors

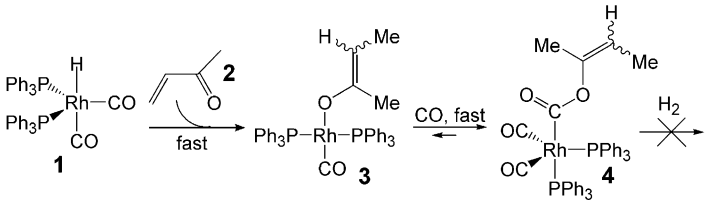
 © 2003 Wiley-VCH Verlag GmbH & Co. KGaA, Weinheim

Contents

Catalyst Deactivation

E. B. Walczuk, P. C. J. Kamer, P. W. N. M. van Leeuwen* — **4665 – 4669**

Dormant States of Rhodium Hydroformylation Catalysts: Carboalkoxyrhodium Complex Formed from Enones in the Alkene Feed



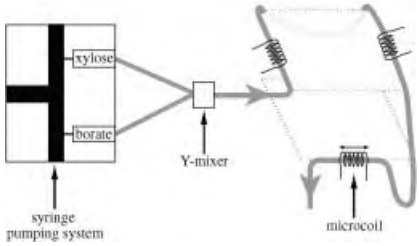
Catalysts get food poisoning: Conversion of the active 1-alkene hydroformylation catalyst **1** with reactive impurities in the feed, such as dienes and enones, into unreactive rhodium intermediates leads to deactivation of **1**. For example, **2** is much more reactive towards **1** than the substrate and transforms it temporarily into **4** blocking the hydroformylation activity.

Continuous-Flow NMR Spectroscopy

L. Ciobanu, D. A. Jayawickrama, X. Zhang, A. G. Webb, J. V. Sweedler* — **4669 – 4672**

Measuring Reaction Kinetics by Using Multiple Microcoil NMR Spectroscopy

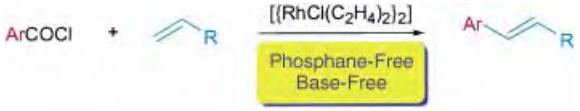
The technique of continuous reactant flow is combined with multiple microcoil NMR detection in a new and efficient approach to obtain kinetic information on reactions that take place on timescales between seconds and minutes. As a model system, xylose–borate reaction kinetics are studied (see picture).



C-C Coupling Reactions

T. Sugihara, T. Satoh, M. Miura,* M. Nomura — **4672 – 4674**

Rhodium-Catalyzed Mizoroki–Heck-Type Arylation of Alkenes with Aroyl Chlorides under Phosphane- and Base-Free Conditions

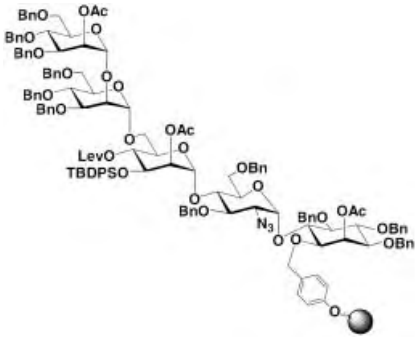


Simple but effective! Even without the addition of any phosphane ligand and base, alkenes efficiently undergo Mizoroki–Heck-type arylation upon treatment with aroyl chlorides in the presence of a rhodium catalyst (see scheme). The products were isolated by a very simple procedure.

Solid-Phase Synthesis of Glycolipids

N.-C. Reichardt, M. Martín-Lomas* — **4674 – 4677**

A Practical Solid-Phase Synthesis of Glycosylphosphatidylinositol Precursors



The conserved pseudo-pentasaccharide structure common to all known GPI-anchors (GPI = glycosylphosphatidylinositol) was assembled on a solid support by using a novel attachment procedure and a optimized deprotection/glycosylation protocol. Orthogonal protection for the main branching points allows access to a variety of GPI-glycan structures from the same precursor molecule.

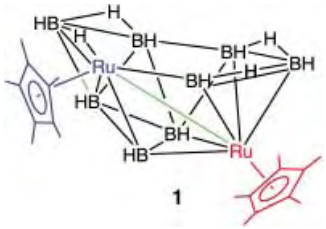
 © 2003 Wiley-VCH Verlag GmbH & Co. KGaA, Weinheim

Metallaboranes

S. Ghosh, A. M. Beatty, T. P. Fehlner* ——— 4678 – 4680

Transition-Metal Variation as a Probe of the Origins of Hypoelectronic Metallaboranes: Eight- and Ten-Vertex Open Ruthenaboranes

Finding skeletons in metallaboranes' closets: Reaction of $[(Cp^*Ru)_2B_4H_8]$ ($Cp^* = C_5Me_5$) with BH_3·THF leads to the formation of 10 skeletal electron pair (sep) compound $[(Cp^*RuH_2)_2B_6H_8]$ and 11 sep, hypoelectronic $[(Cp^*Ru)_2B_8H_{12}]$ (**1**). Compound **1** has the framework of the 12 sep cluster $B_{10}H_{14}$ but modified by a single diamond-square-diamond rearrangement that permits a Ru–Ru interaction (green) between the five-connected (blue) and six-connected (red)



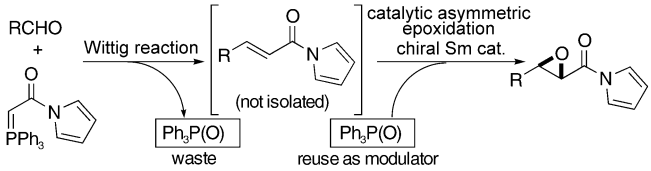
1

{Cp*Ru} fragments which generates an additional unavailable orbital in the ruthenium "t_{2g}" set.

Asymmetric Olefination–Epoxidation

T. Kinoshita, S. Okada, S.-R. Park, S. Matsunaga, M. Shibasaki* ——— 4680 – 4684

Sequential Wittig Olefination–Catalytic Asymmetric Epoxidation with Reuse of Waste $Ph_3P(O)$: Application of α,β-Unsaturated *N*-Acyl Pyrroles as Ester Surrogates



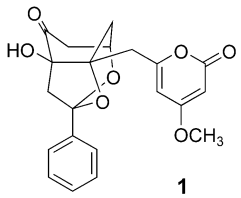
Waste not, want not: Efficient one-pot access to optically active epoxides with 96 to 99.5% *ee* from a variety of aldehydes is described. In a sequential process, the $Ph_3P(O)$ by-product of a Wittig reaction acts as a modulator for the samarium catalyst in the asymmetric epoxidation of the conjugated *N*-acyl pyrrole Wittig product (see scheme). The *N*-acyl pyrrole functionality is key to the high reactivity and selectivity observed. R = alkyl, aryl, vinyl.

Total Synthesis of Polyketides

S. Kirsch, T. Bach* ——— 4685 – 4687

Total Synthesis of (+)-Wailupemycin B

A high functional-group density necessitated the careful choice of protection/deprotection strategy for the successful stereoselective total synthesis of the marine polyketide (+)-wailupemycin B (**1**) from (*S*)-carvone in 6% overall yield. Key to the success of the synthesis was the manipulation of orthogonal protecting groups, two stereoselective additions to highly functionalized cyclohexanones, and mild reliable methods for the oxidation of alcohols.

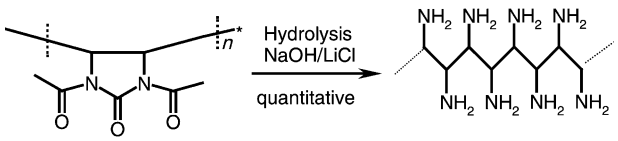


1

Highly Functionalized Polycations

M. Klapper,* C. Hamciuc, R. Dyllick-Brenzinger,* K. Müllen* ——— 4687 – 4690

Poly(methylene amine): A Polymer with the Maximum Possible Number of Amino Groups on a Polymer Backbone



Taken to the limit: The synthesis of a new amino-functionalized polymer containing one amino group on each carbon of the backbone, is presented. This compound, poly(methylene amine), can be considered as the polymer with the highest content of amino functions known.

 © 2003 Wiley-VCH Verlag GmbH & Co. KGaA, Weinheim

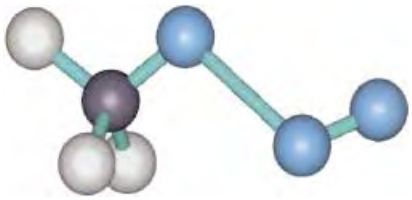
Contents

Generation of the CF_3OOO Radical

S. von Ahsen,* H. Willner,*
J. S. Francisco* ——— **4690 – 4693**

The Trifluoromethyltrioxy Radical, CF_3OOO

Tic-tac-toe, three O's in a row: The trifluoromethyltrioxy radical, CF_3OOO (structure shown), is generated by vacuum flash thermolysis of CF_3O-$C(O)OOC(O)OCF_3$ or $CF_3OC(O)OOCF_3$ in an excess of O_2. The reaction products are quenched as a matrix at low temperatures.

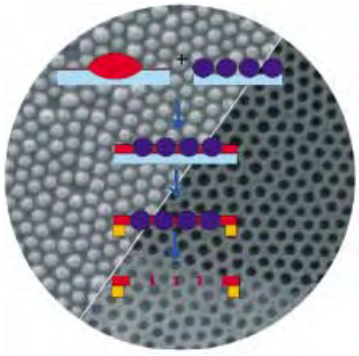


Porous Membranes

H. Xu, W. A. Goedel* ——— **4694 – 4696**

From Particle-Assisted Wetting to Thin Free-Standing Porous Membranes

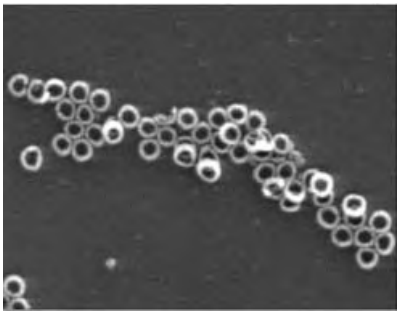
Puncturing polymer membranes: Non-wetting organic liquids (see scheme; red) can form a mesoscopic wetting layer on a water surface (light blue), if they are mixed with suitable particles (dark blue). Photochemical cross-linking of the liquid in the mixed layer and transfer to metal grids or porous supports produces composite membranes. Subsequent removal of the particles yields free-standing porous membranes with uniform pore size and high porosity (see scheme).



Template Synthesis of Micro-Rings

H. Xu, W. A. Goedel* ——— **4696 – 4700**

Mesoscopic Rings by Controlled Wetting of Particle Imprinted Templates

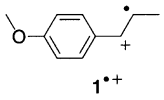


Rings and a few other things: A method for the preparation of uniform mesoscopic titanium dioxide rings that are bound in a periodic array on a substrate, linked to a free-standing membrane, or are dispersed as individual particles (see SEM image) is presented. The technique is based on the selective wetting of the inner surface of a porous membrane.

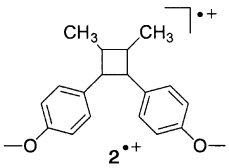
Detection of Transient Radicals

S. Meyer, R. Koch,
J. O. Metzger* ——— **4700 – 4703**

Investigation of Reactive Intermediates of Chemical Reactions in Solution by Electrospray Ionization Mass Spectrometry: Radical Cation Chain Reactions



$1^{\bullet+}$



$2^{\bullet+}$

Transient radicals tracked down: An electrospray ionization mass spectrometer coupled on-line to a microreactor system is useful for investigating reactions in solution and for directly detecting reactive intermediates. The transient radical cations $\mathbf{1}^{\bullet+}$ and $\mathbf{2}^{\bullet+}$ formed in the radical cation chain dimerization of *trans*-anethole were detected unambiguously by MS/MS methods.

Communications labeled with this symbol have been judged by two referees as being "very important papers".

The publication of Communications labeled with this symbol has been accelerated because of their topical or highly competitive nature.

Deadline for recruitment adverts

43/2003	October 16	Publication date:	November 10
44/2003	October 23	Publication date:	November 11

Angewandte Chemie International Edition
Advertising Sales Department:
Marion Schulz
Phone: 0 62 01 – 60 65 65
Fax: 0 62 01 – 60 65 50
E-Mail: MSchulz@wiley-vch.de

Place an advert in the printed version
and have it made available online for 1 month, free of charge!

Service

Keywords ____ *4704*

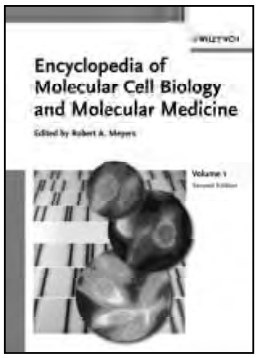
Authors ____ *4705*

Preview ____ *4707*

Corrigendum

In the Communication "Catalytic Asymmetric Allylation of Hydrazano Esters in Aqueous Media by Using ZnF_2–Chiral Diamines" by S. Kobayashi et al. (*Angew. Chem.* **2003**, *115*, 4057; *Angew. Chem. Int. Ed.* **2003**, *42*, 3927) the entry in the last row of Table 2, column 2 should be 3-MeO-2-naphthyl (**12**) and not 8-MeO-2-naphthyl (**12**). The author apologizes for this error.

The Nucleus of Knowledge



2005. Approx. 10,000 pages.
Hardcover.
ISBN 3-527-30542-4
Prepublication price
approx. € 4144.-
valid until March 31, 2004
thereafter approx. € 4944.-

Publication dates:
volumes 1-5 Jan 2004
volumes 6-10 Aug 2004
volumes 11 –16 May 2005

ROBERT A. MEYERS, Ramtech Ltd., Tarzana, CA, USA (ed.)
Encyclopedia of Molecular Cell Biology and Molecular Medicine
16 Volume Set

"*This series is a classic...*" -
Molecular Medicine Today/Trends in Molecular Medicine

The insight of 10 Nobel laureates

The second edition of the bestselling "Encyclopedia of Molecular Biology and Molecular Medicine" provides a one-stop working library of the molecular basis of life, disease diagnosis and therapy with a new focus on the cell level.

It was designed in collaboration with a founding board of 10 Nobel laureates. The encyclopedia is published in 16 volumes containing approximately 425 articles. Each article presents an in-depth treatment accompanied by a key word list with definitions and an extensive bipartite bibliography of primary and secondary papers.

Save € 800,- until March 31st, 2004

http://meyers-emcbmm.de

Register now for the free
WILEY-VCH Newsletter!
www.wiley-vch.de/home/pas

WILEY-VCH • P.O. Box 11 11 61 • D-69451 Weinheim, Germany • Fax: +49 (0) 62 01 - 60 61 84
e-mail: service@wiley-vch.de • www.wiley-vch.de

WILEY-VCH

57503052_kn

 © 2003 Wiley-VCH Verlag GmbH & Co. KGaA, Weinheim

Peptide-Based Ligands

Metal-Ion-Binding Peptides: From Catalysis to Protein Tagging

Giulia Licini and Paolo Scrimin**

Keywords:
combinatorial chemistry · homogeneous catalysis · metal ions · peptides · sensors

Metal ions are among the most important cofactors in proteins. They play a key role in regulating the activity of proteins both at allosteric sites and at catalytic ones. The repertoire of natural amino acids comprises several functional groups in the side arms for the purpose of binding metal ions. Appropriate positioning of these groups in the protein sequence ensures the binding of a diverse range of metal ions, often with remarkable selectivity, according to their nature and their position, as determined by the secondary and tertiary conformation adopted by the polymer. It is thus not surprising that chemists are making more and more use of peptide sequences in their selection of ligands for metal ions for diverse applications.[1] A common approach takes advantage of the natural sequences known to bind a specific metal ion. Chemists, however, have also expanded the supply of coordination motifs provided by natural amino acids by synthesizing new ones and by introducing specific capping units into peptide sequences.[2] The reported applications range from the synthesis of catalysts for reactions not necessarily finding an equivalent in the biological world to obtaining probes for analytical purposes.

One of the important advantages of a peptide sequence over other building blocks is the fact that a solid-phase synthesis, and hence a combinatorial, approach to the preparation of libraries[3] of molecules can be accomplished with ease. The challenge in these cases is to devise methodologies for the screening of the libraries. This approach requires the possibility of estimating the binding strength of the ligands for the metal ions and, depending on the final use of the complexes, to also evaluate their activity as catalysts or sensing devices.

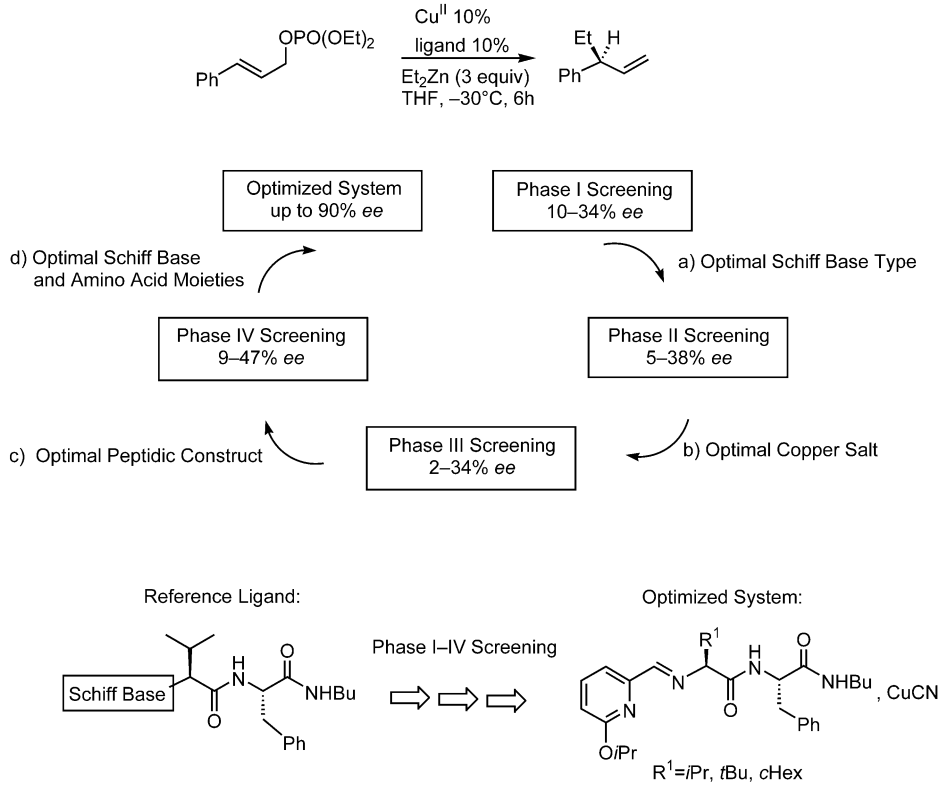
Functional metal peptides are clearly the most appealing targets. Novel peptide-based catalysts were obtained by Francis and Jacobsen from metal-binding combinatorial libraries for the epoxidation of alkenes.[4] A combinatorial approach to the cleavage of phosphates by hydrolytic metallopeptides was reported by Berkessel and Hérault.[5] Their strategy allowed the direct on-beads screening of a 625-member library of undecapeptides with a chromogenic model phosphate. In this way they were able to find active compounds whose efficiency was also tested in homogeneous solution. Combinatorial optimization of the tripeptide Xaa-Xaa-His for complexation to Ni^{2+} ions and deoxyribose-based (oxidative) cleavage of B-form DNA was performed by Long and co-workers.[6] The procedure they have employed is to generate two libraries (by using 18 naturally occurring amino acids and excluding Cys and Trp) in which the first and second position of the ligand were varied. The optimized metallopeptide Ni^{2+}-Pro-Lys-His was found to cleave DNA an order of magnitude better than Ni^{2+}-Gly-Gly-His, the reference compound used as a starting point for the selection process. Interestingly, metal complexation and the T/A-rich site selectivity of the optimized metallopeptide were not altered, while the affinity of DNA binding was only slightly increased. Thus, the observed increased activity is mostly related to the geometry of binding, as suggested by molecular models.

The stereoselective catalysis of a series of rather different reactions was performed by Hoveyda's research group using metallopeptide complexes. In this case, the highly crucial identification of the most effective chiral ligand/metal salt couple for a specific process has been performed by preliminary parallel screening of different metal precursors with readily modifiable (modular) ligands. In all cases, peptide-based Schiff bases with different O, N, or P donors were used in the presence of both early and late transition metal ions: the development of efficient and highly stereoselective C–C bond-forming processes, such as Ti^{IV}-catalyzed CN addition to epoxides[7] and imines,[8] Al^{III}CN addition to ketones,[9] Zr^{IV}-catalyzed dialkyl zinc addition to imines,[10] Cu-catalyzed conjugate addition to enones,[11] and allylic substitution,[12] have been achieved. As an example, pyridinyl peptidic derivatives have been found to be effective chiral ligands for the Cu-catalyzed allylic substitution of di- and trisubstituted alkenes. This catalytic system allowed the synthesis of (*R*)-(−)-sporochnol with 82% *ee* in 82% overall yield.[12]

The strategy towards the selection of the optimal reaction conditions was based on a rational rather than a combinatorial screening approach with the following steps (Scheme 1): a) The identification of the most reactive substrates and metal precursors (allylic phosphates

[*] Prof. Dr. G. Licini, Prof. Dr. P. Scrimin
Department of Organic Chemistry
and ITM-CNR, Padova Section
University of Padova
Via Marzolo, 35131 Padova (Italy)
Fax: (+39) 049-827-5239
E-mail: giulia.licini@unipd.it
paolo.scrimin@unipd.it

 © 2003 Wiley-VCH Verlag GmbH & Co. KGaA, Weinheim DOI: 10.1002/anie.200301668



Scheme 1. The protocol used by Hoveyda and co-workers for the optimization of a peptide-based ligand/Cu salt combination for the asymmetric allylic substitution of alkenes.

and CuCN) as well as the best Schiff base for the addition of Et_2Zn in THF. The two best ligands under these conditions afforded *ee* values of 34% and 26%, which were unimpressive starting points. b) Identification of the best ligand/Cu salt combination using the above-selected ligands and six copper salts. c) The determination of the optimal peptide (number of amino acids in the sequence, nature of the C-terminal group). d) The tuning of the Schiff base and the first amino acid. With this selection process the *ee* values went up to 87% with aryl-disubstituted alkenes and to 90% with the aryl-trisubstituted ones. Similar enantiomeric excesses were obtained by using a nonrational approach based on the screening of parallel libraries of substrates, solvents, and metal ions.[8a,10] This observation may indicate that small, focused libraries may provide results that are as good as a rational, but more time-consuming, approach in the selection of a catalytic system.

An important aspect was raised by Gilbertson et al. in selecting catalysts comprised of peptide-based phosphane ligands and late transition metal ions:[13,14] that of tuning the best chiral ligand/substrate couple. This point underlines the quest for catalysts which are rather specific for a substrate, a property typical of enzymes. By studying the Pd^{II}-catalyzed addition of dimethylmalonate to cyclopentadienyl acetate with catalysts selected from two series of 96- and 40-member peptide libraries, this research group has also addressed the relevance of the secondary conformation of the peptide on the stereoselectivity of the catalytic process. They found that β-turns are better than helical conformations and that the direct screening of the catalysts anchored on the solid support where they had been synthesized is possible in some cases, with results comparable to those obtained in homogeneous solution.

While catalysis has been proven to be an excellent proving ground for testing the potentiality of metallopeptides, a newly emerging application of metallopeptides as fluorescent markers has been reported by Imperiali and coworkers. Previously, they had focused their research on peptide-based fluorescent chemosensors for Zn^{II} ions.[15] The scope of their research has now widened to the discovery of a Ln^{3+}-binding peptide for the rapid detection of tagged proteins. The development of fluorescent proteins as molecular tags may allow complex biochemical processes to be correlated with the function of living cells.[16] The work by Imperiali's group is based on previous studies carried out by other research groups which had focused on the similarities in ionic radii and coordination preferences between Ca^{2+} and Ln^{3+} ions of sequences based on specific loops of calcium-binding proteins.[17] This previous work[18] had pinpointed hot positions that were relevant both for binding and fluorescence enhancing in 14-mer peptides. The screening[19] by Imperiali and co-workers of a large (up to 500000 member) library of peptides of the general sequence Ac-Gly-Xaa-Zaa-Xaa-Zaa-Xaa-Gly-Trp-Zaa-Glu-Zaa-Zaa-Glu-Leu (where Xaa were potential metal-binding residues Asp, Asn, Ser, and Glu and Zaa were hydrophobic amino acids) led to the discovery of a peptide with a K_D value for Tb^{3+} ions as

 © 2003 Wiley-VCH Verlag GmbH & Co. KGaA, Weinheim

low as 0.22 μM. The authors have suggested that these lanthanide-binding tags (LBTs) may constitute a new alternative for expressing fluorescent fusion proteins by routine molecular biological techniques. To test this idea they have appended the most promising sequences to ubiquitin.

As shown in Figure 1, an intervening Gly-Pro-Gly sequence between the N-terminal His tag and LBT tag was introduced as a stop site to allow subsequent removal of the His tag. Very rewardingly, they discovered that protein expression was not diminished by the presence of the LBT. Metal-ion competition experiments established that the LBTs demonstrate good selectivity for Tb^{3+} ions. They have also devised a powerful combinatorial screening[20] on beads to find sequences with an even better binding ability for this lanthanide ion. The methodology utilizes solid-phase split-and-pool combinatorial peptide synthesis where orthogonally cleavable linkers provide the possibility for an efficient two-step screening procedure (Figure 2). The initial screen avoids the interference caused in on-bead screening by photochemically releasing a portion of the peptides into an agarose matrix for evaluation. The secondary screening further characterizes each hit in a defined aqueous solution. It is worth mentioning that this procedure avoids any interference from the solid support, as found in the on-bead screening recently reported by Miller and co-workers[21] and Davis and co-workers[22] in which they looked for products of a reaction produced by a solid-supported catalyst. With this approach, and by further focusing the library, the dissociation constant for Tb^{3+} ions was decreased to 57 nM for a linear peptide and 2 nM when it was cyclized through formation of a disulfide. As a proof of principle, these peptide sequences were used for the determination of the protein concentration and expression profiling. The fluorescence of the lanthanide ion can be exploited for this purpose only if the binding strength is such that it is possible to operate at metal-ion concentrations well below that required by nonspecific binders.

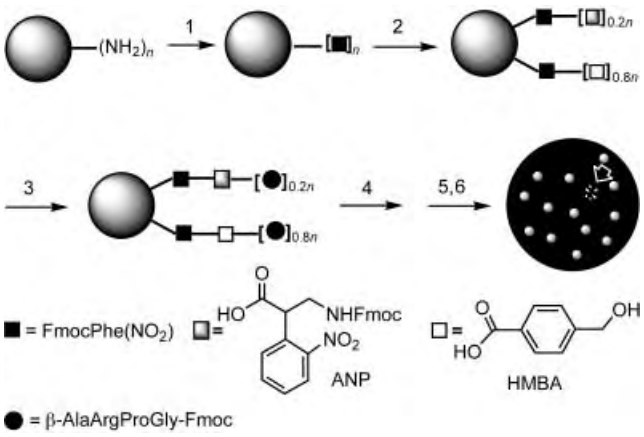


Figure 2. Protocol used by Imperiali and co-workers for the synthesis and screening of Tb^{3+}-binding peptides. 1) Coupling of *N*-α-Fmoc-4-nitrophenylalanine; 2) coupling of ANP:HMBA (1:10); 3) introduction of the spacer sequence; 4) synthesis of a "split-and-pool" library with a mass spectral ladder; 5,6) deprotection of the amino acid side chains followed by casting into agarose with 50 μM Tb^{3+} ions and photolysis. After selection of the beads with luminescent halos and work-up, they are titrated with Tb^{3+} ions and the sequence deconvoluted by MALDI-MS. Fmoc = 9-fluorenylmethoxycarbonyl.

Although ligand peptides[23] have only recently been exploited, nevertheless an impressive amount of useful applications of peptide–metal complexes have already emerged. Functional peptides can not only be screened with a combinatorial approach, but they can also be incorporated into proteins expressed in vivo (with the possibility to encode even unnatural amino acids[24]) and offer the possibility of providing new tools to study proteins and cellular functions and to obtain generations of new synthetic proteins with unusual properties.

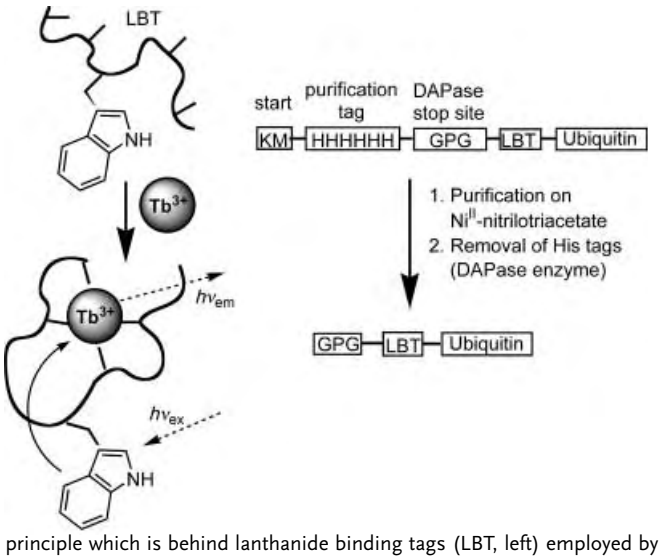


Figure 1. The principle which is behind lanthanide binding tags (LBT, left) employed by Imperiali and co-workers and their general strategy towards LBT-tagged proteins (right). Removal of the His tag can be performed with the TAGZyme protocol (using dipeptidyl aminopeptidase (DAPase) enzyme).

[1] G. Xing, V. J. DeRose, *Curr. Opin. Chem. Biol.* **2001**, *5*, 196–200.
[2] H. Ishida, Y. Inoue, *Rev. Heteroat. Chem.* **1999**, *19*, 79–142.
[3] B. E. Turk, L. C. Cantley, *Curr. Opin. Chem. Biol.* **2003**, *7*, 84–90.
[4] M. B. Francis, E. N. Jacobsen, *Angew. Chem.* **1999**, *111*, 987–991; *Angew. Chem. Int. Ed.* **1999**, *38*, 937–941.
[5] A. Berkessel, D. A. Hérault, *Angew. Chem.* **1999**, *111*, 99–102; *Angew. Chem. Int. Ed.* **1999**, *38*, 102–105.

 © 2003 Wiley-VCH Verlag GmbH & Co. KGaA, Weinheim

[6] X. Huang, M. E. Pieczko, E. C. Long, *Biochemistry* **1999**, *38*, 2160 – 2166.
[7] K. D. Shimizu, B. M. Cole, C. A. Krueger, K. W. Kuntz, M. L. Snapper, A. H. Hoveyda, *Angew. Chem.* **1997**, *109*, 1781 – 1785; *Angew. Chem. Int. Ed. Engl.* **1997**, *36*, 1703 – 1707, and references therein.
[8] C. A. Krueger, K. W. Kuntz, C. D. Dzierba, W. G. Wirschum, J. D. Gleason, M. L. Snapper, A. H. Hoveyda, *J. Am. Chem. Soc.* **1999**, *121*, 4284 – 4285; b) J. R. Porter, W. G. Wirschun, K. W. Kuntz, M. L. Snapper, A. H. Hoveyda, *J. Am. Chem. Soc.* **2000**, *122*, 2657 – 2658.
[9] H. Deng, M. P. Isler, M. Snapper, A. H. Hoveyda, *Angew. Chem.* **2002**, *114*, 1051 – 1054; *Angew. Chem. Int. Ed.* **2002**, *41*, 1009 – 1012.
[10] J. R. Porter, J. F. Traverse, A. H. Hoveyda, M. L. Snapper, *J. Am. Chem. Soc.* **2001**, *123*, 984 – 985.
[11] C. A. Luchaco-Cullis, H. Mizutani, K. E. Murphy, A. H. Hoveyda, *Angew. Chem.* **2001**, *113*, 1504 – 1508; *Angew. Chem. Int. Ed.* **2001**, *40*, 1456 – 1460; b) S. J. Degrado, H. Mizutani, A. H. Hoveyda, *J. Am. Chem. Soc.* **2002**, *124*, 13362 – 13363.
[12] S. J. Degrado, H. Mizutani, A. H. Hoveyda, *J. Am. Chem. Soc.* **2001**, *123*, 755 – 756.
[13] S. R. Gilbertson, S. E. Collibee, A. Agarkov, *J. Am. Chem. Soc.* **2000**, *122*, 6522 – 6523.
[14] S. R. Gilbertson, X. Wang, *Tetrahedron* **1999**, *55*, 11609 – 11618, and references therein.
[15] G. K. Walkup, B. Imperiali, *J. Am. Chem. Soc.* **1997**, *119*, 3443 – 3450.
[16] J. Lippincott-Schwartz, G. H. Patterson, *Science* **2003**, *300*, 87 – 91.
[17] For the use of EF-hand sequences (a Ca-binding motif of calmodulin) as Ln^{III}-based metallonucleases, see J. T. Welch, W. R. Kearney, S. J. Franklin, *Proc. Natl. Acad. Sci. USA* **2003**, *100*, 3725 – 3730, and references therein.
[18] J. P. MacManus, C. W. Hogue, B. J. Marsden, M. Sikorska, A. G. Szabo, *J. Biol. Chem.* **1990**, *265*, 10358 – 10366.
[19] K. J. Franz, M. Nitz, B. Imperiali, *ChemBioChem* **2003**, *4*, 265 – 271.
[20] M. Nitz, K. J. Franz, R. L. Maglathlin, B. Imperiali, *ChemBioChem* **2003**, *4*, 272 – 276.
[21] R. F. Harris, A. J. Nation, G. T. Copeland, S. J. Miller, *J. Am. Chem. Soc.* **2000**, *122*, 11270 – 11271.
[22] M. Müller, T. W. Mathers, A. P. Davis, *Angew. Chem.* **2001**, *113*, 3929 – 3931; *Angew. Chem. Int. Ed.* **2001**, *40*, 3813 – 3815.
[23] R. B. Hill, D. P. Raleigh, A. Lombardi, W. F. DeGrado, *Acc. Chem. Res.* **2000**, *33*, 745 – 754.
[24] L. Wang, P. G. Schultz, *Chem. Commun.* **2002**, 1 – 11.

 © 2003 Wiley-VCH Verlag GmbH & Co. KGaA, Weinheim

Bioelectrocatalysis and Magnets

Magnetic Control of Electrocatalytic and Bioelectrocatalytic Processes

Itamar Willner and Eugenii Katz*

Keywords:
biosensors · electrochemistry · magnetic particles · nanotechnology

Bioelectronics is a rapidly progressing interdisciplinary research field that has important implications for the development of biosensors, biofuel cells, biomaterial-based computers, and bioelectronic devices. Magneto-controlled molecular electronics and bioelectronics are new topics that examine the effect of an external magnetic field on electrocatalytic and bioelectrocatalytic processes of functionalized magnetic particles associated with electrodes. In this article we describe the progress in the developments of magneto-switchable electrocatalytic and bioelectrocatalytic transformations, and the effects of the rotation of the magnetic particles on the electrocatalytic and bioelectrocatalytic processes are discussed. Finally, the implications of the results on the development of biosensors, amplified immunosensors, and DNA sensors are described.

Introduction

Bioelectronics is a rapidly progressing research field that comprises the development of biosensors, for example, enzyme-based sensors[1] immunosensors,[2] and DNA sensors,[3] the assembly of biofuel cell elements,[4] the fabrication of bioelectronic devices[5] and mechanical units,[6] the construction of electronic circuitry,[7] and the use of biomaterials for computer applications.[8]

The possibility of signal triggering by molecular[9] and biomolecular[10] redox functions has incited efforts directed to the development of information-processing devices, logic elements, and molecular-based machines. For example, chemical stimuli such as pH were employed to activate redox functions,[11] and photochemical triggering of switchable redox functions was suggested as a means for the electronic transduction of recorded photonic information.[12] Also, photochemical isomerization of supramolecular assemblies accompanied by the mechanical switching of molecular components between distinct states was suggested as a means for information storage and processing,[13] and preliminary efforts to construct molecular computing devices were reported.[14] Similarly, the photochemical activation of the redox functions of enzymes was accomplished, and biomaterial-based systems capable of electronic transduction of recorded photonic information were studied in detail.[15] For example, the modification of redox proteins with photoisomerizable units[15a] and the reconstitution of apo-proteins with photoisomerizable cofactors[15b,c] were reported to switch the biocatalytic functionalities of the protein between "on" and "off" states. Similarly, photoisomerizable interfaces were used as "command surfaces" for communication between redox proteins and electrode supports as well as for the "on" and "off" stimulation of electron-transfer enzyme cascades.[16]

In this article we review recent scientific accomplishments in the switching and controlling of electrocatalytic and bioelectrocatalytic processes by means of an external magnet. We discuss the possible future applications of such systems in the design of biosensors and generation of new optobioelectronic systems. The use of rotating magnetic fields to enhance electrocatalytic and bioelectrocatalytic transformations is emphasized with the aim to highlight new concepts for amplified biosensing and for the acceleration of biorecognition events. Substantial efforts were directed toward the development of biological sensing assays that use magnetic particles. Ingenious methods for labeling magnetic particles with biomaterials such as antigens/antibodies[17] and nucleic acids[18] for immunosensing and DNA sensing were developed. In these systems the magnetic particles are used as matrices for the formation, isolation, and physical separation of the biorecognition complexes from complex biological

[*] Prof. I. Willner, Dr. E. Katz
Institute of Chemistry
The Hebrew University of Jerusalem
Jerusalem 91904 (Israel)
Fax: (+972) 2-6527-715
E-mail: willnea@vms.huji.ac.il

 © 2003 Wiley-VCH Verlag GmbH & Co. KGaA, Weinheim DOI: 10.1002/anie.200201602

mixtures by means of an external magnet. In other words, the collection of the functionalized magnetic particles by means of an external magnet enables their purification by washing and leads to the concentration of the biological recognition pairs. In contrast to these reports,[17–19] in which the magnetic particles are used as a vehicle for the physical translocation of the linked biomaterials, the present review summarizes recent activities in which electrochemical transformations are coupled to functionalized magnetic particles attracted to electrode supports by an external magnetic field.

Preparation and Reactions of Functionalized Magnetic Particles

Magnetite particles[20] (Fe_3O_4, saturated magnetization ca. 65 emu g^{-1}, ca. 1 μm average diameter) were functionalized with an aminopropylsiloxane film. A series of electroactive relay units—2,3-dichloro-1,4-naphthoquinone (**1**), *N*-ferrocenylmethyl-6-aminohexanoic acid (Fc, **2**), *N*-carboxyundecyl-*N*′-methyl-4,4′-bipyridinium (**3**), the pyrroloquinoline quinone **4** (PQQ), and microperoxidase-11 (MP-11, **5**)—were covalently linked[21] to the magnetite particles (Scheme 1 A and B).

The switching of the electrochemical activities of the functional particles by means of the external magnet is outlined in Scheme 2 A. Attraction of the magnetic particles to the electrode surface by means of the external magnet activates the electrical contact between the redox units, R, and the electrode, and the redox features of the redox components are switched on. Positioning the magnet above the electrochemical cell retracts the magnetic particles from the electrode, and the electrochemical activity of the functional magnetic particles is switched off.

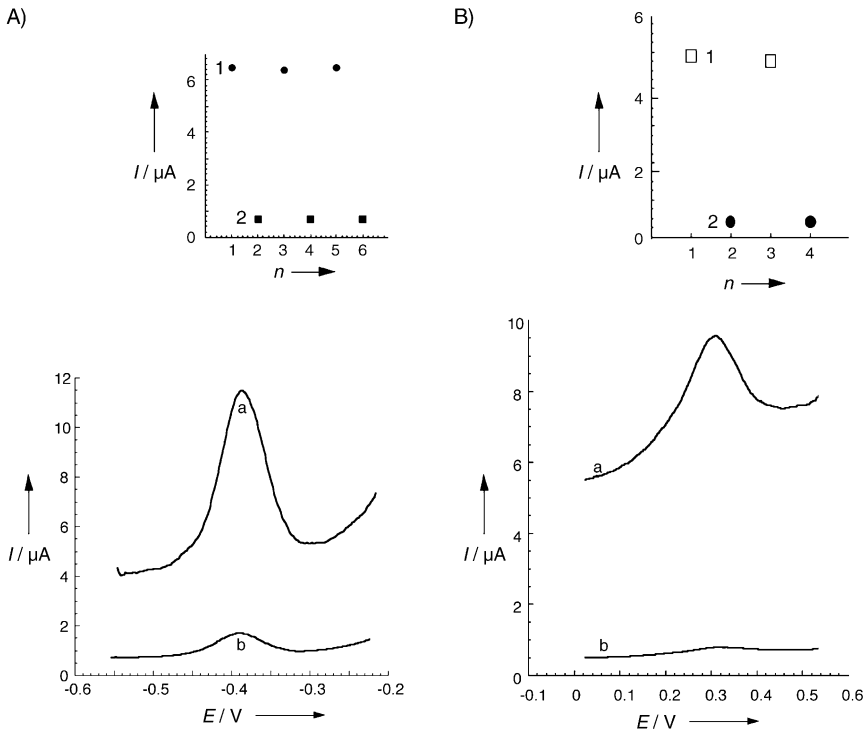


Figure 1. Electrochemistry of relay-functionalized magnetic particles reversibly switched "on" and "off" by means of an external magnet. A) For particles functionalized with aminonaphthoquinone **6**, B) for particles functionalized with ferrocene **2**. Bottom: Differential pulse voltammograms obtained a) when the particles are magnetically attracted to and b) when they are magnetically retracted from the electrode surface. Top: Reversible changes of the peak current of the differential pulse voltammograms upon magnetically switching the redox response of the functionalized particles "on" (1) and "off" (2); n = number of steps. The data were recorded for the functionalized magnetic particles (10 mg) in 0.1 M phosphate buffer, pH 7.0, under argon. The differential pulse voltammograms were measured at a potential scan rate of 20 mV s^{-1} with a pulse height of 5 mV.

Figure 1 shows the results of the reversible magnetic-field-induced contacting and retraction of magnetic particles functionalized with aminonaphthoquinone **6** ($E^0 = -0.39$ V vs. SCE at pH 7.0) and the ferrocene derivative **2** ($E^0 = 0.32$ V vs. SCE). Electrochemical activation of the redox units associated with the magnetic particles enables the secondary magneto-controlled switchable activation and deactivation of electrocatalytic processes. For example, pyrroloquinoline quinone PQQ (**4**, $E^0 = -0.16$ V vs. SCE at pH 8.0) acts as an electrocatalyst for the oxidation of 1,4-dihydro-β-nicotinamide adenine dinucleotide (NADH).[22] Accordingly, PQQ-functionalized magnetic particles (average surface coverage of 7.5×10^3 PQQ units per particle) were employed for

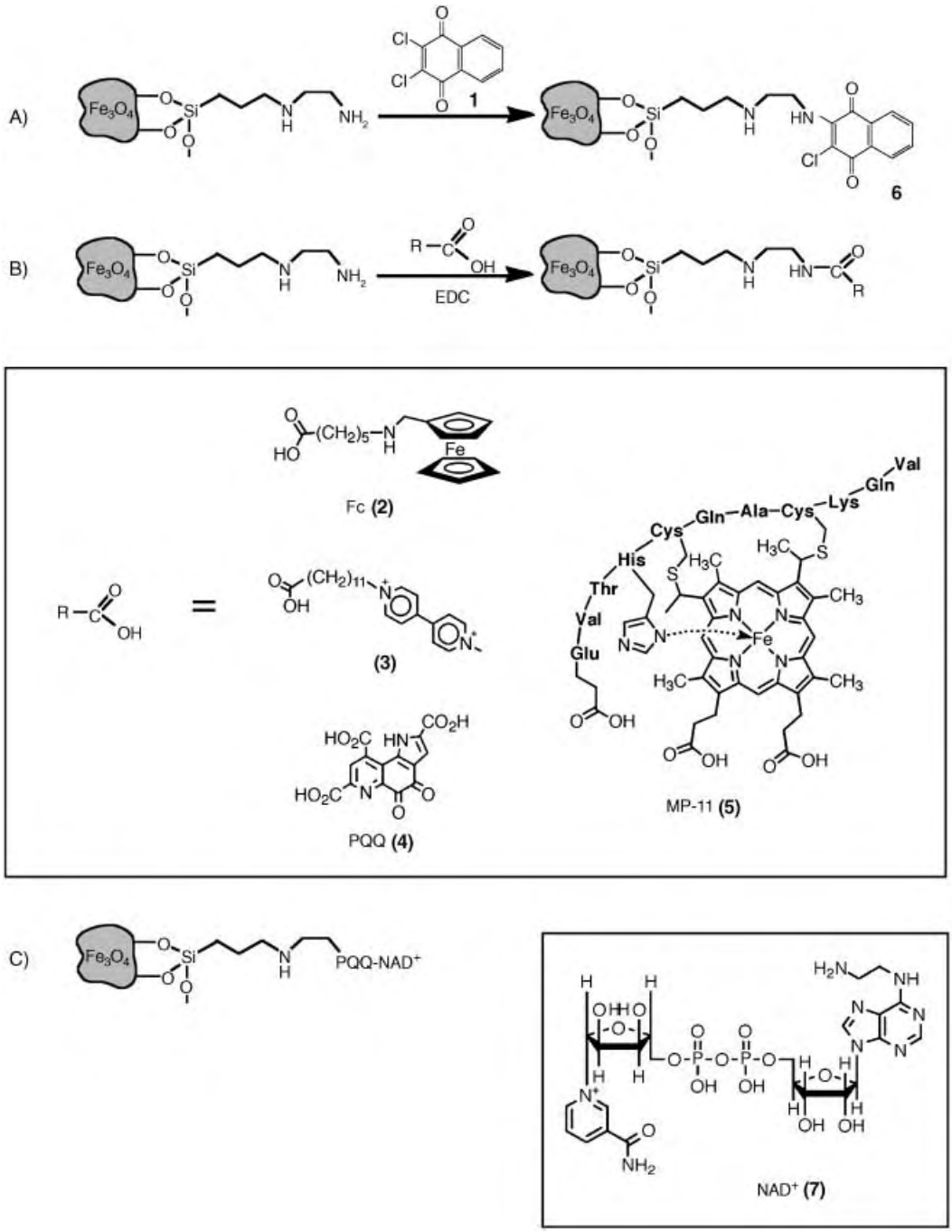


Itamar Willner was born in 1947 and completed his PhD studies in Chemistry in 1978 at The Hebrew University of Jerusalem. After a postdoctoral stay with M. Calvin at the University of California, Berkeley, from 1978 to 1981, he joined the Institute of Chemistry at The Hebrew University of Jerusalem in 1981 and was appointed Professor in 1986. He serves on several editorial boards and is the recipient of the Kolthoff Award, The Max Planck Research Award for International Cooperation, the Israel Chemical Society Award (2001), and the Israel Prize in Chemistry (2002). He is a member of the Israel Academy of Sciences.



Eugenii Katz was born in 1952 in Moscow. He completed his PhD studies in 1983 at the Frumkin Institute of Electrochemistry, Moscow, and until 1991 served as a research associate at the Institute of Photosynthesis, Pushchino, Russia. In 1991 he conducted postdoctoral research with I. Willner at The Hebrew University of Jerusalem and in 1993, as a recipient of the Humboldt scholarship, he worked at the Technische Universität, München, with H.-L. Schmidt. He joined the research group of I. Willner at the Hebrew University in 1994 as a senior research associate.

 © 2003 Wiley-VCH Verlag GmbH & Co. KGaA, Weinheim

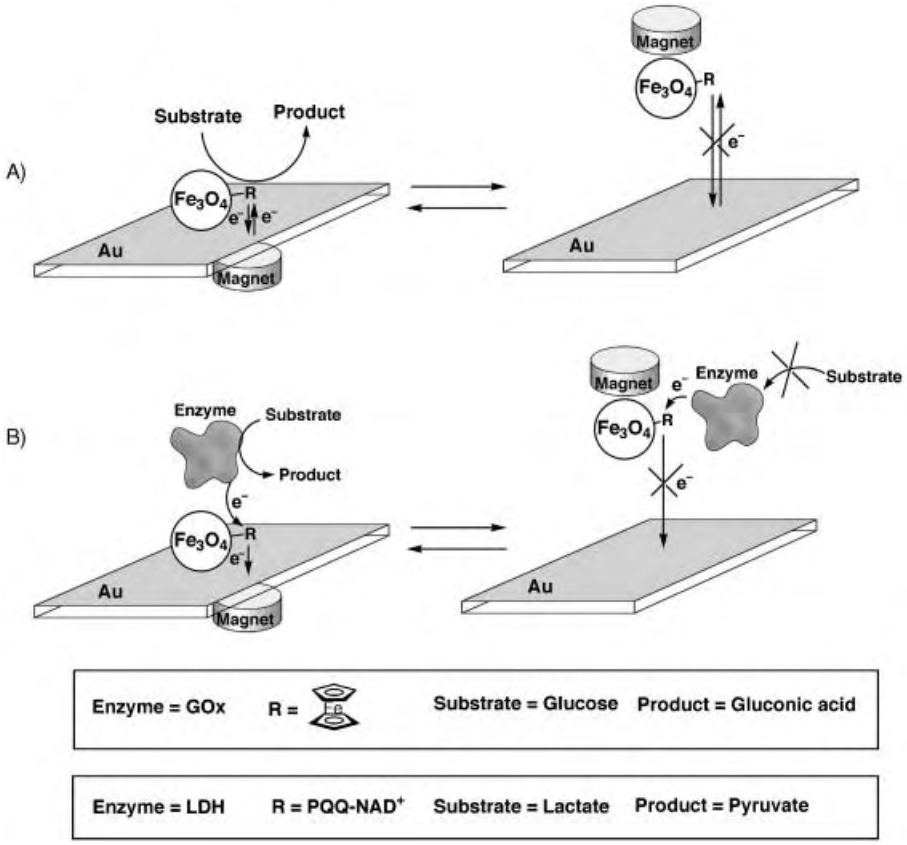


Scheme 1. Synthesis of relay-functionalized magnetic particles by the covalent linkage of redox-active units to magnetic particles functionalized with a [*N*-(2-aminoethyl)-3-aminopropyl]siloxane film: A) Linkage of 2,3-dichloro-1,4-naphthoquinone (**1**) to the particles to yield magnetic particles functionalized with aminonaphthoquinone **6**. B) Carbodiimide coupling of electron-relay carboxylic acid derivatives to the amino groups of the siloxane layer (EDC = 1-[3-(dimethylamino)propyl]-3-ethylcarbodiimide hydrochloride). C) Magnetic particles functionalized with the PQQ–NAD^+ dyad for electrochemical activation of NAD^+-dependent enzymes.

controlling the electrocatalyzed oxidation of NADH by means of the external magnet.[21b] Figure 2 A depicts the cyclic switchable activation and deactivation of the electrocatalytic oxidation of NADH by the PQQ-functionalized particles upon their attraction to the electrode and their retraction from the electrode by means of the external magnet. Similarly, the magnetic particles functionalized with MP-11 (**5**) were employed for magnetically controlled electrocatalytic reduction of hydrogen peroxide.[21b]

Electron-relay units act as electron-transfer mediators that electrically communicate with redox enzymes and electrode supports. For example, ferrocene and bipyridinium redox-relay units were reported to electrically contact oxidative redox enzymes, for example, glucose oxidase (GOx), and

 © 2003 Wiley-VCH Verlag GmbH & Co. KGaA, Weinheim



Scheme 2. Electrochemical, electrocatalytic, and bioelectrocatalytic reactions of functional magnetic particles controlled by means of an external magnet. A) Switching "on" and "off" the electrochemical reaction of the redox-relay groups (R) covalently bound to the magnetic particles and the respective switching of the electrocatalytic function provided by the redox groups. B) Switching "on" and "off" the bioelectrocatalytic oxidation of glucose in the presence of glucose oxidase (GOx) and Fc-functionalized magnetic particles or oxidation of lactate in the presence of lactate dehydrogenase (LDH) and PQQ–NAD^+-functionalized magnetic particles.

reductive biocatalysts, for example, nitrate reductase, respectively.[23] Thus, the activation of the redox functionalities of the relay-modified magnetic particles enables the subsequent switchable activation and deactivation of bioelectrocatalytic transformations by means of the external magnet.[21] Scheme 2B shows the magneto-switchable activation of redox enzymes in the presence of electron-relay-functionalized magnetic particles, for example, the bioelectrocatalyzed oxidation of glucose by glucose oxidase in the presence of the magnetic particles functionalized with the ferrocene derivative Fc (**2**). The attraction of the Fc-functionalized magnetic particles to the electrode results in the oxidation of the ferrocene units to the ferrocenyl cation components. These in turn oxidize the redox center of glucose oxidase and activate the bioelectrocatalyzed oxidation of glucose. Retraction of the magnetic particles from the electrode support by means of the external magnet blocks the electrical communication between the electrode and the ferrocene units and inhibits the secondary bioelectrocatalyzed oxidation of glucose.

Figure 2B shows the results of the magnetic activation of the bioelectrocatalyzed oxidation of glucose, reflected by the electrocatalytic anodic current, due to the attraction of the functional magnetic particles to the electrode. Similarly, the retraction of the magnetic particles from the electrode blocks the bioelectrocatalytic oxidation of glucose. By the reversible concentration and removal of the magnetic particles onto the electrode and from the electrode, respectively, cyclic "on" and "off" activation and deactivation of the bioelectrocatalytic process is accomplished. A similar approach was applied for the magnetic switching of the bioelectrocatalyzed reduction of nitrate to nitrite, in which nitrate

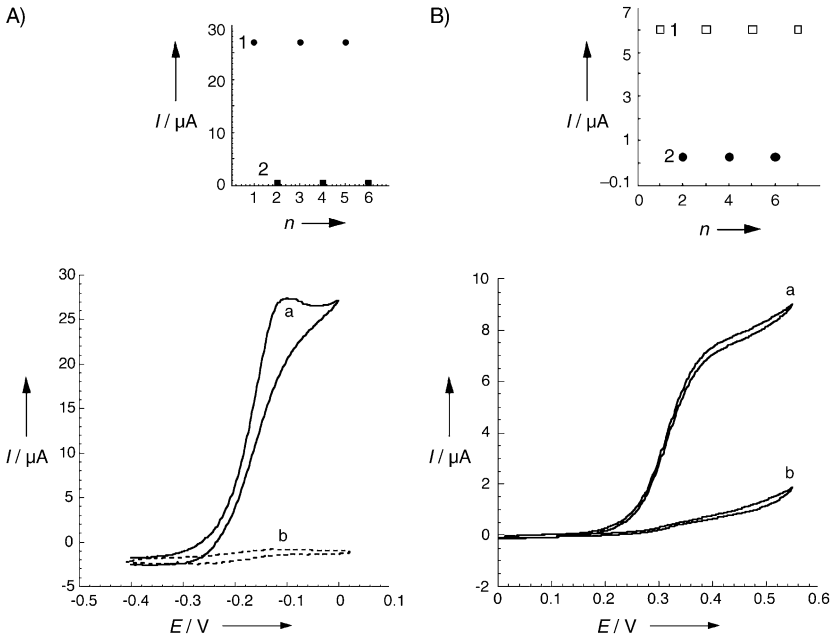


Figure 2. Magneto-switching of the bioelectrocatalyzed transformations corresponding to A) the oxidation of NADH (50 mM) mediated by PQQ-functionalized magnetic particles (10 mg) in the presence of $CaCl_2$ (10 mM), and B) the oxidation of glucose (10 mM) mediated by ferrocene-modified magnetic particles (10 mg) in the presence of GOx (1 mg mL^{-1}). Bottom: Cyclic voltammograms upon a) attraction of the particles to the electrode and b) retraction of the particles from the electrode. Top: Switching of the electrocatalytic currents in the systems upon attraction (1) and retraction (2) of the functionalized magnetic particles to and from the electrode, respectively. Experimental details are given in ref. [21b].

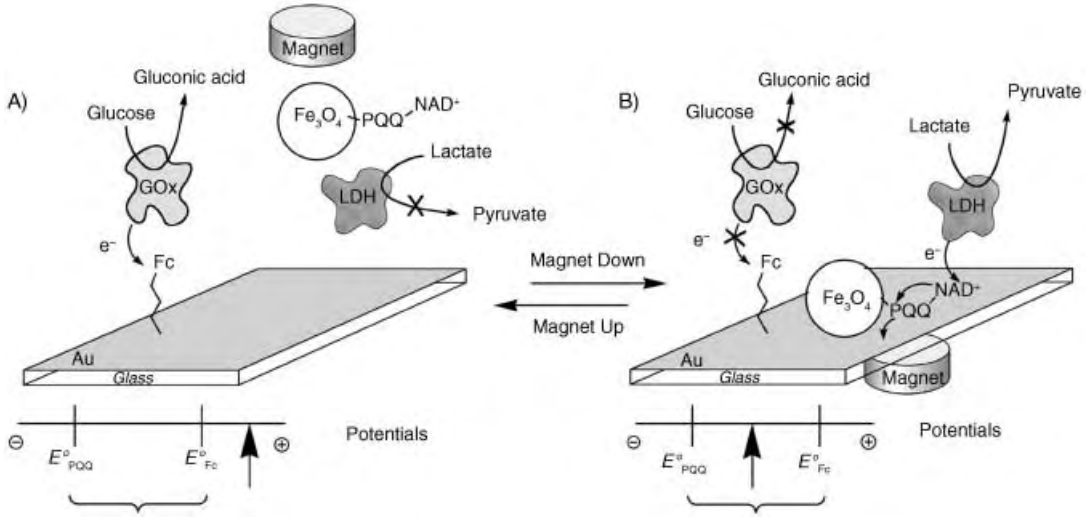
 © 2003 Wiley-VCH Verlag GmbH & Co. KGaA, Weinheim

reductase served as the biocatalyst and magnetic particles functionalized with bipyridinium **3** ($E^0 = -0.57$ V vs. SCE) served as a mediator unit.[21b] Upon attraction of the bipyridinium-functionalized magnetic particles to the electrode and application of a potential of $E = -0.7$ V to the electrode, the bioelectrocatalyzed reduction of nitrate to nitrite mediated by bipyridinium radical cation occurred at a rate corresponding to 6.5×10^{-3} mM min^{-1}, whereas retraction of the particles from the electrode by positioning the magnet above the electrochemical cell blocked the bioelectrocatalytic process. By switching the position of the external magnet below the electrode surface and above the cell, the electrocatalyzed reduction of NO_3^- could be reversibly switched between "on" and "off" states, respectively.

Functional magnetic particles were also employed for the cyclic activation and deactivation of NAD^+-dependent enzymes by means of an external magnet. It was reported[24] that a covalently linked PQQ–NAD^+ monolayer associated with an electrode provided an active interface for the activation of NAD^+-dependent enzymes, for example, lactate dehydrogenase (LDH). The biocatalyzed oxidation of the substrate yields NADH that is oxidized to NAD^+ by PQQ. The resulting $PQQH_2$ is oxidized to PQQ enabling the electrochemically driven biocatalyzed oxidation of the substrate, for example, lactate. Accordingly, PQQ-functionalized magnetic particles were treated with N^6-(2-aminoethyl)-β-nicotinamide adenine dinucleotide (NAD^+, **7**)[25] to yield PQQ–NAD^+-modified particles (Scheme 1 C). The resulting particles were then used for the magneto-switching of the bioelectrocatalytic functions of the NAD^+-dependent enzyme LDH by means of the external magnet (Scheme 2 B). Attraction of the PQQ–NAD^+-functionalized magnetic particles to the electrode in the presence of lactate dehydrogenase (LDH) activates the bioelectrocatalyzed oxidation of lactate to pyruvate. The biocatalyzed reduction of the NAD^+ cofactor unit by lactate is followed by the oxidation of the resulting NADH by the PQQ electrocatalyst. The application of the appropriate potential ($E = 0.05$ V vs. SCE) for oxidation of the resulting $PQQH_2$ regenerates the electrocatalyst. This enables the continuous bioelectrocatalyzed oxidation of lactate to pyruvate in the presence of LDH. The electrocatalytic anodic current developed by the system increases in magnitude as the lactate concentration is elevated, and it levels off to the value of the current density of $i_{max} = 1.8$ μA cm^{-2} at a lactate concentration of 50 mM. Analysis of the electrocatalyzed oxidation of lactate to pyruvate by LDH under steady-state electrolysis indicates that pyruvate is generated at a rate corresponding to 0.13 mM min^{-1}. Retraction of the functionalized magnetic particles from the electrode by means of the external magnet prohibited the bioelectrocatalyzed oxidation of lactate, and by the cyclic positioning of the external magnet below and above the cell, the process could be reversibly switched between "on" and "off" states, respectively.

Dual Biosensing Systems

The ability to control bioelectrocatalytic transformations by means of an external magnet was utilized to develop selective dual biosensing systems.[26] The specific simultaneous electrochemical sensing of two substrates with overlapping redox potentials is a challenging topic in bioelectronics. Scheme 3 outlines the concept for the dual sensing of lactate and glucose in the presence of the two oxidative enzymes LDH and GOx by using PQQ–NAD^+-functionalized magnetic particles and an external magnet. The electrode is modified with a monolayer of Fc **2**, and the PQQ–NAD^+-functionalized magnetic particles, the enzymes LDH and GOx, and the two substrates, lactate and glucose, are included in the system. When a potential $E > 0.32$ V (vs. SCE) is applied to the electrode and the magnetic particles are retracted from the electrode (Scheme 3 A), the ferrocene-mediated bioelectrocatalyzed oxidation of glucose occurs (Figure 3 A, bottom, curve b), whereas the bioelectrocatalyzed oxidation of lactate is blocked (Figure 3 A, top, curve 2). Magnetic attraction of the PQQ–NAD^+-functionalized mag-



Scheme 3. Magneto-controlled dual biosensing of glucose (A) and lactate (B) in the presence of GOx, LDH, magnetic particles functionalized with PQQ–NAD^+, and an Au-electrode modified with a monolayer of ferrocene units.

 © 2003 Wiley-VCH Verlag GmbH & Co. KGaA, Weinheim

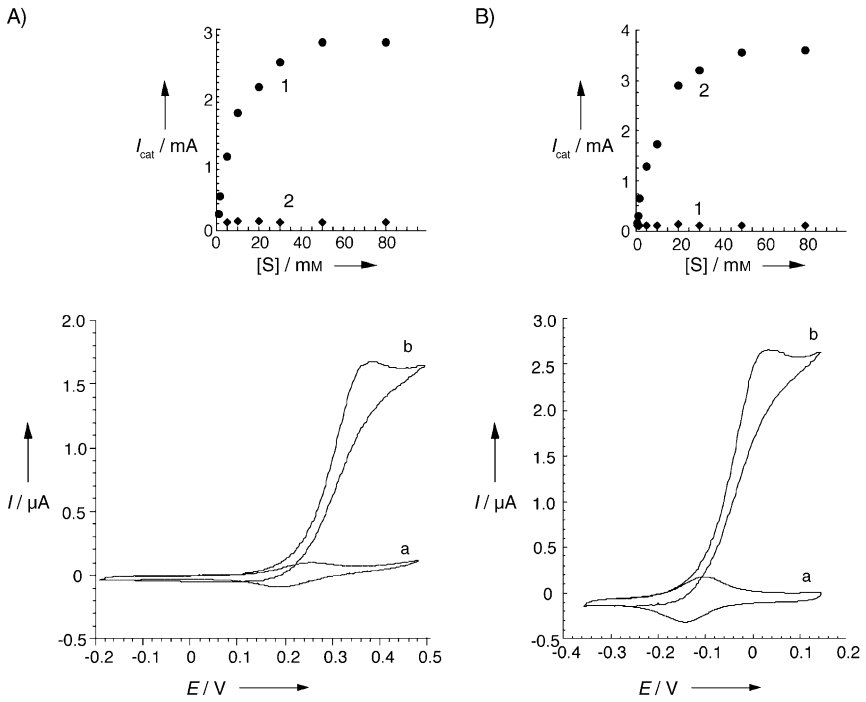


Figure 3. Magneto-controlled dual biosensing of glucose and lactate in the presence of PQQ–NAD^+-functionalized magnetic particles (20 mg) through cyclic voltammetry at a gold electrode functionalized with a ferrocene monolayer in 0.1 M Tris-HCl (under argon, pH 7.0, $CaCl_2$ (10 mM); potential scan rate: 5 $mV s^{-1}$). In (A) the magnetic particles are retracted from, in (B) attracted to the electrode by the external magnet. Bottom: curves a: in the presence of GOx (1 $mg mL^{-1}$) and LDH (2 $mg mL^{-1}$); curves b: in the presence of GOx (1 $mg mL^{-1}$), LDH (2 $mg mL^{-1}$), glucose (50 mM), and lactate (20 mM). Top: Calibration plots of the amperometric responses of the system with the magnet in the up (A) and down (B) position and the applied potential $E = 0.50$ V (vs. SCE) for different concentrations of glucose (curves 1) and lactate (curves 2).

netic particles to the electrode, followed by applying the potential on the electrode in the range of $-0.13\,V < E < 0.32$ V (vs. SCE) allows the PQQ–NAD^+-mediated oxidation of lactate in the presence of the NAD^+-dependent LDH (Scheme 3B). Since the ferrocene units are not oxidized in this potential range, the bioelectrocatalyzed oxidation of glucose is prohibited. Curve b at the bottom of Figure 3B shows the electrocatalytic anodic current resulting from the biocatalyzed oxidation of lactate, and curve 1 in Figure 3B top shows the lack of electrical response of the system to glucose. The specific sensing of lactate is thus achieved by limiting the potential applied on the electrode. Note, however, that the specific analysis of glucose is accomplished only by retraction of the magnetic particles from the electrode by means of the external magnet, since both bioelectrocatalyzed transformations may proceed in the extended potential region.

DNA Sensors

Electronic detection of DNA utilized magnetic particles for the separation and concentration of the target DNA.[27] Avidin-modified magnetic particles were functionalized with a biotinylated DNA probe. The hybridized target DNA was separated from the analyzed sample by means of an external magnet. Release of the hybrid DNA under basic conditions, followed by the chronopotentiometric stripping of the released guanine residue enabled the quantitative analysis of the target DNA. The sequence specific to the breast cancer gene *brca1* was analyzed by this method. The reversible magnetically controlled oxidation of DNA was accomplished in the presence of nucleic acid modified magnetic particles.[28] Avidin-modified magnetic particles were functionalized with the biotinylated probe nucleic acid and subsequently hybridized with the complementary DNA. Two carbon-paste electrodes were patterned on a surface and applied as working electrodes. Spatial deposition of the functionalized magnetic particles on the right (r) or left (l) electrode enabled the magneto-controlled oxidation of the DNA by chronopotentiometric experiments (potential pulse from 0.6 V to 1.2 V, Figure 4).

An interesting approach for the magneto-controlled amplified detection of DNA was introduced by Wang and colleagues by using nucleic acid modified metal[29,30] and semiconductor nanoparticles[31] as tags for the electrochemical detection of DNA. In this approach the nucleic acid functionalized nanoparticle tags associated with the sensing interface undergo electrochemical stripping or chemical dissolution, which enables the electrochemical analysis of the dissolved product. Also, the metal nanoparticle associated with the sensing interface could act as a catalytic site for the deposition of other metals, thus leading to the amplified detection of DNA by the intermediary accumulation of metals that are stripped off, or by generating an enhanced amount of dissolved product that can be electrochemically analyzed.

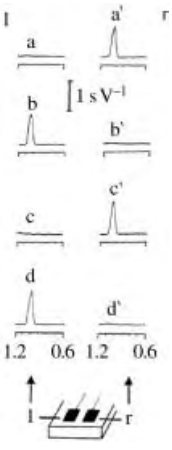
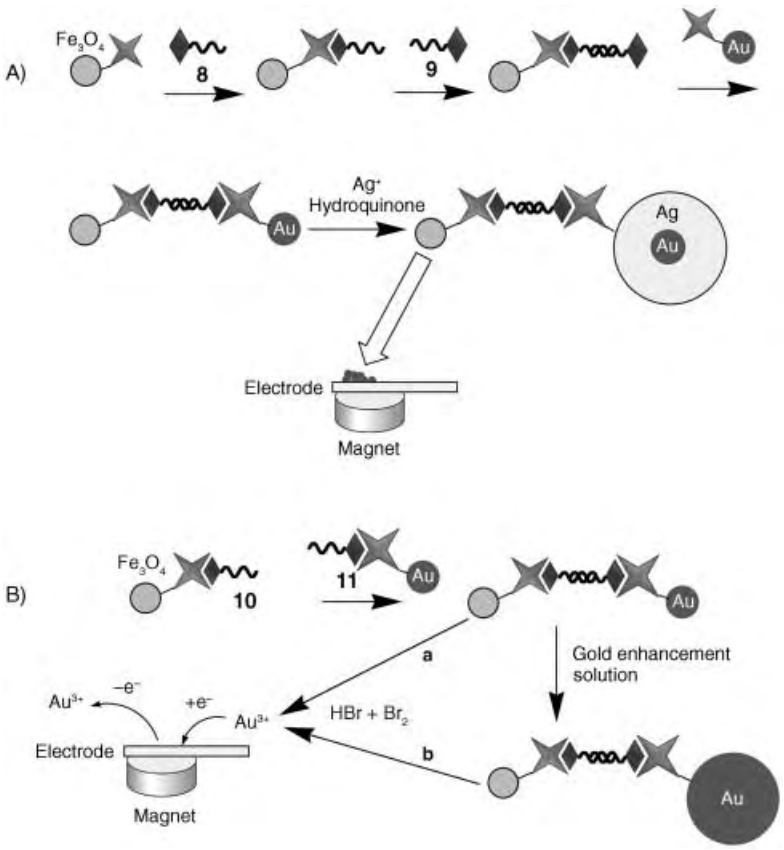


Figure 4. Potentiometric stripping analysis (PSA) for DNA oligomer-functionalized magnetic particles (100 μg) with an assembly containing two carbon-paste electrodes. The signal intensities in $s V^{-1}$ are given as a function of the potential E in V. Potentiograms a–d were measured at the left-hand electrode (l), while potentiograms a′–d′ were measured at the right-hand electrode (r); a, b′, c, and d′ were recorded in the absence of the magnet, while a′, b, c′, and d were recorded in the presence of the magnet (reproduced from ref. [28]).

 © 2003 Wiley-VCH Verlag GmbH & Co. KGaA, Weinheim



Scheme 4. Electrochemical analysis of DNA upon the assembly of DNA molecules at magnetic particles followed by their association with Au nanoparticles. For details see text.

Scheme 4A depicts the amplified detection of DNA by the application of nucleic acid functionalized magnetic beads and Au nanoparticles as catalytic seeds for the deposition of silver.[29] A biotin-labeled nucleic acid (labeled **8** in Scheme 4A) is immobilized on the avidin-functionalized magnetic particles and hybridized with the complementary biotinylated nucleic acid (**9**). The hybridized assembly is then reacted with the Au-nanoparticle–avidin conjugate. Magnetic separation of the particles by an external magnet removes the hybridized assembly from the analyzed sample and reactants. Treatment of the conjugate particles with silver ions in the presence of hydroquinone results in the catalytic deposition of metallic silver on the Au nanoparticles. This process is an amplification route since the accumulation of silver on the Au nanoparticle is triggered by a single DNA-recognition event. The current originating from the potential stripping of the accumulated silver metal provides the electronic signal for the analysis of the target DNA.

In a related system the electrochemical detection of DNA is accomplished by the use of Au nanoparticles as electroactive and catalytic tags (Scheme 4B).[30a] The primer biotinylated nucleic acid (labeled **10**) is linked to the magnetic beads through an avidin bridge. The hybridization of the nucleic acid (**11**) functionalized Au nanoparticle is then followed by the dissolution of the Au nanoparticle in a HBr/Br_2 solution. The resulting Au^{3+} ions are reduced onto the electrode, and this surface-generated gold is then electrochemically stripped (route a in Scheme 4B). This analytical procedure can be further amplified by the intermediary deposition of gold on the Au nanoparticles (route b). The higher gold content after this deposition leads to a higher chronopotentiometric signal. Figure 5 shows the potentiograms corresponding to the stripping of the gold generated on the electrode upon the analysis of the nucleic acid associated with 5-nm Au nanoparticles (route a) and after the deposition of gold on the Au nanoparticles for 10 minutes (route b).

Similarly, CdS semiconductor nanoparticles modified with nucleic acid were employed as tags for the detection of DNA hybridization events.[31] Dissolution of the CdS (in the presence of 1M HNO_3) followed by the electrochemical reduction of the Cd^{2+} ions to Cd^0, which accumulates on the electrode, and the stripping off of this generated Cd^0 (to give Cd^{2+}) provides the electrical signal for the DNA analysis. Figure 6 shows the chronopotentiograms resulting from the analysis of different concentrations of the complementary target DNA in which the modified CdS nanoparticles are used as tags.

In the methods outlined in Scheme 4 the magnetic particles serve as carriers for the metal or semiconductor nanoparticles and as a means to concentrate the analyzed DNA. An interesting aspect of these systems is the future possibility of using a combination of different metal or semiconductor tags linked to different nucleic acids for the simultaneous analysis of different DNA targets (a library) linked to different magnetic beads. In this approach the variable potentials needed to strip off the different metals could act as electrochemical indicators for the nature of the analyzed DNA.

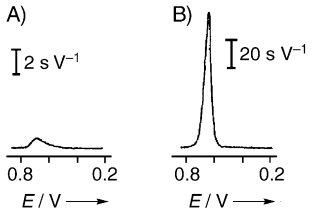


Figure 5. Effect of the gold enhancement upon the stripping response in the analysis of DNA **11** (10 μg mL^{-1}). PSA signal of the Au nanoparticle label A) before and B) after 10 min in the gold enhancement solution. Hybridization time: 25 min; amount of magnetic beads: 90 μg; number of 5-nm avidin-coated gold particles: 7.6×10^{10}; gold oxidation time: 5 min (reproduced from ref. [30a]).

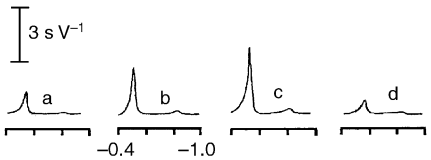


Figure 6. PSA signals vs. *E* in V upon sensing of different concentrations of DNA bound to magnetic particles and labeled with CdS nanoparticles: a) 0.2 mg L^{-1}, b) 0.4 mg L^{-1}, c) 0.6 mg L^{-1} DNA and d) control experiment with noncomplementary DNA (0.6 mg L^{-1}). Amount of magnetic particles: 20 μg; concentration of the DNA-functionalized CdS nanoparticles: 0.01 mg mL^{-1}; hybridization time: 10 min; accumulation potential: −0.9 V; accumulation time: 2 min; stripping current: 1 μA (reproduced from ref. [31]).

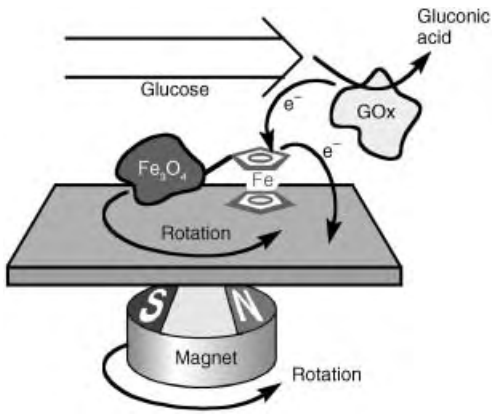
 © 2003 Wiley-VCH Verlag GmbH & Co. KGaA, Weinheim

Electrochemically Driven Chemiluminescence Systems

The magnetic control of electrocatalytic transformations at electrode supports was further employed to develop a magneto-controlled electrochemically driven chemiluminescence system.[32] Magnetic particles functionalized with aminonaphthoquinone **6** were used as the active component for switching the electrochemiluminescent process. Attraction of the particles to the electrode support results in the reduction of the quinone units to the hydroquinone, which catalyzes the reduction of O_2 to H_2O_2.[33] The enzyme horseradish peroxidase (HRP) catalyzes the chemiluminescent process between luminol (3-aminophthalhydrazide, **12**) and H_2O_2, leading to emission of light at $\lambda = 425$ nm (see Scheme 6).[34] Retraction of the magnetic particles from the electrode blocks the light emission process since the quinone units are not coupled to the electrode support. This system represents a magneto-switched optoelectronic system, where electrochemically generated light is switched between "on" and "off" states. Electrochemiluminescent systems have been used extensively as optical labels for biorecognition processes.[35] Thus, the magneto-controlled light emission process may be coupled to biosensing events (vide infra).

Signal Amplification by Rotation of the Magnetic Particles

An important advance in the magnetic control of electrocatalytic and bioelectrocatalytic transformations was accomplished by magnetic attraction of the magnetic particles to the electrode support followed by the rotation of the magnetic particles on the electrode by means of an external rotating magnet.[36] The rotation of the redox-functionalized magnetic particles turns them into circularly rotating microelectrodes. As a result, redox-activated electrocatalytic or bioelectrocatalytic processes mediated by the functional particles are controlled by convection rather than diffusion of the substrate to the microelectrodes. Accordingly, enhanced amperometric responses of the particle-mediated electrocatalytic processes are anticipated, and the resulting currents should be controlled by the rotation speed of the particles. Scheme 5 depicts the amplified amperometric analysis of glucose by the rotation of ferrocene-functionalized magnetic particles on the electrode support. The rotating magnetic particles are functionalized with an electron-transfer mediator, and the interaction with GOx and glucose is convection-controlled. Thus, the resulting electrocatalytic currents should relate to the square root of the rotation speed ($I_{cat} \propto \omega^{1/2}$). Figure 7A shows the bioelectrocatalytic currents obtained in the system when the external magnet is rotated at different speeds. Clearly, the amperometric response increases as the rotation speed is elevated. Figure 7B shows the analysis of variable concentrations of glucose by the particles rotating at two different speeds as compared to the amperometric responses of the system when the particles are not rotating. The rotation of the particles results in an approximately 15-fold increase in the amperometric responses of the bioelectrocatalytic proc-



Scheme 5. Bioelectrocatalytic oxidation of glucose in the presence of GOx and ferrocene-functionalized magnetic particles enhanced upon circular rotation of the particles by means of an external rotating magnet.

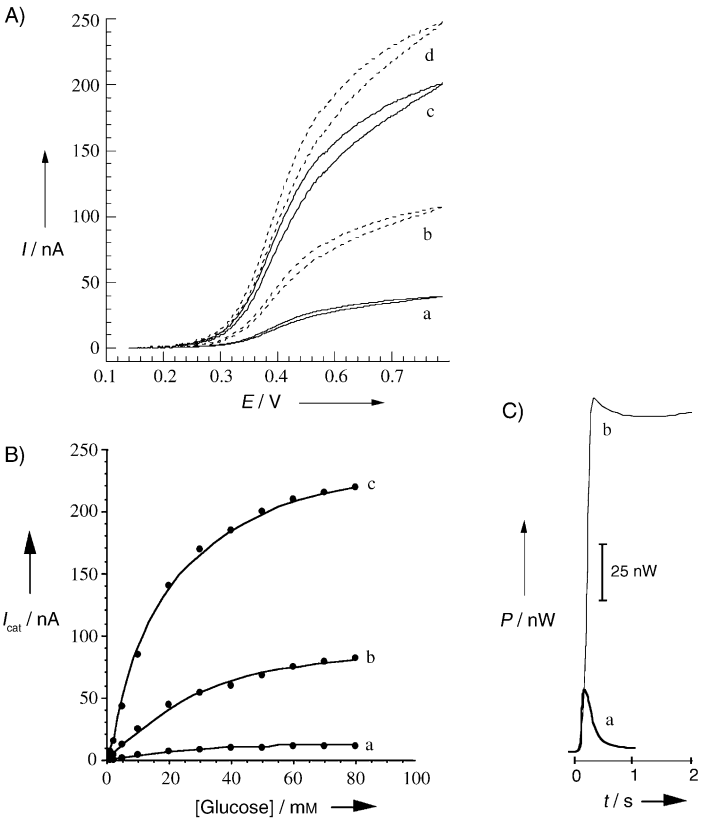


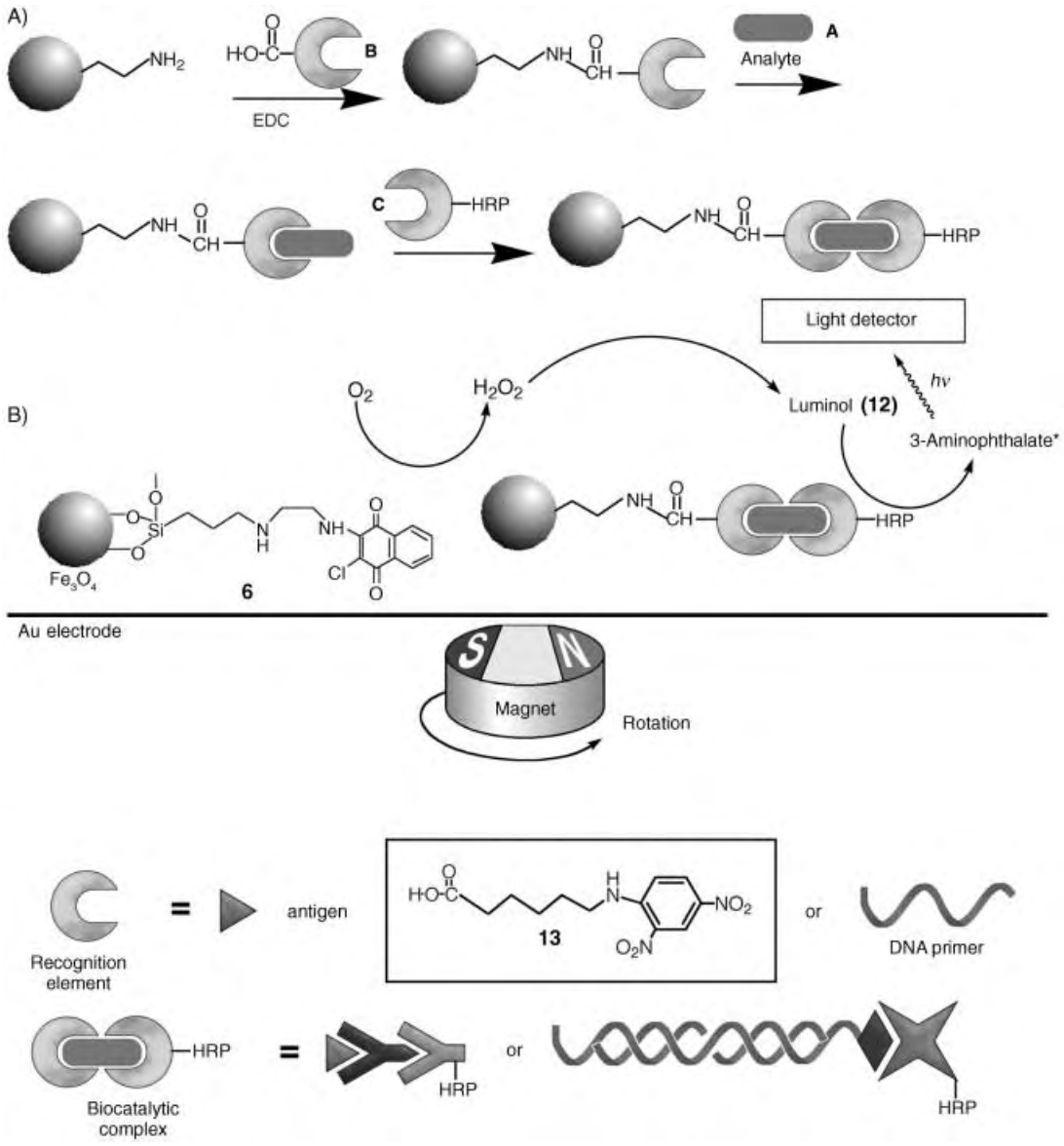
Figure 7. Amplification of sensing events upon rotation of functionalized magnetic particles. A) Cyclic voltammograms from a gold electrode with the magnetically attracted ferrocene-functionalized magnetic particles (6 mg) in the presence of GOx (1×10^{-5} M) and glucose (50 mM) upon rotation of the magnet at a) 0, b) 10, c) 100, and d) 400 rpm. Potential scan rate: 5 $mV s^{-1}$. B) Calibration plots for the amperometric detection of glucose ($E = 0.5$ V vs. SCE) upon rotation of the magnet at a) 0, b) 100, and c) 400 rpm. The data were recorded in 0.1 M phosphate buffer, pH 7.0. C) Radiant power of the electrochemiluminescence enhanced by the rotation of functionalized magnetic particles upon application of potential $E = -0.5$ V (vs. SCE) to the conductive support: a) 0 and b) 400 rpm. The measurements were conducted under air, and the system included aminonaphthoquinone-functionalized magnetic particles (10 mg), HRP (1 $mg mL^{-1}$), and luminol (1×10^{-6} M) in 0.1 M phosphate buffer, pH 7.0.

 © 2003 Wiley-VCH Verlag GmbH & Co. KGaA, Weinheim

ess. Similar results were observed for the electrocatalyzed oxidation of NADH by rotating the PQQ-functionalized electrocatalytic magnetic particles. Also, the rotation of magnetic particles functionalized with aminonaphthoquinone **6** in the presence of HRP and luminol resulted in enhanced electrogenerated chemiluminescence (Figure 7C). The amperometric responses of the electrocatalytic transformations originating from the rotation of the redox-functionalized magnetic particles may be analyzed by using conventional rotating disc electrode (RDE) theory.[37] When the experimental currents obtained at different rotation speeds are analyzed in terms of Levich theory, the interfacial electron-transfer rate constant can be estimated.

The enhanced electrocatalysis and bioelectrocatalysis in the presence of rotating magnetic particles can be used to amplify biosensing events. This is illustrated in Scheme 6A, where an analyte **A** is sensed by magnetic particles that include unit **B**, which is the complementary unit for **A**. Binding of **C**, the second recognition element for **A**, which is conjugated to HRP, yields the biocatalytic "sandwich structure" for analyzing **A**.

The magnetic attraction of a mixture of particles consisting of the magnetic particles functionalized with aminonaphthoquinone **6** together with the sandwich structure generated from the magnetic particles that contain the components **B**/**A**/**C**-HRP enables the amplified detection of the analyte by electrogenerated chemiluminescence. Electroreduction of the aminonaphthoquinone units leads to the electrocatalyzed reduction of O_2 to H_2O_2, which in the presence of luminol and HRP results in the biocatalyzed generation of light (Scheme 6B). Upon rotation of the magnetic particles, O_2 and luminol interact with the two types of functionalized magnetic particles by convection, leading to the amplified generation of chemiluminescence.



Scheme 6. Amplified detection of bioaffinity recognition processes by multilabeled rotating magnetic particles: A) Synthesis of the functionalized magnetic particles for the biorecognition assay. B) Amplified biorecognition assay upon the rotation of the functionalized magnetic particles.

 © 2003 Wiley-VCH Verlag GmbH & Co. KGaA, Weinheim

The biosensing affinity interactions occurring on the magnetic particles may be antigen–antibody, nucleic acid–DNA or any other intermolecular host–guest binding process. In fact, magnetic particles functionalized with biorecognition complexes were previously employed for biosensing in which electrogenerated chemiliminescence served as the means of transduction, and this technology has been successfully commercialized.[38] The ORIGEN method is based on the formation of a biorecognition complex on a magnetic particle that is labeled with $[Ru(bpy)_3]^{2+}$ (bpy = bipyridine) as a electrochemiluminescence-generating component. The electrogenerated $[Ru(bpy)_3]^{3+}$ oxidizes triphenylamine while generating the excited $*[Ru(bpy)_3]^{2+}$, which emits light and transduces the biorecognition events.

Besides the new amplification schemes that will be discussed here for the analysis of antigen–antibody complexes and of DNA, the importance of the rotation of the magnetic particles for amplified biosensing will be discussed. For example, amplified detection of immunological interactions, and the ultrasensitive detection of DNA was accomplished with rotating functionalized magnetic particles.[39]

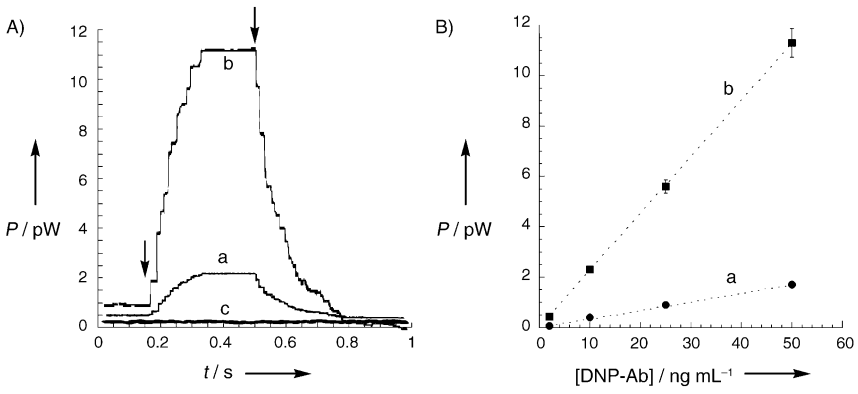


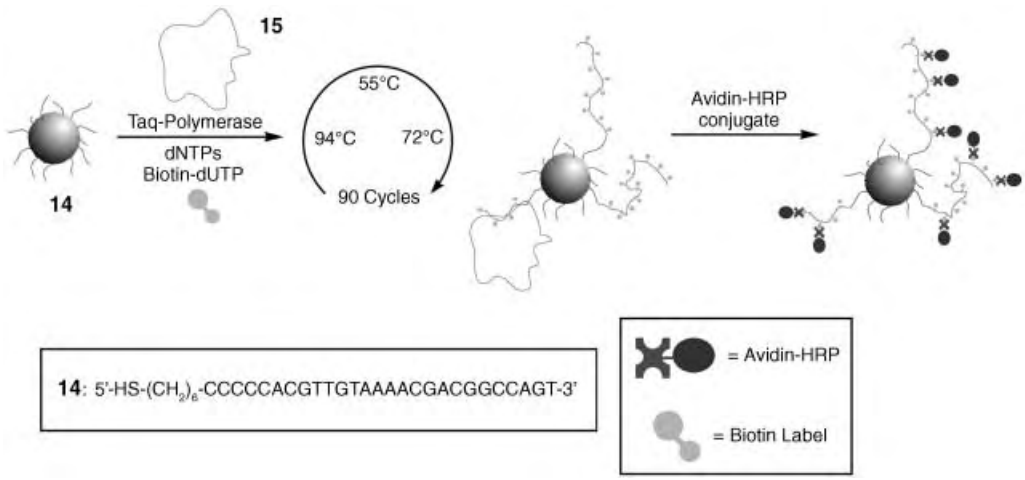
Figure 8. A) Radiant power of the chemiluminescence in the analysis of the DNP-Ab (50 ng mL^{-1}) when the functionalized magnetic particles are rotated at a) 0 and b) 400 rpm; c) in a control experiment without DNP-Ab but with a rotation rate of 400 rpm. b) Peak chemiluminescence intensities observed in the presence of different concentrations of the DNP-Ab at rotation rates of a) 0 and b) 400 rpm. For all the experiments the chemiluminescence signals were produced by applying a potential step on the electrode from 0 V to −0.5 V and back (vs. SCE). Arrows in (A) indicate the times at which the potential was switched to −0.5 V and to 0.0 V. The measurements were conducted under air, and the system included functionalized magnetic particles (10 mg), HRP (1 mg mL^{-1}), and luminol (1×10^{-6} M) in 0.1 M phosphate buffer, pH 7.0.

The approach outlined in Scheme 6 can, for example, be used for the analysis of the dinitrophenyl antibody, DNP-Ab. Magnetic particles functionalized with the dinitrophenyl antigen **13** (as the recognition element) are used as the sensing particles, and added magnetic particles labeled with aminonaphthoquinone **6** act as electrocatalytic particles supplying H_2O_2 for the sensing process (Scheme 6B). In the presence of DNP-Ab, the antigen–antibody complex is formed on the sensing magnetic particles, and this enables the secondary association of the avidin–HRP conjugate. The electrocatalyzed reduction of O_2 by the aminonaphthoquinone-modified particles yields H_2O_2, which, in the presence of luminol and the HRP conjugate, yields chemiluminescence from the system (Scheme 6B). Upon rotation of the particles, the electrocatalyzed reduction of O_2 and the subsequent HRP/luminol-induced generation of chemiluminescence are controlled by the convection of the substrates to the electrode-confined particles. As a result, enhanced chemiluminescence from the system is expected.

Figure 8A shows a plot of the radiant power from the system analyzing the DNP-Ab (50 ng mL^{-1}) at different rotation speeds of the particles. In Figure 8B the radiant power emitted from the system are plotted for different concentrations of the DNP-Ab. As the rotation speed increases, the sensitivity of the detection process is enhanced, and at a rotation speed corresponding to 400 rpm the detection limit for analyzing the DNP-Ab is ca. 1 ng mL^{-1}. The procedure was also used for the analysis of DNA.[39] The target DNA was hybridized with the complementary nucleic acid functionalized magnetic particles, and further hybridized with a biotinylated nucleic acid complementary to a second segment of the target DNA to yield the respective three-component nucleic acid/DNA complex. The association of the avidin–HRP conjugate to the complex and contact of these particles with the aminonaphthoquinone-functionalized particles led to the light emission upon electrochemical reduction of the quinone units (Scheme 6B). When the magnetic particles were rotated, the generation of chemiluminescence was enhanced.

A modification of this scheme for the amplified detection of viral DNA by functional magnetic particles is shown in Scheme 7 with the analysis of the 7229-base M13 phage DNA.[40] The 27-base-pair DNA primer **14** complementary to a segment of the analyte DNA is associated with the magnetic particles. The hybridization of **14** with the M13 phage DNA **15** is followed by a polymerization process in the presence of the dNTP (deoxynucleoside triphosphate) and biotin-labeled dUTP. The replication introduces biotin labels into the replicated nucleic acid on the magnetic particles. This replication process is followed by a sequence of thermal cycles where the M13 phage DNA is dissociated, rehybridized with another primer on the particle, and further replicated with incorporation of the biotin labels. The resulting particles are then treated with the avidin–HRP bioconjugate, and the resulting functionalized magnetic particles are collected by means of the external magnet on the electrode surface, and mixed with the particles labeled with aminonaphthoquinone **6**. The electrocatalyzed reduction of O_2 by the quinone units yields H_2O_2, which leads in the presence of luminol and HRP to the generation of the chemiluminescence, and by the rotation of the particles to the amplified light emission. Figure 9A shows the radiant power of the emitted light upon the analysis of the M13 DNA (8×10^{-9} M) at different rotation speeds of the particles. By means of this method the target DNA could be analyzed with a detection limit of 8×10^{-18} M (Figure 9B). The intensity of the chemiluminescence generated in the system correlates linearly with the square root of the rotation speed ($\omega^{1/2}$), consistent with the fact that the

 © 2003 Wiley-VCH Verlag GmbH & Co. KGaA, Weinheim



Scheme 7. Labeling of the nucleic acid replica on the magnetic particles with biotin units using thermal cycles for amplified detection of viral DNA by multilabeled rotating magnetic particles.

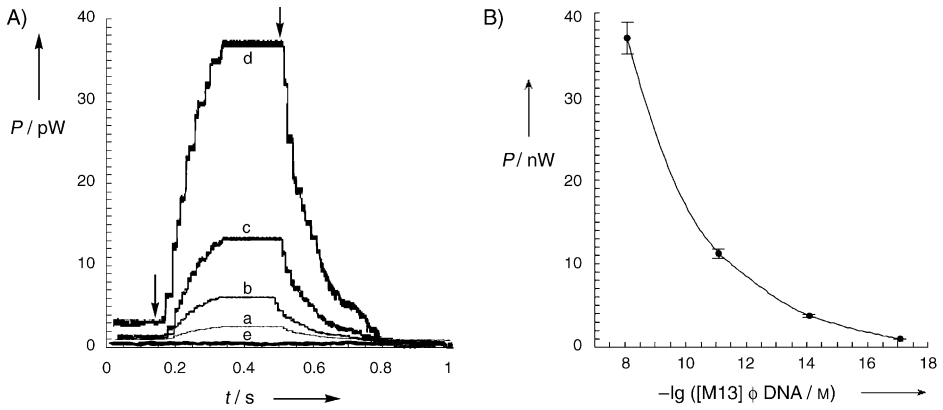


Figure 9. A) Radiant power of the chemiluminescence generated in the analysis of M13 phage DNA (8×10^{-9} M) at rotation rates of a) 0, b) 60, c) 400, and d) 2000 rpm; e) chemiluminescence signal obtained in the absence of M13 phage DNA but with rotation at 2000 rpm. B) Calibration plots of the radiant power of the chemiluminescence in the analysis of different concentrations of M13 phage DNA with a rotation rate of 2000 rpm. For details see legend of Figure 8.

luminescence intensity is controlled by convection of the substrates to the rotating particles. A similar approach was applied to detect single-base mismatches in DNA.[40]

In all the systems in which detection of biorecognition events is amplified by rotation of the magnetic particles the amplification effect is accomplished by controlling the electrogenerated chemiluminescence by the convection of the substrates to the electrode support. Since the chemiluminescence requires the confinement of the biocomponent to the electrode support, simple mixing or stirring of the medium cannot lead to this effect. The amplification effect could, however, be achieved by anchoring the biocomponents to a rotating disc electrode. The advantages of the rotating magnetic particles over the disc electrode configuration are obvious, for example, the high surface area of the magnetic particles acting as microelectrodes, and the possibility for the rapid regeneration of the sensing system by exchanging the functional magnetic particles with the aid of an external magnet.

Conclusions and Perspectives

We have described a recently developed field of research based on the control of electrocatalytic and bioelectrocatalytic transformations through magnets. The magnetic control of electrocatalytic and bioelectrocatalytic transformations may be used in regulating the composition of bioreactors. For example, functional magnetic particles could be coupled to a sensing device, and switchable magneto-controlled electrocatalytic or bioelectrocatalytic transformations could be used to degrade inhibitors or interfering components. Other feasible future applications are the use of magneto-switchable bioelectrocatalytic processes for dual sensing[26] and micropatterning of surfaces.[41]

The use of functional magnetic particles and specifically the external rotation of the magnetic particles provides a novel concept in the development of bioelectrocatalytic systems.[39,40] The attraction of functionalized magnetic particles to surfaces can be used to concentrate and separate the

 © 2003 Wiley-VCH Verlag GmbH & Co. KGaA, Weinheim

ingredients involved in the analytical processes. The localization of redox-functionalized magnetic particles on electrodes enables the electronic transduction of the biosensing events. The rotation of the magnetic particles on the electrode surface may enhance biorecognition processes on the particles or amplify the electronic signal that transduces the biosensing events. These features of the magnetic particles may be used separately or sequentially to improve the performance of bioelectrochemical sensor devices. The coupled enhanced hybridization and amplified electronic, or optoelectronic (chemiluminescent), detection of DNA or DNA–protein interactions at rotating magnetic particles seems to be a powerful future technique for gene analysis. Other future applications of the concept could include the targeted activation of therapeutic compounds using conductive magnetic stents and functional magnetic particles. Furthermore, one could envisage the use of functionalized magnetic particles, on which heterogeneous catalysts are immobilized, as integrated electrocatalytic systems that are triggered by an external magnet. The rotation of such magnetic particles on electrode supports could lead to enhanced electrochemically induced heterogeneous catalysis. At this stage the applications of magneto-switchable electrocatalytic and bioelectrocatalytic systems are in their infancy. However, recent advances suggest that exciting research opportunities exist for chemists, biologists, and material scientists.

Our studies are supported in part by the Israel Science Foundation and by the U.S.–Israel Binational Science Foundation (BSF).

Received: October 17, 2002
Revised: March 11, 2003 [M1602]

[1] a) F. A. Armstrong, G. S. Wilson, *Electrochim. Acta* **2000**, *45*, 2623 – 2645; b) I. Willner, E. Katz, *Angew. Chem.* **2000**, *112*, 1230 – 1269; *Angew. Chem. Int. Ed.* **2000**, *39*, 1180 – 1218; c) I. Willner, E. Katz, B. Willner, *Electroanalysis* **1997**, *13*, 965 – 977; d) L. Habermüller, M. Mosbach, W. Schuhmann, *Fresenius J. Anal. Chem.* **2000**, *366*, 560 – 568; e) A. Heller, *Acc. Chem. Res.* **1990**, *23*, 128 – 134.

[2] a) A. Warsinke, A. Benkert, F. W. Scheller, *Fresenius J. Anal. Chem.* **2000**, *366*, 622 – 634; b) R.-I. Stefan, J. F. van Staden, H. Y. Aboul-Enein, *Fresenius J. Anal. Chem.* **2000**, *366*, 659 – 668.

[3] a) J. Wang, *Chem. Eur. J.* **1999**, *5*, 1681 – 1685; b) I. Willner, E. Katz, B. Willner in *Electroanalytical Methods of Biological Materials* (Eds.: A. Brajter-Toth, J. Q. Chambers), Marcel Dekker, New York, **2002**, pp. 43 – 107; c) I. Willner, B. Willner, *Trends Biotechnol.* **2001**, *19*, 222 – 230.

[4] a) E. Katz, I. Willner, A. B. Kotlyar, *J. Electroanal. Chem.* **1999**, *479*, 64 – 68; b) T. Chen, S. C. Barton, G. Binyamin, Z. Q. Gao, Y. C. Zhang, H. H. Kim, A. Heller, *J. Am. Chem. Soc.* **2001**, *123*, 8630 – 8631; c) E. Katz, A. F. Bückmann, I. Willner, *J. Am. Chem. Soc.* **2001**, *123*, 10752 – 10753.

[5] a) A. B. Kharitonov, M. Zayats, A. Lichtenstein, E. Katz, I. Willner, *Sens. Actuators B* **2000**, *70*, 222 – 231; b) M. Zayats, A. B. Kharitonov, E. Katz, A. F. Bückmann, I. Willner, *Biosens. Bioelectron.* **2000**, *15*, 671 – 680; c) A. B. Kharitonov, J. Wasserman, E. Katz, I. Willner, *J. Phys. Chem. B* **2001**, *105*, 4205 – 4213; d) K. Mitsubayashi, Y. Hashimoto, *Sens. Actuators B* **2002**, *83*, 35 – 40; e) J. Min, H. G. Choi, J. W. Choi, W. H. Lee, *Mol. Cryst. Liq. Cryst. Sci. Technol. Sect. A* **1999**, *327*, 263 – 266.

[6] a) A. M. Moulin, S. J. O'Shea, M. E. Welland, *Ultramicroscopy* **2000**, *82*, 23 – 31; b) J. Fritz, M. K. Baller, H. P. Lang, H. Rothuizen, P. Vettiger, E. Meyer, H. J. Guntherodt, C. Gerber, J. K. Gimzewski, *Science* **2000**, *288*, 316 – 318.

[7] a) E. Braun, Y. Eichen, U. Sivan, G. Ben-Yoseph, *Nature* **1998**, *391*, 775 – 778; b) F. Patolsky, Y. Weizmann, O. Lioubashevski, I. Willner, *Angew. Chem.* **2002**, *114*, 2429 – 2433; *Angew. Chem. Int. Ed.* **2002**, *41*, 2323 – 2327.

[8] a) A. G. Frutos, L. M. Smith, R. M. Corn, *J. Am. Chem. Soc.* **1998**, *120*, 10277 – 10282; b) D. Normile, *Science* **2002**, *295*, 951.

[9] a) A. N. Shipway, I. Willner, *Acc. Chem. Res.* **2001**, *34*, 421 – 432; b) R. Ballardini, V. Balzani, A. Credi, M. T. Gandolfi, M. Venturi, *Acc. Chem. Res.* **2001**, *34*, 445 – 455; c) V. Amendola, L. Fabbrizzi, C. Mangano, P. Pallavicini, *Acc. Chem. Res.* **2001**, *34*, 488 – 493.

[10] a) I. Willner, S. Rubin, *Angew. Chem.* **1996**, *108*, 419; *Angew. Chem. Int. Ed. Engl.* **1996**, *35*, 367 – 385; b) I. Willner, *Acc. Chem. Res.* **1997**, *30*, 347 – 356.

[11] R. A. Bissel, E. Cordova, A. E. Kaifer, J. F. Stoddart, *Nature* **1994**, *369*, 133 – 137.

[12] a) G. M. Tsivgoulis, J.-M. Lehn, *Chem. Eur. J.* **1996**, *2*, 1399 – 1406; b) Z.-F. Liu, K. Morigaki, K. Hashimoto, A. Fujishima, *Anal. Chem.* **1992**, *64*, 134 – 137; c) A. Doron, M. Portnoy, M. Lion-Dagan, E. Katz, I. Willner, *J. Am. Chem. Soc.* **1996**, *118*, 8937 – 8944.

[13] a) A. R. Pease, J. O. Jeppesen, J. F. Stoddart, Y. Luo, C. P. Collier, J. R. Heath, *Acc. Chem. Res.* **2001**, *34*, 433 – 444; b) I. Willner, V. Pardo-Yissar, E. Katz, K. T. Ranjit, *J. Electroanal. Chem.* **2001**, *497*, 172 – 177.

[14] C. P. Collier, G. Mattersteig, E. W. Wong, Y. Luo, K. Beverly, J. Sampaio, F. M. Raymo, J. F. Stoddart, J. R. Heath, *Science* **2000**, *289*, 1172 – 1175.

[15] a) M. Lion-Dagan, E. Katz, I. Willner, *J. Am. Chem. Soc.* **1994**, *116*, 7913 – 7914; b) I. Willner, R. Blonder, E. Katz, A. Stocker, A. F. Bückmann, *J. Am. Chem. Soc.* **1996**, *118*, 5310 – 5311; c) R. Blonder, E. Katz, I. Willner, V. Wray, A. F. Bückmann, *J. Am. Chem. Soc.* **1997**, *119*, 11747 – 11757.

[16] a) E. Katz, B. Willner, I. Willner, *Biosens. Bioelectron.* **1997**, *12*, 703 – 719; b) I. Willner, M. Lion-Dagan, S. Marx-Tibbon, E. Katz, *J. Am. Chem. Soc.* **1995**, *117*, 6581 – 6592; c) M. Lion-Dagan, E. Katz, I. Willner, *J. Chem. Soc. Chem. Commun.* **1994**, 2741 – 2742; d) I. Willner, A. Doron, E. Katz, S. Levi, A. J. Frank, *Langmuir* **1996**, *12*, 946 – 954.

[17] a) J. Lange, R. Kotitz, A. Haller, L. Trahms, W. Semmler, W. Weitschies, *J. Magn. Magn. Mater.* **2002**, *252*, 381 – 383; b) V. Kourilov, M. Steinitz, *Anal. Biochem.* **2002**, *311*, 166 – 170; c) R. Sato, H. Takeyama, T. Tanaka, T. Matsunaga, *Appl. Biochem. Biotechnol.* **2001**, *91*, 109 – 116; d) K. Nishi, S. Nishimura, M. Higashiura, N. Ikeya, H. Ohta, T. Tsuji, M. Nishimura, S. Ohnishi, H. Higashi, *J. Immunol. Methods* **2000**, *240*, 39 – 46; e) Y. Namba, M. Usami, O. Suzuki, *Anal. Sci.* **1999**, *15*, 1087 – 1093; f) M. V. Kiselev, A. K. Gladilin, N. S. Melik-Nubarov, P. G. Sveshnikov, P. Miethe, A. V. Levashov, *Anal. Biochem.* **1999**, *269*, 393 – 398; g) H. Yu, *Anal. Chim. Acta* **1998**, *376*, 77 – 81; h) J. G. Bruno, H. Yu, J. P. Kilian, A. A. Moore, *J. Mol. Recogn.* **1996**, *9*, 474 – 479.

[18] a) J. G. Bruno, J. L. Kiel, *Biotechniques* **2002**, *32*, 178 – 182; b) A. Perrin, T. Martin, A. Theretz, *Bioconjugate Chem.* **2001**, *12*, 678 – 683; c) M. L. Smit, B. A. J. Giesendorf, S. G. Heil, J. A. M. Vet, F. J. M. Trijbels, H. J. Blom, *Biotechnol. Appl. Biochem.* **2000**, *32*, 121 – 125; d) J. G. Bruno, J. L. Kiel, *Biosens. Bioelectron.* **1999**, *14*, 457 – 464.

[19] a) T. Matsunaga, H. Takeyama, *Supramol. Sci.* **1998**, *5*, 391 – 394; b) E. E. Carpenter, *J. Magn. Magn. Mater.* **2001**, *225*, 17 – 20;

 © 2003 Wiley-VCH Verlag GmbH & Co. KGaA, Weinheim

c) G. A. Robinson, H. A. O. Hill, R. D. Philo, J. M. Gear, S. J. Rattle, G. C. Forrest, *Clin. Chem.* **1985**, *31*, 1449 – 1452.
[20] L. Shen, P. E. Laibinis, T. A. Hatton, *Langmuir* **1999**, *15*, 447 – 453.
[21] R. Hirsch, E. Katz, I. Willner, *J. Am. Chem. Soc.* **2000**, *122*, 12053 – 12054; b) E. Katz, L. Sheeney-Haj-Ichia, I. Willner, *Chem. Eur. J.* **2002**, *8*, 4138 – 4148.
[22] a) E. Katz, T. Lötzbeyer, D. D. Schlereth, W. Schuhmann, H.-L. Schmidt, *J. Electroanal. Chem.* **1994**, *373*, 189 – 200; b) I. Willner, A. Riklin, *Anal. Chem.* **1994**, *66*, 1535 – 1539.
[23] P. N. Bartlett, P. Tebbutt, R. G. Whitaker, *Prog. React. Kinet.* **1991**, *16*, 55 – 155.
[24] A. Bardea, E. Katz, A. F. Bückmann, I. Willner, *J. Am. Chem. Soc.* **1997**, *119*, 9114 – 9119.
[25] A. F. Bückmann, V. Wray, *Biotechnol. Appl. Biochem.* **1992**, *15*, 303 – 310.
[26] E. Katz, L. Sheeney-Haj-Ichia, A. F. Bückmann, I. Willner, *Angew. Chem.* **2002**, *114*, 1399 – 1402; *Angew. Chem. Int. Ed.* **2002**, *41*, 1343 – 1346.
[27] J. Wang, A.-N. Kawde, A. Erdem, M. Salazar, *Analyst* **2001**, *126*, 2020 – 2024.
[28] J. Wang, A.-N. Kawde, *Electrochem. Commun.* **2002**, *4*, 349 – 352.
[29] J. Wang, D. Xu, R. Polsky, *J. Am. Chem. Soc.* **2002**, *124*, 4208 – 4209.
[30] a) J. Wang, D. Xu, A.-N. Kawde, R. Polsky, *Anal. Chem.* **2001**, *73*, 5576 – 5581; b) J. Wang, R. Polsky, D. Xu, *Langmuir* **2001**, *17*, 5739 – 5741.
[31] J. Wang, G. Liu, R. Polsky, A. Merkoci, *Electrochem. Commun.* **2002**, *4*, 722 – 726.
[32] L. Sheeney-Haj-Ichia, E. Katz, J. Wasserman, I. Willner, *Chem. Commun.* **2002**, 158 – 159.
[33] G. S. Calabrese, R. W. Buchanan, M. S. Wrighton, *J. Am. Chem. Soc.* **1983**, *105*, 5594 – 5600.
[34] K. A. Fahnrich, M. Pravda, G. G. Guilbault, *Talanta* **2001**, *54*, 531 – 559.
[35] a) M. Aizawa, *Anal. Chim. Acta* **1991**, *250*, 249 – 256; b) M. Tanaka, S. Kamiya, A. Shibue, K. Namba, Y. Ikariyama, M. Aizawa, *Sens. Actuators B* **1993**, *13*, 184 – 187.
[36] E. Katz, I. Willner, *J. Am. Chem. Soc.* **2002**, *124*, 10290 – 10291.
[37] A. J. Bard, L. R. Faulkner, *Electrochemical Methods: Fundamentals and Applications*, Wiley, New York, **1980**.
[38] http://www.igen.com/home.htm.
[39] Y. Weizmann, F. Patolsky, E. Katz, I. Willner, *J. Am. Chem. Soc.* **2003**, *125*, 3452 – 3454.
[40] F. Patolsky, Y. Weizmann, E. Katz, I. Willner, *Angew. Chem.* **2003**, *115*, 2474 – 2478; *Angew. Chem. Int. Ed.* **2003**, *42*, 2372 – 2376.
[41] E. Katz, I. Willner, *Electrochem. Commun.* **2002**, *4*, 201 – 204.

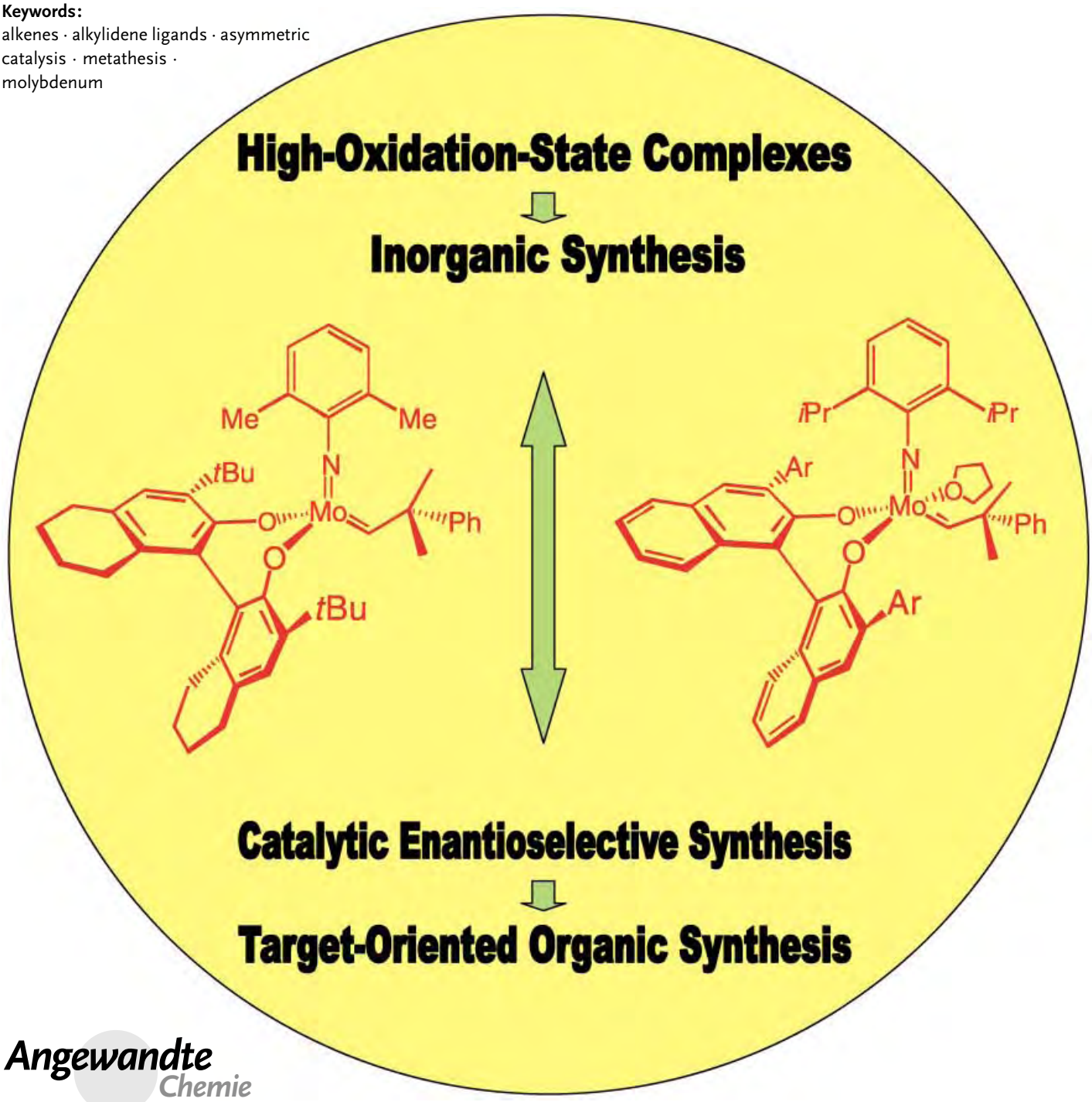
 © 2003 Wiley-VCH Verlag GmbH & Co. KGaA, Weinheim

Olefin-Metathesis Catalysts

Molybdenum and Tungsten Imido Alkylidene Complexes as Efficient Olefin-Metathesis Catalysts

Richard R. Schrock and Amir H. Hoveyda**

Keywords:
alkenes · alkylidene ligands · asymmetric catalysis · metathesis · molybdenum



© 2003 Wiley-VCH Verlag GmbH & Co. KGaA, Weinheim
DOI: 10.1002/anie.200300576

Catalytic olefin metathesis has quickly emerged as one of the most often-used transformations in modern chemical synthesis. One class of catalysts that has led the way to this significant development are the high-oxidation-state alkylidene complexes of molybdenum. In this review key observations that resulted in the discovery and development of molybdenum- and tungsten-based metathesis catalysts are outlined. An account of the utility of molybdenum catalysts in the synthesis of biologically significant molecules is provided as well. Another focus of the review is the use of chiral molybdenum complexes for enantioselective synthesis. These highly efficient catalysts provide unique access to materials of exceptional enantiomeric purity and often without generating solvent waste.

From the Contents

1. Introduction 4593

2. Design and Development of Tungsten- and Molybdenum-Based Alkylidene Complexes for Catalytic Olefin Metathesis 4599

3. Ring-Opening Metathesis Polymerization (ROMP) Catalyzed by Molybdenum-Based Imido Alkylidene Complexes 4608

4. Achiral Molybdenum-Based Olefin-Metathesis Catalysts in Stereoselective Synthesis 4611

5. Enantiomerically Pure Chiral Molybdenum-Based Olefin-Metathesis Catalysts in Asymmetric Synthesis 4619

6. A Few Notes Regarding Molybdenum- Versus Ruthenium-Based Metathesis Catalysts 4627

7. Conclusions and Outlook 4628

1. Introduction

Metal-catalyzed olefin metathesis has had an enormous impact on organic synthesis. A myriad of small-, medium-, and large-ring carbo- and heterocycles, and a wide assortment of acyclic unsaturated molecules are now readily accessible through this important class of reactions.[1–6] Stereoselective methods that utilize catalytic metathesis and successful complex-molecule total syntheses that have strategically benefited from this remarkable transformation are being disclosed in increasing numbers. Reports of new metal complexes that promote selective metathesis reactions that were not feasible before, catalysts that can be applied to large-scale or combinatorial syntheses, or catalysts that are recyclable or deliver unprecedented levels of efficiency and selectivity continue to adorn our leading journals. Much of this "revolution" in organic synthesis is a consequence of the development of well-defined and functional-group tolerant molybdenum- and ruthenium-based catalysts that are now so widely used.

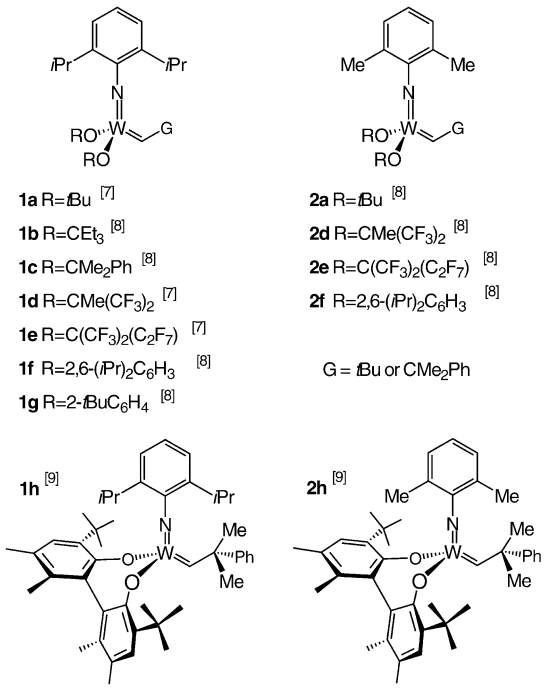


Figure 1. Tungsten-based olefin-metathesis catalysts.

Herein we first provide an account of the journey that eventually resulted in the discovery and development of high-oxidation-state tungsten and then molybdenum imido alkylidene complexes. We will refer to a comprehensive list of tungsten-based (Figure 1[7–9]) and molybdenum-based catalysts throughout this review (Figure 2[10–13] for achiral complexes and Figure 3[14–23] and Figure 4[14–19,24,25] for chiral complexes. In Section 2 of this article we review the design and development of these tungsten and molybdenum-based alkylidene complexes for olefin metathesis, and in Section 3 we discuss the utility of molybdenum-based imido alkylidene

[*] Prof. Dr. R. R. Schrock
Department of Chemistry
Massachusetts Institute of Technology
Cambridge, MA 02139 (USA)
Fax: (+1) 617-253-7670
E-mail: rrs@mit.edu
Prof. Dr. A. H. Hoveyda
Department of Chemistry, Merkert Chemistry Center
Boston College
Chestnut Hill, MA 02467 (USA)
Fax: (+1) 617-552-1442
E-mail: amir.hoveyda@bc.edu

 DOI: 10.1002/anie.200300576 © 2003 Wiley-VCH Verlag GmbH & Co. KGaA, Weinheim

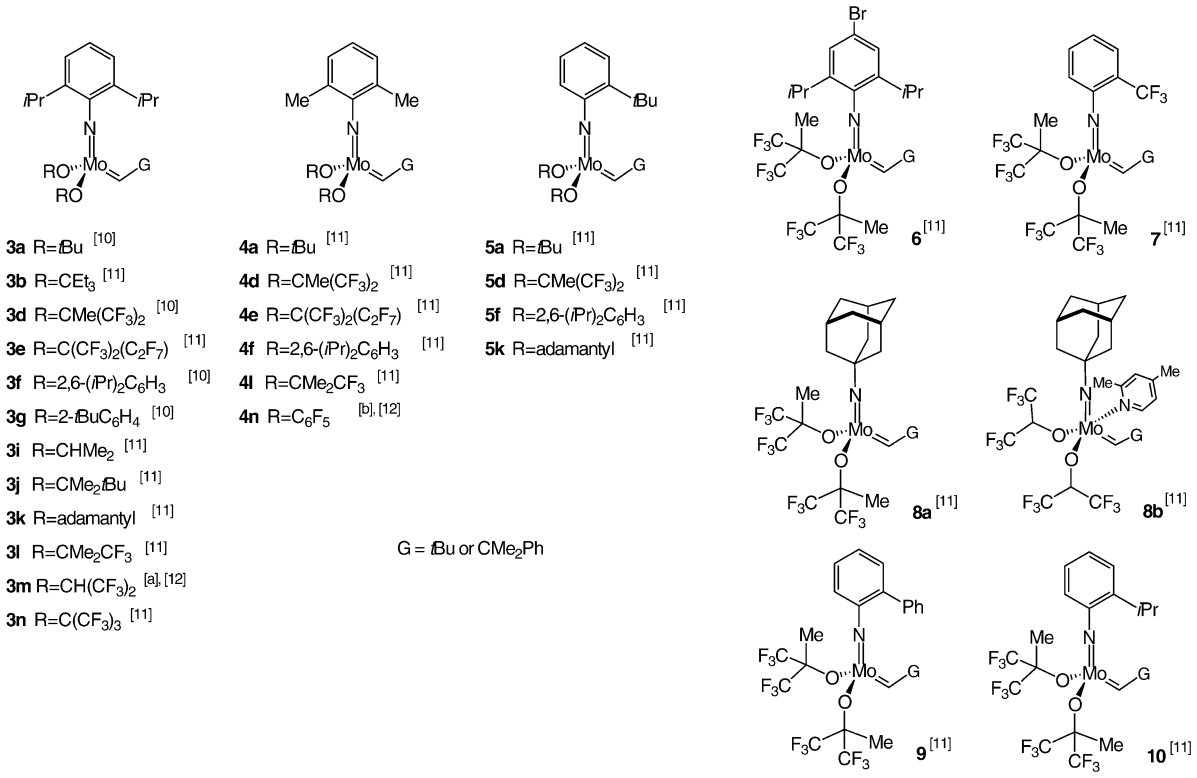


Figure 2. Achiral molybdenum-based olefin-metathesis catalysts. [a] Isolated with an additional 2,4-dimethylpyridine ligand (see **8b**). [b] Isolated with an additional quinuclidine ligand.

complexes as catalysts for ring-opening metathesis polymerization (ROMP). In Section 4, we review the use of achiral molybdenum-based catalysts in the synthesis of relatively complex organic molecules. In Section 5, the ability of enantiomerically pure chiral molybdenum-based catalysts to afford optically pure or enriched organic compounds is presented. When relevant data are available, molybdenum-based and ruthenium-based catalysts will be compared (see also Section 6). For additional details the reader can refer to other articles that cover the discovery and development of high-oxidation-state alkylidene complexes for olefins metathesis[26–33] and their early applications to polymer synthesis.[34–36] The reader may also consult recent reviews concerning olefin metathesis in organic synthesis.[1–6]

1.1. The Basic Process and Key Intermediates in the Catalytic Cycle

The key step in olefin metathesis is a [2+2] addition of an olefin (for example, *trans*-RCH=CHR′; Scheme 1) to a metal–carbon double bond (for example, in **I**) to give a metallacyclobutane complex (for example, **II** in Scheme 1). Metallacyclobutane **II** can decompose in a retro [2+2] reaction either to give **I** and *trans*-RCH=CHR′ again, or to give a new metal alkylidene **I′** and *trans*-R′CH=CHR′, as shown in Scheme 1. Further reaction of **I′** with *trans*-RCH=CHR′ then yields (for example) **II′**, which can decompose to yield *trans*-RCH=CHR and **I**. Metallacycles analogous to **II** (or **II′**) can form in which R′ (or R) substituents on one or both



Richard R. Schrock obtained his B.A. in 1967 from the University of California at Riverside and his Ph.D. at Harvard in 1971 as a student of J. A. Osborn. After a postdoctoral fellowship with Lord Jack Lewis at Cambridge he joined E. I. duPont de Nemours and Company in the group of George Parshall. In 1975 he moved to M.I.T. and became a full professor in 1980. He has received many awards and is a member of the National Academy of Sciences. His interests include developing new imido and amido ligands for early-transition-metal chemistry and catalysts for the living polymerization of terminal olefins.



Amir H. Hoveyda received his B.A. in 1981 at Columbia University where he was introduced to catalytic olefin metathesis in Tom Katz's group. After receiving his Ph.D. in 1986, at Yale with Stuart Schreiber, he joined David Evans at Harvard as a postdoctoral fellow. In 1990, he joined the faculty at Boston College, where he became Professor in 1994. His many honors include an ACS Cope Scholar Award and the ExxonMobil Award for Excellence in Catalysis. His research interests include catalytic enantioselective methods in synthesis, synthesis of natural products, and combinatorial chemistry.

 © 2003 Wiley-VCH Verlag GmbH & Co. KGaA, Weinheim

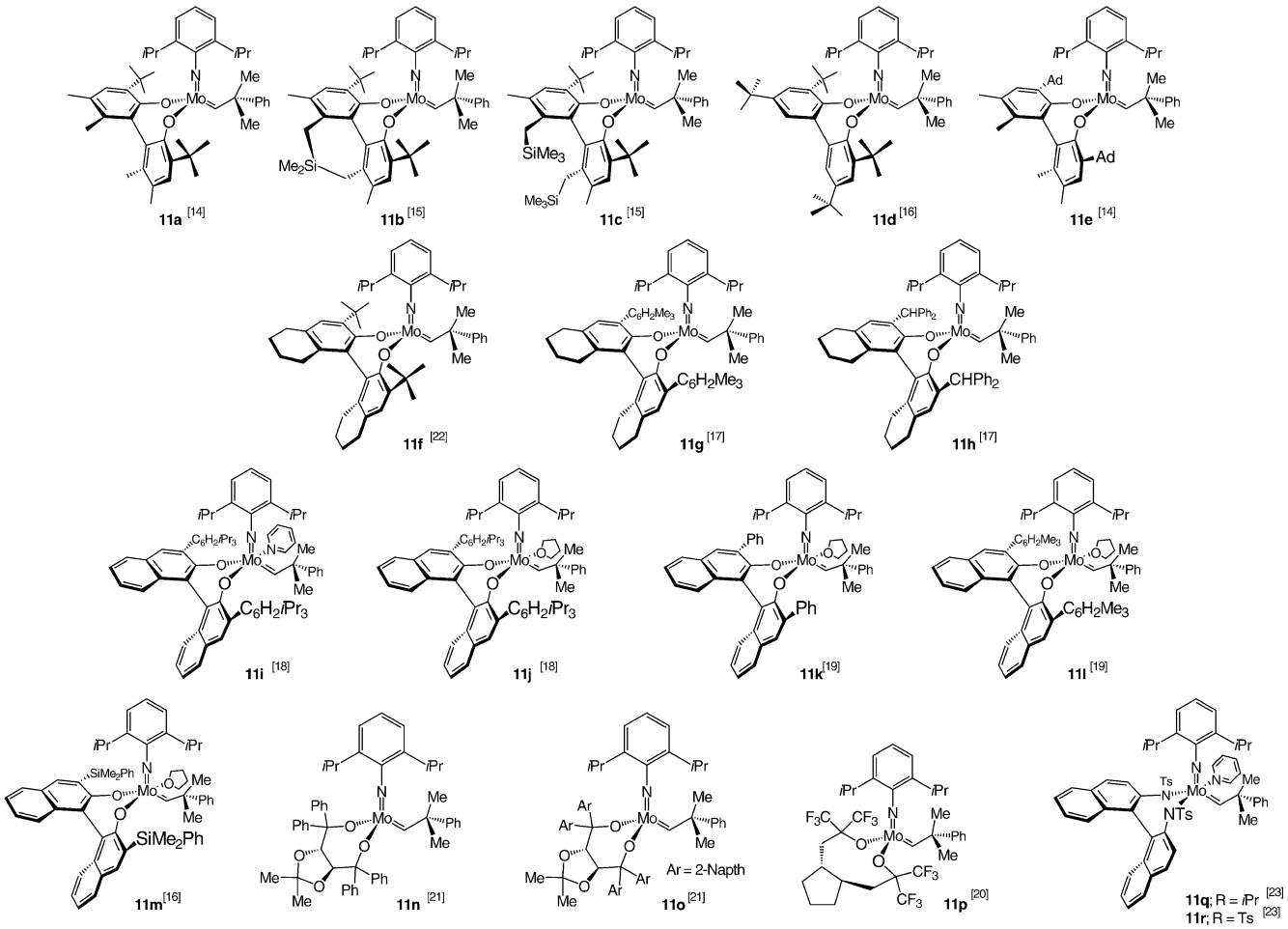


Figure 3. Chiral molybdenum-based catalysts for olefin metathesis bearing a 2,6-diisopropylaryl imido ligand. Complexes **11q** and **11r** to date have not exhibited catalytic metathesis activity and are shown here only for the purpose of discussion. Ad = adamantyl, Ts = tosyl.

α carbon atoms and the β carbon are *cis* to one another. *cis* Olefins can be generated upon cleavage of these metallacycles. Therefore, as shown in Scheme 1, *trans*-RCH=CHR′ would be transformed catalytically into an equilibrium mixture of approximately two parts of RCH=CHR′ (a mixture of *cis* and *trans*) and one part each of R′CH=CHR′ (*cis* and *trans*) and RCH=CHR (*cis* and *trans*).[37–39] Metallacycles that do not lead to new olefins may be formed as well. For example, addition of *trans*-RCH=CHR′ to **I** so that R is on the β carbon atom of the metallacycle and an R′ group is present on each of the α carbon atoms (as opposed to **II** in Scheme 1) would result in a degenerate metathesis reaction, four of which are possible if both *cis* and *trans* olefins are considered. Compounds **I** and **I′** are referred to as the propagating alkylidenes, since they are the two possible alkylidene complexes that can be formed from any alkylidene that initiates the catalytic cycle.

A number of variations of the basic reaction shown in Scheme 1 are known which allow the starting olefin to be converted completely into products. Perhaps the simplest is that in which R′ is a proton, in which case one of the products is ethylene. If ethylene is removed during the reaction, RCH=CH_2 would be consumed completely to give *cis*- and *trans*-RCH=CHR. If an α,ω-diene were employed and if ethylene were removed during the reaction, a cyclic olefin would be formed. These and many other variations form the basic set of transformations that are now used by chemists to access a variety of olefinic products by treatment of readily available alkenes with metal alkylidene initiators.

1.2. A Historical Perspective

1.2.1. Ill-Defined Metathesis Catalysts

Early molybdenum- and tungsten-based homogeneous olefin-metathesis catalysts were prepared in a wide variety of ways from various types of starting materials in which the metal was in an oxidation state between 0 and VI.[37–39] Typical syntheses that began with W^{VI} complexes involved reactions between WCl_6 or $W(O)Cl_4$ in chlorobenzene and an alkylating agent, such as an alkyl aluminum, alkyl lithium, or alkyl stannane. Although such catalytic systems were examined extensively by physical organic techniques (see Section 1.2.2), the oxidation state of the metal and the nature of the ligands were never determined. For this reason, and in contrast to "well-defined" catalysts (isolable and characterizable com-

 © 2003 Wiley-VCH Verlag GmbH & Co. KGaA, Weinheim

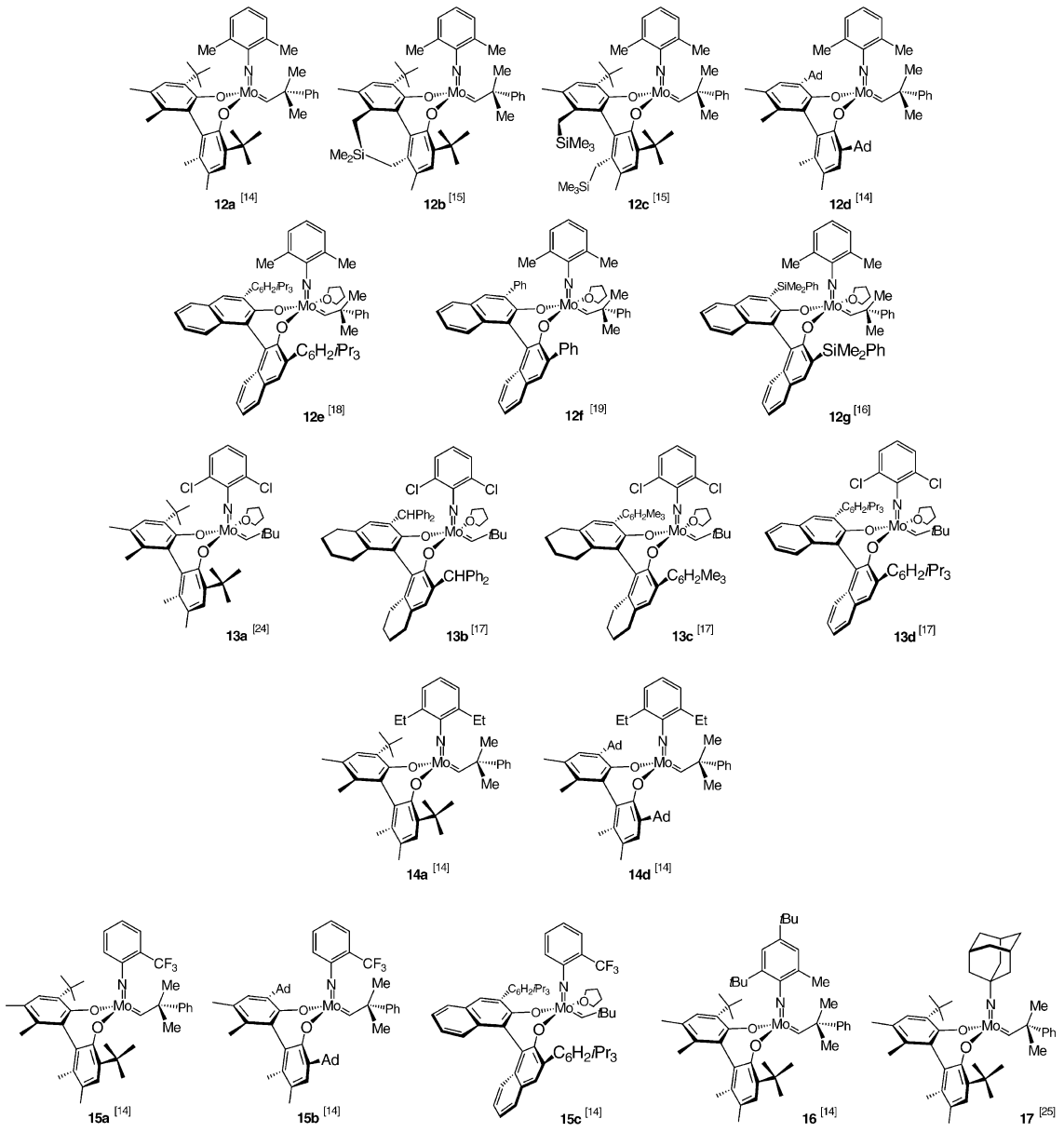
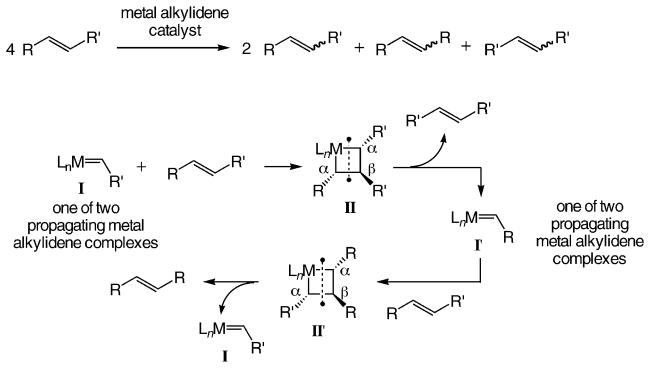


Figure 4. Chiral molybdenum-based catalysts for olefin metathesis bearing various imido ligands.



Scheme 1. A representative metal-catalyzed olefin-metathesis reaction. Metallacyclobutanes **II** and **II′** and the propagating alkylidene complexes **I** and **I′** are key intermediates for productive metathesis. (Only metathesis of a *trans* olefin to give *trans* products is shown.)

plexes that are essentially identical to intermediates in the catalytic reaction), early catalysts now may be considered "ill-defined." Today, a metal-containing compound that provides catalytic activity, but is not directly related to the catalyst that is actually present in the reaction, would be called a "catalyst precursor" or a "precatalyst."

In virtually all ill-defined systems the percentage of metal that is active at any one time is thought to be small ($< 1\,\%$).[37,38] This is one of the reasons why characterization of the active species in these circumstances has not been possible. Many catalysts have been shown to be exceedingly active (> 100 turnovers per second based on metal added), but they are also generally the shortest-lived (minutes). Ill-defined catalysts often tend to produce side products, or are readily deactivated by common Lewis basic functional groups. As a consequence of these features, the activity of ill-defined

 © 2003 Wiley-VCH Verlag GmbH & Co. KGaA, Weinheim

catalysts, even if reproducible, cannot be controlled in a rational manner. In addition, organic molecules frequently undergo side reactions promoted by various requisite metal-containing activators. Therefore, although much was learned about the metathesis reaction, and many applications to polymer synthesis were discovered[37,38] (see Section 3), the use of ill-defined catalysts in the synthesis of organic molecules that contain functional groups is relatively rare.[40–42]

Complications observed in connection with the use of ill-defined catalysts, and the lack of a plausible mechanistic platform that would allow for an interpretation of selectivity and reactivity data, pointed to the preparation of well-defined catalysts as a compelling research objective. Well-defined metathesis catalysts are those that 1) are essentially identical to the active species in terms of metal oxidation state and ligand coordination sphere, 2) react with olefins to yield observable new carbene complexes derived from those olefins, and 3) are stable enough to be characterized through spectroscopic means and preferably also X-ray structural analysis.

1.2.2. Fischer Carbenes as Metathesis Catalysts and Related Mechanistic Studies

In 1964 Fischer and Maasböl reported the reaction of phenyl lithium with $[W(CO)_6]$ to give an anionic complex which contains an acyl ligand.[43] Protonation followed by treatment with diazomethane yielded the first deliberately synthesized "metal carbene" complex, $[(CO)_5W{=}CPh(OMe)]$. This species contains 18 electrons in metal-based orbitals. Reports of hundreds of compounds that bear a heteroatom-stabilized (usually O or N) carbene ligand soon followed.[44] In such species the heteroatom is believed to stabilize a partial positive charge on the carbene carbon atom, thereby leading to their being characterized as "electrophilic carbenes," since the M=C bond would then be polarized with a partial negative charge ($\delta-$) on the metal center and a relative positive charge ($\delta+$) on the carbene carbon atom, that is, ($\delta-$)M=C($\delta+$). It is appropriate to view a carbene ligand that contains one or two heteroatoms bound to the α carbon atom as being neutral with a metal–carbon bond order between one and two. Therefore, $[(CO)_5W{=}CPh(OMe)]$ contains W(0) and this type of complex falls into the category of a carbene complex in which the metal is in a low oxidation state. In the early 1970s a large volume of research on heteroatom-stabilized carbene complexes was carried out and several comprehensive reviews were published.[44–47] Since many Fischer-type carbene complexes had been prepared when interest in olefin metathesis gathered steam in the late 1960s, Fischer carbenes naturally were scrutinized as possible olefin-metathesis catalysts.

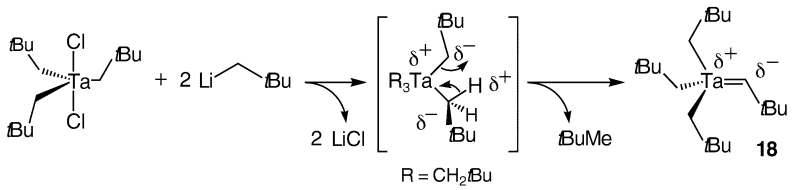
In the 1970s several significant publications concerning the mechanism of olefin metathesis appeared. Some of the most important results were published by the groups of Casey,[48] Chauvin,[49] Dolgoplosk,[50] Grubbs,[51,52] and Katz.[53–55] A detailed discussion of these and related studies can be found in various early reviews[52,55–58] and texts.[37–39] Grubbs et al.,[51] Katz and McGinnis,[53] and Chauvin and Hérisson[49] demonstrated convincingly that metal-catalyzed olefin metathesis is the result of a non-pair-wise exchange of alkylidene fragments. Hérisson and Chauvin are given credit for first proposing in 1971[49,59] the now widely accepted mechanism illustrated in Scheme 1. Casey et al. synthesized $[(CO)_5W{=}CPh_2]$ and showed that it reacts with certain olefins in a manner consistent with the metallacyclobutane mechanism.[48] The expected new carbene could be detected under certain circumstances, but many other products (e.g., cyclopropanes) were also observed, and metathesis products were formed only in substoichiometric quantities. Katz et al.[54] showed that when $[(CO)_5W{=}CPh_2]$ and even $[(CO)_5W{=}CPh(OMe)]$ are added to certain strained cyclic olefins, the cyclic olefins are polymerized slowly to give the polymers expected from ring-opening metathesis polymerization (ROMP; see Section 3 for more details). These investigations collectively provided strong evidence that metal carbene complexes are indeed intermediates in olefin metathesis reactions. However, in spite of the fact that the initial metal complex was well-characterized in many of the above investigations, none rigorously established the nature of the actual catalyst, and no propagating metal carbenes were detected in a catalytic metathesis reaction. Since Casey et al. reported in 1979 that $[(CO)_5W{=}CHPh]$ decomposes above $-60\,^{\circ}C$ and does not yield metathesis products upon reaction with olefins,[60] it seems unlikely that Fischer-type W(0) complexes would be the propagating species in reactions in which some catalytic metathesis activity was observed.[54]

1.3. "High-Oxidation-State" Carbene (or Alkylidene) Complexes of Tantalum

At the time that early examples of metathesis with ill-defined, homogeneous, W and Mo catalysts were known, there were no reports of metathesis reactions promoted by ill-defined tantalum-based catalysts.[37,38] Yet, tantalum-based complexes played a crucial role in our understanding how effective W and Mo catalysts might be designed, since metathesis activity ultimately could be observed with certain newly discovered and carefully tuned "high-oxidation-state" carbene complexes. Therefore, Ta complexes will be considered in this historical perspective.

The events that led to the discovery of the first tantalum-based alkylidene began in 1974 with the synthesis of pentamethyltantalum,[61] the first pentaalkyl complex of Ta. Pentamethyltantalum was found to decompose (sometimes explosively) above $0\,^{\circ}C$ through unidentified intermolecular pathways.[62] To inhibit bimolecular decomposition, attempts were made to synthesize $[Ta(CH_2tBu)_5]$, in which bulky neopentyl groups would replace the much smaller methyl ligands. However, as illustrated in Scheme 2, these attempts did not lead to $[Ta(CH_2tBu)_5]$, but to formation of the tantalum-based carbene **18**, the first example of a stable M=CHR complex, through an intramolecular decomposition of intermediate $[Ta(CH_2tBu)_5]$.[63] The intramolecular decomposition consists of abstraction of an α hydrogen (proton) by a neighboring alkyl group (a base). Compound **18** is unusually robust thermally; it melts at around $70\,^{\circ}C$ and can be distilled

 © 2003 Wiley-VCH Verlag GmbH & Co. KGaA, Weinheim



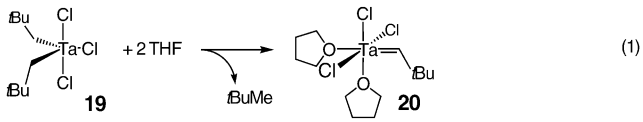
Scheme 2. Formation of the first high-oxidation-state alkylidene complex by α-hydrogen abstraction.

in vacuo. It is sensitive to oxygen, water, and a variety of functionalities, among them ketones and aldehydes, with which it reacts to yield polymeric $[(t\mathrm{BuCH_2})_3\mathrm{Ta{=}O]}_n$ and the expected olefin.[64] Therefore **18** is related to an alkylidene phosphorane,[65] and may be viewed as a Ta(v) alkylidene species. Complex **18** differs sharply in several respects from Fischer-type complexes where a heteroatom is bound to the carbene ligand (see above).[44] Among these differences are the polarities of the M=C bonds (e.g., $(\delta+)\mathrm{Ta{=}C}(\delta-)$ as in Scheme 2 vs. $(\delta-)\mathrm{W{=}C}(\delta+)$ in $[(\mathrm{CO})_5\mathrm{W{=}CPh(OMe)}]$) and the number of electrons in metal-based orbitals (10 for the Ta species versus 18 for the W complex). Note that the 18-electron count in $[(\mathrm{CO})_5\mathrm{W{=}CPh(OMe)}]$ would require that one CO ligand be lost to give a 16-electron species before an olefin can react and form the required metallacyclobutane intermediate. In contrast, no (covalently bound) ligand could be lost from the 10-electron tantalum species under mild conditions, nor would any have to be.

The synthesis of Ta alkylidene **18** established that sterically hindered covalently bound ligands can stabilize electronically unsaturated (< 18 electron) pseudotetrahedral alkylidene complexes towards bimolecular decomposition. Accordingly, further exploitation of the principle of steric protection, and investigation of neopentyl complexes in particular, became critical in the study of high-oxidation-state alkylidene complexes and their development as olefin-metathesis catalysts.

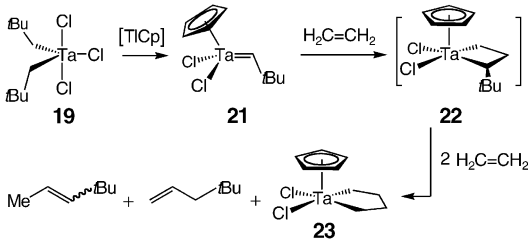
As depicted in Scheme 2, α-hydrogen (proton) abstraction offers an attractive method for the generation of high-oxidation-state alkylidene complexes. In this context, it was demonstrated that such processes can be induced by coordinating solvents.[66] For example, yellow-orange $[\mathrm{Cl_3Ta}(\mathrm{CH_2}t\mathrm{Bu})_2]$[**19**, Eq. (1)] is stable in pentane. In contrast, dissolution of **19** in THF results in formation of purple, 14-electron $[\mathrm{Cl_3(thf)_2Ta{=}CH}t\mathrm{Bu}]$ (**20**).[66]

Compound **19** reacts with [TlCp] (Cp = $\mathrm{C_5H_5}$) to afford $[\mathrm{CpCl_2Ta{=}CH}t\mathrm{Bu}]$ (**21**; Scheme 3), the first of the new alkylidene complexes whose reactivity towards olefins was



(1)

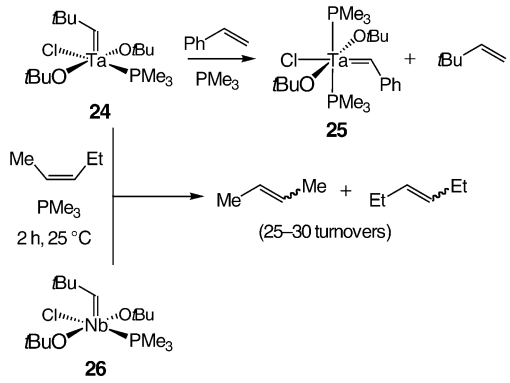
explored in detail.[67] Complex **21** undergoes reaction with terminal olefins to give products derived from β-hydride rearrangement of a tantalacyclobutane intermediate. As shown in Scheme 3 for the reaction between **21** and ethylene, the intermediate (unobservable) tantalacycle **22** rearranges in the presence of ethylene to yield *cis*- and *trans*-4,4-dimethyl-2-pentene, 4,4-dimethyl-1-pentene, and tantalacyclopentane **23**.[68] It is presumed that: 1) the two observed olefin products are bound to Ta in a $[\mathrm{CpTaCl_2(olefin)}]$ complex immediately upon rearrangement of **22**; 2) olefin products are displaced by ethylene to yield $[\mathrm{CpTaCl_2(ethylene)}]$; 3) $[\mathrm{CpTaCl_2}$-(ethylene)] subsequently reacts with ethylene to yield **23**.[68] Olefin complexes and tantalacyclopentanes ultimately were investigated more extensively in the analogous Cp* (η^5-$\mathrm{C_5Me_5}$) system.[68]



Scheme 3. β-Hydride rearrangement of a tantalacyclobutane formed by reaction of a tantalum-based alkylidene complex with ethylene.

The reactions shown in Scheme 3 suggested that although a metallacyclobutane forms when a Ta neopentylidene reacts with ethylene, it rearranges more rapidly than it converts into *tert*-butylethylene and a Ta methylene complex analogous to **21**. It was subsequently shown that complexes such as $[\mathrm{Cl_3(PMe_3)_2Ta{=}CH}t\mathrm{Bu}]$ react with olefins in a similar fashion to afford olefinic products through rearrangement of unobservable tantalacyclobutanes, and that even **20** [Eq. (1)] is a short-lived metathesis catalyst for *cis*-2-pentene.[69] In an important contrast, however, it was demonstrated that $[(\mathrm{PMe_3})(\mathrm{O}t\mathrm{Bu})_2\mathrm{ClTa{=}CH}t\mathrm{Bu}]$ (**24**) reacts with styrene in the presence of $\mathrm{PMe_3}$ to provide the isolable benzylidene complex, $[(\mathrm{PMe_3})_2(\mathrm{O}t\mathrm{Bu})_2\mathrm{ClTa{=}CHPh}]$ (**25**; Scheme 4). In addition, when treated with *cis*-2-pentene in the presence of $\mathrm{PMe_3}$, Ta complex **24** or the analogous Nb system **26** promote the metathesis of *cis*-2-pentene (25–30 turnovers) at room temperature.[69,70] This was the first time that an alkylidene complex analogous to the initial alkylidene species could be isolated upon reaction with an olefin.[71] However, the ethylidene and propylidene intermediates which were formed in the metathesis of *cis*-2-pentene (Scheme 4), apparently rearranged readily to give ethylene and propylene, respectively, and therefore could not be observed. Rearrangement of ethylidene and propylidene intermediates to olefins is one reason why metathesis by **24** or **26** is not long-lived. It was demonstrated later that some tantalacyclobutane and alkylidene complexes derived from them could be observed if three bulky phenoxide ligands were bound to the Ta center.[72–74] Thus, it was clear that bulky alkoxide ligands are beneficial to sustained metathesis reactions involving Ta or Nb alkylidene complexes.

 © 2003 Wiley-VCH Verlag GmbH & Co. KGaA, Weinheim



Scheme 4. The first example of an isolable high-oxidation-state metal alkylidene complex (**25**) formed in a reaction between a well-characterized metal alkylidene catalyst (**24**) and an olefin, and catalytic metathesis with **24** and **26**.

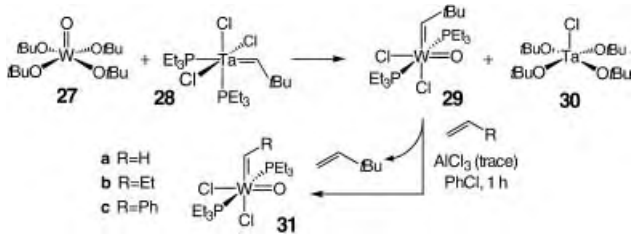
In spite of the above discoveries, the prospects for Ta-based alkylidene complexes as effective catalysts for use in organic synthesis did not appear promising. Tantalum alkylidene complexes do not reform readily from intermediate tantalacyclobutanes relative to the rate at which they rearrange (as shown in Scheme 3), and electron-deficient Ta alkylidene complexes are transformed to an olefin when the alkylidene bears a β proton.[75]

2. Design and Development of Tungsten- and Molybdenum-Based Alkylidene Complexes for Catalytic Olefin Metathesis

Three important findings that emerged from studies involving Ta alkylidene complexes were relevant to alkene metathesis: 1) entirely new (high oxidation state) alkylidene complexes could be prepared and isolated, 2) alkoxides (relative to chlorides as ligands) appeared to promote metathesis, and 3) electron-deficient and sterically crowded pseudotetrahedral alkylidene complexes that contain only covalently bound bulky ligands (including the alkylidene) can be stable. On the basis of the high metathesis activity of ill-defined catalysts described in Section 1.2.1, it seemed likely that some type of high-oxidation-state tungsten- or molybdenum-based alkylidene complexes were the active species. However, exactly what class of metal alkylidene complexes should have been sought or how they might have been prepared was unclear. It was nonetheless appreciated that an alkylidene would have to be stable to bimolecular decomposition if it were to be detected. Moreover, an alkylidene that contains a β proton would have to be stable with respect to rearrangement to an olefin. Finally, loss of an alkylidene α proton to yield an alkylidyne complex, another type of high-oxidation-state species (see Section 2.2),[76] had to be avoided.

2.1. Early Tungsten-Based Metathesis Catalysts

A tungsten-based complex believed to be a plausible target as a well-defined catalyst for olefin metathesis was five-coordinate [(*t*BuO)$_4$W=CH*t*Bu]. (The advantages of a sterically crowded pseudotetrahedral coordination sphere were not appreciated at that time.) The first reaction shown in Scheme 5 (between **27** and **28**) was an attempt to prepare



Scheme 5. Synthesis of tungsten-based oxo alkylidene complexes from a tantalum alkylidene complex.

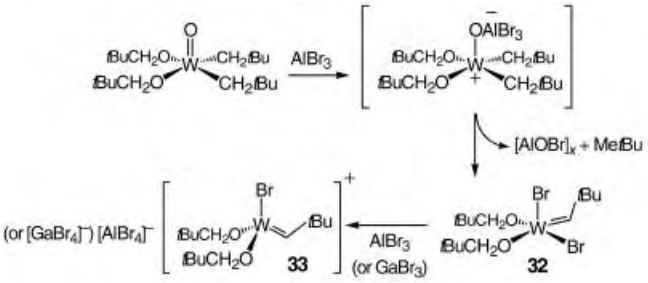
[(*t*BuO)$_4$W=CH*t*Bu] through exchange of an oxo ligand on W with an alkylidene on Ta.[77,78] Instead, the oxo alkylidene [(PEt$_3$)$_2$Cl$_2$W(O)(CH*t*Bu)] (**29**, Scheme 5) and **30** were formed quantitatively. Assembly of **29** suggested that an oxo ligand might help stabilize an alkylidene and that alkylidenes other than a neopentylidene therefore might be observable.

The electron count of the metal center in **29** is 18, since the oxo ligand donates one of its two electron pairs to the metal to create a pseudo triple bond.[79] Therefore it did not seem likely that **29** could react with an olefin unless a phosphane or a chloride ligand were lost to yield a 16-electron species. Nevertheless, it was found that **29** would metathesize terminal and internal olefins very slowly. However, the rate of metathesis was accelerated dramatically in the presence of a trace of AlCl$_3$.[77] It was in this context that the methylene complex [(PEt$_3$)$_2$Cl$_2$W(O)(CH$_2$)] (**31a** in Scheme 5) and new alkylidene complexes that contain β protons, such as **31b**, were observed for the first time.[70] Since it later was demonstrated that addition of one equivalent of AlCl$_3$ (in CH$_2$Cl$_2$) to [(PEt$_3$)$_2$Cl$_2$W(O)(CH*t*Bu)] (**29**, Scheme 5) yielded the 16-electron cationic species [(PEt$_3$)$_2$ClW(O)(CH*t*Bu)][AlCl$_4$],[80] and since [(PEt$_3$)$_2$ClW(O)(CH*t*Bu)][AlCl$_4$] would metathesize terminal and internal olefins (in CH$_2$Cl$_2$; up to ≈100 turnovers in 24 h at room temperature), a small amount of [(PEt$_3$)$_2$ClW(O)(CH*t*Bu)][AlCl$_4$] was believed to be responsible for the metathesis of olefins by [(PEt$_3$)$_2$Cl$_2$W(O)(CH*t*Bu)] in the presence of a trace of AlCl$_3$. Interestingly, the 16-electron complex [(PEt$_3$)Cl$_2$W(O)(CH*t*Bu)] could be isolated and crystallographically characterized and shown to metathesize *cis*-2-pentene for a short time.[77] On the basis of these data, the metal oxidation state that is appropriate for efficient metathesis activity was proposed to be W^{VI}, where the alkylidene is counted as a dianionic ligand. However, it was clear that bimolecular decomposition of alkylidene complexes other than a neopentylidene was still problematic. Decomposition was likely to be most rapid for

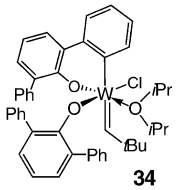
 © 2003 Wiley-VCH Verlag GmbH & Co. KGaA, Weinheim

methylene complexes, since even 18-electron [$Cp_2MeTa{=}CH_2$] had been found to be unstable towards bimolecular decomposition.[81,82]

Related advances were disclosed by Osborn and co-workers,[83–87] who found that addition of various Lewis acids (such as $AlBr_3$) to [$(OCH_2tBu)_2(CH_2tBu)_2W{=}O$] leads to the formation of metathesis catalysts.[84] Accordingly, it was found that oxo-free alkylidene complexes represented by [$(OCH_2tBu)_2Br_2W{=}CHtBu$] (**32**, Scheme 6) could be isolated,[85] and that **32**, in turn, could be transformed by Lewis acids into cations of the type [$(OCH_2tBu)_2BrW{=}CHtBu)]^+$ (**33**). These cations effectively promoted metathesis of internal olefins and gave rise to observable propagating alkylidenes.[85] It should be noted that the above tungsten-based complexes, along with those later discovered by Basset and co-workers (such as **34**),[88,89] are among the few high-oxidation-state metathesis catalysts that do not contain a second multiply bound ligand in addition to the alkylidene. The neopentoxides were found to be crucial to the preparation and reactivity of the class of tungsten-based catalysts discovered by Osborn and aryloxides were found to be critical to the catalysts prepared by Basset.



Scheme 6. Formation of metathesis-active cationic tungsten-based alkylidene complexes.



2.2. Alkylidyne Complexes and Alkyne Metathesis

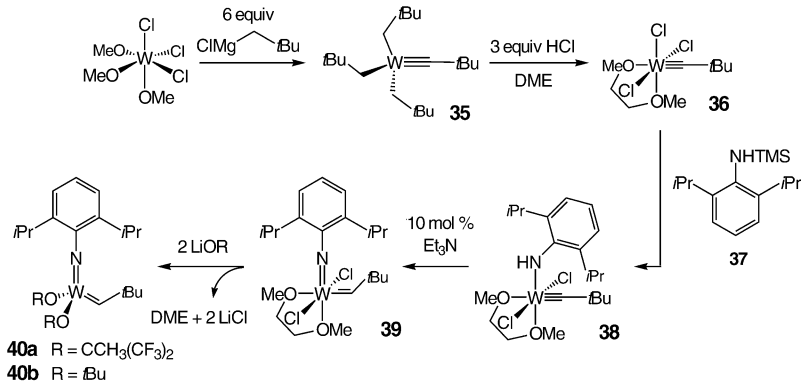
The first reported homogeneous catalysts for alkyne metathesis were prepared from molybdenum hexacarbonyl and a phenol.[90,91] However, reactions promoted by such complexes were slow and the active species and mechanism could not be identified. Katz and McGinnis[53] proposed a catalytic cycle for alkyne metathesis that is analogous to that suggested for alkene metathesis (see Scheme 1), which involves a reversible reaction between a metal–carbon triple bond and an alkyne to give a metallacyclobutadiene. Alkylidyne complexes that were known in the mid 1970s, namely those prepared by Fischer and co-workers,[92,93] such as [$Br(CO)_4W{\equiv}CPh$], did not metathesize alkynes. The discovery of the first high-oxidation-state alkylidynes of Mo and W of the type [$(tBuCH_2)_3M{\equiv}CtBu$] in 1978[94] within a few years led to the development of high-oxidation-state alkylidyne complexes that would metathesize alkynes, and in the process, to an understanding of what might be required to prepare well-defined Mo or W catalysts for olefin metathesis.

The development of well-defined catalysts for alkyne and alkene metathesis took place more or less simultaneously and are strongly linked. For this reason, a brief description of high-oxidation-state Mo and W alkylidyne complexes is provided below.

2.2.1. Synthesis of Well-Defined Tungsten- and Molybdenum-Based Alkylidyne Complexes

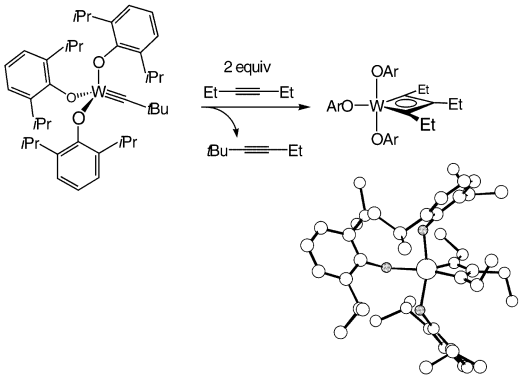
The first practical synthesis of a high-oxidation-state alkylidyne complex of tungsten consists of the reaction between [$W(OMe)_3Cl_3$] and six equivalents of neopentyl magnesium chloride (Scheme 7). Sequential abstraction of two α hydrogen atoms (neopentyl→neopentylidene→neopentylidyne) and complete alkylation at the metal center gives the neopentylidyne complex **35** (Scheme 7).[76,95] The precise sequence of reactions that leads to **35** is not known. Compound **35** is a yellow crystalline compound that melts at approximately 70 °C and can be distilled in vacuo, properties that are reminiscent of [$(tBuCH_2)_3Ta{=}CHtBu$] (**18**, Scheme 2). As shown in Scheme 7, treatment of **35** with three equivalents of HCl in the presence of dimethoxyethane (dme) produces [$(dme)Cl_3W{\equiv}CtBu$] (**36**) quantitatively.

Tungsten-based alkylidyne **36** can be converted readily into a variety of mononuclear compounds with the formula [$(OR)_3W{\equiv}CtBu$], as long as the alkoxide groups are sterically demanding (e.g., OR = O*t*Bu, $OCMe(CF_3)_2$, or O-2,6-$(iPr)_2C_6H_3$).[76,95] Compounds of this type were found to be highly active for alkyne metathesis and were the first well-defined catalysts for this reaction.[29,76,96–98] The expected intermediate alkylidynes could be observed in alkyne meta-



Scheme 7. Synthesis of tungsten-based imido alkylidene complexes from alkylidyne complexes; TMS = Me_3Si.

thesis reactions when bulky electron-withdrawing alkoxides were present, and were isolated and characterized. The structure of intermediate trigonal-bipyramidal (TBP) metallacyclobutadienes could be elucidated by crystallography as well. A representative example of an isolable metallacyclobutadiene is the triaryloxytungstacyclobutadiene shown in Equation (2).[97] This species can act as a catalyst for alkyne



(2)

metathesis since it undergoes a retro [2+2] reaction to yield an alkyne and a triaryloxytungsten alkylidyne complex. Compound **36** (Scheme 7) reacts with an alkyne to afford a five-coordinate trichlorotungstacyclobutadiene analogous to the triaryloxytungstacyclobutadiene shown in Equation (2), but the trichlorotungstacycle reacts further, and irreversibly, with another alkyne equivalent to generate a W^{IV} cyclopentadienyl complex.[99] These studies confirmed that alkoxide ligands promote metathesis-like reactions, while chlorides encourage side reactions that destroy the alkylidyne. On the basis of these studies it was suggested that the most successful tungsten-based olefin-metathesis catalyst might be a pseudotetrahedral species that contains sterically demanding alkoxide ligands.

Pseudotetrahedral molybdenum-based alkylidyne complexes that contain bulky alkoxide ligands were synthesized by techniques similar to those used to prepare the tungsten-based complexes and were shown to be active for alkyne metathesis.[10,95] With alkoxide or phenoxide ligands bound to the Mo center, alkyne metathesis proved to be efficient, while alkyne metathesis could not be detected when halide ligands were present. Intermediate molybdacyclobutadienes appeared to be less stable than the corresponding tungstacyclobutadienes toward loss of alkyne and alkylidyne reformation.

Application of alkyne metathesis to organic synthesis is enjoying increased attention today as a consequence of the development of well-defined high-oxidation-state W and Mo catalysts analogous to those described above.[100] Although alkyne metathesis may not have the scope and potential of alkene metathesis, it is not complicated by the formation of stereoisomers. Controlling the formation of *cis* or *trans* (or *E* or *Z*) isomers in olefin metathesis for the most part remains an unsolved problem.

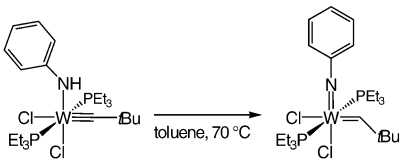
2.3. Development of Imido Alkylidene Complexes as Olefin-Metathesis Catalysts

Tungsten-based complex **29**, shown in Scheme 5, and related systems proved to be fully functional olefin-metathesis catalysts in the presence of $AlCl_3$, which probably removes a chloride to generate an electron-deficient cationic species (< 18 electron). However, metathesis activity was limited by since alkylidene complexes other than the neopentylidene were unstable towards bimolecular decomposition, a process that might include ligand redistribution (e.g., chloride transfer) or alkylidene coupling to give an olefin. The success of using sterically bulky alkoxide ligands in promoting metathesis (of olefins or alkynes) suggested that a complex such as $[W(O)(CHtBu)(OtBu)_2]$ might be a viable target as a well-defined catalyst. Indeed, substitution of the chlorides in **29** with *tert*-butoxide groups led to formation of $[(PEt_3)(OtBu)_2W(O)(CHtBu)]$ but this species decomposed in solution or in the solid state at room temperature.[80] It was thus recognized that an oxo ligand is not sufficiently sterically bulky, that is, it can bridge between metal centers and encourage bimolecular decomposition. Thus, a search for alkylidene complexes that contain an imido ligand in place of an isoelectronic oxo ligand, namely $[W(NR)(CHtBu)(OR')_2]$, was initiated.

To maximize steric protection at the metal center by the imido (NR) group and limit the ability of the imido ligand to bridge between metal centers, complexes bearing N-2,6-$iPr_2C_6H_3$ (NAr) were targeted. Sterically more demanding candidates such as N-2,6-$(tBu)_2C_6H_3$ were rejected on the basis of projected synthetic difficulties. For this reason, a route to $[W(NAr)(CHtBu)(OR')_2]$ species became the immediate goal. An attractive strategy involved alkylidyne complexes, which were being studied intensely at the time. Since neopentylidynes had been prepared by removing two α protons from neopentyl ligands, it seemed possible that one might be able to add a single proton to an alkylidyne to prepare an alkylidene.

2.3.1. Synthesis of Tungsten- and Molybdenum-Based Imido Alkylidene Complexes

The strategy of transferring a proton from an amido nitrogen to an alkylidyne carbon atom was first established in a paper published in 1982.[101] Thus, amido neopentylidyne complexes of the type $[(NHR)Cl_2L_2W{\equiv}CtBu]$ (R = H or Ph; L = PEt_3 or PMe_3) were reported to be transformed into the related imido neopentylidene complexes, $[(NR)Cl_2L_2W{=}CHtBu]$, upon heating or addition of a base, such as triethylamine; an example is shown in Equation (3). Reactions analogous to those in Equation (3) where Ar = 2,6-$iPr_2C_6H_3$ were not attempted. Perhaps the main problem with the



(3)

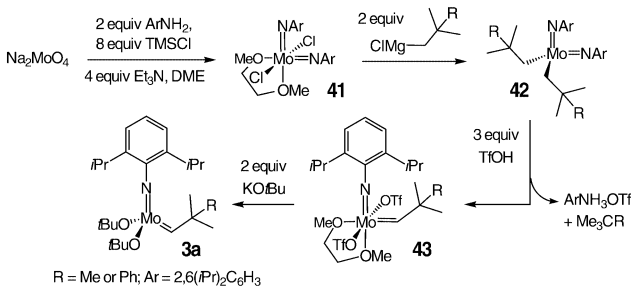
© 2003 Wiley-VCH Verlag GmbH & Co. KGaA, Weinheim

method shown in Equation (3), as far as preparation of the desired [W(NAr)(CH*t*Bu)(OR′)$_2$] is concerned, is that phosphanes could coordinate to the W center and possibly limit high catalytic activity of the resulting [W(NAr)(CH*t*-Bu)(OR′)$_2$] species.

Six years later it was found that analogous transformations could be carried out on dimethoxyethane complexes, as depicted in Scheme 7. The amido alkylidyne complex **38** was prepared by the reaction of **36** with **37**. Upon treatment with a catalytic amount of Et_3N, **38** was transformed quantitatively into **39**.[7] Miscellaneous observations in the last fifteen years suggest that the type of reaction represented by the conversion of **38** into **39** can proceed in the opposite direction.[14,102] Accordingly, the energetic difference between an amido alkylidyne and an imido alkylidene complex (for example, **38** and **39**, respectively, in Scheme 7) must not be large. Proton migrations between anionic C or N centers in d^0 metal complexes of the type described are related to the α-hydrogen (proton) abstraction (Scheme 2) in which a neopentylidene ligand is formed (irreversibly) from two neopentyl ligands.

When the chloride ligands in tungsten-based alkylidene **39** (Scheme 7) are replaced with sterically demanding alkoxide groups, four-coordinate **40a** and **40b** can be isolated; these should be considered as 14-electron complexes, since the imido ligand donates its electron pair to the metal center to form a pseudo triple bond. Dimethoxyethane, which binds to the metal only as a chelating ligand, does not remain bound to the crowded bis(alkoxide) species for steric reasons. The fact that all four ligands in W alkylidene complexes **40** are sterically demanding and covalently attached to the transition-metal center accounts for their stability toward bimolecular decomposition, a theme that harkens back to the stability of [(*t*BuCH$_2$)$_3$W≡C*t*Bu] (**35**, Scheme 7) and [(*t*BuCH$_2$)$_3$Ta=CH*t*Bu] (**18**).

The Mo alkylidyne complex [(*t*BuCH$_2$)$_3$Mo≡C*t*Bu] is prepared less efficiently than the analogous tungsten-based alkylidyne **35** (Scheme 7). Moreover, the alkylidyne pathway to imido alkylidene compounds (Scheme 7) requires that five out of six neopentyl groups are discarded en route to alkylidyne **36**. Accordingly, an alternative synthesis of molybdenum imido alkylidene complexes was sought. Towards this end, it was established that [Mo(NAr)$_2$(dme)Cl$_2$] (**41**, Scheme 8) can be prepared in large quantities from Na_2MoO_4, two equivalents of $ArNH_2$, eight equivalents of Me_3SiCl, and four equivalents of triethylamine in dimethoxyethane. Alkylation of **41** with neopentyl or neophyl Grignard reagents affords **42**, which upon treatment with three equivalents of triflic acid gives the 18-electron bis(triflate) **43**, in which the Mo=C bond survives further attack by the strong acid (cf. **35**→**36** in Scheme 7). In the presence of various alkoxide or aryloxide salts (Li, Na, or K), including even relatively weak nucleophiles, such as LiOCMe(CF$_3$)$_2$, **43** is converted into Mo alkylidene complexes represented by **3a** in Scheme 8.[13] These molybdenum-based bis(alkoxy)aryl imido alkylidene complexes are stable as long as the alkoxide ligand has sufficient steric bulk to prevent bimolecular decomposition. A complete list of Mo complexes of this general type can be found in Figure 2.



Scheme 8. The route for practical synthesis of molybdenum-based alkylidene complexes; OTf = [CF$_3$SO$_3$]$^-$.

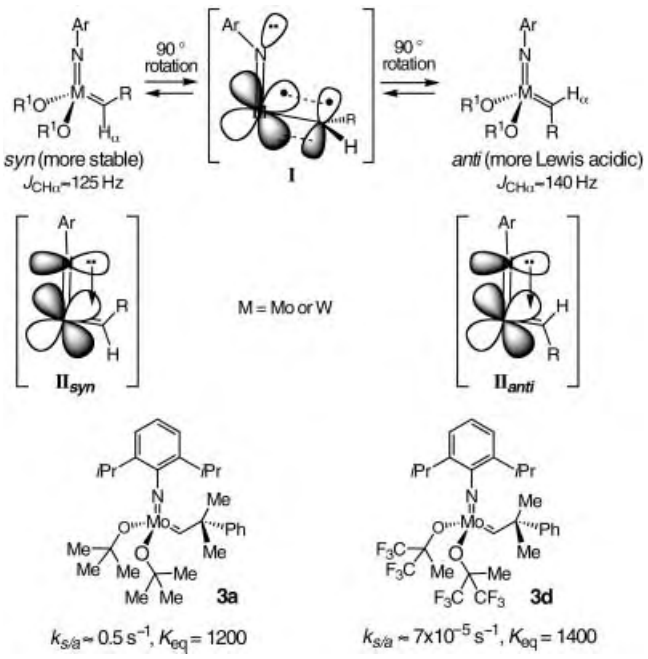
The route outlined in Scheme 8 is the preferred method of synthesizing Mo imido alkylidene complexes. As can be seen from the list in Figure 2, catalysts have been prepared that contain a variety of aryl imido ligands. The only alkyl imido complexes of this general type that have been isolated are 1-adamantylimido species such as **8a** or **8b** (Figure 2). Note that complexes that contain the relatively small OCH(CF$_3$)$_2$ or OC$_6$F$_5$ ligands can be isolated only as adducts with a suitable base (**3m**, **4n**, or **8b**; see also Section 2.3.3). The distinct reactivity and selectivity patterns arising from variations in the aryl imido ligands of molybdenum-based chiral complexes, and the unique attributes of the derived adamantylimido systems, are among the topics discussed below in the context of catalytic asymmetric olefin-metathesis reactions.

Tungsten imido alkylidene complexes can also be prepared by methods related to those shown in Scheme 8, where alkylidyne complexes are not involved.[8]

2.3.2. syn *and* anti *Alkylidene Isomers of Imido Alkylidene Complexes*

In four-coordinate molybdenum- and tungsten-based imido alkylidene complexes (Figures 1–4) the imido ligand is bound to the metal through a pseudo triple bond. That is, the electron pair on the nitrogen atom is donated into an empty d orbital on the metal center. Therefore the M-N-C_{ipso} angle is approximately 180°, and the d orbital on the metal that is involved in the formation of the M=C bond must lie perpendicular to the N-M-C_{ipso} plane. Thus, the metal complex can exist as two stereoisomeric forms. As shown in Scheme 9, one isomer is the *syn* alkylidene, where the substituent R points towards the imido ligand. The other is the *anti* alkylidene, where the substituent points away from the imido nitrogen atom. Studies concerning the structural and reactivity differences of *syn* and *anti* alkylidene complexes of Mo (largely) and W, and the equilibrium between them, have led to a number of important mechanistic insights into olefin metathesis. Selected experimental observations are summarized below. Many of these findings, as well as a number of other details that cannot be explored easily by experimental methods, have been probed by several groups through a variety of theoretical studies.[103]

M=CHR complexes can be detected readily by ^{1}H NMR spectroscopy. In all the complexes in Figures 1–4, the resonance signal of the alkylidene H$_\alpha$ usually is found



Scheme 9. *syn* and *anti* Mo and W alkylidene complexes are interconvertible. The rate constant for *syn* to *anti* conversion ($k_{s/a}$), and the reverse ($k_{a/s}$), are influenced by electronic and steric factors that affect the energy of intermediate **I**.

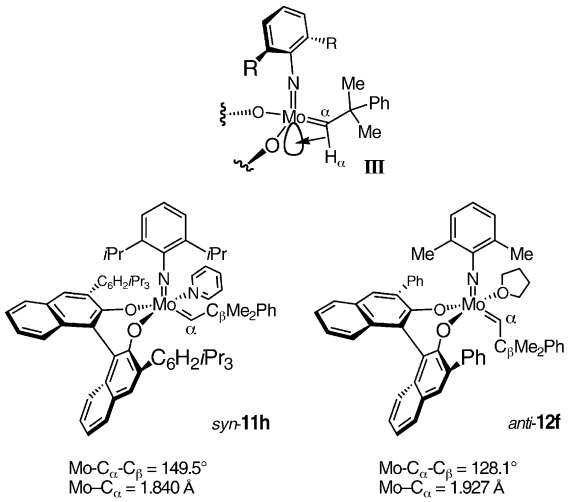
between $\delta = 8$–14 ppm. The resonance that corresponds to the typically minor *anti* isomer, if it can be seen, appears 1–2 ppm downfield of the *syn* H_α resonance. A reasonably reliable method of identifying the isomer is the J_{CH} coupling constant; J_{CH} for the *syn* isomer is typically approximately 125 Hz, while for the *anti* isomer it is typically about 140 Hz. Often only the *syn* isomer can be detected in routine NMR spectra, since so little *anti* isomer is present. However, the minor *anti* isomer is detected in many situations, especially in the aryl oxide complexes shown in Figure 3 and Figure 4.

In 1992, it was demonstrated that Mo complex **3d** (Figure 2, $G = CMe_2Ph$), which exists almost exclusively as its *syn* isomer at 22 °C, can be transformed into an equilibrium 1:2 mixture of *anti* and *syn* alkylidene complexes upon photolysis (360 nm) of the sample in [D_8]toluene at −78 °C (see Scheme 9).[104,105] When the light is turned off and the temperature raised above −78 °C, the *anti* isomer reverts back to the *syn* form in a reaction that is first order in *anti*-**3d**. In this manner, it was determined experimentally that *anti* alkylidenes can interconvert with their *syn* isomers either thermally or photochemically by rotation about the M=C bond.

Rate constants for conversion of the *anti* into the *syn* isomer ($k_{a/s}$) have been determined at temperatures between −78 °C and 22 °C for a variety of Mo complexes. Once the location of the *anti* H_α resonance signal was determined, the equilibrium constant between *syn* and *anti* isomers could be measured at room temperature, although in some cases with difficulty on account of the large magnitude of K_{eq} ($K_{eq} = [syn]/[anti]$). From K_{eq} and $k_{a/s}$ at 22 °C values (measured or calculated from temperature studies), $k_{s/a}$ may be determined at 22 °C ($K_{eq} = k_{a/s}/k_{s/a}$). Values for K_{eq} usually range from approximately 20 to around 2000 and both $k_{a/s}$ and $k_{s/a}$ tend to vary significantly as a function of the alkoxide and the imido ligand. For example, comparison of $k_{s/a}$ for **3a** and **3d**, which have nearly the same K_{eq} values (toluene, 22 °C; Scheme 9), reveals that the *syn* isomer of the *tert*-butoxide complex converts into the *anti* isomer $\approx 10^4$ times more rapidly than in the hexafluoro-*tert*-butoxide analogue.

As illustrated in **I** in Scheme 9, the d orbital in the N-M-C plane, which is involved in the formation of the pseudo triple bond between the imido nitrogen atom and the metal center, also participates in the formation of a M=C bond in the rotated alkylidene. The M-N-C_{ipso} angle therefore is likely to decrease in **I**, although it is not clear whether the imido substituent would point away or towards the alkylidene.[103f] A plausible model that explains the difference in $k_{s/a}$ for **3a** and **3d** is that the electron-withdrawing alkoxide groups in **3d** strengthen the M–N pseudo triple bond, thereby rendering access to the rotated alkylidene **I** (Scheme 9) energetically more costly. The rate of interconversion of *syn* and *anti* isomers often changes with the nature of the imido group, the alkylidene ligand, and the metal center (W versus Mo).[104] If photolysis in [D_8]toluene at −78 °C does not establish an equilibrium between *anti* and *syn* isomers, then spin saturation transfer is a possible alternative method of determining the rate of interconversion of *anti* and *syn* isomers. Spin saturation transfer has been employed in studies involving aryloxide complexes.[14,15]

Stereoelectronic factors are at least partially responsible for the fact that *syn* alkylidenes are energetically favored. As illustrated in **III** in Scheme 10, and supported by theoretical studies,[103] an agostic interaction[106] is proposed to exist between the C_α–H_α bond and the transition-metal center. Such a stabilizing hyperconjugation ($\sigma_{C-H} \rightarrow \sigma^*_{Mo-N}$) increases the π character of the C_α–H_α bond, thereby lowering J_{CH} and increasing the triple-bond character of the Mo=C_α bond. Crystallographic studies support the validity of such interactions. As an example, as illustrated in Scheme 10, the X-ray



Scheme 10. Hyperconjugative effect proposed to be present in the *syn* alkylidene complexes and representative structural consequences.

 © 2003 Wiley-VCH Verlag GmbH & Co. KGaA, Weinheim

structure of *syn*-**11h**[18] is comparable to that of the closely related *anti*-**12f**,[16] except for two significant differences: 1) *anti*-**12f** contains a smaller Mo=C_α–C_β bond angle (128.1(6)°) than *syn*-**11h** (149.5(10)°), and 2) *anti*-**12f** has a longer Mo–C_α bond (1.927(9) Å) than *syn*-**11h** (1.840(12) Å). Such differences can be explained in terms of the aforementioned agostic interaction.

On the basis of the structural differences between *syn* and *anti* isomers discussed above, it is not surprising that the two isomers exhibit disparate reactivity profiles, at least when determination of a difference is possible. For instance, in the case of Mo complex **3d** the *anti* isomer is estimated to be at least 100-times more reactive than the corresponding *syn* alkylidene toward 2,3-bis(trifluoromethyl)norbornadiene ($NBDF_6$) at −78 °C. In contrast, it has been estimated that *anti*-**3a** is possibly 10^5-times more reactive than *syn*-**3a** towards $NBDF_6$ at 22 °C.[104] It is generally presumed that an alkylidene/olefin complex is a transition state on the pathway to formation of a metallacyclobutane intermediate. Accordingly, the lower reactivity of the *syn* isomer might result in part from steric interactions between the alkylidene substituent and the aryl imido groups in **IV** depicted in Figure 5, as compared to those in the *anti* isomer **V**. (See below for further discussion and evidence.) *anti* Alkylidenes may exhibit higher reactivity owing to the increased Lewis acidity of the metal center (more effective association with the π-donor olefin substrate), which is consistent with the hyperconjugative interactions mentioned above (Scheme 10), and the strength of the interaction between the metal center in *anti* alkylidenes and two-electron-donor ligands such as phosphanes (see Section 2.3.3).

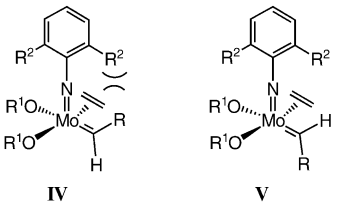
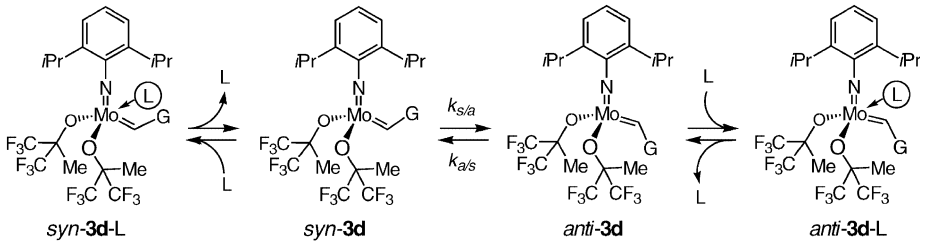


Figure 5. Steric interactions in the square-pyramidal (SP) complex formed upon coordination of olefin substrate may be partly responsible for lower reactivity of *syn* alkylidenes towards an olefin (ethylene used as example).

2.3.3. *Molybdenum and Tungsten Imido Alkylidene Complexes with Various Donor Ligands: Mechanistic Implications*

In general, four-coordinate Mo and W imido alkylidene complexes can form monoadducts with good two-electron-donor ligands, such as THF, PMe_3, pyridine, or quinuclidine (see Figures 3 and 4 and Scheme 10 for THF and pyridine adducts).[107] In all cases reported to date, the donor has been found to add to a CNO tetrahedral face (one of two pseudotetrahedral faces with the imido nitrogen, the alkylidene C_α, and an alkoxide oxygen atom at the corners), to afford a trigonal bipyramidal complex in which the new ligand is bound in the axial position (Scheme 11). When the alkoxide groups are electron-withdrawing, as in **3d** (Scheme 11), and the donor (L) is PMe_3, then the initial adduct contains the alkylidene in the *syn* orientation (e.g., *syn*-**3d**-PMe_3). This is because the phosphane ligand binds tightly to the perdominating *syn* isomer ($K_{eq} \approx 1400$ for **3d**). With time, as illustrated in Scheme 11, the *syn* adduct loses the phosphane to give a small concentration of the base-free species, the alkylidene rotates about the M=C bond (*syn*-**3d**→*anti*-**3d**) in the base-free form, and the phosphane binds again to yield the thermodynamically more stable adduct of the *anti* isomer. Note that the *syn* alkylidene is favored ($K_{eq} = 1400$) in base-free **3d**, while the *anti* alkylidene is the predominant adduct in **3d**-PMe_3. Coordinating bases bind strongly to electron-poor metal centers, as in hexafluoro-*tert*-butoxides, and weakly to relatively electron-rich metal centers, as in *tert*-butoxide complexes; however, the strength of the metal–donor-ligand interactions have not yet been quantified.



Scheme 11. *syn* and *anti* metal alkylidene complexes form adducts with various donor ligands (L). Interconversion between the two isomers, however, requires loss and reassociation of the donor ligand (G=CMe_2Ph).

The crystal structure of *syn*-**3d**-PMe_3 shown in Figure 6 reveals a significant steric repulsion between the *t*Bu group of the alkylidene and one of the *o*-*i*Pr groups of the imido ligand; such a claim is based on essentially identical values (≈156°) for the Mo-N-C_{ipso} angle in the imido ligand, which is normally about 180°, and the Mo-C_α-C_β angle in the neo-

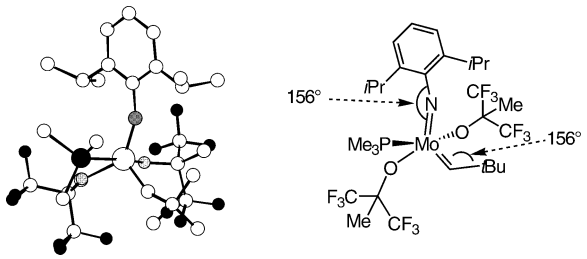


Figure 6. Structure of the PMe_3 adduct of [(NAr){$OCMe(CF_3)_2$}$_2$Mo=CH*t*Bu].

 © 2003 Wiley-VCH Verlag GmbH & Co. KGaA, Weinheim

pentylidene ligand, which is typically around 140°. This effect is the same interaction discussed in Section 2.3.2 and presented in Figure 5. Interaction between an *o*-*i*Pr group and the *syn* alkylidene substituent is probably at least partially responsible for destabilizing the *syn*-L adduct, thus lowering the reactivity of the *syn* alkylidene complex towards two-electron donors, which include olefins. Reactivity differences therefore can depend dramatically on the nature of the substituent on the alkylidene and the nature of the imido ligand. For example, there is evidence that *syn* and *anti* isomers of the 1-adamantylimido Mo complex **8a** (Figure 2) are approximately equally reactive towards $NBDF_6$.[104]

When the alkoxide ligand is relatively small and electron-withdrawing, the derived neopentylidene or neophylidene complex is stable toward bimolecular decomposition only as a Lewis base adduct. As an example, Mo alkylidene **3m** (see Figure 2), where $OR = OCH(CF_3)_2$, can be isolated only as its 2,4-dimethylpyridine complex.[12] Similarly, bis(hexafluoroisopropoxide) Mo alkylidene **8b**, bearing the relatively small adamantylimido ligand, is isolated only as a 2,4-dimethylpyridine complex.[12]

A number of enantiomerically pure Mo systems exist as THF adducts (Figure 3 and Figure 4). It is noteworthy that a base adds to the same diastereotopic CNO face of a complex, regardless of the diolate, imido group, alkylidene isomer, or the donor molecule (see the pyridine complex **11h** in Scheme 10).[17] This trend suggests that one face of an enantiomerically pure catalyst is sterically more accessible (see Section 5 for a detailed discussion).

Among THF-bound chiral Mo complexes are those that bear an electron-withdrawing 2,6-dichlorophenylimido ligand (e.g., **13a–d** in Figure 4). The smaller size of the 2,6-dichlorophenylimido group (compared to the NAr ligand) in combination with its greater electron-withdrawing ability encourages the donor molecule to coordinate to the more electron-poor and sterically accessible metal center. In a similar fashion, complexes that bear diolate ligands which provide a significant amount of space in their chiral pocket (as judged by examination of molecular models) are isolated as pyridine or THF complexes. Representative examples of the latter type are substituted binaphtholate Mo complexes **11i–m** in Figure 3 and **12e** in Figure 4.

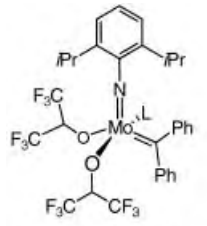
In the presence of coordinating solvents, such as THF (especially at low temperatures), *syn* and *anti* complexes in which the donor solvent is bound to the metal center can usually be detected.[16,18,19,25] In some cases all four diastereomeric solvent adducts can be detected at low temperature, where exchange of the bound THF is slow.[9,19,25] At elevated temperatures, NMR spectroscopic evidence suggests that donor solvent molecules (usually THF) first begin to dissociate from the less Lewis acidic *syn* complexes (see Scheme 9) and subsequently from the more Lewis acidic *anti* complexes.[18] Dissociation of donor solvent molecules is more facile in the case of sterically more demanding chiral ligands, or when bulky and more electron-donating imido groups are present.

If a coordinating solvent dissociates readily from *syn* and *anti* isomers, then interconversion of the two alkylidenes may proceed through rotation about the Mo=C bond. In connection with the effect of a Lewis basic ligand on the efficiency of alkylidene isomerization, it has been determined that the rate of interconversion between *syn* and *anti* isomers of **3d**, a Mo complex that bears electron-withdrawing alkoxide ligands, is significantly slower in $[D_8]$THF than in $[D_8]$toluene.[104] Whereas for most Mo alkylidene complexes the value for $\Delta S^{\neq}$ is aproximately 0 in $[D_8]$toluene, the relatively large and positive value for $\Delta S^{\neq}$ obtained in $[D_8]$THF ($+20$ to $25\ cal\,mol^{-1}\,K^{-1}$) is consistent with a process that requires rate-limiting loss of Lewis basic THF from the metal center.[104] These values also suggest that the alkylidene rotates in four-coordinate species, not five-coordinate base adducts.

On the basis of the discussion so far, one might suspect that five-coordinate base adducts of imido alkylidene complexes cannot react directly with olefins, since the donor ligand effectively blocks coordination of the olefin. All evidence to date suggests that this is the case.

One might question whether an olefin adduct of an alkylidene complex is observable. An alkylidene/olefin complex, distinct from a metallacycle, has been detected in NMR spectra at low temperatures in only one instance, one which involves cationic catalysts of the type studied by Osborn and Kress (see Scheme 6 and the related discussion).[108] Alkylidene/olefin intermediates have not been observed in any imido alkylidene bis(alkoxide) complexes of Mo or W.

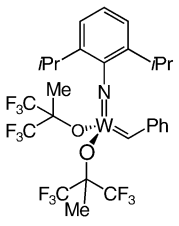
The strength of coordination of a base to an imido alkylidene bis(alkoxide) complex, and the degree to which the base stabilizes that alkylidene complex towards bimolecular decomposition (see Section 2.4.2), depend on the size and electronic characteristics of the alkylidene, alkoxide, and imido ligands, and, of course, the Lewis base. We have discussed primarily adducts of neopentylidene or neophylidene complexes in which the alkoxides and imido ligands are sterically demanding and are inherently relatively stable toward bimolecular coupling of alkylidenes to form a disubstituted olefin (e.g., *trans*-di-*tert*-butylethylene). Therefore, complexes that contain disubstituted alkylidenes should be even more stable toward bimolecular alkylidene coupling. For example, diphenylmethylene complexes (such as **45**[12] that contain small alkoxide groups) which in solution are largely base-free at concentrations of approximately 10 mM, can be isolated. At the other end of the steric scale are methylene complexes, no base-free example of which has been isolated. Thus, while complex **46** has been isolated and characterized,[7] the corresponding methylene species has only been detected as a Lewis base adduct, phosphane complex **47** being one example.[7]



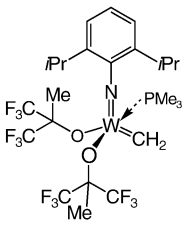
45 L = 2,4-dimethylpyridine

The base adducts of alkylidene complexes can still be reactive, if the base is labile enough to provide a significant concentration of the free alkylidene, under conditions where the alkylidene does not decompose bimolecularly. For example, the 2,4-dimethylpyridine complex **8b** (Figure 2)

 © 2003 Wiley-VCH Verlag GmbH & Co. KGaA, Weinheim



46



47

readily polymerizes (*o*-TMS)phenylacetylene.[12,109] When the base is pyridine, the adduct is virtually inactive toward (*o*-TMS)phenylacetylene, while the 2,5-dimethylpyridine complex analogous to **8b** is unstable as a consequence of the high concentration of the base-free species formed in solution which then decomposes bimolecularly.

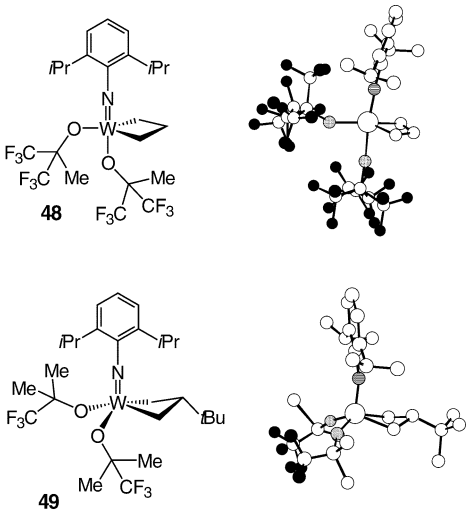


Figure 7. Tungstacycobutanes have been isolated, characterized, and shown to exist as trigonal-bipyramidal (TBP; **48**) or square-pyramidal (SP; **49**) complexes.

2.4. Olefin Metathesis Catalyzed by Imido Alkylidene Complexes

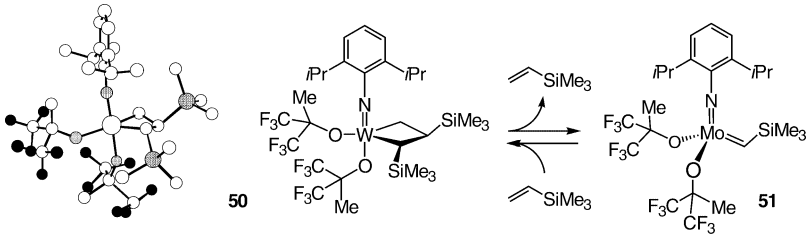
2.4.1. Reactions of Tungsten- and Molybdenum-Based Alkylidene Complexes with Olefins

Alkoxide-bearing W imido alkylidene complexes, such as those illustrated in Figure 1, are highly active catalysts for the metathesis of internal olefins.[7,28,32] Catalyst activity for metathesis of an unfunctionalized internal alkene, such as *cis*-2-pentene (to generate 2-butenes and 2-hexenes), is higher with W complex **1d**, which bears $OCMe(CF_3)_2$ ligands, than with **1a**, which contains O*t*Bu groups. Differences in catalyst activity can be attributed in a general sense to the increased electrophilicity of the metal center in a given isomer (*syn* or *anti*), although the rate of equilibration of *syn* and *anti* isomers, and their relative reactivities are also important aspects of overall reactivity (see Scheme 9 and related discussion).

Two types of tungstacyclobutanes, each of which has distinctive ^1H and ^{13}C NMR spectra, have been observed under a variety of conditions.[7,28] Crystallographic studies indicate that these metallacyclobutanes possess either a trigonal-bipyramidal (TBP, **48**, Figure 7) or a square-pyramidal geometry (SP, **49**, Figure 7). In certain instances, both geometries have been observed in solution and found to interconvert without loss of an olefin. In each type of metallacycle (SP or TBP) the $W-C_\alpha$ bond lengths are relatively short (2.05–2.15 Å) compared to typical $W-C_\alpha$ bond lengths in ordinary W^{VI} alkyl complexes (2.20–2.25 Å). Moreover, it was established that SP complexes are more stable towards loss of olefin when they contain a relatively electron-donating alkoxide group (e.g., O*t*Bu) and TBP systems are most stable when their alkoxide ligands are relatively electron-withdrawing (e.g., $OMe(CF_3)_2$). However, it has not been determined which metallacycle, if either, is formed directly upon reaction of the alkylidene complex with an olefin.

Unsubstituted tungstacycles (illustrated by **48** in Figure 7), can be formed under conditions where ethylene is generated. More unsubstituted than substituted metallacycles have been isolated and characterized, since loss of ethylene occurs more readily from unsubstituted metalacycles than the rate with which substituted metalacyclcles loses alkenes.[28,110] Therefore, unsubstituted metallacycles may be the dominant and detectable species in solution whenever ethylene is generated.[19] Like five-coordinate base adducts of alkylidenes, five-coordinate metallacycles are relatively stable towards bimolecular decomposition and thus can serve as reservoirs for reactive alkylidenes.

Isolation and study of tungstacyclobutanes revealed another noteworthy mechanistic principle: formation of a metallacyclobutane does not necessarily guarantee that an olefin undergoes metathesis. For example, reaction of tungsten-based complexes **1d** with $TMSCH{=}CH_2$ leads to the formation of TBP metallacyclobutane **50** (Scheme 12) which has been isolated and structurally characterized.[7] Complex **50** contains *trans* TMS groups, rendering it a possible intermediate en route to the formation of *trans*-1,2-bis(trimethylsilyl)ethylene (*trans*-TMSCH=CHTMS). Nevertheless, as illustrated in Scheme 12, metallacycle **50** selectively loses vinyltrimethylsilane to afford **51** (not TMSCH=CHTMS and the tungsten-based methylidene species); therefore vinyltrimethylsilane is not metathesized by **1d** to generate



50 51

Scheme 12. Bis(trimethylsilyl)tungstacyclobutane **50**, isolated and characterized by X-ray crystallography, breaks up to afford silylalkylidene complex **51** (not TMSHC=CHTMS), which suggests that not all metallacyclobutanes lead to productive metathesis.

 © 2003 Wiley-VCH Verlag GmbH & Co. KGaA, Weinheim

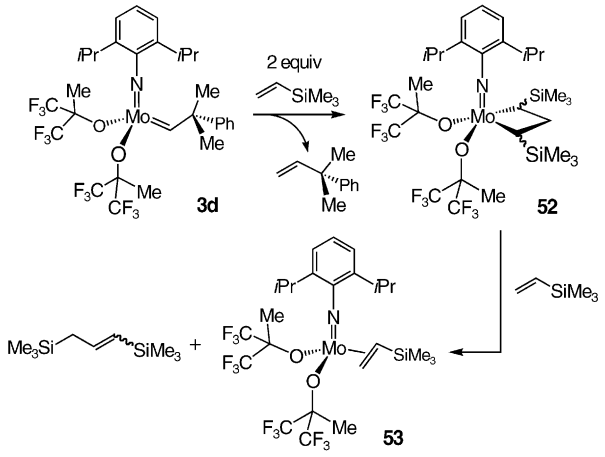
ethylene and TMSCH=CHTMS. This result suggests that transformations between certain terminal olefins might prove to be selective in favor of formation of cross-metathesis products versus those derived from homometathesis reactions.[111–113]

Similar to tungsten-based systems, molybdenum-based complexes (Figures 2–4) are highly active olefin-metathesis catalysts, particularly when electron-withdrawing alkoxide groups are present (e.g., **3d**, Figure 2).[32,33] One advantage of molybdenum-based catalysts is that molybdacyclobutane intermediates appear to break up more readily than their tungsten counterparts. Thus, in a molybdenum-catalyzed metathesis process, an unsubstituted metallacyclobutane is less likely to serve as a reservoir of a Mo=CH_2 complex.

No other anionic ligands in Mo and W imido alkylidene complexes to date have proven to be as successful as alkoxides for sustained metathesis activity.[29] This situation arises either because alternative ligands are not bulky enough to stabilize an electron-deficient metal center and prevent decomposition (e.g., halides) or because such ligands donate too much electron density to the metal in a σ and/or π fashion (e.g., amides). Recent examples of the latter effect are complexes **11q** and **11r** (Figure 3); no reaction was observed between **11q** or **11r** and ethylene or even benzaldehyde.[23]

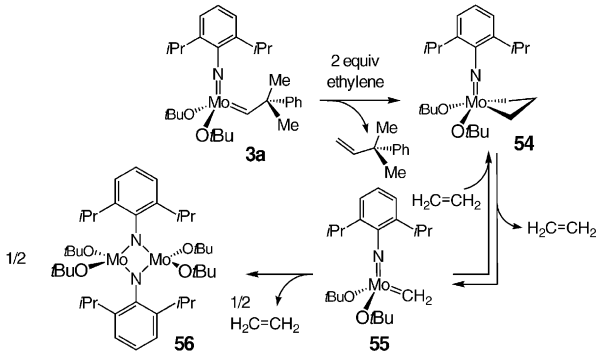
2.4.2. *Pathways that Lead to Catalyst Decomposition*

Two main mechanistically elucidated routes lead to a depletion of catalyst concentration during a typical metathesis reaction; in each of these processes, reduced (Mo^{IV} or W^{IV}) species are generated. Such decomposition pathways are the following: 1) Rearrangement of metallacyclobutanes to olefins. For example, the reaction shown in Scheme 13



Scheme 13. One pathway that results in decomposition of molybdenum-based metathesis catalysts leads to molybdenum(IV) olefin complexes, such as **53**.

involving **3d**, leads to formation of a Mo^{IV} olefin complex **53** as a consequence of β-hydride rearrangement of an intermediate α,α′-disubstituted metallacyclobutane (**52**).[114] 2) Bimolecular decomposition of alkylidene complexes. This pathway, which is fastest for methylene complexes, leads to the formation of olefins as a result of coupling of two alkylidenes (Scheme 14). The *tert*-butoxide complex **3a** upon



Scheme 14. Pathways that lead to the generation of dimeric complexes, such as **56**, also account for decomposition of molybdenum-based metathesis catalysts.

reaction with ethylene is converted into a detectable (by ^{1}H NMR spectroscopy) SP metallacyclobutane (**54**), which in turn decomposes to afford imido-bridged dimeric system **56** via methylene complex **55**.[114] It has been proposed that **56** is formed via an intermediate that contains two bridging methylenes, which subsequently loses ethylene.[114] Bimolecular decomposition of methylene complexes was demonstrated most convincingly for the 18-electron species [$Cp_2(CH_3)Ta{=}CH_2$] early in the development of high-oxidation-state alkylidene complex chemistry.[82]

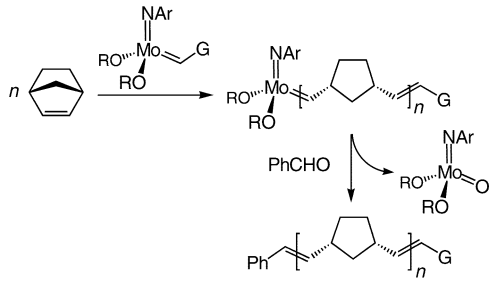
More recent studies involving the enantiomerically pure binaphtholate complexes **11j**, **11k**, and **11l** (see Figure 3) indicate that some propylene is formed as well upon decomposition of unsubstituted molybdacyclobutane species.[19] These investigations suggest that decomposition of unsubstituted molybdacyclobutane compounds derived from binaphtholate complexes is faster in the absence or the presence of ethylene. Accelerated decomposition in the absence of ethylene can be ascribed to displacement of the equilibrium between an unsubstituted metallacyclobutane and a methylene complex (for example, between **54** and **55** in Scheme 14) in favor of the latter, which subsequently decomposes bimolecularly. However, decomposition of an unsubstituted metallacyclobutane to give propylene in the presence of ethylene was unexpected. Clearly, additional mechanistic studies will be required to elucidate decomposition pathways of imido alkylidene complexes and their metallacyclobutane counterparts. Regardless of various mechanistic intricacies, the above findings indicate that since ethylene is generated in a metathesis reaction involving a terminal olefin, it is especially important to consider carefully the conditions under which the transformation is carried out (for example, whether a closed or open vessel is employed).

 © 2003 Wiley-VCH Verlag GmbH & Co. KGaA, Weinheim

3. Ring-Opening Metathesis Polymerization (ROMP) Catalyzed by Molybdenum-Based Imido Alkylidene Complexes

Olefin metathesis has many variations, among them reactions that lead to polymers. Examples include the ring-opening metathesis polymerization (ROMP) reaction,[37,38] polymerization of terminal alkynes,[12,36,115,116] step-growth polymerization of dienes,[117,118] and cyclopolymerization of 1,6-heptadiynes.[119,120] Studies concerned with ROMP of norbornenes has led to an elucidation of the reactivity patterns of *syn* and *anti* alkylidenes. The results of these investigations are detailed below.

ROMP reactions were of great interest to polymer chemists long before questions regarding the exact nature of the active catalyst began to be addressed rigorously.[37,38] The development of well-defined catalysts provided new opportunities for increasing our understanding of the mechanism of ROMP. As illustrated in Scheme 15 for norbornene, in

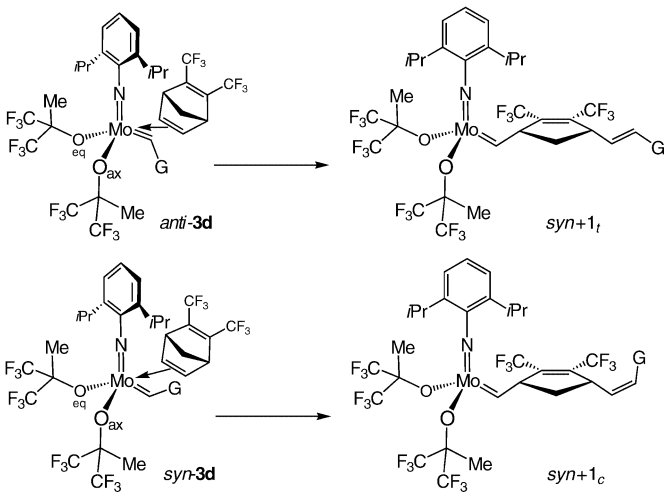


Scheme 15. ROMP and cleavage of the polymer with benzaldehyde in a Wittig-like reaction.

ROMP reactions a cyclic olefin reacts with the alkylidene to give a metallacyclobutane that is ruptured to afford a new alkylidene into which the cyclic species has been incorporated.[34,35,121,122] The new alkylidene may continue to react with the cyclic olefin in a similar manner to form a polymer with repeating units consisting of the "opened" alkene. If intermediates of this type escape decomposition during the process, and if the ring-opening step is irreversible, then such ROMP reactions are referred to as living; another monomer can be added after consumption of the first, which results in the formation of block copolymers. Alternatively, the polymer may be cleaved from W or Mo through reaction with a benzaldehyde. In processes that are not living, ROMP products can equilibrate to deliver mixtures that contain other cyclic or linear olefins formed by secondary metathesis processes.

3.1. Effect of Catalyst Structure (syn and anti Alkylidenes) on Rate of Polymerization and Olefin Stereoselectivity

At −78 °C the *anti* alkylidene isomer of Mo complex *anti*-**3d** (Scheme 16) has been demonstrated to react selectively with 2,3-bis(trifluoromethyl)norbornadiene ($NBDF_6$) to produce the racemic *syn* "first insertion product" bearing a *trans*



Scheme 16. Different alkylidene isomers can lead to polymeric structures with varying backbone olefin stereochemistry (C=CMe$_2$Ph).

olefin (*syn* + 1_t in Scheme 16). This outcome can be explained if $NBDF_6$ approaches one CNO face of the catalyst in the manner illustrated in Scheme 16 (through the *exo* face of the C=C bond), where the bridgehead methylene group of the olefin substrate lies approximately over the "flattened" aryl imido ring and the C=C and Mo=C bonds are approximately parallel to one another.[104] Formation of the derived metallacycle and subsequent ring-opening would then deliver a *trans* alkene. Note that the *syn* + 1_t product now contains a chiral β carbon atom, and that subsequent reaction of the monomer at one or the other CNO face will not be energetically equivalent. It is estimated that $NBDF_6$ reacts with *anti*-**3d** at least 100-times faster than with *syn*-**3d** at −78 °C.

As depicted in Scheme 16, the *syn* alkylidene isomer of the same Mo complexes (*syn*-**3d**) reacts with $NBDF_6$ to afford selectively a *syn* Mo alkylidene that carries a *cis* alkene (*syn* + 1_c). This reaction takes place readily only above 0 °C.

The importance of these findings was underlined by the subsequent discovery of the high *cis* content (≈95 %) of the polymer derived from $NBDF_6$ when **3d** is employed as an initiator.[123] (For **3d** $K_{eq} = [syn]/[anti] = 1400$ at 22 °C in toluene, the *anti* form of the first insertion product, *anti* + 1_c, is not detected in routine NMR spectra; that is, K_{eq} was estimated to be > 100 for *syn* + 1_c and subsequent insertion products.) Accordingly, *syn* alkylidene species are likely to be responsible for the polymerization process. (*anti* Alkylidene propagating species would deliver *trans* alkenes). The near exclusive involvement of the *syn* isomer is the result of two circumstances: 1) The *anti* isomer is not readily accessed through rotation about the Mo=C bond on the time scale of polymerization ($k_{s/a} = 7\text{x}10^{-5}\ s^{-1}$ at 22 °C). 2) Addition of $NBDF_6$ to a *syn* isomer yields another *syn* isomer and a *cis* alkene. Even though the *anti* isomer is the more reactive at ambient temperature by at least two orders of magnitude, it cannot be accessed rapidly and its concentration is low. The modes of approach of substrate to a CNO face shown in Scheme 16 are preferred in aryl imido complexes because the flat aryl ring is expected to lie approximately in the trigonal plane of the TBP transition state (where the incoming olefin

 © 2003 Wiley-VCH Verlag GmbH & Co. KGaA, Weinheim

occupies an axial position) and steric interaction between the incoming substrate and alkoxide ligands can be minimized. Addition of $NBDF_6$ to the Mo=C bond in an orientation 180° to that shown in Scheme 16 would lead to significant interaction of the $NBDF_6$ with the alkoxide ligands. Similar arguments would apply to any alkylidenes formed in the course of the polymerization process.

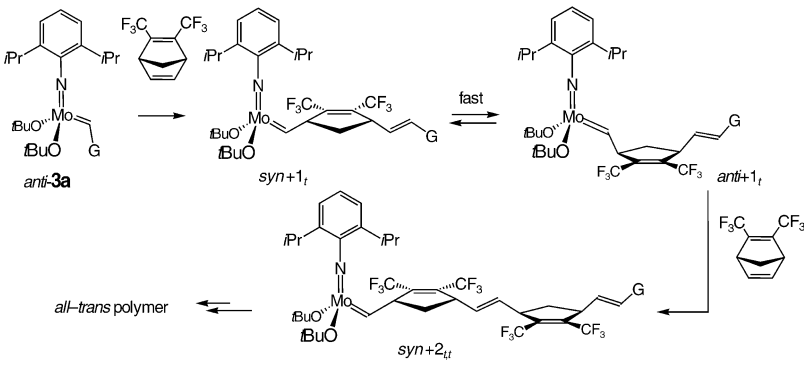
Polymerization of $NBDF_6$ by the less Lewis acidic Mo complexes **3a** (bearing O*t*Bu ligands) affords a polymer in which approximately 98% of its backbone alkene units are *trans*.[124] *trans* Linkages can be formed through reactions involving only *anti* alkylidenes (Scheme 17), if the following assumptions hold:

1) The mode of approach of a monomer to an *anti* alkylidene (Scheme 17) is the same as the proposed mode of approach to a *syn* alkylidene (Scheme 16)
2) The *tert*-butoxide ligands in **3a** deactivate the metal to the point where the *syn* alkylidenes do not react with $NBDF_6$ before the kinetically accessible ($k_{s/a} = 1\ s^{-1}$) *anti* isomer does, in spite of the fact that the concentration of the *syn* alkylidene is nearly a thousand-times higher than the *anti* isomer. Thus, if we assume that $k_a[anti] = 100\ k_s[syn]$ and $K_{eq} = 10^3$, then $k_a = 10^5 k_s$, which indicates that the *anti* alkylidene can be approximately five orders of magnitude more reactive than the corresponding *syn* isomer toward $NBDF_6$.

For a more reactive monomer, such as norbornene, the above mechanistic scenario may not hold and more *cis* linkages can form.

It also has been demonstrated that when Mo complexes **8** are used instead of **3d** (i.e., changing the aryl imido ligand to an adamantylimido group), the initial *syn* and *anti* metal alkylidene complexes appear to be approximately equally reactive toward $NBDF_6$. These findings suggest that the steric and electronic properties of the imido ligand are of fundamental importance in determining polymer *cis*/*trans* structure.

In 1994, Feast, Gibson, and co-workers disclosed an intriguing result demonstrating that the mechanistic pathway for polymerization reactions catalyzed by molybdenum-based catalysts might vary dramatically based on the nature of the substrate.[125,126] These researchers established that 1,7,7-trimethylnorbornene is polymerized slowly by the complexes **3d** in CH_2Cl_2 to give an *all-trans* polymer (not *all-cis* as with $NBDF_6$) at a rate that is independent of substrate concentration and with a rate constant that is essentially equal to the $k_{s/a}$ value measured for the catalyst at 22°C ($7x10^{-5}\ s^{-1}$). These findings are consistent with a rate-limiting conversion of *syn* into *anti* alkylidene. The *anti* alkylidene in turn reacts relatively rapidly with the substrate monomer to afford a *syn* insertion product with a *trans* alkene. Reaction of 1,7,7-trimethylnorbornene with *syn* Mo alkylidenes, even highly reactive **3d**, essentially does not take place, presumably for steric reasons.



Scheme 17. In spite of predominance of the *syn* molybdenum-based alkylidene complexes, the substantially higher reactivity of the *anti* isomers leads to the formation of *all-trans* polymers (G=CMe_2Ph).

3.2. Effect of Catalyst Structure on Polymer Tacticity

3.2.1. Achiral Catalysts and Chain-End Control of Stereochemistry

The ability to control *cis*/*trans* selectivity as well as the relative stereochemistry between monomer units (tacticity) are important features of ROMP with well-defined catalysts. In ROMP reactions of norbornenes or norbornadienes that contain a mirror plane, four stereoregular polymers can be formed, as shown in Figure 8 for a generic disubstituted

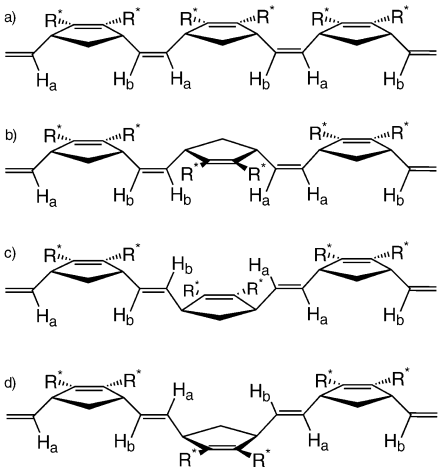
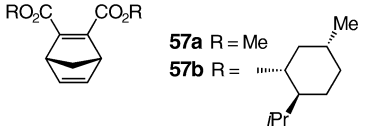


Figure 8. The four possible regular structures of 2,3-disubstituted norbornadienes and the effect of enantiomerically pure auxiliary R* (from reactions of **57b**) on the chemical environments of the inequivalent protons H_a and H_b; a) *cis*, isotactic (*cc*,*mm*), b) *cis*, syndiotactic (*cc*,*rr*), c) *trans*, syndiotactic (*tt*,*rr*), d) *trans*, isotactic (*tt*,*mm*).

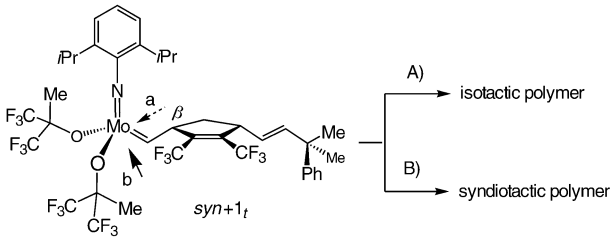
norbornadiene (such as **57a** or **57b**). In a triad, which is a three-monomer unit within the polymer as shown in Figure 8, the central monomer unit in a *cis*, isotactic polymer is flanked by *cis* double bonds and a mirror plane relates the central unit



 © 2003 Wiley-VCH Verlag GmbH & Co. KGaA, Weinheim

to the unit on each side. That is, the polymer has a *cc*,*mm* (*cis*,*cis*,*meso*,*meso*) structure at the triad level of analysis. Therefore, as shown in Figure 8, the *cis*, syndiotactic polymer has a *cc*,*rr* structure (*cis*,*cis*,*racemic*,*racemic*).

The *all-trans* product derived from polymerization of $NBDF_6$ catalyzed by Mo complex **3a** is highly tactic (according to ^{13}C NMR spectroscopy; see below).[124] In contrast, the high *cis* polymer obtained from the reaction of $NBDF_6$ with **3d** (G = *t*Bu) has been shown to be biased toward one tacticity (≈75%, ^{13}C NMR spectroscopy). Any tacticity control under either set of conditions must arise through chain-end control. That is, the chirality of the β carbon atom in the first insertion product determines which diastereotopic face of the M=C bond is approached by the next equivalent of monomer. As summarized in Scheme 18, if the same CNO face is approached in each step in the polymerization process, an isotactic polymer is formed. If alternating CNO faces are approached in each step in the polymerization process, then a syndiotactic polymer is generated. If monomers add randomly to diastereotopic CNO faces then there is no stereocontrol and an atactic polymer results.



Scheme 18. Approach from the two diastereotopic faces of a chiral alkylidene intermediate determines the tacticity of the polymer product. A) monomer approaches one CNO diastereoface (a or b) in each step, B) monomer approaches alternating CNO diastereofaces a and b.

The tacticity of *all-cis*- or *all-trans*-poly($NBDF_6$) is determined by evaluating the C(7) resonance(s) in ^{13}C NMR spectra.[21] As shown in Figure 9a the C(7) resonance in the *all-cis* polymer prepared by treatment of $NBDF_6$ with achiral Mo complex **3d** (G = CMe_2Ph) was found to consist of three resonances at δ = 38.4, 37.6, and 36.5 ppm, with the dominant one being at 38.4 ppm. In atactic, *all-cis* poly($NBDF_6$), the resonances at δ = 38.4, 37.6, and 36.5 ppm would be found in a 1:2:1 ratio, since the center resonance can be ascribed to the C(7) resonance in a *cis*,*cis*,*meso*,*racemic* (*cc*,*mr*) triad. Therefore, the polymer whose C(7) resonance is shown in Figure 9a is biased toward one tacticity that gives rise to the C(7) resonance at approximately δ = 38.4 ppm. However, the tacticities that give rise to C(7) resonances at δ = 38.4 and 36.5 ppm (*cc*,*mm* = isotactic or *cc*,*rr* = syndiotactic; Figure 8) cannot be assigned a priori.

3.2.2. *Chiral Catalysts and Stereochemical Induction by Metal-Complex Asymmetry*

A potential disadvantage of chain-end control is that an error in a tactic polymer can control the next insertion. Such an error is said to be propagated (not corrected). In contrast, the asymmetric nature of a chiral catalyst may control the stereochemistry of monomer addition more efficiently compared to a chiral β carbon atom in a chain-end (Scheme 18), and higher tacticity polymers would be expected. If a chiral metal complex forces the monomer to add to the same CNO face in each ROMP step, an isotactic polymer will be formed.

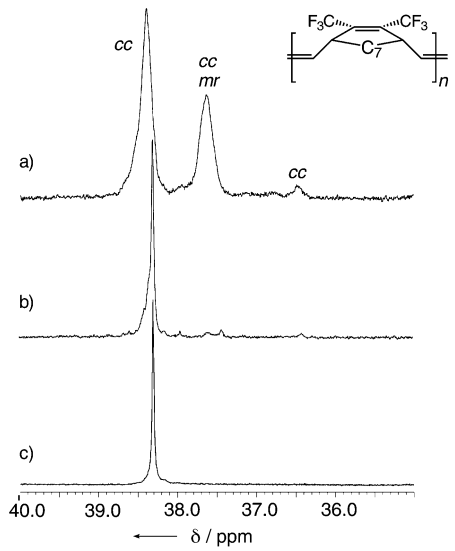


Figure 9. The C(7) resonance(s) in the ^{13}C NMR spectra of *cis* polymers obtained from reactions of $NBDF_6$, where molybdenum-based complexes **3d** (G = CMe_2Ph); spectrum a), **11o** (spectrum b), and **12g** (spectrum c) are used as the catalyst. (*cc mr* = *cis*,*cis*,*meso*,*racemic*; see text for explanation.)

Molybdenum-based complexes **11d**, **11m**, **11n** (enantiomerically pure), and **12g** were employed to examine the control of polymer tacticity by a chiral catalyst (see Figure 3 and Figure 4).[16,21] Except for **11d**, all the other Mo catalysts were obtained and used as their THF-coordinated complexes. The *all-cis* polymers obtained from polymerization of $NBDF_6$ catalyzed by complex **11o** (Figure 9, spectrum b) or especially **12g** (Figure 9, spectrum c) were found to be highly tactic (>99%), with only the δ = 38.4 ppm resonance being visible. The results shown in spectrum c of Figure 9 are particularly striking compared to the low tacticity of the polymer product obtained by chain-end control from reaction of $NBDF_6$ in the presence of **3d** (G = CMe_2Ph) as the catalyst (Figure 9, spectrum a). When **11m** is employed as the catalyst (wherein the N-2,6-$Me_2C_6H_3$ imido ligand of **12g** is replaced with N-2,6-$i Pr_2C_6H_3$), the resulting polymer contains ≈25% *trans* olefins, and therefore is highly irregular with a complex and broad set of resonances (not shown) for C(7). It is likely that additional steric crowding in the *syn* alkylidene isomer of the more sterically hindered **11m** shifts some chain propagation to the *anti* isomer, which promotes the generation of *trans* alkenes. Surprisingly, with biphenolate **11d**, which is used as a base-free complex and bears a ligand that is achiral in its metal-free form, *cis*, tactic poly($NBDF_6$) is again obtained. One would expect that a chiral catalyst encourages monomer addition to the same diastereotopic CNO face and therefore promotes the formation of an isotactic polymer. Therefore

one would expect the $\delta = 38.4$ ppm resonance to be due to *all-cis*-poly($NBDF_6$). However, it is not feasible to prove the tacticity of the *all-cis*, tactic poly($NBDF_6$) made from **12g**, or the *all-trans*, tactic poly($NBDF_6$) made from **3a** (see Section 3.2.1.)

It would be possible to demonstrate the tacticity of *all-cis* or *all-trans* tactic polymers if they were to contain an enantiomerically pure group (R* in Figure 8) in place of the trifluoromethyl group. Fortunately, 2,3-dicarboalkoxynorbornadienes **57a** and **57b** (which contain the required enantiomerically pure group) can be polymerized to give *all-trans*, tactic polymers with catalyst **3a**, and *all-cis*, tactic polymers with **12g**; their ^{13}C NMR spectra are analogous to those discussed for poly($NBDF_6$). As in the case of poly($NBDF_6$) samples, the olefinic region of the ^1H NMR spectra of *all-cis*, tactic poly(**57a**) is sharp and well-resolved. This circumstance made it possible to determine tacticity through analysis of the ^1H NMR spectra of poly(**57b**). Thus, as shown in Figure 8, the two inequivalent olefinic protons (H_a and H_b) in the four regular structures are bound to adjacent olefinic carbon atoms in isotactic, but not syndiotactic, polymers. Therefore, if two olefinic resonances are observed and if the two olefinic protons are coupled, the polymer is isotactic; if the protons are not coupled, the polymer is syndiotactic. As illustrated in Figure 10, the COSY spectra for a product obtained by

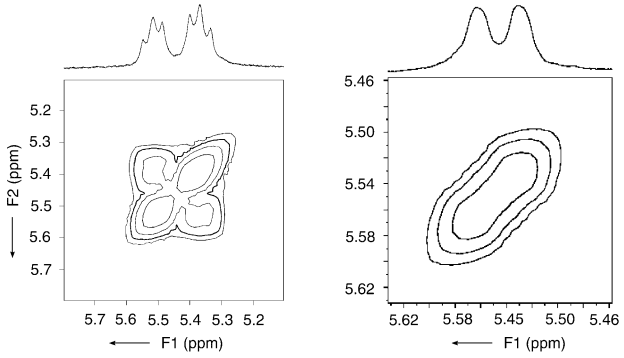


Figure 10. The olefinic regions of the 300 MHz homonuclear COSY NMR spectra of *all-cis*, isotactic (left) and *all-trans*, syndiotactic (right) polymers obtained from polymerization of **57b** ($CDCl_3$ at 25 °C) with **12g** and **3a** as the catalysts, respectively.

polymerization of **57b** show that the olefinic protons are coupled in the *cis* (prepared with **12g** as the catalyst), and not in the *trans* polymer (prepared with **3a** as the catalyst). These findings are consistent with *all-cis*, isotactic polymer being generated through enantiomorphic site control imposed by chiral Mo complex **12g** and *all-trans*, syndiotactic polymer being formed by chain-end control in the presence of **3a**. Although it is not possible to demonstrate the tacticity of *trans* and *cis* poly($NBDF_6$), it seems likely that they are also syndiotactic and isotactic, respectively.

4. Achiral Molybdenum-Based Olefin-Metathesis Catalysts in Stereoselective Synthesis

Only a few years ago incorporation of a transformation involving olefin metathesis in a total synthesis scheme was viewed as a daring application of an interesting but unproven process. Today, metathesis-based approaches, particularly ring-closing metathesis (RCM), are employed with such regularity that their use in a large number of contexts is considered routine.[1–4] In this section, we provide an overview of the use of achiral molybdenum-based complex **3d** in modern organic synthesis. In instances where the use of ruthenium-based catalysts **58**[127] (shown in Figure 11) has also been explored, comparative data are presented.

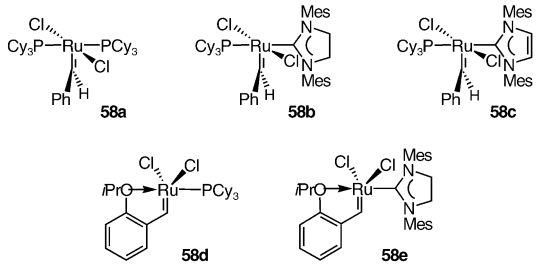
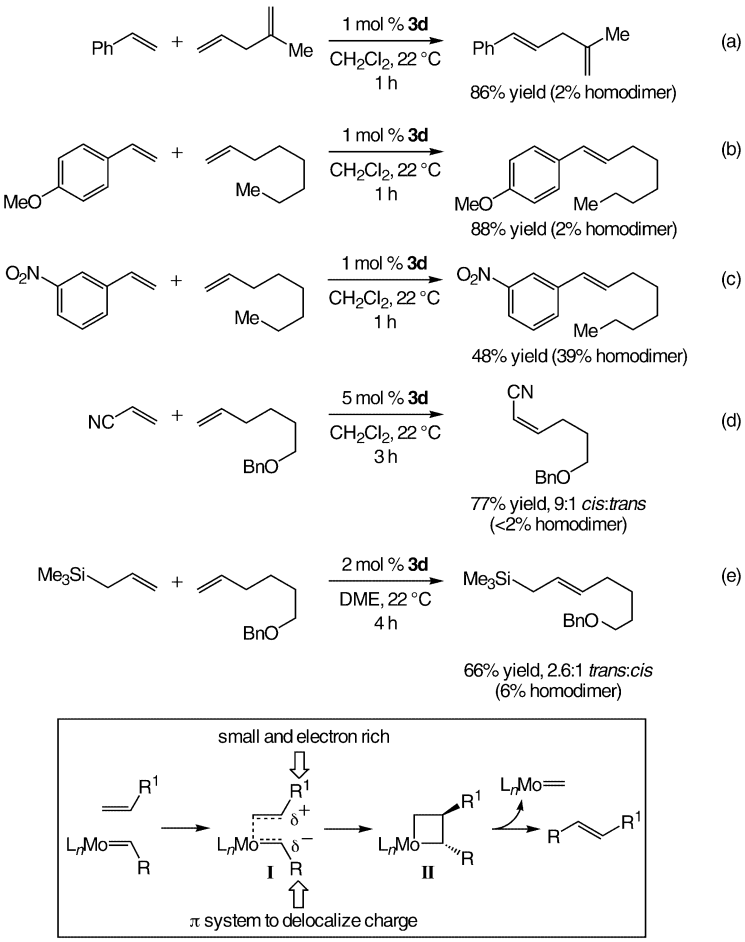


Figure 11. Achiral ruthenium-based olefin-metathesis catalysts. Mes = 2,4,6-$Me_3C_6H_2$.

4.1. Molybdenum-Catalyzed Cross-Metathesis Reactions

One of the earlier applications of Mo catalysts was reported by Crowe and Zhang in 1993 in the context of stereoselective cross metathesis (CM).[111] As the examples in Scheme 19 illustrate [Eq. (a)–(c)], styrenes and terminal aliphatic alkenes undergo CM promoted by Mo complex **3d** (G = CMe_2Ph). Transformations proceed with varying efficiency, depending on the electronic attributes of the aryl olefin. The electron-rich alkene in Equation (b) of Scheme 19 delivers a significantly higher yield of the desired CM product than the electron-poor nitrostyrene [Eq. (c)], with which nearly 40% homodimer is generated. Based on these and additional data, Crowe and Goldberg proposed a model for the molybdenum-catalyzed CM (Scheme 19, bottom).[112] It was suggested that reactions are more efficient when one olefin partner bears a substituent that stabilizes the partial negative charge at the carbon atom of the Mo alkylidene and the other olefin has an electron-donating substituent that can stabilize the developing electron deficiency at the β carbon atom of the incipient metallacyclobutane. The ability of acrylonitrile to participate effectively in molybdenum-catalyzed CM is consistent with this postulate [Eq. (d), Scheme 19]. However, subsequent studies provided instances that cannot be rationalized by the mechanistic picture in Scheme 19; one such case is the efficient catalytic CM between allylsilane and terminal alkenes [Eq. (e) of Scheme 19].[113,128]

 © 2003 Wiley-VCH Verlag GmbH & Co. KGaA, Weinheim



Scheme 19. Top: Molybdenum complex **3d** used in some the first examples of efficient catalytic and stereoselective cross metathesis, bottom: proposed molybdenum-catalyzed cross-metathesis mechanism.

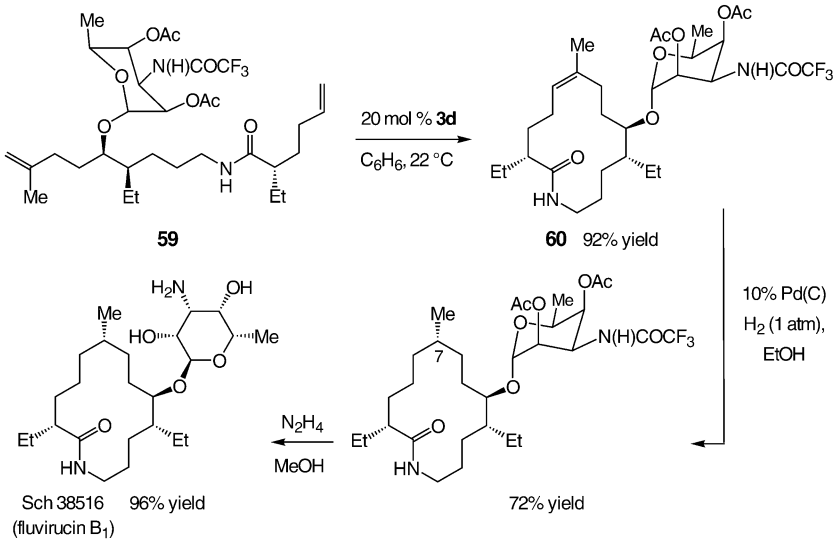
Molybdenum-catalyzed CM was later used by Barrett and co-workers to access optically pure *trans*-disubstituted homoallylic ethers, where the requisite terminal homoallylic alcohol was prepared through enantioselective allylation of aldehydes by an optically pure allylboronate.[129] These researchers later illustrated that, in contrast to ruthenium-based catalyst **58a**, complex **3d** (G = CMe2Ph) does not effect CM reactions with allenes.[130]

4.2. Molybdenum-Catalyzed Ring-Closing Metathesis (RCM) Reactions

4.2.1. Synthesis of Macrocycles by Molybdenum-Catalyzed RCM

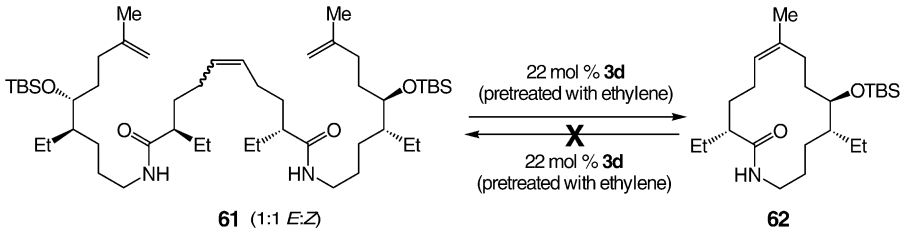
In 1995, in the context of the enantioselective total synthesis of fluvirucin B_1 (or Sch 38516), an efficient molybdenum-catalyzed ring-closing metathesis (RCM) leading to the formation of the desired fourteen-membered lactam was reported (Scheme 20).[131] The catalytic ring closure of fully functionalized diene **59** to afford macrocycle **60** was effected in 92% yield.[132] Facile formation of **60** illustrated that Mo complex **3d** can be employed to prepare macrocyclic structures in the presence of a variety of Lewis basic functional groups. The stereoselective formation of the trisubstituted olefin (> 95% *Z*) proved critical, as the subsequent catalytic hydrogenation of the alkene could then be used to establish the remote C7 stereochemistry (> 98% *de*).

Subsequent studies[133] demonstrated that efficient generation of the fourteen-membered macrolactam and the absence of homodimeric products is probably the result of the reversible nature of metal-catalyzed metathesis.[134] As depicted in Equation (4) (where TBS = *t*BuMe$_2$Si) treatment of homodimeric triene **61** (1:1 *E*:*Z*, obtained from reaction of monomer with Ru catalyst **58a**) with 22 mol% **3d** (G = CMe$_2$Ph) in the presence of ethylene led to the formation of macrolactam **62**. Ethylene was used to ensure exact reaction conditions through generation of the corresponding molybdenum methylidene complex. Furthermore, subjection of **62** to the above conditions did not deliver any monomeric or homodimeric adducts, which suggests that stereoselective olefin formation is kinetically controlled and not a result of a thermodynamic preference for the *Z* alkene. Follow-up investigations showed that conformational preorganization imposed by stereogenic centers in **59** or **61** (1:1 *E*:*Z*) is critical to the efficiency of the catalytic RCM. Removal of stereogenic sites resulted in substantial amounts of homodimers. It would be intriguing to establish the effectiveness of some of the more reactive and



Scheme 20. A key step in the total synthesis of fluvirucin B_1 is the molybdenum-catalyzed RCM that forms a trisubstituted olefin **60** with > 98% *Z* selectivity and generates a fourteen-membered cyclic lactam.

 © 2003 Wiley-VCH Verlag GmbH & Co. KGaA, Weinheim

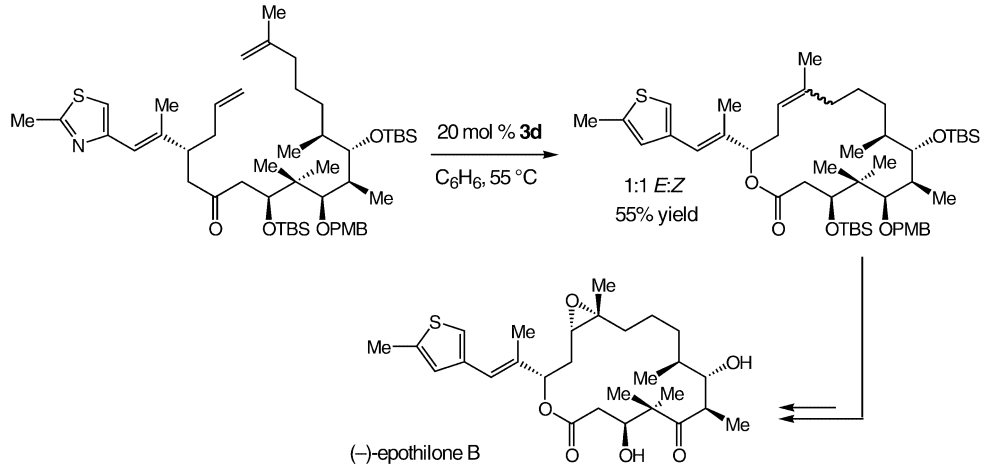


(4)

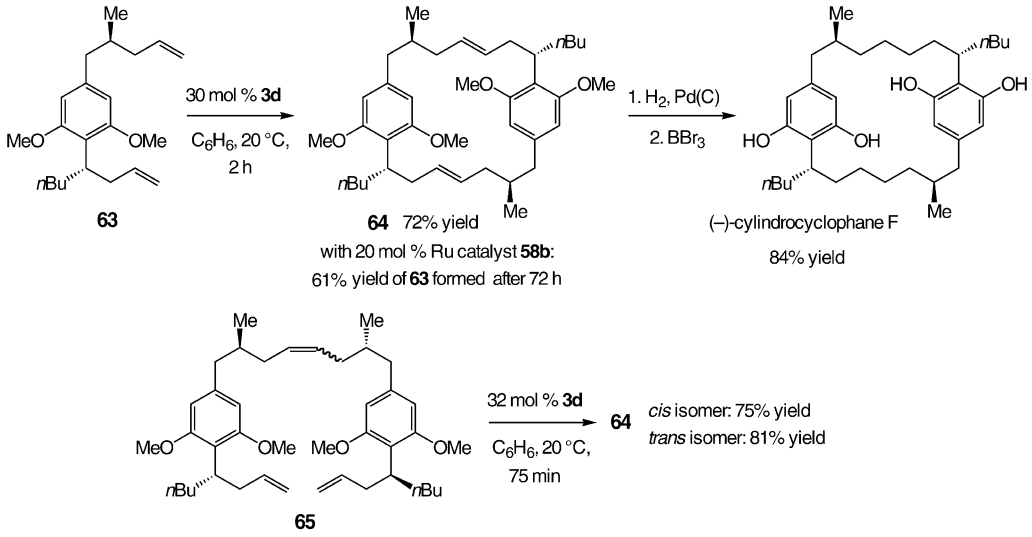
recently developed Ru-based catalysts, such as **58b–d** (Figure 11), in promoting the formation of such trisubstituted cyclic olefins. In general, the same question can be posed in connection to a number of olefin-metathesis processes discussed below.

A more recent molybdenum-catalyzed RCM reaction, where the target is a trisubstituted olefin within a macrolactone olefin, was reported in 1998 in the context of the total synthesis of (−)-epothilone B.[135] As illustrated in Scheme 21, in the presence of 20 mol% **3d** (Figure 2, $G = CMe_2Ph$), the desired product was generated in 55% yield. Unlike the fluvirucin B_1 synthesis, a mixture of *E* and *Z* isomers (1:1) was produced (separated through chromatography on silica gel). Subsequent functional-group manipulations, including oxidation of the appropriate alkene isomer, led to the isolation of the target molecule.

Molybdenum-catalyzed metathesis reactions have been investigated by Smith and co-workers in the context of the total syntheses of (−)-cylindrocyclophanes A and F.[136] Through a tandem molybdenum-catalyzed CM/RCM, as depicted in Scheme 22, acyclic diene **63** is converted into



Scheme 21. Molybdenum-catalyzed RCM affords a macrocyclic lactone bearing the trisubstituted olefin used at a later stage to install the requisite epoxide in the total synthesis of (−)-epothilone B. PMB = *p*-methoxybenzyl.

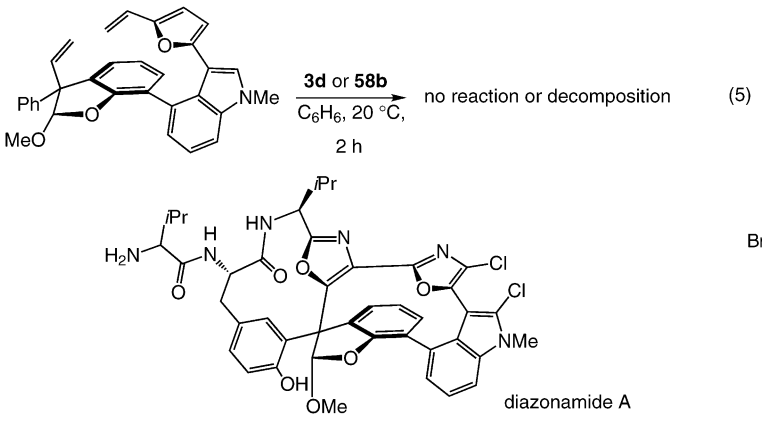


Scheme 22. The molybdenum-catalyzed tandem CM/RCM reaction leads to a regioselective dimerization that serves as the foundation of a total synthesis of (−)-cylindrocyclophanes; control experiments indicate that the initial CM is reversible, which allows the predominant formation of the lower energy head-to-tail macrocycle.

 © 2003 Wiley-VCH Verlag GmbH & Co. KGaA, Weinheim

macrocyclic diene **64** with complete regiocontrol (head-to-tail). The same transformation proved significantly less efficient with Ru catalyst **58b** (Figure 11). The reversible nature of alkene metathesis plays a critical role here as well. As shown by transformation of the head-to-head CM product **65** to **64**, the higher energy pathway required for the RCM of intermediates such as **65**, causes reversion to monomeric compounds.[137,138] Regeneration of the head-to-tail CM adduct and a facile RCM leads to the desired macrocycle.

In the above examples, where catalytic metathesis is used to prepare complex macrocycles, experimental evidence points to the influence of ring size and substrate stereochemistry in reaction efficiency. In this vein, it should be noted that, in the context of the total synthesis of diazonamide A, Nicolaou and co-workers attempted to effect the RCM transformation in Equation (5) with **3d** (Figure 2, G = CMe_2Ph), or various Ru-based catalysts to no avail. This lack of reactivity is likely to be a result of the ring strain associated with the desired target structure.[139]



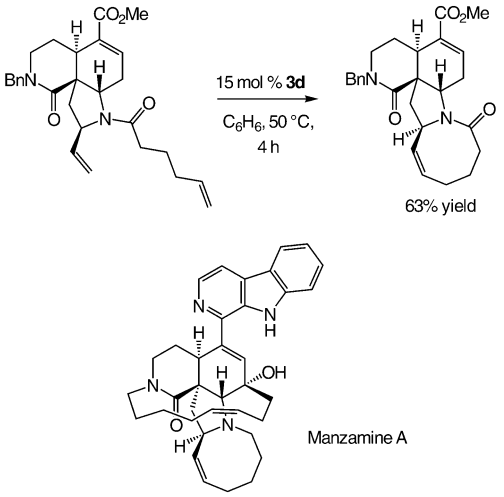
(5)

4.2.2. *Synthesis of Medium Rings by Molybdenum-Catalyzed RCM*

Since a considerable number of medicinally important agents bear seven- and eight-membered-ring carbo- and heterocycles, efficient and selective synthesis of medium rings has been, and remains, a long-standing goal in modern organic synthesis. In this arena also, molybdenum-catalyzed olefin metathesis has made a significant impact.

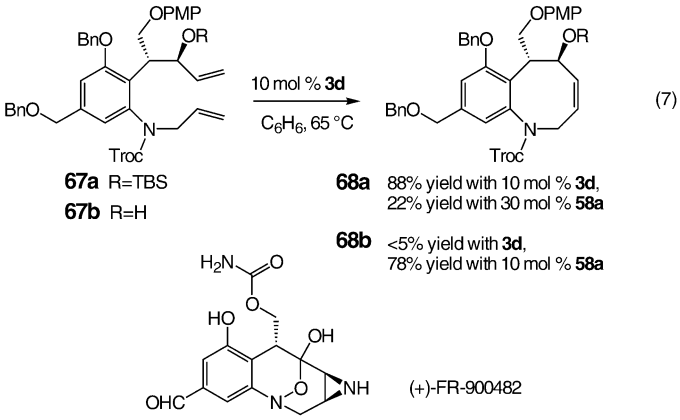
One of the earliest examples (1994) of the use of olefin metathesis to access a medium ring is the molybdenum-catalyzed transformations reported by Martin and co-workers. As depicted in Equation (6) (**3d** Figure 2, G = CMe_2Ph), synthesis of the desired tetracycle, including an eight-membered unsaturated amide proceeds in 63% yield.[140]

Another important early example, disclosed in the context of the total synthesis of antitumor antibiotic (+)-FR900482, is shown in Equation (7).[141] This study is noteworthy as it provides an early illustration of the complementarity of the molybdenum- and ruthenium-based catalysts. Catalytic RCM was effected by 10 mol% **3d** (Figure 2, G = CMe_2Ph), to afford **68a** in 88% yield. When Ru complex **58a** (Figure 11) was used (30 mol%), the desired product was generated in



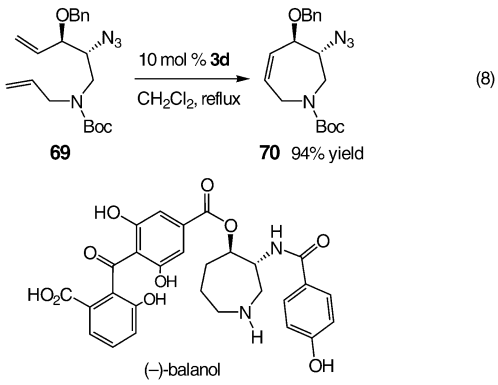
(6)

22% yield (48% recovered starting material). Mo complex **3d** (G = CMe_2Ph) cannot be used with substrates that bear sterically unprotected hydroxy units. However, reaction of the allylic alcohol **67b** was readily promoted by 10 mol% **58a** to provide **68b** in 78% yield. Bicyclic amide **68b** was subsequently utilized to complete the total synthesis.



(7)

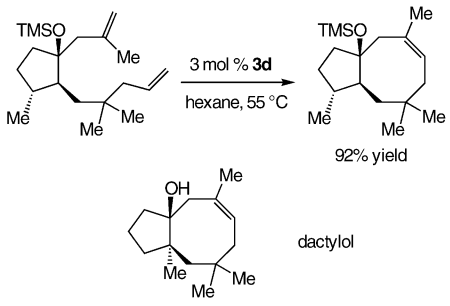
In the course of studies towards the total synthesis of balanol [Eq. (8); Boc = 1,1-dimethylethoxycarbonyl], RCM of diene **69** was effected at 70°C in the presence of Ru complex **58a** (Figure 11), to give a thermally induced non-metathesis product.[142] However, in the presence of 10 mol%



(8)

3d (refluxing CH_2Cl_2), the desired unsaturated seven-membered-ring amine **70** was isolated in 94% yield.

The formation of the trisubstituted olefin in Equation (9) was later disclosed to proceed in 92% yield in the presence of

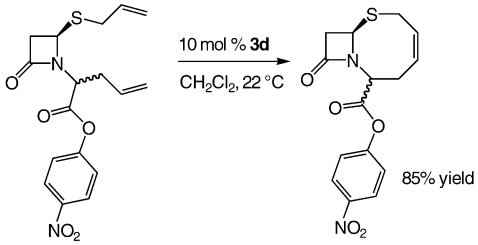


(9)

3 mol % **3d**.[143] The desired bicyclic adduct was subsequently transformed to the target sesquiterpene dactylol.

As depicted in Scheme 23, in the course of synthetic and structure determination of liverwort diterpenes (such as **73**), RCM of **71** was effected by Mo complex **3d** (Figure 2), leading to functionalized cycloheptene **72**. Since the same process was effected with 10 mol % **58a** (Figure 11), it is likely that such high loadings of **3d** are not necessary.[144] As also illustrated in Scheme 23, initial attempts to promote the RCM of the parent ketone was unsuccessful with catalysts **3d** and **58a**; Mo complex **3d** (Figure 2, $G = CMe_2Ph$) is usually incompatible with carbonyl groups[145] and the reaction of **58a** is probably retarded by coordination of the ruthenium carbene unit with the oxygen atom of the neighboring carbonyl group. In support of the latter hypothesis, in the presence of Lewis acidic $Ti(OiPr)_4$ and 30 mol % **58a** some of the desired product was obtained.[146,147]

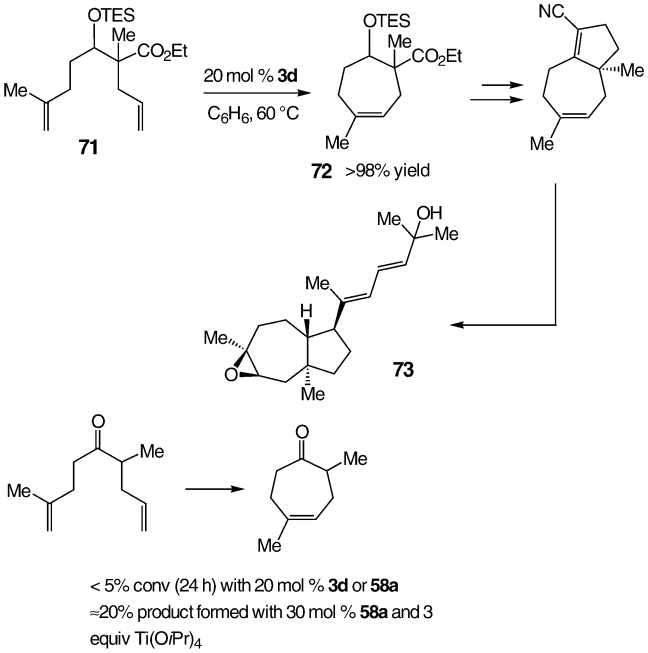
A variety of β-lactam carbocyclic esters have been synthesized by tandem Ireland–Claisen rearrangement/catalytic RCM methods. A notable advantage of molybdenum-based catalysts (versus Ru complexes) was demonstrated in the context of this investigation.[148] Thus, the sulfur-containing diene, shown in Equation (10), was readily converted into



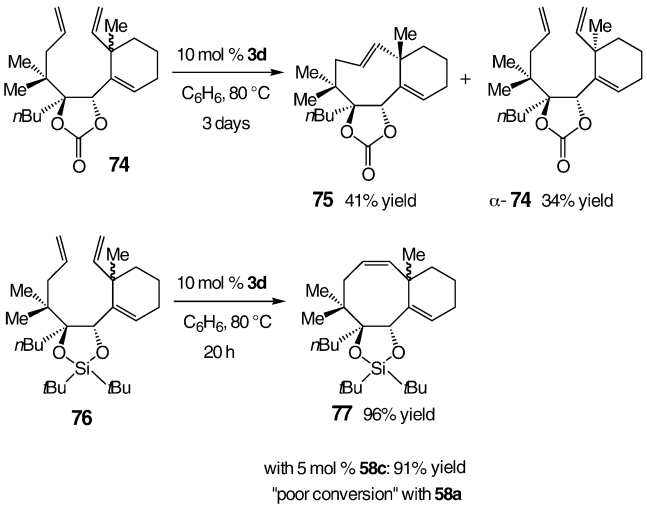
(10)

the desired cyclic product. In contrast, ruthenium-based catalyst **58a** (Figure 11) rapidly decomposes upon exposure to the same substrate.

More evidence regarding the influence of a substrate's stereochemical identity and its conformational properties on the facility of catalytic metathesis was provided in a study by Prunet and co-workers (Scheme 24).[149] Molybdenum-catalyzed RCM of a mixture of two diastereomers of **74** leads to the conversion of only one isomer to provide **75** and recovered α-**74**. Furthermore, it is the *trans* alkene that is generated preferentially; subsequent treatment of *trans*-**74** with **3d** (Figure 2, $G = CMe_2Ph$), and diallyl ether leads to the formation of the thermodynamically favored *cis* alkene through sequential ROM/RCM. The same RCM was effected by Ru complex **58a**, albeit at a slower rate (8 days vs. 3 days



Scheme 23. Molybdenum-catalyzed RCM affords medium-ring carbocycles that can be used in the total synthesis of terpenes such as **73**; TES = Et_3Si.

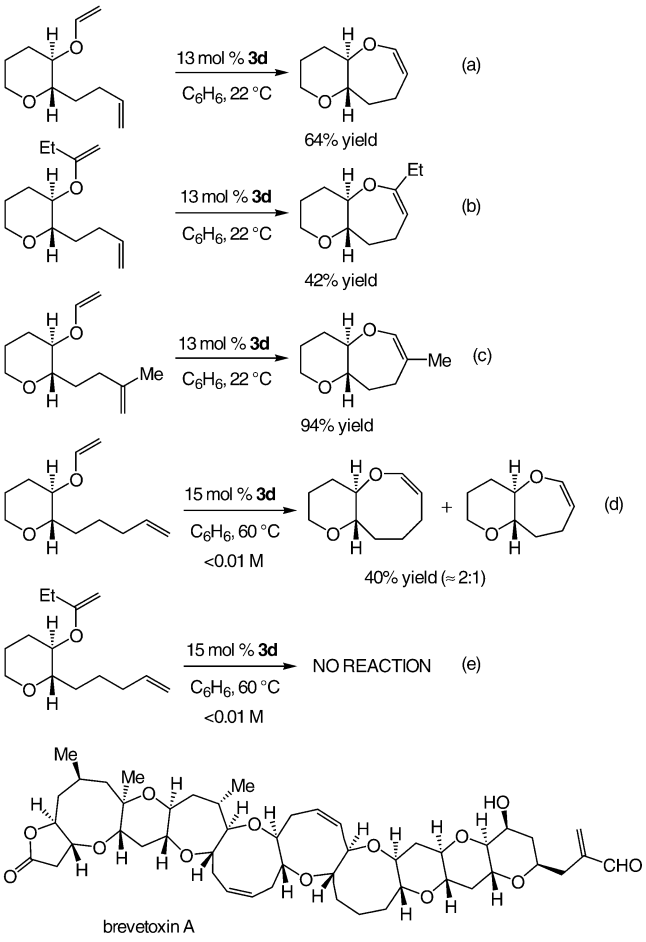


Scheme 24. Functionalities within a substrate and conformational preferences can be critical to the outcome of RCM reactions that afford medium rings.

© 2003 Wiley-VCH Verlag GmbH & Co. KGaA, Weinheim

for **3d**). In contrast, when the cyclic carbonate of **74** was exchanged with a cyclic silyl ether (**76**, Scheme 24), the molybdenum-catalyzed RCM proceeded to completion to afford **77** in 96% yield;[150] Ru complex **58a** delivers "poor conversions," while the more active **58c** (Figure 11) affords **77** in 91% yield.

The discovery of medicinally significant and structurally complex molecules, such as marine neurotoxin brevetoxin A (Scheme 25), has given rise to a number of investigations aimed at the development of efficient syntheses of these polycyclic ethers. Given the remarkable ability of catalytic



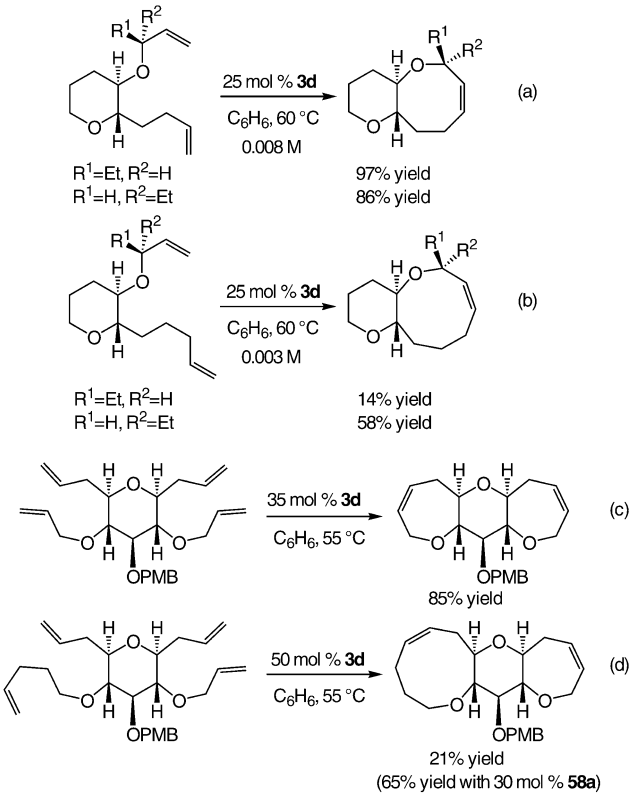
Scheme 25. Molybdenum-catalyzed RCM delivers medium-ring enol ethers that may be used as building blocks in the total synthesis of ichthyotoxins, such as brevetoxin A (**3d**, Figure 2, G = CMe_2Ph).

RCM in yielding medium rings that are otherwise difficult to access, it is not surprising that a number of key studies in this area are based on olefin metathesis.

Some of the more revealing disclosures in this connection are by Clark and Kettle.[151–153] As the results summarized in Scheme 25 indicate, seven- and some eight-membered cyclic enol ethers are accessible through molybdenum-catalyzed RCM. As reactions in Equations (a)–(c) of Scheme 25 illustrate, seven-membered ring enol ethers that bear di- and trisubstituted olefins were synthesized at ambient temperature with 13 mol% **3d**. The efficiency of RCM does vary depending on the substitution pattern of the substrate alkene and enol ether moieties. As illustrated in Equations (d) and (e) of Scheme 25, reactions that lead to eight-membered rings were less efficient; not only were higher dilution conditions required, significant amounts of a seven-membered-ring enol ether were generated as well [Eq. (d) in Scheme 25]. The latter complication presumably involves initial olefin isomerization to the disubstituted internal alkene,[154] followed by RCM.

RCM reactions involving enol ethers cannot typically be promoted by ruthenium-based catalysts. Recent strategies to access such structures through ruthenium-catalyzed RCM of allylic ethers followed by olefin isomerization, although effective in certain settings, may prove to be synthetically limited, particularly in light of mechanistic uncertainties regarding the nature of the isomerization catalyst. Moreover, the latter strategy imposes limitations regarding the presence of other olefin units that might also undergo adventitious isomerization or metathesis reactions.[155]

Related molybdenum-catalyzed RCM of allylic ethers have been outlined by Clark et al. as well (Scheme 26).[156,157] In these transformations, in contrast to the processes involving enol ethers (Scheme 25), eight-membered systems can be prepared efficiently [Eq. (a), Scheme 26]. The difference in the outcome between RCM of the two substrates in Equa-

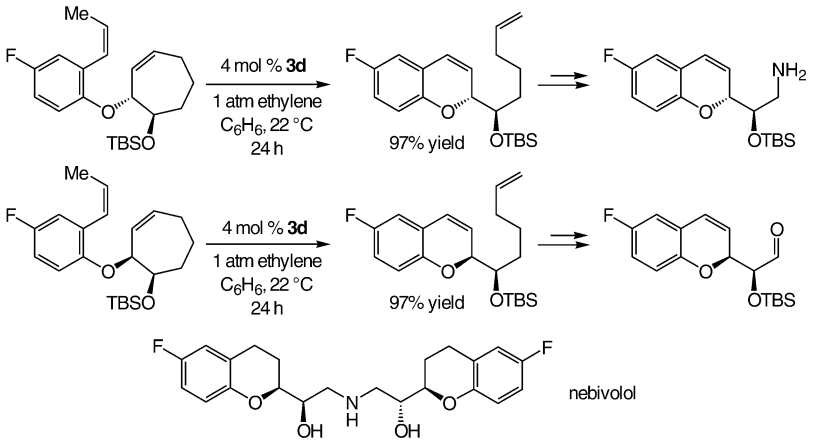


Scheme 26. Molybdenum-catalyzed RCM affords eight- and nine-membered-ring allylic ethers; reaction facility depends on the relative stereochemistry of substrate structures (**3d**, Figure 2, G = CMe_2Ph).

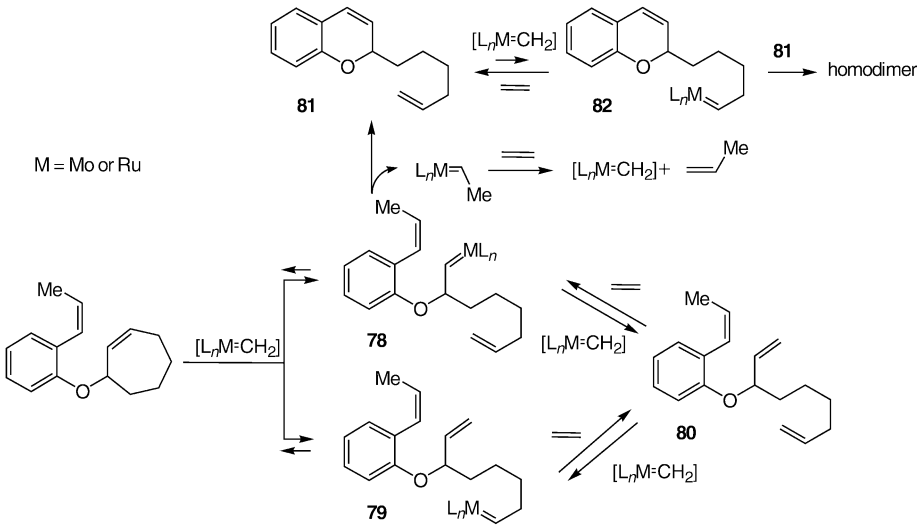
tion (b) of Scheme 26 provides another illustration of the significance of a substrate's stereochemical identity on reaction efficiency. Also noteworthy is the formation of the nine-membered ring [Eq. (d) of Scheme 26]; this product can be accessed more efficiently in the presence of Ru complex **58a**.

4.2.3. *Synthesis of Five- and Six-Membered Rings by Molybdenum-Catalyzed Metathesis*

Catalytic olefin metathesis has made a significant impact on methods for synthesis of five- and six-membered rings. As the examples below illustrate, the availability of Mo complex **3d** (Figure 2 G = CMe_2Ph) has led to the development of effective strategies that have allowed for unorthodox retrosynthetic analyses, which give rise to substantially more concise synthesis routes.In 1997, a catalytic conversion of various carbocyclic styrenyl ethers into the corresponding 2-substituted chromenes, building blocks found in a wide range of medicinally important agents, was reported (Scheme 27).[127f] These ring-opening/ring-closing metathesis (ROM/RCM) transformations proceed effectively with substrates bearing a terminal styrene with both **3d** and Ru catalyst **58a** (Figure 11). However, with disubstituted styrenes, such as those shown in Scheme 27, only **3d** is sufficiently reactive. It should be noted that disubstituted styrenes are required for effective zirconium-catalyzed kinetic resolutions[158,159] that deliver the requisite disubstituted styrenes in the optically pure form (terminal styrenes cannot be resolved by the same method). The tandem zirconium-catalyzed kinetic resolution/molybdenum-catalyzed ROM/RCM was subsequently employed in the enantioselective total synthesis of antihypertensive agent nebivolol.[160]



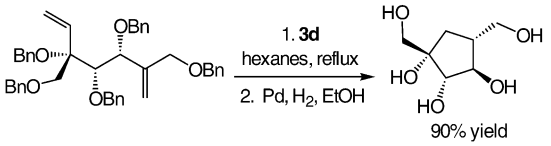
Scheme 27. Molybdenum-catalyzed ROM/CM used to prepare functionalized chromenes en route to the total synthesis of antihypertensive agent nebivolol (**3d**, Figure 2, G = CMe_2Ph).



Scheme 28. Reaction pathway for the molybdenum-catalyzed (or ruthenium-catalyzed) reactions of disubstituted styrenyl ethers in the presence of ethylene atmosphere.

In the course of the total synthesis of nebivolol, it was established that unless the ROM/CM reactions are carried out under an atmosphere of ethylene (with both Mo- and Ru-based catalysts), products would be obtained in low yield along with formation of significant amounts of homodimeric compounds. Mechanistic studies[127g] indicated that the presence of ethylene is critical to efficiency of metathesis reactions for three reasons: 1) Ethylene rapidly converts the initial metal complexes into the more reactive methylidene complexes ([$L_nMo{=}CH_2$] in Scheme 28), thus enhancing initiation rates. 2) Rapid reaction of the metal alkylidene derived from the terminal alkene of **82** (Scheme 28) with ethylene leads to minimization of dimerization products. 3) Since reactions have been shown to be initiated at the cycloalkene site (versus the styrene olefin) and such ROM processes are not likely to be regioselective (**78** and **79** in Scheme 28 are formed nonselectively), ethylene converts the "wrong" metal alkylidene **79** into an olefin **78** which can then be converted into the desired chromene. This simple but effective strategy has been subsequently adopted successfully in a number of other related studies.[161]

Molybdenum complex **3d** has been employed in the synthesis of highly functionalized smaller ring structures. One example is illustrated in Equation (11) (**3d**, catalyst loading



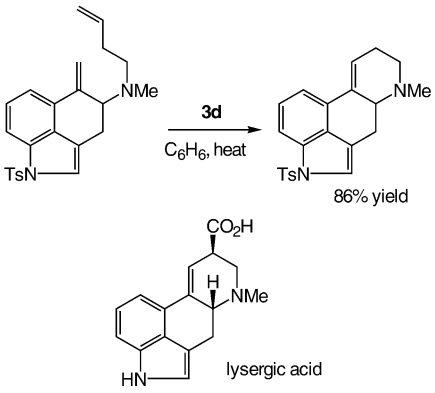
(11)

and reaction temperature not specified), where catalytic RCM occurs efficiently between a 1,1-disubstituted olefin and

 © 2003 Wiley-VCH Verlag GmbH & Co. KGaA, Weinheim

a sterically hindered terminal alkene. The resulting product was subsequently transformed to a fructofuranose derivative.[162]

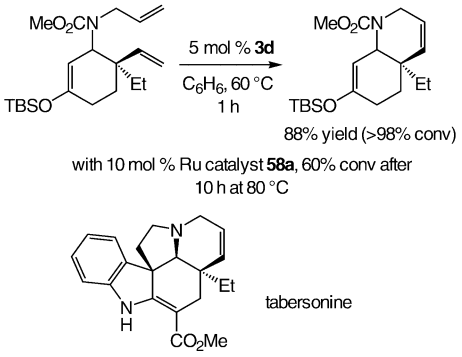
Molybdenum-based catalysts are tolerant of amine functional groups, as demonstrated in the transformation in Equation (12) (**3d** Figure 2, $G = CMe_2Ph$; catalyst loading



(12)

and reaction temperature not specified). These studies were disclosed by Martin and co-workers in the context of the total synthesis of the *ergot* alkaloid lysergic acid.[163] In contrast, use of the ruthenium-based catalyst **58a** provided "small quantities" of the desired product. (For studies regarding enantioselective olefin metathesis involving tertiary amines, see Section 5).

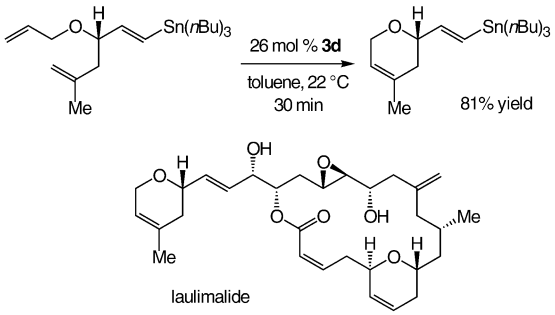
A trademark of molybdenum-based metathesis catalysts is their often unparalleled reactivity. One telling recent example is the RCM reaction reported by Rawal in the course of the total synthesis of tabersonine. As illustrated in Equation (13) (**3d** Figure 2, $G = CMe_2Ph$) an allylic amide



(13)

and a sterically encumbered terminal olefin adjacent to a quaternary carbon center undergo efficient ring-closure to deliver the desired compound.[164,165]

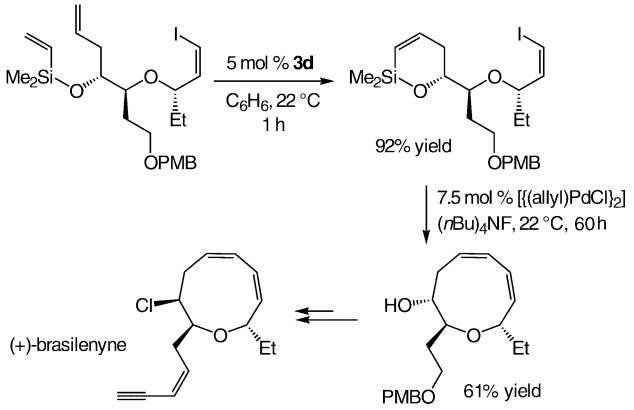
Although highly reactive, Mo complex **3d** can be used to promote site-selective transformations. A revealing example is shown in Equation 14, involving a regioselective process that excludes participation by the more hindered vinyl stannane.[166] The unreacted C–Sn bond was subsequently converted into the derived Grignard reagent and used by



(14)

Nelson et al. in a key diastereoselective C–C bond-forming reaction en route to the total synthesis of laulimalide.

Another site-selective molybdenum-catalyzed RCM has recently been reported by Denmark and Yang in the context of the total synthesis of antifeedant (+)-brasilenyne (Scheme 29).[167] The vinyl iodide moiety, used in the follow-

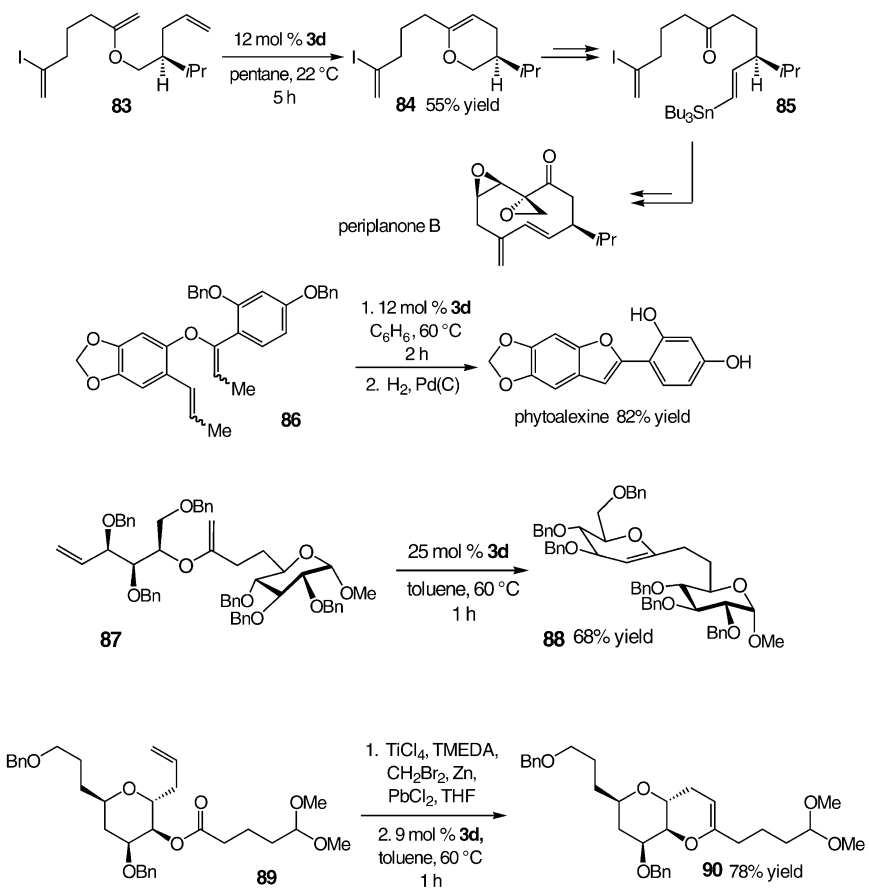


Scheme 29. Cyclic vinylsilane obtained from molybdenum-catalyzed RCM is used in a subsequent palladium-catalyzed intramolecular cross-coupling to afford a nine-membered-ring structure en route to the total synthesis of brasilenyne.

up palladium-catalyzed cross-coupling, does not participate in the catalytic RCM process.

A variety of small-ring enol ethers have been accessed through molybdenum-catalyzed RCM. Four examples are depicted in Scheme 30. The first instance involves the regioselective ring-closure of **83** to afford vinyl iodide **84** in the course of synthetic studies towards periplanone B.[168] Similar to the case in Scheme 29 or analogous to the vinyl stannane in Equation (14), the vinyl iodide moiety was later utilized to effect an intramolecular Stille coupling (via **85**). The molybdenum-catalyzed RCM involving **86** proceeds smoothly with two highly congested olefin partners to deliver phytoalexine.[169]

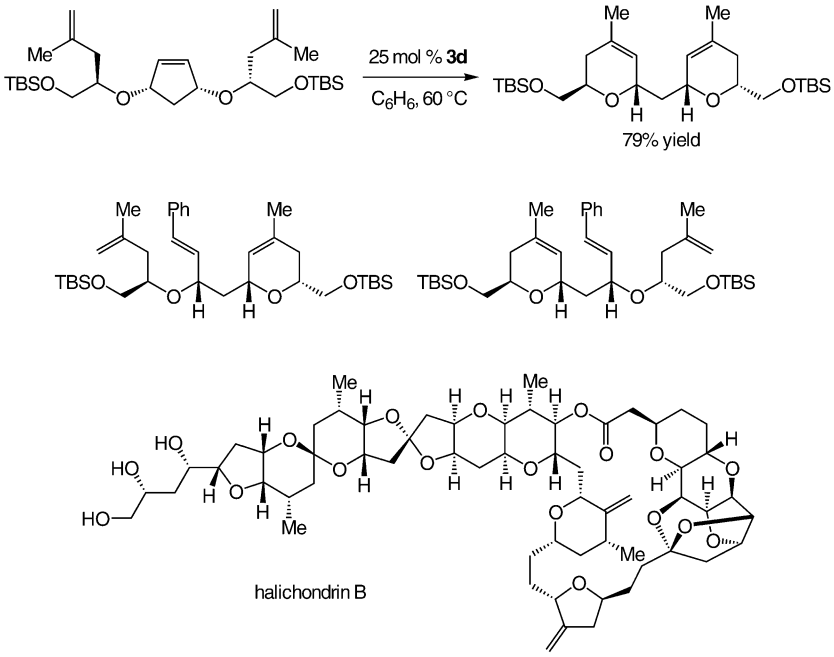
Another RCM transformation that underlines the unique reactivity and functional group compatibility of **3d** (Figure 2, $G = CMe_2Ph$) is the conversion of **87** into β-C-disaccharide **88**.[170–172] Note that formation of compounds such as **88** are inefficient with Ru catalyst **58a**. With the more reactive complexes **58b** or **58c** (see Figure 11) similar loadings are



Scheme 30. Molybdenum-catalyzed RCM can be used in target-oriented synthesis to access a variety of complex cyclic enol ethers; TMEDA = *N*,*N*,*N*′,*N*′-tetramethyl 1,2-ethanediamine. Compound **88** is also formed with 25 mol% **58b** (added in portions under Ar).

required but catalysts must be added in portions (under Ar) to drive the reaction to completion. The last example shown in Scheme 30 (**89**→**90**) has been reported by Rainier et al. who has utilized catalytic RCM of highly functionalized enol ethers to access intermediates to be used in the total synthesis of brevitoxins.[173–175]

The molybdenum-catalyzed transformation illustrated in Scheme 31 is an efficient sequential ROM/RCM/RCM reported by Burke et al. as part of studies aimed at the total synthesis of halichondrin B.[176] Attempts to effect this transformation with Ru complex **58a** resulted in the formation of monopyrans shown in Scheme 31. These undesired compounds are likely derived from a ROM/RCM process, where the initial transformation deposits the benzylidene of the catalyst structure within the product. Addition of ethylene to circumvent the above complication proved unsuccessful.



Scheme 31. Molybdenum-catalyzed (**3d** Figure 2, G = CMe_2Ph) ROM/RCM provides access to bis(dihydropyran) structures that may be used as intermediates in the total synthesis of halichondrin B. With 25 mol% of Ru complex **58a** as the catalyst (80 °C, C_6H_6) the two byproducts shown in the middle of the scheme are formed in 21% yield.

5. Enantiomerically Pure Chiral Molybdenum-Based Olefin-Metathesis Catalysts in Asymmetric Synthesis

With regard to the synthesis of optically pure materials, catalytic olefin metathesis has generally served a supporting role. In cases where RCM is required, as the examples discussed in Section 4 illustrate, an already optically pure diene is treated with an achiral metal catalyst so that a nonracemic product is isolated (e.g., Scheme 20, Scheme 21, Scheme 22). Alternatively, there are examples where optically enriched cyclic alkenes are employed in instances where ROM is needed (e.g., Scheme 27). Although such strategies have led to noteworthy accomplishments, there are several unique attributes of olefin metathesis that can only be realized with chiral optically pure catalysts.

One of the most useful characteristics of metathesis reactions is their ability to promote skeletal rearrangements, where simple achiral substrates are transformed into more complex chiral molecules. As will be seen below, in numerous instances, products that are rendered available by a chiral

 © 2003 Wiley-VCH Verlag GmbH & Co. KGaA, Weinheim

metathesis catalyst would only be accessible, and often less selectively, by a longer route if alternative synthetic methods were to be used.

5.1. The First Enantiomerically Pure Chiral Catalysts for Olefin Metathesis

As mentioned before (Section 3.2.2), the first enantiomerically pure chiral metathesis catalysts were molybdenum-based complexes **11 m**, **11 n**, and **12 g** (Figure 3 and Figure 4), which were synthesized to address tacticity control in ROMP processes.[16,21] The eventual application of such catalysts to enantioselective synthesis of small organic molecules was adumbrated in a statement that appeared in the 1993 publication that such chiral catalysts "could selectively …. ring close one enantiomer in a racemic mixture."[21]

The constitution of molybdenum-based catalysts, such as those shown in Figure 2, provides an attractive opportunity for development of chiral metathesis catalysts. In addition to their high activity, these complexes possess a modular structure involving imido and alkoxide moieties that do not dissociate from the metal center during the catalytic cycle. Structural alterations may therefore be implemented so that the desired effect on selectivity and reactivity is attained. As with the first chiral complexes mentioned above, alkoxide moieties offer an excellent opportunity for incorporation of chirality.

5.2. Molybdenum-Catalyzed Asymmetric Ring-Closing Metathesis (ARCM)

5.2.1. Catalytic Kinetic Resolution with a Chiral Hexafluoro Molybdenum Catalyst[177]

The preparation and utility of chiral complex **11p** (Figure 3) in kinetic resolution of various dienes was disclosed in 1996 by Grubbs and Fujimura.[178–180] As the case regarding the resolution of shown in Figure 12 indicates, levels of enantiodifferentiation proved to be low ($k_{rel} < 3$).

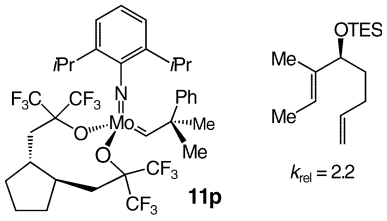


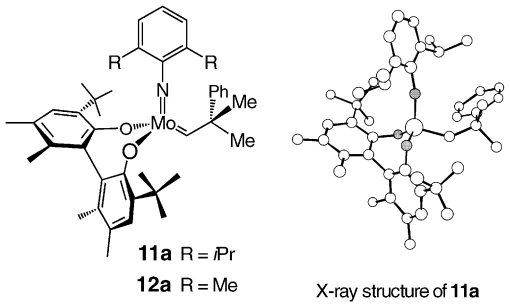
Figure 12. The first attempt at kinetic resolution through molybdenum-catalyzed ARCM.

5.2.2. The First Effective Chiral Metathesis Catalysts

During the past seven years, numerous chiral Mo catalysts and two chiral tungsten-based complexes (Figure 1, Figure 3, and Figure 4), have been developed for use in asymmetric RCM (ARCM).[181] As will be discussed below, the structural modularity of these chiral high-oxidation-state alkylidene complexes has proven critical to their potential utility in organic synthesis; preparation and screening of catalyst pools can thus be carried out,[182] so that optimal reactivity and selectivity levels are identified.

5.2.3. Chiral biphen Molybdenum Catalysts

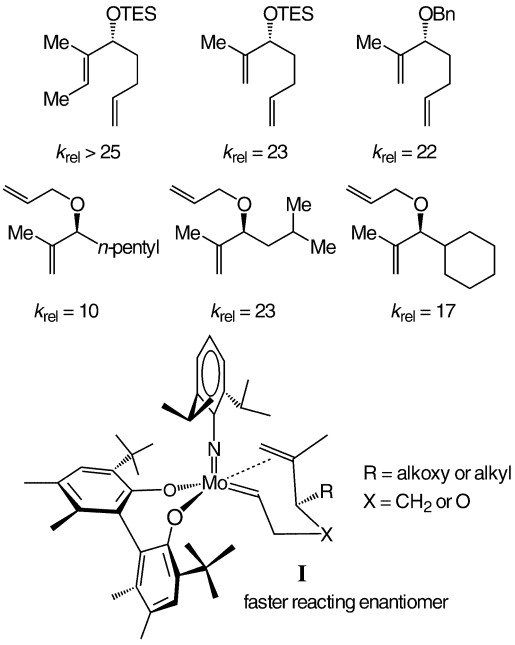
Enantiomerically pure chiral Mo complexes **11a** and **12a** were synthesized in 1997 and their ability to effect ARCM was probed.[14,183] It was established that these Mo catalysts



initiate olefin metathesis with excellent asymmetric induction owing to their rigidity and the sterically based differentiation imposed on the binding pocket of the chiral complex. Complexes **11a** and **12a** are orange solids and indefinitely stable when kept under an atmosphere of N_2.

5.2.4. Catalytic Kinetic Resolution by Molybdenum-Catalyzed ARCM

Catalytic kinetic resolution of various dienes through ARCM can be carried out efficiently at 22 °C in the presence of 5 mol % **11a**.[183] As the data in Scheme 32 illustrate, 1,6-



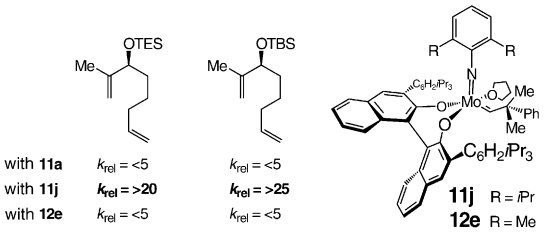
Scheme 32. Effective molybdenum-catalyzed kinetic resolution of 1,6-dienes through ARCM promoted by **11a**.

dienes[184] and allylic ethers[185] that afford five-membered-ring structures upon ring closure have been resolved with levels of enantioselectivity ($k_{rel} > 10$, see Scheme 32) that are superior to those observed with **11p** (see Figure 12).

The high levels of enantioselectivity attained with chiral Mo complex **11a** (vs. **11p**) are likely to be due to the intermediacy of the more reactive *anti* alkylidenes, such as **I** (Scheme 32; see Section 2.3.2 for reactivity of *syn* versus *anti* alkylidenes[104]). The stereochemistry of the metal–olefin complex arises from coordination of the Lewis basic olefin to the CNO face,[28] so that the olefinic π orbital can properly overlap with the molybdenum-centered LUMO (see Figure 5).[103] Moreover, this mode of olefin–metal association is consistent with the stereochemistry of coordination of various donor ligands with Mo complexes shown in Figures 6, 3, and 4 (see Section 2.3.3). The 1,1-disubstituted olefin thus interacts with the metal center while pointing away from the protruding diolate *t*Bu and the *i*Pr groups of the imido ligands.

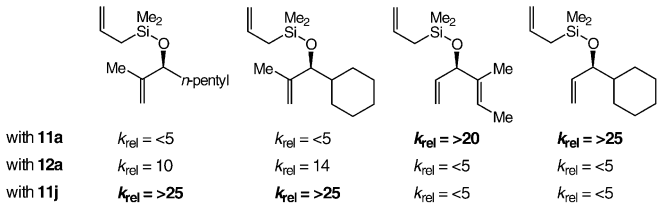
5.2.5. Modularity of Chiral Molybdenum Complexes and Optimization of Catalytic ARCM Reactions

In spite of the high enantioselectivity observed in the molybdenum-catalyzed ARCM of 1,6-dienes, when **11a** and **12a** are used in transformations involving 1,7-dienes, inferior asymmetric induction is obtained ($k_{rel} < 5$). Representative examples are shown in Scheme 33. To address this shortcoming, the modular character of the Mo complexes was exploited and a range of chiral complexes were synthesized and tested as catalysts. It was accordingly discovered (Scheme 33) that binol (2,2′-dihydroxy-1,1′-biphenyl) based complex **11j** promotes the RCM of 1,7-dienes with outstanding selectivity ($k_{rel} > 20$).[18] Binol-based catalyst **12e**, bearing the (dimethyl)phenylimido ligand, appears to be less efficient in promoting the resolution of this class of substrates.



Scheme 33. Molybdenum-catalyzed kinetic resolution of 1,7-dienes and the importance of structural modification of the chiral catalysts.

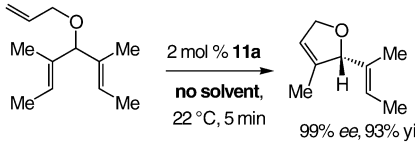
The above findings underline the significance of the availability of a diverse set of chiral catalysts. It should however be noted that, as the data in Scheme 34 illustrate, although binol-based complexes (e.g., **11j**) typically promote ARCM of 1,7-dienes with higher selectivity than the biphen-based catalysts (e.g., **11a**), such a trend does not always hold. Thus, each catalyst may not be optimal in every instance, but efficient resolution of a wide range of chiral oxygenated 1,6- and 1,7-dienes can be achieved once the appropriate catalyst, from a small set of two to four possibilities, is identified.



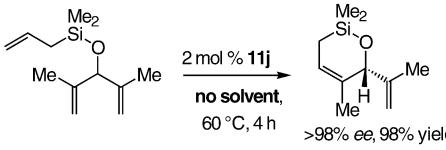
Scheme 34. Small structural changes within the substrate structure can alter the identity of the optimum chiral Mo catalyst.

5.2.6. Enantioselective Synthesis of Small Rings without use of Solvents: Molybdenum-Catalyzed Enantioselective Desymmetrization

The arena in which catalytic asymmetric olefin metathesis can have a significant impact on organic synthesis is the desymmetrization of achiral molecules. Formation of the unsaturated furan in Equation (15) is promoted with 5 mol% **11a** in 99% *ee* and 93% yield;[185] the reaction is complete within five minutes at 22 °C and can be carried out without solvent. As the example in Equation (16) illustrates, enantioselective synthesis of unsaturated six-membered-ring heterocycles is catalyzed by **11j** with exceptional efficiency and selectivity and, again, without need for solvents.[186] Moreover, although 5 mol% catalyst is typically used, 1–2 mol% loading often delivers equally efficient and selective transformations. It must be noted that the ARCM reaction in Equation (15) is less efficient with **11j** (< 5% conversion in 18 h). With **11a** as the catalyst, the transformation in Equation (16) proceeds only to 50% conversion in 24 h to afford the desired siloxane in only 65% *ee*. In the latter transformation, even in a 0.1 M solution, the major product is that formed through homometathesis of the terminal alkenes. The lack of homodimer generation when **11j** is used as the catalyst, particularly in the absence of solvent, bears testimony to the remarkable degree of catalyst–substrate specificity in these asymmetric transformations. Finally, it has been reported recently that chiral tungsten-based catalysts **1h** and **2h** (see Figure 1) promote the reactions shown in Equations (15) and (16) with yields and enantioselectivities similar to the analogous molybdenum-based catalysts.[9]



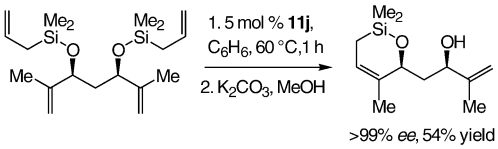
(15)



(16)

© 2003 Wiley-VCH Verlag GmbH & Co. KGaA, Weinheim

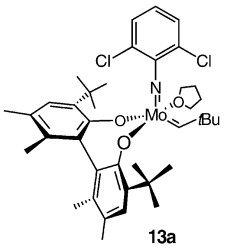
The catalytic desymmetrization depicted in Equation (17) involves ARCM of a *meso*-tetraene.[24] The unaffected siloxy

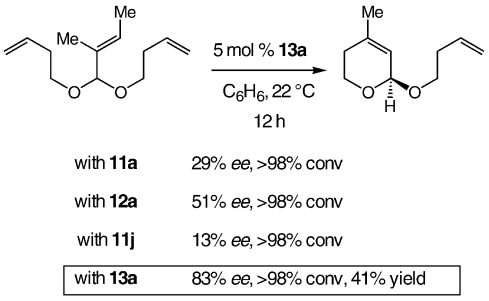


(17)

ether moiety can be subsequently removed to deliver the derived carbinol. In this enantioselective desymmetrization, alkylidenes of both enantiotopic terminal alkenes are likely to be generated. Since alkylidene formation is reversible, the major product arises from the rapid RCM of the "matched" segment of the tetraene. If any of the "mismatched" RCM takes place, a subsequent and more facile matched RCM leads to the formation of the *meso*-bicyclized product. Such a byproduct is absent from the unpurified mixture, which highlights the exceptionally high degree of stereodifferentiation induced by the chiral catalyst. As before, in contrast to **11j**, Mo complex **11a** is ineffective in facilitating the ARCM depicted in Equation (17).

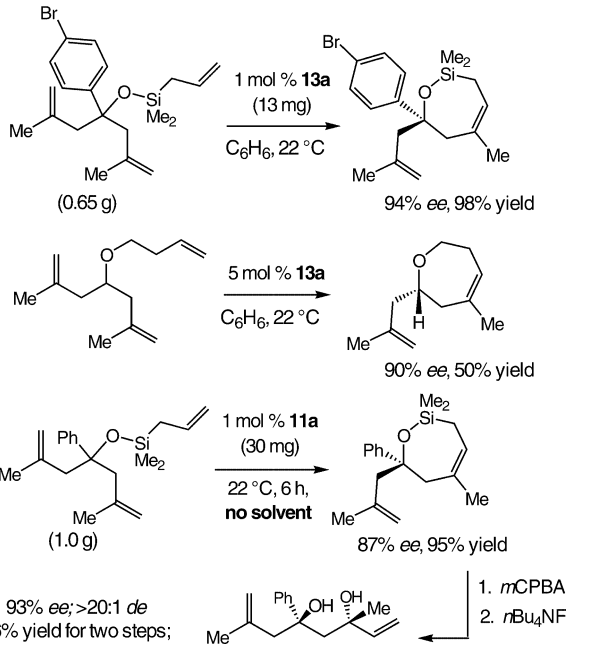
Incorporation of electron-withdrawing groups within either the imido or diolate moieties of a chiral Mo complex can result in enhanced Lewis acidity of the metal center and higher catalyst activity. As the examples in Scheme 35 outline,





Scheme 35. Chiral complex **13a** is the catalyst of choice for asymmetric synthesis of acetals.

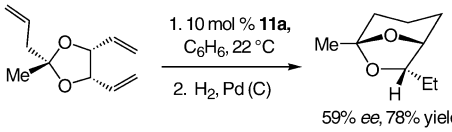
such structural modifications can have an effect on enantioselectivity as well. In the desymmetrization of the acetal substrate in Scheme 36, dichlorophenylimido complex **13a** provides higher asymmetric induction than the biphen- or binol-based catalysts that carry 2,6-dialkylphenylimido ligands (e.g., **11a** and **11j**). Note that cyclic unsaturated



Scheme 36. Molybdenum-catalyzed tandem ARCM can be used to synthesize enantioenriched seven-membered heterocycles in a practical and efficient manner; *m*CPBA = *m*-chloro peroxybenzoic acid.

acetals of this type retain their stereochemical integrity through various laboratory operations (such as chromatography on silica gel) and can be functionalized to deliver a range of chiral nonracemic functionalized heterocycles.

Molybdenum-catalyzed ARCM has been utilized by Burke et al. in a brief and enantioselective total synthesis of *endo*-brevicomin [Eq. (18)]; the key step is a catalytic



(18)

enantioselective desymmetrization of a triene.[187] It is possible that screening of additional molybdenum-based catalysts, unavailable at the time of this study, could lead to significantly higher asymmetric induction.

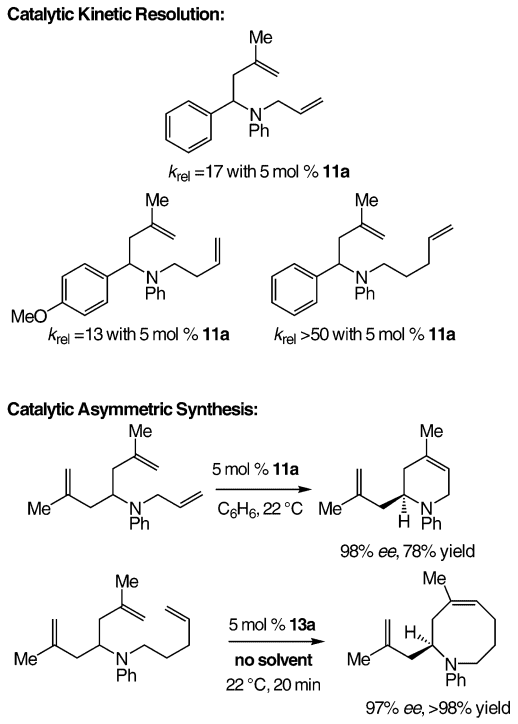
5.2.7. *Enantioselective Synthesis of Medium-Ring Ethers; Use of Solvent not Required*

As the examples in Scheme 36 (see also Scheme 37) indicate, molybdenum-catalyzed ARCM has been applied to the enantioselective synthesis of medium ring heterocycles.[188] These processes are effected efficiently in preparative scale, at low catalyst loading and without use of solvent. Moreover, as the last example in Scheme 36 illustrates, the optically enriched siloxanes obtained by molybdenum-catalyzed ARCM can be stereoselectively functionalized to afford compounds that are otherwise difficult to synthesize.

 © 2003 Wiley-VCH Verlag GmbH & Co. KGaA, Weinheim

5.2.8. Enantioselective Synthesis of Acyclic and Small- and Medium-Ring Amines; Use of Solvent not Required

The functional group tolerance of chiral molybdenum-based catalysts is underlined in ARCM reactions illustrated in Scheme 37. Acyclic and cyclic tertiary amines are synthesized with high enantiopurity through catalytic kinetic resolution or asymmetric synthesis.[189] The facility and selectivity with which medium-ring unsaturated amines are obtained is noteworthy. Catalytic enantioselective synthesis of the eight-membered-ring amine (Scheme 37) proceeds efficiently, with excellent enantioselectivity and in the absence of solvent.



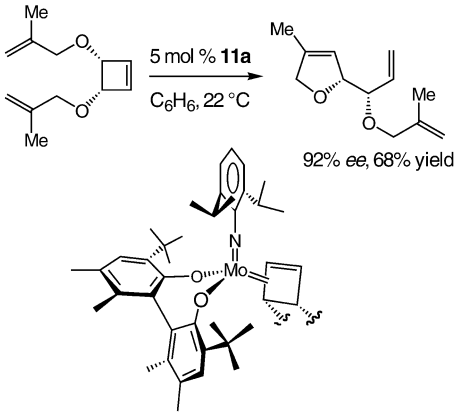
Scheme 37. Enantioselective synthesis of amines through molybdenum-catalyzed ARCM.

5.3. Molybdenum-Catalyzed Asymmetric Ring-Opening Metathesis (AROM)

Catalytic ROM transformations—although less explored than RCM processes—offer unique and powerful approaches to selective organic synthesis.[190] Moreover, chiral Mo alkylidene complexes that are products of AROM may be trapped either intramolecularly (by RCM) or intermolecularly (by CM) to generate an assortment of versatile optically enriched compounds.

5.3.1. Molybdenum-Catalyzed Tandem Ring-Opening/Ring-Closing Metathesis Reactions (AROM/RCM)

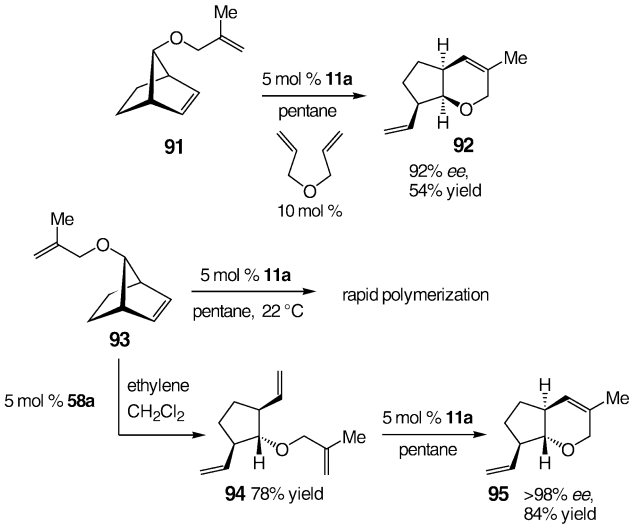
Transformations described in this section are the first reported examples of catalytic asymmetric ring-opening (AROM). In 2000, it was disclosed that *meso*-triene substrate in Equation (19) can be converted into a chiral heterocyclic triene in 92% *ee* and 68% yield in the presence of 5 mol% **11a**.[191] It has been proposed that, as illustrated, stereo-



(19)

selective approach of the more reactive cyclobutenyl alkene leads to the enantioselective formation of the observed dihydrofuran enantiomer.

Another early example of AROM, shown in Scheme 38, involves the net rearrangement of *meso*-bicycle **91** to **92** in 92% *ee*. The reaction is promoted by 5 mol% **11a** and



Scheme 38. Efficiency of catalytic AROM processes can depend on the stereochemical identity of the substrate.

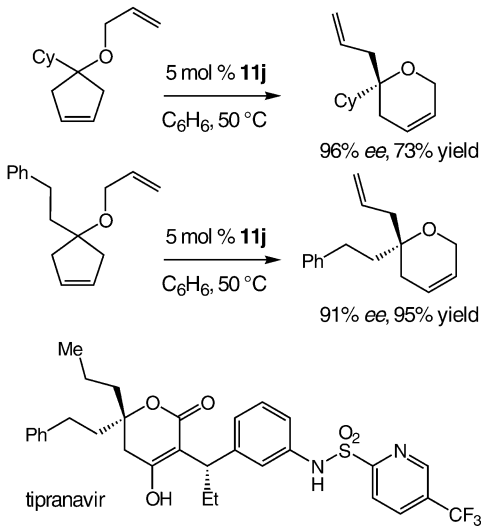
requires the addition of diallyl ether.[127g] As mentioned previously (see Scheme 28), initial reaction of diallyl ether with neophylidene **11a** most likely leads to the formation of the substantially more reactive chiral Mo=CH_2 complex, which can react with the sterically hindered norbornyl alkene to initiate the catalytic cycle.

In contrast to **91**, diastereomer **93** undergoes rapid polymerization in the presence of **11a** (Scheme 38), presumably because of its more exposed strained olefin. The less-reactive Ru catalyst **58a** (Figure 11) can, however, be used

 © 2003 Wiley-VCH Verlag GmbH & Co. KGaA, Weinheim

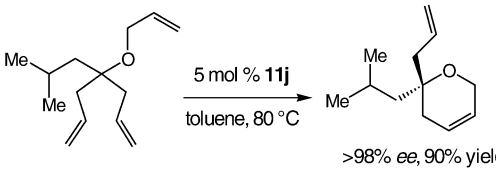
under an atmosphere of ethylene to effect a tandem ROM/CM to generate *meso*-**94**. The resulting triene may be subsequently induced to undergo molybdenum-catalyzed ARCM to afford optically pure **95**, the AROM/RCM product that would be directly obtained from **93**.

The molybdenum-catalyzed transformations shown in Scheme 39 might be viewed as examples of tandem AROM/RCM.[192] It is however possible that initiation occurs at the terminal olefin, followed by an ARCM involving the cyclic alkene. The enantioselective rearrangements shown in Scheme 39, catalyzed by binaphtholate-based catalyst **11j**, deliver unsaturated pyrans bearing a tertiary ether site with excellent enantioselectivity. Biphenolate Mo catalysts, such as **11a**, deliver significantly lower *ee* values. This class of heterocycles would not be accessible by an asymmetric synthesis of the precursor diene, followed by RCM promoted by an achiral catalyst. The enantioselective synthesis of the pyran portion of the anti-HIV agent tipranavir (Scheme 39) demonstrates the potential of the method in asymmetric synthesis of biomedically important agents.[193]



Scheme 39. Molybdenum-catalyzed enantioselective rearrangement of cyclopentenes to unsaturated pyrans. Cy = cyclohexyl.

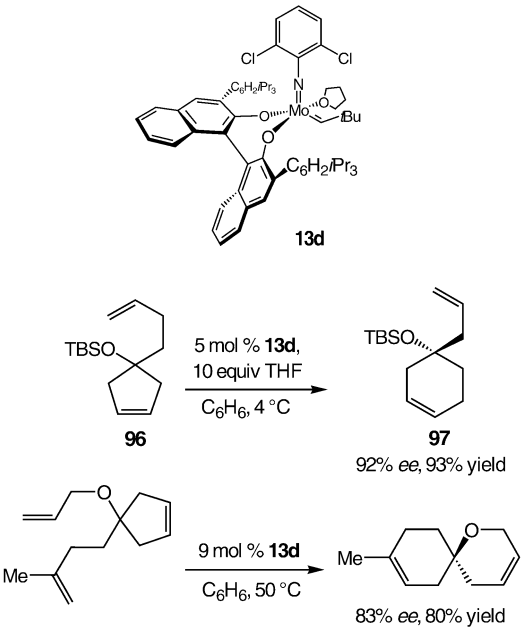
The nonracemic pyrans shown in Scheme 39 can be obtained by molybdenum-catalyzed ARCM of trienes as well. The example shown in Equation (20) is illustrative.



(20)

Elevated temperatures are required for high enantioselectivity; under conditions shown in Scheme 39, (50 °C) the triene substrates are converted into the desired pyrans in significantly lower *ee* values.

A related process to those discussed above is the asymmetric molybdenum-catalyzed synthesis of cyclohexenyl ethers (**96**→**97**, Scheme 40).[194] An unusual attribute of this class of reactions is that higher levels of enantioselectivity are obtained when substrate THF is added to the reaction mixture. As an example, **97** is formed in only 58% *ee* in the absence of THF (< 5% conversion when THF is used as solvent). As also shown in Scheme 40, enantioenriched spirocycles are accessed easily by a similar approach; in this case, additive effects are not observed.[195]



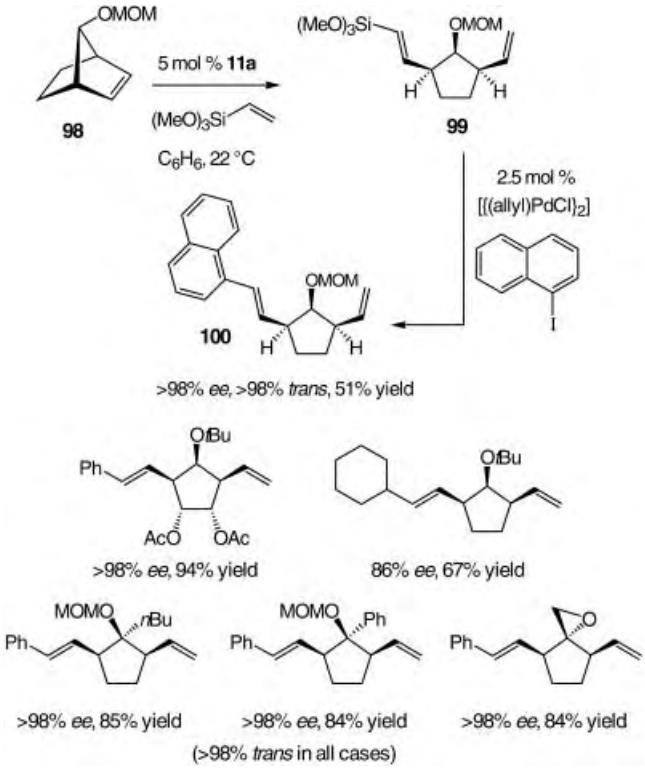
Scheme 40. Enantioselective synthesis of carbocyclic tertiary ethers and spirocycles through molybdenum-catalyzed asymmetric olefin metathesis.

5.3.2. Molybdenum-Catalyzed Tandem Asymmetric Ring-Opening/Cross Metathesis Reactions (AROM/CM)

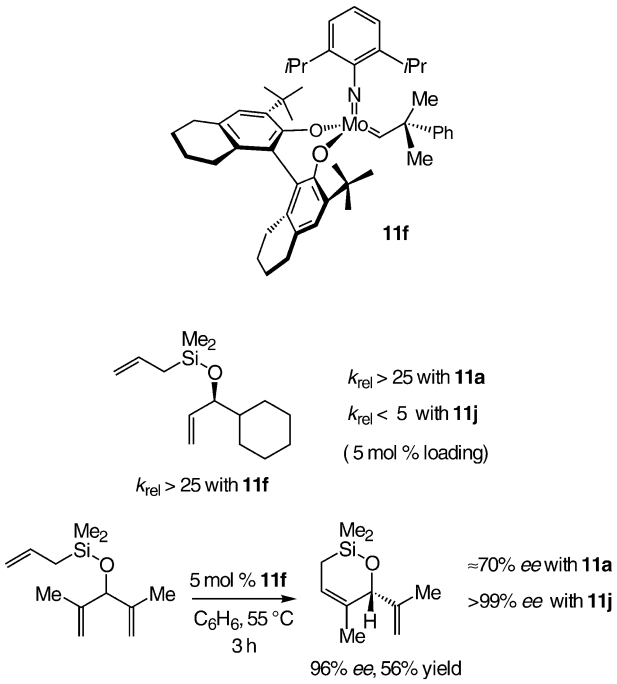
The chiral molybdenum alkylidene complex derived from AROM of a cyclic olefin may participate in an intermolecular cross metathesis. As depicted in Scheme 41, treatment of **98** with a solution of 5 mol% **11a** and two equivalents of vinylsiloxane leads to the formation of optically pure **99**.[196] Subsequent palladium-catalyzed cross-coupling delivers optically pure **100** in 51% yield (> 98% *trans*).[197]

As the representative products illustrated in Scheme 41 indicate, the molybdenum-catalyzed AROM/CM may be performed on functionalized norbornenes and aryl or aliphatic terminal alkenes. These are optically pure and easily functionalizable organic molecules that cannot be easily prepared by other methods. It should be noted that the relative orientation of the heteroatom substituent versus the reacting olefin has a significant influence on reaction efficiency (see Sections 5.6 and for a discussion of complementarity of Mo and Ru catalysts).

 © 2003 Wiley-VCH Verlag GmbH & Co. KGaA, Weinheim



Scheme 41. Molybdenum-catalyzed tandem AROM/CM proceeds with high enantioselectivity and olefin stereocontrol; MOM = methoxymethyl.



Scheme 42. Chiral complex **11 f** represents a hybrid between biphen- and binol-based catalysts and provides a unique selectivity profile.

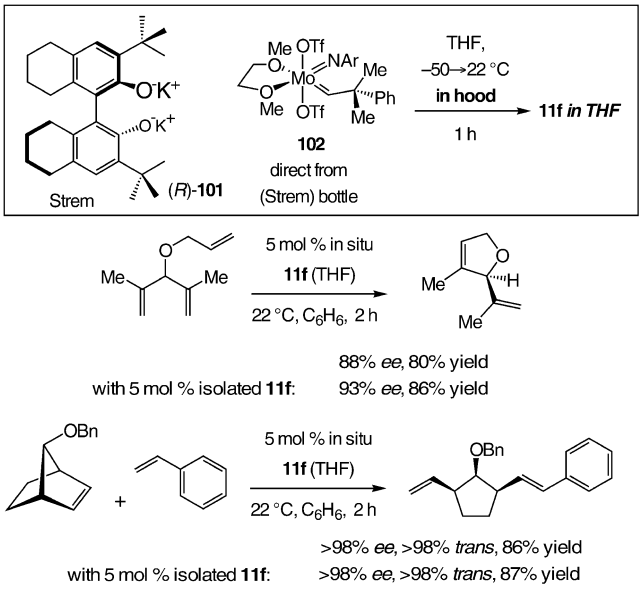
5.4. Towards more User-Friendly and Practical Chiral Molybdenum-Based Catalysts for Olefin Metathesis

The issue of practicality is a critical aspect of research regarding the development of practical molybdenum-based metathesis catalysts. Two related key advances have recently been reported. One is in connection to the in situ preparation of commercially available Mo catalysts from commercially available compounds, and the other is related to the development of a recyclable polymer-supported chiral Mo catalyst.

5.4.1. Chiral Molybdenum Catalysts Prepared In Situ: Catalyst Isolation not Required

From a practical point of view, binaphthol-based catalysts such as **11 j** have an advantage over the biphenol complexes represented by **11 a**. The synthesis of the optically pure diolate begins from the inexpensive and commercially available (*R*)- or (*S*)-binaphthol. Access to the optically pure biphenol ligand in **11 a** and its derivatives requires resolution of the racemic material by fractional crystallization of phosphorus(v) mentholates.[14] Enantiomerically pure **11 f**,[22] shown in Scheme 42, is a catalyst that bears a "biphenol-type" ligand but is synthesized from the readily available optically pure binaphthol. Complex **11 f** shares structural features with both the biphen- and binol-based catalysts and represents an intriguing possibility regarding the range of reactions for which it can serve as a suitable catalyst.[22] Two examples are depicted in Scheme 42. Note that in many, but not all, instances, **11 f** delivers compounds of high optical purity where either biphen- or binol-based catalysts are ineffective.

Not only is Mo complex **11 f** easier to prepare than biphenolate **11 a**, it is also simpler to use. As outlined in Scheme 43, a solution of **11 f**, obtained by the reaction of bis(potassium salt) **101** (commercially available from Strem) and Mo triflate **102** (commercially available from Strem), can be used directly to promote enantioselective metathesis.[22] Similar reactivity and selectivity is observed with in situ **11 f** as with isolated and purified **11 a** or **11 f**. Moreover, asymmetric



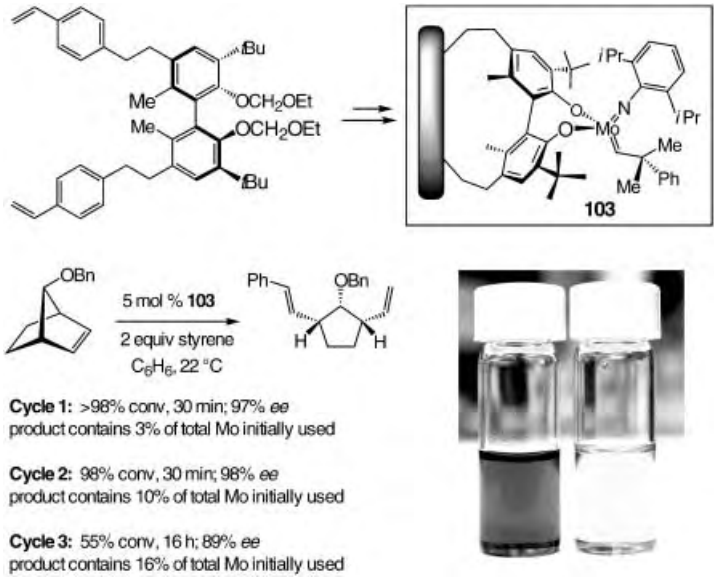
Scheme 43. In situ preparation and utility of chiral metathesis catalyst **11 f**.

 © 2003 Wiley-VCH Verlag GmbH & Co. KGaA, Weinheim

olefin metatheses proceed with equal efficiency and enantioselectivity with the same stock solutions of (*R*)-**101** and **102** after two weeks, which makes the use of glovebox, Schlenk equipment, or vacuum lines no longer mandatory. It has subsequently been demonstrated that the in situ catalyst preparation procedure can be readily applied to other chiral Mo complexes as well.[194]

5.4.2. The First Enantiomerically Pure Solid-Supported Catalyst for Olefin Metathesis

Synthesis and catalytic activity of the first supported chiral catalyst for olefin metathesis was disclosed in 2002.[198] As illustrated in Scheme 44, supported catalyst **103** efficiently promotes a range of ARCM and AROM processes. Reactions are slower than with the corresponding monomeric complex **11a**, but often similar enantioselectivity is observed. Although **103** must be kept under dry and oxygen-free conditions, it can be recycled. Moreover, the unpurified product solution, after simple filtration, contains significantly lower levels of metal impurity than detected when using the monomeric catalysts, where >90% of the Mo used is found in the unpurified product (ICP-MS analysis). The lower levels of activity exhibited by **103** might be due to inefficient diffusion of substrate molecules into the polymer. On the other hand, the supported catalyst is also expected to be less susceptible to bimolecular decomposition of methylidene intermediates (see Scheme 14).[114]



Scheme 44. The first recyclable and supported chiral catalyst for olefin metathesis delivers reaction products that contain significantly less metal impurity. The two dram vials show unpurified product from a reaction catalyzed by **11a** (left) and **103** (right).

5.5. The First Enantiomerically Pure Alkyl Imido Molybdenum Catalyst

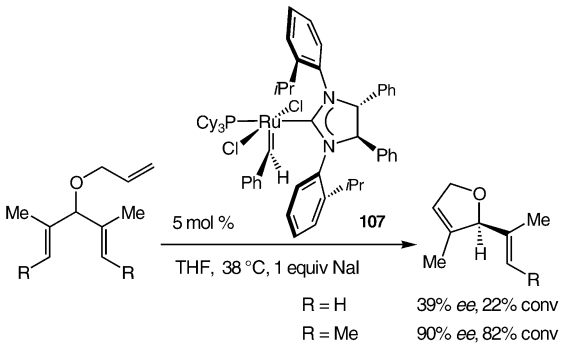
In spite of the advances discussed above regarding chiral molybdenum-based complexes, a large number of problems in selectivity and reactivity cannot be addressed by the available chiral catalysts. Accordingly, recent efforts have been directed towards the development of structurally distinct chiral catalysts. Such initiatives have resulted in the synthesis, characterization, and study of the catalytic activity of the first enantiomerically pure molybdenum-based alkyl imido complex (Scheme 45).[25] Enantiomerically pure alkylidene complex **17** exists almost exclusively in its *syn* form (≈0.5% *anti* alkylidene at 22 °C) and can be easily prepared on multigram scale. Importantly, the adamantylimido complex exhibits unique reactivity and selectivity profiles not available through the use of aryl imido systems. One representative example, where **17** promotes an AROM/CM substantially more efficiently than any molybdenum-based catalysts, is presented in Scheme 45.

5.6. Comparison with Chiral Ruthenium Catalysts

Two different types of chiral ruthenium-based catalysts have been disclosed. Although these Ru systems complement enantiomerically pure Mo catalysts, the latter class of catalysts have so far proven to be superior in scope.

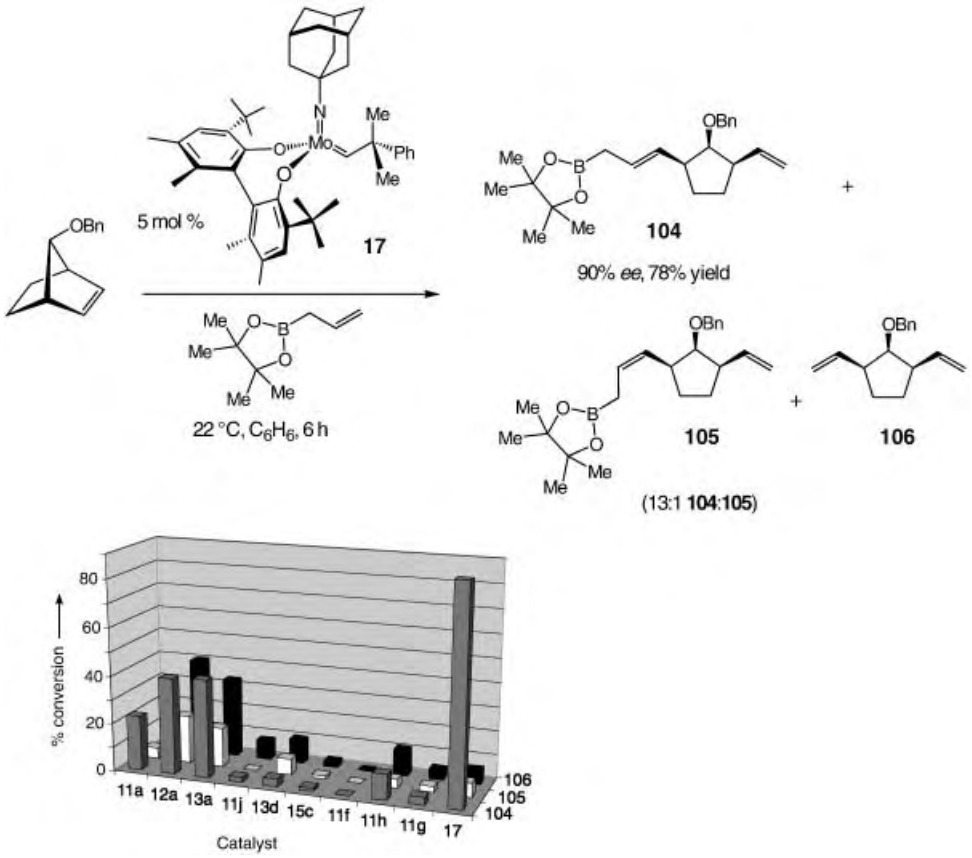
In 2001, Grubbs and co-workers reported the first chiral Ru catalyst for olefin metathesis **107** [Eq. (21)].[199] The reactions illustrated in Equation (21) include the highest *ee* value reported in that study (13–90% *ee*). Asymmetric induction is lower than that obtained with molybdenum-based catalysts [see Eq. (15) for comparison] and is dependent on the degree of olefin substitution. As is the case with nearly all catalytic enantioselective reactions,[182] the identity of the optimal catalyst depends on the substrate being used. A number of chiral Ru catalysts were therefore synthesized and screened before **107** was identified as the most suitable.

Early in 2002, the synthesis, characterization and catalytic activity of chiral ruthenium-based carbene **108** was disclosed (Scheme 46).[200] Catalyst **108** is stereogenic at the metal center, can be prepared in >98% diastereoselectivity and

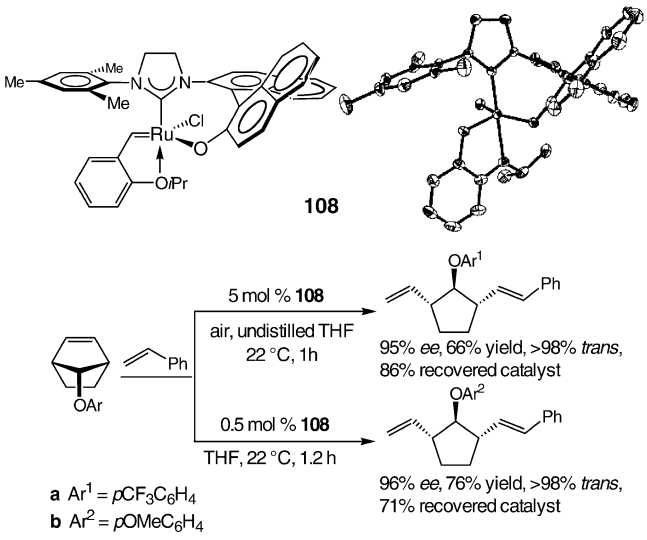


(21)

 © 2003 Wiley-VCH Verlag GmbH & Co. KGaA, Weinheim



Scheme 45. The adamantylimido chiral catalyst **17** can offer levels of reactivity and selectivity that are not available by the corresponding aryl imido catalysts.



Scheme 46. Air stable chiral ruthenium-based catalyst for olefin metathesis can be used to promote AROM/CM reactions.

purified by chromatography on silica gel with undistilled solvents. This styrene ether Ru complex, which is based on complexes represented by **58d,e** (Figure 11) which were first reported in 1997,[127f–i] catalyzes RCM and ROM reactions. Moreover, **108** is air stable and recyclable. As the representative cases in Scheme 46 illustrate, this chiral Ru catalyst is highly effective (0.5–10 mol % loading) in promoting AROM/CM. These enantioselective transformations can be effected in air and with unpurified solvents air (see Scheme 46). It should be noted that the substrates illustrated in Scheme 46 undergo rapid polymerization in the presence of chiral molybdenum-based catalysts.

6. A Few Notes Regarding Molybdenum- Versus Ruthenium-Based Metathesis Catalysts

6.1. Are Molybdenum Catalysts "Functional-Group Tolerant?"

Statements that simplify a complicated field of research often gain rapid popularity. One claim that is frequently stated by users of olefin metathesis is that "unlike ruthenium-based catalysts, high-oxidation-state complexes are not functional-group tolerant." Such a statement tends to marginalize important data and can lead to unwise decisions in experimental design.

In contrast to the ruthenium-based catalysts, such as those shown in Figure 11, Mo complexes are relatively sensitive to moisture and air, and should be handled under inert atmosphere and used in anhydrous solvents. The early-transition-metal complexes are incompatible with carboxylic acids, ketones, aldehydes, most alcohols and primary amines.

 © 2003 Wiley-VCH Verlag GmbH & Co. KGaA, Weinheim

However, Mo catalysts are effective in the presence of phosphanes[201] and thioethers [see Eq. (10)],[202,203] functional groups that readily decompose Ru complexes. Molybdenum catalysts also have been shown to be active in the presence of nitriles[112] and a sterically protected free alcohol.[204] There are numerous reported examples, including several discussed above (see Scheme 37), where Mo catalysts not only show high catalytic activity in the presence of amines, they deliver unparalleled enantioselectivity.[205] Molybdenum catalyst **3d** (Figure 2, $G = CMe_2Ph$) is active in the presence of metal–carbonyl compounds.[206] Thus the response to a statement that a particular class of catalysts are "not functional-group tolerant" should be: exactly which functional groups are being discussed?

6.2. Do Molybdenum catalysts still Offer the Highest Levels of Reactivity?

Although recent generations of ruthenium-based catalysts, such as **58b,c** and **58e** (Figure 11), provide significantly improved activity compared to their precursors **58a** and **58d**, Mo catalysts can still offer unique levels of reactivity. As an example, the ROM/CM in Scheme 43, which occurs within minutes with 5 mol% **11a**, does not proceed, even at 70 °C, in the presence of catalytic or stoichiometric amounts of "second generation" Ru catalysts **58b** or **58e**.[207]

One important lesson that the field of catalysis has taught us is that simple generalizations, in spite of their lure, are best avoided. Blanket statements regarding reactivity or selectivity often carry as many (if not more) cases that are exceptions as agreements, particularly since higher activity of a catalyst is often claimed based on data collected regarding a narrow field of substrates (at times a single starting material is used).

As discussed above, molybdenum- and ruthenium-based catalysts offer complementary degrees of efficiency and stereoselectivity. Superior activity of a Mo catalyst in one case does not mean that such is true in all cases.

7. Conclusions and Outlook

The journey from a new high-oxidation-state Ta alkylidene to asymmetric Mo catalysts for the metathesis of olefins required twenty-five years. Investigations of high-oxidation-state Ta alkylidene chemistry led to the finding that bulky alkoxide ligands slow the rearrangement of tantalacyclobutane rings to olefins and promote olefin metathesis. Studies concerned with alkylidyne complexes of W and Mo confirmed that bulky alkoxide ligands are most desirable for efficient metathesis of alkynes and revealed that trigonal-bipyramidal metallacyclobutadienes are intermediates in alkyne metathesis reactions. Neopentylidene or neophylidene complexes of W or Mo can be isolated when sterically demanding aryl imido and alkoxide ligands are present and serve as effective olefin-metathesis catalysts, especially when the alkoxide is the relatively electron-withdrawing hexafluoro-*tert*-butoxide group. Moreover, several new alkylidenes derived from olefins and metallacyclobutane intermediates have been observed and isolated. Studies regarding ROMP have resulted in the realization that *syn* and *anti* isomers can be present in imido alkylidene complexes, and that their reactivities and rates of interconversion may vary dramatically with the nature of the alkoxide and imido ligands. Finally, the success at controlling ROMP structure with chiral biphenolates culminated with the synthesis of enantiomerically pure imido alkylidene catalysts which can be employed in asymmetric metathesis reactions.

The exciting results of the investigations described in the preceding sections clearly indicate that the modular construct of molybdenum- and tungsten-based imido alkylidene complexes can be exploited to generate a range of highly efficient and selective catalysts for olefin metathesis. A variety of ring-closing, ring-opening, and cross metathesis reactions can be promoted by high-oxidation-state complexes to obtain products that are typically unavailable by other methods or can only be accessed by significantly longer routes.

Molybdenum-based catalysts, although more sensitive to moisture and air than the related ruthenium-based systems, often provide complementary reactivity and selectivity patterns and offer the most effective chiral catalysts that can be used in asymmetric synthesis. Achiral catalyst **3d** and chiral complex **11a** (both antipodes and racemic) are commercially available from Strem, Inc. Molybdenum-based complexes can be handled on a large scale and in the significant number of cases, reactions proceed readily to completion in the presence of 1 mol% loading. In many cases, optically pure materials can be synthesized within minutes without the need for solvents.

The advent of protocols for in situ preparation of chiral Mo catalysts and the emergence of supported and new generations of easily recyclable complexes augur well for future developments towards truly practical molybdenum- and tungsten-based metathesis catalysts. The above attributes and ongoing research efforts will hopefully lead to the arrival of even more efficient catalysts that can be used in organic synthesis.

The authors are grateful to the NIH and NSF for generously funding their programs in catalytic olefin metathesis, and to all the graduate and postdoctoral students who have been involved in the work described here. Recent support has been provided by NIH grant GM-59426 to R. R. S. and A. H. H. and NSF grants CHE-9988766 to R. R. S. and CHE-0213009 to A. H. H.

Received: February 4, 2003 [A576]

[1] A. Fürstner, *Angew. Chem.* **2000**, *112*, 3140–3172; *Angew. Chem. Int. Ed.* **2000**, *39*, 3012–3043.
[2] M. Schuster, S. Blechert, *Angew. Chem.* **1997**, *109*, 2124–2145; *Angew. Chem. Int. Ed. Engl.* **1997**, *36*, 2036–2056.
[3] R. H. Grubbs, S. Chang, *Tetrahedron* **1998**, *54*, 4413–4450.
[4] A. Fürstner, in *Topics in Organometallic Chemistry; Alkene Metathesis in Organic Synthesis, Vol. 1* (Ed.: A. Fürstner), Springer, Berlin, **1998**, pp. 37–72.
[5] A. J. Phillips, A. D. Abell, *Aldrichimica Acta* **1999**, *32*, 75–89.
[6] D. L. Wright, *Curr. Org. Chem.* **1999**, *3*, 211–240.

 © 2003 Wiley-VCH Verlag GmbH & Co. KGaA, Weinheim

[7] R. R. Schrock, R. DePue, J. Feldman, C. J. Schaverien, J. C. Dewan, A. H. Liu, *J. Am. Chem. Soc.* **1988**, *110*, 1423 – 1435.
[8] R. R. Schrock, R. T. DePue, J. Feldman, K. B. Yap, D. C. Yang, W. M. Davis, L. Y. Park, M. DiMare, M. Schofield, J. Anhaus, E. Walborsky, E. Evitt, C. Krüger, P. Betz, *Organometallics* **1990**, *9*, 2262 – 2275.
[9] W. C. P. Tsang, K. C. Hultzsch, J. B. Alexander, P. J. Bonitatebus, Jr., R. R. Schrock, A. H. Hoveyda, *J. Am. Chem. Soc.* **2003**, *125*, 2591 – 2596.
[10] J. S. Murdzek, R. R. Schrock, *Organometallics* **1987**, *6*, 1373 – 1374.
[11] J. H. Oskam, H. H. Fox, K. B. Yap, D. H. McConville, R. O'Dell, B. J. Lichtenstein, R. R. Schrock, *J. Organomet. Chem.* **1993**, *459*, 185 – 198.
[12] R. R. Schrock, S. Luo, J. J. C. Lee, N. C. Zanetti, W. M. Davis, *J. Am. Chem. Soc.* **1996**, *118*, 3883 – 3895.
[13] R. R. Schrock, J. S. Murdzek, G. C. Bazan, J. Robbins, M. DiMare, M. O'Regan, *J. Am. Chem. Soc.* **1990**, *112*, 3875 – 3886.
[14] J. B. Alexander, R. R. Schrock, W. M. Davis, K. C. Hultzsch, A. H. Hoveyda, J. H. Houser, *Organometallics* **2000**, *19*, 3700 – 3715.
[15] K. C. Hultzsch, P. J. Bonitatebus, Jr., J. Jernelius, R. R. Schrock, A. H. Hoveyda, *Organometallics* **2001**, *20*, 4705 – 4712.
[16] K. M. Totland, T. J. Boyd, G. G. Laovie, W. M. Davis, R. R. Schrock, *Macromolecules* **1996**, *29*, 6114 – 6125.
[17] R. R. Schrock, J. Y. Jamieson, S. J. Dolman, S. A. Miller, P. J. Bonitatebus, Jr., A. H. Hoveyda, *Organometallics* **2002**, *21*, 409 – 417.
[18] S. S. Zhu, D. R. Cefalo, D. S. La, J. Y. Jamieson, W. M. Davis, A. H. Hoveyda, R. R. Schrock, *J. Am. Chem. Soc.* **1999**, *121*, 8251 – 8259.
[19] W. C. P. Tsang, R. R. Schrock, A. H. Hoveyda, *Organometallics* **2001**, *20*, 5658 – 5669.
[20] O. Fujimura, F. J. De la Mata, R. H. Grubbs, *Organometallics* **1996**, *15*, 1865 – 1871.
[21] D. H. McConville, J. R. Wolf, R. R. Schrock, *J. Am. Chem. Soc.* **1993**, *115*, 4413 – 4414.
[22] S. L. Aeilts, D. R. Cefalo, P. J. Bonitatebus, J. H. Houser, A. H. Hoveyda, R. R. Schrock, *Angew. Chem.* **2001**, *113*, 1500 – 1504; *Angew. Chem. Int. Ed.* **2001**, *40*, 1452 – 1456.
[23] J. Y. Jamieson, R. R. Schrock, W. M. Davis, P. J. Bonitatebus, S. S. Zhu, A. H. Hoveyda, *Organometallics* **2000**, *19*, 925 – 930.
[24] G. S. Weatherhead, J. H. Houser, J. G. Ford, J. Y. Jamieson, R. R. Schrock, A. H. Hoveyda, *Tetrahedron Lett.* **2000**, *41*, 9553 – 9559.
[25] W. C. P. Tsang, J. A. Jernelius, A. G. Cortez, G. S. Weatherhead, R. R. Schrock, A. H. Hoveyda, *J. Am. Chem. Soc.* **2003**, *125*, 2652 – 2666.
[26] R. R. Schrock, in *Reactions of Coordinated Ligands* (Ed.: P. R. Braterman), Plenum, New York, **1986**, pp. 221 – 283.
[27] R. R. Schrock, *Pure Appl. Chem.* **1994**, *66*, 1447 – 1454.
[28] J. Feldman, R. R. Schrock, *Prog. Inorg. Chem.* **1991**, *39*, 1 – 74.
[29] R. R. Schrock, *Polyhedron* **1995**, *14*, 3177 – 3195.
[30] R. R. Schrock, *J. Chem. Soc. Dalton Trans.* **2001**, 2541 – 2550.
[31] R. R. Schrock, *Chem. Rev.* **2001**, *101*, 145 – 180.
[32] R. R. Schrock, in *Topics in Organometallic Chemistry. Alkene Metathesis in Organic Synthesis, Vol. 1* (Ed.: A. Fürstner), Springer, Berlin, **1998**, pp. 1 – 36.
[33] R. R. Schrock, *Tetrahedron* **1999**, *55*, 8141 – 8153.
[34] R. R. Schrock, in *Ring-Opening Polymerization* (Ed.: D. J. Brunelle), Hanser, Munich, **1993**, pp. 129 – 156.
[35] R. R. Schrock, in *Metathesis Polymerization of Olefins and Polymerization of Alkynes* (Ed.: Y. Imamoglu), Kluwer, Dordrecht, **1998**, pp. 1 – 27.
[36] R. R. Schrock, in *Metathesis Polymerization of Olefins and Polymerization of Alkynes* (Ed.: Y. Imamoglu), Kluwer, Dordrecht, **1998**, pp. 357 – 380.
[37] K. J. Ivin, J. C. Mol, *Olefin Metathesis and Metathesis Polymerization*, Academic Press, San Diego, **1997**.
[38] K. J. Ivin, *Olefin Metathesis*, Academic, New York, **1983**.
[39] V. Dragutan, A. T. Balaban, M. Dimonie, *Olefin Metathesis and Ring-Opening Polymerization of Cyclo-Olefins*, 2nd ed., Wiley, New York, **1985**.
[40] S. R. Wilson, D. E. Schalk, *J. Org. Chem.* **1976**, *41*, 3928 – 3929.
[41] D. Villemin, *Tetrahedron Lett.* **1980**, *21*, 175 – 178.
[42] J. Tsuji, S. Hashiguchi, *Tetrahedron Lett.* **1980**, *21*, 2955 – 2958.
[43] E. O. Fischer, A. Maasböl, *Angew. Chem.* **1964**, *76*, 645.
[44] a) E. O. Fischer, *Pure Appl. Chem.* **1970**, *42*, 407 – 423; b) E. O. Fischer, *Pure Appl. Chem.* **1972**, *44*, 353 – 372; c) E. O. Fischer, *Adv. Organomet. Chem.* **1976**, *14*, 1 – 32.
[45] D. J. Cardin, B. Cetinkaya, M. F. Lappert, *Chem. Rev.* **1972**, *72*, 545 – 574.
[46] F. A. Cotton, C. M. Lukehart, *Prog. Inorg. Chem.* **1972**, *16*, 487 – 613.
[47] D. J. Cardin, B. Cetinkaya, M. J. Doyle, M. F. Lappert, *Chem. Soc. Rev.* **1973**, *2*, 99 – 144.
[48] a) C. P. Casey, T. J. Burkhardt, *J. Am. Chem. Soc.* **1973**, *95*, 5833 – 5834; b) C. P. Casey, T. J. Burkhardt, *J. Am. Chem. Soc.* **1974**, *96*, 7808 – 7809; c) C. P. Casey, H. E. Tuinstra, M. C. Saemen, *J. Am. Chem. Soc.* **1976**, *98*, 608 – 609; d) C. P. Casey, T. J. Burkhardt, C. A. Bunnell, J. C. Calabrese, *J. Am. Chem. Soc.* **1977**, *99*, 2127 – 2134.
[49] J. L. Hérisson, Y. Chauvin, *Makromol. Chem.* **1971**, *141*, 161 – 176.
[50] B. A. Dolgoplosk, K. L. Makovetsty, T. G. Golenko, Y. V. Korshak, E. I. Timyakova, *Eur. Polym. J.* **1974**, *10*, 901 – 904.
[51] R. H. Grubbs, D. D. Carr, C. Hoppin, P. L. Burk, *J. Am. Chem. Soc.* **1976**, *98*, 3478 – 3483.
[52] R. H. Grubbs, *Prog. Inorg. Chem.* **1978**, *24*, 1 – 50.
[53] T. J. Katz, J. McGinnis, *J. Am. Chem. Soc.* **1975**, *97*, 1592 – 1594.
[54] a) T. J. Katz, S. J. Lee, N. Acton, *Tetrahedron Lett.* **1976**, *17*, 4247 – 4250; b) T. J. Katz, R. Rothchild, *J. Am. Chem. Soc.* **1976**, *98*, 2519 – 2526; c) T. J. Katz, N. Acton, *Tetrahedron Lett.* **1976**, *17*, 4251 – 4254; d) T. J. Katz, J. McGinnis, C. Altus, *J. Am. Chem. Soc.* **1976**, *98*, 606 – 608; e) T. J. Katz, J. McGinnis, *J. Am. Chem. Soc.* **1977**, *99*, 1903 – 1912; f) T. J. Katz, W. H. Hersh, *Tetrahedron Lett.* **1977**, *18*, 585 – 588; g) J. McGinnis, T. J. Katz, S. Hurwitz, *J. Am. Chem. Soc.* **1976**, *98*, 605 – 606.
[55] T. J. Katz, *Adv. Organomet. Chem.* **1977**, *16*, 283 – 317.
[56] R. H. Grubbs, in *Comprehensive Organometallic Chemistry, Vol. 8* (Eds.: G. Wilkinson, F. G. A. Stone, E. W. Abel), Pergamon, New York, **1982**, pp. 499 – 551.
[57] D. S. Breslow, *Prog. Polym. Sci.* **1993**, *18*, 1141 – 1195.
[58] N. Calderon, J. P. Lawrence, E. A. Ofstead, *Adv. Organomet. Chem.* **1979**, *17*, 449 – 492.
[59] This reference is often quoted as a 1970 paper, a consequence of a mistake in the running header in the volume 141, **1971** issue.
[60] C. P. Casey, S. W. Polichnowski, A. J. Shusterman, C. R. Jones, *J. Am. Chem. Soc.* **1979**, *101*, 7282.
[61] R. R. Schrock, P. Meakin, *J. Am. Chem. Soc.* **1974**, *96*, 5288 – 5290.
[62] R. R. Schrock, *J. Organomet. Chem.* **1976**, *122*, 209 – 225.
[63] R. R. Schrock, *J. Am. Chem. Soc.* **1974**, *96*, 6796 – 6797.
[64] R. R. Schrock, *J. Am. Chem. Soc.* **1976**, *98*, 5399 – 5400.
[65] H. Schmidbaur, *Adv. Organomet. Chem.* **1976**, *14*, 205 – 243.
[66] G. A. Rupprecht, L. W. Messerle, J. D. Fellmann, R. R. Schrock, *J. Am. Chem. Soc.* **1980**, *102*, 6236 – 6244.
[67] C. D. Wood, S. J. McLain, R. R. Schrock, *J. Am. Chem. Soc.* **1979**, *101*, 3210 – 3222.
[68] S. J. McLain, C. D. Wood, R. R. Schrock, *J. Am. Chem. Soc.* **1979**, *101*, 4558 – 4570.
[69] S. M. Rocklage, J. D. Fellmann, G. A. Rupprecht, L. W. Messerle, R. R. Schrock, *J. Am. Chem. Soc.* **1981**, *103*, 1440 – 1447.

 © 2003 Wiley-VCH Verlag GmbH & Co. KGaA, Weinheim

[70] R. R. Schrock, S. M. Rocklage, J. H. Wengrovius, G. Rupprecht, J. Fellmann, *J. Mol. Catal.* **1980**, *8*, 73 – 83.

[71] Tebbe et al. reported in 1979 that Ti complexes that contain a bridging methylene ligand would react with olefins to undergo methylene exchange, leading to a degenerate metathesis reaction. See: F. N. Tebbe, G. W. Parshall, D. W. Ovenall, *J. Am. Chem. Soc.* **1979**, *101*, 5074 – 5075.

[72] K. C. Wallace, J. C. Dewan, R. R. Schrock, *Organometallics* **1986**, *5*, 2162 – 2164.

[73] K. C. Wallace, R. R. Schrock, *Macromolecules* **1987**, *20*, 448 – 450.

[74] K. C. Wallace, A. H. Liu, J. C. Dewan, R. R. Schrock, *J. Am. Chem. Soc.* **1988**, *110*, 4964 – 4977.

[75] Although rare, tantalum alkylidene complexes that contain 18 electrons and do not contain ligands that can dissociate from the metal are stable when β protons are present. An example is $[(\eta^5\text{-}C_5H_5)_2MeTa{=}CHMe]$; see P. R. Sharp, R. R. Schrock, *J. Organomet. Chem.* **1979**, *171*, 43 – 51.

[76] R. R. Schrock, *Acc. Chem. Res.* **1986**, *19*, 342 – 348.

[77] J. H. Wengrovius, R. R. Schrock, M. R. Churchill, J. R. Missert, W. J. Youngs, *J. Am. Chem. Soc.* **1980**, *102*, 4515 – 4516.

[78] M. R. Churchill, A. L. Rheingold, W. J. Youngs, R. R. Schrock, *J. Organomet. Chem.* **1981**, *204*, C17 – C20.

[79] W. A. Nugent, J. M. Mayer, *Metal-Ligand Multiple Bonds*, Wiley, New York, **1988**.

[80] J. H. Wengrovius, R. R. Schrock, *Organometallics* **1982**, *1*, 148 – 155.

[81] R. R. Schrock, *J. Am. Chem. Soc.* **1975**, *97*, 6577 – 6578.

[82] R. R. Schrock, P. R. Sharp, *J. Am. Chem. Soc.* **1978**, *100*, 2389 – 2399.

[83] J. R. M. Kress, M. J. M. Russell, M. G. Wesolek, J. A. Osborn, *J. Chem. Soc. Chem. Commun.* **1980**, 431 – 432.

[84] J. Kress, M. Wesolek, J.-P. Le Ny, J. A. Osborn, *J. Chem. Soc. Chem. Commun.* **1981**, 1039 – 1040.

[85] J. Kress, M. Wesolek, J. A. Osborn, *J. Chem. Soc. Chem. Commun.* **1982**, 514 – 516.

[86] J. Kress, A. Aguero, J. A. Osborn, *J. Mol. Catal.* **1986**, *36*, 1 – 12.

[87] M. T. Youinou, J. Kress, J. Fischer, A. Aguero, J. A. Osborn, *J. Am. Chem. Soc.* **1988**, *110*, 1488 – 1493.

[88] F. Lefebvre, M. Leconte, S. Pagano, A. Mutch, J.-M. Basset, *Polyhedron* **1995**, *14*, 3209 – 3226.

[89] J. L. Couturier, C. Paillet, M. Leconte, J. M. Basset, K. Weiss, *Angew. Chem.* **1992**, *104*, 622 – 624; *.Angew. Chem. Int. Ed. Engl.* **1992**, *31*, 628 – 631.

[90] A. Mortreux, J. C. Delgrange, M. Blanchard, B. Labochinsky, *.J. Mol. Catal.* **1977**, *2*, 73 – 82.

[91] A. Mortreux, M. Blanchard, *J. Chem. Soc. Chem. Commun.* **1974**, 786 – 787.

[92] See H. Fischer, P. Hofmann, F. R. Kreissl, R. R. Schrock, U. Schubert, K. Weiss, *Carbyne Complexes*, VCH, New York, **1988**.

[93] E. O. Fischer, G. Kreis, C. G. Kreiter, J. Müller, G. Huttner, H. Lorenz, *Angew. Chem.* **1973**, *85*, 618 – 620; *Angew. Chem. Int. Ed. Engl.* **1973**, *12*, 564 – 565.

[94] D. N. Clark, R. R. Schrock, *J. Am. Chem. Soc.* **1978**, *100*, 6774 – 6776.

[95] J. S. Murdzek, R. R. Schrock, in *Carbyne Complexes*, VCH, New York, **1988**, pp. 148 – 203.

[96] J. H. Wengrovius, J. Sancho, R. R. Schrock, *J. Am. Chem. Soc.* **1981**, *103*, 3932 – 3934.

[97] M. R. Churchill, J. W. Ziller, J. H. Freudenberger, R. R. Schrock, *Organometallics* **1984**, *3*, 1554 – 1562.

[98] J. H. Freudenberger, R. R. Schrock, M. R. Churchill, A. L. Rheingold, J. W. Ziller, *Organometallics* **1984**, *3*, 1563 – 1573.

[99] S. F. Pedersen, R. R. Schrock, M. R. Churchill, H. J. Wasserman, *J. Am. Chem. Soc.* **1982**, *104*, 6808 – 6809.

[100] a) A. Fürstner, G. Seidel, *Angew. Chem.* **1998**, *110*, 1758 – 1760; *Angew. Chem. Int. Ed.* **1998**, *37*, 1734 – 1736; b) A. Fürstner, C. Mathes, C. W. Lehmann, *J. Am. Chem. Soc.* **1999**, *121*, 9453 – 9454; c) U. H. F. Bunz, L. Kloppenburg, *Angew. Chem.* **1999**, *111*, 503 – 505; *Angew. Chem. Int. Ed.* **1999**, *38*, 478 – 481; d) A. Fürstner, O. Guth, A. Rumbo, G. Seidel, *J. Am. Chem. Soc.* **1999**, *121*, 11108 – 11113; e) A. Fürstner, K. Grela, *Angew. Chem.* **2000**, *112*, 1292 – 1294; *Angew. Chem. Int. Ed.* **2000**, *39*, 1234 – 1236; f) A. Fürstner, G. Seidel, *J. Organomet. Chem.* **2000**, *606*, 75 – 78; g) N. G. Pschirer, W. Fu, R. D. Adams, U. H. F. Bunz, *Chem. Commun.* **2000**, 87 – 88; h) Y. C. Tsai, P. L. Diaconescu, C. C. Cummins, *Organometallics* **2000**, *19*, 5260 – 5262; i) G. Brizius, N. G. Pschirer, W. Steffen, K. Stitzer, H.-C. zur Loye, U. H. F. Bunz, *J. Am. Chem. Soc.* **2000**, *122*, 12435 – 12440; j) W. Zhang, S. Kraft, J. S. Moore *Chem. Commun.* **2003**, 832 – 833; k) B. Aguilera, L. B. Wolf, P. Nieczypor, F. Rutjes, H. S. Overkleeft, J. C. M. van Hest, H. E. Schoemaker, B. Wang, J. C. Mol, A. Fürstner, M. Overhand, G. A. van der Marel, J. H. van Boom, *J. Org. Chem.* **2001**, *66*, 3584 – 3589; l) K. Eder, E. Reichel, H. Schottenberger, C. G. Huber, M. R. Buchmeiser, *Macromolecules* **2001**, *34*, 4334 – 4341; m) A. Fürstner, A. Rumbo, *J. Org. Chem.* **2000**, *65*, 2608 – 2611; n) A. Fürstner, T. Dierkes, *Org. Lett.* **2000**, *2*, 2463 – 2465; o) A. Fürstner, K. Grela, C. Mathes, C. W. Lehmann, *J. Am. Chem. Soc.* **2000**, *122*, 11799 – 11805; p) A. Fürstner, C. Mathes, K. Grela, *Chem. Commun.* **2001**, 1057 – 1059; q) A. Fürstner, C. Mathes, C. W. Lehmann, *Chem. Eur. J.* **2001**, *7*, 5299 – 5317; r) A. Fürstner, A. S. Castanet, K. Radkowski, C. W. Lehmann, *J. Org. Chem.* **2002**, *67*, 1521 – 1528; s) K. Grela, J. Ignatowska, *Org. Lett.* **2002**, *4*, 3747 – 3749; t) T. Lindel, *Nachr. Chemie* **2000**, *48*, 1242 – 1244; u) O. S. Miljanic, K. P. C. Vollhardt, G. D. Whitener, *Synlett* **2003**, 29 – 34.

[101] S. M. Rocklage, R. R. Schrock, M. R. Churchill, H. J. Wasserman, *Organometallics* **1982**, *1*, 1332 – 1338.

[102] R. R. Schrock; unpublished results. See also: R. R. Schrock, J. Y. Jamieson, J. P. Araujo, P. J. Bonitatebus, Jr., A. Sinha, P. H. J. Lopez, *J. Organomet. Chem*, in press.

[103] a) D. S. Marynick, C. M. Kirkpatrick, *J. Am. Chem. Soc.* **1985**, *107*, 1993 – 1994; b) M. Sodupe, J. M. Lluch, A. Oliva, J. Bertran, *Organometallics* **1989**, *8*, 1837 – 1841; c) T. Upton, A. K. Rappe, *J. Am. Chem. Soc.* **1985**, *107*, 1206 – 1218; d) J. Ushio, H. Nakatsuji, T. Yonezawa, *J. Am. Chem. Soc.* **1984**, *106*, 5892 – 5901; e) M. Sodupe, J. M. Lluch, A. Oliva, J. Bertran, J. *Nouv. J. Chim.* **1991**, *15*, 321 – 325; f) Y.-D. Wu, Z.-H. Peng, *J. Am. Chem. Soc.* **1997**, *119*, 8043 – 8049; g) K. Monteyne, T. Ziegler, *Organometallics* **1998**, *17*, 5901 – 5907; h) S.-H. Choi, Z. Lin, Z. Xue, *Organometallics* **1999**, *18*, 5488 – 5495; i) E. Folga, T. Ziegler, *Organometallics* **1993**, *12*, 325 – 337; j) O. Eisenstein, R. Hoffmann, A. R. Rossi, *J. Am. Chem. Soc.* **1981**, *103*, 5582 – 5584; k) T. R. Cundari, M. S. Gordon, *J. Am. Chem. Soc.* **1991**, *113*, 5231 – 5243; l) T. R. Cundari, M. S. Gordon, *J. Am. Chem. Soc.* **1992**, *114*, 539 – 548; m) T. R. Cundari, M. S. Gordon, *Organometallics* **1992**, *11*, 55 – 63; n) H. H. Fox, M. H. Schofield, R. R. Schrock, *Organometallics* **1994**, *13*, 2804 – 2815; o) S. F. Vyboishchikov, G. Frenking, *Chem. Eur. J.* **1998**, *4*, 1428 – 1438; p) S. F. Vyboishchikov, G. Frenking, *Chem. Eur. J.* **1998**, *4*, 1439 – 1448; q) R. J. Goddard, R. Hoffmann, E. D. Jemmis, *J. Am. Chem. Soc.* **1980**, *102*, 7667 – 7676.

[104] J. H. Oskam, R. R. Schrock, *J. Am. Chem. Soc.* **1993**, *115*, 11831 – 11845.

[105] J. H. Oskam, R. R. Schrock, *J. Am. Chem. Soc.* **1992**, *114*, 7588 – 7589.

[106] M. Brookhart, M. L. H. Green, L. Wong, *Prog. Inorg. Chem.* **1988**, *36*, 1 – 124.

 © 2003 Wiley-VCH Verlag GmbH & Co. KGaA, Weinheim

[107] R. R. Schrock, W. E. Crowe, G. C. Bazan, M. DiMare, M. B. O'Regan, M. H. Schofield, *Organometallics* **1991**, *10*, 1832 – 1843.
[108] J. Kress, J. A. Osborn, *Angew. Chem.* **1992**, *104*, 1660 – 1662; *Angew. Chem. Int. Ed. Engl.* **1992**, *31*, 1585 – 1587.
[109] R. R. Schrock, S. Luo, N. Zanetti, H. H. Fox, *Organometallics* **1994**, *13*, 3396.
[110] J. Feldman, W. M. Davis, J. K. Thomas, R. R. Schrock, *Organometallics* **1990**, *9*, 2535 – 2548.
[111] W. E. Crowe, Z. J. Zhang, *J. Am. Chem. Soc.* **1993**, *115*, 10998 – 10999.
[112] W. E. Crowe, D. R. Goldberg, *J. Am. Chem. Soc.* **1995**, *117*, 5162 – 5163.
[113] W. E. Crowe, D. R. Goldberg, Z. J. Zhang, *Tetrahedron Lett.* **1996**, *37*, 2117 – 2120.
[114] J. Robbins, G. C. Bazan, J. S. Murdzek, M. B. O' Regan, R. R. Schrock, *Organometallics* **1991**, *10*, 2902 – 2907.
[115] T. Masuda, H. Tachimori, *J. Macromol. Sci. Pure Appl. Chem. A* **1997**, *34*, 1977 – 1995.
[116] H. Shirakawa, T. Masuda, K. Takeda, in *The Chemistry of Triple-Bonded Functional Groups, Supplement C2*(Ed.: S. Patai), Wiley, **1994**, pp. 945 – 1016.
[117] a) J. Konzelman, K. B. Wagener, *Macromolecules* **1995**, *28*, 4686 – 4692; b) J. Konzelman, K. B. Wagener, *Macromolecules* **1996**, *29*, 7657 – 7660; c) K. B. Wagener, K. Brzezinska, J. D. Anderson, T. R. Younkin, K. Steppe, W. DeBoer, *Macromolecules* **1997**, *30*, 7363 – 7369.
[118] a) E. Thorn-Csanyi, K. P. Pflug, *Makromol. Chem. Rapid Commun.* **1993**, *14*, 619 – 624; b) E. Thorn-Csanyi, P. Kraxner, *Macromol. Rapid Commun.* **1995**, *16*, 147 – 153.
[119] S.-K. Choi, Y.-S. Gal, S.-H. Jin, H. K. Kim, *Chem. Rev.* **2000**, *100*, 1645 – 1682.
[120] H. H. Fox, M. O. Wolf, R. O' Dell, B. L. Lin, R. R. Schrock, M. S. Wrighton, *J. Am. Chem. Soc.* **1994**, *116*, 2827 – 2843.
[121] R. H. Grubbs, W. Tumas, *Science* **1989**, *243*, 907 – 915.
[122] M. R. Buchmeiser, *Chem. Rev.* **2000**, *100*, 1565 – 1604.
[123] W. J. Feast, V. C. Gibson, E. L. Marshall, *J. Chem. Soc. Chem. Commun.* **1992**, 1157 – 1158.
[124] G. Bazan, E. Khosravi, R. R. Schrock, W. J. Feast, V. C. Gibson, M. B. O'Regan, J. K. Thomas, W. M. Davis, *J. Am. Chem. Soc.* **1990**, *112*, 8378 – 8387.
[125] W. J. Feast, V. C. Gibson, K. J. Ivin, A. M. Kenwright, E. Khosravi, *J. Mol. Catal.* **1994**, *90*, 87 – 99.
[126] W. J. Feast, V. C. Gibson, K. J. Ivin, A. M. Kenwright, E. Khosravi, *J. Chem. Soc. Chem. Commun.* **1994**, 1399 – 1400.
[127] Ru-based complex **58a**: a) P. Schwab, R. H. Grubbs, J. W. Ziller, *J. Am. Chem. Soc.* **1996**, *118*, 100 – 110; catalyst **58b**: b) M. Scholl, S. Ding, C. W. Lee, R. H. Grubbs, **1999**, *1*, 953 – 956; complex **58c**: c) M. Scholl, T. M. Trnka, J. P. Morgan, R. H. Grubbs, *Tetrahedron Lett.* **1999**, *40*, 2247 – 2250; d) J. Huang, E. D. Stevens, S. P. Nolan, J. L. Petersen, *J. Am. Chem. Soc.* **1999**, *121*, 2647 – 2678; e) L. Ackermann, A. Fürstner, T. Weskamp, F. J. Kohl, W. A. Herrmann, *Tetrahedron Lett.* **1999**, *40*, 4787 – 4790; complex **58d**: f) J. P. A. Harrity, M. S. Visser, J. D. Gleason, A. H. Hoveyda *J. Am. Chem. Soc.* **1997**, *119*, 1488 – 1489; g) J. P. A. Harrity, D. S. La, D. R. Cefalo, M. S. Visser, A. H. Hoveyda *J. Am. Chem. Soc.* **1998**, *120*, 2343 – 2351; h) J. S. Kingsbury, J. P. A. Harrity, P. J. Bonitatebus, Jr., A. H. Hoveyda, *J. Am. Chem. Soc.* **1999**, *121*, 791 – 799; complex **58e**: i) S. B. Garber, J. S. Kingsbury, B. L. Gray, A. H. Hoveyda, *J. Am. Chem. Soc.* **2000**, *122*, 8168 – 8179.
[128] For a recent study of molybdenum-catalyzed CM, see: T. Yasuda, J. Abe, H. Yoshida, T. Iyoda, T. Kawai, *Adv. Synth. Catal.* **2002**, *344*, 705 – 711.
[129] A. G. M. Barrett, J. C. Beall, V. C. Gibson, M. R. Giles, G. L. P. Walker, *Chem. Commun.* **1996**, 2229 – 2230.
[130] M. Ahmed, T. Arnauld, A. G. M. Barrett, D. C. Braddock, K. Flack, P. A. Procopiou, *Org. Lett.* **2000**, *2*, 551 – 553.
[131] A. F. Houri, Z. M. Xu, D. A. Cogan, A. H. Hoveyda, *J. Am. Chem. Soc.* **1995**, *117*, 2943 – 2944.
[132] Z. M. Xu, C. W. Johannes, S. S. Salman, A. H. Hoveyda, *J. Am. Chem. Soc.* **1996**, *118*, 10926 – 10927.
[133] Z. Xu, C. W. Johannes, A. F. Houri, D. S. La, D. A. Cogan, G. E. Hofilena, A. H. Hoveyda, *J. Am. Chem. Soc.* **1997**, *119*, 10302 – 11016.
[134] For a study regarding the reversible nature of Ru-catalyzed olefin-metathesis reactions, see: N. J. Marsella, H. D. Maynard, R. H. Grubbs, *Angew. Chem.* **1997**, *109*, 1147 – 1150; *Angew. Chem. Int. Ed. Engl.* **1997**, *36*, 1101 – 1103.
[135] S. A. May, P. A. Grieco, *Chem. Commun.* **1998**, 1597 – 1598.
[136] A. B. Smith, S. A. Kozmin, C. M. Adams, D. V. Paone, *J. Am. Chem. Soc.* **2000**, *122*, 4984 – 4985.
[137] A. B. Smith, C. M. Adams, S. A. Kozmin, *J. Am. Chem. Soc.* **2001**, *123*, 990 – 991.
[138] A. B. Smith, C. M. Adams, S. A. Kozmin, D. V. Paone, *J. Am. Chem. Soc.* **2001**, *123*, 5925 – 5937.
[139] K. C. Nicolaou, S. A. Snyder, K. B. Simonsen, A. E. Koumbis, *Angew. Chem.* **2000**, *112*, 3615 – 3620; *Angew. Chem. Int. Ed.* **2000**, *39*, 3473 – 3478.
[140] S. F. Martin, Y. S. Liao, Y. L. Wong, T. Rein, *Tetrahedron Lett.* **1994**, *35*, 691 – 694.
[141] a) I. M. Fellows, D. E. Kaelin, Jr., S. F. Martin, *J. Am. Chem. Soc.* **2000**, *122*, 10781 – 10787; b) S. F. Martin, H.-J. Chen, A. K. Courtney, Y. Liao, M. Patzel, M. N. Ramser, A. S. Wagman, *Tetrahedron* **1996**, *52*, 7251 – 7264; c) J. M. Humphrey, Y. Liao, A. Ali, T. Rein, Y.-L. Wong, H.-J. Chen, A. K. Courtney, S. F. Martin, *J. Am. Chem. Soc.* **2002**, *124*, 8584 – 8592; For Ru-catalyzed RCM reactions aimed towards the total synthesis of manzamine A, see: d) B. C. Borer, S. Deerenberg, H. Bieraugel, U. K. Pandit, *Tetrahedron Lett.* **1994**, *35*, 3191 – 3194.
[142] A. Fürstner, O. R. Thiel, *J. Org. Chem.* **2000**, *65*, 1738 – 1742.
[143] A. Fürstner, K. Langemann, *J. Org. Chem.* **1996**, *61*, 8746 – 8749.
[144] K. Nakashima, K. Inoue, M. Sono, M. Tori, *J. Org. Chem.* **2002**, *67*, 6034 – 6040.
[145] O. Fujimura, G. C. Fu, P. W. K. Rothemund, R. H. Grubbs, *J. Am. Chem. Soc.* **1995**, *117*, 2355 – 2356.
[146] A. Fürstner, K. Langemann, *J. Am. Chem. Soc.* **1997**, *119*, 9130 – 9136.
[147] A. K. Ghosh, J. Cappielo, D. Shin, *Tetrahedron Lett.* **1998**, *39*, 4651 – 4654.
[148] A. G. M. Barrett, M. Ahmed, S. P. Baker, S. P. D. Baugh, D. C. Braddock, P. A. Procopiou, A. J. P. White, D. J. Williams, *J. Org. Chem.* **2000**, *65*, 3716 – 3721.
[149] D. Bourgeois, A. Pancrazi, L. Ricard, J. Prunet, *Angew. Chem.* **2000**, *112*, 741 – 744; *Angew. Chem. Int. Ed.* **2000**, *39*, 726 – 728.
[150] D. Bourgeois, J. Mahuteau, A. Pancrazi, S. P. Nolan, J. Prunet, *Synthesis* **2000**, 869 – 882.
[151] J. S. Clark, J. G. Kettle, *Tetrahedron Lett.* **1997**, *38*, 123 – 126.
[152] J. S. Clark, J. G. Kettle, *Tetrahedron Lett.* **1997**, *38*, 127 – 130.
[153] J. S. Clark, J. G. Kettle, *Tetrahedron* **1999**, *55*, 8231 – 8248.
[154] For examples of adventitious olefin isomerization observed with molybdenum-catalyzed olefin-metathesis reactions, see: D. Joe, L. E. Overman, *Tetrahedron Lett.* **1997**, *38*, 8635 – 8638, and ref. [153].
[155] For representative studies on Ru-catalyzed olefin isomerization in conjunction with olefin metathesis, see: a) S. J. Miller, H. E. Blackwell, R. H. Grubbs, *J. Am. Chem. Soc.* **1996**, *118*, 9606 – 9614; b) L. Ackermann, D. El Tom, A. Fürstner, *Tetrahedron* **2000**, *56*, 2195 – 2202; c) L. A. Paquette, I. Efremov, *J. Am. Chem. Soc.* **2001**, *123*, 4492 – 4501; d) M. Gurjar, P. Yakambram, *Tetrahedron Lett.* **2001**, *42*, 3633 – 3636; e) C. Cadot, P. Dalko, J. Cossy, *Tetrahedron Lett.* **2002**, *43*, 1839 – 1841; f) A. E. Sutton,

 © 2003 Wiley-VCH Verlag GmbH & Co. KGaA, Weinheim

B. A. Seigal, D. F. Finnegan, M. L. Snapper, *J. Am. Chem. Soc.* **2002**, *124*, 13390 – 13391; g) M. Arisawa, Y. Terada, M. Nakagawa, A. Nishida, *Angew. Chem.* **2002**, *114*, 4926 – 4928; *Angew. Chem. Int. Ed.* **2002**, *41*, 4732 – 4734.

[156] J. S. Clark, O. Hamelin, R. Hufton, *Tetrahedron Lett.* **1998**, *39*, 8321 – 8324.

[157] J. S. Clark, O. Hamelin, *Angew. Chem.* **2000**, *112*, 380 – 382; *Angew. Chem. Int. Ed.* **2000**, *39*, 372 – 374.

[158] J. P. Morken, M. T. Didiuk, M. S. Visser, A. H. Hoveyda, *J. Am. Chem. Soc.* **1994**, *116*, 3123 – 3124.

[159] M. S. Visser, N. M. Heron, M. T. Didiuk, J. F. Sagal, A. H. Hoveyda, *J. Am. Chem. Soc.* **1996**, *118*, 4291 – 4298.

[160] C. W. Johannes, M. S. Visser, G. S. Weatherhead, A. H. Hoveyda, *J. Am. Chem. Soc.* **1998**, *120*, 8340 – 8347.

[161] For example, see: a) J. A. Smulik, S. T. Diver, *Org. Lett.* **2000**, *2*, 2271 – 2274; b) M. J. Bassindale, P. Hamley, J. P. A. Harrity, *Tetrahedron Lett.* **2001**, *42*, 9055 – 9057; c) D. Banti, M. North, *Tetrahedron Lett.* **2002**, *43*, 1561 – 1564; d) M. Mori, Y. Kuzuba, T. Kitamura, Y. Sato, *Org. Lett.* **2002**, *4*, 3855 – 3858; e) D. Meng, D. L. Parker, Jr., *Tetrahedron Lett.* **2002**, *43*, 9035 – 9038.

[162] a) M. Seepersaud, Y. Al-Abed, *Org. Lett.* **1999**, *1*, 1463 – 1465; for a related example, see: b) O. Sellier, P. V. de Weghe, D. Le Nouen, C, Strehler, J. Eustache, *Tetrahedron Lett.* **1999**, *40*, 853 – 856.

[163] K. L. Lee, J. B. Goh, S. F. Martin, *Tetrahedron Lett.* **2001**, *42*, 1635 – 1638.

[164] S. A. Kozmin, V. H. Rawal, *J. Am. Chem. Soc.* **1998**, *120*, 13523 – 13524.

[165] S. A. Kozmin, T. Iwama, Y. Huang, V. H. Rawal, *J. Am. Chem. Soc.* **2002**, *124*, 4628 – 4641.

[166] S. G. Nelson, W. S. Cheung, A. J. Kassick, M. A. Hilfike, *J. Am. Chem. Soc.* **2002**, *124*, 13654 – 13655.

[167] S. E. Denmark, S.-M. Yang, *J. Am. Chem. Soc.* **2002**, *124*, 15196 – 15197.

[168] D. M. Hodgson, A. M. Foley, L. T. Boulton, P. J. Lovell, G. N. Maw, *J. Chem. Soc. Perkin Trans. 1* **1999**, 2911 – 2922.

[169] O. Fujimura, G. C. Fu, R. H. Grubbs, *J. Org. Chem.* **1994**, *59*, 4029 – 4031.

[170] D. Calimente, M. H. D. Postema, *J. Org. Chem.* **1999**, *64*, 1770 – 1771.

[171] L. Liu, M. H. D. Postema, *J. Am. Chem. Soc.* **2001**, *123*, 8602 – 8603.

[172] M. H. D. Postema, D. Calimente, L. Liu, T. L. Behrmann, *J. Org. Chem.* **2000**, *65*, 6061 – 6068.

[173] J. D. Rainier, S. P. Allwein, J. M. Cox, *Org. Lett.* **2000**, *2*, 231 – 234.

[174] J. D. Rainier, J. M. Cox, S. P. Allwein, *Tetrahedron Lett.* **2001**, *42*, 179 – 181.

[175] J. D. Rainier, S. P. Allwein, J. M. Cox, *J. Org. Chem.* **2001**, *66*, 1380 – 1386.

[176] S. D. Burke, K. J. Quinn, V. J. Chen, *J. Org. Chem.* **1998**, *63*, 8626 – 8627.

[177] Throughout this article, the identity of the enantiomer formed is that which is obtained with the catalyst antipode illustrated. Transformations with binol-based complexes (e.g., **11**) were carried out with the opposite antipode of the catalyst versus that illustrated. Because (*S*)-biphen and (*R*)-binol complexes were employed in our studies, this adjustment has been made to facilitate comparison between biphen- and binol-based catalysts.

[178] O. Fujimura, R. H. Grubbs, *J. Org. Chem.* **1998**, *63*, 824 – 832.

[179] O. Fujimura, R. H. Grubbs, *J. Am. Chem. Soc.* **1996**, *118*, 2499 – 2500.

[180] For a review of metal-catalyzed kinetic resolution, see: A. H. Hoveyda, M. T. Didiuk, *Curr. Org. Chem.* **1998**, *2*, 537 – 574.

[181] For an earlier overview of molybdenum-catalyzed asymmetric olefin metathesis, see: A. H. Hoveyda, R. R. Schrock, *Chem. Eur. J.* **2001**, *7*, 945 – 950.

[182] For discussions regarding combinatorial approaches to catalyst discovery and the issue of "catalyst generality," see: A. H. Hoveyda, *Handbook of Combinatorial Chemistry*, (Eds.: K. C. Nicolaou, R. Hanko, W. Hartwig), Wiley-VCH, Weinheim, **2002**, pp. 991 – 1016.

[183] J. B. Alexander, D. S. La, D. R. Cefalo, A. H. Hoveyda, R. R. Schrock, *J. Am. Chem. Soc.* **1998**, *120*, 4041 – 4042.

[184] The value for k_{rel} is calculated by the equation reported by Kagan and Fiaud: H. B. Kagan, J. C. Fiaud, *Top. Stereochem.* **1988**, *53*, 708 – 710.

[185] D. S. La, J. B. Alexander, D. R. Cefalo, D. D. Graf, A. H. Hoveyda, R. R. Schrock, *J. Am. Chem. Soc.* **1998**, *120*, 9720 – 9721.

[186] All transformations promoted by chiral Mo catalysts can be carried out in toluene (in addition to benzene) or alkanes (e.g., *n*-pentane) with equal efficiency. See text for specific examples.

[187] S. D. Burke, N. Muller, C. M. Beudry, *Org. Lett.* **1999**, *1*, 1827 – 1829.

[188] A. F. Kiely, J. A. Jernelius, R. R. Schrock, A. H. Hoveyda, *J. Am. Chem. Soc.* **2002**, *124*, 2868 – 2869.

[189] S. J. Dolman, E. S. Sattely, A. H. Hoveyda, R. R. Schrock, *J. Am. Chem. Soc.* **2002**, *124*, 6991 – 6997.

[190] For representative studies regarding non-asymmetric ROM reactions, see: a) M. L. Randall, J. A. Tallarico, M. L. Snapper, *J. Am. Chem. Soc.* **1995**, *117*, 9610 – 9611; b) M. L. Snapper, J. A. Tallarico, M. L. Randall, *J. Am. Chem. Soc.* **1997**, *119*, 1478 – 1479; c) W. J. Zuercher, M. Hashimoto, R. H. Grubbs *J. Am. Chem. Soc.* **1996**, *118*, 6634 – 6640; d) see ref. [127f]; e) M. F. Schneider, N. Lucas, J. Velder, S. Blechert, *Angew. Chem.* **1997**, *109*, 257 – 259; *Angew. Chem. Int. Ed. Engl.* **1997**, *36*, 257 – 259; f) F. D. Cuny, J. Cao, J. R. Hauske, *Tetrahedron Lett.* **1997**, *38*, 5237 – 5240; g) M. Michaut, J.-L. Parrain, M. Santelli, *Chem. Commun.* **1998**, 2567 – 2568; h) H. Katayama, H. Urushima, T. Nishioka, C. Wada, M. Nagao, F. Ozawa, *Angew. Chem.* **2000**, *112*, 4687 – 4689; *Angew. Chem. Int. Ed.* **2000**, *39*, 4513 – 4515.

[191] G. S. Weatherhead, J. G. Ford, E. J. Alexanian, R. R. Schrock, A. H. Hoveyda, *J. Am. Chem. Soc.* **2000**, *122*, 1828 – 1829.

[192] D. R. Cefalo, A. F. Kiely, M. Wuchrer, J. Y. Jamieson, R. R. Schrock, A. H. Hoveyda, *J. Am. Chem. Soc.* **2001**, *123*, 3139 – 3140.

[193] For a subsequent catalytic enantioselective approach to tipranavir, see: B. M. Trost, N. G. Andersen, *J. Am. Chem. Soc.* **2002**, *124*, 14320 – 14321.

[194] X. Teng, D. R. Cefalo, R. R. Schrock, A. H. Hoveyda, *J. Am. Chem. Soc.* **2002**, *124*, 10779 – 10784.

[195] For synthesis of spirocyclic structures through catalytic olefin metathesis, see: a) ref. [161b]; b) D. J. Wallace, J. M. Goodman, D. J. Kennedy, A. J. Davies, C. J. Cowden, M. S. Ashwood, I. F. Cottrell, U.-H. Dolling, P. J. Reider, *Org. Lett.* **2001**, *3*, 671 – 674; c) D. J. Wallace, P. G. Bulger, D. J. Kennedy, M. S. Ashwood, I. F. Cottrell, U.-H. Dolling, *Synlett.* **2001**, 357 – 360.

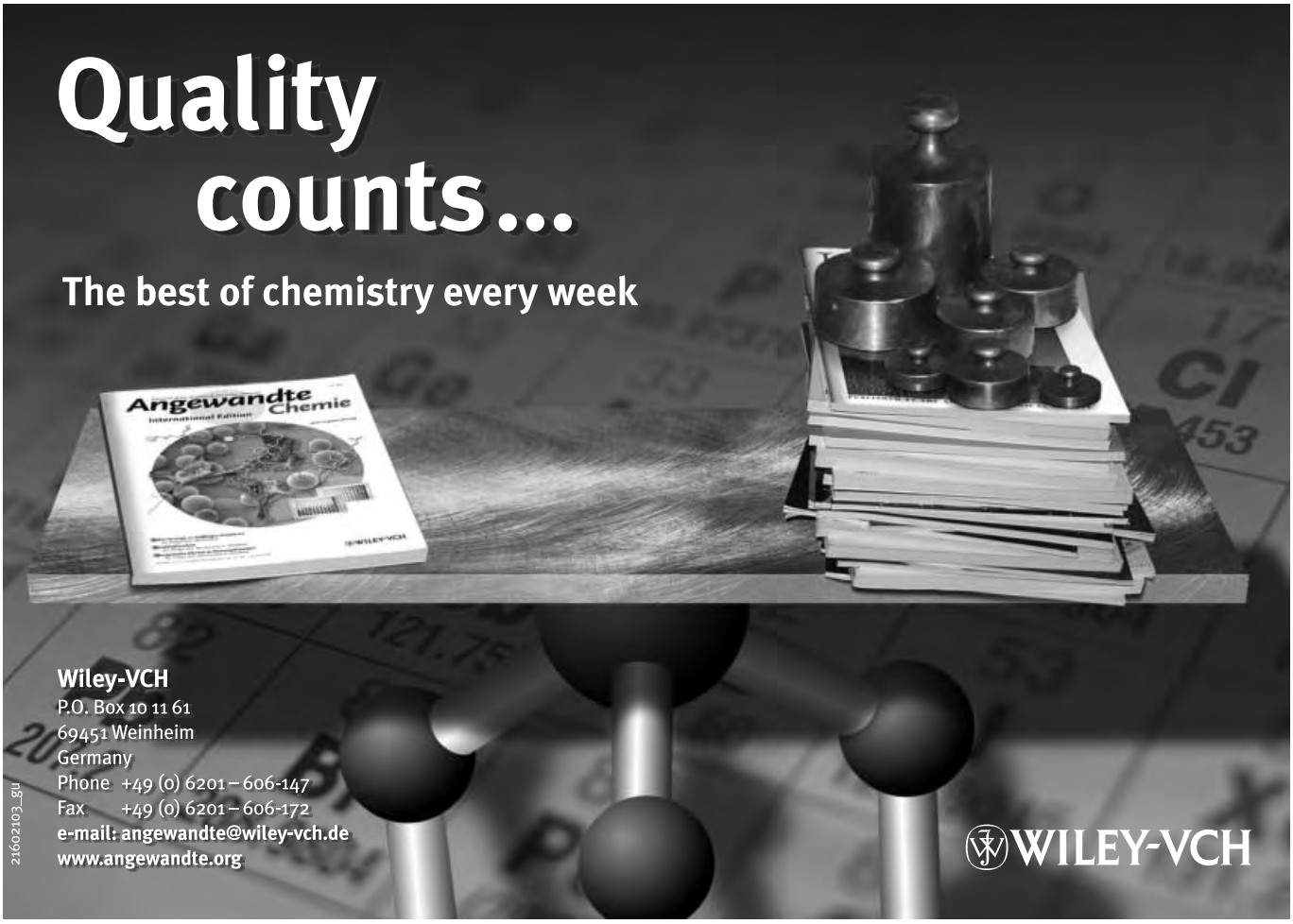
[196] a) D. S. La, J. G. Ford, E. S. Sattely, J. P. J. Bonitatebus, R. R. Schrock, A. H. Hoveyda, *J. Am. Chem. Soc.* **1999**, *121*, 11603 – 11604; b) D. S. La, E. S. Sattely, J. G. Ford, R. R. Schrock, A. H. Hoveyda, *J. Am. Chem. Soc.* **2001**, *123*, 7767 – 7778.

[197] The chiral Mo alkylidene most likely approaches norbornyl alkenes from the exo face. For the X-ray structure of a related molybdacyclobutane, see: G. C. Bazan, J. H. Oskam, H. Cho, L. Y. Park, R. R. Schrock, *J. Am. Chem. Soc.* **1991**, *113*, 6899 – 6907.

[198] K. C. Hultzsch, J. A. Jernelius, A. H. Hoveyda, R. R. Schrock, *Angew. Chem.* **2002**, *114*, 609 – 613; *Angew. Chem. Int. Ed.* **2002**, *41,* 589 – 593.

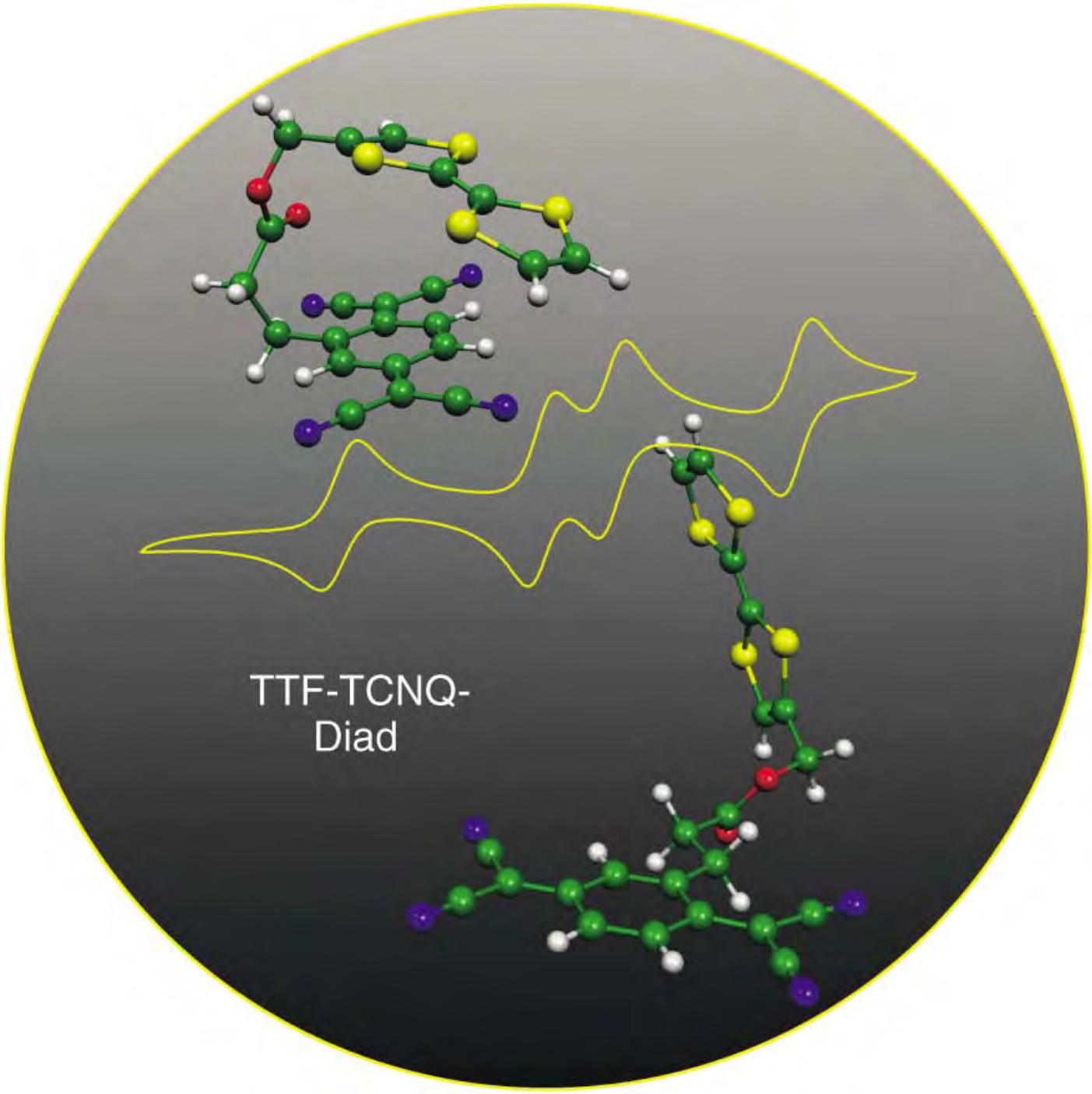
 © 2003 Wiley-VCH Verlag GmbH & Co. KGaA, Weinheim

[199] T. J. Seiders, D. W. Ward, R. H. Grubbs, *Org. Lett.* **2001**, *3*, 3225 – 3228.
[200] a) J. J. Van Veldhuizen, S. B. Garber, J. S. Kingsbury, A. H. Hoveyda, *J. Am. Chem. Soc.* **2002**, *124*, 4954 – 4955; b) J. J. Van Veldhuizen, D. G. Gillingham, S. B. Garber, O. Katoka, A. H. Hoveyda, *J. Am. Chem. Soc.* **2003**, *125*, in press.
[201] Z. Wu, D. R. Wheeler, R. H. Grubbs, *J. Am. Chem. Soc.* **1992**, *114*, 146 – 151.
[202] S. K. Armstrong, B. A. Christie, *Tetrahedron Lett.* **1996**, *37*, 9373 – 9376.
[203] Y. S. Shon, T. R. Lee, *Tetrahedron Lett.* **1997**, *38*, 1283.
[204] G. C. Fu, R. H. Grubbs, *J. Am. Chem. Soc.* **1993**, *115*, 3800 – 3801.
[205] See also: K. L. Lee, J. B. Goh, S. F. Martin, *Tetrahedron Lett.* **2001**, *42*, 1635 – 1638.
[206] J. A. Burlison, J. M. Gray, D. G. J. Young, *Tetrahedron Lett.* **2001**, *42*, 5363 – 5365.
[207] J. S. Kingsbury, A. H. Hoveyda; unpublished results.



 © 2003 Wiley-VCH Verlag GmbH & Co. KGaA, Weinheim

Communications



Two conformers of a covalently linked diad that incorporates donor tetrathiafulvalene (TTF) and acceptor tetracyanoquinodimethane (TCNQ) moieties are described in the Communication by M. R. Bryce and co-workers on the following pages. The molecule exhibits a remarkably low HOMO–LUMO energy gap and thermoexcited electron transfer.

DOI: 10.1002/anie.200351876
© 2003 Wiley-VCH Verlag GmbH & Co. KGaA, Weinheim

Covalent TTF–TCNQ Diad

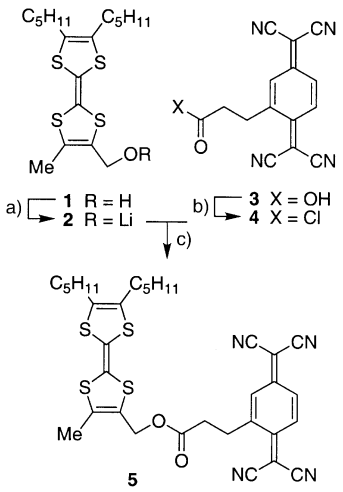
A Covalent Tetrathiafulvalene–Tetracyanoquinodimethane Diad: Extremely Low HOMO–LUMO Gap, Thermoexcited Electron Transfer, and High-Quality Langmuir–Blodgett Films**

Dmitrii F. Perepichka, Martin R. Bryce, Christopher Pearson, Michael C. Petty, Eric J. L. McInnes, and Jing P. Zhao*

The challenge of covalently linking an electron donor tetrathiafulvalene (TTF) moiety to an electron acceptor tetracyano-*p*-quinodimethane (TCNQ) moiety was initiated in a theoretical paper by Aviram and Ratner published in 1974,[1] shortly after the first report[2] of metallic conductivity in the intermolecular 1:1 charge-transfer complex (CTC) formed between TTF and TCNQ. It was proposed that a single donor–acceptor molecule (specifically a TTF-σ-TCNQ diad) when aligned between two electrodes could serve as a rectifier of electric current, because the $TTF^{+\bullet}$-σ-$TCNQ^{-\bullet}$ state (supporting direct electron flow) is highly preferable over $TTF^{-\bullet}$-σ-$TCNQ^{+\bullet}$ (which is required for reverse electron flow).[1] Since then numerous attempts to synthesize TTF–TCNQ hybrid molecules have been undertaken. Such covalent diads have also been sought as a means of controlling the unpredictable stoichiometry of CTCs to obtain organic metals[3] and energy-harvesting materials for solar cells.[4] However, the task of covalently coupling a strong π-electron donor to a strong π-electron acceptor (which is required to achieve the unusual electronic properties in the diad, including rectification behavior[5]) is extremely difficult,[4b,6] although many different acceptor moieties with moderate electron affinity have been attached to TTF.[4b,7] For example, TTF has been linked to tetracyanoanthraquinodimethane (TCNAQ)[8], which is not a "true" TCNQ system due to the much weaker acceptor properties that result from its buckled structure. Several TTF–benzoquinone diads have been identified as potential precursors to TTF–TCNQ, but all attempts at converting the quinone moiety to the corresponding TCNQ derivative have been unsuccessful[7] due to the sensitivity of the TTF nucleus to the acidic conditions ($TiCl_4$) of this reaction.

In the first report in 1976 claiming covalent linkage of TTF and TCNQ, Hertzler described the reaction of a TTF–diisocyanate with a TCNQ–dialcohol which could reasonably form a TTF–TCNQ polyurethane.[9] However, the only characterization data reported for the intractable reaction product were elemental analysis ($\delta > 1\,\%$) and electrical conductivity ($\sigma_{rt} = 10^{-7}\,S\,cm^{-1}$). In 1984 Panetta et al. reported that the coupling of suitably functionalized TTF and TCNQ units gave EPR-active products, the structures of which were not convincingly established.[10] In particular, the absence of TCNQ reduction waves in cyclic voltammetry (CV) experiments seems inconsistent with the proposed TTF–TCNQ diad structure. No further experimental investigation has been published, although the structures of postulated TTF–TCNQ diads have recurred in several review articles.[4b,7,11] We recently reported TTF-σ-polynitrofluorene diads which are highly electrochemically amphoteric systems ($E^0_{ox} - E^0_{red} \approx 0.3$ V).[12] We now present the first well-characterized TTF-σ-TCNQ diad, and describe the unusual physical properties of this compound.

The key idea allowing a covalent coupling of TTF and TCNQ moieties was to use highly reactive functionalities (an acid chloride and an alkoxide anion), which can compete with the electron-transfer and following side reactions (Scheme 1).



Scheme 1. Synthesis of TTF-σ-TCNQ diad: a) *n*BuLi, THF, −78 °C, 30 min; b) $(COCl)_2$, 20 °C, 72 h; c) **2** + **4**, THF, −100 °C→20 °C, 12 h.

The reagents for our synthesis are TTF derivative **1**[12] (the pentyl chains were chosen for increased processibility) and TCNQ derivative **4**, which was obtained from the acid precursor **3**[13] by reaction with oxalyl chloride. The lithium alkoxide salt **2**[12] was generated in situ and reacted with compound **4** to give analytically pure product **5** in 27 % yield

[*] Prof. M. R. Bryce, Dr. D. F. Perepichka
Department of Chemistry and Centre for Molecular and Nanoscale Electronics
University of Durham, Durham, DH1 3LE (UK)
Fax: (+44) 191-384-4737
E-mail: m.r.bryce@durham.ac.uk
Dr. D. F. Perepichka
INRS-Énergie et Matériaux
Université du Québec
Varennes, Quebec H3H 1X1 (Canada)
Dr. C. Pearson, Prof. M. C. Petty
School of Engineering and
Centre for Molecular and Nanoscale Electronics
University of Durham, Durham, DH1 3LE (UK)
Dr. E. J. L. McInnes, Dr. J. P. Zhao
The EPSRC EPR Service Centre, Department of Chemistry
The University of Manchester, Manchester M13 9PL (UK)

[**] We thank the EPSRC and the NSERC for funding this work, and Dr. Michael Bendikov for helpful discussions of the calculation results.

Supporting information for this article is available on the WWW under http://www.angewandte.org or from the author.

 © 2003 Wiley-VCH Verlag GmbH & Co. KGaA, Weinheim DOI: 10.1002/anie.200351876

as a stable dark-brown powder. The purity of the compound was established by HPLC and elemental analysis, and its structure was proved beyond doubt by NMR and HRMS data.

In CV experiments compound **5** shows reversible amphoteric redox behavior consisting of two, single-electron reduction waves (from the TCNQ moiety), and two, single-electron oxidations (from the TTF fragment) thus revealing five stable redox states (Figure 1). The mutual effect of the donor and acceptor moieties on the redox properties of their counter-

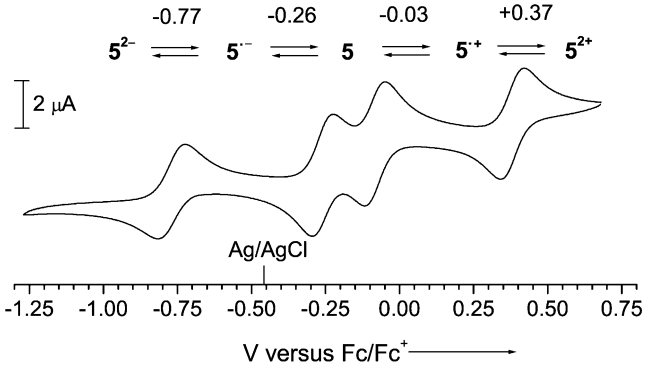


Figure 1. Cyclic voltammetry of compound **5** in MeCN (0.1 M Bu_4NPF_6), scan rate 100 mV s^{-1}, 20 °C.

parts is small due to the isolating nature of the linker; there is a 20 mV shift of the first reduction and oxidation potentials, compared to separate TTF and TCNQ molecules and, in contrast to our expectations based on TTF–fluorene diads,[12] the separation between the first and second redox process increases in the diad **5** (benzoyl-**1**: $E^0_{1ox} = -0.11$ V, $E^0_{2ox} = +0.43$ V; **3**: $E^0_{1red} = -0.24$ V, $E^0_{2red} = -0.72$ V. Remarkably, the difference between the first oxidation and first reduction potentials ($E^0_{1ox} - E^0_{1red}$) of compound **5** is only 170 mV, presenting the lowest known electrochemical HOMO–LUMO gap (0.17 eV) in an organic molecule. Such a small difference for $E^0_{1ox} - E^0_{1red}$ is expected[14] to lead to a high degree (> 0.7) of charge transfer in the solid state. Indeed, the C≡N stretching frequency in the IR spectra (KBr pellet, see Supporting Information) of **5** ($\tilde{\nu}_{CN} = 2187$ cm^{-1}) is between those of neutral and radical anion TCNQ ($\tilde{\nu}_{CN} = 2225$ and 2180 cm^{-1}, respectively),[15] which is consistent with ≈85% charge transfer.[14]

In solution, intramolecular charge transfer (ICT) in compound **5** is manifested by a broad absorption band in the near-IR region of its electronic spectra with $\lambda_{max} =$ 1630 nm (0.75 eV; $\varepsilon = 3600$ M^{-1}cm^{-1}) and a red edge at ≈2700 nm (0.45 eV) (see Supporting Information). Its intramolecular nature was established by a linear concentration dependence in the range 2×10^{-4}–3×10^{-3} M. Taking into account the density functional theory (DFT) calculations (B3LYP/6-31G*) for a homologue **5′**, which suggest the coexistence of linear and intramolecularly complexed head-to-tail conformations[16] we attribute the ICT band to π–π through-space charge transfer (Figure 2). The discrepancy between the electrochemically and spectroscopically deter-

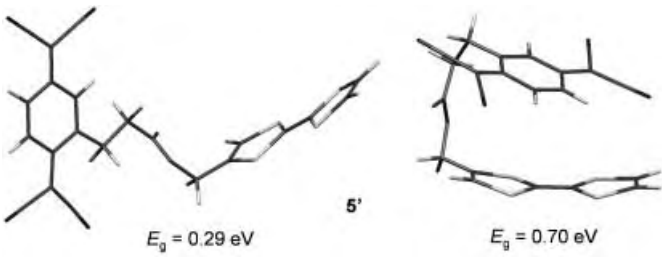


Figure 2. Geometries and HOMO–LUMO gaps (E_g) of an extended (left) and a head-to-tail intramolecularly complexed (right) conformation of a model TTF–TCNQ diad **5′**, and calculated at the B3LYP/6-31G(d) level.

mined HOMO–LUMO gaps (0.17 eV and 0.75 eV, respectively) is due to the fact that the optical HOMO–LUMO transition occurs only in the head-to-tail conformation (where the HOMO and LUMO orbitals are in close proximity), whereas CV experiments characterize an extended, "uncomplexed" state of the compound, which is easier to reduce/oxidize (because the charge-transfer interaction in the head-to-tail conformation decreases HOMO and increases LUMO energies, see Supporting Information). This conclusion is in full agreement with the calculation results, which predict HOMO–LUMO gaps of 0.29 eV and 0.70 eV for two conformations of **5′** (Figure 2). In powdered samples the CT band maximum shifts bathochromically by ≈300 nm as a result of intermolecular complexation[17] (see Supporting Information), and its tail is seen in the FTIR spectra down to 2000 cm^{-1}. Such a low energy band is usually indicative of electrical conductivity; accordingly, two-probe measurements on pressed pellets of **5** gave a value of $\sigma_{rt} \approx 10^{-6}$ S cm^{-1}.

Compounds for which color and transparency in the visible and near-IR region can be changed by applying various potentials are of great interest.[18] Although conducting polymers are currently the most studied materials in this respect, the majority of polymer electrochromic devices can operate only in on/off mode. Molecular electrochromic materials[19] bring the advantage of multicolor switching using a single material. Evaluation of the electrochromic properties of **5** revealed that stepwise application of various redox potentials to a brown solution of neutral **5** results in complete disappearance of the near-IR ICT band at 1630 nm, and subsequently turns the solution green (**5**$^{\cdot+}$ at +0.5 V versus Pt wire), orange (**5**$^{2+}$ at +1 V), blue (**5**$^{\cdot-}$ at −0.5 V), and red (**5**$^{2-}$ at −1.4 V; Figure 3 and Supporting Information). All four redox processes are completely reversible, that is, the initial spectrum of **5** returned after resetting the potential to +0.2 V, which demonstrates that this compound is a promising multicolor electrochromic material for the visible/near-IR region.

The EPR spectrum of a solution of **5** in CH_2Cl_2 at 290 K comprises two signals, which can be well simulated assuming a 1:1 ratio of TTF radical cation ($g = 2.0080$, $\Delta B_{p\text{-}p} = 2.5$ G) and TCNQ radical anion ($g = 2.0045$, $\Delta B_{p\text{-}p} = 4.5$ G) (Figure 4). Spin-quantification experiments under these conditions show ≈1.4 mol% of radical species, that is, approximately 0.7% of the compound exists in solution in a biradical state. The shape of the spectra is essentially unchanged on cooling the solution

 © 2003 Wiley-VCH Verlag GmbH & Co. KGaA, Weinheim

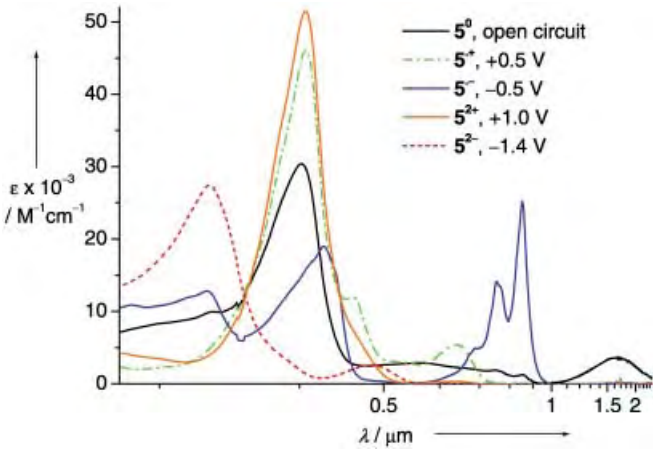


Figure 3. Spectroelectrochemistry of compound **5** in CH_2Cl_2 (0.1 M Bu_4NPF_6); potentials are versus a Pt wire quasi-reference electrode.

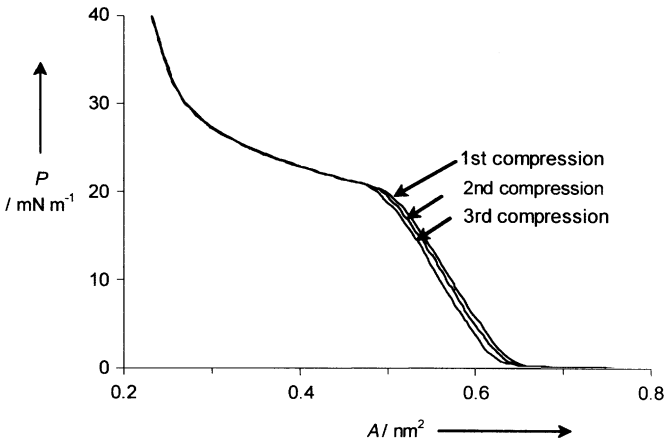


Figure 5. Surface pressure (*P*) versus area per molecule (*A*) isotherms for compound **5**.

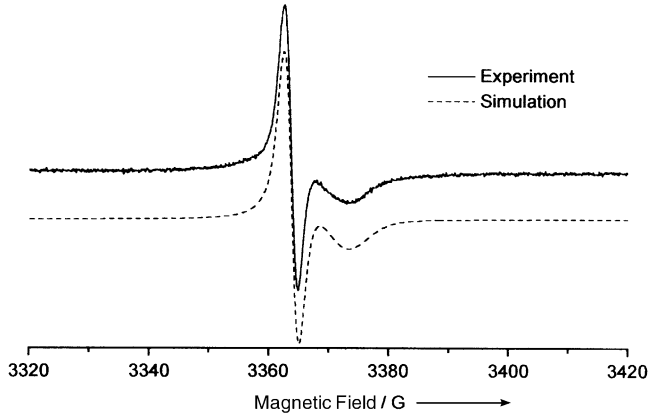


Figure 4. EPR spectrum of compound **5** in CH_2Cl_2 solution at 290 K and a simulation line.

from 290 to 175 K, but the intensity of the signal drops by a factor of about three (see Supporting Information). This is evidence for the first observation of a thermoexcited electron transfer in a donor–acceptor diad.[20] Calculation of the concentration of the thermoexcited biradical state $[D^{\bullet+}A^{\bullet-}]$ from the Arrhenius equation ($K=[D^{\bullet+}A^{\bullet-}]/[DA]=e^{-\Delta E/kT}$, where $\Delta E=E^0_{1ox}-E^0_{1red}$) predicts 0.12% of the biradical state at 290 K, which is somewhat lower than the observed value of 0.7%, presumably due to the influence of intramolecular[21] head-to-tail complexation of **5**.

To approach molecular electronics applications, we prepared Langmuir–Blodgett (LB) films of **5**. Surface pressure versus area isotherms for the first, second, and third compressions are almost identical, which indicates the high reversibility of the LB film formation (Figure 5). The initial rise of the surface pressure (at an area of $\approx 0.65\ nm^2$ molecule^{-1}) is followed by a region of relative stability (with a pressure of 20–25 mN m^{-1}) and then a rapidly increasing pressure below a surface area $\approx 0.3\ nm^2$ molecule^{-1}. Multilayer LB deposition was attempted at two different surface pressure values, either side of the surface pressure "plateau", 35 and 15 mN m^{-1} (hereafter called high and low pressure, respectively). At high pressure, only poor-quality patchy films could be deposited, which precluded their further investigation. At low pressure, however, Y-type deposition (that is, film transfer on both the downward and upward movements of the substrate through the air/water interface) was achieved and high-quality uniform films could be transferred onto different substrates with a transfer ratio close to unity (up to 240 layers).

Film-thickness measurements by low-angle X-ray reflection, ellipsometry, and surface profiling over the range of 20 to 240 layers indicate a layer thickness of 1.39 ± 0.08 nm. Absence of a CT band in the optical spectra of **5**-LB films and a shift of the CN stretching peak to 2218 cm^{-1} (close to the value of a noninteracting TCNQ moiety, see Supporting Information) suggest that a specific molecular conformation (and the interlayer architecture, Y-type deposition) prevent a donor–acceptor interaction between TTF and TCNQ fragments. The in-plane conductivity of a 20-layer film on a glass substrate was less than 10^{-7} S cm^{-1}, and very little change was evident after exposure to iodine vapor. The out-of-plane current versus voltage curves for a 240-layer film were symmetrical for different polarities of applied voltage. The dc conductivity was estimated to be very small, less than 2×10^{-11} S cm^{-1}, and ac voltage (1 MHz) measurements gave a value of 3.6 ± 0.2 for the relative permittivity of the organic film. These data are consistent with the neutral state of **5** in the film. To date, our attempts to measure the out-of-plane conductivity for a single monolayer of **5** (that is, to investigate molecular rectification) have been unsuccessful due to the difficulty of establishing reliable metallic top contacts. However, we are currently exploring alternative strategies.

The molecular area of **5** on the water surface, the transferred layer thickness, the absence of charge transfer, and the poor conductivity of the multilayer LB film (compared to other amphiphilic charge-transfer LB materials)[22] can be explained by the molecular orientation comprised of the TCNQ moiety lying on the surface and the TTF units making an angle with the surface of ≈45° (calculated molecular area of $\approx 0.7\ nm^2$ and the monolayer thickness of ≈1.4 nm, see Supporting Information). This molecular

 © 2003 Wiley-VCH Verlag GmbH & Co. KGaA, Weinheim

arrangement prevents close face-to-face stacking of either the TCNQ or TTF units, and accounts for the low dc conductivities in both the in-plane and through-plane directions. The region in the isotherm in Figure 5 above the surface pressure plateau could correspond to the formation of a bilayer floating film, with the TTF units interleaved.

In conclusion, we report the first synthesis of a well-characterized TTF–TCNQ diad **5**. The electrochemistry is characteristic of both donor and acceptor moieties, which result in five stable redox states, each with a distinctive color, suggesting the use of **5** as a multichannel electrochromic material. The extremely low HOMO–LUMO gap in **5** leads to facile electron transfer, which may occur in solution at room temperature with thermal excitation. Compound **5** gives high-quality LB films, which are poorly conductive due to the specific film structure.

Experimental Section

5: Compound **3**[13] (32 mg, 0.117 mmol) was stirred in oxalyl chloride (0.8 mL) for 72 h at 20 °C. The mixture was filtered and the filtrate was evaporated in vacuo to give acid chloride **4** as a yellow powder. ^{1}H NMR (300 MHz, $CDCl_3$): $\delta = 7.65$ (1H, d, $J = 9.5$ Hz), 7.49 (1H, d, $J = 9.5$ Hz), 7.37 (1H, s), 3.43 (2H, t, $J = 6$ Hz), 3.36 ppm (2H, t, $J = 6$ Hz). *n*BuLi (1.6 M solution in hexane; 65 μL, 0.104 mmol) was added to a solution of compound **1**[12b] (39 mg, 0.100 mmol) in anhydrous THF (10 mL) at −78 °C, stirred for 30 min and a solution of **4** in anhydrous MeCN (4 mL) was added dropwise over 10 min at −100 °C. The reaction mixture was stirred at −78 °C for 5 h and left to warm to 20 °C overnight. The solvent was removed in vacuo, the residue was dissolved in ethyl acetate, washed with water, dried over $MgSO_4$ and the solvent was removed in vacuo. The residue was redissolved in ethyl acetate (0.3 mL), diluted with hexane (0.3 mL) and quickly filtered through a 1 cm pad of silica, eluting with ethyl acetate/hexane (1:1 v/v). Flash chromatography of the filtrate (silica; eluent: ethyl acetate/hexane 1:4 v/v) afforded pure compound **5** as a dark-brown powder (18 mg, 27%), m.p. 152–154 °C. ^{1}H NMR (300 MHz, [D_6]acetone): $\delta = 2.91$ (2H, br), 1.61 (4H, br), 1.37 (8H, br), 0.89 ppm (6H, m); three aromatic protons, three CH_2 groups, and one CH_3 group adjacent to the TTF and TCNQ nuclei are unobservable due to paramagnetic broadening (see Supporting Information). IR (KBr): $\tilde{\nu} = 2187$ (CN), 1734 (CO), 1348, 1279, 1165 cm^{-1}. MS (FAB): *m/z* 646 (M^+, 65%), 388 (35%), 371 (100%). HRMS (EI): 646.1539; calcd for $C_{33}H_{34}N_4O_2S_4$: 646.1564. Elemental analysis calcd (%): C 61.27, H 5.30 N 8.66; found: C 61.01, H 5.28, N 8.55.

Supporting information for this article is available on the WWW under http://www.angewandte.com or from the authors, comprising experimental details; extended discussion of quantum-mechanical calculations, spectroelectrochemical, EPR, low-angle X-ray reflection and AFM experiments; the ^{1}H NMR spectrum of **5**; UV/Vis/NIR spectra of **5** in solution, powder, and LB film; FTIR spectra of **5** in powder and LB film; EPR spectra of **5** in powder and frozen solution; temperature dependence of the EPR signal of a solution of **5**; AFM images of LB films of **5**; diagram of a proposed structure of **5** in LB films; X-ray reflection data for compound **5**; correlation of the LB film thickness measured by different methods; diagram of HOMO and LUMO orbitals of **5′**.

Received: May 12, 2003
Revised: July 29, 2003 [Z51876]

Keywords: cyclic voltammetry · donor–acceptor complexes · electron transfer · tetracyanoquinodimethane · tetrathiafulvalene

[1] A. Aviram, M. A. Ratner, *Chem. Phys. Lett.* **1974**, *29*, 277.
[2] J. Ferraris, D. O. Cowan, V. V. Walatka, J. H. Perlstein, *J. Am. Chem. Soc.* **1973**, *95*, 948.
[3] a) J. Y. Becker, J. Bernstein, S. Bittner, N. Levi, S. S. Shaik, *J. Am. Chem. Soc.* **1983**, *105*, 4468; b) V. Khodorkovsky, J. Y. Becker in *Organic Conductors: Fundamentals and Applications* (Ed: J. P. Farges), Marcel Dekker, New York, **1994**, chap. 3, p. 75.
[4] a) T. J. Meyer, *Acc. Chem. Res.* **1989**, *22*, 163; b) J. L. Segura, N. Martín, *Angew. Chem.* **2001**, *113*, 1416; *Angew. Chem. Int. Ed.* **2001**, *40*, 1372.
[5] K. Stokbro, J. Taylor, M. Brandbyge, *J. Am. Chem. Soc.* **2003**, *125*, 3674.
[6] C. A. Panetta, N. E. Heimer, C. L. Hussey, R. M. Metzger, *Synlett* **1991**, 301.
[7] Reviews: a) M. R. Bryce, *Adv. Mater.* **1999**, *11*, 11; b) M. R. Bryce, *J. Mater. Chem.* **2000**, *10*, 589.
[8] D. F. Perepichka, M. R. Bryce, J. A. K. Howard, A. O. Cuello, M. Gray, V. M. Rotello, *J. Org. Chem.* **2001**, *66*, 4517.
[9] W. R. Hertzler, *J. Org. Chem.* **1976**, *41*, 1412.
[10] C. A. Panetta, J. Baghdadchi, R. M. Metzger, *Mol. Cryst. Liq. Cryst.* **1984**, *107*, 103.
[11] a) R. M. Metzger, R. R. Schumaker, M. P. Cava, R. K. Laidlaw, C. A. Panetta, E. Torres, *Langmuir* **1988**, *4*, 298; b) "Molecular and Biomolecular Electronics": R. M. Metzger in *Advances in Chemistry Series, Vol. 240*, (Ed.: R. R. Birge), American Chemical Society, Washington, DC, **1994**, chap. 5, p. 81.
[12] a) D. F. Perepichka, M. R. Bryce, E. J. L. McInnes, J. P. Zhao, *Org. Lett.* **2001**, *3*, 1431; b) D. F. Perepichka, M. R. Bryce, A. S. Batsanov, E. J. L. McInnes, J. P. Zhao, R. D. Farley, *Chem. Eur. J.* **2002**, *8*, 4656.
[13] J. Baghdadchi, C. A. Panetta, *J. Org. Chem.* **1983**, *48*, 3352. Numerous attempts to attach TCNQ moiety **3** to TTF are reported to have been unsuccessful[6] and we are not aware of any other derivatives of the acid **3**.
[14] V. Kampar, O. Neilands, *Russ. Chem. Rev.* **1986**, *55*, 334.
[15] J. S. Chappell, A. N. Bloch, W. A. Bryden, M. Maxfield, T. O. Poehler, D. O. Cowan, *J. Am. Chem. Soc.* **1981**, *103*, 2442.
[16] Geometry optimization of a model homologue of **5** lacking three alkyl substituents on TTF using DFT suggests that linear and folded "head-to-tail" conformations, where intramolecular π–π interactions can take place are energetically almost equal: $E = -1\,761\,805.8$ and $-1\,761\,807.2$ kcal mol^{-1}, respectively, see Supporting Information.
[17] A similar band (λ_{max} 1585 nm, absorption 0.31 in 1 mm cuvette) is seen in the solution spectrum of the intermolecular complex of $CH_3(C_5H_{11})_2$TTF and TCNQ (1.0×10^{-2} M of each in MeCN); this band vanishes rapidly on dilution, and is not observable at concentrations $< 10^{-3}$ M due to complex dissociation.[12]
[18] R. J. Mortimer, *Chem. Soc. Rev.* **1997**, *26*, 147.
[19] S. Hünig, M. Kemmer, H. Wenner, I. F. Perepichka, P. Bäuerle, A. Emge, G. Gescheid, *Chem. Eur. J.* **1999**, *5*, 1969.
[20] The in situ prepared metalorganic complex [Eu^{3+}···quinone-σ-ferrocene] which was recently claimed to be the first donor–acceptor diad with thermal electron transfer is actually a ground-state radical (S. Fukuzumi, K. Okamoto, H. Imahori, *Angew. Chem.* **2002**, *114*, 642; *Angew. Chem. Int. Ed.* **2002**, *41*, 620).
[21] The contribution of the intermolecular complex to the EPR signal at 290 K is low, since no concentration dependence of the signal was found in the concentration range 1–3 mM.
[22] Reviews: a) M. R. Bryce, M. C. Petty, *Nature* **1995**, *374*, 771; b) T. Bjørnholm, T. Hassenkam, N. Reitzel, *J. Mater. Chem.* **1999**, *9*, 1975.

 © 2003 Wiley-VCH Verlag GmbH & Co. KGaA, Weinheim

Delivering Anticancer Agents

Design of Environment-Sensitive Supramolecular Assemblies for Intracellular Drug Delivery: Polymeric Micelles that are Responsive to Intracellular pH Change**

*Younsoo Bae, Shigeto Fukushima, Atsushi Harada, and Kazunori Kataoka**

The recent development of biomolecular devices that function within the living body has required the integration of capabilities for sensing in vivo chemical stimuli, generating detectable signals, and effecting suitable responses into a single molecule or molecular complex.[1] In particular, biopharmaceutical systems which interact with intracellular components or events such as ions, proteins, enzymes, and pH changes are becoming important for implementing programmed functions that respond to signatures of the body.[2–6] Supramolecular chemistry is attracting attention as it offers methods for assembling different constituents capable of structural and dynamic changes into single molecules.[7] Herein we demonstrate the intracellular localization of a pH-sensitive supramolecular assembly that changes its structure and fluorescences when activated to induce mortality of malignant cells.

There are many difficulties in the clinical use of some biomolecular devices, these problems include phagocytic clearance during blood circulation, systemic spread causing toxic side effects, and exclusion from the cell by membrane transporters. In general, the cells selectively permeable membranes prevent the access of biomolecular devices that have not been appropriately designed. Therefore, the creation of biomolecular devices that are sensitive to the intracellular environment has been suggested as a method to overcome these physiological bottlenecks.[8,9]

From self-assembling acid-sensitive amphiphilic block copolymers we have prepared a polymeric micelle that is activated by the intracellular pH value (Figure 1). The polymeric micelle is a supramolecular assembly with characteristic properties, such as a core-protecting double-layer structure that is tens of nanometers in diameter, low toxicity in the human body, and has a prolonged circulation in the blood owing to its high water-solubility, thus avoiding phagocytic and renal clearance.[10] In addition, the functionality of the micelles can be modified simply by changing the chemical structures of the block copolymers,[11] and materials such as drugs,[12–14] proteins,[15] and DNAs,[16–18] can be selectively delivered to solid tumors in the body.[19,20] Site-specific tumor targeting in the body is achieved by the enhanced permeability and retention (EPR) effect, proposed by Maeda and Matsumura.[21] According to their report, solid tumors have abnormal blood vessels with loose junction and insufficient lymphatic drainage, so that the micelles easily escape from the blood vessel and accumulate in tumor tissues but they hardly return to the blood stream again. In general, cells take up large materials, such as the micelles, by folding the cell membrane inwardly, surrounding the materials to be ingested. The material is then engulfed in small bubble-like endocytic vesicles. This is called the endocytosis process that allows supramolecular assemblies to sneak into intracellular regions avoiding the cell-membrane transporters. After the micelles are taken up to the cell interior through endocytosis, the substance transport occurs. The endocytic vesicles change from early and late endosomes and finally to lysosomes in which the proton concentration is 100-times lower (pH 5.0) than the physiological condition (pH 7.4), which is an important in vivo chemical stimuli that can be used to trigger functional biomolecular devices.[22]

An amphiphilic block copolymer, poly(ethylene glycol)–poly(aspartate–hydrazone–adriamycin) (PEG–p(Asp–Hyd–ADR)), was synthesized using the aspartic acid of poly(ethylene glycol)–poly(β-benzyl-L-aspartate) (PEG–PBLA) as a convenient template (Scheme 1). PEG–PBLA was synthesized from the ring-opening polymerization of β-benzyl-L-aspartate *N*-carboxy-anhydride (BLA–NCA). Poly-

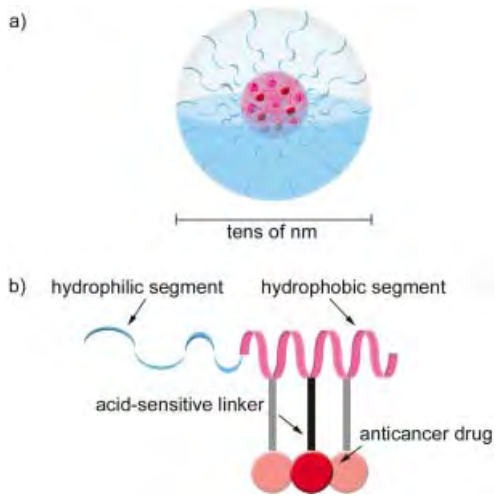


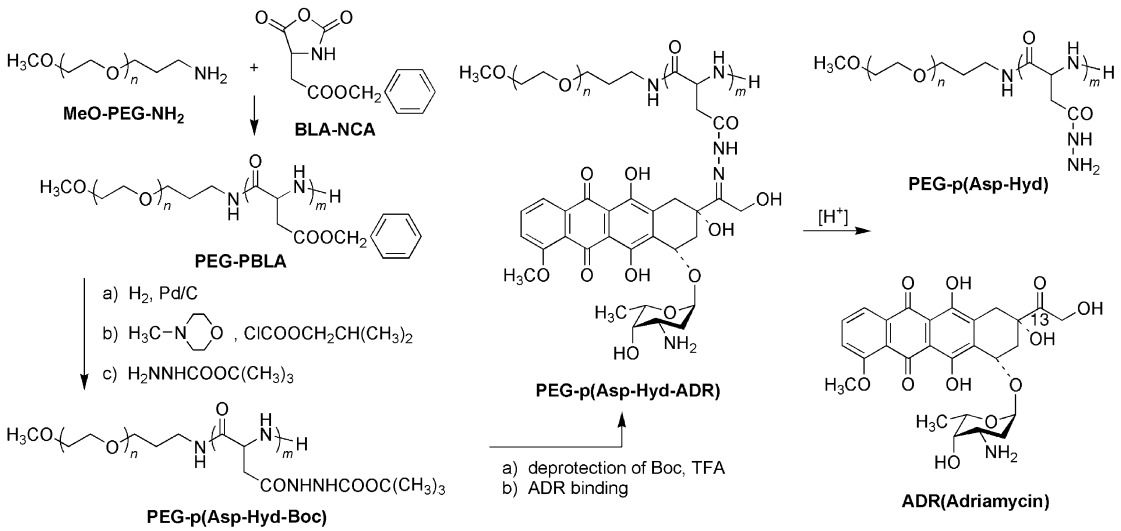
Figure 1. The polymeric micelles (a), were prepared from self-assembling acid-sensitive amphiphilic block copolymers (b), in aqueous solution. A supramolecular structure of the micelles has the advantage of site-specific targeting in the body, protecting reactive functional moieties with the hydrophilic outer shell during blood circulation.

[*] Prof. Dr. K. Kataoka, Y. Bae, S. Fukushima, A. Harada
Department of Material Science and Engineering
Graduate School of Engineering
The University of Tokyo
7-3-1 Hongo, Bunkyo-ku, Tokyo 113-8656 (Japan)
Fax: (+81) 3-5841-7139
E-mail: kataoka@bmw.t.u-tokyo.ac.jp

[**] This work is financially supported by a Grant-in-Aid for Scientific Research from the Ministry of Education, Culture, Sports, Science and Technology (MEXT), Japan, and by Core Research for Evolutional Science and Technology (CREST), Japan Science and Technology Corporation (JST). The authors acknowledge the National Cancer Center Research Institute, Japan, for supplying a human small cell lung cancer cell line SBC-3. Y.B. acknowledges financial support from the Japanese Monbusho's scholarship program.

Supporting information for this article is available on the WWW under http://www.angewandte.org or from the author.

 © 2003 Wiley-VCH Verlag GmbH & Co. KGaA, Weinheim DOI: 10.1002/anie.200250653



Scheme 1. Synthesis of PEG–p(Asp–Hyd–ADR) block copolymers. The Schiff base formed between the C13 ketone of ADR and the hydrazide groups of the PEG–p(Asp–Hyd) block polymer are most effectively cleavable under acidic conditions around pH 5.0, which correspond to that of the lysosomes in the cells. Boc = *tert*-butoxycarbonyl, TFA = trifluoroacetic acid.

merization of BLA–NCA was initiated by the terminal primary amino group of α-methoxy-ω-amino poly(ethylene glycol) under argon atmosphere in distilled dimethylformamide. After deprotection of the benzyl groups of PEG–PBLA, hydrazide groups were attached to the end of the aspartate side chains of the block copolymer by an acid anhydride reaction which is a modification of the synthetic method suggested by T. Kaneko et al.[23] ^{1}H NMR measurements in [D$_6$]DMSO at 80 °C reveal that the numbers of repeating units of P(Asp) block and hydrazide groups were 37 and 28, respectively (see Supporting Information). Adriamycin (ADR) was then conjugated to the polymer backbone through an acid-labile hydrazone bond between C13 of ADR and the hydrazide groups of the PEG–p(Asp–Hyd) block copolymer. Subsequently, the polymeric micelles were prepared by a dialysis method which brought the organic components into an aqueous environment. The micelles were about 65 nm in diameter and of uniform size, as confirmed by dynamic light-scattering measurements (DLS; Supporting Information). ADR is an anticancer agent and suppresses cell growth by binding with DNA strands in the cell nucleus. Despite its efficacy, ADR use is frequently accompanied by toxic side effects. However, its activity is suspended by binding to materials such as polymers, antibodies, and molecular complexes.[24] In addition, the detectable fluorescence of ADR allows it to be used as a fluorescence probe in this study.

The acid-sensitivity of the micelles was evaluated by reversed-phase liquid chromatography (RPLC) (Supporting Information). As shown in Figure 2, the micelles release ADR both time- and pH-dependently as the pH value decreases from pH 7.4 to 3.0. The micelles were stable over 72 h in region A (Figure 2), which corresponds to physiological and early endosomal conditions. On the other hand, the release of ADR gradually increases and reaches equilibrium as the pH decreases in regions B and C. The ADR release profile in region B is notable considering that the pH values in

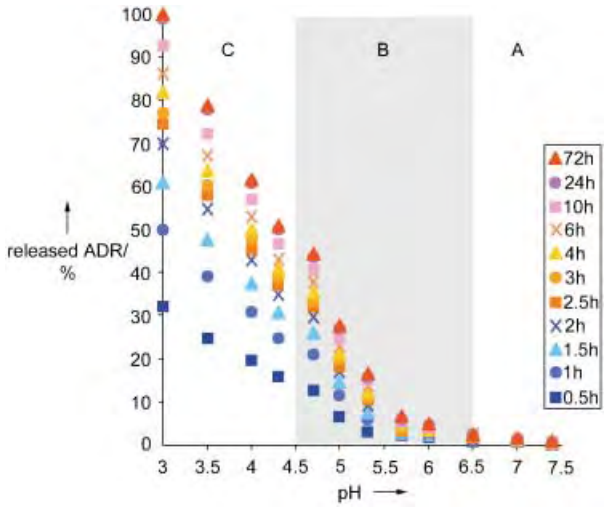


Figure 2. Time and pH-dependent ADR release profile of the micelles. The micelles selectively released ADR under the pH conditions of regions A and B which correspond to outer and intracellular conditions, respectively. The amount of loaded ADR on the micelles was calculated at pH 3.0 in region C, where the release was the maximum.

late endosomes and/or lysosomes in the cells are around 5.0 where the acid-sensitive hydrazone bonds can be cleaved most effectively. Because the formation of reversible hydrazone bonds is hindered by strong acidity, the loading content of ADR on the micelles was calculated from the maximum ADR release at pH 3.0 in region C (Supporting Information). The calculation revealed that the micelles consisted of the block copolymers containing ADR with 67.6 % mol substitution with respect to aspartate units of PEG–p(Asp–Hyd–ADR).

Measurement of fluorescence intensity reveals that the micelles are stable under physiological conditions and fluorescence only occurs when the ADR is released under acidic

 © 2003 Wiley-VCH Verlag GmbH & Co. KGaA, Weinheim

conditions (Supporting Information). The micelles and free ADR were incubated in cell culture medium, Dulbecco's Modified Eagle's Medium (DMEM) supplemented with 10% fetal bovine serum for 24 h. Ion and pH levels are controlled in DMEM, which is very similar to physiological condition in the body. Concentrations of ADR and the ADR bound in the micelles were adjusted to be equivalent (100 $\mu g\,mL^{-1}$). Samples were excited with the wavelength of 485 nm, and the fluorescence at 590 nm was monitored by a spectrofluorometer. Compared with the intense fluorescence of free ADR, the fluorescence intensity of the ADR-bound in the micelles remained low and no significant change in intensity was observed after 24 h monitoring. Like most fluorescence materials, the fluorescence of ADR is quenched in a high concentration in solution. This phenomenon also occurs in the micelle core where ADR molecules are confined at high local concentrations. The fluorescence remains quenched as long as the ADR is incorporated in the micelle core and a change in fluorescence reflects the, release of the ADR from the micelles. Thus, the pH sensitive structural change of the micelles can be detected through the change in fluorescence.

Observations using confocal laser scanning microscopy (CLSM) reveal the intracellular localization of micelles that were incubated with human small cell lung cancer cell SBC-3. As shown in Figure 3, a time-dependent fluorescence change in intensity was observed over 24 h. After 1 h exposure, an increase in fluorescence intensity was observed for SBC-3 incubated with ADR (Figure 3a), but no such increase was detected with the micelles (Figure 3c). On the other hand, a considerable fluorescence change was observed in the cells exposed to the micelles after 24 h incubation (Figure 3d), which clearly demonstrates intracellular distribution of the micelles and the released ADR. Compared with Figure 3b which shows that ADR is only accumulated in cell nuclei, Figure 3d indicates that the localized fluorescence is dot-shaped within the cytoplasm suggesting the presence of the micelles trapped in the endocytic vesicles. In general, it is very difficult to distinguish between the fluorescence material ADR and its polymer conjugates in solution because both exhibit intense fluorescence. However, the micelles solve this problem because of their characteristic fluorescence quenching effects.

As a system releasing bioactive molecules, the micelles are required to maintain the ability of the loaded ADR to suppresses cell growth by binding with DNA strands in the cell nucleus. Figure 4 shows the growth-inhibition effects of

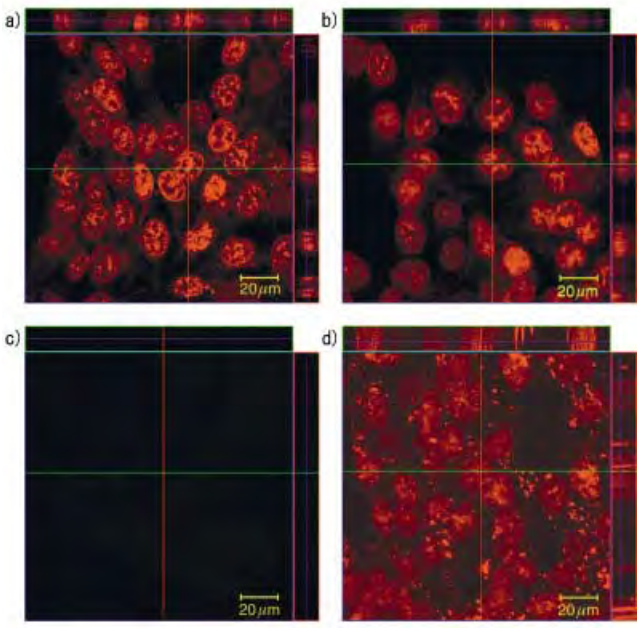


Figure 3. CLSM images of the SBC-3 cells incubated with ADR and the micelles (10 $\mu g\,mL^{-1}$). In contrast to free ADR, the fluorescence of the ADR in the micelles is only detected when they are activated. A series of optical sections was stacked (Z-stacked) by moving the focal plane of the instrument step-by-step through the depth of the cell. The Z-stacked images clearly reveal that the micelles are localized within the cytoplasm with a dotlike shape, assumed to be micelles in acidic lysosomal compartments, while most of the ADR released from the micelles is in the cell nucleus. a) free ADR after 1 h exposure, b) free ADR after 24 h incubation, c) micelles after 1 h exposure, d) micelles after 24 h incubation.

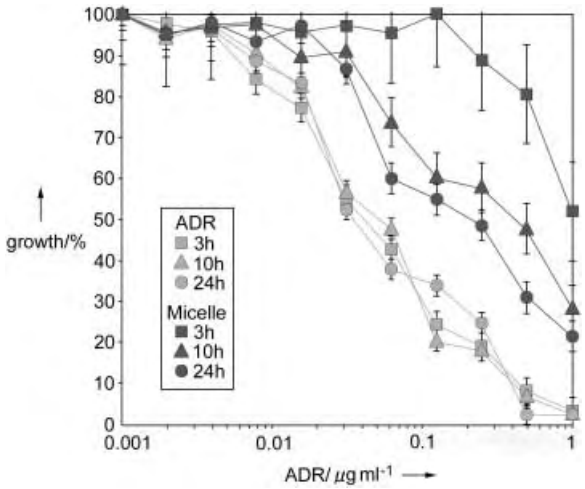


Figure 4. Growth inhibition assay results on human small lung cancer cells SBC-3 with different ADR concentrations and exposure times. As time elapses, the curve indicating the inhibition effect of the ADR-containing micelles approached that of free ADR.

the micelles on SBC-3 cells. The results obtained with the micelles gradually approach those of free ADR, which demonstrates that the ADR released from the micelles is pharmaceutically active. Therefore, we conclude that ADR accumulates in the cell nuclei after release from the micelles localized within the cytoplasm.

In summary, we have shown the intracellular localization of pH-sensitive polymeric micelles whose functions are controlled by live cells. As a multifunctional biomolecular device, the micelles undergo dynamic changes in structure and/or function in response to environmental stimuli (pH value). Furthermore, the ADR released from the micelles fluorescences which allows its localization within the living cells to be detected. CLSM reveals that the micelles are trapped in lysosomes where they are programmed to function by responding to low pH, and the released ADR

 © 2003 Wiley-VCH Verlag GmbH & Co. KGaA, Weinheim

accumulates in the cell nuclei and effectively suppresses the synchronizing cell viability of cancer cells. These results suggest that highly controlled functional biomolecular devices have become available.

Received: November 28, 2002
Revised: April 25, 2003 [Z50653]

Keywords: anticancer agents · micelles · polymers · self-assembly · supramolecular chemistry

[1] D. S. Goldin, C. A. Dahl, K. L. Olsen, L. H. Ostrach, R. D. Klausner, *Science* **2001**, *292*, 443 – 444.
[2] H. R. Ihre, O. L. Padilla de Jesus, F. C. Szoka, Jr., M. J. Fréchet, *Bioconjugate Chem.* **2002**, *13*, 443 – 452.
[3] H. Stephan, H. Spies, B. Johannsen, C. Kauffmann, F. Vögtle, *Org. Lett.* **2000**, *2*, 2343 – 2346.
[4] M. Kramer, J. F. Stumbe, H. Turk, S. Krause, A. Komp, L. Delineau, S. Prokhovova, H. Kautz, R. Haag, *Angew. Chem.* **2002**, *114*, 4426 – 4431; *Angew. Chem. Int. Ed.* **2002**, *41*, 4252 – 4256.
[5] D. E. Dishcher, A. Eisenberg, *Science* **2002**, *297*, 967 – 973.
[6] R. Langer, *Science* **2001**, *293*, 58 – 59.
[7] J. M. Lehn, *Science* **2002**, *295*, 2400 – 2403.
[8] A. Tang, P. Kopeckova, J. Kopecek, *Pharm. Res.* **2003**, *20*, 360 – 367.
[9] H. Shen, A. Eisenberg, *Angew. Chem.* **2000**, *112*, 3448 – 3450; *Angew. Chem. Int. Ed.* **2000**, *39*, 3310 – 3312.
[10] K. Kataoka, A. Harada, Y. Nagasaki, *Adv. Drug Delivery Rev.* **2001**, *47*, 113 – 131.
[11] Y. Nagasaki, T. Okada, C. Scholz, M. Lijima, M. Kato, K. Kataoka, *Macromolecules* **1998**, *31*, 1473 – 1479.
[12] M. Yokoyama, M. Miyauchi, N. Yamada, T. Okano, Y. Sakurai, K. Kataoka, S. Inoue, *J. Controlled Release* **1990**, *11*, 269 – 278.
[13] M. Yokoyama, T. Okano, Y. Sakurai, H. Ekimoto, C. Shibazaki, K. Kataoka, *Cancer Res.* **1991**, *51*, 3229 – 3236.
[14] K. Kataoka, G. S. Kwon, M. Yokoyama, T. Okano, Y. Sakurai, *J. Controlled Release* **1993**, *24*, 119 – 132.
[15] A. Harada, K. Kataoka, *Macromolecules* **1998**, *31*, 288 – 294.
[16] K. Kataoka, H. Togawa, A. Harada, K. Yasugi, T. Matsumoto, S. Katayose, *Macromolecules* **1996**, *29*, 8556 – 8557.
[17] S. Katayose, K. Kataoka, *Bioconjugate Chem.* **1997**, *8*, 702 – 707.
[18] Y. Kakizawa, A. Harada, K. Kataoka, *J. Am. Chem. Soc.* **1999**, *121*, 11 247 – 11 248.
[19] G. S. Kwon, S. Suwa, M. Yokoyama, T. Okano, Y. Sakurai, K. Kataoka, *J. Controlled Release* **1994**, *29*, 17 – 23.
[20] T. Nakanishi, S. Fukushima, K. Okamoto, M. Suzuki, Y. Matsumura, M. Yokoyama, T. Okano, Y. Sakurai, K. Kataoka, *J. Controlled Release* **2001**, *74*, 295 – 302.
[21] H. Maeda, Y. Matsumura, *Crit. Rev. Ther. Drug Carrier Syst.* **1989**, *6*, 193 – 210.
[22] R. Duncan, *Anti-Cancer Drugs* **1992**, *3*, 175 – 210.
[23] T. Kaneko, D. Willner, I. Monkovic, J. O. Knipe, G. R. Braslawsky, R. S. Greenfield, D. M. Vyas, *Bioconjugate Chem.* **1991**, *2*, 133 – 141.
[24] M. Yokoyama, T. Okano, Y. Sakurai, S. Fukushima, K. Okamoto, K. Kataoka, *J. Drug Targeting* **1999**, *7*, 171 – 186.

 © 2003 Wiley-VCH Verlag GmbH & Co. KGaA, Weinheim

O_2 Insertion and Epoxidation

First Structurally Authenticated Zinc Alkylperoxide: A Model System for the Epoxidation of Enones**

Janusz Lewiński, Zbigniew Ochal, Emil Bojarski, Ewa Tratkiewicz, Iwona Justyniak, and Janusz Lipkowski*

It is over 150 years since the high reactivity of zinc alkyl species towards oxygen was noted by Frankland in his pioneering studies on dialkyl zinc compounds, R_2Zn.[1] Since then the interaction of zinc alkyl complexes with O_2 has been of continuous interest from the fundamental and practical point of view as well as an ubiquitous side reaction in the preparation and handling of organozinc compounds.[2] In 1890 Demuth and Meyer[3] postulated for the first time the formation of the alkylperoxide [EtZnOOEt] as the result of the insertion of an O_2 molecule into the Zn–C bond. On the other hand, the most spectacular application of the reaction of zinc alkyl complexes with O_2 is the epoxidation of enones, where the alkylperoxide [ZnOOR] species is prepared in situ and acts as an efficient epoxidizing reagent.[4,5] Recently, there has also been an increased interest in various radical addition reactions initiated by the R_2Zn/O_2 system.[6] However, despite the long history of studies on the reaction of organozinc compounds with dioxygen, there have been no reports of the structurally authenticated zinc alkylperoxide; controlling and understanding the reactivity of zinc alkyl complexes with dioxygen is a demanding task. It should be also noted that the structural data for main-group metal alkylperoxides are very limited because of the high reactivity and often low stability of this group of compounds.[7]

Our recent studies have been directed towards designing main-group complexes as model species for investigations of the relationship between the molecular geometry and reactivity or other property of interest.[7a,b,8] Thus, investigations on the reactivity of aluminum alkyl species with molecular oxygen have shown that the key feature in the oxygenation reaction is the O_2 attack on the four-coordinate metal center, followed by an insertion of O_2 into the Al–C bond to generate an Al–OOR moiety.[7a,b] As an extension of these studies we turned our attention to the design of zinc alkyl complexes as model species with which a better understanding of dioxygen activation by organometallic compounds could be gained. The

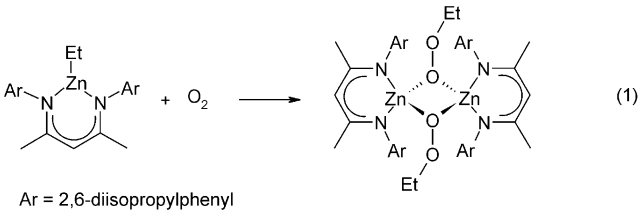
[*] Dr. J. Lewiński, Z. Ochal, E. Bojarski, E. Tratkiewicz
Department of Chemistry
Warsaw University of Technology
Noakowskiego 3, 00–664 Warsaw (Poland)
Fax: (+48) 22-6607-279
E-mail: lewin@ch.pw.edu.pl
Dr. I. Justyniak, Prof. Dr. J. Lipkowski
Institute of Physical Chemistry
Polish Academy of Sciences
Kasprzaka 44/52, 01-224 Warsaw (Poland)

[**] This work was supported by the State Committee for Scientific Research (No 3 T09A 066 19).

 DOI: 10.1002/anie.200351940 © 2003 Wiley-VCH Verlag GmbH & Co. KGaA, Weinheim

choice of ligand, 2-[(2,6-diisopropylphenyl)amino]-4-[(2,6-diisopropylphenyl)imino]-pent-2-ene (BDI-H), was dictated by the recent successful use of such bulky β-diketiminates in the stabilization of unique main-group metal species[9] and of well-defined single-site catalysts.[10] We report herein the synthesis and structural characterization of the zinc alkylperoxide derived from the insertion of dioxygen into the Zn–Et bond, and the high reactivity of the resulting compound in the epoxidation of enones.

The reaction of $[Et_2Zn]$ with BDI-H leads to the well-defined three-coordinate complex [(BDI)ZnEt] (**1**).[10b,c] When the toluene solution of **1** was exposed to an excess of dry dioxygen at 0 °C for approximately 5 min. and then stored at −20 °C, a white crystalline precipitate of $[\{(BDI)Zn\text{-}OOEt\}_2]$ (**2**) deposited in good yield [Eq. (1)].[11] The room



(1)

Ar = 2,6-diisopropylphenyl

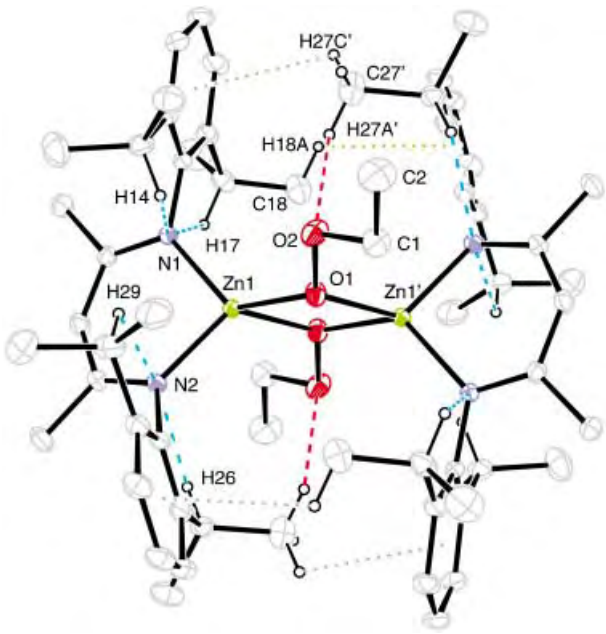


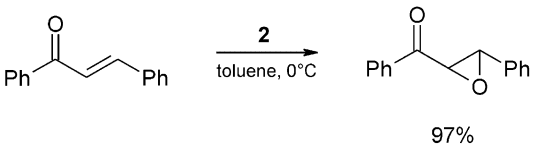
Figure 1. The molecular structure of **2**. Thermal ellipsoids are set at 40% probability, and only selected hydrogen atoms are shown for clarity.

temperature ^{1}H NMR spectrum of the final mixture reveals the presence of an ethyl group bound to oxygen and the lack of the Zn–Et group, which implies the complete oxygenation of the Zn–C bond [Eq. (1)]. The IR spectrum of **2** exhibits a moderate absorption at 854 cm^{-1} attributable to the characteristic peroxidic $\tilde{\nu}$(O–O) stretching vibration.

The molecular structure of **2** was determined by a single-crystal X-ray diffraction (Figure 1).[12] Most notably, the structure reveals **2** to be a dinuclear aggregate with monomeric {(BDI)ZnOOEt} units joined by the μ_2-bridging ethylperoxide groups. The central $\{ZnN_2O_2\}$ core in **2** has a similar structure to that observed for recently characterized alkoxides $[\{(BDI)ZnOR\}_2]$ (where R = Me, *i*Pr).[10a,b,e] The molecule has crystallographic C_i symmetry and the geometry about the zinc centers is distorted tetrahedral. The six-membered ZnNCCCN ring adopts a sofa conformation, and the zinc atom is displaced 0.532(2) Å out of the almost flat ligand plane. The Zn–Zn separation is 3.179 Å and Zn1–O1 and Zn1–O1′ bonds (1.971(1) and 2.044(1) Å) all are slightly larger than those in the alkoxide compounds $[\{(BDI)Zn\text{-}OR\}_2]$. This observation correlates well with both the relatively wide Zn1-O1-Zn1′ angle (104.69(6)°) and narrow O1-Zn1-O1′ angle (75.31(6)°) when compared to the related values in the alkoxide $\{Zn_2O_2\}$ cores.[10a,b,e] The peroxo O1–O2 bond of 1.451(2) Å is close to that found for alkylperoxides coordinated to main-group metal centers and transition-metals.[7,13] While the bridging oxygen atom in the alkoxides $[\{(BDI)ZnOR\}_2]$ is planar, the oxygen atom of the ethylperoxo group in **2** shows the expected pyramidal stereochemistry.[14] The ethylperoxo ligand is oriented in an eclipsed–staggered conformation, to minimize lone-pair repulsion on the oxygen atoms. It should be noted that the relative orientation of this ligand with respect to the central $\{Zn_2O_2\}$ ring (the torsion angles for COOZn1 and COOZn1′ are 167.3(1) and −57.3(2)°) is distinct from that observed for other compounds containing μ_2-bridging alkylperoxide groups, all of which are essentially perpendicular to the central core.[7d,f,14,15] However, a detailed inspection of the molecular structure of **2** indicates that a complex system of weak intramolecular hydrogen bonds plays a substantial role in the determination of the molecular shape (Figure 1). The analysis of intramolecular contacts shows a pair of C–H···π interactions between the C18 and C27′ methyl groups and the proximal aryl ring of adjacent ligand (the intermolecular H···(ring centroid) contacts are 2.85 and 2.96 Å) as well as the C–H···O interaction between the C27′ methyl groups and the ethylperoxide oxygen atom (C-H27A′···O2 2.67 Å).[16] The orientation of the *i*Pr groups in the 2,6-diisopropylphenyl substituents also indicates the presence of intramolecular C–H···N interactions between the *i*Pr group methine hydrogen atoms and the nitrogen atoms (2.41–2.50 Å). Therefore we presume that although the structure of the central core is dictated by the strong Zn–O bonds, the observed conformational preferences in **2** result from the cooperative non-covalent interactions.[17]

The epoxidation of electron-deficient olefins remains a challenging task in organic chemistry[5] and, as we mentioned above, zinc alkylperoxides are very promising reagents for this process. Thus, we assume that compound **2** may be a useful model compound for the epoxidation of enones. Indeed, the epoxidation of *trans*-chalcone revealed that **2** is a highly reactive oxidizing reagent, the reaction being complete in several minutes at 0 °C, to give the *trans*-epoxide in very good yield [Eq. (2)]. For comparison, epoxidation of chalcone with an Et_2Zn/O,N-H/O_2 system (where O,N-H =

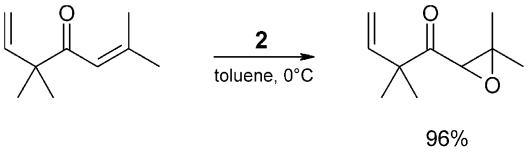
 © 2003 Wiley-VCH Verlag GmbH & Co. KGaA, Weinheim



97% (2)

aminoalcohol as the auxiliary ligand) was completed after 16 h under similar conditions.[4b]

Furthermore, despite the high reactivity of **2** towards enones, the regio- and chemoselective epoxidation of artemisia ketone is feasible as illustrated in Equation (3). Thus, **2**



96% (3)

is highly selective for the electron-deficient alkene unit in the presence of β-functionalized unconjugated alkene. Based on these initial studies we anticipate that using **2** will allow the epoxidation of a wide range of enones.

Further studies on the interaction of zinc alkyl complexes with dioxygen and the reactivity of zinc alkylperoxides are in progress along with developing the epoxidation of enones.

Experimental Section

2: A stirred solution of [(BDI)ZnEt] (1.02 g, 2 mmol) in toluene (5 cm^3) was cooled to 0 °C, then an excess of dry dioxygen (1 atm) was introduced. After 5 min the excess of O_2 was removed (the reaction mixture was cooled to −78 °C, then the system was purged with nitrogen using a vacuum/nitrogen line). The mixture was stored at −20 °C and white crystalline product deposited; yield: 90 %. ^{1}H NMR (400 MHz, C_6D_6): $\delta = 1.02$ (t, $J = 6.8$ Hz, 6H, OCH_2CH_3) 1.15 (d, $J =$ 7.0 Hz, 24H, $CH(CH_3)_2$), 1.20 (d, $J = 7.0$ Hz, 24H, $CH(CH_3)_2$), 1.66 (s, 12H, CCH_3), 3.31 (m, 8H, $CH(CH_3)_2$), 3.84 (q, $J = 6.8$ Hz, 4H, OCH_2CH_3), 4.88 (s, 2H, CH), 7.12 ppm (m, 16H, Ar); IR (Nujol): $\tilde{\nu} =$ 1547 (m), 1526 (s), 1462 (s), 1436 (s), 1407 (s), 1317 (s), 1265 (m), 1253 (m), 1235 (w), 1180 (m), 1160 (w), 1137 (w), 1107 (w), 1100 (w), 1058 (w), 1036 (w), 1022 (w),937 (w), 854 (w), 796 (m), 760 (m), 729 (m), 694 (w), 638 (w), 563 (w), 529 cm^{-1} (w); elemental analysis (%) calcd for $C_{62}H_{92}N_4O_4Zn_2 \cdot 0.95$ toluene: C70.21, H 8.54, N 4.75; found: C 70.12, H 8.56, N 4.78.

Epoxidation of enones: To a stirred solution of **2** (2 mmol) in toluene (5 cm^3) was added the corresponding enone (1.9 mmol) at 0 °C and the reaction mixture was stirred for 15 min and the crude mixture was analyzed by ^{1}H NMR. Then the solution was treated with KF (3.5 g, 60 mmol) and water (1.2 mL, 67 mmol). The organic products formed were extracted with ethyl ether and the conversion was analyzed by liquid chromatography (HPLC) and ^{1}H NMR. Additionally, the α,β-epoxyketones were isolated by flash chromatography.

Received: May 21, 2003
Revised: June 25, 2003 [Z51940]

Keywords: asymmetric epoxidation · enones · N ligands · peroxides · zinc

[1] E. Frankland, *Justus Liebigs Ann. Chem.* **1849**, *71*, 171.
[2] a) G. Sosnovsky, J. H. Brown, *Chem. Rev.* **1966**, *66*, 529; b) A. G. Davies, B. P. Roberts, *Acc. Chem. Res.* **1972**, *5*, 387; c) G. Boche, J. C. W. Lohrenz, *Chem. Rev.* **2001**, *101*, 697; d) D. Seyferth, *Organometallics* **2001**, *20*, 2940.
[3] R. Demuth, V. Meyer, *Ber. Dtsch. Chem. Ges.* **1890**, *23*, 394.
[4] a) K. Yamamoto, N. Yamamoto, *Chem. Lett.* **1989**, 1149; b) D. Enders, J. Zhu, G. Raabe, *Angew. Chem.* **1996**, *109*, 1827; *Angew. Chem. Int. Ed. Engl.* **1996**, *35*, 1725; c) D. Enders, J. Zhu, L. Kramps, *Liebigs Ann.* **1997**, 1101; d) D. Enders, L. Kramps, J. Zhu, *Tetrahedron: Asymmetry* **1998**, *9*, 3959; e) H.-B. Yu, H.-F. Zheng, Z.-M. Lin, Q.-S. Hu, W.-S. Huang, L. Pu, *J. Org. Chem.* **1999**, *64*, 8149.
[5] For a recent review on the asymmetric epoxidation of electron-deficient olefins see: M. J. Porter, J. Skidmore, *Chem. Commun.* **2000**, 1215.
[6] Selected recent examples: a) S. Bazin, L. Feray, D. Siri, J. V. Naubron, M. P. Bertrand, *Chem. Commun.* **2002**, 2506; b) K. Yamada, H. Fujihara, Y. Yamamoto, Y. Miwa, T. Taga, K. Tomioka, *Org. Lett.* **2002**, *4*, 3509; c) T. Shinohara, S. Fujioka, H. Kotsuki, *Heterocycles* **2001**, *52*, 237; d) H. van der Deen, R. M. Kellogg, B. L. Feringa, *Org. Lett.* **2000**, *2*, 1593; e) M. P. Bertrand, L. Feray, R. Nouguier, P. Perfetti, *J. Org. Chem.* **1999**, *64*, 9189; f) I. Ryu, F. Araki, S. Minakata, M. Komatsu, *Tetrahedron Lett.* **1998**, *39*, 6335.
[7] a) J. Lewiński, J. Zachara, P. Gos, E. Grabska, T. Kopec, I. Madura, W. Marciniak, I. Prowotorow, *Chem. Eur. J.* **2000**, *6*, 3215; b) J. Lewiński, J. Zachara, E. Grabska, *J. Am. Chem. Soc.* **1996**, *118*, 6794; c) G. Boche, K. Möbus, K. Harms, J. C. W. Lohrenz, M. Marsch, *Chem. Eur. J.* **1996**, *2*, 604; d) M. B. Power, J. W. Ziller, A. R. Barron, *Organometallics* **1993**, *12*, 4908; e) A. L. Balch, C. R. Cornman, M. M. Olmstead, *J. Am. Chem. Soc.* **1990**, *112*, 2963; f) W. M. Cleaver, A. R. Barron, *J. Am. Chem. Soc.* **1989**, *111*, 8967; g) V. E. Shklover, Yu. T. Struchkov, V. A. Dodonov, T. I. Zinoveva, V. L. Antonovskii, *Metalloorg. Khim.* **1988**, *1*, 1140; h) Z. A. Starikowa, T. M. Shchegoleva, V. K. Trunov, I. E. Pokrovskaya, E. N. Kanunnikova, *Kristallografiya* **1979**, *24*, 1211.
[8] a) J. Lewiński, J. Zachara, I. Justyniak, *Chem. Commun.* **2002**, 1586; b) J. Lewiński, J. Zachara, P. Horeglad, D. Glinka, J. Lipkowski, I. Justyniak, *Inorg. Chem.* **2001**, *40*, 6086; c) J. Lewiński, J. Zachara, T. Kopec, K. B. Starowieyski, J. Lipkowski, I. Justyniak, E. Kolodziejczyk, *Eur. J. Inorg. Chem.* **2001**, 1123; d) C. S. Branch, J. Lewiński, I. Justyniak, S. G. Bott, J. Lipkowski, A. R. Barron, *J. Chem. Soc. Dalton Trans.* **2001**, 1253.
[9] Selected recent examples: a) P. L. Holland, W. B. Tolman, *J. Am. Chem. Soc.* **1999**, *121*, 7270; b) C. M. Cui, H. W. Roesky, H. G. Schmidt, M. Noltemeyer, H. J. Hao, F. Cimpoesu, *Angew. Chem.* **2000**, *112*, 4444; *Angew. Chem. Int. Ed.* **2000**, *39*, 4274; c) N. J. Hardman, B. E. Eichler, P. P. Power, *Chem. Commun.* **2000**, 1991; d) V. C. Gibson, J. A. Segal, A. J. P. White, D. J. Williams, *J. Am. Chem. Soc.* **2001**, *122*, 7120; e) D. J. E. Spencer, A. M. Reynolds, P. L. Holland, B. A. Jazdzewski, C. Duboc-Toia, L. Le Pape, S. Yokota, Y. Tachi, S. Ito, W. B. Tolman, *Inorg. Chem.* **2002**, *41*, 6307.
[10] Selected recent examples: a) B. M. Chamberlain, M. Cheng, D. R. Moore, T. M. Ovitt, E. B. Lobkovsky, G. W. Coates, *J. Am. Chem. Soc.* **2001**, *123*, 3229; b) M. Cheng, D. R. Moore, J. J. Reczek, B. M. Chamberlain, E. B. Lobkovsky, G. W. Coates, *J. Am. Chem. Soc.* **2001**, *123*, 8738; c) J. Prust, A. Stasch, W. J. Zheng, H. W. Roesky, E. Alexopoulos, I. Uson, D. Bohler, T. Schuchardt, *Organometallics* **2001**, *20*, 3825; d) A. P. Dove, V. C. Gibson, E. L. Marshall, A. J. P. White, D. J. Williams, *Chem. Commun.* **2001**, 283; e) D. R. Moore, M. Cheng, E. B. Lobovsky, G. W. Coates, *Angew. Chem.* **2002**, *114*, 27119; *Angew. Chem. Int. Ed.* **2002**, *41*, 2599.

 © 2003 Wiley-VCH Verlag GmbH & Co. KGaA, Weinheim

[11] We have not observed an oxidative degradation of the β-diketiminate ligand under these condition as found for other inorganic Zn^{II} complexes supported by this type ligands: S. Yakota, Y. Tachi, S. Itoh, *Inorg. Chem.* **2002**, *41*, 1342.

[12] Crystal data for **2**·toluene, $C_{69}H_{100}N_4O_4Zn_2$: $M_r = 1180.27$, crystal dimensions $0.42 \times 0.36 \times 0.16$ mm^3, triclinic, space group $P\bar{1}$ (no. 2), $a = 11.0610(2)$, $b = 13.0220(2)$, $c = 13.5830(2)$ Å, $\alpha = 97.5150(10)$, $\beta = 112.3750(10)$, $\gamma = 108.3870(10)°$, $V = 1645.14(5)$ Å^3, $Z = 1$, $F(000) = 634$, $\rho_{calcd} = 1.191$ g m^3, $T = 150(2$ K, $\mu(Mo_{K\alpha}) = 4.19$ mm^{-1}, Nonius Kappa-CCD diffractometer, $\theta_{max} = 27.5°$, 7530 unique reflections. The structure was solved by direct methods using the SHELXS86[18] program and was refined by full-matrix least-squares on F^2 using the program SHELXL97.[19] The peroxide moiety was refined as a disordered group. The disorder was modeled in terms of two sets of (OOEt) atoms with refined occupancy factors. The group showing SOF = 0.131(4) was refined isotropically with geometrical restraints assuming that chemically equivalent distances in both groups were nearly equal. Hydrogen atoms were included in idealized positions and refined isotropically. Refinement converged at $R1 = 0.0509$, $wR2 = 0.0906$ for all data and 398 parameters ($R1 = 0.0383$, $wR2 = 0.0866$ for 6360 reflections with $I_o > 2\sigma(I_o)$). The GoF on F^2 was equal 1.026. A weighting Scheme $w = [\sigma^2(F_o^2 + (0.0418P)^2 + 3.1964P]^{-1}$ where $P = (F_o^2 + 2F_c^2)/3$ was used in the final stage of refinement. The residual electron density = +0.54/−0.48 e Å^{-3}. CCDC-210720 (**2**) contains the supplementary crystallographic data for this paper. These data can be obtained free of charge via www.ccdc.cam.ac.uk/conts/retrieving.html (or from the Cambridge Crystallographic Data Centre, 12 Union Road, Cambridge CB2 1EZ, UK; fax: (+44) 1223-336-033; or deposit@ccdc.cam.ac.uk).

[13] H. Mimoun, *Comprehensive Coordination Chemistry, Vol. 6* (Eds.: G. Wilkinson, R. D. Gillard, J. A. McCleverty), Pergamon, Oxford, **1988**, chap. 1.

[14] H. Mimoun, R. Charpentier, A. Mitscher, J. Fischer, R. Weiss, *J. Am. Chem. Soc.* **1980**, *102*, 1047.

[15] For a detailed discussion on the observed coordination modes of alkylperoxo moieties to main group metals see ref. [7a].

[16] The observed intramolecular contacts are within the accepted distance range for this type of interaction; G. R. Desiraju, T. Steiner, *The Weak Hydrogen Bond in Structural Chemistry and Biology*, Oxford University Press, Oxford, **1999**.

[17] A consideration of the space-filling representation showed that there is the lack of significant steric interactions within the dimer. It seems likely that the effectiveness of β-diketiminate ligands in both the stabilization of unique metal species and catalysis is due to a useful range of noncovalent interactions, in addition to the steric and electronic properties, provided by this class of ligands.

[18] G. M. Sheldrick, *Acta Crystallogr. Sect A* **1990**, *46*, 467.

[19] G. M. Sheldrick, SHELXL 97, Program for Refinement of Crystal Structures, University of Göttingen, Göttingen (Germany), **1993**.

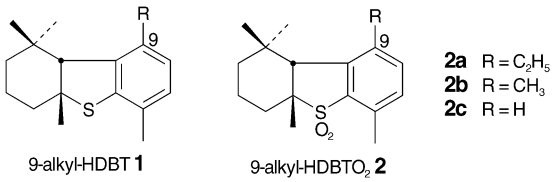
 © 2003 Wiley-VCH Verlag GmbH & Co. KGaA, Weinheim

Organosulfur Compounds in Fuels

Terpenoid-Derived Sulfides as Ultimate Organic Sulfur Compounds in Extensively Desulfurized Fuels**

Armelle Charrié-Duhaut, Christine Schaeffer, Pierre Adam, Pascal Manuelli, Pierre Scherrer, and Pierre Albrecht**

The desulfurization of fuels (for example, diesel oil) is a major concern of the petroleum industry worldwide because of the consequences for human health and the environment of high levels of sulfur dioxide emissions. In this context, a major problem encountered in refineries is the elimination of organosulfur components resistant to hydrodesulfurization processes. Although it has been shown that a substantial fraction of the organic sulfur compounds remaining after hydrodesulfurization is composed of mono- and polyalkylated dibenzothiophenes (mainly 4,6-dialkyldibenzothiophenes),[1] the lack of knowledge concerning the structures of residual highly resistant organic sulfur compounds still appears to be the greatest handicap in progressing towards higher degrees of hydrodesulfurization. We report here the identification of a series of novel, terpenoid-derived, non-dibenzothiophenic polycyclic sulfides from highly desulfurized diesel oils. These 1,1,4a,6-tetramethyl-9-alkyl-1,2,3,4,4a,9b-hexahydrodibenzothiophenes **1** (9-alkyl HDBT) were isolated from the aromatic fraction after oxidation to the corresponding sulfones **2** (9-alkyl-HDBTO$_2$).[2–4] The 9-ethyl homologue was unambiguously identified by mass spectrometry and NMR studies.



9-alkyl-HDBT **1** 9-alkyl-HDBTO$_2$ **2**

Organic sulfur compounds were studied in diesel oils from various origins and desulfurized on a mini-pilot scale to

[*] Dr. P. Adam, Dr. P. Albrecht, Dr. A. Charrié-Duhaut
Laboratoire de Géochimie Bioorganique, ECPM
Université Louis Pasteur
UMR 7509-CNRS, 25 rue Becquerel, 67200 Strasbourg (France)
Fax: (+33) 3-90-24-26-35
E-mail: padam@chimie.u-strasbg.fr
albrecht@chimie.u-strasbg.fr

Dr. C. Schaeffer
Laboratoire de Spectrométrie de Masse Bioorganique
ECPM, Université Louis Pasteur, UMR 7509-CNRS
25 rue Becquerel, 67200 Strasbourg (France)

Dr. P. Manuelli, Dr. P. Scherrer
Centre de Recherche, TotalFinaElf
BP 27, 76700 Harfleur (France)

[**] This work was supported by TotalFinaElf and the Centre National de la Recherche Scientifique. We thank E. Mastio-Motsch, P. Wehrung, and R. Graff for their assistance in MS and NMR measurements.

 © 2003 Wiley-VCH Verlag GmbH & Co. KGaA, Weinheim DOI: 10.1002/anie.200351426

different levels of residual sulfur, which ranged from 400 to less than 10 ppm. They exclusively occur in the aromatic fractions of the oils (generally in the 10–30% range), which were separated by silica gel column chromatography. The difficulty of the analytical problem was circumvented by transforming the sulfides into their more polar sulfone counterparts by using the persulfate-based oxidant oxone ($2\,KHSO_5{\cdot}KHSO_4{\cdot}K_2SO_4$).[2–4] This reagent was not only extremely selective, barely affecting aromatic hydrocarbons, but also gave quasi-quantitative reactions, even for extremely low concentrations. The resulting mixture of sulfones was easily separated from the untouched hydrocarbon matrix by chromatography on silica gel. GC-MS investigation[5] of the sulfone fractions revealed the presence of a series of unknown sulfur compounds besides the usually predominant 4,6-dialkyldibenzothiophene 5,5-dioxides. The EIMS spectra of all homologues are characterized by a major fragment at $m/z = 109$ and molecular ions ranging from $m/z = 278$ to 334 and corresponding to the general formula $C_{16+n}H_{22+2n}SO_2$ ($n = 0$–4). Since no further structural information could be obtained from the fragmentation pattern in the mass spectrum, these new compounds were isolated as sulfones from a diesel oil strongly depleted in sulfur compounds (50 ppm S) by a combination of liquid chromatography on silica gel and reversed-phase HPLC,[4] which gave pure **2a**–**c**.

About 1 mg of pure **2a** was obtained, and this enabled its complete characterization by 1D and 2D NMR studies including homonuclear ($^1H,^1H$ COSY and NOESY) and heteronuclear ($^1H,^{13}C$ HSQC and HMBC) correlation experiments. These studies permitted us to unambiguously establish the structure and relative configuration of 9-ethyl-HDBTO$_2$ (**2a**) and to assign the signals of all protons and carbon atoms (Table 1).

The ^{13}C NMR, ^1H-noise-decoupled, and DEPT spectra indicate the presence of an aromatic ring bearing one methyl, one ethyl, and two vicinal protons, as well as an aliphatic part composed of two quaternary carbon atoms, and one methine, three methylene, and three methyl groups. The carbon skeleton of 9-ethyl-HDBTO$_2$ was finally established mainly on the basis of a long-range ($^{2,3}J$) correlation experiment (Figure 1a) and $^1H,^1H$ COSY and heteronuclear $^1H,^{13}C$ (^1J) correlation experiments. The presence of a nuclear Overhauser effect (NOE) between H-9b and protons of the C-4a-methyl group clearly indicates a *cis* junction between the cyclohexane ring and the sulfurized five-membered ring (Figure 1b). The NOEs observed between H-9b and protons respectively located on C-2 and C-4 indicate the axial position of H-9b on the cyclohexane ring. Consequently, the C-4a-methyl group must be equatorial.

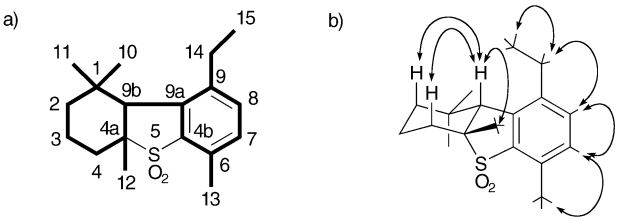


Figure 1. a) Carbon sequence (bold) established from the inverse long-range $^1H,^{13}C$ correlation experiment; b) spatial representation of **2a** showing the most important NOEs observed.

Two lower homologues **2b** and **2c**, showing the typical fragmentation pattern of 9-alkyl-HDBTO$_2$ in their mass spectra,[6] were isolated in small amounts that enabled 1D ^1H NMR studies. The ^1H NMR spectrum[6] of **2b** has numerous similarities to that of **2a** and shows a singlet methyl signal with a chemical shift characteristic of a benzylic position, which replaces the ethyl group on C-9 of **2a**. This ^1H NMR spectrum allowed us to propose the structure of 9-methyl-HDBTO$_2$ for compound **2b**. The structure of 9-dealkylated-HDBTO$_2$ could be assigned to compound **2c**, since its ^1H NMR spectrum[6] shows the same aliphatic part and the signals of three aromatic protons (one triplet, two doublets) and of one benzylic methyl group.

Other homologues and isomers belonging to this novel series were detected in trace amounts by GC-MS in the fractions enriched in 9-alkyl-HDBTO$_2$ by HPLC from a diesel oil with 50 ppm residual sulfur. These compounds were identified on the basis of their mass spectra, which show the typical fragmentation pattern of 9-alkyl-HDBTO$_2$ dominated by the $m/z = 109$ fragment. In particular, we were able to detect and tentatively identify higher homologues with multiple substitution or longer side chains, in particular 9-(iso)propyl ($m/z = 320$ [M^+]) and 9-(iso)butyl-HDBTO$_2$ ($m/z = 334$ [M^+]), in accordance with the biological origin proposed below.

It clearly appears that the structures of these compounds are not the result of extensive molecular reorganization, as might be the case for dibenzothiophene-type structures, but are directly inherited from biological precursors related to terpenoids. These biological precursors could be derived from an unsaturated diterpenoid such as retinol or more likely from carotenoid precursors, which give rise to numerous molecular fossil counterparts[7] and in this case may

Table 1: ^1H (500.1 MHz) and ^{13}C (125.8 MHz) NMR spectroscopic data for compound **2a** (Bruker ARX 500; in CD_2Cl_2, δ in ppm relative to TMS).

C	$\delta(^{13}C)$ [ppm]	$\delta(^1H)$	C	$\delta(^{13}C)$ [ppm]	$\delta(^1H)$ [ppm]
1	36.4		9	140.6	
2	40.1	1.52 (m, α, eq)–1.38 (m, β, ax)	9a	138.5	
3	18.7	2.01 (m, α, ax)–1.54 (m, β, eq)	9b	55.1	3.04 (s, β, ax)
4	30.4	2.44 (m, α, eq)–1.59 (m, β, ax)	10	35.1	1.07 (s, 3H, eq Me)
4a	62.3		11	22.5	0.54 (s, 3H, ax Me)
4b	136.0		12	30.5	1.23 (s, 3H)
6	133.4		13	16.6[a]	2.54 (s, 3H)
7	130.9	7.17 (d, $^3J = 7.5$ Hz)	14	25.7	2.67 (dq, $^2J = 14.0$ Hz, $^3J = 7.0$ Hz) 2.84 (dq, $^2J = 14.0$ Hz, $^3J = 7.0$ Hz)
8	133.2	7.36 (d, $^3J = 7.5$ Hz)	15	16.5[a]	1.13 (t, $^3J = 7.0$ Hz, 3H)

[a] Values may be interchanged.

 © 2003 Wiley-VCH Verlag GmbH & Co. KGaA, Weinheim

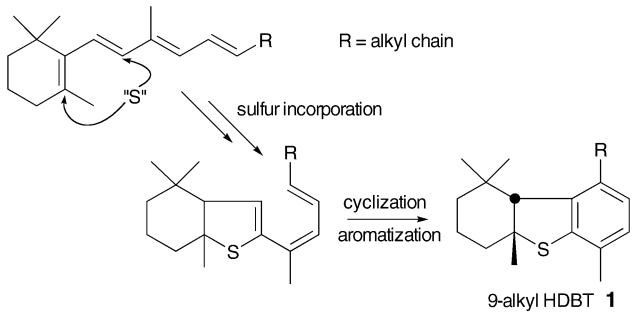


Figure 2. Possible mode of formation of 9-alkyl-HDBT **1** from biological terpenoids (e.g., carotenoids).

have undergone sulfurization followed by cyclization and aromatization (Figure 2).

In a first step, the sulfurized five-membered ring could have been formed by early diagenetic reactions of double bonds of the precursor lipid with reduced inorganic sulfur species formed by bacterial sulfate reduction.[8] In a later stage, formation of the fused aromatic ring might be explained by cyclization and aromatization of polyunsaturated intermediates following a process often observed in sediments and petroleum and leading, for instance, from functionalized hopanoid precusors to sedimentary benzohopanoids[9] or from biological carotenoids to sedimentary polycyclic aromatic carotenoid derivatives.[7a] Oxidation reactions or biodegradation occurring in the early stages of diagenesis, as well as thermal processes involving cracking reactions at a later stage of burial, might explain the partial or total loss of the side chain leading to HDBT series **1**. Since these compounds are derived from biological molecules, their presence and distribution in diesel oils may be strongly dependent on the origin of the parent crude oil and may eventually be used as geochemical source indicators.

Comparison of the distribution of 9-alkyl-HDBTO$_2$ by GC-MS in diesel oils of the same origin, but desulfurized to different levels, clearly showed their relative increase as the amount of residual sulfur decreased, which shows that they are extremely resistant to hydrodesulfurization. In highly desulfurized fuels, 9-alkyl-HDBTs **1** can clearly become the predominant organosulfur compounds, even more abundant than 4,6-dimethyldibenzothiophene (Figure 3).

The reactivity of organic sulfur compounds towards hydrodesulfurization is significantly influenced by steric hindrance and the electron density on the sulfur atom.[10] These factors explain, for example, the known resistance of 4,6-dimethyldibenzothiophene towards hydrodesulfurization. In the case of 9-alkyl-HDBT, the presence of methyl groups at the 4a- and 6-positions, as well as the *cis* ring junction, could hinder the S atom sterically and thus prevent its interaction with the solid catalyst surface. This would explain the survival of these organic sulfur compounds under extreme hydrodesulfurization conditions. Their removal and hence the production of highly or even totally desulfurized fuels will require adaptation of existing hydrodesulfurization processes (e.g., new catalysts) or development of new desulfurization methods working under economically viable conditions,[11] a goal which can now be pursued based on precise knowledge of their structures.

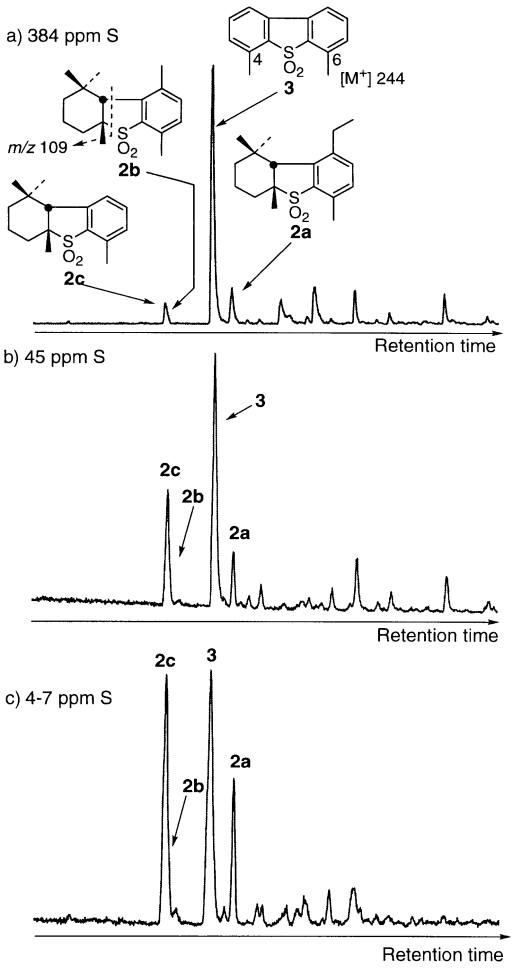


Figure 3. Sum of the partial mass chromatograms $m/z = 109$ (tentatively assigned) and $m/z = 244$ (GC-MS, EI 70 eV, MAT TSQ 700 mass spectrometer connected to a Varian 3400 gas chromatograph, conditions as in ref. [5]) showing the distribution of HDBTO$_2$ and 4,6-dimethyldibenzothiophene-5,5′-dioxide (**3**) in the organic sulfur compounds isolated as sulfones from the same diesel oil desulfurized to three different levels: a) 384 ppm, b) 45 ppm c) 4–7 ppm residual sulfur. The observed relative intensities are very similar to those measured by gas chromatography (flame ionization detector), that is, they reflect the relative amounts.

Received: March 18, 2003 [Z51426]

Keywords: carotenoids · desulfurization · fuels · oxidation · sulfur heterocycles

[1] a) J. T. Andersson, *J. Chromatogr.* **1991**, *585*, 376–377; b) J. M. Girgis, B. C. Gates, *Ind. Eng. Chem. Res.* **1991**, *30*, 2021–2058; c) J. T. Andersson, K. Sielex, *J. High Resolut. Chromatogr.* **1996**, *19*, 49–53.

[2] B. M. Trost, D. P. Curran, *Tetrahedron Lett.* **1981**, *22*, 1287–1290.

[3] Typically, 2.00 g of oxone (Aldrich) in 20 mL water was added to a mixture of acetone (20 mL) and 1.00 g of aromatic fraction isolated from a diesel oil by chromatography on a silica gel column ($0.05 < R_f < 0.90$, TLC, SiO$_2$/hexane). The reaction

 © 2003 Wiley-VCH Verlag GmbH & Co. KGaA, Weinheim

mixture was stirred and heated to reflux for 4 h. After addition of water, extraction with CH_2Cl_2, and removal of the solvent under reduced pressure, the crude mixture was fractionated on a silica gel column (CH_2Cl_2) to give the sulfone fraction.

[4] After oxidation of the aromatic fraction isolated from a diesel oil with 50 ppm residual sulfur and separation of the sulfone fraction, **2a–c** were obtained by a sequence of chromatographic separations involving liquid chromatography on silica gel and reverse-phase HPLC steps (DuPont Zorbax ODS, 7 μm, 9.4 × 250 mm, CH_3OH/H_2O 9:1).

[5] GC-MS analyses were performed on a Finnigan MAT TSQ 700 mass spectrometer, connected to a Varian 3400 gas chromatograph (on-column injector, J&W DB-5 column, 60 m × 0.25 mm, 0.1 μm film thickness). Mass spectra were recorded at 70 eV; helium was used as carrier gas.

[6] **2a**: for NMR see Table 1, MS (Finnigan MAT TSQ 700, EI, 70 eV): *m*/*z* (%): 306 (100) [M^+] ($C_{18}H_{26}SO_2$), 289 (32), 224 (57), 185 (35), 179 (38), 157 (37), 109 (99). **2b**: ^{1}H NMR (500 MHz, CD_2Cl_2, 25 °C): $\delta = 0.58$ (s, 3H, H-11), 1.08 (s, 3H, H-10), 1.21 (s, 3H, H-12), 2.36 (s, 3H, H-14), 2.54 (s, 3H, H-13), 3.01 (s, 1H, H-9b), 7.13 (d, ^3J(H,H) = 7.5 Hz, 2H, H-7 or H-8), 7.30 ppm (d, ^3J(H,H) = 7.5 Hz, 2H, H-7 or H-8); MS (EI, 70 eV): *m*/*z* (%): 292 (100) [M^+] ($C_{17}H_{24}SO_2$), 275 (29), 210 (42), 171 (35), 165 (41), 157 (24), 109 (98). **2c**: ^{1}H NMR (500 MHz, CD_2Cl_2, 25 °C): $\delta = 0.71$ (s, 3H, H-11), 1.16 (s, 3H, H-10), 1.21 (s, 3H, H-12), 2.73 (s, 3H, H-13), 6.99 (d, ^3J (H,H) = 7.5 Hz, 1H, H-9 or H-7), 7.18 (d, ^3J (H,H) = 7.5 Hz, 1H, H-7 or H-9), 7.27 ppm (t, ^3J (H,H) = 7.5 Hz, 1H, H-8). MS (EI, 70 eV): *m*/*z* (%): 278 (79) [M^+] ($C_{16}H_{22}SO_2$,), 261 (8), 179 (10), 157 (25), 143 (19), 109 (100).

[7] a) J. S. Sinninghe Damsté, J. Köster, M. Baas, M. P. L. Koopmans, H. M. E. van Kaam-Peters, J. A. J. Geenevasen, C. Kruk, *J. Chem. Soc. Chem. Commun.* **1995**, 187–188; b) P. Schaeffer, P. Adam, P. Wehrung, P. Albrecht, *Tetrahedron Lett.* **1997**, *38*, 8413–8416; c) J. S. Sinninghe Damsté, M. Baas, M. P. Koopmans, J. A. J. Geenevasen, *Tetrahedron Lett.* **1997**, *38*, 2347–2350; d) J. S. Sinninghe Damsté, M. P. Koopmans, *Pure Appl. Chem.* **1997**, *69*, 2067–2074.

[8] a) J. S. Sinninghe Damsté, J. W. de Leeuw, *Org. Geochem.* **1990**, *16*, 1077–1101; b) J. Poinsot, P. Schneckenburger, P. Adam, P. Schaeffer, J. M. Trendel, P. Albrecht, *Chem. Commun.* **1997**, 2191–2192; c) J. Poinsot, P. Schneckenburger, P. Adam, P. Schaeffer, J. M. Trendel, A. Riva, P. Albrecht, *Geochim. Cosmochim. Acta* **1998**, *62*, 805–814.

[9] a) G. Hussler, P. Albrecht, G. Ourisson, M. Cesario, J. Guilhem, C. Pascard, *Tetrahedron Lett.* **1984**, *25*, 1179–1182; b) T. Carrillo-Hernandez, P. Schaeffer, P. Albrecht, *Chem. Commun.* **2001**, 1976–1977.

[10] a) X. Ma, K. Sakanishi, I. Mochida, *Ind. Eng. Chem. Res.* **1994**, *33*, 218–222; b) X. Ma, K. Sakanishi, T. Isoda, I. Mochida, *Energy Fuels* **1995**, *9*, 33–37; c) X. Ma, K. Sakanishi, I. Mochida, *Ind. Eng. Chem. Res.* **1996**, *35*, 2487–2494; d) G. F. Froment, G. A. Depauw, V. Vanrysselberghe, *Stud. Surf. Sci. Catal.* **1997**, *106*, 83–97.

[11] See, for example, a) G. Castorena, C. Suarez, I. Valdez, G. Amador, L. Fernandez, S. Le Borgne, *FEMS Microbiol. Lett.* **2002**, *215*, 157–161; b) C. Song, X. Ma, *Appl. Catal. B* **2003**, *41*, 207–238; c) I. V. Babich, J. A. Moulijn, *Fuel* **2003**, *82*, 607–631; d) H. Mei, B. W. Mei, T. F. Yen, *Fuel* **2003**, *82*, 405–414.

 © 2003 Wiley-VCH Verlag GmbH & Co. KGaA, Weinheim

Hierarchically Ordered Porous Silica

One-Pot Synthesis of Hierarchically Ordered Porous-Silica Materials with Three Orders of Length Scale

Tapas Sen, Gordon J. T. Tiddy, John L. Casci, and Michael W. Anderson**

Porous, solid materials occur widely in nature and are the subject of intense study owing to their unique properties. The pore sizes can vary from Ångstroms in zeolite minerals to nanometers in leaf cellular structures to microns in diatom skeletons. The pores can be very uniform in shape and size with near delta function for the pore size distribution or can cover a wide range of pore sizes. The wall structure can be highly organized (crystalline) or highly disorganized (amorphous). Finally, the chemistry (composition) of the wall can vary enormously from oxide structures to functionalized polymers. In synthetic inorganic porous materials a Rubicon was crossed in 1992 by researchers at Mobil[1] who devised a method by using molecular self-association templating to synthesize materials with well defined pores on a nanometer scale. That is, they used the well-known phenomenon of self-organization of surfactant molecules into mesostructures such that the combined assembly of organic molecules acted as a template around which an inorganic material could be formed. Previously, in zeolite synthesis in which pores are formed on an Ångstrom scale, individual organic molecules rather than collections of organic molecules were used. Such a macromolecular templating is almost certainly the root of many complex inorganic porous structures in nature. However, the work of the Mobil researchers demonstrated, for the first time, that such a general synthetic philosophy could be used to control the porosity and chemistry of a multitude of porous materials. Since 1992 several thousand publications have reported extensions of the Mobil work.

Armed with this knowledge one important avenue that can be pursued is the creation of hierarchically ordered porous materials. That is, materials with several different degrees of porosity incorporated into one composite material. Nature produces such hierarchically ordered porous structures for example, diatoms, lumbar vertebra, lungs for optimal transport of fluids and gases. There are a number of reasons why this is important. For a porous material to be used in

[*] Dr. T. Sen, Prof. M. W. Anderson
UMIST Centre for Microporous Materials
Department of Chemistry, UMIST
P.O. Box 88, Manchester M60 1QD (UK)
Fax: (+44) 161-236-7677
E-mail: m.anderson@umist.ac.uk
Prof. G. J. T. Tiddy
Department of Chemical Engineering
UMIST
P.O. Box 88, Manchester M60 1QD (UK)
Prof. J. L. Casci
Synetix
P.O. Box 1, Billingham, Cleveland TS23 1LB (UK)

 DOI: 10.1002/anie.200351479 © 2003 Wiley-VCH Verlag GmbH & Co. KGaA, Weinheim

bulk-chemistry applications such as catalysis, in which reactant molecules need to readily access the interior pore structure but at the same time the internal surface area is maximized, a ramified pore structure with large pores leading to smaller and then smaller pores is desired (similar to the structure of lungs). Indeed it can be shown that the largest pores should form a 3D grid with the grid sections subdivided by a subgrid of smaller pores, and so on.[2] Consequently, there is a desire to have complete control not only of the pore sizes at each dimension but also the interconnectivity of these pores. Furthermore for bulk applications it is important that the preparation of such materials is facile, scalable and ultimately fairly inexpensive. In a recent paper,[3] we showed how some of these criteria could be met through a combination of using natural, inexpensive macroporous diatomaceous earth that is coated with a microporous zeolite. Herein, we adopt a different strategy that is entirely synthetic to achieve porosity with 3D interconnectivity of pores controlled on three length scales in a one-pot synthesis. Furthermore, at the macro- and mesoscale both ordering and size is controlled whilst at the microscale only the interconnectivity is controlled. We draw upon a number of different methodologies developed by others (most importantly the Mobil researchers) but also on the efforts to use a variety of templates such as synthetic opals,[4] latex spheres,[5] block copolymers,[6] emulsion droplets,[7] foams,[8] vesicles,[9] and bacteria.[10] Most of these papers report materials with a porous structure on one scale. However, Stein and co-workers[11] reported an ordered macroporous material with a crystalline microporous (silicalite-1) wall structure or disordered mesoporous structure.[12] Also, recently Danumah et al.[13] reported the synthesis of materials containing ordered macropores with cubic mesoporous (MCM-48) wall structure. Neither report demonstrated 3D interconnectivity between the pores. Stucky, Whitesides and co-workers[14] have concentrated on an approach, which involves stamping a sol–gel designed to produce mesopores with a 2D macroporous architecture. This process is tailored to produce films for optoelectronic applications but is not suitable for bulk chemical applications. Our strategy uses synthetic latex spheres to produce a controlled three-dimensionally interconnected macroporosity (300 nm–1 μm), block copolymer macromolecular templating to produce a mesoscale porosity (≈10 nm) and individual polymer templating to produce micropores (≈1 nm). These materials which are the subject of a recent patent[15] could be potential candidates as supports for heterogeneous catalysis with bulky molecules.

Monodispersity, sphere packing, and void size of the polystyrene sphere monoliths were determined by SEM and Hg-porosimetry experiments and are presented in Figure 1. Two distinct voids (Figure 1b) are present in the monoliths owing to octahedral (O_h; left peak) and tetrahedral interstitial sites (T_d; right peak). The position of the peaks due to the O_h and T_d interstitial sites are well matched with the theoretically calculated values from radius-ratio rules for a cubic close-packed arrangement.

The ordering of macropore structure of the silica materials is evidenced from SEM (Figure 2a) This shows a material where the latex spheres have been removed by toluene

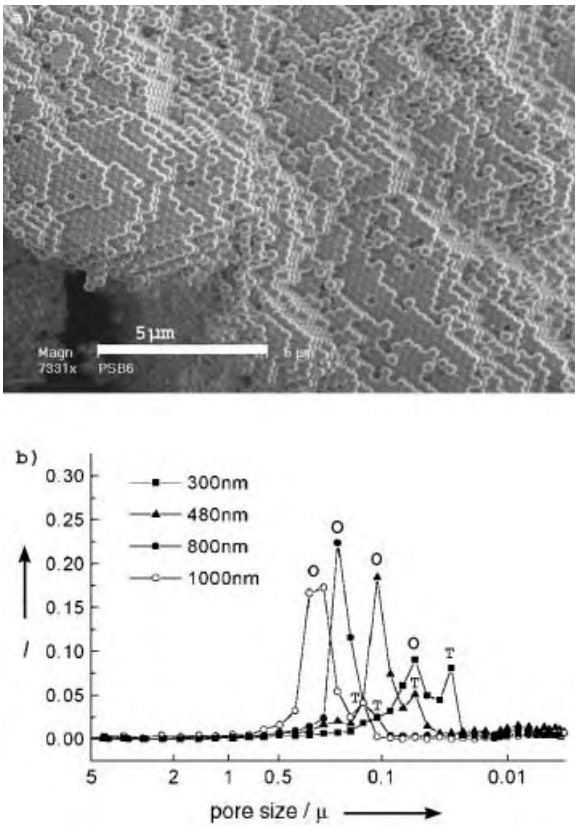


Figure 1. a) SEM of polystyrene latex sphere monolith, b) Hg intrusion curves over polystyrene latex spheres of various sizes. O = octahedral, T = tetrahedral, *I* = intensity (arbitrary units).

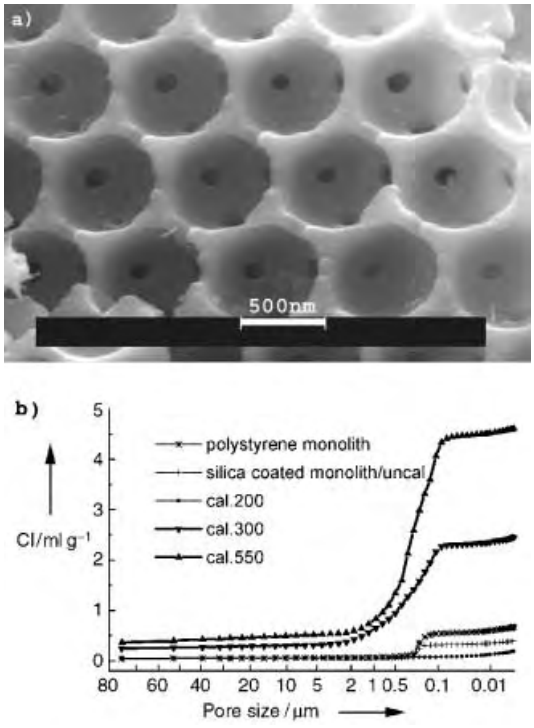


Figure 2. a) SEM of silica material synthesized by using triblock copolymer F127 and cosurfactant butanol. The latex was removed with toluene; b) Hg cumulative intrusion curves of macoporous monoliths at various stages of preparation. CI = cumulative intrusion.

 © 2003 Wiley-VCH Verlag GmbH & Co. KGaA, Weinheim

extraction followed by calcination. This is the optimum route and yields exceptionally well-ordered macroporous silicas as can be seen in Figure 2a. The macropores are uniform (200–800 nm depending upon initial sphere size) with interconnected windows (70–130 nm). Removal of the latex by calcination alone retains the macroporosity, however, the macro-spheres are somewhat deformed (not shown). The progressive formation of the ordered macroporous structure can be followed conveniently with Hg porosimetry (Figure 2b). The starting monolith (without silica, sphere size = 805 nm) has Hg intrusion of 0.5 ml g^{-1} due to the O_h and T_d interstitial voids. After silica condensation this value decreases to 0.2 ml g^{-1}, thus indicating that the silica coats the latex spheres and does not completely fill the voids. If the polystyrene latex is removed by calcination alone first the Hg intrusion drops to zero at 200 °C owing to latex melting but then increases finally to 3.3 ml g^{-1} after calcination at 550 °C. The high Hg intrusion is due to the void volume created by the removal of polystyrene latexes and confirms the presence of interconnecting windows.

The details of the wall structure are determined through a combination of X-ray diffraction (XRD), transmission electron microscopy (TEM) and nitrogen adsorption. The single XRD peak ($d = 8$ nm to 10.2 nm), not shown, in the low-angle region indicates the presence of mesoscopic ordering. The TEM images of a sample synthesised with F127 block copolymer and butanol as cosurfactant exhibits well defined mesostructure with an apparent square arrangement of pores with repeat distance ≈ 9.9 nm and pore sizes of 8.2 nm (see Figure 3a). In the presence of P123 block copolymer the TEM suggests a layered structure although it is impossible to determine the detailed structure from this information alone (see Figure 3c). A careful examination of the TEM images provides three important points: 1) the presence of macroscale interconnecting windows ≈ 100 nm; 2) ordered mesopores ≈ 8.2 nm with 10 nm repeat distance; 3) an amorphous region around the macropore windows. The 10 nm repeat distance for the mesostructure from TEM correlates well with the d spacing from low angle XRD.

The surface area and mesopore volume of the materials were low (46 $m^2 g^{-1}$, 0.053 ml g^{-1}) when the polystyrene latex was removed by direct calcination at 550 °C (Figure 4a). However, removal of the latex by toluene extraction followed by calcination at 450 °C resulted in a very high total surface area 531 $m^2 g^{-1}$ (Figure 4b). The total pore volume of pores less than 72 nm diameter is 0.29 mL g^{-1}. The BJH desorption cumulative pore volume due to the mesopores is 0.19 mL g^{-1}. The high uptake of N_2 (Figure 4b) at low relative p/p_0 clearly indicates the presence of micropores (< 2 nm) and this is further supported by a positive slope in the t-plot analysis (volume added versus thickness determined by Harkins–Jura methods; not shown, micropore surface area = 293 $m^2 g^{-1}$, micropore volume = 0.1 mL g^{-1}). The narrow mesopore size distribution is due to the high ordering on the mesoporous length scale. In summary: mesopore volume ≈ 0.19 mL g^{-1}, surface area ≈ 240 $m^2 g^{-1}$; micropore volume ≈ 0.1 mL g^{-1}, surface area ≈ 291 $m^2 g^{-1}$.

The presence of micropores in a mesoporous sample prepared by using triblock copolymers (F127 or P123) was

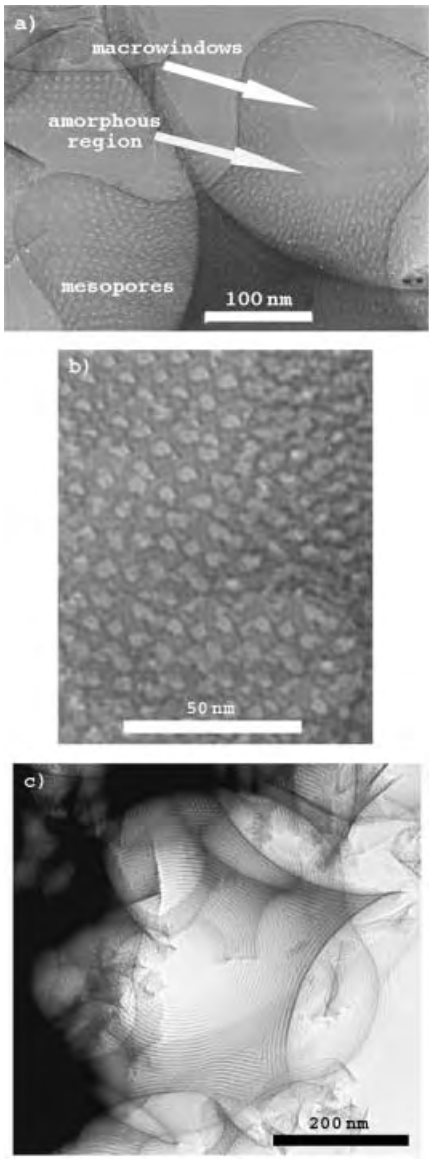


Figure 3. TEM images of silica materials synthesized by using triblock copolymer: a) F127 b) enlarged form of selected region of (a), c) P123.

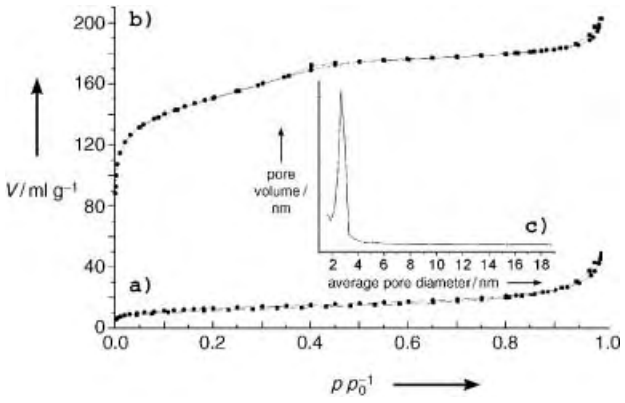


Figure 4. N_2 adsorption isotherms of a) silica material prepared by calcination alone, and b) silica material prepared by toluene extraction followed by calcination with c) associated desorption pore size distribution. circle adsorption and square desorption.

 © 2003 Wiley-VCH Verlag GmbH & Co. KGaA, Weinheim

reported earlier.[16,17] As a comparison with the bulk materials synthesised with P123 mentioned in these references typical micropore volumes are 0.1 $mL\,g^{-1}$ and mesopore volumes are 0.5–0.6 $mL\,g^{-1}$. The micropore volume is similar to our material but the mesopore volume is substantially larger. Consequently, the formation of a thin silica membrane around the latex spheres has resulted in a lower mesoporosity. This will in part be due to the thinness of the silica membrane ($\approx$100 nm from TEM) which results in a different organization of the block copolymer over the latex in comparison to a bulk synthesis.

The formation of macrospheres, interconnecting windows, mesoporous wall structure, amorphous region around windows, and microporosity is explained diagrammatically in the Figure 5. The macrospheres and interconnecting windows are

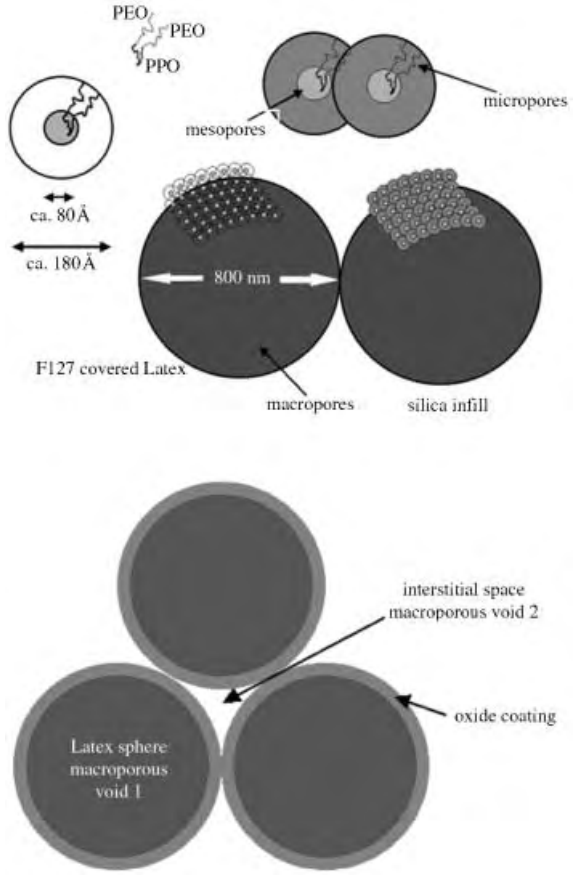


Figure 5. Diagrammatic presentation of macro-, meso-, and micropores formation.

formed due to the removal of polystyrene spheres. The formation of windows is due to the close-packed arrangement of polystyrene spheres (touching points). The meso- and microporosity is generated by the micelle formation of the EO–PO–EO (EO: ethylene oxide, PO: propylene oxide) block copolymer in the presence of cosurfactant butanol or pentanol. Owing to the hydrophobic nature of PO and hydrophilic nature of EO, the PO forms a solid impenetrable core and the EO tails project more loosely around this core. The PO core consequently templates the mesoporous structure and the EO tails individually template the microporous structure. The diameter (8 nm) of the micellar core correlates well with the mesopore sizes (8.2 nm) from the TEM results. The formation of micelles is excluded in regions near where polystyrene spheres touch resulting in the amorphous region around the windows.

In conclusion, hierarchically ordered porous silica materials are prepared with ordering on three different scales, that is, macropores (200–800 nm), interconnecting windows (70–130 nm), ordered mesoporous walls (80 nm) with narrow micropores <2 nm in the presence of multiple templates, that is, polystyrene latex spheres, surfactants (triblock copolymers) and cosurfactants (butanol or pentanol). This method of synthesis will extend the preparation of inorganic composites with tunable pores over various length scales with ordering in three dimensions.

Experimental Section

Noncross-linked, monodisperse polystyrene spheres were synthesized by using emulsifier-free polymerization techniques according to literature procedures.[12] Styrene (105 mL, Fluka, $>$99% purity) was washed in a separating funnel five times with 100 mL of 0.1M NaOH (BDH, 99% purity) then five times with 100 mL deionised water. After this step the colorless styrene became pale yellow and the NaOH solution became pink. A five necked, 2000 mL round bottom flask was filled with the required amount of deionised water and heated to 70°C with an isopad heating isomantle before washed styrene (100 mL) was added. One neck of the flask was attached with stirrer glands (quickfit) connected with a PTFE stirring rod. The stirring rod was fitted with an electric motor with a display of the rotation speed (Heidolph RZR2051). The other four necks had a water condenser, thermometer, septum, and a pasteur pipette connected to a N_2 cylinder by a rubber tube. In a separate 100 mL polypropylene beaker, the required amount of potassium persulfate (initiator, Sigma, 99% purity) was dissolved in water (50 mL) and heated to 70°C. The persulfate solution was added to the reaction flask containing the mixture of deionised water and washed styrene at 70°C. The whole mixture was stirred at a specific stirring speed for 28 h. The temperature was kept at 70°C during the reaction. The product was collected with a syringe for particle size distribution measurement. The final reaction mixture was milky white and transferred into a polypropylene bottle. The colloidal solution of polystyrene spheres was cooled down to room temperature before storage in a refrigerator at 4°C. A close-packed latex sphere monolith was produced by centrifugation at 4000 rpm, which was dried at 60°C.

The one-pot synthesis of hierarchically ordered porous silica materials was carried out as follows: a required quantity of HCl was diluted by the required amount of deionised water in a polypropylene beaker at room temperature. A required amount of tetramethyl ortho silicate (Aldrich) was added to the acidic solution. The tetramethyl orthosilicate (TMOS) was vigorously reacted with acidic solution and the temperature of the mixture was increased to 60°C. The mixture was stirred for 15 minutes during which time the solution temperature decreased to 30°C. In a separate polypropylene beaker the required amount of tri-block copolymer P123 (BSF) or F127 (Sigma) was mixed with the required amount of pentanol or butanol (Aldrich). The TMOS solution was added to the surfactant solution and stirred for 5 minutes. The molar composition of the silica gel is given in the following:

Surfactant:H_2O:Co-Surfactant:HCl:TMOS = 0.003–0.007:6.47:0.335:0.01625:1.

 © 2003 Wiley-VCH Verlag GmbH & Co. KGaA, Weinheim

4 gm of polystyrene latex monolith was added to the silica gel and stirred gently for another 15 minutes at room temperature. Finally the monolith was separated from the gel by filtration. The uncalcined materials were dried at 60 °C before calcination at 550 °C at a rate of 1 °C/minute in air. Alternatively templates were removed by toluene extraction at room temperature followed by calcination at 450 °C in air.

Sample preparation for SEM and TEM: The SEM micrographs were recorded on a Philips XL30 with a field emission gun. The samples were prepared by sprinkling the powder materials onto double-sided sticky tape and mounted on a microscope stub. This was then coated with a thin carbon film to increase the conductivity. The TEM micrographs were recorded on a Phillips CM20 200 kV. The sample was crushed (a few mg was used) and then dispersed in acetone. The mixture was then placed onto a copper grid using a dropping pipette.

Received: March 25, 2003
Revised: June 27, 2003 [Z51479]

Keywords: macroporous materials · mesoporous materials · microporous materials · porosity · silica

[1] C. T. Kresge, M. E. Leonowicz, W. J. Roth, J. C. Vartuli, J. S. Beck, *Nature* **1992**, *359*, 710.
[2] U. A. El-Nafaty, R. Mann, *Chem. Eng. Sci.* **1999**, *54*, 3475.
[3] M. W. Anderson, S. M. Holmes, N. Hanif, C. S. Cundy, *Angew. Chem.* **2000**, *112*, 2819; *Angew. Chem. Int. Ed.* **2000**, *39*, 2707.
[4] A. V. Blaaderen, *Science* **1998**, *282*, 887.
[5] O. D. Velev, T. A. Jede, R. F. Lobo, A. M. Lenhoff, *Nature* **1997**, *389*, 448.
[6] D. Zhao, J. Feng, Q. Huo, N. Melosh, G. H. Fredrickson, B. F. Chelmka, G. D. Stucky, *Science* **1998**, *279*, 548.
[7] A. Imhof, J. Pine, *Nature* **1997**, *389*, 948.
[8] P. Sepulveda, G. P. Binner, *J. Eur. Ceram. Soc.* **1999**, *19*, 2059.
[9] D. M. Antonelli, *Microporous Mesoporous Mater.* **1999**, *33*, 209.
[10] S. A. Davis, S. L. Burkett, N. H. Mendelson, S. Mann, *Nature* **1997**, *385*, 420.
[11] B. T. Holland, L. Abrams, A. Stein, *J. Am. Chem. Soc.* **1999**, *121*, 4308.
[12] B. T. Holland, C. F. Blanford, T. Do, A. Stein, *Chem. Mater.* **1999**, *11*, 795.
[13] C. Danumah, S. Vaudreuil, L. Bonneviot, M. Bousmina, S. Giasson, S. Kaliaguine, *Microporous Mesoporous Mater.* **2001**, *44*, 241.
[14] P. Yang, T. Deng, D. Zhao, P. Feng, D. Pine, B. F. Chmelka, G. M. Whitesides, G. D. Stucky, *Science* **1998**, *279*, 548.
[15] "A macroporous–mesoporous–microporous silica material with ordered mesoporosity influenced by alcohol cosurfactant": T. Sen, M. W. Anderson, J. L. Casci, C. C. Egger, G. J. T. Tiddy, UK patent GB 0201951.1, **2002**.
[16] M. Imperor-Clerc, P. Davidson, A. Davidson, *J. Am. Chem. Soc.* **2000**, *122*, 11925.
[17] R. Ryoo, C. H. Ko, M. Kruk, V. Antochshuk, M. Jaroniec, *J. Phys. Chem. B* **2000**, *104*, 11465.

 © 2003 Wiley-VCH Verlag GmbH & Co. KGaA, Weinheim

Single-Molecule Magnets

Synthesis and Characterization of a Cobalt(II) Single-Molecule Magnet**

Mark Murrie, Simon J. Teat, Helen Stœckli-Evans, and Hans U. Güdel**

Single-molecule magnets (SMMs) provide a tantalizing glimpse of the future possibilities for data storage technology.[1] The well-defined molecular size of SMMs has also proved ideal for the observation of quantum effects such as tunneling of the magnetization.[2] The requirements for SMM behavior are well established: the presence of a large-spin ground state (S) and an Ising-type magnetic anisotropy ($D<0$) leads to an energy barrier (ΔE) to reorientation of the magnetization, where $\Delta E = S^2 D$ for integer-spin ground states. Consequently, if the available thermal energy is small compared to the barrier height, slow magnetic relaxation can occur. The prototype SMM $[Mn_{12}O_{12}(OAc)_{16}(H_2O)_4]$ still possesses the largest energy barrier of 66 K due to its $S=10$ ground state and large negative D parameter.[3] Thus, many current routes to SMMs culminate in manganese(III) containing complexes, to exploit the associated large single-ion anisotropy.[4] Another promising candidate ion for the isolation of SMMs with a large anisotropy is cobalt(II). Despite this, there is only one report of a cobalt(II) cluster which displays slow magnetic relaxation.[5] Slow magnetic relaxation has been observed in a one-dimensional chain compound, which comprises cobalt(II) ions and nitronyl nitroxide radicals.[6]

We have developed a route to nickel(II) spin clusters using the citrate ligand ($cit^{4-} = [C(O^-)(CO_2^-)(CH_2CO_2^-)_2]$).[7] A nickel(II) citrate cluster, which contains 21 metal centers, displays SMM behavior as shown by the appearance of frequency-dependent out-of-phase signals in the ac susceptibility below 800 mK.[8] To isolate spin clusters with a larger

[*] Dr. M. Murrie, Prof. H. U. Güdel
Departement für Chemie und Biochemie
Universität Bern
Freiestrasse 3, 3000 Bern 9 (Switzerland)
Fax: (+41) 31-631-4399
E-mail: mark.murrie@iac.unibe.ch
hans-ulrich.guedel@iac.unibe.ch
Dr. S. J. Teat
CCLRC
Daresbury Laboratory
Warrington, Cheshire WA4 4AD (UK)
Prof. Dr. H. Stœckli-Evans
Institut de Chimie
Université de Neuchâtel
Avenue de Bellevaux 51, 2000 Neuchâtel (Switzerland)

[**] This work was supported by the Swiss National Science Foundation (NRP47 Supramolecular Functional Materials), the European Community (Fifth Framework Programme MOLNANOMAG HPRN-CT-1999-00012) and the EPSRC (UK).

Supporting information for this article is available on the WWW under http://www.angewandte.org or from the author.

 DOI: 10.1002/anie.200351753 © 2003 Wiley-VCH Verlag GmbH & Co. KGaA, Weinheim

magnetic anisotropy, and thus higher blocking temperatures, we have extended our synthetic approach to cobalt(II). Herein, we report the synthesis and characterization of a new hexanuclear cobalt(II) SMM.

Slow diffusion of ethanol into a neutral aqueous solution containing Co^{II} and citrate ions in the presence of NMe_4^+ and Na^+ ions gives pale-pink rodlike crystals of $[(NMe_4)_3Na\{Co_4(cit)_4[Co(H_2O)_5]_2\}]\cdot 11H_2O$ (**1**·11 H_2O; see Experimental Section). The single-crystal X-ray structure of **1**·11 H_2O reveals a hexanuclear cluster based on a $\{Co_4O_4\}$ core, where each oxygen atom is derived from a tridentate citrate alkoxide group (Figure 1).[9] The four citrate ligands are

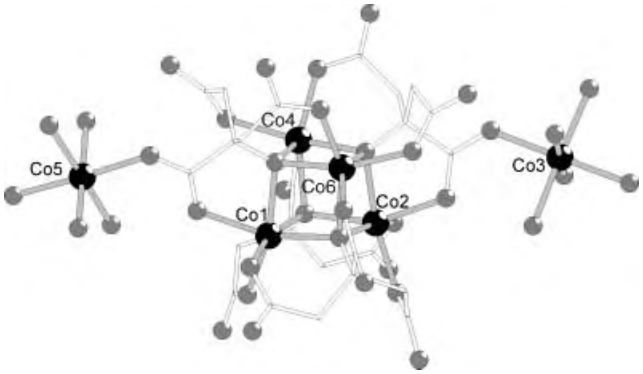


Figure 1. The structure of the anion in **1** (Co, black sphere; O, gray sphere; C, rods; H omitted for clarity). Bond length ranges [Å; average esd = 0.006 Å] Co-O: 2.075–2.142 (citrate O^-), 2.055–2.157 (citrate CO_2^-); bond angle ranges [°; average esd = 0.2°] Co-O-Co: 95.9–100.3.

tetradeprotonated, in contrast to previously reported mono- and dinuclear cobalt(II) complexes which contain the tride-protonated ligand $Hcit^{3-}$.[10] The three carboxylate groups of each ligand cap the Co^{II} centers bridged by the alkoxide group. Each cobalt(II) center within the core is hexacoordinated, and displays a twisted trigonal-prismatic geometry. Two of the ligands are each bonded to a further octahedral Co^{II} center,[11] through carboxylate groups in an *anti–syn* bridging mode; this is the first time this bonding motif has been observed for the citrate ligand. The bonding mode of the two citrate ligands which bridge three metal centers (e.g., Co1-Co2-Co6) has been identified in nickel and iron complexes.[7,12] Water molecules complete the coordination sphere of Co3 and Co5; the $\{Co(O_2CR)Co(H_2O)_5\}$ fragment is unusual but has been observed in $[Co_2(H_2O)_5(pdc)_2]$ (H_2pdc is pyrdidine-2,6-dicarboxylic acid).[13] One Na^+ and three NMe_4^+ ions balance the overall negative charge on the cluster.

If the synthesis is carried out in the absence of Na^+ ions, small needlelike crystals of **2**·16 H_2O are obtained. These were found to be unsuitable for single-crystal X-ray diffraction due to multiple twinning. However, IR data and elemental analysis of **2**·16 H_2O are consistent with a compound, which contains the $\{Co_6\}$ cluster found in **1**·11 H_2O with the charge balanced by four NMe_4^+ ions, that is, $[(NMe_4)_4\{Co_4(cit)_4[Co(H_2O)_5]_2\}]\cdot 16H_2O$ (see Experimental Section and Supporting Information).

For a fully solvated sample, **1**·11 H_2O, at 300 K χT = 17.5 $cm^3 mol^{-1} K$, consistent with six noninteracting Co^{II} centers with $S_i = 3/2$ and an average g value of 2.5 (Figure 2, ○).[14] χT reaches a local minimum at 20 K, then increases to reach a value of 16.5 $cm^3 mol^{-1} K$ at 10 K, before dropping sharply to 13.2 $cm^3 mol^{-1} K$ at 1.8 K. At 1.8 K, the magnetization $M/N\mu_B$ is not saturated in a field of 5 T and reaches a value of 11.2 (Figure 2, inset). For a fully solvated sample (**2**·16 H_2O), χT (Figure 2, +) and $M/N\mu_B$ are practically

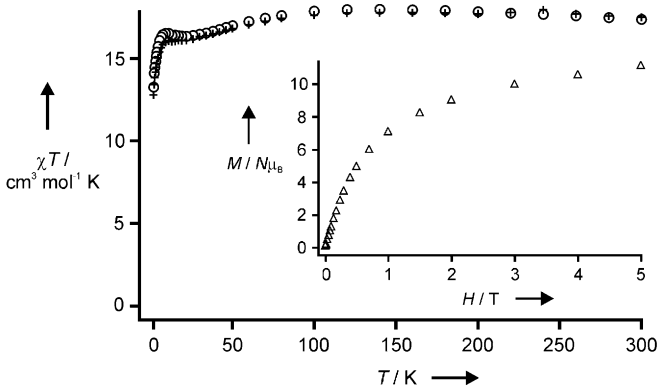


Figure 2. Temperature dependence of χT for **1**·11 H_2O (○) and **2**·16 H_2O (+). Inset shows the field dependence of the magnetization for **1**·11 H_2O at 1.8 K.

identical to those of **1**·11 H_2O. The magnetic behavior of partially desolvated samples **1**·7 H_2O and **2**·6 H_2O is shown in Figure 3.[15] The behavior is very similar to the fully solvated samples between 300 K and 50 K, (compare with Figure 2). Below 50 K there are slight differences, in particular the maximum in χT found in the fully solvated samples is no longer observed. As found for solvated samples, $M/N\mu_B$ is not saturated in a field of 5 T at 1.8 K (Figure 3, inset). It is difficult to perform a quantitative analysis of magnetic susceptibility data obtained for polycrystalline cobalt(II) compounds due to the large orbital contribution. At very low temperatures, each Co^{II} center may be treated as an effective spin $S' = 1/2$ center with anisotropic g values.[16] Using this approximation, the values obtained for $M/N\mu_B$ in all the four samples, are consistent with an effective value for

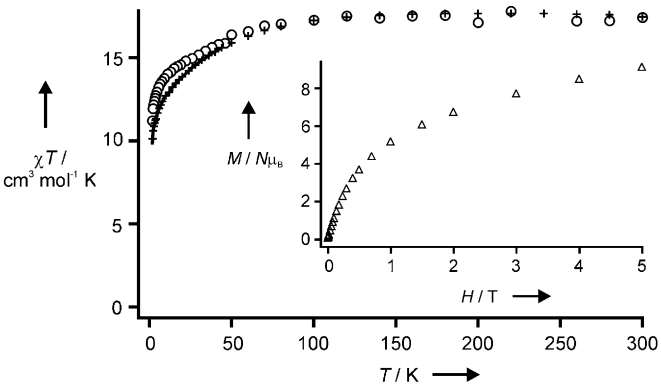


Figure 3. Temperature dependence of χT for partially solvated samples: **1**·7 H_2O (○) and **2**·6 H_2O (+). Inset shows the field dependence of the magnetization for **1**·7 H_2O at 1.8 K.

 © 2003 Wiley-VCH Verlag GmbH & Co. KGaA, Weinheim

$S'_{cluster}$ of 3 and an average g value >3 for the new $\{Co_6\}$ cluster.

In ac susceptibility measurements, fully solvated samples **1**·11 H_2O and **2**·16 H_2O show the onset of a frequency-dependent out-of-phase ac signal (χ'') below 6 K, although no χ'' peaks are observed above 1.8 K. In contrast, for the partially desolvated samples, well-resolved peaks for χ'' are observed. Figure 4 shows the in-phase and out-of-phase components of the ac susceptibility of **1**·7 H_2O and **2**·6 H_2O, measured at three different frequencies. An Arrhenius analysis yields the parameters: $\Delta E/k_B = 26$ K (18 cm^{-1}) and $\tau_0 = 8.2 \times 10^{-9}$ s for **1**·7 H_2O and $\Delta E/k_B = 32$ K (22 cm^{-1}) and $\tau_0 = 2.1 \times 10^{-9}$ s for **2**·6 H_2O.[17] The magnitude of χ'' compared to χ' at the peak position, and the values obtained for $\Delta E/k_B$ and τ_0 are entirely consistent with SMM behavior. Hence, the $\{Co_6\}$ cluster found in compounds **1** and **2**, is a new example of a cobalt(II) SMM. Furthermore, the energy barriers obtained for **1**·7 H_2O and **2**·6 H_2O are the highest energy barriers found for a non-manganese based SMM (compared with $[Fe_8O_2(OH)_{12}(tacn)_6]^{8+}$, $S = 10$, $\Delta E/k_B = 24.5$ K, tacn = triazacyclononane; determined from ac susceptibility measurements).[18]

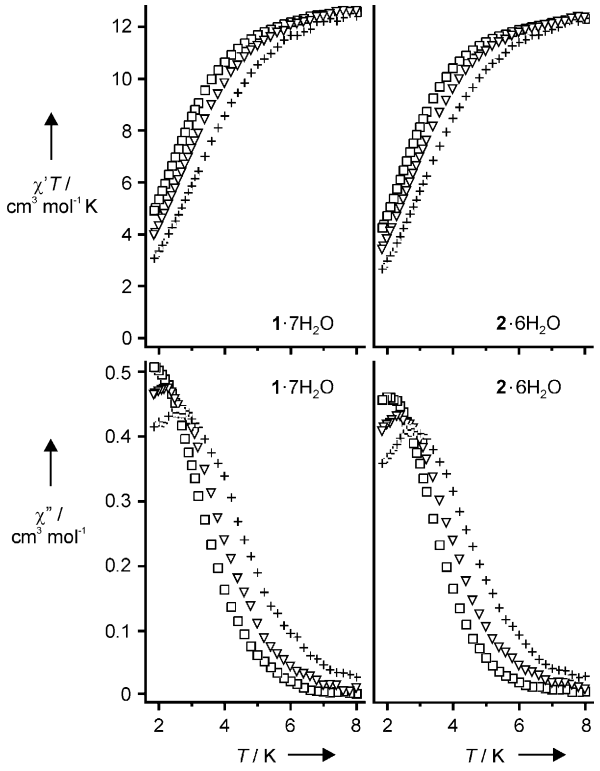


Figure 4. The in-phase and out-of-phase components of the ac susceptibility shown as $\chi'T$ versus T and χ'' versus T measured at 48 (□), 248 (△), and 1302 Hz (+) for samples of **1**·7 H_2O and **2**·6 H_2O.

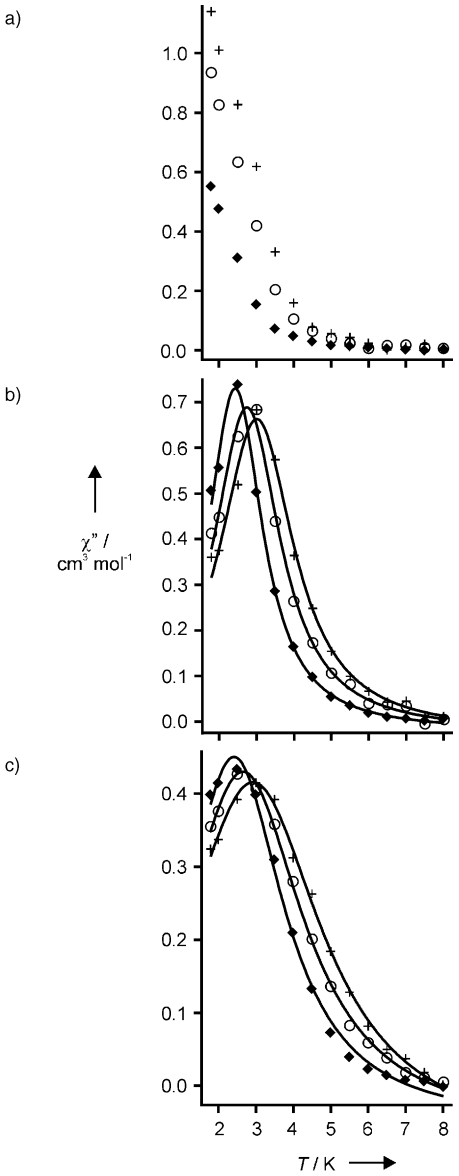


Figure 5. The out-of-phase component of the ac susceptibility χ'' versus T measured at 124 (◆), 496 (○), and 1302 Hz (+) for samples of **2**: a) fully solvated; b) dried in vacuo for 15 min; c) dried in vacuo for 3 h. Solid lines are least-squares fits to the data, yielding the following parameters: b) $\Delta E/k_B = 29$ K, $\tau_0 = 8.0 \times 10^{-9}$ s; c) $\Delta E/k_B = 32$ K, $\tau_0 = 2.1 \times 10^{-9}$ s.

Figure 5 shows the effect of solvent loss upon the out-of-phase ac component for **2**. Fully solvated samples show the onset of a frequency-dependent out-of-phase signal below 6 K (see Figure 5 a). Figure 5 b shows that after drying in vacuo for 15 min, peaks are observed for χ''. An Arrhenius analysis yields the parameters $\Delta E/k_B = 29$ K (20 cm^{-1}) and $\tau_0 = 8.0 \times 10^{-9}$ s, comparable to those found for samples of **1**·7 H_2O and **2**·6 H_2O after drying for 3 h. The shift in position of the χ'' signals for both **1** and **2** when moving from fully, to partially solvated samples is interesting. A similar shift in position of χ'' with respect to the amount of lattice solvent has been noted for manganese-based SMMs.[19] Upon solvent loss from the lattice, distortions in the cluster geometry will occur. This may be especially important at the two outer cobalt centers, which are each bonded to the central tetranuclear core by a monodentate carboxylate oxygen donor. Structural changes can affect the activation energy ΔE in two ways. We see from Figure 1 that the $\{Co_6\}$ cluster does not have axial symmetry. A change in the cluster geometry can therefore affect both the

 © 2003 Wiley-VCH Verlag GmbH & Co. KGaA, Weinheim

barrier height and the tunneling probability. Slightly different molecular geometries thus account for the difference in the $\Delta E/k_B$ parameters obtained for $\mathbf{1}\cdot 7H_2O$ and $\mathbf{2}\cdot 6H_2O$.

In conclusion, we have synthesized a new hexanuclear cobalt(II) spin cluster using the tetradeprotonated form of the proligand citric acid. Magnetic measurements show that this cluster behaves as a single-molecule magnet, displaying the largest energy barrier to reorientation of the magnetization for a non-manganese based SMM. Hence, this study highlights the potential for creating improved SMMs by using cobalt(II) ions as metal centers.

Experimental Section

Addition of citric acid monohydrate (1.518 g, 7.2 mmol) to an aqueous solution (10 mL) of $CoSO_4\cdot 7H_2O$ (2.030 g, 7.2 mmol) gave a solution with pH 1.46. The pH value was raised to 7.0 using $NMe_4OH\cdot 5H_2O$ (4.65 g, 25.7 mmol). 0.2 mL aliquots of this solution were taken, mixed with a solution of Na_2SO_4 (0.01 g in 0.2 mL H_2O) and layered with EtOH (1.6 mL). After one month, well-formed rodlike crystals of $\mathbf{1}\cdot 11H_2O$ could be isolated. Yield per aliquot: 4 mg (16% based on Co); elemental analysis (after drying for 3 h in vacuo) calcd(%)for $\mathbf{1}\cdot 7H_2O$ ($C_{36}H_{86}Co_6N_3NaO_{45}$): C 26.08, H 5.23, N 2.53; found: C 26.25, H 5.02, N 2.36. Selected IR data (KBr): $\tilde{\nu}=3434$ (s), 1573 (s), 1489 (m), 1385 (m), 1292 (w), 1242 (w), 1087 (w), 1057 (w), 950 (w), 920 (w), 850 (w), 689 (w), 648 cm^{-1} (w). For the synthesis of **2**, 0.2 mL aliquots of the solution at pH 7.0 were taken, mixed with H_2O (0.2 mL) and then EtOH (1.9 mL) and kept in sealed sample tubes. After two weeks needlelike crystals of **2** could be isolated: elemental and thermogravimetric analysis on fully solvated samples are consistent with 16 water molecules of crystallization. Yield per aliquot: 8 mg (29% based on Co); elemental analysis (after drying for 3 h in vacuo) calcd(%) for $\mathbf{1}\cdot 6H_2O$ ($C_{40}H_{96}Co_6N_4O_{44}$): C 28.41, H 5.72, N 3.31; found: C 28.59, H 5.76, N 3.27. Selected IR data (KBr): $\tilde{\nu}=3437$ (s), 1577 (s), 1489 (m), 1384 (m), 1289 (w), 1241 (w), 1094 (w), 1057 (w), 950 (w), 922 (w), 850 (w), 689 (w), 650 cm^{-1} (w).

Received: April 28, 2003 [Z51753]

Keywords: citric acid · cobalt · magnetic properties · O ligands · single-molecule magnets

[1] R. Sessoli, H.-L. Tsai, A. R. Schake, S. Wang, J. B. Vincent, K. Folting, D. Gatteschi, G. Christou, D. N. Hendrickson, *J. Am. Chem. Soc.* **1993**, *115*, 1804 – 1816.

[2] a) J. R. Friedman, M. P. Sarachick, J. Tejada, R. Ziolo, *Phys. Rev. Lett.* **1996**, *76*, 3830 – 3833; b) L. Thomas, F. Lionti, R. Ballou, D. Gatteschi, R. Sessoli, B. Barbara, *Nature* **1996**, *383*, 145 – 147.

[3] I. Mirebeau, M. Hennion, H. Casalta, H. Andres, H. U. Güdel, A. V. Irodova, A. Caneschi, *Phys. Rev. Lett.* **1999**, *83*, 628 – 631.

[4] a) C. Boskovic, W. Wernsdorfer, K. Folting, J. C. Huffman, D. N. Hendrickson, G. Christou, *Inorg. Chem.* **2002**, *41*, 5107 – 5118; b) E. K. Brechin, M. Soler, J. Davidson, D. N. Hendrickson, S. Parsons, G. Christou, *Chem. Commun.* **2002**, 2252 – 2253.

[5] E. C. Yang, D. N. Hendrickson, W. Wernsdorfer, M. Nakano, L. N. Zakharov, R. D. Sommer, A. L. Rheingold, M. Ledezma-Gairaud, G. Christou, *J. Appl. Phys.* **2002**, *91*, 7382 – 7384.

[6] A. Caneschi, D. Gatteschi, N. Lalioti, R. Sessoli, L. Sorace, V. Tangoulis, A. Vindigni, *Chem. Eur. J.* **2002**, *8*, 286 – 292.

[7] M. Murrie, H. Stoeckli-Evans, H. U. Güdel, *Angew. Chem.* **2001**, *113*, 2011 – 2014; *Angew. Chem. Int. Ed.* **2001**, *40*, 1957 – 1960.

[8] S. T. Ochsenbein, M. Murrie, E. Rusanov, H. Stoeckli-Evans, C. Sekine, H. U. Güdel, *Inorg. Chem.* **2002**, *41*, 5133 – 5140.

[9] Crystal structure analysis: Intensity data were collected using a Bruker AXS SMART CCD area detector attached to Station 9.8 at the CCLRC Daresbury synchrotron radiation source ($\lambda=0.6932$ Å). The structure was solved by direct methods using the SHELXS-97 program. The refinement and all further calculations were carried out using SHELXL-97. The H-atoms were included in calculated positions and treated as riding atoms using SHELXL default parameters. The non-H atoms were refined anisotropically, using weighted full-matrix least-squares on F^2. After the location of three tetramethylammonium cations and two possible positions for the sodium cation (occupancy 0.5 each site), giving four cations in all, the SQUEEZE routine in PLATON was used (488 electrons for a volume of 1660.8 Å). The disordered solvent of crystallization was equated to 11 water molecules per molecule of complex (per asymmetric unit). The crystal structure was refined in the noncentrosymmetric space group $Pna2_1$ as a racemic twin, refined x factor = 0.409(19). Crystal data for $\mathbf{1}\cdot 11H_2O$: $0.14\times 0.02\times 0.02$ mm; $C_{36}Co_6H_{94}N_3NaO_{49}$, $M_r=1729.10$; orthorhombic, space group $Pna2_1$, $a=23.093(3)$, $b=14.3843(18)$, $c=21.691(3)$ Å, $\alpha=\beta=\gamma=90°$, $V=7205.2(16)$ Å^3, $Z=4$, $\rho_{calcd}=1.595$ g cm^{-3}, $T=150$ K, $1.66<\theta<24.06°$; $F(000)=3504$. Refinement by full-matrix least-squares methods gave final $R_1(F_o)=0.0565$, $wR_2(F_o^2)=0.1590$ for 9701 reflections with $I>2\sigma(I)$ and 632 parameters; max/min residual electron density 0.662/−0.681 e Å^{-3}. CCDC-209085 (**1**) contains the supplementary crystallographic data for this paper. These data can be obtained free of charge via www.ccdc.cam.ac.uk/conts/retrieving.html (or from the Cambridge Crystallographic Data Centre, 12, Union Road, Cambridge CB21EZ, UK; fax: (+44) 1223-336-033; or deposit@ccdc.cam.ac.uk).

[10] a) M. Matzapetakis, M. Dakanali, C. P. Raptopoulou, V. Tangoulis, A. Terzis, N. Moon, J. Giapintzakis, A. Salifoglou, *J. Biol. Inorg. Chem.* **2000**, *5*, 469 – 474; b) N. Kotsakis, C. P. Raptopoulou, V. Tangoulis, A. Terzis, J. Giapintzakis, T. Jakusch, T. Kiss, A. Salifoglou, *Inorg. Chem.* **2003**, *42*, 22 – 31.

[11] All six metal centers are divalent as confirmed by bond valence sum analysis. W. Liu, H. H. Thorp, *Inorg. Chem.* **1993**, *32*, 4102 – 4105.

[12] A. Bino, I. Shweky, S. Cohen, E. R. Bauminger, S. J. Lippard, *Inorg. Chem.* **1998**, *37*, 5168 – 5172.

[13] L. C. Nathan, T. D. Mai, *J. Chem. Crystallogr.* **2000**, *30*, 509 – 518.

[14] Variable-temperature magnetic measurements were recorded using a SQUID magnetometer (Quantum Design). Crushed single crystals were restrained between the two halves of a gelatine capsule by inverting the top half.

[15] After drying in vacuo at ambient temperature for three hours, samples analyzed as $\mathbf{1}\cdot 7H_2O$ and $\mathbf{2}\cdot 6H_2O$.

[16] O. Kahn, *Molecular Magnetism*, VCH, Weinheim, **1993**, p. 38.

[17] Peak positions were extracted from the χ'' data obtained at frequencies between 124 and 1302 Hz, by least-squares fitting to a Lorentzian function.

[18] C. Sangregorio, T. Ohm, C. Paulsen, R. Sessoli, D. Gatteschi, *Phys. Rev. Lett.* **1997**, *78*, 4645 – 4648.

[19] C. Boskovic, E. K. Brechin, W. E. Streib, K. Folting, J. C. Bollinger, D. N. Hendrickson, G. Christou, *J. Am. Chem. Soc.* **2002**, *124*, 3725 – 3736.

 © 2003 Wiley-VCH Verlag GmbH & Co. KGaA, Weinheim

Vancomycin–Oligosaccharide Library

A Programmable One-Pot Oligosaccharide Synthesis for Diversifying the Sugar Domains of Natural Products: A Case Study of Vancomycin

*Thomas K. Ritter, Kwok-Kong T. Mong, Haitian Liu, Takuji Nakatani, and Chi-Huey Wong**

Drug discovery relies heavily on the pool of natural products for the identification of lead compounds. Numerous natural products are glycosylated, and their peripheral carbohydrate moieties are the key recognition elements and often define their biological activities.[1] Yet, efficient methods to systematically alter these essential carbohydrate ligands are still lacking. There are several strategies for the one-pot synthesis of oligosaccharides.[2] In particular, programmed one-pot oligosaccharide synthesis facilitates the convenient assembly of glycan structures[3] and has been used in the synthesis of such complex molecules as Globo H,[4] Lewis Y,[5] and fucosyl GM_1.[6] Desired glycan structures three to six residues in length can be constructed by choosing building blocks with suitable reactivities from the Optimer database.[7] Furthermore, the one-pot glycosylation methodology may provide a unique opportunity for convenient assembly of glycosylation libraries of natural products (Figure 1). Libraries of this type have been shown to facilitate elucidation of glycan function as well as the discovery of new compounds with interesting activities.[8]

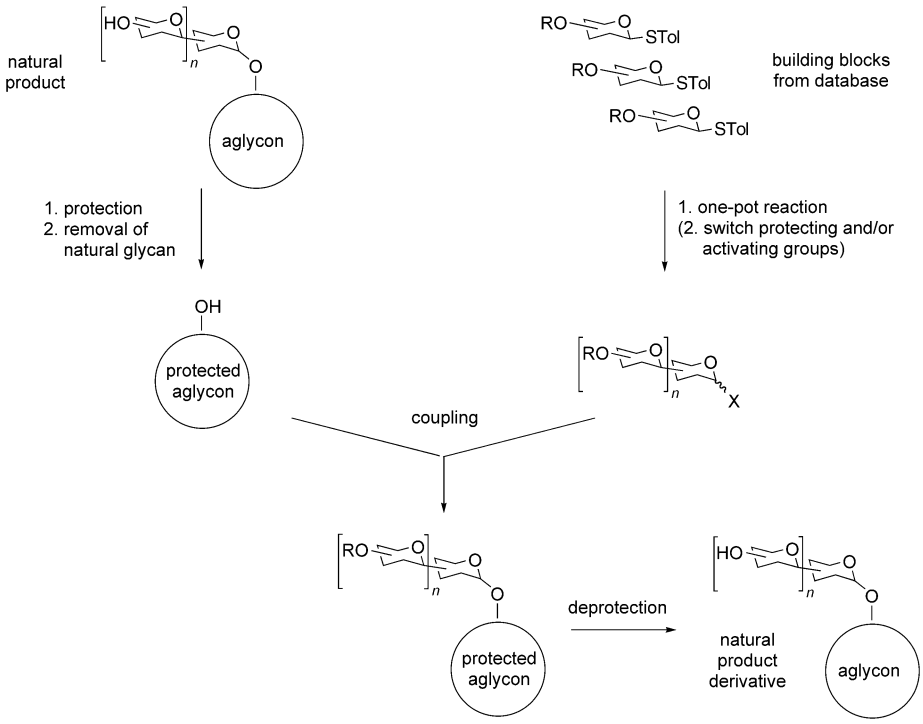


Figure 1. Strategies for the synthesis of libraries of glycosylated natural products by the direct one-pot glycosylation (left) or the coupling of preformed oligosaccharides (right).

The notoriously difficult glycosylation of vancomycin as well as the clinical importance of this antibiotic prompted us to choose vancomycin as a test case for the strategy outlined in Figure 1. Vancomycin is the most important member of the glycopeptide class of antibiotics and is considered the drug of last resort for the treatment of methicillin-resistant *Staphylococcus aureus* infections. Due to the emergence of vancomycin-intermediate-resistant *S. aureus* (VISA) and vancomycin-resistant enterococci (VRE), there is currently great interest in improving the efficacy of vancomycin. Vancomycin inhibits peptidoglycan biosynthesis in the bacterial cell wall by binding to the terminal peptide fragments of immature cell walls. In VRE a change in the peptide substrate weakens its affinity for the vancomycin binding pocket. Although the hydrogen-bonding interactions between the vancomycin aglycon and the peptidoglycan precursor are well understood, reengineering of the binding pocket by replacing internal amino acids would be a very complex synthetic endeavor. However, dramatic increases in activity against resistant strains were achieved by attaching hydrophobic groups to vancomycin's terminal sugar residue, vancosamine.[9] This increased activity was originally rationalized by the enhancing effects the substituents might have on dimerization and membrane anchoring.[10] More detailed studies suggest that the new vancomycin derivatives inhibit peptidoglycan biosynthesis by directly interfering with the enzymes catalyzing transglycosylation.[11–13]

In order to further investigate the role of the glycan portion, an efficient strategy for the glycosylation of the vancomycin aglycon is required. Enzymatic glycosylation procedures are restricted by the substrate tolerance of the glycosyltransferases and the availability of the nucleotide-sugar donors.[14–16] Previous chemical protocols suffer from poor yields in the glycosylation step[17] or lengthy protection/deprotection procedures.[18] A solid-support approach was reported, greatly simplifying workup and purification procedures.[19] However, only monoglycosylated derivatives resulted from this work. In a different approach, a short ethylene glycol linker was placed between the glycan and the aglycon, simplifying the coupling step significantly.[20] Yet, no

[*] Prof. Dr. C.-H. Wong, Dr. T. K. Ritter, Dr. K.-K. T. Mong, H. Liu, Dr. T. Nakatani
Department of Chemistry and
The Skaggs Institute of Chemical Biology
The Scripps Research Institute
10550 N. Torrey Pines Road, La Jolla, CA 92037 (USA)
Fax: (+1) 858-784-2409
E-mail: wong@scripps.edu

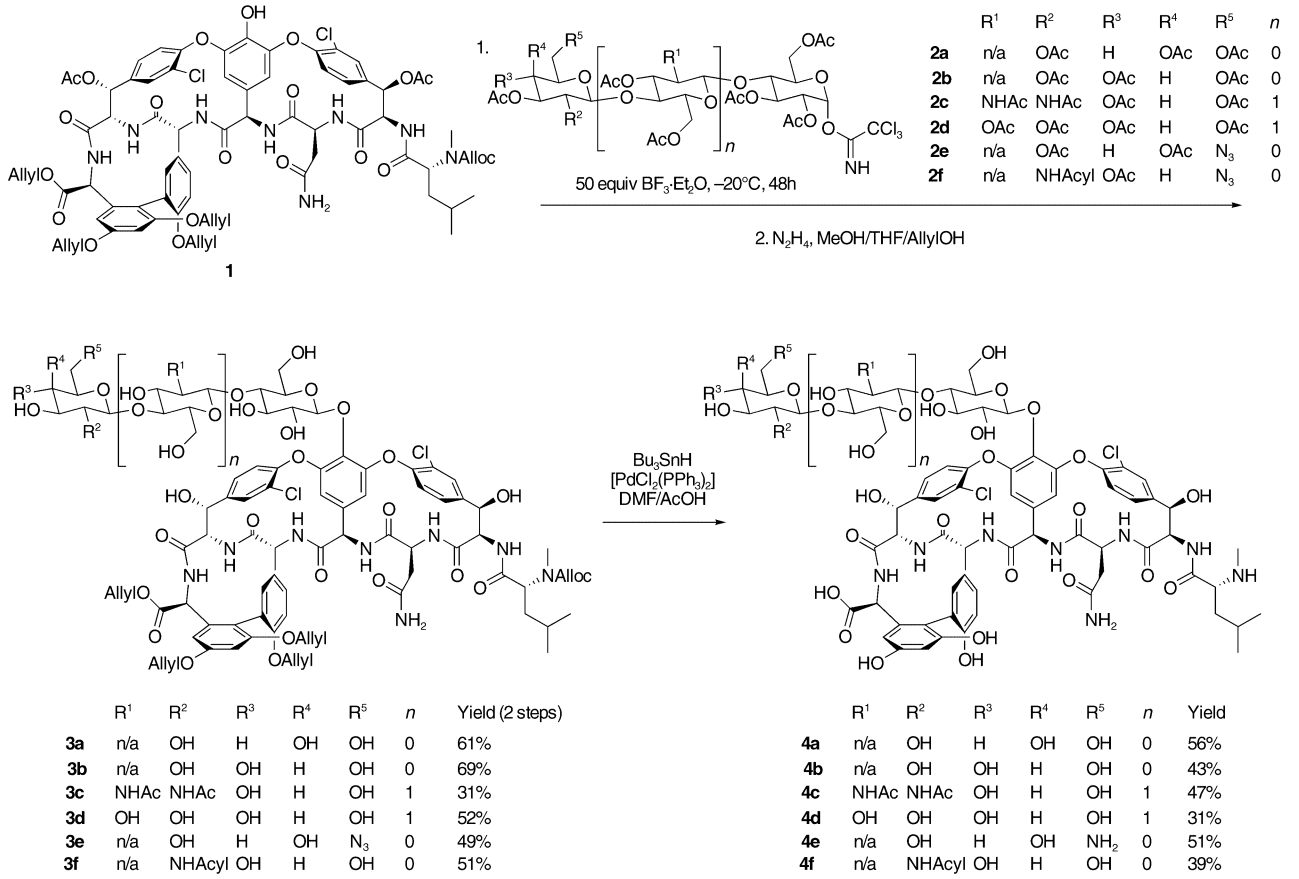
 DOI: 10.1002/anie.200351534 © 2003 Wiley-VCH Verlag GmbH & Co. KGaA, Weinheim

examples of direct chemical glycosylation of the aglycon to provide vancomycin derivatives bearing nonnatural di- or oligosaccharide substituents have been reported. By implementing a programmable one-pot oligosaccharide strategy, we hoped to construct a set of such derivatives.

In order to investigate the feasibility of our approach, it was necessary to establish an efficient glycosylation procedure for attaching oligosaccharides to a protected vancomycin aglycon. Di-*O*-acetyl-*N*-alloc-tri-*O*-allyl vancomycin aglycon allyl ester **1** was obtained in seven steps from commercially available vancomycin.[17] Glycosylation of **1** with thioglycoside donors could not be achieved under a variety of conditions, including different promoters such as *N*-iodosuccinimide and dimethyl(methylthio)sulfonium trifluoromethanesulfonate (DMTST). Therefore, glycosylation with peracetylated imidate donors **2a** and **2b** was performed and proceeded in good yields after optimization (Scheme 1). The acetate and allyl protecting groups were subsequently removed by reaction with hydrazine and palladium-catalyzed reduction, respectively,[17] providing the vancomycin derivatives **4a** and **4b**.[21]

The successful synthesis of oligosaccharides by the one-pot strategy relies on the generation of significant differences in reactivity between the individual thioglycoside donors. New nitrogen-containing building blocks were designed by fine-tuning reactivities through various electron-donating and -withdrawing protecting groups (Figure 2). Relative reactivity values (RRV) of these compounds were determined as described previously.[7] As shown in Scheme 2, the reactivity differences of the new donors and building blocks available from our database are in a suitable range for successful one-pot syntheses. The oligosaccharides were assembled according to the standard coupling protocol of the programmable one-pot synthesis (*N*-iodosuccinimide, triflic acid). Following the synthesis of the oligosaccharides, the protecting groups were exchanged for acetates. This operation minimizes the number of deprotection steps required after coupling of the glycans to the vancomycin aglycon. The peracetylated oligosaccharides were activated as trichloroacetimidates **2c–f** by a two-step procedure: deprotection of the anomeric hydroxy groups (hydrazine/acetate in the case of anomeric acetate, *N*-bromosuccinimide in the case of anomeric thioglycosides) followed by conversion to their corresponding trichloroacetimidates with trichloroacetonitrile and cesium carbonate. Compounds **2c–f** were then coupled to the vancomycin aglycon by using the conditions developed for the couplings of **2a** and **b**, and the protecting groups were removed. Deallylation of **3e** occurred with concomitant reduction of the C6 azide on the terminal sugar residue by means of a radical-mediated reduction mechanism through a Sn–N bond-forming process.

The biological activities of the vancomycin derivatives were investigated by determination of their minimum inhibitory concentrations (MIC) against a vancomycin-sensitive



	R1	R2	R3	R4	R5	n
2a	n/a	OAc	H	OAc	OAc	0
2b	n/a	OAc	OAc	H	OAc	0
2c	NHAc	NHAc	OAc	H	OAc	1
2d	OAc	OAc	OAc	H	OAc	1
2e	n/a	OAc	H	OAc	N_3	0
2f	n/a	NHAcyl	OAc	H	N_3	0

	R1	R2	R3	R4	R5	n	Yield (2 steps)
3a	n/a	OH	H	OH	OH	0	61%
3b	n/a	OH	OH	H	OH	0	69%
3c	NHAc	NHAc	OH	H	OH	1	31%
3d	OH	OH	OH	H	OH	1	52%
3e	n/a	OH	H	OH	N_3	0	49%
3f	n/a	NHAcyl	OH	H	OH	0	51%

	R1	R2	R3	R4	R5	n	Yield
4a	n/a	OH	H	OH	OH	0	56%
4b	n/a	OH	OH	H	OH	0	43%
4c	NHAc	NHAc	OH	H	OH	1	47%
4d	OH	OH	OH	H	OH	1	31%
4e	n/a	OH	H	OH	NH_2	0	51%
4f	n/a	NHAcyl	OH	H	OH	0	39%

Scheme 1. Coupling of various oligosaccharides to vancomycin aglycon and deprotection of the resulting vancomycin derivatives. n/a = not available. Alloc = allyloxycarbonyl.

 © 2003 Wiley-VCH Verlag GmbH & Co. KGaA, Weinheim

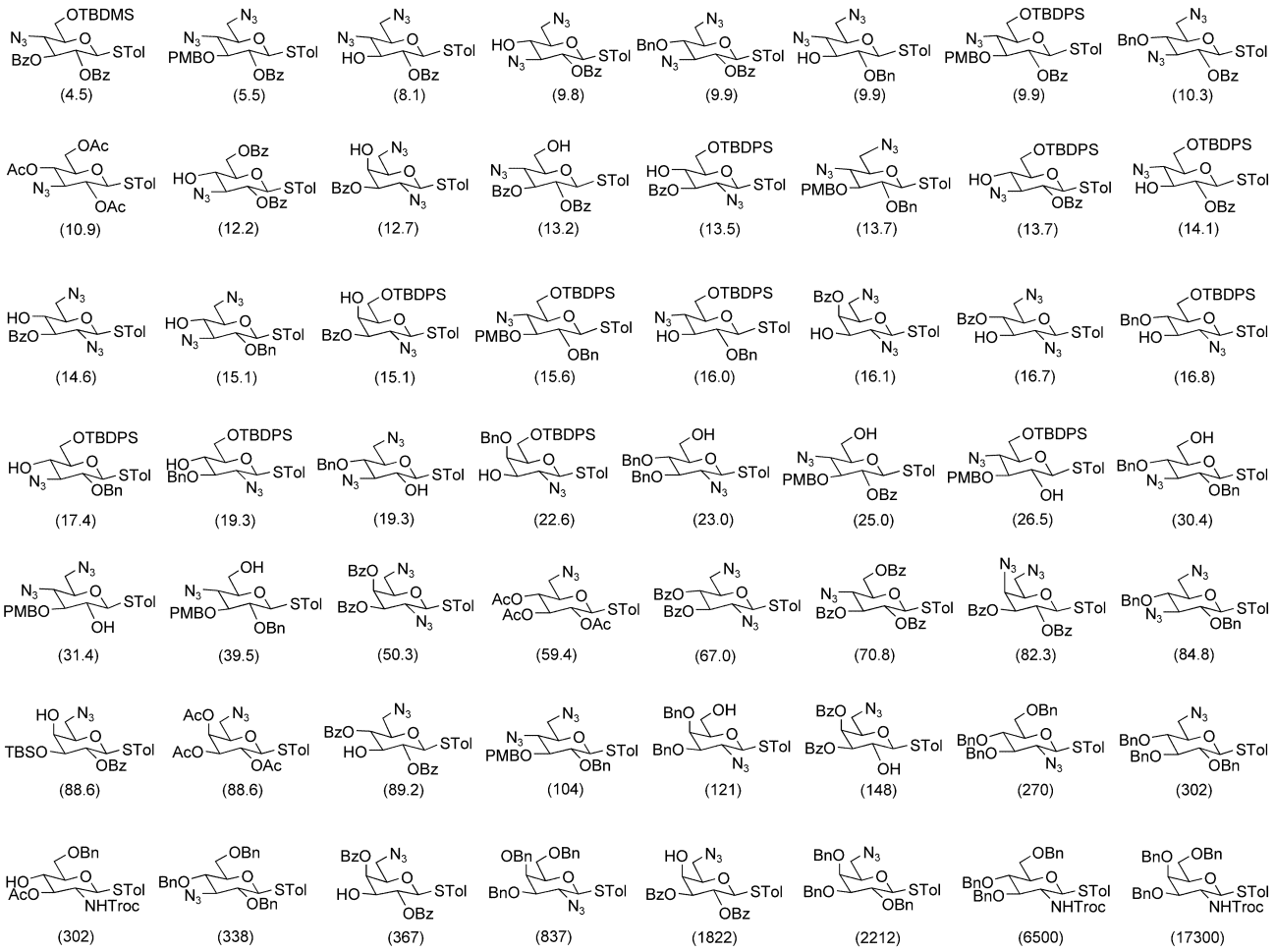


Figure 2. New nitrogen-containing building blocks for the Optimer database. Relative reactivity values are in parentheses. Bn = Benzyl, PMB = *para*-methoxybenzyl, TBDMS = *tert*-butyldimethylsilyl, TBDPS = *tert*-butyldiphenylsilyl, Tol = toluene.

(*E. faecalis* 29212, MIC(vancomycin) = 2 μg mL^{-1}) and a Van A vancomycin-resistant strain (*E. faecalis* BM4166, MIC(vancomycin) = 2000 μg mL^{-1}). Compounds **4e–f** were shown to inhibit growth of vancomycin-sensitive bacteria at a concentration of 5 μg mL^{-1}, whereas compounds **4a–d** showed no growth inhibition at concentrations up to 40 μg mL^{-1}. This result and other data (not shown) indicate the importance of the amino functionality on the terminal sugar for antibacterial activity. Growth inhibition of the Van A strain by **4a–f** was not observed at concentrations up to 100 μg mL^{-1}.

In conclusion, by combining an efficient oligosaccharide segment glycosylation with a straightforward deprotection scheme, we have developed a method for the facile synthesis of vancomycin derivatives bearing different sugar substituents. Compounds **4a–f** are the first products of the one-step chemical glycosylation of the vancomycin aglycon with non-natural oligosaccharides. Their biological evaluation demonstrates the importance of the glycan portion for activity, in particular the requirement for a terminal amino sugar residue. The chemistry developed sets the stage for a more detailed, systematic exploration of glycan function. Furthermore, this study constitutes the first implementation of the programmable one-pot glycosylation towards the synthesis of a set of natural product derivatives. This new strategy, that is, rapid creation of oligosaccharide sets by one-pot glycosylation followed by conversion to peracetylated trichloroacetimidate donors and coupling to an aglycon, should be generally applicable towards the construction of glycosylation libraries of natural products and the exploration of the varied biological functions of their carbohydrate substituents.

Received: March 31, 2003 [Z51534]

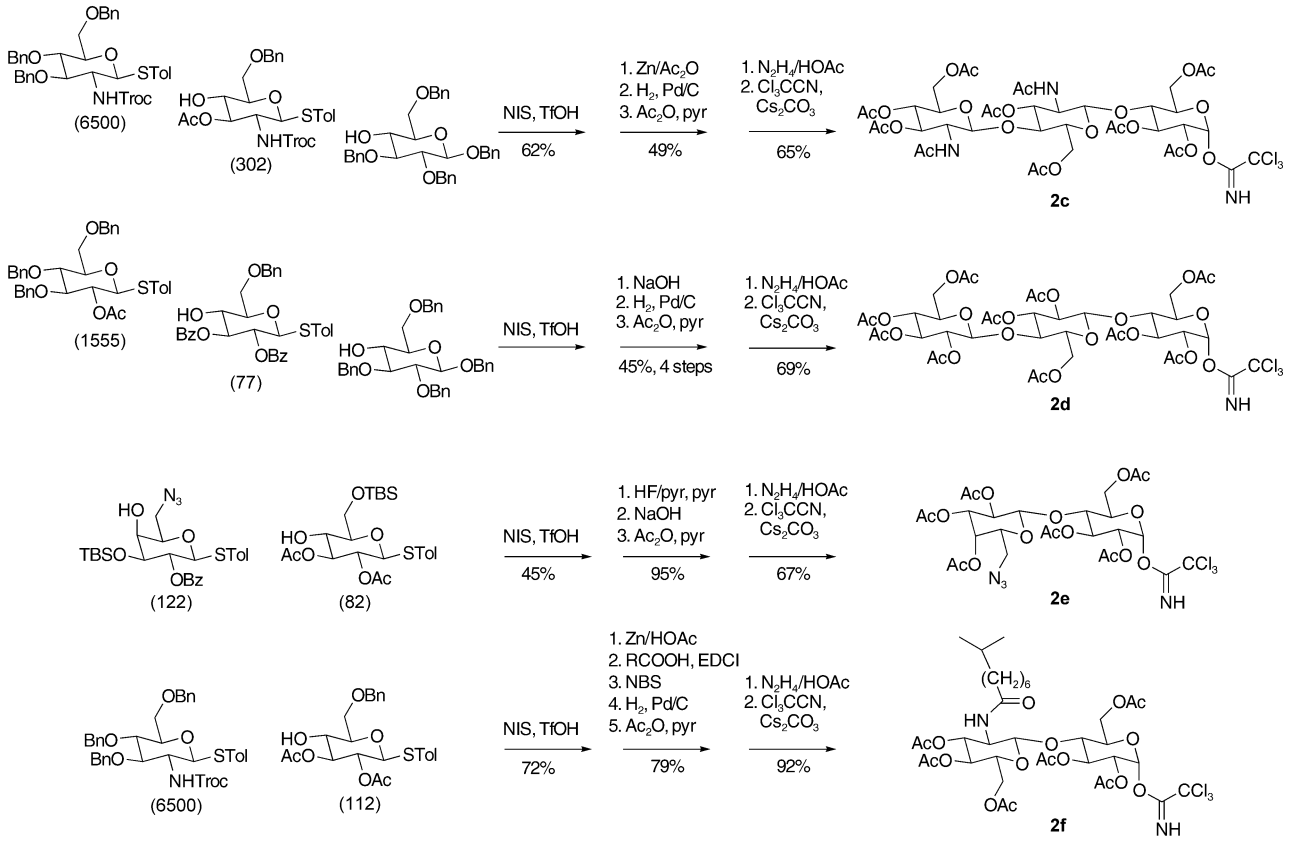
Keywords: antibiotics · carbohydrates · glycosylation · oligosaccharides · vancomycin

[1] T. K. Ritter, C.-H. Wong, *Angew. Chem.* **2001**, *113*, 3616–3641; *Angew. Chem. Int. Ed.* **2001**, *40*, 3508–3533.

[2] a) S. Raghavan, D. Kahne, *J. Am. Chem. Soc.* **1993**, *115*, 1580–1581; b) H. Yamada, T. Harada, T. Takahashi, *J. Am. Chem. Soc.* **1994**, *116*, 7919–7920; c) S. V. Ley, H. W. M. Priepke, *Angew. Chem.* **1994**, *106*, 2412–2414; *Angew. Chem. Int. Ed. Engl.* **1994**, *33*, 2292–2294.

[3] P. Sears, C.-H. Wong, *Science* **2001**, *291*, 2344–2350.

 © 2003 Wiley-VCH Verlag GmbH & Co. KGaA, Weinheim



Scheme 2. Programmable one-pot oligosaccharide synthesis, followed by switching of protecting groups and activation as trichloroacetimidates. EDCI = 1-ethyl-3-[3-(dimethylamino)propyl]carbodiimide hydrochloride, pyr = pyridine, TBS = *tert*-butyldimethylsilyl, Tf = trifluoromethanesulfonyl, Troc = 2,2,2-trichloroethoxycarbonyl.

[4] F. Burkhart, Z. Zhang, S. Wacowich-Sgarbi, C.-H. Wong, *Angew. Chem.* **2001**, *113*, 1314; *Angew. Chem. Int. Ed.* **2001**, *40*, 1274 – 1277.

[5] K.-K. T. Mong, C.-H. Wong, *Angew. Chem.* **2002**, *114*, 4261 – 4264; *Angew. Chem. Int. Ed.* **2002**, *41*, 4087 – 4090.

[6] K.-K. T. Mong, H.-K. Lee, S. G. Durón, C.-H. Wong, *Proc. Natl. Acad. Sci. USA* **2003**, *100*, 797 – 802.

[7] Z. Zhang, I. R. Ollmann, X.-S. Ye, R. Wischnat, T. Baasov, C.-H. Wong, *J. Am. Chem. Soc.* **1999**, *121*, 734 – 753.

[8] C. J. Thomas, A. O. Chizhov, C. J. Leitheiser, M. J. Rishel, K. Konishi, Z.-F. Tao, S. M. Hecht, *J. Am. Chem. Soc.* **2002**, *124*, 12926 – 12927.

[9] R. Nagarajan, A. A. Schabel, J. L. Occolowitz, F. T. Counter, J. L. Ott, A. M. Felty-Duckworth, *J. Antibiot.* **1989**, *42*, 63 – 72.

[10] D. H. Williams, B. Bardsley, *Angew. Chem.* **1999**, *111*, 1264 – 1286; *Angew. Chem. Int. Ed.* **1999**, *38*, 1173 – 1193.

[11] M. Ge, Z. Chen, H. R. Onishi, J. Kohler, L. L. Silver, R. Kerns, S. Fukuzawa, C. Thompson, D. Kahne, *Science* **1999**, *284*, 507 – 511.

[12] R. C. Goldman, E. R. Baizman, C. B. Longley, A. A. Branstrom, *FEMS Microbiol. Lett.* **2000**, *183*, 209 – 214.

[13] R. Sinha Roy, P. Yang, S. Kodali, Y. Xiong, R. M. Kim, P. R. Griffin, H. R. Onishi, J. Kohler, L. L. Silver, K. Chapman, *Chem. Biol.* **2001**, *8*, 1095 – 1106.

[14] P. J. Solenberg, P. Matsushima, D. R. Stack, S. C. Wilkie, R. C. Thompson, R. H. Baltz, *Chem. Biol.* **1997**, *4*, 195 – 202.

[15] H. C. Losey, M. W. Peczuh, Z. Chen, U. S. Eggert, S. D. Dong, I. Pelczer, D. Kahne, C. T. Walsh, *Biochemistry* **2001**, *40*, 4745 – 4755.

[16] S. D. Dong, M. Oberthuer, H. C. Losey, J. W. Anderson, U. S. Eggert, M. W. Peczuh, C. T. Walsh, D. Kahne, *J. Am. Chem. Soc.* **2002**, *124*, 9064 – 9065.

[17] C. Thompson, M. Ge, D. Kahne, *J. Am. Chem. Soc.* **1999**, *121*, 1237 – 1244.

[18] K. C. Nicolaou, H. J. Mitchell, N. F. Jain, N. Winssinger, R. Hughes, T. Bando, *Angew. Chem.* **1999**, *111*, 253 – 255; *Angew. Chem. Int. Ed.* **1999**, *38*, 240 – 244.

[19] K. C. Nicolaou, S. Y. Cho, R. Hughes, N. Winssinger, C. Smethurst, H. Labischinski, R. Endermann, *Chem. Eur. J.* **2001**, *7*, 3798 – 3823.

[20] B. Sun, Z. Chen, U. S. Eggert, S. J. Shaw, J. V. LaTour, D. Kahne, *J. Am. Chem. Soc.* **2001**, *123*, 12722 – 12723.

[21] **4a**: ^{1}H NMR (600 MHz, D_2O, 330 K): δ = 8.04 (d, 1H), 8.01 (s, 1H), 7.92–7.85 (m, 2H), 7.56 (d, 1H), 7.46 (s, 1H), 7.18–7.15 (m, 2H), 6.87 (s, 1H), 6.86 (s, 1H), 6.25 (s, 2H), 6.16 (s, 1H), 5.95 (s, b, 1H), 5.88 (s, 1H), 5.75 (s, 1H), 5.71 (d, 1H), 5.67 (d, 1H), 5.08 (s, 1H), 4.84 (d, 1H), 4.54 (s, 1H), 4.41 (t, 1H), 4.28–4.22 (m, 3H), 4.19 (t, 1H), 4.13–4.05 (m, 6H), 4.02–3.98 (m, 2H), 3.88 (dd, 1H), 3.17–3.15 (m, 1H), 3.11 (s, 1H), 2.59–2.52 (m, 1H), 2.13–2.12 (m, 1H), 2.05–2.01 (m, 1H), 1.90–1.88 (m, 1H), 1.19 (d, 3H), 1.16 ppm (d, 3H); HRMS (MALDI) *m/z* calcd for $C_{65}H_{72}Cl_2N_8O_{27}Na$ $[M+Na]^+$: 1489.3776, found: 1489.3703; HPLC (C_{18} reverse-phase, 5–80% CH_3CN in H_2O + 0.1% TFA, 0–30 min) t_R = 10.6 min.

 © 2003 Wiley-VCH Verlag GmbH & Co. KGaA, Weinheim

α-Fucosidase Inhibitors

Rapid Diversity-Oriented Synthesis in Microtiter Plates for In Situ Screening: Discovery of Potent and Selective α-Fucosidase Inhibitors**

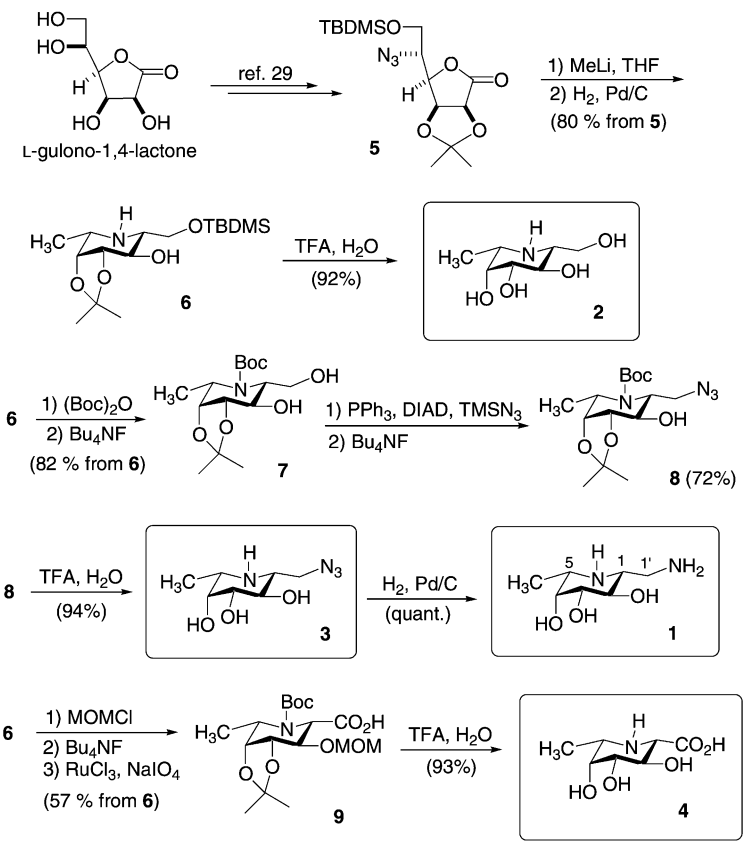
Chung-Yi Wu, Chuan-Fa Chang, Jenny Szu-Yu Chen, Chi-Huey Wong, and Chun-Hung Lin**

Polyhydroxypiperidines and pyrrolidines (also called iminocyclitols or aza-sugars) have attracted increasing attention because of their inhibitory activity against various glycosidases.[1,2] The glucose-type iminocyclitol deoxynojirimycin (DNJ), for example, has been used for the treatment of non-insulin-dependent diabetes (miglitol, targeting the intestinal disaccharidases).[3] Recent studies further indicate that DNJ and its derivatives are effective against hepatitis B[4,5] and C,[6] as well as glycosphingolipid storage disorders (such as Gaucher disease).[7,8] The efficacy of iminocyclitols is attributed to their mimicry of the transition state of enzymatic glycosidic cleavage.

Of the members of the glycosidase family, α-fucosidase is involved in the hydrolytic degradation of numerous fucose-containing glycoconjugates. The existence of this enzyme is associated with a variety of essential functions. For example, the abnormal accumulation of fuco-glycoconjugates, which results from the absence or deficiency of α-fucosidase, leads to the genetic neurovisceral storge disease fucosidosis.[9] An aberrant distribution of intracellular and extracellular α-fucosidase is also found in cystic fibrosis[10,11] and colon–rectal cancer.[12,13] Though the physiological functions of α-fucosidase are not completely understood, potent fucosidase inhibitors may be used as probes for the study of fucosidases with regard to their functions and for the development of potential therapeutic agents.

Recently we have established a novel combinatorial approach to five-membered iminocyclitols based on reductive amination and the Strecker reaction,[14] and a potent inhibitor has been identified from the library. The process, that is, synthesis and isolation of individual compounds for testing, is however very slow. To further facilitate the discovery of new glycosidase inhibitors, we aimed to develop a new method for the rapid derivatization of an iminocyclitol core designed for a specific glycosidase family (for example, fuconojirimycin derivatives for fucosidases in this study) without protecting group manipulation and under such conditions that the product could be used directly for screening in situ without isolation. This concept was first demonstrated by the development of new HIV protease inhibitors.[15] Herein we report the generation of a library based on fuconojirimycin (FNJ) in a microtiter plate, followed by the direct in situ evaluation of these reaction mixtures as fucosidase inhibitorse without product isolation. This approach has led to the discovery of the most potent inhibitors of α-fucosidases from bovine kidney and *Corynebacterium sp*.

Previous work on the development of glycosidase inhibitors indicated the existence of an additional binding component in the inhibitor.[2,16–25] This study was thus aimed at generating an FNJ derivative **1** (Scheme 1) as a core structure to mimic the transition state of the fucose moiety. A β-aminomethyl group was attached to the C1-position for identification of a new binding component throught the subsequent in situ amide-bond formation and screening. Since 1-deoxy-FNJ has been shown to be a potent inhibitor against α-fucosidases ($K_i = 9.8$ nM for the α-fucosidase from human neutrophil and 6.2 nM from bovine epididymal),[26]



Scheme 1. Synthesis of fuconojirimycin derivatives **1**–**4**. TBDMS = *tert*-butyldimethylsilyl, TFA = trifluoroacetic acid, Boc = *tert*-butoxycarbonyl, DIAD = diisopropyl-azodicarboxylate, TMS = trimethylsilyl, MOM = methoxymethyl.

[*] Prof. C.-H. Wong, Prof. C.-H. Lin, Dr. C.-Y. Wu, Dr. C.-F. Chang, J. S.-Y. Chen
The Genomics Research Center and
Institute of Biological Chemistry
Academia Sinica
No. 128 Academia Road Section 2, Nan-Kang, Taipei, 11529 (Taiwan)
Fax: (+886) 2-2651-4705
E-mail: chunhung@gate.sinica.edu.tw
Prof. C.-H. Wong
Department of Chemistry and
the Skaggs Institute for Chemical Biology
The Scripps Research Institute
10550 North Torrey Pines Road, La Jolla, CA 92037 (USA)
Fax: (+1) 858-784-2409
E-mail: wong@scripps.edu

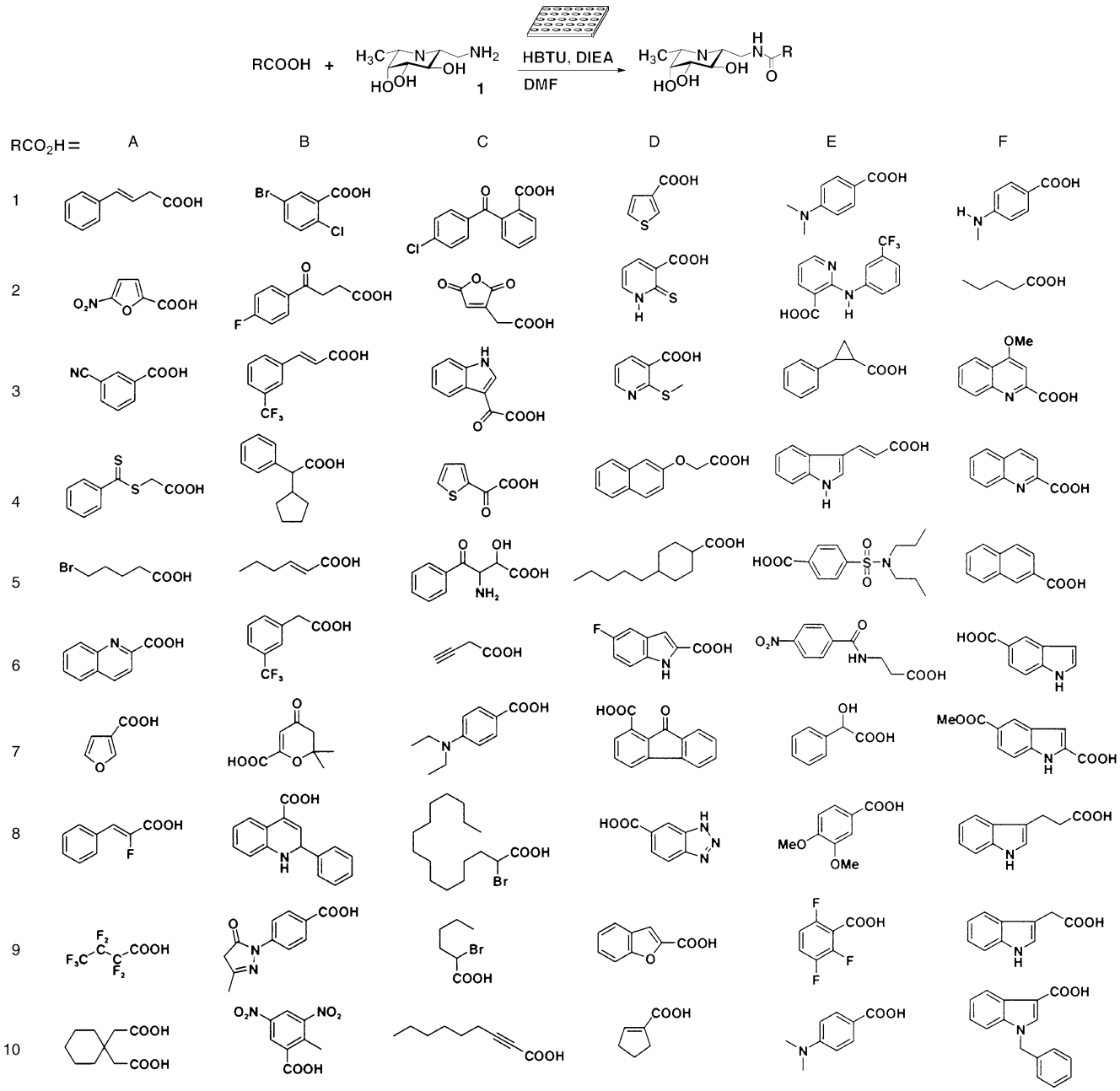
[**] This work was supported by Academia Sinica, Taipei, Taiwan.
Supporting information for this article is available on the WWW under http://www.angewandte.org or from the author.

 DOI: 10.1002/anie.200351823 © 2003 Wiley-VCH Verlag GmbH & Co. KGaA, Weinheim

further derivatization of this core may lead to a better and more-selective inhibitor of a specific fucosidase. In addition, it has been suggested that the inhibitory potency of **1**, in comparison with that of FNJ, was not affected by the tether extending from C1 or the anomeric stereochemistry,[27] and the β-linked FNJ amine may also be used for the identification of GDP-β-fucose (the glycosyl donor of α-fucosyltransferases) mimics as fucosyltransferase inhibitors.[28]

As shown in Scheme 1, FNJ analogues **1**–**4** were synthesized from L-gulono-1,4-lactone by a modified procedure developed by Fleet et al.,[27,29,30] and azido-lactone **5** was prepared in four steps in an overall 40% yield.[29] The nucleophilic addition of methyllithium and subsequent reductive amination afforded **6** with an exclusive new *S* stereogenic center in 80% yield (two steps from **5**). β-Homofuconojirimycin **2** was obtained in 92% yield by acidic deprotection. To selectively convert the C1′-hydroxy group into another functionality, compound **6** was transformed to diol **7**. Mitsunobu reaction of **7** to transform the primary alcohol to an azide and removal of the trimethylsilyl group afforded the desired product **8** (72% in two steps). Deprotection followed by reduction gave 1-aminomethyl-FNJ (**1**). In addition, compound **6** was converted into the carboxyl derivative **4** through protection and oxidation with $RuCl_3/NaIO_4$ (54% from **6**).

The α-fucosidase from bovine kidney[31] was chosen for the inhibition studies of iminocyclitols **1**–**4**. Compounds **1**–**3** showed strong inhibitory effects with IC_{50} values of 25, 30, and



Scheme 2. The reaction of 1-aminomethyl-FNJ (**1**) with a library of 60 carboxylic acids in a microtiter plate for direct screening of fucosidase inhibition in situ.

 © 2003 Wiley-VCH Verlag GmbH & Co. KGaA, Weinheim

24 nM, respectively, in contrast to the three- to fourfold lower activity of the carboxylic analogue **4** (92 nM). Compound **1** was then used for the subsequent diversity-oriented reaction with various acids in the presence of (1*H*-benzotriazole-1-yl)-1,1,3,3-tetramethyluronium hexafluorophosphate (HBTU, 1 equiv) and diisopropyl ethylamine (DIEA, 2 equiv) in DMF, followed by aqueous dilution and screening without purification. Each assay was performed in a well of a microtiter plate containing 10 nM of the reaction mixture, and the remaining enzyme activity was measured spectroscopically by detection of the released *p*-nitrophenol at 400 nm in the presence of *p*-nitrophenyl-α-L-fucopyranoside (the substrate).

Of the 60 compounds generated from the amide-forming reaction (Scheme 2), several potent inhibitors were found. For the purpose of easy understanding, the potency was expressed as % inhibition at one concentration of the reaction product. As shown in the inhibition profile of these reaction products (Figure 1), the

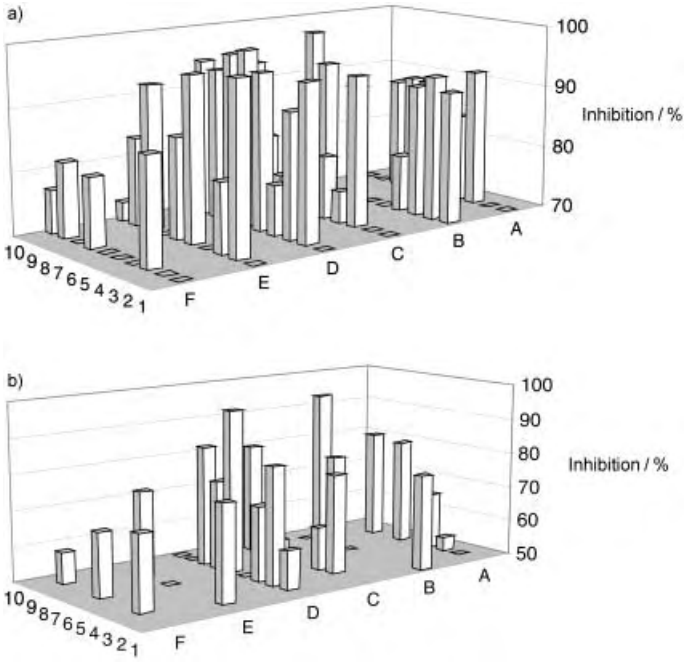
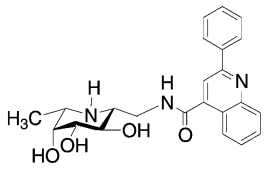


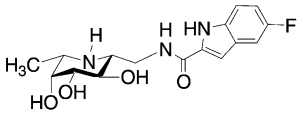
Figure 1. Inhibition profile of the reactions of **1** with 60 different acids at concentartions of a) 50 nM and b) 10 nM.

enzyme indeed prefers a hydrophobic aglycon to a hydrophilic one (for example, the product with B1 versus the one with C5). About two thirds of the reaction products were more potent than or comparable to **1**. The α-fucosidase inhibition was thus greatly enhanced by introduction of an appropriate hydrophobic moiety. Furthermore, the inhibitory results suggest that the enzyme is more interactive with an aromatic than an alkyl aglycon (for example, the reaction with B5 or A10) or partially alkyl derivative (for example, the reaction with B4 or C5). The enzyme seems to prefer a hetroaromatic component (especially a nitrogen-containing hetrocycle such as a quinoline type (for example, A6 and B8) and an indole type (D6)), as well as a fused aromatic ring (for example, the reaction with D4 or D7).

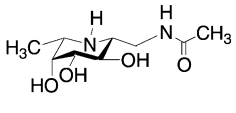
As a consequence of the strongest inhibitory potency exhibited by the aforementioned screening, the acids B8 and D6 were treated with 1-aminomethyl-FNJ **1**, and the products were chromatographed to afford **10** and **11**, respectively. The



10



11



12

inhibitions of **10** and **11** were studied and the K_i values were determined to be 0.50 and 0.60 nM, respectively; thus both are competitive against the nitrophenyl substrate. Neither acid B8 nor acid D6 alone showed any significant inhibition. The coupling reagents (HBTU and *N*-hydroxybenzotriazole (HOBT)) used for the formation of an amide bond and the reaction side product showed little inhibition.[32] Both **10** and **11** were also examined as inhibitors of glycosidases, including α- and β-glucosidases, α- and β-galactosidases, as well as α- and β-mannosidases (Table 1), and no significant inhibition were observed, thus indicating their high selectivity for α-fucosidase.

Previous reports indicated that the inhibition activity was diminished to a great extent when the *exo*-cyclic amino group was converted into an amide by acylation.[20,33] To understand

Table 1: Inhibition activity against various glycosidases.

Enzyme	Inhibitor	% Inhibition at 1 mM
α-fucosidase[a]	**10**	100[h] (K_i = 0.50 nM)
	11	100[h] (K_i = 0.60 nM)
	1	K_i = 25 nM
α-glucosidase[b]	**10**	20
	11	n.i.
	1	6
β-glucosidase[c]	**10**	20
	11	n.i.
	1	3
α-galactosidase[d]	**10**	18
	11	36
	1	46
β-galactosidase[e]	**10**	n.i.
	11	9
	1	n.i.
α-mannosidase[f]	**10**	41
	11	19
	1	n.i.
β-mannosidase[g]	**10**	2
	11	2
	1	n.i.

[a] Bovine kidney (Sigma Co. or Glyko Inc.). [b] *Saccharomyces sp.* (Toyobo Co.). [c] *Caldocellum saccharolyticum*, a recombinant protein (Sigma Co.). [d] *Aspergillus niger* (Sigma Co.). [e] *Escherichia coli* (Toyobo Co.). [f] Jack beans (Sigma Co.). [g] Snail acetone powder (Sigma Co.). [h] 100% inhibition was observed when the inhibitor concentration is equal to or higher than 12 nM. n.i. = no inhibition

 © 2003 Wiley-VCH Verlag GmbH & Co. KGaA, Weinheim

if the amide played a role in the inhibition, amide **12** was prepared (in quantitative yield by reaction of compound **1** with acetyl chloride) and found to have a fourfold lower activity ($K_i = 100$ nM). This result illustrates that the enzyme inhibition can be significantly enhanced by introduction of a hydrophobic amide group, even though the existence of an alkyl-amide bond has a negative effect.

The α1,2-fucosidase from *Corynebacterium sp.* was then investigated with the same library. The results revealed a preferred aglycon of fused (for example, D4, F4, F5, and F9) or polarized aromatic compounds (for example, B6, D7, and E6), with the exception of D5. The most potent inhibitions were found in the reaction with D7 ($IC_{50} = 5.6$ nM), F4 ($IC_{50} = 4.1$ nM), and F9 ($IC_{50} = 6.3$ nM). Compounds **10** and **11**, the best inhibitors previously described, are less active than the positive control **1** in this study. To obtain more sensitive detection in the enzyme assay, 4-methylumbelliferyl-α-L-fucopyranoside was also used to confirm the previous results. The compound was found to be a better substrate for the bacterial α1,2-fucosidase ($K_m = 12$ μM) than *p*-nitrophenyl-α-L-fucopyranoside ($K_m = 35$ μM), but inactive toward the bovine kidney α-fucosidase.[34] Similar IC_{50} values were obtained for the α1,2-fucosidase from *Corynebacterium sp.*

In conclusion, the method described here represents the first rapid search for an optimal group attached to the core of a common transition-state mimic to bind the hydrophobic site of a glycosyltransfer enzyme using a simple amide-bond forming reaction followed by screening in situ without product isolation. The two compounds (**10** and **11**) are the most potent and selective inhibitors reported so far ($K_i = 0.50$ and 0.60 nM, respectively). The same library was screened for inhibitors of the *Corynebacterium* fucosidase and a different group of inhibitors was identified. This approach is thus proven to be very effective and simple for the rapid identification of selective potent inhibitors of enzymes within the same family.

Received: May 6, 2003 [Z51823]

Keywords: combinatorial chemistry · iminocyclitol · inhibitors · microreactors

[1] A. E. Stütz, *Iminosugars as Glycosidase Inhibitors—Norjirimycin and Beyond*, Wiley-VCH, Weinheim, **1999**.
[2] V. H. Lillelund, H. H. Jensen, X. Liang, M. Biols, *Chem. Rev.* **2002**, *102*, 515 – 553.
[3] A. Mitrakou, N. Tountas, A. E. Raptis, R. J. Bauer, H. Schulz, S. A. Raptis, *Diabetic Med.* **1998**, *15*, 657 – 660.
[4] T. M. Block, X. Lu, F. M. Platt, G. R. Foster, W. H. Gerlich, B. S. Blumberg, R. A. Dwek, *Proc. Natl. Acad. Sci. USA* **1994**, *91*, 2235 – 2239.
[5] A. Mehta, S. Carrouee, B. Conyers, R. Jordan, T. Butters, R. A. Dwek, T. M. Block, *Hepatology* **2001**, *33*, 1488 – 1495.
[6] D, Durantel, N. Branza-Nichita, S. Carrouee-Durantel, T. D. Butters, R. A. Dwek, N. Zitzmann, *J. Virol.* **2001**, *75*, 8987 – 8998.
[7] T. Cox, R. Lachmann, C. Hollak, J. Aerts, S. van Weely, M. Hrebicek, F. Platt, T. Butters, R. A. Dwek, C. Moyses, I. Gow, D. Elstein, A. Zimran, *Lancet* **2000**, *355*, 1481 – 1485.
[8] For a detailed review about the recent development, see R. A. Dwek, T. D. Butters, F. M. Platt, N. Zitzmann, *Nat. Rev. Drug Discovery* **2002**, *1*, 65 – 75.
[9] a) G. H. Thomas, A. L. Beaudet, in *The Metabolic Basis of Inherited Diseases* (Eds.: C. R. Scriver, A. L. Beaudet, W. S. Sly, D. Valle), McGraw-Hill, New York, 7th ed., **1995**, pp. 2529 – 2561; b) J. C. Michalski, A. Klein, *Biochim. Biophys. Acta* **1999**, *1455*, 69 – 84.
[10] M. C. Glick, V. A. Kothari, A. Liu, L. I. Stoykova, T. F. Scanlin, *Biochimie* **2001**, *83*, 743 – 747.
[11] T. F. Scanlin, M. C. Glick, *Biochim. Biophys. Acta* **1999**, *1455*, 241 – 253.
[12] D. Ayude, J. Fernandez-Rodriguez, F. J. Rodriguez-Berrocal, V. S. Martinez-Zorzano, A. de Carlos, E. Gil, M. P. de La Cadena, *Oncology* **2000**, *59*, 310 – 316.
[13] J. Fernandez-Rodriguez, D. Ayude, M. P. de La Cadena, V. S. Martinez-Zorzano, A. de Carlos, A. Caride-Castro, G. de Castro, F. J. Rodriguez-Berrocal, *Cancer Detect. Prev.* **2000**, *24*, 143 – 149.
[14] C. Saotome, C.-H. Wong, O. Kanie, *Chem. Biol.* **2001**, *8*, 1061 – 1070.
[15] A. Brik, Y.-C. Lin, J. Elder, C.-H. Wong, *Chem. Biol.* **2002**, *9*, 891 – 896.
[16] M. Kleban, P. Hilgers, J. N. Greul, R. D. Kugler, J. Li, S. Picasso, P. Vogel, V. Jager, *ChemBioChem* **2001**, *2*, 365 – 368.
[17] J. N. Greul, M. Kleban, B. Schneider, S. Picasso, P. Vogel, V. Jager, *ChemBiochem* **2001**, *2*, 368 – 370.
[18] O. Boss, E. Leroy, A. Blaser, J.-L. Reymond, *Org. Lett.* **2000**, *2*, 151 – 154.
[19] M. Nakata, C. Chong, Y. Niwata, K. Toshima, K. Tatsuta, *J. Antibiot.* **1993**, *46*, 1919 – 1922.
[20] J. N. BeMiller, R. J. Gilson, R. W. Myers, M. M. Santoro, M. P. Yadav, *Carbohydr. Res.* **1993**, *250*, 93 – 100.
[21] A. Blaser, J.-L. Reymond, *Helv. Chim. Acta* **1999**, *82*, 760 – 768.
[22] A. Blaser, J.-L. Reymond, *Org. Lett.* **2000**, *2*, 1733 – 1736.
[23] Y. Nishimura, E. Shitara, F. Kojima, T. Takeuchi, *Bioorg. Med. Chem.* **1999**, *7*, 1241 – 1246.
[24] Y. Nishimura, E. Shitara, T. Takeuchi, *Tetrahedron Lett.* **1999**, *40*, 2351 – 2354.
[25] S. Ogawa, M. Mori, G. Takeuchi, F. Doi, M. Watanabe, Y. Sakata, *Bioorg. Med. Chem. Lett.* **2002**, *12*, 2814 – 2822.
[26] D. M. Andrews, M. I. Bird, M. M. Cunningham, P. Ward, *Bioorg. Med. Chem. Lett.* **1993**, *3*, 2533 – 2536.
[27] G. W. J. Fleet, S. K. Namgoong, C. Barker, S. Baines, G. S. Jacob, B. Winchester *Tetrahedron Lett.* **1989**, *30*, 4439 – 4442.
[28] We have developed a number of α1,3-fucosyltransferase inhibitors, see a) M. L. Mitchell, F. Tian, L. V. Lee, C.-H. Wong, *Angew. Chem.* **2002**, *114*, 3167 – 3170; *Angew. Chem. Int. Ed.* **2002**, *41*, 3041 – 3044; b) M. Takayanagi, T. Flessner, C.-H. Wong, *J. Org. Chem.* **2000**, *65*, 3811 – 3815; c) B. W. Murray, V. Wittmann, M. D. Burkart, S.-C. Hung, C.-H. Wong, *Biochemistry* **1997**, *36*, 823 – 831.
[29] G. W. J. Fleet, N. G. Ramsden, D. R. Witty, *Tetrahedron* **1989**, *45*, 319 – 326.
[30] J. P. Shilvock, G. W. J. Fleet, *Synlett* **1998**, 554 – 556.
[31] It was reported that the enzyme is able to hydrolyze the nonreducing fucose residues with α1,2-, α1,3-, α1,4-, and α1,6-linkages, and the cleavage of α1,6- linkage is more efficient than other fucose linkages. Please see the catalogue of Glyko Inc. or find the information at the webside: http://www.glyko.com/.
[32] The IC_{50} values of HBTU and HOBt were measured to be 0.5 and 1.0 mM, respectively.
[33] W. Guo, J. Hiratake, K. Ogawa, M. Yamamoto, S.-J. Ma, K. Sakata, *Bioorg. Med. Chem. Lett.* **2001**, *11*, 467 – 470.
[34] *p*-Nitrophenyl-α-L-fucopyranoside has a K_m value of 310 μM for the α-fucosidase from bovine kidney.

 © 2003 Wiley-VCH Verlag GmbH & Co. KGaA, Weinheim

Catalyst Deactivation

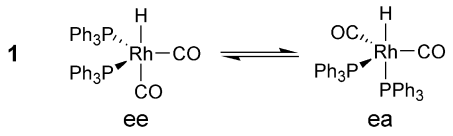
Dormant States of Rhodium Hydroformylation Catalysts: Carboalkoxyrhodium Complex Formed from Enones in the Alkene Feed**

*Edyta B. Walczuk, Paul C. J. Kamer, and Piet W. N. M. van Leeuwen**

The stability, deactivation, and regeneration of the catalyst are, along with activity and selectivity, important issues in homogeneous catalysis.[1] The turnover number (TON) of a catalyst, a reflection of the catalyst stability, is one of the pivotal parameters for implementation of a process. Deactivation can occur in many ways, but sometimes deactivation is only temporary and the catalyst activity is restored. For long-term catalyst performance in the hydroformylation reaction, avoiding deactivation of the catalyst caused by reactive impurities in alkene feeds is of great importance. Such impurities may trap active rhodium catalysts either in a temporary or a permanent inactive state. Dienes and alkynes are poisons for many catalytic processes involving alkenes.[1] Since hydroformylation of dienes is much slower than that of alkenes,[2] diene impurities might thus slow down 1-alkene hydroformylation, if the resting state of the catalytic cycle of the diene is appropriate.[3] Examples of such deactivation are reported in patent literature.[4]

We have studied the deactivation of hydroformylation catalysts by controlled reaction with the most likely impurities in alkene feeds, such as dienes, alkynes, and enones. The hydrido rhodium complex, the common resting state in hydroformylation, at which the catalytic cycle starts, was prepared in a high-pressure (HP)-IR autoclave under syn gas (CO/H_2), from the catalyst precursor, $[Rh(acac)(CO)_2]$ (acac = 2,4-pentadione) and excess of PPh_3 at 80 °C. After complete conversion of $[Rh(acac)(CO)_2]$ into $[RhH(CO)_2(PPh_3)_2]$ (**1**), a substrate or a mixture of substrates was added to the reaction mixture from a separately pressurized reservoir. We have used in situ high-pressure IR spectroscopy in conjunction with (high-pressure) NMR spectroscopy to detect and characterize the catalyst under actual catalytic conditions.[5] Employing NMR spectroscopy studies Brown and Kent have shown that **1** exists as a mixture of two rapidly equilibrating trigonal-bipyramidal isomers in a diequatorial (ee) to equatorial-apical (ea) isomer ratio of 85:15 (Scheme 1).[6]

The HP-IR spectrum of **1** has four carbonyl bands (at $\tilde{\nu}$ = 2043, 1997, 1986, and 1953 cm^{-1}) that have been assigned to the two isomers.[7] HP-IR studies of the hydroformylation of 1-octene showed that, while 1-octene was present in the reaction mixture, the main species observed was **1**. Minor decomposition of **1** was due to the formation of an inactive dimer.[8] New bands, characteristic of the dimer, appeared in the IR spectrum at $\tilde{\nu}$ = 2023, 1972, and 1957 cm^{-1}.



Scheme 1. Compound **1** as a mixture of two trigonal-bipyramidal isomers.

Several linear dienes, 2,4-hexadiene, 1,5-hexadiene, and 1,3-pentadiene were tested as inhibitors of the catalyst. The addition of 2,4-hexadiene to **1** formed in situ resulted in the slow growth of two new bands in the IR spectrum (Table 1) at the cost of the four absorption bands characteristic of **1**, but these four initial bands did not disappear completely. 1,5-Hexadiene underwent fast hydroformylation and its addition to the reaction mixture did not change the nature of the resting state of the rhodium complex and it did not influence the rate of 1-octene hydroformylation either.

Table 1: Influence of poisons/inhibitors on the Rh-C=O bands of **1** under syn gas.

1 + poison/inhibitor	Rh-C=O bands [cm^{-1}]
–	1953, 1986, 1997, 2043
2,4-hexadiene	1967, 2016[a]
1,3-pentadiene	1949 (w), 1957 (s), 2016 (s)
1-octyne	1946, 1988, 2020, 2042, 2073, 2120[a]
trans-3-nonen-2-one	1946 (w), 1984 (vs)
3-buten-2-one (MVK, **2**)	1946 (w), 1984 (vs)

[a] Weak bands from **1** also present.

Addition of the conjugated 1,3-pentadiene to **1**, however, resulted in the immediate formation of new bands in the IR spectrum (Table 1). A 60-fold excess of diene gave complete conversion of **1** and new bands were observed immediately after addition of the diene (Figure 1). When the ratio of diene:Rh is 20:1, the signals of **1** did not disappear completely. After 10 min the concentration of **1** was about 50% of its initial value. In both cases 1,3-pentadiene underwent hydroformylation to a mixture of aldehydes.

Addition of 1,3-cyclohexadiene or cyclopentadiene to **1** did not affect the IR spectrum. Both the cyclic dienes underwent fast hydroformylation and new bands characteristic of the corresponding unsaturated aldehydes appeared in the IR spectra.

Internal and terminal alkynes proved to have completely different effects on **1**. Addition of 3-hexyne did not affect the nature of **1**, whereas the addition of 1-octyne immediately caused irreversible formation of new rhodium species, as indicated by several new bands (Table 1), which remained present throughout the experiment (Figure 2). Furthermore,

[*] Prof. Dr. P. W. N. M. van Leeuwen, Dr. E. B. Walczuk, Dr. P. C. J. Kamer
Institute of Molecular Chemistry
University of Amsterdam
Nieuwe Achtergracht 166, 1018 WV Amsterdam (The Netherlands)
Fax: (+31) 20-525-6456
E-mail: pwnm@science.uva.nl

[**] We are indebted to Sasol Technology Ltd. for financial support and to Dr. M. J. Green and co-workers for stimulating discussions.

 DOI: 10.1002/anie.200351884 © 2003 Wiley-VCH Verlag GmbH & Co. KGaA, Weinheim

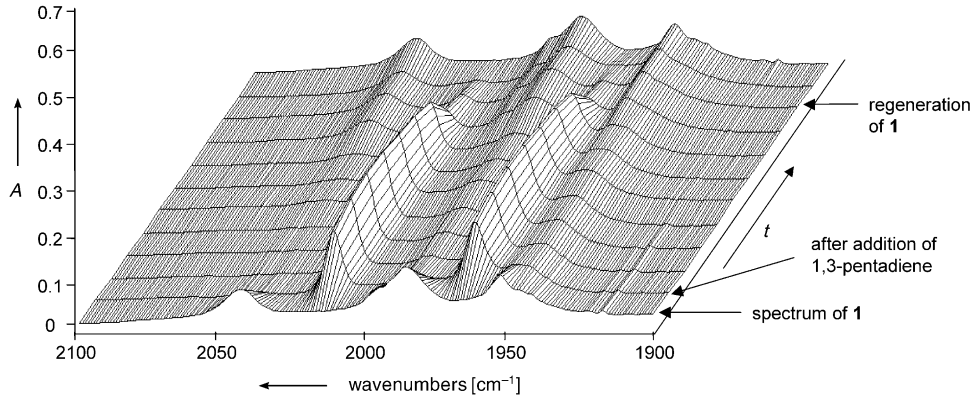


Figure 1. In situ HP-IR study of hydroformylation of 1,3-pentadiene catalyzed by **1** (1,3-pentadiene:**1** = 60:1).

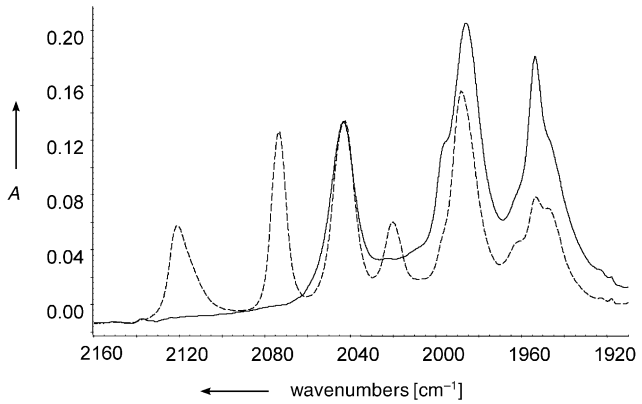


Figure 2. In situ HP-IR study of hydroformylation of 1-octyne catalyzed by **1**; —— spectrum of **1**, ----- spectrum after the addition of 1-octyne.

1-octyne underwent slow hydroformylation to a mixture of products.

Addition of unsaturated ketones, such as *trans*-3-nonen-2-one and 3-buten-2-one (MVK, **2**), to a solution of **1** immediately gave rise two new bands in the IR spectrum (Table 1) and the disappearance of the four bands characteristic of **1** (Figure 3).

Note that when most of **2** had reacted, **1** was regenerated and became again the predominant species. The addition of 2-cyclohexen-1-one to **1** had the same effect as the addition of the linear α,β unsaturated ketones. The branched unsaturated ketone, mesityl oxide (4-methyl-3-penten-2-one), did not lead to a decrease of the concentration of **1**.

The large impact of **2** on the concentration of **1** prompted us to perform a detailed study of the temporary deactivation. A high initial concentration of **2** in the reaction mixture gave a very slow initial hydroformylation of 1-octene as measured by syn-gas consumption. At low concentration of **2**, only minor inhibition occurred and the normal rates of the hydroformylation of 1-octene were observed (Figure 4).

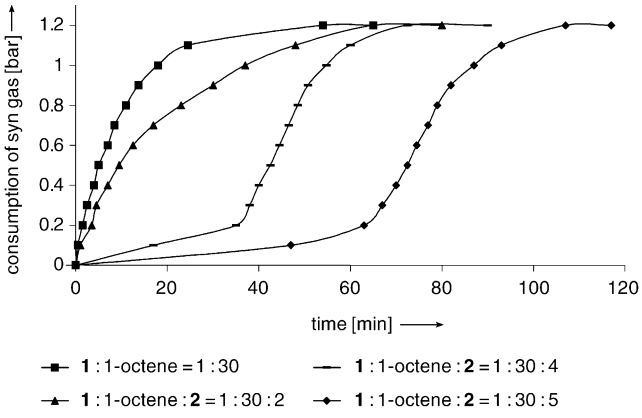


Figure 4. Comparison of the rates of hydroformylation of 1-octene and mixtures of 1-octene and **2** catalyzed by **1**.

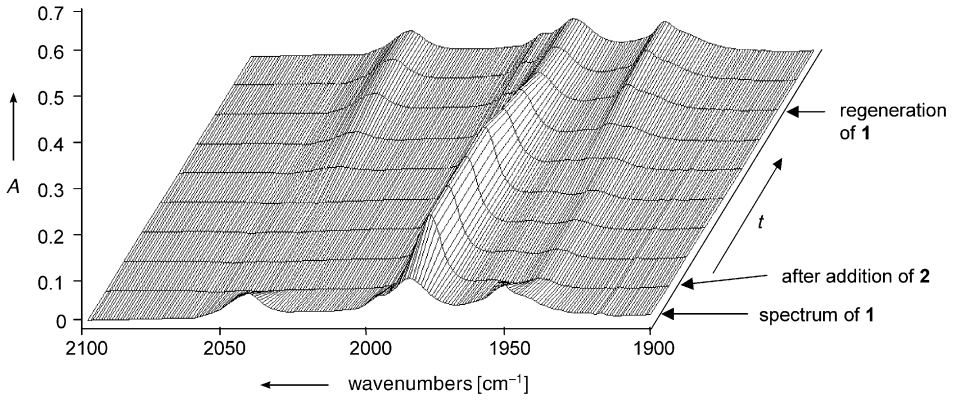


Figure 3. In situ HP-IR study of the reaction of **2** with **1**.

 © 2003 Wiley-VCH Verlag GmbH & Co. KGaA, Weinheim

Similar competition experiments were carried out with the other substrates 1-octyne, 1,3-pentadiene, cyclopentadiene, and 2-cyclohexen-1-one. The substrates 1-octyne, 2-cyclohexen-1-one, and **2** changed the nature of the resting state of the rhodium species. When these new rhodium species were present in the reaction mixture, hydroformylation of 1-octene stopped or was retarded. When most of the inhibitor was converted and its concentration reached a certain lower level, the hydrido complex **1** again became the predominant species and hydroformylation of 1-octene resumed. Compounds not changing the resting state (cyclopentadiene, 2-cycloocten-1-one (not shown)) or that are converted very quickly (1,3-pentadiene) did not influence the rate of the 1-octene hydroformylation (Figure 5).

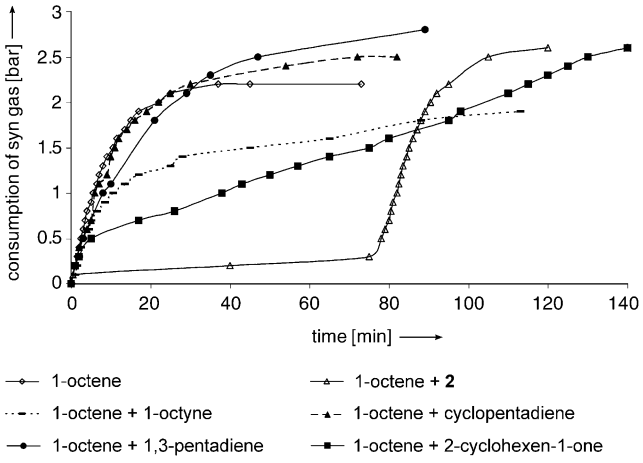
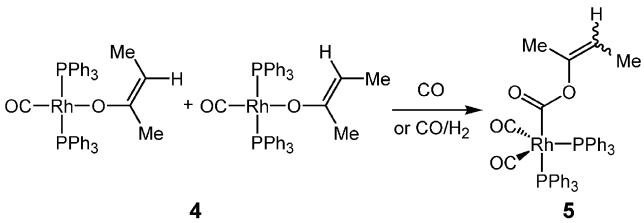


Figure 5. Comparison of the rates of hydroformylation of 1-octene and mixtures of 1-octene and other substrates catalyzed by **1**.

HP ^{1}H and ^{31}P NMR spectroscopy was employed to study the intermediate products. However, the reaction between **1** and **2** at room temperature was very fast giving a mixture containing many new compounds, which we did not attempt to identify. As a model catalyst we then used $[RhH(CO)(PPh_3)_3]$ (**3**) in the reaction with **2** in a ratio of 1:1.2. The reaction was initially monitored at −80 °C and then the reaction mixture was gradually heated to −20 °C while ^{1}H and ^{31}P NMR spectra were recorded. Subsequently, the NMR tube was cooled to −60 °C and ^{1}H, COSY, ^{31}P{^{1}H}, and ^{13}C{^{1}H} NMR spectra were recorded. ^{31}P NMR showed complete conversion of **3** and two new doublets at $\delta = 26.74$ and 29.99 ppm and a signal assigned to one equivalent of free PPh_3 at $\delta = -6.26$ ppm were observed. This result indicates formation of two isomeric insertion products, both containing two equivalent triphenylphosphane units. Because of their extremely unstable nature attempts to isolate the intermediates were not successful, but they could be identified in situ. Their structure was unambiguously determined by NMR spectroscopy.[9] Two η^1-oxygen bound rhodium enolate complexes (**4**; Scheme 2) were identified and characterized by IR spectroscopy they give a carbonyl band at $\tilde{\nu} = 1968\ cm^{-1}$. The two carbonyl bands at $\tilde{\nu} = 1690$ and $1719\ cm^{-1}$ characteristic of **2** disappear.

When the reaction of **3** with **2** was complete and a mixture of **4a** and **4b** was formed, CO/H_2 or CO was bubbled through the reaction mixture for 6 min at −60 °C. The reaction of **4** with CO was studied by NMR (^{1}H, ^{31}P{^{1}H}, ^{13}C{^{1}H}, COSY, ^{31}P–^{31}P correlation, ^{31}P–^{13}C correlation and ^{31}P–^{103}Rh correlation) and HP-IR spectroscopy.

^{1}H and ^{31}P{^{1}H} spectra taken after the reaction showed complete conversion of **4** and formation of new species (**5**; Scheme 3) which we characterized using HP-IR and several NMR spectroscopy techniques.



4 **5**

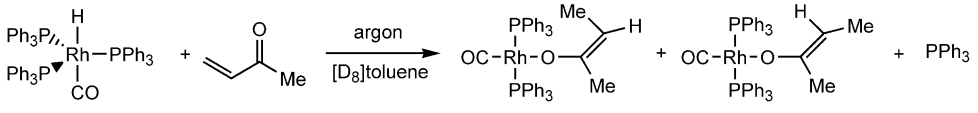
Scheme 3. Reaction of **4** with CO.

The ^{31}P{^{1}H} spectrum changed totally when CO was present in the reaction mixture. The two doublets characteristic of **4** disappeared and two new doublets of doublets at $\delta =$ 26.15 and 28.53 ppm were observed. The data were confirmed by simulation of the spectrum of **5** (Figure 6).[10]

According to the ^{31}P–^{31}P correlation spectra these two doublets of doublets belong to two inequivalent phosphorus atoms bonded to the same rhodium(I) species. This result was confirmed by ^{31}P–^{103}Rh correlation spectroscopy.

^{1}H NMR spectroscopy showed formation of two *E*/*Z* isomers that differed in the vinyl part in a ratio of 30:70. The *E* isomer (**5a**) gave three resonance signals at $\delta = 0.8$, 1.35, and 2.6 ppm. Another set of three signals at $\delta = 1.28$, 1.50, and 4.15 ppm was assigned to the *Z* isomer (**5b**). The phenyl groups of both isomers gave overlapping signals at $\delta = 6.8$–7.8 ppm. The two isomers could not be distinguished by ^{31}P NMR spectroscopy.

A more detailed examination of the structure of **5** was carried out employing ^{13}CO instead of ^{12}CO, which was bubbled through the solution of the rhodium enolate complexes **4**. The ^{13}C{^{1}H} spectrum taken at −40 °C showed one



3 **2** **4a** **4b**

Scheme 2. Reaction of **3** with **2** under argon.

 © 2003 Wiley-VCH Verlag GmbH & Co. KGaA, Weinheim

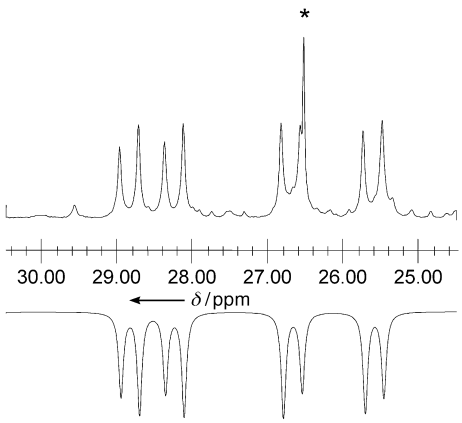


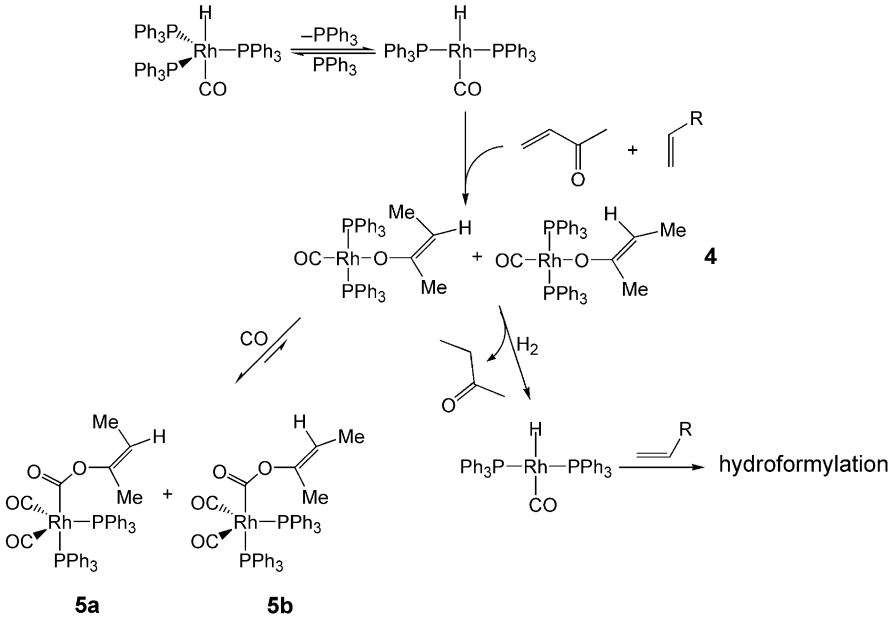
Figure 6. Top: $^{31}P\{^1H\}$ spectrum obtained after bubbling CO/H_2 through the solution containing the rhodium enolate complexes **4**, * $O{=}PPh_3$; bottom: simulation of this spectrum.

resonance for an acyl group at 235.5 ppm and one resonance for rhodium-bound carbonyl group at 198 ppm. Coupling of the acyl carbon with the rhodium ($J(Rh,C) = 22$ Hz) and phosphorus nuclei ($J(P,C) = 80$ Hz) was observed. The terminal carbonyl groups are coupled to the rhodium nucleus ($J(Rh,C) = 76$ Hz). The ^{31}P–^{13}C correlation spectrum showed strong cross-peaks for the two double doublets occurring in the $^{31}P\{^1H\}$ NMR spectrum and for the signal of a carbonyl ligand at 198 ppm and that of a rhodium-acyl resonance at 235.5 ppm. Therefore, we conclude that the two signals present in the $^{13}C\{^1H\}$ NMR spectrum and two double doublets in the $^{31}P\{^1H\}$ NMR spectrum belong to the same carboalkoxyrhodium complex, which exists as a mixture of *E*/*Z* isomers.

The reaction of **4** with CO was also performed in the HP-IR autoclave. When **2** was added to a cyclohexane solution of **3** the bands in the IR spectrum characteristic of the rhodium hydride complex ($\tilde{\nu} = 2011$ and 1938 cm^{-1}) disappeared and a new band characteristic of **4** appeared at $\tilde{\nu} = 1968$ cm^{-1}. Then CO/H_2 or CO was added to the reaction mixture and the latter band disappeared and new bands at $\tilde{\nu} = 1984$ and 1946 cm^{-1} were observed, indicative of coordination of two carbonyl ligands. The positions of these bands in the IR spectrum were exactly the same as those observed after addition of **2** to the solution of **1** under CO/H_2 (Figure 3).

The NMR and IR spectroscopy studies have shown that addition of CO to the solution of **4** results in coordination of a CO molecule to the rhodium center and insertion of a second one to the rhodium–oxygen bond forming five coordinate rhodium(I) complexes (**5**; Scheme 4).[6,11] Structurally analogous carboalkoxy complexes of iridium, which are formed upon carbonylation of four-coordinate iridium alkoxides, have been reported.[12]

The formation of **5** is the cause for slow or no hydroformylation of 1-octene when **2** is present in the reaction mixture. The unsaturated ketone is much more reactive towards **1** than the alkene and forms carboalkoxy complexes with rhodium thus blocking its activity for the 1-octene hydroformylation. Catalyst **1** for the hydroformylation of 1-octene is only restored after the enone has been converted into 2-butanone. The formation of formate esters from the enone substrate was not detected by GC-MS and HP-NMR spectroscopy. The analysis of the reaction mixture confirmed that the only organic product present after the reaction was 2-butanone. The rhodium enolate complexes react very fast with CO leading to the formation of **5**, which does not react with H_2 as formate formation is apparently very slow. Instead, a de-insertion has to occur to allow for hydrogenation of **4**,



Scheme 4. Deactivation mechanism of the rhodium hydride complex by **2**.

which results in butanone formation. In equilibrium, during a catalytic reaction, the concentration of **4** is too low to detect by HP-IR spectroscopy. When most of **2** has been converted into butanone, the hydroformylation of 1-octene can proceed. (Scheme 4).

In conclusion unsaturated impurities in the alkene feed, such as enones, dienes, and alkynes, deactivate the hydroformylation catalyst. Enones transform the "active" **1** temporarily into an inactive dormant state by formation of carboalkoxyrhodium complex. The hydroformylation catalyst is reformed by hydrogenation, which explains why the inhibiting effect can be reduced by high H_2 pressure.[3]

Experimental Section

High-pressure IR experiments were performed in an SS-316 50-mL autoclave equipped with IRTRAN windows (ZnS, transparent above

 © 2003 Wiley-VCH Verlag GmbH & Co. KGaA, Weinheim

700 cm^{-1}, $\varnothing = 10$ mm, optical path length = 0.4 mm), a mechanical stirrer, a temperature controller, and a pressure device. In a typical experiment, $[Rh(CO)_2(acac)]$ (0.008 g, 3.0×10^{-5} mol) and PPh_3 (6.0×10^{-4} mol) of were dissolved in cyclohexane (15 mL) under argon. The solution was brought into the autoclave and after flushing and pressurizing with CO/H_2, the HP-IR cell was placed into a Nicolet 510 FTIR spectrometer. Then the reaction mixture was heated to 80 °C. A substrate or a mixture of substrates were added to the reaction mixture from a separately pressurized reservoir by means of overpressure once the active catalyst, $[RhH(CO)_2(PPh_3)_2]$ (**1**), was formed. The IR spectra were recorded while the samples were stirred.

4: A solution of $[RhH(CO)(PPh_3)_3]$ (**3**; 0.05 g, 5.4×10^{-5} mol; Strem) in $[D_8]$toluene was prepared in a 5-mm NMR tube under argon. The tube was placed in a NMR machine and cooled to −60 °C. The NMR tube was then ejected and 3-butene-2-one (**2**, 5.5 μL, 6.5×10^{-5} mol) was added and the tube placed back in the precooled NMR machine and the NMR spectra were recorded. *E* isomer (**4a**): ^{1}H NMR (300 MHz, C_7D_8, −60 °C): $\delta = 1.49$ (s, =C(CH_3), 3H), 2.15 (d, J(H,H) = 6 Hz, 3H, =CH(CH_3)), 3.97 (q, J(H,H) = 6 Hz, 1H, =CH(CH_3)), 6.8–7.5 ppm (m, 30H, PPh_3); ^{31}P{^{1}H} NMR (121.5 MHz, C_7D_8, −60 °C): $\delta = 26.74$ ppm (d, J(Rh,P) = 145.00 Hz); ^{13}C{^{1}H} NMR (75.4 MHz, C_7D_8, −60 °C): $\delta = 14.95$ (s, CH_3), 29.21 (s, CH_3), 92.15 (s, =CH), 159.03 (s, Rh-O-C), 191.46 ppm (dt, Rh-CO); *Z* isomer (**4b**): ^{1}H NMR (300 MHz, C_7D_8, −60 °C): $\delta = 1.36$ (s, 3H, =C(CH_3)), 1.53 (d, J(H,H) = 6 Hz, 3H, =CH(CH_3)), 4.63 (q, J(H,H) = 6 Hz, 1H, =CH(CH_3)), 6.8–7.5 ppm (m, 30H, PPh_3); ^{31}P{^{1}H} NMR (121.5 MHz, C_7D_8, −60 °C): $\delta = 29.99$ ppm (d, J(Rh,P) = 146.25 Hz); ^{13}C{^{1}H} NMR (75.4 MHz, C_7D_8, −60 °C): $\delta = 14.29$ (s, CH_3), 28.95 (s, CH_3), 88.17 (s, =CH), 160.36 (s, Rh-O-C), 191.46 ppm (dt, Rh-CO); **4a** and **4b**: IR (C_5H_{12}): 1968 cm^{-1} (s).

5: First a mixture of **4** was prepared in a 5-mm NMR tube according to the description given above. Then CO or CO/H_2 was bubbled through the solution for 6 min at −60 °C and the NMR spectra were recorded. *E* isomer (**5a**): ^{1}H NMR (300 MHz, C_7D_8, −60 °C): $\delta = 0.8$ (d, J(H,H) = 7.2 Hz, 3H, =CH(CH_3)), 1.35 (s, 3H, =C(CH_3)), 2.6 (q, J(H,H) = 7.2 Hz, 1H, =CH(CH_3)), 6.8–7.8 ppm (m, 30H, PPh_3); *Z* isomer (**5b**): ^{1}H NMR (300 MHz, C_7D_8, −60 °C): $\delta =$ 1.28 (d, J(H,H) = 6.9 Hz, 3H, =CH(CH_3)), 1.50 (s, 3H, =C(CH_3)), 4.15 (q, J(H,H) = 6.9 Hz, 1H, =CH(CH_3)), 6.8–7.8 ppm (m, 30H, PPh_3); **5a** and **5b**: ^{31}P{^{1}H} NMR (121.5 MHz, C_7D_8, −60 °C): $\delta = 26.15$ (dd, J(Rh,P) = 132 Hz, J(P,P) = 30 Hz), 28.53 ppm (dd, J(Rh,P) = 72 Hz, J(P,P) = 30 Hz); ^{13}C{^{1}H} NMR (75.4 MHz, C_7D_8, −40 °C): $\delta = 198$ (d, J(Rh,C) = 76 Hz, Rh-CO), $\delta = 235.5$ ppm (dd, J(Rh,C) = 22 Hz, J(P,C) = 80 Hz, Rh-COO); IR (C_5H_{12}): 1984 (vs), 1946 (w), 1652 cm^{-1} (w).

Received: May 13, 2003 [Z51884]

Keywords: high-pressure spectroscopy · homogeneous catalysis · hydroformylation · reaction mechanisms · rhodium

[1] P. W. N. M. van Leeuwen, *Appl. Catal. A* **2001**, *212*, 61.
[2] a) P. W. N. M. van Leeuwen, C. F. Roobeek, *J. Mol. Catal.* **1985**, *31*, 345; b) A. van Rooy, J. N. H. de Bruijn, C. F. Roobeek, P. C. J. Kamer, P. W. N. M. van Leeuwen, *J. Organomet. Chem.* **1996**, *507*, 69.
[3] K. F. Muilwijk, P. C. J. Kamer, P. W. N. M. van Leeuwen, *J. Am. Oil Chem. Soc.* **1997**, *74*, 223.
[4] E. Billig, A. G. Abatjoglou, D. R. Bryant, R. E. Murray, J. M. Maher (Union Carbide Corporation), US Pat. 4,717,775, **1988**; [*Chem. Abstr.* **1989**, *109*, 233177].
[5] M. Diéguez, C. Claver, A. M. Masdeu-Bultó, A. Ruiz, P. W. N. M. van Leeuwen, G. C. Schoemaker, *Organometallics* **1999**, *18*, 2107.
[6] J. M. Brown, A. G. Kent, *J. Chem. Soc. Perkin Trans. 2* **1987**, 1597.
[7] a) L. A. van der Veen, M. D. K. Boele, F. R. Bregman, P. C. J. Kamer, P. W. N. M. van Leeuwen, K. Goubitz, J. Fraanje, H. Schenk, C. Bo, *J. Am. Chem. Soc.* **1998**, *120*, 11616; b) A. Castellanos-Páez, S. Castillón, C. Claver, P. W. N. M. van Leeuwen, W. G. J. de Lange, *Organometallics* **1998**, *17*, 2543.
[8] a) D. Evans, G. Yagupsky, G. Wilkinson, *J. Chem. Soc. A* **1968**, 2660; b) A. S. C. Chan, H.-S. Shieh, J. R. Hill, *J. Chem. Soc. Chem. Commun.* **1983**, 688.
[9] a) G. A. Slough, R. G. Bergman, C. H. Heathcock, *J. Am. Chem. Soc.* **1989**, *111*, 938; b) G. A. Slough, R. Hayashi, J. R. Ashbaugh, S. L. Shamblin, A. M. Aukamp, *Organometallics* **1994**, *13*, 890; c) G. A. Slough, J. R. Ashbaugh, L. A. Zannoni, *Organometallics* **1994**, *13*, 3587; d) S. Sato, I. Matsuda, Y. Izumi, *Chem. Lett.* **1985**, 1875.
[10] The spectra were simulated using gNMR 4.1; P. H. M. Budzelaar, Ivory Soft, Cherwell Scientific Publishers, Oxford, **1999**.
[11] a) J. Zhang, M. Poliakoff, M. W. George, *Organometallics* **2003**, *22*, 1612; b) K. Fagnou, M. Lautens, *Chem. Rev.* **2003**, *103*, 169; c) S. C. van der Slot, P. C. J. Kamer, P. W. N. M. van Leeuwen, J. A. Iggo, B. T. Heaton, *Organometallics* **2001**, *20*, 430.
[12] a) W. M. Ress, J. D. Atwood, *Organometallics* **1985**, *4*, 402; b) W. M. Ress, M. R. Churchil, Y.-J. Li, J. D. Atwood, *Organometallics* **1985**, *4*, 1162; c) W. M. Ress, M. R. Churchil, J. C. Fettinger, J. D. Atwood, *Organometallics* **1985**, *4*, 2179; d) M. R. Churchil, J. C. Fettinger, W. M. Ress, J. D. Atwood, *J. Organomet. Chem.* **1986**, *304*, 227.

 © 2003 Wiley-VCH Verlag GmbH & Co. KGaA, Weinheim

Continuous-Flow NMR Spectroscopy

Measuring Reaction Kinetics by Using Multiple Microcoil NMR Spectroscopy**

*Luisa Ciobanu, Dimuthu A. Jayawickrama, Xiaozhong Zhang, Andrew G. Webb, and Jonathan V. Sweedler**

Knowledge of kinetics is an important component in investigating reaction mechanisms. Such information greatly benefits drug design,[1] drug metabolism,[2] and a variety of industrial processes.[3] A number of different analytical techniques can be employed to investigate kinetic data. Spectroscopic tools are particularly useful because, besides

[*] Prof. J. V. Sweedler, Dr. D. A. Jayawickrama
Department of Chemistry and Beckman Institute
University of Illinois at Urbana-Champaign
600 South Mathews Avenue, Urbana, IL 61801 (USA)
Fax: (+1) 217-244-8068
E-mail: sweedler@scs.uiuc.edu
Dr. L. Ciobanu, X. Zhang, Prof.0, A. G. Webb
Department of Electrical and Computer Engineering and Beckman Institute
University of Illinois at Urbana-Champaign
1406 West Green Street, Urbana, IL 61801 (USA)

[**] This work was supported by the U.S.A. NIH (8R01EB002343-07), the NSF and the Alexander von Humboldt Stiftung (AGW).

Supporting information for this article is available on the WWW under http://www.angewandte.org or from the author.

 DOI: 10.1002/anie.200351901 © 2003 Wiley-VCH Verlag GmbH & Co. KGaA, Weinheim

reaction rates, they can provide chemical information at the molecular level. Nuclear magnetic resonance (NMR) is one of the most information-rich techniques, able to provide a high degree of structural information. However, poor sensitivity and subsequent long measurement times often preclude the acquisition of real-time NMR data for chemical reactions involving small amounts of material. A simple and effective approach to improve the mass sensitivity of NMR is to employ solenoidal NMR microcoil detectors. It has been shown both theoretically and experimentally that reducing the diameter of the coil increases its sensitivity,[4] thus allowing the analysis of pL to μL sample volumes. Since the introduction of high-resolution microcoil NMR probes[5] a number of applications have been demonstrated. NMR microcoils have been successfully used as online detectors in capillary separation[6] and for protein-unfolding kinetics.[7]

NMR has been used for the direct observation of short-lived species in chemical reactions by using rapid injection[8] and continuous-flow techniques.[9] In the present study we combine the technique of continuous reactant flow with multiple microcoil NMR detection in a new and efficient approach to obtain kinetic information on reactions that take place on timescales between seconds and minutes. As a model system we have studied xylose–borate reaction kinetics.

Two fluid flows that contain the reactants are mixed and this mixture passes through a capillary around which are wound multiple, physically distinct NMR detector coils. The distance between the mixer and each individual NMR coil, together with the flow rate used, determines the post-reaction-time point. Signal averaging can be performed for as long as necessary to obtain an adequate signal-to-noise ratio, as the time of the data measurement and the reaction time are decoupled through this experimental method. However, the longer the required total data-acquisition time, the greater the amount of reactants are needed. The use of multiple small-volume microcoils, three in this case, (Figure 1), minimizes this amount.

The ^{1}H NMR spectra of D-xylose (300 mM) and the equilibrium mixture D-xylose plus borate (400 mM, pD 10) solutions are shown in Figure 2 a and b, respectively, with no flow present. The NMR line broadens as the flow rate increases[10] and also its intrinsic shape changes. With no flow the lineshape was measured to be a pure Lorentzian with a full-width-half-maximum (FWHM) of 2.5 Hz. As the flow rate was increased to 18 μL min^{-1}, the nominal linewidth increases to ≈6 Hz, with a lineshape described by a Voigt function, defined by the convolution of Gaussian and Lorentzian functions.[11] The fractional Lorentzian linewidth was 44% and Gaussian linewidth 56%. Given the substantial alterations in NMR lineshape with flow, the most robust method of data analysis is to measure the ratio of signal areas of product and reactants by using specific resonances as shown in Figure 2. The use of these ratios also enables us to combine data acquired from the three different radio-frequency (RF) coils, which may have slightly different line widths and sensitivities.

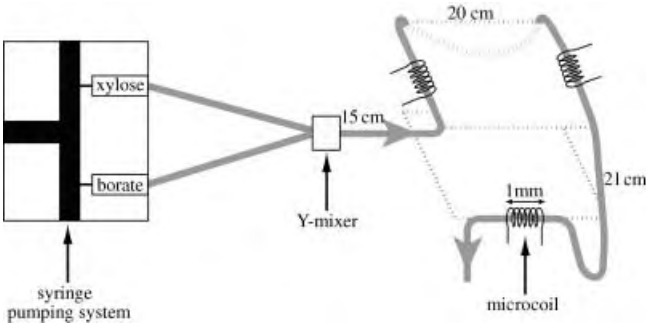


Figure 1. Schematic of the experimental setup. Two syringes on the pump inject the reactants into two capillaries. The reactants are mixed rapidly at the Y-mixer. After mixing, the solution flows through the microcoils while data are being acquired.

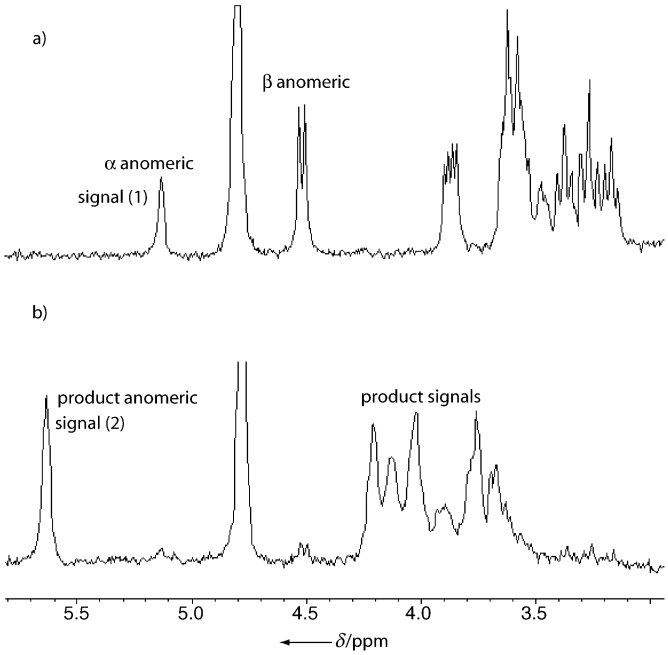
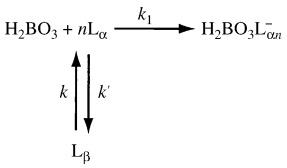


Figure 2. ^{1}H NMR spectra of 300 mM a) D-xylose in D_2O and b) D-xylose plus 400 mM borate at pD 10. The spectrum in b) corresponds to the equilibrated product mixture. Chemical shifts are referenced to HDO at 4.78 ppm.

The formation of stable borate–sugar complexes has been the subject of numerous studies.[12] The reaction kinetics model for the D-xylose-borate reaction is represented in Scheme 1, in which L_α and L_β represent the α and β forms of D-xylose, $H_2BO_3^-$ the borate ion and $H_2BO_3L_{\alpha n}^-$ the 1:*n* borate–xylose complexes. The NMR signals shown in Figure 2 b correspond to the reaction product under equilibrium conditions. Weak background signals arise from D-xylose. "On-flow" time resolved or stopped-flow NMR measurements do not provide evidence for significant back reaction.



Scheme 1. The reaction kinetics model for the D-xylose-borate reaction.

 © 2003 Wiley-VCH Verlag GmbH & Co. KGaA, Weinheim

Therefore, it can be safely assumed the D-xylose–borate reaction is effectively irreversible at the pD value of 10 used in these experiments. In the presence of borate, the conversion of L_β to L_α is fast, and one can therefore assume that $L_\alpha = \text{const}\, L_{total}$. Experiments were performed in which the initial borate concentration was higher than the D-xylose concentration, which allowed the consideration of only 1:1 complexes ($H_2BO_3L^-_{\alpha n}$). Thus, the reaction is described by the following set of differential equations (based on the assumption of a second-order reaction) [Eq. (1)]:

$$\begin{cases} -\frac{d[L_\alpha]}{dt} = k_1[B^-][L_\alpha] \\ -\frac{d[B^-]}{dt} = k_1[B^-][L_\alpha] \\ \frac{d[BL^-_\alpha]}{dt} = k_1[B^-][L_\alpha] \end{cases} \quad (1)$$

By solving the system above the time dependence of the ratio $[H_2BO_3L^-_{\alpha n}]/[L_\alpha]$ is found to be [Eq. (2)]:

$$\frac{[H_2BO_3L^-_{\alpha n}]}{L_\alpha} = \frac{m_2 + m_3 \exp(m_1 k_1 t)}{m_1} \quad (2)$$

in which the reaction rate constant k_1 and the coefficients m_1, m_2 and m_3 are to be estimated from the experimental data.

As the reaction progresses, a decrease in the height of the α and β anomeric peaks and the appearance of a new peak (denoted product anomeric in Figure 2b), at 5.55 ppm, were observed. NMR spectra that correspond to successive reaction times were recorded independently and simultaneously with all three RF coils. The results from a quantitative analysis of the spectra are presented in Figure 3. The data from all three probes are plotted on the same axis in this figure and fall on the same curve, thus validating the use of distinct NMR coils at multiple locations along the capillary/reaction-time coordinate. The ratio of the signal heights, height of signal (2)/height of signal (1) (Figure 2) is plotted as a function of time. By fitting the experimental data to the theoretical $[BL^-_{\alpha n}]/[L_\alpha]$ ratio given by Equation (2), a reaction rate constant, $k_1 = 0.077 \pm 0.004\ s^{-1}\ mol^{-1}\ L$, for the second order reaction was obtained.

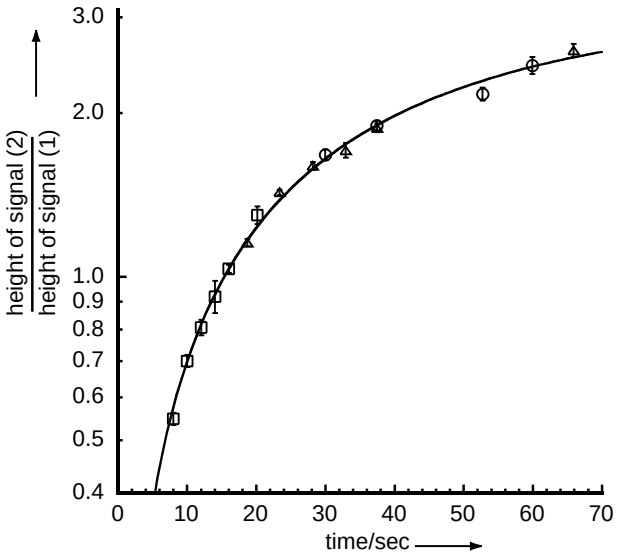


Figure 3. The ratio of the signal amplitudes, height of signal (2)/height of signal (1), as a function of time. □ coil 1; △ coil 2; ○ coil 3. The error bars represent the standard error from ten measurements. The fit parameters, Equation (2), are: $m_1 = -0.316$, $m_2 = -1$ and $m_3 = 0.994$.

In summary, this work demonstrates the possibility of using NMR as an analytical tool to study chemical kinetics of small amounts of materials with reaction times of a few seconds or longer by using continuous-flow NMR with multiple microreceiver coil detection. Continuous flow decouples the total data-measurement time from the reaction time, and the use of multiple microcoils decreases the amount of sample required to obtain the data. Highly reproducible results from a xylose–borate system, which show excellent agreement with the predicted mathematical model, validate this approach and demonstrate its utility for obtaining kinetic information on chemical species difficult to measure using other detection modalities. Moreover, the method can also be used to perform continuous-flow 2D NMR experiments at a particular reaction time,[13] which demonstrates the ability to examine intermediate species. A further expansion of the probehead to include four to six coils appears possible, with a concomitant reduction in the total amount of material needed for a kinetic study.

Experimental Section

Experiments were carried out at 300 MHz on a wide bore (89 mm) magnet by using a four-receiver channel Apollo Tecmag console. RF pulses were transmitted from a single frequency source through a power-splitter to each coil. The NMR probe consisted of three identical 370 μm diameter solenoidal RF microcoils, constructed of 50 μm copper wire wrapped around polyimide tubing.[14] Each coil was about 1 mm long and had seventeen turns. The sample flowed through a 200 μm internal diameter capillary, which resulted in a detection volume of ≈31 nL. The three-coil-probe assembly was immersed in FC-43 to minimize susceptibility-mismatch distortions.[15] FWHM linewidths of 1–2 Hz were obtained for HDO (2% H_2O in D_2O) for single coils. Simultaneous data acquisition performed by using optimized shimming for all three coils yielded linewidths of 4–6 Hz.

Interactions between different coils were measured both electrically and by NMR. Table 1 lists the S_{21} parameters for the three-coil configuration, while Table 2 contains the NMR measurements of

Table 1: S_{21} parameter (in dB) for intercoil coupling.

Coil	1	2	3
1	–	−40	−34
2	−40	–	−45
3	−34	−45	–

Table 2: NMR signal bleedthrough between coils measured using the S/N of the HDO peak.

Coil	1	2	3
1	–	0.0035	0.0050
2	0.0035	–	0.0022
3	0.0050	0.0022	–

 © 2003 Wiley-VCH Verlag GmbH & Co. KGaA, Weinheim

signal cross-contamination. The S_{21} parameter, with suitably impedance-matched loads, measures the ratio of the output voltage across one coil when an input voltage is applied to a second coil; for zero intercoil coupling this value should be $-\infty$ dB. All the microcoils gave values between -30 and -50 dB, thus indicating extremely high isolation. To measure the NMR intercoil signal bleedthrough the system was configured to transmit on only one coil and receive on all three coils. A total of 100 scans were acquired with a relaxation delay of 750 ms, and the signal to noise (S/N) of the HDO signal was measured for each coil. The numbers displayed in Table 2 were obtained by dividing the S/N values for each coil pair. The results show a very small degree of cross talk in agreement with the electrical measurements.

D-xylose and borate solutions were mixed rapidly by using a Y-mixer. The mixed solution flowed continuously from the Y-mixer through all three RF coils. The reaction times at which the measurements were made were defined by the physical separation of the detection coils from the micromixer and the flow rate used. The distances between the three detection points are shown in Figure 1. Flow rates ranging from 17.6 $\mu L\,min^{-1}$ to 5 $\mu L\,min^{-1}$, which correspond to reaction times between 8 s and 66 s, respectively, were used (as there are two capillaries entering the Y-mixer, a flow rate f delivered by the syringe pump corresponds to an effective flow rate $2f$ in the capillary running through the NMR coils).

Received: May 12, 2003
Revised: July 4, 2003 [Z51901]

Keywords: analytical methods · kinetics · NMR spectroscopy · reaction mechanisms

[1] R. Almog, C. A. Waddling, F. Maley, G. F. Maley, P. Van Roey, *Protein Sci.* **2001**, *10*, 988.
[2] J. M. Hutzler, T. S. Tracy, *Drug Metab. Dispos.* **2002**, *30*, 355.
[3] X. S. Chai, Q. Luo, J. Y. Zhu, *J. Chromatogr. A* **2002**, *946*, 177.
[4] A. Abragam, *The Principles of Nuclear Magnetism*, Clarendon Press, Oxford, **1961**.
[5] D. L. Olson, T. L. Peck, A. G. Webb, R. L. Magin, J. V. Sweedler, *Science* **1995**, *270*, 1967.
[6] M. E. Lacey, Z. J. Tan, A. G. Webb, J. V. Sweedler, *J. Chromatogr. A* **2001**, *922*, 139; M. E. Lacey, A. G. Webb, J. V. Sweedler, *Anal. Chem.* **2000**, *72*, 4991; A. M. Wolters, D. A. Jayawickrama, C. K. Larive, J. V. Sweedler, *Anal. Chem.* **2002**, *74*, 4191.
[7] M. Kakuta, D. A. Jayawickrama, A. M. Wolters, A. Manz, J. V. Sweedler, *Anal. Chem.* **2003**, *75*, 956.
[8] J. F. McGarrity, C. A. Ogle, Z. Brich, H.-R. Loosli, *J. Am. Chem. Soc.* **1985**, *107*, 1810.
[9] C. A. Fyfe, S. W. H. Damji, A. Koll, *J. Am. Chem. Soc.* **1979**, *101*, 951; C. A. Fyfe, M. Cocivera, S. W. H. Damji, *J. Am. Chem. Soc.* **1975**, *97*, 5707; K. Albert, E.-L. Dreher, H. Straub, A. Rieker, *Magn. Reson. Chem.* **1987**, *25*, 919.
[10] *On-line LC-NMR and Related Techniques* (Ed.: K. Albert), Wiley, West Sussex, **2002**.
[11] T. Ida, M. Ando, H. Toraya, *J. Appl. Crystallogr.* **2000**, *33*, 1311.
[12] S. Chapelle, J. F. Verchere, *Tetrahedron* **1988**, *44*, 4469; J. F. Verchere, M. Hlaibi, *Polyhedron* **1987**, *6*, 1415.
[13] For continuous-flow 2D NMR experiments see Supporting Information.
[14] R. A. Kautz, M. E. Lacey, A. M. Wolters, F. Foret, A. G. Webb, B. L. Karger, J. V. Sweedler, *J. Am. Chem. Soc.* **2001**, *123*, 3159.
[15] Y. Li, A. M. Wolters, P. V. Malawey, J. V. Sweedler, A. G. Webb, *Anal. Chem.* **1999**, *71*, 4815.

 © 2003 Wiley-VCH Verlag GmbH & Co. KGaA, Weinheim

C-C Coupling Reactions

Rhodium-Catalyzed Mizoroki–Heck-Type Arylation of Alkenes with Aroyl Chlorides under Phosphane- and Base-Free Conditions

Toru Sugihara, Tetsuya Satoh, Masahiro Miura, and Masakatsu Nomura*

The arylation of alkenes with aryl halides (ArX) is well-known as the Mizoroki–Heck reaction and is now recognized to be of genuine synthetic utility for preparing aromatic fine chemicals.[1] Besides the halides, various synthetic equivalents, including ArOTf and ArCOX can also be employed as the arylating reagents. One of the substantial problems in the reaction comes from an acidic by-product (HX), which requires the addition of stoichiometric amounts of base. Recently, the use of aromatic carboxylic acid anhydrides[2] and aryl esters[3] allowed the reaction to be conducted under base-free conditions. Although these methods are useful, additional workup procedures such as fractional distillation and acid–base extraction are required to obtain pure coupling products owing to the corresponding organic by-products.

Aryl and aroyl halides are also capable of undergoing oxidative addition toward certain rhodium(I) complexes to form aryl rhodium(III) species, and a number of useful catalytic processes involving this step have been developed.[4,5] We previously demonstrated that aroyl chlorides efficiently react with terminal and internal alkynes in the presence of a rhodium–phosphane catalyst to produce the corresponding vinyl chloride and indenone derivatives, accompanied by decarbonylation and dehydrochlorination, respectively.[5a] The coupling with alkenes in place of alkynes was successful when norbornenes were used in the presence of a disilane, giving aroylarylation products.[5b] Herein we report our new findings that styrene and acrylate ester can also be arylated by using an appropriate phosphane-free rhodium catalyst.[6] Thus, the alkenes efficiently undergo Mizoroki–Heck-type coupling with aroyl chlorides in the absence of any base and phosphane ligand; the by-products (CO and HCl) are readily removed.[7] The simple conditions make the product-isolation procedure significantly simple, as described below.

In an initial attempt, benzoyl chloride (**1a**) was treated with styrene (**2**; 1 equiv) in a batch reactor with an N_2 balloon under conditions similar to those employed for the reaction with internal alkynes. In the presence of $[\{RhCl(cod)\}_2]$ (1 mol%), PPh_3 (2 mol%), and Na_2CO_3 (1 equiv) in refluxing *o*-xylene for 24 h,[5a] (*E*)-stilbene (**3a**) was formed in only 7%

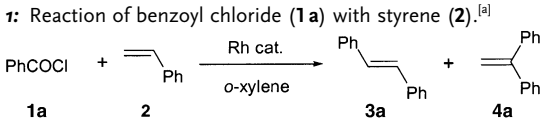
[*] Prof. Dr. M. Miura, T. Sugihara, Dr. T. Satoh, Prof. Dr. M. Nomura
Department of Applied Chemistry
Faculty of Engineering, Osaka University
Suita, Osaka 565-0871 (Japan)
Fax: (+81) 6-6879-7362
E-mail: miura@chem.eng.osaka-u.ac.jp

Supporting information for this article is available on the WWW under http://www.angewandte.org or from the author.

 © 2003 Wiley-VCH Verlag GmbH & Co. KGaA, Weinheim DOI: 10.1002/anie.200351905

yield (Table 1, entry 1). Fortunately, it was found that an ethylene complex $[\{RhCl(C_2H_4)_2\}_2]$ exhibits significantly higher activity than $[\{RhCl(cod)\}_2]$. Thus, the yield of **3a** was improved to 69%; a minor amount of 1,1-diphenylethylene (**4a**) was detected, as was the case in the palladium-catalyzed Mizoroki–Heck reaction (Table 1, entry 2).[2,3] Interestingly, the reaction proceeded much more smoothly in the absence of the phosphane ligand and base. As a result, **3a** was obtained in 82% yield within 4 h (Table 1, entry 4). Under the same conditions, $[\{Rh(acac)(cod)\}_2]$ and $[\{RhCl(nbd)\}_2]$ showed lower activities (Table 1, entries 5 and 6). In the latter case, however, prolonged reaction time led to a satisfactory product yield (Table 1, entry 7). Although a decrease in the amount of $[\{RhCl(C_2H_4)_2\}_2]$ to 0.25 mol% resulted in a slight decrease in the product yield (Table 1, entry 8), **3a** was obtained in 87% yield within 2 h when 1.2 equivalents of **2** was used (Table 1, entry 9).

Table 1: Reaction of benzoyl chloride (**1a**) with styrene (**2**).[a]



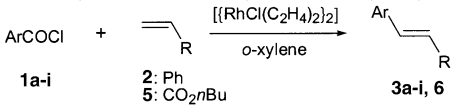
Entry	Rh cat. (mol%)	Time [h]	Yield [%][b]	
			3a	**4a**
1[c]	$[\{RhCl(cod)\}_2]$ (1)/PPh_3 (2)	24	7	
2[c]	$[\{RhCl(C_2H_4)_2\}_2]$ (1)/PPh_3 (2)	23	69	8
3	$[\{RhCl(C_2H_4)_2\}_2]$ (1)/PPh_3 (2)	23	69	7
4	$[\{RhCl(C_2H_4)_2\}_2]$ (1)	4	82	8
5	$[\{Rh(acac)(cod)\}_2]$ (1)	26	36	3
6	$[\{RhCl(nbd)\}_2]$ (1)	4	33	2
7	$[\{RhCl(nbd)\}_2]$ (1)	18	88	6
8	$[\{RhCl(C_2H_4)_2\}_2]$ (0.25)	4	72	10
9[d]	$[\{RhCl(C_2H_4)_2\}_2]$ (0.25)	2	87	9
10[d,e]	$[\{RhCl(C_2H_4)_2\}_2]$ (0.25)	8	75	7

[a] Unless noted, the reaction of **1a** (1 mmol) with **2** (1 mmol) was conducted in refluxing *o*-xylene (5 mL) under N_2 (balloon). [b] Yield determined by GC based on the amount of **1a** used. [c] With Na_2CO_3 (1 mmol). [d] **2** (1.2 mmol) was used. [e] With LiCl (0.04 mmol).

Table 2 summarizes the results for the syntheses of stilbenes **3a–i** and cinnamate **6** by the reactions of 4-substituted benzoyl chlorides **1a–g**, 2-naphthoyl chloride (**1h**), or anthraquinone-2-carbonyl chloride (**1i**) with **2** and of **1a** with *n*-butyl acrylate (**5**). The reactions were carried out under a slow stream of N_2 to effectively remove HCl and CO evolved. It can be seen from Table 2 that various functional groups are tolerated under the present conditions.[8] It should be emphasized that essentially pure stilbenes **3** were isolated after a simple workup procedure, that is, only filtration, evaporation, and washing with an appropriate solvent such as methanol (see Experimental Section). The cinnamate **6** was isolated by Kugelrohr distillation.[9] The reactions in Table 2, entries 1, 2, 4, 6, and 13 were carried with use of 10 mmol of **1**. Even on a relatively larger scale and with a higher substrate/catalyst ratio (**1**/Rh = 2000), the products were obtained with good yields after reasonable reaction times.

The initial step of the present reaction appears to involve oxidative addition of **1** to a Rh^ICl species to generate

Table 2: Reaction of aroyl chlorides with styrene or *n*-butyl acrylate.[a]



Entry	**1**	Ar	[mmol]	Alkene	[mmol]	*t* [h]	Product	Yield [%][b]
1	**a**	Ph	10	**2**	15	6	**3a**	86
2	**b**	4-MeC_6H_4	10	**2**	15	7	**3b**	79
3	**c**	4-$MeOC_6H_4$	1	**2**	1.2	4	**3c**	51
4	**d**	4-BrC_6H_4	10	**2**	15	6	**3d**	81
5	**e**	4-NCC_6H_4	1	**2**	1.5	6	**3e**	73
6	**f**	4-$O_2NC_6H_4$	10	**2**	15	10	**3f**	75
7	**g**	4-$MeO_2CC_6H_4$	1	**2**	1.5	24	**3g**	75
8	**h**	2-naphthyl	1	**2**	1.2	3	**3h**	83
9	**i**	2-AQ[c]	1	**2**	1.2	12	**3i**	69
10[d]	**a**	Ph	1	**5**	1.2	7	**6**	(73)[e] (95:5)[f]
11[d,g]	**a**	Ph	1	**5**	1.2	9	**6**	(81) (93:7)[f]
12[d,h]	**a**	Ph	1	**5**	1.2	9	**6**	(98) (96:4)[f]
13[h]	**a**	Ph	10	**5**	12	48	**6**	72 (93:7)[f]

[a] Unless noted, the reaction was carried out with $[\{RhCl(C_2H_4)_2\}_2]$ (2.5 μmol) in refluxing *o*-xylene (5 mL) under a slow stream of N_2. [b] Yield of isolated product based on the amount of **1** used. Value in parenthesis is determined by GC. [c] 2-AQ-COCl = Anthraquinone-2-carbonyl chloride. [d] With $[\{RhCl(C_2H_4)_2\}_2]$ (0.01 mmol). [e] No increase in the yield after 24 h. [f] *E*/*Z* ratio. [g] With $Me(nC_8H_{17})_3NCl$ (0.04 mmol). [h] With LiCl (0.04 mmol).

$[ArCORh^{III}Cl_2]$, which then undergoes decarbonylation to give $[ArRh^{III}Cl_2]$ as the key intermediate.[5,10] The subsequent insertion of the alkene and β-hydride elimination as in the Mizoroki–Heck reaction affords the coupling product and $Rh^{III}(H)Cl_2$. The latter may release HCl, regenerating Rh^ICl. Dienes such as cod and nbd on the catalyst precursors may retard the reaction by their stronger coordination ability relative to that of the alkene substrates. The success with the bromide **1d** seems to be due to the fact that oxidative addition of aryl halides under the present conditions is difficult to take place. Notably, the addition of a chloride source such as an alkylammonium chloride or lithium chloride considerably improved the reaction efficiency with the acrylate ester (Table 2, entry 10 vs. entries 11 and 12), whereas no positive effect was observed in the case of styrene (Table 1, entry 10). Thus, it is possible that the enhancement is due to the generation of anionic rhodium species by the coordination of chloride. The electron-poor alkene may preferably interact with the metal center.

In summary, we have demonstrated that the Mizoroki–Heck-type arylation of alkenes can be performed using benzoyl chlorides in the presence of a rhodium catalyst without the addition of any phosphane ligand and base. Not only does the reaction proceed efficiently, but also the workup procedure is significantly simple. Thus, this protocol seems to provide a new, convenient route to vinyl-substituted aromatic compounds.

Experimental Section

Typical procedure: A mixture of **1a** (10 mmol, 1.41 g), **2** (15 mmol, 1.56 g), and $[\{RhCl(C_2H_4)_2\}_2]$ (2.5 μmol, 1 mg) in refluxing *o*-xylene (5 mL) was stirred under N_2 flow (in a draft chamber). The effluent

 © 2003 Wiley-VCH Verlag GmbH & Co. KGaA, Weinheim

gas was led to water during the reaction, so that HCl could be recovered as hydrochloric acid. After 6 h, the mixture was cooled to room temperature, Et_2O (30 mL) was added, and a small amount of insoluble material was removed by filtration through filter paper. After evaporation of the solvents under vacuum, MeOH (10 mL) was added, and the resulting mixture was filtered to give white crystals of **3a** (1.54 g, 86%). Characterization data of products are summarized in the Supporting Information.

Received: May 15, 2003 [Z51905]

Keywords: aromatic substitution · C–C coupling · Heck reaction · homogeneous catalysis · rhodium

[1] a) R. F. Heck, *Palladium Reagents in Organic Syntheses*, Academic Press, New York, **1985**; b) J. Tsuji, *Palladium Reagents and Catalysts*, Wiley, Chichester, **1995**; c) W. Cabri, I. Candiani, *Acc. Chem. Res.* **1995**, *28*, 2; d) S. Bräse, A. de Meijere in *Metal-Catalyzed Cross-Coupling Reactions* (Eds.: F. Diederich, P. J. Stang), Wiley-VCH, Weinheim, **1998**, p. 99; e) I. P. Beletskaya, A. V. Cheprakov, *Chem. Rev.* **2000**, *100*, 3009.

[2] M. S. Stephan, A. J. J. M. Teunissen, G. K. M. Verzijl, J. G. de Vries, *Angew. Chem.* **1998**, *110*, 688; *Angew. Chem. Int. Ed.* **1998**, *37*, 662.

[3] L. J. Gooßen, J. Paetzold, *Angew. Chem.* **2002**, *114*, 1285; *Angew. Chem. Int. Ed.* **2002**, *41*, 1237.

[4] a) T. Mizuno, H. Alper, *J. Mol. Catal. A* **1997**, *123*, 21; b) K. M. Hossain, K. Takagi, *Chem. Lett.* **1999**, 1241; c) T. Ishiyama, J. F. Hartwig, *J. Am. Chem. Soc.* **2000**, *122*, 12043; d) M. Murata, M. Ishikura, M. Nagata, S. Watanabe, Y. Masuda, *Org. Lett.* **2002**, *4*, 1843; e) R. B. Bedford, S. J. Coles, M. B. Hursthouse, M. E. Limmert, *Angew. Chem.* **2003**, *115*, 116; *Angew. Chem. Int. Ed.* **2003**, *42*, 112; f) T. Morimoto, M. Fujioka, K. Fuji, K. Tsutsumi, K. Kakiuchi, *Chem. Lett.* **2003**, 154.

[5] a) K. Kokubo, K. Matsumasa, M. Miura, M. Nomura, *J. Org. Chem.* **1996**, *61*, 6941; b) K. Kokubo, K. Matsumasa, M. Miura, M. Nomura, *J. Organomet. Chem.* **1998**, *560*, 217.

[6] For an example of the Mizoroki–Heck reaction in which a Wilkinson complex is used as catalyst, see: S. Iyer, *J. Organomet. Chem.* **1995**, *490*, C27; however, we failed to reproduce the reported reaction.

[7] We also reported that the iridium-catalyzed coupling of aroyl chlorides with internal alkynes can proceed under base-free conditions: T. Yasukawa, T. Satoh, M. Miura, M. Nomura, *J. Am. Chem. Soc.* **2002**, *124*, 12680.

[8] The reaction of **1a** with *N-tert*-butylacrylamide, however, was not successful; an undesired acyl exchange took place to give *N-tert*-butylbenzamide as the major product.

[9] In the reaction with **5**, only a trace amount of α-phenylated product was detected by GC-MS.

[10] For an example of a Mizoroki–Heck-type reaction involving an arylrhodium(I) intermediate, see: a) M. Lautens, A. Roy, K. Fukuoka, K. Fagnou, B. Martín-Matute, *J. Am. Chem. Soc.* **2001**, *123*, 5338; b) A. Mori, Y. Danda, T. Fujii, K. Hirabayashi, K. Osakada, *J. Am. Chem. Soc.* **2001**, *123*, 10774.

 © 2003 Wiley-VCH Verlag GmbH & Co. KGaA, Weinheim

Solid-Phase Synthesis of Glycolipids

A Practical Solid-Phase Synthesis of Glycosylphosphatidylinositol Precursors**

*Niels-Christian Reichardt and Manuel Martín-Lomas**

Glycosylphosphatidylinositol (GPI) anchors serve to attach proteins to cellular membranes through a covalent linkage.[1] These glycolipids have been a subject of sustained interest for the last fifteen years.[2] Besides the anchoring function, GPIs are involved in important biological events. They act as a targeting signal to the secretion and insertion of proteins to distinct membrane domains[3] and seem to play a role in transmembrane signaling.[4] GPIs function as a malarial toxin as well[5] and anti-GPI vaccination was shown to prevent malaria in an animal model.[6]

As a general rule, all reported GPI structures present a linear myoinositol containing oligosaccharide backbone. (Figure 1).

While this general structure is conserved, there is a considerable diversity within the GPI anchor family, which is reflected on the nature and the location of branching groups in this pseudo-pentasaccharide skeleton. These branching groups are species-specific carbohydrate side chains, additional phosphoethanolamine units, and variations in the lipid moiety. As for the location, positions 2 and 3 of the proximal mannose unit and positions 2 and 6 of the distal mannose unit seem to invariably constitute the branching points.[1]

Because of their biochemical significance, their biomedical interest, and the challenges involved in their total synthesis, GPIs have received a lot of attention from synthetic chemists, and have been chosen as a target to test methods and strategies in complex oligosaccharide synthesis. .[1–7] Consequently, a number of total syntheses of specific GPIs were reported.[7] However, a general strategy that supports the synthesis of a diversity of GPI structures from a common precursor has not been reported so far.

The development of conditions for the efficient solid-phase synthesis of complex oligosaccharides on automated synthesizers may constitute a key step in deciphering many outstanding questions in Glycobiology.[8] An effective strategy for the synthesis of GPI on solid support that allows the access to a diversity of GPI structures from a common pseudo-pentasaccharide construct is, therefore, highly desirable. With only one exception,[9] all described syntheses of

[*] Prof. Dr. M. Martín-Lomas, N.-C. Reichardt
Grupo de Carbohidratos
Instituto de Investigaciones Químicas, CSIC
Américo Vespucio s/n, Isla de La Cartuja, 41092 Sevilla (Spain)
Fax: (+34) 95-446-0565
E-mail: manuel.martin-lomas@iiq.csic.es

[**] This work was supported by the Ministerio de Ciencia y Tecnología (Grant BQU 2002–03734). N.-C. R. thanks the European Union for a fellowship (Grant HRN-CT-2000–00001/Glycotrain).

Supporting information for this article is available on the WWW under http://www.angewandte.org or from the author.

 © 2003 Wiley-VCH Verlag GmbH & Co. KGaA, Weinheim DOI: 10.1002/anie.200351950

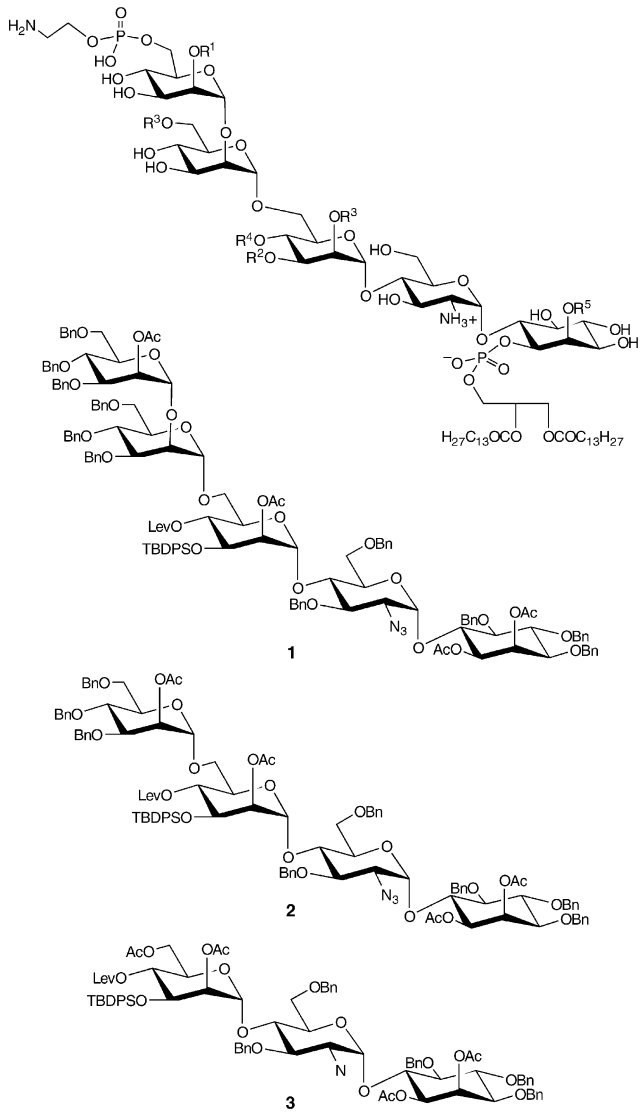


Figure 1. GPI-anchor structures, R^1: Man or not-determined glycan, R^2: Gal_n, GalNAc, GalNAc-Gal-NANA, P-Man, $PEtNH_2$, GlcNAc-Gal, $(GalNAc\text{-}Gal)_9$, GalNAc-Glc, R^3 extra phosphoethanaolamine, R^4: GalNAc, NANA-Gal-GalNAc, R^5: Acyl (not substrate to PI3-Kinase); synthetic GPI-glycan-strucures **1**, **2** and **3**. Man = mannose, Gal = galactose.

GPI structures have been carried out in solution. Because of our long-standing interest in the role of GPI-like molecules in insulin signaling,[10] we have been aiming at an efficient solid-phase step-by-step construction of the GPI pseudo-pentasaccharide backbone. Such a synthesis should permit the introduction of a variety of side chains at the main branching positions by using commercially available linkers and supports, and standard experimental conditions. We have now developed such synthetic procedure, which is reported herein.

After extensive investigations on the compatibility of all parameters involved such as the type of solid support, linker, attachment strategy, capping procedure, glycosylation method, and protecting group strategy, we chose the following system:

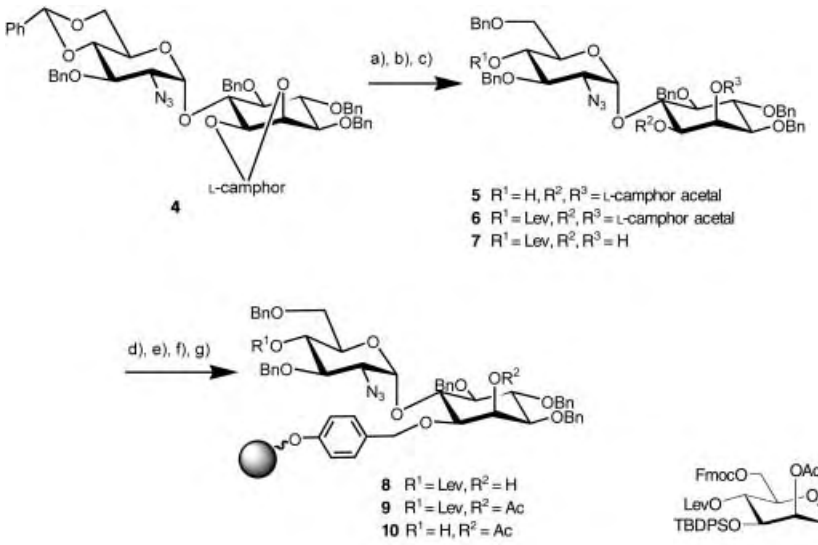
1) A polyethylene glycol (PEG)-grafted polystyrene resin functionalized with a Wang-Cl linker. These flexible PEG grafts provide a solutionlike environment for bound molecules, which results in fast reaction rates and permits the obtainment of high resolution NMR spectra.[11]
2) A Wang-type linker readily cleavable under acidic media but stable to low-temperature-glycosylation conditions with catalytic Lewis acid promoters, and highly stable to basic conditions.[12]
3) A mild experimental procedure for the attachment of the substrate to the solid support through stannylidene activation.
4) *O*-Glycosyl trichloroacetimidates as donors that allow glycosylation under the above conditions.[13]
5) Lev/Fmoc[14] and TBDPS/Lev[15] as orthogonal protecting groups for the construction of the pseudo-pentasaccharide backbone and the establishment of branching points.
6) A fast and traceless cleavage of the target molecule and intermediates.[12]

Under these general conditions pseudo-oligosaccharides **1**, **2** and **3** have been prepared by sequential glycosylation starting from pseudodisaccharide **4**. Compound **4** can be obtained in multigram quantities.[10b,c] The formation of the glucosamine α1→6 myoinositol linkage with complete selectivity is difficult to achieve.[10b,d,e] Therefore, building block **4** was synthesized in solution.

After attempting different strategies, we decided to attach the pseudo-disaccharide glycosyl acceptor to the solid support through the myoinositol moiety. The scarce differences of reactivity among the myoinositol hydroxyl groups may complicate the anchoring process, but results of previous experiments prompted us to use this strategy instead of an alternative attachment through C6-OH of the D-glucosamine unit. Thus, compound **4** was transformed into diol **7** by the regioselective opening of the benzylidene acetal (→**5**), addition of the levulinate group (→**6**) and removal of the L-camphor ketal (→**7**). The attachment of **7** to the solid support was performed by stannylidene acetal-mediated activation of the diol system followed by the reaction with the linker functionalized resin (→**8**) (Scheme 1); the loading was 0.31 mmol g^{-1}. Unreacted linker sites were capped by quenching with methanol or by transforming the hydrolized benzyl chloride functionality into the corresponding trichloroacetimidate and subsequent methylation with methanol in the presence of BF_3OEt_2.[16] Acetylation (→**9**) and subsequent removal of the levuline group afforded **10**. ^1H NMR analysis of a cleaved sample showed a 2:1 C1-OH/C2-OH regioselectivity for the attachment process. This is of no consequence for the solid phase synthesis of the oligosaccharide skeleton herein described but has to be taken into account for the further solution phase installation of the lipid moiety.

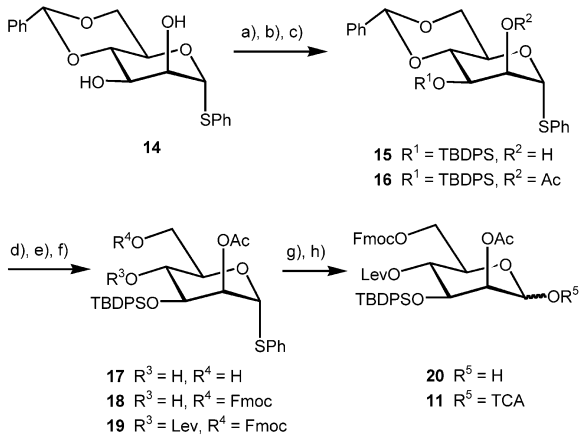
Mannopyranosyl trichloroacetimidates **11**, **12**[17] and **13**[18a,b,c] have been sequentially used in the step-by-step construction of the orthogonally protected pseudo-oligosaccharide backbone **1**. The highly functionalized glycosyl donor **11** was designed as to permit selective deprotection at C3, C4, and C6 for further attachment of branching groups. It contains a combination of acetyl, silyl, levulinoyl and Fmoc orthogonal protecting groups[14,15] and could be obtained in a

 © 2003 Wiley-VCH Verlag GmbH & Co. KGaA, Weinheim



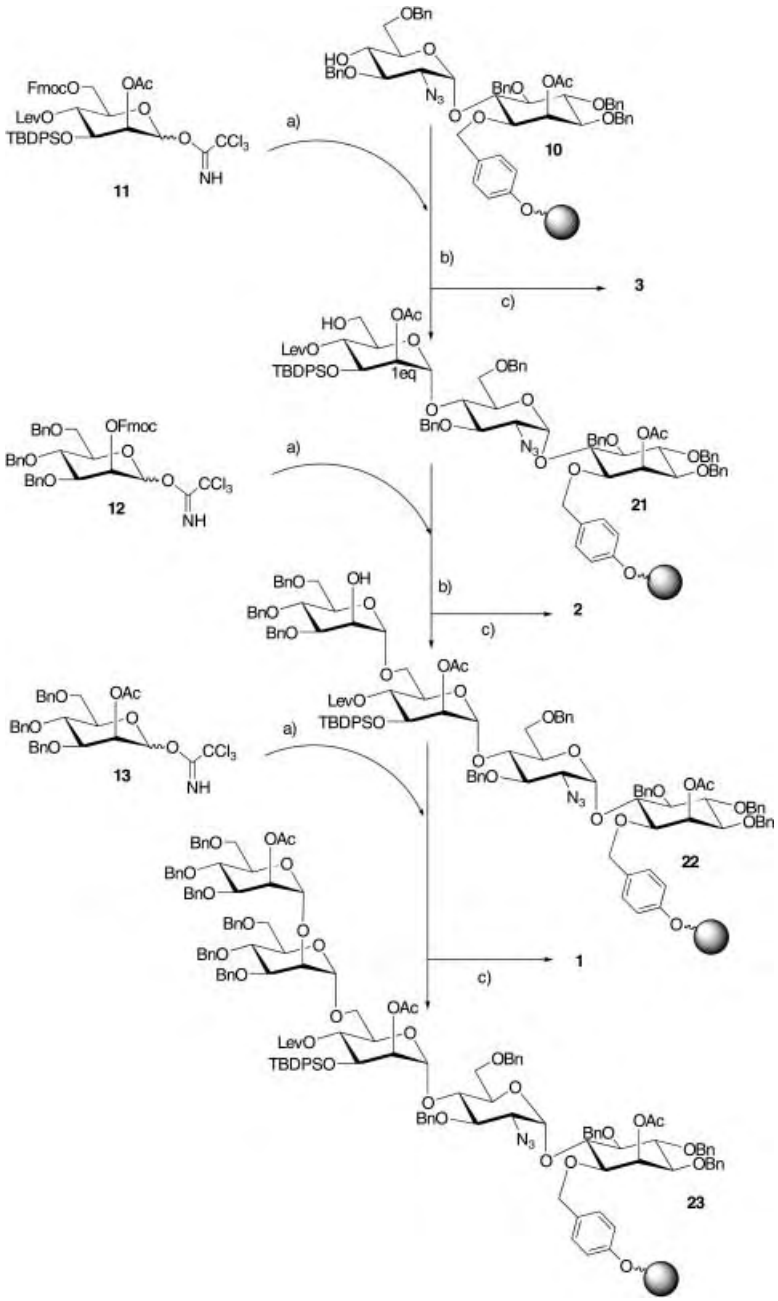
Scheme 1. Preparation and attachment of pseudodisaccharide **5** to resin. a) $NaCNBH_3$, HCl (1 M sol. in Et_2O), THF, 10 min, 81%; b) LevOH, DCC, DMAP, CH_2Cl_2, 1 h, 95%; c) TFA 20% in $CHCl_3$, 80%; d) Bu_2SnO, MeOH, reflux, 3 h; e) resin Argo-Gel-Wang-Cl, [21] (0.43 mmol g^{-1}), TBAI, CsF, MeCN, 70–80%, 1-OH/2-OH 1:2; f) Ac_2O, py, DMAP, CH_2Cl_2, 1.5 h, quant.; g) N_2H_4:AcOH, CH_2Cl_2, 20 h, quant. Lev = $RCOCH_2CH_2COCH_3$ DCC = dicyclohexylcarbodiimide, DMAP = 4-dimethylaminopyridine, TFA = trifluoroacetic acid, TBAI = tetrabutylammonium iodide, py = pyridine.

straightforward manner (Scheme 2). Stannylidene acetal mediated silylation of thioglycoside **14**[19] gave the 3-*O*-silyl derivative **15**. Conventional acetylation afforded **16**. Cleavage of the benzylidene acetal in **16** yielded diol **17** that was selectively protected as a 6-Fmoc ester to give **18**. The levulinic ester group was then installed (→**19**). Mild hydrolysis gave **20** that was activated as trichloroacetimidate **11** (Scheme 3).[20]



Scheme 2. Synthesis of key mannose donor **7**. a) Bu_2SnO, MeOH, reflux, 1 h; b) TBDPSCl, DMF, TBAI, 16 h, 71%; c) Ac_2O, py, DMAP, 2 h, 95%; d) BF_3OEt_2, EtSH, CH_2Cl_2, 92%; e) FmocCl, MeCN, py, DMAP, 1 h, 85%; f) LevOH, DCC, DMAP, 1.5 h, 85%; g) NBS, acetone, H_2O, −20 °C, 2 h, 90%; h) Cl_3CCN, NaH, 40 min, 79%. TBDPS = *tert*-butyldiphenylsilyl, DMF = dimethylformamide, Fmoc = 9-fuorenylmethoxycarbonyl, NBS = *N*-bromosuccinimide.

The synthesis of the pseudopentasaccharide skeleton started with the glycosylation of acceptor **10** with donor **11** in the presence of TMSOTf to afford the corresponding resin-bound trisaccharide. A preparative sample was cleaved from the resin, submitted to treatment with triethylamine to release the Fmoc group, and acetylated to give pseudotrisaccharide **3** that was fully characterized. Glycosyl acceptor **21** was obtained after hydrolysis of the Fmoc group and then glycosylated with glycosyl donor **12**[17] in the previously established conditions. Again a preparative



Scheme 3. Assembly of glycan structure on solid support a) TMSOTf (0.1 equiv), CH_2Cl_2, −20 °C, 2 h; b) Et_3N, CH_2Cl_2, room temperature, 4 h; c) 1. TFA 10% in $CHCl_3$, room temperature, 2 h, 2. Ac_2O, py, DMAP, 0 °C, 2 h. TMS = Trimetylsilyl, Tf = trifluoromethanesulfonate.

 © 2003 Wiley-VCH Verlag GmbH & Co. KGaA, Weinheim

sample was cleaved and acetylated to give pseudotetrasaccharide **2** the ^{1}H NMR spectrum of which was fully assigned. The final assembly was performed by generating the glycosyl acceptor as above and performing a further glycosylation step with donor **13**[18a–c] to afford **23**. Compound **1** was obtained after releasing from the resin and acetylation. The overall yield for the target structure **1** was 20% after a ten steps synthesis with an average 85% per step.

The above results describe a practical solid phase strategy for the assembly of GPI precursor structures that combines a solution like environment and a fully orthogonal protecting-group pattern with the efficiency of the trichloroacetimidate method for stereoselective glycosylation. The use of a PG-grafted resin permits high resin loadings without affecting the performance of the coupling reactions. The attachment of the pseudodisaccharide unit to the resin using a mild stannylene activation constitutes a convenient and original procedure for highly functionalized derivatives. The biosynthetically inspired linear construction of the GPI backbone permits to access to GPI-like intermediates from the same precursor. The described system allows for the construction of a diversity of structures in a combinatorial manner and for the generation of a small library of GPI precursors.

Received: May 22, 2003
Revised: July 1, 2003 [Z51950]

Keywords: carbohydrates · glycolipids · glycosylation · protecting groups · solid-phase synthesis

[1] For reviews on GPI anchors see: a) M. A. J. Ferguson, *Biochem. Soc. Trans.* **1992**, *20*, 243–256; b) P. T. Englund, *Annu. Rev. Biochem.* **1993**, *62*, 121–138; c) M. J. McConville, M. A. J. Ferguson, *Biochem. J.* **1993**, *294*, 305–324; d) V. L. Stevens, *Biochem. J.* **1995**, *310*, 361–370; e) M. A. J. Ferguson, *Philos. Trans. R. Soc. London Ser. B* **1997**, *352*, 1295–1302.

[2] M. A. J. Ferguson, S. W. Homans, R. A. Dwek, T. W. Rademacher, *Science* **1988**, *239*, 753–759.

[3] R. G. Anderson, *Sem. Immunol.* **1994**, *6*, 89–95.

[4] a) A. R. Saltiel, *Philos. Trans. R. Soc. London Ser. B* **1988**, *320*, 29–41; b) G. N. Gaulton, J. C. Pratt, *Sem. Immunol.* **1994**, *6*, 97–104.

[5] a) L. Schofield, F. Hackett, *J. Exp. Med.* **1993**, *177*, 145–153; b) D. S. Tachado, L. Schofield, *Biochem. Biophys. Res. Commun.* **1994**, *205*, 984–991; c) S. D. Tachado, P. Gerold, M. J. McConville, T. Baldwin, D. Quilici, R. T. Scwarz, L. Schofield, *Proc. Natl. Acad. Sci. USA* **1997**, *94*, 4022–4027.

[6] L. Schofield, M. C. Hewitt, K. Evans, M. Simons, P. H. Seeberger, *Nature* **2002**, *418*, 785–789.

[7] a) T. Ogawa, C. Murakata, *Tetrahedron Lett.* **1991**, *32*, 671–674; b) T. Ogawa, C. Murakata, *Carbohydr. Res.* **1992**, *235*, 95–114; c) T. G. Mayer, B. Kratzer, R. R. Schmidt, *Angew. Chem.* **1994**, *106*, 2289–2293; *Angew. Chem. Int. Ed. Engl.* **1994**, *33*, 2177–2181; d) B. Fraser-Reid, A. S. Campbell, *J. Am. Chem. Soc.* **1995**, *117*, 10387–10388; e) T. G. Mayer, R. R. Schmidt, *Eur. J. Org. Chem.* **1999**, 1153–1165; f) D. Tailler, V. Ferriers, K. Pekari, R. R. Schmidt, *Tetrahedron Lett.* **1999**, *40*, 679–682; g) D. A. Baeschlin, A. R. Chaperon, L. G. Green, M. G. Hahn, S. J. Ince, S. W. Ley, *Chem. Eur. J.* **2000**, *6*, 172–186; h) D. K. Baeschlin, L. G. Green, M. G. Hahn, B. Hinzen, S. J. Ince, S. V. Ley, *Tetrahedron: Asymmetry* **2000**, *11*, 173–174.

[8] a) P. H. Seeberger, W.-C. Haase, *Chem. Rev.* **2000**, *100*, 4349–4393; b) O. J. Plante, E. R. Palmacci, P. H. Seeberger, *Science* **2001**, *291*, 1523–1527; c) E. R. Palmacci, O. J. Plante, P. H. Seeberger, *Eur. J. Org. Chem.* **2002**, 595–606.

[9] M. C. Hewitt, A. A. Synder, P. H. Seeberger, *J. Am. Chem. Soc.* **2002**, *124*, 13434–13436.

[10] a) N. Khiar, M. Martín-Lomas in *Carbohydrate Mimics. Concepts and Methods* (Ed.: Y. Chapleur), Wiley-VCH, Weinheim, **1998**, pp. 443–462, and references therein; b) H. Dietrich, J. F. Espinosa, J. L. Chiara, J. Jiménez-Barbero, Y. León, I. Varela-Nieto, J. M. Mato, F. H. Cano, C. Foces-Foces, M. Martín-Lomas, *Chem. Eur. J.* **1999**, *5*, 320–336; c) M. Martín-Lomas, N. Khiar, S. García, J.-L. Koessler, P. M. Nieto, T. W. Rademacher, *Chem. Eur. J.* **2000**, *6*, 3608–3621.

[11] T. L. Deegan, O. W. Gooding, S. Baudart, J. A. Porco Jr. , *Tetrahedron Lett.* **1997**, *38*, 4973–4976.

[12] a) H. Shimizu, Y. Ito, O. Kanie, T. Ogawa, *Bioorg. Med. Chem. Lett.* **1996**, *6*, 2841–2846; b) S. Hanessian, H. K. Huynh, *Synlett* **1999**, 102–104.

[13] L. Knerr, R. R. Schmidt in *Solid support oligosaccharide synthesis and combinbatorial carbohydrate libraries* (Eds.: P. H. Seeberger), Wiley Intersccience, Weinheim, **2001**, pp. 67–116, and references therein.

[14] a) T. Zhu, G.-J. Boons, *Tetrahedron: Assymetry* **2000**, *11*, 199–205; b) T. Zhu, G.-J. Boons, *J. Am. Chem. Soc.* **2000**, *122*, 10222–10223; c) T. Zhu, G.-J. Boons, *Chem. Eur. J.* **2001**, *7*, 2382–2389; d) F. Roussel, M. Takhi, R. R. Schmidt, *J. Org. Chem.* **2001**, *66*, 8540–8548.

[15] TBDPS-cleavage was achieved on resin by repeated treatment with excess TBAF/AcOH in THF at 40°C, without effecting the Lev-group, N. Reichardt, unpublished results.

[16] S. Hanessian, X. Fang, *Tetrahedron Lett.* **1998**, *39*, 733–736.

[17] M. Grathwohl, R. R. Schmidt, *Synthesis* **2001**, *15*, 2263–2272.

[18] a) H. Paulsen, B. Helpap, *Carbohydr. Res.* **1991**, *216*, 289–313; b) T. G. Mayer, B. Kratzer, R. R. Schmidt, *Angew. Chem.* **1994**, *106*, 2289–2293; *Angew. Chem. Int. Ed. Engl.* **1994**, *33*, 2177–2181.

[19] K. Kohata, T. Konno, H. Meguro, *Tetrahedron Lett.* **1980**, *21*, 3771–3774.

[20] F. Roussel, L. Knerr, M. Grathwohl, R. R. Schmidt, *Org. Lett.* **2000**, *2*, 3043–3046.

[21] Argo-Gel-Wang-Cl, commercial resin, Argonaut Technologies, San Carlos, USA.

 © 2003 Wiley-VCH Verlag GmbH & Co. KGaA, Weinheim

Metallaboranes

Transition-Metal Variation as a Probe of the Origins of Hypoelectronic Metallaboranes: Eight- and Ten-Vertex Open Ruthenaboranes**

*Sundargopal Ghosh, Alicia M. Beatty, and Thomas P. Fehlner**

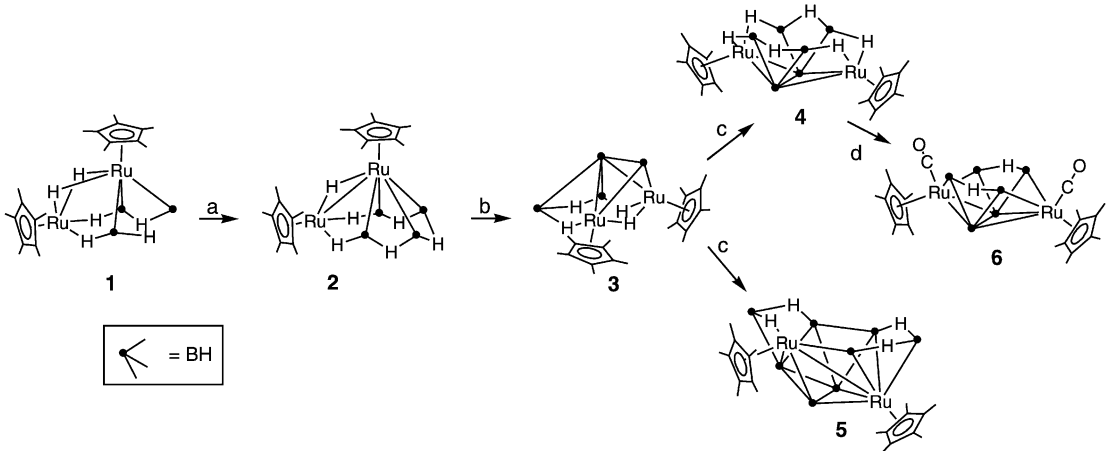
Recently we described a homologous series of closo-rhenaboranes, $[(Cp^*Re)_2B_nH_n]$, $n = 6$–10 ($Cp^* = \eta^5$-C_5Me_5), of unusual shape and skeletal electron count.[1,2] Although related to a larger set of "disobedient" clusters,[3] these compounds are particularly significant as they demonstrate systematic and large deviations from the cluster shape/electron count principle, which has proven satisfactory for understanding the structures of a majority of borane and transition-metal clusters.[4,5] An analysis of this rhenaborane series relative to existing models of electronic structure has appeared.[6] Herein we show that an ability to vary metal identity at near constant stoichiometry provides insight into the role of the metal fragments in the electronic structure of main-group/transition-element clusters.

The thermodynamic control implied by the reaction conditions in the hypoelectronic rhena- and tungstaborane systems,[7] suggests other metallaboranes containing extra hydrogen atoms should be susceptible to condensation. The {Cp*Ru} fragment drew our renewed attention as it has one more electron than the {Cp*Re} fragment and one less electron than the ideal two-electron {Cp*M} fragment, M = Group 9 metal. Loss of the two "extra" metal hydride units from $[(Cp^*RuH)_2B_3H_7]$ (**1**),[8,9] hydrides which are required to make up the seven skeletal electron pairs (sep) associated with the square-pyramidal geometry, might yield compounds with structures bridging the behavior patterns of the Group 7 and Group 9 compounds.

The reactions in Scheme 1 in which **1** is converted into $[(Cp^*Ru)_2B_4H_{10}]$, (**2**) and then $[(Cp^*Ru)_2B_4H_8]$ (**3**), have been discussed earlier.[8] Vigorous heating of **3** with BH_3·THF leads to good yields of two new, stable diruthenaborane clusters. Single-crystal X-ray structure determinations define the cluster geometries which are in full accord with the solution spectroscopic data. The structures of $[(Cp^*RuH_2)_2B_6H_8]$ (**4**) and $[(Cp^*Ru)_2B_8H_{12}]$ (**5**), are shown in Figure 1 and 2.[10] We have been unable to convert **4** into **5** by the addition of borane.

In contrast to most of the dirhenaboranes,[11] **4** and **5** retain bridging hydrogen atoms in the product frameworks and the structures are reminiscent of those of 10 sep B_8H_{12} and 12 sep $B_{10}H_{14}$, respectively.[12] Considering a {Cp*Ru} fragment as a three-orbital, one-electron fragment, the formal electron counts are 10 sep for **4** and 11 sep for **5**: the structure of the former follows the borane analogy whereas the latter is formally one pair short. Note that like **1**, complex **4** contains one "extra" H per {Cp*Ru} fragment relative to the analogous borane whereas **5** does not.

The view of **4** as an "obedient" metallaborane can be tested. For example, we have previously shown that the addition of CO to unsaturated five sep compound



Scheme 1. Stepwise conversion of **1** into $[(Cp^*RuH_2)_2B_6H_8]$ (**4**), $[(Cp^*Ru)_2B_8H_{12}]$ (**5**), and $[(Cp^*RuCO)_2B_6H_8]$ (**6**). Conditions: a) 60°, BH_3·THF; b) 90°; c) 95°, BH_3·THF; d) 55°, $[Co_2(CO)_8]$. The structures shown are schematic representations, −H− indicates an H-bridged bond.

[*] Prof. Dr. T. P. Fehlner, Dr. S. Ghosh, Dr. A. M. Beatty
Department of Chemistry and Biochemistry
University of Notre Dame
Notre Dame, IN 46556 (USA)
Fax: (+1) 574-631-6652
E-mail: fehlner.1@nd.edu

[**] The support of the National Science Foundation (CHE99-86880) is gratefully acknowledged. We thank Prof. Bruce King for helpful discussions.

$[(Cp^*Cr)_2B_4H_8]$ leads to saturated six sep compound $[(Cp^*CrCO)_2B_4H_6]$[13] whereas addition of CO to saturated six sep $[(Cp^*ReH_2)_2B_4H_4]$ leads to saturated six sep compound $[(Cp^*ReCO)(Cp^*ReH_2)B_4H_4]$.[14] If **4** is indeed a 10 sep saturated cluster, addition of two CO units should lead to $[(Cp^*RuCO)_2B_6H_8]$, which is analogous to $C_2B_6H_{10}$, that is, a {Cp*RuCO} fragment is generated that functions as a three-orbital, three-electron fragment ("into the t_{2g} set").[15] As

 © 2003 Wiley-VCH Verlag GmbH & Co. KGaA, Weinheim DOI: 10.1002/anie.200352101

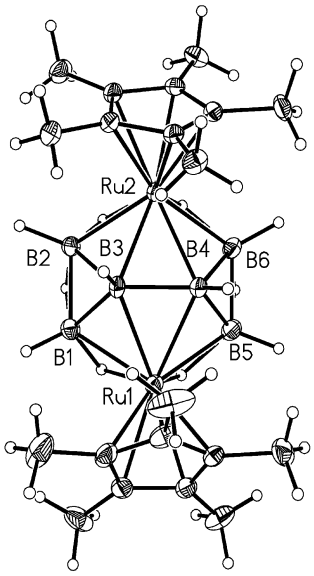


Figure 1. Molecular structure of **4**. Selected bond lengths [Å]: Ru1-B5 2.208(5), B1-B2 1.734(6), Ru2-B2 2.200(4).

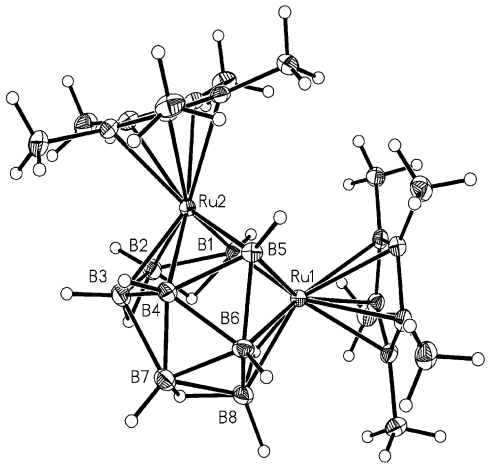


Figure 2. Molecular structure of **5**. Selected bond lengths [Å]: Ru1-B1 2.158(2), Ru1-B8 2.207(2), Ru1-B6 2.288(2), Ru1-Ru2 2.8897(2), B3-B4 1.758(3), B3-B7 2.014(3).

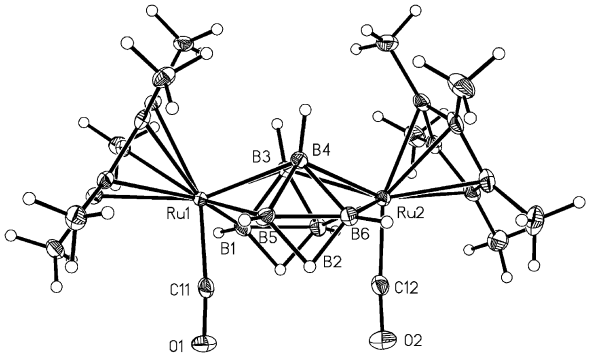


Figure 3. Molecular structure of **6**. Selected bond lengths [Å]: Ru1-B1 2.174(3), Ru1-B4 2.277(3), B2-B3 1.726(4), B5-B6 1.693(4). The torsion angle between Ru1-C11 and Ru2-C12 is −0.8°

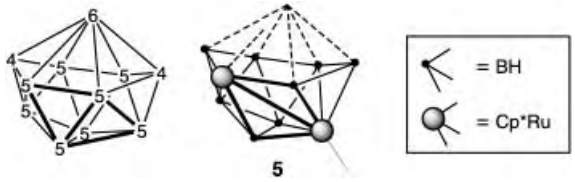


Figure 4. The observed geometry of **5** is generated by removing the connectivity-six vertex from an octadecahedron and by performing one dsd rearrangement.

shown in Scheme 1, addition of CO to **4** does lead to $[Cp^*RuCO)_2B_6H_8]$ (**6**; Figure 3) corroborating the assignment of the {Cp*Ru} fragment in **4** as a three-orbital, one-electron fragment.

This analysis of **4** serves as a basis for understanding **5**. The framework geometry of **5** resembles that of $B_{10}H_{14}$ except that the diamond in the cluster framework containing the two ruthenium atoms has undergone a diamond-square-diamond (dsd) rearrangement thereby increases the connectivity of the ruthenium sites to five and six and decreases the connectivities of the two boron sites correspondingly (Figure 4).[16] Based on our previous analysis of $[(Cp^*Cr)_2B_4H_8]$,[17,18] we suggest that a pair of occupied "t_{2g}" ruthenium orbitals of bonding symmetry interact to form a lower-energy filled bonding and higher-energy unfilled antibonding orbital without strongly perturbing the energies of orbitals of high boron content. It is the dsd rearrangement that makes possible the utilization of a pair of metal "t_{2g}" orbitals.

Earlier analyses of metallaboranes with low sep and geometries related by dsd rearrangements to geometries of analogous boranes has led to competing descriptions which differ in the manner in which the valence electron density is partitioned. One, with the designation iso- (closo, nido, or arachno), requires the normal cluster-electron count to be met.[3,19,20] To do so, the metal fragment utilizes one of its nonbonding sets; something that is seen to occur in organometallic compounds.[15,21] The second description, with the designation hyper-closo, requires the metals to be restricted to a three-orbital contribution to cluster bonding.[22] In this case it is the change in shape that adjusts the number of cluster bonding orbitals or, more precisely, the number of unfilled antibonding orbitals.[23,24] The analysis of **5** can be equally well described as the generation of another unavailable orbital (the M–M antibonding orbital) or as the generation of another pair of electrons for the cluster bonding network from the "t_{2g}" set albeit involving both metals (the M–M bonding orbital). The approaches are the same and can both be described by the term hypoelectronic.[16,25]

Diruthenaborane **5** possesses two {Cp*Ru} fragments which must be counted differently if the electron-counting rules are to be satisfied. This flaw originates in partitioning electrons between cluster bonding and all other filled orbitals by using a main-group-atom model. Transition-metal fragments will not be constrained to the monolithic behavior of main-group fragments.

 © 2003 Wiley-VCH Verlag GmbH & Co. KGaA, Weinheim

Experimental Section

Synthesis of **4** and **5**: $[(Cp^*Ru)_2B_4H_8]$ (**3**; 0.15 g, 0.28 mmol) in toluene (15 mL) was heated with sixfold excess of BH_3·THF (1.73 mL, 1.73 mmol) at 95 °C for 16 h. After filtration, the residue was subjected to thin layer chromatography (TLC) on silica gel plates. Elution with hexane:CH_2Cl_2 (75:25 v/v) yielded two well-separated bands: yellow **4** (0.08 g, 52 %); red **5** (0.05 g, 36 %).

Selected data for **4**: MS (FAB) P^+(max) 547 (isotopic pattern for 2 Ru and 6 B atoms), $^{12}C_{20}{}^{1}H_{42}{}^{11}B_6{}^{101}Ru_2$, calcd: 550.1775; obsd: 550.1797 (exact mass calculated for $[M^+-2]$); ^{11}B NMR (C_6D_6, 400 MHz, 22 °C): $\delta = 37.87$ (d, $J_{B\text{-}H} = 110$ Hz, 4 B), 1.19 ppm (d, $J_{B\text{-}H} = 116$ Hz, 2 B); ^{1}H NMR (C_6D_6, 400 MHz, 22 °C): $\delta = 6.39$ (partially collapsed quartet (pcq), 4 BH_t (t = terminal)), 2.33 (pcq, 2 BH_t), 1.67 (s, 30 H, 2 Cp*), −0.67 (s, br, 2 B-H-B), −13.55 ppm (s, br, 4 Ru-H-B); IR (hexane): $\tilde{\nu} = 2529$ w, 2449 cm^{-1} w (B-H_t).

Selected data for **5**: MS (FAB) P^+(max) 567 (isotopic pattern for 2 Ru and 8 B atoms), $^{12}C_{20}{}^{1}H_{42}{}^{11}B_8{}^{101}Ru_2$, calcd: 571.1805; obsd: 571.1851 (exact mass calculated for $[M^+-4]$); ^{11}B NMR (C_6D_6, 400 MHz, 22 °C): $\delta = 109.17$ (d, $J_{B\text{-}H} = 145$ Hz, 1 B), 63.11 (d, $J_{B\text{-}H} = 125$ Hz, 1 B), 33.66 (d, $J_{B\text{-}H} = 123$ Hz, 1 B), 16.22 (d, $J_{B\text{-}H} = 114$ Hz, 1 B), 13.51 (d, $J_{B\text{-}H} = 125$ Hz, 1 B), 9.13 (d, $J_{B\text{-}H} = 128$ Hz, 1 B), 2.16 (d, $J_{B\text{-}H} = 137$ Hz, 1 B), −27.24 ppm (d, $J_{B\text{-}H} = 136$ Hz, 1 B); ^{1}H NMR (C_6D_6, 400 MHz, 22 °C): $\delta = 9.86$ (pcq, 1 BH_t), 6.18 (pcq, 1 BH_t), 5.56 (pcq, 1 BH_t), 5.36 (pcq, 1 BH_t), 3.41 (pcq, 1 BH_t), 3.05 (pcq, 1 BH_t), 2.58 (pcq, 1 BH_t), 1.28 (pcq, 1 BH_t), 1.60 (s, 15 H, 1 Cp*), 1.44 (s, 15 H, 1 Cp*), 0.83 (s, br, 1 B-H-B), −0.41 (s, br, 1 B-H-B), −2.40 (s, br, 1 B-H-B), −17.09 ppm (s, br, 1 Ru-H-B): IR (hexane): 2494 w, 2449 cm^{-1} w (B-H_t).

6: **4** (0.15 g, 0.27 mmol) in hexane (15 mL) was stirred with $[Co_2(CO)_8]$ (0.47 g, 1.36 mmol) for 5 h at 55 °C. Extraction in hexane, filtration through silica gel, and TLC (hexane:CH_2Cl_2 7:3) yielded **6** (0.07 g, 44 %). MS (FAB) P^+(max) 600 (isotopic pattern for 2 Ru and 6 B atoms), $^{12}C_{22}{}^{1}H_{38}{}^{11}B_6{}^{101}Ru_2{}^{16}O_2$, calcd: 604.1517, obsd: 604.1534; ^{11}B NMR (C_6D_6, 400 MHz, 22 °C): $\delta = 52.54$ (d, $J_{B\text{-}H} = 135$ Hz, 4 B), 6.68 ppm (d, $J_{B\text{-}H} = 115$ Hz, 2 B); ^{1}H NMR (C_6D_6, 400 MHz, 22 °C): = 7.18 (pcq, 4 BH_t), 1.53 (pcq, 2 BH_t), 1.66 (s, 30 H, 2 Cp*), −0.05 ppm (s, br, 2 B-H-B); ^{13}C NMR (C_6D_6, 300 MHz, 22 °C): $\delta = 201.5$ (Ru-CO), 100.8 ($C_5(CH_3)_5$), 9.6 ppm ($C_5(CH_3)_5$); IR (hexane): $\tilde{\nu} = 2488$ w, 2415 w (B-H_t), 1967.1 s, 1942.9 cm^{-1} w (Ru-CO) with calculated dihedral angle between the CO units = 20°.

Received: June 10, 2003 [Z52101]

Keywords: boranes · cluster compounds · electronic structure · metallaboranes · ruthenium

[1] S. Ghosh, M. Shang, Y. Li, T. P. Fehlner, *Angew. Chem.* **2001**, *113*, 1159; *Angew. Chem. Int. Ed.* **2001**, *40*, 1125.
[2] S. Ghosh, A. M. Beatty, T. P. Fehlner, *J. Am. Chem. Soc.* **2001**, *123*, 9188.
[3] J. D. Kennedy in *The Borane, Carborane, Carbocation Continuum* (Ed.: J. Casanova), Wiley, New York, **1998**, p. 85.
[4] K. Wade, *Adv. Inorg. Chem. Radiochem.* **1976**, *18*, 1.
[5] D. M. P. Mingos, D. J. Wales, *Introduction to Cluster Chemistry*, Prentice Hall, New York, **1990**.
[6] H. Wadepohl, *Angew. Chem.* **2002**, *114*, 4394; *Angew. Chem. Int. Ed.* **2002**, *41*, 4220.
[7] A. S. Weller, M. Shang, T. P. Fehlner, *Organometallics* **1999**, *18*, 853.
[8] X. Lei, M. Shang, T. P. Fehlner, *J. Am. Chem. Soc.* **1999**, *121*, 1275.
[9] Y. Kawano, H. Matsumoto, M. Shimoi, *Chem. Lett.* **1999**, 489.
[10] CCDC-211168, CCDC-211169, and CCDC-211884 contain the supplementary crystallographic data for this paper. These data can be obtained free of charge via www.ccdc.cam.ac.uk/conts/retrieving.html (or from the Cambridge Crystallographic Data Centre, 12 Union Road, Cambridge CB21EZ, UK; fax: (+44) 1223-336-033; or deposit@ccdc.cam.ac.uk).
[11] S. Ghosh, A. L. Rheingold, T. P. Fehlner, *Chem. Commun.* **2001**, 895.
[12] R. E. Williams in *The Borane, Carborane, Carbocation Continuum* (Ed.: J. Casanova), Wiley-Interscience, New York, **1997**, p. 3.
[13] J. Ho, K. J. Deck, Y. Nishihara, M. Shang, T. P. Fehlner, *J. Am. Chem. Soc.* **1995**, *117*, 10292.
[14] S. Ghosh, X. Lei, C. L. Cahill, T. P. Fehlner, *Angew. Chem.* **2000**, *112*, 3022; *Angew. Chem. Int. Ed.* **2000**, *39*, 2900.
[15] R. Hoffmann, *Science* **1981**, *211*, 995.
[16] T. P. Fehlner, *Adv. Chem.* **2002**, *822*, 49.
[17] T. P. Fehlner, *J. Organomet. Chem.* **1998**, *550*, 21.
[18] T. P. Fehlner, *J. Chem. Soc. Dalton Trans.* **1998**, 1525.
[19] J. D. Kennedy, *Inorg. Chem.* **1986**, *25*, 111.
[20] R. B. King, I. Silaghi-Dumitrescu, A. Kun, *Inorg. Chem.* **2001**, *40*, 2450.
[21] C. Elschenbroich, A. Salzer, *Organometallics*, VCH, New York, **1989**.
[22] R. T. Baker, *Inorg. Chem.* **1986**, *25*, 109.
[23] R. L. Johnston, D. M. P. Mingos, *Inorg. Chem.* **1986**, *25*, 3321.
[24] R. L. Johnston, D. M. P. Mingos, P. Sherwood, *New J. Chem.* **1991**, *15*, 831.
[25] J. D. Corbett, *Struct. Bonding (Berlin)* **1997**, *87*, 157.

 © 2003 Wiley-VCH Verlag GmbH & Co. KGaA, Weinheim

Asymmetric Olefination–Epoxidation

Sequential Wittig Olefination–Catalytic Asymmetric Epoxidation with Reuse of Waste $Ph_3P(O)$: Application of α,β-Unsaturated *N*-Acyl Pyrroles as Ester Surrogates**

*Tomofumi Kinoshita, Shigemitsu Okada, Sun-Ryung Park, Shigeki Matsunaga, and Masakatsu Shibasaki**

The catalytic asymmetric epoxidation of α,β-unsaturated carbonyl compounds is an important transformation in organic synthesis.[1] Although we[2] and others[1] have developed efficient catalytic asymmetric epoxidations of α,β-unsaturated ketones, there are only limited examples of the use of α,β-unsaturated esters as substrates with a salen–Mn complex[3] or a chiral ketone[4] as the catalyst. In both cases,

[*] Prof. Dr. M. Shibasaki, T. Kinoshita, S. Okada, S.-R. Park, S. Matsunaga
Graduate School of Pharmaceutical Sciences
The University of Tokyo
Hongo, Bunkyo-ku, Tokyo 113-0033 (Japan)
Fax: (+81) 3-5684-5206
E-mail: mshibasa@mol.f.u-tokyo.ac.jp

[**] This work was partially supported by RFTF and a Grant-in-Aid for the Encouragement of Young Scientists (B) (to S.M.) from the JSPS.

Supporting information for this article is available on the WWW under http://www.angewandte.org or from the author.

 © 2003 Wiley-VCH Verlag GmbH & Co. KGaA, Weinheim DOI: 10.1002/anie.200352509

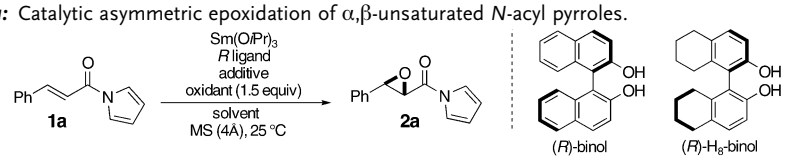
except for the recent report of Shi and co-workers,[4a] only β-aryl-substituted α,β-unsaturated esters were used. Although Shi and co-workers reported excellent results for a few β-alkyl-substituted substrates, *trans*-β-alkyl-substituted α,β-unsaturated esters could not be used, thus leaving room for improvement in substrate generality. We recently reported the catalytic asymmetric epoxidation of α,β-unsaturated 4-phenylcarboxylic acid imidazolides[5,6] and morpholinyl amides[6] as ester surrogates. Although moderate to high enantioselectivities were observed for substrates with β-aryl or β-alkyl substituents (imidazolide: 79–94% *ee*, amide: 99% *ee*), from a practical viewpoint many problems remained: a) a catalyst loading of 10 mol% was essential for good conversion, b) explosive *tert*-BuOOH (TBHP) was essential as the oxidant for good reactivity, and c) the preparation of β-alkyl α,β-unsaturated carboxylic acid imidazolides from aldehydes was lengthy. To address these issues, we report herein the application of α,β-unsaturated *N*-acyl pyrroles, which were found to be highly reactive and versatile substrates, as ester surrogates. Furthermore, these substrates were used in a one-pot sequential Wittig-olefination–catalytic-asymmetric-epoxidation process in which the $Ph_3P(O)$ formed in the Wittig step was reused in the second step. This process provided efficient access to optically active pyrrolyl epoxides from a variety of aldehydes in high yields and with high enantioselectivities. The versatility of the pyrrolyl epoxide products was also demonstrated.

Although the potential of *N*-acyl pyrroles as ester surrogates was reported two decades ago,[7] it was only recently that the unique reactivity of *N*-acyl pyrroles was recognized and utilized in organic synthesis, for example, in asymmetric catalysis.[8] A recent report by Evans et al.[9] on the unique properties of *N*-acyl pyrroles prompted us to investigate the use of α,β-unsaturated *N*-acyl pyrroles as ester surrogates. As summarized in Table 1, the catalytic asymmetric epoxidation of **1a** proceeded smoothly. When the Sm–(*R*)-binol complex (10 mol%)[10] and $Ph_3As(O)$ (10 mol%)[11] were used, the reaction was complete within 0.5 h and afforded **2a** in 93% yield and with 94% *ee* (Table 1, entry 1). The reaction rate was much faster than for a carboxylic acid imidazolide or a morpholinyl amide, and as fast as for an enone. The reaction also proceeded smoothly in the presence of 5 mol% of the catalyst (Table 1, entry 2: 85% yield, 96% *ee*). Various binol derivatives were screened in an attempt to improve the enantioselectivity of the reaction, and it was found that H_8-binol gave the best results. The superior performance of the H_8-binol complex over that of the binol complex is probably a result of the large bite angle in the former complex.[12] Compound **2a** was formed with 99% *ee* in the presence of the novel Sm–(*R*)-H_8-binol complex (Table 1, entry 3). $Ph_3P(O)$ was also an effective additive in the reaction of substrate **1a**[11] (Table 1, entries 4–6). A THF/toluene solvent mixture led to better results than THF alone, and **2a** was obtained with 96–99% *ee*, depending on the amount of $Ph_3P(O)$ added (Table 1, entries 7–9). Both the reaction rate and the selectivity were highest when 100 mol% of the $Ph_3P(O)$ additive was used (Table 1, entry 9). Under the best conditions (THF/toluene, $Ph_3P(O)$ (100 mol%)) the reaction proceeded smoothly with a low catalyst loading (1 mol%) to afford **2a** in 94% yield and with 99% *ee* within 0.3 h (Table 1, entry 10). Cumene hydroperoxide (CMHP), which is less explosive and less reactive than TBHP, could also be used. The reaction reached completion in the presence of this oxidant within 0.2 h with 5 mol% of the catalyst (Table 1, entry 11: 91% yield, >99.5% *ee*).[13]

One reason that α,β-unsaturated *N*-acyl pyrroles have not been widely used as acceptors in 1,4-addition reactions, despite their high reactivity, might be the lack of an efficient method for their preparation under mild conditions.[14] A Wittig reaction of the ylide **3** with aldehydes was examined as a general synthetic approach to a range of functionalized α,β-unsaturated *N*-acyl pyrroles. The ylide **3** was synthesized efficiently in 98% yield in one step from 1,1′-carbonyldipyrrole and methylenetriphenylphosphorane.[15] The Wittig reaction of **3** with benzaldehyde (**4a**) proceeded smoothly to afford **1a** in 97% yield, along with a stoichiometric amount of waste $Ph_3P(O)$ (Scheme 1).

Although the functional-group tolerance of the Wittig reaction is good because of the mild conditions, this olefination is generally considered to be somewhat inefficient as a result of the production of $Ph_3P(O)$ as a by-product. We hypothesized that the reuse of waste $Ph_3P(O)$ in the epoxidation reaction as a modulator for the Sm–H_8-binol complex would partially compensate this disadvantage of the Wittig reaction. Thus, a sequential Wittig olefination–catalytic asymmetric epoxidation was designed in which the $Ph_3P(O)$ produced in the first (Wittig) reac-

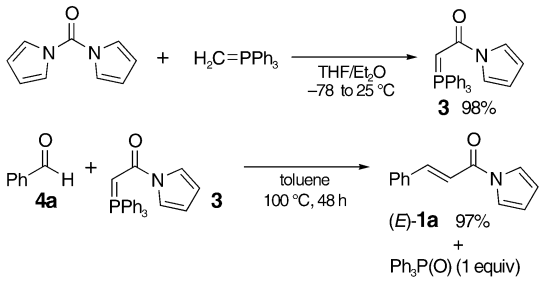
Table 1: Catalytic asymmetric epoxidation of α,β-unsaturated *N*-acyl pyrroles.



Entry	Ligand (mol%)[a]	Additive (mol%)	Solvent	Oxidant	*t* [h]	Yield [%][b]	*ee* [%][c]
1	binol (10)	$Ph_3As(O)$ (10)	THF	TBHP	0.5	93	94
2	binol (5)	$Ph_3As(O)$ (5)	THF	TBHP	0.5	85	96
3	H_8-binol (5)	$Ph_3As(O)$ (5)	THF	TBHP	0.5	94	99
4	H_8-binol (5)	$Ph_3P(O)$ (15)	THF	TBHP	0.5	84	94
5	H_8-binol (5)	$Ph_3P(O)$ (50)	THF	TBHP	0.5	88	98
6	H_8-binol (5)	$Ph_3P(O)$ (100)	THF	TBHP	0.5	85	97
7	H_8-binol (5)	$Ph_3P(O)$ (15)	THF/toluene	TBHP	0.4	85	96
8	H_8-binol (5)	$Ph_3P(O)$ (50)	THF/toluene	TBHP	0.5	92	99
9	H_8-binol (5)	$Ph_3P(O)$ (100)	THF/toluene	TBHP	0.2	97	99
10	H_8-binol (1)	$Ph_3P(O)$ (100)	THF/toluene	TBHP	0.3	94	99
11	H_8-binol (5)	$Ph_3P(O)$ (100)	THF/toluene	CMHP	0.2	91	>99.5

[a] Sm(O*i*Pr)$_3$/ligand 1:1. [b] Yield of isolated product. [c] Determined by HPLC analysis on a chiral phase.

 © 2003 Wiley-VCH Verlag GmbH & Co. KGaA, Weinheim

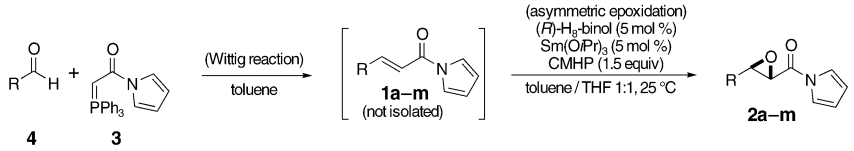


Scheme 1. Synthesis of the ylide **3** and Wittig reaction.

tion was reused as an additive in the second (epoxidation) reaction. When **4a** was subjected to this olefination–epoxidation sequence, **2a** was produced in 96% yield (two steps) and with 99.8% *ee* (Scheme 2a). As expected, the selectivity and reactivity were much lower when the reaction was performed in two separate steps and no $Ph_3P(O)$ was added in the second step (75.2% *ee*, Scheme 2b). When $Ph_3P(O)$ (15 mol% or 50 mol%) was added in the second step after isolation of intermediate **1a** and removal of the $Ph_3P(O)$ by-product (1 equiv) as waste, **2a** was obtained with 96.8% *ee* or 98.8% *ee*, respectively (Scheme 2b). These results suggested that $Ph_3P(O)$ did indeed function as an effective additive to improve the yield and enantioselectivity of the epoxidation reaction, but that only 0.5–1 equivalent of $Ph_3P(O)$ was required to promote high enantioselectivity. The fact that only one purification step was required in the one-pot process (Scheme 2a), in contrast to the two required in the reaction sequence in Scheme 2b, clearly shows the higher total efficiency of the one-pot sequential process for the synthesis of the epoxide **2a** from the aldehyde **4a**. The total efficiency of this system is also superior to previous results with carboxylic acid imidazolides[5,6] and morpholinyl amides,[6] which were synthesized and purified prior to use.

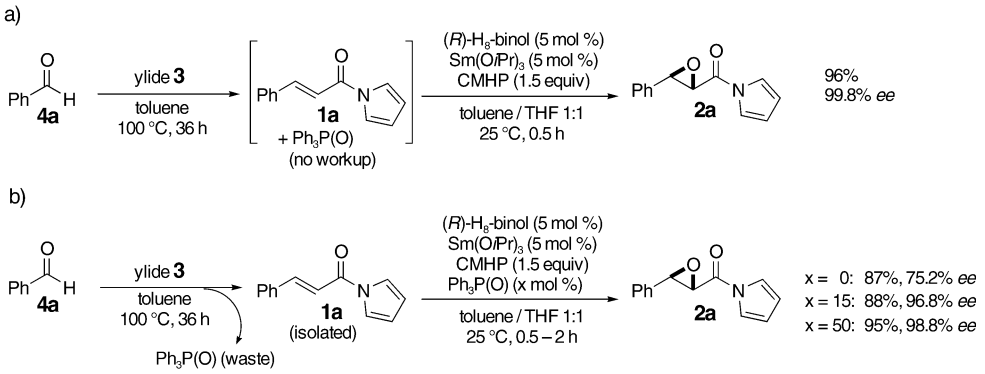
As summarized in Table 2, the sequential reaction described herein has broad substrate generality and affords the desired epoxides with excellent enantioselectivities (96 to >99.5% *ee*) and in good yields (Table 2, entries 1–13: 72–96% yield from the corresponding aldehydes). Aromatic aldehydes with various substituents (Table 2, entries 1–7), functionalized aliphatic linear and branched aldehydes (Table 2, entries 8–12), and α,β-unsaturated aldehydes (Table 2, entry 13) were all suitable substrates. The reaction proceeded chemoselectively with the aldehyde **4l**, which contains a methyl ketone (Table 2, entry 12). In many examples, less explosive CMHP was used as the oxidant instead of TBHP, which demonstrates an additional practical benefit of this methodology. When the chiral aldehyde **4n** was used, the sequential reaction proceeded in an almost com-

Table 2: Sequential Wittig olefination–catalytic asymmetric epoxidation with achiral aldehydes.



Entry	R		Wittig reaction T [°C]	Wittig reaction t [h]	Epoxidation t [h]	Yield [%][a]	*ee* [%][b]
1	C_6H_5-	**4a**	100	48	0.5	96	>99.5
2	*p*-Me-C_6H_4-	**4b**	100	48	2.5	92	99
3	*p*-Cl-C_6H_4-	**4c**	100	24	0.5	100	99
4[c]	*p*-MeO-C_6H_4-	**4d**	110	84	0.5	87	98
5[c]	*o*-ClC_6H_4-	**4e**	100	24	0.5	83	97
6	2-naphthyl	**4f**	100	48	2	100	99
7	1-naphthyl	**4g**	100	48	0.5	85	99
8	$C_6H_5CH_2CH_2$-	**4h**	80	24	0.5	84	97
9	$PMBOCH_2CH_2$-	**4i**	80	24	0.5	91	97
10	CH_2=$CH(CH_2)_8$-	**4j**	100	25	0.5	82	96
11	*c*-C_6H_{11}	**4k**	100	72	2	75	98
12	$CH_3C(O)CH_2CH_2$-	**4l**	80	36	0.5	93	96
13[c,d]	*trans*-$CH_3(CH_2)_2CH$=CH-	**4m**	100	72	2	72	96

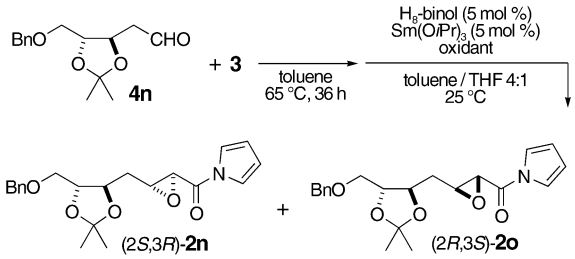
[a] Yield of the isolated product **2** (from **4**). [b] Determined by HPLC analysis on a chiral phase. [c] *t*BuOOH was used as the oxidant. [d] Catalyst: 10 mol%.



Scheme 2. Wittig olefination–catalytic asymmetric epoxidation as a) a one-pot sequential process and b) a stepwise process with isolation of the Wittig product and addition of external $Ph_3P(O)$.

 © 2003 Wiley-VCH Verlag GmbH & Co. KGaA, Weinheim

pletely catalyst-controlled manner (Scheme 3 and Table 3). The epoxide was obtained in a **2n**/**2o** ratio of >99:1 with the *R*-configured catalyst (matched pair, Table 3, entry 1) and in a **2n**/**2o** ratio of 1:36 with the *S*-configured catalyst (mismatched pair, Table 3, entry 3). When achiral epoxidation systems were used, much lower selectivity was observed (d.r. 54:46).[16]



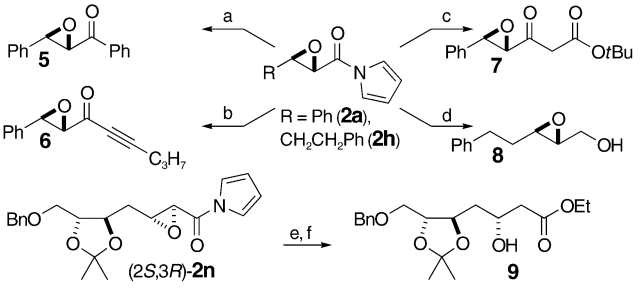
Scheme 3. Sequential Wittig olefination–catalytic asymmetric epoxidation with the chiral aldehyde **4n**.

Table 3: Sequential Wittig olefination–catalytic asymmetric epoxidation with the chiral aldehyde **4n**.

Entry	Ligand	*t* [h]	Oxidant	Yield [%][a]	d.r.[b] (**2n**/**2o**)
1	(*R*)-H_8-binol	0.7	CMHP	80	>99:1
2	(*S*)-H_8-binol	0.9	CMHP	60	1:56
3	(*S*)-H_8-binol	0.7	TBHP	78	1:36

[a] Yield of the isolated product **2n** (from **4n**). [b] Determined by HPLC analysis.

The versatility of the pyrrolyl epoxide products was demonstrated by transformations of **2** into compounds **5**–**9** (Scheme 4). The addition of various carbon nucleophiles followed by treatment with DBU afforded **5**–**7** in good yields.[17] The epoxy alcohol **8** was obtained by the stepwise reduction of **2h** with $LiBH_4$ and $NaBH_4$. After the epoxide opening of **2n**, EtSLi in EtOH was determined to be a suitable reagent for the conversion of the *N*-acyl pyrrole into the corresponding ethyl ester **9** in high yield at room temperature.



Scheme 4. Various transformations of the pyrrolyl epoxides **2**. a) PhLi, THF; then DBU, CH_2Cl_2, 88%; b) BuLi, 1-pentyne, THF; then DBU, CH_2Cl_2, 84%; c) *tert*-butyl acetate, LDA, THF; then DBU, CH_2Cl_2, 74%; d) $LiBH_4$, THF; then $NaBH_4$, 72%; e) $(PhSe)_2$, $NaBH_4$, EtOH/AcOH, 94%; f) EtSLi, EtOH, 92%. DBU = 1,8-diazabicyclo[5.4.0]undec-7-ene, LDA = lithium diisopropylamide.

In summary, we have developed a sequential Wittig-olefination–catalytic-asymmetric-epoxidation process, which utilizes *N*-acyl pyrroles as ester surrogates and provides efficient one-pot access to optically active epoxides. Good yields and excellent enantioselectivities were observed for a broad range of aldehyde substrates. The $Ph_3P(O)$ produced in the first step is used to modulate the second step, and CMHP, which is less explosive and thus more practical than TBHP, can be used as the oxidant. The reaction of the ylide **3** with aldehydes proved to be an efficient method for the synthesis of a variety of functionalized α,β-unsaturated *N*-acyl pyrroles, which should also be suitable substrates for asymmetric 1,4-addition reactions.

Experimental Section

Benzaldehyde (**4a**; 50.8 μL, 0.5 mmol) was added to a stirred suspension of the ylide **3** (139.1 mg, 0.65 mmol) in toluene (1.25 mL) at 25 °C. The mixture was stirred for a further 36 h at 100 °C, then cooled to 25 °C. Toluene (1.25 mL) and a suspension of the catalyst prepared from $Sm(OiPr)_3$ (125 μL, 0.025 mmol, 0.2 M in THF), (*R*)-H_8-binol (7.4 mg, 0.025 mmol), CMHP (231 μL, 0.75 mmol, 3.25 M in toluene), and molecular sieves (4 Å) were added to the reaction mixture at 25 °C. The mixture was stirred for a further 0.5 h at 25 °C, then the reaction was quenched with aqueous citric acid (2.5%), and the mixture was filtered through celite. The filtrate was extracted three times with ethyl acetate, and the combined organic layers were washed with saturated, aqueous $NaHCO_3$, then brine, and dried over $MgSO_4$. The solvent was evaporated, and the resulting crude residue was purified by flash column chromatography (silica gel, ethyl acetate/hexane 1:20) to afford **2a** (102.4 mg, 96% yield, >99.5% *ee*).

Received: July 29, 2003 [Z52509]
Published Online: September 11, 2003

Keywords: asymmetric catalysis · epoxidation · samarium · synthetic methods · Wittig reactions

[1] For recent reviews, see: a) M. J. Porter, J. Skidmore, *Chem. Commun.* **2000**, 1215; b) T. Nemoto, T. Ohshima, M. Shibasaki, *J. Synth. Org. Chem. Jpn.* **2002**, *60*, 94; poly(amino acid) catalysis: c) M. J. Porter, S. M. Roberts, J. Skidmore, *Bioorg. Med. Chem.* **1999**, *7*, 2145; catalysis by a chiral ketone: d) M. Frohn, Y. Shi, *Synthesis* **2000**, 1979; for selected leading references, see also: e) D. Enders, J. Zhu, G. Raabe, *Angew. Chem.* **1996**, *108*, 1827; *Angew. Chem. Int. Ed. Engl.* **1996**, *35*, 1725; f) C. L. Elston, R. F. W. Jackson, S. J. F. MacDonald, P. J. Murray, *Angew. Chem.* **1997**, *109*, 379; *Angew. Chem. Int. Ed. Engl.* **1997**, *36*, 410.

[2] a) M. Bougauchi, S. Watanabe, T. Arai, H. Sasai, M. Shibasaki, *J. Am. Chem. Soc.* **1997**, *119*, 2329; for the effects of $Ph_3As(O)$ and $Ph_3P(O)$ as additives, see: b) T. Nemoto, T. Ohshima, K. Yamaguchi, M. Shibasaki, *J. Am. Chem. Soc.* **2001**, *123*, 2725; c) K. Daikai, M. Kamaura, J. Inanaga, *Tetrahedron Lett.* **1998**, *39*, 7321.

[3] E. N. Jacobsen, L. Deng, Y. Furukawa, L. E. Martinez, *Tetrahedron* **1994**, *50*, 4323.

[4] a) X.-Y. Wu, X. She, Y. Shi, *J. Am. Chem. Soc.* **2002**, *124*, 8792; b) A. Armstrong, Hayter, B. R. *Chem. Commun.* **1998**, 621; c) A. Solladié-Cavallo, L. Bouérat, *Org. Lett.* **2000**, *2*, 3531; d) M. Seki, T. Furutani, R. Imashiro, T. Kuroda, T. Yamanaka, N. Harada, H. Arakawa, M. Kusama, T. Hashiyama, *Tetrahedron*

 © 2003 Wiley-VCH Verlag GmbH & Co. KGaA, Weinheim

Lett. **2001**, *42*, 8201; see also: e) D. Yang, Y.-C. Yip, M.-W. Tang, M.-K. Wong, J.-H. Zheng K.-K. Cheung, *J. Am. Chem. Soc.* **1996**, *118*, 491.

[5] a) T. Nemoto, T. Ohshima, M. Shibasaki, *J. Am. Chem. Soc.* **2001**, *123*, 9474; b) T. Nemoto, S. Tosaki, T. Ohshima, M. Shibasaki, *Chirality* **2003**, *15*, 306.

[6] S. Tosaki, T. Nemoto, T. Ohshima, M. Shibasaki, *Org. Lett.* **2003**, *5*, 495.

[7] S.-D. Lee, M. A. Brook, T.-H. Chan, *Tetrahedron Lett.* **1983**, *24*, 1569.

[8] a) D. A. Evans, D. S. Johnson, *Org. Lett.* **1999**, *1*, 595; b) D. A. Evans, K. A. Scheidt, J. N. Johnston, M. C. Willis, *J. Am. Chem. Soc.* **2001**, *123*, 4480; see also: c) Y. Arai, T. Matsuda, Y. Masaki, *Chem. Lett.* **1997**, 145; d) Y. Arai, M. Kasai, K. Ueda, Y. Masaki, *Synthesis* **2003**, 1511, and references therein; e) B. L. Hodous, G. C. Fu, *J. Am. Chem. Soc.* **2002**, *124*, 10006.

[9] D. A. Evans, G. Borg, K. A. Scheidt, *Angew. Chem.* **2002**, *114*, 3320; *Angew. Chem. Int. Ed.* **2002**, *41*, 3188.

[10] Among the lanthanide metals screened (La, Pr, Nd, Sm, Gd, Er, and Yb), Sm showed the best reactivity and selectivity. The use of La, Pr, Nd, Gd, and Er complexes also afforded **2a** with >90% *ee* and in >80% yield. Yb was not suitable for this reaction with **1a**.

[11] Standard conditions for asymmetric epoxidations with lanthanide complexes: $Ln(OiPr)_3$/binol/$Ph_3As(O)$ 1:1:1 and $Ln(OiPr)_3$/binol/$Ph_3P(O)$ 1:1:3; see references [2], [5], and [6]. When an imidazolide or an amide was the substrate, a catalyst loading of 10 mol% was essential for the reaction to reach completion.

[12] For a review on the use of H_8-binol in asymmetric catalysis, see: T.-L. A.-Y. Terry, S.-S. Chan, A. S. C. Chan, *Adv. Synth. Catal.* **2003**, *345*, 537.

[13] With less reactive CMHP as the oxidant, the reaction of the corresponding 4-phenylcarboxylic acid imidazolide resulted in a low chemical yield (18 h, 47% yield with 10 mol% of the catalyst); see reference [5b].

[14] The preparation of α,β-unsaturated *N*-acyl pyrroles from the corresponding α,β-unsaturated amides was reported by Evans et al.; see reference [9] and references therein. The reaction of lithiated pyrrole with an acyl halide did not proceed cleanly, although the equivalent reaction of 2-substituted pyrroles has been described; see reference [8c].

[15] For the preparation and reactivity of 1,1′-carbonyldipyrrole, see reference [9]. For related reactions of *N*-acyl imidazoles with methylenetriphenylphosphorane to afford alkanoyl triphenylphosphoranes, see: M. Miyano, M. A. Stealey, *J. Org. Chem.* **1975**, *40*, 2840.

[16] Use of the system Et_2Zn/*o*-methoxyphenol/*t*BuOOH led to the epoxide in 76% yield in 18 h at 25°C with low selectivity (d.r. 54:46). Other conditions, such as H_2O_2–urea with a base, *m*CPBA, or aqueous NaClO with a phase-transfer catalyst either resulted in the decomposition of the enone or afforded the product in low yield (<20%).

[17] For reactions of the *N*-acyl pyrrole unit, see reference [9] and references therein.

 © 2003 Wiley-VCH Verlag GmbH & Co. KGaA, Weinheim

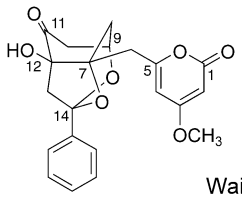
Total Synthesis of Polyketides

Total Synthesis of (+)-Wailupemycin B**

*Stefan Kirsch and Thorsten Bach**

Dedicated to Professor Reinhard W. Hoffmann on the occasion of his 70th birthday

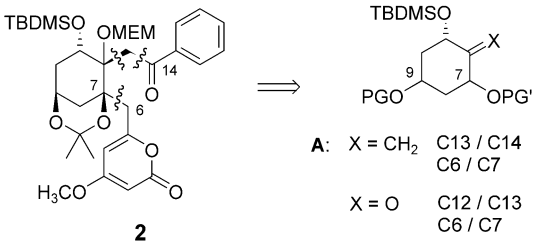
Wailupemycin B (**1**), an α-pyrone-containing metabolite, was isolated together with two structurally related compounds (wailupemycin A and C) by Davidson and co-workers from



Wailupemycin B (**1**)

Streptomyces maritimus. The organism was found at Wailupe Beach Park along the southeast coast of Oahu (Hawaii).[1] Because of the limited supply from natural sources, the antiinfective potential of the natural product has not been fully evaluated. Owing to its unique structural features, wailupemycin B was considered an attractive target for synthesis, not only because of its novel structure, but because a flexible de novo approach would allow a variation of the peripheral cyclic substituents. The natural product is a polyketide-derived cyclohexanone structure characterized by a high density of functional groups. Although the biosynthesis of the wailupemycins has been studied intensively, no total synthesis of any wailupemycin has, to our knowledge, been reported.[2] Herein, we describe the first total synthesis of (+)-wailupemycin B.

Wailupemycin B (**1**) is the cyclic acetal of a ketone (C14) and a *cis*-1,3-cyclohexanediol (C7, C9). Davidson and co-workers already mentioned its lability to acids.[1] We planned to postpone the oxidation at C11 to the final step of the synthesis. This strategy avoids chemoselectivity problems that could arise from a possible competitive oxidation at C9. We reckoned that the hydroxy group at C11 would have to adopt an axial position to allow smooth and selective acetal formation. Along this retrosynthetic analysis we considered cyclohexane **2** (Scheme 1; TBDMS = *tert*-butyldimethylsilyl, MEM = methoxyethoxymethyl) as a key intermediate that



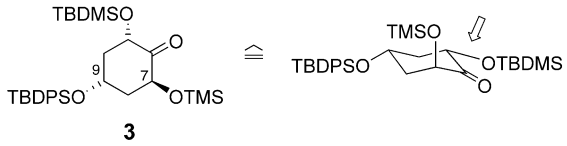
2

Scheme 1. Retrosynthetic disconnection of key intermediate **2**. PG, PG′ = protecting groups.

contains all stereogenic centers with the correct configuration. We further envisioned a flexible strategy for the introduction of the peripheral substituents which should establish the stereogenic centers with high stereoselectivity. Cyclohexanes of type **A**, derived from carvone,[3] could conveniently be used as key building blocks.

Powerful nucleophiles are required to create the C13–C14 bond by reaction with an epoxide derived from **A** (X = CH_2) or to form the C12–C13 bond by addition to a ketone **A** (X = O). To avoid the risk of competing attack at the α-pyrone (Scheme 1), the formation of the C6–C7 bond was postponed to a later stage of the synthesis. Another approach was based on the formation of the C4–C5 bond followed by cyclization and was a possible alternative for the introduction of the α-pyrone moiety.[4]

Preliminary studies also suggested that the presence of a dithiane-protected ketone at C14, which was obtained by opening of an epoxide ring, inhibits addition to C7 and C5 carbonyl groups. We consequently decided to establish the relevant bonds starting from ketone **A** (X = O) in the sequence C12–C13 and C6–C7. Further preliminary experiments indicated that the configuration at C7 and C9 has a significant effect on the facial diastereoselectivity of the C12–C13 bond formation. Bulky groups at C9 and C11 effectively lock the molecule into a chair conformation. Sufficiently large nucleophiles attack cyclohexanone derivatives **3** (TBDPS = *tert*-butyldiphenylsilyl, TMS = trimethylsilyl) in an equatorial



3

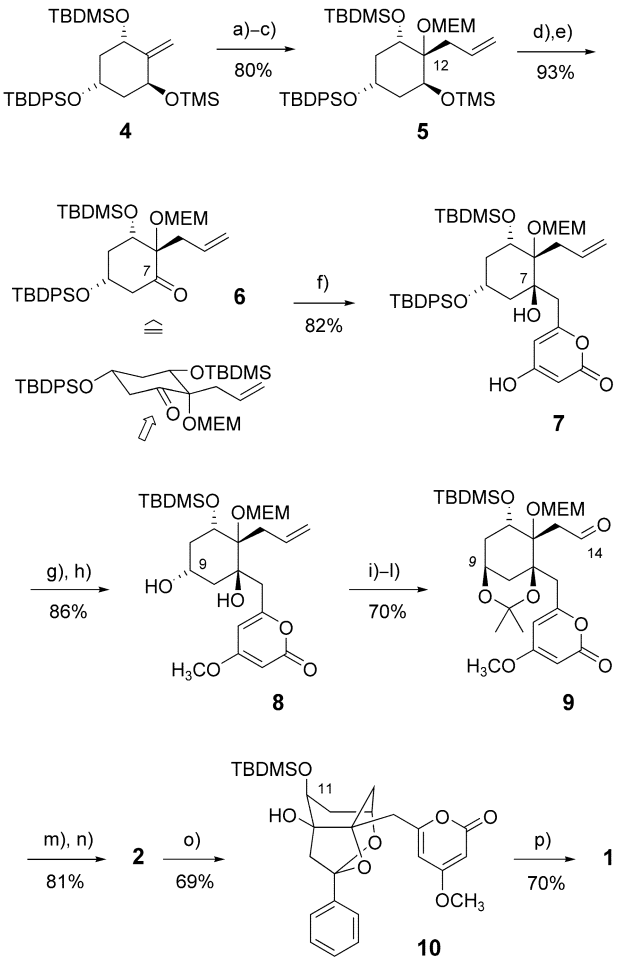
fashion, as represented schematically. Epimers of compound **3** with the desired absolute configuration at C9 either showed worse diastereoselectivities or did not react at all.

Advanced intermediate **4** (Scheme 2) was readily generated in 42% overall yield from commercially available (*S*)-(+)-carvone according to literature procedures.[5] Ozonolytic cleavage of the exocyclic C–C double bond and reductive workup resulted in the formation of the orthogonally protected ketone **3**, which was treated with allylmagnesium bromide (whose use is justified below). The reaction proceeded with good diastereoselectivity (d.r. = 90:10). Protection of the tertiary hydroxy group at C12 as a MEM ether

[*] Prof. Dr. T. Bach, Dipl.-Chem. S. Kirsch
Lehrstuhl für Organische Chemie I
Technische Universität München
Lichtenbergstrasse 4, 85 747 Garching (Germany)
Fax: (+49) 89-2891-3315
E-mail: thorsten.bach@ch.tum.de

[**] Financial support from Bayer AG (Wuppertal) is gratefully acknowledged. We thank Olaf Ackermann for excellent technical assistance.

 DOI: 10.1002/anie.200351455 © 2003 Wiley-VCH Verlag GmbH & Co. KGaA, Weinheim



Scheme 2. Total synthesis of (+)-wailupemycin B (**1**). Yields refer to isolated, purified, and fully characterized compounds. a) O_3, MeOH in CH_2Cl_2, −78 °C; then Me_2S, −78 °C→RT, quant.; b) CH_2CHCH_2MgBr (1.5 equiv) in THF, −20 °C, 1 h, quant. (d.r. = 90:10); c) MEMCl (2.0 equiv), Et*N*iPr_2 (3.0 equiv) in DCE, 70 °C, 4 h, 80% (d.r. = > 95:5); d) K_2CO_3 in MeOH (3% w/v), room temperature, 12 h, 95%; e) IBX (2.0 equiv) in DMSO, room temperature, 5 h, 98%; f) 4-hydroxy-6-methylpyran-2-one (2.5 equiv), *t*BuLi (5.3 equiv) in THF, −85 °C→0 °C; then **6** in THF, −85 °C, 2 d, 82%; g) dimethyl sulfate (2.0 equiv), K_2CO_3 (10.0 equiv) in acetone, room temperature, 6 h, 92% (d.r. = > 95:5); h) HF·py in THF, 0 °C→RT, 12 h, 94%; i) IBX (1.5 equiv) in DMSO, room temperature, 4 h, 96%; j) L-Selectride (1.0 equiv) in THF, −78 °C, 1 h, 97%; k) 2-methoxypropene (2.0 equiv), PPTS (cat.) in DCE, room temperature, 3 h, 90%; l) OsO_4 (0.2 equiv), $NaIO_4$ (2.4 equiv), NaOAc (24.0 equiv) in THF/H_2O (1:1 v/v), room temperature, 4 h, 83%; m) PhMgBr (1.5 equiv) in THF, −78 °C, 1 h, 89%; n) DMP (2.0 equiv), $NaHCO_3$ (14.0 equiv) in CH_2Cl_2, room temperature, 3 h, 91%; o) TFA/HOAc/H_2O/THF (1:2:2:4 v/v), room temperature; 1.5 h, 69%; p) 1) TBAF (1.0 equiv) in THF, 0 °C, 25 min; 2) IBX (5.0 equiv) in EtOAc, 77 °C, 4 h, 70%. Abbreviations not defined in text: DMSO = dimethyl sulfoxide, *t*BuLi = *tert*-butyllithium, L-Selectride = lithium tri(*sec*-butyl)borohydride, PPTS = pyridinium *p*-toluenesulfonate, TBAF = tetrabutylammonium fluoride.

proceeded smoothly only at elevated temperature in 1,2-dichloroethane (DCE) as the solvent.[6,7] Selective deprotection of the secondary TMS ether, followed by oxidation with 2-iodoxybenzoic acid (IBX)[8–10] yielded ketone **6**. Introduction of the pyrone fragment was achieved with the dianion[11] derived from 4-hydroxy-6-methylpyran-2-one. The addition of the dianion to the carbonyl group at C7 in **6** proceeded with very good facial diastereoselectivity. The preferential formation of the desired diastereoisomer can be understood by an equatorial approach of the dianion to a chairlike conformation of ketone **6** (Scheme 2). This result confirmed our retrosynthetic considerations concerning the configuration of intermediate **3** and the choice of protecting groups. Subsequent *O*-methylation of the resulting hydroxypyrone with dimethyl sulfate followed by selective cleavage of the TBDPS ether with HF·py (py = pyridine) furnished alcohol **8**. The high chemoselectivity of desilylation was to be expected as the TBDMS ether at C11 is highly shielded. In fact, removal of the TBDMS protecting group could only be effected after cleavage of the MEM group.

The inversion of the C9 stereogenic center was achieved by oxidation and subsequent reduction. As expected, the hydride reagent approached the conformationally locked substrate equatorially. This sequence was followed by simultaneous protection of the free hydroxy groups as an isopropylidene acetal and subsequent introduction of the phenyl group at C14. At first sight, the late introduction of the phenyl group is surprising, and a direct addition of 2-phenylpropenylmagnesium bromide to **3** in step b) (Scheme 2) might appear to be a more direct alternative. Our decision to introduce the allyl group instead was driven by the desire to gain flexibility for the installation of other substituents at C14 at the end of the synthesis. Furthermore, the bulky phenyl group retards or prevents simple reactions at the densely functionalized cyclohexanone framework. Lemieux–Johnson oxidation[12] gave the corresponding aldehyde **9**, which was then treated with phenylmagnesium bromide at low temperature to provide the two C14 epimers. Surprisingly, but in line with the above-mentioned reactivity associated with the sterically demanding phenyl group, exposure of a mixture of C14 epimers to several standard oxidation reactions either resulted in no reaction or gave rise to a series of uncharacterizable products. In this respect, we were delighted to find that key intermediate **2** was readily accessed upon treatment with Dess–Martin periodinane (DMP)[13] in the presence of sodium bicarbonate.[14] The following step involved removal of the MEM protecting group, hydrolytic cleavage of the acetonide ring, and conversion into the internal ketal **10**, an objective which was accomplished by exposing **2** to a mixture of TFA (trifluoroacetic acid), acetic acid, water, and THF (1:2:2:4). Finally, precursor **10** was converted into wailupemycin B (**1**) by initial deprotection of the secondary silyl ether followed by oxidation with IBX without isolation of the intermediate unstable axial alcohol. Based on spectroscopic data[16] the synthetic material was identical to natural wailupemycin B. The absolute configuration of wailupemycin B was proven by comparison of the optical rotations ($[\alpha]_D^{20} = +79.0$ ($c = 0.09$, MeOH), natural product[1]: $[\alpha]_D^{24} = +77.7$ ($c = 0.07$, MeOH)), which also confirmed the absolute configuration proposed by Davidson and co-workers.

In conclusion, we have described an expedient, stereocontrolled synthesis of wailupemycin B (16 steps, 14% overall yield from **4**). The stereogenic centers were formed with high facially diastereoselective control. Furthermore, our flexible

 © 2003 Wiley-VCH Verlag GmbH & Co. KGaA, Weinheim

approach should provide access to a variety of new analogues by incorporating different substituents at the periphery. Applications of the newly developed synthetic strategy and investigations into the biological activity of wailupemycin B and its derivatives are currently underway.

Received: March 24, 2003 [Z51455]

Keywords: antibiotics · asymmetric synthesis · ketones · polyketides · total synthesis

[1] N. Sitachitta, M. Gadepalli, B. S. Davidson, *Tetrahedron* **1996**, *52*, 8073 – 8080.

[2] a) B. S. Moore, C. Hertweck, *Nat. Prod. Rep.* **2002**, *19*, 70 – 99; b) L. Xiang, J. A. Kalaitzis, G. Nilsen, L. Chen, B. S. Moore, *Org. Lett.* **2002**, *4*, 957 – 960; c) J. Piel, C. Hertweck, P. R. Shipley, D. M. Hunt, M. S. Newman, B. S. Moore, *Chem. Biol.* **2000**, *7*, 943 – 955; d) C. Hertweck, B. S. Moore, *Tetrahedron* **2000**, *56*, 9115 – 9120; e) J. Piel, K. Hoang, B. S. Moore, *J. Am. Chem. Soc.* **2000**, *122*, 5415 – 5416.

[3] a) J. Wang, R. Busson, N. Blaton, J. Rozenski, P. Herdewijn, *J. Org. Chem.* **1998**, *63*, 3051 – 3058; b) S. Hatakeyama, H. Numata, K. Osanai, S. Takano, *J. Org. Chem.* **1989**, *54*, 3515 – 3517; c) K. A. Parker, A. Dermatakis, *J. Org. Chem.* **1997**, *62*, 6692 – 6696.

[4] T. Bach, S. Kirsch, *Synlett* **2001**, 1974 – 1976.

[5] Starting from (*S*)-(+)-carvone, we mostly followed the procedures given in reference [3b]. Reduction to the desired diastereoisomer was achieved with $NaBH_4/CeCl_3$ according to reference [3b], footnote 13.

[6] E. J. Corey, J.-L. Gras, P. Ulrich, *Tetrahedron Lett.* **1976**, 809 – 812.

[7] For examples of the use of 1,2-dichloroethane at elevated temperatures, see: a) H. Paulsen, B. Mielke, *Liebigs Ann. Chem.* **1990**, 169 – 180; b) D. A. Clark, F. De Riccardis, K. C. Nicolaou, *Tetrahedron* **1994**, *50*, 11391 – 11426; c) P. A. Procopiou, E. J. Bailey, C. Chan, G. G. A. Inglis, M. G. Lester, A. R. P. Srikantha, P. J. Sidebottom, N. S. Watson, *J. Chem. Soc. Perkin Trans. 1* **1995**, 1341 – 1348.

[8] For the synthesis of IBX, see: a) C. Hartmann, V. Meyer, *Ber. Dtsch. Chem. Ges.* **1893**, *26*, 1727 – 1732; b) M. Frigerio, M. Santagostino, S. Sputore, *J. Org. Chem.* **1999**, *64*, 4537 – 4538.

[9] a) M. Frigerio, M. Santagostino, *Tetrahedron Lett.* **1994**, *35*, 8019 – 8022; b) S. De Munari, M. Frigerio, M. Santagostino, *J. Org. Chem.* **1996**, *61*, 9272 – 9279; c) J. D. More, N. S. Finney, *Org. Lett.* **2002**, *4*, 3001 – 3003.

[10] For a review on IBX oxidations, see: T. Wirth, Angew. Chem. **2001**, *113*, 2893 – 2895; *Angew. Chem. Int. Ed.* **2001**, *40*, 2812 – 2814.

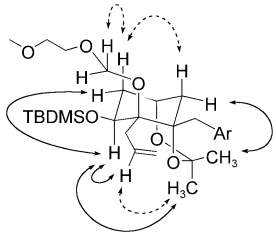
[11] a) M. P. Wachter, T. M. Harris, *Tetrahedron* **1970**, *26*, 1685 – 1694; b) G. A. Poulton, T. D. Cyr, *Can. J. Chem.* **1982**, *60*, 2821 – 2829; c) W. C. Groutas, M. A. Stanga, M. J. Brubaker, T. L. Huang, M. K. Moi, R. T. Carroll, *J. Med. Chem.* **1985**, *28*, 1106 – 1109.

[12] a) R. Pappo, D. S. Allen, R. U. Lemieux, W. S. Johnson, *J. Org. Chem.* **1956**, *21*, 478 – 479; b) C.-Y. Chen, D. J. Hart, *J. Org. Chem.* **1993**, *58*, 3840 – 3849; c) P. Wipf, Y. Kim, D. M. Goldstein, *J. Am. Chem. Soc.* **1995**, *117*, 11106 – 11112.

[13] a) D. B. Dess, J. C. Martin, *J. Org. Chem.* **1983**, *48*, 4155 – 4156; b) D. B. Dess, J. C. Martin, *J. Am. Chem. Soc.* **1991**, *113*, 7277 – 7287; c) R. K. Boeckman, Jr., P. Shao, J. J. Mullins, *Org. Synth.* **1999**, *77*, 141 – 149.

[14] For examples of Dess–Martin oxidations in the presence of sodium bicarbonate, see: a) T. I. Richardson, S. D. Rychnovsky, *Tetrahedron* **1999**, *55*, 8977 – 8996; b) K. C. Nicolaou, J. Jung, W. H. Yoon, K. C. Fong, H.-S. Choi, Y. He, Y.-L. Zhong, P. S. Baran, *J. Am. Chem. Soc.* **2002**, *124*, 2183 – 2189.

[15] The relative configurations and conformations of various intermediates were been determined throughout the synthesis by NOESY experiments. The rigid precursor to compound **2**, which already contains all stereogenic centers of the natural product, offered a chance to check the relative configuration. The most important NOE data (----- = medium, —— = strong) are given in the illustration (Ar = 4-methoxy-6-oxopyran-2-yl).



[16] Spectroscopic data for **1**: ^{1}H NMR (600 MHz, $CDCl_3$, 25 °C): δ = 1.62 (d, ^2J = 13.3 Hz, 1H; $H_{8a}H_b$), 2.41 (ddd, ^2J = 13.3 Hz, ^3J = 5.0 Hz, ^4J = 2.6 Hz, 1H; H_aH_{8b}), 2.55 (d, ^2J = 13.6 Hz, 1H; $H_{13a}H_b$), 2.74 (dd, ^2J = 18.7 Hz, ^3J = 5.3 Hz, 1H; $H_{10a}H_b$), 2.76 (d, ^2J = 13.6 Hz, 1H; H_aH_{13b}), 2.85 (d, ^2J = 14.9 Hz, 1H; H_6H_b), 3.03 (d, ^2J = 14.9 Hz, 1H; H_aH_{6b}), 3.14 (br d, ^2J = 18.7 Hz, 1H; H_aH_{10b}), 3.80 (s, 3H; OCH_3), 4.01 (br s, 1H; OH), 4.76 (virt. t, ^3J = 5.0 Hz, 1H; H_9), 5.43 (d, ^4J = 2.0 Hz, 1H; H_2), 6.02 (d, ^4J = 2.0 Hz, 1H; H_4), 7.36–7.41 (m, 3H; CH_{ar}), 7.59 ppm (d, ^3J = 7.0 Hz, 2H; CH_{ar}); ^{13}C NMR (90 MHz, $CDCl_3$, 25 °C): δ = 36.1, 38.7, 43.7, 54.7, 55.8, 69.0, 85.0, 85.4, 88.2, 103.2, 105.9, 125.0, 128.3, 128.9, 138.5, 160.5, 164.3, 171.0, 208.9 ppm; MS (EI, 70 eV): *m*/*z* (%): 384 (18) [M^+], 356 (48), 209 (51), 140 (100), 125 (50), 105 (92), 77 (33).

 © 2003 Wiley-VCH Verlag GmbH & Co. KGaA, Weinheim

Highly Functionalized Polycations

Poly(methylene amine): A Polymer with the Maximum Possible Number of Amino Groups on a Polymer Backbone**

Markus Klapper, Corneliu Hamciuc, Rainer Dyllick-Brenzinger,* and Klaus Müllen**

One of the most demanding challenges in research is exploring the theoretical limits of properties. A good example of these limitations comes from polymers containing many amino functions on the polymer backbone. These polymers have become increasingly important in industrial applications, which make use of their ability to form stable amino–

[*] Dr. M. Klapper, Prof. Dr. K. Müllen, Dr. C. Hamciuc
Max Planck Institut für Polymerforschung
Ackermannweg 10, 55128 Mainz (Germany)
Fax: (+49) 6131-379-100
E-mail: klapper@mpip-mainz.mpg.de
muellen@mpip-mainz.mpg.de
Dr. R. Dyllick-Brenzinger
BASF Aktiengesellschaft
67056 Ludwigshafen (Germany)
Fax: (+49) 621-60-40855
E-mail: rainer.dyllick-brenzinger@basf-ag.de

[**] Financial support from the BASF AG, Ludwigshafen is gratefully acknowledged.

 DOI: 10.1002/anie.200351500 © 2003 Wiley-VCH Verlag GmbH & Co. KGaA, Weinheim

metal complexes[1] or to form aggregates by interaction of amino groups with surfaces, for example, in waste-water management.[2] Other applications include their use as flocculants in the paper industry.[3] However, existing amino polymers, such as poly(ethylene imine) synthesized by cationic ring-opening polymerization[4] or poly(vinyl amine) prepared from vinylformamide[5] have just one amino group per two carbon atoms. Although low-molecular-mass compounds which are functionalized on each carbon atom are known from nature (carbohydrates), or from some examples in organic chemistry (for example, 1,2,3,4,5-penta-*n*-aminopentane),[6] to date an increased incorporation of "active" amino groups in polymers to improve the efficiency of additives for applications mentioned above has not been achieved.

Herein we present the first synthesis of poly(methylene amine) (**1**), a new amino-functionalized polymer containing one amino group per carbon atom. This polymer has the highest content of functionality possible and allows, after protonation, for the generation of a cationic polymer with the highest charge density known on a polymer to date.

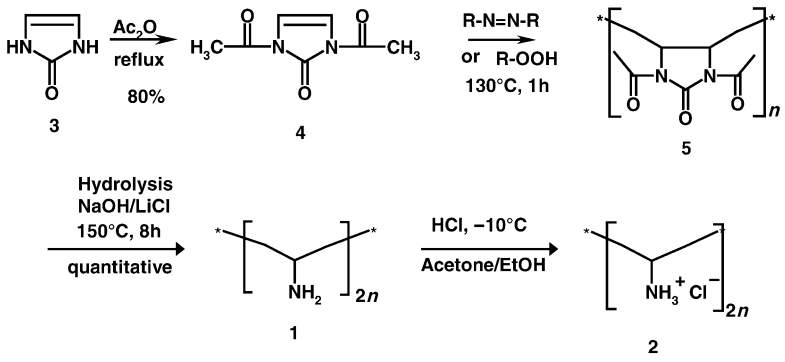
Clearly, **1** cannot be obtained by a direct polymerization of, for example, 1,2-diaminoethylene as a tautomerization of the monomer will lead to the formation of a nonpolymerizable azomethine structure. As in the synthesis of poly(vinyl amine)[5] where *N*-vinylformamide is used as the monomer the amino groups must be protected. We initially tried to polymerize *N*,*N*′-diacetyl-1,2-diaminoethylene[7] but this monomer was not polymerizable. This lack of reactivity might be due to steric reasons as the protecting acetyl groups are shielding the polymerizable double bond. Therefore, we investigated the polymerization of cyclic monomers based on imidazoline-2-one. First experiments using 1,3-2*H*-4-imidazoline-2-one (**3**)[8] (Scheme 1) were performed in solvents such as DMF or NMP (methylpyrrolidone). However, only small amounts of oligomers were obtained. Polymerizations in bulk were also unsuccessful owing to partial decomposition of the monomer at the elevated temperature required to obtain a melt (m.p. of **3**: 242 °C). One possible explanation for the low reactivity of **3** towards radical polymerization is the generation of a stable 2-hydroxyimidazol radical which shows no tendency to polymerize owing to its "aromatic" character.[9]

Instead, we investigated 1,3-diacetyl-4-imidazolin-2-one (**4**) as another symmetrical monomer which can be prepared from **3** by acetylation.[8] The acetyl groups not only protect the amino groups, but they also lower the melting point allowing bulk polymerization at reasonable temperatures. Furthermore, the ring structure of the monomer limits the rotation of the acetyl groups in comparison to the "open" *N*,*N*′-diacetyl-1,2-aminoethylene mentioned above, which minimizes their shielding effect.

The resulting monomer **4** can be homopolymerized by radical polymerization using azo initiators or peroxides (Scheme 1). However, it was found that reasonable number-molecular-weight averages (M_n) and weight-molecular-weight averages (M_w) of **5** (poly(1,3-diacetyl-1,3-dihydro-2*H*-imidazol-2-one) are only obtained by bulk polymerization. With increasing amounts of solvents M_n rapidly decreases (Table 1, entries 3–5). This effect could be due to precipitation of the product at an early stage of the polymerization or be due to radical transfer reactions to the solvents (DMF or NMP). As the melting temperature of **4** is still rather high the polymerization in bulk has to be performed at around 130 °C. We found that the highest molecular masses of **5** ($M_n = 104\,000$, Table 1, entry 2) can be obtained with the relatively slowly decomposing initiator 1,1′-azo-bis-(1-cyanocyclohexane).[10]

The most challenging step in the synthesis of **1** is the hydrolysis of the cyclic urea units (Scheme 1). We investigated several reaction conditions with different solvents, bases, and acids and concluded that the best results are obtained under basic conditions using ethylene glycol as solvent and NaOH as base. LiCl was added to improve the solubility of the polymer. Although, the acetyl groups can easily be hydrolyzed, cleavage of the cyclic urea requires harsh conditions (see the Experimental Section).

In the ^{1}H NMR spectrum of **1** a broad singlet at $\delta = 2.85$ ppm clearly indicates the presence of only the backbone CH protons. The NH_2 protons are not detected because of proton exchange with D_2O solvent. The IR spectrum of **1** shows the complete disappearance of the carbonyl



Scheme 1. Synthesis of poly(methylene amine) (**1**).

Table 1: Polymerization of **4** to **5** with 1,1′-azobis-(1-cyancyclohexane) (ACC) as initiator.

Entry	ACC [mg]	ACC:**4**	*T* [°C]	Solvent	M_n [g mol^{-1}][a]	M_w [g mol^{-1}][a]	Time [h]	Yield [%]
1	2.46	1:500	130	in bulk	29 800	94 100	1	91
2	0.73	1:2000	130	in bulk	104 000	263 000	1	93
3	1.46	1:1000	125	0.1 mL DMF	66 000	172 000	1	90
4	1.46	1:1000	125	0.7 mL DMF	13 000	34 500	1	85
5	1.46	1:1000	125	4 mL DMF	3200	4000	10	65

[a] Determined by GPC in THF, polystyrene standard.

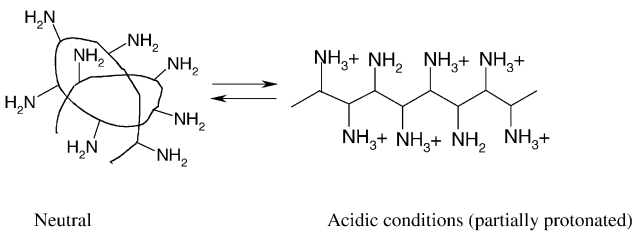
 © 2003 Wiley-VCH Verlag GmbH & Co. KGaA, Weinheim

groups, but the signals arising from the C–N bonds (1595 cm^{-1}) and the NH_2 groups (3420 cm^{-1}) are clearly visible.

We were unable to determine the M_n of **1** by gel permeation chromatography (GPC) because of the strong interaction of the polar polymer with the GPC columns. However, as there is no evidence of any degradation during the hydrolysis process, we can calculate the M_n for **1** from that of the starting material **5**. After cleavage of the protecting groups the mass is reduced to 34%, which means a precursor polymer of $M_n = 104\,000$ will result in a poly(methylene amine) of $M_n \approx 35\,000$.

To study the basicity of the polymer we titrated a solution of 15 mg of **1** in 10 mL of H_2O with aqueous hydrochloric acid (0.1N) (Potentiograph E536, Electrode Metrohm 6.0203.100). Remarkably up to pH 1, we did not observe a quantitative protonation and the titration curve was very flat. The degree of protonation at pH 1 can be estimated as 70%. This result is in agreement with that for 1,2,3,4,5-penta-*n*-aminopentane, where 80% protonation at pH 1 was observed.[11] This behavior can be explained by the increasing charge density on the polymeric backbone. Quantum mechanical calculations on fragments of poly(methylene amine) show that total protonation of all primary amino groups is unlikely in aqueous systems.[12] The protonation can be monitored by ^{1}H NMR spectroscopy (in D_2O) where the resonance of the CH proton shifts continuously from 2.85 ppm (pH 12) to 3.84 ppm (pH 1.5) during the addition of 1N HCl in D_2O.

As GPC measurements failed we investigated **1** by viscosimetry in H_2O. The inherent viscosity (η_{inh}) of a solution of neutral **1** (10 g L^{-1} in H_2O, 20°C; $M_n = 10\,100$, obtained by hydrolysis of a polymer with $M_n = 29\,800$, Table 1, entry 1) was determined to $\eta_{inh} = 0.182$ g L^{-1}. In contrast, the inherent viscosity of a 10 g L^{-1} solution of the corresponding "charged" poly(methylene amine hydrochloride) (**2**) in H_2O was found to have $\eta_{inh} = 0.45$ g L^{-1}. This change of the inherent viscosity corresponds to a strong polyelectrolyte effect, typical for polycations or polyanions.[13] For the neutral polymer the low viscosity indicates a random-coil structure. With increasing charge density, there is an increasing repulsion of the charges along the polymer-chain backbone. This effect causes the polymer-chain conformation to become more and more extended changing from a random-coil structure to a stretched and linear conformation (see Scheme 2), which results in the increased viscosity of the solution. However, this change in the chain conformation can be reversed by adding salts to a solution of such a polyelectrolyte, as a result the charges are shielded from each other by the added ions. When the NaCl concentration is increased from 0 to 1 mol L^{-1} the viscosity decreases as a result of the shielding effect from $\eta_{inh} = 0.45$ g L^{-1} to 0.11 g L^{-1}.



Scheme 2. Schematic representation of the changes caused by the polyelectrolyte effect on the conformation of **1**.

We have achieved the first synthesis of poly(methylene amine) (**1**), a new type of amino functionalized polymer containing a primary amino group on each carbon atom of the backbone. This system is highly basic, can be protonated to a high degree and therefore, this structure may be considered as the highest charged polymer known. Polymer **1** marks a borderline in terms of the amount of functionalization and, in its protonated form, in charge density. From studying this polymer one can expect to gain fundamental insights into the behavior of charged synthetic as well as natural polymers. We are presently investigating the polyelectrolyte effect in solution by scattering methods and viscosity measurements. Owing to the high concentration of amino groups, complex formation with metal ions or the interaction with surfaces, essential for the applications mentioned above, should be improved in comparison to the commercial polyamines.[2,3] Furthermore, this polymer can be of interest as fuel-cell membrane material as it should show a very high proton conductivity. Finally, poly(methylene amine) should undergo transformations of the amino groups, such as alkylations, acylations, or cyclizations, which would result in a broad variety of new polymers.

Experimental Section

5: 1,3-Diacetyl-4-imidazoline-2-one (**4**; 1 g)) and the initiator 1,1′-azo-1-bis(cyclohexanecarbonitrile) (1.46 mg), and the corresponding amount of DMF (Table 1) were mixed under argon (flushing the flask with argon for 15 min.). The mixture was kept at 130°C for 1 h. The polymerization was fast and exothermic. The resulting polymer was dissolved in DMF and precipitated in methanol. The solid was filtered and dried. (Yield in Table 1 and molecular weights see Table 1): ^{1}H NMR (300 MHz, [D$_6$]DMSO): $\delta = 2.5$ (s, 6H, CH_3); 4.1 ppm (m, 2H, CH-CH); M_n determined by GPC (in THF, using polystyrene as standard).

2: Hydrolysis of **5**: A mixture of poly(1,3-diacetyl-1,3-dihydro-2*H*-imidazoline-2-one) (**5**; 2.5 g), lithium chloride (0.6 g), ethylene glycol (7 mL), water (4 mL), and NaOH (6 g) was heated under vigorous reflux at 150–155°C for 8 h. After cooling and dilution with water (20 mL), the resulting polymer was soluble in water and was precipitated as the chlorohydrate. For this step the basic aqueous solution was acidified with concentrated HCl (37%) to obtain a 6N HCl solution. This mixture was cooled to −10°C and acetone (100 mL) was added. The chlorohydrate of **1** precipitated (10 g), was collected by filtration, and washed with acetone and dried. This precipitate was placed in a flask with NaOH (1 g) and ethanol (100 mL) and stirred for 10 h. HCl was added to obtain a pH value of approximately 7 and the solution was filtered. The ethanolic filtrate was evaporated until the volume was around 50 mL and to this a solution of HCl (37%, 50 mL) was added. A precipitate formed which was collected by filtration, washed with acetone, and dried to yield pure **2** as the hydrochloride. ^{1}H NMR (250 MHz, D_2O, pH 2.5): $\delta =$ 3.84 ppm (s, 1H, CH); ^{13}C NMR (D_2O, 125 MHz, 1,4 dioxane as standard): $\delta = 56.0$ ppm (CH, broad).

1 from **2**: **2** (1 g) was dissolved in water (25 mL) and filtered through an ion exchange column (Amberlite IRA 400 (Cl) Aldrich). Polymer **1** is isolated from the filtrate by freeze-drying. Residual traces of water were removed under high vacuum. ^{1}H NMR (250 MHz, D_2O, pH 10.2): $\delta = 2.85$ ppm (s, 1H, CH) (pH 10.2);

 © 2003 Wiley-VCH Verlag GmbH & Co. KGaA, Weinheim

^{13}C NMR (D_2O, 125 MHz, 1,4-dioxane as standard, pH 10.2): $\delta =$ 51.3 ppm (CH, broad).

Received: March 27, 2003
Revised: July 6, 2003 [Z51500]

Keywords: polyamines · polyelectrolyte effect · polymerization · protonation

[1] B. L. Rivas, G. V. Seguel, K. E. Geckeler, *Angew. Makromol. Chem.* **1997**, *251, 97*.
[2] a) "Flocculants": H. Burkert, J. Hartmann in *Ullmanns Encyclopedia of Industrial Chemistry, Vol. 14*, Wiley-VCH, Weinheim, **2003**, pp. 201 – 212; b) "Polyethyleneimine—Physical Properties and Applications:" D. Horn in *Polymeric Amines and Ammonium Salts* (Ed.: E. J. Goethals), Pergamon, New York, **1980**, p. 330; c) I. Voigt, F. Simon, H. Komber, H.-J. Jacobasch, S. Spange, *J. Coll. Polym. Sci.* **2000**, *278*, 48; d) I. Voigt, F. Simon, K. Estel, S. Spange, *Langmuir* **2001**, *17*, 3080.
[3] F. Linhart, *Grundlagen der Chemie für Papieringenieure*, Papiertechnische Stiftung, München, **1990**.
[4] T. Saegusa, Y. Chujo, *Makromol. Chem. Macromol. Symp.* **1990**, *33*, 31.
[5] a) R. B. Pinschmidt, Jr., W. L. Renz, W. E. Carroll, K. Yacoub, J. Drescher, A. F. Nordquist, N. Chen, *J. Macromol. Sci. Pure Appl. Chem.* **1997**, *34*, 1885; b) S. Spange, A. Madl, U. Eismann, J. Utecht, *Makromol. Chem. Rapid Commun.* **1997**, *18*, 1075; c) A. Madl, S. Spange, *Macromol. Symp.* **2000**, *161*, 149.
[6] G. J. Reiss, A. Zimmer, K. Hegetschweiler, *Acta Crystallogr. Sect. C* **2000**, *56*, 284.
[7] P. Ruggli, R. Ratti, E. Henzi, *Helv. Chim. Acta* **1929**, *12*, 332; C. Grundmann, H. Ulrich, *J. Org. Chem.* **1959**, *24*, 271.
[8] a) R. Duschinsky, L. A. Dolan, *J. Am. Chem. Soc.* **1946**, *68*, 2350; b) D. R. Haines, N. J. Leonard, D. F. Wiemer, *J. Org. Chem.* **1982**, *47*, 474.
[9] A. Samuni, P. Neta, *J. Phys. Chem.* **1973**, *77*, 1629.
[10] *Polymer Handbook*, 4th ed., (Eds.: J. Brandrup, E. H. Immergut, E. A. Grulle), Wiley, New York, **1999**, p. II/87.
[11] A. Zimmer, Ph.D. thesis, Saarbrücken, **2000**, p. 143.
[12] A. Schäfer, BASF AG personal communication. Quantum mechanical calculations for 1,2,3,4,5,6-hexaamino-*n*-hexane using the density functional theory (DFT) were performed. Molecular structures were optimized by applying the functional B-P86 (J. P. Perdew, *Phys. Rev. B* **1986**, *33*, 8822) and a split valence basis (A. Schäfer, H. Horn, R. Ahlrichs, *J. Chem. Phys.* **1992**, *97*, 2571) with polarization functions on C and N atoms. The calculations were performed with the software program TURBOMOLE (M. von Arnim, R. Ahlrichs, *J. Comput. Chem.* **1998**, *19*, 1746) using an RI-J approximation. (K. Eichkorn, O. Treutler, H. Öhm, M. Häser, R. Ahlrichs, *Chem. Phys. Lett.* **1995**, *242*, 652). It could be shown that definite conformations with typical hydrogen-bonding patterns are favored.
[13] M. Antonietti, S. Förster, M. Zisenis, J. Conrad, *Macromolecules* **1995**, *28*, 2270.

 © 2003 Wiley-VCH Verlag GmbH & Co. KGaA, Weinheim

Generation of the CF_3OOO Radical

The Trifluoromethyltrioxy Radical, CF_3OOO**

Stefan von Ahsen, Helge Willner,* and Joseph S. Francisco**

Oxygen-containing radicals play an important role in atmospheric and synthetic chemistry.[1] While the chemistry of oxy radicals RO and peroxy radicals ROO (R = H, F, CH_3, CF_3) is well studied,[1–5] that of the trioxy radicals ROOO is less well known. The HOOO trioxy radical was identified first in the gas phase[6] and then by matrix isolation.[7] More recently, the radical FOOO was generated in an argon matrix containing F atoms trapped with ozone.[8] The experimental isolation and characterization of ROOO radicals with organic substituents (CH_3) and fluorinated substituents (CF_3) have not been reported. However, the existence of CF_3OOO in atmospheric oxidation processes and in the formation of higher oxides has been discussed in mechanistic studies.[9,10] UV measurements on $FS(O)_2O_x$ species show absorptions of a previously unrecognized species proposed to be the $FS(O)_2OOO$ radical.[11] However, a definitive characterization was not provided. Furthermore, the CF_3OOO trioxy radical has been suggested as an intermediate in an important ozone-depletion reaction in which CF_3 reacts with O_3, but the proposed intermediate was not characterized.[12–14] In the 1960s trioxy radicals were invoked to explain patterns in the ESR spectra of solutions of CF_3O[15] and $(CH_3)_3CO$ radicals in liquid oxygen at −196 °C.[16]

In this communication we describe the nearly quantitative formation of CF_3OOO and its isolation in an oxygen matrix at low temperatures. Fundamental vibrational frequencies of the CF_3OOO radical have been observed and assigned with the aid of quantum-chemical calculations. In addition, the UV spectrum of this species is reported.

Either $CF_3OC(O)OOCF_3$ or $CF_3OC(O)OOC(O)OCF_3$[17] were flash thermolyzed in an excess of gaseous oxygen, and the reaction mixture was subsequently quenched as a matrix at low temperatures. The IR spectra of the matrix-isolated reaction products show no bands of the precursors, and new

[*] Dr. S. von Ahsen, Prof. Dr. H. Willner
Fakultät für Naturwissenschaften, Anorganische Chemie
Universität Duisburg-Essen
Lotharstrasse 1, 47048 Duisburg (Germany)
Fax: (+49) 203-379-2231
E-mail: von.ahsen@uni-duisburg.de
willner@uni-duisburg.de

Prof. Dr. J. S. Francisco
Department of Chemistry, Earth and Atmospheric Sciences
Purdue University, 1393 H. C. Brown Building
West Lafayette 47907 IN (USA)
Fax: (+1)-765-494-0239
E-mail: francisc@purdue.edu

[**] This work was supported by the Deutsche Forschungsgemeinschaft and the Fonds der Chemischen Industrie. J.S.F. expresses his thanks to the Alexander von Humboldt Foundation for a research award for senior U.S. scientists.

 © 2003 Wiley-VCH Verlag GmbH & Co. KGaA, Weinheim DOI: 10.1002/anie.200351909

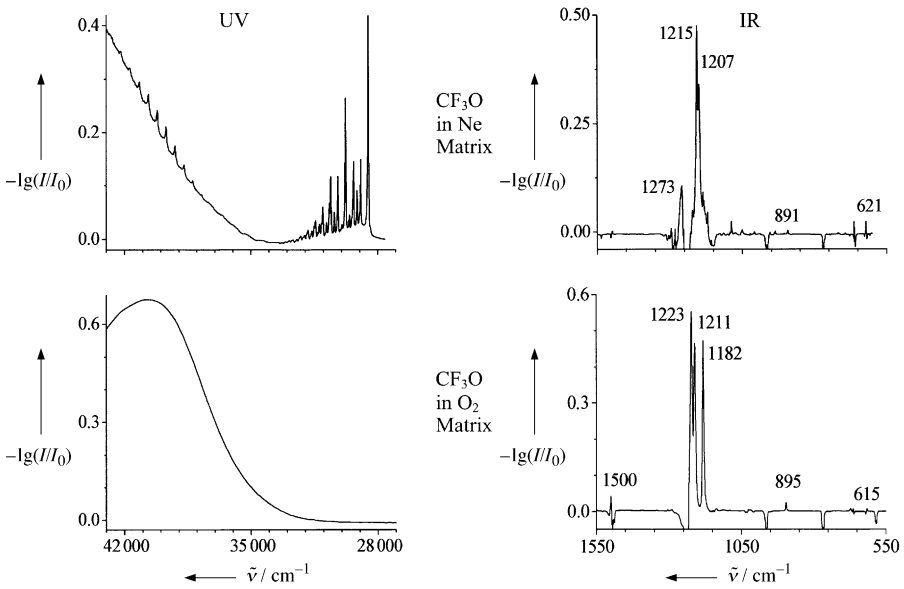


Figure 1. UV (left) and IR (right) spectra of CF_3O isolated in Ne matrix (top)[18] and in O_2 matrix (bottom, this work). The IR spectra were obtained from the difference in the IR spectra before and after UV photolysis. Negative bands indicate photolysis products.

absorptions appear. Figure 1 depicts the IR and UV spectra of the thermolysis products of $CF_3OC(O)OOC(O)OCF_3$ or $CF_3OC(O)OOCF_3$ isolated in an oxygen matrix along with the spectra from the analogous reaction with an excess of neon. There are significant differences in both the IR and UV spectra. The vacuum flash pyrolysis in neon yields the CF_3O radical,[17] whereas the analogous reaction in oxygen leads to a new compound with distinct absorption features that are attributed to the CF_3OOO trioxy radical. Its formation is described by Equations (1) and (2).

$$CF_3OC(O)OOCF_3 \rightarrow 2\,CF_3O + CO_2 \quad (1)$$

$$CF_3O + O_2(+M) \rightarrow CF_3OOO(+M) \quad (2)$$

Equation (1) is confirmed by literature data as occurring in the a flash thermolysis in an excess of neon; no further reaction occurs and CF_3O was characterized spectroscopically.[18] To confirm the formation of the trioxy radical according Equation (2), the matrix containing the new species was irradiated with UV light from a mercury high-pressure lamp. Upon irradiation, all bands of the new species disappear, while absorptions of COF_2 and FOO appear. Moreover, the correlation of growing bands of COF_2 and FOO with the disappearance of the new species suggests that the former arise directly from the latter [Eq. (3)]. Therefore

$$CF_3OOO + h\nu \rightarrow COF_2 + FOO \quad (3)$$

the new species must contain one carbon atom, three oxygen atoms, and three fluorine atoms, which is consistent with the CF_3OOO trioxy radical.

The UV spectrum of CF_3OOO shows no fine structure and therefore differs from that of CF_3O, which shows a vibrational structure in its UV band system (Figure 1). This indicates, together with the results of the photolysis experiments, that the excited state of the trioxy radical is dissociative. A characteristic feature of CF_3OOO is the appearance of an IR absorption band at 1500 cm^{-1} assigned to the OO stretching mode of the terminal O_2 moiety. It appears in the same spectral region as the absorption of matrix-isolated O_2 (1548 cm^{-1}, IR-active in matrix). The red shift of 48 cm^{-1} indicates the formation of a species having a strong terminal O–O bond. This is further support for the given connectivity of the CF_3OOO radical; the strong bond within the terminal O_2 unit and a weaker CF_3O–O_2 bond is in agreement with a complex between CF_3O and O_2.

Results from quantum-chemical calculations predict the structure of the trioxy radical shown in Figure 2. The use of either density functional (B3LYP6-311G(d,p))[19] or coupled cluster (QCISD/6-31G(d))[20] methods yield the trioxy radical as a complex between CF_3O and O_2.[21] The central O–O_2 bond is quite long (2.184 Å with B3LYP and

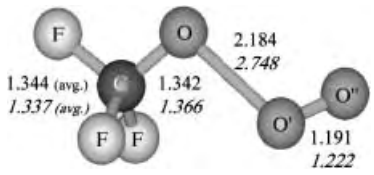


Figure 2. Calculated structure of CF_3OOO (distances in Å). The first value is from B3LYP6-311G(d,p) calculations, the second (in italics) is from QCISD/6-31G(d) calculations.

2.748 Å with QCISD), which indicates a weak bond binding the CF_3OOO radical together. The bonding energies (ΔH_{Diss} under standard conditions) with respect to dissociation into CF_3O and ground-state O_2 are 10.2 kJ mol^{-1} (B3LYP) and 7.5 kJ mol^{-1} (QCISD). The calculations are consistent with the spectra of a weakly bound species; the stretching vibration of this central bond is predicted and found in the far-IR region. The calculations aid the assignment of other features in the IR spectra of the CF_3OOO radical. This includes C–O and C–F stretches and one CF_3 umbrella motion. The OO stretch in the terminal O_2 moiety is calculated by DFT calculations to be at 1644 cm^{-1} (B3LYP; for O_2 $\tilde{\nu}_{OO}$ = 1641 cm^{-1}), while the QCSID method predicts this mode at 1521 cm^{-1}, which is closer to the experimental value of 1500 cm^{-1} observed for the CF_3OOO trioxy radical. Moreover, the IR spectrum of CF_3OOO indicates the lowering of the CF_3O symmetry in the free radical CF_3O from C_s close to C_{3v}[18] (due to the Jahn–Teller effect) to C_1 as proposed by quantum-chemical calculations.

 © 2003 Wiley-VCH Verlag GmbH & Co. KGaA, Weinheim

We performed an additional experiment with $^{18}O_2$ as the matrix material to get more insight into the bonding in the CF_3OOO trioxy radical. The results are gathered in Table 1 together with the assignment of the vibrations of the natural CF_3OOO. From the isotopic shifts when going from $CF_3{}^{16}O^{16}O^{16}O$ to $CF_3{}^{16}O^{18}O^{18}O$, the degree of coupling between the CF_3O and O_2 units becomes visible. Small but significant red-shifts are evident for all observed vibrations, which is in variance with the calculated data, where only a few fundamentals are expected to show an isotopic shift. These data suggest that the calculations underestimate the strength of the central O–O_2 bond.

The trioxy radical can exist in a doublet state, CF_3-$O^{\downarrow}$-$^{\uparrow}$O-$O^{\uparrow}$, or a quartet state, CF_3-$O^{\uparrow}$···$^{\uparrow}$O-$O^{\uparrow}$. Plots of the potential vs. the R(O–O_2) distance were calculated for CF_3OOO in the doublet and quartet states (Figure 3). While the doublet state shows a minimum stabilized by 14.8 kJ mol^{-1} ($E_{\mathrm{UB+HF-LYP}}$, no zero-point corrections included), the quartet state, which can be seen as a van der Waals complex of CF_3O with molecular oxygen in its triplet state, has a very flat potential with a maximum stabilization of 1.9 kJ mol^{-1}. The B3LYP O–O_2 distances at the minima are 2.184 Å for doublet-CF_3OOO (as mentioned above) and 3.130 Å for quartet-CF_3OOO. The calculations predict that intercrossing points exist at O–O_2 distances around 4 Å, as also seen in Figure 3. This intercrossing allows a reorganization of the electron spin, yielding the doublet state when an O_2 molecule comes into contact with a trifluoromethoxy radical.

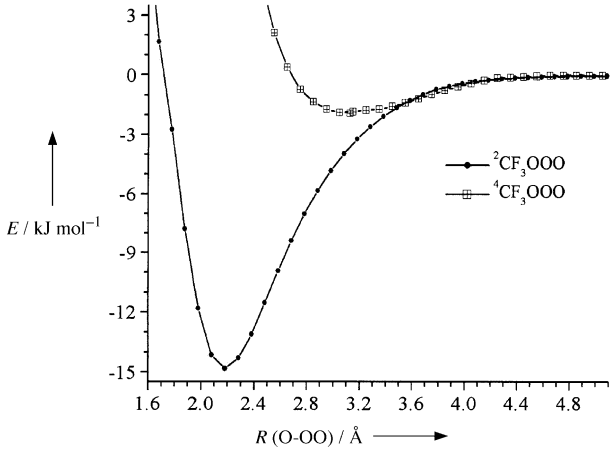


Figure 3. Calculated B3LYP6-311G(d,p) energies for doublet-CF_3OOO and quartet-CF_3OOO versus the O–O_2 distance.

The CF_3OOO trioxy radical has not been included in any atmospheric models of CF_3O_x chemistry. Nevertheless, it could be relevant in the atmospheric chemistry of CF_3O radicals. For example, a reaction of CF_3O radicals with CO yielding CF_3OCO in the gas phase requires a third body to carry off the reaction excess energy and is therefore statistically not favored. However, the reaction of the CF_3OOO trioxy radical with CO in a two-body reaction via Equation (4) could be a more favored reaction.

$$CF_3OOO + CO \rightarrow CF_3OCO + O_2 \qquad (4)$$

Note that these reactions describe a chaperon mechanism, the impact of which increases with the stabilization energy of the "complex" CF_3OOO. Besides this stabilization energy, the electron-spin distribution implies high spin density[22] not only on the terminal oxygen, but on all O atoms, thus providing more than one reactive center. Hence, any reaction of CF_3OOO with other atmospheric species at the carbon-bound oxygen atom yields the same products as those from reactions of free CF_3O. It is possible that the presence of O_2 may enhance the reactivity of CF_3O radicals by opening reaction pathways via the CF_3OOO radical.

If one considers these results in a more general discussion on ROOO species, our findings on CF_3OOO substantiates claims of a ClOOO radical in atmospheric chemistry. There has been a gap in our understanding of the underlying chemistry to explain the effect that O_2 has on suppressing chlorine-photosensitized ozone loss.[23] Prasad suggested that

Table 1: Experimental and calculated fundamental vibrations of CF_3OOO.

$CF_3{}^{16}O^{16}O^{16}O$					$CF_3{}^{16}O^{18}O^{18}O$		
O_2 matrix		B3LYP6-311G(d,p)			Mode, description	$^{18}O_2$ matrix	B3LYP6-311G(d,p)
$\tilde{\nu}$ [cm^{-1}]	I_{rel}	$\tilde{\nu}$ [cm^{-1}]	I [km mol^{-1}]			$\Delta\tilde{\nu}$ [cm^{-1}][a]	$\Delta\tilde{\nu}$ [cm^{-1}][a]
1548		1641	–		O_2 (matrix)	86.1	94.1
1500	16	1644	133	ν_1	O′O″ stretch	69.1	93.1
1223	100	1239	549	ν_2	CO stretch	1.0	0.9
1211	64	1179	393	ν_3	CF stretch, antisym.	4.8	0.0
1182	57	1158	346	ν_4	CF stretch, antisym.	5.0	0.0
895	3.9	887	25	ν_5	CF stretch, sym.	0.5	0.0
615	1.4	620	12	ν_6	CF_3 umbrella	0.6	0.2
		606	2.1	ν_7	CF_3 deformation		0.0
581	0.4	594	7.3	ν_8	CF_3 deformation		0.1
450	1.2	437	9.4	ν_9	CF_3 scissor		0.6
		408	0.05	ν_{10}	OCF deformation		0.1
239	0.1	265	5.0	ν_{11}	OOO bend		12.8
219	0.2	126	5.0	ν_{12}	O–O′ stretch		4.1
		90	0.09	ν_{13}	OOC bend		2.7
		50	0.39	ν_{14}	OOCF torsion		1.1
		17	0.04	ν_{15}	OOOC torsion		0.4

[a] $\Delta\nu = \nu(CF_3{}^{16}O^{16}O^{16}O) - \nu CF_3{}^{16}O^{18}O^{18}O)$ or $\nu(^{16}O_2) - \nu(^{18}O_2)$.

 © 2003 Wiley-VCH Verlag GmbH & Co. KGaA, Weinheim

a ClOOO radical might play an important role.[24] Atmospheric modeling studies[25] have shown that the existence of the ClOOO radical may enhance formation of the ClO dimer with O_2 acting as a chaperon. Recent experimental evidence for ClOOO[26] is consistent with studies of Prasad and Lee.[27] Moreover, our results on CF_3OOO have broader implications for more general ROOO species and new roles for the interaction of O_2 with radicals in atmospheric chemistry.

Experimental Section

$CF_3OC(O)OOCF_3$ and $CF_3OC(O)OOC(O)OCF_3$ were prepared as described in the literature.[17] Small amounts of $CF_3OC(O)OOCF_3$ or $CF_3OC(O)OOC(O)OCF_3$ were diluted (1:500) with an excess of oxygen (Messer-Griesheim, Krefeld, Germany). The gas mixture was stored in a stainless-steel container and passed through a vacuum line connected by a stainless-steel capillary with the heated nozzle in front of the matrix support. For the thermolysis of $CF_3OC(O)OOCF_3$ and $CF_3OC(O)OOC(O)OCF_3$ the oven temperature was adjusted to 310°C and 260°C, respectively. Photolysis experiments on the matrices were undertaken in the UV region using a high-pressure mercury lamp (TQ 150, Heraeus, Hanau, Germany) in combination with cut-off or interference filters (Schott, Mainz, Germany). Details of the matrix apparatus are given elsewhere.[28,29]

Matrix IR spectra were recorded on a IFS 66 v/S FTIR spectrometer (Bruker, Ettlingen, Germany) with a resolution of 0.3 cm^{-1} in the range of 5000 to 400 cm^{-1} in reflectance mode with a transfer optic. A DTGS detector and a KBr/Ge beam splitter were used, and 64 scans were coadded for each spectrum. A far-IR DTGS detector together with a 6-μm Mylar/Ge beam splitter were used in the 600–80-cm^{-1} region. A total of 64 scans were coadded for each spectrum with an apodized resolution of 1.2 cm^{-1}. Matrix UV spectra were recorded with a Perkin-Elmer Lambda 900 UV/Vis spectrometer (Perkin-Elmer, Norwalk, CT, U.S.) with a stepwidth of 1 nm (slit 1 nm, integration time 1 s). The spectra were measured in reflectance mode with two quartz fibers and special condenser optics (Hellma, Jena, Germany).

Received: May 15, 2003 [Z51909]

Keywords: atmospheric chemistry · density functional calculations · reaction mechanisms · trioxy radicals · vibrational spectroscopy

[1] J. S. Francisco, M. M. Maricq, *Adv. Photochem.* **1995**, *20*, 79.
[2] R. Atkinson, *J. Phys. Chem. Ref. Data* **1997**, *26*, 215.
[3] R. Atkinson, *Atmos. Environ.* **2000**, *34*, 2063.
[4] M. D. King, C. E. Canosa-Mas, R. P. Wayne, *Atmos. Environ.* **2001**, *35*, 2081.
[5] P. D. Lightfoot, R. A. Cox, J. N. Crowley, M. Destriau, G. D. Hayman, M. E. Jenkin, G. K. Moortgat, F. Zabel, *Atmos. Environ. Part A* **1992**, *28*, 1805.
[6] F. Cacace, G. de Petris, F. Pepi, A. Trojani, *Science* **1999**, *285*, 81.
[7] B. Nelander, A. Engdahl, T. Svensson, *Chem. Phys. Lett.* **2000**, *332*, 403.
[8] E. Y. Misochko, A. V. Akimov, C. A. Wight, *J. Phys. Chem. A* **1999**, *103*, 7972.
[9] T. W. P. Jungkamp, J. H. Seinfeld, *Chem. Phys. Lett.* **1996**, *263*, 371.
[10] X. Xu, R. P. Müller, W. A. Goddard III, *Proc. Natl. Acad. Sci. USA* **2002**, *99*, 3376.
[11] A. E. Croce, C. J. Cobos, E. Castellano, *J. Fluorine Chem.* **1997**, *82*, 91.
[12] J. S. Francisco, I. H. Willams, *Int. J. Chem. Kinet.* **1988**, *20*, 455.
[13] M. K. W. Ko, N. D. Sze, J. M. Rodriguez, D. K. Weistenstein, C. W. Heisey, R. P. Wayne, P. Biggs, C. E. Canosa-Mas, H. Sidebottom, *Geophys. Res. Lett.* **1994**, *21*, 101.
[14] P. Biggs, C. E. Canosa-Mas, D. E. Shallcross, A. Vipond, R. P. Wayne, *J. Chem. Soc. Faraday Trans.* **1997**, *93*, 2477.
[15] R. W. Fessenden, *J. Chem. Phys.* **1968**, *48*, 3725.
[16] M. C. R. Symons, *J. Am. Chem. Soc.* **1969**, *91*, 5924.
[17] G. A. Argüello, H. Willner, F. E. Malanca, *Inorg. Chem.* **2000**, *39*, 1195.
[18] G. A. Argüello, H. Willner, *J. Phys. Chem. A* **2001**, *105*, 3466.
[19] A. D. Becke, *Phys. Rev. A* **1988**, *38*, 3098.
[20] J. A. Pople, M. Head-Gordon, *J. Chem. Phys.* **1987**, *87*, 5968.
[21] Gaussian 98 (Revision A.7), M. J. Frisch, G. W. Trucks, H. B. Schlegel, G. E. Scuseria, M. A. Robb, J. R. Cheeseman, V. G. Zakrzewski, J. A. Montgomery, R. E. Stratmann, J. C. Burant, S. Dapprich, J. M. Millam, A. D. Daniels, K. N. Kudin, M. C. Strain, O. Farkas, J. Tomasi, V. Barone, M. Cossi, R. Cammi, B. Mennucci, C. Pomelli, C. Adamo, S. Clifford, J. Ochterski, G. A. Petersson, P. Y. Ayala, Q. Cui, K. Morokuma, D. K. Malick, A. D. Rabuck, K. Raghavachari, J. B. Foresman, J. Cioslowski, J. V. Ortiz, B. B. Stefanov, G. Liu, A. Liashenko, P. Piskorz, I. Komaromi, R. Gomperts, R. L. Martin, D. J. Fox, T. Keith, M. A. Al-Laham, C. Y. Peng, A. Nanayakkara, C. Gonzalez, M. Challacombe, P. M. W. Gill, B. G. Johnson, W. Chen, M. W. Wong, J. L. Andres, M. Head-Gordon, E. S. Replogle, J. A. Pople, Gaussian, Inc., Pittsburgh, PA, **1998**.
[22] The calculated spin densities for $CF_3OO'O''$ are −0.79 (O), +0.85 (O′), and +0.98 (O″).
[23] R. G. W. Norrish, *J. Chem. Soc.* **1934**, 1864.
[24] S. S. Prasad, *Nature* **1980**, *285*, 152.
[25] D. T. Shindell, *J. Atmos. Chem.* **1997**, *20*, 323.
[26] R. Kopitzky, H. Grothe, H. Willner, *Chem. Eur. J.* **2002**, *8*, 5601.
[27] S. S. Prasad, T. J. Lee, *J. Geophys. Res. [Atmos.]* **1994**, *99*, 8225.
[28] H. Schnöckel, H. Willner in *Infrared and Raman Spectroscopy, Methods and Applications* (Ed.: B Schrader), VCH, Weinheim, **1994**, p. 297.
[29] S. von Ahsen, J. Hufen, H. Willner, J. S. Francisco, *Chem. Eur. J.* **2001**, *8*, 1189.

 © 2003 Wiley-VCH Verlag GmbH & Co. KGaA, Weinheim

Porous Membranes

From Particle-Assisted Wetting to Thin Free-Standing Porous Membranes**

*Hui Xu and Werner A. Goedel**

Membranes with small uniform pores are important in applications as simple as ultrafiltration or as sophisticated as the protection of implanted xenogenic cells from the immune reaction of a living organism.[1,2] Thin membranes with precisely controlled pores of uniform size are often prepared using standard top-down lithography techniques. However, porous materials can be made in much simpler ways by the selective removal of one component out of structured solids. Such solids can be prepared by ion-bombardment of polymers,[3] spinodal demixing of glasses,[4] self-assembly of block copolymers,[5,6] and embedding of surfactant arrays, emulsion droplets, and colloidal crystals into a continuous matrix.[7–15] These structured materials are usually cast onto solid substrates or in a thin layer between two solid plates and have to be separated from these plates if a free-standing membrane is desired. This separation is especially difficult in the production of sub-micrometer thin membranes, but can be circumvented completely by producing membranes on fluid surfaces. We have reported the fabrication of thin free-standing porous membranes on the air–water interface by using polymeric monolayers and colloidal particles.[16] However, to overcome the inability of organic matter to wet the air–water interface, we needed specially prepared amphiphilic polymers that are not readily available. Herein we report the use of a new principle, particle-assisted wetting,[17,18] to prepare high-quality thin porous membranes by spreading mixtures of particles and commercially available polymerizable liquids on a water surface. The resulting membranes bear a high density of uniform pores and can be transferred easily to any desired continuous or macroporous substrate. A representation of the membrane fabrication is shown in Figure 1, the corresponding experimental observations are shown in Figure 2 and Figure 3.

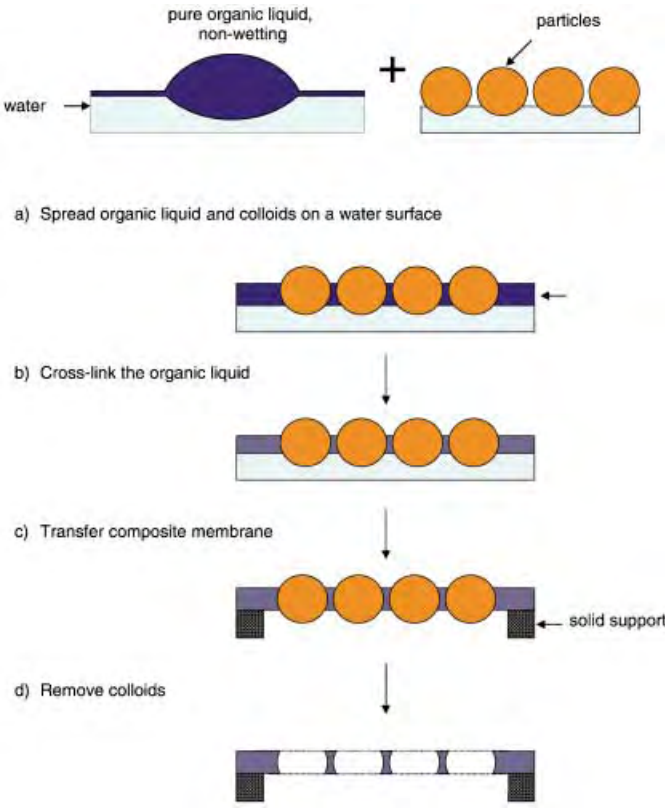


Figure 1. Schematic representation of the preparation of thin free-standing porous membranes.

The membrane fabrication starts with the formation of a mixed layer made up of colloidal particles and a nonvolatile polymerizable organic liquid on a water surface. Like most organic liquids, the nonvolatile organic liquid used here (trimethylolpropane trimethacrylate (TMPTMA)) does not wet the air–water interface to form a uniform wetting layer, instead it forms micrometer to millimeter-sized lenses (Figure 2a). On the other hand, the hydrophobized silica colloids used here form homogeneous monolayers on the air–water interface. Scanning electron microscopy (SEM) images (Figure 2b) and the recorded lateral-pressure versus area isotherms (Figure 2c) indicate, that the particles form nearly close-packed two-dimensional monolayers, which are similar to colloidal monolayers reported the literature.[19]

If a mixture of the polymerizable liquid TMPTMA with the hydrophobized silica particles is spread onto the air–water interface a mixed wetting layer is formed (Figure 1a). SEM images of the top (Figure 2d) and bottom interface (inset of Figure 2d) of the wetting layer obtained after solidification of the liquid and transfer to mica substrates show that the colloids are embedded in a continuous polymer layer and penetrate through both interfaces of this layer. Comparing the SEM pictures (Figure 2b and Figure 2d) and the lateral-pressure versus area isotherms in Figure 2c, shows the

[*] Priv.-Doz. Dr. W. A. Goedel,[+] H. Xu
Organic and Macromolecular Chemistry, OC III
University of Ulm
89069 Ulm (Germany)
Fax: (+49) 731-50-22883
E-mail: werner.goedel@chemie.uni-ulm.de

[+] BASF Aktiengesellschaft
Polymer Research
Department of Polymer Physics
67056 Ludwigshafen (Germany)
Fax: (+49) 620-60-72660
E-mail: werner.goedel@basf-ag.de

[**] The support by M. Möller and B. Rieger (University of Ulm) and H. Auweter and R. Iden (BASF) is greatly appreciated. We thank C. van Kats, J. Wijnhoven, A. Philipse, and A. van Blaaderen, (Utrecht Colloid Synthesis Facility, Van't Hoff Laboratory for Physical and Colloid Chemistry, Utrecht University, The Netherlands) for providing the silica colloids and valuable discussions, and P. Walther for help in electron microscopy. H.X. thanks the Alexander von Humboldt Stiftung for support. This work was funded by the Deutsche Forschungsgemeinschaft within the framework of the SFB 569 and the SPP 1052.

 © 2003 Wiley-VCH Verlag GmbH & Co. KGaA, Weinheim DOI: 10.1002/anie.200351427

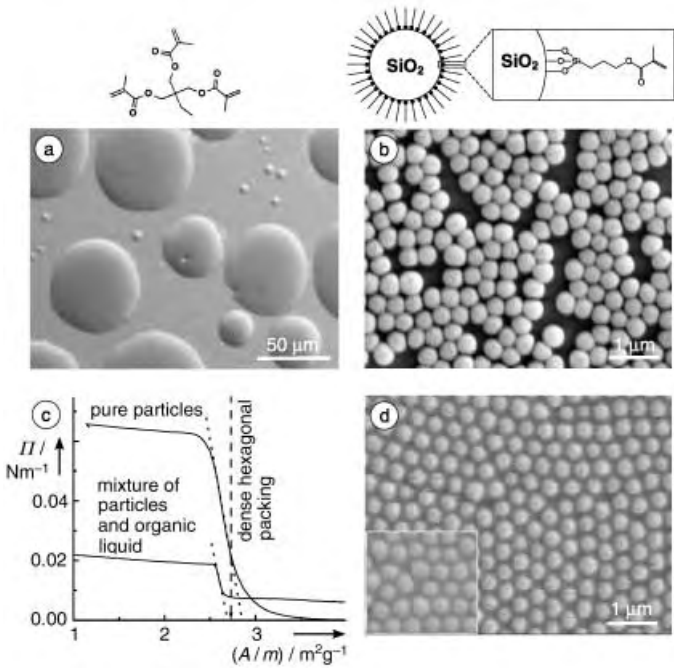


Figure 2. Particle-assisted wetting. a) SEM image of the liquid lenses of TMPTMA substrate. b) SEM image of a monolayer of hydrophobized silica particles. c) Lateral pressure (π) versus area-per-mass (A/m) isotherms of a pure colloidal monolayer and of a mixed layer of colloids and the liquid TMPTMA. d) SEM image, top view. of the mixed layer; the inset is a bottom view of the mixed layer. Images (a), (b), and (d) were all taken after spreading on a water surface, photopolymerization, and transfer to mica substrate.

polymerizable liquid facilitates an even denser packing of the colloids. This denser packing could be due to the capillary forces, similar to that discussed for wet colloidal monolayers on a solid surface.[20,21] It is also possible that the liquid enables the particles to better slide past one another and so pack closer together.

The polymerizable liquid used in our case does not wet the air–water interface in absence of particles, but rather retracts into small lenses. Thus, one might be surprised that it homogeneously spreads on the air–water interface when mixed with suitable particles. However, this effect can be explained by a reduction in the total interfacial energy which occurs on partial wetting of the particles by the hydrophobic polymerizable liquid. Since this effect has been described in more detail elsewhere,[17,18] we focus herein on utilizing the resulting wetting layers for the preparation of thin porous membranes.

The solidified mixed layers can easily be transferred to a variety of different solid substrates ranging from smooth substrates such as mica to macroporous supports and electron microscope grids. The silica particles can easily be removed by hydrofluoric acid vapor, either before or after transfer, which leaves the polymer matrix behind as a porous membrane. SEM images of such a thin free-standing porous membrane transferred onto a gold grid are shown in Figure 3a and b. The grid with 100-μm wide openings was completely covered by the thin membrane. When viewed from above, the underlying gold grid can even be seen through the pores of the membrane (see left part of Figure 3b), which indicates that the pores pass through the membrane. The top view and bottom view of the membrane look very similar, suggesting a nearly symmetric structure of the pores. This interpretation is confirmed by the high-resolution scanning electron microscopy images shown in Figure 3c. The thickness of the membrane can be estimated from Figure 3c to be approximately 150 nm, which is smaller than the diameter of the pores (approximately 250 nm on top and bottom surface and 300 nm in middle of the pore). Image analysis based on transmission electron microscopy (TEM) images of the membrane (Figure 3d) yields a pore density of 9×10^8 pores cm^{-2}, a pore size of 300 nm and a standard deviation of the pores sizes of 6%. The pore size and size distribution is reminiscent of the size of the templating colloids, which indicates that the pore size could be tuned by choosing colloids of different sizes.

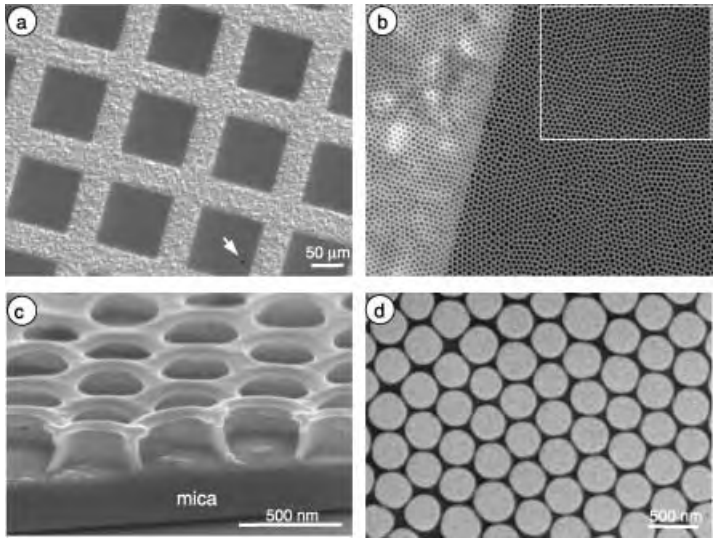


Figure 3. Porous membranes. a), b) SEM images of thin free-standing porous membranes that cover a gold grid with 100-μm wide openings. The small hole in (a), indicated by a white arrow shows the contrast to a not-covered area, inset in (b) is a bottom view of the same membrane. c) High-resolution scanning electron microscopy image of a side view of the porous membrane supported on mica. d) TEM image of a free-standing porous membrane.

The process introduced here is based on the fact that colloidal particles can assist the wetting of organic liquids on air–water interfaces to form a uniform composite layer. The resulting porous membrane is of a high quality in terms of uniformity of pores and pore ordering. In this respect they are comparable to those porous materials obtained by casting colloidal crystals onto solid plates or into solid molds.[22–24] Moreover, an additional advantage of our method is that the membranes can easily be manipulated and transferred to any desired substrate including grids and porous supports. The membrane is thin but still robust to form a stable free-standing membrane. Note that the lateral dimensions of the membrane are only limited by the size of the air–water interface and, if a continuous process is used, can be made unlimited in size. The preparation process is simple, rapid and has potential for large-scale production. A number of unique applications can be foreseen for this porous membrane:

 © 2003 Wiley-VCH Verlag GmbH & Co. KGaA, Weinheim

supports for the electron microscopy of biological molecules, masks or molds for nanolithography, and as "separation layers" in asymmetric membranes for ultrafiltration, sterilization, and bio-encapsulation.

Experimental Section

The photopolymerizable organic liquid trimethylolpropane trimethacrylate (TMPTMA; Aldrich) was made inhibitor-free before use by passing the liquid through a column filled with Al_2O_3. Photoinitiator benzoinisobutylether (Aldrich; 3–5 wt% of the liquid) was added into the liquid TMPTMA to initiate its photopolymeriztion. Silica colloids (average diameter of 320 nm, polydispersity of 6%, hydrophobized by treatment with methacryloxypropyltrimethoxysilane as described in ref. [25]) were obtained as dispersions in ethanol from the Utrecht Colloid Synthesis Facility, The Netherlands. Mixtures of TMPTMA and/or the colloid dispersions in chloroform and ethanol (the final solution contained 20% ethanol and approximately 1 wt% of TMPTMA and silica colloid particles) were added to a Langmuir trough filled with water (equipment was identical to that described in ref. [26]). After evaporation of the solvent and lateral compression to a surface pressure of $15–20 \times 10^{-3}$ N m^{-1}, the structures were solidified by photopolymerization (irradiation with UV-A light of 360 nm wavelength), and transferred to solid substrates such as gold electron microscope grids by horizontal transfer.[27] The particles were removed by exposure of the membranes to hydrofluoric acid vapor for 1–3 min. SEM images were taken using a Zeiss DSM 962 scanning electron microscope (Zeiss, Germany), or a field-emission scanning electron microscope (S-5200, Hitachi, Japan). TEM was measured on an EM 400T microscope (Philips, The Netherlands).

Received: March 18, 2003 [Z51427]

Keywords: nanostructures · particle-assisted wetting · polymers · porous membranes

[1] T. A. Desai, D. Hansford, M. Ferrari, *J. Membr. Sci.* **1999**, *159*, 221–231.
[2] F. A. Lim, M. Sun, *Science* **1980**, *210*, 908–910.
[3] M. Yoshida, M. Asano, T. Suwa, N. Reber, R. Spohr, R. Katakai, *Adv. Mater.* **1997**, *9*, 757–758.
[4] R. J. Tonucci, B. L. Justus, A. J. Campillo, C. E. Ford, *Science* **1992**, *258*, 783–785.
[5] T. Thurn-Albrecht, J. Schotter, C. A. Kastle, N. Emley, T. Shibauchi, L. Krusin-Elbaum, K. Guarini, C. T. Black, M. T. Tuominen, T. P. Russell, *Science* **2000**, *290*, 2126–2129.
[6] V. Z.-H. Chan, J. Hoffman, V. Y. Lee, H. Iatrou, A. Avgeropoulos, N. Hadjichristidis, R. D. Miller, E. L. Tomas, *Science* **1999**, *286*, 1716–1719.
[7] D. W. Breck, *Zeolite Molecular Sieves*, Krieger, Florida, **1984**.
[8] C. T. Kresge, M. E. Leonowicz, W. J. Roth, J. C. Vartuli, J. S. Beck, *Nature* **1992**, *359*, 710–712.
[9] N. K. Raman, M. T. Anderson, C. J. Brinker, *Chem. Mater.* **1996**, *8*, 1681–1701.
[10] O. D. Velev, A. M. Lenhoff, *Curr. Opin. Colloid Interface Sci.* **2000**, *5*, 56–63.
[11] O. D. Velev, T. A. Jede, R. F. Lobo, A. M. Lenhoff, *Nature* **1997**, *389*, 447–448.
[12] B. T. Holland, C. F. Blanford, A. Stein, *Science* **1998**, *281*, 538–540.
[13] J. E. G. J. Wijnhoven, W. L. Vos, *Science* **1998**, *281*, 802–804.
[14] P. Jiang, K. S. Hwang, D. M. Mittleman, J. F. Bertone, V. L. Colvin, *J. Am. Chem. Soc.* **1999**, *121*, 11630–11637.
[15] S. A. Johnson, P. J. Ollivier, T. E. Mallouk, *Science* **1999**, *283*, 963–965.
[16] H. Xu, W. A. Goedel, *Langmuir* **2002**, *18*, 2363–2367.
[17] H. Xu, W. A. Goedel, *Langmuir* **2003**, *19*, 4950–4952.
[18] W. A. Goedel, *Europhys. Lett.* **2003**, *42*(4), 607–613.
[19] K. U. Fulda, B. Tieke, *Adv. Mater.* **1994**, *6*, 288–290.
[20] P. A. Kralchevsky, N. D. Denkov, *Curr. Opin. Colloid Interface Sci.* **2001**, *6*, 383–401.
[21] N. D. Denkov, O. D. Velev, P. A. Kralchevsky, I. B. Ivanov, H. Yoshimura, K. Nagayama, *Langmuir* **1992**, *8*, 3183–3190.
[22] S. H. Park, Y. N. Xia, *Langmuir* **1999**, *15*, 266–273.
[23] S. H. Park, Y. N. Xia, *Chem. Mater.* **1998**, *10*, 1745–1747.
[24] S. I. Matsushita, T. Miwa, D. A. Tryk, A. Fujishima, *Langmuir* **1998**, *14*, 6441–6447.
[25] A. P. Philipse, A. Vrij, *J. Colloid Interface Sci.* **1989**, *128*, 121–136.
[26] W. A. Goedel, R. Heger, *Langmuir* **1998**, *14*, 3470–3474.
[27] T. Araki, S. I. Oinuma, K. Iriyama, *Langmuir* **1991**, *7*, 738–744.

 © 2003 Wiley-VCH Verlag GmbH & Co. KGaA, Weinheim

Template Synthesis of Micro-Rings

Mesoscopic Rings by Controlled Wetting of Particle Imprinted Templates**

*Hui Xu and Werner A. Goedel**

Decreasing the feature size of microelectronic, -optical, and -mechanical building blocks allows us to integrate more and more complex functions into a single device, as well as to investigate and utilize size-dependent physical effects. However, conventional structuring techniques, such as photo- and electron-beam lithography, are limited in spatial resolution or writing speed. A number of recent investigations overcome these limitations by using the self-organization of block

[*] W. A. Goedel,[+] H. Xu
Organic and Macromolecular Chemistry, OC III
University of Ulm
89069 Ulm (Germany)
Fax: (+49) 731-50-22883
E-mail: werner.goedel@chemie.uni-ulm.de

[+] BASF Aktiengesellschaft
Polymer Research, Department of Polymer Physics
67056 Ludwigshafen (Germany)
Fax: (+49) 6201-60-72660
E-mail: werner.goedel@basf-ag.de

[**] The support by M. Möller and B. Rieger (University of Ulm) and H. Auweter and R. Iden (BASF), is greatly appreciated. We thank C. van Kats, J. Wijnhoven, A. Philipse, and A. van Blaaderen, (Utrecht Colloid Synthesis Facility, Van 't Hoff Laboratory for Physical and Colloid Chemistry, Utrecht University, The Netherlands) for providing the silica colloids and valuable discussions, P. Walther for help in electron microscopy, K. Thonke, M. Haupt, and A. Ladenburger for support in the preparation of the zinc oxide rings and for providing the image in the inset of Figure 2 D. H.X. thanks the Alexander von Humboldt Foundation for a fellowship. This work was funded by the Deutsche Forschungsgemeinschaft within the framework of the SFB 569 and the SPP 1052.

 © 2003 Wiley-VCH Verlag GmbH & Co. KGaA, Weinheim DOI: 10.1002/anie.200351428

copolymers, micelles, or particles to generate regular two- and three-dimensional patterns of submicrometer periodicity.[1–5] Most of these investigations used spherical particles. However, the self-organization of spheres gives rise only to highly symmetric hexagonal or cubic lattices. For certain applications, such as the generation of materials with photonic band gaps, however, there are advantages in less symmetric spatial arrangements, which in principle can be generated by the self-organization of non-spherical particles, for example, discs or rings. On the other hand, non-spherical particles themselves are of interest for their special physical properties. For example, the trapping of a magnetic flux in the interior of an electrically conducting ring can lead to "persistent currents"[6–8] and the photoluminescence of a semiconducting ring can couple to electron-transfer processes.[9] While there is an extensive literature on the synthesis of spheres[10–13] and rods,[14–21] only a few papers report the synthesis of prolate or oblate particles of defined size.[22–24] There are several reports on the nonconventional generation of ring-like structures bound to a planar support using unconventional dewetting processes,[25,26] selective wetting of substrates decorated with colloidal monolayers,[27,28] advanced lithography in combination with colloidal masks[29] and selective decomposition of core–shell particles.[30] Furthermore, polydisperse isolated ring-shaped particles, which are suspended in a liquid can be synthesized by ring closure of nanotubes[31] or ribbons,[32] or through the necklace-like aggregation of magnetic particles.[33,34] However, as far as we known, there are no reports of the synthesis of suspended (that is, not substrate bound) rings of narrow size distribution.

Herein, we present a method for the fabrication of mesoscopic rings, which can either be arranged as a regular array on a solid substrate, as a free-standing membrane of connected rings, or be dispersed as isolated rings in a liquid. This method is based on the selective wetting of the interior surfaces of a porous membrane, which itself was prepared by colloidal imprinting (Figure 1).

As described in ref. [35] mixtures of coated silica colloids and a polymerizable liquid form mesoscopic wetting layers on a water surface, in which the colloids are partially embedded in a layer of liquid, but penetrate through this layer at the top and the bottom surface (Figure 2A). Subsequent polymerization of the organic liquid by UV illumination and removal of the silica colloids with hydrofluoric acid (HF) yields a porous polymeric layer (Figure 2B), which can be transferred to any desired substrate or converted into a freely suspended membrane by transferring it across openings in a porous support.

If this porous layer deposited on a mica substrate is dipped into a 5 wt% solution of tetraethyloxy titanium ($Ti(OEt)_4$) in ethanol, then withdrawn from the solution, and dried in the ambient air to allow the hydrolysis and condensation of $Ti(OEt)_4$ into TiO_2, a reduction in the pore diameter is observed (changing from 250 nm to 200 nm, see Figure 2C). After removing the organic polymer by heating, two-dimensional arrays of titanium oxide rings of 300 nm outer diameter, 75 nm height and 140 nm inner diameter remain on the substrate (see SEM and SFM images in Figure 2D–F). The dimensions and polydispersity (6%) of the rings are similar to the size of the original colloids used in the preparation of the porous membrane.

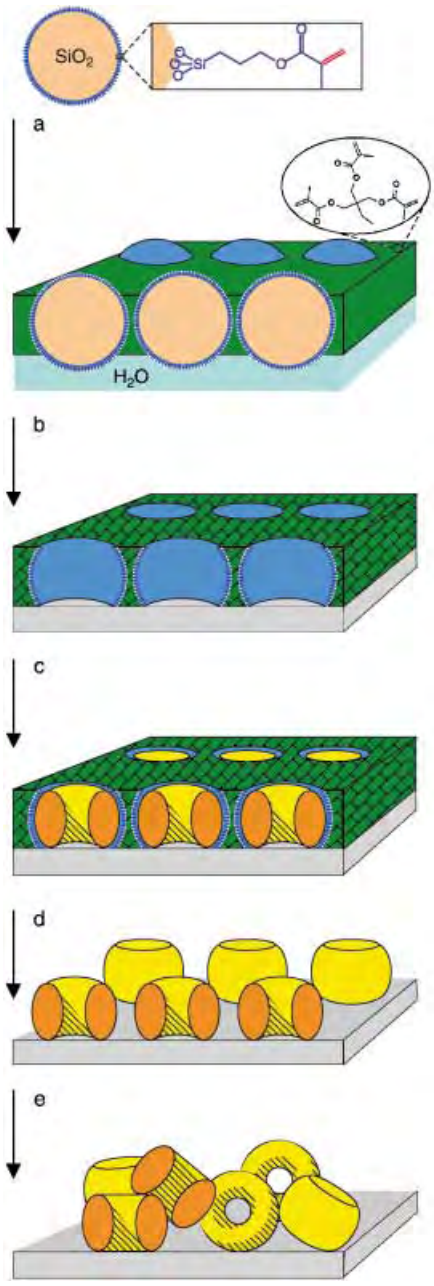


Figure 1. Schematic representation of the casting of rings into a porous membrane that was structured by particle imprinting. a) Spreading of coated silica particles and polymerizable organic liquid onto a water surface, b) polymerization of the organic liquid, removal of the particles, transfer of the resulting composite membrane, c) partial filling of the pores with tetraethoxy titanium, conversion of tetraethoxy titanium to titanium dioxide, d) remove polymer, e) detach rings from surface

The process can be extended to other precursor solutions, for example, the inset of Figure 2D shows zinc oxide rings made by using a solution of zinc acetate ($50\,g\,L^{-1}$) as a precursor in the dipping process.[36] The shape of the structures that remain on the surface after removing the

 © 2003 Wiley-VCH Verlag GmbH & Co. KGaA, Weinheim

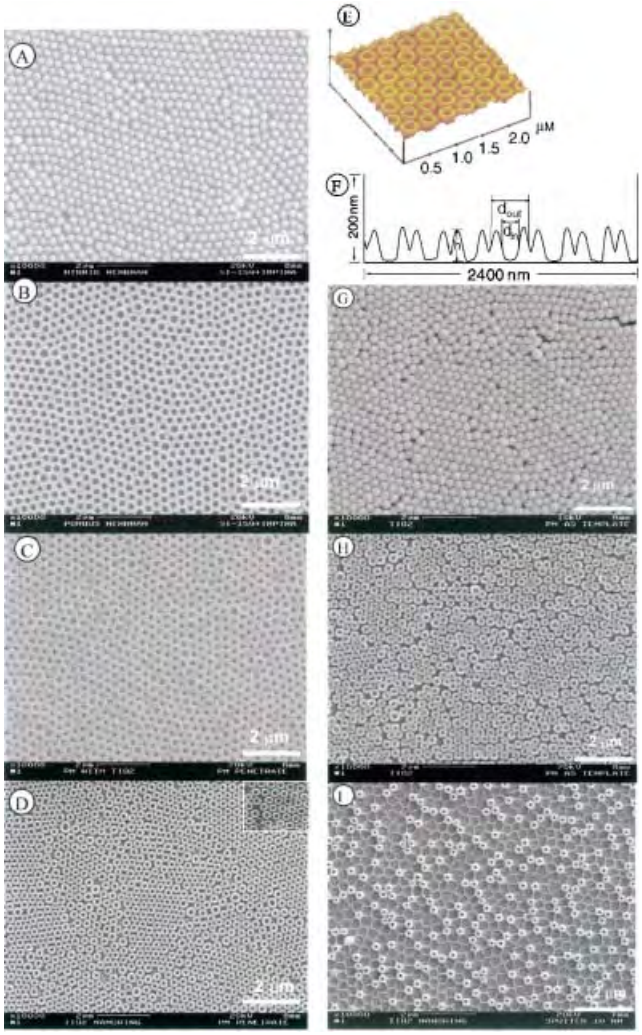


Figure 2. SEM images A) a composite membrane made from coated silica colloids of 320 nm diameter that are partially embedded in a layer of cross-linked organic polymer, B) the precursor porous membrane prepared from the composite membrane by removing the silica colloids, C) the porous membrane supported by a mica substrate after dipping, under dry nitrogen atmosphere, into a solution of $Ti(OEt)_4$ (5 wt% in ethanol) and exposure to ambient air to allow evaporation of the ethanol and the hydrolysis and condensation of $Ti(OEt)_4$ into TiO_2, D) array of TiO_2 rings on a mica surface after removing the porous precursor membrane. The inset shows zinc oxide rings prepared by dipping into a zinc acetate solution, E) Scanning force microscopy (SFM) image of an array of titanium dioxide rings on mica surface, F) cross-section of image (E) indicating the height ($h = 75$ nm), outer, and inner diameter ($d_{out} = 300$ nm; $d_{in} = 140$ nm), G–I) surface structures obtained by dipping a precursor membrane on mica into solutions of decreasing concentration of $Ti(OEt)_4$ (20 wt% (G), 10 wt% (H), and 2 wt% (I)).

organic polymer can be varied by changing the concentration of the precursor solution used in the dipping process: at higher concentrations of the dipping solution, hemispheres and cuplike structures (Figure 2G,H) are formed, at lower concentrations the formation of thin web-like structures is observed (Figure 2I).

The surface properties of the substrate also influences the shape of the nanostructures on the surface. A mica substrate favors cuplike structures, while oxide-free GaAs and silicon substrates preferentially give rise to rings. If the porous membrane used in the dipping process is free-standing (e.g. supported by an electron microscopy grid instead of a continuous solid substrate), free-standing membranes of interconnected rings are obtained (Figure 3A–C) after pyrolysis of the polymer. The rings are flexible enough that they can be deformed by lateral shearing, without substantial damage (see Figure 3C).

While the rings in the free-standing membrane are interconnected, the rings on a solid substrate seem to be isolated from each other. Thus, it should be possible to detach the rings from the surface to obtain a dispersion of isolated rings. This indeed can be achieved by washing the titanium dioxide rings from a silicon surface with dilute hydrofluoric acid. Figures 3D and E show a pile of these detached rings left behind after a drop of a dispersion of rings was placed on a carbon substrate and dried. Arrows indicate rings in the pile that are positioned in such a way that one can see underlying rings through the central hole.

Several elegant publications already describe the preparation of solid and hollow particles by the filling of porous materials[37–37] or of gaps between particles and a planar support.[25,28] For example, tubes and hollow spheres have been generated by deposition of oxides, metal, or polymers onto the walls of cylindrical or spherical pores in filtration membranes[38] and inverse opals.[37] In these investigations the whole interior and exterior surface of the porous template is uniformly coated with a thin solid layer and the hollow objects are interconnected. In our investigations we observe selective coating of the inner surfaces of the pores only, while the outer planar surfaces of the porous membrane are almost free of the titanium oxide layer. This selective wetting might be of purely geometrical origin. However, it is of note, that the coating of the particles contains polymerizable methacroyl groups and thus is covalently linked to the polymer matrix during the polymerization process and remains linked to it even after removal of the particles. We believe that this surface coating generates a chemical contrast between the inner and outer surface of the membrane and promotes the selective wetting of the pore walls by the titanium alkoxide solution. Thus the observations made here might be similar to the well-established field of molecular imprinting (sacrificial templates imprint not only their shape, but a specific chemical functionality into a matrix, which can subsequently be used to selectively interact with other materials, for example, in chromatography).[40–42] However, the process used here is working on a mesoscopic rather than on a molecular length scale.

The generation of rings is rather simple and can be performed in any laboratory without sophisticated clean room or vacuum equipment; it is easy to control the size and the morphology of the rings by using appropriate templates; the rings can be fabricated on different substrates and can be made from different materials. Thus, we anticipate that the technique can be exploited in various applications requiring ringlike structures, for example, in microelectronics, -mechanics and -optics.

 © 2003 Wiley-VCH Verlag GmbH & Co. KGaA, Weinheim

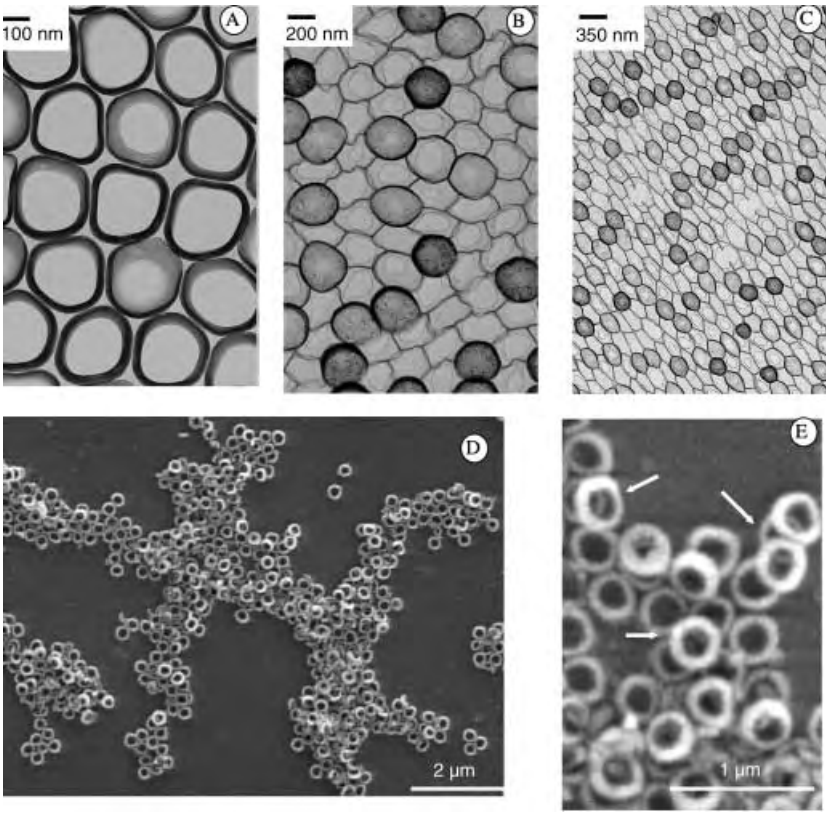


Figure 3. A–C) TEM images of membranes of interconnected titanium dioxide rings made by dipping a free-standing porous membrane into a solution of $Ti(OEt)_4$ (exposure to ambient air and burning off the polymer (at 450 °C). The membrane shown in (A) was dipped in a solution of higher concentration than (B) and (C). The membrane imaged in (C) was deformed by shearing the supporting electron-microscopy grid. D) and E) Isolated titanium dioxide rings detached from a silicon substrate by washing with dilute HF acid. Arrows indicate rings which are positioned in such a way that one can see underlying rings through the central hole.

Experimental Section

Equipment and materials used for the preparation of the porous membranes are identical to those used refs. [43] The photopolymerizable organic liquid trimethylolpropane trimethacrylate (TMPTMA; Aldrich) was made inhibitor-free before use by passing the liquid through a column filled with Al_2O_3. Photoinitiator benzoinisobutylether (Aldrich; 3–5 wt % of the liquid) was added into the liquid TMPTMA to initiate photopolymerization. Silica colloids (average diameter of 320 nm, polydispersity of 6 %, hydrophobized by treatment with methacryloxypropyltrimethoxysilane as described in ref. [44] were obtained as dispersions in ethanol from the Utrecht Colloid Synthesis Facility, The Netherlands. Absolute ethanol (Merck) and ethanol solution of $Ti(OEt)_4$ (Aldrich) were used as received. Zinc acetate (Aldrich) was dissolved in absolute ethanol by heating under reflux for 3 h. The silica particles were removed by exposure to the vapor of hydrofluoric acid (37 % aqueous solution) for 1–3 min. Mica substrates and gold grids were purchased from Plano GmbH. The polymer precursor membrane was removed by heating in air at 450 °C for 5 min. SEM images were taken using a Zeiss DSM 962 (Zeiss, Germany). TEM was measured on an EM 400T (Philips, The Netherlands). SFM was measured on a Nanoscope III (Digital, Santa Babara, USA) at tapping mode.

Received: March 18, 2003
Revised: July 7, 2003 [Z51428]

Keywords: mesoscopic structures · nanostructures · particle-assisted wetting · template synthesis · titanium dioxide

[1] T. Hashimoto, K. Tsutsumi, Y. Funaki, *Langmuir* **1997**, *13*, 6869–6872.
[2] M. Templin, A. Franck, A. Du Chesne, H. Leist, Y. Zhang, R. Ulrich, V. Schädler, U. Wiesner, *Science* **1997**, *278*, 1795–1798.
[3] M. Haupt, S. Miller, A. Ladenburger, R. Sauer, K. Thonke, J. P. Spatz, S. Riethmüller, M. Möller, F. Banhart, *J. Appl. Phys.* **2002**, *91*, 6057–6059.
[4] N. D. Denkov, O. D. Velev, P. A. Kralchevsky, I. B. Ivanov, H. Yoshimura, K. Nagayama, *Langmuir* **1992**, *8*, 3183–3190.
[5] A. van Blaaderen, R. Ruel, P. Wiltzius, *Nature* **1997**, *385*, 321–324.
[6] M. Büttiker, Y. Imry, R. Landauer, *Phys. Lett. A* **1983**, *96*, 365–367.
[7] D. Mailly, C. Chapelier, A. Benoit, *Phys. Rev. Lett.* **1993**, *70*, 2020–2023.
[8] A. Lorke, R. J. Luyken, A. O. Govorov, J. P. Kotthaus, J. M. Garcia, P. M. Petroff, *Phys. Rev. Lett.* **2000**, *84*, 2223–2226.
[9] R. J. Warburton, C. Schäflein, D. Haft, F. Bickel, A. Lorke, K. Karrai, J. M. Garcia, W. Schoenfeld, P. M. Petroff, *Nature* **2000**, *405*, 926–929.
[10] *Nanoparticles and Nanostructured Films: Preparation, Characterization and Applications* (Ed.: J. H. Fendler), Wiley-VCH, Weinheim, **1998**.
[11] W. P. McConnell, J. P. Novak, L. C. Brousseau, R. R. Fuierer, R. C. Tenent, D. L. Feldheim, *J. Phys. Chem. B* **2000**, *104*, 8925–8930.
[12] N. Toshima, T. Yonezawa, *New J. Chem.* **1998**, *22*, 1179–1201.
[13] M. Möller, J. P. Spatz, *Curr. Opin. Colloid Interface Sci.* **1997**, *2*, 177–187.
[14] H. A. Klok, K. A. Jolliffe, C. L. Schauer, L. J. Prins, J. P. Spatz, M. Möller, *J. Am. Chem. Soc.* **1999**, *121*, 7154–7155.
[15] A. P. Philipse, A. M. Wierenga, *Langmuir* **1998**, *14*, 49–54.
[16] M. L. Sandrock, C. A. Foss, *J. Phys. Chem. B* **1999**, *103*, 11398–11406.
[17] X. F. Duan, Y. Huang, Y. Cui, J. F. Wang, C. M. Lieber, *Nature* **2001**, *409*, 66–69.
[18] T. Thurn-Albrecht, J. Schotter, C. A. Kastle, N. Emley, T. Shibauchi, L. Krusin-Elbaum, K. Guarini, C. T. Black, M. T. Tuominen, T. P. Russell, *Science* **2000**, *290*, 2126–2129.
[19] Y. Cui, C. M. Lieber, *Science* **2001**, *291*, 851–853.
[20] S. Iijima, *Nature* **1991**, *354*, 56–58.
[21] "Fullerenes and related structures": M. Terrones, W. K. Hsu, H. W. Kroto, D. R. M. Walton, *Top. Curr. Chem.* **1999**, *199*, 189–234.
[22] C. C. Ho, A. Keller, J. A. Odell, R. H. Ottewill, *Colloid Polym. Sci.* **1993**, *271*, 469–479.
[23] C. C. Ho, R. H. Ottewill, L. Yu, *Langmuir* **1997**, *13*, 1925–1930.
[24] T. van Dillen, A. van Blaaderen, W. Fukarek, A. Polman, *Appl. Phys. Lett.* **2001**, *78*, 910–912.
[25] A. P. H. J. Schenning, F. B. G. Benneker, H. P. M. Geurts, X. Y. Liu, R. J. M. Nolte, *J. Am. Chem. Soc.* **1996**, *118*, 8549–8552.
[26] J. Liu, H. J. Dai, J. H. Hafner, D. T. Colbert, R. E. Smalley, S. J. Tans, C. Dekker, *Nature* **1997**, *385*, 780–781.

 © 2003 Wiley-VCH Verlag GmbH & Co. KGaA, Weinheim

[27] M. Winzer, M. Kleiber, N. Dix, R. Wiesendanger, *Appl. Phys. A* **1996**, *63*, 617 – 619.
[28] J. Boneberg, F. Burmeister, C. Schäfle, P. Leiderer, D. Reim, A. Frey, S. Herminghaus, *Lanmguir* **1997**, *13*, 7080 – 7084.
[29] J. Aizpurua, P. Hanarp, D. S. Sutherland, M. Kall, G. W. Bryant, F. Garcia de Abajo, *Phys. Rev. Lett.* **2003**, *90*, 057401-04.
[30] D. K. Yi, D. Y. Kim, *Nano Lett.* **2003**, *3*, 207 – 211.
[31] M. Sano, A. Kamino, J. Okamura, S. Shinkai, *Science* **2001**, *293*, 1299 – 1301.
[32] Z. J. Li, X. L. Chen, H. J. Li, Q. Y. Tu, Z. Yang, Y. P. Xu, B. Q. Hu, *Appl. Phys. A* **2001**, *72*, 629 – 632.
[33] K. V. P. M. Shafi, I. Felner, Y. Mastai, A. Gedanken, *J. Phys. Chem. B* **1999**, *103*, 3358 – 3360.
[34] S. L. Tripp, S. V. Pusztay, A. E. Ribbe, A. Wei, *J. Am. Chem. Soc.* **2002**, *124*, 7914 – 7915.
[35] H. Xu, W. A. Goedel, *Angew. Chem.* **2003**, *115*, 4842 – 4844; *Angew. Chem. Int. Ed.* **2003**, *42*, 4694 – 4696.
[36] See also: A. Ladenburger, M. Haupt, R. Sauer, K. Thonke, H. Xu, W. A. Goedel, *Phys. E* **2003**, *17*, 489.
[37] P. Jiang, J. F. Bertone, V. L. Colvin, *Science* **2001**, *291*, 453 – 457.
[38] S. de Vito, C. R. Martin, *Chem. Mater.* **1998**, *10*, 1738 – 1741.
[39] M. Steinhart, J. H. Wendorff, A. Greiner, R. B. Wehrspohn, K. Nielsch, J. Schilling, J. Choi, U. Gösele, *Science* **2002**, *296*, 1997 – 1997.
[40] G. Wulff, A. Sarhan, *Angew. Chem.* **1972**, *84*, 364; *Angew. Chem. Int. Ed. Engl.* **1972**, *11*, 341.
[41] O. Norrlow, M. Glad, K. Mosbach, *J. Chromatogr.* **1984**, *299*, 29 – 41.
[42] G. Wulff, *Angew. Chem.* **1995**, *107*, 1958 – 1979; *Angew. Chem. Int. Ed. Engl.* **1995**, *34*, 1812 – 1832.
[43] W. A. Goedel, R. Heger, *Langmuir* **1998**, *14*, 3470 – 3474.
[44] A. P. Philipse, A. Vrij, *J. Colloid Interface Sci.* **1989**, *128*, 121 – 136.

Detection of Transient Radicals

Investigation of Reactive Intermediates of Chemical Reactions in Solution by Electrospray Ionization Mass Spectrometry: Radical Cation Chain Reactions**

*Sven Meyer, Rainer Koch, and Jürgen O. Metzger**

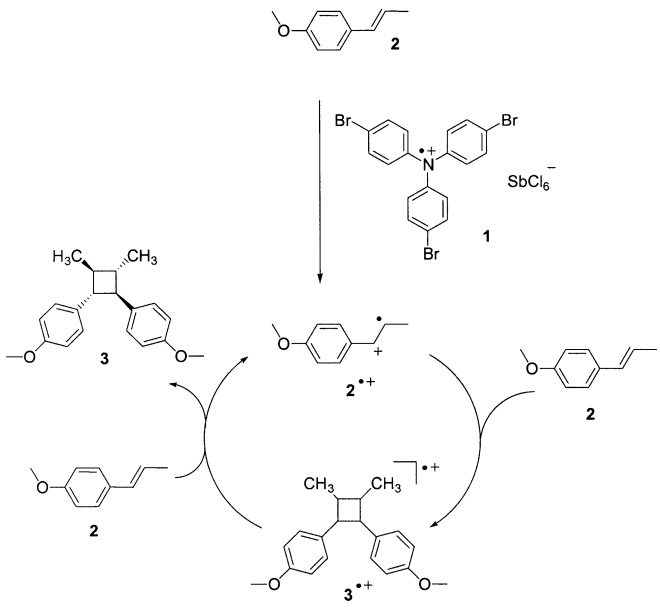
Dedicated to Professor Helmut Schwarz on the occasion of his 60th birthday

Simple methods for the direct detection of reactive intermediates, if possible under the conditions of the preparative reaction, are essential for elucidating and understanding the mechanisms of synthetically important reactions in solution. Electrospray ionization mass spectrometry (ESI-MS),[1] and atmospheric pressure chemical ionization mass spectrometry (APCI-MS)[2] can be used to study liquid-phase solutions by mass spectrometry. We reported recently that transient radicals in preparatively important tributyltin-mediated radical chain reactions can be investigated directly by using a simple microreaction system coupled online to the ESI source.[3] The transient carbon radicals were detected unambiguously and characterized by ESI-MS/MS. Now we report on investigations of a preparatively important radical cation chain reaction and the direct detection of the transient radical cations.

In 1981 Bauld et al. showed that triarylaminium salts like the commercially available tris(*p*-bromophenyl)aminium hexachloroantimonate ($\mathbf{1}^{\bullet+}SbCl_6^-$) can oxidize suitable substrates to give radical cations, thus initiating in catalytic quantities radical cation chain reactions.[4] Preparatively interesting radical cation initiated cycloadditions of alkenes to cyclobutanes and Diels–Alder reactions have been reviewed recently.[5]

We have now studied an important and often investigated cycloaddition by using a microreactor coupled to an ESI mass spectrometer. The highly stereo- and regioselective dimerization of *trans*-anethole (**2**) to give the head-to-head *trans,anti,trans*-cyclobutane **3** initiated by aminium salt $\mathbf{1}^{\bullet+}SbCl_6^-$ proceeds by a radical cation chain mechanism (Scheme 1) as shown by kinetic investigations.[5,6] A solution of $\mathbf{1}^{\bullet+}SbCl_6^-$ (5 mol %) in dichloromethane was added to a solution of substrate **2** at 0 °C, and the product **3** was obtained in 45 % yield after less than 10 minutes.[7]

Aminium salt $\mathbf{1}^{\bullet+}SbCl_6^-$ oxidizes substrate **2** to give radical cation $\mathbf{2}^{\bullet+}$, which adds to **2** to give the dimer radical cation $\mathbf{3}^{\bullet+}$.



Scheme 1. The radical cation chain reaction of *trans*-anethole (**2**) initiated by $\mathbf{1}^{\bullet+}SbCl_6^-$ to give *trans,anti,trans*-1,2-bis-(4-methoxyphenyl)-3,4-dimethyl cyclobutane (**3**) via the reactive intermediates $\mathbf{2}^{\bullet+}$ and $\mathbf{3}^{\bullet+}$.[5,6]

[*] Prof. Dr. J. O. Metzger, Dipl.-Chem. S. Meyer, Dr. R. Koch
Institute for Pure and Applied Chemistry
Carl von Ossietzky University Oldenburg
Carl-von-Ossietzky-Strasse 9–11, 26111 Oldenburg (Germany)
Fax: (+49) 441-798-3329
E-mail: juergen.metzger@uni-oldenburg.de

[**] We thank the German Research Association (DFG) and the Heinz Neumüller Foundation, Oldenburg, for financial support.

Supporting information for this article is available on the WWW under http://www.angewandte.org or from the author.

 © 2003 Wiley-VCH Verlag GmbH & Co. KGaA, Weinheim DOI: 10.1002/anie.200352044

This adduct is finally reduced by substrate **2** to yield cycloaddition product **3**. Up until now, the two radical cations could not be detected directly in this chain reaction. However, radical cation $\mathbf{2}^{\bullet+}$ could be detected and characterized in pulse radiolysis of anethole (**2**) by UV spectroscopy,[8–10] in photoinduced electron transfer from **2** to triplet quinone by CIDNP (chemically induced dynamic nuclear spin polarization),[11] as well as in zeolite Na ZSM-5 by ESR spectroscopy and CIDNP,[12] and also by cyclic voltammetry.[13] Despite considerable effort, radical cation $\mathbf{3}^{\bullet+}$ could not be detected directly in solution by any method so far.[8,9]

For the mass-spectrometric investigation of this reaction separate solutions of **2** (1.0 mM) and $\mathbf{1}^{\bullet+}SbCl_6^-$ (0.1 mM) in absolute dichloromethane were prepared.[14] The two solutions were injected with a dual syringe pump into an effective micromixer,[15] which was coupled directly to the ion source of the mass spectrometer. The reacting solution was pumped directly and continuously into the mass spectrometer.[16] The reacting solution was first examined by APCI-MS. The APCI mass spectrum shows substrate $[\mathbf{2}+H]^+$ (*m*/*z* 149) and product $[\mathbf{3}+H]^+$ (*m*/*z* 297) in addition to radical cation $\mathbf{1}^{\bullet+}$ (*m*/*z* 481/483), proving that a reacting solution is being introduced into the ion source of the mass spectrometer and being ionized.[17] For comparison compounds **2** and **3** were examined separately by APCI-MS, and the respective quasimolecular ions were observed.[17] Remarkably, the APCI mass spectrum also shows signals of the radical cations $\mathbf{2}^{\bullet+}$ and $\mathbf{3}^{\bullet+}$, which are formed by the APCI process, besides the quasimolecular ions $[\mathbf{2}+H]^+$ and $[\mathbf{3}+H]^+$. The radical cations $\mathbf{2}^{\bullet+}$ and $\mathbf{3}^{\bullet+}$ were characterized unambiguously by APCI-MS/MS (Figure 1).

If one assumes the radical cation chain mechanism, both transient radical cations $\mathbf{2}^{\bullet+}$ and $\mathbf{3}^{\bullet+}$ must be present under steady-state conditions in low concentrations in the reacting solution of $\mathbf{1}^{\bullet+}SbCl_6^-$ and **2**. Because the ESI method in contrast to APCI normally releases ions preformed in solution, it can be expected that the ions $\mathbf{2}^{\bullet+}$ and $\mathbf{3}^{\bullet+}$ should be detectable by ESI-MS/MS in the reacting solution despite the presence of other species.

The ESI mass spectrum (Figure 2a) of the reacting solution shows accordingly an intensive signal for radical cation $\mathbf{1}^{\bullet+}$ (*m*/*z* 481/483). In contrast substrate **2** and product **3** are not present as preformed ions and should not be ionized by the ESI process; not surprisingly, no intensive signals for $\mathbf{2}^{\bullet+}$ (*m*/*z* 148) and $\mathbf{3}^{\bullet+}$ (*m*/*z* 296) are observed. However, very weak ion currents appear at these *m*/*z* values (Figure 2a). By using the MS/MS technique,[1] which allows the separation of the ions of interest from all other ions, and by collision-induced dissociation (CID) their mass-spectrometric characterization, we could detect and identify both radical cations $\mathbf{2}^{\bullet+}$ (Figure 2b) and $\mathbf{3}^{\bullet+}$ (Figure 2c) clearly by comparison with the MS/MS spectra of the species $\mathbf{2}^{\bullet+}$ (Figure 1a) and $\mathbf{3}^{\bullet+}$ (Figure 1b) produced by APCI. The fragmentation of the ions at *m*/*z* 148 and *m*/*z* 296, which were examined under ESI-MS/MS conditions, agrees very well with that of the authentic ions $\mathbf{2}^{\bullet+}$ and $\mathbf{3}^{\bullet+}$, respectively, which were characterized by APCI-MS/MS.[18]

Finally, to prove that $\mathbf{2}^{\bullet+}$ and $\mathbf{3}^{\bullet+}$ are not generated in small amounts by the ESI process itself, control experiments in the absence of $\mathbf{1}^{\bullet+}SbCl_6^-$ were performed. The solution of **2** used

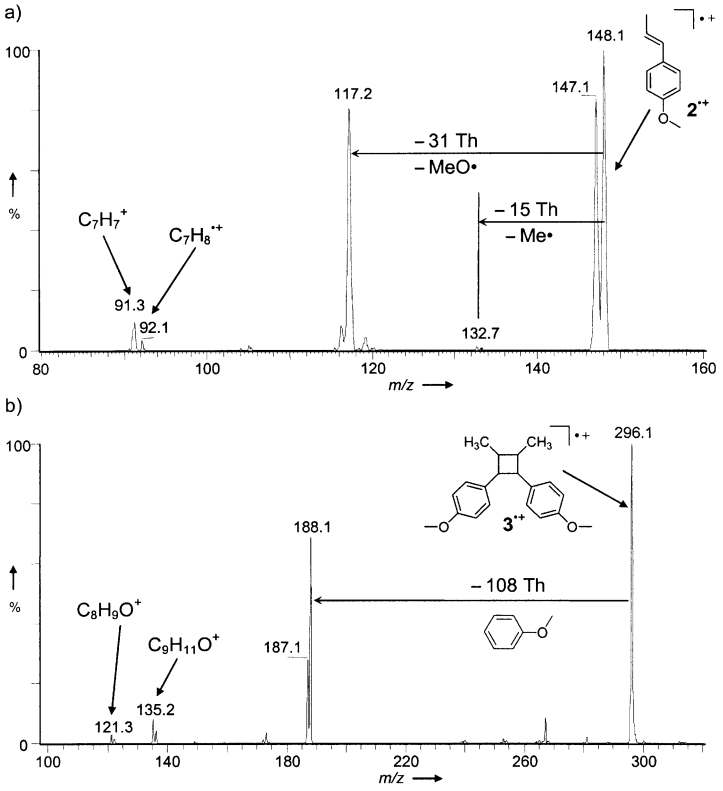


Figure 1. a) MS/MS spectrum of the molecular ion of $\mathbf{2}^{\bullet+}$ (*m*/*z* 148), produced by APCI of the solution of **2** in dichloromethane. CID of $\mathbf{2}^{\bullet+}$ results in ion *m*/*z* 147 by loss of hydrogen (−1 Th). Furthermore the cleavage of methyl radical (−15 Th) and methoxy radical (−31 Th) to give the respective daughter ions *m*/*z* 133 and *m*/*z* 117 is observed as characteristic fragmentations. In addition the ions $C_7H_7^+$ (*m*/*z* 91) and $C_7H_8^{\bullet+}$ (*m*/*z* 92) are formed. b) MS/MS spectrum of the molecular ion of $\mathbf{3}^{\bullet+}$ (*m*/*z* 296), produced by APCI of the solution of **3** in dichloromethane. CID of $\mathbf{3}^{\bullet+}$ gives mainly the ions *m*/*z* 188 und *m*/*z* 187, which correspond to the neutral loss of methoxybenzene C_7H_8O (−108 Th) and $C_7H_9O^{\bullet}$ (−109 Th), respectively. Minor fragmentations form the ions $C_8H_9O^+$ (*m*/*z* 121) and $C_9H_{11}O^+$ (*m*/*z* 135).[18]

was examined by ESI-MS/MS for the presence of the radical cations $\mathbf{2}^{\bullet+}$ and $\mathbf{3}^{\bullet+}$. In the same way product **3** was analyzed. In the respective MS/MS experiments $\mathbf{2}^{\bullet+}$ and $\mathbf{3}^{\bullet+}$ could not be observed. Thus, the ESI process neither oxidizes substrate **2** to $\mathbf{2}^{\bullet+}$ nor product **3** to $\mathbf{3}^{\bullet+}$. These experiments give clear evidence that radical cations $\mathbf{2}^{\bullet+}$ and $\mathbf{3}^{\bullet+}$ (Figure 2b, c) detected in the reacting solution, as described above, are generated in the radical cation chain reaction and are not formed by a mass-spectrometric ionization process in the ESI source.

It has often been debated whether radical cation $\mathbf{3}^{\bullet+}$ exists as a distonic ion or as a cyclobutane radical cation.[5] Under our experimental conditions the cyclobutane radical cation is observed exclusively. A distonic open-chain radical cation can be excluded since fragmentation to *m*/*z* 148 ($\mathbf{2}^{\bullet+}$) is not evident.[20]

Quantum-mechanical calculations confirm these findings. They predict the addition of **2** to $\mathbf{2}^{\bullet+}$ to be exothermic by 88 kJ mol^{-1}. The radical cation $\mathbf{3}^{\bullet+}$ (Figure 3) is calculated to be 52 kJ mol^{-1} lower in energy than the distonic 1,4-butanediyl radical cation (UMP2/6-311 + G(d,p)//UB3LYP6-31G(d)).[21] The barrier for ring closure of the latter radical

 © 2003 Wiley-VCH Verlag GmbH & Co. KGaA, Weinheim

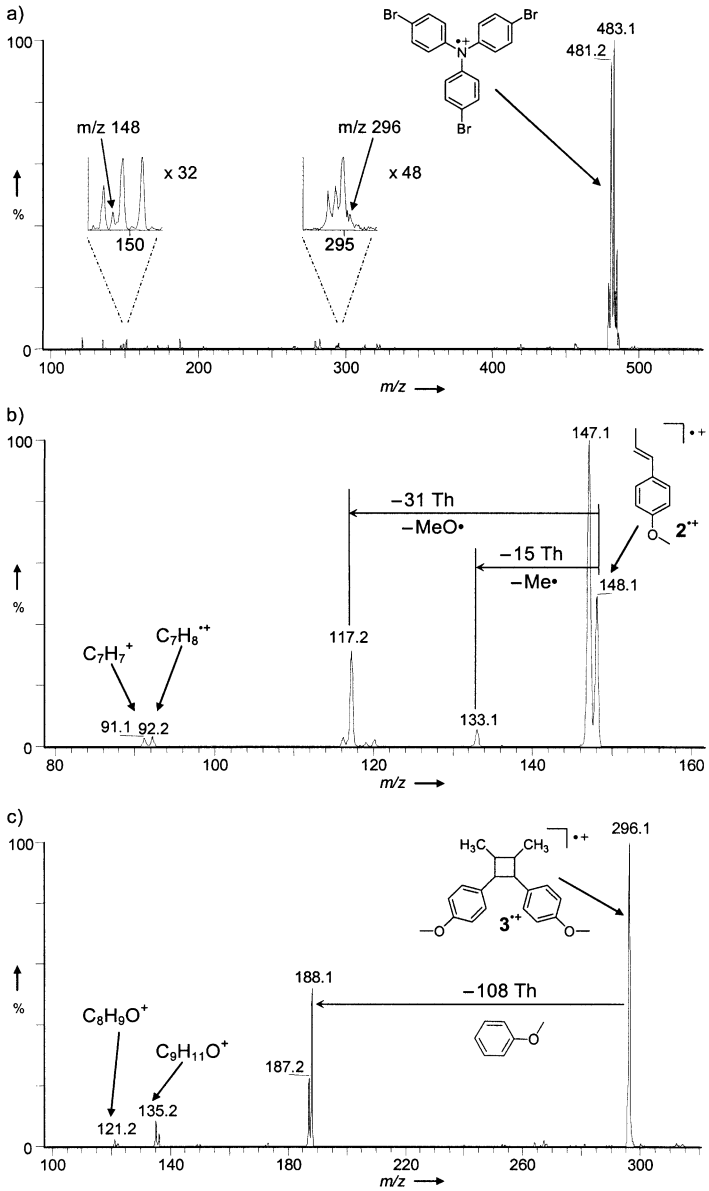


Figure 2. a) Positive ESI mass spectrum of the reacting solution of **2** and $\mathbf{1}^{+\bullet}SbCl_6^-$ in dichloromethane (reaction time ca. 7 s). The spectrum displays only the intensive signal of $\mathbf{1}^{+\bullet}$ (*m*/*z* 481/483). The transient radical cations $\mathbf{2}^{\bullet+}$ (*m*/*z* 148) and $\mathbf{3}^{\bullet+}$ (*m*/*z* 296) are not immediately evident in the spectrum. When the signal is intensified, very weak signals can be recognized at the *m*/*z* values expected for the radical cations. b) ESI-MS/MS spectrum of the ion at *m*/*z* 148 of the same reacting solution, which shows fragmentations identical to those in the APCI-MS/MS spectrum of the authentic radical cation $\mathbf{2}^{\bullet+}$ (see Figure 1a). c) ESI-MS/MS spectrum of the ion at *m*/*z* 296 of the same reacting solution, which shows fragmentations identical to those in the APCI-MS/MS spectrum of the authentic radical cation $\mathbf{3}^{\bullet+}$ (see Figure 1b).

cation to give $\mathbf{3}^{\bullet+}$ is about 10 kJ mol^{-1}, which is small enough to allow spontaneous cyclization. A prediction whether the cycloaddition may be concerted or stepwise[5] is not possible based on these results.

The newly formed diaryl-substituted C–C bond in $\mathbf{3}^{\bullet+}$ is about 0.1 Å longer than the analogous bond in the neutral cyclobutane derivative **3** (1.669 Å vs. 1.571 Å). NBO analysis shows that the charge in $\mathbf{3}^{\bullet+}$ is well delocalized in the aromatic

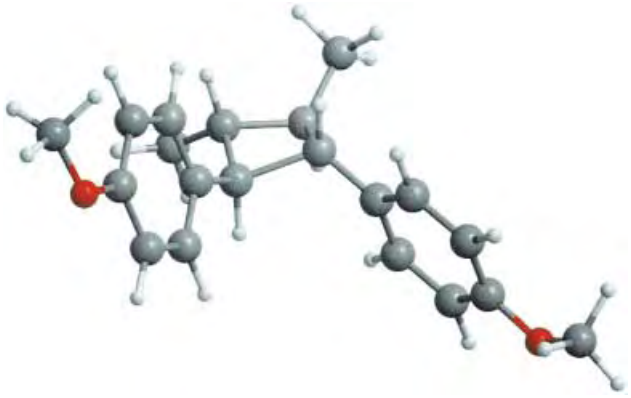


Figure 3. UB3LYP6-31G(d)-optimized structure of $\mathbf{3}^{\bullet+}$.

substituents. No centers with significantly increased partial charges can be identified.

With the method described, transient radical cations could be detected for the first time conveniently and unambiguously in a radical cation chain reaction of synthetic interest under conditions comparable to those of the preparative reaction. The reactions were studied by online coupling of a microreactor system to APCI- and ESI-MS. The transient radical cations were detected and characterized by ESI-MS/MS. This method is also of very general importance since it can be applied to detect transient species in principle in any reaction in solution, presuming that these intermediates are ionic or can be ionized.

Received: June 3, 2003 [Z52044]

Keywords: cycloadditions · mass spectrometry · microreactors · radical ions · reactive intermediates

[1] *Electrospray Ionization Mass Spectrometry—Fundamentals, Instrumentation and Applications* (Ed.: R. B. Cole), Wiley, New York, **1997**.
[2] a) A. G. Harrison, *Chemical Ionization Mass Spectrometry*, CRC, 2nd ed., Boca Raton, **1992**, pp. 53–55; b) W. D. Lehmann, *Massenspektrometrie in der Biochemie*, Spektrum Akademischer Verlag, Heidelberg, **1996**, pp. 48–52.
[3] J. Griep-Raming, S. Meyer, T. Bruhn, J. O. Metzger, *Angew. Chem.* **2002**, *114*, 2863–2866; *Angew. Chem. Int. Ed.* **2002**, *41*, 2738–2742.
[4] D. J. Bellville, D. D. Wirth, N. L. Bauld, *J. Am. Chem. Soc.* **1981**, *103*, 718–720.
[5] N. L. Bauld, D. Gao, The Electron-Transfer Chemistry of Carbon–Carbon Multiple Bonds in *Electron Transfer in Chemistry, Vol. II, Part 1* (Eds.: V. Balzani, J. Mattay), Wiley-VCH, Weinheim, **2001**, pp. 133–205.
[6] a) N. L. Bauld, D. J. Bellville, R. Pabon, R. Chelsky, G. Green, *J. Am. Chem. Soc.* **1983**, *105*, 2378–2382; b) K. T. Lorenz, N. L. Bauld, *J. Am. Chem. Soc.* **1987**, *109*, 1157–1160.
[7] N. L. Bauld, R. Pabon, *J. Am. Chem. Soc.* **1983**, *105*, 633–634.
[8] F. D. Lewis, M. Kojima, *J. Am. Chem. Soc.* **1988**, *110*, 8664–8670.
[9] O. Brede, F. David, S. Steenken, *J. Chem. Soc. Perkin Trans. 2* **1995**, 23–32.
[10] S. Tojo, S. Toki, S. Taramuku, *J. Org. Chem.* **1991**, *56*, 6241–6243.

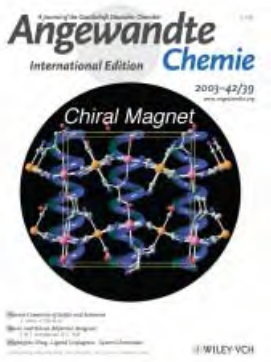
 © 2003 Wiley-VCH Verlag GmbH & Co. KGaA, Weinheim

[11] a) G. Eckert, M. Goez, *J. Am. Chem. Soc.* **1994**, *116*, 11999 – 12009; b) M. Goez, G. Eckert, *J. Am. Chem. Soc.* **1996**, *118*, 140 – 154.
[12] H. D. Roth, H. Weng, D. Zhon, P. S. Lakkaraja, *Acta Chem. Scand.* **1997**, *51*, 626 – 635.
[13] C. Demaille, A. J. Bard, *Acta Chem. Scand.* **1999**, *53*, 842 – 848.
[14] Solutions of $\mathbf{1}^{\bullet+}SbCl_6^-$ (1.6 mg, 2 μmol) and of **2** (3.0 mg, 20 μmol) were prepared with freshly distilled dichloromethane and kept in absence of light. The two solutions were injected with the same flow rate with a dual syringe pump into an effective micromixer that was coupled directly to the ion source of the mass spectrometer, and the reacting solution was pumped continuously into the MS. The flow rate can be varied in the range of 2.5 to 100 $\mu L\,min^{-1}$. When the microreactor is connected directly to the spray capillary, reaction times from 0.7 to 28 s can be covered.
[15] Micromixer Alltech PEEK Mixing Tee. The microreactor was connected to the LCQ-APCI source through a fused-silica transfer capillary. The microreactor was connected to the ESI source directly through the stainless-steel spray capillary.
[16] All experiments were performed using a Finnigan LCQ (Thermo Finnigan, San José, CA, USA) quadrupole ion trap mass spectrometer equipped with a standard ESI and APCI ion source. The standard ESI source of the LCQ was used with a stainless-steel metal capillary (110 μm ID, 240 μm OD, 120.5 mm in length, Metal Needle Kit, Thermo Finnigan).
[17] See Supplementary Information.
[18] The ESI mass spectrum of the reacting solution (Figure 2a) shows a signal at *m*/*z* 295, which contributes with its ^{13}C isotopomer to the signal of the radical cation $\mathbf{3}^{\bullet+}$ (*m*/*z* 296). This contribution was calculated to be approximately 30% by comparison of the relative intensities of *m*/*z* 188 and *m*/*z* 187 in the APCI-MS/MS spectrum (Figure 2b) and in the ESI-MS/MS spectrum (Figure 3c). In case of CID fragmentation of radical cation $\mathbf{3}^{\bullet+}$ the cleavage of methoxybenzene (anisole) C_7H_8O is in agreement with the elimination of benzene from a 1,2-diphenylethane radical cation.[19] An additional fragmentation of $C_7H_9O^{\bullet}$ is remarkable. Furthermore, it is surprising that no daughter ion *m*/*z* 148 and therefore no cycloreversion can be observed. For that reason we also generated radical cation $\mathbf{3}^{\bullet+}$ by EI from **3**. Under these conditions the daughter ions *m*/*z* 188 and *m*/*z* 187 are observed unambiguously in the MS/MS spectrum. Ion *m*/*z* 148 is formed with low intensity.
[19] D. Kuck, A. Bruder, D. V. Ramana, *Int. J. Mass Spectrom. Ion Processes* **1997**, *167*/168, 55 – 68.
[20] G. S. Groenewold, E. K. Chess, M. L. Gross, *J. Am. Chem. Soc.* **1984**, *106*, 539 – 543.
[21] All geometries were optimized spin-unrestricted at the B3LYP6-31G(d) level of theory. No spin contamination was observed. Unrestricted MP2/6-311 + G(d,p) single-point energies, based on the DFT geometries, are even more reliable; however, no significant deviations were found. The calculations employed the program package Gaussian 98 and NBO 3.1 included therein.

 © 2003 Wiley-VCH Verlag GmbH & Co. KGaA, Weinheim

Cover Picture

Katsuya Inoue,* Koichi Kikuchi, Masaaki Ohba, and Hisashi Ōkawa



Chiral magnets exhibit two important optical properties: intrinsic optical activity and the Faraday effect. Two-dimensional chiral magnets reveal these effects at higher critical temperatures than their one-dimensional counterparts. On page 4810 ff., K. Inoue and co-workers describe the structure and magnetic properties of such a chiral molecular magnet in which Mn^{II} and Cr^{III} ions are shown to interact ferrimagnetically; the magnetic transition occurs at 38 K.

Contents

Angewandte EarlyView

The following articles are available online (in Wiley InterScience). You can find them at www.angewandte.org, under Full Text, Early View.

Z. Machova, R. von Eggelkraut-Gottanka, N. Wehofsky, F. Bordusa, A. G. Beck-Sickinger:*
Expressed Enzymatic Ligation for the Semisynthesis of Chemically Modified Proteins
DOI: 10.1002/anie.200351774
Published online: September 30, 2003

A. W. G. Burgett, Q. Li, Q. Wei, P. G. Harran:*
A Concise and Flexible Total Synthesis of (−)-Diazonamide A
DOI: 10.1002/anie.200352577
Published online: September 30, 2003

P. Brunet, E. Demers, T. Maris, G. D. Enright, J. D. Wuest:*
Designing Permeable Molecular Crystals that React with External Agents To Give Crystalline Products
DOI: 10.1002/anie.200352252
Published online: September 19, 2003

Articles judged by the referees or the editor as being either very important or very urgent are immediately edited, proof-read, and electronically published once the manuscript has arrived in the editorial office in final form. As long as there is no page number available these articles should be cited in the following manner:

Author(s) *Angew. Chem. Int. Ed.*, online publication date, DOI.

Web Sites

http://engineering.rowan.edu/~polikar/WAVELETS/WTtutorial.html ____ **4722**	A New Tool for Chemical-Signal Processing	*X.-G. Shao, F.-T. Chau*

Books

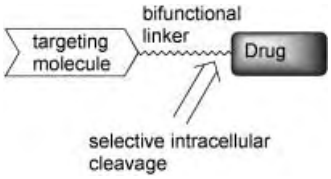
NMR Spectroscopy of Glycoconjugates ____ **4723**	Jesús Jiménez-Barbero, Thomas Peters	*reviewed by Hans Vliegenthart*
Nitride Semiconductors ____ **4724**	Pierre Ruterana, Martin Albrecht, Jörg Neugebauer	*reviewed by Stefan Kaskel*

Highlights

Drug–Ligand Conjugates

W. Maison,* J. V. Frangioni* **4726 – 4728**

Improved Chemical Strategies for the Targeted Therapy of Cancer

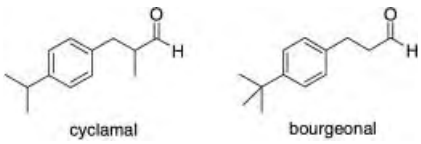


One of the prerequisites for the successful treatment of cancer is selective or "targeted" therapy. Particularly important in this respect are recent advances in the conjugation of cytotoxic compounds to tumor-specific targeting molecules (see picture). The current trend is aimed at minimizing the size of the conjugates.

Sperm Chemotaxis

S. Bartram, W. Boland* ____ **4729 – 4731**

The Arduous Way to the Egg: Follow the Nose



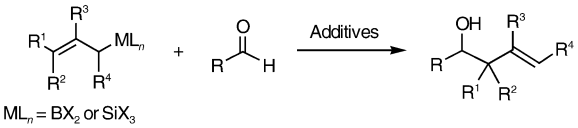
The scent of success! On their way to the ovum, human sperms are guided by chemical signals, which may be related to the scent of the lily of the valley. *para*-Substituted 3-phenylpropanals such as cyclamal and bourgeonal are recognized by an olfactory receptor of the sperm and trigger an influx of Ca^{2+} ions via cAMP as a second messenger. The signal modulates the swimming behavior and speed of the sperm. Undecanal acts as an antagonist and makes the sperm cells slow and disoriented.

Minireviews

Allylation Reagents

J. W. J. Kennedy, D. G. Hall* **4732 – 4739**

Recent Advances in the Activation of Boron and Silicon Reagents for Stereocontrolled Allylation Reactions



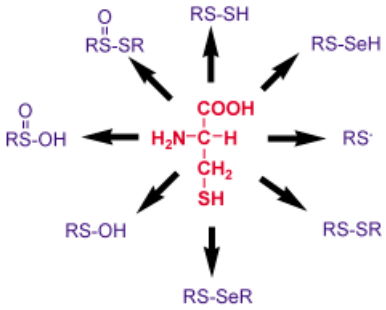
The activation of allyl boron and allyl silicon reagents is a subject of much current interest. Recent strategies are based on increasing the reactivity of the reagents by varying the remaining substituents on the boron or silicon center, or by using a Lewis acid or a Lewis base additive to accelerate reactions with carbonyl compounds or imine derivatives to make homoallylic alcohols and amines in a stereocontrolled fashion (see scheme).

Reviews

Chalcogen-Containing Proteins

C. Jacob,* G. I. Giles, N. M. Giles, H. Sies* **4742 – 4758**

Sulfur and Selenium: The Role of Oxidation State in Protein Structure and Function



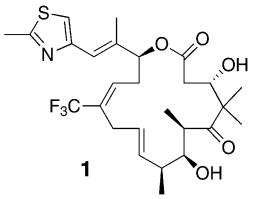
Biochemical chameleon: Chalcogen-containing amino acids play an important role in biological redox chemistry. The oxidation state of sulfur in cysteine varies from −2 to +6, and therefore cysteine can participate in a wide range of redox reactions, such as atom-, electron-, and hydride transfer, as well as radical and exchange reactions (see scheme). Mechanistic, structural, and functional aspects of sulfur- and selenium-containing proteins are discussed.

Communications

Epothilones: Synthesis and Activity

T.-C. Chou, H. Dong, A. Rivkin, F. Yoshimura, A. E. Gabarda, Y. S. Cho, W. P. Tong, S. J. Danishefsky* **4762 – 4767**

Design and Total Synthesis of a Superior Family of Epothilone Analogues, which Eliminate Xenograft Tumors to a Nonrelapsable State



1

Unusually promising profiles of antitumor activity are displayed by 26-trifluoro-(*E*)-9,10-dehydro-dEpoB (**1**), the design and practical total synthesis of which is described. This compound promotes tumor shrinkage and disappearance in human xenografts in nude mice at well-tolerated doses, with complete remission for over two months and early rapid recovery of body weight to the pretreatment control levels.

For the USA and Canada:
ANGEWANDTE CHEMIE International Edition (ISSN 1433-7851) is published weekly by Wiley-VCH PO Box 191161, D 69451 Weinheim, Germany. Air freight and mailing in the USA by Publications Expediting Inc. 200 Meacham Ave., Elmont, NY 11003. Periodicals postage paid at Jamaica NY 11431. US POSTMASTER: send address changes to *Angewandte Chemie*, Wiley-VCH, 111 River Street, Hoboken, NJ 07030. Annual institutional subscription price for institutions: Europe € 3430.00/3118.00. Outside Europe US$ 4499.00/4090.00 (valid for print and electronic/print or electronic delivery); for individuals who are personal members of a national chemical society, or whose institution already subscribes, or who are retired or self-employed consultants, print only. Europe € 248.00/Outside Europe US$ 378.00. Postage and handling charges included. All Wiley-VCH prices are exclusive VAT.

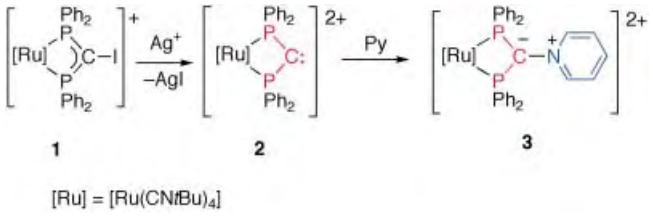
 © 2003 Wiley-VCH Verlag GmbH & Co. KGaA, Weinheim

Contents

Carbene Chemistry

J. Ruiz,* M. E. G. Mosquera, G. García, E. Patrón, V. Riera, S. García-Granda, F. Van der Maelen _____ **4767 – 4771**

Trapping Highly Electrophilic Metalladiphosphanylcarbenes

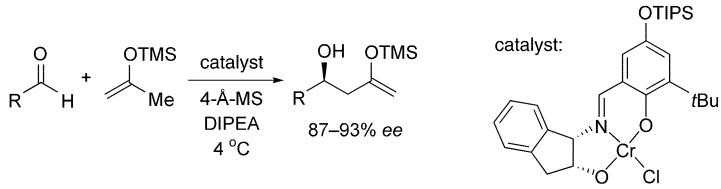


A nonstandard method of carbene generation is provided by reaction of **1** with $AgBF_4$ to give the transient metalladiphosphanylcarbene **2**. This unique dicationic singlet carbene can be trapped with bases (pyridine (Py) for example, see scheme) showing its electrophilic character, which is also confirmed by DFT calculations.

Hetero-Ene Reaction

R. T. Ruck, E. N. Jacobsen* _____ **4771 – 4774**

Asymmetric Hetero-Ene Reactions of Trimethylsilyl Enol Ethers Catalyzed by Tridentate Schiff Base Chromium(III) Complexes

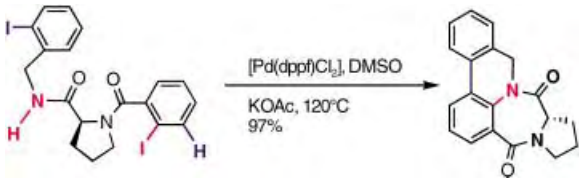


A concerted ene reaction between silyl enol ethers and simple aldehydes is catalyzed by chiral (Schiff base) Cr^{III} complexes with high stereoselectivity (see scheme). This method leads directly to enantioenriched β-hydroxy silyl enol ether derivatives, which are known to be useful intermediates for the stereocontrolled synthesis of substituted polyol frameworks.

Versatile Domino Cyclizations

G. Cuny, M. Bois-Choussy, J. Zhu* _____ **4774 – 4777**

One-Pot Synthesis of Polyheterocycles by a Palladium-Catalyzed Intramolecular N-Arylation/C–H Activation/Aryl–Aryl Bond-Forming Domino Process

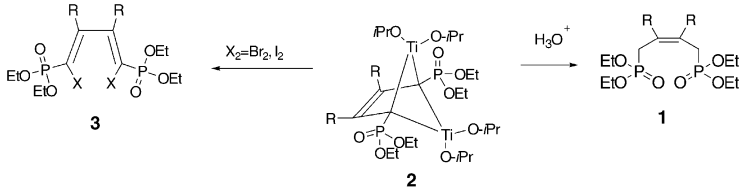


A catalytic domino reaction involving intramolecular N-arylation, C–H activation, and aryl–aryl bond formation provides access to the first dihydroazaphenanthrenes fused with medium-sized and macrocyclic ring systems (see scheme). While $[Pd(dppf)Cl_2]$ catalyzes the transformation efficiently, the "ligand-free" palladium catalyst $Pd(OAc)_2$ was shown to be equally effective (dppf = 1,1′-bis(diphenylphosphanyl)ferrocene).

Bisallylphosphonates

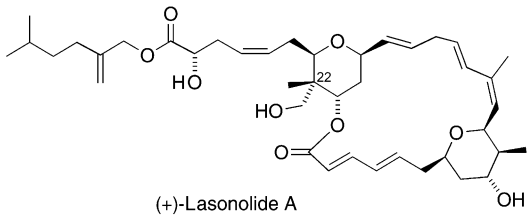
A. A. A. Quntar, O. Baum, A. Shibli, V. M. Dembitsky, M. Srebnik* _____ **4777 – 4779**

Substituted 1,4-Bisallylphosphonates: Preparation from 1-Alkynylphosphonates and $Ti(OiPr)_4/2\,iPrMgCl$



Unexpectedly 1-Alkynylphosphonates react with two equivalents of $Ti(OiPr)_2$ to give phosphonates **1**. Deuterium labeling suggests a dinuclear titanium intermediate **2**. The reaction is general for nonhindered 1-alkynylphosphonates. Addition of Br_2 or I_2 to **2** produces compounds **3**.

 © 2003 Wiley-VCH Verlag GmbH & Co. KGaA, Weinheim



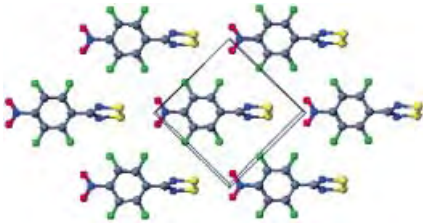
(+)-Lasonolide A

The diastereoselective differentiation of two methylene groups of a cyclic acetal is a unique feature of a highly enantioselective total synthesis of natural (+)-lasonolide A (see picture), which is used to create the C22 quaternary asymmetric center. Other key strategies are the use of a sulfone–sulfide as a three-carbon fragment with two latent *trans* double bonds and macrocyclization through an intramolecular Horner–Emmons reaction.

Natural Product Synthesis

S. H. Kang,* S. Y. Kang, C. M. Kim, H.-w. Choi, H.-S. Jun, B. M. Lee, C. M. Park, J. W. Jeong —— **4779 – 4782**

Total Synthesis of Natural (+)-Lasonolide A



The sulfur–nitrogen radical *p*-$O_2NC_6F_4CNSSN^{\bullet}$ (see packing diagram) provides a rare example of an organic radical that orders ferromagnetically above 1 K. It is suggested that the near orthogonal nature of the singly occupied molecular orbitals of neighboring molecules is important for such behavior to be observed.

Organic Ferromagnetism

A. Alberola, R. J. Less, C. M. Pask, J. M. Rawson,* F. Palacio, P. Oliete, C. Paulsen, A. Yamaguchi, R. D. Farley, D. M. Murphy —— **4782 – 4785**

A Thiazyl-Based Organic Ferromagnet

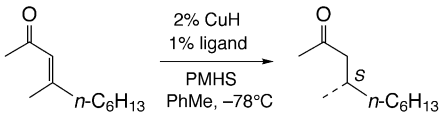
Arrays of nanoscale polymer brushes have been synthesized on both metallic and insulating substrates by a combination of dip-pen nanolithography and surface-initiated ring-opening metathesis polymerization (see atomic force microscopy image). This approach provides control over patterned polymer feature size, brush length, and composition. The technique points towards a way of rapidly making combinatorial libraries of functional polymer nanostructures.



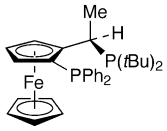
Nanoscale Polymer Brushes

X. Liu, S. Guo, C. A. Mirkin* **4785 – 4789**

Surface and Site-Specific Ring-Opening Metathesis Polymerization Initiated by Dip-Pen Nanolithography



95%; 99% *ee*



A powerful new reaction has been developed for the asymmetric 1,4-reduction of prochiral enones (see scheme). The key ingredients in this exceedingly mild and straightforward procedure are catalytic quantities of CuH, a readily available nonracemic phosphane ligand such as that shown, and inexpensive polymethylhydrosiloxane (PMHS) as the stoichiometric source of hydride.

Asymmetric 1,4-Reduction of Enones

B. H. Lipshutz,* J. M. Servesko —— **4789 – 4792**

CuH-Catalyzed Asymmetric Conjugate Reductions of Acyclic Enones

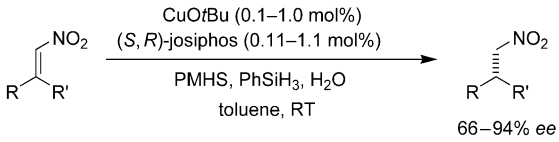
 © 2003 Wiley-VCH Verlag GmbH & Co. KGaA, Weinheim

Contents

Chiral Nitroalkanes

C. Czekelius,
E. M. Carreira* ——— **4793 – 4795**

Catalytic Enantioselective Conjugate Reduction of β,β-Disubstituted Nitroalkenes

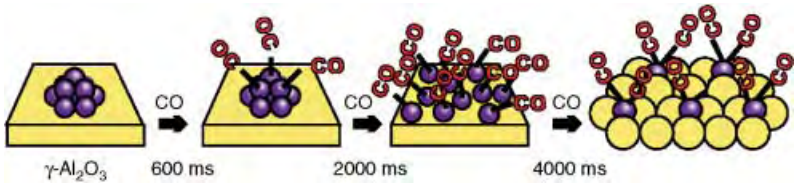


Efficient addition: Bisphosphane–Cu^{I} complexes catalyze the enantioselective reduction of β,β-disubstituted nitroalkenes, giving chiral β,β-disubstituted nitroalkanes in useful yields and selectivities (see scheme). The reaction can be carried out with as little as 0.1 mol% of complex, rendering the process among one of the more efficient methods for conjugate addition chemistry.

Mechanism Elucidation by EXAFS

A. Suzuki, Y. Inada, A. Yamaguchi, T. Chihara, M. Yuasa, M. Nomura, Y. Iwasawa* ——— **4795 – 4799**

Time Scale and Elementary Steps of CO-Induced Disintegration of Surface Rhodium Clusters

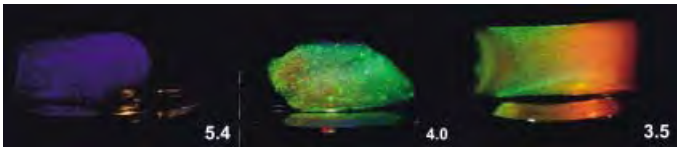


The disintegration of Rh clusters on an Al_2O_3 surface induced by CO, the elementary steps, and timescale of the reaction are analyzed for the first time by energy-dispersive X-ray absorption fine structure (DXAFS) at a time resolution of 100 ms (see picture). This study by the improved time-resolved DXAFS technique provides a new research area of structural dynamics of catalytically active materials at surfaces.

Targeted Hydrogel Synthesis

Z. Hu,* G. Huang ——— **4799 – 4802**

A New Route to Crystalline Hydrogels, Guided by a Phase Diagram

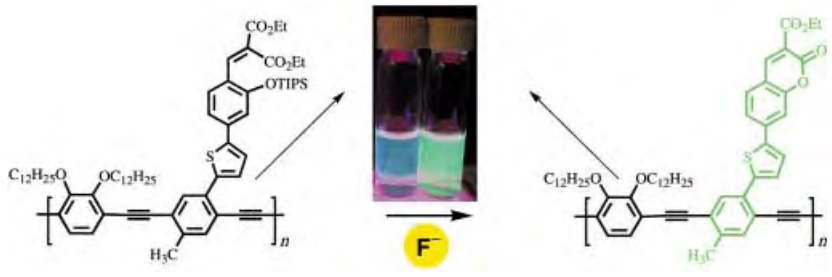


Iridescent crystalline hydrogels with high polymer concentration were synthesized by initiating crystallization of a colloidal fluid near the melting point but stabilizing the crystalline structure below the glass-transition temperature under the guidance of a phase diagram. The iridescent colors of such hydrogels shift from blue to red as the polymer concentration decreases from 5.4 to 3.5 wt% in water, as shown in the photographs.

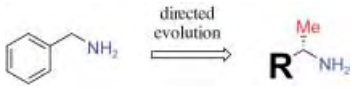
Ion Sensors

T.-H. Kim, T. M. Swager* ——— **4803 – 4806**

A Fluorescent Self-Amplifying Wavelength-Responsive Sensory Polymer for Fluoride Ions



A glowing response: Novel fluoride-selective sensors, utilizing fluoride-induced lactonization to highly fluorescent coumarin derivatives, are reported. The incorporation of this sensory system into a conjugated polymer amplifies the fluorescence response which can be detected visually, see scheme; TIPS = triisopropylsilyl.

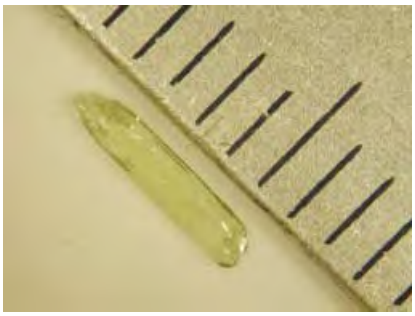


Evolving enzymes: Directed evolution of the amine oxidase from *Aspergillus niger*, by using (*S*)-α-methylbenzylamine as the target substrate, resulted in a variant enzyme (Asn336Ser) possessing both broad substrate specificity and high *S* enantioselectivity towards a wide range of chiral amines (see scheme).

Directed Evolution

R. Carr, M. Alexeeva, A. Enright, T. S. C. Eve, M. J. Dawson, N. J. Turner* ——— **4807 – 4810**

Directed Evolution of an Amine Oxidase Possessing both Broad Substrate Specificity and High Enantioselectivity



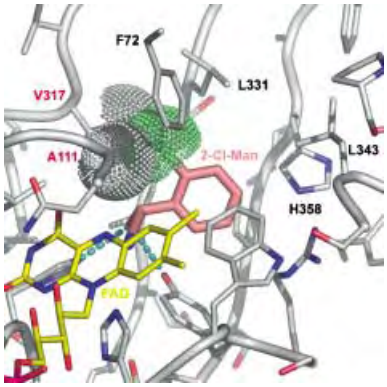
Large single crystals of the chiral ferrimagnet [{$Cr(CN)_6$}{Mn(*S*)-pnH-(H_2O)}](H_2O) can be recovered from the reaction between $K_3[Cr(CN)_6]$, $Mn(ClO_4)_2$, and (*S*)-1,2-diaminopropane dihydrochloride (see picture). Magnetic measurements of the complex show that Mn^{II} and Cr^{III} ions interact ferrimagnetically, with a magnetic transition occurring at 38 K.

Chiral Ferrimagnetism

K. Inoue,* K. Kikuchi, M. Ohba, H. Ōkawa ——— **4810 – 4813**

Structure and Magnetic Properties of a Chiral Two-Dimensional Ferrimagnet with T_C of 38 K

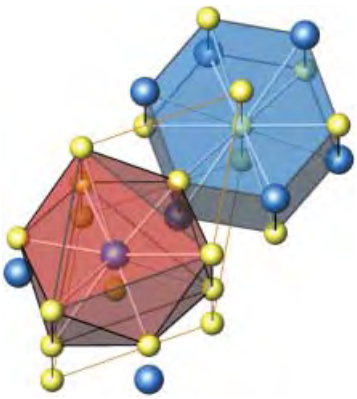
A custom-made enzyme: The gene and protein sequence of a new (*R*)-hydroxynitrile lyase from *Prunus amygdalus* was cloned and engineered for recombinant production on a large scale. The enzyme is stable and active at low pH values. A rationally designed active-site mutant now permits the rapid and stereoselective synthesis of sterically hindered cyanohydrins such as *ortho*-chloromandelonitrile (see picture).



Tailor-Made Enzyme Catalyst

A. Glieder,* R. Weis, W. Skranc, P. Poechlauer, I. Dreveny, S. Majer, M. Wubbolts, H. Schwab, K. Gruber ——— **4815 – 4818**

Comprehensive Step-by-Step Engineering of an (*R*)-Hydroxynitrile Lyase for Large-Scale Asymmetric Synthesis



Relatively ionic: The new platinide Cs_2Pt is dark red and transparent. The calculated band structure shows a complete transfer of the valence electrons from cesium to platinum, which exists as a Pt^{2-} ion. This result is further experimental evidence for a relativistic lowering of the 6s orbital energy. The crystal structure, a Ni_2In structure type (see picture; Cs yellow, Pt blue), is a high-pressure polymorph of the CaF_2 structure. Hence, according to the pressure-homologue rule Cs_2Pt can be considered as a homologue of the alkali-metal chalcogenides.

Stable Platinum Anions

A. Karpov, J. Nuss, U. Wedig, M. Jansen* ——— **4818 – 4821**

Cs_2Pt: A Platinide(-II) Exhibiting Complete Charge Separation

 © 2003 Wiley-VCH Verlag GmbH & Co. KGaA, Weinheim

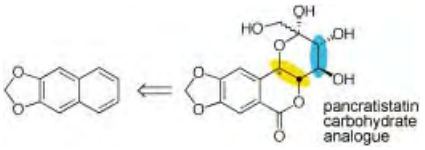
Contents

Pancratistatin Analogues

A. N. Phung, M. T. Zannetti, G. Whited, W.-D. Fessner* ——— **4821 – 4824**

Stereospecific Biocatalytic Synthesis of Pancratistatin Analogues

A two-stage enzymatic sequence of dihydroxylation (at the site labelled in yellow) and aldolization (blue) reactions, which has been developed for the synthesis of analogues of the cytotoxic pancratistatin pharmacophore, converts a naphthalene core into a hybrid arene–carbohydrate structure, with simultaneous creation of four contiguous stereocenters. From the multitude of possible equilibrating product isomers, mild bromine oxidation locks the carbohydrate chain into fixed bicyclic lactones of high molecular complexity.

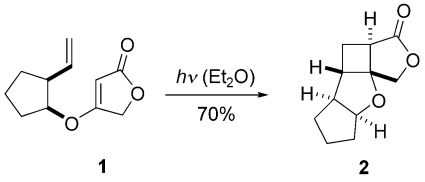


Diastereoselective Photoaddition

M. Kemmler, T. Bach* ——— **4824 – 4826**

[2+2] Photocycloaddition of Tetronates

Previously unknown in photochemistry was the [2+2] photocycloaddition of tetronates. The facial and simple diastereoselectivity of the reaction is excellent, as exemplified by the intramolecular photocycloaddition of the tetronate **1** to give the tetracycle **2**. If the alkoxy group of the tetronic acid is not incorporated in the cyclic skeleton, the cyclobutane in the cycloaddition product may be induced to undergo ring opening in a retroaldol reaction.

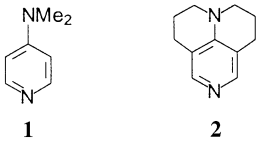


Powerful Acylation Catalyst

M. R. Heinrich, H. S. Klisa, H. Mayr, W. Steglich,* H. Zipse ——— **4826 – 4828**

Enhancing the Catalytic Activity of 4-(Dialkylamino)pyridines by Conformational Fixation

Six times more active than DMAP (**1**), the tricyclic DMAP analogue **2** catalyzes the acetylation of a tertiary alcohol with acetic anhydride. The experimental results can be rationalized by quantum chemical calculations.



VIP Communications labeled with this symbol have been judged by two referees as being "very important papers".

The publication of Communications labeled with this symbol has been accelerated because of their topical or highly competitive nature.

Sources

Product and Company Directory

You can start the entry for your company in "Sources" in any issue of *Angewandte Chemie*.

If you would like more information, please do not hesitate to contact us.

Wiley-VCH Verlag – Advertising Department
Tel.: 0 62 01 - 60 65 65
Fax: 0 62 01 - 60 65 50
E-Mail: MSchulz@wiley-vch.de

Service

Keywords ——— *4830*

Authors ——— *4831*

Angewandte's Sister Journals ——— *4832 – 4833*

Preview ——— *4835*

Corrigenda

In the Communication "Template Synthesis of Uniform 1D Mesostructured Silica Materials and Their Arrays in Anodic Alumina Membranes" by Z. Yang, Y. Lu et al. (*Angew. Chem.* **2003**, *115*, 4333 – 4335; *Angew. Chem. Int. Ed.* **2003**, *42*, 4201 – 4023), the Experimental Section incorrectly refers to the reagent "octachlorosilane". The correct reagent is "octyltrichlorosilane".

In the Communication "Structural Evaluation of Systematically Enumerated Hypothetical Uninodal Zeolites" by R. G. Bell, J. Klinowski, and co-workers (*Angew. Chem.* **2003**, *115*, 4025 – 4029; *Angew. Chem. Int. Ed.* **2003**, *42*, 3895 – 3899), identical diagrams were published as parts c) and d) of Figure 5. The corrected version of Figure 5 is reproduced below:

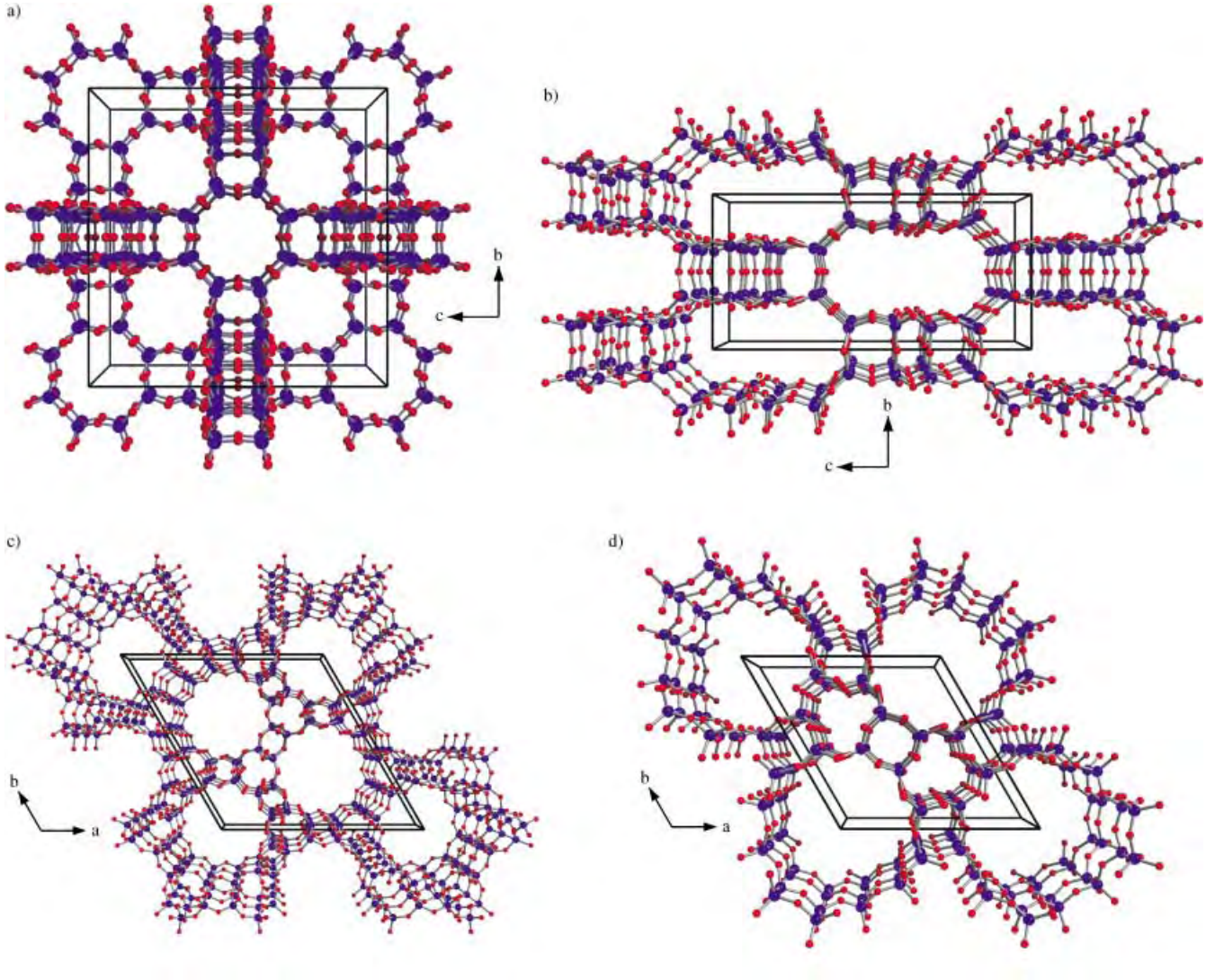


Figure 5. a) Structure 11 consists of cages connected by 4- and 8-membered rings; b) structure 14 contains two systems of elongated channels outlined by 12-membered rings (5.3×9.3 Å) running along the *a* and *b* directions of the unit cell; c) structure 71 consists of layers of 12-membered rings (7.2×7.2 Å) connected by 4- and 6-membered rings; d) structure 73 contains large channels of 12-membered rings, and narrower channels of 4- and 6-membered rings. When viewed along the *c* axis, the structure is similar to that of AFI, although the rings are connected in a different fashion along the *a* and *b* axes.

 © 2003 Wiley-VCH Verlag GmbH & Co. KGaA, Weinheim

Drug–Ligand Conjugates

Improved Chemical Strategies for the Targeted Therapy of Cancer**

Wolfgang Maison and John V. Frangioni**

Keywords:
antitumor agents · bifunctional linkers · chemical conjugation · peptides · tumor targeting

The selective targeting of a compound to tumors, or for that matter to any structure in the body, requires high stability of the compound in blood, biodistribution to the target site, adequate contact time with the target, adequate retention by the target, maintenance of drug potency, and adequate clearance of nontargeted compound. For over two decades, antibodies have been the scaffold of choice for delivering contrast agents and chemotherapeutics to tumor cells since they are stable in blood, typically have nanomolar affinities for their target, and, because binding and nonbinding domains are separated physically, tolerate substitution with contrast agents and chemotherapeutics.[1]

Although monoclonal antibodies (mAbs) are typically tolerant to the conjugation of chemotherapeutics, the agents themselves often lose potency in the conjugated form. Therefore, novel chemical strategies are required for releasing the cytotoxic agent, either after binding to the cancer cell surface or after endocytosis into the cell.[2] A compelling example of this comes from the antitumor antibiotic calicheamicin. When conjugated to a tumor-targeting mAb through an amide linkage, the conjugate is accumulated by the tumor, but has no appreciable cytotoxicity.[3] In contrast, when conjugated by using a pH-sensitive bifunctional linker that permits release of calicheamicin intracellularly[4] (Figure 1), the conjugate shows potent antitumor activity. Indeed, gemtuzumab ozogamicin ("gem-ozo", Mylotarg), a conjugate of a CD33-specific mAb and calicheamicin, which utilizes this bifunctional linker, is already approved for the treatment of certain acute myeloid leukemias.[4]

The taxanes are a class of potent chemotherapeutics that possess a complex chemical structure.[5] Recently, two different strategies have been employed to conjugate taxanes to tumor-targeting monoclonal antibodies, while retaining chemotherapeutic potency. In conjugate mAb-**1** (Scheme 1), an enzymatically cleavable glutarate ester bond[6] is placed between the amide linkage to

[*] Dr. W. Maison
Institut für Organische Chemie
Universität Hamburg
Martin-Luther-King-Platz 6
20146 Hamburg (Germany)
Fax: (+49) 40-42838-2495
E-mail: maison@chemie.uni-hamburg.de
Prof. J. V. Frangioni
Harvard Medical School
Beth Israel Deaconess Medical Center
SL-BO5
330 Brookline Avenue, Boston, MA 02215 (USA)
Fax: (+1) 617-667-0981
E-mail: jfrangio@bidmc.harvard.edu

[**] W.M. is supported by the Deutsche Forschungsgemeinschaft and the Fonds der Chemischen Industrie. J.V.F. is supported by the Department of Energy (Office of Biological and Environmental Research) grant no. DE-FG02-01ER63188, a Clinical Scientist Development Award from the Doris Duke Charitable Foundation, and grants from the National Institutes of Health nos. R21/33 CA-88245 and R21 CA-88870 (National Cancer Institute) and R21/R33 EB-00673 (National Institute of Biomedical Imaging and Bioengineering).

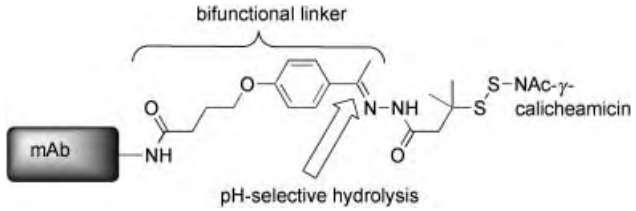
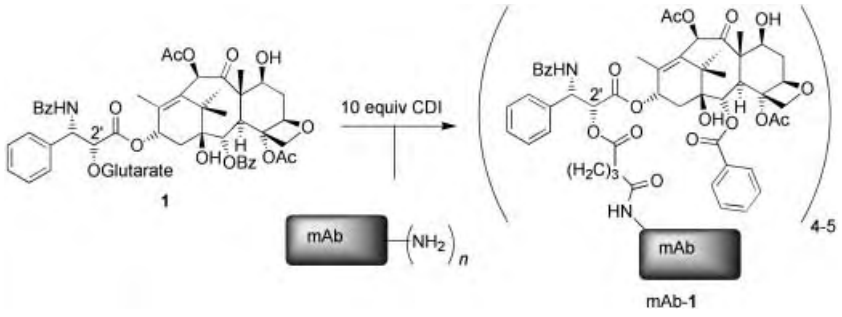


Figure 1. Cleavable bifunctional linker for the conjugation of calicheamicin to monoclonal antibodies.



Scheme 1. Conjugation of paclitaxel derivative **1** to monoclonal antibodies. CDI: *N*,*N*-carbonyldiimidazole.

 © 2003 Wiley-VCH Verlag GmbH & Co. KGaA, Weinheim DOI: 10.1002/anie.200301666

the mAb, and the 2′ position of a first-generation taxane such as paclitaxel (Taxol).[7] After endocytosis of the paclitaxel/mAb conjugate, nonspecific cellular esterases release free paclitaxel, which can diffuse out of endosomes, and into the cytosol, where it exerts its biological effect.[7]

As shown in Scheme 2, the second-generation taxane **2** (SB-T-110131, IDN5109; BAY59-8862) was conjugated at position 10, under mild conditions, by using a methyldisulfanyl alkanoyl (MDS) linker,[8] to mAbs specific for the epidermal growth factor (EGFR), which is known to be overexpressed in several human squamous cell cancers. The anti-EGFR mAbs were modified with *N*-succinimidyl-4-(2-pyridyldithio)-pentanoate to attach 4-pyridyldithio pentanoyl groups and subsequently coupled to taxoid **2** through a disulfide linkage. After endocytosis of the conjugate, the reducing environment of the cell would be expected to release the taxane from the antibody. Antitumor activities of two anti-EGFR mAb-**2** conjugates (KS61-**2** and KS77-**2**) were evaluated against human tumor xenografts in severe combined immune deficiency mice.[8] Both conjugates showed remarkable antitumor activity and it was demonstrated that the dose of mAb–taxoid conjugate used were nontoxic to the mice.

A very interesting and more general linker system based on enzymatic activation was recently reported by Shabat and co-workers.[9] The central core of this "chemical adapter" is a 4-hydroxymandelic acid unit with three functional groups that are suitable for conjugation to a targeting molecule, a cytotoxic moiety, and an enzyme substrate (Figure 2). The underlying concept is that the targeting molecule will guide the conjugate to the tumor site, where an enzymatic reaction with the enzyme substrate would trigger a spontaneous reaction that releases the cytotoxic molecule. The release mechanism proceeds by enzymatic cleavage of the enzyme substrate, subsequent elimination of a cyclic dimethylurea derivative, and formation of an intermediate quinone methide, which releases the cytotoxic molecule as a carbamic acid that decarboxylates spontaneously to yield the active drug (Figure 2). The concept has been proven for a conjugate consisting of a *N*-(2-hydroxypropyl)methacrylamide (HPMA) copolymer[10] as a targeting molecule, etoposide as a cytotoxic molecule, and a substrate for a retro-aldol retro-Michael sequence that is catalyzed by the antibody 38C2 as the cleaving enzyme. However, it has not yet been tested in vivo.

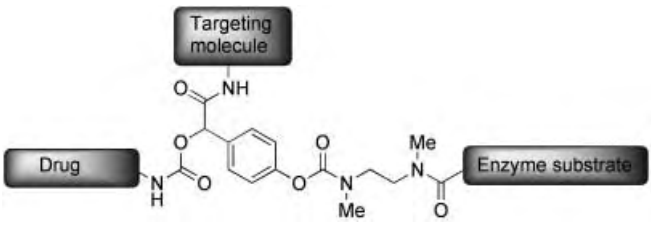
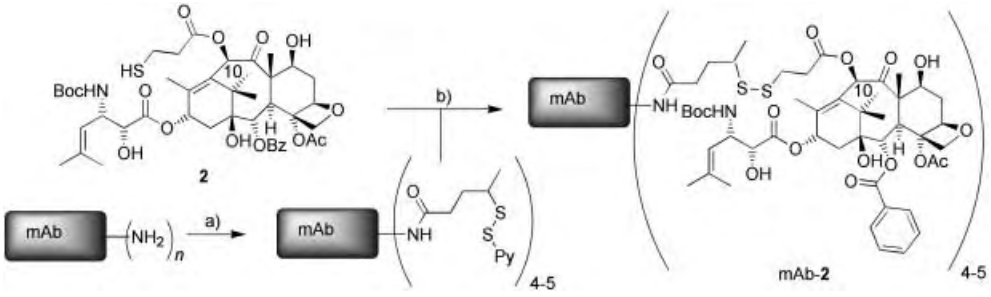


Figure 2. Chemical adapter system based on 4-hydroxymandelic acid.

Although the chemical strategies described above have been typically applied to mAbs, the advantages of mAbs come with a high cost in terms of biodistribution and pharmacokinetics. Immunoglobulin G (IgG) has a molecular weight (M_W) of about 150000 Da, corresponding to a hydrodynamic diameter (HD) of about 10.4 nm. Such macromolecules require over 24 h to reach equilibrium with the extracellular space, exhibit a half-life of two to three days, and typically require up to seven days for complete clearance from the body. Furthermore, the high hydrostatic pressure found in many solid tumors resists penetration of IgG.[11] Finally, although the apparent affinity of antibodies is high, this is achieved by divalency. Indeed, most single-chain antibodies do not possess an affinity high enough for effective targeting in vivo.

Recently, there has been a trend towards replacing the antibody scaffold with low molecular weight ligands. Conceptually, these ligands are similar to an antibody in that they possess one or more binding domains for tumor targeting, and a nonbinding domain for conjugation to functional molecules such as contrast agents and/or chemotherapeutics. Unlike mAbs, their low molecular weight and small hydrodynamic diameter permit rapid clearance, usually via the kidney and liver. The challenge is to engineer low molecular weight ligands such that they are "modular", that is, that they retain tumor binding even after substitution with a molecule that may be of similar, or larger, size.

Natural peptide ligands bind their receptors with high specificity, and with



Scheme 2. Conjugation of monoclonal antibodies to the second-generation taxane **2** (SB-T-110131; Boc = *tert*-butoxycarbonyl). a) *N*-succinimidyl-4-(2-pyridyldithio)pentanoate, 50 mM phosphate buffer, 50 mM NaCl, pH 6.5, 2 mM EDTA, 90 min; b) 50 mM phosphate buffer, 50 mM NaCl, pH 6.5, 2 mM EDTA, 1.7 equiv **2**, 24 h.

 © 2003 Wiley-VCH Verlag GmbH & Co. KGaA, Weinheim

affinities often in the nanomolar or subnanomolar range. Since a number of peptide receptors are overexpressed on human cancer cells, they make attractive targets for therapy. Peptides such as somatostatin, substance P, gastrin, bombesin, α-melanocyte stimulating hormone (α-MSH), neurotensin, and vasoactive intestinal peptide (VIP), or analogues thereof,[12] are being studied as low molecular weight ligands in the preclinical and clinical phases.[13] In fact, radiolabeled derivatives of these peptides already constitute a large class of peptidic agents used for imaging.[14] Among them the ^{111}In-labeled somatostatin analogue OctreoScan is approved for clinical use and a large number of patients have been screened successfully with this analogue.[15]

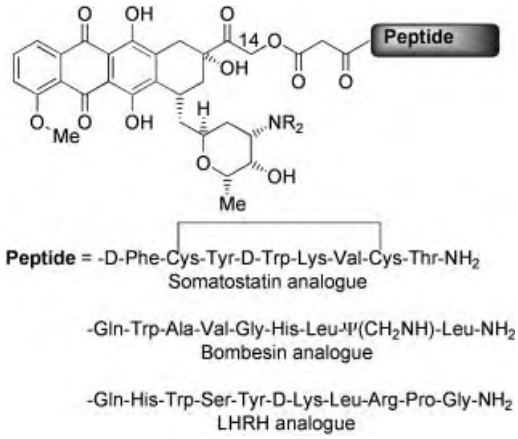


Figure 3. Conjugates of doxorubicin with different targeting peptides.

Conjugation of cytotoxic moieties to tumor-targeting low molecular weight ligands has also been successfully performed.[16] For example, a number of doxorubicin conjugates with analogues of somatostatin, bombesin, and luteneinizing hormone-releasing hormone (LHRH) as targeting molecules have been developed (Figure 3) and tested against various human cancers. Conjugation of the cytotoxic agent to the targeting peptide was done through the 14-*O*-glutaryl esters of doxorubicin, which have been previously reported to be effective antitumor agents.[17] Many of these peptides are also amenable to solid-phase synthesis. Certain LHRH conjugates were extensively investigated in preclinical studies and are planned to be tested in clinical trials soon.[16]

Selective targeting of malignant cells with monoclonal antibodies and low molecular weight ligands is rapidly gaining importance in cancer detection and treatment. For effective therapy, a chemical method for releasing the cytotoxic agent in a bioactive form, and at the appropriate subcellular location, is necessary. We have highlighted some of the newer strategies for effective chemical linkage between targeting molecule and cytotoxic agent, and have identified a trend toward designing more compact targeting molecules, with improved biodistribution and clearance. Such compounds hold great promise for cancer diagnosis and treatment in the future.

[1] R. O. Dillman, *Cancer Invest.* **2001**, *19*, 833 – 841.

[2] F. M. Huennekens, *Adv. Enzyme Regul.* **1997**, *37*, 77 – 90.

[3] A phase 2 study of the cytotoxic immunoconjugate CMB-401 (hCTM01-calicheamicin) in patients with platinum-sensitive recurrent epithelial ovarian carcinoma. S. Y. Chan, A. Gordon, R. Coleman, J. Hall, M. Berger, M. Sherman, C. Eten, N. Finkler, *Cancer Immunol. Immunother.* **2003**, *52*, 243 – 248.

[4] The pH stability of the hydrazone linkage can be triggered by the choice of linker; *para*-substituted acetophenone derivatives such as that in Figure 1 give the best results. They are stable at 37 °C in pH 7.4 buffer (simulating blood circulation conditions) and are rapidly hydrolyzed at pH 4.5 (simulating lysosomal conditions). P. R. Hamann, L. M. Hinman, I. Hollander, C. F. Beyer, D. Lindh, R. Holcomb, W. Hallett, H.-R. Tsou, J. Upeslacis, D. Shochat, A. Mountain, D. A. Flowers, I. Bernstein, *Bioconjugate Chem.* **2002**, *13*, 47 – 58.

[5] Structure–activity relationships of second-generation taxoids: I. Ojima, J. C. Slater, E. Michaud, S. D. Kuduk, P.-Y. Bounaud, P. Vrignaud, M.-C. Bissery, J. Veith, P. Pera, R. J. Bernacki, *J. Med. Chem.* **1996**, *39*, 3889 – 3896.

[6] a) N. F. Magri, D. G. I. Kingston, *J. Nat. Prod.* **1988**, *51*, 298 – 301; b) H. M. Deutsch, J. A. Glinski, M. Hernandez, R. D. Haugwitz, V. L. Narayanan, M. Suffness, Leon H. Zalkow, *J. Med. Chem.* **1989**, *32*, 788 – 792.

[7] V. Guillemard, H. U. Saragovi, *Cancer Res.* **2001**, *61*, 694 – 699.

[8] I. Ojima, X. Geng, X. Wu, C. Qu, C. P. Borella, H. Xie, S. D. Wilhelm, B. A. Leece, L. M. Bartle, V. S. Goldmacher, R. V. J. Chari, *J. Med. Chem.* **2002**, *45*, 5620 – 5623.

[9] A. Gopin, N. Pessah, M. Shamis, C. Rader, D. Shabat, *Angew. Chem.* **2003**, *115*, 341 – 346; *Angew. Chem. Int. Ed.* **2003**, *42*, 327 – 332.

[10] *N*-(2-Hydroxypropyl)methacrylamide (HPMA) copolymers are known to accumulate selectively at tumor sites due to the enhanced permeability and retention effect, which is a consequence of angionesis. H. Maeda, J. Wu, T. Sawa, Y. Matsumura, K. Hori, *J. Controlled Release* **2000**, *65*, 271 – 284.

[11] R. K. Jain, *Int. J. Radiat. Biol.* **1991**, *60*, 85 – 100.

[12] A recent approach to modular dipeptide mimetics: W. Maison, D. Küntzer, D. Grohs, *Synlett* **2002**, 1795 – 1798.

[13] M. Langer, A. G. Beck-Sickinger, *Curr. Med. Chem. Anti Cancer Agents* **2001**, *1*, 71 – 93.

[14] Synthesis of radiolabeled peptides for diagnostic imaging: J. Fichna, A. Janecka, *Bioconjugate Chem.* **2003**, *14*, 3 – 17.

[15] E. P. Krenning, D. J. Kwekkeboom, W. H. Bakker, W. A. Breeman, P. P. Krooij, H. Y. Oei, M. van Hagen, P. T. Postema, M. de Jong, J. C. Reubi, *Eur. J. Nucl. Med.* **1993**, *20*, 716 – 725.

[16] A. V. Schally, A. Nagy, *Life Sci.* **2003**, *72*, 2305 – 2320.

[17] A. Nagy, A. Plonowski, A. V. Schally, *Proc. Natl. Acad. Sci. USA* **2000**, *97*, 829 – 834.

 © 2003 Wiley-VCH Verlag GmbH & Co. KGaA, Weinheim

Sperm Chemotaxis

The Arduous Way to the Egg: Follow the Nose

*Stefan Bartram and Wilhelm Boland**

Keywords:
bourgeonal · chemotaxis · odorants · receptors · signal cascades

The fertilization of a human ovum by a spermatozoon is a remarkably wasteful but nevertheless highly complicated process. Only 200–300 spermatozoids (1 of approximately 25000!) manage the long way from the vagina to the ovum; that is less than 0.004% of the ejaculated sperm cells ($4–40 \times 10^7$). A spermatozoid with a length of about 60 µm has to cross the uterus (ca. 70–80 mm) and at its end find the opening of the fallopian tube (diameter ca. 0.2–0.5 mm). After another 50–80 mm the sperm cells reach the egg (diameter 0.1 mm) coated by a layer of cumulus cells.[1] The sperm cells are transported quite comfortably through the uterus in cervical mucus droplets. Directional peristaltic movements of the organ transport them up to the opening of the active oviduct.[2] Overall a sperm travels a distance more than 3000 times its own length until it reaches a viable oocyte waiting to be fertilized within a few hours. In terms of human dimensions this is equivalent to navigating to a transiently available target of 3 m in diameter at a distance of 4–5 km in complete darkness and through a rugged landscape. Without additional guidance the fusion of sperm cells with a mature oocyte would be a completely random process. Although in the last few decades many chemical messengers from more primitive organisms (sea urchins, algae, corals, fish) were identified that facilitate a directed navigation of the sexual cells towards each other,[3] there was for a long time no considerable progress in the field of mammals.

In the early 1990s, a remarkable breakthrough happened in what at first glance appeared to be a not directly related field. Buck and Axel reported the isolation of a multigene family of odorant receptors (OR) from the olfactory epithelium of rats. All ORs proved to be G-protein coupled and tandem-arranged with a signal transduction pathway.[4] Today, we know that for all organisms studied to date the initial chemoelectric signal transduction is based on analogous receptor–ligand interactions that are followed by different intracellular amplification cascades. Such cascades may involve the activation of adenylate cyclases leading to the production of cyclic adenosine-3′-monophosphate (cAMP) and/or the activation of a phospholipase C, which hydrolyzes membrane-bound phosphatidyl inositol to 1,4,5-triphosphate (IP_3) and diacylglycerol (Figure 1). Each of these cascades generates a receptor potential via specifically associated ion channels, which, among other effects, leads to a transient increase of cytosolic Ca^{2+}.[4–6] The latter can be elegantly visualized by modern ratiofluorometric imaging techniques.[7]

The actual receptor proteins consist of approximately 300 amino acid residues and possess seven transmembrane units (7TM-proteins). The coding region of the epithelial ORs has some conserved amino acid sequences in common that separate them from other 7TM proteins and facilitate their identification. Hypervariable regions are located in the transmembrane segments between the 2nd and 6th unit (Figure 2). The lipophilic odorant molecules are most likely bound in these segments in which the high local structural diversity allows selective interactions with different odorant molecules.[4,6]

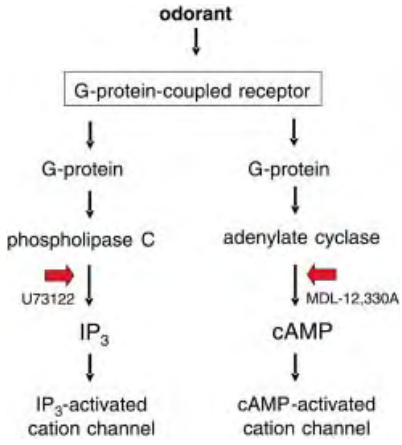


Figure 1. Alternative signal cascades associated with olfactory receptors. Olfactory receptors (OR) act through associated G-proteins and cyclic AMP (typically for vertebrates) or by activation of a phospholipase C, which converts phosphatidyl inositol to IP_3 (invertebrates, fish, crustaceans, and insects). Both cascades activate specifically associated ion channels. The cascades can operate individually (as for example, the expression system of the embryonic kidney cell HEK293) or mutually interact in a complex fashion (e.g. antagonistic). U73122 and MDL-12,330A are specific inhibitors of the two signaling pathways.

Within the human genome 17 different gene families exist that code for ORs and lie distributed on almost all chromosomes with the exception of chromosome 20 and Y. With their approximately 1000 separate genes (only about 350 genes are functional, all others are pseudogenes), they represent up to 1% of the human genome.[6,8] However, very few are exclusively or preferentially expressed in spermatogenic cells. A first OR was previously localized by antibodies on the flagellum of mature dog sperm,[9] and also ion channels with a comparable structure and function to

[*] Prof. Dr. W. Boland, Dr. S. Bartram
Max Planck Institute for Chemical Ecology
Bioorganic Chemistry
Hans-Knöll Strasse 10
07745 Jena (Germany)
Fax: (+49) 3641-57-1202
E-mail: boland@ice.mpg.de

DOI: 10.1002/anie.200301676
© 2003 Wiley-VCH Verlag GmbH & Co. KGaA, Weinheim

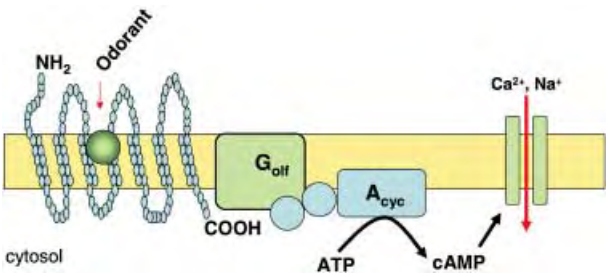


Figure 2. Schematic representation of an olfactory receptor (OR). The binding of the odorant molecule is assumed to occur at the hypervariable transmembrane segments of the OR protein. This activates the adenylate cyclase (A_{cyc}) through the associated olfactory G-protein (G_{olf}). Cyclic AMP (cAMP) is produced and stimulates the influx of Ca^{2+} and Na^+ through specifically associated ion channels.

olfactory cells were already reported to occur on human sperm cells.[10]

Using sequence data of a novel testicular OR-gene (hOR17-4) from chromosome 17, Hatt et al. recently demonstrated for the first time the functional importance of an OR for the navigation (chemotaxis) of human sperm.[11] Since binding of odorants usually occurs in the transmembrane domains of the 7TM-proteins (see Figure 2), a part of the cloned hOR17-4 (II–VII transmembrane segments) was transferred into embryonic human kidney cells (HEK293). In this recombinant system the activation of the receptor complex leads via an associated IP_3-signal cascade (see Figure 1) to a transient increase of cytosolic Ca^{2+}.[7] Although the natural signal of the mature ovum (or its environment) is still unknown, the authors could limit the structural diversity of bioactive candidates by exposing the cells to a mixture of 100 chemically very different odorants (Henkel 100) and their subfractions to identify potential ligands for hOR174. Only one component of this mixture, namely cyclamal (Figure 3) led to an increase of the Ca^{2+} concentration. The ligand tolerance of the receptor was studied next by assays with structurally related compounds and revealed bourgeonal as the most effective compound (bourgeonal and cyclamal represent synthetic lily of the valley scents). An aromatic aldehyde of the type 3-phenylpropanal (Figure 3) was identified as a lead structure. Additional methyl groups in the side chain are tolerated, isopropyl- or *tert*-butyl substituents at the *para* position of the ring amplify the effect. Polar substituents (see helional), or a double bond in the side chain, leave the molecule inactive.

Unexpected results were obtained with Henkel Mix 10/2. Although this mixture contained bourgeonal, no increase of cytosolic Ca^{2+} was observed. Finally it turned out that undecanal, another component of the test mixture, had completely suppressed the Ca^{2+} response. Kidney cells with the completely expressed receptor protein hOR17-4 led to identical results. Most importantly, the observations could be transferred to viable human sperm without restrictions. Although sperm cells are about 100 times more sensitive to bourgeonal than the recombinant HEK-cells, they respond in exactly the same way to the structural features of the test substances. Coapplication of bourgeonal and an inhibitor of the adenylate cyclase (50 μM MDL-12,330A, see Figure 1) suppressed the Ca^{2+} increase, while an inhibitor of phospholipase C (50 μM U73122) showed no effect. These results identify hOR17-4 as a G-protein-coupled receptor operating by means of an cAMP-controlled signal cascade that finally leads to a transient increase of cytosolic Ca^{2+}.

Computer-assisted video analysis of the movement pattern of the sperm cells swimming in a concentration gradient of bourgeonal showed a distinct orientation toward the increasing gradient (chemotaxis) and revealed, in addition, an enhanced speed of the sperm cells, if the concentration exceeded 10^{-8} M. If bourgeonal and undecanal (10–100 nM) were simultaneously present, the bourgeonal response was completely suppressed (Figure 4). Undecanal acts as a competitive antagonist at the binding site of bourgeonal and prevents triggering of the associated signal cascade (competitive antagonist): The sperm cells become slow and disorientated.

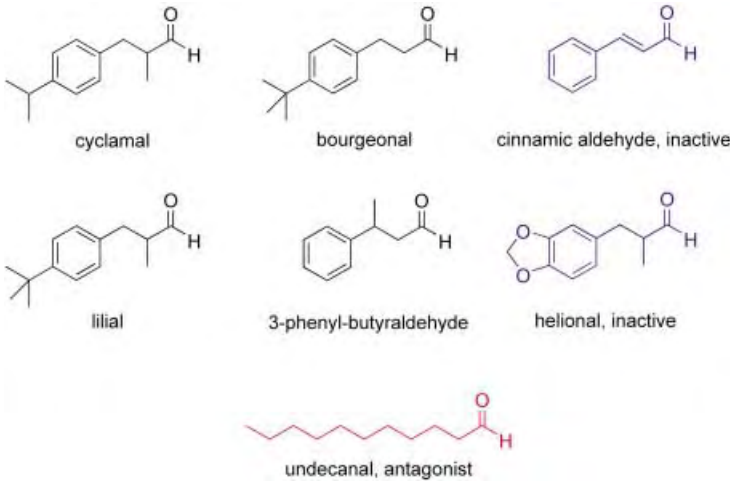


Figure 3. 3-Phenylpropanals acting as signals for human spermatozoids. A double bond in the side chain or polar substituents at the ring are not tolerated. A second substituent has to be placed at the *para* position. Undecanal competes as a strong antagonist for the binding site of hOR17-4.

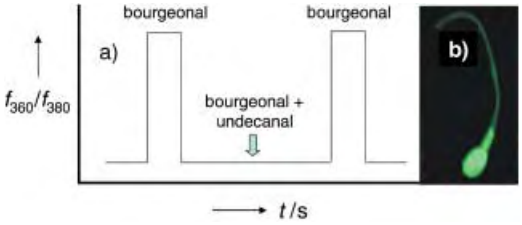
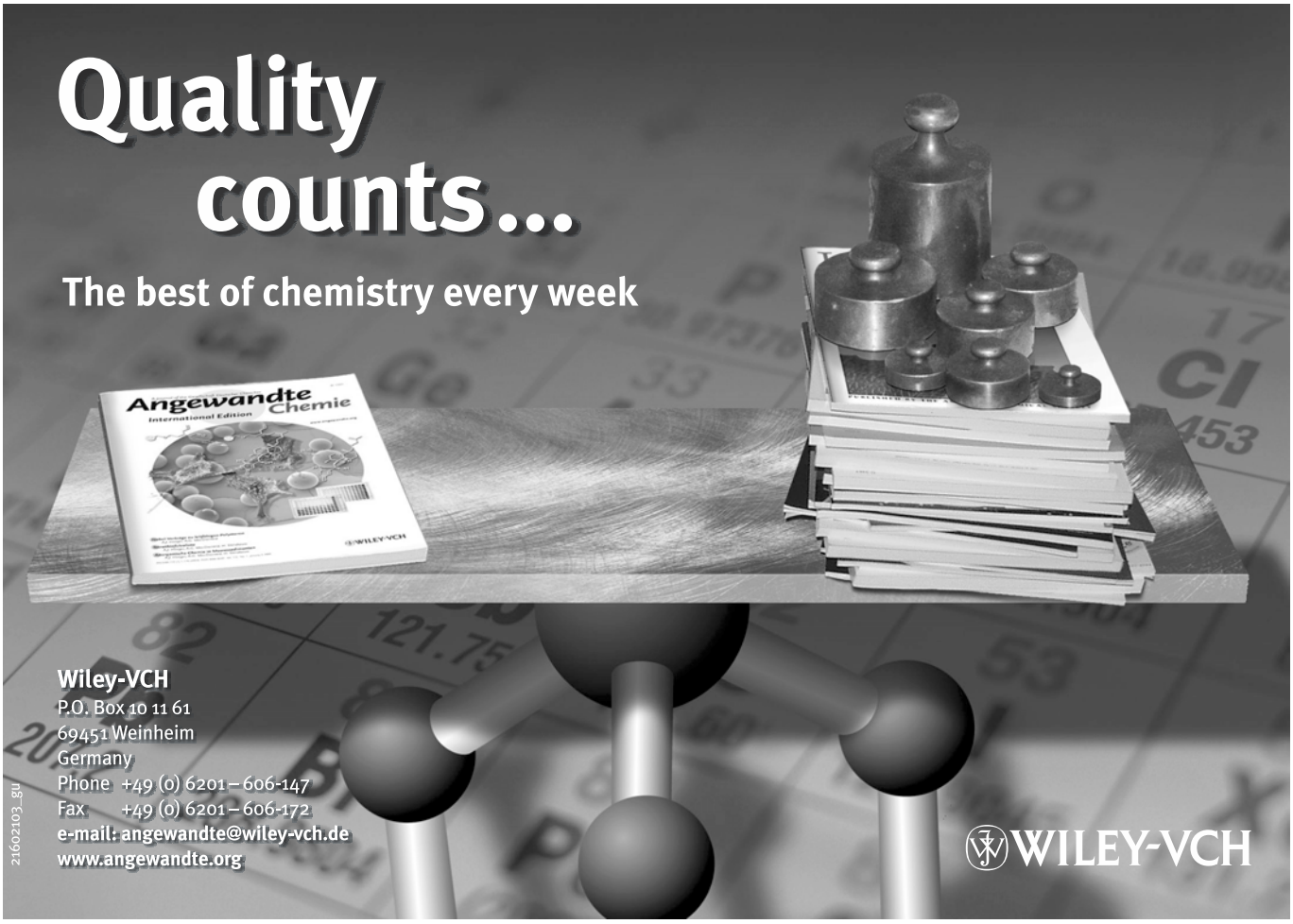


Figure 4. a) Schematic presentation of the response of bourgeonal-stimulated spermatozoids. The transient accumulation of cytosolic Ca^{2+} is monitored by the fluorescence of sperms pretreated with Fura-2 (Ca^{2+}-sensitive fluorescence dye). Bourgeonal induces a reproducible and concentration-dependent influx of Ca^{2+} ions. No influx of Ca^{2+} ions is observed if bourgeonal and undecanal are applied simultaneously. b) Fluorescing sperm cell.

 © 2003 Wiley-VCH Verlag GmbH & Co. KGaA, Weinheim

Although these new results still have to be confirmed by in vivo studies, they create already fascinating perspectives for the future of reproductive medicine. It appears that the success of fertilization could be influenced positively or negatively by local application of signaling compounds. Novel and nontoxic contraceptives, avoiding interactions with the sensitive hormone balance of women, are conceivable. The existence of an agonist and an antagonist competing for the binding site of hOR17-4 suggests that similar phenomena may exist in other olfactory systems and, eventually, could be used for their control. Finally, it remains a major challenge to identify the natural signal(s) of the mature egg or its cellular environment. Whether these signals are the same or closely related for all mammals or whether they share structural features only within limited groups remains an exciting question.

[1] M. Eisenbach, I. Tur-Kaspa, *Bioessays* **1999** *21*, 203 – 210.
[2] G. Kunz, D. Beil, H. Deininger, L. Wildt, G. Leyendecker, *Hum. Reprod.* **1996**, *11*, 627 – 632.
[3] M. Eisenbach, *Rev. Reprod.* **1999**, *4*, 56 – 66.
[4] L. Buck, R. Axel, *Cell* **1991**, *65*, 175 – 187.
[5] J. Krieger, H. Breer, *Science* **1999**, *286*, 720 – 723.
[6] P. Mombaerts, *Science* **1999**, *286*, 707 – 711.
[7] C. H. Wetzel, M. Oles, C. Wellerdieck, M. Kuczkowiak, G. Gisselmann, H. Hatt, *J. Neurosci.* **1999**, *19*, 7426 – 7433.
[8] G. Glusman, I. Ynani, I. Rubin, D. Lancet, *Genome Res.* **2001**, *11*, 685 – 702.
[9] P. Vanderhaeghen, S. Schurmans, G. Vassart, M. Parmentier, *J. Cell Biol.* **1993**, *123*, 1441 – 1452.
[10] I. Weyand, M. Godde, S. Frings, J. Weiner, F. Müller, W. Altenhofen, H. Hatt, U. B. Kaupp, *Nature* **1994**, *368*, 859 – 863.
[11] M. Spehr, G. Gisselmann, A. Poplawski, J. A. Riffell, C. H. Wetzel, R. K. Zimmer, H. Hatt, *Science* **2003**, *299*, 2054 – 2058.



 © 2003 Wiley-VCH Verlag GmbH & Co. KGaA, Weinheim

Allylation Reagents

Recent Advances in the Activation of Boron and Silicon Reagents for Stereocontrolled Allylation Reactions

*Jason W. J. Kennedy and Dennis G. Hall**

Keywords:
activation · allylation · boron · silicon · stereocontrol

Despite the popularity of boron and silicon allylation reagents in stereocontrolled synthesis, they suffer from a number of inherent limitations that have slowed down their development as synthetic tools for nucleophilic additions to carbonyl compounds and imine derivatives. These limitations are the low reactivity and diastereoselectivity of allyl trialkylsilane reagents, and the lack of catalytic systems for the activation and substoichiometric control of enantioselectivity in the additions of allyl boron reagents. To develop more efficient and general methods for the control of absolute stereochemistry in the resulting homoallylic alcohols, new approaches aimed at solving the problem of activation of allylic boron and silicon reagents are needed. This Minireview describes a number of recent approaches that have been devised to address this problem.

1. Introduction

Semimetallic allylic reagents of boron, silicon, and tin have found widespread use in organic synthesis.[1] Their regioselective addition to carbonyl compounds provides stereocontrolled access to functionalized homoallylic alcohols, a highly prized class of synthetic intermediates for the construction of a wide variety of complex natural products.[2] The popularity of these allylation reagents stems mainly from their ease of formation and their stability. From a structural standpoint, allylic boron/silicon/tin compounds share several common features (Figure 1). The metal atom has at least one transferable allylic group, and a number of variable alkyl (R) or heteroatom-containing (X) substituents to complete its valence shell. There are, however, significant mechanistic characteristics and stereochemical consequences that distinguish these different allylation reagents from each other and define their respective advantages and limitations.

A classification system for allylation reagents that takes into account the postulated nature of the mechanism of addition to carbonyl compounds was proposed by Denmark and Weber in the early 1980's.[3] Allyl boron reagents belonging to the type I class (Scheme 1; M = B) are involved in closed, six-membered cyclic chairlike transition states that are characterized by internal activation of the carbonyl group by the boron atom.[4] This mechanism contrasts with the type II reagents, exemplified by most allyl trialkylsilane and allyl trialkylstannane analogues (M = Si or Sn), which generally react with aldehydes under the activation of an external Lewis

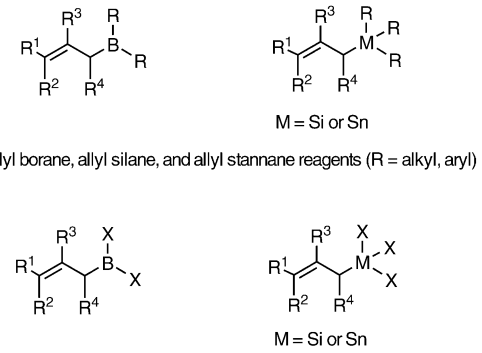
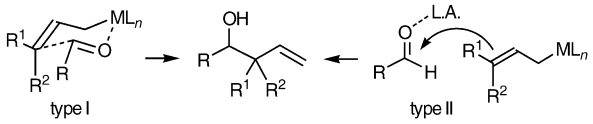


Figure 1. Generic structures for allylic boron, silicon, and tin reagents.



Scheme 1. Postulated mechanistic pathways for type I and type II allylation reagents.[3] L.A. = Lewis acid.

[*] Prof. D. G. Hall, J. W. J. Kennedy
Department of Chemistry, Gunning–Lemieux Chemistry Centre
University of Alberta
Edmonton, Alberta T6G 2G2 (Canada)
Fax: (+1) 780-492-8231
E-mail: dennis.hall@ualberta.ca

 © 2003 Wiley-VCH Verlag GmbH & Co. KGaA, Weinheim DOI: 10.1002/anie.200301632

acid, and proceed by way of open transition structures. Allyl trialkyl tin reagents may also behave as type I reagents in the absence of a Lewis acid, albeit only at high temperatures.[5] Because of their compact and organized transition structure, aldehyde allylborations with γ-substituted reagents tend to demonstrate a level of diastereoselectivity superior to that of the corresponding type II silicon and tin reagents. Furthermore, the stereochemistry of the homoallylic products is predictable from the type I model. For example, (*E*)- and (*Z*)-crotylboron reagents reliably provide the *anti* and *syn* addition products, respectively.

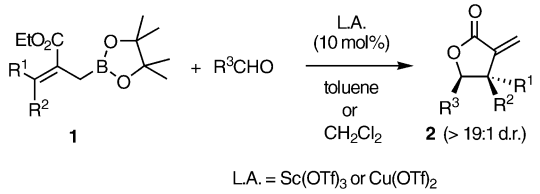
Although allylic tin reagents demonstrate high reactivity under Lewis acid catalysis, the high toxicity associated with tin compounds has prompted some reluctance in their use. Allylic boron and silicon reagents are environmentally friendlier, yet a number of fundamental problems have slowed down their development as synthetic tools. As a consequence of their typical behavior as type II reagents, γ-substituted allyl trialkylsilanes tend to demonstrate a lack of diastereoselectivity. Although the requirement for an external Lewis acid may allow for catalytic enantioselective additions, the traditionally used trimethylsilyl allylic reagents suffer from a lack of reactivity that calls for the use of strong Lewis acids for effective activation. In the case of allyl boranes and allyl boronates, low reactivity is usually not a problem as it can be modulated quite easily by varying the two remaining boron substituents (i.e., R or X in Figure 1). Whereas diastereoselection with γ-substituted allyl boron reagents is generally high, impetus for developing catalytic enantioselective variants did not exist until recently because Lewis acids were thought unsuitable for catalyzing allyl boron additions to aldehydes.

To develop more efficient and general methods for the control of absolute stereochemistry in the resulting homoallylic alcohols, new approaches aimed at solving the problem of activation of allylic boron and silicon reagents are needed. This Minireview describes a number of strategies published over the past five years that have been devised to address this problem. These new strategies can be classified as internal, typically through increasing the reactivity of the reagent by varying the remaining substituents on the metal center, or external, using a Lewis acid or a Lewis base additive to accelerate the reaction with carbonyl compounds or imine derivatives. These strategies may be directed at activating either the allylic reagent or the carbonyl (imine) substrate, or both simultaneously.

2. Lewis Acid-Catalyzed Activation of Allyl Boronates

Despite its enormous utility, carbonyl allylboration remained one of the few important organic reactions devoid of a catalytic system to provide activation and substoichiometric control of enantioselectivity. Because the carbonyl group is internally activated in the transition state by the boron atom itself, there was no apparent reason to believe that these reactions could be accelerated by an external Lewis acid. Moreover, by potentially inducing a changeover from a type I mechanism towards open transition structures, the use of Lewis acids could be detrimental to the diastereoselectivity of the reaction. These perspectives have recently changed since we disclosed the first examples of Lewis acid-catalyzed additions of allyl boronates.[6] Allyl boron pinacolates constitute a particularly attractive class of reagents, which are conveniently purified by chromatography; however, their stability comes at the expense of a mitigated reactivity. Using isomerically pure tetrasubstituted allyl boron pinacolates **1** (Scheme 2),[7] we reported that some metal triflates catalyze the addition of these reagents to aldehydes to give γ-lactone products **2** at temperatures almost 100 °C lower than the corresponding uncatalyzed reactions.

The use of 10 mol % $Cu(OTf)_2$ or $Sc(OTf)_3$ in either dichloromethane or toluene was optimal for providing the fastest rate of formation of α-exomethylene γ-lactone **2**, leading to a complete reaction within 12 h for a wide variety



Scheme 2. Lewis acid-catalyzed additions of tetrasubstituted β-alkoxycarbonyl allyl boronates **1**.[6]



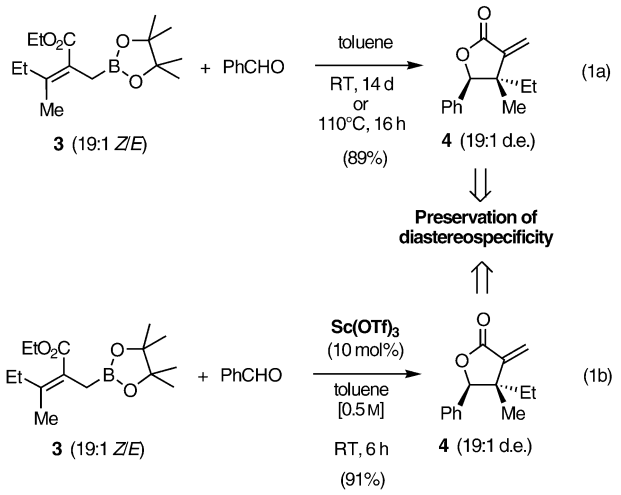
Dennis Hall, born in 1968 in Baie-Comeau (Canada), obtained his PhD in 1995 with Prof. P. Deslongchamps (Sherbrooke) and from 1995 to 1997 was a postdoctoral fellow with Prof. P. G. Schultz (Berkeley). August 1997 saw him take a faculty position at the University of Alberta (promoted to Associate level in 2001). His research focuses on the development of new synthetic and biological applications of organoboronic acid derivatives, with projects including stereocontrolled synthetic methodology and combinatorial chemistry. He received a Boehringer Ingelheim Young Investigator Award for Organic Chemistry (1999), an AstraZeneca Award in Chemistry (2003), and a Petro-Canada Young Innovator Award (2003).



Jason Kennedy, born in 1973 in St. John's (Canada), completed his BSc(Honours) with Prof. G. J. Bodwell in 1995 (Memorial University of Newfoundland), and obtained an MSc under the supervision of Prof. J. M. Chong (Waterloo) in 1998. His PhD studies with Prof. D. G. Hall center on the development of new organoboron-mediated asymmetric reactions. He will soon join the group of Prof. Dr. A. Fürstner (Max-Planck-Institut für Kohlenforschung, Mülheim an der Ruhr) as an NSERC (Canada) postdoctoral fellow.

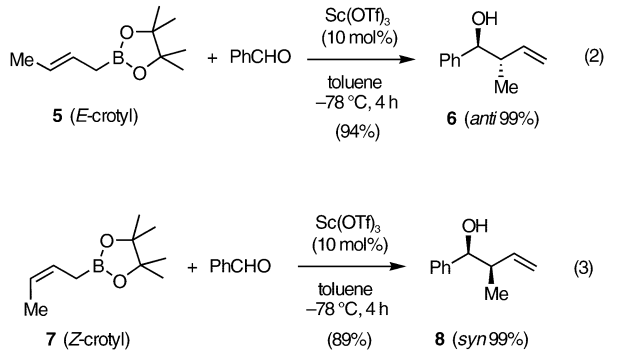
 © 2003 Wiley-VCH Verlag GmbH & Co. KGaA, Weinheim

of aliphatic and aromatic aldehydes. Quite surprisingly, the stereospecificity observed in the uncatalyzed allylborations is preserved, which suggests that type I behavior is maintained in this new catalytic reaction manifold. Furthermore, the rate enhancement is considerable. Indeed, to reach completion without a catalyst,[7] the allylboration between **3** and benzaldehyde required 14 days at room temperature or 16–24 h at 110 °C [Eq. (1a)]! Comparative kinetic experiments showed



that $Sc(OTf)_3$-promoted catalysis provided a 35-fold increase in the reaction rate for the formation of lactone **4** [Eq. (1b)].[6] Provided that the chiral ligands do not appreciably deactivate the metal center, such a level of rate enhancement should be sufficient to allow high selectivity in catalytic asymmetric allylborations. Prospects towards the use of chiral catalysts are thus very promising.

In a related study, Ishiyama, Ahiko, and Miyaura independently reported that the reaction of (*E*)- or (*Z*)-crotylboron pinacolates **5** and **7** could also be greatly accelerated by strong Lewis acids (e.g., $AlCl_3$, $BF_3{\cdot}OEt_2$) as well as with $Sc(OTf)_3$ at −78 °C [Eqs. (2) and (3)].[8] In fact, it is claimed



that aldehyde additions with **5** and **7** do not proceed at this temperature in the absence of the catalyst. The formation of the respective *anti* and *syn* propionate products **6** and **8** also confirmed our findings that the metal-catalyzed allylboration occurs with preservation of diastereospecificity, and that the presence of a 2-carboxyester group on the allyl boronate moiety is not essential for providing a rate enhancement.

Although relatively few ligand systems were attempted, preliminary investigations using chiral aluminum and scandium catalysts provided modest though encouraging levels of enantioselectivity. Altogether, these recent results pave the way for the development of a regio- and diastereospecific, and highly enantioselective catalytic aldehyde allylation system. Provided that broad substrate generality could be demonstrated both for the allyl boronate and the aldehyde components, such a system would constitute an ideal carbon–carbon bond-formation methodology. To reach this objective, a better mechanistic understanding of this new allylboration process is desirable. Unfortunately, the exact mode of Lewis acid promoted activation remains quite hypothetical at this stage. The fact that the catalyzed allylborations preserve the stereospecificity of the uncatalyzed process suggests that a cyclic type I transition structure is favored over open transition structures. Of particular interest is the intriguing question concerning the binding site of the metal ion. Electrophilic boronate activation via coordination of the oxygen atom(s) (Figure 2, **A**), possibly with assistance of the ester in the case of allyl boronates **1**, or double coordination of the aldehyde (Figure 2, **B**) both appear as reasonable possibilities at this stage.

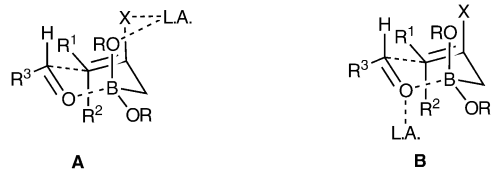


Figure 2. Possible transition structures for the Lewis acid-catalyzed additions of allyl boronates to aldehydes (X = CO_2R' or noncoordinated H).[6] L.A. = Lewis acid.

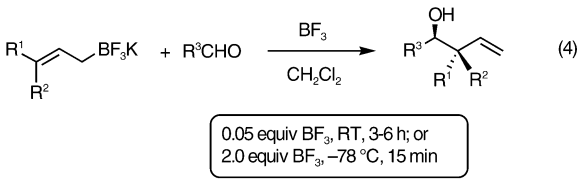
In the former hypothesis (**A**), coordination of the metal to one of the boronate oxygen atoms would suppress n_O–p_B overlap and increase the acidic character of the boron atom, which would compensate by strengthening its interaction with the aldehyde at the transition-state level. This assumption is in agreement with the experimental demonstration by Brown et al. that the electrophilicity of boron is determinant to the reactivity of allyl boronates.[9] Further support also comes from recent MO calculations, which concluded that the strength of boron–carbonyl coordination is the main factor lowering the activation energy of allylborations.[10,11] Double coordination of the aldehyde has been hypothesized to explain the stereochemical outcome in particular cases of aldol condensations.[12] In the present case, double-coordination of the aldehyde in structure **B** would superactivate the carbonyl group to facilitate the formation of a new carbon–carbon bond and concomitantly accelerate the reaction. At first sight, this second hypothesis appears less likely as calculations show only a small degree of C–C bonding character in the allylboration transition state.[10,11] However,

 © 2003 Wiley-VCH Verlag GmbH & Co. KGaA, Weinheim

since other modes of activation may also be possible, further studies are required to elucidate the precise mechanistic nature of these Lewis acid-catalyzed allylborations.

3. Activation of Allyl Boranes by Electronic Modulation of Boron Substituents: Allyl Trifluoroborate Salts

It has long been known that the reactivity of allyl boron reagents can be modulated with the steric and electronic properties of the two remaining boron substituents. In particular, a decrease in the electron-donating ability of the boron substituents is generally translated into an increase of reactivity.[9] The use of more reactive allyl boron reagents is advantageous on the standpoint of stereoselectivity because their reactions may be carried out at a lower temperature. The more reactive allyl boranes and allyl boronates, however, tend to be unstable to air and moisture and thus cannot be easily handled and purified. A few years ago, Batey et al. succeeded at combining stability and reactivity as desirable attributes in a single class of allyl boranes. Inspired by the work of Vedejs et al.,[13] they reported the preparation and additions of a series of allyl trifluoroborate salts [Eq. (4)].[14] These reagents



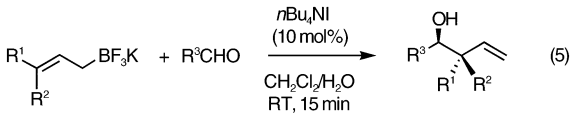
9 (R^1=Me, R^2=H) **6** (R^3=Ph) > 98:2 d.r.

10 (R^1=H, R^2=Me) **8** (R^3=Ph) > 98:2 d.r.

are readily available from the reaction of the corresponding allyl boronic acids with aqueous KHF_2, and they can be purified by recrystallization and stored as air- and water-stable solids for extended periods of time at room temperature.

Allyl trifluoroborate salts are inert to carbonyl compounds until activated by an external Lewis acid, at which point they become extremely effective allylating agents that produce homoallylic alcohols in high yields. This new method of activation is thought to involve a rather unusual mechanism whereby the electrophilic additive (usually $BF_3{\cdot}OEt_2$) strips off a fluoride ion from the trifluoroborate salt. The putative product of this equilibrium is a highly electrophilic tricoordinate allylic difluoroborane. Although the actual allylation species has not been identified, it was anticipated that allylic difluoroboranes should react with aldehydes through the usual type I pathway.[10] Consistent with this hypothesis, the *E*- and *Z*-crotyl reagents **9** and **10** provided, in over 90% yield, the respective *anti* and *syn* aldol-like adducts expected from a cyclic, chairlike transition structure [Eq. (4)]. While the reaction is usually carried out using two equivalents of $BF_3{\cdot}OEt_2$ at −78 °C, it can also be performed with as little as 5 mol% of the same additive, albeit at room temperature. The latter procedure is noteworthy because it provides the first formal example of a catalyzed allylboration.

Even though this new strategy constitutes an appealing methodology to perform diastereoselective allylations, it presents little hope for applications in absolute stereocontrol since neither the activating agent (BF_3) nor the allyl boron substituents (fluoride) are readily modified to incorporate chiral directing groups. Towards this end, the same group recently reported the use of allyl trifluroborate salts in water and in biphasic aqueous media [Eq. (5)].[15] While water alone



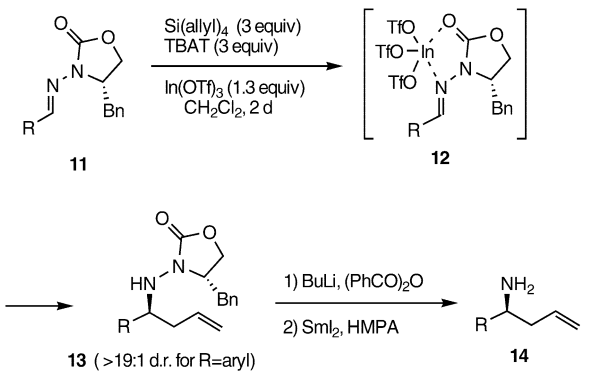
accelerates the allylation of water-soluble aldehydes, the reactions in biphasic media were found to be greatly accelerated by the phase-transfer agent nBu$_4$NI. Although the exact mechanism for this interesting procedure remains to be determined, control experiments revealed a pronounced common-ion effect, which points to the same mechanism described above involving reversible fluoride-ion dissociation rather than direct addition of the allyl trifluoroborate salts. The reaction is thought to occur at the interface of the aqueous and organic phases where all reactive species can coexist at a high effective concentration.

Multinuclear NMR investigations suggest that the reaction occurs on the organic side of the solvent interface. Consistent with these studies, Batey and Thadani have suggested that the added quaternary ammonium salt accelerates the reaction by transporting the water-soluble allyl trifluoroborate anion into the organic phase. Unfortunately, the authors noted that the use of chiral quaternary ammonium salts in this new aldehyde allylation system did not result in enantioselective additions.[15]

4. Dual Activation of Allylsilanes

Allyl trialkylsilane reagents generally require activation of the aldehyde substrate by a strong Lewis acid before they can undergo an addition reaction. One potential drawback to this requirement is that some substrates may not tolerate these conditions. A clever approach to this problem is to use a strategy of dual activation, in which the allylation is promoted by two mild activators rather than a single strong one.[16] This dual activation approach is elegantly demonstrated by the recent work of Friestad and Ding (Scheme 3).[17] Here, chiral *N*-acyl hydrazones **11** were shown to undergo highly stereoselective additions with tetraallylsilane in the presence of both indium triflate and tetrabutylammonium triphenyldifluorosilicate (TBAT). These reaction conditions are compatible with a wide range of aldehydes to afford chiral allylamine derivatives **13** in high yield and good stereoselectivity. Aromatic hydrazones gave the best results, and a single example with an aliphatic hydrazone provided good, if somewhat lower, yield and selectivity. α,β-Unsaturated hy-

 © 2003 Wiley-VCH Verlag GmbH & Co. KGaA, Weinheim

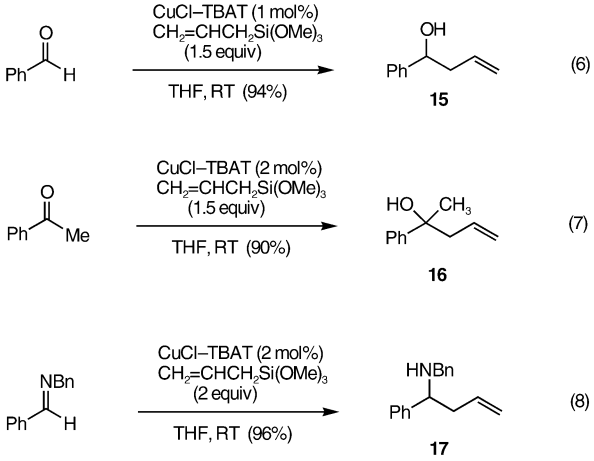


Scheme 3. Dual activation strategy for tetraallylsilane additions onto chiral hydrazones.[17] TBAT = tetrabutylammonium triphenyldifluorosilicate; HMPA = hexamethyl phosphoramide.

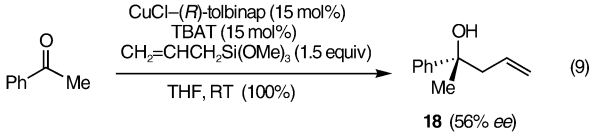
drazones underwent regioselective 1,2-addition. After reaction, the hydrazones can be reductively cleaved with SmI_2 to give enantioenriched α-branched allylamines **14**.

The authors proposed that the reaction proceeds through the attack of a fluoride-activated hypervalent silane on an indium-complexed hydrazone **12**. The indium center serves not only to activate the hydrazone but also to rigidify the substrate, effectively shielding the *Re* face of the C–N double bond. All of the stereochemical results reported can be explained by *Si*-face attack of the allylsilane on the putative chelate **12**. Consistent with the proposed dual-activation effect, reaction in the presence of either TBAT or $In(OTf)_3$ alone proceeded in much lower yield and selectivity.

Shibasaki and co-workers recently reported another example of a dually activated system, in which an allylsilane is activated by both a metal salt and a fluoride anion source.[18] In this study, allyltrimethoxysilane was shown to effectively allylate aldehydes, ketones, and imines in the presence of catalytic amounts of CuCl and TBAT [Eqs. (6)–(8)]. These



conditions appear to be quite general, with cyclic, acyclic, aliphatic, and aromatic substrates, as well as electron-rich and electron-poor compounds all reacting well. As above, α,β-unsaturated enones chemoselectively underwent 1,2-addition. The allylating species generated in this system behaves like a true type II reagent (see below), as both (*E*)- and (*Z*)-crotylsilanes gave the same diastereomeric ratio of products. The authors offer a single enantioselective example, where acetophenone is allylated using a catalytic system derived from (*R*)-binap, CuCl, and TBAT to give tertiary alcohol **18** in 100% yield and 56% enantiomeric excess [Eq. (9)]. Although the enantioselectivity is quite modest, this example marks the first report of a catalytic enantioselective allylsilylation of a ketone.

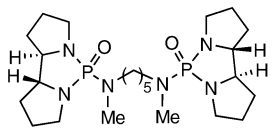


This new activation approach to allylsilylations is suspected to be mechanistically different from that of Friestad and Ding (see above), and its exact nature remains quite speculative. The currently available data points to a complicated mechanism in which the Cu^I species, fluoride ion, and allyltrimethoxysilane all play an active role in the catalytic cycle. NMR studies showed that copper chloride, TBAT, and the allylsilane react in several steps to produce allylfluorodimethoxysilane. However, the authors showed that this tetracoordinate fluorosilane does not allylate benzaldehyde but instead reacts further with another molecule of allyltrimethoxysilane to generate the true allylating species. While the authors cannot at this stage determine if this is an allyl copper species or a hyperactive allyl silicon reagent, they note that the currently available evidence favors the intermediacy of a silicon-based species. They also found that the regioselective 1,2-addition of allyltrimethoxysilane onto benzalacetone (*trans*-4-phenyl-3-buten-2-one) under these conditions is different from the behavior of independently generated allyl copper reagents. Furthermore, as mentioned above, the similar diastereomeric ratio of products originating from both (*E*)- and (*Z*)-crotyltrimethoxysilanes under these conditions is consistent with the outcome expected from typical type II allylsilane reagents.

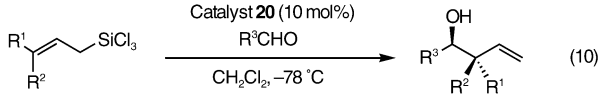
5. Lewis Base Activation of Allyl Trichlorosilanes with Bisphosphoramides

Another approach towards activating allylsilanes comes from Denmark and Fu,[19] who have exploited prior knowledge on the ability of some basic solvents (e.g., DMF) to accelerate the additions of allylic halosilanes.[20] Hexamethylphosphoramide, even employed in substoichiometric amounts, was found to be an effective promoter, and this strategy has now reached the stage where it can be successfully applied in absolute stereocontrol.[21] In the latest advance, treatment of an allyltrichlorosilane **19** with a dimeric chiral phosphoramide catalyst **20** generates a highly reactive silane species which then allylates aldehydes to give homoallylic alcohols in high stereoselectivity [Eq. (10)].[22]

 © 2003 Wiley-VCH Verlag GmbH & Co. KGaA, Weinheim



(*R*, *R*) - **20**

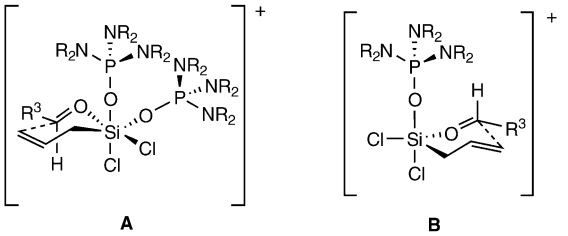


19 (10)

15 (R^1=H, R^2=H, R^3=Ph)	85%, 87% *ee*
21 (R^1=H, R^2=H, R^3=4-MeO-C_6H_4)	84%, 88% *ee*
22 (R^1=H, R^2=H, R^3=4-CF_3-C_6H_4)	79%, 80% *ee*
6 (R^1=Me, R^2=H, R^3=Ph)	82%, 86% *ee* (99:1 d.r.)
8 (R^1=H, R^2=Me, R^3=Ph)	89%, 94% *ee* (99:1 d.r.)
23 (R^1=Me, R^2=Me, R^3=Ph)	89%, 96% *ee*
24 (R^1=Ph, R^2=Me, R^3=Ph)	64%, 94% *ee* (99:1 d.r.)

Under these conditions, unsaturated aldehydes react smoothly to give homoallylic alcohols in good yields and high enantioselectivities. Selectivities range from 80–95% *ee*, with electron-rich aldehydes (e.g., **21**) tending to the higher end of this range and electron-poor aldehydes (e.g., **22**) to the lower.[23] The high diastereoselectivity and the dependence of product stereochemistry on the geometry of γ-substituted reagents, as exemplified by the formation of **6** and **8**, indicates that these allyltrichlorosilanes react through the type I pathway. This behavior is consistent with other base-promoted additions of highly acidic allylic silanes containing electronegative substituents.[1] A significant extension of this work was demonstrated in the synthesis of the serotonin agonist LY426965, where a γ,γ-disubstituted silane underwent effective catalyzed addition to give key intermediate **24** containing an enantioenriched quaternary carbon center.[24]

Silicon has the ability to reach high coordination numbers (up to six) with different geometries and conformations.[25] Mechanistically, the current reaction is believed to proceed via a hexacoordinate silicon species (Figure 3).[26]

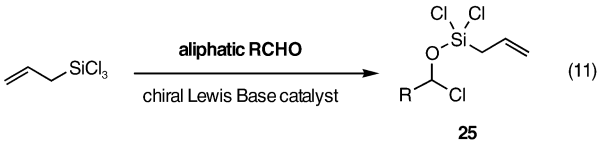


A **B**

Figure 3. Proposed transition structure in the phosphoramide-promoted additions of allyltrichlorosilanes to aromatic and α,β-unsaturated aldehydes.[26]

In this case, both phosphoramide oxygen atoms chelate to the highly acidic trichlorosilyl group, which causes ionization through the loss of one chloride ion. This ionization process generates a cationic, octahedral silane (Figure 3, **A**) which then undergoes reaction with the aldehyde via a closed chairlike type I mechanism. The use of a bisphosphoramide ligand is essential for suppressing competing pathways and obtaining high enantioselectivities in the reaction. Chiral monophosphoramides also catalyze a selective reaction in an analogous manner to the bisphosphoramides, however, they also promote a less selective catalytic addition cycle via a pentacoordinate cationic silane (Figure 3, **B**) where only one phosphoramide group binds to the silicon. Tethering the two phosphoramides together (i.e., using a bisphosphoramide) effectively shuts down this competing process.

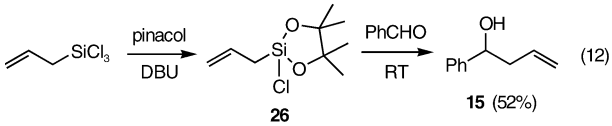
A significant limitation to this approach is that it is currently not applicable to aliphatic aldehydes. Instead of producing the desired homoallylic alcohols, saturated aldehydes react with the ionized chloride (see above) to yield α-chloro silyl ethers (**25**) [Eq. (11)]. Conditions are yet to have been found to allow the use of aliphatic substrates.



25 (11)

6. Strain-Induced Activation of Allylsilanes by Modulation of Silicon Substituents

Yet another approach for the activation of allylsilanes takes advantage of the fact that constraining silicon in a small ring increases its Lewis acidity.[27] In these systems, where unusually small bond angles are imposed on a four-coordinate silicon center, coordination of an additional ligand (e.g., a carbonyl oxygen atom) induces a rehybridization to a more favorable trigonal-bipyramidal geometry that helps release the ring strain. Thus, by reacting allyltrichlorosilane with 1,2-diols, diamines, and aminoalcohols, allylchlorosilanes are generated in which the silicon is part of a strained heterocyclic five-membered ring. Pioneering work by Wang and co-workers showed that stereoselective additions of tartrate-derived allylsilanes to aldehydes occur in the presence of a large excess of a Lewis base.[28] Kira and co-workers observed that these allylsilanes are able to react with aldehydes without an external promoter, and implied that the internal coordination of one of the tartrate esters to the silicon center is important for the reaction to proceed.[29] Unfortunately, the yields and enantioselectivities in both of these processes were quite modest. A significant advance in this methodology was recently reported by Leighton and co-workers, who used pinacol-derived tetrahedral allylchlorodioxasilacyclopentane **26** to clearly demonstrate that strained cyclic allylsilanes are capable of adding to aldehydes without the need for further inter- or intramolecular activation of the silicon atom ([Eq. (12)]; DBU = 1,8-diazabicyclo[5.4.0]undec-7-ene).[30] The authors argue that this enhanced reactivity is due, at least partly, to the strain induced by the small ring since

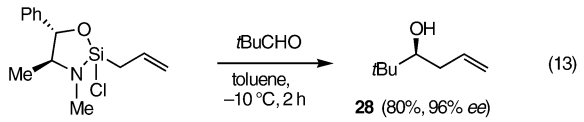


26 **15** (52%) (12)

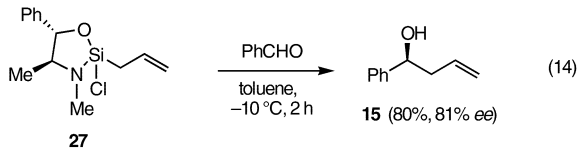
 © 2003 Wiley-VCH Verlag GmbH & Co. KGaA, Weinheim

neither an acyclic nor a six-membered analogue of **26** reacts with aldehydes. The independence of these allylsilanes from a secondary activator sets them apart from the other allylation reagents discussed in this Minireview.

The most interesting aspect of this recent work comes from allylsilanes bearing chiral 1,2-aminoalcohols and 1,2-diamines as substituents instead of pinacol. For example, use of pseudoephedrine affords **27**, a chiral version of **26**, as a 2:1 mixture of diastereomeric oxazasilacyclopentanes. This mixture provides a surprisingly effective allylating agent that reacts with both aliphatic and unsaturated aldehydes to give products in moderate-to-high yields and with good levels of enantioselectivity [Eqs. (13) and (14)].[30] This wider reactivity

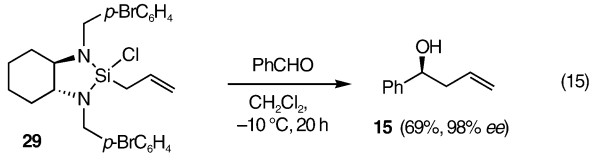


(13)



(14)

profile contrasts with the methodology of Denmark et al. described in the previous section. Although the allylsilanes of Leighton and co-workers are effective with both saturated and unsaturated aldehydes, selectivities are generally higher with saturated substrates (*ee* ~ 90%) than with aromatic and unsaturated aldehydes (*ee* ~ 80%). However, in a recent improvement, reactions with the novel diamine-modified allylsilane **29** are exceptionally selective for a broad range of aldehydes, including unsaturated and aromatic examples [Eq. (15)].[31] This higher level of selectivity helps compensate



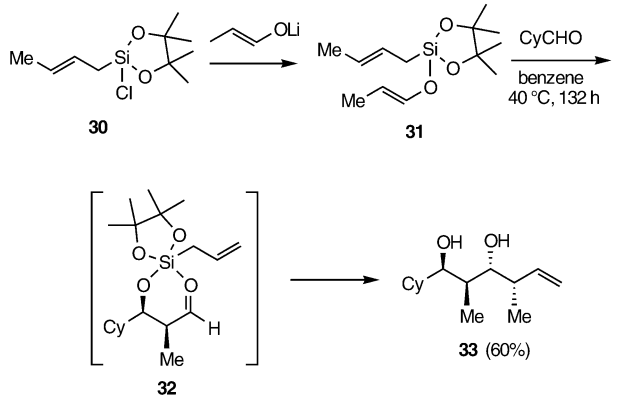
(15)

for the longer reaction times with these reagents, compared to those derived from pseudoephedrine, as well as for the fact that the required diamine precursor is not commercially available.

In spite of their remarkable reactivity towards aldehydes, these novel reagents are stable, easy to handle, and possess a long shelf life. Furthermore, they feature shorter reaction times and significantly higher enantioselectivities than additions with the earlier tartrate-derived analogues.[28,29]

The detailed mechanism and the mode of stereoinduction of this novel allylation system are not yet known. The authors propose that the aldehyde complexes to the strained allylsilane to give a pentacoordinate siliconate species prior to allyl transfer. Although this proposal suggests that these allylsilanes follow a closed transition structure common to type I reagents, no examples with crotyl derivatives were reported to probe this issue. However, the related tartrate-modified crotylsilanes are known to operate as type I reagents.[29] Another complicating factor is that the pseudoephedrine-derived allylsilane is used as a diastereomeric mixture, which to date has proven inseparable, and it is not yet known if both diastereomers react in an identical or a complementary manner. The authors also note that the selectivity of the reaction increases as the temperature is lowered to −10 °C, but then further cooling results in a loss of selectivity, an observation which further suggests that a complex mechanism is at work.

An important extension of this concept, reported by the same group,[32] is an elegant tandem aldol–allylation process, exemplified in Scheme 4. Chlorosilane **30** is first combined



Scheme 4. Tandem aldol/allylation process using strained allylsilanes.[32]

with the (*E*)-lithium enolate of propionaldehyde to give a stable bifunctional allylenolsilane **31**. Treatment of this (*E*)-enol-(*E*)-crotylsilane with cyclohexanecarboxaldehyde resulted first in an aldol reaction followed by an intramolecular allylsilylation of the intermediate aldehyde **32** to give 1,3-diol **33** as the major diastereomer. Although not yet an enantioselective process, the fact that a polyketide structure bearing four contiguous stereogenic centers can be prepared in one step from relatively simple starting materials is testimony to the power and promise of this novel methodology.

7. Summary and Outlook

This Minireview described a number of recent, innovative strategies devised to address the problem of activation of boron and silicon allylation reagents. The ultimate goal of these efforts is the development of more efficient, highly practical, and general methods for the control of both diastereoselectivity and absolute stereochemistry, preferably using a catalytic system, in the resulting homoallylic alcohol products. While these novel methodologies may not yet have reached this stage, the prospects are very promising in this

 © 2003 Wiley-VCH Verlag GmbH & Co. KGaA, Weinheim

important area of investigation and more breakthroughs are to be expected.

The authors acknowledge the support of the Natural Sciences and Engineering Research Council (NSERC) of Canada and the University of Alberta. J.W.J.K. thanks NSERC, the Alberta Heritage Foundation for Medical Research (AHFMR), and the University of Alberta for graduate scholarships.

Received: January 28, 2003 [M1632]

[1] S. E. Denmark, N. G. Almstead in *Modern Carbonyl Chemistry* (Ed.: J. Otera), Wiley-VCH, Weinheim, **2000**, chap. 10, pp. 299–402.
[2] S. R. Chemler, W. R. Roush in *Modern Carbonyl Chemistry* (Ed.: J. Otera), Wiley-VCH, Weinheim, **2000**, chap. 11, pp. 403–490.
[3] S. E. Denmark, E. J. Weber, *Helv. Chim. Acta* **1983**, *66*, 1655–1660.
[4] Y. Li, K. N. Houk, *J. Am. Chem. Soc.* **1989**, *111*, 1236–1240.
[5] A. J. Pratt, E. J. Thomas, *J. Chem. Soc. Chem. Commun.* **1982**, 1115.
[6] J. W. J. Kennedy, D. G. Hall, *J. Am. Chem. Soc.* **2002**, *124*, 11586–11587.
[7] J. W. J. Kennedy, D. G. Hall, *J. Am. Chem. Soc.* **2002**, *124*, 898–899.
[8] T. Ishiyama, T.-a. Ahiko, N. Miyaura, *J. Am. Chem. Soc.* **2002**, *124*, 12414–12415.
[9] H. C. Brown, V. S. Racherla, P. J. Pellachia, *J. Org. Chem.* **1990**, *55*, 1868–1874.
[10] K. Omoto, H. Fujimoto, *J. Org. Chem.* **1998**, *63*, 8331–8336.
[11] J. J. Gajewski, W. Bocian, N. L. Brichford, J. L. Henderson, *J. Org. Chem.* **2002**, *67*, 4236–4240.
[12] J. D. White, R. G. Carter, K. F. Sundermann, M. Wartmann, *J. Am. Chem. Soc.* **2001**, *123*, 5407–5413, and references therein.
[13] E. Vedejs, R. W. Chapman, S. C. Fields, S. Lin, M. R. Schrimpf, *J. Org. Chem.* **1995**, *60*, 3020–3027.
[14] a) R. A. Batey, A. N. Thadani, D. V. Smil, *Tetrahedron Lett.* **1999**, *40*, 4289; b) R. A. Batey, A. N. Thadani, D. V. Smil, A. J. Lough, *Synthesis* **2000**, 990–998.
[15] A. N. Thadani, R. A. Batey, *Org. Lett.* **2002**, *4*, 3827–3830.
[16] For a similar concept of dual activation of allyltrimethylsilane involving a single metal fluoride catalyst, see: a) B. L. Pagenkopf, E. M. Carreira, *Chem. Eur. J.* **1999**, *5*, 3437–3442, and references therein. For a recent use of allyltrimethoxysilane involving aqueous acceleration, see: b) N. Aoyama, T. Hamada, K. Manabe, S. Kobayashi, *Chem. Commun.* **2003**, 676–677.
[17] G. K. Friestad, H. Ding, *Angew. Chem.* **2001**, *113*, 4623–4625; *Angew. Chem. Int. Ed.* **2001**, *40*, 4491–4493.
[18] S. Yamasaki, K. Fujii, R. Wada, M. Kanai, M. Shibasaki, *J. Am. Chem. Soc.* **2002**, *124*, 6536–6537.
[19] S. E. Denmark, J. Fu, *Chem. Commun.* **2003**, 167–170.
[20] a) S. Kobayashi, K. Nishio, *Tetrahedron Lett.* **1993**, *34*, 3453–3456; b) S. Kobayashi, K. Nishio, *J. Org. Chem.* **1994**, *59*, 6620–6628.
[21] S. E. Denmark, D. M. Coe, N. E. Pratt, B. D. Griedel, *J. Org. Chem.* **1994**, *59*, 6161–6163.
[22] S. E. Denmark, J. Fu, *J. Am. Chem. Soc.* **2001**, *123*, 9488–9489.
[23] For a similar approach using axially chiral 2,2′-bipyridine *N,N′*-dioxides, see: T. Shimada, A. Kina, S. Ikeda, T. Hayashi, *Org. Lett.* **2002**, *4*, 2799–2801.
[24] S. E. Denmark, J. Fu, *Org. Lett.* **2002**, *4*, 1951–1953.
[25] C. Chuit, R. J. P. Corriu, C. Reye, J. C. Young, *Chem. Rev.* **1993**, *93*, 1371–1448.
[26] a) S. E. Denmark, J. Fu, *J. Am. Chem. Soc.* **2000**, *122*, 12021–12022; b) S. E. Denmark, J. Fu, *J. Am. Chem. Soc.* **2003**, *125*, 2208–2216.
[27] E. F. Perozzi, R. S. Michalak, G. D. Figuly, W. H. Stevenson, D. B. Dess, M. R. Ross, J. C. Martin, *J. Org. Chem.* **1981**, *46*, 1049–1053.
[28] D. Wang, Z. G. Wang, M. W. Wang, Y. J. Chen, L. Liu, Y. Zhu, *Tetrahedron: Asymmetry* **1999**, *10*, 327–338.
[29] L. C. Zhang, H. Sakurai, M. Kira, *Chem. Lett.* **1997**, 129–130.
[30] J. W. A. Kinnaird, P. Y. Ng, K. Kubota, X. Wang, J. L. Leighton, *J. Am. Chem. Soc.* **2002**, *124*, 7920–7921.
[31] K. Kubota, J. L. Leighton, *Angew. Chem.* **2003**, *115*, 976–978; *Angew. Chem. Int. Ed.* **2003**, *42*, 946–948.
[32] X. Wang, Q. Meng, A. J. Nation, J. L. Leighton, *J. Am. Chem. Soc.* **2002**, *124*, 10672–10673.

 © 2003 Wiley-VCH Verlag GmbH & Co. KGaA, Weinheim

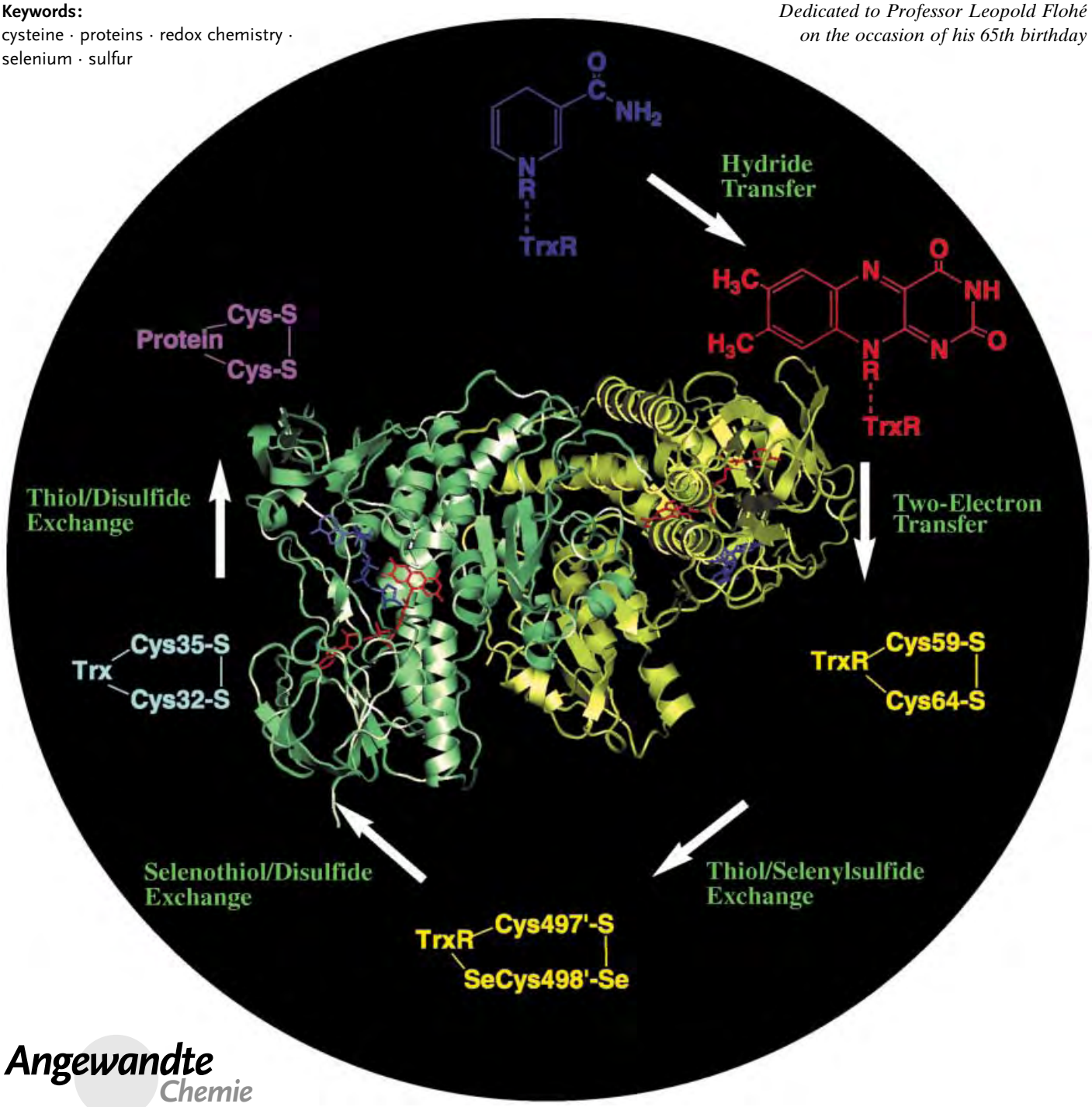
Chalcogen-Containing Proteins

Sulfur and Selenium: The Role of Oxidation State in Protein Structure and Function

Claus Jacob, Gregory I. Giles, Niroshini M. Giles, and Helmut Sies**

Keywords:
cysteine · proteins · redox chemistry · selenium · sulfur

Dedicated to Professor Leopold Flohé on the occasion of his 65th birthday



© 2003 Wiley-VCH Verlag GmbH & Co. KGaA, Weinheim
DOI: 10.1002/anie.200300573

Sulfur and selenium occur in proteins as constituents of the amino acids cysteine, methionine, selenocysteine, and selenomethionine. Recent research underscores that these amino acids are truly exceptional. Their redox activity under physiological conditions allows an amazing variety of posttranslational protein modifications, metal free redox pathways, and unusual chalcogen redox states that increasingly attract the attention of biological chemists. Unlike any other amino acid, the "redox chameleon" cysteine can participate in several distinct redox pathways, including exchange and radical reactions, as well as atom-, electron-, and hydride-transfer reactions. It occurs in various oxidation states in the human body, each of which exhibits distinctive chemical properties (e.g. redox activity, metal binding) and biological activity. The position of selenium in the periodic table between the metals and the nonmetals makes selenoproteins ideal catalysts for many biological redox transformations. It is therefore apparent that the chalcogen amino acids cysteine, methionine, selenocysteine, and selenomethionine exhibit a unique biological chemistry that is the source of exciting research opportunities.

From the Contents

1. Introduction 4743
2. Cysteine-Based Redox Proteins 4743
3. Beyond Cystine: Disulfide-S-Oxides, S-Sulfates, Sulfoxides, and Sulfones in Proteins 4749
4. Metal-Binding Properties of Cysteine, Sulfinic Acids, and Sulfoxides 4751
5. Cysteine Dehydrogenases and Proteases 4753
6. From Sulfur to Selenium—Similarities and Differences 4754
7. Summary and Outlook 4756

1. Introduction

The chalcogen ("ore-generating") elements oxygen, sulfur, and selenium fulfill a wide range of essential biological functions. All three elements are constituents of functional groups in biomolecules that participate in redox reactions in vivo. The fundamental importance of chalcogen-based redox systems in biology becomes apparent when redox-active proteins as a whole are considered.[1–5] Most proteins rely on organic or inorganic cofactors (e.g. metal ions, NAD^+, FAD) for redox activity. In contrast, the chalcogen-containing amino acids cysteine and methionine (Cys and Met, both of which contain sulfur), selenocysteine and selenomethionine (SeCys and SeMet, which contain selenium), and tyrosine (Tyr, which contains redox-active oxygen) endow proteins with a powerful redox chemistry based on the side chains of the amino acids. Moreover, while most redox active metal cofactors occur in just two or three oxidation states in vivo, sulfur in cysteine has been found to occur in up to ten (i.e. from $+6$ to -2, including fractional oxidation states).[6] Figure 1 provides an overview of the most common cysteine, methionine, selenocysteine, and selenomethionine modifications that have thus far been identified in biological systems. Considering that each of them also represents a separate posttranslational protein modification with specific properties (e.g. redox activity, metal binding), the full complexity of this chalcogen biochemistry becomes apparent.

This Review will explore the field of chalcogen biochemistry from the perspective of different oxidation states with a focus on eukaryotic biochemistry. Section 2 deals with the ability of cysteine to undergo posttranslational redox modifications and considers its ability to react through different redox mechanisms, while Section 3 addresses the biological redox chemistry of disulfides and methionine, whose redox transformations during oxidative stress have recently received increased attention. Section 4 explores metal binding as an important property of these individual modifications. Paradoxically, not all redox enzymes have redox-active residues or metals at their active site, and Section 5 discusses dehydrogenase enzymes that contain redox-inactive cysteine or zinc–cysteine complexes. The distinctive redox behavior of selenocysteine and selenomethionine is briefly addressed in Section 6.

2. Cysteine-Based Redox Proteins

Any review of the biological redox chemistry of cysteine is confronted with the complexity of this subject.[7] To provide systematic guidance, it might be worthwhile to classify the redox behavior of cysteine along the lines of underlying redox mechanisms. Sulfur has an electron configuration of $3s^2 3p^4$, which allows oxidation states between $+6$ and -2. In cysteine the element is fully reduced (the oxidation state of -2 is assigned), and its thiol group can undergo a range of reactions under physiological conditions, some of which are illustrated in Scheme 1.

Cysteine in proteins participates in a range of different redox reactions that do not directly involve, but can be

[*] Dr. C. Jacob, Dr. G. I. Giles, Dr. N. M. Giles
School of Chemistry, University of Exeter
Stocker Road, Exeter EX4 4QD (UK)
Fax: (+44) 1392-26-3434
E-mail: C.Jacob@ex.ac.uk
Prof. Dr. H. Sies
Institute for Biochemistry and Molecular Biology I
Heinrich-Heine-Universität Düsseldorf
Postfach 101 007, 40001, Düsseldorf (Germany)
E-mail: sies@uni-duesseldorf.de

 DOI: 10.1002/anie.200300573 © 2003 Wiley-VCH Verlag GmbH & Co. KGaA, Weinheim

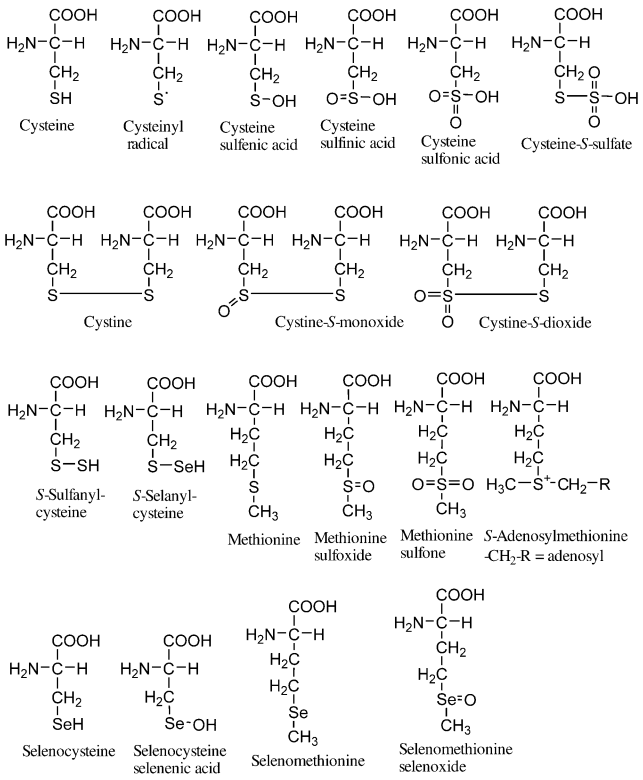
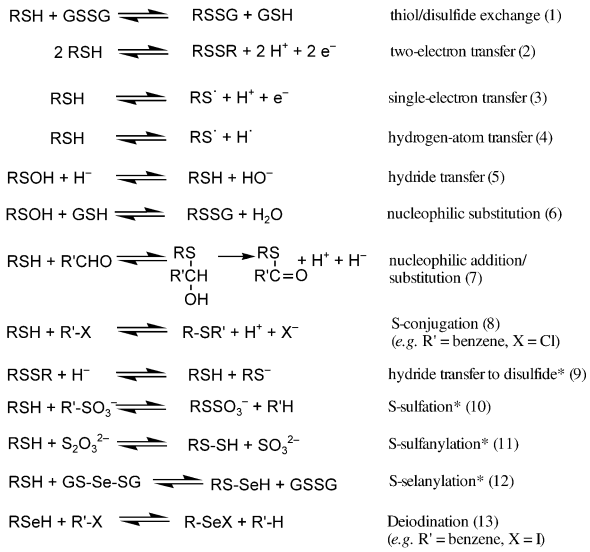


Figure 1. Common modifications of cysteine, selenocysteine, methionine, and selenomethionine in proteins. These modifications have been confirmed or postulated to occur in vivo.



Scheme 1. Redox mechanisms and reactions of cysteine. Details of these mechanisms and their occurrence in vivo are discussed in the text. The asterisk (*) marks reaction sequences theoretically possible in cysteine redox chemistry, but not yet confirmed in vivo. The protonation state of sulfur species in these reactions might vary.

coupled to, electron transfer. This has far-reaching implications for the redox activity of sulfur in vivo, exemplified by the tripeptide glutathione (γ-Glu-Cys-Gly, GSH). GSH is a vital intra- and extracellular mammalian peptide with many biological functions,[8–13] among them maintenance of the intracellular redox balance. GSH ($E^{o'}$(GSSG/2 GSH) ≈ −250 mV (NHE)) is readily oxidized to glutathione disulfide



Claus Jacob (born 1969) is a lecturer in inorganic chemistry at the University of Exeter. He received a BSc degree in Chemistry from University of Leicester in 1993, a DPhil in bioinorganic chemistry from the University of Oxford in 1997, and a Magister Artium degree in Philosophy, History, and Psychology from Hagen University in 1998. His research interests include the biological redox chemistry of the chalcogens, rational drug design, bioelectrochemistry, and philosophy of chemistry. He is Chairman and a Director of Exeter Antioxidant Therapeutics Ltd.



Dr. Helmut Sies (born 1942) is a Professor at Heinrich-Heine-Universität Düsseldorf (Germany) and Chairman of the Department of Biochemistry and Molecular Biology I at the Faculty of Medicine. He received an MD degree from the Ludwig-Maximilians-Universität in München (Germany) in 1967, where he completed his Habilitation for physiological chemistry and physical biochemistry in 1972. He was President of the International Society for Free Radical Research (1998–2000) and is President of the Nordrhein-Westfälischen Akademie der Wissenschaft. His research interests include oxidative stress (oxidants and antioxidants) as well as micronutrients and vitamins.



Dr. Gregory Giles (born 1974) is a research fellow at the University of Exeter. He received a BSc degree in Chemistry from the University of Durham in 1996 and a PhD in bioorganic chemistry from the University of Southampton in 2000. His research interests include redox biochemistry and the design of enzyme mimics. He is also a Director of Exeter Antioxidant Therapeutics Ltd.



Dr. Niroshini Giles, née Silva (born 1974) is a research fellow at the University of Exeter. She received a BSc (Hons) degree in Biochemistry from the Imperial College of Science, Technology and Medicine in 1996 and is an Associate of the Royal College of Science. She received a PhD from the University of Southampton in 1999 for her work on enzyme kinetics. Her research involves structural and mechanistic aspects of inflammation, antioxidants, redox signaling, and cancer therapy.

 © 2003 Wiley-VCH Verlag GmbH & Co. KGaA, Weinheim

(GSSG) and the GSH/GSSG ratio adjusts the global intracellular thiol redox potential. Most healthy cells have a GSH/GSSG ratio in the range of 100:1.[10,11] This ratio decreases during oxidative stress (Sections 3 and 4) and disturbance of the GSH/GSSG ratio may affect cellular proteins, DNA, and membranes.

Mechanistically, GSH can participate in electron-transfer, atom-transfer, and thiol/disulfide-exchange reactions. As a consequence, it reacts with a wide spectrum of cellular oxidants, while its regeneration involves thiol/disulfide-exchange reactions. GSH and its associated redox proteins can therefore be seen as the "switchboard" of cellular redox chemistry that integrates various different cellular redox pathways.[12,13] These distinct redox mechanisms will now be discussed in more detail.

2.1. Thiol/Disulfide-Exchange Reactions

Thiol/disulfide-exchange reactions are nucleophilic substitutions of a thiol or thiolate nucleophile (RSH or RS^-) on a disulfide bond (RS–SR), which leads to the formal oxidation of the nucleophile and reduction of the "exchanged" leaving group (Reaction (1) in Scheme 1). These reactions are among the most common redox reactions of cysteine residues in vivo. They are, for example, used to form structural disulfides in peptides and proteins which are reversible to maintain the cellular redox balance, to regulate enzyme activity (*S*-thiolation or *S*-glutathionylation, see Section 2.2), to allow oxidative cell-signaling pathways, and to provide powerful redox catalysis. In proteins, the two-electron redox potential of the cysteine/cystine couple is influenced by adjacent amino acid residues and can vary from approximately -125 mV in the case of *Escherichia coli* (*E. coli*) disulfide-bond-promoting product of gene *dsbA* (DsbA) to -270 mV for thioredoxin Trx-1 (Table 1). This diversity in potentials is mirrored by the diverse role that these thiol/disulfide oxidoreductase proteins play in vivo, ranging from protein reduction to disulfide bond formation. Notably, although potentials can formally be measured for the thiol/disulfide couple of these proteins, this does not imply that electron transfer is necessarily part of their redox cycles in vivo.

The thioredoxin-motif Cys-Xaa1-Xaa2-Cys (Xaa = amino acid, see Table 1) is a typical thiol/disulfide redox motif present at the active site of thioredoxins (Trx), glutaredoxins (Grx), tryparedoxins (TXN), and DsbA and protein disulfide isomerases (PDI). Although these proteins fulfill different biological roles, their redox reactions follow a mechanism similar to that of Trx.

The ubiquitous 12 kDa thioredoxins are part of redox chains that play various roles in the reduction of proteins. Human Trx proteins, for example, may be involved in activation and binding of transcription factors and in the activity of redox enzymes and may also play a major role during oxidative stress and apoptosis.[14] They reduce disulfides in proteins through a thiol/disulfide-exchange mechanism, and in the process form an intramolecular disulfide at the active site. All Trx proteins have a similar tertiary structure, which consists of a central core of five strands forming one β sheet enclosed by four α helices. The active site of human Trx1 contains the conserved amino acid sequence Cys32-Gly-Pro-Cys35. The two cysteine residues are in close vicinity, thereby allowing the reversible oxidation of the SH to the S-S redox state. The thiol group of the N-terminal Cys32 has a low pK_a value (6.7) and acts as a nucleophile for the reduction of disulfides in target proteins. This reaction results in the intermediate formation of a mixed disulfide (Cys32-S-SR), followed by a rapid thiol/disulfide exchange with Cys35, which results in the thioredoxin forming a disulfide (Cys32-S-S-Cys35) and concomitantly generating two reduced cysteines in the target protein.[15] Oxidized Trx relies on thioredoxin reductase (TrxR) for regeneration of its reduced state in a process that consumes NADPH (see Section 2.3).

Thiol/disulfide-exchange reactions are not only used to break (i.e. reduce) disulfide bonds in proteins, but also to generate them. Disulfide bridges contribute significantly to protein folding and stability and this process is catalyzed by enzymes such as PDI and DsbA, which are located in the endoplasmic reticulum of eukaryotic cells or in the periplasm of prokaryotes, respectively. Although DsbA and PDI have an active-site motif similar to that of Trx (Table 1), their considerably more positive redox potentials (-125 mV and -127 mV, respectively) allow them to function as thiol/disulfide oxidoreductases and to facilitate correct disulfide bond formation.

2.2. Conjugation and S-Thiolation/S-Glutathionylation

The nucleophilic properties of the cysteine residue in glutathione (and proteins) are used in both conjugation and

Table 1: Thiol/disulfide oxidoreductases. The cysteine redox potential is fine-tuned in these proteins and ultimately influences their biological activity.

Protein	Motif in active site	Redox potential [mV versus NHE][a]	Biological function
Thioredoxin (12 kDa)	-Cys-Gly-Pro-Cys-	-270	protein reduction[14]
Glutaredoxin (9 kDa)	-Cys-Pro-Tyr-Cys-	-233 (Grx-1); -198 (Grx-3)	catalyzes reduction of ribonucleotide reductase by GSH[132]
Tryparedoxin (16 kDa)	-Cys-Pro-Pro-Cys-	-249	utilizes trypanothione in place of GSH[133,134]
Protein disulfide isomerases (57 kDa)	-Cys-Gly-His-Cys-	-127	catalyzes reduction and reformation of disulfide bonds[135]
DsbA (21 kDa)	-Cys-Pro-His-Cys-	-125	catalyzes formation/rearrangement of protein disulfide bonds from thiols/misformed disulfide bonds[136]

[a] Reaction: $RSSR + 2e^- + 2H^+ \rightarrow 2RSH$.

 © 2003 Wiley-VCH Verlag GmbH & Co. KGaA, Weinheim

thiol/disulfide-exchange reactions. Reversible *S*-thiolation/*S*-glutathionylation is frequently observed in proteins; together with reversible *S*-nitrosylation and irreversible oxidation, this oxidative modification plays an important regulatory role.[16–19] Mechanistically, *S*-thiolation can occur by a range of different physiological processes, among them thiol/disulfide-exchange reactions (e.g. *S*-glutathionylation of a thiol group of a cysteinyl residue in a protein through slow reaction with GSSG), oxidation (e.g. reaction of a protein cysteinyl sulfenic acid with GSH), and reactions of nitrosylated species (e.g. reaction of a protein cysteinyl group with *S*-nitrosoglutathione (GSNO) leading to the formation of a mixed disulfide). Although resting levels of *S*-thiolated proteins in cells are only around 1%, oxidative stress (see Section 3) leads to a significant increase in *S*-thiolation, as observed for neutrophil and monocyte proteins, such as carbonic anhydrase III just minutes after the oxidative burst.[20] *S*-Thiolation modulates enzyme activity,[16–18] but is reversible and might ultimately protect proteins from irreversible oxidative damage.

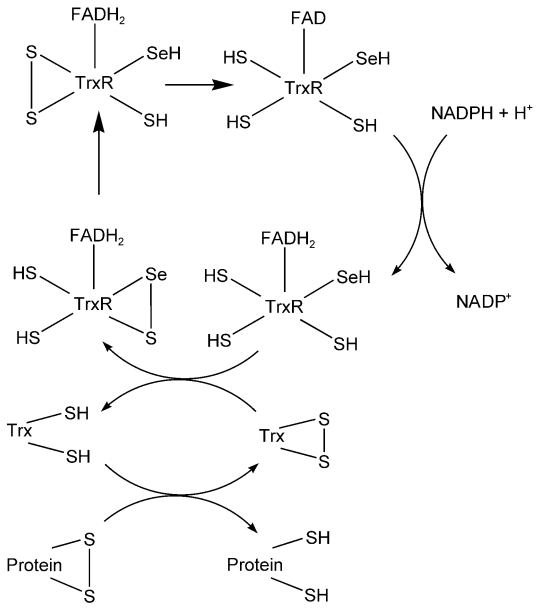
Cysteine takes part in related nucleophilic substitution reactions not considered as redox reactions. Such thioether-formation reactions (also called *S*-conjugation), for example, substitution of GSH for chloride in chlorobenzene, are irreversible processes that enhance excretion of toxic hydrophobic substances (such as halobenzenes) from the body by increasing their hydrophilicity.[8,21] These reactions are catalyzed by the glutathione *S*-transferase (GST) enzymes that contain cysteine residues in the active site (Reaction (7) in Scheme 1). Although GST enzymes do not catalyze redox reactions, they are redox-sensitive.[22–25]

2.3. Two-Electron Transfer Reactions

Although thiol/disulfide-exchange reactions are essential in maintaining the cellular redox balance and keeping proteins in their active reduced state, they do not lower the total number of disulfides in the cell. Reduction of disulfides without subsequent formation of other disulfides is achieved by the enzymes GSSG reductase ("glutathione reductase", GR), lipoamide dehydrogenase (LipDH), and thioredoxin reductase (TrxR). These proteins contain active-site cysteine residues that integrate the thiol/disulfide exchange with the electron-transfer mechanism and provide continuous reduction of disulfides by NADPH (Reaction (2) in Scheme 1).[26]

Human glutathione reductase regenerates GSH from GSSG, oxidizing NADPH in the process. This 104-kDa dimeric enzyme contains two redox systems per subunit, that is, a thiol/disulfide redox system based on two cysteine residues (Cys58 and Cys63) and a flavin cofactor. GSSG is reduced to two GSH units through thiol/disulfide exchange that initially leads to a mixed disulfide Cys58-S-SG and ultimately to an intramolecular disulfide Cys58-S-S-Cys63 in GR.[27] This disulfide is reduced by direct two-electron transfer from $FADH_2$ (Cys58-S-S-Cys63 + $FADH_2$ → Cys58-SH + Cys63-SH + FAD). FAD is subsequently reduced by hydride transfer from NADPH (FAD + NADPH + H^+ → $FADH_2$ + $NADP^+$). Glutathione reductase, therefore, integrates thiol/disulfide exchange, electron transfer, and hydride transfer, whereas Cys58 and Cys63 participate in two different types of redox reaction. In the yeast enzyme, Cys50 and FAD form a charge-transfer complex with an absorbance at 540 nm.[28] The relatively large difference in redox potential between the GSSG/2GSH ($E^{o\prime} = -241$ mV) and $NADP^+$/NADPH ($E^{o\prime} = -327$ mV) couples and the high ratio of NADPH/$NADP^+$ in healthy cells lead to extensive reduction of GSSG and the high GSH/GSSG ratio mentioned above.

Whereas glutathione reductase reduces GSSG to GSH, thioredoxin reductase enzymes form part of the cellular protein disulfide reduction machinery by reducing the disulfide in the active site of Trx in the presence of NADPH. Their catalytic mechanisms resemble that of GR with one major difference: Human TrxR is a 100–130-kDa dimeric flavoprotein that contains a Gly-Cys-SeCys-Gly sequence per subunit and—unlike GR—initially operates with a (thiol, selenol)/selenylsulfide (SH, SeH/S-Se) couple rather than a (thiol, thiol)/disulfide (2SH/S-S) redox couple (Scheme 2).[29] The selenocysteine and adjacent cysteine



Scheme 2. Reduction of protein disulfides by the thioredoxin–thioredoxin reductase redox chain. A chain of thiol/disulfide-exchange reactions drives the reduction of disulfides in proteins. TrxR couples thiol/disulfide exchange to intramolecular electron and hydride transfer.[15]

make up the redox-active site of the enzyme that reduces the Trx disulfide through a (thiol, selenol)/disulfide-exchange mechanism, forming a selenylsulfide in the process. The latter is re-reduced to the selenol and thiol through a (thiol, thiol)/selenylsulfide-exchange reaction involving two cysteine residues in an additional redox center located in the other subunit of the dimer. As in GR, electron transfer from $FADH_2$ then reduces the disulfide formed in the exchange reaction. Although the precise redox potentials of all redox couples involved (e.g. the (SH, SeH)/Se-S couple) have not yet been determined, reduction of Trx by NADPH seems to occur in a relatively small potential range from approximately

 © 2003 Wiley-VCH Verlag GmbH & Co. KGaA, Weinheim

-327 mV ($NADP^+$/NADPH) to -283 mV (unbound FAD/$FADH_2$)[30] to -270 mV (for Trx, Cys-S-S-Cys/2 Cys-SH). The significant difference between the redox potentials of cysteine (-233 mV) and selenocysteine (-488 mV) is shown in Figure 2. In human TrxR, the selenylsulfide–disulfide redox

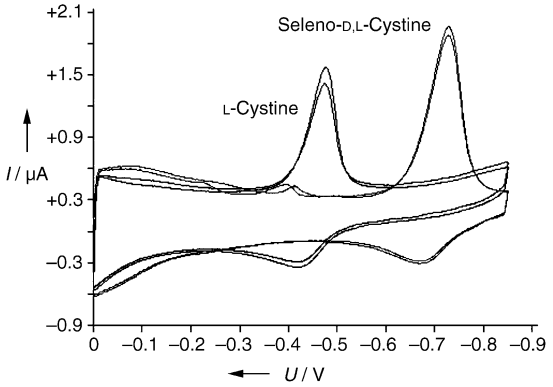


Figure 2. Cyclic voltammograms of cystine and selenocystine. Voltammograms of L-cystine (100 µM) and D,L-selenocystine (50 µM) were recorded in potassium phosphate buffer (pH 7.0; 200 mM) at 25 °C and at a scan rate of 500 mVs^{-1} with a dropping mercury working electrode, a standard silver reference electrode (SSE), and a platinum counterelectrode. The significant difference in redox potential of about 250 mV between selenocysteine/selenocystine (-710 mV versus SSE, i.e., -488 mV versus NHE) and cysteine/cystine (-455 mV versus SSE, -233 versus NHE) confers considerably more reducing properties to selenocysteine.

chain seems to play an essential role, which might become fully apparent once the potentials of all redox couples involved are determined.

Moreover, the activity of human TrxR can be reversed to reduce mediators of oxidative stress in the presence of reduced Trx, depending on the substrates. With peroxynitrite, TrxR acts as a peroxynitrite reductase, as was demonstrated by using the selenoorganic compound ebselen (2-phenyl-1,2-benzoisoselenazol-3[2*H*]-one) as a reductant.[31] Ebselen then acts as a "superfast" Trx oxidant.[32] Again in this case the presence of selenium might play a decisive role (see Section 6.).

Although known mammalian TrxR enzymes operate by direct two-electron transfer to the disulfide of the active site, two sequential one-electron transfers are theoretically possible. This reduction route is observed in plants and bacteria for ferredoxin-thioredoxin reductase (FTR). FTR is briefly discussed here, since it provides unique insight into the redox behavior of disulfides and thiyl radicals (other iron/sulfur proteins have been extensively reviewed elsewhere[33]). Spinach FTR is a 30-kDa heterodimeric enzyme that contains a redox-active disulfide (Cys 54-Cys 84) and an $[4Fe\text{-}4S]^{2+}$ ($S = 0$) iron–sulfur cluster in its 13-kDa catalytic β subunit.[34] This enzyme is unique in that it is the only known iron/sulfur protein that can reduce a disulfide bond in the presence of reduced [2Fe-2S] ferredoxin (the latter replaces the NADPH that is used as an electron source for mammalian TrxR enzymes). The reduced $[2Fe\text{-}2S]^{2+}$ cluster of ferredoxin acts as a one-electron donor that reduces Cys 54-S-S-Cys 84 to Cys 54-S^- and a thiyl radical (Cys 84-$S^\bullet$).[35] Cys 54-S^- then forms a heterodisulfide with Trx in a mechanistic step analogous to that of mammalian TrxR. The thiyl radical is deactivated and stabilized by coordinating to an iron center of the $[4Fe\text{-}4S]^{2+}$ ($S = 0$) cluster of FTR, forming an intermediate species with a formally oxidized $[4Fe\text{-}4S]^{3+}$ ($S = {}^1/_2$) cluster with one pentacoordinated iron center and a formally reduced Cys 84-S^- ligand.[36] A second ferredoxin molecule then supplies another electron to this intermediate species to generate Cys 84-S^- and $[4Fe\text{-}4S]^{2+}$ at the active site. Cys 84-S^- then attacks the mixed disulfide between FTR and Trx, resulting in fully reduced Trx and regeneration of the disulfide in the active site.

In general, the reduction potential for the one-electron reduction of a disulfide is experimentally inaccessible. By examination of the potentials for the available two-electron reduction, however, it is apparent that electron transfer from ferredoxin ($E^{o\prime} = -350$ mV) to Trx ($E^{o\prime} = -210$ mV) through the disulfide of the active site of FTR ($E^{o\prime} = -230$ mV) is thermodynamically favorable.[34] Unlike NADH, ferredoxin is only a one-electron donor, which prohibits the normal two-electron reduction pathway and requires the formation of a highly reactive thiyl radical as an intermediate. FTR uses the iron–sulfur cluster ($E^{o\prime} = -650$ mV for $[4Fe\text{-}4S]^{3+/2+}$) to stabilize this otherwise transient radical species. FTR therefore provides an elegant solution to a considerable mechanistic challenge (one- versus two-electron transfer) by amalgamating the redox and metal-binding properties of cysteine to enable its unique function.

As has been shown for spinach FTR, electron transfer to disulfides can result in the formation of thiyl radicals as intermediates. This leads us to consider the role of sulfur-based radicals in mammalian biology, in which the thiyl radical directly participates in electron- and atom-transfer reactions.

2.4. Radical Reactions

Radical-formation and -transfer mechanisms provide enzymes with additional cysteine-based redox pathways that involve redox processes distinctly different from exchange and electron-transfer reactions. The thiol/thiyl radical redox couple occurs in important enzymes such as the ribonucleotide reductase (RNRase) superfamily, pyruvate formate lyase (PFL), and benzylsuccinate synthase (BSS). In these enzymes the thiyl radical is formed by two alternative pathways: long-range one-electron transfer from the thiol (with subsequent loss of H^+ (Reaction (3) in Scheme 1) and short-range hydrogen-atom abstraction from the thiol (Reaction (4) in Scheme 1).

Long-range one-electron transfer is found in aerobic Fe-dependent (class I) RNRase from *E. coli*, which generates a thiyl radical by electron transfer from cysteine to an oxygen-centered tyrosyl radical.[37] In contrast, the formation of the thiyl radical in anaerobic formate-dependent (class III) RNRase (ARR) from bacteriophage T4 and in anaeorobic pyruvate formate lyase (PFL) from *E. coli* proceeds through a short-range hydrogen-atom transfer from cysteine to a (carbon-centered) glycyl radical.[38]

 © 2003 Wiley-VCH Verlag GmbH & Co. KGaA, Weinheim

The formation of the glycyl radical in ARR requires a range of components, including a flavodoxin reductase system, NADPH, *S*-adenosylmethionine (SAM), and dithiothreitol (DTT).[39] The [4Fe-4S] iron/sulfur cluster of ARR reduces SAM to methionine and the 5′-deoxyadenosyl radical by one-electron transfer. This is followed by a hydrogen-abstraction step from glycine by the adenosyl radical, resulting in the formation of 5′-deoxyadenosine and the glycyl radical, which then forms the thiyl radical. Similarly, PFL is catalytically activated by PFL activase (which also contains an iron/sulfur center) utilizing SAM and generating a glycyl radical (Gly 734 in PFL from *E. coli*), methionine, and 5′-deoxyadenosine. A nucleophilic thiyl radical at Cys 418 in this enzyme is then formed by a sequential hydrogen abstraction from Cys 419 by the glycyl radical.

Once formed, these thiyl radicals are highly reactive (i.e. oxidizing) and are reduced to thiols by hydrogen-atom-abstraction reactions, the hallmark reaction of thiyl radicals. In RNRases the hydrogen atom is abstracted either from external dithiols or formate (in the case of ARR), which are ultimately oxidized to disulfides or CO_2, respectively. In *E. coli* PFL, the Cys 418 radical attacks the carbonyl carbon atom of the pyruvate substrate to form an unstable, covalent *S*-acetyl-PFL radical species that rapidly fragments to produce the (nonradical) acylthioester of Cys 418 and a formate radical, which then abstracts a hydrogen atom from Cys 419. The Cys 419 radical, in turn, abstracts a hydrogen atom from Gly 734 to recycle the glycyl radical. The *S*-acetyl-PFL form reacts with coenzyme A (CoA) to form acetyl-CoA and the recycled enzyme. Overall, this reaction generates acetyl-CoA and formate from CoA and pyruvate, all of which are nonradical species.[40]

A glycyl–thiyl radical chain is also found in benzylsuccinate synthase (BSS) from *Thauera aromatica* which catalyzes the initial step in the degradation of toluene to benzylsuccinate. This BSS contains an active-site glycyl radical at Gly 825. Abstraction of a hydrogen atom from the methyl group of toluene results in the formation of a benzyl radical, which attaches to the double bond of fumarate to form a benzylsuccinate radical intermediate. This species is then reduced to benzylsuccinate by hydrogen abstraction from the thiolate of Cys 489, which in turn abstracts the hydrogen atom from Gly 825 to regenerate the initial glycyl radical.[41]

Hydrogen-atom-transfer reactions represent one example of "atom-transfer reactions" that cysteine can undergo in vivo. Whereas hydrogen-atom transfer is a radical reaction, other atom-transfer reactions that involve cysteine (such as hydride transfer) proceed through nonradical mechanisms. These transfer reactions frequently occur as part of the same catalytic cycle and are therefore discussed together.

2.5. Atom-Transfer Reactions

Antioxidant enzymes such as glutathione reductase and thioredoxin reductase are frequently evaluated for additional catalytic activity. The peroxynitrite reductase activity of TrxR, for example, has already been mentioned. Peroxidation of thiols often leads to a distinct oxidation state of sulfur, with chemical properties that differ dramatically from those of the disulfide state: the sulfenic acid (Figure 1). This cysteine modification is only stable, however, in the absence of additional thiol groups (the latter would react with sulfenic acid to form a disulfide and water). In human GR, for example, oxidation with H_2O_2 results in the formation of the Cys 58-S-S-Cys 63 disulfide, an enzyme that exhibits poor peroxidase activity.[42]

In contrast, redox enzymes such as NADH peroxidase (Npx), NADH oxidase (Nox), and peroxiredoxins (Prx)[43] function through a cysteine (Cys-SH)/cysteine sulfenic acid (Cys-SOH) redox couple that allows effective peroxidation catalysis. These enzymes contain a catalytic cysteine residue that is oxidized to cysteine sulfenic acid, a highly reactive (i.e. oxidizing) cysteine species whose reduction can proceed through two distinct mechanisms both of which occur in vivo: either through an exchange reaction involving two thiol equivalents or through hydride transfer (Reaction (5) in Scheme 1).

Npx from *Streptococcus* (*Enterococcus*) *faecalis* is a tetramer of 46 kDa per subunit and belongs to the family of pyridine nucleotide–disulfide oxidoreductases. Unlike other cysteine-based oxidoreductases (e.g. GR), it contains just one cysteine residue in the active site of each subunit that catalyzes the reduction of H_2O_2 in the presence of NADH. The reduced thiolate nucleophile attacks H_2O_2 to form Cys 42-SOH and water. Hydride transfer from NADH to Cys 42-SOH then occurs through FAD. Structural data show that the flavin is located in the enzyme between the reducing NADH and the Cys 42-SH/Cys 42-SOH redox center to optimize hydride transfer.

This redox mechanism has been supported by mutagenesis experiments that were used to test if and how many cysteine residues are essential for this peroxidase activity. Mutagenesis of Cys 42 to serine or alanine results in a low turnover rate, emphasizing the importance of the cysteine redox center.[44,45] Introduction of an additional cysteine residue (Cys 40) at the active site, however, almost completely eliminates catalytic activity (k_{cat} of mutant is about 0.1 % of the value of that of wild-type Npx[42]). These results illustrate both the significance of the sulfenic acid state in peroxidases and the importance of avoiding the disulfide state in these enzymes as the formation of the Cys 40-S-S-Cys 42 disulfide from Cys 40-SH and Cys 42-SOH is detrimental to the activity.

Hydride transfer (e.g. from NADH or $FADH_2$) to disulfides—a mechanism possible in theory—does not seem (yet) to have been observed in proteins (Reaction (9) in Scheme 1); this is also true for electron transfer to sulfenic acids.

The redox mechanism of Nox from *Streptococcus* (*Enterococcus*) *faecalis* is closely related to that of Npx (Nox has 44 % sequence identity with Npx and the Cys-SH/Cys-SOH redox couple is conserved in both enzymes). Nox catalyzes the reduction of molecular oxygen to water with the consumption of four electrons (i.e. 2 mol equivalents of NADH). It is a dimeric enzyme (50 kDa per subunit) and each subunit contains one cysteine residue (Cys 42) and one FAD redox center. O_2 is first activated by reaction with $FADH_2$ to form peroxyflavin ($FADH_2O_2$). The latter reacts

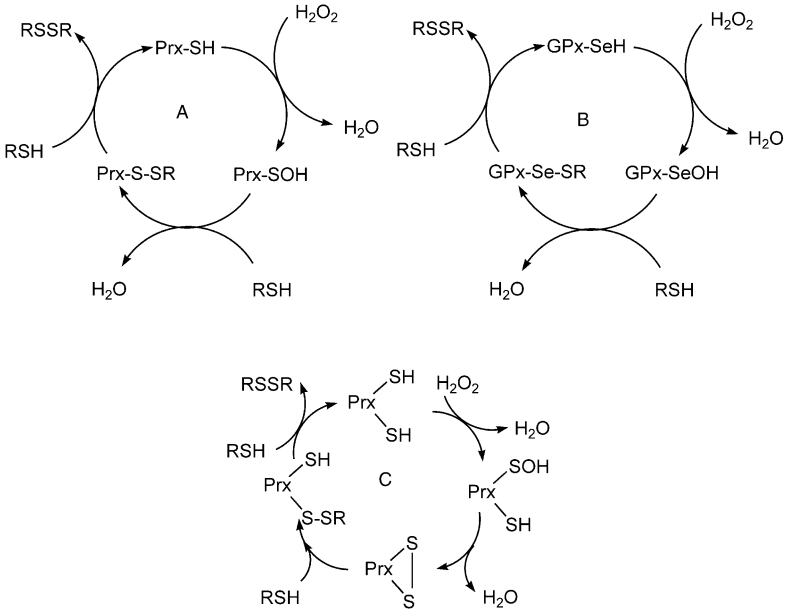
with the thiolate of Cys42[46] in a reaction that resembles the peroxidation step of the Npx cycle to form Cys42-SOH and FADHOH. The FADHOH then eliminates water to generate FAD, which is reduced by 1 equivalent of NADH to $FADH_2$. Cys42-SOH is re-reduced to the thiol by hydride transfer from $FADH_2$. The FAD formed in this reaction is reduced to $FADH_2$ by another equivalent NADH to regenerate the fully reduced thiol and $FADH_2$ for the next round of catalysis.

As in the case of Npx, mutagenesis experiments strongly support this redox mechanism. Replacement of Cys42 by serine (i.e. removal of one of the two redox centers) results in an enzyme that reduces O_2 to H_2O_2 by using 1 mol equivalent of NADH. Although the flavin center still maintains its function, the lack of the sulfur redox center prevents reduction of H_2O_2 to water.[46]

From a biochemical point of view, the sulfur-based redox mechanism of Nox is even more interesting when the overall reaction is considered from a different perspective. Nox catalyzes the reduction of oxygen by NADH, a reaction not dissimilar to processes that occur in the human mitochondrial respiratory chain. Whereas metal-based redox centers in proteins such as iron/sulfur proteins, the Rieske center, cytochrome *c*, and cytochrome *c* oxidase are responsible for the reduction of oxygen during respiration, Nox accomplishes a chemically related task by using exclusively nonmetal redox systems.

Although the catalytic cycles of Npx and Nox are closely related, the sulfenic acids contained in human peroxiredoxin enzymes exhibit a different redox mechanism that resembles that found in the well-known selenium enzyme glutathione peroxidase (GPx, see Section 6.). As is the case for GPx, Prx enzymes catalyze the reduction of H_2O_2 and alkyl hydroperoxides to water or the corresponding alcohol, oxidizing thiols to disulfides in the process. The cysteine residue (Cys47) in the active site of the human 1-Cys-Prx (hORF6) reacts with peroxide in a substitution reaction similar to those of Npx and Nox, in which the thiol(ate) forms a S–O bond and releases hydroxide. In marked contrast to Npx and Nox, however, Cys47-SOH is not reduced by hydride transfer (Prx is not a flavin protein) but reacts with 2 equivalents of thiols to regenerate the reduced form of Cys47 and a disulfide (Scheme 3). Reduction of the sulfenic acid therefore proceeds through exchange reactions that involve the substitution of OH^- by RS^- with subsequent formation of a mixed disulfide.

Although we have mentioned that the presence of two cysteine residues in close vicinity would prevent the formation of a stable sulfenic acid, 2-Cys-Prx enzymes use a redox pathway that involves disulfide formation from a sulfenic acid and a thiol (Scheme 3).[47] The disulfide formed is then reduced through a thiol/disulfide-exchange mechanism. This disulfide has been observed in the crystal structure of the 2-Cys-Prx heme-binding protein (HBP-23) as a disulfide bond that forms between Cys52 on one subunit and Cys173 on the second subunit.[48] The precise oxidation state of the cysteine residue in the active site has yet to be assigned unambiguously. The crystal structure of decameric peroxiredoxin TPx-B from human erythrocytes was recently determined with a resolution of 1.7 Å. Interestingly, this shows the Cys51 in the active site exists as a cysteine sulfinic acid (Cys-SO_2H), which is buried within the active-site pocket.[49] The presence of a sulfinic rather than a sulfenic acid in this enzyme and the precise meaning of this finding are still controversial. Unlike sulfenic acids, sulfinic acids cannot easily be reduced by GSH or other thiols, and as a consequence the presence of a second cysteine in close vicinity to the sulfinic acid might not lead to the formation of disulfide.[25]



Scheme 3. Catalytic cycles of 1-Cys and 2-Cys peroxiredoxins and glutathione peroxidase. Although they use different chalcogens for their catalysis, 1-Cys Prx (A) and GPx (B) have comparable redox cycles.[43,111] Peroxidation of the thiol (selenol) by H_2O_2 generates highly reactive sulfenic (selenenic) acids. Reduction occurs through exchange reactions in which 2 equivalents of substrate thiols (e.g. GSH, dithiothreitol) are consumed. The redox cycle of 2-Cys-Prx involves condensation of Cys-SOH and Cys-SH to form either an intramolecular disulfide or, as in case of the more common oligomeric Prxs, an intersubunit disulfide (C).[47] In vivo, these thiols and selenols are in equilibrium with corresponding thiolates and selenolates.

The growing interest in redox-active cysteine does not imply, however, that the biological redox chemistry of sulfur is limited to reactions of the thiol group. Less-well-known oxidized sulfur species in proteins (e.g. disulfide-*S*-oxides, methionine-*S*-oxides, persulfides) have only recently attracted attention. The next section discusses some of these biochemically more "exotic" and sometimes speculative species.

3. Beyond Cystine: Disulfide-S-Oxides, S-Sulfates, Sulfoxides, and Sulfones in Proteins

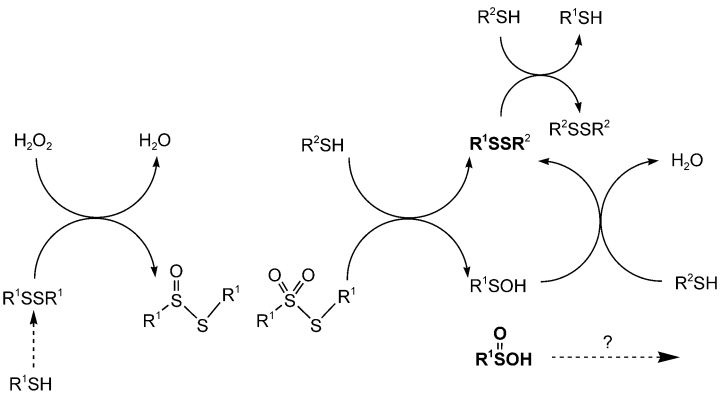
The ability of sulfur to occur in many oxidation states and to form sulfur–oxygen, sulfur–sulfur and sulfur–selenium bonds results in a range of less-well-known cysteine modifications. Whereas some of these species, such as cysteine *S*-sulfate (Cys-S-SO_3^-) are formed through transfer pathways, other species form as a result of oxidative stress.

 © 2003 Wiley-VCH Verlag GmbH & Co. KGaA, Weinheim

Oxidative stress, a biochemical condition initially defined in 1985,[50–52] is associated with many human diseases ranging from neurodegenerative and autoinflammatory conditions such as Alzheimer's disease and rheumatoid arthritis to diabetes and cancer. This pathological condition is characterized by an imbalance between cellular oxidizing and reducing species and provides unusual oxidizing conditions in vivo characterized by the presence of reactive oxygen species that can cause oxidative damage to biomolecules. Owing to the accessibility of its oxidation states, cysteine is a prime target of many of these oxidants, and the harsh oxidizing conditions present during oxidative stress promote the formation of cysteine and methionine species that are found in considerably smaller amounts in healthy cells (Figure 1). It should be emphasized from the outset that many of the modifications discussed in this section have only recently been discovered in vivo and that their biochemistry (if any) is still controversial.

3.1. Disulfide-S-oxides

Disulfides are not necessarily the end products of the oxidation of cysteine under oxidative stress. Oxidation of disulfides can lead to highly reactive disulfide-*S*-monoxides (thiosulfinates, RS(O)SR) and disulfide-*S*-dioxides (thiosulfonates, $RS(O)_2SR$). Disulfides such as cystamine and GSSG are easily oxidized to disulfide-*S*-oxides.[53,54] These "activated" disulfides rapidly react with thiols in proteins and enzymes and deactivate the enzymes in the process. Disulfide-*S*-oxides provide a cysteine redox pathway leading to redox cascades that also involve sulfenic and sulfinic acids and glutathionylation of proteins. One such sulfur redox cascade involving disulfide-*S*-oxides is shown in Scheme 4. Although these species have primarily been discussed in the context of small reactive sulfur species and oxidative stress, new evidence also points to the presence of disulfide-*S*-oxides in proteins.[53–58] As these cysteine modifications are highly reactive and have virtually no distinct spectroscopic or chemical properties, their identification in proteins is difficult.



Scheme 4. Redox cascade of oxidized cysteine species. Oxidation of disulfides (RSSR) to disulfide-*S*-oxides with subsequent stepwise reduction reactions involving protein thiols (RSH) have been postulated to occur in vivo during oxidative stress.[55,83] Species in bold denote the likely end products of these cascades. The redox activity of sulfinic acids in vivo is still under investigation.[55]

Future developments in X-ray protein crystallography, mass spectrometry, and NMR spectroscopy might provide deeper insight into oxidative cystine modifications in proteins.

3.2. S-Sulfocysteine, Persulfides, and Selenopersulfides

S-sulfated cysteines, the so-called *S*-sulfocysteines (Cys-S-SO_3^-, Figure 1), are also found in vivo and these species can be considered a disulfide modification. Species such as *S*-sulfocysteine and *S*-sulfoglutathione ($GSSO_3H$) occur during enzyme-catalyzed detoxification of sulfite in humans. GSSG initially reacts with sulfite to form $GSSO_3H$ and GSH. The $GSSO_3H$ is then enzymatically hydrolyzed to sulfocysteinylglycine and, finally, to *S*-sulfocysteine.[59] These *S*-sulfated metabolites readily react with proteins. $GSSO_3H$, for example, is a competitive inhibitor of glutathione S-transferase (GST), which is active in the detoxification of carcinogens; this inhibition could thus be responsible for the carcinogenic properties of SO_2.[60] Although posttranslational modification of whole proteins by *S*-sulfation in humans has not yet been reported, *O*-sulfation (sulfate transfer from 3′-phosphoadenosine 5′-phosphosulfate to free hydroxy groups such as those of tyrosine residues in proteins) was recently described as a possible biochemical alternative to *O*-phosphorylation in signaling and regulatory pathways.[61,62]

Whereas *S*-sulfocysteine contains one highly oxidized sulfur atom, *S*-sulfanylcysteine (Cys-S-SH) is a persulfide species. This catenation event is found, for example, at the active site of sulfurtransferases such as bovine liver rhodanese.[63] This enzyme was recently used to generate an active site *S*-selanylcysteine (Cys-S-SeH) in vitro in a reaction involving selenite and GSH.[64] Although the relevance of this modification in vivo remains to be demonstrated, a chemically similar species, glutathione selenopersulfide (GSSeH), is an integral part of selenocysteine metabolism. An *S*-selanylcysteine residue was also postulated to exist in CO dehydrogenase from the aerobic bacterium *Oligotropha carboxidovorans*,[65] although this claim has now been withdrawn.[66] *S*-selanylation and its underlying mechanism (Reaction (12) in Scheme 1) are still highly controversial, but would provide an elegant pathway to introduce selenium into proteins that would not rely on the elaborate expression machinery required for the incorporation of selenocysteine (see Section 6.).

3.3. Sulfoxides and Sulfones—Biological Redox Chemistry of Methionine

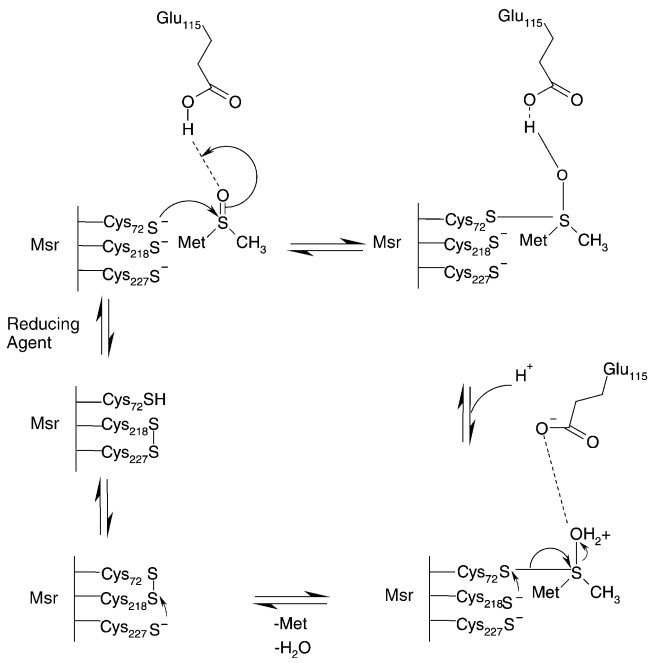
Methionine is encoded by the start codon AUG, which sets the reading frame for protein synthesis and is therefore present in most proteins. Like disulfides, its dialkyl sulfide (thioether) group (Figure 1) is susceptible to oxidation with subsequent formation of sulfoxides and sulfones. The oxidation of methionine in proteins to methionine sulfoxide has a biochemical and physiological role.[67,68] Methionine exhibits antioxidant properties,[69,70] and their significance in vivo is presently under investigation.

 © 2003 Wiley-VCH Verlag GmbH & Co. KGaA, Weinheim

Methionine residues on protein surfaces provide a high concentration of antioxidant residues that can act as protection against oxidation of other residues that are vital for activity. On the basis of a protein with just eight modifiable methionine residues and a spherical diameter of 60 Å, the concentration of methionine within that volume would be approximately 100 mM, about ten times the cytosolic concentration of GSH.[69] This protective role of methionine has been supported by recent experimental evidence. For example, oxidation of 8 of the 16 methionine residues in glutamine synthetase to the sulfoxide can occur per enzyme subunit without significantly affecting enzyme activity,[71] and methionine residues at or near the active site of this enzyme may prevent autoxidation by the substrate, products, or cofactors.

The discovery of the human enzyme methionine sulfoxide reductase (Msr) has added weight to the notion of redox-active methionine in proteins and enzymes. Whereas most sulfoxides do not spontaneously react with GSH, Msr ensures that sulfoxide formation is reversible in the presence of NADPH.

Reduction of the sulfoxide is also interesting from a mechanistic point of view (Scheme 5). Two possible reaction mechanisms have been proposed for Msr activity, proceeding either through a chain of thiol/disulfide-exchange steps or



Scheme 5. Mechanism of methionine sulfoxide reductase. Nucleophilic attack of cysteine at the oxidized sulfur atom leads to the formation of a tetravalent intermediate. Proton transfer and attack of Cys 218 on Cys 72 facilitate loss of water and collapse of the intermediate to release methionine. The active site is regenerated by thiol/disulfide exchange with Trx.[72]

utilizing a sulfenic acid intermediate. A catalytic mechanism has been reported for bovine MsrA (bMsrA), which has an 88% sequence similarity to that of human MsrA.[72] The Cys 72 residue in the active site of bMsrA forms a thiolate anion and its nucleophilic attack on the sulfoxide sulfur atom of Met(O) leads to the formation of a tetrahedral disulfide-*S*-oxide intermediate. Attack of Cys 218 on Cys 72, followed by proton transfer to the oxygen atom of the sulfoxide then leads to loss of water and to the formation of methionine and of a disulfide bond between Cys 72 and Cys 218. The reduced state is restored through thiol/disulfide exchange first between Cys 227 and Cys 218, followed by reduction by an external thiol substrate.[72]

An alternative mechanism has been proposed for *E. coli* MsrA catalysis. In this case the Cys 51 attacks the sulfur atom of the sulfoxide substrate with the formation of a tetrahedral intermediate that rearranges to form a sulfenic acid at Cys 51, releasing methionine in the process (i.e. a net oxygen-atom transfer from methionine sulfoxide to cysteine). Cys 198 then attacks the sulfur atom of the Cys 51 sulfenic acid to form a disulfide bond and water. The active site is fully reduced by thiol/disulfide exchange, initially through an adjacent cysteine residue (Cys 206) and then an external thiol.[73]

The biological role of methionine sulfone (Figure 1) is less apparent. The modified amino acid itself has been found to exhibit antiinflammatory properties. Interestingly, this highly oxidized form of methionine is more active than the sulfoxide but less active than methionine, thus showing no correlation between oxidation state of sulfur and this kind of antioxidant activity.[70] This result is comparable to recent investigations of disulfide-*S*-oxides that have also shown no direct correlation between the oxidation state of sulfur and in vitro reactivity.[53,55] As with these disulfide-*S*-oxides, methionine sulfoxide and sulfone might play a significant role during oxidative stress, either as antioxidants or as reactive sulfur species.[53–55]

Apart from sulfoxide and sulfone modifications, methionine is also able to form a trivalent sulfonium species (Figure 1) found in the biological methylating agent *S*-adenosylmethionine (SAM). Sulfonium formation represents another modification of methionine that frequently occurs in vivo and exhibits its own, unique reactivity (the methyl group attached to the sulfur is highly electrophilic).

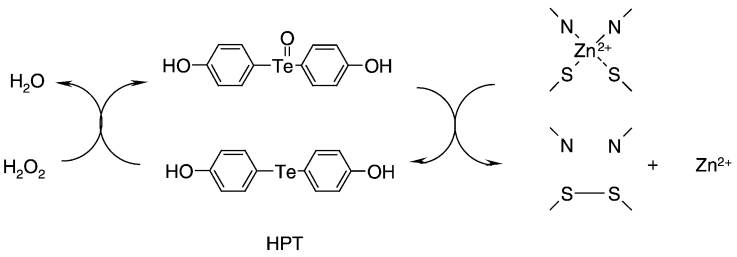
Oxidation of cysteine, cystine, and methionine in proteins has consequences reaching far beyond redox catalysis or antioxidant protection. For example, it was recently suggested that posttranslational cysteine modifications in proteins might be linked to enzyme regulation and signaling,[74] and sulfenic acid formation has been implied in the redox regulation of transcription factors such as OxyR and AP-1. A discussion of all of these redox-controlled processes is beyond the scope of this Review.

4. Metal-Binding Properties of Cysteine, Sulfinic Acids, and Sulfoxides

The thiolate group in cysteine is not only redox-active, but also forms coordinative bonds with a wide range of metal ions such as iron, zinc, cadmium, mercury, cobalt, and copper, but not group 1 or group 2 metal ions. Numerous proteins contain zinc/sulfur sites with structural (e.g. zinc finger proteins of transcription factors), catalytic (e.g. alcohol dehydrogenase and metallolactamases), and regulatory/inhibitory properties (e.g. glyceraldehyde 3-phosphate dehydrogenase).

 © 2003 Wiley-VCH Verlag GmbH & Co. KGaA, Weinheim

Once the two main properties of the thiol group (i.e. metal binding and redox activity) are considered together, cysteine-linked reactions open the door to redox control of metal binding and metal control of sulfur redox activity in biological systems.



HPT

Scheme 6. Redox control of metal binding by organotellurium compounds in a catalytic cycle that mimics the function of GPx. The tellurium center of 4,4′-dihydroxydiphenyltelluride (HPT) is initially oxidized by hydrogen peroxide to form the telluroxide. This highly reactive species is then reduced by a zinc finger motif to regenerate the telluride. Oxidation of the zinc finger results in zinc release owing to the formation of the disulfide.[83]

4.1. Redox Control of the Cysteine Ligand

The interdependence between metal binding and redox activity of cysteine has been extensively studied for the zinc/sulfur protein metallothionein (MT).[75–78] MT is a major intracellular zinc-binding protein with a significant regulatory role in zinc uptake, distribution, storage, and release. Mammalian MT is a single polypeptide chain of approximately 60 amino acids, of which 20 are cysteine residues. Despite the lack of secondary structure, these cysteines together bind seven zinc ions with an exceptionally high metal-binding constant ($K(Zn^{2+}) = 3.2 \times 10^{13}\,M^{-1}$ at pH 7.4)[79] in two zinc/sulfur clusters (Zn_4Cys_{11} and Zn_3Cys_9).[79] MT readily participates in intermolecular metal-exchange and metal-transfer reactions.[75,77] Metal transfer from MT to proteins is greatly enhanced in the presence of other metal-binding agents such as GSH and citrate,[77] but also by oxidizing agents that release zinc from MT.[77,78,80] Oxidation of the thiol(ate) ligands in MT eliminates metal binding, which might be an important in vivo trigger for metal release and transfer to other proteins.[81]

A similar redox control exists for a number of transcription factors that contain a zinc finger motif. Transcription factors bind to DNA, initiating the initial stages of gene expression. The DNA-binding domains of these transcription factors are frequently built out of zinc fingers, motifs of approximately 30 amino acids in length containing a zinc ion. The zinc is ligated either by a pair of histidine and a pair of cysteine residues (CCHH), three cysteine groups and one histidine moiety (CCCH), or four cysteine residues (CCCC). The key feature of this structure is that the cysteine residue must be in its reduced form to allow coordination of zinc.[82] If the redox balance is altered such that the cysteine ligands are oxidized and can no longer bind zinc, the structural motif will collapse, leaving the transcription factor unable to bind DNA, thus modulating mRNA synthesis and gene expression.

Although the full in vivo implications of these findings are still under discussion, redox control of transcription factors in cancer cells has already attracted considerable interest among biochemists and might even serve as the target for catalytic redox drugs.[83] Whereas zinc finger motifs and MT only react slowly with oxidative stressors such as hydrogen peroxide, small quantities of sulfur-specific peroxidation catalysts that mimic GPx activity (Scheme 6) effectively destroy these proteins and significantly increase the stressor-induced cell damage in neuronal cell culture.

The reverse effect, that is, the use of metal ions to control the redox activity of sulfur, has equally important biochemical implications. Thionein, the metal-free (apo) form of MT, is considerably more reactive toward oxidizing agents than MT itself, a well-known fact that has recently been underlined.[76] A similar control mechanism is found in metal-poisoned cysteine enzymes (inhibitory or regulatory zinc/sulfur sites). Inhibition by zinc occurs in many enzymes, including mammalian liver fructose-1,6-bisphosphatase, muscle glyceraldehyde 3-phosphate dehydrogenase (GAPDH), muscle enolase, human caspase-3, human T cell protein tyrosine phosphatase, and yeast aldehyde dehydrogenase (ALDH).[84] In some instances, inhibition occurs at nanomolar concentrations of zinc in vitro, indicating the importance of metal-regulated cysteine residues. Notably, thionein is able to remove zinc from inhibitory (but not catalytic) protein sites, hinting at the existence of a complex feedback mechanism between cysteine redox activity and metal binding.[84]

There is, however, an interesting twist to redox control of metal binding: the recent discovery of sulfinic acid ligands bound to metal ions in enzymes has added another dimension to this issue.[43,85,86]

4.2. Sulfinic Acids and Sulfoxides as Ligands

Cysteine sulfinic acid has recently been found in metalloenzymes such as bacterial nitrile hydratase (NHase), in which the sulfinic acid binds to metals such as iron through the oxygen atom. These NHases catalyze the hydration of nitriles to the corresponding amides and can coordinate either a low-spin, non-heme Fe^{III} or non-corrinoid Co^{III}. Recent X-ray crystallographic analysis shows that iron-containing NHase from *Rhodococcus sp. N-771* has an unusual Cys109-Ser-Leu-Cys112-Ser-Cys114 metal-binding sequence.[85] It is suggested that in the active form of the enzyme, Cys112 and Cys114 are modified to the respective sulfinic ($Cys\text{-}SO_2H$) and sulfenic acids (Cys-SOH) and contribute to iron coordination. Other studies have confirmed that the sulfinic acid is present in both the active and inactive forms of the enzyme, whereas the existence of the sulfenic acid residue of the Cys114 in the active NHase is still controversial.[86] Further studies have shown that the Cys114 and Cys112 are modified together during posttranslational modification of the enzyme.[87] Oxidized cysteine acids that can act as ligands are also being investigated in some transcription factors such as BPV-1 E2 protein, activator protein-1,[43] and cobalt-containing NHase from *Pseudonacardia thermophila*

 © 2003 Wiley-VCH Verlag GmbH & Co. KGaA, Weinheim

JCM 3095. The crystal structure of this NHase was recently resolved to 1.8 Å, and Cys 111 and Cys 113 were found to be modified to the sulfinic and sulfenic acids, respectively, and coordinated to Co^{III}.[88]

Metal binding of oxidized cysteine species is therefore very different from the metal binding of reduced cysteine. To date, bacterial NHases are the only examples of sulfinic acid ligands in metalloenzymes. However, these results are still controversial as the sulfenic and sulfinic acid might well be formed during the isolation and characterization of the enzyme. If posttranslational modification of cysteine to sulfenic and sulfinic acid is confirmed in NHase and other proteins, it might provide a mechanism to create types of metal-binding sites in proteins that have so far been mostly overlooked. A "redox switch" in metal preference from zinc (thiol) to iron (sulfenic/sulfinic acid) could also be important in oxidative stress, in which the antioxidant response of a protein to oxidation would be the release of the "antioxidant" metal zinc and subsequent binding of the "pro-oxidant" iron.

Methionine also plays a role in metal binding and there is evidence of redox-dependent metal binding to this amino acid. Reduced methionine readily coordinates to toxic metals such as lead, cadmium, and mercury, aiding in their excretion from the body.[89–91] It is also found as a metal ligand in many proteins such as ascorbate oxidase (copper)[92] and various cytochromes (iron).[93] As an example for oxidized methionine, the bacterial catalase from *Proteus mirablis PR* (a peroxide-resistant 56-kDa enzyme) contains a heme group found to interact with a methionine sulfone, which could prevent access of large substrates or inhibitors to the iron-containing active site.[94]

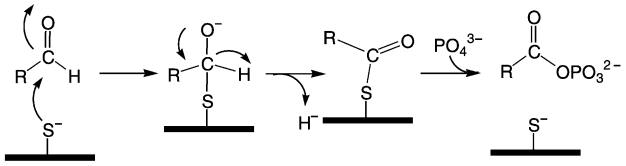
Metal binding to cysteine leads us to another group of redox enzymes that contain redox-inactive cysteine residues at the active site. The following section completes our discussion of cysteine-based redox catalysis with a look at dehydrogenases.

5. Cysteine Dehydrogenases and Proteases

Table 2 illustrates the mechanistic diversity available to cysteine in enzymes that catalyze the oxidation/reduction of NADPH. Whereas GR contains two redox-active cysteine residues that oxidize NADPH by hydride transfer to FAD with subsequent two-electron transfer to the disulfide, Npx oxidizes NADH by hydride transfer to a sulfenic acid through FAD. In contrast, the cysteine dehydrogenase GAPDH contains a cysteine that facilitates hydride transfer between aldehyde and NAD^+, whereas the human liver alcohol dehydrogenase (ADH) contains a zinc/cysteine coordination site that facilitates reversible hydride transfer between ethanol and NAD^+ without a change in the oxidation states of cysteine or zinc.

5.1. Thioether Formation and Breakage of C–H and C–N Bonds

Mammalian muscle GAPDH catalyzes the oxidation and subsequent phosphorylation of aldehydes to acyl phosphates, while reducing NAD^+ to NADH. Its catalytic cycle involves a crucial hydride-transfer step that requires an activated aldehyde substrate. The active site of the enzyme contains a cysteine residue (Cys 149) that attacks the aldehyde to form an activated, highly reactive, tetravalent thioether intermediate (Scheme 7). A hydride ion is transferred to NAD^+ to form



Scheme 7. Cysteine-catalyzed dehydrogenation. Dehydrogenases use cysteine to form a tetravalent thioether that facilitates hydride transfer. A similar mechanism is found in cysteine proteases.[84]

a thioester at the active site. The latter is cleaved by nucleophilic attack of phosphate, resulting in the formation of a phosphoester with regeneration of the cysteine residue in the active site. Importantly, cysteine itself acts as a nucleophile in this redox cycle and does not directly take part in the redox mechanism. It merely facilitates hydride abstraction from the aldehyde by forming the tetravalent thioether intermediate. Related enzymes such as ALDH follow a similar redox mechanism. These enzymes are inhibited by oxidizing agents such as reactive sulfur species,[55] peroxynitrite,[95] and zinc ions, emphasizing the importance of the

Table 2: Cysteine and NAD(P)H. Mechanistic diversity of hydride transfer involving cysteine in the active site.

Enzyme	Active site	Redox mechanism	Oxidation states
Glutathione disulfide reductase (GR)	cysteine	two-electron transfer from $FADH_2$ to disulfide, then hydride transfer from NADPH to FAD[27]	−2 (thiol), −1 (disulfide)
Thioredoxin reductase (TrxR)	cysteine, selenocysteine	selenylsulfide exchanges thiol to form disulfide, then as for GR[29,131]	−2 (thiol, selenol), −1 (disulfide, selenylsulfide)
NADH peroxidase (Npx)	cysteine	hydride transfer from NADH to cysteine sulfenic acid through FAD[43]	−2 (thiol), 0 (sulfenic acid)
Glyceraldehyde 3-phosphate dehydrogenase (GAPDH)	cysteine	nucleophilic attack of thiolate on carbonyl group of aldehyde facilitates hydride transfer from aldehyde to $NADP^+$[84]	−2 (thiolate, thioether, thioester)
Alcohol dehydrogenase (ADH)	zinc/cysteine complex	coordination of ethanol to zinc facilitates (reversible) hydride transfer to $NAD(P)^+$[99]	−2 (thiol), +2 (zinc)

 © 2003 Wiley-VCH Verlag GmbH & Co. KGaA, Weinheim

reduced and "metal-free" state of the cysteine residue in the active site.[84]

Interestingly, the thioether intermediate is not only a feature of dehydrogenases but is also found in another class of functionally entirely unrelated enzymes, the cysteine proteases such as papain, cathepsin B, and human caspases.[96] Rather than attacking the carbonyl group of an aldehyde, the nucleophilic thiolate function of the cysteine residue in the protease attacks the carbonyl group of its substrate amide. The tetrahedral thioether formed in this process then eliminates an amine RNH^- (compared to H^- in GAPDH), leading to the formation of a thioester acyl enzyme intermediate, which is subsequently hydrolyzed with release of the carboxylic acid and regeneration of free enzyme.

In cysteine proteases, cysteine does not directly take part in a redox process, and zinc ions strongly inhibit these enzymes.[84] In contrast, there are numerous proteases and dehydrogenases that are only active when zinc is tightly bound to their active-site cysteine residues.

5.2. The Role of Zinc/Sulfur Coordination in Breaking C–H and C–N Bonds

Mammalian ADH is an important dimeric 80-kDa enzyme that catalyzes the oxidation of ethanol to acetaldehyde under alkaline conditions, reducing NAD^+ to NADH in the process (at lower pH values, the enzyme catalyzes the oxidation of NADH in the presence of aldehyde).[97] It is essential for human alcohol tolerance and inhibition of the enzyme has been used in the treatment of alcoholism. Each of the two subunits of the enzyme has one binding site for NAD^+ and two binding sites for Zn^{2+}. Only one of the zinc ions is involved directly in catalysis. It is coordinated to Cys 46, His 67, Cys 174, and an exchangeable water molecule that forms a hydrogen bond to Ser 48. The other zinc ion plays a structural role as part of a $ZnCys_4$ site. The crystal structure of human liver ADH[98] has revealed that in the enzyme–NAD^+–alcohol active ternary complex, the OH group of ethanol binds to the zinc through an inner coordination sphere, with the side chains of Ser 48 and Phe 93 effectively locking the alcohol into a position that promotes hydride transfer from the alcohol to the NAD^+.[99] During hydride transfer (oxidizing ethanol and reducing NAD^+), neither the cysteine ligands in the active site nor the zinc ion change their oxidation states. ADH is, however, sensitive to cysteine oxidation, which releases the zinc ions and deactivates the enzyme.[53–55,80]

As is the case for the dehydrogenases, protease enzymes can utilize cysteine either directly as a catalytic residue or indirectly as a ligand to a catalytically active zinc ion. For example, matrix metalloproteases (MMPs) are zinc-dependent endopeptidases present in plants, invertebrates, and vertebrates. Cysteine acts in a regulatory role as ligand to the catalytically active zinc ion. In the active form of the enzyme, zinc is coordinated to three highly conserved histidine residues with a vacant coordination site for the peptide substrate. In the inactive propeptide, however, this fourth coordination site is occupied by a highly conserved cysteine residue in a sequence that caps the active site and is cleaved from the MMP upon proteolytic activation of the enzyme.[100]

Similarly, tissue inhibitors of metalloproteinases (TIMPs), peptides of approximately 20 kDa, contain several conserved cysteine residues (12 in the case of TIMP-1 and TIMP-2), which are essential not only for structural integrity but are directly involved in MMP inhibition. The crystal structure of the MMP3–TIMP-1 complex between human stromelysin-1 (MMP-3) and human TIMP-1 shows a cysteine residue near the active-site zinc of MMP-3, probably blocking its activity.[101]

6. From Sulfur to Selenium—Similarities and Differences

The role of selenium in biology is currently of considerable interest, and there are several recent reviews on this topic.[4,102–105] The aim of this section is not to provide a comprehensive review of the biological role of selenium, but rather to focus on the redox chemistry of the selenium-containing amino acids, their redox mechanisms, oxidation states, and metal-binding properties in proteins in comparison with cysteine and methionine.

6.1. Natural Occurrence of Selenium in Proteins

The element selenium is located below sulfur on the periodic table, and thus there are close similarities, but also striking differences, between these two elements in terms of their chemistry and biochemistry. The abundance of selenium in the earth's crust is about four orders of magnitude lower than that of sulfur, and this is also reflected in the natural abundance of these elements in biological systems. Whereas sulfur occurs in the human body in quantities similar to those of potassium (140 g in an adult), selenium is a trace element present in milligram amounts, primarily as selenocysteine, selenomethionine, and, at a much lower content, their metabolic precursors (e.g. GS-Se-SG, GSSeH, selenophosphate). Mammalian selenium-containing proteins can be divided into three groups: 1) specific selenocysteine-containing selenoproteins, 2) proteins that contain nonspecifically incorporated selenium, and 3) specific selenium-binding proteins. Selenoproteins with known functions identified so far include several glutathione peroxidases, two deiodinases, several thioredoxin reductases, and selenophosphate synthetase-2. A biological function of selenoprotein P (i.e. its important role in delivering hepatic selenium to specific tissues) was recently confirmed in gene knockout experiments in mice.[106,107] Selenoprotein W, a 15-kDa protein, an 18-kDa protein, and several selenoproteins identified in silico from nucleotide sequence databases contain selenocysteine, but their functions are not fully known. The current state of knowledge on these proteins has recently been reviewed.[4] Incorporation of selenocysteine into these proteins requires an elaborate translation machinery.[108] In contrast, selenomethionine is randomly incorporated into proteins in place of methionine.

 © 2003 Wiley-VCH Verlag GmbH & Co. KGaA, Weinheim

6.2. Selenocysteine and Selenomethionine: Oxidation States, Redox Catalysis, and Antioxidant Activity

A major difference between selenocysteine and cysteine residues is a significantly lower pK_a value of the selenol group in selenocysteine (p$K_a = 5.2$) relative to that of the thiol group of cysteine (p$K_a = 8.3$).[109] As a consequence, selenols in selenocysteine-containing proteins are normally present as selenolates at physiological pH, whereas thiols in cysteine-containing proteins are usually present as undissociated thiols. There are, of course, notable exceptions, such as NADH oxidase and human thiol transferase. The dissociation states were found to be similar when cysteine replaced selenocysteine in the active site GPx mutant of phospholipid hydroperoxide GPx.[110] Furthermore, selenocysteine occurs mainly in the reactive selenol and selenenic acid oxidation states (Scheme 3) and, unlike disulfides, reactive diselenides have not yet been found in proteins. The redox cycle of GPx exemplifies the redox mechanism of these peroxidases: Selenocysteine is oxidized by oxygen-atom transfer, and reduction of selenenic acid occurs through an exchange reaction involving two GSH equivalents.[111]

Although diselenides have not been found in proteins yet, selenylsulfides are present in GPx and human TrxR. The redox behavior of selenocysteine in these proteins is rather interesting from a mechanistic point of view. Reduction of disulfides can proceed through exchange as well as electron-transfer reactions (see Section 2). Theoretically, the selenylsulfide in human TrxR would therefore also lend itself to reduction through electron transfer from $FADH_2$ (the disulfide subsequently formed in human TrxR is reduced by two-electron transfer). Electron transfer to the selenylsulfide does not occur in human TrxR and reduction follows a more elaborate pathway (Scheme 2): The selenylsulfide is first reduced by cysteine in an exchange reaction, and the resulting disulfide is then reduced by electron transfer. Common cysteine redox mechanisms such as electron transfer, hydride transfer, and radical reactions have not been observed for selenocysteine in proteins.

The occurrence of selenol, selenylsulfide, and selenenic acid in selenoproteins does not mean, however, that other selenium oxidation states are principally absent in vivo. The selenocysteine/selenocystine redox potential of -488 mV (Figure 2) indicates that diselenide formation is possible under physiological redox conditions. However, few proteins have two selenocysteine residues in close enough proximity to facilitate diselenide formation (perhaps with the exception of selenoprotein P, which contains up to 10 selenocysteine residues). A range of additional selenium oxidation states occurs during selenium metabolism: selenite (SeO_3^{2-}) is reduced stepwise by GSH to form H_2Se and ultimately selenophosphate. This process involves selenium species in various oxidation states ranging from $+4$ to -2. Excretion pathways of excess H_2Se also involve a trivalent selenonium species in the form of trimethylselenonium, which is excreted in urine. Although not yet known to take part in protein mechanisms, species such as seleninic acids could exist under physiological conditions and are known to be redox-active in the presence of zinc/thiolate coordination centers.[78]

Whereas selenocysteine is specifically incorporated into proteins,[112,113] selenomethionine occurs apparently randomly in proteins in place of methionine, depending on the supply of selenomethionine. Like methionine, selenomethionine is readily oxidized to the corresponding selenoxide.[114] Unlike methionine sulfoxide, which requires a sulfoxide reductase for reduction (see Section 3.3), selenomethionine selenoxide is nonenzymatically reduced by 2 equivalents of GSH.[115] Selenomethionine might, therefore, serve as a line of defense against permanent oxidative damage in proteins, because the funneling of oxidative challenge into a repairable site of damage can be advantageous over introducing nonrepairable damage sites, which require proteolytic degradation of the protein. Whether this strategy is utilized to a major extent in vivo is being debated.[116]

This distinctive feature of selenoxide is also used in effective synthetic antioxidants that mimic glutathione peroxidase activity, such as ebselen.[117] Whereas selenols are frequently oxidized to "dead end" diselenides, dialkyl, diaryl, and alkylaryl selenides cannot form diselenides and are among the best peroxidase redox catalysts; their activity is only surpassed by that of diaryl tellurides.[83,118–120] This rapidly growing field of research into selenoorganic compounds that carry out catalytic functions mimicking those of selenoproteins has recently been reviewed.[121]

Another interesting family of selenocysteine-containing enzymes are the deiodinases, which function in thyroxine metabolism.[122] The catalytic mechanism of these enzymes in vivo might be rather unusual and possibly involves nucleophilic substitution of an iodine atom of an aryl iodide (Reaction (13) in Scheme 1).[123] The selenolate of the selenocysteine (SeCys-Se^-) in the active site acts as a nucleophile that attacks an iodine atom of 3,3′,5,5′-tetraiodo-L-thyronine (prohormone L-thyroxine). An oxidized selenenyl iodide intermediate (SeCys-Se-I) is formed, and the reduced aromatic hormone 3,3′,5-triiodo-L-thyronine is protonated and released. The reduced form of selenocysteine is regenerated by reduction with dithiols (the latter are oxidized to disulfides in this process). A comparison with the S-conjugation reactions catalyzed by glutathione transferase enzymes is interesting: Whereas selenocysteine in the deiodinases attacks the halogen atom with the (reduced) aromatic ring as leaving group, cysteine in the GST enzymes attacks the ring with the reduced halide as leaving group.

6.3. Selenium and Metal Binding

Metal binding is a common feature of cysteine, and a range of metal–selenium sites might be expected in proteins. Surprisingly, this is not the case, as examples of selenocysteine–metal complexes have been observed in a few selenoproteins. Unexpectedly, in cases in which they have been observed, the selenocysteine is bound to the hard and intermediate rather than to the soft heavy-metal ions. A selenium–molybdenum bond was found in formate dehydrogenase from *E. coli*[124] and a selenium–tungsten bond was recently identified in formate dehydrogenase from *Desulfovibrio gigas*.[125] Although selenocysteine is essential for

 © 2003 Wiley-VCH Verlag GmbH & Co. KGaA, Weinheim

formate dehydrogenase activity, the role of selenium in these proteins is unclear. The genus *Desulfovibrio* also contains an intermediate metal ligation in the form of a selenium–nickel coordination, found in the nickel–(iron/sulfur)–selenium-containing hydrogenases.[126] Genetic engineering has shown that it is possible for selenium to bind a soft heavy metal in a protein, by substituting selenocysteine for the cysteine ligand of copper in azurin.[127] A similar selenium–copper bond has yet to be observed in vivo. Metal binding to selenenic acids or selenomethionine, although chemically possible, has not yet been observed in proteins.

Metal binding to selenocysteine underlines the dichotomy between the chemically possible and biochemically realized. Selenium species in unusual oxidation states and metal–selenium interactions in proteins are areas for future investigation.

7. Summary and Outlook

This Review delineates the complex biological chemistry of cysteine, methionine, selenocysteine, and selenomethionine, discussing biological examples from the perspective of their redox chemistry. During protein synthesis, cysteine is incorporated as one of the 21 mammalian proteinogenic amino acids (with selenocysteine as the 21st amino acid).[108,128] A variety of posttranslational modifications ensure that this one amino acid is present in the form of about 10 different species, which exhibit unique chemical and biochemical properties. Thus, cysteine may be considered as the most diverse amino acid building block in proteins.

Whereas redox-active metals transfer electrons, NAD(P)H transfers hydride ions, oxoanions transfer oxygen atoms, FAD transfers hydride ions or electrons, and tyrosine forms radicals in biological systems, cysteine carries out all of these and other redox reactions, for example, long-range electron and short-range hydrogen-atom transfer and thiol/disulfide-exchange reactions. There are probably no other chemical species in biological systems that can occur in as many different oxidation states, allow for as many different posttranslational protein side-chain modifications, provide as many different redox pathways, generate such a variety of structurally distinct metal-binding sites, and fulfill a multitude of different biological functions as the "redox chameleon" sulfur in the amino acid cysteine.

With the identification of different oxidation states of sulfur in methionine, the discovery of a sulfoxide reductase, and the postulation of methionine–metal bonds in proteins, the biological redox chemistry of methionine is also becoming increasingly important.

Recent developments in genomics and bioinformatics have revealed genomic sequences that should lead to the identification of novel sulfur- and selenium-containing proteins. Similarly, the emerging discipline of proteomics will facilitate the discovery of new posttranslational modifications. Our knowledge of Nature's use of oxidation state to regulate protein structure and function is in its infancy; the recent developments outlined in this Review give an indication of possible unidentified pathways and reaction mechanisms that may be operating within the cell. For example, exciting new developments in the study of the oxidation states of sulfur have shown that disulfide-*S*-oxides can be formed under physiological conditions. In addition to their own reaction pathways, these oxidizing species can be "activated" by reduction, forming highly reactive sulfenic acids. Ongoing investigations into this redox metabolism of sulfur point to the existence of multiple redox sulfur cascades within the cell which influence protein activity and signaling.

A further topic of interest is the possibility of a metal-binding role of sulfenic/sulfinic acids and their potential importance in protein functions. Interestingly, the first cysteine persulfide coordinated to heme was recently identified in the active site of SoxAX, a *c*-type cytochrome from *Rhodovulum sulfidophilum*, which has provided insight into the bacterial sulfur cycle.[129] New posttranslational sulfur modifications are expected to be uncovered. At the same time, synthetic enzyme mimics may find applications in rational drug design, as shown by the use of organochalcogen GPx catalysts in therapy for cerebral ischemia,[130] and by promising leads from electrochemical and other in vitro and cell-culture studies with regard to cancer and dementia.[83,120]

This work was supported by the Wellcome Trust, the Leverhulme Trust, DAART, Exeter Antioxidant Therapeutics Ltd., and by the Deutsche Forschungsgemeinschaft (Schwerpunktsprogramm Selenoproteine Si 255/11-2). C.J. is Chairman of EAT Ltd. and H.S. is a Fellow of the National Foundation for Cancer Research. We also thank Professor G. Buettner (Iowa City), Dr. L.-O. Klotz (Düsseldorf), Prof. J. A. Littlechild (Exeter), Professor W. Stahl (Düsseldorf), and Professor J. Thomas (Ames) for helpful discussions.

Received: January 24, 2003 [A573]

[1] *Thiol Metabolism and Redox Regulation of Cellular Functions* (Eds.: A. Pompella, G. Bahegyi, M. Wellman-Rousseau), IOS Press, Amsterdam, **2002**, pp. 1–348.
[2] *Cellular Implications of Redox Signalling* (Eds.: C. Gitler, A. Danon), World Scientific, Singapore, **2003**.
[3] *Antioxidant and Redox Regulation of Genes* (Eds.: C. K. Sen, H. Sies, P. A. Baeuerle), Academic Press, San Diego, **2000**, pp. 1–556.
[4] *Protein Sensors and Reactive Oxygen Species, Part A: Selenoproteins and Thioredoxin* (Eds.: H. Sies, L. Packer), Academic Press, San Diego, **2002**, pp. 1–461.
[5] *Protein Sensors and Reactive Oxygen Species, Part B: Thiol Enzymes and Proteins* (Eds.: H. Sies, L. Packer), Academic Press, San Diego, **2002**, pp. 1–364.
[6] Y.M Torchinsky, *Sulfur in Proteins*, Pergamon, Oxford, **1981**, pp. 1–277.
[7] P. C. Jocelyn, *Biochemistry of the SH Group*, Academic Press, London, **1972**.
[8] *Glutathione Conjugation: Mechanisms and Biological Significance* (Eds.: H. Sies, B. Ketterer), Academic Press, London, **1988**, pp. 1–470.
[9] W. J. Lees, G. M. Whitesides, *J. Org. Chem.* **1993**, *58*, 642–647.
[10] T. P. Akerboom, M. Bilzer, H. Sies, *J. Biol. Chem.* **1982**, *257*, 4248–4252.
[11] R. C. Fahey, *Adv. Exp. Med. Biol.* **1977**, *86A*, 1–30.
[12] H. Sies, *Free Radical Biol. Med.* **1999**, *27*, 916–921.

 © 2003 Wiley-VCH Verlag GmbH & Co. KGaA, Weinheim

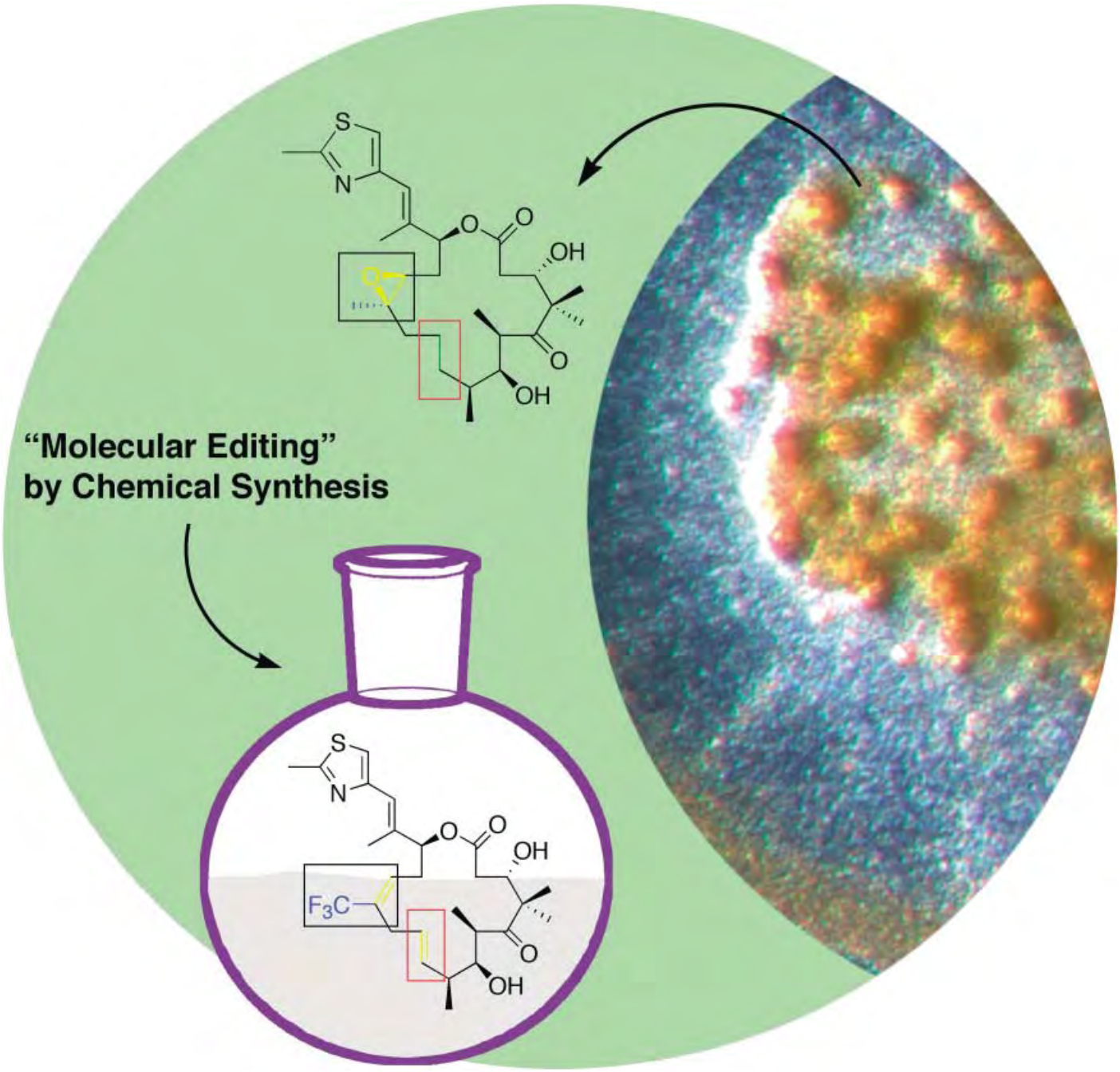
[13] F. Q. Schäfer, G. R. Buettner, *Free Radical Biol. Med.* **2001**, *30*, 1191 – 1212.
[14] Y. Nishinaka, H. Masutani, H. Nakamura, J. Yodoi, *Redox Rep.* **2001**, *6*, 289 – 295.
[15] A. Holmgren, *Struct. Bonding (Berlin)* **1995**, *3*, 239 – 243.
[16] R. Brigelius, in *Oxidative Stress* (Ed.: H. Sies), Academic Press, London, **1985**, pp. 243 – 272.
[17] D. M. Ziegler, *Annu. Rev. Biochem.* **1985**, *54*, 305 – 329.
[18] J. A. Thomas, R. Mallis, H. Sies in *Cellular Implications of Redox Signalling* (Eds.: C. Gitler, A. Danon), World Scientific, Singapore, **2003**, pp. 141 – 174.
[19] G. I. Giles, C. Jacob, *Biol. Chem.* **2002**, *383*, 375 – 388.
[20] Y. C. Chai, S. Hendrich, J. A. Thomas, *Arch. Biochem. Biophys.* **1994**, *310*, 273 – 281.
[21] L. F. Chasseaud, *Adv Cancer Res.* **1979**, *29*, 175 – 274.
[22] J. P. Ploemen, M. L. van Iersel, L. W. Wormhoudt, J. N. Commandeur, N. P. Vermeulen, P. J. van Bladeren, *Biochem. Pharmacol.* **1996**, *52*, 197 – 204.
[23] R. Morgenstern, J. W. DePierre, L. Ernster, *Biochem. Biophys. Res. Commun.* **1979**, *87*, 657 – 663.
[24] R. Rinaldi, E. Eliasson, S. Swedmark, R. Morgenstern, *Drug Metab. Dispos.* **2002**, *30*, 1053 – 1058.
[25] Y. Ji, B. M. Bennett, *Mol. Pharmacol.* **2003**, *63*, 136 – 146.
[26] L. D. Arscott, S. Gromer, R. H. Schirmer, K. Becker, C. H. Williams, Jr., *Proc. Natl. Acad. Sci. USA* **1997**, *94*, 3621 – 3626.
[27] E. F. Pai, G. E. Schulz, *J. Biol. Chem.* **1983**, *258*, 1752 – 1757.
[28] L. D. Arscott, D. M. Veine, C. H. Williams, Jr., *Biochemistry* **2000**, *39*, 4711 – 4721.
[29] D. Mustacich, G. Powis, *Biochem. J.* **2000**, *346*, 1 – 8.
[30] J. T. Spence, M. J. Barber, L. P. Solomonson, *Biochem. J.* **1988**, *250*, 921 – 923.
[31] G. E. Arteel, K. Briviba, H. Sies, *Chem. Res. Toxicol.* **1999**, *12*, 264 – 269.
[32] R. Zhao, H. Masayasu, A. Holmgren, *Proc. Natl. Acad. Sci. USA* **2002**, *99*, 8579 – 8584.
[33] D. C. Rees, *Annu. Rev. Biochem.* **2002**, *71*, 221 – 246.
[34] C. R. Staples, E. Ameyibor, W. Fu, L. Gardet-Salvi, A. L. Stritt-Etter, P. Schurmann, D. B. Knaff, M. K. Johnson, *Biochemistry* **1996**, *35*, 11425 – 11434.
[35] S. Dai, C. Schwendtmayer, P. Schurmann, S. Ramaswamy, H. Eklund, *Science* **2000**, *287*, 655 – 658.
[36] G. N. Jameson, E. M. Walters, W. Manieri, P. Schurmann, M. K. Johnson, B. H. Huynh, *J. Am. Chem. Soc.* **2003**, *125*, 1146 – 1147.
[37] A. L. Persson, M. Sahlin, B.M Sjöberg, *J. Biol. Chem.* **1998**, *273*, 31016 – 31020.
[38] X. Sun, S. Ollagnier, P. P. Schmidt, M. Atta, E. Mulliez, L. Lepape, R. Eliasson, A Gräslund, M. Fontecave, P. Reichard, B. M. Sjöberg, *J. Biol. Chem.* **1996**, *271*, 6827 – 6831.
[39] S. Ollagnier, E. Mulliez, P. P. Schmidt, R. Eliasson, J. Gaillard, C. Deronzier, T. Bergman, A. Gräslund, P. Reichard, M. Fontecave, *J. Biol. Chem.* **1997**, *272*, 24216 – 24223.
[40] P. A. Frey, *Annu. Rev. Biochem.* **2001**, *70*, 121 – 148.
[41] J. A. Gerlt, P. C. Babbitt, *Annu. Rev. Biochem.* **2001**, *70*, 209 – 246.
[42] H. Miller, S. S. Mande, D. Parsonage, S. H. Sarfaty, W. G. Hol, A. Claiborne, *Biochemistry* **1995**, *34*, 5180 – 5190.
[43] A. L. Claiborne, T. C. Mallett, J. I. Yeh, J. Luba, D. Parsonage, *Adv. Protein Chem.* **2001**, *58*, 215 – 276.
[44] S. S. Mande, D. Parsonage, A. Claiborne, W. G. Hol, *Biochemistry* **1995**, *34*, 6985 – 6992.
[45] D. Parsonage, A. Claiborne, *Biochemistry* **1995**, *34*, 435 – 441.
[46] T. C. Mallett, A. Claiborne, *Biochemistry* **1998**, *37*, 8790 – 8802.
[47] B. Hofmann, H. J. Hecht, L. Flohé, *Biol. Chem.* **2002**, *383*, 347 – 364.
[48] S. Hirotsu, Y. Abe, K. Okada, N. Nagahara, H. Hori, T. Nishino, T. Hakoshima. *Proc. Natl. Acad. Sci. USA* **1999**, *96*, 12333 – 12338.
[49] E. Schröder, J. Littlechild, A. Lebedev, N. Errington, A. Vagin, M. Isupov, *Struct. Bonding (Berlin)* **2000**, *8*, 605 – 615.
[50] H. Sies in *Oxidative Stress* (Ed.: H. Sies), Academic Press, London, UK, **1985**, pp. 1 – 8.
[51] H. Sies, *Angew. Chem.* **1986**, *98*, 1061 – 1075; *Angew. Chem. Int. Ed. Engl.* **1986**, *25*, 1058 – 1071.
[52] H. Sies in *Encyclopedia of Stress, Vol. III*, (Ed.: G. Fink), Academic Press, San Diego, **2000**, pp. 102 – 105.
[53] G. I. Giles, K. M. Tasker, C. Jacob, *Free Radical Biol. Med.* **2001**, *31*, 1279 – 1283.
[54] G. I. Giles, K. M. Tasker, C. Jacob, *Gen. Physiol. Biophys.* **2002**, *21*, 65 – 72.
[55] G. I. Giles, K. M. Tasker, C. Collins, N. M. Giles, E. O'Rourke, C. Jacob, *Biochem. J.* **2002**, *364*, 579 – 585.
[56] T. Okamoto, T. Akaike, T. Sawa, Y. Miyamoto, M. A. van der Vliet, H. Maeda, *J. Biol. Chem.* **2001**, *276*, 29596 – 29602.
[57] J. Li, F. L. Huang, K. P. Huang, *J. Biol. Chem.* **2001**, *276*, 3098 – 3105.
[58] G. Nöhammer in *Thiol Metabolism and Redox regulation of Cellular Functions* (Eds.: A. Pompella, G. Banhegyi, M. Wellman-Rousseau), IOS Press, Amsterdam, **2002**, pp. 48 – 60.
[59] B. Kagedal, M. Kallberg, B. Sorbo, *Biochem. Biophys. Res. Commun.* **1986**, *136*, 1036 – 1041.
[60] D. A. Keller, D. B. Menzel, *Chem.-Biol. Interact.* **1989**, *21*,145 – 156.
[61] C. D. Klaassen, J. W. Boles, *FASEB J.* **1997**, *11*, 404 – 418.
[62] M. Negishi, L. G. Pedersen, E. Petrochenko, S. Shevtsov, A. Gorokhov, Y. Kakuta, L. C. Pedersen, *Arch. Biochem. Biophys.* **2001**, *390*, 149 – 157.
[63] F. Gliubich, R. Berni, M. Colapietro, L. Barba, G. Zanotti, *Acta Crystallogr. Sect. D* **1998**, *54*, 481 – 486.
[64] Y. Ogasawara, G. Lacourciere, T. C. Stadtman, *Proc. Natl. Acad. Sci. USA* **2001**, *98*, 9494 – 9498.
[65] H. Dobbek, L. Gremer, O. Meyer, R. Huber, *Proc. Natl. Acad. Sci. USA* **1999**, *96*, 8884 – 8889.
[66] H. Dobbek, L. Gremer, R. Kiefersauer, R. Huber, O. Meyer, *Proc. Natl. Acad. Sci. USA* **2002**, *99*, 15971 – 15976.
[67] N. Brot, H. Weissbach, *Arch. Biochem. Biophys.* **1983**, *223*, 271 – 281.
[68] W. Vogt, *Free Radical Biol. Med.* **1995**, *18*, 93 – 105.
[69] R. L. Levine, B. S. Berlett, J. Moskovitz, L. Mosoni, E. R. Stadtman, *Mech. Ageing Dev.* **1999**, *10*, 323 – 332.
[70] M. K. Unnikrishnan, M. N. Rao, *Agents Actions* **1990**, *31*, 110 – 112.
[71] R. L. Levine, L. Mosoni, B. S. Berlett, E. R. Stadtman, *Proc. Natl. Acad. Sci. USA* **1996**, *93*, 15036 – 15040.
[72] W. T. Lowther, N. Brot, H. Weissbach, B. W. Matthews, *Biochemistry* **2000**, *39*, 13307 – 13312.
[73] S. Boschi-Müller, S. Azza, S. Sanglier-Cianferani, F. Talfournier, A. Van Dorsselear, G. Branlant, *J. Biol. Chem.* **2000**, *275*, 35908 – 35913.
[74] T. Finkel, *FEBS Lett.* **2000**, *476*, 52 – 54.
[75] W. Maret, *Proc. Natl. Acad. Sci. USA* **1994**, *91*, 237 – 241.
[76] S. Zhang, J. Li, C.-C. Wang, C.-L. Tsou, *FEBS Lett.* **1999**, *462*, 383 – 386.
[77] C. Jacob, W. Maret, B. L. Vallee, *Proc. Natl. Acad. Sci. USA* **1998**, *95*, 3489 – 3494.
[78] C. Jacob, W. Maret, B. L. Vallee, *Proc. Natl. Acad. Sci. USA* **1999**, *96*, 1910 – 1914.
[79] J. D. Otvos, D. H. Petering, C. F. Shaw, *Comments Inorg. Chem.* **1989**, *1*, 1 – 35.
[80] C. Jacob, W. Maret, B. L. Vallee, *Biochem. Biophys. Res. Commun.* **1998**, *248*, 569 – 573.

 © 2003 Wiley-VCH Verlag GmbH & Co. KGaA, Weinheim

[81] W. Maret, B. L. Vallee, *Proc. Natl. Acad. Sci. USA* **1998**, *95*, 3478 – 3482.
[82] S. Lee, W. Maret, *Antioxid. Redox Signaling* **2001**, *3*, 531 – 534.
[83] N. M. Giles, N. J. Gutowski, G. I. Giles, C. Jacob, *FEBS Lett.* **2003**, *535*, 179 – 182.
[84] W. Maret, C. Jacob, B. L. Vallee, E. H. Fischer, *Proc. Natl. Acad. Sci. USA* **1999**, *96*, 1936 – 1940.
[85] M. Tsujimura, N. Dohmae, M. Odaka, M. Chijimatsu, K. Takio, M. Yohda, M. Hoshino, S. Nagashima, I. Endo, *J. Biol. Chem.* **1997**, *272*, 29454 – 29459.
[86] D. Bonnet, J. M. Stevens, R. Alves de Sousa, M. Sari, D. Mansuy, I. Artuad, *J. Biochem.* **2001**, *130*, 227 – 233.
[87] T. Murakami, M. Nojiri, H. Nakayama, M. Odaka, M. Yohda, N. Dohmae, K. Takio, T. Nagamune, I. Endo, *Protein Sci.* **2000**, *9*, 1024 – 1030.
[88] A. Miyanaga, S. Fushinobu, K. Ito, T. Wakagi, *Biochem. Biophys. Res. Commun.* **2001**, *288*, 1169 – 1174.
[89] D. N. Kachru, S. Khandelwal, S. K. Tandon, *Biomed. Environ. Sci.* **1989**, *2*, 265 – 270.
[90] A. C. Esteves, J. Felcman, *Biol. Trace Elem. Res.* **2000**, *76*, 19 – 30.
[91] Y. Kajiwara, A. Yasutake, T. Adachi, K. Hirayama, *Arch. Toxicol.* **1996**, *70*, 310 – 314.
[92] A. Messerschmidt, A. Rossi, R. Ladenstein, R. Huber, M. Bolognesi, G. Gatti, A. Marchesini, R. Petruzzelli, A. Finazzi-Agro, *J. Mol. Biol.* **1989**, *206*, 513 – 529.
[93] R. O. Louro, E. C. de Waal, M. Ubbink, D. L. Turner, *FEBS Lett* **2002**, *510*, 185 – 188.
[94] A. Buzy, V. Bracchi, R. Sterjiades, J. Chroboczek, P. Thibault, J. Gagnon, H. M. Jouve, G. Hudry-Clergeon, *J. Protein Chem.* **1995**, *14*, 59 – 72.
[95] D. P. Buchczyk, K. Briviba, F. U. Hartl, H. Sies, *Biol. Chem.* **2000**, *381*, 121 – 126.
[96] For a comprehensive review of these proteases, see: K. Brocklehurst, A. B. Watts, M. Patel, C. Verma, E. W. Thomas in *Comprehensive Biological Catalysis, Vol. 2* (Ed.: M. L. Sinnott), Academic Press, London, **1998**, pp. 381 – 423.
[97] J. D. Shore, H. Gutfreund, R. L. Brooks, D. Santiago, P. Santiago, *Biochemistry* **1974**, *13*, 4185 – 4191.
[98] H. Eklund, B. V. Plapp, J. P. Samama, C. I. Branden, *J. Biol. Chem.* **1982**, *257*, 14349 – 14358.
[99] Y. Pocker, *Chem.-Biol. Interact.* **2001**, *33*, 383 – 393.
[100] I. Massova, L. P. Kotra, R. Fridman, S. Mobashery, *FASEB J.* **1998**, *12*, 1075 – 1095.
[101] F. X. Gomis-Ruth, K. Maskos, M. Betz, A. Bergner, R. Huber, K. Suzuki, N. Yoshida, H. Nagase, K. Brew, G. P. Bourenkov, H. Bartunik, W. Bode, *Nature* **1997**, *389*, 77 – 81.
[102] M. P. Rayman, *Lancet* **2000**, *356*, 233 – 241.
[103] T. C. Stadtman, *Ann. N. Y. Acad. Sci.* **2000**, *899*, 399 – 402.
[104] M. Birringer, S. Pilawa, L. Flohé, *Nat. Prod. Rep.* **2002**, *19*, 693 – 718.
[105] G. E. Arteel, H. Sies, *Environ. Toxicol. Pharmacol.* **2001**, *10*, 153 – 158.
[106] L. Schomburg, U. Schweizer, B. Holtmann, L. Flohé, M. Sendtner, J. Köhrle, *Biochem. J.* **2003**, *370*, 397 – 402.
[107] K. E. Hill, J. Zhou, W. J. McMahan, A. K. Motley, J. F. Atkins, R. F. Gesteland, R. F. Burk, *J. Biol. Chem.* **2003**, *278*, 13640 – 13646.
[108] M. Thanbichler, A. Böck, *Methods Enzymol.* **2002**, 347, 3 – 16.
[109] R. E. Huber, R. S. Criddle, *Arch. Biochem. Biophys.* **1967**, *122*, 164 – 173.
[110] M. Maiorino, K. D. Aumann, R. Brigelius-Flohé, D. Doria, J. van den Heuvel, J. McCarthy, A. Roveri, F. Ursini, L. Flohé, *Biol. Chem. Hoppe-Seyler* **1995**, *376*, 651 – 660.
[111] P. Mauri, L. Benazzi, L. Flohé, M. Maiorino, P. G. Pietta, S. Pilawa, A. Roveri, F. Ursini, *Biol. Chem.* **2003**, *384*, in press.
[112] J. Köhrle, R. Brigelius- Flohé, A. Böck, R. Gartner, O. Meyer, L. Flohé, *Biol. Chem.* **2000**, *381*, 849 – 864.
[113] A. Böck, *BioFactors* **2000**, *11*, 77 – 78.
[114] A. Assmann, M. Bonifacic, K. Briviba, H. Sies, D. Asmus, *Free Radical Res.* **2000**, *32*, 371 – 376.
[115] A. Assmann, K. Briviba, H. Sies, *Arch. Biochem. Biophys.* **1998**, *349*, 201 – 203.
[116] R. J. Hondal, A. K. Motley, K. E. Hill, R. F. Burk, *Arch. Biochem. Biophys.* **1999**, *371*, 29 – 34.
[117] A. Müller, E. Cadenas, P. Graf, H. Sies, *Biochem. Pharmacol.* **1984**, *33*, 3235 – 3239.
[118] C. Jacob, G. E. Arteel, T. Kanda, L. Engman, H. Sies, *Chem. Res. Toxicol.* **2000**, *13*, 3 – 9.
[119] K. Briviba, R. Tamler, L. O. Klotz, L. Engman, I. A. Cotgreave, H. Sies, *Biochem. Pharmacol.* **1998**, *55*, 817 – 823.
[120] G. I. Giles, K. M. Tasker, R. J. Johnson, C. Jacob, C. Peers, K. N. Green, *Chem. Commun.* **2001**, *23*, 2490 – 2491.
[121] For a review, see: G. Mugesh, W.-W. du Mont, H. Sies, *Chem. Rev.* **2001**, *101*, 2125 – 2179.
[122] J. Köhrle, *Mol. Cell. Endocrinol.* **1999**, *151*, 103 – 119.
[123] J. Köhrle in *Protein Sensors and Reactive Oxygen Species, Part A: Selenoproteins and Thioredoxin* (Eds.: H. Sies, L. Packer), Academic Press, San Diego, **2002**, pp. 125 – 167.
[124] V. N. Gladyshev, S. V. Khangulov, M. J. Axley, T. C. Stadtman, *Proc. Natl. Acad. Sci. USA* **1994**, *91*, 7708 – 7711.
[125] H. Raaijmakers, S. Macieira, J. M. Dias, S. Teixeira, S. Bursakov, R. Huber, J. J. Moura, I. Moura, M. J. Romão, *Struct. Bonding (Berlin)* **2002**, *10*, 1261 – 1272.
[126] G. Fauque, H. D. Peck, J. J. G. Moura, B. H. Huynh, Y. Berlier, D. V. Dervartanian, M. Teixeira, A. E. Przybyla, P. A. Lespinat, I. Moura, J. Legall, *FEMS Microbiol. Rev.* **1988**, *4*, 299 – 344.
[127] S. M. Berry, M. D. Gieselman, M. J. Nilges, W. A. van Der-Donk, Y. Lu, *J. Am. Chem. Soc.* **2002**, *124*, 2084 – 2085.
[128] J. F. Atkins, R. F. Gesteland, *Science* **2002**, *296*, 1409 – 1410.
[129] V. A. Bamford, S. Bruno, T. Rasmussen, C. Appia-Ayme, M. R. Cheesman, B. C. Berks, A. M. Hemmings, *EMBO J.* **2002**, *21*, 5599 – 5610.
[130] M. Parnham, H. Sies, *Expert Opin. Invest. Drugs* **2000**, *9*, 607 – 619.
[131] T. Sandalova, L. Zhong, Y. Lindqvist, A. Holmgren, G. Schneider, *Proc. Natl. Acad. Sci. USA* **2001**, *98*, 9533 – 9538.
[132] F. Åslund, K. D. Berndt, A. Holmgren, *J. Biol. Chem.* **1997**, *272*, 30780 – 30786.
[133] E. Nogoceke, D. U. Gommel, M. Kiess, H. M. Kalisz, L. Flohe, *Biol. Chem.* **1997**, *378*, 827 – 836.
[134] N. Reckenfelderbaumer, R. L. Krauth-Siegel, *J. Biol. Chem.* **2002**, *277*, 17548 – 17555.
[135] J. Lundstrom, A. Holmgren, *Biochemistry* **1993**, *32*, 6649 – 6655.
[136] J. F. Collett, J. C. Bardwell, *Mol. Microbiol.* **2002**, *44*, 1 – 8.

 © 2003 Wiley-VCH Verlag GmbH & Co. KGaA, Weinheim

Communications



Molecular editing of epothilone B (isolated from a myxobacterium) led to the discovery of a 26-trifluoro analogue that is remarkably active in treating xenograft tumors in nude mice. These findings underscore the potential of directed multistep total synthesis in the quest for new drugs, as discussed by S. J. Danishefsky and co-workers on the following pages.

DOI: 10.1002/anie.200352361
© 2003 Wiley-VCH Verlag GmbH & Co. KGaA, Weinheim

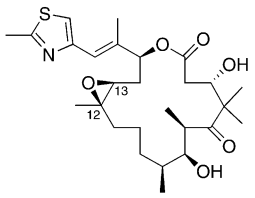
Epothilones: Synthesis and Activity

Design and Total Synthesis of a Superior Family of Epothilone Analogues, which Eliminate Xenograft Tumors to a Nonrelapsable State**

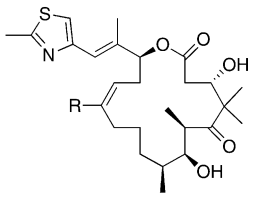
*Ting-Chao Chou, Huajin Dong, Alexey Rivkin, Fumihiko Yoshimura, Ana E. Gabarda, Young Shin Cho, William P. Tong, and Samuel J. Danishefsky**

The epothilone macrolides, first discovered by Höfle et al. in fermentation broths, have elicited a great deal of interest as potential agents in cancer chemotherapy.[1–8] A key paper of Bollag et al.[9] seeded the now multicenter epothilone initiative. This disclosure revealed the cellular target of the epothilones to be microtubule stabilization, which is the same mode of action as the established, clinically useful taxoids exhibit. Moreover, the epothilones were shown to manifest virtual imperviousness to the defenses of otherwise multidrug-resistant (MDR) cells.[10] As susceptibility to disablement by MDR cells is one of the main liabilities of the taxoid drugs, the robustness of the epothilones in this regard is of particular significance. Following extensive multidisciplinary research into the biology, chemistry, pharmacology, toxicology, and biosynthesis of the structurally new epothilones, three agents, including compound **2** (see below), have already been advanced to late phase I and phase II clinical trials, and additional structural variants are being made ready to be approved for investigation.[11]

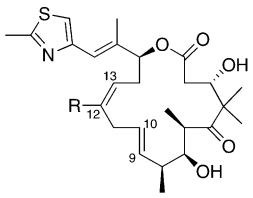
A governing concept in our laboratory had been the notion that the 12,13-oxido linkage of the epothilones is a site of non-tumor-selective toxicity.[12] Therefore, this linkage was "edited", initially through chemical synthesis, to provide 12,13-desoxyEpoB (dEpoB, **2**) and related desoxy congeners.[13,14] Although it is significantly less cytotoxic than epothilone B (EpoB, **1**) itself, in xenograft models dEpoB is roughly equipotent with paclitaxel (taxol)[15] and taxotere, the currently leading tubulin-directed anticancer drugs. dEpoB benefits from a much broader therapeutic index in xenograft models than taxoids or other epothilones, which contain epoxides. The major advantage of dEpoB over paclitaxel in these nude-mouse xenograft models is its particularly dramatic activity against resistant tumors. dEpoB has been entered into human clinical trials.[11]



1



2: R = Me
3: R = CF_3



4: R = Me
5: R = CF_3

In a second-generation 12,13-desoxyepothilone drug candidate, we hoped to recover some of the loss of potency that had been sustained by deletion of the oxido linkage from EpoB. For further development, we also required a second-generation epothilone to exhibit a clinically and readily exploitable therapeutic index, and in particular to lead to complete and nonreversible cures in xenograft models. This standard is seldom, if ever, set in the search for new anticancer drugs. We also hoped to produce an agent type of greater pharmacostability in humans than dEpoB, which has a potentially vulnerable macrolide (cyclic ester) linkage.

By a combination of chemical synthesis, molecular modeling, and spectroscopic analysis, we discovered that the introduction of an *E*-9,10 double bond (see compound **4**) leads to an approximately 10-fold enhancement of drug potency in xenograft experiments with drug-resistant MX-1 tumors.[16] It was apparent from the correlation of in vitro and in vivo experiments focused on MX-1 tumor types that **4** is inherently more cytotoxic than **1**. A second contributing factor is that the lactone functionality in the 9,10-dehydro series is significantly more stable in mouse and human plasma than that in the 9,10-saturated congeners. The sum of these two complementary effects was to render **4** capable of complete tumor suppression in a variety of xenografts at 3 mg kg^{-1}, in contrast to the 30 mg kg^{-1} dose required for **2**.

However, along with this much-enhanced antitumor activity in **4**, significant non-tumor-specific toxicity was observed, which sorely complicated the full eradication of its tumor targets. As with other potent chemotherapeutic

[*] Prof. S. J. Danishefsky, Dr. A. Rivkin, Dr. F. Yoshimura, Dr. A. E. Gabarda, Dr. Y. S. Cho
Laboratory for Bioorganic Chemistry
Sloan-Kettering Institute for Cancer Research
1275 York Avenue, New York, NY 10021 (USA)
Fax: (+1) 212-772-8691
E-mail: s-danishefsky@ski.mskcc.org
and
Department of Chemistry, Columbia University
Havemeyer Hall, 3000 Broadway, New York, NY 10027 (USA)
Dr. T.-C. Chou, Dr. H. Dong
Preclinical Pharmacology Core Facility
Sloan-Kettering Institute for Cancer Research
1275 York Avenue, New York, NY 10021 (USA)
Dr. W. P. Tong
Analytical Pharmacology Core Facility
Sloan-Kettering Institute for Cancer Research
1275 York Avenue, New York, NY 10021 (USA)

[**] This work was supported by the National Institutes of Health (CA-28824). F.Y. is a Uehara Memorial Foundation Fellow. A.R. is a NIH Cancer Pharmacology Fellow (T32-CA62948). A.E.G. is a MSKCC Experimental Therapeutics Center Fellow. We thank Sylvi Rusli (NMR Core Facility, CA-02848) and Anna Dudkina for mass-spectral analyses. We thank Dr. Klaus Gerth and Dr. Rolf Müller of GBF, Germany for the picture of *Sorangium cellulos* that is part of the frontispiece design.

Supporting information for this article is available on the WWW under http://www.angewandte.org or from the author.

 © 2003 Wiley-VCH Verlag GmbH & Co. KGaA, Weinheim DOI: 10.1002/anie.200352361

agents, easily perceptible tumors reappeared in some fraction of the animals upon suspension of treatment. Accordingly, fully synthetic **4** does not, at least at present, qualify as having a highly favorable effective therapeutic index and causing elimination of tumors to a nonrelapsing state, as we had aimed for in a second-generation drug candidate.

These findings directed our attention to the consequences of substituting the three hydrogen atoms of the 26-methyl group of **4** with three fluorine atoms. We anticipated that incorporation of fluorine atoms at this position could lead to improved stability of the C12–C13 double bond toward oxidation.[17] Previous experience had pointed to some attenuation of cytotoxicity when polar groups were placed near the C12–C13 double bond.[16] Herein we report on the total synthesis and antitumor activity of 9,10-dehydro-26-trifluoroepothilones, with particular emphasis on the unique biological activity of the parent structure **5**.

The therapeutic efficacy of dEpoB (30 mg kg^{-1}), paclitaxel (20 mg kg^{-1}), and F_3-deH-dEpoB (**5**, 20 and 30 mg kg^{-1}) against human-mammary-carcinoma MX-1 xenografts was closely studied in terms of tumor disappearance and relapse (Table 1). Each dose group consisted of four or more nude mice. "Body weight" refers to total body weight minus tumor weight. Tumor disappearance was observed for all three compounds. On the 10th day after suspension of treatment, 5/10 (dEpoB), 2/7 (paclitaxel), and 0/4 (compound **5**) mice relapsed. Extended observation following suspension of treatment with 20 mg kg^{-1} dosages of **5** showed a long-term absence of tumors until day 27, at which point 2/4 mice relapsed. Remarkably, treatment with dosages of **5** of 30 mg kg^{-1} resulted in complete tumor disappearance and the absence of any relapse for over two months after suspension of treatment.

When the dose of agent **5** was lowered to 10 mg kg^{-1} (Q2Dx12 = administered every other day, 12 doses in total), nine doses were required for tumor disappearance to be observed (Figure 1a). As an added challenge, chemotherapeutic treatment was delayed until the size of the tumor reached 0.5 g (~2.3% of body weight). Treatment with dosages of 25 mg kg^{-1} (Q2Dx7 = administered every other day, 7 doses in total) of **5** then caused all four of the mouse tumors to disappear. By contrast, dosages of 30 mg kg^{-1} (Q2Dx8) of dEpoB were required to induce the disappearance of tumors in 3/4 mice. Furthermore, the apparent tumor disappearance that occurred following treatment with dEpoB was subject to relapse with time (Figure 1b).

The fact that agent **5** completely suppressed the growth of the human-mammary-carcinoma MX-1 xenografts, shrank the tumors, and eliminated the tumors for as long as 64 days is impressive. Moreover, following the cures by **5** (20 mg kg^{-1} or 30 mg kg^{-1} Q2Dx6, six-hour intravenous infusion, Table 2), body weight returned to pretreatment control level within 12–18 days after the suspension of treatment. This finding suggests a lack of vital-organ damage. Most remarkably, at a curative low dosage of 10 mg kg^{-1}, Q2Dx12 (Figure 1a), the maximal decrease in body weight was only 12%, with a gain in body weight of 6% during the last three doses. The body weight recovered to the pretreatment control level only three days after the cessation of treatment. Table 2 shows that the animals could survive body-weight losses of as much as 27%.

Table 1: Therapeutic effect of dEpoB (**2**), paclitaxel, and F_3-deH-dEpoB (**5**) against an MX-1 xenograft in nude mice.[a]

Drug	Dosage [mg kg^{-1}]	Change in body weight [%][b] day 4	day 8	Tumor-free after treatment period	Tumor reappearance[c]
2	30	−25.3 ± 2.1	−9.1 ± 4.1	10/10	5/10
paclitaxel	20	−23.9 ± 3.7	−8.7 ± 0.7	7/7	2/7
5	20	−22.4 ± 0.6	−7.3 ± 0.7	4/4	0/4[d]
5	30	−27.1 ± 2.7	−17.4 ± 5.5	4/4	0/4[e]

[a] Human-mammary-carcinoma MX-1 xenograft tissue (50 mg) was implanted subcutaneously on day 0. The treatment (Q2Dx6 6-h intravenous infusion) was started on day 8 and stopped on day 18. [b] Change in body weight on day 4 and day 8 of treatment, measured after administration of the drug. [c] Number of mice in sample in which tumor reappeared on the 10th day after the end of the treatment period. [d] Detectable tumor reappearance in 2/4 mice on the 27th day after treatment was stopped. No further tumor reappearance between the 28th and 64th days after treatment was stopped. [e] No tumor reappearance during 64 days after treatment was stopped, at which point the experiment was terminated.

Table 2: Profile of dEpoB derivatives.

Compound	IC_{50} [nM][a]	Maximal drop in body weight without death [%]	Stability half-life Mouse plasma [min]	Human-liver S9 fraction [h]	Solubility in water [μg mL^{-1}]	Lipophilicity octanol/water partition (POW)	Therapeutic dose regimen [mg kg^{-1}][b]	Relative therapeutic index at MTD[c]
1	0.53 ± 0.2	15	57	15.8	n.d.	n.d.	0.6–0.8	+++
2	5.6 ± 2.8	32	46 ± 7	1.0 ± 0.1	9.4	4.4	25–30	++++
4	0.90 ± 0.40	29	84 ± 6	4.9 ± 0.7	27	3.3	3–4	++++
3	9.3 ± 5.2	22	66 ± 7	1.6 ± 0.4	8	4.1	15–20	++
5	3.2 ± 0.3	33	212 ± 88	10.5 ± 2.3	20	3.3	10–30	+++++

[a] IC_{50} values are for CCRF-CEM leukemic cells. Values are the range of two experiments. All values are obtained from eight time points. n.d. = not determined. [b] Therapeutic dose regimen for Q2D 6-h intravenous infusion. [c] Graded relative therapeutic index (TI) at MTD (maximal tolerated dose): + Tumor growth suppressed by 25–50%. ++ Tumor growth suppressed by 50–100%. +++ Tumor shrinkage but no tumor disappearance. ++++ Tumor disappearance in some or all nude mice with slow body-weight recovery and/or with relapse in some mice within one week after treatment was stopped. +++++ Tumor disappearance in all nude mice with rapid body-weight recovery and/or without relapse. The therapeutic effects of epothilones against human xenografts in nude mice, such as MX-1, were studied in references [15] and [27].

 © 2003 Wiley-VCH Verlag GmbH & Co. KGaA, Weinheim

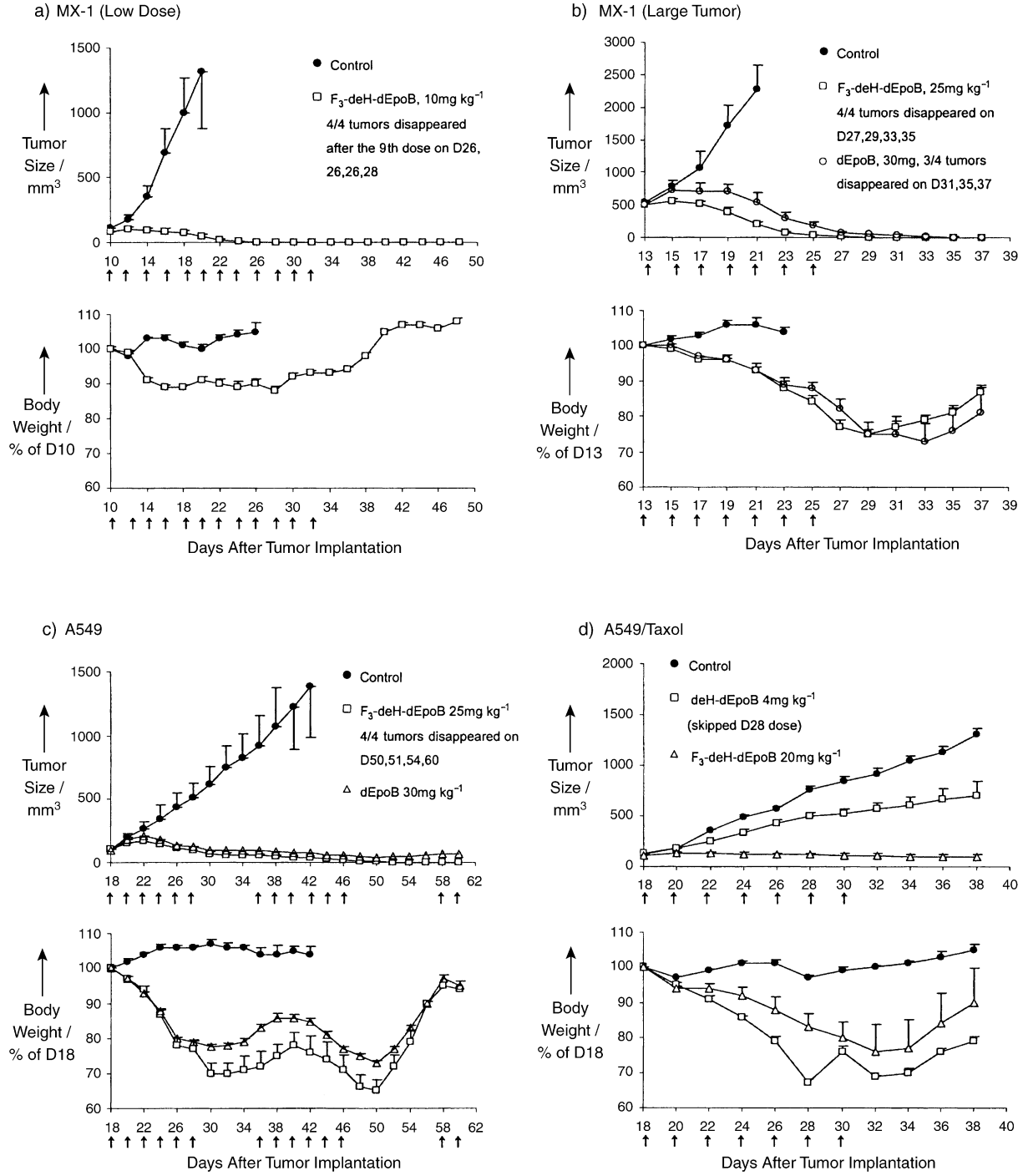


Figure 1. Chemotherapeutic effect against human tumor xenografts in nude mice. Tumor tissue (40–50 mg) was implanted subcutaneously on day 0. Treatment was started when tumor size reached about 100 mm^3 or larger, as indicated. All treatments, indicated by arrows, were carried out by six-hour intravenous infusion into the tail vein with a minicatheter and programmable pump as described previously.[7,14] Each dose group consisted of four or more mice. "Body weight" refers to the total body weight minus the tumor weight, with the assumption that 1 mm^3 of tumor tissue has a weight of 1 mg. a) Mammary-carcinoma MX-1 xenograft treated with a low dose of **5** (10 $mg\,kg^{-1}$) relative to the experiments in Table 1 (20 $mg\,kg^{-1}$ and 30 $mg\,kg^{-1}$). b) MX-1 large xenografts (500 mm^3) treated with **5** (25 $mg\,kg^{-1}$) and dEpoB (30 $mg\,kg^{-1}$). c) Slow-growing A549 lung-carcinoma xenograft treated with **5** (25 $mg\,kg^{-1}$) and dEpoB (30 $mg\,kg^{-1}$). d) A549/taxol (44-fold resistance to paclitaxel in vitro) xenograft treated with **5** (20 $mg\,kg^{-1}$) and **4** (4 $mg\,kg^{-1}$). The treatment with deH-dEpoB on day 28 was skipped as a result of marked and rapid decreases in body weight. D = day.

The therapeutic safety margin observed in this work is remarkably broad for a curative therapeutic agent against cancer. The therapeutic efficacy of **5** against human-lung-carcinoma xenograft (A549) and the paclitaxel-resistant human-lung-carcinoma A549/taxol xenografts was also evaluated (Figure 1c,d). The slow-growing lung-carcinoma xenografts A549 were treated with **5** (25 $mg\,kg^{-1}$, Q2Dx6, twice, eight days apart), which resulted in 99.5 % tumor suppression

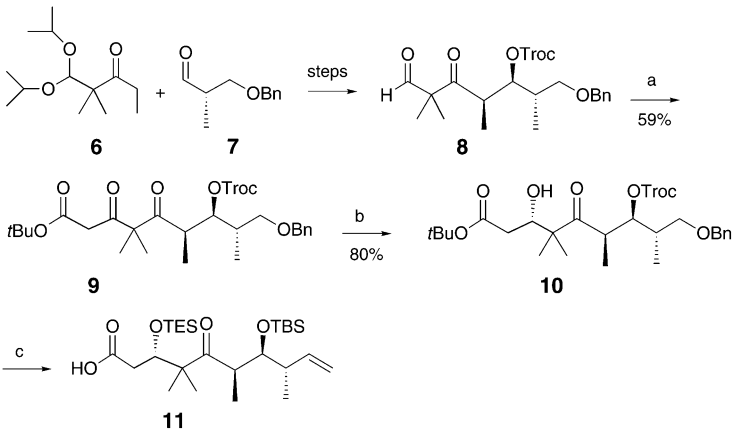
 © 2003 Wiley-VCH Verlag GmbH & Co. KGaA, Weinheim

with the eventual complete eradication of all four tumors after two more doses (Figure 1c). Interestingly, the body weight of the mice decreased as much as 35% without any lethality, and suspension of the treatment led to rapid body-weight recovery to near the pretreatment control level (Figure 1c). In contrast, a parallel study with dEpoB (30 mg kg^{-1}, Q2Dx6) resulted in 97.6% tumor suppression but led to no tumor eradication. In an additional study of **5** (dosage: 20 mg kg^{-1}) against A549/taxol-resistant xenografts (Figure 1d), tumor growth was totally suppressed, and the tumor was eventually reduced by 24.4% of the pretreatment control. During this study, the maximal body weight decreased by 24%. However, upon suspension of drug treatment the body weight returned to 90% of the pretreatment control. In a comparison study with (*E*)-9,10-dehydro-dEpoB (**4**, 4 mg kg^{-1}), tumor growth was suppressed by 41.6%.

We wanted to assess the factors responsible for the remarkable therapeutic index of compound **5**. The pertinent data for this analysis in conjunction with corresponding data for closely related congeners are provided in Table 2. A whole order of magnitude is lost in moving from EpoB(**1**) to dEpoB (**2**) in terms of inherent cytotoxicity. About 60% of this loss is restored in the case of 9,10-dehydro-dEpoB (**4**). Some of this inherent cytotoxicity is forfeited by the inclusion of the CF_3 group in **5**, which is ~1.8 times as cytotoxic as the benchmark compound **2**, at least in the cell.

Among the 12,13-dehydroepothilones, **5** exhibited by far the highest stability in mouse plasma and was also the most stable in human liver S9 plasma. We also observed that in the two sets of 12,13-dehydro isomers, the 26-trifluoromethyl substituent gives rise to decreased lypophilicity and somewhat increased water solubility. It would appear that the excellent therapeutic activity of **5** arises from improvements in serum stability and bioavailability.

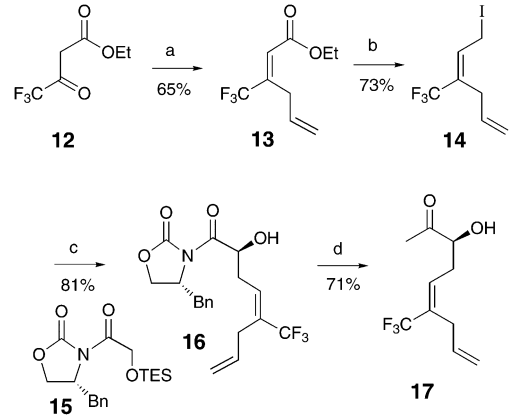
All of the agents **2**–**5** were initially discovered through total synthesis. A practical synthesis of **2** has been described previously.[13,14] First-generation discovery-level routes to **4** and **5** have also been described.[16,18–20] Selective reduction of the C9–C10 double bond of **5** afforded **3**. The remarkable results obtained from the xenograft studies described above for **5**, which is currently the most promising compound, clearly called for its advancement to detailed toxicology and pharmacokinetic studies in higher animals, and from there, if appropriate, to human clinical trials. Such prospects completely altered the nature of the synthetic challenge from the preparation of probe samples to the preparation of multigram quantities of these new epothilone derivatives. We carried out a major revamp of our previous routes, which were initially conceived and demonstrated in a discovery setting. In particular, our new protocols allowed major simplifications in the stereospecific elaboration of the C3 and C26 centers. Aldehyde **8** was prepared as described previously (Scheme 1).[16] In the new synthesis, the stereocenters C6, C7, and C8 are derived from the readily available ketone **6** and aldehyde **7**. Condensation of the aldehyde **8** with *tert*-butyl acetate, as shown, afforded an aldol-like product. As the condensation is not diastereomerically controlled, it was followed by oxidation of the resulting 1:1 mixture of C3



Scheme 1. Synthesis of the acyl sector **11**. Reagents and conditions: a) 1. LDA, *tert*-butyl acetate, THF, 80%; 2. Dess–Martin periodinane, 74%; b) Noyori catalyst (10 mol%), MeOH/HCl, H_2, 1200 psi, 80%; c) 1. TESCl, imidazole, 77%; 2. Zn, AcOH, THF, 99%; 3. TBSOTf, 2,6-lutidine, 82%; for remaining steps, see reference [16]. Troc = trichloroethoxycarbonyl, LDA = lithium diisopropylamide, TES = triethylsilyl, TBS = *tert*-butyldimethylsilyl.

epimers to the ketone **9**, which was then subjected to a highly successful Noyori reduction[21] under the conditions shown. The C3 alcohol product **10** was converted into the acid **11** in a few additional simple steps, as shown.

A new, straightforward synthesis, which can be scaled up readily, has also been developed for **17** (Scheme 2). The synthesis starts with the reaction of the commerically available trifluorinated β-ketoester **12** with allyl indium bromide. The key step in the synthesis is the regio- and stereospecific dehydration of the resulting tertiary alcohol to produce **13** in 65% yield from **12**. We surmise that the stereoselectivity observed in this reaction arises from a "dipolar effect", whereby a *trans* orientation of the strongly electron-withdrawing CF_3 and CO_2Et groups is favored, with respect to the double bond that is forming. The required iodide **14** was obtained in two steps from **13**. Alkylation of the

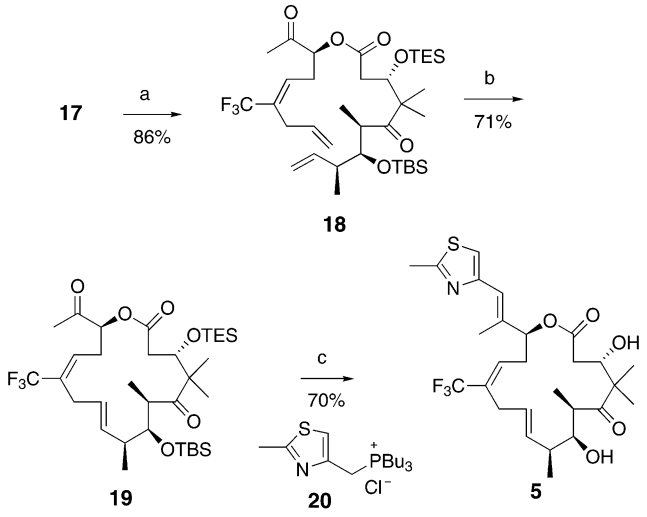


Scheme 2. Synthesis of the alkyl sector **17**. Reagents and conditions: a) 1. Allyl bromide, In, THF/H_2O (3:1), 48 °C, 85%; 2. $SOCl_2$, pyridine, 55 °C, 77%; b) 1. DIBAL-H, CH_2Cl_2, −78 °C→RT, 99%; 2. I_2, PPh_3, imidazole, CH_2Cl_2, 74%; c) 1. LiHMDS, THF, −78 °C→RT; 2. HOAc/THF/H_2O (3:1:1), 81% for two steps; d) 1. $AlMe_3$, MeONHMe, THF, 0 °C→RT, 97%; 2. MeMgBr, THF, 0 °C, 53% (73% based on recovered starting material). DIBAL-H = diisobutylaluminium hydride, HMDS = hexamethyldisilazide.

 © 2003 Wiley-VCH Verlag GmbH & Co. KGaA, Weinheim

previously reported lithium enolate of **15** with iodide **14** in THF, followed by removal of the silyl protecting group, afforded **16** in 81% yield and with high diastereoselectivity (d.r. > 25:1). Compound **16** was advanced in two steps to **17** as shown.

With **11** and **17** in hand, the route to **5** was clear based on chemistry first developed in our discovery phase.[16] The key ring-closing metathesis reaction of **18** was carried out in toluene in the presence of the second-generation Grubbs catalyst (Scheme 3).[22–26] The reaction afforded the *trans*



Scheme 3. Final steps of the synthesis of **5**. Reagents and conditions: a) EDCI, DMAP, CH_2Cl_2, **11**, 0 °C→RT, 86% based on **11**; b) second-generation Grubbs catalyst, toluene, 110 °C, 20 min, 71%; c) 1. KHMDS, **20**, THF, −78 °C→−20 °C, 70%; 2. HF·pyridine, THF, 98%. EDCI = 1-[3-(dimethylamino)propyl]-3-ethylcarbodiimide hydrochloride, DMAP = 4-(dimethylamino)pyridine.

isomer **19** exclusively in 71% yield. Installation of the thiazole moiety, as shown in Scheme 3, was followed by removal of the two silyl protecting groups with HF·pyridine to give **5**. Compound **5** was converted into **3** in high yield by reduction of the C9–C10 double bond. Gram quantities of these structurally novel epothilones have been prepared by total synthesis in our laboratory.

At the moment there are no grounds on which to argue that the strikingly superior performance of **5** arises from factors other than the significantly improved pharmacokinetic and bioavailability features that were designed into the molecule through the medium of chemical synthesis. However, the possibility that the results reflect new (or enhanced) drug–target interactions is the object of continuing study. New areas of analogue synthesis are accessible through permutations of the late-stage olefination (e.g. **19** + **20**) by the use of other phosphonates. In this way, new design features that result in enhanced pharmaceutical properties are being explored further.

It is important to keep in mind that the ultimate purpose of the chemotherapeutic arm of cancer research is to provide clinically valuable treatment for patients with neoplastic diseases. Only progression to clinical trials can establish the value of any of the new epothilone agents with regard to this central goal.

This study serves to underscore the potential applicability of directed total synthesis, even in a multistep setting, in the quest for new substances of material clinical benefit. The current research environment tends to favor recourse to massive numbers of compounds for screening, in preference to smaller numbers of more carefully crafted, hypothesis-driven candidate structures. However, there is much to be learnt from natural products, and these warrant close and continuing study.

Received: July 11, 2003 [Z52361]
Published Online: September 11, 2003
Please note: Minor changes have been made to this manuscript since its publication in *Angewandte* Early View. The Editor.

Keywords: antitumor agents · conformation analysis · epothilones · natural products · structure–activity relationships

[1] G. Höfle, N. Bedorf, K. Gerth, H. Reichenbach (GBF), DE-B 4138042, **1993**.
[2] G. Höfle, N. Bedorf, H. Steinmetz, D. Schumburg, K. Gerth, H. Reichenbach, *Angew. Chem.* **1996**, *108*, 1671; *Angew. Chem. Int. Ed. Engl.* **1996**, *35*, 1567.
[3] K. Gerth, N. Bedorf, G. Höfle, H. Irschik, H. Reichenbach, *J. Antibiot.* **1996**, *49*, 560.
[4] K. C. Nicolaou, A. Ritzén, K. Namoto, *Chem. Commun.* **2001**, *17*, 1523.
[5] K. H. Altmann, M. Wartmann, T. O'Reilly, *Biochim. Biophys. Acta* **2000**, *1470*, M79.
[6] C. R. Harris, S. J. Danishefsky, *J. Org. Chem.* **1999**, *64*, 8434.
[7] K. C. Nicolaou, F. Roschangar, D. Vourloumis, *Angew. Chem.* **1998**, *110*, 2120; *Angew. Chem. Int. Ed.* **1998**, *37*, 2014.
[8] G. A. Orr, S. B. Horwitz, *Drug Discovery Today* **2001**, *6*, 1153.
[9] D. M. Bollag, P. A. Mcqueney, J. Zhu, O. Hensens, L. Koupal, J. Liesch, M. Goetz, E. Lazarides, C. M. Woods, *Cancer Res.* **1995**, *55*, 2325.
[10] T.-C. Chou, X. G. Zhang, C. R. Harris, S. D. Kuduk, A. Balog, K. A. Savin, J. R. Bertino, S. J. Danishefsky, *Proc. Natl. Acad. Sci. USA* **1998**, *95*, 9642.
[11] For more information about clinical trials of dEpoB, visit: www.kosan.com.
[12] D.-S. Su, A. Balog, D. Meng, P. Bertinato, S. J. Danishefsky, Y.-H. Zheng, T.-C. Chou, L. He, S. B. Horwitz, *Angew. Chem.* **1997**, *109*, 2178; *Angew. Chem. Int. Ed. Engl.* **1997**, *36*, 2093.
[13] C. R. Harris, S. D. Kuduk, A. Balog, K. Savin, P. W. Glunz, S. J. Danishefsky, *J. Am. Chem. Soc.* **1999**, *121*, 7050.
[14] D. Meng, P. Bertinato, A. Balog, D.-S. Su, T. Kamenecka, E. J. Sorensen, *J. Am. Chem. Soc.* **1997**, *119*, 10073.
[15] T.-C. Chou, X. G. Zhang, C. R. Harris, S. D. Kuduk, A. Balog, K. A. Savin, J. R. Bertino, S. J. Danishefsky, *Proc. Natl. Acad. Sci. USA* **1998**, *95*, 15798.
[16] A. Rivkin, F. Yoshimura, A. E. Gabarda, T.-C. Chou, H. Dong, W. P. Tong, S. J. Danishefsky, *J. Am. Chem. Soc.* **2003**, *125*, 2899.
[17] B. E. Smart, *J. Fluorine Chem.* **2001**, *109*, 3.
[18] J. D. White, R. G. Carter, K. F. Sundermann, M. Wartmann, *J. Am. Chem. Soc.* **2001**, *123*, 5407.
[19] F. Yoshimura, A. Rivkin, A. E. Gabarda, T.-C. Chou, H. Dong, G. Sukenick, F. F. Morel, R. E. Taylor, S. J. Danishefsky, *Angew. Chem.* **2003**, *115*, 2622; Angew . *Chem. Int. Ed.* **2003**, *42*, 2518.
[20] A. Rivkin, J. T. Njardarson, K. Biswas, T.-C. Chou, S. J. Danishefsky, *J. Org. Chem.* **2002**, *67*, 7737.
[21] R. Noyori, T. Ohkuma, M. Kitamura, H. Takaya, N. Sayo, H. Kumobayashi, S. Akutagawa, *J. Am. Chem. Soc.* **1987**, *109*, 5856.

 © 2003 Wiley-VCH Verlag GmbH & Co. KGaA, Weinheim

[22] R. H. Grubbs, S. J. Miller, G. C. Fu, *Acc. Chem. Res.* **1995**, *28*, 446.
[23] T. M. Trnka, R. H. Grubbs, *Acc. Chem. Res.* **2001**, *34*, 18.
[24] *Alkene Metathesis in Organic Chemistry* (Ed.: A. Fürstner), Springer, Berlin, **1998**.
[25] A. Fürstner, *Angew. Chem.* **2000**, *112*, 3140; *Angew. Chem. Int. Ed.* **2000**, *39*, 3012.
[26] R. R. Schrock, *Top. Organomet. Chem.* **1998**, *1*, 1.
[27] T.-C. Chou, O. A. O'Connor, W. P. Tong, Y. Guan, Z.-G. Zhang, S. J. Stachel, C. Lee, S. J. Danishefsky, *Proc. Natl. Acad. Sci. USA* **2001**, *98*, 8113 – 8118.

 © 2003 Wiley-VCH Verlag GmbH & Co. KGaA, Weinheim

Carbene Chemistry

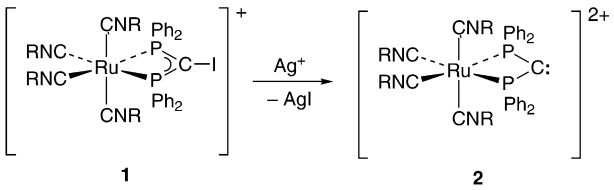
Trapping Highly Electrophilic Metalladiphosphanylcarbenes**

Javier Ruiz, Marta E. G. Mosquera, Gabriel García, Elena Patrón, Víctor Riera, Santiago García-Granda, and Francisco Van der Maelen*

In recent years much attention has been paid to the study of nucleophilic carbenes of Arduengo type (N-heterocyclic carbenes)[1] and related diaminocarbenes $(R_2N)_2C$:[2] which are stabilized by the presence of two π-donor nitrogen atoms bonded to the carbene carbon atom. The synthesis of the first push-pull phosphanylsilylcarbene of formula $(R_2P)(SiMe_3)C$: ($R = NiPr_2$) by Bertrand and co-workers was also a milestone in carbene chemistry.[3] Mixed-substituent aminophosphanylcarbenes have recently been prepared.[4] Of great interest are also the analogous diphosphanylcarbenes $(R_2P)_2C$:, although they are only known as transient species,[5] which have been investigated by ab initio calculations.[6] Interestingly, their protonated phosphoniumphosphanylcarbene derivatives $[(R_2P)(R_2PH)C:]^+$ ions are known to be stable.[7]

We report herein on the generation and trapping reactions of the transient highly electrophilic metalladiphosphanylcarbene $[Ru(CNtBu)_4(PPh_2)_2C:]^{2+}$ (**2**).[8] The electrophilic character of **2** has been confirmed experimentally and by density functional theory (DFT) calculations.[9]

Transient carbene **2** is formed from the cationic complex $[Ru(CNtBu)_4\{(PPh_2)_2CI\}]^+$ (**1**)[10] by iodide abstraction with silver(I) salts ($AgClO_4$ or $AgBF_4$) (Scheme 1), a nonstandard method of carbene generation. Thus the formally anionic diphosphanyliodomethanide ligand $\{(PPh_2)_2CI\}^-$ is converted into the neutral ligand $(PPh_2)_2C$: Coordination of the diphosphanylcarbene $(PPh_2)_2C$: to the metal fragment



1 2

Scheme 1. Formation of the transient metalladiphosphanylcarbene **2**. R = *t*Bu.

through the phosphorus atoms avoids dimerization to form the corresponding $1\lambda^5,3\lambda^5$-diphosphete derivative,[11] or even 1,2-migration of a phenyl group to give the phosphaalkene,[5b] and enhances the electrophilicity of the carbene as the phosphorus lone pairs can no longer be used for π donation to the carbene carbon atom. Owing to its high electrophilicity (see calculated electron affinities (EA) values in Table 1) **2** is very unstable and instantaneously decomposes, unless a trapping reagent is added. Thus, reaction of **1** with $AgBF_4$ in CH_2Cl_2 as solvent in the presence of pyridine (Py) gives complex **3**, the pyridine adduct of carbene **2** (Scheme 2).[12] Complex **3** cocrystallizes with the silver complex salt $[Ag(Py)_2]BF_4$ giving suitable crystals for X-ray analysis (Figure 1).[13] In the new pyridinium diphosphanylylide ligand the C1–N1 bond is slightly shortened with respect to single bond, and the pyridinium plane is coplanar with the P1-P2-C1 plane allowing a π interaction of the ylide carbon atom C1 with the π system in the ring. The P1–C1 and P2–C1 bonds are appreciable shorter than single bonds indicating that the negative charge at the ylide carbon atom is also shared with both coordinated phosphorus atoms, thus stabilizing the ylide structure. Another adduct of carbene **2** is formed by treatment of **1** with $AgBF_4$ in the presence of tetrahydrothiophene (tht). The reaction occurs readily to give complex **4** (Scheme 2).[14] The ^1H NMR spectrum of **4** shows three resonance signals for the CH_2 groups of tht (see Experimental Section), as the two protons of each α-CH_2 unit are inequivalent owing to its different orientation respect to the

Table 1: Calculated structural parameters, singlet–triplet splittings (ΔE_{ST}), and electron affinities (EA) of **2b**.

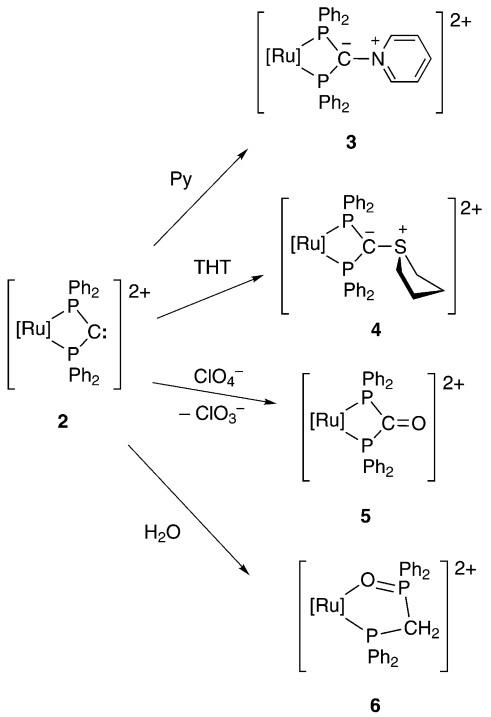
	B3LYP6-31G*,LanL2DZ[a]	B3LYP6-31G*,3-21G	B3LYP6-31G**,3-21G*	B3LYP6-311++G**,3-21+G*
C-P [Å]	1.673	1.681	1.682	1.662
P-C-P [°]	134.3	129.2	129.3	137.9
ΔE_{ST} [kcal mol^{-1}]	−8.96	−9.86	−10.00	−10.80
EA [eV]			8.94	8.99

[a] Second basis for Ru, first basis for all the other atoms.

[*] Dr. J. Ruiz, Dr. M. E. G. Mosquera, G. García, E. Patrón, Prof. Dr. V. Riera
Departamento de Química Orgánica e Inorgánica
Facultad de Química
Universidad de Oviedo
33071 Oviedo (Spain)
Fax: (+34) 98-5103-446
E-mail: jruiz@sauron.quimica.uniovi.es
Dr. S. García-Granda, Dr. F. Van der Maelen
Departamento de Química Física y Analítica
Facultad de Química
Universidad de Oviedo
33071 Oviedo (Spain)

[**] This work was supported by the Spanish DGES (Project 1FD97-0750) and by the Principado de Asturias (Project PR-01-GE-7).

 DOI: 10.1002/anie.200219604 © 2003 Wiley-VCH Verlag GmbH & Co. KGaA, Weinheim



Scheme 2. Trapping reactions of carbene **2**. [Ru] = [Ru(CN*t*Bu)$_4$], tht = tetrahydrothiophene.

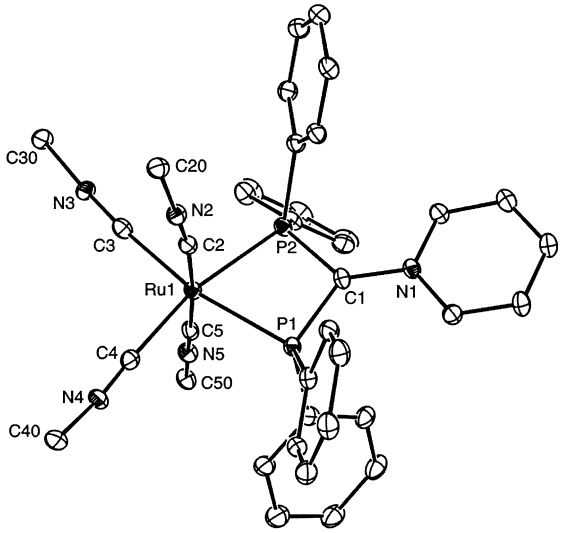


Figure 1. A view of the structure of the cation **3** (thermal ellipsoids set at 20% probability). Methyl groups in the CN*t*Bu ligands are omitted for clarity. Selected bond lengths [Å] and angles [°]: Ru1-P1 2.355(2), Ru1-P2 2.359(2), P1-C1 1.761(9), P2-C1 1.756(10), N1-C1 1.428(10); P1-Ru1-P2 70.48(9), N1-C1-P2 128.9(7), N1-C1-P1 129.8(7), P2-C1-P1 101.3(4).

lone pair of sulfur. The solid-state structure of **4** was solved by X-ray analysis (Figure 2), and clearly shows a tht solvent molecule stabilizing carbene **2** with a rather strong C–S interaction (C1-S1 1.707(6) Å).

When carbene **2** is generated by treatment of **1** with an excess of $AgClO_4$, the diphosphanylketone complex

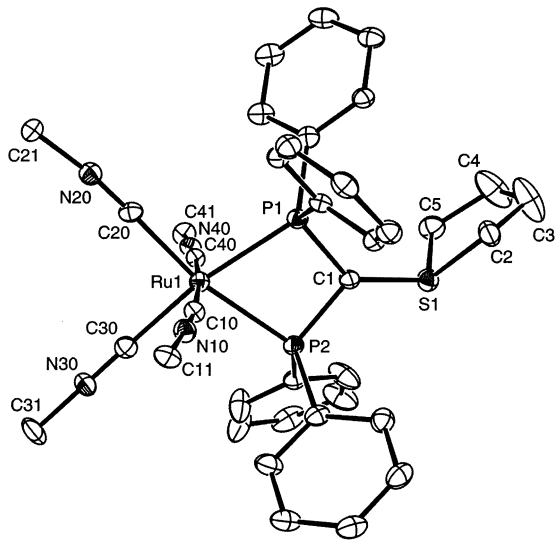


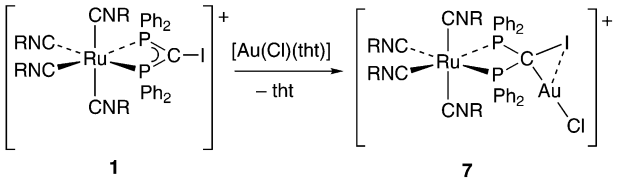
Figure 2. A view of the structure of the cation **4** (thermal ellipsoids set at 20% probability). Methyl groups in the CN*t*Bu ligands are omitted for clarity. Selected bond lengths [Å] and angles [°]: P1-C1 1.774(6), P2-C1 1.771(6), S1-C1 1.707(6), S1-C2 1.820(7), S1-C5 1.812(7); P1-Ru1-P2 70.51(5), S1-C1-P2 124.5(3), S1-C1-P1 134.9(4), C1-S1-C2 114.2(3), C1-S1-C5 109.8(3).

$[Ru(CN\mathit{t}Bu)_4\{(PPh_2)_2C{=}O\}]^{2+}$ (**5**) is obtained, after precipitation of AgI (Scheme 2). This result implies the transfer of an oxygen atom from the ClO_4^- group to the transient carbene **2**, which probably proceeds through nucleophilic attack of the oxoanion to the carbene carbon atom. The IR spectrum of **5** reveals the presence of the ketone group ($\tilde{\nu}CO = 1721\ cm^{-1}$ (m)), as well as the $^{13}C\{^1H\}$ NMR spectrum which shows a triplet at $\delta = 216.6$ ppm ($^1J(P,C) = 16$ Hz) for the P_2CO carbon atom.[15] The solid structure of **5** has also been confirmed by X-ray analysis (not shown).

The formation of carbene **2** by treatment of **1** with $AgBF_4$ in the presence of H_2O yields the cationic complex $[Ru(CN\mathit{t}Bu)_4\{(O{=}PPh_2)(PPh_2)CH_2\}]^{2+}$ (**6**; Scheme 2), which contains a mono-oxidized methylenebis[(diphenyl)phosphane] (dppm) ligand arising from activation of both O–H bonds in the water molecule by the carbene. The structure of **6** has been confirmed by ^{31}P and ^1H NMR spectroscopy (see Experimental Section) and by X-ray analysis. On the basis of the known trapping reactions of transient diphosphanylcarbenes with alcohols,[5a] the formation of **6** could proceed through insertion of carbene **2** into a O–H bond of water, followed by a 1,2-shift of the OH group to a phosphorus atom and further proton migration to the central carbon atom.

To investigate the iodide abstraction leading to carbene **2** we treated **1** with some soluble silver(I) and gold(I) complexes. With the silver derivative $Ag(ClO_4)(PPh_3)$, the interaction with iodide is so strong that formation of $[\{AgI(PPh_3)\}_4]$ is immediately observed with parallel formation of $[Ru(CN\mathit{t}Bu)_4\{(PPh_2)_2CH_2\}]^{2+}$ as decomposition product of the carbene. Fortunately, treatment of **1** with [AuCl(tht)] allowed the isolation of the complex $[Ru(CN\mathit{t}Bu)_4(PPh_2)_2C(AuCl)I]^+$ (**7**; Scheme 3). The structure of this cation (Figure 3) shows the AuCl unit bonded to the methanide carbon atom, but also a close Au···I contact of 3.35 Å which is shorter than the sum of

 © 2003 Wiley-VCH Verlag GmbH & Co. KGaA, Weinheim



Scheme 3. Formation of the heterometallic ruthenium(II)/gold(I) complex **7**. R = *t*Bu.

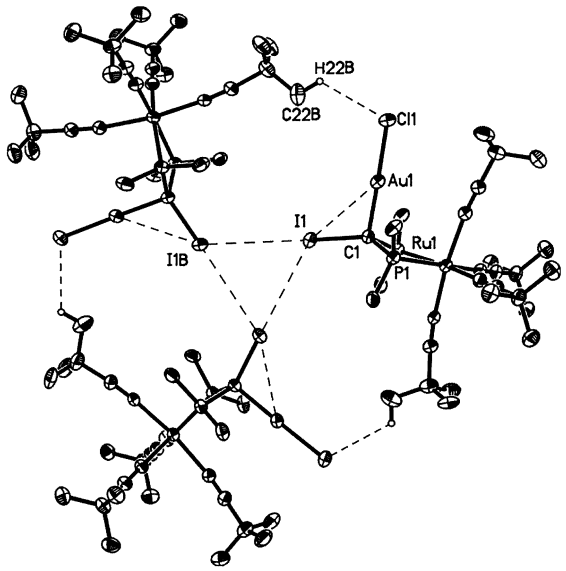


Figure 3. A view of the structure of the cation **7** (thermal ellipsoids set at 20% probability) showing a three-cation aggregate. Phenyl groups are omitted for clarity. Selected bond lengths [Å] and angles [°]: Au1-C1 2.100(19), Au1-Cl1 2.326(5), C1-I1 2.171(18), C1-P1 1.837(12); P1-Ru1-P1 71.48(18), C1-Au1-Cl1 178.7(5), P1-C1-P1 97.4(9), P1-C1-Au1 104.4(7), P1-C1-I1 122.4(6), Au1-C1-I1 103.7(8).

van der Waals radii of both atoms (3.64 Å). Some activation is also observed in the C–I bond in **7** (2.177(18) Å) compared to coordinated diphosphanyliodomethanide (2.115(4) Å).[16] All these structural data indicate that **7** can be considered an isolated intermediate for the formation of transient carbene **2** by halide abstraction from **1** with metal fragments. Additionally the solid structure of **7** is of interest in forming supramolecular triangular aggregates, with central I···I contacts and peripheral C–H···Cl hydrogen bonds (Figure 3).

Table 1 shows some selected results of the calculations performed on the carbene $[Ru(CNH)_4(PH_2)_2C{:}]^{2+}$ (**2b**), a model structure obtained from **2** by replacing *t*Bu and Ph substituents by hydrogen atoms.[9] The optimized structure shows a perfect C_{2v} symmetry in the highest levels of calculation, both for singlet and triplet states, although for the triplet state P–C distances are clearly longer (1.788 Å) and P-C-P angles are much smaller (113.1°) than for the singlet ground state (the values of which are shown in Table 1). These results are much in line with those found for other symmetrically substituted cyclic diphosphanylcarbenes,[6b] and clearly differ from symmetrically substituted acyclic diphosphanylcarbenes,[6a] which prefer an asymmetric P–C multiple-bond phosphorus vinyl ylide structure.

In conclusion we have present an approach to generate a unique dicationic singlet carbene (**2**), whose electrophilic character has been confirmed experimentally and by DFT calculations. This new type of carbene, as well as its isolated pyridine and tetrahydrothiophene adducts, show promise as reaction intermediates for the preparation of new functionalized diphosphane ligands, as exemplified with the synthesis of the diphosphanylketone derivative **5**.

Experimental Section

All reactions and manipulations were performed under a atmosphere of dry nitrogen by using standard Schlenk and glovebox techniques. Solvents were distilled over appropriate drying agents under dry nitrogen prior to use. Chemical shifts of the NMR spectra are referenced to internal $SiMe_4$ (^1H and ^{13}C) or external H_3PO_4 (^{31}P).

3-$(BF_4)_2$·0.5{[$Ag(Py)_2$]BF_4}: Pyridine (81 μL, 1 mmol) was added to a solution of [Ru(CN*t*Bu)$_4${(PPh_2)$_2$Cl}]I (**1**-I; 0.11 g, 0.1 mmol) in CH_2Cl_2 (20 mL). This solution was transferred by canula to a Schlenk containing $AgBF_4$ (0.08 g, 0.4 mmol) previously cooled to −75 °C and covered to protect from the light. The mixture was stirred for 10 min and then allowed to warm to room temperature and stirred for a further hour. Filtration of the mixture gave a clear yellow solution. Half of the solvent was removed in vacuo and diethyl ether (15 mL) was carefully added. Storage at −18 °C for 4 days afforded yellow crystals, yield: 0.094 g (67%). Elemental analysis (%) calcd for $C_{55}H_{66}N_7Ag_{0.5}B_{2.5}F_{10}N_6P_2Ru$: C 53.05, H 5.34, N 6.75; found: C 52.53, H 5.10, N 6.77; IR (CH_2Cl_2): $\tilde{\nu}$ = 2215 (w), 2180 cm^{-1} (s) (CN*t*Bu); $^{31}P\{^1H\}$ NMR (121.5 MHz, CD_2Cl_2): δ = 10.5 ppm; ^1H NMR (300 MHz, CD_2Cl_2): δ = 8.1–7.3 (35H), 1.53 (s, 18H, CN*t*Bu), 0.95 ppm (s, 18H, CN*t*Bu); ^{13}C NMR (75.5 MHz, CD_2Cl_2): δ = 133.5–126.3 (Ph and Py), 59.7 (s, CN*C*(CH_3)$_3$), 59.0 (s, CN*C*(CH_3)$_3$), 61.8 (t, ^1J(P,C) = 49, P_2CPy, 30.7 (s, CNC(CH_3)$_3$) 29.9 ppm (s, CNC(CH_3)$_3$). Resonance for *C*NC(CH_3)$_3$ not observed.

4-$(BF_4)_2$: A solution of **1**-I (0.1 g, 0.093 mmol) and THT (1 mL) in THF (30 mL) was added through a canula to a Schlenk containing $AgBF_4$ (0.062 g, 0.318 mmol). The mixture was stirred for 20 min and then filtered and the filtrate concentrated to 15 mL to afford white crystals of the compound, yield: 0.056 g (56%). Elemental analysis (%) calcd for $C_{49}H_{64}N_4B_2F_8P_2RuS$: C 54.61, H 5.99, N 5.20; Found: C, 54.32; H, 5.96; N, 5.09; IR (CH_2Cl_2): $\tilde{\nu}$ = 2214 (m), 2172 cm^{-1} (vs) (CN*t*Bu); $^{31}P\{^1H\}$ NMR (121.5 MHz, CD_2Cl_2): δ = 0.38 ppm; ^1H NMR (300 MHz, CD_2Cl_2): δ = 7.7–7.6 (20H, Ph), 3.46 (m, 2H, tht), 1.85 (m, 2H, tht), 1.82 (m, 4H, tht) 1.55 (s, 18H, CN*t*Bu), 1.15 ppm (s, 18H, CN*t*Bu).

5-$(ClO_4)_2$: $AgClO_4$ (0.025 g, 0.12 mmol) was added to a solution of **1**-I (0.05 g, 0.048 mmol) in CH_2Cl_2 (10 mL). The mixture was stirred for 10 min in the absence of light. After filtration, the solvent was removed from the filtrate in vacuo and the residue recrystallized from CH_2Cl_2/diethyl ether affording yellow crystals, yield: 0.036 g (73%). Elemental analysis (%) calcd for $C_{45}H_{56}N_4Cl_2O_9P_2Ru$: C 52.43, H 5.47, N 5.43; Found: C, 52.35; H, 5.31; N, 5.29; IR (CH_2Cl_2): $\tilde{\nu}$ = 2230 (w), 2190 cm^{-1} (s) (CN*t*Bu), 1721 cm^{-1} (m) (CO); $^{31}P\{^1H\}$ NMR (121.5 MHz, CD_2Cl_2): δ = 76.2 ppm; ^1H NMR (300 MHz, CD_2Cl_2): δ = 7.8–7.4 (20H, Ph), 1.76 (s, 18H, CN*t*Bu), 0.95 ppm (s, 18H, CN*t*Bu); ^{13}C NMR (75.5 MHz, CD_2Cl_2): δ = 134–126 (Ph), 216.6 (t, ^1J(P,C) = 16 Hz) P_2CO, 61.4 (s, CN*C*(CH_3)$_3$), 60.6 (s, CN*C*(CH_3)$_3$), 30.5 (s, CNC(*C*H_3)$_3$) 29.3 ppm (s, CNC(*C*H_3)$_3$). Resonance for *C*NC(CH_3)$_3$ not observed.

6-$(BPh_4)_2$: A solution containing **1**-I (0.09 g, 0.08 mmol) and water (4 μL, 0.22 mmol) in CH_2Cl_2 (20 mL) was added through a canula to $AgBF_4$ (0.08 g, 0.4 mmol) placed in a Schlenk previously cooled to −75 °C and covered from the light. The mixture was stirred for 10 min and then allowed to warm to room temperature and stirred for a further hour. Filtration of the solution and evaporation of the solvent from the filtrate afforded a white solid of **6**-$(BF_4)_2$ Yield:

 © 2003 Wiley-VCH Verlag GmbH & Co. KGaA, Weinheim

0.086 g (70%). To obtain suitable crystals for an X-ray diffraction study, a metathesis of the anion was performed by treating a CH_2Cl_2/MeOH solution of the compound with an excess of $NaBPh_4$. Elemental analysis (%) calcd for $C_{93}H_{98}N_4B_2OP_2Ru$: C 75.86, H 6.70, N 3.80; Found: C 75.79; H 6.45, N 4.02; IR (CH_2Cl_2): $\tilde{\nu}=2223$ (w), 2181 (s), 2164 cm^{-1} (sh) (CN*t*Bu); $^{31}P\{^1H\}$ NMR (121.5 MHz, CD_2Cl_2): $\delta=67.7$ (d, $^2J(P,P)=29$ Hz), 41.4 ppm (d, $^2J(P,P)=29$ Hz); ^1H NMR (300 MHz, CD_2Cl_2): $\delta=8.0$–7.4 (60H, Ph), 4.01 (dd, $^2J(P,H)=11$, $^2J(P,H)=9$ Hz, 2H, CH_2), 1.73 (s, 9H, CN*t*Bu), 1.53 (s, 9H, CN*t*Bu), 1.10 ppm (s, 18H, CN*t*Bu).

7-[Au(Cl)(I)]: [Au(Cl)(tht)] (0.031 g, 0.096 mmol) was added to a solution of **1**-I (0.050 g, 0.048 mmol) in THF (12 mL) and the resulting mixture stirred for 10 min. The solution was then concentrated to 6 mL and let to stand over night to afford yellow crystals, yield: 0.065 g (90%). IR (CH_2Cl_2):$\tilde{\nu}=2215$ (s), 2177 cm^{-1} (vs) (CN*t*Bu); $^{31}P\{^1H\}$ NMR (121.5 MHz, CD_2Cl_2): $\delta=13.4$ ppm; ^1H NMR (300 MHz, CD_2Cl_2): $\delta=7.7$–7.4 (20H, Ph), 1.63 (s, 18H, CN*t*Bu), 1.44 (s, 9H, CN*t*Bu), 0.99 ppm (s, 9H, CN*t*Bu).

Received: June 24, 2002
Revised: June 23, 2003 [Z19604]

Keywords: carbene ligands · density functional calculations · P ligands · ruthenium

[1] For recent reviews see: a) A. J. Arduengo, *Acc. Chem. Res.* **1999**, *32*, 913; b) D. Bourissou, O. Guerret, F. P. Gabbaï, G. Bertrand, *Chem. Rev.* **2000**, *100*, 39–91; c) W. A. Herrmann, *Angew. Chem.* **2002**, *114*, 1326; *Angew. Chem. Int. Ed.* **2002**, *41*, 1290.

[2] a) R. W. Alder, P. R. Allen, M. Murray, A. G. Orpen, *Angew. Chem.* **1996**, *108*, 1211; *Angew. Chem. Int. Ed. Engl.* **1996**, *35*, 1121; b) A. J. Arduengo, J. R. Goerlich, W. J. Marshall, *J. Am. Chem. Soc.* **1995**, *117*, 11027; c) M. K. Denk, A. Thadani, K. Hatano, A. J. Lough, *Angew. Chem.*, **1997**, *109*, 2719; *Angew. Chem. Int. Ed. Engl.* **1997**, *36*, 2607; d) D. Enders, K. Breuer, G. Raabe, J. Runsink, J. H. Teles, J. Melder, K. Ebel, S. Brode, *Angew. Chem.* **1995**, *107*, 1119; *Angew. Chem. Int. Ed. Engl.* **1995**, *34*, 1021–1023.

[3] A. Igau, A. Baceiredo, G. Trinquier, G. Bertrand, *Angew. Chem.* **1989**, *101*, 617; *Angew. Chem. Int. Ed. Engl.* **1989**, *28*, 621. For a review on phosphanylcarbenes see: D. Bourissou, G. Bertrand, *Adv. Organomet. Chem.* **1999**, *44*, 175.

[4] N. Merceron, K. Miqueu, A. Baceiredo, G. Bertrand, *J. Am. Chem. Soc.* **2002**, *124*, 6806–6807.

[5] a) A. Baceiredo, A. Igau, G. Bertrand, M. J. Menu, Y. Dartiguenave, J. J. Bonnet, *J. Am. Chem. Soc.* **1986**, *108*, 7868; b) M. Soleilhavoup, A. Baceiredo, G. Bertrand, *Angew. Chem.* **1993**, *105*, 1245; *Angew. Chem. Int. Ed. Engl.* **1993**, *32*, 1167.

[6] a) O. Treutler, R. Ahlrichs, M. Soleilhavoup, *J. Am. Chem. Soc.* **1993**, *115*, 8788; b) W. W. Schoeller, *Eur. J. Inorg. Chem.* **2000**, 369.

[7] M. Soleilhavoup, A. Baceiredo, O. Treutler, R. Ahlrichs, M. Nieger, G. Bertrand, *J. Am. Chem. Soc.* **1992**, *114*, 10959.

[8] Similar Mn^I carbenes are apparently implicated in the formation of diphosphanylketenimines, which open routes to an unprecedented phosphaheterocycles chemistry: a) J. Ruiz, V. Riera, M. Vivanco, M. Lanfranchi, A. Tiripicchio, *Organometallics* **1998**, *17*, 3835; b) J. Ruiz, F. Marquínez, V. Riera, M. Vivanco, S. García-Granda, M. R. Díaz, *Angew. Chem.* **2000**, *112*, 1891; *Angew. Chem. Int. Ed.* **2000**, *39*, 1821; c) J. Ruiz, F. Marquínez, V. Riera, M. Vivanco, S. García-Granda, M. R. Díaz, *Chem. Eur. J.* **2002**, *8*, 3872–3878.

[9] The calculations were performed with the Gaussian 98 program package.[17a] The experimental geometry of **3** was used as a starting point for **2b** and a preliminary calculation using the HF/LanL2DZ level of theory converged to the first optimized structures for both singlet and triplet states. Further calculations were made by using DFT methods with the B3LYP hybrid functional[17b] and increasing the size of the basis set from the quasi-relativistic pseudo-potential LanL2DZ basis set[17c] for Ru and the standard 6-31G* basis set[17d] for all the other atoms (C, H, N, and P), used in a first round, to the 3-21+G*[17e] basis set for the former and the 6-311++G** basis set[17f,g] for the latter used in the final round. All calculated structures represent real minima as harmonic frequencies calculated at the same levels of theory showed no imaginary frequencies. Scaled zero-point energies (ZPE) were added to the final electronic energies to obtain singlet–triplet splittings (ΔE_{ST}) and electron affinities (EA). Scale factor used for ZPE: 0.9804.[17h]

[10] Compound **1**-I was prepared from $[Ru(CN\mathit{t}Bu)_4\{(PPh_2)_2CH_2\}\text{-}(ClO_4)_2]$ in a similar way to that described for the synthesis of $[Mn(CO)_4\{(PPh_2)_2Cl\}]$: J. Ruiz, V. Riera, M. Vivanco, S. García-Granda, M. R. Díaz, *Organometallics* **1998**, *17*, 4562.

[11] H. Keller, G. Maas, M. Regitz, *Tetrahedron Lett.* **1986**, *27*, 1903.

[12] Carbene–pyridine adducts have been spectroscopically characterized and used as evidence for the formation of carbenes: J. L. Wang, J. P. Toscano, M. S. Platz, V. Nikolaev, V. Popik, *J. Am. Chem. Soc.* **1995**, *117*, 5477; J. P. Toscano, M. S. Platz, V. Nikolaev, V. Popic, *J. Am. Chem. Soc.* **1994**, *116*, 8146.

[13] Crystal data for $[\mathbf{3}\text{-}(BF_4)_2]_2\cdot[(AgPy_2)\cdot(BF_4)]\cdot(CH_2Cl_2)_3\cdot(H_2O)_2$ ($C_{113}H_{142}AgB_5Cl_6F_{20}N_{12}O_2P_4Ru_2$): $M_r=2781.03$, monoclinic, space group $P2_1/n$, $a=16.8409(1)$, $b=14.9234(2)$, $c=53.8328(5)$ Å, $B=93.830(1)°$, $V=13499.2(2)$ Å^3, $Z=4$, $\rho_{calcd}=1.368\ g\,cm^{-3}$, $F(000)=5688$, $Cu_{K\alpha}$ radiation ($\lambda=1.5418$ Å), $\mu=5.134\ mm^{-1}$; crystal dimensions $0.42\times0.17\times0.27$ mm. Data collection was performed at 120(2) K on a Nonius KappaCCD single crystal diffractometer. Crystal structure was solved by direct methods (SHELXS-97) and refined using full-matrix least squares on F^2 (SHELXL-97). Non-hydrogen atoms were anisotropically refined, except for some atoms on three disordered anions and the solvent molecules. Hydrogen atoms were geometrically placed and left riding on their parent atoms. Some restrains on the disordered anions and one solvent molecule were applied. wR_2 ($F^2>2\sigma(F^2)$) = 0.1889, conventional R [on F values for 24246 reflections] ($F^2>2\sigma(F^2)$) = 0.0695 for 1452 parameters. Crystal data for **4**-$(BF_4)_2$ ($C_{49}H_{64}B_2F_8N_4P_2RuS$): $M_r=1077.73$, monoclinic, space group $P2_1/c$, $a=14.5238(5)$, $b=20.9879(8)$, $c=17.9357(6)$ Å, $\beta=99.508(2)°$, $V=5392.1(3)$ Å3, $Z=4$, $\rho_{calcd}=1.328\ g\,cm^{-3}$, $F(000)=2232$, $Cu_{K\alpha}$ radiation ($\lambda=1.5418$ Å), $\mu=3.816\ mm^{-1}$; crystal dimensions $0.25\times0.10\times0.10$ mm. Data collection was performed at 120(2) K on a Nonius KappaCCD single crystal diffractometer. Crystal structure was solved by direct methods and refined using full-matrix least squares on F^2. All non-hydrogen atoms were anisotropically refined. Hydrogen atoms were geometrically placed and left riding on their parent atoms. $wR2$ ($F^2>2\sigma(F^2)$) = 0.2001, conventional R [on F values for 9838 reflections] ($F^2>2\sigma(F^2)$) = 0.0773 for 604 parameters. Crystal data for **7**-[AuICl]·THF ($C_{49}H_{64}Au_2Cl_2I_2N_4OP_2Ru$): $M_r=1606.69$, hexagonal, space group $P63/m$, $a=28.7293(5)$, $b=28.7293(5)$, $c=14.9542(3)$ Å, $V=10689.2(3)$ Å^3, $Z=6$, $\rho_{calcd}=1.489\ g\,cm^{-3}$, $F(000)=4596$, $Cu_{K\alpha}$ radiation ($\lambda=1.5418$ Å), $\mu=17.422\ mm^{-1}$; crystal dimensions $0.23\times0.17\times0.16$ mm. Data collection was performed at 120(2) K on a Nonius KappaCCD single crystal diffractometer. Crystal structure was solved by direct methods and refined using full-matrix least squares on F^2. All non-hydrogen atoms were anisotropically refined, except for the chlorine atom in the counteranion which is disordered in three positions. In the counteranion the gold atom shows positional disorder. Hydrogen atoms were geometrically placed and left riding on their parent atoms. Some restrains on a phenyl group and the solvent molecule were applied. wR2 ($F^2>2\sigma(F^2)$) = 0.2498, conventional R [on F values for 6792 reflections] ($F^2>2\sigma(F^2)$) = 0.0864

 © 2003 Wiley-VCH Verlag GmbH & Co. KGaA, Weinheim

for 322 parameters. CCDC-187344 (**3**), CCDC-211797 (**4**), CCDC-187345 (**5**), and CCDC-211798 (**7**) contain the supplementary crystallographic data for this paper. These data can be obtained free of charge via www.ccdc.cam.ac.uk/conts/retrieving.html (or from the Cambridge Crystallographic Data Centre, 12 Union Road, Cambridge CB2 1EZ, UK; fax: (+44) 1223-336-033; or deposit@ccdc.cam.ac.uk).

[14] Reactions of electrophilic singlet carbenes with sulfides to afford sulfonium ylides are well established: A. Padwa, S. F. Hornbuckle, *Chem. Rev.* **1991**, *91*, 263–309.

[15] It has been reported that the ketone $(PPh_2)_2C{=}O$ can be prepared by reaction of phosgene with Me_3SiPPh_2 at −110 °C, but this compound was poorly characterized owing to its thermal instability above −60 °C: H. J. Becher, E. Larger, *Angew. Chem.* **1973**, *85*, 910; *Angew. Chem. Int. Ed. Engl.* **1973**, *12*, 842.

[16] J. Ruiz, R. Araúz, V. Riera, M. Vivanco, S. García-Granda, A. Menéndez-Velázquez, *Organometallics* **1994**, *13*, 4162.

[17] a) Gaussian 98 (Revision A.7), M. J. Frisch, G. W. Trucks, H. B. Schlegel, G. E. Scuseria, M. A. Robb, J. R. Cheeseman, V. G. Zakrzewski, J. A. Montgomery, R. E. Stratmann, J. C. Burant, S. Dapprich, J. M. Millam, A. D. Daniels, K. N. Kudin, M. C. Strain, O. Farkas, J. Tomasi, V. Barone, M. Cossi, R. Cammi, B. Mennucci, C. Pomelli, C. Adamo, S. Clifford, J. Ochterski, G. A. Petersson, P. Y. Ayala, Q. Cui, K. Morokuma, D. K. Malick, A. D. Rabuck, K. Raghavachari, J. B. Foresman, J. Cioslowski, J. V. Ortiz, B. B. Stefanov, G. Liu, A. Liashenko, P. Piskorz, I. Komaromi, R. Gomperts, R. L. Martin, D. J. Fox, T. Keith, M. A. Al-Laham, C. Y. Peng, A. Nanayakkara, C. Gonzalez, M. Challacombe, P. M. W. Gill, B. G. Johnson, W. Chen, M. W. Wong, J. L. Andres, M. Head-Gordon, E. S. Replogle, J. A. Pople, Gaussian, Inc., Pittsburgh, PA, **1998**; b) A. D. Becke, *J. Chem. Phys.* **1993**, *98*, 5648; c) P. J. Hay, W. R. Wadt, *J. Chem. Phys.* **1985**, *82*, 299, and references therein; d) R. C. Binning Jr., L. A. Curtiss, *J. Comput. Chem.* **1990**, *11*, 1206, and references therein; e) K. D. Dobbs, W. J. Hehre, *J. Comput. Chem.* **1987**, *8*, 880, and references therein; f) A. D. MacLean, G. S. Chandler, *J. Chem. Phys.* **1980**, *72*, 5639; g) R. Krishnan, J. S. Binkley, R. Seeger, J. A. Pople, *J. Chem. Phys.* **1980**, *72*, 650; h) C. W. Bauschlicher, Jr., H. Partridge, *J. Chem. Phys.* **1995**, *103*, 1788.

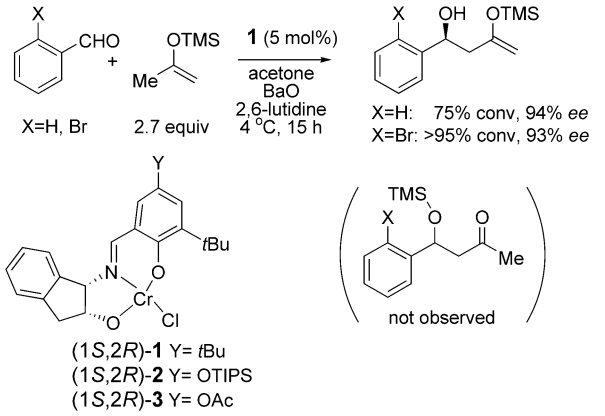
 © 2003 Wiley-VCH Verlag GmbH & Co. KGaA, Weinheim

Hetero-Ene Reaction

Asymmetric Hetero-Ene Reactions of Trimethylsilyl Enol Ethers Catalyzed by Tridentate Schiff Base Chromium(III) Complexes**

*Rebecca T. Ruck and Eric N. Jacobsen**

Asymmetric hetero-ene reactions between aldehydes and enol ethers provide convenient access to a wide variety of chiral β-hydroxycarbonyl derivatives from stable, readily available precursors. Recently, we demonstrated that the tridentate Schiff base chromium(III) complex **1** catalyzes hetero-ene reactions between 2-methoxypropene and benzaldehyde derivatives to provide the corresponding β-aryl β-hydroxymethylenol ether products in high enantioselectivities and yields.[1] Promising reactivity and enantioselectivity were also uncovered in reactions of 2-trimethylsilyloxyproprene with aromatic aldehydes to generate highly enantioenriched β-hydroxytrimethylsilyl enol ether products (Scheme 1).



Scheme 1. TIPS = triisopropylsilyl, TMS = trimethylsilyl.

None of the corresponding β-silyloxyketone products attributable to Mukaiyama aldol pathways were detected in the latter case, suggesting a concerted pericyclic reaction mechanism.[2] Intrigued by the potential of this unusual silyl enol ether ene methodology,[3] we have investigated it more deeply and discovered it to be far more broadly applicable than the corresponding alkyl enol ether methodology first reported.

[*] Prof. E. N. Jacobsen, R. T. Ruck
Department of Chemistry and Chemical Biology
Harvard University
Cambridge, MA 02138 (USA)
Fax: (+1) 617-496-1880
E-mail: jacobsen@chemistry.harvard.edu

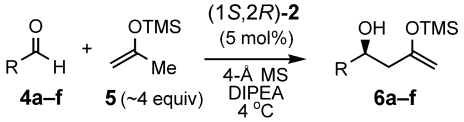
[**] This work was supported by the NIH (GM-59316) and by a predoctoral fellowship from the National Science Foundation and an graduate fellowship from the ACS Division of Organic Chemistry sponsored by Albany Molecular Research, Inc. to R.T.R.

Supporting information for this article is available on the WWW under http://www.angewandte.org or from the author.

 DOI: 10.1002/anie.200351591 © 2003 Wiley-VCH Verlag GmbH & Co. KGaA, Weinheim

We report here its successful application to highly enantioselective and diastereoselective reactions of prochiral and chiral aliphatic aldehydes.

Aliphatic aldehydes **4a–f** proved to be excellent substrates for enantioselective hetero-ene reactions catalyzed by Cr^{III} complex **2**, undergoing reaction with 2-trimethylsilyloxypropene to generate the β-hydroxytrimethylsilyl enol ether products **6a–f** in high yields and enantioselectivities (Table 1).



(1)

Table 1: Hetero-ene reactions between aliphatic aldehydes and 2-trimethylsilyloxypropene [Eq. (1)].[a,b]

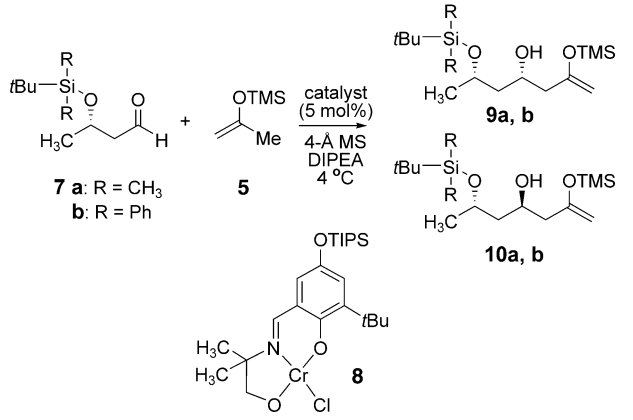
Product	R	*t* [h]	Yield [%][c]	*ee* [%]
6a	*n*Pr	65	87	89[e]
6b	*i*Pr	72	83	90[e]
6c	*i*Bu	72	77	87[e]
6d	cyclopropyl	72	47[f]	93[e]
6e	$TBDPSOCH_2CH_2$[d]	20	90	93[g]
6f	$TBDPSOCH_2CH_2CH_2$[d]	40	87	90[g]

[a] Reactions were carried out with 1.0 mmol of aldehyde, ~4 mmol of **5** (480 μL of 93–94% purity), 0.05 mmol of **2** (28.4 mg), powdered 4-Å molecular sieves (400 mg), and DIPEA (25 μL) at 4°C. [b] Absolute stereochemistry was determined by hydrolysis of **6c** to the β-hydroxyketone and comparison of the optical rotation to the known literature value.[5] [c] Net yield of crude product contaminated with residual catalyst (see text). [d] TBDPS = *tert*-butyldiphenylsilyl. [e] Enantiomeric excess was determined by hydrolysis to the β-hydroxyketone and analysis by chiral GC (γ-TA) or HPLC (Whelk-01). [f] This reaction proceeded only to 55% conv. of substrate. [g] Enantiomeric excess determined for the TMS enol ether, which was analyzed by chiral HPLC on a Whelk-01 column.

Catalysts **1** and **2** afforded similar enantioselectivities, but rates were 1.5–2 times faster with the more soluble complex **2**. Reactions were conducted under solvent-free conditions in the presence of 4-Å molecular sieves, with 2-trimethylsilyloxypropene and aldehyde in a 4:1 molar ratio. Addition of substoichiometric amounts of diisopropylethylamine (DIPEA) served to inhibit an unselective pathway promoted, most likely, by trace amounts of Brønsted acid associated to the catalyst.[4] The β-hydroxytrimethylsilyl enol ether products were unreactive as ene partners under the reaction conditions.

The enantioselectivity and rate of the ene reactions displayed little dependence on the steric properties of the aldehydes, except in the extreme case of pivalaldehyde, which proved almost completely unreactive. Butyraldehyde (**4a**) underwent catalyst-induced trimerization under standard reaction conditions, but this could be avoided by slow addition of **4a** to a solution of the other reaction components, with no deleterious effect on enantioselectivity or reaction rate. Reaction of β- or γ-silyloxy-substituted aldehydes (**4e, 4f**) proceeded with similar enantioselectivities but measurably faster rates than the unfunctionalized counterparts.[6]

The high reactivity and enantioselectivity observed with aldehyde **4e** suggested that chiral β-silyloxyaldehydes might serve as useful substrates for doubly diastereoselective ene reactions to generate monoprotected *syn*- or *anti*-1,3-diols. Enantiopure 3-hydroxybutyraldehyde derivatives **7a** and **7b** were both subjected to ene reactions with 2-trimethylsilyloxypropene (**5**), and the selectivities obtained with each enantiomer of catalyst **2** were compared with those generated with the achiral variant **8** (Scheme 2, Table 2). Achiral catalyst **8**



Scheme 2.

Table 2: Doubly diastereoselective ene reactions.

Aldehyde	Catalyst	**9**:**10**[a]	Conv. [%][b]
7a	**8**	2.8:1	n.d.
7a	(*R*,*S*)-**2**	>46:1	92
7a	(*S*,*R*)-**2**	1:14.4	92
7b	**8**	1:2.6	n.d.
7b	(*R*,*S*)-**2**	3.8:1	51
7b	(*S*,*R*)-**2**	1:>160	91

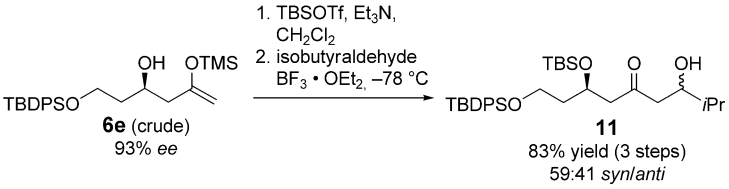
[a] *Syn*:*anti* ratios were determined by GC analysis. [b] Conversions determined by ^{1}H NMR spectroscopy; n.d. = not determined.

provided a modest 2.8:1 diastereoselectivity in the ene reaction between **7a** and **5**, favoring the enantiopure *syn*-diol derivative **9a**. This substrate-based selectivity was enhanced to a significant extent with "matched" catalyst (1*R*,2*S*)-**2** (>46:1). The "mismatched" catalyst (1*S*,2*R*)-**2** provided a synthetically useful diastereoselectivity of 14.4:1 in favor of the enantiopure *anti*-diol derivative **10a**. The substrate-induced selectivity with the bulkier aldehyde **7b** reversed to favor *anti*-diol derivative **10b** in a 2.6:1 ratio. The now-"matched" catalyst (1*S*,2*R*)-**2** provided a >160:1 d.r. in favor of the *anti* product **10b**, whereas "mismatched" catalyst (1*R*,2*S*)-**2** afforded a modest 3.8:1 selectivity favoring the *syn* isomer **9b**. Thus, the highly selective generation of either *syn*- or *anti*-1,3-diol derivatives was possible through appropriate choice of catalyst enantiomer and silyl protecting group.

The crude β-hydroxytrimethylsilylenol ether products were obtained by filtration of the reaction mixtures through Celite to remove the 4-Å molecular sieves followed by concentration in vacuo.[7] Analysis of the brown residue by ^{1}H NMR spectroscopy indicated the presence of ene adduct as the only diamagnetic component. Yields were calculated

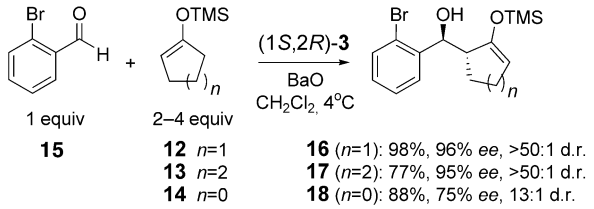
 © 2003 Wiley-VCH Verlag GmbH & Co. KGaA, Weinheim

assuming that the crude product retains 100% of the catalyst by subtracting the mass of catalyst **2** used from the mass of crude product obtained. Purification by chromatography led to significant losses due to product decomposition, and clean products were obtained by flash chromatography in only ca. 35% yield.[8] However, we found that the crude mixture of catalyst and product could be employed in a variety of useful transformations. For example, crude β-hydroxytrimethylsilyl enol ether **6e** was protected as the *tert*-butyldimethylsilyl (TBS) ether,[9] and then a Mukaiyama aldol reaction was carried out with isobutyraldehyde in the presence of $BF_3 \cdot OEt_2$ to generate enantiopure adduct **11** in 83% yield over three steps and a 59:41 *syn*/*anti* ratio of diastereomers (Scheme 3).[10]



Scheme 3.

More sterically hindered silyl enol ether derivatives were also found to undergo asymmetric ene reactions, albeit with significant limitations on the scope of useful aldehyde substrates. While aliphatic aldehydes were unreactive in ene reactions with trimethylsilylenol ethers derived from cyclopentanone (**12**) or cyclohexanone (**13**), 2-bromobenzaldehyde (**15**) underwent clean and highly stereoselective reactions with these enophiles in the presence of catalyst **3** (Scheme 4).[11] High *anti* diastereoselectivity was observed in



Scheme 4.

both reactions, indicating that the ene reaction of the cyclic (*E*)-enol ether proceeds selectively through an endo transition state, as is the case in Cr^{III}-catalyzed hetero-Diels–Alder reactions.[2] Reaction of 2-bromobenzaldehyde (**15a**) with 1-trimethylsilyloxycyclobutene (**14**) as the ene component was also catalyzed by **3**, although the product (**18**) was generated with only moderate enantio- and diastereoselectivity. The trisubstituted trimethylsilyl enol ether products displayed increased stability toward silica gel chromatography, and their purification and full characterization was accomplished after simple filtration of the crude reaction mixture through a small pad of silica gel to remove catalyst.

In summary, tridentate Schiff base chromium(III) complexes **1**–**3** catalyze a wide range of hetero-ene reactions between aromatic or aliphatic aldehydes and silyl enol ether derivatives to generate β-hydroxytrimethylsilyl enol ethers in high enantioselectivities and yields. Current efforts are directed toward elucidation of the mechanism of this process and toward synthetic extensions and applications of this promising methodology.

Received: April 7, 2003 [Z51591]
Published Online: September 23, 2003

Keywords: aldehydes · asymmetric catalysis · chromium · ene reaction · Schiff bases

[1] R. T. Ruck, E. N. Jacobsen, *J. Am. Chem. Soc.* **2002**, *124*, 2882–2883.
[2] The hetero-Diels–Alder reactions reported using a similar catalyst also appear to proceed by a concerted mechanism: a) A. G. Dosseter, T. F. Jamison, E. N. Jacobsen, *Angew. Chem.* **1999**, *111*, 2549–2552; *Angew. Chem. Int. Ed.* **1999**, *38*, 2398–2400; b) K. Gademann, D. E. Chavez, E. N. Jacobsen, *Angew. Chem.* **2002**, *114*, 3185–3187; *Angew. Chem. Int. Ed.* **2002**, *41*, 3059–3061.
[3] The lone previous example of an asymmetric silyl enol ether ene transformation was reported by Mikami et al. and involved reaction of 2-*tert*-butyldimethylsilyloxypropene and glyoxylate derivatives: K. Mikami, S. Matsukawa, M. Nagashima, H. Funabashi, H. Morishima, *Tetrahedron Lett.* **1997**, *38*, 579–582.
[4] The procedure for the preparation of catalysts **1**–**3**[1] incorporates a late-stage workup step with HCl, which is the likely source of acidic impurities.
[5] B. List, P. Pojarliev, C. Castello, *Org. Lett.* **2001**, *3*, 573–576.
[6] In contrast, aldehydes bearing silyloxy α-substituents underwent ene reactions in good yields but low enantioselectivities. For example, the reaction between *tert*-butyldiphenylsilyloxyacetaldehyde and **5** proceeded in a comparatively low 53% *ee*. Similarly, $TBSOCH_2CHO$ underwent the hetero-ene reaction with 2-methoxypropene in the presence of **1** in 54% *ee*. These results stand in sharp contrast to those obtained in hetero-Diels–Alder reactions with analogous Cr^{III} catalysts, where substrates such as $TBSOCH_2CHO$ afforded outstanding results (> 99% *ee*) in cycloadditions with alkoxy- or silyloxydiene derivatives. See ref. [2a], and: P. Liu, E. N. Jacobsen, *J. Am. Chem. Soc.* **2001**, *123*, 10772–10773.
[7] The crude β-hydroxytrimethylsilyl enol ether products listed in Table 1 were characterized by ^1H NMR spectroscopy; the purified β-hydroxyketone hydrolysis products were fully characterized.
[8] Separation of the products from the nonpolar catalyst was difficult and required careful chromatography. The low recovery of the silyl enol ether products is attributable to partial hydrolysis due to prolonged exposure to the chromatographic support.
[9] The unprotected β-hydroxy silyl enol ethers underwent competitive elimination and/or hydrolysis reactions under a variety of Lewis acid catalyzed conditions.
[10] The stereochemical assignment is tentative and based on closely related reactions: a) D. A. Evans, P. J. Coleman, B. Cote, *J. Org. Chem.* **1997**, *62*, 788–789; b) I. Paterson, K. R. Gibson, R. M. Oballa, *Tetrahedron Lett.* **1996**, *37*, 8585–8588.
[11] Electron-deficient benzaldehyde derivatives bearing *ortho* substituents provided the best rates and enantioselectivities in this reaction, similar to observations made in ene reactions with 2-methoxypropene. See ref. [1].

 © 2003 Wiley-VCH Verlag GmbH & Co. KGaA, Weinheim

[12] The relative stereochemistry was determined by hydrolysis of the product to the β-hydroxyketone and comparison of the coupling constant between the two methine protons ($J = 9.3$ Hz) to that of the previously reported parent phenyl analogue: S. E. Denmark, R. A. Stavenger, K.-T. Wong, *Tetrahedron* **1998**, *54*, 10389 – 10402.

 © 2003 Wiley-VCH Verlag GmbH & Co. KGaA, Weinheim

Versatile Domino Cyclizations

One-Pot Synthesis of Polyheterocycles by a Palladium-Catalyzed Intramolecular N-Arylation/C–H Activation/Aryl–Aryl Bond-Forming Domino Process**

*Guylaine Cuny, Michèle Bois-Choussy, and Jieping Zhu**

There has been considerable interest in developing novel cyclization methodologies for organic synthesis.[1] Indeed, many complex natural products and drugs are cyclic in nature, and a ring closure reaction is very often the crucial step in a multistep synthesis. In connection with our ongoing project on the synthesis of macrocycles with an *endo* aryl–aryl bond,[2] we examined the cyclization of diamide **1** under modified Miyaura–Suzuki conditions.[3] However, heating a solution of **1** in DMSO in the presence of [$PdCl_2$(dppf)] (5.0 mol%; dppf = 1,1′-bis(diphenylphosphanyl)ferrocene), KOAc (3.0 equiv), and bis(pinacolato)diboron (**2**, 1.2 equiv) did not provide macrocycle **4**. Instead, polyheterocycle **3** was produced in about 50% yield (Scheme 1). Formally, one C_{aryl}–N and one C_{aryl}–C_{aryl} bond were created with concurrent formation of a nine-membered and a six-membered ring. While intramolecular N-arylation leading to five- and six-membered rings is well-established, attempts to access medium-sized and macrocyclic ring systems by the same reaction were, to the best of our knowledge, unsuccessful.[4,5] Intrigued by the potential synthetic power of this novel catalytic domino process,[6] we set out to examine in detail this unprecedented transformation and report herein our preliminary results.

A survey of reaction conditions with variation of the palladium source, the ligand, the temperature, the base, and the solvent is summarized in Table 1. Mechanistically, a domino process involving a sequence of intramolecular Buchwald–Hartwig amination,[4,5] C–H activation, and aryl–aryl bond formation[7] could account for the production of polyheterocycle **3** from linear diamide **1**. This speculative analysis suggested that the diboron reagent **2** is redundant, and a similar yield of **3** was indeed obtained in its absence under otherwise identical conditions (entry 1). The reaction temperature was found to have dramatic effect on the reaction, and higher yields were obtained when the reaction was performed at higher temperature (entries 1 and 2). In contrast to previous studies on the intramolecular N-arylation of amides,[8,9] the present domino process is much less sensitive to the ligands used. Both bidendate phosphanes such as dppf (entries 2, 6) and binap (entries 7, 10, 11) and the monodentate ligand Ph_3P (entry 15) were suitable, although tBu$_3$P (entries 12, 13) seemed to be less efficient.[8i,10] Potassium acetate (entry 2) was more effective than cesium carbonate (entry 5) as base, while DMSO was a better solvent than DMF (entry 3) and toluene (entry 4). The highest yield was obtained with a catalyst prepared in situ from $Pd(OAc)_2$ and binap in a molar ratio of 1:2, but we chose [$PdCl_2$(dppf)] as the catalyst for the subsequent studies for simplicity of manipulation and product purification ([$PdCl_2$(dppf)], KOAc, DMSO, 120 °C, concentration of substrate = 0.02 M).

Table 1: Palladium-catalyzed cyclization of **1**: survey of reaction conditions.[a]

Entry	Catalyst[b]	Solvent	Base	T [°C]	Yield of **3** [%][c]
1	[$PdCl_2$(dppf)]	DMSO	KOAc	80	48
2	[$PdCl_2$(dppf)]	DMSO	KOAc	120	65
3	[$PdCl_2$(dppf)]	DMF	KOAc	120	32
4	[$PdCl_2$(dppf)]	Toluene	KOAc	reflux	0
5	[$PdCl_2$(dppf)]	DMSO	Cs_2CO_3	120	25
6	[$Pd(dba)_2$]/dppf (1:1)	DMSO	KOAc	120	51
7	[$Pd(dba)_2$]/binap (1:1)	DMSO	KOAc	120	60
8	[$Pd(dba)_2$]/tBu$_3$P (1:1)	DMSO	KOAc	120	50
9	[$Pd(dba)_2$]/tBu$_3$P (1:2)	DMSO	KOAc	120	40
10	$Pd(OAc)_2$/binap (1:1)	DMSO	KOAc	120	62[d]
11	$Pd(OAc)_2$/binap (1:2)	DMSO	KOAc	120	77[d]
12	$Pd(OAc)_2$/tBu$_3$P (1:1)	DMSO	KOAc	120	44
13	$Pd(OAc)_2$/tBu$_3$P (1:2)	DMSO	KOAc	120	44
14	[$PdCl_2$(dppf)]/dppf (1:1)	DMSO	KOAc	120	46
15	$[Pd(PPh)_3]_4$	DMSO	KOAc	120	60

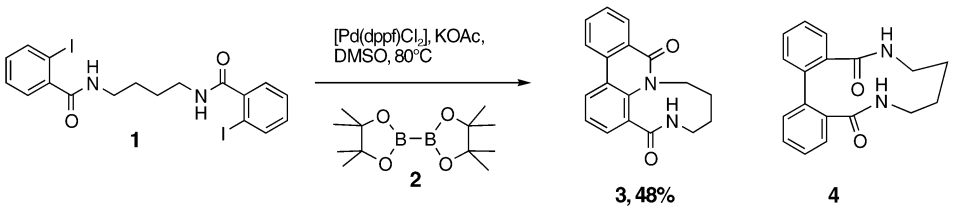
[a] Concentration: 0.02 M, reaction time: 16 h, in the absence of bis(pinacolato)diboron. [b] 5 mol% of catalyst was used; binap = [1,1′-binaphthalene]-2,2′-diylbis(diphenylphosphane), dba = dibenzylideneacetone, dppf = 1,1′-bis(diphenylphosphanyl)ferrocene. [c] Yields refer to the average of two runs. [d] Contains a small amount of binap derivatives.

As shown in Figure 1, this novel catalytic domino process can be applied to the construction of azaphenanthrenes fused with an 8-membered (**5**), 10-membered (**6**), 11-membered (**7**), and 13-membered lactam motif (**8**), in addition to the 9-

[*] Dr. J. Zhu, G. Cuny, Dr. M. Bois-Choussy
Institut de Chimie des Substances Naturelles
CNRS
91198 Gif-sur-Yvette Cedex (France)
Fax: (+33) 1-6907-7247
E-mail: zhu@icsn.cnrs-gif.fr

[**] We thank CNRS for financial support. A doctoral fellowship from this institute to G.C. is gratefully acknowledged. We thank Professor J.-Y. Lallemand for his interest in this work.

 © 2003 Wiley-VCH Verlag GmbH & Co. KGaA, Weinheim DOI: 10.1002/anie.200351923



Scheme 1. Catalytic domino process leading to polyheterocycles.

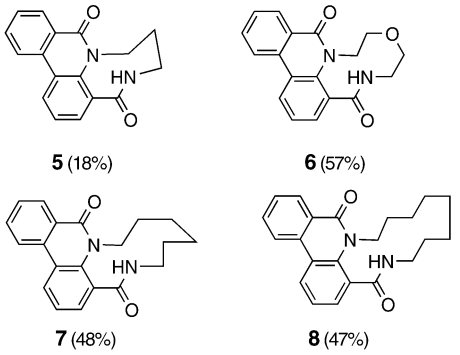
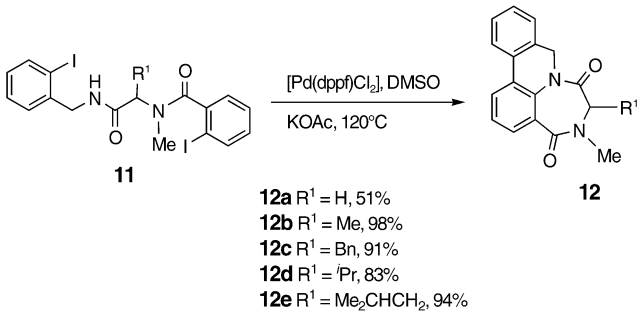


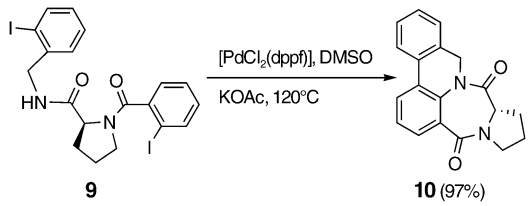
Figure 1. Structure of dihydroazaphenanthrenes fused with a macrocyclic ring.



Scheme 3. Synthesis of substituted 5,6-dihydro-8*H*-[5,7-*a*]diazacycloheptа[*jk*]phenanthrene-4,7-diones.

membered polyheterocycle **3**. To the best of our knowledge, these are the first examples where an intramolecular Buchwald–Hartwig amidation has been successfully applied to the synthesis of medium-sized ring systems and macrocycles.

To further exploit the generality of this catalytic domino process, we synthesized proline derivative **9** by standard procedures and subjected it to the cyclization conditions. The catalytic domino cyclization occurred smoothly to give the desired pentacyclic compound **10** in 97% yield of isolated product (Scheme 2). Double cyclization of *ent*-**9**, prepared

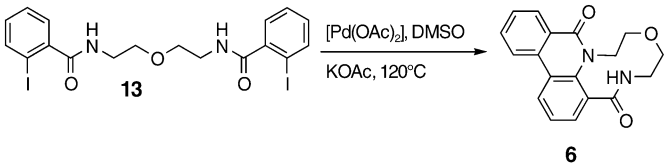


Scheme 2. One-pot synthesis of a pentacyclic compound.

from D-proline, provided *ent*-**10** (structure not shown) in a similar yield. Its optical rotation was opposite in sign and nearly equal in magnitude to that of **10**. Chiral HPLC analysis shown that the enantiomeric excesses of **10** and *ent*-**10** are both greater than 98%.

The scope of this reaction was further examined by applying the optimized conditions to differently substituted amides **11** (Scheme 3). The 1,4-benzodiazepine-2,5-dione derivatives incorporating sarcosine (**12a**), *N*-methylalanine (**12b**), *N*-methylphenylalanine (**12c**), *N*-methylvaline (**12d**), and *N*-methyl leucine (**12e**) can be prepared in good-to-excellent yields. The ready accessibility of the starting material and the generality of this process clearly indicated its potential in the diversity-oriented synthesis of this family of compounds.[11,12]

Synthesis of simple seven-membered rings by palladium-catalyzed intramolecular N-arylation of aryl halides with xantphos and 2-methoxy-2′-diphenylphosphanyl-1,1′binaphthyl (MOP) as ligands has been reported,[8c] but application of this reaction to the synthesis of medium-sized and larger rings was unsuccessful.[8] The efficiency of the present domino process is thus intriguing. A template effect due to the chelation of the metal by two amido groups leading to conformational preorganization could be a reasonable explanation. Such a template effect would require at least one open coordination site of the putative Pd^{II} oxidative adduct. This consideration prompted us to examine the "ligand-free" palladium acetate as a catalyst for this transformation.[13] To our delight, treatment of a solution of **13** in DMSO in the presence of $Pd(OAc)_2$ and KOAc provided the tetracyclic compound **6** (Scheme 4) in a yield (55%) comparable to that obtained with [$PdCl_2$(dppf)]. Similarly, **10** was obtained in 90% yield from **9** with $Pd(OAc)_2$ as catalyst. To the best of our knowledge, these are the first examples in which a ligand-free palladium catalyst was employed for the amidation



Scheme 4. "Ligand-free" palladium-catalyzed domino cyclization.

 © 2003 Wiley-VCH Verlag GmbH & Co. KGaA, Weinheim

process. It has been established that low-coordinate Pd^{II}–amido complexes should favor the competitive β-hydrogen elimination process and thus reduce the yield of the desired amidation product.[14] This trend is apparently not observed in the present catalytic domino process, probably due to the internal ligation.[15]

To probe the structural requirement for this interesting domino cyclization, we synthesized an amide (structure not shown) in which a simple benzyl group replaced the *ortho*-iodobenzyl group of **11b**. To our surprise, subjecting this monoiodide derivative to the cyclization conditions ([$PdCl_2$(dppf)], DMSO, KOAc, 120 °C) did not provide the corresponding 1,4-benzodiazepine-2,5-dione. The surprising result of this control experiment was indicative of the crucial rule of the bisiodido functionality. Since two chemical bonds are formed in the present process by way of a formal Buchwald–Hartwig amidation and C–H activation/aryl–aryl bond-forming processes, we surmised that there is some kind of cooperative effect in these two distinct palladium catalyzed bond-forming processes.[16] Further studies will be necessary to determine the mechanistic features of the reaction.

In conclusion, we have established a novel catalytic domino process.[17] The reaction generates significant molecular complexity from simple and readily accessible starting materials. We are exploring the scope, mechanism, and synthetic utility of this reaction.

Experimental Section

Typical procedure: Freshly distilled DMSO was added to a flask containing molten KOAc (3 equiv), [$PdCl_2$(dppf)] (0.05 equiv), and diamide (concentration of the substrate: 0.02 M). The mixture was degassed and stirred at 120 °C under argon for 12–36 h. After cooling to room temperature, the reaction mixture was extracted with ethyl acetate. The combined organic extracts were washed with brine, dried over Na_2SO_4, and concentrated on a rotary evaporator. The crude material was purified by flash chromatography to afford the desired polyheterocycle. **10**: $R_f = 0.26$ (toluene/methanol 10:1); m.p. 95 °C; $[\alpha]_D = +589.1$ ($c = 1.1$ in $CHCl_3$); IR ($CHCl_3$): $\tilde{\nu} = 3004$, 1679, 1633, 1474, 1434, 1392, 1228, 1167, 983 cm^{-1}; ^1H NMR (300 MHz, $CDCl_3$, 293 K, TMS): $\delta = 1.95$–2.17 (m, 4H), 2.70–2.75 (m, 1H), 3.56–3.65 (m, 1H), 3.83–3.90 (m, 1H), 4.04 (d, 1H, $^1J = 15.0$ Hz), 5.81 (d, 1H, $^1J = 15.0$ Hz), 7.35–7.43 (m, 3H), 7.40 (t, 1H, $^1J = 7.4$ Hz), 7.77 (d, 1H, $^1J = 7.4$ Hz), 7.95 ppm (d, 2H, $^1J = 7.4$ Hz); ^{13}C NMR (75 MHz, $CDCl_3$): $\delta = 23.6$, 26.6, 43.9, 46.8, 56.4, 123.6, 125.9, 126.1, 127.5, 128.4, 128.7, 129.2, 129.8, 131.1, 133.8, 134.7, 164.9, 168.5 ppm; MS (ESI): $m/z = 327$ [M+Na], 305 [M+H]. HRMS calcd for $C_{19}H_{16}N_2O_2$+H: 305.1290; found: 305.1304. *ent*-**10**: $\alpha_D = -589.8$ ($c = 0.8$ in $CHCl_3$). HPLC (chiral AD column, hexane/2-propanol 9:1): retention times of **10** and *ent*-**10**: 46.69 and 22.69 min, respectively.

Received: May 19, 2003 [Z51923]

Keywords: C–C coupling · C–H activation · cyclization · domino reactions · palladium

[1] Reviews: a) C. J. Roxburgh, *Tetrahedron* **1995**, *51*, 9767–9822; b) R. H. Grubbs, S. J. Miller, G. C. Fu, *Acc. Chem. Res.* **1995**, *28*, 446–452; c) J. Zhu, *Synlett* **1997**, 133–144; d) A. Fürstner, *Angew. Chem.* **2000**, *112*, 3140–3172; *Angew. Chem. Int. Ed.* **2000**, *39*, 3012–3043; e) K. E. Krakowiak, R. M. Izatt, J. S. Bradshaw, *J. Heterocycl. Chem.* **2001**, *38*, 1239–1248; Recent examples from this group: f) G. Zhao, X. Sun, H. Bienaymé, J. Zhu, *J. Am. Chem. Soc.* **2001**, *123*, 6700–6701; g) P. Janvier, M. Bois-Choussy, H. Bienaymé, J. Zhu, *Angew. Chem.* **2003**, *115*, 845–847; *Angew. Chem. Int. Ed.* **2003**, *42*, 811–814, and references therein.

[2] A. C. Carbonnelle, J. Zhu, *Org. Lett.* **2000**, *2*, 3477–3480.

[3] N. Miyaura, A. Suzuki, *Chem. Rev.* **1995**, *95*, 2457–2483.

[4] a) J. P. Wolfe, S. Wagaw, J. F. Marcoux, S. F. Buchwald, *Acc. Chem. Res.* **1998**, *31*, 805–818; b) B. H. Yang, S. L. Buchwald, *J. Organomet. Chem.* **1999**, *576*, 125–146.

[5] a) J. F. Hartwig, *Angew. Chem.* **1998**, *110*, 2154–2177; *Angew. Chem. Int. Ed.* **1998**, *37*, 2046–2067; b) J. F. Hartwig in "*Modern Amination Methods* (Ed. A. Ricci), Wiley-VCH, Weinheim, **2000**, Chap. 7.

[6] a) L. F. Tietze, *Chem. Rev.* **1996**, *96*, 115–136; b) A. Padwa, M. D. Weingarten, *Chem. Rev.* **1996**, *96*, 223–269.

[7] Reviews: a) G. Dyker, *Angew. Chem.* **1999**, *111*, 1808–1822; *Angew. Chem. Int. Ed.* **1999**, *38*, 1698–1712; b) V. Ritleng, C. Sirlin, M. Pfeffer, *Chem. Rev.* **2002**, *102*, 1731–1769; c) M. Catellani, *Synlett* **2003**, 298–313; Recent examples: d) Harayama, T. K. Shibaike, *Heterocycles* **1998**, *49*, 191–195; e) T. Harayama, T. Akiyama, H. Akamatsu, K. Kawano, H. Abe, Y. Takeuchi, *Synthesis* **2001**, *3*, 444–450; f) T. Harayama, T. Akiyama, Y. Nakano, H. Nishioka, H. Abe, Y. Takeuchi, *Chem. Pharm. Bull.* **2002**, *50*, 519–522; g) F. Kakiuchi, S. Kan, K. Igi, N. Chatani, S. Murai, *J. Am. Chem. Soc.* **2003**, *125*, 1698–1699; h) A. Mori, A. Sekiguchi, K. Masui, T. Shimada, M. Horie, K. Osakada, M. Kawamoto, T. Ikeda, *J. Am. Chem. Soc.* **2003**, *125*, 1700–1701.

[8] a) J. P. Wolfe, R. A. Rennels, S. L. Buchwald, *Tetrahedron* **1996**, *52*, 7525–7546; b) S. Wagaw, R. A. Rennels, S. L. Buchwald, *J. Am. Chem. Soc.* **1997**, *119*, 8451–8458; c) B. H. Yang, S. L. Buchwald, *Org. Lett.* **1999**, *1*, 35–37; d) A. Abouabdellah, R. H. Dodd, *Tetrahedron Lett.* **1998**, *39*, 2119–2122; e) K. Yamada, T. Kubo, H. Tokuyama, T. Fukuyama, *Synlett* **2002**, 231–234; f) M. Qadir, R. E. Priestley, T. W. D. F. Rising, T. Gelbrich, S. J. Coles, M. B. Hursthouse, P. W. Sheldrake, N. Whittall, K. K. Hii, *Tetrahedron Lett.* **2003**, *44*, 3675–3678; g) G. Evindar, R. A. Batey, *Org. Lett.* **2003**, *5*, 133–136; h) B. J. Margolis, J. J. Swidorski, B. N. Rogers, *J. Org. Chem.* **2003**, *68*, 644–647; i) K. Nozaki, K. Takahashi, K. Nakano, T. Hiyama, H. Z. Tang, M. Fujiki, S. Yamaguchi, K. Tamao, *Angew. Chem.* **2003**, *115*, 2097–2099; *Angew. Chem. Int. Ed.* **2003**, *42*, 2051–2053; j) R. Omar-Amrani, A. Thomas, E. Brenner, R. Schneider, Y. Fort, *Org. Lett.* **2003**, *5*, 2311–2314.

[9] For an elegant application in natural product synthesis, see F. He, B. M. Foxman, B. B. Snider, *J. Am. Chem. Soc.* **1998**, *120*, 6417–6418.

[10] Efficient arylamination procedure using tBu$_3$P as ligand: M. K. Hooper, M. Utsunomiya, J. F. Hartwig, *J. Org. Chem.* **2003**, *68*, 2861–2873. For a recent review, see A. F. Littke, G. C. Fu, *Angew. Chem.* **2002**, *114*, 4350–4386; *Angew. Chem. Int. Ed.* **2002**, *41*, 4176–4211.

[11] S. L. Schreiber, *Science* **2000**, *287*, 1964–1968.

[12] a) S. Bräse, C. Gil, K. Knepper, *Bioorg. Med. Chem.* **2002**, *10*, 2415–2437; b) C. Hulme, V. Gore, *Curr. Med. Chem.* **2003**, *10*, 51–80; c) D. A. Horton, G. T. Bourne, M. L. Smythe, *Chem. Rev.* **2003**, *103*, 893–930.

[13] "Ligand-free" palladium-catalyzed cross-coupling reaction: a) Review: I. P. Beletskaya, *Bull. Acad. Sci. USSR Div. Chem. Sci. (Engl. Transl.)* **1991**, *40*, 2013–2028; Recent examples: b) T. I. Wallow, B. M. Novak, *J. Org. Chem.* **1994**, *59*, 5034–5037; c) M. Moreno-Mañas, F. Pajuelo, R. Pleixats, *J. Org. Chem.* **1995**, *60*, 2396–2397; d) D. Badone, M. Baroni, R. Cardamone, A. Ielmini, U. Guzzi, *J. Org. Chem.* **1997**, *62*, 7170–7173; e) C. G. Blettner, W. A. König, W. Stenzel, T. Schotten, *J. Org. Chem.*

 © 2003 Wiley-VCH Verlag GmbH & Co. KGaA, Weinheim

1999, *64*, 3885 – 3890; f) N. E. Leadbeater, M. Marco, *Org. Lett.* **2002**, *4*, 2973 – 2976; g) R. B. Bedford, M. E. Blake, C. P. Butts, D. Holder, *Chem. Commun.* **2003**, 466 – 467.

[14] a) G. M. Whitesides, J. F. Gaasch, E. R. Stedronsky, *J. Am. Chem. Soc.* **1972**, *94*, 5258 – 5270; b) J. F. Hartwig, S. Richards, D. Baranãno, F. Paul, *J. Am. Chem. Soc.* **1996**, *118*, 3626 – 3633; c) J. F. Marcoux, S. Wagaw, S. L. Buchwald, *J. Org. Chem.* **1997**, *62*, 1568 – 1569.

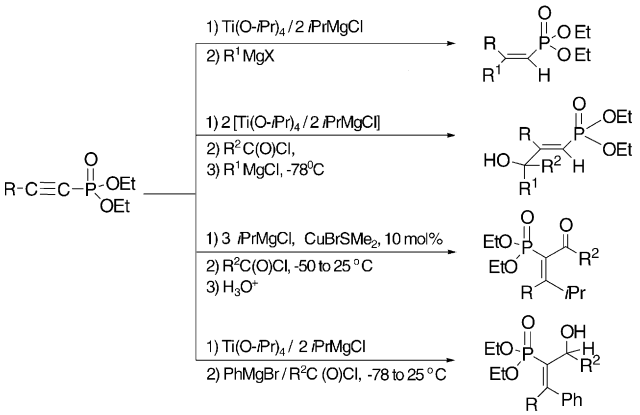
[15] DMF as ligand: a) J. M. Gioria, B. P. Susz, *Helv. Chim. Acta* **1971**, *54*, 2251 – 2256; b) C. Amatore, A. A. Bahsoun, A. Jutand, G. Meyer, A. N. Ntepe, L. Richard, *J. Am. Chem. Soc.* **2003**, *125*, 4212 – 4222.

[16] It is also possible that the formation of an Ar-Pd-Ar′ intermediate proceeded Ar–N bond formation, as proposed by one of the referees. We are further investigating this mechanistic issue.

[17] Intermolecular N-arylation followed by aryl–aryl bond formation leading to five-membered carbazoles was recently reported: R. B. Bedford, S. J. Cazin, *Chem. Commun.* **2002**, 2310 – 2311. Sequential intra- and intermolecular N-arylation leading to functionalized 1-aminoindoles: M. Watanabe, T. Yamamoto, M. Nishiyama, *Angew. Chem.* **2000**, *112*, 2620 – 2623; *Angew. Chem. Int. Ed.* **2000**, *39*, 2501 – 2504.

 © 2003 Wiley-VCH Verlag GmbH & Co. KGaA, Weinheim

mides and triethyl phosphite,[4] the Michaelis–Baker synthesis,[3,5] and catalytic cross-coupling of 1,4-diiodobutadiene with two equivalents of diethyl phosphite.[6] Recently, we began exploring the chemistry of titanacycle alkoxides.[7] These intermediates undergo a series of reactions with electrophiles that depends on the 1:2 stoichiometry of $Ti(OiPr)_4$ and *i*PrMgCl and of additives, such as $CuBrSMe_2$. A variety of di- and trisubstituted vinylphosphonates may be prepared in a regio- and stereoselective manner (Scheme 1).



Scheme 1. Synthesis of di- and trisubstituted vinylphosphonates.

Bisallylphosphonates

Substituted 1,4-Bisallylphosphonates: Preparation from 1-Alkynylphosphonates and $Ti(OiPr)_4$/2 *i*PrMgCl**

*Abed Al Aziz Quntar, Ofir Baum, Amal Shibli, Valery M. Dembitsky, and Morris Srebnik**

Bisphosphonates have wide range of applications,[1] Among the various types of bisphosphonates, the 1,4-bisphosphonates are potent inhibitors of yeast glyceraldehyde-3-phosphate dehydrogenase, and phosphoglycerate kinase,[2,3] which disturbs the production of ATP and causes cardiovascular respiratory disorders. Surprisingly, the methods of synthesis of 1,4-bisphosphonates are limited. Among these methods is the Michaelis–Arbuzov reaction of the appropriate alkylbro-

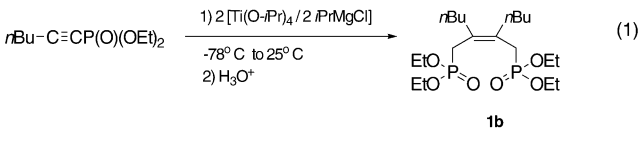
[*] Prof. Dr. M. Srebnik, A. A. A. Quntar, O. Baum, A. Shibli, Dr. V. M. Dembitsky
Department of Medicinal Chemistry and Natural Products
School of Pharmacy
Hebrew University
Jerusalem 91120 (Israel)
Fax: (+972) 2-675-8201
E-mail: msrebni@md.huji.ac.il

[**] This work was supported by the Israel Science Foundation and by the Kamea Fund (VMD)

Supporting information (NMR spectroscopic data and MS data for **1**, **2**, and **5**) for this article is available on the WWW under http://www.angewandte.org or from the author.

Indeed, these titanacycles display a much richer chemistry than the corresponding zirconacycles. Thus, whereas the titanacycles react with imines, the corresponding zirconacycles do not.[8] The reactions of the zirconacyclopropenes with the various nucleophiles took place at room temperature.[9] On the other hand, nucleophiles added to the titanacyclopropenes at low temperature (−30 °C to −50 °C). In addition, a longer time was required for the reactions of zirconacycles than for those with Ti^{II} complexes. Warming the reactions of 1-alkenylphosphonate zirconacycles to room temperature produced *cis*-vinylphosphonate after hydrolysis.[9d] In general, titanacyclopropenes generated from Grignard reagents are not stable at temperatures above −30 °C.[10] However, herein we offer evidence that under certain conditions Ti^{II} complexes generated from Grignard reagents are stable and report the synthesis of novel 1,4-bisphosphonates by a straightforward one-pot reaction.

When the diethyl 1-hexynylphosphonate was treated with two equivalents of the $Ti(OiPr)_4$/2 *i*PrMgCl reagent,[11] allowed to warm to 25° C, and hydrolyzed, an unexpected compound was formed. Dimerization had occurred which gave, not the expected 1,3-butadienylphosphonate but rather the 1,4-bisallylphosphonate **1b** which was isolated as the only product in about 75 % yield [Eq. (1)].

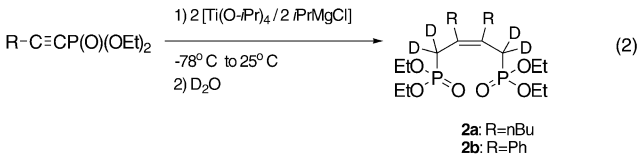


(1)

1b

 DOI: 10.1002/anie.200351974 © 2003 Wiley-VCH Verlag GmbH & Co. KGaA, Weinheim

To explore the formation of **1b**, the reaction mixture was quenched with D_2O. GC-MS analysis of the D_2O quenched product **2a** indicated that four atoms of deuterium had been incorporated [Eq. (2)]. The phenyl analogue **2a** also showed



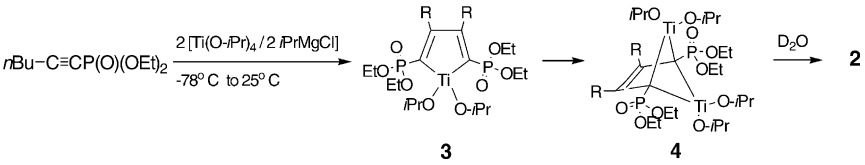
(2)

incorporation of four deuterium atoms (Table 1). The symmetry of deuterium incorporation is consistent with the ^{1}H NMR and ^{13}C NMR spectra.

Table 1: Yields and select ^{31}P NMR spectroscopic data for the deuterated compounds **2**.

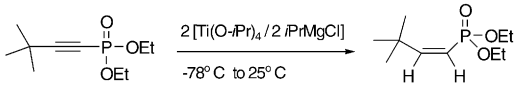
2	R	^{31}P NMR δ	$^2J_{PH}$	Yield % NMR (isolated)
a	Ph	27.49	–	80 (65)
b	*n*Bu	29.15	–	82 (68)

To explain the incorporation of four deuterium atoms, four C–Ti bonds are required. This situation requires that two Ti atoms are incorporated into the intermediate leading to **1** or **2**. A possible structure accounting for the deuterium incorporation would be the dinuclear complex **4** which could be generated from the initial cyclization product, **3**, by addition of another equivalent of the Ti(O*i*Pr)$_4$ (Scheme 2). The nature of dinuclear titanocene complexes depends on the stoichiometry and nature of the reaction conditions.[12] However, to our knowledge, dinuclear titanium alkoxide complexes have not been reported. Repeated attempts to isolate and characterize **4** have thus far been unsuccessful.



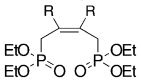
Scheme 2. proposed intermediate in the formation of **2**.

The formation of compounds **1** was investigated with several 1-alkynylphosphonates. The results are shown in Table 2. The reaction is very clean and yields are high. The only failure was when (3,3-dimethyl-but-1-ynyl)-phosphonic acid diethyl ester was used. Only the corresponding *cis*-vinylphosphonate was isolated [Eq. (3)].



(3)

Table 2: Yields and select ^{31}P NMR spectroscopic data of **1**.



1	R	^{31}P NMR δ	$^2J_{PH}$	Yield % NMR (isolated)
a	*n*Pentyl	29.06	19.2	95 (76)
b	*n*Bu	28.97	20.2	93 (75)
c	Ph	27.65	18.9	85 (71)
d	Cl-$CH_2CH_2CH_2$	28.39	19.2	85 (72)
e	*m*-F_3CPh	26.44	19.5	80 (63)

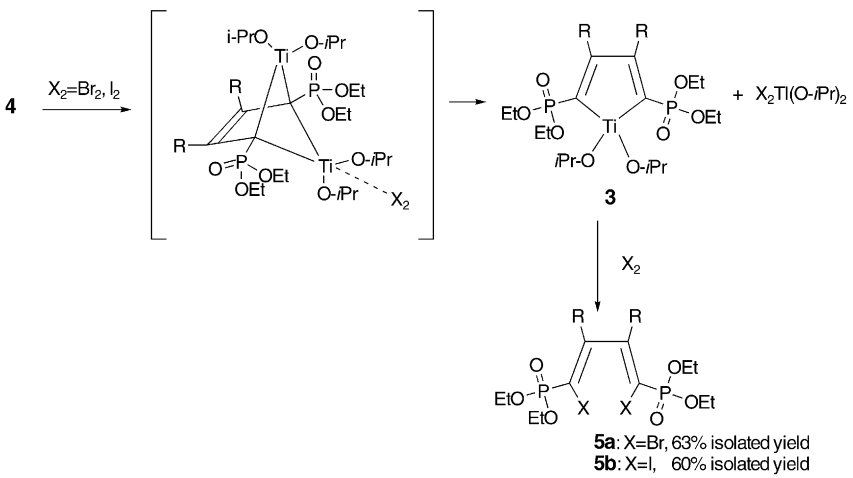
The structure of compounds **1** was determined by GC-MS, LC-MS, and NMR spectroscopic data (Table 2). The presence of only one phosphorus resonance signal in the ^{31}P NMR, and phosphorus couplings in the ^{1}H NMR and ^{13}C NMR spectra, all indicated that compounds **1** had a symmetrical structure in which homo coupling occurred on C2. The ^{31}P resonances for the different compounds **1** lie in the range $\delta = 26.4$–29.06 and are indicative that the phosphorus is coupled to an sp^3 carbon. Usually, when the phosphorus is coupled to an sp^2 carbon, it resonates in the range $\delta \approx 10$–20 ppm, and when coupled to an sp carbon, it resonates in the range -8 – 0 ppm. The doublets found in the range $\delta = 2.69$–3.37 ppm with $^2J_{PH}$ (18.9–20.2 Hz) in the ^{1}H NMR spectra are consistent with the presence of a methylene group adjacent to phosphorus. (The doublet is absent in compounds **2**, Table 2). This assignment is corroborated by the doublet in the ^{13}C NMR spectrum at $\delta \approx 29.5$ ppm, with $^1J_{PC}$ 133.3–140.3 Hz (see Supporting Information). Furthermore, the intensity of the signal at $\delta \approx 129$ ppm is consistent with the presence of two symmetrical vinylic carbon atoms.

Several other electrophiles were investigated. Bromine and iodine gave products **5**.[13] This reaction can be explained by initial complexation of the halogen with one of the titanium atoms of **4**, followed by oxidative elimination to **3** and $X_2Ti(OiPr)_2$ (Scheme 3).[14] The latter alkoxide then is halogenated in the usual manner.

In conclusion, the formation of **1** is very facile. Even with one equivalent of Ti(O*i*Pr)$_4$/2 *i*PrMgCl, only **1** and starting material were obtained at 25 °C. However, the reaction with one equivalent of Ti(O*i*Pr)$_4$/2 *i*PrMgCl and alkynylphosphonate at −30 °C resulted in the formation of *cis*-vinylphosphonates after workup at −30 °C. Thus, although zirconium and titanium belong to the same group differences in reactivity between Zr^{II} and Ti^{II} complexes were observed in the present reaction. The same reaction conditions using [$ZrCp_2Cl_2$]/2 *n*BuLi (Negishi's reagent; Cp = C_5H_5) resulted only in *cis*-vinylphosphonate formation, that is, no homo-coupling products were detected. This result is probably due to the larger steric requirements of the zirconocene complex.

Received: May 26, 2003
Revised: July 10, 2003 [Z51974]

 © 2003 Wiley-VCH Verlag GmbH & Co. KGaA, Weinheim



Scheme 3. Proposed mechanism for preparation of **5**.

Keywords: alkoxides · alkynes · C—C coupling · phosphonates · titanium

[1] The following reviews are representative: a) Treatment of osteoporosis H. J. Hauselmann, R. Rizzoli, *Osteoporosis Int.* **2003**, *14*, 2; b) treatment of prostate cancer G. M. Oades, J. Coxon, K. W. Colston, *Prostate Cancer Prostatic Dis.* **2002**, *5*, 264; c) treatment of multiple myeloma J. R. Berenson, B. E. Hillner, R. A. Kyle, K. Anderson, A. Lipton, G. C. Yee, J. S. Biermann, *J. Clin. Oncol.* **2002**, *20*, 3719; d) breast-cancer management L. M. Pickering, J. L. Mansi, *Curr. Med. Res. Opin.* **2002**, *18*, 284.

[2] Y. Li, L. Byers, *Biochim. Biophys. Acta* **1993**, *1164*, 17.

[3] D. Jakeman, A. Ivory, M. Williamson, G. Blackburn, *J. Med. Chem.* **1998**, *41*, 4439.

[4] T. Morita, Y. Okamoto, H. Sakurai, *Tetrahedron Lett.* **1978**, 2523.

[5] Y. Nagaoka, K. Tomioka, *Org. Lett.* **1999**, *1*, 1467.

[6] I. G. Trostyanskaya, D. Yu. Titskiy, E. A. Anufrieva, A. A. Borisenko, M. A. Kazankova, I. P. Beletskaya, *Izv. Ross. Akad. Nauk Ser. Khim.* **2001**, 2003.

[7] A. A. Quntar, M. Srebnik, *Chem. Commun.* **2003**, 58.

[8] A. A. Quntar, V. M. Dembitsky, M. Srebnik, *Org. Lett.* **2003**, *5*, 357.

[9] a) A. A. Quntar, A. Melman, M. Srebnik, *J. Org. Chem.* **2002**, *67*, 3769; b) A. A. Quntar, A. Melman, M. Srebnik, *Synlett* **2002**, 61; c) A. A. Quntar, M. Srebnik, *J. Org. Chem.* **2001**, *66*, 6650; d) A. A. Quntar, M. Srebnik, *Org. Lett.* **2001**, *3*, 1379.

[10] However, Ti^{II} complexes derived from *n*BuLi are stable at room temperature: J. J. Eisch, J. N. Gitua, P. O. Otieno, X. Shi, *J. Organomet. Chem.* **2001**, *624*, 229.

[11] a) O. G. Kulinkovitch, S. V. Sviridov, D. A. Vasilevski, *Synthesis* **1991**, 234; b) O. G. Kulinkovitch, A. de Meijere, *Chem. Rev.* **2000**, *100*, 2789; c) F. Sato, H. Urabe, S. Okamoto, *Synlett* **2000**, 753.

[12] a) U. Rosenthal, P.-M. Pellny, F. G. Kirchbauer, V. V. Burlakov, *Acc. Chem. Res.* **2000**, *33*, 119, and references therein; b) R. Choukroun, P. Cassoux, *Acc. Chem. Res.* **1999**, *32*, 494, and references therein; c) H. Lang, D. S. A. George, G. Rheilwald, *Coord. Chem. Rev.* **2000**, *206–207*, 102; d) U. Rosenthal, V. V. Burlakov in *Titanium and Zirconium in Organic Synthesis* (Ed.: I. Marek), Wiley-VCH, Weinheim, **2002**, p. 355.

[13] a) S. Yamaguchi, R.-Z. Jin, K. Tamao, F. Sato, *J. Org. Chem.* **1998**, *63*, 10060; b) E. Block, M. Birringer, C. He, *Angew. Chem.* **1999**, *111*, 1710; *Angew. Chem. Int. Ed.* **1999**, *38*, 1604.

[14] We thank one of the referees for helpful suggestions on the mechanism.

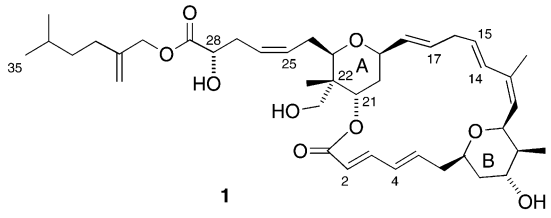
 © 2003 Wiley-VCH Verlag GmbH & Co. KGaA, Weinheim

Natural Product Synthesis

Total Synthesis of Natural (+)-Lasonolide A**

Sung Ho Kang, Suk Youn Kang, Chul Min Kim, Hyeong-wook Choi, Hyuk-Sang Jun, Byeong Moon Lee, Chul Min Park, and Joon Won Jeong*

The novel 20-membered macrolide lasonolide A (**1**) was isolated from the Caribbean marine sponge *Forcepia* sp.[1] Lasonolide A displayed antitumor activity by inhibiting the



1

in vitro proliferation of A-549 human lung carcinoma cells and interdicting cell adhesion in a cell assay for the detection of signal-transduction agents.[2] The relative stereochemistry of lasonolide A was originally proposed incorrectly based on extensive 2D NMR spectroscopic studies. Its structure was

[*] Prof. Dr. S. H. Kang, S. Y. Kang, C. M. Kim, H.-w. Choi, H.-S. Jun, B. M. Lee, C. M. Park, J. W. Jeong
Department of Chemistry
Center for Molecular Design and Synthesis
School of Molecular Science (BK 21)
Korea Advanced Institute of Science and Technology
Daejeon 305-701 (Korea)
Fax: (+82) 42-869-2810
E-mail: shkang@kaist.ac.kr

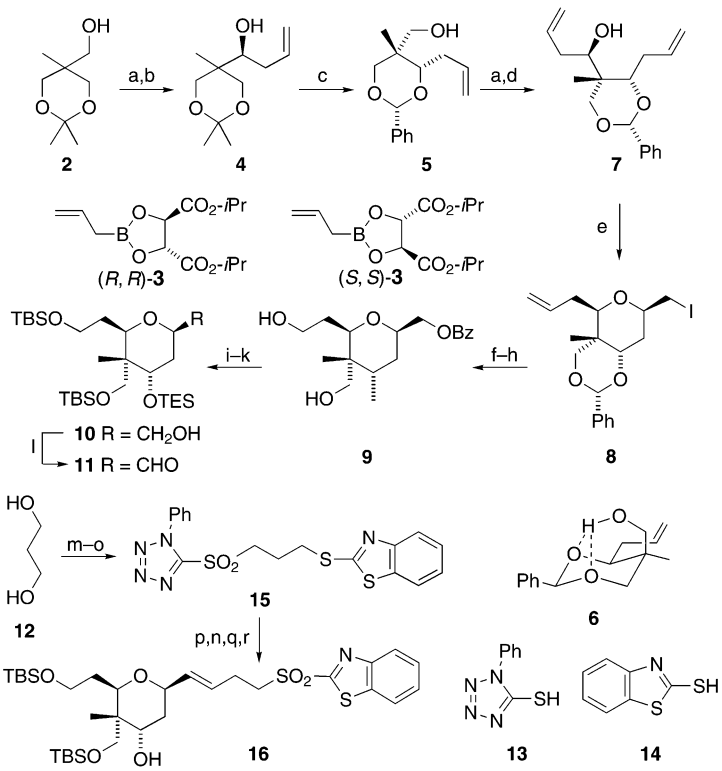
[**] This work was supported by a grant from the Korea Research Foundation (KRF-2002–070-C00058).

 DOI: 10.1002/anie.200352016 © 2003 Wiley-VCH Verlag GmbH & Co. KGaA, Weinheim

later revised as **1**, with the stereochemistry of the hydroxy-substituted epimerizable C28 center and the absolute configuration shown, based on synthetic studies.[3,4] The intriguing structural features and significant biological activity of this natural product led us to undertake its total synthesis. Herein, we describe a highly enantioselective total synthesis of the natural (+)-lasonolide A (**1**).

Retrosynthetically, we envisaged that double bonds could be introduced at C25 by a Wittig olefination of **27**, at C2 by an intramolecular Horner–Emmons reaction of the α,β-unsaturated aldehyde derived from **25**, and at C14 and C17 by the Julia–Kocieński sulfone-coupling protocol[5] (Scheme 3). Formation of the two *cis*-2,6-disubstituted tetrahydropyran rings by iodoetherification of **7** in the case of the A ring (Scheme 1) and by the intramolecular Michael addition of **19** in the case of the B ring (Scheme 2) was planned, and the choice of protecting groups turned out to be crucial for high stereoselectivity to be observed in these transformations. It was planned to install the C22 quaternary chiral center through the thermodynamic equilibration of **4**.

To secure subunit **16** with the tetrahydropyran ring A, the known alcohol **2**[6] was oxidized and then allylated with the allylboronate (*R*,*R*)-**3** of Roush et al.[7] to give the homoallylic alcohol **4** with 78% *ee* (Scheme 1). The next step was contrived to differentiate the two methylene groups of the 1,3-dioxane ring diastereoselectively and put in place the C22 quaternary stereogenic center. Based on the presumed increased thermodynamic stability caused by hydrogen bonding between the axial hydroxymethyl group and the two oxygen atoms of the acetal as suggested in **6**, the tandem conversion of **4** into the benzylidene **5** was explored extensively under a variety of acidic conditions. A remarkable result was observed when **4** was treated with benzaldehyde in the presence of trifluoroacetic acid (4 equiv). This reaction furnished a 5:1 separable mixture of the desired benzylidene **5** and the diastereomeric acetal with the hydroxymethyl group in an equatorial position, in 72% combined yield. Two other diastereomers in which the benzylidene acetal was formed with the two primary hydroxy groups were produced in 24% combined yield. After one recycling step with the undesired diastereomeric benzylidenes, compound **5** was produced in a total yield of 82%. Swern oxidation[8] of **5**, followed by a second asymmetric allylation, this time with (*S*,*S*)-**3**, gave the alcohol **7** with an enhanced *ee* value of 91%. It was found that the cyclic acetal protecting group was beneficial for the stereoselective formation of ring A. Compound **7** underwent cyclization in the presence of iodine to afford a 27:1 mixture of the *cis*-2,6-disubstituted tetrahydropyran **8** and the corresponding *trans* isomer. The iodide **8** was subjected to a reaction sequence involving substitution, ozonolysis, a reductive workup, and removal of the benzylidene group by hydrogenolysis. The primary and secondary hydroxy groups of the resulting triol **9** were differentially silylated with TBSCl and TESOTf, respectively, and the benzoate group was then hydrolyzed to provide the alcohol **10**.



Scheme 1. a) $(COCl)_2$, DMSO, CH_2Cl_2, −78 °C, then Et_3N, −78→0 °C; b) (*R*,*R*)-**3**, 4-Å MS, PhMe, −78 °C→RT; 2 N NaOH, 0 °C, 86% (for steps a and b); c) PhCHO (3 equiv), CF_3CO_2H (4 equiv), PhMe, −20→0 °C, 82% (after one recycling step); d) (*S*,*S*)-**3**, 4-Å MS, PhMe, −78 °C→RT; 2 N NaOH, 0 °C, 77% (for steps a and d); e) I_2, K_2CO_3, MeCN, −30→−20 °C, 95%; f) BzONa, NMP, 100 °C, 97%; g) O_3, $NaHCO_3$, MeOH, −78 °C; $NaBH_4$, 0 °C, 96%; h) H_2, 10% Pd/C, HOAc, MeOH, room temperature, 89%; i) TBSCl, imidazole, DMF, 0 °C, 95%; j) TESOTf, 2,6-lutidine, CH_2Cl_2, 0 °C, 98%; k) K_2CO_3, MeOH, room temperature, 91%; l) Dess–Martin periodinane, pyridine, CH_2Cl_2, room temperature; m) **13**, DEAD, Ph_3P, THF, 0 °C, 81%; n) $(NH_4)_6Mo_7O_{24}\cdot 4H_2O$, H_2O_2, phosphate buffer (pH 7.6), THF, EtOH, room temperature; o) **14**, DEAD, Ph_3P, THF, 0 °C, 75% (for steps n and o); p) KHMDS, DME, −70 °C→RT, 95% (for steps l and p); q) *p*-TsOH·H_2O, MeOH, room temperature; r) TBSCl, imidazole, DMF, room temperature, 88% (for steps n, q, and r). DMSO = dimethyl sulfoxide, MS = molecular sieves, Bz = benzoyl, NMP = 1-methyl-2-pyrrolidinone, TBS = *tert*-butyldimethylsilyl, DMF = *N*,*N*-dimethylformamide, TES = triethylsilyl, Tf = trifluoromethanesulfonyl, DEAD = diethyl azodicarboxylate, HMDS = bis(trimethylsilyl)amide, DME = 1,2-dimethoxyethane, Ts = toluenesulfonyl.

We chose the disulfone equivalent **15** as a suitably functionalized substrate for the introduction of the three carbon atoms required in the target fragment in addition to those present in the alcohol **10** and the later introduction of the *trans* double bonds at C14 and C17. The diol **12** was treated with the tetrazolethiol **13** under Mitsunobu conditions, and the product was oxidized to the corresponding sulfone and then converted into the sulfone–sulfide **15** through a second Mitsunobu reaction with the thiazolethiol **14**. The coupling of the aldehyde **11**, derived from **10**, with **15** was carried out in the presence of KHMDS to give the expected diastereomeric alkenes (*trans*/*cis* 31:1), which were

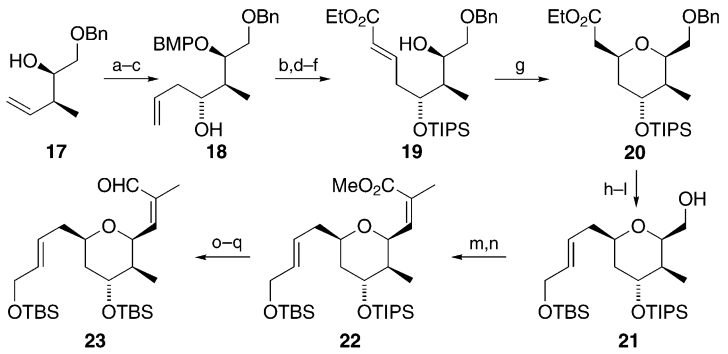
 © 2003 Wiley-VCH Verlag GmbH & Co. KGaA, Weinheim

separated by chromatography. The synthesis of the subunit **16** was completed by oxidation and protecting-group manipulation of the *trans* olefinic sulfide. Whereas the heptamolybdate oxidation of the sulfide to the sulfone under normal conditions[9] proceeded very slowly with partial desilylation, the reaction in the presence of a phosphate buffer was efficient and reached completion within a few hours.

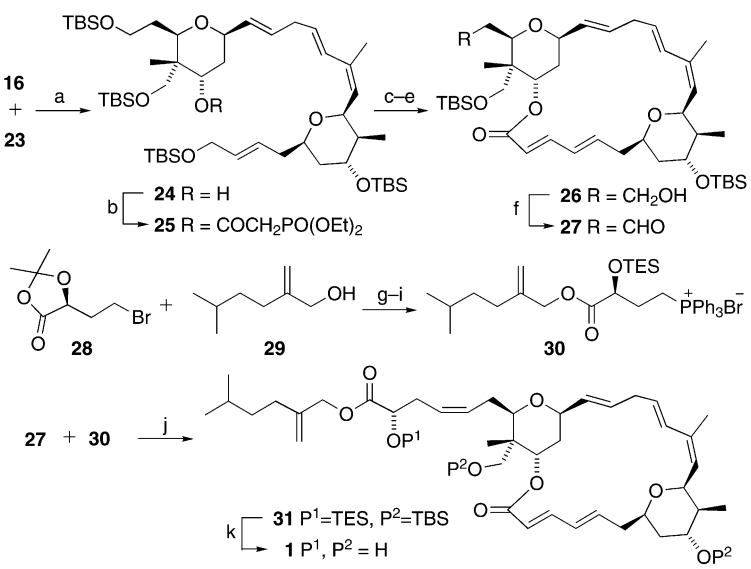
The synthesis of subunit **23**, which contains tetrahydropyran B, started with the *p*-methoxybenzylation of the known alcohol **17**,[10] followed by oxidative cleavage and asymmetric allylation according to the method of Brown et al.[11] to yield the homoallylic alcohol **18**, no diastereoisomers of which could be isolated in appreciable amounts (Scheme 2). After oxidative cleavage of the double bond and conversion of the resulting aldehyde into conjugated ethyl esters (*trans*/*cis* 24:1), the *trans* isomer was subjected to silylation of the alcohol functionality and oxidative removal of the PMB protecting group to furnish the hydroxyester **19**. The intramolecular Michael addition of **19** produced the *cis*-2,6-disubstituted tetrahydropyran **20** as a single stereoisomer. Compound **20** was reduced to the corresponding aldehyde and then treated under olefination conditions to give the expected conjugated esters (*trans*/*cis* 22:1). The *trans* isomer was then sequentially reduced, debenzylated, and monosilylated to afford the alcohol **21**. Swern oxidation of **21** followed by olefination with the trifluoroethyl phosphonate of Still and Gennari[12] provided the conjugated ester **22** (*cis*/*trans* 6.6:1). As all attempts at the desilylation of TIPS-protected lasonolide A proved abortive in the last stage of our synthesis, the TIPS group of the *cis* conjugated ester **22** was exchanged for a TBS group, and the resulting ester was reduced to the aldehyde to yield the tetrahydropyran subunit **23**.

A mixture of the C3–C14 and C15–C25 subunits **16** and **23** was treated with LiHMDS to give a mixture of the coupling product **24** and its *cis* isomer at the newly formed double bond in a $>20{:}1$ ratio (Scheme 3). As the *trans*,*trans*-2,4-dienyl carboxylic acid prepared from **24** and substituted with a hydroxy group at C21 was resistant to macrolactonization in our hands, compound **24** was converted into the phosphonoacetate **25** so that a Horner–Emmons olefination could be employed for the macrocyclization. After removal of the two sterically less hindered TBS groups of **25**, the resulting diol was subjected to allylic oxidation and cyclization mediated by K_2CO_3 in the presence of [18]crown-6[13] to furnish the macrolactone **26** smoothly. Compound **26** was then oxidized to the aldehyde **27**. The C26–C35 side chain required for the construction of the complete lasonolide A skeleton was obtained as the phosphonium salt **30** from the known acetonide **28**[14] and alcohol **29**[15] by acid-mediated esterification, followed by silylation and nucleophilic substitution with PPh_3. The Wittig olefination of **27** and **30** was most effective in the presence of KHMDS, and the protected lasonolide A **31** was desilylated uneventfully to produce the natural (+)-lasonolide A (**1**), all physical and spectroscopic data of which were identical to those reported in the literature.[1,3]

In summary, we have reported a highly enantioselective total synthesis of natural (+)-lasonolide A. The synthesis is characterized by a diastereoselective differentiation step to create the C22 quaternary asymmetric center, the development of the sulfone–sulfide **15** as a three-carbon fragment with two latent *trans* double bonds, cyclizations to form the two *cis*-2,6-disubstituted tetrahydropyrans, and an intramolecular Horner–Emmons reaction to effect macrocyclization.



Scheme 2. a) NaH, PMBCl, nBu$_4$NI, DMF, THF, room temperature, 97%; b) OsO_4, $NaIO_4$, H_2O, THF, room temperature; c) (−)-Ipc$_2$BCH$_2$CH=CH$_2$, Et_2O, −78 °C; 3 N NaOH, H_2O_2, room temperature, 74% (for steps b and c); d) Ph_3P=CHCOOEt, PhH, reflux, 87% (for steps b and d); e) TIPSOTf, 2,6-lutidine, CH_2Cl_2, 0 °C, 98%; f) DDQ, H_2O, CH_2Cl_2, room temperature, 87%; g) NaH, THF, −78→−20 °C, 81%; h) DIBAL, CH_2Cl_2, −78 °C; i) $EtO_2CCH_2PO(OEt)_2$, NaH, THF, −78 °C, 89% (for steps h and i); j) DIBAL, CH_2Cl_2, −78 °C, 91%; k) Li, NH_3 (*liq*), THF, −78 °C, 87%; l) NaH, TBSCl, THF, 0 °C, 94%; m) $(COCl)_2$, DMSO, CH_2Cl_2, −78 °C, then Et_3N, −78→0 °C; n) $MeO_2CCH(Me)PO(OCH_2CF_3)_2$, KHMDS, [18]crown-6, THF, −78 °C, 79% (for steps m and n); o) TBAF, THF, room temperature; p) TBSOTf, 2,6-lutidine, CH_2Cl_2, 0 °C; q) DIBAL, CH_2Cl_2, −78 °C, 88% (for steps o–q). PMB = *p*-methoxybenzyl, Ipc = isopinocamphenyl, TIPS = triisopropylsilyl, DDQ = 2,3-dichloro-5,6-dicyano-1,4-benzoquinone, DIBAL = diisobutylaluminum hydride, TBAF = tetrabutylammonium fluoride.



Scheme 3. a) LiHMDS, DME, −70 °C→RT, 82%; b) $HO_2CCH_2PO(OEt)_2$, DCC, DMAP, CH_2Cl_2, room temperature, 94%; c) PPTS, MeOH, room temperature, 91%; d) MnO_2, EtOAc, room temperature; e) K_2CO_3, [18]crown-6, PhMe, 70→80 °C, 71% (for steps d and e); f) Dess–Martin periodinane, pyridine, CH_2Cl_2, room temperature; g) *p*-TsOH·H_2O, PhMe, room temperature, 85%; h) TESOTf, 2,6-lutidine, CH_2Cl_2, 0 °C; i) Ph_3P, MeCN, reflux, 88% (for steps h and i); j) KHMDS, THF, −60 °C, 86% (for steps f and j); k) HF·py, pyridine, THF, room temperature, 87%. DCC = 1,3-dicyclohexylcarbodiimide, DMAP = 4-dimethylaminopyridine, PPTS = pyridinium *p*-toluenesulfonate, py = pyridine.

 © 2003 Wiley-VCH Verlag GmbH & Co. KGaA, Weinheim

The longest linear synthetic sequence exploited the ready availability of the alcohol **17** in 26 steps and 7.4% overall yield.

Received: May 30, 2003 [Z52016]

Keywords: allylation · macrolides · natural products · olefination · total synthesis

[1] P. A. Horton, F. E. Koehn, R. E. Longley, O. J. McConnell, *J. Am. Chem. Soc.* **1994**, *116*, 6015.
[2] R. E. Longley, D. Harmody, *J. Antibiot.* **1991**, *44*, 93.
[3] E. Lee, H. Y. Song, J. W. Kang, D.-S. Kim, C.-K. Jung, J. M. Joo, *J. Am. Chem. Soc.* **2002**, *124*, 384.
[4] For other synthetic approaches, see: a) H. Beck, H. M. R. Hoffmann, *Eur. J. Org. Chem.* **1999**, 2991; b) M. Nowakowski, H. M. R. Hoffmann, *Tetrahedron Lett.* **1997**, *38*, 1001; c) M. K. Gurjar, A. Chakrabarti, B. V. Rao, P. Kumar, *Tetrahedron Lett.* **1997**, *38*, 6885; d) M. K. Gurjar, P. Kumar, B. V. Rao, *Tetrahedron Lett.* **1996**, *37*, 8617.
[5] a) P. R. Blakemore, W. J. Cole, P. J. Kocieński, A. Morley, *Synlett* **1998**, 26; b) J. B. Baudin, G. Hareau, S. A. Julia, R. Lorne, O. Ruel, *Bull. Soc. Chim. Fr.* **1993**, *130*, 856.
[6] V. W. Gash, *J. Org. Chem.* **1972**, *37*, 2197.
[7] W. R. Roush, A. E. Walts, L. K. Hoong, *J. Am. Chem. Soc.* **1985**, *107*, 8186.
[8] a) T. T. Tidwell, *Org. React.* **1990**, *39*, 297; b) A. J. Mancuso, D. Swern, *Synthesis* **1981**, 165.
[9] D. R. Williams, D. A. Brooks, M. A. Berliner, *J. Am. Chem. Soc.* **1999**, *121*, 4924.
[10] K. C. Nicolaou, A. P. Patron, K. Ajito, P. K. Richter, H. Khatuya, P. Bertinato, R. A. Miller, M. J. Tomaszewski, *Chem. Eur. J.* **1996**, *2*, 847.
[11] a) H. C. Brown, P. K. Jadhav, K. S. Bhat, T. Perumal, *J. Org. Chem.* **1986**, *51*, 432; b) H. C. Brown, P. K. Jadhav, *J. Am. Chem. Soc.* **1983**, *105*, 2092.
[12] W. C. Still, C. Gennari, *Tetrahedron Lett.* **1983**, *24*, 4405.
[13] a) M. L. Morin-Fox, M. L. Lipton, *Tetrahedron Lett.* **1993**, *34*, 7899; b) K. C. Nicolaou, S. P. Seitz, M. R. Pavia, *J. Am. Chem. Soc.* **1982**, *104*, 2030.
[14] H.-O. Kim, C. Lum, M. S. Lee, *Tetrahedron Lett.* **1997**, *38*, 4935.
[15] I. Fleming, I. Paterson, A. Pearce, *J. Chem. Soc. Perkin Trans. 1* **1981**, 25.

 © 2003 Wiley-VCH Verlag GmbH & Co. KGaA, Weinheim

Organic Ferromagnetism

A Thiazyl-Based Organic Ferromagnet**

Antonio Alberola, Robert J. Less, Christopher M. Pask, Jeremy M. Rawson, Fernando Palacio, Patricia Oliete, Carley Paulsen, Akira Yamaguchi, Robert D. Farley, and D. M. Murphy*

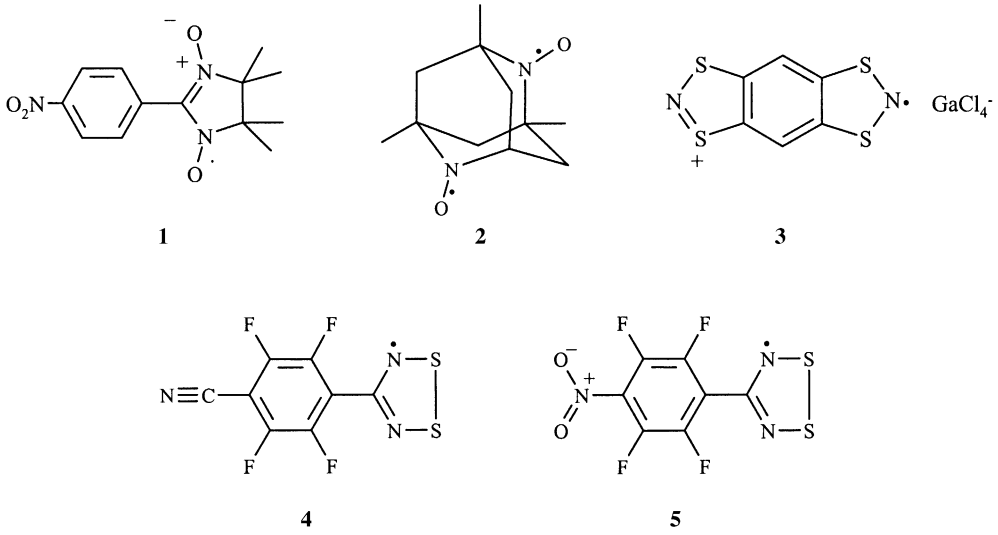
In 1928 Heisenberg proposed[1] that bulk ferromagnetic order would only ever be achieved in systems containing heavy atoms, that is, metals, their oxides, and related derivatives. Indeed it was not until 1991 that the first organic ferromagnet was reported; the β-polymorph of the *para*-nitrophenyl nitronyl nitroxide radical (*p*-NPNN, **1**; Scheme 1) was shown to order below 0.6 K.[2] Since then a number of other purely organic radicals have been found to undergo bulk ferromagnetic order, although the majority order below 1 K. Exceptions include the radical cation salts $[C_{60}][TDAE]$[3] (TDAE = tetrakis(dimethylamino)ethylene) and [BBDTA]-$GaCl_4$[4] (**3**; BBDTA = benzobis(1,3,2-dithiazolyl), which order as ferromagnets at 16 and 6.7 K, respectively. Of the neutral radicals, only the nitroxide-based diradical DOTMDAA (**2**; DOTMDAA = *N,N′*-dioxy-1,3,5,7-tetramethyl-2,6-diazaadamantane) orders ferromagnetically above 1 K (T_c = 1.48 K),[5] although the dithiadiazolyl radical *p*-$NCC_6F_4CNSSN^{\bullet}$ (**4**) orders as a weak ferromagnet at 36 K under ambient pressure,[6] the highest reported temperature for magnetic ordering in an organic radical. We have sought to prepare new dithiadiazolyl radicals, closely related to **4**, in which small structural changes may lead to new magnetically ordered systems. Here we report the structure and magnetic properties of **5**, which is only the second neutral organic radical to order as a ferromagnet above 1 K.

[*] Dr. J. M. Rawson, A. Alberola, Dr. R. J. Less, C. M. Pask
The Department of Chemistry, The University of Cambridge
Lensfield Road, Cambridge CB2 1EW (UK)
Fax: (+44) 1223-336-362
E-mail: jmr31@cus.cam.ac.uk
Prof. F. Palacio, Dr. P. Oliete
Instituto de Ciencia de Materials de Aragon
CSIC-Universidad de Zaragoza, 50009 Zaragoza (Spain)
Prof. Dr. C. Paulsen
CRTBT – CNRS
BP 166, 38042 Grenoble Cedex 9 (France)
Prof. Dr. A. Yamaguchi
7-3-1 Hongo, Bunkyo-ku, Tokyo 113-8654 (Japan)
Dr. R. D. Farley, Dr. D. M. Murphy
Department of Chemistry, The University of Cardiff
PO Box 912, Cardiff CF10 3TB (UK)

[**] We would like to thank the EPSRC (A.A., R.J.L., C.M.P., and R.D.F.), the CICYT (grant MAT2001-3507-C02-02), and the Gates Cambridge Trust (A.A.) for financial support, and the ESF program "Molecular Magnets" for partial support to the collaborative activities. We are grateful to Dr. N. Feeder for X-ray data collection and analysis and preparation of crystallographic data for deposit.

Supporting information for this article is available on the WWW under http://www.angewandte.org or from the author.

 © 2003 Wiley-VCH Verlag GmbH & Co. KGaA, Weinheim DOI: 10.1002/anie.200352194



Scheme 1. Organic molecular magnets **1**–**5**.

The radical, p-$O_2NC_6F_4CNSSN^{\bullet}$ (**5**), was synthesized from p-$O_2NC_6F_4CN$ utilizing standard synthetic procedures. X-ray diffraction studies revealed an asymmetric unit[7] comprising half a molecule of **5** located about a crystallographic twofold axis. The molecular dimensions are of unexceptional geometry[8] with a twist angle between the two ring planes of 58.1°. The packing of **5** (Figure 1) can be described in terms of

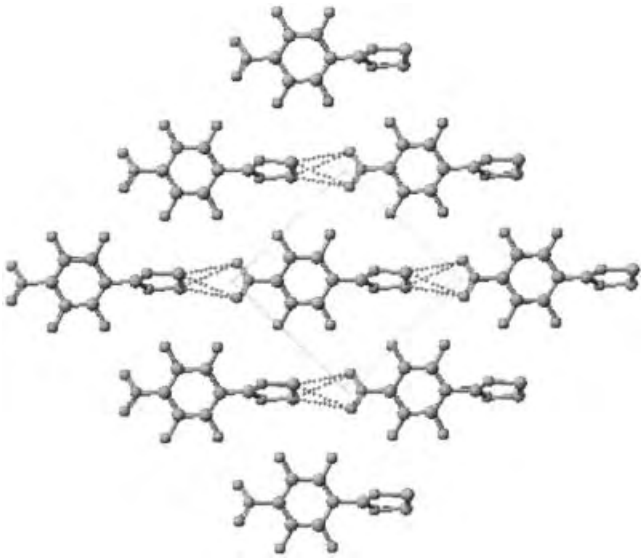


Figure 1. Crystal structure of the p-$O_2NC_6F_4CNSSN^{\bullet}$ radical in the *ab* plane.

chains of molecules linked through electrostatic $S^{\delta+}\cdots O^{\delta-}$ interactions in the [110] plane. These chains are reminiscent of the favorable $CN^{\delta-}\cdots S^{\delta+}$ contacts observed in **4**.[6] Whilst chains in **4** align co-parallel throughout the structure, polar sheets of **5** are related via a 4_1 screw axis down the crystallographic *c* axis, with each molecule forming four symmetry-equivalent S···N contacts of 3.681 Å to neighboring heterocycles, which are nearly orthogonal ($\theta = 97.3°$; Figure 2).

X- and Q-band EPR studies on **5** exhibit hyperfine coupling to the two heterocyclic N atoms and superhyperfine coupling to the two *ortho* F atoms of the phenyl substituent.

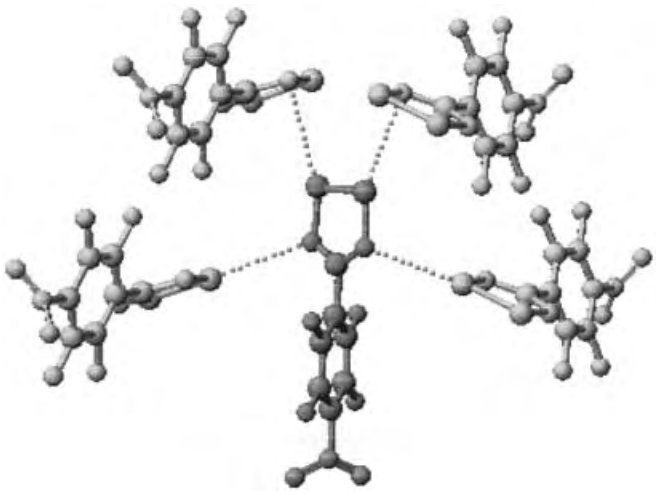


Figure 2. Crystal structure of the p-$O_2NC_6F_4CNSSN^{\bullet}$ radical illustrating close intermolecular S···N contacts between layers.

The coupling constants are similar to those reported for other perfluorophenyl dithiadiazolyl radicals[9,10] and are consistent with substantial localization of the spin density on the dithiadiazolyl ring. The spin-density distribution in **5** extracted from the anisotropic EPR spectra (≈24% on each dithiadiazolyl N atom and less than 0.1% on each of the *ortho* F atoms) is in good agreement with previous DFT calculations.[10]

The magnetic behavior of a polycrystalline sample of **5** (0.104 g) was measured between 1.8 and 300 K using a Quantum Design SQUID magnetometer in an applied field

 © 2003 Wiley-VCH Verlag GmbH & Co. KGaA, Weinheim

of 10 kOe. The sample was corrected for diamagnetism ($\chi_d = -114 \times 10^{-6}$ emu Oe^{-1} mol^{-1}) using Pascal's constants. The compound exhibits Curie–Weiss behavior down to approximately 10 K (Figure 3) with $\theta = +1.6(\pm 0.1)$ K and a Curie constant $C = 0.368$ emu K mol^{-1} Oe^{-1} (compared with 0.375

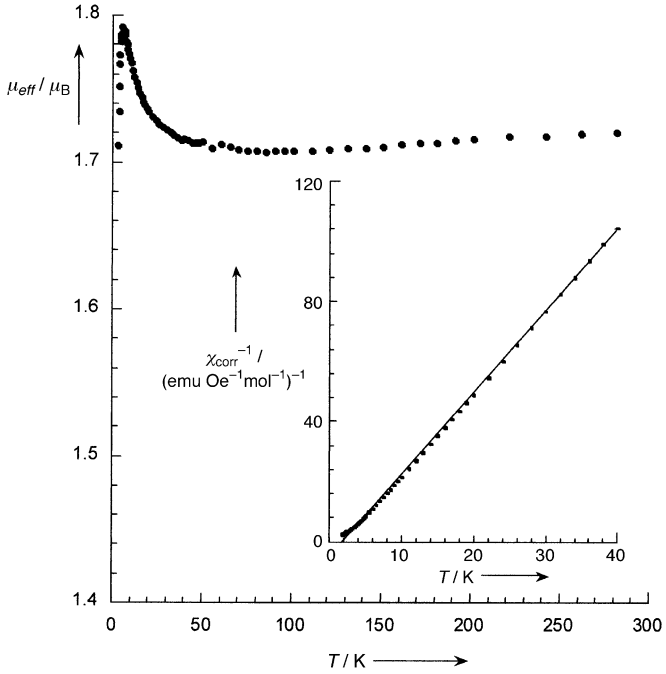


Figure 3. Temperature dependence (5–280 K) of the effective magnetic moment of the *p*-$O_2NC_6F_4CNSSN^{\bullet}$ radical measured in an applied field of 10 kOe. The appearance of the maximum is a consequence of the suppression of the ferromagnetic state by the applied field. Inset: A plot of $1/\chi$ versus *T*.

for an $S = 1/2$ paramagnet). The positive value of θ is consistent with ferromagnetic exchange interactions between $S = 1/2$ centers with an upper limit to the ferromagnetic ordering temperature of 1.6 K, based on mean field theory. Below 10 K the data begins to deviate from Curie–Weiss behavior, as expected in the region of T_c because of short-range interactions. The maximum observed in μ_{eff} is due to saturation effects of the applied field on a ferromagnet and cannot be compared with measurements made at very low field (see below).

Low-temperature ac susceptibility measurements on a single crystal of **5** were made between 0.6 and 2.5 K on a low-field SQUID magnetometer in a field of approximately 2 G. The crystal, when oriented both perpendicular and parallel to the [001] axis, showed an abrupt increase in the out-of-phase ac susceptibility below 1.4 K, reaching a maximum at 1.3 K, consistent with the onset of bulk ferromagnetic order with $T_c = 1.32 \pm 0.02$ K (Figure 4). Little anisotropy in *M* versus *H* or χ versus *T* data was observed. The difference in the data corresponding to the crystal orientations shown in Figure 4 is attributed to demagnetizing effects arising from the sample geometry.

Previous magnetic studies on thiazyl radicals[6,11–15] have shown that magnetic interactions propagate through inter-

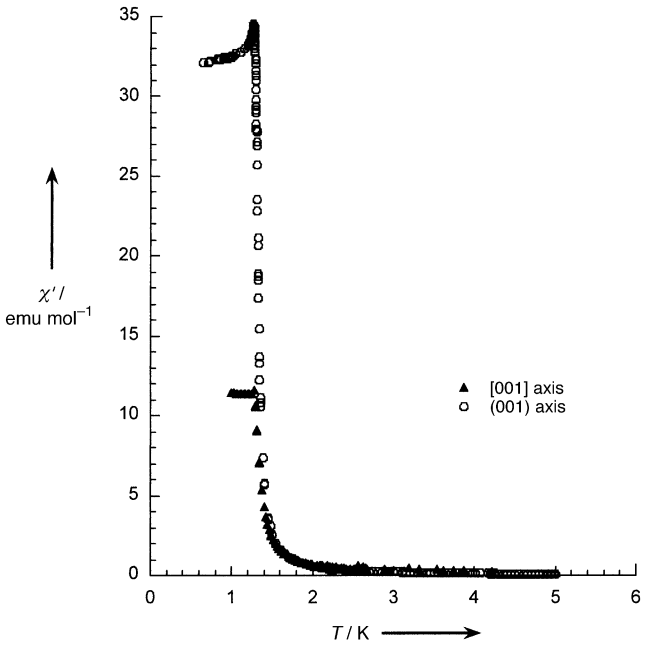


Figure 4. Single-crystal ac susceptibility of the *p*-$O_2NC_6F_4CNSSN^{\bullet}$ radical in an applied field of 2 G and at 1.11 Hz.

molecular S···N contacts. In the case of **5**, the near orthogonal nature of the singly occupied molecular orbitals on neighboring molecules would appear to lead to a ferromagnetic interaction.[16]

These studies provide clear evidence of ferromagnetic order in an organic radical above 1 K. Detailed analysis of the spin-density distribution by polarized neutron diffraction, EPR/ENDOR, and DFT studies, coupled with a determination of the magnetic structure through single-crystal neutron diffraction experiments, a theoretical analysis of the exchange pathway, and determination of the critical exponents of the magnetic behavior will be the subjects of future reports.

Experimental Section

5: *p*-$O_2NC_6F_4CN$ (500 mg, 2.27 mmol) was added to a solution of $Li[N(SiMe_3)_2]$ (380 mg, 2.27 mmol) in dry Et_2O (40 mL). The reaction mixture turned red and was stirred for 18 h at room temperature. SCl_2 (0.40 mL, 660 mg, 5.11 mmol) was then added to the solution at 0 °C. The solution was allowed to warm to room temperature and stirred for a further 5 h. The resultant yellow precipitate was filtered, washed (2×10 mL of dry Et_2O), and dried in vacuo. The yellow salt ([*p*-$O_2NC_6F_4CNSSN$]Cl) was stirred with Ag powder (245 mg, 2.27 mmol) in liquid SO_2 for 18 h, and the purple SO_2 extracts were sublimed (100 °C, 10^{-3} Torr) to yield lustrous black blocks (70 mg, 10%). Positive EI-MS: *m*/*z* 297.9 (M^+), 252.0 (M^+–SN). Elemental analysis (%) calcd: C 28.19, N 14.09; found: C 28.52, N 14.17. X-band EPR (THF, $T = 298$ K): $g = 2.011$, $a_N = 5.2$ G, $a_F = 1.3$ G.

Received: June 23, 2003 [Z52194]
Published Online: September 23, 2003

Keywords: ferromagnetism · magnetic properties · molecular magnetism · radical ions · radicals

 © 2003 Wiley-VCH Verlag GmbH & Co. KGaA, Weinheim

[1] W. Heisenberg, *Z. Phys.* **1928**, *49*, 619.
[2] M. Tamura, Y. Nakazawa, D. Shiomi, K. Nozawa, Y. Hosokoshi, M. Ishikawa, M. Takahashi, M. Kinoshita, *Chem. Phys. Lett.* **1991**, *186*, 401.
[3] M. P. Allemand, K. C. Khemani, A. Koch, F. Wudl, K. Holczer, S. Donovan, G. Grüner, J. D. Thompson, *Science* **1991**, *253*, 301.
[4] W. Fujita, K. Awaga, *Chem. Phys. Lett.* **2002**, *357*, 385.
[5] R. Chiarelli, M. A. Novak, A. Rassat, J. L. Tholance, *Nature* **1993**, *363*, 147.
[6] A. J. Banister, N. Bricklebank, I. Lavender, J. M. Rawson, C. I. Gregory, B. K. Tanner, W. Clegg, M. R. J. Elsegood, F. Palacio, *Angew. Chem.* **1996**, *108*, 2648; *Angew. Chem. Int. Ed. Engl.* **1996**, *35*, 2533.
[7] Crystal data for **4**. A crystal of **4** was studied on a Nonius Kappa 4 CCD diffractometer equipped with an Oxford Instruments Cryostream [$T = 220(2)$ K] using $Mo_{K\alpha}$ radiation ($\lambda = 0.71069$ Å). Crystal structure solution utilized SHELXTL software. All atoms were refined anisotropically. Chemical Formula: $C_7F_4N_3O_2S_2$, $M_r = 298.22$, tetragonal, space group $P4_12_12$, $a = 8.1380(4)$, $b = 8.1380(4)$, $c = 15.0490(12)$ Å, $Z = 4$, $\rho_{calcd} = 1.987\ g\,cm^{-3}$, $\mu = 0.592\ mm^{-1}$, $F(000) = 588$. All 1145 unique reflections of the 3046 reflections measured, were used in refinement yielding refinement indices wR_2 (all data) $= 0.080$ and R_1 [$I > 2\sigma(I)$] $= 0.035$. The Flack parameter of $-0.18(14)$ is indicative of the correct absolute structure determination. The largest residual electron density was within $\pm 0.3\ e\,Å^{-3}$. CCDC-210990 contains the supplementary crystallographic data for this paper. These data can be obtained free of charge via www.ccdc.cam.ac.uk/conts/retrieving.html (or from the Cambridge Crystallographic Data Centre, 12, Union Road, Cambridge CB21EZ, UK; fax: (+44) 1223-336-033; or deposit@ccdc.cam.ac.uk).
[8] J. M. Rawson, A. J. Banister, I. Lavender, *Adv. Heterocycl. Chem.* **1995**, *62*, 137.
[9] S. A. Fairhurst, L. H. Sutcliffe, K. F. Preston, A. J. Banister, A. S. Partington, J. M. Rawson, J. Passmore, M. J. Schriver, *Magn. Reson. Chem.* **1993**, *31*, 1027.
[10] P. J. Alonso, G. Antorrena, J. I. Martinez, J. J. Novoa, F. Palacio, J. M. Rawson, J. N. B. Smith, *Appl. Magn. Reson.* **2001**, *20*, 231.
[11] G. Antorrena, J. E. Davies, M. Hartley, F. Palacio, J. M. Rawson, J. N. B. Smith, A. Steiner, *Chem. Commun.* **1999**, 1393.
[12] P. J. Langley, J. M. Rawson, J. N. B. Smith, M. Schuler, R. Bachmann, A. Schweiger, F. Palacio, G. Antorrena, G. Gescheidt, A. Quintel, P. Rechsteiner, J. Hulliger, *J. Mater. Chem.* **1999**, *9*, 1431.
[13] G. D. McManus, J. M. Rawson, N. Feeder, F. Palacio, P. Oliete, *J. Mater. Chem.* **2000**, *10*, 2001.
[14] G. D. McManus, J. M. Rawson, N. Feeder, J. van Duijn, E. J. L. McInnes, J. J. Novoa, R. Burriel, F. Palacio, P. Oliete, *J. Mater. Chem.* **2001**, *11*, 1992.
[15] H. I. Süss, T. Wuest, A. Sieber, R. Althaus, F. Budde, H.-P. Luthi, G. D. McManus, J. M. Rawson, *CrystEngComm* **2002**, *4*, 2106.
[16] K. Awaga in *Magnetic Properties of Organic Materials* (Ed.: P. M. Lahti), Marcel Dekker, New York, **1999**, chap. 25.

 © 2003 Wiley-VCH Verlag GmbH & Co. KGaA, Weinheim

Nanoscale Polymer Brushes

Surface and Site-Specific Ring-Opening Metathesis Polymerization Initiated by Dip-Pen Nanolithography**

*Xiaogang Liu, Shouwu Guo, and Chad A. Mirkin**

Patterned polymeric structures have attracted significant interest for possible applications in the development of sensors, catalysis, and optical devices.[1,2] Thus far, several strategies, based upon photolithography, electron beam lithography, and microcontact printing have been developed for generating polymer arrays.[2] While useful for many applications, these methods do not allow one to control nanostructure composition in a site-specific manner and, therefore, do not allow one to fabricate complex multicomponent polymer arrays over the nano- to micrometer length scales. Having the capability to generate multicomponent arrays with nanoscopic features could afford one the opportunity to construct and study high-density combinatorial libraries of novel macromolecular systems.

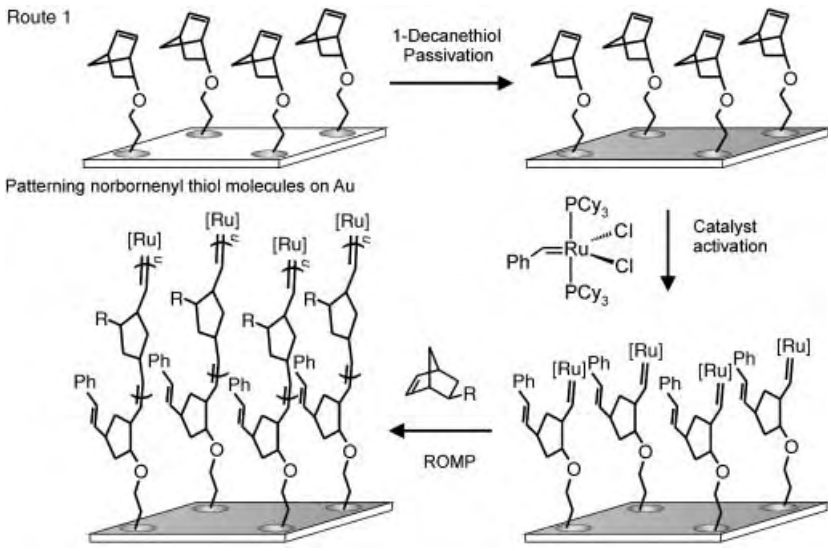
Herein, we report a novel approach, based upon dip-pen nanolithography (DPN)[3] and ring-opening metathesis polymerization (ROMP),[4–6] to the fabrication of polymer brush arrays on the nanometer length scale.[7] The combined approach utilizes the attributes of DPN and ROMP for synthesizing high-density polymer brush arrays with control over feature size (on the nanometer length scale), shape, and interfeature distance. Furthermore, the capability of directly delivering monomers through a standard AFM microcantilever will allow one to generate small, but diverse, libraries of nanoscale polymer brushes that comprise large numbers of structurally distinct compounds by assembling many possible combinations of small building monomers containing desired active functionalities.

To explore the potential of the combined approach and provide the basis for the studies leading to the design of combinatorial polymer libraries, two complementary routes have been developed for synthesizing arrays of the nanoscale polymer brushes based on DPN and ROMP. Route 1 is an approach based on growing polymers from a DPN-patterned template (Scheme 1). To test the viability of this route, 10-(*exo*-5-norbornen-2-oxy)decane-1-thiol molecules were patterned on a gold substrate by bringing a tip coated with norbornenylthiol in contact with the substrate. The *exo* isomer rather than the corresponding *endo* isomer was used to optimize ROMP reactivity.[8] Subsequently, the substrate

[*] Prof. C. A. Mirkin, X. Liu, Dr. S. Guo
Department of Chemistry and Institute for Nanotechnology
Northwestern University
2145 Sheridan Road, Evanston, IL 60208-3113 (USA)
Fax: (+1) 847-491-7713
E-mail: camirkin@chem.northwestern.edu

[**] We acknowledge the AFOSR, DARPA through ARO (no. DAAD19-03-1-0065), and NSF for support of this research. We thank P. A. Bertin and J. M. Gibbs for providing the norbornenyl monomers.

 DOI: 10.1002/anie.200352309 © 2003 Wiley-VCH Verlag GmbH & Co. KGaA, Weinheim



Scheme 1. Graphical representation of surface-initiated ROMP by DPN.

was dipped into a solution of 1-decanethiol (0.005 M) in acetonitrile for 1 min to form a passivating layer on the gold surface around the norbornenylthiol nanostructures. After the samples had been rinsed with acetonitrile and dried with compressed difluoroethane, they were further immersed in a solution of Grubbs' first generation catalyst ($[(PCy_3)_2Cl_2Ru{=}CHPh]$ (Cy = cyclohexyl), 0.1 M) in dichloromethane for 20 min. The surface was then rinsed with dry dichloromethane several times to remove excess catalyst. Finally, exposure of the catalyst-initiated wafers to a solution of norbornenyl-functionalized monomers (0.05 M) for a period of 10–240 min resulted in polymer brush arrays.

Line and dot arrays of the polymer brushes comprised of *exo*-5-norbornen-2-ol were constructed according to the method in Scheme 1. Topographic AFM images show the height of the polymer structures and provide insight into the uniformity of the polymer growth process (Figure 1 a–c). For example, the average diameter of each polymer brush dot is 78(± 4) nm and the average height is 5(± 1) nm (Figure 1 d).[9] It should be noted that polymer brush nanostructures with different feature sizes (many micrometer to sub-100 nm-length scale), shapes (dots, lines, and other types of geometries), and compositions could be routinely generated by controlling the feature size and shape of the norbornenylthiol template (by DPN), the polymerization reaction time (10–240 min), and the choice of the norbornenyl-functionalized monomers. In addition, the feature height of the polymer nanostructures can be controlled over the 1–10 nm range by adjusting the polymerization reaction time (Figure 2). However, under these conditions the polymer growth stopped after about 240 min, presumably because of deactivation of the immobilized catalyst.[2e] Arrays of nanoscale polymer brush patterns consisting of the electrochemically active monomers *exo*-5-norbornen-2-yl ferrocenecarboxylate (**1**) and *exo*-5-norbornen-2-ylferrocenyl acetate (**2**) were synthesized on gold electrodes by the above-mentioned procedure as a control experiment. Differential pulse voltammetry (DPV) measurements on the patterns that consist of the polymerized monomer **1** show an anodic peak at 185 mV versus the ferrocene/ferrocenium couple (FcH/FcH^+), which is consistent with the solution DPV measurements of the oxidation potential for the norbornenyl ferrocenyl derivative (E_{pa} =

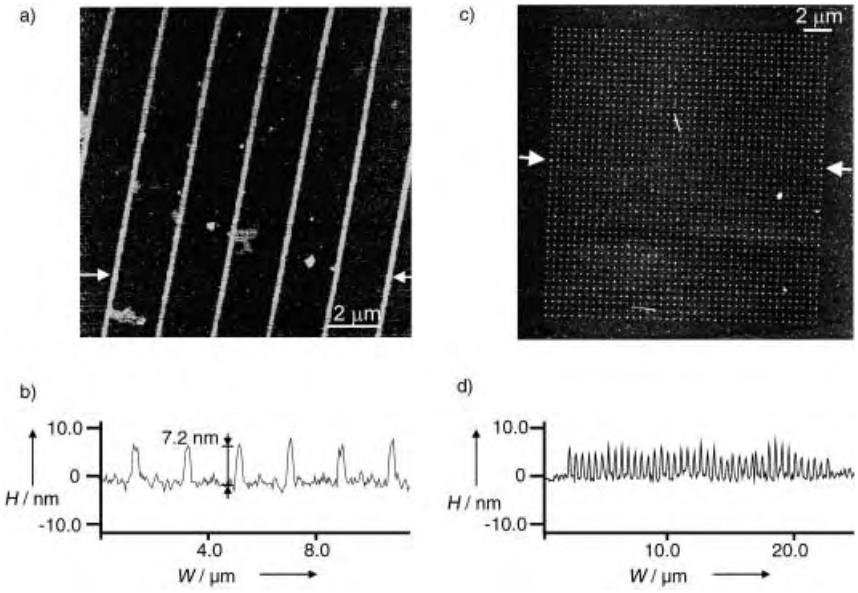


Figure 1. Polymer brush nanostructures prepared according to Scheme 1: a) Topographic AFM image of polymer brush lines. The speed of norbornenylthiol deposition, polymerization time, and measured average full-width at half-maximum (FWHM) values are 0.02 μm s^{-1}, 60 min, and 480 nm, respectively; b) cross-sectional topography trace for a selected line from Figure 1 a; c) topographic AFM image of a polymer brush dot array. The norbornenylthiol deposition and polymerization times are 1 s and 30 min, respectively; d) cross-sectional topography trace for a selected line from Figure 1 c.

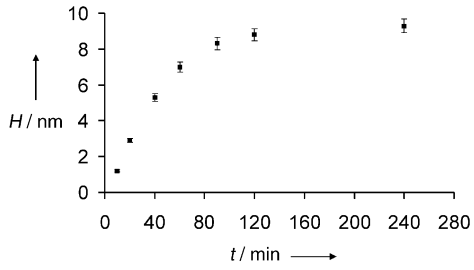


Figure 2. The height of poly-*exo*-5-norbornen-2-ol brush nanostructures plotted as a function of polymerization reaction time.

 © 2003 Wiley-VCH Verlag GmbH & Co. KGaA, Weinheim

180 mV versus FcH/FcH^+, Figure 3a). In contrast, DPV measurements on the diblock copolymer patterns consisting of two blocks of electrochemically distinct ferrocenyl monomers **1** and **2** exhibit two anodic peaks at −50 mV and 190 mV, which correspond to the sequential oxidations of the two different types of ferrocenyl moieties (Figure 3b). Taken together, the data presented here unambiguously confirm that the polymers indeed grow from the catalyst-initiated patterns generated by DPN.

An alternative procedure (Route 2) that involves transporting the norbornenyl monomers to catalyst-activated substrates with an AFM microcantilever was developed (Scheme 2) in an effort to evaluate the potential of generating a polymer brush array where each dot is a different polymer with a different degree of polymerization. These types of arrays could be useful in the generation of combinatorial libraries of nanoscale polymer features. To generate a substrate suitable for catalyst activation, a silicon oxide substrate was modified with 5-(bicycloheptenyl)trichlorosilane and immersed in a solution of Grubbs' first-generation catalyst in dichloromethane for 20 min. After being washed several times with dichloromethane to remove excess catalyst, the catalyst-tethered substrate was immediately used for generating polymer brushes with a monomer-coated AFM tip. Thus, in principle, a wide range of polymers with various numbers of repeating monomer units can be easily

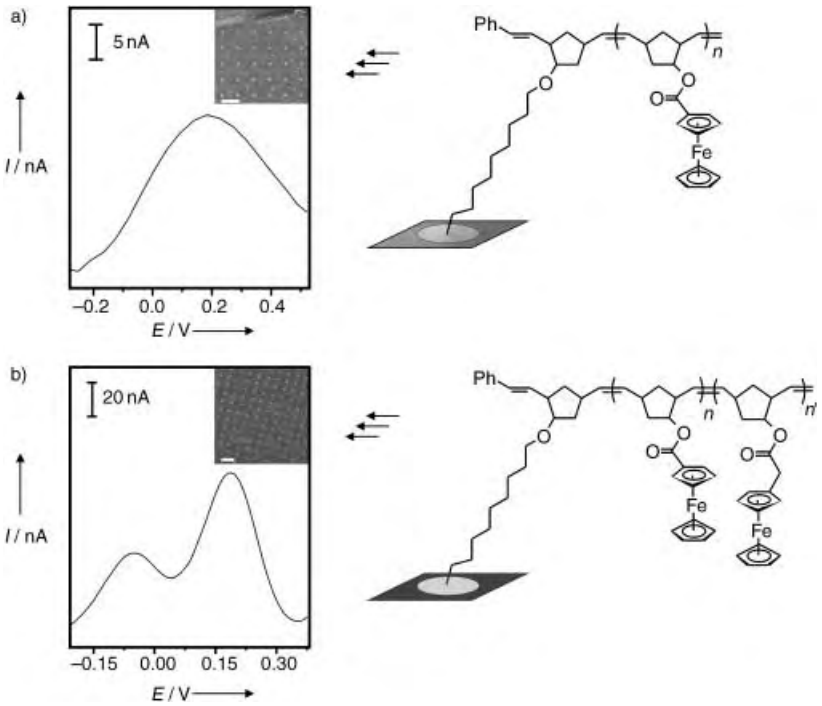
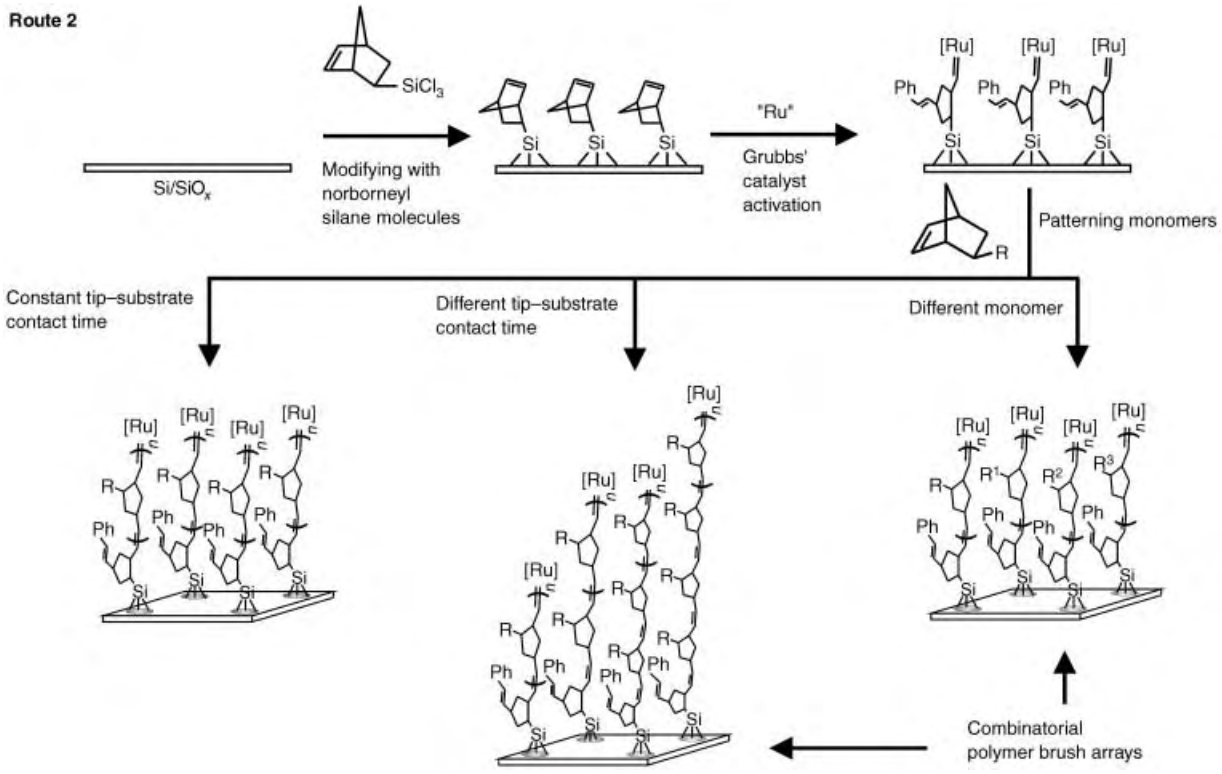


Figure 3. a) DPV of an electrode (0.28 mm^2) patterned with poly-**1** by DPN and ROMP (inset: AFM topography image of the poly-**1** pattern. The scale bar is 2 μm); b) DPV of an electrode patterned with diblock copolymers consisting of monomer **1** and **2** by DPN and ROMP (inset: AFM topography image of the diblock copolymer brush pattern. The scale bar is 2 μm). For DPV experiments: scan rate = 50 $mV s^{-1}$; pulse period = 200 ms; pulse amplitude = 50 $mV s^{-1}$; and pulse width = 50 ms.



Scheme 2. Graphical representation of ROMP initiated by DPN and a monomer-coated tip.

 © 2003 Wiley-VCH Verlag GmbH & Co. KGaA, Weinheim

generated by deliberately controlling the tip–substrate contact time. Significantly, a high-density two-dimensional array of polymer brushes that consists of different norbornenyl monomer entities in different spatially defined regions can be generated by this approach (Scheme 2).

As proof-of-concept, the monomer, *exo*-5-norbornen-2-ol, was delivered to a catalyst-activated silicon oxide substrate by an AFM tip and polymerized in situ. In a typical patterning experiment, a conventional silicon nitride AFM microcantilever coated with a solution of the monomer in dichloromethane was brought into contact with the substrate to generate an array of polymers in a glove box (N_2 atmosphere). An AFM topographic image of such an array comprising *exo*-5-norbornen-2-ol as the chain-propagating monomer shows that features of controlled height (22 ± 1 nm) can be reproducibly generated (Figure 4a). An important feature of this

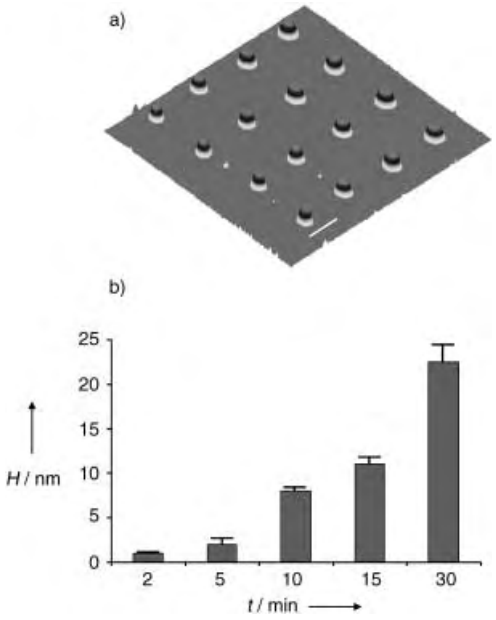


Figure 4. a) Three-dimensional topographic AFM image of an array of polymer brush dots generated according to the method in Scheme 2 (the scale bar is 2 μm); b) a plot of nanostructure height (poly-*exo*-5-norbornen-2-ol) as a function of tip-induced polymerization reaction time (as measured by tip–substrate contact time). The data points are the averaged measurements, and the vertical bars correspond to the standard deviation.

monomer–DPN approach is the ability to monitor and control the living polymerization process on the catalyst-tethered surface with the monomer-coated microcantilever.[10] As anticipated, the height of the polymer brush nanostructures increases with tip–substrate contact time (Figure 4b). It is noted that the polymer growth rate in the monomer–DPN approach (Scheme 2) is much faster than that under comparable bulk conditions (Scheme 1). This can be attributed, in part, to the higher local concentration of the monomer accessible to the catalyst-activated sites on the patterned substrate. Indeed, the polymerizable ink is confined to the region near the tip and point of contact with the catalyst.

In conclusion, a novel approach for synthesizing arrays of nanoscale polymer brushes, based upon a combination of DPN and a surface-initiated ROMP method, has been demonstrated on metallic and insulating substrates. These approaches are important because they point towards a route to combinatorial libraries of functional polymer nanostructures of almost limitless chemical complexity, which can be constructed in situ. The capabilities demonstrated by these single-pen experiments will be dramatically facilitated through the use of multipen arrays that do not require the step-by-step changing of inks and pens during a conventional DPN experiment.[3e,n]

Experimental Section

Exo-5-norbornen-2-ol, 10-(*exo*-5-norbornen-2-oxy)decane-1-thiol, *exo*-5-norbornen-2-yl ferrocenecarboxylate, and *exo*-5-norbornen-2-ylferrocenyl acetate were synthesized according to literature procedures.[5b,11] All other reagents were purchased from the Aldrich Chemical Company and used without further purification. All solvents were distilled under nitrogen and saturated with nitrogen prior to use. All reactions were performed in a dry nitrogen atmosphere or in a glove box unless otherwise noted. Silicon oxide wafers were cut into 0.5×0.5 cm^2 slides and sonicated sequentially in dichloromethane, methanol, and nanopure water for 10 min. The wafers were then immersed in freshly mixed ammonia peroxide solution ($NH_3 \cdot H_2O$:H_2O_2:H_2O (v:v:v) = 1:1:5) for 1 h at about 100 °C, after which time they were rinsed with nanopure water followed by ethanol. The gold substrates were prepared by coating a Si wafer coated with silicon oxide with a Ti adhesion layer (5 nm) followed by 50 nm of gold using an Edwards Auto 306 evaporator. DPN experiments were carried out in a glove box (23 °C, N_2 atmosphere) with a Thermomicroscopes CP AFM driven by customer lithography software (NanoInk, Inc., Chicago, IL) and commercial Si_3N_4 cantilevers (Thermomicroscopes Sharpened Microcantilever A, force constant: 0.05 N m^{-1}). To minimize piezo tube drift problems, a 90-μm scanner with closed loop scan control was used for all DPN experiments. AFM topography images were acquired using a Digital Instruments Multimode Nanoscope IIIa with an extender electronics module in tapping mode. Electrochemical experiments were performed with a Bioanalytical Systems (BAS) Model 100B using Au disk electrodes with a Pt wire counter electrode and a silver wire reference electrode.

Received: July 4, 2003 [Z52309]

Keywords: lithography · nanostructures · polymers · ring-opening polymerization · scanning probe microscopy

[1] a) J. M. J. Fréchet, E. Eichler, H. Ito, C. G. Willson, *Polymer* **1983**, *24*, 995; b) O. Prucker, J. Rühe, *Macromolecules* **1998**, *31*, 592; c) S. L. Clark, P. T. Hammond, *Adv. Mater.* **1998**, *10*, 1515; d) Y. Xu, J. T. Watson, M. L. Bruening, *Anal. Chem.* **2003**, *75*, 185; e) A. Pogantsch, G. Trattnig, G. Langer, W. Kern, U. Scherf, H. Tillmann, H.-H. Hörhold, E. Zojer, *Adv. Mater.* **2002**, *14*, 1722; f) C.-H. Jang, B. D. Stevens, P. R. Carlier, M. A. Calter, W. A. Ducker, *J. Am. Chem. Soc.* **2002**, *124*, 12114.

[2] a) W. M. Lackowski, P. Ghosh, R. M. Crooks, *J. Am. Chem. Soc.* **1999**, *121*, 1419; b) T. A. von Werne, D. S. Germack, E. C. Hagberg, V. V. Sheares, C. J. Hawker, K. R. Carter, *J. Am. Chem. Soc.* **2003**, *125*, 3831; c) B. Rowan, M. A. Wheeler, R. M. Crooks, *Langmuir* **2002**, *18*, 9914; d) B. Domercq, R. D. Hreha, Y.-D. Zhang, N. Larribeau, J. N. Haddock, C. Schultz, S. R. Marder, B. Kippelen, *Chem. Mater.* **2003**, *15*, 1491; e) N. Y. Kim, N. L. Jeon, I. S. Choi, S. Takami, Y. Harada, K. R. Finnie, G. S. Girolami, R. G. Nuzzo, G. M. Whitesides, P. E. Laibinis, *Macromolecules* **2000**, *33*, 2793; f) M. Husemann, D. Mecerreyes, C. J.

 © 2003 Wiley-VCH Verlag GmbH & Co. KGaA, Weinheim

Hawker, J. L. Hedrick, R. Shah, N. L. Abbott, *Angew. Chem.* **1999**, *111*, 685; *Angew. Chem. Int. Ed.* **1999**, *38*, 647; g) M. Weck, J. J. Jackiw, R. R. Ross, P. S. Weiss, R. H. Grubbs, *J. Am. Chem. Soc.* **1999**, *121*, 4088; h) U. Schmelmer, R. Jordan, W. Geyer, W. Eck, A. Gölzhäuser, M. Grunze, A. Ulman, *Angew. Chem.* **2003**, *115*, 577; *Angew. Chem. Int. Ed.* **2003**, *42*, 559; i) D. M. Jones, W. T. S. Huck, *Adv. Mater.* **2001**, *13*, 1256.

[3] For selected examples, see a) R. D. Pine, J. Zhu, F. Xu, S. Hong, C. A. Mirkin, *Science* **1999**, *283*, 661; b) S. Hong, J. Zhu, C. A. Mirkin, *Science* **1999**, *286*, 523; c) H. Zhang, S.-w. Chung, C. A. Mirkin, *Nano Lett.* **2003**, *3*, 43; d) L. M. Demers, D. S. Ginger, S.-J. Park, Z. Li, S.-W. Chung, C. A. Mirkin, *Science* **2002**, *296*, 5574; e) M. Zhang, D. Bullen, S.-W. Chung, S. Hong, K. S. Ryu, Z. Fan, C. A. Mirkin, C. Liu, *Nanotechnology* **2002**, *13*, 212; f) Y. Li, B. W. Maynor, J. Liu, *J. Am. Chem. Soc.* **2001**, *123*, 2105; g) B. W. Maynor, Y. Li, J. Liu, *Langmuir* **2001**, *17*, 2575; h) A. Noy, A. E. Miller, J. E. Klare, B. L. Weeks, B. W. Woods, J. J. DeYoreo, *Nano Lett.* **2002**, *2*, 109; i) R. McKendry, W. T. S. Huck, B. Weeks, M. Fiorini, C. Abell, T. Rayment, *Nano Lett.* **2002**, *2*, 713; j) L. A. Porter, Jr., H. C. Choi, J. M. Schmeltzer, A. E. Ribbe, L. C. C. Elliott, J. M. Buriak, *Nano Lett.* **2002**, *2*, 1369; k) P. E. Sheehan, L. J. Whitman, *Phys. Rev. Lett.* **2002**, *88*, 156104; l) G. Agarwal, R. R. Naik, M. O. Stone, *J. Am. Chem. Soc.* **2003**, *125*, 7408; m) P. Manandhar, J. Jang, G. C. Schatz, M. A. Ratner, S. Hong, *Phys. Rev. Lett.* **2003**, *90*, 115505; n) P. Belaubre, M. Guirardel, G. Garcia, J. B. Pourciel, V. Leberre, A. Dagkessamanskaia, E. Trévisiol, J. M. Francois, *Appl. Phys. Lett.* **2003**, *82*, 3122; o) C. L. Cheung, J. A. Camarero, B. W. Woods, T. Lin, J. E. Johnson, J. J. De Yoreo, *J. Am. Chem. Soc.* **2003**, *125*, 6848.

[4] "Ring Opening Metathesis Polymerisation and Related Chemistry:" , *NATO Sci. Ser. II* **2002**, *56*.

[5] a) A. G. M. Barrett, B. T. Hopkins, J. Köbberling, *Chem. Rev.* **2002**, *102*, 3301; b) K. J. Watson, J. Zhu, S. T. Nguyen, C. A. Mirkin, *J. Am. Chem. Soc.* **1999**, *121*, 462; c) M. R. Buchmeiser, G. Seeber, M. Mupa, G. K. Bonn, *Chem. Mater.* **1999**, *11*, 1533.

[6] T. M. Trnka, R. H. Grubbs, *Acc. Chem. Res.* **2001**, *34*, 18.

[7] For other examples of SPM-based lithography, see a) I. W. Lyo, P. Avouris, *Science* **1991**, *253*, 173; b) W. T. Muller, D. L. Klein, T. Lee, J. Clarke, P. L. Mceuen, P. G. Schultz, *Science* **1995**, *268*, 1995; c) S. L. Brandow, W. J. Dressick, C. S. Dulcey, T. S. Koloski, L. M. Shirey, J. Schmidt, J. M. Calvert, *J. Vac. Sci. Technol. B* **1997**, *15*, 1818; d) S. S. Wong, E. Joselevich, A. T. Woolley, C. L. Cheung, C. M. Lieber, *Nature* **1998**, *394*, 52; e) R. Maoz, E. Frydman, S. R. Cohen, J. Sagiv, *Adv. Mater.* **2000**, *12*, 424; f) H, Sugimura, N. Nakagiri, *J. Vac. Sci. Technol. B* **1996**, *14*, 1223; g) G.-Y. Liu, S. Xu, Y. L. Qian, *Acc. Chem. Res.* **2000**, *33*, 457; h) C.-H. Jang, B. D. Stevens, P. R. Carlier, M. A. Calter, W. A. Ducker, *J. Am. Chem. Soc.* **2002**, *124*, 12114; i) A. Bruckbauer, L. Ying, A. M. Rothery, D. Zhou, A. I. Shevchuk, C. Abell, Y. E. Korchev, D. Klenerman, *J. Am. Chem. Soc.* **2002**, *124*, 8810.

[8] J. D. Rule, J. S. Moore, *Macromolecules* **2002**, *35*, 7878.

[9] Note that the error was determined by analyzing the highest point of each dot in a 20×20 array and not from the height profile in Figure 1 d.

[10] Note that in a typical DPN experiment a molecule-coated AFM cantilever can be used not only for transporting molecules onto a substrate, but also for imaging the nanostructures in contact mode to determine whether or not the molecules have been deposited. High scan rates (> 6 Hz) do not lead to appreciable ink deposition. All nanostructures were subsequently imaged separately with a Digital Instruments Multimode Nanoscope in the tapping mode.

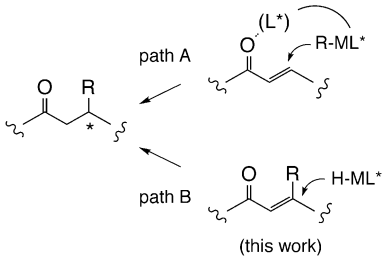
[11] G. H. Posner, J. S. Ting, C. M. Lentz, *Tetrahedron* **1976**, *32*, 2281.

 © 2003 Wiley-VCH Verlag GmbH & Co. KGaA, Weinheim

CuH-Catalyzed Asymmetric Conjugate Reductions of Acyclic Enones**

Bruce H. Lipshutz and Jeff M. Servesko*

Strategies for controlling absolute stereochemistry at a site β to an electrophilic center, in particular a ketone, usually rely on organometallic-based Michael additions (Scheme 1, path A).[1] Processes that are catalytic in both the transition metal (M) and the associated nonracemic ligand (L*) are



Scheme 1. Control of stereochemistry β to a ketone.

most desirable, and outstanding progress continues to be made with several different Michael donors[1,2] and acceptors.[1,3] Acyclic enones have proven to be particularly challenging substrates in this regard, although breakthrough methodologies based on copper-catalyzed additions of organozinc reagents have recently been disclosed.[4] Far greater success, on the other hand, has been realized with unsaturated esters.[5] The alternative approach, wherein a nonracemic source of hydride is delivered to a preformed, unsymmetrical β,β-disubstituted enone (path B) would offer an attractive means of accomplishing the same net transformation, thereby doubling the number of potential routes to a selected target. To the best of our knowledge, there is no general procedure for effecting this type of reduction on acyclic unsaturated enones in both high yields and enantioselectivities.[6] In this report we disclose results from our preliminary studies which

[*] Prof. B. H. Lipshutz, J. M. Servesko
Department of Chemistry
University of California
Santa Barbara, CA 93106 (USA)
Fax: (+1) 805-893-8265
E-mail: lipshutz@chem.ucsb.edu

[**] We thank the NSF for financial support (CHE 0213522), and in particular Jeff Zira (UCSB) for outstanding technical assistance. We are indebted to many colleagues who generously supplied us with the ligands used in this study (Solvias "kit": Drs. H.-U. Blaser and M. Thommen, Solvias; BIPHEP: Drs. R. Schmid and M. Scalone, Roche; SEGPHOS: Dr. T. Saito and H. Shimizu, Takasago; BoPhoz: Dr. N. Boaz, Eastman; Phanephos: Dr. P. J. Pye, Merck; BITIANP: Prof. F. Sannicolo, University of Milan; TaniaPhos: Prof. P. Knochel, Ludwig-Maximilian University, Munich).

Supporting information for this article is available on the WWW under http://www.angewandte.org or from the author.

 DOI: 10.1002/anie.200352313 © 2003 Wiley-VCH Verlag GmbH & Co. KGaA, Weinheim

suggest that a solution to this long-standing problem may be in hand. We considered nonracemic biaryl ligands such as Roche's BIPHEP[7] and Takasago's SEGPHOS[8] (see Figure 1) for screening in the presence of CuH[9a,b] generated

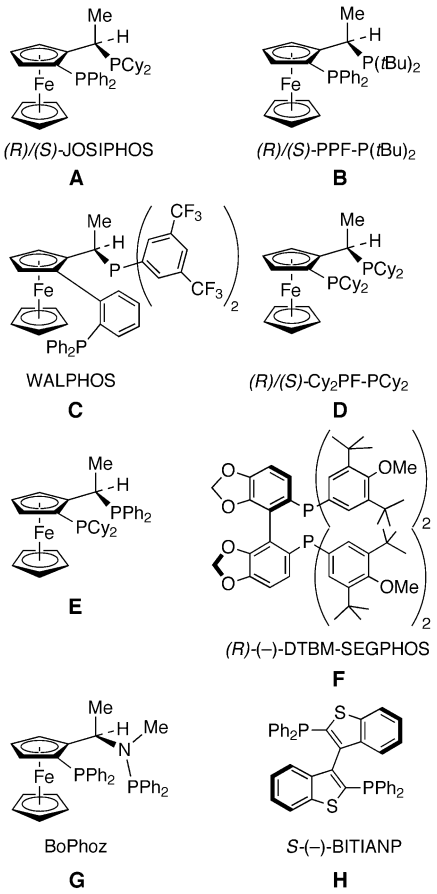
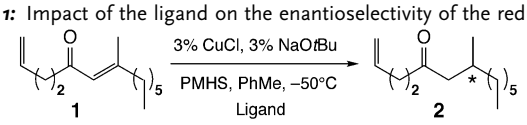


Figure 1. Ligands screened with cat. CuH/PMHS.

in situ,[9c] along with stoichiometric polymethylhydrosiloxane (PMHS)[10] based on their exceptional influence on aryl ketones undergoing asymmetric hydrosilylation.[11] Also taken into account were the significant improvements in asymmetric 1,4-reductions of hindered β,β-disubstituted cyclic enones found when the latter reagent combination (i.e., cat. CuH·DTBM-SEGPHOS/PMHS) was used.[9c,12] As indicated in Table 1, however, neither the SEGPHOS-based system (ligand **F** in Figure 1, entry 1 in Table 1) nor any of several other ligands of recent vintage[13] afforded useful levels of enantioselectivity in reactions with acyclic enone **1**. On the other hand, use of JOSIPHOS[14] (ligand **A**, Figure 1), as supplied within the Solvias "kit", led to an excellent reaction both in terms of educt consumption (100%) and enantioselectivity (91% *ee* at −50°C, 92% *ee* at −78°C) giving keto product **2** after hydrolytic workup of the presumed polymeric silyl enol ether. Remarkably, the mono-(di-*tert*-butyl)phosphane analogue of JOSIPHOS (ligand *ent*-**B**) was even more effective at the same temperature (93% *ee*), while at −78°C ketone **2** was isolated in good yield (94%) and with an even higher enantioselectivity (97% *ee*).

Table 1: Impact of the ligand on the enantioselectivity of the reduction.

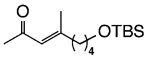
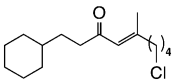
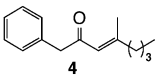
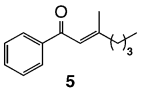
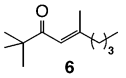
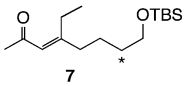


Ligand[a]	Conv. [%]	*ee* [%][b]	Yield [%][c]	*R*/*S*[d]
F	100	35	–	*S*
G	100	0	–	–
H	95	23	–	*R*
Phanephos[e]	20	23	–	*S*
A	100	91[f]	95	*S*
ent-**B**	100	97[g]	94	*R*

[a] Cf. Figure 1. [b] By capillary GC. [c] Yield of isolated product. [d] Stereochemistry of product ketone. [e] Cf. ref [16]. [f] 92% *ee* at −78°C. [g] Reaction conducted at −78°C.

Table 2 gives a survey of reactions run in toluene at −78°C with additional substrates and mainly PPF-P(*t*Bu)$_2$ (**B** or *ent*-**B**, Figure 1) as the ligand of choice on copper. With **3** as a representative enone, the 1,4-adduct was obtained in 98% *ee* (entry 2). Conducting the same experiment at 0°C decreased the level of induction, although an *ee* of 90% was still

Table 2: Asymmetric 1,4-hydrosilylations of acyclic enones.[a]

Entry	Substrate (enone)[b]	Ligand	Yield [%][c]	*ee* [%][d]	*R*/*S*
1		**A**	94	94	*S*
2		**B**	96	98	*S*
3		*ent*-**B**	96	98	*R*
4	**3**	**B**	95	90[e]	*S*
5		**D**	95	55	–[f]
6		**E**	97	35	–[f]
7		*ent*-**B**	93	99	*R*
8		**A**	91	91	*S*
9	 **4**	**B**	88	90	*S*
10		**B**	96	87	*R*
11	**5**	**C**	91	91	*S*
12	 **6**	**C**	93	95[g]	*R*
13		*ent*-**B**	95	96	*R*
14	**7**	**C**	95	97	*R*

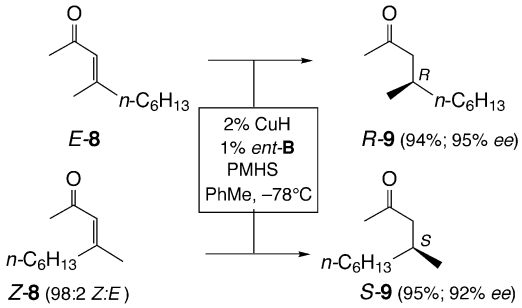
[a] Conditions: 2% CuCl, 2% NaO*t*Bu, 1% ligand, PMHS, 1.0 M in toluene, −78°C, 6–9 h. [b] TBS = *tert*-butyldimethylsilyl. [c] Yield of keto product isolated and purified by chromatography. [d] By capillary GC. [e] Reaction conducted at 0°C. [f] Not determined. [g] Reaction time 60 h.

observed (entry 4). Curiously, while the switch from cyclohexyl groups on phosphorus in JOSIPHOS (**A**) to *tert*-butyl residues in **B** enhances the level of stereodifferentiation, replacing the phenyl residues on phosphorus for cyclohexyl groups (as in ligands **D** and **E**, entries 5 and 6) significantly lowers the enantioselectivity of the reaction. In the sequence

 © 2003 Wiley-VCH Verlag GmbH & Co. KGaA, Weinheim

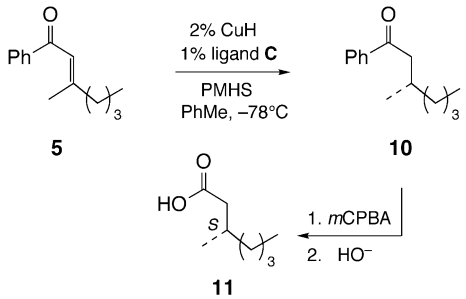
of substrates with alkyl, then benzylic (**4**, entry 9), and aryl (**5**, entry 10) substituents, the enantioselecitivities dropped from >95 to $\leq 90\%$ *ee*, suggesting an influential stereoelectronic effect or perhaps arene–arene or arene–metal coordination. Switching to WALPHOS (ligand **C**, Figure 1) in the case of the phenyl enone **5** (entry 11) raised the enantioselectivity of the reaction back to the $>90\%$ *ee* level. Further evidence that steric factors do not seem to play a major role in determining the enantioselectivity comes from conjugate reduction of *tert*-butyl enone **6** (entry 12) which, although slow, was both efficient and highly enantioselective. Indeed, in a direct comparison in reactions with the alkyl enone **7**, it was ligand **C** that appeared to be slightly more effective (entries 13 and 14). The high level of facial discrimination exemplified with educt **7**, where the reagent must recognize differences in olefin substitution three carbons removed from the β-site (cf. starred carbon in **7**) is especially noteworthy.

The tentative assignment of stereochemistry for all non-aromatic keto products is based on comparison of the optical rotation of product ketone **9** with that in the literature.[15] Thus, ligand *ent*-**B**, in the case of educt *E*-**8**, leads to product **9** with *R* stereochemistry (Scheme 2). Inverting the geometry of the enone as in *Z*-**8**, under otherwise identical reaction conditions, inverts the stereochemical outcome to give *S*-**9**, as expected. Employing ligand **B** in the reaction of enone *E*-**8**, likewise gives rise to enantiomeric keto product *S*-**9** (Scheme 3). Thus, on the basis of either ligand stereochemistry or geometry of the enone double bond, the newly formed stereocenter β to the product ketone is readily controlled. Interestingly, in reactions with aryl ketones the induction proceeds in the opposite sense, as indicated by the processing of product ketone **10** obtained from enone **5** (cf. Table 2, entries 10 and 11). Thus, treatment of **10** with *meta*-chloroperbenzoic acid (*m*CPBA) followed by aqueous base and an acidic workup led to the known[17] carboxylic acid **11** (Scheme 4).



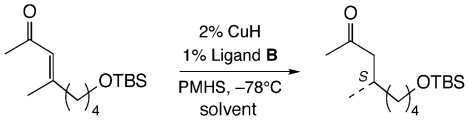
Scheme 2. Effect of substrate geometry on the stereochemistry of the conjugate reduction.

The impact of solvent on reaction rate and enantioselectivity was also determined with substrate enone **3** (Table 3), since these reductions (cf. Table 1 and Table 2) were routinely run in toluene (1.0 M). THF appears to cause a slight decrease in stereoinduction, while reactions run in CH_2Cl_2 are substantially less selective. The best solvent appears to be Et_2O, which led to a stereospecific conjugate reduction within our limits of detection. No significant effect on reaction rate was noted, as all the reactions required between four and six hours to reach completion. Substrate-to-ligand (S/L) ratios of 100:1 were typically used in the above reactions, mainly on the basis of convenience. However, the amount of ligand could be substantially reduced. As illustrated in Scheme 5, complete reduction of 1.64 grams of enone **3** could be achieved in high yield and with excellent optical purity even when only two milligrams of ligand **B** were used (i.e., S/L = 1650:1). The actual limits for the S/L ratio, however, have yet to be ascertained.



Scheme 4. Conversion of product **10** to the known carboxylic acid **11**.

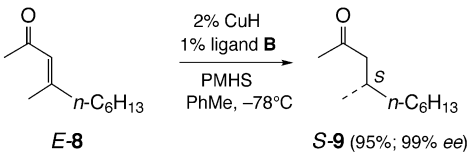
Table 3: Impact of solvent on the enantioselecitivity of the reduction.



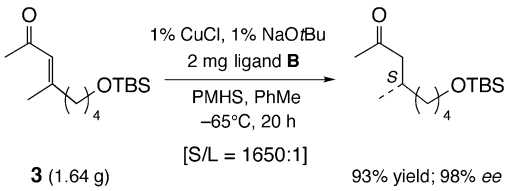
Solvent	*ee* [%][a]	Yield [%][b]
THF	91	94
PhMe	98	95
Et_2O	>99	96
CH_2CH_2	80	95

[a] By capillary GC. [b] Yield of isolated product.

In summary, a powerful new reaction has been developed in which, for the first time, asymmetric 1,4-reductions of



Scheme 3. Effect of the ligand on the stereochemistry of the conjugate reduction.



Scheme 5. Increasing the substrate/ligand ratio.

 © 2003 Wiley-VCH Verlag GmbH & Co. KGaA, Weinheim

prochiral enones provides access to compounds with highly stereodefined centers β to acyclic ketones. Reliance on catalytic quantities of a base metal in the form of CuH, along with readily available nonracemic ferrocenyl ligands and inexpensive PMHS as the stoichiometric source of hydride, all combine to offer an exceedingly mild and straighforward procedure.[18] New technologies utilizing this initial CuH-based 1,4-reduction/transmetalation protocol but which rely on boranes[19] (in place of silanes), thereby providing entries to subsequent aldol reactions, α-arylations, etc., will be reported in due course.

Received: July 4, 2003 [Z52313]
Published Online: September 23, 2003

Keywords: conjugate reductions · copper hydride · enones · hydrosilylation · phosphane ligands

[1] N. Krause, A. Hoffmann-Roder, *Synthesis* **2001**, 171.
[2] a) B. L. Feringa, R. Naasz, R. Imbos, L. A. Arnold in *Modern Organocopper Chemistry* (Ed.: N. Krause), Wiley-VCH, Weinheim, **2002**; b) K. Yoshida, M. Ogasawara, T. Hayashi, *J. Org. Chem.* **2003** *68*, 1901; c) Y. Iguchi, R. Itooka, N. Miyaura, *Synthesis* **2003**, 1040; d) K. Yoshida, M. Ogasawara, T. Hayashi, *J. Am. Chem. Soc.* **2002**, *124*, 10984; e) R. Amengual, R. Michelet, J.-P. Genet, *Synlett* **2002**, 1791; f) M. Pucheault, S. Darses, J.-P. Genet, *Eur. J. Org. Chem.* **2002**, 3552; g) M. Kuriyama, K. Nagai, K. Yamada, Y. Miwa, T. Taga, K. Tomioka, *J. Am. Chem. Soc.* **2002**, *124*, 8932; h) S. Sakuma, N. Miyaura, *J. Org. Chem.* **2001**, *66*, 8944; i) S. M. W. Bennett, S. M. Brown, A. Cunningham, M. R. Dennis, J. P. Muxworthy, M. A. Oakley, S. Woodward, *Tetrahedron* **2000**, *56*, 2847.
[3] M. Shibasaki, H. Sasai, T. Arai, *Angew. Chem.* **1997**, *109*, 1290; *Angew. Chem. Int. Ed. Engl.* **1997**, *36*, 1236.
[4] a) H. Mizutani, S. J. Degrado, A. H. Hoveyda, *J. Am. Chem. Soc.* **2002**, *124*, 779; b) S. J. Degrado, H. Mizutani, A. H. Hoveyda, *J. Am. Chem. Soc.* **2002**, *124*, 13362; c) J.-G. Boiteau, R. Imbos, A. J. Minnaard, B. L. Feringa, *Org. Lett.* **2003**, *5*, 681; d) I. H. Escher, A. Pfaltz, *Tetrahedron* **2000**, *56*, 2879; e) A. Alexakis, C. Benhaim, S. Rosset, M. Humam, *J. Am. Chem. Soc.* **2002**, *124*, 5262; f) A. Alexakis, C. L. Winn, F. Guillen, J. Pytkowicz, S. Roland, P. Mangeney, *Adv. Synth. Catal.*. **2003**, *345*, 345; g) A. Alexakis, C. Benhaim, *Eur. J. Org. Chem.* **2002**, 3221.
[5] D. H. Appella, Y. Moritani, R. Shintani, E. M. Ferreira, S. L. Buchwald, *J. Am. Chem. Soc.* **1999**, *121*, 9473.
[6] Due to the lack of any suitable means of effecting such asymmetric conjugate reductions, this strategy is usually not even considered an option for the control of stereochemistry at a site β to a ketone.[1] For early hydrogenation studies on enones using nonracemic ruthenium and cobalt complexes, see V. Massonneau, P. Le Maux, G. Simonneaux, *J. Organomet. Chem.* **1987**, *327*, 269; P. Le Maux, V. Massonneau, G. Simonneaux, *J. Organomet. Chem.* **1985**, *284*, 101.
[7] a) R. Schmid, E. A. Broger, M. Cereghetti, Y. Crameri, J. Foricher, M. Lalonde, R. K. Muller, M. Scalone, G. Schoettel, U. Zutter, *Pure. Appl. Chem.* **1996**, *68*, 131; b) R. Schmid, J. Foricher, M. Cereghetti, P. Schonholzer, *Helv. Chim. Acta* **1991**, *74*, 370.
[8] T. Saito, T. Yokozawa, T. Ishizaki, T. Moroi, N. Sayo, T. Miura, H. Kumobayashi, *Adv. Synth. Catal.* **2001**, *343*, 264.
[9] a) J.-X. Chen, J. F. Daeuble, D. M. Brestensky, J. M. Stryker, *Tetrahedron* **2000**, *56*, 2153; b) W. S. Mahoney, J. M. Stryker, *J. Am. Chem. Soc.* **1989**, *111*, 8818. c) For in situ generation of CuH, see ref. [5] and Y. Moritani, D. H. Appella, V. Jureakauseas, S. L. Buchwald, *J. Am. Chem. Soc.* **2000**, *122*, 6797.
[10] N. J. Lawrence, M. D. Drew, S. M. Bushell, *J. Chem. Soc. Perkin Trans. 1* **1999**, 3381. Although four equivalents of hydride were used in these experiments, we have since found that only two equivalents are actually needed.
[11] a) B. H. Lipshutz, K. Noson, W. Chrisman, A. Lower, *J. Am. Chem. Soc.* **2003**, *125*, 8779; b) B. H. Lipshutz, K. Noson, W. Chrisman, *J. Am. Chem. Soc.* **2001**, *123*, 12917.
[12] Y. Moritani, D. H. Appella, V. Jurkauskas, S. L. Buchwald, *J. Am. Chem. Soc.* **2000**, *122*, 6797. See also, B. H. Lipshutz, J. M. Servesko, P. Papa, T. Petersen, A. Lover, in preparation.
[13] a) *S*-(−)-BITIANP: T. Benincori, E. Brenna, F. Sannicolo, L. Trimarco, P. Antognazza, E. Cesarotti, F. Demartin, T. Pilati, *J. Org. Chem.* **1996**, *61*, 6244; b) *R,S*-(−)-BoPhoz: N. W. Boaz, S. D. Debenham, E. B. Mackenzie, S. E. Large, *Org. Lett.* **2002**, *4*, 2421; c) TaniaPhos: T. Ireland, K. Tappe, G. Grossheimann, P. Knochel, *Chem. Eur. J.* **2002**, *8*, 843 (only 2% conversion after 7 h).
[14] a) A. Togni, C. Breutel, A. Schnyder, F. Spindler, H. Landert, A. Tijani, *J. Am. Chem. Soc.* **1994**, *116*, 4062; b) H.-U. Blaser, W. Brieden, B. Pugin, F. Spindler, M. Studer, A. Togni, *Top. Catal.* **2002**, *19*, 3.
[15] Product *S*-**9** gave a negative rotation ($[\alpha]_{546}^{20} = -6.0$ ($c = 1.8$, $CHCl_3$), whereas *R*-**9** gave an equal and opposite (positive) rotation, as expected for these known compounds; cf. G. Bram, D. Caberet, N. Maigrot, J.-P. Mazaleyrat, Z. Welvart, *J. Chem. Res. Synop.* **1979**, 196; D. Caberet, N. Maigrot, Z. Welvart, *Tetrahedron Lett.* **1981**, *22*, 5279.
[16] P. J. Pye, K. Rossen, R. A. Reamer, N. N. Tsou, R. P. Volante, P. J. Reider, *J. Am. Chem. Soc.* **1997**, *119*, 6207.
[17] S. Norsikian, I. Marek, S. Klein, J. F. Poisson, J. F. Normant, *Chem. Eur. J.* **1999**, *5*, 2055.
[18] Represenative procedure (Table 3, entry 2): To a 5-mL round-bottom flask flame-dried and purged with argon was added $CuH{\cdot}PPh_3$ (2 mg, 0.006 mmol) and ligand *ent*-**B** (5.42 mg, 0.003 mmol). Toluene (0.3 mL) was added and the solution cooled to −78 °C. PMHS (78 μL, 1.21 mmol) was introduced dropwise by syringe and then the enone was added (neat; 82 mg, 0.304 mmol). The reaction mixture was stirred for 6 h at −78 °C until the reaction was complete by TLC (2% Et_2O:ligroin). It was then quenched at −78 °C with 3 M NaOH, warmed to room temperature, diluted with Et_2O/H_2O, and stirred for 2 h. The aqueous layer was extracted twice with Et_2O, and the combined organic layers were washed with brine, dried over anhydrous $MgSO_4$, filtered, and concentrated by rotary evaporation. The residue was purified by flash chromatography (2% Et_2O:ligroin) to afford the product ketone (78 mg, 95%) as a clear oil. The product ($R_f = 0.27$, 10% Et_2O/ligroin) was analyzed by chiral GC (BDM 110) which indicated an *ee* of 98%. IR (neat): $\tilde{\nu} =$ 2929, 1718, 1255, 1097, 835, 774 cm^{-1}; ^1H NMR (400 MHz, C_6D_6): $\delta = 0.08$ (s, 6H), 0.82 (d, $J = 6.4$ Hz, 3H), 1.00 (s, 9H), 1.14–1.24 (m, 2H), 1.24–1.37 (m, 2H), 1.43 (m, 2H), 1.66 (s, 3H), 1.80 (dd, $J = 17.5$, 6.8 Hz, 1H), 1.95 (m, 1H), 1.98 (dd, $J = 17.5$, 5.7 Hz, 1H), 3.54 ppm (t, $J = 6.1$ Hz, 2H); EIMS: *m*/*z* (%): 215 (40) [M^+−Bu], 171 (64), 115 (29), 75 (100); HR-EIMS calcd for $C_{15}H_{32}O_2Si{\cdot}C_4H_9$: 215.1467; found 215.1470. Additional data for all new compounds can be found in the Supporting Information.
[19] B. H. Lipshutz, P. Papa, *Angew. Chem.* **2002**, *114*, 4762; *Angew. Chem. Int. Ed.* **2002**, *41*, 4580.

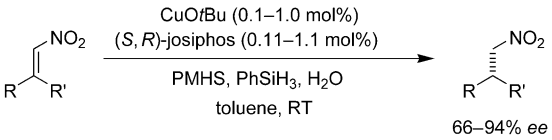
 © 2003 Wiley-VCH Verlag GmbH & Co. KGaA, Weinheim

Chiral Nitroalkanes

Catalytic Enantioselective Conjugate Reduction of β,β-Disubstituted Nitroalkenes**

*Constantin Czekelius and Erick M. Carreira**

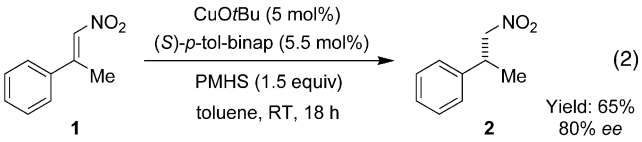
Optically active nitroalkanes are versatile precursors for a wide range of useful building blocks for fine-chemical synthesis. However, only a few effective methods for their preparation are available.[1–3] Despite recent advances in the addition of dialkyl zinc reagents to α,β-unsaturated nitroolefins, the complementary method involving metal-catalyzed enantioselective reduction of β,β-disubstituted nitroalkenes has not been reported.[2] Herein we document such an approach in which bisphosphane–Cu complexes (with tol-binap or josiphos[4]) catalyze the enantioselective reduction of β,β-disubstituted nitroalkenes, giving optically active β,β-disubstituted nitroalkanes in useful yields and selectivities [Eq. (1)].[5] Of additional mechanistic and practical importance is the observation we have made regarding the inhibitory effect of halides; thus, in their absence the reductions can be carried out with as little as 0.1 mol% of complex, rendering the process among one of the more efficient methods for conjugate addition chemistry.



(1)

We had previously reported that a complex prepared from tol-binap and CuO*t*Bu effectively catalyzes the addition of dienolates to aldehydes involving a metalloenolate intermediate.[6] A related complex derived from tol-binap, CuCl, and NaO*t*Bu mediates the enantioselective reduction of α,β-unsaturated esters and ketones.[7,8] As part of our ongoing investigations of copper–phosphane complexes for asymmetric synthesis, we have tested such systems in the reduction of β,β-disubstituted nitroalkenes, which are not only easily prepared (i.e., addition of N_2O_4 to alkenes and subsequent elimination[1,9]) but also whose reductions are unprecedented in small-molecule catalysis.[10]

In our initial investigations on the reduction of (*E*)-1-nitro-2-phenyl-1-propene (**1**) with PMHS, we employed the published procedure for the preparation of the catalyst formed between CuCl, tol-binap, and NaO*t*Bu. Under these conditions, the reaction proceeded rather sluggishly: 5 mol% of catalyst led to 18% conversion after 22 h at 25°C. Additionally, isomerization of **1** to the β,γ-unsaturated nitroalkene (14%) was observed. We then investigated the catalyst prepared from tol-binap and CuO*t*Bu which we had originally formulated for mechanistic studies in aldol addition chemistry. In the presence of 5 mol% of this catalyst, full conversion of **1** into **2** (65% yield, 80% *ee*) within 18 h at room temperature was observed [Eq. (2)].[11] Interestingly, at this stage the reduction appeared to be quite general as 2-methyl-3-nitro-prop-2-en-1-ol provided the corresponding nitroalkane in 58% yield and 56% *ee*.[12]



(2)

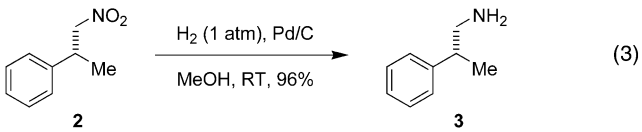
These results along with subsequent investigations led us to the significant conclusion that the presence of NaCl inhibits the activity of the Cu–phosphane complex, a premise which is supported by the finding that the addition of various inorganic salts (e.g. LiCl, NEt_4Cl, KCN) always leads to diminished reaction rates.

We subsequently looked to variation of the silane component in the reaction in an effort to increase turnover frequency and lower catalyst loading.[13] We found that the use of diphenylsilane or phenylsilane in the reaction resulted in increased reaction rates, with the highest acceleration observed when a combination of PMHS (0.1 equiv) and phenylsilane (1.2 equiv) was employed. Nevertheless, under these conditions, substantial amounts of 2-phenyl-propional-dehydeoxime (38%) were isolated.[14] However, the addition of 1.2 equivalents of water to the reaction mixture resulted in complete suppression of this overreduction.[15] An important consequence of these conditions is the fact that in the presence of tol-binap and josiphos, the catalyst loadings can be further substantively decreased to the level of 0.1 mol% [Eq. (1), Table 1].

As shown in Table 1 aromatic and aliphatic substrates are reduced to give adducts in useful selectivity. Both protected and unprotected alcohol functionalities as well as heterocyclic substrates are tolerated. The reduction of *E* and *Z* olefins (Table 1, entries 7 and 8) resulted in the formation of opposite enantiomers with similar high levels of enantioselectivity.[17] This observation is in accordance with those in conjugate reductions of unsaturated carbonyls.[8a,18]

The nitroalkane products provide entry to valuable chiral amines that are otherwise not easily accessed. In this respect, reduction of **2** (Pd/C, H_2) serves to exemplify the convenience with which amines can be accessed in high yield [Eq. (3)].[19]

In conclusion, we have developed a novel copper-catalyzed, asymmetric reduction of substituted nitroolefins that



(3)

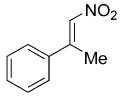
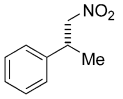
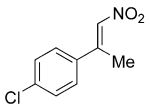
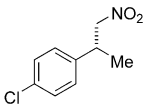
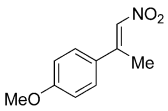
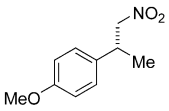
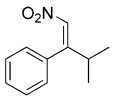
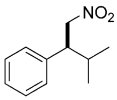
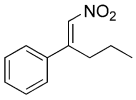
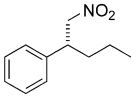
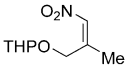
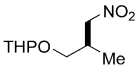
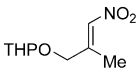
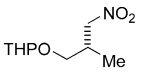
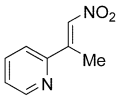
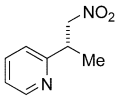
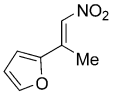
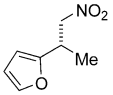
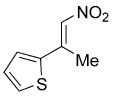
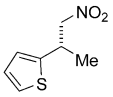
[*] Prof. Dr. E. M. Carreira, C. Czekelius
Laboratorium für Organische Chemie
ETH Hönggerberg, HCI H335
8093 Zürich (Schweizerland)
Fax: (+41) 1-632-1328
E-mail: carreira@org.chem.ethz.ch

[**] This research was supported by Sumika Fine Chemicals, Japan. C.C. was supported by a fellowship of the Fonds der Chemischen Industrie (Germany).

Supporting information for this article is available on the WWW under http://www.angewandte.org or from the author.

 DOI: 10.1002/anie.200352175 © 2003 Wiley-VCH Verlag GmbH & Co. KGaA, Weinheim

Table 1: Conjugate reduction in the presence of CuO*t*Bu, PMHS, and $PhSiH_3$.

Entry	Substrate	Product	Ligand	Catalyst [mol%]	*t* [h]	Yield [%]	*ee* [%]
1			(*S*)-tol-binap	0.1	24	60	78
			(*S*,*R*)-josiphos	0.1	24	77	88
2			(*S*,*R*)-josiphos	1	5	89	90
			(*S*,*R*)-josiphos	0.1	24	88	90
3			(*S*,*R*)-josiphos	1	5	94	90
4			(*S*,*R*)-josiphos	1	12	83	94
5			(*S*,*R*)-josiphos	1	12	86	92
6			(*S*)-tol-binap	1	5	60	86
			(*S*,*R*)-josiphos	1	5	66	90
			(*S*,*R*)-josiphos	0.3	24	55	86
7			(*S*)-tol-binap	1	5	76	66[b]
			(*S*,*R*)-josiphos	0.1	24	81	86[b]
8			(*S*,*R*)-josiphos	1	5	82	68[b]
			(*S*,*R*)-josiphos	0.1	24	77	66[b]
9			(*S*,*R*)-josiphos	1	12	55	72
10			(*S*,*R*)-josiphos	1	12	72	90
11			(*S*,*R*)-josiphos	1	12	75	84

[a] Reactions were run at 0.2 M of olefin in toluene with $PhSiH_3$ (1.2 equiv), PMHS (0.1 equiv), and water (1.2 equiv) at room temperature. [b] See reference [16].

provides access to optically active β,β-disubstituted nitroalkanes. Importantly, we have documented means by which such reductions can be carried out under operationally convenient conditions with as little as 0.1 mol% of catalyst (CuO*t*Bu, tol-binap, or josiphos). The method described represents the first such report, ultimately providing access to optically active amines. Given the increased importance of copper-catalyzed processes for asymmetric synthesis, of additional significance is the observation that halides can inhibit such catalytic processes. Further work is continuing with the aim of better understanding the mechanism of the reaction and ultimately identifying ligands that lead to further improvement in the selectivity.

Received: June 23, 2003 [Z52175]

Keywords: asymmetric catalysis · copper · hydrosilylation · nitro compounds · reduction

 © 2003 Wiley-VCH Verlag GmbH & Co. KGaA, Weinheim

[1] For the transformation of aliphatic nitro compounds, see: a) V. V. Perekalin, E. S. Lipina, V. M. Berestovitskaya, D. A. Efremov, *Nitroalkenes*, Wiley, Chichester, **1994**; b) N. Ono, *The Nitro Group in Organic Synthesis*, Wiley-VCH, New York, **2001**.

[2] a) For an excellent review, see: O. M. Berner, L. Tedeschi, D. Enders, *Eur. J. Org. Chem.* **2002**, 1877; b) H. Schäfer, D. Seebach, *Tetrahedron* **1995**, *51*, 2305; c) N. Sewald, V. Wendisch, *Tetrahedron: Asymmetry* **1998**, *9*, 1341; d) S. Ongeri, U. Piarulli, R. F. W. Jackson, C. Gennari, *Eur. J. Org. Chem.* **2001**, 803; e) C. Luchaco-Cullis, A. H. Hoveyda, *J. Am. Chem. Soc.* **2002**, *124*, 8192; f) A. Alexakis, C. Benhaim, S. Rosset, M. Humam, *J. Am. Chem. Soc.* **2002**, *124*, 5262; g) A. Duursma, A. J. Minnaard, B. L. Feringa, *J. Am. Chem. Soc.* **2003**, *125*, 3700.

[3] For related additions of organoboronic acids, see: a) T. Hayashi, T. Senda, M. Ogasawara, *J. Am. Chem. Soc.* **2000**, *122*, 10716; b) T. Hayashi, *Synlett* **2001**, 879.

[4] josiphos = 1-[2-(diphenylphosphanyl)ferrocenyl]ethyldicyclohexylphosphane

[5] PMHS = poly(methylhydrosiloxane); for a review, see: N. J. Lawrence, M. D. Drew, S. M. Bushell, *J. Chem. Soc. Perkin Trans. 1* **1999**, 3381.

[6] a) B. L. Pagenkopf, J. Krüger, A. Stojanovic, E. M. Carreira, *Angew. Chem.* **1998**, *110*, 3312; *Angew. Chem. Int. Ed.* **1998**, *37*, 3124; b) for the preparation of CuO*t*Bu, see: T. Tsuda, T. Hashimoto, T. Saegusa, *J. Am. Chem. Soc.* **1972**, *94*, 658.

[7] For the use of achiral copper hydride reducing agents, see: a) W. S. Mahoney, J. M. Stryker, *J. Am. Chem. Soc.* **1989**, *111*, 8818; b) A. Mori, A. Fujita, H. Kajiro, Y. Nishihara, T. Hiyama, *Tetrahedron* **1999**, *55*, 4573; c) B. H. Lipshutz, W. Chrisman, K. Noson, P. Papa, J. A. Slafani, R. W. Vivian, J. M. Keith, *Tetrahedron* **2000**, *56*, 2779.

[8] a) D. H. Appella, Y. Moritani, R. Shintani, E. M. Ferreira, S. L. Buchwald, *J. Am. Chem. Soc.* **1999**, *121*, 9473; b) Y. Moritani, D. H. Appela, V. Jurkauskas, S. L. Buchwald, *J. Am. Chem. Soc.* **2000**, *122*, 6797; c) J. Yun, S. L. Buchwald, *Org. Lett.* **2001**, *3*, 1129; d) V. Jurkauskas, S. L. Buchwald, *J. Am. Chem. Soc.* **2002**, *124*, 2892; e) B. H. Lipshutz, K. Noson, W. Chrisman, *J. Am. Chem. Soc.* **2001**, *123*, 12917; f) B. H. Lipshutz, A. Lower, K. Noson, *Org. Lett.* **2002**, *4*, 4045; g) J. Courmarcel, N. Mostefaï, S. Sirol, S. Choppin, O. Riant, *Isr. J. Chem.* **2001**, *41*, 231.

[9] a) P. Knochel, D. Seebach, *Synthesis* **1982**, 1017; b) W.-W. Lin, Y.-J. Jang, Y. Wang, J.-T. Liu, S.-R. Hu, L.-Y. Wang, C.-F. Yao, *J. Org. Chem.* **2001**, *66*, 1984; c) H. Baldock, N. Levy, C. W. Scaife, *J. Chem. Soc.* **1949**, 2627 and references therein; d) R. Schneider, P. Gerardin, B. Loubinoux, *Tetrahedron* **1993**, *49*, 3117; e) J. Zindel, A. de Meijere, *Synthesis* **1993**, 190.

[10] For the enzyme-catalyzed reduction of β,β-disubstituted nitroalkenes, see: a) H. Ohta, K. Ozaki, G.-i. Tsuchihashi, *Chem. Lett.* **1987**, 191; b) H. Ohta, N. Kobayashi, K. Ozaki, *J. Org. Chem.* **1989**, *54*, 1802.

[11] The stereochemistry of **2** was assigned by comparison with reference [10b].

[12] Reduction of (*E*)-2-methyl-3-nitro-prop-2-en-1-ol provided (*R*)-2-methyl-3-nitro-propan-1-ol. The absolute stereochemistry of the product was assigned by reduction to the aminoalcohol (Pd/C, H_2) and comparison with R. A. Barrow, T. Hemscheidt, J. Liang, S. Paik, R. E. Moore, M. A. Tius, *J. Am. Chem. Soc.* **1995**, *117*, 2479.

[13] a) D. A. Evans, F. E. Michael, J. S. Tedrow, K. R. Campos, *J. Am. Chem. Soc.* **2003**, *125*, 3534; b) B. Tao, G. C. Fu, *Angew. Chem.* **2002**, *114*, 4048; *Angew. Chem. Int. Ed.* **2002**, *41*, 3892; c) A. Mori, T. Kato, *Synlett* **2002**, *7*, 1167.

[14] For the problem of overreduction of nitroalkenes, see a) H. Shechter, D. E. Ley, E. B. Roberson, Jr., *J. Am. Chem. Soc.* **1956**, *78*, 4984; b) B. C. Ranu, R. Chakraborty, *Tetrahedron*, **1992**, *48*, 5317.

[15] We believe that in the presence of water, the first formed silyl nitronate undergoes protonation faster than it is reduced to the oxime.

[16] Owing to the presence of the THP group, the products of the reduction are diastereomers. The diastereomeric ratio was determined to be 1:1 and the *ee* value for each identical, indicating that the acetal stereocenter has no effect on the stereochemical outcome of the conjugate reduction.

[17] In the synthesis of the nitroalkene starting materials, olefins were obtained as single isomers in most cases (*E* for entries 1, 2, 3, 5, 6, 9, 10, and 11 and *Z* for entry 4).

[18] a) U. Leutenegger, A. Madin, A. Pfaltz, *Angew. Chem.* **1989**, *101*, 61; *Angew. Chem. Int. Ed. Engl.* **1989**, *28*, 60; b) P. von Matt, A. Pfaltz, *Tetrahedron: Asymmetry* **1991**, *2*, 691; c) M. Misun, A. Pfaltz, *Helv. Chim. Acta* **1996**, *79*, 961; d) T. Yamada, Y. Ohtsuka, T. Ikeno, *Chem. Lett.* **1998**, 1129.

[19] It was shown by analysis of the Mosher amide that no erosion of enantiomeric purity occurred in the course of the reduction.

 © 2003 Wiley-VCH Verlag GmbH & Co. KGaA, Weinheim

Mechanism Elucidation by EXAFS

Time Scale and Elementary Steps of CO-Induced Disintegration of Surface Rhodium Clusters**

*Akane Suzuki, Yasuhiro Inada, Aritomo Yamaguchi, Teiji Chihara, Makoto Yuasa, Masaharu Nomura, and Yasuhiro Iwasawa**

While the reaction kinetics and dynamics of molecules adsorbed on catalyst surfaces have been extensively studied, little is known about the dynamic structural change of active

[*] Prof. Dr. Y. Iwasawa, A. Suzuki
Department of Chemistry
Graduate School of Science
the University of Tokyo
Hongo, Bunkyo-ku, Tokyo, 113-0033 (Japan)
Fax: (+81) 3-5800-6892
E-mail: iwasawa@chem.s.u-tokyo.ac.jp

Dr. Y. Inada
Graduate School of Science
Nagoya University
Chikusa, Nagoya (Japan)

Dr. A. Yamaguchi, Prof. Dr. M. Yuasa
Faculty of Science and Technology
Tokyo University of Science
Noda, Chiba (Japan)

Dr. T. Chihara
RIKEN
Wako, Saitama 351-01 (Japan)

Prof. Dr. M. Nomura
Photon Factory
Institute of Materials Structure Science, KEK
Ibaraki 305-0801 (Japan)

[**] This study was supported by a Grant-in-aid for The 21st Century COE Program for Frontiers in Fundamental Chemistry from the Ministry of Education, Culture, Sports, Science and Technology.

Supporting information for this article is available on the WWW under http://www.angewandte.org or from the author.

 DOI: 10.1002/anie.200352318 © 2003 Wiley-VCH Verlag GmbH & Co. KGaA, Weinheim

metal sites in supported metal cluster/nanoparticle catalysts, such as the time scale of formation and disintegration of the active structure induced by reaction gases and the sequence of bond rearrangements involved in the dynamic event on the surfaces. The in situ time-resolved structural characterization of surface metal clusters and nanoparticles by energy-dispersive X-ray absorption fine structure (DXAFS) is essential to document their dynamic property on an atomic basis, which has been a long-term challenge to be addressed. We have succeeded in observing the CO-induced disintegration process of Rh clusters on an Al_2O_3 surface by DXAFS every 100 ms. Previous static studies on the similar surface phenomenon have been performed by IR,[1–3] XAFS,[4,5] and STM,[5,6] which revealed the structural modification of highly dispersed Rh nanoparticles/Al_2O_3 catalysts that leads to the formation of isolated $Rh(CO)_2$ species by CO adsorption. The DXAFS technique has been developed and improved to provide in situ structural information on dispersed catalytic materials at a time resolution of 1 s—several 10 s.[7–25] Herein, we report novel issues found by the time-resolved DXAFS characterization of the structural disintegrity of Rh clusters on an Al_2O_3 surface, namely, the time scale and sequence of dynamic bond rearrangements in the clusters and at the interface.

Figure 1 shows XANES (XANES = X-ray absorption near-edge spectroscopy) spectra at the Rh Kedge during the carbonylation process of the Rh/Al_2O_3 catalyst under 26.7 kPa of CO at 298 K. The DXAFS spectra were recorded

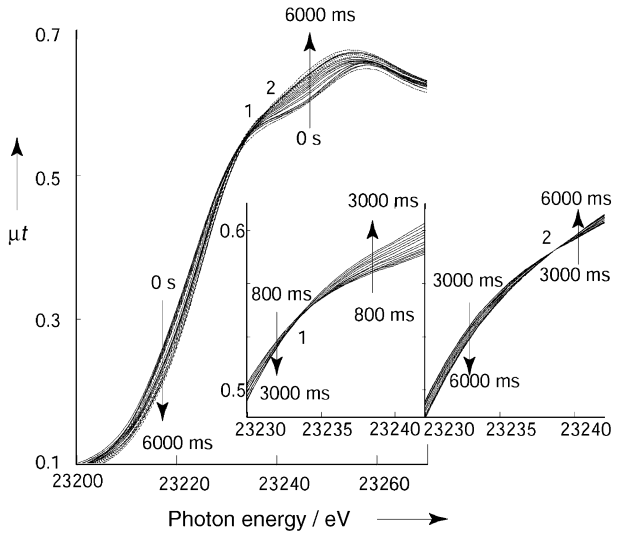


Figure 1. A series of XANES spectra at the Rh *K* edge during the carbonylation of Rh/Al_2O_3 under CO (26.7 kPa) at 298 K. The acquisition time of each spectrum is 100 ms, Cat.weight (wafer) = 80 mg.

every 100 ms. There is an isosbestic point at 23.234 keV (point **1**) in the serial XANES spectra during the period of 0.8–3 s as shown in the inset of Figure 1, thus indicating a direct change from a Rh species to another Rh species in its time scale. The spectra at the beginning of CO adsorption (0–600 ms) did not pass the isosbestic point. The k^3-weighted EXAFS oscillations at the Rh K edge during the carbonylation process are shown in Figure 2a. The amplitude of extended X-ray absorption fine structures (EXAFS) oscillations did not change significantly at 0–600 ms, but a remarkable decrease in the amplitude in the higher k range was observed from 600 ms till 3000 ms. This indicates that the observation of the isosbestic point is due to a structural change in the Rh clusters. The second isosbestic point was observed at

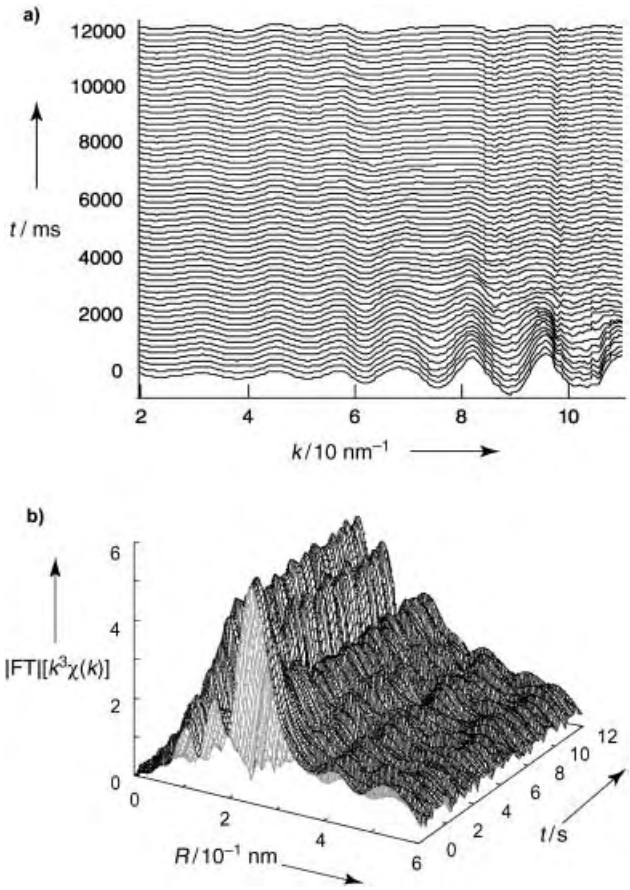


Figure 2. a) The k^3-weighted EXAFS oscillations and b) their Fourier transformed functions for Rh/Al_2O_3 at the Rh K-edge during the carbonylation process at 298 K measured by DXAFS every 100 ms.

23.239 keV (point **2**) after 3 s as shown in the inset of Figure 1. The existence of the isosbestic point different from the first one means that another structural change occurred as a sequential process during the period of 3–6 s. Two distinct peaks in the FT at 0.174 and 0.248 nm (phase-shift uncorrected), which are assigned to Rh–O and Rh–Rh, respectively, were observed at $t = 0$ as shown in Figure 2b. After CO adsorption an FT peak due to the formation of the Rh–C–(O) bond appeared at 0.123 nm (phase-shift uncorrected) within the first 200 ms, while the FT peaks for Rh–O and Rh–Rh remained unchanged over 600 ms. A drastic change in the FT was observed at 800–3000 ms, and the Rh–Rh peak completely disappeared at 3000 ms. The quality of the DXAFS spectra observed every 100 ms was good enough for the structural analysis. The values of the coordination numbers (C.N.) and bond length (R) determined by the curve fitting

 © 2003 Wiley-VCH Verlag GmbH & Co. KGaA, Weinheim

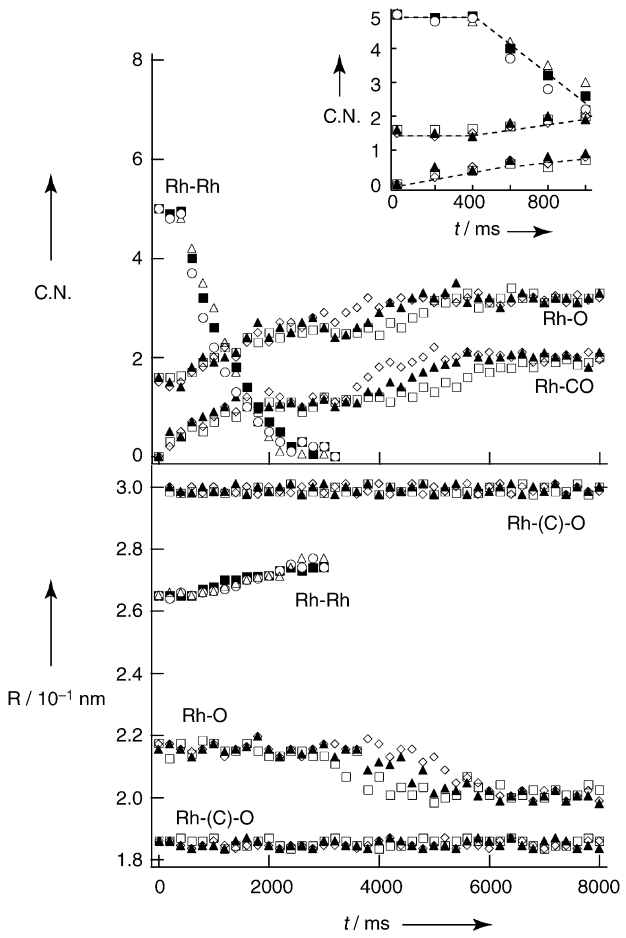


Figure 3. The values of coordination number (C.N.) and bond length (*R*) determined by the curve fitting as a function of CO exposure time at 298, 333, and 353 K. 298 K: Rh-Rh 298 (■), 333 (△), 353 (○); Rh-CO 298(□), 333 (▲), 353 (◇); Rh-O 298 (□), 333 (▲), 353 (◇).

Table 1: Structural parameters for the 2 wt% Rh/γ-Al_2O_3 catalyst.[a]

abs.-scat	C.N.	*R* [10^{-1} mm]	σ^2 [10^{-2} nm^2]
(Species A) after reduction at 593 K (flow of H_2) (0 s)			
($\Delta E_0 = 2.6$ eV, $R_f = 2.8\%$, *R* range = 0.15–0.3 nm)			
Rh-Rh	5.0 ± 0.4	2.65 ± 0.02	6.7 ± 0.2
Rh-O	1.6 ± 0.5	2.13 ± 0.02	13.7 ± 1
(Intermediate B) CO adsorption at 298 K (600 ms)			
($\Delta E_0 = 2.4$ eV, $R_f = 30\%$, *R* range = 0.10–0.32 nm)			
Rh-Rh	5.0 ± 0.4	2.65 ± 0.02	6.7 ± 0.2
Rh-O	1.6 ± 0.5	2.12 ± 0.02	13.7 ± 2
Rh-C	0.7 ± 0.6	1.85 ± 0.03	8.0 ± 3
Rh-(C)-O	0.7 ± 0.6	3.00 ± 0.04	9.7 ± 3
(Intermediate C) CO adsorption at 298 K (300 ms)			
($\Delta E_0 = 2.8$ eV, $R_f = 4.8\%$, *R* range = 0.10–0.32 nm)			
Rh-O	2.5 ± 0.5	2.13 ± 0.03	10.9 ± 2
Rh-C	1.2 ± 0.6	1.86 ± 0.03	8.0 ± 3
Rh-(C)-O	1.2 ± 0.6	2.99 ± 0.04	9.7 ± 3
(Species D) adsorption at 298 K (7000 ms)			
($\Delta E_0 = 1.8$ eV, $R_f = 4.5\%$, *R* range = 0.10–0.32 nm)			
Rh-O	3.2 ± 0.5	2.00 ± 0.03	10.9 ± 2
Rh-C	1.9 ± 0.6	1.87 ± 0.03	8.0 ± 3
Rh-(C)-O	1.9 ± 0.6	3.00 ± 0.04	9.7 ± 3

[a] **A** after reduction at 593 K (flow of H_2), and three intermediate **B, C** and **D** during CO adsroption at 298 K by DXAFS (see Figure 4).

were plotted as a function of CO exposure time at 298, 333, and 353 K in Figure 3. There were no changes in the Rh–Rh and Rh–O parameters at 0–600 ms, but the C.N. values for Rh–CO increased from 0 to 0.7 at 600 ms. After the interval of 600 ms, the C.N. of Rh–Rh bond decreased uniformly during the period of 800–3000 ms, accompanied by elongation of the Rh–Rh bond length and an increase of the C.N. for Rh–O from 1.6 to 2.5 at 3000 ms. The C.N. values for Rh–O and Rh–CO were almost constant at 2000–3000 ms, thus indicating the existence of a semistable structural state for CO-adsorbed Rh clusters on Al_2O_3. After 3000 ms the C.N. for Rh–O increased from 2.5 to 3.2 and for Rh–CO from 1.2 to 1.9 as shown in Figure 3; the *R* of Rh–O also decreased from 0.213 to 0.200 nm. The rate of the change was greater with an increase temperature. The observed and fitted FTs for the samples at 0 ms, 600 ms, 3000 ms, and 7000 ms are shown in the Supporting Information and the determined structural parameters are given in Table 1. The change in the C.N. values determined by the DXAFS analysis was in excellent accordance with the result of volumetric measurements (see Supporting Information); the amount of adsorbed CO molecules is plotted as a function of CO exposure time at 298 K.

Thus the time-resolved DXAFS analysis reveals three elementary steps for the surface dynamic structural rearrangement of Rh clusters involving two intermediate states as depicted in Figure 4. Before CO exposure ($t = 0$) Rh atoms in

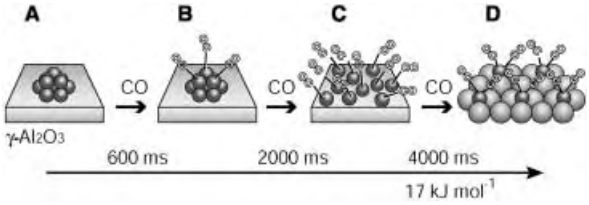


Figure 4. An illustrative mechanism, with times given as taken from the beginning of the reaction, of three elementary steps at 298 K for the disintegration of Rh clusters on Al_2O_3 during CO adsorption by time-resolved DXAFS.

the cluster interact with the surface oxygen atoms of Al_2O_3 at the distance of 0.213 nm. The C.N. (5.0) and *R* (0.265 nm) of Rh–Rh (Table 1) are in good agreement with those determined by conventional XAFS (4.9 and 0.264 nm). These structural parameters assume that the Rh cluster consists of seven atoms in the first layer and three atoms in the second layer as shown in Figure 4, which shows the C.N. of 5.4 for Rh–Rh bond. The C.N. value of 1.6 for Rh–O indicates that each Rh atom in the lower layer interacts with two O atoms of the Al_2O_3 surface. At the first step of the dynamic processes (0–600 ms) CO rapidly adsorbs on the Rh cluster to give a C.N. of 0.7 for Rh–CO, which indicates that one CO molecule adsorbs on each Rh atom of the second layer. At this stage no Rh–Rh bond breaking occurs. At the second step after 600 ms the Rh–Rh bonds become weaker by further CO adsorption and the Rh cluster is completely disintegrated at 3000 ms, at which point the ratio of adsorbed CO to Rh is one (see

 © 2003 Wiley-VCH Verlag GmbH & Co. KGaA, Weinheim

Supporting Information). The existence of the isosbestic point (**1**) in Figure 1 indicates that the second step consists of a one-to-one direct conversion, namely from $[Rh_{10}(CO)_3]$ (**B**) to $[Rh{-}CO]_{10}$ (**C**) in Figure 4. The [Rh–CO] can migrate across the Al_2O_3 surface to react with OH groups. The fragmentation of the Rh cluster permits the adsorption of further CO molecules on the Rh atoms at the third step (3000–6000 ms) to form $[Rh(CO)_2]$, which interacts with three surface O atoms as shown in Figure 4. This process is also a direct transformation process as evidenced by the second isosbestic point (**2**), in which the Rh atoms more strongly interact with the surface because of a decrease in the Rh–O distance from 0.213 to 0.200 nm (Table 1). The $[Rh(CO)_2]$ monomers form on the Cl-free Rh/Al_2O_3 catalyst, which is in contrast to the situation previously reported.[26]

The [Rh–CO] species and the $[Rh(CO)_2]$ species were also confirmed by in situ FTIR. The FTIR spectra were recorded as difference spectra on a JASCO FTIR 230 spectrometer in a transmission mode. In FTIR spectra (see Supporting Information) a peak at 2060 cm^{-1} is assigned to ν_{CO} for a terminal CO molecule on a Rh atom, while two peaks around 2095 and 2023 cm^{-1} are assigned to symmetric and asymmetric ν_{CO} for Rh discarbonyl species. After the 1.5 s CO exposure, the peak intensity at 2060 cm^{-1} increased at first, followed by the development of peaks at 2095 and 2023 cm^{-1} (4.5 s). Only these two bands were observed at 10.5 s. The formation of Rh dicarbonyl species is in accordance with the previous reports.[1–3]

We have carried out the DXAFS measurements at three different temperatures. The rates of the first and second steps were independent of the temperature at the present conditions. In contrast, the rate of the third step clearly depended on the temperature and the activation energies were estimated to be 15 ± 2, 17 ± 2, and 19 ± 2 kJ mol^{-1} for the changes in the C.N. of Rh–CO, the C.N. of Rh–O, and the *R* of Rh–O, respectively, which are in good agreement with each other. By CO adsorption, the Rh–Rh bond distance increased from 0.26 nm for the incipient Rh clusters to 0.27 nm for the $[Rh{-}CO]_{10}$ species, while the Rh cluster framework disintegrated during the Rh–Rh elongation. Thus the [Rh–CO] species can move off from the cluster at the surface without any significant energy barrier. The slowest step in the cluster disintegration with the energy barrier of 17 kJ mol^{-1} is the formation of $[Rh(CO)_2]$ monomers, which occurs concertedly with the bond rearrangement (C.N. and *R* of Rh–O) at the interface and probably with the oxidation of Rh^0 to Rh^+ by surface OH groups.

In summary we have shown the time scale and bond sequence in the dynamic structural disintegration of Rh clusters on the γ-Al_2O_3 surface, which proceeds through two intermediate states and is detected by time-resolved DXAFS every 100 ms. The present time-resolved structural analysis provides crucial structural aspects to elucidate the mechanism for dynamic surface processes and contributes to a new area of structural dynamics of metal clusters/nanoparticles dispersed at surfaces.

Experimental Section

A 2 wt% Rh/γ-Al_2O_3 catalyst was prepared by an incipient wet-impregnation method with an aqueous solution of $RhCl_3 \cdot 3H_2O$, followed by drying at 393 K for 30 h to remove the solvent. The obtained sample of 80 mg was pressed to a disk (4 mmϕ) and placed at a holder of an in situ DXAFS cell, and reduced at 613 K for 1.5 h under a flow of hydrogen, followed by evacuation at 573 K for 1 h. It is noteworthy that the amount of residual Cl in the Rh/Al_2O_3 sample was below detection limits by XRF and elemental analysis.

DXAFS measurements in the energy range 23.0–24.2 keV were carried out at BL-9C in KEK-PF. A four-point supporting crystal bender was newly developed for a Si(311) bent-crystal polychromator (Bragg-type) to obtain elliptical optics for focusing incident X-rays on the sample. A self-scanning photodiode array (PDA: 1024 sensing elements: 25 μm width and 2.5 mm height for each element) manufactured by HAMAMATSU Photonics (S3904-1024FX SPL3402) was used as a position-sensitive linear detector. A fiber optical plate embrocated by a CsI(Tl) fluorescent was directly coupled at the active area of PDA to convert X-ray to visible light. The energy calibration at each sensing element of the PDA was performed by comparison with an XAFS spectrum of a Rh foil recorded by using an Si(311) channel-cut monochromator. The in situ DXAFS cell was made of stainless steel and had two slit windows with capton films to measure the incident and transmitted X-rays. The obtained XAFS spectra were analyzed by using the UWXAFS program.[27] After the background subtraction by the AUTOBK program,[28] the Fourier transformation for the k^3-weighted EXAFS oscillation was performed, and the structural parameters were determined by a curve fitting procedure in the *R* space by using the FEFFIT program involving multiple scattering effects.[29] The back scattering amplitude and phase shift functions, and the mean free paths were generated by the FEFF8 code that accounted for energy resolution of the DXAFS spectrometer (4.0 eV). The time-resolved DXAFS spectra were fitted by using a model function composed of four shells, that is, Rh–C–(O) and Rh–(C)–O for carbonyl ligands, Rh–Rh for Rh clusters, and Rh–O at the interface between the Rh cluster and the Al_2O_3 surface. The coordination numbers of Rh–C–(O) and Rh–(C)–O bonds were fixed to be the same. The Debye–Waller factors of all the contributions were fixed at the values obtained by conventional XAFS to reduce the number of independent parameters in the fitting procedure.[30] The validity of this procedure was confirmed for stable Rh species by comparing the Debye–Waller factors obtained by the DXAFS and conventional XAFS. The residual factors for the fitting were typically 4%.

Received: July 8, 2003 [Z52318]
Published Online: September 25, 2003

Keywords: EXAFS spectroscopy · heterogeneous catalysis · reaction mechanisms · solid-state structures · time-resolved spectroscopy

[1] A. C. Yang, C. W. Garland, *J. Phys. Chem.* **1957**, *61*, 1504.
[2] R. R. Cavanagh, T. Yates, Jr., *J. Chem. Phys.* **1981**, *74*, 4150.
[3] P. Basu, D. Panayotov, J. T. Yates, Jr., *J. Am. Chem. Soc.* **1988**, *110*, 2074.
[4] H. D. J. van't Blik, J. B. A. D. van Zon, T. Huizunga, J. C. Koningsberger, R. Prins, *J. Am. Chem. Soc.* **1985**, *107*, 11; H. D. J. van't Blik, J. B. A. D. van Zon, T. Huizunga, J. C. Koningsberger, R. Prins, *J. Am. Chem. Soc.* **1985**, *107*, 3140.
[5] A. Berko, G. Menesi, F. Solymosi, *J. Phys. Chem.* **1996**, *100*, 17732.
[6] A. Berko, F. Solymosi, *J. Catal.* **1999**, *183*, 91.
[7] T. Matsushita, R. P. Phizackerley, *Jpn. J. Appl. Phys.* **1981**, *20*, 2223.

 © 2003 Wiley-VCH Verlag GmbH & Co. KGaA, Weinheim

[8] A. M. Flank, A. Fontaine, A. Jucha, M. Lemonnier, C. Williams, *J. Phys. Lett.* **1982**, *43*, L315.
[9] D. Bazin, H. Dexpert, P. Lagarde, P. Bournonville, *J. Catal.* **1988**, *110*, 209.
[10] A. Fontaine, E. Dartyge, J. P. Itie, A. Jucha, A. Polian, H. Tolentino, G. Tourillon, *Top. Curr. Chem.* **1989**, *151*, 179.
[11] J. W. Couves, J. M. Thomas, D. Waller, R. H. Jones, A. J. Dent, G. E. Derbyshire, G. N. Greaves, *Nature* **1991**, *354*, 465.
[12] G. Sanker, J. M. Thomas, D. Waller, J. W. Couves, C. R. A. Catlow, G. N. Greaves, *J. Phys. Chem.* **1992**, *96*, 7485.
[13] T. Ressler, M. Hagelstein, U. Hatje, W. Metz, *J. Phys. Chem. B* **1999**, *101*, 6680.
[14] N. Hilbrandt, R. Frahm, M. Martin, *J. Phys. IV* **1997**, *7*, 727.
[15] S. G. Fiddy, M. A. Newton, A. J. Dent, G. Salvini, J. M. Corker, S. Turin, T. Campbell, J. Evans, *Chem. Commun.* **1999**, 851.
[16] A. Yamaguchi, T. Shido, Y. Inada, T. Kogure, K. Asakura, M. Nomura, Y. Iwasawa, *Catal. Lett.* **2000**, *68*, 139.
[17] A. Yamaguchi, A. Suzuki, T. Shido, Y. Inada, K. Asakura, M. Nomura, Y. Iwasawa, *Catal. Lett.* **2001**, *71*, 203.
[18] A. Yamaguchi, T. Shido, Y. Inada, T. Kogure, K. Asakura, M. Nomura, Y. Iwasawa, *Bull. Chem. Soc. Jpn.* **2001**, *74*, 801.
[19] S. G. Fiddy, M. A. Newton, C. T. Campbell, J. M. Corker, S. Turin, J. Evans, A. J. Dent, I. Harvey, G. Salvini, *Chem. Commun.* **2001**, 445.
[20] M. A. Newton, D. G. Burnaby, A. J. Dent, S. Diaz-Moreno, J. Evans, S. G. Fiddy, T. Neisius, S. Pascaralli, S. Turin, *J. Phys. Chem. A* **2001**, *105*, 5965.
[21] A. Yamaguchi, A. Suzuki, T. Shido, Y. Inada, K. Asakura, M. Nomura, Y. Iwasawa, *J. Phys. Chem. B* **2002**, *106*, 2415.
[22] M. A. Newton, A. J. Dent, S. Diaz-Moreno, S. G. Fiddy, J. Evans, *Angew. Chem.* **2002**, *114*, 2699; *Angew. Chem. Int. Ed.* **2002**, *41*, 2587.
[23] A. J. Dent, *Top. Catal.* **2002**, 27.
[24] C. Lamberti, C. Prestipino, F. Bonino, L. Capello, S. Bordiga, G. Spoto, A. Zecchina, S. Diaz-Moreno, B. Cremaschi, M. Garilli, A. Marsella, D. Carmello, S. Vidotto, G. Leofanti, *Angew. Chem.* **2002**, *114*, 2447; *Angew. Chem. Int. Ed.* **2002**, *41*, 2341.
[25] F. Meneau, G. Sankar, N. Morgante, R. Winter, C. R. A. Catlow, G. N. Greaves, J. M. Thomas, *Faraday Discuss.* **2003**, *122*, 203.
[26] P. Johnston, R. W. Joyner, *J. Chem. Soc. Faraday Trans.* **1993**, 863.
[27] E. A. Stern, M. Newville, B. Ravel, Y. Yacoby, D. Haskel, *Phys. B* **1995**, *208*, 117.
[28] M. Newville, P. Livins, Y. Yacoby, E. A. Stern, J. J. Rehr, *Phys. Rev. B* **1993**, *47*, 14126.
[29] A. L. Ankudinov, B. Ravel, J. J. Rehr, S. D. Conradson, *Phys. Rev. B* **1998**, *58*, 7565.
[30] E. A. Stern, *Phys. Rev. B* **1993**, *48*, 9825.

 © 2003 Wiley-VCH Verlag GmbH & Co. KGaA, Weinheim

Targeted Hydrogel Synthesis

A New Route to Crystalline Hydrogels, Guided by a Phase Diagram**

Zhibing Hu and Gang Huang*

Monodisperse colloidal systems have been used as models for the study of phase transitions and as templates for the fabrication of photonic crystals.[1–7] Most investigations on colloids are primarily focused on hard-sphere-like particles such as polymethylmethacrylate, silica, or polystyrene.[7] It was found recently that wet and soft poly-*N*-isopropylacrylamide (PNIPAM) nanoparticles can self-assemble into a crystalline array in water.[8–14] However, uses of PNIPAM colloidal dispersions that exploit their crystalline structure are limited because the structure can be easily destroyed by any external disturbance, such as small vibrations. To solve this problem, Asher et al. developed a method for embedding a polystyrene colloidal crystalline array inside a PNIPAM gel.[8,14] Hu et al. demonstrated that the crystalline structure of PNIPAM nanoparticles can be stabilized by bonding the particles into a network.[15,16] The latter approach has the restriction that the particle-linking reaction must be carried out in a harsh environment (pH 12) that could encumber loading with protein drugs. Furthermore, the mechanical strength of the bonded particle assembly was low due to its low polymer concentration. Here we show a new route for the fabrication of crystalline hydrogels that follows a phase diagram. The central idea is to synthesize monodisperse nanoparticles of PNIPAM-*co*-allylamine and measure the phase diagram of their water dispersion. By exploiting the fact that thermally sensitive nanoparticles in colloidal glasses can be converted into ordered crystals by particle-based volume transition, as reported by Lyon et al.,[10] a crystalline hydrogel could be obtained by initiating the crystallization process near the colloidal crystal melting temperature while subsequently bonding the PNIPAM-*co*-allylamine particles below the glass-transition temperature. This can increase the polymer concentration and result in a crystalline hydrogel with higher mechanical strength. Furthermore, allylamine has amino groups that can be covalently bonded in water at neutral pH, but it does not significantly affect the volume phase transition of the PNIPAM polymer. Hydrogels are well known for their unique hydrophilic and environmentally responsive properties, which lead to fascinating applications that include controlled drug delivery, artificial muscles, devices, and sensors.[17–25] Tailoring hydrogels with periodic

[*] Prof. Dr. Z. Hu, G. Huang
Departments of Physics and Chemistry
University of North Texas
P. O. Box 311427, Denton, TX 76203 (USA)
Fax: (+1) 940-565-4824
E-mail: zbhu@unt.edu

[**] This work is supported by the National Science Foundation, the U.S. Army Research Office, the Texas Advanced Technology Program, and Access Pharmaceuticals, Inc. We thank Dr. J. Gao for helpful discussion.

 DOI: 10.1002/anie.200351326 © 2003 Wiley-VCH Verlag GmbH & Co. KGaA, Weinheim

structures under mild synthesis conditions could open a new avenue for these applications.

Monodisperse *N*-isopropylacrylamide (NIPA)-*co*-allylamine colloidal spheres were synthesized by using a precipitation polymerization method.[26] These particles showed phase behavior similar to that of pure PNIPAM gel[27] with a slightly higher volume phase transition temperature around 35 °C. The average hydrodynamic radius of the particles is about 140 nm at 23 °C and shrinks to about 80 nm at 36 °C.

The dispersions with polymer concentrations ranging from 2 to 4 wt % exhibit iridescent colors (Figure 1 a), which

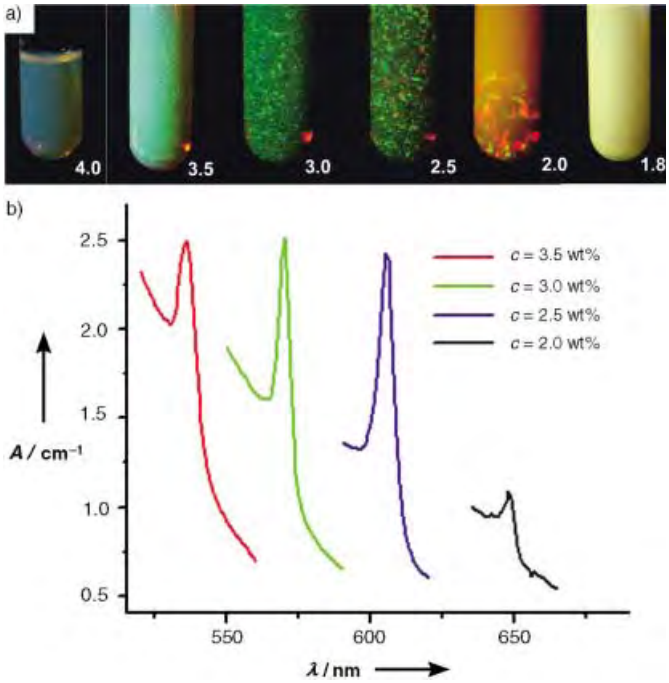


Figure 1. a) Photographs of PNIPAM-*co*-allylamine nanoparticle dispersions at various polymer concentrations at 23 °C. From left to right: 4.0, 3.5, 3.0, 2.5, 2.0, and 1.8 wt %. Here the average hydrodynamic radius of the particles in water at 23 °C is 140 nm. The diameter of the tubes is 1 cm. b) Turbidity versus wavelength curves measured with a UV/Vis spectrophotometer. The Bragg diffraction peak shifts to lower wavelength as the polymer concentration increases. From left to right: 3.5, 3.0, 2.5, and 2.0 wt %.

indicate that the particles self-assemble into an ordered arrangement. As the polymer concentration increases, the crystalline grain size decreases, and the color shifts to shorter wavelengths. When the concentration exceeds 4.5 wt %, the crystals are too small to be observed, and the assemblies are in a glass phase. When the concentration is below 1.8 wt %, the dispersions become cloudy because the particles are well separated and scatter light randomly.

The color observed in the dispersions is due to diffraction from ordered colloidal arrays with a lattice spacing on the order of the wavelength of visible light according to the Bragg law: $2nd\sin\theta = m\lambda$, where n is the mean refractive index of the dispersion, θ the diffraction angle, d the lattice spacing, m the diffraction order, and λ the wavelength of diffracted light.[8] Figure 1 b shows the turbidity of the PNIPAM-*co*-allylamine nanoparticle dispersions as a function of wavelength. The sharp peak is due to Bragg diffraction and shifts from 640 to 530 nm as the polymer concentration increases from 2.0 to 3.5 wt %. This shift is due to the decrease in the interparticle distance with increasing polymer concentration.

Figure 2 a and b show the temperature-dependent turbidity of the PNIPAM-*co*-allylamine colloidal dispersions at 2.5 and 3.0 wt %, respectively. The initial increase in the intensity of the Bragg peak when the temperature is increased above

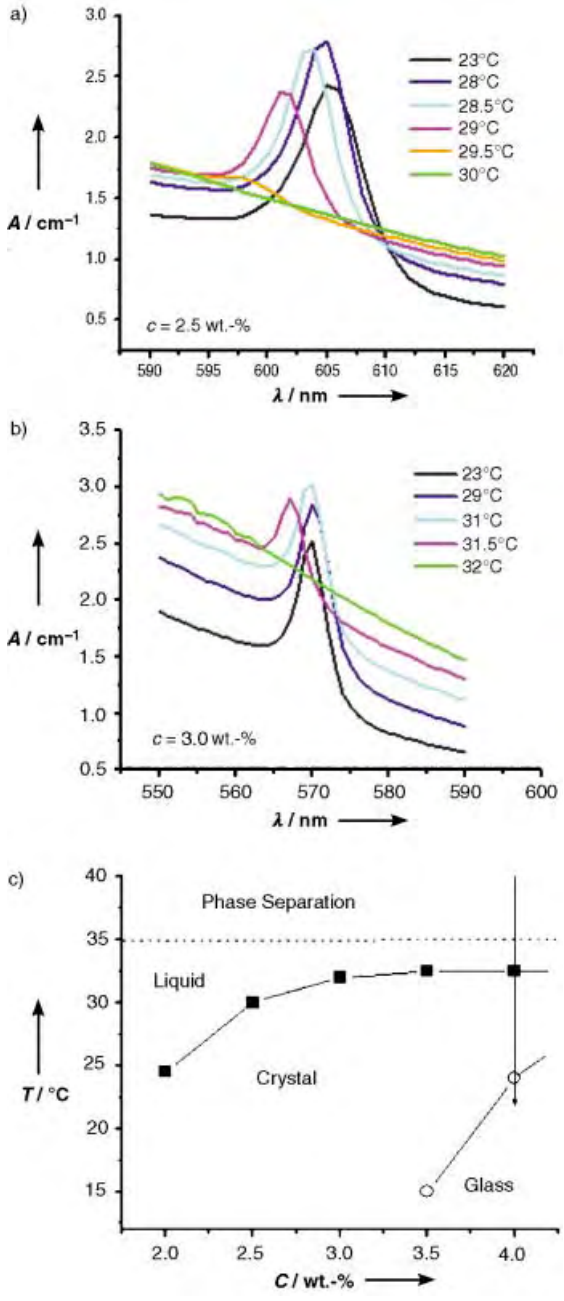
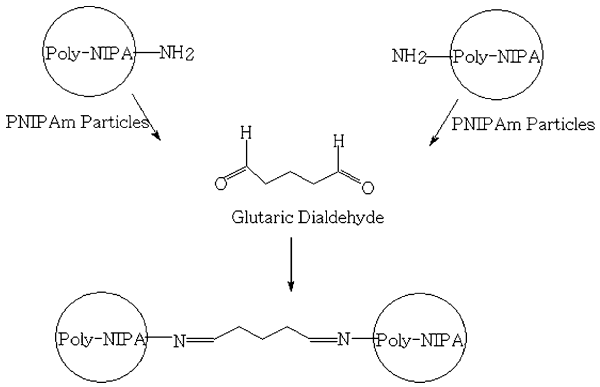


Figure 2. Temperature-dependent phase behavior of the PNIPAM-*co*-allylamine nanoparticle dispersions. a) Turbidity versus wavelength curves at various temperatures for 2.5 wt % dispersion and b) for 3.0 wt % dispersion. c) Phase diagram: the volume phase transition (T_c) of the PNIPAM-*co*-allylamine particles (-----), melting temperature (T_m, ■), and the glass-transition temperature (T_g, ○) are denoted.

 © 2003 Wiley-VCH Verlag GmbH & Co. KGaA, Weinheim

room temperature indicates that heating can facilitate the formation of an ordered structure. As the sample is heated further, the Bragg peak broadens, shifts to shorter wavelength, and eventually disappears at the melting temperature T_m. The value of T_m increases with increasing polymer concentration. This phase behavior is summarized in Figure 2c. Here T_c (dashed line) is the volume phase transition temperature of PNIPA–allylamine particles, T_m (solid squares) is the melting temperature, and T_g (open circles) is the glass-transition temperature.

Guided by this diagram, we engineered a crystalline hydrogel with higher polymer concentration. We started with a PNIPAM-*co*-allylamine particle dispersion of 4.0 wt%, in which the viscosity is too high to allow the particles to form a periodic structure at room temperature. This system was heated from 23 to 40 °C and then cooled back to 23 °C at a rate of about 0.4 K min^{-1}. As indicated by the arrow in Figure 2c, when the sample was cooled to below T_m, crystallization started. Here the dispersion had low viscosity since the particles were only partially swollen. This gave the spheres enough freedom to self-assemble into an ordered array. When the sample was cooled further to below T_g, the particle size and viscosity increased considerably. As a result, the crystalline structure formed at the higher temperature was "frozen" or preserved. Then, the particle assembly with a crystalline structure was fully stabilized by a cross-linking reaction at neutral pH (Scheme 1) over about two days. As a result of the



Scheme 1. The amino groups on the PNIPAM-*co*-allylamine nanoparticles react with glutaric dialdehyde to form a network in water at neutral pH and room temperature.

higher mechanical strength of this crystalline hydrogel, it is easier to remove from the tube than the previous sample formed at room temperature in an aqueous solution at a high pH value.[16] It is apparent that a combination of a covalent bonding process and a heating–cooling process that yields a crystalline structure at a high polymer concentration can significantly improve the mechanical strength of a crystalline hydrogel.

This fabrication process leads to the formation of crystalline hydrogels with different iridescent color patterns. Figure 3 shows blue, green, and red iridescent hydrogels with polymer concentrations of 5.4, 4.0, and 3.5 wt%, respectively. With increasing polymer concentration, the interparticle

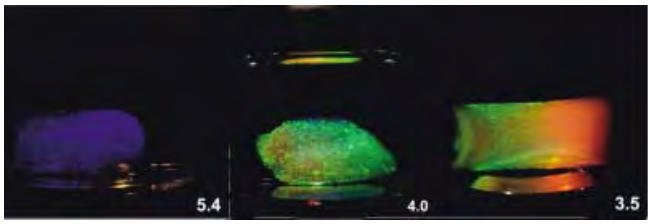


Figure 3. Iridescent colors of the PNIPAM-*co*-allylamine crystal hydrogels made according to Scheme 1 change with polymer concentration in water at pH 7. From left to right: 5.4, 4.0, and 3.5 wt%. The average hydrodynamic radius for the three samples in water at 23 °C is about 140 nm. The diameter of the vial is 2.73 cm.

distance decreases, and a blue shift in the iridescent color results. The angular dependence of the scattering was investigated. The color changes from red to blue when the angle varies from back-scattering to 90°.

Creating crystalline hydrogels allows us to obtain useful functionalities, not only from the periodic structure, but also from the constituent building blocks. Because the building blocks here are environmentally responsive colloidal spheres, their size as well as the lattice spacing should be tunable by external stimuli. Thus, the crystalline hydrogel can serve as an optical sensor to visually reveal environmental changes. An examples is shown in Figure 4a. The crystalline hydrogel at room temperature is bright green. With increasing temper-

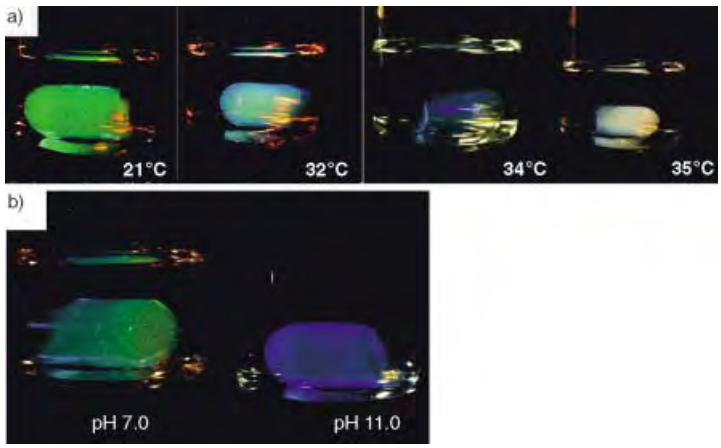


Figure 4. a) The PNIPAM-*co*-allylamine crystal hydrogel changes its iridescent color with temperature. The diameter of the vial is 2.73 cm. From left to right: 21, 32, 34, and 35 °C. b) pH-responsive property of the PNIPAM-*co*-allylamine crystalline hydrogel at pH 7 and pH 11.

ature, the color changes from green to blue at 32 °C, and eventually to milky white at 35 °C, just above the volume phase transition temperature of the particles. When the temperature is decreased to room temperature again, the color and volume of the gel are restored. This process is fully reversible. The color change is due to the decreasing particle size with increasing temperature, which causes a decrease in interparticle spacing. We note that the current hydrogel has iridescent speckles that indicate the existence of large

 © 2003 Wiley-VCH Verlag GmbH & Co. KGaA, Weinheim

crystalline domains, in contrast to previous thermally tunable hydrogels, which have only a uniform color.[15,16]

As a consequence of the presence of basic NH_2 groups on the PNIPAM-*co*-allylamine building blocks, the swelling capacity of the hydrogel can be changed by controlling the pH of the medium. As shown in Figure 4b, the color of the hydrogel shifts from green to blue as the pH changes from 7 to 11. Partial ionization of the amino groups on the particles in water at neutral pH results in swelling of the particles. At higher pH values, ionization of the NH_2 groups is inhibited, and the particles shrink. This variation in size of the building block with pH value changes the lattice spacing and results in a color change.

In summary, monodisperse PNIPAM-*co*-allylamine colloidal spheres have been synthesized by precipitation polymerization. The phase diagram of this system was determined by UV/Vis spectrophotometry. By following the phase diagram, a new route to a crystalline structure with a high polymer concentration was discovered by initiating crystallization near T_m but stabilizing the crystalline structure below T_g. The stabilization is achieved by bonding the PNIPAM-*co*-allylamine spheres with glutaric dialdehyde as a cross-linker at room temperature at neutral pH. The hydrogel with a higher polymer concentration has better mechanical strength, while the mild synthesis at pH 7 makes this material particularly useful for biomedical applications, such as loading biomolecules between the particles for controlled drug delivery. The crystalline hydrogels exhibit iridescent patterns that are tunable by changing the temperature or pH value. Such soft and wet hydrogels with periodic structures may lead to new sensors, devices, and displays that operate in the aqueous solutions in which most biological and biomedical systems reside.

Experimental Section

Hydrogel nanoparticles: NIPA monomer (3.845 g), allylamine monomer (0.2 g, 10% molar ratio), methylene bisacrylamide (0.1315 g; cross-linker), sodium docecyl sulfate (0.0755 g; surfactant), and deionized water (230 mL) were mixed in a reactor. The solution was heated to 60 °C with nitrogen bubbling for about 40 min, and potassium persulfate (0.155 g) dissolved in deionized water (20 mL) was added to initiate the reaction. The reaction was carried out at 60 °C for 5 h. The resulting particle dispersions were dialyzed for 7 days to remove small molecules and surfactants.

Light-scattering: The temperature-dependent average hydrodynamic radius and its distribution of the PNIPAM-*co*-allylamine particles in dilute dispersions were measured on a light-scattering spectrometer (ALVCo., Germany) at a scattering angle of 60°.

UV/Vis spectrophotometry: The PNIPAM-*co*-allylamine particle dispersions were condensed in an ultracentrifuge at 40000 rpm for 2 h. The polymer concentration of a dispersion was obtained by completely drying the dispersion at 60 °C and then weighing it. The turbidity of the PNIPAM-*co*-allylamine nanoparticle dispersions as a function of the wavelength was determined on a UV/Vis spectrophotometer (Agilent 8453).[12]

Synthesis of crystalline hydrogels: A 4.0 wt% PNIPAM-*co*-allylamine particle dispersion was heated from 23 to 40 °C and then cooled back to 23 °C at a rate of about 0.4 K min^{-1}. Then glutaric dialdehyde (0.04 g) was added to the top of the dispersion to act as a cross-linker. This reagent diffused through the dispersion and covalently bonded the particles together at neutral pH as illustrated in Scheme 1. The particle assembly with a crystalline structure was stabilized by the cross-linking reaction over about 2 days, and removed from the test tube by injecting water into the bottom of the tube with a syringe.

Received: March 4, 2003 [Z51326]

Keywords: colloids · gels · nanostructures · phase diagrams · self-assembly

[1] P. N. Pusey in *Liquid, Freezing, and the Glass Transition* (Eds.: J. P. Les Houches, H. D. Levesque, J. Zinn-Justin), Elsevier, Amsterdam, **1990**, pp. 763–942.
[2] A. V. Blaaderen, R. Ruel, P. Wiltzius, *Nature* **1997**, *385*, 321.
[3] Z. Cheng, W. B. Russel, P. M. Chaikin, *Nature* **1999**, 401, 893.
[4] P. Jiang, J. F. Bertone, V. L. Colvin, *Science* **2001**, *291*, 453.
[5] J. M. Jethmalani, H. B. Sunkara, W. T. Ford, S. L. Willoughby, B. J. Ackerson, *Langmuir* **1997**, *13*, 2633, and references therein.
[6] C. Lellig, W. Hartl, J. Wagner, R. Hempelmann, *Angew. Chem.* **2002**, *114*, 108; *Angew. Chem. Int. Ed.* **2002**, *41*, 102.
[7] Y. Xia, B. Gates, Y. Yin, Y. Lu, *Adv. Mater.* **2000**, *12*, 693; Y. Xia, *Adv. Mater.* **2001**, *13*, 369.
[8] J. M. Weissman, H. B. Sunkara, A. S. Tse, S. A. Asher, *Science* **1996**, 274, 959.
[9] H. Senff, W. Richtering, *Langmuir* **1999**, *15*, 102.
[10] J. D. Debord, L. A. Lyon, *J. Phys. Chem. B* **2000**, *104*, 6327; J. D. Debord, S. Eustis, S. B. Debord, M. T. Lofye, L. A. Lyon, *Adv. Mater.* **2002**, *14*, 658.
[11] T. Hellweg, C. D. Dewhurst, E. Bruckner, K. Kratz, W. Eimer, *Colloid Polym. Sci.* **2000**, *278*, 972.
[12] J. Gao, Z. B. Hu, *Langmuir* **2002**, *18*, 1360.
[13] J. Z. Wu, B. Zhou, Z. B. Hu, *Phys. Rev. Lett.* **2003**, *90*, 048304; J. Z. Wu, G. Huang, Z. B. Hu, *Macromolecules* **2003**, *36*, 440.
[14] J. H. Holtz, S. A. Asher, *Nature* **1997**, *389*, 829.
[15] Z. B. Hu, X. H. Lu, J. Gao, C. J. Wang, *Adv. Mater.* **2000**, *12*, 1173.
[16] Z. B. Hu, X. H. Lu, J. Gao, *Adv. Mater.* **2001**, *13*, 1708.
[17] N. A. Peppas, R. Langer, *Science* **1994**, *263*, 1715.
[18] T. Tanaka, I. Nishio, S. T. Sun, S. Ueno-Nishio, *Science* **1982**, *218*, 467.
[19] R. A. Siegel, B. A. Firestone, *Macromolecules* **1988**, *21*, 3254.
[20] Y. Osada, H. Okuzaki, H. Hori, *Nature* **1992**, *355*, 242.
[21] G. Chen, A. S. Hoffman, *Nature* **1995**, *373*, 49.
[22] Y. Osada, J. P. Gong, *Adv. Mater.* **1998**, *10*, 827.
[23] M. J. Snowden, M. J. Murray, B. Z. Chowdry, *Chem. Ind.* **1996**, 531.
[24] C. Wang, R. J. Stewart, J. Kopecek, *Nature* **1999**, *397*, 417.
[25] A. Lendlein, S. Kelch, *Angew. Chem.* **2002**, *114*, 2138; *Angew. Chem. Int. Ed.* **2002**, *41*, 2034.
[26] R. H. Pelton, P. Chibante, *Colloids Surf.* **1986**, *20*, 247.
[27] Y. Hirotsu, T. Hirokawa, T. Tanaka, *J. Chem. Phys.* **1987**, *87*, 1392.

 © 2003 Wiley-VCH Verlag GmbH & Co. KGaA, Weinheim

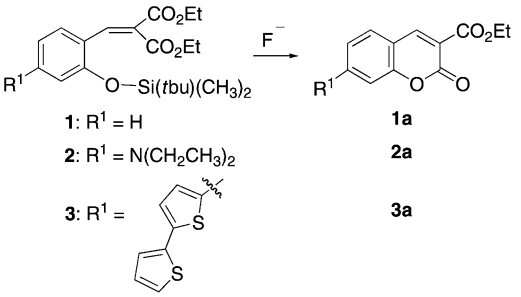
Ion Sensors

A Fluorescent Self-Amplifying Wavelength-Responsive Sensory Polymer for Fluoride Ions**

*Tae-Hyun Kim and Timothy M. Swager**

Fluoride, the smallest anion, has unique chemical properties and its recognition and detection are of growing interest because it is associated with nerve gases and the refinement of uranium used in nuclear weapons manufacture. As a result, there is a need to develop new selective and sensitive methods for fluoride detection in environments that are not easily served by conventional ion-selective electrodes. Most of the emerging detection methods have focused on receptors that differentiate fluoride from other anions, such as chloride, phosphate, or nitrate and convert the binding into an electrochemical or optical response.[1] These efforts have enjoyed success and in some cases have resulted in the ability to visually detect fluoride ions.[2–4]

An approach to greater sensitivity in fluorescence detection schemes is to use the exciton-transporting properties of semiconducting polymers to amplify perturbations (transduction events) produced by analyte binding. These methods were originally demonstrated using electron-transfer quenching[5a] and variations on this scheme have been used to create a number of chemical and biological sensory methods, most of which involve changes in the emission intensities.[5] In spite of these successes, it is generally preferable for a fluorescence sensory signal to involve a new emission at a different wavelength rather than a modulation of an existing signal. The advantage of the latter approach is that a new signal is inherently easier to detect than an intensity change. Furthermore, nonspecific chemical interactions are more likely to produce intensity changes than new signals, hence we can also expect specificity gains in properly designed sensors that create new emissions. Fluorescence resonance energy transfer (FRET) is broadly used to produce new emissive signals and the amplification of these processes through intramolecular energy transfer from conjugated polymers has been demonstrated.[6] New analyte-triggered emissions, if optimally deployed, offer high specificity and low background. In consideration of how to best construct such a system for the selective detection of fluoride ions we have decided to explore schemes using the unique chemical reactivity of fluoride ions with silicon,[7] rather than elaborate receptors. In a fusion of these different elements, we report herein a fluoride-sensing system in which a fluoride triggered Si–O bond cleavage results in the formation of a highly fluorescent coumarin [Eq. (1)] and show how the interconnection of this transduction element to a conjugated polymer produces a 100-fold sensitivity enhancement.



(1)

Our decision to focus on the fluoride-ion-triggered formation of coumarins, was based upon the fact that coumarins are laser dyes with high radiative quantum yields.[8] To this end we synthesized a series of coumarin derivatives with varying electron-donating groups in the 7-position of the coumarin to tune the absorption and emission wavelengths as shown (compounds **1a**–**3a** in Table 1). The synthesis of the indicators involved a two-step sequence, namely silylation of the corresponding 2-hydroxy benzaldehyde, followed by a condensation reaction under the modified Knoevenagel conditions.[9] The *tert*-butyldimethylsilyl (TBS) group was chosen as the protecting group for the phenols to promote selectivity to fluoride by rendering indicator **2** stable (unreactive) to likely interferents. Indeed **2** is stable in THF solutions containing an excess of chloride ions (tetrabutylammonium salt). To avoid a possible problematic *trans–cis* isomerization of the double bond, we used diethyl malonate to introduce symmetrically substituted double bonds in **1, 2**, and **3**.

Table 1: Photophysical data in dichloromethane.

Compound	Abs. max.[a] ($\log\varepsilon$)	Emission max.[a]	Φ [%][b]
1	322 (3.66)	–	<0.01
2	386 (4.31)	450	0.2
3	384 (4.43)	489	0.8
4	378 (4.76)[c]	482	12
1a	334 (3.71)	415	12
2a	417 (4.39)	450	81
3a	412 (4.64)	529	37
4a	396 (4.80)[c]	517	30

[a] Given in nanometers. [b] Determined with quinine sulfate as a standard. [c] Per monomer unit.

The cyclization reaction is irreversible and produces a time-dependent dosimetric response that is controlled by the reaction kinetics. The rate of the cyclization of **2** to **2a** in THF solution was monitored by fluorescence and found to be first order in **2**, independent of fluoride (tetrabutylammonium salt, TBAF), and relatively slow with a rate constant of $k = 2 \times 10^{-4}\ s^{-1}$. The rate constants do not change for the ranges from

[*] Prof. Dr. T. M. Swager, Dr. T.-H. Kim
Department of Chemistry
Massachusetts Institute of Technology
Cambridge, MA 02139 (USA)
Fax: (+1) 617-253-7929
E-mail: tswager@mit.edu

[**] We are grateful for research funding from the Department of Energy, Nuclear Nonproliferation Program.

Supporting information for this article is available on the WWW under http://www.angewandte.org or from the author.

 DOI: 10.1002/anie.200352075 © 2003 Wiley-VCH Verlag GmbH & Co. KGaA, Weinheim

0.5 to 3 molar ratio of fluoride ion relative to **2**. Hence it appears that the silyl cleavage (or fluoride association with the silyl) is fast and that the cyclization is the slow step. With a higher 10-fold excess of fluoride ion there is an enhancement in the rate, and a saturation of the emission intensity is observed in approximately 2 h (Figure 1 a). The rate acceleration at high fluoride concentrations suggests additional ionic associations with the tetrabutylammonium fluoride (TBAF) salt. The non-innocence of excess fluoride is further revealed by additional peaks in absorbance spectra of **2a** (Figure 1 a inset) that are present at high TBAF concentration but absent after an aqueous extraction.

To impart greater sensitivity to our fluoride-induced-lactonization detection scheme, we designed semiconductor-polymer–indicator conjugates that could amplify the response. Amplification of a turn-on sensor can in principle be performed by bringing a chromophore of the proper spectral characteristics near to the polymer to achieve FRET. Indeed our purpose in synthesizing **3a** which has a longer-wavelength emission was to enable this type of detection scheme. However, in spite of our chromophore engineering, the cyclized coumarins lacked the proper energy matching with poly(phenylene ethynylene)s (PPEs), whose optical and electronic properties are well suited for this fluorescent sensory application.[5]

To overcome the constraints of FRET we pursued a potentially more powerful approach wherein the electronic character of the indicator is strongly electronically coupled to the band structure of the polymer. This approach enables an additional energy-transfer mechanism (known as Dexter energy transfer for small molecules) wherein activation of an indicator locally perturbs the band gap of the polymer. This approach is further attractive because detailed fluorescence-depolarization studies have shown that the strong electronic coupling (band structure) in PPEs contributes more to energy transfer than Förster energy transfer, the basis of FRET schemes.[10] Hence in strongly electronically coupled conjugation schemes a few cyclization events triggered by fluoride ions will produce local minima in the band gap that trap mobile excitons to give a new emission (Figure 2).[11] The facile transport of excitons in semiconductive organic polymers allow these polymers to sample many potential transduction sites and thereby dramatically increase the probability of emission from a lower-energy-trapping (cyclized) site. The result is an amplified turn-on sensory scheme.

In designing PPE-conjugates we sought to develop a general scheme that could be exploited for future indicator systems. In addition, band-gap engineering by the interconnection of pendant chro-

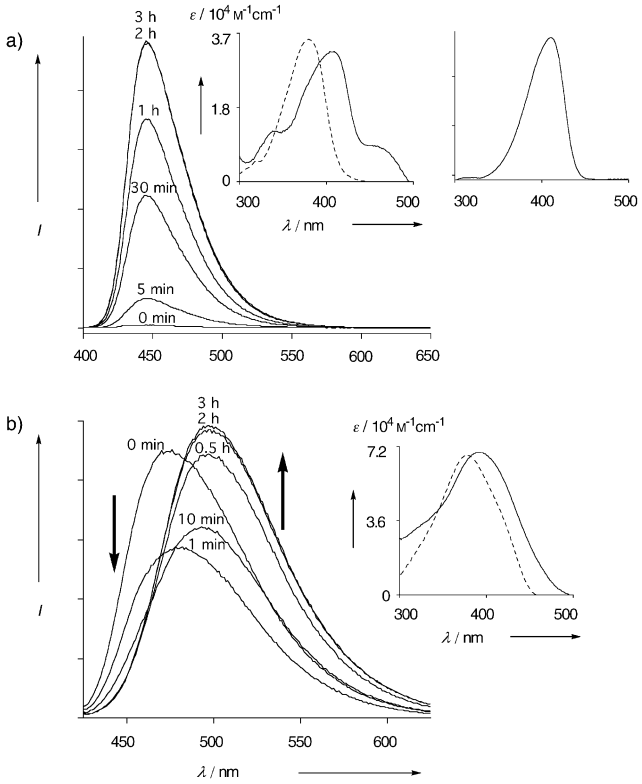


Figure 1. Emission changes of indicator **2** (a) and sensory polymer **4** (b) upon addition of TBAF. The insets show the respective absorption spectra of the initial solution (0 min, -----) and after exposure to TBAF (2 h, ——). The second inset (top right) is the absorption spectrum of **2a** after aqueous extraction, which removes absorptions that appear to be the result of interactions with fluoride ion. Experimental conditions: 298 K in all cases. a) **2**, 3.2×10^{-6} M in THF and TBAF, 33×10^{-6} M; b) **4**, 1.5×10^{-6} M in CH_2Cl_2 (repeating group concentration) and TBAF, 1.6×10^{-7} M. For the polymer **4** $\lambda_{max}=378$ nm, $\varepsilon=57\,600\ M^{-1}cm^{-1}$; emission $\lambda_{max}=482$ nm and **4a** $\lambda_{max}=396$ nm, $\varepsilon=63\,400\ M^{-1}cm^{-1}$; emission $\lambda_{max}=517$ nm.

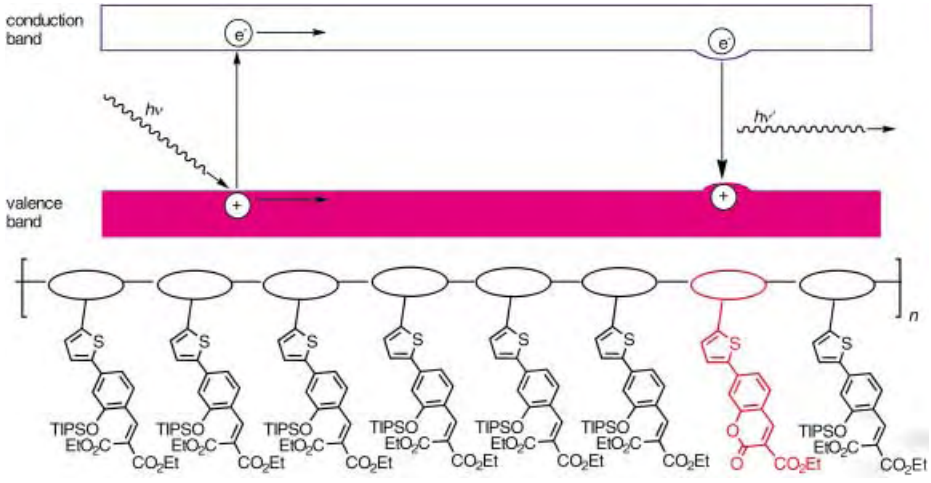


Figure 2. Schematic band diagram illustrating the mechanism by which a semiconductive polymer can produce an enhancement in a new fluorescence chemosensory response. The horizontal dimension represents the position along the polymer backbone shown schematically at the bottom. Excitons are created by absorption of a photon ($h\nu$) and then migrate along the backbone. Fluoride-induced lactonization in the side-chains produces a trapping site with a smaller band gap (E_g) and recombination of excitons at that site results in a new amplified emission.

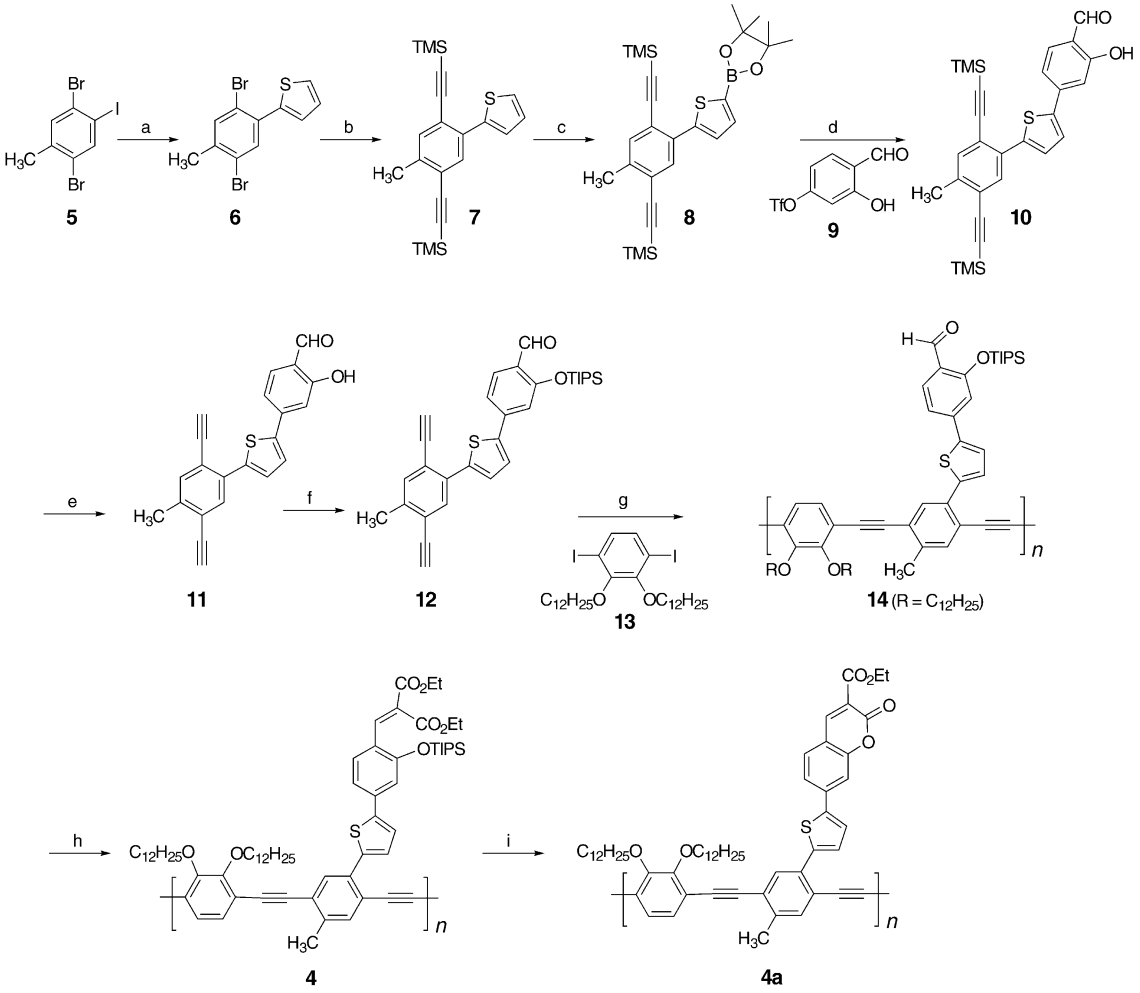
 © 2003 Wiley-VCH Verlag GmbH & Co. KGaA, Weinheim

mophores to semiconducting polymers is applicable to other electrooptical technologies. Our semiconductive-sensory-polymer designs have focused on the PPE-based material **4** (Scheme 1), in which a thiophene-bridge connects the sensory *o*-silyloxybenzylidene malonate moiety with the polymer backbone.[12] Thiophene is the linkage of choice because its strong π-electron delocalizing nature will relay electronic perturbations in the side-chains to the conjugated backbone and it is synthetically versatile.

The synthesis of sensory polymer **4** is shown in Scheme 1.[13] Bis(trimethylsilylethynyl)phenyl thiophene **7**, obtained from **5** by selective Stille cross-coupling and subsequent Sonogashira cross-coupling reactions, was derivatized to the corresponding dioxaborolane **8**. A further cross-coupling reaction with the appropriate triflate **9**[14] produced the thiophene-bridged diaryl compound **10**. Desilylation of diethynylenes using TBAF, followed by silylation of phenol with TIPSCl, gave the monomer **12**.[15] A Sonogashira cross-coupling polymerization provided polymer **14**.[16] As a final step we modified polymer **14** using a titanium-mediated Knoevenagel reaction with diethyl malonate to produce the desired sensory polymer **4**.

The effect of coumarin formation on the band gap of polymer **4** is readily apparent by inspection of the absorption and emission spectra before and after quantitative conversion into **4a** by treatment with an excess of TBAF. As expected, both absorbance and emission spectra of the coumarin-containing form **4a** in dichloromethane solution were red-shifted compared to those of its precursor **4** (Figure 1b). Moreover, the emission change from blue to blue-green is readily detected visually. Cyclization also caused a significant increase in the fluorescence quantum yield of the conjugated polymer (**4**: $\Phi = 0.12$; **4a**: $\Phi = 0.30$). These results indicate that we can trigger a strong change in photophysical properties of PPEs using an electronic perturbation from the appended indicator. The gel permeation chromatography (GPC) analysis of the polymer **4** and **4a** revealed molecular weights of $M_n = 1.06 \times 10^4$ and $M_n = 1.05 \times 10^4$, respectively.

Fluorescence studies reveal that our amplification scheme is highly effective. Kinetic studies for the polymer **4** were not



Scheme 1. Reagents and conditions: a) 2-tributylstannylthiophene, $[PdCl_2(PPh_3)_2]$, DMF, 80 °C, 12 h, 76%; b) TMSA, $[Pd(PPh_3)_4]$, CuI, toluene/DIPA 4:1, 80 °C, 20 h, 76%; c) *t*BuLi, THF, −70 °C, 90 min, then 2-isopropoxy-4,4,5,5-tetramethyl-1,3,2-dioxaborolane, RT, 4 h, 59%; d) $[Pd(PPh_3)_4]$, triethylamine, DMF, 100 °C, 24 h, 64%; e) TBAF, THF, RT, 1 h; f) TIPSCl, imidazole, DMF, RT, 2 h, 75% over two steps; g) $[Pd(PPh_3)_4]$, CuI, toluene/DIPA 4:1, 65 °C, 24 h, 43%; h) $TiCl_4$ in CCl_4 to THF, 0 °C, then **14** and diethylmalonate in THF, then pyridine in THF, 0 °C, 1 h and RT, 2 h, 88%; i) TBAF, THF, RT, 3 h, 98%. TMSA = trimethylsilylacetylene, DIPA = diisopropylamine.

 © 2003 Wiley-VCH Verlag GmbH & Co. KGaA, Weinheim

possible in the same way as for the small molecule **2**, because the fluorescence quantum yield of the polymer varies as a function of conversion and at low conversion we observe less efficient emission. Nevertheless, it is clear that the polymer **4** has a faster response to fluoride ion (Figure 1b). The enhanced fluoride sensitivity of **4** relative to **2** is clearly evident when one considers that exposure of **4** (1.5×10^{-6} M based upon the repeating group) to fluoride (1.6×10^{-7} M, TBAF in THF) results in a complete transformation of the fluorescence intensity maximum of **4** in 2 h, whereas **2** required a 100-fold higher fluoride concentration to achieve a complete fluorescence transformation over the same time with all other conditions the same (Figure 1). Hence we conclude that **4** is approximately 100-times more sensitive than its small-molecule-based counterpart **2**. This amplification factor is in accord with our previous determination of exciton diffusion in isolated polymers.[5a] We further note that energy migration within isolated polymers (i.e. dilute solutions) is inherently inefficient owing to the one-dimensional exciton diffusion.[17] Thin films that display two- and three-dimensional transport characteristics exhibit more favorable transport statistics and also benefit from improved Förster energy-transfer process between polymer chains. Unfortunately **4** is strongly quenched in thin films, however, it should be possible to generate related indicator materials with desirable solid-state properties and much larger amplification factors in the future.

In summary, we have introduced a new system for the detection of fluoride ion and successfully amplified the response using exciton migration in a semiconducting organic polymer. In contrast to most semiconductive-polymer sensor schemes that rely on changes in emission intensity, this sensory system utilizes a new fluorescence signal. The approach of directly interconnecting the indicator electronically with the polymer's band structure is a promising alternative to FRET schemes and we intend to apply this approach to other analytes of interest.

Received: June 6, 2003 [Z52075]
Published Online: September 23, 2003

Keywords: fluorescence · fluorides · materials science · polymers · sensors

[1] a) C. Dusemund, K. R. A. S. Sandanayake, S. Shinkai, *J. Chem. Soc. Chem. Commun.* **1995**, 333; b) H. Yamamoto, A. Ori, K. Ueda, C. Dusemund, S. Shinkai, *Chem. Commun.* **1996**, 407; c) C. R. Cooper, N. Spencer, T. D. James, *Chem. Commun.* **1998**, 1365; d) M. Nicolas, B. Fabre, J. Simonet, *Chem. Commun.* **1999**, 1881; e) C. B. Black, B. Andrioletti, A. C. Try, C. Ruiperez, J. L. Sessler, *J. Am. Chem. Soc.* **1999**, *121*, 10438, and references therein; f) H. Miyaji, W. Sato, J. L. Sessler, *Angew. Chem.* **2000**, *112*, 1847; *Angew. Chem. Int. Ed.* **2000**, *39*, 1777; g) S. Mason, J. M. Llinares, M. Morton, T. Clifford, K. Bowman-James, *J. Am. Chem. Soc.* **2000**, *122*, 1814; h) M. Takeuchi, T. Shioya, T. M. Swager, *Angew. Chem.* **2001**, *113*, 3476; *Angew. Chem. Int. Ed.* **2001**, *40*, 3372; i) For a recent review on anion recognition, see: P. D. Beer, P. A. Gale, *Angew. Chem.* **2001**, *113*, 502; *Angew. Chem. Int. Ed.* **2001**, *40*, 486.

[2] a) H. Miyaji, J. L. Sessler, *Angew. Chem.* **2001**, *113*, 158; *Angew. Chem. Int. Ed.* **2001**, *40*, 154.

[3] a) J. J. Lavigne, E. V. Anslyn, *Angew. Chem.* **1999**, *111*, 3903; *Angew. Chem. Int. Ed.* **1999**, *38*, 3666.

[4] S. Yamaguchi, S. Akiyama, K. Tamao, *J. Am. Chem. Soc.* **2001**, *123*, 11372.

[5] a) Q. Zhou, T. M. Swager, *J. Am. Chem. Soc.* **1995**, *117*, 12593; b) J.-S. Yang, T. M. Swager, *J. Am. Chem. Soc.* **1998**, *120*, 5321; c) J.-S. Yang, T. M. Swager, *J. Am. Chem. Soc.* **1998**, *120*, 11864; d) T. M. Swager, *Acc. Chem. Res.* **1998**, *31*, 201; e) D. T. McQuade, A. E. Pullen, T. M. Swager, *Chem. Rev.* **2000**, *100*, 2537; f) for a recent review, see: T. M. Swager, J. H. Wosnick, *MRS Bull.* **2002**, *27*, 446.

[6] D. T. McQuade, A. H. Hegedus, T. M. Swager, *J. Am. Chem. Soc.* **2000**, *122*, 12389.

[7] For another sensor approach that used the affinity of fluoride to silicon see: S. Yamaguchi, S. Akiyama, K. Tamao, *J. Am. Chem. Soc.* **2000**, *122*, 6793.

[8] K. D. Drexhage in *Dye Lasers, Vol. 1* (Ed.: F. P. Schäfer), Springer, New York, **1977**.

[9] a) W. Lehnert, *Tetrahedron Lett.* **1970**, 4723; b) M. Black, J. I. G. Cadogan, H. McNab, A. D. MacPherson, V. P. Roddam, C. Smith, H. R. Swenson, *J. Chem. Soc. Perkin Trans. 1* **1997**, 2483.

[10] A. Rose, C. G. Lugmair, T. M. Swager, *J. Am. Chem. Soc.* **2001**, *123*, 11298.

[11] T. M. Swager, C. J. Gil, M. S. Wrighton, *J. Phys. Chem.* **1995**, *99*, 4886.

[12] The alternative approach to develop PPE based on the 3,6-diethynyl-2-hydroxy-benzaldehyde was not pursued, as *o*-phenoxyacetylenes could undergo tandem cyclization to the corresponding benzofuran by use of TBAF or CsF, for example, see: A. Sakai, T. Aoyama, T. Shioiri, *Heterocycles* **2000**, *52*, 643.

[13] See Supporting Information for details.

[14] 2-Hydroxy-4-(trifluoromethanesulfonyl) benzaldehyde (**9**) was obtained by treating 4-hydroxy-2-methoxybenzaldehyde with triflic anhydride in pyridine (95%), followed by demethylation involving BBr_3 in CH_2Cl_2 at −40 °C (79%). See also Supporting Information.

[15] Triisopropylsilyl group (TIPS) was used instead of *tert*-butyldimethylsilyl (TBS) as the thermal polymerization conditions required a more stable protecting group for phenol.

[16] 1,4-Diiodobenzene with *ortho*-dialkoxy side-chains **13** was chosen as a comonomer to produce a sensory polymer with higher frequencies (blue-shifted). Z. Zhu, T. M. Swager, *Org. Lett.* **2001**, *3*, 3471.

[17] I. A. Levitsky, J. Kim, T. M. Swager, *J. Am. Chem. Soc.* **1999**, *121*, 1466.

 © 2003 Wiley-VCH Verlag GmbH & Co. KGaA, Weinheim

Directed Evolution

Directed Evolution of an Amine Oxidase Possessing both Broad Substrate Specificity and High Enantioselectivity**

*Reuben Carr, Marina Alexeeva, Alexis Enright, Tom S. C. Eve, Michael J. Dawson, and Nicholas J. Turner**

Enantiomerically pure chiral amines are of increasing value in organic synthesis, especially as resolving agents,[1] chiral auxiliaries/chiral bases,[2] and catalysts for asymmetric synthesis.[3] In addition, chiral amines often possess pronounced biological activity in their own right and hence are in demand as intermediates for agrochemicals and pharmaceuticals.[4] Current methods for the preparation of enantiomerically pure chiral amines are largely based upon the resolution of racemates, either by recrystallization of diastereomeric salts[5] or by enzyme-catalyzed kinetic resolution of racemic substrates using lipases and acylases.[6] To develop more efficient methods, attention is turning towards asymmetric approaches or their equivalent, for example, the asymmetric hydrogenation of imines[7] or the conversion of ketones into amines by using transaminases.[8] Attempts to develop dynamic kinetic resolutions, which employ enzymes in combination with transition-metal catalysts, have unfortunately been hampered by the harsh conditions required to racemize amines.[9]

Recently we reported a novel catalytic method for the preparation of optically active chiral amines by deracemization of the corresponding racemic mixture (Figure 1).[10] The deracemization approach relies upon coupling an enantioselective amine oxidase with a nonselective reducing agent to effect stereoinversion of the *S* to *R* enantiomer via the intermediate achiral imine.

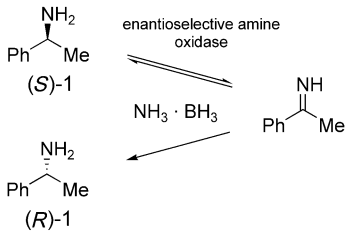


Figure 1. Deracemization of α-methylbenzylamine using an enantioselective amine oxidase in combination with ammonia·borane as the reducing agent.

The *S* enantiomer selective amine oxidase used for the deracemization of (*R/S*)-α-methylbenzyl amine was identified from a library of variants of the wild-type enzyme, from *Aspergillus niger*, by using a high-throughput colorimetric screen to guide selection.[10] The library of variants was generated by randomly mutating the plasmid harboring the amine oxidase gene by using the *E. coli* XL1-Red mutator strain. Using (*S*)-α-methylbenzylamine as the target substrate we were able to identify a variant (Asn336Ser) that possessed significantly improved catalytic activity (47 fold) and enantioselectivity (sixfold) towards this particular substrate compared to the wild type enzyme. To explore the opportunities for using this variant amine oxidase to deracemize other racemic chiral amines we decided to undertake a more detailed study of its substrate specificity. Herein we show that the Asn336Ser variant possesses broad substrate specificity and high enantioselectivity towards a wide range of chiral amines.

Prior to carrying out further studies with the Asn336Ser amine oxidase, an additional mutation was introduced into the sequence (Met348Lys) that resulted in a variant enzyme (hereafter referred to as Asn336Ser) with higher specific activity and expression levels although its substrate specificity appeared unchanged (data not shown). Incorporation of an *N*-terminal histidine tag into the amine oxidase allowed facile purification of both the wild-type and Asn336Ser variant in one step, by a nickel-affinity column, to yield protein of $>90\,\%$ purity as evidenced by gel electrophoresis (Figure 2, see Experimental Section). Solutions of the amine oxidases prepared in this manner were used for all the subsequent substrate specificity studies.

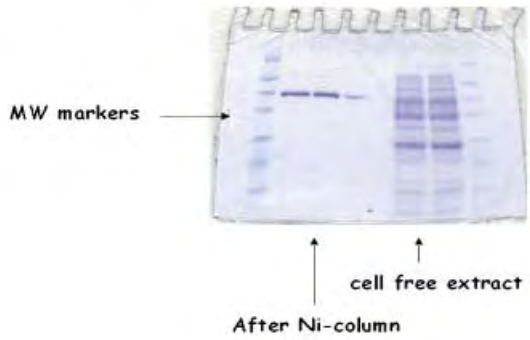


Figure 2. Polyacrylamide gel of amine oxidase enzyme after affinity purification on a nickel column.

A panel of amine substrates **1**–**51**, with broad structural features, was selected to characterize both the wild-type amine oxidase and Asn336Ser variant (Figure 3). Each substrate was screened individually, at 10 mM substrate concentration, against the partially purified wild-type and mutant amine oxidase in 96-well microtitre plate format using a UV/Vis plate-reader. The rate of oxidation was monitored by measuring hydrogen peroxide production by using a coupled enzyme assay.[11] For each substrate the k_{cat} and K_m values were calculated but for clarity only the relative activities are shown. These values have been calculated by

[*] Prof. Dr. N. J. Turner, R. Carr, M. Alexeeva, Dr. A. Enright, T. S. C. Eve
School of Chemistry
The University of Edinburgh
King's Buildings, West Mains Road, Edinburgh EH9 3JJ (UK)
Fax: (+44) 131 650 4717
E-mail: n.j.turner@ed.ac.uk
Dr. M. J. Dawson
GlaxoSmithKline R&D
Medicines Research Centre
Gunnels Wood Road, Stevenage, Hertfordshire, SG1 2NY (UK)

[**] We are grateful to the BBSRC and GlaxoSmithKline for funding a postdoctoral fellowship (MA) and CASE awards (RC, AE). We also thank the Wellcome Trust for financial support.

 DOI: 10.1002/anie.200352100 © 2003 Wiley-VCH Verlag GmbH & Co. KGaA, Weinheim

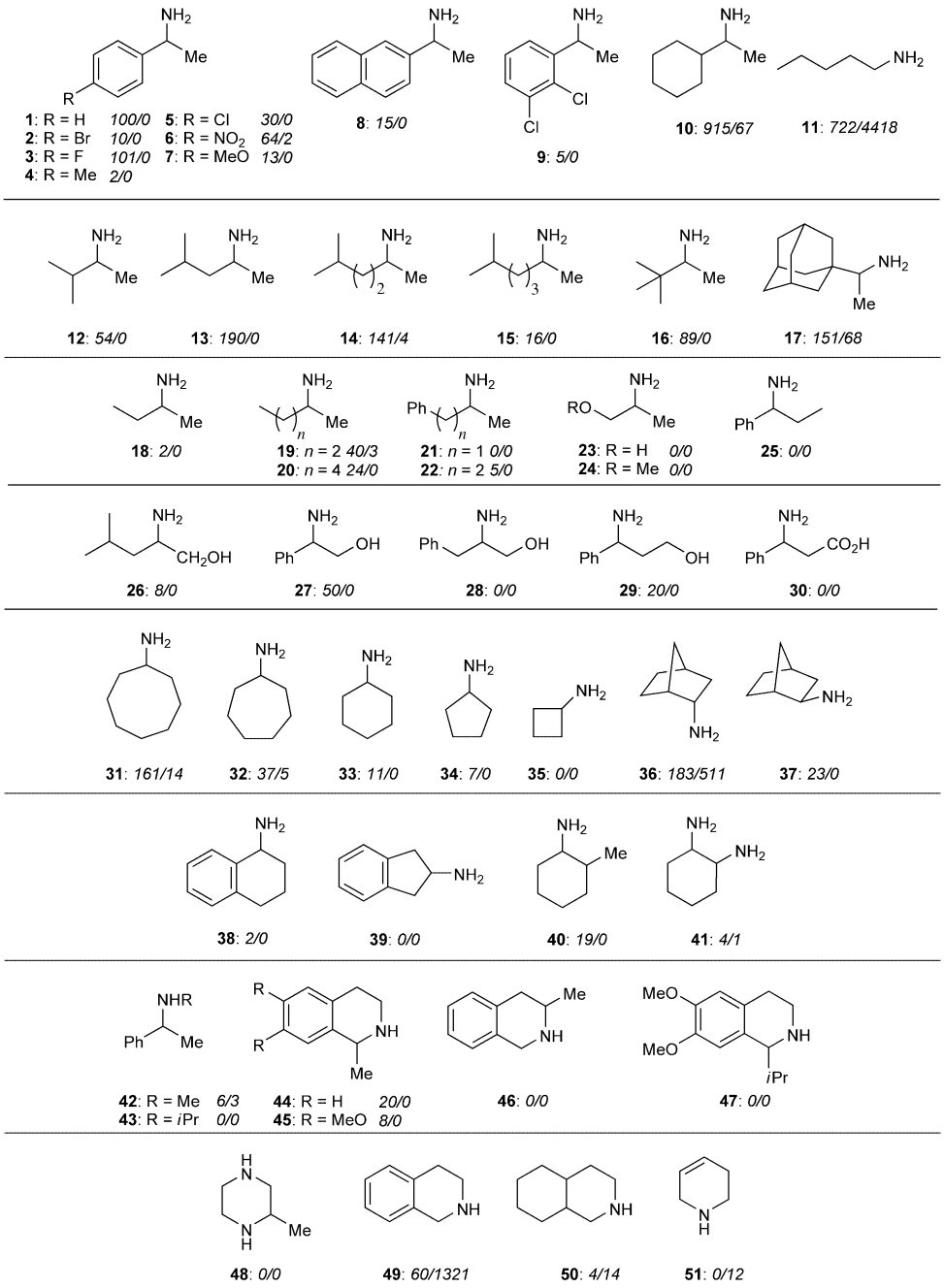


Figure 3. Panel of amines used in the screening experiments. Numbers in italics beneath the structures refer to relative rates of oxidation for Asn336Ser mutant/wild-type enzyme compared to α-methylbenzylamine.

setting the activity of the Asn336Ser variant towards α-methylbenzylamine as 100% and reporting all other rates as relative values. In addition, for a number of the chiral racemic substrates which gave positive assay results, the individual *R* and *S* enantiomers were also examined to determine the enantioselectivity of the reaction.

The wild-type amine oxidase was found to be inactive towards most of the amines shown in Figure 3. Of the 51 substrates examined, only nine gave relative activities of over 5%. The wild-type enzyme is most active towards simple straight-chain amines (e.g. pentylamine (**11**)) and generally shows poor activity towards more sterically demanding branched amines. By comparison, however, the Asn336Ser variant amine oxidase showed a quite different substrate profile with significant activity (≧5%) towards more than half of the substrates examined (33 out of 51). Eight of the substrates tested (**3**, **10**, **11**, **13**, **14, 17**, **31**, and **36**) were more reactive than α-methylbenzylamine itself with 1-cyclohexylethylamine (**10**) reacting approximately nine-times faster. The Asn336Ser variant amine oxidase showed high reactivity towards certain classes of chiral amines, particularly substituted phenethylamines (**2**, **3**, **5**–**8**) and 1-alkylethylamines (**12**–**17**, **19, 20**). Secondary amines reacted more slowly (cf. **42** versus **1**) although 2-methyltetrahydroisoquinoline **44** was

 © 2003 Wiley-VCH Verlag GmbH & Co. KGaA, Weinheim

oxidized with a relative activity of 20% and the dimethoxy derivative **45** with a relative activity of 8%. Other substrates of interest that showed good activity were 2-phenyl-2-aminoethanol (**27;** rel. activity = 50%), *endo*-1-amino-norbornane (**36**; 183%), and 3-amino-3-phenylpropanol (**29**; 20%).

The enantioselectivity of the Asn336Ser variant towards 11 selected chiral amine substrates was then examined and the results are shown in Figure 4 and Table 1. The enantio-

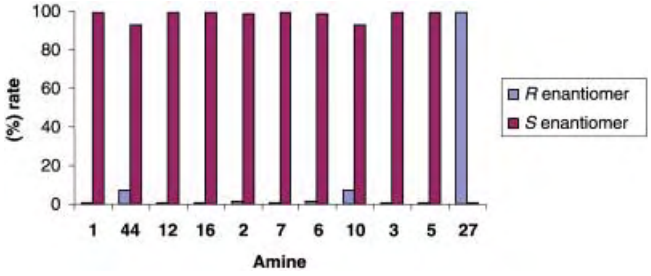


Figure 4. Graph showing relative rate of oxidation of individual *S* and *R* enantiomers by Asn336Ser amine oxidase. The rate of each substrate has been normalized to 100%.

Table 1: Enantioselectivity of Asn336Ser mutant towards selected chiral amines.[a]

Amine	*E*	Amine	*E*
1	199	**6**	86
44	13	**10**	13
12	142	**3**	275
16	96	**5**	110
2	84	**27**	270
7	184		

[a] The numbers reported refer to the enantiomeric ratio (*E*) for the individual substrates.

meric ratio *E*[12] for α-methylbenzylamine was very high ($E = 199$) and was in general maintained with most of the other chiral amines. Such *E* values translate to *ee* values of around 97→99%. Only 1-methyltetrahydroisoquinoline (**44**) and 1-cyclohexylethylamine (**10**) gave significantly lower values (both $E = 13$) although even these values would equate to an *ee* value of about 85%. Significantly, in all cases the Asn336Ser variant amine oxidase was found to be selective for the *S* enantiomer of the amine substrate (note that for **27** the *R* enantiomer is oxidized owing to the change in priority of the substituents).

For secondary amine substrates, for example, **42**, **44**, **45**, **49**, and **50** the possibility arose as to the regioselectivity of oxidation with respect to the amine functionality. Thus **44** could, in principle undergo oxidation to yield either imine **A** or **B**, or a mixture of both (Figure 5). To establish that the former pathway operated at least to some extent, we carried out the Asn336Ser amine oxidase catalyzed oxidation of (*S*)-**44** in the presence of the reducing agent ammonia·borane which we have previously shown to be effective for reduction of the intermediate imine.[10] Analysis of the chiral HPLC profile clearly showed that after 90 h significant production of (*R*)-**44** had occurred. The formation of (*R*)-**44** from (*S*)-**44** can only occur via the achiral imine **A** and not the chiral imine **B** (see Experimental Section).

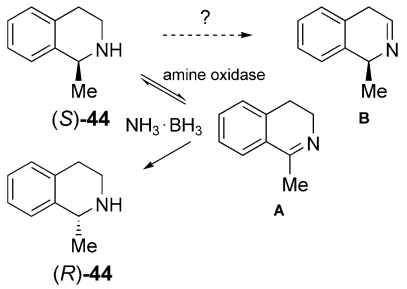


Figure 5. Stereoinversion of (*S*)-**44** to (*R*)-**44**, via imine **A**, by using Asn336Ser amine oxidase with ammonia borane.

In summary, we have shown that a directed evolution approach, based initially upon screening a library of mutant amine oxidases for activity against one enantiomer of a specific substrate ((*S*)-α-methylbenzyl amine), has lead to the identification of an enzyme possessing much broader substrate specificity whilst retaining high enantioselectivity. The Asn336Ser variant shows highest activity towards substrates containing a primary amine group flanked by a methyl group and a bulky alkyl/aryl group (Figure 6). In all cases so far examined the variant enzyme is selective for the *S* enantiomer

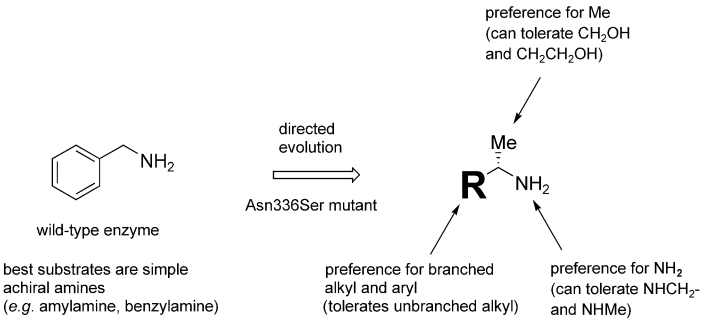


Figure 6. Comparison of substrate specificity of wild-type and Asn336Ser mutant amine oxidase.

of the chiral amine substrate. Other groups have also reported the identification of highly enantioselective enzymes by screening against single enantiomer substrates.[13] Although the *A. niger* Asn336Ser amine oxidase is suitable at present for small-scale deracemization reactions,[10] we are continuing to evolve this enzyme to develop an enzyme that has the required characteristics (e.g. stability, activity, selectivity) to be used for large-scale applications.

The development of enzymes possessing broad substrate specificity combined with high enantioselectivity remains an important goal in biocatalysis. Previous studies have demonstrated that directed evolution can be used to alter the substrate specificity and enantioselectivity of enzymes and moreover such variant enzymes often possess broader specificity when compared with the wild-type enzyme.[14] The results described herein represent the most in-depth study to date of how the substrate specificity of an enzyme can be dramatically altered by a point-mutation. The ability to select for such enzymes, using appropriate high-throughput screens, is critical to success in this area and highlights the need for new methods to enable the detection of a wider range of enzyme activities than is currently possible.[15]

 © 2003 Wiley-VCH Verlag GmbH & Co. KGaA, Weinheim

Experimental Section

Expression and purification of amine oxidase: BL21 star was transformed with the wild-type/mutant amine oxidase gene and plated onto LB (70 μg mL^{-1} ampicillin) petri dishes. A single colony was added to LB media (6 × 300 ml) containing ampicillin and grown at 30 °C for 24 h. The cells were spun and the cell pellet stored at −20 °C. Lysis of the cells was performed in 25 mM Tris/HCl pH 7.8, 10 mM imidazole, 1 mM β-mercaptoethanol, 1 mM phenylmethanesulfonyl fluoride (PMSF), and 300 mM NaCl and the lysate centrifuged. The cell-free extract from a 1 g pellet was loaded onto a 1-mL Ni-*N*,*N*-bis(carboxymethyl) glycine (nitrilotriacetic acid (NTA)) column. Column wash (five column volumes); 25 mM Tris/HCl pH 7.8, 60 mM imidazole, 1 mM β-mercaptoethanol, 1 mM PMSF, and 300 mM NaCl. Protein elution (the amine oxidase elutes in ≈2nd–7th 1 ml fractions); 25 mM Tris/HCl pH 7.8, 200 mM imidazole, 1 mM β-mercaptoethanol, 1 mM PMSF, and 300 mM NaCl. The protein was desalted in 25 mM Tris/HCl pH 7.8, 1 mM threo-1,4-dimercapto-2,3-butanediol (dithiothreitol (DTT)), 1 mM PMSF, and 300 mM NaCl using a Pharmacia PD10 column. Samples were stored frozen at −80 °C and thawed prior to use.

*Stereoinversion of (*S*)-**44***: A solution (600 μL) containing 20 mM (*S*)-**44**, 400 mM $NH_3{\cdot}BH_3$, 25 mM Tris/HCl pH 7.8, 1 mM DTT, 1 mM PMSF, and 300 mM NaCl aqueous buffer was held at 30 °C with shaking for 2 h. A 100-μL aliquot was removed and analyzed by HPLC as a $t = 0$ sample. amine oxidase (0.215 mg) in 500 μL of 25 mM Tris/HCl pH 7.8, containing 1 mM DTT, 1 mM PMSF and 300 mM NaCl was added to the remaining 500 μL of the (*S*)-**44** solution. The mixture was shaken at 30 °C and after $t = 90$ h a 100 μL aliquot was removed and analyzed by HPLC. Some precipitation was observed over the course of the reaction.

HPLC sample preparation: An aliquot (100 μL) of the reaction mixture was extracted with hexane (2 × 150 μL). The combined hexane extracts were analyzed directly by HPLC: Chiracel OD-H column 46 cm, eluent hexane:ethanol 98:2 (v/v), flow rate = 0.5 ml min^{-1}, column temperature = 0 °C; retention times, imine **A** = 18.7 min, (*S*)-**44** = 22.4 min, (*R*)-**44** = 26.2 min.

Received: June 10, 2003 [Z52100]

Keywords: amines · deracemization · directed evolution · enzymes

[1] J. W. Nieuwenhuijzen, R. F. P. Grimbergen, C. Koopman, R. M. Kellogg, T. R. Vries, K. Pouwer, E. van Echten, B. Kaptein, L. A. Hulshof, Q. B. Broxterman, *Angew. Chem.* **2002**, *114*, 4457; *Angew. Chem. Int. Ed.* **2002**, *41*, 4281.

[2] K. W. Henderson, W. J. Kerr, J. H. Moir, *Chem. Commun.* **2000**, 479.

[3] M. F. A. Adamo, V. K. Aggarwal, M. A. Sage, *J. Am. Chem. Soc.* **2000**, *122*, 8317.

[4] M. Berger, B. Albrecht, A. Berces, P. Ettmayer, W. Neruda, M. Woisetschläger, *J. Med. Chem.* **2001**, *44*, 3031.

[5] T. R. Vries, H. Wynberg, E. van Echten, J. Koek, W. ten Hoeve, R. M. Kellogg, Q. B. Broxterman, A. Minnaard, B. Kaptein, S. van der Sluis, L. A. Hulshof, J. Kooista, *Angew. Chem.* **1998**, *110*, 2491; *Angew. Chem. Int. Ed.* **1998**, *37*, 2349.

[6] F. Messina, M. Botta, F. Corelli, M. P. Schneider, F. Fazio, *J. Org. Chem.* **1999**, *64*, 3767; M. I. Youshko, F. van Rantwijk, R. A. Sheldon, *Tetrahedron: Asymmetry* **2001**, *12*, 3267; A. Luna, I. Alfonso, V. Gotor, *Org. Lett.* **2002**, *4*, 3627.

[7] S. Kainz, A. Brinkmann, W. Leitner, A. Pfaltz, *J. Am. Chem. Soc.* **1999**, *121*, 6421.

[8] J.-S. Shin, B.-G. Kim, *Biosci. Biotechnol. Biochem.* **2001**, *65*, 1782.

[9] M. T. Reetz, K. Schimossek, *Chimia* **1996**, *50*, 668; Y. K. Choi, M. J. Kim, Y. Ahn, M.-J. Kim, *Org. Lett.* **2001**, *3*, 4099; O. Pamies, A. H. Ell, J. S. M. Samec, N. Hermanns, J.-E. Bäckvall, *Tetrahedron Lett.* **2002**, *43*, 4699.

[10] M. Alexeeva, A. Enright, M. J. Dawson, M. Mahmoudian, N. J. Turner, *Angew. Chem.* **2002**, *114*, 3309; *Angew. Chem. Int. Ed.* **2002**, *41*, 3177.

[11] M. Braun, J. M. Kim, R. D. Schmid, *Appl. Biochem. Biotechnol.* **1992**, *37*, 594.

[12] For the definition of enantiomeric ratio (*E*) see; C. S. Chen, Y. Fujimoto, G. Girdaukas, C. J. Sih, *J. Am. Chem. Soc.* **1982**, *104*, 7294; C. S. Chen, S. H. Wu, G. Girdaukas, C. J. Sih, *J. Am. Chem. Soc.* **1987**, *109*, 2812.

[13] B. Lingen, J. Grötzinger, D. Kolter, M.-R. Kula, M. Pohl, *Protein Eng.* **2002**, *15*, 585.

[14] L. Sun, T. Bulter, M. Alcalde, I. P. Petrounia, F. H. Arnold, *ChemBioChem* **2002**, *3*, 781; O. May, P. T. Nguye, F. H. Arnold, *Nat. Biotechnol.* **2000**, *18*, 317; D. Zha, S. Wilensek, M. Hermes, K.-E. Jaeger, M. T. Reetz, *Chem. Commun.* **2001**, 2664; G. J. Williams, S. Domann, A. Nelson, A. Berry, *Proc. Natl. Acad. Sci. USA* **2003**, *100*, 3143; M. Wada, C.-C. Hsu, D. Franke, M. Mitchell, A. Heine, I. Wilson, C.-H. Wong, *Bioorg. Med. Chem.* **2003**, *11*, 2091.

[15] N. J. Turner, *Trends Biotechnol.* **2003**, *21*, in press.

 © 2003 Wiley-VCH Verlag GmbH & Co. KGaA, Weinheim

Chiral Ferrimagnetism

Structure and Magnetic Properties of a Chiral Two-Dimensional Ferrimagnet with T_C of 38 K**

Katsuya Inoue, Koichi Kikuchi, Masaaki Ohba, and Hisashi Ōkawa*

The construction of molecule-based magnetic materials, which possess additional properties such as conductivity,[1] photoreactivity,[2] or optical properties,[3–5] is currently a

[*] Prof. Dr. K. Inoue
Department of Applied Molecular Science I
Institute for Molecular Science, Okazaki National Institutes
Myoudaiji, Okazaki, 444-8585 (Japan)
Fax: (+81) 564-54-2254
E-mail: kino@ims.ac.jp
Prof. Dr. K. Kikuchi
Department of Chemistry
Tokyo Metropolitan University
Hachioji, Tokyo 192-0367 (Japan)
Dr. M. Ohba
Department of Chemistry
Graduate School of Science, Kyushu University
Fukuoka 812-8581 (Japan) and
PRESTO, Japan Science and Technology Corporation (JST)
Prof. Dr. H. Ōkawa
Department of Chemistry
Graduate School of Science, Kyushu University
Fukuoka 812-8581 (Japan)

[**] This work is supported by a program entitled "Research for the Future(RFTF)" of the Japan Society of the Promotion of Science(99P01201). We also thank Prof. M. Kurmoo (IPCMS, Strasbourg, France) for helpful discussions.

Supporting information for this article is available on the WWW under http://www.angewandte.org or from the author.

 © 2003 Wiley-VCH Verlag GmbH & Co. KGaA, Weinheim DOI: 10.1002/anie.200351888

challenging target. Specific goals aimed for the latter two molecule-based magnets include: 1) The ability to design the molecular building blocks and to organize them in the solid for desired dimensionality, and 2) optical transparency.[3] The physical aspects of the current interest is centered on optical properties, particularly with respect to optical activity. When a magnet is characterized by optical transparency and chiral structure, there is a great possibility that the crystals have a chiral spin structure. These magnets display asymmetric magnetic anisotropy and magnetochiral dichroism.[4] This category of materials is not only of academic interest; they also afford the potential of being used in new devices. When chiral molecule-based magnets are constructed, chirality must be controlled in the molecular structure as well as in the entire crystal structure. As a consequence of this difficulty, only few examples of this type of magnet exist. Until now, most of the reported chiral magnets have low-dimensional magnetic structures, in which the magnetic ordering temperatures are below 10 K.[5] To afford a high-T_C magnet, dimensionality of the magnetic structure must be extended. When magnetic building blocks with more than three connections are introduced, two or three-dimensional magnets might be prepared. In 2001, we reported a three-dimensional (3D) chiral complex that was prepared by using this strategy.[8] Here we report on the crystal structure and optical and magnetic properties of a new 2D chiral ferrimagnet; $[\{Cr(CN)_6\}\{Mn(S)\text{-}pnH(H_2O)\}](H_2O)$ (**1**); ((*S*)-pn = (*S*)-1,2-diaminopropane).

The complex **1**[6] was obtained as green needle-shaped crystals by the reaction of a solution of $K_3[Cr(CN)_6]$, $Mn(ClO_4)_2$, and (*S*)-1,2-diaminopropane dihydrochloride ((*S*)-pn·2 HCl) in a 1:1:1 molar ratio in methanol/H_2O (1:1), adjusted to pH 6–7 with KOH under an argon atmosphere. X-ray structural analysis found an orthorhombic unit cell and the structure revealed the formation of a two-dimensional chiral network (Figure 1).[7] Four cyanide groups in the $[Cr(CN)_6]^{3-}$ ion are ligated to Mn^{2+} ions to form a bimetallic square, which is arranged almost perpendicular to the *c* axis. Each unit has one chiral (*S*)-pn ligand and two water molecules between the sheets. The (*S*)-pn ligand and one of the water molecules coordinates to an Mn^{2+} ion and separates the sheets. The two shortest intersheet metal separations are observed between the Mn and Cr atoms (7.3105(4) and 7.7701(4) Å, respectively), which describe a ferromagnetic interaction between 2D sheets from the point of view of a magnetic dipole interaction, while the shortest intersheet homometallic contacts are greater than 8 Å.

The magnetic behavior of the complex was measured using a SQUID magnetometer. The temperature dependence of $\chi_{mol}T$ values are displayed in Figure 2. The $\chi_{mol}T$ value is 5.01 emu K mol^{-1} (6.33 μ_B) at 300 K, and decreases with decreasing temperature down to a minimum value of 3.65 emu K mol^{-1} (5.41 μ_B) at 85 K. The extrapolated value of the effective magnetic moment (7.07 μ_B) is in good agreement with the spin-only theoretical value. (Figure 2; inset: Paramagnetic spin of 5/2 + 3/2 → 7.07 μ_B) Upon further cooling, the $\chi_{mol}T$ value increases and diverges. In both the field-cooled (FC) and zero-field-cooled (ZFC) cycles, and with a low applied field (5 Oe) in the temperature range of 5–100 K, a long-range magnetic ordering is observed below 38 K (Figure 3). As shown in Figure 4, the magnetization (*M*) increases sharply with applied field and is saturated rapidly.

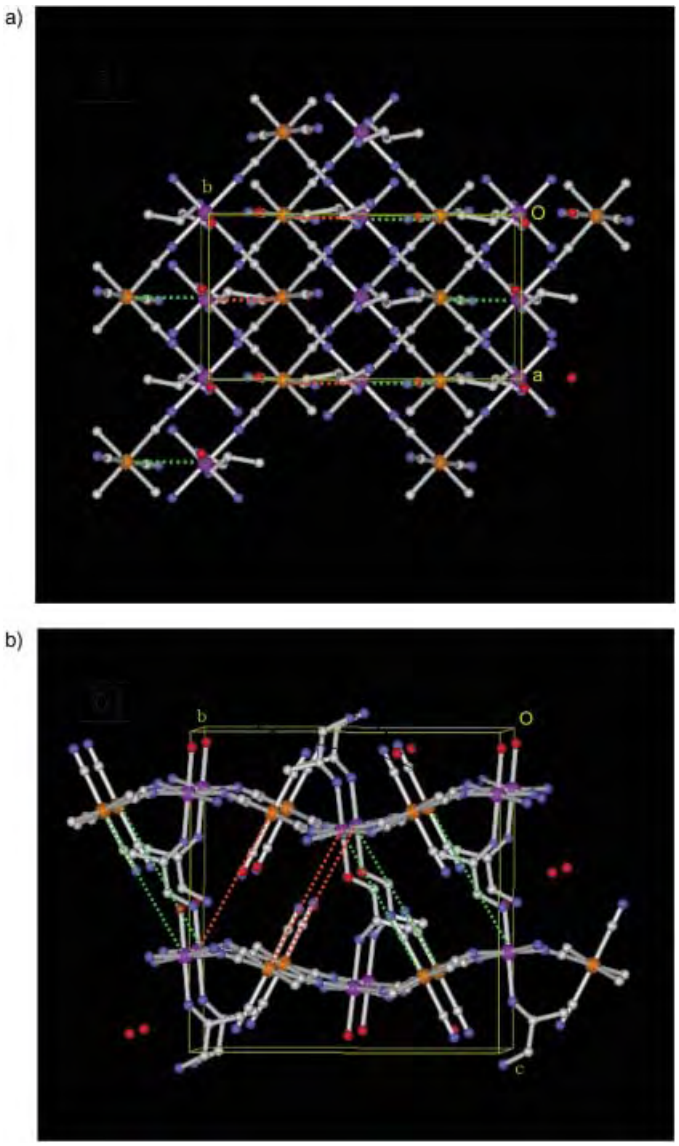


Figure 1. X-ray crystal structure of **1**. Atoms: Mn (purple), Cr (orange), N (blue), and C (gray).

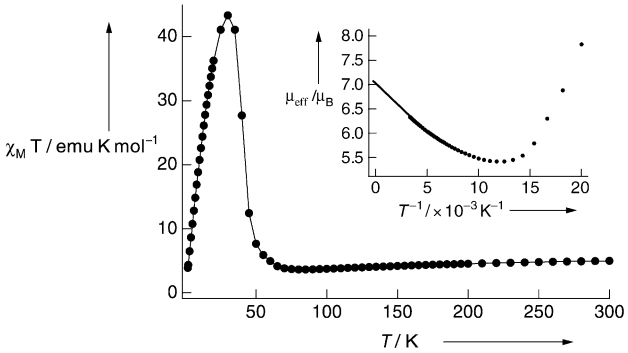


Figure 2. Temperature dependence of $\chi_{mol}T$ for **1**. Inset: Plot of μ_{eff} versus T^{-1}.

 © 2003 Wiley-VCH Verlag GmbH & Co. KGaA, Weinheim

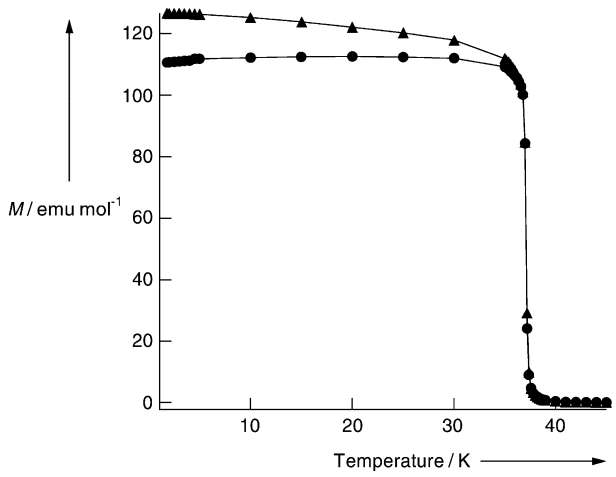


Figure 3. Temperature dependence of magnetization for a polycrystalline sample of **1** at 5 Oe: Zero-field-cooled (ZFC, ●) and field-cooled magnetization (FC, ▲).

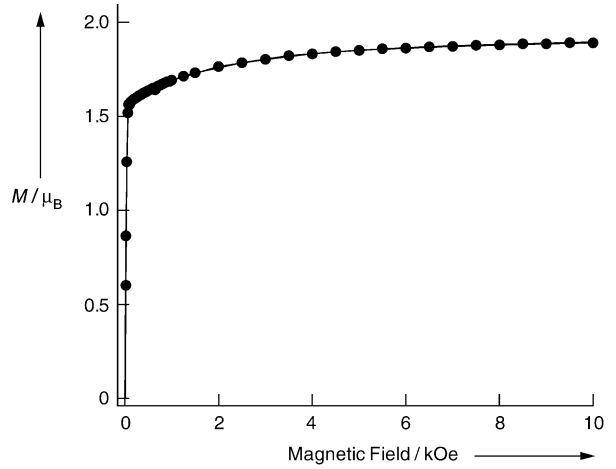


Figure 4. Field dependence of the magnetization of a polycrystalline sample of **1** at 5 K.

The saturation magnetization is $M_S = 2\ \mu_B$. This value is in good agreement with the theoretical value of antiferromagnetic coupling between Cr^{3+} and Mn^{2+} ions. $(5/2-3/2=1)$ A hysteresis loop (with a remnant magnetization of 1800 emu G mol^{-1} and a coercive field of 10 Oe) was observed at 5 K, which suggests a soft magnetic behavior.

(Magnetic) circular dichroism ((M)CD) spectra of complex **1** were measured within a pressed KBr disk in a magnetic field of 0–10 kOe, and in the temperature range of 10–300 K. The temperature dependence of the MCD spectra at 10 kOe is shown in Figure 5. The MCD spectra enhanced at around the critical temperature T_C.(Figure 5B) This behavior originates from Faraday effect that is exhibited by this material. The field dependence of the MCD spectra at 6 K is shown in Figure 6; hysteresis is observed at this temperature.

In summary, we have successfully constructed and structurally characterized the first two-dimensional, fully chiral ferrimagnet. Furthermore, the magnetic transition temperature of this complex is relatively high (38 K) among the

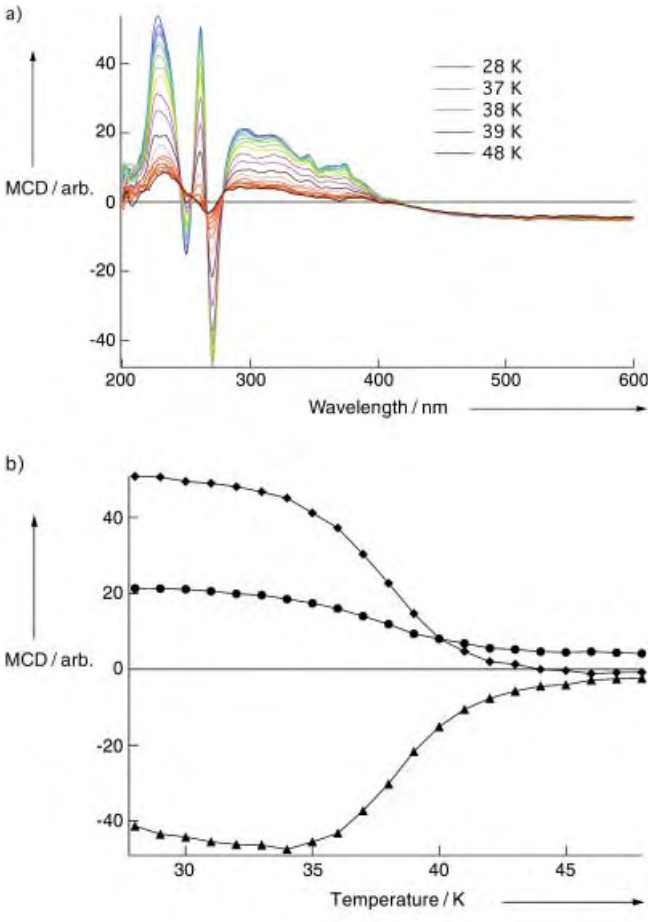


Figure 5. a) Temperature-dependent (28–48 K) MCD spectra of **1** (KBr disk) at 1 kOe; b) Temperature dependence of the MCD intensity at 295 (●), 270 ▲, and 261 nm ◆.

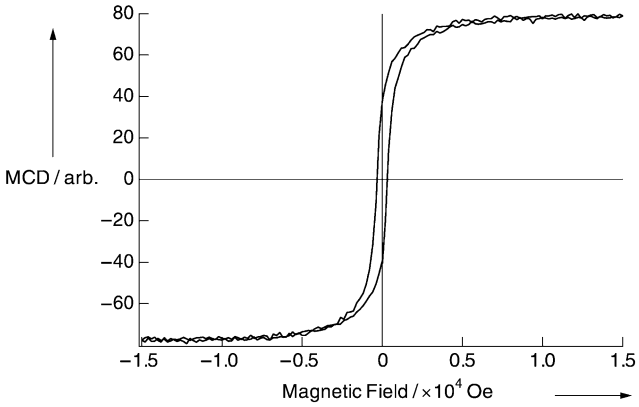


Figure 6. Field dependence of the MCD intensity at 6 K.

known molecule-based magnets. We believe that this complex is a potential candidate for novel magneto-optical phenomena. In the future, these complexes should lead to the development of a novel group of molecule-based magnetic materials.

Received: May 13, 2003 [Z51888]
Published Online: August 1, 2003

 © 2003 Wiley-VCH Verlag GmbH & Co. KGaA, Weinheim

Keywords: chiral resolution · chromium · circular dichroism · magnetic properties · manganese

[1] M. Kurmoo, A. W. Graham, P. Day, S. J. Coles, M. B. Hursthouse, J. L. Caulfield, J. Singleton, F. L. Pratt, W. Hayes, L. Ducasse, P. Guionneaul, *J. Am. Chem. Soc.* **1995**, *117*, 12209; L. Balicas, J. S. Brooks, K. Storr, S. Uji, M. Tokumoto, H. Tanaka, H. Kobayashi, A. Kobayashi, V. Barzykin, L. P. Gor'kov, *Phys. Rev. Lett.* **2001**, *87*, 067002; S. Uji, H. Shinagawa, T. Terashima, T. Yakabe, Y. Terai, M. Tokumoto, A. Kobayashi, H. Tanaka, H. Kobayashi, *Nature* **2001**, *410*, 908; E. Coronado, J. R. Galan-Mascaros, C. J. Gomez-Garcia, V. Laukhin, *Nature* **2000**, *408*, 447.

[2] O. Sato, T. Iyoda, A. Fujishima, K. Hashimoto, *Science* **1996**, *272*, 704; S. Karasawa, H. Kumada, N. Koga, H. Iwamura, *J. Am. Chem. Soc.* **2001**, *123*, 9685.

[3] C. Bellitto, P. Day, *J. Chem. Soc. Chem. Commun.* **1978**, 511; "Supramolecular Engneering of Synthetic Metallic Materials Conductors and Magnets": P. Day, *NATO ASI Ser. Ser. C* **1999**, *518*, 253.

[4] G. Wagniere, A. Mejer, *Chem. Phys. Lett.* **1984**, *110*, 546; G. L. J. A. Rikken, E. Raupach, *Nature* **1997**, *390*, 493.

[5] A. Caneschi, D. Gatteschi, P. Ray, R. Sessoli, *Inorg. Chem.* **1991**, *30*, 3936; M. Hernáez-Molina, F. Lloret, C. Ruiz-Pérez, M. Julve, *Inorg. Chem.* **1998**, *37*, 4131; H. Kumagai, K. Inoue, *Angew. Chem.* **1999**, *111*, 1694; *Angew. Chem. Int. Ed.* **1999**, *38*, 1601; R. Andres, M. Brissard, M. Gruselle, C. Train, J. Vaissermann, B. Malezieux, J. P. Jamet, M. Verdaguer, *Inorg. Chem.* **2001**, *40*, 4633; E. Coronado, J. R. Galan-Mascaros, C. J. Gomez-Garcia, J. M. Martinez-Agudo, *Inorg. Chem.* **2001**, *40*, 113.

[6] IR in KBr (Supporting Information): $\tilde{\nu}_{CN} = 2157.0$ (Cr-CN-Mn), 2137.7 cm^{-1} (Cr–CN, terminal).

[7] Crystal data for [{$Cr(CN)_6$}{Mn(*S*)-pnH(H_2O)}](H_2O): green needle, $C_9H_{14}CrMnN_8O_2$, $M_r = 374.22$, orthorhombic, space group $P2_12_12_1$, $a = 7.6280(17)$, $b = 14.510(3)$, $c = 14.935(3)$ Å, $V = 1653.1(6)$ $Å^3$, $Z = 4$, crystal size $0.2 \times 0.05 \times 0.05$ mm^3, $\mu(Mo_{K\alpha}) = 1.436$ mm^{-1}. Data were collected with a Bruker SMART-APEX three-circle diffractometer, equipped with a CCD area detector (graphite-monochromated $Mo_{K\alpha}$ radiation, $\lambda = 0.71073$ Å, ω-scan mode (0.3° steps), semi-empirical absorption correction on Laue equivalents). The structures were solved by direct methods and refined by full-matrix least-squares against F^2 of all data using SHELXTL software. Hydrogen atoms were included in calculated positions but not refined. All non-H atoms were refined anisotropically. The refinement converges with $R_1 = 0.0265$ for 2377 data ($I > 2\sigma(I)$), $wR_2 = 0.0709$ for 2383 unique data ($2.73 \geq \theta \geq 23.28°$), Flack parameter = 0.01(3), max/min residual electron density 0.108/−0.683 e $Å^3$. CCDC-172588 contains the supplementary crystallographic data for this paper. These data can be obtained free of charge via www.ccdc.cam.ac.uk/conts/retrieving.html (or from the Cambridge Crystallographic Data Centre, 12, Union Road, Cambridge CB21EZ, UK; fax: (+44) 1223-336-033; or deposit@ccdc.cam.ac.uk).

[8] K. Inoue, H. Imai, P. S. Ghalsasi, K. Kikuchi, M. Ohba, H. Ōkawa, J. V. Yakhmi, *Angew. Chem.* **2001**, *113*, 4372; *Angew. Chem. Int. Ed.* **2001**, *40*, 4242.

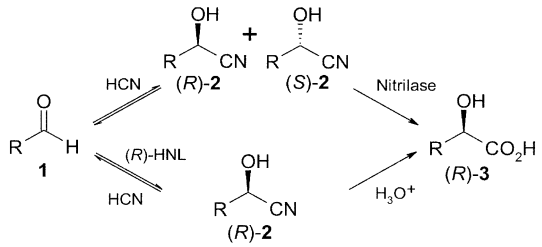
 © 2003 Wiley-VCH Verlag GmbH & Co. KGaA, Weinheim

Tailor-Made Enzyme Catalyst

Comprehensive Step-by-Step Engineering of an (*R*)-Hydroxynitrile Lyase for Large-Scale Asymmetric Synthesis**

Anton Glieder, Roland Weis, Wolfgang Skranc, Peter Poechlauer, Ingrid Dreveny, Sandra Majer, Marcel Wubbolts, Helmut Schwab, and Karl Gruber*

Optically active α-hydroxyacids, such as mandelic acid, and their derivatives are important building blocks for the production of pharmaceuticals.[1] Attractive synthetic routes are made available by hydroxynitrile lyases (HNLs). These enzymes catalyze the asymmetric addition of HCN to aldehydes to provide cyanohydrins in high yields and with high selectivities (Scheme 1).[2,3] The cyanohydrin products



Scheme 1. Enantioselective synthesis of (*R*)-α-hydroxycarboxylic acids (*R*)-**3** from aldehydes **1** by the nitrilase and the hydroxynitrile lyase (HNL) routes. Other methods, such as the hydrolytic resolution of cyanohydrins in the absence of an additional catalyst, are limited to a maximum yield of 50%.

undergo chemical hydrolysis under acidic conditions at elevated temperature to give the corresponding α-hydroxy-acids without racemization.[1] An alternative route, which involves enantioselective nitrilases,[4,5] should also theoretically lead to quantitative yields through substrate racemization in situ at high pH values. However, many nitrilases suffer from low turnover frequencies (TOF), low stereoselectivity, and rapid deactivation at high substrate concentrations.

(*R*)-2-Chloromandelic acid (**3b**) is a key intermediate for the production of a widely administered anticoagulant that reduces the risk of cardiovascular events in patients with acute coronary syndromes. However, o*rtho*-substituted substrates perform poorly in all known syntheses of chiral cyanohydrins, and their use results in low yields, low TOF values, and/or low *ee* values.[4,6–9] Furthermore, the conversion of aromatic aldehydes into cyanohydrins with the only reported recombinant (*R*)-hydroxynitrile lyase (*Lu*HNL, cloned from *Linum usitatissimum*) does not reach completion.[10] (*R*)-HNL from *Prunus amygdalus* (*Pa*HNL), which shows a broad substrate specificity, is only available from very limited natural sources, and the recombinant production of any active FAD (flavin adenine dinucleotide)-containing HNL was previously unsuccessful.[11] Herein we report the first recombinant *Pa*HNL that retains its activity under process conditions and can be used in emulsion systems at low pH values. We also demonstrate the success of a generally applicable engineering concept, which could be used to improve the productivity of this enzyme during the fermentation process, and which led to a high TOF value for the challenging substrate **1b**. Our goal was to develop a commercially viable biocatalyst for the production of (*R*)-**3b** by the HNL route, or in other words to make the production of optically pure (*R*)-**2b** possible in high yield in the presence of a small quantity of a robust enzyme.

A considerable amount of data from preparative reactions and from biochemical and structural studies[2,3,12–17] are available for *Pa*HNL. We cloned the *Pa_hnl5* gene from *Prunus amygdalus* to have unlimited access to *Pa*HNL. This gene was very similar to *hnl* genes from *Prunus dulcis* (*mdl*1, 99% identity) and *Prunus serotina* (*mdl*5, 94% identity), which are expressed specifically in floral tissues. By overexpressing the *Pa_hnl5* gene, including its native plant secretory-signal sequence, in the methylotrophic yeast *Pichia pastoris*, we obtained 250 mg of the active secreted enzyme per liter of culture supernatant. The highly glycosylated enzyme showed a specific activity of 295 ± 30 μmol min^{-1} mg for the cleavage of **2a**, which is twice as high as the specific activity of *Pa*HNL isolated from almond seeds (Sigma M-6782, Lot41H4016; 160 ± 30 μmol min^{-1} mg^{-1}). The activity of the recombinant isoenzyme *Pa*HNL5 did not change significantly over the range pH 2.5–6.5. *Pa*HNL5 was surprisingly stable under acidic conditions (Figure 1), under which the competitive chemical reaction is suppressed[18,19] and the enantiomerically pure cyanohydrin product is also stable. This extremely important technical feature of HNL reactions in emulsion systems makes the production of pure enantiomers possible even from substrates that react slowly and facilitates effective enzyme recycling. No other HNL is known to be so stable at low pH values. Although the molecular foundation for this property is still unclear, overglycosylation by *Pichia* can be excluded as the only cause, as deglycosylation of recombinant *Pa*HNL5 by endoglycosidase H in a nondenaturing buffer at 37°C to leave just one *N*-acetylglucosamine substituent on each of the modified Asn residues did not lead to instability at

[*] Dr. A. Glieder, S. Majer, Prof. Dr. H. Schwab
Institut für Biotechnologie, Technische Universität Graz
Petersgasse 12, 8010 Graz (Austria)
Fax: (+43) 316-873-8434
E-mail: glieder@glieder.com
R. Weis, Prof. Dr. K. Gruber
Research Centre Applied Biocatalysis
Steyrergasse 17, 8010 Graz (Austria)
Dr. I. Dreveny, Prof. Dr. K. Gruber
Institut für Chemie, Karl-Franzens-Universität Graz
Heinrichstrasse 28, 8010 Graz (Austria)
Dr. W. Skranc, Dr. P. Poechlauer, Dr. M. Wubbolts
R & D Center Linz
DSM Fine Chemicals Austria Nfg. GmbH & Co KG
St.-Peter-Strasse 25, 4021 Linz (Austria)

[**] We thank the SFB Biokatalyse (F0101), the TIG, the province of Styria, SFG, and the city of Graz for financial support.

Supporting information for this article is available on the WWW under http://www.angewandte.org or from the author.

 DOI: 10.1002/anie.200352141 © 2003 Wiley-VCH Verlag GmbH & Co. KGaA, Weinheim

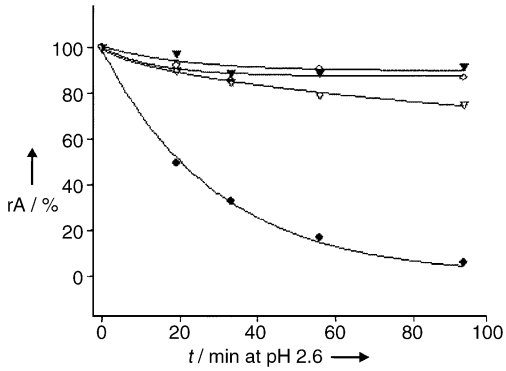


Figure 1. Plot of the relative activities (rA) of a series of enzymes for the cleavage of **2a** at pH 5.0 after incubation at pH 2.6. *Pa*HNL5 (H21, ○), which was expressed in *Pichia pastoris* with the signal sequence of the α mating factor of *S. cerevisiae*, and its A111G variant (▼) showed remarkable stability at low pH values. The deglycosylated enzyme (H21_deglyco, ▽) was slightly less stable. The commercially available native *Pa*HNL from almond seeds (Sigma; ●) is shown for comparison.

pH 2.6, in contrast to the significant denaturation observed for a *Pa*HNL preparation from almond seeds (Sigma) under the same conditions (Figure 1). The deglycosylated enzyme showed a slight decrease in stability after treatment at 37 °C. The estimated deactivation half-life values of the recombinant protein *Pa*HNL5_L1Q (H21), the enzyme with the additional mutation (A111G), the deglycosylated enzyme (H21_deglyco), and the native enzyme from almond seeds (Sigma) under these conditions were determined from the deactivation curves as ≈530, 530, 250, and 20 min, respectively (Figure 1).

In the next step, the enzyme productivity was increased 4–4.5-fold by changing the first amino acid of the mature protein (leucine to glutamine; L1Q) and replacing the native plant secretion-signal peptide with the α-mating-factor prepro leader from *Saccharomyces cerevisiae*. The secretion of near-pure enzyme into the culture supernatant and the production of 1 g of enzyme per liter of supernatant ensures almost unlimited availability of this novel biocatalyst.

High enantioselectivity was observed for the synthesis of the commercially interesting intermediate (*R*)-**2b** catalyzed by the pH-stable recombinant *Pa*HNL isoenzyme 5. The TOF values were more than 10–15 times lower than those observed in the reaction with the natural unsubstituted substrate **1a** (Table 1). No effective method for the stereoselective conversion of *ortho*-substituted mandelonitrile or benzaldehyde derivatives into cyanohydrins has yet been reported. The observations made for the reaction of native *Pa*HNL from natural sources,[9] for the conversion of **2b** by nitrilases,[4] and for the nonbiocatalytic route with titanium or vanadium catalysts[6,7,20] were similar to those for the reaction of *Pa*HNL isoenzyme 5. To minimize unfavorable steric interactions within the active site, alanine 111 and valine 317 were replaced by smaller glycine residues through site-directed mutagenesis. Computer substrate-docking simulations of (*R*)-**2b**, (*R*)-**2c**, and (*R*)-**2d** in the active site of a homology model of *Pa*HNL5 (based on the known structure of the homologous isoenzyme *Pa*HNL1[15] from almond seeds) allowed the identification of amino acid residues situated near the chloro substituents of the substrate (Figure 2). In the case of (*R*)-**2b**, the side chains of A111 and V317 are in close contact with the chlorine atom at the *ortho* position of the aromatic ring. Steric interactions with these two residues, particularly between A111 and (*R*)-**2b**, are probably responsible for the decreased enzymatic performance observed with this substrate. A chloro substituent in the *meta* position did not cause any noticeable steric problems (Figure 2).

Table 1: Enantioselective synthesis and cleavage of chloro-substituted mandelonitrile derivatives.[a]

Entry	R	Substrate	Product	Mutation	Specific activity[b] [μmol min^{-1} mg]
1	Ph	**1a**	(*R*)-**2a**		1450 ± 400
2	Ph	**1a**	(*R*)-**2a**	A111G	1150 ± 400
3	Ph	**1a**	(*R*)-**2a**	V317G	295 ± 50
4	*o*-Cl-Ph	**1b**	(*R*)-**2b**		67 ± 25
5	*o*-Cl-Ph	**1b**	(*R*)-**2b**	A111G	409 ± 60
6	*o*-Cl-Ph	**1b**	(*R*)-**2b**	V317G	< 5
7	*m*-Cl-Ph	**1c**	(*R*)-**2c**		155 ± 30
8	*m*-Cl-Ph	**1c**	(*R*)-**2c**	A111G	390 ± 100
9	*m*-Cl-Ph	**1c**	(*R*)-**2c**	V317G	290 ± 50
10	*p*-Cl-Ph	**1d**	(*R*)-**2d**		298 ± 50
11	*p*-Cl-Ph	**1d**	(*R*)-**2d**	A111G	566 ± 40
12	*p*-Cl-Ph	**1d**	(*R*)-**2d**	V317G	26 ± 13
13	Ph	**2a**	(*S*)-**2a** + **1a**		325 ± 30
14	Ph	**2a**	(*S*)-**2a** + **1a**	A111G	8 ± 2
15	Ph	**2a**	(*S*)-**2a** + **1a**	V317G	6 ± 1.5

[a] All synthetic reactions were performed with 15 mM substrate and 0.5 mg of the purified enzyme in an emulsion of citrate buffer (50 mM, 3.8 mL), *tert*-butyl methyl ether (2.1 mL), and HCN (1.2 mL) at 10 °C and pH 3.4. All *Pa*HNL variants were based on PaHNL5 with the mutation L1Q. The cleavage activity for **2a** was determined photometrically within the first 3 min of a linear increase in product concentration ($\lambda = 280$ nm; $T = 25$ °C; substrate concentration: 12 mM; phosphate–citrate buffer (0.1 M; pH 5). [b] The specific activity is based on protein concentrations determined by a Lowry assay with *Pa*HNL from Sigma as a standard and on product-formation rates within the first 15 min (**1b**) or 5–10 min (**1a**–**d**). In these time periods 5–20% of the product was formed.

For both mutations, A111G and V317G, a dramatic decrease in activity to just 2–5% was observed in the cleavage of **2a** (Table 1). This nearly total loss of activity was not surprising, as there is a very high risk of destroying enzymatic activity when highly conserved amino acid residues in the hydrophobic cavity of the enzyme are changed. However, a completely different situation arose in the synthetically more important HCN addition reaction. Whereas the mutant V317G also showed poor reactivity in the synthesis of (*R*)-**2a**, (*R*)-**2b**, and (*R*)-**2d**, the A111G variant retained high hydrocyanating activity. Turnover rates of the A111G variant with the natural substrate **1a** were only ≈20–30% lower than those of *Pa*HNL5_L1Q. Moreover, the activity of the enzyme in the synthesis of (*R*)-**2b** was strongly enhanced through this single mutation (specific activity of A111G: 409 μmol mg^{-1}-min; TOF: 390 sec^{-1}; six times faster than with the wildtype enzyme). Both mutants catalyzed the conversion of compound **1c** at higher rates than the native enyzme and with excellent enantioselectivity (> 99% *ee*). The synthesis of (*R*)-

 © 2003 Wiley-VCH Verlag GmbH & Co. KGaA, Weinheim

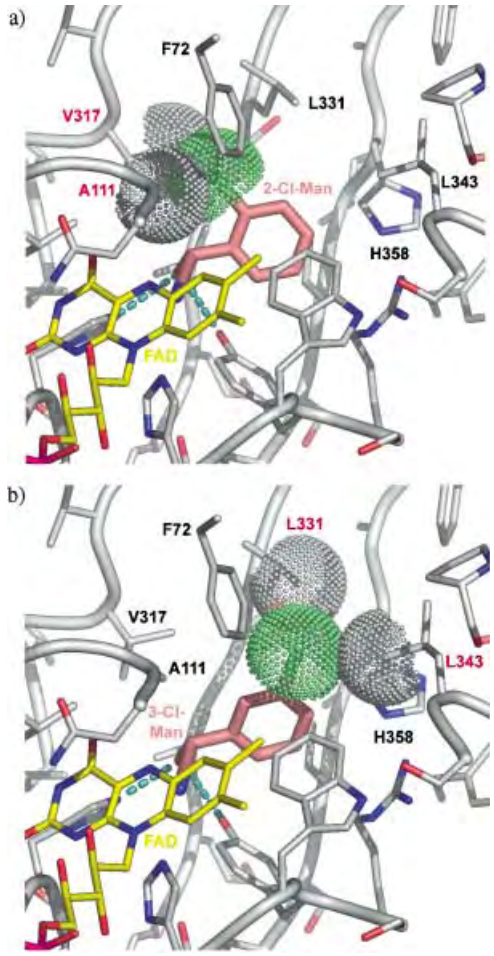


Figure 2. The active site of *Pa*HNL5 with (*R*)-**2b** (2-Cl-Man) and (*R*)-**2c** (3-Cl-Man). a) Steric interactions between the *ortho* chloro substituent (green area) of the substrate 2-Cl-Man and A111 and V317 (gray areas). b) Close contact of L343 and L331 (gray areas) with the *meta*-chloro substituent (green area) of 3-Cl-Man.

2d was slightly improved through the mutation A111G. In a reaction with a high concentration of aldehyde (3 M based on the volume of the aqueous phase), **1b** (150 mmol) was converted in the presence of the enzyme (≈5 mg) at pH 3.4 into (*R*)-**2b** (21.1 g); 2.9% of the starting aldehyde **1b** was also recovered. This result corresponds to 95.9% of the theoretical yield of (*R*)-**2b**. No by-products were observed after a reaction time of 7 h and extraction with *tert*-butyl methyl ether. The *R* enantiomer was obtained in 96.5% *ee*. This represents a tremendous improvement in the synthesis of (*R*)-**2b** by the HNL route. In the best case reported previously,[9] an *ee* value of 83% was observed at pH 3.3 when ≈25 times as much native enzyme was used (based on calculations with the specific enzyme activity of the most commonly used native *Pa*HNL in the cleavage reaction of **2a** (160 μmol min^{-1} mg)). In spite of significant advances, the use of non-enzymatic catalysts in these asymmetric synthetic steps led to only ≈80% *ee*, low yields for *ortho*-substituted substrates,[7,20,21] and the necessity for a recrystallization step to obtain **3b** with high optical purity.

An *ee* value as high as that observed with the A111G variant (97% *ee*) was described for the enzymatic step of the nitrilase route,[22] albeit with low substrate concentrations. Furthermore, the specific activity reported was more than 100 times lower, with only 3 μmol of product per minute per mg of nitrilase I. Protein folding and protein stability are often adversely affected by mutations of active-site residues, which frequently impedes the generation of useful mutants. Our A111G variant was also expressed well when the fermentation was scaled up and showed high stability at low pH values.

*Pa*HNL was the first biocatalyst described for asymmetric synthesis.[23] However, its instability at low pH values (conditions under which the competitive chemical reaction is suppressed), limited availability from relatively expensive natural sources, and low activity and selectivity in reactions with *ortho*-substituted aryl aldehydes have contributed to the fact that *Pa*HNL has not yet found application in industrial processes. We believe that variation in the fractions of the individual isoenzymes in enzyme preparations from different batches and suppliers are the reason for the varying enantioselectivities and conversion rates observed by Gotor and coworkers.[24] Through the cloning and expression engineering of the gene that encodes HNL isoenzyme 5 from *Prunus amygdalus* we have established the foundation for a cheap and unlimited supply of a recombinant *Pa*HNL with novel technological features. Rational engineering of the active site led to the adaptation of the enzyme for the difficult stereoselective conversion of the unnatural, industrially interesting substrate **1b** into (*R*)-**2b** with high enantioselectivity. Thus, almost 100 years after the discovery of the first stereoselective biocatalyst, an industrial application of this type of enzyme on a multiton scale is now within reach, as a result of a comprehensive molecular-engineering program.

Received: June 13, 2003 [Z52141]
Published Online: September 29, 2003

Keywords: asymmetric synthesis · C—C coupling · enzyme catalysis · protein design · protein engineering

[1] H. Groger, *Adv. Synth. Catal.* **2001**, *343*, 547–558.
[2] F. Effenberger, S. Forster, H. Wajant, *Curr. Opin. Biotechnol.* **2000**, *11*, 532–539.
[3] D. V. Johnson, A. A. Zabelinskaja-Mackova, H. Griengl, *Curr. Opin. Chem. Biol.* **2000**, *4*, 103–109.
[4] G. Desantis, Z. Zhu, W. A. Greenberg, K. Wong, J. Chaplin, S. R. Hanson, B. Farwell, L. W. Nicholson, C. L. Rand, D. P. Weiner, D. Robertson, M. J. Burk, *J. Am. Chem. Soc.* **2002**, *124*, 12922.
[5] M. Ress-Loeschke, B. Hauer, R. Mattes, D. Engels (BASF, A.-G.), DE 10010149, **2000** [*Chem. Abstr.* **2001**, *135*, 223444].
[6] C. Bensoussan, M. C. Bontoux, P. M. Gelo, F. Foray (Rhodia Chimie), Fr 4014[2822460], **2001** [*Chem. Abstr.* **2002**, *137*, 368675].
[7] A. J. Blacker, I. N. Houson (Avecia Limited), WO GB667[0266410], **2002** [*Chem. Abstr.* **2002**, *137*, 201079].
[8] B. Kirschbaum, G. Wilbert, F. Effenberger (Clariant), US 4600[20020052523], **2001** [*Chem. Abstr.* **2002**, *136*, 355075].
[9] B. Kirschbaum, R. Fell, (Clariant), WO EP6681[0305010], **2002** [*Chem. Abstr.* **2003**, *138*, 106498].
[10] K. Trummler, J. Roos, U. Schwaneberg, F. Effenberger, S. Forster, K. Pfizenmaier, H. Wajant, *Plant Sci.* **1998**, 139, 19–27.

 © 2003 Wiley-VCH Verlag GmbH & Co. KGaA, Weinheim

[11] D. V. Johnson, A. A. Zabelinskaja-Mackova, H. Griengl, *Curr. Opin. Chem. Biol.* **2000**, *4*, 103 – 109.
[12] K. R. Baerwald, L. Jaenicke, *FEBS Lett.* **1978**, *90*, 255 – 260.
[13] W. Becker, U. Benthin, E. Eschenhof, E. Pfeil, *Angew. Chem.* **1963**, *75*, 93; *Angew. Chem. Int. Ed. Engl.* **1963**, *2*, 44 – 45.
[14] J. Butenuth, E. Pfeil, *Hoppe-Seyler's Z. Physiol. Chem.* **1972**, *353*, 698 – 699.
[15] I. Dreveny, K. Gruber, A. Glieder, A. Thompson, C. Kratky, *Structure* **2001**, *9*, 803 – 815.
[16] I. Dreveny, C. Kratky, K. Gruber, *Protein Sci.* **2002**, *11*, 292 – 300.
[17] M. Schmidt, H. Griengl, *Top. Curr. Chem.* **1999**, 200, 193 – 226.
[18] M. Bauer, R. Geyer, M. Boy, H. Griengl, W. Steiner, *J. Mol. Catal. B* **1998**, *5*, 343 – 347.
[19] U. Kragl, U. Niedermeyer, M. R. Kula, C. Wandrey, *Ann. N. Y. Acad. Sci.* **1990**, *613*, 167 – 175.
[20] Y. N. Belokon', M. North, T. Parsons, *Org. Lett.* **2000**, *2*, 1617 – 1619.
[21] Y. N. Belokon', S. Caveda-Cepas, B. Green, N. S. Ikonnikov, V. N. Khrustalev, V. S. Larichev, M. A. Moscalenko, M. North, C. Orizu, V. I. Tararov, M. Tasinazzo, G. I. Timofeeva, L. V. Yashkina, *J. Am. Chem. Soc.* **1999**, *121*, 3968 – 3973.
[22] G. Desantis, Z. Zhu, W. A. Greenberg, K. Wong, J. Chaplin, S. R. Hanson, B. Farwell, L. W. Nicholson, C. L. Rand, D. P. Weiner, D. E. Robertson, M. J. Burk, *J. Am. Chem. Soc.* **2002**, *124*, 9024 – 9025.
[23] L. Rosenthaler, *Biochem. Z.* **1909**, *14*, 238 – 253.
[24] G. de Gonzalo, R. Brieva, V. Gotor, *J. Mol. Catal. B* **2002**, *8*, 223 – 230.

 © 2003 Wiley-VCH Verlag GmbH & Co. KGaA, Weinheim

Stable Platinum Anions

Cs_2Pt: A Platinide(-II) Exhibiting Complete Charge Separation**

*Andrey Karpov, Jürgen Nuss, Ulrich Wedig, and Martin Jansen**

Dedicated to Professor Bernt Krebs on the occasion of his 65th birthday

The chemical-bonding characteristics of an atom are basically determined by the energy, symmetry, and extension of its valence orbitals. These values vary in a characteristic fashion with the nuclear charge, its influence on the valence electrons is modified by screening effects of the core shells. This interplay leads to the well-known relationship between position of an element in the periodic system and its bonding properties. The importance of relativistic effects, which had already been introduced into calculations of electronic structures by Dirac,[1] grows with increasing atomic number. One of the most important consequences is the contraction of the occupied s and p orbitals, and the concomitant expansion of the d and f orbitals.[2] The associated shifts in the spectrum of orbital energies become rather prominent when reaching the 6th period. The effects are particularly noticeable for gold, which exhibits the highest electron affinity among all metals (2.31 eV[3]), and the Au^- ion is stabile in the gas phase, in solution,[4] and in the solid state.[5] Furthermore the crystal-chemical parallels[6] to the halogenides, and a reactivity partly analogous to the halogens, for example, the base-induced disproportionation,[7] have found a straightforward explanation in the relativistic stabilization of the Au^- ion.

Platinum is the metal with the second highest electron affinity (2.13 eV[3]), which agrees well with calculations by Pyykkö and Desclaux showing that platinum exhibits the second largest 6s-contraction.[2] It is remarkable, that the electron affinity of platinum exceeds that of sulfur (2.08 eV), the highest value in the chalcogen group, the members of which, as typical nonmetals, readily form negatively charged dianions. Based on these facts it appears promising to attempt the synthesis of platinides containing platinum with a negative ionic charge.[8] Although the Pt^{2-} ion, as with every twofold negatively charged anion, is expected to be unstable in the free state, our goal from the beginning has been to realize this closed-shell valence state. After numerous failures we have now succeeded in obtaining Cs_2Pt, unexpectedly through a high-temperature synthesis: cesium and platinum sponge are sealed in a tantalum ampoule, reacted at 973 K and then slowly cooled down to room temperature. The Cs_2Pt crystals grow in the shape of dark-red transparent hexagonal columns, which could be mechanically separated from the excess of liquid cesium for structure analysis.[9] The compound is extremely air and moisture sensitive, but thermally stable up to about 473 K. At this temperature it decomposes to a previously unknown phase containing less cesium. It proved to be difficult to remove the excess of cesium by distillation without a simultaneous partial decomposition of the product phase.

According to the results of X-ray single-crystal structure analysis,[9] Cs_2Pt crystallizes in the Ni_2In-type of structure. This structure type (Figure 1) exhibits no variable positional parameters, thus all structure–chemical properties are fully determined by the values of the lattice constants, in particular the *c*/*a* ratio. A platinum center is surrounded by nine cesium atoms (328 (3×) and 404 (6×) pm) in the form of a tricapped trigonal prism, with two additional neighbors at a distance of 474 pm. The environments of the two independent cesium atoms differ significantly: Cs1 is coordinated by six Pt and six Cs2 atoms at the same distance of 404 pm, Cs2 by three Pt (328 pm) and six Cs1 (404 pm). Nevertheless, in an ionic picture (Cs^+, Pt^{2-}) both cesium atoms are energetically balanced, with respect to their partial Madelung energies.[10]

The Ni_2In structure type is currently regarded as the end member of a series of polymorph modifications, adopted by compounds in the fluorite structure type (CaF_2) under increased hydrostatic pressure.[11] Recently, we reported that the sequence fluorite→cotunnite→Ni_2In structure type is

[*] Prof. Dr. M. Jansen, Dipl.-Chem. A. Karpov, Dr. J. Nuss, Dr. U. Wedig
Max-Planck-Institut für Festkörperforschung
Heisenbergstrasse 1, 70569 Stuttgart (Germany)
Fax: (+49) 711-689-1502
E-mail: m.jansen@fkf.mpg.de

[**] We thank the Fonds der Chemischen Industrie for continuous financial support.

 © 2003 Wiley-VCH Verlag GmbH & Co. KGaA, Weinheim DOI: 10.1002/anie.200352314

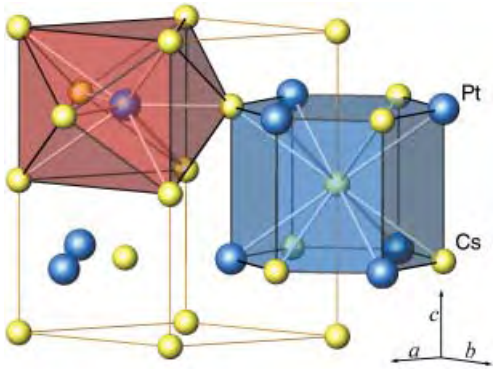


Figure 1. Perspective representation of the crystal structure of Cs_2Pt (red: $PtCs_9$ polyhedron, blue: $(Cs1)Pt_6(Cs2)_6$ polyhedron, orange lines: elementary cell edges).

also achieved for the alkali-metal monochalcogenides.[12] Of note is the close structural relationship between the $PbCl_2$ and Ni_2In structure types (Figure 2), which can be transformed into each other by a displacive rearrangement mechanism. This relationship explains why ionic solids can also crystallize in the Ni_2In structure. In accordance with the pressure-homologue rule, Cs_2S, Cs_2Se, and Cs_2Te already exist under normal pressure in the $PbCl_2$ structure type. Rb_2Te[13] marks a transition, since it exists in the CaF_2, $PbCl_2$, and, at high temperatures, in the Ni_2In structure. In this sense the Pt^{2-} ion might be considered as a higher homologue of the chalcogenides.

Hence, we take the structure–chemical affiliation of Cs_2Pt to the family of alkali-metal monochalcogenides as a first indication of an ionic nature of this compound. However, the Ni_2In structure is encountered both in (polar) intermetallic phases and in ionic crystals. Therefore, its adoption by Cs_2Pt is not a sufficient evidence for an ionic character of Cs_2Pt.

A strong and unambiguous sign for the charge separation is the red color and the transparency of the crystals, which indicate the existence of a band gap. Calculations in both the density-functional approach[14,15] and the Hartree–Fock approximation[15] confirm this, independently. The values for the band gap, found using the LMTO program, lie between 1.3 eV and 1.8 eV, depending on the functional used (local[16] or gradient corrected (Perdew–Wang[17])), the choice of Muffin–Tin radii,[18] and the treatment of the 5s and 5p orbitals (core or valence region). Bands shown in Figure 3 were calculated by using the gradient-corrected functional, the radii variant B, and Cs 5p valence orbitals. In the fat-band representation the widths exhibit the contributions of an individual atomic orbital to the corresponding bands. Bands with exclusively Pt 5d character lie below the Fermi-level. The rather small splitting and dispersion of the bands indicates a basically closed d shell. Bands mainly consisting of Pt 6s orbitals reside below the ones mentioned above.

If the one-particle equations within the Muffin–Tin spheres are evaluated nonrelativistically, the s and d bands interchange their positions, while the band gap contracts by 45%. Nevertheless, the ionic character remains. Clearly, the relativistic contraction of the 6s orbital of platinum atoms is not responsible by itself for the stability of crystalline Cs_2Pt.

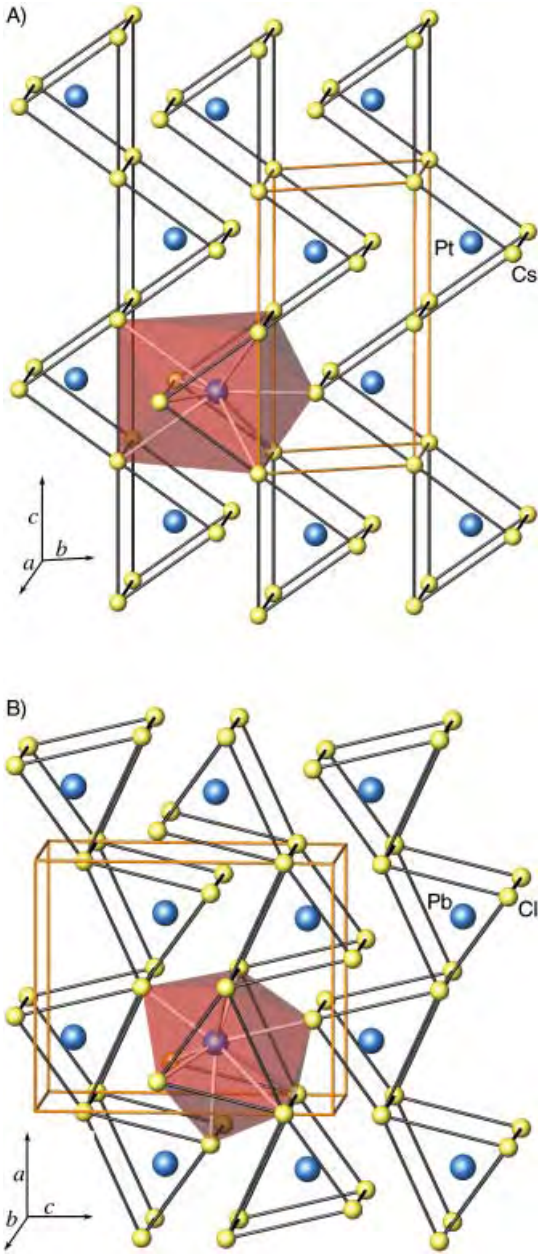


Figure 2. Comparison of crystal structures of Cs_2Pt (A) and $PbCl_2$ (B), red polyhedron: tricapped trigonal prism ($PtCs_9$ (A) and $PbCl_9$ (B), black lines correspond to the edges of the trigonal prisms, orange lines mark elementary cells.

The domains of the electron-localization function (ELF),[19] shown in Figure 4, show the strong polarization both of the Pt^{2-} ions and the Cs^+ ions, in particular within the hexagonal Cs2–Pt layers. Static as well as dynamic polarization interactions contribute significantly to the bonding. Theoretical investigations of the hypothetical Cs_2Pt molecule,[20,21] at a more accurate level of calculations with respect to basis sets and correlation methods, support this point of view. No bonding is realized assuming the cesium 5s–5p shell is frozen. For a correct description of the bonding in the molecule, the static polarization (including the corresponding functions for the Cs 5s and 5p shells), the dispersion interaction

 © 2003 Wiley-VCH Verlag GmbH & Co. KGaA, Weinheim

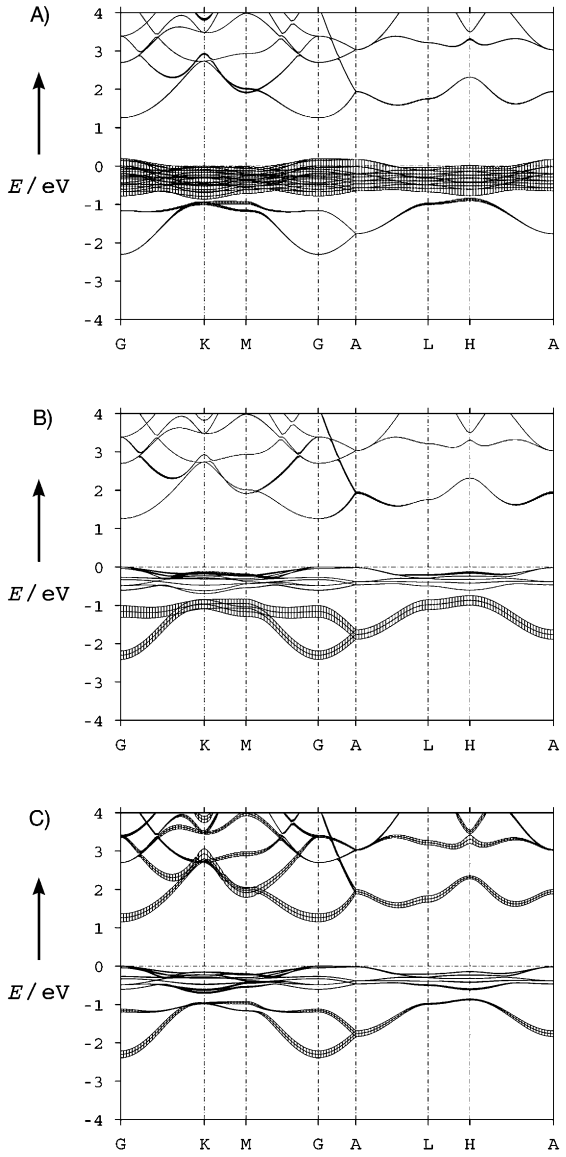


Figure 3. TB-LMTO-ASA band structure of Cs_2Pt. The widths of the bands shows the contributions of different atom orbitals: A) Pt 5d, B) Pt 6s, C) s and p orbitals of Cs1 and Cs2.

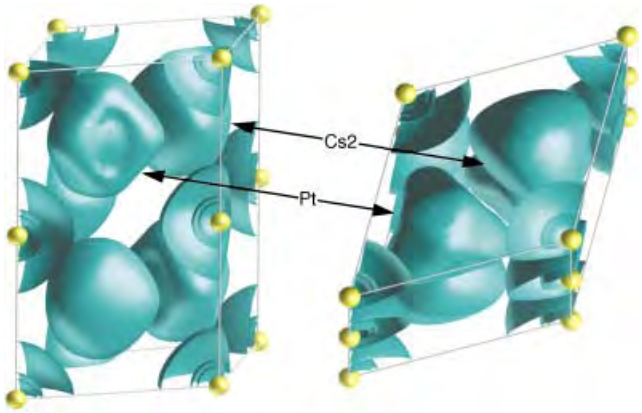


Figure 4. Domains of the electron localization function (ELF = 0.35) in Cs_2Pt.

(CCSD(T)), and relativistic effects (quasi-relativistic pseudopotentials) have to be taken into account. All three effects almost equally contribute to an increase of the charge separation. The molecule appears to be a good model with which to understand the bonding within the hexagonal Cs2–Pt layers in the crystal. Independently of the method used, the effective partial charge in the crystal at the Pt atom amounts to at least −1.3.

The results of our investigations on Cs_2Pt yield a consistent picture. The structural–chemical relation to the alkali-metal monochalcogenides and a band gap in the visible region of the electromagnetic spectrum suggest an ionic arrangement consisting of Cs^+ and Pt^{2-} ions. This view is supported by quantum chemical calculations, which indicate a complete charge separation. Even if the stability of Cs_2Pt is due in a considerable degree to dispersion forces, this compound provides further experimental evidence for the relativistic stabilization of the $6s^2$ state.

Experimental Section

Cs_2Pt was prepared by reaction of cesium (synthesized from CsCl by a reduction with calcium and distilled two times under vacuum)[22] with platinum sponge (ChemPur, 99.9%, dried before the use at 673 K in vacuum at 10^{-6} bar) in a 3:1 ratio. The mixture (2–3 g) was sealed under Ar in a tantalum ampoule, annealed for 2 days at 973 K, and then cooled to room temperature with a rate of 10 K h^{-1}. Dark-red transparent hexagonal columns ($0.2 \times 0.2 \times 0.4$ mm^3) of Cs_2Pt were separated from an excess of liquid cesium in a glove box, mechanically fixed in glass capillaries which were subsequently sealed. The attempts to distil the excess of Cs at 393 K in vacuum lead to a two-phase mixture of Cs_2Pt and a further phase containing more Pt (energy dispersive X-ray spectroscopy (EDX): Cs/Pt ≈ 1/2).

Received: July 4, 2003 [Z52314]

Keywords: cesium · charge separation · platinum · relativistic effects · solid-state structures

[1] P. A. M. Dirac, *Proc. R. Soc. London Ser. A* **1928**, *117*, 610–624; P. A. M. Dirac, *Proc. R. Soc. London Ser. A* **1928**, *118*, 351–361; P. A. M. Dirac, *Proc. R. Soc. London Ser. A* **1929**, *123*, 714–733; P. A. M. Dirac, *Proc. R. Soc. London Ser. A* **1932**, *136*, 453–464.
[2] P. Pyykkö, J. P. Desclaux, *Acc. Chem. Res.* **1979**, *12*, 276–281.
[3] T. Andersen, H. K. Haugen, H. Hotop, *J. Phys. Chem. Ref. Data* **1999**, *28*, 1511–1533.
[4] A.-V. Mudring, M. Jansen, J. Daniels, S. Krämer, M. Mehring, J. P. P. Ramalho, A. H. Romero, M. Parrinello, *Angew. Chem.* **2002**, *114*, 128–132; *Angew. Chem. Int. Ed.* **2002**, *41*, 120–124; P. D. C. Dietzel, M. Jansen, *Chem. Commun.* **2001**, 2208–2209.
[5] A. H. Sommer, *Nature* **1943**, *152*, 215; W. E. Spicer, A. H. Sommer, J. G. White, *Phys. Rev.* **1959**, *115*, 57–62; C. Feldmann, M. Jansen, *Angew. Chem.* **1993**, *105*, 1107–1108; *Angew. Chem. Int. Ed. Engl.* **1993**, *32*, 1049–1050; C. Feldmann, M. Jansen, *J. Chem. Soc. Chem. Commun.* **1994**, 1045–1046; A. Pantelouris, G. Küper, J. Hormes, C. Feldmann, M. Jansen, *J. Am. Chem. Soc.* **1995**, *117*, 11749–11753.
[6] C. Feldmann, M. Jansen, *Z. Anorg. Allg. Chem.* **1995**, *621*, 1907–1912.
[7] A.-V. Mudring, M. Jansen, *Angew. Chem.* **2000**, *112*, 3194–3196; *Angew. Chem. Int. Ed.* **2000**, *39*, 3066–3067; A.-V. Mudring, J. Nuss, U. Wedig, M. Jansen, *J. Solid State Chem.* **2000**, *155*, 29–36.

 © 2003 Wiley-VCH Verlag GmbH & Co. KGaA, Weinheim

[8] Diploma thesis A.-V. Mudring, Rheinische Friedrich-Wilhelms-University, Bonn, **1995**.
[9] Crystal data of Cs_2Pt: hexagonal, spacegroup $P6_3/mmc$ (No. 194), $a = 567.6(1)$, $c = 947.1(3)$ pm, $V = 264.3(1) \times 10^6$ pm^3, $\rho_{calcd} = 5.783$ g cm^{-3}, $Z = 2$, $\mu Mo_{K\alpha} = 39.86$ mm^{-1}, $F(000) = 376$, $\lambda = 71.073$ pm, Bruker AXS Smart-APEX-difractometer, graphite monochromator, $T = 293$ K, ω-Scan, 3711 measured reflexes, 243 symmetry independent reflexes ($2\theta_{max} = 68°$), 8 refined parameters. Semiempirical absorption correction (SADABS[23]). The structure solution and refinement have been performed using SHELXTL:[24] $R_1 = 0.0221$ and $wR_2 = 0.0524$. Further details on the crystal-structure investigations may be obtained from the Fachinformationszentrum Karlsruhe, 76344 Eggenstein-Leopoldshafen, Germany (fax: (+49) 7247-808-666; e-mail: crysdata@fiz-karlsruhe.de), on quoting the depository number CSD-413241.
[10] R. Hoppe, *Angew. Chem.* **1966**, *78*, 52 – 63; *Angew. Chem. Int. Ed. Engl.* **1966**, *5*, 95 – 106.
[11] J. M. Leger, J. Haines, A. Atouf, O. Schulte, S. Hull, *Phys. Rev. B* **1995**, *52*, 13247 – 13256.
[12] A. Grzechnik, A. Vegas, K. Syassen, I. Loa, M. Hanfland, M. Jansen, *J. Solid State Chem.* **2000**, *154*, 603 – 611; A. Vegas, A. Grzechnik, K. Syassen, I. Loa, M. Hanfland, M. Jansen, *Acta Crystallogr. Sect. B* **2001**, *57*, 151 – 156; A. Vegas, A. Grzechnik, M. Hanfland, C. Mühle, M. Jansen, *Solid State Sci.* **2002**, *4*, 1077 – 1081.
[13] K. Stöwe, S. Appel, *Angew. Chem.* **2002**, *114*, 2849 – 2854; *Angew. Chem. Int. Ed.* **2002**, *41*, 2725 – 2730.
[14] R. W. Tank, O. Jepsen, A. Burkhardt, O. K. Andersen, TB-LMTO-ASA-Programm, Version 4.7, Max-Planck-Institut für Festkörperforschung, Stuttgart, **1998**.
[15] V. R. Saunders, R. Dovesi, C. Roetti, M. Causa, N. M. Harrison, R. Orlando, C. M. Zicovich-Wilson, CRYSTAL98 Users Manual, University of Torino, Torino, **1998**.
[16] U. von Barth, L. Hedin, *J. Phys. C* **1972**, *5*, 1629 – 1642.
[17] J. P. Perdew, Y. Wang, *Phys. Rev. B* **1986**, *33*, 8800 – 8802; J. P. Perdew, Y. Wang, *Phys. Rev. B* **1989**, *40*, 3399; J. P. Perdew, Y. Wang, *Phys. Rev. B* **1992**, *45*, 13244 – 13249; J. P. Perdew, *Electronic Structure of Solids*, Akademie Verlag, Berlin, **1991**.
[18] Variant A: R(Pt) = 3.34 a.u., R(Cs1) = 4.99 a.u., R(Cs2) = 3.73 a.u. (standard values); variant B: R(Pt) = 3.73 a.u., R (Cs1) = 4.99 a.u., R (Cs2) = 3.34 a.u.
[19] A. Savin, A. D. Becke, J. Flad, R. Nesper, H. Preuß, H. G. von Schnering, *Angew. Chem.* **1991**, *103*, 421 – 424; *Angew. Chem. Int. Ed. Engl.* **1991**, *30*, 409 – 412; A. Savin, O. Jepsen, J. Flad, O. K. Andersen, H. Preuß, H. G. von Schnering, *Angew. Chem.* **1992**, *104*, 186 – 188; *Angew. Chem. Int. Ed. Engl.* **1992**, *31*, 187 – 188.
[20] U. Wedig, M. Jansen, unpublished results.
[21] Cs_2Pt molecule: calculated with Gaussian 98;[25] quasi-relativistic pseudopotentials: Pt, 18 valence electrons,[26] Cs, 9 valence electrons,[27] basis set: Pt [6s5p4d2f], Cs [5s4p2d1f]; CCSD(T); C_{2v}; $R_{Cs-Pt} = 296.1$ pm; $\Theta_{Cs\text{-}Pt\text{-}Cs} = 132.7°$; $D_e = 4.12$ eV (with correction of the basis superposition errors); harmonic frequencies: 22.9 cm^{-1}, 95.7 cm^{-1} (A_1), 101.2 cm^{-1} (B_2); Mulliken-charge (SCF density) Pt: −1.48, Cs: +0.74.
[22] G. Brauer, *Handbuch der Präparativen Anorganischen Chemie, vol. 2*, Ferdinand Enke, Stuttgart, **1978**, pp. 938 – 942.
[23] G. M. Sheldrick, Bruker AXS, Inc. Madison, USA, SADABS version 2.0, program for absorption correction, **2001**.
[24] G. M. Sheldrick, Bruker AXS, Inc. Madison, USA, SHELXTL version 6.12, program package for crystal structure solution and refinement, **2000**.
[25] Gaussian 98 (Revision A.7), M. J. Frisch, G. W. Trucks, H. B. Schlegel, G. E. Scuseria, M. A. Robb, J. R. Cheeseman, V. G. Zakrzewski, J. A. Montgomery, R. E. Stratmann, J. C. Burant, S. Dapprich, J. M. Millam, A. D. Daniels, K. N. Kudin, M. C. Strain, O. Farkas, J. Tomasi, V. Barone, M. Cossi, R. Cammi, B. Mennucci, C. Pomelli, C. Adamo, S. Clifford, J. Ochterski, G. A. Petersson, P. Y. Ayala, Q. Cui, K. Morokuma, D. K. Malick, A. D. Rabuck, K. Raghavachari, J. B. Foresman, J. Cioslowski, J. V. Ortiz, B. B. Stefanov, G. Liu, A. Liashenko, P. Piskorz, I. Komaromi, R. Gomperts, R. L. Martin, D. J. Fox, T. Keith, M. A. Al-Laham, C. Y. Peng, A. Nanayakkara, C. Gonzalez, M. Challacombe, P. M. W. Gill, B. G. Johnson, W. Chen, M. W. Wong, J. L. Andres, M. Head-Gordon, E. S. Replogle, J. A. Pople, Gaussian, Inc., Pittsburgh, PA, **1998**.
[26] D. Andrae, U. Haeussermann, M. Dolg, H. Stoll, H. Preuss, *Theor. Chim. Acta* **1990**, *77*, 123 – 141.
[27] T. Leininger, A. Nicklass, W. Küchle, H. Stoll, M. Dolg, A. Bergner, *Chem. Phys. Lett.* **1996**, *255*, 274 – 280.

 © 2003 Wiley-VCH Verlag GmbH & Co. KGaA, Weinheim

Pancratistatin Analogues

Stereospecific Biocatalytic Synthesis of Pancratistatin Analogues**

*Anh Nga Phung, Maria Teresa Zannetti, Gregg Whited, and Wolf-Dieter Fessner**

The *Amaryllidaceae* alkaloids constitute an important class of natural compounds.[1] Particularly, pancratistatin (**1**) and its closely related anhydro and deoxy congeners narciclasine (**3**), lycoricidine (**4**), and *trans*-dihydrolycoricidine (**2**) have been isolated from roots of the Hawaiian plant *Hymenocallis littoralis*.[2] These compounds have attracted considerable attention due to their interesting biological properties, such as potent cytotoxic, antiviral, and insect antifeedant activity.[1–3] Current knowledge suggests a mechanism that involves a disruption of protein biosynthesis through inhibition of ribosomal tRNA binding.[4] Thus, the unique, highly oxygenated phenanthridone skeleton constitutes a promising lead for new anticancer drugs.

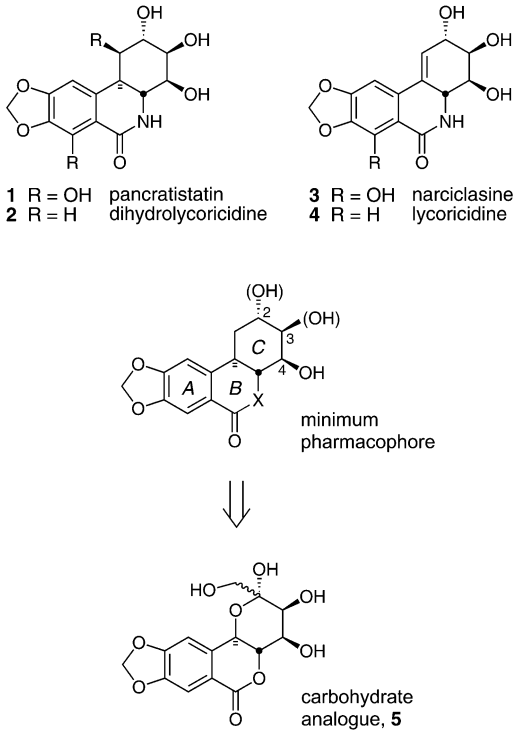
The structures **1**–**4** have been the subject of several elegant total syntheses[5,6] that centered around the major difficulty of a controlled installation of the five to six

[*] Prof. Dr. W.-D. Fessner, A. N. Phung, Dr. M. T. Zannetti
Institut für Organische Chemie und Biochemie
Technische Universität Darmstadt
Petersenstrasse 22, 64287 Darmstadt (Germany)
Fax: (+49) 6151-16-6666
E-mail: fessner@tu-darmstadt.de
Dr. G. Whited
Genencor International
925 Page Mill Road, Palo Alto, CA 94304 (USA)

[**] This study was supported by a grant (SFB 380/B25) from the Deutsche Forschungsgemeinschaft and by the Fonds der Chemischen Industrie. M.T.Z. thanks the Alexander von Humboldt Foundation for a postdoctoral fellowship.

Supporting information for this article is available on the WWW under http://www.angewandte.org or from the author.

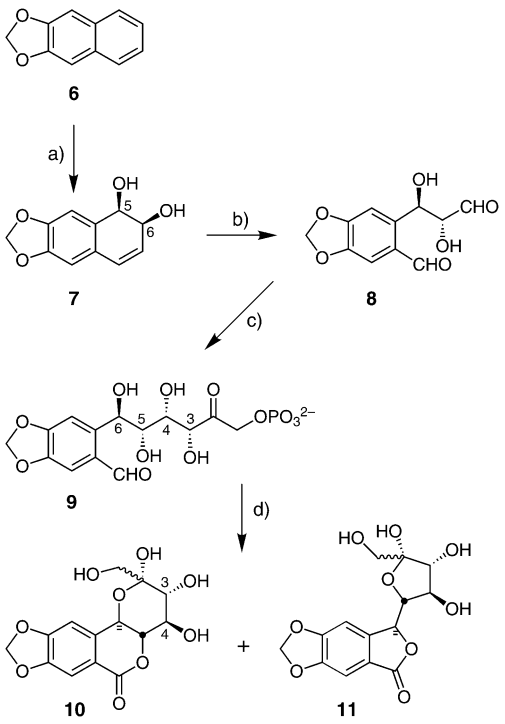
 DOI: 10.1002/anie.200352023 © 2003 Wiley-VCH Verlag GmbH & Co. KGaA, Weinheim



contiguous stereogenic centers, including the B/C ring junction. Systematic investigations to establish the minimum structure of the pharmacophore have been performed only very recently,[6–9] however, due to the limited natural supply and the complexity of the structural core. From these structure–activity studies it may be concluded that the crucial features for biological activity reside in 1) the piperonyl-type ring A, 2) the *trans* stereochemistry of the B/C ring junction that adjusts 3) the correct spatial orientation of peripheral hydroxy functions in the aminocyclitol-type ring C. Among the latter, it appears that at least the correctly positioned 4-OH and either or both of the 2-/3-hydroxyl groups are obligatory for the minimum pharmacophore.[9] While oxygenated seco-derivatives were found to be inactive,[6,8] however, a requirement for the lactam nature of ring B has not been demonstrated yet.

On the assumption of such a hypothetical minimum structure, we reasoned that replacement of the cyclitol moiety by a carbohydrate ring structure might be a permissible structural variation due to the fact that most hexoaldoses and -ketoses preferentially adopt a cyclic pyranoid structure in aqueous solution. In addition to the anomeric hydroxy group, which would mimic the 2-OH group of pancratistatin, a ketose unit as in **5** would further offer the possibility that the primary CH_2OH moiety may be positioned in a way to replace hydrophilic contacts made by the extra 1-OH in **1** upon effector binding. Thus, the B-ring lactone analogue **5** is an interesting synthetic target (as well as related stereoisomers). The major advantage of such a synthetic strategy lies in the rather simple task of attaching the aromatic nucleus to a linear carbohydrate side chain. The carbohydrate fragment itself could be established enzymatically by an aldolase reaction, which would effect a chain extension by a dihydroxyacetone fragment with simultaneous adjustment of the desired absolute configuration.[10] In this respect, the well-characterized dihydroxyacetone phosphate dependent aldolases[11] have been shown to accept an unusually broad variety of aldehyde acceptors in place of the natural substrate but maintain complete stereocontrol over the asymmetric centers at the newly formed C–C bond.

Retrosynthetically, this strategy called for an aldehyde acceptor component of type **8** that in turn might be generated by ozonolytic ring cleavage of the unsaturated *cis*-diol precursor **7** (Scheme 1). Dihydroarene-*cis*-diols, derived



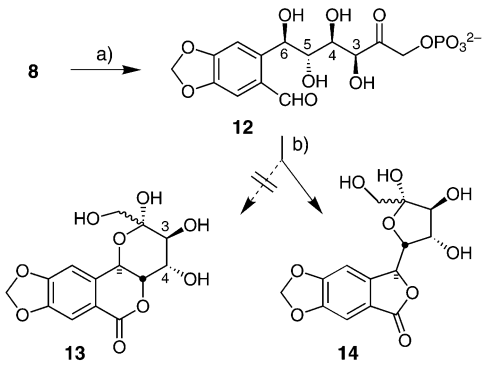
Scheme 1. Sequence of enzymatic dihydroxylation and aldolization to create four contiguous stereocenters. a) Naphthalene dioxygenase (*E. coli*), aeration, 24 h at 37 °C; 64% yield (85% based on conversion). b) O_3, −78 °C, MeOH; then Me_2S, room temperature. c) Rhamnulose 1-phosphate aldolase, dihydroxyacetone phosphate, pH 7.0, room temperature, two days. d) Acid phosphatase, pH 5.9, three days, then Br_2/$BaCO_3$; product ratio 1:1, flash chromatography; 10% overall yield (four steps from **7**).

from oxidative microbial arene degradation, have recently been developed as synthetically valuable building blocks.[12] Particularly, naphthalene dioxygenases[13] from *Pseudomonas* strains have been shown to be highly effective for dihydroxylation of polycyclic arenes and derivatives. The dioxole **6** required for this study, however, posed a considerable challenge owing to its linearly extended substrate structure, because known biocatalysts prefer angular substrates.[12,14] Screening experiments revealed that toluene dioxygenases were ineffective but that indeed a naphthalene dioxygenase from *Pseudomonas putida* G7 was able to oxidize **6**. Preparative whole-cell biooxidation, using recombinant *E. coli* cells that harbored the gene for dioxygenase overproduction,[15] was performed on multigram scale to produce the desired diol

 © 2003 Wiley-VCH Verlag GmbH & Co. KGaA, Weinheim

7 in enantiopure form (>98% *ee*) which was isolated by extraction and flash chromatography.[16] The compound was found to be rather sensitive to traces of acid, which causes decomposition to the corresponding naphthol and diminished total yields (85% based on conversion). The absolute (5*R*,6*S*) configuration of **7** follows from its positive sign of optical rotation that is shared by all related *cis*-dihydrodiol metabolites from polycyclic aromatic hydrocarbons, and by the notion that such metabolites had previously been shown to have an identical configuration, independent from the type and source of enzyme.[12]

Enediol **7** had to be ozonized under carefully controlled conditions because of its tendency for naphthol formation and facile overoxidation of the electron-rich arene by excess ozone. Without further purification, the aqueous solution of dialdehyde **8** (mixture of several hydrate constitutional isomers according to ^{1}H NMR analysis) was immediately treated with a solution of dihydroxyacetone phosphate[17] in the presence of an aldolase. Both the stereocomplementary fructose 1,6-bisphosphate (FruA)[11b] and rhamnulose 1-phosphate (RhuA))[11a] aldolases were found to accept **8** as a substrate to produce monophosphorylated products (TLC control). Conversion was rather sluggish and remained incomplete, which is probably due to the poor solubility of **8** in water that limits the effective substrate concentration. Regiospecific aldolase-catalyzed addition to the aliphatic aldehyde moiety was expected because of the excellent substrate quality of hydroxyaldehydes and the known unreactivity of aromatic carbaldehydes.[10] Spectroscopic analysis of the aldol adducts **9** and **12** gave complex spectra that were inconclusive for product identification, likely because of intramolecular cyclization to equilibrating five- or six-membered-ring hemiacetals of varying diastereomeric composition. Therefore, after enzymatic dephosphorylation, analysis was simplified by mild oxidation to furnish stable lactones. Interestingly, from the RhuA-catalyzed reaction both the desired pyranoid isomer **10** along with an equal fraction of the furanoid isomer **11** were formed (10% overall yield from **7**),[16] while from the FruA-catalyzed reaction only the undesired furanoid product **14** (10% overall yield) but no δ-lactone **13** resulted (Scheme 2). As a plausible explanation, in the case of the FruA-induced configuration the 3-/4-OH groups of **13** become enforced in a diaxial orientation, which destabilizes pyranose formation in favor of the competing furanoid structures. Furthermore, oxidation of furanoid hemiacetals may be at a certain kinetic advantage and thus favor the formation of γ-lactones.



Scheme 2. γ-Lactone formation from FruA-catalyzed aldolization. a) Fructose 1,6-bisphosphate aldolase, dihydroxyacetone phosphate, pH 7.0, room temprature, two days. b) Acid phosphatase, pH 5.9, three days, then Br_2/$BaCO_3$; 10% yield (four steps from **7**).

The δ-lactone **10** resembles (+)-pancratistatin in overall absolute configuration but deviates at 3-OH which is inverted. Correct overall configuration **5** (3/4-OH *cis*-vicinal) would call for catalysis by a tagatose 1,6-diphosphate aldolase (TagA). However, known TagA enzymes show low stereoselectivity for non-natural substrate analogues,[10,18] which currently renders such an option not viable but requires screening for new stereoselective aldolases.[19] Chemical inversion at this position would probably be rather difficult because of its low steric accessibility. Thus, **10** seems the so far best approximation that is accessible by this approach.

In summary, we have developed a new strategy for the stereospecific synthesis of novel pancratistatin analogues. Our study demonstrates that structures of high molecular complexity, incorporating a manifold of contiguous chiral centers, can be readily prepared in a few synthetic steps by a combination of enzymatic dihydroxylation and aldolization, without recourse to protective group manipulations. Screening of the new compounds for their biological activity, particularly with respect to anti-neoplastic effectivity, is currently in progress and will be reported in due course.

Received: June 2, 2003 [Z52023]

Keywords: aldol reaction · antitumor agents · asymmetric synthesis · carbohydrates · enzyme catalysis

[1] a) S. F. Martin in *The Alkaloids, Vol. 40* (Ed.: A. R. Brossi), Academic Press, New York, **1987**, pp. 251–376; b) O. Hoshino in *The Alkaloids, Vol. 51* (Ed.: G. A. Cordell), Academic Press, New York, **1998**, pp. 324–424.

[2] a) G. R. Pettit, V. Gaddamidi, D. L. Herald, S. B. Singh, G. M. Cragg, J. M. Schmidt, F. E. Boettner, M. Williams, Y. Sagawa, *J. Nat. Prod.* **1986**, *49*, 995–1002; b) G. R. Pettit, G. R. Pettit III, R. A. Backhaus, M. R. Boyd, A. W. Meerow, *J. Nat. Prod.* **1993**, *56*, 1682–1687.

[3] a) B. Gabrielsen, T. P. Monath, J. W. Huggins, D. F. Kefauver, G. R. Pettit, G. Groszek, M. Hollingshead, J. J. Kirsi, W. M. Shannon, E. M. Schubert, *J. Nat. Prod.* **1992**, *55*, 1569–1581; b) M. Ouarzane-Amara, J.-F. Franetich, D. Mazier, G. R. Pettit, L. Meijer, C. Doerig, I. Desportes-Livage, *Antimicrob. Agents Chemother.* **2001**, *45*, 3409–3415.

[4] a) L. Carrasco, M. Fresno, D. Vazquez, *FEBS Lett.* **1975**, *52*, 236–239; b) A. Mondon, K. Krohn, *Chem. Ber.* **1975**, *108*, 445–463; c) A. Jimenez, L. Sanchez, D. Vazquez, *FEBS Lett.* **1975**, *60*, 66–70; d) A. Baez, D. Vazquez, *Biochim. Biophys. Acta* **1978**, *518*, 95–103.

[5] R. Polt in *Organic Synthesis: Theory and Applications, Vol. 3* (Ed.: T. Hudlicky), JAI, Greenwich, CT, **1997**, pp. 109–148.

[6] T. Hudlicky, U. Rinner, D. Gonzalez, H. Akgun, S. Schilling, P. Siengalewicz, T. A. Martinot, G. R. Pettit, *J. Org. Chem.* **2002**, *67*, 8726–8743, zit. Lit.

[7] a) A. Evidente, O. Arrigoni, R. Liso, G. Calabrese, G. Randazzo, *Phytochemistry* **1986**, *25*, 2739–2743; b) G. R. Pettit, N. Melody, D. L. Herald, J. M. Schmidt, R. K. Pettit, J.-C. Chapuis, *Heterocycles* **2002**, *56*, 139–155.

 © 2003 Wiley-VCH Verlag GmbH & Co. KGaA, Weinheim

[8] F. Chretien, S. I. Ahmed, A. Masion, Y. Chapleur, *Tetrahedron* **1993**, *49*, 7463 – 7478.
[9] J. McNulty, J. Mao, R. Gibe, R. Mo, S. Wolf, G. R. Pettit, D. L. Herald, M. R. Boyd, *Bioorg. Med. Chem. Lett.* **2001**, *11*, 169 – 172.
[10] a) W.-D. Fessner, C. Walter, *Top. Curr. Chem.* **1996**, *184*, 97 – 194; b) W.-D. Fessner in *Stereoselective Biocatalysis* (Ed.: R. N. Patel), Marcel Dekker, New York, **2000**, S. 239 – 265.
[11] a) W.-D. Fessner, G. Sinerius, A. Schneider, M. Dreyer, G. E. Schulz, J. Badía, J. Aguilar, *Angew. Chem.* **1991**, *103*, 596 – 599; *Angew. Chem. Int. Ed. Engl.* **1991**, *30*, 555 – 558; b) M. T. Zannetti, C. Walter, M. Knorst, W. D. Fessner, *Chem. Eur. J.* **1999**, *5*, 1882 – 1890; c) A. C. Joerger, C. Gosse, W.-D. Fessner, G. E. Schulz, *Biochemistry* **2000**, *39*, 6033 – 6041; d) M. Kroemer, G. E. Schulz, *Acta Crystallogr. Sect. D* **2002**, *58*, 824 – 832.
[12] a) H. A. J. Carless, *Tetrahedron: Asymmetry* **1992**, *3*, 795 – 826; b) S. M. Brown, T. Hudlicky, in *Organic Synthesis: Theory and Applications, Vol. 2* (Ed.: T. Hudlicky), JAI, Greenwich, CT, **1993**, S. 113 – 176; c) D. R. Boyd, G. N. Sheldrake, *Nat. Prod. Rep.* **1998**, *15*, 309 – 324; d) T. Hudlicky, D. Gonzalez, D. T. Gibson, *Aldrichimica Acta* **1999**, *32*, 35 – 62.
[13] A. Karlsson, J. V. Parales, R. E. Parales, D. T. Gibson, H. Eklund, S. Ramaswamy, *Science* **2003**, *299*, 1039 – 1042.
[14] D. R. Boyd, N. D. Sharma, J. S. Harrison, M. A. Kennedy, C. C. R. Allen, D. T. Gibson, *J. Chem. Soc. Perkin Trans. 1* **2001**, 1264 – 1269.
[15] a) W.-C. Suen, D. T. Gibson, *Gene* **1994**, *143*, 67 – 71; b) C. M. Serdar, D. C. Murdock, B. D. Ensley, U.S. Patent 5 173 425, **1992** [*Chem. Abstr.* **1993**, *118*, 100551].
[16] Selected data for new compounds: **7**, m.p. 132–133 °C; $[\alpha]_D^{20} = +180.6°$ ($c = 1$, $CHCl_3$); ^{1}H NMR (300 MHz, CD_3OD, TMS): $\delta = 5.66$, 5.31 (2 s, 1-,4-H), 5.08 (dd, 7-H), 4.66 (s, 2H, CH_2), 4.59 (dd,8-H), 3.19 (d, 5-H), 2.97 ppm (dt, 6-H), $J_{5,6} = 4.9$, $J_{6,7} = 0.8$, $J_{6,8} = 4.0$, $J_{7,8} = 9.7$ Hz; ^{13}C NMR (75 MHz, CD_3OD, TMS): $\delta =$ 147.2, 147.1 (C-2,-3), 130.4 (C-4a), 128.1, 126.9 (C-1,-4), 126.5 (C-1a), 108.0, 107.0 (C-7,-8), 101.0 (CH_2), 70.6, 67.8 ppm (C-5,-6); ESI-MS: m/z: 206 (17) $[M]^+$, 188 (100) $[M-H_2O]^+$. **10**, ^{1}H NMR (500 MHz, D_2O, TSP): $\delta = 7.18$, 7.13 (2 s, $2H_{ar}$), 6.05 (s, 2H, OCH_2O), 5.24 (d, 6-H), 3.89 (t, 4-H), 3.74 (d, 1-H_a), 3.71 (d, 3-H), 3.68 (t, 5-H), 3.54 ppm (d, 1-H_b), $J_{1a,1b} = 11.8$, $J_{3,4} = 9.6$, $J_{4,5} = 9.4$, $J_{5,6} = 10.0$ Hz; ^{13}C NMR (125.6 MHz, D_2O, TSP): $\delta = 188.4$ (C=O), 151.2, 150.5 ($2OC_{ar}$), 132.4, 118.6 ($2C_{ar}$), 115. 5, 111.4 ($2HC_{ar}$), 105.1 (OCH_2O), 101.0 (C-2), 76.9 (C-5), 76.5 (C-4), 75.6 (C-6), 73.4 (C-3), 66.5 ppm (C-1); ESI-MS: m/z: 349 (100) $[M+Na]^+$. **11**, ^{1}H NMR (500 MHz, D_2O, TSP): $\delta = 7.16$, 7.12 (2 s, $2H_{ar}$), 6.17 (s, 2H, OCH_2O), 5.60 (d, 6-H), 4.25 (t, 4-H), 4.13 (d, 3-H), 4.00 (dd, 5-H), 3.65 (d, 1-H_a), 3.60 ppm (d, 1-H_b), $J_{1a,1b} =$ 12.1, $J_{3,4} = 7.9$, $J_{4,5} = 6.8$, $J_{5,6} = 5.8$ Hz; ^{13}C NMR (125.6 MHz, D_2O, TSP): $\delta = 175.6$ (C=O), 157.0, 152.4 ($2OC_{ar}$), 147.1, 121.2 ($2C_{ar}$), 106.5, 106.2 ($2HC_{ar}$), 106.1 (OCH_2O), 104.9 (C-2), 83. 7 (C-6), 83.4 (C-5), 78.3 (C-3), 77.7 (C-4), 65.5 ppm (C-1); ESI-MS: m/z: 349 (100) $[M+Na]^+$.
[17] W.-D. Fessner, G. Sinerius, *Angew. Chem.* **1994**, *106*, 217 – 220; *Angew. Chem. Int. Ed. Engl.* **1994**, *33*, 209 – 212.
[18] W.-D. Fessner, O. Eyrisch, *Angew. Chem.* **1992**, *104*, 76 – 78; *Angew. Chem. Int. Ed. Engl.* **1992**, *31*, 56 – 58.
[19] E. Gonzalez-Garcia, V. Helaine, G. Klein, M. Schuermann, G. A. Sprenger, W.-D. Fessner, J.-L. Reymond, *Chem. Eur. J.* **2003**, *9*, 893 – 899.

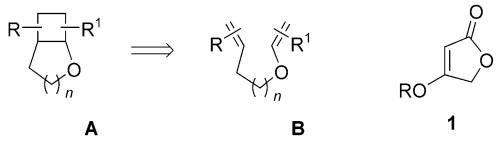
 © 2003 Wiley-VCH Verlag GmbH & Co. KGaA, Weinheim

Diastereoselective Photoaddition

[2+2] Photocycloaddition of Tetronates**

*Michael Kemmler and Thorsten Bach**

In connection with the synthesis of 2-oxabicyclo[3.2.0]heptanes ($n = 1$) and related oxygen-containing heterocycles of the general formula **A**, we postulated that a Cu-catalyzed intramolecular [2+2] photocycloaddition[1] of enol ethers **B** might provide a general approach to this class of compounds (Scheme 1). In contrast to simple homoallyl vinyl ethers,



Scheme 1. Synthesis of 2-oxabicyclo[3.2.0]heptanes by intramolecular [2+2] photocycloaddition.

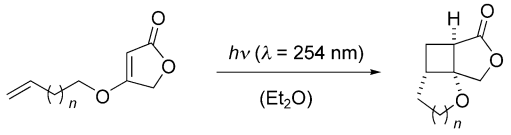
which have been shown to undergo Cu-catalyzed [2+2] photocycloadditions,[2] the more highly substituted substrates of type **B** that we tested did not react as desired, but decomposed in the presence of the copper salts. As an alternative to enol ethers we examined derivatives of tetronic acid[3] (**1**, R = H) in direct [2+2] photocycloaddition reactions and found that these building blocks deliver excellent results under irradiation conditions. Although the [2+2] photocycloaddition of 3[2*H*]-furanones[4] and 2[5*H*]-furanones[5] is well known, to the best of our knowledge no study of tetronates in [2+2] photocycloaddition reactions has yet been conducted. Herein, we report the first [2+2] photocycloaddition reactions of these compounds.

Tetronates of the general formula **2** are readily available from tetronic acid or its derivatives and ω-alkenols by nucleophilic substitution.[6] In a first series of experiments we investigated the intramolecular [2+2] photocycloaddition of the O-bridged dienes **2** (Scheme 2). The reactions proceeded smoothly[7,8] to produce the tetrahydrofuran **3a** and the tetrahydropyran **3b** with excellent simple diastereoselectivity. In each case a single product was observed in diastereomerically pure form. The relative configuration was unambiguously assigned by NOESY experiments and X-ray crystallographic analysis. The light source in the irradiation experiments was either a TNN 15/32 (Original

[*] Prof. Dr. T. Bach, Dipl.-Chem. M. Kemmler
Lehrstuhl für Organische Chemie I
Technische Universität München
Lichtenbergstrasse 4, 85747 Garching (Germany)
Fax: (+49) 89-2891-3315
E-mail: thorsten.bach@ch.tum.de

[**] This project was supported by the Deutsche Forschungsgemeinschaft (Ba 1372-6/1) and the Fonds der Chemischen Industrie.

 © 2003 Wiley-VCH Verlag GmbH & Co. KGaA, Weinheim DOI: 10.1002/anie.200352171

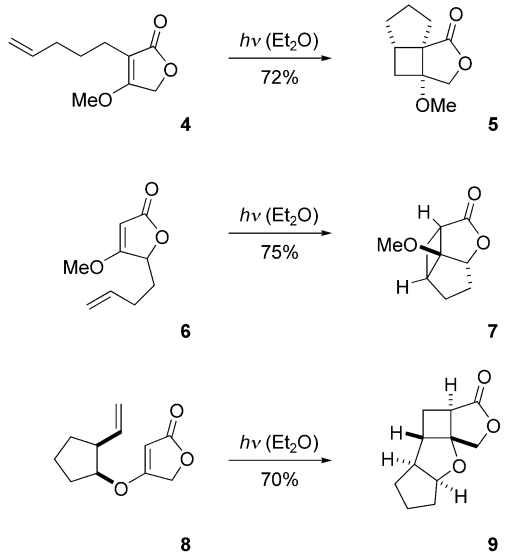


2a	*n* = 1	74%	**3a**
2b	*n* = 2	71%	**3b**

Scheme 2. Intramolecular [2+2] photocycloaddition of ω-alkenyl tetronates **2**.

Hanau, Heraeus Noblelight) low-pressure mercury arc or lamps of the type RPR-2437 Å (Rayonet).

Analogous experiments in acetone as the solvent or with a triplet sensitizer (benzophenone, acetophenone) in diethyl ether or acetonitrile were less successful and led to the formation of side products. The intramolecular photocycloaddition is not restricted by the position of the alkenyl side chain. In compound **4** the ω-alkenyl chain is attached at C3, in compound **6** at C5 (Scheme 3). The cyclization of these

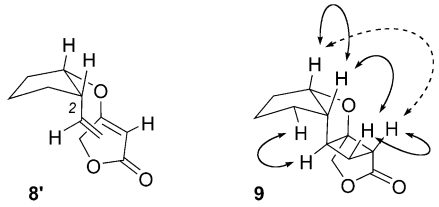


4 **5** **6** **7** **8** **9**

Scheme 3. Intramolecular [2+2] photocycloaddition of further substituted tetronates.

substrates gave the structurally interesting tricyclic products **5** and **7** with high chemo-, regio-, and stereoselectivity. Thus, this represents a new and efficient approach to the bicyclo[3.2.0]heptane scaffold, which is frequently encountered in natural products.[9] In all cases (**3, 5, 7**), a single product was formed in which the cyclobutane ring and the annelated five- or six-membered rings are connected in a *cis* fashion (simple diastereoselectivity). The facial diastereoselectivity in the reaction **6**→**7** can be understood as the attack of the terminal alkene to the face of the tetronate to which the alkyl chain is directed by the stereogenic center at C5.

For the synthesis of the tricyclic skeleton of punctaporonin C[10] we investigated the intramolecular [2+2] photocycloaddition of the tetronate **8** (Scheme 3), which was readily prepared from the known compound *trans*-2-vinyl-1-cyclopentanol[11] by a Mitsunobu reaction with tetronic acid. The photocycloaddition again proceeded smoothly to provide the tetracycle **9** as the sole product with perfect facial diastereoselectivity. The configuration of **9** was assigned by NOESY experiments (Figure 1). In this case the observed face differentiation is more difficult to explain, and arguments that have been put forward previously to interpret stereochemical results in a series of carbocyclic tricyclo[6.2.0.0^{2,6}]-decanes[12] have to be considered. These suggest that the



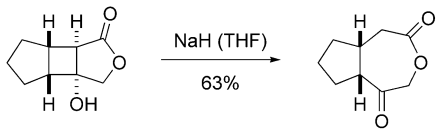
8' **9**

Figure 1. Preferred conformation **8′** of compound **8** in the reaction to form **9** and NOESY contacts in the tetracyclic compound **9** (----- medium, —— strong).

cyclopentane ring prefers an envelope conformation in which the tetronate group occupies a pseudoequatorial and the vinyl group a pseudoaxial position (**8′**, Figure 1). Free rotation about the bond connecting the vinyl substituent with the cyclopentane ring at C2 is restricted by steric interactions at the double bond (1,2- versus 1,3-allylic strain). A conformation in which the vinyl group and the H atom at C2 of the cyclopentane are arranged synperiplanar is favored, because 1,3-allylic strain is thus minimized.

Not only are the molecular frameworks that are accessible through tetronate photocycloaddition suitable for direct synthetic applications, but we felt it would be interesting to expand the methodology to use the cyclobutane ring in the products for subsequent fragmentation reactions. In this context, we investigated the retroaldol reaction and applied this strategy to the product of an intermolecular [2+2] photocycloaddition as a model system. As the reaction of free tetronic acid proceeded sluggishly, the methoxyethoxymethyl (MEM)-protected derivative (**1**, R = MEM, Scheme 1) was used, and the product of its photocycloaddition with cyclopentene was subsequently deprotected to give the alcohol **10** [a) MEM-Cl, NEt_3, CH_2Cl_2; b) cyclopentene, $\lambda = 254$ nm, *t*BuOH; c) $TiCl_4$, CH_2Cl_2; overall yield 41 %]. Upon treatment with a base, **10** was readily converted into the ketolactone **11** (Scheme 4).

Although this fragmentation step has not yet been optimized, the reaction sequence described indicates that the tetronate photocycloaddition products are amenable to



10 **11**

Scheme 4. Retroaldol reaction of the photocycloaddition product **10**.

 © 2003 Wiley-VCH Verlag GmbH & Co. KGaA, Weinheim

ring expansion. In analogy with the de Mayo reaction,[13,14] which is conducted with 1,3-diketones, a stereoselective lactone annelation appears to be possible. We are currently investigating the scope and potential of the tetronate photocycloaddition reaction and the application of this methodology to the synthesis of target compounds.

Received: June 18, 2003 [Z52171]

Keywords: cycloaddition · diastereoselectivity · lactones · oxygen heterocycles · photochemistry

[1] Reviews: a) R. G. Salomon, *Tetrahedron* **1983**, *39*, 485 – 575; b) J. Mattay, R. Conrads, R. Hoffmann in *Methoden der Organischen Chemie (Houben-Weyl), 4th ed., 1952–, Vol. E21c* **1995**, pp. 3085 – 3132; c) P. Margaretha in *Methoden der Organischen Chemie (Houben-Weyl), 4th ed., 1952–, Vol. E17e*, **1997**, pp. 159 – 162.

[2] a) S. R. Raychaudhuri, S. Ghosh, R. G. Salomon, *J. Am. Chem. Soc.* **1982**, *104*, 6841 – 6842; b) S. Ghosh, S. R. Raychaudhuri, R. G. Salomon, *J. Org. Chem.* **1987**, *52*, 83 – 90; c) D. Patra, S. Ghosh, *J. Org. Chem.* **1995**, *60*, 2526 – 2531; d) S. Ghosh, D. Patra, S. Samajdar, *Tetrahedron* **1998**, *54*, 1789 – 1800.

[3] T. Meul, R. Miller, L. Tenud, *Chimia* **1987**, *41*, 73 – 76.

[4] a) P. Margaretha, *Tetrahedron* **1973**, *29*, 1317 – 1319; b) P. Margaretha, *Chimia* **1975**, *29*, 203 – 209; c) S. W. Baldwin, M. T. Crimmins, P. M. Gross, *Tetrahedron Lett.* **1978**, *19*, 4197 – 4200; d) S. W. Baldwin, T. J. Mazzuchelli, *Tetrahedron Lett.* **1986**, *27*, 5975 – 5978; e) J. Patjens, P. Margaretha, *Helv. Chim. Acta* **1989**, *72*, 1817 – 1824; f) R.-C. Gebel, P. Margaretha, *Chem. Ber.* **1990**, *123*, 855 – 858; g) R.-C. Gebel, P. Margaretha, *Helv. Chim. Acta* **1992**, *75*, 1633 – 1638; h) T. Sano, N. Koseki, T. Saitoh, Y. Horiguchi, J. Toda, F. Kiuchi, Y. Tsuda, *Chem. Pharm. Bull.* **1997**, *45*, 608 – 612; i) T. Bach, M. Kemmler, E. Herdtweck, *J. Org. Chem.* **2003**, *68*, 1994 – 1997, and references therein.

[5] a) K. Ohga, T. Matsuo, *Bull. Chem. Soc. Jpn.* **1970**, *43*, 3505 – 3510; b) H. Kosugi, H. Uda, *Bull. Chem. Soc. Jpn.* **1980**, *53*, 160 – 168; c) E. Anklam, P. Margaretha, *Helv. Chim. Acta* **1983**, *66*, 1466 – 1474; d) K. Tomioka, M. Tanaka, K. Koga, *Chem. Pharm. Bull.* **1989**, *37*, 1201 – 1207; e) N. Hoffmann, H. Buschmann, G. Raabe, H.-D. Scharf, *Tetrahedron* **1994**, *50*, 11167 – 11186; f) M. Tanaka, K. Tomioka, K. Koga, *Tetrahedron* **1994**, *50*, 12829 – 12842; g) R. Alibés, J. L. Bourdelande, J. Font, A. Gregori, T. Parella, *Tetrahedron* **1996**, *52*, 1279 – 1292; h) F. Busqué, P. de March, M. Figuerdo, J. Font, P. Margaretha, J. Raya, *Synthesis* **2001**, 1143 – 1148, and references therein.

[6] a) H. Zimmer, A. Amer, C. Van Pham, D. Grob-Schmitt, *J. Org. Chem.* **1988**, *53*, 3368 – 3370; b) J. S. Bajwa, R. C. Anderson, *Tetrahedron Lett.* **1990**, *31*, 6973 – 6976; c) T. Sato, K. Yoshimatsu, J. Otera, *Synlett* **1995**, 843 – 844; d) F. F. Paintner, L. Allmendinger, G. Bauschke, *Synlett* **2003**, 83 – 86.

[7] Representative experimental procedure: Compound **2a** (78 mg, 0.5 mmol) was dissolved in dry, degassed diethyl ether (500 mL) and irradiated in a quartz apparatus at $\lambda = 254$ nm (Rayonet RPR-2437 Å or Original Hanau TNN 15/32) for 1 h at room temperature. When the reaction was complete the solvent was removed on a rotary evaporator, and the crude cycloaddition product **3a** (75 mg, 96%) was obtained as a pale yellow oil, in > 90% purity according to NMR spectroscopic analysis. The crude product was further purified by flash chromatography (silica, pentane/ethyl acetate 6:1) to give compound **3a** (58 mg, 74%) as a colorless, crystalline solid. ^{1}H NMR (500 MHz, $CDCl_3$): $\delta = 1.78$ (dd, $J = 5.6$, 12.8 Hz, 1H, C*H*HCH$_2$O), 1.94–2.03 (m, 2H, C*H*H, CH*H*CH$_2$O), 2.22 (ddd, $J = 4.2$, 8.4, 12.8 Hz, 1H, CH*H*), 2.95 (ddd, $J = 1.3$, 4.2, 10.1 Hz, 1H, CHCOO), 2.98 (pseudo q, $J \approx 8.4$ Hz, 1H, CH), 3.96 (ddd, $J = 5.6$, 9.0, 11.5 Hz, 1H, C*H*HO), 4.25 (pseudo t, $J \approx 9.0$ Hz, 1H, CH*H*O), 4.26 (d, $J = 10.2$ Hz, 1H, COOC*H*H), 4.33 ppm (d, $J = 10.2$ Hz, 1H, COOCH*H*); ^{13}C NMR (90 MHz, $CDCl_3$): $\delta = 25.0$ (CH_2), 31.7 (CH_2CH_2O), 40.4 (*C*HCOO), 41.6 (*C*H), 68.8 (CH_2O), 72.5 (COO*C*H$_2$), 86.5 (*C*OCH$_2$), 177.9 ppm (*C*OOCH$_2$).

[8] The corresponding allyl tetronate (**2**, $n = 0$) did not react in an intramolecular [2+2] photocycloaddition. Instead, carbon radicals generated by hydrogen abstraction from the solvent (Et_2O, THF, or *i*PrOH) added to the terminal double bond.

[9] For a review, see: T. V. Hansen, Y. Stenstrøm in *Organic Synthesis: Theory and Applications, Vol. 5* (Ed.: T. Hudlicky), JAI, Greenwich, **2001**, pp. 1 – 38.

[10] J. R. Anderson, R. L. Edwards, J. P. Poyser, A. J. S. Whalley, *J. Chem. Soc. Perkin Trans. 1* **1988**, 823 – 831.

[11] R. W. Hoffmann, G. Niel, *Liebigs Ann. Chem.* **1991**, 1195 – 1201.

[12] T. Bach, A. Spiegel, *Eur. J. Org. Chem.* **2002**, 645 – 654.

[13] P. De Mayo, *Acc. Chem. Res.* **1970**, *3*, 41 – 47.

[14] For reviews on ring-opening reactions of cyclobutanes, see: a) H. N. C. Wong, K. L. Lau, K. F. Tam, *Top. Curr. Chem.* **1986**, *133*, 83 – 157; b) H. N. C. Wong, G. Mann, H. M. Muchall, L. Fitjer, M. Heuschmann in *Methoden der Organischen Chemie (Houben-Weyl), 4th ed., 1952–, Vol. E17e*, **1997**, pp. 470 – 610; c) J. C. Namyslo, D. E. Kaufmann, *Chem. Rev.* **2003**, *103*, 1485 – 1537.

 © 2003 Wiley-VCH Verlag GmbH & Co. KGaA, Weinheim

Powerful Acylation Catalyst

Enhancing the Catalytic Activity of 4-(Dialkylamino)pyridines by Conformational Fixation**

Markus R. Heinrich, Heike Sabine Klisa, Herbert Mayr, Wolfgang Steglich, and Hendrik Zipse*

Dedicated to Professor Heinrich Nöth on the occasion of his 75th birthday

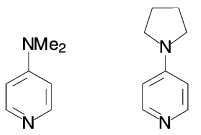
4-(Dimethylamino)pyridine (DMAP, **1**) was introduced to synthetic chemistry as a powerful nucleophilic group-transfer catalyst more than three decades ago[1,2] and has become a standard reagent[3] for acylation, esterification,[4] macrolactonization,[5] and silylation reactions,[6] to mention only a few applications. DMAP has since served as a basis for several research groups for the development of chiral acylation catalysts.[7] Herein we report on the enhanced

[*] Prof. Dr. W. Steglich, Dr. M. R. Heinrich, H. S. Klisa, Prof. Dr. H. Mayr, Prof. Dr. H. Zipse
Department Chemie, Ludwig-Maximilians-Universität München
Butenandtstrasse 5–13, 81377 München (Germany)
Fax: (+49) 89-2180-77756
E-mail: wos@cup.uni-muenchen.de

[**] We thank Sabine Voss for valuable experimental support.

Supporting information for this article is available on the WWW under http://www.angewandte.org or from the author.

 © 2003 Wiley-VCH Verlag GmbH & Co. KGaA, Weinheim DOI: 10.1002/anie.200352289

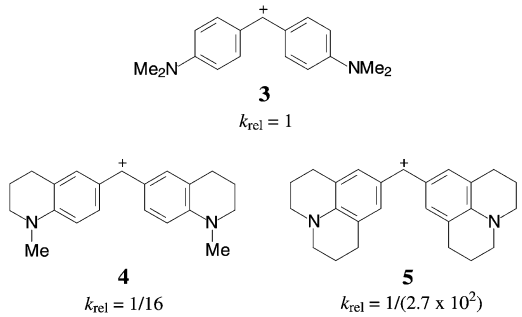


1 **2**

catalytic activity of 4-(dialkylamino)pyridines in which the 4-amino group is conformationally fixed in a ring fused to the pyridine ring.

Previous work showed that 4-pyrrolidinopyridine (PPY, **2**)[3a,8,9] is a more effective acylation catalyst than DMAP. Evidently the catalytic activity depends on the stabilization of the *N*-acyl pyridinium ion by interaction with the lone pair of electrons of the 4-amino group.[10] Therefore, an increase in this interaction should lead to enhanced catalytic performance.

Studies on 4,4′-bis(dialkylamino)benzhydryl cations showed a dramatic increase in stabilization when the nitrogen atom was part of a conformationally fixed ring system. This is illustrated by the series of benzhydryl cations **3**–**5** (Scheme 1),

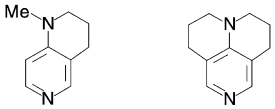


3 $k_{rel} = 1$

4 $k_{rel} = 1/16$ **5** $k_{rel} = 1/(2.7 \times 10^2)$

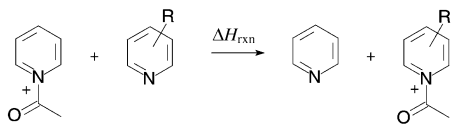
Scheme 1. Relative reactivities of benzhydryl cations derived from the rate constants of their reactions with π nucleophiles (20 °C).[11]

in which the bisjulolidinyl derivative **5** is about 300 times less electrophilic than the simple bis(dimethylamino) derivative **3**.[11] We reasoned that conformational fixation combined with the inductive electron-donating effect of an alkyl group in the *meta* position might have a similar effect on the corresponding (4-dialkylamino)pyridines and cause an increase in electron density at the pyridine nitrogen atom, thus resulting in stabilization of the *N*-acyl pyridinium ion derivative. We used the 4-(dialkylamino)pyridines **6** and **7** for this study.



6 **7**

The expected enhanced stability of the *N*-acyl intermediates derived from the DMAP analogues **6** and **7** can be verified through theoretical evaluation of the reaction enthalpies for the acetyl-transfer reaction shown in Equation (1). Reaction enthalpies at 298 K were calculated for a



(1)

number of DMAP derivatives at the B3LYP/6-311 + G(d,p)// B3LYP/6-31G(d) level of theory,[12] whereby more negative values indicate better stabilization of the acetyl group relative to pyridine (Table 1). As expected, a strongly negative

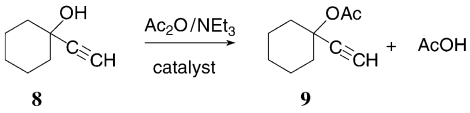
Table 1: Calculated reaction enthalpies ΔH_{rxn} for the acetyl-transfer reaction (1) and experimental half-lives $t_{1/2}$ for the reference reaction (2).

	DMAP (**1**)	PPY (**2**)	**6**	**7**
ΔH_{rxn} [kJ mol^{-1}]	−82.1	−93.1	−96.0	−108.9
$t_{1/2}$ [min]	151	69	63	26

reaction enthalpy was calculated for DMAP, which confirms the special properties of this compound from the viewpoint of the stability of the acyl intermediate. Reaction enthalpies more negative by 11–14 kJ mol^{-1} were predicted for the singly annulated DMAP analogue **6** and PPY (**2**). Annulation of an additional six-membered ring as in **7** lowers the reaction enthalpy by 27 kJ mol^{-1}. These results suggest that the DMAP derivative **7** may be a significantly better acyl-transfer catalyst than DMAP itself or even **2**.

The known pyridonaphthyridine derivative **7**[13] was prepared from 1,6-naphthyridine in four steps according to a literature procedure.[13b] The bicyclic analogue **6** was synthesized by reaction of the *ortho*-lithiated derivative of 4-(*tert*-butoxycarbonylamino)pyridine[7e] with 1-chloro-3-iodopropane and reduction of the resulting *tert*-butoxycarbonyl (Boc) derivative[14] with diisobutylaluminum hydride.[15]

To test the catalytic activity of the 4-aminopyridines **1, 2, 6**, and **7**, the acetylation of 1-ethynylcyclohexanol (**8**) with acetic anhydride in the presence of triethylamine as the auxiliary base was studied in $CDCl_3$ at 20 °C [standard reaction, Eq. (2)].[3a] The reaction was monitored by



8 **9** (2)

^{1}H NMR spectroscopy under the conditions described, based on the increase in the intensity of the CH_3CO signals. The results are illustrated in Figure 1 and summarized in Table 1.

The results indicate that the incorporation of the 4-amino group in one single six-membered ring (as in **6**) leads to an enhancement of the catalytic activity similar to that observed for **2** relative to **1**. Compound **7**, in which the amino group is incorporated in two six-membered rings, exhibits a substantial increase in activity and appears to be about six times more active than DMAP (**1**). It even outperforms PPY (**2**), until now the best catalyst known for this transformation, by a factor of 2.5. The acylation of the sterically hindered alcohol **8** was complete within 2 to 3 h under the catalysis of **7**, whereas the DMAP- or PPY-catalyzed reactions were far from completion after the same amount of time (Figure 1).[16]

In conclusion, we have shown that it is possible to develop nucleophilic acylation catalysts that are superior to the

 © 2003 Wiley-VCH Verlag GmbH & Co. KGaA, Weinheim

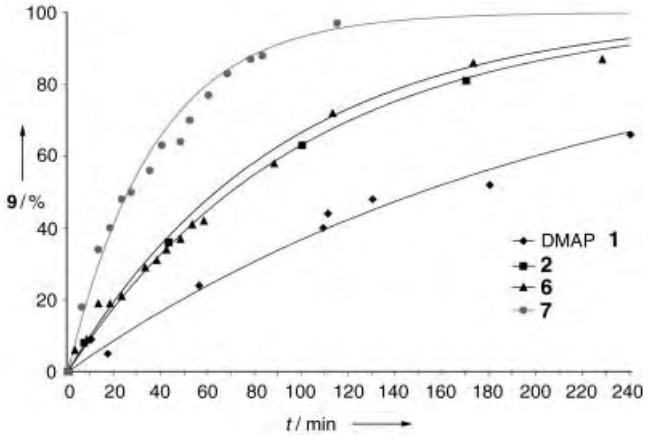


Figure 1. Acetylation of **8** ($c = 0.2$ mol L^{-1}) with Ac_2O ($c = 0.4$ mol L^{-1}) in the presence of NEt_3 ($c = 0.6$ mol L^{-1}) and various (4-dialkylamino)-pyridine catalysts ($c = 0.02$ mol L^{-1}) in $CDCl_3$ at 20 °C.

familiar DMAP. Compounds such as **7** are of potential value for acylations that proceed in low yields because of undesired side reactions when the less active catalysts **1** or **2** are used. Moreover, the annulated derivative **7** provides a rigid, highly reactive scaffold upon which new generations of chiral DMAP derivatives can be built.

Received: July 2, 2003 [Z52289]

Keywords: ab initio calculations · acylation · dimethylaminopyridine · kinetics

[1] a) W. Steglich, G. Höfle, *Angew. Chem.* **1969**, *81*, 1001; *Angew. Chem. Int. Ed. Engl.* **1969**, *8*, 981; b) G. Höfle, W. Steglich, *Synthesis* **1972**, 619 – 621.

[2] For kinetic evidence for the high catalytic activity of DMAP in the benzoylation of aryl amines, see: L. M. Litvinenko, A. I. Kirichenko, *Dokl. Akad. Nauk SSSR Ser. Khim.* **1967**, *176*, 97 – 100.

[3] For reviews, see: a) G. Höfle, W. Steglich, H. Vorbrüggen, *Angew. Chem.* **1978**, *90*, 602 – 615; *Angew. Chem. Int. Ed. Engl.* **1978**, *17*, 569 – 583; b) E. F. V. Scriven, *Chem. Soc. Rev.* **1983**, *12*, 129 – 161; c) A. Hassner in *Encyclopedia of Reagents for Organic Synthesis, Vol. 3* (Ed.: L. A. Paquette), Wiley, Chichester, **1995**, pp. 2022 – 2024.

[4] a) B. Neises, W. Steglich, *Angew. Chem.* **1978**, *90*, 556 – 557; *Angew. Chem. Int. Ed. Engl.* **1978**, *17*, 552; b) A. Hassner, V. Alexanian, *Tetrahedron Lett.* **1978**, 4475 – 4478.

[5] a) J. Inanaga, K. Hirata, H. Saeki, T. Katsuki, M. Yamaguchi, *Bull. Chem. Soc. Jpn.* **1979**, *52*, 1989 – 1993; b) E. P. Boden, G. E. Keck, *J. Org. Chem.* **1985**, *50*, 2394 – 2395.

[6] S. K. Chaudhary, O. Hernandez, *Tetrahedron Lett.* **1979**, 99 – 102.

[7] a) E. Vedejs, X. Chen, *J. Am. Chem. Soc.* **1996**, *118*, 1809 – 1810; b) J. C. Ruble, G. C. Fu, *J. Org. Chem.* **1996**, *61*, 7230 – 7231; c) T. Kawabata, M. Nagato, K. Takasu, K. Fuji, *J. Am. Chem. Soc.* **1997**, *119*, 3169 – 3170; d) B. Tao, J. C. Ruble, D. A. Hoic, G. C. Fu, *J. Am. Chem. Soc.* **1999**, *121*, 5091 – 5092; e) A. C. Spivey, T. Fekner, S. E. Spey, H. Adams, *J. Org. Chem.* **1999**, *64*, 9430 – 9443, and references therein; f) A. C. Spivey, T. Fekner, S. E. Spey, *J. Org. Chem.* **2000**, *65*, 3154 – 3159; g) A. C. Spivey, A. Maddaford, T. Fekner, A. J. Redgrave, C. S. Frampton, *J. Chem. Soc. Perkin Trans. 1* **2000**, 3460 – 3468; h) G. C. Fu, *Acc. Chem. Res.* **2000**, *33*, 412 – 420, and references therein; i) A. C. Spivey, A. Maddaford, T. Fekner, D. P. Leese, A. J. Redgrave, C. S. Frampton, *J. Chem. Soc. Perkin Trans. 1* **2001**, 1785 – 1794; j) G. Priem, B. Pelotier, S. J. F. Macdonald, M. S. Anson, I. B. Campbell, *J. Org. Chem.* **2003**, *68*, 3844 – 3848; k) S. France, D. J. Guerin, S. J. Miller, T. Lectka, *Chem. Rev.* **2003**, *103*, 2985 – 3012.

[8] W. Steglich, G. Höfle, *Tetrahedron Lett.* **1970**, *54*, 4727 – 4730.

[9] A. Hassner, L. R. Krepski, V. Alexanian, *Tetrahedron* **1978**, *34*, 2069 – 2076.

[10] Compare the analogous effects in the enamine series: a) S. Hünig, H. Hoch, *Fortschr. Chem. Forsch.* **1970**, *14*, 235 – 293; b) B. Kempf, N. Hampel, A. R. Ofial, H. Mayr, *Chem. Eur. J.* **2003**, *9*, 2209 – 2218.

[11] a) H. Mayr, T. Bug, M. F. Gotta, N. Hering, B. Irrgang, B. Janker, B. Kempf, R. Loos, A. R. Ofial, G. Remennikov, H. Schimmel, *J. Am. Chem. Soc.* **2001**, *123*, 9500 – 9512; b) H. Mayr, B. Kempf, A. R. Ofial, *Acc. Chem. Res.* **2003**, *36*, 66 – 77.

[12] All structures were first optimized at the Becke3LYP/6-31G(d) level of theory. Zero-point vibrational energies and thermochemical corrections to enthalpies at 298 K were calculated based on the rigid-rotor/harmonic-oscillator model at the same level of theory. Single-point energies were then calculated at the Becke3LYP/6-311 + G(d,p) level of theory. Combination of the Becke3LYP/6-311 + G(d,p) total energies with the previously calculated thermochemical data yielded the enthalpies termed "B3LYP/6-311 + G(d,p)//B3LYP/6-31G(d)" in the text. Boltzmann averaging of enthalpies was performed for those systems that display more than one low-energy conformation. All calculations were performed with the Gaussian 98 (Rev. A.7) package.[17] Energy data and structural parameters for pyridine, the pyridine bases **1, 2, 6**, and **7**, and their *N*-acetyl derivatives are given in the Supporting Information.

[13] a) K. Tsuda, S. Saeki, S. Imura, S. Okuda, Y. Sato, H. Mishima, *J. Org. Chem.* **1956**, *21*, 1481 – 1486; b) T. Sakomoto, N. Miura, Y. Kondo, H. Yamanaka, *Chem. Pharm. Bull.* **1986**, *34*, 2018 – 2023.

[14] J. N. Reed, J. Rotchford, D. Strickland, *Tetrahedron Lett.* **1988**, *29*, 5725 – 5728.

[15] The synthesis of **6** and the spectroscopic data of compounds **6** and **7** are described in the Supporting Information.

[16] The importance of the auxiliary base is illustrated by the fact that the half-life for the acetylation of **8** under the catalysis of **7** is increased from 151 to 465 min if pyridine is used instead of triethylamine.

[17] Gaussian 98 (Revision A.7), M. J. Frisch, G. W. Trucks, H. B. Schlegel, G. E. Scuseria, M. A. Robb, J. R. Cheeseman, V. G. Zakrzewski, J. A. Montgomery, R. E. Stratmann, J. C. Burant, S. Dapprich, J. M. Millam, A. D. Daniels, K. N. Kudin, M. C. Strain, O. Farkas, J. Tomasi, V. Barone, M. Cossi, R. Cammi, B. Mennucci, C. Pomelli, C. Adamo, S. Clifford, J. Ochterski, G. A. Petersson, P. Y. Ayala, Q. Cui, K. Morokuma, D. K. Malick, A. D. Rabuck, K. Raghavachari, J. B. Foresman, J. Cioslowski, J. V. Ortiz, B. B. Stefanov, G. Liu, A. Liashenko, P. Piskorz, I. Komaromi, R. Gomperts, R. L. Martin, D. J. Fox, T. Keith, M. A. Al-Laham, C. Y. Peng, A. Nanayakkara, C. Gonzalez, M. Challacombe, P. M. W. Gill, B. G. Johnson, W. Chen, M. W. Wong, J. L. Andres, M. Head-Gordon, E. S. Replogle, J. A. Pople, Gaussian, Inc., Pittsburgh, PA, **1998**.

 © 2003 Wiley-VCH Verlag GmbH & Co. KGaA, Weinheim

Cover Picture



Nis Halland, Tore Hansen, and Karl Anker Jørgensen*

Optically active anticoagulants are formed in a new one-step organocatalytic asymmetric Michael reaction. The synthesis of the optically active warfarin from simple starting materials is shown. The background is a CT-scanning image of the lungs, where thrombosis can occur. The other images show a heart with a thrombus (left), and the same heart after surgery and treatment with anticoagulant (right), these images can be seen as films in the Supporting Information. Full details are in the Communication by K. A. Jørgensen et al. on page 4955 ff.

Contents

Angewandte EarlyView

The following articles are available online (in Wiley InterScience). You can find them at www.angewandte.org, under Full Text, Early View.

A. Müller, S. K. Das, S. Talismanov, S. Roy, E. Beckmann, H. Bögge, M. Schmidtmann, A. Merca, A. Berkle, L. Allouche, Y. Zhou, L. Zhang:*
Trapping Cations in Specific Positions in Tuneable "Artificial Cell" Channels: New Nanochemistry Perspectives
DOI: 10.1002/anie.200352358
Published online: October 8, 2003

S. Arndt, T. P. Spaniol, J. Okuda:*
Homogeneous Ethylene-Polymerization Catalysts Based on Alkyl Cations of the Rare-Earth Metals: Are Dicationic Mono(alkyl) Complexes the Active Species?
DOI: 10.1002/anie.200352532
Published online: October 8, 2003

R. Fasel, M. Parschau, K.-H. Ernst*:*
Chirality Transfer from Single Molecules into Self-Assembled Monolayers
DOI: 10.1002/anie.200352232
Published online: October 6, 2003

L. E. Cheruzel, M. S. Pometun, M. R. Cecil, M. S. Mashuta, R. J. Wittebort, R. M. Buchanan:*
Structures and Solid-State Dynamics of One-Dimensional Water Chains Stabilized by Imidazole Channels
DOI: 10.1002/anie.200352157
Published online: October 6, 2003

Articles judged by the referees or the editor as being either very important or very urgent are immediately edited, proof-read, and electronically published once the manuscript has arrived in the editorial office in final form. As long as there is no page number available these articles should be cited in the following manner:

Author(s) *Angew. Chem. Int. Ed.*, online publication date, DOI.

News

Spotlight on RSC Award Winners — **4850**

Books

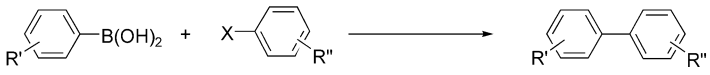
Solvent-free Organic Synthesis — **4851**	Koichi Tanaka	*reviewed by G. Kaupp*
High Pressure Chemistry — **4852**	Rudi van Eldik, Frank-Gerrit Klärner	*reviewed by L. M. Harwood*
Alkaloids — **4852**	Manfred Hesse	*reviewed by F. von Nussbaum*

Highlights

Aryl–Aryl Coupling Reactions

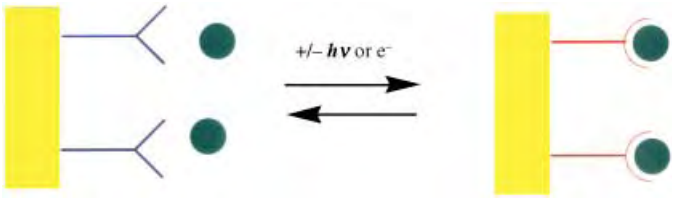
C.-J. Li* — **4856 – 4858**

Suzuki Reaction Takes a "Naked Hot Bath": Coupling in High-Temperature Water without Transition Metals



Hot stuff: The Suzuki reaction of arylboronic derivatives with aryl halides is the most important method for generating aryl–aryl coupling products. Now such couplings have become easier and cleaner in hot water without the need of a transition-metal catalyst (see scheme).

Minireviews



Solid progress: The transfer of responsive supramolecular systems from the solution to the solid state by immobilizing their components onto surfaces is an attractive method for developing systems with molecular electronics and device applications (see scheme). The ability to coherently interface these systems with the outside world may pave the way for their implementation as novel components within the emerging advanced materials and nanotechnology industries.

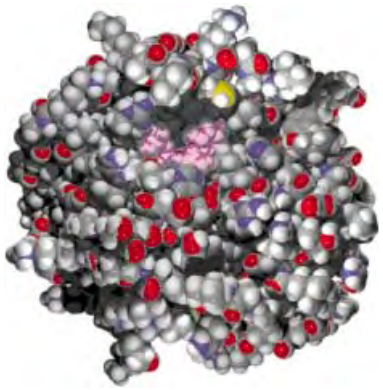
Interfacial Host–Guest Complexes

G. Cooke* _____ **4860 – 4870**

Electrochemical and Photochemical Control of Host–Guest Complexation at Surfaces

Reviews

Statistically shown: Complexes of enzymes and catalytic antibodies with their substrates and cyclodextrins, synthetic hosts, and albumins with organic molecules all have similar association constants (K_a) of 10^1–10^6 M^{-1}. Antibody–antigen and enzyme–inhibitor complexes achieve tighter binding ($K_a = 10^4$–10^{12} M^{-1}) and enzyme–transition-state binding is much stronger ($K_a = 10^{10}$–10^{20} M^{-1}). The origins of these differences, the role of enthalpy/entropy compensation, and the relationships between the size of the buried solvent-accessible surface areas of the guest and binding affinities are analyzed.



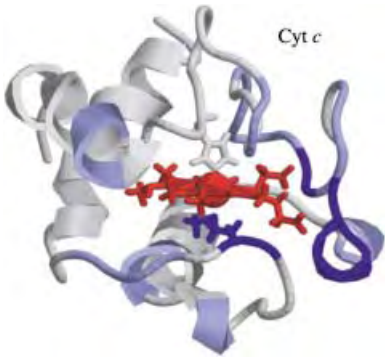
Thermodynamic Organic Complexes

K. N. Houk,* A. G. Leach, S. P. Kim, X. Zhang _____ **4872 – 4897**

Binding Affinities of Host–Guest, Protein–Ligand, and Protein–Transition-State Complexes

Communications

Selectively cleaved: Under appropriate experimental conditions, electrospray ionization mass spectrometry produces fragment ions that directly indicate noncovalent protein–heme interaction sites in native Cytochrome *c* (see picture). The proposed mechanism involves asymmetric charge partitioning in gaseous protein dimer ions, which causes electron transfer and subsequent backbone-cleavage.



MS Shows Tertiary Structure

K. Breuker,* F. W. McLafferty _____ **4900 – 4904**

Native Electron Capture Dissociation for the Structural Characterization of Noncovalent Interactions in Native Cytochrome *c*

For the USA and Canada:
ANGEWANDTE CHEMIE International Edition (ISSN 1433-7851) is published weekly by Wiley-VCH PO Box 191161, D 69451 Weinheim, Germany. Air freight and mailing in the USA by Publications Expediting Inc. 200 Meacham Ave., Elmont, NY 11003. Periodicals postage paid at Jamaica NY 11431. US POSTMASTER: send address changes to *Angewandte Chemie*, Wiley-VCH, 111 River Street, Hoboken, NJ 07030. Annual institutional subscription price for institutions: Europe € 3430.00/3118.00. Outside Europe US$ 4499.00/4090.00 (valid for print and electronic/print or electronic delivery); for individuals who are personal members of a national chemical society, or whose institution already subscribes, or who are retired or self-employed consultants, print only. Europe € 248.00/Outside Europe US$ 378.00. Postage and handling charges included. All Wiley-VCH prices are exclusive VAT.

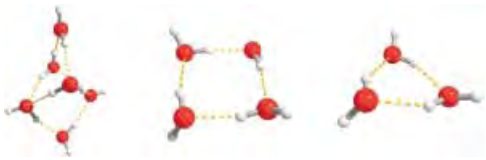
 © 2003 Wiley-VCH Verlag GmbH & Co. KGaA, Weinheim

Contents

Water Clusters

T. Köddermann, F. Schulte, M. Huelsekopf, R. Ludwig* ——— **4904 – 4908**

Formation of Water Clusters in a Hydrophobic Solvent



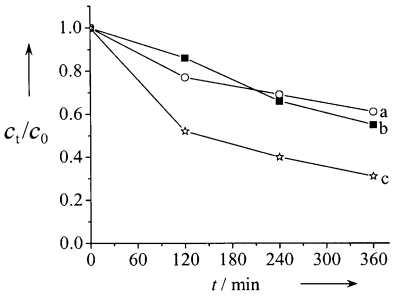
And not a drop to drink: Hydrogen-bonded water clusters could be detected in CCl_4 by IR spectroscopy. The comparison between measured and calculated frequencies along with the characteristic temperature behavior of band intensities suggests that cyclic clusters are formed up to the tetramer (see picture).

Titanium Dioxide Photocatalysts

S. Sakthivel, H. Kisch* ——— **4908 – 4911**

Daylight Photocatalysis by Carbon-Modified Titanium Dioxide

Green titana: Carbon-doped titanium dioxide, supported onto filter paper, photocatalyzes the gas-phase degradation of the atmospheric pollutants benzene (a), acetaldehyde (b) and carbon monoxide (c) in diffuse indoor visible light (see picture).

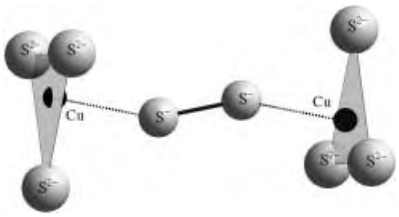


Lanthanum Copper Chalcogenides

S. Strobel, T. Schleid* ——— **4911 – 4913**

La_2CuS_4: A Lanthanum Copper Sulfide with Discrete Anion Triples $[S_3Cu\cdots S{-}S\cdots CuS_3]^{12-}$ Based on $La_4[Cu_2S_6(S_2)]$

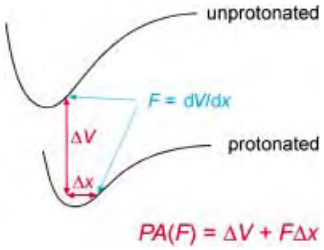
A unique structure: In the crystalline state the lanthanum copper sulfide La_2CuS_4 comprises discrete anion triples. These are composed of almost planar triangular $[CuS_3]^{5-}$ units, which consist of Cu^+ and S^{2-} ions linked through a $^-S{-}S^-$-dumbbell to form the $[S_3Cu\cdots S{-}S\cdots CuS_3]^{12-}$ anion (see picture).



Force-Induced Affinity Changes

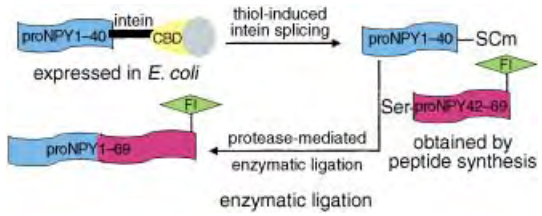
M. K. Beyer* ——— **4913 – 4915**

Coupling of Mechanical and Chemical Energy: Proton Affinity as a Function of External Force



Small action, large effect: The proton affinity has been defined as a function of an external mechanical force and its applicability as a chemical concept is explored (see scheme). It is shown that forces in the sub-nN to nN range change the proton affinity of small model molecules by values ranging from kT up to several 10 kJ mol^{-1}, which suggests that these affinity changes are chemically significant.

 © 2003 Wiley-VCH Verlag GmbH & Co. KGaA, Weinheim

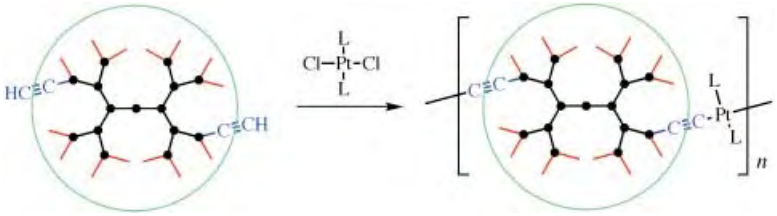


Synthesis of Modified Proteins

Z. Machova, R. von Eggelkraut-Gottanka, N. Wehofsky, F. Bordusa, A. G. Beck-Sickinger* ——— **4916 – 4918**

Expressed Enzymatic Ligation for the Semisynthesis of Chemically Modified Proteins

Enzymatic synthesis and expressed protein ligation were combined in a method for protein synthesis in which protein thioesters with specific leaving groups could be used by protease V8 from *Staphylococcus aureus* to catalyze the formation of peptide bonds. This method was applied to the synthesis of fluorescence-labeled (Fl) analogues of proneuropeptide Y (proNPY; see scheme). CBD = chitin binding domain.

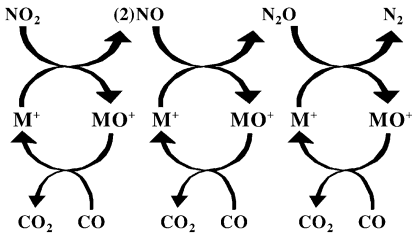


A Chain of Dendrimers

H.-F. Chow,* C.-F. Leung, W. Li, K.-W. Wong, L. Xi ——— **4919 – 4923**

Synthesis and Characterization of Dendritic Necklaces: A Class of Outer-Sphere–Outer-Sphere Connected Dendronized Organoplatinum Polymers

Molecular jewelry! Up to 880 dendrimer beads can be joined together with Pt complexes to make a long "necklace" of dendrimers (see picture). The polymerization of dendrimers that contain reactive functional subunits on the dendrimer surface opens a new route to a novel class of dendronized polymers of high molecular weights and in good yields.



Catalyzed Reduction of N Oxides

V. Blagojevic, M. J. Y. Jarvis, E. Flaim, G. K. Koyanagi, V. V. Lavrov, D. K. Bohme* ——— **4923 – 4927**

Gas-Phase Reduction of Oxides of Nitrogen with CO Catalyzed by Atomic Transition-Metal Cations

A novel catalytic role for transition-metal cations in the homogeneous conversion of the nitrogen oxides NO_2, NO, or N_2O and CO into N_2 and CO_2 is demonstrated by thermodynamic and kinetic studies of gas-phase reactions of 29 transition-metal cations and some of their oxides (see scheme). Fe^+, Os^+, and Ir^+ ions are shown to be most effective. The chemistry identified may have practical applications in new designs of catalytic converters.



Enantioselective Alcohol Synthesis

M. Locatelli, P. G. Cozzi* ——— **4928 – 4930**

Effective Modular Iminooxazoline (IMOX) Ligands for Asymmetric Catalysis: [Zn(IMOX)]-Promoted Enantioselective Reduction of Ketones by Catecholborane

Closing the door to nucleophilic attack on one face of the substrate by using a bulky substituent (see schematic formula) was the key to obtaining high enantiomeric excesses in the reduction of methyl ketones by catecholborane with promotion by zinc complexes of new chiral iminooxazoline (IMOX) ligands. The modular nature, simple design, and possibility to produce tailored IMOX ligands could be advantages in designing the next generation of these chiral ligands.

 © 2003 Wiley-VCH Verlag GmbH & Co. KGaA, Weinheim

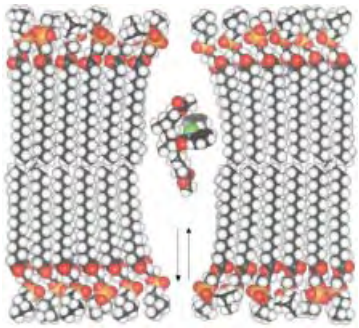
Contents

Membrane Transport

A. V. Koulov, T. N. Lambert, R. Shukla, M. Jain, J. M. Boon, B. D. Smith,* H. Li, D. N. Sheppard,* J.-B. Joos, J. P. Clare, A. P. Davis* ____ **4931 – 4933**

Chloride Transport Across Vesicle and Cell Membranes by Steroid-Based Receptors

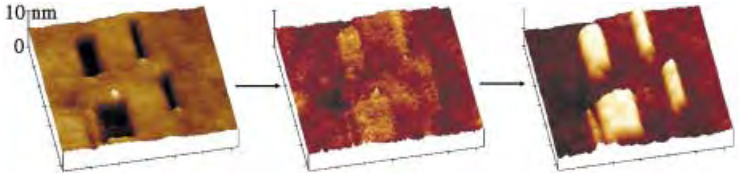
Crossing the barriers: Membrane transport, a well-established phenomenon for neutral cation receptors such as valinomycin, has been demonstrated for the anion-binding "cholapods". The cholapods promote chloride efflux from vesicles by an antiport mechanism and mediate anion flow through live cells grown as epithelia (see schematic representation).



DNA Hybridization Detection

D. Zhou, K. Sinniah, C. Abell,* T. Rayment* ____ **4934 – 4937**

Label-Free Detection of DNA Hybridization at the Nanoscale: A Highly Sensitive and Selective Approach Using Atomic-Force Microscopy

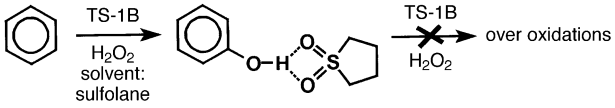


Less than 10^{-21} mol of label-free probe DNA with high sequence specificity can be quantitatively detected on a surface by using AFM to create nanofeatures of single-stranded DNA and monitor the topographic changes upon exposure to a complimentary DNA (see scheme).

Oxidation of Benzene to Phenol

L. Balducci, D. Bianchi,* R. Bortolo, R. D'Aloisio, M. Ricci, R. Tassinari, R. Ungarelli ____ **4937 – 4940**

Direct Oxidation of Benzene to Phenol with Hydrogen Peroxide over a Modified Titanium Silicalite

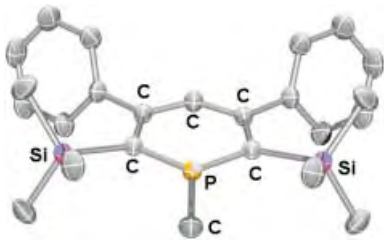


Stopping the rot! The selective oxidation of benzene to phenol with hydrogen peroxide is achieved by using a new zeolite catalyst (TS-1B), obtained by the modification of titanium silicalite with NH_4HF_2 and H_2O_2 (see scheme). The new catalyst, used in presence of a particular cosolvent (sulfolane) protects the produced phenol from overoxidation and dramatically enhances the selectivity of the reaction.

Phosphininium Compounds

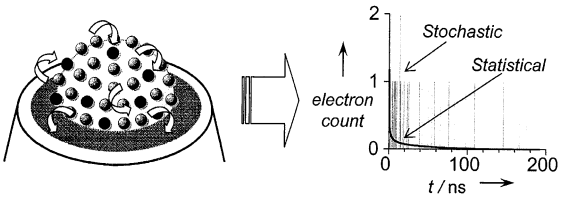
A. Moores, L. Ricard, P. Le Floch* ____ **4940 – 4944**

A 1-Methyl-Phosphininium Compound: Synthesis, X-Ray Crystal Structure, and DFT Calculations



A tetravalent phosphorus atom in an aromatic system! A 1-methylphosphininium tetrachlorogallate is synthesized and fully characterized (see structure). This compound has aromatic properties like those of phosphinine, pyridine, and pyridinium salts. These features were asserted and quantified by DFT calculations. This phosphininium salt reacts easily with an alkyne to yield a phosphabarellenium salt through a Diels–Alder reaction.

 © 2003 Wiley-VCH Verlag GmbH & Co. KGaA, Weinheim



The behavior of a limited number of molecules is expected to show a profound stochastic character and therefore to significantly differ from the usual chemical kinetic laws. This dichotomy is investigated theoretically within an electrochemical framework by considering the specific example of the oxidation of a PAMAM redox dendrimer caped by 64 ruthenium bis-terpyridine centers (see picture). Thus the maximum number of adsorbed molecules at which the observation of the intrinsic stochastic nature of the phenomenon should remain observable can be evaluated, either by itself, or when instrumental distortions are involved.

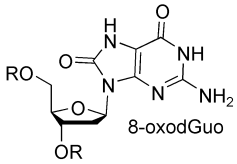
Electrochemistry on a Few Molecules

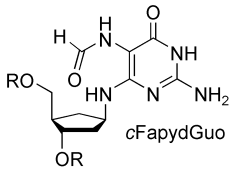
C. Amatore,* F. Grün, E. Maisonhaute ——— **4944 – 4947**

Electrochemistry within a Limited Number of Molecules: Delineating the Fringe Between Stochastic and Statistical Behavior

---

A stable analogue (*c*FapydGuo) of the major oxidative DNA lesion FapydGuo was prepared. The direct comparison of the pairing properties of the oxidative lesion β-8-oxodGuo and β-*c*FapydGuo (see formulae) revealed significant differences in base pairing, indicative of unexpected mutagenic differences.



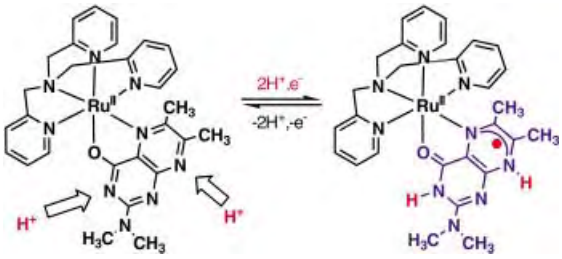


DNA Lesions

M. Ober, U. Linne, J. Gierlich, T. Carell* ——— **4947 – 4951**

The Two Main DNA Lesions 8-Oxo-7,8-dihydroguanine and 2,6-Diamino-5-formamido-4-hydroxypyrimidine Exhibit Strongly Different Pairing Properties

---



Coupled to coenzymes: Ruthenium(II) complexes having a pterin as a ligand, which is a redox-active heteroaromatic coenzyme, are synthesized and characterized to reveal that the complexes showed reversible proton-dependent redox behavior (see scheme). The pterin ligand undergoes proton-coupled electron transfer to form a ruthenium(II)-coordinated monohydropterin radical upon one-electron reduction.

Ruthenium Pterin Radical Complex

T. Kojima,* T. Sakamoto, Y. Matsuda, K. Ohkubo, S. Fukuzumi ——— **4951 – 4954**

A Ruthenium Pterin Complex Showing Proton-Coupled Electron Transfer: Synthesis and Characterization

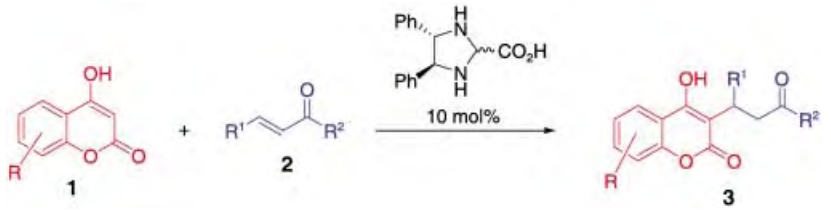
 © 2003 Wiley-VCH Verlag GmbH & Co. KGaA, Weinheim

Contents

Asymmetric Michael Addition

N. Halland, T. Hansen, K. A. Jørgensen* ——— **4955 – 4957**

Organocatalytic Asymmetric Michael Reaction of Cyclic 1,3-Dicarbonyl Compounds and α,β-Unsaturated Ketones—A Highly Atom-Economic Catalytic One-Step Formation of Optically Active Warfarin Anticoagulant

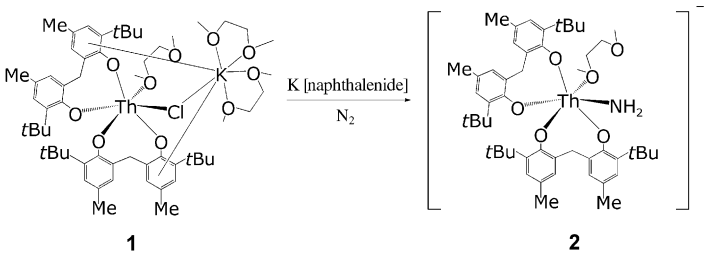


A broad range of Michael adducts **3** were obtained by the organocatalytic asymmetric Michael addition of cyclic 1,3-dicarbonyl compounds **1** to α,β-unsaturated ketones **2**. The reaction allows a one-step synthesis of the optically active anticoagulant warfarin and several analogues **3** on a kilogram scale in up to 99% yield with 88% *ee* (>99.9% *ee* after a single recrystallization).

Low-Valent Thorium Complexes

I. Korobkov, S. Gambarotta,* G. P. A. Yap ——— **4958 – 4961**

Amide from Dinitrogen by In Situ Cleavage and Partial Hydrogenation Promoted by a Transient Zero-Valent Thorium Synthon



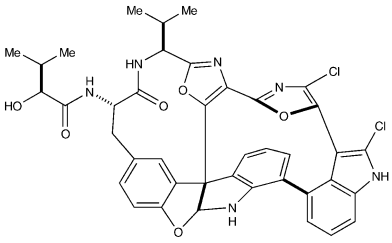
Reduction through cleavage: The reduction of a tetravalent thorium–bisdiaryloxide complex **1** with [K(naphthalenide)] leads to the cleavage of dinitrogen and partial hydrogenation via the probable formation of a zero-valent thorium–amide synthon (**2**; see scheme).

Natural Product Synthesis

A. W. G. Burgett, Q. Li, Q. Wei, P. G. Harran* ——— **4961 – 4966**

A Concise and Flexible Total Synthesis of (−)-Diazonamide A

The remarkable action of an I^{III} species on a tripeptide containing acyclic tyrosine/tryptophan is the key step in a total synthesis of (−)-diazonamide A. The completed preparation of this new antimitotic is concise, multiply convergent, and amenable to diversification of intermediates.



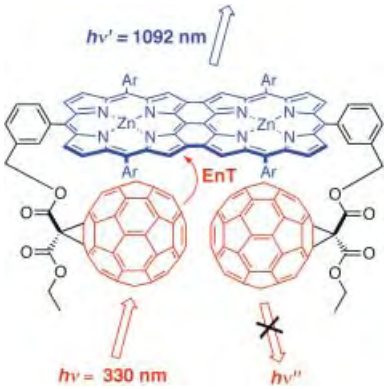
diazonamide A

Porphyrin–C60 Conjugates

D. Bonifazi, M. Scholl, F. Song, L. Echegoyen,* G. Accorsi, N. Armaroli,* F. Diederich* ——— **4966 – 4970**

Exceptional Redox and Photophysical Properties of a Triply Fused Diporphyrin–C_{60} Conjugate: Novel Scaffolds for Multicharge Storage in Molecular Scale Electronics

Up to fifteen electrons are reversibly accommodated in a triply fused porphyrin dimer conjugated to two [60]fullerene moieties. Its photophysical properties differ completely from those of the many known porphyrin–fullerene dyads: Photoexcitation of the C_{60} moieties results in quantitative sensitization of the low-lying (about 1 eV) and very short lived lowest singlet level of the porphyrin sheet (see scheme).



 © 2003 Wiley-VCH Verlag GmbH & Co. KGaA, Weinheim

Communications labeled with this symbol have been judged by two referees as being "very important papers".

The publication of Communications labeled with this symbol has been accelerated because of their topical or highly competitive nature.

Looking for outstanding employees?

Do you need another expert for your excellent team?
...Chemists, PhD Students, Managers, Professors, Sales Representatives...

Place an advert in the printed version and have it made available online for 1 month, free of charge!

Angewandte Chemie International Edition
Advertising Sales Department: Marion Schulz
Phone: 0 62 01 - 60 65 65
Fax: 0 62 01 - 60 65 50
E-Mail: MSchulz@wiley-vch.de

Service

Keywords ____ *4972*

Authors ____ *4973*

Angewandte's Sister Journals ____ *4974 – 4975*

Preview ____ *4977*

Corrigendum

In the communication "6-Amino-3-Pyridinols: Towards Diffusion-Controlled Chain-Breaking Antioxidants" by D. A. Pratt, L. Valgimigli, G. F. Pedulli, N. A. Porter and co-workers (*Angew. Chem.* **2003**, *115*, 4506–4509; *Angew. Chem. Int. Ed.* **2003**, *42*, 4370–4373), on page 4370 there is an error in the sentence "Calculations predicted that incorporation of two nitrogen atoms at the 3- and 5-positions of the phenolic ring significantly raises the IP and greatly improves the stability of the compound in air while only minimally lowering the O–H BDE.[4]" the word "lowering" should be "increasing". The authors apologize for this error.

 © 2003 Wiley-VCH Verlag GmbH & Co. KGaA, Weinheim



RSC Awards

In this issue we present some more recipients of Royal Society of Chemistry (RSC, UK) awards…



D. Boger

An Adrien Albert Lectureship has been awarded to **Dale Boger** for the use of heterocyclic chemistry to improve biological activity. Boger completed his PhD in 1980 at Harvard University (Massachusetts, USA), then went on to Kansas and Purdue (Indiana, USA) before becoming professor at The Scripps Research Institute (California, USA) in 1991. His research includes new synthetic methods, the total synthesis of natural products,[1a] and the interaction of DNA and proteins with drugs.[1b]



A. Fürstner

Alois Fürstner has been distinguished with a Centenary Lectureship for his pioneering work in the development of new synthetic methods, in particular diene and diyne metathesis and its use in natural product synthesis. He completed his PhD in 1987 at the Technische Universität Graz (Austria) with H. Weidmann and his habilitation there in 1992 following a postdoctoral period with W. Oppolzer (Geneva, Switzerland). Since 1993 he has led a research group at the Max-Planck-Institut für Kohlenforschung (MPI, Mülheim/Ruhr, Germany). His Review on roseophilin and prodigiosin alkaloids was the cover-picture article in issue 31/2003 of *Angewandte Chemie*.[2] Fürstner is on the Academic Advisory Board of *Advanced Synthesis & Catalysis*.



E. Solomon

Edward Solomon has also been awarded a Centenary Lectureship. Solomon uses spectroscopy and MO calculations to study the electronic structure of copper and iron centers in proteins. These sites are responsible for electron transfer and the activation of oxygen.[3] He also studies highly symmetrical transition-metal complexes. Solomon completed his PhD in 1972 at Princeton University under the guidance of D. S. McClure and was professor at the Massachusetts Institute of Technology (MIT, USA) until 1982, when he moved to Stanford University (California, USA).

Alexander Pines completed his PhD in 1972 at the MIT and then took up a position as professor of chemistry at the University of California in Berkeley. He has been awarded a Faraday Lectureship for his work on NMR spectroscopy—experiment and theory. Pines was a leading figure in the introduction of high-resolution solid-state NMR spectroscopy of dilute spins (^{13}C, ^{15}N) by using cross-polarization. His recent work includes multiple-quantum NMR spectroscopy. He is on the Editorial Board of *Chemistry—A European Journal*.



A. Pines

This year the Merck Research Lectureship has been awarded to **Dudley Williams** for his contributions to biological chemistry, in particular for his determination of the structures and modes of action of the vancomycin group of antibiotics.[4] Williams completed his PhD in 1961 at the University of Leeds (UK), then carried out postdoctoral research at Stanford University. He has been professor of biological chemistry at the University of Cambridge since 1964.



D. Williams

Another chemistry professor at the University of Cambridge is the recipient of a Robert Robinson Lectureship, awarded to **Ian Paterson** for improving our understanding of the stereochemistry of symmetrical reactions and for the total synthesis of a variety of biologically active compounds.[5] Paterson completed his PhD in 1979 with Ian Fleming in Cambridge and then took up a postdoctoral position with Gilbert Stock (New York, USA). He was at University College London from 1981 to 1983.



I. Paterson

[1] a) D. L. Boger, M. W. Ledeboer, M. Kume, Q. Jin, *Angew. Chem.* **1999**, *111*, 2533; *Angew. Chem. Int. Ed.* **1999**, *38*, 2424; b) D. L. Boger, J. Desharnais, K. Capps, *Angew. Chem.* **2003**, *115*, 470; *Angew. Chem. Int. Ed.* **2003**, *42*, 4138.

[2] A. Fürstner, *Angew. Chem.* **2003**, *115*, 3706; *Angew. Chem. Int. Ed.* **2003**, *42*, 3582.

[3] E. I. Solomon, P. Chen, M. Metz, S.-K. Lee, A. E. Palmer, *Angew. Chem.* **2001**, *113*, 4702; *Angew. Chem. Int. Ed.* **2001**, *40*, 4570.

[4] D. H. Williams, B. Bardsley, *Angew. Chem.* **1999**, *111*, 1264; *Angew. Chem. Int. Ed.* **1999**, *38*, 1172.

[5] a) K.-S. Yeung, I. Paterson, *Angew. Chem.* **2002**, *114*, 4826; *Angew. Chem. Int. Ed.* **2002**, *41*, 4632; b) I. Paterson, M. Tudge, *Angew. Chem.* **2003**, *115*, 357; *Angew. Chem. Int. Ed.* **2003**, *42*, 343.

 © 2003 Wiley-VCH Verlag GmbH & Co. KGaA, Weinheim

Aryl–Aryl Coupling Reactions

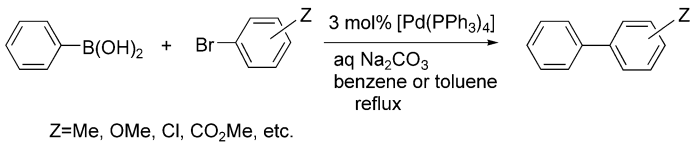
Suzuki Reaction Takes a "Naked Hot Bath": Coupling in High-Temperature Water without Transition Metals

*Chao-Jun Li**

Keywords:
C–C coupling · microwave reactions · reaction mechanisms · water chemistry

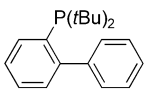
Since the discovery of the Ullmann reaction over a century ago,[1] the metal-mediated and -catalyzed formation of aryl–aryl coupling products has played an important role in the synthesis of natural products, pharmaceutical and agrochemical products, specialty chemicals, and organic photo/electronic materials.[2] The developments of palladium-catalyzed Stille,[3] Suzuki,[4] and Kumada–Tamao–Hiyama[5] couplings have profoundly advanced the synthesis of bi- and polyaryl compounds. The Suzuki reaction of arylboronic derivatives with aryl halides has become the most important method for generating aryl–aryl coupling products because of its higher stability, its wide range of functional-group tolerance, and the low toxicity associated with boron compounds.

The reaction was discovered in the early 1980s and was initially carried out in benzene under an inert atmosphere catalyzed by 3 mol% of $[Pd(PPh_3)_4]$ (Scheme 1).[6] While the reaction showed a good tolerance of a range of functional groups, such as halides and carbonyls, its limitation is the high air-sensitivity of $[Pd(PPh_3)_4]$ and the use of toxic benzene as a solvent, especially for large-scale reactions. The high air-sensitivity makes the catalyst recycling/recovery difficult, which (together with the relatively high loading of the expensive catalyst) increases the application cost. The contamination of the product by the catalyst, albeit in minute amounts, is also a concern in cases such as pharmaceutical agents. Progress has been made to overcome such limitations because of both economical concerns and increased environmental awareness.[7]



Scheme 1. Suzuki coupling of phenylboronic acid with aryl bromides.

Recently, a major study on Suzuki reactions has focused on increasing the activity of the catalyst and decreasing the catalyst loading; this has included the use of additives, the modification of the catalyst, and changing the solvents. A major advance achieved by increasing the catalytic activity is the extension of the Suzuki reaction to unactivated aryl chlorides, as noted by the research groups of Buchwald,[8] Fu,[9] and Herrmann,[10] as well as several other groups. The key for such an increase in catalytic activity was the use of more electron-rich ligands such as **1**, which provides



1

excellent yields of Suzuki products at room temperature, even with unactivated aryl chlorides.[8]

Another major focus has been the use of environmentally benign media. Suzuki reactions in supercritical CO_2,[11] in ionic liquids,[12] solventless,[13] and in water[14] have all been developed. The use of water as a solvent for chemical reactions clearly has both economical and environmental advantages because it is inexpensive, abundant, nontoxic, nonflammable, and readily separable from organic compounds.[15] An additional advantage of performing the Suzuki reaction in water is the ready tuning of the pH of the media, which has a critical influence on the rate of reaction. It has also been shown that Suzuki reactions in water are frequently better in the absence of a phosphane ligand[16] and have increased stability in air.[17] Mechanistic studies have shown that the formation of borate intermediates (for example, by the addition of base or a fluoride salt) can facilitate the reactions.[18] Badone et al. reported a great acceleration of a Suzuki coupling catalyzed by "ligand-free" palladium acetate by the addition of one equivalent of tetrabutylammonium bromide (TBAB) in water.[19] Interestingly, aryl bromides appeared more reactive than aryl iodide under these reaction conditions. The role of TBAB was explained as acting as a phase-transfer catalyst and facilitating the formation of a borate intermediate $[ArB(OH)_3]^-$.

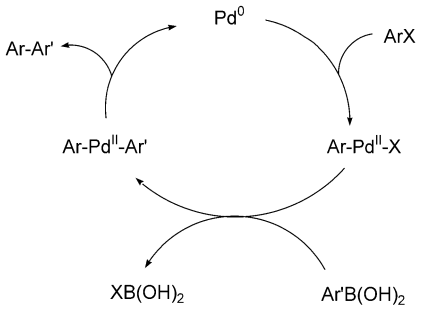
Microwave heating has recently been shown to be an effective method in promoting the Suzuki reaction. Lar-

[*] C.-J. Li
Department of Chemistry
McGill University
801 Sherbrooke St. West, Montreal, PQ H3A 2K6 (Canada)
and
Department of Chemistry
Tulane University
New Orleans, LA 70118 (USA)
Fax: (+1) 504-865-5596
E-mail: cjli@tulane.edu

 © 2003 Wiley-VCH Verlag GmbH & Co. KGaA, Weinheim DOI: 10.1002/anie.200301672

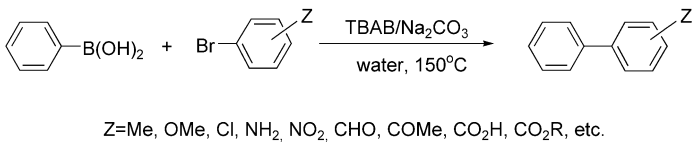
hed and Halleberg reported a microwave-accelerated Suzuki coupling in aqueous 1,2-dimethoxyethane (DME),[20] while Schotten and co-workers showed that the Suzuki reaction can be catalyzed by "ligand-free" palladium acetate with poly(ethylene glycol) as the soluble support and phase-transfer catalyst.[21] The reaction time was shortened from 2 h to 2–4 min by using microwave irradiation. The effect of microwave heating on achieving a rapid Suzuki coupling of sodium tetraphenylborate in water or methylformamide was demonstrated by Villemin et al.[22] Leadbeater and Marco reported the coupling of a range of aryl halides, including aryl chlorides with phenylboronic acid in neat water with palladium acetate as the catalyst and TBAB as an additive, by using microwave heating.[23]

The commonly recognized mechanism for the Suzuki reaction (and other related aryl–aryl couplings) involves oxidative addition-transmetalation-reductive elimination sequences with the oxidative addition often being the rate-limiting step (Scheme 2).[4] With such a



Scheme 2. Mechanism of the Suzuki reaction.

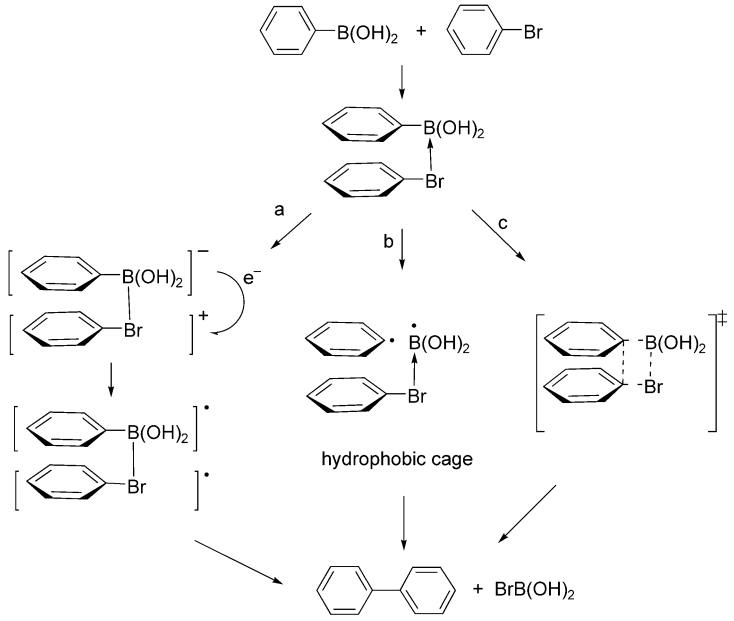
general consensus in the chemical community, the discovery by Leadbeater and Marco of a Suzuki-type coupling of boronic acid with aryl halides in hot water in the presence of TBAB without a palladium or any other transition-metal catalyst is a most surprising development in the Suzuki reaction (Scheme 3).[24] Optimum yields of the product were obtained at 150 °C in a sealed tube when the ratio of aryl bromide to boronic acid was 1:1.3. The excess amount of boronic acid required was attributed to some protodeboronation of the boronic acid, which gave benzene. The reactions of various aryl



Scheme 3. Suzuki coupling of phenylboronic acid with aryl bromides.

bromides bearing both electron-donating and electron-withdrawing groups proceeded readily. Aryl bromides provided better yields than aryl iodides or aryl chlorides; the latter showed no reactivity under the reaction conditions. Sterically demanding aryl bromides were also coupled in good yields. The reaction was also found to be regiospecific with respect to both the aryl bromide and the boronic acid, and the reaction of 4-bromoacetophenone with 4-methylbenzeneboronic acid produced the desired coupling product in excellent yield. Microwave heating for 5 min provided yields comparable to that obtained by conventional heating with 4-bromoacetophenone for 5 h. Conventional heating is not sufficient for unactivated and deactivated aryl bromides, even after 16 h. New glassware, apparatus, and reagents were used to show that the reaction was truly metal-free. No palladium was detected down to 0.1 ppm by analysis of the crude reaction mixture. Induced coupled plasma atomic absorption (ICP-AA) spectroscopy analysis did not show the presence of other possible catalytic metals above the detection limit of the apparatus (0.5–1 ppm).

This unexpected finding seemingly defies our long understanding of the mechanism of aryl–aryl couplings of aryl halides, in which a transition metal is required to break the strong sp^2 aryl C–X bond, as it is unlikely to involve a direct S_N2 reaction with aryl halide derivatives. The reduced reactivity of the aryl iodides is also not in accord with an S_N2 mechanism. On the other hand, most organic reaction mechanisms are based on studies carried out in organic solvents. While a microwave provided focused heating,[25] it is unlikely to be the critical factor for the onset of the reaction. While it may be too early to pin down the exact mechanism of this new reactivity, it nevertheless leads to various speculations. One possibility is that the reaction occurred through a radical mechanism (Scheme 4). The me-



Scheme 4. Possible pathways for the Suzuki reaction without a transition-metal catalyst in high-temperature water.

 © 2003 Wiley-VCH Verlag GmbH & Co. KGaA, Weinheim

dium, water, provides an enhanced π stacking as a result of the hydrophobic effect.[26] Then, either an internal electron transfer to generate a diradical species (route a) or an external diradical formation within the substrate "cage" leads to the product formation (route b). Another possibility is through a σ-bond metathesis of a borate complex (route c). Clearly, further studies are needed to understand the mechanistic rationale for the coupling. If the reactivity is general, this may open the door to a new opportunity of possibly performing other transition-metal-catalyzed reactions under similar conditions without using transition metals (a frequent environmental concern).

Evidently, the discovery that the Suzuki reaction can be performed in hot water without using a transition metal is another fascinating, but unexpected, result of organic reactions in water. It also demonstrates the fertile novelty of chemistry when going beyond the conventional organic media and standard conditions. However, the findings need to be corroborated with more experimental results. The study of unconventional chemistry is not performed in order to abandon traditional chemistry but to enrich our knowledge and synthetic tools. There will always be a need for transition-metal-catalyzed Suzuki reactions because of its versatility, chemo- and regio-selectivity, functional-group tolerance, and mild conditions.

[1] F. Ullmann, J. Bielecki, *Ber. Dtsch. Chem. Ges.* **1901**, *34*, 2174 – 2185.

[2] J. Hassan, M. Sévignon, C. Gozzi, E. Schulz, M. Lemaire, *Chem. Rev.* **2002**, *102*, 1359 – 1470.

[3] J. K. Stille, *Angew. Chem.* **1986**, *98*, 504 – 519; *Angew. Chem. Int. Ed. Engl.* **1986**, *25*, 508 – 524.

[4] N. Miyaura, A. Suzuki, *Chem. Rev.* **1995**, *95*, 2457 – 2483.

[5] Y. Hatanaka, T. Hiyama, *Synlett* **1991**, 845 – 853.

[6] N. Miyaura, T. Yanagi, A. Suzuki, *Synth. Commun.* **1981**, *11*, 513 – 519.

[7] P. T. Anastas, J. C. Warner, *Green Chemistry: Theory and Practice*, Oxford University Press, Oxford, **1998**.

[8] D. W. Old, J. P. Wolfe, S. L. Buchwald, *J. Am. Chem. Soc.* **1998**, *120*, 9722 – 9723; J. P. Wolfe, S. L. Buchwald, *Angew. Chem.* **1999**, *111*, 2570 – 2573; *Angew. Chem. Int. Ed.* **1999**, *38*, 2413 – 2416.

[9] A. F. Little, G. C. Fu, *Angew. Chem.* **1998**, *110*, 3586 – 3587; *Angew. Chem. Int. Ed.* **1998**, *37*, 3387 – 3388.

[10] W. A. Herrmann, V. P. W. Böhm, C. P. Reisinger, *J. Organomet. Chem.* **1999**, *576*, 23 – 41.

[11] R. S. Gordon, A. B. Holmes, *Chem. Commun.* **2002**, 640 – 641.

[12] C. J. Mathews, P. J. Smith, T. Welton, *Chem. Commun.* **2000**, 1249 – 1250.

[13] G. W. Kabalka, R. M. Pagni, C. M. Hair, *Org. Lett.* **1999**, *1*, 1423 – 1425.

[14] A. L. Casalnuovo, J. C. Calabrese, *J. Am. Chem. Soc.* **1990**, *112*, 4324 – 4330; J. P. Genêt, E. Blart, M. Savignac, *Synlett* **1992**, 715 – 717; N. A. Bumagin, V. V. Bykov, *Tetrahedron* **1997**, *53*, 14437 – 14450.

[15] C. J. Li, T. H. Chan, *Organic Reactions in Aqueous Media*, Wiley, New York, **1997**; *Organic Synthesis in Water* (Ed.: P. A. Grieco), Thomson Science, Glasgow, **1998**; *Aqueous-Phase Organometallic Catalysis, Concepts and Applications* (Eds.: B. Cornils, W. A. Herrmann), Wiley-VCH, Weinheim, **1998**.

[16] T. I. Wallow, B. M. Novak, *J. Org. Chem.* **1994**, *59*, 5034 – 5037.

[17] S. Venkatraman, C. J. Li, *Org. Lett.* **1999**, *1*, 1133 – 1135; S. Venkatraman, T. S. Huang, C. J. Li, *Adv. Synth. Catal.* **2002**, *344*, 399 – 405.

[18] G. B. Smith, G. C. Dezeny, D. L. Hughes, A. O. King, T. R. Verhoeven, *J. Org. Chem.* **1994**, *59*, 8151 – 8156.

[19] D. Badone, M. Baroni, R. Cardamone, A. Ielmini, U. Guzzi, *J. Org. Chem.* **1997**, *62*, 7170 – 7173.

[20] M. Larhed, A. Halleberg, *J. Org. Chem.* **1996**, *61*, 9582 – 9584.

[21] C. G. Blettner, W. A. König, W. Stenzel, T. Schotten, *J. Org. Chem.* **1999**, *64*, 3885 – 3890.

[22] D. Villemin, M. J. Gómez-Escalonilla, J. F. Saint-Clair, *Tetrahedron Lett.* **2001**, *42*, 635 – 637.

[23] N. E. Leadbeater, M. Marco, *Org. Lett.* **2002**, *4*, 2973 – 2976.

[24] N. E. Leadbeater, M. Marco, *Angew. Chem.* **2003**, *42*, 1407 – 1409; *Angew. Chem. Int. Ed.* **2003**, *42*, 1407 – 1409.

[25] R. S. Varma in *Microwaves in Organic Synthesis* (Ed.: A. Loupy), Wiley-VCH, Weinheim, **2002**, chap. 6, pp. 181–218.

[26] R. Breslow, *Acc. Chem. Res.* **1991**, *24*, 159 – 164.

 © 2003 Wiley-VCH Verlag GmbH & Co. KGaA, Weinheim

Interfacial Host–Guest Complexes

Electrochemical and Photochemical Control of Host–Guest Complexation at Surfaces

*Graeme Cooke**

Keywords:
electrochemistry · molecular recognition · monolayers · photochemistry · supramolecular chemistry

The application of electrochemistry or photochemistry to modulate supramolecular interactions between host–guest systems in solution is a burgeoning field. In particular, the speed and reversibility associated with electrochemically or photochemically actuated supramolecular interactions has allowed the creation and modulation of novel solution-based devices. In recent years, great advances have been made in transferring these systems from the solution to the solid state, to facilitate the development of molecular-electronics components that can operate in unison under the influence of an externally applied stimulus. These studies pave the way for the creation of responsive surfaces with advanced materials and nanotechnology applications.

1. Introduction

Self-assembled monolayers (SAMs),[1] Langmuir monolayers, and Langmuir–Blodgett[2] multilayer films have become ubiquitous as methods of organizing and depositing molecules at interfaces. In particular, these systems have afforded platforms for developing pragmatic sensors and devices,[3] as well as systems with biological applications.[4] Immobilization of such systems allows the transition from the solution to the solid state, thus offering a method of fabricating well-defined and, on occasion, robust and stable structures that can operate in unison. Furthermore, molecules organized in this manner offer a convenient means of connecting these systems to the macroscopic world. As a result, molecular-recognition events between immobilized host–guest complexes can be detected by an external means (for example, voltammetry),[5] which may facilitate the development of novel chemosensors.[6] However, increased attention has been directed towards controlling the assembly/disassembly of these systems to form responsive surfaces with device applications, in which the binding efficiency (Figure 1a), assembly/disassembly (Figure 1b), or molecular motion (Figure 1c) can be modulated at the solid–liquid interface. Arguably, the most promising methods of modulating host–guest interactions at surfaces are those which utilize electrochemically or photochemically controlled supramolecular interactions. The former method greatly simplifies the reversible fabrication and actuation of devices, as electronic input (from the potentiostat) is used directly to allow near seamless electronic interfacing to contemporary input/output (I/O) systems, whilst the latter offers convenient actuation using a readily available stimulus. This Minireview focuses upon some of the recent applications

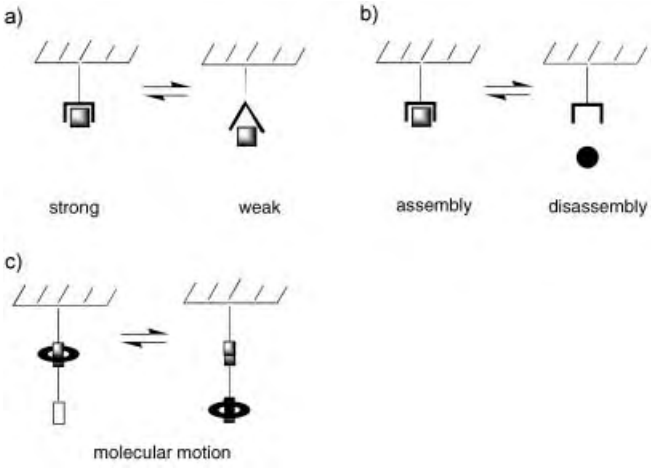


Figure 1. Schematic representation of some of the possible methods of modulating host–guest interactions at interfaces: a) Modulation of binding efficiency; b) control of assembly/disassembly; c) control of molecular motion.

[*] Dr. G. Cooke
Centre for Biomimetic Design & Synthesis
Chemistry, William H. Perkin Building
School of Engineering & Physical Sciences
Heriot–Watt University, Riccarton, Edinburgh EH14 4AS (UK)
Fax: (+44) 131-451-3180
E-mail: g.cooke@hw.ac.uk

 © 2003 Wiley-VCH Verlag GmbH & Co. KGaA, Weinheim DOI: 10.1002/anie.200301636

of redox and photochemically controlled supramolecular interactions to modulate host–guest complexation at the solid/liquid interface.

2. Redox Control of Host–Guest Interactions

As hydrogen bonds are essentially electrostatic in nature, the application of electrochemistry to control the electrostatic properties between complementary donor and acceptor sites of hydrogen-bonded host–guest dyads is a rapidly developing field within supramolecular chemistry.[7] For example, Rotello and co-workers have shown that electrochemical reduction of the flavin moiety of the hydrogen-bonded dyad formed between isobutylflavin (**1**) and 2,6-diethylamidopyridine (**2**), results in a 500-fold increase in the binding efficiency of the complex in solution (Figure 2a).[8] In a series of further studies, they have exploited the redox-controlled hydrogen-bonding interactions between **1** and diamidopyridine derivatives immobilized onto gold nanoparticle scaffolds to provide a colloidal receptor **3** with electrochemically controllable binding properties (Figure 2b).[9] The recognition properties of this receptor with flavin guest **1** were similar to those observed for diamidopyridine hosts in solution ($CDCl_3$), with an association constant of $196\,M^{-1}$ for the complex with neutral flavin **1**. However, upon electrochemical reduction of the flavin guest to its radical anionic state ($\mathbf{1}^{\bullet-}$), the increase in the electron density at the oxygen atoms of the flavin resulted in a 20-fold increase in host–guest binding efficiency.

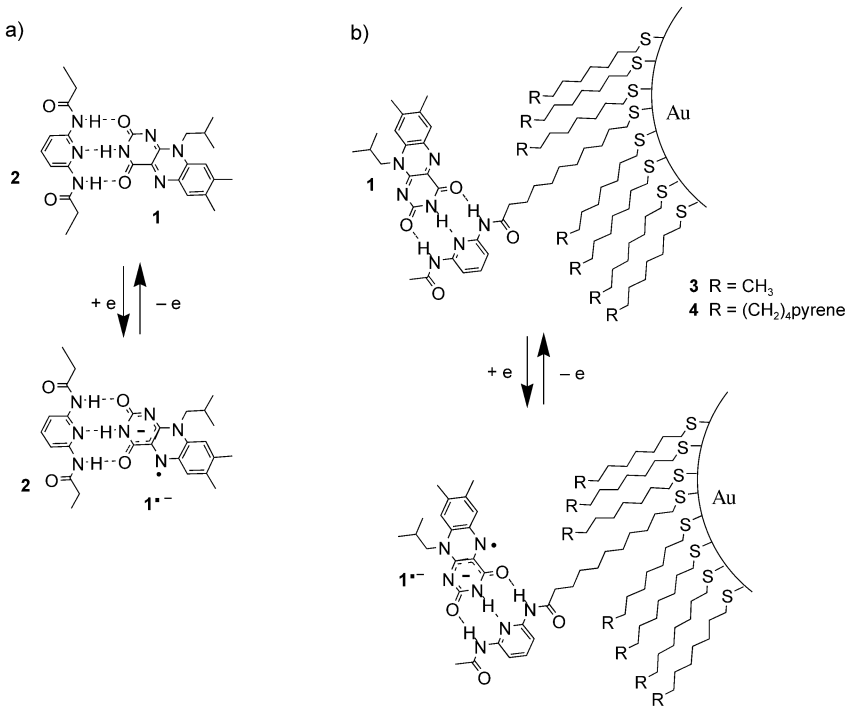


Figure 2. Electrochemically controlled hydrogen-bonding interactions between flavin (**1**) and diamidopyridine (**2**) moieties: a) in solution; b) at a nanoparticle–solution interface.

In a subsequent study by the same group, diamidopyridine thiols were place-exchanged onto a colloid containing pyrene units to afford colloidal receptor **4**.[10] The addition of pyrene units to the gold colloid substantially increased the hydrogen-bonding efficiency between the immobilized pyridine unit and the neutral flavin moiety in solution (compared to colloid **3** in $CDCl_3$ (**1**·**3** $K_a = 196\,M^{-1}$; **1**·**4** $K_a = 320\,M^{-1}$)). This stabilization of the complex (0.3 kcal mol^{-1}) was principally a result of the aromatic stacking interactions between the electron-deficient flavin and electron-rich pyrene subunits. In contrast, electrochemical reduction of flavin guest **1** to the $\mathbf{1}^{\bullet-}$ state transformed the electron-deficient nature of **1** to the more electron-rich $\mathbf{1}^{\bullet-}$ state, which evokes unfavorable interactions between the reduced flavin and the pyrene subunits. Indeed, a significant (0.6 kcal mol^{-1}) reduction in the redox-enhanced binding efficiency was observed (relative to **3** in CH_2Cl_2 ($\mathbf{1}^{\bullet-}$·**3** $K_a = 6400\,M^{-1}$; $\mathbf{1}^{\bullet-}$·**4** $K_a = 2300\,M^{-1}$)).

By using an alternative approach, Smith and co-workers have explored the electrochemically controllable hydrogen-bonding interactions between a surface-deposited redox-active host, in the form of a phenathrenequinone (PQ)-modified glassy carbon electrode, and urea guests.[11] It has previously been shown by the same group that reduction of the phenanthrenequinone component of the hydrogen-bonded complex **5**·**6**, formed in polar (DMF) and nonpolar (CH_2Cl_2) solvents, resulted in a significant increase in the hydrogen-bonding efficiency of the dyad (Figure 3a).[12] In transferring this system to a surface, the authors chose to electropolymerize the pyrrole derivative **7** onto a glassy carbon working electrode, which ensured a more direct electrical contact between the potentiostat and the redox-active component (Figure 3b). Very large positive shifts (+107 mV) in the half-wave potentials for the redox wave of the immobilized PQ derivative were observed upon the addition of **6** to the cyclic voltammetry (CV) cell, which indicated the formation of strong hydrogen-bonding interactions between the immobilized $PQ^{\bullet-}$ moiety and the urea unit. It is noteworthy that the subsequent increase in binding efficiency, as suggested by the large shift in half-wave potential values, occurred in a fairly polar solvent (i.e., CH_3CN). Thus, the data suggest that reduction leads to the formation of hydrogen-bonded systems with reasonable



Graeme Cooke received his PhD (Univ. of Durham) in 1992, working on Langmuir–Blodgett films with Profs. M. R. Bryce and M. C. Petty. After postdoctoral work with Prof. R. Pettit (Arizona State), he became Senior Demonstrator at the Univ. of East Anglia (1994–96). Following lectureships at the Univs. of Teesside and Northumbria, he was appointed Lecturer of Organic Chemistry at Heroit–Watt University in 2000. His research focuses on using supramolecular chemistry to create systems with advanced materials, biomimetic, and nanotechnological applications.

 © 2003 Wiley-VCH Verlag GmbH & Co. KGaA, Weinheim

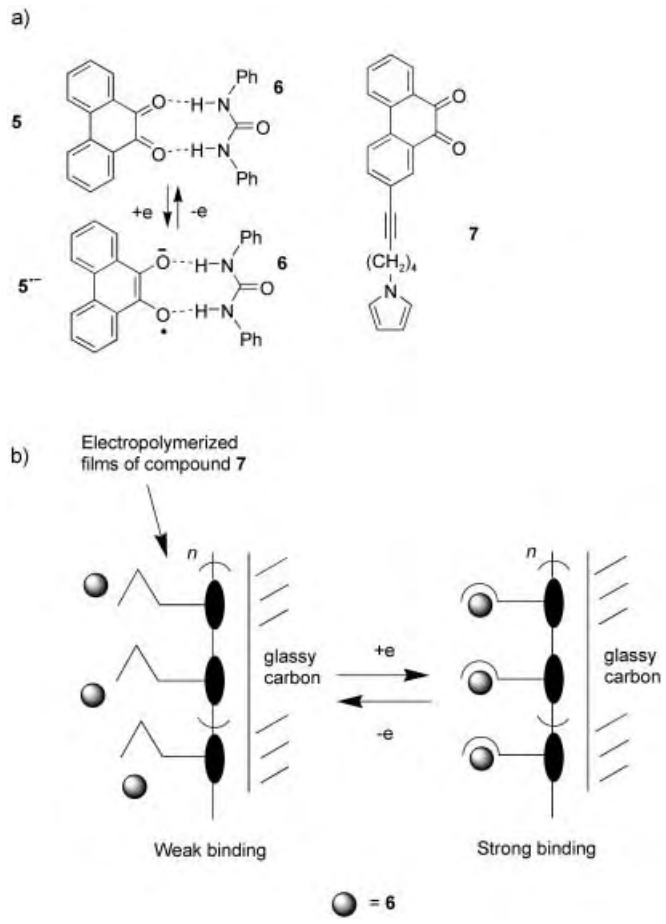


Figure 3. Electrochemically controllable hydrogen-bonding interactions between diphenylurea (**6**) and: a) Phenanthrenequinone (**5**, PQ) in solution; b) a PQ-modified electrode.

environmental robustness, which is one of the key requirements for subsequent sensor and device applications. Unfortunately, the stability of the electrochemically controlled interactions was offset by the poor longevity of the electroactive monolayer, as a significant loss of material from the electrode surface was shown to occur upon repeated redox cycling. However, as the magnitude of the shift in half-wave potential was shown to be independent of electrode coverage, and only upon the concentration of **6**, the sensor applications of these systems were not significantly impaired.

Astruc and co-workers have adopted a similar approach by immobilizing the redox-active component of the host–guest dyad onto gold nanoparticles.[13] However, their approach focused upon the use of immobilized ferrocene units as the electroactive component, which allows the switching of binding efficiency to be modulated at positive potentials, and thus overcomes the problems associated with the instability of reduced species (e.g., radical anions) to oxygen (Figure 4a). In these studies, the electrochemically controlled hydrogen-bonding interactions between the amidoferrocenyl moieties of gold colloids **8** or **9** and $H_2PO_4^-$ ions have been investigated (Figure 4b). The addition of $H_2PO_4^-$ ions to a CH_2Cl_2 solution of **8** or **9** resulted in a gradual disappearance of the original ferrocene oxidation wave and the appearance of a new wave that was shifted by over −210 mV, which is characteristic of strong hydrogen-bonding interactions between the amidoferrocenium-functionalized nanoparticles and $H_2PO_4^-$ ions. In both cases, the original oxidation wave disappeared when one equivalent of $H_2PO_4^-$ ions (per amidoferrocenyl branch) was added. This indicates that each amidoferrocenium moiety of the colloid forms a 1:1 complex with the $H_2PO_4^-$ ions. The shift in the redox wave was consistent with more than a 5000-fold increase in binding efficiency between the immobilized ferrocene species and the $H_2PO_4^-$ ions. Furthermore, the shifts were shown to be significantly larger than those observed for analogous nonimmobilized monomeric amidoferrocenyl units in solution.

The binding efficiency of metal–ligand coordination complexes, like their hydrogen-bonded counterparts, can also be modulated by oxidizing or reducing the components of the complex.[14] Tender and co-workers have exploited this principle by investigating the electrochemically controlled metal–ligand coordination between the immobilized electroactive peptide microperoxidase-11 (**10**) and imidazole (**11**; Figure 5a).[15] As the heme center of **10** has only one available coordination site, it was reasoned that immobilized **10**, in the

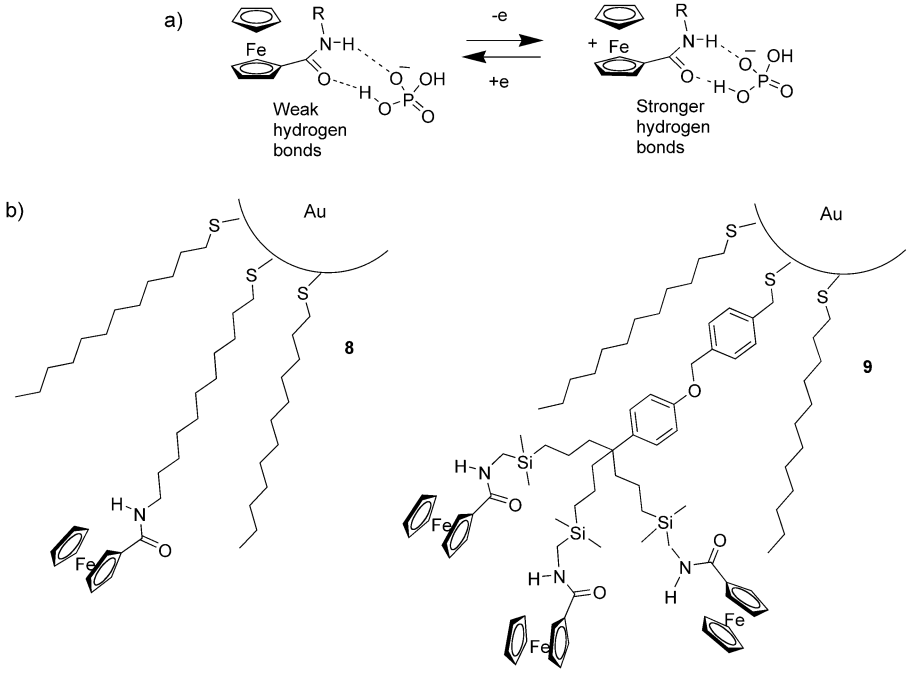


Figure 4. Schematic representations of: a) the electrochemically controlled binding between $H_2PO_4^-$ ions and amidoferrocenyl units; b) the ferrocene-functionalized gold nanoparticles **8** and **9**.

 © 2003 Wiley-VCH Verlag GmbH & Co. KGaA, Weinheim

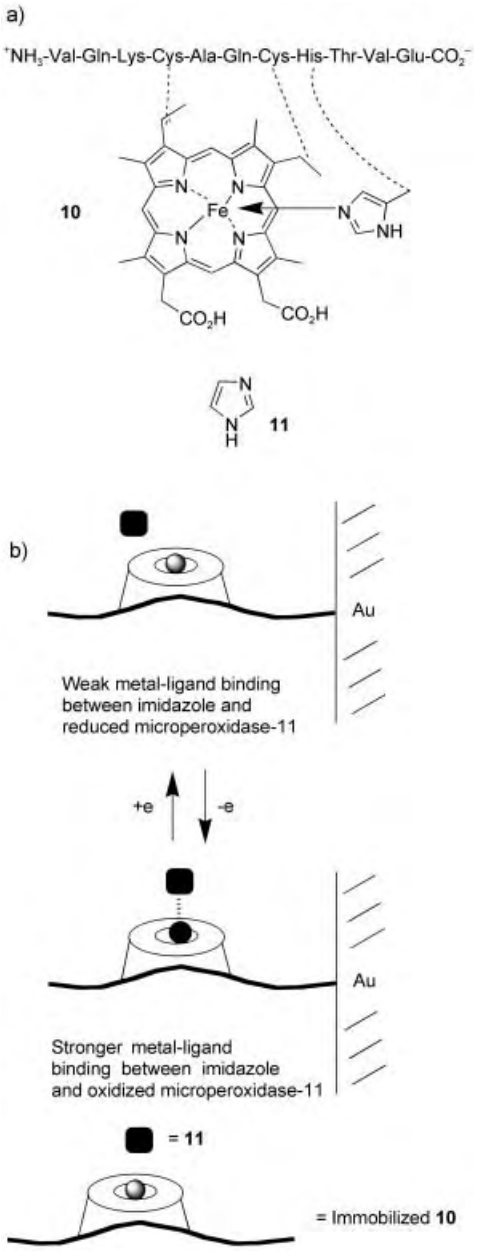


Figure 5. a) A representation of microperoxidase-11 (**10**) and imidazole (**11**); b) the electrochemically controlled metal–ligand coordination between immobilized **10** and **11**.

form of a SAM upon a gold electrode, could serve as an integrated recognition switch and transduction unit (Figure 5b). In particular, the ligation of weak base **11** to the iron redox center could be controlled by varying the electrode potential, which could in turn be reported by the shift in the Fe^{II}/Fe^{III} redox couple of the heme unit. The incremental shift in the formal redox potential of immobilized **10** was monitored upon the addition of imidazole, which from the resulting negative shift revealed that imidazole binding stabilizes the oxidized iron center of the heme unit of **10**. Furthermore, by using electrochemical simulations, immobilized **10** was shown to have a higher binding affinity for imidazole in the oxidized state ($K_a = 6250\,M^{-1}$) compared to the reduced state ($K_a = 1890\,M^{-1}$).

The miniaturization of devices and machines down to molecular dimensions is receiving an enormous amount of attention.[16] It is likely that immobilizing these systems onto surfaces will prove to be the most promising method of transforming these systems from academic curiosities to commercially viable devices. Stoddart and co-workers have recently developed very interesting switching devices based upon interlocked molecules.[17] By utilizing chemical and electrochemical redox reactions, they have been able to induce molecular motion within catenane, pseudorotaxane, and rotaxane-based supramolecules in solution, and more recently in the solid state. For example, they have developed a [2]catenane **12** that displays chemically and electrochemically controlled switching properties in solution (Figure 6a).[18] The tetrathiafulvalene (TTF) moiety of **12a** was shown to preferentially reside within the cavity of the tetracationic cyclophane cyclobis(paraquat-*p*-phenylene). However, upon electrochemical oxidation of the TTF unit to its positively charged radical cation, coulombic repulsion between the latter and the tetracationic cyclophane resulted in a circumrotation of the macrocyclic polyether chain (with respect to the tetracationic cyclophane). This process resulted in the neutral 1,5-dioxynaphthalene moiety being positioned inside the tetracationic cyclophane, thus affording structure **12b**. Upon reduction of the TTF moiety of **12b** to its neutral state, another circumrotation occurred to regenerate the original structure **12a**.

To develop solid-state devices from this bistable catenane, Langmuir monolayers were fabricated onto a photolithographically patterned polysilicon electrode, which was facilitated by replacing the PF_6^- counterions with amphiphilic dimyristoylphosphatidyl ($DMPA^-$) anions.[19] The patterning of the polysilicon substrate allowed the Langmuir film to be deposited along parallel lines on the electrode surface. Following monolayer deposition, metallic top electrodes were deposited onto the film to afford a sandwich-type structure. The top electrodes were arranged orthogonally to the bottom electrodes, which allowed the construction of an array of junctions that could be individually addressed. Conduction was shown to occur by electron tunneling through the one-molecule-thick layer between the junction electrodes. Therefore, perturbations in the electronic characteristics of the device would affect the tunneling efficiency and resistance of the junction. A series of voltage pulses between $+2.0$ and -2.0 V were applied to the device, and the subsequent current through the device was read at a nonperturbing voltage. The resulting hysteretic current–voltage curves allowed the mechanochemical mechanism of the device to be interpreted, as indicated in Figure 6b. By applying the appropriate bias voltage to oxidize the TTF component of the ground-state (switch-open) device, a similar voltage-driven circumrotation of the macrocyclic polyether component occurred to that which was observed in solution. When the voltage of the device was reduced to a near-zero bias, so that the TTF moiety became neutral, the electron-deficient cyclophane was shown to reside over the 1,5-dioxynaphthalene moiety of the macrocyclic polyether component (switch-closed state). However, to regenerate the original structure, partial reduction of the electron-deficient cyclophane unit was required. This finding

 © 2003 Wiley-VCH Verlag GmbH & Co. KGaA, Weinheim

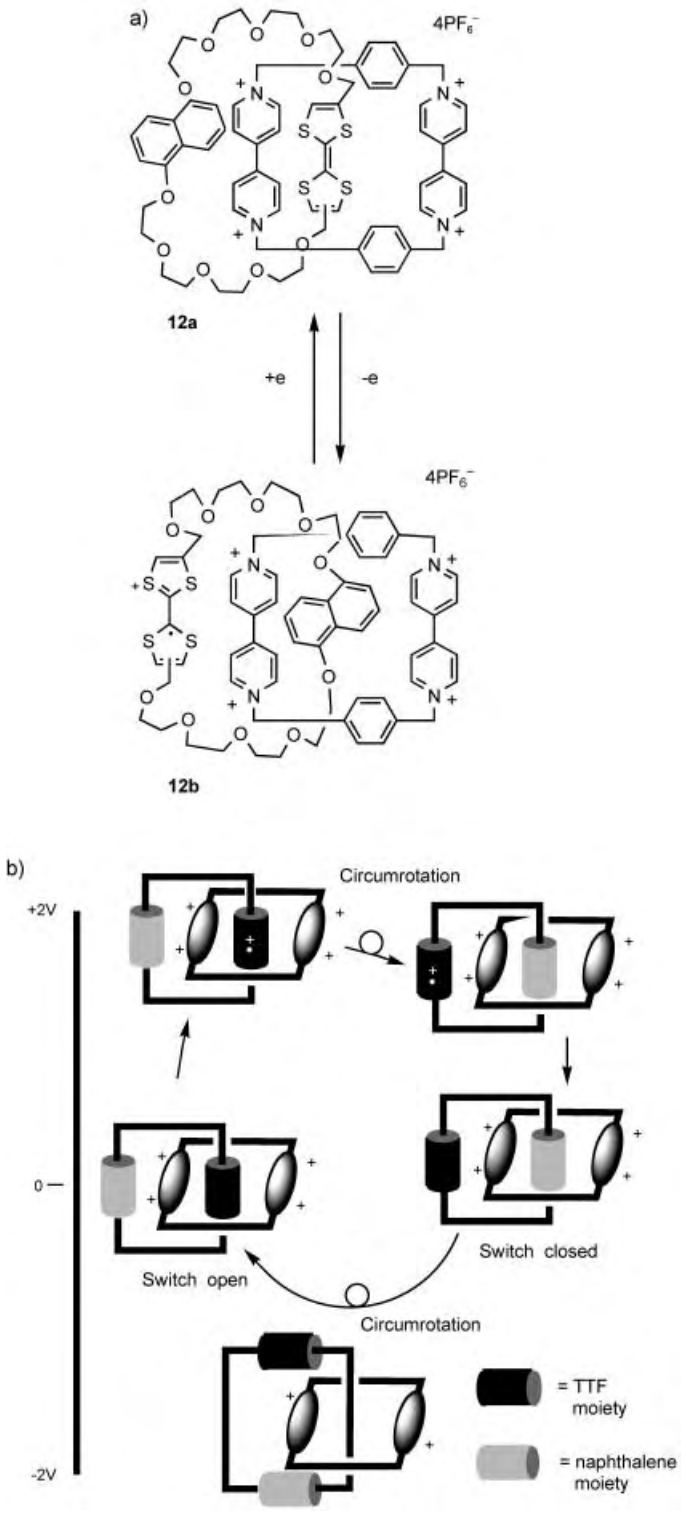


Figure 6. Schematic representations of the redox-induced switching characteristics of a [2]catenane: a) in solution; b) in the solid state.

is in contrast with the same process in solution, where reduction of the oxidized TTF unit was required to regenerate the switch-open state. The voltage-driven circumrotation process of the solid-state device was shown to be reversible, as it could be cycled at least a few hundred times.

In an evolutionary process starting from the [2]catenane-based device described above, Stoddart, Heath, and co-workers have used the amphiphilic [2]rotaxane **13** to fabricate a two-dimensional (2D) crossbar device that displays both memory and logic functions (Figure 7a).[20] Although the previous example provided an encouraging precedent to develop solid-state molecular-electronics devices from interlocked supramolecules, it was argued that the [2]catenane would have limited use in the fabrication of 2D crossbar circuits, principally because of its poor switching magnitude and low current levels through the device. Moreover, the electrochemically active component of the device, the [2]catenane, was positioned near the polysilicon electrode, with much of the gap between the electrodes being bridged by the electrochemically inactive $DMPA^-$ counterions. It was reasoned that the rotaxane nature of **13** would place the redox-active components more centrally between the electrodes, which in turn would increase the resonant tunneling current. Furthermore, the large footprint of the rotaxane architecture should help to prevent the formation of domains within the films, which negates domain switching and thus allows the molecules to act individually within the device.

Device fabrication from **13** was achieved using a similar method to that described for the [2]catenane-based device above. However, by utilizing a scalable fabrication process it was possible to fabricate 2D crossbars with micrometer and nanometer-scale patterning. Bias voltages were applied to the polysilicon electrode, whilst the top electrode was grounded through a preamplifier. A relay-switching matrix was used to achieve independent control over every wire. The voltages required to open and close the device were -2.0 and $+2.0$ V, respectively, and these values remained constant as the devices were repeatedly cycled between the closed and open states. As the mechanism of the 2D-crossbar device was not directly measured, the mechanistic arguments shown in Figure 7b were postulated from known solution-based data. Interestingly, by using micrometer-scale devices fabricated from **13**, the authors were able to show point addressabilty in a 64-junction 2D crossbar by creating a 64-bit random access memory circuit. Moreover, as the aforementioned 2D-crossbar circuits only lacked diode character for logic operations, it was possible to experimentally approximate a 2D logic crossbar containing diodes by selectively hard-wiring 1D circuits into the crossbar. For example, it was shown that a simple half-adder function could be configured from the 2D crossbar by building in a diode response into the junctions. This pioneering work paves the way for the future development of a machine that allows logic and memory to communicate with each other and the macroscopic world, thereby demonstrating the feasibility of a molecular computing machine.

3. Photochemical Control of Host–Guest Interactions

In an extensive range of studies, Willner and co-workers have produced surfaces with molecular information and bioelectronic applications.[21] This work has been underpinned

 © 2003 Wiley-VCH Verlag GmbH & Co. KGaA, Weinheim

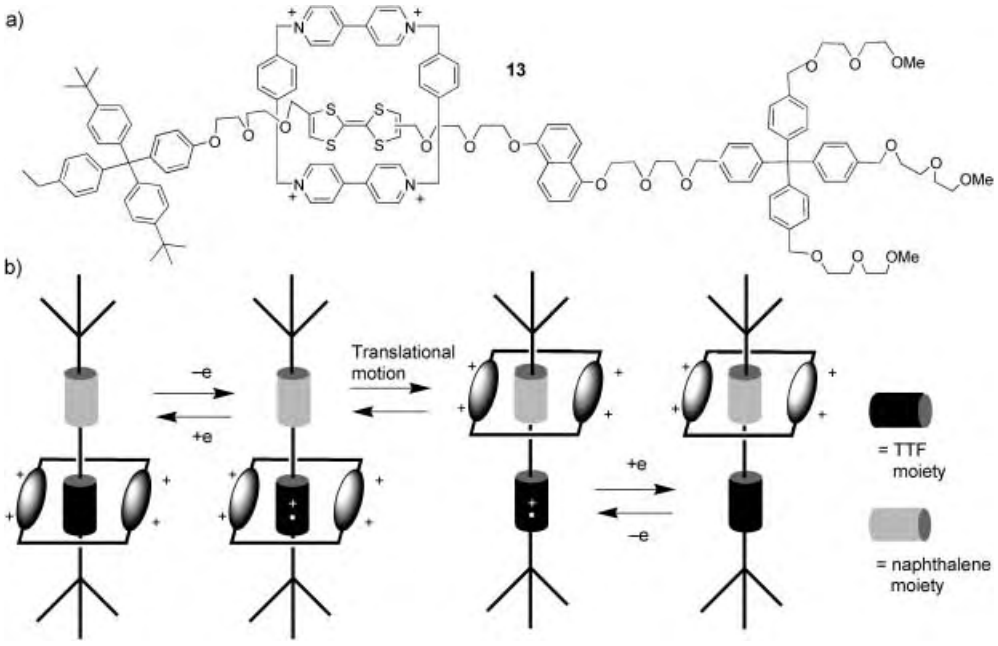


Figure 7. a) A representation of the amphiphilic [2]rotaxane **13**; b) a schematic representation of its electrochemically controlled translational motion within a 2D crossbar device.

by the development of photoisomerizable surfaces that have the propensity to control the association and dissociation of a species, both to and from an electrode. For example, the photoisomerization of a nitrospiropyran surface has been exploited to produce surfaces that can selectively bind to either positively or negatively charged species in solution (Figure 8).[22] Irradiation of the neutral monolayer with light of wavelength $320 < \lambda < 350$ nm (at pH 7) resulted in the photoisomerism of the neutral nitrospiropyran **14** (SP) state to the positively charged nitromerocyanine **15** (MRH^+) state. This isomerization proved to be reversible, as irradiation at $\lambda > 495$ nm regenerated the original SP state of the monolayer. This light-induced reversible transformation of the neutral-to-positively charged interface (and vice versa) allowed the control of electrostatic interactions between the immobilized units and charged electroactive species in solution to occur. For example, by reversibly switching between states **14** and **15**, the binding between the negatively charged 3,4-dihydroxyphenylacetic acid (DHPAA, **16**) was controlled by modulating the attractive interactions between these molecules. By monitoring the redox properties of DHPAA using CV studies, a substantially higher current for this redox process was observed for the MRH^+ state than the SP state, which is consistent with the electrostatic attraction between the electroactive DHPAA unit and the positively charged MRH^+-functionalized surface.

Extending this work, Willner and co-workers have exploited the photoisomerization of a related dinitrospiropyran-functionalized monolayer to control the binding to a dinitrophenyl antibody (DNP-Ab) (Figure 9). Dinitrospiropyran is an effective antigen for DNP-Ab, however, upon photoisomerization to the positively charged dinitromerocyanine state the affinity for this antibody is lost. Accordingly, a dinitrospiropyran-functionalized monolayer **18** displayed a high affinity for DNP-Ab, whilst photoisomerization to the positively charged dinitromerocyanine monolayer **17** reduced the affinity of the surface for the antibody, and as a result, the biomacromolecule was released from the surface. Interestingly, whilst the antibody was bound to the surface, the electrode was insulated from an electroactive species in solution (e.g., **16**), thus creating a novel method of blocking the diffusion (and thus oxidation) of **16** to the electrode surface. However, upon photoisomerization to the dinitromerocyanine state, the antibody was released from the surface and the electrochemical oxidation of DHPAA was again observed.

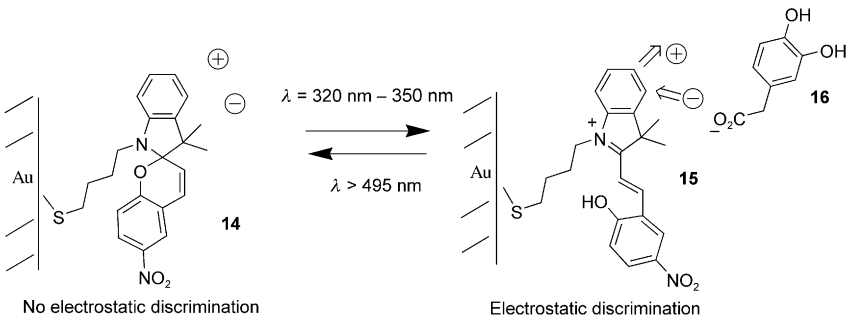


Figure 8. Photochemical control of electrostatic interactions between a nitrospiropyran monolayer and DHPAA (**16**).

The photochemically controlled "on/off" binding between appropriately functionalized surfaces and other biomacromolecules has also been observed. Using nitrospiropyran monolayer **19** (also containing self-assembled pyridinethiol

 © 2003 Wiley-VCH Verlag GmbH & Co. KGaA, Weinheim

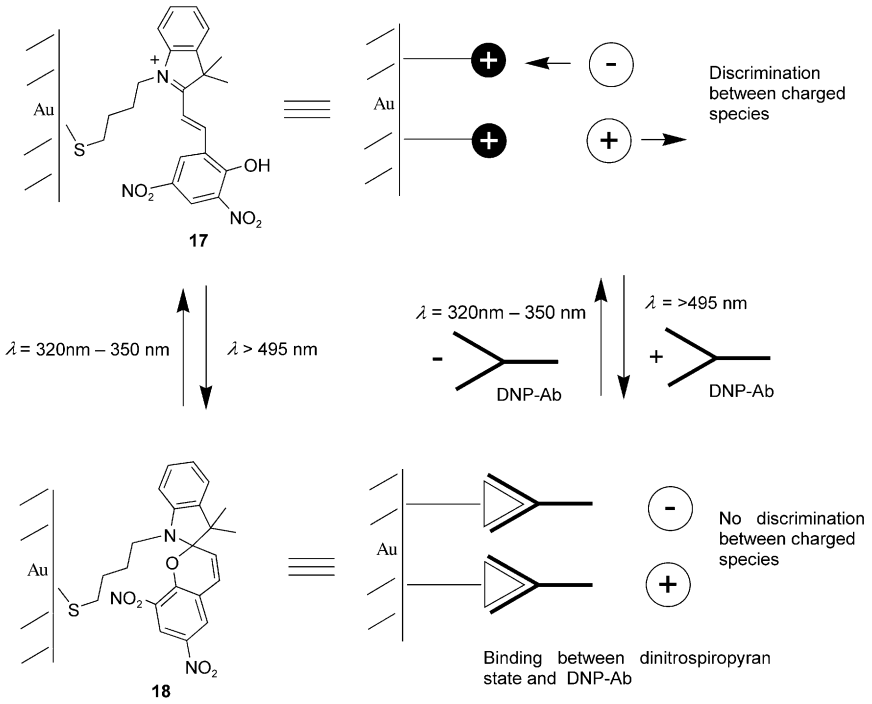


Figure 9. Photochemically controlled binding between a dinitrospiropyran-functionalized monolayer and the dinitrophenyl antibody DNP-Ab.

units), Willner and co-workers have utilized photoisomerization to control the attraction and repulsion of cytochrome c to an electrode surface (Figure 10).[23] CV studies performed on the nitrospiropyran-functionalised monolayer gave a quasi-reversible redox wave for the cytochrome unit, which indicated that pyridinethiol units helped to promote attractive interactions between cytochrome c and the electrode surface. However, the photoisomerization of nitrospiropyran-functionalized monolayer **19** to the positively charged merocyanine state **20** caused the positively charged cytochrome c molecules to be repelled from the electrode surface. This resulted in electrical contact between the electrode surface and the heme protein being blocked, and the corresponding loss of the heme redox wave in the cyclic voltammogram. This redox response was monitored during the photochemical cycling of the monolayer between the **19** and **20** states, and was consistent with reversible "on/off" binding between the pyridine-functionalized SAM and cytochrome c.

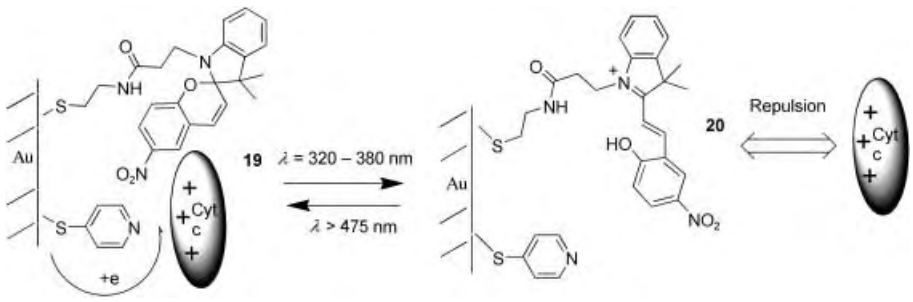


Figure 10. Photochemical control of electrostatic interactions between a nitrospiropyran monolayer (**19**) and cytochrome c.

Photochemistry offers a facile means of modulating the supramolecular interactions between components of molecular machines, and thus affords an attractive method for controlling the self-assembly of the complementary units both in solution and, more importantly in the context of this Minireview, in the solid state. For example, Stoddart, Zink, and co-workers have developed photochemically controlled supramolecular machines based upon pseudorotaxane systems immobilized upon a sol–gel surface.[24] The pseudorotaxane nature of these systems allows the wheel component to reversibly thread/dethread from the immobilized axle unit under the influence of an external stimulus, which offers the exciting possibility of developing responsive surfaces with photochemically controlled binding properties. Here, the axle moiety of the pseudorotaxane incorporated the electron-rich 1,5-dialkyloxynaphthalene unit **21**, which was immobilized onto a silicon substrate upon which a 150-nm thick layer of a sol–gel had been deposited (Figure 11). The derivatized films were immersed into an aqueous solution of $CBPQT^{4+}$ (**22**), which resulted in near quantitative formation of the pseudorotaxane **21**·**22** (only 4% of the monolayer remained unthreaded, based upon emission intensity measurements). The pseudorotaxane films were then irradiated with light at $\lambda = 365$ nm (in the presence of a photosensitiser and a sacrificial reagent), which photochemically reduced the $CBPQT^{4+}$ unit and nullified the charge-transfer (CT) and C–H···O interactions, causing the components of the pseudorotaxane to dethread. In addition to the photochemically induced dethreading process, it was also shown that re-equilibration processes were responsible for some of the units becoming dethreaded. Some degree of reversibility was reported for this system, however, the relative amount of the photochemically induced dethreaded species was shown to diminish slightly with each cycle.

In contrast to the previous example, which utilized photochemistry to modulate electrostatic interactions between the components of a surface-bound pseudorotaxane, Willner and co-workers have utilized the photochemically driven isomerization of azobenzene unit **23** to bring about threading/dethreading of an immobilized pseudorotaxane (Figure 12a). In particular, they have developed surfaces with photochemically controllable binding properties from a β-cyclodextrin (CD) modified gold electrode **24** and photoisomerizable electroactive azobenzene **23**.[25] The electro-inactive CD host unit **24** afforded a cavity into which the *trans* form of the azobenzene unit ($\mathbf{23}_{trans}$) could effectively form a pseudorotaxane (Figure 12b). The electroactive nature of the latter was exploited to establish the degree of host–guest complexation at the liquid/solid interface of the SAM by monitoring

 © 2003 Wiley-VCH Verlag GmbH & Co. KGaA, Weinheim

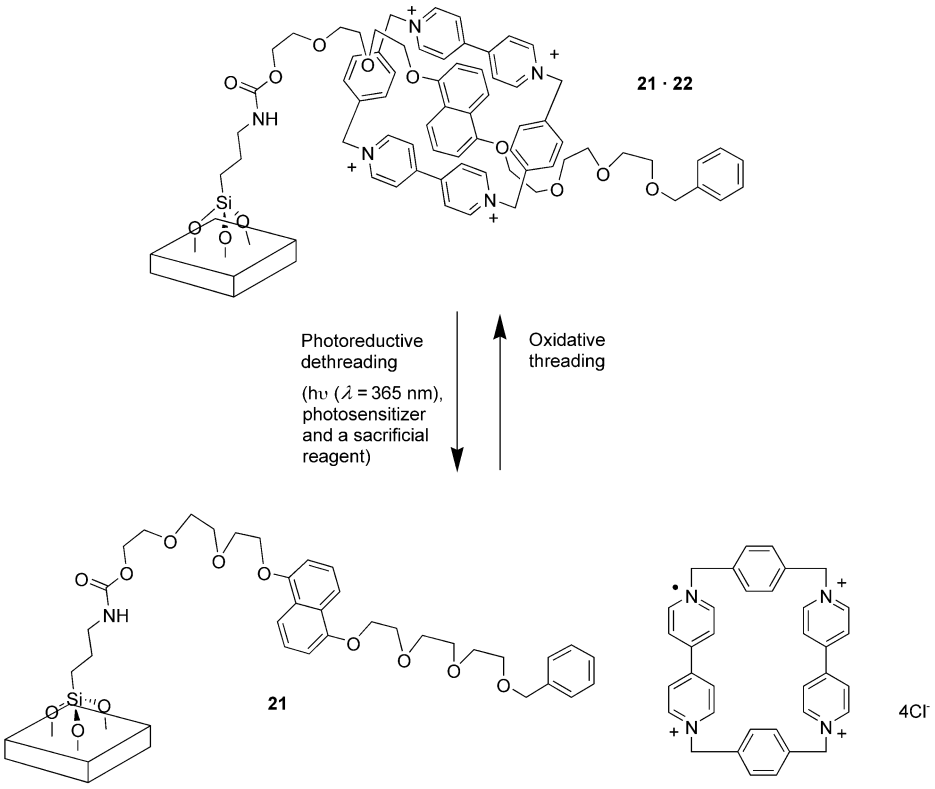


Figure 11. The photochemically driven threading/dethreading of a pseudorotaxane immobilized onto a sol–gel surface.

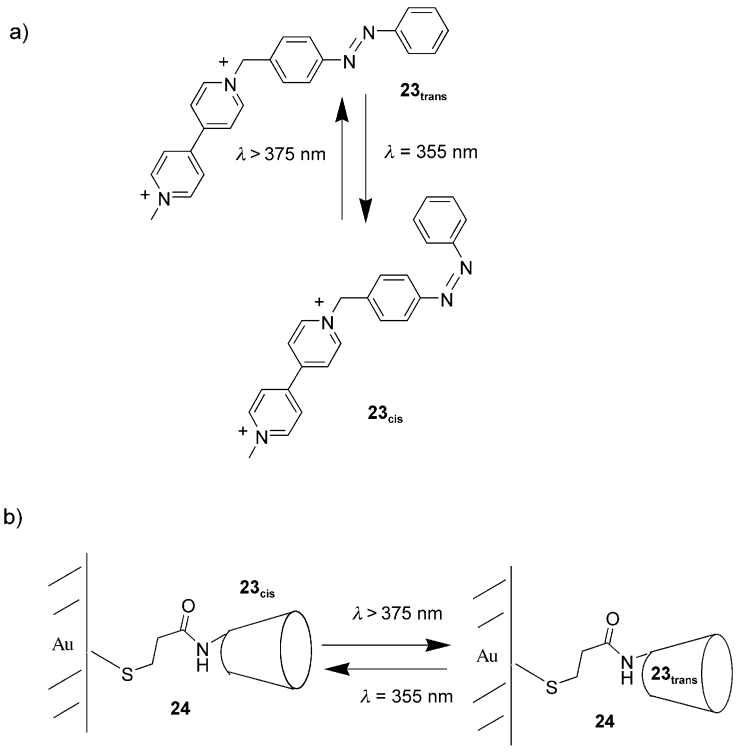


Figure 12. a) An electroactive azobenzene; b) the photochemically controlled pseudorotaxane formation between this unit and an immobilized β-cyclodextrin.

the CV data of this unit upon inclusion within the CD cavity. A high amperometric response was observed for the one-electron reduction of the *trans* bipyridinium species. Moreover, the peak currents of this redox wave displayed a linear increase with scan rate, which is consistent with a surface-confined redox-active unit. However, upon irradiation with light of $\lambda = 355$ nm, the resulting *trans*-to-*cis* isomerization of the azobenzene unit resulted in a considerably lower amperometric response. By comparison with data obtained using control experiments, it was deduced that photoisomer $\mathbf{23}_{trans}$ displayed a large amperometric response due to its higher affinity for the CD binding site, whereas the lower redox signal of the $\mathbf{23}_{cis}$ state was due to the correspondingly lower binding affinity of the *cis* form. Repeated photoisomerization of the azobenzene unit resulted in cyclic high and low amperometric signals, consistent with reversible association and dissociation of the components of the pseudorotaxane.

A potentially useful approach to develop surfaces with controllable complexation properties is to tailor the size and shape of specific recognition sites within the monolayer by utilizing imprinting methodologies. Indeed, imprinted recognition sites within monolayer-functionalised electrodes will undoubtedly lead to the future development of novel devices, sensors, and biomimetic systems. For example, Willner and co-workers have developed a photochemical method to imprint molecular-recognition sites in SAMs, which allow the development of surfaces with controllable binding properties to guest species in solution (Figure 13).[26] Mixed monolayers of 1-tetradecanethiol and thiol-functionalized naphthacene quinone were deposited onto a gold electrode to afford **25**. Irradiation of the monolayer with light of wavelength $320 < \lambda < 380$ nm, resulted in the photoisomerization of the quinone moiety to its redox-inactive *ana*-quinone form **26**. Subsequent exposure of the monolayer to butylamine resulted in cleavage of the *ana*-quinone moiety from the monolayer, which left behind a well-defined empty binding pocket. The phenol residue of **27** remained as part of the monolayer, and thus had the propensity to act as a recognition element within the SAM. Coulometry and CV experiments performed on the monolayer-hole-imprinted electrode showed that a

 © 2003 Wiley-VCH Verlag GmbH & Co. KGaA, Weinheim

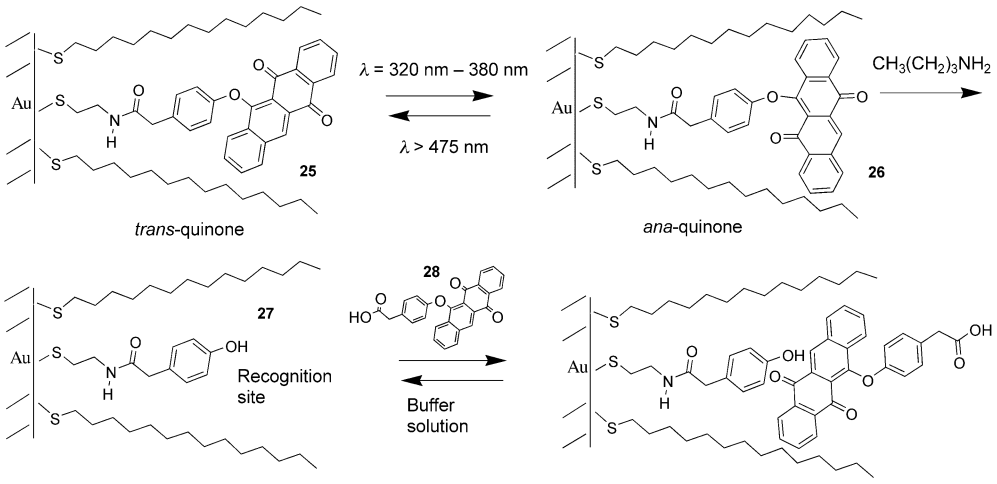


Figure 13. Photochemically imprinted molecular-recognition sites in monolayers assembled on gold.

gradual diffusion of added electroactive *trans*-quinone **28** into the pocket occurred. Moreover, quartz-crystal-microbalance measurements corroborated the association of **28** to the electrode surface, and revealed that subsequent exposure of the electrode to a pure buffer solution resulted in the slow diffusion of **28** from the recognition sites. The recognition sites displayed high selectivity for the *trans*-quinone unit, presumably due to a combination of good structural fit and complementary hydrophobic and hydrogen-bonding interactions between the *trans*-quinone unit and the imprinted recognition sites.

Usually the photoswitching of "on" and "off" binding characteristics of surfaces has been actuated by direct irradiation of the photosensitive moiety of the monolayer with the appropriate wavelength. However, Cook, Russell, and co-workers have adopted an alternative strategy by utilizing an evanescent field to control the coordination of zinc tetraphenylporphyrin (ZnTPP) to an 4-(arylazo)pyridine-containing SAM.[27] Monolayers of an 4-(arylazo)pyridine-containing disulfide were deposited onto a thin film of gold (8 nm) deposited onto a quartz slide, to produce the mixed monolayer $\mathbf{29}_{\mathbf{trans}}$ shown schematically in Figure 14. The waveguided photoisomerization (*trans*-to-*cis*) of the azobenzene moiety was achieved by irradiating the edge of the shorter side of the quartz slide with light ($\lambda = 365$ nm). Subsequent irradiation of the photoisomerized SAM $\mathbf{29}_{\mathbf{cis}}$ with light of $\lambda = 439$ nm led to approximately 95% recovery of an absorption band characteristic of the $\mathbf{29}_{\mathbf{trans}}$ form of the azobenzene moiety. When the as-deposited films ($\mathbf{29}_{\mathbf{trans}}$) were exposed to a solution of ZnTTP, UV/Vis spectroscopy indicated that the pyridine moiety of the SAMs had the propensity to coordinate to the zinc atom of the porphyrin unit. Waveguided light of $\lambda = 365$ nm was then applied to the slide, which resulted in a significant decrease in the Soret band of the SAM-bound ZnTPP (80% after 10 h). A much smaller diminution (15%) of this band was observed without irradiation, and it was thus deduced that *trans*-to-*cis* isomerization (of ZnTPP-coordinated and uncoordinated units) was the likely cause for the release of ZnTPP from the film by the creation of an unfavorable metal–ligand binding geometry. It

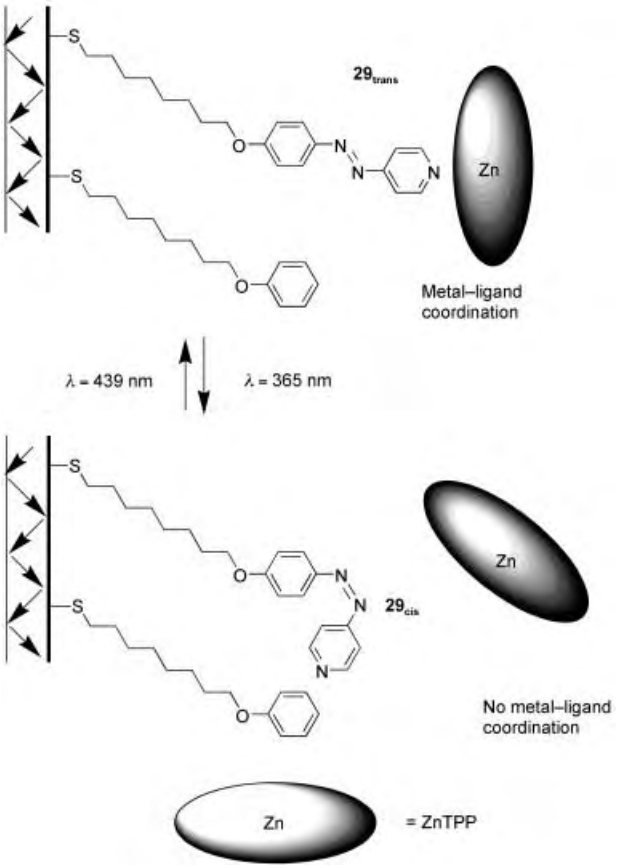


Figure 14. Control of the coordination and release of ZnTPP from a 4-(arylazo)pyridine-containing SAM by utilizing an evanescent field.

was suggested that isomerization of uncoordinated units could reduce the number of binding sites within the film, thus helping to control the equilibrium between bound and unbound ZnTPP units.

As was mentioned previously, redox-induced translocation within a rotaxane architecture has been utilized to create

 © 2003 Wiley-VCH Verlag GmbH & Co. KGaA, Weinheim

novel molecular-electronic devices. Photochemistry also offers an attractive method of actuating the shuttling of the wheel component along the axle of an immobilized rotaxane. For example, Willner et al. have developed a light-driven rotaxane-based molecular shuttle organized on a gold electrode surface.[28] Here, the shuttle was fabricated from a ferrocene-functionalized β-cyclodextrin (Fc-β-CD) wheel threaded upon an immobilized monolayer axle. The latter consisted of an azobenzene unit stoppered at one end with a bulky anthracene unit to prevent dethreading of the rotaxane architecture (Figure 15). The Fc-β-CD moiety was shown to preferentially reside over the *trans*-azobenzene moiety of the axle to form $\mathbf{30}_{\mathbf{trans}}$. However, when the system was irradiated with light of wavelength $320 < \lambda < 380$ nm, the resulting

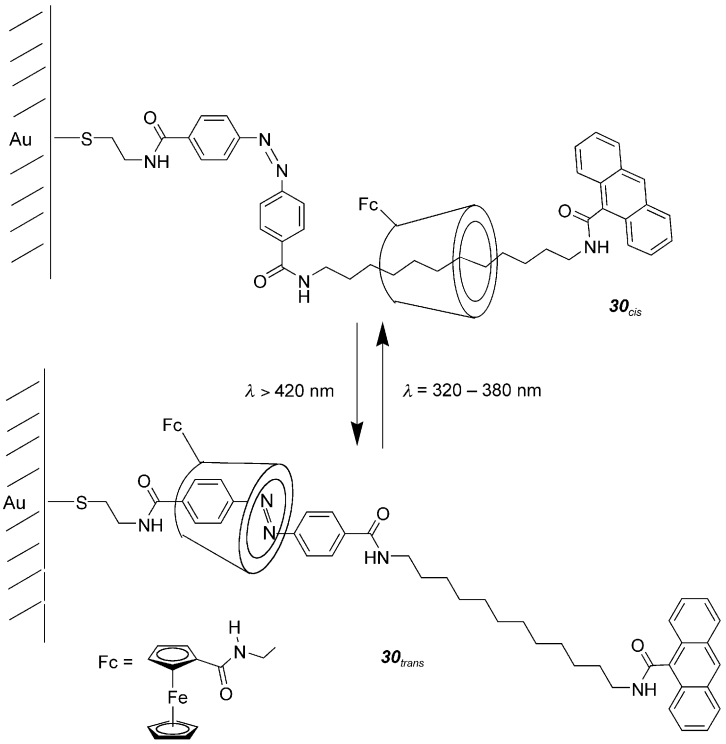


Figure 15. Light-stimulated translocation of a β-cyclodextrin wheel along an immobilized azobenzene axle.

photoisomerization of the azobenzene unit from the $\mathbf{30}_{\mathbf{trans}}$ to the $\mathbf{30}_{\mathbf{cis}}$ state caused translocation of the Fc-β-CD unit to the alkyl-chain component of the rotaxane. The redox-active nature of the Fc-β-CD wheel moiety allowed chronoamperometric measurements to determine that the Fc-β-CD unit, whilst complexed with the *trans*-azobenzene unit, was in close proximity to the electrode surface, thus giving rise to rapid interfacial electron transfer. However, photoisomerization of the monolayer to the *cis* state allowed the wheel to move away from the electrode surface to the alkyl portion of the axle, and as a result, gave rise to slower electron-transfer rates. By monitoring the current response for the *cis* and the *trans* states of the axle unit, it was deduced that the Fc-β-CD moiety reversibly shuttles between the azobenzene and alkyl stations upon photoisomerization of the axle component.

4. Conclusions and Outlook

It is clear from this Minireview that great strides have been made in transferring supramolecules with controllable recognition properties from the solution to the solid state. For example, considerable success in using electrochemistry to tune the effectiveness of hydrogen-bonding interactions between weak and stronger states has been achieved. However, the future development of surfaces with nanotechnological applications will undoubtedly require the development of host–guest systems with true "on/off" binding properties. Systems with binary complexation capabilities of this type will afford controllable surfaces with near-defect-free binding capabilities, thus maximizing their potential future role as novel molecular-electronics components. Pseudorotaxane systems with electrochemically or photochemically reversible threading/dethreading cycles have achieved this aim to some extent, and could provide a means to produce responsive surfaces with properties and functions that can be controlled through binding to an appropriate complementary modifier in solution. However, the reversibility and longevity of the pseudorotaxane architecture may be an issue for their future transformation into useable devices. On the other hand, photochemically and electrochemically driven molecular motion within immobilized, covalently interlocked catenane and rotaxane systems, with their more stable and reversible architectures, will likely prove to be the best candidates for developing commercially viable components for the emerging molecular electronics and nanotechnology industries.

Received: February 11, 2003 [M1636]

[1] A. Ulman, *An Introduction to Ultrathin Films: From Langmuir–Blodgett to Self-Assembly*, Academic Press, San Diego, **1991**.

[2] M. C. Petty, *Langmuir–Blodgett Films: An Introduction*, Cambridge University Press, Cambridge, **1996**.

[3] For examples of reviews focusing on sensor and device applications of monolayers see: a) L. H. Dubois, R. G. Nuzzo, *Annu. Rev. Phys. Chem.* **1992**, *43*, 437–463; b) A. R. Bishop, R. G. Nuzzo, *Curr. Opin. Colloid Interface Sci.* **1996**, *1*, 127–136; c) C. J. Zong, M. D. Porter, *Anal. Chem.* **1995**, *67*, 709A–715A; d) S. Flink, F. C. J. M. van Veggel, D. N. Reinhoudt, *Adv. Mater.* **2000**, *12*, 1315–1328; e) R. M. Crooks, A. J. Ricco, *Acc. Chem. Res.* **1998**, *31*, 219–227; f) A. E. Kaifer, *Isr. J. Chem.* **1996**, *36*, 389–397; g) A. N. Shipway, I. Willner, *Chem. Commun.* **2001**, 2035–2045.

[4] For examples of reviews that focus upon biological applications of monolayers see: a) T. Wink, S. J. van Zuilen, A. Bult, W. P. van Bennekom, *Analyst* **1997**, *122*, 43R–50R; b) C. M. Niemeyer, *Angew. Chem.* **2001**, *113*, 4254–4287; *Angew. Chem. Int. Ed.* **2001**, *40*, 4128–4158; c) M. Mrksich, *Curr. Opin. Chem. Biol.* **2002**, *6*, 794–797.

[5] For examples of the application of electrochemistry to detect host–guest complexation at surfaces see: a) J. Liu, W. Ong, E. Román, M. J. Lynn, A. E. Kaifer, *Langmuir* **2000**, *16*, 3000–3002; b) L. Zhang, L. Godínez, T. Lu, G. W. Gokel, A. E. Kaifer, *Angew. Chem.* **1995**, *107*, 236–237; *Angew. Chem. Int.*

 © 2003 Wiley-VCH Verlag GmbH & Co. KGaA, Weinheim

Ed. Engl. **1995**, *34*, 235 – 237; c) M. T. Rojas, R. Königer, J. F. Stoddart, A. E. Kaifer, *J. Am. Chem. Soc.* **1995**, *117*, 336 – 343.

[6] For an example of a review which focuses upon voltammetric sensors organized at the solid/liquid interface see: L. M. Goldenberg, M. R. Bryce, M. C. Petty, *J. Mater. Chem.* **1999**, *9*, 1957 – 1974.

[7] For reviews see: a) A. E. Kaifer, M. Gómez-Kaifer, *Supramolecular Electrochemistry*, Wiley-VCH, Weinheim, **1999**; b) P. L. Boulas, M. Gomez-Kaifer, L. Echegoyen, *Angew. Chem.* **1998**, *110*, 226 – 258; *Angew. Chem. Int. Ed.* **1998**, *37*, 216 – 247; c) V. M. Rotello, A. Niemz, *Acc. Chem. Res.* **1999**, *32*, 44 – 52; d) A. E. Kaifer, *Acc. Chem. Res.* **1999**, *32*, 62 – 71; e) J. H. R. Tucker, S. R. Collinson, *Chem. Soc. Rev.* **2002**, *31*, 147 – 156.

[8] E. Breinlinger, A. Niemz, V. M. Rotello, *J. Am. Chem. Soc.* **1995**, *117*, 5379 – 5380.

[9] A. K. Boal, V. M. Rotello, *J. Am. Chem. Soc.* **1999**, *121*, 4914 – 4915.

[10] a) A. K. Boal, V. M. Rotello, *J. Am. Chem. Soc.* **2000**, *122*, 734 – 735; b) A. K. Boal, V. M. Rotello, *J. Am. Chem. Soc.* **2002**, *124*, 5019 – 5024.

[11] Y. Ge, D. K. Smith, *Anal. Chem.* **2000**, *72*, 1860 – 1865.

[12] a) Y. Ge, R. R. Lilienthal, D. K. Smith, *J. Am. Chem. Soc.* **1996**, *118*, 3976 – 3977; b) Y. Ge, L. Miller, T. Ouimet, D. K. Smith, *J. Org. Chem.* **2000**, *65*, 8831 – 8838.

[13] a) A. Labande, D. Astruc, *Chem. Commun.* **2000**, 1007 – 1008; b) M.-C. Daniel, J. Ruiz, S. Nlate, J. Palumbo, J.-C. Blais, D. Astruc, *Chem. Commun.* **2001**, 2000 – 2001.

[14] A. M. Allgeier, C. A. Mirkin, *Angew. Chem.* **1998**, *110*, 936 – 952; *Angew. Chem. Int. Ed.* **1998**, *37*, 894 – 908.

[15] H. M. Goldston, A. N. Scribner, S. A. Trammell, L. M. Tender, *Chem. Commun.* **2002**, 416 – 417.

[16] For recent reviews and books focusing upon molecular electronics and devices see: a) V. Balzani, M. Venturi, A. Credi, *Molecular Devices and Machines—A Journey into the Nanoworld*, Wiley-VCH, Weinheim, **2003**; b) R. L. Carroll, C. B. Gorman, *Angew. Chem.* **2002**, *114*, 4556 – 4579; *Angew. Chem. Int. Ed.* **2002**, *41*, 4378 – 4400.

[17] A. R. Pease, J. O. Jeppesen, J. F. Stoddart, Y. Luo, C. P. Collier, J. R. Heath, *Acc. Chem. Res.* **2001**, *34*, 433 – 444.

[18] a) M. Asakawa, P. R. Ashton, V. Balzani, A. Credi, C. Hamers, G. Mattersteig, M. Montalti, A. N. Shipway, N. Spencer, J. F. Stoddart, M. S. Tolley, M. Venturi, A. J. P. White, D. J. Williams, *Angew. Chem.* **1998**, *110*, 357 – 361; *Angew. Chem. Int. Ed.* **1998**, *37*, 333 – 337; b) V. Balzani, A. Credi, G. Mattersteig, O. A. Matthews, F. M. Raymo, J. F. Stoddart, M. Venturi, A. J. P. White, D. J. Williams, *J. Org. Chem.* **2000**, *65*, 1924 – 1936.

[19] a) M. Asakawa, M. Higuchi, G. Mattersteig, T. Nakamura, A. R. Pease, F. M. Raymo, T. Shimizu, J. F. Stoddart, *Adv. Mater.* **2000**, *12*, 1099 – 1102; b) C. P. Collier, G. Mattersteig, E. W. Wong, Y. Luo, K. Beverly, J. Sampaio, F. M. Raymo, J. F. Stoddart, J. R. Heath, *Science* **2000**, *289*, 1172 – 1175; c) C. P. Collier, J. O. Jeppersen, Y. Luo, J. Perkins, E. W. Wong, J. R. Heath, J. F. Stoddart, *J. Am. Chem. Soc.* **2001**, *123*, 12632 – 12641.

[20] Y. Luo, C. P. Collier, J. O. Jeppesen, K. A. Nielsen, E. Delonno, G. Ho, J. Perkins, H.-R. Tseng, T. Yamamoto, J. F. Stoddart, J. R. Heath, *ChemPhysChem* **2002**, *3*, 519 – 524.

[21] a) A. N. Shipway, I. Willner, *Acc. Chem. Res.* **2001**, *34*, 421 – 432; b) I. Willner, E. Katz, *Angew. Chem.* **2000**, *112*, 1230 – 1269; *Angew. Chem. Int. Ed.* **2000**, *39*, 1180 – 1218.

[22] A. Doron, E. Katz, G. Tao, I. Willner, *Langmuir* **1997**, *13*, 1783 – 1790.

[23] M. Lion-Dagan, E. Katz, I. Willner, *J. Chem. Soc. Chem. Commun.* **1994**, 2471 – 2472.

[24] S. Chia, J. Cao, J. F. Stoddart, J. I. Zink, *Angew. Chem.* **2001**, *113*, 2513 – 2517; *Angew. Chem. Int. Ed.* **2001**, *40*, 2447 – 2451.

[25] M. Lahav, K. T. Ranjit, E. Katz, I. Willner, *Chem. Commun.* **1997**, 259 – 260.

[26] M. Lahav, E. Katz, A. Doron, F. Patolsky, I. Willner, *J. Am. Chem. Soc.* **1999**, *121*, 862 – 863.

[27] M. J. Cook, A.-M. Nygård, Z. Wang, D. A. Russell, *Chem. Commun.* **2002**, 1056 – 1057.

[28] I. Willner, V. Pardo-Yissar, E. Katz, K. T. Ranjit, *J. Electroanal. Chem.* **2001**, *497*, 172 – 177.

 © 2003 Wiley-VCH Verlag GmbH & Co. KGaA, Weinheim

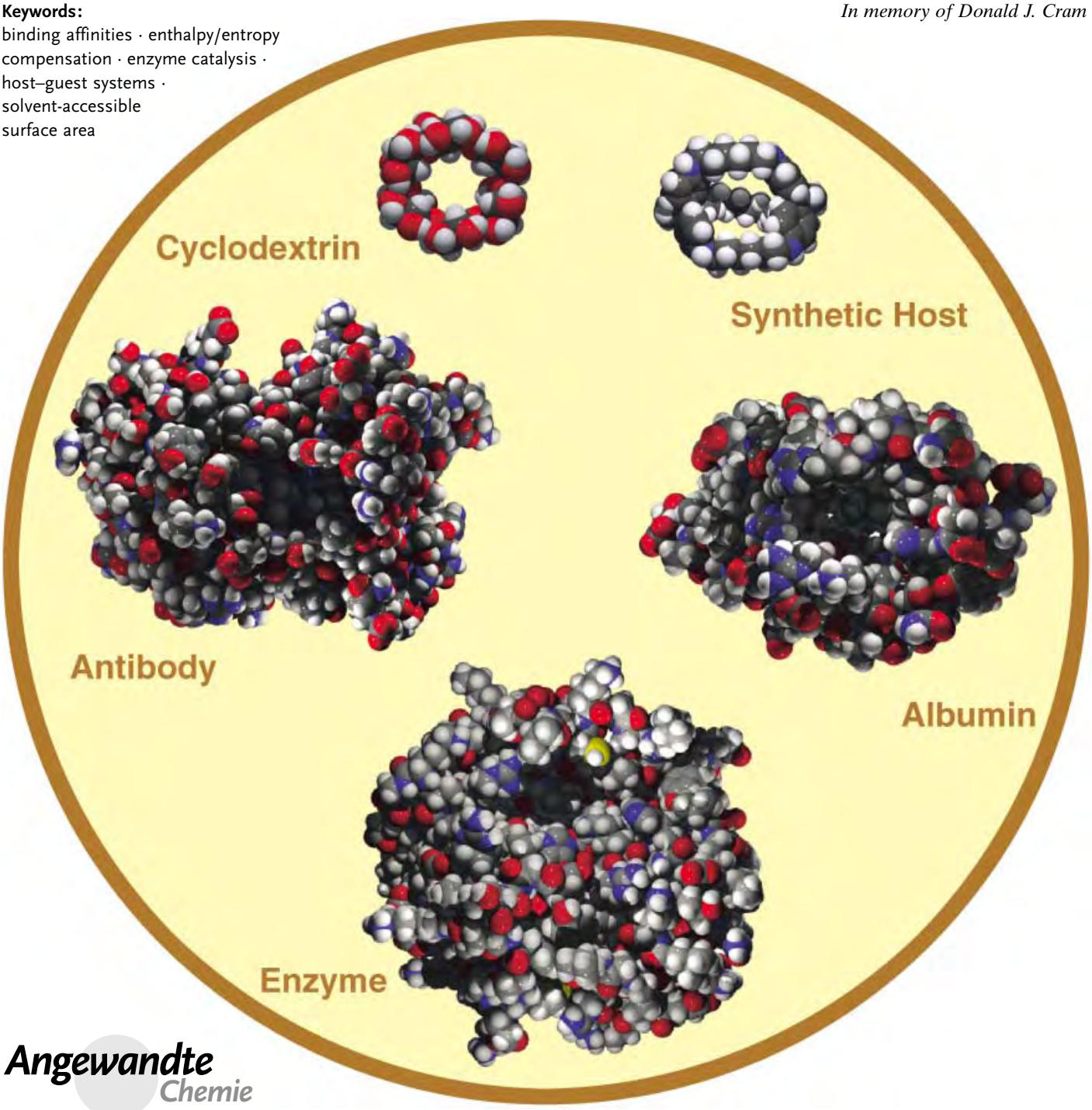
Thermodynamic Organic Complexes

Binding Affinities of Host–Guest, Protein–Ligand, and Protein–Transition-State Complexes

K. N. Houk, Andrew G. Leach, Susanna P. Kim, and Xiyun Zhang*

Keywords:
binding affinities · enthalpy/entropy compensation · enzyme catalysis · host–guest systems · solvent-accessible surface area

In memory of Donald J. Cram



© 2003 Wiley-VCH Verlag GmbH & Co. KGaA, Weinheim
DOI: 10.1002/anie.200200565

The affinities of hosts—ranging from small synthetic cavitands to large proteins—for organic molecules are well documented. The average association constants for the binding of organic molecules by cyclodextrins, synthetic hosts, and albumins in water, as well as of catalytic antibodies or enzymes for substrates are $10^{3.5\pm2.5}\,M^{-1}$. Binding affinities are elevated to $10^{8\pm2}\,M^{-1}$ for the complexation of transition states and biological antigens by antibodies or inhibitors by enzymes, and to $10^{16\pm4}\,M^{-1}$ for transition states with enzymes. The origins of the distributions of association constants observed for the broad range of host–guest systems are explored in this Review, and typical approaches to compute and analyze host–guest binding in solution are discussed. In many classes of complexes a rough correlation is found between the binding affinity and the surface area that is buried upon complexation. Enzymes transcend this effect and achieve transition-state binding much greater than is expected from the surface areas.

From the Contents

1. Introduction 4873
2. Trends in the Magnitudes of Binding Constants 4874
3. The Origins and Limits of Binding Affinities 4885
4. Relationship between Average Binding Constants and the Average Surface Areas Buried upon Binding 4890
5. Why Are Transition States Bound so Tightly Relative to Substrates by Enzymes? 4893
6. Summary and Outlook 4894

1. Introduction

Molecular recognition is a term used to describe noncovalent interactions between molecules. The field encompasses host–guest chemistry, as defined by Cram, and supramolecular chemistry, as defined by Lehn, and incorporates both theory and experiment.[1] Whether it is sequestration, sensing, crystallization, catalysis, solubility, self-assembly, distribution ratios in immiscible solvents, or drug–receptor interactions, the nature and strength of interactions between molecules creates many of the phenomena of contemporary interest in chemistry, biology, and materials science.

Much of the research in molecular recognition aims to control selectivities or to maximize host–guest binding energies. Both discrimination among hosts and high binding constants are sought for sequestering and sensor applications, as well as to control the architectures of supramolecular constructs.[1] Antibodies are nature's versatile binders, and the immune system can select a binding array suitable to meet most antigenic challenges.[2] Antibodies have also been developed as catalysts, although strong and selective binding of transition states by antibodies is still an elusive goal, which has been accomplished in only a few cases.[3] By contrast, nature's evolved catalysts, the enzymes, are remarkably selective and potent binders of transition states.[4] Although chemists have attempted to design and synthesize catalysts based on transition-state binding, none of these are competitive with enzymes or even with the best of the antibody catalysts.[5] Contemporary medicinal chemistry employs a broad arsenal of techniques, from rational structure-based design to combinatorial chemistry and high-throughput screening, to discover selective enzyme inhibitors as well as receptor agonists and antagonists.[6] Much progress has already been made in the understanding and quantifying of host–guest binding,[1,7,8] but much remains to be learned.

To move closer to a quantitative understanding of molecular recognition, we have compared and contrasted the binding energies of host–guest complexes of all types, including protein hosts (albumins, antibodies, enzymes). We have identified patterns in the binding constants of organic molecules with synthetic hosts, antibodies, and enzymes. We have established limits on the strength of binding constants that have been, or are likely to be, achieved in each host system, and established what may be considered normal binding energies for that host type.

The hosts and guests are usually neutral organic molecules, although carboxylates or protonated amines are sometimes present, especially in the protein hosts and receptors. We have intentionally excluded complexes involving metal ions, although the data for enzymes do include some metalloenzymes. The binding constants are usually measured in water, although the stability of complexes in organic solvents is also discussed.

This Review surveys the average binding energies and range of complex stabilities for many types of hosts. The classes reviewed are cyclodextrin and synthetic non-cyclodextrin hosts in water and in organic solvents, albumins and other binding proteins with organic molecules, antibodies with biomolecules and nonbiological organic molecules, and enzymes with substrates. The binding of transition states and

[*] Prof. Dr. K. N. Houk, Dr. A. G. Leach, S. P. Kim, X. Zhang
Department of Chemistry and Biochemistry
University of California, Los Angeles
Los Angeles, CA 90095-1569 (USA)
Fax: (+1) 310-206-1843
E-mail: houk@chem.ucla.edu

 DOI: 10.1002/anie.200200565 © 2003 Wiley-VCH Verlag GmbH & Co. KGaA, Weinheim

transition-state analogues by catalytic antibodies and enzymes is also documented.

The review first summarizes and presents graphical and statistical representations of the binding energies for each class of the host–guest complexes. The binding constants for the organic hosts and some proteins have been experimentally determined; those for catalytic antibodies and enzymes are mainly derived by Michaelis–Menten kinetics, which give approximate dissociation constants K_M. To facilitate ready comparison, the binding energies of all host–guest complexes mentioned in this Review are discussed in terms of association constants, with the units M^{-1}. Specifically, the constants K_d, K_M, K_I (inhibition constant), and K_{tx} (Wolfenden's transition-state dissociation constant) are all stated in their reciprocal forms, while K_a values are unchanged. Each graph presented in this Review depicts the number of host–guest complexes from each host class that fall within a particular range of K_a. The average K_a value and the standard deviation from that average are then determined from the data used to construct the graphs. Plots of ΔH versus ΔS were constructed for certain host classes where data was available. These graphs show whether a correlation between enthalpy and entropy exists and whether that correlation has extra-thermodynamic significance.

In the latter part of the Review we describe the origins of the observed trends in the magnitude of binding. Enthalpy/entropy compensation, hydrophobic effects, and the contribution that these effects make to the binding phenomenon are discussed. A direct comparison of the host–guest surface area buried upon binding to complex stability is made, and a simple method for the rough prediction of binding affinities for various host–guest systems based on buried surface area is described.

2. Trends in the Magnitudes of Binding Constants

2.1. Binding Constants of Organic Hosts

2.1.1. Cyclodextrins

Cyclodextrins are water-soluble hosts that contain a hydrophobic cavity which are able to accommodate a variety of small organic molecules.[9] α-Cyclodextrin is composed of six glucose residues, while β-cyclodextrin has seven and γ-cyclodextrin has eight. This means that each type of cyclodextrin provides a cavity with slightly different geometric properties and a preference for particular-sized molecules (Figure 1).

Figure 2 shows the CPK model of the crystal structure of the α-cyclodextrin–(*p*-hydroxybenzoic acid) complex.[10a] This is a typical cyclodextrin complex formed in aqueous solution. The hydrophobic cavity encircles the aromatic ring, and the polar substituent projects into the water. This complex has an association constant K_a of $10^3\,M^{-1}$,[10b] which is often referred to as a millimolar dissociation constant ($K_d = 10^{-3}$ M). The corresponding free energy of binding in water (ΔG_a) is -4.1 kcal mol^{-1}.

In fact, many neutral guests that are small enough to fit into cyclodextrins exhibit similar binding energies. Figure 3 shows a plot of the frequency of occurrence of complexes with specific values of K_a for α-, β-, and γ-cyclodextrins.[11,12] This and subsequent frequency plots show the number of equilibrium constants lying within each 0.25 range of pK_a unit for the entire range for which data are available. Connors previously reported and discussed individual plots of this nature for α-, β-, and γ-cyclodextrins.[8] The guests are typically substituted benzenes, adamantanes, and other small organic molecules with hydrophobic and polar parts.



K. N. Houk is Professor of theoretical and physical organic chemistry at the University of California, Los Angeles. He has published extensively on cycloadditions, stereoselectivity, and molecular recognition and uses the tools of computational chemistry to solve problems in organic and biological chemistry. He is a Fellow of the American Academy of Arts and Sciences and will receive the 2003 American Chemical Society Computers in Chemistry and Pharmaceutical Research Award.



Andrew Leach is from Chester, UK. He studied Natural Sciences at Cambridge and remained at Cambridge to pursue a PhD entitled "New Techniques for Combinatorial Chemistry" with Prof. S. V. Ley. He was a post-doctoral fellow at UCLA with Prof. K. N. Houk in the area of computational organic chemistry. He was the recipient of a Fulbright–AstraZeneca post-doctoral fellowship and of the Amgen award for post-doctoral research in chemistry from UCLA. Since October 2003 he has worked for AstraZeneca. He is a keen brass bandsman and played with the Golden State British Brass Band.



Susanna P. Kim was an undergraduate majoring in Microbiology at the University of California, Los Angeles, where she did research in the research group of K. N. Houk. She is currently a graduate student in Pharmacy at the University of Illinois, Chicago.



Xiyun Zhang grew up in Chongqing, China and received her B.S. from Beijing Normal University in 1997. After spending three more years at Beijing Normal University she received her M.S. in organic synthesis, working in the research group of Prof. Qinghua Chen. She is currently working towards her Ph.D. in the research group of Prof. Houk. Her research focuses on theoretical studies of enzyme- and antibody-catalyzed organic reactions using a combination of quantum-mechanical calculations and molecular-dynamics simulations.

 © 2003 Wiley-VCH Verlag GmbH & Co. KGaA, Weinheim

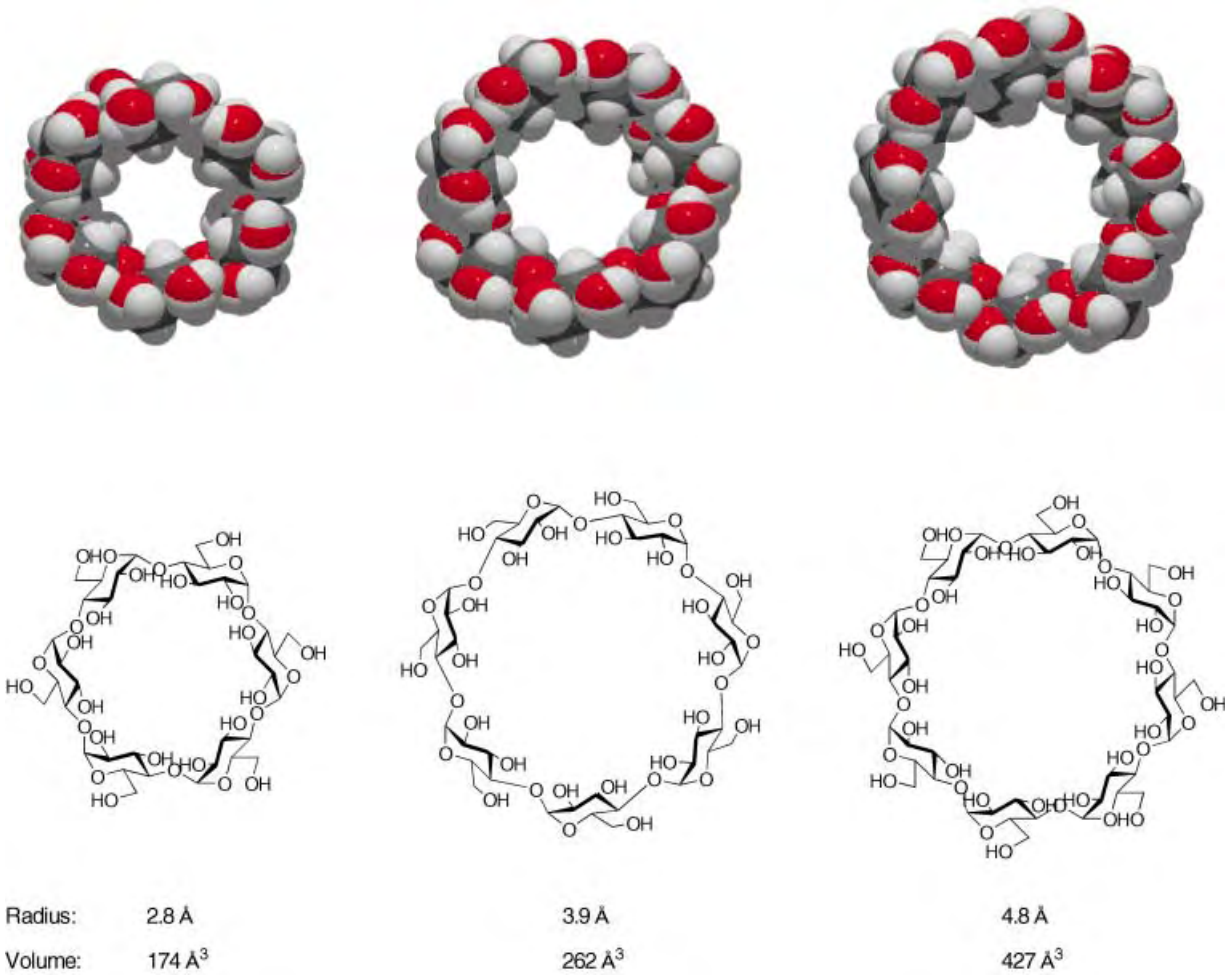


Figure 1. The structures of α- (left), β- (middle), and γ-cyclodextrins (right). The dimensions are measured between points on the van der Waals surfaces of the molecules.

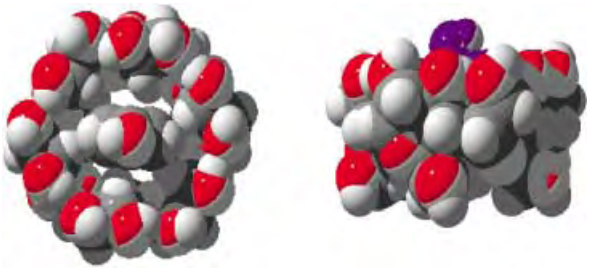


Figure 2. Top (left) and side views (right) of the complex formed between α-cyclodextrin and *p*-hydroxybenzoic acid.

The average free energy of binding for all 1257 examples plotted here is -3.5 ± 1.4 kcal mol^{-1}, and the corresponding K_a value is $10^{2.5\pm1.1}$ M^{-1}. The ranges given here for the ΔG and K_a values are standard deviations. Another way to state the range is that 68% (encompassing one standard deviation) of the complexes fall in the $10^{2.5\pm1.1}$ M^{-1} ($10^{1.4}$–$10^{3.6}$ M^{-1}) range and 95% of the complexes lie in a range of two standard deviations, that is, $10^{2.5\pm2.2}$ M^{-1}, or a range of about $K_a = 1$–10^5 M^{-1}. While this range might be considered to be narrow, it does allow for a considerable selectivity of 10^5 in the dynamic range of binding affinities.

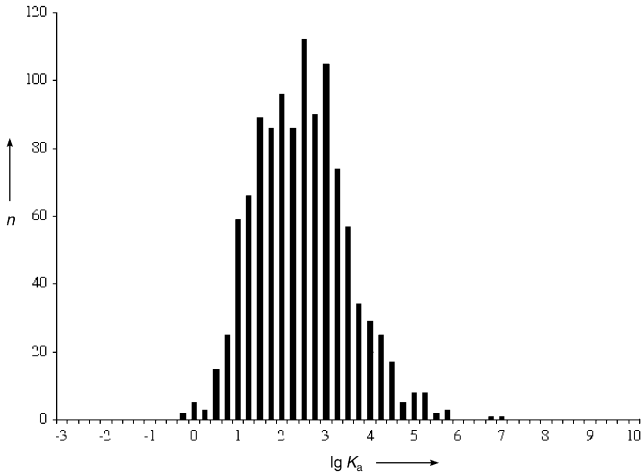


Figure 3. Distribution of α-, β-, and γ-cyclodextrin complexes within a particular range of lg K_a values ($K_a = 10^{2.5\pm1.1}$ M^{-1}, n = number of complexes).[11,12]

In spite of this relatively narrow range of free energies of -3.5 ± 1.4 kcal mol^{-1}, the enthalpies of complexation (ΔH) vary over a very wide range, from -20 to 5 kcal mol^{-1}.

© 2003 Wiley-VCH Verlag GmbH & Co. KGaA, Weinheim

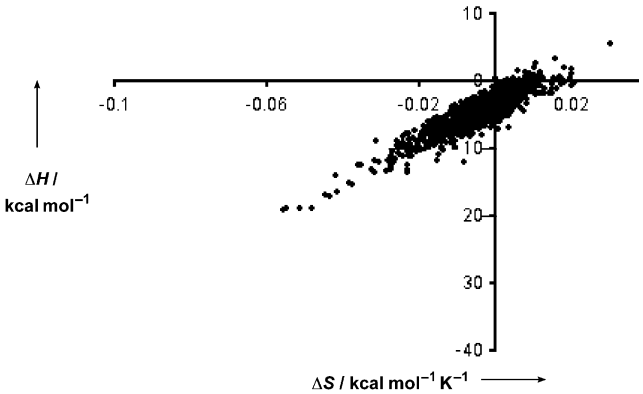


Figure 4. Plot of ΔH versus ΔS for α-, β-, and γ-cyclodextrin complexes;[11] the linear regression gives $\Delta H = 281.8(\pm 4.1)\,\Delta S - 3.3(\pm 0.0)$.

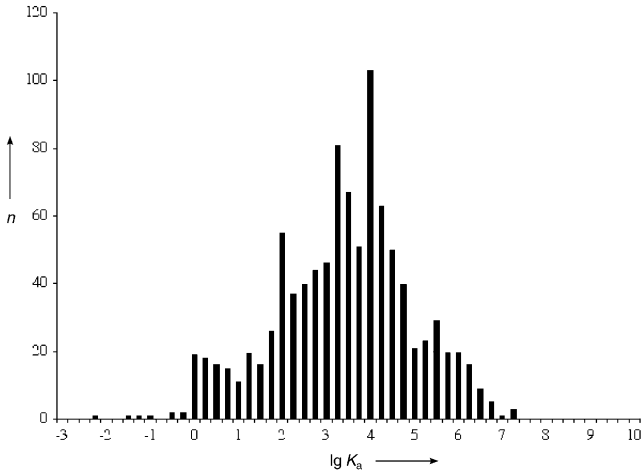


Figure 5. Plot of the number of complexes with non-cyclodextrin organic hosts within a particular range of $\lg K_a$ values in aqueous solution ($K_a = 10^{3.4\pm1.6}\,\text{M}^{-1}$).[13–27]

Figure 4 shows a plot of the ΔH values versus the ΔS values measured experimentally for 1121 of the complexes plotted in Figure 3.[11] There is a strong enthalpy/entropy compensation, such that the free energy of complexation remains around -3.5 kcal mol^{-1}. These types of plots were made earlier by Connors for individual classes of cyclodextrins.[8] Such a plot may reflect an intimate relationship between the tightness of binding and the values of ΔH and ΔS. Alternatively, the fundamental principle may be that all ΔG values for complexation are approximately -3.5 kcal mol^{-1}, and since $\Delta G = \Delta H - T\Delta S$, then ΔH must be approximately $(T\Delta S - 3.5)$ kcal mol^{-1}. If the temperature dependence of K_a is not measurable with high precision over a large temperature range, then experimental error, rather than any fundamental principle, may be responsible for the apparent correlation between ΔH and ΔS. This topic will be discussed in more detail in Section 3.2.

2.1.2. *Synthetic Hosts*

Data have also been collected from the literature for many other neutral host–guest complexes formed in water.[13–27] Figure 5 shows a frequency plot of $\lg K_a$ values for all the 973 complexes, whose aqueous association constants were reported in references [13–27]. Complexes involving metal-containing hosts and/or charged guests have been excluded. The guests are, for the most part, small and uncharged organic molecules ranging from benzene derivatives to steroids.

The hosts include many of the most familiar organic receptors, some of which required special substituents to make them water-soluble: resorcinols,[13] resorcinarenes,[14] cyclophanes,[15] azacyclophanes,[16] ammonium cyclophanes,[17] crown ethers and their nitrogen analogues (macrocyclic polyamines),[18] calixarenes,[19] the cyclophanes of Dougherty and co-workers,[20] a macrocyclic derivative of Tröger's base,[21] flavinophanes,[22] metal-free porphyrins,[23] cyclotetrachromotropylene,[24] the aromatic hosts of Lehn and coworkers,[25] hexapus,[26] and cucurbituril[27] (Figure 6). The K_a values are mostly within the range of 1 to $10^7\,\text{M}^{-1}$ (see Figure 5). Statistically, the K_a values are $10^{3.4\pm1.6}\,\text{M}^{-1}$, which corresponds to a ΔG value of -4.6 ± 2.1 kcal mol^{-1}. The average binding energy for these synthetic hosts in water is only about 1 kcal mol^{-1} stronger than that of cyclodextrins, and the range is somewhat broader for this diverse set of hosts.

There are some apparent exceptions to these generalizations. For example, Whitesides and co-workers reported a very strong binding of a synthetic host–guest complex of $K_a = 10^{17}\,\text{M}^{-1}$.[28] However, the host consists of three vancomycin units tethered to an aromatic nucleus and the guest has three peptide units which bond to vancomycin. The binding energy *per unit* was essentially the same as that of a single vancomycin–peptide complex.[28] Each individual host–guest interaction in this and other polyvalent systems fits the above generalization.

The entropy/enthalpy compensation for the 58 systems for which thermodynamic data have been reported is similar to that found for cyclodextrins (Figure 7). The scatter in these data is considerably larger than that found for cyclodextrins, and this may be a function of the diversity of the hosts. Nevertheless, the narrow range of binding constants is remarkable considering the structural variety of the hosts.

2.1.3. *Organic Host–Guest Complexes in Non-Aqueous Solvents*

Figure 8 shows the frequency of occurrence of binding constants for complexes formed between organic hosts and small neutral organic guests.[29] The binding constants for the 1710 complexes examined are $K_a = 10^{2.2\pm1.6}\,\text{M}^{-1}$, which correspond to a binding free energy of -3.1 ± 2.2 kcal mol^{-1}. The range is similar to that in aqueous solution, but the binding constants are on average about 10-times less. Examples of these hosts, and the solvent for which binding energies were measured, are given in Figure 9. These are similar to the water-soluble hosts mentioned in Section 2.1.2. The average difference between the binding free energies in water and organic solvents of 1.5 kcal mol^{-1} is evidence for the importance of hydrophobic effects in the complexes. Entropy/enthalpy compensation is observed also for the 276 cases in which such data have been reported (Figure 10).[29]

 © 2003 Wiley-VCH Verlag GmbH & Co. KGaA, Weinheim

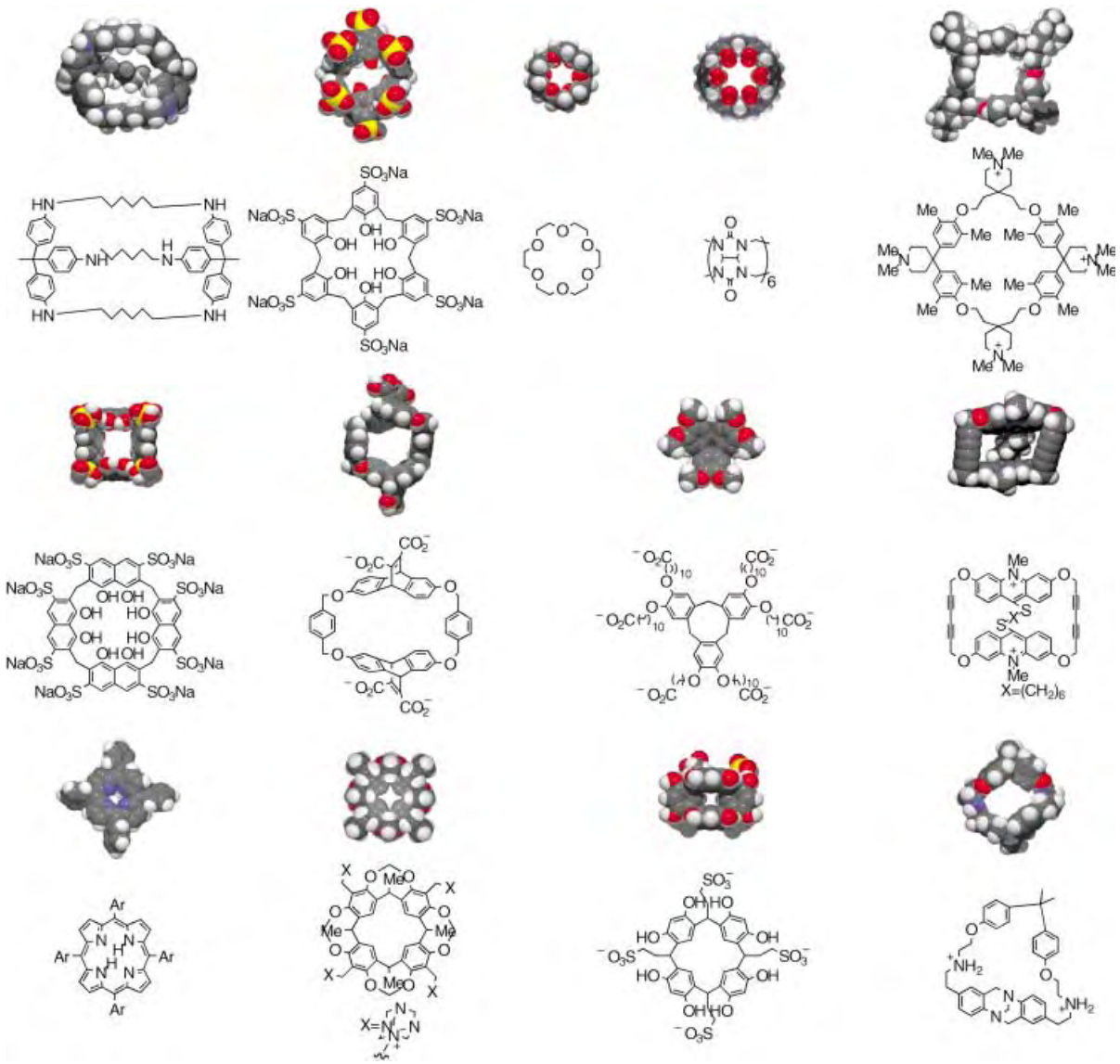


Figure 6. Examples of non-cyclodextrin water-soluble hosts for organic molecules.[13–27]

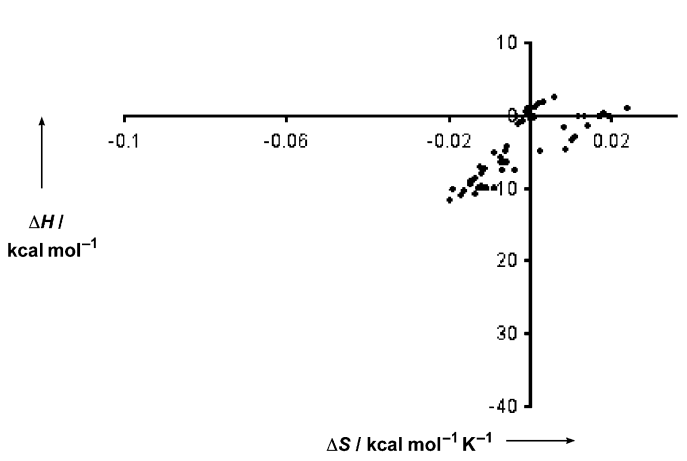


Figure 7. Plot of ΔH versus ΔS for non-cyclodextrin organic host–guest complexes in aqueous solution;[13–27] linear regression gives $\Delta H = 310.7(\pm 33.2)\,\Delta S - 3.3(\pm 0.4)$.

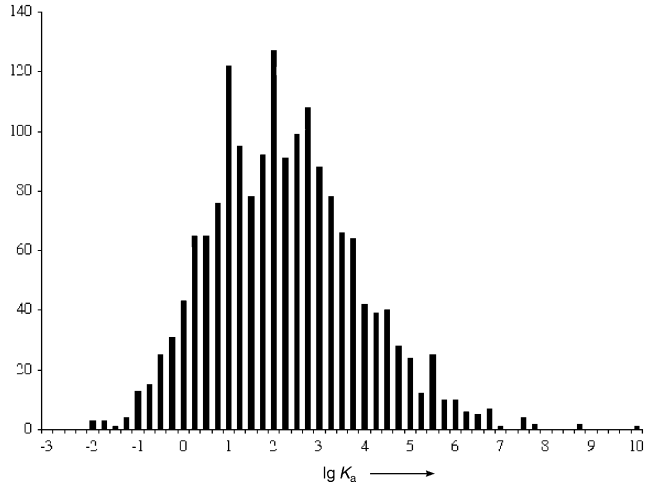


Figure 8. Plot of the number of organic host complexes with a particular range of lg K_a values in non-aqueous solvents ($K_a = 10^{2.2\pm1.6}\,\text{M}^{-1}$).[29]

© 2003 Wiley-VCH Verlag GmbH & Co. KGaA, Weinheim

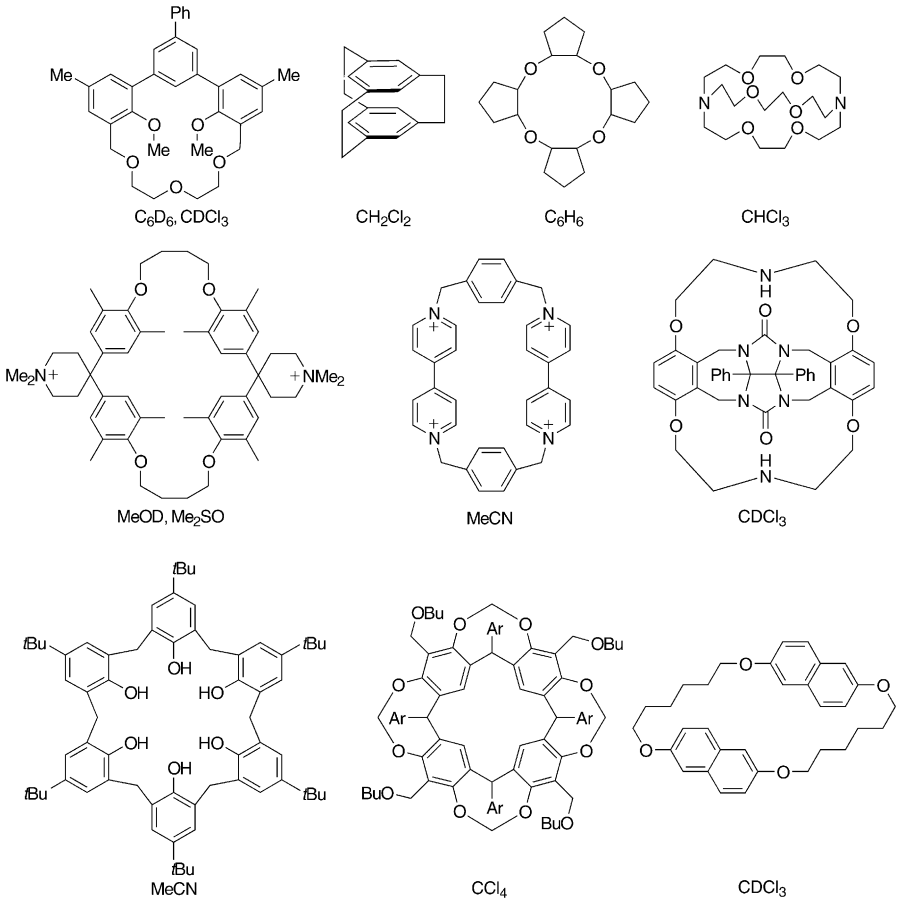


Figure 9. Examples of hosts for organic molecules in non-aqueous solution. The solvents in which the equilibrium constants were measured are listed.[29]

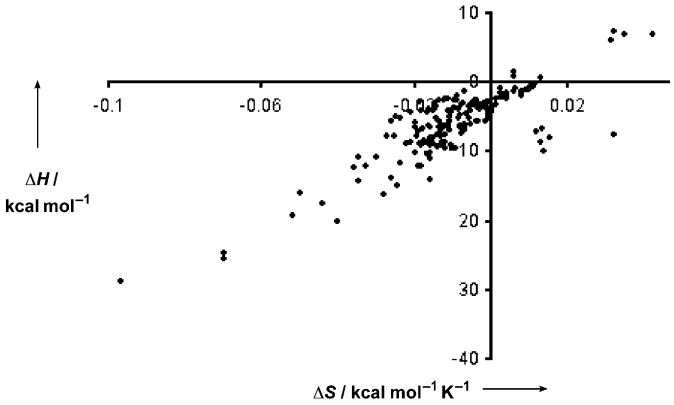


Figure 10. Plot of ΔH versus ΔS for organic host–guest complexes in non-aqueous solution;[29] regression analysis gives $\Delta H = 229.9(\pm 11.0)\,\Delta S - 3.2(\pm 0.2)$.

2.2. Binding Constants of Proteins

2.2.1. Antibody–Antigen Complexes

Antibodies are produced by the mammalian immune system to bind and mark foreign substances and fragments of bacteria and viruses for removal and destruction. The six hypervariable loops of such antibody binding pockets contain about 100 amino acid residues. The affinities (K_d^{-1}) of mature antibodies for natural antigens (predominantly immunogenic organic molecules, protein, carbohydrate, and nucleic acid fragments) fall in a wide range of 10^4–$10^{14}\,M^{-1}$; in the most favorable cases these ΔG values reach as high as -19 kcal mol^{-1}.[30]

Frequency plots similar to those for the systems described previously have been compiled based on a limited set of available data.[31] These antibody binding data were divided into two types: the binding constants for antibody complexes with organic molecules are shown in Figure 11, while those for antibody–protein and antibody–oligosaccharide complexes are shown in Figure 13. The repertoire of antibody types includes whole immunoglobulins (specifically, immunoglobulin G, IgG), Fab regions, and single-chain F_V regions. There has been no attempt to exclude all potentially charged haptens from these graphs.

K_a values of $10^{7.3\pm1.9}\,M^{-1}$ are typical for complexes of organic molecules with antibodies. This represents a binding free energy of -10 ± 3 kcal mol^{-1}, which is about double that of cyclodextrins and synthetic hosts described in Section 2.1.1.

Figure 12 shows a typical antibody binding pocket, both with and without a bound hapten.[32] The dimensions of the

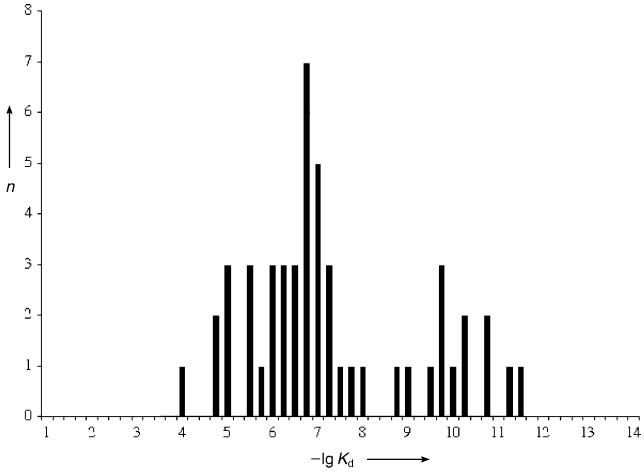


Figure 11. Plot of the number of antibody–antigen complexes found to fall within a particular range of $-\lg K_d$ ($=\lg K_a$) values ($K_a = 10^{7.3\pm1.9}\,M^{-1}$).[31] The antigens here are relatively small organic molecules, and data for proteins and carbohydrates are excluded.

 © 2003 Wiley-VCH Verlag GmbH & Co. KGaA, Weinheim

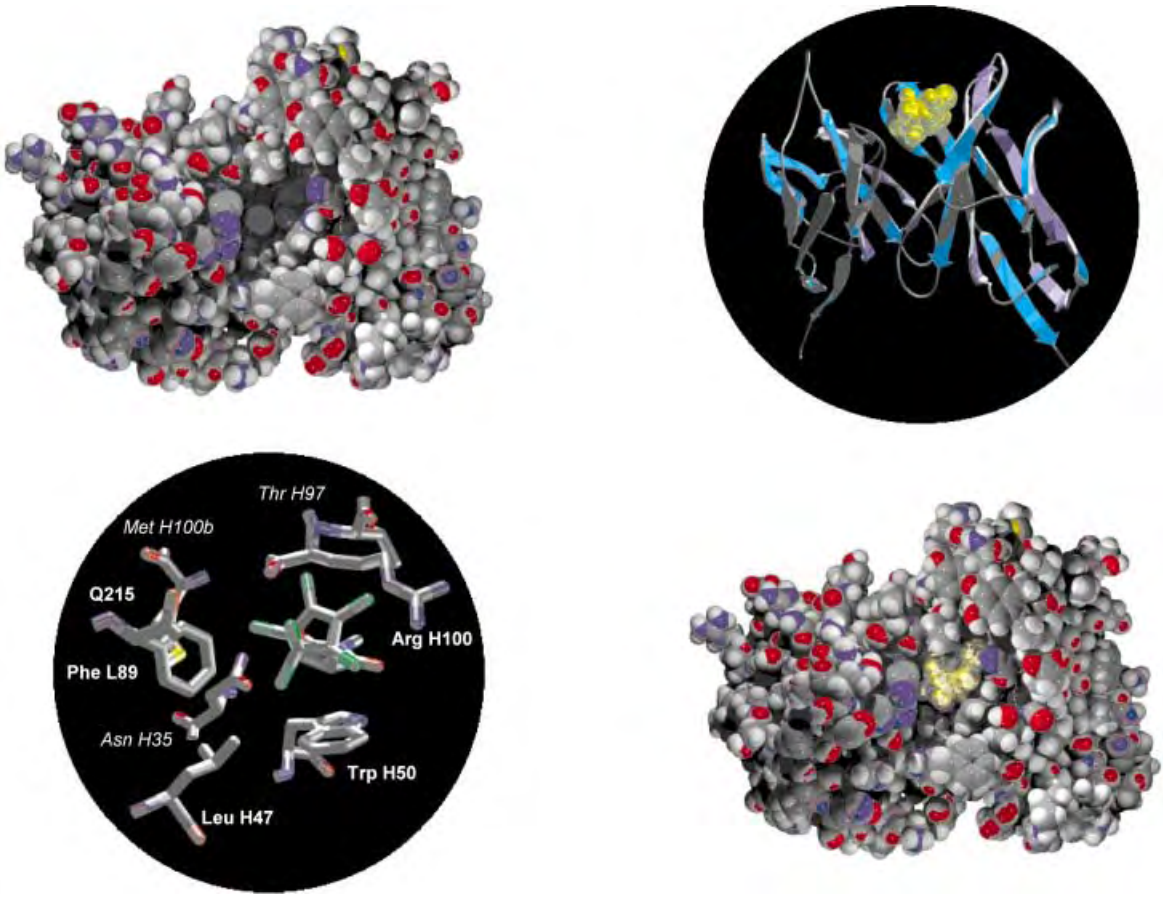


Figure 12. Different renderings of catalytic antibody 1E9. Top left: space-filling model of the hollow binding site; top right: a ribbon rendering of the antibody with a space-filling model of the bound hapten; bottom left: the binding site with the bound organic hapten; and bottom right: space-filling model of the binding site with a yellow space-filling model of the bound hapten.[32]

Fab region of an antibody exceed those of the synthetic hosts described earlier, but otherwise the cavities of the hosts are similar: they both consist mainly of hydrophobic residues.

Stronger binding ($K_a = 10^{8.9\pm1.7}\,M^{-1}$) is found for antibody–protein and antibody–oligosaccharide complexes (Figure 13).

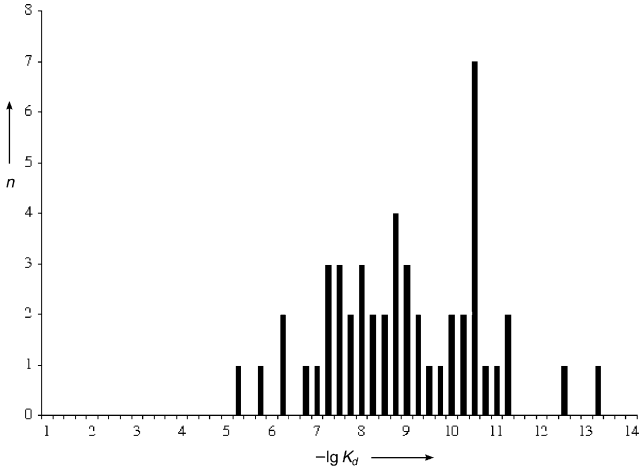


Figure 13. Plot of the number of antibody–antigen complexes of proteins and carbohydrates found to fall within a particular range of $-\lg K_d$ ($=\log K_a$) values ($K_a = 10^{8.9\pm1.7}\,M^{-1}$).[31]

These types of fragments are the typical natural ligands for antibodies in vivo. The binding sites of antibodies for proteins and carbohydrates are larger and flatter than for small organic molecules.[2,33] Binding constants K_a can be dissected into rates of binding (k_1) and rates of release (k_{-1}), such that $K_a = k_1 k_{-1}^{-1}$. It has been found that k_1 is typically $10^6\,M^{-1}s^{-1}$ for antibodies;[2] thus, binding is about 100-times slower than diffusion in water, but still very rapid when it is considered that the binding pocket must be desolvated and reorganized at least to some extent for binding. Typically, k_{-1} is $10^{-1}\,s^{-1}$,[34a] thus the range of common binding constants for this set of antibody–antigen complexes is 10^7–$10^{12}\,M^{-1}$.

Entropy/enthalpy compensation operates in the binding of antibodies for the very limited set of 30 cases for which these data are available (Figure 14). For those complexes for which the temperature dependence of binding has been determined, the ΔH of binding varies from -28 to -8 kcal mol^{-1}, but entropy/enthalpy compensation limits the association energies. The temperature range at which the binding constants have been measured is small, so a considerable lack of precision is expected in these data, a factor that may contribute to apparent entropy/enthalpy compensation (see Section 3.2).

Catalytic antibodies, such as 1E9 (Figure 12), are produced by the immune response to small stable molecules

 © 2003 Wiley-VCH Verlag GmbH & Co. KGaA, Weinheim

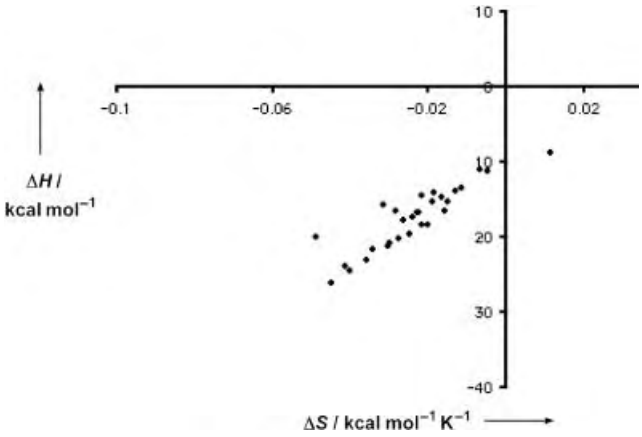


Figure 14. Plot of ΔH versus ΔS for antibody–antigen complexes; linear regression gives $\Delta H = 296.9(\pm 28.2)\,\Delta S - 10.5(\pm 0.8)$.[31]

(haptens) that are analogues of transition states of organic reactions. Haptens are attached to proteins such as keyhole limpet hemocyanin or bovine serum albumin and then used to induce antibody production. Some of these antibodies may show selective binding for transition states and function as catalysts. Catalytic antibodies have been prepared to effect diverse types of organic reactions.[3] Kinetic studies of these species involve the measurement of Michaelis–Menten kinetic parameters. The Michaelis constant K_M is an upper limit to the dissociation constant of the substrate. If follows that $K_M = (k_{-1} + k_{cat.})\,k_1^{-1}$, while $K_d = k_{-1}\,k_1^{-1}$. If the rate constant for the reaction of the protein–substrate complex ($k_{cat.}$) is small compared to that for dissociation k_{-1}, then K_M is a good approximation for K_d; otherwise the actual K_d value will be smaller than the observed K_M value. The values of K_M^{-1} for catalytic antibodies (Figure 15) are $10^{3.5\pm1.0}\,M^{-1}$, based upon 175 data points obtained from the review by Blackburn et al.[3a] This is the same magnitude of binding demonstrated earlier for simpler cyclodextrin and synthetic host–guest systems in water.

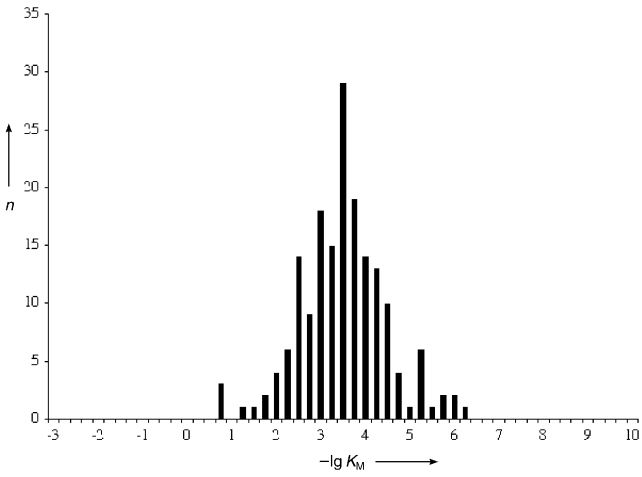


Figure 15. Plot of the number of complexes formed between catalytic antibodies and substrates having a value of $-\lg K_M$ falling within a particular range ($K_a = 10^{3.5\pm1.0}\,M^{-1}$).[3a]

Wolfenden described the "catalytic proficiency" by the quantity K_{tx}^{-1}, where $K_{tx}^{-1} = k_{cat.}\,K_m^{-1}\,k_{uncat.}^{-1}$. The proficiency has the units M^{-1} and reflects the hypothetical binding affinity that an antibody or enzyme develops for the transition state.[34b] K_{tx} is interpreted as the dissociation constant for the complex formed between the transition state and the enzyme. Since transition states have a lifetime of only 10^{-13} s, no equilibrium between a transition state in water and a transition state with the enzyme is possible, yet, the hypothetical equilibrium can be determined from a thermodynamic cycle, which is in turn derived from the kinetics of the catalyzed and uncatalyzed reactions.

Figure 16 shows the binding constants (K_{tx}^{-1}) of transition states of antibody-catalyzed reactions, also derived from the data in the review by Blackburn et al.[3a] The average

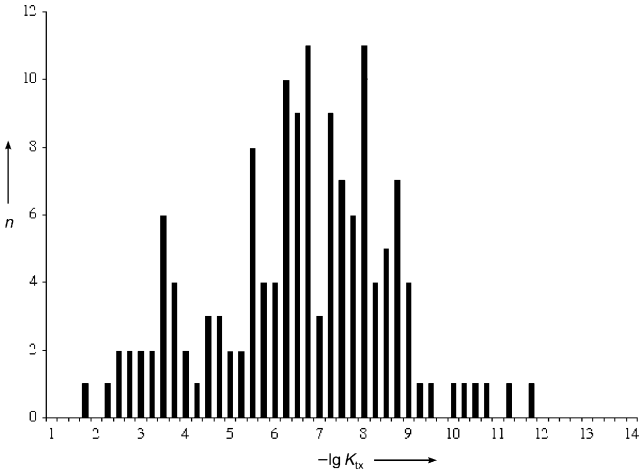


Figure 16. Plot of the binding constants of complexes formed between catalytic antibodies and transition states having a $-\lg K_{tx}$ ($\lg K_a$) value within a given range ($K_a = 10^{6.6\pm2.0}\,M^{-1}$).[3a]

K_{tx}^{-1} value is $10^{6.6\pm2.0}\,M^{-1}$, and the corresponding binding energy is -9.0 ± 2.7 kcal mol^{-1}. Thus, the transition states for typical antibody-catalyzed reactions are bound about 10^3 times more strongly than the substrates; this is the average value of the reaction acceleration by catalytic antibodies obtained from comparing their averages. When individual antibodies are compared, the average acceleration is still about 10^3. The binding of transition states is slightly weaker than that found for antibodies and small immunogenic organic haptens ($10^{7.3}\,M^{-1}$).

2.2.2. *Albumin–Ligand and Other Protein–Ligand Complexes*

Albumins are proteins that bind and transport small molecules in the bloodstream.[35] Such transport proteins must both bind and release readily to facilitate transport, and these do not have especially large binding constants relative to the artificial organic host–guest systems discussed in Section 2.1.2. A survey of the experimentally measured binding constants for albumins is given in Figure 17. The values of the binding constants are typically $10^{4.6\pm0.9}\,M^{-1}$, although only 59 data points are available.

 © 2003 Wiley-VCH Verlag GmbH & Co. KGaA, Weinheim

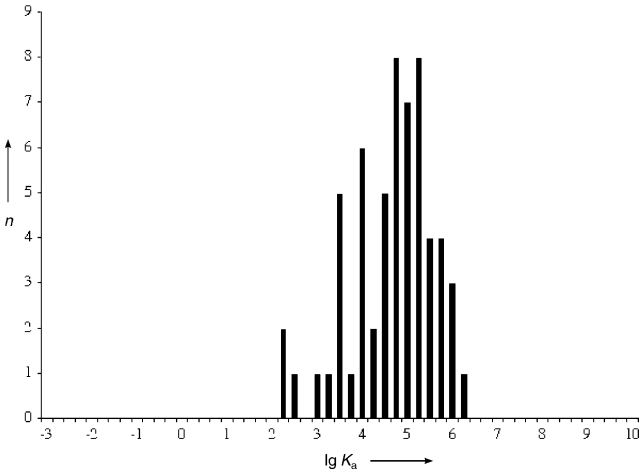


Figure 17. Plot of the number of albumin–guest complexes within a particular range of lg K_a values ($K_a = 10^{4.6\pm0.9}\ \text{M}^{-1}$).[35]

Binding by albumins has been shown to be relatively unspecific, and a typical albumin binding site is shown in Figure 18.[36] In fact, albumins generally have a number of different binding sites on the same protein structure. One of the six identified binding pockets in the binding of the fatty acid myristic acid by human serum albumin is highlighted in Figure 18. The global structure of this protein, including all of these binding sites, is also shown.

Protein–ligand binding is the subject of a developing field of science; only a few famous or very strong protein–ligand interactions are discussed here, to contrast with other data in this Review. The strongest and best known complexes of protein and relatively simple organic molecules involve biotin binding by avidin and streptavidin (Figure 19).[37] The association constant for the complex of streptavidin with biotin is $2.5 \times 10^{13}\ \text{M}^{-1}$, and the free energy of binding is $-18\ \text{kcal mol}^{-1}$. The ΔG value for the complex of avidin with biotin is even larger, $-21\ \text{kcal mol}^{-1}$.[38] This binding is accompanied by an important flap motion of the protein, which facilitates binding of the biotin ligand.

The pregnane xenobiotic receptor (PXR) is a nuclear binding receptor that has received much recent attention because it is a relatively promiscuous binder of drugs of various types.[37] PXR is involved in drug–drug interactions, and a crystal structure was recently obtained.[38b] This protein has a large cavity and variable flaps, and binds a variety of guests. Typical dissociation constants of 27 nM, which corresponds to a free energy of binding of $-11\ \text{kcal mol}^{-1}$, have been measured for ligands such as hyperforin (Figure 19).[38]

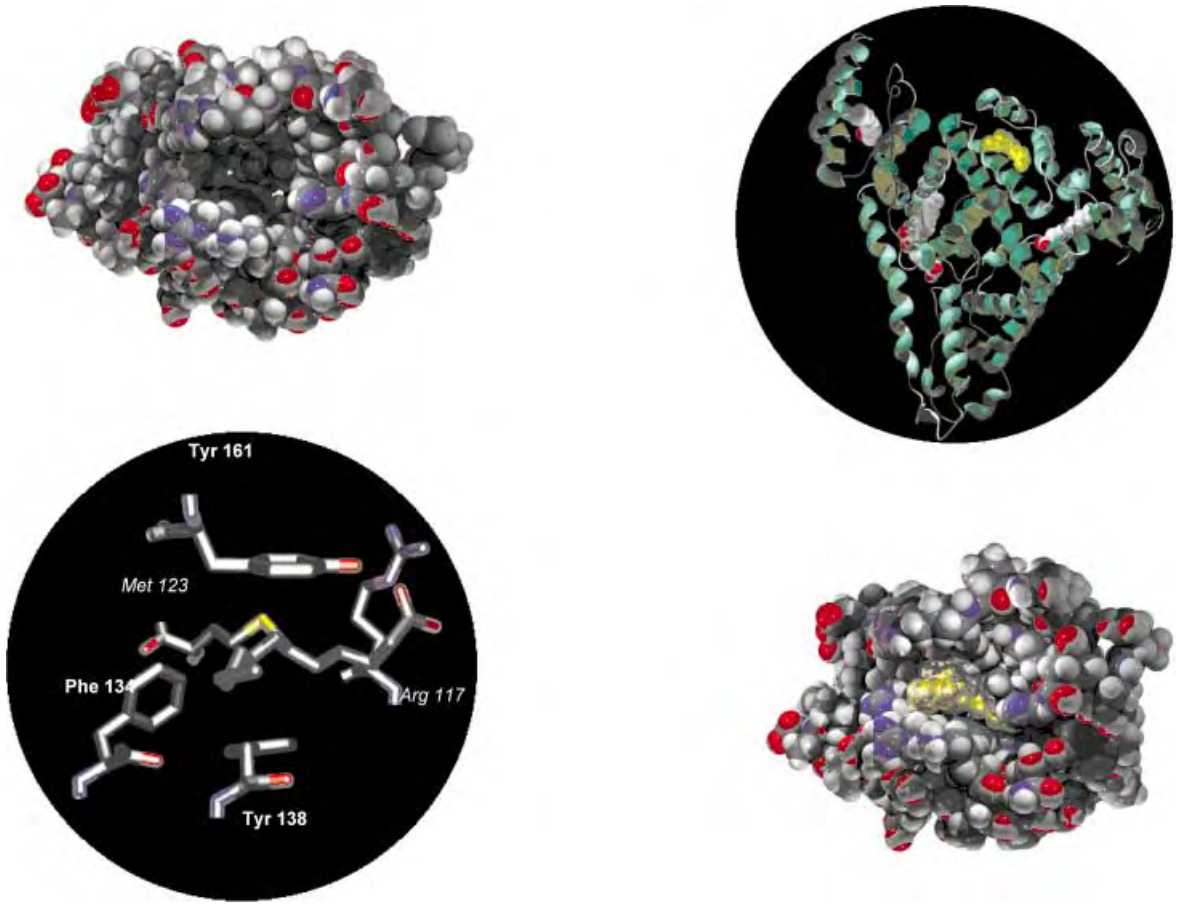


Figure 18. Different views of albumin. Top left: space-filling model of the hollow binding site; top right: a ribbon rendering of albumin with a space-filling model of the ligand, myristic acid, bound in various binding pockets; bottom left: the binding site with the bound myristic acid; and bottom right: space-filling model of the binding site with a yellow space-filling model of the bound myristic acid.[36]

 © 2003 Wiley-VCH Verlag GmbH & Co. KGaA, Weinheim

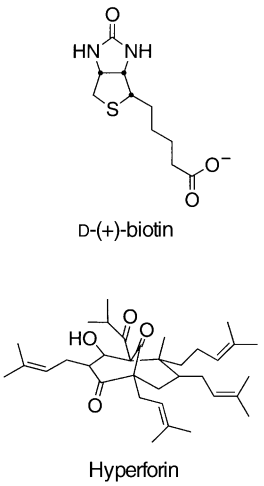


Figure 19. Chemical formulas of biotin and hyperforin.

2.2.3. *Enzyme–Substrate Complexes*

Dissociation constants for the enzyme–substrate complexes, $K_S = [\text{enzyme}][\text{substrate}][\text{enzyme-substrate}]^{-1}$, have not been obtained experimentally in many cases, but Michaelis–Menten kinetics have been reported for most enzymes. As with the earlier discussion of catalytic antibody data, the K_M values of enzymes are used here to approximate dissociation constants of substrates.

A survey of about 22 000 enzyme K_M values is available.[39] Figure 20 shows the frequency of given values of K_M^{-1}, which is a measure of enzyme–substrate association. The distribution that is by now familiar for organic host–guest binding is found even for these enzyme–substrate complexes. No attempt has been made to exclude charged substrates from this list, and metal ions are sometimes present in these binding sites.

Enzymes do not show any outstanding binding properties for their substrates compared to other hosts. The average value of K_M^{-1} is $10^{3.7\pm1.3}\,\text{M}^{-1}$, and $K_M^{-1} = 10^1$–$10^6\,\text{M}^{-1}$ ($K_M =$ 100 mM–1 μM) for 95% of all the values surveyed. The free energies of binding of substrates by enzymes are therefore -5.1 ± 1.7 kcal mol^{-1}. This quantity is a powerful reminder that the ability of enzymes to catalyze reactions arises from transition-state binding, not substrate binding (see Section 2.2.4).

It has been proposed that enzymes have evolved to have K_M values in the mM–μM range, to match the low concentrations of substrates [S] present under physiological conditions. As long as K_M is larger than [S], the rate of the catalyzed reaction is determined by the free energy of the enzyme–transition-state complex relative to the separated enzyme and substrate in solution.[4b]

2.2.4. *Transition-State and Transition-State-Analogue Binding by Enzymes and Receptor–Drug Binding*

The association constants of the systems described so far are for the most part in the range of 10^1–$10^6\,\text{M}^{-1}$, with an average value of $10^{3.5}\,\text{M}^{-1}$. The antibody–antigen complexes are exceptions, especially for proteins and carbohydrates, and frequently exhibit larger binding constants in the range of 10^6–$10^{12}\,\text{M}^{-1}$.

Transition states must be bound better than substrates or stable molecules for catalysis to be effective.[4c] As described earlier, the K_{tx}^{-1} value for catalytic antibodies is $10^{6.6\pm2.0}\,\text{M}^{-1}$ (see Figure 16, Section 2.2.1),[3] while K_M^{-1} is $10^{3.5\pm1.0}\,\text{M}^{-1}$ (Figure 15). By using these average values of K_M^{-1} and K_{tx}^{-1}, the average acceleration of an antibody-catalyzed process is 10^3.

Although the $k_{cat.}$ values for thousands of enzymes are available from the BRENDA database,[39] many fewer values of $k_{uncat.}$ have been measured. Wolfenden and co-workers have compiled and measured many of these, and they provide most of the data that allow calculation of the K_{tx}^{-1} values plotted in Figure 21.[40] The average value of K_{tx}^{-1} for enzymes of $10^{16.0\pm4.0}\,\text{M}^{-1}$ corresponds to an average free energy of binding of 22 kcal mol^{-1}, but can range up to 32 kcal mol^{-1}.[34b,40] The value of $k_{cat.}\,k_{uncat.}^{-1}$ can be estimated

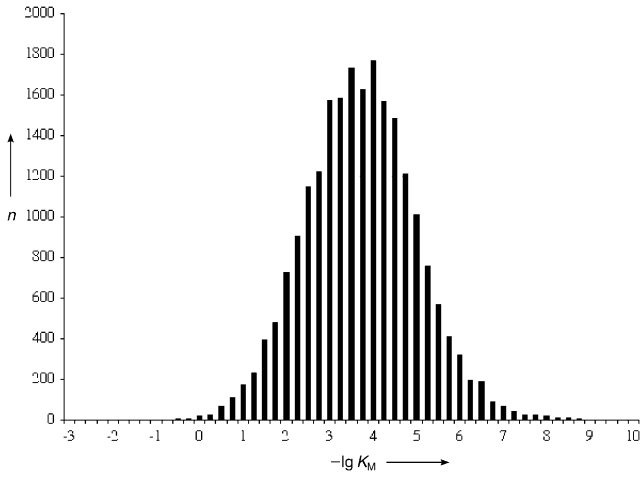


Figure 20. Plot of the number of enzyme–substrate complexes within a particular range of $-\lg K_M$ values ($K_a = 10^{3.7\pm1.3}\,\text{M}^{-1}$).[39]

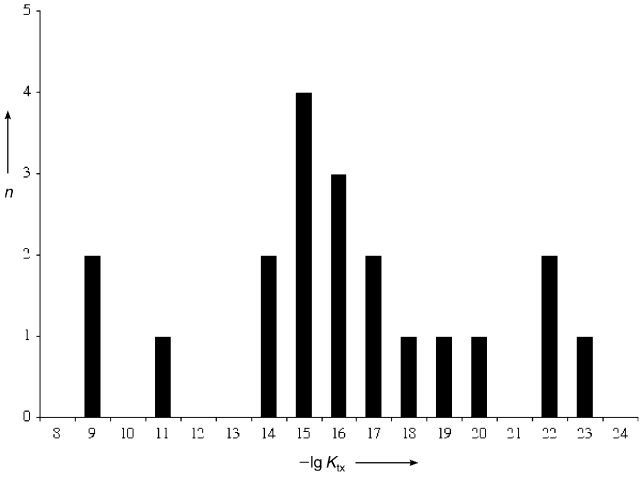


Figure 21. Plot of the number of complexes formed between enzymes and transition states with values of $-\lg K_{tx}$ falling within a particular range ($K_a = 10^{16.0\pm4.0}\,\text{M}^{-1}$).[40]

as $K_M K_{tx}^{-1}$. From our previous discussion, the average value of K_M is $10^{-3.7}$ M. Therefore, the average value of $k_{cat.} k_{uncat.}^{-1}$ of 10^{12} reflects that the binding free energies of transition states are 13 kcal mol^{-1} higher than those of substrates by enzymes. The possible origins of this difference are discussed in Section 5.

Transition-state mimics serve as enzyme inhibitors and can also show exceptionally high binding affinities. Figure 22 is a frequency curve for the occurrence of different values of

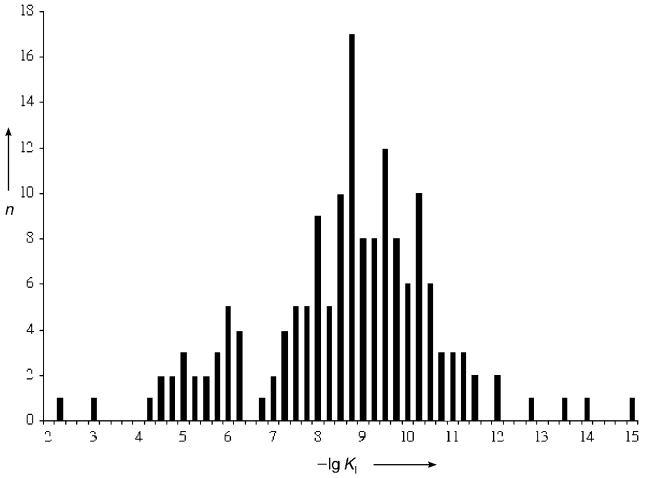


Figure 22. Plot of the number of enzyme–inhibitor combinations having a value of $-\lg K_I$ falling within a particular range ($K_a = 10^{8.6\pm2.1}$ M^{-1}).[41a] These data are for the tightest-binding inhibitors known for a wide range of proteins.

the dissociation constant K_I for an enzyme–inhibitor complex determined kinetically. These data are expressed as reciprocal values K_I^{-1} to reflect the association of inhibitors with enzymes. The values were measured for especially good inhibitors.[41a] Many inhibitors that bind with lower affinities are not included on this graph, so that a truly statistical analysis would include many more substances with low binding affinities. However, this graph reflects the binding by stable neutral substances that successfully mimic transition states and bind to the active sites. The association constant for this set of good inhibitors is typically $10^{8.6\pm2.1}$M^{-1}, with a range of 10^5–10^{13} M^{-1} accounting for 91% of the complexes. Kollman, Kuntz, and co-workers noted that the "maximal affinity of ligands" (drugs and inhibitors) to receptors and enzymes corresponds to a ΔG binding energy of about -15 kcal mol^{-1} ($K_I^{-1} = 10^{11}$M^{-1}). They found that approximately 1.5 kcal mol^{-1} of binding free energy is available per heavy (non-H) atom in the ligand for molecules with 10 or fewer heavy atoms, but the ΔG value per heavy atom drops off with larger molecules and reaches a maximum of 15 kcal mol^{-1} with only a few well-known exceptions, such as the biotin–streptavidin complex discussed earlier.[41a] The average maximal-affinity inhibitor binds to enzymes 10^6 times more weakly than the average transition state.

Gilli et al. collected the thermodynamic data on the binding of 136 drugs by 13 receptors (ten membrane receptors, two enzymes, and a DNA molecule).[41b] The data from Gilli et al. has been compiled and the frequency plot of 176 receptor–drug complexes is shown in Figure 23. The average association constant, $K_I^{-1} = 10^{7.3\pm1.5}$ M^{-1}, is somewhat lower than the values obtained from the preceeding Kuntz et al. data. Gilli et al. chose the data set based upon the availability of thermodynamic data obtained from van't Hoff plots.

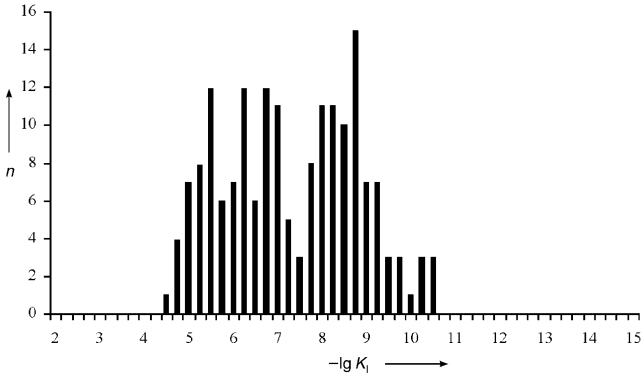


Figure 23. Plot of the number of receptor–drug complexes with values of $-\lg K_I$ falling within a particular range ($K_a = 10^{7.3\pm1.5}$ M^{-1}).[41b]

The plot of ΔH versus ΔS for these complexes is shown in Figure 24. The average binding energy for these drugs is -9.5 kcal mol^{-1}, which corresponds to a $-\lg K_d$ value of 7, while binding affinities range from $-\lg K_d = 4$ ($\Delta G = -5.4$ kcal mol^{-1}) to $-\lg K_d = 11$ ($\Delta G = -15.0$ kcal mol^{-1}). Gilli et al. proposed that the maximum achievable K_d^{-1} value is 10^{-11}M^{-1}, because of enthalpy/entropy compensation.[41b]

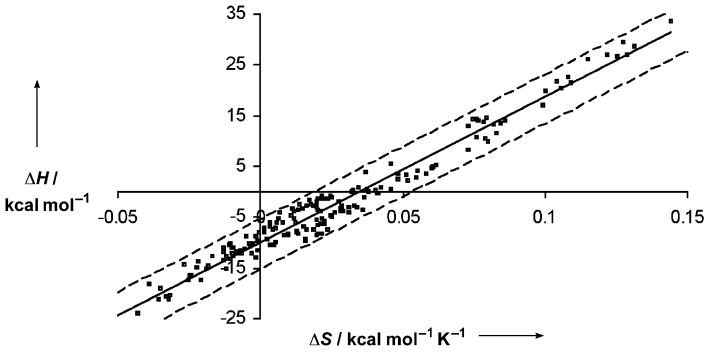


Figure 24. Plot of the standard enthalpies ΔH versus standard entropies ΔS from Gilli et al.[41b] The data come from van't Hoff plots of binding equilibria for 176 receptor–drug complexes. The two dashed lines indicate the loci of the points for which the macromolecule–ligand dissociation constants K_d are 10 pM and 100 μM; the continuous line is a linear regression ($\Delta H = 285.6(\pm3.9)\,\Delta S - 9.9(\pm0.2)$ and has a correlation of 0.981.[41b] Reprinted with permission from *J. Phys. Chem.* **1994**, *98*, 1515–1518. Copyright 1994, American Chemical Society.

2.3. Summary of Host–Guest Binding

2.3.1. Trends in the Magnitude of Binding Constants

Table 1 summarizes all the data presented in the distribution diagrams (Figures 3, 5, 8, 11, 13, 15–17, 20–23). Figure 25 presents this in graphic form, excluding only the non-aqueous

 © 2003 Wiley-VCH Verlag GmbH & Co. KGaA, Weinheim

Table 1: Summary of binding constants of synthetic hosts, antibodies, proteins, and enzymes with neutral organic compounds.

Host type	Guest type	Mean lg K_a	Standard deviation[a]	$-\Delta G$ [kcal mol^{-1}]
organic host[b]	organic molecule	2.2	1.6	3.1 ± 2.2
cyclodextrin	organic molecule	2.5	1.1	3.5 ± 1.4
organic host [c]	organic molecule	3.4	1.6	4.6 ± 2.1
catalytic antibody	substrate	3.5	1.0	4.8 ± 1.3
enzyme	substrate	3.7	1.3	5.1 ± 1.7
albumin	organic molecule	4.6	0.9	6.3 ± 1.3
catalytic antibody	transition state	6.6	2.0	9.0 ± 2.7
receptor	drug	7.3	1.5	9.5 ± 2.1
antibody	antigen	8.1	2.0	11.1 ± 2.7
enzyme	inhibitor	8.6	2.1	11.7 ± 2.8
enzyme	transition state	16.0	4.0	21.9 ± 5.4

[a] In units of lg K_a; 68% of cases fall within one standard deviation of the mean value, 95% within two standard deviations for a normal distribution. [b] In non-aqueous solvent. [c] In aqueous solvent.

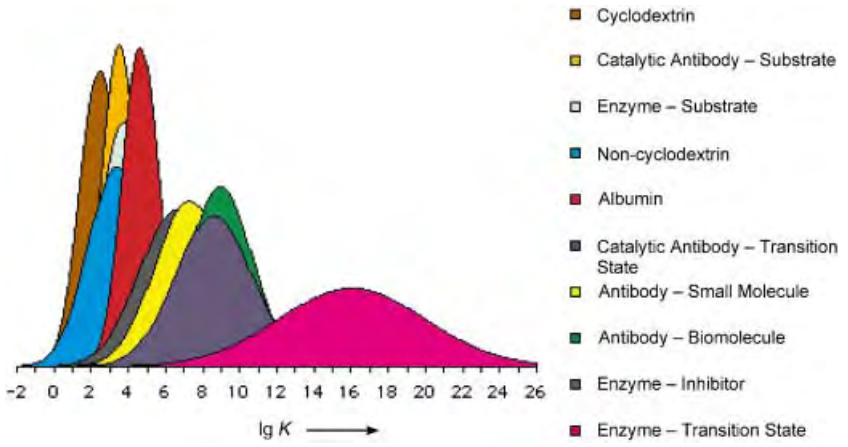


Figure 25. Summary of the average binding constants for host–guest complexes.

data (Figure 8). For each class of hosts discussed earlier, the binding distribution is represented in Figure 25 by an idealized normal distribution. Each curve is normalized to have the same area, the maximum occurs at the average value of K_a, and the standard deviation is used to set the width of the curve.

The association constants for this diverse set of hosts fall into several well-defined regions. Complexes of cyclodextrins, synthetic hosts in water, catalytic antibodies and enzymes with substrates, as well as albumin–organic guest complexes have dissociation constants between $10^{-2.4}$ and $10^{-4.6}$ M. We refer to these as the "millimolar binders". The vast majority of complexes involving such hosts and neutral organic molecules have dissociation constants in the decimolar (10^{-1} M) to micromolar (10^{-6} M) range, centered at millimolar values (10^{-3} M). The second group of complexes falls in the $10^{-6.6}$–$10^{-8.6}$ M range and includes complexes of catalytic antibodies with transition states, antibodies with small organic and biomolecules, receptor–drug complexes, and enzyme–inhibitor complexes. These relatively strong binding constants are reflected in their dissociation constants in the micromolar to nanomolar range. For purposes of classification, the antibody–hapten and transition-state binding is roughly micromolar, the antibody–biomolecule and enzyme–inhibitor binding is roughly nanomolar, and receptor–inhibitor binding is intermediate. Finally, the strongest binding—in a class distinctly separated from the others—involves enzymes and transition states. With an average association constant of $10^{16\pm4}$ M^{-1}, most enzyme–transition-state complexes have dissociation constants in the picomolar (10^{-12} M) to zeptomolar (10^{-21} M) range. These in general can be considered to be "femtomolar" (10^{-15} M). These amazingly large binding constants are the result of billions of years of evolution to produce effective catalysts to sustain life. These binding constants reflect dynamic processes such as "induced fit"[42] and strong electrostatic interactions that contribute to binding, but evolution is probably not able to achieve zeptomolar binding only from many noncovalent interactions and dynamic processes. Instead, enzymes often take advantage of charged residues, metal cofactors, acid–base chemistry, and covalent interactions between the enzyme and transition state. A good example of the advantage of covalent attachment is the recent report by Meares and co-workers of "antibodies with infinite affinity," where covalent attachment of the substrate and protein results in very high binding energies.[43]

2.3.2. *Selectivity in Host–Guest Binding*

The relatively narrow ranges of binding constants observed for different classes of hosts and proteins have been emphasized here. Nevertheless, significant selectivity is possible within these ranges of observed binding affinities. First, there are a variety of molecules that do not form complexes at all with given host molecules, and these are not included in our statistics. Hosts in general exhibit strong preferences for a relatively limited set of guests that fit into the binding cavity of the host. Among those guest molecules that fit into a host, a binding energy difference of only 1.7 kcal mol^{-1} between the binding energy of the target molecule and the next best binder would produce 95:5 selectivity for the better guest at room temperature. Most of the host classes exhibit a range of K_a values of at least 10^4 M^{-1}, so that very high selectivity is possible when comparing the strongest and weakest complexes in a particular class. Such selectivities are the source of much research attention, since selective sensors, catalysts, and inhibitors are sought for a variety of applications. Furthermore, the understanding of such subtle, yet chemically very significant, energy differences is a challenge to theory that has been taken up by many research groups. Our generalizations about binding constants provide an easy way to predict rough binding affinities of guests with many types of hosts, but these rules of thumb do not address the subtle yet profound differences that lead to selectivity.

 © 2003 Wiley-VCH Verlag GmbH & Co. KGaA, Weinheim

3. The Origins and Limits of Binding Affinities

3.1. General Considerations

There are two features of the survey of binding data that are particularly striking: average binding constants are quite modest and, generally, 95% of the binding constants fall in a range of about $10^4\,\text{M}^{-1}$. For complexes of cyclodextrins, synthetic hosts, antibodies, and enzymes with small organic molecules, a binding constant of $10^{3.5\pm2.5}\,\text{M}^{-1}$ in water can be predicted for any water-soluble organic guest molecule able to fit into the host binding cavity.

There are some experimental limitations on the binding affinities that can be measured. This issue has been discussed by Kuntz et al. in their article on maximal ligand binding affinities.[41a] The types of molecules that have been studied as guests are limited in part by practical experimental factors. Gases usually have low-molecular weights and are expected to have very low binding affinities, thus they are seldom studied. By contrast, high-molecular-weight molecules are often insoluble and cannot be studied. In general, few data have been reported for very small or very large guests, which are expected to have very small binding constants. There may also be experimental limits of detection as well as convenient ranges of measurement that are applied to the determination of equilibrium constants. Part of the narrowness of the distributions in various graphs in Section 2 may be the result of these factors. On the other hand, the regular shift of average complex stability to a higher value with the size of the host (see later) shows that the frequency plots described here reveal a more fundamental nature of host–guest complexation.

3.2. Enthalpy/Entropy Compensation

Enthalpy/entropy compensation is commonly observed for many types of host–guest complexes.[44] The enthalpy/entropy plots presented in Section 2 show correlations of varying quality, but all are consistent with increasingly negative entropies of complexation paralleling increasingly negative complexation enthalpies. This correlation may be the result of a real physical relationship, a so-called extra-thermodynamic relationship in which tighter binding leads to both more negative ΔH (favorable) and more negative ΔS values (unfavorable). Alternatively, experimental uncertainties in van't Hoff plots used to determine the ΔH and ΔS values may lead to accidental correlations with no statistical significance.

Many authors have noted that as the enthalpy of guest binding gets greater, and the enthalpy becomes more negative, the motions of the host are restricted, and the entropy becomes more negative as well.[44a] While this is reasonable, there is no thermodynamic reason that this relationship should be linear. If there is a linear (or other functional) correlation, it has extra-thermodynamic, not fundamentally thermodynamic, origins.

There have been suggestions of functional relationships between the enthalpy and entropy of binding. Dunitz discussed enthalpy/entropy compensation in terms of thermodynamic functions, whereby an association was treated in terms of an increase in the force constant for interaction;[45] that is, translation and rotation of two molecules with respect to each other can be considered as vibrations with very weak force constants. As the molecules associate with each other, these force constants become larger and larger. The corresponding entropy becomes more negative in a functional way.

Williams and Westwell proposed that there is a general relationship between the exothermicity of an association reaction ($\Delta H°$) and the entropic cost ($-298\Delta S°$) of association. This relationship, shown in Figure 26,[46b] is based on qualitative thermodynamic considerations related to the Dunitz derivation.[45] The data analyzed by Williams and Westwell belong to the same set of data included in our Figures 7 and 10. The idealized graph shown in Figure 26 is meant to convey the idea that for very weak interactions $\Delta H°$ slowly becomes more negative (for example, in van der Waals associations), but entropy changes rapidly as translational motion is eliminated. In this region $\Delta G°$ is greater than 0. For intermediate regions $\Delta H° \approx T\Delta S°$ and there is the type of linear relationship shown in many graphs. Finally, when association is very tight, as in the formation of a covalent bond, the $\Delta S°$ value changes little, while $\Delta H°$ of binding continues to increase. The utility of this relationship has been illustrated through analyzing the thermodynamic data for the interactions of macrocycles with neutral molecules, where the contribution of $\Delta H°$ and $\Delta S°$ to binding can be measured separately.[46a,b]

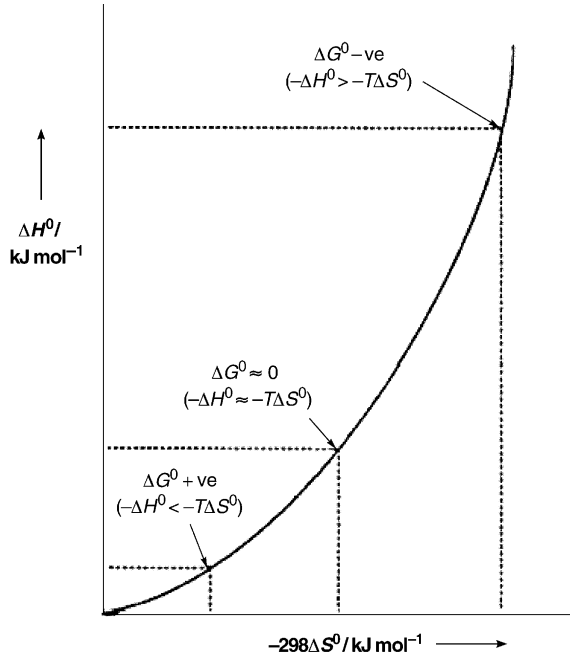


Figure 26. The general form of the extent of the exothermicity of association ($\Delta H°$) A + B → A–B as a function of the entropic cost ($\Delta S°$) at 298 K. There is a limit in the price in entropy to be paid (arising from the loss of translational and rotational freedom) and this limit is approached before covalent bond strength is approached.[46b] Reproduced with permission from The Royal Society of Chemistry.

 © 2003 Wiley-VCH Verlag GmbH & Co. KGaA, Weinheim

This relationship represents the proposal that weak noncovalent binding is associated with restriction of translation and rotation which can reduce entropy by as much as 10 e.u. or 3 kcal mol^{-1} at room temperature in terms of $T\Delta S$, while only formation of a covalent bond can produce a further reduction of 30–40 e.u. (or 9–12 kcal mol^{-1}); the latter range is characteristic of bimolecular reactions. Three translational and three rotational degrees of freedom of the host plus a guest are converted into vibrations upon association. These vibrations are very low frequency motions and the entropies are still quite large for very weak associations. For example, the formation of a van der Waals complex from an average-sized host and guest changes the entropy by about -10 e.u. Covalent binding produces very strong force constants, and the change in ΔS for average systems is about -45 e.u.[46c] The situation is complicated because the entropy of solvation may change as well. An overall positive entropy of association may occur if solvent molecules originally inside a host cavity, or solvating a guest molecule, are released upon host–guest association.

Williams et al. have also discussed enthalpy/entropy compensation in terms of positive and negative cooperativity.[7,47]

Gilli et al. studied the thermodynamics of drug–receptor binding, and have suggested that enthalpy/entropy compensation limits the K_d value to about 10 pM (Figure 24).[41b] A careful analysis of errors was made, which led the authors to conclude that the $\Delta H/\Delta S$ relationship is not really statistically significant, since the compensation temperature or slope (278($\pm$4) K in the study by Gilli et al.,[41b] and 286($\pm$4) K in our plot of their data in Figure 24) is too close to the average measurement temperature (290 K). On the other hand, they did suggest that a common mechanism of binding, especially hydrogen bonding, could account for some of the correlation; tighter hydrogen bonds lead to less freedom of motion and more unfavorable entropy.[46]

An apparent enthalpy/entropy relationship may arise from experimental errors in measurement. This is particularly true when van't Hoff plots are used to determine the ΔH and ΔS values and when the temperature range of the measurements is small. Such determinations are based upon an assumption that ΔH and ΔS are constant over the temperature range of the experiments. In addition, it is often assumed that measurements involve two states, unbound and bound only, whereas a number of intermediate states are possible. In addition, a change of protonation state may confound the determination of the ΔH and ΔS values. Exner has urged caution in the use of plots of ΔH versus $T\Delta S$, especially the attribution of physical significance to such a correlation, in part because of their systematic errors, but also as a result of random errors in measurement.[48]

Sharp recently pointed out how the significance of a plot of ΔH versus ΔS could be evaluated.[49d] A statistical test that was developed more than 25 years ago[50] shows that a ΔH versus ΔS correlation has no statistical significance (at 95% confidence level) if the average experimental temperature of the experiments T lies within the 95% confidence level ($\pm 2\sigma$) of T_C, where T_C is the slope of the ΔH versus ΔS plot. In other words, if T_C is within 20% of the average temperature of measurement, the correlation is unlikely to be significant.

Authentic examples of enthalpy/entropy compensation were also discussed by Sharp. For example, there is a correlation between the ΔH and ΔS values for alkane solvation in water.[49b] For these data, the average temperature for the measurements is 298 K, but $T_C = 163 \pm 6$ K and $\Delta G = 7 \pm 2.5$ kcal mol^{-1}. Hydrophobic solvation shows a significant correlation between ΔH and ΔS.[49c] The correlations between ΔH and ΔS values in Figures 4, 7, 10, 14, and 24 could be influenced by solvation effects of this type.

The values of $T_C \pm 2\sigma$ obtained from the ΔH versus $T\Delta S$ graphs in Figures 4 (cyclodextrins), 7 (non-cyclodextrin organic hosts), 10 (organic hosts in non-aqueous solvents), 14 (antibody–antigen complexes), and 24 (Gilli's receptor–drug data) are 282 ± 8, 311 ± 66, 230 ± 22, 297 ± 56, and 286 ± 8 K, respectively.[41b] The equilibrium constants are measured around room temperature (298 K) or lower for the Gilli data. According to the Sharp criterion, the plots for cyclodextrins in water (Figure 4) and the organic hosts in non-aqueous solvent (Figure 10) show correlations with slight extra-thermodynamic significance. Note that these plots have intercepts of -3.3, -3.3, -3.2, -10.5, and -9.9, respectively, which is approximately the average association free energy deduced from the frequency graphs, as expected.

The statistical test arises from the fact that a random set of ΔH and ΔS values, constrained only to produce a nearly constant ΔG value at some temperature, will give a linear correlation, but it will have no physical significance. This was demonstrated beautifully by Cornish-Bowden for activation parameters,[51] but the same analysis applies here. A random set of 100 points with uniform distribution of E_a and $\ln k$ values within certain ranges was created (Figure 27a).[51] The E_a and $\ln k$ values of each point were then employed to derive the $\Delta H^{\neq}$ and $\Delta S^{\neq}$ values through Arrhenius plots.

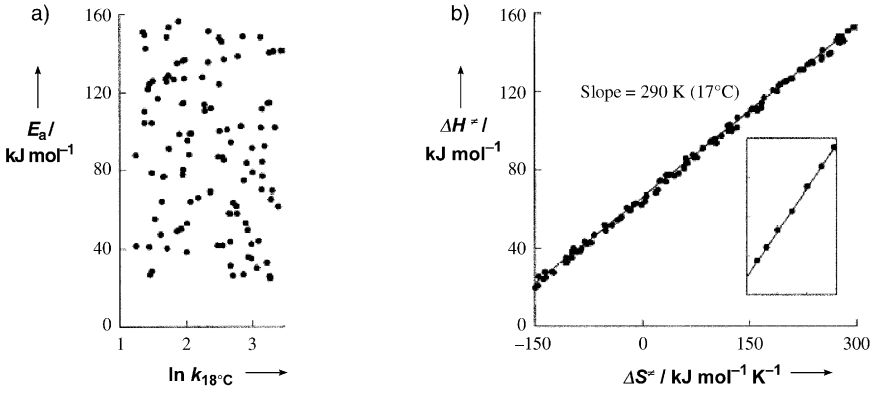


Figure 27. a) A random set of 100 points ($k_{18°C} = 2.3 \pm 1.15$; $E_a = 30$–160 kJ mol^{-1}); b) enthalpy/entropy compensation plot: the $\Delta H^{\neq}$ and $\Delta S^{\neq}$ values for each of the points are estimated based on the Arrhenius plot analysis of a corresponding point in (a).[51] Reprinted with permission from *J. Biosci.* **2002**, *27*, 121–126. Copyright 2002, Indian Academy of Science.

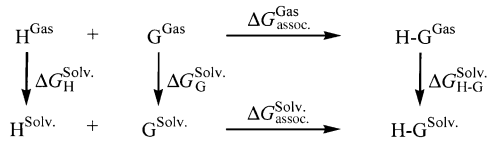
 © 2003 Wiley-VCH Verlag GmbH & Co. KGaA, Weinheim

Remarkably good enthalpy/entropy compensation was observed for the scattered 100 points (Figure 27b). The same exercise with ΔG and $\lg K_a$ values, and van't Hoff plots would show how $\Delta H/\Delta S$ correlations can occur accidentally.

This analysis suggests that the enthalpy/entropy compensation observed for a given type of host–guest complex may be a manifestation of approximately constant ΔG values, rather than the cause. That is, if ΔG is constant and since $\Delta G = \Delta H - T_C\Delta S$, then $\Delta H = T_C\Delta S +$ constant, where T_C is the average slope of the correlation. The linear relationship between ΔH and ΔS is really just a statement that ΔG is a constant in such cases.

3.3. Computational Approaches: Quantitative Models of Host–Guest Binding

The free energy of host–guest binding in solution, $\Delta G^{Solv.}_{H\text{-}G}$ can be analyzed according to the following thermodynamic cycle involving binding energies in the gas phase ΔG^{Gas} and the solvation energies $\Delta G^{Solv.}$ of host (H), guest (G), and the host–guest complex (H-G, Scheme 1). This cycle allows



Scheme 1. Cyclic process for the analysis of Host–Guest (H-G) interactions.

analysis of direct host–guest interactions, and of the role of solvation on binding. Quantum mechanical methods can be used for the quantitative evaluation of the binding of relatively small molecules in the gas phase. Modern quantum mechanical methods are able to compute interaction energies very accurately in the gas phase to precisions of a few tenths of a kcal mol^{-1}, which is well within common experimental errors.[52] However, the sizes of the systems discussed in this article preclude the use of such high accuracy methods; rarely have systems of more than 10 heavy atoms been treated by such methods.

The calculation of the binding free energies of larger flexible hosts and guests requires not just computation of the minimum energy of a complex but averaging over all accessible conformations of the host and of the host–guest complex. This statistical problem becomes even more severe for the proper computation of solvation; accurate results require averaging over a huge number of possible solvent–solute configurations. Recent calculations suggest what might be possible in the future,[53] and direct quantum dynamics techniques, such as the Car–Parrinello method, are applied more and more frequently to phenomena occurring during solvation.[54] Nevertheless, highly accurate quantum mechanical treatments of host–guest complexes in solution are currently impossible.

Although high-accuracy quantum mechanics cannot be used to compute solvation and host–guest binding, a variety of approximate methods have been developed. Polarizable continuum models (PCM) for solvation have been developed to circumvent the problems of dealing with tens to millions of solvent molecules.[55] Here, a solute is surrounded by a continuum with a specified dielectric constant, and this is allowed to polarize in response to the charge distribution of the solute. Excellent results have been obtained for many systems, but no entirely general high-accuracy method yet exists.

Empirical force-field methods have been combined with statistical mechanics for quantitative studies of host–guest complexes. Empirical force fields are classical descriptions of interaction energies that have been parameterized to reproduce a set of experimental data. The most commonly used force fields for energetic descriptions of host–guest interactions are AMBER which was developed by Kollman and co-workers[56] and OPLS of Jorgensen et al.[57] The intermolecular interactions in such force-fields are computed from van der Waals and Coulombic effects, as shown in Equation (1).

$$\Delta E_{inter} = \sum_{i,j} (A/r_{ij}^{12} - B/r_{ij}^{6}) + \sum_{i,j} q_i\, q_j/r_{ij}\ (i \neq j) \qquad (1)$$

The first summation in this equation is the Lennard–Jones potential for the van der Waals attraction and repulsion between pairs of atoms i and j. A and B are constants for given atom pairs which represent the repulsive and attractive part of the van der Waals potential, respectively. The second summation corresponds to Coulomb's Law and provides the energies resulting from electrostatic interactions. The quantities q_i and q_j are partial charges on atoms i and j of the two molecules, while r_{ij} is their separation.

These intermolecular potentials can be used to optimize the geometries of complexes, and solution energetics can be computed approximately by including solvation energies using solvent cavity models such as the generalized Born/solvent-accessible surface area (GB/SA) model developed by Still and co-workers which is an empirical model that gives solvation free energies.[58] Calculations can also be done with explicit water (or other solvent) molecules, using these empirical potentials.

Jorgensen and co-workers have demonstrated the value of Monte Carlo simulations with the OPLS force field for the study of complexes in solution,[59] while Kollman and co-workers have used AMBER and molecular dynamics methods to study organic complexes in solution as well as protein–inhibitor complexes.[60]

Intermolecular interactions are mainly comprised of electrostatic interactions, dispersive interactions, inductive interactions, and exchange repulsions, the combination of which determines the geometries and energetics of the complexes. Theoretical calculations, including quantum mechanics and force-field calculations, help examine the magnitudes as well as the origins of interaction energies.[61a] Many research groups have developed empirical functions that compute interaction energies in terms of groups present on the surfaces of the host and guest. Such approaches are intended to lead to the types and magnitudes of interactions that influence complex stabilities in solution.

 © 2003 Wiley-VCH Verlag GmbH & Co. KGaA, Weinheim

Williams and co-workers are pioneers in the empirical analysis of peptide–receptor binding constants in aqueous solution. The complexes of peptides with vancomycin antibiotics have been used to obtain the relative magnitudes of the interactions that they consider important [Eq. (2)].[61b,c] This equation is representative of such empirical analyses.

$$\Delta G = \Delta G_{t+r} + \Delta G_r + \Delta G_{conf} + \sum \Delta G_p + \Delta G_{vdw} + \Delta G_h \quad (2)$$

Here, ΔG_{t+r} is unfavorable free energy arising from the restriction of translational and rotational entropy upon converting the host and guest into a complex; ΔG_r is the unfavorable free energy resulting from restrictions of internal rotations; ΔG_{conf} is the free energy cost of any conformational energy change required for binding; $\Sigma\Delta G_p$ is the free energy of polar interactions, such as hydrogen bonds and ionic interactions; ΔG_{vdw} is the van der Waals free energy change; and ΔG_h is the hydrophobic binding free energy.

This free energy function contains both intermolecular interaction terms ($\Sigma\Delta G_p$, ΔG_{vdw}) and terms involving solvation (ΔG_h), as described previously. It also includes terms involving the constraint of reactants into complex geometries: ΔG_r and ΔG_{conf} for internal restrictions, and ΔG_{t+r} for the confinement of the host and guest into a single molecular complex. Inclusion of ΔG_r, ΔG_{conf}, and ΔG_{t+r} into the equation is an attempt to account for entropic consequences of binding a flexible guest into a specific conformation in a host–guest complex. Closely related empirical free energy functions have been developed by other research groups.[59,60] For example, Böhm developed a well-known function used in the program LUDI [Eq. (3)].[62]

$$\Delta G_{binding} = \Delta G_o + \Delta G_{hb} f_1(\Delta R) f_2(\Delta\alpha) + \Delta G_{ionic} \sum_{\text{ionic int.}} f_1(\Delta R) f_2(\Delta\alpha) + \Delta G_{lipo} + \Delta G_{rot} \mathrm{NROT} \quad (3)$$

ΔG_o is the unfavorable free energy change resulting from decreased entropy upon the binding of two entities into one. ΔG_{hb} is the hydrogen-bonding free energy; it is given a maximum value for the ideal geometries of interactions of two groups and is reduced for deviations of distances from the ideal (ΔR) and/or deviation of angles from the ideal ($\Delta\alpha$). ΔG_{ionic} represents ionic interactions, which are again reduced by f_1 and f_2 when the distance and angle differ from the ideal values. ΔG_{lipo} represents lipophilic (or hydrophobic) interactions resulting from the interactions of hydrocarbon residues and is a function of the lipophilic surface areas of the host and guest. ΔG_{rot} is the free energy associated with freezing out each of the NROT free rotations in the host. In the program LUDI, contact points are defined for each functional group of the protein, and these rules are used to determine the strength of various interactions. The program is used for the de novo design of drugs and generally is considered to provide reasonable estimates of total interaction energy.[62]

The ideal values of the ΔG parameters obtained for protein–ligand complexes, are:

$\Delta G_o = +1.3$ kcal mol^{-1} for the entropy loss upon association (corresponding to $\Delta S = -4$ e.u. at 25 °C). $\Delta G_{hb} = -1.2$ kcal mol^{-1} for an ideal hydrogen bond, with H···O/N = 1.9 Å, $\alpha = 180°$. $\Delta G_{ionic} = -2$ kcal mol^{-1} for an ideal ionic interaction, for example, in a salt bridge. $\Delta G_{lipo} = -0.04$ kcal mol^{-1} Å^{-2} for removal of a hydrocarbon surface area from water. $\Delta G_{rot} = +0.3$ kcal mol^{-1} per rotatable bond that is fixed in the complex. Systematic measurements using a series of compounds produced similar values for ΔG_{rot}.[63]

These parameters were calibrated with inhibition constants of $K_I = 10^{-1.5}$ to $10^{-13.5}$ M (kinetically determined dissociation constants) for 45 complexes of proteins with small molecules. The predicted values had a standard deviation of $\pm 10^{1.4}$ or 2 kcal mol^{-1} from those of the test set.

A remarkable feature of the LUDI potential function is the relatively small value of binding energy arising from ionic and hydrogen-bonding interactions (ca. 2 and 1 kcal mol^{-1}, respectively). This is more or less equal to the lipophilic contribution of the face of a benzene ring and a methyl group, respectively. This contribution arises because the cost of removing ions or hydrogen-bonding groups from water is barely compensated for by binding interactions. Typical small functional groups thus contribute 1–2 kcal mol^{-1} to binding, regardless of their nature. This is part of the reason that the gross surface area buried upon binding can provide a reasonable estimate of the binding constant without differentiating the specific atom types.

Many authors have described the binding energies of host–guest complexes as the sum of the contributions of hydrophobic, hydrogen bonding, electrostatic, and van der Waals interactions [Eq. (4)].[42,64]

$$\Delta G = \Delta\Delta G_{hydrophobic} + \Delta G_{H\text{-}bonding} + \Delta G_{electrostatic} + \Delta G_{vdw} \quad (4)$$

This equation treats aqueous solvation by the term $\Delta\Delta G_{hydrophobic}$, while the remaining terms distinguish different complexes by the hydrogen bonds, electrostatic interactions, and van der Waals interactions that occur between the host and guest. The separation in this way is somewhat arbitrary, since aqueous solvated guest and host containing water in the binding cavity both have hydrogen-bond, electrostatic, and van der Waals interactions with water solvent molecules. In Equation (4), the guest and host interactions with water are included in the $\Delta\Delta G_{hydrophobic}$ term.

Connors has developed even simpler empirical models to predict the equilibrium constant for the binding of organic molecules by cyclodextrins.[8a] The model is a phenomenologically based Equation (5).

$$\lg K_a = -1.74 - [Z] - 0.032(\Delta SAHSA_H) \quad (5)$$

In this equation, [Z] includes solvent–solute and host–guest interaction energies arising from specific hydrogen bonds and electrostatic interactions. $SAHSA_H$ is the solvent-accessible hydrophobic surface area of the host, and $\Delta SAHSA_H$ is the change in this accessible surface area of the host when it binds to a guest in the host–guest complex. The negative sign illustrates that the solvent-accessible surface area decreases during complexation. This model separates the direct interaction of guest atoms with the host atoms from other effects related only to surface area.[8a]

 © 2003 Wiley-VCH Verlag GmbH & Co. KGaA, Weinheim

For cyclodextrins, the Connors model was found to predict K_a values to within an order of magnitude for 95% of the 569 cases examined.[8] For almost all of the cases examined by Connors, [Z] is an order of magnitude smaller than $0.032\,\Delta SAHSA_H$ and in general less than 1 kcal mol^{-1}.[8]

A variety of other correlations have been proposed for the binding energies of complexes based on surface areas. For example, Eisenberg et al. proposed a hydrophobicity function based on the accessible surface areas of proteins to predict modes of protein folding and binding in solution.[65a,b]

Luque and Freire have recently developed an empirical relationship between binding enthalpy of a number of inhibitors of HIV-1 protease [Eq. (6)], and buried surface

$$\Delta H_{binding} = 5.9(\pm1.3) - 0.007(\pm0.002)\,\Delta ASA_{nonpolar} + 0.031(\pm0.006)\,\Delta ASA_{polar} \quad (6)$$

area. They have applied this to the calculation of binding energies for six different proteins.[65c] In the Equation, the constant contains conformational changes in the protein and substrate required to achieve binding. $\Delta ASA_{nonpolar}$ and ΔASA_{polar} refer to the change in solvent-accessible surface area of nonpolar and polar parts of the surface, respectively. The main quantity corresponding to binding here is the burying of nonpolar surface, since the conformational energies and burying of polar surface area is unfavorable.

3.4. Hydrophobic Effects

Hydrophobic interactions are often thought to play a dominant role in the binding stability of host–guest complexes involving organic substances in water.[66,67] The hydrophobic effect refers to the fact that nonpolar substances are less soluble in water than in organic solvents. Simply stated, nonpolar organic compounds avoid water and prefer a nonpolar environment. The concept of the hydrophobic effect was originally based on the observation that hydrocarbon molecules spontaneously aggregate to minimize the exposed solvent-accessible surface in aqueous solution. It is considered to be one of the most significant factors controlling protein folding.[65,68]

The hydrophobic effect at room temperature is now generally attributed in large part to entropic effects.[64,69] The total entropy of a nonpolar solute in water is less than that of a nonpolar solute in a nonpolar solvent.[64] This is often rationalized as a result of reduced order of the water molecules in the bulk solvent than in the vicinity of a nonpolar solute. Around a nonpolar solute, water becomes ordered into "icebergs".

The hydrophobic effect is present at all temperatures, but although it has an entropic origin around room temperature it becomes enthalpic at high temperature.[70] This occurs because the transfer of a nonpolar solute into water is accompanied by a large positive change in the heat capacity (ΔC_p). The relationship between heat capacity and ΔH or ΔS [Eq. (7)] shows that as the temperature increases, the enthalpic contribution to the free energy of solvation increases, but the entropic contribution ($-T\Delta S$) becomes smaller, since ΔS starts negative and becomes less negative.

$$\Delta C_p = (d\Delta H/dT)_p = T\,(d\Delta S/dT)_p \quad (7)$$

A variety of models have been proposed and quantitatively tested for the hydrophobic effect, and a consensus view of the effect has been offered by Southall et al.[70] It also gives insight into hydrophobic effects in general, and is described here.

When small nonpolar solutes are transferred to water, a cavity is opened and the water molecules are ordered around it. Producing the cavity is unfavorable for water and, indeed, for all solvents. The ordering of water around the cavity in hot water is diminished, and unfavorable entropy is minimized. However, the unfavorable enthalpy of interaction of water with a nonpolar solute rather than with other water molecules becomes the dominant effect.[70] Large solutes disrupt the hydrogen bonding between water even more, which leads to an additional enthalpic contribution to the hydrophobic effect. At room temperature, "it takes about 25 cal mol^{-1} Å^{-2} to transfer small oil molecules into water", while it costs three times this (per surface area) to form an oil–water interface.[70] That is, the hydrophobic effect depends on the surface area of the solute in a nonlinear fashion.

Hydrophobic effects, or solvophobic effects in general, are sometimes analyzed in terms of the two factors alluded to above: 1) the cavitation energy, which corresponds to the unfavorable energy required to make a cavity in water; 2) the interaction energy between the solute and solvent, which corresponds to the energy required to put a solute into an appropriately sized and solvent-surrounded cavity. Both factors are directly related to the surface area of the guest. In fact, it is generally found that the hydrophobic effect on binding correlates with the change of the exposed surface area that occurs upon binding [Eq. (8)].

$$\Delta\Delta G_{hydrophobic} = \gamma\Delta SAHSA_{H+G} \quad (8)$$

Here, γ is the free energy/surface area coefficient, while $\Delta SAHSA_{H+G}$ is the difference between the accessible hydrophobic surface area of the host–guest complex and that of the separate host and guest molecules. The value of γ is frequently cited as 0.025 kcal mol^{-1} Å^{-2},[69] but sometimes this is stated for the hydrophobic surface area (C or CH groups on the surface) or sometimes for the total surface. Many different values of γ have been reported (Table 2).[61b,c] The value of γ varies from 0.02 to 0.2 kcal mol^{-1} Å^{-2} depending on the types of measurement and methods of calculating the surface area. This range of values corresponds to the burial of 7 to 50 Å^2 of the hydrophobic surface area for each

Table 2: Dependence of the coefficient γ (Gibbs energy of the buried hydrophobic surface area) on the measurement method.[61b,c]

Method of measurement	γ [kcal^{-1} mol^{-1} Å^{-2}]
solvent transfer	0.02–0.05
ligand binding	0.03–0.06
protein engineering	0.02–0.2
calculation	0.02–0.03

© 2003 Wiley-VCH Verlag GmbH & Co. KGaA, Weinheim

kcal mol^{-1} of binding energy. In terms of equilibrium constants at room temperature, each 10–70 Å^2 of buried surface area is worth a factor of 10 in the equilibrium constant as a result of hydrophobic effects. Values of $\gamma = 0.02$–0.05 were obtained from solvent transfer, which is a direct measure of the difference of the free energy of solvation in water and in a hydrocarbon solvent. Here, the total surface area of the solute is taken for $\Delta SAHSA_{H+G}$. Ligand binding and protein engineering values are obtained from measurements of changes in the binding energy upon altering the hydrophobic surface area in a ligand or in the protein. For example, the surface area increases by 22–35 Å^2 when a methyl substituent replaces a hydrogen atom and the measurable change in binding free energy was used to determine the γ value. In a recent article by Meyer, Castellano, and Diederich, a large enthalpic driving force partially compensated by an unfavorable complexation entropy has been addressed for apolar complexation in aqueous solution, which has been named as the "nonclassical hydrophobic effect".[44a,b] The nonclassical hydrophobic effect is normally encountered when arenes bind to cyclodextrins, synthetic hosts, or biological receptors (enzymes and DNA). Based on the calorimetric studies they had surveyed and performed, Diederich et al. identified favorable changes in solvent cohesive interactions and a gain in dispersion interactions as the origins of the nonclassical hydrophobic effect.

4. Relationship between Average Binding Constants and the Average Surface Areas Buried upon Binding

The hydrophobic surface area buried upon complexation is a quantity often used in empirical calculations of binding energies. For each of the classes of host–guest complexes discussed in Section 2, the solvent-accessible surface areas of guests buried upon complexation were computed or estimated by methods that are described below.

The total, not just hydrophobic, buried surface area of the guest is the difference between the solvent-accessible surface area of the free guest and the bound guest. For many of the complexes discussed previously, the total accessible surface of guest molecules and of the host–guest complexes were computed with a 1.4 Å radius probe, essentially the radius of a water molecule. The crevices that are not penetrated by the probe do not contribute to the surface area. Unlike some other treatments of binding energies and surface areas, these calculations do not limit the surface area to only those parts of the surface that are hydrophobic or nonpolar. The calculations are performed with NACCESS or GRASP on X-ray crystal structures,[71] or on AMBER-optimized structures for cases when the X-ray structure was not available.[56]

Table 3 lists the solvent-accessible surface areas of 20 different simple organic guests (free and complexed inside α-cyclodextrin) and the buried surface areas after complexation.[72] The guests represent the range of observed binding affinities. The buried surface areas of guests are in the range of 170 ± 18 Å^2, while $\lg K_a$ values from these guests range from 0.7 to 3.8.

Table 4 shows solvent-accessible and buried surface areas of nine free guest molecules and of bound guests inside β-cyclodextrin. The buried surface areas of guests are in the range of 192 ± 19 Å^2, while the $\lg K_a$ values range from 0.7 to 2.7. The average buried surface areas of guests inside β-cyclodextrin are slightly larger than those in α-cyclodextrin.

Table 3: Solvent-accessible surface areas (SASA, in Å^2) of the free and bound guest inside α-cyclodextrin, as well as the buried surface areas (ΔSASA) of the bound guest.

Guest	SASA, bound	SASA, free	ΔSASA	Experimental binding constant ($\lg K_a$)
ethanol	27.7	172.5	145	0.83
1-propanol	52.2	199.8	148	1.46
1-butanol	74.9	225.9	151	1.22
1-pentanol	89.9	251.2	161	2.5
1-hexanol	92.8	275.5	183	2.96
hexanoic acid	72.4	276.8	204	2.91
cyclobutanol	57.1	205.5	148	1.2
cyclopentanol	68.1	223.8	156	1.56
cyclohexanol	91.0	245.2	154	2.7
benzene	39.9	222.6	183	1.5
phenol	58.0	235.8	178	1.57
pyridine	37.6	218.7	181	2.2
benzoic acid	79.2	266.4	187	2.4
2-chlorophenol	90.9	263.9	173	2.3
3-chlorophenol	84.2	265.7	188	2.3
4-chlorophenol	77.5	267.0	190	2.4
3-nitrophenol	96.5	277.7	181	2.1
4-nitrophenol	99.3	278.5	179	2.6
4-methylphenol	77.8	261.6	194	1.75
acetic acid	26.4	180.8	154	3.8
acetonitrile	32.5	173.8	141	0.72

Table 4: Solvent-accessible surface areas (SASA, in Å^2) of free and bound guest inside β-cyclodextrin, as well as the buried surface areas (ΔSASA) of the bound guest.

Guest	SASA, bound	SASA, free	ΔSASA	Experimental binding constant ($\log K_a$)
1-propanol	42.8	197.5	155	0.65
1-butanol	50.1	223.8	174	1.22
1-hexanol	85.9	279.5	194	2.34
cyclohexanol	54.0	245.0	191	2.7
benzene	40.6	225.1	185	2.23
benzoic acid	54.1	267.0	213	2.4
4-methylphenol	61.3	264.0	203	2.4
3-nitrophenol	67.9	277.6	210	2.44
2-chlorophenol	62.2	264.0	202	2.3

 © 2003 Wiley-VCH Verlag GmbH & Co. KGaA, Weinheim

Table 5: Solvent-accessible surface areas (SASA, in Å^2) of free and bound guest in albumins and buried surface areas (ΔSASA) of the bound guests.

PDB code	Molecular formula of guest[a]	SASA, bound	SASA, free ligand	ΔSASA
1E7A	$C_{12}O$	97	363	266
	$C_{12}O$	106	367	261
1E7B	C_2F_3ClBr	74	209	135
	C_2F_3ClBr	64	210	146
	C_2F_3ClBr	65	211	146
1E7C	$C_{11}O_2$	88	420	332
	$C_{11}O_2$	102	426	324
	$C_{11}O_2$	108	427	319
	$C_{13}O_2$	124	472	348
	$C_{14}O_2$	144	505	361
	C_2F_3ClBr	68	209	141
	C_2F_3ClBr	71	209	138
	C_2F_3ClBr	79	209	130
	C_2F_3ClBr	59	210	151
	C_2F_3ClBr	68	210	142
	C_2F_3ClBr	54	211	157
	C_2F_3ClBr	98	211	113
	C_2F_3ClBr	104	211	107
1E7E	C_7O_2	102	316	214
	C_8O_2	107	343	236
	C_9O_2	138	367	229
	C_9O_2	98	369	271
	C_9O_2	101	373	272
	$C_{10}O_2$	97	396	299
	$C_{10}O_2$	138	397	259
	$C_{10}O_2$	101	398	297
	C_8	92	312	220
	C_{10}	68	351	283
1E7F	$C_{11}O_2$	142	420	278
	$C_{11}O_2$	116	425	309
	$C_{11}O_2$	120	425	305
	$C_{12}O_2$	117	440	323
	$C_{12}O_2$	128	446	318
	$C_{12}O_2$	137	449	312
	C_{10}	110	366	256
	C_{12}	96	382	286
1E7G	$C_{11}O_2$	93	423	330
	$C_{11}O_2$	104	424	320
	$C_{12}O_2$	124	447	323
	$C_{14}O_2$	136	502	366
	$C_{14}O_2$	142	502	360
	$C_{14}O_2$	147	502	355
	C_{10}	91	367	276
	C_{12}	100	413	313
1E7H	$C_{11}O_2$	109	419	310
	$C_{15}O_2$	142	507	365
	$C_{15}O_2$	162	533	371
	$C_{16}O_2$	160	552	392
	$C_{16}O_2$	133	556	423
	$C_{16}O_2$	137	558	421
	C_{10}	94	358	264
1E7I	$C_{13}O_2$	128	461	333
	$C_{17}O_2$	162	550	388
	$C_{17}O_2$	156	580	424
	$C_{17}O_2$	146	586	440
	$C_{18}O_2$	293	608	315
	$C_{18}O_2$	180	609	429
	$C_{18}O_2$	302	609	307
	C_{11}	86	386	300
1H9Z	$C_{14}O_2$	124	477	353
	$C_{14}O_2$	120	483	363
	$C_{14}O_2$	133	492	359
	$C_{14}O_2$	134	502	368
	$C_{14}O_2$	148	502	354
	$C_{14}O_2$	98	506	408
	$C_{19}O_4$	161	508	347
1H9Z	$C_{14}O_2$	140	478	338
	$C_{14}O_2$	126	484	358
	$C_{14}O_2$	140	490	350
	$C_{14}O_2$	130	502	372
	$C_{14}O_2$	148	504	356
	$C_{14}O_2$	117	509	392
	$C_{19}O_4$	151	494	343

[a] H is excluded.

Table 5 shows accessible and buried surface areas of 73 guests bound by albumins for which crystal structures are available.[73] The values of the binding constants for all of these complexes have not been reported. Consequently, the average binding energies and standard deviations reported earlier (Figure 25) are compared to these surface areas.

Table 6 shows solvent-accessible and buried surface areas of 15 guest molecules (free and bound guests inside catalytic antibodies, see also Figure 28).[74] These are, in general, relatively small organic molecules but are larger than the cyclodextrin guests noted above. The buried surface areas of guests are in the range of 420 ± 80 Å^2. The average buried surface areas of guests inside catalytic antibodies are nearly double that in α or β-cyclodextrins. K_d values have been reported for 11 of these complexes for which there are crystal structures available. In these complexes, the average bound surface area was found to be 400 ± 79 Å^2. The data for this set of 15 structures were assumed to be representative of the substrates for catalytic antibodies, and these have been compared to the binding constants noted earlier ($10^{3.5\pm1.0}$ M^{-1}). Padlan's survey of crystal structures led to the generalization that antibody–hapten complexes have a surface contact area of 190–350 Å^2. This contact area is much larger (400–900 Å^2) for antibody complexes of protein antigens.[75]

Thermodynamic data for protein–substrate complexes have been well documented, but the accessible surface areas have not been systematically classified. Jones and Thornton reported that the mean buried SASA ($[\Delta\Sigma ASA_H + \Delta\Sigma ASA_G]/2$) is 777 ± 135 Å^2 for enzyme–inhibitor complexes for which X-ray structures are available, and 785 ± 75 Å^2 for antibody–protein complexes.[76] Table 7 summarizes the average buried surface areas and average binding constants for α-

© 2003 Wiley-VCH Verlag GmbH & Co. KGaA, Weinheim

Table 6: Solvent-accessible surface areas (SASA, in Å^2) of free and the bound guest in catalytic antibodies, as well as the buried surface areas (ΔSASA) of the bound spieces (hapten or products; see Figure 28).

PDB code	Antibody	SASA, bound	SASA, free	ΔSASA	K_d
1a4k	39A11	222.8	638.1	415	10 nM
1aj7	48G7[a]	93.9	489.1	395	135 μM
1c5c	21D8	75.1	469.4	394	110 nM
1cf8	HA5-19A4	209.9	708.3	498	1.4 μM
1c1e	1E9	38.4	442.6	404	1 nM
1ct8	7C8	327.2	794.3	467	0.3 μM
1f3d	4B2	41.7	403.6	362	n.a.[b]
1 gaf	48G7[c]	78.5	484.1	406	45 nM
1kel	28B4	110.5	519.4	409	52 nM
1yef	D2.3	60.3	549.3	489	n.a.
1yeg	D2.3	27.3	303.4	276	50 μM
25c8	5C8	75.4	588.0	513	n.a.
35c8	5C8	74.4	580.0	506	n.a.
3fct	7G12	349.4	842.7	493	49 μM[d]
43ca	43C9	23.4	270.9	248	1 μM

[a] Germline antibody. [b] Not available. [c] Mature antibody. [d] K_M.

and β-cyclodextrins, catalytic antibodies, enzyme–inhibitors, and antibody–protein complexes. The range of buried surface areas and binding energies for a given host type are also shown in the Table or with error bars in Figure 29, which shows the plot of the binding affinities versus buried surface areas.

A clear trend between the buried areas of the guests and binding affinities is found. A linear fit gives a slope of 0.011, which corresponds to a γ value of 0.007 kcal mol^{-1} Å^{-2} in the equation $\Delta G = \gamma \Delta \Sigma SASA$, where the total ΔSASA of the host plus guest is now used to correspond to the conventional meaning of γ. This means that 67 Å^2 of accessible surface area of guest is buried for 1 kcal mol^{-1} binding energy. This value corresponds to about 90 Å^2 per lg K_a unit. For example, the approximate 200 Å^2 of surface area buried upon binding in α-cyclodextrins corresponds to an average binding constant of about $10^{2.2}$ M^{-1}. The ΔSASA of 800 Å^2 for enzymes binding with inhibitors relates to K_a values of about 10^9 M^{-1}. The γ value of 0.007 found in this way is considerably smaller than the previously reported values of 0.02–0.15 kcal mol^{-1} Å^{-2} described before (the most widely quoted value of γ is 0.025 kcal mol^{-1} Å^{-2} for ΔHSASA[69]), but most of the literature values are based on buried hydrophobic surface area only, whereas Figure 29 compares the binding energy to total buried surface area of the guest. The value of γ is the same as that determined by Luque and Freire for the calculation of ΔH from nonpolar surface area only.[65c] On the other hand, our results suggest a correlation between the buried hydrophobic surface area and total buried surface area of the guest. These results suggest

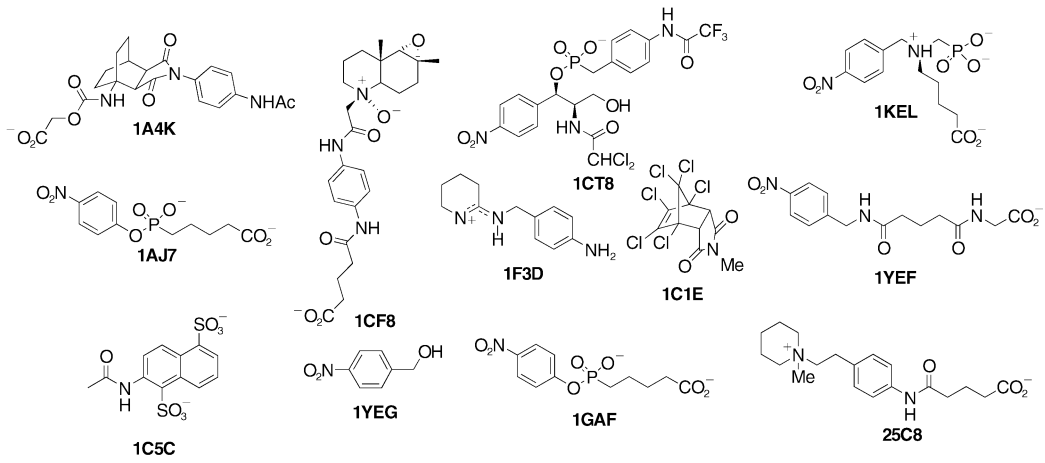


Figure 28. Hapten structures for catalytic antibodies discussed in Table 6.

Table 7: Summary of mean buried surface areas of the guests (ΔSASA, in Å^2) and lg K_a for various classes of host–guest complexes in water; standard deviations (σ) are also given.

System	Mean ΔSASA	σ (ΔSASA)	Source	Mean lg K_a	σ(lg K_a)	Source
α-cyclodextrin–organic guests	170	18	Table 3	2.0	0.8	Table 3
β-cyclodextrin–organic guests	192	19	Table 4	2.1	0.7	Table 4
catalytic antibodies–substrates	418	80	Table 6	3.5	1.0	Table 1
catalytic antibodies–inhibitors	400	79	Table 6	6.3	1.6	Table 6
albumins–organic guests	300	85	Table 5	4.6	0.9	Table 5
enzymes–inhibitors	777	135	[64]	8.6	2.1	Table 1
antibodies–proteins	785	75	[76]	8.9	1.7	Table 1

 © 2003 Wiley-VCH Verlag GmbH & Co. KGaA, Weinheim

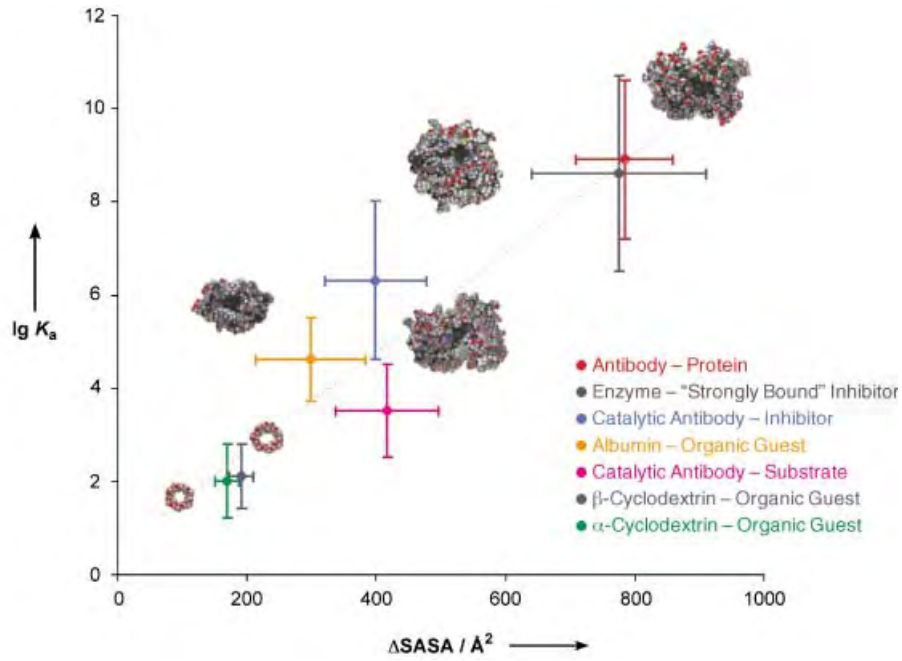


Figure 29. Plot of average lg K_a versus average buried solvent-accessible surface area.

that the average binding constants for host–guest complexes in water are a result of the relatively small surface areas that are removed from water and placed in contact in typical host–guest complexes.

The reasonable correlation between the ΔSASA and binding constant in water suggests that the average values of association constants are predictable from the size of the host cavity and the amount of surface area of the guest that comes into contact with the host upon binding. This emphasizes the important role of the hydrophobic effect in binding. While the average association constant is readily explained by the buried surface area, the range in binding constants requires a more detailed explanation. The range can be attributed to variations in direct host–guest interactions resulting from specific hydrogen bonding, electrostatic, and van der Waals interactions. These are the factors that provide selectivity for a given type of hydrophobic binding cavity and cause significant deviations from a simple relationship based upon surface area. A variety of other factors have been invoked to rationalize selectivity; for example, that the most stable complexes are formed when the guest maintains mobility inside the host.[77]

Recently, the main theoretical and empirical approaches for predicting binding affinities in enzymes and protein receptors were summarized by Gohlke and Klebe.[78a] They found that the standard deviations for regression-based approaches (empirical scoring functions) normally range from 0.5 to 2.5 kcal mol^{-1}. The average standard deviation of these scoring functions, 1.3 kcal mol^{-1}, is about one third of 3.5 kcal mol^{-1}, the standard deviation of a simple ΔSASA correlation. A new scoring function, which combines several to obtain a consensus energy, also has a standard deviation of 2.2 kcal mol^{-1}.[78b] Furthermore, in a recent review by Davis et al.,[78c] the root-mean-square error (RMSE) of a knowledge-based scoring function (SmoG2001) is 1.69 log unit, and the RMSE of SCORE1 (LUDI) is 3.47 log unit. All these interesting comparisons suggest that the correlation between ΔSASA and the binding constant in water obtained from our surveys and calculations can provide a simplified and semiquantitative way to predict binding affinities based solely on the solvent-accessible surface area buried upon binding.

A dramatic exception to simple ΔG/ΔSASA relationships is found in the data for enzymes: The binding constant for enzyme–substrate complexes is $10^{3.7\pm1.3}\,\mathrm{M}^{-1}$, while complexes formed between enzymes and transition states have a binding constant of $10^{16.0\pm4.0}\,\mathrm{M}^{-1}$, even though the surface area of the substrate and transition state cannot be vastly different. Enzyme–substrate complexes give the same type of ΔG/ΔSASA correlation found for complexes formed between catalytic antibodies and substrates. Here, average buried surface areas are about 420 Å^2, binding constants are about $10^{3.5}\,\mathrm{M}^{-1}$, and free energies of binding are about 5 kcal mol^{-1}. The "transition-state binding" is much greater than this, in spite of similar buried surface areas.

5. Why Are Transition States Bound so Tightly Relative to Substrates by Enzymes?

As noted earlier, enzyme–substrate complexes have $K_M{}^{-1}$ values of $10^{3.7\pm1.3}\,\mathrm{M}^{-1}$, yet enzyme–transition-state binding is $K_{tx}{}^{-1} = 10^{16.0\pm4.0}\,\mathrm{M}^{-1}$. Many factors have been invoked to explain the origin of catalysis, but among the more compelling are the following:

A. Chemical Effects

a) Perhaps the most apparent factor is that readily reversible host–guest complexation involves noncovalent interactions, while many, if not all, enzymes act by covalent, metal–ligand, or acid–base catalysis. Covalent interactions can provide much more powerful interactions than the noncovalent effects governing the stabilities of many host–guest complexes.

b) Charge development in the transition state can increase Coulombic interactions. Strong electrostatic interactions can occur in transition states, whereas the neutral substrates are bound more modestly. Warshel has emphasized the role of oriented dipoles specifically arranged (through evolution) in the binding site to stabilize the transition state.[79] The energy to arrange these dipoles

 © 2003 Wiley-VCH Verlag GmbH & Co. KGaA, Weinheim

unfavorably but complementary to the transition state is afforded by the protein folding.

c) The binding of phosphate or other polar groups that seem secondary to the reaction may be very strong in the transition state. Wolfenden and co-workers have determined an effect of 17 kcal mol^{-1} for phosphate binding for ODCase,[80] while Aymes et al. determined that the preferential binding of phosphate in the transition state by triosephosphate isomerase contributes 14 kcal mol^{-1} to the reduction in the transition-state energy.[81] Such multisite binding can lead to the "Circe effect".[34b]

B. Effects of Enzyme and Transition-State Complementarity

d) According to Koshland's induced-fit mechanism, the catalyst modifies its shape to fit the transition state and provide complementarity.[42,82] This can provide at most a small increase in ΔSASA, but might enhance specific electrostatic interactions.

e) Large-scale motions of protein loops can provide constrictive binding of the transition state, or at least can increase the surface area for binding.

f) Dynamic coupling between protein fluctuations and movement of atoms in the transition state could accelerate reactions. This effect has attracted considerable attention recently, but these dynamic coupling effects are usually found to be small, except when tunneling occurs.[83]

g) H_2O release from the binding pocket as the transition state is formed can provide favorable entropy for the reaction. This can also occur in ground-state substrate binding but could be tuned for maximum effect on the transition state.[84]

It is quite likely that any or all of these effects operate in specific types of transition states.[85] Current studies in our and many other laboratories are designed to quantitate the role of these factors in enzymatic catalysis.

6. Summary and Outlook

The binding energy ranges discussed here make it possible to estimate within several orders of magnitude the binding constants for neutral molecules in water with a variety of hosts, with the magnitude of the constants depending upon the size of host cavity and the guest surface area. More quantitative computational methods should be able to give predictions with greater precision than these generalizations, but will necessitate a great deal of expense in terms of computer resources and time.

The magnitudes and ranges of noncovalent binding in water are determined by hydrophobic effects and the relationships to surface areas. The origins of the average binding energies are now understood, but the understanding and quantitation of exceptions and specific values remains a significant challenge. Finally, transition states are bound by enzymes to an astonishing degree, and the understanding of the combination of chemical effects responsible remains a significant challenge.

We are grateful to the National Institute of General Medical Sciences, the National Institutes of Health for financial support of this research, and to the Fulbright Commission and AstraZeneca for a fellowship to A.G.L. We thank Dr. Jiangang Chen for discussions and for the techniques used for the computation of surface areas. We appreciate helpful discussions with Professors François Diederich, Dudley H. Williams, William L. Jorgensen, Hans-Jörg Schneider, Ronald K. Castellano, and Dr. W. Bruce Turnbull. We also thank Professor D. Schomburg, Institut für Biochemie, Universität zu Köln for assistance in acquiring enzyme K_M data.

Received: December 4, 2002 [A565]

[1] a) F. Vögtle, *Supramolecular Chemistry*, Wiley, New York, **1991**; b) J. M. Lehn, *Supramolecular Chemistry*, VCH, Weinheim, **1995**; c) *Comprehensive Supramolecular Chemistry, Vol. 11* (Eds.: J. L. Atwood, J. E. D. Davies, D. D. MacNicol, F. Vögtle), Pergamon, Oxford, **1996**; d) H.-J. Schneider, *Angew. Chem.* **1991**, *103*, 1419–1439; *Angew. Chem. Int. Ed. Engl.* **1991**, *30*, 1417–1436; e) H.-J. Schneider, A. Yatsimirsky, *Principles and Methods in Supramolecular Chemistry*, Wiley, Chichester, **2000**; f) C. A. Schalley, J. Rebek in *Stimulating Concepts in Chemistry* (Eds.: F. Vögtle, J. F. Stoddart, M. Shibasaki), Wiley-VCH, Weinheim, **2000**, pp. 199–210; g) M. C. T. Fyfe, J. F. Stoddart, *Acc. Chem. Res.* **1997**, *30*, 393–401; h) J. H. Hartley, T. D. James, C. J. Ward, *J. Chem. Soc. Perkin Trans. 1* **2000**, 3155–3184; i) T. H. Webb, C. S. Wilcox, *Chem. Soc. Rev.* **1993**, *22*, 383–395; j) J. C. Ma, D. A. Dougherty, *Chem. Rev.* **1997**, *97*, 1303–1324; k) S. L. McKay, B. Haptonstall, S. H. Gellman, *J. Am. Chem. Soc.* **2001**, *123*, 1244–1245.

[2] J. S. Huston, M. N. Margolies, E. Haber in *Advances in Protein Chemistry, Vol. 49* (Eds.: F. M. Richards, D. E. Eisenberg, P. S. Kim), Academic Press, San Diego, **1996**, pp. 330–450.

[3] a) G. M. Blackburn, A. Datta, H. Denham, P. Wentworth, Jr., *Adv. Phys. Org. Chem.* **1998**, *31*, 249–392; b) J.-L. Reymond, *Top. Curr. Chem.* **1999**, *200*, 59–93.

[4] a) A. R. Fersht, *Structure and Mechanism in Protein Science*, W. H. Freeman, New York, **2000**; b) T. C. Bruice, S. J. Benkovic, *Biochemistry* **2000**, *39*, 6267–6274; c) the use of the word "bound" here requires some comment, since some, notably Bruice and Benkovic, have objected to this description.[4b] The term is used here to mean the lower free energy of the enzyme–transition-state complex ($E{\cdot}S^{\ddagger}$) than for the enzyme plus the transition state in water ($E + S^{\ddagger}$), which corresponds to Wolfenden's constant K_{tx}. The objection to the terminology "bound" arises from the fact that "transition-state binding energy" cannot be measured directly, and often, as a result of covalent mechanisms, the transition state of the uncatalyzed reaction in water differs in composition from that in the enzyme.

[5] a) A. J. Kennan, H. W. Whitlock, *J. Am. Chem. Soc.* **1996**, *118*, 3027–3028, and references therein; b) J. Suh, *Adv. Supramol. Chem.* **2000**, *6*, 245–286; c) Y. Murakami, J. Kikuchi, Y. Hisaeda, O. Hayashida, *Chem. Rev.* **1996**, *96*, 721–758.

[6] P. J. Gane, P. M. Dean, *Curr. Opin. Struct. Biol.* **2000**, *10*, 401–404.

[7] C. T. Calderone, D. H. Williams, *J. Am. Chem. Soc.* **2001**, *123*, 6262–6267, and references therein.

[8] a) K. A. Connors, *Chem. Rev.* **1997**, *97*, 1325–1357; b) K. A. Connors, *J. Pharm. Sci.* **1995**, *84*, 843–848.

 © 2003 Wiley-VCH Verlag GmbH & Co. KGaA, Weinheim

[9] *Chem. Rev.* **1998**, *98*, 1741 – 2076 (a special edition on cyclodextrins).
[10] a) K. Harata, *Bull. Chem. Soc. Jpn.* **1977**, *50*, 1416 – 1424; b) K. Harata, *Bioorg. Chem.* **1981**, *10*, 388 – 398.
[11] M. V. Rekharsky, Y. Inoue, *Chem. Rev.* **1998**, *98*, 1875 – 1917.
[12] a) D. H. Macartney, A. W. Roszak, K. C. Smith, *Inorg. Chim. Acta* **1999**, *291*, 354 – 371; b) S. Nepogodiev, J. F. Stoddart, *Chem. Rev.* **1998**, *98*, 1959 – 1976; c) Y. Inoue, K. Yamamoto, T. Wada, S. Everitt, X. Gao, Z. Hou, L. Tong, S. Jiang, H. Wu, *J. Chem. Soc. Perkin Trans. 2* **1998**, 1807 – 1816; d) Y. Liu, B. Han, S. Sun, T. Wada, Y. Inoue, *J. Org. Chem.* **1999**, *64*, 1487 – 1493; e) A. Abou-Hamdan, P. Bugnon, C. Saudan, P. G. Lye, A. E. Merbach, *J. Am. Chem. Soc.* **2000**, *122*, 592 – 602; f) G. Castronuovo, V. Elia, A. Iannone, M. Niccoli, F. Velleca, *Carbohydr. Res.* **2000**, *325*, 278 – 286; g) J. C. Morales, D. Zurita, S. Penadés, *J. Org. Chem.* **1998**, *63*, 9212 – 9222; h) M. Rekharsky, Y. Inoue, *J. Am. Chem. Soc.* **2000**, *122*, 10949 – 10955.
[13] a) K. Kobayashi, Y. Asakawa, Y. Kato, Y. Aoyama, *J. Am. Chem. Soc.* **1992**, *114*, 10307 – 10313; b) K. Kobayashi, M. Tominaga, Y. Asakawa, Y. Aoyama, *Tetrahedron Lett.* **1993**, *34*, 5121 – 5124.
[14] a) D.-R. Ahn, T. W. Kim, J.-I. Hong, *Tetrahedron Lett.* **1999**, *40*, 6045 – 6048; b) M. H. B. Grote Gansey, F. K. G. Bakker, M. C. Feiters, H. P. M. Geurts, W. Verboom, D. N. Reinhoudt, *Tetrahedron Lett.* **1998**, *39*, 5447 – 5450; c) R. Yanagihara, M. Tominaga, Y. Aoyama, *J. Org. Chem.* **1994**, *59*, 6865 – 6867; d) T. Haino, D. M. Rudkevich, A. Shivanyuk, K. Rissaanen, J. Rebek, Jr., *Chem. Eur. J.* **2000**, *6*, 3797 – 3805.
[15] a) S. B. Ferguson, E. M. Sanford, E. M. Seward, F. Diederich, *J. Am. Chem. Soc.* **1991**, *113*, 5410 – 5419; b) F. Diederich, K. Dick, D. Griebel, *Chem. Ber.* **1985**, *118*, 3588 – 3619; c) S. B. Ferguson, E. M. Seward, F. Diederich, E. M. Sanford, A. Chou, P. Inocencio-Szweda, C. B. Knobler, *J. Org. Chem.* **1988**, *53*, 5593 – 5595; d) F. Diederich, K. Dick, *Tetrahedron Lett.* **1982**, *23*, 3167 – 3170; e) F. Diederich, K. Dick, *Chem. Ber.* **1985**, *118*, 3817 – 3829; f) K. Koga, K. Odashima, *J. Inclusion Phenom. Mol. Recognit. Chem.* **1989**, *7*, 53 – 60; g) K. Odashima, T. Soga, K. Koga, *Tetrahedron Lett.* **1981**, *22*, 5311 – 5314; h) F. Diederich, K. Dick, *Angew. Chem.* **1984**, *96*, 789 – 790; *Angew. Chem. Int. Ed. Engl.* **1984**, *23*, 810 – 812; i) H.-J. Schneider, D. Güttes, U. Schneider, *J. Am. Chem. Soc.* **1988**, *110*, 6449 – 6454; j) H.-J. Schneider, D. Güttes, U. Schneider, *Angew. Chem.* **1986**, *98*, 635 – 636; *Angew. Chem. Int. Ed. Engl.* **1986**, *25*, 647 – 649; k) F. Diederich, D. Griebel, *J. Am. Chem. Soc.* **1984**, *106*, 8037 – 8046; k) F. Diederich, K. Dick, *J. Am. Chem. Soc.* **1984**, *106*, 8024 – 8036; m) F. Diederich, K. Dick, D. Griebel, *J. Am. Chem. Soc.* **1986**, *108*, 2273 – 2286; n) M. R. Hester, M. A. Uyeki, F. Diederich, *Isr. J. Chem.* **1989**, *29*, 201 – 212; o) Y. Murakami, J. Kikuchi, T. Ohno, O. Hayashida, M. Kojima, *J. Am. Chem. Soc.* **1990**, *112*, 7672 – 7681; p) O. Manabe, K. Asakura, T. Nishi, S. Shinkai, *Chem. Lett.* **1990**, 1219 – 1222; q) D. R. Carcanague, F. Diederich, *Angew. Chem.* **1990**, *102*, 836 – 838; *Angew. Chem. Int. Ed. Engl.* **1990**, *29*, 769 – 771; r) B. R. Peterson, P. Wallimann, D. R. Carcanague, F. Diederich, *Tetrahedron* **1995**, *51*, 401 – 421; s) F. Diederich, *Angew. Chem.* **1988**, *100*, 372 – 396; *Angew. Chem. Int. Ed. Engl.* **1988**, *27*, 362 – 386.
[16] a) Y. Murakami, J.-I. Kikuchi, T. Ohno, T. Hirayama, *Chem. Lett.* **1989**, 881 – 884; b) Y. Murakami, J.-I. Kikuchi, *Pure Appl. Chem.* **1988**, *60*, 549 – 554; c) R. Fornasier, F. Reniero, P. Scrimin, U. Tonellato, *J. Inclusion Phenom.* **1988**, *6*, 175 – 181; d) Y. Murakami, T. Ohno, O. Hayashida, Y. Hisaeda, *J. Chem. Soc. Chem. Commun.* **1991**, 950 – 952; e) Y. Murakami, J.-I. Kikuchi, T. Ohno, T. Hirayama, Y. Hisaeda, H. Nishimura, J. P. Snyder, K. Steliou, *J. Am. Chem. Soc.* **1991**, *113*, 8229 – 8242; f) Y. Hisaeda, T. Ihara, T. Ohno, Y. Murakami, *Tetrahedron Lett.* **1990**, *31*, 1027 – 1030; g) Y. Murakami, T. Ohno, O. Hayashida, Y. Hisaeda, *Chem. Lett.* **1991**, 1595 – 1598; h) J. Franke, F. Vögtle, *Angew. Chem.* **1985**, *97*, 224 – 225; *Angew. Chem. Int. Ed. Engl.* **1985**, *24*, 219 – 222; i) S. Kumar, H.-J. Schneider, *J. Chem. Soc. Perkin Trans. 2* **1989**, 245 – 250.
[17] a) H.-J. Schneider, R. Kramer, I. Theis, M.-Q. Zhou, *J. Chem. Soc. Chem. Commun.* **1990**, 276 – 278; b) H. Kawakami, O. Yoshino, K. Odashima, K. Koga, *Chem. Pharm. Bull.* **1985**, *33*, 5610 – 5613; c) K. Odashima, H. Kawakami, A. Miwa, I. Saski, K. Koga, *Chem. Pharm. Bull.* **1989**, *37*, 257 – 259; d) H.-J. Schneider, J. Pöhlmann, *Bioorg. Chem.* **1987**, *15*, 183 – 193; e) H.-J. Schneider, T. Blatter, S. Simova, I. Theis, *J. Chem. Soc. Chem. Commun.* **1989**, 580 – 581; f) H.-J. Schneider, I. Theis, *Angew. Chem.* **1989**, *101*, 757 – 759; *Angew. Chem. Int. Ed. Engl.* **1989**, *28*, 753 – 754.
[18] a) C. J. van Stavern, V. M. L. J. Aarts, P. D. J. Crootenhuis, W. J. H. Droppers, J. van Eerden, S. Harkema, D. N. Reinhoudt, *J. Am. Chem. Soc.* **1998**, *120*, 8134 – 8144; b) S. G. Mairanovskii, S. K. Erbekov, R. U. Vakhobova, *Elektrokhimiya* **1990**, *26*, 88 – 90; c) E. Kimura, A. Watanabe, M. Kodama, *J. Am. Chem. Soc.* **1983**, *105*, 2063 – 2066; d) E. Kimura, T. Koike, M. Kodama, *Chem. Pharm. Bull.* **1984**, *32*, 3569 – 3578; e) E. Kimura, *J. Inclusion Phenom. Mol. Recognit. Chem.* **1989**, *7*, 183 – 191; f) O. V. Kulikov, I. V.; Terekhova, *Russ. J. Coord. Chem.* **1998**, *24*, 821 – 823; g) D. Sun, J. Chen, W. Lu, X. Zheng, *J. Solution Chem.* **1998**, *27*, 1097 – 1107.
[19] a) S. Shinkai, *J. Inclusion Phenom. Mol. Recognit. Chem.* **1989**, *7*, 193 – 201; b) C. D. Gutsche, I. Alam, *Tetrahedron* **1988**, *44*, 4689 – 4694; c) C. D. Gutsche, I. Alam, M. Iqbal, T. Mangiafico, K. C. Nam, J. Rogers, K. A. See, *J. Inclusion Phenom. Mol. Recognit. Chem.* **1989**, *7*, 61 – 72; d) I. Alam, C. D. Gutsche, *J. Org. Chem.* **1990**, *55*, 4487 – 4489; e) S. Shinkai, H. Koreishi, S. Mori, T. Sone, O. Manabe, *Chem. Lett.* **1985**, 1033 – 1036; f) S. Shinkai, *Pure Appl. Chem.* **1986**, *58*, 1523 – 1528; g) S. Shinkai, S. Mori, H. Koreishi, T. Tsubaki, O. Manabe, *J. Am. Chem. Soc.* **1986**, *108*, 2409 – 2416; h) S. Shinkai, H. Kawabata, T. Arimura, T. Matsuda, H. Satoh, O. Manube, *J. Chem. Soc. Perkin Trans. 1* **1989**, 1073 – 1074; i) L. Zhang, A. Macías, T. Lu, J. I. Gordon, G. W. Gokel, A. E. Kaifer, *J. Chem. Soc. Chem. Commun.* **1993**, 1017 – 1019; j) G. Arena, A. Casnati, A. Contino, F. G. Gulino, D. Sciotto, R. Ungaro, *J. Chem. Soc. Perkin Trans. 2* **2000**, 419 – 423; k) R. Castro, L. A. Godínez, C. M. Criss, A. E. Kaifer, *J. Org. Chem.* **1997**, *62*, 4928 – 4935; l) G. Arena, A. Casnati, A. Contino, G. G. Lombardo, D. Sciotto, R. Ungaro, *Chem. Eur. J.* **1999**, *5*, 738 – 744; m) S. Shinkai, K. Araki, T. Matsuda, O. Manabe, *Bull. Chem. Soc. Jpn.* **1989**, *62*, 3856 – 3862.
[20] a) T. H. Webb, H. Suh, C. S. Wilcox, *J. Am. Chem. Soc.* **1991**, *113*, 8554 – 8555; b) D. A. Stauffer, R. E. Barrans, Jr., D. A. Dougherty, *J. Org. Chem.* **1990**, *55*, 2762 – 2767; c) T. J. Shepodd, M. A. Petti, D. A. Dougherty, *J. Am. Chem. Soc.* **1988**, *110*, 1983 – 1985; d) P. C. Kearney, L. S. Mizoue, R. A. Kumpf, J. E. Forman, A. McCurdy, D. A. Dougherty, *J. Am. Chem. Soc.* **1993**, *115*, 9907 – 9919; e) A. McCurdy, L. Jimenez, D. A. Stauffer, D. A. Dougherty, *J. Am. Chem. Soc.* **1992**, *114*, 10314 – 10321.
[21] C. S. Wilcox, M. D. Cowart, *Tetrahedron Lett.* **1986**, *27*, 5563 – 5566.
[22] E. M. Seward, R. B. Hopkins, W. Sauerer, S.-W. Tam, F. Diederich, *J. Am. Chem. Soc.* **1990**, *112*, 1783 – 1790.
[23] K. Kano, T. Hayakawa, S. Hashimoto, *Bull. Chem. Soc. Jpn.* **1991**, *64*, 778 – 784.
[24] a) B.-L. Poh, L.-S. Koay, *Tetrahedron Lett.* **1990**, *31*, 1911 – 1914; b) B.-L. Poh, C. S. Lim, L.-S. Koay, *Tetrahedron* **1990**, *46*, 6155 – 6160.
[25] S. Claude, J.-M. Lehn, F. Schmidt, J.-P. Vigneron, *J. Chem. Soc. Chem. Commun.* **1991**, 1182 – 1185.
[26] F. M. Menger, M. Takeshita, J. F. Chow, *J. Am. Chem. Soc.* **1981**, *103*, 5938 – 5939.
[27] R. Neugebauer, W. Knoche, *J. Chem. Soc. Perkin Trans. 2* **1998**, 529 – 534.

 © 2003 Wiley-VCH Verlag GmbH & Co. KGaA, Weinheim

[28] a) J. Rao, J. Lahiri, R. M. Weis, G. M. Whitesides, *J. Am. Chem. Soc.* **2000**, *122*, 2698 – 2710; b) a general review of polyvalent interactions is also available: M. Mammen, S.-K. Choi, G. M. Whitesides, *Angew. Chem.*, **1998**, *110*, 2908 – 2953; *Angew. Chem. Int. Ed.* **1998**, *37*, 2754 – 2794.
[29] R. M. Izatt, J. S. Bradshaw, K. Pawlak, R. L. Brening, B. J. Tarbet, *Chem. Rev.* **1992**, *92*, 1261 – 1354.
[30] A. J. Portmann, S. A. Levison, W. B. Dandliker, *Immunochemistry* **1975**, *12*, 461 – 466.
[31] a) F. Schwesinger, R. Ros, T. Strunz, D. Anselmetti, H.-J. Güntherodt, A. Honegger, L. Jermutus, L. Tiefenauer, A. Plückthun, *Proc. Natl. Acad. Sci. USA* **2000**, *97*, 9972 – 9977; b) O. Siiman, A. Burshteyn, *Cytometry* **2000**, *40*, 316 – 326; c) E. T. Boder, K. S. Midelfort, K. D. Wittrup, *Proc. Natl. Acad. Sci. USA* **2000**, *97*, 10701 – 10705; d) H. Torigoe, T. Nakayama, M. Imazato, I. Schimada, Y. Arata, A. Sarai, *J. Biol. Chem.* **1995**, *270*, 22218 – 22222; e) J. B. Pitner, W. F. Beyer, T. M. Venetta, C. Nycz, M. J. Mitchell, S. L. Harris, J. R. Mariño-Albernas, F.-I. Auzanneau, F. Forooghian, B. M. Pinto, *Carbohydr. Res.* **2000**, *324*, 17 – 29; f) D. M. Shaw, M. J. Embleton, C. Westwater, M. G. Ryan, K. A. Myers, S. M. Kingsman, M. W. Carroll, P. L. Stern, *Biochim. Biophys. Acta* **2000**, *1524*, 238 – 246; g) J. E. Smallshaw, F. Georges, J. S. Lee, E. B. Waygood, *Protein Eng.* **1999**, *12*, 623 – 630; h) D. A. Dougan, R. L. Malby, L. C. Gruen, A. A. Kortt, P. J. Hudson, *Protein Eng.* **1998**, *11*, 65 – 74; i) K. Dill, C. Poteras, C. Fraser, D. G. Hafemann, J. C. Owicki, J. D. Olson, *Anal. Biochem.* **1994**, *217*, 127 – 138; j) N. H. H. Heegaard, O. J. Bjerrum, *Anal. Biochem.* **1991**, *195*, 319 – 326; k) N. V. Visser, I. E. Smit-Kingma, *Spectrochim. Acta Part A* **1999**, *55*, 2271 – 2279; l) "Thermodynamic Data for Protein–Ligand Interaction": H. Wiesinger, H.-J. Hinz in *Thermodynamic Data for Biochemistry and Biotechnology* (Ed.: H.-J. Hinz), Springer, New York, **1986**, pp. 211 – 226.
[32] J. Xu, Q. Deng, J. Chen, K. N. Houk, J. Bartek, D. Hilvert, I. A. Wilson, *Science* **1999**, *286*, 2345 – 2348.
[33] a) I. A. Wilson, R. L. Stanfield, *Curr. Opin. Struct. Biol.* **1993**, *3*, 113 – 118; b) R. L. Stanfield, I. A. Wilson, *Curr. Opin. Struct. Biol.* **1995**, *5*, 103 – 113.
[34] a) J. Foote, H. N. Eisen, *Proc. Natl. Acad. Sci. USA* **1995**, *92*, 1254 – 1256; b) B. G. Miller, R. Wolfenden, *Annu. Rev. Biochem.* **2002**, *71*, 847 – 885.
[35] a) A. Mazzini, P. Cavatorta, M. Iori, R. Favilla, G. Sartor, *Biophys. Chem.* **1992**, *42*, 101 – 109; b) J. L. Sohl, A. G. Splittgerber, *J. Chem. Educ.* **1991**, *68*, 262 – 264; c) K. Murakami, *Bull. Chem. Soc. Jpn.* **1993**, *66*, 2808 – 2813; d) K. Murakami, *Biophys. Chem.* **1991**, *41*, 253 – 261; e) N. Okabe, M. Hozake, *Chem. Pharm. Bull.* **1991**, *39*, 478 – 480; f) N. Okabe, Y. Sagimori, M. Hozake, *Chem. Pharm. Bull.* **1991**, *39*, 2115 – 2116; g) I. N. Bojesen, E. Bojesen, *J. Lipid Res.* **1994**, *35*, 770 – 778; h) S. Watanabe, T. Sato, *Biochim. Biophys. Acta* **1996**, *1289*, 385 – 396.
[36] S. Curry, P. Brick, N. P. Franks, *Biochim. Biophys. Acta* **1999**, *1441*, 131 – 140.
[37] a) M. J. Swamy, *Biochem. Mol. Biol. Int.* **1995**, *36*, 219 – 225; b) B. Kuhn, P. A. Kollman, *J. Am. Chem. Soc.* **2000**, *122*, 3909 – 3916.
[38] a) L. B. Moore, B. Goodwin, S. A. Jones, G. B. Wisely, C. J. Serabjit-Singh, T. M. Willson, J. L. Collins, S. A. Skiewer, *Proc. Natl. Acad. Sci. USA* **2000**, *97*, 7500 – 7502; b) R. E. Watkins, G. B. Wisely, L. B. Moore, J. L. Collins, M. H. Lambert, S. P. Williams, T. M. Willson, S. A. Kliewer, M. R. Redinbo, *Science* **2001**, *292*, 2329 – 2333.
[39] BRENDA online database of enzyme metabolic data: http://www.brenda.uni-koeln.de (accessed in February 2001).
[40] a) A. Radzicka, R. Wolfenden, *J. Am. Chem. Soc.* **1996**, *118*, 6105 – 6109; b) R. Wolfenden, X. Lu, G. Young, *J. Am. Chem. Soc.* **1998**, *120*, 6814 – 6815; c) A. Radzicka, R. Wolfenden, *Science* **1995**, *267*, 90 – 93; d) E. A. Taylor, D. R. J. Palmer, J. A. Gerlt, *J. Am. Chem. Soc.* **2001**, *123*, 5824 – 5825; e) R. A. R. Bryant, D. E. Hansen, *J. Am. Chem. Soc.* **1996**, *118*, 5498 – 5499.
[41] a) I. E. Kuntz, K. Chen, K. A. Sharp, P. A. Kollman, *Proc. Natl. Acad. Sci. USA* **1999**, *96*, 9997 – 10002; b) P. Gilli, V. Ferretti, G. Filli, P. A. Borea, *J. Phys. Chem.* **1994**, *98*, 1515 – 1518.
[42] D. E. Koshland, Jr., *Proc. Natl. Acad. Sci. USA* **1958**, *44*, 98 – 104.
[43] A. J. Chmura, M. S. Orton, C. F. Meares, *Proc. Natl. Acad. Sci. USA* **2001**, *98*, 8480 – 8484.
[44] a) E. A. Meyer, R. K. Castellano, F. Diederich, *Angew. Chem.* **2003**, *115*, 1244 – 1287; *Angew. Chem. Int. Ed.* **2003**, *42*, 1210 – 1250; b) E. Grunwald, C. Steel, *J. Am. Chem. Soc.* **1995**, *117*, 5687 – 5692; c) A. F. D. de Namor, M.-C. Ritt, M.-J. Schwing-Weill, F. Arnaud-Neu, D. F. V. Lewis, *J. Chem. Soc. Faraday Trans.* **1991**, *87*, 3231 – 3239.
[45] J. D. Dunitz, *Chem. Biol.* **1995**, *2*, 709 – 712.
[46] a) M. S. Westwell, M. S. Searle, J. Klein, D. H. Williams, *J. Phys. Chem.* **1996**, *100*, 16000 – 16001; b) D. H. Williams, M. S. Westwell, *Chem. Soc. Rev.* **1998**, *27*, 57 – 63; c) M. I. Page, W. P. Jencks, *Gazz. Med. Ital.* **1987**, *117*, 455 – 460.
[47] D. H. Williams, C. T. Calderone, D. P. O. Brien, R. Zerella, *Chem. Commun.* **2002**, *12*, 1266 – 1267.
[48] O. Exner, *Prog. Phys. Org. Chem.* **1973**, *10*, 411 – 482.
[49] a) K. Sharp, *Protein Sci.* **2001**, *10*, 661 – 667; b) A. Ben-Naim, Y. Marcus, *J. Chem. Phys.* **1984**, *81*, 2016; c) N. T. Southall, K. A. Dill, A. D. J. Haymet, *J. Phys. Chem. B* **2002**, 106, 521 – 533.
[50] a) R. Krug, W. Hunter, R. Grieger, *Nature* **1976**, *261*, 566 – 567; b) R. Lumry, S. Rajender, *Biopolymers* **1970**, *9*, 1125 – 1227.
[51] A. C. Bowden, *J. Biosci.* **2002**, *27*, 121 – 126.
[52] a) L. A. Curtiss, K. Raghavachari, P. C. Redfern, G. S. Kedziora, J. A. Pople, *J. Phys. Chem. A* **2001**, *105*, 227 – 228; b) J. A. Montgomery, M. J. Frisch, J. W. Ochterski, G. A. Petersson, *J. Chem. Phys.* **1999**, *110*, 2822 – 2827; c) J. M. L. Martin, G. de Oliveira, *J. Chem. Phys.* **1999**, *111*, 1843 – 1856.
[53] S. Raugei, M. L. Klein, *J. Am. Chem. Soc.* **2001**, *123*, 9484 – 9485.
[54] M. C. Payne, M. P. Teter, D. C. Allan, *J. Chem. Soc. Faraday Trans.* **1990**, *86*, 1221 – 1226.
[55] J. Tomasi, R. Cammi, B. Mennucci, *Int. J. Quantum Chem.* **1999**, *75*, 783 – 803.
[56] W. D. Cornell, P. Cieplak, C. I. Bayly, I. R. Gould, K. M. Merz, Jr., D. M. Ferguson, D. C. Spellmeyer, T. Fox, J. W. Caldwell, P. A. Kollman, *J. Am. Chem. Soc.* **1995**, *117*, 5179 – 5197.
[57] W. L. Jorgensen, D. S. Maxwell, J. Tirado-Rives, *J. Am. Chem. Soc.* **1996**, *118*, 11225 – 11236.
[58] a) D. Qiu, P. S. Shenkin, F. P. Hollinger, W. C. Still, *J. Phys. Chem. A* **1997**, *101*, 3005 – 3014; b) W. C. Still, A. Tempczyk, R. C. Hawley, T. Hendrickson, *J. Am. Chem. Soc.* **1990**, *112*, 6127 – 6129.
[59] a) R. C. Rizzo, J. Tirado-Rives, W. L. Jorgensen, *J. Med. Chem.* **2001**, *44*, 145 – 154; b) M. L. P. Price, W. L. Jorgensen, *J. Am. Chem. Soc.* **2000**, *122*, 9455 – 9466.
[60] a) C. M. Reyes, R. Nifosi, A. D. Frankel, P. A. Kollman, *Biophys. J.* **2001**, *80*, 2833 – 2842; b) P. A. Kollman, I. Massova, C. Reyes, B. Kuhn, S. Huo, L. Chong, M. Lee, T. Lee, Y. Duan, W. Wang, O. Donini, P. Cieplak, J. Srinivasan, D. A. Case, T. E. Cheatham III, *Acc. Chem. Res.* **2000**, *33*, 889 – 897.
[61] a) K. S. Kim, P. Tarakeshwar, J. Y. Lee, *Chem. Rev.* **2000**, *100*, 4145 – 4186; b) D. H. Williams, B. Bardsley, *Perspect. Drug Discovery Des.* **1999**, *17*, 43 – 59; c) M. S. Searle, D. H. Williams, U. Gerhard, *J. Am. Chem. Soc.* **1992**, *114*, 10697 – 10704.
[62] H.-J. Böhm, *J. Comput.-Aided Mol. Des.* **1994**, *8*, 243 – 256, 623 – 632.
[63] a) F. Eblinger, H.-J. Schneider, *Angew. Chem.* **1998**, *110*, 821 – 824; *Angew. Chem. Int. Ed.* **1998**, *37*, 826 – 829; b) A. Hossain, H.-J. Schneider, *Chem. Eur. J.* **1999**, *5*, 1284 – 1290.
[64] K. A. Dill, *J. Biol. Chem.* **1997**, *272*, 701 – 704.

 © 2003 Wiley-VCH Verlag GmbH & Co. KGaA, Weinheim

[65] a) D. Eisenberg, A. D. McLachlan, *Nature* **1986**, *319*, 199–203; b) L. Wesson, D. Eisenberg, *Protein Sci.* **1992**, *1*, 227–235; c) I. Luque, E. Freire, *Proteins Struct. Funct. Genet.* **2002**, *49*, 181–190.

[66] a) C. Tanford, *The Hydrophobic Effect: Formation of Micelles and Biological Membranes*, Wiley, New York, **1980**; b) W. Blokzijl, J. B. F. N. Engberts, *Angew. Chem.* **1993**, *105*, 1610–1648; *Angew. Chem. Int. Ed. Engl.* **1993**, *32*, 1545–1579; c) T. Lazaridis, *Acc. Chem. Res.* **2001**, *34*, 931–937.

[67] Ref. [15s].

[68] K. A. Dill, *Biochemistry* **1990**, *29*, 7133–7155.

[69] See, for example: T. M. Raschke, J. Tsai, M. Levitt, *Proc. Natl. Acad. Sci. USA* **2001**, *98*, 5965–5969.

[70] Ref. [49c].

[71] a) R. Hubbard, J. Thornton, NACCESS, **1993**, Department of Biochemistry and Molecular Biology, University College London; b) A. Nicholls, K. A. Sharp, B. Honig, *Proteins Struct. Funct. Genet.* **1991**, *11*, 281–296.

[72] Since the buried surface area depends on the binding mode, conformational searching is first carried out with MacroModel using the AMBER* force field. The Merck molecular force field is used for nitrophenol since no suitable AMBER* force-field parameter has been found. The lowest energy conformation is chosen as the input for NACCESS.[71a]

[73] a) A. Bhattacharya, T. Grüne, S. Curry, *J. Mol. Biol.* **2000**, *303*, 721–732; b) I. Petitpas, A. A. Bhattacharya, S. Twine, M. East, S. Curry, *J. Biol. Chem.* **2001**, *276*, 22804–22809; c) A. A. Bhattacharya, S. Curry, N. P. Franks, *J. Biol. Chem.* **2000**, *275*, 38731–38738.

[74] a) F. E. Romesberg, B. Spiller, P. G. Schultz, R. C. Stevens, *Science* **1998**, *279*, 1929–1933; b) G. J. Wedemayer, P. A. Patten, L. H. Wang, P. G. Schultz, R. C. Stevens, *Science* **1997**, *276*, 1665–1669; c) K. Hotta, H. Lange, D. J. Tantillo, K. N. Houk, D. Hilvert, I. A. Wilson, *J. Mol. Biol.* **2000**, *302*, 1213–1225; d) C. M. Paschal, J. Hasserodt, T. Jones, R. A. Lerner, K. D. Janda, D. W. Christianson, *Angew. Chem.* **1999**, *111*, 1859–1864; *Angew. Chem. Int. Ed.* **1999**, *38*, 1743–1747; e) J. Hasserodt, K. D. Janda, R. A. Lerner, *J. Am. Chem. Soc.* **1997**, *119*, 5993–5998; f) B. Gigant, T. Tsumuraya, I. Fujii, M. Knossow, *Structure* **1999**, *7*, 1385–1393; g) B. Golinelli-Pimpaneau, O. Gonçalves, T. Dintinger, D. Blanchard, M. Knossow, C. Tellier, *Proc. Natl. Acad. Sci. USA* **2000**, *97*, 9892–9895; h) P. A. Patten, N. S. Gray, P. L. Yang, C. B. Marks, G. J. Wedemayer, J. J. Boniface, R. C. Stevens, P. G. Schultz, *Science* **1996**, *271*, 1086–1091; i) L. C. Hsieh-Wilson, P. G. Schultz, R. C. Stevens, *Proc. Natl. Acad. Sci. USA* **1996**, *93*, 5363–5367; j) B. Gigant, J.-B. Charbonnier, Z. Eshhar, B. S. Green, M. Knossow, *Proc. Natl. Acad. Sci. USA* **1997**, *94*, 7857–7861; k) K. Gruber, B. Zhou, K. N. Houk, R. A. Lerner, C. G. Shelvin, I. A. Wilson, *Biochemistry* **1999**, *38*, 7062–7074; l) F. E. Romesberg, B. D. Santarsiero, B. Spiller, J. Yin, D. Barnes, P. G. Schultz, R. C. Stevens, *Biochemistry* **1998**, *37*, 14404–14409; m) A. G. Cochran, P. G. Schultz, *Science* **1990**, *249*, 781–783; n) M. M. Thayer, E. H. Olender, A. S. Arvai, C. K. Koike, I. L. Canestrelli, J. D. Stewart, S. J. Benkovic, E. D. Getzoff, V. A. Roberts, *J. Mol. Biol.* **1999**, *291*, 329–345.

[75] E. A. Padlan, *Adv. Protein Chem.* **1990**, *49*, 57–133.

[76] S. Jones, J. M. Thornton, *Proc. Natl. Acad. Sci. USA* **1996**, *93*, 13–20.

[77] a) H.-J. Schneider, T. Blatter, S. Simova, *J. Am. Chem. Soc.* **1991**, *113*, 1996–2000; b) L. Garel, B. Lozach, J.-P. Dutasta, A. Collet, *J. Am. Chem. Soc.* **1993**, *115*, 11652–11653.

[78] a) H. Gohlke, G. Klebe, *Angew. Chem.* **2002**, *114*, 2764–2798; *Angew. Chem. Int. Ed.* **2002**, *41*, 2644–2676; b) R. Wang, L. Lai, S. Wang, *J. Comput.-Aided Mol. Des.* **2002**, *16*, 11–26; c) A. M. Davis, S. J. Teague, G. J. Kleywert, *Angew. Chem.* **2003**, *115*, 2822–2841; *Angew. Chem. Int. Ed.* **2003**, *42*, 2718–2736.

[79] A. Warshel, *Computer Modeling of Chemical Reactions in Enzymes and Solutions*, Wiley, New York, **1991**.

[80] B. G. Miller, M. J. Snider, S. A. Short, R. Wolfenden, *Biochemistry* **2000**, *39*, 8113–8118.

[81] T. L. Aymes, A. C. O'Donoghue, J. P. Richard, *J. Am. Chem. Soc.* **2001**, *123*, 11325–11326.

[82] a) D. E. Koshland, Jr., *Angew. Chem.* **1994**, *106*, 2467–2472; *Angew. Chem. Int. Ed. Engl.* **1994**, *33*, 2375–2378; b) D. Herschlag, *Bioorg. Chem.* **1988**, *16*, 62–96.

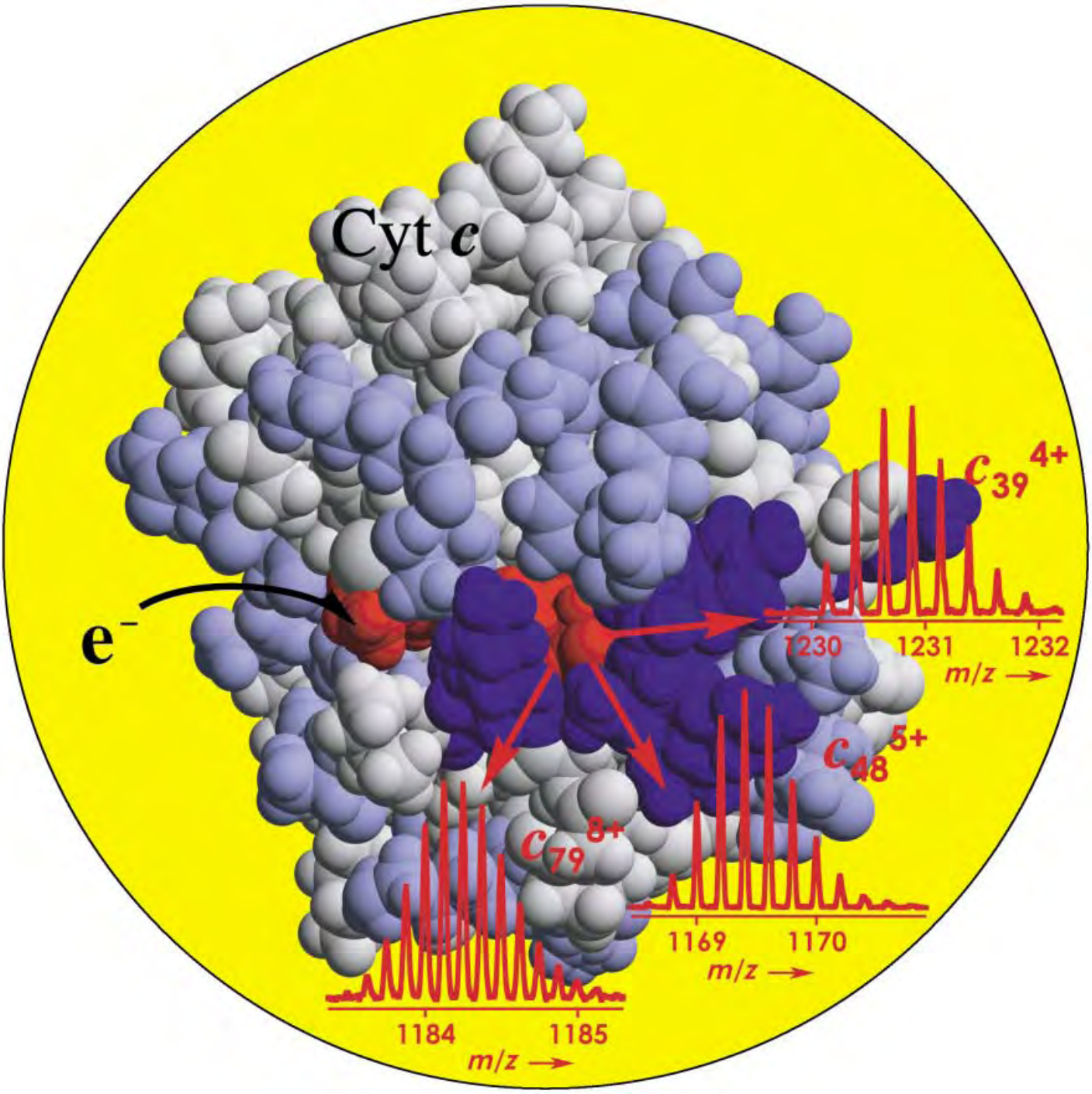
[83] a) A. Kohen, J. P. Klinman, *Chem. Biol.* **1999**, *6*, R191–R198; b) W. R. Cannon, S. J. Benkovic, *J. Biol. Chem.* **1998**, *273*, 26257–26260; c) E. Y. Lau, T. C. Bruice, *J. Am. Chem. Soc.* **1998**, *120*, 12387–12394; d) J. L. Radkiewicz, C. L. Brooks III, *J. Am. Chem. Soc.* **2000**, *122*, 225–231; e) M. Karplus, *J. Phys. Chem. B* **2000**, *104*, 11–27.

[84] G. Ujaque, D. J. Tantillo, Y. Hu, K. N. Houk, K. Hotta, D. Hilvert, *J. Comput. Chem.* **2002**, *24*, 98–110.

[85] M. J. Field, *J. Comput. Chem.* **2000**, *23*, 48–58.

 © 2003 Wiley-VCH Verlag GmbH & Co. KGaA, Weinheim

Communications



Native electron capture dissociation (NECD) is a new mass-spectrometric method for the structural investigation of noncovalent interactions in native proteins such as Cytochrome *c*. In contrast to conventional ECD techniques no external electrons are added because highly asymmetrical charge distribution (charge partitioning) occurs on dissociation of protein dimers and results in electron transfer.

DOI: 10.1002/anie.200351705
© 2003 Wiley-VCH Verlag GmbH & Co. KGaA, Weinheim

MS Shows Tertiary Structure

Native Electron Capture Dissociation for the Structural Characterization of Noncovalent Interactions in Native Cytochrome *c***

Kathrin Breuker and Fred W. McLafferty*

Recent efforts in biomolecular mass spectrometry (MS) are directed towards life-science problems beyond molecular-weight determination and protein identification,[1] for example, the study of noncovalent protein complexes[2] and protein folding.[2b,3] From electrospray ionization (ESI) MS experiments, the stoichiometry of binding partners within protein–protein, protein–ligand, and protein–nucleic acid complexes can be derived,[2] given that any changes in noncovalent bonding on entrance into the gas phase do not affect this stoichiometry. However, extensive studies show that hydrophobic and hydrogen bonds are weakened and strengthened, respectively, in the gas phase, and that gaseous tertiary structures can differ dramatically from those in solution.[4] The most detailed information on the structurally transformed gas-phase conformers from ESI has come recently from electron capture dissociation (ECD).[4d,g,h,5] We report herein what appear to be ECD mass spectra that instead reflect the *native* structure of the protein, formed *without* the experimental addition of electrons. We term this new technique "native ECD" (NECD).

Cytochrome *c* (Cyt *c*), a small electron-transfer protein with an almost spherical shape in its native state (Figure 1),[6] is among the proteins most thoroughly investigated with respect to structure and folding in the gas phase.[2c,3,4a–4f] After ESI of Cyt *c* solutions retaining the native structure (pH 3.5, 4.5) into a Fourier transform (FT) mass spectrometer, ECD of the 8+ and 9+ molecular ions (MS/MS) gave no product ions from backbone fragmentation; the nonergodic ECD cleaves the protein-ion backbone without rupture of the noncovalent bonding of the tertiary structure[4d,g,h] After denaturation of the molecular ions by gentle collisional activation,[5d] the ECD spectrum demonstrates cleavage of 69 of the 103 inter-residue bonds in the Cyt *c* backbone (see Figure 2a). In agreement with the radical mechanism of ECD (Scheme 1) unique products ***c***, ***z****, and ***a**** (as well as ***y*** ions) are obtained; conventional ion-dissociation spectra from energetic cleavage (e.g., collisionally activated dissociation (CAD), or infrared multiphoton dissociation (IRMPD)) of protein ions instead show ***b*** ($RC{\equiv}O^+$) as well as ***y*** ions. Thus we were surprised to find ***c*** ions in an ESI spectrum of Cyt *c* (Figure 2b) run without added electrons under conditions of ion activation that produced no ***b*** ions. The other products in Figure 2b were ***y*** ions that generally arose by cleavages between the same amino acids that gave the ***c*** ions. Figure 2b and a show little resemblance; the most favored cleavage, between Lys 79 and Met 80, of Figure 2b is among the least favored in Figure 2a. Under the same conditions, but after rigorous stirring of the Cyt *c* solutions, spectra like those in Figure 2c were obtained;

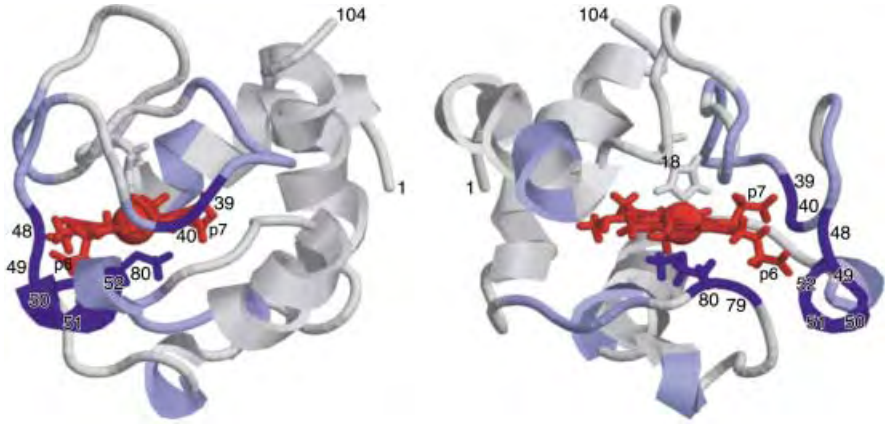
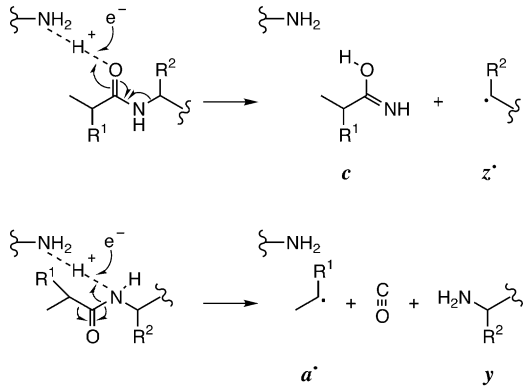


Figure 1. Band and stick representation of native (Fe^{III}) Cyt *c* (solution structure from the protein data base (PDB file 1AKK[11a]).[17] Red: heme; blue: residues 39, 40, 48–52, 79, 80 framing major NECD cleavages shown in Figure 2b, c; light blue: residues 11–13, 26–28, 33–38, 41, 45–47, 53–55, 68, 69, 72, 73, 82–85 framing minor NECD cleavages. The images differ by a 120° rotation around the vertical axis.

[*] Dr. K. Breuker
Institute of Organic Chemistry
Innsbruck University
Innrain 52a, 6020 Innsbruck (Austria)
Fax: (+43) 512-507-2892
E-mail: kbreuker@gmx.net
Prof. Dr. F. W. McLafferty
Department of Chemistry and Chemical Biology
Baker Laboratory
Cornell University, Ithaca, NY 14853-1301 (USA)

[**] The authors acknowledge generous funding from the Austrian Science Foundation (FWF grant P15767 to KB) and the National Institutes of Health (NIH grant GM16609 to FWM), and thank Dr. Rich Knochenmuss, Prof. Dr. Bernhard Kräutler, Huili Zhai, Dr. Vlad Zabrouskov, Dr. Cheng Lin, and Xuemei Han for discussions and Pieter Dörrestein for recording solution UV/Vis spectra.



Scheme 1. Mechanism of ECD fragmentation, with the proton originally on an adjacent basic amino acid residue.

 © 2003 Wiley-VCH Verlag GmbH & Co. KGaA, Weinheim DOI: 10.1002/anie.200351705

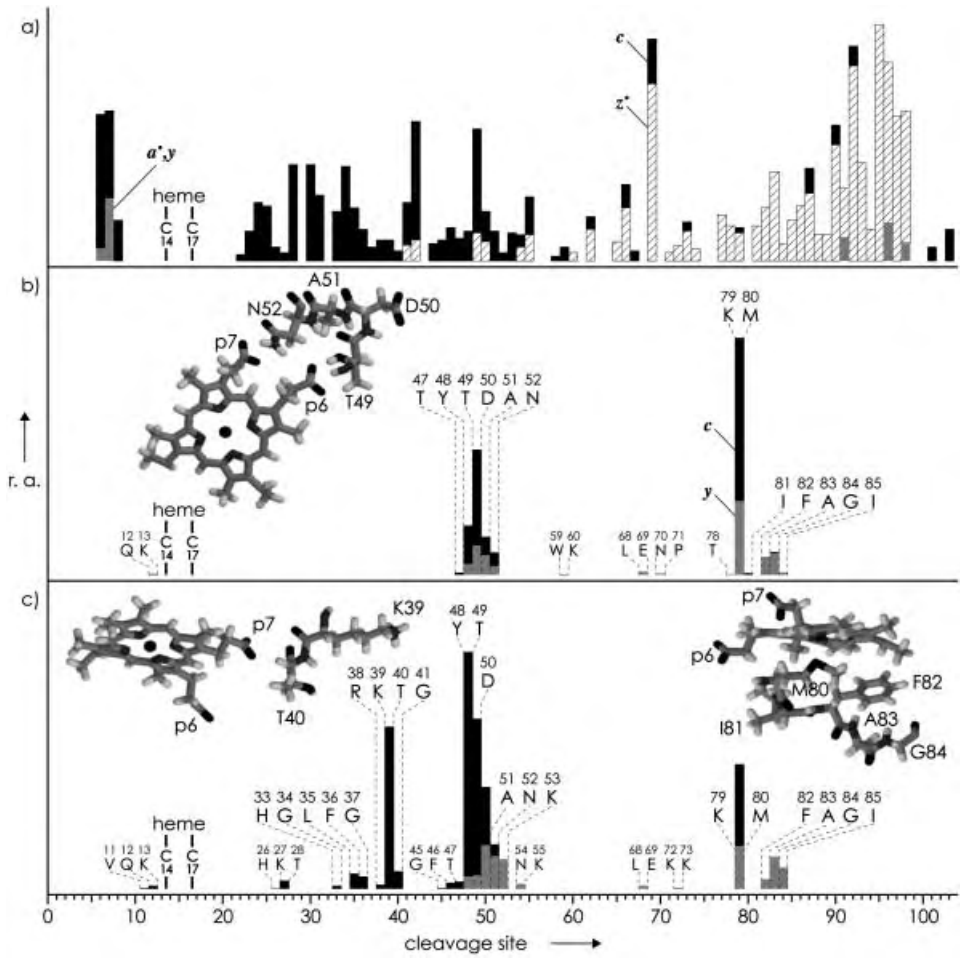


Figure 2. Relative abundances (r.a.) of Cyt*c* fragment ions: a) spectrum after conventional ECD of molecular ions from ESI of a 10 μM, pH 3.5 aqueous solution (in-beam collisional activation);[5d] b, c) ESI of a 75 μM, pH 4.5 aqueous solution without the external addition of electrons, both 36% NECD yield, with partial structures of heme and neighboring residues of native (Fe^{III}) Cyt*c*; c) spectrum after 1 h additional stirring of the ESI solution with a Vortex mixer. ***c*** ions: black bars, ***y*** ions (***a***+**y*** in (a)): gray bars, ***z**** ions: striped bars.

these spectra appear to be the sum of the spectrum in Figure 2b plus a new one, whose formation is still under investigation. Although no extra electrons were added experimentally, the 36% yield of these ***c***, ***y*** product ions is high compared to that of early ECD studies.[5a]

The effect of the concentration of the ESI solution on fragment-ion yield is dramatic (Figure 3). In recent fluorescence studies, evidence for Cyt*c* dimerization in electrospray droplets was found for solution concentrations above 33 μM.[7] The corresponding increase shown in Figure 3 suggests that dimers are essential for the formation of ***c*** and ***y*** (although no dimer ions were detected in any of these spectra). The fragment yield decreases above 100 μM, presumably because of competitive formation of aggregates larger than dimers. Solution acidity also affects yield; for 100 μM aqueous solutions the following yields were obtained, pH 2.5, 5% (0% in 70% MeOH); pH 3.5, 13%; pH 4.5, 16%, and pH 5.5, 7% (adding 1% glycerol[8] did not affect the yield). These data are consistent with the decreasing denaturation of native Cyt*c* from pH 2.5 to 4.5,[9] with higher pH values (lower H^+ concentration) decreasing overall protonation during ESI. The yield was also strongly influenced by the temperature of the capillary through which the ESI ions enter the mass spectrometer. At 75 μM, pH 5, a reduction from 43 to 28°C decreased ***c*** and ***y*** formation from 21% to 2% (Figure 4) of the remaining molecular ions; lowering the pH to 3.5 at 30°C gave a yield of 31%. Formation of the ***c*** and ***y*** ions must occur in this capillary region, before extensive solvent removal ($\approx 10^{-4}$ Torr), and requires significantly more energy than

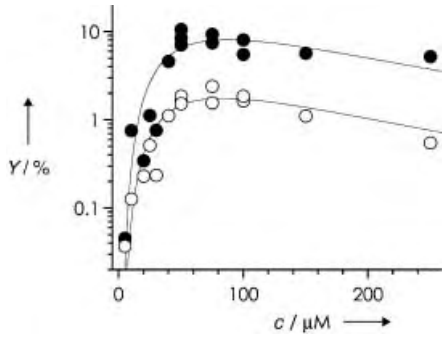


Figure 3. Yield (*Y*) of ***c*** and ***y*** (●) and $\boldsymbol{c}_{79}$ (○) ions from ESI of (Fe^{III}) Cyt*c* in H_2O as a function of solution concentration at pH 5.5. The solid line is to guide the eye.

 © 2003 Wiley-VCH Verlag GmbH & Co. KGaA, Weinheim

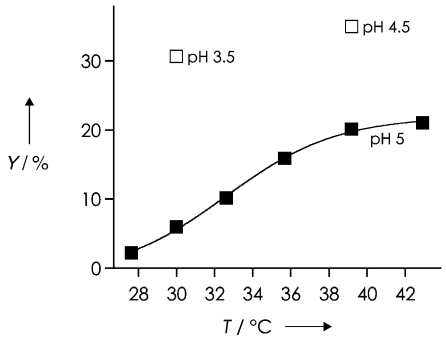


Figure 4. Yield (*Y*) of ***c*** and ***y*** ions from ESI of 75 μM (Fe^{III})Cyt *c* aqueous solutions as a function of capillary temperature (measured at the capillary orifice where ions enter the mass spectrometer); temperatures inside the capillary are proportionally higher by an estimated factor of two. Solid line is to guide the eye.

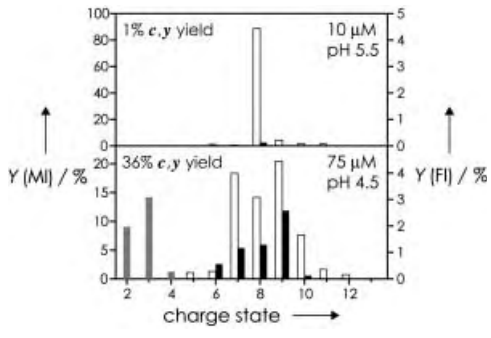


Figure 5. Yield (*Y*) of molecular ions $[M+(n-1)H]^{n+}$ (MI, open bars), and $(c_{79}+nH)^{n+}$ and $(y_{25}+nH)^{n+}$ fragment ions (FI, black and gray bars, respectively) from ESI of aqueous (Fe^{III}) Cyt *c* solutions (10 μM, pH 5.5 and 75 μMM, pH 4.5) versus charge state.

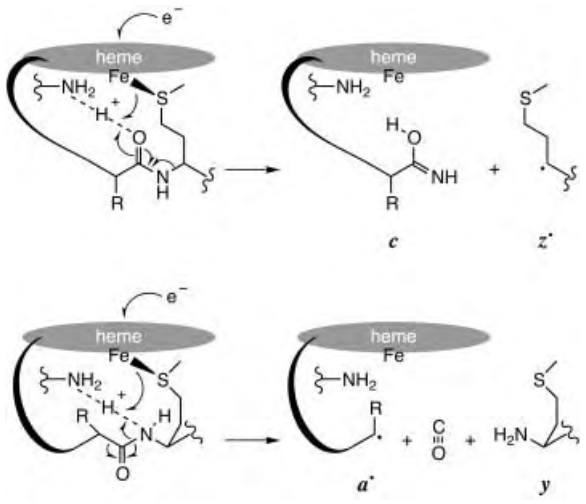
molecular-ion desolvation does. However, changing the instrumental parameters in lower pressure regions, such as the nozzle–skimmer voltage or related ion-lens potentials, had no effect.

The ***c***, ***y*** fragmentation pattern of (Fe^{II})Cyt *c*[10] electrosprayed from 100 μM aqueous solution at pH 4.5 (data not shown) was, within experimental error, the same as that of (Fe^{III})Cyt *c*; the Fe^{III} and Fe^{II} native forms differ mainly in the reorientation of a few side chains.[11] Further, all the ***c*** products that include the heme unit covalently bound to Cys 14 and Cys 17, obtained from both Fe^{III} and Fe^{II} solutions, have *m*/*z* values that indicate reduction to Fe^{II}. This result suggests that there is facile electron transfer in forming the Fe^{II} products from the Fe^{III} precursors. This same source could also supply an electron to effect ECD and form the observed ***c*** and ***y*** products, although the spectra in Figure 2 b, c show none of the expected complementary $z^{\bullet}$ and $a^{\bullet}$ products (Scheme 1). However, these highly reactive and thermally labile radical species[4g] should undergo many energetic collisions in passage through the capillary region.

An unusual MS/MS dissociation of stable gaseous Cyt *c* dimer ions electrosprayed from non-denaturing solutions and trapped in a FT-MS cell was recently elucidated by Williams and Jurchen.[12] Although with weak MS/MS (CAD) activation the dimer ions predominantly dissociate into monomers with equal charges, higher energies for activation result in asymmetric charge partitioning. This also appears to be the case for our dimer ions, which dissociate in the capillary region (Figure 5). ESI at 10 μM, a concentration at which little dimer or ***c*** and ***y*** ions are formed, produces almost exclusively 8+ monomer ions. ESI at 75 μM, a concentration favorable for formation of both dimers and ***c*** and ***y***, instead shows asymmetric charge partitioning with monomer charge states as high as 12+. An even higher charge is indicated for the precursors of the ***c*** and ***y*** ions (Figure 5, below); the sum of the average charges of the quasi-complementary fragments c_{79} (+8.48) and y_{25} (+2.66), together with the two electrons for ECD and heme-iron-center reduction, is consistent with an approximate 13+ charge for their monomeric precursor. This precursor must have depleted the charge of the other monomer to 3+ or 4+, which indicates a huge charge asymmetry prior to dimer dissociation that could have caused the electron transfers producing the ***c***(Fe^{II}), ***y*** products. Williams and Jurchen give convincing evidence that this charge asymmetry in protein dimer ions following activation results from the unfolding of one of the monomers.[12] The increased separation of the basic amino acid residues greatly increases their proton affinity, which attracts protons from the other monomer.

Because the ***c*** and ***y*** ions are found only from ESI of the native Cyt *c*, does its structure[6] also provide a mechanistic rationalization for the highly specific ***c*** and ***y*** ion formation shown in Figure 2 b,c? At least one of the transferred electrons, that forming the Fe^{II} product, must go to the heme ligand. In both native Fe^{II} and Fe^{III} structures the heme is also noncovalently bound to amino acid residues at which a second electron transfer could cause protein-backbone cleavage (Figure 2 b,c).[11] These residues are all positioned close to the exposed edge of the heme (Figure 1), thought to be the site of biological electron transfer.[13] The most prominent fragments arise from cleavage on the N-terminal side of Met 80 whose sulfur atom distally coordinates the heme iron center (Figure 1 and 2). Other abundant products originate from cleavages next to Thr 40, Thr 49, and Asn 52, which are hydrogen bonded to the carboxylate units of heme propionates 7, 6, and 7, respectively, in (Fe^{III})Cyt *c* (Asn 52 is hydrogen bonded to p6 in (Fe^{II})Cyt *c*).[11] The only other products, making up less than 1% of the total, are from cleavages close to the heme, such as near Lys 13 and in the 68–71 region. His 18, which is coordinated to the Fe center opposite to Met 80, exhibits no neighboring ECD. The proposal outlined in Scheme 2 supports the assumption that these cleavages, which occur during "gentle" ESI without external electron addition, actually involve the conventional ECD mechanism of Scheme 1. As the dimer passes through the inlet capillary, one of its monomers partially unfolds. The high-energy transition state in solution unfolding involves denaturation of the 3–14 and 90–101 terminal helices (Figure 1, right image, left side) by cleavage of the hydrophobic Phe 10–Leu 94 interhelix bond. These helices contain eight of the 21 basic residues in the monomer. Of the estimated eight protons on the monomer originally, around

 © 2003 Wiley-VCH Verlag GmbH & Co. KGaA, Weinheim



Scheme 2. Proposed mechanism of NECD fragmentation near Met80.

three of them should be found on these helices. Partial denaturation attracts five protons from the other monomer, enough for protonation of the newly exposed basic sites and to give a total of eight protons on these terminal helices. In response to this huge charge asymmetry, the other monomer gives up electrons to the partially unfolded monomer, with one electron reducing the Fe^{III} center and another electron being transferred to the heme to effect the ECD process shown in Scheme 2.

Cyt *c* native molecular ions are stabilized significantly by hydrophobic bonding;[14] complete desolvation accompanying ESI causes their denaturation. Previous ECD experiments[4d] have shown that after denaturation gaseous Cyt *c* ions refold into more stable gaseous ion structures quite different from the native solution structure.[4g] Although ESI of native Cyt *c* solutions can give $\leq 8+$ molecular ions whose collision-cross-section values agree with those calculated for the native structure,[4e] our evidence indicates that they have unfolded and refolded during transfer to the gas phase. This possibility should be considered seriously before using conventional ESI mass spectra as evidence of noncovalent binding in solution.[2]

We have shown that NECD is a promising new MS technique for the structural probing of noncovalent interactions in native proteins. Charge partitioning in protein dimer dissociation can apparently be so asymmetric that it causes intermolecular electron transfer and ECD of the protein backbone. For Cyt *c*, the resulting fragment ions directly correlate with noncovalent protein–heme interaction sites in the native structure. Although this appears to be the most detailed evidence reported to date of native conformation retained in transfer to the gas phase, NECD also shows that this conformation is a transient structure even during "gentle" ESI.

Experimental Section

Experiments were carried out on a 6-Tesla FT mass spectrometer described elsewhere.[5c] Ions formed by ESI at atmospheric pressure entered the instrument through a heated capillary and are transferred into the FT-ICR cell ($< 10^{-9}$ torr, N_2 pulse trapping) through quadrupole ion guides. ESI utilized homemade emitters of $\approx 5\,\mu m$ tip internal diameter, flow 200–500 $nL\,min^{-1}$, and 1 kV spray potential. Horse heart Cyt *c* (Sigma, St. Louis, MO, USA) was dissolved in water (nanopure, pH 5.5), lower pH values were obtained by addition of acetic acid. For (Fe^{II}) Cyt *c*, ascorbic acid was added to give pH 4.5.[10,4c,15] Spectral interpretation utilized the automated THRASH program.[16]

Received: April 23, 2003 [Z51705]
Published Online: September 23, 2003

Keywords: cytochrome *c* · electron capture dissociation · electron transfer · mass spectrometry · noncovalent interactions

[1] R. Aebersold, M. Mann, *Nature* **2003**, *422*, 198–207; F. Meng, B. J. Cargile, S. M. Patrie, J. R. Johnson, S. M. McLoughlin, N. L. Kelleher, *Anal. Chem.* **2002**, *74*, 2923–2929; G. E. Reid, S. A. McLuckey *J. Mass Spectrom.* **2002**, *37*, 663–675.

[2] a) J. A. Loo, *Mass Spectrom. Rev.* **1997**, *16*, 1–23; b) R. L. Winston, M. C. Fitzgerald, *Mass Spectrom. Rev.* **1997**, *16*, 165–179; c) B. N. Pramanik, P. L. Bartner, U. A. Mirza, Y.-H. Liu, A. K. Ganguly, *J. Mass Spectrom.* **1998**, *33*, 911–920; d) J. A. Loo, *Int. J. Mass Spectrom.* **2000**, *200*, 175–186; e) F. Sobott, C. V. Robinson, *Curr. Opin. Struct. Biol.* **2002**, *12*, 729–734.

[3] U. A. Mirza, S. L. Cohen, B. T. Chait, *Anal. Chem.* **1993**, *65*, 1–6; C. S. Hoaglund-Hyzer, A. E. Counterman, D. E. Clemmer, *Chem. Rev.* **1999**, *99*, 3037–3079; M. F. Jarrold, *Annu. Rev. Phys. Chem.* **2000**, *51*, 179–207; I. A. Kaltashov, S. J. Eyles, *Mass Spectrom. Rev.* **2002**, *21*, 37–71.

[4] a) D. Suckau, Y. Shi, S. C. Beu, M. W. Senko, J. P. Quinn, F. M. Wampler III, F. W. McLafferty, *Proc. Natl. Acad. Sci. USA* **1993**, *90*, 790–793; b) D. E. Clemmer, R. R. Hudgins, M. F. Jarrold, *J. Am. Chem. Soc.* **1995**, *117*, 10141–10142; c) F. W. McLafferty, Z. Guan, U. Haupts, T. D. Wood, N. L. Kelleher, *J. Am. Chem. Soc.* **1998**, *120*, 4732–4740; d) D. M. Horn, K. Breuker, A. J. Frank, F. W. McLafferty, *J. Am. Chem. Soc.* **2001**, *123*, 9792–9799; e) E. R. Badman, C. S. Hoaglund-Hyzer, D. E. Clemmer, *Anal. Chem.* **2001**, *73*, 6000–6007; f) R. Grandori, *Protein Sci.* **2002**, *11*, 453–458; g) K. Breuker, H.-B. Oh, D. M. Horn, B. A. Cerda, F. W. McLafferty, *J. Am. Chem. Soc.* **2002**, *124*, 6407–6420; h) H.-B. Oh, K. Breuker, S.-K. Sze, Y. Ge, B. K. Carpenter, F. W. McLafferty, *Proc. Natl. Acad. Sci. USA* **2002**, *99*, 15863–15868.

[5] a) R. A. Zubarev, N. L. Kelleher, F. W. McLafferty, *J. Am. Chem. Soc.* **1998**, *120*, 3265–3266; b) R. A. Zubarev, N. A. Kruger, E. K. Fridriksson, M. A. Lewis, D. M. Horn, B. K. Carpenter, F. W. McLafferty, *J. Am. Chem. Soc.* **1999**, *121*, 2857–2862; c) R. A. Zubarev, D. M. Horn, E. K. Fridriksson, N. L. Kelleher, N. A. Kruger, M. A. Lewis, B. K. Carpenter, F. W. McLafferty, *Anal. Chem.* **2000**, *72*, 563–573; d) D. M. Horn, Y. Ge, F. W. McLafferty, *Anal. Chem.* **2000**, *72*, 4778–4784.

[6] L. Banci, M. Assfalg in *Handbook of Metalloproteins, Vol. 1* (Eds: A. Messerschmidt, R. Huber, T. Poulos, K. Wieghardt), Wiley, New York, **2002**, pp. 33–43.

[7] S. E. Rodriguez-Cruz, J. T. Khoury, J. H. Parks, *J. Am. Soc. Mass Spectrom.* **2001**, *12*, 716–725.

[8] A. T. Iavarone, E. R. Williams, *J. Am. Chem. Soc.* **2003**, *125*, 2319–2327.

[9] Y. Goto, Y. Hagihara, D. Hamada, M. Hoshino, I. Nishii, *Biochemistry* **1993**, *32*, 11878–11885; Y. O. Kamatari, T. Konno, M. Kataoka, K. Akasaka, *J. Mol. Biol.* **1996**, *259*, 512–523.

[10] Cyt *c* molecular-ion *m*/*z* values from electrospray of reducing aqueous solutions (ascorbic acid, Cyt *c* oxidation state confirmed by UV/Vis spectroscopy) were $[M+nH]^{n+}$, consistent with Fe^{II}; ESI of (Fe^{III}) Cyt *c* gave $[M+(n-1)H]^{n+}$.

 © 2003 Wiley-VCH Verlag GmbH & Co. KGaA, Weinheim

[11] a) L. Banci, I. Bertini, H. B. Gray, C. Luchinat, T. Reddig, A. Rosato, P. Turano, *Biochemistry* **1997**, *36*, 9867 – 9877; b) L. Banci, I. Bertini, J. G. Huber, G. A. Spyroulias, P. Turano, *J. Biol. Inorg. Chem.* **1999**, *4*, 21 – 31.
[12] J. C. Jurchen, E. R. Williams, *J. Am. Chem. Soc.* **2003**, *125*, 2817 – 2826.
[13] J. Rawlings, S. Wherland, H. B. Gray, *J. Am. Chem. Soc.* **1976**, *98*, 2177 – 2180; A. J. Ahmed, F. Millett, *J. Biol. Chem.* **1981**, *256*, 1611 – 1615; W. H. Koppenol, E. Margoliash, *J. Biol. Chem.* **1982**, *257*, 4426 – 4437; H. S. Pappa, T. L. Poulos, *Biochemistry* **1995**, *34*, 6573 – 6580.
[14] L. Hoang, S. Bédard, M. M. G. Krishna, Y. Lin, S. W. Englander, *Proc. Natl. Acad. Sci. USA* **2002**, *99*, 12173 – 12178.
[15] F. He, C. L. Hendrickson, A. G. Marshall, *J. Am. Soc. Mass Spectrom.* **2000**, *11*, 120 – 126; K. A. Johnson, B. A. Shira, J. L. Anderson, I. J. Amster, *Anal. Chem.* **2001**, *73*, 803 – 808.
[16] D. M. Horn, R. A. Zubarev, F. W. McLafferty, *J. Am. Soc. Mass Spectrom.* **2000**, *11*, 320 – 332.
[17] H. M. Berman, J. Westbrook, Z. Feng, G. Gilliland, T. N. Bhat, H. Weissig, I. N. Shindyalov, P. E. Bourne, *Nucleic Acids Res.* **2000**, *28*, 235 – 242.

Water Clusters

Formation of Water Clusters in a Hydrophobic Solvent**

*Thorsten Köddermann, Frank Schulte, Markus Huelsekopf, and Ralf Ludwig**

Water is of fundamental importance for all forms of life and plays an important role in many biological and chemical processes.[1,2] The exploration of the structural and binding properties of small water complexes provides a key to the understanding of bulk water in its liquid and solid phases.[3–5] As a result, considerable attention has been given to the theoretical[6–11] and experimental[12–23] study of small water complexes.

Modern methods of laser spectroscopy have generated a wealth of information regarding the intricate details of how water molecules interact. Recent experiments have yielded detailed information about structural and dynamic aspects of small clusters.[12–23] Up to the pentamer the clusters occur as nearly planar ring structures,[14,18,19] whereas three-dimensional arrangements are energetically favored if the number of water molecules exceeds five.[17] Large intermolecular zero-point energies of the hydrogen bonds become crucial, and can alter the energy ordering of the low-lying hexamer structures.[9] This is the reason why the cage hexamer is found in the gas phase[17] and the quasi planar ring hexamer in liquid helium.[20] Clearly the physical and chemical environment strongly determines the occurrence of different isomers.

The study of water clusters usually requires high sophisticated equipment and very low temperatures. Herein we use standard FTIR spectroscopy to detect the formation of small water clusters in the hydrophobic solvent CCl_4. To our knowledge this is the first demonstration of the presence of water clusters in solution at room temperature. Beside the water monomer we found a dimer, a cyclic trimer, a cyclic tetramer, and a large hydrogen-bonded structure, which we suppose to be a cage hexamer. To date these water clusters could only be found with complicated methods under conditions that are expensive to achieve. Additionally the formation process of the clusters can be monitored as a function of temperature and thus we can say something about their enthalpic and entropic stability.

The infrared spectra obtained for the O–H stretching region of water clusters formed in CCl_4 as a function of temperature are shown in Figure 1. Because of the solvent

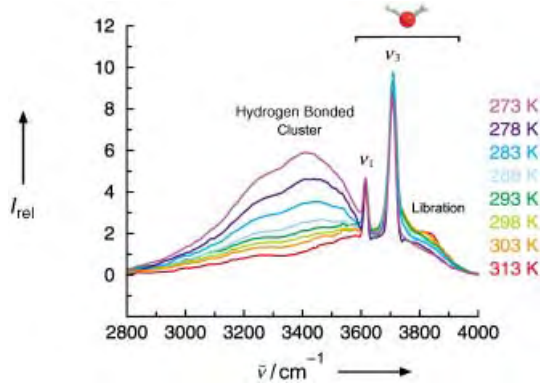


Figure 1. Experimental IR spectra of water clusters in CCl_4 as a function of temperature (O–H stretching vibrations region). At high temperatures the spectra are dominated by the vibrational motion (ν_1 and ν_3) and a librational contribution (hindered rotation by collision with the solvent molecules) of the water monomer. Decreasing temperature leads to formation of hydrogen-bonded water clusters as indicated by the red-shifted bands.

effects and high temperatures the vibrational bands of the water clusters overlap and are not well resolved. But characteristic shape-changes with temperature allows the deconvolution of the spectral bands into a number of Voigt profiles and thus the identification of small complexes. The evolving nature of the spectroscopic data acquired from a system subjected to continuously increasing temperature, means no assumptions are necessary regarding the number of species or peak shape in the resolution process. The spectra

[*] Priv.-Doz. Dr. R. Ludwig, Dipl.-Chem. T. Köddermann, Dipl.-Chem. F. Schulte, Dipl.-Chem. M. Huelsekopf
Physikalische Chemie
Fachbereich Chemie der Universität Dortmund
Otto-Hahn-Strasse 6, 44221 Dortmund (Germany)
Fax: (+49) 231-755-3937
E-mail: ludwig@pc2a.chemie.uni-dortmund.de

[**] This work is supported by the Deutsche Forschungsgemeinschaft (DFG-Forschergruppe 436) and the Fonds der Chemischen Industrie. We thank the John von Neumann Institut für Computing, Jülich, for the generous amount of computer time.

Supporting information for this article is available on the WWW under http://www.angewandte.org or from the author.

 © 2003 Wiley-VCH Verlag GmbH & Co. KGaA, Weinheim DOI: 10.1002/anie.200351438

provide evidence for the number of distinct water structures existing in CCl_4 together with some clues as to the composition of these structures.

All the spectra could be fitted simultaneously by a fixed set of Voigt functions over the whole temperature range (see Supporting Information 1). The decomposed spectrum at 273 K is given as an example in Figure 2. The spectrum could

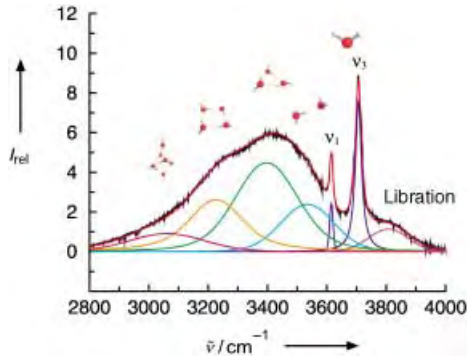


Figure 2. The deconvoluted IR spectrum of water in CCl_4 at 273 K. The spectrum could be fitted by seven Voigt profiles. Three bands having the highest wave numbers represent the vibrational motion (ν_1 and ν_3) and librational contribution of the water monomer.[24] The four red-shifted bands are attributed to the hydrogen-bonded dimer, the cyclic trimer and tetramer, as well as the cage hexamer (Table 1).

be described by seven Voigt functions. Three bands at the highest wave numbers can be attributed to the symmetric and asymmetric O–H stretch (ν_1:$\tilde{\nu} = 3616\ cm^{-1}$ and ν_3:$\tilde{\nu} = 3707\ cm^{-1}$) as well as to a librational contribution ($\tilde{\nu} = 3808\ cm^{-1}$) of the monomer which is associated with the ν_3 mode. This assignment is known from studies of Danten et al.[24] who investigated the pure water monomer in CCl_4. In a nice combination of infrared spectroscopy and molecular dynamics (MD) simulations these authors could show that the librational dynamics of water is primarily governed by "collisional" interactions with the neighboring solvent molecules.[24] The other four Voigt profiles in our spectrum are red shifted indicating the formation of hydrogen-bonded water clusters. We attribute these bands to the hydrogen-bonded dimer, the cyclic trimer, the cyclic tetramer, and a cage hexamer (Table 1).

Our assignment of the experimental data is from comparing the observed frequency shifts with the calculated frequency shifts. By using density functional (B3LYP) and Møller-Plesset second-order perturbation (MP2) calculations the vibrational frequencies for water clusters up to the cyclic and cage hexamers were calculated. The frequency shifts vary smoothly with cluster size (Figure 3), and for the dimer, the

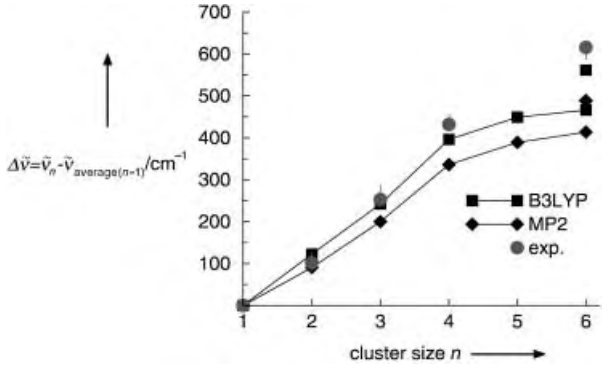


Figure 3. B3LYP (■) and MP2 (◆) calculated vibrational red shifts for the water dimer and cyclic water clusters from the trimer to the hexamer. Measured red shifts (●). The red shift of the cage hexamer is stronger than for the cyclic structure. $\nu_{average(n=1)}$ = the average of the symmetric and asymmetric O–H stretches of the monomer. For full details see text.

cyclic trimer, and cyclic tetramer the measured and deconvoluted peaks lie where expected from calculations. There may be also contributions of cyclic pentamers, but the difference in the calculated red shifts for the cyclic tetramer and the cyclic pentamer is so small, that both species can not be resolved properly in the measured spectra. Better agreement than this is probably not expected, given that the theoretical values are based on harmonic frequency calculations and that our measurements take place in solution.

Although these cyclic clusters all have multiple O–H vibrational bands, the most intense ones for each cluster size (the ring stretches) are close in frequency and thus merge into a single band, which is particularly intense. Indeed, calculations show that the intensities of the O–H modes of clusters in which the molecules are inequivalent, are much smaller than for the cyclic structures. The band with the strongest red shift in our spectra could be attributed neither to the cyclic pentamer nor to the cyclic hexamer but to the average of the two most intense peaks of the cage hexamer as characterized in the gas phase.[17]

Except for the clear monomer contributions, our IR spectra for water in a hydrophobic solvent look quite similar to the Raman spectra for liquid water. In the latter a broad band in the region of the hydrogen-bonded structures has been interpreted as a convolution of two subbands assigned to "ice-like" and "liquid-like" hydrogen-

Table 1: Comparison of the proton-donor O-H stretching frequencies of $(H_2O)n$ in the gas phase, in liquid helium droplets, in solid para hydrogen (p-H_2) and in CCl_4.

Gas phase	Liquid helium	Solid p-H_2	CCl_4[f]	CCl_4[g]	CCl_4 [i]	Assignment
3756[a]	3754[c]	3743	3709[f]	3708	3706–3709	ν_3
3657[a]			3616[f]	3616	3615–3616	ν_1
3601[a]	3597[c,d] 3545,[c] 3544[d]	3579[e]		3553	3535–3587	$(H_2O)_2$
3533[a]	3532[c] 3528[d]	3518[e] 3531[e]		3409	3395–3433	*cyc*-$(H_2O)_3$
3416[a]	3394[d]	3379[e]		3229	3221–3254	*cyc*-$(H_2O)_4$
3220[b]	3229[d]	3222[e]		3046	3043–3074	cage-$(H_2O)_6$

[a] Huisken (1996).[19] [b] Paul (1997).[21] [c] Fröchtenicht (1996).[20] [d] Nauta (2000).[18] [e] Fajardo (2001).[23] [f] Danten (1995).[24] [g] This work: simultaneous fit for all temperatures. [i] This work: separate fit for each temperature.

 © 2003 Wiley-VCH Verlag GmbH & Co. KGaA, Weinheim

bonding modes. The higher-energy band around 3450 cm^{-1} is assigned to the vibrational motion of liquid-like water as in the so-called "Walrafen pentamer",[25] in which a water molecule is surrounded by nearby molecules in a tetrahedral fashion. Such a bulk structure cannot be expected for very small clusters in a low water concentration in a hydrophobic solvent, such as CCl_4, as in this case water molecules tend to form as many hydrogen-bonds as possible.

The band at 3200 cm^{-1} in the Raman spectrum is assigned to full tetrahedral network with all the water molecules involved in hydrogen bonding, such as in hexagonal ice.[26] In our sample, such extended structures are not expected, however, the most red-shifted cluster species, the largest one that we observe, the cage hexamer, gives comparable frequencies. This situation can be explained in that the cage hexamer has a three-dimensional, "extended" hydrogen-bond structure in which, the water molecule giving rise to the lowest vibrational frequencies is bound in a tetrahedral hydrogen-bond network similar to that of ice.

Beside our simultaneous fit we also deconvoluted the spectra separately for each temperature (see Supporting Information 2). Whereas the monomer contributions slightly rise with the temperature, the intensities of the hydrogen-bonded cluster species decrease (Figure 4). Clearly the larger

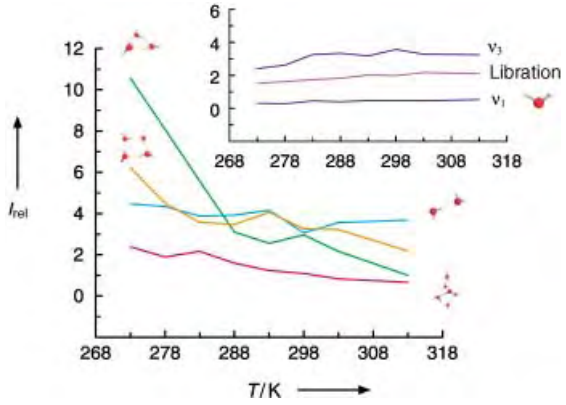


Figure 4. Integral band intensities of the O–H stretching bands of the water clusters as a function of temperature. The monomer contributions increase slightly with temperature (inset). At the same time the intensity of the hydrogen-bonded water structures declines. The contribution of the cyclic trimer (green) decreases most rapidly with temperature because of its unfavorable bent hydrogen-bonds.[25,26]

hydrogen-bonded clusters successively breakdown into smaller species and finally into monomers. The strongest change in intensity can be observed for the structure assigned to the cyclic trimer. Its temperature behavior can be explained on the basis of the calculated binding energies and vibrational frequencies of the hydrogen-bonded clusters. On entropic and enthalpic grounds, strained geometries leading to significantly nonlinear hydrogen bonds are disfavored. Such entropy effects are particularly evident in small cyclic structures. On enthalpic grounds the cyclic water trimer has marginally higher average hydrogen-bond strengths than the dimer since cyclic cooperativity is able to overcome the losses resulting from the strain. Thus the thermal dependence of the trimer might be expected to compete favorably with that of the dimer. However, the trimer concentration decreases more rapidly with temperature. Rotation about the hydrogen-bond axis, which is virtually free in the larger ring structures, is hindered in the strained trimer leading to IR bands at higher frequencies and an entropic penalty.[27,28] In Table 2 the three lowest frequencies of the calculated water clusters are given (see also Supporting Information 3).

Table 2: BSSE corrected binding energies per molecule ΔE_b^{corr} and the three lowest-lying frequencies for the water clusters, calculated at the B3LYP6-311++G** and MP2/6-311++G** levels.

	B3LYP		MP2	
Cluster	ΔE_b^{corr} [kJ mol^{-1}]	$\tilde{\nu}$ [cm^{-1}]	ΔE_b^{corr} [kJ mol^{-1}]	$\tilde{\nu}$ [cm^{-1}]
$(H_2O)_2$	−10.48	136.2	−9.32	135.2
		164.1		171.1
		171.7		176.5
cyc-$(H_2O)_3$	−21.52	184.4	−18.91	177.5
		189.4		184.5
		198.5		198.3
cyc-$(H_2O)_4$	−28.58	56.6	−24.60	52.2
		92.2		85.2
		212.3		202.9
cyc-$(H_2O)_5$	−30.13	22.8	−25.86	21.7
		46.0		46.2
		71.9		71.5
cyc-$(H_2O)_6$	−31.26	26.7	−26.88	32.3
		26.7		32.3
		52.7		53.2
cage-$(H_2O)_6$	−30.44	22.76	−26.49	48.1
		46.00		56.6
		71.94		81.6

How does cluster growth in CCl_4 take place? At the highest temperature (313 K) the monomer is the dominant species. As the intensities of the hydrogen-bonded clusters are up to 100-times higher than for the water monomer, the hydrogen-bonded clusters are only present in trace amounts. On cooling, the intensities of the hydrogen-bonded clusters increase smoothly. We suggest that a cyclic trimer is formed when a monomer combines with a dimer and that larger clusters form correspondingly. When a fourth molecule binds to a preformed cyclic trimer the ring has to open. In liquid helium there is a low-barrier pathway, which allows the insertion of a water molecule into a trimer ring. For methanol clusters in liquid helium Buck and co-workers[29] showed that once the cyclic trimer is formed and cooled, insertion of the fourth molecule into the ring is inhibited by the lack of energy available to open the ring. In our study cyclic trimers and tetramers are formed, but the formation of larger cyclic structures is not seen. Instead we find significant intensity at a frequency, which is calculated for the two most intensive bands of the cage hexamer. In principle the formation process from the cyclic tetramer to the cage hexamer is possible and can be thought as follows: Insertion of molecules into the ring tetramer is prevented by the lack of available energy to open the ring. Instead the ring tetramer is bridged by two water molecules forming the cage hexamer.[17]

 © 2003 Wiley-VCH Verlag GmbH & Co. KGaA, Weinheim

Deconvoluting the spectra separately leads to the expected slightly temperature-dependent shifts for the frequencies of the hydrogen-bonded clusters (Figure 5, Table 1). Whereas the frequencies for the monomer asymmetric and symmetric stretch as well as the libration stay constant, the

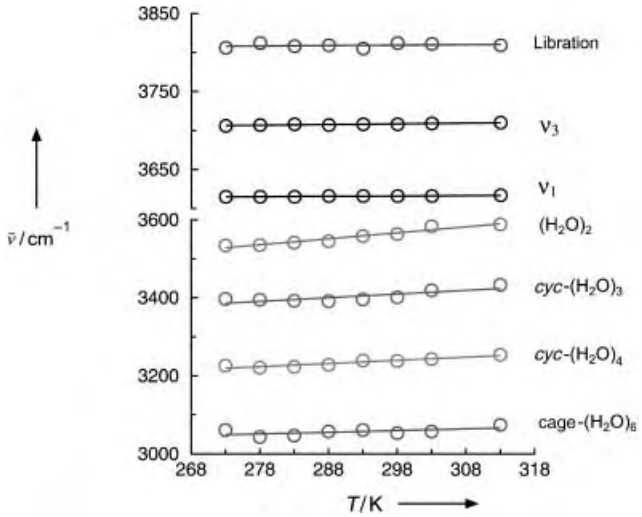


Figure 5. Temperature-dependent shifts of the vibrational bands. Whereas the monomer contributions mainly stay constant (top), the frequencies of the hydrogen-bonded clusters red shift with decreasing temperature because the hydrogen bonds are strengthened leading to weaker O–H bonds.

frequencies of the band maxima for the hydrogen-bonded clusters decrease with decreasing temperature. Cooling the system leads to more stable clusters and thus further red-shifted frequencies. Note that the temperature dependent red shift decreases with increasing cluster size. Naturally all the hydrogen-bonded clusters display free O–H stretching vibrations, which also contribute to the broad feature assigned to the asymmetric stretch ν_3 of the monomer. However, the concentration of the hydrogen-bonded clusters is so low compared to the monomer concentration that the free O–H stretches of these species and their temperature behavior have only a minor impact on the shape and the frequency of the monomer profile.

The present study suggests a series of experiments which, if combined with the corresponding theoretical calculations, could throw light on the cluster formation of hydrogen-bonded systems in solution. It could help to answer the question of whether chainlike and cyclic structures are preferred. Also information regarding cluster formation as a function of isotopic substitution can be expected.

Experimental Section

The solutions were prepared by mixing ultra-pure water with CCl_4 (Aldrich, purity +99%), dehydrated for several days over molecular sieves. The solutions were carefully checked to ensure they were properly equilibrated by repeating measurements until the spectra did not show further changes. The reproducibility of the measurements indicates that the solutions were saturated in water (at room temperature ($\approx$298 K) molar fraction 8.4×10^{-4} [30]).

IR measurements were performed with a Bruker Vector 22 FT-IR spectrometer. An L.O.T.-Oriel variable-temperature cell equipped with CaF_2 windows, path length of 1.0 mm, was used for the variable temperature experiments. The sample chamber was purged with dry nitrogen during data collection to minimize spectral contributions from atmospheric gases. Temperatures were maintained with an external Hake C25P cryostat and were monitored with a thermocouple attached directly to the cell. For each spectrum 256 scans were recorded (resolution 1 cm^{-1}). Solvent subtraction was carried out by using reference spectra obtained at the same temperatures as the sample spectra.

The spectra were deconvoluted simultaneous as well as separately into a number of Voigt profiles (convolution of Lorentzian and Gaussian functions) following the Levenberg–Marquardt procedure.[31] The Voigt profile has four parameters: the intensity, the frequency, the half-width of the Lorentzian, and the half-width of the Gaussian, which is normalized. Thus there are 28 parameters for deconvoluting the spectra into seven bands. As the three monomer contributions (ν_1, ν_3, librational contribution) are well separated and clearly assigned, this reduces the number of critical parameters to 16. We also gain additional information from a simultaneous deconvolution as a function of temperature. Despite lowering the number of parameters we concede that the configuration is probably not unique. Thus several other configurations have been tried, without leading to a minimum of the sum of square deviations or without giving a reasonable temperature behavior for the integrated intensities. We want to emphasize that at least seven functions per spectrum are needed to deconvolute all the spectra simultaneously, and that the Levenberg–Marquardt algorithm normally fails if too many functions are used.

Ab initio calculations have been performed at the density functional (B3LYP) and the second-order Møller–Plesset perturbation (MP2) levels with the Gaussian 98 program[32] using the internal stored 6-311++G(d,p) basis set. The basis set supperposision errors (BSSE), corrected binding energies, and the three lowest vibrational frequencies of the water clusters are given in Table 2 (see also Supporting Information 3). We are aware that numerous calculations of water clusters are available.[6–11] But for a reliable comparison of all the water clusters taken we recalculated them at the same level of theory.

Received: March 18, 2003
Revised: April 30, 2003 [Z51438]

Keywords: cluster compounds · hydrogen bonds · IR spectroscopy · water chemistry

[1] *Water—A comprehensive Treatise, Vol. 1–7* (Ed.: F. Franks), Plenum, New York, **1972–1982**.
[2] F. H. Stillinger, *Science* **1980**, *209*, 451–457.
[3] U. Buck, F. Huisken, *Chem. Rev.* **2000**, *100*, 3863–3890.
[4] F. N. Keutsch, R. Saykally, *Proc. Natl. Acad. Sci. USA* **2001**, *98*, 10533–10540.
[5] R. Ludwig, *Angew. Chem.* **2001**, *113*, 1856–1876; *Angew. Chem. Int. Ed. Engl.* **2001**, *40*, 1808–1827.
[6] S. S. Xantheas, *J. Chem. Phys.* **1994**, *100*, 7523–7534.
[7] S. S. Xantheas, *J. Chem. Phys.* **1995**, *102*, 4505–4517.
[8] S. S. Xantheas, *J. Chem. Phys.* **1996**, *104*, 8821–8824.
[9] J. Kim, K. S. Kim, *J. Chem. Phys.* **1998**, *109*, 5886–5895.
[10] J. Kim, D. Majumbur, H. M. Lee, K. S. Kim, *J. Chem. Phys.* **1999**, *110*, 9128–9134.
[11] K. Kim, K. D. Jordan, T. S. Zwier, *J. Am. Chem. Soc.* **1994**, *116*, 11568–11569.
[12] N. Pugliano, R. J. Saykally, *Science* **1992**, *257*, 1937–1940.

 © 2003 Wiley-VCH Verlag GmbH & Co. KGaA, Weinheim

[13] J. D. Cruzan, L. B. Braly, K. Liu, M. G. Brown, J. G. Loeser, R. J. Saykally, *Science* **1996**, *271*, 59 – 62.
[14] K. Liu, M. G. Brown, J. D. Cruzan, R. J. Saykally, *Science* **1996**, *271*, 62 – 64.
[15] K. Lui, J. D. Cruzan, R. J. Saykally, *Science* **1996**, *271*, 929 – 933.
[16] J. K. Gregory, D. C. Clary, K. Liu, M. G. Brown, R. J. Saykally, *Science* **1997**, *275*, 814 – 817.
[17] K. Liu, M. G. Brown, C. Carter, R. J. Saykally, J. K. Gregory, D. C. Clary, *Nature* **1996**, *381*, 501 – 503.
[18] K. Nauta, R. E. Miller, *Science* **2000**, *287*, 293 – 295.
[19] F. Huisken, M. Kaloudis, A. Kulcke, *J. Chem. Phys.* **1996**, *104*, 17 – 25.
[20] R. Fröchtenicht, M. Kaloudis, M. Koch, F. Huisken, *J. Chem. Phys.* **1996**, *105*, 6128 – 6140.
[21] J. B. Paul, C. P. Collier, R. J. Saykally, J. J. Scherer, A. O. O'Keefe, *J. Phys. Chem. A* **1997**, *101*, 5211 – 5214.
[22] J. B. Paul, R. A. Provencal, C. Chapo, K. Roth, R. Casaes, R. J. Saykally, *J. Phys. Chem. A* **1999**, *103*, 2972 – 2974.
[23] M. E. Fajardo, S. Tam, *J. Chem. Phys.* **2001**, *115*, 6807 – 6810.
[24] Y. Danten, T. Tassaing, M. Besnard, *J. Phys. Chem. A* **2000**, *104*, 9415 – 9427.
[25] G. E. Walrafen, *J. Chem. Phys.* **1967**, *47*, 114 – 126.
[26] D. Eisenberg, W. Kauzmann, *The Structure and Properties of Water*, Oxford University Press, New York, **1969**.
[27] F. Weinhold, *THEOCHEM* **1997**, *399*, 181 – 197.
[28] F. Weinhold, *J. Chem. Phys.* **1998**, *109*, 367 – 372; F. Weinhold, *J. Chem. Phys.* **1998**, *109*, 373 – 384.
[29] M. Behrens, R. Fröchtenicht, M. Hartmann, J.-G. Siebers, U. Buck, F. C. Hagemeister, *J. Chem. Phys.* **1999**, *111*, 2436 – 2443.
[30] S. Goldman, *Can. J. Chem.* **1974**, *52*, 1668 – 1680; S. Goldman, *J. Phys. Chem.* **1981**, *85*, 2975 – 2979.
[31] *Numerical Recipies in FORTRAN: The Art of Scientific Computing*, 2nd ed. (Eds.: W. H. Press, S. A. Teukolsky, W. T. Vetterling, B. P. Flannery), Cambridge University Press, Cambridge, **1994**.
[32] Gaussian 98 (Revision A.7), M. J. Frisch, G. W. Trucks, H. B. Schlegel, G. E. Scuseria, M. A. Robb, J. R. Cheeseman, V. G. Zakrzewski, J. A. Montgomery, R. E. Stratmann, J. C. Burant, S. Dapprich, J. M. Millam, A. D. Daniels, K. N. Kudin, M. C. Strain, O. Farkas, J. Tomasi, V. Barone, M. Cossi, R. Cammi, B. Mennucci, C. Pomelli, C. Adamo, S. Clifford, J. Ochterski, G. A. Petersson, P. Y. Ayala, Q. Cui, K. Morokuma, D. K. Malick, A. D. Rabuck, K. Raghavachari, J. B. Foresman, J. Cioslowski, J. V. Ortiz, B. B. Stefanov, G. Liu, A. Liashenko, P. Piskorz, I. Komaromi, R. Gomperts, R. L. Martin, D. J. Fox, T. Keith, M. A. Al-Laham, C. Y. Peng, A. Nanayakkara, C. Gonzalez, M. Challacombe, P. M. W. Gill, B. G. Johnson, W. Chen, M. W. Wong, J. L. Andres, M. Head-Gordon, E. S. Replogle, J. A. Pople, Gaussian, Inc., Pittsburgh, PA, **1998**.

 © 2003 Wiley-VCH Verlag GmbH & Co. KGaA, Weinheim

Titanium Dioxide Photocatalysts

Daylight Photocatalysis by Carbon-Modified Titanium Dioxide**

*Shanmugasundaram Sakthivel and Horst Kisch**

In memory of Dieter Sellmann

Semiconductor photocatalysis is an efficient method for the chemical utilization of solar energy. It is based on the surface trapping of light-generated charges which induce interfacial electron-transfer reactions with a great variety of substrates. Titanium dioxide, the most promising photocatalyst is already used in various practical applications, such as self-cleaning paints and window panes.[1] However, because of its large band gap of 3.20 eV only the small UV fraction of solar light, about 2–3 %, can be utilized. Therefore many attempts have been made to sensitize titanium dioxide for the much larger visible fraction.

In previous work we have shown that incorporation of a few weight percent of a transition-metal chloride either in the bulk or at the surface of titanium dioxide leads to visible-light photocatalysis.[2] Especially the materials modified by chemisorbed platinum(IV) chloride were very active and sustained photomineralization of the ubiquitous pollutant 4-chlorophenol by visible light ($\lambda \geq 455$ nm) for several days.[2e] Different from modification by metal complexes, we recently found that a coke-containing titanium dioxide was active also with visible light. This material was prepared by a sol–gel method using various titanium alkoxide precursors.[3] Since its activity, especially at low light intensity was much smaller than the platinum(IV) chloride modified titanium dioxide, we searched for improvement. This was achieved during work on nitrogen-doped titanium dioxide[4a] in which we hydrolyzed titanium tetrachloride with nitrogen bases, such as tetrabutylammonium hydroxide. At the subsequent calcination step we observed that prolonged heating at 400 °C afforded an anatase material which contained carbon instead of nitrogen. This preparation method has an excellent reproducibility and greater applicability than the oxidation of a titanium metal sheet to a carbon-doped rutile layer in a natural gas flame.[5,6] In the degradation of 4-chlorophenol by artificial light ($\lambda \geq$ 455 nm) these new, blackish-brown powders are five times more active than nitrogen-doped titanium dioxide. Herein we report the preparation, photoelectrochemical, and photo-

[*] Prof. Dr. H. Kisch, Dr. S. Sakthivel
Institut für Anorganische Chemie
Universität Erlangen-Nürnberg
Egerlandstrasse 1, 91058 Erlangen (Germany)
Fax: (+49) 9131-852-7363
E-mail: kisch@chemie.uni-erlangen.de

[**] This work was supported by Deutsche Forschungsgemeinschaft (SFB 583).

Supporting information for this article is available on the WWW under http://www.angewandte.org or from the author.

 © 2003 Wiley-VCH Verlag GmbH & Co. KGaA, Weinheim DOI: 10.1002/anie.200351577

catalytic properties of carbon doped TiO_2 under direct artificial and diffuse natural light.

The samples TiO_2-C1a, TiO_2-C1b, and TiO_2-C2 containing 2.98, 0.42, and 0.03 % carbon were prepared by the hydrolysis of titanium tetrachloride with tetrabutylammonium hydroxide followed by calcination at 400 °C for 0.25 h (TiO_2-C1a) and 1 h (TiO_2-C1b), and at 550 °C for 4 h (TiO_2-C2). Unmodified TiO_2 was prepared by the same procedure but replacing the nitrogen base by sodium hydroxide. Except for TiO_2-C1a, which contained traces of nitrogen, the three other samples were nitrogen-free. According to X-ray diffraction (XRD) measurements all the materials were in the anatase modification except TiO_2-C2 which contained trace quantities of the rutile phase.

X-ray photoelectron spectroscopy (XPS) measurements of the C1 binding energy indicated the complete absence of carbon in the undoped sample, whereas for TiO_2-C1b, peaks at 285.6, 287.5, and 288.5 eV were found.[7] The first value arises from adventitious elemental carbon,[8,9] the latter two values suggest the presence of a carbonate species.[8] This assumption is supported by the IR spectrum of TiO_2-C1b which exhibits low-intensity peaks at 1738, 1096, and 798 cm^{-1} which are indicative for the carbonate ion.[10,11] In contrast to these results, it was proposed that in the rutile layer, prepared by flame oxidation, carbon partially substitutes the oxide ion.[6]

Diffuse reflectance spectra reveal that the new absorption at 400–700 nm is related to the carbon content. It is stronger for TiO_2-C1a than for TiO_2-C1b and completely absent in TiO_2-C2 (Figure 1, Table 1), which was calcined at 550 °C. Assuming the materials to be indirect semiconductors, like TiO_2, a plot of the modified Kubelka–Munk function versus the energy of exciting light[12,13] affords band-gap energies of 3.16, 3.02, 3.11, and 3.17 eV for TiO_2, TiO_2-C1a, TiO_2-C1b, and TiO_2-C2, respectively (Figure 1, Table 1).[14] The maximum band-gap narrowing of 0.14 eV is comparable with the value of 0.05 eV recently observed for nitrogen-doped TiO_2.[4a,c]

To understand whether a shift of the valence or conduction band edge is responsible for this decrease of the band-gap energy, the position of the flat-band potential (U_{fb}) was determined by the "slurry method"[15,16] through measuring the photovoltage[16] as a function of the suspension pH value (Figure 2). The inflection point corresponds to the pH_0 value from which the flat-band potential can be calculated (Table 1). The value of −0.52 V measured for TiO_2 at pH 7 is in good agreement with the −0.58 reported for an anatase single crystal and measured by the Mott–Schottky method[17] and −0.47 V for anatase powder also measured by the slurry method.[18] As observed for the band gap, the change in flat-band potential is also related to the carbon content. Whereas the potential of −0.54 V, found for the low-carbon sample TiO_2-C2, does not differ significantly from that of unmodified TiO_2 (−0.52 V) it is shifted to −0.39 and −0.48 V for TiO_2-C1a and TiO_2-C1b, respectively. The anodic shifts of 130 and

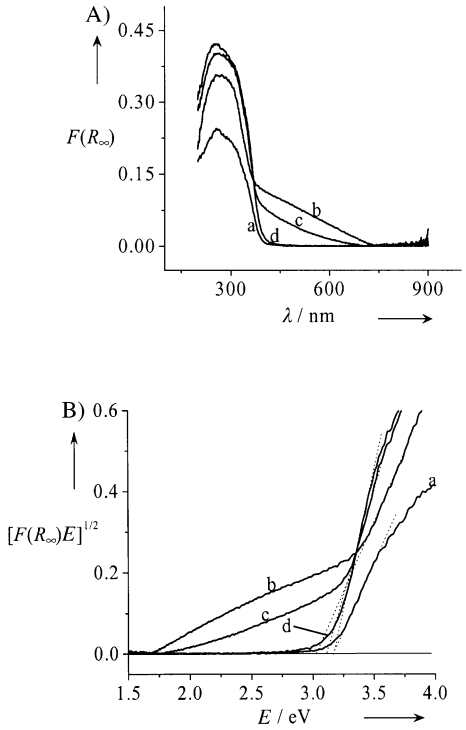


Figure 1. A) Diffuse reflectance spectra of modified and pure TiO_2; B) Plot of transformed Kubelka–Munk function versus the energy of the light absorbed; a) TiO_2, b) TiO_2-C1a, c) TiO_2-C1b, d) TiO_2-C2.

Table 1: Carbon content, photoelectrochemical data, band-gap energies, and initial disappearance rates (r_i) of 4-chlorophenol.

Catalyst	C [%]	pH_0[a]	E_{bg} [eV][b]	U_{fb} (NHE)[a] [V][c]	r_i [10^{-8} mol L^{-1} s^{-1}][d]
TiO_2	0.00	5.80	3.16	−0.52	0.10
TiO_2-C1a	2.98	7.90	3.02	−0.39	3.75
TiO_2-C1b	0.42	6.40	3.11	−0.48	7.65
TiO_2-C2	0.03	5.44	3.17	−0.54	0.13

[a] Measured according to ref. [16] and calculated for pH 7. [b] Reproducibility was better than ±0.01 eV. [c] Reproducibility was better than ±0.01 V. [d] Obtained by measuring the decrease of absorbance at 224 nm; $\lambda_{irr} \geq 455$ nm.

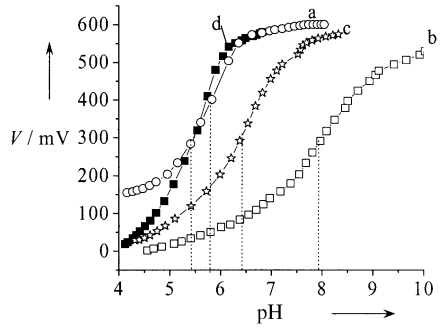


Figure 2. Variation of photovoltage with pH value for the suspension of catalyst in the presence of methyl viologen a) TiO_2, b) TiO_2-C1a, c) TiO_2-C1b, d) TiO_2-C2.

© 2003 Wiley-VCH Verlag GmbH & Co. KGaA, Weinheim

40 mV may be compared with the value of 50 mV found for nitrogen-doped TiO_2.[4a] Assuming that the distance between flat-band potential and the conduction band edge is vanishing for these probably highly doped n-type semiconductor materials, the position of the valence-band edge can be located from the corresponding band-gap energies as +2.63 V for all samples.

Since the carbon-modified samples start absorbing at about 735 nm (1.70 eV; Figure 1) a variety of surface states must exist. To determine their approximate energy, the wavelength dependence of OH-radical formation by TiO_2-C1b was investigated in the presence of two different electron acceptors and benzoic acid as OH scavenger.

In the presence of oxygen, salicylic acid was produced irrespective of exciting TiO_2-C1b at $\lambda \geq 320$ (3.88 eV), 455 (2.73 eV), and 495 nm (2.51 eV). This can be rationalized by recalling that the reduction potential of the O_2/O_2^- couple at pH 7 is −0.16 V.[19] If light absorption at the longest wavelength would occur from the valence band to a surface state close to the conduction band, the resulting potential of the trapped electron should be located at about +0.12 V and reduction of oxygen und subsequent OH-radical formation is not feasible. Contrary, this process becomes possible when absorption occurs from a surface state located near the valence band to the conduction band, since now the trapped electron potential is −0.39 V. In accord with this explanation, upon replacement of oxygen by tetranitromethane as an electron acceptor, salicylic acid formation proceeded only for the short wavelength irradiation. Under these band-to-band absorption conditions the OH-radical formation occurs directly through hole-oxidation of water or surface hydroxy groups (Figure 3). This significant difference suggests the presence of surface states close to the valence-band edge, as was also concluded from theoretical calculations.[4c]

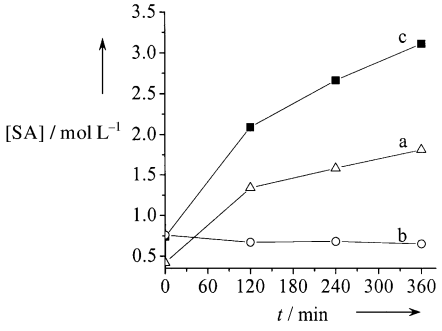


Figure 3. Formation of salicylic acid (SA) upon irradiation of TiO_2-C1b in the presence of benzoic acid; a) $\lambda \geq 495$ nm, under O_2, b,c) $\lambda \geq 495$ nm, under Ar and in the presence of tetranitromethane c) $\lambda \geq 320$ nm, under Ar and in the presence of tetranitromethane.

To explore the photocatalytic activity of the new materials, the degradation of some typical pollutants in water and air by artificial and natural light was investigated. Figure 4 A illustrates the photomineralization of the ubiquitous water pollutant 4-chlorophenol with visible light ($\lambda = 455$ nm) in the presence of the various photocatalysts. TiO_2-C1a and TiO_2-C1b induced complete mineralization after 210 and 180 min,

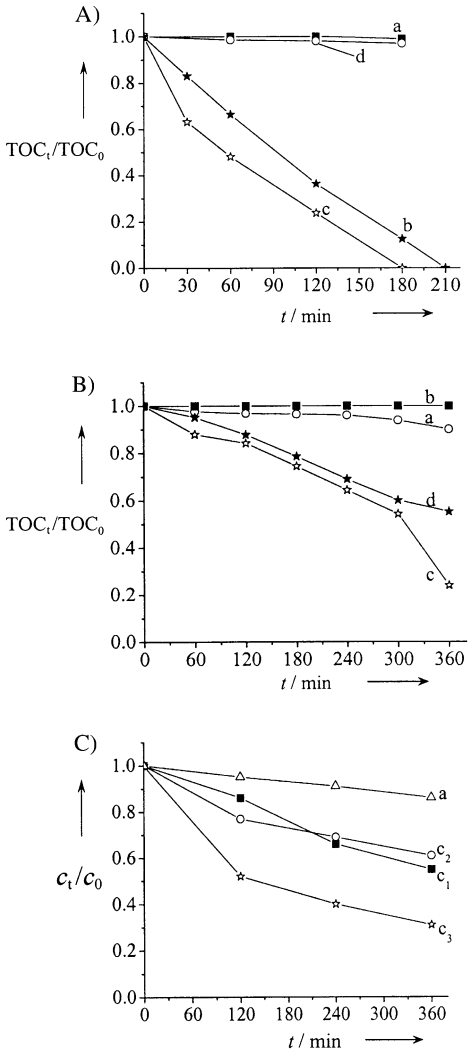


Figure 4. A) Photomineralization of 4-chlorophenol with artificial visible light ($\lambda = 455$ nm; TOC_0 and TOC_t = total organic carbon content at times 0 and t); a) TiO_2, b) TiO_2-C1a, c) TiO_2-C1b, d) TiO_2-C2. B) Diffuse indoor daylight degradation of 4-chlorophenol (4-CP) and remazol red in the presence of pure TiO_2 and TiO_2-C1b; a) TiO_2/4-CP, b) TiO_2/remazol red, c) TiO_2-C1b/4-CP, d) TiO_2-C1b/remazol red. C) Gas-phase photodegradation of acetaldehyde (a and c_1, 5 vol%), benzene (c_2, 5 vol%), and carbon monoxide (c_3, 5 vol%) in air through diffuse indoor light in the presence of pure TiO_2 (a) and TiO_2-C1b (c).

respectively (curves b, c). In contrast, TiO_2-C2 and unmodified TiO_2 did not significantly change the total organic carbon value (curves a, d). However, they induced a small reduction in the concentration of 4-chlorophenol as measured by UV absorption spectroscopy. The corresponding rates found for TiO_2-C1a and TiO_2-C1b were about 30 and 60 times larger (Table 1). The twofold rate enhancement induced by TiO_2-C1b relative to TiO_2-C1b although the latter contains more carbon may be due to the higher crystallinity of TiO_2-C1a as suggested by XRD spectra.

The superior photocatalytic activity of the carbon-doped materials is demonstrated by illumination experiments in diffuse indoor daylight. In solution 4-chlorophenol and the azo dye remazol red are efficiently mineralized only by TiO_2-

 © 2003 Wiley-VCH Verlag GmbH & Co. KGaA, Weinheim

C1b (Figure 4B, curves c, d) whereas unmodified TiO_2 is almost inactive (curves a, b). Furthermore TiO_2-C1b supported on filter paper, photocatalyzes the oxidation of gaseous acetaldehyde, benzene, and carbon monoxide (Figure 4C).

Experimental Section

Preparation of photocatalysts: A solution of tetrabutylammonium hydroxide (0.25 mol L^{-1}) was added dropwise to 0.25 M $TiCl_4$ (200 mL) at 0 °C until a pH value of 5.5 was reached. After ageing the suspension for 24 h at room temperature, the precipitate was collected by filtration and dried under air at 70 °C. The residue was crushed into a fine powder and calcined in a muffle furnace at 400 °C for 0.25 and 1 h, and at 550 °C for 4 h. Calcination temperatures were attained at a heating rate of about 5 °C min^{-1}.

Photochemical experiments: Photomineralizations in the aqueous phase were carried out with catalyst powder (15 mg) suspended in a water-cooled cylindrical 15-mL quartz cuvette; the suspension was stirred magnetically. Appropriate cut-off filters were inserted before irradiating with an Osram XBO 150 W xenon arc lamp. Salicylic acid was measured through its intense fluorescence at 400–420 nm as described elsewhere.[2d] Daylight experiments were performed in the laboratory by exposing the reaction system to the diffuse radiation arriving through the window (4–10 W m^{-2} at 400–1200 nm). Solution experiments were conducted in an Erlenmeyer flask containing TiO_2-C1b (50 mg) and solutions of 4-chlorophenol (50 mL; 2.5×10^{-4} mol L^{-1}) or solutions of remazol red (50 mL; 1×10^{-4} mol L^{-1}). Gas-phase experiments were conducted in a 1-L round bottom flask containing a filter paper of 11-cm diameter onto which the catalyst (12 mg) was supported; concentration change and CO_2 formation were measured by IR spectroscopy.

Received: April 4, 2003 [Z51577]
Publication delayed at authors request

Keywords: carbon · doping · photocatalysis · semiconductor · titanium dioxide

[1] a) D. A. Tryk, A. Fujishima, K. Honda, *Electrochim. Acta* **2000**, *45*, 2363.
[2] a) H. Kisch, L. Zang, C. Lange, W. F. Maier, C. Antonius, D. Meissner, *Angew. Chem.* **1998**, *110*, 3201; *Angew. Chem. Int. Ed.* **1998**, *37*, 3034; b) L. Zang, C. Lange, W. F. Maier, I. Abraham, S. Storck, H. Kisch, *J. Phys. Chem. B* **1998**, *102*, 10765; c) L. Zang, W. Macyk, C. Lange, W. F. Maier, C. Antonius, D. Meissner, H. Kisch, *Chem. Eur. J.* **2000**, *6*, 379; d) W. Macyk, H. Kisch, *Chem. Eur. J.* **2001**, *7*, 1862; e) G. Burgeth, H. Kisch, *Coord. Chem. Rev.* **2002**, *230*, 41.
[3] C. Lettmann, K. Hildenbrand, H. Kisch, W. Macyk, W. F. Maier, *Appl. Catal. B* **2001**, *32*, 215.
[4] a) S. Sakthivel, H. Kisch, *ChemPhysChem*, **2003**, *4*, 487; for other preparations see: b) S. Sato, *Chem. Phys. Lett.* **1986**, *123*, 126; c) R. Asahi, T. Morikawa, T. Ohwaki, A. Aoki, Y. Taga, *Science* **2001**, *293*, 269; d) T. Morikawa, R. Asahi, T. Ohwaki, A. Aoki, Y. Taga, *Jpn. J. Appl. Phys.* **2001**, *40*, 561.
[5] A. Fujishima, K. Kohayakawa, K. Honda, *J. Electrochem. Soc.* **1975**, *122*, 1487.
[6] S. U. M. Khan, M. Al-Shahry, W. B. Ingler, Jr., *Science* **2002**, *297*, 2243.
[7] Relevant atomic percentages are C1s 5.70, O1s 62.66, Ti2p 32.63%. We are highly indebted to Prof. P. Schmuki for these measurements.
[8] E. Papirer, R. Lacroix, J.-B. Donnet, G. Nanse, P. Fioux, *Carbon* **1995**, *33*, 63.
[9] C. S. Gopinath, S. G. Hegde, A. V. Ramaswamy, S. Mahapatra, *Mater. Res. Bull.* **2002**, *37*, 1323.
[10] It is noted that hydrolysis with sodium carbonate does not afford a photocatalyst active in the visible.
[11] S. Gablenz, H.-P. Abicht, E. Pippel, O. Lichtenberger, J. Woltersdorf, *J. Eur. Ceram. Soc.* **2000**, *20*, 1053.
[12] J. Tauc, R. Grigorovici, A. Vanuc, *Phys. Status Solidi* **1966**, *15*, 627.
[13] B. Karvaly, I. Hevesy, *Z. Naturforsch. A* **1971**, *26*, 245.
[14] This corresponds to absorption onsets of 392, 411, 399, and 391 nm.
[15] J. R. White, A. J. Bard, *J. Phys. Chem.* **1985**, *89*, 1947.
[16] A. M. Roy, G. C. De, N. Sasmal, S. S. Bhattacharyya, *Int. J. Hydrogen Energy* **1995**, *20*, 627. The powders (30 mg) were suspended in 50 mL of 0.1 M KNO_3 containing 6 mg of methylviologen dichloride; $\lambda_{irr} = 320$ nm.
[17] L. Kavan, M. Grätzel, S. E. Gilbert, C. Klemenz, H. J. Scheel, *J. Am. Chem. Soc.* **1996**, *118*, 6716.
[18] M. D. Ward, J. R. White, A. J. Bard, *J. Am. Chem. Soc.* **1983**, *105*, 27.
[19] D. T. Sawyer, J. S. Valentine, *Acc. Chem. Res.* **1981**, *14*, 393.

 © 2003 Wiley-VCH Verlag GmbH & Co. KGaA, Weinheim

Lanthanum Copper Chalcogenides

La_2CuS_4: A Lanthanum Copper Sulfide with Discrete Anion Triples $[S_3Cu\cdots S{-}S\cdots CuS_3]^{12-}$ Based on $La_4[Cu_2S_6(S_2)]$**

*Sabine Strobel and Thomas Schleid**

Some unusual material properties of solid-state compounds are due to the special coordination geometry of the ions in the crystal structure. For example, the superconductivity of $YBa_2Cu_3O_{7-\delta}$ $(0 \leqslant |\delta| \leqslant 1)$[1] is, in part, the result of the valence of the copper ions being greater than +II and their coordination by oxygen atoms in many different ways: Certain Cu^+ cations are surrounded by O atoms in a square-pyramidal arrangement, whereas others adopt an almost square-planar (for $\delta = 0$) or linear coordination geometry (for $\delta = 1$). The properties of these rare-earth copper oxides change when oxygen is substituted by other chalcogens such as sulfur. Thus, studies of rare-earth/copper/sulfur systems should provide results on new ternary or quaternary rare-earth copper chalcogenides. Mainly those substances that exhibit both unusual oxidation states and coordination geo-

[*] Prof. Dr. T. Schleid, S. Strobel
Institut für Anorganische Chemie, Universität Stuttgart
Pfaffenwaldring 55, 70569 Stuttgart (Germany)
Fax: (+49) 711-685-4241
E-mail: schleid@iac.uni-stuttgart.de

[**] This research was supported financially by the federal state of Baden-Württemberg. The authors thank Dr. Falk Lissner for the X-ray single-crystal-structure data collection.

 DOI: 10.1002/anie.200351641 © 2003 Wiley-VCH Verlag GmbH & Co. KGaA, Weinheim

metries are of interest. Experience has shown that in many cases, compounds with "normal" coordination properties and uncommon oxidation states are observed, for example, $K_3Cu_8S_6$, $Na_3Cu_4S_4$, $BaCu_{5.65}S_{4.5}$,[2] and $La_5Cu_6O_4S_7$,[3] in which copper has an non-integer oxidation state between +1 and +2. Cu^+ cations usually prefer a tetrahedral coordination of sulfur (in the S^{2-} state). Nevertheless, compounds are known in which copper is coordinated by only three S^{2-} anions. The binary copper sulfide Cu_2S (chalcosite type),[4] for example, consists mainly of $[CuS_3]$ triangles. Out of 24 crystallographically different Cu^+ cations, 21 are surrounded by three S^{2-} anions, whereas just two with CN = 2+1 (CN = coordination number) deviate from the ideal triangle, and only one with CN = 3+1 exhibits a distorted tetrahedral coordination geometry. The crystal structure of the ternary copper sulfide $Bi_4Cu_4S_9$[5] shows similar $[CuS_3]$ units of Cu^+ cations and S^{2-} anions, two of which are joined by a bridging disulfide unit. However, the displacement of the Cu^+ cations of almost 80 pm above the triangular face is so evident that this structure fragment can also be described as two disulfide-bridged $[CuS_4]$ tetrahedra. In $Bi_4Cu_4S_9$, the $[S_3Cu\cdots S{-}S\cdots CuS_3]$ units are interconnected and linked by additional three-coordinate Cu^+ cations to form a puckered layer. To actualize the empirical formula $Bi_4Cu_4S_9$, Bi^{3+} and extra Cu^+ cations with CN = 3+1 are integrated. Even though $[S_3Cu\cdots S{-}S\cdots CuS_3]$-like units exist as building blocks in further linked structures, no solid-state compounds that include discrete anion triples of this kind are known.

For the first time, La_2CuS_4, a ternary lanthanum(III) copper(I) sulfide with discrete $[S_3Cu\cdots S{-}S\cdots CuS_3]$ units, has been synthesized by direct reaction of elementary lanthanum, copper, and sulfur in a molar ratio of 2:1:4. The X-ray single-crystal structure analysis[6] indicates that these units comprise two almost planar $[CuS_3]^{5-}$ triangles bridged by a disulfide anion ($[S_2]^{2-}$). Thus an anionic contact-ion triple based on $[S_3Cu]^{5-}\cdots[S_2]^{2-}\cdots[CuS_3]^{5-}$ is formed in which the Cu^+ cations are displaced slightly above the $[CuS_3]^{5-}$ triangular faces by 13 pm (Figure 1). Whereas in La_2CuS_4 the sulfur–sulfur

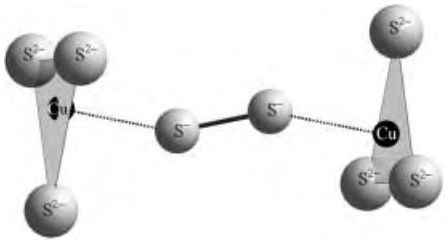


Figure 1. Configuration of a $[S_3Cu]^{5-}\cdots[S{-}S]^{2-}\cdots[CuS_3]^{5-}$ contact-ion triple in the crystal structure of La_2CuS_4 ($\equiv La_4[Cu_2S_6(S_2)]$).

distance within the disulfide anion $[S_2]^{2-}$ ($d(S^-{-}S^-) = 211$ pm) corresponds very well with that in LaS_2,[7] the distances between the Cu^+ cations and the three S^{2-} anions range from 224 to 226 pm and are shorter than those known for copper in tetrahedral arrangements (e.g. $CuLaS_2$:[8] average distance $\bar{d}(Cu{-}S) = 243$ pm). They rather match those found for copper with triangular coordination (average distance $\bar{d}(Cu{-}S) = 233$ pm in Cu_2S[4]).

On the other hand, the distance to both S^- anions (bearing only one negative charge) in the bridging disulfide unit (296 pm) is longer than that in $Cu_4Bi_4S_9$.[5] Similarly, the distance of 230 pm between the Cu^+ cations and $(S_2)^{2-}$ anions in the binary copper sulfide CuS[9] (which consists of Cu-S_2-Cu layers in which $[CuS_4]$ tetrahedra are linked through bridging S_2^{2-} dianions and of Cu–S layers formed by corner-shared $[CuS_3]$ triangles) is clearly shorter than in La_2CuS_4. This indicates that the Coulomb repulsion of the single fragments in $[S_3Cu]^{5-}\cdots[S_2]^{2-}\cdots[CuS_3]^{5-}$ impairs the common attractive interactions between Cu^+ cations and S^- anions. In the crystal structure, the $[S_3Cu\cdots S{-}S\cdots CuS_3]^{12-}$ building blocks are layered along [001]. The contact-ion triples of one layer orientate in the same direction and those of the following layer are rotated by 90° (Figure 2). The incorporation of two

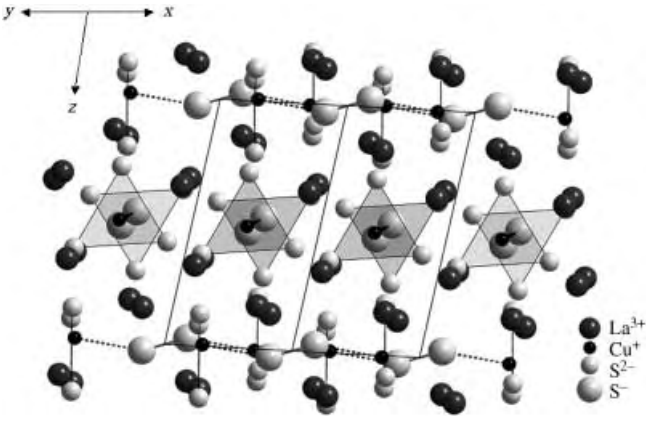


Figure 2. Section of the crystal structure of La_2CuS_4 viewed along [001].

crystallographically different La^{3+} cations results in the formation of a three-dimensional crystal structure. The linkage within one layer is formed solely by La^{3+}–S^{2-} contacts, whereas $[S_2^{2-}]$ anions are only involved in interconnecting layers. However, the distance of 362 pm between the $[S_2^{2-}]$ anions and a La^{3+} cation in the next layer exceeds that in other lanthanum–sulfur bonds, which range between 286 and 342 pm. If the disulfide groups are treated as single $[S_2]^{2-}$ anions, both crystallographically different lanthanum cations are surrounded by a bicapped trigonal prism of sulfur (Figure 3).

Although the formula La_2CuS_4 by analogy to La_2CuO_4[10] suggests an oxidation state of +II for copper, the compound exclusively contains copper as *singly* charged cations. Charge balance results from the mixed valance in the anionic part of the structure such that two sulfide anions are substituted by one disulfide unit ($[S_2^{2-}]$) based on $(La^{3+})_4(Cu^+)_2(S^{2-})_6[S_2]^{2-}$ ($\equiv 2 \times La_2CuS_4$). The low oxidizing potential of sulfur towards copper may be primarily responsible for this observation. There are also copper sulfides such as $K_3Cu_8S_6$, $Na_3Cu_4S_4$ or $BaCu_{5.65}S_{4.5}$,[2] in which the charge of copper is greater than +1. Thus it appears, that cations of the highly electropositive alkali and alkaline-earth metals are apt to stabilize these charges, whereas the large trivalent cations of the 6th period tend to form $[S_3Cu\cdots S{-}S\cdots CuS_3]$ building blocks, as is the case

 © 2003 Wiley-VCH Verlag GmbH & Co. KGaA, Weinheim

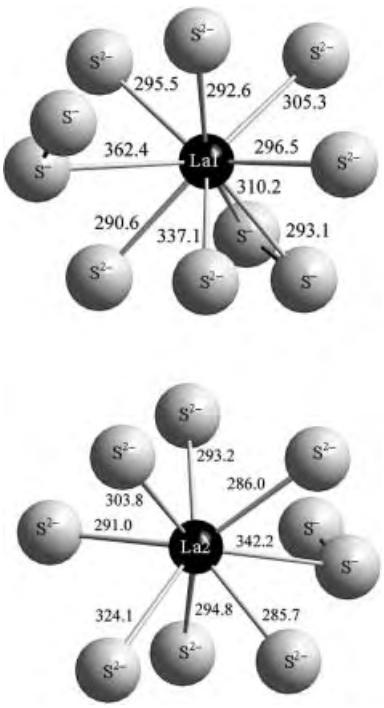


Figure 3. Coordination polyhedra of the two crystallographically different La^{3+} cations in the crystal structure of La_2CuS_4.

with $Bi_4Cu_4S_9$[5] and La_2CuS_4. When the trivalent transition metal lanthanum is used, even discrete $[S_3Cu]^{5-}\cdots[S_2]^{2-}\cdots[CuS_3]^{5-}$ contact-ion triples exist within the crystal structure. It has so far not been clarified whether the lanthanoids stabilize similar structure fragments.

Experimental Section

Light-red and translucent coarse single crystals of La_2CuS_4 were obtained by direct oxidation of metallic lanthanum and copper with sulfur. The addition of CsBr as fluxing agent promoted the crystal growth significantly, but LaS_2[7] and $LaCuS_2$[8] were formed as undesired by-products. In the presence of CsI as fluxing agent, the yield of La_2CuS_4 increased, although no pure product was obtained with this method. Likewise, variations of temperature (optimum: 700 °C) and of molar ratios did not yield by-product-free La_2CuS_4 samples.

Received: April 11, 2003 [Z51641]

Keywords: copper · crystal structure · lanthanum · polyanions · sulfur

[1] a) G. Calestani, C. Rizzoli, *Nature* **1987**, *328*, 606 – 607; b) H.-J. Meyer in *Moderne Anorganische Chemie*, 1st ed. (Ed.: E. Riedel), de Gruyter, Berlin, **1999**, pp. 462 – 467; c) F. Schwaigerer, B. Sailer, J. Glaser, H.-J. Meyer, *Chem. Unserer Zeit* **2002**, *36*, 108 – 124; d) M. K. Wu, J. R. Ashburn, C. J. Torng, P. H. Hor, R. L. Meng, L. Gao, Z. J. Huang, Y. Q. Wang, C. W. Chu, *Phys. Rev. Lett.* **1987**, *58*, 908 – 910; e) M. T. Weller in *Basistext Chemie: Anorganische Materialien, Vol. 11* (Eds.: S. G. Davis, R. G. Compton, J. Evans), VCH, Weinheim, **1996**, pp. 82 – 86.

[2] a) $K_3Cu_8S_6$: C. Burschka, *Z. Naturforsch. B* **1979**, *34*, 675 – 677; b) $Na_3Cu_4S_4$: C. Burschka, *Z. Naturforsch. B* **1979**, *34*, 396 – 397; c) $BaCu_{5.65}S_{4.5}$: J. S. Chang, H. Y.-P. Hong, G. H. Lee, Y. Wang, *Mater. Res. Bull.* **1990**, *25*, 863 – 869.

[3] F. Q. Huang, P. Brazis, C. R. Kannewurf, J. A. Ibers, *J. Solid State Chem.* **2000**, *155*, 366 – 371.

[4] a) H. T. Evans, Jr., *Nature* **1971**, *232*, 69 – 70; b) H. T. Evans, Jr., *Z. Kristallogr.* **1979**, *150*, 299 – 320.

[5] Y. Takéuchi, T. Ozawa, *Z. Kristallogr.* **1975**, *141*, 217 – 232.

[6] Crystal data of La_2CuS_4: monoclinic, space group $P2_1/c$ (no. 14), $a = 775.65(6)$, $b = 753.32(6)$, $c = 1081.13(9)$ pm, $\beta = 103.950(8)°$, $V_m = 92.301\ cm^3\,mol^{-1}$, $\rho_{calcd} = 5.088\ g\,cm^{-3}$, $Z = 4$, $\mu(Mo_{K\alpha}) = 18.34\ mm^{-1}$, $F(000) = 828$, Nonius-κ-CCD diffractometer, $Mo_{K\alpha}$ radiation ($\lambda = 71.069$ pm, graphite monochromator), $T = 293$ K, 27426 measured reflections, 2694 independent reflections, numerical absorption correction (HABITUS), $R_{int} = 0.0456$ ($R_\sigma = 0.0234$). The crystal structure was solved by direct methods (SHELX-97) and refined anisotropically with least-squares methods against F^2 with all data and 65 free parameters to $R_1 = 0.0227$, $wR_2 = 0.0387$, and GoF = 1.115. Further details on the crystal structure investigation may be obtained from the Fachinformationszentrum Karlsruhe, 76344 Eggenstein-Leopoldshafen, Germany (fax: (+49) 7247-808-666; e-mail: crysdata@fiz-karlsruhe.de), on quoting the depository number CSD-412900 (La_2CuS_4).

[7] J. Dugué, D. Carré, M. Guittard, *Acta Crystallogr. Sect. B* **1978**, *34*, 403 – 406.

[8] M. Julien-Pouzol, S. Jaulmes, A. Mazurier, M. Guittard, *Acta Crystallogr. Sect. B* **1981**, *37*, 1901 – 1903.

[9] a) F. Hulliger, *Struct. Bonding (Berlin)* **1968**, *4*, 83 – 229; b) H. J. Gotsis, A. C. Barnes, P. Strange, *J. Phys. Condens. Matter* **1992**, *4*, 10461 – 10468.

[10] B. Grande, H. Müller-Buschbaum, M. Schweizer, *Z. Anorg. Allg. Chem.* **1977**, *428*, 120 – 124.

 © 2003 Wiley-VCH Verlag GmbH & Co. KGaA, Weinheim

Force-Induced Affinity Changes

Coupling of Mechanical and Chemical Energy: Proton Affinity as a Function of External Force

*Martin K. Beyer**

The proton affinity of a molecule as a function of an external mechanical force is defined as a new thermochemical quantity. To explore its applicability as a chemical concept, it is evaluated with the help of density-functional calculations, using gas-phase dimethyl ether as a model system.

Recent experimental studies have measured the mechanical force that a covalent bond can withstand before it breaks,[1–3] and theoretical works have corroborated the

[*] Dr. M. K. Beyer
Institut für Physikalische und Theoretische Chemie
Technische Universität München
Lichtenbergstrasse 4, 85747 Garching (Germany)
Fax: (+49) 89-289-13416
E-mail: beyer@ch.tum.de

 DOI: 10.1002/anie.200351748 © 2003 Wiley-VCH Verlag GmbH & Co. KGaA, Weinheim

experimental findings.[1,4–6] Dynamic force spectroscopy in general has been described in theoretical works by Evans, Grubmüller, Schulten, and their co-workers.[7] A recent example of mechanochemistry is the mechanically induced isomerization of thiolate–gold clusters.[8] Besides simple homolytic bond breaking, it is conceivable that the application of an external force may also modify the course and outcome of more complex chemical reactions involving multiple reactants. Aktah and Frank showed in a recent study that ether bonds in aqueous solution undergo heterolytic cleavage under mechanical stress.[5b] The first step in a reaction commonly is the binding of an attacking moiety to a reactive site. With a general concept about how this binding is affected by the presence of mechanical strain, we may better understand how mechanical forces activate covalent bonds and how they promote or hinder chemical reactions. In turn, we would gain a view from a completely different angle on problems ranging from wear and tear of materials under long-term mechanical stress to the mechanisms of supramolecular catalysts and enzymes.

Let V_u and V_p be the potential functions of a molecule in its unprotonated and protonated form, respectively. An external force F stretches the unprotonated molecule to a length x_u, which is defined by $dV_u(x_u)/dx = F$. At this lengthening, the negative gradient of the potential, which is the force exerted by the stretched molecule, exactly balances the external force. As soon as a proton binds, the molecule takes on the new length x_p with $dV_p(x_p)/dx = F$. A positive external force F in this definition means a stretching force. The energy released upon binding is the difference between the potential energies and the mechanical work performed during the geometry change. This defines the proton affinity (PA) as a function of an external mechanical force F [Eq. (1)]:

$$PA(F) = -[V_p(x_p) - V_u(x_u)] + (x_p - x_u)F \quad (1)$$

The first minus sign in Equation (1) is necessary because the potentials are negative, whereas proton affinity is defined as a positive value. Figure 1 illustrates the meaning of this

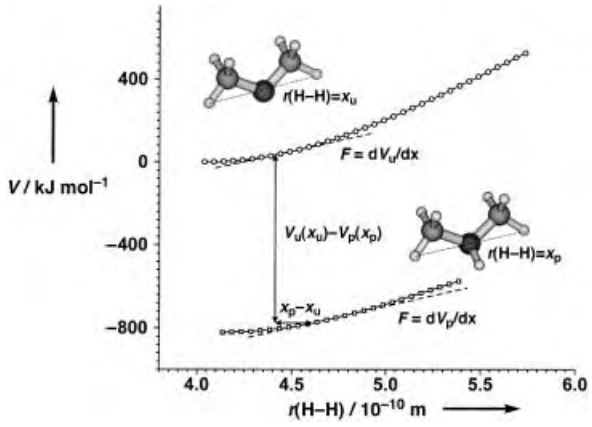


Figure 1. COGEF potentials for dimethyl ether V_u (open circles) and protonated dimethyl ether V_p (open squares). When an external force F is applied, the unprotonated and protonated molecules are elongated to distances r(H-H) $= x_u$ and x_p, respectively. Proton affinity as a function of force consists of the potential difference $V_p(x_p) - V_u(x_u)$ and the mechanical work performed by the force F over a distance $(x_p - x_u)$.

equation; dimethyl ether is chosen as a simple model system. COGEF (constrained geometry simulates external force)[4] potentials of dimethyl ether in its unprotonated and protonated form are used as V_u and V_p, respectively, which have been calculated with Gaussian 98[9] as described previously.[4] $PA(F)$ consists of a chemical contribution, the difference between the potential functions $(V_u - V_p)$, and a purely mechanical contribution, the force acting over the length increase $(x_p - x_u)$. This mechanical contribution is supplied by the environment, for example, by the force exerted through the cantilever of an atomic force microscope (AFM).

The COGEF potentials are estimated with a fourth-order polynomial fit. These can be used to calculate the $PA(F)$ for dimethyl ether according to Equation (1). It is, however, more instructive to calculate the force-induced change in proton affinity, $\Delta PA(F)$ [Eq. (2)]:

$$\Delta PA(F) = PA(F) - PA(0) \quad (2)$$

The result is displayed graphically in Figure 2. For small values of F, the function is almost linear. This region is dominated by the $(x_p - x_u)F$ contribution, which to a good

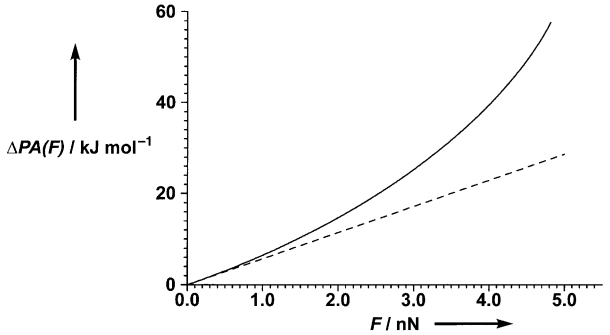


Figure 2. Force-induced change in proton affinity $\Delta PA(F)$ (solid line) of dimethyl ether. In the low-force limit, the mechanical work $\Delta PA(F)_{LF} = (x_{p,0} - x_{u,0})F$ (dashed line) is an excellent approximation. For higher forces, the softening of the bonds upon protonation becomes important. The same force stretches the protonated more than the unprotonated molecule. When both effects act together (the softening of the bond and the lengthening of the molecule upon protonation), they lead to a drastic increase in proton affinity of up to 60 kJ mol^{-1} under the influence of an external force.

approximation is the difference in length between the protonated and unprotonated unstretched molecule $(x_{p,0} - x_{u,0})$ multiplied by the applied force. The reason for this simply is that small forces do not lead to a significant geometry change. The dominant contribution is the change in length induced by the protonation itself. In the low-force limit, the force-induced change in proton affinity, $\Delta PA(F)_{LF}$ is described by [Eq. (3)]:

$$\Delta PA(F)_{LF} = (x_{p,0} - x_{u,0})F \quad (3)$$

In plain mathematical language, Equation (3) states that the proton affinity changes with force, even if the force is too small to induce a geometry change in the molecule. Forces of

 © 2003 Wiley-VCH Verlag GmbH & Co. KGaA, Weinheim

a few 100 pN are actually present in macromolecules such as enzymes.[10,11] Figure 2 suggests that Equation (3) is valid up to 500 pN, which covers the full range of entropic forces and forces induced by the tertiary structure of a macromolecule. As soon as the change in proton affinity is in the range of kT, it is likely to affect the rate of a reaction that is initiated by the attack of the proton, or to change equilibrium constants. At room temperature, kT amounts to 2.5 kJ mol^{-1}, which is reached at a force of $F = 420$ pN for dimethyl ether.

Another immediate consequence of Equation (3) is that the change in proton affinity is proportional to the geometry change upon protonation in the low-force limit. In dimethyl ether, the length increase is caused mostly by an increase in the COC bond angle. It is conceivable that the effect will be more pronounced if the bond order changes upon protonation. To achieve a kT change in proton affinity with a force of 200 pN, a length increase of only 0.2 Å is required according to Equation (3).

It is now straightforward to formulate a mechanochemical aspect of enzyme catalysis: Upon binding of the first substrate, the enzyme is deformed. Instead of being dissipated as heat and lost, a fraction of the substrate-binding energy is stored as mechanical energy in the enzyme, just in the same way that mechanical energy is stored in a deformed spring. Binding of the second substrate, for example, a proton, is promoted by the release of the stored mechanical energy. Equations (1) and (3) can be used to quantify this effect. The deformations of the enzyme are governed rather by a Gibbs free energy landscape G, than a potential-energy landscape V. This landscape, however, generates the force F. The proposed concept thus describes the effect of the complex, multidimensional free-energy landscape through the mechanical force it exerts on the substrate.

At higher forces, the softening of the molecule upon protonation becomes more important: The protonated molecule is stretched more than the unprotonated molecule, and this results in a deviation from the initially linear behavior. The gas-phase proton affinity changes by more than 60 kJ mol^{-1} until the maximum force is reached, which is given by the maximum slope of V_p. At this point, the molecule inevitably breaks. Bond breaking mathematically means that the bond length approaches infinity ($x_p \rightarrow \infty$), whereas the unprotonated molecule is still intact. Under these circumstances, $V_u(x_u)$ is constant, as well as F and x_u in Equation (1). $V_p(x_p)$ goes against the energy of the fully relaxed fragments of the model molecule, again a constant value. It then follows from Equation (1) that $PA(F) \rightarrow \infty$ if $x_p \rightarrow \infty$.

Chemically, $PA(F) \rightarrow \infty$ means that stretching an unprotonated molecule in a protic solvent inevitably leads to protonation, which is followed by bond breaking as soon as the breaking force of the protonated molecule is reached. Application of a mechanical force thus activates the protonation site and forces protonation: The proton is pulled out of the solvent, as shown in quantum molecular-dynamics simulations by Aktah and Frank.[5b] Equation (1) gives a conceptual explanation for this behavior.

So far, the influence of an external force on chemical reactions was seen mostly as imposing geometry constraints on the reactants. The definition of thermochemical quantities such as proton affinity as a function of force provides a quantitative and at the same time intuitive description for the coupling of mechanical and chemical energy. Clearly, the definition in Equation (1) also holds for electron affinities, as well as for the binding energies of larger attacking moieties as a function of mechanical force. The results in the low-force limit suggest that small forces modify the energy profile of a reaction, even if they are too small to induce a significant geometry change.

Received: April 25, 2003 [Z51748]

Keywords: enzymes · hydrolysis · mechanochemistry · protonation · theoretical chemistry

[1] M. Grandbois, M. Beyer, M. Rief, H. Clausen-Schaumann, H. E. Gaub, *Science* **1999**, *283*, 1727 – 1730.
[2] T. Wang, A. Ikai, *Jpn. J. Appl. Phys.* **1999**, *38*, 3912 – 3917.
[3] L. Garnier, B. Gauthier-Manuel, E. W. van der Vegte, J. Snijders, G. J. Hadziioannou, *J. Chem. Phys.* **2000**, *113*, 2497 – 2503.
[4] M. K. Beyer, *J. Chem. Phys.* **2000**, *112*, 7307 – 7312.
[5] a) U. F. Rohrig, I. Frank, *J. Chem. Phys.* **2001**, *115*, 8670 – 8674; b) D. Aktah, I. Frank, *J. Am. Chem. Soc.* **2002**, *124*, 3402 – 3406.
[6] a) D. Krüger, H. Fuchs, R. Rousseau, D. Marx, M. Parrinello, *J. Chem. Phys.* **2001**, *115*, 4776 – 4786; b) D. Krüger, H. Fuchs, R. Rousseau, D. Marx, M. Parrinello, *Phys. Rev. Lett.* **2002**, *89*, 186402.
[7] a) E. Evans, K. Ritchie, *Biophys. J.* **1997**, *72*, 1541 – 1555; b) S. Izrailev, S. Stepaniants, M. Balsera, Y. Oono, K. Schulten, *Biophys. J.* **1997**, *72*, 1568 – 1581; c) B. Heymann, H. Grubmüller, *Phys. Rev. Lett.* **2000**, *84*, 6126 – 6129.
[8] D. Krüger, R. Rousseau, H. Fuchs, D. Marx, *Angew. Chem.* **2003**, *115*, 2353 – 2355; *Angew. Chem. Int. Ed.* **2003**, *42*, 2251 – 2253.
[9] Gaussian 98 (Revision A.7), M. J. Frisch, G. W. Trucks, H. B. Schlegel, G. E. Scuseria, M. A. Robb, J. R. Cheeseman, V. G. Zakrzewski, J. A. Montgomery, R. E. Stratmann, J. C. Burant, S. Dapprich, J. M. Millam, A. D. Daniels, K. N. Kudin, M. C. Strain, O. Farkas, J. Tomasi, V. Barone, M. Cossi, R. Cammi, B. Mennucci, C. Pomelli, C. Adamo, S. Clifford, J. Ochterski, G. A. Petersson, P. Y. Ayala, Q. Cui, K. Morokuma, D. K. Malick, A. D. Rabuck, K. Raghavachari, J. B. Foresman, J. Cioslowski, J. V. Ortiz, A. G. Baboul, B. B. Stefanov, G. Liu, A. Liashenko, P. Piskorz, I. Komaromi, R. Gomperts, R. L. Martin, D. J. Fox, T. Keith, M. A. Al-Laham, C. Y. Peng, A. Nanayakkara, C. Gonzalez, M. Challacombe, P. M. W. Gill, B. G. Johnson, W. Chen, M. W. Wong, J. L. Andres, M. Head-Gordon, E. S. Replogle, J. A. Pople, Gaussian, Inc., Pittsburgh, PA, **1998**. The B3LYP density functional was used in combination with the 6-311++G(3df,3pd) basis set.
[10] M. Rief, M. Gautel, F. Oesterhelt, J. M. Fernandez, H. E. Gaub, *Science* **1997**, *276*, 1109 – 1112.
[11] T. Hugel, M. Seitz, *Macromol. Rapid Commun.* **2001**, *22*, 989 – 1016.

 © 2003 Wiley-VCH Verlag GmbH & Co. KGaA, Weinheim

Synthesis of Modified Proteins

Expressed Enzymatic Ligation for the Semisynthesis of Chemically Modified Proteins**

*Zuzana Machova, Regula von Eggelkraut-Gottanka, Nicole Wehofsky, Frank Bordusa, and Annette G. Beck-Sickinger**

Chemical synthesis is the most powerful way to assemble selectively modified proteins and is a tool for engineering proteins that are inaccessible by standard site-directed mutagenesis. A number of methods for the chemical synthesis of proteins have been developed, of which native chemical ligation (NCL)[1] is currently the most widely applied. This ligation approach is based on the chemoselective reaction of a C-terminal peptide thioester with a peptide that has a cysteine residue at its N terminus and results in the formation of a native peptide bond. Various attempts have been made to overcome the requirement for the cysteine residue at the ligation site. However, although some of these were successful, for example, with glycine[2] or selenocysteine[3] in place of cysteine, this feature still limits the flexibility of NCL.

Expressed protein ligation (EPL)[4] has opened up a whole new dimension in terms of accessible protein targets, because it applies recombinant techniques. However, this method suffers from restrictions similar to those of native ligation. Proteases that are used as ligation catalysts tolerate greater structural diversity at the coupling site. However, the limited primary substrate specificity of these enzymes reduces the scope of their use in synthesis. In the subtiligase-catalyzed fragment-condensation strategy (SCFC), which is one of the most successful enzymatic ligation methods to date, a genetically optimized enzyme is used for the synthesis of native and modified ribonuclease A.[5] Although this method increased the size of synthetic targets to entire proteins, it still suffers from the typical requirement for the careful selection of suitable coupling sites, because of limited enzyme specificity. Thus, despite significant progress in protein synthesis, alternative ligation strategies with broader applicability are still needed.

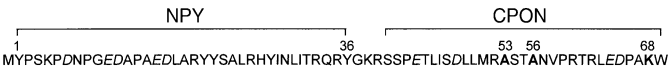
[*] Prof. Dr. A. G. Beck-Sickinger, Dr. Z. Machova, Pharm. R. von Eggelkraut-Gottanka
Institut für Biochemie der Universität Leipzig
Brüderstrasse 34, 04103 Leipzig (Germany)
Fax: (+49) 341-97-36-909
E-mail: beck-sickinger@uni-leipzig.de
Dr. N. Wehofsky, Dr. F. Bordusa
Max-Planck-Forschungsstelle für Enzymologie der Proteinfaltung
06120 Halle (Germany)

[**] This research was supported by the Deutsche Forschungsgemeinschaft (SFB 610/projects A1 and A3) and the Fonds der Chemischen Industrie. The authors thank Regina Reppich for recording the MALDI mass spectra.

Supporting information for this article is available on the WWW under http://www.angewandte.org or from the author.

Herein we report a further step toward this ambitious aim—expressed enzymatic ligation (EEL), which combines the advantages of EPL with those of the substrate-mimetic-mediated ligation strategy. The latter eliminates the specificity problem of classical protease-catalyzed synthesis through the attachment of an active-site-specific ester leaving group at the C-terminus of a nonspecific peptide moiety.[6] This combined approach also takes advantage of the recombinant expression of long-chain peptide thioesters, which can then act as substrate mimetics. Through this technique, peptide coupling can be carried out by an ordinary protease, for example, the Glu/Asp-specific serine protease V8 from *Staphylococcus aureus*, at nonspecific ligation sites, regardless of the specificity of the enzyme.

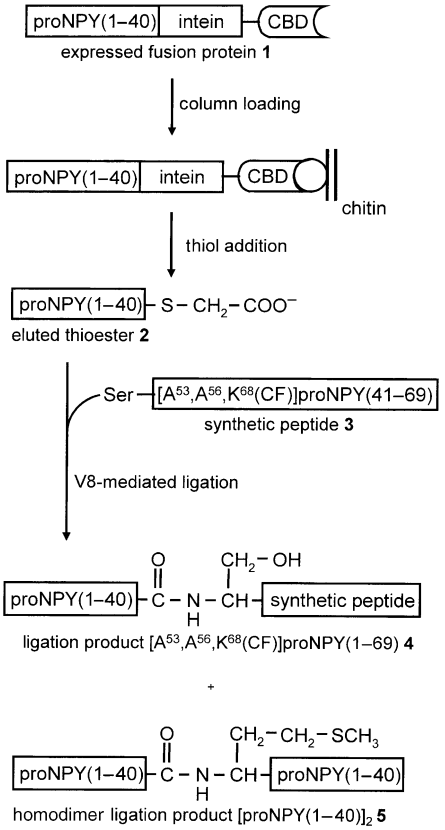
The feasibility of EEL has been demonstrated through the synthesis of a cysteine-free carboxyfluorescein (CF)-labeled analogue of the 69-mer prohormone neuropeptide Y (proNPY; Scheme 1). ProNPY processing leads to one of the most abundant neuropeptides in the brain, neuropeptide Y (NPY), which is involved in numerous biological events, such as the regulation of food intake and dealing with stress.[7]



Scheme 1. Sequence of the proNPY-derived analogue synthesized by EEL. Alanine substitutions were performed at positions 53 and 56. Exchange of Met 68 for lysine allowed site-specific incorporation of a CF label into the target sequence. The Glu-X and Asp-X peptide bonds are italicized as potential cleavage sites. The additional N-terminal methionine residue is derived from the translation initiation codon in all bacterially expressed N-terminal segments.

Our synthetic strategy is illustrated schematically in Scheme 2. The thioester substrate mimetic was generated by intein-mediated purification with a chitin-binding affinity tag (IMPACT system). All recombinantly expressed proteins were obtained with an additional methionine residue at their N terminus.[8] ProNPY(1–40) was cloned and expressed in *E. coli* as a fusion precursor with a C-terminal intein–chitin-binding-domain (CBD) tag. Under optimized conditions, the expression level of the proNPY(1–40)–intein–CBD protein **1** was high (≈ 270 mg of soluble protein per liter of cell culture). After the immobilization of **1** on chitin beads, thiol-induced self-cleavage of the intein resulted in the formation of very pure thioester **2** (40 mg per liter of bacterial culture), which could be used directly for enzymatic ligation. The selection of 2-sulfanylacetic acid (HSCm) as the intein-splicing agent was based on its previously reported ability to mediate the acceptance of nonspecific (containing neither Glu nor Asp) acyl moieties by protease V8.[9] A processing activity of the intein-fusion protein of up to 95% was observed with this untypical thiol under optimized conditions (for details, see Supporting Information). The C-terminal proNPY(41–69)-derived fragment **3** was synthesized by standard Fmoc (9-fluorenylmethoxycarbonyl) solid-phase peptide synthesis. Fragment **3** contains the natural serine residue at the N terminus. Alanine substitutions were made at positions 53 and 56, and Met 68 was exchanged for lysine, the side chain of which was modified with CF.

 © 2003 Wiley-VCH Verlag GmbH & Co. KGaA, Weinheim DOI: 10.1002/anie.200351774



Scheme 2. Course of EEL. The target protein proNPY(1–40) was expressed in bacteria with a C-terminal intein–CBD tag. After purification of the fusion protein **1** on chitin beads, intein cleavage was induced by the addition of 2-sulfanylacetic acid (HSCm). The eluted thioester **2**, which contains the specific leaving group ($S{-}CH_2{-}COO^-$), was used in the ligation with the synthetic proNPY(41–69)-derived peptide **3**, which bears an N-terminal serine residue. In addition to the corresponding ligation product **4** (60% yield), the homodimer **5** was obtained in 6% yield. The proteins **2, 4**, and **5** bear an additional N-terminal methionine residue (derived from the translation initiation codon).

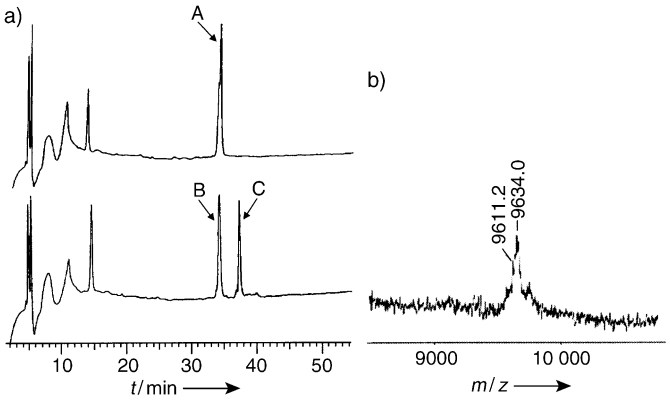


Figure 1. Analysis of the protease V8-catalyzed dimerization of proNPY(1–40) by reversed-phase HPLC. a) HPLC profiles of the ligation reaction mixture at the start of the reaction (top) and after 9 h (bottom) at 220 nm. Analysis was carried out on a C18 column with trifluoroactetic acid (TFA; 0.08%) in acetonitrile and TFA (0.1%) in water as the elution system (gradient: 0 to 100% acetonitrile over 90 min at a flow rate of 0.6 mL min^{-1}). The proNPY(1–40)–SCm thioester **2** (peak A) served as both the acyl donor and the acyl acceptor in the ligation. After termination of the enzymatic reaction, the hydrolyzed ester (peak B) and the homodimer **5** (peak C) were detected. The remaining peaks correspond to free HSCm and the buffer background. b) Identification of **5** by MALDI mass spectrometry: m/z_{calcd}: 9610.8, m/z_{found}: 9634.0 ($+Na^+$). The proteins **2, 4**, and **5** bear an additional N-terminal methionine residue.

Initially, the ability of protease V8 to accept the thioester **2** as a substrate was investigated. For this purpose, **2** was dissolved in an ammonium bicarbonate buffer in a final concentration of 1.2 mM and incubated with 0.24 μM enzyme. The bicarbonate buffer was used because it suppresses the cleavage of Glu–X bonds.[10] Protease V8 was also preincubated with HSCm to minimize its proteolytic-cleavage activity. HPLC analysis revealed that an incubation time of 9 h led to complete consumption of the ester, which illustrates the general acceptance of **2** by the enzyme. Under these conditions, no undesired proteolytic cleavage at the two glutamic acid and three aspartic acid residues of **2** could be detected (Figure 1a). Interestingly, the enzyme catalyzed the dimerization of the thioester to the 82-mer **5** nearly as fast as it catalyzed its hydrolysis (Figure 1a, peaks B and C).

Next, the ligation reaction of **2** and **3** was performed under similar conditions, with each reactant in a concentration of 1.2 mM. The reaction could be monitored easily at 450 nm because of the CF label present in **3**. After 9 h and complete consumption of the ester, the reaction was terminated, and the reaction mixture was analyzed by HPLC. The selected HPLC profiles in Figure 2 show that a number of products were formed in the reaction. These products were identified by mass spectrometry. The most intense product peaks B correspond to the desired CF-containing product **4**, which was formed in a yield of nearly 60%. Interestingly, the ester dimer **5** was formed in only 6% yield. Peaks C correspond to truncated peptide fragments, which result from competitive cleavage reactions of **3** in approximately 20% combined yield. Although the final product **4** is derived from a partially cleavage-sensitive fragment, it was found to be remarkably stable even after extended incubation times of up to one day.

In summary, these findings confirm that EEL represents a powerful alternative to NCL and SCFC, which does not rely on the presence of thiol-containing or enzyme-specific amino acid residues at the ligation junction. The EPL strategy, which we applied in parallel for the synthesis of proNPY analogues,[11] required the incorporation of an artificial cysteine residue in the protein sequence. This considerable limitation can be elegantly bypassed in EEL by using specific thioester substrate mimetics for enzyme-mediated ligation. The successful coupling that leads to the products **4** and **5**, which contain a Ser and a Met residue at the coupling site, respectively, strongly suggests that a broader range of N-terminal amino acid residues are accepted by protease V8. Additional coupling reactions with model peptides that contain an N-terminal tyrosine or isoleucine residue as the acyl acceptor supported this assumption (see Supporting Information). Further significant evidence for this hypothesis comes from our previously reported screening studies on the effect of substrate mimetics on the flexibility of protease V8

 © 2003 Wiley-VCH Verlag GmbH & Co. KGaA, Weinheim

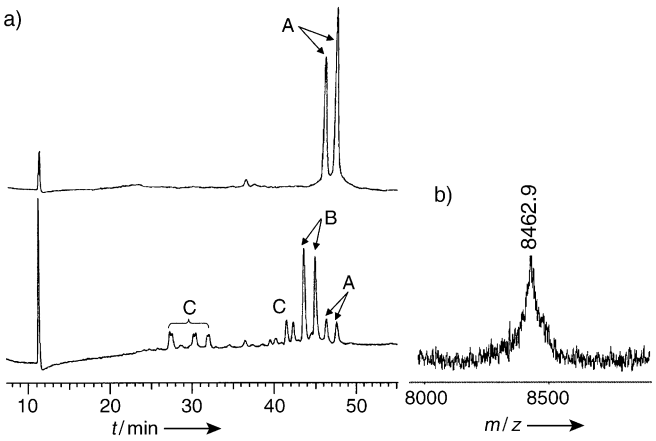


Figure 2. Analysis of the protease V8-catalyzed synthesis of [A^{53},A^{56},K^{68}(CF)]proNPY(1–69) (**4**) by reversed-phase HPLC. a) HPLC profiles of the ligation reaction mixture at the start of the reaction (top) and after 9 h (bottom) at 450 nm. Analysis was carried out on a C18 column with TFA (0.08%) in acetonitrile and TFA (0.1%) in water as the elution system (gradient: 0 to 100% acetonitrile over 90 min at a flow rate of 0.6 mL min^{-1}). The thioester **2** served as the acyl donor, and [A^{53},A^{56},K^{68}(CF)]proNPY(41–69) (**3**; peaks A) was used as the acyl acceptor. In addition to the intrinsic cleavage products of **3** (peaks C), the ligation product **4** was easily identified by making use of the CF label (peaks B). Because of the CF label, which consists of two isomers, the substrate **3** and the product **4** were detected as two separate peaks. b) Identification of the ligation product **4** (with an N-terminal methionine residue) by MALDI mass spectrometry: m/z_{calcd}: 8423.6, m/z_{found}: 8462.9 ($+K^+$).

for peptide synthesis.[12] These results led to the conclusion that the enzyme has broad tolerance toward the sequence and length of the acyl acceptor. This also holds for the acyl donor component, through mediation by the substrate mimetic. The findings presented herein suggest that expressed enzymatic ligation has significant potential for improving the flexibility of existing methods for protein synthesis. Further attempts to modify proteins, for example, by insertion of spin-resonance probes and noncanonical amino acids into selected target sequences or through photoaffinity labeling, are in progress.

Received: April 29, 2003 [Z51774]
Published Online: September 30, 2003

Keywords: enzymatic ligation · fluorescent probes · neuropeptide Y · protein modifications · substrate mimetics

[1] P. E. Dawson, T. W. Muir, I. Clark-Lewis, S. B. Kent, *Science* **1994**, *266*, 776–779.
[2] C. Marinzi, S. J. Bark, J. Offer, P. E. Dawson, *Bioorg. Med. Chem.* **2001**, *9*, 2323–2328.
[3] R. J. Hondal, R. T. Raines, *Methods Enzymol.* **2002**, *347*, 70–83.
[4] T. W. Muir, R. M. Hofmann, *Curr. Opin. Biotechnol.* **2002**, *13*, 297–303.
[5] D. Y. Jackson, J. Burnier, C. Quan, M. Stanley, J. Tom, J. A. Wells, *Science* **1994**, *266*, 243–247.
[6] F. Bordusa, *Curr. Protein Pept. Sci.* **2002**, *3*, 159–180.
[7] D. R. Gehlert, *Neuropeptides* **1999**, *33*, 329–338.
[8] S. Chong, F. B. Mersha, D. G. Comb, M. E. Scott, D. Landry, L. M. Vence, F. B. Perler, J. Benner, R. B. Kucera, C. A. Hirvonen, J. J. Pelletier, H. Paulus, M. Q. Xu, *Gene* **1997**, *192*, 271–281.
[9] N. Wehofsky, F. Bordusa, *FEBS Lett.* **1999**, *443*, 220–224.
[10] J. J. Birktoft, K. Breddam, *Methods Enzymol.* **1994**, *244*, 114–126.
[11] R. A. von Eggelkraut-Gottanka, Z. Machova, E. Grouzmann, A. G. Beck-Sickinger, *ChemBioChem* **2003**, *4*, 425–433.
[12] N. Wehofsky, J. Wissmann, M. Alisch, F. Bordusa, *Biochim. Biophys. Acta* **2000**, *1479*, 114–122.

 © 2003 Wiley-VCH Verlag GmbH & Co. KGaA, Weinheim

A Chain of Dendrimers

Synthesis and Characterization of Dendritic Necklaces: A Class of Outer-Sphere–Outer-Sphere Connected Dendronized Organoplatinum Polymers**

Hak-Fun Chow, Cham-Fai Leung, Wei Li, Kai-Wai Wong, and Luan Xi*

Some years ago Newkome and Vögtle proposed the concept of dendritic networks[1] whereby simple dendrimer/dendron subunits could be connected together to form macromolecular assemblies with nanoscopic dimensions.[2] At about the same time, Schlüter and co-workers began to report their pioneering works on the synthesis and characterization of a special kind of dendritic networks, also known as cylindrical dendronized polymers,[3,4] based on an inner-sphere–inner-sphere connection[2] approach, that is, the resulting dendronized polymers may be viewed as constructed from the connection of individual dendrons through their internal focal-point functional groups. A large number of such inner-sphere–inner-sphere connected dendronized polymers were reported. Some of them were shown to have cylindrical geometry[4] while some were known to self-assemble into spherical nanostructures.[5] To our surprise, examples of dendritic networks created by the alternative outer-sphere–outer-sphere connection strategy[2] are less studied. A few examples were already reported but invariably they all involve a random polymerization of dendrimer subunits that have a large number of reactive functional groups on the dendrimer surface.[6] We report herein a new variant of the outer-sphere–outer-sphere connection strategy that allows us to prepare a novel class of nanoscopic dendritic networks (hereafter called dendritic necklaces because of their structural resemblance to untied necklaces) by the controlled polymerization of dendrimer subunits containing only two reactive surface functional moieties (Figure 1).[7] We also show that the resulting dendritic necklaces, in contrast to randomly connected dendritic networks, can be fully characterized by solution techniques such as NMR, MS, GPC and laser light scattering (LLS) to enable a thorough assessment of their structural identity and purity. Employing organo-

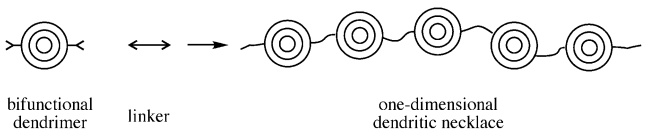
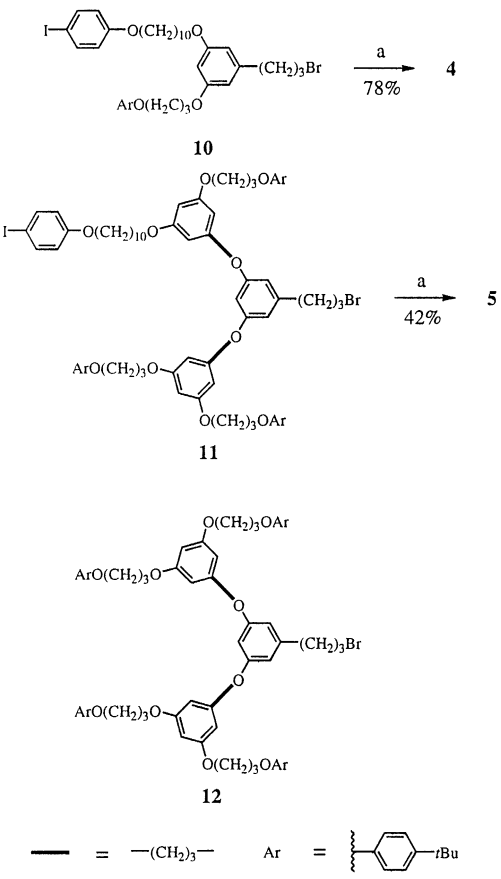


Figure 1. Synthesis of dendritic necklaces by outer-sphere–outer-sphere connection of bifunctional dendrimers.

platinum coordination chemistry as a method for the polymerization of bis(ethynyl) surface-functionalized G1–G3 dendritic beads **1**–**3**, we demonstrate that higher-order 1D dendritic necklaces with high degree-of-polymerization values (DP, from 30–880) could be prepared in high yields. We also describe a general synthetic protocol for the construction of dendrimers that contain a limited number of functional groups on the surface sector.

Because bis(ethynyl) polyether-based dendrimers readily form *trans*-dialkynyl organoplatinum(II) complexes upon treatment with *trans*-$[(Et_3P)_2PtCl_2]$, this reaction was chosen to link the dendrimers **1**–**3** together.[8] To avoid random polymerization of the dendritic beads, only two of the surface moieties were functionalized with "reactive" long chain 10-(4-ethynylphenoxy)decyloxyl residues while the rest were decorated with "inert" 3-(4-*tert*-butylphenoxy)propoxy groups.

The synthesis of the target dendritic monomers **1**–**3** required the availability of three bromo-dendrons **10**, **11**, and **12**[9] (Scheme 1). Hence, the G1-dendrimer **4** and G2-



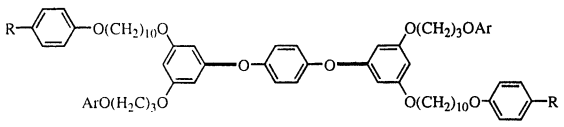
Scheme 1. Reagents and conditions: a) hydroquinone (0.45 equiv), Cs_2CO_3, dibenzo-24-crown-8, DMF, 110°C, 2 h.

[*] Prof. Dr. H.-F. Chow, C.-F. Leung, W. Li
Department of Chemistry
The Chinese University of Hong Kong
Shatin, NT (Hong Kong SAR)
Fax: (+852) 26035057
E-mail: hfchow@cuhk.edu.hk
Dr. K.-W. Wong, L. Xi
Department of Physics
The Chinese University of Hong Kong
Shatin, NT (Hong Kong SAR)

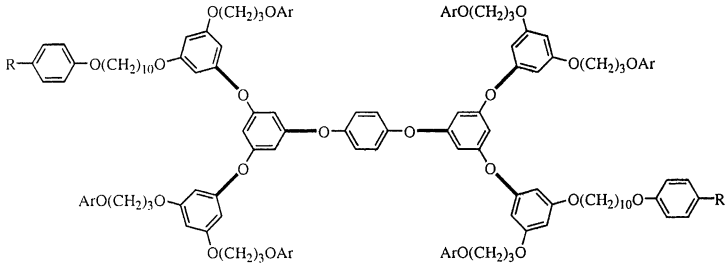
[**] We thank the Research Grants Council, HKSAR (CUHK4201/99P) for the financial support, Prof. D. T. W. Chan for mass spectral and Prof. C. Wu and Mr. T. Ngai for LLS measurements

Supporting information for this article is available on the WWW under http://www.angewandte.org or from the author.

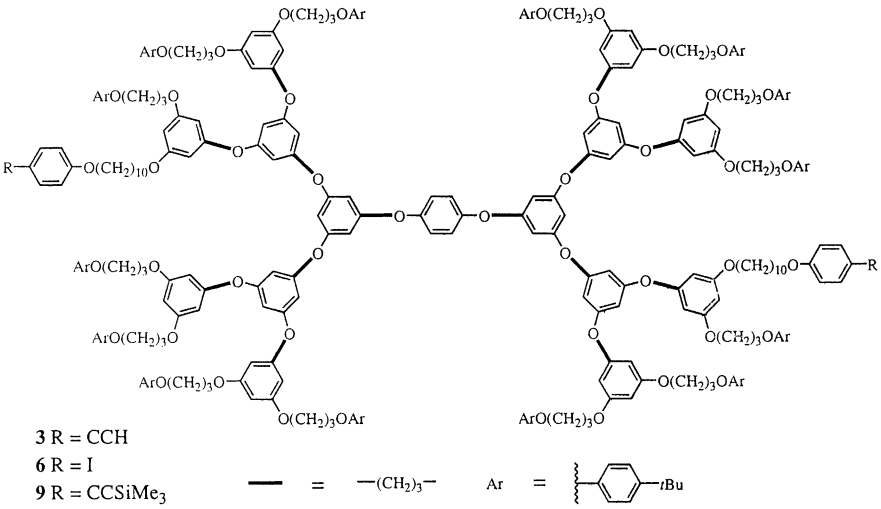
 DOI: 10.1002/anie.200351613 © 2003 Wiley-VCH Verlag GmbH & Co. KGaA, Weinheim



1 R = CCH
4 R = I
7 R = $CCSiMe_3$



2 R = CCH
5 R = I
8 R = $CCSiMe_3$



3 R = CCH
6 R = I
9 R = $CCSiMe_3$

The G1–G3 diiodide surface-functionalized dendrimers **4–6** were then converted to the corresponding bis(trimethylsilylethynyl) dendrimers **7–9**, respectively, by the Sonogashira coupling reaction with 1-trimethylsilylethyne. The trimethylsilyl groups were then removed under basic conditions to afford the target bifunctional dendrimers **1–3**, respectively, from compounds **7–9**. The structures of the target monomers **7–9** were confirmed by ^{1}H and ^{13}C NMR and mass spectroscopic measurements,[9] and their purity and homogeneity (polydispersity index (PDI) = 1.04) were also evaluated by GPC analysis (Figure 2).

Copolymerization reactions of a 1:1 molar ratio (20–30 mM) of the bifunctional dendrimers **1–3** and *trans*-$[(Et_3P)_2PtCl_2]$ were conducted in the presence of CuI, diisopropylamine in CH_2Cl_2 to afford G1–G3 dendritic necklaces **17–19**, respectively (Scheme 3). The light yellow organoplatinum products were isolated by successive precipitation from the addition of a CH_2Cl_2 solution to acetone and to methanol and their structures were characterized by ^{1}H, ^{13}C and ^{31}P NMR spectroscopy. Figure 3 showed the ^{1}H NMR spectra of the G2-monomer **2** and the resulting G2-dendritic necklace **18**. Prior to Pt complexation, the terminal acetylenic proton gave a sharp singlet at $\delta =$ 3.0 ppm and an AB system ($\delta = 7.4$ and 6.8 ppm) due to the aromatic protons of the 4-ethynylphenoxy surface groups. After complexation, the positions of the AB system were shifted upfield ($\delta = 7.2$ and 6.7 ppm) while the signal of the acetylenic proton due to the end group could hardly be observed because of the high degree of polymerization (DP $\approx$ 90, see below). The $^{31}P\{^{1}H\}$ NMR spectra of the G1-**17** and G2- **18** dendritic necklaces consisted of one ^{31}P signal located at about $\delta = 17.5$ ppm with two ^{195}Pt satellite signals [$^{1}J(Pt,P) \approx 2380$ Hz] of

dendrimer **5** containing two aryl iodide surface moieties were constructed by anchoring the mono-iodo surface-functionalized[10] G1-bromide **10** (2.2 equiv) and G2-bromide **11** (2.2 equiv), respectively, to a hydroquinone core in the presence of Cs_2CO_3 in reasonable yields. Conversely, a differentially (methoxymethyl (MOM) and benzyl) protected hypercore **13**[9] was used in the synthesis of the diiodo surface-functionalized G3-dendrimer **6** (see Scheme 2). Hence, the two MOM groups were cleaved under acidic conditions to afford a bis(phenol) intermediate **14**, which was then treated first with 2.2 equivalents of the symmetrical G2-bromide **12** to give a partially constructed G3-dendrimer **15**. The benzyl groups were then removed and the product **16** was reacted with 2.2 equivalents of the unsymmetrical G2-bromide **11** to give the G3-dendrimer **6**.

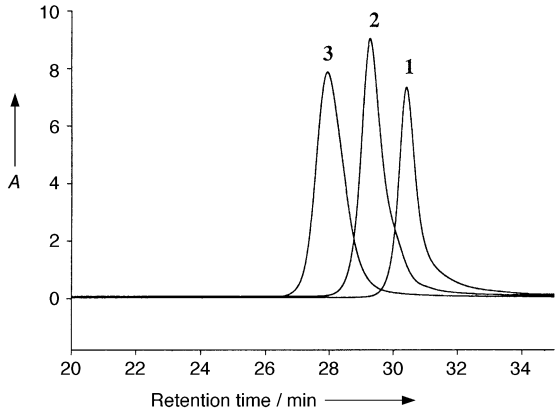
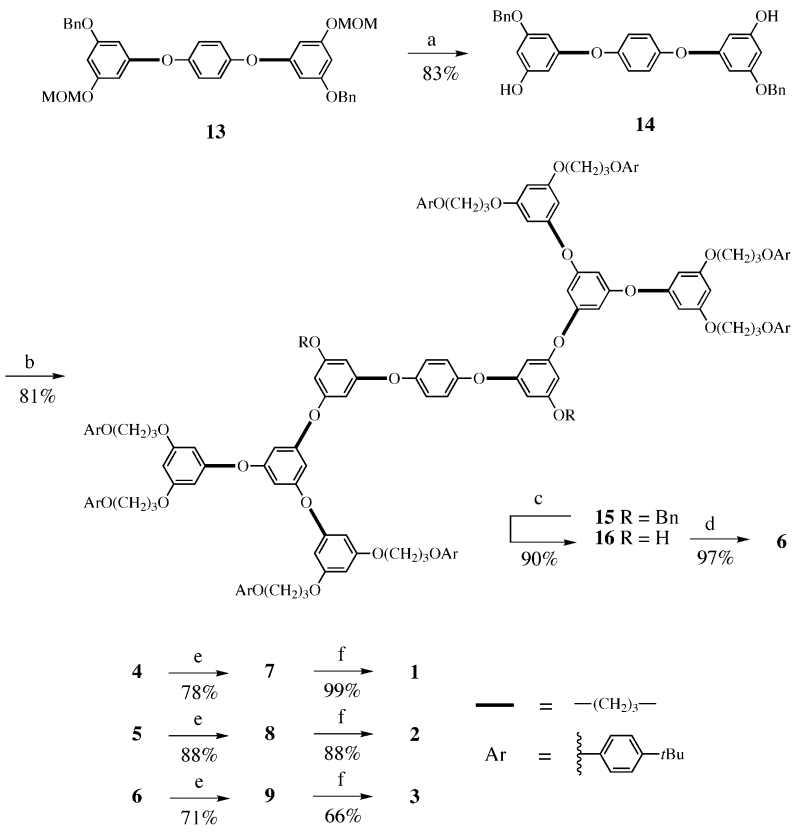


Figure 2. GPC chromatograms of bis(ethynyl) surface-functionalized dendrimers **1–3**. *A* = UV absorbance, arbitrary units.

 © 2003 Wiley-VCH Verlag GmbH & Co. KGaA, Weinheim



Scheme 2. Reagents and conditions: a) HCl, EtOH, THF, 0 °C, 1 h; b) **12** (2.2 equiv), Cs_2CO_3, dibenzo-24-crown-8, DMF, 60 °C, 3 h; c) H_2 (1 atm), 10% Pd/C, EtOH, EtOAc (1:1), 25 °C, 6 h; d) **11** (2.2 equiv), Cs_2CO_3, dibenzo-24-crown-8, DMF, 60 °C, 3 h; e) TMSC≡CH, $[Pd(PPh_3)_2Cl_2]$, CuI, NEt_3, PPh_3, toluene, 60 °C, 24 h; f) K_2CO_3, MeOH, THF, 25 °C, 1.5 h.

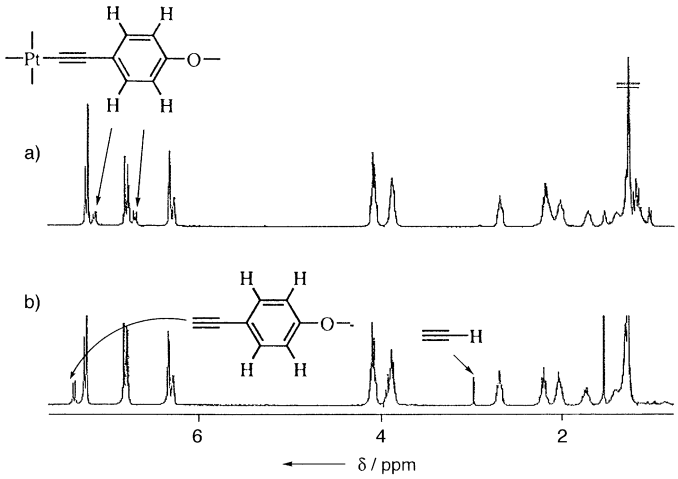
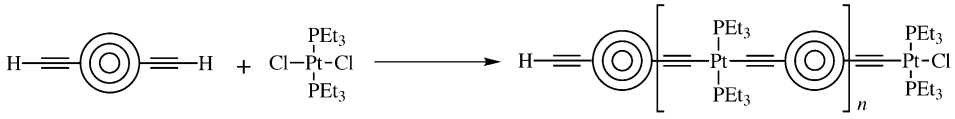


Figure 3. ^1H NMR (300 MHz, $CDCl_3$) spectra of a) G2-dendritic necklace **18** and b) G2-dendrimer **2**.

one sixth intensity (Figure 4). Conversely, the $^{31}P\{^1H\}$ NMR spectrum of the G3 dendritic necklace **19** consisted of one major ^{31}P signal at about the same position ($\delta = 16.3$ ppm). However, two additional ^{31}P signals ($\delta = 20.2$ and 14.0 ppm) of lower intensities were also noted. These signals probably arose from ^{31}P resonances of the end group, which became more evident due to the lower DP value (≈ 30) of the G3-dendritic necklace **19**.

The molecular weights and distributions of the necklaces **17**–**19** in THF were determined by LLS and GPC studies (Table 1) and the measured values were not influenced by the monomer concentration used in the copolymerization. Furthermore, the molecular-weight values of the G1-dendritic necklace **17** obtained from GPC studies were also independent of the sample concentration used in the measurements,[11] which suggests the values in Table 1 reflect the molecular weights of individual dendritic necklaces and not those of the aggregates. The PDI values obtained were rather large (≈ 2.0) and were independent of dendrimer generation. Examination of the LLS data indicated that this new outer-sphere–outer-sphere connection strategy could produce large nanoscopic-sized ($R_g \approx$ 100 nm) dendritic necklaces of high molecular weights ($\bar{M}_w > 1.8 \times 10^5$). It was also noted that the copolymerization was sensitive to steric inhibition as the DP value dropped significantly from 880 to 30 on going from the first to the third generation. Nonetheless, the DP values were still comparable to the high-end values of dendronized polymers obtained from inner-sphere–inner-sphere connection strategy.[4c] Furthermore, GPC measurements tended to produce much smaller $\bar{M}_w$ values as polystyrenes were not good calibration standards for dendritic polymers. The ratio of the $\bar{M}_w$ values obtained from LLS and GPC, values that indicated how much the GPC results underestimated the real molar mass of the tested compounds, showed a gradual decrease (from 14.0 to 1.5) from the G1- to the G3-dendritic necklace. The ratios are much greater than unity as the hyperbranched dendritic necklaces are expected to have a much larger mass per unit length than polystyrene. However, as the size of the dendritic beads was getting larger for the G3-necklace, the long hydrocarbon linker groups were



1-3 (G1-G3) **17-19** dendritic necklaces G1-G3

Scheme 3. Reagents and conditions: $HN(iPr)_2$, CuI, CH_2Cl_2, 25 °C, 12 h.

 © 2003 Wiley-VCH Verlag GmbH & Co. KGaA, Weinheim

Table 1: LLS and GPC data of G1-G3 dendritic necklaces **17–19**.

Dendritic necklaces	Yield % [a]	LLS[b]			GPC[c]		$\bar{M}_w$ (DLLS)/
		$\bar{M}_w \times 10^3$	DP[d]	R_g [nm]	$\bar{M}_w \times 10^3$	PDI	$\bar{M}_w$ (GPC)
G1 **17**	88	1500 (1.7)[e]	8.8×10^2	170	107[f]	1.9	14.0
G2 **18**	78	290 (3.1)	0.9×10^2	76	82[g]	1.7	3.5
G3 **19**	58	180 (5.8)	0.3×10^2	124	117[g]	2.0	1.5

[a] Yield after precipitation from solvents. [b] Solvent: THF. [c] Solvent: THF. Polystyrenes were used as calibration standards. [d] Calculated from $\bar{M}_w$ determined by LLS. [e] Values in brackets are the calculated molecular weights of the repeating unit. [f] Sample concentration = 2.7 mg mL^{-1}. [g] Sample concentration = 0.54 mg mL^{-1}.

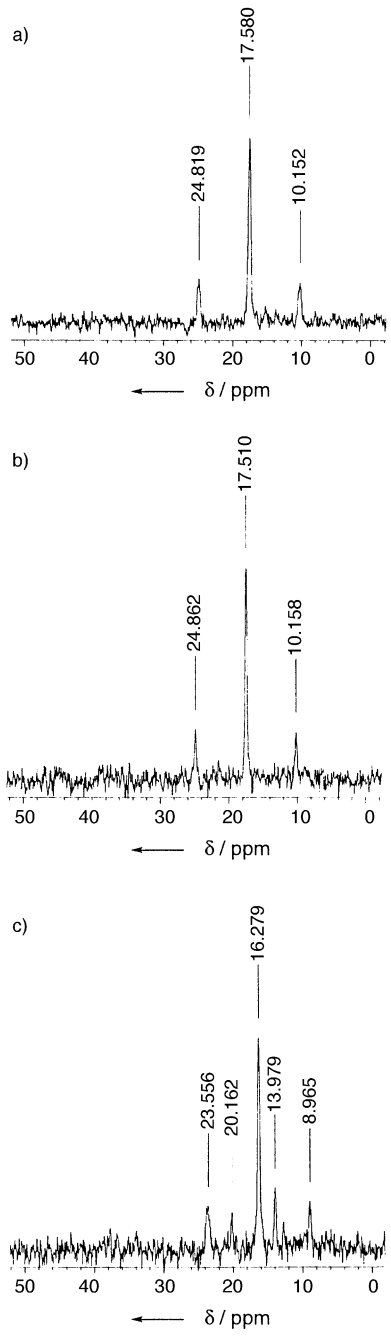


Figure 4. $^{31}P\{^1H\}$ NMR (161.9 MHz, $CDCl_3$) spectra of dendritic necklaces a) G1 **17**, b) G2 **18**, and c) G3 **19**.

expected to stiffen and result in an increase of hydrodynamic volume and hence a decrease of the ratio.

A scanning tunneling microscopic (STM) study on spin-casted (3000 rpm) samples of dendritic necklaces **17–19** from diluted THF solutions ($\approx 10\ \mu g\,mL^{-1}$) on highly oriented pyrolytic graphite (HOPG) showed that the necklaces existed in aggregate form and adopted a coiled structure. An increase in the spin-casting speed to 5000 rpm facilitated the rate of solvent evaporation and prevented aggregate formation, and the dendritic necklaces were found across the steps of the freshly cleaved HOPG surface as thin threads (Figure 5). The mean cross-section

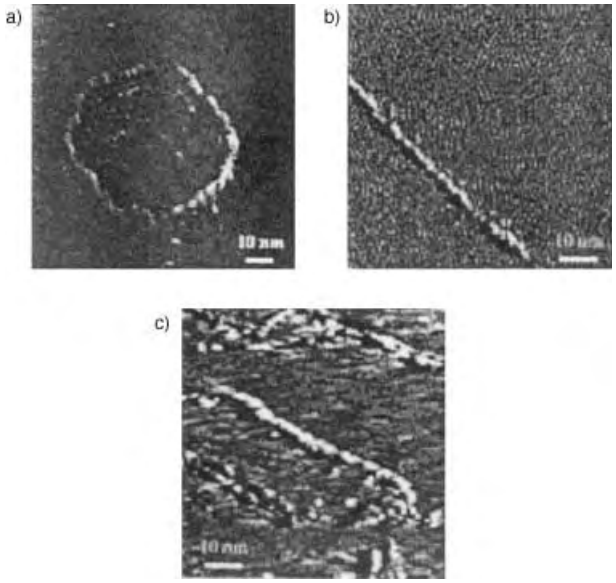


Figure 5. STM images of dendritic necklaces a) **17** b) **18** and c) **19** spin-casted (5000 rpm) on HOPG.

diameter of the individual threads was found to increase from 1.1 to 1.6 and then to 2.0 nm on going from G1–G3, thus showing that the size of the dendritic beads also played a role in controlling the molecular dimensions of these dendritic necklaces.

In summary, we report here a general method for the synthesis of functional dendrimers that contain a limited number of reactive functional groups on the dendritic surface and also a new strategy for the construction of a novel class of structurally defined dendritic necklaces by using an outer-sphere–outer-sphere connection strategy. One notable feature of this method is that the dendritic necklaces thus obtained have a very high degree of polymerization. We believe this new method offers a new entry towards the construction of nanoscale shape-controlled polymers. Two important structural elements in this strategy are the length of the linker groups and the size of the dendrimer beads, which

 © 2003 Wiley-VCH Verlag GmbH & Co. KGaA, Weinheim

are expected to be the key variables that can be used to control the three dimensional morphology of the dendritic networks. Hence, dendritic necklaces that have tight packing dendrimer subunits may be realized by using shorter linker molecules and larger dendrimer beads. Furthermore, multi-block dendritic necklaces that have segregated regions can also be constructed from dendrimer beads and linker units that are of different physical properties.

Received: April 8, 2003 [Z51613]

Keywords: dendrimers · nanostructures · platinum · polymers

[1] The term "networks" coined by Newkome and Vögtle has a different conception from that used in polymer chemistry. In polymer chemistry, networks are generally referred to highly cross-linking systems while dendritic networks do not necessarily have a cross-linking architecture.

[2] a) G. R. Newkome, C. N. Moorefield, F. Vögtle, *Dendritic Molecules. Concepts. Syntheses. Perspectives*, Wiley-VCH, Weinheim, **1996**, chap. 9; b) G. R. Newkome, C. N. Moorefield, F. Vögtle, *Dendrimers and Dendrons. Concepts, Syntheses, Applications*, Wiley-VCH, Weinheim, **2001**, chap. 9.

[3] a) R. Freudenberger, W. Claussen, A.-D. Schlüter, H. Wallmeier, *Polymer* **1994**, *35*, 4496 – 4501; b) W. Claussen, N. Schulte, A.-D. Schlüter, *Macromol. Rapid Commun.* **1995**, *16*, 89 – 94.

[4] For reviews and highlights on cylindrical dendronized polymers, see a) A. D. Schlüter, *Top. Curr. Chem.* **1998**, *197*, 165 – 191; b) H. Frey, *Angew. Chem.* **1998**, *110*, 2313 – 2318; *Angew. Chem. Int. Ed.* **1998**, *37*, 2193 – 2197; c) A. D. Schlüter, J. R. Rabe, *Angew. Chem.* **2000**, *112*, 860 – 880; *Angew. Chem. Int. Ed.* **2000**, *39*, 864 – 883.

[5] V. Percec, C.-H. Ahn, G. Ungar, D. J. P. Yeardley, M. Möller, S. S. Sheiko, *Nature* **1998**, *391*, 161 – 164.

[6] a) S. Watanabe, S. L. Regen, *J. Am. Chem. Soc.* **1994**, *116*, 8855 – 8856; b) J. Li, D. R. Swanson, D. Qin, H. M. Brothers, L. T. Piehler, D. Tomalia, D. J. Meier, *Langmuir* **1999**, *15*, 7347 – 7350; c) D. J. Díaz, G. D. Storrier, S. Bernhard, K. Takada, H. D. Abruña, *Langmuir* **1999**, *15*, 7351 – 7354; d) M. T. Reetz, D. Giebel, *Angew. Chem.* **2000**, *112*, 2614 – 2617; *Angew. Chem. Int. Ed.* **2000**, *39*, 2498 – 2501.

[7] A recent paper describing the synthesis of G1- and G2-dendritic monomers that have bifunctional surface moieties for outer-sphere–outer-sphere connection had appeared. However, no polymerization study was disclosed, see R. N. Ganesh, J. Shraberg, P. G. Sheridan, S. Thayumanavan, *Tetrahedron Lett.* **2002**, *43*, 7217 – 7220.

[8] K. Sonogashira, Y. Fujikura, T. Yatake, N. Toyoshima, S. Takahashi, N. Hagihara, *J. Organomet. Chem.* **1978**, *145*, 101 – 108.

[9] See Supporting Information for details of synthetic procedures and physical data.

[10] The methodology used in the synthesis of the surface-functionalized G1-bromide **10** and G2-bromide dendrons **11** was similar to that described in the literature, see K. L. Wooley, C. J. Hawker, J. M. J. Fréchet, *J. Chem. Soc. Perkin Trans. 1* **1991**, 1059 – 1076 for details.

[11] The estimated GPC mass-average molar mass ($\bar{M}_w$) of the G1-dendritic necklace **17** at concentrations 0.11, 0.54, and 2.70 mg mL^{-1} were 1.05×10^5, 1.04×10^5 and, 1.07×10^5 respectively.

 © 2003 Wiley-VCH Verlag GmbH & Co. KGaA, Weinheim

Catalyzed Reduction of N Oxides

Gas-Phase Reduction of Oxides of Nitrogen with CO Catalyzed by Atomic Transition-Metal Cations**

*Voislav Blagojevic, Michael J. Y. Jarvis, Eric Flaim, Gregory K. Koyanagi, Vitali V. Lavrov, and Diethard K. Bohme**

Catalytic conversion of harmful gases, such as the oxides of nitrogen produced in fossil-fuel combustion into nitrogen and carbon dioxide, is of utmost importance, both environmentally and economically. CO was one of the first gases investigated for eliminating NO from automobile exhaust gas: the reaction of NO with CO [Eq. (1)] is one of the most

$$NO + CO \rightarrow {}^{1}/_{2}N_2 + CO_2 \quad (1)$$

important reactions occurring in automotive catalytic converters where both reactants are undesirable pollutants.[1]

Base-metal oxides, mixed metal-oxide compounds such as perovskites, supported metal catalysts, metal zeolites, and alloys have all been investigated as heterogeneous catalysts for this reaction, which does not occur directly in the gas phase at room temperature to any measurable extent.[1] For example, copper in the $+2$ oxidation state has been found to be active both as a base-metal-oxide catalyst and in a metal-supported or perovskite form.

We report here the first example of homogeneous catalysis by the reaction described in Equation (1), which occurs in the gas phase with atomic transition-metal cations serving as catalysts. The catalysis occurs in two steps in which NO is first reduced to N_2O. An analogous three-step catalytic reduction of NO_2, in which NO_2 is first reduced to NO, was also discovered.

The overall catalytic scheme that was established in the study reported here consists of the three catalytic cycles shown in Figure 1. These three cycles were characterized with laboratory measurements of reactions of each of the three nitrogen oxides NO_2, NO, and N_2O with up to 29 different transition-metal cations M^+ [Eqs. (2)–(4)]:

[*] Prof. D. K. Bohme, V. Blagojevic, M. J. Y. Jarvis, E. Flaim, G. K. Koyanagi, V. V. Lavrov
Department of Chemistry
York University
Toronto, ON, M3J 1P3 (Canada)
Fax: (+1) 416-736-5936
E-mail: dkbohme@yorku.ca

[**] Support for this research by the Natural Sciences and Engineering Research Council of Canada is greatly appreciated. Also, we acknowledge support from the National Research Council, the Natural Science and Engineering Research Council, and MDS SCIEX in the form of a Research Partnership grant. As holder of a Canada Research Chair in Physical Chemistry, D.K.B. thanks the contributions of the Canada Research Chair Program to this research. We also thank Dr. I. Kretzschmar for helpful discussions.

 DOI: 10.1002/anie.200351628 © 2003 Wiley-VCH Verlag GmbH & Co. KGaA, Weinheim

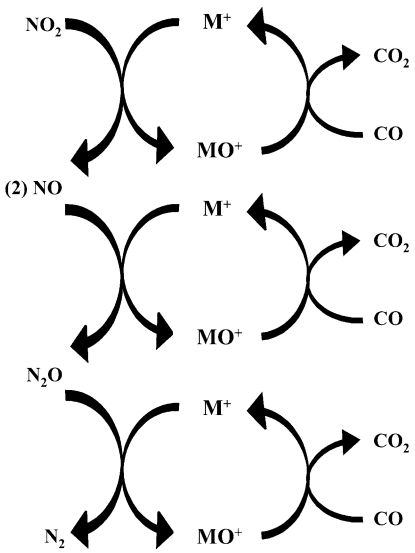


Figure 1. Catalytic cycles for the homogeneous reduction of nitrogen oxides by carbon monoxide, mediated by atomic transition-metal cations.

$$M^+ + NO_2 \rightarrow MO^+ + NO \quad (2)$$

$$M^+ + NO + NO \rightarrow MO^+ + N_2O \quad (3)$$

$$M^+ + N_2O \rightarrow MO^+ + N_2 \quad (4)$$

These reactions lead to the reduction of the corresponding nitrogen oxide as well as the oxidation of M^+ to MO^+. Also, metal-oxide cations, MO^+, were reacted with CO. These reactions lead to the reduction of MO^+ to M^+ as well as the oxidation of CO to CO_2 according to Equation (5), where the catalyst

$$MO^+ + CO \rightarrow M^+ + CO_2 \quad (5)$$

M^+, which reduces the three nitrogen oxides, is regenerated:

Two modes were observed for the reactions of M^+ with NO. M^+ ions with a high O-atom affinity, $OA\ (M^+) > OA\ (N) = 151$ kcal mol^{-1},[2] were found to abstract an O atom from NO exothermically according to Equation (6) with high efficiency, $k > 10^{-10}$ cm^3 molecule^{-1} s^{-1}.

$$M^+ + NO \rightarrow MO^+ + N \quad (6)$$

The bimolecular reaction shown in Equation (6) was observed with $M^+ = Sc^+$, Ti^+, Y^+, Zr^+, Nb^+, La^+, Hf^+, Ta^+, and W^+ (see Table 1 for values of $OA\ (M^+)$). Second-order NO reactions of the type shown in Equation (3) were observed at high NO flows for $M^+ = V^+$, Cr^+, Mn^+, Fe^+, Co^+, Ni^+, Mo^+, Ru^+, Re^+, Os^+ and Ir^+. The reaction given in Equation (6) is endothermic for these latter ions (see Table 1) but that in Equation (3), driven by N–NO bond formation, is exothermic since $OA\ (M^+) > OA\ (N) - D\ (N\text{-}NO) = 36$ kcal mol^{-1}.[2] Figure 2 (top left) presents experimental data obtained for the second-order (in NO) reduction of NO by Fe^+. With V^+, Cr^+, Mn^+ and Mo^+, this reaction occurs in competition with the second-order ionization of NO [Eq. (7)], driven by the formation of the stable metal nitrosyl molecule MNO.

$$M^+ + NO + NO \rightarrow NO^+ + MNO \quad (7)$$

Cu^+, Rh^+, Pd^+, Ag^+, Cd^+, and Pt^+ ions were observed to react only by second-order ionization of NO (as well as by NO addition in some cases). Reactions of the metal-oxide MO^+ ions with CO [Eq. (5)] are exothermic if $OA\ (M^+) < OA\ (CO) = 127$ kcal mol^{-1}.[2] Of those ions with $OA\ (M^+) < 127$ kcal mol^{-1} (see Table 1) that have been observed to react measurably with N_2O according to Equation (4), only Fe^+, Os^+, and Ir^+ have been observed to undergo the reaction given in Equation (5), with $k > 2.6 \times 10^{-11}$ cm^3 molecule^{-1} s^{-1}. Figure 2 (top right) shows experimental data obtained for the reduction of FeO^+ by CO, which is exothermic by 47 kcal mol^{-1}.

The reactions described by Equations (3) and (5) taken together in principle constitute the catalytic cycle shown in Scheme 1 (and the middle of Figure 1), which leads to the reduction of NO to N_2O and requires that $36 < OA\ (M^+) < 127$ kcal mol^{-1}. Also, the ionization energy of the metal and metal oxide must be less than that of NO, E_i (M) and E_i (MO) $< E_i$ (NO) $= 9.26$ eV,[2] to avoid competition with

Table 1: O-atom affinities, $OA = D_0$ (M^+-O) [kcal mol^{-1}],[3] and ionization energies, E_i (M) and E_i (MO) [eV],[2] for transition-metal cations.

	First Row				Second Row				Third Row			
M^+	$OA\ (M^+)$	E_i (M)	E_i (MO)	M^+	$OA\ (M^+)$	E_i (M)	E_i (MO)	M^+	$OA\ (M^+)$	E_i (M)	E_i (MO)
Sc^+	164.6 ± 1.4	6.56		Y^+	167.0 ± 4.2	6.22	5.85	La^+	206 ± 4	5.58	4.9
Ti^+	158.6 ± 1.6	6.75	6.56	Zr^+	178.9 ± 2.5	6.63	6.1	Hf^+	173 ± 5	6.83	7.55
V^+	134.9 ± 3.5	6.77	7.5	Nb^+	164.4 ± 2.5	6.76	6.1	Ta^+	188 ± 15	7.55	7.92
Cr^+	85.8 ± 2.8	7.43	7.85	Mo^+	116.7 ± 0.5	7.09	8	W^+	126 ± 10[a]	7.86	9.1
Mn^+	68.0 ± 3.0	7.43	8.65					Re^+	115 ± 15	7.83	
Fe^+	80.0 ± 1.4	7.9	8.9	Ru^+	87.9 ± 1.2	7.36	8.7	Os^+	100 ± 12	8.44	
Co^+	74.9 ± 1.2	7.88	8.9	Rh^+	69.6 ± 1.4	7.46	9.3	Ir^+	59[b]	8.97	10.1
Ni^+	63.2 ± 1.2	7.64	9.5	Pd^+	33.7 ± 2.5	8.34	9.1	Pt^+	77	8.96	10.1
Cu^+	37.4 ± 3.5	7.72		Ag^+	28.4 ± 1.2	7.58		Au^+		9.23	
Zn^+	38.5 ± 1.2	9.39		Cd^+		8.99		Hg^+		10.4	

[a] This value for OA (W^+) is too low according to our observation of the fast reaction $W^+ + NO \rightarrow WO^+ + N$, $k = 5.0 \times 10^{-10}$ cm^3 molecule^{-1} s^{-1}. [b] This value for OA (Ir^+) is also too low according to our observation of the reaction $Ir^+ + NO_2 \rightarrow IrO^+ + NO$ (see Table 2).

 © 2003 Wiley-VCH Verlag GmbH & Co. KGaA, Weinheim

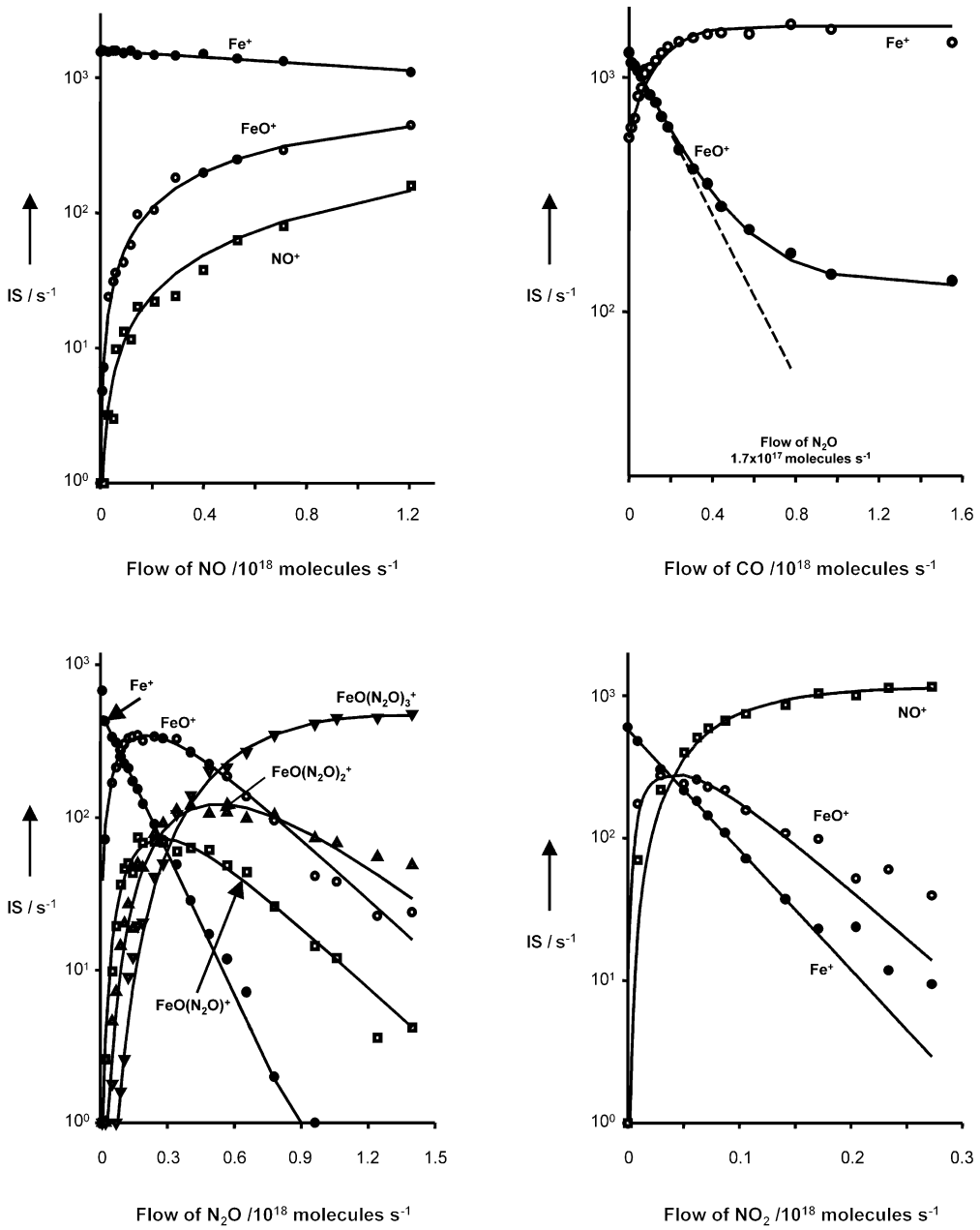


Figure 2. Top left: Experimental data for the second-order (in NO) reduction of NO by Fe^+ ions. The product FeO^+ reacts further in this case with NO by electron transfer. Top right: Data for the reduction of FeO^+ by CO. The decay of FeO^+ (solid line) is slowed down due to the reoxidation of Fe^+ by N_2O added upstream into the flow tube. Bottom left: Data for the reduction of N_2O by Fe^+ ions. The FeO^+ product adds to N_2O sequentially at high flows of N_2O. Bottom right: Data for the reduction of NO_2 by Fe^+ ions. The FeO^+ product reacts further to produce $NO^+ + FeO_2$. IS = Ion signal.

$$\begin{array}{l} 2\,NO + M^+ \rightarrow MO^+ + N_2O \\ MO^+ + CO \rightarrow M^+ + CO_2 \\ \hline 2\,NO + CO \rightarrow N_2O + CO_2 \end{array}$$

Scheme 1. Catalytic cycle for the homogeneous reduction of nitric oxide by carbon monoxide, mediated by atomic transition-metal cations.

bimolecular electron transfer, which we have observed to predominate in exothermic reactions.

The further reduction of N_2O to N_2 [Eq. (4)] can be achieved with transition-metal ions with $OA\ (M^+) > OA\ (N_2) = 40$ kcal mol^{-1}.[2] We have surveyed the transition-metal cations in the periodic table and, of the M^+ ions observed to undergo the reaction in Equation (3), we have observed the reaction described in Equation (4) with $k > 1 \times 10^{-12}$ cm^3 molecule^{-1} s^{-1} for $M^+ = V^+$, Fe^+, Co^+, Os^+, and Ir^+. Experimental data obtained for the reduction of N_2O by Fe^+ ions are shown in Figure 2 (bottom left). FeO^+ is seen to add N_2O at high concentrations of N_2O in sequential N_2O addition reactions.

The reactions described by Equations (4) and (5) taken together in principle constitute the catalytic cycle shown in Scheme 2 (and the bottom of Figure 1), which leads to the

 © 2003 Wiley-VCH Verlag GmbH & Co. KGaA, Weinheim

$$M^+ + N_2O \rightarrow MO^+ + N_2$$
$$MO^+ + CO \rightarrow M^+ + CO_2$$
$$N_2O + CO \rightarrow N_2 + CO_2$$

Scheme 2. Catalytic cycle for the homogeneous reduction of nitrous oxide by carbon monoxide, mediated by atomic transition-metal cations.

reduction of N_2O to N_2 and requires that $40 < OA\ (M^+) < 127$ kcal mol^{-1} and E_i (M) and E_i (MO) $< E_i$ (N_2O) = 12.886 eV.[3] Figure 2 (top right) shows catalytic data for M = Fe.

The reaction shown in Equation (4) has commonly been used in the gas phase to produce transition-metal oxide cations[4] and previous measurements using ion cyclotron resonance (ICR) spectroscopy actually have demonstrated that Fe^+ ions will catalyze the oxidation of CO to CO_2 by N_2O under ICR conditions according to Scheme 2 (and that the five transition-metal cations Ti^+, Zr^+, V^+, Nb^+, and Cr^+ fail to do so).[5]

Scheme 1 and Scheme 2 taken together lead to the conversion of NO and CO to N_2 and CO_2 according to the overall reaction [Eq. (8)], which is the equivalent of Equation (1):

$$2\,NO + 2\,CO \rightarrow N_2 + 2\,CO_2 \qquad (8)$$

The M^+ catalyst must satisfy the thermodynamic requirements that $40 < OA\ (M^+) < 127$ kcal mol^{-1} and E_i (M) and E_i (MO) $< E_i$ (NO) = 9.26 eV. This requirement is met (see Table 1) by the transition metals Fe, Os, and Ir, all of which have been observed to undergo the reactions given in Equations (3), (4), and (5) with $k > 1 \times 10^{-11}$ cm^3 molecule^{-1} s^{-1} (see Table 2). Mo^+ and Ru^+ ions meet this requirement, but their reaction with N_2O gives only addition (no MO^+ formation). Co^+ and Cr^+ ions also meet this requirement but the reaction in Equation (4) was too slow to produce enough MO^+ species to measure the results of the following reaction [Eq. (5)].

Finally, NO_2 has also been observed to be reduced by certain transition-metal ions according to Equation (2), often in competition with formation of NO^+ (see Table 2). Figure 2 (bottom right) shows experimental data for the reduction of NO_2 by Fe^+ [Eq. (9)], followed by Equation (10):

$$Fe^+ + NO_2 \rightarrow FeO^+ + NO \qquad (9)$$

$$FeO^+ + NO_2 \rightarrow NO^+ + FeO_2 \qquad (10)$$

The reactions described in Equations (2) and (5) taken together in principle constitute the catalytic cycle shown in Scheme 3 (and the top of Figure 1), which leads to the reduction of NO_2 to NO.

$$M^+ + NO_2 \rightarrow MO^+ + NO$$
$$MO^+ + CO \rightarrow M^+ + CO_2$$
$$NO_2 + CO \rightarrow NO + CO_2$$

Scheme 3. Catalytic cycle for the homogeneous reduction of nitrogen dioxide by carbon monoxide, mediated by atomic transition-metal cations.

Schemes 1, 2, and 3 taken together lead to the conversion of NO_2 and CO to N_2 and CO_2 according to Equation (11):

$$2\,NO_2 + 4\,CO \rightarrow N_2 + 4\,CO_2 \qquad (11)$$

The M^+ catalyst must satisfy the thermodynamic requirements that $73.5 < OA(M^+) < 127$ kcal mol^{-1} and E_i (M) and E_i (MO) $< E_i$ (NO) = 9.26 eV. Of the 29 transition-metal ions that were surveyed only Fe, Os, and Ir[2] meet this requirement (see Table 1) and have been observed to undergo all the reactions in Equations (2)–(5), with $k > 1 \times 10^{-11}$ cm^3 molecule^{-1} s^{-1} (see Table 2).

Os^+ and Ir^+ ions produce higher oxides in sequential reactions with NO_2 and N_2O (but not NO) according to the reactions given in Equations (12a,b) and (13) up to $n = 3$ and

$$MO_n^+ + NO_2 \rightarrow MO_{n+1}^+ + NO \quad (n = 0-3) \qquad (12a)$$

$$\rightarrow NO^+ + MO_{n+1} \quad (n = 0) \qquad (12b)$$

$$MO_n^+ + N_2O \rightarrow MO_{n+1}^+ + N_2 \quad (n = 0-3) \qquad (13)$$

$n = 2$ for M = Os and Ir, respectively. Figure 3 shows results for Os^+ in which NO^+ is produced primarily by the reaction of OsO^+ with NO_2 in competition with OsO_2^+ formation.

Os^+ and Ir^+ ions react sequentially with N_2O according to Equation (13). The bare metal cation is recovered by sequential reactions with CO molecules according to Equation (14) as shown in Figure 3 for OsO_n^+:

$$MO_n^+ + CO \rightarrow MO_{n-1}^+ + CO_2 \quad (n = 1-4) \qquad (14)$$

This demonstrates that the catalytic cycle will not be inhibited if higher oxides are formed, that is, the transition-metal oxide cations MO_n^+ formed in each step of the catalytic cycle are reverted back to bare metal cations by reaction with CO.

In conclusion, we have reported a detailed and comprehensive thermodynamic and kinetic investigation of a novel role for transition-metal cations in the homogeneous catalytic conversion of nitrogen oxides and carbon monoxide to nitrogen and carbon dioxide. Fe^+, Os^+, and Ir^+ ions are

Table 2: Rate coefficients, k [cm^3 molecule^{-1} s^{-1}], and products observed for reactions with M = Fe, Os, and Ir at room temperature in helium buffer at 0.35 Torr.

Reaction	Fe		Os		Ir	
	Products	k[a]	Products	k[a]	Products	k[a]
$M^+ + NO + NO$	$FeO^+ + N_2O$	1.6×10^{-11}	$OsO^+ + N_2O$	1.5×10^{-11}	$IrO^+ + N_2O$	1.5×10^{-11}
$M^+ + N_2O$	$FeO^+ + N_2$	3.7×10^{-11}	$OsO^+ + N_2$	5.8×10^{-11}	$IrO^+ + N_2$	2.9×10^{-10}
$M^+ + NO_2$	$FeO^+ + NO$	9.1×10^{-10}	$OsO^+ + NO$ (0.8) $NO^+ + OsO$ (0.2)	7.3×10^{-10}	$IrO^+ + NO$ (0.6) $NO^+ + IrO$ (0.4)	7.9×10^{-10}
MO^+[b] $+ CO$	$Fe^+ + CO_2$	$>3.7\times10^{-10}$	$Os^+ + CO_2$	$>4.6\times10^{-11}$[c]	$Ir^+ + CO_2$	$>2.6\times10^{-11}$[c]

[a] Apparent bimolecular rate coefficient with an estimated accuracy of ±30%. [b] Produced from the reaction of M^+ with N_2O (M = Fe, Os, Ir) and of MO_2^+ with CO (M = Os, Ir). [c] Determined from a fit to the production and loss of MO^+.

 © 2003 Wiley-VCH Verlag GmbH & Co. KGaA, Weinheim

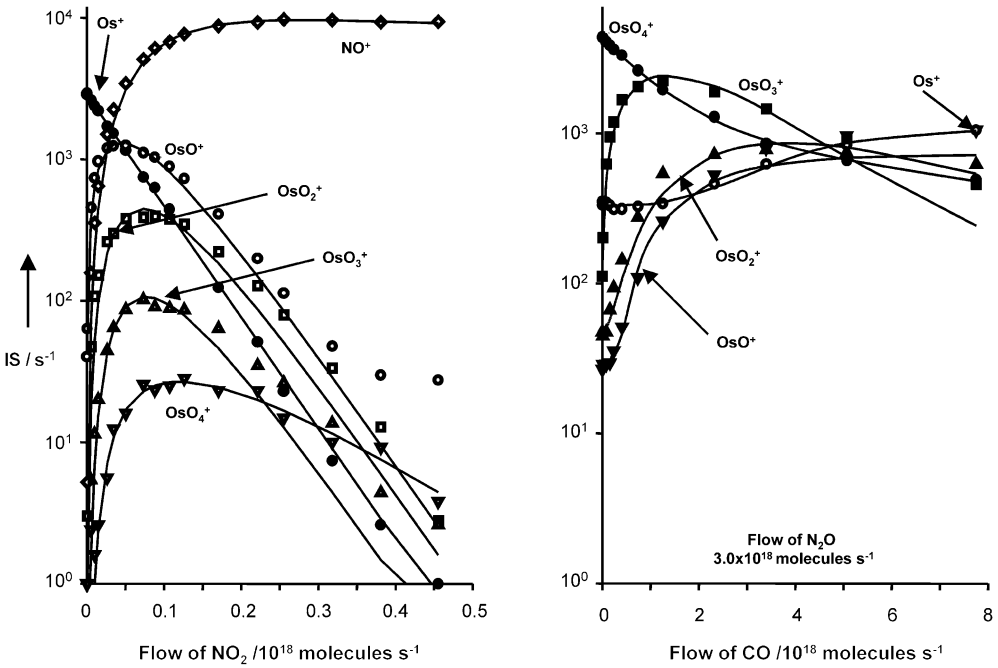


Figure 3. Experimental data for the sequential oxidation of Os^+ ions by NO_2 (left) and the reduction of oxides of Os^+ by CO (right). The NO^+ formation (left) competes with the further oxidation of OsO^+. IS = Ion signal.

shown to be most effective. The catalytic conversion has been demonstrated in principle but it remains to be seen whether the catalytic cycles shown in Figure 1 have applications in practical catalysis; they may provide the basis of new designs of catalytic converters in automobiles through the use, for example, of cold cathode discharges. For the most part the reactions measured are clean (single-channel) reactions so that the specific catalytic cycles that are proposed in principle have a turnover number of infinity. The two exceptions are the NO_2 cycles involving Ir^+ and Os^+ ions that show both MO^+ and NO^+ production in their reactions with NO_2 (60% and 80% MO^+ production for Ir^+ and Os^+, respectively). These two cycles have turnover numbers of 1.5 and 4, respectively. Of course in a practical device that exploits the catalytic cycles that we have proposed, the turnover numbers can be further reduced by secondary reactions, competing reactions with impurities or surfaces, or other losses.

Experimental Section

The reactions were investigated in an inductively coupled plasma/selected-ion flow tube (ICP/SIFT) tandem mass spectrometer.[6] The transition-metal ions were produced from their metal-salt solutions, which were sprayed into an argon plasma operating at atmospheric pressure and $\approx$5500 K. The ions are then mass selected by a quadrupole mass filter and injected into a flow tube flushed with He buffer gas at 0.35 Torr and 294 $\pm$ 3 K. The ions cool by radiation and collision with argon and helium from their point of origin to the entrance of the reaction region.[7] The reagent gas (NO, NO_2, or N_2O) was added into the reaction region downstream into the flow tube and the reacting mixture was sampled by a second quadrupole mass spectrometer. Reaction-rate coefficients were derived from the measured variation of the ion signal intensities with the reagent flow with an estimated accuracy of $\pm$30%. In the study of metal-oxide cation chemistry, the metal-oxide cation was produced upstream from the reaction of the metal ion with N_2O. CO was introduced into the reaction region further downstream into the flow tube.

Received: April 10, 2003
Revised: August 4, 2003 [Z51628]

Keywords: cations · homogeneous catalysis · kinetic measurements · nitrogen oxides · transition metals

[1] V. I. Parvulescu, P. Grange, B. Oelmon, *Catal. Today* **1998**, *46*, 233–317.
[2] Taken or calculated from thermochemical data found in S. G. Lias, J. E. Bartmess, J. F. Liebman, J. L. Holmes, R. D. Levin, W. G. Mallard, *J. Phys. Chem. Ref. Data* **1988**, *17*, Suppl. 1.
[3] D. Schröder, H. Schwarz, S. Shaik, *Struct. Bonding (Berlin)* **2000**, *97*, 91.
[4] a) M. M. Kappas, R. H. Staley, *J. Phys. Chem.* **1981**, *85*, 942–944; b) D. Schröder, H. Schwarz, *Angew. Chem.* **1995**, *107*, 2126–2150; *Angew. Chem. Int. Ed. Engl.* **1995**, *34*, 1973–1995.
[5] M. M. Kappas, R. H. Staley, *J. Am. Chem. Soc.* **1981**, *103*, 1286–1287.
[6] a) G. K. Koyanagi, V. Lavrov, V. I. Baranov, D. Bandura, S. D. Tanner, J. W. McLaren, D. K. Bohme, *Int. J. Mass Spectrom.* **2000**, *194*, L1–L5; b) G. K. Koyanagi, V. I. Baranov, S. D. Tanner, D. K. Bohme, *J. Anal. At. Spectrom.* **2000**, *15*, 1207–1210.
[7] G. K. Koyanagi, D. Caraiman, V. Blagojevic, D. K. Bohme, *J. Phys. Chem. A* **2002**, *106*, 4581–4590.

 © 2003 Wiley-VCH Verlag GmbH & Co. KGaA, Weinheim

Enantioselective Alcohol Synthesis

Effective Modular Iminooxazoline (IMOX) Ligands for Asymmetric Catalysis: [Zn(IMOX)]-Promoted Enantioselective Reduction of Ketones by Catecholborane**

*Manuela Locatelli and Pier Giorgio Cozzi**

Chiral catalysts based on readily available chiral ligands are widely used in academia and industry for the synthesis of enantioenriched precursors of materials, sensors, and drugs.[1] The C_2-symmetric bisoxazoline (BOX) ligands (Figure 1)

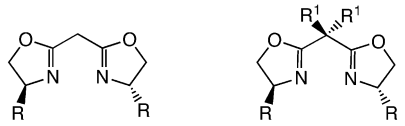


Figure 1. Bisoxazoline (BOX) ligands.

were introduced into asymmetric catalysis by Pfaltz et al.[2] in their seminal work on semicorrins, and have since been applied to a wide variety of asymmetric transformations.[3] Indeed, Diels–Alder, aldol, ene, amination, Friedel–Crafts, and other Lewis acid catalyzed reactions are all effectively promoted by chiral metal BOX complexes.[4] The underlying feature of the aforementioned reactions is substrate activation by two-point binding to the chiral metal BOX complex. Chiral information seems to be poorly transmitted when the two-point binding criterion is not met (i.e., one-point binding).[5] Hence, the development of a new family of chiral N,N ligands capable of general substrate activation by one-point binding would be a significant advance in the field of Lewis acid/BOX-mediated reactions.

Earlier we showed that a new catalyst system capable of reducing α-alkoxyketones with up to 82% *ee* is obtained by combining BOX ligands and $Zn(OTf)_2$ in the presence of catecholborane.[6] Unfortunately, the reduction of nonchelating ketones led to racemic products, a typical symptom of BOX-mediated processes with two-point binding. We tackled this problem by designing a new family of novel modular[7] oxazoline/imine ligands that simulate BOX-type N,N coordination. We first focused on the commercial availability of the necessary chiral building blocks **A**–**D** containing the oxazoline framework (Figure 2). Aromatic, heterocyclic, and ferrocenyl oxazolines are readily available and can be further functionalized without difficulty. We reasoned that introduction of a bulky group near the imino moiety would be the key to efficiently blocking one face of the chiral metal complexes (Figure 3). In addition, free coordination sites on the complex

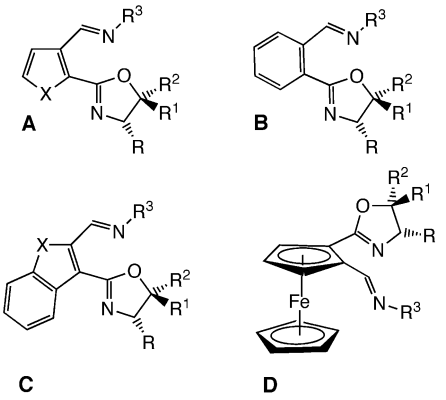


Figure 2. Readily available oxazoline frameworks.

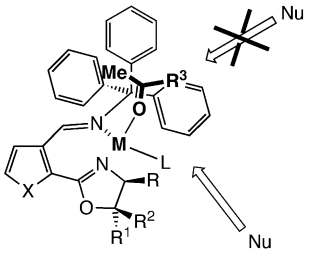


Figure 3. Blocking one face of the chiral complex with a bulky group.

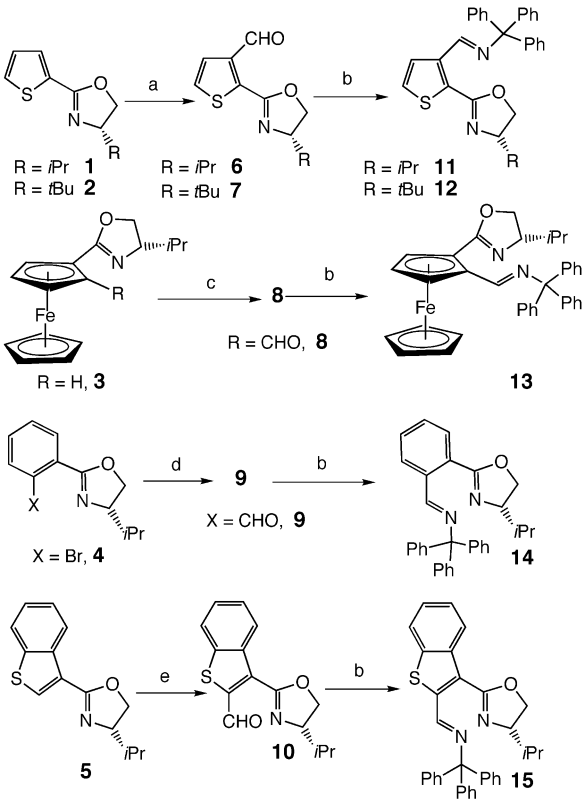
could be controlled by subtle conformational changes of the bulky group. Hence, we employed a hindered amine bearing aromatic rings, namely, tritylamine, as a bulky group in the synthesis of a variety of iminooxazoline (IMOX) ligands. Oxazolines **1**–**5** were prepared without difficulty by known procedures.[8] The aldehyde moiety near the oxazoline ring was introduced by reaction of the corresponding lithium derivatives with DMF (Scheme 1). Facile metalation of benzothienyl- and thienyloxazolines occured with *n*BuLi, whereas ferrocenyloxazolines required *n*BuLi/TMEDA. Metalation was achieved by lithium/bromine exchange in the case of the oxazoline obtained from 2-bromobenzonitrile. Aldehydes **6**–**10** were thus obtained in fair to good yields. To the best of our knowledge, syntheses of **6**–**10** have not been reported in the literature. This was quite surprising, given the potential utility of aldehyde oxazolines for the preparation of a variety of chiral ligands.[9] The IMOX ligands **11**–**15** were obtained by adding tritylamine to a solution of aldehydes **6**–**10** in CH_2Cl_2 in the presence of magnesium sulfate as a

[*] Prof. Dr. P. G. Cozzi, Dr. M. Locatelli
Dipartimento di Chimica "G. Ciamician"
Università di Bologna
Via Selmi 2, 40126 Bologna (Italy)
Fax: (+39) 051-2099-456
E-mail: pgcozzi@ciam.unibo.it

[**] We thank CNR (Rome), MIUR (Rome) "Progetto Stereoselezione in Chimica Organica – Metodologie ed Applicazioni", and the University of Bologna (funds for selected research topics) for financial support of this research. P.G.C. thanks Dr. Nicole End (Ciba Research Group, Basel) for the generous gift of benzo[*b*]-thiophene oxazolines. Prof. Kenny Lipkowitz is acknowledged for preliminary calculations on metal IMOX complexes.

Supporting information for this article is available on the WWW under http://www.angewandte.org or from the author.

 © 2003 Wiley-VCH Verlag GmbH & Co. KGaA, Weinheim DOI: 10.1002/anie.200351754



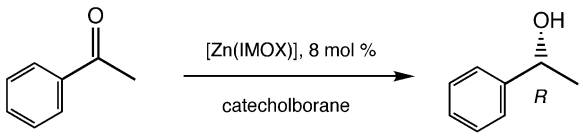
Scheme 1. Preparation of the IMOX ligands: a) *n*BuLi, Et_2O, −78 °C 30 min, 0 °C 30 min, then DMF, −78 °C; b) TritylNH$_2$, $MgSO_4$, CH_2Cl_2, RT; c) *n*BuLi, TMEDA, −78 °C, DMF, −78 °C; d) *n*BuLi, −78 °C, THF, then DMF, −78 °C; e) *n*BuLi, Et_2O, −78 °C, then DMF, −78 °C. TMEDA = *N*,*N*,*N*′*N*′-tetramethyethylenediamine.

dehydrating agent (Scheme 1).[10] The IMOX ligands were isolated after purification by chromatography on triethylamine-deactivated silica gel. However, even under these mild isolation conditions, purification of **14** was complicated by ligand decomposition. Our preliminary studies with the novel IMOX ligands were carried out on the reduction of acetophenone as model substrate with modification of the solvent and the reaction temperature (Table 1, Scheme 2). The

Table 1: Enantioselective reduction of acetophenone promoted by [Zn(IMOX)] complexes.[a]

Entry	IMOX	Yield [%][b]	*T* [°C]	*ee* [%][c]
1	**11**	86	0	84
2	**12**	88	0	84
3	**11**	77	−15	89
4	**12**	75	−15	90
5	**14**	–[d]	−15	86
6	**13**	–[d]	−15	20
7	**11**	60[e]	0	56
8	**11**	76[f]	0	77

[a] All the reactions were carried out in anhydrous CH_2Cl_2 at the indicated temperature for 48 h. [b] Yield of isolated product after chromatographic purification. [c] Determined by chiral GC analysis (see Supporting Information for details). The absolute configurations of the products were determined by comparison with analytical data reported in the literature. [d] Not determined. [e] The reaction was performed in Et_2O. [f] The reaction was performed in toluene.



Scheme 2. Asymmetric reduction of acetophenone with catecholborane with promotion by chiral [Zn(IMOX)] complexes.

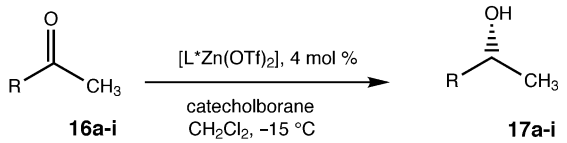
IMOX ligands gave high enantioselectivities with this nonchelating substrate. The reaction conditions were further optimized with the most readily available ligand **11**, by varying the number of equivalents of reducing agent, temperature, and catalyst loading. A reaction temperature of −15 °C with 1.4 equiv of catecholborane[11] and 4 mol % [Zn(IMOX)](OTf)$_2$ catalyst were found to be optimal. The generality of these optimal conditions is shown in Table 2 and

Table 2: Enantioselective reduction of methylketones catalyzed by [Zn(IMOX)] complexes.

Entry[a]	Ligand	Ketone	Yield [%][b]	*ee* of **17** [%][c]
1	**15**	**16a**	76	92 (*R*)
2	**12**	**16b**	80	89 (*R*)
5	**15**	**16b**	57	93 (*R*)
3	**11**	**16c**	84	88 (*R*)
4	**12**	**16d**	83	87 (*R*)
8	**12**	**16e**	81	86 (*R*)
2	**11**	**16f**	62	87 (*R*)
3	**15**	**16f**	70	91 (R)
9	**11**	**16g**	85	86 (*R*)
10	**11**	**16h**	54	92 (*R*)[d]
11	**11**	**16i**	92	53 (*R*)[d]

[a] All reactions were performed at −15 °C in a freezer without stirring. [b] Yield of isolated product after flash chromatography. [c] Determined by chiral GC analysis (see Supporting Information for details). [d] Determined by chiral HPLC analysis (Chiralcel OD column).

Scheme 3. Various aromatic methylketones were reduced in good-to-excellent yields and with excellent enantiomeric excesses. Other aromatic alkyl ketones were also reduced in good yield, although the results were inferior in terms of enantioselectivity.[12] High *ee* values (86–93 %) were obtained with *p*-substituted aromatic acetyl ketones. Electron-withdrawing groups accelerate the reactions considerably, while



16a R = Ph,
16b R = *p*-F-Ph,
16c R = *p*-Cl-Ph,
16d R = *p*-Br-Ph,
16e R = *p*-CF_3-Ph,
16f R = *p*-Me-Ph,
16g R = α-Naphtyl,
16h R = CH=CHPh,
16i R = CH_2CH_2Ph,

Scheme 3. Asymmetric reduction of methyl ketones promoted by IMOX ligands **11**, **12**, and **15**.

 © 2003 Wiley-VCH Verlag GmbH & Co. KGaA, Weinheim

electron-donating groups decrease the reaction rates. It is noteworthy that IMOX ligands **11** and **12** give virtually identical enantiomeric excesses in the reduction of acetophenone. Hence, these ligands were used interchangeably throughout our work. Benzo[*b*]thiophene-derived ligand **15** appeared to give slightly better results, but its synthesis is more laborious than those of **11** and **12**. Unsaturated ketones are chemoselectively and enantioselectively reduced by this system (Table 2, entry 10). We believe that the new IMOX ligands create a suitable chiral pocket in which the methylketones are coordinated such that nonbonding interactions are minimized (Figure 3, R^3 = aryl). The trityl group serves to control the size of the pocket and hinder the approach of the reducing agent to one face of the substrate.[13] Our work suggests that hindered aromatic amines can be effectively used as elements of stereocontrol in the design of effective, novel catalysts.

In summary we have synthesized, in a modular fashion, a novel class of chiral iminooxazoline (IMOX) ligands capable of effectively promoting enantioselective reductions of aromatic methyl ketones with good enantioselectivity (86–93% *ee*). This facile synthetic approach to IMOX ligands may lend itself to the creation of large libraries of these compounds. The application of IMOX ligands to other asymmetric transformations is currently under investigation in our laboratories.

Received: April 28, 2003
Revised: July 16, 2003 [Z51754]

Keywords: alcohols · asymmetric catalysis · enantioselectivity · ligand design · reduction

[1] H.-U. Blaser, *Chem. Commun.* **2003**, 293–296.
[2] A. Pfaltz, *Synlett* **1999**, 835–843.
[3] T. P. Yoon, E. N. Jacobsen, *Science* **2003**, *299*, 1691–1693.
[4] For recent examples of C_2 bisoxazoline–Lewis acid complexes as catalysts, see a) J. S. Johnson, D. A. Evans, *Acc. Chem. Res.* **2000**, *33*, 325–335; b) N. Gathergood, W. Zhuang, K. A. Jørgensen, *J. Am. Chem. Soc.* **2000**, *122*, 12517–12522; c) K. B. Jensen, J. Thorhauge, R. G. Hazell, K. A. Jørgensen, *Angew. Chem.* **2001**, *113*, 164–167; *Angew. Chem. Int. Ed.* **2001**, *40*, 160–163; d) H. Audrain, K. A. Jørgensen, *J. Am. Chem. Soc.* **2000**, *122*, 11543–11544; e) K. Juhl, N. Gathergood, K. A. Jørgensen, *Angew. Chem.* **2001**, *113*, 3083–3085; *Angew. Chem. Int. Ed.* **2001**, *40*, 2995–2997; f) K. R. Knudsen, T. Risgaard, N. Nishiwaki, K. V. Gothelf, K. A. Jørgensen, *J. Am. Chem. Soc.* **2001**, *123*, 5843–5844; g) N. Nishiwaki, K. R. Knudsen, K. V. Gothelf, K. A. Jørgensen, *Angew. Chem.* **2001**, *113*, 3080–3083; *Angew. Chem. Int. Ed.* **2001**, *40*, 2992–2995; h) K. Juhl, K. A. Jørgensen, *J. Am. Chem. Soc.* **2002**, *124*, 2420–2421; i) J. Thorhauge, M. Roberson, R. G. Hazell, K. A. Jørgensen, *Chem. Eur. J.* **2002**, *8*, 1888–1898; j) D. A. Evans, M. C. Kozlowski, J. A. Murry, C. S. Burgey, K. R. Campos, B. T. Connell, R. J. Staples, *J. Am. Chem. Soc.* **1999**, *121*, 669–685; k) D. A. Evans, C. S. Burgey, M. C. Kozlowski, S. W. Tregay, *J. Am. Chem. Soc.* **1999**, *121*, 686–699; l) D. A. Evans, K. A. Scheidt, J. N. Johnston, M. C. Willis, *J. Am. Chem. Soc.* **2001**, *123*, 4480–4491; m) D. A. Evans, D. M. Barnes, J. S. Johnson, T. Lectka, P. von Matt, S. J. Miller, J. A. Murry, R. D. Norcross, E. A. Shaughnessy, K. R. Campos, *J. Am. Chem. Soc.* **1999**, *121*, 7582–7594; n) D. A. Evans, S. J. Miller, T. Lectka, P. von Matt, *J. Am. Chem. Soc.* **1999**, *121*, 7559–7573; o) D. A. Evans, T. Rovis, M. C. Kozlowski, J. S. Tedrow, *J. Am. Chem. Soc.* **1999**, *121*, 1994–1995.
[5] Copper–PyBOX complexes promote enantioselective Diels–Alder reactions of monodentate dienophiles.[4m]
[6] M. Bandini, P. G. Cozzi, M. DeAngelis, A. Umani-Ronchi, *Tetrahedron Lett.* **2000**, *41*, 1601–1605.
[7] For efficient modular ligands, see a) H. Deng, M. P. Isler, M. L. Snapper, A. H. Hoveyda, *Angew. Chem.* **2002**, *114*, 1051–1054; *Angew. Chem. Int. Ed.* **2002**, *41*, 1009–1012; b) C. A. Luchaco-Cullis, H. Mizutani, K. E. Murphy, A. H. Hoveyda, *Angew. Chem.* **2001**, *113*, 1504–1508; *Angew. Chem. Int. Ed.* **2001**, *40*, 1456–1460; c) K. D. Shimizu, B. M. Cole, C. A. Krueger, K. W. Kuntz, M. L. Snapper, A. H. Hoveyda, *Angew. Chem.* **1996**, *108*, 1776–1779; *Angew. Chem. Int. Ed. Engl.* **1996**, *35*, 1668–1674; d) I. Chataigner, C. Gennari, U. Piarulli, S. Ceccarelli, *Angew. Chem.* **2000**, *112*, 953–956; *Angew. Chem. Int. Ed.* **2000**, *39*, 916–918; e) J. Blankenstein, A. Pfaltz, *Angew. Chem.* **2001**, *113*, 4577–4579; *Angew. Chem. Int. Ed.* **2001**, *40*, 4445–4447.
[8] Oxazoline **3:** M. Peer, J. C. de Jong, M. Kiefer, T. Langer, H. Rieck, H. Schell, P. Sennhenn, J. Sprinz, H. Steinhagen, B. Wiese, G. Helmchen, *Tetrahedron* **1996**, *52*, 7547–7583. Oxazoline **4:** C. J. Richards, A. W. Mulvaney, *Tetrahedron: Asymmetry* **1996**, *7*, 1419–1430. Oxazolines **1, 2**, and **5**: a) P. G. Cozzi, F. Menges, S. Kaiser, *Synlett* **2003**, 833–836; b) L. F. Tietze, J. K. Lohmann, *Synlett* **2002**, 2083–2085.
[9] Modular ligands described by Hoveyda, Snapper, et al. were prepared by condensation between aldehydes bearing a coordinating group and chiral amines.[7] See also a) N. S. Josephsohn, M. L. Snapper, A. H. Hoveyda, *J. Am. Chem. Soc.* **2003**, *125*, 4018–4019; b) K. E. Murphy, A. H. Hoveyda, *J. Am. Chem. Soc.* **2003**, *125*, 4690–4691.
[10] We have obtained a preliminary crystal structure for IMOX ligand **13**. The absolute planar chiral configuration was assigned on the basis of the crystal structure (P. G. Cozzi, M. Monari, S. Selva, unpublished results).
[11] Other reducing agents (silanes, BH_3, poly(methylhydroxysiloxane) (PMSH)) were also studied. However, racemic products or low enantiomeric excesses were obtained in the reduction of acetophenone. For enantioselective reduction of ketones by metal complexes and catecholborane, see a) W.-S. Huang, Q.-S. Hu, L. Pu, *J. Org. Chem.* **1999**, *64*, 7940–7956; b) A. J. Blake, A. Cunningham, A. Ford, A. J. Teat, S. Woodward, *Chem. Eur. J.* **2000**, *6*, 3586–3594; c) I. Sarvary, F. Almqvist, T. Frejd, *Chem. Eur. J.* **2001**, *7*, 2158–2166.
[12] The following aromatic ketones were reduced under the optimized reaction conditions: phenyl isopropyl ketone (60% yield, 49% *ee*), isovalerophenone (82% yield, 78% *ee*), α-bromoacetophenone (76% yield, 76% *ee*), and butyrophenone (84% yield, 85% *ee*).
[13] To stress the importance of the hindered trityl group next to the imino moiety, IMOX ligands prepared from different aromatic and aliphatic amines were studied in the enantioselective reduction of acetophenone under the optimized reaction conditions. However, only racemic products or low enantiomeric excesses were obtained (see Supporting Information).

 © 2003 Wiley-VCH Verlag GmbH & Co. KGaA, Weinheim

Membrane Transport

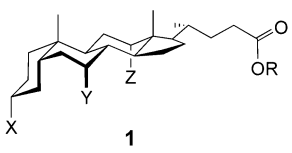
Chloride Transport Across Vesicle and Cell Membranes by Steroid-Based Receptors**

Atanas V. Koulov, Timothy N. Lambert, Rameshwer Shukla, Mahim Jain, J. Middleton Boon, Bradley D. Smith, Hongyu Li, David N. Sheppard,* Jean-Baptiste Joos, John P. Clare, and Anthony P. Davis**

It is well-established that molecules which transport cations across cell membranes (cationophores) can have potent biological effects.[1] Anion flux is also important to the cell and, correspondingly, anion carriers may be capable of biological activity. Indeed, chloride transporters have direct medical potential as treatments for cystic fibrosis and other diseases caused by defective channel proteins.[2] Despite this motivation, there have been relatively few reports of anionophore natural products[3] or of anion transport by synthetic systems.[4] Most, moreover, have involved cationic centers,[5] which can assist anion passage through the formation of an ion pair.[4a–g] Anion transport by purely electroneutral systems is still quite rare.[4j–l] The recently described "cholapod" anion receptors **1** are intrinsically lipophilic, potentially membrane-soluble, and tuneable to very high affinities.[6] Certain cholapods have proved capable of "flippase" activity, that is, they can convey polar head groups across phospholipid membranes.[7] We therefore supposed that electroneutral cholapods might transport inorganic anions by a "shuttle" mechanism, in the manner of cationophores such as valinomycin. We now report that cholapods **2** are indeed capable of transporting chloride ions across liposomal membranes and also across live cells grown as polarized epithelia.

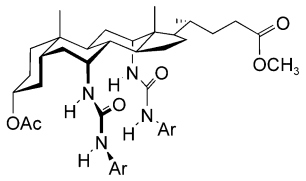
[*] Prof. Dr. B. D. Smith, A. V. Koulov, T. N. Lambert, R. Shukla, M. Jain, J. M. Boon
Department of Chemistry and Biochemistry and
Walther Cancer Research Center
University of Notre Dame
Notre Dame, IN 46556 (USA)
Fax: (+1) 574-631-6652
E-mail: smith.115@nd.edu
Dr. D. N. Sheppard, Dr. H. Li
Department of Physiology
School of Medical Sciences
University of Bristol
University Walk, Bristol BS8 1TD (UK)
Fax: (+44) 117-928-8923
E-mail: d.n.sheppard@bristol.ac.uk
Prof. Dr. A. P. Davis, Dr. J.-B. Joos, J. P. Clare
School of Chemistry
University of Bristol
Cantock's Close, Bristol BS8 1TS (UK)
Fax: (+44) 117-929-8611
E-mail: anthony.davis@bristol.ac.uk

[**] Financial support for this work was provided by the EPSRC (GR/R04584/01), the University of Bristol, the CF Trust, the NKRF, the NSF (USA), the Walther Cancer Institute, and the Royal Society.
Supporting information for this article is available on the WWW under http://www.angewandte.org or from the author.

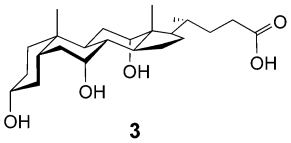


1

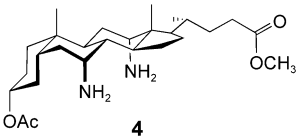
X,Y, and/or Z contain H-bond donor functional groups



2a Ar = 4-methoxyphenyl
2b Ar = 3-methoxyphenyl
2c Ar = 4-methylphenyl
2d Ar = phenyl
2e Ar = 4-nitrophenyl



3



4

Receptors **2** were prepared from cholic acid **3** by conversion into diamine **4**[8] and treatment with appropriate isocyanates. Initially, their anion-transport properties were studied by following chloride efflux from unilamellar vesicles using a chloride-selective electrode. More specifically, 30 mM unilamellar vesicles (200 nm mean diameter) were prepared by extruding a 7:3 mixture of 1-palmitoyl-2-oleoyl-*sn*-glycero-3-phosphocholine (POPC) and cholesterol[9] in aqueous NaCl (500 mM). This stock vesicle dispersion was dialyzed against aqueous $NaNO_3$ (500 mM) to replace the external chloride ions with nitrate and then diluted with 500 mM $NaNO_3$ to give a 1 mM total lipid concentration. As shown in Figure 1, addition of a solution of **2a–e** in THF (4.0 μM final cholapod concentration) caused chloride efflux from the inner phase of the vesicles. The initial rates of chloride efflux and the association constants of **2a–e** for $Et_4N^+Cl^-$ and $Et_4N^+NO_3^-$ in

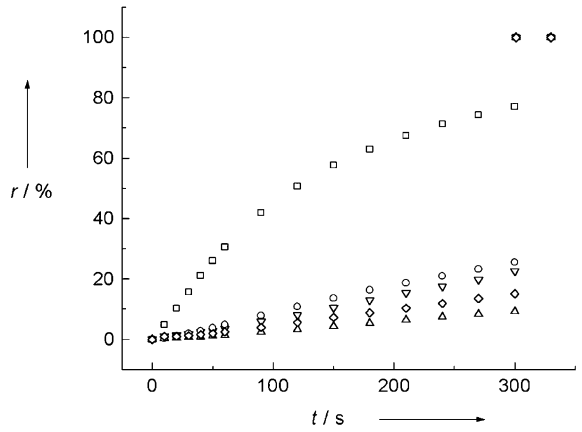


Figure 1. Chloride release (*r*) upon addition of **2e** (□), **2d** (○), **2c** (▽), **2b** (◇), and **2a** (△). At time 0 s cholapod (4 μM) was added to vesiclesn (1 mM total lipid) containing NaCl (500 mM) dispersed in $NaNO_3$ (500 mM). The detergent (polyoxythylene(8) lauryl ether) was added at time 300 s to disrupt the vesicles and release remaining chloride ions.

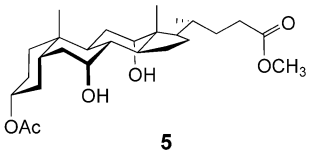
 DOI: 10.1002/anie.200351957 © 2003 Wiley-VCH Verlag GmbH & Co. KGaA, Weinheim

Table 1: Initial rates of Cl^- release from vesicles and affinity constants.

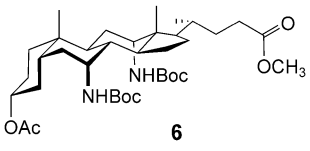
Compound	Initial rate of efflux [% s^{-1}][a]	K_a ($Et_4N^+Cl^-$) [M^{-1}][b]	K_a (Et_4N^+ NO_3^-) [M^{-1}][b]
2a	0.031	3.4×10^6	2.1×10^6
2b	0.051	1.2×10^7	8.8×10^6
2c	0.075	6.3×10^6	5.1×10^6
2d	0.085	1.5×10^7[c]	1.0×10^7[c]
2e	0.52	5.2×10^8	1.7×10^8

[a] For details see text and legend to Figure 1. [b] Average of two measurements. [c] Determinations made on the corresponding eicosyl ester to avoid overlap of NMR signals.

water-saturated $CHCl_3$, as measured by extraction, are listed in Table 1.[6b] The efflux rates correlate reasonably well with the association constants, thus indicating that a hydrogen-bonding recognition event controls the transport process. As expected, compounds **5** and **6** (Boc = *tert*-butoxycarbonyl) with very weak chloride affinity produced no measurable efflux.



5



6

Further studies were performed on **2d** to clarify the mechanism of transport. Firstly, chloride efflux was shown to be unaltered upon changing the entrapped countercation from sodium to either potassium or caesium (see the Supporting Information), which indicates that the metal cation is not involved in the transport process. Secondly, the external anion was varied. As shown in Figure 2, the effect was substantial. For example, replacement of the external NO_3^- with HCO_3^- ions lowered transport rates by about 80%, while substitution with SO_4^{2-} ions prevented chloride efflux altogether. Addition of external NO_3^- ions to this latter experiment restored transport (see the Supporting Information). These results clearly indicate an anion antiport mechanism; substantial chloride efflux can only occur if there is corresponding influx of an external anion. Cholapod **2d** transports both Cl^- and NO_3^- ions, but is less effective for the more hydrophilic HCO_3^- and SO_4^{2-} ions. In the case of external sulfate, a small amount of chloride transport (undetectable using the Cl^- electrode) creates a transmembrane potential difference, after which further efflux cannot occur. In support of this mechanism, cholapod **2d** induced an electric potential (inside negative) across vesicle membranes partitioning Na_2SO_4 (inside) and NaCl (outside), as judged by fluorescence experiments using the potential-sensitive dye safranin O (see the Supporting Information).[4l]

The ability of **2e** to transport chloride ions into vesicles was detected by using ^{35}Cl NMR spectroscopy. In this case, vesicles were formed in 300 mM NaBr solution and then dialyzed against aqueous NaCl (300 mM) containing $CoCl_2$ (10 mM) as a ^{35}Cl NMR shift reagent.[4a,10] Internalized chloride ions were detected as an unshifted ^{35}Cl NMR resonance after addition of **2e** (Figure 3). Separate resonance peaks for the internal and external chloride ions were observed for at least 24 h, thus showing that the vesicle membranes remain unperturbed by the cholapod.

In principle, cholapods **2** might act as mobile carriers or through formation of multicomponent channels. To date, there are two pieces of evidence suggesting the former. First,

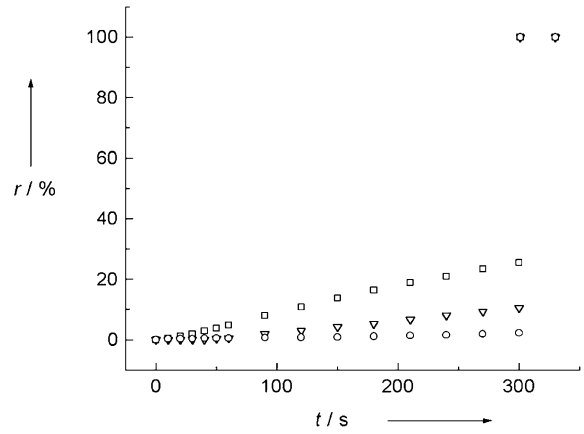


Figure 2. Dependence of the chloride release (*r*) induced by **2d** on external anions. The vesicles containing NaCl (500 mM) were dispersed in isotonic $NaNO_3$ (□), $NaHCO_3$ (▽), or Na_2SO_4 (○). See Figure 1 for other details.

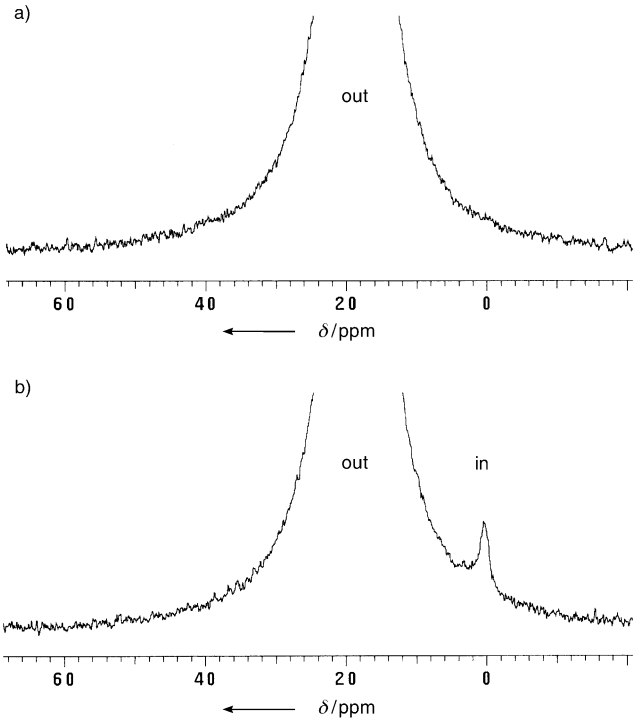


Figure 3. ^{35}Cl NMR spectra of vesicles (30 mM total lipid) containing 300 mM NaBr dispersed in a solution of 300 mM NaCl and 10 mM $CoCl_2$. Spectra were obtained a) before and b) 24 h after addition of **2e** (4 μM). Signals corresponding to chloride ions outside and inside the vesicles are labeled accordingly.

 © 2003 Wiley-VCH Verlag GmbH & Co. KGaA, Weinheim

efflux rates with **2d** increased just 3.2-fold when the receptor concentration was increased from 4 to 40 μM (see the Supporting Information). This less than first-order dependence suggests the formation of inactive, rather than active, aggregates at the higher concentration.[11] Second, there is no cholapod-mediated efflux of chloride ions from vesicles composed of dipalmitoylphosphatidylcholine (DPPC) at room temperature (gel phase), but facilitated efflux occurs above the temperature for the gel/liquid crystalline phase transition (fluid phase). This is signature behavior of a mobile carrier (for example, monensin) whose activity depends on membrane viscosity; in contrast, channel activity should not show this effect.[12]

Finally, cholapod-mediated Cl^- transport was demonstrated in live cells by using Madin Darby canine kidney (MDCK) epithelia and the Ussing chamber technique.[13] The method involves growing an oriented layer of cells on a filter support and placing it between current- and voltage-measuring electrodes. Endogenous active transport systems generate a potential difference across the cell membranes. Addition of a passive chloride transporter causes discharge of the electrochemical gradient, which is detected as a flow of current. Receptor **2e** (80 μM) did indeed produce this effect (see the Supporting Information). As expected, the response was anion-dependent; replacement of chloride by gluconate anions on either side of the membrane reduced the signal by about 80%. Moreover, the response was different from that induced by activators of native chloride channels found in MDCK epithelia (see the Supporting Information).

In conclusion, cholapods **2** have been shown by three techniques (electrochemical, NMR, and fluorescence) to transport chloride ions across vesicle membranes. The data favors an antiport mechanism with the cholapod more likely acting as a mobile carrier than a channel. The cholapod does not disrupt the bilayer membrane and is able to convert a chloride concentration gradient into a transmembrane electrical potential. Facilitated chloride transport has also been demonstrated in polarized epithelial cells, which augurs well for future applications in biochemistry and medicine.

Received: May 22, 2003 [Z51957]

Keywords: anions · membranes · receptors · steroids · supramolecular chemistry

[1] M. Dobler in *Comprehensive Supramolecular Chemistry, Vol. 1* (Ed.: G. W. Gokel), Pergamon, Oxford, **1996**, p. 267.
[2] J. R. Broughman, L. P. Shank, W. Takeguchi, B. D. Schultz, T. Iwamoto, K. E. Mitchell, J. M. Tomich, *Biochemistry* **2002**, *41*, 7350, and references therein.
[3] The prodigiosin family of antibiotics have been shown to be H^+Cl^- cotransporters; for a leading reference, see K. Tanigaki, T. Sato, Y. Tanaka, T. Ochi, A. Nishikawa, K. Nagai, H. Kawashima, S. Ohkuma, *FEBS Lett.* **2002**, *524*, 37.
[4] Leading references: a) A. V. Koulov, J. M. Mahoney, B. D. Smith, *Org. Biomol. Chem.* **2003**, *1*, 27; b) L. A. J. Chrisstoffels, F. de Jong, D. N. Reinhoudt, *Chem. Eur. J.* **2000**, *6*, 1376; c) L. A. J. Chrisstoffels, F. de Jong, D. N. Reinhoudt, S. Sivelli, L. Gazzola, A. Casnati, R. Ungaro, *J. Am. Chem. Soc.* **1999**, *121*, 10142; d) J. L. Sessler, W. E. Allen, *Chemtech* **1999**, *29*, 16; e) M. Merritt, M. Lanier, G. Deng, S. L. Regen, *J. Am. Chem. Soc.* **1998**, *120*, 8494; f) N. Sakai, S. Matile, *Tetrahedron Lett.* **1997**, *38*, 2613; g) B. Dietrich, T. M. Fyles, M. W. Hosseini, J.-M. Lehn, K. C. Kaye, *J. Chem. Soc. Chem. Commun.* **1988**, 691; h) D. P. Wallace, J. M. Tomich, J. W. Eppler, T. Iwamoto, J. J. Grantham, L. P. Sullivan, *Biochim. Biophys. Acta* **2000**, *1464*, 69; i) K. E. Mitchell, T. Iwamoto, J. Tomich, L. C. Freeman, *Biochim. Biophys. Acta* **2000**, *1466*, 47; j) P. H. Schlesinger, R. Ferdani, J. Liu, J. Pajewska, R. Pajewski, M. Saito, H. Shabany, G. W. Gokel, *J. Am. Chem. Soc.* **2002**, *124*, 1848; k) V. Sidorov, F. W. Kotch, G. Abdrakhmanova, R. Mizani, J. C. Fettinger, J. T. Davis, *J. Am. Chem. Soc.* **2002**, *124*, 2267; l) V. Sidorov, F. W. Kotch, J. L. Kuebler, Y. F. Lam, J. T. Davis, *J. Am. Chem. Soc.* **2003**, *125*, 2840.
[5] Present in the transporter itself or in cotransported countercations.
[6] a) A. P. Davis, J. J. Perry, R. P. Williams, *J. Am. Chem. Soc.* **1997**, *119*, 1793; A. J. Ayling, M. N. Pérez-Payán, A. P. Davis, *J. Am. Chem. Soc.* **2001**, *123*, 12716; b) A. J. Ayling, S. Broderick, J. P. Clare, A. P. Davis, M. N. Pérez-Payán, M. Lahtinen, N. J. Nissinen, K. Rissanen, *Chem. Eur. J.* **2002**, *8*, 2197.
[7] T. N. Lambert, J. M. Boon, B. D. Smith, M. N. Pérez-Payán, A. P. Davis, *J. Am. Chem. Soc.* **2002**, *124*, 5276; J. M. Boon, T. N. Lambert, A. L. Sisson, A. P. Davis, B. D. Smith, *J. Am. Chem. Soc.* **2003**, *125*, 8195.
[8] A. P. Davis, M. N. Pérez-Payán, *Synlett* **1999**, 991.
[9] The 7:3 ratio of POPC to cholesterol mimics that present in animal cell membranes. Vesicles composed only of POPC were disrupted by the receptors, as determined by carboxyfluorescein leakage assay.
[10] F. G. Riddell in *Encyclopedia of Spectroscopy and Spectrometry* (Eds.: J. C. Lindon, G. E. Tranter, J. L. Holmes), Academic Press, London, **1999**, p. 1584.
[11] NMR spectra of **2d** in $CDCl_3$ showed concentration dependence, which confirmed the tendency for aggregation in nonpolar media.
[12] G. Deng, T. Dewa, S. L. Regen, *J. Am. Chem. Soc.* **1996**, *118*, 8975.
[13] D. N. Sheppard, M. R. Carson, L. S. Ostedgaard, G. M. Denning, M. J. Welsh, *Am. J. Physiol.* **1994**, *266*, L405.

 © 2003 Wiley-VCH Verlag GmbH & Co. KGaA, Weinheim

DNA Hybridization Detection

Label-Free Detection of DNA Hybridization at the Nanoscale: A Highly Sensitive and Selective Approach Using Atomic-Force Microscopy**

Dejian Zhou, Kumar Sinniah, Chris Abell, and Trevor Rayment**

The hybridization of oligonucleotides in solution to surface-immobilized DNA is of crucial importance to microarray-based genetic diagnostic devices.[1–3] Most microarray-based approaches rely on the labeling of samples with a fluorophore or a radioactive tag. This allows for very sensitive detection but can be time-consuming and expensive. Alternative label-free methods, using a quartz crystal microbalance,[4] surface plasmon resonance (SPR),[5–9] and cantilever arrays[10] have been shown to be capable of detecting DNA quantitatively, however, their relatively large detection areas have limited their detection sensitivity. To date, the highest sensitivity for the detection of label-free DNA probes by these methods is in the femto to attomol range.[8,10] Attomol-scale sensitivity was achieved by modifying the probe strand with gold colloids.[11]

Atomic-force microscopy (AFM) is a powerful tool in nanotechnology not only because of its ability to detect surface topography at sub-nanometer precision, but also because it may be used for nanoscale construction and manipulation. AFM has been used to measure DNA surface coverage, layer thickness,[12,13] and to construct and read DNA and protein micro- or nanoarrays.[14–19] The recent development of AFM-based nanolithography techniques, nanoshaving and nanografting,[20] make it possible to produce surface features as small as $2 \times 4\ nm^2$, and follow their evolution in situ.[21] A wide range of surface features have been constructed from alkyl thiols,[20,22] DNA,[23,24] protein,[25] and active enzymes.[26] We have recently used nanoshaving to produce and manipulate DNA nanofeatures through hybridization and chemical treatment.[24] Herein, we show this method can be used to detect label-free DNA hybridization quantitatively and follow the hybridization dynamics at the nanoscale. We also show the successful construction of multisequenced DNA nanofeatures on a single surface through sequential nanoshaving and self-assembly, which can selectively detect unlabeled target DNA in the presence of 100-fold excess of nonmatching DNA. This approach can detect less than 10^{-21} mol of label-free probe DNA, which makes it one of the most sensitive methods for the detection of DNA hybridization with label-free DNA.

The experimental approach involved the following steps: 1) A self-assembled monolayer (SAM) resist of a 12-mer thiolated double-stranded (ds) DNA was prepared on a template-stripped gold (TSG) surface.[24] TSG was selected as the substrate because its extreme flatness made it possible to detect small changes in topography by AFM. A resist coating of DNA was selected in favor of conventional alkyl thiols because self-assembled monolayers of DNA may be removed by a soft cantilever, thereby improving sensitivity, and because of its biocompatibility.[24] 2) Nanoshaving[20] was used to remove the dsDNA resist at preselected nanoareas to create reactive surface domains. 3) The nanoholes were filled with a 20-mer thiolated single-stranded DNA (ssDNA) by self-assembly to obtain ssDNA (target) nanofeatures. 4) Finally the surface was incubated with a solution of a 24-mer nonthiolated ssDNA whose sequence is complementary to that of the ssDNA nanofeatures. The topographic changes of the DNA nanofeatures were monitored as a function of time. Hybridization of the probe strands in solution with complementary target strands tethered on the Au surface within the nanofeature led to the formation of rigid dsDNA that "stood up" and aligned more perpendicular from the surface. This occurs since extra space is needed to hold the extra volume of the newly introduced probe DNA. The resulting increase in the height of the DNA nanofeatures was detected in situ and measured by AFM. Hybridization was highly sequence specific, no detectable nonspecific adsorption of probe DNA onto the dsDNA resist background was observed (Figure 1).

Table 1 lists the DNA sequences used in this study. A DNA SAM resist was prepared by incubation of a freshly prepared TSG surface with a 2 μM solution of HS-dsDNA-0 in tris(hydroxymethyl)aminomethane (Tris) buffer (pH 7.5) for 48–72 h.[24] An AFM topographic image showed the formation of a complete SAM. Nanoholes created within the dsDNA resist SAM by nanoshaving had a depth of 2.8 ± 0.3 nm (Figure 1a). After incubation of the surface with HS-DNA-1 (1 μM) for 60 minutes, the holes were filled and the average height of the protrusions was approximately 0.5 nm above the background (Figure 1b). When the surface was incubated with a solution of the complementary probe DNA (DNA-1C) at concentrations between 10 nM to 1 μM, height increases as a result of hybridization were observed on the

Table 1: The DNA sequences and their nomenclatures.

Name		Sequence
HS-dsDNA-0	$HS\text{-}C_6H_{12}$-	5′-GATCCTCATCGA-3′
		3′-CTAGGAGTAGCT-5′
HS-dsDNA-1	HSC_6H_{12}-	5′-CTCTAGACATATGGGTACCG-3′
		3′-GAGATCTGTATACCCATGGCTTAA-5′
HS-DNA-1	HSC_6H_{12}-	5′-CTCTAGACATATGGGTACCG-3′
DNA-1C		3′-GAGATCTGTATACCCATGGCTTAA-5′
HS-DNA-2	HSC_6H_{12}-	5′-CGTGCACCCATGGCTCGAGA-3′
DNA-2C		3′-GCACGTGGGTACCGAGCTCTTCGA-5′
DNA-3		3′-GGAATTCTCTAGAGACGTCCCTAG-5′

[*] Prof. C. Abell, Dr. T. Rayment, Dr. D. Zhou, Dr. K. Sinniah
Department of Chemistry
University of Cambridge
Lensfield Road, Cambridge CB2 1EW (UK)
Fax: (+44) 1223-336-362
E-mail: ca26@cam.ac.uk
tr22@cam.ac.uk

[**] We thank the Leverhulme Trust (UK) for funding this project, and Mr. Jon Lee for his help in preparation of the template-stripped gold. K.S. thanks Calvin College and the Burroughs–Wellcome Fund for sabbatical support.

 © 2003 Wiley-VCH Verlag GmbH & Co. KGaA, Weinheim DOI: 10.1002/anie.200352178

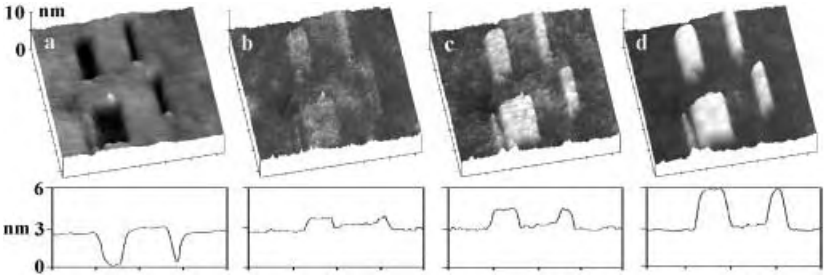


Figure 1. Representative AFM topographic images showing the hybridization process of HS-DNA-1 nanofeatures. All images were in the same *x*-, *y*- ($1.25\times1.25\ \mu m^2$), and *z*-scales. a) A series of nanoholes (20×300, 50×400, 100×400, and $200\times400\ nm^2$) created within the HS-dsDNA-0 SAM by nanoshaving. b) After incubation with 1 μM HS-DNA-1 for 60 mins, the holes were filled and protruded by about 0.5 nm above the background. Incubation of the surface with the complementary DNA-1C (1 μM) for c) 15 and d) 140 mins. The height of the features increased to 1.5, and 3.0 nm above the background, respectively. Longer incubation times resulted in no further height increase of the nanofeatures. The corresponding averaged line-scan profiles across the top two DNA features in the AFM images are shown underneath each image. All line scans are in the same z-scale. The standard deviation on the measured DNA feature height is about ±0.2 nm.

DNA nanofeatures in all cases. Representative images are shown in Figure 1 c–h. The changes in feature height versus incubation time at a variety of DNA-1C concentrations are shown in Figure 2 a.

It is clear that the rate of increase in height and the maximum height increase are strongly dependent on the DNA-1C concentration. For example,, saturation was not reached until over 400 minutes at 10 nM, with a maximum height increase of only 1.1 nm, while saturation was observed within 100 minutes using a more concentrated DNA-1C solution (1 μM), and the height increase was 2.5 nm. It took longer to reach saturation in these experiments than has been reported in SPR or cantilever array studies, most probably because a flow system was used in those experiments.[7–10] Quantitative analysis of these data is possible if it is assumed that the height increase is linearly proportional to hybridization efficiency. Normalized hybridization efficiencies were obtained by division of the increase in the saturated height by the difference in the thickness between SAMs of HS-DNA-1 (0% hybridization) and HS-dsDNA-1 (100% hybridization, which is 7.0 ± 0.8 nm thick).[24] The parameters of a Langmuir adsorption model were fitted to the data to derive a thermodynamic surface–solution equilibrium dissociation constant K_d. If it is assumed that the target–probe bindings are independent of the surface coverage (hybridization efficiency) the Langmuir isotherm can be described as hybridization efficiency $= a\,c/(K_d + c)$,[10] where c is the concentration of the target DNA-1C, and a is the maximum hybridization efficiency under the above conditions (not all surface-tethered ssDNA strands are available for hybridization).[7–10] The plot of the reciprical hybridization efficiency versus the reciprical concentration (Figure 1 b) gives a linear fit ($R = 0.992$), which yields $K_d = 19$ nM and $a = 0.69$. The K_d value for the 20-mer is in good agreement with values obtained from SPR studies and cantilever arrays, (for example, $K_d = 17$ nM for a 25-mer, 33 nM for a 18-mer,[7] and 41 nM for a 12-mer[10]). The maximum hybridization efficiency of 69% for the HS-DNA-1 nanofeatures observed in this study is higher than those reported from SPR studies.[6–8] Perhaps the much smaller feature size and longer incubation time permit greater accessibility to the complementary strand.

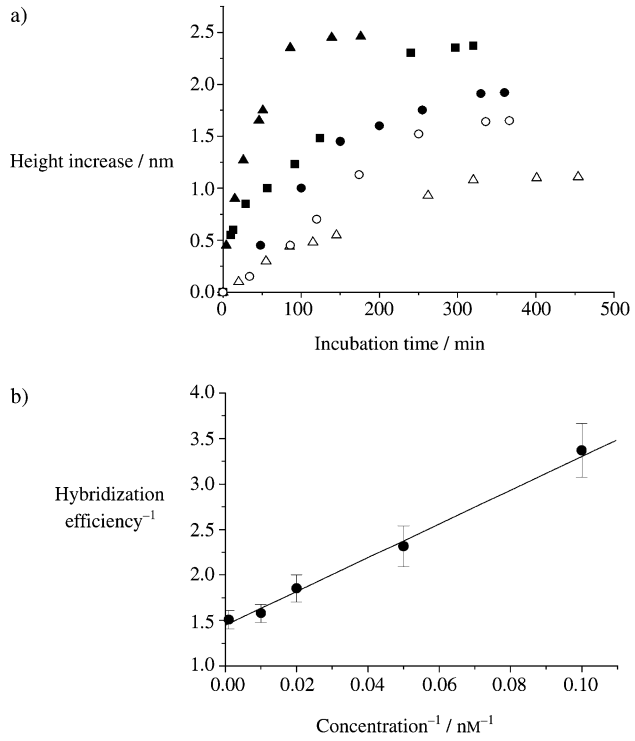


Figure 2. a) Plot of the height changes for the HS-DNA-1 nanofeatures versus the incubation time of the DNA-1C at 1 μM (▲), 100 nM (■), 50 nM (●), 20 nM (○), and 10 nM (△). b) Plot of the hybridization efficiency^{-1} versus concentration^{-1} of the probe DNA.

Experiments have been conducted on smaller-sized HS-DNA-1 features, typically $20\times300\ nm^2$ (Figure 1) which have an area more than six orders of magnitude smaller than those used in SPR hybridization experiments (typically $500\times500\ \mu m^2$)[5] or cantilever arrays ($100\times500\ \mu m^2$).[10] In a $20\times300\ nm^2$ feature there are only about 1500 HS-DNA-1 molecules.[27] A hybridization efficiency of 20%, which corresponds to about 300 hybridized molecules (5×10^{-22} mol), produces significant, readily detectable topographic changes (Figure 1). This is the most sensitive method for detection of label-free DNA through hybridization so far reported.[8,10]

It is important that a hybridization experiment exhibits selectivity. To demonstrate sequence specificity, we employed nanoshaving[20] to produce multisequenced DNA features on a single surface. Nanoshaving was used first to produce two nanoholes (2.5-nm deep) within the DNA resist layer (Figure 3 a). After incubation with the HS-DNA-1 (1 μM) for 1 h, the holes were filled and the features protruded by

 © 2003 Wiley-VCH Verlag GmbH & Co. KGaA, Weinheim

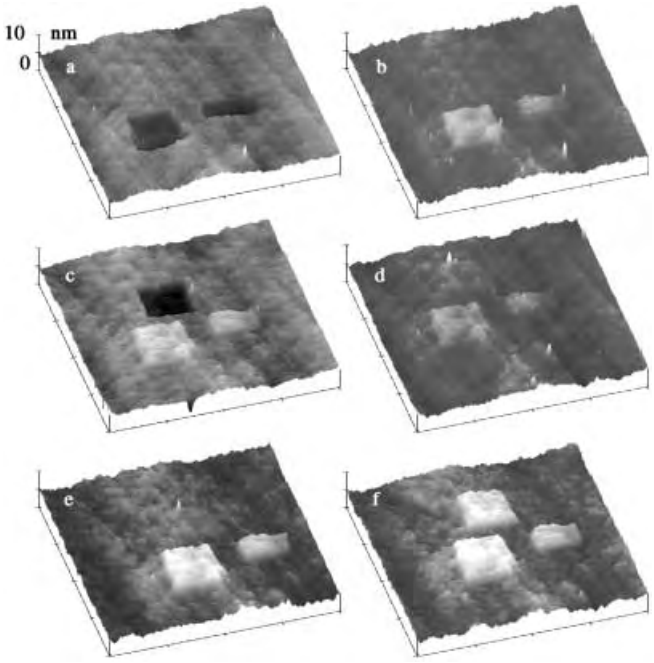


Figure 3. AFM topographic images showing the process for the construction of multisequenced ssDNA nanofeatures on a single surface and selective DNA sequence detection. All images are in the same *x*-, *y*- ($2\times2\ \mu m^2$) and *z*-scales. a) Two nanoholes (400×400 and $400\times200\ nm^2$) were made within HS-dsDNA-0 SAM resist. b) After incubation with HS-DNA-1 (1 μM) for 1 h. c) A new hole was constructed. d) Incubation with HS-DNA-2 (1 μM) for 1 h. No detectable changes were observed upon exposure of the surface to a noncomplementary DNA-3 (10 μM) for 1 h. e) After incubation of the surface with 91 nM DNA-1C in the presence of 9.1 μM DNA-3 for 4 h. f) After introducing 0.5 μM DNA-2C into the incubation solution and incubating for 80 minutes.

about 1 nm above the DNA resist background (Figure 3b). A new hole was produced at a different location of the surface with a depth of 3.0 nm (Figure 3c), and filled by further incubation with HS-DNA-2 (1 μM) for 1 h. The new feature protruded by about 0.4 nm above the DNA background (Figure 3d). No topographic changes were observed on exposure of this surface to a solution of the noncomplementary DNA-3 (10 μM) for 1 h. However, when the surface was exposed to a solution containing the complementary DNA-1C (91 nM) in the presence of 100-fold excess of DNA-3 (9.1 μM) for 4 h, a height increase of about 1.2 nm was observed for the HS-DNA-1 features, with no observable topographic changes from the HS-DNA-2 feature (Figure 3e). Following the introduction of 0.5 μM DNA-2C (complementary to HS-DNA-2), the height of the ssDNA-2 feature was found to have increased by about 2 nm after incubation for 80 minutes (Figure 3f). This observation confirmed that the integrity of the HS-DNA-2 feature had been maintained, and no detectable exchange of thiolated DNA had occurred during the sequential nanoshaving and self-assembly processes. These results demonstrate that the multisequenced DNA nanofeatures have a high selectivity towards probe sequences, which can specifically detect probe sequences even in the presence of a 100-fold excess of noncomplementary strands.

In summary, this work demonstrates the use of AFM as a tool for systematic and quantitative studies of the DNA hybridization dynamics by monitoring the topographic changes of the DNA nanofeatures produced by nanoshaving and self-assembly. This method is extremely sensitive. We have demonstrated that it is possible to image approximately 300 molecules of unlabeled DNA and detect hybridization from 10 nM solutions in situ. We have also demonstrated the use of sequential nanoshaving and self-assembly to produce multisequenced DNA nanofeatures on the same surface, which can selectively detect probe DNA sequences in the presence of 100-fold excess of noncomplementary DNA.

Experimental Section

All single-stranded (ss) DNAs were purchased from MWG Biotech AG (Ebersberg, Germany) and their sequences are listed in Table 1. MilliQ water (resistance $>18\ M\Omega\,cm$) was used to make the Tris buffer (10 mM Tris·HCl, 100 mM NaCl, 10 mM $MgCl_2$, pH 7.5). TSG surfaces were prepared following the literature procedure.[24] Once prepared, the TSG surfaces were immediately used to minimize contamination. Prehybridized dsDNA was prepared following the literature procedure,[24] and diluted to a working concentration with the Tris buffer.

All AFM experiments were carried out on a Digital Instrument (Veeco, CA, USA) Dimension 3100 AFM with a Nanoscope IV controller and a fluid cell under Tris buffer at $24\pm1\,°C$ in contact mode.[24] Standard oxide-sharpened Si_3N_4 probes (DI, spring constant: $0.12\ N\,m^{-1}$) were used in all image collections and nanoshaving experiments. Images were collected at 2 Hz, and analyzed using the Nanoscope image analyzing software with first-order flattening. Before conducting the nanoshaving experiment, the dsDNA SAM resist surface was first imaged under minimum loading force (0.2–0.5 nN) to select a suitable small flat area that avoided domain boundaries. The chosen area was repeatedly scanned at 4–5 Hz under high loading forces (30–50 nN) to scratch away the DNA resist till the gold interatomic steps were clearly visible.[24] The AFM tip was then fully retracted from the surface, zoomed out to a bigger scan area, then re-engaged with minimum force to take topographic images. After each manipulation, the remaining unreacted solution was removed from the fluid cell, and the surface was thoroughly washed with Tris buffer, before a new DNA solution (ca. 150 μL) was introduced and incubated.

Received: June 23, 2003 [Z52178]

Keywords: DNA structures · monolayers · nanolithography · scanning probe microscopy · self-assembly

[1] C. M. Niemeyer, D. Blohm, *Angew. Chem.* **1999**, *111*, 3039; *Angew. Chem. Int. Ed.* **1999**, *38*, 2865.
[2] S. V. Tillib, A. Mirzabekov, *Curr. Opin. Biotechnol.* **2001**, *12*, 53.
[3] E. Southern, K. Mir, M. Shchepinov, *Nat. Genet.* **1999**, *21*, 5.
[4] F. Caruso, E. Rodda, D. F. Furlong, K. Niikura, Y. Okahata, *Anal. Chem.* **1997**, *69*, 2043.
[5] B. P. Nelson, T. E. Grimsrud, M. R. Liles, R. M. Goodman, R. M. Corn, *Anal. Chem.* **2001**, *73*, 1.
[6] A. W. Peterson, R. J. Heaton, R. M. Georgiadis, *Nucleic Acids Res.* **2001**, *29*, 5163.
[7] A. W. Peterson, L. K. Wolf, R. M. Georgiadis, *J. Am. Chem. Soc.* **2002**, *124*, 14601.

 © 2003 Wiley-VCH Verlag GmbH & Co. KGaA, Weinheim

[8] F. Y. Song, F. M. Zhou, J. Wang, N. J. Tao, J. Q. Lin, R. L. Vellanoweth, Y. Morquecho, J. Wheeler-Laidman, *Nucleic Acids Res.* **2002**, *30*, e72.
[9] R. Georgiadis, K. P. Peterlinz, A. W. Peterson, *J. Am. Chem. Soc.* **2000**, *122*, 3166.
[10] R. McKendry, J. Y. Zhang, Y. Arntz, T. Strunz, M. Hegner, H. P. Lang, M. K. Baller, U. Certa, E. Meyer, H. J. Guntherodt, C. Gerber, *Proc. Natl. Acad. Sci. USA* **2002**, *99*, 9783.
[11] L. He, M. D. Musick, S. R. Nicewarner, F. G. Salinas, S. J. Benkovic, M. J. Natan, C. D. Keating, *J. Am. Chem. Soc.* **2000**, *122*, 9071.
[12] S. O. Kelley, J. K. Barton, N. M. Jackson, L. D. McPherson, A. B. Potter, E. M. Spain, M. J. Allen, M. G. Hill, *Langmuir* **1998**, *14*, 6781.
[13] M. Sam, E. M. Boon, J. K. Barton, M. G. Hill, E. M. Spain, *Langmuir* **2001**, *17*, 5727.
[14] R. D. Piner, J. Zhu, F. Xu, S. H. Hong, C. A. Mirkin, *Science* **1999**, *283*, 661.
[15] J. C. O'Brien, J. T. Stickney, M. D. Porter, *J. Am. Chem. Soc.* **2000**, *122*, 5004.
[16] J. R. Kenseth, J. A. Harnisch, V. W. Jones, M. D. Porter, *Langmuir* **2001**, *17*, 4105.
[17] K. B. Lee, S. J. Park, C. A. Mirkin, J. C. Smith, M. Mrksich, *Science* **2002**, *295*, 1702.
[18] L. M. Demers, D. S. Ginger, S. J. Park, Z. Li, S. W. Chung, C. A. Mirkin, *Science* **2002**, *296*, 1836.
[19] S. J. Park, T. A. Taton, C. A. Mirkin, *Science* **2002**, *295*, 1503.
[20] G. Y. Liu, S. Xu, Y. L. Qian, *Acc. Chem. Res.* **2000**, *33*, 457.
[21] G. Y. Liu, N. A. Amro, *Proc. Natl. Acad. Sci. USA* **2002**, *99*, 5165.
[22] X. Z. Wang, D. J. Zhou, T. Rayment, C. Abell, *Chem. Commun.* **2003**, 474.
[23] M. Z. Liu, N. A. Amro, C. S. Chow, G. Y. Liu, *Nano Lett.* **2002**, *2*, 863.
[24] D. J. Zhou, K. Sinniah, C. Abell, T. Rayment, *Langmuir* **2002**, *18*, 8278.
[25] K. Wadu-Mesthrige, N. A. Amro, J. C. Garno, S. Xu, G. Y. Liu, *Biophys. J.* **2001**, *80*, 1891.
[26] C. H. Jang, B. D. Stevens, P. R. Carlier, M. A. Calter, W. A. Ducker, *J. Am. Chem. Soc.* **2002**, *124*, 12114.
[27] A HS-DNA-1 SAM prepared on a TSG surface under identical condition (1 μM in Tris, 1 h) has a dry DNA thickness of 1.6 ± 0.4 nm from the ellipsometry measurement, which corresponds to $2.6 \pm 0.7 \times 10^{13}$ DNA cm^{-2} assuming a DNA density of 1.7 g cm^{-3} (see Y. K. Cho, S. Kim, G. Lim, S. Granick, *Langmuir* **2001**, *17*, 7732). The value is in very good agreement with XPS and radiolabeling data (see D. Y. Petrovykh, H. Kimura-Suda, L. J. Whitman, M. J. Tarlov, *J. Am. Chem. Soc.* **2003**, *125*, 5219; A. B. Steel, R. L. Levicky, T. M. Herne, M. J. Tarlov, *Biophys. J.* **2000**, *79*, 975).

 © 2003 Wiley-VCH Verlag GmbH & Co. KGaA, Weinheim

Oxidation of Benzene to Phenol

Direct Oxidation of Benzene to Phenol with Hydrogen Peroxide over a Modified Titanium Silicalite

Luigi Balducci, Daniele Bianchi, Rossella Bortolo, Rino D'Aloisio, Marco Ricci, Roberto Tassinari, and Raffaele Ungarelli*

Phenol is one of the most important intermediates of the chemical industry. Nearly all its current production is based upon the cumene process, which also represents the most important route to acetone, coproduced in 1:1 molar ratio with respect to phenol. However, as the expected market growth is quite different for phenol and acetone, much effort is currently being devoted to decouple their productions. In this context, a long-standing goal is the development of an effective process for the direct oxidation of benzene to phenol with hydrogen peroxide. This reaction, however, is often affected by a poor selectivity, due to the lack of kinetic control. Indeed, phenol is more reactive toward oxidation than benzene itself, and substantial formation of over-oxygenated by-products (catechol, hydroquinone, benzoquinones, and tars) usually occurs.[1]

In our continuing effort aimed at discovering new processes for a one-step, by-product-free synthesis of phenol,[2] we report herein that by combining a suitable solvent and a modified titanium silicalite catalyst (TS-1 B), satisfactory selectivities and yields can be achieved in the direct oxidation of benzene to phenol with hydrogen peroxide.

In the first stage of this study, the hydroxylation of benzene was investigated by using titanium silicalite (TS-1)[3] as the catalyst, on the basis of its well established efficiency in a series of oxidation processes with hydrogen peroxide, such as alkenes epoxidation,[4] alkanes oxidation,[5] alcohol oxidation,[6] cyclohexanone ammoximation,[7] and phenol hydroxylation.[8] The reactions were carried out with different cosolvents to homogenize the hydrophobic substrate and the aqueous hydrogen peroxide in the liquid phase.

As expected, the selectivity to phenol (expressed as moles of produced phenol/moles of reacted benzene $\times 100$) rapidly dropped when with conventional solvents such as acetone, acetonitrile, and *tert*-butanol, even at low benzene conversion (Figure 1). With these solvents, under the reaction conditions described in Table 1 (H_2O_2/benzene molar ratio $= 0.1$), the selectivity based on benzene was lower than 50% with a selectivity based on hydrogen peroxide (expressed as moles of produced phenol/moles of reacted $H_2O_2 \times 100$) lower than

[*] Dr. D. Bianchi, Dr. L. Balducci, Dr. R. Bortolo, R. D'Aloisio, Dr. M. Ricci, R. Tassinari, R. Ungarelli
Polimeri Europa S.p.A.
Istituto Guido Donegani
Via Fauser 4, 28100 Novara (Italy)
Fax: (+39) 0321-447-425
E-mail: daniele.bianchi@polimerieuropa.com

 DOI: 10.1002/anie.200352184 © 2003 Wiley-VCH Verlag GmbH & Co. KGaA, Weinheim

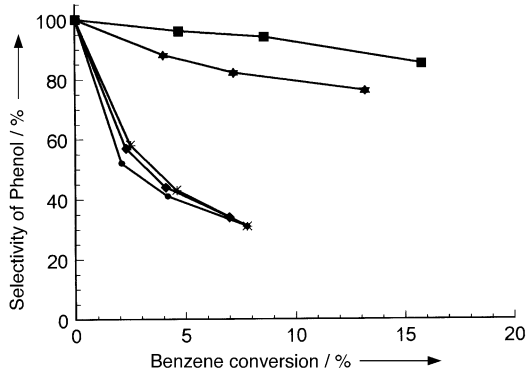


Figure 1. Effect of the solvent on benzene oxidation. (●) acetone, (*) acetonitrile, (◆) *tert*-butanol, (✱) sulfolane, (■) sulfolane/TS-1B. Reaction conditions: benzene/solvent = 2/8 w/w, TS-1/benzene = 0.1 w/w, temperature = 100 °C. An aqueous solution of H_2O_2 (30% w/w) was gradually added in 2 h up to a hydrogen peroxide/benzene molar ratio = 0.2.

Table 1: Effect of the solvent and the catalyst treatment on benzene oxidation.

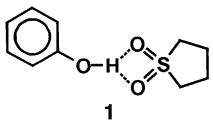
	Solvent[a]	Benzene Conversion [%]	H_2O_2 Conversion [%]	Selectivity to phenol based on benzene[b]	based on H_2O_2[c]
1	acetone	4.2	90	41	19
2	acetonitrile	4.6	93	43	21
3	*tert*-butanol	4.1	90	44	20
4	sulfolane	7.8	97	83	67
5	sulfolane/ TS-1B[d]	8.6	97	94	83

[a] Reaction conditions: benzene/solvent = 2:8 w/w, H_2O_2/benzene molar ratio = 0.1, TS-1/benzene = 0.1:1 w/w, temperature = 100 °C. [b] Moles of phenol/moles of reacted benzene × 100. [c] Moles of phenol/moles of reacted H_2O_2 × 100. [d] Reaction carried out using the TS-1B (TS-1 modified with NH_4HF_2 and H_2O_2).

20%, mainly owing to the formation of dioxygenated products and tars. Even worse results were obtained with methanol and 2-propanol, which were oxidized in competition with benzene to give formaldehyde dimethyl acetal and acetone, respectively, or with nitrogen-containing solvents (dimethylformamide and *N*-methylpyrrolidone) the reaction afforded only negligible yields of phenol.

Conversely, as shown in Figure 1, a dramatic improvement of selectivity was observed by using tetrametilene sulfone (sulfolane) as a cosolvent, which allowed a conversion of benzene close to 8% with a selectivity of phenol higher than 80% (Table 1, entry 4). In this case the detected by-products were catechol (7%), hydroquinone (4%), 1,4-benzoquinone (1%), and tars (5%).

Sulfolane is a solvent with high dipole moment (4.81 debye) and dielectric constant (43.26), thus having the peculiar property of being able to form complexes with phenolic compounds. These complexes are not stable enough to be isolated but were identified in solution by IR spectroscopy.[9] In the case of phenol, the formation of the complex **1** was reported.[10]



1

The increased selectivity observed by performing the benzene oxidation in sulfolane may be due to the formation of this sterically hindered species, which can not enter the titanium silicalite pores, thus allowing phenol to remain relatively protected towards further oxidation.[11] This effect was confirmed by calculating the loading of the free phenol molecule and the phenol–sulfolane complex (expressed as number of loaded molecules in a crystal elementary unit of TS-1), by using the program Sorption,[15] which turned out to be 13.6 for phenol and 0.8 for the phenol–sulfolane complex.

The protective effect exerted by sulfolane can be also evaluated by measuring the reaction rate, expressed as turnover frequency (TOF: moles of reacted substrate/moles of Ti × hour) for the oxidation of benzene and phenol, carried out separately in acetone and sulfolane as cosolvents. In the case of acetone, the phenol oxidation rate (TOF = 190) was ten times faster with respect to that measured for benzene (TOF = 19), conversely, when the reaction was performed in sulfolane the rate measured for phenol (TOF = 51) was only 1.6 times faster than that measured for benzene (TOF = 31), according to the higher value of the observed selectivity. However, the formation of over-oxidation by-products, such as 1,4-benzoquinone and tars, suggests the possible presence of a heterogeneous population of catalytic sites on TS-1, which differ in reactivity and shape-selectivity and some of these are accessible to sterically hindered catechol and hydroquinone. It was reported that titanium atoms are not equally distributed in the 12 crystallographically independent sites of the MFI framework of TS-1, but are hosted in four preferential positions[12] which, in principle, might display different catalytic properties.

With the aim to remove the less selective catalytic sites, we studied a new post-synthesis treatment of TS-1. What we found was a method that can remove selectively a fraction of titanium atoms leaving unchanged the crystalline structure of the zeolite. The treatment was carried out at 80 °C in an aqueous solution of NH_4HF_2 and H_2O_2 with a F/Ti molar ratios = 7 and a H_2O_2/Ti molar ratios = 30. In these conditions up to 75% of titanium was removed as $(NH_4)_3TiF_5O_2$, as confirmed by UV/Vis, IR, and Raman spectroscopy. Only a negligible fraction of silica (1%) was removed as $(NH_4)_2SiF_6$. As shown in Figure 2, both the catalytic activity and the selectivity of the modified catalyst increased at lower residual titanium concentration. After removal of 75% of the initial titanium, the TOF of the residual metal, measured for the oxidation of benzene, increased from 31 to 80, while the selectivity to phenol was raised from 83 to 94% (Table 1, entry 5), with formation of catechol (4%), and hydroquinone (2%) as the only by-products, without any evidence of further oxidation reactions.

A preliminary characterization of the modified catalyst (residual titanium = 29%), carried out by UV/Vis spectroscopy[13] (Figure 3), showed: a) the titanium atoms that had a tetrahedral coordination environment, $[Ti(OSi)_4]$, and absorbed at 48000–50000 cm^{-1} (as the majority of atoms present in the starting TS-1), were almost completely removed; b) the

 © 2003 Wiley-VCH Verlag GmbH & Co. KGaA, Weinheim

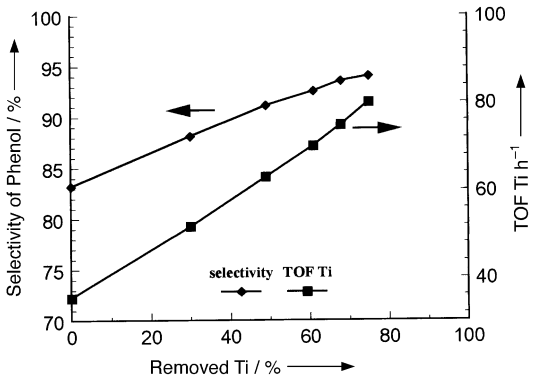


Figure 2. Effect titanium removal on the catalyst activity and selectivity. (◆) Selectivity to phenol = moles of phenol/moles of reacted benzene × 100 (■) TOF Ti = moles of reacted benzene/moles of Ti × hour. The reactions were carried out as previously described in Figure 1.

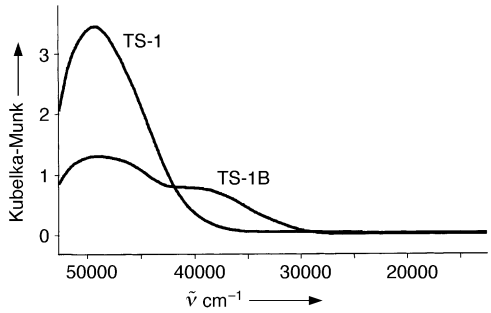


Figure 3. UV/Vis DRS (Diffuse Reflectance Spectroscopy) of TS-1 and TS-1 B. Spectra were recorded starting from on a TS-1 sample containing 2.8% w/w of TiO_2, totally free of amorphous extraframework titanium. After the treatment, the TiO_2 content of the resulting TS-1 B was reduced to 0.8%.

formation of amorphous extraframework titanium species (TiO_2) that absorbed at 30000–35000 cm^{-1} was not observed; c) a new titanium species that absorbed at 40000 cm^{-1} was generated by the treatment.

After the treatment, titanium atoms in tetrahedral coordination decreased by 87%, as quantitatively determined by IR spectroscopy (960 cm^{-1} band):[14] 71% of them were removed and the remaining 16% transformed in the new species. The formation of this new species, the characterization of which is currently in progress, makes the treated catalyst a completely new material, now named TS-1 B, with respect to the starting TS-1, and can explain the different catalytic properties, such as the increased activity, that cannot be a consequence of the simple removal of the titanium sites with low shape selectivity.

In a further development study, the oxidation of benzene to phenol was carried out under continuous operation, by using a continuous stirred tank reactor (CSTR) equipped with filter, to maintain the catalyst inside the vessel. At 100°C, only a negligible loss of catalytic activity was observed after 100 h of continuous operation.

In conclusion, the simplicity of this one-step process, the high selectivity value achieved, and the demonstrated possibility of a continuous operation process in CSTR reactors, make this methodology particularly attractive for a possible industrial development.

Experimental Section

Titanium silicalite containing 3.6% (w/w) of TiO_2 was synthesised according to a literature procedure.[3] All other chemicals (Aldrich) were used as purchased.

Postsynthesis modification of titanium silicalite: Titanium silicalite (10 g, containing 4.5 mmol of Ti, corresponding to 3.6% w/w of TiO_2) was suspended in an aqueous solution (300 mL) containing NH_4HF_2 (0.9 g, 15.8 mmol) at 80°C. A 30% (w/w) aqueous solution of hydrogen peroxide (15.4 g, 135.5 mmol) was added and the suspension was mechanically stirred for 4 h. The mixture was then cooled at 25°C and the catalyst filtered off and washed with 100 mL of water. The wet catalyst was dried at 100°C and calcinated in air at 550°C for 4 h. The TiO_2 content of the modified titanium silicalite (TS-1B) was 0.9% (w/w) determined by XRF and ICP analysis.

Benzene oxidation (general procedure): Titanium silicalite (either TS-1 or TS-1 B, 5 g) was suspended in a solution of benzene (40 g, 512.8 mmol) and one of a cosolvent (acetone, acetonitrile, *tert*-butanol, sulfolane; 160 g). The suspension was added into a stainless steel autoclave, and pressurised at 5 bar with nitrogen. Then, an aqueous solution of 30% w/w hydrogen peroxide (5.8 g, 51.3 mmol) was fed stepwise within one hour under mechanical stirring, while the reaction was kept at 100°C. At the end of the reaction, the hydrogen peroxide concentration in the aqueous phase was determined by titration with potassium permanganate and the oxidation products concentration in both the aqueous and organic phases was determined by HPLC analysis.

TOF determination: The initial turn over frequency of the titanium was expressed as moles of reacted substrate/(moles of Ti × hour). The TOF were determined carrying out the oxidation reactions as described above, but the total amount of hydrogen peroxide was added at the beginning of the reaction and the reaction was stopped (by filtering off the catalyst and fast cooling) at an oxidant conversion lower that 20%.

Received: June 23, 2003 [Z52184]

Keywords: benzene · hydroxylation · solvent effects · titanium · zeolites

[1] a) R. A. Sheldon, J. K. Kochi in *Metal-Catalyzed Oxidations of Organic Compounds*, Academic Press, New York, **1981**, pp. 329–333; b) G. Goor in *Catalytic Oxidations with Hydrogen Peroxide as Oxidant* (Ed.: G. Strukul), Kluver, Dordrecht, **1992**, pp. 29–31.

[2] D. Bianchi, R. Bortolo, R. Tassinari, M. Ricci, R. Vignola, *Angew. Chem.* **2000**, *112*, 4491–4493; *Angew. Chem. Int. Ed.* **2000**, *39*, 4321–4323.

[3] M. Taramasso, G. Perego, B. Notari, US Patent 4410501, **1983** [*Chem. Abstr.* **1981**, *95*, 206272].

[4] M. G. Clerici, P. Ingallina, *J. Catal.* **1993**, *140*, 71–83.

[5] M. G. Clerici, *Appl. Catal.* **1991**, *68*, 249–261.

[6] F. Maspero, U. Romano, *J. Catal.* **1994**, *146*, 476–482.

[7] M. A. Mantegazza, G. Petrini, G. Spanò, R. Bagatin, F. Rivetti, *J. Mol. Catal. A* **1999**, *146*, 223–228.

[8] A. Esposito, M. Taramasso, C. Neri, US Patent 4396783, **1983** [*Chem. Abstr.* **1982**, *96*, 199290].

[9] V. V. Prezhdo, O. V. Prezhdo, E. V. Vaschenko, *J. Mol. Struct.* **1995**, *356*, 7–13.

[10] R. S. Drago, B. Wayland, R. L. Carlson, *J. Am. Chem. Soc.* **1963**, *85*, 3125–3128.

[11] This phenol protection by sulfolane, which reduces its overoxidation, is reminiscent to some extent of other means to trap phenol, for example, by sequestration in a biphasic system (reference [2]) or even by protonation in superacidic medium (G. A. Olah, R. Ohnishi, *J. Org. Chem.* **1978**, *43*, 865–867).

 © 2003 Wiley-VCH Verlag GmbH & Co. KGaA, Weinheim

[12] C. Lamberti, S. Bordiga, A. Zecchina, G. Artioli, G. Marra, G. Spanò, *J. Am. Chem. Soc.* **2001**, *123*, 2204 – 2212.
[13] A. Zecchina, G. Spoto, S. Bordiga, A. Ferrero, G. Petrini, M. Padovan, G. Leofanti, *Stud. Surf. Sci. Catal.* **1991**, *69*, 251 – 258.
[14] M. R. Boccuti, K. M. Rao, A. Zecchina, G. Leofanti, G. Petrini, in *Structure and Reactivity of Surfaces* (Ed.: C. Monterra), Elsevier, Amsterdam **1989**, pp. 133 – 153.
[15] Sorption program, Cerius 2, Accelrys Inc., S. Diego)

 © 2003 Wiley-VCH Verlag GmbH & Co. KGaA, Weinheim

Phosphininium Compounds

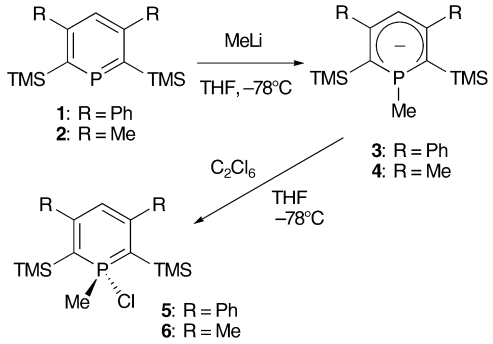
A 1-Methyl-Phosphininium Compound: Synthesis, X-Ray Crystal Structure, and DFT Calculations**

*Audrey Moores, Louis Ricard, and Pascal Le Floch**

It is well established that the replacement of nitrogen by phosphorus in aromatic structures results in profound modifications of electronic properties.[1] One of the most representative examples is provided by phosphinines, the phosphorus equivalent of pyridines. In these heterocycles, the lone pair at the phosphorus center, which features a significant amount of 3s character (63.8% vs 29.1% in pyridine), is only weakly basic.[2] Conversely, phosphinines are relatively inert towards electrophilic attacks at the phosphorus atom. An illustration of this peculiar electronic situation is given by several unsuccessful attempts to produce 1-R-phosphininium (R = alkyl, aryl, or H). For example, direct protonation of phosphorus with CF_3SO_3H did not yield the expected 1-H-phosphininium and the gas-phase proton affinity of phosphinine, determined by ion-cyclotron resonance techniques, was found to be slightly higher than that of PH_3.[3,4]

Though phosphininiums were thought to be involved as intermediates in many transformations leading to λ^5-phosphinines, only a few data are available on their structure, reactivity, and electronic properties.[5] In 1984, Dimroth and co-workers reported the successful preparation of a 1-phenylphosphinium, from the reaction of $AlCl_3$ with a λ^5-1-phenyl-1-fluorophosphinine, but this compound was only partially characterized (^{31}P and ^1H NMR spectroscopy).[6] In view of the potential synthetic utility of phosphininium compounds in heterocyclic phosphorus chemistry, we reinvestigated their synthesis. Herein, we report the characterization by NMR spectroscopy and X-ray crystallography of a 1-methylphosphininium gallium tetrachloride adduct and its electronic structure.

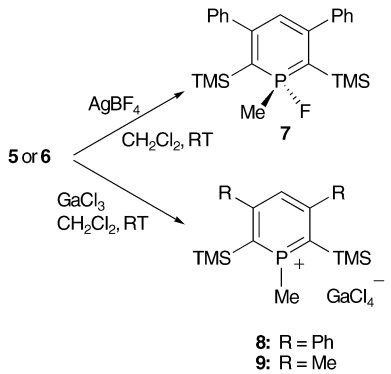
λ^5-1-methyl-1-chlorophosphinines **5** and **6** were chosen as starting precursors for this study. Their syntheses rely on the oxidation of anions **3** and **4** that were conventionally produced by treating methyllithium with phosphinines **1**[7] and **2**,[8] respectively (Scheme 1).[9]



Scheme 1. Synthesis of compounds **5** and **6**. TMS = $SiMe_3$.

We tried to duplicate the strategy reported by Dimroth and co-workers, and therefore compounds **5** and **6** were treated with $AlCl_3$ in CH_2Cl_2 at room temperature. In both cases, a reaction took place and the ^{31}P NMR spectrum showed broad signals at $\delta = 133.5$ and 137.0 ppm, respectively. Suspecting that an exchange could occur between the counterion $AlCl_4^-$ and the phosphininium, we investigated the use of different reagents as chloride abstractor ($AgBF_4$, $AgBPh_4$, $TlBPh_4$ and $GaCl_3$). Whereas no reaction occurred when **5** or **6** were treated with tetraphenylborate salts salts, treatment of **5** with $AgBF_4$ resulted in the exchange of the halogen atom at phosphorus to afford the fluoro derivative **7**. More convincing results were obtained when **5** and **6** were treated with $GaCl_3$ in CH_2Cl_2 at room temperature. In both cases, a clean reaction took place to produce 1-methylphosphininium compounds **8** and **9** which were isolated as moisture sensitive powders (Scheme 2).

Both compounds were successfully characterized by NMR spectroscopy and elemental analysis. The formation of the



Scheme 2. Synthesis of compounds **7**, **8**, and **9**.

[*] Dr. P. Le Floch, A. Moores, Dr. L. Ricard
Laboratoire "Hétéroéléments et Coordination" UMR CNRS 7653 (DCPH)
Département de Chimie, Ecole Polytechnique
91128 Palaiseau cedex (France)
Fax: (+33) 1-6933-4570
E-mail: lefloch@poly.polytechnique.fr

[**] This work was supported by the CNRS and the Ecole Polytechnique.

Supporting information for this article is available on the WWW under http://www.angewandte.org or from the author.

 © 2003 Wiley-VCH Verlag GmbH & Co. KGaA, Weinheim DOI: 10.1002/anie.200352230

phosphininium is evidenced by a strong downfield shift in ^{31}P NMR (from $\delta = 63.7$ in **5** to $\delta = 160.2$ ppm for **8** and from $\delta = 64.7$ in **6** to $\delta = 156.9$ ppm for **9**). The aromaticity of the ring is also apparent in the ^{13}C NMR spectra from the chemical shifts of the C2 and C4 carbon atoms that are strongly deshielded (from $\delta = 88.8$ in **5** to $\delta = 140.3$ in **8** for C2 and from $\delta = 117.4$ to $\delta = 134.7$ for C4). The formulation of **8** was definitively established by an X-ray crystal-structure analysis.[10] A view of one molecule of **8** is presented in Figure 1. The structure consists of two discrete units containing the phosphininium cation, the $GaCl_4^-$ ion and two molecules of THF. One THF molecule is located far away above the ring (P–O separation: 3.174(5) Å), the oxygen atom pointing in the direction of the phosphorus atom. The phosphinine ring is not rigorously planar and both phosphorus and the C4 carbon atoms escape from the mean plane (C2-C3-C3′-C2′) by 3.8° and 1.7°, respectively. But, the most significant data are given by the internal bond distances which are significantly modified in comparison to those of a λ^3-phosphinine: the two internal P–C bond lengths are significantly shortened from 1.734(5) Å in the reference compound[11] to 1.697(2) Å in **8**,[12] whilst the internal C2-P1-C2′ angle changes from 106.3(2)° to 117.7(1)°. These two pieces of data clearly suggest that the phosphorus atom has gained a significant amount of sp^2 character. This result is peculiar as it has always been believed that phosphorus could not undergo such a rehybridization within a six-membered ring, which accounted for the low basicity of phosphinine moieties.[4,13]

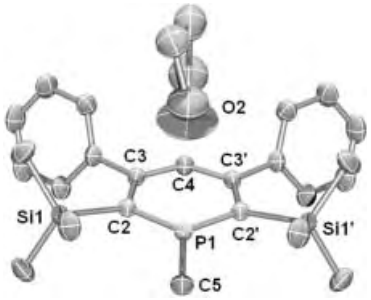
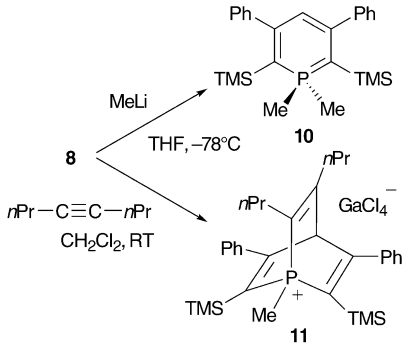


Figure 1. Molecular structure of **8** without hydrogen atoms. Selected bond lengths [Å] and angles [°]: P1-C2 1.697(2), C2-C3 1.415(3), C3-C4 1.407(2), Si1-C2 1.921(2), P1-C5 1.790(3); C2-P1-C2′ 117.7(1), C2-P1-C5 120.80(6), P1-C2-C3 113.1(1), C2-C3-C4 24.7(2), C3-C4-C3′ 126.5(2).

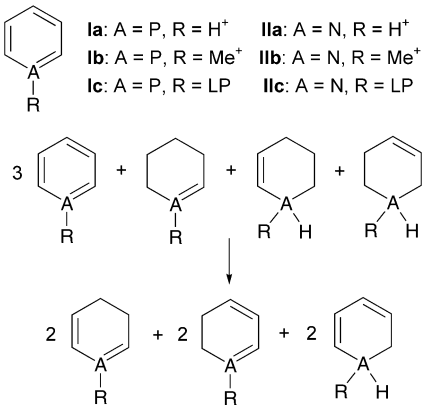
Phosphininium intermediates are known to be highly reactive towards nucleophiles and we found that compound **8** rapidly reacts with methyllithium in THF at low temperature to afford the λ^5-dimethylphosphinine **10** (Scheme 3). We also found that the dienic character of the ring is significantly enhanced compared to λ^3-phosphinines. Reaction of **8** with 4-octyne at room temperature for 24 h cleanly yielded the phosphabarrelenium salt **11** which was isolated as beige solid and fully characterized by NMR spectroscopy and elemental analysis (Scheme 3).

A theoretical study was undertaken; calculations were carried out on the unsubstituted 1-H **Ia** and 1-Me- **Ib** derivatives by using a combination of the B3LYP functional with the 6-311 + G(d,p) basis set.[14] The calculated geometry



Scheme 3. Reactivity of phosphoninium **8**.

of **Ib** was found to be close to that of the experimental structure. The shortening of the two P=C bonds (1.698 Å in **Ib** vs 1.743 Å in the parent phosphinine **Ic**; Scheme 4) as well as the widening of the internal angle C2-P1-C2′ angle (110.67° in **Ib** vs 100.02° in **Ic**) are reproduced.[15] An NBO analysis[16] reveals that the phosphorus atom bears a significant positive charge (1.017 in **Ia** and 1.285 in **Ib** vs 0.642 in **Ic**) and has gained a substantial sp^2 character. Thus the contribution of



Scheme 4. Structures used as the basis for calculations and the aromatic stabilization energy equation; LP = lone pair.

the 3s orbital in a P–C bond changes from 19.42 % in **Ic** to 33.30 % in **Ib**. Useful data were obtained by calculating the ASE (aromatic stabilization energy) using the equation depicted in Scheme 4.[17] To draw an efficient comparison, similar calculations were also carried out on the 1-H **IIa**, 1-Me **IIb** pyridinium cations and pyridine **IIc**. Nuclear independent chemical shift (NICS; *N*-iodosuccinimide) at 1 Å above the ring were calculated at the 6-311 + G** level (Table 1).[18] The aromaticity of the phosphininium is close to that of the free phosphinine (94.3 % in **Ia** and 99.2 % in **Ib**). On the contrary, the two pyridiniums were found to be slightly more aromatic than pyridine (109.3 % in **IIa** and 105.9 % in **IIb**). NICS values do not reproduce exactly the same trends, but confirm the strong aromaticity of the six molecules. In view of these data, it seems evident that the high reactivity of **8** towards 4-octyne does not result from a disruption of aromaticity within the ring. Therefore, the reaction paths of the [4+2] cycloaddition

 © 2003 Wiley-VCH Verlag GmbH & Co. KGaA, Weinheim

Table 1: Calculated aromatic stabilization energy of compound **Ia–c**, **IIa–c**.

Compound	Ia	Ib	Ic	IIa	IIb	IIc
ASE [kcal mol^{-1}] ZPE corrected	26.5	27.87	28.09	32.29	31.29	29.55
NICS (1 Å)	−11.6128	−11.4749	−10.7827	−10.7212	−10.7446	−11.1321

process of **Ib** and **Ic** with acetylene (to give **IIIb** and **IIIc**) were modeled (Figure 2). These calculations which were conducted at the B3LYP6-311 + G(d,p) level of theory indicate that the formation of the phosphabarrelenium is strongly exothermic (−23.03 kcal mol^{-1} and only requires a weak activation energy

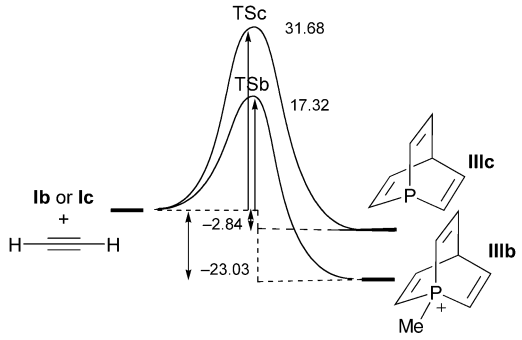


Figure 2. Calculated reaction profile of Diels–Alder reaction on phosphinine or phosphininium (energies, zero-point energy (ZPE) corrected, are in kcal mol^{-1}).

(E_{TSb} = 17.32 kcal mol^{-1}; TS = transition state). In good agreement with experimental data, the formation of the phosphabarrelene from **Ic** is only weakly exothermic and involves a high activation barrier (E_{TSc} = 31.68 kcal mol^{-1}).

These results are fully consistent with the relative energies of frontier orbitals in **Ib** and **Ic** (calculated at the MP2/6-311 + G(d,p) level of theory using B3LYP geometries). As expected, the introduction of a methyl group at the phosphorus atom does not modify the shape of frontier orbitals, which, having a π symmetry, can not interact with methyl group molecular orbitals (MOs). On the contrary, energies of the MOs are significantly lowered because of orbital contraction. As can be seen in Figure 3, reaction of **Ic** with acetylene is a classical [4+2] cycloaddition process in which the phosphinine acts as the diene and reacts through its HOMO. On the contrary, in phosphininium **Ib** its low-lying LUMO reacts with the HOMO of the alkyne (inverse electron demand process).

In conclusion, we have established the existence of 1-methyl-phosphininium compounds. We believe that these cations will find interesting applications in the synthesis of new phosphorus heterocycles.

Experimental Section

All work was carried out under nitrogen or argon using Schlenk techniques. The solvents used were freshly distilled, dried, and saturated with nitrogen or argon.

5: A solution of MeLi in diethyl ether (80 μL, 0.127 mmol, 1.6 M) was added to a solution of 50 mg of phosphinine (**1** or **2**, 0.127 mmol)

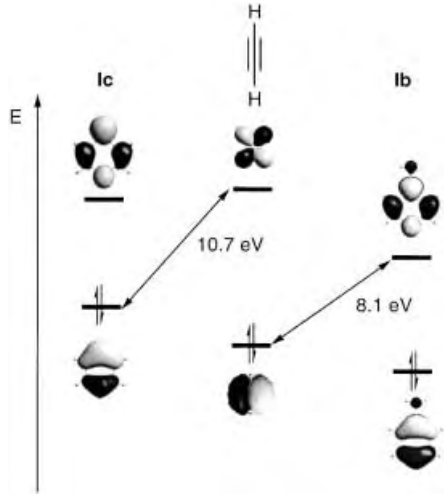


Figure 3. Shape and level of frontier orbitals of phosphinine, phosphininium, and acetylene.

in THF (2 mL) at −78 °C. The solution turned from colorless to red and was warmed to room temperature. Completion of the reaction was checked by ^{31}P NMR spectroscopy. Hexachloroethane (30 mg, 0.127 mmol) was added at −78 °C. The solution was warmed to room temperature, solvent was removed in vacuo, and the resulting brown solid was extracted with hexane (3 × 2 mL). The product was recovered as a yellow oil, yield 49 mg (87 %); **5** was too air sensitive to give satisfactory elemental data. Selected data: ^{1}H NMR (300 MHz, C_6D_6, 25 °C): δ = 0.14 (s, 18 H, $Si(CH_3)_3$), 2.51 (d, ^{2}J(H,P) = 15.7 Hz, 3 H, PCH_3), 6.07 (d, ^{4}J(H,P) = 4.7 Hz, 1 H, H4), 7.01–7.30 ppm (m, 10 H, Ph); ^{31}P NMR (121.5 MHz, C_6D_6, 25 °C, 85 % H_3PO_4 as external standard): δ = 63.7 ppm (s).

6: A solution of MeLi in diethyl ether (100 μL; 0.149 mmol, 1.6 M) was added to a solution of phosphinine (40 mg 0.149 mmol) in hexane (2 mL) at −78 °C. The solution turned from colorless to bright yellow. The solution was warmed to room temperature and completion of the reaction was checked by ^{31}P NMR spectroscopy. Hexachloroethane (35 mg, 0.149 mmol) was added at −78 °C. The solution was warmed to room temperature, solvent was removed in vacuo, and the solution filtered to remove the salts. The product was recovered from the filtrate as a yellow oil, yield 38 mg (80 %); **6** was too air sensitive to give satisfactory elemental data. Selected data: ^{1}H NMR (300 MHz, C_6D_6, 25 °C): δ = 0.39 (s, 18 H, $Si(CH_3)_3$), 2.12 (d, ^{4}J(H,P) = 0.9 Hz, 6 H, C3-CH_3), 2.24 (d, ^{2}J(H,P) = 16.3 Hz, 3 H, PCH_3), 5.67 ppm (d, ^{4}J(H,P) = 5.0 Hz, 1 H, H4); ^{31}P NMR (121.5 MHz, C_6D_6, 25 °C, 85 % H_3PO_4 as external standard): δ = 64.69 ppm (s).

7: $AgBF_4$ (22 mg, 0.111 mmol) was added to a solution of **5** (0.111 mmol, 49 mg) in THF (2 mL) at room temperature. This solution was stirred for 24 h. Completion of the reaction was checked by ^{31}P NMR spectroscopy. Solvent was removed in vacuo and the resulting brown solid was extracted with hexane (3 × 2 mL). The product was recovered as a pale brown oil, yield 35 mg (74 %); **7** was too air sensitive to give satisfactory elemental data. Selected data: ^{1}H NMR (300 MHz, C_6D_6, 25 °C): δ = 0.11 (s, 18 H, $Si(CH_3)_3$), 1.96 (d, ^{2}J(H,P) = 14.7 Hz, 3 H, PCH_3), 5.90 (dd, ^{4}J(H,P) = 7.0 Hz, ^{5}J(H,P) = 0.6 Hz, 1 H, H4), 7.04–7.31 ppm (m, 10 H, Ph); ^{31}P NMR (121.5 MHz,

 © 2003 Wiley-VCH Verlag GmbH & Co. KGaA, Weinheim

THF, 25 °C 85 % H_3PO_4 as external standard): $\delta = 80.09$ ppm (d, $^1J(P,F) = 1043.2$ Hz).

8: A solution of $GaCl_3$ (21 mg, 0.119 mmol) in CH_2Cl_2 (1 mL) was added to a solution of **5** (48 mg, 0.108 mmol) in CH_2Cl_2 (2 mL) room temperature. After stirring for 5 min, solvent was removed and, the product was recovered as a beige powder, yield 62 mg (93 %). Crystallization of **8** at −18 °C in a mixture of CH_2Cl_2 and hexane afforded colorless crystals. Elemental analysis (%) calcd: C 46.55, H 5.21; found: C 46.53, H 5.22; ^{1}H NMR (300 MHz, C_6D_6, 25 °C): $\delta =$ 0.21 (s, 18 H, $Si(CH_3)_3$), 3.20 (d, $^2J(H,P) = 20.8$ Hz, 3 H, PCH_3), 7.32–7.48 (m, 10 H, Ph), 7.63 ppm (d, $^4J(H,P) = 6.1$ Hz, 1 H, H4); ^{13}C NMR (75.5 MHz, C_6D_6, 25 °C): $\delta = 1.68$ (d, $^3J(C,P) = 3.4$ Hz, $Si(CH_3)_3$), 12.77 (d, $^1J(C,P) = 51.5$ Hz, PCH_3), 128.46 (s, *o*-C of Ph), 128.54 (s, *m*-C of Ph), 129.40 (s, *p*-C of Ph), 134.72 (d, $^3J(C,P) = 51.3$ Hz, C4), 140.34 (d, $^1J(C,P) = 22.4$ Hz, C2-TMS), 142.29 (d, $^2J(C,P) = 18.9$ Hz, C3), 162.45 ppm (d, $^3J(C,P) = 14.9$ Hz, C_{ipso} of Ph); ^{31}P NMR (121.5 MHz, THF, 25 °C, 85 % H_3PO_4 as external standard): $\delta =$ 160.23 ppm (s).

9: A solution of $GaCl_3$ (23 mg, 0.131 mmol) in CH_2Cl_2 (1 mL) was added to a solution of **6** (38 mg, 0.119 mmol) in CH_2Cl_2 (2 mL) at room temperature. After stirring for 5 min, solvent was removed and the product was recovered as a light brown powder, yield 52 mg (88 %). Elemental analysis (%) calcd: C 33.97; H 5.70; found: C 33.93, H 5.68; ^{1}H NMR (300 MHz, C_6D_6, 25 °C): $\delta = 0.55$ (s, 18 H, $Si(CH_3)_3$), 2.71 (d, $^2J(H,P) = 2.4$ Hz, 3 H, PCH_3), 3.03 (d, $^2J(H,P) = 20.9$ Hz, 3 H, PCH_3), 7.50 ppm (d, $^4J(H,P) = 6.1$ Hz, 1 H, H4); ^{13}C NMR (75.5 MHz, C_6D_6, 25 °C): $\delta = 0.97$ (d, $^3J(C,P) = 3.7$ Hz, $Si(CH_3)_3$), 10.91 (d, $^1J(C,P) = 53.6$ Hz, PCH_3), 26.92 (d, $^1J(C,P) = 17.1$ Hz, PCH_3), 134.72 (d, $^3J(C,P) = 53.2$ Hz, C4), 136.46 (d, $^2J(C,P) = 30.2$ Hz, C2), 158.94 ppm (d, $^2J(C,P) = 15.4$ Hz, C3); ^{31}P NMR (121.5 MHz, THF, 25 °C, 85 % H_3PO_4 as external standard): $\delta = 156.86$ ppm (s).

10: MeLi in diethyl ether (70 μL; 0.111 mmol, 1.6 M) was added to a crude solution of **8** (0.111 mmol) in THF at −78 °C. The solution was stirred for 10 min, then allowed to warm to room temperature, solvent was removed in vacuo, and the product extracted in hexane (2 × 2 mL) and recovered as a pale yellow powder, yield 41 mg (88 %). Selected data: elemental analysis (%) calcd for: C 71.04, H 8.35; found: C 71.07, H 8.36; ^{1}H (300 MHz, C_6D_6, 25 °C): $\delta = -0.06$ (s, 18 H, $Si(CH_3)_3$), 1.29 (d, $^2J(H,P) = 12.1$ Hz, 6 H, PCH_3), 5.57 (d, $^4J(H,P) =$ 1.5 Hz, 1 H, H4), 7.02–7.35 ppm (m, 10 H, Ph); ^{31}P (121.5 MHz, C_6D_6, 25 °C 85 % H_3PO_4 as external standard): $\delta = 10.5$ ppm (s).

11: An equimolar amount of dried 4-octyne (17 μL, 0.111 mmol) was added to a crude solution of **8** (0.111 mmol) in CH_2Cl_2. The resulting mixture was stirred at room temperature in the glove box for 24 h. After removing of the solvent in vacuo, the product was recovered as a beige powder, yield 71 mg (86 %). Selected data: elemental analysis (%) calcd for: C 53.32, H 6.51; found: C 53.28, H 6.51; ^{1}H NMR (300 MHz, CD_2Cl_2, 25 °C): $\delta = 0.04$ (s, 18 H, $Si(CH_3)_3$), 0.78 (t, $^3J(H,H) = 7.3$ Hz, 3 H, CH_3 of propyl), 0.92 (t, $^3J(H,H) =$ 7.3 Hz, 3 H, CH_3 of propyl), 1.12–1.23 (m, 2 H, CH_2 of propyl), 1.41–1.50 (m, 2 H, CH_2 of propyl), 2.34–2.39 (m, 2 H, CH_2 of propyl), 2.45–2.58 (m, 2 H, CH_2 of propyl), 2.70 (d, $^2J(H,P) = 13.9$ Hz, 3 H, PCH_3), 5.52 (d, $^4J(H,P) = 6.0$ Hz, 1 H, H4) 6.93–7.00 (m, 5 H, Ph), 7.32–7.48 ppm (m, 5 H, Ph); ^{31}P (121.5 MHz, CD_2Cl_2, 25 °C 85 % H_3PO_4 as external standard): $\delta = 4.36$ ppm (s).

Received: June 26, 2003 [Z52230]

Keywords: aromaticity · density functional calculations · Diels–Alder reactions · phosphininium compounds · phosphorus

[1] K. B. Dillon, F. Mathey, J. F. Nixon, *Phosphorus: The Carbon Copy*, Wiley, Chischester, **1998**.

[2] G. Frison, A. Sevin, N. Avarvari, F. Mathey, P. Le Floch, *J. Org. Chem.* **1999**, *64*, 5524 – 5529; P. Le Floch in *Phosphorus—Carbon Heterocyclic Chemistry: The Rise of a New Domain* (Ed.: F. Mathey), Pergamon, Oxford, **2001**, pp. 485 – 533.

[3] H. Oehling, A. Schweig, *Phosphorus Relat. Group V Elem.* **1971**, *1*, 203 – 205; R. V. Hodges, J. L. Beauchamp, A. J. Ashe, W. T. Chan, *Organometallics* **1985**, *4*, 457 – 461.

[4] A. J. Ashe, *Acc. Chem. Res.* **1978**, *11*, 153 – 157.

[5] C. C. Price, T. Parasaran, T. V. Lakshminarayan, *J. Am. Chem. Soc.* **1966**, *88*, 1034 – 1037; G. Märkl, A. Merz, *Tetrahedron Lett.* **1969**, 1231 – 1234; G. Märkl, A. Merz, H. Rausch, *Tetrahedron Lett.* **1971**, 2989 – 2992.

[6] T. N. Dave, H. Kaletsch, K. Dimroth, *Angew. Chem* **1984**, *96*, 984 – 985; *Angew. Chem. Int. Ed. Engl.* **1984**, *23*, 989 – 990.

[7] N. Avarvari, P. Le Floch, L. Ricard, F. Mathey, *Organometallics* **1997**, *16*, 4089 – 4098; N. Avarvari, P. Le Floch, F. Mathey, *J. Am. Chem. Soc.* **1996**, *118*, 11978 – 11979.

[8] L. Cataldo, S. Choua, T. Berclaz, M. Geoffroy, N. Mezailles, L. Ricard, F. Mathey, P. Le Floch, *J. Am. Chem. Soc.* **2001**, *123*, 6654 – 6661.

[9] A. Moores, L. Ricard, P. Le Floch, N. Mézailles, *Organometallics* **2003**, *22*, 1960 – 1966.

[10] Crystal data for **8**; $C_{32}H_{48}Cl_4GaO_2PSi_2$; $M_r = 763.37$; 0.20 × 0.20 × 0.20 mm; orthorhombic; space group $Cmc2_1$; $a = 15.9430(10)$, $b = 12.8210(10)$, $c = 18.7420(10)$ Å; $V = 3831.0(4)$ Å^3; $Z = 4$; $_{calcd} = 1.324$ g cm^{-3}; $\theta_{max} = 30.02°$; $Mo_{K\alpha}$ radiation (0.71069 Å); φ and ω scans; $T = 150.0(1)$ K; 8344 measured, 4963 unique, 4612 used reflections, criterion $I > 2\sigma(I)$; Refinement: least-squares (full matrix) on F^2; $F(000) = 1592$, $\mu = 1.128$ cm^{-1}, KappaCCD diffractometer; $R_{int} = 0.0226$; Absorption corrections : multiple scans, 0.8058 min, 0.8058 max; 235 parameters refined; $R_1 =$ 0.0271; $wR2 = 0.0751$, GoF = 1.084; Flack's parameter 0.001(7); difference peak/hole: 0.426(0.047)/−0.358(0.047) e Å^{-3}. CCDC-212930 (**8**) contains the supplementary crystallographic data for this paper. These data can be obtained free of charge via www.ccdc.cam.ac.uk/conts/retrieving.html (or from the Cambridge Crystallographic Data Centre, 12 Union Road, Cambridge CB2 1EZ, UK; fax: (+44) 1223-336-033; or deposit@ccdc.cam.ac.uk).

[11] A silacalix-[4]-phosphinines was taken as a reference compound: N. Avarvari, N. Mezailles, L. Ricard, P. Le Floch, F. Mathey, *Science* **1998**, *280*, 1587 – 1589.

[12] This value is intermediate between P–C single bond and P–C double bond in methylene phosphenium: H. Grützmacher, H. Pritzkow, *Angew. Chem.* **1992**, *104*, 92 – 94; *Angew. Chem. Int. Ed. Engl.* **1992**, *31*, 99 – 101; A. Igau, A. Baceiredo, H. Grutzmacher, H. Pritzkow, G. Bertrand, *J. Am. Chem. Soc.* **1989**, *111*, 6853 – 6854.

[13] D. J. Berger, P. P. Gaspar, J. F. Liebman, *Theochem J. Mol. Struct.* **1995**, *338*, 51 – 70; A. J. Ashe, M. K. Bahl, K. D. Bomben, W. T. Chan, J. K. Gimzewski, P. G. Sitton, T. D. Thomas, *J. Am. Chem. Soc.* **1979**, *101*, 1764 – 1767.

[14] A. D. Becke, *Phys. Rev. A* **1988**, *38*, 3098 – 3108; Gaussian 98 (Revision A.11), M. J. Frisch, G. W. Trucks, H. B. Schlegel, G. E. Scuseria, M. A. Robb, J. R. Cheeseman, V. G. Zakrzewski, J. A. Montgomery, R. E. Stratmann, J. C. Burant, S. Dapprich, J. M. Millam, A. D. Daniels, K. N. Kudin, M. C. Strain, O. Farkas, J. Tomasi, V. Barone, M. Cossi, R. Cammi, B. Mennucci, C. Pomelli, C. Adamo, S. Clifford, J. Ochterski, G. A. Petersson, P. Y. Ayala, Q. Cui, K. Morokuma, D. K. Malick, A. D. Rabuck, K. Raghavachari, J. B. Foresman, J. Cioslowski, J. V. Ortiz, B. B. Stefanov, G. Liu, A. Liashenko, P. Piskorz, I. Komaromi, R. Gomperts, R. L. Martin, D. J. Fox, T. Keith, M. A. Al-Laham, C. Y. Peng, A. Nanayakkara, C. Gonzalez, M. Challacombe, P. M. W. Gill, B. G. Johnson, W. Chen, M. W. Wong, J. L. Andres, M. Head-Gordon, E. S. Replogle, J. A. Pople, Gaussian, Inc., Pittsburgh, PA, **1998**; J. P. Perdew, *Phys. Rev. B* **1986**, *33*, 8822 – 8832.

 © 2003 Wiley-VCH Verlag GmbH & Co. KGaA, Weinheim

[15] This trend has already been observed for compound **Ia** at the HF/4.31G level: L. L. Lohr, H. B. Schlegel, K. Morokuma, *J. Phys. Chem.* **1984**, *88*, 1981 – 1987.
[16] A. E. Reed, L. A. Curtiss, F. Weinhold, *Chem. Rev.* **1988**, *88*, 899 – 926.
[17] ASE equations, which consider the different isomers of dihydro and tetrahydrophosphinine compounds, compensate for ring strain: L. Nyulaszi, *Chem. Rev.* **2001**, *101*, 1229 – 1246; P. von R. Schleyer, P. K. Freeman, H. J. Jiao, B. Goldfuss, *Angew. Chem.* **1995**, *107*, 332 – 335; *Angew. Chem. Int. Ed. Engl.* **1995**, *34*, 337 – 340.
[18] P. von R. Schleyer, C. Maerker, A. Dransfeld, H. J. Jiao, N. J. Hommes, *J. Am. Chem. Soc.* **1996**, *118*, 6317 – 6318.

 © 2003 Wiley-VCH Verlag GmbH & Co. KGaA, Weinheim

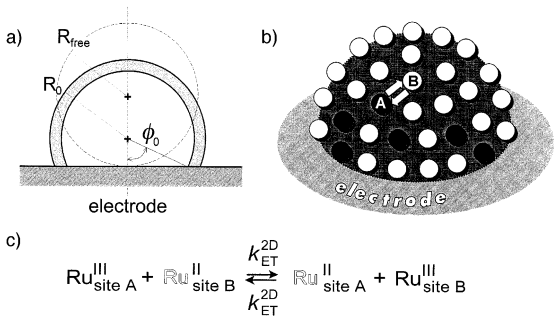


Figure 1. a) Schematized redox continuum showing the cross-section of an average PAMAM dendrimer molecule adsorbed onto a platinum ultra-microelectrode surface. The shaded area represents the thin shell ($d = 1.4$ nm) into which the 64 ruthenium redox centers are dispersed and where electron hopping diffusion takes place. The white zone located inside features the dendrimer covalent tethers. The circle shown in dashed line represents the size of the free dendrimer molecule in solution for comparison. b) Representation of the equivalent diffusion by electron hopping from a reduced (Ru^{II}, white, site B) towards an oxidized (Ru^{III}, black, site A) ruthenium bis-terpyridine moiety over the dendrimer hemispherical surface. c) Electron exchange reaction occurring between the Ru^{II} (white) and Ru^{III} (black) redox centers shown in (b).

Electrochemistry on a Few Molecules

Electrochemistry within a Limited Number of Molecules: Delineating the Fringe Between Stochastic and Statistical Behavior**

Christian Amatore, Frédéric Grün, and Emmanuel Maisonhaute*

Single molecule experiments attract an increasing interest in physical chemistry.[1,2] Indeed, the expectation of replacement of silicon by single molecules has stimulated investigations of molecular components.[3,4] In this context, electrochemistry provides an exceptional tool for monitoring electron transfer responses of a limited number of molecules.[2]

In this context, by using ultrafast voltammetry, we could recently analyze the dynamics of electron hopping inside an electroactive fourth-generation PAMAM dendrimer capped with 64 ruthenium(II) bis-terpyridine redox moieties.[5,6] In that case, each dendrimer could be oxidized progressively by the propagation of the electrochemical perturbation over the 64 redox centers distributed on its surface (Figure 1). However, about 10^6 molecules were adsorbed onto the ultramicroelectrode of micrometric radius, so that the analysis involved the averaging of about 64×10^6 individual events occurring in parallel. In a seminal experiment, Bard and coworkers reported the measurement of the electrochemical current provided by a single molecule trapped between two electrodes.[1] Even so, in this spectacular experiment a different kind of averaging was involved. Indeed, considering the time scale (about 1 s) of the method, this single molecule was involved in an electrochemical recycling during which it was continuously oxidized and reduced about 10^6 times so that the current resulted from the temporal averaging of a large series of fast sequential individual events. Both experiments involved temporal or spatial averaging of a large number of events so that in each case classical electrochemical formulations based on Fick's laws of diffusion could be used to analyze the experimental data. As electrodes of nanometer dimensions are presently available,[7–9] and considering that the electrochemical detection limits are continuously decreasing, one may expect soon the detection of electrochemical signals provided by a single molecule or a few ones. For example, in the "chronoamperograms" presented below (see Figure 2 and Figure 3), half of the charge (i.e. 32 electrons for each dendrimer), is passed within 25 ns, which would correspond to an average current of about 200 pA per dendrimer molecule. However, in the stochastic mode, and without any instrumental constraint the exchange of each electron should correspond to a much larger instant current, that is, $e/\Delta\tau_{et}$, where e is the charge of an electron and $\Delta\tau_{et}$ the life-time of the event. In the best electrochemical practice, the shortest sampling times, $\Delta\tau_{sampl}$, are in the range of a few nanoseconds[5,6] and are therefore expected to exceed most values of $\Delta\tau_{et}$. It follows that the largest instant currents in the stochastic mode are expected to be in the range of $e/\Delta\tau_{sampl}$, namely about 100 pA.

Under such conditions, the stochastic nature of each electrochemical event should be observable, thus leading to important deviations from the usual collective electrochemical laws (namely, statistical ones). Experimental investigation of such stochastic information is clearly warranted since it contains precious information about how molecules explore their phase domains, either concerning its transport or its reactivity.

[*] Prof. Dr. C. Amatore, F. Grün, Dr. E. Maisonhaute
Ecole Normale Supérieure
Département de Chimie
UMR CNRS-ENS-UPMC 8640 "PASTEUR"
24 rue Lhomond, 75231 Paris Cedex 05 (France)
Fax: (+33) 1-4432-3863
E-mail: christian.amatore@ens.fr

[**] This work has been supported in parts by the CNRS (UMR 8640), the French Ministry of Research and by Ecole Normale Supérieure.

 © 2003 Wiley-VCH Verlag GmbH & Co. KGaA, Weinheim DOI: 10.1002/anie.200352353

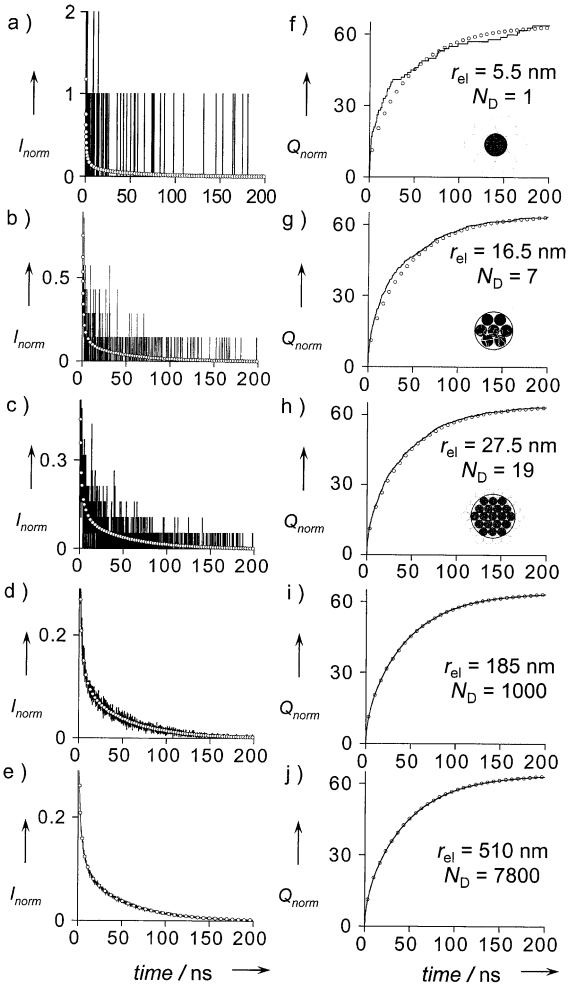


Figure 2. (a–e) Vertical thin lines: predicted variations of the normalized stochastic current (I_{norm}) versus time as a function of the number of dendrimers molecules adsorbed onto the electrode surface without considering any instrumental distortions. In each panel, $I_{norm} = I/N_D$ represents the current, I, normalized by the number of dendrimers, N_D. Vertical units are chosen so that one electron transferred during the time window interval of the simulation gives a current $I_{norm} = 1$ for $N_D = 1$, so that I_{norm} reflects the sequential electron count for the average "single" molecule during one 0.1 ns time window. These variations are superimposed onto the statistical electrochemical normalized current predicted for an infinite number of adsorbed dendrimers (open circles; same curve in each panel a–e). (f–j) Same as (a–e) but the electrochemical Faradaic charge ($Q_{norm} = ne/N_D$) normalized per dendrimer is considered, in which ne is the actual number of electrons transferred from the beginning of the experiment. $N_D = 1$ (a,f), 7 (b,g), 19 (c,h), 1000 (d,i), 7800 (e,j); see picture and/or legend in (f–j).

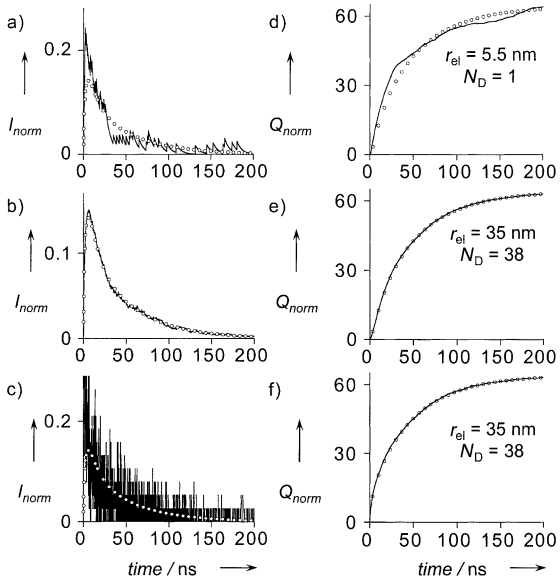


Figure 3. Effect of instrumental distortions. Solid lines: current (a–b) or charge (d–e) versus time variations considering an ultrafast potentiostat with a 6 ns time constant.[5,6,13,14] $N_D = 1$ (a,d), or 38 (b,e), see legend in (d–f). In (c, f) are shown the current and charge variations versus time in the absence of any instrumental distortion for $N_D = 38$ to emphasize the effect of instrumental filtering by comparison to (b, e) respectively. On each panel is superimposed the predicted result for an infinite population of dendrimers when the same instrumental distortion applies (open circles). Vertical current axis (namely, I_{norm} and Q_{norm}) in (a–c) are defined as in Figure 2.

Herein, we wish therefore to address theoretically this fundamental question through estimating the maximal number of events to be sampled so that stochastic electrochemical signatures may be detected within a determined experimental accuracy. We wish to develop this work in consideration of the specific example of our previous study on PAMAM redox dendrimers,[5,6] as this system is virtually commutable from completely statistical to totally stochastic, simply by decreasing the size of the electrode on which the array of dendrimers is adsorbed. Indeed, this controls directly the number of molecules addressable electrochemically.[7] To simplify the presentation we assume a perfect hexagonal pavement of the electrode though the true 2D-array is slightly distorted.[10] In solution, the dendrimer has a spheroidal shape with a diameter of approximately 10 nm, its 64 [$Ru^{II/III}$-(terpy)$_2$] (terpy = terpyridine) redox sites being distributed over its surface.[10] Upon adsorption, the dendrimer resembles a near hemisphere of radius R_0 and half angle $\phi_0 = 1.2$ rd, as described in Figure 1.[5,6] In each dendrimer molecule, all the 64 redox sites are covalently fixed to the dendrimer core by their dendritic polyamidoamide branches, so that they cannot diffuse "physically" to and from the electrode surface. Electrochemical contact between the dendrimer and the electrode may therefore only occur through the few redox sites distributed along the ring of the dendrimer shell in close contact with the electrode (see Figure 1 b). Propagation of the electrochemical perturbation over the dendrimer surface occurs then by "electron hopping"[11,12] between adjacent Ru^{II}/Ru^{III} redox centers (Figure 1 b,c). Thus, the status of the center (namely, Ru^{II} versus Ru^{III}) is propagated over the dendrimer shell by electron transfer between adjacent ruthenium centers without displacement of the centers themselves.[5,6]

Each center has several possibilities to cross-talk with its neighbors of appropriate redox state, so that the system is equivalent to the random-walk displacement of a fake particle representing the site status (Figure 1 b,c). Based on the Nernst-Schmoluchovski relationship between diffusion and random walk, this phenomenon is equivalent to diffusion over

 © 2003 Wiley-VCH Verlag GmbH & Co. KGaA, Weinheim

the dendrimer shell.[6] Within one dendrimer molecule, these events are necessarily stochastic and are finite as there are only 64 centers and the phenomenon stops when all centers have their redox state commuted (namely, from Ru^{II} to Ru^{III} during an oxidative polarization, or from Ru^{III} to Ru^{II} during a reductive one). However, when an infinite array of dendrimer is adsorbed onto the electrode,[5,6,10] the series of events occurring within each dendrimer take place in parallel, so that a continuous statistical formulation becomes valid (Figure 1 a).[5,6] Conversely, upon decreasing the size of the electrode, the number of adsorbed dendrimers decreases and one may be able to evidence the basic stochastic nature of the phenomenon. Electrodes with radii of several tens of nanometers are now available,[7–9] so that the fundamental problem considered here is not far from being addressable experimentally.

To stress the effect related to the number of adsorbed dendrimers, we consider chronoamperometry, the simplest electrochemical technique. At $t = 0$, the electrode potential is poised at a value high enough to ensure a sufficient driving force so that at the electrode–dendrimer junction the commutation time can be considered as being instantaneous compared to the time required for propagation over the whole dendrimer shell, namely, several tens of ns. In agreement with the physical reality of the propagation phenomenon, we used a random-walk algorithm to account for the discrete nature of charge displacement, and we treated the processes occurring within each dendrimer through an individual simulation. Any selected number of simulations may be gathered together afterwards to account for the exact number of dendrimers supposedly adsorbed onto an electrode surface of any specific surface area.

We wished first to focus on the physicochemical significance of the measured current as a function of number of adsorbed dendrimers. We therefore assumed that the electrochemical equipment is perfect, that is, that there is no distortion of the signal. For only one adsorbed dendrimer, the electrochemical current shows a random and discontinuous succession of single electron-transfer events (Figure 2 a). Obviously each simulation produces a different pattern, however, Figure 2 a is representative of the most frequent ones. For a larger electrode, namely, where seven dendrimers can be adsorbed (Figure 2 b, which corresponds to an electrode of about 16.5 nm in radius), one still observes an important stochastic "noise" in the current though the classical shape of a chronoamperogram becomes already recognizable, with an increased probability of three or two simultaneous (namely, occurring within the same 0.1 ns sampling time window) events at initial times. This trend is pursued as the number of molecules increases (Figure 2 c–e), the current function approaches more and more closely the statistical one. For example, for an array of 7800 dendrimers (namely, an electrode of about 500 nm in radius) the stochastic nature of the phenomenon is no more clearly discernable. It amounts only to the introduction of a $\pm 10\,\%$ noise added onto the would-be classical electrochemical current, though observation of this later would require an infinite population.[5,6] (compare Figure 2 e). When one observes the electrochemical charge instead of the current (Figure 2 f–j) the stochastic noise is reflected by a series of staircase steps (e.g., Figure 2 f) whose fine structure rapidly vanishes when the number of adsorbed dendrimers approaches 20 (see Figure 2 h). This reflects the smoothing of the stochastic noise that arises from the integration. Nevertheless, the stochastic nature of the phenomenon is still reflected by a systematic misfit versus the statistical charge variation predicted for an infinite number of dendrimers, though this misfit is almost impossible to observe as soon as about 20 molecules are examined in parallel (Figure 2 h).

To be observed experimentally, the above results would require a perfect electrochemical instrumentation so that the apparatus did not introduce any filtering of its own. However, even with the fastest potentiostat available today,[13,14] a minimal time constant of about 6 ns is imposed by the electrochemical instrumentation.[14] This constant is obviously negligible with respect to the overall duration of the whole phenomenon (namely, a few 100 ns, see Figure 2, and Figure 3) but introduces a significant exponential tail[15] on each individual electron-transfer event as evidenced by the comparison between Figure 2 a and Figure 3 a. In this case, the stochastic noise becomes about $\pm 10\,\%$ of the statistical chronoamperogram for only 38 adsorbed dendrimers (Figure 3 b), although it is seen in Figure 3 c that for such a small number of molecules the real stochastic nature of the phenomenon would be definitely observable in absence of any instrumental distortions. Evidently, the same is true when the electrochemical charge is considered (Figure 3 d–f). Noteworthy, even for a single molecule the staircase nature of the charge variations is no more observable (Figure 3 d), though the stochastic reality of the phenomenon is still reflected by the deviation from the statistical curve. Therefore, experimentally, one may be led to believe that the electrochemical signal observed for a very minute quantity of molecules is very close to the average signal, though this would be an artifact reflecting only the characteristics of the apparatus and its distortions.

In conclusion, this particular example demonstrates that one should constantly bear in mind that a smooth current–time variations closely identical to that predicted by Fick's laws may not mean that the electrochemical signal for a few molecules is essentially similar to the usual statistical behavior, but may simply reflect instrumental distortions. Such considerations seem fundamental for subsequent analysis of experimental data relative to electrochemistry with limited number of molecules.

Experimental Section

In the random walk simulations, individual particle positions over the dendrimer shell (Figure 1) are referred by their spherical angular coordinates θ and ϕ. At each time iteration a direction is randomly chosen while Δl, the length of displacement, is maintained constant. The sampling frequency was fixed at $1/\Delta t = 10^{10}\ s^{-1}$, and the length of displacements of individual particles was chosen so that they agree altogether (namely, $\Delta l = 2(D\Delta t)^{1/2}$ with $D = 5 \times 10^{-6}\ cm^2 s^{-1}$) with the average equivalent diffusion coefficient value, D, which was measured experimentally for an array of about 10^6 adsorbed dendrimers.[5,6] D and k_{ET}^{2D}, the 2D-bimolecular rate constant of electron exchange (see its definition in Figure 1 c) are related by Equation (1):[5,6]

 © 2003 Wiley-VCH Verlag GmbH & Co. KGaA, Weinheim

$$D = \frac{2\,k_{ET}^{2D}}{3\pi d} \quad (1)$$

in which d is the diameter of a ruthenium redox center (1.4 nm). Validity of the random-walk procedure was checked by two methods. First it was verified that without electrochemical reaction (namely, upon tracking the particle walks but without modifying the Ru^{II} or Ru^{III} status along the particle walk), the average population on the truncated sphere remained homogeneous when particles were allowed to move for duration times exceeding by several times the maximal times considered here. Second, the chronoamperometric current resulting from the averaging of 10^6 individual simulations (taken here as an infinite population) was compared to the statistical one obtained by solving the continuous analytical Fick's laws by finite differences as described elsewhere for voltammetry[5,6] though a chronoamperometric condition was imposed at the electrode dendrimer interface (namely, at $\phi = \phi_0$ in Figure 1 a). A perfect match was obtained except for the very first few events close to $t = 0$ where either the random walk or the finite differences solutions are not accurate by construction. It has to be underlined that a great advantage of this random walk formulation is to allow almost any further refinement of the model, that is, by incorporating real dynamics of the redox centers within their potential wells over the dendrimer surface which affects the local probabilities of electron exchange.[5,6] This was however outside the scope of the present paper.

Received: July 10, 2003 [Z52353]

Keywords: dendrimers · electrochemistry · electron transfer · redox chemistry · single-molecule studies

[1] a) A. J. Bard, F. R. F. Fan, *Acc. Chem. Res.* **1996**, *29*, 572; b) F. R. F. Fan, J. Kwak, A. J. Bard, *J. Am. Chem. Soc.* **1996**, *118*, 9669.
[2] J. Park, A. N. Pasupathy, J. I. Goldsmith, C. Chang, Y. Yaish, J. R. Petta, M. Rinkoski, J. P. Sethna, H. D. Abruna, P. L. McEuen, D. C. Ralph, *Nature* **2002**, *417*, 722.
[3] A. Aviram, *J. Am. Chem. Soc.* **1988**, *110*, 5687.
[4] H. X. He, C. Z. Li, N. J. Tao, *Appl. Phys. Lett.* **2001**, *78*, 811.
[5] C. Amatore, Y. Bouret, E. Maisonhaute, J. I. Goldsmith, H. D. Abruna, *ChemPhysChem* **2001**, *2*, 130.
[6] C. Amatore, Y. Bouret, E. Maisonhaute, J. I. Goldsmith, H. D. Abruna, *Chem. Eur. J.* **2001**, *7*, 2206.
[7] J. J. Watkins, J. Chen, H. S. White, H. D. Abruna, E. Maisonhaute, C. Amatore, *Anal. Chem.* **2003**, *accepted*.
[8] C. E. Gardner, J. V. Macpherson, *Anal. Chem.* **2002**, *74*, 576A.
[9] B. Ballesteros Katemann, W. Schuhmann, *Electroanalysis* **2002**, *14*, 22.
[10] D. J. Diaz, G. D. Storrier, S. Bernhard, K. Takada, H. D. Abruna, *Langmuir* **1999**, *15*, 7351.
[11] H. J. Dams, *J. Phys. Chem.* **1968**, *72*, 362.
[12] I. Ruff, V. J. Friedrich, *J. Phys. Chem.* **1971**, *75*, 3297.
[13] C. Amatore, E. Maisonhaute, G. Simonneau, *Electrochem. Commun.* **2000**, *2*, 81.
[14] C. Amatore, E. Maisonhaute, G. Simonneau, *J. Electroanal. Chem.* **2000**, *486*, 141.
[15] C. Amatore, C. Lefrou, *J. Electroanal. Chem.* **1992**, *324*, 33.

 © 2003 Wiley-VCH Verlag GmbH & Co. KGaA, Weinheim

DNA Lesions

The Two Main DNA Lesions 8-Oxo-7,8-dihydroguanine and 2,6-Diamino-5-formamido-4-hydroxypyrimidine Exhibit Strongly Different Pairing Properties**

*Matthias Ober, Uwe Linne, Johannes Gierlich, and Thomas Carell**

Dedicated to Professor R. W. Hoffmann on the occasion of his 70th birthday

DNA damage generated by the reaction of DNA with reactive oxygen species is one of the major reasons for mutations and carcinogenesis.[1–4] Additionally, oxidative DNA damage is believed to play a major role in the pathogenesis of ageing.[5–9] Reactive oxygen species (ROS) are generated as side products during aerobic respiration, a process that involves the stepwise reduction of molecular oxygen to water. One of the most dangerous reaction products is the OH radical, which is a potent electrophilic oxidant able to oxidize DNA.[4] In DNA, the OH radical reacts preferentially with guanine. Guanine is also the major target for general oxidative damage because it has the lowest oxidation potential among the four bases.

In the last decade, a large number of guanine-derived genome lesions produced either by direct oxidation or reaction with OH radicals were isolated and characterized.[10,11] 8-Oxo-7,8-dihydroguanine (8-oxodGuo) and 2,6-diamino-5-formamido-4-hydroxypyrimidine (FapydGuo, Scheme 1) were found as two main degradation products.[12,13] They are currently believed to be predominantly responsible for the biological effect of oxidative and OH-radical-induced DNA damage.[14]

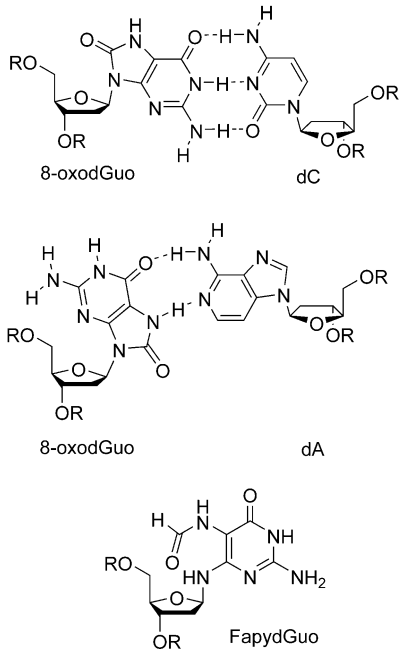
To study repair and the mutagenic effect of both lesions it is essential to prepare oligonucleotides that contain these lesions in defined positions. To this end, lesion phosphoramidites are needed, which allow their incorporation into DNA by using machine-assisted DNA synthesis.[15] The guanine derivative 8-oxodGuo is a stable compound, which early on allowed its chemical synthesis and incorporation into DNA.[16,17] Consequently, a wealth of chemical and biochemical data are now available on this important lesion.[18,19]

Investigation of the FapydGuo lesion, in contrast, is strongly hindered owing to its instability.[20,21] We recently reported the synthesis of the FapydGuo lesion in a protected form and discovered that the compound is relatively stable

[*] Prof. Dr. T. Carell, Dipl.-Chem. M. Ober, Dr. U. Linne, Dipl.-Chem. J. Gierlich
Department of Chemistry, Philipps-Universität Marburg
Hans-Meerwein Strasse, 35032 Marburg (Germany)
Fax: (+49) 6421-282-2189
E-mail: carell@staff.uni-marburg.de

[**] The work was generously supported by the Volkswagen Stiftung, the Fonds der Chemischen Industrie, and the Deutsche Forschungsgemeinschaft. We thank the Boehringer Ingelheim Fonds for a predoctoral fellowship to M.O.

 DOI: 10.1002/anie.200351287 © 2003 Wiley-VCH Verlag GmbH & Co. KGaA, Weinheim



Scheme 1. Depiction of the oxidative DNA lesion 8-oxodGuo base paired with dC and with dA, together with the oxidative DNA lesion FapydGuo.

under physiological conditions.[22] However, the compound was found to anomerize rapidly under conditions generally required for chemical DNA synthesis. Greenberg and coworkers published the synthesis of a dinucleotide building block, which allowed the incorporation of the FapydGuo lesion as an α/β-mixture into DNA.[23,24] Over the last two years, this achievement has allowed initial information to be gathered on how FapydGuo affects the stability of DNA duplexes and how it is replicated by polymerases.[25]

Herein we report the synthesis of a stabilized bioisosteric FapydGuo analogue,[26] which can be inserted in DNA as the pure "β" anomer. The mutagenic potential of all DNA lesions is strongly connected to their base-pairing properties, which can be estimated by using melting-temperature studies. Such melting-point data of the 8-oxodGuo lesion showed efficient base pairing with dC and dA.[27] A crystal structure for the 8-oxodGuo in DNA opposite dA clarified that the lesion pairs with dA if the N–glycoside bond adopts the unusual *syn* conformation as shown in Scheme 1.[28]

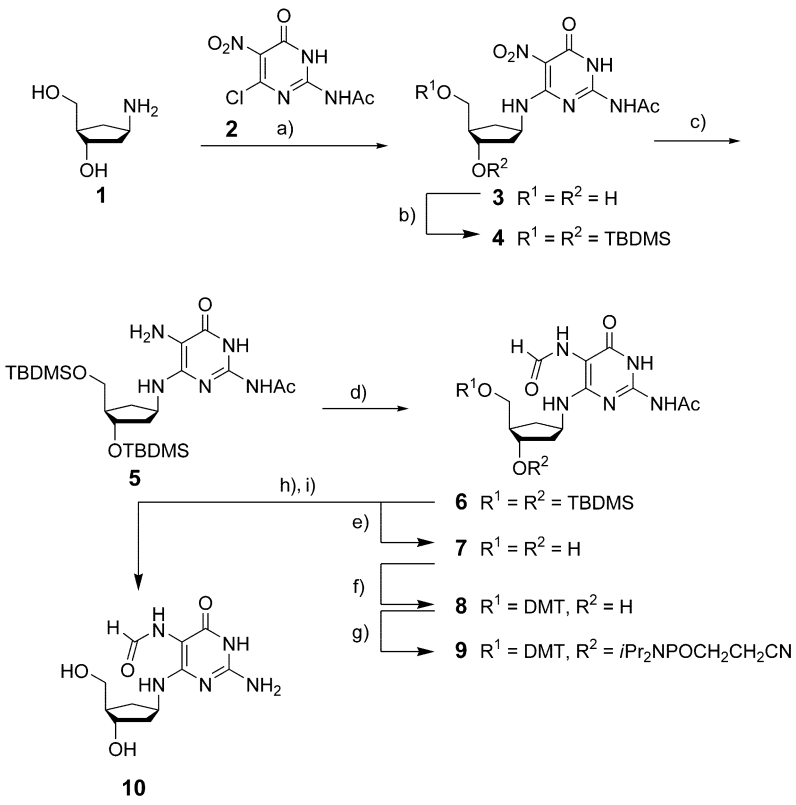
The structural similarity of 8-oxodGuo and FapydGuo, manifested in the C8=O carbonyl group present in both lesions, led to the suggestion that both lesions might have very similar base-pairing properties. This belief was recently supported by melting-point data obtained with α/β-FapydGuo-containing DNA.[24,27] In contrast, our experiments show that FapydGuo has a pairing behavior very different from that of 8-oxodGuo. This result suggests a completely different mutagenic effect of FapydGuo.

To circumvent the anomerization problem, we prepared a stabilized, strictly bioisosteric lesion analogue, which contains a cyclopentane skeleton instead of the 2′-deoxyribose sugar backbone.[29] Replacement of the 2′-deoxyribose oxygen atom by a methylene group leaves the heteroatom structure and therefore the base-pairing properties of the lesion fully intact. For the standard nucleotides, it was proven that the oxygen-to-methylene chemical mutation has a negligible effect on duplex stability and duplex structure.[29–31] To analyze possible effects of the O-to-CH_2 chemical mutation on the *syn*/*anti* conformational equilibrium, which is so critical for the mutagenic potential of the 8-oxodGuo, we performed molecular modeling and density functional calculations.[32] In both cases we obtained almost the same, very small differences between the *syn* and *anti* conformations of only about 5 to 32 kJ mol^{-1}, indicating that the heterocycle rotates in both compounds freely around the C1′–N glycoside bond. The *anti* conformation is energetically somewhat more favorable, in agreement with NOESY experiments performed with compound **6** in $CDCl_3$. The NOESY showed stronger cross-peaks between the C1′-N*H* and the *endo* protons at C2′, C3′, and C5′, thus indicating a larger population of the *anti* conformation. Most important, however, is the result that the O-to-CH_2 chemical mutation has, if at all, only a minor effect on the *syn*/*anti* conformational equilibrium.

For the synthesis of the *c*FapydGuo analogue (Scheme 2), we started with the enantiomerically pure cyclopentylamine **1**, which was prepared in six steps by following the synthetic route recently reported by Cullis and Dominguez.[33] Coupling of this building block with the acetyl-protected 2-amino-6-chloro-5-nitro-4-oxopyrimidine (**2**)[34–36] furnished the cyclopentane derivative **3**. Protection of the hydroxy groups with TBDMSCl yielded compound **4**. The following steps included reduction of the nitro group to the amine **5** and transformation of the amine into the formamide **6**.[22] Cleavage of the TBDMS groups was performed with HCl in ethyl acetate. Conversion of the carbocyclic analogue of the β-FapydGuo lesion **7** into the phosphoramidite **9** was possible by using standard procedures. The fully deprotected *c*FapydGuo lesion **10** was synthesized in two steps from **6**. Deacetylation of compound **6** was performed with a 0.05 M solution of K_2CO_3 in methanol. Desilylation required treatment of the product with HCl in THF. The building block **9** was finally incorporated into oligonucleotides using slightly modified standard DNA synthesis procedures, which will be described in due course. The coupling of the *c*FapydGuo unit was found to be above 98%. Cleavage of the fully assembled DNA from the solid support and of all protecting groups present at the various nucleotides was performed by using a saturated solution of ammonia in water/ethanol (3:1) at 15 °C. Intensive studies with the monomer **6** showed that at 15 °C, cleavage of the acetyl protecting group is highly selective. All DNA strands that contained *c*FapydGuo were finally purified by reversed-phase HPLC.

Analysis of the DNA was carried out by analytical HPLC and MALDI-TOF mass spectrometry. The obtained data proved that the *c*FapydGuo-containing oligonucleotides were prepared in excellent yields. The oligonucleotides had, after preparative HPLC purification, a final purity of >98%, necessary for detailed melting-point studies. Final proof that the *c*FapydGuo was correctly inserted into the DNA strand was obtained by an HPLC/MS/MS experiment. To this end, the *c*FapydGuo-containing DNA strand was fully digested in an enzyme mixture of phosphodiesterase II, nuclease P1,

 © 2003 Wiley-VCH Verlag GmbH & Co. KGaA, Weinheim



5'-d(GCGAT**X**TAGCG)-3' X = FaPydGuo, Y=T,C,A,G
3'-d(CGCTA**Y**ATCGC)-5' X = 8-oxodGuo, Y=T,C,A,G
X = G, Y=T,C,A,G

Scheme 2. Synthesis of the *c*FapydGuo lesion analogue phosphoramidite **9** and depiction of the DNA double strands prepared for melting-point studies. a) DIPEA, DMF, 70°C, 1.5 h, 72%; b) TBDMSCl, imidazole, DMF, 20°C, 3 h, 88%; c) Pd/C, H_2, EtOH, 20°C, 2.5 h; d) HCOOH, EDC, DIPEA, DMF, 20°C, 36 h, 70% for two steps; e) HCl/EtOAc (5%), 0→20°C, 1.5 h, 95%; f) DMTCl, lutidine, DMF, 0°C, 3 h, 49%; g) DIPEA, $iPr_2NPOCH_2CH_2CN^+Cl^-$, THF, 0°C, 30 min, 86%; h) K_2CO_3 (0.05 M)/MeOH, 20°C, 2 h, 90%; i) HCl/THF (5%), 0→20°C, 1.5 h, 95%. DIPEA = diisopropylethylamine, DMF = *N*,*N*-dimethylformamide, TBDMS = *tert*-butyldimethylsilyl, EDC = 1-ethyl-3-(3-dimethylaminopropyl)carbodiimide hydrochloride, DMT = 4,4′-dimethoxytrityl.

phosphodiesterase I, and alkaline phosphatase.[37] The HPLC chromatogram obtained after the digestion showed five peaks, of which four could be assigned to the four nucleobases A, T, G, and C by mass spectrometry. The fifth, small and broad peak, which almost co-eluted with cytosine, was assigned to the *c*FapydGuo. The peak showed the same retention time as the co-injected compound **10**. The molecular weight corresponding to the new peak was found to be identical to that of compound **10**, and finally also the fragmentation patterns of **10** and of the new HPLC peak were identical. Thus, the reported DNA synthesis procedure and the availability of the building block **9** in large amounts allowed the preparation of stable *c*FapydGuo-containing oligonucleotides in quantities sufficient for detailed physicochemical and structural investigations.

To analyze the melting behavior and hence the pairing properties of β-*c*FapydGuo, we prepared the DNA double strands depicted in Scheme 2. The DNA duplexes contain either the canonical base dG, the *c*FapydGuo lesion analogue **7**, or the 8-oxodGuo lesion and all four canonical bases as counterbases. All 12 double strands gave CD spectra, which are typical for B-helical DNA.[38] The differences in the CD spectra were found to be very small, thus confirming that the compounds FapydGuo and 8-oxodGuo have only a very small effect on the overall duplex structure.

The melting temperatures measured for all DNA double strands are summarized in Table 1. As expected, the guanine-containing strand shows the highest melting temperature in the matching dG:dC situation. All mismatches strongly destabilize the duplex by at least 14°C. The two lesions 8-oxodGuo and *c*FapydGuo destabilize the double strands, regardless of the counterbase. However, in agreement with previous reports, 8-oxodGuo pairs relatively well with both dC and dA.[27] Both base pairs provide double strands with melting points that are only 6°C lower than that of the undisturbed dG:dC duplex. The 8-oxodGuo lesion is therefore able to form the expected ^{anti}8-oxodGuo:dC and ^{syn}8-oxodGuo:dA base pairs, also in the oligonucleotide duplexes analyzed in this study. Our data therefore support the base-pairing schemes shown in Scheme 1.

In contrast to currently accepted theory, we find that the melting behavior of the *c*FapydGuo is drastically different to that of 8-oxodGuo. First, the destabilization of the duplexes in the presence of this lesion is much more pronounced. This is surprisingly also the case if dC functions as the counterbase. For the *c*FapydGuo:dC base pair, the melting temperature measured was similar to that associated with a mismatch! The data show that *c*FapydGuo double strands have the highest melting point with the counterbase dT.[39] In fact, the *c*FapydGuo:dT base pair seems to be as stable as the 8-oxodGuo:dC and 8-oxodGuo:dA base pairs.

In addition, all the double strands in which *c*FapydGuo faces one of the two purine bases feature an unusual double sigmoidal melting behavior. The curves obtained for the double strands *c*FapydGuo:dA and *c*FapydGuo:dG (red

Table 1: List of the melting temperatures measured for the twelve DNA duplexes shown in Scheme 1.[a]
5′-d(GCGAT**X**TAGCG)-3′
3′-d(CGCTA**Y**ATCGC)-5′

	T_m [°C]		
	X = dG	X = 8-oxodGuo	X = *c*FapydGuo
Y = dA	33.9	46.0	16.1 (54.9)
Y = dC	51.8	45.6	36.9
Y = dG	37.9	31.4	16.1 (54.9)
Y = dT	35.8	36.7	45.0

[a] Conditions: Tris /HCl, pH 7.4 (0.01 M), NaCl (0.15 M), DNA (3 μM).

 © 2003 Wiley-VCH Verlag GmbH & Co. KGaA, Weinheim

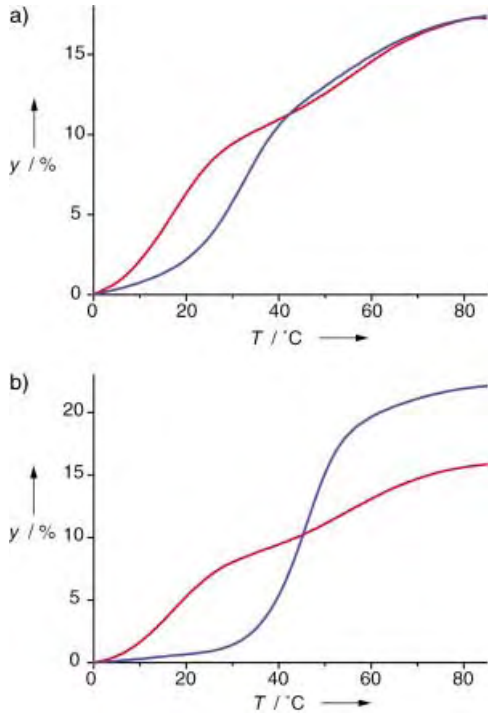


Figure 1. Melting curves of a) the two oligonucleotide double strands containing a *c*FapydGuo:dG (red) and an 8-oxodGuo:dG (blue) base pair and b) of the oligonucleotide double strands containing a *c*FapydGuo:dA (red) and an 8-oxodGuo:dA (blue) base pair.

curves), together with the corresponding melting curves of 8-oxodGuo:dG and 8-oxodGuo:dA (blue curves) are depicted in Figure 1. For *c*FapydGuo:dG and *c*FapydGuo:dA a first very low melting point is observed at about 16 °C, which is not observed in the experiments performed with the 8-oxodGuo lesion. A second, much weaker transition is observed at higher temperatures. This second transition cannot be explained currently. One explanation could be that the strongly destabilizing *c*FapydGuo:purine pairs induce local melting of the duplex around the lesion site at 16 °C. Full melting of the duplex would then explain the second higher transition temperature. Alternatively, this second transition could arise from the melting of an intramolecular hairpinlike structure. Whatever the reason for the second melting curve may be, it is clear that the *c*FapydGuo:purine-containing duplexes show a first very low melting temperature indicative of a strongly destabilized duplex structure. Most interesting are, however, the dramatically different melting curves obtained for the *c*FapydGuo:dA and 8-oxodGuo:dA duplexes as depicted in Figure 1b. These curves clearly show that in contrast to 8-oxodGuo, pairing of FapydGuo with dA gives rise to strongly destabilized duplexes. We therefore conclude that FapydGuo is unable to form proper base pairs with dC and dA, which pair so well with 8-oxodGuo. In contrast, the lesion FapydGuo seems to recognize dT.[39]

In summary, the main oxidative DNA lesions 8-oxodGuo and FapydGuo, predominantly responsible for the mutagenic and cell toxic effect of oxidative DNA damage, have dramatically different pairing properties, which suggests that their mutagenic properties vary as well.

Received: February 27, 2003
Revised: May 21, 2003 [Z51287]

Keywords: DNA damage · DNA · electron transfer · nucleotides · oxidative lesions

[1] a) T. Lindahl, *Nature* **1993**, *362*, 709; b) for a recent Review on DNA damage and repair, see: O. D. Schärer, *Angew. Chem.* **2003**, *115*, 3052; *Angew. Chem. Int. Ed.* **2003**, *42*, 2946.
[2] E. C. Friedberg, G. C. Walker, W. Siede, *DNA Repair and Mutagenesis*, ASM Press, Washington, DC, **1995**.
[3] C. Richter, J.-W. Park, B. N. Ames, *Proc. Natl. Acad. Sci. USA* **1988**, *85*, 6465.
[4] A. P. Breen, J. A. Murphy, *Free Radical Biol. Med.* **1995**, *18*, 1033.
[5] M. L. Hamilton, Z. M. Guo, C. D. Fuller, H. Van Remmen, W. F. Ward, S. N. Austad, D. A. Troyer, I. Thompson, A. Richardson, *Nucleic Acids Res.* **2001**, *29*, 2117.
[6] R. S. Sohal, R. Weindruch, *Science* **1996**, *273*, 59.
[7] D. Harman, *J. Gerontol.* **1957**, *2*, 298.
[8] P. Hasty, J. Campisi, J. Hoeijmakers, H. van Steeg, J. Vijk, *Science* **2003**, *299*, 1355.
[9] S. Hekimi, L. Guarente, *Science* **2003**, *299*, 1351.
[10] C. J. Burrows, J. G. Muller, *Chem. Rev.* **1998**, *98*, 1109.
[11] J. Cadet, M. Berger, T. Douki, B. Morin, S. Raoul, J.-L. Ravanat, S. Spinelli, *Biol. Chem.* **1997**, *378*, 1275.
[12] J. Cadet, T. Delatour, T. Douki, D. Gasparutto, J.-P. Pouget, J.-L. Ravanat, S. Sauvaigo, *Mutat. Res.* **1999**, *424*, 9.
[13] T. Douki, S. Spinelli, J. L. Ravanat, J. Cadet, *J. Chem. Soc. Perkin Trans. 2* **1999**, 1875.
[14] T. Finkel, N. J. Holbrook, *Nature* **2000**, *408*, 239.
[15] J. Butenandt, L. T. Burgdorf, T. Carell, *Synthesis* **1999**, 1085.
[16] V. Bodepudi, S. Shibutani, F. Johnson, *Chem. Res. Toxicol.* **1992**, *5*, 608.
[17] V. Bodepudi, C. R. Iden, F. Johnson, *Nucleosides Nucleotides* **1991**, *10*, 755.
[18] J. C. Fromme, G. L. Verdine, *Nat. Struct. Biol.* **2002**, *9*, 544
[19] S. D. Bruner, D. P. G. Norman, G. L. Verdine, *Nature* **2000**, *403*, 859.
[20] M. Berger, J. Cadet, *Z. Naturforsch. B* **1985**, *40*, 1519.
[21] B. Tudek, *J. Biochem. Mol. Biol.* **2003**, *36*, 12.
[22] L. T. Burgdorf, T. Carell, *Chem. Eur. J.* **2002**, *8*, 293.
[23] K. Haraguchi, M. M. Greenberg, *J. Am. Chem. Soc.* **2001**, *123*, 8636.
[24] K. Haraguchi, M. O. Delaney, C. J. Wiederholt, A. Sambandam, Z. Hantosi, M. M. Greenberg, *J. Am. Chem. Soc.* **2002**, *124*, 3263.
[25] C. J. Wiederholt, M. M. Greenberg, *J. Am. Chem. Soc.* **2002**, *124*, 7278.
[26] M. O. Delaney, M. M. Greenberg, *Chem. Res. Toxicol.* **2002**, *15*, 1460.
[27] G. E. Plum, F. Johnson, A. P. Grollman, K. Breslauer, *Biochemistry* **1995**, *34*, 16148.
[28] M. Kouchakdjian, V. Bodepudi, S. Shibutani, M. Eisenberg, F. Johnson, A. P. Grollman, D. J. Patel, *Biochemistry* **1991**, *30*, 1403.
[29] M. Ferrero, V. Gotor, *Chem. Rev.* **2000**, *100*, 4319.
[30] F. Johnson, G. Dorman, R. A. Rieger, R. Marumoto, C. R. Iden, R. Bonala, *Chem. Res. Toxicol.* **1998**, *11*, 193.
[31] S. Smirnov, F. Johnson, R. Marumoto, C. de los Santos, *J. Biomol. Struct. Dyn.* **2000**, *17*, 981.
[32] The energies were calculated with Gaussian 98 (Revision A.7), M. J. Frisch, G. W. Trucks, H. B. Schlegel, G. E. Scuseria, M. A. Robb, J. R. Cheeseman, V. G. Zakrzewski, J. A. Montgomery,

 © 2003 Wiley-VCH Verlag GmbH & Co. KGaA, Weinheim

R. E. Stratmann, J. C. Burant, S. Dapprich, J. M. Millam, A. D. Daniels, K. N. Kudin, M. C. Strain, O. Farkas, J. Tomasi, V. Barone, M. Cossi, R. Cammi, B. Mennucci, C. Pomelli, C. Adamo, S. Clifford, J. Ochterski, G. A. Petersson, P. Y. Ayala, Q. Cui, K. Morokuma, D. K. Malick, A. D. Rabuck, K. Raghavachari, J. B. Foresman, J. Cioslowski, J. V. Ortiz, B. B. Stefanov, G. Liu, A. Liashenko, P. Piskorz, I. Komaromi, R. Gomperts, R. L. Martin, D. J. Fox, T. Keith, M. A. Al-Laham, C. Y. Peng, A. Nanayakkara, C. Gonzalez, M. Challacombe, P. M. W. Gill, B. G. Johnson, W. Chen, M. W. Wong, J. L. Andres, M. Head-Gordon, E. S. Replogle, J. A. Pople, Gaussian, Inc., Pittsburgh, PA, **1998** at the B3LYP/6-31G* level of theory. The starting geometries were obtained through torsional screening around C1′–NH using Tripos SYBYL8.6 with the MMFF94 force field.

[33] B. M. Dominguez, P. M. Cullis, *Tetrahedron Lett.* **1999**, *40*, 5783.

[34] H. S. Forrest, R. Hull, H. J. Rodda, A. R. Todd, *J. Chem. Soc.* **1951**, 3.

[35] W. Pfleiderer, H. Walter, *Justus Liebigs Ann. Chem.* **1964**, *677*, 113.

[36] J. C. Temple, B. H. Smith, J. A. Montgomery, *J. Org. Chem.* **1975**, *40*, 3141.

[37] T. Douki, J. Cadet, *Photochem. Photobiol. Sci.* **2003**, *2*, 433.

[38] W. C. Johnson, Jr, *Determination of the Conformation of Nucleic Acids by Electronic CD*, Plenum, New York, **1996**.

[39] P. Cysewski, R. Oliński, *Z. Naturforsch. C* **1999**, *54*, 239.

 © 2003 Wiley-VCH Verlag GmbH & Co. KGaA, Weinheim

Ruthenium Pterin Radical Complex

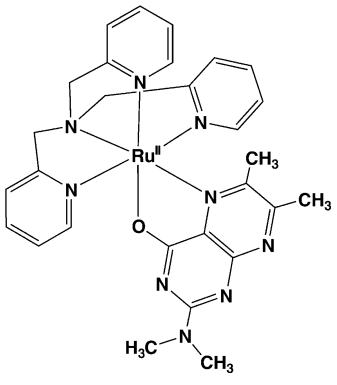
A Ruthenium Pterin Complex Showing Proton-Coupled Electron Transfer: Synthesis and Characterization**

Takahiko Kojima, Taisuke Sakamoto, Yoshihisa Matsuda, Kei Ohkubo, and Shunichi Fukuzumi*

Pterins are responsible for many aspects of biological events,[1] many of which are also related to diseases.[2] Such biological significance leads many researchers to pursue the properties and reactivity of pterin derivatives not only in vivo but also in vitro.[3] Pterins, as versatile redox-active heteroaromatics, are coenzymes which participate in a wide variety of enzyme-catalyzed oxidation and/or reduction processes.[4] In these processes, pterins undergo proton-coupled electron transfer (PCET) involving four electrons and four protons. The enzymes involved often contain metal-ion cofactors, such as the molybdenum-pterin cofactors (molybdopterin cofactors; Mo-co) of all the oxo-molybdenum enzymes,[5] non-heme iron[6] and copper cofactors[7] of the phenylalanine hydroxylases and heme-containing nitric oxide synthases.[8] Along this line, many pterin-metal complexes have been reported to model Mo-co,[9] tungstopterins,[10,11] and copper-containing pterin-dependent enzymes.[12] The coordination chemistry of ruthenium pterin complexes has also been investigated.[13–15] However, the PCET process of metal pterin complexes has yet to be clarified. The lack of the crystal structures together with low stability in redox processes of metal complexes with pterin ligands has precluded elucidation of the PCET mechanism of metal pterin complexes.

We report herein the synthesis and characterization of novel ruthenium(II) complexes containing a bidentate, deprotonated pterin derivative and tripodal, tetradentate pyridylamine ligands, as well unprecedented PCET behavior to give a coordinated monohydropterin radical. The successful detection by ESR of the monohydropterin radical coordinated to the ruthenium(II) center provides valuable information about the PCET process.

$[Ru(dmdmp)(TPA)]ClO_4$ (**1**)[16] (Hdmdmp = 3-(*N*,*N*-dimethyl)-6,7-dimethylpterin, TPA = tris(2-pyridylmethyl)-amine) and $[Ru(dmdmp)(5\text{-}Me_3\text{-}TPA)]ClO_4$ (**2**) were prepared by the reaction of Hdmdmp with bis-μ-chloro dimeric $[\{RuCl(TPA)\}_2](ClO_4)_2$[17] and $[\{RuCl(5\text{-}Me_3\text{-}TPA)\}_2](ClO_4)_2$ by refluxing in methanol in the presence of NEt_3 under N_2, respectively. Recrystallization from methanol gave crystals suitable for X-ray crystallography (Figure 1).[18]. This is the first crystallographically characterized ruthenium pterin complex. The geometry around the ruthenium center is distorted octahedral with 164.4(3)° for N1-Ru1-N3 which is the meridional coordination of the TPA unit. The pterin ligand binds to the Ru^{II} center as a monoanion in a common fashion through the O1-N5 atoms. There is severe steric hindrance



1

[*] Dr. T. Kojima, T. Sakamoto, Prof. (Emeritus) Y. Matsuda
Department of Chemistry, Graduate School of Sciences
Kyushu University
Hakozaki, Higashi-Ku, Fukuoka 812-8581 (Japan)
Fax: (+81) 92-642-2570
E-mail: cosyscc@mbox.nc.kyushu-u.ac.jp
Dr. K. Ohkubo, Prof. S. Fukuzumi
Department of Material and Life Science
Faculty of Engineering and
CREST, JST, Osaka University, Suita, Osaka 565-0871 (Japan)

[**] We are grateful to Dr. Mikio Yasutake (Kyushu University) for his expertise in X-ray crystallography, Dr. Yasuhiro Funahashi (Nagoya Institute of Technology) for his help in preparing Hdmdmp, Prof. Kazuya Uezu (The University of Kita-Kyushu) for his help on DFT calculations, and Prof. Kazuhiro Takahashi (Kyushu University) for his help in electrolysis. We also thank financial support by a Grant-in-Aid (No. 11740373 to T.K.) from the Ministry of Education, Science, Sports, and Culture of Japan.

Supporting information for this article is available on the WWW under http://www.angewandte.org or from the author.

 DOI: 10.1002/anie.200352111 © 2003 Wiley-VCH Verlag GmbH & Co. KGaA, Weinheim

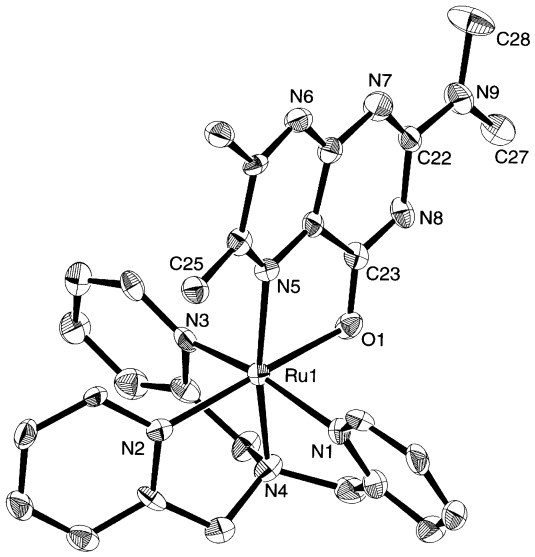
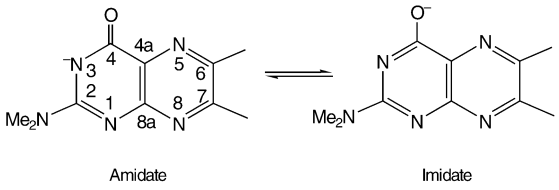


Figure 1. An ORTEP drawing of the cation of **1**. Selected bond lengths [Å] and angles [°]: Ru1-O1 2.083(5), Ru1-N1 2.082(7), Ru1-N2 2.086(6), Ru1-N3 2.050(8), Ru1-N4 2.041(7), Ru1-N5 2.107(6), O1-C23 1.272(10), N8-C23 1.322(10), N9-C22 1.369(9); O1-Ru1-N5 80.3(2), N1-Ru1-N4 81.2(3), N2-Ru1-N4 80.8(3), N3-Ru1-N4 83.4(3), N2-Ru1-N5 109.8(2), N1-Ru1-N3 164.4(3), O1-Ru1-N2 166.1(3), N4-Ru1-N5 169.4(2).

between one methyl group (C25) of pterin ligand ($dmdmp^-$) at the 6-position and the pyridine group including N2 (Figure 1), as indicated by the large N2-Ru-N5 angle of 109.8(2). This hindrance pushes away the pyrazine moiety of the $dmdmp^-$ ligand which results in the long Ru1-N5 bond and tilts the N5-containing ring out of the pterin plane towards the equatorial pyridine moiety including N3 (dihedral angle of 39.4(3)° between the pyrazine plane and the axial N5-pyridine-ring plane). Concerning the deprotonated amide moiety of the $dmdmp^-$ ligand two possible tautomers can be considered (Scheme 1). For **1**, the structure should be



Scheme 1. Possible tautomers of coordinated $dmdmp^-$ ligand with general numbering scheme for pterins.

described as an imidate rather than an amidate, based on the bond lengths of 1.272(10) Å for O1–C23 and 1.322(10) Å for N8–C23. In addition, the imidate nitrogen atoms forms hydrogen bonds with a water molecule of crystallization (N8···O8, 2.927(9) Å; not shown). The imidate coordination has been observed in $[M(NDMP^-)_2(MeOH)_2]$ (M = Fe, Co, Ni; HNDMP = 2-dimethylamino-4(3*H*)-pteridinone)[13] and [Cu(tppb)(pterin)] (tbbp = tris(3-phenylpyrazolyl)hydroborate).[19] In contrast, Yamauchi and co-workers have reported that Hdmdmp coordinates to a Cu^{II} center in $[Cu(NO_3)_2(Hdmdmp)_2]$[20] as a neutral ligand and Burgmayer et al. have also demonstrated that the amide is not deprotonated upon coordination in their Mo^{VI} pterin complexes.[9] This difference probably stems from the interactions of pterins with metal d orbitals and the Lewis acidity of the Ru–TPA unit, in which three pyridine moieties act as π acceptors to increase the acidity on the metal center which facilitates the deprotonation of Hdmdmp, and which results in the imidate binding.

The cyclic voltammogram (CV) of **1** was measured in CH_3CN. A free Hdmdmp exhibits irreversible redox waves at $E_{pc} = 0.59$ V and $E_{pa} = 0.34$ V ($\Delta E = 0.25$ V) relative to ferrocene/ferrocenium (Fc/Fc^+) redox couple in DMF. In sharp contrast, complex **1** exhibits three reversible redox waves for one-electron redox processes at −2.07 V ($\Delta E = 100$ mV) and 0.27 V ($\Delta E = 60$ mV), and at 0.51 V ($\Delta E = 50$ mV), the last of these is scan-rate dependent (see Supporting Information S1). The scan-rate dependency of the second oxidation process suggests that reorganization of the geometrical and electronic structures takes place and that the reorganization process is slow on the CV time scale at the scan rate of 500 mV s^{-1}. We assigned this latter redox wave to the coordinated $dmdmp^-$/$dmdmp^{\bullet}$ redox couple. Clarke and co-workers have reported a reversible one-electron redox process for Ru^{II}-coordinated neutral 3,6,7-Me_3-pterin at −0.85 V (vs. Fc/Fc^+) in an acidic DMF solution, however, the assignment of this redox process has yet to be made.[15a] In our case, coordinated pterin ligands without methylation at the 3-N position exhibit reversible redox behavior (see Supporting Information S1).

The redox behavior of **1** was investigated by UV/Vis spectroscopy. Upon oxidation at 0.41 V (vs. Fc/Fc^+; CH_3CN), the absorption spectrum of **1** shows loss of intensity for both the ligand-to-metal charge transfer (LMCT) band (459 nm) and the metal-to-ligand charge transfer (MLCT) band (407 nm), and the π–π* transition of pyridine rings of the TPA ligand at 249 nm is also weakened and red-shifted to 259 nm, accompanied by appearance of a new absorption band at 335 nm (Figure 2). This spectral change exhibits three isosbestic points at 243 (not shown), 362, and 540 nm,

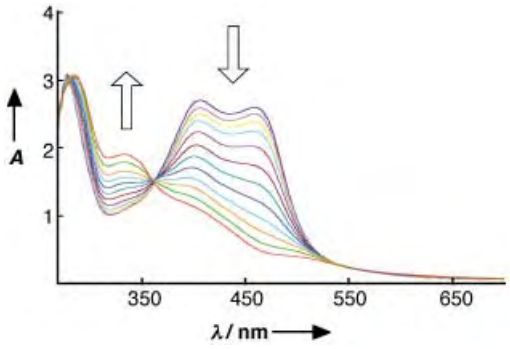


Figure 2. Spectral change in the course of electrolysis of **1** in CH_3CN containing 0.1 M Bu_4NClO_4 at an applied potential of 0.41 V at room temperature. Spectra taken at 1 hour intervals.

 © 2003 Wiley-VCH Verlag GmbH & Co. KGaA, Weinheim

suggesting that one-to-one electrochemical conversion takes place in this redox process.

The ESR spectrum of the one-electron oxidation product exhibits a typical $S = 1/2$ spectrum with a large spin-orbit coupling affording anisotropic g factors of 2.465, 2.304, and 1.730 (see Supporting Information S2). Thus, the first oxidation occurs at the Ru center to produce $[Ru^{III}(dmdmp)(TPA)]^{2+}$. The ESR spectra showed no temperature dependence between 173–223 K. This result indicates that no valence-tautomerization takes place for $[Ru^{III}(dmdmp)(TPA)]^{2+}$. The second oxidation process was thus assigned to the coordinated $dmdmp^-/dmdmp^\bullet$ redox couple.

Protonation–deprotonation behavior is indicated by the UV/Vis spectra of **1** and **2** (see below). In a neutral CH_3CN solution, the UV/Vis spectra of **1** has an LMCT band at 459 nm arising from a transition from the imidate oxygen atom to the Ru^{II} center and an MLCT band at 407 nm from transfer from the Ru^{II} center to the pyrazine moiety, (Figure 3; trace a). Upon addition of $HClO_4$ (60% aq), the

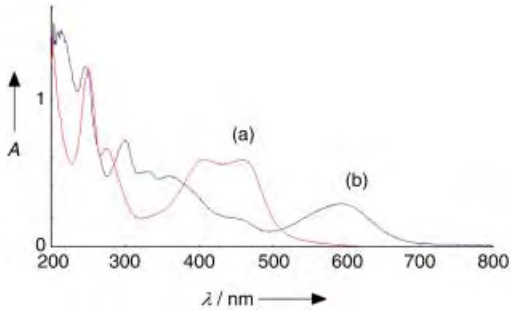


Figure 3. UV/Vis spectra of **1** in CH_3CN in the absence (a) and presence (b) of $HClO_4$ (10 equiv).

orange **1** turns to blue with a new absorption at 595 nm, which is assigned to a MLCT band arising from a transition from the Ru^{II} center to a protonated pterin ligand, and a new absorption in the range of 330–430 nm resulting from a π–π* transition of coordinated H_2dmdmp^+ (Figure 3; trace b).[15a]

We determined the pK_a values of the two-step protonation of **1** in an aqueous solution as $pK_{a1} = 5.21$ and $pK_{a2} = 0.45$ by spectrophotometric titration. The original spectrum was recovered by adding NEt_3, which indicates that this protonation–deprotonation is reversible even though the positively charged pterin cation is bound to the Ru^{II} center as a ligand. This reversibility is due to the strong π backbonding to the pterin cation from the Ru^{II} center as demonstrated by the intense MLCT band for the protonated complex.

Upon protonation, the reversible one-electron reduction of the pterin ligand in **1** exhibits a large positive shift from −2.07 V ($dmdmp^-/dmdmp^{2-\bullet}$) to −0.58 V ($H_2dmdmp^{+}/H_2dmdmp^\bullet$) upon protonation (see Supporting Information S1). The reversible one-electron oxidation (Ru^{II}/Ru^{III}) potential is also positively shifted from 0.51 to 0.65 V (see Supporting Information). Similarly, the redox events arising from the Ru^{II}/Ru^{III} and $H_2dmdmp^+/H_2dmdmp^\bullet$ couples of **2** are observed at 0.62 and −0.60 V, respectively. These results clearly indicate that the redox property of the pterin ligand is drastically altered by the presence of proton.

ESR spectroscopy was applied to detect the one-electron reduced species and we succeeded in detecting an eight-line signal at $g = 2.0008$ (Figure 4a).[21] We assigned this signal to a

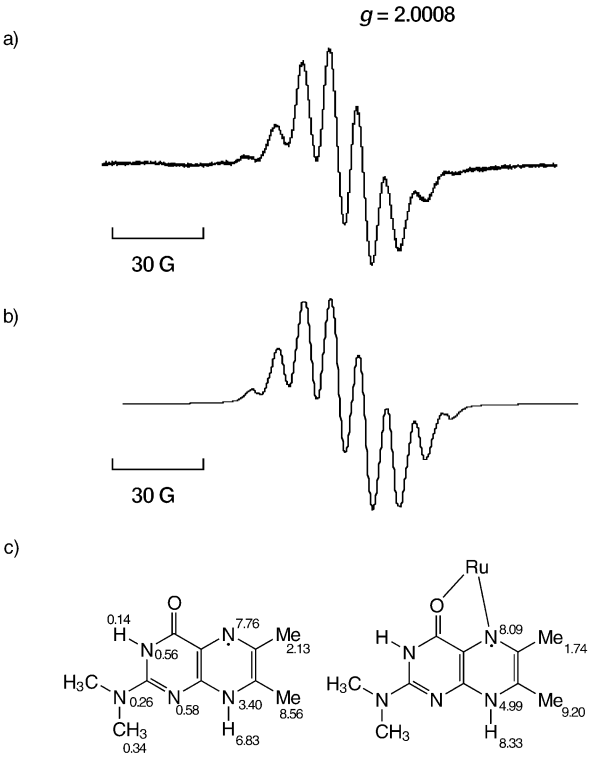


Figure 4. a) ESR spectrum of one-electron reduced species of $[Ru(H_2dmdmp)(TPA)]^{3+}$ (1.0×10^{-3} M) generated by electrolysis at −0.9 V (vs $Ag/AgNO_3$) in CH_3CN containing 0.1 M Bu_4NClO_4 in the presence of $HClO_4$ (5.0×10^{-3} M) at 253 K. b) The computer simulated spectrum. c) The calculated hfc values (in gauss) of the free-ligand radical obtained by DFT calculation and the observed hfc values determined from the observed ESR spectrum by the computer simulation ΔH_{msl}(maximum slope linewidth = 1.8 G.

ruthenium(II)-coordinated monohydropterin radical, which is an intermediate in the PCET reactions of pterins. The g value is smaller than the free spin value (2.0023), which indicates the presence of spin-orbit coupling between the unpaired electron and the Ru^{II} center. This result lends credence to the proposed coordination of the radical to the Ru center. The computer simulation for the spectrum based on DFT calculations (UB3LYP6-31G*) of the ligand-radical moiety gave fairly good agreements (Figure 4b), which allowing us to determine the hyperfine coupling constants (hfc; Figure 4c). The hfc values indicate that the unpaired electron is delocalized on the PCET region (N5, C6, C7, and N8 in Scheme 1) of the pyrazine moiety of the pterin. Kaim and coworkers have reported a one-electron reduced species of $[Ru(DMA)(bpy)_2](PF_6)_2$ in THF (DMA = 1,3-dimethylalloxazine; bpy = 2,2′-bipyridine).[22] In their system, ruthenium-coordinated $DMA^{\bullet-}$ has been reported to show an ESR signal

 © 2003 Wiley-VCH Verlag GmbH & Co. KGaA, Weinheim

with superhyperfine coupling owing to the Ru center at $g = 1.9990$, this value is smaller than the g value in Figure 4a.[22] The g value closer to the free-spin value and no observation of superhyperfine coupling owing to the Ru^{II} center in the present case indicates the interaction of the neutral radical H_2dmdmp$^{\bullet}$ with the Ru^{II} center is smaller than the case of the negatively charged DMA$^{\bullet-}$ ligand.

In conclusion, we have prepared a novel ruthenium(II) pterin complexes and determined the first crystal structure of a ruthenium pterin complex. The complex has unique redox and protonation–deprotonation behavior which is reflected by spectroscopic and electrochemical measurements. We have also investigated the redox characteristics of these complexes and succeeded in detecting the coordinated monohydropterin radical.

Experimental Section

Preparation of Complex **1**: $[\{RuCl(TPA)\}_2](ClO_4)_2$ (81 mg, 0.077 mmol) and Hdmdmp (34 mg, 0.16 mmol) were suspended in methanol under N_2 and triethylamine (43 μL, 0.31 mmol) was added. The mixture was heated under reflux for 6 h under N_2 and then cooled to room temperature. Red crystalline materials precipitated and were collected, washed with diethyl ether, and then dried in vacuo (yield: 51%). Elemental analysis of **1** (%) calcd for $C_{28}H_{30}N_9O_5Cl$-$Ru{\cdot}1.5\,H_2O$: C 45.68, H 4.52, N 17.12; found: C 45.88, H 4.45, N 17.11. Complex **2** was also synthesized by the same procedure except using $[\{RuCl(5\text{-}Me_3\text{-}TPA)\}_2](ClO_4)_2$ instead of $[\{RuCl(TPA)\}_2]$-$(ClO_4)_2$. Elemental analysis of **2** (%) calcd for $C_{31}H_{36}N_9O_5ClRu{\cdot}H_2O$: C 48.40, H 4.98, N 16.39; found: C 48.57, H 5.40, N 16.27.

Received: June 10, 2003 [Z52111]

Keywords: cofactors · N ligands · protonation · redox chemistry · ruthenium

[1] C. G. B. Hamon, J. A. Blair in *Rodd's Chemistry of Carbon Compounds, Vol. 4*, 2nd ed. (Ed.: M. F. Ansell), Elsevier, New York, **1988**, pp. 129–154.

[2] a) A. R. Berro, B. Nare, D. Freedman, L. Hardy, S. M. Beverley *Proc. Natl. Acad. Sci. USA* **1994**, *91*, 11442–11446; b) H. A. Denz, K. Grünewald, J. Thaler, H. Huber, *Pteridines* **1989**, *1*, 167–170; c) K. Ito, S. Kawakami, *Biochemistry* **1997**, *36*, 1774–1781.

[3] a) A. M. Bobst, *Nature* **1968**, *220*, 164–165; b) J. A. Blair, A. J. Pearson, *J. Chem. Soc. Perkin Trans. 2* **1974**, 80–88; c) G. Eberlein, T. C. Bruice, R. A. Lazarus, R. Henrie, S. J. Benkovic, *J. Am. Chem. Soc.* **1984**, *106*, 7916–7924; d) D. M. A. M. Luykx, J. A. Duine, S. de Vries, *Biochemistry* **1998**, *37*, 11366–11375; e) J. Vásquez-Vivar, J. Whitsett, P. Martásek, N. Hogg, B. Kalyanaraman, *Free Radical Biol. Med.* **2001**, *31*, 975–985.

[4] a) M. J. Romão, M. Archer, I. Moura, J. J. G. Moura, J. LeGall, R. Engh, M. Schneider, P. Hof, R. Huber, *Science* **1995**, *270*, 1170–1176; b) H. Schindelin, C. Kisker, J. Hilton, K. V. Rajagopalan, D. C. Rees, *Science* **1996**, *272*, 1615–1621; c) S. V. Khangulov, V. N. Gladyshev, G. C. Dismukes, T. C. Stadtman, *Biochemistry* **1998**, *37*, 3518–3528; d) M. J. Almendra, C. D. Brondino, O. Gavel, A. S. Pereira, P. Tavares, S. Bursakov, R. Duarte, J. Caldeira, J. J. G. Moura, I. Moura, *Biochemistry* **1999**, *38*, 16366–16372.

[5] R. Hille, *Chem. Rev.* **1996**, *96*, 2757–2816.

[6] T. J. Kappock, J. P. Caradonna, *Chem. Rev.* **1996**, *96*, 2659–2756.

[7] T. A. Dix, S. J. Benkovic, *Acc. Chem. Res.* **1988**, *21*, 101–107.

[8] a) B. R. Crane, A. S. Arvai, S. Ghosh, E. D. Getzoff, D. J. Stuehr, J. A. Tainer, *Biochemistry* **2000**, *39*, 4608–4621; b) H. Li, C. S. Raman, C. B. Glaser, E. Blasko, T. A. Young, J. F. Perkinson, M. Whitlow, T. L. Poulos, *J. Biol. Chem.* **1999**, *274*, 21276–21284.

[9] a) S. J. N. Burgmayer, M. R. Arkin, L. Bostick, S. Dempster, K. M. Everett, H. L. Layton, K. E. Paul, C. Rogge, A. L. Rheingold, *J. Am. Chem. Soc.* **1995**, *117*, 5812–5823; b) B. Fischer, H. Schmalle, E. Dubler, A. Schäfer, M. Viscontini, *Inorg. Chem.* **1995**, *34*, 5726–5734; c) H. L. Kaufmann, L. Liable-Sands, A. L. Rheingold, S. J. N. Burgmayer, *Inorg. Chem.* **1999**, *38*, 2592–2599; d) H. L. Kaufmann, P. J. Carroll, S. J. N. Burgmayer, *Inorg. Chem.* **1999**, *38*, 2600–2609; e) S. J. N. Burgmayer, H. L. Kaufmann, G. Fortunato, P. Hug, B. Fisher, *Inorg. Chem.* **1999**, *38*, 2607–2613.

[10] R. U. Meckenstock, R. Krieger, S. Ensign, P. M. H. Kroneck, B. Schink, *Eur. J. Biochem.* **1999**, *264*, 176–182.

[11] F. M. Hornung, W. Kaim, *J. Chem. Soc. Faraday Trans.* **1994**, *90*, 2909–2912.

[12] a) T. Kohzuma, H. Masuda, O. Yamauchi, *J. Am. Chem. Soc.* **1989**, *111*, 3431–3433; b) J. Perkinson, S. Brodie, K. Mosny, P. J. Carroll, T. V. Morgan, S. J. N. Burgmayer, *Inorg. Chem.* **1991**, *30*, 719–727; c) A. Odani, H. Masuda, K. Inukai, O. Yamauchi, *J. Am. Chem. Soc.* **1992**, *114*, 6294–6300; d) Y. Funahashi, T. Kohzuma, A. Odani, O. Yamauchi, *Chem. Lett.* **1994**, 385–388.

[13] Y. Funahashi, Y. Hara, H. Masuda, O. Yamauchi, *Inorg. Chem.* **1997**, *36*, 3869–3875.

[14] W. Kaim, B. Schwederski, O. Heilmann, F. M. Hornung, *Coord. Chem. Rev.* **1999**, *182*, 323–342.

[15] a) A. Abelleira, R. D. Galang, M. J. Clarke, *Inorg. Chem.* **1990**, *29*, 633–639; b) C. Bessenbacher, C. Vogler, W. Kaim, *Inorg. Chem.* **1989**, *28*, 4645–4648.

[16] UV/Vis (in CH_3CN), λ_{max} [nm] (ε ($M^{-1}cm^{-1}$)): 460 (1.40×10^4), 408 (1.46×10^4); ^1H NMR (270 mHz, CD_3CN): $\delta = 2.72$ (s, 7-CH_3, 3H), 3.02 (s, -$N(CH_3)_2$, 6H), 3.14 (s, 6-CH_3, 3H), 4.51 (s, -CH_2-, 2H), 4.94 and 5.17 (ABq, $J_{AB} = 16$ Hz, -CH_2-, 2H), 6.94 (td, $J = 7$ and 2 Hz, py-H5(ax), 1H), 7.06 (t, $J = 6$ Hz, py-H5 (eq), 2H), 7.14 (d, $J = 7$ Hz, py-H3(ax), 1H), 7.31 (d, $J = 8$ Hz, py-H3(eq), 2H), 7.41 (td, $J = 8$ and 1 Hz, py-H4(ax), 1H), 7.62 (td, $J = 8$ and 2 Hz, py-H4(eq), 2H), 8.08 (dd, $J = 5$ and 2 Hz, py-H6(eq), 2H), 8.88 ppm (d, $J = 5$ Hz, py-H6(ax), 1H).

[17] a) T. Kojima, T. Amano, Y. Ishii, M. Ohba, Y. Okaue, Y. Matsuda, *Inorg. Chem.* **1998**, *37*, 4076–4085; b) T. Kojima, H. Matsuo, Y. Matsuda, *Inorg. Chim. Acta* **2000**, *300–302*, 661–667.

[18] A single crystal of **1** was obtained from recrystallization from its methanolic solution. X-ray data for **1**: monoclinic, $P2_1/c$ (No. 14), $a = 17.768(4)$, $b = 11.202(3)$, $c = 17.723(5)$ Å, $\beta = 115.531(8)°$, $V = 3182$ (1) Å^3, $T = -180$ °C, $Z = 4$, $R(Rw) = 0.085$ (0.143) ($I > 3\sigma(I)$), GOF = 1.47. CCDC-215178 contains the supplementary crystallographic data for this paper. These data can be obtained free of charge via www.ccdc.cam.ac.uk/conts/retrieving.html (or from the Cambridge Crystallographic Data Centre, 12 Union Road, Cambridge CB2 1EZ, UK; fax: (+44) 1223-336-033; or deposit@ccdc.cam.ac.uk).

[19] J. Perkinson, S. Brodie, K. Yoon, K. Mosny, P. J. Carroll, T. V. Morgan, S. J. N. Burgmayer, *Inorg. Chem.* **1991**, *30*, 719–727.

[20] O. Yamauchi, A. Odani, H. Masuda, Y. Funahashi, In *Bioinorganic Chemistry of Copper* (Eds.: K. D. Karlin, Z. Tyeklár), Chapman & Hall, New York, **1993**, p. 363.

[21] Trials for deuteration of the radical have been unsuccessful and no change has been observed for the spectrum even in CD_3CN in the presence of $DClO_4$.

[22] F. M. Hornung, O. Heilmann, W. Kaim, S. Zalis, J. Fiedler, *Inorg. Chem.* **2000**, *39*, 4052–4058.

 © 2003 Wiley-VCH Verlag GmbH & Co. KGaA, Weinheim

Asymmetric Michael Addition

Organocatalytic Asymmetric Michael Reaction of Cyclic 1,3-Dicarbonyl Compounds and α,β-Unsaturated Ketones—A Highly Atom-Economic Catalytic One-Step Formation of Optically Active Warfarin Anticoagulant**

*Nis Halland, Tore Hansen, and Karl Anker Jørgensen**

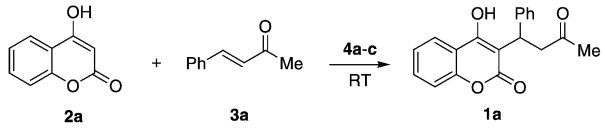
As optically active drugs become increasingly important for the treatment of diseases in patients, still more enantiopure drugs are introduced to the market either as new drugs or as the result of a racemic switch. An important goal for asymmetric catalysis is to develop new reactions that afford optically active compounds from simple and easily available starting materials and catalysts. However, the ultimate goal would be if the new reaction could be used directly for a one-step synthesis of optically active molecules that have important biological and pharmaceutical activities. Herein we present such an advance and its direct application in an atom-economic synthesis of optically active drugs based on the development of a new organocatalytic enantioselective Michael addition of cyclic 1,3-dicarbonyl compounds to α,β-unsaturated ketones.[1]

The present development leads to a catalytic enantioselective one-step procedure for the formation of one of the most widely used anticoagulants, warfarin (coumadin), and related important compounds. Warfarin has been prescribed as a racemate for more than 40 years and it is well-known that the anticoagulant activity of the *S* enantiomer is about 5–8 times higher than of the *R* enantiomer.[2] Furthermore, the enantiomers are metabolized by different pathways, which is reflected by the different half-lives in the human body, 21–43 and 37–89 h, for (*S*)- and (*R*)-warfarin, respectively.[2] Due to these very different half-lives, one of the major problems with racemic warfarin is the delivery and maintenance of a stable dose as too high doses might lead to internal hemorrhages in the patient. The dosage problem is further complicated by the fact that the peak pharmacological effect of a single dose is not achieved until after approximately 48 h, and the pharmacological effect lasts 4–5 days. As patients respond differently, it is expected that treatment of patients with optically pure warfarin will reduce the dosage problem. Another advantage of optically pure warfarin would be that weakened patients unable to tolerate the stronger racemic or (*S*)-warfarin could be treated with the milder (*R*)-warfarin.[3] However, probably the most important advantage of administering optically pure warfarin is the possibility of eliminating drug–drug interactions, which represents another serious problem with racemic warfarin, as enzymes that are responsible for metabolizing warfarin also metabolize many other drugs.[2]

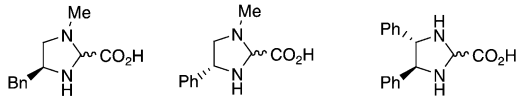
Three different approaches towards the synthesis of optically active warfarin have been reported: Demir et al. used a diastereoselective Michael addition in which chiral enamines of 4-hydroxycoumarin were treated with benzylideneacetone in the presence of LDA and superstoichiometric amounts of Lewis acid to obtain warfarin in moderate yield and enantiomeric excess.[4] Li and co-workers at DuPont Merck Pharmaceutical Company obtained enantioenriched warfarin from racemic warfarin through an oxidation procedure and subsequent asymmetric hydrogenation.[5] The diastereoselective synthesis by Cravotto et al. involved a tandem Knoevenagel/hetero-Diels–Alder approach; however, yields were low owing to the somewhat lengthy synthesis.[6]

Herein we present, besides the development of a new organocatalytic enantioselective reaction, a simple, effective and highly atom-economical synthesis of optically active warfarin (**1a**) from 4-hydroxycoumarin (**2a**) and benzylideneacetone (**3a**) in the presence of imidazolidine catalysts (Table 1).[7] Furthermore, the scope and potential of this new one-step, organocatalytic enantioselective Michael addition is demonstrated by the formation of a number of important

Table 1: Screening of catalysts for the organocatalytic asymmetric formation of **1a**.[a]



2a **3a** **1a**



4a **4b** (*S*,*S*)-**4c**

Entry	Catalyst	[mol%]	Solvent	*t* [h]	Yield [%][b]	*ee* [%][c]
1	(*S*)-proline	50	DMSO	15	85	0
2	**4a**	10	CH_2Cl_2	70	77	62 (*S*)
3	**4a**	5	THF	70	85	70 (*S*)
4	**4a**	10	EtOH	70	69	47 (*S*)
5	**4a**	10	H_2O	90	22	49 (*S*)
6	**4b**	10	THF	130	83	56 (*R*)
7	(*R*,*R*)-**4c**	10	CH_2Cl_2	150	96	82 (*R*)[d]
8	(*S*,*S*)-**4c**	10	THF	130	90	80 (*S*)[d]

[a] Experimental conditions: A mixture of **3a** (0.5 mmol), **2a** (0.525 mol, 1.05 equiv), and the catalyst was stirred at ambient temperature for the time indicated. The crude mixture was then purified by flash chromatography. [b] Yield of product isolated after flash chromatography. [c] Enantiomeric excess determined by CSP-HPLC. The absolute configuration of the major enantiomer is indicated in parentheses. [d] Enantiomeric purity increased to >99.9% by a single recrystallization in acetone/water.

[*] Prof. Dr. K. A. Jørgensen, Dr. N. Halland, Dr. T. Hansen
The Danish National Research Foundation:
Center for Catalysis, Department of Chemistry
Aarhus University
8000 Aarhus C (Denmark)
Fax: (+45) 8919-6199
E-mail: kaj@chem.au.dk

[**] We are grateful to Dr. A. Lohse and Dr. N. Jacobsen at Cheminova for performing the scale-up reactions and providing compounds **2d,f** and to Dr. R. G. Hazell for X-ray crystallographic analysis of compounds **1a,b**. This work was made possible by a grant from The Danish National Research Foundation.

Supporting information for this article (including films of hearts before and after treatment) is available on the WWW under http://www.angewandte.org or from the author.

 DOI: 10.1002/anie.200352136 © 2003 Wiley-VCH Verlag GmbH & Co. KGaA, Weinheim

optically, biologically, and pharmaceutically active compounds.

We envisioned that the imidazolidine catalysts **4a–c**[8] would be efficient catalysts for the addition of cyclic 1,3-dicarbonyl compounds to α,β-unsaturated carbonyl compounds. Table 1 shows some screening results for the reaction of **2a** with **3a**.

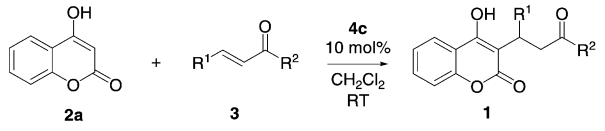
Initially, (*S*)-proline was investigated as the organocatalyst, but only racemic warfarin (**1a**) was obtained (Table 1, entry 1). We then turned our attention to the amino acid derived imidazolidine catalysts **4a,b**. To our delight we found that when the reaction was catalyzed by **4a**, optically active **1a** was formed in high yields with up to 70% *ee* (Table 1, entries 2–5). However, organocatalyst **4c**, formed by the condensation of 1,2-diphenylethanediamine with glyoxylic acid, proved to be superior to **4a,b**, and **1a** was obtained with up to 82% *ee* (Table 1, entries 7 and 8). In all cases the reaction proceeded smoothly at ambient temperature in the absence of an external base and without the formation of any by-products. To improve the enantiomeric purity of the Michael adduct, a single recrystallization from a water/acetone mixture provided the enantiopure (>99.9% *ee*) warfarin **1a** when starting from a sample with 79% *ee*.

This new organocatalytic asymmetric Michael reaction also proceeds on a kilogram scale when catalyzed by imidazolidine **4a** without any decrease in yield or enantioselectivity. Recycling of the catalyst was also possible, and thus the reaction provides very easy and inexpensive access to large quantities of enantiopure warfarin.

The scope of the present organocatalytic asymmetric Michael reaction using catalyst **4c** was extended to various α,β-unsaturated enones and the results are given in Table 2. The results in Table 2 demonstrate that the Michael addition of **2a** to a number of α,β-unsaturated enones **3b–i** that bear alkyl, branched alkyl, as well as various aromatic and heteroaromatic R^1 substituents proceeds smoothly to afford Michael adducts **1b–i** in high yields and enantioselectivities. The ketone substituent (R^2) could also be varied from methyl to ethyl and isopropyl; although a slightly lower yield of the Michael adduct **1k** was obtained, good enantioselectivities were maintained.

To extend the scope of the reaction further, several other cyclic 1,3-dicarbonyl compounds were utilized as Michael donors in the reaction with benzylideneacetone (**3a**) in the presence of catalyst **4c** (Table 3). The Michael reaction proceeded in good yields and with high enantioselectivities when using 4-hydroxycoumarin bearing either electron-withdrawing or electron-donating substituents (Table 3, entries 1–4), as well as when using 1-thio-4-hydroxycoumarin **2f**

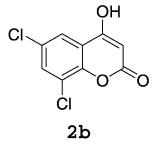
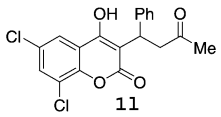
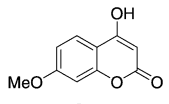
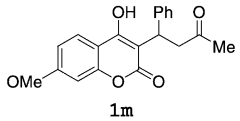
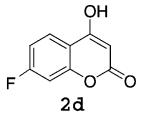
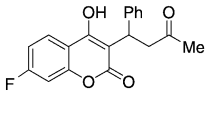
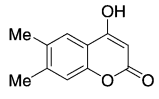
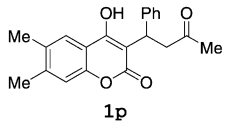
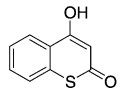
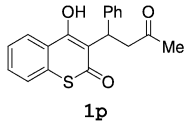
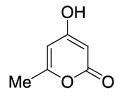
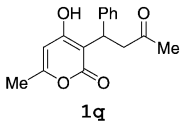
Table 2: Organocatalytic asymmetric Michael addition of **2a** to α,β-unsaturated enones **3b–k**.[a]



Entry	R^1	R^2	**3**	Catalyst	*t* [h]	**1**	Yield [%]	*ee* [%][b]
1	4-ClPh	Me	**b**	(*S*,*S*)-**4c**	130	**b**	86	82 (*S*)[c]
2[d]	4-ClPh	Me	**b**	(*S*,*S*)-**4c**	200	**b**	68	87 (*S*)
3	4-NO_2Ph	Me	**c**	(*S*,*S*)-**4c**	130	**c**	81	83 (*S*)
4	4-MeOPh	Me	**d**	(*S*,*S*)-**4c**	160	**d**	91	82 (*S*)[e]
5	2-Np	Me	**e**	(*S*,*S*)-**4c**	130	**e**	81	83 (*S*)[e]
6	*n*Bu	Me	**f**	(*R*,*R*)-**4c**	60	**f**	99	84 (*S*)[e]
7	*i*Pr	Me	**g**	(*S*,*S*)-**4c**	90	**g**	77	83 (*S*)[e]
8	2-thienyl	Me	**h**	(*R*,*R*)-**4c**	150	**h**	78	79 (*R*)[e]
9	2-furyl	Me	**i**	(*R*,*R*)-**4c**	150	**i**	75	75 (*R*)[e]
10	Ph	Et	**j**	(*S*,*S*)-**4c**	130	**j**	84	88 (*S*)[e]
11	Ph	*i*Pr	**k**	(*S*,*S*)-**4c**	180	**k**	71	85 (*S*)[e]

[a] Experimental conditions: The reaction mixture was treated with catalyst **4c** (10 mol%) in CH_2Cl_2 at ambient temperature for the time indicated. [b] Enantiomeric excess determined by CSP-HPLC. The absolute configuration of the major enantiomer is indicated in parentheses. [c] Enantiomeric purity increased to >99.9% *ee* after a single recrystallization in acetone/water. [d] Performed at 10°C. [e] Absolute stereochemistry assigned by analogy to **1a–c**.

Table 3: Organocatalytic asymmetric Michael addition of Michael donors **2b–g** to dibenzylideneacetone (**3a**).[a]

Entry	Michael donor	Michael adduct	Yield [%][b]	*ee* [%][c]
1[d]	 **2b**	 **1l**	65	79
2	 **2c**	 **1m**	81	85
3	 **2d**	 **1n**	68	83
4	 **2e**	 **1p**	84	85
5	 **2f**	 **1p**	84	78
6	 **2g**	 **1q**	76	85

[a] Reaction conditions: The reaction mixture was treated with catalyst (*S*,*S*)-**4c** (10 mol%) in CH_2Cl_2 at ambient temperature for 150 h. [b] Yield of product isolated after flash chromatography. [c] Enantiomeric excess determined by CSP-HPLC. [d] Performed in THF.

 © 2003 Wiley-VCH Verlag GmbH & Co. KGaA, Weinheim

(Table 3, entry 5) and 4-hydroxy-6-methylpyrone **2g** (Table 3, entry 6) as Michael donors.

The absolute configuration of coumachlor (**1b**) was determined by X-ray crystallographic analysis (see Supporting Information)[9] and by comparison of optical rotation for warfarin (**1a**)[10a] and acenocoumarin (**1c**).[10b] The observed stereochemical outcomes of the reactions catalyzed by **4a** is in accordance with previously proposed iminium-ion intermediates for the imidazolidine-catalyzed Michael reaction.[7g,h] For the imidazolidine catalyst (*S,S*)-**4c**, both an iminium-ion and an aminal intermediate species can be envisaged. Optimization using PM3 calculations show very little shielding of the alkene for the iminium-ion intermediate (Figure 1a).[11] On

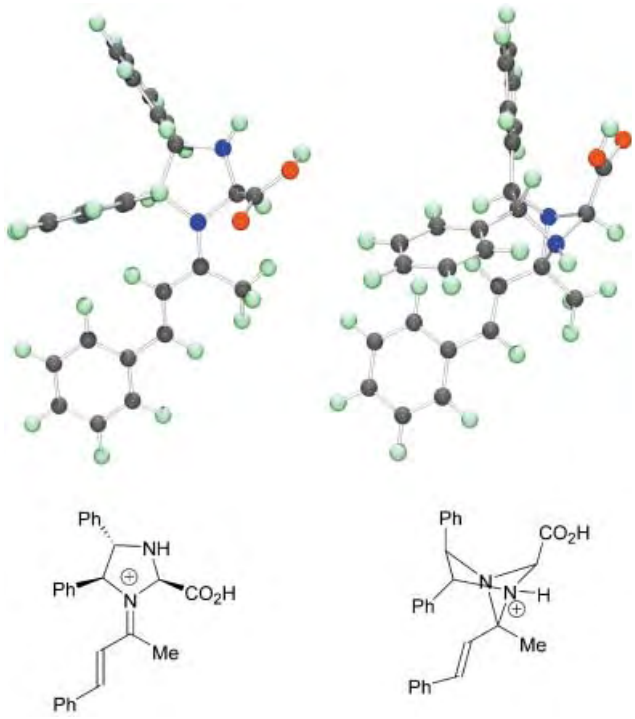


Figure 1. Possible intermediates for imidazoline-catalyzed Michael reaction. Left: iminium ion intermediate. Right: aminal intermediate.

the other hand, the bicyclic protonated aminal intermediate, formed by a nucleophilic displacement of the hemiaminal species, shows very good shielding of the *Re* face of the alkene (Figure 1b). The alkene fragment in the latter intermediate is activated[11] for addition of the 1,3-dicarbonyl compound and thus provides a possible explanation for the observed stereochemistry in the reaction.

In summary we have developed the first organocatalytic asymmetric Michael addition of cyclic 1,3-dicarbonyl compounds to α,β-unsaturated enones. This versatile and environmentally friendly Michael reaction affords warfarin and other Michael adducts in high yields and enantioselectivities in the presence of an easily available organic catalyst. Furthermore, it was demonstrated that enantiopure products could be obtained by a single recrystallization.

Received: June 13, 2003 [Z52136]
Published Online: September 29, 2003

Keywords: asymmetric catalysis · enones · Michael addition · natural products · synthetic methods

[1] For general reviews of asymmetric conjugate addition reactions, see: a) *Comprehensive Asymmetric Catalysis*, (Eds.: E. N. Jacobsen, A. Pfaltz, H. Yamamoto), Springer, Berlin, **1999**; b) M. P. Sibi, S. Manyem, *Tetrahedron* **2000**, *56*, 8033; c) N. Krause, A. Hoffmann-Röder, *Synthesis* **2001**, 171.

[2] For example, see: a) R. A. O'Reilly, *N. Engl. J. Med.* **1976**, *295*, 354; b) L. B. Wingard, R. A. O'Reilly, G. Levy, *Clin. Pharmacol. Ther.* **1978**, *23*, 212; c) H. P. Rang, M. M. Dale, J. M. Ritter, P. Gardner, *Pharmacology, 4th ed.*, Churchill Livingstone, Philadelphia, **2001**.

[3] H. J. Bardsley, A. K. Daly, PCT patent WO 00/43003, 2000.

[4] A. S. Demir, C. Tanyeli, V. Gülbeyaz, H. Akgün, *Turk. J. Chem.* **1996**, *20*, 139.

[5] See, for example: a) A. Robinson, H.-Y. Li, J. Feaster, *Tetrahedron Lett.* **1996**, *37*, 8321; b) H.-Y. Li, A. Robinson, US patent 5,856,525, 1999.

[6] G. Cravotto, G. M. Nano, G. Palmisano, S. Tagliapietra, *Tetrahedron: Asymmetry* **2001**, *12*, 707.

[7] For iminium-ion-promoted asymmetric conjugate additions, see: a) S. P. Brown, N. C. Goodwin, D. W. C. MacMillan, *J. Am. Chem. Soc.* **2003**, *125*, 1192; b) N. A. Paras, D. W. C. MacMillan, *J. Am. Chem. Soc.* **2002**, *124*, 7894; c) N. A. Paras, D. W. C. MacMillan, *J. Am. Chem. Soc.* **2001**, *123*, 4370; d) J. F. Austin, D. W. C. MacMillan, *J. Am. Chem. Soc.* **2002**, *124*, 1172; e) N. Halland, P. S. Aburel, K. A. Jørgensen, *Angew. Chem.* **2003**, *115*, 685; *Angew. Chem. Int. Ed.* **2003**, *42*, 661; f) N. Halland, R. G. Hazell, K. A. Jørgensen, *J. Org. Chem.* **2002**, *67*, 8331; see also: g) M. Yamaguchi, T. Shiraishi, M. Hirama, *J. Org. Chem.* **1996**, *61*, 3520; h) M. Yamaguchi, Y. Igarashi, R. S. Reddy, T. Shiraishi, M. Hirama, *Tetrahedron* **1997**, *53*, 11223; i) M. Yamaguchi, T. Shiraishi, Y. Igarashi, M. Hirama, *Tetrahedron Lett.* **1994**, *35*, 8233; j) M. Yamaguchi, T. Shiraishi, M. Hirama, *Angew. Chem.* **1993**, *105*, 1243; *Angew. Chem. Int. Ed. Engl.* **1993**, *32*, 1176; k) A. Kawara, T. Taguchi, *Tetrahedron Lett.* **1994**, *35*, 8805.

[8] Catalysts were formed by condensation of commercially available glyoxylic acid with the corresponding diamine (see Supporting Information).

[9] CCDC-212540 and 212541 contain the supplementary crystallographic data for this paper (**1a** and **1b**, respectively). These data can be obtained free of charge via www.ccdc.cam.ac.uk/conts/retrieving.html (or from the Cambridge Crystallographic Data Centre, 12, Union Road, Cambridge CB21EZ, UK; fax: (+44) 1223-336-033; or deposit@ccdc.cam.ac.uk).

[10] a) B. D. West, S. Preis, C. H. Schroeder, K. P. Link, *J. Am. Chem. Soc.* **1961**, *83*, 2676; b) C. R. Wheeler, W. F. Trager, *J. Med. Chem.* **1979**, *22*, 1122.

[11] PM3 calculations were performed by using the PC Spartan software. The alkene part in the hemiaminal species is significantly more activated (lower LUMO energy) towards nucleophilic addition than the alkene part in benzylideneacetone.

 © 2003 Wiley-VCH Verlag GmbH & Co. KGaA, Weinheim

Low-Valent Thorium Complexes

Amide from Dinitrogen by In Situ Cleavage and Partial Hydrogenation Promoted by a Transient Zero-Valent Thorium Synthon**

Ilia Korobkov, Sandro Gambarotta, and Glenn P. A. Yap*

Current research efforts in the field of dinitrogen activation/fixation generally target N_2 cleavage and the incorporation of either nitrides or reduced N_2 moieties into organic substrates.[1] In the sequence of transformations discovered so far (cleavage,[2] incorporation of nitrides into substrates,[3] coordinated N_2 partial hydrogenation,[4] and nitride protonation[5]), the reactions are typically performed in a series of steps. The main challenge towards developing catalytic processes involving N_2 is posed by finding multiple transformations, as in the case of the nitrogenase enzyme, that combines electrons from an ancillary reducing system with protons from the solvent (water) to form ammonia in a catalytic fashion and under mild reaction conditions.[6] A major breakthrough in this direction is the recent discovery of a catalytic cycle for reduction to ammonia obtained by using an ammonium salt as a protonating agent, chromocene as a reductant, and a Mo complex as a N_2 coordinating agent.[7]

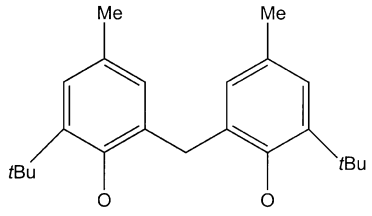
In this paper, we wish to present a novel, metal-promoted reduction of N_2 that was obtained during attempts to prepare a low-valent Th species. The reaction resulted in both dinitrogen cleavage and hydrogen abstraction to directly form an $-NH_2$ functionality.

Recently, actinides also entered the arena of N_2 activation with an example of reversible fixation[8a] and two-electron reduction.[8b] Furthermore, a trivalent uranium complex of a calix[4]tetrapyrrole ligand system, while in the presence of a strong reductant, afforded N_2 cleavage among a variety of other transformations.[9] The use of the same ligand and reducing agent afforded with Th an unprecedented divalent synthon.[10] In both cases, the ability of the ligand to work as both a σ and π donor is most likely the factor that provides sufficient stability to these highly reactive species. With the aim of increasing the reactivity even further, we have now attempted the synthesis of a low-valent Th complex/synthon supported by a robust σ-donor-based ligand system. In particular, we regarded the rare trivalent state of this metal[11] as particularly promising given that the possible $6d^1$ electronic configuration[12] may well provide an exceedingly reactive radical-type species. Herein we describe our findings.

[*] Prof. S. Gambarotta, Dr. I. Korobkov, Dr. G. P. A. Yap
Department of Chemistry
University of Ottawa
Ottawa, Ontario, K1N 6N5 (Canada)
Fax: (+1) 613-5672-5170
E-mail: sgambaro@science.uottawa.ca

[**] This work was supported by the Natural Sciences and Engineering Council of Canada (NSERC).

The reaction of $[ThCl_4(dme)_2]$ with the dipotassium salt of the diphenol **1** afforded the corresponding mononuclear complex **2** (Scheme 1). The crystal structure of the complex does not display any particularly significant features. The



1

octahedral coordination environment of the metal is defined by the four O donor atoms of the two diphenolate dianions, one dangling DME molecule, and one chlorine atom, which in turn bridges a potassium atom (Figure 1). The connection of the K cation to the Th-containing moiety is realized not only

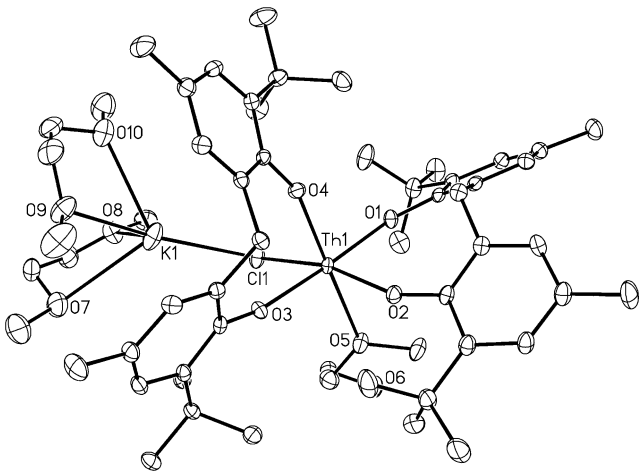
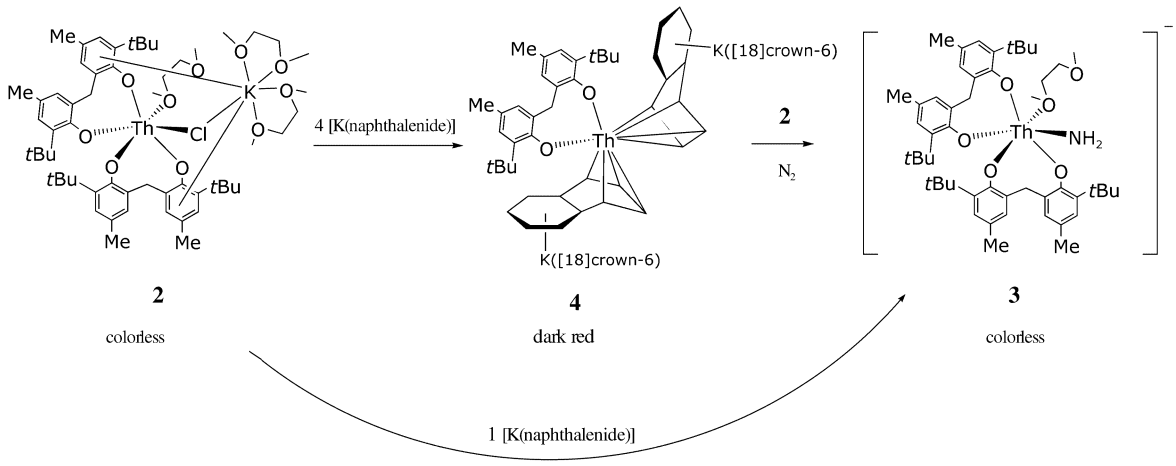


Figure 1. Thermal ellipsoid plot of **2**; bond lengths [Å] and angles [°]: Th-O1 2.209(3), Th-O2 2.208(3), Th-O3 2.240(3), Th-O4 2.197(3), Th-O5 2.613(3), Th-Cl 2.7941(11), Cl-K 3.1274(17); O1-Th-O2 87.56(10), O1-Th-O3 175.49(10), O1-Th-O4 90.33(10), O1-Th-O5 85.44(10), O1-Th-Cl 93.90(7), O2-Th-O3 91.61(10), O2-Th-O4 101.21(11), O2-Th-O5 84.48(10), O2-Th-Cl 164.20(8), O3-Th-O4 85.48(10), O3-Th-O5 98.91(10), O3-Th-Cl 88.10(7), O4-Th-O5 172.78(10), O4-Th-Cl 94.51(8), O5-Th-Cl 79.97(7).

via the bridging chlorine atom but also through π coordination to one of the two aromatic rings of each of the diphenolate anions. Spectroscopic and analytical data in agreement with the formulation were also obtained. The only noticeable NMR feature is the resonance of the CH_2 group connecting the two phenyl rings, which displayed two sharp and well-separated doublets at $\delta = 5.02$ and 3.52 ppm ($J = 13.3$ Hz) coupled to the same C atom at 35.05 ppm.

Attempts to reduce **2** to the trivalent state were carried out by treating it with one equivalent of [K(naphthalenide)] in DME (Scheme 1). The reaction afforded a dark-red solution upon mixing. While the reaction carried out under Ar gave

 © 2003 Wiley-VCH Verlag GmbH & Co. KGaA, Weinheim DOI: 10.1002/anie.200352205



Scheme 1.

only intractable, dark-colored materials, reaction mixtures kept under nitrogen slowly discolored after about two days. Standard work up of the resulting colorless solution afforded the amide complex **3**, which was isolated as colorless crystals in reasonable yield (47%). The very low percentage of nitrogen in the molecule made analytical values inconclusive although they were in excellent agreement with the proposed formulation obtained from the single-crystal X-ray structure. The arrangement around the thorium atom is very similar to that in **2** (Figure 2) showing the presence of the two diaryloxide ligands with comparable bond lengths and angles. The dangling DME molecule is also present in a *cis* position with respect to the NH_2 group. However, no direct connection is present with the K counterion, which is solvated by four molecules of DME and well separated from its anionic counterpart.

The identification of the amide atom as nitrogen was initially suggested by optimization of the refinement of the thermal parameters. However, the most conclusive evidence about the identity of the nitrogen atom and its origin from gaseous nitrogen was provided by NMR spectroscopy. An identical reaction carried out under $^{15}N_2$ afforded the ^{15}N-labeled **3** in crystalline form. Its ^{15}N NMR spectrum clearly showed the presence of a sharp triplet centered at 155.01 ppm ($J = 57.2$ Hz) coupled to a doublet at $\delta = 2.00$ ppm in the ^{1}H NMR spectrum (broad singlet in the ^{14}N sample). Furthermore, the proton resonance at $\delta = 2.00$ ppm did not show coupling with any carbon atom. This indicates without doubt the presence of an -NH_2 function generated from dinitrogen. All other spectral features were as expected and similar to those of **2**.

The formation of the -NH_2 function is very surprising and implies the participation of several equivalents of reductant, since N_2 cleavage alone requires six electrons. In addition, the acquisition of the two H atoms by the N atom in a non-protic solvent such as DME most likely implies radical-type hydrogen abstraction. In an attempt to clarify this unprecedented and complex transformation, we have focused on the transient red intermediate formed in the initial stage of the reaction. The intense dark color possibly indicates the formation of a low-valent species or synthon, while the slow discoloration in the presence of nitrogen gas indicates that this species is capable of further reaction with N_2. Immediate work-up of the dark-red reaction mixture, or even of identical reactions with two and four equivalents of [K(naphtalenide)], which did not discolor after several days, afforded the same

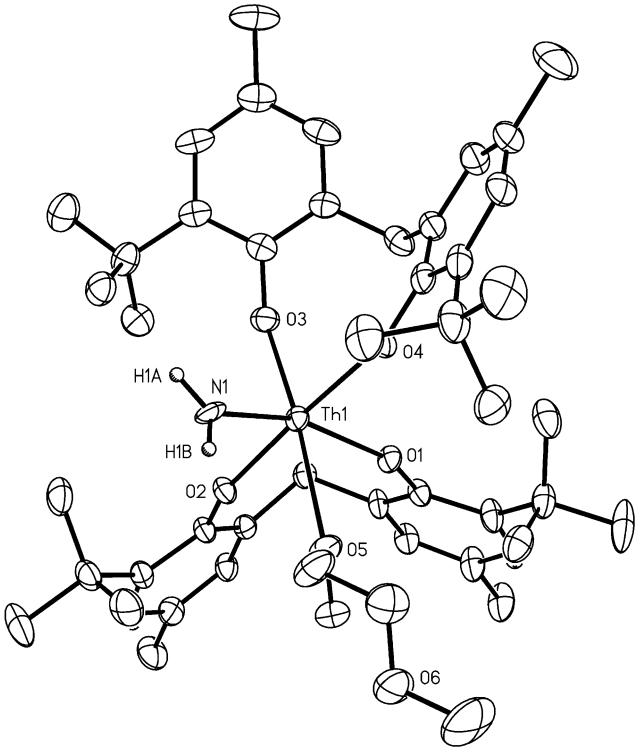


Figure 2. Thermal ellipsoid plot of the anionic moiety of **3**; bond lengths are [Å] and angles [°]: Th-N1 2.2431(6), Th-O1 2.265(4), Th-O2 2.254(4), Th-O3 2.217(5), Th-O4 2.279(4), Th-O5 2.620(5); O1-Th-O2 85.96(14), O1-Th-O3 99.96(16), O1-Th-O4 88.92(15), O1-Th-O5 81.24(15), O1-Th-N1 160.52(18), O2-Th-O3 91.83(16), O2-Th-O4 174.57(14), O2-Th-O5 82.64(16), O2-Th-N1 92.98(16), O3-Th-O4 87.29(17), O3-Th-O5 174.27(16), O3-Th-N1 99.52(17), O4-Th-O5 98.36(17), O4-Th-N1 92.45(17), O5-Th-N1 79.33(17).

 © 2003 Wiley-VCH Verlag GmbH & Co. KGaA, Weinheim

very air-sensitive crystalline compound **4** in low yield. As expected, the reaction with four equivalents of reductant gave the best yield (30%). Despite treatment with [18]crown-6 to improve solubility and crystallinity, compound **4** could not be isolated in an analytically pure form as it was always contaminated by red crystals of [(naphthalene){K([18]-crown-6)}$_2$] and colorless crystals of a new Th complex (not yet identified), thus preventing a complete characterization. The formulation was yielded only by an X-ray analysis (Figure 3). The structure consists of one thorium atom in a

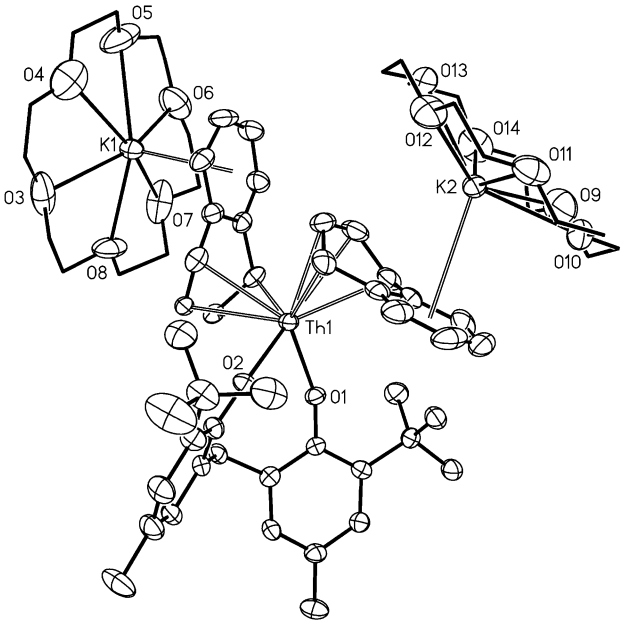


Figure 3. Thermal ellipsoid plot of the anionic moiety of **4**; bond lengths [Å] and angles [°]: Th-O1 2.284(5), Th-O2 2.258(5), Th-C24 2.737(8), Th-C25 2.745(7), Th-C26 2.732(7), Th-C27 2.710(8), Th-C34 2.671(8), Th-C35 2.760(9), Th-C36 2.784(8); O1-Th-O2 83.49(17).

pseudotetrahedral environment with the coordination sphere defined by two oxygen atoms of one diaryloxide ligand and the two centroids of two rings of two separate naphthalene molecules. Similar to the case of the calix-tetrapyrrole–naphthalene divalent synthon recently reported,[10] the π-bonding mode of the metal center to one of the two naphthalene rings causes a major ring distortion towards a diene-type arrangement. The other ring of each naphthalene group coordinates one potassium atom, which is in turn coordinated to the six oxygen atoms of one molecule of crown ether.

The presence of only one diaryloxide ligand and two potassium atoms around the thorium center assigns a formal zero-valent state to the thorium atom. However, the severe distortion of the two naphthalene rings clearly indicates that the extent of back-bonding is substantial and that complex **4** most likely should be regarded as a tetravalent species or a zero-valent synthon. Its formation, through a reaction with a 1:1 stoichiometric ratio that requires four electrons, confirms that the reaction initially affords **4** through a very rapid process. While this accounts for the transient intense red color observed during the formation of **3**, the lack of reductant necessarily leaves behind a substantial amount of unreacted **2**. The fact that the formation of **3** is not observed in the reactions carried out with larger amounts of [K(naphthalenide)] possibly suggests that it is the reaction of **2** with **4** that triggers a process through which dinitrogen is coordinated, cleaved, and partly hydrogenated, to afford the colorless **3**.

Obviously, a complete rationalization of this remarkable reaction is premature at this stage. We are currently focusing on the working hypothesis that a trivalent Th synthon, either directly formed as a transient intermediate or via comproportionation between **2** and **4**, may react with dinitrogen. Subsequent reaction of the dinitrogen complex with **4** may afford both cleavage and hydrogenation from the solvent via H abstraction. Further work to test this hypothesis is being actively pursued at the moment.

Experimental Section

2: A solution of ligand **1** (0.65 g, 1.92 mmol) in DME (10 mL) was treated with KH (0.15 g, 3.84 mmol). A vigorous reaction took place accompanied by gas evolution. After stirring the mixture for an additional 60 min, a solution of [$ThCl_4(dme)_2$] (0.53 g, 0.96 mmol) in DME (5 mL) was added. The resulting pale-brown suspension was stirred for an additional 4 h then centrifuged to eliminate KCl, concentrated to a small volume, and heptane was added. The solution was allowed to stand at −30 °C overnight, upon which colorless crystals of **2** were formed (1.03 g, 0.82 mmol, 86%). Elemental analysis calcd (%) for $C_{58}H_{90}O_{10}KClTh$: C 55.56, H 7.23; found: C 55.41, H 7.17. ^{1}H NMR (500 MHz, [D$_8$]THF, 25 °C): $\delta = 7.35$ and 7.07 (d, CH phenyl ring, 4H each), 5.02 and 3.52 (d, CH_2 (ligand), 2H each), 3.73 (s, CH_2 (DME), 12H), 3.58 (s, CH_3 (DME), 18H), 2.49 (s, Me (ligand), 12H), 1.76 ppm (br s, *t*Bu (ligand), 36H); ^{13}C NMR (125.72 MHz, [D$_8$]THF, 25 °C): $\delta = 162.19$, 137.01, 134.90, 35.54 (quat C), 129.27 and 124.98 (CH aromatic), 72.71 (CH_2 (DME)), 58.97 (Me (DME)), 35.05 (CH_2 (ligand)), 31.20 (*t*Bu), 21.35 ppm (Me (ligand)).

3: A solution of **2** (0.76 g, 0.61 mmol) in DME (5 mL) was reacted at room temperature with a solution of [K(naphthalenide)] in DME, which was prepared by dissolving K (0.024 g, 0.61 mmol) with naphthalene (0.078 g, 0.61 mmol) in DME (5 mL), to afford a dark-red mixture. Stirring was continued for 72 h upon which the color slowly faded forming a nearly colorless solution. The suspension was filtered and layered with heptane at room temperature for two days, upon which colorless crystals of **3** were formed (0.45 g, 0.29 mmol, 47%). Elemental analysis calcd (%) for $C_{76}H_{120}NO_{14}KTh$: C 59.16, H 7.84, N 0.91; found: C 59.09, H 7.77, N 1.03. ^{1}H NMR (500 MHz, [D$_8$]THF, 25 °C): $\delta = 8.09$ and 7.70 (m, naphthalene, 4H each), 7.25 and 6.98 (d, CH phenyl ring, 4H each), 4.99 and 3.35 (d, CH_2 (ligand), 2H each), 3.69 (s, CH_2 (DME), 12H), 3.54 (s, CH_3 (DME), 18H), 2.41 (s, Me (ligand), 12H), 2.00 (br s, NH_2, 2H), 1.73 ppm (s, *t*Bu (ligand), 36H). ^{13}C NMR (125.72 MHz, [D$_8$]THF, 25 °C): $\delta = 162.71$, 137.01, 134.54, 123.25, 35.55 (quat C), 129.28 and 125.00 (CH aromatic), 128.64 and 126.55 (naphthalene), 72.78 (CH_2 (DME)), 58.94 (Me (DME)), 34.51 (CH_2 (ligand)), 30.85 (*t*Bu), 21.39 ppm (Me (ligand)). ^{15}N NMR (50.66 MHz, [D$_8$]THF, 25 °C): $\delta = 155.01$ ppm (t, $J =$ 57.2 Hz).

4: A solution of **2** (1.02 g, 0.81 mmol) in DME (10 mL) was reacted at room temperature with a solution of K(naphthalenide) in DME, which was prepared by dissolving K (0.13 g, 3.3 mmol) with naphthalene (0.41 g, 3.5 mmol) in DME (7 mL) affording a dark-red mixture. The dark-red suspension was immediately centrifuged and the supernatant concentrated to about half of the volume and treated with a solution of [18]crown-6 (0.38 g, 1.5 mmol) in toluene. The solution was placed in a freezer for one day at −30 °C and afforded dark-red crystals of **4** contaminated by [(naphthalene){K([18]crown-

 © 2003 Wiley-VCH Verlag GmbH & Co. KGaA, Weinheim

6)}$_2$] and another unidentidfied tetravalent thorium complex (approximately 30%).

Crystal data for **2**: $C_{58}H_{90}O_{10}KClTh$, $M_r = 1253.89$, monoclinic, $P21/m$, $a = 15.015(2)$, $b = 20.836(3)$, $c = 19.740(3)$ Å, $\beta = 99.144(3)°$, $V = 6096.9(17)$ Å^3, $Z = 4$, $\rho_{calcd} = 1.366$ Mg m^{-3}; absorption coefficient 2.610 mm^{-1}, $F(000) = 2576$, reflections collected 43472, independent reflections 14178, GOF = 1.006, $R = 0.0417$, $wR^2 = 0.0839$.

Crystal data for **3**: Two crystallographically independent but chemically equivalent molecules were found in the asymmetric unit. $C_{152}H_{240}N_2O_{28}K_2Th_2$, $M_r = 3085.74$, monoclinic, $P21/c$, $a = 25.9697(12)$, $b = 21.0627(9)$, $c = 30.5093(15)$ Å, $\beta = 99.895(2)°$, $V = 16440.1(13)$ Å^3, $Z = 4$, $\rho_{calcd} = 1.247$ Mg m^{-3}; absorption coefficient 1.921 mm^{-1}, $F(000) = 6432$, reflections collected 47999, independent reflections 32316, GOF = 1.008, $R = 0.0572$, $wR^2 = 0.1520$.

Crystal data for **4**: The data for this compound is not unquestionable due to the very poor crystal quality observed. For example, in spite of the β angle being equal to 90°, the systematic absences clearly indicate a monoclinic symmetry rather than orthorhombic; a chemically meaningful solution was obtained for a treatment in the monoclinic system. $C_{74}H_{102}O_{14}K_2Th$, $M_r = 1525.80$, monoclinic, $P21/m$, $a = 17.391(9)$, $b = 21.163(11)$, $c = 19.701(11)$ Å, $\beta = 90.000(9)°$, $V = 7251(7)$ Å^3, $Z = 4$, $\rho_{calcd} = 1.398$ Mg m^{-3}; absorption coefficient 2.233 mm^{-1}, $F(000) = 3144$, reflections collected 45100, independent reflections 12764, GOF = 1.031, $R = 0.0561$, $wR^2 = 0.1152$.

Crystallographic data (excluding structure factors) for the structures reported in this paper have been deposited with the Cambridge Crystallographic Data Centre as supplementary publication. CCDC-213059 (**2**) -213060 (**3**), and -213061 (**4**) contain the supplementary crystallographic data for this paper. These data can be obtained free of charge via www.ccdc.cam.ac.uk/conts/retrieving.html (or from the Cambridge Crystallographic Data Centre, 12, Union Road, Cambridge CB21EZ, UK; fax: (+44) 1223-336-033; or deposit@ccdc.cam.ac.uk).

Received: June 23, 2003 [Z52205]
Published Online: September 29, 2003

Keywords: nitrogen · O ligands · subvalent compounds · synthons · thorium

[1] See for example: a) M. Hidai, Y. Mizobe, *Met. Ions Biol. Syst.* **2002**, *39*, 121; b) M. D. Fryzuk, S. A. Johnson, *Coord. Chem. Rev.* **2000**, *200*, 379; c) T. A. Bazhenova, A. E. Shilov, *Coord. Chem. Rev.* **1995**, *144*, 69; d) C. J. Pickett, *J. Biol. Inorg. Chem.* **1996**, *1*, 601; e) S. Gambarotta, *Inorganic Chemistry Highlights* (Eds.: G. Meyer, D. Naumann, L. Wesemann), Wiley-VCH, Weinheim, **2002**; a) M. Hidai, *Coord. Chem. Rev.* **1999**, *185*, 99; b) M. Hidai, Y. Mizobe, *Pure Appl. Chem.* **2001**, *73*, 261.

[2] See for example: a) C. E. Laplaza, C. C. Cummins, *Science* **1995**, *268*, 861; b) G. K. B. Clentsmith, V. M. E. Bates, P. B. Hitchcock, F. G. N. Cloke, *J. Am. Chem. Soc.* **1999**, *121*, 10444; c) H. Kawaguchi, T. Matsuo, *Angew. Chem.* **2002**, *114*, 2916; *Angew. Chem. Int. Ed.* **2002**, *41*, 2792; d) A. Caselli, E. Solari, R. Scopelliti, C. Floriani, N. Re, C. Rizzoli, A. Chiesi-Villa, *J. Am. Chem. Soc.* **2000**, *122*, 3652; e) E. Solari, C. D. Silva, B. Iacono, J. Hesschenbrouck, C. Rizzoli, R. Scopelliti, C. Floriani, *Angew. Chem.* **2001**, *113*, 4025; *Angew. Chem. Int. Ed.* **2001**, *40*, 3907; f) Y. C. Tsai, M. J. A. Johnson, D. J. Mindiola, C. C. Cummins, W. T. Klooster, J. F. Koetzle, *J. Am. Chem. Soc.* **1999**, *121*, 10426.

[3] a) M. D. Fryzuk, C. M. Kozak, M. R. Bowdridge, B. O. Patrick, S. J. Rettig, *J. Am. Chem. Soc.* **2002**, *124*, 8389; b) M. D. Fryzuk, B. A. MacKay, B. O. Patrick, *J. Am. Chem. Soc.* **2003**, *125*, 3234; c) M. D. Fryzuk, B. A. MacKay, S. A. Johnson, B. O. Patrick, *Angew. Chem.* **2002**, *114*, 3861; *Angew. Chem. Int. Ed.* **2002**, *41*, 3709.

[4] M. D. Fryzuk, J. B. Love, S. J. Rettig, V. G. Young, *Science* **1997**, *275*, 1445.

[5] a) D. V. Yandulov, R. R. Schrock, *J. Am. Chem. Soc.* **2002**, *124*, 6252; b) M. B. O'Donoghue, W. M. Davis, R. R. Schrock, W. M. Reiff, *Inorg. Chem.* **1999**, *38*, 243.

[6] a) J. Kim, D. C. Rees, *Science* **1992**, *257*, 1677; b) J. Kim, D. C. Rees, *Nature*, **1992**, *360*, 563.

[7] D. V. Yandulov, R. R. Schrock, *Science* **2003**, *301*, 76.

[8] a) P. Roussel, P. Scott, *J. Am. Chem. Soc.* **1998**, *120*, 1070; b) F. G. N. Cloke, P. B. Hitchcock, *J. Am. Chem. Soc.* **2002**, *124*, 9352.

[9] I. Korobkov, S. Gambarotta, G. P. A. Yap, *Angew. Chem.* **2002**, *114*, 3583; *Angew. Chem. Int. Ed.* **2002**, *41*, 3433.

[10] I. Korobkov, S. Gambarotta, G. P. A. Yap, *Angew. Chem.* **2003**, *115*, 838; *Angew. Chem. Int. Ed.* **2003**, *42*, 814.

[11] a) J. S. Parr, F. G. N. Cloke, S. J. Coles, M. B. Hursthouse, *J. Am. Chem. Soc.* **1999**, *121*, 6867; b) P. C. Blake, M. F. Lappert, J, . L. Atwood, H. Zhang, *J. Chem. Soc. Chem. Commun.* **1986**, 1148; c) R. W. Broach, A. J. Schultz, J. M. Williams, G. M. Brown, J. M. Manriquez, P. J. Fagan, T. J. Marks, *Science* **1979**, *203*, 172.

[12] M. Dolg, P. Fulde, H. Stoll, H. Preuss, A. Chang, R. M. Pitzer, *Chem. Phys.* **1995**, *195*, 71.

 © 2003 Wiley-VCH Verlag GmbH & Co. KGaA, Weinheim

Natural Product Synthesis

A Concise and Flexible Total Synthesis of (−)-Diazonamide A**

*Anthony W. G. Burgett, Qingyi Li, Qi Wei, and Patrick G. Harran**

Diazonamide A is a potently antimitotic natural product whose structure was originally assigned as polycycle **1** (Figure 1).[1] We recently synthesized this material—only to discover that **1** is neither a natural substance nor, in fact, stable.[2] A reinterpretation of published spectroscopic and X-ray crystallographic data led to the proposal that diazonamide A was actually hydroxy isovaleramide-containing aminal **2**.[3] This revision has been recently confirmed through synthesis.[4] We felt that the differences between **1** and **2**, while seemingly subtle, provided for a very different synthetic problem. Therefore, minor adaptations of the route used to prepare **1** were not pursued. Rather, we developed and

[*] Prof. P. G. Harran, A. W. G. Burgett, Q. Li, Q. Wei
Department of Biochemistry
University of Texas
Southwestern Medical Center at Dallas
Dallas, TX 75390-9038 (USA)
Fax: (+1) 214-648-6455
E-mail: pharra@biochem.swmed.edu

[**] Funding provided by the NIH (RO1-GM60591), the Howard Hughes Medical Institute, the Robert A. Welch Foundation, and unrestricted research awards from AstraZeneca, Eli Lilly, and Pfizer are gratefully acknowledged. P.H. is a fellow of the Alfred P. Sloan Foundation. A.B. thanks the medicinal chemistry section of the ACS for a predoctoral fellowship (sponsor: Aventis Pharmaceuticals). We are indebted to Dr. Nigam Rath (University of Missouri at St. Louis) for his crystallographic analysis of aminal **15**.

 DOI: 10.1002/anie.200352577 © 2003 Wiley-VCH Verlag GmbH & Co. KGaA, Weinheim

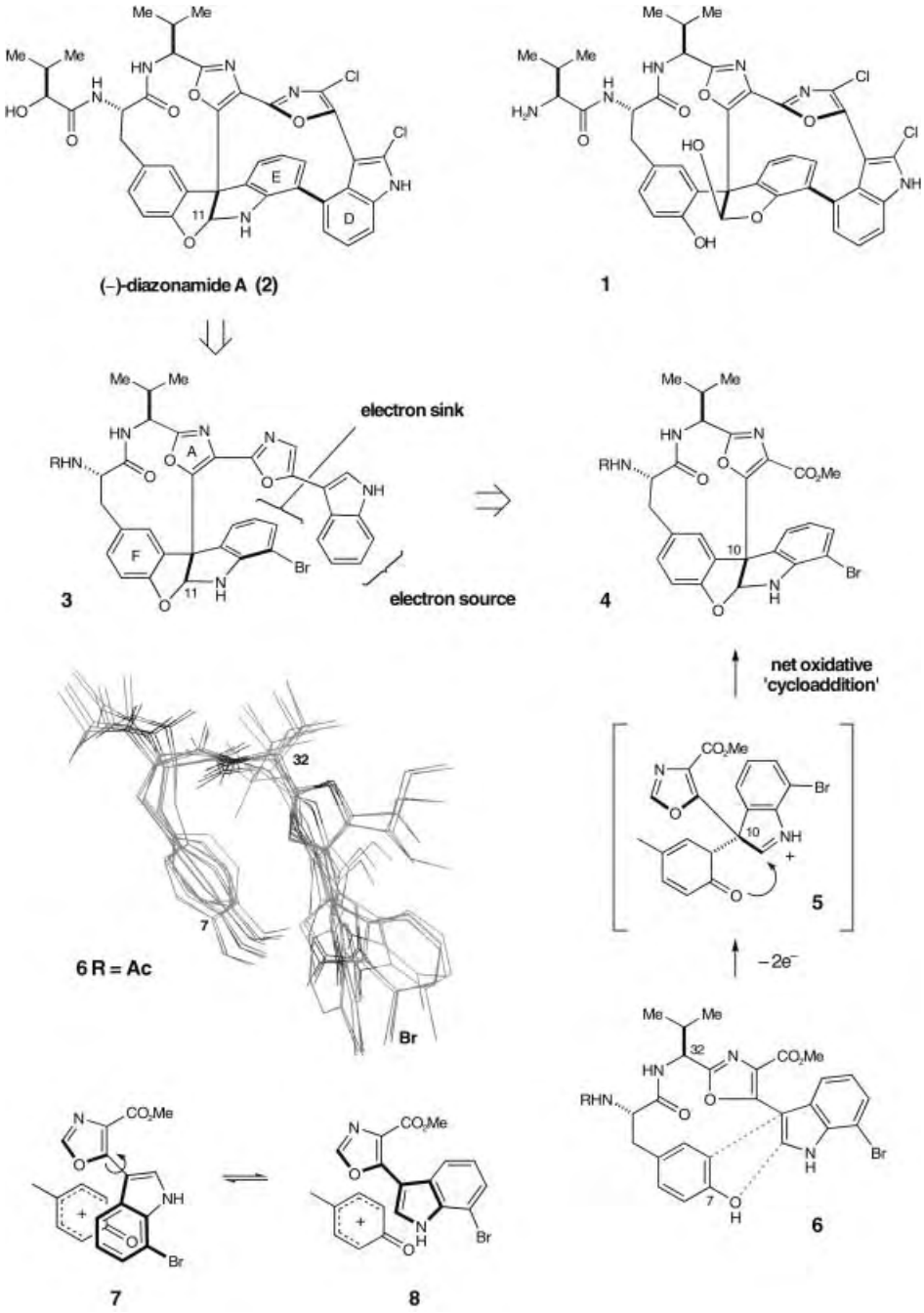


Figure 1. Diazonamide A structure and primary retrosynthesis.

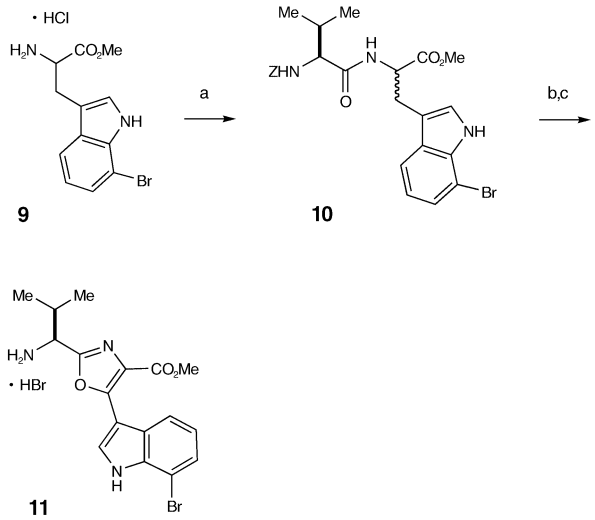
describe here a new sequence—one that generates natural diazonamide A in a particularly concise manner and along lines possibly relevant to its biosynthesis.

Lessons learned from earlier work proved valuable. Peripheral halogenation and acyl substitution can be installed late on a diazonamide core. In addition, we knew that potentially complicating issues of atropisomerism[5] during assembly of this core could be avoided by forming the D/E biaryl bond intramolecularly in the context of a pre-existing, correctly configured A/F macrolactam. This implicated seco halide **3** as a penultimate target—a position from which photoinduced electron transfer mediated elimination of HBr could complete the diazonamide ring system.[2] From **3**, the problem simplifies to central aminal **4**. The dihydrobenzofuro[2,3b]indole subunit of this molecule is viewed as a remnant of oxidation. In particular, of a linear peptidyl precursor (e.g. **6**) wherein, for example, heterolytic oxidation of the phenol could initiate an annulation involving phenoxenium ion capture by the tethered indole and ring closure (as indicated) within the resultant cyclohexadienone-linked indoleninium species.[6] With respect to stereoinduction in this scheme, calculated conformational preferences for **6** (Figure 1[7]) indicate a left handedness to the display of Cα substituents in its dipeptide segment. To the extent that these computations and, for that matter ground state conformational preference, would be predictive[8]—an electron deficient

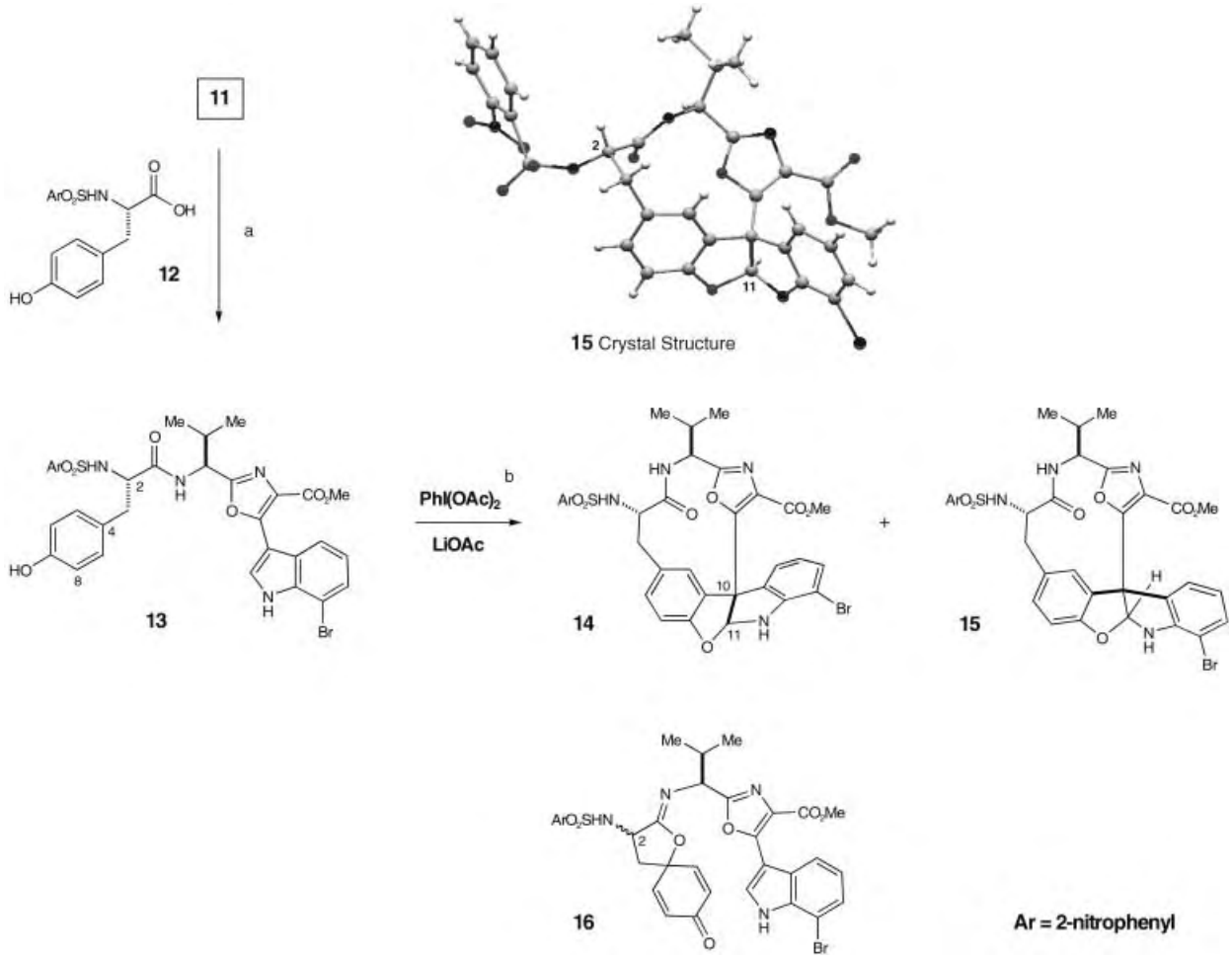
 © 2003 Wiley-VCH Verlag GmbH & Co. KGaA, Weinheim

intermediate generated from the phenol would situate itself beneath (as shown in Figure 1) the indole unit as they approached within the bonding distance. Kinetic C10 stereochemistry in **5** would thus reflect whether nucleophilic attack (by the indole at its 3-position[9]) had occurred from *s-cis* rotamer **8** or its *trans* counterpart **7**; the former producing a desired result. While our ability to predict such a preference was limited, the construction itself could be evaluated readily.

An oxidation substrate was synthesized beginning with racemic 7-bromotryptophan methyl ester[10] (Scheme 1). Treatment of this material with the acid chloride derived from N-Z-[L]-Val-OH[11] provided an epimeric mixture of dipeptides **10**. Yonemitsu oxidation[12] of the mixture gave one 3-oxazoylindole product whose carbamate then degraded in HBr/AcOH to give crystalline amine salt **11**. Condensation of **11** with L-tyrosine-derived sulfonamide **12**[13] subsequently completed the content of a diazonamide aminal (Scheme 2)—a fact made strikingly clear by the observation that adding **13** to a cold trifluoroethanol solution of $PhI(OAc)_2$ is sufficient to generate target lactam **14**—presumably through mechanistic events related to those outlined in Figure 1. As currently performed, aminal **14** is produced alongside its C10-(*R*),C11-(*S*) diastereoisomer **15** (≈3:1 favoring **14**[14])



Scheme 1. Reaction conditions: a) N-Z-[L]-Val-OH, 1-chloro-*N*,*N*-2-trimethyl-1-propen-1-amine, CH_2Cl_2 then **9** (0.95 equiv), py (2.0 equiv), 0°C (76%). b) DDQ (2.3 equiv), THF, 70°C, 2 h (90%). c) 33% HBr in glacial AcOH, room temperature, 10 min (94%). DDQ = 2,3-dichloro-5,6-dicyano-1,4-benzoquinone, py = pyridine.

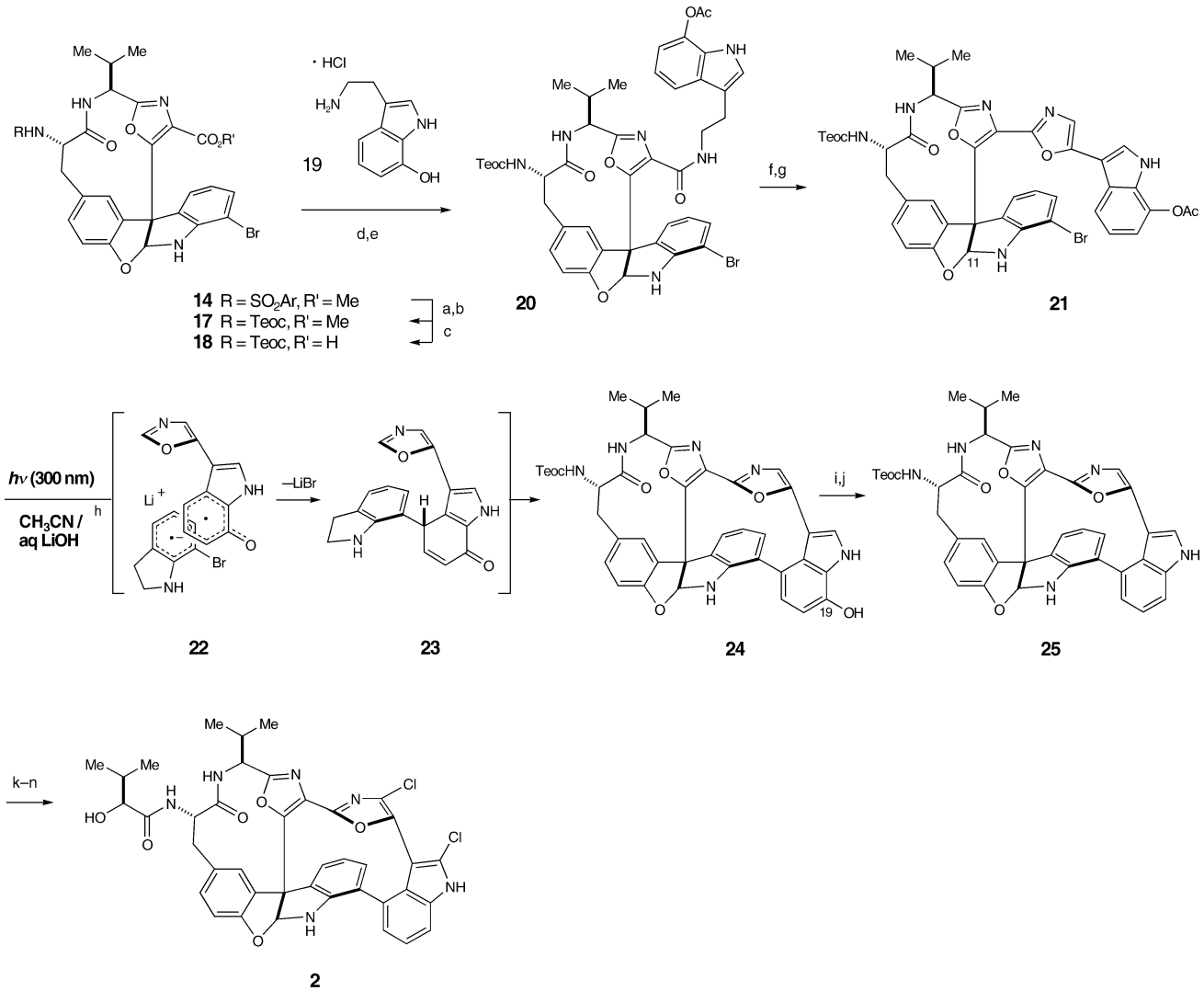


Scheme 2. Reaction conditions: a) TBTU, $(iPr)_2NEt$, DMF, room temperature (91%). b) $PhI(OAc)_2$ (1.1 equiv), LiOAc (2.0 equiv), 2,2,2-trifluoroethanol, inverse addition, −20°C, 10 min. (20–25% **14**, 7–8% **15**, ~15% **16** (1:1)). TBTU = 2-(1H-benzotriazol-1-yl)-1,1,3,3-tetramethyluronium tetrafluoroborate.

 © 2003 Wiley-VCH Verlag GmbH & Co. KGaA, Weinheim

and comparable amounts of epimeric spirodienones **16**.[15] Notably, C2-epi-**13** (derived from D-tyrosine) does not cyclize similarly nor does **16** convert to **14**/**15** when resubjected to the reaction conditions. These data are consistent with the (**14** + **15**)/**16** ratio being a result of kinetic competition between nucleophilic attack at C8 and C4 of an intervening phenoxenium ion.[16] Populated conformations of **13** evidently permit macrolactam formation to compete[17] with an ostensibly favored, more conventional medium-ring spiroannulation manifold. The latter has been exploited in various contexts following Kita's seminal demonstrations of the method.[18]

The above five-step synthesis of **14** quickly moved our effort to its advanced stages. Three functional group manipulations[19] prepared the molecule to serve as an acylating agent for 7-hydroxytryptamine **19**.[20] Condensation of **17** and **19**, acetylation of the product, and a two-step benzylic oxidation/cyclodehydration sequence[2,21] afforded bis(oxazoyl)indole **21** (Scheme 3). Compound **21** was then dissolved in aqueous CH_3CN that contained LiOH and allowed to stand for 20 minutes. The resultant lithium phenoxide solution was degassed and photolyzed (Rayonet, 300 nm) to produce biaryl **24** (single atropdiastereomer) in good yield. This result is a significant improvement over our earlier D/E biaryl bond synthesis.[2] As in that photochemistry, we rationalize the chemistry in terms of photoinduced electron transfer[22] between the indole chromophore and the adjacent bromoarene—leading initially to a radical ion pair capable of mesolytic elimination of bromide. The incipient biradical can then internally collapse and the resultant indolenone (**23**) tautomerize to generate **24**. Additional electron density in the indole subunit benefits the process tremendously, in fact, more than enough to justify bringing an otherwise superfluous



Scheme 3. Reaction conditions: a) PhSH, Na_2CO_3, DMF, room temperature. b) Teoc-Cl, CH_2Cl_2, aqueous K_2CO_3 (80%—2 steps). c) LiOH, aqueous MeOH (99%). d) **19** (1.1 equiv), TBTU, $(iPr)_2NEt$ (2 equiv), DMF, (91%). e) Ac_2O, py, CH_2Cl_2/THF (95%). f) DDQ (2.2 equiv), 9:1 THF/H_2O (86%). g) PPh_3, $(CCl_3)_2$, Et_3N, CH_2Cl_2, 15 min (55%). h) *hν* (300 nm), 3.0 mM in argon-purged CH_3CN/H_2O (3:1) that contained LiOH (2 equiv), room temperature, 3 h (72%). i) 4-nitrophenyltriflate, K_2CO_3, DMF (87%). j) 20% $Pd(OH)_2$/C, 1 atm H_2, EtOAc/MeOH, room temperature (96%). k) diallyldicarbonate, Et_3N, THF, room temperature; add Teoc-Cl, Et_3N, room temperature; add $[Pd(PPh_3)_4]$ (5 mol%), morpholine (5 equiv), 0°C, 20 min (78% overall). l) 2,3,4,5,6,6-hexachloro-2,4-cyclohexadien-1-one (2.5 equiv), DMF, room temperature, 24 h (30–50%). m) $(Me_2N)_3SSiMe_3F_2$ (5 equiv), DMF, room temperature (95%). n) (*S*)-α-hydroxy isovaleric acid (1.1 equiv), $(EtO)_2P(O)CN$, *N*-methylmorpholine, THF, room temperature (90%).

 © 2003 Wiley-VCH Verlag GmbH & Co. KGaA, Weinheim

substituent into the synthesis. After reductive removal of this spectator phenol (at C19, through its triflate[23]), the molecule was differentially acylated, carefully chlorinated on its right periphery with perchloro-2,4-cyclohexadien-1-one,[24] and treated with tris(dimethylamino)sulfur trimethyldifluorosilicate[25] to afford desbromo diazonamide B. Phosphoryl cyanide-mediated condensation with commercial (*S*)-α-hydroxy isovaleric acid then delivered (−)-diazonamide **2**. Synthetic **2** has identical spectroscopic characteristics and co-elutes with a sample of natural material[26] when a pre-mixture is analyzed by LC/MS.

The synthesis of (−)-diazonamide A described herein converges on the target from five segments in a total of 19 operations (longest linear sequence is nine steps). We have evidence that **2** blocks mitotic cell division by an unprecedented mechanism[27] and this preparation will provide sufficient material and derivatives to explore diazonamide pharmacology in depth.

Received: August 6, 2003 [Z52577]
Published Online: September 30, 2003

Keywords: antimitotic agents · natural products · oxidation · photochemistry · total synthesis

[1] a) N. Lindquist, W. Fenical, G. D. Van Duyne, J. Clardy, *J. Am. Chem. Soc.* **1991**, *113*, 2303 – 2304; b) N. Lindquist, Ph.D. thesis, University of California San Diego (USA), **1989**.

[2] J. Li, S. Jeong, L. Esser, P. G. Harran, *Angew. Chem.* **2001**, *113*, 4901 – 4904; *Angew. Chem. Int. Ed.* **2001**, *40*, 4765 – 4770.

[3] J. Li, A. W. G. Burgett, L. Esser, C. Amezcua, P. G. Harran, *Angew. Chem.* **2001**, *113*, 4905 – 4909; *Angew. Chem. Int. Ed.* **2001**, *40*, 4770 – 4773.

[4] a) K. C. Nicolaou, P. Bheema Rao, J. Hao, M. V. Reddy, G. Rassias, X. Huang, D. Y.-K. Chen, S. A. Snyder, *Angew. Chem.* **2003**, *115*, 1795 – 1800; *Angew. Chem. Int. Ed.* **2003**, *42*, 1753 – 1758; b) K. C. Nicolaou, M. Bella, D. Y.-K. Chen, X. Huang, T. Ling, S. A. Snyder, *Angew. Chem.* **2002**, *114*, 3645 – 3649; *Angew. Chem. Int. Ed.* **2002**, *41*, 3495 – 3499; c) For a review of efforts aimed at diazonamide synthesis (through 2001) see: T. Ritter, E. M. Carreira, *Angew. Chem.* **2002**, *114*, 2601 – 2606; *Angew. Chem. Int. Ed.* **2002**, *41*, 2489 – 2494; More recent contributions include: d) T. Sawada, D. E. Fuerst, J. L. Wood, *Tetrahedron Lett.* **2003**, *44*, 4919 – 4921; e) I. D. Hills, G. C. Fu, *Angew. Chem.* **2003**, *115*, 4216 – 4219; *Angew. Chem. Int. Ed.* **2003**, *42*, 4082 – 4085.

[5] a) E. Vedejs, M. A. Zajac, *Org. Lett.* **2001**, *3*, 2451 – 2454; b) K. C. Nicolaou, S. A. Snyder, K. B. Simonsen, A. E. Koumbis, *Angew. Chem.* **2000**, *112*, 3615 – 3620; *Angew. Chem. Int. Ed.* **2000**, *39*, 3473 – 3478.

[6] Ring closure in **5** could also occur via its phenol tautomer.

[7] Geometry optimization of **6** (R = Ac) was performed by using the Amber force field within Macromodel v7.0 (Schrödinger). The result was subjected to a Monte Carlo molecular dynamics simulation. Figure 1 depicts rigid superimposition of the ten lowest energy conformations calculated from this exercise.

[8] J. I. Seeman, *Chem. Rev.* **1983**, *83*, 83 – 134.

[9] a) A. H. Jackson, A. E. Smith, *Tetrahedron* **1968**, *24*, 403 – 413; b) A. H. Jackson, B. Naidoo, P. Smith, *Tetrahedron* **1968**, *24*, 6119 – 6129.

[10] Prepared in two steps from 7-bromoindole and methyl 3-bromopyruvate oxime. See: a) Y. Konda-Yamada, C. Okada, K. Yoshida, Y. Umeda, S. Arima, N. Sato, T. Kai, H. Takayanagi, Y. Harigaya, *Tetrahedron* **2002**, *58*, 7851 – 7861; b) D. E. Davies, T. L. Gilchrist, T. G. Roberts, *J. Chem. Soc. Perkin Trans. 1* **1983**, 1275 – 1280; c) T. F. Jamison, Ph.D. thesis, Harvard University, **1997**.

[11] U. Schmidt, M. Kroner, U. Beutler, *Synthesis* **1988**, 475 – 477.

[12] Y. Oikawa, T. Yoshioka, K. Mohri, O. Yonemitsu, *Heterocycles* **1979**, *12*, 1457 – 1462.

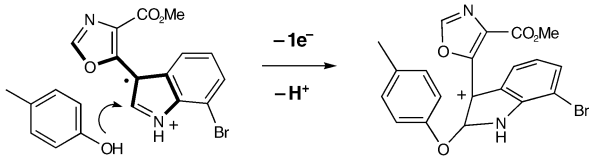
[13] Prepared from L-tyrosine methyl ester hydrochloride in two steps: 1) 2-nitrophenylsulfonyl chloride, pH 9.0 phosphate buffer/CH_2Cl_2; 2) KOH, aq MeOH (70 %—2 steps).

[14] C11 stereochemistry, relative to C10, is governed by geometry. Only two *cis*-fused dihydrobenzofuro[2,3b] indole diastereomers are formed. C10-(*R*), C11-(*S*) diastereomer **15** has been characterized by X-ray diffraction (Scheme 2). CCDC-218220 (**15**) contains the supplementary crystallographic data for this paper. These data can be obtained free of charge via www.ccdc.cam.ac.uk/conts/retrieving.html (or from the Cambridge Crystallographic Data Centre, 12 Union Road, Cambridge CB2 1EZ, UK; fax: (+44) 1223-336-033; or deposit@ccdc.cam.ac.uk).

[15] Analytical HPLC analyses of crude oxidation mixtures show that **14, 15**, and epimers **16** are formed in the ratio 3:1:0.7:0.7. Spirodienones **16** can be purified by preparative HPLC (C_{18}, CH_3CN/H_2O gradient) but partially degrade during flash chromatography on silica gel.

[16] L. Kürti, P. Herczegh, J. Visy, M. Simonyi, S. Antus, A. Pelter, *J. Chem. Soc. Perkin Trans. 1* **1999**, 379 – 380.

[17] We are mindful of another explanation. It is possible that **14** and **15** form as a result of an indolic oxidation. The (**14** + **15**)/**16** ratio may actually reflect two separate pathways operating rather than bifurcation through a common intermediate. For example, one electron oxidation of the indole subunit in **13** would produce a radical cation (e.g. **I**). This species could trap the tethered phenol, relinquish a second electron (to either I^{III} or I^{II}) and the



I **II**

resultant ion (**II**) undergo an internal Friedel-Crafts type alkylation to afford **14**/**15**. While experiments to test these ideas are ongoing, we do note examples of I^{III} oxidations for which related mechanisms might be invoked: a) Y. Kishi, S. Nakatsuka, T. Fukuyama, M. Havel, *J. Am. Chem. Soc.* **1973**, *95*, 6493 – 6495; b) N. A. Braun, M. Ousmer, J. D. Bray, D. Bouchu, K. Peters, E.-M. Peters, M. A. Ciufolini, *J. Org. Chem.* **2000**, *65*, 4397 – 4408.

[18] a) Y. Kita, H. Tohma, K. Kikuchi, M. Inagaki, T. Yakura, *J. Org. Chem.* **1991**, *56*, 435 – 438; b) Y. Tamura, T. Yakura, J. Haruta, Y. Kita, *J. Org. Chem.* **1987**, *52*, 3927 – 3930; c) P. Wipf, Y. Kim, *Tetrahedron Lett.* **1992**, *33*, 5477 – 5480; d) G. Scheffler, H. Seike, E. J. Sorensen, *Angew. Chem.* **2000**, *112*, 4783 – 4785; *Angew. Chem. Int. Ed.* **2000**, *39*, 4593 – 4596.

[19] Cleavage of the 2-nitrophenylsulfonamide: T. Fukuyama, C.-K. Jow, M. Cheung, *Tetrahedron Lett.* **1995**, *36*, 6373 – 6374.

[20] Prepared just prior to use by hydrogenolyzing commercial 7-benzyloxy tryptamine (Biosynth AG, Switzerland) over $Pd(OH)_2/C$ (1 equiv ethereal HCl, EtOH, 1 atm H_2, >95 % yield).

[21] P. Wipf, F. Yokokawa, *Tetrahedron Lett.* **1998**, *39*, 2223 – 2226.

[22] a) O. Yonemitsu, P. Cerutti, B. Witkop, *J. Am. Chem. Soc.* **1966**, *88*, 3941 – 3945; b) H. G. Theuns, H. B. M. Lenting, C. A. Salemink, H. Tanaka, M. S. Shibata, K. Ito, R. J. J. C. Lousberg,

 © 2003 Wiley-VCH Verlag GmbH & Co. KGaA, Weinheim

Heterocycles **1984**, *22*, 2007 – 2011; c) J. Mattay, *Synthesis* **1989**, 233 – 252.
[23] A. P. Kozikowski, W. Tuckmantel, C. George, *J. Org. Chem.* **2000**, *65*, 5371 – 5381.
[24] A. Guy, M. Lemaire, J.-P. Guetté, *Tetrahedron* **1982**, *38*, 2339 – 2346.
[25] a) W. R. Roush, D. S. Coffey, D. J. Madar, *J. Am. Chem. Soc.* **1997**, *119*, 11331 – 11332; b) R. Noyori, I. Nishida, J. Sakata, M. Nishizawa, *J. Am. Chem. Soc.* **1980**, *102*, 1223 – 1225.
[26] We are grateful to Professor William Fenical (Scripps Oceanographic Institute) for a generous gift of natural (−)-diazonamide A.
[27] G. Wang, A. W. G. Burgett, X. Wang, P. G. Harran, unpublished results.

Porphyrin–C60 Conjugates

Exceptional Redox and Photophysical Properties of a Triply Fused Diporphyrin–C_{60} Conjugate: Novel Scaffolds for Multicharge Storage in Molecular Scale Electronics**

Davide Bonifazi, Markus Scholl, Fayi Song, Luis Echegoyen, Gianluca Accorsi, Nicola Armaroli,* and François Diederich**

Dedicated to Professor Manfred T. Reetz on the occasion of his 60th birthday

The expansion and functionalization of π-conjugated molecular architectures to enhance the optoelectronic properties of the resulting chromophores is a topic of broad current interest.[1] Fascinating examples are the molecular tapes consisting of triply fused porphyrins, reported by Osuka and co-workers, which exhibit exceptionally low-energy electronic states and hold great potential as molecular wires in nanoscale electronics devices.[2]

The past decade has seen the construction of a great variety of electron donor–acceptor dyads, frequently featuring C_{60} as the electron-accepting component because of its three-dimensional structure and six easily accessible reduction states in solution.[3] In a biomimetic fashion, many of these dyads feature porphyrin donors which lose their characteristic luminescence properties as a result of light-induced energy and/or electron transfer to the fullerene acceptor.[4,5]

Since the chemical functionalization of the triply fused porphyrin sheets is largely unexplored[6] and the nature of their interactions with redox- and photoactive chromophores, such as fullerenes, unknown, we decided to prepare conjugate **1** with two C_{60} spheres covalently attached to a triply fused porphyrin dimer (Scheme 1). Here, we describe the synthesis and the exceptional physical properties of **1**. The first full electrochemical study on triply fused porphyrin sheets shows that **1** is capable of undergoing as many as fifteen reversible electron-transfer processes. Moreover, photophysical investigations demonstrate that **1** does not exhibit at all the classical[7] behavior documented for numerous porphyrin–fullerene dyads. Rather, photoexcitation of the fullerene units results in quantitative sensitization of the weakly emitting lowest singlet level of the porphyrin sheet while the fullerene emission is quenched.

The functionalized triply fused porphyrin dimer **2** on the way to **1** was obtained following two routes (Scheme 1). Dimerization of diarylporphyrin **3** with $AgPF_6$, followed by silver-mediated iodination and subsequent Suzuki coupling with phenylboronic ester **4**,[8] afforded the biaryl-type dimer **5**. Dimer **5** was converted into **2** (11% yield over four steps) following the protocol by Tsuda and Osuka[2c] for oxidative ring closure (DDQ and $Sc(OTf)_3$). As a better alternative, monoiodination of **3** afforded **6** and Suzuki coupling with **4** gave **7**. Oxidative ring closure of **7** directly led to **2** (39% yield over three steps). Reduction of **2** (DIBAL-H) provided dialdehyde **8** which was reduced ($NaBH_4$) to the corresponding bis(benzyl alcohol). Esterification with EtO_2CCH_2COCl yielded bismalonate **9**, and Bingel reaction with C_{60} gave the target conjugate **1**.

The redox properties of **1, 2, 5**, and comparison compounds **10**,[9] **11**,[9] and **12** were examined by cyclic (CV) and differential pulse (DPV) voltammetry (Table 1, Figures 1 and 2).

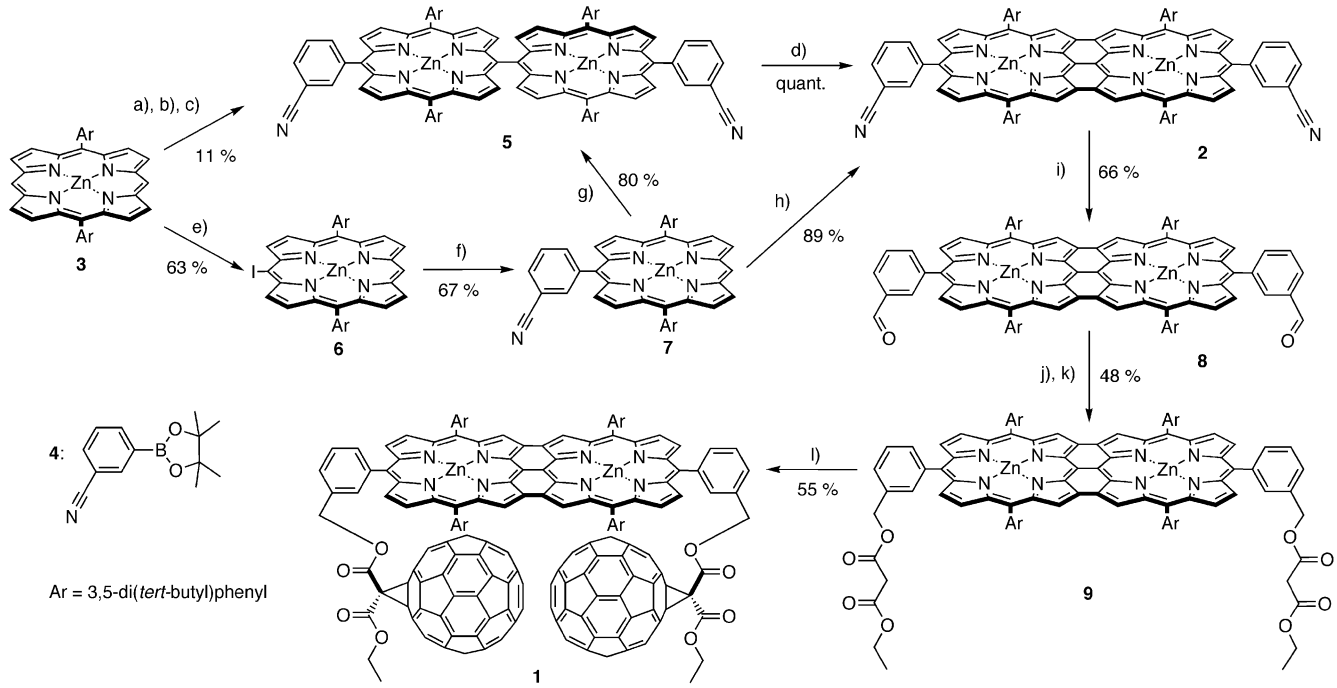
The cyclic voltammogram of **5** (Table 1) features two partially overlapped reduction couples at −1.75 and −1.86 V (difference of 0.11 V). The first 1-e$^-$ oxidation of the two porphyrin moieties appears as separated couples at 0.38 and 0.51 V whereas the second oxidation of both rings also gives two couples at 0.78 and 1.10 V. Seven reversible redox couples with identical current for each peak were observed for the triply fused porphyrin dimer **2** in CH_2Cl_2 (Figure 1b). The first and second reduction couples correspond to two-step, 1-e$^-$ per porphyrin ring reductions. Likewise, the first and the

[*] Prof. Dr. L. Echegoyen, Dr. F. Song
Department of Chemistry
Clemson University
219 Hunter Laboratories, Clemson SC 29634 (USA)
Fax: (+1) 864-656-6613
E-mail: luis@clemson.edu
Dr. N. Armaroli, Dr. G. Accorsi
Istituto per la Sintesi Organica e la Fotoreattività
40129 Bologna (Italy)
Fax: (+39) 051-6399844
E-mail: armaroli@isof.cnr.it
Prof. Dr. F. Diederich, D. Bonifazi, M. Scholl
Laboratorium für Organische Chemie
ETH-Hönggerberg, HCI
8093 Zürich (Switzerland)
Fax: (+41) 1-632-1109
E-mail: diederich@org.chem.ethz.ch

[**] We thank Rolf Häfliger for the mass spectrometric measurements. This research was supported by the Swiss National Science Foundation and the NCCR "Nanoscale Science", the Spinner Agency (Regione Emilia-Romagna, Italy), and the US National Science Foundation (CHE-0135786).

Supporting information for this article (selected physical and spectral data of **1** and **2**, cyclic voltammograms of **1, 2**, and **11**, luminescence spectra of **11** compared to reference compounds **5** and **13**, UV/Vis data of **1, 2, 9**, and **13**) is available on the WWW under http://www.angewandte.org or from the author.

 © 2003 Wiley-VCH Verlag GmbH & Co. KGaA, Weinheim DOI: 10.1002/anie.200352265



Scheme 1. Synthesis of conjugate **1**. a) $AgPF_6$, $CH_3CN/CHCl_3$ 1:6, RT, 15 h; b) $AgPF_6$, I_2, pyridine/$CHCl_3$ 1:60, RT; c) **4**, Cs_2CO_3, $[Pd(PPh_3)_4]$, toluene, reflux, 18 h; d) DDQ, $Sc(OTf)_3$, toluene, reflux, 30 min; e) $AgPF_6$, I_2, pyridine/$CHCl_3$ 1:60, RT; f) **4**, Cs_2CO_3, $[Pd(PPh_3)_4]$, toluene, reflux, 18 h; g) $AgPF_6$, $CH_3CN/CHCl_3$ 1:6, RT, 15 h; h) DDQ, $Sc(OTf)_3$, toluene, reflux, 30 min; i) DIBAL-H, CH_2Cl_2, −78 °C→RT, 2.5 h; j) $NaBH_4$, THF/EtOH 1:1, 0 °C→RT, 4 h; k) EtO_2CCH_2COCl, Et_3N, CH_2Cl_2, RT, 16 h; l) C_{60}, I_2, DBU, toluene, RT, 1.5 h. DDQ = 2,3-dichloro-5,6-dicyano-*p*-benzoquinone; DIBAL-H = di(*iso*-butyl)aluminum hydride; DBU = 1,8-diazabicyclo[5.4.0]undec-7-ene; Tf = trifluoromethanesulfonyl.

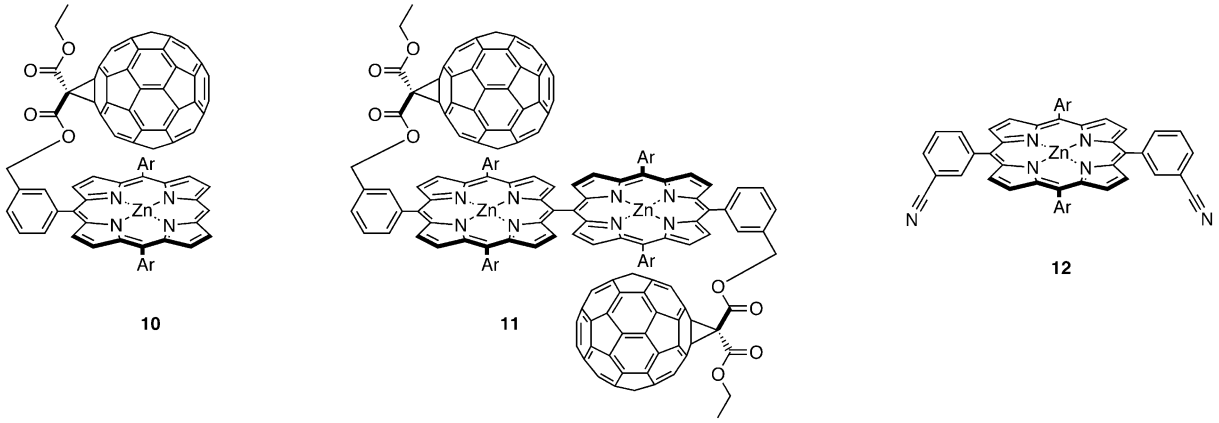


Table 1: Cyclic voltammetry data in CH_2Cl_2 (+0.1 M nBu_4NPF_6).[a]

	$E^{1/2}_{red,1}$	$E^{1/2}_{red,2}$	$E^{1/2}_{red,3}$	$E^{1/2}_{red,4}$	$E^{1/2}_{ox,1}$	$E^{1/2}_{ox,2}$	$E^{1/2}_{ox,3}$	$E^{1/2}_{ox,4}$
12	−1.71 (1 e⁻)	−2.09 (1 e⁻)	–	–	0.44 (1 e⁻)	0.74 (1 e⁻)	–	–
5	−1.75 (1 e⁻)	−1.86 (1 e⁻)	−2.20 (1 e⁻)	–	0.38 (1 e⁻)	0.51 (1 e⁻)	0.78 (1 e⁻)	1.10 (1 e⁻)
2[b]	−1.06 (1 e⁻)	−1.40 (1 e⁻)	−2.29 (1 e⁻)	−2.59 (1 e⁻)	0.15 (1 e⁻)	0.47 (1 e⁻)	0.92 (1 e⁻)	–
2	−1.01 (1 e⁻)	−1.26 (1 e⁻)	−2.18 (1 e⁻)	–	0.09 (1 e⁻)	0.37 (1 e⁻)	0.83 (1 e⁻)	1.10 (1 e⁻)
10	−1.06 (1e⁻)	−1.41 (1 e⁻)	−1.84 (2 e⁻)	–	0.36 (1 e⁻)	0.74 (1 e⁻)	–	–
11	−0.98 −1.06 (2 e⁻)	−1.41 (2 e⁻)	−1.84 (4 e⁻)	–	0.37 (1 e⁻)	0.50 (1 e⁻)	0.73 (1 e⁻)	0.84 (1 e⁻)
1	−0.99 −1.09 (3 e⁻)	−1.40 (3 e⁻)	−1.87 (2 e⁻)	−2.29 (3 e⁻)	0.03 (1 e⁻)	0.34 (1 e⁻)	0.82 (1 e⁻)	1.09 (1 e⁻)

[a] Potentials versus Fc/Fc^+. Working electrode: glassy carbon electrode; counter electrode: Pt; reference electrode: Ag/AgCl. Scan rate: 0.1 Vs^{-1}. $E^{1/2} = (E_{pa} + E_{pc})/2$, where E_{pc} and E_{pa} = cathodic and anodic peak potentials, respectively. [b] Solvent: THF.

 © 2003 Wiley-VCH Verlag GmbH & Co. KGaA, Weinheim

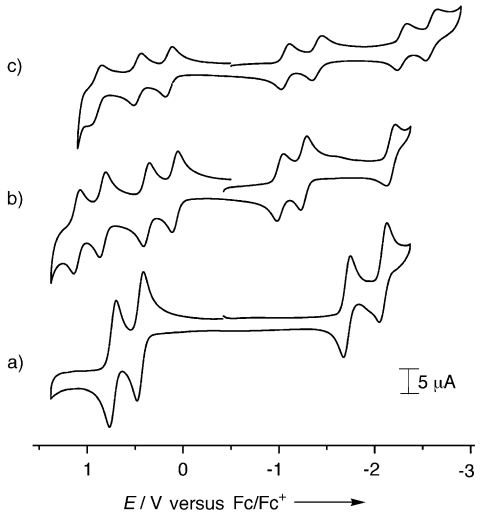


Figure 1. Cyclic voltammograms of a) **12** in CH_2Cl_2, b) **2** in CH_2Cl_2, and c) **2** in THF at 20±2°C (+0.1 M nBu_4NPF_6).

second oxidation peaks each correspond to a 1-e⁻ process, one per porphyrin ring. Relative to **12**, the first 1-e⁻ reduction potential of **2** is shifted positively by 0.7 V whereas the first 1-e⁻ oxidation potential is shifted negatively by 0.35 V. The fourth reduction peak was not observed because of the limited potential window in CH_2Cl_2. However, CV and DPV measurements in THF revealed the presence of the fourth reduction peak (Figure 1c). These results confirm that each redox couple for **12** splits into two couples for **2**.

Conjugation of two C_{60} moieties to the triply bridged porphyrin dimer in **1** results in nine reversible redox processes involving a total of fifteen electrons (Figure 2b). The four oxidation peaks correspond to the four 1-e⁻ oxidation steps centered at the porphyrin units, and the first oxidation peak is cathodically shifted relative to **2** (Figure 2a) by 60 mV. The two partially overlapped peaks at −1.0 V correspond to the first reduction of the two C_{60} units and a 1-e⁻ process for the porphyrin system (a 3-e⁻ net process). The peak at −1.38 V corresponds, likewise, to the second reduction of the two C_{60} units and a second reduction of the porphyrin sheet (again, a net 3-e⁻ process). The smaller peak at −1.85 V is attributed to the third 1-e⁻ reduction of each of the two C_{60} moieties (a 2-e⁻ process). The peak at −2.28 V corresponds to the fourth 1-e⁻ reduction of the fullerene moieties and the third 1-e⁻ reduction of the porphyrin (a 3-e⁻ net process). The cyclic voltammogram of biaryl-type dimer **11** features the first porphyrin-based oxidation peak potential anodically shifted by 300 mV relative to **1** (Figure 2c). Furthermore, the first two porphyrin-centered reduction steps in **11** are shifted cathodically by 850 mV relative to the corresponding first reduction couple in **1**.

The photophysical properties of the two conjugates **1** and **11** also differ dramatically. The absorption spectrum (toluene)

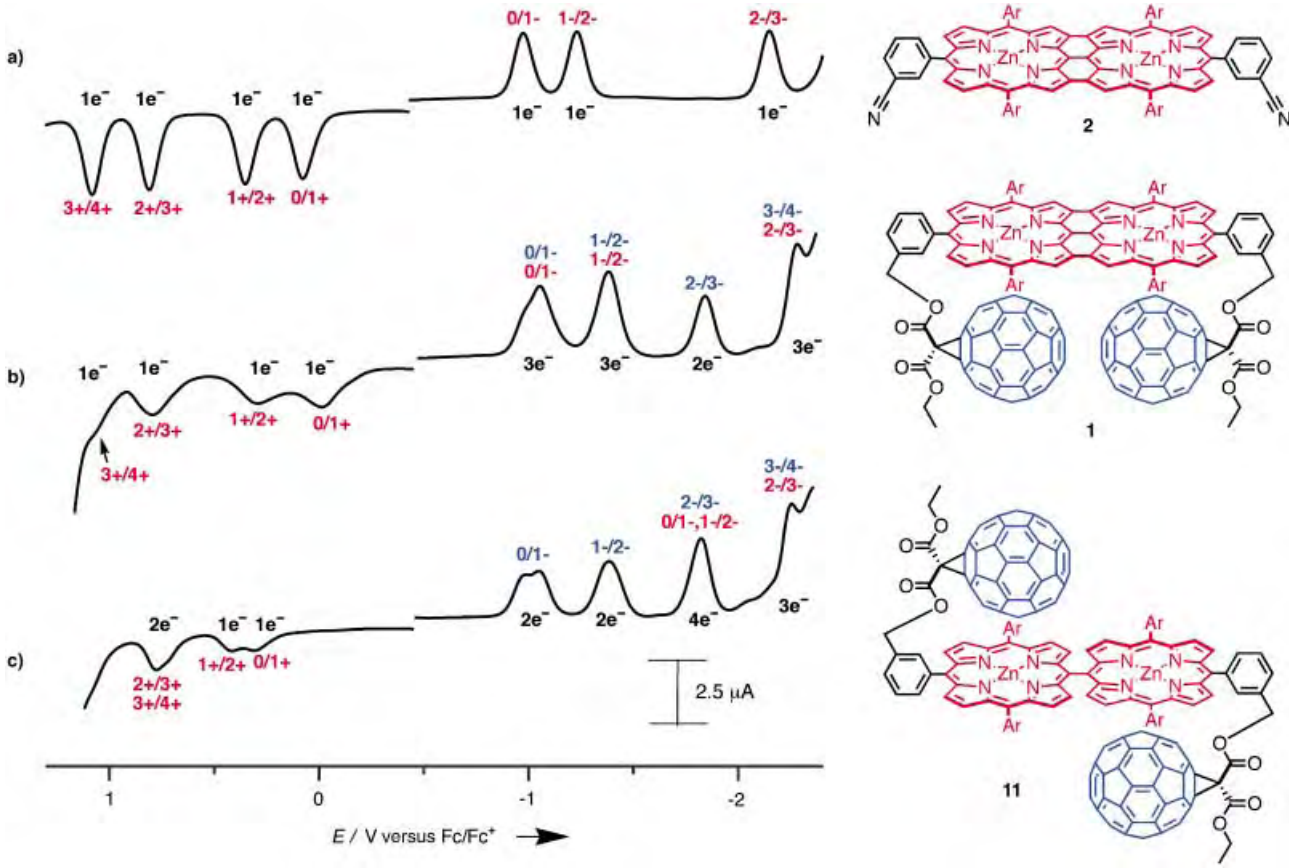
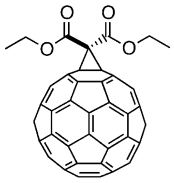


Figure 2. Differential pulse voltammograms of a) **2**, b) **1**, and c) **11** in CH_2Cl_2 at 20±2°C.

 © 2003 Wiley-VCH Verlag GmbH & Co. KGaA, Weinheim



13

of conjugate **11** with the biaryl-type porphyrin dimer does not match the sum spectrum of its component units (**5** and 2 × **13**; Figure 3), particularly in the Soret-band region, which is split as a result of exciton coupling.[10] This result is attributed to strong face-to-face electronic interactions between the porphyrin and fullerene chromophores.[11] Only the 630–800-nm region of the spectrum of **11** is more intense than its calculated counterpart, which suggests the occurrence of sizeable interchromophoric charge transfer interactions.[12] An emissive charge-transfer

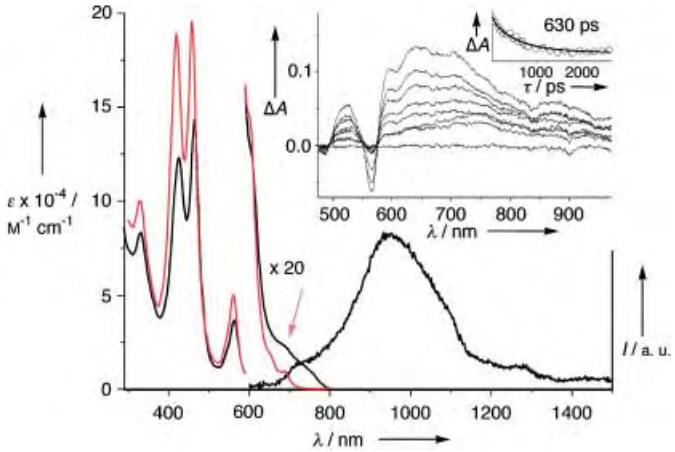


Figure 3. Red line: sum of the electronic absorption spectra of **5** and two fullerenes **13**. Black line: Absorption and (from 600 nm) emission spectra (λ_{exc} = 330 nm) of **11.** Inset: Transient absorption spectrum of **11** at λ_{exc} = 532 nm and spectral time decay at 660 nm. All spectra were recorded in toluene at 298 K.

(CS) state is detected in the NIR region (λ_{max} = 950 nm, Figure 3). The transient absorption spectrum of **11** in toluene (λ_{exc} = 532 nm, Figure 3) exhibits the diagnostic broad band of the Zn^{II}–porphyrin radical cation with a maximum at 640 nm, thus indicating that photoinduced electron transfer from the porphyrin to the fullerene moieties occurs.[12] The lifetime of the CS state is 630 ps. Porphyrin singlet and triplet excited states are dramatically quenched as shown from fluorescence and phosphorescence spectra at 298 and 77 K, respectively. In contrast, some residual excited-state features of the fullerene are detected (that is, a tail of fullerene fluorescence above 700 nm and a very weak fullerene triplet absorption trace at λ_{max} = 740 nm), which are accompanied by a very minor amount of singlet oxygen luminescence (Figure 3). All the above results indicate that the local excited states of **11** centered on the porphyrin and fullerene moieties are deactivated to a lower lying luminescent charge-separated state that is localized at about 1.4 eV, as derived from electrochemical (Table 1, CH_2Cl_2) and luminescence data (Figure 3, toluene). The residual localized excited states of the fullerene are attributed to a minority (< 10 %) of loose molecules where strong donor–acceptor porphyrin–fullerene attractions are not established.[12b]

The steady-state absorption spectrum of **9** is characterized by splitting of the Soret band as a result of exciton coupling between the two fused porphyrin units and a shift of the Q-band envelope into the NIR region (Figure 4).[13] The comparison of the absorption spectrum of **1** with the sum of its component units (**9** + 2 × **13**) shows two small but relevant differences: a) a 3-nm red shift and a very small decrease in

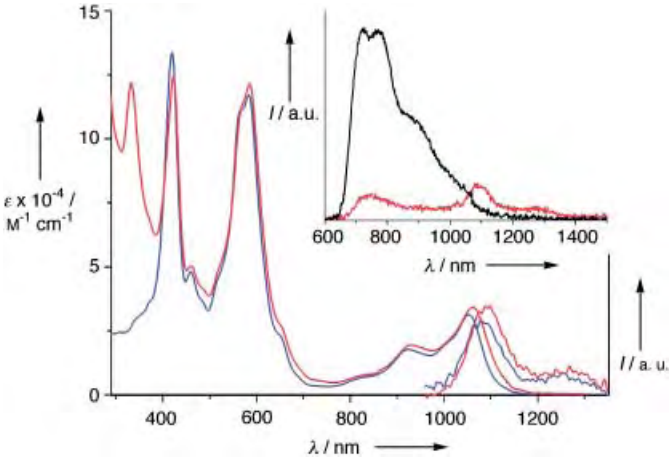


Figure 4. Absorption and (from 960 nm) fluorescence spectra (λ_{exc} = 420 nm, A = 0.20) of **9** (blue) and **1** (red). Inset: fluorescence spectra of **13** (black) and **1** (red), λ_{exc} = 330 nm, A = 0.30. All fluorescence spectra were recorded from air-purged samples.

the intensity of the highest energy Soret band and b) a 10-nm shift to lower energy of the most intense Q-band in the NIR domain. These spectral changes are smaller than those observed for **11** or other conjugates with face-to-face alignment of porphyrin and C_{60} moieties,[12] thus suggesting weaker electronic interchromophoric interactions.

Dimer **9** exhibits an emission band in the NIR region (λ_{max} = 1080 nm) at all excitation wavelengths. This is a mirror image of the profile of the Q bands (Figure 4), and is unambiguously assigned to fluorescence from the lowest singlet excited state. The NIR emission band is observed also for **1** upon selective excitation of the porphyrin chromophore (420 or 585 nm). This band is shifted by 12 nm (λ_{max} = 1092 nm) relative to that in **9**, and is in line with the trend seen in the absorption spectra. Preferential excitation of the C_{60} chromophores in **1** at 330 nm (≥ 80 %) shows a dramatic quenching of the fullerene fluorescence relative to **13**, whereas a pure porphyrin fluorescence band is detected in the NIR region (Figure 4, inset). According to the electrochemical data in CH_2Cl_2, the charge-separated state, which corresponds to the reduction of a fullerene unit and oxidation of the porphyrin moiety, is located at about 1.0 eV.[14] This energy value is comparable to the singlet level of the porphyrin, as estimated from the wavelength of the fluorescence band (Figure 4). Thus, in principle, both energy and electron transfer may be responsible for the observed quenching of the fullerene luminescence. Two experimental results helped to unravel the quenching mechanism: 1) the picosecond transient absorption of **1** with a time resolution of 35 ps shows only (at early times) the spectral features of the fused porphyrin dimer, and 2) the porphyrin fluorescence

 © 2003 Wiley-VCH Verlag GmbH & Co. KGaA, Weinheim

quantum yield is identical, within experimental uncertainty, for **1** and **9** ($\Phi_F = 3.5 \times 10^{-4}$, $\lambda_{exc} = 330$ nm). We conclude that excitation of the fullerene chromophore results in quantitative sensitization of the lowest singlet state of the porphyrin, and that the role of the nearly isoenergetic charge-separated state in toluene solution, if any, is not relevant.

In summary, despite the fact that triply fused porphyrin dimers are much better electron donors than simple porphyrins, their low-lying and very short lived (4.5 ps)[13] singlet level offers an extremely competitive deactivation pathway and acts as a sink for the higher energy electronic levels. Hence, the photoinduced process in **1** (C_{60}→porphyrin energy transfer) is completely different from that in the biaryl-type bisporphyrin conjugate **11** (porphyrin→C_{60} electron transfer) while, notably, both molecules are NIR emitters.

Received: June 30, 2003 [Z52265]

Keywords: electrochemistry · electron transfer · fullerenes · luminescence · porphyrinoids

[1] a) J. M. Tour, *Acc. Chem. Res.* **2000**, *33*, 791 – 804; b) R. E. Martin, F. Diederich, *Angew. Chem.* **1999**, *111*, 1440 – 1469; *Angew. Chem. Int. Ed.* **1999**, *38*, 1351.

[2] a) A. Tsuda, H. Furuta, A. Osuka, *Angew. Chem.* **2000**, *112*, 2649 – 2652; *Angew. Chem. Int. Ed.* **2000**, *39*, 2549 – 2552; b) A. Tsuda, H. Furuta, A. Osuka, *J. Am. Chem. Soc.* **2001**, *123*, 10304 – 10321; c) A. Tsuda, A. Osuka, *Science* **2001**, *293*, 79 – 82.

[3] L. Echegoyen, F. Diederich, L. E. Echegoyen, *Fullerenes: Chemistry and Physics & Technology* (Eds.: K. M. Kadish, R. S. Ruoff), Wiley, New York, **2000**, pp. 1 – 51.

[4] Recent reviews: a) H. Imahori, Y. Mori, Y. Matano, *J. Photochem. Photobiol. C* **2003**, *3*, 55 – 83; b) N. Armaroli, *Photochem. Photobiol. Sci.* **2003**, *2*, 73 – 87; c) D. Gust, T. A. Moore, A. L. Moore, *Acc. Chem. Res.* **2001**, *34*, 40 – 48; d) D. A. K. Burrell, D. L. Officer, P. G. Pflieger, D. C. W. Reid, *Chem. Rev.* **2001**, *101*, 2751 – 2796; e) D. M. Guldi, *Chem. Commun.* **2000**, 321 – 327; f) D. M. Guldi, M. Prato, *Acc. Chem. Res.* **2000**, *33*, 695 – 703.

[5] Some selected publications: a) H. Imahori, N. V. Tkachenko, V. Vehmanen, K. Tamaki, H. Lemmetyinen, Y. Sakata, S. Fukuzumi, *J. Phys. Chem. A* **2001**, *105*, 1750 – 1756; b) D. Sun, F. S. Tham, C. A. Reed, P. D. W. Boyd, *Proc. Natl. Acad. Sci. USA* **2002**, *99*, 5088 – 5092.

[6] I. M. Blake, A. Krivokapic, M. Katterle, H. L. Anderson, *Chem. Commun.* **2002**, 1662 – 1663.

[7] D. M. Guldi, *Chem. Soc. Rev.* **2002**, *31*, 22 – 36.

[8] L. Sebo, V. Gramlich, F. Diederich, *Helv. Chim. Acta* **2000**, *83*, 93 – 113.

[9] D. Bonifazi, F. Diederich, *Chem. Commun.* **2002**, 2178 – 2179.

[10] N. Aratani, A. Osuka, H. S. Cho, D. Kim, *J. Photochem. Photobiol. C* **2002**, *3*, 25 – 52.

[11] The interchromophoric ground-state interaction in **10** and **11** was quantified as about 12 kJ mol^{-1} (toluene, 298 K), see ref. [9]. In contrast, interchromophoric interactions in **1** are weaker (see text). Thus, the conformation of **1** depicted in Scheme 1 is only one of many possible; conformers with the carbon spheres nesting on opposite faces of the porphyrin dimer or turned away from the heterocycle are of equal probability.

[12] a) N. Armaroli, G. Marconi, L. Echegoyen, J.-P. Bourgeois, F. Diederich, *Chem. Eur. J.* **2000**, *6*, 1629 – 1645; b) N. Armaroli in *Fullerenes: From Synthesis to Optoelectronic Properties* (Eds.: D. M. Guldi, N. Martin), Kluwer, Dordrecht, **2002**, pp. 137 – 162.

[13] H. S. Cho, D. H. Jeong, S. Cho, D. Kim, Y. Matsuzaki, K. Tanaka, A. Tsuda, A. Osuka, *J. Am. Chem. Soc.* **2002**, *124*, 14642 – 14654.

[14] The use of the electrochemical data in CH_2Cl_2 to estimate the energy of the CS state of **1** in toluene is a reasonable approximation in light of the good accord found between the energy of the CS state calculated by luminescence data (toluene) and electrochemistry (CH_2Cl_2) for the similar system **11**.

 © 2003 Wiley-VCH Verlag GmbH & Co. KGaA, Weinheim

Cover Picture

Ludwig L. Böhm*



Fifty years ago Karl Ziegler and co-workers discovered the now-famous process for the catalytic production of polyethylene at moderate temperatures and pressures. The cover of the patent gives November 18, 1953 as the priority date. Today, 50 years on, as a result of highly active catalysts and a detailed understanding of the system on all scales, it is still an extremely viable process. In his Review on page 5010 ff. L. L. Böhm describes the current industrial process based on Ziegler catalysts.

Contents

Angewandte EarlyView

The following articles are available online (in Wiley InterScience). You can find them at www.angewandte.org, under Full Text, Early View.

X. Wang, L. Andrews:*
Gold Is Noble but Gold Hydride Anions Are Stable
DOI: 10.1002/anie.200351780
Published online: October 14, 2003

F. Dumestre, B. Chaudret, C. Amiens, M. Respaud, P. Fejes, P. Renaud, P. Zurcher:*
Unprecedented Crystalline Super-Lattices of Monodisperse Cobalt Nanorods
DOI: 10.1002/anie.200352090
Published online: October 14, 2003

J. P. Camden, H. A. Bechtel, R. N. Zare:*
Dynamics of the Simplest Reaction of a Carbon Atom in a Tetrahedral Environment
DOI: 10.1002/anie.200352642
Published online: October 14, 2003

Articles judged by the referees or the editor as being either very important or very urgent are immediately edited, proof-read, and electronically published once the manuscript has arrived in the editorial office in final form. As long as there is no page number available these articles should be cited in the following manner:

Author(s) *Angew. Chem. Int. Ed.*, online publication date, DOI.

News

Awards for John M. Thomas and Tobin J. Marks _____ **4992**

Books

Structural Bioinformatics _____ **4993** — Philip E. Bourne, Helge Weissig — *reviewed by Lars-Oliver Essen*

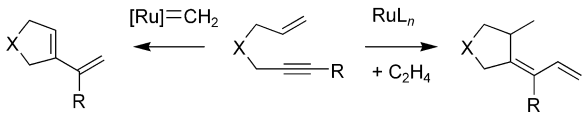
DNA and RNA Binders _____ **4994** — Martine Demeunynck, Christian Bailly, W. David Wilson — *reviewed by Oliver Seitz*

Highlights

Cyclizations

B. Schmidt* _____ **4996 – 4999**

Ruthenium-Catalyzed Cyclizations: More than Just Olefin Metathesis!



From unexpected side products to new catalytic cyclizations: Numerous ruthenium-catalyzed cyclization reactions that probably proceed via five-membered ruthenium metallacycles and do not involve olefin metathesis have been described recently. The border between metathesis and nonmetathesis cyclization pathways is not always clearly defined. This phenomenon can lead to the discovery of new ruthenium-catalyzed reactions (see scheme; X = CR_2, NR).

Essays

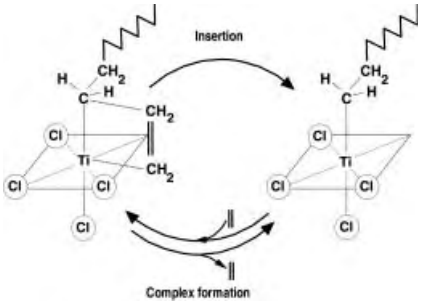
Fifty Years of Ziegler Catalysts

G. Wilke* _____ **5000 – 5008**

Fifty Years of Ziegler Catalysts: Consequences and Development of an Invention

In October, 1953 an experiment was carried out in the Max Planck Institut für Kohlenforschung in Mülheim an der Ruhr, that even today has a huge influence on the chemical industry: the catalytic polymerization of ethylene under normal pressure carried out with what at the time was known as the Mülheim mixed catalyst. The story of what is know known as the Ziegler catalyst reveals its discovery to be the result of the meticulous analysis of apparently failed experiments.

Reviews



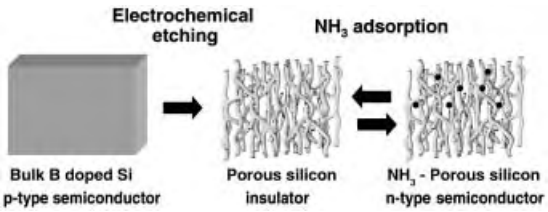
Happy birthday! 50 years after the discovery of the catalytic polymerization of ethylene with Ziegler catalysts (see scheme) this process is still a vital, modern, industrial process. Based on high-performance catalysts and a broad process knowledge, products with excellent combinations of properties for a wide-range of applications can be produced in an economical environmentally friendly and resources saving way.

Fifty Years of Ziegler Catalysts

L. L. Böhm* ——— **5010 – 5030**

The Ethylene Polymerization with Ziegler Catalysts: Fifty Years after the Discovery

Communications



Gas works wonders! Conduction-band electrons can be generated in p^+-type mesoporous crystalline silicon through the adsorption of ammonia (see scheme). Free-carrier concentration increases with increasing NH_3 adsorption to a critical value, where a reversible insulator-to-metal transition occurs.

Electronic Transitions in Silicon VIP

M. Chiesa, G. Amato, L. Boarino, E. Garrone, F. Geobaldo, E. Giamello* ——— **5032 – 5035**

Reversible Insulator-to-Metal Transition in p^+-Type Mesoporous Silicon Induced by the Adsorption of Ammonia



Thin CdSe layers ("quantum shells") were epitaxially grown onto CdS nanocrystal templates. Their optical properties are dominated by the shell thickness despite the different bandgap and size of the templates. The emission of the CdSe quantum shells, which can be tuned by varying the shell thickness, ranges from 520 to 650 nm (see Figure), and the emission quantum yield can be increased to over 40% by coating the quantum shells with epitaxially grown CdS thin layers (CdSe colloidal "quantum wells").

CdSe Quantum Shells and Wells

D. Battaglia, J. J. Li, Y. Wang, X. Peng* ——— **5035 – 5039**

Colloidal Two-Dimensional Systems: CdSe Quantum Shells and Wells

For the USA and Canada:
ANGEWANDTE CHEMIE International Edition (ISSN 1433-7851) is published weekly by Wiley-VCH PO Box 191161, D 69451 Weinheim, Germany. Air freight and mailing in the USA by Publications Expediting Inc. 200 Meacham Ave., Elmont, NY 11003. Periodicals postage paid at Jamaica NY 11431. US POSTMASTER: send address changes to *Angewandte Chemie*, Wiley-VCH, 111 River Street, Hoboken, NJ 07030. Annual institutional subscription price for institutions: Europe € 3430.00/3118.00. Outside Europe US$ 4499.00/4090.00 (valid for print and electronic/print or electronic delivery); for individuals who are personal members of a national chemical society, or whose institution already subscribes, or who are retired or self-employed consultants, print only. Europe € 248.00/Outside Europe US$ 378.00. Postage and handling charges included. All Wiley-VCH prices are exclusive VAT.

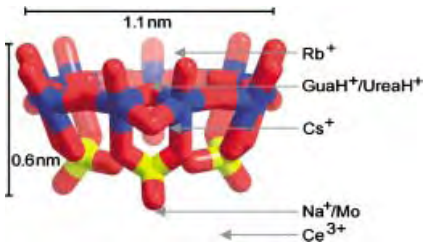
 © 2003 Wiley-VCH Verlag GmbH & Co. KGaA, Weinheim

Contents

"Nano-ion Chromatograph"

A. Müller,* S. K. Das, S. Talismanov, S. Roy, E. Beckmann, H. Bögge, M. Schmidtmann, A. Merca, A. Berkle, L. Allouche, Y. Zhou, L. Zhang ——— **5039 – 5044**

Trapping Cations in Specific Positions in Tuneable "Artificial Cell" Channels: New Nanochemistry Perspectives

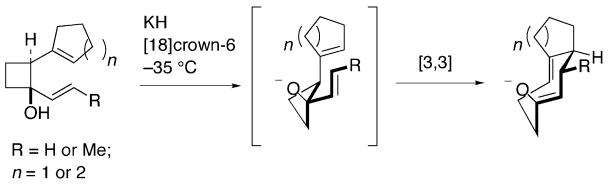


A decision-making capsule! Where cation trafficking comes to a halt is predetermined, with the process corresponding to a "nano-ion chromatograph" in action: starting from pores the route may end in a finely sculpturable interior of a stable, soluble spherical capsule but in many cases it ends in between in channels that exhibit a variety of cation-capturing functionalities at different positions (one of the twenty channels is shown with the residing cations).

Oxy-Cope Reaction Mechanism

P. Maurin, S.-H. Kim, S. Y. Cho, J. K. Cha* ——— **5044 – 5047**

On the Mechanism of the Anionic Oxy-Cope Rearrangement of *trans*-1,2-Dialkenylcyclobutanols

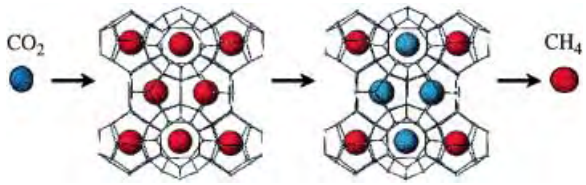


A concerted mechanism involving a chairlike transition state (see scheme) and no appreciable loss of enantiopurity was concluded for the anionic oxy-Cope rearrangement of sterically unencumbered *trans*-1,2-dialkenylcyclobutanols from a study employing nonracemic substrates containing vinyl and propenyl groups with evaluation of the enantio- and diastereofacial selectivity.

CH_4 from Methane Hydrate

H. Lee, Y. Seo, Y.-T. Seo, I. L. Moudrakovski, J. A. Ripmeester* ——— **5048 – 5051**

Recovering Methane from Solid Methane Hydrate with Carbon Dioxide

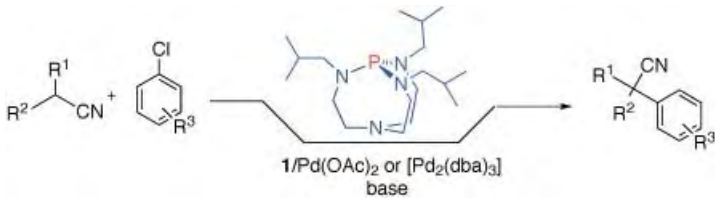


CO_2 in, CH_4 out! From NMR spectroscopic measurements of composition and kinetics, it can be shown that the recovery of methane from methane hydrate is possible through its reaction with CO_2 (see diagram), even though the yield is less than that expected from kinetic and thermodynamic arguments.

Arylation of Nitriles

J. You, J. G. Verkade* ——— **5051 – 5053**

A General Method for the Direct α-Arylation of Nitriles with Aryl Chlorides



The long-standing challenge of developing a general method for the title methodology is met for a broad range of aryl chlorides through the use of bicyclic P(*i*BuNCH$_2$CH$_2$)$_3$N (**1**) as a bulky electron-rich ligand for palladium (see scheme, dba = dibenzylideneacetone).

 © 2003 Wiley-VCH Verlag GmbH & Co. KGaA, Weinheim

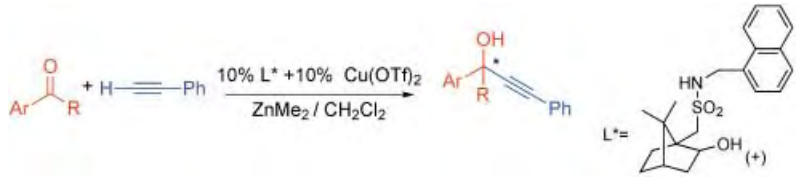


A key role for sulfur and the potential for $N_{ax} \rightarrow P$ intrabridgehead interactions are invoked to explain the impressive effect of the cocatalyst (shown in color) in the $TiCl_4$-mediated Baylis–Hillman reaction [Eq. (1)]. Even sterically hindered and electronically deactivated aldehydes such as *o*-anisaldehyde can be coupled under these conditions. EWG = electron-withdrawing group, RT = room temperature.

Baylis–Hillman Reaction

J. You, J. Xu, J. G. Verkade* . **5054 – 5056**

A Highly Active and Selective Catalyst System for the Baylis–Hillman Reaction

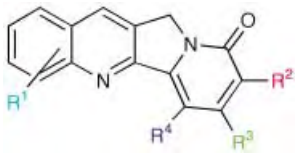


The smooth addition of phenylacetylene to aromatic ketones in the presence of catalytic amounts of $Cu(OTf)_2$ and camphorsulfonamide provides the corresponding tertiary propargylic alcohols in high yields and with up to 97% *ee*. This reaction represents a highly enantioselective catalytic addition of dialkynyl zinc reagents to simple ketones.

Enantioselective Alkynylation

G. Lu, X. Li, X. Jia, W. L. Chan, A. S. C. Chan* _____ **5057 – 5058**

Enantioselective Alkynylation of Aromatic Ketones Catalyzed by Chiral Camphorsulfonamide Ligands

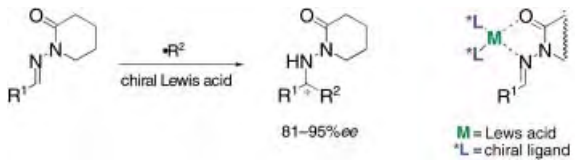


A general route to oxoindolizino quinolines, such as nothapodytine A, mappicine, camptothecin, and several chemotherapeutic derivatives, is illustrated by the synthesis of the antiviral natural product from *Nothapodytes foetida*, mappicine ketone ($R^1 = R^4 = H$, $R^2 = CH_3$, $R^3 = COC_2H_5$). A wide range of new camptothecinoids should now be readily available for biological testing.

Synthesis of Quinoline Alkaloids

G. B. Raolji, S. Garçon, A. E. Greene,* A. Kanazawa* _____ **5059 – 5061**

A Modular Approach to Oxoindolizino Quinolines: Efficient Synthesis of Mappicine Ketone (Nothapodytine B)



A radical concept: In the presence of chiral Cu^{II}–bisoxazoline complexes, the addition of alkyl radicals to achiral *N*-acyl hydrazones, which have a two-point-binding motif, proceeded with high enantioselectivity. Evidence of catalyst turnover was demonstrated, providing the first example of asymmetric catalysis in radical additions to C=N bonds.

Radical Additions to C = N Bonds

G. K. Friestad,* Y. Shen, E. L. Ruggles _____ **5061 – 5063**

Enantioselective Radical Addition to *N*-Acyl Hydrazones Mediated by Chiral Lewis Acids

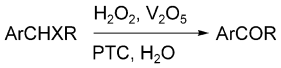
 © 2003 Wiley-VCH Verlag GmbH & Co. KGaA, Weinheim

Contents

Green Chemistry

C. Li,* P. Zheng, J. Li, H. Zhang, Y. Cui, Q. Shao, X. Ji, J. Zhang, P. Zhao, Y. Xu ——— 5063 – 5066

The Dual Roles of Oxodiperoxovanadate Both as a Nucleophile and an Oxidant in the Green Oxidation of Benzyl Alcohols or Benzyl Halides to Aldehydes and Ketones



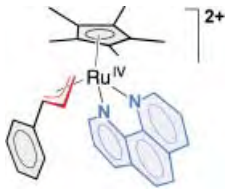
One catalyst, two roles: $VO(O_2)_2^-$ reacts as a nucleophilic oxidant under acidic conditions towards benzyl alcohols. Altogether 15 alcohols have been oxidized, in the absence of organic solvent, in excellent yields. Benzyl halides are also oxidized by H_2O_2 in water catalyzed by oxodiperoxovanadate and a phase transfer catalyst into aromatic aldehydes and ketones (see scheme). This reaction is the first green oxidation of benzyl halides.

Regioselective Allylic Substitution

M. D. Mbaye, B. Demerseman,* J.-L. Renaud, L. Toupet, C. Bruneau* ——— 5066 – 5068

[Cp*(η^2-bipy)(MeCN)Ru^{II}][PF_6] Catalysts for Regioselective Allylic Substitution and Characterization of Dicationic [Cp*-(η^2-bipy)(η^3-allyl)Ru^{IV}][PF_6]$_2$ Intermediates

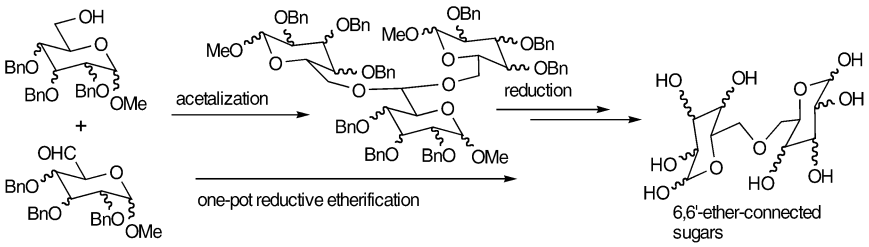
The coordination of a 2,2′-bipyridyl derivative to a $(C_5Me_5)Ru^{II}$ fragment provides both a facile route to unprecedented dicationic (allyl)Ru^{IV} complexes (see picture) and new highly efficient catalysts for the regioselective allylic substitution from unsymmetrical allylic carbonates.



Dipyranose Ethers

H. Takahashi, T. Fukuda, H. Mitsuzuka, R. Namme, H. Miyamoto, Y. Ohkura, S. Ikegami* ——— 5069 – 5071

Development of a Novel Sugar Linkage: 6,6′-Ether-Connected Sugars



Unusual sugar dimers: The synthesis of 6,6′-ether-connected pyranoses by an acetalization–reduction procedure is described (see scheme). Structure–activity-relationship studies of these novel carbohydrate dimers suggested that the natural product coyolosa, which has been shown to have a significant effect on fasting blood-glucose levels, may have a different structure from the one previously reported.

Catalytic Methanol Oxidation

H. Liu, N. Bayat, E. Iglesia* 5072 – 5075

Site Titration with Organic Bases During Catalysis: Selectivity Modifier and Structural Probe in Methanol Oxidation on Keggin Clusters

The selective and permanent titration of protons with organic bases (2,6-di-*tert*-butylpyridine or pyridine) provides an accurate measure of the dispersion of Keggin structures during catalytic oxidation of methanol. Titration allows the systematic control of the redox and acid properties of $H_{3+n}PV_nMo_{12-n}O_{40}$ ($n = 0$–4) Keggin clusters and leads to unprecedented selectivity in the formation of dimethoxymethane (> 80%) and high yields.

 © 2003 Wiley-VCH Verlag GmbH & Co. KGaA, Weinheim

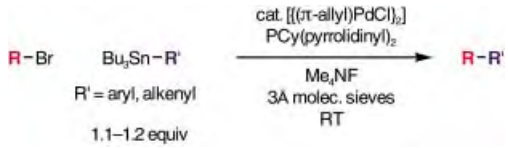


Easily accessible, the tris(alkyl) complexes of rare-earth elements [Ln(CH_2SiMe_3)$_3$(thf)$_2$] are activated by [NMe_2HPh][$B(C_6F_5)_4$] in the presence of Al*i*Bu$_3$ to catalyze homogeneous ethylene polymerization. Model reactions show that the bis(alkyl) yttrium monocation is converted into the mono(alkyl) dication (see picture), which appears to be the active species in ethylene polymerization.

Efficient Ethylene Polymerization

S. Arndt, T. P. Spaniol, J. Okuda* ——— **5075 – 5079**

Homogeneous Ethylene-Polymerization Catalysts Based on Alkyl Cations of the Rare-Earth Metals: Are Dicationic Mono(alkyl) Complexes the Active Species?

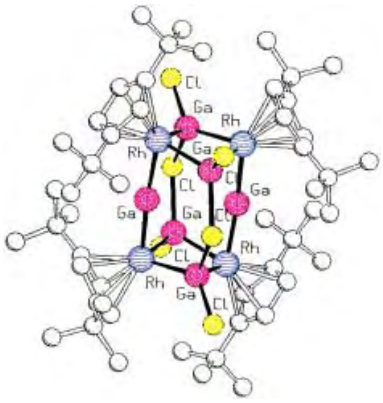


Alkyldiaminophosphanes (PR(NR'$_2$)$_2$) are a new class of ligands for palladium-catalyzed cross-couplings of alkyl halides (see scheme). In comparison with trialkylphosphanes, alkyldiaminophosphanes furnish more versatile catalysts for Stille reactions of alkyl bromides and achieve efficient couplings with both vinyl and aryl stannanes. Furthermore, Pd/PR(NR'$_2$)$_2$ provides the first method for accomplishing Stille cross-couplings of simple alkyl iodides that bear β-hydrogen atoms.

Expanding the Stille Coupling

H. Tang, K. Menzel, G. C. Fu* ——— **5079 – 5082**

Ligands for Palladium-Catalyzed Cross-Couplings of Alkyl Halides: Use of an Alkyldiaminophosphane Expands the Scope of the Stille Reaction

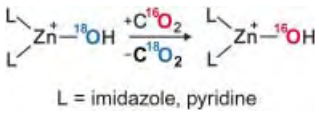


Mild reduction with metals: Elemental gallium is used as mild reducing agent for transition-metal halides to generate subvalent GaCl ligands in novel clusters. In the reaction of Ga with [{Cp''RhCl2}] (Cp'' = η^5-1,3-C_5H_3tBu$_2$), clusters with GaCl ligands and with unprecedented two-coordinate Ga centers in a multicenter–multiple-bonding interaction between two rhodium centers are formed (see picture).

Cluster Chemistry

M. Scheer,* M. Kaupp,* A. V. Virovets, S. N. Konchenko* ——— **5083 – 5086**

Elemental Gallium as a Source of Subvalent Gallium Units in Gallium–Rhodium Clusters



Masses of evidence: Mass spectrometry combined with ^{18}O labeling reveals that the imidazole and pyridine complexes [L_nZnOH]$^+$ (n = 1, 2) are capable of activating carbon dioxide, under thermal conditions. These gas-phase reactions thus provide a simple mimic for the function of the active site in carbonic anhydrase.

Carbon Dioxide Activation

D. Schröder,* H. Schwarz, S. Schenk, E. Anders ——— **5087 – 5090**

A Gas-Phase Reaction as a Functional Model for the Activation of Carbon Dioxide by Carbonic Anhydrase

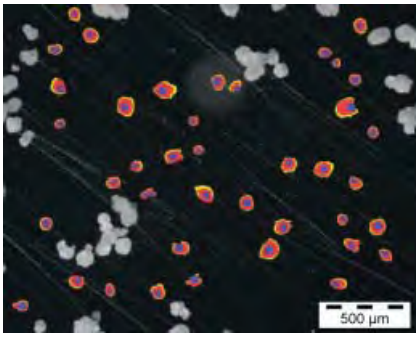
 © 2003 Wiley-VCH Verlag GmbH & Co. KGaA, Weinheim

Contents

Kinetics of Olefin Polymerization

S. Knoke, D. Ferrari, B. Tesche, G. Fink* ——— **5090 – 5093**

Microkinetic Videomicroscopic Analysis of Olefin Polymerization with a Supported Metallocene Catalyst

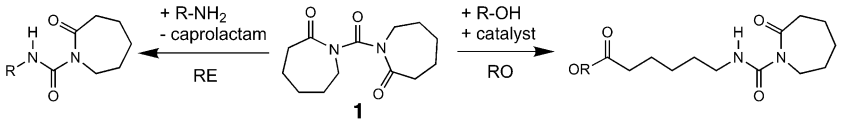


Picture this: The simultaneous growth of many single grains of catalyst culminating in polymer particles can be observed by videomicroscopy, and single-grain kinetics can be studied. The gas-phase polymerization of ethylene on 40 particles was examined in an autoclave equipped with a glass window by automatic image processing. The picture shows the overlap of three different stages of the polymerization after 0 (blue), 60 (red), and 180 (yellow) minutes.

Blocked Isocyanate Equivalents

S. Maier, T. Loontjens, B. Scholtens, R. Mülhaupt* ——— **5094 – 5097**

Carbonylbiscaprolactam: A Versatile Reagent for Organic Synthesis and Isocyanate-Free Urethane Chemistry



The power of the rings: The reactions of carbonylbiscaprolactam (CBC, **1**) with amines and alcohols proceed either by ring elimination (RE) or by ring opening (RO). The conversion and selectivity of these reactions were optimized in studies with various hydroxy and amino compounds, catalysts, reaction temperatures, and ratios of **1**/nucleophile.

Sources

Product and Company Directory

You can start the entry for your company in "Sources" in any issue of *Angewandte Chemie*.

If you would like more information, please do not hesitate to contact us.

Wiley-VCH Verlag – Advertising Department
Tel.: 0 62 01 - 60 65 65
Fax: 0 62 01 - 60 65 50
E-Mail: MSchulz@wiley-vch.de

Service

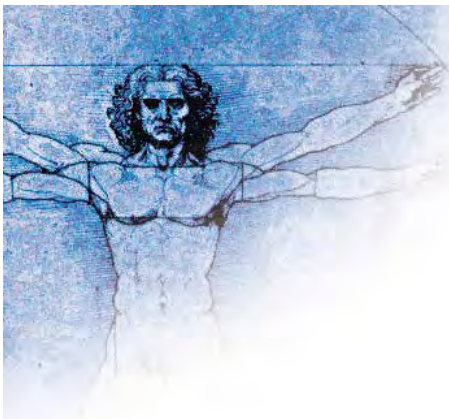
Keywords ——— *5098*

Authors ——— *5099*

Sources ——— *A59*

Vacancies ——— *A61*

Preview ——— *5101*



John M. Thomas Receives Natta Medal

John Meurig Thomas, Honorary Professor in solid-state chemistry at the Department of Materials Science of the University of Cambridge and Emeritus Professor of Chemistry at the Davy Faraday Research Laboratory in London, has been awarded the Giulio Natta Gold Medal of the Italian Chemical Society for his pioneering work in pure and applied catalysis. Earlier this year he was the first European chemist to be awarded the Linus Pauling Gold Medal of Stanford University (California, USA) for his contributions to the advancement of science. Thomas is renowned both as a pioneer of solid-state and materials chemistry and for his wide-ranging studies in the design of new catalysts[1] and the development of in situ techniques for their characterization.[2]



J. M. Thomas

Thomas studied chemistry at the University of Wales, Swansea and completed his PhD in 1958 at Queen Mary College, London. For 20 years he taught and carried out research at the University of Wales, Bangor (1958-69) and Aberystwyth (1969-78), where, as Head of Chemistry, he established one of the most active centers of solid-state science in Europe. He was invited to succeed J. W. Linnett as Head of the Department of Physical Chemistry in Cambridge in 1978, where he introduced many new techniques (such as high-resolution electron microscopy,[3] electron-energy-loss spectroscopy (EELS) neutron scattering, and magic-angle-spinning (MAS) NMR spectroscopy) that are now routinely used in condensed-matter chemistry. In recognition of his contributions to geochemistry, the International Mineralogical Association named a new mineral "meurigite" in 1995, an honor rarely bestowed on living scientists.

Thomas succeeded Sir George (later Lord) Porter as Director of the Royal Institution of Great Britain and of the Davy Faraday Laboratory in 1986. There he extended his research to open-structure catalysts and devised synchrotron-based methods of structural elucidation of catalysts under operating conditions. In 1993 he returned to the University of Cambridge as Master of its oldest college, Peterhouse, founded in 1284.

Thomas was knighted in 1991 for his services to chemistry and the popularization of science. He has received numerous other honors: the Davy Medal of the Royal Society, the Faraday Medal of the Royal Society of Chemistry, the Willard Gibbs Gold Medal of the American Chemical Society, and the Semenov Centenary Medal of the Russian Academy of Sciences. Later this year the Honourable Society of Cymmrodorion, a body founded in London by eminent Welshmen over 250 years ago, will confer its gold medal upon him for services to Welsh culture and British public life. A prolific author, he has also produced a definitive text (with his namesake) on heterogeneous catalysis.[4] He is a founding editor of *Advanced Materials*.

Karl Ziegler Prize to Tobin J. Marks

The Karl Ziegler Prize, one of the most prestigious German awards for chemistry, is awarded by the Gesellschaft Deutscher Chemiker (GDCh). The Prize recognizes diverse contributions to areas of research in which Ziegler was active, that is, organic and inorganic chemistry, catalysis, and polymer chemistry. This broadness of research interests certainly applies to the recipient for 2003, who has been recognized for his preparative work and mechanistic studies on new catalyst systems of the d- and f-block elements and new cocatalysts.



T. J. Marks

Tobin J. Marks completed his undergraduate degree at the University of Maryland (USA) and his PhD in 1970 at the Massachusetts Institute of Technology (MIT, USA). He then began his career at Northwestern University in Evanston, Illinois (USA). His research is focused on catalysis with lanthanoids, in particular on polymerization catalysis with metallocenes. In this work Marks could show that the interaction between the catalyst and the cocatalyst has a fundamental influence on the activity of the catalyst and the stereochemistry of the reaction. A second focal point of his research is materials science, for example, materials for nonlinear optics[5] and molecular electronics, and polymeric organic semiconductors.[6]

The Prize was presented at the annual general meeting of the GDCh on October 7 in Munich. Marks's lecture at the presentation ceremony was entitled "Catalysis as a Route to Useful New Materials. Single- and Multiple-Site Olefin Polymerization Catalysts".

[1] J. M. Thomas, *Angew. Chem.* **1999**, *111*, 3800; *Angew. Chem. Int. Ed.* **1999**, *38*, 3588.

[2] a) J. M. Thomas, G. N. Greaves, *Science* **1994**, *265*, 1675; b) J. M. Thomas, *Chem. Eur. J.* **1997**, *3*, 1557.

[3] J. M. Thomas, O. Terasaki, P. L. Gasi, W. Zhou, J. Gonzalez-Calbet, *Acc. Chem. Res.* **2001**, *34*, 583; J. M. Thomas, W. Zhou, *ChemPhysChem*, **2003**, *4*, 927.

[4] J. M. Thomas, W. J. Thomas, *Principles and Practices of Heterogeneous Catalysis*, Wiley-VCH, Weinheim, **1997**.

[5] T. J. Marks, M. A. Ratner, *Angew. Chem.* **1995**, 107, 167; *Angew. Chem. Int. Ed. Engl.* **1995**, *34*, 155.

[6] A. Facchetti, M.-H. Yoon, C. L. Stern, H. E. Katz, T. J. Marks, *Angew. Chem.* **2003**, *115*, 4030; *Angew. Chem. Int. Ed.* **2003**, *42*, 3900.

 © 2003 Wiley-VCH Verlag GmbH & Co. KGaA, Weinheim

Cyclizations

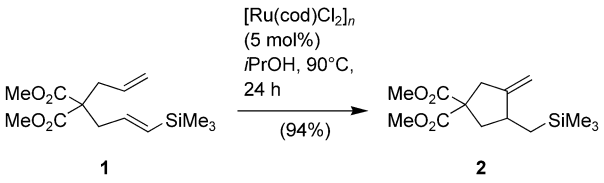
Ruthenium-Catalyzed Cyclizations: More than Just Olefin Metathesis!

*Bernd Schmidt**

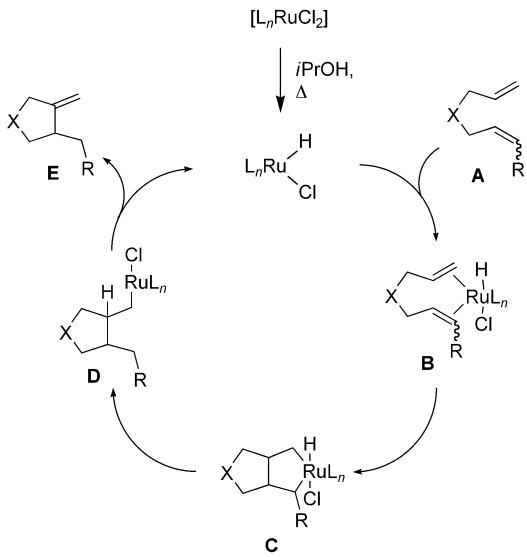
Keywords:
alkenes · alkynes · cyclizations · metathesis · ruthenium

The great interest in ruthenium-based metathesis catalysts[1] has recently resulted in the discovery of more and more nonmetathesis reaction types mediated by these same complexes.[2] Frequently this reactivity has been confirmed upon inspection of the side products from the metathesis reaction. The isomerization of double bonds, for instance, can often occur if the olefin metathesis proceeds slowly. In this special case, there is evidence that the isomerization is mediated by a ruthenium hydride species that is generated under the reaction conditions or that is present as an impurity in the precatalyst.[3] These findings and others led to the development of a synthetically useful olefin-metathesis–isomerization sequence, in which a metathesis catalyst is converted into an effective isomerization catalyst upon completion of the metathesis.[4]

During the past few years examples have been described of competition between the ring-closing metathesis and the cycloisomerization of α,ω-dienes.[5] Although transition-metal-catalyzed cycloisomerizations of α,ω-dienes have been known for some time,[6] the application of ruthenium catalysts in this transformation has only recently been examined by Itoh and co-workers.[7] An example of this is the conversion of the unsymmetrical diallyl malonate **1** into the exo-methylenecyclopentane **2** in good yield and with high selectivity (Scheme 1). Itoh and co-workers found evidence that a ruthenium hydride generated in situ is the active catalytic species in this transformation. However, they observed regioselectivities different from those initially expected. The combination of these discoveries led to the postulation of a new type of mechanism for ruthenium-catalyzed cycloisomerizations.[8] It is assumed that the active catalytic species, a ruthenium hydride complex, is formed through the reaction of the precatalyst with the isopropyl alcohol solvent. The coordination of substrate **A** leads to the π complex **B**, which undergoes oxidative cyclization to produce the ruthenacyclopentane **C**. Reductive elimination to the alkyl ruthenium species **D** and β-hydride elimination to give **E** complete the catalytic cycle (Scheme 2).



Scheme 1. Ruthenium-catalyzed cyclization of the unsymmetrical diallyl malonate **1**.



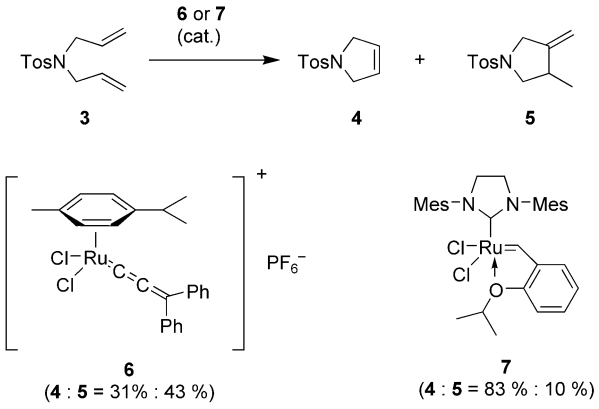
Scheme 2. Suggested mechanism for ruthenium-catalyzed cycloisomerizations. X = CR_2, NR.

It is not clear whether this mechanism comes into play when cycloisomerization products are formed as by-products of olefin metathesis reactions. Fürstner et al.[9] attributed side products observed in the reaction of *N*-tosyldiallylamine (**3**) with the cationic allene–ylidine complex **6** to the intrinsic reactivity of the precatalyst. When Connon and Blechert used the precatalyst **7** in the same transformation, they suggested on the basis of NMR spectroscopic experiments that another species generated from **7** during the course of the reaction catalyzes a cycloisomerization instead of the desired metathesis (Scheme 3).[10]

Whereas the metathesis and the cycloisomerization pathways can be dis-

[*] Priv.-Doz. Dr. B. Schmidt
Fachbereich Chemie—Organische Chemie, Universität Dortmund
Otto-Hahn-Strasse 6, 44227 Dortmund (Germany)
E-mail:
bschmidt@chemie.uni-dortmund.de

 © 2003 Wiley-VCH Verlag GmbH & Co. KGaA, Weinheim DOI: 10.1002/anie.200301688

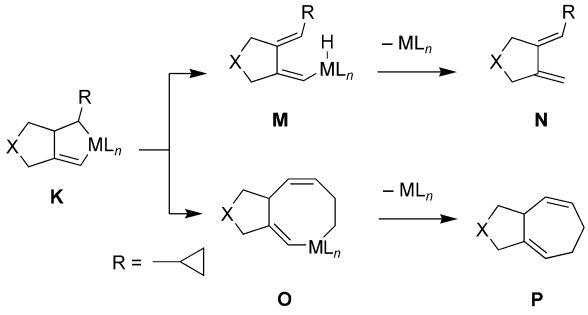


Scheme 3. A cycloisomerization product **5** as a by-product of olefin metathesis. Mes = 2,4,6,-trimethylphenyl, Tos = *p*-toluenesulfonyl.

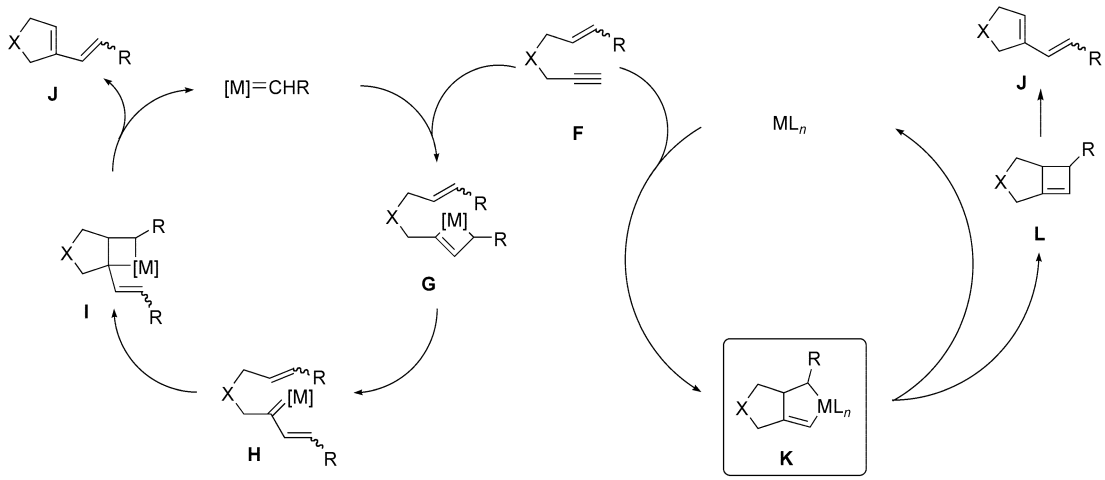
tinguished based on the product distribution in the cyclization of α,ω-dienes, the situation is more complicated in enyne metathesis. Enyne metathesis is understood as the cyclization of an enyne to give a vinyl cycloalkene or a vinyl heterocycloalkene. Thus, unlike in olefin or alkyne metathesis, the cyclization product is an isomer of the starting material. The first cyclization of this type was reported by Katz and Sivavec in 1985. They described the catalytic activity of Fischer carbene complexes of tungsten in this transformation.[11] Trost and Tanoury later reported palladium complexes with an entirely different structure that mediate the same cyclization.[12] In the following years, other catalysts for enyne metathesis were discovered. These catalysts can be divided into two main groups: transition-metal–carbene complexes (in particular the molybdenum and ruthenium precatalysts known from olefin metathesis) and those catalysts that do not possess a carbene ligand (e.g. $[Pt(PPh_3)_2(OAc)_2]$,[13] $[\{RuCl_2(CO)_3\}_2]$,[14] $PtCl_2$,[15] and $[IrCl(CO)_3]_n$[16]). It is generally assumed that a different catalytic cycle applies to each of these two groups of catalyst precursors (Scheme 4).[17]

For metal–carbene complexes, a mechanism is proposed that is similar to that of olefin metathesis in that it is based on a sequence of formal [2+2]-cycloaddition and [2+2]-cycloreversion steps (Scheme 4, left). Metallacyclobutenes **G** are formed as intermediates. Electrocyclic ring opening results in a new carbene complex **H**, which undergoes a cyclization similar to a ring-closing metathesis reaction.[18] The alternative mechanism (Scheme 4, right) is believed to dominate when the catalyst is not a metal–carbene complex. This mechanism is very similar to that involved in the cycloisomerization of α,ω-dienes (Scheme 2), in that a metallacyclopentene **K** is generated as a result of an oxidative cyclization. However, in contrast to diene cycloisomerization, the metallacycle intermediate **K** undergoes reductive elimination to afford a strained cyclobutene derivative **L**, the electrocyclic ring opening of which then leads to the vinyl cycloalkene **J**. Thus, two different mechanistic pathways, which are dependent on the structure of the catalytic system, lead to the same metathesis product **J**. Furthermore, there is evidence supporting the existence of yet a third mechanism arising from use of $PtCl_2$ as the catalyst.[19].

The metallacyclopentene **K** lies at an important crossroads in the cyclization of enynes (Scheme 5). For example, this intermediate can take part in an ene-type cycloisomerization,[6] in which β-hydride elimination from **K** to give the metal hydride **M** is followed by reductive elimination to form the diene **N**. The synthetic utility of enyne cyclizations can be improved through insertion



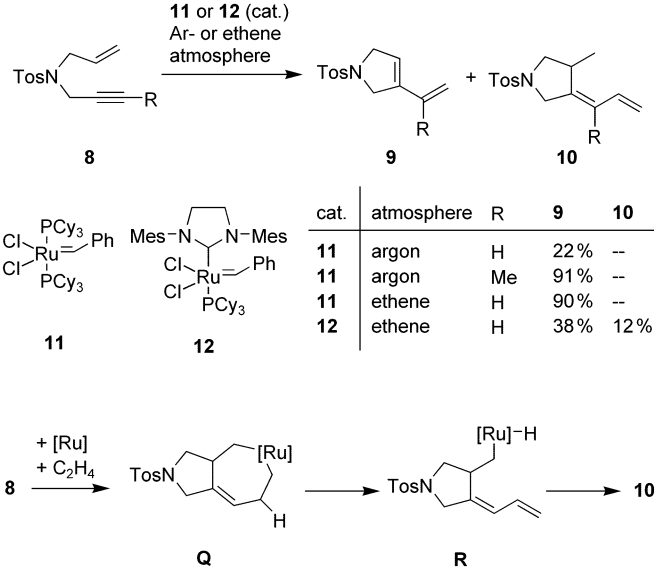
Scheme 5. The metallacyclopentene **K** is a versatile intermediate in the enyne cyclization with catalysts that do not contain a carbene ligand.



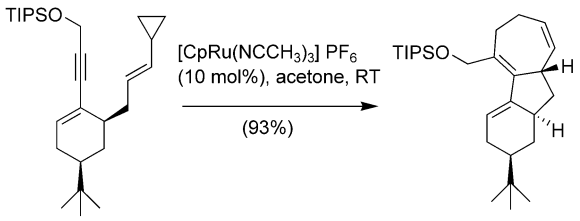
Scheme 4. Enyne metathesis: Different precatalysts lead to different catalytic cycles. Left: transition-metal complexes with a carbene ligand; right: transition-metal complexes without a carbene ligand. [M] = Metal-complex fragment.

 © 2003 Wiley-VCH Verlag GmbH & Co. KGaA, Weinheim

reactions of the metallacyclopentene intermediate **K**. An especially instructive example of this is the [5+2] cycloaddition developed by Wender et al., in which a cyclopropylenyne undergoes cycloisomerization in the presence of a rhodium(I) catalyst.[20] If the metallacyclopentene **K** has a cyclopropyl substituent R, insertion of the cyclopropane ring into the metal–carbon bond occurs with formation of the metallacyclooctadiene **O** (Scheme 5). Reductive elimination then yields the bicyclic cycloheptadiene **P**.[21] Trost and Shen showed recently that a cationic ruthenium complex catalyzes the [5+2] cycloaddition efficiently at room temperature. This transformation facilitates the stereoselective construction of polycyclic systems in good yields and with excellent diastereoselectivities (Scheme 6).[22]



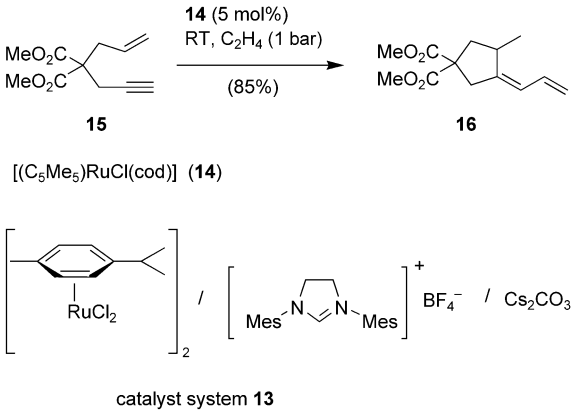
Scheme 7. Enyne metathesis with the Grubbs catalysts **11** and **12**.



Scheme 6. An example of the use of the ruthenium-catalyzed [5+2] cycloaddition in the stereoselective synthesis of polycyclic systems. TIPS = triisopropylsilyl.[22]

The use of ruthenium–carbene complexes (Grubbs catalysts), such as **11**, in enyne metathesis was first described by Kinoshita and Mori in 1994 (Scheme 7).[23] As for other metal–carbene complexes, the metallacyclobutene mechanism (Scheme 4, left) is assumed to be involved. Mori and co-workers have examined this transformation extensively and have noticed a significant reactivity dependence on substrate substitution patterns.[24] Whereas enynes with internal triple bonds react smoothly to give the expected metathesis products, low conversions are observed when enynes with terminal triple bonds are used. Mori explained this phenomenon as resulting from inhibition of the catalytically active species by the product, and subsequently solved the problem by performing the reactions under an ethene atmosphere instead of an inert atmosphere.[25] When the more reactive second-generation Grubbs catalyst **12** was used, the same research group obtained not only the expected metathesis product **9** (R = H), but also the unexpected by-product **10** (R = H), whose formation can not be explained by the metallacyclobutene mechanism (Scheme 7).[26] Instead a mechanism has been postulated that proceeds through an oxidative cyclization via a ruthenacyclopentene (Scheme 4, right). Similar to the [5+2] cycloaddition, an insertion takes place into the metal–carbon bond. In this case, ethene apparently reacts selectively with the Ru–C(sp^2) bond to produce a ruthenacycloheptene **Q**. The mechanistic difference to the [5+2] cycloaddition first appears in the next step. β-Hydride elimination from the intermediate **Q** is apparently much more facile than the expected reductive elimination that would lead to a cycloaddition product.[27] A new ruthenium hydride species **R** is probably formed, reductive elimination from which produces the product **10** (Scheme 7).

On the basis of this mechanistic assumption, Mori and co-workers developed an experimental protocol that optimizes the chemo-, regio-, and *E*/*Z* selectivity of the alkenylative cyclization to give the by-product **10**. Ruthenium complexes were investigated as catalyst precursors that were likely to react by an oxidative cyclization pathway in enyne cyclization reactions. Dixneuf and co-workers found that the catalyst system **13** (Scheme 8) catalyzed the cycloisomerization of *N*-tosyldiallylamine (**3**; Scheme 3) to yield the pyrrolidine **5** with high selectivity.[28] Indeed, the reaction of the enyne **15** in the presence of this catalyst under an ethene atmosphere afforded the cyclization product **16** in moderate yields. Further studies showed that the N-heterocyclic carbene



Scheme 8. Ruthenium-catalyzed enyne cyclizations by the oxidative-cyclization mechanism.

 © 2003 Wiley-VCH Verlag GmbH & Co. KGaA, Weinheim

ligand in this example had no effect on the reaction. The pentamethylcyclopentadienyl complex [$C_5Me_5RuCl(cod)$] (**14**; cod = cyclooctadiene) catalyzed the cyclization of enynes with incorporation of ethene in good to very good yields and was found to be the precatalyst of choice. Itoh and co-workers had shown previously that **14** is also able to efficiently catalyze [2+2+2] cycloadditions of α,ω-diynes with alkenes or alkynes. In this case, an oxidative cyclization probably also initiates the catalytic cycle.[29]

It is not yet possible to say whether the key observation that led to the development of this new enyne cyclization refutes the generally accepted theory that metal–carbene complexes can only catalyze enyne metathesis by means of the metallacyclobutene mechanism. Nor is it clear at present whether the reported formation of nonmetathesis by-products is catalyzed by the metathesis catalyst itself, by an impurity present in the precatalyst, or by a decomposition product of the catalyst. However, these mechanistically diverse ruthenium-catalyzed C–C bond-forming reactions[30] open up more possibilities for the development of new catalytic reactions and reaction sequences.

[1] For reviews, see: S. K. Armstrong, *J. Chem. Soc. Perkin Trans. 1* **1998**, 371–388; R. H. Grubbs, S. Chang, *Tetrahedron* **1998**, *54*, 4413–4450; M. Schuster, S. Blechert, *Angew. Chem.* **1997**, *109*, 2124–2144; *Angew. Chem. Int. Ed. Engl.* **1997**, *36*, 2036–2055; A. Fürstner, *Angew. Chem.* **2000**, *112*, 3140–3172; *Angew. Chem. Int. Ed.* **2000**, *39*, 3013–3043.

[2] B. Alcaide, P. Almendros, *Chem. Eur. J.* **2003**, *9*, 1259–1262.

[3] A. Fürstner, L. Ackermann, B. Gabor, B. R. Goddard, C. W. Lehmann, R. Mynott, F. Stelzer, O. R. Thiel, *Chem. Eur. J.* **2001**, *7*, 3236–3253.

[4] a) A. E. Sutton, B. A. Seigal, D. F. Finnegan, M. L. Snapper, *J. Am. Chem. Soc.* **2002**, *124*, 13390–13391; b) B. Schmidt, *Eur. J. Org. Chem.* **2003**, 816–819; c) B. Schmidt, *Chem. Commun.* **2003**, 1656–1657.

[5] B. Çetinkaya, S. Demir, I. Özdemir, L. Toupet, D. Sémeril, C. Bruneau, P. H. Dixneuf, *New J. Chem.* **2001**, *25*, 519–521.

[6] B. M. Trost, M. J. Krische, *Synlett* **1998**, 1–16.

[7] Y. Yamamoto, N. Ohkoshi, M. Kameda, K. Itoh, *J. Org. Chem.* **1999**, *64*, 2178–2179.

[8] Y. Yamamoto, Y. Nakagai, N. Ohkoshi, K. Itoh, *J. Am. Chem. Soc.* **2001**, *123*, 6372–6380.

[9] A. Fürstner, M. Liebl, C. W. Lehmann, M. Picquet, R. Kunz, C. Bruneau, D. Touchard, P. H. Dixneuf, *Chem. Eur. J.* **2000**, *6*, 1847–1857.

[10] S. J. Connon, S. Blechert, *Bioorg. Med. Chem. Lett.* **2002**, *12*, 1873–1876.

[11] T. J. Katz, T. M. Sivavec, *J. Am. Chem. Soc.* **1985**, *107*, 737–738.

[12] B. M. Trost, G. J. Tanoury, *J. Am. Chem. Soc.* **1988**, *110*, 1636–1637.

[13] B. M. Trost, V. K. Chang, *Synthesis* **1993**, 824–832.

[14] N. Chatani, T. Morimoto, T. Muto, S. Murai, *J. Am. Chem. Soc.* **1994**, *116*, 6049–6050.

[15] N. Chatani, N. Furukawa, H. Sakurai, S. Murai, *Organometallics* **1996**, *15*, 901–903.

[16] N. Chatani, H. Inoue, T. Morimoto, T. Muto, S. Murai, *J. Org. Chem.* **2001**, *66*, 4433–4436.

[17] For reviews on enyne metathesis, see: M. Mori, *Top. Organomet. Chem.* **1998**, *1*, 133–154; C. S. Poulsen, R. Madsen, *Synthesis*, **2003**, 1–18.

[18] For a discussion of the mechanisms of enyne metathesis reactions catalyzed by carbene complexes, see: M. P. Schramm, D. S. Reddy, S. A. Kozmin, *Angew. Chem.* **2001**, *113*, 4404–4407; *Angew. Chem. Int. Ed.* **2001**, *40*, 4274–4277.

[19] A. Fürstner, H. Szillat, B. Gabor, R. Mynott, *J. Am. Chem. Soc.* **1998**, *120*, 8305–8314.

[20] P. A. Wender, H. Takahashi, B. Witulski, *J. Am. Chem. Soc.* **1995**, *117*, 4720–4721.

[21] C. Aubert, O. Buisine, M. Malacria, *Chem. Rev.* **2002**, *102*, 813–834.

[22] B. M. Trost, H. C. Shen, *Angew. Chem.* **2001**, *113*, 2375–2378; *Angew. Chem. Int. Ed.* **2001**, *40*, 2313–2316.

[23] A. Kinoshita, M. Mori, *Synlett* **1994**, 1020–1022.

[24] T. Kitamura, Y. Sato, M. Mori, *Adv. Synth. Catal.* **2002**, *344*, 678–693.

[25] M. Mori, N. Sakakibara, A. Kinoshita, *J. Org. Chem.* **1998**, *63*, 6082–6083.

[26] M. Mori, N. Saito, D. Tanaka, M. Takimoto, Y. Sato, *J. Am. Chem. Soc.* **2003**, *125*, 5606–5607.

[27] M. Lautens, W. Klute, W. Tam, *Chem. Rev.* **1996**, *96*, 49–92.

[28] D. Sémeril, C. Bruneau, P. H. Dixneuf, *Helv. Chim. Acta* **2001**, *84*, 3335–3341.

[29] Y. Yamamoto, R. Ogawa, K. Itoh, *Chem. Commun.* **2000**, 549–550.

[30] B. M. Trost, F. D. Toste, A. B. Pinkerton, *Chem. Rev.* **2001**, *101*, 2067–2096.

 © 2003 Wiley-VCH Verlag GmbH & Co. KGaA, Weinheim

Fifty Years of Ziegler Catalysts

Fifty Years of Ziegler Catalysts: Consequences and Development of an Invention**

*Günther Wilke**

Keywords:
biography · history of science · polymerization · Ziegler catalysts · Ziegler, Karl

On October 26, 1953 an experiment was carried out in the Max Planck Institut für Kohlenforschung in Mülheim an der Ruhr that was to become the basis of a patent with the priority of November 18, 1953—a patent that would cause a revolution in the chemical industry and, within a short time, provide a strong impetus to basic research around the world. The inventors were Karl Ziegler, Heinz Breil, Erhard Holzkamp, and Heinz Martin. The title of the German patent was a "Process for Preparing High-Molecular Polyethylenes" (Figure 1).[1]

Now, a half century later, it is well worth looking back at the developments that would to lead to the award of a Nobel Prize[2] and bring great financial rewards to the Institute in Mülheim, particularly because the story is a prime example relevant to the current political discussion on the funding of basic research and innovation for industry.

When looking at the biography of Karl Ziegler, one cannot help noticing that the years ending in a "3" represent major landmarks in his life. 1923 was the year of his habilitation under the guidance of his doctoral advisor, Karl von Auwers. In 1933 his first publication on "*Vielgliedrige Ringsysteme*" (large ring systems)[3] appeared—this presents the fundamentals of the Ruggli–Ziegler dilution principle, as it was later called. In 1943 he took over as director of the Kaiser Wilhelm Institut für Kohlenforschung in Mülheim an der Ruhr as successor to Franz Fischer. 1953 saw the discovery of the so-called Mülheim mixed catalysts, which were later described in a patent of Giulio Natta as "Ziegler catalysts", a name which is still used today. The award of the Nobel Prize in 1963 can rightly be regarded as the peak of Karl Ziegler's academic career. On August 11, 1973, four months before his 75th birthday, Karl Ziegler died Mülheim.



BUNDESREPUBLIK DEUTSCHLAND

AUSGEGEBEN AM 14. APRIL 1960

DEUTSCHES PATENTAMT

PATENTSCHRIFT

Nr. 973 626

KLASSE 39c GRUPPE 25 01

INTERNAT. KLASSE C 08 f

Z 3799 IV b / 39 c

Dr. Dr. e. h. Karl Ziegler, Mülheim/Ruhr,
Dr. Heinz Breil, Oberhausen (Rhld.), Dr. Erhard Holzkamp, Düsseldorf,
und Dr. Heinz Martin, Mülheim/Ruhr
sind als Erfinder genannt worden

Dr. Dr. e. h. Karl Ziegler, Mülheim/Ruhr

Verfahren zur Herstellung von hochmolekularen Polyäthylenen

Patentiert im Gebiet der Bundesrepublik Deutschland vom 18. November 1953 an
Patentanmeldung bekanntgemacht am 4. Oktober 1956
Patenterteilung bekanntgemacht am 24. März 1960

In der deutschen Patentschrift 878 560 werden Versuche beschrieben, bei denen hochmolekulare Polyäthylene aus Äthylen und Aluminiumtrialkyl allein erhalten werden. Hierbei ist es in gewissen Grenzen möglich, den Polymerisationsgrad durch die Wahl des Mengenverhältnisses Aluminiumtrialkyl zu Äthylen zu beeinflussen. Es hat sich ergeben, daß nach dem Verfahren dieses Patentes Polyäthylen mit einem Molekulargewicht höher als einige Tausend nur sehr schwer zu erhalten ist, was unter anderem auch daran liegt, daß man für die Erzeugung sehr hochmolekularer Produkte extrem wenig Aluminiumtrialkyl nehmen müßte, beispielsweise für ein Molekulargewicht von rund 28 000 nur 1 % Aluminiumtriäthyl von der verwandten Äthylenmenge. Damit werden diese Versuche aber außerordentlich empfindlich gegen Spuren von Verunreinigungen im Äthylen, wie Sauerstoff oder Wasserdampf, die die Aluminiumtrialkyle zersetzen. Außerdem laufen die Versuche sehr langsam, weil die Menge des Katalysators in der gesamten Reaktionsmischung zu klein ist.

In der belgischen Patentschrift 527 736 ist die Beobachtung beschrieben worden, daß man den Verlauf der in der deutschen Patentschrift 878 560 beschriebenen Reaktion zwischen Aluminiumalkylen

Figure 1. Copy of the first page of the German Patent DBP 973 626.

Karl Ziegler's Scientific Work from 1923 to 1949

When relating the story of the discovery of the organometallic mixed catalysts—I am deliberately using the term first used by Karl Ziegler himself—

[*] Prof. Dr. G. Wilke
Max Planck Institut für Kohlenforschung
Kaiser Wilhelm Platz 1, 45470 Mülheim an der Ruhr (Germany)
Fax: (+ 49) 208-389-9761
E-mail: guenther.wilke@t-online.de

[**] Karl Ziegler's Nobel Lecture had the Title "Consequences and Developments of an Invention".[2]

 © 2003 Wiley-VCH Verlag GmbH & Co. KGaA, Weinheim DOI: 10.1002/anie.200330056



Figure 2. The Professors and Lecturers from the Chemical Institute in Heidelberg (January 1928): Max Trautz, Ernst Müller, Hans Kautsky, Karl Freudenberg, Walter Hieber, Hausorth (guest), Robert Stollé, and Karl Ziegler.

then one must ask what led Karl Ziegler into organometallic chemistry in the first place. The answer can be found in a paper published in 1923, the same year as his habilitation, in which he reported "On Alkali Metals as Reagents for Weakened Valencies ("*abgeschwächte Valenzen*") in Organic Compounds".[4]

In the course of investigations into tetraarylallyl radicals, which can be trapped by alkali metals, it was discovered that certain ethers can be cleaved very easily by alkali metals, particularly with sodium–potassium alloy. In addition to the alcoholates, organometallic compounds of the alkali metals were obtained, which were thus formed both by cleaving the ether and by trapping the free radicals. The tetraarylallyl radicals were the starting point of a long series of papers that appeared under the collective title of "Studies on'Trivalent' Carbon". This research is reported in the years up to 1950 in no fewer than 24 papers which belong to Ziegler's most fascinating publications. They earned him the reputation of being one of the first "physical organic chemists", even in the late 1920s he was already using physico-chemical methods in his organic chemical studies, carrying out studies of kinetics and determining dissociation and activation energies at a time when most organic chemists still had little idea of the possibilities they presented. In a footnote to the first paper[4] he commented that "I gave a short review of this interesting group of compounds on April 21, 1923, in Heidelberg at the Conference of Lecturers of the South-West German Universities." Three years later, Karl Freudenberg brought the young lecturer to Heidelberg (Figure 2).

In the context of the studies on radicals, the organometallic compounds of the alkali metals at first appeared to be mere by-products, but Karl Ziegler soon recognized that the high reactivity of these compounds opened up completely new synthetic possibilities. His work in this field led to a further series of 18 publications titled "Investigations into Organo–Alkali-Metal Compounds", which likewise appeared up to the year 1950.

For the time being, however, the investigations concentrated on new ways of synthesizing the ethane derivatives required to study their dissociation into tetraarylallyl radicals. It was discovered that when the organometallic compounds of the alkali metals formed during the course of the ether cleavage, particularly the potassium compounds, were treated with tetramethylethylene bromide, the corresponding ethanes were formed very smoothly.[5] It was during this project[6] that 2-phenylisopropyl potassium was prepared by ether cleavage: the study of this deep red compound, which is readily soluble in ether, was soon to lead to very fundamental discoveries. It required considerable experimental skill to handle such highly reactive organometallic compounds successfully. Solutions of 2-phenylisopropyl potassium in ether are exceptionally sensitive test reagents for impurities in gases such as ethylene, since the deep red solutions lose their color immediately in the presence of, for example, water or oxygen.

In a preliminary communication, Karl Ziegler and Kurt Bähr described the addition of 2-phenylisopropyl potassium to stilbene.[7] In the introduction to this paper they wrote that

"the polymerizing effect of the alkali metals on unsaturated hydrocarbons has been known for a long time. ... . The mechanism of this characteristic property of the alkali metals was previously completely unknown ... . During the course of experiments being carried out with completely different aims, we found by chance a reaction that is most probably of great significance for the occurrence of the polymerizations described: alkali metal alkyls undergo addition reactions with conjugated double bonds or double bonds adjacent to a benzene ring. ... . This reaction was discovered while attempting to prepare dipotassium diphenylethane by reacting stilbene with 2-phenylisopropyl potassium as follows:

$$C_6H_5.CH:CH.C_6H_5 + 2\,C_6H_5.C(CH_3)_2K = C_6H_5.CH(K).CH(K).C_6H_5 + C_6H_5.(CH_3)_2C.C(CH_3)_2.C_6H_5$$

These substances did not react with each other in the way that was intended. Instead it was observed that 2-phenylisopropyl potassium undergoes an addition reaction with stibene.

"It was the first example of the addition of an organometallic compound to a C=C double bond, a reaction that was hitherto completely unknown. Just a single series of experiments sufficed to show that this reaction was clearly a general one with a wide range of applicability."

$$C_6H_5.(CH_3)_2C....K + C_6H_5.CH:CH.C_6H_5 \text{ ----- } C_6H_5.CH.CH.C_6H_5$$
$$C_6H_5.(CH_3)_2.C \quad K$$

 © 2003 Wiley-VCH Verlag GmbH & Co. KGaA, Weinheim

Based on this fundamental discovery, Karl Ziegler formulated at once a method for polymerizing butadiene to 1,2 polybutadiene.[7] The "further investigation of this addition reaction" were "planned".

The above quotations reveal the characteristic way in which Karl Ziegler thought and worked—to recognize immediately the general significance of a new and unexpected result and then to follow this up systematically. "In the course of this project we have made a comprehensive study of the reactions between unsaturated hydrocarbons and alkali metals and report on these in the following." Just $1^1/_2$ years after the preliminary communication he submitted an extended three-part publication on the "Reactions between Unsaturated Hydrocarbons and Alkali-Metal Alkyl Species." in which Ziegler observed that "the reactivity of the alkali-metal compounds have something capricious about them, so we are not yet able to formulate general rules that are valid for all our experimental data."[8]

The extension of these studies to include lithium alkyl compounds was to influence their development in a big way. Lithium alkyl compounds still had to be prepared by treating lithium metal with mercury alkyls—a not particularly satisfactory method! "This remarkable procedure is not exactly convenient." All the same, very significant results were obtained. Just a year later, Karl Ziegler and Herbert Colonius published "A Convenient Synthesis of Simple Lithium Alkyl Species".[9] They were able to show that by working in benzene and keeping the temperature to 35 °C, butyllithium could be prepared from butyl chloride and lithium metal in yields of between 80 % and 100 %. This process was then patented, since it could clearly be of industrial value. However, attempts to distil butyllithium were unsuccessful because it decomposed at higher temperature. This observation was re-examined years later and would then lead to unexpected consequences.

Karl Ziegler's postulate on the polymerization of butadiene[7] was followed by detailed experimental studies on the "Mechanism of the Polymerization of Unsaturated Hydrocarbons by Alkali Metals and Alkyls."[10] "As is well known, these reactions are the basis of the formation of the so-called "sodium-rubbers", of which sodium-butadiene rubber has gained a certain amount of attention in the industrial field."

The most important results to emerge from this work are that butadiene in ether is polymerized rapidly by butyllithium, that when the reaction is stopped abruptly by adding water, unsaturated hydrocarbons with the general formula $C_4H_9(C_4H_6)_nH$ $(n=1–6)$ are obtained, and that the first step in this organometallic synthesis can be trapped by the reaction of triphenylmethyl sodium and butadiene in the presence of dicyclohexylamine:[11]

$$(C_6H_5)_3CNa + Bu \rightarrow (C_6H_5)_3CCH_2CH{=}CHCH_2Na + (C_6H_{11})_2NH \rightarrow (C_6H_5)_3CCH_2CH{=}CHCH_3 + (C_6H_{11})_2NNa$$

At first, triphenylmethane had been used to try to trap the primary addition product. Ziegler wrote that "the principle of working at high dilution to detect less favored reaction paths was first used for this reaction at about the same time as for the recently published experiments to prepare large ring systems."[3] However, the trapping reactions proved to be too slow, so dicyclohexylamine was used instead.

The proof was finally found by a method analogous to that used to investigate the polymerization of butadiene induced by sodium and lithium metals:[12]

"However, clear conclusions on the nature of the initial reaction products can be reached based upon the results of two groups of experiments. It was the study of the reaction of butadiene with alkali metals in the presence of trapping reagents and the surprisingly clear reaction between certain butadienes and lithium metal that finally gave us the missing pieces of evidence required to clear up all remaining hypothetical assumptions."

The investigations also produced the important realization that[12]

"our results produced no evidence at all for the formation of radical intermediates in the course of the alkali metal polymerization. We emphasize this particularly in view of the statements made by Midgley and Henne[13] and Wagner-Jauregg.[14] On the contrary, all the evidence obtained to date speaks for these processes being entirely due to organometallic syntheses."

Without doubt, Karl Ziegler's habilitation thesis, which he submitted to the Faculty in Marburg and which was published in the *Annalen der Chemie*, provided the basis for the work that he then carried out during a short stay at the Johann-Wolfgang-Goethe-University in Frankfurt and particularly in Heidelberg after that. He soon achieved international recognition, but because of his clearly discernible rejection of National Socialism he had to wait before he received a call to a university chair. Finally, in 1936, he could be overlooked no longer. The call to the Chair at the University of Halle an der Saale opened up new ways of widening his research and led to further contacts with industry.

His investigations on the polymerization of butadiene continued to gain in importance with the construction of the Buna Works nearby at Schkopau. Thus it is not surprising that two major review articles on the polymerization of butadiene[15,16] were published during his time in Halle together with an original publication[17] in which he reported on experiments to steer the polymerization towards either 1,2- polybutadiene or 1,4 polybutadiene. His paper concluded:

"In summary, of all the factors, namely (1) temperature, (2) rate of addition of butadiene, (3) the solvent chosen, and (4) the type of alkali metal, the temperature alone determines the constitution of the polymer formed."

At −70 °C a nearly pure 1,2-polybutadiene is formed, while at 150 °C the 1,4-polymer is obtained. This steered polymerization was the result of pure basic research, but its technical importance is clear, since the industrial properties of the rubber are determined by the structure of the polymer constituents.

In 1943 came the call to the Kaiser Wilhelm Institut für Kohlenforschung in Mülheim an der Ruhr as successor of Franz Fischer. The Institute derived its

 © 2003 Wiley-VCH Verlag GmbH & Co. KGaA, Weinheim

support from the Kaiser-Wilhelm-Gesellschaft, the coal mining industry, and the town of Mülheim.

Karl Ziegler recounted his first reaction to this offer as follows:[18]

"In early 1943 I received a letter in my office at the Chemistry Institute of the University of Haale an der Saale from the unforgotten President of the Kaiser Wilhelm Gesellschaft, A. Vögler, asking me if I would be prepared to take over as director of the Kaiser-Wilhelm-Institut für Kohlenforschung in Mülheim an der Ruhr. I must freely admit that my immediate reaction was completely negative. There were good reasons for this: in my scientific career I had experienced happy years in which my work was guided purely by the pleasure of working on the problems that I had chosen myself, even though this was within the framework of the modest resources of a university professor of chemistry. Moreover, the period of directed research immediately preceding had made it clear to me that I was less suited for projects with predetermined aims. With just a few exceptions, my research had developed from observations that had been made during the immediately preceding work. I was very convinced of the fruitfulness of the policy of allowing my work to develop from the interaction of observation, theoretical interpretation and new experiments, without regard to the fields into which this would lead me. It is therefore quite natural that I was disturbed that the name of the institute being offered to me expressed its purpose. However, in the course of the negotiations that now took place I found that both the President of the Kaiser-Wilhelm-Gesellschaft and the Chairman of the Institute's Board of Governors, Generaldirektor Bergassessor H. Kellermann, showed great understanding for the condition I placed on going to Mülheim an der Ruhr: I insisted that I must be given complete freedom to pursue the entire field of compounds of carbon ("organic chemistry") irrespective of whether a clear relationship could be recognized between my work and coal, or not."

Even at that time as the German Reich headed for defeat, Ziegler's conditions were accepted. This decision should also prove instructive for the present day, whenever decisions have to be made about granting support for research.

Karl Ziegler accepted the call to Mülheim and between 1943 and 1945 he shuttled back and forth between Halle and Mülheim as he had to supervise both institutes. His family did not finally move to Mülheim until 1945. Although most of Mülheim had been destroyed by aerial bombing, the Institute remained undamaged, so that the research work there could carry on at a modest rate.

Mülheim also offered contacts with industry, since his work on the polymerization of butadiene was as interesting for the Chemische Werke Hüls in Marl as for the Bunawerke in Schkopau. In the following decades the Chemische Werke Hüls would take licenses from the Institute in Mülheim for a very wide range of processes.

In 1950, the last original publication in the series about butadiene and its polymerization appeared,[19] and the lithium alkyls once again became the focus of the organometallic investigations. Attention turned afresh to the behavior that was observed when butyllithium is distilled. Decomposition took place at the temperature required to distil it and the liquid became cloudy as lithium hydride precipitated out. The distillation was finally achieved in special equipment under high vacuum.[20] Ethyllithium proved to be more stable than butyllithium, but it, too, decomposed at higher temperature:

$$C_2H_5Li \rightarrow CH_2{=}CH_2 + LiH$$

Remarkably, small amounts of butene were detected in the gas produced, which indicated that some of the ethylene formed in the primary process had dimerized. Apparently ethyllithium was able to undergo an addition reaction with ethylene. Karl Ziegler and Hans-Georg Gellert immediately undertook systematic experiments to discover more about this and they were able to show that at elevated temperature lithium alkyls react with ethylene under pressure to form longer chains:[21]

$$C_4H_9Li + n\,CH_2{=}CH_2 \rightarrow C_4H_9(CH_2CH_2)_nLi$$

"It is evident that this addition of ethylene to lithium alkyls is probably the simplest and at the same time the most effective way of lengthening the chain using organometallic reagents. When starting with any lithium alkyl having an even number of carbon atoms, then alkyl chains with an even number of carbon atoms are obtained, while starting with lithium alkyl compounds having an odd number produces alkyl chains with an odd number of carbon atoms."

As interesting as these observations were from a scientific point of view, Karl Ziegler asked himself[22]

"whether, in the very difficult period after the war, one could really justify continuing investigations in a coal research institute into the properties of exotic materials with no industrial significance whatsoever—something that appeared to be the pursuit of private pleasure?"

The answer came in the successes that soon followed.

"Various observations led us to conclude that these elimination reactions are basically reversible, so that one should actually write:

$$CH_3{-}CH_2{-}Li \rightleftarrows CH_2{=}CH_2{+}LiH$$

An extensive series of experiments aimed at observing this reverse reaction, for example, the addition of lithium hydride to ethylene, was unsuccessful. Lithium hydride is completely insoluble and is therefore unable to react with the ethylene. "It appeared at first that this part of our work on organolithium compounds was heading for a dead end."[21]

 © 2003 Wiley-VCH Verlag GmbH & Co. KGaA, Weinheim

1949—The Beginning of Organoaluminum Chemistry

The turn-around came about in 1949. More or less as a last resort, Hans-Georg Gellert, who had worked with Karl Ziegler for many years, treated ethylene under pressure with a solution of lithium aluminum hydride, a material that had just recently been discovered, in ether at 180–200°C. The pressure fell rapidly and the product isolated was identified as a mixture of pure α-olefins. It appeared that the lithium hydride in the form of soluble $LiAlH_4$ had not only added to ethylene in the manner being sought, but that in addition an "Aufbau" (chain growth) reaction had occurred: the aluminum component had apparently rendered the reagent soluble. However, it soon became clear that aluminum hydride itself could undergo an addition reaction with ethylene, indeed that the triethylaluminum formed as the primary product of this reaction was itself undergoing the Aufbau reaction.[22,23]

This discovery was fundamental, because it was now possible to employ metal alkyl species of a common metal, aluminum, and this finding appeared to open up the way even to industrial applications. Pure α-olefins could now be prepared by a homogeneous catalytic process. When the reaction was carried out at high temperature the olefins were formed by chain formation then cleavage. The cleavage, later called elimination, could be suppressed by lowering the temperature at which the reaction was carried out from 180–200°C to 100°C. The chain-forming process produced higher aluminum alkyls, which on hydrolysis gave straight-chain (unbranched) paraffins. Thus, a method had been found of polymerizing ethylene under very mild conditions. At the same time, however, even under the most favorable circumstances it produced waxy products with molecular weights of up to 5000: polyethylenes with true plastic properties could apparently not yet be prepared in this way because, after about a hundred addition steps, the chain formation was terminated by an elimination reaction.

Thus, when triethylaluminum was used as the initial catalyst, ethylene, under pressure at high temperature, yielded mixtures of α-olefins, a class of substances of industrial interest since they could not prepared in a pure form before. At normal pressure and temperatures of around 170°C, a smooth dimerization of the ethylene to butene-1 was achieved. We will come back to this process later. With typical thoroughness, Karl Ziegler had the reactions of triethylaluminum with propylene or butene-1 tested to see what reactions occurred. The result was a smooth dimerization to 2-methyl-1-pentene and 2-ethyl-1-hexene, respectively, since a further extension of the chain did not occur with either of these olefins. The 2-methyl-1-pentene later found use as the starting material for the large-scale industrial synthesis of isoprene, while the 2-ethyl-1-hexene opened up the way to terephthalic acid, since the aromatization of the 2-ethylhexene leads to the formation of *para*-xylene.

Initially, these reactions of aluminum alkyl species with potential industrial applications all suffered a grave disadvantage—aluminum alkyl compounds were difficult to prepare. Although the syntheses known at that time could be used to obtain these compounds on a small laboratory scale, they were unsuitable for production on an industrial scale. I remember how valuable the small amounts of triethylaluminum were that had been prepared in the Institute. It was vitally important to find a way of preparing it on the kilogram scale. The reaction of aluminum with ethyl bromide to give so-called ethylaluminum sesquibromide, an equimolar mixture of diethylaluminum bromide and ethylaluminum dibromide, was known but the ethyl bromide starting material was expensive. Whereas ethyl chloride is cheap, either it does not react under similar conditions or decomposition occurs. I finally discovered that the reaction of aluminum with ethyl chloride can be catalyzed by the sesquibromide prepared in situ. The reaction then proceeds so smoothly that in the end we were able to use 100-litre vessels, since we also had to show that such compounds that ignite in the air and explode with water can be handled safely on this a scale:

$$2\,Al + 3\,C_2H_5Cl \xrightarrow{cat.} (C_2H_5)_2AlCl + C_2H_5AlCl_2$$

The sesquichloride, which was later to play a role in the development of the Ziegler catalysts, had to be dehalogenated to obtain triethylaluminum. Metallic sodium was found to be the best material for doing this: when pieces of sodium metal are added to ethylaluminum sesquichloride at around 170°C the sodium takes up the chlorine, aluminum is precipitated, and the triethylaluminum is formed:

$$(C_2H_5)_3Al_2Cl_3 + 3\,Na \rightarrow (C_2H_5)_3Al + 3\,NaCl + Al$$

In 1952 we synthesized in the pilot plant of our Institute our first 20 kg batch of triethylaluminum—a material that could hitherto be prepared only in small quantities.

I have mentioned quite deliberately that we synthesized the triethylaluminum on the kilogram scale, since this leads me to comment on present day conditions. Nowadays, if one were to work in a research institute like ours under conditions that were normal in 1952, the institute's director would be in court faster than at the patent office. The overregulation as regards safety would without doubt hinder or presumably prevent progress in such work altogether. I am not making a case here for carelessness but against the exaggerated ordinances of bureaucrats.

On May 14, 1952, Karl Ziegler gave his first comprehensive report on the new work under the title "Novel Catalytic Conversion of Olefins".[22] Just a few days later, on May 19, he lectured on "Organoaluminum Synthesis in the Field of Olefinic Hydrocarbons" at the Annual Meeting of the Gesellschaft Deutscher Chemiker (GDCh, German Chemical Society) at the Achema in Frankfurt.[24]

The First Licenses are Granted

This second lecture in particular was to have far reaching consequences, since Giulio Natta and Sir Robert Robinson were in the audience. They had close connections with industry, Natta with Montecatini in Italy and Sir Robert with Petrochemicals in Manchester. Both were convinced by Ziegler's presenta-

 © 2003 Wiley-VCH Verlag GmbH & Co. KGaA, Weinheim

tion that what they had heard could be of importance for the future development of these companies. The lecture created general excitement, and an invitation to give a lecture in Milan, the contents of which had already been published in Italian in *La Chimica & Industria* in September 1952,[25] resulted in negotiations soon being opened with Montecatini for a license for the processes that had been presented. An initial comprehensive license was granted in January 1953 covering the new organoaluminum reactions and further developments in this field. The contract was a major financial success for the Institute, since the so-called "down payment" was DM 600000, an enormous sum in those days.

In 1952, Karl Ziegler, who was an enthusiastic climber, reached another summit in the truest sense of the word—the ascent and traverse of the Matterhorn starting from Hörnligrat in Switzerland and descent via the ridge on the Italian side to Cervinia (Figure 3). He was accompanied by his son Erhard and me. Unfortunately, we were caught in a sudden change of weather which forced us to stay overnight in the Cabanne Luigi Amadeo at an altitude of 3900 m. On the summit there was no glorious view, just a driving snow.

On the way back home through the Aosta valley we made a short detour to Champoluc, where the Natta family had a large holiday house. We were given a friendly welcome as their guests and with a large circle of their friends enjoyed a multilingual evening—Signora Natta was fluent in no fewer than four languages.

On the basis of the license contract, two young chemists, Paulo Chini and Roberto Magri, and an engineer, Giovanni Crespi, came from Montecatini to Mülheim in early 1953 to gain experience in the field of organoaluminum chemistry. Paulo Chini and Roberto Magri came to me in my laboratory, since I had the syntheses of aluminum alkyl compounds and the dimerization of ethylene at normal pressure running continuously in small glass apparatus. Giovanni Crespi went to the pilot plant, where Dr. Zosel had a larger apparatus for the continuous dimerization of propylene under pressure. The guests were also highly interested in the experiments



Figure 3. The mountaineer Karl Ziegler.

on the Aufbau reaction being carried out by Dr. Gellert and Dipl.-Chem. Erhard Holzkamp.

About the same time, contracts were made with Farbwerke Höechst, and the companies Petrochemicals in England and Hercules Powder Co., USA. Dr. A. Glasebrook from Hercules Powder came as a guest to the laboratory of Erhard Holzkamp. The purely organoaluminum syntheses reported in the Frankfurt lecture were now the focus of attention of industry.

The reaction of triethylaluminum with ethylene under pressure, the Aufbau reaction, had at this time already been studied systematically in long series of experiments. Depending upon the conditions, higher aluminum alkyl species could be prepared. Since it was clear that no high molecular weight polyethylene could be prepared this way, Karl Ziegler had the splendid idea of using this process industrially in a completely different way. The chain growth must be steered to give an average length of 6–8 ethylene molecules. When the aluminum alkyls were subsequently oxidized in the air, the corresponding aluminum alcoholates were obtained, which on hydrolysis yielded primary alcohols.[26] These compounds are an ideal starting material for bio-degradable detergents. This did not remain just an idea—a few years later large-scale production plants produced hundreds of thousands of tons of primary alcohols on the basis of the Mülheim process. However, this process really only got going after the elegant direct syntheses of aluminum alkyl compounds, in particular that of triethylaluminum, had been developed.[27]

In the case of triethylaluminum the synthesis has to be carried out in two steps because otherwise the Aufbau reaction takes place:

$$2\,Al(C_2H_5)_3 + 1\tfrac{1}{2}\,H_2 + Al \rightarrow 3\,HAl(C_2H_5)_2$$

$$3\,HAl(C_2H_5)_2 + 3\,CH_2{=}CH_2 \rightarrow 3\,Al(C_2H_5)_3$$

$$1\,Al + 1\tfrac{1}{2}\,H_2 + 3\,CH_2{=}CH_2 \rightarrow Al(C_2H_5)_3$$

The synthesis of triisobutylaluminum was achieved in a one-step reaction because with this compound, olefin chain-growth cannot occur.[27] Today, many thousand tons of aluminum trialkyls are produced annually by direct synthesis in large-scale industrial plants.

The Nickel Effect and Its Consequences

As already described, a long series of experiments had shown that the Aufbau reaction could always be reproduced exactly. However, early in 1953 something odd happened. Instead of obtaining the higher aluminum alkyls expected, Erhard Holzkamp observed in the course of experiments for his doctoral work that when ethylene reacted with triethylaluminum under the usual conditions, a smooth dimerization of the ethylene to butene occurred instead. He was able to repeat the experiment time and again using triethylaluminum from the same charge. Understandably, what was at first was regarded as an annoying mishap caused considerable excitement. Somewhat bad tempered, Karl Ziegler came to me and said "Now we have these large quantities of triethylaluminum that are useless. I warned right from the beginning about using sodium for the dehalogenation." The real reason for these problems was not found until some weeks later. It was not the trie-

 © 2003 Wiley-VCH Verlag GmbH & Co. KGaA, Weinheim

thylaluminum that was to blame but traces of nickel compounds that had been left behind after the V2A autoclaves had been cleaned. The mishap soon proved to be a piece of luck, because it marked the beginning of a completely new chapter in catalysis.[28]

The method of dimerizing ethylene that Holzkamp had discovered was much more effective than the one at normal pressures that I had developed. The development of the new process, particularly as regards its industrial application, was much too large a topic for a doctoral study, so Karl Ziegler put me in charge of the further development up to the stage of a continuously running pilot plant. At that time the catalytic dimerization of ethylene opened up a new route to butene, which was not yet available from refinery production. However, first of all Holzkamp's experiments had to be reproduced and here again unexpected difficulties arose: the very first attempts to repeat the nickel cocatalysis went wrong and instead of continuously producing butene I was obtaining longer chain products again! After several further experiments it was discovered that Holzkamp had used technical-grade ethylene whereas I had used ethylene purified with sodium aluminum tetraethyl. Gas analyses revealed that the technical grade ethylene contained about 0.5 % acetylene and we discovered that these traces of acetylene stabilized the nickel cocatalyst.[28] Thus began our "organonickel chemistry".[29]

The discovery of the "nickel effect", as it has become known in the chemical literature,[28] appeared to be only the beginning of a new wide-ranging line of research that would far exceed the bounds of a doctoral study. Nevertheless, as early as May 1953 Karl Ziegler told Erhard Holzkamp to carry out initial experiments with chromium compounds to see whether other metals had a similar cocatalytic effect to nickel. At first these experiments proceeded without a clear direction, since in addition to olefins, small amounts of solid products (which were possibly polyethylene) were obtained. The systematic investigation did not begin until after the summer holidays. Another diploma student, Heinz Breil, was brought in, as it was clear that they would have to work through the whole Periodic Table to see if there were any other metals that were equally effective. Experiments using the acetylacetonates of chromium, manganese, vanadium, and platinum did not produce any spectacular results.

The revolution in the chemistry of polymers began quite unexpectedly on October 26, 1953 when Heinz Breil carried out the experiment using zirconium acetylacetonate. In comparison with the conditions required to produce the high-pressure polyethylene known at that time (300 °C, 1500–2000 bar), he obtained under sensationally mild conditions (ca. 100 °C, 100 bar) a polyethylene that could be compressed into a foil. One needs little fantasy to imagine the excitement that went round the Institute! The further development could not rest on the shoulders of one diploma student, Heinz Breil, alone.

For a long time Dr. Heinz Martin had been trying to find conditions under which the Aufbau reaction would, after all, produce chains of 1000 ethylene molecules or more, which could ultimately have led to the formation of a plastic polyethylene. The latest results had shown that influences, such as the nickel effect, had to be excluded by all means possible. Therefore, experiments were in progress at that time using aluminum-lined autoclaves. Now, however, it was important develop systematically the sensational results of Heinz Breil as rapidly as possible so that they could be patented. Understandably, this assignment was given to Heinz Martin, who had already been working on the preparation of a polyethylene, although from different direction. The situation was similar to mine in the case of the ethylene dimerization.

It should be mentioned at this point that almost 40 years later Heinz Martin was indeed able to prepare high molecular-weight polyethylene using triethylaluminum alone. At room temperature triethylaluminum really does react with ethylene under pressure, albeit extremely slowly, without the chain formation being interrupted by an elimination reaction to form an olefin. Thus, in principle, the original aim had been achieved. This observation is of scientific interest but, of course, of no value industrially.[30]

Heinz Breil's first polymerization experiments with titanium tetrachloride as the transition metal component in combination with triethylaluminum showed that titanium catalysts that are considerably more efficient than zirconium. He observed a highly exothermic reaction, a rapid fall in pressure in the autoclave, and the only product was high-molecular-weight polyethylene. With the help of further variation in the catalyst, Heinz Martin finally achieved the so-called normal-pressure polymerization, which he was able to carry out in a large glass for home preserves modified for the purpose. This experiment was later demonstrated to numerous license holders and guests and it never ceased to amaze them. It has even been recorded on film. In a further important development, it was discovered how the molecular weight of the polyethylene being produced could be varied at will.

As early as November 17, 1953 Karl Ziegler submitted a patent application to the German Patent Office that he had prepared himself[31]—the Institute's patent lawyer was away on business at the time. The main claim of the application is:

"1. A method of preparing high-molecular polyethylene using aluminum trialkyls as catalysts, characterized by bringing together ethylene at pressures greater than 10 atmospheres and temperatures above 50 °C with mixtures of aluminum trialkyls and compounds of the metals of groups IVa to VIa of the Periodic Table with the atomic numbers 22 to 74 (namely titanium, zirconium, hafnium, niobium, tantalum, chromium, molybdenum, and tungsten)."

The clear limitation of the claim to ethylene was to cause the Institute considerable problems in later years, but at that time Karl Ziegler claimed only what had been demonstrated experimentally. Although Heinz Breil had already carried out an experiment with propylene, he had not been able to isolate any polypropylene, a material that was not yet known. Thus, Heinz Martin was the first to show that the new catalysts were also able to polymerize propylene.[33]

The sensational news spread like wildfire around the world when Karl Ziegler first reported the low-pressure polymerization of ethylene at the IUPAC Congress in Zurich on July 22,

 © 2003 Wiley-VCH Verlag GmbH & Co. KGaA, Weinheim

1955. Giulio Natta also announced at the same conference the stereospecific polymerization of olefins to isotactic polymers with the aid of Ziegler catalysts without, however, naming them in detail. Natta had had access to all the relevant information through the license contract between Ziegler and Monticatini, so that he was one of the first outside the Institute in Mülheim to be able to work in the new field. On September 14, 1955 Karl Ziegler held the same lecture as in Zürich at the Main Meeting of the Gesellschaft Deutscher Chemiker in Munich.[32]

In 1954 Karl Ziegler was able to grant further license contracts. It became clear what an advantage it was that he was able to act as both director of the Institute and at, the same time, as managing director of the Studiengesellschaft Kohle m.b.H., which was the trustee for the Institute. The licensees got to know him as a versed business man. Based on these first licenses, the whole field also developed outside the Institute with enormous speed, resulting in numerous patent applications. From the Institute came the homopolymerization of propylene and of butene,[33] a clear proof that propylene too could be polymerized. Without going into details about where further processes were developed, I will just list the milestones of the further development. In the USA it was found how isoprene could be polymerized with Ziegler catalysts to form either a natural rubber-like material (*cis*-1,4-polyisoprene) or guttapercha (*trans*-1,4-polyisoprene). With the new catalyst butadiene formed either *cis*- or *trans*-1,4-polybutadiene. I myself found at the same time as Natta how to produce 1,2-polybutadiene[34] and then, completely unexpectedly, the cyclotrimerization of butadiene to give *trans,trans,cis*-1,5,9-cyclododecatriene,[35] which opened up the way novel polyamides.

The business of licensing flourished. Leaving the chronological report for a moment, it should be mentioned that between 1953 and 1990 no less than 80–90 contracts were agreed, bringing the Institute income that guaranteed its complete financial independence for more than 40 years and freeing the Max Planck Society from having to fund it. Thus the financial benefits continued to flow for more than 20 years after Karl Ziegler retired as director of the Institute. The licenses and income were one side of the coin, the other was, however, the numerous infringements of the Institute's patents, which led to numerous lawsuits, particularly in the USA. One of these cases ran for no less than 18 years until finally a judgment was made in favor of the Institute. As managing director of the Studiengesellschaft Kohle m. b. H., to which he was appointed in 1970, along with his role as a scientist, Heinz Martin was engaged full time in looking after the interests of the Institute both in the granting of licenses and in the defense of the patent rights. As the major co-inventor of the polypropylene process together with Karl Ziegler, he was ideally equipped both as a scientist and through the experience that he had gained as an insider in the world of patents. In his book "Polymere und Patente" published in 2002[36] he gives a fascinating detailed account of both sides of the coin. Particularly worth reading is his account of the unique situation regarding the classification of the pioneering Mülheim patents in the USA, since this judgment provided income to the Institute on the basis of the 1954 basic patent until 1995. It is estimated that today about 25–30 million tons of polypropylene, 10–12 million tons of low-pressure polyethylene, and 15000 tons of aluminum alkyl compounds are produced every year using the Mülheim processes.

After 30 years of basic research came the great breakthrough in industrial chemistry, but the scientific success was in no way less important. The honors bestowed upon Karl Ziegler are legion.[37] After 1953 excitement grew in the Institute every year in the period leading up to the annual announcement of the new Nobel Prize winners, since everyone was convinced that one day Karl Ziegler would be awarded the Nobel Prize. Outside the Institute others were of the same opinion. Surprisingly, he had to wait for ten years until the Prize Committee honored him—surprising in as far as, according to the constitution of the Nobel Foundation, the prize should be awarded to the person that has done the most for humanity in the previous year. There was great elation and it was all the greater for Hans-Georg Gellert, Heinz Martin, and myself, and for our wives, as Karl Ziegler invited us to accompany him and his family to Stockholm (Figure 4). What a difference it made to be present at the festivities rather than just watching them on television!

This pinnacle of success cannot be better documented than by the following sentences taken from the Nobel Prize Committee's document giving the grounds for awarding the Nobel Prize to Karl Ziegler and Giulio Natta, since they were made after a careful analysis of the contributions of the laureates.[38]



Figure 4. Picture from the Nobel Prize ceremony in Stockholm (1963) left King Gustav VI. Adolf, right Karl Ziegler.

 © 2003 Wiley-VCH Verlag GmbH & Co. KGaA, Weinheim

"However, Professor Ziegler has found entirely new methods of polymerization. Ziegler catalysts, now widely used, have simplified and rationalized polymerization processes, and given us new and better synthetic materials.
However, Professor Natta has found that certain types of Ziegler catalysts lead to stereoregular macromolecules, i.e., macromolecules with spatially uniform structure. In such chains, all the side chains point to right or to left."

This Essay is intended to keep alive the memory of a development in chemistry that is almost unique—a development that arose from basic research but the industrial success of which around the world was a result of recognizing its potential and systematically following it up. The quotations from Karl Ziegler's publications are intended to give our young chemists an insight into the especially successful way of thinking of this great research scientist. But above all, I hope that this Highlight will remind everyone who has to make political decisions on research that truly novel developments can only emerge from unfettered basic research.

[1] K. Ziegler, H. Breil, E. Holzkamp, H. Martin, DBP No. 973626, **1960**.
[2] K. Ziegler, *Angew. Chem.* **1964**, *76*, 545–553.
[3] K. Ziegler, H. Eberle, H. Ohlinger, *Justus Liebigs Ann. Chem.* **1933**, *504*, 94–130.
[4] K. Ziegler, F. Thielmann, *Ber. Dtsch. Chem. Ges.* **1923**, *56*, 1740–1745.
[5] K. Ziegler, *Justus Liebigs Ann. Chem.* **1923**, *434*, 34–78 (Habilitation thesis).
[6] K. Ziegler, B. Schnell, *Justus Liebigs Ann. Chem.* **1924**, *437*, 227–255.
[7] K. Ziegler, K. Bähr, *Ber. Dtsch. Chem. Ges.* **1928**, *61*, 253–263.
[8] K. Ziegler, F. Crössmann, H. Kleiner, O. Schäfer, *Justus Liebigs Ann. Chem.* **1929**, *473*, 1–35.
[9] K. Ziegler, H. Colonius, *Justus Liebigs Ann. Chem.* **1930**, *479*, 135–149.
[10] K. Ziegler, F. Dersch, H. Wollthan, *Justus Liebigs Ann. Chem.* **1934**, *511*, 13–44.
[11] K. Ziegler, L. Jakob, *Justus Liebigs Ann. Chem.* **1934**, *511*, 45–63.
[12] K. Ziegler, L. Jakob, H. Wollthan, A. Wenz, *Justus Liebigs Ann. Chem.* **1934**, *511*, 64–88.
[13] T. Midgley, Jr., A. L. Henne, *J. Am. Chem. Soc.* **1929**, *51*, 1294.
[14] T. Wagner-Jauregg, *Justus Liebigs Ann. Chem.* **1932**, *496*, 52–77.
[15] K. Ziegler, *Chem.-Ztg.* **1938**, *62*, 125–127.
[16] K. Ziegler, *Handbuch der Katalyse, Vol. VII*, Springer, Heidelberg, **1943**, pp. 106–135.
[17] K. Ziegler, H. Grimm, R. Willer, *Justus Liebigs Ann. Chem.* **1939**, *542*, 90–122.
[18] "Das Kohlenforschungsinstitut in Mülheim a.d. Ruhr zehn Jahre lang unter neuer Leitung": K. Ziegler, *Aus der Deutschen Forschung*, Georg Thieme, Stuttgart, **1956**. See also G. Wilke, *Justus Liebigs Ann. Chem.* **1975**, 804–833.
[19] K. Ziegler, E. Eimers, W. Hechelhammer, H. Wilms, *Justus Liebigs Ann. Chem.* **1950**, *567*, 43–96.
[20] K. Ziegler, H.-G. Gellert, *Justus Liebigs Ann. Chem.* **1950**, *567*, 179–184.
[21] K. Ziegler, H.-G. Gellert, *Justus Liebigs Ann. Chem.* **1950**, *567*, 195–203.
[22] K. Ziegler, *Brennst.-Chem.* **1952**, *33*, 193–200.
[23] K. Ziegler, H.-G. Gellert, H. Martin, K. Nagel, J. Schneider, *Justus Liebigs Ann. Chem.* **1954**, *589*, 91–162. First paper in the series "Metallorganische Verbindungen" (*Organometallic Compounds*) XIX–XLII, which continued the series "Alkaliorganische Verbindungen" (*Organometallic Compounds of the Alkali Metals*) I–XVII.
[24] K. Ziegler, *Angew. Chem.* **1952**, *64*, 323–329.
[25] K. Ziegler, *Chim. Ind.* **1952**, *34*, 520–527.
[26] K. Ziegler, F. Krupp, K. Zosel, *Angew. Chem.* **1955**, *67*, 425–426.
[27] K. Ziegler, H.-G. Gellert, H. Lehmkuhl, W. Pfohl, K. Zosel, *Justus Liebigs Ann. Chem.* **1960**, *629*, 1–13.
[28] K. Ziegler, H.-G. Gellert, E. Holzkamp, G. Wilke, *Brennst.-Chem.* **1954**, *35*, 321–325.
[29] G. Wilke, *Angew. Chem.* **1988**, *100*, 189–211; *Angew. Chem. Int. Ed. Engl.* **1988**, *27*, 189–211.
[30] H. Martin, *Makromol. Chem.* **1992**, *193*, 1283–1288.
[31] Ref. [1].
[32] K. Ziegler, *Angew. Chem.* **1955**, *67*, 541–547.
[33] K. Ziegler, H. Breil, H. Martin, E. Holzkamp, Deutsche Patentschrift 1257430.
[34] G. Wilke, *Angew. Chem.* **1956**, *68*, 306–307.
[35] G. Wilke, *Angew. Chem.* **1957**, *69*, 397–398.
[36] H. Martin, *Polymere und Patente*, Wiley-VCH, Weinheim, **2002**.
[37] G. Wilke, *Justus Liebigs Ann. Chem.* **1975**, 804–833.
[38] *Nobel-Lectures, Chemistry*, Elsevier Publishing Company, Dordrecht, **1972**.

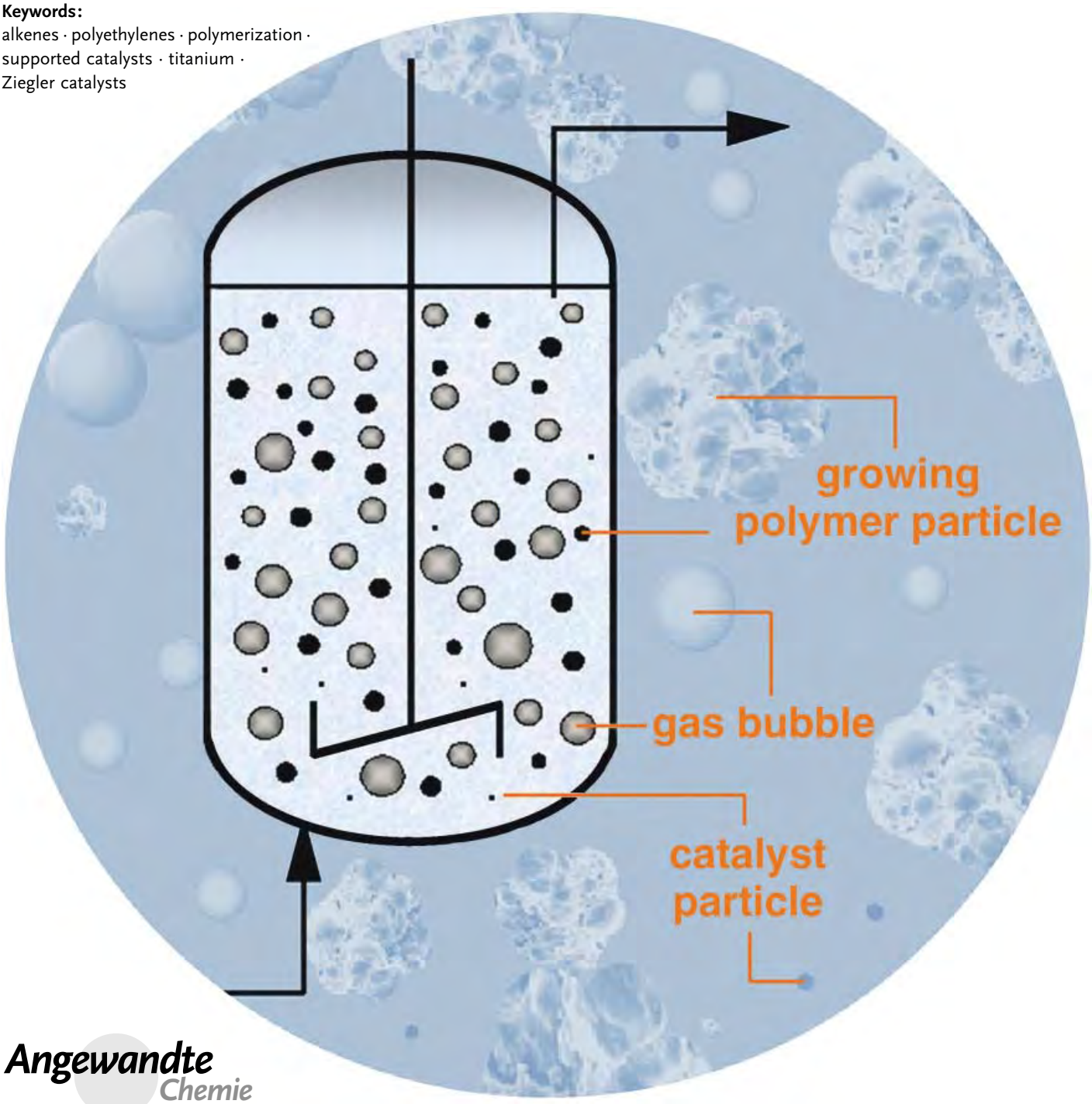
 © 2003 Wiley-VCH Verlag GmbH & Co. KGaA, Weinheim

Fifty Years of Ziegler Catalysts

The Ethylene Polymerization with Ziegler Catalysts: Fifty Years after the Discovery

*Ludwig L. Böhm**

Keywords:
alkenes · polyethylenes · polymerization · supported catalysts · titanium · Ziegler catalysts



 © 2003 Wiley-VCH Verlag GmbH & Co. KGaA, Weinheim DOI: 10.1002/anie.200300580

Fifty years ago, Karl Ziegler and his co-workers discovered the synthesis of polyethylenes at low pressures and moderate high temperatures with transition-metal catalysts of the 4th group and aluminum organic compounds as cocatalysts. The last 50 years represent a story of innovations in science and industry in the development of high-activity catalysts and processes based on a detailed understanding of all relevant chemical and physical processes on all scales. Catalysts, technologies, and products are still under further development, which shows that the potential of this polymerization process is not fully exploited. Today's targets include achieving better product properties at lower production costs and the substitution of other materials, such as glass, paper, steel, and concrete in certain fields because polyethylenes deliver better resource-saving solutions.

From the Contents

1. Introduction 5011
2. Active Sites, Polymerization Mechanism, High-Activity Catalysts 5012
3. Precipitation Polymerization, Particle-Forming Process, Microreactors 5016
4. Modelling of the Polymerization Reactor: Macro-, Meso-, Microscale 5019
5. Tailored High-Density Polyethylenes 5023
6. Outlook 5026

1. Introduction

In his Nobel prize lecture,[1] Karl Ziegler reflected on the discovery of the catalytic polymerization of ethylene in the following way: "The new development began at the end of 1953 when I, together with Holzkamp, Breil, and Martin, discovered within a few days in a nearly dramatic way that gaseous ethylene was polymerized quickly to high-molecular plastics at low pressures of 100, 20, 5 atm and even at normal pressure using simple producible catalysts." With this discovery,[2,3] based on fundamental investigations of the reaction between ethylene and organometallic compounds, especially aluminum compounds, Ziegler has changed the world in a twofold way: He initiated many scientific studies in the field of catalysis using organometallic compounds and his discovery was of outstanding relevance for the industrial synthesis of polyolefins.[4–6]

The production of polyethylenes by polymerization of ethylene under normal pressure or pressures up to 5 MPa and moderate high temperatures (up to 90 °C) using organometallic catalysts formed by mixing alkyl aluminum compounds and transition-metal chlorides, such as $TiCl_4$,in a hydrocarbon diluent (diesel oil or petrol) was transferred into an industrial process within a few months. This industrial process came on stream so quickly because this was an new polyethylene. At the time when Ziegler and co-workers discovered this new way to polymerize ethylene, the high-pressure process working at pressures up to 300 MPa and at temperatures up to 300 °C was well known and had been in operation since 1938.[7] The catalytic polymerization process opened the door to an new "hard" polyethylene with higher crystallinity and stiffness (elastic modulus) compared to the high-pressure-process polyethylene. This high-density polyethylene was introduced into the market as a "new polyethylene"—mainly known under the trade name Hostalen—because, owing to its higher stiffness, it offered new possibilities for applications. However, there were other properties in processing and the final products. The polyethylene with high density (HDPE) has not replaced the polyethylene with low density (LDPE) and both materials are still produced commercially, in some cases they are even blended to improve properties.

The industrial polymerization process was a scale-up of the laboratory process presented by Ziegler in his Nobel prize lecture.[1] However, the target was to transfer this process into a continuous industrial process. For this reason, the transfer from laboratory to industrial scale was realized within a few months.[9,10] After start-up of the industrial process, it became clear that there were opportunities for further developments. The catalysts described by Ziegler and co-workers suffered from a low activity. The catalyst productivity was so low that the catalyst components had to be destroyed and the residues had to be removed from the polyethylene to achieve marketable products. The most important challenge was to develop high-activity catalysts which produced such a low level of residues that they no longer needed to be destroyed and removed. This problem was solved in a convincing way.[11]

The process had also to be modified to get better products for known applications as well as for new ones. The catalytic polymerization process has a remarkable flexibility and potential for modifications. The polymer properties can be modified by copolymerization with 1-alkenes,[12,13] and with hydrogen the average chain length can be easily varied over a wide range and even set as desired.[14] Consequently, starting from easy-to-handle compounds, such as ethylene, 1-alkenes, and hydrogen, a broad range of polyethylenes with different density and average molecular mass can be produced. The product portfolio covers oligomers and waxes with average molecular mass between 1000 and 10000 $g\,mol^{-1}$ up to

[*] Prof. Dr. L. L. Böhm
Basell Polyolefine GmbH
Industriepark Höchst, 65926 Frankfurt (Germany)
Fax: (+49) 69-305-3305
E-mail: ludwig.boehm@basell.com

 DOI: 10.1002/anie.200300580 © 2003 Wiley-VCH Verlag GmbH & Co. KGaA, Weinheim

ultrahigh molecular-mass polyethylenes with average molecular mass beyond 1 000 000 g mol^{-1}.

The development of the current process and the achievable product portfolio was realized step by step, based on results from basic research and innovations from industrial research and development. Both have influenced and cross-fertilized each other. The Ziegler slurry process has now reached a volume of 8 Mt per annum and is operated worldwide alongside the high-pressure process and other low-pressure processes (Philipps slurry process, gas-phase process, solution process).[15]

2. Active Sites, Polymerization Mechanism, High-Activity Catalysts

In his Nobel prize lecture,[1] Ziegler reported on the preparation of the catalyst in the following way: "The catalyst used in the shown experiment is formed by mixing triethylaluminum or diethylaluminum chloride with titanium tetrachloride." This reaction in diesel oil or petrol results in a dark brown precipitate mainly consisting of $TiCl_3$.[16] Besides this $TiCl_3$, there are also further alkyl aluminum compounds in the reaction mixture. It was not known at which active center the polymer chain was built up. The polymerization reaction could run at the titanium or aluminum compound, or at a titanium–aluminum complex. Understandably, this outstanding discovery aroused the interest of many research groups, and discussion started on how these catalysts can transform ethylene into polyethylene. Different models and reaction mechanisms were developed.[17] Since it was shown that titanium compounds in combination with $TiCl_3$ or $TiCl_2$ are active for polymerization in the absence of alkyl aluminum compounds, it was generally agreed that the monomer inserted into a Ti–C bond.[18] Natta had stressed this idea at a very early stage.[4] Thus the polymer chain is formed at a titanium-based active site. Cossee[19] developed a model to explain the catalytic polymerization process of ethylene or 1-alkenes at a titanium center. The catalytic cycle (Figure 1) starts with the side-on complexation of ethylene which activates the C–C double bond. This step followed by the insertion into the Ti–C bond via a cyclic transition state. The polymer chain is lengthened by one monomer unit. At the same time, the vacant site becomes free for complexation of the monomer molecule again.

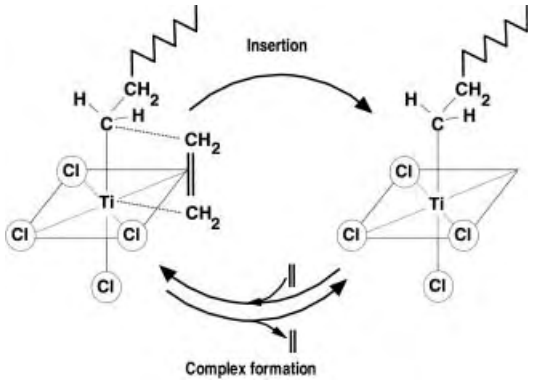


Figure 1. Catalytic cycle for ethylene polymerization at a heterogeneous $TiCl_3$ catalyst according to Cossee and Arlman.

Together with Arlman, Cossee explained how active sites are formed at the surface of $TiCl_3$ by the reaction with alkyl aluminum compounds.[20] The chlorine anions form a close-packed array with interstices in which the much smaller titanium cations sit. In this $TiCl_3$ crystal, each titanium cation is surrounded octahedrally by six chlorine anions. At the surface, titanium centers and chlorine anions are exposed (Figure 2), and thus accessible to other components. One chlorine ion is exposed in such a way that it can react with alkyl aluminum compounds and be replaced by an alkyl group. In this way, a Ti–C bond is generated at the surface of the $TiCl_3$ particle. Ethylene can insert into this Ti–C bond provided there is a vacant site for ethylene complexation. On complexation of one ethylene molecule to the titanium center, the complex shown in Figure 2 is formed. In Figure 2, the three chlorine ions at the surface of the $TiCl_3$ particle are shown together with the CH_2 group of the growing chain; the nearest-neighbor chlorine ion inside the crystal cannot be seen. The sixth titanium coordination site is occupied by an ethylene molecule. Starting from this transition state, ethylene is inserted into the Ti–C bond. One catalytic cycle, as

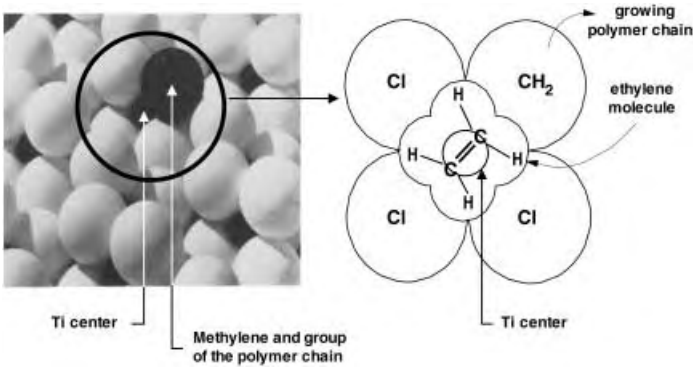


Figure 2. Topology of the δ-$TiCl_3$ surface (left; the titanium-bound methylene end group of the alkyl chain is shown in black) and structure of the active center with a complexed ethylene molecule (right).



Ludwig Böhm, born 1941 in Friedrichshafen on lake Constance, studied chemistry in Mainz. Following his Ph.D. with Prof. G. V. Schulz on anionic polymerization of styrene he moved to Hoechst AG in 1972 and worked on polyolefins. In 1988 he completed his habilitation at the RWTH Aachen on highly active Ziegler catalysts, and has since then lectured on industrial polymerization processes. Currently he works in research and development for Basell Polyolefine.

 © 2003 Wiley-VCH Verlag GmbH & Co. KGaA, Weinheim

shown in Figure 1, is thus completed. The polymer chain grows out of the surface of the heterogeneous catalyst.

The model for the catalytic polymerization of ethylene with heterogeneous titanium catalysts and alkyl aluminum cocatalysts proposed by Cossee and Arlman is in line with the Rideal mechanism for heterogeneous catalytic processes.[21] The Rideal mechanism teaches that the reaction at the surface of the heterogeneous catalyst takes place between a covalently bound atom or radical, and a complexed molecule. The main point is that the covalent bond remains or is transformed into another covalent bond to re-establish the vacant site. The polymerization of ethylene as shown in Figure 1 follows this mechanism. In each insertion step of the activated complexed monomer into the Ti–C bond, a new Ti–C bond is formed, and the vacant site is regenerated for complexation of the next monomer molecule.

In addition to the main reaction, chain propagation (with the monomer as the reaction partner), there are further reactions at the active site, such as the β-hydride elimination which leads to removal of the polymer chain from the active center along with the formation of a vinyl group at the chain end, or chain-transfer reactions with hydrogen and alkyl aluminum compounds. The reaction scheme is shown in Figure 3.[22] For a clearer presentation, "Cat" represents the active site. Cat comprises all parts of the active complex at the surface of the heterogeneous catalyst except the vacant site and the Ti–C bond as shown in Figure 4.

All reactions of the scheme in Figure 3 follow the Rideal mechanism.[21]. Complexation and activation of ethylene, a reversible reaction (1), the monomer is inserted into the Ti–C bond (2) or, to a minor extent a β-H elimination reaction transferring a hydrogen atom from the β position of the polymer chain to the ethylene molecule generating a vinyl-

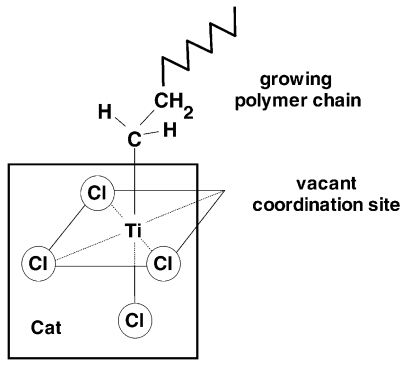


Figure 4. Active center "Cat" (see Figure 3).

group-terminated polymer chain and an ethyl group at the titanium site (3). The insertion reaction is represented as irreversible. This is because the concentration of ethylene, dissolved in a hydrocarbon and in equilibrium with solid, partially crystalline polyethylene, can be calculated based on thermodynamic data to be 10^{-7} mol dm^{-3} at 80 °C.[23,24]

The vinyl chain end group can either leave the active site (5) finishing the chain-propagation process, or insert into the Ti–C bond of the ethyl group (4) to form an ethyl branch in the growing polymer chain. The ratio of chain propagation to β-H elimination is around 10^4:1 at 80 °C.[25] These two reactions lead to different, covalently bound alkyl groups at the titanium center (Figure 3).

In addition to these reactions, there are a variety of chain-transfer reactions running in a second cycle. These reactions are with alkyl aluminum compounds (6,7), by β-H elimination and formation of a Ti–H bond (8,9) followed by conversion of this Ti–H bond into a Ti–C bond by insertion

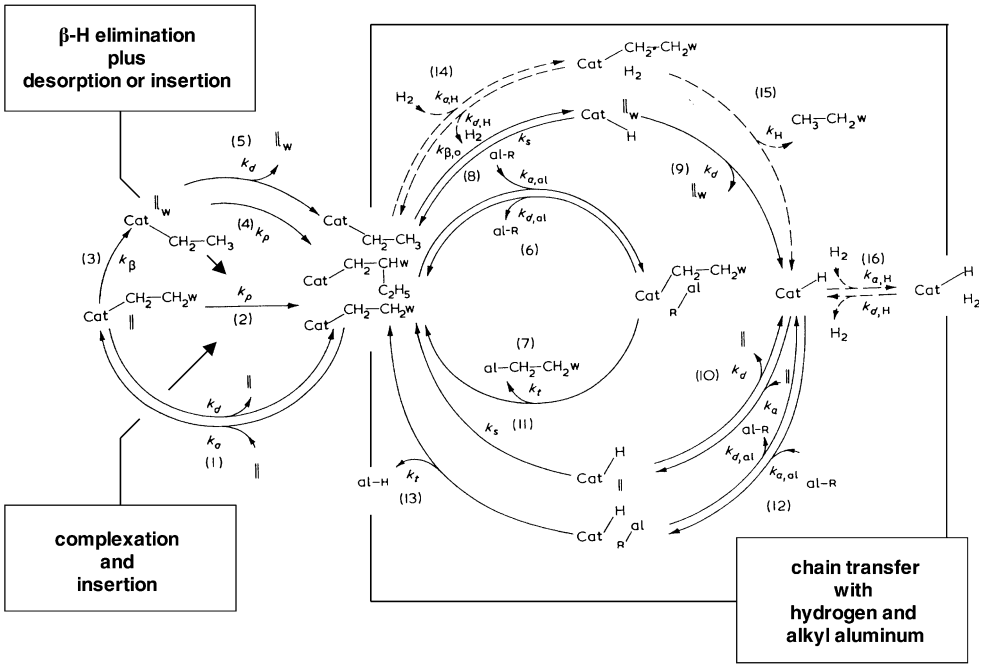


Figure 3. Mechanism of the catalytic polymerization of ethylene with a titanium catalyst. al = $^1/_3$ Al, R = $(CH_2)_nCH_3$, w = growing polymer chain, ‖ = ethylene molecule; all the constants are assigned to elementary processes.

 © 2003 Wiley-VCH Verlag GmbH & Co. KGaA, Weinheim

of ethylene (10,11), or by the exchange of the hydrogen atom by an alkyl group of the alkyl aluminum compound (12,13). By far, the most important and, for the industrial process, most relevant chain-transfer reaction takes place with hydrogen (14,15).[14] The generated Ti–H bond can be converted back into a Ti–C bond by the reactions (10,11) or (12,13). This Ti–C bond then enters into the chain-propagation cycle again. Reaction (16) is the reversible inhibition of the active center by hydrogen, this is an important side reaction because it significantly reduces catalyst activity.

This scheme shown in Figure 3 describes the catalytic polymerization process with a Ziegler titanium-based catalyst and alkyl aluminum compounds as cocatalysts in a comprehensive way.[21] All the reaction cycles follow the Rideal mechanism,[21] and the regulation of chain length with hydrogen is included. It describes only the homopolymerization process, however, it can be extended to the copolymerization of ethylene and 1-alkenes. This extension was carried out for the binary copolymerization. With equations derived from this scheme, and its extension to the copolymerization process, it is possible to describe this process and to determine kinetic parameters based on experimental data.[25,26]

Because the only active titanium sites are at the surface of the heterogeneous $TiCl_3$ catalyst, only a minor amount of titanium atoms can participate in the polymerization process. Of the total number of titanium cations in a $TiCl_3$ crystal of 1 μm only around 10^{-3} equivalents mol^{-1} are accessible; this means that only one titanium site out of 1000 can be part of the catalytic process. With such catalysts, catalyst productivity[11] remains below 10 kg g^{-1} leading to a titanium content in the polymer of 100 ppm. This high Ti content combined with a high content of chlorine anions from $TiCl_3$ and alkyl aluminum chlorides means that on contact with humidity such polyethylenes release hydrochloric acid which leads to corrosion of the extrusion line and the moulds during pelletization and processing. It was thus necessary to decompose catalyst and cocatalyst residues, and to remove the reaction products from the polyethylene. This was a complicated procedure with high costs.[11]

The catalyst productivity had to be increased by a factor of 100 or better more, but how? In principle, there were the following ways to go: increase the number of active sites at the surface of the heterogeneous catalyst by a factor of 100 or increase the overall propagation rate constant by the same factor. A combination of both ways could also lead to success.

To make more titanium centers accessible at the surface of the catalyst, the specific surface had to be increased. This route could be realized in two different ways. On treating isoprenylaluminum with $TiCl_4$ at 0 °C in petrol, a $TiCl_3$ catalyst precipitates which has much higher activity than those $TiCl_3$ catalysts prepared with $TiCl_4$ and other alkyl aluminum compounds at higher temperatures.[27] Isoprenylaluminum[28] is a organoaluminum compound of higher molecular mass, which on reaction with $TiCl_4$ forms a $TiCl_3$ precipitate with smaller crystallites and much higher specific surface area. This catalyst does not fully reach the targets, but it shows a clear activity increase, and it can be prepared in a simple, one-step way. The catalyst productivity[11] is around 20 kg g^{-1} in the industrial process.

The preparation of more active $TiCl_3$ catalysts also be achieved by the precipitation of $TiCl_3$ from the reaction of $TiCl_4$ in petrol with diethylaluminum chloride again at 0 °C. The precipitated $TiCl_3$ contains high amounts of $AlCl_3$. This $AlCl_3$ can be extracted afterwards by treatment with long chain diethers, such as diisoamylether. This approach generates a porous particle structure with crystallites in the range of 5 to 10 nm. Then, a further treatment with $TiCl_4$ follows.[20] In this way, the activity can be increased by a factor of up to 10 in the industrial process.[30] Bonding of $TiCl_4$ onto inorganic supports again resulted in activity increase but not of the required magnitude.[31] The production of highly active catalysts (high-mileage catalysts) was possible by binding $TiCl_4$ to the surface of anhydrous $MgCl_2$.[11,32] The outstanding success of $MgCl_2$ is because δ-$MgCl_2$ and δ-$TiCl_3$ have the same crystal structure and the nearly identical ionic radii and lattice distances (Table 1).The coverage of the $MgCl_2$ particle surface with the titanium component, and the conversion of this titanium component into active sites corresponding the Cossee/Arlman model, can be represented as shown in Figure 5–7.[33]

Table 1: Crystallographic data for δ-$MgCl_2$ and δ-$TiCl_3$.

δ-$MgCl_2$	δ-$TiCl_3$
hexagonal close packing of the Cl^- ions	
$a = b = 3.63$ Å	$a = b = 3.54$ Å
$c = 5.93$ Å	$c = 5.86$ Å
Cation coordination: octahedral	
Mg-Cl = 1.23 Å	Ti-Cl = 1.25 Å
$Mg^{2+} = 0.65$ Å	$Ti^{4+} = 0.68$ Å
	$Ti^{3+} = 0.76$ Å

Along the axis [100] and [110] $TiCl_4$ can be absorbed (Figure 5). Over several steps, the active sites are formed (Figure 6). In the first step, one chlorine ligand at the titanium center is exchanged for an alkyl group of the alkyl aluminum compound. In the next step, Ti^{4+} is reduced to Ti^{3+} by splitting off an alkyl radical. This alkyl radical is deactivated by reaction with a further alkyl radical. By these two reaction steps, the vacant site at the titanium center is formed, which is necessary to complex and activate the ethylene molecule.

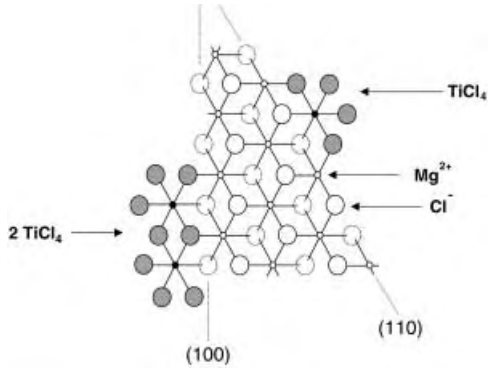


Figure 5. Epitaxial binding of $TiCl_4$ on to the surface of δ-$MgCl_2$.

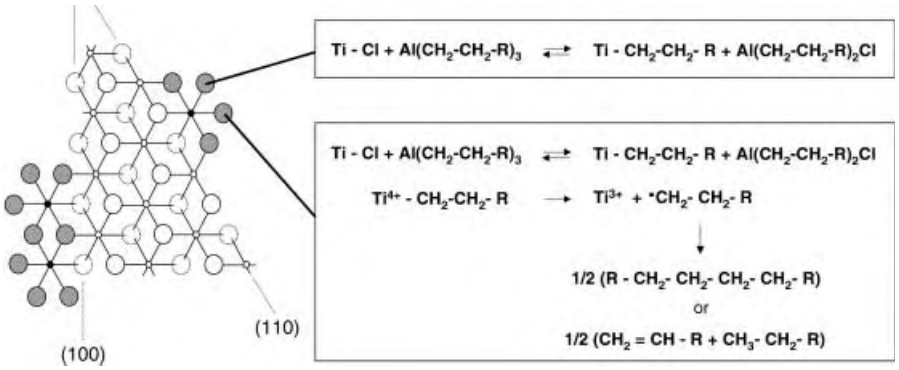


Figure 6. Formation of the active center on the surface of the $MgCl_2$–titanium catalyst.

By the exchange of a further chlorine ligand by an alkyl group, again by reaction with the alkyl aluminum compound, the Ti–C bond is introduced that is necessary for the insertion of ethylene. The structure of these active sites corresponds to the structure of active sites for the polymerization of ethylene as postulated by Cossee and Arlman.

All steps 1 to 3, as shown on Figure 7, can take place in the polymerization reactor or can be part of the catalyst synthesis. Then the catalyst is activated by the cocatalyst (steps 1 and 2) followed, if necessary, by a prepolymerization step with ethylene (step 3—(see also Section 3, Particle-Forming Process).

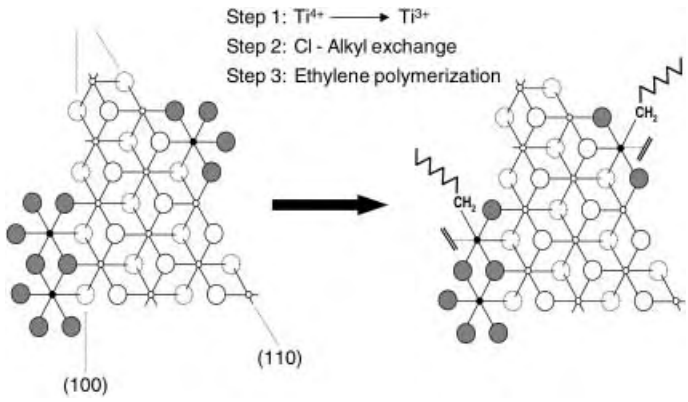


Figure 7. Reactions at the active center on the surface of the $MgCl_2$–titanium catalyst.

In the industrial process, these catalysts achieve the targeted catalyst productivities[11,33] of 100 kg g^{-1} and more. The chain length of the polymer can be regulated with hydrogen, and there is sufficient activity with higher 1-alkenes to vary the copolymer composition and thus achieve the targeted product properties. It was shown that the activity increase is mainly caused by the increase of equivalents of active sites reaching a level of 0.8 equivalents mol (Ti)$^{-1}$. The propagation rate constants remain at the same level known for $TiCl_3$ catalysts (ca. 100 dm^3 mol^{-1} s^{-1} at 80 °C).[26]

For industrial use, it is of utmost importance to find simple routes for catalyst synthesis to realize a cost level of not more than 20 € for the catalyst and cocatalyst to produce 1 t of polyethylene. A further challenge was to gain access to $MgCl_2$ supports with the requires particle morphology (the particle morphology plays a key role in industrial processes because it influences reactor loading (see Section 4)). Today, four industrially viable synthetic routes are used to fulfill the requirements.

1. Solid $MgCl_2$ is ball-milled with liquid $TiCl_4$ ($TiCl_4/MgCl_2 < 0.15$) under inert gas.[32] This procedures results in a significant increase in the specific surface area of the solid. Catalyst particles are formed composed of very small crystallites. This process can be monitored by X-ray diffraction which shows a broadening of the some typical peaks.[32] At the surface of $MgCl_2$ crystallites, $TiCl_4$ is fixed as already described (see Figure 5). The titanium content of the catalyst is in the range of 4 wt %. By generating titanium centers at the surface of $MgCl_2$ with high specific-surface-area catalysts are formed having high catalyst productivity of nearly a factor of 100 compared to other already optimized $TiCl_3$ catalysts.[34] The most important disadvantage of this procedure is the insufficient particle morphology which cannot be manipulated as requested.
2. By precipitation of $MgCl_2$ out of an alcoholic solution into a hydrocarbon mixture (paraffin oil) at higher temperatures droplets of $MgCl_2$ complexes with *n* molecules of C_2H_5OH are formed. After solidification of these droplets to spherical particles by rapid cooling, they are treated with $TiCl_4$. Excess titanium compounds are afterwards washed out with petrol. The titanium content can be adjusted between 1–4 wt %. The essential advantage of this process is the formation of spherical particles. The particle size and the particle morphology (specific surface area and porosity) can be fine-tuned.[35]
3. Treating Grignard compounds with alkyl chlorides in petrol.[36] Excellent catalysts with spherical particle shape can be synthesized using BOMAG (butyloctylmagnesium, an industrial product known as BOMAG-A) with for example, $CHCl_3$ or CCl_4. During this reaction, a solid component is precipitated in petrol, mainly consisting of $MgCl_2$ but also containing alkyl groups. The precipitation process can be performed so as to generate spherical particles with average size between 10 and 50 μm. The precipitate is washed with excess petrol before being treated with $TiCl_4$. Between 1 and 4 wt % of titanium is fixed at this support. Excess titanium compounds are removed by washing with petrol.
4. The reaction of magnesium alcoholate compounds, such as $Mg(OC_2H_5)_2$, with $TiCl_4$ in petrol.[11,37] With this process, high-activity catalysts are formed in a one or multistep, one-pot synthesis. Magnesium alcoholate compounds consist of crystals with layers of magnesium cations and alcoholate anions with loose layers of alkyl chains of the alcoholate groups in between.[38] As known from silicates with layer structures, solvents can penetrate

 © 2003 Wiley-VCH Verlag GmbH & Co. KGaA, Weinheim

into these loose layers. These layers swell and the bonds are weakened.[39] For magnesium alcoholate compounds, hydrocarbons are incorporated. During the reaction with $TiCl_4$, a reaction with $TiCl_4$ takes place in this layer to form $MgCl_2$ and $TiCl_{4-n}(OC_2H_5)_n$ compounds. The in petrol suspended magnesium ethanolate is transformed into the $MgCl_2$ support and at the same time, $TiCl_4$ is absorbed. The soluble $TiCl_{4-n}(OC_2H_5)_n$ compounds are removed by washing with petrol. Between 5 and 6 wt % of titanium is fixed on these catalysts.

$MgCl_2$-supported titanium catalysts are today the preferred catalysts for the slurry polymerization process in petrol for producing polyethylenes. They represent the state-of-the-art. All the catalysts are insoluble in petrol and they are applied as a finely dispersed slurry in the industrial process. They fulfill all the requirements with respect to activity as the catalyst productivity reaches 100 kg g^{-1} and more under industrial process conditions. They are also cost efficient (< € 20 per ton of polyethylene), they can be regulated with hydrogen, and they can be copolymerized with 1-alkenes to adjust the product properties.

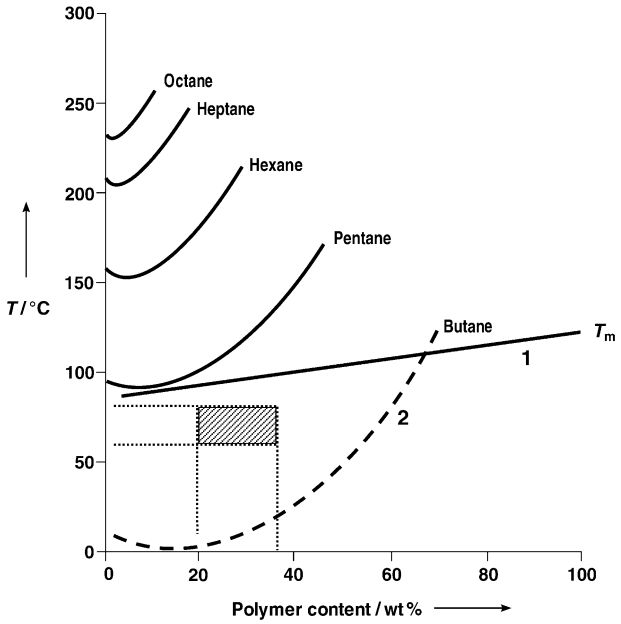


Figure 8. Phase diagram for polyethylene and aliphatic hydrocarbons.

3. Precipitation Polymerization, Particle-Forming Process, Microreactors

Ziegler described the precipitation polymerization process in the following way: "The gas is quickly absorbed. In two liters of the diluent, around 300–400 litres of ethylene is consumed in an hour. After that time, the mixture becomes pulpy and can hardly be stirred. If the brown catalyst is destroyed by alcohol and air, then the precipitate turns to a white powder which can be isolated by filtration. The end result is between 300–500 g of this dry white powder."[1] This experiment shows that the formed polyethylene is insoluble in diesel oil or petrol and precipitates during polymerization as a powder. It further shows that increasing polymer content leads to problems in mixing of the slurry. Both observations have a high relevance for the industrial process.

The phase diagram of polyethylenes and saturated aliphatic hydrocarbon diluents (petrol, diesel oil) is presented on Figure 8.[40] There is a turbidity line (1), at temperatures below this line the polymer becomes insoluble in hydrocarbon diluents. The location of this turbidity line (1) depends on the melting point of the polymer T_m. Depending on the melting point, the turbidity line moves up or down.[41]

For the slurry process, lower critical solution temperature curves (2) are not relevant. Under these conditions, a solution of polyethylene in a hydrocarbon diluent separates into a polymer-rich liquid phase (gel) and diluted polymer phase (sol). These lines (2) show a strong dependence on the chain length of the hydrocarbon diluent. In contrast, turbidity curves (1) are independent of this parameter.

The industrial slurry process is operated at temperatures below the turbidity line (see the area on Figure 8). In this area, the polymer precipitates during polymerization. This process allows high polymer contents to be obtained independent of the average molecular mass of the polyethylene because the viscosity of the slurry increases only slightly. High polymer contents can be obtained in industrial processes if the polymer forms a separate phase in the liquid or gaseous phase. These processes are called heterogeneous processes.[42,43] In this slurry polymerization process, the catalyst is suspended in petrol and is so introduced into the reactor. The polymerization takes place at the surface of the catalyst particle, and the polymer chains propagate at this surface (see Section 2) forming a solid crystalline phase. In this way the catalyst particles are transformed into polymer particles. This process is called the particle-forming process. The catalyst becomes part of the polymer particle and remains totally inside the polymer. It leaves the polymerization reactor with the polymer. To keep the polymerization process running, fresh catalyst must be steadily fed into the polymerization reactor.

As described in Section 2, the $MgCl_2$- supported titanium catalysts consist of particles which average between 10 and 100 μm in diameter. The average particle size can be adjusted during the catalyst synthesis. The catalyst particle is composed of much smaller particles with a size in the nm range. These particles are called primary particles. By agglomeration of many primary particles, a catalyst particle with high porosity and high specific surface area is formed. The pore volume is in the range of 0.3 to more than 1 cm^3 g^{-1}. The specific surface area reaches values between 50–300 m^2 g^{-1}.[26,34]

These catalyst particles are transformed into polymer particles during polymerization. When polymerization starts at the surface of the primary particles, the primary particle agglomerate is disrupted. The polymeric phase is formed around each catalyst fragment, growing larger and larger by polymer formation. In this way these catalyst fragments are distributed more homogeneously in the growing particle (Figure 9).

 © 2003 Wiley-VCH Verlag GmbH & Co. KGaA, Weinheim

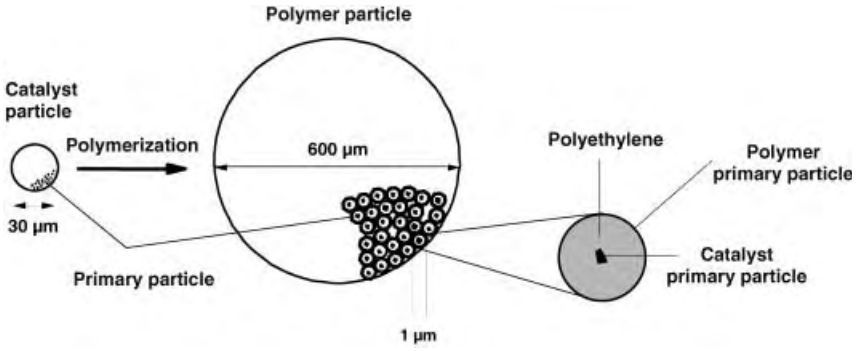


Figure 9. The particle-forming process: conversion of a catalyst particle into a polymer particle.

The catalyst particle shape is replicated in the polymer particle shape. This means that particle shapes and particle size distributions are the same for the catalyst and the polymer (Figure 10).[33] The particle grows in diameter by a factor of 10 to 25 corresponding to a volume increase by a factor of 10^3 to 10^4. Both the particle size of the catalyst and the polymer are adjusted as required for the industrial polymerization process as well as for the extrusion of the polymer powder.

The particle-forming process is very complicated. It is influenced by the catalyst-particle structure and the reaction conditions for polymerization. Because of the complexity of this particle-forming process, there are different models to describe it.[44] The simplest model for this process using high-activity catalysts is the "polymeric flow model" (Figure 11).[45] It is assumed that the growing particle is spherical and all the active sites are distributed evenly over the particle which can be regarded as being quasi-homogeneous. This condition means that the diffusion rate constant of ethylene can be shown as an effective value, without taking into account that there is a difference of ethylene diffusion in the pores filled with petrol and in the petrol-swollen amorphous polyethylene formed during polymerization.

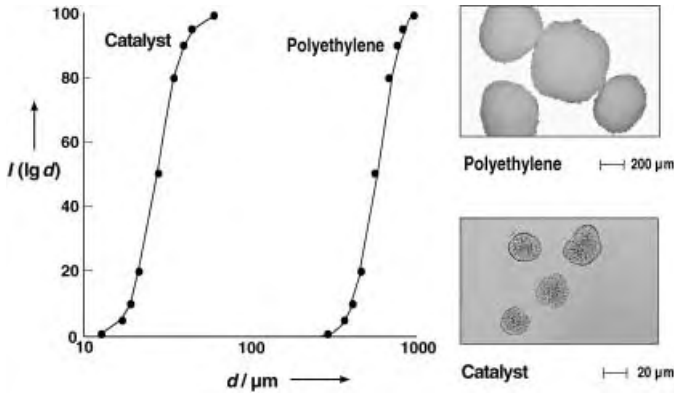


Figure 10. Size distribution of catalyst and polyethylene particles.

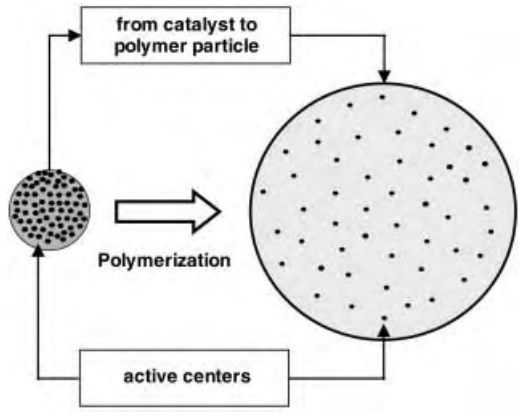


Figure 11. The "polymeric flow model" of the particle-forming process.

The Equations (1), (2) for the description of the particle-forming process are only valid when the temperature is the same over the whole polymerizing particle.[45,46] Equation (1)

$$\frac{d^2c_{1.P}}{dr^2}+\frac{2}{r}\frac{dc_{1.P}}{dr}\cdot\frac{(\bar{k}pf)(n_k/V_K)R_o^3}{D_{eff}R^3}c_{1.P}=0 \quad \text{with } \frac{dc_{1.P}}{dr}=0 \text{ for } r=0 \text{ and } c_{1.P}=c_1 \text{ for } r=R \tag{1}$$

describes consumption of ethylene by polymerization and the ethylene feed by diffusion inside the polymerizing particle. Equation (2) describes how the particle size increase with

$$\frac{dR}{dt}=\frac{M_1}{d_P}D_{eff}\left(\frac{dc_{1.P}}{dr}\right)_{r=R} \quad \text{with } R=R_o \text{ for } t=0 \tag{2}$$

time by solid-polymer formation ($c_{1.P}$ = ethylene concentration, r = particle radius; $\bar{k}p$ = overall propagation rate constant, f = catalyst efficiency ($0<f\leq 1$), D_{eff} = diffusion rate constant of ethylene, n_K = amount of titanium in the catalyst particle with the volume V_K; R_0 = radius of the catalyst particle, R = radius of the polymer particle, d_P = density of the polymer particle, M_1 = molecular mass of ethylene, t = reaction time).

The polymeric flow model can be described with only two parameters: $\bar{k}pf$ and D_{eff}. With this model, it is possible to determine under which conditions this process is kinetically controlled, that is, when the consumption of ethylene by polymerization is the relevant process, or when the diffusion of ethylene inside the polymerizing particle is the rate-determining step.[47–49] These ranges, known as the kinetically controlled and diffusion-controlled range, respectively, are shown in Figure 12. The preferred range in the industrial process is the kinetically controlled range as it is here that the catalyst productivity reaches the highest value. In this range all the active sites are involved in the same way in the polymerization process because in the growing polymer particle, all the active sites have full access to ethylene.

Each of these polymerizing particles can be regarded as a small reactor with its own mass and heat balance and for this reason they are called microreactors. There are models for catalytic processes with low-molecular-mass compounds,

 © 2003 Wiley-VCH Verlag GmbH & Co. KGaA, Weinheim

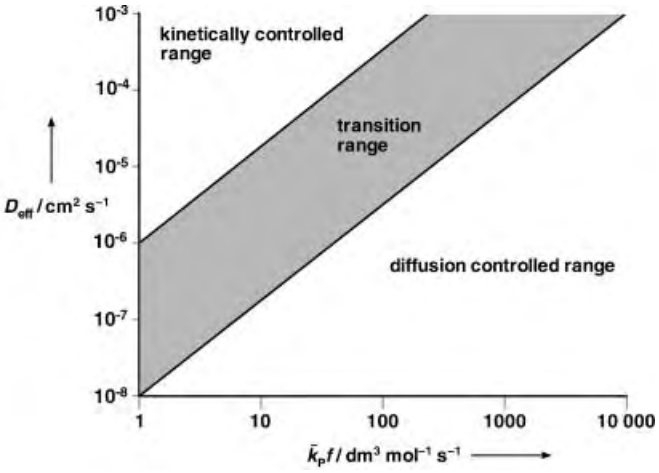


Figure 12. Polymerization in microreactors: kinetic- and diffusion-controlled regions.

mainly developed by Wicke[50] and Eigenberger.[51] These investigations show that these microreactors can strongly heat up if large amounts of heat produced by a rapidly running chemical reaction cannot be transferred to the environment. The same effect can also exist in such a polymerizing microreactor.

For the polymerization process, it is essential that, first, the temperature of each microreactor remains close to that of the surrounding medium, and second, that inside and at the outer surface of the microreactor there are only minor concentration gradients for ethylene (kinetically controlled range). The heat of the strong exothermic polymerization reaction (≈100 kJ per mol of reacted ethylene) produced inside the microreactor must be removed through the surface of the polymer particle. If the heat-transfer line (Figure 13) is steep and cuts the heat-production line at the lower stable process point, then the temperature of the microreactor remains slightly above the environmental temperature (ca. 1–2 K; Figure 13).[49–51] On the other hand, when the heat-transfer line is flat and cuts the heat production line at the upper stable process point, then the temperature of the microreactor jumps up to a much higher temperature in relation to the environment (> 20 K; Figure 13).[52] This can

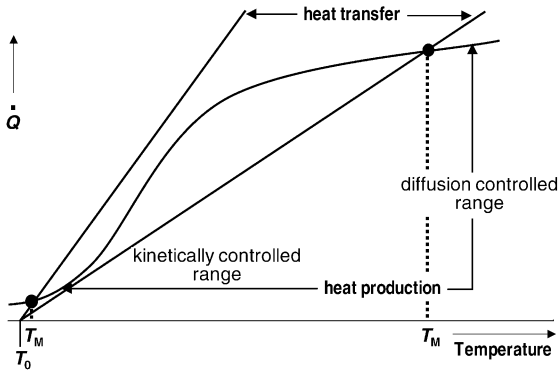


Figure 13. Heat transfer and heat production at microreactors.

lead to melting or swelling and even dissolving of the polymer particle.

If there is a very fast polymerization reaction inside such particles, the ethylene feed into the microreactor can become the rate-determining step. Then a concentration gradient is formed at the surface and inside the microreactor. The concentration gradient inside the particle can be calculated using the Thiele equation.[46] At the outer surface, it is assumed that the concentration gradient is linear.

Thus the microreactor can take on two significantly different steady states. In one case the gradients for temperature and ethylene concentration are very small, in the other instance they are very large (Figure 14). The favored steady

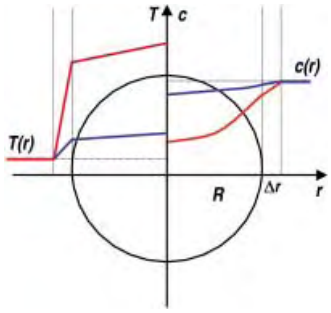


Figure 14. Temperature and ethylene-concentration gradients at and in microreactors.

state in the industrial process is the one in which there are small gradients for both parameters. Particularly important is the strong heating of the polymer particle about the temperature of the surrounding environment (formation of hot spots). When this process occurs over a large volume of the polymerization reactor, then many particles can clump together, which inevitably leads to the shut down of the reactor as the contents of the reactor can no longer be mixed homogeneously and the whole process then runs out of control. This critical state occurs especially with small-diameter particles, that is, at the start of polymerization in a catalyst particle.[52] In this case a very large number of active centers are present in a small reaction space, and the correspondingly small surface of the microreactors is not sufficient to dissipate the heat generated into the surrounding medium.

various strategies are available to prevent the overheating of microreactors. At the beginning of polymerization the heat production in the microreactor can be held under the heat transfer curve if at the start of the reaction the rate of polymerization is low and increases only with the increasing volume of the microreactor (Figure 15). With a high initial rate of polymerization (curve 2; Figure 15), satisfactory heat transfer only occurs above R_{crit}, and in small particles overheating of the microreactors occurs.

Figure 16 shows the polymerization behavior of an optimized catalyst with a slowly increasing polymerization activity. The polymerization activity in the microreactor begins at a very low level and increases over 30 min with the increasing volume to a maximum value. When the

 © 2003 Wiley-VCH Verlag GmbH & Co. KGaA, Weinheim

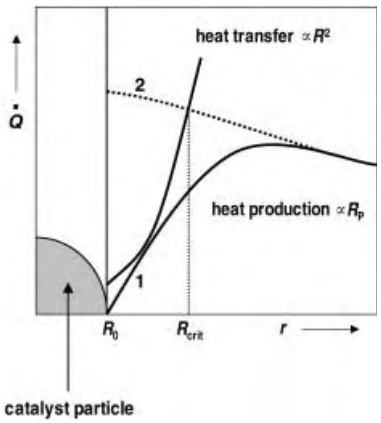


Figure 15. Heat balance at microreactors.

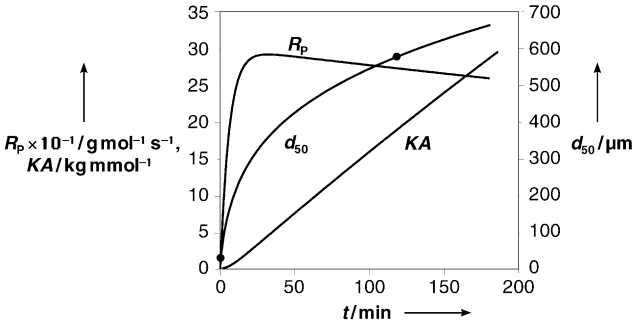


Figure 16. Polymerization with an optimized catalyst: R_P = rate of polymerization, KA = catalyst productivity, d_{50} = average particle diameter; all amounts are based on titanium. For sample size distribution, see Figure 10.

polymerization activity only decreases a little over the average time the particles are in the polymerization reactor, up to three hours, then the catalyst excellently fulfills the industrial requirements. Optimized industrial catalysts typically show this behavior.

If it is not possible to optimize a catalyst in this way, than the formation of over-heated particles can be suppressed by slowly treating the particles with ethylene, outside the polymerization reactor, and thus forcing a slow polymerization. As a result the particles expand without the development of hot spots.[53] When the particle size exceeds the critical R_{crit} (at R_{crit} the heat production from polymerization and the heat transfer through the outer surface are equivalent) then the prepolymerized catalyst is added to the polymerization reactor and the particle-forming process proceeds as usual.

In summary, it can be concluded that there are two essential points for an optimized particle forming process: 1) a homogeneous temperature distribution inside the microreactor together with a temperature of this microreactor close to the temperature of the diluent, and 2) the same ethylene concentration throughout the microreactor and only a small concentration gradient at its surface during overall high catalyst productivity under industrial process conditions.

4. Modelling of the Polymerization Reactor: Macro-, Meso-, Microscale

For the description and modeling of industrial polymerization processes, Ray[54] divided the reaction space into different scales. This principle is of great value. The slurry polymerization process can be scaled on these three levels (Figure 17).

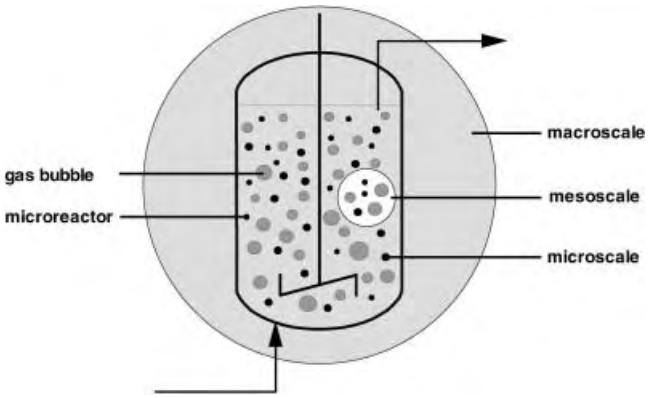


Figure 17. Scales of the polymerization reaction according to Ray.[54]

The reaction space in which the polymerization runs is the polymerization reactor (macroscale). Provided there is good mixing by turbines it can be regarded as a continuous stirred tank reactor (CSTR). Good mixing means that both the material and temperature distributions inside this reactor are homogeneous, and that all growing polymer particles are moving randomly and independent of each other in the slurry. This condition is realized if the volume fraction of the polymer in the slurry stays below the volume fraction of the bulk polymer powder Φ_o. In this case, the relative viscosity increase of the slurry remains low.[43] The volume fraction of the bulk polymer powder Φ_o can be calculated using the bulk density and the density of the polyethylene ($d = 0.950\ g\,cm^{-3}$). The relative viscosity increase of the slurry can be described by the Mooney equation (Figure 18).

The relative viscosity of the slurry increases sharply when the volume fraction of the polymer powder Φ approaches Φ_o. Then the slurry becomes, as Ziegler put it, "pulpy" and it can no longer mixed homogeneously.[1] To run the polymerization reactor at high polymer contents, Φ_o must be as high as possible, and the powder morphology must be adjusted to the process.

The components petrol, catalyst, cocatalyst, ethylene, 1-alkene, (in this case, 1-butene), and hydrogen are continuously fed in under nitrogen, and the polymer leaves the polymerization reactor with petrol and residual starting materials. There are three phases, petrol as the liquid phase which contains finely dispersed gas bubbles of the reaction partners ethylene, 1-butene, hydrogen, and nitrogen, as well the solid phase which comprises the polymer with the catalyst residues. In this reaction space, steady-state reaction conditions, such as temperature, pressure, partial pressures, space-time yield, average residence time, and others are set

 © 2003 Wiley-VCH Verlag GmbH & Co. KGaA, Weinheim

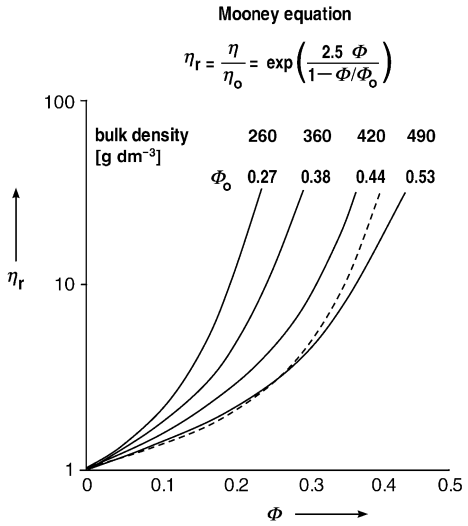


Figure 18. Increase in the relative viscosity (η_r) of a polyethylene–petrol suspension as a function of the volume fraction of Polyethylene (Φ); —— measured, – – – calculated.

to ensure that the polymerization process generates the targeted polyethylenes.

The modeling of the polymerization reactor on the macroscale is carried out on the basis of a mass balance for all components (ethylene, 1-alkene, and hydrogen). These components are either introduced into the reactor as a gas or liquid (1-butene). They flow from the gas phase through the liquid phase to the polymerizing microreactors. There they are converted into the polymer or take part in the polymerization process. The mass balance can be written as Equation 3 (c_i = concentration of component i, J = amount of

$$c_{i.g}^{in}\dot{V}_g^{in} = c_{i.g}^{out}\dot{V}_g^{out} + J_i \tag{3}$$

component consumed, $\dot{V}$ = volume stream, indices: 1 = ethylene, 2 = comonomer, 3 = hydrogen, 4 = nitrogen, in = feed into the reactor, out = leaving the reactor, g = gaseous, l = liquid; α = Ostwald solubility coefficient).[55]

Equation (3) shows that the amount component i, $c_{i.g}^{in}\dot{V}_g^{in}$, entering by the gas inlet flows through the liquid phase (petrol) into the microreactors where it is consumed. A small amount of substance, $c_{i.g}^{out}\dot{V}_g^{out}$, leaves the reactor as gas. The amount of substance transferred into the diluent reacts to a large extent, but a certain amount leaves the reactor dissolved in petrol [Eq. (4) and (5)].

$$J_i = c_{i.l}^{out}\dot{V}_l^{out} + \dot{n}_{i.p} \tag{4}$$

$$c_{i.l}^{out} = \alpha_i\, c_{i.g}^{out} \tag{5}$$

Equation (6a) describes the amount-of-substance balance

$$\frac{c_{i.g}^{in}\dot{V}_g^{in} - c_{i.g}^{out}\dot{V}_g^{out}}{c_{i.g}^{in}\dot{V}_g^{in}} = \alpha_i \frac{\dot{V}_l^{out}}{\dot{V}_g^{out}}\left(1 + \frac{\dot{n}_{i.p}}{c_{i.l}^{out}\dot{V}_l^{out}}\right) \tag{6a}$$

of the component i and gives the amount consumed by polymerization in relation to the amount unreacted. The relevant dimensionless value is the Damköhler number 1 (Da) as given in Equation (6b).[56] This number describes the

$$Da_{I,i} = \frac{\dot{n}_{i.p}}{c_{i.l}^{out}\dot{V}_l^{out}} \tag{6b}$$

ratio of the polymerized amount of substance ($\dot{n}_{i.p}$) and the amount of substance leaving the reactor.

If in Equation (6a) index i is replaced by 1 for ethylene, then the equation describes the amount of substance balance for ethylene. The Damköhler number 1 can be written as Equation 7.

$$Da_{I.1} = \bar{k}p\, f \frac{n_K}{V_l}\tau \tag{7}$$

$Da_{I.1}$ is calculated by multiplying the overall propagation rate constant $\bar{k}p$ and the catalyst efficiency f ($0 < f \leq 1$; f is the number of active sites taking part in the polymerization in relation to the number of titanium centers), the catalyst content n_K in the reaction volume V_l (which in this case is the volume of the slurry, that is, the sum of the petrol volume and the solid polymer volume), and the average residence time τ. This number describes the activity of the catalyst in the industrial process.

For the other components, such as the comonomer (1-butene) and hydrogen, similar equations can be formulated. It is essential that all the equations contain the Damköhler number for ethylene because the consumption is either related by the Mayo-Lewis equation[57] for the comonomer or by the Mayo equation[58] for the molecular-weight regulating hydrogen, which is coupled to the consumption of ethylene [Eq. (8) and (9a, b)].

$$\frac{\dot{n}_{2.p}}{\dot{n}_{1.p}} = \left(\frac{n_2}{n_1}\right)_P = \frac{1}{r_1}\frac{c_{2.l}^{out}}{c_{1.l}^{out}} \tag{8}$$

$$\frac{\dot{n}_{2.p}}{c_{2.l}^{out}\dot{V}_l^{out}} = \frac{1}{r_1}\frac{\dot{n}_{1.p}}{c_{1.l}^{out}\dot{V}_l^{out}} \tag{9a}$$

$$Da_{I.2} = \frac{1}{r_1} Da_{I.1} \tag{9b}$$

Equation (8) with only one Mayo–Lewis parameter r_1 is valid because for this copolymerization process, the r parameters differ by orders of magnitude.[59] The reason is the large differences of the overall propagation rate constants for ethylene (index 1) and 1-butene (index 2; Table 2).[13] There are great differences for these values because for this

Table 2: r-Parameters and growth constants for the binary copolymerization of ethylene und 1-butene.[a]

T [°C]	r_1	r_2	k_{11}	k_{12}	k_{21}	k_{22}
120	50	0.04	200	4	22	0.82
85	80	0.08	100	1.3	14	1.1
65	110	0.10	70	0.64	11	1.1
50	130	0.10	60	0.46	10	1.0

[a] [k_{ij}] = dm^3 mol^{-1} s^{-1} $\Delta r_1 = \pm 15\%$; $\Delta r_2 = \pm 30\%$; Δr_1 (85 °C) = $\pm 10\%$.

 © 2003 Wiley-VCH Verlag GmbH & Co. KGaA, Weinheim

process the activation enthalpies for all the propagation steps of the binary copolymerization are nearly the same. On the other hand, the activation entropies calculated using the Eyring equation[60] are highly different (Table 3).[13]

Table 3: Entropy and enthalpy values for the polymerization of ethylene and 1-butene.[a]

Reaction	Entropy [J K^{-1} mol^{-1}]	Enthalpy [kJ mol^{-1}]
$n\,M_{1.s} \rightarrow 1/n\,(M_{1.s})_c$	−128	−100
$n\,M_{1.s} \rightarrow 1/n\,(M_{1.s})_a$	−100	−92
$wM_1\text{-Cat} + M_{1.s} \rightarrow wM_1\text{-Cat}$	−160[b]	15[b]
$wM_1\text{-Cat} + M_{2.s} \rightarrow wM_2\text{-Cat}$	−210[b]	12[b]
$n\,M_{2.s} \rightarrow 1/n\,(M_{2.s})_{c.isot}$	−94	−79
$mM_2\text{-Cat} + M_{2.s} \rightarrow mM_2\text{-Cat}$	−210[b]	12[b]
$mM_2\text{-Cat} + M_{1.s} \rightarrow mM_1\text{-Cat}$	−200[b]	9[b]

[a] 1 = ethylene, 2 1-butene; s = 1 M ideal solution, a = amorphous solid polyethylene, c = crystalline solid polyethylene; isot = isotactic, Cat = active center. [b] Calculated from the kinetic data.

The most relevant chain-transfer reaction takes place with hydrogen. For the average-molecular-mass regulation with hydrogen, all other chain-transfer reactions shown in the reaction scheme (Figure 3) can be ignored. Hydrogen and ethylene consumption are connected by the average chain length of the copolymer (P_n) as given by Equation (10).

$$\frac{\dot{n}_{3.p}}{\dot{n}_{1.p}} = \frac{1}{P_n} = \left(A + B\frac{c_{2.l}^{out}}{c_{1.l}^{out}}\right)\frac{c_{3.l}^{out}}{c_{1.l}^{out}} \tag{10}$$

Because there are two different chain ends (ethylene and 1-butylene) bound to the active site, the equation contains two chain-transfer constants A and B [Eq. (11a,b)].

$$\frac{\dot{n}_{3.p}}{c_{3.l}^{out}\dot{V}_l^{out}} = \left(A + B\frac{r_1}{(n_1/n_2)_P}\right)\frac{\dot{n}_{1.p}}{c_{1.l}^{out}\dot{V}_l^{aus}} \tag{11a}$$

$$Da_{I.3} = \left(A + B\frac{r_1}{(n_1/n_2)_P}\right)Da_{I.1} \tag{11b}$$

To complete the modeling of the polymerization reactor on the macroscale, in addition to the equations for ethylene (index 1), 1-butene (index 2), and hydrogen (index 3), a further equation for nitrogen (index 4) is needed. This equation is needed because the polymerization reactor is filled with nitrogen as an inert atmosphere (see Figure 20) and therefore, nitrogen influences gas phase composition in the polymerization reactor. With these four equations (12) to (15), the behavior of the polymerization reactor can be described.

$$\frac{c_{1.g}^{in}\dot{V}_g^{in} - c_{1.g}^{out}\dot{V}_g^{out}}{c_{1.g}^{out}\dot{V}_g^{out}} = \alpha_1\frac{\dot{V}_l^{out}}{\dot{V}_g^{aus}}\left(1 + \frac{\dot{n}_{1.p}}{c_{1.l}^{out}\dot{V}_l^{out}}\right) = \alpha_1\frac{\dot{V}_l^{out}}{\dot{V}_g^{out}}(1 + Da_{I.1}) \tag{12}$$

$$\frac{c_{2.g}^{in}\dot{V}_g^{in} - c_{2.g}^{out}\dot{V}_g^{out}}{c_{2.g}^{out}\dot{V}_g^{out}} = \alpha_2\frac{\dot{V}_l^{out}}{\dot{V}_g^{out}}\left(1 + \frac{\dot{n}_{2.p}}{c_{2.l}^{out}\dot{V}_l^{out}}\right) = \alpha_2\frac{\dot{V}_l^{out}}{\dot{V}_g^{out}}\left(1 + \frac{1}{r_1}Da_{I.1}\right) \tag{13}$$

$$\frac{c_{3.g}^{in}\dot{V}_g^{in} - c_{3.g}^{out}\dot{V}_g^{out}}{c_{3.g}^{out}\dot{V}_g^{out}} = \alpha_3\frac{\dot{V}_l^{out}}{\dot{V}_g^{out}}\left(1 + \frac{\dot{n}_{3.p}}{c_{3.l}^{out}\dot{V}_l^{out}}\right) = \alpha_3\frac{\dot{V}_l^{out}}{\dot{V}_g^{out}}\left(1 + \left(A + B\frac{r_1}{(n_1/n_2)_P}\right)Da_{I.1}\right) \tag{14}$$

$$\frac{c_{4.g}^{in}\dot{V}_g^{in} - c_{4.g}^{out}\dot{V}_g^{out}}{c_{4.g}^{out}\dot{V}_g^{out}} = \alpha_4\frac{\dot{V}_l^{out}}{\dot{V}_g^{out}} \tag{15}$$

On the mesoscale, in the homogeneous, stirred reaction mixture, there is the transfer of ethylene from the gas bubbles into the diluent and from there to the microreactors. The ethylene concentrations in the different phases cannot be regarded as equilibrium concentrations. They are steady state concentrations because at the phase boundaries there are resistances to the flow of ethylene. For hydrogen and for the comonomer 1-butene, equilibrium concentrations can be assumed because consumption during polymerization is smaller by one or more orders of magnitude compared to ethylene, and for hydrogen the diffusion processes are much faster. 1-butene is mainly dissolved in petrol, therefore, the transfer from the gas phase is not significant.

According to Satterfield[61] and others[62] the overall resistance is the sum of separate resistances. In Equation (16), two resistances are notable, these are, the transition of

$$\frac{S}{1-S} = \frac{k_L a}{\bar{k}_P f} = \left(1 + \frac{\bar{k}_P f}{k_S F}\right)\frac{V_l}{n_K} \tag{16}$$

ethylene from gas bubbles into petrol ($k_L a$) and its transition from petrol into the microreactors ($k_S F$). Both contributions have to be related to the consumption of ethylene by polymerization in the microreactors ($\bar{k}_P f$). If these resistances are known, the degree of saturation S ($0 < S \leq 1$) for ethylene in petrol can be calculated for the steady state as a function of catalyst content in the reaction space n_k/V_l.[55]

The saturation curve (Figure 19) at 83 °C, is calculated using the following data: $k_L a = 0.025\ s^{-1}$; $\bar{k}_P f = 36$ dm^3 mol^{-1} s^{-1}, and $(\bar{k}_P f/k_S F) \approx 0$ because $k_S F$ is much higher than $\bar{k}_P f$. For the steady state the degree of saturation S is 0.85 which is in agreement with data from the production line. This means that the Ostwald solubility coefficient must be multiplied with this degree of saturation S to describe the steady state correctly.[55]

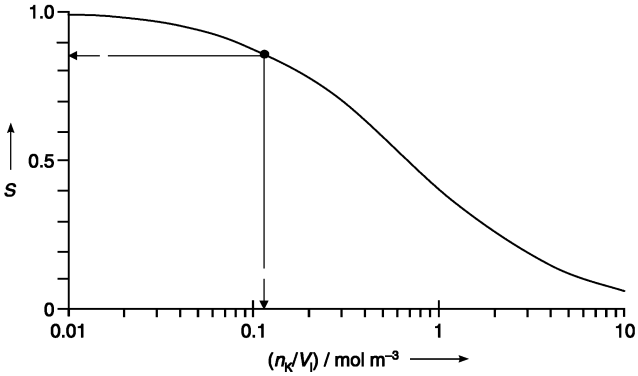


Figure 19. Saturation curve of ethylene as a function of the catalyst content in the reaction volume. $T = 83$ °C, $k_L a = 0.025\ s^{-1}$, $\bar{k}_p f = 36$ dm^3 mol^{-1} s^{-1}.

 © 2003 Wiley-VCH Verlag GmbH & Co. KGaA, Weinheim

On the microscale, the processes at, and inside, the polymerizing particles are considered. It is important that these processes inside the microreactors are running as already described, and that each catalyst particle is transformed into a polymer particle.

Equations (12) to (16) describe the steady state of the polymerization reactor. Using these equations, it is possible to calculate the process data of the reaction partners and nitrogen and petrol in the reactor, together with the two most relevant pieces of product data, the average degree of polymerization P_n and copolymer composition $(n_1/n_2)_P$, as functions of the Damköhler number $Da_{I,1}$ (Figure 20).[55] The calculated curves and the experimental data at the steady state with $Da_{I,1} = 53$ are in very good agreement.

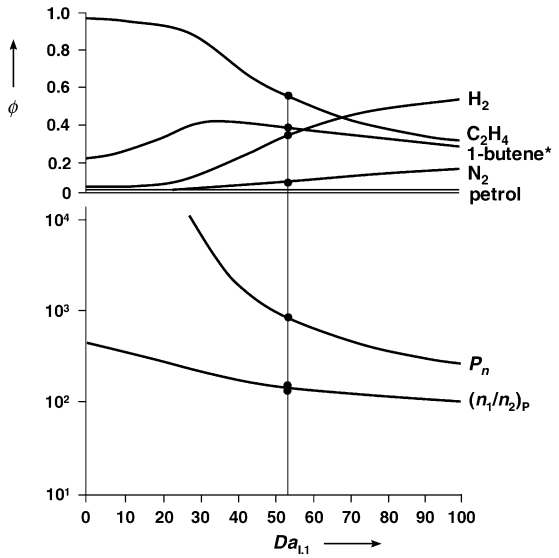


Figure 20. Steady-state working condition of the polymerization reactor: gas-phase composition (volume fraction ϕ), average degree of polymerization P_n and copolymer composition $(n_1/n_2)_P$. $T = 83\,°C$, $p = 0.68$ MPa, $r_1 = 80$, $A = 0.00944$, $B = 0.0177$. * The curve for 1-butene is magnified by a factor of 10.

This set of equations can be used for process simulations, to determine, for example, which macroscale variables control the polymer properties on the microscale and to what extent. Figure 21 shows a simulation for the ethylene feed ($c^{in}_{1.g}\dot{V}^{in}_g$). The values for the average degree of polymerization P_n and for the copolymer composition $(n_1/n_2)_P$ can be converted into the melt flow rate (*MFR 190/5*) and density (d), values which are used in industry for product characterization. The melt flow rate is determined according to ISO 1133, the density according to ISO 1183. For these calculations, Equations (17) and (18) are used.

$$\log MFR\,190/5 = 9.24 - 3.10 \log P_n \qquad (17)$$

for $2000 > P_n > 200$

$$d = 0.952 - 1.50\,(n_1/n_2)_P + 0.00815 \log MFR\,190/5 \qquad (18)$$

for $400 > (n_1/n_2) > 80$ and $100 > MFR\,190/5 > 0.1$.

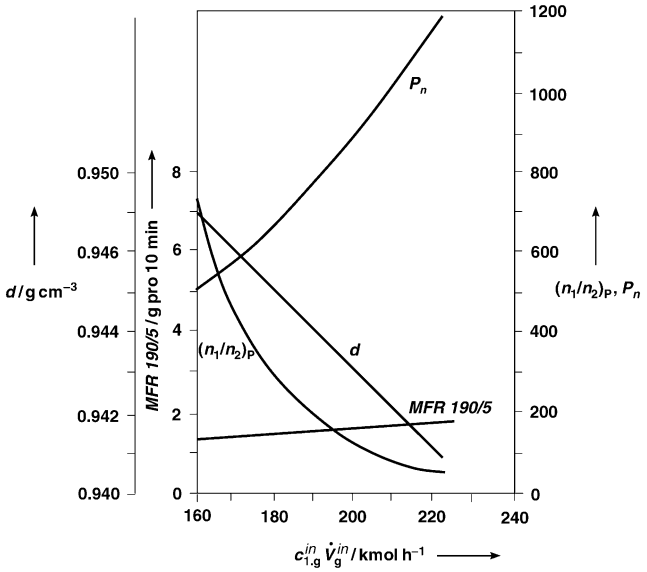


Figure 21. Process simulation: product data as a function of the ethylene feed flow; $T = 83\,°C$.

The result of these simulations (Figure 21) shows that both of the most important product data rely on a well-defined number of intensive (not depending on reactor size) and extensive (depending on reactor size) process data. The simulation further delivers the quantitative dependences and consequently the sensitivities of these product data on the process data on the macroscale (Figure 22).[55] To observe, control, and regulate this process in the required ranges, instruments to measure the process data given in Figure 22 have been installed. All the instruments have a sensitivity higher than a factor of 10 for the deviations given in Figure 22.

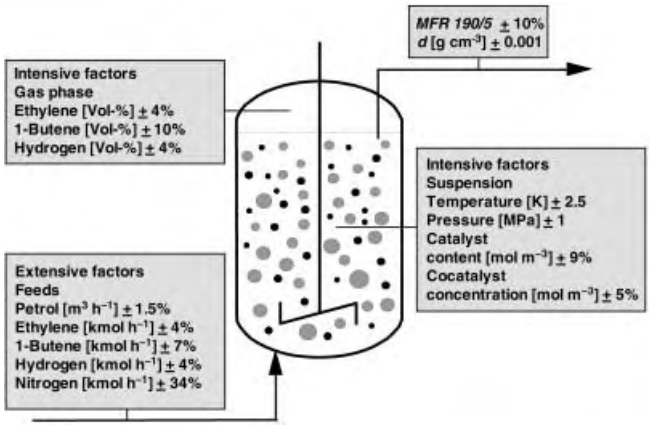


Figure 22. Intensive and extensive process parameters.

This steady-state-process model was further extended to a state observer.[63] With this state observer, melt flow rate and density of the just-formed polymer in the microreactor can be evaluated. Because it is possible to look into the polymerization process and because what happens there at any time

 © 2003 Wiley-VCH Verlag GmbH & Co. KGaA, Weinheim

and at all scales is known, this reactor is called a transparent reactor.[64] It is the basis for an advanced process control system using FUZZY logic.[63]

As all products are produced in large volumes and go into commodity applications, in this case especially for packaging, high-density polyethylenes are under tough price pressure leading to pressure on production costs (that is, the costs over and above ethylene). Production costs can be reduced by increasing plant scale, a practice that has been on-going for a long time.[65] Today, production facilities are built with capacities up to 320 000 t per annum. Based on a precise understanding of the process on all scales—macro-, meso-, and microscale—and the knowledge of the relevant intensive and extensive process parameters, a scale-up can be planned and realized.

The polymerization reactor consists of identical zones with a turbine for mixing. In Figure 23, two reactors are shown. The smaller one has three zones; the larger one has

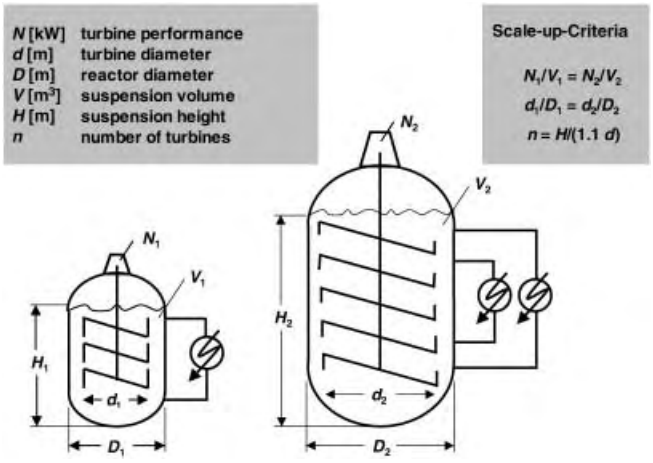


Figure 23. Criteria for the scale-up of the polymerization reactor.

five zones. In each zone, the conditions must the same for the intensive-process parameters. This is achieved by strong mixing within and between these zones. Because of the different pressures in these zones, the concentrations of the compounds are also different. From the bottom to the top of the reactor there is a decrease in the ethylene concentration in petrol. This gradient is caused by the decrease of the ethylene partial pressure. Therefore, there is higher polymerization rate at the bottom of the reactor and a higher heat production as well. This leads to a temperature gradient from bottom to top (< 5 K). The heat to be removed increases with the number of zones and with increasing ethylene throughput. Because the heat removal via the reactor walls is not sufficient, the reactor content must be pumped through heat exchangers with a large surface area, and this surface must be increased accordingly. The dimensioning of the reactor is based on the criteria given in Figure 23.

The polyethylene leaves the polymerization reactor as powder. The commercial product is pelletized. These pellets are formed by melting the powder and, in the extruder, mixing in additives and, if needed, other compounds, such as carbon black, pigments, or fillers. Again, this process is of great relevance for product quality, and all parts of the polymer melt must have the same composition. The different sizes of polymer molecules and the low-molecular-mass additives must be molecularly dispersed. All heterophasic compounds like pigments or carbon black must be homogeneously dispersed. This is a difficult homogenizing task at throughputs of 40 t h^{-1}.[66]

5. Tailored High-Density Polyethylenes

Catalysts and the polymerization process are the basis for the production of polymers. However, to produce tailored products or even products with new, as yet unknown combinations of properties, knowledge must be available about the relation between polymer structure and polymer properties in the melt (important to tailor the processing behavior) and in the solid state (to reach the targeted final product properties). Knowledge of catalysts, processes, and the structure–property relations are fundamental to improve products for known applications and to develop products for new applications.

High-density polyethylenes comprise low-molecular-mass, easy-flowing grades as well as high-molecular-mass, heavy-flowing grades, and are used for injection-molded articles, containers of all size, film, tapes, fibers, monofilaments, and pipes. The product portfolio is shown on Figure 24.

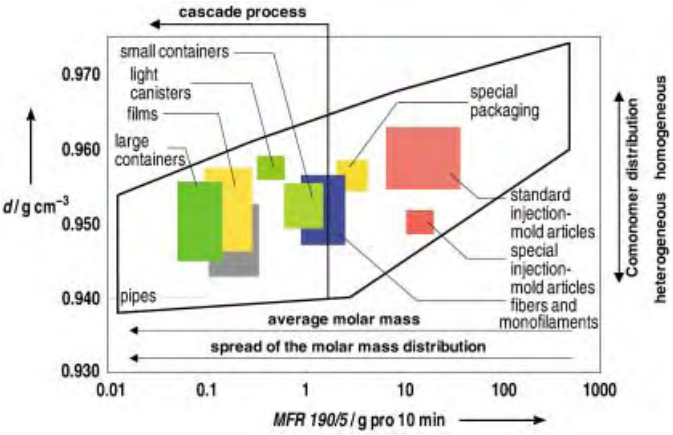


Figure 24. Product portfolio of high-density polyethylene (HDPE).

The product fields are indicated in the density, flowing behavior (melt flow rate) diagram. Flowing behavior is the throughput of the polymer melt through a specified die under defined conditions, such as temperature and load. The standard designation ISO 1133 defines this testing method and the determination of the melt flow rate. The test measures the mass of the polymer melt that passes the die in 10 minutes. The products in the portfolio differ not only in density and melt flow behavior but also in other characteristics, such as molecular mass and comonomer distribution. An efficient production technology must be able to generate the whole product range with outstanding, at least standard qualities.

 © 2003 Wiley-VCH Verlag GmbH & Co. KGaA, Weinheim

One way to reach this target is the variation of the industrial process while using only one catalyst/cocatalyst system. This means that there is always the same system, and that the chemistry for the catalytic process is not changed. This approach brings a high flexibility for the development of new grades and for the optimization of existing ones. Such a catalyst must fulfill a lot of conditions: The molecular-mass distribution must be narrow, the average molecular mass must be varied over a wide range with hydrogen, and 1-alkenes, such as 1-butene, must be copolymerizable with ethylene in the required amounts. At all process conditions there must be sufficient catalyst productivity to hold catalyst residues in the polymer below 5 ppm titanium. The specific catalyst costs must remain below € 20 per ton.

$MgCl_2$-supported Ti catalysts fulfill these demands in an outstanding way.[33] The average molecular mass can be adjusted with hydrogen over a wide range in a simple way without a significant loss in activity (Figure 25). These catalyst systems show acceptable copolymerization behavior with 1-butene (Figure 26). Because of the very different rate constants of ethylene (high r_1 parameter) in relation to 1-butene (small r_2 parameter), the industrial process must be heavily loaded with the comonomer. However, this can be handled because the comonomer dissolved in petrol is recycled into the polymerization reactor.

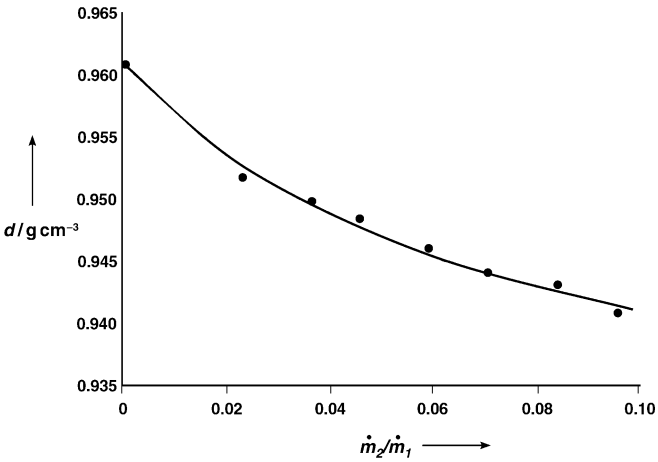


Figure 26. Density as a function of the 1-butene feed ($\dot{m}_2$) in relation to the ethylene feed ($\dot{m}_1$); $\dot{m}_i$ in mol h^{-1}.

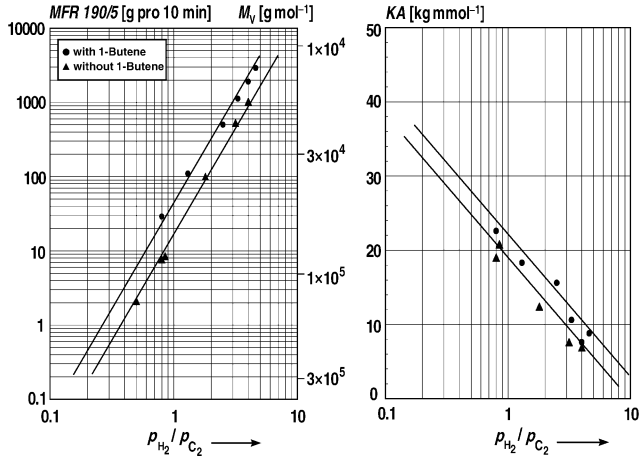


Figure 25. Control of the melt flow rate *MFR 190/5* with hydrogen and influencing the catalyst productivity *KA*; $T = 85\,^{\circ}C$.

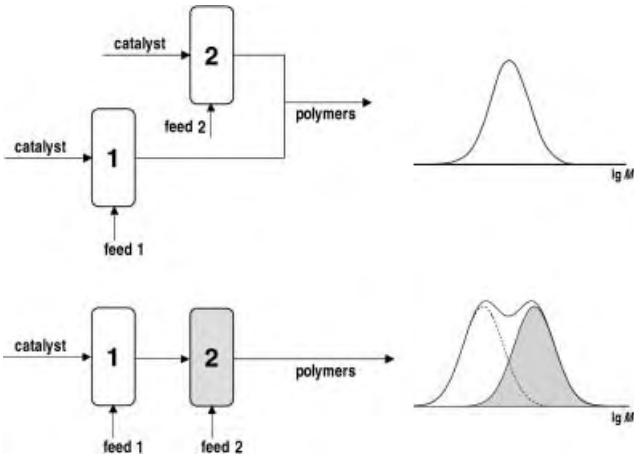


Figure 27. Reactor setup to control the molar mass distribution.

Easy flowing, low-molecular-mass products (*MFR 190/5* > 5) must have narrow molecular-mass distributions; heavy or heavier flowing products (*MFR 190/5* < 5) must have broad to very broad molecular-mass distributions. To manipulate the molecular-mass distribution as requested, two polymerization reactors are operated in different ways.[67,68] To get products with narrow-molecular-mass distribution both reactors are run parallel under the same process conditions. Also, the feeds of both reactors 1 and 2 are the same (Figure 27, top). To get polymers with broad to very broad molecular-mass distributions, the reactors are run in a cascade and at very different process conditions (Figure 27, bottom). The feeds 1 and 2 are also different. The catalyst is fed only into the first polymerization reactor and is then passed through both reactors during polymer-particle formation.[67]

In the cascade process, in the first reactor, high amounts of hydrogen are fed with ethylene. This process leads to the formation of low-molecular-mass polyethylenes. The second reactor is loaded with much less hydrogen to form a high- or very high-molecular-mass polyethylene. By variation of average molecular mass and the mass ratio in both reactors, there are two independent parameters with which to tune the molecular-mass distribution (Figure 28).

The cascade process allows a further essential product modification: the incorporation of comonomer in the long polymer chains within the second reactor. This way a polymer blend is formed with a low-molecular-mass ethylene homopolymer and a high-molecular-mass ethylene-1-alkene copolymer. These products build up a polymer alloy in the solid state consisting of crystalline regions (crystal lamella) and amorphous regions in between. The crystalline regions are mainly formed by the low-molecular-mass homopolyethylene. The high-molecular-mass copolymers form the amorphous regions and act as tie molecules that connect the

 © 2003 Wiley-VCH Verlag GmbH & Co. KGaA, Weinheim

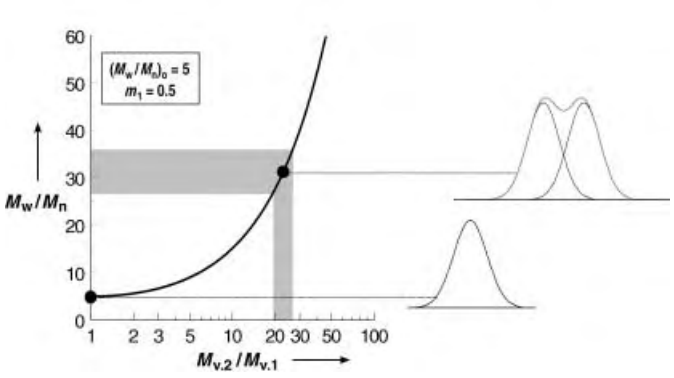


Figure 28. Altering the molar mass distribution by cascade processes; $M_{v,1}$, $M_{v,2}$ viscometric average of the molar mass in reactor 1 and 2, respectively .

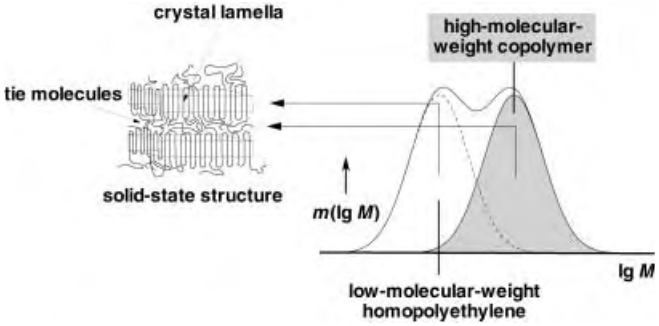


Figure 29. Bimodal polyethylene and its solid-state structure.

crystal lamella. In this way, a physical network is formed (Figure 29).[69,70]

These polymer-blend products show outstanding combinations of properties which result from the bimodal molecular-mass distribution and the heterogeneous comonomer distribution. This can be demonstrated with polymer products for drinking-water-, sewage-, and gas-pipe applications (Figure 30).[71,72]

Pipes made out of this polyethylene have a high stiffness (elastic modulus) because of the high density. But the main point is the high resistance against slow crack propagation

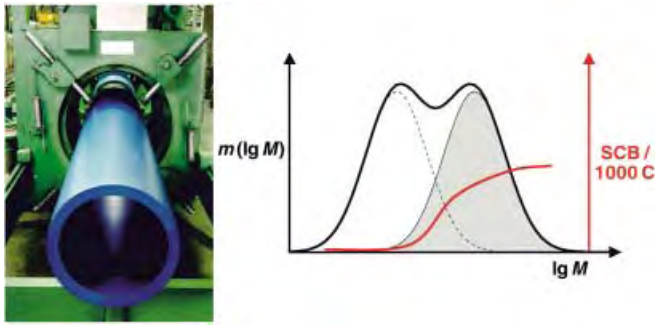


Figure 30. Drinking-water pipe and molecular construction of the polyethylene; SCB = number of side chains (in this case ethyl groups) per 1000 backbone carbon atoms.

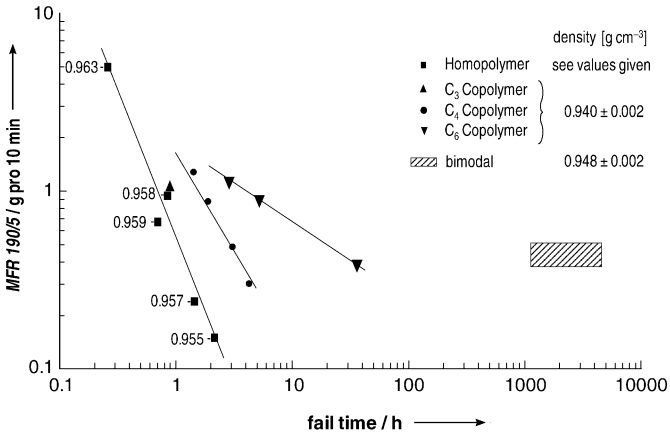


Figure 31. Fail-time test (FNCT-Test) and product data for polymer blends.

under stress.[73] These values can be measured with a laboratory-scale test (full notch creep test; Figure 31).[74]

The high resistance against slow crack growth is further determined by the internal pressure creep rupture test.[75] At 20 °C, these pipes can have a life time of 50 years and more under operation.[76] The extrapolated lines at 20 °C for a life time of 100 years deliver a hope stress of >10 MPa (see standard ISO 12162) which means that this pipe belongs to the class PE 100.

These polyethylene blends are also an excellent materials for gas-distribution systems. Such pipes are used under a permanent gas pressure. If the pipe is damaged, a crack can grow very quickly over a long range driven by the stored energy in the pipe, which leads to a failure of the gas-distribution line. Therefore, these pipes must have a high resistance against rapid crack propagation. This behavior is measured with the S4 (small scale steady state) test (see standard ISO 13477). Again, these polyethylene blends show an improved behavior. The rapid crack growth starts at much higher pressures compared to older polyethylene products. Therefore, the use of this polyethylene increases safety (Figure 32).

For testing, two different polyethylene pipes are welded together. Then, a crack is cut into the pressurized pipe surface of the older material to start rapid crack growth. When this crack enters into the pipe of the new polyethylene, growth stops immediately (Figure 33).

With this polymerization technology, products for other applications with new combinations of properties are also possible. For packaging, the weight of containers can be reduced owing to the high stiffness (density increase) combined with high stress-crack resistance,[77] noted as ESCR (Environmental Stress Crack Resistance) and measured according to DIN 55457. These product developments and the developments of the processing technology over the past 25 years have cut container weight in half (Figure 34).

The cascade technology is further used to produce film grades for very thin films (below 10 μm). These films are made using the film-blowing process (Figure 35). There are demands on the rheology of the polymer melt under shear and strain for this process.[78] Very thin films can be produced

 © 2003 Wiley-VCH Verlag GmbH & Co. KGaA, Weinheim

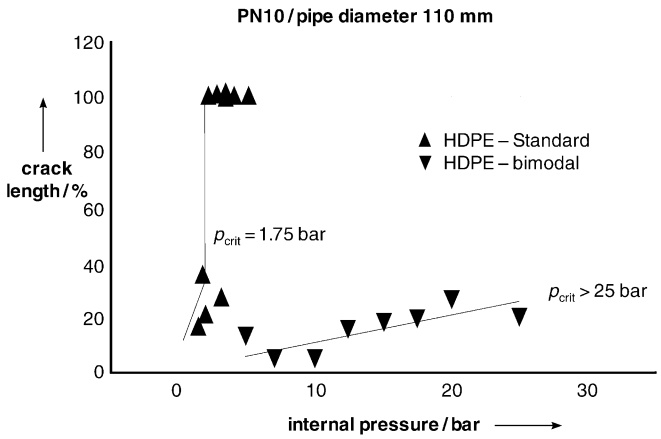


Figure 32. Rapid crack propagation (S4-Test)for pipes with unimodal molar mass distribution (standard) and pipes with bimodal molar mass distribution.

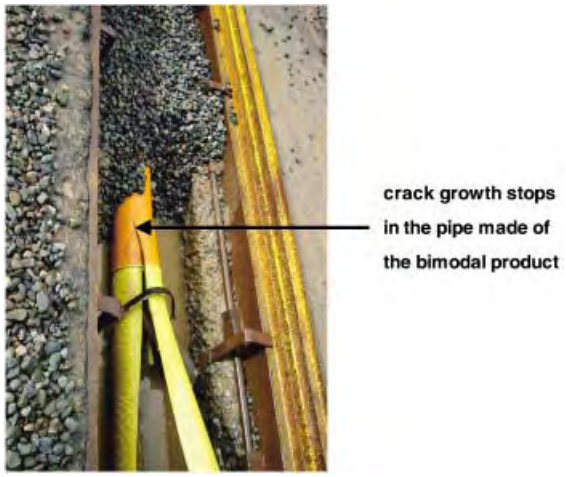


Figure 33. Rapid crack propagation test (Advantica Technologies Ltd.).

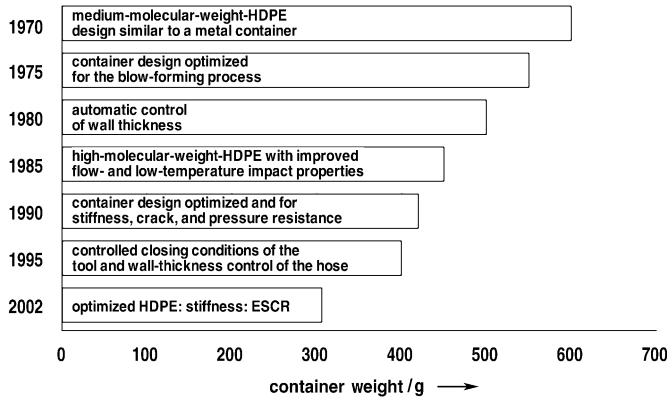


Figure 34. Reduction in container weight for 10-L containers.

only if there is a sufficient strain hardening of the polymer melt. This effect stabilizes the film bubble and guarantees a safe processing over long time because the film bubble is not disrupted. The film-blowing process shown in Figure 35 shows

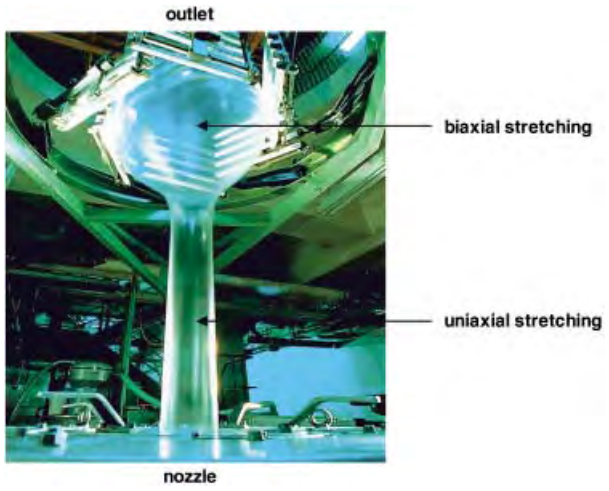


Figure 35. Extrusion and blowing process for the production of thin films.

that the tube is drawn upwards after leaving the die (uniaxial extension) and is then inflated (biaxial extension). The drawing out of the polymer melt must be stable at high throughputs which means that the shape of the bubble must be stable.

These films have an increased toughness. This property means that thinner films can serve the same purpose as the heavier films of the past. Therefore, for the same application, the amount of material can be significantly reduced (Table 4).[79]

Table 4: Thicknesses of LDPE and HDPE films with the same usage properties.

Film thickness [μm]		Volume [dm^3]	Net weight [kg][a]
LDPE	HDPE		
55	20	50	12.5
60	20	70	17.5
60	25	110	27.5
100	35	175	43.75

[a] According to DIN 55 456.

All product developments are targeted to either generate products for new applications or to improve existing products to achieve the same properties with less material, to achieve higher throughputs, or to achieve both.

6. Outlook

This process—The Mülheimer Normaldruck–Polyäthylen–Verfahren (the Mülheim normal-pressure process)[8]—was developed over a number of years into a high-standard, industrial and commercial polymerization process for the production of high-density polyethylenes with unusual combinations of properties. The developments rest on the availability of optimized catalyst/cocatalyst systems, the further development of the polymerization technology

 © 2003 Wiley-VCH Verlag GmbH & Co. KGaA, Weinheim

including the knowledge of physical and chemical processes on all scales, and the understanding of structure–property relationships for processing the polymer melt and for the final injection-molded, extruded, or blown articles.

The construction of new plants today means that this process will run at least for another 15 years or even longer. During this time, this polymerization process will continue to be the subject of further research and development. All indicators point to new results that will extend the product portfolio beyond those that exist today, with better products being developed for processing and application.

Polyethylenes have been so successful in competition with other materials because they have clear advantages. Of special note are their excellent chemical resistance, high impact strength, and stiffness even at low temperatures. Therefore, polyethylenes have the highest production volumes of all synthetic polymers.[81]

The production of all synthetic polymers adds up to 220 Mt per annum. Around 60 Mt per annum are polyethylenes with around 8 Mt per annum produced with this process.[81–84] The high amount of polyethylenes in relation to all polymers can be explained by some key success factors typical for polyethylenes. First is the raw material basis. Ethylene is a industrial product produced in large quantities and is available at reasonable costs. The industrial processes are mature. They are working at low costs and are environmental friendly. Using ethylene combined with 1-alkenes, a large number of products for a broad range of applications can be produced at low costs. These products are environmental friendly. They do not contaminate air, water, or soil. When they are collected from the environment nothing remains. These products contribute to sustainability because they have better life-cycle assessments than other materials for different applications.[85–87] For small containers (bottles), the energy consumption for the life-cycle related to 1000 objects is 1140 MJ for high-density polyethylene, 3160 MJ for polyethylene terephthalate (PET), and 8310 MJ for glass. For packaging, there is a clear advantage of high-density polyethylene over paper. Consider 1000 grocery sacks: high-density polyethylene has much better energy balance data (139 MJ) than paper (621 MJ).[87] The specific energy consumption (MJ kg^{-1}) for high-density-polyethylene production is low compared to other materials, such as metals, glass, paper, and the energy content of polyethylenes is similar to crude oil or other energy delivers.[88] When polyethylenes have lost their performance, they can be used for energy production. In the garbage-burning process, polyethylenes are desired as materials for energy generation. However, polyethylene can also be recycled like other thermoplastic materials.

In summary, it can be concluded that polyethylenes will play an important role as materials in the future.[89,90] Polyethylene pipes will help to guarantee fresh water supply, an important point in the future according to a recent Delphi study.[91] These pipes are further used to renew or install sewage water lines at an acceptable level of capital expenditure.

Product properties will be essential success factors and all production technologies (slurry, gas-phase, solution, high-pressure)[92] will be evaluated as to whether they can achieve the desired product properties or not. In this competition, the process with the best performance will be the winner. The slurry process has an excellent chance competing with others even after 50 years because it delivers excellent products at competitive conditions.

To the described developments, many colleagues have made contributions in different fields. I want to express my thanks for these contributions to Dr. J. Berthold, Dr. D. Bilda, Dr. W. Breuers, Dr. H.-F. Enderle, Dr. M. Fleißner, Dr. R. Franke, Dipl.-Ing. P. Göbel, Dipl.-Ing. L.-G. Heinicke, Dr. H. F. Herrmann, Dr. R. Lecht, Dr. O. Lorenz, Dr. H. Lüker, Dr. P. R. Schöneborn, Dipl.-Ing. H. Seintsch, Dipl.-Ing. R. H. Schubbach, Dipl.-Ing. U. Schulte, Dr. T. Tauchnitz, Dr. G. Thum.

Received: February 7, 2003 [A580]

[1] K. Ziegler, *Angew. Chem.* **1964**, *76*, 545 – 553.
[2] K. Ziegler, E. Holzkamp, H. Breil, H. Martin, *Angew. Chem.* **1955**, *67*, 426.
[3] K. Ziegler, H. Breil, E. Holzkamp, H. Martin, DE 973626, **1953** [*Chem. Abstr.* **1960**, *54*, 14794].
[4] With these catalysts Natta and co-workers polymerized propylene to isotactic polypropylene (i-PP). They discovered the principles of the regio- and stereospecific polymerization of 1-alkenes: G. Natta, *Angew. Chem.* **1956**, *68*, 869 – 887; G. Natta, *Angew. Chem.* **1964**, *76*, 553 – 566; and references therein.
[5] The process to synthesize isotactic polypropylene was again transferred into a industrial process within a few years because an new polymer (polypropylene) with new properties was accessible: A. Bosoni, G. Guzzetta, I. Ronzoni, F. Sabbioni, *Mater. Plast.* **1956**, *12*, 1010 – 1022; G. Lombardo, *Mater. Plast.* **1957**, *13*, 409 – 414; G. Ballabio, *Mater. Plast.* **1957**, *13*, 415 – 419; R. Pozzo, S. Compostella, *Mater. Plast.* **1957**, *13*, 425 – 434.
[6] These catalysts can also be used for the copolymerization of ethylene and propylene to produce ethylene–propylene elastomers; again these were new polymers: G. Crespi, A. Valvassori, G. Sartori in *High Polymers, Vol. 18* (Ed.: G. E. Ham), Wiley-Interscience, New York, **1964**, pp. 231 – 274.
[7] E. W. Fawcett, R. U. Gibson, M. W. Perrin, J. G. Paton, E. G. Williams (ICI), GB 471590, **1936** [*Chem. Abstr.* **1938**, *32*, 1362]; *Polyethylenes 1933–1983: Past, Present, Future*, The Plastics and Rubber Institute, London, **1983**.
[8] In the first *Hostalen* brochure [Ed. *Farbwerke Hoechst AG*, **1956**] the introduction states: "The properties are in part very different compared to polyethylenes produced with the high-pressure process". This point was stressed in further publications: K. Ziegler, *Angew. Chem.* **1955**, *67*, 541 – 547; E. Grams, E. Gaube, *Angew. Chem.* **1955**, *67*, 548 – 556; G. Schulz, K. Mehnert, *Kunststoffe* **1955**, 45, 410 – 414; *Kunststoff-Praxis* **1955**, *12*, P101–P107; W. Kneip, *Chem. Ind.* **1955**, *7*, 297 – 298.
[9] This polymerization process was transferred into a industrial process which was the same as the laboratory-scale procass. As early as the end of 1955 the production was on stream E. Bäumler, *Farben, Formen, Forscher, Hoechst und die Geschichte der industriellen Chemie in Deutschland*, Piper, München, **1989**, pp. 335 – 340.
[10] This new process was seen as a technological breakthrough, and therefore it was presented at the world exhibition at Brussels in 1958. The visitors could see how gaseous ethylene was converted into a white powder, and how this powder was molten and injection molded into a badge which they could take with them: S. Sommer, S. Wagener, H. Ebner, *Kunststoffe* **1959**, *49*,500 – 502;

 © 2003 Wiley-VCH Verlag GmbH & Co. KGaA, Weinheim

this plant was presented to Deutsches Museum at München after the world exhibition.

[11] The catalysts discovered by Ziegler and co-workers and further developed in industry show a catalyst productivity in the range below 5 kg polyethylene per g of titanium: B. Diedrich, *Appl. Polym. Symp.* **1975**, *26*, 1–11; The catalyst used today achieve values of 100 kg polyethylene per g titanium. Catalyst productivity means the amount (mass) of polyethylene in kg related to the amount (mass) of catalyst in g titanium under industrial reaction conditions of temperature, ethylene partial pressure, average residence time, space time yield, and others. This value is thus a number for the catalyst activity under well-defined industrial process conditions. With this number the performance of catalysts can be compared.

[12] Y. V. Kissin, *Adv. Polym. Sci.* **1974**, *15*, 91–155.

[13] L. L. Böhm, *Angew. Makromol. Chem.* **1980**, *89*, 1–32; L. L. Böhm, *J. Appl. Polym. Sci.* **1984**, *29*, 279–289.

[14] G. Natta, G. Mazzanti, P. Longi, F. Bernardini, *Chim. Ind.* **1959**, 41, 519–526; E. J. Vandenberg (Hercules Powder Co.), US 3051690, **1962** [*Chem. Abstr.* **1959**, *53*, 13660]; A. S. Hofmann, B. A. Fries, P. C. Condit, *J. Polym. Sci. Part C* **1963**, *4*, 109–126.

[15] K. S. Whiteley, T. G. Heggs, H. Koch, R. L. Mawer, W. Immel in *Ullmann's Encyclopedia of Industrial Chemistry, Vol. A21*, VCH, Weinheim, **1992**, pp. 487–577; and references therein.

[16] There are 4 modifications of $TiCl_3$ (α, β, γ, δ). For all modifications the chlorine ions form a spherical close packaging. The different modifications follow from the different arrangement of the chlorine-ion layers. The δ modification is the preferred one for catalysts. In this case the layers are random. For the α and γ modification the layers are periodic. The β modification has another structure: G. Natta, P. Corradini, G. Allegra, *J. Polym. Sci.* **1961**, *51*, 399–410; T. Keii, *Kinetics of Ziegler-Natta Polymerzation*, Kodansha, Tokyo, **1972**, pp. 44–45.

[17] H. Uelzmann, *J. Polym. Sci.* **1958**, *32*, 457–476; F. Patat, H. J. Sinn, *Angew. Chem.* **1958**, *70*, 496–500; G. Natta, I. Pasquon, *Adv. Catal.* **1959**, *11*, 1–66; G. Natta, G. Mazzanti, *Tetrahedron* **1960**, 86–100; M. L. Huggins, *J. Polym. Sci.* **1960**, *48*, 473–475; G. Natta, I. Pasquon, A. Zambelli, G. Gatti, *J. Polym. Sci.* **1961**, *51*, 387–398; F. Danusso, D. Sianesi, *Chim. Ind.* **1962**, *44*, 474–482.

[18] C. Beermann, H. Bestian, *Angew. Chem.* **1959**, *71*, 618–623.

[19] P. Cossee, *J. Catal.* **1964**, *3*, 80–88; E. J. Arlman, *J. Catal.* **1964**, *3*, 89–98; E. J. Arlman, P. Cossee, *J. Catal.* **1964**, *3*, 99–104.

[20] The complexes shown in Figure 1 for the catalytic cycle are derived from the crystal structure of δ-$TiCl_3$ (see also Figure 2). Whether and how the structure of the complex is changed by exchange of one chlorine anion by an alkyl chain and by the side-on-complexation of a monomer, such as ethylene, is discussed in detail in the literature: P. J. T. Tait, N. D. Watkins in *Comprehensive Polymer Science, Vol. 4* (Eds.: G. Allen, J. C. Bevington), Pergamon, Oxford, **1989**, pp. 533–573; for the formation of active sites in titanium catalysts supported on $MgCl_2$ see P. Corradini, V. Busico, G. Guerra in *Transition Metals and Organometallics as Catalysts for Olefin Polymerization* (Eds.: W. Kaminsky, H. Sinn), Springer, Berlin, **1988**, pp. 337–348; P. Corradini, V. Busico, G. Guerra in *Comprehensive Polymer Science, Vol. 4* (Eds.: G. Allen, J. C. Bevington), Pergamon, Oxford, **1989**, pp. 29–50; G. Monaco, M. Toto, G. Guerra, P. Corradini, L. Cavallo, *Macromolecules* **2000**, *33*, 8953–8962; for the structure of these complexes see also: H. Weiss, M. Boero, M. Parrinello, *Macromol. Symp.* **2001**, *173*, 137–147.

[21] E. K. Rideal, *Proc. Cambridge Philos. Soc.* **1939**, *35*, 130–132.

[22] L. L. Böhm, *Polymer* **1978**, *19*, 545–552.####

[23] For the polymerization of ethylene dissolved in petrol or diesel oil ethylene (1-molar, ideal solution) to give solid crystalline (c) or amorphous (a) polyethylene the following thermodynamic data are known: $\Delta H_c = -100\ kJ\,mol^{-1}$, $\Delta S_c = -128\ J\,K^{-1}\,mol^{-1}$, $\Delta H_a = -92\ kJ\,mol^{-1}$ and $\Delta S_a = -110\ J\,K^{-1}\,mol^{-1}$: S. Dainton, D. M. Evans, F. E. Hoare, T. P. Melia, *Polymer* **1962**, *3*, 286–296; B. Wunderlich, *J. Chem. Phys.* **1962**, *37*, 1203–1207; T. R. Das, N. R. Kuloor, *Indian J. Technol.* **1967**, *5*, 86–91; K. Goldmann in *The Physical Properties of Ethylene* (Ed.: S. A. Miller), Ernest Benn, London, **1969**, pp. 150–168; K. J. Ivin in *Polymer Handbook* (Eds.: J. Brandrup, E. H. Immergut), Wiley, New York, **1975**, p. 11.

[24] With these data given in ref. [23] for a degree of crystallinity of 50% the equilibrium concentrations of ethylene at 80°C can be calculated: F. S. Dainton, K. J. Ivin, *Q. Rev. (London)* **1958**, *12*, 61–92.

[25] L. L. Böhm, *Polymer* **1978**, *19*, 562–566.

[26] L. L. Böhm, *Polymer* **1978**, *19*, 553–561.

[27] B. Diedrich, K. D. Keil (Farbwerke Hoechst AG), DE 1595666, **1966**.

[28] Isoprenylaluminum is formed by the reaction of triisobutylaluminum with isoprene. In this process a higher molecular, partially branched alkyl aluminum compound is formed. The structure depends on the amounts of the C_4 and C_5 components. The composition can be determined by analyzing the gaseous components after alcoholysis and hydrolysis. Isoprenylaluminum is a industrial product: H. Hoberg, M. Martin, R. Rienäcker, K. Zosel, K. Ziegler, *Brennst.-Chem.* **1969**, *50*, 217–221.

[29] J. P. Hermans, P. Henrioulle (Solvay et Cie.), DE 2213086, **1980** [*Chem. Abstr.* **1973**, 78, 16791].

[30] The physico-chemical processes of the catalyst preparation are described in detail: R. P. Nielson in *Transition Metal Catalyzed Polymerizations* (Eds.: R. P. Quirk, H. L. Hsieh, G. B. Klingensmith, P. J. T. Tait), harwood academic publishers, London, **1983**, pp. 47–82.

[31] B. Diedrich, K. Rust, K. D. Keil (Farbwerke Hoechst AG), DE 1770727, **1972** [*Chem. Abstr.* **1972**, *77*, 75821]; B. Diedrich, K. D. Keil, K. Rust (Farbwerke Hoechst AG), DE 1770730, **1972** [*Chem. Abstr.* **1972**, *77*, 75819]; U. Giannini, P. Longi, D. Deluca, A. Cassata (Montecatini Edison S.p.A.), DE 1905583, **1969** [*Chem. Abstr.* **1969**, *71*, 125184].

[32] P. Galli, E. Susa, G. Di Drusco (Montecatini Edison S.p.A.), DE 2000585, **1970** [*Chem. Abstr.* **1970**, *73*, 56566]; A. Mayr, E. Susa, G. Di Drusco (Montecatini Edison S.p.A.), DE 2013730, **1970** [*Chem. Abstr.* **1970**, *73*, 121062]; P. Galli, L. Luciani, G. Cecchin, *Angew. Makromol. Chem.* **1981**, *94*, 63–90; P. C. Barbé, G. Cecchin, L. Noristi, *Adv. Polym. Sci.* **1986**, *81*, 1–81; F. Auriemma, G. Talarico, P. Corradini in *Progress and Development of Catalytic Olefin Polymerization* (Eds.: T. Sano, T. Uozumi, H. Nakatani, M. Terano), Technology and Education Publishers, Tokyo, **2000**, pp. 7–15.

[33] L. L. Böhm, *Macromol. Symp.* **2001**, *173*, 55–63.

[34] L. Luciani, N. Kashiwa, P. Barbé, A. Toyota (Montedison, Mitsui Petrochemical), US 4226714, **1975** [*Chem. Abstr.* **1977**, *87*, 68693]; N. Kashiwa, *Polym. J.* **1980**, *12*, 603–608; N. Kashiwa, J. Yoshitake, T. Tsutsui in *Transition Metals and Organometallics as Catalysts for Olefin Polymerization* (Ed.: W. Kaminsky, H. J. Sinn), Springer, Berlin, **1988**, pp. 33–43.

[35] M. Ferraris, F. Rosati, S. Parodi, E. Giannetti, G. Motroni, E. Albizzati (Montedison S.p.A.), DE 2933997, **1980** [*Chem. Abstr.* **1980**, *92*, 199055].

[36] G. Thum (Hoechst AG), DE 3620060, **1987** [*Chem. Abstr.* **1988**, *108*, 205257]; W. Breuers, R. Lecht, L. Böhm (Hoechst AG), EP 0613909, **1994** [*Chem. Abstr.* **1995**, *122*, 134146].

[37] L. Böhm (Hoechst AG), DE 4017661, **1990** [*Chem. Abstr.* **1992**, *116*, 84398].

[38] N. J. Turowa, B. A. Popowkin, A. W. Nowoselowa, *Z. Anorg. Allg. Chem.* **1969**, *365*, 100–112.

[39] G. Lagally in *Fließverhalten von Stoffen und Stoff-gemischen* (Ed.: W.-M. Kulicke), Hüthig & Wepf, Basel, **1986**, pp. 147–186.

 © 2003 Wiley-VCH Verlag GmbH & Co. KGaA, Weinheim

[40] R. B. Richards, *Trans. Faraday Soc.* **1946**, *42*, 10 – 28; F. Hamada, K. Fujisawa, A. Nakajima, *Polym. J.* **1973**, *4*, 316 – 322; H. Horacek, *Makromol. Chem. Suppl.* **1975**, *1*, 415 – 439; Y. Kodama, F. L. Swinton, *Br. Polym. J.* **1978**, *10*, 191 – 200; Y. Kodama, F. L. Swinton, *Br. Polym. J.* **1978**, *10*, 201 – 204.

[41] L. Mandelkern in *Comprehensive Polymer Science, Vol. 2* (Eds.: G. Allen, J. C. Bevington), Pergamon, Oxford, **1989**, pp. 363 – 414 (see also pp. 397–399).

[42] This concerns pearl, suspension, emulsion, and Gas-phase polymerization: H. Gerrens in *Ullmanns Encyclopädie der technischen Chemie, Vol. 19* (Eds.: E. Bartholomé, E. Bieckert, H. Hellmann, H. Ley, M. Weigert, E. Weise), Verlag Chemie, Weinheim, **1980**, pp. 107 – 165; H. Gerrens, *Chem. Ing. Tech.* **1982**, *52*, 477 – 488.

[43] For the slurry polymerization process the viscosity of the slurry depends only on physical data, such as particle size, particle shape, bulk density, and the volume fraction in petrol. It is not dependent on average molecular mass of polyethylene. Therefore with this process ultrahigh molecular-mass polyethylene can be produced: M. Mooney, *J. Colloid Sci.* **1951**, *6*, 162 – 170; T. B. Lewis, L. E. Nielson, *Trans. Soc. Rheol.* **1968**, *12*, 421 – 443; R. Michael, K. H. Reichert, *Chem. Ing. Tech.* **1984**, *56*, 48 – 50.

[44] W. R. Schmeal, J. R. Street, *AIChE J.* **1971**, *17*, 1188 – 1197; E. J. Nagel, V. A. Kirillov, W. H. Ray, *Ind. Eng. Chem. Prod. Res. Dev.* **1880**, *19*, 372 – 379; T. W. Taylor, K. Y. Choi, H. Yuan, W. H. Ray in *Transition Metal Catalyzed Polymerization* (Ed.: R. P. Quirk), Harwood, London, **1983**, pp. 191 – 222; R. A. Hutchinson, C. M. Chen, W. H. Ray, *J. Appl. Polym. Sci.* **1992**, *44*, 1389 – 1414.

[45] L. Böhm, *Chem. Ing. Tech.* **1984**, *58*, 674 – 684; L. L. Böhm, R. Franke, G. Thum in *Transition Metals and Organometallics as Catalysts for Olefin Polymerization* (Eds.: W. Kaminsky, H. Sinn), Springer, Berlin, **1988**, pp. 391 – 403; this particle-forming process can also be described with other models, such as the "multigrain model": R. A. Hutchinson, C. M. Chen, W. H. Ray, *J. Appl. Polym. Sci.* **1992**, *44*, 1389 – 1414; the simpliest model is the "polymeric flow model"; it describes the particle-forming process in a simple and clear way, the calculated and experimental data correspond well, therefore it is of importance still today: T. Mc Kenna, V. Mattioli, *Macromol. Symp.* **2001**, *173*, 149 – 162.

[46] Thiele has used such equations to describe the synthesis of low-molecular-mass compounds in catalyst particles: E. W. Thiele, *Ind. Eng. Chem.* **1939**, *21*, 916 – 920; in contrast to the polymerization process described in this review, for the catalytic processes described by Thiele, the size and structure of the catalyst particle remains unchanged.

[47] S. Floyd, K. J. Choi, T. W. Taylor, W. H. Ray, *J. Appl. Polym. Sci.* **1986**, *32*, 2935 – 2960; S. Floyd, G. E. Mann, W. H. Ray in *Studies in Surface Science and Catalysis, Vol. 25* (Eds: T. Keii, K. Soga), Kodansha Tokyo, **1986**, pp. 339 – 367.

[48] H.-F. Herrmann, L. L. Böhm, *Polym. Commun.* **1991**, *32*, 58 – 61.

[49] S. Floyd, T. Heiskanen, T. W. Taylor, G. E. Mann, W. H. Ray, *J. Appl. Polym. Sci.* **1987**, *33*, 1021 – 1065; T. F. Mc Kenna, F. Barbotin, R. Spitz, *J. Appl. Polym. Sci.* **1996**, *62*, 1835 – 1841.

[50] E. Wicke, *Chem. Ing. Tech.* **1974**, *46*, 365 – 374.

[51] G. Eigenberger, *Chem. Ing. Tech.* **1978**, *50*, 924 – 933.

[52] R. A. Hutchinson, W. H. Ray, *J. Appl. Polym. Sci.* **1987**, *34*, 657 – 676; R. A. Hutchinson, W. H. Ray, *J. Appl. Polym. Sci.* **1990**, *41*, 51 – 81.

[53] J. T. M. Pater, G. Weickert, W. P. M. van Swaaij, *DECHEMA Monogr.* **2001**, *137*, 383 – 389.

[54] W. H. Ray, *Ber. Bunsen-Ges.* **1986**, *90*, 947 – 955.

[55] L. L. Böhm, P. Göbel, P.-R. Schöneborn, *Angew. Makromol. Chem.* **1990**, *174*, 189 – 203.

[56] E. Fitzer, W. Fritz, *Technische Chemie*, Springer, Berlin, **1975**, pp. 264; G. Damköhler in *Der Chemie-Ingenieur, Vol. 3* (Eds.: A. Eucken, M. Jakob), Akademische Verlagsgesellschaft, Leipzig, **1937**, pp. 359 – 485.

[57] F. R. Mayo, F. M. Lewis, *J. Am. Chem. Soc.* **1944**, *66*, 1594 – 1601.

[58] F. R. Mayo, *J. Am. Chem. Soc.* **1943**, *65*, 2324 – 2329; W. V. Smith, *J. Am. Chem. Soc.* **1946**, *68*, 2069 – 2071; T. Alfrey, V. Hardy, *J. Polym. Sci.* **1948**, *3*, 500 – 502.

[59] W. Cooper in *Comprehensive Chemical Kinetics, Vol. 15* (Eds.: C. H. Bamford, C. F. H. Tipper), Elsevier Scientific, Amsterdam, **1976**, pp. 133 – 257.

[60] H. Eyring, E. M. Eyring in *Selected Topics in Modern Chemistry* (Eds.: H. H. Sisler, C. A. Van der Werf), Reinhold, Chapman&-Hall, London, **1963**, pp. 1 – 114.

[61] C. N. Satterfield, *Mass Transfer in Heterogeneous Catalysis*, MIT Press, Cambridge, MA, **1970**.

[62] K.-H. Reichert, R. Michael, H. Meyer, *Stud. Surf. Sci. Catal.* **1986**, *25*, 369 – 386.

[63] L. L. Böhm, P. Göbel, O. Lorenz, T. Tauchnitz, *DECHEMA Monogr.* **1992**, *127*, 257 – 273; L. L. Böhm, P. Göbel, P.-R. Schöneborn, T. Tauchnitz, *Proceedings Fourth World Congress of Chemical Engineering* (Karlsruhe, June 16 – 21, **1991**), Dechema, Frankfurt (M), **1992**, pp. 605–619.

[64] L. L. Böhm, P. Göbel, T. Tauchnitz, *Chem. Ind. (Duesseldorf)* **1990**, *6* (90), 24 – 25.

[65] B. Schmitt, W. Prätorius, K. Mühlbach, T. Plesnig, *Kunststoffe* **1999**, *89*, 24 – 31.

[66] L. Böhm, D. Fischer, *Anforderungsgerechte Materialeigenschaften*, VDI, Düsseldorf, **2000**, pp. 205 – 225.

[67] L. L. Böhm in *Progress and Development of Catalytic Olefin Polymerization* (Eds.: T. Sano, T. Uozumi, H. Nakatani, M. Terano), Technology and Education Publishers, Tokyo, **2000**, pp. 256 – 263.

[68] F. P. Alt, L. L. Böhm, H.-F. Enderle, J. Berthold, *Macromol. Symp.* **2001**, *163*, 135 – 143.

[69] L. L. Böhm, H. F. Enderle, M. Fleißner, *Adv. Mater.* **1992**, *4*, 234 – 235.

[70] L. L. Böhm, D. Bilda, W. Breuers, H. F. Enderle, R. Lecht in *Ziegler Catalysts* (Eds.: G. Fink, R. Mülhaupt, H. H. Brintzinger), Springer, Berlin, **1995**, pp. 387 – 400.

[71] J. Scheirs, L. L. Böhm, J. C. Boot, P. S. Leevers, *Trends Polym. Sci.* **1996**, *4*, 408 – 415.

[72] H. Lüker, U. Schulte, *Kunststoffe* **1995**, *85*, 1127 – 1128; R. Weinlein, V. Lackner, *Plastics Special* **1997**, issue 11, 4 – 10; U. Schulte, R. Lecht, *Swiss Plast.* **1998**, *20* (6), 15 – 22.

[73] K. Richard, G. Diedrich, *Kunststoffe* **1956**, *46*, 183 – 190; K. Richard, E. Gaube, G. Diedrich, *Kunststoffe* **1959**, *49*, 516 – 525; E. Gaube, G. Diedrich, W. Müller, *Kunststoffe* **1976**, *66*, 2 – 8.

[74] M. Fleißner, *Kunststoffe* **1987**, *77*, 45 – 50; M. Fleißner, *Polym. Eng. Sci.* **1998**, *38*, 330 – 340.

[75] M. Ifwarson, *Kunststoffe* **1989**, *79*, 525 – 529; M. Ifwarson, H. Leijstrom, *Proc. Plastic Pipes VII*, paper C171 (Eindhoven, The Netherlands, September 21 – 24, **1992**), Plastics and Rubber Institute, London).

[76] U. Schulte, *Kunststoffe* **1997**, *87*, 203 – 206; U. Schulte, *BBR Wasser und Rohrbau*, **1999**, issue 11, 14 – 21.

[77] R. Bergner, *Blasformen'97, Innovationen und Perspektiven*, VDI, Düsseldorf, **1997**, pp. 3 – 27; R. Kaps, R. Schubbach, *Blasformen'97, Innovationen und Perspektiven*, VDI, Düsseldorf, **1997**, pp. 29 – 48.

[78] M. Fleißner, *Int. Polym. Process.* **1988**, *2*, 229 – 233.

[79] L. L. Böhm, H. F. Enderle, M. Fleißner, *Plastics, Rubber and Composites Process. Appl.* **1998**, *27*, 25 – 29.

[80] W. Prätorius, *Kunststoffe* **2000**, *90*, 22 – 25.

[81] Wirtschaftsdaten und Graphiken zu Kunststoffen **2003** (Eds. Verband Kunststofferzeugende Industrie e.V., Frankfurt (M)), http://www.vke.de.

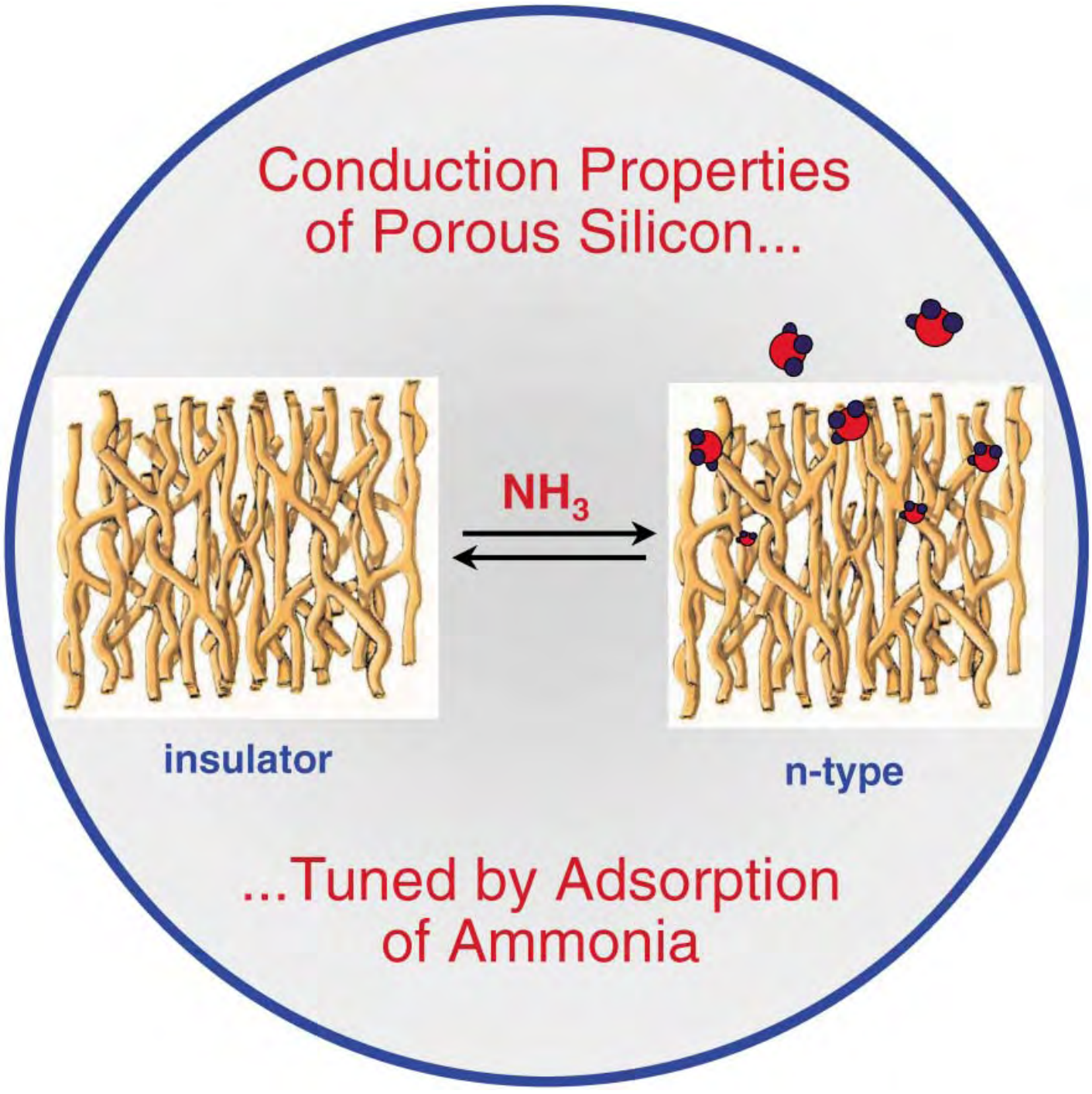
[82] L. A. Utracki, *Polym. Eng. Sci.* **1995**, *35*, 2 – 17.

 © 2003 Wiley-VCH Verlag GmbH & Co. KGaA, Weinheim

[83] L. L. Böhm, J. Berthold, H. F. Enderle, M. Fleissner in *Organometallic Catalysts for Synthesis and Polymerization* (Ed.: W. Kaminsky), Springer, Berlin, **1999**, pp. 3 – 13.
[84] IK Industrieverband Kunststoffverpackungen e.V., *Mitglieder-Zeitschrift* **1998**, 9 – 10.
[85] *Plastics in Packaging* **2001**; *Environmental Benefits* **2001** (Eds. APME, Association of Plastics Manufacturers in Europe), http://www.apme.org.
[86] *Verpacken mit Kunststoffen. Argumente, Fakten, Perspektiven* (Eds. BASF AG, Ludwigshafen, Germany).
[87] *Survey Report on Life Cycle Assessment (LCA) for Plastics and other Packaging Materials*, Plastic Waste Management Institute, Japan, **1995**.
[88] H. Kindler, A. Nikles, *Kunststoffe* **1980**, *70*, 802 – 807; R. Mülhaupt, *Plastverarbeiter* **1999**, *50*, 68 – 86.
[89] G. Beer, H. R. Schmidt, *Kunststoffe* **1998**, *88*, 1668 – 1672; G. Beer, M. Flosdorff, R. Kaps, U. Schulte, R. Seintsch, *Kunststoffe* **1999**, *89*, 34 – 40; G. Beer, H. Danz, S. Justus, R. Mantel, F. Schnorr, M. Vogt, A. Weber, *Kunststoffe* **2002**, *92*, 36 – 42.
[90] J. Brandrup in *Blasformen'97, Innovationen und Perspektiven*, VDI, Düsseldorf, **1997**, pp. 131 – 156.
[91] H. Eschwey, K. Cuhls, *Die Kunststoffindustrie im 21. Jahrhundert*, Frauenhofer Institut Systemtechnik und Innovationsforschung, Karlsruhe, **1999**.
[92] *Polyolefins Planning Service*, CHEM SYSTEMS (Nexant) London, **2001**.

 © 2003 Wiley-VCH Verlag GmbH & Co. KGaA, Weinheim

Communications



The adsorption of ammonia leads to a remarkable increase in the electron population of the conduction band of mesoporous silicon. This effect, and the insulator-to-metal transition that is observed at high NH_3 doses, is detailed in the Communication by E. Giamello and co-workers on the following pages.

DOI: 10.1002/anie.200352114
© 2003 Wiley-VCH Verlag GmbH & Co. KGaA, Weinheim

Electronic Transitions in Silicon

Reversible Insulator-to-Metal Transition in p^+-Type Mesoporous Silicon Induced by the Adsorption of Ammonia

*Mario Chiesa, Giampiero Amato, Luca Boarino, Edoardo Garrone, Francesco Geobaldo, and Elio Giamello**

Several "classic" functional materials, when prepared in nanostructured forms, exhibit unique physical properties that present opportunities for new applications.[1–3] This is the case for mesoporous silicon, a material widely investigated for its peculiar photoluminescence, optical, and electronic properties.[4] These properties have been harnessed for a variety of challenging chemical sensor applications,[5] such as the quantification of reactive pollutant gases (for example, NO_2).[6] The present article reports the observation of a dramatic increase in the conduction-electron population in mesoporous silicon, which occurs upon adsorption of ammonia onto the surface. This effect has been monitored by EPR spectroscopy and is interpreted in terms of a reversible change from Langevin to Pauli paramagnetism, which corresponds to an insulator-to-metal transition.

Mesoporous silicon (m-PS) is prepared by electrochemically etching B-doped p^+-type crystalline silicon in HF solutions, where the boron content is typically of the order of 10^{19}–10^{20} atoms cm^{-3}. It possesses a dendritic structure, comprised of Si nanowires with diameters ranging from 5–12 nm and a specific surface area up to 600 $m^2 cm^{-3}$.

Despite the number of papers devoted to m-PS in recent years, a number of questions are still unanswered, for example, concerning the hole-based electrical conductivity of B-doped Si, which drops by several orders of magnitude upon the formation of pores, and renders the PS nearly an insulator. This loss of conductivity cannot be ascribed to any preferential removal of boron atoms during etching. The disappearance of the great majority of free holes has been interpreted by various, sometimes conflicting hypotheses.[7–11] There are a few examples of experiments in which the conductivity of porous Si samples increases. For example, contact between porous silicon and polar liquids causes such an increase, and this observation has been interpreted as the removal of carrier constriction.[12] Most interpretations of this phenomenon postulate that the reactivation of "trapped" holes is due to an increase in dielectric constant when the liquid fills the porous structure.[13] In the present work, it will be shown that the free carriers generated by NH_3 adsorption on B-doped porous silicon are indeed electrons. This interpretation is in agreement with the observation of Poindexter and co-workers[14] for the case of p- and n-type porous silicon when in contact with acetone.

Freshly prepared p^+ layers only show a weak EPR spectrum due to P_b centers (silicon dangling bonds at the Si/SiO_2 interface).[15] These centers have been thoroughly investigated in the past[16,17] and will not be commented upon further here. On dosing m-PS at room temperature with an amount of NH_3 corresponding to 2.7×10^{20} molecules per cm^3 of m-PS, and cooling the cell down to 77 K, a symmetric, intense EPR signal is observed. This signal

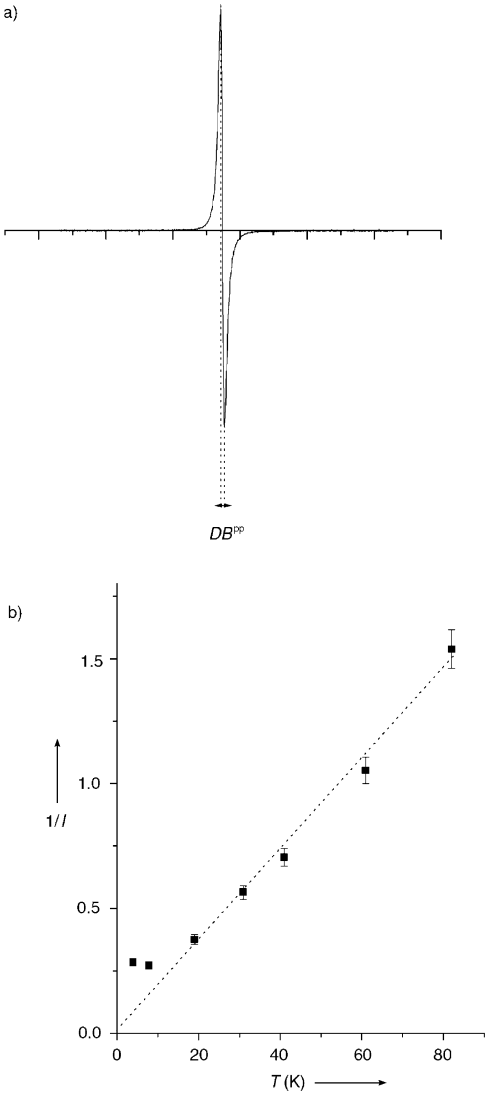


Figure 1. a) EPR spectrum of mesoporous silicon (m-PS) dosed with ammonia (2.7×10^{20} molecules per cm^3 m-PS) measured at 10 K (B^{PP} = peak-to-peak separation); b) the temperature dependence of the paramagnetic susceptibility χ, measured in terms of $1/I$ versus T.

[*] Prof. Dr. E. Giamello, Dr. M. Chiesa
Dipartimento di Chimica IFM, Università di Torino
Istituto Nazionale per la Fisica della Materia
via P. Giuria 7, 10125 Torino (Italy)
Fax: (+39) 011-6707-855
E-mail: elio.giamello@unito.it
Dr. G. Amato, Dr. L. Boarino
Quantum Res. Lab.
Istituto Elettrotecnico Nazionale Galileo Ferraris
Strada delle Cacce 91, 10135 Torino (Italy)
Prof. Dr. E. Garrone, Prof. Dr. F. Geobaldo
Dipartimento di Scienza dei Materiali e Ingegneria Chimica
Politecnico di Torino
Corso Duca degli Abruzzi 24, 10129 Torino (Italy)

 © 2003 Wiley-VCH Verlag GmbH & Co. KGaA, Weinheim DOI: 10.1002/anie.200352114

disappears upon removal of the adsorbate and it can be regenerated with a fresh dose of NH_3. The temperature dependence of this EPR signal has been investigated. The spectrum at 10 K is shown in Figure 1 a; the resonance has an isotropic g value of 1.9984 ± 0.0003, independent of temperature, and a Lorentzian line-shape. The peak-to-peak line width ($\Delta H_{pp} = 10$ G at 10 K) linearly decreases in the range 100–30 K while it remains constant from 30 to 4 K. The broadening of the line prevents observation of the signal at temperatures above 130 K. The intensity I of the EPR signal is a measure of the pure paramagnetic susceptibility of the sample (χ): Figure 1 b reports the temperature dependence of χ in the range 4–100 K, as a plot $1/I$ versus T. The data displays Langevin–Curie behavior down to about 20 K. A spin–lattice relaxation time of $(2.5 \pm 1) \times 10^{-6}$ s was derived from the saturation trend observed in the resonance at 10 K. This value is typical of conduction electrons in Si-based semiconductors.[18] The spin concentration (see Experimental Section) is estimated to be $5 \pm 3 \times 10^{17}$ spins cm^{-3}. The line shape, g value, and temperature dependence indicate that the EPR signal is associated with conduction-band (CB) electrons, as described by Poindexter et al.[14] for the case of p- and n-type porous silicon treated with acetone. The signal reported in Figure 1 a is therefore a true conduction electron spin resonance (CESR) signal. Any role that holes might have in determining such a signal is excluded, as is the case in silicon-based semiconductors, where holes are EPR-inactive unless a strong mechanical stress is applied to the solid.[19]

The intensity of the Lorentzian line has been studied as a function of the amount of adsorbed NH_3 in the range between 1×10^{19}–4×10^{20} molecules cm^{-3} of PS (data not reported), and a linear dependence is observed. A dramatic change in the EPR spectrum occurs when higher doses of NH_3 are adsorbed. The spectrum recorded at 77 K upon dosing of 6×10^{20} molecules cm^{-3} is displayed in Figure 2 a. Under these conditions a marked asymmetry in the resonance line is observed, corresponding to a Dysonian line-shape. The g value of the resonance is the same as that measured at lower ammonia doses and is constant with temperature. The Dyson profile is typically ascribed to the magnetic resonance of electrons in conducting materials when the electron concentration is high enough to produce the so-called "skin-depth effect". In this case the resonance of electrons is observed in a limited external portion of the material (skin) whose depth is given by:

$$\delta = \left(\frac{2 c^2 \varepsilon_0 \rho}{\omega} \right)^{1/2} \quad (1)$$

where ρ is the electrical resistivity and ω is the angular frequency of the radiation. The symmetric Lorentzian line shape gives way to the asymmetric Dysonian absorption when δ becomes small in comparison to the sample thickness.[20] In other words the line shape is expected to change from Lorentzian to Dysonian when the electrical conductivity of the material increases.

The above observations are consistent with the paramagnetic susceptibility reported in Figure 2 b. In parallel with the onset of the transition to a Dysonian line shape, a

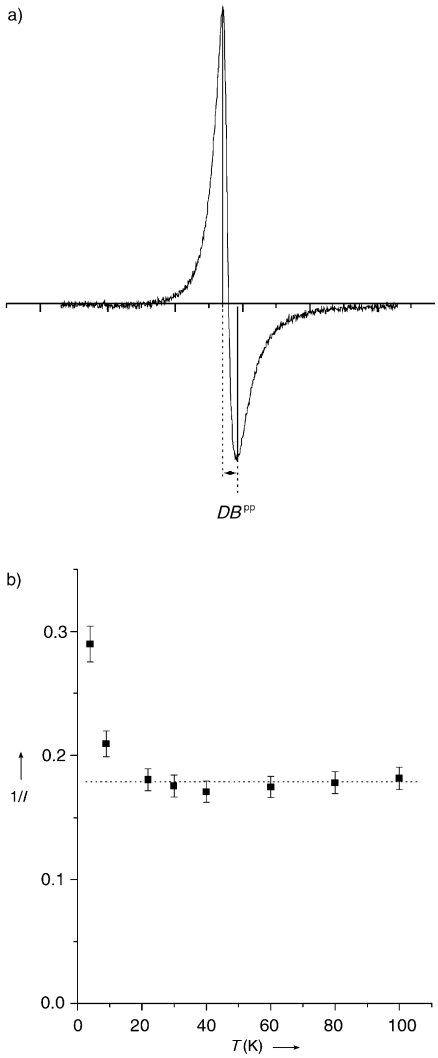


Figure 2. a) EPR spectrum of mesoporous silicon (m-PS) with a higher ammonia dosage (6×10^{20} molecules per cm^3 m-PS) measured at 77 K; b) the temperature dependence of the paramagnetic susceptibility χ, measured in terms of $1/I$ versus T.

temperature-independent (in the range 20–100 K) Pauli-like behavior is observed for χ. Below 20 K a deviation from linearity occurs, as observed in the case of low ammonia coverage (Figure 1 b), which could be ascribed to a magnetic phase transition. This phenomenon is currently under investigation in our laboratories.

According to standard formulas,[21] degeneracy of a free-electron gas and the concomitant onset of Pauli paramagnetism is expected to occur at about 100 K for an electron concentration of the order of 10^{19} cm^{-3}. Such a value can be considered a reasonable estimate of the electron density in m-PS in the conditions corresponding to the onset of the Dysonian ESR line. The generation of free carriers in the present samples is induced by the adsorption of ammonia. Remarkably, these free carriers are electronic in nature and their concentration depends on the amount of adsorbed ammonia. The coverage in ammonia is estimated to be of the order of a monolayer under circumstances leading to the

 © 2003 Wiley-VCH Verlag GmbH & Co. KGaA, Weinheim

Dysonian line shape; note that the whole adsorbed amount in such conditions (40 mbar NH_3 pressure in the cell before cooling to 77 K) corresponds to about 4% of the porous volume. This rules out any explanation of the observed phenomena in terms of capillary condensation into the pores, and consequent changes in the dielectric properties of the sample. The remarkable changes observed are ascribed to effects associated with the chemical interaction between the porous system and the adsorbed molecules. Similarly, increases in absorption by free carriers have been observed by means of IR spectroscopy in the case of NO_2 acting as an adsorbate.[6]

Modifications of the surface conductivity in insulators and semiconductors brought about by redox interactions between the solid and an adsorbate are not unusual.[22] This implies the development of space charge in the solid, band bending, and possibly Fermi-level pinning to the energy of the surface state. The case described in the present paper has peculiar features in that: a) the modification of the electron population seems to involve all of the solid; b) the chemical properties of ammonia (a typical Lewis base) are very different from those of the molecules or ions which have previously been shown to modify surface conductivity.[23] In these latter cases, the molecules or ions involved are usually redox active with suitable electrochemical potential.

Regardless of the exact nature of the NH_3–porous silicon interaction, the phenomenon reported here is remarkable considering that the starting material (p^+ crystalline silicon) is a p-type semiconductor, which becomes pratically an insulator upon etching (p^+ mesoporous silicon) and, in turn, an n-type semiconductor upon adsorption of ammonia (Figure 3). Moreover the remarkable peculiarity of the case

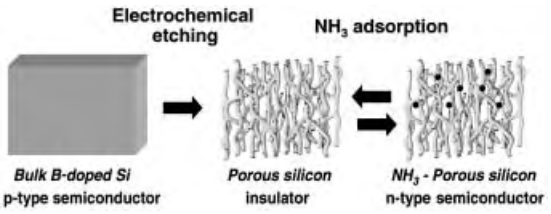


Figure 3. The electronic behavior of mesoporous silicon on the adsorption of ammonia.

here described is that the conversion is triggered by adsorption of a gas (a low-energy reversible process) and that, in principle, the electronic (and magnetic) properties of the solid can be tuned simply by varying the amount of adsorbed gas. The phenomenon is also intriguing considering that it has already been demonstrated that adsorption of an electron scavenger like NO_2 on the same type of m-PS employed in the present work, restores the original hole conductivity of the bulk B-doped Si.[11,12] Thus, the possibility of creating an n–p junction by gas adsorption appears very exciting.

In summary, we report evidence for the generation of conduction-band electrons in p^+-type porous silicon by the adsorption of NH_3 molecules. The g value of the observed CESR signal ($g = 1.9984$) is, within the experimental error, the same as that of conduction electrons in crystalline, polycrystalline, and porous silicon.[14–25] The number of free carriers increases with increasing NH_3 adsorption and, beyond a critical value, a true reversible insulator-to-metal transition[26] is observed with the onset of both a skin-depth effect and transition from a Langevin to Pauli paramagnetism.

Experimental Section

Porous silicon membranes were prepared in 25% HF/25% H_2O/50% EtOH solutions by anodization of boron-doped p^+-type c-Si(100) substrates ($B \cong 3 \times 10^{19}$ atoms cm^{-3}; resistivity = 5–15 mΩ cm). Etching was carried out at a current density of 250 mA cm^{-2} to produce $\approx$60% porosity membranes. At the end of anodization, the membrane was detached by means of a high-current pulse.

Measurements were performed with a Bruker ESP-300 spectrometer operating in the X-band mode (9.5 GHz). The sample (typically 5 mg) was cooled with a gas-flow cryostat operated from $T = 4.0$ to 300 K. DPPH ($g = 2.0036$) and a solid solution of Mn^{2+} ions in MgO ($g = 2.0064$) were used as standards for g-value calibration and quantitative evaluation of the number of carriers. The intensity of the EPR signal was obtained as the absorption curve area by a numerical integration of the data. In order to measure the number of molecules interacting with the solid, the volume of the EPR cell was carefully evaluated by means of a volumetric vacuum manifold.

Received: June 11, 2003 [Z52114]
Published Online: August 25, 2003

Keywords: ammonia · EPR spectroscopy · insulators · semiconductors · silicon

[1] K. D. Hirschman, L. Tsybeskov, S. P. Duttagupta, P. M. Fauchet, *Nature* **1996**, *384*, 338.
[2] G. Ledoux, O. Guillois, D. Porterat, C. Reynaud, F. Huisken, B. Kohn, V. Paillard, *Phys. Rev. B* **2000**, *62*, 15942.
[3] J. Kong, N. R. Franklin, C. Zhou, M. G. Chapline, S. Peng, K. Cho, H. Dai, *Science* **2000**, *287*, 622.
[4] L. T. Canham, *Appl. Phys. Lett.* **1990**, *57*, 1046; Y. Kanemitsu, *Phys. Rep.* **1995**, *263*, 3.
[5] M. Sailor in *Properties of Porous Silicon* (Ed.: L. T. Canham), EMIS Data review series, INSPEC, London, **1997**, p. 364, and references therein.
[6] F. Geobaldo, B. Onida, P. Rivolo, S. Borini, L. Boarino, A. Rossi, G. Amato, E. Garrone, *Chem. Commun.* **2001**, 2196.
[7] V. Lehmann, F. Hofmann, F. Möller, U. Grüning, *Thin Solid Films* **1999**, *255*, 20.
[8] M. Ben-Chorin in *Properties of Porous Silicon* (Ed.: L. T. Canham), EMIS Data review series, INSPEC, London, **1997**, p. 165, and references therein.
[9] L. A. Balagurov, D. G. Yarkin, E. A. Petrova, *Mater. Sci. Eng. B* **2000**, *69–70*, 127.
[10] G. Polisski, D. Kovalev, G. Dollinger, T. Sulima, F. Koch, *Phys. B* **1999**, *273–274*, 951.
[11] L. Boarino, F. Geobaldo, S. Borini, A. M. Rossi, P. Rivolo, M. Rocchia, E. Garrone, G. Amato, *Phys. Rev. B* **2001**, *64*, 205308.
[12] V. Y. Timoshenko, T. Dittrich, V. Lysenko, M. G. Lisachenko, F. Koch, *Phys. Rev. B* **2001**, *64*, 085314.
[13] V. Y. Timoshenko, T. Dittrich, F. Koch, *Phys. Status Solidi B* **2000**, *222*, R1.
[14] C. F. Young, E. H. Poindexter, G. J. Gerardi, *J. Appl. Phys.* **1997**, *81*, 7468.

 © 2003 Wiley-VCH Verlag GmbH & Co. KGaA, Weinheim

[15] E. H. Poindexter, P. J. Caplan, B. E. Deal, R. R. Razouk, *J. Appl. Phys.* **1981**, *52*, 879.
[16] H. J. von Bardeleben, D. Stievenard, A. Grosman, C. Ortega, J. Siejka, *Phys. Rev. B* **1993**, *47*, 10899.
[17] F. C. Rong, J. F. Harvey, E. H. Poindexter, G. J. Gerardi, *Appl. Phys. Lett.* **1993**, *63*, 920.
[18] C. Malten, J. Muller, F. Finger, *Phys. Status Solidi B* **1997**, *201*, R15.
[19] G. Feher, J. C. Hensel, E. A. Gere, *Phys. Rev. Lett.* **1960**, 5, 309.
[20] F. J. Dyson, *Phys. Rev.* **1955**, 98, 349.
[21] H. Kodera, *J. Phys. Soc. Jpn.* **1966**, *21*, 1040.
[22] F. Maier, M. Riedel, B. Mantel, J. Ristein, I. Ley, *Phys. Rev. Lett.* **2000**, *85*, 3472.
[23] S. Roy Morrison in *The Chemical Physics of Surfaces*, Plenum, New York, **1977**.
[24] G. Feher, *Phys. Rev.* **1959**, *114*, 1219.
[25] C. F. Young, E. H. Poindexter, G. J. Gerardi, W. L. Warren, D. J. Keeble, *Phys. Rev. B* **1997**, *55*, 16245.
[26] P. P. Edwards, M. J. Sienko, *Acc. Chem. Res.* **1982**, *15*, 87; N. Mott, *Proc. R. Soc. London Ser. A* **1982**, *382*, 1; P. P. Edwards, R. L. Johnston, F. Hensel, C. N. R. Rao, D. P. Tunstall, *Solid State Phys.* **1999**, *52*, 229.

 © 2003 Wiley-VCH Verlag GmbH & Co. KGaA, Weinheim

CdSe Quantum Shells and Wells

Colloidal Two-Dimensional Systems: CdSe Quantum Shells and Wells**

*David Battaglia, Jack J. Li, Yunjun Wang, and Xiaogang Peng**

Nanometer-sized structures with at least one dimension smaller than the critical size for a given property of a material have attracted considerable attention recently,[1–5] because of their size-dependent properties. Zero-dimensional (0D) and one-dimensional (1D) structures have recently been chemically synthesized and studied quite explicitly. On the other hand, 2D systems are rare. In fact, most of the properties of 2D semiconductor systems have not yet been demonstrated. Here we report a class of 2D colloidal semiconductor structures, ultrathin layers of semiconductors with a narrow bandgap, epitaxially grown onto a nanocrystal template with a substantially wider bandgap. The absorption and emission properties of these new structures strongly depend on the shell thickness but not on the size of the nanocrystal templates, which indicates quantum confinement only occurs along the radial direction (quantum shells).

Although there have been no reports on synthesizing colloidal semiconductor discs or sheets whose emission color is tunable in the visible color window, 2D semiconductor thin films are routinely grown onto single-crystal substrates through molecular beam epitaxy (MBE) with a precise control of the thickness.[6] This encouraged us to mimic the MBE-grown 2D semiconductor structures in solution, with the aim to grow a few monolayers of a narrow bandgap semiconductor onto a nanocrystal template with a wide bandgap. To do so, the perimeter of the shell should be larger than the diameter of the exciton of the shell semiconductor. Several research groups have attempted to grow such structures, and a significant red-shift of the absorption band edge has been observed.[7–11] The best studied system comprises one monolayer of HgS sandwiched between a CdS core and several layers of CdS overcoating.[8,9] After being activated in basic solutions, CdS/HgS/CdS emitted a red band-edge emission, which must originate from the HgS layer. Unfortunately, the poor quality of the core nanocrystals and underdeveloped growth methods for the shell layers made it difficult to observe the expected properties of 2D semiconductor structures, such as solely thickness-dependent absorption and emission, staircase-like electronic band structures (predicted by a simple model for 2D systems),[2] and good emission efficiency. In addition to the quality of the nanocrystals, the diameter of the HgS exciton may be too big to be only confined along the radial direction.

The accurate control of film thickness in MBE 2D structures and other thin film structures has been achieved through atomic layer epitaxy (ALE)[6] and successive ion layer asorption and reaction (SILAR).[12] Recently, we have demonstrated that a modified SILAR technology can be extended to the growth of core/shell semiconductor nanocrystals with precise thickness control.[13] The key feature of the newly developed SILAR method is that the precursors of the anionic and cationic components of the shell compound semiconductor are introduced in an alternating fashion. Importantly, only two subsequent additions are required for the growth of a layer of the shell semiconductor. X-ray diffraction (XRD), transmission electron microscopy (TEM), X-ray photoelectron spectroscopy (XPS), and optical spectroscopy revealed that the shell growth of the CdSe/CdS core/shell system was nearly precisely controlled, homogeneous, and epitaxial.[13] This success motivated us to apply this new technique for growing quantum shells.

CdSe was chosen as the first quantum shell system partly because the corresponding quantum dots and rods are the most understood systems, and they exhibit tunable emission colors covering most of the visible optical window.[14,15] The diameter of the bulk exciton of CdSe is about 11 nm, which is smaller than the outer perimeter of all of the core/shell structures with more than two monolayers of the CdSe shell

[*] Prof. X. Peng, D. Battaglia, J. J. Li
Dept. of Chemistry and Biochemistry
University of Arkansas
Fayetteville, AR 72701 (USA)
Fax: (1) 501-575-4049
E-mail: xpeng@uark.edu
Y. Wang
Nanomaterials and Nanofabrication Laboratories (NN-Labs),
Fayetteville, AR 72704

[**] Financial support of this work by the University of Arkansas and the NSF is acknowledged. J.J.L. is grateful for the graduate fellowship provided by CSTAR, and Y.W. is supported by NSF SBIR programs (Nos. 0215254 and 0232976).

Supporting information for this article is available on the WWW under http://www.angewandte.org or from the author.

 DOI: 10.1002/anie.200352120 © 2003 Wiley-VCH Verlag GmbH & Co. KGaA, Weinheim

shown in this report. Thus, we suspect that the exciton should only experience quantum confinement along the radial direction. CdS nanocrystals were chosen as the nanocrystal templates since CdSe/CdS core/shell nanocrystals have been well studied, and epitaxial and uniform growth in solution between these two materials can easily be achieved by the SILAR technique.[13] In addition, CdS quantum dots with a quality that compares well with that of the standard CdSe nanocrystals can be readily synthesized using the newly developed alternative routes in noncoordinating solvents.[16]

For this specific system, SILAR temperatures between 180 and 200 °C were found to yield nanocrystals with the required thickness (about 0.7 nm increase in diameter per layer) and crystallinity, characterized by standard techniques used for the CdSe/CdS regular core/shell nanocrystals.[13] All experimental evidence indicates that the CdSe quantum shells are epitaxially grown on the CdS nanocrystal templates, similar to the reversed system, epitaxially grown CdSe/CdS core/shell nanocrystals. Figure 1 provides a selective-area electron diffraction (SAED) pattern and four TEM images that show the 3.7 nm CdS nanocrystal template before growth is initiated, and then after the growth of three (3-layer), five (5-layer), and seven monolayers (7-layer) of CdSe shells. The sizes of the dot-shaped quantum shells in Figure 1 approximately match the theoretical thicknesses predicted by the SILAR process.

Several CdS nanocrystal templates with diameters between 2.5 and 5.0 nm were used for the growth of the quantum shells, with the absorption peak ranging from 380 (3.26 eV) to 440 nm (2.82 eV). It should be noted that the amounts of cadmium and selenium precursors added for the growth of a monolayer of a CdSe shell on differently sized CdS templates varied significantly. For example, for the growth of the second monolayer of CdSe onto 2.5, 2.7, 3.7, and 5 nm CdS templates, 0.21, 0.23, 0.36, and 0.58 mL of the cadmium and selenium injection solutions (0.04 mol L^{-1}) were respectively injected into growth solutions with the same particle concentration. This shows that the volume increase of a monolayer of a dot-shaped crystal is strongly associated with the diameter of the dots.

Despite the large difference in the energy bandgap, the size of the templates used, and the volume increase of the CdSe shells on differently sized templates, the resulting CdSe quantum shell nanocrystals with the same shell thickness on differently sized templates have great similarities in their photoluminescence (PL) and absorption properties. For all quantum shells with a thickness equal to or greater than two monolayers, the position of the PL peak and the color of the emission were all strongly dependent on the thickness of the quantum shells (Figure 2). As a comparison, the influence of the size and the energy bandgap of the template nanocrystals on the PL position of a given shell thickness was found to be small, within ± 8 nm or ± 0.03 eV (Figure 2). The highest PL quantum yield (QY) of the band-edge emission of the CdSe quantum shells was about 20 %.

The absorption onset and the overall contour of the absorption spectra of the quantum shells are also mainly determined by the shell thickness (Figures 2 and 3). In addition, multiple staircase-like states in the absorption spectra were resolved in the absorption and photoluminescence excitation (PLE) spectra (Figures 2 and 3) if the shell thickness was two or more monolayers. The energy bandgap of the CdS template nanocrystals showed some local influence at the energy window close to the original absorption peak of the CdS templates, especially for thin layers. Furthermore, this influence increased as the size (energy gap) of the nanocrystal templates increased (decreased). When the shell thickness reached five monolayers, this influence became insignificant for all cases (Figure 2) due to the dominant volume fraction of the shell material. This fact is further demonstrated by the PLE spectra (Figure 3). The

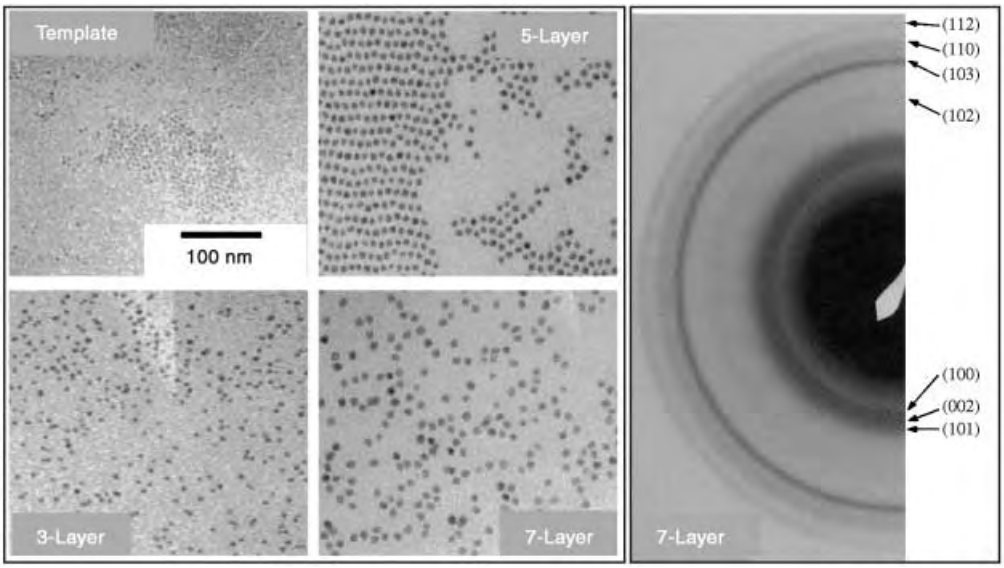


Figure 1. Left: TEM images of CdSe quantum shells with different thickness grown on 3.7-nm CdS nanocrystal templates; right: a SAED pattern of the 7-layer CdSe quantum shells and the indices of each diffraction ring, which are indicative of a wurtzite structure.

 © 2003 Wiley-VCH Verlag GmbH & Co. KGaA, Weinheim

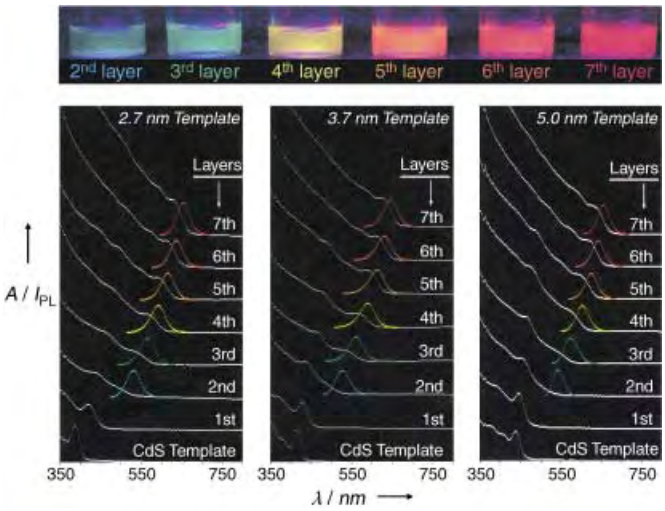


Figure 2. Bottom: Absorption and PL spectra of the CdSe quantum shells grown on three different-sized CdS templates, 2.7 nm (left), 3.7 nm (middle), and 5.0 nm (right). The number of CdSe monolayers is marked on the right for each sample; top: emission colors of CdS/CdSe quantum shells with different shell thicknesses.

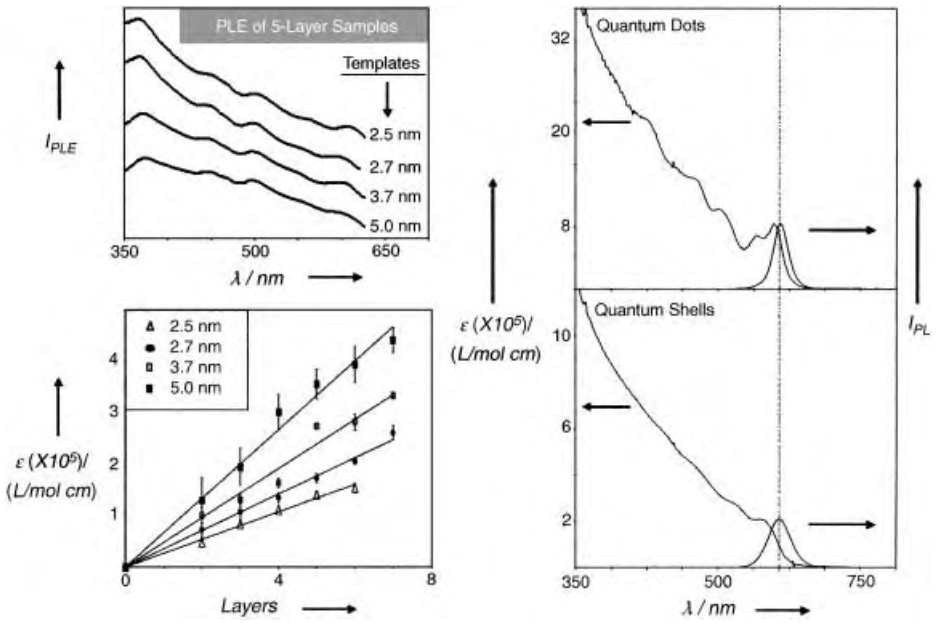


Figure 3. Top left: A collection of photoluminescence excitation (PLE) spectra for the 5-layer CdSe quantum shells grown on four different-sized CdS nanocrystal templates; bottom Left: a plot of the extinction coefficients (ε) at the first absorption feature of the quantum shells versus the number of monolayers of CdSe grown on four different-sized CdS nanocrystal templates. The error bars account the uncertainty of the peak position of the first absorption feature. The solid lines are a linear fit of the experimental data for the four series of CdSe quantum shells; right: a spectroscopic comparison between CdSe quantum shells (below) and high-quality CdSe quantum dots (above). Note: The scales of the y axis for the two plots are different.

overall size (including the CdS templates) of the four 5-layer quantum shells shown in Figure 3 ranged approximately from 6.0 to 8.5 nm depending on the size of the templates.

The extinction coefficient per mole of the nanocrystals (ε) at the first absorption feature position was found to be approximately proportional to the shell thickness for a given sized template (Figure 3, bottom left). Regardless of the template sizes, the ε values were found to be proportional to the CdSe units per particle (see Supporting Information). This is similar to some of the results reported in literature.[17–19] In addition, all four straight lines shown in the plot go through the origin, which indicates that the absorption feature is indeed caused by the CdSe shells. The ε values of the CdSe quantum shells at the emitting peak position are significantly lower than that of CdSe quantum dots with the same PL peak position (Figure 3), which makes the quantum shells potentially ideal emitters when a high concentration of particles is needed, such as for LEDs,[20,21] lasers,[22] and multiple or high-density bio-labeling.[23,24] Under these circumstances, reabsorption and Forster energy transfer may cause serious quenching of the PL[14] and electroluminescence (EL)[20] since the particles are in close proximity with each other.

The optical properties of the 1-layer structures have typically not fully developed into 2D systems, in contrast to those with thicker layers. This was true for CdS/CdSe and other systems (see Supporting Information) with a variety of template sizes. Typically, the absorption spectra are dominated by the slightly red-shifted absorption of the CdS template nanocrystals with a tail on the low energy side (Figure 2). PL spectra of all 1-layer structures display mainly the deep-trap emission of the nanocrystals. If the ε value of the first absorption feature of the 1-layer structure falls onto the linear trend lines shown in Figure 3, the oscillator strength of the narrow bandgap semiconductor is extremely low in comparison to that of the CdS template nanocrystals. As a result, the energy states contributed by the single monolayer of the narrow bandgap semiconductor may mostly act as the deep-trap states of the core CdS structures, causing deep-trap emissions.

The emission properties of quantum shells can be improved through inorganic passivation by additional epitaxial growth of a high-bandgap semiconductor on the surface of the quantum shells in a one-pot approach. The resulting nanocrystals structurally and electronically resemble the MBE quantum wells, thus we denote those structures as colloidal quantum wells. Figure 4 shows the optical spectra before and after the epitaxial growth of four monolayers of CdS onto a CdSe quantum shell sample. As expected, the PL QY increased

 © 2003 Wiley-VCH Verlag GmbH & Co. KGaA, Weinheim

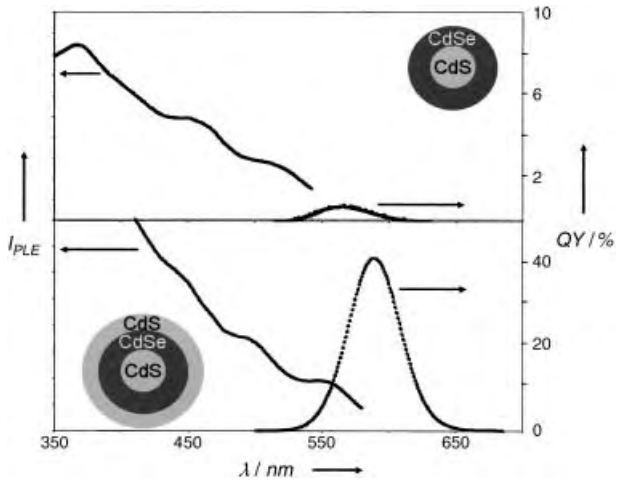


Figure 4. PLE and PL spectra of CdSe quantum shells before (top) and after (bottom) the expitaxial growth of four monolayers of CdS shell on the outer surface. Note: The scales for PL quantum yield (QY) for the quantum shells (top) and the colloidal quantum wells (bottom) are different.

significantly after inorganic overcoating and the PL peak position was red-shifted. To inorganically passivate quantum shells with CdS, it was seen that using fatty acids (such as oleic acid) as ligands yielded nanocrystals with higher quantum yields than when using amines. When fatty acids were used as the ligands, the CdSe quantum shells before inorganic passivation did not emit well but did grow the desired monolayers on the CdS templates. This is consistent with the observation that fatty acids are better passivation ligands for CdS surfaces, while amines are better for CdSe surfaces.[13,16,25,26] However, one issue became apparent when fatty acids were employed: There was a possibility that the nanocrystals might become insoluble during or after growth. Typically, reactions performed with short fatty acids had a strong tendency to form insoluble species but did yield CdS/CdSe/CdS colloidal quantum wells with the highest quantum yields.

In summary, CdSe quantum shells with necessary control over the shell thickness and the size distribution of the nanocrystals have been synthesized. Preliminary results revealed that other quantum shells, such as CdS/InP (see Supporting Information), can also be grown in a similar manner. The experimental results of the inorganically passivated quantum shells reveal that even more complex systems can be conveniently built with the SILAR technique. The synthesis of quantum shells and other complex systems will eventually add many new materials to the colloidal semiconductor nanocrystal family. The unique properties described above and the ones to be discovered for such new systems should greatly promote the fundamental understanding of semiconductor nanocrystals, especially for 2D systems. High-quality quantum shells and colloidal quantum wells are optically comparable to high-quality quantum dots and rods, with reasonably high PL quantum yields (over 20% for the CdSe quantum shells and over 40% for the CdS/CdSe/CdS colloidal quantum wells), relatively narrow emission bands, and tunable emission colors from about 520 to 650 nm. These optical features coupled with their low extinction coefficients at the emission position warrant their potential applications as desired emitters when high densities of nanocrystals are needed, such as for LEDs, lasers, and certain biomedical applications.

Experimental Section

High-quality CdS nanocrystals of a size ranging between 2.5 and 5 nm were synthesized and purified using a scheme modified from previously reported methods.[16] The growth of CdSe quantum shells was achieved by following the established SILAR method.[13] For a typical SILAR process, the Cd injection solution (CdO dissolved with oleic acid in octadecene (ODE)) and the Se injection solution (Se powder dissolved with tributylphosphane in ODE) were injected in an alternate fashion at 185 °C. The quantity of shell precursors added into the growth solution for each monolayer was based on the size of the nanocrystal templates, the concentration of the nanocrystals, and the lattice constants of the crystal system. Control experiments without the presence of CdS nanocrystal templates revealed that a trace amount of CdSe nanocrystals with a peak at around 550 nm were slowly formed under the reaction conditions, which typically did not show any noticeable photoluminescence. The extinction coefficient per particle (ε) at the first absorption feature of the quantum shells was obtained by diluting a certain amount of reaction mixture in a given volume of solvent. Since the concentration of the CdS nanocrystal templates in the reaction mixture was known, the concentration of the quantum shells in the diluted solution could be readily determined for the calculation of ε. For the quantum shells grown on different sized templates, the emission color of samples with the same shell thickness was observed to be approximately the same. The emission for taking PL images was generated while the nanocrystals were illuminated by a handheld UV lamp (365 nm). The formation of CdS/CdSe/CdS colloidal quantum wells was achieved by alternating injections of Cd (0.04 M) and S (0.04 M in ODE) precursor solutions after growth of the quantum shells by using fatty acids as the ligands. It was found that a higher reaction temperature (230–240 °C) was necessary for the formation of the outer CdS layers than for the CdSe layers. Up to five layers of CdS were found to give the best emission efficiencies for the nanocrystals; purification of the nanocrystals always led to an increase in the emission efficiency of the nanocrystals.

Received: June 11, 2003
Revised: August 12, 2003 [Z52120]

Keywords: cadmium · colloids · nanostructures · selenium · semiconductors

[1] L. Brus, *J. Phys. Chem.* **1986**, *90*, 2555.
[2] A. P. Alivisatos, *Science* **1996**, *271*, 933.
[3] C. M. Lieber, *Solid State Commun.* **1998**, *107*, 607.
[4] R. E. Smalley, B. I. Yakobson, *Solid State Commun.* **1998**, *107*, 597.
[5] S. A. Empedocles, R. Neuhauser, K. Shimizu, M. G. Bawendi, *Adv. Mater.* **1999**, *11*, 1243.
[6] M. A. Herman, H. Sitter, *Molecular Beam Epitaxy: Fundamentals and Current Status, Second Revised and Updated Edition*, Springer, Berlin, **1996**.
[7] A. R. Kortan, R. Hull, R. L. Opila, M. G. Bawendi, M. L. Steigerwald, P. J. Carroll, L. E. Brus, *J. Am. Chem. Soc.* **1990**, *112*, 1327.

 © 2003 Wiley-VCH Verlag GmbH & Co. KGaA, Weinheim

[8] A. Mews, A. Eychmueller, M. Giersig, D. Schooss, H. Weller, *J. Phys. Chem.* **1994**, *98*, 934.
[9] A. Mews, A. V. Kadavanich, U. Banin, A. P. Alivisatos, *Phys. Rev. B* **1996**, *53*, R13242.
[10] Y. Tian, T. Newton, N. A. Kotov, D. M. Guldi, J. H. Fendler, *J. Phys. Chem.* **1996**, *100*, 8927.
[11] R. B. Little, M. A. El-Sayed, G. W. Bryant, S. Burke, *J. Chem. Phys.* **2001**, *114*, 1813.
[12] S. Park, B. L. Clark, D. A. Keszler, J. P. Bender, J. F. Wager, T. A. Reynolds, G. S. Herman, *Science* **2002**, *297*, 65.
[13] J. Li, Y. A. Wang, W. Guo, X. Peng, J. Am. Chem. Soc, in press.
[14] C. B. Murray, C. R. Kagan, M. G. Bawendi, *Annual Rev. Mater. Sci.* **2000**, *30*, 545.
[15] X. Peng, L. Manna, W. D. Yang, J. Wickham, E. Scher, A. Kadavanich, A. P. Alivisatos, *Nature* **2000**, *404*, 59.
[16] W. W. Yu, X. Peng, *Angew. Chem.* **2002**, *114*, 2474; *Angew. Chem. Int. Ed.* **2002**, *41*, 2368.
[17] O. Schmelz, A. Mews, T. Basche, A. Herrmann, K. Mullen, *Langmuir* **2001**, *17*, 2861.
[18] A. Striolo, J. Ward, J. M. Prausnitz, W. J. Parak, D. Zanchet, D. Gerion, D. Milliron, A. P. Alivisatos, *J. Phys. Chem. B* **2002**, *106*, 5500.
[19] W. W. Yu, X. Peng, *Chem. Mater.* **2003**, in press.
[20] M. C. Schlamp, X. G. Peng, A. P. Alivisatos, *J. Appl. Phys.* **1997**, *82*, 5837.
[21] H. Mattoussi, L. H. Radzilowski, B. O. Dabbousi, E. L. Thomas, M. G. Bawendi, M. F. Rubner, *J. Appl. Phys.* **1998**, *83*, 7965.
[22] V. I. Klimov, A. A. Mikhailovsky, S. Xu, A. Malko, J. A. Hollingsworth, C. A. Leatherdale, H. J. Eisler, M. G. Bawendi, *Science* **2000**, *290*, 314.
[23] M. Bruchez, M. Moronne, P. Gin, S. Weiss, A. P. Alivisatos, *Science* **1998**, *281*, 2013.
[24] W. C. W. Chan, S. M. Nie, *Science* **1998**, *281*, 2016.
[25] D. Talapin, A. L. Rogach, A. Kornowski, M. Haase, H. Weller, *Nano Lett.* **2001**, *1*, 207.
[26] L. Qu, X. Peng, *J. Am. Chem. Soc.* **2002**, *124*, 2049.

 © 2003 Wiley-VCH Verlag GmbH & Co. KGaA, Weinheim

"Nano-ion Chromatograph"

Trapping Cations in Specific Positions in Tuneable "Artificial Cell" Channels: New Nanochemistry Perspectives**

Achim Müller, Samar K. Das, Sergei Talismanov, Soumyajit Roy, Eike Beckmann, Hartmut Bögge, Marc Schmidtmann, Alice Merca, Alois Berkle, Lionel Allouche, Yunshan Zhou, and Lijuan Zhang*

Dedicated to Professor Ram Rao on the occasion of his 70th birthday

Molecular dimensioned holes can serve as filters but also trap molecules with well-defined shapes. Whereas a large number of porous materials with cages and tunnels exist as extended structures,[1] as yet not much is known about well-defined, discrete (molecular) nanoporous species. Processes that refer to the entrance of substrates (e.g. of cations) are of particular interest if the affinity of *specific* substrates to *specific* capsule areas can be predicted. This is now possible for nanosized spherical capsules based on the robust fundamental skeleton $(pent)_{12}(linker)_{30} \cong \{(Mo)Mo_5O_{21}(H_2O)_6\}_{12}\{Mo_2O_4(ligand)\}_{30}$[2,3] which has sizeable pores, finely sculpturable interiors and, in between, tuneable functionalized channels with unprecedented molecular-scale filter properties. These will be discussed here for the first time. Most importantly, the channel functionalities as well as the capsule size and charge can be extensively varied, while charge modulations lead to related changes in the affinity to cations! Herein we show that different substrates/cations can be fixed at well-defined positions above, below, and especially in the channels.[3] This situation allows us to study, in principle, new types of molecular transport phenomena, including osmotic-type ones, on the nanoscale, and shows properties of a "nano-ion chromatograph".[4] Additionally, one can construct new geometries such as interpenetrating solids from entering cations owing to the fact that we have a multitude of different as well as equivalent sites in the channels, pores, and in the interior (see also ref. [3b]). This also allows us to study properties of matter under confined conditions.

For the investigations into the uptake of cations and substrates, we used the known capsule **1a**[3] as well as the new

[*] Prof. Dr. A. Müller, Dr. S. K. Das, Dr. S. Talismanov, S. Roy, E. Beckmann, Dr. H. Bögge, M. Schmidtmann, A. Merca, A. Berkle, Dr. L. Allouche, Dr. Y. Zhou, Dr. L. Zhang
Lehrstuhl für Anorganische Chemie I
Fakultät für Chemie der Universität
Postfach 100131, 33501 Bielefeld (Germany)
Fax: (+49) 521-106-6003
E-mail: a.mueller@uni-bielefeld.de

[**] The authors gratefully acknowledge the financial support of the Deutsche Forschungsgemeinschaft, the Fonds der Chemischen Industrie, and the Volkswagen Stiftung. S.R. and A.M. thank the "Graduiertenkolleg Strukturbildungsprozesse", Universität Bielefeld, for their fellowships and L.A. thanks the European Union for a grant (HRPN-CT-1999-0012).

 DOI: 10.1002/anie.200352358 © 2003 Wiley-VCH Verlag GmbH & Co. KGaA, Weinheim

capsule **2a**[5] (both can be easily obtained from **3a**; see Experimental Section) that exhibits the above-mentioned skeleton. As they contain the neutral linker units $\{Mo_2O_4(SO_4)\}$ and $\{Mo_2O_4(HPO_4)\}$, the overall cluster charge corresponds to that of the 12 pentagonal units, that is, $12\times(6-)=72-$.

$(NH_4)_{72-n}[\{(H_2O)_{81-n}+(NH_4)_n\}\subset\{(Mo^{VI})Mo_5^{VI}O_{21}(H_2O)_6\}_{12}$-
$\{Mo_2^{V}O_4(SO_4)\}_{30}]\cdot\approx 200\,H_2O\equiv(NH_4)_{72-n}$-**1a**$\cdot\approx 200\,H_2O$ **1**[2]

$Na_{10}(NH_4)_{62}[\{(Mo^{VI})Mo_5^{VI}O_{21}(H_2O)_6\}_{12}\{Mo_2^{V}O_4(HPO_4)\}_{30}]\cdot$
$\approx[2\,Na^+ + 2\,NH_4^+ + 4\,H_2PO_4^- + 300\,H_2O]$
$\equiv Na_{10}(NH_4)_{62}$-**2a**$\cdot$[crystal ingredients] **2**

$(NH_4)_{42}[\{(Mo^{VI})Mo_5^{VI}O_{21}(H_2O)_6\}_{12}\{Mo_2^{V}O_4(CH_3COO)\}_{30}]\cdot$
$\approx[10\,CH_3COONH_4+300\,H_2O]$
$\equiv(NH_4)_{42}$-**3a**$\cdot$[crystal ingredients] **3**[2b]

The reaction of **1a** and **2a** with different substrates/cations such as Na^+, Cs^+, Ce^{3+}, and $OC(NH_2)NH_3^+$ in aqueous solution leads to the formation of compounds **4**–**7**, respectively, which exhibit well-defined cation separations at, above, or below the capsule's channel-landscapes ("nano-ion chromatography" principle). All compounds were characterized in the solid state by elemental analyses, thermogravimetry (to determine the amount of water of crystallization), single-crystal X-ray diffraction analyses[6] (including bond valence sum (BVS) calculations), IR spectroscopy,[7a] and ^{31}P solid-state NMR[7b] studies.

$Cs_{10}(NH_4)_{52-n}[\{Cs_{10}+(H_2O)_{81-n}+(NH_4)_n\}$
$\subset\{(Mo^{VI})Mo_5^{VI}O_{21}(H_2O)_6\}_{12}\{Mo_2^{V}O_4(SO_4)\}_{30}]\cdot\approx 200\,H_2O$
$\equiv Cs_{10}(NH_4)_{52-n}$-**4a**$\cdot\approx 200\,H_2O$ **4**

$Ce_3(NH_4)_{54}[Ce_3\subset\{(Mo^{VI})Mo_5^{VI}O_{21}(H_2O)_6\}_{12}\{Mo_2^{V}O_4(SO_4)\}_{30}]\cdot$
$\approx 300\,H_2O$
$\equiv Ce_3(NH_4)_{54}$-**5a**$\cdot\approx 300\,H_2O$ **5**

$(NH_3CONH_2)_{28}Na_{11}[\{(NH_3CONH_2)_{20}+Na_{13}\}$
$\subset\{(Mo^{VI})Mo_5^{VI}O_{21}(H_2O)_6\}_{12}\ \{Mo_2^{V}O_4(SO_4)\}_{30}]\cdot\approx 200\,H_2O$
$\equiv(NH_3CONH_2)_{28}Na_{11}$-**6a**$\cdot\approx 200\,H_2O$ **6**

$(NH_4)_{52}[H_{15}\{(Mo^{VI})Mo_5^{VI}O_{21}(H_2O)_6\}_{12}\{Mo_2^{V}O_4(HPO_4)\}_{30}\{Mo^{VI}O_3H\}_5]\cdot$
$\approx[8\,NH_4H_2PO_4+300\,H_2O]$
$\equiv(NH_4)_{52}$-**7a**$\cdot$[crystal ingredients] **7**

$\{(NH_2)_3C\}_{32}[\{(NH_2)_3C)_{20}+(H_2O)_{100}\}\subset\{(Mo^{VI})Mo_5^{VI}O_{21}$-
$(H_2O)_6\}_{12}\{Mo_2^{V}O_4(SO_4)\}_{10}\{Mo_2^{V}O_4(H_2PO_2)\}_{20}]\cdot\approx 100\,H_2O$
$\equiv\{(NH_2)_3C\}_{32}$-**8a**$\cdot\approx 100\,H_2O$ **8**[8]

Whereas the basic skeleton $\{(Mo)Mo_5O_{21}(H_2O)_6\}_{12}\{Mo_2O_4(ligand)\}_{30}$ of the capsule of the precursors **1a** (see refs [2,3]) and **2a** and of the resulting species **4a**–**7a** is the same, **4a**–**7a** show after cation uptake the expected different interiors (Figure 1, 2); this is a situation for molecular materials never observed before. The uptake leads to stoichiometric preferences when the cations are fixed in the higher channel areas, that is, if the $\{Mo_9O_9\}$ pores can function like a type of crown ether. Non-stoichiometric situations can also occur there, but especially below the pore area. In these cases the uptake can be increased by increasing related concentrations and the capsule charge. Whereas the large, stoichiometrically bound, protonated urea cations in **6a** fit reasonably well into the $\{Mo_9O_9\}$ rings/pores (see below), the somewhat smaller Cs^+ ions are not found exactly at the pore centers, but slightly shifted. The even smaller Rb^+ ions show complicated "chameleonic" behavior and are found at several different capsule functionalities, including positions outside the capsule, as there are no characteristic complementary sites available: the Rb^+ ion is too small to be fixed inside the $\{Mo_9O_9\}$ rings and seems to be too large to enter into the channels (see Figure 1). Finally, the much smaller Ce^{3+} ions can enter easily into the capsule interior through the whole channel areas as in **5a**. Comparing the Ce^{3+} behavior with that of Na^+ is especially instructive: Na^+ ions are trapped within the lower part of the channels as they fit exactly into a well-defined site spanned by three oxygen atoms of three SO_4^{2-} ligands (Figure 1 and 2); on the other hand, Ce^{3+} ions are found below the channels and each is coordinated symmetrically in a bidentate fashion to only one SO_4^{2-} ligand. The 30 equivalent Ce^{3+}-type positions span an icosidodecahedron (see below). Importantly, the protonated urea cations in **6a** and also the guanidinium cations in **8a**[8] are noncovalently coordinated to the oxygen atoms of the $\{Mo_9O_9\}$ pores through hydrogen bonds in the usual way known in supramolecular chemistry;[9] a guanidinium cation analogue based on a crown-ether structure has already been described.[9]

The channels of the clusters are lined with nucleo-/hydrophilic chemical groups conducive to the passage of electrophilic (i.e., positively charged) ions:[10] ligands such as sulfate and phosphate promote cation diffusion leading to selectivity and mechanisms controlling the flux. There is also the option of different substrates coordinating simultaneously in the higher and lower parts of the "channels" along the C_3 axes in the direction of the capsule center if the cations are simultaneously present. This offers, in principle, also the possibility to study novel types of cooperativity interactions between different types of encapsulated, fixed cationic centers including paramagnetic ones. When the usual reaction system forming **1a**[2a] is treated with a strong electrolyte solution, such as NaCl in the presence of urea, the cluster anion **1a** "takes up" Na^+ ions before channel "closing" with protonated urea, and forming **6a**. This remarkable preferential trafficking depends specifically on the activity of different functional groups of the capsule.

As the channels' "clothes" can be modified by exchanging ligands attached to the 30 linkers the option exists to use different related functionalities. This is nicely demonstrated by the reaction of **3a** with phosphate ions at different pH values. At about pH 5, the acetate groups are replaced by phosphate groups leading to the formation of **2a**. But if the same reaction is performed at a lower pH (ca. 2; which leads to a partial decomposition of **2a**, that is, with some "molybdate formation"), a novel type of cavity-internal reaction occurs: a nucleation process between the phosphate ligands and the molybdate—released through the preceding reaction—takes place below the $\{Mo_9O_9\}$ rings by linking $\{MoO_3H\}$ groups to phosphate ligands under formation of

 © 2003 Wiley-VCH Verlag GmbH & Co. KGaA, Weinheim

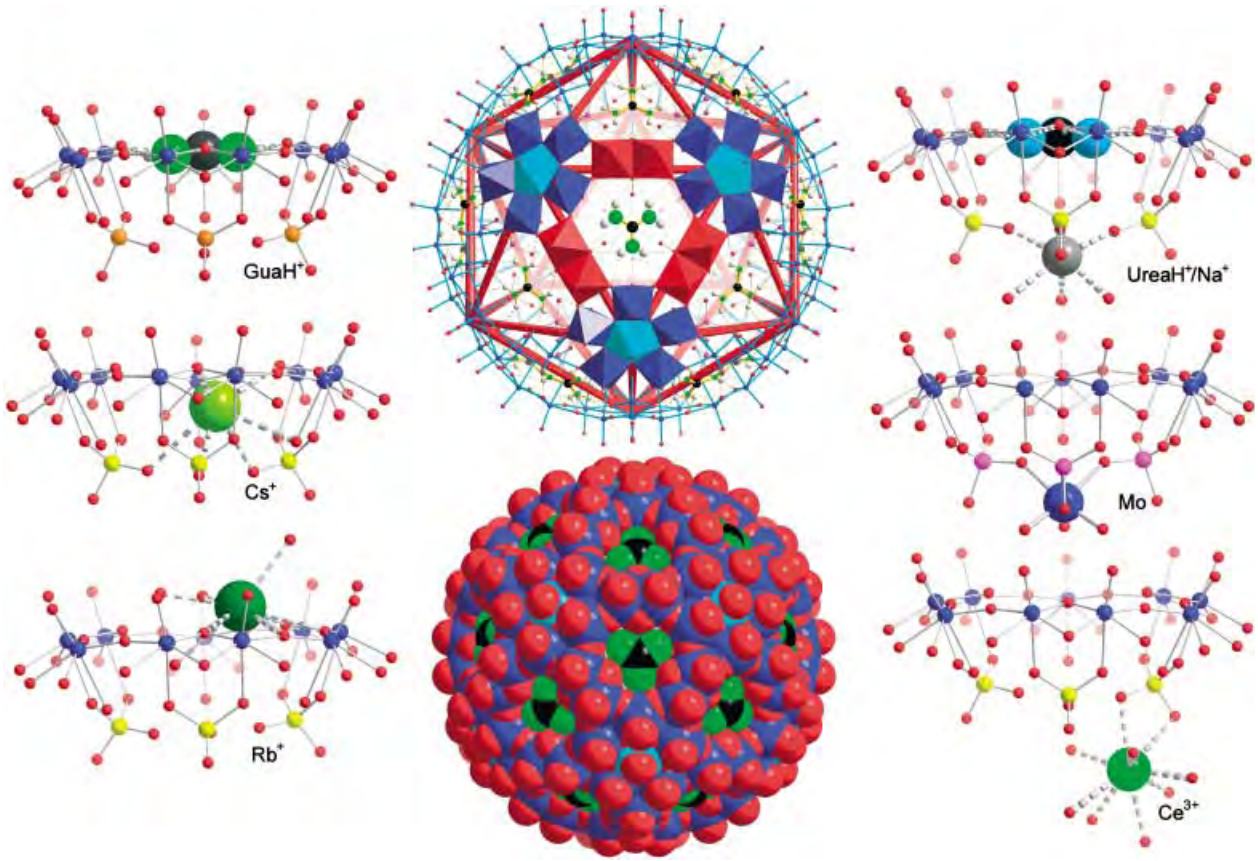


Figure 1. Cations residing at well-defined positions of the capsule of the type $[\{(Mo)Mo_5O_{21}(H_2O)_6\}_{12}\{Mo_2O_4(ligand)\}_{30}]$ with 20 pores and channels. Bottom middle: one whole capsule with guanidinium guests (space-filling); top middle: the main entering portion of one of the 20 $\{Mo_9O_9\}$ pores (with a guanidinium guest) placed on one of the 20 faces of the icosahedron spanned by the 12 central Mo atoms of the pentagonal units in polyhedral representation (see also ref. [3a]). Left and right rows: within the $\{Mo_9O_9\}$ rings/pores the protonated urea (**6a**, top right) and guanidinium cations (**8a**, top left), below, Na^+ within a channel in an environment spanned by three O atoms of three sulfate ligands (**6a**, top right), further below three O atoms of the related phosphate ligands that "fix" the Mo atom of the $\{MoO_3H\}$ group (**7a**, middle right); whereas the rather large Cs^+ ions are found approximately in the pore centers (**4a**, middle left), the small Ce^{3+} ions are positioned below the channels (**5a**, bottom right). As no specific positions are available for Rb^+ ions, these are found in a complicated distribution (only one of which is shown) at several positions even outside the capsule (bottom left). Color code: Mo blue, O red, S yellow, P violet, P/S (of **8**) brown, C black, N green; other respective substrates/cations in different colors.

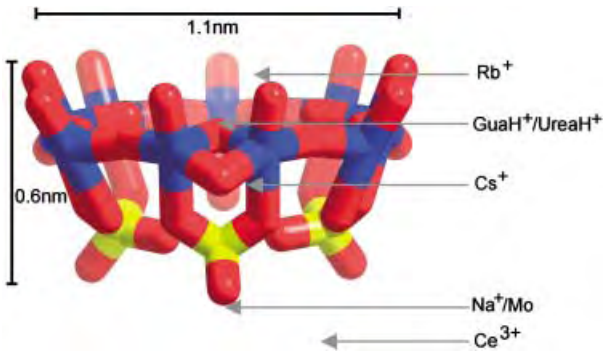


Figure 2. The relative positions of all the fixed substrates in one of the 20 channels (wire-frame representation; color code as in Figure 1).

7a.[11] As geometric constraints allow only for accommodation of up to eight $\{MoO_3H\}$ moieties exactly positioned at the C_3 axes (but according to the underoccupation only five $\{MoO_3H\}$ groups are found), this leads to the generation of a new type of interpenetrating solids in a confined spherical geometry: a cube spanned by eight characteristic $\{MoO_3H\}$-type positions inscribed within a dodecahedron (Figure 3; see also ref. [3b]). The reaction would not occur in case of **1a** with the sulfate channel type, since the relevant anion has a lower electron density at the O atoms and therefore a lower affinity to protonation which is a necessary precondition for a condensation process.

Summary and perspectives: Our capsules can be considered as nanoscale laboratories[12] with a variety of functionalities that enable the positioning of substrates/cations under controlled conditions. Additionally, cation trapping in the 20 pores and channels can be achieved stepwise and several times, respectively, with the consequence that the affinity of the positive substrates to the sites of the negative capsule changes with each cation trapping event due to the decrease of negative charge, a phenomenon which can be regarded as one of the hallmarks of nanotechnology. Interestingly, also capsules with relatively small charges (like that of **3a**) may attract cations, provided that they have a larger charge than the monopositive ones mentioned above: $[M(H_2O)_6]^{2+}$ (M =

 © 2003 Wiley-VCH Verlag GmbH & Co. KGaA, Weinheim

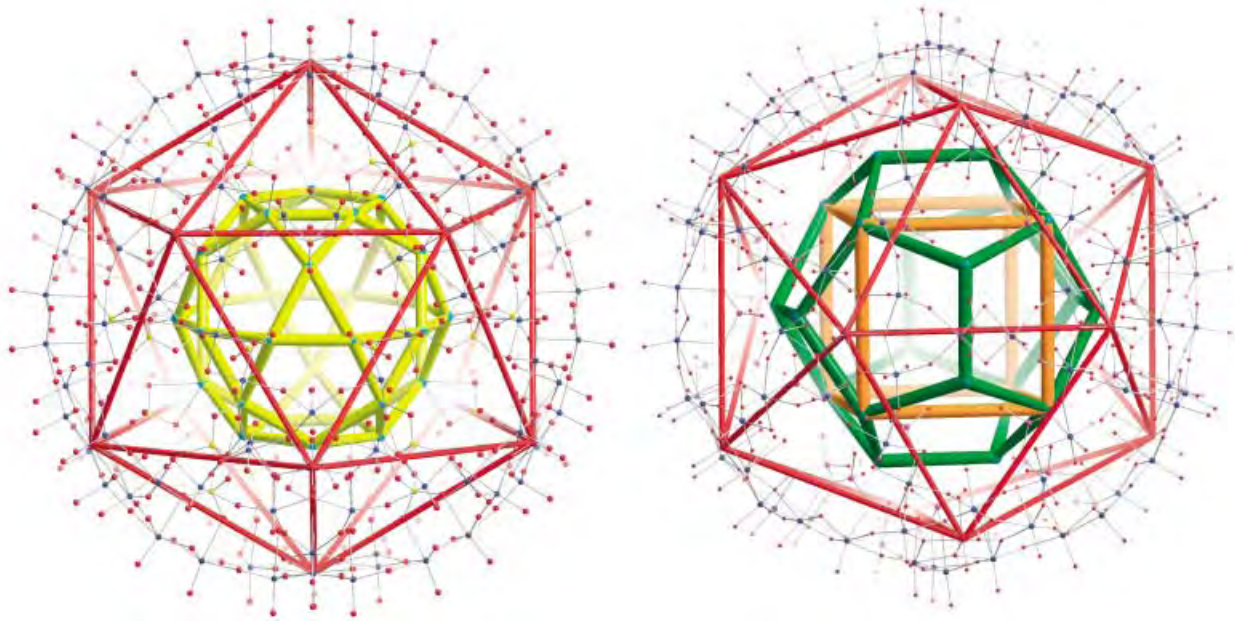


Figure 3. Interpenetrating solids within the capsules of **5a** and **7a** (ball-and-stick model; color code as in Figure 1). Right: a cube (orange) with eight (possible) $\{MoO_3H\}$-type positions as part of the 20 vertices of a dodecahedron (green) spanned by all 20 symmetry-related channel positions on the C_3 axes in **7a** (see also ref. [3b]); left: an icosidodecahedron (yellow) formed by the characteristic Ce^{3+} ion positions of **5a** which are related here to the icosahedron (red) spanned by the 12 central Mo atoms of the pentagonal units—deliberately shown in spite of underoccupation to demonstrate the option of generating different interpenetrating solids.

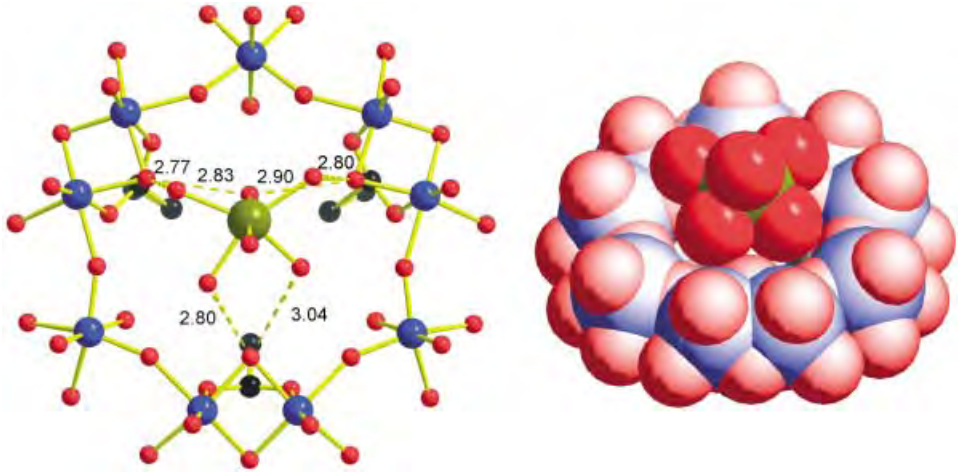


Figure 4. Ball-and-stick (with distances (Å), left) and space-filling representation (right) of one of the $[Ni(H_2O)_6]^{2+}$ complexes interacting through hydrogen bonds with one of the $\{Mo_9O_9\}$ pores of the acetate-type capsule **3a**, leading to the formation of a novel supramolecular cluster arrangement (in the compound about 16 of the 42 NH_4^+ ions of **3a** are replaced by the Ni units; color code as in Figure 1, Ni olive green).

Mg, Ca, Ni) complexes in solution[13] are attracted and fixed through formation of hydrogen bonds between their H_2O ligands and the O atoms in the capsule pores[14] (see Figure 4, which also shows relevant distances). The Ni–O–H···O interactions, that is, second-sphere coordinations, might be considered as an interesting supramolecular cluster phenomenon with perspectives for further investigations.[14] Importantly, the separation of cations in aqueous solution allows, in principle, the option of fabricating a "nano-ion chromatograph", as the "artificial cells" respond to their solute/solvent environment in a specific way. For instance, well-defined, hydrated metal ions such as the above complexes are blocked by the pores because of their size. As the reactions are performed under the conditions of nanocapsule confinement while the capsule size and charge can be precisely generated, new and basic processes may emerge that need not necessarily agree with those observed in bulk materials though also offering new insight into related bulk reactions. For example, it was found very recently that at least five water molecules were necessary to observe dissociation of HBr.[15] Our systems can, generally speaking, provide insight into the influence of geometric confinement on different substrate positionings but especially allow—because of the multitude of different types of equivalent sites—the generation of novel nanoscopic

 © 2003 Wiley-VCH Verlag GmbH & Co. KGaA, Weinheim

architectures, for example, with interpenetrating solids like a cube in a dodecahedron (see Figure 3 and refs. [3b,11]).

Experimental Section

3: Compound **3** was prepared as reported in ref. [5].

2: Compound **3** (3.0 g, 0.11 mmol) was added under constant stirring to a solution of NaH_2PO_4 (3 g, 25 mmol) and NH_4Cl (3 g, 56 mmol) in H_2O (200 mL). The pH was adjusted to ~5 with NH_4OH. The red-brown crystals that precipitated from the solution after five days were filtered off and dried at room temperature. Yield: 1.5 g. Elemental analyses (%) calcd: Na 0.9, N 3.1, P 3.6; found: Na 0.8, N 3.0, P 3.6.

4: A solution of **3** (4.0 g, 0.14 mmol) in H_2O (350 mL) was treated with cesium sulfate (16.5 g, 45.6 mmol) and was stirred at 80 °C for 3 h. The resulting reaction mixture was kept at room temperature for 24 h. The precipitated microcrystalline solid was filtered, washed with water, and dried at room temperature. After the solid was suspended in an ammonium sulfate solution (10.0 g in 350 mL), the suspension was heated at 80 °C for 10–12 min, whereby a clear solution was obtained. The solution was filtered and kept at room temperature for one week in an open 1 L beaker, and red-brown crystals of **4** precipitated. To obtain "better" crystals, the precipitate was redissolved by subsequent warming on a hot plate at 70–80 °C in the same mother liquor by adding water (130 mL), and the resulting clear solution was kept in the same open beaker for one week. The precipitated brown rhombohedral crystals, which are more suitable for a structure determination than the first precipitated crystals crystallizing in the cubic space group showing a problematical disorder, were filtered, washed with 2-propanol, and dried at room temperature. Yield: 2.1 g. Elemental analyses (%) calcd: Cs 8.7, N 2.4, S 3.1; found: Cs 8.7, N 2.5, S 3.4.

5: $CeCl_3{\cdot}7H_2O$ (10.0 g, 26.8 mmol) was added after 1.5 h to a refluxing solution of **3** (5.0 g, 0.18 mmol) and ammonium sulfate (15.0 g, 113.5 mmol) in H_2O (400 mL). The resulting solution was refluxed for 30 min and filtered hot. The dark brown crystals of **4** that precipitated after one day were filtered, washed with ice-cold 2-propanol, and dried in air. Yield: 4.4 g. Elemental analyses (%) calcd: Ce 2.9, N 2.6, S 3.2; found: Ce 2.6, N 3.0, S 3.6.

6: A mixture of **3** (0.5 g, 0.02 mmol), urea (1.0 g, 16.7 mmol), $(NH_4)_2SO_4$ (2.5 g, 18.9 mmol), H_2O (40 mL), and 16% HCl (8 mL) in a 100-mL Erlenmeyer flask (covered with a watch-glass) was heated to 60–70 °C. After 90 min, NaCl (3.0 g, 51.3 mmol) was added and the solution was heated for 90 min and then kept at room temperature. After 3–4 days brown rhombohedral crystals of **6** were filtered off, washed with a small amount of ice-cold water, then with ice-cold 2-propanol, and dried in air. Yield: 0.35 g. Elemental analyses (%) calcd: Na 1.9, C 1.9, N 4.6; found: Na 2.1, C 1.8, N 4.6.

7: Compound **3** (3.0 g, 0.11 mmol) was added under constant stirring (15 min) to a solution of $NH_4H_2PO_4$ (3 g, 26 mmol), NH_4Cl (3 g, 56 mmol) and HCl (15 mL, 1M) in H_2O (200 mL). After the solution was kept in an open beaker at room temperature for seven days, the precipitated red-brown crystals of **7** were filtered off and dried at room temperature. Yield: 2.0 g. Elemental analyses (%) calcd: N 2.8, P 3.9; found: N 2.8, P 3.9.

The chemical formulas refer to the maximum number of water molecules in the crystal, which is in agreement with the cell volume. According to the observed loss of water the analytical data, however, refer to this number of crystal water molecules minus 50.

Received: July 11, 2003 [Z52358]
Published Online: October 8, 2003

Keywords: confined geometries · encapsulation · ion transport/uptake · nanotechnology · porous materials

[1] a) *Handbook of Porous Solids* (Eds.: F. Schüth, K. S. W. Sing, J. Weitkamp), Wiley-VCH, Weinheim, **2002**; b) M. A. White, *Properties of Materials*, Oxford University Press, New York, **1999**, chap.: Inclusion Compounds; c) G. Férey, *Science* **2001**, *291*, 994–995.

[2] a) A. Müller, E. Krickemeyer, H. Bögge, M. Schmidtmann, B. Botar, M. O. Talismanova, *Angew. Chem.* **2003**, *115*, 2131–2136; *Angew. Chem. Int. Ed.* **2003**, *42*, 2085–2090; b) A. Müller, E. Krickemeyer, H. Bögge, M. Schmidtmann, F. Peters, *Angew. Chem.* **1998**, *110*, 3567–3571; *Angew. Chem. Int. Ed.* **1998**, *37*, 3360–3363.

[3] a) A. Müller, P. Kögerler, C. Kuhlmann, *Chem. Commun.* **1999**, 1347–1358; b) A. Müller, *Science* **2003**, *300*, 749–750. c) The term stability refers here to the fact that at least in the final product always the same type of well-defined capsules are found with the expected functionalities after reactions have taken place in solution. But, in principle, it cannot be excluded that in solution the pores, that is, the $\{Mo_9O_9\}$ rings, are opened slightly during uptake. Related solution NMR studies concerning the stability and reaction pathways are currently possible and are in progress (F. Taulelle, M. Henry, A. Müller; see also ref. [5]).[16]

[4] See also related discussion in: M. Gross, *Chem. Br.* **2003**, *39* (August Issue), p. 18. As the cations entering through the gates are not randomly distributed in the cell interior but fixed at functionalities according to their specific properties, thus relatively reducing the whole capsule system entropy, a situation results that is formally comparable to that of "Maxwell's Demon", but acting in a closed system (the related Gedanken experiment is for instance explained in textbooks of Statistical Thermodynamics and even in *The New Encyclopaedia Britannica, Vol. 23*, 15th ed., Encyclopaedia Britannica, Chicago, **2002**, p. 692, including the statement: "The hypothetical intelligent being known as Maxwell's demon was a factor in the development of information theory"). See also: M. Gross, *Travels to the Nanoworld: Miniature Machinery in Nature and Technology*, Perseus Publishing, Cambridge, Massachusetts, **2001** (Chapter: Maxwell's demon—a predecessor of nanotechnology?); D. E. H. Jones, *Nature* **1995**, *374*, 835–837.

[5] Both are formed by ligand exchange from **3a**, which is available in facile syntheses according to: L. Cronin, E. Diemann, A. Müller in *Inorganic Experiments* (Ed.: J. D. Woollins), 2nd ed., Wiley-VCH, Weinheim, **2003**, pp. 340–346 and A. Müller, S. K. Das, E. Krickemeyer, C. Kuhlmann, *Inorg. Synth.* **2003**, *34*, in press. The sulfate cluster anion **1a**[2a] with the high charge of 72− is formed from **3a** in situ in solution during the processes leading to **4a, 5a**, and **6a**, which can also be obtained by starting from solutions of crystalline **1**. Important in context with footnote [3] is that **1a** can be obtained by ligand exchange from **3a** without heating, that is at room temperature and under low pH conditions which supports the release of the leaving group acetic acid.

[6] Crystal data for **2**: $H_{1038}Mo_{132}N_{64}Na_{12}O_{880}P_{34}$, $M_r = 30015.89\ g\,mol^{-1}$, cubic space group $Fm\bar{3}$, $a = 45.6162(12)$ Å, $V = 94920(4)$ Å^3, $Z = 4$, $\rho = 2.100\ g\,cm^{-3}$, $\mu = 1.862\ mm^{-1}$, $F(000) = 58848$, crystal size $= 0.24 \times 0.24 \times 0.24\ mm^3$. A total of 120764 reflections ($0.77 < \Theta < 25.02°$) were collected, of which 7311 reflections were unique ($R(int) = 0.0578$). $R = 0.0832$ for 4974 reflections with $I > 2\sigma(I)$, $R = 0.1464$ for all reflections, max./min. residual electron density 1.316 and $-1.715\ e\,Å^{-3}$. Crystal data for **4**: $H_{914}Cs_{20}Mo_{132}N_{52}O_{845}S_{30}$, $M_r = 31453.91\ g\,mol^{-1}$, rhombohedral space group $R\bar{3}$, $a = 32.7258(8)$, $c = 73.664(3)$ Å, $V = 68323(3)$ Å^3, $Z = 3$, $\rho = 2.293\ g\,cm^{-3}$, $\mu = 2.725\ mm^{-1}$, $F(000) = 45486$, crystal size $= 0.25 \times 0.20 \times 0.15\ mm^3$. A total of 188827 reflections ($0.77 < \Theta < 30.01°$) were collected, of which 44291 reflections were unique ($R(int) = 0.0564$). $R = 0.0498$ for 32184 reflections with

 © 2003 Wiley-VCH Verlag GmbH & Co. KGaA, Weinheim

$I > 2\sigma(I)$, $R = 0.0789$ for all reflections, max./min. residual electron density 2.369 and $-1.403\ e\,Å^{-3}$. Crystal data for **5**: $H_{960}Ce_6Mo_{132}N_{54}O_{864}S_{30}$, $M_r = 30014.82\ g\,mol^{-1}$, rhombohedral space group $R\bar{3}$, $a = 32.7411(7)$, $c = 73.682(2)$ Å, $V = 68404(3)$ Å^3, $Z = 3$, $\rho = 2.186\ g\,cm^{-3}$, $\mu = 2.229\ mm^{-1}$, $F(000) = 43866$, crystal size $= 0.40 \times 0.25 \times 0.20\ mm^3$. A total of 136090 reflections ($0.77 < \Theta < 27.02°$) were collected, of which 33123 reflections were unique ($R(\text{int}) = 0.0277$). $R = 0.0424$ for 27495 reflections with $I > 2\sigma(I)$, $R = 0.0559$ for all reflections, max./min. residual electron density 2.242 and $-1.215\ e\,Å^{-3}$. Crystal data for **6**: $C_{48}H_{784}Mo_{132}N_{96}Na_{24}O_{812}S_{30}$, $M_r = 29881.35\ g\,mol^{-1}$, rhombohedral space group $R\bar{3}$, $a = 32.8028(5)$, $c = 73.948(2)$ Å, $V = 68910(2)$ Å^3, $Z = 3$, $\rho = 2.160\ g\,cm^{-3}$, $\mu = 1.933\ mm^{-1}$, $F(000) = 43584$, crystal size $= 0.25 \times 0.25 \times 0.15\ mm^3$. A total of 190772 reflections ($0.77 < \Theta < 30.02°$) were collected, of which 44749 reflections were unique ($R(\text{int}) = 0.0358$). $R = 0.0395$ for 36437 reflections with $I > 2\sigma(I)$, $R = 0.0556$ for all reflections, max./min. residual electron density 2.527 and $-1.426\ e\,Å^{-3}$. Crystal data for **7**: $H_{1050}Mo_{137}N_{60}O_{911}P_{38}$, $M_r = 30795.64\ g\,mol^{-1}$, cubic space group $Fm\bar{3}$, $a = 45.6587(12)$ Å, $V = 95186(4)$ Å^3, $Z = 4$, $\rho = 2.149\ g\,cm^{-3}$, $\mu = 1.925\ mm^{-1}$, $F(000) = 60328$, crystal size $= 0.24 \times 0.24 \times 0.24\ mm^3$. A total of 118119 reflections ($0.77 < \Theta < 25.03°$) were collected, of which 7327 reflections were unique ($R(\text{int}) = 0.0643$). $R = 0.0883$ for 5296 reflections with $I > 2\sigma(I)$, $R = 0.1371$ for all reflections, max./min. residual electron density 1.701 and $-1.782\ e\,Å^{-3}$. Crystals of **2, 4, 5, 6**, and **7** were removed from the mother liquor and immediately cooled to 173–193 K on a Bruker AXS SMART diffractometer (three-circle goniometer with 1 K CCD detector, $Mo_{K\alpha}$ radiation, graphite monochromator; hemisphere data collection in ω at 0.3° scan width in three runs with 606, 435, and 230 frames ($\phi =$ 0, 88, and 180°) at a detector distance of 4.0–5.0 cm). For all structures empirical absorption corrections were performed by using equivalent reflections with the program SADABS 2.03. The structures were solved with the program SHELXS-97 and refined by using SHELXL-93. (SHELXS/L, SADABS from G. M. Sheldrick, University of Göttingen (Germany) **1993/97**; structure graphics with DIAMOND 2.1 from K. Brandenburg, Crystal Impact GbR, **2001**). Further details of the crstal structure investigations can be obtained from the Fachinformationszentrum Karlsruhe, 76344 Eggenstein-Leopoldshafen, Germany, (fax: (+49)7247-808-666; e-mail: crysdata@fiz.karlsruhe.de) on quoting the depository numbers CSD-413251 (**2**), CSD 413252 (**4**), CSD 413253 (**5**), CSD 413254 (**6**) and CSD 413255 (**7**).

[7] a) Characteristic IR bands (solid, KBr pellet, $\tilde{\nu}$) for compounds **1–8** due to presence of the [{(Mo)Mo_5}$_{12}${Mo_2}$_{30}$]-type skeleton (variations $\pm 3\ cm^{-1}$): 970s, [ν(Mo=O)], 860m, 800vs, 725vs, 570s; **2** shows additionally bands at 1107, 1050, 1009 [ν(P–O)] and **4, 5, 6** at 1140 (m), 1035 cm^{-1} (w–m, $\nu_{as}(SO_4)$); **6** shows weak urea bands and **2, 4, 5, 7** the $\delta(NH_4)$ bands at $\approx 1400\ cm^{-1}$. b) ^{31}P MAS NMR spectra allow us to distinguish between the "phosphates" coordinated as ligands and those abundant in the crystal lattice.

[8] A. Müller, E. Krickemeyer, H. Bögge, M. Schmidtmann, S. Roy, A. Berkle, *Angew. Chem.* **2002**, *114*, 3756–3761; *Angew. Chem. Int. Ed.* **2002**, *41*, 3604–3609.

[9] J.-M. Lehn, *Supramolecular Chemistry: Concepts and Perspectives*, VCH, Weinheim, **1995**, p. 28.

[10] For the transport of the cations through biological membranes, negatively charged amino acids play a key role; see: D. Voet, J. G. Voet, *Biochemistry*, 2nd ed., Wiley, New York, **1995**, chap. 18.

[11] The situation is comparable to the formation of P-O-Mo bonds during the synthesis of the $[PMo_{12}O_{40}]^{3-}$ Keggin anion at low pH values. In **7a** the phosphate ligands, instead of being positioned exactly below the {Mo_2} groups, "are oriented" slightly towards the {MoO_3H} group. Consequently, a {MoO_3H} moiety is not found in all 20 channels/sites, hence not a dodecahedron is generated by 20 {MoO_3H} groups but "only" a cube with eight of these can be formed. (This can be visualized as only two of each of the dodecahedral pentagon vertices can be involved as sites for {MoO_3H}. As three pentagonal faces are connected at each vertex this leads to a total number of $8 = (12 \times 2)/3$ positions; see Figure 3).

[12] For related topics see: a) K. E. Drexler, *Nanosystems: Molecular Machinery, Manufacturing, and Computation*, Wiley, New York, **1992**; b) *Recent Advances in the Chemistry of Nanomaterials* (Eds.: C. N. R. Rao, A. Müller, A. K. Cheetham), Wiley-VCH, Weinheim, in press; c) P. Ball, *Made to Measure*: *New Materials for the 21st Century*, Princeton University Press, Princeton, **1997**; regarding the importance of pores see also: d) J. Tersoff, *Nature* **2001**, *412*, 135–136.

[13] D. T. Richens, *The Chemistry of Aqua Ions*, Wiley, Chichester, **1997** (Ni^{2+} has a well-defined, rather strongly bonded primary hydration sphere in aqueous solution, for example, compared to Ce^{3+}).

[14] The phenomenon of trapping aqueous solutes/complexes will be studied separately: A. Müller, Y. Zhou, L. Zhang, L. Toma, H. Bögge, M. Schmidtmann, unpublished results.

[15] A. F. Voegele, K. R. Liedl, *Angew. Chem.* **2003**, *115*, 2162–2164; *Angew. Chem. Int. Ed.* **2003**, *42*, 2114–2116.

[16] **Note added in proof** (Setember 24, 2003): According to new NMR investigations (F. Taulelle, M. Henry, A. Müller) the stability of the capsule in solution is very high. Furthermore the exchange of the acetate ligands of the starting material **3a** is easily possible under low pH conditions (see also ref. [5]).

 © 2003 Wiley-VCH Verlag GmbH & Co. KGaA, Weinheim

Oxy-Cope Reaction Mechanism

On the Mechanism of the Anionic Oxy-Cope Rearrangement of *trans*-1,2-Dialkenylcyclobutanols**

*Philippe Maurin, Se-Ho Kim, Sung Yun Cho, and Jin Kun Cha**

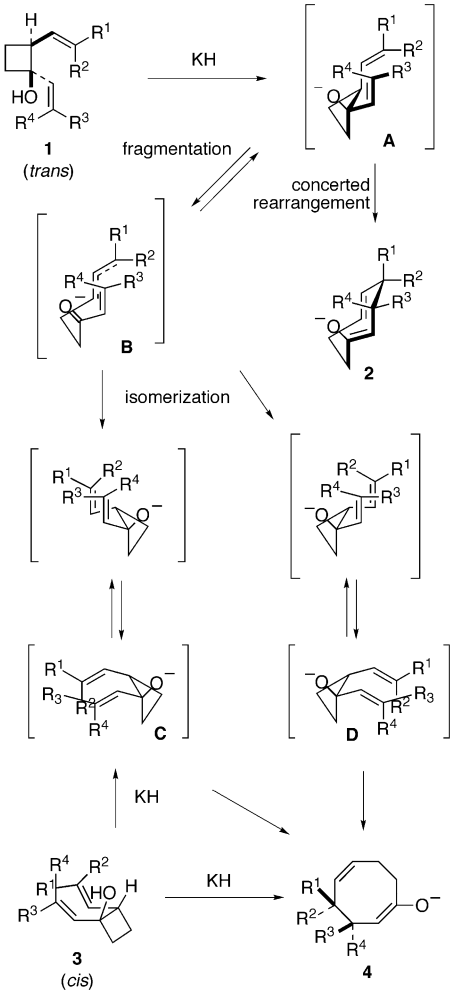
Sigmatropic rearrangements have frequently been utilized in the stereoselective construction of multiple stereocenters of easily predictable relative and absolute configurations. Among them, the anionic oxy-Cope rearrangement has evolved as a powerful tool for stereoselective syntheses because of dramatic rate acceleration.[1–3] Of particular note is the variant for ring expansion leading to medium-sized rings

[*] Prof. J. K. Cha, Dr. P. Maurin, S.-H. Kim, S. Y. Cho
Department of Chemistry
University of Alabama
Tuscaloosa, AL 35487
and
Department of Chemistry
Wayne State University
Detroit, MI 48202 (USA)
Fax: (+1) 313-577-8822
E-mail: jcha@chem.wayne.edu.

[**] This work was supported by the National Institutes of Health (GM35956) and the National Science Foundation (CHE02-09321).

 © 2003 Wiley-VCH Verlag GmbH & Co. KGaA, Weinheim DOI: 10.1002/anie.200350988

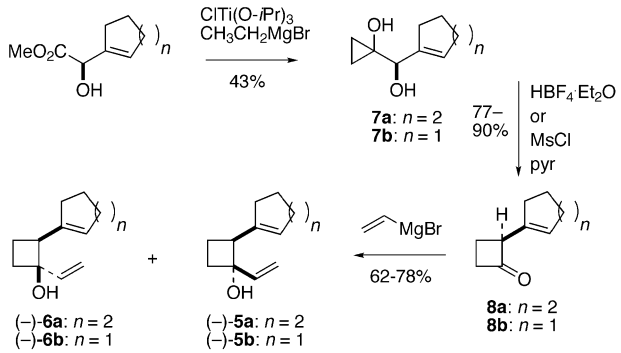
by employing 1,2-dialkenylcycloalkanols.[4] Adaptation of this variant to smaller rings (e.g., cyclopropanols and cyclobutanols) has provided unique avenues for the stereocontrolled construction of seven- and eight-membered rings.[5,6] A majority of ingenious and notable applications have relied on *cis*-1,2-dialkenylcyclopropanols and -cyclobutanols (**3**→**C**→**4**; Scheme 1).[1] In sharp contrast, only a handful of



Scheme 1. Concerted and stepwise pathways of the anionic oxy-Cope rearrangement of *trans*-1,2-dialkenylcyclobutanols.

examples are known for anionic oxy-Cope rearrangements of *trans*-cyclobutanols;[6] the feasibility of a concerted rearrangement (**1**→**A**→**2**) was considered by Gadwood et al., but discounted on the basis of the apparent difficulty of bringing the reacting termini within bonding distance.[6a,7] It has since become generally accepted that rearrangement of *trans*-1,2-dialkenylcyclobutanols to 4-cyclooctenones proceeds by a stepwise mechanism involving initial isomerization to the *cis* isomers (**A**→**B**→**C** and/or **A**→**B**→**D**) and subsequent anionic oxy-Cope rearrangement (**C** and/or **D**→**4**). However, there is no conclusive stereochemical information available. Here we report a stereochemical study which employs nonracemic *trans*-1,2-dialkenylcyclobutanols and supports a concerted anionic oxy-Cope rearrangement.

Nonracemic **5a,b** and **6a,b** were chosen to probe the key issue of the concertedness of the rearrangement. If a stepwise pathway were operative in the anionic oxy-Cope rearrangement of *trans*-1,2-dialkenylcyclobutanols, the products could become racemic, as the *trans*→*cis* isomerization step might proceed (via **B**) with racemization.[8] Additionally, the stereochemistry of the products (e.g., **2** versus **4**) should provide decisive insight into the reaction mechanism. The cyclohexene and cyclopentene rings were chosen as one of the alkenyl groups in the stereochemical studies, since eight-membered carbocyclic rings that are found in bioactive natural products are typically embedded in fused polycyclic systems.[9] 2-Cycloalkenylcyclobutanones **8a,b** were prepared by titanium-mediated cyclopropanation of enantiomerically enriched α-hydroxy esters with ethylmagnesium bromide, followed by a pinacol-type rearrangement of the resulting cyclopropanols **7a,b** (Scheme 2).[10] Treatment of ketone **8a**

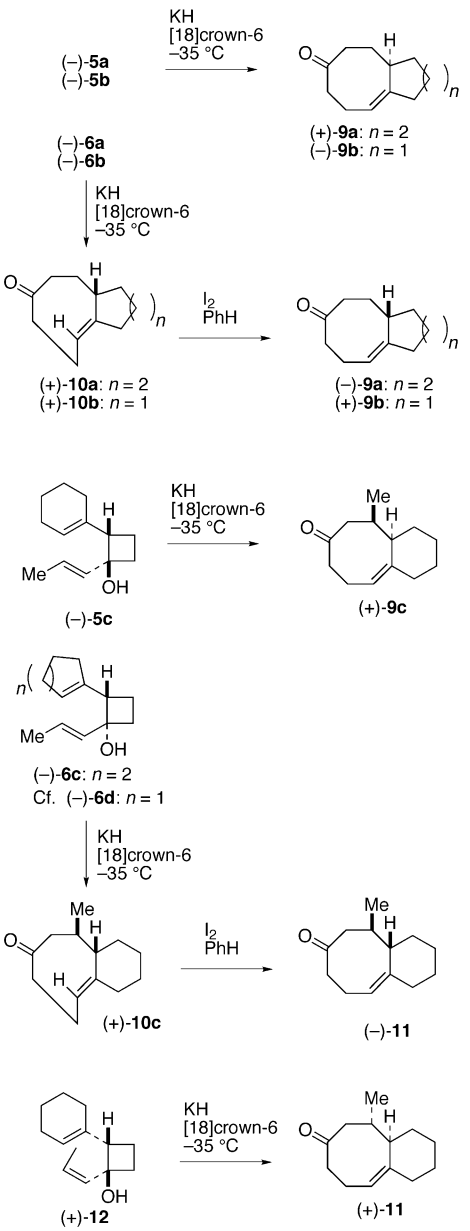


Scheme 2. Preparation of *cis*- and *trans*-1,2-dialkenylcyclobutanols.

with vinylmagnesium bromide in THF at −40 °C afforded an easily separable 1:25 mixture of (−)-**5a** and (−)-**6a** in 78% yield and 92% *ee* (Chiralcel). Similarly, a 1:20 mixture of (−)-**5b** and (−)-**6b** was obtained in 62% yield from **8b**.[11] As a control experiment, anionic oxy-Cope rearrangement of (−)-*cis*-**5a** was first carried out (5.0 equiv KH, 2.5 equiv [18]crown-6, THF, 5 min) at −35 °C to furnish (+)-**9a** ($[\alpha]_D = +83.4$, $c = 0.3$ in CH_2Cl_2) in 75–79% yield and 92% *ee* (Scheme 3).[12,13a] Sigmatropy of *cis*-1,2-dialkenylcyclobutanes and cyclobutanols has been well established to favor boatlike transition states in a concerted reaction. Under similar conditions, the rearrangement of (−)-**6a** gave (+)-**10a** ($[\alpha]_D = +103.0$, $c = 1.1$ in CH_2Cl_2) in 84–90% yield and 88% *ee* (i.e., 96% chirality transfer from (−)-**6a** of 92% *ee*). The absolute configuration of (+)-**10a** was determined by its facile isomerization (91%) by treatment with I_2 (ambient light) to (−)-**9a** ($[\alpha]_D = -80.9$, $c = 1.0$ in CH_2Cl_2). The latter product was thus enantiomeric to the rearrangement product of (−)-**5a**.[14]

The cognate rearrangement of (−)-**5b** and (−)-**6b** was next examined. Analogous to the anionic oxy-Cope rearrangement of (−)-**5a**, that of (−)-**5b** afforded (−)-**9b**,[13b] in 70% yield and 92% *ee*. Under the same conditions, rearrangement of (−)-**6b** yielded a 4.7:1:0.2 mixture (GC-MS) of (+)-**10b** ($[\alpha]_D = +43.4$, $c = 0.5$ in CH_2Cl_2; 89% *ee*, 97% chirality transfer), racemic **9b**, and an unidentified by-product

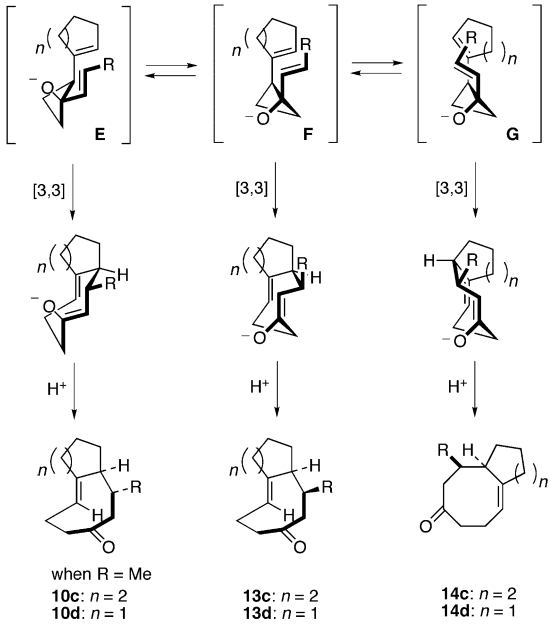
 © 2003 Wiley-VCH Verlag GmbH & Co. KGaA, Weinheim



Scheme 3. Anionic oxy-Cope rearrangements of *cis*- and *trans*-dialkenylcyclobutanols.

in a total yield of 63–68 %.[15a,b] The product ratios of (+)-**10b** to (±)-**9b** appeared to be kinetic in origin, since the reaction time (e.g., 30 s and 2 min at −35 °C) had only a small influence on these ratios. Additionally, (+)-**10b** remained unchanged when resubjected to the rearrangement conditions. Finally, treatment of (+)-**10b** with I_2 resulted in facile isomerization to (+)-**9b**. Formation of (±)-**9b** indicates that initial isomerization to the *cis*-dialkenylcyclobutanol isomer is accompanied by racemization (**A**→**B**→**C** and **D**). The observations that the oxyanionic Cope rearrangement of (−)-**6b** gave (+)-**10b** with no loss of enantiopurity, yet racemic **9b** was formed, raises an interesting question about the epimerization step: Does fragmentation/recombination lead to exclusive formation of the *cis* isomer with racemization, or to the cogeneration of both *cis* and *trans* isomers, but with different degrees of racemization?[16] As reversion of **B** to the starting alkoxide would require very little motion or rotation of bonds, **B** may well revert to **A** with no loss of enantiopurity.[8]

High degrees of chirality transfer in the above-mentioned formation of (+)-**10a** and (+)-**10b** from (−)-**6a** and (−)-**6b**, respectively, provides strong evidence for a concerted mechanism. Among three possible transition states **E, F**, and **G** (Scheme 4), the observed *E* double-bond geometry of (+)-



Scheme 4. Analysis of three possible transition states **E**–**G**.

10a and (+)-**10b** ruled out the involvement of **G** (Scheme 4). To distinguish between the two remaining transition states **E** and **F**, diastereoselectivity was next examined by employing an (*E*)-propenyl substituent. Thus, (−)-**5c**, (−)-**6c**, (−)-**6d**, and (+)-**12** were prepared from **8a,b** in a manner analogous to Scheme 2. The anionic oxy-Cope rearrangement of (−)-**5c** afforded (+)-**9c** ($[\alpha]_D = +56.7$, $c = 0.7$ in CH_2Cl_2) in 78 % yield and with 92 % *ee* (≈100 % chirality transfer) under the above-mentioned conditions, whereas that of (−)-**6c** gave an approximately 2:1 mixture of (+)-**10c** (38 %; $[\alpha]_D = +29.1$, $c = 0.6$ in CH_2Cl_2; 91 % *ee* ≡ 99 % chirality transfer) and **9c** (20 %; ≈10 % *ee* by comparison of $[\alpha]_D$ values). The relative configuration of (+)-**10c** was unequivocally determined by X-ray analysis,[17] and its absolute configuration was established by its facile isomerization (91 %) to (−)-**11** ($[\alpha]_D = -28.1$, $c = 0.3$ in CH_2Cl_2) on exposure to I_2 (ambient light). This product was diastereomeric to (+)-**9c**, but enantiomeric to the rearrangement product (+)-**11** ($[\alpha]_D = +30.2$, $c = 0.6$ in CH_2Cl_2; 83 % yield) of the (*Z*)-propenyl substrate (+)-**12**. The diastereoselective formation of (+)-**10c** provides compelling evidence for the involvement of a chairlike transition state **E** (cf. **A**).[18]

Surprisingly, the anionic oxy-Cope rearrangement of (−)-**6d** failed to provide the (*E*)-cyclooctenone product, but the (Z)-cyclooctenone isomer (43 %; ≈32 % *ee*) was instead isolated, along with a product of [1,3]-sigmatropic rearrange-

 © 2003 Wiley-VCH Verlag GmbH & Co. KGaA, Weinheim

ment (10%). The above-mentioned angle strain and the methyl substituent might conspire to alter the mechanism in favor of a stepwise rearrangement pathway. With an increasing number of substituents at the double bonds, the difference in activation barrier between a concerted rearrangement and a stepwise pathway appears to become smaller; a delicate balance between the two mechanisms seems to depend on substitution patterns of the double bonds and could be easily tipped toward the latter mechanism for sterically hindered substrates. Further corroboration of the substituent effects is being sought by employing acylic alkenyl substituents.

In summary, we have shown that the anionic oxy-Cope rearrangement of sterically unencumbered *trans*-1,2-dialkenylcyclobutanols proceeds by a concerted mechanism with an excellent degree of chirality transfer, attributable to a chair-like transition state. On the other hand, the presence of substituents in the reacting termini results in partitioning between the concerted and stepwise pathways.

Experimental Section

Preparation of (+)-**10a**: A solution of (−)-**6a** (69 mg, 0.39 mmol) and [18]crown-6 (255 mg, 0.97 mmol) in THF (10 mL) was added to a suspension of potassium hydride (washed in hexane; 68 mg, 1.94 mmol) in THF (10 mL) at −35 °C. The reaction mixture was stirred for 10–15 min at the same temperature and then quenched with saturated aqueous NH_4Cl at −60 °C. The resulting mixture was allowed to warm to 0 °C and extracted with diethyl ether. The combined extracts were washed with H_2O, dried with $MgSO_4$, filtered, and concentrated. Purification of the concentrate by column chromatography (4% diethyl ether in hexane) afforded 59 mg (86%) of (+)-**10a**: $[\alpha]_D = +103.0$ ($c = 1.1$ in CH_2Cl_2); IR (neat): $\tilde{\nu} = 1699, 1449, 1432, 1098\ cm^{-1}$; ^1H NMR (360 MHz, $CDCl_3$, TMS): $\delta = 5.81$ (br d, $J(H,H) = 11.8$ Hz; 1H), 2.93–2.80 (m, 2H), 2.52 (td, $J(H,H) = 12.9, 1.7$ Hz; 1H), 2.40–2.14 (m, 5H), 2.07 (dd, $J(H,H) = 12.9, 5.6$ Hz; 1H), 1.78–1.41 (m, 7H), 1.15 ppm (m, 1H); ^{13}C NMR (90 MHz, $CDCl_3$): $\delta = 214.3, 141.5, 125.6, 48.6, 44.8, 44.3, 31.9, 28.9$ (two peaks), 26.2, 25.2, 21.5 ppm; HRMS [M^+] calcd for $C_{12}H_{18}O$: 178.1358; found: 178.1341.

Received: January 22, 2003 [Z50988]

Keywords: diastereoselectivity · reaction mechanisms · sigmatropic rearrangement · substituent effects · transition states

[1] For recent reviews, see a) L. A. Paquette, *Tetrahedron* **1997**, *53*, 13971; b) L. A. Paquette, *Chem. Soc. Rev.* **1995**, *24*, 9.
[2] a) J. J. Bronson, R. L. Danheiser in *Comprehensive Organic Synthesis, Vol. 5* (Eds.: B. M. Trost, I. Fleming), Pergamon, Oxford, **1991**, pp. 999–1035; b) S. R. Wilson, *Org. React.* **1993**, *43*, 93.
[3] D. A. Evans, A. M. Golob, *J. Am. Chem. Soc.* **1975**, *97*, 4765.
[4] a) W. C. Still, *J. Am. Chem. Soc.* **1977**, *99*, 4186; b) W. C. Still, *J. Am. Chem. Soc.* **1979**, *101*, 2493.
[5] a) J. P. Marino, T. Kaneko, *J. Org. Chem.* **1974**, *39*, 317; b) P. A. Wender, M. A. Eissenstat, M. P. Filosa, *J. Am. Chem. Soc.* **1979**, *101*, 2196; c) E. Piers, H. E. Morton, I. Nagakura, R. W. Thies, *Can. J. Chem.* **1983**, *61*, 1226; d) J. Lee, H. Kim, J. K. Cha, *J. Am. Chem. Soc.* **1995**, *117*, 9919.
[6] a) R. C. Gadwood, R. M. Lett, *J. Org. Chem.* **1982**, *47*, 2268; b) R. C. Gadwood, R. M. Lett, J. E. Wissinger, *J. Am. Chem. Soc.* **1986**, *108*, 6343; c) S. A. Miller, R. C. Gadwood, *J. Org. Chem.* **1988**, *53*, 2214; d) T. A. Lyle, H. B. Mereyala, A. Pascual, B. Frei, *Helv. Chim. Acta* **1984**, *67*, 774; e) P. A. Zucker, J. A. Lupia, *Synlett* **1990**, 729. See also f) M. Kahn, *Tetrahedron Lett.* **1980**, *21*, 4547; g) S. G. Levine, R. L. McDaniel, Jr., *J. Org. Chem.* **1981**, *46*, 2199; h) R. Huston, M. Rey, A. S. Dreiding, *Helv. Chim. Acta* **1982**, *65*, 451; i) R. L. Danheiser, S. K. Gee, H. Sard, *J. Am. Chem. Soc.* **1982**, *104*, 7670.
[7] The respective cyclobutanes were found to be recalcitrant toward the Cope rearrangement, but reacted predominantly by a [1,3]-sigmatropic rearrangement at elevated temperatures. a) J. A. Berson, P. B. Dervan, *J. Am. Chem. Soc.* **1972**, *94*, 7597; b) J. A. Berson, P. B. Dervan, *J. Am. Chem. Soc.* **1972**, *94*, 8949; c) J. A. Berson, P. B. Dervan, *J. Am. Chem. Soc.* **1973**, *95*, 267 and J. A. Berson, P. B. Dervan, *J. Am. Chem. Soc.* **1973**, *95*, 269.
[8] In light of our recent observation of an oxyanionic [1,3]-sigmatropic rearrangement of nonracemic *cis*-2-(1-cyclohexenyl)cyclobutanols, however, there is the intriguing possibility that the *trans*→*cis* isomerization step might possibly take place with retention of configuration at the allylic carbon atom: S.-H. Kim, S. Y. Cho, J. K. Cha, *Tetrahedron Lett.* **2001**, *42*, 8769.
[9] a) N. A. Petasis, M. A. Patane, *Tetrahedron* **1992**, *48*, 5757; b) G. Mehta, V. Singh, *Chem. Rev.* **1999**, *99*, 881.
[10] a) S. Y. Cho, J. K. Cha, *Org. Lett.* **2000**, *2*, 1337; b) Unless pinacol rearrangement of **7a,b** was performed under carefully controlled conditions, a varying degree of racemization was observed. See also c) H. Nemoto, K. Fukumoto, *Synlett* **1997**, 863.
[11] a) On a silica gel column or on standing at room temperature, **6b** slowly underwent retro-ene ring opening. However, the retro-ene reaction was readily curtailed by storage at −25 °C or below. See also b) J. P. Barnier, J. Ollivier, J. Salaun, *Tetrahedron Lett.* **1989**, *30*, 2525; c) R. D. Rieke, M. S. Sell, H. Xiong, *J. Am. Chem. Soc.* **1995**, *117*, 5429.
[12] An excess of KH was employed to ensure reliable reproducibility. All rearrangement reactions were performed at least three times. Ranges or averages of these multiple experiments are given for yields and optical rotations.
[13] The spectroscopic data for (+)-**9a** and (+)-**9b** were identical to those reported for racemic compounds: **9a**: a) C. M. G. Phillippo, N. H. Vo, L. A. Paquette, *J. Am. Chem. Soc.* **1991**, *113*, 2762; L. A. Paquette, C. M. G. Phillippo, N. H. Vo, *Can. J. Chem.* **1992**, *70*, 1356; **9b**: b) W. A. Kinney, M. J. Coghlan, L. A. Paquette, *J. Am. Chem. Soc.* **1985**, *107*, 7352.
[14] Comparable results (chirality transfer and yield) were also obtained by using *N,N*-dimethyl-*N,N'*-propylene urea (DMPU) instead of [18]crown-6. Even in the absence of a complexing agent, the rearrangement took place smoothly, but small amounts of other unidentified by-products were obtained.
[15] a) Because of the UV absorption of (+)-**10a**, (+)-**10b**, and (+)-**10c**, their enantiomeric purity was readily determined by HPLC analysis (Chiralcel OB column). b) The surprisingly unfavorable product ratio in the rearrangement of (−)-**6b** might be in part attributable to the higher activation energy leading to **10b** compared to **10a**, which is a consequence of the greater angle strain of the double bond exocyclic to the cyclopentane ring, compared to that for a cyclohexane ring.
[16] We thank Prof. Edwin Vedejs (University of Michigan) for insightful comments.
[17] We thank Dr. Fook Tham (University of California, Riverside) for X-ray structural analysis of **10c**.
[18] *trans,trans*-Cyclooctadiene is known to be stable: a) G. M. Whitesides, G. L. Goe, A. C. Cope, *J. Am. Chem. Soc.* **1969**, *91*, 2608; b) D. Boeckh, R. Huisgen, H. Nöth, *J. Am. Chem. Soc.* **1987**, *109*, 1248.

 © 2003 Wiley-VCH Verlag GmbH & Co. KGaA, Weinheim

CH_4 from Methane Hydrate

Recovering Methane from Solid Methane Hydrate with Carbon Dioxide**

*Huen Lee, Yongwon Seo, Yu-Taek Seo, Igor L. Moudrakovski, and John A. Ripmeester**

The discovery of vast hydrocarbon resources in hydrate form on the continental margins and in permafrost regions has sparked an interest in the possible recovery of relatively clean-burning methane gas,[1] especially in resource-poor national economies. At the same time, it has been proposed that CO_2, obtained as a by-product of combustion processes, possibly could be stored either in the deep ocean as liquid, or as a solid hydrate,[2] in order to reduce the release of greenhouse gas into the atmosphere. As such, the conversion of methane hydrate to CO_2 hydrate with the net recovery of methane seems quite attractive.[3] The limiting equilibrium composition of the mixed hydrate and the kinetics of conversion then become of primary interest in assessing this potential technology. In this communication we address these various issues, which have been considered so far only from a macroscopic point of view, by following not only kinetics, but also the distribution of guests over different cages using solid-state NMR methods. This combined approach allows the derivation of thermodynamic and kinetic information and also gives a molecular-level rationale for the observations; thus it is a powerful way of studying solid-state reactions.

Both CO_2 and CH_4 form a structure I (sI) hydrate,[4] as do mixtures of these gases,[5] with an icelike framework that consists of hydrogen-bonded water molecules. It has eight cagelike guest sites in the unit cell, including two pentagonal dodecahedra (5^{12}) and six tetrakaidecahedra ($5^{12}6^2$) consisting of 12 pentagonal and two hexagonal faces. The ideal unit cell can be written as $2\,M_S{\cdot}6\,M_L{\cdot}46\,H_2O$ with an ideal hydration number $M{\cdot}5^3/_4H_2O$ if a single type of guest is present. However, sI hydrates are non-stoichiometric, and the actual hydration numbers usually lie somewhere between 6 and 8.[4] The latter can be measured by the careful application of direct methods,[6] and also from cage occupancies obtained from structures derived by single crystal X-ray diffraction,[7] or from spectroscopy[8] where the cage occupancy ratio can be linked to the hydration number by using the van der Waals–-Platteeuw,[9] or related, models.

To observe favorable exchange between CO_2 and methane hydrate, there must be preferential partitioning of CO_2 and CH_4 between the gas and the hydrate solid phases. The only way this can arise is if CO_2 has a preference for the large cage ($5^{12}6^2$) in the hydrate, as the larger cages outnumber the smaller by a factor of three. This premise was investigated by examining the distribution of methane over the two cage sites by MAS ^{13}C NMR for hydrate samples prepared from gas mixtures (Figure 1). One can see that for pure methane

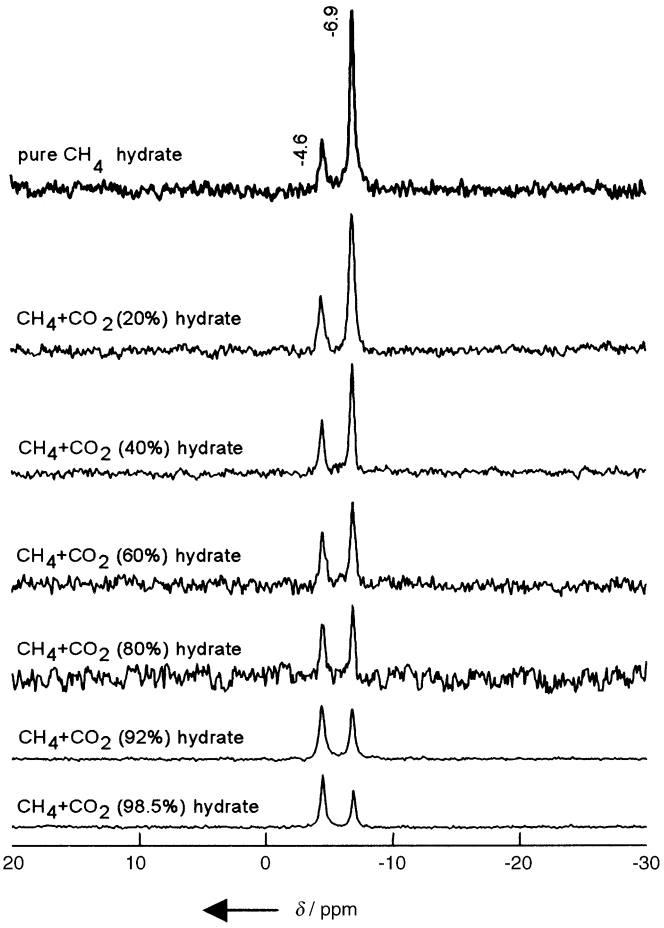


Figure 1. ^{13}C HPDEC MAS NMR spectra of an sI hydrate prepared using CH_4/CO_2 mixtures with compositions as indicated.

hydrate $\theta_{L,CH_4}/\theta_{S,CH_4}$ is ≈ 1.26, so that the small cage is occupied to a smaller degree than the larger cage, as reported before for synthetic and natural methane hydrates.[8,10] With increasing CO_2 in the gas mixture, the ratio declines steadily to a value that shows that now fewer than half as many large as small cages are filled with methane. This behavior can be explained in terms of the molecular sizes of CO_2 and CH_4. The size of CO_2 is almost the same as the cavity diameter of the small 5^{12} cage in the sI hydrate, the molecular diameter to cavity diameter ratio being 1.00 for CO_2 and 0.855 for CH_4. For CO_2 hydrate, NMR and diffraction techniques have

[*] Dr. J. A. Ripmeester, Dr. I. L. Moudrakovski
Steacie Institute for Molecular Sciences
National Research Council Canada
100 Sussex Drive, Ottawa, Ontario K1A 0R6 (Canada)
Fax: (+1) 613-998-7833
E-mail: john.ripmeester@nrc.ca
Prof. H. Lee, Dr. Y. Seo, Dr. Y.-T. Seo
Department of Chemical & Biomolecular Engineering
Korea Advanced Institute of Science and Technology
373-1, Guseong-dong, Yuseong-gu, Daejeon, 305-701 (Korea)

[**] This research was carried out in part for the Carbon Dioxide Reduction & Sequestration Center, one of 21 Century Frontier R&D Programs funded by the Ministry of Science and Technology of Korea and also partially supported by the Brain Korea 21 Project. The NRC researchers gratefully acknowledge partial support for this research by the Institute of Applied Energy (Japan)

 © 2003 Wiley-VCH Verlag GmbH & Co. KGaA, Weinheim DOI: 10.1002/anie.200351489

indicated that the 5^{12} cages have smaller fractional occupancies than the large cages. Hydration numbers of ≈ 6.0 for methane and 6.2 for CO_2 hydrate are consistent with fractional occupancies of the small cages θ_S of ≈ 0.8 and ≈ 0.7, respectively. Thus, when CO_2 competes with CH_4 in occupying the small cage of the sI hydrate, CO_2 is a relatively poorer guest, so that the occupancy ratio for CH_4 ($\theta_{L,CH_4}/\theta_{S,CH_4}$) becomes lower at higher CO_2 compositions because CO_2 preferentially occupies the large $5^{12}6^2$ cage in the mixed CH_4/CO_2 hydrate. Another aspect to be noted is that the equilibrium occupancy ratios ranged from 1.26 (100% CH_4) to 0.23 (very dilute CH_4). Thus when the CH_4 concentration becomes infinitely dilute, the value of 0.23 for $\theta_{L,CH_4}/\theta_{S,CH_4}$ shows that there is a limit to the degree of substitution that one can expect under equilibrium conditions, even when the gas composition approaches 100% CO_2. A second plot (Figure 2) shows the composition of the hydrate as a function

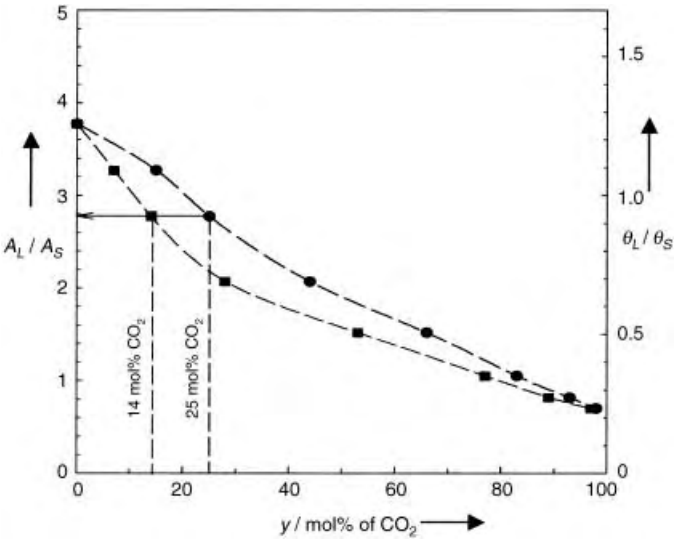


Figure 2. Equilibrium composition of the sI hydrate as a function of the composition of the source gas in mol% CO_2. The circles show the hydrate phase composition at the corresponding vapor phase composition of the source gas, as represented by squares. A_L/A_S is the intensity ratio of the ^{13}C MAS NMR resonance lines of methane molecules in large and small cages. θ_L/θ_S is the occupancy ratio of methane molecules in large and small cages, as calculated from the intensity ratio.

of the corresponding gas composition at equilibrium. Considerable enrichment in CO_2 of the hydrate with respect to the gas occurs for concentrations between ≈ 10 and 70% CO_2. When considering the data in Figure 1 and Figure 2, along with some assumptions,[11] a limiting composition of the mixed hydrate can be estimated showing that at least 64% of methane should be recoverable from a hydrate of composition $CH_4 \cdot 6.05\,H_2O$, which after reaction with CO_2 gives a product hydrate with a CO_2/CH_4 ratio of 1.8 or greater.

The kinetics of transformation are also a key element in considering the feasibility of the gas-replacement reaction. First of all we follow the reaction of CO_2 with powdered ice by measuring the intensity of the ^{13}C CO_2 powder pattern as a function of time. This reaction is remarkably slow at 268 K, with the reaction incomplete after 30 h (rate $k_1 \approx 0.0026\ min^{-1}$ at 268 K, $k_1 \approx 0.0025\ min^{-1}$ at 270 K, $P = 58$ bar).[12] Similarly, the reaction of methane with powdered ice is very slow (rate $k_1 \approx 0.0009\ min^{-1}$ at 270 K, $P = 215$ bar). On the other hand, when methane hydrate is exposed to CO_2 gas, the guest replacement reaction appears to be complete in less than 5 h (rate $k_1 \approx 0.01\ min^{-1}$ at 270 K). The amount of methane obtained from the reaction is about half of the total methane present in the initial hydrate (Figure 3), which indicates that

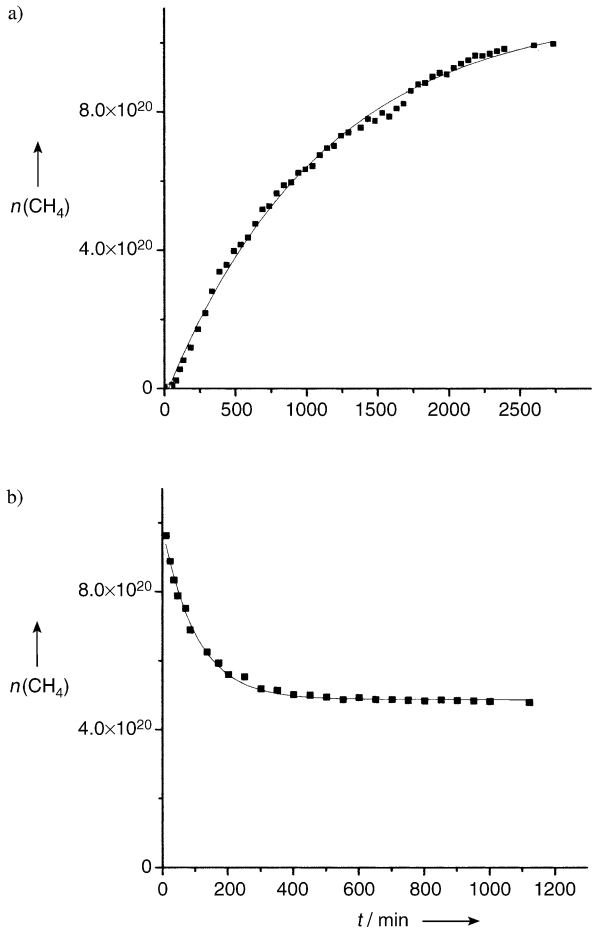


Figure 3. Formation and conversion of sI methane hydrate: a) Integrated intensity of the ^1H NMR signal during formation of sI methane hydrate from CH_4 and powdered ice (268 K, 215 bar). The solid line represents an exponential fit with a rate constant of $9\times10^{-4}\ min^{-1}$; b) conversion of the sI methane hydrate with CO_2, as obtained from the integrated ^{13}C powder-pattern intensity due to CO_2 in the large cage of sI hydrate (60 bar $^{13}CO_2$ at 270 K). The solid line is an exponential fit with a rate constant of $0.97\times10^{-2}\ min^{-1}$.

the product is a hydrate with a CO_2/methane ratio of ≈ 1. This suggests that the conversion is limited by considerations other than thermodynamics, as this predicted a product with a CO_2/methane ratio of ≈ 1.8.[11] It is likely that sample morphology plays an important part, where the conversion reaction proceeds so as to isolate volumes of pure methane hydrate surrounded by the converted hydrate. Sample grinding clearly would allow the reaction to proceed to equilibrium rather than to the pseudo-equilibrium state observed in this study.

 © 2003 Wiley-VCH Verlag GmbH & Co. KGaA, Weinheim

We note that the reaction of CO_2 hydrate with methane, on the other hand, is again very slow (Figure 4), with a steady state established after ≈ 60 h. We note that this experiment

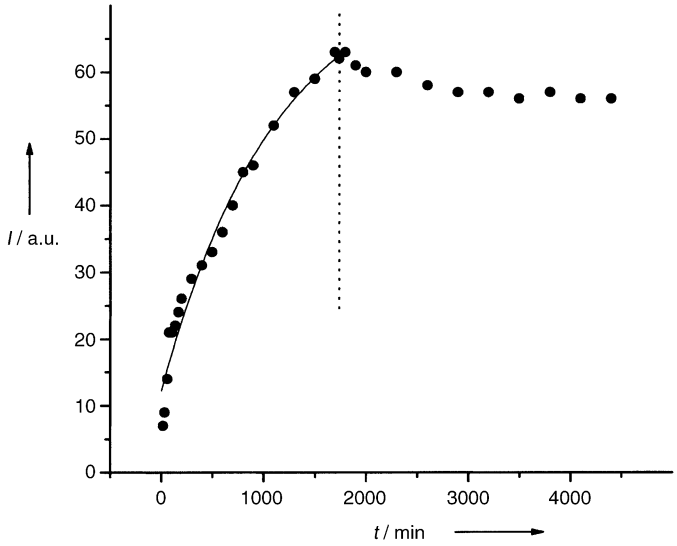


Figure 4. Intensity of the ^{13}C NMR signal due to CO_2 in the large cages of the sI hydrate shown as a function of time during the formation of sI CO_2 hydrate (on the left side of the dotted vertical line; $T = 268$ K, $P = 58$ bar) and after exposure of the material to CH_4 (152 bar; points on the right side of the dotted line).

reports only the replacement of CO_2 in the large cages, so that just over 10% of the large cages in the product contain methane. The reaction of CO_2 with methane hydrate and the reverse reaction of methane with CO_2 hydrate are obviously completely different. One may argue that since CO_2 is a much better large-cage guest than methane, two factors that control the kinetics may be identified. From an equilibrium point of view, it appears that CO_2 should replace methane rather easily, but this requires the lattice to be disrupted completely, as it involves changing the guests in a majority of the $5^{12}6^2$ cages, which are the major constituents of the hydrate lattice. So, the process is likely to lead relatively easily to the pseudo-equilibrium composition, with the replacement of methane by CO_2 accomplished as the hydrate particles recrystallize from the outside in. On the other hand, CO_2 at the hydrate particle surface apparently is not easily replaced by methane, as it is the favored guest only in the small cages; only ≈ 10% of the CO_2 in the large cages is replaced. The hydrate crystal likely remains largely intact, so that methane can only find its way to the interior sites by diffusing through a near-intact hydrate lattice; such a process must be very inefficient.

The results presented here show that, at least in a laboratory setting, the replacement of CH_4 by CO_2 is favored both from the points of view of equilibrium thermodynamics and kinetics. Reaction rates and the total yield of the replacement reaction in actual natural gas hydrate deposits will depend on a variety of factors, such as the degree of hydrate dispersion in sediment, hydrate particle size[12], and gas transport.

Experimental Section

For composition studies, pure and mixed-phase hydrates were prepared in porous silica gel (Aldrich, pore size = 15 nm) to facilitate the rapid equilibration of hydrates. ^{13}C NMR spectra were recorded at 200 K by placing the hydrate samples in a 4-mm diameter Zr-rotor that was loaded into the variable-temperature (VT) probe on a Bruker 400 MHz solid-state NMR spectrometer. All spectra were recorded at a Larmor frequency of 100.6 MHz with magic-angle spinning (MAS) at about 2–4 kHz under high-power proton decoupling (HPDEC). A pulse length of 2 μs and pulse repetition delay of 20 s with radio-frequency field strengths of 50 kHz corresponding to 90° pulses of 5 μs duration were used. The downfield carbon resonance peak of adamantane, assigned a chemical shift of 38.3 ppm at 300 K, was used as an external chemical shift reference. For the mixed hydrate samples of CO_2 compositions over 80 mol%, $^{13}CH_4$ gas was used to obtain higher intensity CH_4 peaks.

Kinetic studies of the reaction of powdered solids (deuterated ice or hydrate, particle size 5–50 μm) with gases were carried out in a high-pressure NMR cell connected to a gas handling system. For CO_2, the reactions were followed by measuring the integrated ^{13}C powder pattern, characteristic of the guest in the large cage of the sI hydrate, as a function of time. The variation of methane content in the hydrate with time was obtained from the integrated ^1H NMR signal. The absolute amount of product was obtained by comparing the signal with that of known samples.

Received: March 26, 2003 [Z51489]

Keywords: carbon dioxide · hydrates · kinetic measurements · methane · thermodynamic measurements

[1] C. Ji, G. Ahmadi, D. H. Smith, *Chem. Eng. Sci.* **2001**, *56*, 5801; B. Deka, S. K. Barnwal, *Chem. Eng. World* **1997**, *32*, 75; C. Taylor, R. S. Cherry, K. Millheim, J. Kwan, W. Maurer, *Prepr. Am. Chem. Soc. Div. Pet. Chem. P.* **2002**, *47*, 344; J. A. Majorowicz, P. K. Hannigan, K. G. Osadetz, *Nat. Resour. Res.* **2002**, *11*, 79; M. Max, W. P. Dillon, *Chem. Ind.* **2000**, 16.

[2] P. G. Brewer, G. Friederich, E. T. Peltzer F. M. Orr, Jr., *Science* **1999**, *284*, 943; P. G. Brewer, C. Goyet, G. Friederich, *Proc. Natl. Acad. Sci. USA* **1997**, *94*, 8308; P. G Brewer, E. T Peltzer, G. Friederich, I. Aya, K. Yamane, *MariChem* **2000**, *72*, 83; J. Lee, M.-K. Chun, K.-M. Lee, Y.-J. Kim, H. Lee, *Korean J. Chem. Eng.* **2002**, *19*, 673.

[3] R. P. Warzinski, R. M. Enick, D. H. Smith, K. S. Seshadri, *Prepr. Am. Chem. Soc. Div. Pet. Chem.* **2000**, *45*, 786; S. Hirohama, Y. Shimoyama, A. Wakabayashi, S. Tatsuta, N. Nishida, *J. Chem. Eng. Jpn.* **1996**, *29*, 1014; K. Ohgaki, K. Takano, H. Sangawa, T. Matsubara, S. Nakano, *J. Chem. Eng. Jpn.* **1996**, *29*, 478.

[4] D. W. Davidson in *Water. A Comprehensive Treatise* (Ed.: F. Franks), Plenum, New York, **1972**, p. 115.

[5] S. Adisasmito, R. J. Frank II, E. D. Sloan, Jr., *J. Chem. Eng. Data* **1991** 36, 68.

[6] Y. P. Handa, *J. Chem. Thermodyn.* **1986**, *18*, 891; **1986**, *18*, 915.

[7] K. A. Udachin, C. I. Ratcliffe, J. A. Ripmeester, *J. Phys. Chem. B* **2001**, *105*, 4200–4204.

[8] J. A. Ripmeester, C. I. Ratcliffe, *J. Phys. Chem.* **1988**, *97*, 337; A. K. Sum, R. C. Burrus, E. D. Sloan, *J. Phys. Chem. B* **1997**, *101*, 7371.

[9] J. H. van der Waals, J. C. Platteeuw, *Adv. Chem. Phys.* **1959**, *2*, 1.

[10] C. A. Tulk, C. I. Ratcliffe, J. A. Ripmeester, *Bull. Geol. Surv. Can.* **1999**, *544*, 251.

[11] For sI hydrates of a single guest component, the large cage occupancies are essentially indistinguishable from 1, thus $\theta_L = 1$, giving $\theta_S = 0.8$, and a hydration number of 6.05, well within the range of measured values. Therefore, in a mixed hydrate, θ_S for

 © 2003 Wiley-VCH Verlag GmbH & Co. KGaA, Weinheim

methane will never be greater than 0.8, the value for the pure hydrate, thus giving a maximum of 1.6 small cages per unit cell of methane. Since θ_L/θ_S is 0.23, then there will be at most 1.12 large cages per unit cell filled with methane, which leaves 4.88 large cages filled with CO_2. So the limiting composition for the mixed hydrate is $4.9\,CO_2 \cdot 2.7\,CH_4 \cdot 46\,H_2O$. If we assume that this represents the minimum amount of CO_2 in the mixed hydrate at equilibrium, the minimum expected recovery level for methane is 64%.

[12] The kinetics of conversion can be described roughly as exponential, and does not have significant pressure dependence in the range of pressures used. On the other hand, the ice-particle size has a profound effect on the conversion rate. When the experiments on ice to CO_2 hydrate conversion were performed at the same pressure and temperature but with ≈ 0.1 mm rather than 50 μm particles, the conversion rate dropped by nearly a factor of three. Our preliminary measurements indicate that the substitution rate of methane with carbon dioxide has only a small dependence on the pressure of CO_2, as long as it is kept above the pressure of CO_2 hydrate formation at a given temperature.

 © 2003 Wiley-VCH Verlag GmbH & Co. KGaA, Weinheim

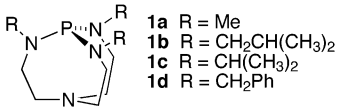
Arylation of Nitriles

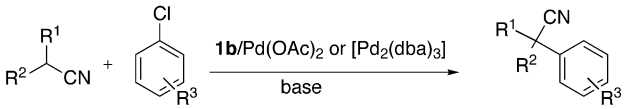
A General Method for the Direct α-Arylation of Nitriles with Aryl Chlorides**

*Jingsong You and John G. Verkade**

α-Aryl-substituted nitriles are not only important building blocks for constructing pyridines, carboxylic acids, primary amines, bicyclic amidines, lactones, aldehydes, and esters,[1] but also for synthesizing biologically active compounds.[2] However, the synthesis of α-aryl nitriles by direct α-arylation of nitriles has been sufficiently difficult, that the development of chemistry that could emanate from a successful method for such a process has been seriously inhibited. Only a few reports have appeared describing uncatalyzed couplings of nitrile carbanions with aryl halides possessing another electron-withdrawing group,[3] or with unactivated aryl fluorides,[4] or for transition-metal-catalyzed α-arylations with aryl iodides[5] or bromides.[6] Although aryl chlorides are both more abundant and less expensive than their corresponding iodides, bromides, and fluorides, they are much less reactive, and to date the addition of a nitrile anion to an aryl chloride has been achieved only with relatively acidic cyanoacetates in the presence of a palladium/$P(t\mathrm{Bu})_3$ or $Ph_5C_5FeC_5H_4P(t\mathrm{Bu})_2$ catalytic systems.[6b,c]

Herein, we describe a general solution to this long-standing challenge by employing bicyclic **1b** as a ligand for palladium in Equation (1) (dba = dibenzylideneacetone) which leads to efficient coupling of an array of nitriles with a broad range of aryl chlorides.





(1)

Ever since the bicyclic proazaphosphatranes **1** (of which **1a–c** are commercially available[7]) were first synthesized in our laboratories, they have continued to find uses as versatile nonionic very strong bases and potent catalysts for a variety of useful transformations.[8] These reactions appear to be quite dependent upon the occurrence (and in many cases the postulated occurrence) of transannulation of the bridgehead nitrogen center's lone pair to the phosphorus, which enhances the basicity of these proazaphosphatranes and also the stability of reaction intermediates formed with them. Moreover, the frameworks of compounds such as **1a–d** are fairly rigid but strain-free in a bicyclic (approximately C_{3v}) structure, thus favoring augmentation of the lone-pair electron density at phosphorus.[9,10] Additionally, the electronic and steric properties of these molecules can be easily fine tuned by introducing suitable organic substituents at each PN_3 nitrogen center. Very recently, we discovered that **1b** serves as a particularly effective ligand for palladium-catalyzed Suzuki-type cross-coupling[11] and aryl aminations[12] with a wide array of aryl chlorides, bromides and iodides. Those results prompted us to examine the use of **1** in α-arylations of nitriles with aryl chlorides.[13]

Our initial exploration of reaction conditions for the palladium-catalyzed α-arylation of nitriles focused on the coupling of isobutyronitrile with chlorobenzene (Table 1, entries 1–5). After screening **1a–1d** and $P(NMe_2)_3$, the more bulky **1b** was found to be a particularly effective ligand, while **1a** and **1c** provided only trace amounts of the cross-coupling product and **1d** gave only a moderate yield.[11,12,14] As expected, non-cyclic $P(NMe_2)_3$ did not afford the anticipated α-arylated product (Table 1, entry 5). The best results were obtained with α-arylations of isobutyronitrile at 90 °C in toluene using $NaN(SiMe_3)_2$[15] as a base, and a catalyst system generated in situ from 2 mol % of $Pd(OAc)_2$ and 4 mol % of **1b**.[16] Under our optimized reaction conditions, α-arylations of isobutyronitrile in high yields were accomplished with a wide array of aryl chlorides including electron-rich, electron-poor, electron-neutral, and sterically hindered examples (Table 1, entries 2 and 6–8).

We have determined that not only a broad spectrum of aryl chlorides, but also a diverse set of nitriles (Table 2),

[*] Prof. Dr. J. G. Verkade, Dr. J. You
Department of Chemistry
Iowa State University
Ames, IA 50011 (USA)
Fax: (+1) 515-294-0105
E-mail: jverkade@iastate.edu

[**] The authors are grateful to the National Science Foundation for grant support.

 DOI: 10.1002/anie.200351954 © 2003 Wiley-VCH Verlag GmbH & Co. KGaA, Weinheim

Table 1: Catalytic α-arylation of isobutyronitrile with aryl chlorides by $Pd(OAc)_2$/**1**.[a]

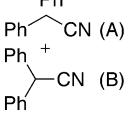
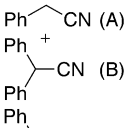
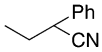
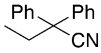


(2)

Entry	Ligand	Aryl chloride	Yield [%][b]
1	**1a**	C_6H_5Cl	10
2	**1b**	C_6H_5Cl	82
3	**1c**	C_6H_5Cl	15
4	**1d**	C_6H_5Cl	40
5	$P(NMe_2)_3$	C_6H_5Cl	0
6	**1b**	2-MeC_6H_5Cl	81
7[c]	**1b**	4-NCC_6H_5Cl	92
8	**1b**	4-$MeOC_6H_5Cl$	70

[a] Reaction conditions: 1.0 mmol of aryl chloride, 1.2 mmol of isobutyronitrile, 1.4 mmol of $NaN(SiMe_3)_2$, 0.02 mmol of $Pd(OAc)_2$, and 0.04 mmol of **1** in 2.0 mL of toluene at 90°C for 8 h under Ar atmosphere. [b] Yields (average of two runs) based on aryl chloride. [c] Reaction time: 2 h.

Table 2: Catalytic α-arylation of nitriles with chlorobenzene by $Pd(OAc)_2$/**1b**.[a]

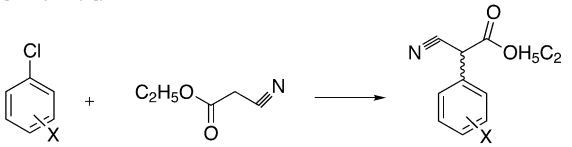
Entry	Nitrile	Product	*t*	Yield [%][b]
1			8 h	82
2	CH_3CN		15 h	50(A) 20(B)
3[c]	CH_3CN		15 h	70(A) 10(B)
4			6 h	91
5[d]			6 h	83
6			3 h	90
7[e]	$PhSO_2CH_2CN$	$PhSO_2CH(Ph)CN$	4 h	96
8			6 h	81

[a] Reaction conditions: 1.0 mmol of chlorobenzene, 1.2 mmol of nitrile, 1.4 mmol of $NaN(SiMe_3)_2$, 0.02 mmol of $Pd(OAc)_2$ and 0.04 mmol of **1b** in 2.0 mL of toluene at 90°C under Ar atmosphere. [b] Yields (average of two runs) based on chlorobenzene. [c] 2.0 mmol of CH_3CN. [d] 0.04 mmol of $Pd(OAc)_2$ and 0.08 mmol of **1b**. [e] Dioxane as a solvent, 1.4 mmol of KO-*t*Bu as a base.

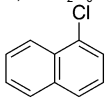
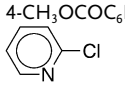
participate efficiently in α-arylations of nitriles in the presence of $Pd(OAc)_2$/**1b**. For these transformations we chose to use chlorobenzene as the aryl chloride. The coupling of primary nitriles, such as benzyl nitrile, *n*-butyronitrile, and $PhSO_2CH_2CN$ with chlorobenzene afforded the corresponding monoarylated product almost exclusively in 91%, 83% and 96% yields, respectively, (entries 4, 5, and 7). The monoarylated product of *n*-butyronitrile was found to couple with a second equivalent of chlorobenzene to form the corresponding diarylated product (entry 6). However, acetonitrile afforded a mixture of di- and monoarylated product under the same conditions (entry 2). By increasing the amount of acetonitrile, however, the yield of the monoarylated product was improved (entry 3). In addition, a cyclic secondary nitrile, such as cyclohexanecarbonitrile, was efficiently coupled with chlorobenzene, affording monoarylated product in good yield (entry 8).

α-Aryl cyanoacetates are useful intermediates in the preparation of amino alcohols, β-amino acids, and arylacetic acids.[17] Thus, it was gratifying to discover that a catalyst system, generated from $[Pd_2(dba)_3]$/**1b** in dioxane using KO-*t*Bu as a base, effectively facilitated the α-arylation of ethyl cyanoacetate with a broad range of aryl chlorides (Table 3). Whether the aryl chlorides are electron-rich (entry 7), electron-poor (entries 8–10), electron-neutral (entries 1–6), or sterically hindered (entries 3, 5, and 6), all of them afforded excellent product yields under our conditions.

Table 3: Catalytic α-arylation of ethyl cyanoacetate with aryl chlorides by $[Pd_2(dba)_3]$/**1b**.[a]



(3)

Entry	Aryl chloride	Yield [%][b]
1	C_6H_5Cl	93
2[c]	C_6H_5Cl	91
3	2-MeC_6H_5Cl	92
4	4-MeC_6H_5Cl	93
5	2,5-$Me_2C_6H_5Cl$	90
6		92
7	4-$MeOC_6H_5Cl$	90
8	4-$F_3CC_6H_5Cl$	92
9[d]	4-NCC_6H_5Cl	96
10	4-$CH_3OCOC_6H_5Cl$	87
11		91

[a] Reaction conditions: 1.0 mmol of aryl chloride, 1.1 mmol of ethyl cyanoacetate, 2.0 mmol of KO-*t*Bu, 0.02 mmol of $[Pd_2(dba)_3]$ and 0.08 mmol of **1b** in 2.0 mL of dioxane at 90°C under Ar atmosphere for 5 h. [b] Yields (average of two runs) based on aryl chloride. [c] 0.005 mmol of $[Pd_2(dba)_3]$ and 0.02 mmol of **1b**. [d] Temperature: 80°C.

Limitations on the structures of aryl halides were encountered when $Pd/Ph_5C_5FeC_5H_4P(tBu)_2$ or $Pd/P(tBu)_3$ catalyst systems were employed.[6c] For example, cyanoacetate esters did not couple with pyridyl halides or with aryl halides possessing electron-withdrawing groups, such as esters or nitriles.[6c] In contrast, our catalytic system tolerates a broad variety of aryl halides. Thus the arylation of ethyl cyanoacetate with 4-chlorobenzonitrile, methyl-4-chlorobenzoate, and 2-chloropyridine gave the desired products in 96, 87, and 91% yields, respectively, (entries 9–11).

 © 2003 Wiley-VCH Verlag GmbH & Co. KGaA, Weinheim

Although not yet investigated in detail, α-arylations of ethyl cyanoacetate also occurred with substantially lower catalyst loading than with our standard condition of 2 mol% of $[Pd_2(dba)_3]$. As shown in entry 2 of Table 3, the reaction of ethyl cyanoacetate with chlorobenzene occurred in 91% yield with 1 mol% of palladium precursor at 90°C.

In summary, we have described a solution to the long-standing challenge of developing a general method for the direct α-arylation of nitriles with aryl chlorides. With the catalytic system generated from palladium and commercially available **1b**, it is now possible to effect direct α-arylation of a wide variety of nitriles with a broad range of aryl chlorides.

Received: May 22, 2003 [Z51954]

Keywords: α-arylation · homogeneous catalysis · nitriles · P ligands · palladium

[1] a) H. Leader, R. M. Smejkal, C. S. Payne, F. N. Padilla, B. P. Doctor, R. K. Gordon, P. K. Chiang, *J. Med. Chem.* **1989**, *32*, 1522–1528; b) B. K. Trivedi, A. Holmes, T. L. Stoeber, C. J. Blankey, W. H. Roark, J. A. Picard, M. K. Shaw, A. D. Essenburg, R. L. Stanfield, B. R. Krause, *J. Med. Chem.* **1993**, *36*, 3300–3307; c) M. A. Convery, A. P. Davis, C. J. Dunne, J. W. MacKinnon, *Tetrahedron Lett.* **1995**, *36*, 4279–4282; d) M. Tiecco, L. Testaferri, M. Tingoli, D. Bartoli, *Tetrahedron* **1990**, *46*, 7139–7150; e) C. Pascal, J. Dubois, D. Guénard, L. Tchertanov, S. Thoret, F. Guéritte, *Tetrahedron* **1998**, *54*, 14737–14756; f) E. J. Bush, D. W. Jones, *J. Chem. Soc. Perkin Trans. 1* **1997**, 3531–3536.

[2] a) S. M. Bromidge, F. Brown, F. Cassidy, M. S. G. Clark, S. Dabbs, J. Hawkins, J. M. Loudon, B. S. Orlek, G. J. Riley, *Bioorg. Med. Chem. Lett.* **1992**, *2*, 791–796; b) S. Dei, M. N. Romanelli, S. Scapecchi, E. Teodori, A. Chiarini, F. Gualtieri, *J. Med. Chem.* **1991**, *34*, 2219–2225; c) K. Mitani, S. Sakurai, T. Suzuki, E. Morikawa, H. Kato, Y. Ito, T. Fujita, *Chem. Pharm. Bull.* **1988**, *36*, 4121–4135; d) L. J. Theodore, W. L. Nelson, *J. Org. Chem.* **1987**, *52*, 1309–1315.

[3] When activated aryl halides including fluorides, chlorides, bromides, and iodides were used as substrates, the uncatalyzed coupling of nitriles focused only on phenylacetonitrile derivatives and cyanoacetates as reactants: a) M. Makosza, M. Jagusztyn-Grochowska, M. Ludwikow, M. Jawdosiuk, *Tetrahedron* **1974**, *30*, 3723–3735; b) A. Loupy, N. Philippon, P. Pigeon, J. Sansoulet, H. Galons, *Synth. Commun.* **1990**, *20*, 2855–2864; c) M. B. Sommer, M. Begtrup, K. P. Bogeso, *J. Org. Chem.* **1990**, *55*, 4817–4821; d) X.-M. Zhang, D.-L. Yang, Y.-C. Liu, *J. Org. Chem.* **1993**, *58*, 224–227; e) M. Makosza, R. Podraza, A. Kwast, *J. Org. Chem.* **1994**, *59*, 6796–6799; f) R. G. Plevey, P. Sampson, *J. Chem. Soc. Perkin Trans. 1* **1987**, 2129–2136.

[4] For unactivated aryl fluorides, limitations were encountered on the structures of the nitriles found suitable for reaction. For example, only the anions of secondary nitriles underwent substitution, and ethyl cyanoacetate and primary nitriles were unreactive: S. Caron, E. Vazquez, J. M. Wojcik, *J. Am. Chem. Soc.* **2000**, *122*, 712–713.

[5] a) K. Okuro, M. Furuune, M. Miura, M. Nomura, *J. Org. Chem.* **1993**, *58*, 7606–7607; b) M. Uno, K. Seto, S. Takahashi, *J. Chem. Soc. Chem. Commun.* **1984**, 932–933; c) M. Uno, K. Seto, M. Masuda, S. Takahashi, *Synthesis* **1985**, 506–508.

[6] a) T. Sataoh, J. Inoh, Y. Kawamura, Y. Kawamura, M. Miura, M. Nomura, *Bull. Chem. Soc. Jpn.* **1998**, *71*, 2239–22467; b) S. R. Stauffer, N. A. Beare, J. P. Stambuli, J. F. Hartwig, *J. Am. Chem. Soc.* **2001**, *123*, 4641–4642; c) N. A. Beare, J. F. Hartwig, *J. Org. Chem.* **2002**, *67*, 541–555; d) D. A. Culkin, J. F. Hartwig, *J. Am. Chem. Soc.* **2002**, *124*, 9330–9331; e) D. Culkin, J. F. Hartwig, *Acc. Chem. Res.* **2003**, *36*, 234–245.

[7] Aldrich and Fluka for **1a, 1b, 1c**; Strem for **1b**.

[8] For a recent review, see J. G. Verkade, *Top. Curr. Chem.* **2003**, *233*, 1–44.

[9] For discussions of the electronic structure of tris(alkylamino)-phosphanes, see: a) A. H. Cowley, M. Lattman, P. M. Stricklen, J. G. Verkade, *Inorg. Chem.* **1982**, *21*, 543–549; b) K. G. Molloy, J. L. Petersen, *J. Am. Chem. Soc.* **1995**, *117*, 7696–7710; c) S. K. Xi, H. Schmidt, C. Lensink, S. Kim, D. Wintergrass, L. M. Daniels, R. A. Jacobson, J. G. Verkade, *Inorg. Chem.* **1990**, *29*, 2214–2220; d) S. M. Socol, R. A. Jacobson, J. G. Verkade, *Inorg. Chem.* **1984**, *23*, 88–94; e) C. Romming, J. Songstad, *Acta Chem. Scand. Ser. A* **1980**, *34*, 365–373; f) C. Romming, J. Songstad, *Acta Chem. Scand. Ser. A* **1979**, *33*, 187–197.

[10] An X-ray structural study of **1c** showed that the bonding environment around the PN_3 nitrogen center is rather planar, the sum of angles being 354.9, 356.6, and 357.5°: A. E. Wroblewski, J. Pinkas, J. G. Verkade, *Main Group Chem.* **1995**, *1*, 69–79.

[11] S. Urgaonkar, M. Nagarajan, J. G. Verkade, *Tetrahedron Lett.* **2002**, *43*, 8921–8924.

[12] a) S. Urgaonkar, M. Nagarajan, J. G. Verkade, *J. Org. Chem.* **2003**, *68*, 452–459; b) S. Urgaonkar, M. Nagarajan, J. G. Verkade, *Org. Lett.* **2003**, *5*, 815–818.

[13] General experimental: A dried Schlenk flask equipped with a magnetic stirring bar was charged with $Pd(OAc)_2$ or $[Pd_2(dba)_3]$ (0.02–0.04 mmol) and KO-*t*Bu (2.0 mmol) or $NaN(SiMe_3)_2$ (1.4 mmol) inside a nitrogen-filled glove box. The flask was capped with a rubber septum and removed from the glove box. Toluene or dioxane (2 mL), **1b** (0.04–0.08 mmol in toluene or dioxane (0.5–0.7 mL)) and aryl halide (1.0 mmol) were then added successively. After stirring for 20 min at room temperature, a nitrile (1.1 or 1.2 mmol) was added and the reaction mixture was stirred under the conditions indicated in Tables 1–3. The mixture was then quenched by addition of aqueous 1N HCl and extracted with diethyl ether. The isolated organic phase was dried over Na_2SO_4, filtered, concentrated in vacuo, and purified by column chromatography on silica gel eluting with ethl acetate/hexane or dichloromethane/hexane.

[14] Control experiments showed that either in the absence of a Pd source or in the absence of proazaphosphatrane, no reaction was observed.

[15] After screening a variety of bases (i.e., Na_3PO_4, K_3PO_4, Na_2CO_3, Cs_2CO_3, NaH, $NaN(SiMe_3)_2$, KO-*t*Bu, and NaO-*t*Bu), we found that $NaN(SiMe_3)_2$ gave the best results. In the presence of a weaker base, such as Na_3PO_4, K_3PO_4, Na_2CO_3 or Cs_2CO_3, no reaction was observed.

[16] A 1:2 palladium-to-ligand ratio gave faster reaction rates and better product yields than a 1:1 ratio.

[17] a) C. Cativiela, M. D. Diaz-de-Villegas, J. A. Galvez, *J. Org. Chem.* **1994**, *59*, 2497–2505; b) S. Abele, D. Seebach, *Eur. J. Org. Chem.* **2000**, 1–15; c) H. Brunner, P. Schmidt, *Eur. J. Org. Chem.* **2000**, 2119–2133.

 © 2003 Wiley-VCH Verlag GmbH & Co. KGaA, Weinheim

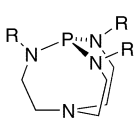
Baylis–Hillman Reaction

A Highly Active and Selective Catalyst System for the Baylis–Hillman Reaction**

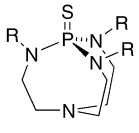
*Jingsong You, Juhua Xu, and John G. Verkade**

The Baylis–Hillman (BH) reaction, i.e., coupling of an activated alkene or alkyne with an aldehyde or ketone, has recently become a very attractive goal.[1] These reactions usually require Lewis bases as catalysts, such as tertiary phosphanes or tertiary amines, among which 1,4-diazabicyclo[2.2.2]octane (DABCO) is the most popular. However, this approach suffers from slow reaction rates (reaction times of weeks and even months[1,2]) which limit the scope of substrates. Numerous chemical and physical methods have been developed to accelerate BH reactions.[1,3] One of the Lewis acids typically used to activate the carbonyl group[4] is $TiCl_4$, used with or without additives (e.g., quaternary ammonium salts, an organic chalcogenide, phosphanes, a diol or a bisoxazoline).[1,4,5] Although the rates of BH reactions are improved significantly with the assistance of $TiCl_4$, the yields are generally only moderate, and limitations are encountered on the structures of the Michael acceptors and the aldehydes which undergo addition, frequently producing complex mixtures.[5–7]

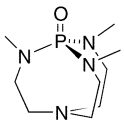
The commercially available bicyclic proazaphosphatranes **1a**–**1c**, first synthesized in our laboratories, have attracted considerable interest in recent years as versatile, exceedingly strong nonionic bases and as catalysts for a variety of useful transformations.[8] Recently, we reported that in the presence of proazaphosphatrane **1c**, activated allylic compounds such as acrylonitrile react efficiently with aromatic aldehydes to afford BH adducts as the only product.[9] However, when activated alkenes (cyclohex-1-en-1-one, vinyl ketones, acrylates, and allyl cyanide) were used as substrates in the presence of **1a**–**1c**, the BH reactions failed whether with or without a Lewis acid ($TiCl_4$ or $AlCl_3$) present. Herein we report the surprising discovery that the proazaphosphatrane sulfide **2a**, easily prepared from commercially available **1a**, facilitates unparalleled speed and selectivity in BH reactions catalyzed by $TiCl_4$.



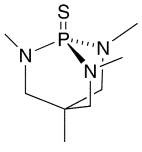
1a R = Me
1b R = *i*Bu
1c R = *i*Pr



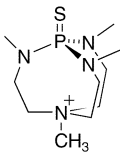
2a R = Me
2b R = *i*Bu
2c R = *i*Pr



3



4



5

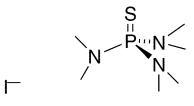
[*] Prof. J. G. Verkade, Dr. J. You, Dr. J. Xu
Department of Chemistry
Iowa State University
Ames, IA 50011 (USA)
Fax: (+1) 515-294-0105
E-mail: jverkade@iastate.edu

[**] The authors are grateful to the National Science Foundation for grant support.

Initially, we examined the model reaction of *p*-nitrobenzaldehyde (1 mmol) with comparatively unreactive cyclohex-2-en-1-one (3 mmol) in CH_2Cl_2 (2 mL) under argon at room temperature.[10] When 20 mol% catalyst **2a** was employed without any additives, this reaction gave only a 5% product yield (based on the aldehyde) after four days. However, we found that the rate improved remarkably when one equivalent of some Lewis acids was added. After screening a variety of such acids (e.g., $MgSO_4$, $BF_3{\cdot}OEt_2$, BCl_3, $SnCl_4$, $AlCl_3$, $Ti(OiPr)_4$, and $TiCl_4$), we found that $TiCl_4$ gave the best results. The model reaction carried out in the presence of 20 mol% **2a** and 1.0 equiv of $TiCl_4$ gave a 95% yield of the product in only 5 min at room temperature.[11] Even with as little as 5 mol% **2a**, a 94% yield was observed in 10 min at room temperature. Proazaphosphatrane sulfides **2b** and **2c** showed slightly reduced activities over the same time period (perhaps due to steric hindrance of the R group), giving yields of 85 and 78%, respectively. To our knowledge, **2a**/$TiCl_4$ is the most effective catalyst system thus far reported for BH reactions.

To shed light on the possible origin of the remarkable activity of **2a** in $TiCl_4$-promoted BH reactions, proazaphosphatrane oxide **3** was first chosen for comparison. The BH reaction catalyzed by 0.05 equiv of **3** proceeded in 48% yield in only 10 minutes, similar to the yield realized with 1 equiv of $TiCl_4$ by itself (44%) over 2 h. This finding suggests a key role for the sulfur atom in **2a** in its catalytic activity. Interestingly, reactions catalyzed by 0.05 equivalents of the analogous bases **4**, lacking the bridgehead nitrogen of **2a**, and **5** led to dramatic decreases in yield (69 and 55%, respectively) after a reaction time of 10 minutes, and the acyclic analogue **6** (0.05 equiv) showed only moderate activity (59% yield) compared with that of **2a** over the same time period. The stronger cocatalytic activity of **2a** compared with that of **4**–**6** appears to be associated with the potential for $N_{ax}{\rightarrow}P$ intrabridgehead interactions, which enhances reaction rates and the nucleophilicity of the sulfur atom. Although the molecular structure of **2a** reveals an $N_{ax}{\rightarrow}P$ distance only 3% shorter than the sum of van der Waals radii of the P and N atoms (3.34 Å),[12] it is conceivable that additional shortening of this distance occurs during the reaction.

The first mechanism suggested for BH reactions mediated by a chalcogenide/metal halide catalyst system involved attack of the sulfur atom from R_2S on the activated alkene.[6a] However, it is currently believed that these reactions proceed by attack of a halide ion released from a Lewis acid by R_2S.[7b] Supporting evidence for this was the unsuccessful use of $BF_3{\cdot}OEt_2$ as the Lewis acid, from which release of a halide ion is far less likely.[6] Very recently a BH reaction of methyl vinyl ketone with aldehydes mediated by tetrahydrothiophene/$BF_3{\cdot}OEt_2$ was developed which gave moderate product yields, indicating the unambiguous requirement of the sulfide for attack on the activated alkene.[13] In accord with these observations, the use of 1.0 equiv of $BF_3{\cdot}OEt_2$ in the reaction of cyclohex-2-en-1-one with *p*-nitrobenzaldehyde in the presence of **2a** (0.2 equiv) at room temperature gave a



6

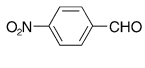
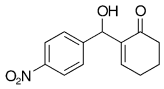
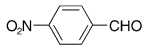
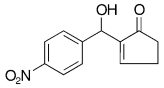
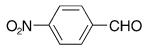
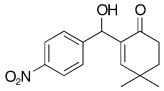
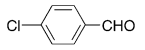
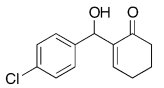
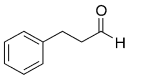
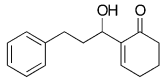
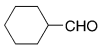
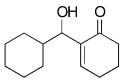
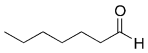
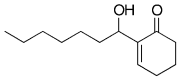
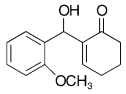
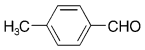
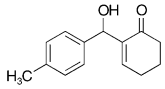
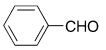
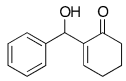
 © 2003 Wiley-VCH Verlag GmbH & Co. KGaA, Weinheim DOI: 10.1002/anie.200352233

50% yield of the BH adduct in four hours, while no desired adduct was isolated in the absence of **2a**.[14] It is reasonable to suggest that coordination of BF_3 to the carbonyl oxygen of the alkene activating group is followed by attack of the sulfur atom of **2a** on the carbon β to the carbon of the activating groups of the alkene, with a concomitant $N_{ax} \rightarrow P$ intrabridgehead interaction that electronically enriches the carbon α to the activating group[15] for nucleophilic attack on the aldehyde carbon. The low yield (53%) of BH product achieved in 10 min in the reaction of *p*-nitrobenzaldehyde with 3-methylcyclohex-2-ene-1-one in the presence of $TiCl_4$ (1 equiv) and 0.05 equiv of **2a** is also in agreement with attack of **2a** (although impeded by the methyl group) at the 3-position of the 3-substituted enone.[16]

BH reactions mediated by **2a**/$TiCl_4$ tolerate a relatively wide scope of Michael acceptors and aldehydes at room temperature. As is evident in Table 1, cyclic enones (which are less reactive than acyclic analogues) were efficiently coupled with a wide variety of aldehydes to give BH adducts. Additionally, reactions of electron-deficient aromatic aldehydes afforded excellent yields in very short times (Table 1, entries 1–4). We were also delighted to find that electron-neutral aromatic aldehydes such as *p*-methylbenzaldehyde and benzaldehyde gave BH adducts with cyclohex-2-en-1-one in 91% and 90% yields, respectively, in only 10 min (entries 9 and 10). Surprisingly, the reaction of the notoriously recalcitrant hindered and deactivated *o*-anisaldehyde with cyclo-hex-2-en-1-one proceeded in 88% yield (entry 8). In sharp contrast, BH reactions of inactive aromatic aldehydes such as this are sluggish with other reported catalyst systems, and the related reactions with cyclic enones are generally limited to the use of aromatic aldehydes with strong electron-withdrawing groups.[6] Whereas BH reactions with simple aliphatic aldehydes using $TiCl_4$/Lewis base copromoters often give low product yields,[6] our catalytic system provided very good yields (entries 5–7).

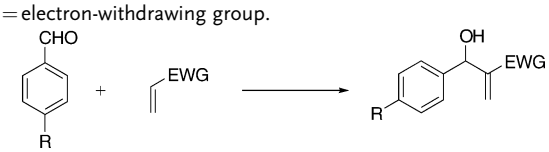
Noncyclic Michael-type acceptors were also examined under our aforementioned conditions (Table 2). Methyl vinyl

Table 1: Baylis–Hillman reactions of aldehydes with cyclic enones catalyzed by **2a**/$TiCl_4$.[a]

Entry	Aldehyde	Enone	Product	*t* [min]	Yield [%][b]
1				10	94
2				10	92
3				10	91
4				10	94
5				10	88
6				30	81
7				30	89
8				10	88
9				10	91
10				10	90

[a] The reactions were carried out with 1.0 mmol of aldehyde and 3.0 mmol of enone in the presence of **2a** (0.05 mmol) and $TiCl_4$ (1.0 mmol) in CH_2Cl_2 under Ar at room temperature. [b] Yield of isolated product based on aldehydes.

Table 2: Baylis–Hillman reactions of aromatic aldehydes with acyclic Michael-type acceptors catalyzed by **2a**/$TiCl_4$.[a] EWG = electron-withdrawing group.



Entry	Aldehyde	EWG	*t* [min]	Yield [%][b]
1	4-$O_2NC_6H_4CHO$	$COCH_3$	5	92
2	C_6H_5CHO	$COCH_3$	5	85
3	4-$O_2NC_6H_4CHO$	$COOC_2H_5$	10	92
4	4-$O_2NC_6H_4CHO$	$COOCH_3$	10	92
5	4-ClC_6H_4CHO	$COOCH_3$	10	92
6	C_6H_5CHO	$COOCH_3$	10	88
7	4-$CH_3OC_6H_4CHO$	$COOCH_3$	10	87
8	C_6H_5CHO	CN	20	95
9	4-$O_2NC_6H_4CHO$	CN	10	88

[a] The reactions were carried out with 1.0 mmol of aldehyde and 3.0 mmol of alkene in the presence of **2a** (0.05 mmol) and $TiCl_4$ (1.0 mmol) in CH_2Cl_2 under Ar at room temperature. [b] Yield of isolated product based on aldehyde.

 © 2003 Wiley-VCH Verlag GmbH & Co. KGaA, Weinheim

ketone gave exclusively BH products in high yields (entries 1 and 2), and side products were not observed by ^{1}H NMR spectroscopy. This result remarkably contrasts previous findings that reactions of α,β-unsaturated acyclic ketones with aldehydes mediated by metal and non-metal halides resulted in complex reaction mixtures.[7] Acrylates are normally very unreactive in Lewis acid catalyzed BH reactions, and very low to zero yields of coupling products are obtained.[6b,7c,7d] Interestingly, our new methodology works very well for both electron-poor and electron-rich aromatic aldehydes, giving excellent yields of Baylis–Hillman products in only 10 min (entries 3–7). When acrylonitrile was employed, reactions with aromatic aldehydes also gave high product yields (entries 8 and 9).

In summary, we have developed a highly active and selective catalyst system (**2a**/$TiCl_4$) for the BH reaction, which to our knowledge is the most generally effective one so far described. Our protocol is applicable to activated alkenes such as enones (including less reactive β-substituted derivatives), acrylonitrile, and acrylates. We believe that $N_{ax}\rightarrow P$ intrabridgehead interaction in **2a** may play an important role in stabilizing a **2a**/activated alkene/$TiCl_4$ intermediate in the reaction pathway. Further development of this methodology, including its application to asymmetric reactions using chiral proazaphosphatrane sulfides, is in progress.

Received: June 26, 2003 [Z52233]

Keywords: Baylis–Hillman reaction · heterocycles · Lewis bases · titanium

[1] For recent reviews see: a) D. Basavaiah, A. J. Rao, T. Satyanarayana, *Chem. Rev.* **2003**, *103*, 811 – 891, and references therein; b) P. Langer, *Angew. Chem.* **2000**, *112*, 3177 – 3180; *Angew. Chem. Int. Ed.* **2000**, *39*, 3049 – 3052.

[2] a) S. Matsumoto, Y. Okubo, K. Mikami, *J. Am. Chem. Soc.* **1998**, *120*, 4015 – 4016; b) Y. Fort, M. C. Berthe, P. Caubere, *Tetrahedron* **1992**, *48*, 6371 – 6384.

[3] a) C. Yu, B. Liu, L. Hu, *J. Org. Chem.* **2001**, *66*, 5413 – 5418; b) W.-D. Lee, K.-S. Yang, K. Chen, *Chem. Commun.* **2001**, 1612 – 1613; c) J. Cai, Z. Zhou, G. Zhao, C. Tang, *Org. Lett.* **2002**, *4*, 4723 – 4725; d) V. K. Aggarwal, D. K. Dean, A. Mereu, R. Williams, *J. Org. Chem.* **2002**, *67*, 510 – 514; e) C. Yu, L. Hu, *J. Org. Chem.* **2002**, *67*, 219 – 223; f) V. K. Aggarwal, I. Emme, S. Y. Fulford, *J. Org. Chem.* **2003**, *68*, 692 – 700.

[4] a) W. Pei, H.-X. Wei, G. Li, *Chem. Commun.* **2002**, 1856 – 1857; b) W. Pei, H.-X. Wei, G. Li, *Chem. Commun.* **2002**, 2412 – 2413; c) D. Balan, H. Adolfsson, *J. Org. Chem.* **2002**, *67*, 2329 – 2334; d) V. K. Aggarwal, A. Mereu, G. J. Tarver, R. McCague, *J. Org. Chem.* **1998**, *63*, 7183 – 7189; e) K. Yang, W. Lee, J. Pan, K. Chen, *J. Org. Chem.* **2003**, *68*, 915 – 919; f) T. Iwamura, M. Fujita, T. Kawakita, S. Kinoshita, S. Watanabe, T. Kataoka, *Tetrahedron* **2001**, *57*, 8455 – 8462; g) M. Shi, C. Wang, *Helv. Chim. Acta* **2002**, *85*, 841 – 846.

[5] a) G. Li, H.-X. Wei, J. J. Gao, T. D. Caputo, *Tetrahedron Lett.* **2000**, *41*, 1 – 5; b) A. Patra, S. Batra, B. S. Joshi, R. Roy, B. Kundu, A. P. Bhaduri, *J. Org. Chem.* **2002**, *67*, 5783 – 5788.

[6] a) T. Kataoka, T. Iwama, S. Tsujiyama, *Chem. Commun.* **1998**, 197 – 198; b) T. Kataoka, T. Iwama, S. Tsujiyama, T. Iwamura, S. Watanabe, *Tetrahedron* **1998**, *54*, 11 813 – 11 824; c) T. Iwama, H. Kinoshita, T. Kataoka, *Tetrahedron Lett.* **1999**, *40*, 3741 – 3744; d) T. Kataoka, H. Kinoshita, T. Iwama, S. Tsujiyama, T. Iwamura, S. Watanabe, O. Muraoka, G. Tanabe, *Tetrahedron* **2000**, *56*, 4725 – 4731; e) T. Kataoka, H. Kinoshita, S. Kinoshita, T. Iwamura, S. Watanabe, *Angew. Chem.* **2000**, *112*, 2448 – 2450; *Angew. Chem. Int. Ed.* **2000**, *39*, 2358 – 2360.

[7] a) S. Uehira, Z. Han, H. Shinokubo, K. Oshima, *Org. Lett.* **1999**, *1*, 1383 – 1385; b) M. Shi, J.-K. Jiang, *Tetrahedron* **2000**, *56*, 4793 – 4797; c) M. Shi, J.-K. Jiang, Y.-S. , Feng, *Org. Lett.* **2000**, *2*, 2397 – 2400; d) M. Shi, Y.-S. Feng, *J. Org. Chem.* **2001**, *66*, 406 – 411; e) G. Li, J. Gao, H.-X. Wei, M. Enright, *Org. Lett.* **2000**, *2*, 617 – 620.

[8] a) J. G. Verkade, *Top. Curr. Chem.* **2003**, *233*, 1 – 44, and references therein; b) P. B. Kisanga, J. G. Verkade, *Tetrahedron Reports*, **2003**, in press.

[9] P. B. Kisanga, J. G. Verkade, *J. Org. Chem.* **2002**, *67*, 426 – 430.

[10] An excess of α,β-unsaturated ketone required for complete consumption of aldehyde and optimized yields.

[11] Typical procedure for the BH reaction: To a solution of aldehyde (1.0 mmol), activated alkene (3.0 mmol), and **2a** (0.05 mmol) in anhydrous dichloromethane (2.0 mL) was added $TiCl_4$ (1.0 mmol) under an Ar atmosphere at room temperature. The mixture was stirred for 10 min and then it was quenched with saturated aqueous $NaHCO_3$ (5.0 mL). The inorganic precipitate was filtered through Celite. The organic phase was dried over Na_2SO_4 and concentrated in vacuo to give the crude product, which was purified by column chromatography on silica gel (ethyl acetate/hexane 1:3).

[12] S. K. Xi, H. Schmidt, C. Lensink, S. Kim, D. Wintergrass, L. M. Jacobson, J. G. Verkade, *Inorg. Chem.* **1990**, *29*, 2214 – 2220.

[13] L. M. Walsh, C. L. Winn, J. M. Goodman, *Tetrahedron Lett.* **2002**, *43*, 8219 – 8222.

[14] Under the same conditions the reaction of methyl vinyl ketone with *p*-nitrobenzaldehyde gave the BH adduct in 75% yield.

[15] Attempts to detect this intermediate by NMR spectroscopy have thus far failed.

[16] Electron-rich aromatic aldehydes such as anisaldehyde do not provide BH adducts when a more sterically hindered 3-substituted cyclohex-2-en-1-one is used.

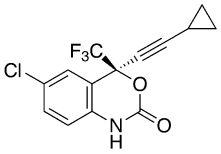
 © 2003 Wiley-VCH Verlag GmbH & Co. KGaA, Weinheim

Enantioselective Alkynylation

Enantioselective Alkynylation of Aromatic Ketones Catalyzed by Chiral Camphorsulfonamide Ligands**

*Gui Lu, Xingshu Li, Xian Jia, Wing Lai Chan, and Albert S. C. Chan**

Chiral tertiary propargylic alcohols are important pharmaceutical intermediates. The synthesis of these compounds by the catalytic asymmetric addition of carbon nucleophiles to ketones has met with only very limited success, although methods to promote the alkynylation of aldehydes are well-studied.[1–6] Grabowski and co-workers[7–10] and Jiang and Feng[11] realized the addition of lithium cyclopropylacetylide to a *p*-methoxybenzyl-protected ketoaniline in 98–99% *ee*. The reaction is a key step in the manufacturing of efavirenz (DMP 266), a drug used in the treatment of AIDS.[12]



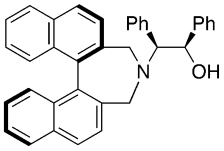
Efavirenz

However, large amounts of catalysts and the protection/deprotection of the aniline moiety are necessary. Grabowski and co-workers reported the direct alkynylation of ketoanilines (up to 99% *ee*) by alkynyl lithium or alkynyl magnesium reagents with *stoichiometric* amounts of chiral amino-alcohol and dialkyl zinc reagents.[13]

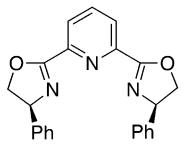
Carreira and co-workers developed a practical method for the synthesis of optically active secondary propargylic alcohols from terminal alkynes and aldehydes in the presence of $Zn(OTf)_2$ and Et_3N.[14–16] This method was applied to the alkynylation of ketoesters,[17] which exhibited reactivities between those of aldehydes and ketones. Kozlowski and DiMauro demonstrated the addition of diethylzinc reagents to α-ketoesters with chiral salen catalysts to give moderate enantiomeric excess.[18]

Organozinc reagents are also highly selective in nucleophilic addition to carbonyl compounds.[1–2] They can tolerate the presence of many functional groups that are reactive towards organolithium and -magnesium reagents, therefore may offer a useful alternative to these highly reactive nucleophiles. However, the low reactivities of organozinc species have limited their synthetic utility. Although three systems for the asymmetric addition of alkyl zinc reagents to ketones have been reported,[19–22] to the best of our knowledge, there was only one report of the catalytic, enantioselective addition of alkynyl zinc reagents to ketones.[23] From both fundamental and practical standpoints, it is highly desirable to develop new methods for the nucleophilic alkynylation of ketones with good stereocontrol.

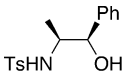
Our attempts to apply chiral binaphthol, titanium tetraisopropoxide, and alkynyl zinc reagents (which are known to be effective catalyst systems for the addition of alkynyl groups to aldehydes[3–6]) to the asymmetric alkynylation of ketones were unsuccessful, and no reaction was observed. The difficulty was mainly due to the inertness of ketones towards this reaction. With the expectation that the reactivity of ketones might be improved by using a stronger Lewis acid, we found that a considerable amount of tertiary propargylic alcohol was obtained by using $Cu(OTf)_2$ as a promoter in the reaction. In a preliminary screening study, we found that when chiral binaphthol, amino alcohol **1**, pybox **2**, and sulfonamide **3** were used as ligands, either poor enantioselectivity or undesired side products were obtained. On the other hand, the use of camphorsulfonamide ligand **4a** gave



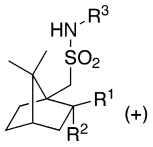
(*R,S,R*)-**1**



(*R,R*)-**2**



(*R,S*)-**3**



4a R^1= OH, R^2= H, R^3= benzyl (90% yield, 82% *ee*)
4b R^1= H, R^2= OH, R^3= benzyl (49% yield, 13% *ee*)
4c R^1= OH, R^2= H, R^3= 1-naphthylmethyl (92% yield, 88% *ee*)
4d R^1= OH, R^2= H, R^3= phenyl (32% yield, 61% *ee*)
4e R^1= OH, R^2= H, R^3= 1-naphthyl (51% yield, 65% *ee*)

90% yield of the product with 82% *ee*. This interesting result prompted us to examine the use of camphor derivatives in the enantioselective reaction. It was found that a sterically hindered ligand such as **4c** gave better yields, whereas ligand **4b** with the hydroxy group in the *endo* position gave very poor *ee*.

The asymmetric alkynylation of acetophenone in the presence of chiral ligand **4a** (**4c** in entries 8–11) in different solvents and with different copper salt/substrate ratios was examined (Table 1). The results revealed that CH_2Cl_2 was the best solvent and the optimum ratio of copper salt to acetophenone was 0.10.

The results of the addition of phenylacetylene to a variety of aromatic ketones catalyzed by chiral camphorsulfonamide **4a** and **4c** are summarized in Table 2. It appeared that electron-donating and electron-withdrawing substituents have little effect on the *ee* of the product. For example, 3′-methyl and 3′-bromoacetophenone gave products with 86 and 82% *ee*, respectively (Table 2, entries 8 and 10). 4′-Methyl- and 4′-bromoacetophenone also showed a similar trend (Table 2 entries 9 and 11).

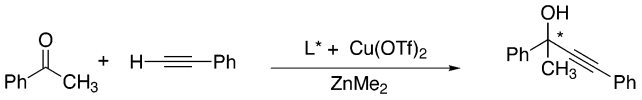
[*] Prof. A. S. C. Chan, G. Lu, Dr. X. Li, X. Jia, Dr. W. L. Chan
Open Laboratory of Chirotechnology
Institute of Molecular Technology for Drug Discovery and Synthesis
and
Department of Applied Biology and Chemical Technology
The Hong Kong Polytechnic University
Hong Kong (China)
Fax: (+852)-2364-9932
E-mail: bcachan@polyu.edu.hk

[**] We thank the University Grants Committee Areas of Excellence Scheme (AoE P/10-01) and The Hong Kong Polytechnic University ASD for the financial support for this study.

Supporting information for this article is available on the WWW under http://www.angewandte.org or from the author.

 DOI: 10.1002/anie.200352013 © 2003 Wiley-VCH Verlag GmbH & Co. KGaA, Weinheim

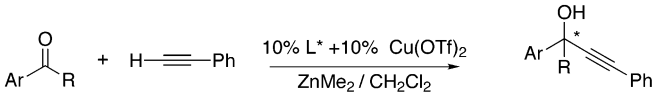
Table 1: The effect of reaction conditions on the enantioselectivity of the alkynylation of acetophenone.[a]



Entry	Solvent	Ligand	Copper triflate/substrate	Yield [%][b]	*ee* [%][c]
1	THF	**4a**	0.10	0	–
2	toluene	**4a**	0.10	87	36 (+)
3	CH_3OH	**4a**	0.10	0	–
4	acetone	**4a**	0.10	0	–
5	hexane	**4a**	0.10	39	13 (+)
6	Et_2O	**4a**	0.10	0	–
7	CH_2Cl_2	**4a**	0.10	90	82 (+)
8	CH_2Cl_2	**4c**	0.20[d]	80	85 (+)
9	CH_2Cl_2	**4c**	0.10	92	88 (+)
10	CH_2Cl_2	**4c**	0.05	88	86 (+)
11	CH_2Cl_2	**4c**	0.01	48	36 (+)

[a] **4a** or **4c** as chiral ligand, acetophenone/phenylacetylene/Me_2Zn = 0.4:1.04:1.2 (molar ratio), 0 °C, 2 mL solvent, 48 h. [b] Yields of isolated products. [c] The enantiomeric excess was determined by HPLC analysis of the alcohols. The sign of rotation of the predominant enantiomer is indicated in parentheses. [d] A large amount of CH_2Cl_2 (4 mL) was used to dissolve the $Cu(OTf)_2$.

Table 2: Enantioselective additions of phenylacetylene to aromatic ketones.[a]



Entry	Substrate	Ligand	Yield [%][b]	*ee* [%][c]
1	acetophenone	**4a**	90	82 (+)
2	acetophenone	**4c**	92	88 (+)
3	2′-bromoacetophenone	**4a**	39	87 (−)
4	2′-bromoacetophenone	**4c**	65	96 (−)
5	2′-chloroacetophenone	**4c**	94	97 (−)
6	2′-fluoroacetophenone	**4c**	91	96 (−)
7	2′-methylacetophenone	**4c**	49	96 (−)
8	3′-bromoacetophenone	**4c**	80	82 (+)
9	4′-bromoacetophenone	**4c**	75	91 (+)
10	3′-methylacetophenone	**4c**	83	86 (+)
11	4′-methylacetophenone	**4c**	77	92 (+)
12	2′-naphthacetophenone	**4c**	75	85 (+)
13	propiophenone	**4c**	57	71 (+)

[a] **4a** or **4c** as chiral ligand, ketone/ligand/$Cu(OTf)_2$/Me_2Zn = 0.4:0.04:0.04:1.2 (molar ratio), CH_2Cl_2 as solvent, 0 °C, 48 h. [b] Yields of isolated products. [c] The enantiomeric excess was determined by HPLC analysis of the alcohols. The sign of rotation of the predominant enantiomer is indicated in parentheses.

Substituents at the *ortho* position of the substrate had a favorable effect on the enantioselectivity. Both 2′-methyl, 2′-fluoro, 2′-chloro, and 2′-bromoacetophenone gave excellent enantioselectivities (Table 2, entries 4–7). The best enantioselectivity (97% *ee*) was obtained in the alkynylation of 2′-chloroacetophenone in the presence of chiral ligand **4c**. It is possible that the proper steric hindrance of the *ortho* substituents restricts the orientation of the substrates and thus results in higher enantioselectivities for the alkynylation of such ketones.

For the alkynylation of α,β-unsaturated ketones, such as *trans*-4-phenyl-3-buten-2-one, moderate selectivity (85% yield, 73% *ee*) was obtained. The reactions of aliphatic terminal alkynes with acetophenone gave low enantioselectivity (54% *ee* when using trimethylsilylacetylene).

In conclusion, camphorsulfonamides are effective chiral catalysts for the production of tertiary propargylic alcohols with good to excellent enantioselectivities. This work represents a highly enantioselective catalytic addition of alkynyl zinc reagents to simple ketones. Further studies on the scope and mechanism of this reaction are underway.

Received: May 30, 2003 [Z52013]

Keywords: alkynylation · asymmetric catalysis · enantioselectivity · ketones · nucleophilic addition

[1] K. Soai, S. Niwa, *Chem. Rev.* **1992**, *92*, 833–856.
[2] L. Pu, H.-B. Yu, *Chem. Rev.* **2001**, *101*, 757–824.
[3] G. Lu, X. Li, W. L. Chan, A. S. C. Chan, *Chem. Commun.* **2002**, 172–173.
[4] X. Li, G. Lu, W. H. Kwok, A. S. C. Chan, *J. Am. Chem. Soc.* **2002**, *124*, 12636–12637.
[5] D. Moore, L. Pu, *Org. Lett.* **2002**, *4*, 1855–1857.
[6] G. Gao, D. Moore, R.-G. Xie, L. Pu, *Org. Lett.* **2002**, *4*, 4143–4146.
[7] A. Thompson, E. G. Corley, M. F. Huntington, E. J. J. Grabowski, *Tetrahedron Lett.* **1995**, *36*, 8937–8940.
[8] A. Thompson, E. G. Corley, M. F. Huntington, E. J. J. Grabowski, J. F. Remenar, D. B. Collum, *J. Am. Chem. Soc.* **1998**, *120*, 2028–2038.
[9] M. E. Pierce, R. L. Parsons, Jr., L. A. Radesca, Y. S. Lo, S. Silverman, J. R. Moore, Q. Islam, A. Choudhury, J. M. D. Fortunak, D. Nguyen, C. Luo, S. J. Morgan, W. P. Davis, P. N. Confalone, C.-y. Chen, R. D. Tillyer, L. Frey, L. Tan, F. Xu, D. Zhao, A. Thompson, E. G. Corley, E. J. J. Grabowski, R. Reamer, P. J. Reider, *J. Org. Chem.* **1998**, *63*, 8536–8543.
[10] F. Xu, R. A. Reamer, R. Tillyer, J. M. Cummins, E. J. J. Grabowski, P. J. Reider, D. B. Collum, J. C. Huffman, *J. Am. Chem. Soc.* **2000**, *122*, 11212–11218.
[11] B. Jiang, Y. Feng, *Tetrahedron Lett.* **2002**, *43*, 2975–2977.
[12] J. W. Corbett, S. S. Ko, J. D. Rodgers, S. Jeffrey, L. T. Bacheler, R. M. Klabe, S. Diamond, C. M. Lai, S. R. Rabel, J. A. Saye, S. P. Adams, G. L. Trainor, P. S. Anderson, S. K. Erickson-Viitanen, *Antimicrob. Agents Chemother.* **1999**, *43*, 2893–2897.
[13] L. Tan, C.-y. Chen, R. D. Tillyer, E. J. J. Grabowski, P. J. Reider, *Angew. Chem.* **1999**, *111*, 724–727; *Angew. Chem. Int. Ed.* **1999**, *38*, 711–713.
[14] D. E. Frantz, R. Fassler, C. S. Tomooka, E. M. Carreira, *Acc. Chem. Res.* **2000**, *33*, 373–381.
[15] D. E. Frantz, R. Fassler, E. M. Carreira, *J. Am. Chem. Soc.* **2000**, *122*, 1806–1807.
[16] D. Boyall, F. López, H. Sasaki, D. Frantz, E. M. Carreira, *Org. Lett.* **2000**, *2*, 4233–4236.
[17] B. Jiang, Z. Chen, X. Tang, *Org. Lett.* **2002**, *4*, 3451–3453.
[18] E. F. DiMauro, M. C. Kozlowski, *Org. Lett.* **2002**, *4*, 3781–3784.
[19] P. I. Dosa, G. C. Fu, *J. Am. Chem. Soc.* **1998**, *120*, 445–446.
[20] D. J. Ramón, M. Yus, *Tetrahedron Lett.* **1998**, *39*, 1239–1242.
[21] D. J. Ramón, M. Yus, *Tetrahedron* **1998**, *54*, 5651–5666.
[22] C. Garcia, L. K. LaRochelle, P. J. Walsh, *J. Am. Chem. Soc.* **2002**, *124*, 10970–10971.
[23] After acceptance of this Communication, an enantioselective Zn(salen)-catalyzed alkynylation of ketones with moderate enantioselectivities (up to 80%) was reported: P. G. Cozzi, *Angew. Chem.* **2003**, *115*, 3001–3004; *Angew. Chem. Int. Ed.* **2003**, *42*, 2895–2898.

 © 2003 Wiley-VCH Verlag GmbH & Co. KGaA, Weinheim

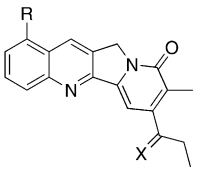
Synthesis of Quinoline Alkaloids

A Modular Approach to Oxoindolizino Quinolines: Efficient Synthesis of Mappicine Ketone (Nothapodytine B)**

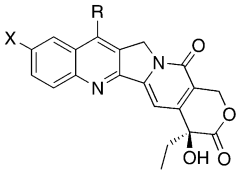
Gajendra B. Raolji, Stéphanie Garçon, Andrew E. Greene, and Alice Kanazawa**

In memory of Patrick Léon

Oxoindolizino quinolines include the natural products mappicine ketone (nothapodytine B, **1a**),[1] nothapodytine A (**1b**),[1] mappicine (**1c**),[2] and camptothecin (**2a**),[3] as well as several chemotherapeutic derivatives of camptothecin, such as topotecan (**2b**) and irinotecan (**2c**).[3] While the



1a: Mappicine ketone (nothapodytine B) (R = H, X = O)
1b: Nothapodytine A (R = OCH_3, X = O)
1c: Mappicine (R = H, X = α-OH,β-H)

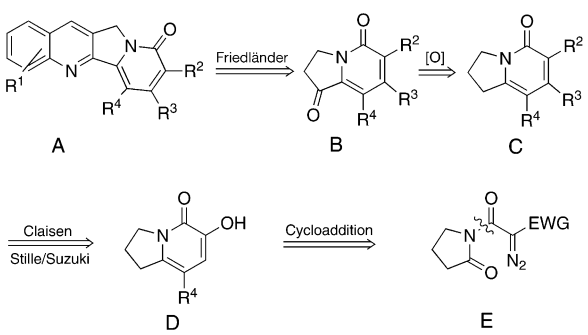


2a: Camptothecin (X = R = H)
2b: Topotecan (X = OH, R = $CH_2N(CH_3)_2 \cdot HCl$)
2c: Irinotecan (X = OCOPipPip, R = C_2H_5)

importance of these and related alkaloids has already fostered many synthetic approaches, beginning with that by Stork and Schultz[4] some 30 years ago, additional, and in particular, efficient and flexible routes remain highly desirable for discovering derivatives with improved biological profiles.

Our envisioned modular approach to these compounds is shown in retrosynthetic form in Scheme 1. A Friedländer condensation, which is ideal for accessing diversely substituted quinolines, was planned for the formation of the tetracyclic framework of the oxoindolizino quinolines.[5] The requisite ketones **B** were viewed as products of benzylic-type oxidation of pyridones **C**, which would originate from various Claisen and Stille/Suzuki transformations of hydroxypyridones **D**.[6] Hydroxypyridones **D** are easily available through cycloaddition of the isomünchnone dipoles derived from diazo imides **E**.[7]

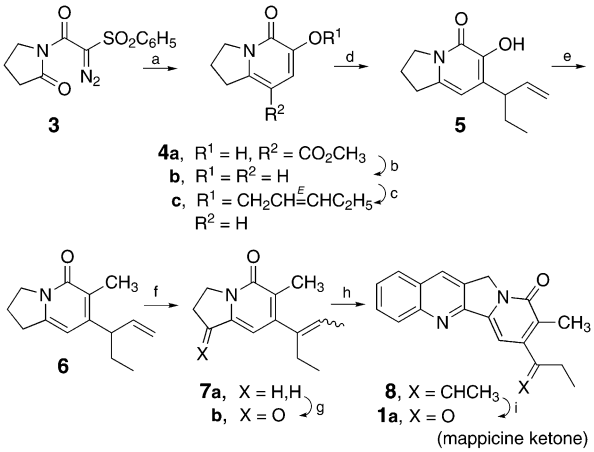
We now illustrate the feasibility of this general strategy by way of an effective synthesis of mappicine ketone (**1a**). Mappicine ketone, present in small amounts in *Nothapodytes foetida* (a plant found in India),[1] and formed by thermolysis of camptothecin,[8] displays strong, selective activity against



Scheme 1. Retrosynthesis of oxoindolizino quinolines **A**.

herpes viruses (HSV-1 and HSV-2, including Acyclovir-resistant forms) and human cytomegalovirus.[9,10]

The synthesis of **1a** began with the formation of the known adduct **4a** by cycloaddition of the carbonyl ylide derived from **3** with methyl acrylate (Scheme 2).[11] This



Scheme 2. Synthesis of **1a**. a) $[Rh(OCOCH_3)_2]_2$, $H_2C{=}CHCO_2CH_3$, C_6H_6, 90 °C, 14 h (81 %); b) 48 % aq HBr, 140 °C, 14 h (82 %); c) (*E*)-$BrCH_2CH{=}CHC_2H_5$, Cs_2CO_3, DMF, 70 °C, 1 h; d) C_6H_5Cl, reflux, 24 h (74 %, 2 steps); e) $C_6H_5NTf_2$, $N(C_2H_5)_3$, CH_2Cl_2, 0→20 °C, 18 h (94 %); $Sn(CH_3)_4$, $[PdCl_2\{P(C_6H_5)_3\}_2]$, LiCl, DMF, 110 °C, 2 h (89 %); f) $RhCl_3$, C_2H_5OH, 100 °C, 0.5 h (91 %); g) NaHMDS, O_2, $P(OC_2H_5)_3$, THF, −78 °C, 2 h (76 %); PDC, 4 Å molecular sieves, CH_2Cl_2, 0 °C, 2 h (81 %); h) *o*-$NH_2C_6H_4CHO$, *p*-TsOH, $C_6H_5CH_3$, reflux, 20 h (73 %); i) O_3, CH_2Cl_2-CH_3OH, −78 °C; $(CH_3)_2S$, −78→20 °C, 16 h (60 %). NaHMDS = sodium hexamethyldisilazide, PDC = pyridinium dichromate.

multistep sequence proceeded smoothly and in high yield when catalyzed by rhodium(II) acetate. Hot aqueous hydrobromic acid then effected decarbomethoxylation of **4a** to give **4b** in 82 % yield.[11] Etherification of **4b** with commercially available (*E*)-1-bromo-2-pentene and cesium carbonate in dimethylformamide produced the expected substitution product, which cleanly underwent Claisen rearrangement[6a] in refluxing chlorobenzene to afford the desired derivative **5** in 74 % overall yield. This transformation is a rare example of a Claisen rearrangement in a hydroxypyridone system.[12]

The α-hydroxypyridone **5** was converted into its triflate derivative under standard conditions. This was followed by Stille coupling[6b] with tetramethyltin to provide α-methyl-

[*] Dr. A. E. Greene, Dr. A. Kanazawa, Dr. G. B. Raolji, S. Garçon
Chimie Recherche (LEDSS)
Université Joseph Fourier de Grenoble
38041 Grenoble Cedex 9 (France)
Fax: (+33) 4-7651-4494
E-mail: andrew.greene@ujf-grenoble.fr
alice.kanazawa@ujf-grenoble.fr

[**] We thank Prof. P. Dumy and Drs. B. Hartmann and J.-P. Vors for their interest in our work, Ms. B. Escudé for technical help, and Aventis and the CNRS (UMR 5616) for financial support.

 DOI: 10.1002/anie.200352094 © 2003 Wiley-VCH Verlag GmbH & Co. KGaA, Weinheim

pyridone **6** in 84% yield. In the presence of rhodium(III) chloride in hot ethanol,[13] **6** rapidly isomerized to olefin **7a** (91%). The success of this key transformation derives from the carbon symmetry of the β substituent in pyridone **6**. Oxidation[14] of **7a** in two steps then selectively generated the Friedländer substrate **7b**, which reacted with *o*-aminobenzaldehyde to give oxoindolizino quinoline **8** in 73% yield. Pleasingly, ozone in dichloromethane/methanol at −78 °C accomplished selective double-bond cleavage in **8** to provide mappicine ketone (m.p. 233–234 °C), with spectroscopic and chromatographic properties identical to those of the naturally derived material (m.p. 231–232 °C).[8b]

In summary, a concise, efficient synthesis of mappicine ketone has been used to demonstrate a modular approach to oxoindolizino quinolines. By virtue of the variations that are possible in the substituents R^1–R^4 (Scheme 1), a wide range of new camptothecinoids should be easily available for biological testing. Continuing efforts are being directed toward the preparation of irinotecan and derivatives by this approach.

Experimental Section

8: A mixture of ketone **7b** (200 mg, 0.86 mmol), *o*-aminobenzaldehyde (126 mg, 1.04 mmol), and *p*-toluenesulfonic acid monohydrate (8 mg, 0.04 mmol) in toluene (10 mL) was refluxed (Dean–Stark trap) for 20 h. The solvent was then removed under reduced pressure, and the crude product was purified by column chromatography on silica gel to yield 200 mg (73%) of quinoline **8** as a mixture of *E* and *Z* isomers. FTIR: $\tilde{\nu}$ = 1650, 1590, 1375, 1226, 968, 834, 755, 725 cm^{-1}; ^1H NMR ($CDCl_3$, 300 MHz, major isomer): δ = 8.31 (s, 1H), 8.16 (d, J = 8.4 Hz, 1H), 7.87 (d, J = 8.1 Hz, 1H), 7.76 (m, 1H), 7.59 (m, 1H), 7.12 (s, 1H), 5.41 (q, J = 6.9 Hz, 1H), 5.25 (s, 2H), 2.45 (q, J = 7.6 Hz, 2H), 2.21 (s, 3H), 1.79 (d, J = 6.9 Hz, 3H), 0.94 ppm (t, J = 7.6 Hz, 3H); ^{13}C NMR ($CDCl_3$, 75.5 MHz, major isomer): δ = 162.0, 153.7, 153.5, 148.8, 141.5, 140.9, 130.7, 130.2, 129.5, 128.9, 128.1, 127.9, 127.3, 126.8, 124.2, 103.2, 49.8, 23.7, 14.2, 13.3, 12.5 ppm; HRMS calcd for $[C_{21}H_{20}N_2O+H]^+$: 317.1654; found: 317.1661.

Selected data for other compounds: **4c**: FTIR: $\tilde{\nu}$ = 1653, 1599, 1285, 1248, 1219, 1185, 1054 cm^{-1}; ^1H NMR ($CDCl_3$, 300 MHz): δ = 6.60 (d, J = 7.4 Hz, 1H), 5.89 (d, J = 7.4 Hz, 1H), 5.88 –5.72 (m, 1H), 5.65–5.54 (m, 1H), 4.41 (d, J = 5.9 Hz, 2H), 4.01 (t, J = 7.1 Hz, 2H), 2.93 (t, J = 7.7 Hz, 2H), 2.14–2.04 (m, 2H), 2.02–1.98 (m, 2H), 0.92 ppm (t, J = 7.5, 3H); ^{13}C NMR ($CDCl_3$, 75.5 MHz): δ = 157.4, 146.7, 140.9, 137.1, 123.5, 116.5, 99.0, 69.7, 48.6, 30.7, 25.1, 22.0, 13.0 ppm; HRMS calcd for $[C_{13}H_{17}NO_2+H]^+$: 220.1338; found: 220.1319. **5**: m.p. 120–121 °C; FTIR: $\tilde{\nu}$ = 3245, 1662, 1634, 1595, 1291, 1237 cm^{-1}; ^1H NMR ($CDCl_3$, 300 MHz): δ = 6.68 (br s, 1H), 5.94 (s, 1H), 5.91–5.82 (m, 1H), 5.09–5.01 (m, 2H), 4.11 (t, J = 7.2 Hz, 2H), 3.55 (q, J = 7.4 Hz, 1H), 2.96 (t, J = 7.6 Hz, 2H), 2.21–2.11 (m, 2H), 1.73–1.55 (m, 2H), 0.85 ppm (t, J = 7.4 Hz, 3H); ^{13}C NMR ($CDCl_3$, 75.5 MHz): δ = 157.0, 141.0, 139.7, 138.3, 131.4, 115.0, 100.8, 48.5, 43.9, 30.7, 26.4, 22.3, 11.9 ppm; HRMS calcd for $[C_{13}H_{17}NO_2+H]^+$: 220.1338; found: 220.1345. **6**: m.p. 76–77 °C; FTIR: $\tilde{\nu}$ = 1641, 1581, 1537, 1184, 1009, 920, 824, 756, 680 cm^{-1}; ^1H NMR ($CDCl_3$, 300 MHz): δ = 5.95 (s, 1H), 5.86–5.74 (m, 1H), 5.09–4.98 (m, 2H), 4.10 (t, J = 7.3 Hz, 2H), 3.38 (q, J = 7.4, 1H), 2.99 (t, J = 7.7 Hz, 2H), 2.17–2.07 (m, 2H), 2.11 (s, 3H), 1.73–1.52 (m, 2H), 0.85 ppm (t, J = 7.4 Hz, 3H); ^{13}C NMR ($CDCl_3$, 75.5 MHz): δ = 162.4, 152.0, 145.9, 139.8, 122.6, 115.2, 99.8, 48.7, 47.0, 31.5, 27.0 , 21.5, 11.9, 11.7 ppm; HRMS: calcd for $[C_{14}H_{19}NO+H]^+$: 218.1545; found: 218.1558. **7a**: m.p. 74–75 °C; FTIR: $\tilde{\nu}$ = 1646, 1570, 1541, 1314, 1209, 1168, 1050, 947, 834, 772, 665 cm^{-1}; ^1H NMR ($CDCl_3$, 300 MHz, major isomer): δ = 5.86 (s, 1H), 5.25 (q, J = 6.9 Hz, 1H), 4.10 (t, J = 7.2 Hz, 2H), 2.99 (t, J = 7.4 Hz, 2H), 2.30 (q, J = 7.5 Hz, 2H), 2.18–2.08 (m, 2H), 2.02 (s, 3H), 1.72 (d, J = 6.9 Hz, 3H), 0.87 ppm (t, J = 7.5 Hz, 3H); ^{13}C NMR ($CDCl_3$, 75.5 MHz, major isomer): δ = 162.8, 153.1, 145.4, 141.3, 123.2, 120.2, 102.9, 48.8, 31.5, 23.8, 21.7, 13.7, 13.3, 12.5 ppm; HRMS: calcd for $[C_{14}H_{19}NO+H]^+$: 218.1545; found: 218.1561. **7b**: m.p. 70–71 °C; FTIR: $\tilde{\nu}$ = 1735, 1644, 1603, 1360, 1314, 1267, 1200, 1116, 838, 763, 668 cm^{-1}; ^1H NMR ($CDCl_3$, 300 MHz, major isomer): δ = 6.68 (s, 1H), 5.32 (q, J = 6.8 Hz, 1H), 4.25 (t, J = 6.9 Hz, 2H), 2.85 (t, J = 6.9 Hz, 2H), 2.34 (q, J = 7.6 Hz, 2H), 2.16 (s, 3H), 1.75 (d, J = 6.8 Hz, 3H), 0.87 ppm (t, J = 7.6 Hz, 3H); ^{13}C NMR ($CDCl_3$, 75.5 MHz, major isomer): δ = 197.2, 162.0, 152.3, 140.0, 135.9, 133.2, 124.9, 105.9, 41.8, 33.8, 23.6, 14.7, 13.3, 12.3 ppm; HRMS: calcd for $[C_{14}H_{17}NO_2+H]^+$: 232.1338; found: 232.1329. **1a**: m.p. 233–234 °C; FTIR: $\tilde{\nu}$ = 3087, 1702, 1654, 1619, 1599, 1379, 1185, 933, 838, 762 cm^{-1}; ^1H NMR ($CDCl_3$, 300 MHz, major isomer): δ = 8.34 (s, 1H), 8.17 (d, J = 8.5 Hz, 1H), 7.90 (d, J = 8.0 Hz, 1H), 7.79 (m, 1H), 7.62 (m, 1H), 7.22 (s, 1H), 5.27 (s, 2H), 2.88 (q, J = 7.3 Hz, 2H), 2.28 (s, 3H), 1.23 ppm (t, J = 7.3 Hz, 3H); ^{13}C NMR ($CDCl_3$, 75.5 MHz): δ = 205.5, 161.7, 152.9, 148.8, 148.2, 143.4, 131.0, 130.4, 129.6, 128.6, 128.1, 128.0, 127.7, 127.0, 97.9, 50.2, 36.0, 13.6, 7.8 ppm; HRMS: calcd for $[C_{19}H_{16}N_2O_2+H]^+$: 305.1290; found: 305.1313.

Received: June 10, 2003 [Z52094]

Keywords: cross-coupling · cycloaddition · isomerization · rearrangement · total synthesis

[1] T.-S. Wu, Y.-Y. Chan, Y.-L. Leu, C.-Y. Chern, C.-F. Chen, *Phytochemistry* **1996**, *42*, 907 – 908.
[2] T. R. Govindachari, K. R. Ravindranath, N. Viswanathan, *J. Chem. Soc. Perkin Trans. 1* **1974**, 1215 – 1217.
[3] Reviews on camptothecin and derivatives: a) *Camptothecins: New Anticancer Agents* (Eds.: M. Potmesil, H. Pinedo), CRC, Boca Raton, **1995**; b) S. Sawada, T. Yokokura, T. Miyasaka, *Curr. Pharm. Des.* **1995**, *1*, 113 – 132; c) M. Torck, M. Pinkas, *J. Pharm. Belg.* **1996**, *51*, 200 – 207; d) C. R. Hutchinson, *Tetrahedron* **1981**, *37*, 1047 – 1065.
[4] G. Stork, A. G. Schultz, *J. Am. Chem. Soc.* **1971**, *93*, 4074 – 4075.
[5] Review on Friedländer quinoline synthesis: C.-C. Cheng, S. J. Yan, *Org. React.* **1982**, *28*, 37 – 201.
[6] a) Reviews on the Claisen rearrangement: S. J. Rhoads, N. R. Raulins, *Org. React.* **1975**, *22*, 1 – 252; S. Blechert, *Synthesis* **1989**, 71 – 82; b) Review on Stille coupling: V. Farina, V. Krishnamurthy, W. J. Scott, *Org. React.* **1997**, *50*, 1 – 652; c) Reviews on Suzuki coupling: N. Miyaura, A. Suzuki, *Chem. Rev.* **1995**, *95*, 2457 – 2483; S. R. Chemler, D. Trauner, S. J. Danishefsky, *Angew. Chem.* **2001**, *113*, 4676 – 4701; *Angew. Chem. Int. Ed.* **2001**, *40*, 4544 – 4568.
[7] Reviews on carbonyl ylide cycloaddition: a) M. C. McMills, D. Wright in *The Chemistry of Heterocyclic Compounds*: *Synthetic Applications of 1,3-Dipolar Cycloaddition Chemistry Toward Heterocycles and Natural Products* (Eds.: A. Padwa, W. H. Pearson), Wiley, New York, **2002**, pp. 253 – 314; b) G. Mehta, S. Muthusamy, *Tetrahedron* **2002**, *58*, 9477 – 9504.
[8] a) J. M. D. Fortunak, A. R. Mastrocola, M. Mellinger, J. L. Wood, *Tetrahedron Lett.* **1994**, *35*, 5763 – 5764; b) B. Das, P. Madhusudhan, A. Kashinatham, *Bioorg. Med. Chem. Lett.* **1998**, *8*, 1403 – 1406; c) See also W. D. Kingsbury, *Tetrahedron Lett.* **1988**, *29*, 6847 – 6850; B. Das, P. Madhusudhan, A. Kashinatham, *Tetrahedron Lett.* **1998**, *39*, 431 – 432.
[9] a) I. Pendrak, S. Barney, R. Wittrock, D. M. Lambert, W. D. Kingsbury, *J. Org. Chem.* **1994**, *59*, 2623 – 2625; b) I. Pendrak, R. Wittrock, W. D. Kingsbury, *J. Org. Chem.* **1995**, *60*, 2912 – 2915.
[10] Previous syntheses of mappicine ketone: L. Carles, K. Narkunan, S. Penlou, L. Rousset, D. Bouchu, M. A. Ciufolini, *J. Org. Chem.* **2002**, *67*, 4304 – 4308, and references therein.

 © 2003 Wiley-VCH Verlag GmbH & Co. KGaA, Weinheim

[11] A. Padwa, S. M. Sheehan, C. S. Straub, *J. Org. Chem.* **1999**, *64*, 8648 – 8659.
[12] Two other examples: a) B. B. Jarvis, C. B. Anderson, *J. Heterocycl. Chem.* **1983**, *20*, 471 – 473; b) K. C. Majumdar, A. K. Kundu, P. Chatterjee, *J. Chem. Res. Synop.* **1995**, 386 – 387.
[13] a) J. Andrieux, D. H. R. Barton, H. Patin, *J. Chem. Soc. Perkin Trans. 1* **1977**, 359 – 363; b) P. A. Grieco, N. Marinovic, *Tetrahedron Lett.* **1978**, 2545 – 2548.
[14] a) E. J. Corey, H. E. Ensley, *J. Am. Chem. Soc.* **1975**, *97*, 6908 – 6909; b) W. Shen, C. A. Coburn, W. G. Bornmann, S. J. Danishefsky, *J. Org. Chem.* **1993**, *58*, 611 – 617.

 © 2003 Wiley-VCH Verlag GmbH & Co. KGaA, Weinheim

Radical Additions to C=N Bonds

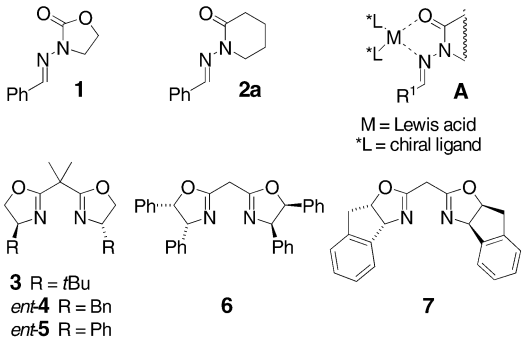
Enantioselective Radical Addition to *N*-Acyl Hydrazones Mediated by Chiral Lewis Acids**

Gregory K. Friestad, Yuehai Shen, and Erik L. Ruggles*

Radical addition reactions can generate new carbon–carbon bonds under mild, nonbasic conditions that may be compatible with a broad range of functionality within either the radical precursor or acceptor.[1] In recent years, campaigns toward achieving enantioselectivity in these processes have achieved some remarkable success, particularly in additions to C=C bonds.[2,3] Reductive radical addition to C=N bonds of imino radical acceptors generates chiral α-branched amines,[4] a class of compounds ubiquitous in biochemistry, medicinal chemistry, and natural product synthesis. The nonbasic character of alkyl radicals takes on particular importance in this case because the use of strongly basic nucleophiles may be compromised by the presence of acidic or electrophilic functionalities. Despite the very recent development of the reaction methodology, intermolecular radical addition to C=N bonds can already be carried out with acyclic stereocontrol through 1,2-asymmetric induction[5] or by using chiral auxiliaries covalently attached to either the carbon branch[6] or the nitrogen substituent.[7,8] We now report the first highly enantioselective radical additions to imino acceptors mediated by chiral Lewis acids, and also present the first evidence for chiral catalyst turnover in radical additions to C=N bonds.

Recently, asymmetric induction with chiral Lewis acids has been documented for radical addition to glyoxylate imines,[6b,9] but no catalytic cycle was evident judging from the low yield and/or high catalyst loading.[10] In these reactions, the two-point-binding glyoxylate moiety places an undesirable restriction on structural variations to the radical acceptor. We envisioned that incorporating the potential of chelation within the nitrogen substituent of the imine radical acceptor might be the foundation for a more versatile approach; the two-point-binding motif of the imine substrate (i.e. **A**, Scheme 1) would then be completely independent of its aldehyde precursor. With this in mind, we chose *N*-acyl hydrazones as a class of substrates for the development of the first asymmetric catalytic radical addition to C=N bonds.

Chiral oxazolidinone-derived *N*-acyl hydrazones are effective radical acceptors, but only upon activation with Lewis acids.[8,11] This fact gave rise to the expectation that achiral oxazolidinone **1** (Scheme 1) would not compete as a radical acceptor in the presence of its corresponding chelate **A** activated by a chiral Lewis acid. Our initial experiments, involving a screening of several chiral ligands (1 equiv) and Lewis acids (1 equiv) in the addition of isopropyl iodide to **1** using Et_3B/O_2 initiation at room temperature, met with disappointment. Although $ZnCl_2$ and $InCl_3$ had previously proved effective in activating the related chiral oxazolidinone-derived hydrazones,[8] significant enantioselectivity was never observed with **1**, and yields of the reductive isopropyl addition product were modest at best.



Scheme 1. *N*-Acyl hydrazones, selected bisoxazoline ligands, and their predicted binding mode (**A**) with Lewis acids.

Surprisingly, though, with valerolactam-derived *N*-acyl hydrazone acceptor **2a**,[12] we found a dramatic improvement in the selectivity of isopropyl addition (Scheme 2).[13] With 1 equivalent each of $ZnCl_2$ and bisoxazoline ligand **3**, a reasonable yield of reductive addition product **8a** was obtained (64%), but there was still no stereocontrol (Table 1, entry 1).[14] $InCl_3$ and $Mg(ClO_4)_2$ offered only modest yields (Table 1, entries 2 and 3), but we were gratified to find 57 and 66% *ee*, respectively, with these Lewis acids. Before any optimization, these results offered higher enantioselectivity than previously reported for any radical addition to a C=N bond.

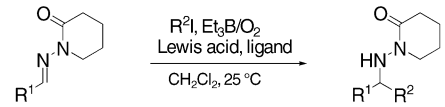
Interestingly, in further variations of the Lewis acid, we found that copper(II) trifluoromethanesulfonate ($Cu(OTf)_2$) gave promising results (41% yield, 59% *ee*). In optimization studies, we tested the effect of a less polar medium, which we assumed would facilitate the assembly of a ternary complex of ligand, Lewis acid, and substrate. In contrast to $Mg(ClO_4)_2$[15] $Cu(OTf)_2$ did not exhibit a reversal of selectivity upon

[*] Prof. G. K. Friestad, Dr. Y. Shen, Dr. E. L. Ruggles
Department of Chemistry, University of Vermont
Burlington, VT 05405 (USA)
Fax: (+1) 802-656-8705
E-mail: gregory.friestad@uvm.edu

[**] We thank the National Science Foundation (CHE-0096803), Research Corporation, and the Petroleum Research Fund for generous support of this work.

Supporting information for this article is available on the WWW under http://www.angewandte.org or from the author.

 DOI: 10.1002/anie.200352104 © 2003 Wiley-VCH Verlag GmbH & Co. KGaA, Weinheim



2a R^1 = Ph
2b R^1 = *p*-C_6H_4OMe
2c R^1 = *p*-C_6H_4Cl

8a–c (R^2=*i*Pr)
9 (R^2=Et)
10 (R^2=*c*-C_5H_9)
11 (R^2=*c*-C_6H_{11})
12 (R^2=CH_2Cl)

Scheme 2. Enantioselective radical addition to *N*-acyl hydrazones.

Table 1: Studies of Lewis acids, reaction medium, and chiral ligand structure in the addition of the isopropyl radical to **2a** (Scheme 2).[a]

Entry	Chiral Ligand	Lewis acid	Solvent	Yield[b] (**8a**) [%]	*ee*[c] [%]
1	**3**	$ZnCl_2$	CH_2Cl_2	64	< 5 (*R*)
2	**3**	$InCl_3$	CH_2Cl_2	33	57 (*R*)
3	**3**	$Mg(ClO_4)_2$	CH_2Cl_2	41	66 (*R*)
4	**3**	$Mg(ClO_4)_2$	PhH/CH_2Cl_2 (2:1)	21	30 (*S*)
5	**3**	$Cu(OTf)_2$	CH_2Cl_2	41	59 (*R*)
6[d,e]	**3**	$Cu(OTf)_2$	PhH/CH_2Cl_2 (2:1)	67	84 (*R*)
7[d–f]	**3**	$Cu(OTf)_2$	PhH/CH_2Cl_2 (2:1)	66	**95** (*R*)
8[d–g]	**3**	$Cu(OTf)_2$	PhH/CH_2Cl_2 (2:1)	**94**	86 (*R*)
9[d,e]	**4**	$Cu(OTf)_2$	PhH/CH_2Cl_2 (2:1)	47	5 (*S*)
10[d,e]	**5**	$Cu(OTf)_2$	PhH/CH_2Cl_2 (2:1)	74	72 (*S*)
11[d,e]	**6**	$Cu(OTf)_2$	PhH/CH_2Cl_2 (2:1)	73	94 (*S*)
12[d,e]	**7**	$Cu(OTf)_2$	PhH/CH_2Cl_2 (2:1)	38	< 1

[a] Reaction conditions: Lewis acid (1 equiv), chiral ligand (1 equiv), 2-iodopropane (6 equiv), Et_3B/O_2 (6 equiv), 25 °C. For details see Experimental Section. [b] Yield of isolated product. [c] Enantiomeric excess by HPLC (95:5 hexane/2-propanol, Chiralcel OD or AD). Configuration of major product indicated in parentheses. [d] Et_3N was added after the reaction to facilitate isolation of the product. [e] In the presence of powdered molecular sieves (4 Å). [f] Preformed aquo complex [Cu(**3**)$(H_2O)_2(OTf)_2$] was used. [g] Larger amounts (10 equiv) of 2-iodopropane and Et_3B were used.

changing to benzene/CH_2Cl_2, and in this less polar medium, very good (*R*) enantioselectivity[16] was observed (Table 1, entries 3–6). Powdered molecular sieves (4 Å) had little effect on selectivity or yield. This facilitated the use of the preformed aquo complex [Cu(**3**)$(H_2O)_2(OTf)_2$], which can be activated by molecular sieves in situ as reported by Evans et al.[17] This latter modification (Table 1, entry 7) gave enhanced operational simplicity and raised the selectivity to 95% *ee* (66% yield). The yield improved with the use of larger amounts of 2-iodopropane and Et_3B (Table 1, entry 8), but this came at the expense of some selectivity.

Other bisoxazoline ligands were next examined.[18] Neither **4** nor **7** afforded enantioselectivity (Table 1, entries 9 and 12), but ligand **5** gave fairly good stereocontrol (Table 1, entry 10). The more highly substituted bisoxazoline **6** gave very high enantioselectivity with an improved yield relative to ligand **3** (compare Table 1, entries 7 and 11).

High enantioselectivity was maintained with variations to both radical precursor and acceptor (Table 2). Without further ligand optimization, additions of isopropyl to hydrazones **2b,c**[12] and additions of various radicals to **2a** were all highly enantioselective (Table 2, entries 1–6).[19] Importantly, the chloromethyl group of **12** (Table 2, entry 6) offers additional functionality for further synthetic transformations.

Table 2: Scope of radical addition to hydrazones **2a–2c** promoted by [Cu(**3**)$(H_2O)_2(OTf)_2$] and effects of Cu^{II} catalyst loading.[a]

Entry	Halide	**2**	Catalyst [equiv]	Product	Yield [%][b]	*ee* [%][c]
1	*i*PrI	**b**	1	(+)-**8b**	46	90
2	*i*PrI	**c**	1	(+)-**8c**	53	81
3	EtI[d]	**a**	1	(+)-**9**	88	83
4	*c*-C_5H_9I[d]	**a**	1	(+)-**10**	86	84
5	*c*-$C_6H_{11}I$[d]	**a**	1	(+)-**11**	84	89
6	$ClCH_2I$[d]	**a**	1	(+)-**12**	44[e]	95
7	*i*PrI	**a**	1	(*R*)-(+)-**8a**	66	95
8	*i*PrI	**a**	0.5	(*R*)-(+)-**8a**	71	81
9	*i*PrI	**a**	0.2	(*R*)-(+)-**8a**	83	58
10	*i*PrI	**a**	0.1	(*R*)-(+)-**8a**	74	46

[a] Reaction conditions: see Table 1, entry 7. [b] Yield of isolated product. [c] Enantiomeric excess (hexane/2-propanol, Chiralcel OD or AD). Enantiomer resolution by HPLC was confirmed by comparison with racemic control samples in all cases. [d] Alkyl halide: 10 equiv. [e] Unreacted **2a** recovered: 56%.

Finally, to test the potential for development of asymmetric catalysis, we checked for turnover by lowering the catalyst loading (Table 2, entries 7–10). The yield remained high, while enantioselectivity decreased. With 46% *ee* and 74% yield at 10 mol% catalyst loading, a catalytic cycle involving **3** is implied.[20] This is the first evidence of asymmetric catalysis in radical additions to C=N bonds.

In comparison with other carbon–carbon bond constructions for amine synthesis, such as the Strecker and the Mannich reactions, methodology for intermolecular radical addition to C=N bonds has only emerged recently. Levels of induction reported herein establish the viability of asymmetric catalysis in radical addition approaches to asymmetric synthesis of amines, and warrant continued development of these intriguing reactions.

Experimental Section

General procedure: A mixture of [Cu((*S,S*)-*t*Bu-box)$(H_2O)_2$-(OTf)](OTf)[17] and the hydrazone in CH_2Cl_2 (ca. 0.1 M) was stirred with powdered molecular sieves (4 Å; 4 g per mmol of catalyst) at room temperature for 30 min. Benzene was added to achieve a 2:1 ratio with CH_2Cl_2, followed by the iodide (3–10 equiv), and triethylborane (6 equiv, 1 M in hexane). A syringe pump was used to add oxygen (40 mL mmol^{-1} hydrazone) over approximately 2 h through a syringe needle in the headspace above the reaction mixture. If necessary (TLC), additional aliquots of oxygen were added to achieve higher conversion. After 10–38 h, the reaction mixture was diluted with EtOAc/Et_3N (5:1) and adsorbed onto silica gel by concentration to a dry, free-flowing powder. Flash chromatography (hexane/EtOAc) afforded the radical addition products with yields and enantiomeric purities indicated in Tables 1 and 2.

Received: June 10, 2003 [Z52104]

Keywords: amines · asymmetric catalysis · enantioselectivity · hydrazones · radical reactions

[1] For reviews of basic principles and applications of radical reactions, see *Radicals in Organic Synthesis* (Eds.: M. P. Sibi, P. Renaud), Wiley-VCH, New York, **2001**.

 © 2003 Wiley-VCH Verlag GmbH & Co. KGaA, Weinheim

[2] For reviews of enantioselective radical reactions, see: a) M. P. Sibi, N. A. Porter, *Acc. Chem. Res.* **1999**, *32*, 163 – 171; b) M. P. Sibi, T. R. Rheault in *Radicals in Organic Synthesis* (Eds.: M. P. Sibi, P. Renaud), Wiley-VCH, New York, **2001**, pp. 461 – 478.
[3] For recent developments in enantioselective radical reactions, see: a) M. P. Sibi, Y. Asano, J. B. Sausker, *Angew. Chem.* **2001**, *113*, 1333 – 1336; *Angew. Chem. Int. Ed.* **2001**, *40*, 1293 – 1296; b) Y. Watanabe, N. Mase, R. Furue, T. Toru, *Tetrahedron Lett.* **2001**, *42*, 2981 – 2984; c) M. Murakata, H. Tsutsui, O. Hoshino, *Org. Lett.* **2001**, *3*, 299 – 302; d) M. Kurihara, T. Hayashi, N. Miyata, *Chem. Lett.* **2001**, 1324 – 1325; e) D. Yang, S. Gu, Y.-L. Yan, N.-Y. Zhu, K.-K. Cheung, *J. Am. Chem. Soc.* **2001**, *123*, 8612 – 8613; f) M. P. Sibi, J. Chen, *J. Am. Chem. Soc.* **2001**, *123*, 9472 – 9473; g) M. P. Sibi, J. B. Sausker, *J. Am. Chem. Soc.* **2002**, *124*, 984 – 991; h) Y. D. Cai, B. P. Roberts, D. A. Tocher, *J. Chem. Soc. Perkin Trans. 1* **2002**, 1376 – 1386; i) M. P. Sibi, S. Manyem, *Org. Lett.* **2002**, *4*, 2929 – 2932; j) D. Yang, S. Gu, Y.-L. Yan, H.-W. Zhao, N.-Y. Zhu, *Angew. Chem.* **2002**, *114*, 3140 – 3143; *Angew. Chem. Int. Ed.* **2002**, *41*, 3014 – 3017; k) A. Gansäuer, H. Bluhm, B. Rinker, S. Narayan, M. Schick, T. Lauterbach, M. Pierobon, *Chem. Eur. J.* **2003**, *9*, 531 – 542.
[4] For reviews of radical additions to C=N bonds, see: G. K. Friestad, *Tetrahedron* **2001**, *57*, 5461 – 5496; A. G. Fallis, I. M. Brinza, *Tetrahedron* **1997**, *53*, 17543 – 17594.
[5] H. Miyabe, K. Fujii, T. Naito, *Org. Lett.* **1999**, *1*, 569 – 572.
[6] a) H. Miyabe, C. Ushiro, T. Naito, *Chem. Commun.* **1997**, 1789 – 1790; b) H. Miyabe, C. Ushiro, M. Ueda, K. Yamakawa, T. Naito, *J. Org. Chem.* **2000**, *65*, 176 – 185; c) H. Miyabe, N. Yoshioka, M. Ueda, T. Naito, *J. Chem. Soc. Perkin Trans. 1* **1998**, 3659 – 3660.
[7] M. P. Bertrand, L. Feray, R. Nouguier, L. Stella, *Synlett* **1998**, 780 – 782; M. P. Bertrand, L. Feray, R. Nouguier, P. Perfetti, *Synlett* **1999**, 1148 – 1150; M. P. Bertrand, S. Coantic, L. Feray, R. Nouguier, P. Perfetti, *Tetrahedron* **2000**, *56*, 3951 – 3961.
[8] G. K. Friestad, J. Qin, *J. Am. Chem. Soc.* **2000**, *122*, 8329 – 8330; G. K. Friestad, J. Qin, *J. Am. Chem. Soc.* **2001**, *123*, 9922 – 9923.
[9] N. Halland, K. A. Jørgensen, *J. Chem. Soc. Perkin Trans. 1* **2001**, 1290 – 1295.
[10] Enantioselectivities in the two precedents were 52% *ee* (1 equiv Lewis acid, 97% yield)[6b] and 30% *ee* (20 mol% Lewis acid, 5% yield).[9]
[11] For discussions of the effects of Lewis acids in radical reactions, see: P. Renaud, M. Gerster, *Angew. Chem.* **1998**, *110*, 2704 – 2722; *Angew. Chem. Int. Ed.* **1998**, *37*, 2562 – 2579; B. Guerin, W. W. Ogilvie, Y. Guindon in *Radicals in Organic Synthesis* (Eds.: M. P. Sibi, P. Renaud), Wiley-VCH, New York, **2001**, pp. 441 – 460.
[12] Hydrazones **2** were prepared from 1-amino-2-piperidinone and aldehydes by established procedures: P. A. S. Smith, H. G. Pars, *J. Org. Chem.* **1959**, *24*, 1325 – 1332; M. Hajimu, M. Takezawa, H. Shibai, T. Okawara, M. Furukawa, *Agric. Biol. Chem.* **1986**, *50*, 1757 – 1764.
[13] The analogous pyrrolidinone-derived hydrazone was inferior, suggesting that the differences in reactivity between **1** and **2** were not solely attributable to electronic effects. For examples of the effects of achiral templates on enantioselective reactions, see references [3c] and [3g].
[14] Under the conditions of Table 1 without chiral Lewis acid, the racemic adduct **8a** was obtained in 75% yield, suggesting that Et_3B could promote addition to **2a**.
[15] Reversal of selectivity suggests a change in the coordination geometry of the Lewis acid upon changing the solvent. For a related discussion, see: M. P. Sibi, M. Liu, *Curr. Org. Chem.* **2001**, *5*, 719 – 755.
[16] The *R* configuration of (+)-**8a** (see Supporting Information for proof), is consistent with a distorted square-planar Lewis acid coordination geometry[17] and addition to the more sterically exposed hydrazone *Re* face, although further mechanistic study is required.
[17] D. A. Evans, J. S. Johnson, E. J. Olhava, *J. Am. Chem. Soc.* **2000**, *122*, 1635 – 1649. D. A. Evans, G. S. Peterson, J. S. Johnson, D. M. Barnes, K. R. Campos, K. A. Woerpel, *J. Org. Chem.* **1998**, *63*, 4541 – 4544.
[18] Because ligands **4**–**7** are pseudoenantiomeric to **3**, compound **8a** obtained from these ligands has the opposite configuration.
[19] Small amounts (0–4%) of ethyl adducts (from Et_3B) were detected in some cases, and were separable by flash chromatography.
[20] The detailed mechanism is under investigation. Preliminary infrared spectroscopy shows increased intensity of N–H absorbance after workup. Because turnover of the chiral Lewis acid catalyst has been demonstrated, we speculate that the product before workup contains an N-BEt_2 moiety, which may suppress binding of product to catalyst. For related mechanistic proposals, see references [7] and [6c].

 © 2003 Wiley-VCH Verlag GmbH & Co. KGaA, Weinheim

Green Chemistry

The Dual Roles of Oxodiperoxovanadate Both as a Nucleophile and an Oxidant in the Green Oxidation of Benzyl Alcohols or Benzyl Halides to Aldehydes and Ketones

Chunbao Li, Pengwu Zheng, Jie Li, Hang Zhang, Yi Cui, Qiyun Shao, Xiujie Ji, Jian Zhang, Pengying Zhao, and Yanli Xu*

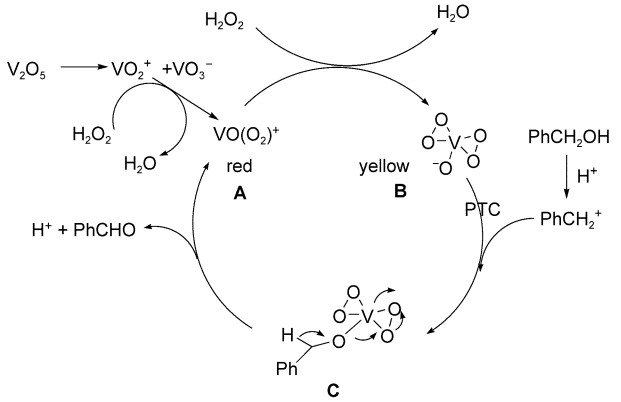
Sulfoxides and tertiary amine oxides have similar structures in that the oxygen atom is partially negatively charged. Both can react as a nucleophilic oxidant toward halides, which are converted into aldehydes or ketones. Recently, we found that dimethylsulfoxide (DMSO) is capable of oxidizing benzyl alcohols to benzaldehydes in high yields when catalyzed by acid. DMSO is believed to function as a nucleophilic oxidant.[1] Traditionally, Mn^{+4}, Mn^{+6}, Cr^{+6}, and Fe^{+6} reagents are the commonly used oxidants for alcohols.[2,3] These reagents must be used in stoichiometric amounts and yield side products that require costly disposal. In these oxidations, the metal oxides or metalates react as an electrophile toward the alcohols in most of the cases.[3] Similarly, the peroxides of $NaMoO_4$ and Na_2WO_4, which are excellent catalysts in the oxidation of alcohol by H_2O_2, were proposed to act as an electrophile towards alcohols.[4]

Vanadium peroxide was reported to be involved in a number of reactions[5] such as the oxidation of ethanol to

[*] Dr. C. Li, P. Zheng, J. Li, H. Zhang, Y. Cui, Q. Shao, X. Ji, J. Zhang, P. Zhao, Y. Xu
Department of Chemistry
School of Sciences
Tianjin University
Tianjin 300072 (China)
Fax: (+86) 22-2740-3475
E-mail: lichunbaosyn@sohu.com

 DOI: 10.1002/anie.200351902 © 2003 Wiley-VCH Verlag GmbH & Co. KGaA, Weinheim

acetaldehyde, and 2-propanol to acetone with H_2O_2 and $VO(OiPr)_3$,[6] the oxidation of alcohols to aldehydes or ketones by using H_2O_2 and vanadium silicate xerogel,[7] and the aerobic oxidation of propargylic alcohols to ketones catalyzed by $VO(acac)_2$ (Hacac = acetylacetone).[8] The discovery of vanadium bromoperoxidase (V–BrPO) in marine organisms has stimulated more active research on vanadium peroxide chemistry.[5,8–12] Although it is well documented that under acidic conditions V_2O_5 can be oxidized by H_2O_2 into vanadium peroxide,[5] there is no report of the oxidation of alcohols with H_2O_2 catalyzed by V_2O_5. We envisioned that $VO(O_2)_2^-$ could behave in a similar way to DMSO as a nucleophilic oxidant toward alcohols (Scheme 1). But this type of reaction has never been reported in the literature for metalates.



Scheme 1. Proposed mechanism for the oxidation of alcohols with H_2O_2 catalyzed by V_2O_5 and PTC.

In addition, the oxidation of benzyl halides to aldehydes is a significant reaction because aromatic aldehydes are used widely. For example, benzaldehyde alone produced in the United States, Western Europe, and Japan in 1983 amounted to 19500 tons.[13] There are two major methods of production of aromatic aldehydes in use. The first method is the hydrolysis of benzal chloride. The problem is that benzal chloride is often contaminated by benzyl chloride and trichloromethyl benzene. In addition, benzal chloride is toxic and carcinogenic.[13] The second method is the oxidation of the methyl group on the aromatic ring, which involves the use of complicated equipment and catalysts. The yield for benzaldehyde is only 40–60% and side products such as maleic anhydride, citraconic anhydride, phthalic anhydride, anthraquinone, CO and CO_2 are produced.[13]

Several oxidations of organic halides to carbonyl compounds are known. These include the Hass–Bender reaction,[14] the Sommelet reaction,[15] the Krohnke reaction,[16] the Kornblum reaction,[17] oxidations by using amine N-oxide,[18] the Masaki photooxidation,[19] and oxidations by using $NaIO_4$.[20] Stoichimetric amount of oxidants have to be used in most of these oxidations. Although the Masaki photooxidation offers the advantage that oxygen is used as the oxidant, volatile organic solvents such as acetone or CH_2Cl_2 are also used in the oxidation.

To solve these existing problems, we started our research by treating benzyl alcohol with dilute H_2O_2, V_2O_5 (0.05 equiv), and BTEAB (benzyltriethylammonium bromide; 0.05 equiv) as the catalysts. The reaction did not take place at room temperature or at reflux. On acidification to pH 4 with HBr, HCl, H_2SO_4, or H_3PO_4, the oxidation of benzyl alcohol to benzaldehyde readily took place at 60 °C. Above pH 5 there was almost no oxidation. A plot of TOF against pH indicates that the reaction rate increases with the acidity of the reaction mixture (Figure 1). The reaction mixture was initially red and became yellow as the reaction proceeded. In the work up, the vanadium reagents were removed by simply washing with aqueous NaOH. A total of 15 liquid alcohols were oxidized by dilute aqueous H_2O_2 (1.2 to 2.8 equiv), with V_2O_5 (0.05 equiv), and BTEAB (0.05 equiv) catalysts at 60 °C at pH 2 without the use of any organic solvents. Table 1 presents the reaction times and

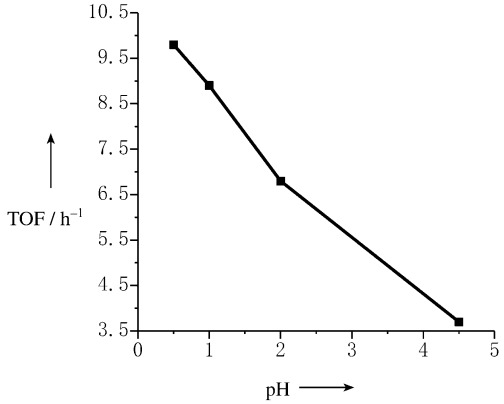


Figure 1. Plot of TOF (h^{-1}) against pH in the oxidation of benzyl alcohol to benzaldehyde using H_2O_2 catalyzed by V_2O_5 and PTC.

Table 1: BTEAB and V_2O_5 catalyzed oxidation of benzyl alcohols to aldehydes or ketones by H_2O_2.

Entry	Alcohol	Time [h]	Yield [%][a]
1	$PhCH_2OH$	6.0	84
2	$PhCH(OH)CH_3$	2.0	81
3	$PhCH(OH)(CH_2)_3CH_3$	1.5	81
4	*p*-$MeOC_6H_4CH_2OH$	8.0	83
5	*p*-$ClC_6H_4CH_2OH$	7.0	84
6	*o*-$ClC_6H_4CH_2OH$	7.5	82
7	*p*-$MeC_6H_4CH_2OH$	10.0	83
8	*o*-$BuOC_6H_4CH_2OH$	7.0	90
		34.0	81
10	2,5-$Br_2C_6H_3CH_2OH$	8.5	87
11	Ph_2CHOH	2.5	88
12	*p*-$ClC_6H_4CH(OH)(CH_2)_3Me$	2.4	85
13	*p*-$MeC_6H_4CH(OH)(CH_2)_3Me$	2.2	87
14	cyclohexanol	30.0	84
15	menthol	36.0	88
16	Menthol[b]	40	0
17	BnCl[c]	6	85

[a] A mixture of benzyl alcohol (0.5 g), H_2O (10 mL), V_2O_5 (0.05 equiv), H_2O_2 (30%, 1.2–2.8 equiv), and BTEAB (0.05 equiv) adjusted to pH 4 with H_2SO_4 and was heated to reflux for the indicated time. After the reaction mixture was cooled to room temperature, it was added to aqueous NaOH (20%, 5 mL) and extracted with ether three times. The organic layer was combined and dried and the solvents were removed by evaporation to give the desired product, which was analyzed by IR and ^{1}HNMR. [b] Aliquat 336 (0.05 equiv) used instead of BTEAB. [c] Benzaldehyde as product.

 © 2003 Wiley-VCH Verlag GmbH & Co. KGaA, Weinheim

yields for these reactions. All the alcohols were oxidized into the corresponding aldehydes or ketones with excellent yields. The benzyl alcohols are oxidized much faster than aliphatic alcohols (entries 14 and 15) and secondary alcohols are oxidized faster than primary alcohols (entries 1, 4–8 versus entries 2 and 3). The presence of the electron-withdrawing group on the aromatic ring (entry 9) leads to a lower rate of oxidation of the *m*-nitrobenzyl alcohol.

When the oxidation was performed under a nitrogen atmosphere, a similar reaction rate was observed. The reaction did not proceed under an oxygen atmosphere when hydrogen peroxide was not present. These results indicate that oxygen is not the oxidant in these reactions, although this was proposed by Conte et al. in the oxidation of alcohols by $VO(OiPr)_3$ and oxygen.[21] To determine the effect of bromide, we used *n*-butoxybenzylalcohol as the substrate and replaced BTEAB with Aliquat 336 (0.05 equiv) in both the absence and presence of potassium bromide (0.05 equiv). Both reactions proceeded at almost the same rate (8.5 h), but without the catalytic amount of V_2O_5, the oxidation was very sluggish. This suggests that the primary function of BTEAB is a phase transfer catalyst (PTC) and the oxidation of alcohol by bromine can be ignored.

As indicated in Table 1, the oxidation rate of *m*-nitrobenzyl alcohol is only one fifth that of benzyl alcohol (entry 9 versus entry 1). This suggests that this oxidation does not occur by a radical pathway but most probably by a nucleophilic oxidation pathway (Scheme 1). Under acidic conditions, benzyl alcohol is protonated and produces a benzyl cation, which is attacked by $VO(O_2)_2^-$ to form intermediate **C**. Losing a proton, intermediate **C** decomposes into benzaldehyde. The rate-determining step is the formation of benzyl cation. This is supported by the fact that the secondary benzyl alcohols are oxidized three to four times faster than the primary benzylalcohols and 16 times faster than the aliphatic alcohols.

To further prove the mechanism, we subjected benzyl chloride to the same oxidation conditions. Benzaldehyde was formed in 85% yield in 6 h. Therefore it is easy to understand why the oxidations of menthol and cyclohexanol occur at much lower reaction rates. When menthol was treated with H_2O_2 (2.5 equiv) catalyzed by V_2O_5 at pH 2 in the presence of Aliquat 336 (0.05 equiv) instead of BTEAB, no reaction took place after 40 h (entry 16). This result suggests that the low concentration of bromine is the oxidant here (entry 15) and $VO(O_2)_2^-$ is not a good enough nucleophile to substitue efficiently the protonated hydroxyl group of aliphatic alcohols. Our attempt at trapping $VO(O_2)_2^-$ with TrCl or TsCl failed, which suggests that $-OV(O_2)_2$ is a very good leaving group and intermediate **C** is extremely unstable.

Therefore, we have for the first time demonstrated the dual roles of $VO(O_2)_2^-$ both as a nucleophile and oxidant toward alcohols. This reaction mechanism is rare among metal oxides and metalate oxidants. We have established a new green oxidation procedure of alcohols with H_2O_2 catalyzed by V_2O_5 and BTEAB. Although several green oxidation procedures of alcohols are known,[22] in most cases expensive metals such as Ru,[23] Pd,[24] Pt,[25] Ir[26] and Rh[27] are used as catalysts. This makes the oxidation process an expensive one. We used H_2O_2 as the oxidant because it has high oxygen content, is inexpensive and stable. V_2O_5 is also inexpensive and stable. Unfortunately, this oxidation is limited to benzyl alcohol because of the unique mechanism related to oxodiperoxovanadate.

To broaden the potential application of oxodiperoxovanadate, we oxidized both primary and secondary benzyl chlorides and bromides to aldehydes and ketones in boiling water using H_2O_2 (1.5 equiv) catalyzed by V_2O_5 (0.05 or 0.1 equiv) and Aliquat 336 (0.05 equiv). The 22 organic halides (Table 2) were all oxidized in good yields to the corresponding aldehydes or ketones. The oxidation is compatible with amides (entry 9), esters (entries 8 and 11), ethers (entries 5, 6, 7 and 13), aryl halides (entries 2, 3, 10, 18 and 11) and phenolic (entries 4 and 12) groups. Primary halide are oxidized faster than secondary halides, which suggests that the $OV(O_2)_2^-$ anion is a bulky nucleophile and is sensitive to steric hindrance. The reaction is faster with benzyl chlorides than with benzyl bromides. A possible reason is that $-OV(O_2)_2$ is such a good leaving group that it is more easily substituted by the better nucleophile, bromide ion, than by the chloride ion. The following equilibrium exists [Eq. (1)].

$$ArCH_2Br + VO(O_2)_2^- \rightleftharpoons ArCH_2OV(O_2)_2 + Br^- \quad (1)$$

A comparative experiment was carried out to verify this. When benzyl chloride was oxidized by H_2O_2 (1.5 equiv) catalyzed by V_2O_5 (0.05 equiv) and Aliquat 336 (0.05 equiv)

Table 2: Oxidation of benzyl halides to aldehydes and ketones by H_2O_2 catalyzed by V_2O_5 and Aliquat 336.[a]

Entry	Benzyl Halide	Time [h]	Yield [%][b]
1	$PhCH_2Cl$	6.0(3.5)	70(90)
2	*p*-$ClC_6H_4CH_2Cl$	6.0 (3.5)	73(90)
3	*o*-$ClC_6H_4CH_2Cl$	7.0	75
4	*o*-$HOC_6H_4CH_2Cl$	5.0	81
5	*o*-$BnOC_6H_4CH_2Cl$	6.0	87
6	*o*-*n*$BuOC_6H_4CH_2Cl$	8.0	82
7	*o*-*i*$BuOC_6H_4CH_2Cl$	11.0	80
8	*o*-$BzOC_6H_4CH_2Cl$	8.0	73
9	*p*-$AcNHC_6H_4CH_2Cl$	6.0	83
10	2,5-$Br_2C_6H_3CH_2Cl$	10.0	82
11	*p*-$BzOC_6H_4CH_2Cl$	8.0	76
12	1-chloromethyl-2-hydroxynaphthalene	13.0	80
13	1-benzyloxy-2-chloromethylnaphthalene	12.0	82
14	PhCHClMe	10.0	77
15	PhCHClEt	10.0	72
16	PhCHClBu	12.0	81
17	*p*-$MeC_6H_4CHClBu$	10.0	78
18	*p*-$ClC_6H_4CHClBu$	12.0	81
19	$PhCH_2Br$[c]	14.0	84
20	*p*-$BrC_6H_4CH_2Cl$	15.0	85
21	1-bromomethylnaphthalene	20.0	75
22	PhCHBrMe	24.0	75

[a] Typical procedure: A mixture of *p*-chlorobenzyl halide (10 g), H_2O (10 mL), H_2O_2 (30%, 1.5 equiv), V_2O_5 (0.005 equiv) and Aliquat 336 (0.05 equiv) was refluxed for 6 h. After cooling to room temperature, the oil layer was separated and distillated to give pure *p*-chlorobenzaldehyde in 73% yield. The aqueous phase was reused for the subsequent oxidation. For the eight subsequent oxidations, the reaction time was 3.5 h and the yield was more than 90%. [b] The conversion for chlorides was quantitative. [c] 0.1 equivalents of V_2O_5 were used for bromide.

 © 2003 Wiley-VCH Verlag GmbH & Co. KGaA, Weinheim

and KBr (1.0 equiv), the reaction took 2 h longer than in the absence of KBr (entry 1). In addition, this result agrees well with the fact that the $OV(O_2)_2^-$ anion could not be trapped with TrCl (see above). We also found that $OV(O_2)_2^-$ ion is an excellent catalyst. The separated aqueous phase containing $OV(O_2)_2^-$ ions and PTC was used in the subsequent eight oxidation runs. In the first run of the oxidation of benzyl chloride and *p*-chlorobenzyl chloride, the yield was 70% and 73% respectively, the reaction time was 6 h. In the subsequent eight runs the yield was 90% and the reaction time was shortened to 3.5 h. The reaction is self-accelerated by the accumulated HCl. In the catalytic oxidation of *p*-chlorobenzyl chloride, the substrate/catalyst ratio reached 1000:5 and the reaction rates and the yields remained unchanged.

In our oxidation, only water was used to dilute the H_2O_2, no organic solvents were used in the whole process. This represents the first green oxidation of benzyl halides, which is operationally simple and produces high yields and is well suited for a variety of functionalized benzyl halides. Our new green oxidation reaction provides a better solution for the existing problems in the oxidation of benzyl halides. The conversion of organic chlorides to aromatic aldehydes is quantitative. The yields are more than 90%. The whole process does not need any organic solvents. The two waste products are water and HCl. The latter provides acidic conditions to accelerate the reaction. The catalysts (V_2O_5 and Aliquat 336) are inexpensive, stable and efficient (S/C 1000:5) and can be reused without losing its efficiency.

Received: May 14, 2003
Revised: August 18, 2003 [Z51902]

Keywords: alcohols · green chemistry · oxidation · vanadium

[1] C. Li, Y. Xu, M. Lu, Z. Zhao, L. Liu, Z. Zhao, Y. Cui, P. Zheng, X. Ji, G. Gao, *Synlett* **2002**, 2041.
[2] R. C. Larock, *Comprehensive Organic Transformations, Vol. 1*, Wiley, New York, **1999**, pp. 1205–1261.
[3] M. Hudlicky, *Oxidations in Organic Chemistry*, American Chemical Society, Woshington, DC, **1990**, pp. 114–159.
[4] K. Sato, M. Aoki, J. Takagi, K. Zimmermann, R. Noyori, *Bull. Chem. Soc. Jpn.* **1999**, *72*, 2287.
[5] A. Butler, M. J. Clague, G. E. Meister, *Chem. Rev.* **1994**, *94*, 625.
[6] O. Bortolini, V. Conte, F. Di Furia, G. Modena, *Nouv. J. Chim.* **1985**, *9*, 147.
[7] R. Neumann, M. Levin-Elad, *Appl. Catal. A* **1995**, *122*, 85.
[8] Y. Maeda, N. Kakiuchi, S. Matsumura. T. Nishimura. T. Kawamura, S. Uemura, *J. Org. Chem.* **2002**, *67*, 6718.
[9] R. Wever, M. B. E. Krenn in *Vanadium in Biological System* (Ed.: N. D. Chasteen), Kluwer Academic Publishers, Dordrecht, The Netherlands, **1990**, p. 81.
[10] U. Bora, G. Bose. M. K. Chaudhurl, S. S. Dahr, R. Gopinath, A. T. Khan, B. K. Patel, *Org. Lett.* **2000**, *2*, 247.
[11] H. Kelm, H.-J. Krueger, *Inorg. Chem.* **1996**, *35*, 3553.
[12] G. J. Colpas, B. J. Hamstra, J. W. Kampf, V. L. Pecoraro, *J. Am. Chem. Soc.* **1996**, *118*, 3469.
[13] *Ullmann's Encyclopedia of Industrial Chemistry*, 7th ed., Electronic release, Wiley, VCH, **2003**.
[14] R. A. Sheldon, I. W. C. E. Arends, A, Dijksman, *Catal. Today* **2000**, *57*, 157.
[15] R. C. Larock, *Comprehensive Organic Transformations, Vol. 2*, Wiley, New York, **1999**, pp. 1222–1225.
[16] T. Nishimura, T. Onoue, K. Ohe, S. Uemura, *J. Org. Chem.* **1999**, *64*, 6750.
[17] N. Kornblum, W. J. Jones, G. J. Anderson, *J. Am. Chem. Soc.* **1959**, *81*, 4113.
[18] M. G. Edwards, J. M. J. Williams, *Angew. Chem.* **2002**, *114*, 4934; *Angew. Chem. Int. Ed.* **2002**, *41*, 4740.
[19] A. Itoh, T. Kodana, S. Inagaki, Y. Masaki, *Org. Lett.* **2000**, *2*, 2455.
[20] H. B. Hass, M. L. Bender, *J. Am. Chem. Soc.* **1949**, *71*, 1767.
[21] V. Conte, F. Di Furia, G. Modena, *J. Org. Chem.* **1988**, *53*, 1665.
[22] F. Kröhnke, *Angew. Chem.* **1963**, *75*, 317; *Angew. Chem. Int. Ed. Engl.* **1963**, *2*, 380.
[23] a) H. Ji, T. Mizugaki, K. Ebitani, K. Kaneda, *Tetrahedron Lett.* **2002**, *43*, 7179; b) K. Yamaguchi, N. Mizuno, *Angew. Chem.* **2002**, *114*, 4720; *Angew. Chem. Int. Ed.* **2002**, *41*, 4538.
[24] S. Suzuki, T. Onishi, Y. Fujita, H. Misawa, J. Otera, *Bull. Chem. Soc. Jpn.* **1986**, *59*, 3287.
[25] C.-G. Jia, F.-Y. Jing, W.-D. Hu, M.-Y. Huang, Y.-Y. Jiang, *J. Mol. Catal.* **1994**, *91*, 139.
[26] S. Das, A. K. Panigrahi, G. C. Maikap, *Tetrahedron Lett.* **2003**, *44*, 1375.
[27] J. Martin, C. Martin, M. Faraj, J.-M. Bregeault, *Nouv. J. Chim.* **1984**, *8*, 141.

 © 2003 Wiley-VCH Verlag GmbH & Co. KGaA, Weinheim

Regioselective Allylic Substitution

$[Cp^*(\eta^2\text{-bipy})(MeCN)Ru^{II}][PF_6]$ Catalysts for Regioselective Allylic Substitution and Characterization of Dicationic $[Cp^*(\eta^2\text{-bipy})(\eta^3\text{-allyl})Ru^{IV}][PF_6]_2$ Intermediates**

Mbaye D. Mbaye, Bernard Demerseman, Jean-Luc Renaud, Loïc Toupet, and Christian Bruneau**

Ruthenium catalysts such as $[Cp(cod)RuCl]/NH_4PF_6$ or $[Cp^*(cod)RuCl]$ (cod = 1,5-cyclooctadiene) have gradually disclosed an increasing efficiency in assisting allylic substitution reactions.[1] In light of the advantage of the unusual regioselectivity provided by ruthenium catalysts, an efficient access to antidepressant drugs was recently reported by using

[*] Dr. B. Demerseman, Dr. C. Bruneau, M. D. Mbaye, Dr. J.-L. Renaud
Institut de Chimie de Rennes
Organométalliques et Catalyse, UMR-CNRS 6509
Université de Rennes 1
35042 Rennes Cedex (France)
Fax: (+33) 2-2323-6939
E-mail: bernard.demerseman@univ-rennes1.fr
christian.bruneau@univ-rennes1.fr

Dr. L. Toupet
Institut de Chimie de Rennes
Groupe Matière Condensée et Matériaux, UMR-CNRS 6626
Université de Rennes 1
35042 Rennes Cedex (France)

[**] This work was supported by CNRS. The authors are grateful to the European Union COST Program Action D24/0005/02 for support. $Cp^* = C_5Me_5$, bipy = 2,2′-bipyridyl derivative.

Supporting information for this article is available on the WWW under http://www.angewandte.org or from the author.

 © 2003 Wiley-VCH Verlag GmbH & Co. KGaA, Weinheim DOI: 10.1002/anie.200352257

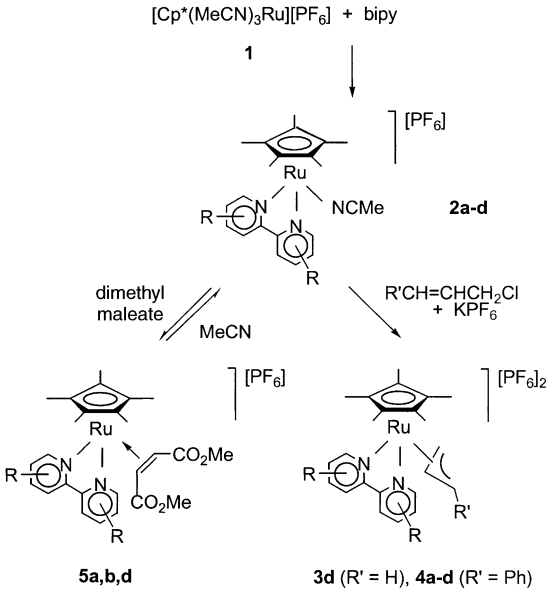
$[Cp^*(MeCN)_3Ru][PF_6]$ as the catalyst precursor.[2] Although the additional coordination of donors such as phosphanes or nitrogen ligands at the ruthenium center stabilize the (η^3-allyl)Ru^{IV} complexes, they also result in a markedly reduced catalytic activity.[1a,3] Thus, a robust cyclopentadienyl–ruthenium fragment associated solely to labile ligands such as cod or acetonitrile is apparently a required key for the design of ruthenium catalysts. However, we recently observed that coordinatively stabilized Cp*(α-diimine)Ru complexes exhibited a noteworthy catalytic activity.[4] Undoubtedly, our observation needed a better understanding because allylic substitution catalyzed by organometallic complexes represents an important tool for organic synthesis.[5] We report herein the synthesis of the new $[Cp^*(\eta^2\text{-bipy})(CH_3CN)Ru^{II}][PF_6]$ (bipy = bipyridyl derivative, see Scheme 1) complexes **2a–d**, and show their catalytic activity in allylic substitution to regioselectively form carbon–carbon or carbon–heteroatom bonds under mild conditions. Furthermore, the dicationic $[Cp^*(\eta^2\text{-bipy})(\eta^3\text{-allyl})Ru^{IV}][PF_6]_2$ derivatives **3d** and **4a–d**, were isolated and appear as key intermediates in the catalytic process.

The purple complexes, **2a–d**, were nearly quantitatively obtained by reacting $[Cp^*Ru(CH_3CN)_3Ru][PF_6]$ **1**, in solution in acetonitrile with a commercial 2,2′-bipyridine derivative (Scheme 1).

The addition of allyl chloride or cinnamyl chloride to a (highly colored) solution of **2a–d** in acetonitrile resulted in a pale-brown solution within 1 h. When the reaction was performed in the presence of KPF_6, subsequent workup afforded pale-yellow crystals of **3d** or orange–yellow crystals of **4a–d**, in 71–88% yield (Scheme 1). Complexes **2–4** are stable in air at the solid state and were characterized by ^1H and $^{13}C\{^1H\}$ NMR spectroscopy and representative elemental analysis. The NMR data collected for **3d** showed as expected a symmetrical allylic fragment as also indicated by the observation of equivalent pyridyl groups. Structural information was also provided by an X-ray study of **4d**·MeCN that showed the ruthenium atom to be coordinated by a π-bonded C_5Me_5 ring, a two σ-N-bonded phenanthroline chelate, and to an η^3-$CH_2CHCHPh$ allylic fragment that has an *endo* orientation (see Figure 1).[6]

The two Ru–N bond lengths (Ru1–N1 = 2.119(3), Ru1–N2 = 2.118(3) Å, are close to the Ru–N bond lengths (2.094 and 2.097 Å) reported for the Ru^{II} complex [Cp*(2,2′-bipyridine)(η^2-EtO_2C–CH = CH–CO_2Et)Ru][PF_6].[7] These observations emphasized the σ-donor character of the N-coordination of the rigid phenanthroline chelate. The Ru1–C11 (2.196(3) Å) and Ru1–C12 (2.197(3) Å) bond lengths are very similar. Significantly longer is the Ru1–C13 (2.398(3) Å) bond and it should be noted that the C12-C13-C14 angle, 123.9(3)°, is very close to 120°. Thus, the coordination of the allyl group in **4d** may be coarsely depicted as an intermediate between an allylic coordination and, with a minor contribution, an olefinic coordination of a formal CH_2=CH-C^+HPh ligand. Indeed, complexes **2** in dichloromethane solution easily exchange their labile acetonitrile ligand for dimethyl maleate to afford complexes **5a,b,d** (Scheme 1). Complexes **5** were characterized by ^1H NMR spectroscopy in CD_2Cl_2. The ^1H NMR spectra of solutions of **5** in CD_3CN showed a mixture of **2**, **5**, and dimethyl maleate, thus indicating a reversible reaction. Such a behavior suggests that the formation of the ruthenium(IV) complexes **3** and **4** from **2** involved a preliminary π-coordination of the allyl chloride followed by an intramolecular oxidative-addition step.

The addition of diethylamine to a yellow solution of **4** in acetonitrile immediatly resulted in an intense violet solution, thus suggesting the recovery of **2** and providing straightforward evidence for an electrophilic reactivity of complexes **4**.



Scheme 1. Synthesis of the new complexes. Bipy = a) 2,2′-bipyridine, b) 4,4′-dimethyl-2,2′-bipyridine, c) 4,4′-di-tert-butyl-2,2′-bipyridine, d) 1,10-phenanthroline.

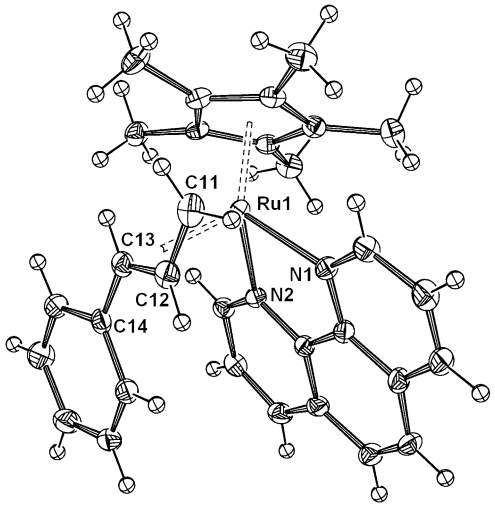
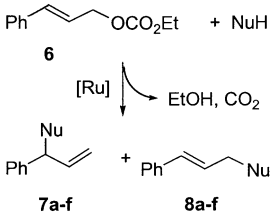


Figure 1. ORTEP view of **4d** showing thermal ellipsoids set at the 50% probability level. Selected bond distances (Å) bonds and angles (°): Ru(1)-C(11) 2.196(3), Ru(1)-C(12) 2.197(3), Ru(1)-C(13) 2.398(3), C(11)-C(12) 1.412(5), C(12)-C(13) 1.402(5), C(13)-C(14) 1.464(5), Ru(1)-N(1) 2.119(3), Ru(1)-N(2) 2.118, C(11)-Ru(1)-C(12) 37.50(13), C(12)-Ru(1)-C(13) 35.18(12), C(11)-Ru(1)-C(13) 63.29(13), C(11)-C(12)-C(13) 118.3(3), C(12)-C(13)-C(14) 123.9(3), N(1)-Ru-N(2) 77.04(10). The two PF_6 anions and the solvent molecule are omitted for clarity.

 © 2003 Wiley-VCH Verlag GmbH & Co. KGaA, Weinheim

Consequently, the reactivity of complexes **2** as catalyst precursors for allylic substitution was then investigated. The catalytic activity of complexes **2** was checked by treating the cinnamyl carbonate **6** with various nucleophiles (Scheme 2) and selected experiments are listed in Table 1.



Scheme 2. Ruthenium-catalyzed nucleophilic allylic substitution. Nu = a) $CH(CO_2Me)_2$, b) $CH(COMe)_2$, c) $N(CH_2)_5$, d) NEt_2, e) $N(CH_2)_4$, f) OMe.

Table 1: Selected ruthenium-catalyzed allylic substitution reactions.

Entry[a]	Catalyst	Nucleophile	Solvent	Products	Branched/Linear[b]
1	**2b**	$NaCH[CO_2Me]_2$	THF	**7a**	
2	**2b**	$CH_2[CO_2Me]_2$	MeCN	**7a, 8a**	25:1
3	**2c**	$CH_2[CO_2Me]_2$	MeCN	**7a, 8a**	20:1
4	**2d**	$CH_2[COMe]_2$	MeCN	**7b, 8b**	55:1
5	**2c**	piperidine	MeCN	**7c, 8c**	27:1
6	**2b**	Et_2NH	MeCN	**7d, 8d**	8:1
7	**2c**	pyrrolidine	MeOH	**7e, 8e**	50:1
8	**2a**	MeOH	MeOH	**7f, 8f**	32:1
9	**2d**	MeOH	MeOH	**7f, 8f**	26:1

[a] conditions: 0.5 mmol of cinnamyl carbonate, 0.6 mmol of nucleophile, 0.015 mmol of catalyst (3 mol%), in 4 mL of solvent, 16 h, room temperature. [b] All reactions led to complete conversion of **6**, the branched/linear ratio was determined by ^1H NMR spectroscopy.

Thus, the reaction of **6** with dimethyl sodiomalonate (1.2 equiv) in the presence of 3 mol% of **2b** in THF at room temperature led to the quantitative formation of the branched isomer **7a** (entry 1). Remarkably, because rare when using a ruthenium catalyst,[8] the nucleophilic substitution by dimethyl malonate that has not been deprotonated also runs when acetonitrile is used as the solvent (entries 2,3). Similarly, acetylacetone reacted as a carbonucleophile with **6** to afford the branched isomer **7b** in more than 98% selectivity (entry 4). The amination with secondary amines showed that the regioselectivity of the reaction was strongly influenced by the nature of the amine: the branched/linear ratio obtained with diethylamine was 8:1 (entry 6), whereas piperidine offered a better regioselectivity of 27:1 (entry 5). The reaction with pyrrolidine was sluggish in acetonitrile, but occurred in methanol to afford the branched allylic amine with a high regioselectivity (entry 7). In the absence of an amine, methanol itself served as a nucleophile. The branched allylic methyl ether **7f** was obtained with a very high regioselectivity (entries 8,9), and it is especially worth mentioning that no reaction occurred when **1** was tested as the catalyst precursor.

In conclusion, the facile synthesis of complexes **2** provides novel efficient catalysts for regioselective allylic substitution from unsymmetrical allylic carbonates. The addition of a wide range of nitrogen-, oxygen-, or carbon-nucleophiles under mild conditions has been achieved with good yields and high regioselectivities in favor of the branched isomer. The characterization of allyl bipyridine–ruthenium(IV) complexes which can also be used as catalyst precursors, brings evidence of the involvement of the bipyridine ligand in the catalytic process.

Experimental Section

2a: A solution of 2,2′ bipyridine (0.69 g, 4.42 mmol) in toluene (90 mL) was added to a solution of **1** (2.20 g, 4.36 mmol) in acetonitrile (30 mL). The reaction mixture was stirred for 1 h after which the solution was slowly concentrated under vacuum to obtain dark-purple crystals that were collected then washed with diethyl ether. Yield: 2.49 g, 95%. **4d**·MeCN**:** Cinnamyl chloride (0.40 mL, 2.87 mmol) was added to a stirred mixture of **2d** (1.50 g, 2.49 mmol) and KPF_6 (0.50 g, 2.72 mmol) in acetonitrile (30 mL). After 1 h, the solvent was completely removed by evaporation. Then water (30 mL) and diethyl ether (30 mL) were added to the residue, and this mixture was stirred to obtain a yellow precipitate, which was collected by filtration. The solid was dissolved in acetonitrile (40 mL) and diethyl ether (120 mL) was added to the resulting solution to obtain orange–yellow crystals. Yield: 1.90 g, 88%. A suitable crystal was selected for the X-ray study.

Received: June 30, 2003 [Z52257]

Keywords: allyl complexes · homogeneous catalysis · ligand effects · N ligands · ruthenium

[1] a) Y. Morisaki, T. Kondo, T. Mitsudo, *Organometallics* **1999**, *18*, 4742–4746; b) T. Kondo, Y. Morisaki, S. Uenoyama, K. Wada, T. Mitsudo, *J. Am. Chem. Soc.* **1999**, *121*, 8657–8658; c) T. Kondo, H. Ono, N. Satabe, T. Mitsudo, Y. Watanabe, *Organometallics* **1995**, *14*, 1945–1953.

[2] B. M. Trost, P. L. Fraisse, Z. T. Ball, *Angew. Chem.* **2002**, *114*, 1101–1103; *Angew. Chem. Int. Ed.* **2002**, *41*, 1059–1061.

[3] a) H. Kondo, Y. Yamaguchi, H. Nagashima, *Chem. Commun.* **2000**, 1075–1076; b) E. Rüba, W. Simanko, K. Mauthner, K. M. Soldouzi, C. Slugovc, K. Mereiter, R. Schmid, K. Kirchner, *Organometallics* **1999**, *18*, 3843–3850.

[4] J.-L. Renaud, C. Bruneau, B. Demerseman, *Synlett* **2003**, 408–410.

[5] J. Tsuji in *Transition Metal Reagents and Catalysts. Innovations in Organic Synthesis*, Wiley, Chichester, **2000**, pp. 109–168.

[6] Crystal data**:** $C_{33}H_{35}F_{12}N_3P_2Ru$, $M_r = 864.65$, crystal size $0.35 \times 0.32 \times 0.30$, monoclinic, space group $P2_1/c$, $Z = 4$, $a = 10.2255(1)$ Å, $b = 11.2593(1)$ Å, $c = 29.3790(4)$ Å, $\beta = 97.243(1)°$, $U = 3355.47(6)$ Å^3, $\delta_{calcd} = 1.712$ g cm^{-3}, $T = 120(1)$ K, $F(000) = 1744$, $Mo_{K\alpha}$ radiation ($\lambda = 0.71069$ Å), $\mu = 0.660$ mm^{-1}, 7583 reflexions measured in the range $2.30° \le \theta \le 27.48°$, 7583 unique, ($R_{int} = 0.038$) which were used in all calculations. The structure was refined by using full-matrix least-squares on F^2 to $R_1 = 0.047$, $wR_2 = 0.128$, $S = 0.985$, for 6559 reflections ($> 2\sigma$) and 460 refined parameters, R_1(all data) 0.055, wR_2(all data) = 0.137, goodness-of-fit on $F^2 = 1.011$. CCDC-213659 contains the supplementary crystallographic data for this paper. These data can be obtained free of charge via www.ccdc.cam.ac.uk/conts/retrieving.html (or from the Cambridge Crystallographic Data Centre, 12 Union Road, Cambridge CB21EZ, UK; fax: (+44) 1223-336-033; or deposit@ccdc.cam.ac.uk).

[7] G. A. Balavoine, T. Boyer, C. Livage, *Organometallics* **1992**, *11*, 456–459.

[8] An example was recently reported in reference [3a].

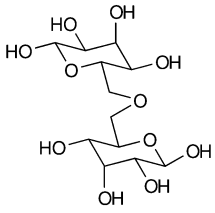
 © 2003 Wiley-VCH Verlag GmbH & Co. KGaA, Weinheim

Dipyranose Ethers

Development of a Novel Sugar Linkage: 6,6′-Ether-Connected Sugars**

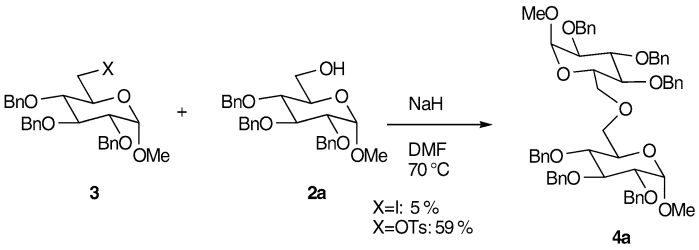
*Hideyo Takahashi, Toshimitsu Fukuda, Haruhiko Mitsuzuka, Rie Namme, Hidetoshi Miyamoto, Yasufumi Ohkura, and Shiro Ikegami**

In 1997, Pérez et al. reported the structure **1** for coyolosa, a natural product isolated from the root of *Acrocomia mexicana*[1] that was shown to have a significant effect on fasting blood-glucose levels.[2] Coyolosa may well be a new candidate in the search for drugs to combat diabetes. Upon examination of the NMR spectroscopic data of Pérez et al. for this unique carbohydrate in which two pyranose groups are connected as a 6,6′-ether, we found it unlikely that coyolosa had the proposed structure **1**.[3] Although there can be no doubt that two pyranose rings linked through their 6-positions form the structure of coyolosa,[4] it is less evident that the stereochemistry of the pyranose moieties corresponds to that shown in **1**. Herein, we report a novel synthesis of 6,6′-ether-connected pyranoses and propose an absolute configuration for coyolosa based on structure–activity-relationship (SAR) studies that is different to the one originally suggested.



1

Little has been reported to date on sugars linked by ether bonds. In preliminary studies, we treated the methyl α-D-*gluco*-pyranoside **2a** with the iodide and the tosylate corresponding to **3** under basic conditions in an attempted Williamson etherification. The desired ether **4a** was only obtained in low to moderate yields (Scheme 1), as the anomeric position was unstable under the Williamson conditions, and the competing elimination could not be avoided.

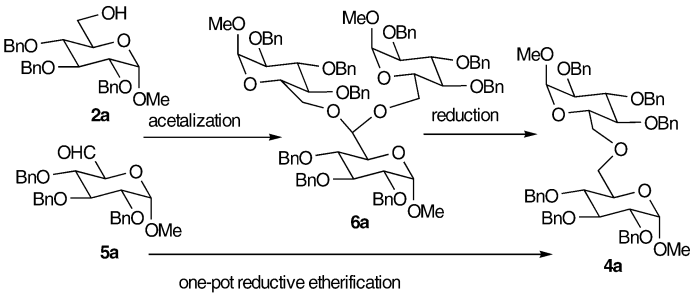


3 + **2a** → (NaH, DMF, 70 °C) → **4a**

X=I: 5%
X=OTs: 59%

Scheme 1. Synthesis of 6,6′-ether-connected pyranoses by the Williamson etherification. DMF = *N*,*N*-dimethylformamide, Tos = *p*-toluenesulfonyl.

As the Williamson etherification had proved unsuccessful in our attempt to synthesize 6,6′-ether-connected pyranoses, we instead adopted an acetalization–reduction approach, as shown in Scheme 2. In this method, a 6-aldehyde **5** is treated with a 6-alcohol **2** under mild acid-catalyzed conditions to provide an intermediate acetal derivative **6**. The treatment of



2a → (acetalization) → **6a** → (reduction) → **4a**

5a → (one-pot reductive etherification) → **4a**

Scheme 2. Proposed synthetic routes to 6,6′-ether-connected pyranoses **4** (shown for **4a**).

6 with a reducing agent then furnishes the desired product **4**. As a two-step procedure is inconvenient, a one-pot reductive etherification,[5] which is a more reliable method for the preparation of ethers under nonbasic conditions, was also envisaged.

A large number of studies have been carried out on reductive etherification, that is, the reduction of oxocarbenium ions or acetals generated in situ to provide ethers. In particular, Lewis acid catalyzed reactions of these compounds with alkoxy silanes or hydrosilanes have proved useful for the efficient synthesis of unsymmetrical ethers.[5e–j] Although the reaction of simple carbonyl compounds (e.g. benzaldehyde) with various alcohols has already been reported, there are few methods[4j] suitable for carbonyl compounds substituted with bulky or multifunctional carbohydrates.

Acetal formation was investigated first. An equimolar amount of the methyl α-D-*gluco*-pyranoside **2a** reacted with the aldehyde **5a** very slowly to give the acetal derivative **6a** in poor yield. However, when an excess of **2a** was used in the presence of trimethylsilyl trifluoromethanesulfonate (TMSOTf) at 0 °C, **6a** was isolated in 91% yield. It had been anticipated that the acetal derivative, which contains three bulky pyranosides, would be relatively unstable. However, we found that **6a** was so stable that it could be purified without difficulty by silica-gel column chromatography. The structure of this acetal derivative is unusual and has many features that remain to be investigated.[6]

The reactions of the D-*gluco*-, D-*galacto*-, D-*manno*-, and D-*allo*-pyranosides **2a, 2b, 2c**, and **2d**, respectively, with the

[*] Prof. S. Ikegami, Dr. H. Takahashi, T. Fukuda, H. Mitsuzuka, R. Namme
School of Pharmaceutical Sciences, Teikyo University
Sagamiko, Kanagawa 199-0195 (Japan)
Fax: (+81) 426-85-3729
E-mail: shi-ike@pharm.teikyo-u.ac.jp
Dr. H. Miyamoto, Dr. Y. Ohkura
Department of Pharmacology, Research Laboratories
KOTOBUKI Pharmaceutical Co., Ltd.
6351 Sakaki, Nagano 389-0697 (Japan)

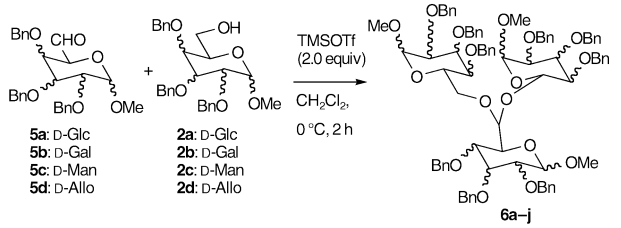
[**] We thank J. Shimode and M. Kitsukawa for spectroscopic measurements. Partial financial support for this research from the Ministry of Education, Culture, Sports, Science, and Technology is gratefully acknowledged. Support from the Takeda Science Foundation to H.T. is also acknowledged.

Supporting information for this article is available on the WWW under http://www.angewandte.org or from the author.

 DOI: 10.1002/anie.200352388 © 2003 Wiley-VCH Verlag GmbH & Co. KGaA, Weinheim

aldehyde derivatives **5a–d**[7] under similar conditions afforded the corresponding acetal derivatives **6a–j** (Table 1). The excess of the pyranoside **2** was recovered quantitatively in each case and reused in other reactions.

Table 1: Acetalization of aldehydes **5** with alcohols **2** catalyzed by TMSOTf.[a]

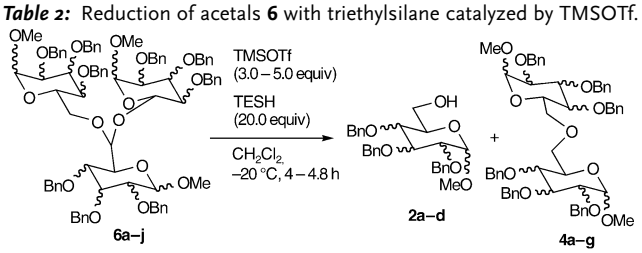


Entry	5	2 (6-OH)	6	Yield [%][b]
1	**a** (Glc)	**a** (Glc)	**a** (Glc-Glc-Glc)	91
2	**a** (Glc)	**b** (Gal)	**b** (Gal-Glc-Gal)	81
3	**a** (Glc)	**c** (Man)	**c** (Man-Glc-Man)	93
4	**b** (Gal)	**a** (Glc)	**d** (Glc-Gal-Glc)	93
5	**b** (Gal)	**b** (Gal)	**e** (Gal-Gal-Gal)	76
6	**b** (Gal)	**c** (Man)	**f** (Man-Gal-Man)	84
7	**c** (Man)	**a** (Glc)	**g** (Glc-Man-Glc)	75
8	**c** (Man)	**b** (Gal)	**h** (Gal-Man-Gal)	76
9	**c** (Man)	**c** (Man)	**i** (Man-Man-Man)	80
10	**d** (All)	**d** (All)	**j** (All-All-All)	69

[a] Reactions were conducted with 10 equivalents of **2**. [b] Yield of isolated product.

With the desired intermediates **6** in hand, we then investigated the reduction step with triethylsilane (TESH) as the reducing agent. It was found that TMSOTf accelerated the reduction of **6** with TESH efficiently to give the desired 6,6′-ether-connected pyranosides **4**. The acetals **6a–j** were successfully converted into the corresponding pyranosides **4a–g** and the excess of the alcohol **2** could be recovered quantitatively and reused (Table 2). This is the first example

Table 2: Reduction of acetals **6** with triethylsilane catalyzed by TMSOTf.

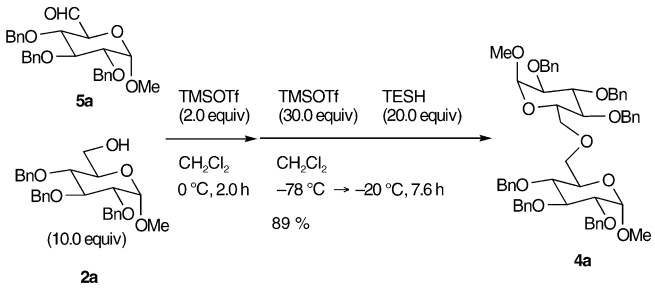


Entry	6	4	Yield [%][a]
1	**a** (Glc-Glc-Glc)	**a** (Glc-Glc)	96
2	**b** (Gal-Glc-Gal)	**b** (Glc-Gal)	79
3	**c** (Man-Glc-Man)	**c** (Glc-Man)	95
4	**d** (Glc-Gal-Glc)	**b** (Gal-Glc)	75
5	**e** (Gal-Gal-Gal)	**d** (Gal-Gal)	82
6	**f** (Man-Gal-Man)	**e** (Gal-Man)	73
7	**g** (Glc-Man-Glc)	**c** (Man-Glc)	73
8	**h** (Gal-Man-Gal)	**e** (Man-Gal)	69
9	**i** (Man-Man-Man)	**f** (Man-Man)	64
10	**j** (All-All-All)	**g** (All-All)	56

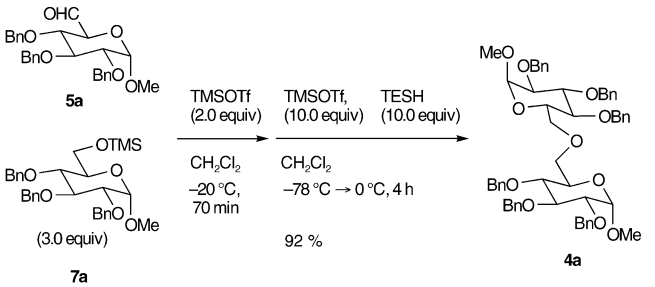
[a] Yield of isolated product.

of the synthesis of these types of carbohydrates, which are connected through the 6,6′-positions by an ether linkage rather than by the usual glycoside linkage.[8]

Having established the required acetalization–reduction procedures, we next turned our attention to the development of a more convenient, one-pot synthesis. First, the one-pot etherification of **2a** with **5a** was investigated. Their acetalization in the presence of TMSOTf was carried out at 0 °C for 2 h, and subsequent addition of TMSOTf and TESH to this system led to the conversion of the acetal into **4a** in 89 % yield (Scheme 3). However, in this case an excess of **2a** and the other reagents was required for the reaction to reach completion. To establish a more efficient synthetic method, we examined the possibility of decreasing the amount of **2a** required by substituting it in the reaction with its 6-OTMS derivative **7a**. After surveying a variety of conditions, we found that 3 equivalents of **7a** were sufficient to provide **4a** in 92 % yield (Scheme 4). The 6-OTMS group may play a role in decreasing the degree of coordination between **7a** and TMSOTf or TESH.



Scheme 3. One-pot acetalization–reduction reaction of **2a** and **5a** with triethylsilane in the presence of trimethylsilyl trifluoromethanesulfonate.



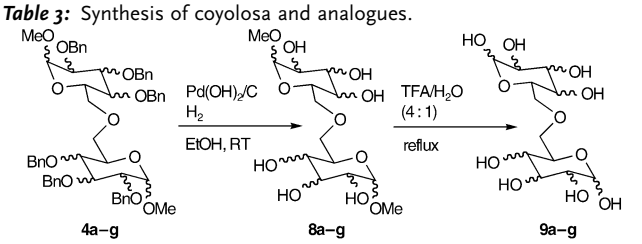
Scheme 4. One-pot acetalization–reduction of **5a** and **7a** with triethylsilane in the presence of trimethylsilyl trifluoromethanesulfonate. TMS = trimethylsilyl.

To complete the synthesis of coyolosa and its analogues we still needed to unmask the hydroxy groups in **4**. Removal of the benzyl groups of **4a–g** by hydrogenolysis furnished the corresponding pyranosides **8a–g**. Treatment of **8a–g** with trifluoroacetic acid then gave the desired 6,6′-ether-connected pyranoses **9a–g** in moderate to good yields (Table 3).

We inspected the spectral data[9] of **9a–g** for confirmation of their structure and reconsidered the possibility of the proposed structure **1** of coyolosa based on structure–activity-relationship (SAR) studies. According to the procedure reported,[1] the biological activity of all synthetic 6,6′-ether-

 © 2003 Wiley-VCH Verlag GmbH & Co. KGaA, Weinheim

Table 3: Synthesis of coyolosa and analogues.



Entry	4	9	Yield [%][a]
1	**a** (Glc-Glc)	**a**	78
2	**b** (Glc-Gal)	**b**	50
3	**c** (Glc-Man)	**c**	72
4	**d** (Gal-Gal)	**d**	59
5	**e** (Gal-Man)	**e**	76
6	**f** (Man-Man)	**f**	37
7	**g** (All-All)	**g**	59

[a] Yield from **4**.

connected pyranoses **9a**–**g** on glucose tolerance in alloxane-induced diabetic rats was investigated. Surprisingly, **9f** demonstrated the most favorable effect on fasting blood-glucose levels, which was similar to that of coyolosa, as reported by Pérez et al.[1,10] We therefore tentatively propose that the structure of coyolosa might be the mannose-derived isomer **9f**, if this natural product is indeed a 6,6′-ether-connected carbohydrate.

In conclusion, we have developed a novel synthesis of 6,6′-ether-connected pyranoses through an acetalization–reduction procedure. For convenience, a one-pot synthesis was also established. Based on an SAR study, we suggest that the structure of coyolosa might be the 6,6′-ether-connected mannose. Additional synthetic and biological studies on ether-connected carbohydrates are currently underway in our laboratory.

Experimental Section

General procedure for acetalization: TMSOTf (46 μL, 0.25 mmol) was added to a mixture of **5a** (58.9 mg, 0.13 mmol) and **2a** (592 mg, 1.30 mmol) in CH_2Cl_2 (2.5 mL) at 0 °C. The reaction mixture was stirred for 2 h then poured into a saturated solution of $NaHCO_3$. The mixture was extracted with CH_2Cl_2, and the organic phase was dried over Na_2SO_4 and concentrated in vacuo. The residual oil was subjected to silica-gel column chromatography (toluene/AcOEt 2:1), and the excess of **2a** was recovered quantitatively. Silica-gel column-chromatographic purification (hexane/Et_2O 1:1) of the remaining material afforded **6a** (159.7 mg, 0.12 mmol, 91 %) as an oil.

General procedure for acetal reduction: TMSOTf (21 μL, 0.12 mmol) and triethylsilane (123 μL, 0.77 mmol) were added successively to a solution of **6a** (52.8 mg, 0.038 mmol) in CH_2Cl_2 (0.4 mL) at −78 °C. The reaction mixture was stirred at −20 °C for 4 h then poured into a saturated solution of $NaHCO_3$. The mixture was extracted with CH_2Cl_2, and the organic phase was dried over Na_2SO_4 and concentrated in vacuo. The residual oil was subjected to silica-gel column chromatography (toluene/AcOEt 2:1), and the excess of **2a** was recovered quantitatively. Silica-gel column-chromatographic purification (hexane/AcOEt 4:1) of the remaining material afforded the desired product **4a** (33.5 mg, 0.037 mmol, 96 %) as a colorless solid.

One-pot procedure for the synthesis of 4: TMSOTf (79 μL, 0.44 mmol) was added to a solution of **5a** (20.3 mg, 0.044 mmol) and **7a** (70.7 mg, 0.13 mmol) in CH_2Cl_2 (0.2 mL) at −78 °C. The reaction mixture was stirred at −20 °C for 70 min, then triethylsilane (70 μL, 0.44 mmol) was added at −20 °C. The reaction mixture was stirred at 0 °C for 4 h then poured into a saturated solution of $NaHCO_3$. The mixture was extracted with CH_2Cl_2, and the organic phase was dried over Na_2SO_4 and concentrated in vacuo. The residual oil was purified by silica-gel column chromatography (toluene/AcOEt 2:1), and the excess of **2a** was recovered quantitatively. Silica-gel column-chromatographic purification (hexane/AcOEt = 4:1) of the remaining material afforded the desired product **4a** (36.8 mg, 0.042 mmol, 92 %) as a colorless solid.

Received: July 18, 2003 [Z52388]
Published Online: October 6, 2003

Keywords: antidiabetic agents · carbohydrates · ethers · structure–activity relationships · synthetic methods

[1] S. Pérez, G. R. M. Pérez, G. C. Pérez, G. M. A. Zavala, S. R. Vargas, *Pharm. Acta Helv.* **1997**, *72*, 105 – 111.
[2] It was reported that coyolosa showed a significant blood-sugar-lowering effect on normal and alloxane-induced diabetic mice when administered at doses of 2.5–40 mg kg^{-1} i.p. (intraperitoneal); see reference [1].
[3] It was reported by Pérez et al. that the NMR spectrum of coyolosa was measured as a solution in $CDCl_3$; however, it is impossible to dissolve unprotected pyranoses in $CDCl_3$. Therefore, we believe there may be an error in the description given in the report. We were unsuccessful in our attempts to contact the authors and were therefore unable to obtain a sample of the natural product from them.
[4] The structure was determined mainly by mass spectrometry, which is a reliable medium.
[5] a) M. P. Doyle, D. J. Debruyn, S. J. Donnelly, D. A. Kooistra, A. A. Odubela, C. T. West, S. M. Zonnebelt, *J. Org. Chem.* **1974**, *39*, 2740; b) M. P. Doyle, C. T. West, S. J. Donnelly, C. C. McOsker, *J. Organomet. Chem.* **1976**, *117*, 129; c) M. B. Sassaman, G. K. Prakash, G. A. Olah, *Tetrahedron* **1988**, *44*, 3771; d) M. P. Doyle, D. J. Debruyn, D. A. Kooistra, *J. Am. Chem. Soc.* **1972**, *94*, 3659; e) K. C. Nicolaou, C.-K. Hwang, D. A. Nugiel, *J. Am. Chem. Soc.* **1989**, *111*, 4136; f) J.-I. Kato, N. Iwasawa, T. Mukaiyama, *Chem. Lett.* **1985**, 743 – 746; g) S. Hatakeyama, H. Mori, K. Kitano, H. Yamada, M. Nishizawa, *Tetrahedron Lett.* **1994**, *35*, 4367 – 4370; h) K. Miura, K. Ootsuka, S. Suda, H. Nishikiori, A. Hosomi, *Synlett* **2002**, 313 – 315; i) X. Jiang, J. S. Bajwa, J. Slade, K. Prasad, O. Repic, T. J. Blacklock, *Tetrahedron Lett.* **2002**, *43*, 9225 – 9227; j) C.-C. Wang, J.-C. Lee, S.-Y. Luo, H.-F. Fan, C.-L. Pai, W.-C. Yang, L.-D. Lu, S.-C. Hung, *Angew. Chem.* **2002**, *114*, 2466 – 2468; *Angew. Chem. Int. Ed.* **2002**, *41*, 2360 – 2362; k) T. Suzuki, K. Ohashi, T. Oriyama, *Synthesis* **1999**, 1561 – 1563; l) M. Wada, S. Nagayama, K. Mizutani, R. Hiroi, N. Miyoshi, *Chem. Lett.* **2002**, 248 – 249; m) S. H. Lee, Y. J. Park, C. M. Yoon, *Tetrahedron Lett.* **1999**, *40*, 6049 – 6050; n) M. J. Verhoef, E. J. Creyghton, J. A. Peters, H. V. Bekkum, *Chem. Commun.* **1997**, 1989 – 1990.
[6] Further investigations are in progress.
[7] A. J. Mancuso, D. Swern, *Synthesis* **1981**, 165 – 168.
[8] No nomenclature has been established as yet by the IUPAC for these types of pyranoses connected by ether bonds. Hence, we hesitate to assign them names.
[9] Spectral (^{1}H NMR, ^{13}C NMR) and analytical (HRMS) data showed **9a**–**g** to be the 6,6′-ether-connected pyranoses. See Supporting Information.
[10] A dosage of 60 mg kg^{-1} of **9f** caused a maximum blood-sugar lowering of 26 % in 2 h in alloxane-induced diabetic rats.

 © 2003 Wiley-VCH Verlag GmbH & Co. KGaA, Weinheim

Catalytic Methanol Oxidation

Site Titration with Organic Bases During Catalysis: Selectivity Modifier and Structural Probe in Methanol Oxidation on Keggin Clusters**

*Haichao Liu, Nader Bayat, and Enrique Iglesia**

Catalytic reactions often require several types of sites with distinct functions, and the relative abundance of these sites influences the rate and selectivity of desired reactions. Heteropolyacid clusters with Keggin structures, which contain acid and redox functions,[1,2] have recently emerged as interesting catalysts for organic reactions involving bifunctional pathways.

We recently discovered a selective one-step synthesis of dimethoxymethane ($CH_3OCH_2OCH_3$, DMM, methylal) by oxidation of methanol at low temperatures (453–493 K) on unsupported and SiO_2-supported $H_{3+n}PV_nMo_{12-n}O_{40}$ ($n = 0$–4) Keggin clusters.[3] The yields and selectivities (based on the absence of dimethyl ether) of DMM resemble those obtained using supported ReO_x catalysts, the only catalysts that enable the formation of DMM in substantial yields.[4] Redox and Brønsted acid sites are required for DMM synthesis, and the reaction involves oxidative dehydrogenation of CH_3OH to formaldehyde (HCHO), acid-catalyzed acetalization of CH_3OH/HCHO mixtures, and condensation of hemiacetal or methoxymethanol intermediates (formed in acetalization reactions)[5,6] with CH_3OH to form DMM.

Brönsted acidity is required to complete the synthesis of DMM, but reaction rates are predominately controlled by the initial formation of HCHO on redox sites, the density and reactivity of which were varied in our studies by changing the dispersion and V/Mo ratio of the Keggin structures, with consequent changes in the rates of DMM synthesis. These compositional changes led to concurrent changes in the number of acid sites, because of the stoichiometry required to balance the charge. DMM selectivity is decreased by side reactions involving CH_3OH dehydration. These reactions are catalyzed by strongly acidic protons in $H_{3+n}PV_nMo_{12-n}O_{40}$ and lead to the undesired formation of dimethyl ether (DME). The latter product ultimately converts into HCHO and DMM products, and can even re-form CH_3OH, but forms DMM more slowly than CH_3OH.[3] Thus, the formation of DME through these side reactions necessitates longer residence times to achieve high yields of DMM from CH_3OH.

We report here the selective titration of protons with organic bases to control the densities of acid sites in Keggin clusters and to measure their dispersion; in both cases we do this during the catalytic reaction, a requirement imposed by the dynamic changes in accessibility that arise from reactions of polar molecules on Keggin clusters.[1,2] In this manner we are able to measure turnover rates (per exposed Keggin unit; KU) and to control the redox and acid properties independently for a given composition of Keggin cluster. This approach has led to unprecedented DMM selectivities (> 80 %) and to a family of stable organic–inorganic composites that provide effective bifunctional catalysts for broad classes of redox–acid bifunctional reactions.

The dispersion of Keggin structures was measured by titration of Brønsted acid sites with a sterically hindered pyridine (2,6-di-*tert*-butylpyridine) during catalytic reactions of mixtures of CH_3OH and O_2. This 2,6-di-*tert*-butylpyridine titrant can protonate Brønsted acid sites, but it cannot interact with Lewis acid sites because of steric constraints near the N atom.[7] Its essentially hydrophobic character also prevents its dissolution and migration into secondary structures of Keggin clusters. This result is in contrast with more polar pyridine titrants, which dissolve and penetrate into these secondary structures.[1] Thus, uptake of 2,6-di-*tert*-butylpyridine during CH_3OH reactions (per KU) reflects the number of accessible protons, and for a given $H_{3+n}PV_nMo_{12-n}O_{40}$ stoichiometry, the fraction of the Keggin structures accessible at external surfaces in supported and unsupported secondary structures. We note that such titrations must be carried out during the reaction, because of the known ability of various reactants to solvate and expose internal regions within secondary packing structures of Keggin clusters to varying degrees.

The number of 2,6-di-*tert*-butylpyridine molecules adsorbed during reactions of CH_3OH and O_2 at 453 K on $H_5PV_2Mo_{10}O_{40}/SiO_2$ (0.28 KU nm^{-2} surface density on SiO_2) increased with time and reached saturation at 1.2 H^+ per KU after about 12×10^3 s (Figure 1). This value corresponds to a nominal fractional dispersion of 0.24, on the basis of the expected H^+/KU stoichiometry; we note, however, that some of the protons in the stoichiometric starting cluster may have been removed during condensation reactions of OH groups in solvated Keggin clusters with silanols on anchoring to SiO_2.

H^+/KU ratios decreased from 1.6/1 to 0.7/1, which corresponds to a decrease in fractional KU dispersion from 0.32 to 0.15, as the KU surface densities increased from 0.1 to 0.65 KU nm^{-2} on $H_5PV_2Mo_{10}O_{40}/SiO_2$ samples. This value was 0.02 H^+ per KU for bulk $H_5PV_2Mo_{10}O_{40}$. The rates of DMM synthesis (per KU) decreased in parallel with this decrease in fractional KU dispersion as the surface density increased from 0.1 to 0.65 KU nm^{-2} (Figure 2). This excellent correlation between rates and titrant uptake for all samples, including an unsupported version of this Keggin composition, indicates that 2,6-di-*tert*-butylpyridine predominately titrates those Keggin structures that participate in bifunctional DMM

[*] Prof. Dr. E. Iglesia, Dr. H. Liu, N. Bayat
Department of Chemical Engineering
University of California at Berkeley, and Chemical Sciences Division,
E.O. Lawrence Berkeley National Laboratory
Berkeley, CA 94720 (USA)
Fax: (+1) 510-642-4778
E-mail: iglesia@cchem.berkeley.edu

[**] This work was supported by BP as part of the Methane Conversion Cooperative Research Program at the University of California at Berkeley. This work was also supported in part by the Director, Office of Basic Energy Sciences, Chemical Sciences Division of the U.S. Department of Energy under contract DE-AC03-765F00098. We acknowledge helpful technical discussions with Dr. Theo Fleisch of BP.

 © 2003 Wiley-VCH Verlag GmbH & Co. KGaA, Weinheim DOI: 10.1002/anie.200352393

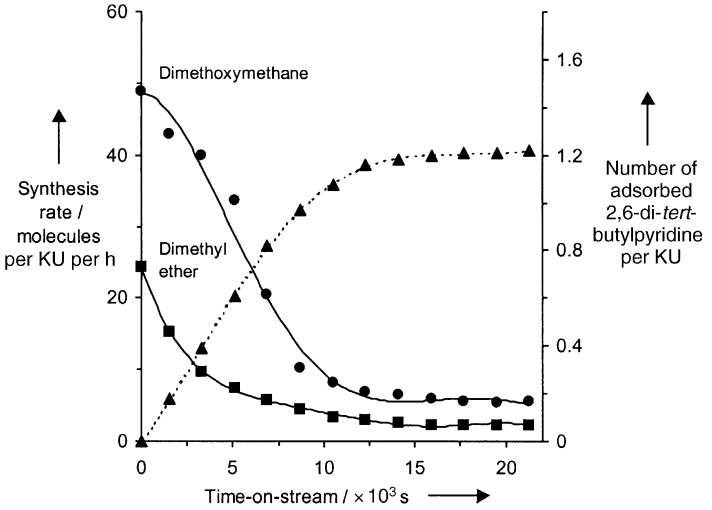


Figure 1. Adsorption uptakes (▲) and rates of DMM (●) and DME synthesis (■) as a function of time-on-stream during addition of 2,6-di-*tert*-butylpyridine to $H_5PV_2Mo_{10}O_{40}/SiO_2$ (0.28 KU nm^{-2}, 453 K, 4 kPa CH_3OH, 9 kPa O_2, CH_3OH/2,6-di-*tert*-butylpyridine (mol) = 1110/1).

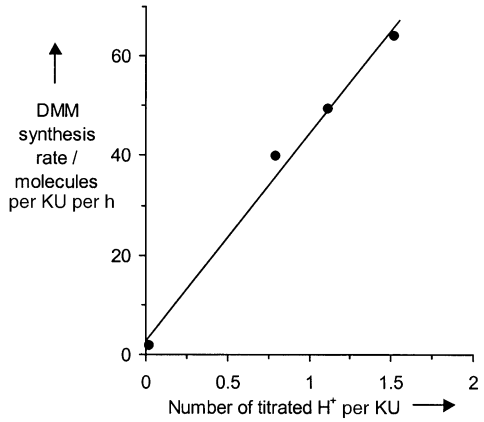


Figure 2. Rates of DMM synthesis as a function of the number of protons (per KU) titrated with 2,6-di-*tert*-butylpyridine on unsupported and SiO_2-supported (0.1–0.65 KU nm^{-2}) $H_5PV_2Mo_{10}O_{40}$ (453 K, 4 kPa CH_3OH, 9 kPa O_2, CH_3OH/2,6-di-*tert*-butylpyridine (mol) = 1110/1).

synthesis pathways. A slight inaccuracy arises from the ability of polar CH_3OH reactants to penetrate secondary Keggin structures to a small extent, as we discuss below.

The rates (per KU) for both the bifunctional DMM and monofunctional DME pathways decreased as the 2,6-di-*tert*-butylpyridine titrated the H^+ sites in $H_5PV_2Mo_{10}O_{40}/SiO_2$ (Figure 1); they reached non-zero constant values after saturation adsorption of 2,6-di-*tert*-butylpyridine (1.2 H^+ per KU; Figure 1), probably because CH_3OH can continue to reach a small number of protons that are inaccessible to 2,6-di-*tert*-butylpyridine (ca. 10–15%). The titration of protons led to lower DME selectivities, but the small number of residual protons not reached by 2,6-di-*tert*-butylpyridine prevents the attainment of DME selectivities lower than 25%. Therefore, we chose instead to examine the effect of titration with pyridine, which can penetrate secondary Keggin structures;[1] this property makes it unsuitable for KU dispersion measurements, but a more effective titrant to suppress residual pathways leading to DME synthesis.

Figure 3 shows the rates of DMM and DME synthesis at 453 K and their ratio on $H_5PV_2Mo_{10}O_{40}/SiO_2$ (0.1 KU nm^{-2}) as a function of the number of H^+ sites per KU titrated by pyridine. The products HCHO and methyl formate (MF) were detected at low selectivities (< 4%) and these data are not included in the figures. Titration with pyridine during the reaction decreased the rates of both DME and DMM synthesis, but the ratio of the DMM/DME rates increased from 1.9/1 to 7.5/1 as the number of titrated protons increased from 0 to 0.6 H^+ per KU. In effect, the loss of acid sites by titration of 0.6 H^+ per KU led to small changes in the rates of DMM synthesis (from 63.9 to 49.9 KU^{-1}h^{-1}), but decreased the rates of DME synthesis by more than a factor of five (34.2 to 6.6 KU^{-1}h^{-1}; Figure 3). Both DME and DMM reaction products became undetectable after titration of about 2.0 H^+ per KU, thus confirming that all the sites accessible to the reactants are titrated by pyridine.

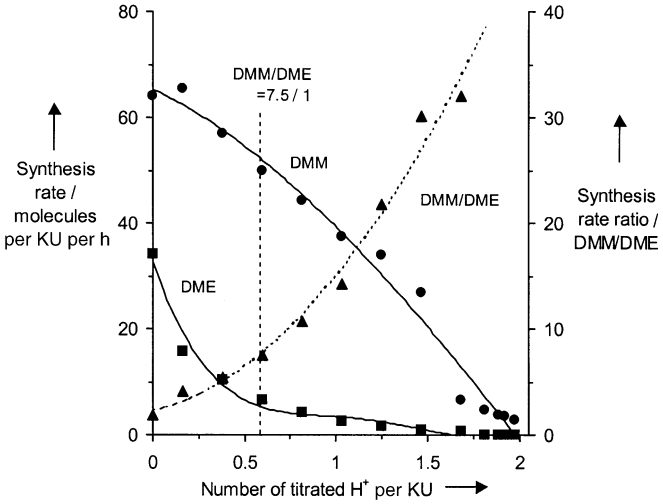


Figure 3. Rates of DMM (●) and DME synthesis (■) and their ratios of DMM/DME (▲) as a function of the number of protons (per KU) titrated with pyridine on $H_5PV_2Mo_{10}O_{40}/SiO_2$ (0.1 KU nm^{-2}, 453 K, 4 kPa CH_3OH, 9 kPa O_2, CH_3OH/pyridine (mol) = 800/1).

These data confirm that the number of Brønsted acid sites can be systematically controlled by partial titration of Keggin structures during reaction, which has marked and beneficial consequences for the selectivity of bifunctional redox–acid catalytic reactions. Selectivities can be modified significantly and, as we discuss shortly, permanently, over the time-scale of typical catalytic use. In the catalytic system used in this proof-of-concept study, the acid-catalyzed steps (acetalization and condensation) required for bifunctional reactions leading to DMM synthesis are near thermodynamic equilibrium, while redox pathways leading to HCHO intermediates limit the overall rates of DMM synthesis.[3] In contrast, CH_3OH dehydration reactions leading to DME are far from equili-

 © 2003 Wiley-VCH Verlag GmbH & Co. KGaA, Weinheim

brium and monofunctional in character; thus, they are much more strongly influenced by the number of available Brønsted acid sites, which can be accurately, flexibly, and permanently controlled by titration with organic bases during the reaction.

These specific results for $H_5PV_2Mo_{10}O_{40}/SiO_2$ are representative of those obtained for all V/Mo ratios (0–0.5/1) and KU surface densities and dispersions (Table 1). In all cases, the titration of 0.5–0.9 H^+ per KU with pyridine significantly decreased the rates of DME synthesis (by factors of 4.5–8), while only slightly decreasing the rates of DMM synthesis (by factors of 1.2–1.3); these combined effects led to much greater DMM selectivities (DMM/DME ratios $>6/1$) than on each corresponding composition unmodified by pyridine titrants (DMM/DME ratios ca. 2/1). These titration methods led to organic–inorganic composite materials with unprecedented selectivity to DMM ($>80\%$) and extremely low DME ($<12\%$) selectivity, without any significant decrease in DMM yields over those obtained without pyridine titrants.

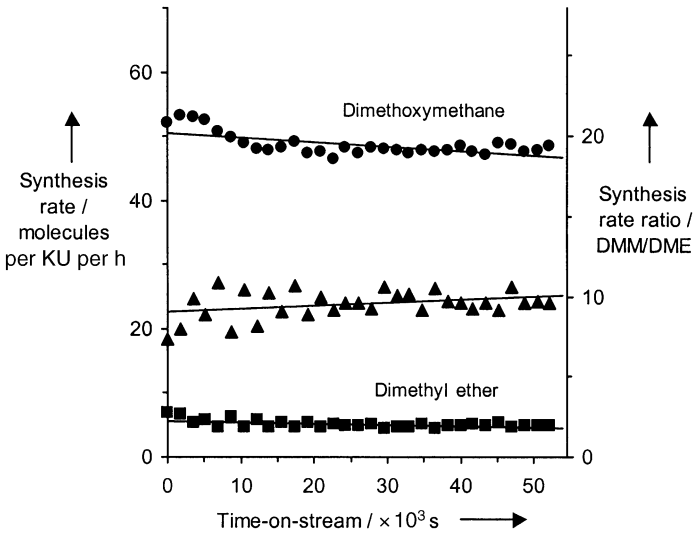


Figure 4. Rates of DMM (●) and DME synthesis (■) and their ratios of DMM/DME (▲) as a function of time-on-stream after titration of 0.6 H^+ per KU and stop of pyridine injection on $H_5PV_2Mo_{10}O_{40}/SiO_2$ (0.1 KU nm^{-2}, 453 K, 4 kPa CH_3OH, 9 kPa O_2, CH_3OH/pyridine (mol) = 800/1).

Table 1: Rates of DMM and DME synthesis and ratios of DMM/DME rate on SiO_2-supported $H_{3+n}PV_nMo_{12-n}O_{40}$ ($n = 0, 1, 2, 4$; ca. 0.1 KU nm^{-2}) and $H_5PV_2Mo_{10}O_{40}/SiO_2$ with varying surface densities of Keggin units (KU; 0.1–0.65 KU nm^{-2}) before and after titration of 0.5–0.9 H^+ per KU.[a]

Catalyst [KU nm^{-2}]	Before titration [molecules KU^{-1} h^{-1}]			After titration [molecules KU^{-1} h^{-1}]		
	DMM	DME	DMM/DME	DMM	DME	DMM/DME
$H_3PMo_{12}O_{40}$ (0.1)	60.7	35.7	1.7/1	43.1	7.0	6.2/1
$H_4PVMo_{11}O_{40}$ (0.1)	72.6	31.5	2.3/1	51.7	6.4	8.1/1
$H_5PV_2Mo_{10}O_{40}$ (0.1)	63.9	34.2	1.9/1	49.9	6.6	7.5/1
$H_6PV_4Mo_8O_{40}$ (0.1)	43.4	20.7	2.1/1	33.5	4.7	7.1/1
$H_5PV_2Mo_{10}O_{40}$ (0.28)	49.3	25.4	1.9/1	39.8	6.2	6.4/1
$H_5PV_2Mo_{10}O_{40}$ (0.65)	40.8	26.1	1.6/1	27.2	3.1	8.8/1

[a] 453 K, 4 kPa CH_3OH, 9 kPa O_2, CH_3OH/pyridine (mol) = 800/1, balance He; ca. 17–22% CH_3OH conversion.

Finally, we established the permanence of these titrant–KU complexes during extended catalytic reactions of CH_3OH and O_2 at 453 K. Figure 4 shows the rates of DMM and DME synthesis on $H_5PV_2Mo_{10}O_{40}/SiO_2$ (0.1 KU nm^{-2}) for a period of 15 h after removal of pyridine from the inlet stream; these data were obtained after about 0.6 H^+ per KU titration by pyridine. The rates of DMM and DME synthesis did not change during catalytic reactions of CH_3OH and O_2 over this period of time. We conclude, therefore, that pyridine–KU hybrid structures remain unchanged during the reaction, and that titration is permanent at these reaction conditions. Similar stability was confirmed for other compositions of Keggin structures; it is consistent with the strong interaction between pyridine rings and protons in Keggin structures detected by temperature-programmed desorption in this study, and from infrared spectra and thermal desorption data in previous studies.[8,9]

These stable organic–inorganic composites represent a novel class of materials that have significant implications for selectivity control in bifunctional redox–acid catalysis. Pyridine has been used to measure the number of available acid sites in fresh samples (not during catalytic reactions),[8–10] but we have found no previous studies describing the intentional use of organic bases as selectivity modifiers for these types of materials. Pyridine–KU complexes have been previously synthesized in efforts to form secondary Keggin structures, for which subsequent removal of pyridine during thermal treatments and before reaction may lead to specific pore morphologies or reduced addenda atoms.[11,12]

In summary, the selective and permanent titration of protons with organic bases (2,6-di-*tert*-butylpyridine or pyridine) provides an accurate measure of the dispersion of Keggin structures during catalysis and absolute values for the turnover rates of CH_3OH oxidation. This method also led to the independent and systematic control of redox and acid properties in $H_{3+n}PV_nMo_{12-n}O_{40}$ ($n = 0–4$) Keggin clusters and to unprecedented DMM selectivities ($>80\%$) and yields. This approach provides a novel and effective general framework for the in situ design of hybrid organic–inorganic catalysts for chemical reactions requiring controlled densities and reactivities of redox and acid sites. It appears to be generally applicable to reactions that take place at temperatures below those required for the desorption of the chosen titrant. Our current studies aim to extend these methods to bifunctional reactions of alkanes, alkenes, and higher alcohols, which often involve multiple redox, acidic, and basic catalytic functions.

 © 2003 Wiley-VCH Verlag GmbH & Co. KGaA, Weinheim

Experimental Section

Supported heteropolyacid catalysts were prepared by incipient wetness impregnation of SiO_2 (Cab-O-Sil, 288 $m^2 g^{-1}$) with methanolic (Merck, 99.98 %) solutions of $H_{3+n}PV_nMo_{12-n}O_{40}{\cdot}30\,H_2O$ ($n = 0$, 1, 2, 4; Japan New Metals Co.) at 298 K for 5 h, followed by drying in ambient air at 398 K overnight.

Methanol and titration reactions were carried out at 453 K in a fixed-bed quartz microreactor containing catalyst powders (0.1–0.3 g). Samples were treated in flowing 20 % O_2/He (O_2, Praxair, 99.999 %; He, Airgas, 99.999 %; 0.67 $cm^3 s^{-1}$) at 553 K for 1.0 h before catalytic reaction measurements. The Keggin structures of these materials before and after the thermal treatment were characterized by Raman spectroscopy.[3] No structural changes were detected for thermal treatments below 673 K. The reactant mixture consisted of 4 kPa CH_3OH (Merck, 99.99 %), 9 kPa O_2, 1 kPa N_2 (Praxair, certified O_2/N_2 mixture), and 86 kPa He (Airgas, 99.999 %). Methanol or mixtures of methanol with pyridine (Fisher Scientific, 99.9 %) or 2,6-di-*tert*-butylpyridine (Aldrich, 97 %) at a molar ratio of CH_3OH/pyridine = 800/1 or CH_3OH/2,6-di-*tert*-butylpyridine = 1110/1 were introduced by continuous injection using a syringe pump. Reactants and products were analyzed by on-line gas chromatography (Hewlett–Packard 6890GC) using a methylsilicone capillary column and a Porapak Q packed column connected to flame-ionization and thermal conductivity detectors, respectively. Rates are reported as the number of CH_3OH molecules converted into a given product per Keggin unit per hour.

Received: July 16, 2003 [Z52393]

Keywords: cluster compounds · heterogeneous catalysis · methanol · organic bases · oxidation

[1] T. Okuhara, N. Mizuno, M. Misono, *Adv. Catal.* **1994**, *41*, 113.
[2] M. Misono, *Chem. Commun.* **2001**, 1141.
[3] H. Liu, E. Iglesia, *J. Phys. Chem. B*, in press.
[4] Y. Yuan, T. Shido, Y. Iwasawa, *J. Phys. Chem. B* **2002**, *106*, 4441.
[5] I. E. Wachs, R. J. Madix, *Surf. Sci.* **1978**, 76, 531.
[6] C. Louis, J.-M. Tatibouet, M. Che, *J. Catal.* **1988**, *109*, 354.
[7] J. G. Santiesteban, J. C. Vartuli, S. Han, R. D. Bastian, C. D. Chang, *J. Catal.* **1997**, *168*, 431.
[8] E. M. Serwicka, E. Broclawik, K. Bruckman, J. Haber, *Catal. Lett.* **1989**, 351.
[9] G. A. Tsigdinos, C. J. Hallada, *Inorg. Chem.* **1968**, *7*, 137.
[10] J. G. Highfield, J. B. Moffat, *J. Catal.* **1984**, *89*, 185.
[11] J. M. Tatibouet, *Appl. Catal. A* **1999**, *182*, 357.
[12] M. E. Davis, C. J. Dillon, J. H. Holles, J. Labinger, *Angew. Chem.* **2002**, *114*, 886; *Angew. Chem. Int. Ed.* **2002**, *41*, 858.

 © 2003 Wiley-VCH Verlag GmbH & Co. KGaA, Weinheim

Efficient Ethylene Polymerization

Homogeneous Ethylene-Polymerization Catalysts Based on Alkyl Cations of the Rare-Earth Metals: Are Dicationic Mono(alkyl) Complexes the Active Species?**

*Stefan Arndt, Thomas P. Spaniol, and Jun Okuda**

Cationic alkyl complexes of Group 4 metals, for example, alkyl zirconocenium ions, currently play a pivotal role as single-site catalysts in homogeneous olefin-polymerization reactions.[1] The first cationic alkyl rare earth metal complex $[La(\eta^5\text{-}C_5Me_5)\{CH(SiMe_3)_2\}(thf)_x]^+[BPh_4]^-$ ($x = 0$ or 3) was reported in 1992,[2a] and since then, there has only been one report with evidence that such a complex, a scandium dimethyl cation, polymerizes ethylene.[2b] A number of cationic alkyl complexes of the rare-earth metals $[Ln(L)R]^+$ supported by monoanionic ancillary noncyclopentadienyl ligands L, such as the amido-functionalized triazacyclononane,[3] β-diketiminate,[4] or benzamidinate[5] were surmised to also catalyze ethylene polymerization. We reported that the thermally sensitive tris(trimethylsilylmethyl) complexes $[Ln(CH_2SiMe_3)_3(thf)_2]$ (Ln = Lu, Y)[6] can be transformed into robust monocationic bis(alkyl) complexes $[Ln(CH_2SiMe_3)_2(thf)_x]^+$ by the reaction with BPh_3.[7] Herein we report that the tris(alkyl) complexes $[Ln(CH_2SiMe_3)_3(thf)_2]$ without any ancillary ligand L can act as precursors for highly active catalysts for homogeneous ethylene polymerization. There is evidence that the active species are the dications $[Ln(CH_2SiMe_3)(solv)_z]^{2+}$, which are formed by the protonolysis of $[Ln(CH_2SiMe_3)_3(thf)_2]$ via the dialkyl monocations $[Ln(CH_2SiMe_3)_2(solv)_y]^+$.

Toluene solutions of the alkyl complexes $[Ln(CH_2SiMe_3)_3(thf)_2]$ (Ln = Tm, Er, Y, Ho, Dy, Tb) efficiently catalyze ethylene polymerization upon activation with the Brønsted acid $[NMe_2HPh][B(C_6F_5)_4]$ in the presence of $Al\mathit{i}Bu_3$. After short run times (10 min) at 5 bar of ethylene pressure, linear polyethylenes with molecular weights $\bar{M}_n = 3500$–$45\,000$ and polydispersities $\bar{M}_w/\bar{M}_n = 2$–6 were produced with activities up to $899\ kg\,mol^{-1}\,h^{-1}\,bar^{-1}$ (Table 1). As illustrated in Figure 1, the catalyst performance can be adjusted by the choice of the rare-earth metal as the activity is well correlated

[*] Prof. Dr. J. Okuda,[+] Dipl.-Chem. S. Arndt, Dr. T. P. Spaniol
Institut für Anorganische Chemie und Analytische Chemie
Johannes Gutenberg-Universität Mainz
Duesbergweg 10–14, 55099 Mainz (Germany)
Fax: (+49) 6131-39-25605
E-mail: okuda@mail.uni-mainz.de

[+] New address:
Institute of Inorganic Chemistry
Aachen University of Technology (RWTH)
Prof.-Pirlet-Strasse 1, 52056 Aachen (Germany)

[**] Financial support by the Deutsche Forschungsgemeinschaft and the Fonds der Chemischen Industrie is gratefully acknowledged. We thank Prof. Dr. U. Englert for recording the crystallographic data, Dr. S. Matsui for GPC analysis, and Dipl.-Chem. K. Beckerle for DSC analysis.

 DOI: 10.1002/anie.200352532 © 2003 Wiley-VCH Verlag GmbH & Co. KGaA, Weinheim

Table 1: Ethylene polymerization with $[Ln(CH_2SiMe_3)_3(thf)_2]$ as catalyst precursor.[a]

Ln	R[b] [Å]	Yield [g]	Activity [kg mol^{-1} h^{-1} bar^{-1}]	$\bar{M}_n$ [g mol^{-1}]	$\bar{M}_w/\bar{M}_n$	T_m [°C]
Sc[c]	0.89	0.03	1	–	–	–
Lu[c]	1.00	traces	–	–	–	–
Yb	1.01	–	–	–	–	–
Tm	1.02	0.76	183	22033	4.1	136.7
Er	1.03	0.85	205	13430	5.3	134.7
Y[d]	1.04	0.91	272	14150	2.9	135.5
Ho	1.04	1.15	275	44847	1.7	132.5
				3446[e]	1.8	
Dy	1.05	3.51	842	3652	3.6	126.3
Tb	1.06	3.74	899	3816	2.9	126.3

[a] $[NMe_2HPh][B(C_6F_5)_4]$ as activator in the presence of Al*i*Bu$_3$. Conditions: 5 μmol Ln; B:Ln = 5:1, Al:Ln = 200:1, T = 25 °C, p = 5 bar, t = 10 min, V = 30 mL (toluene). [b] Effective ionic radius of Ln^{3+} for CN = 6, see reference [8]. [c] t = 60 min. [d] t = 8 min. [e] Bimodal molecular weight distribution.

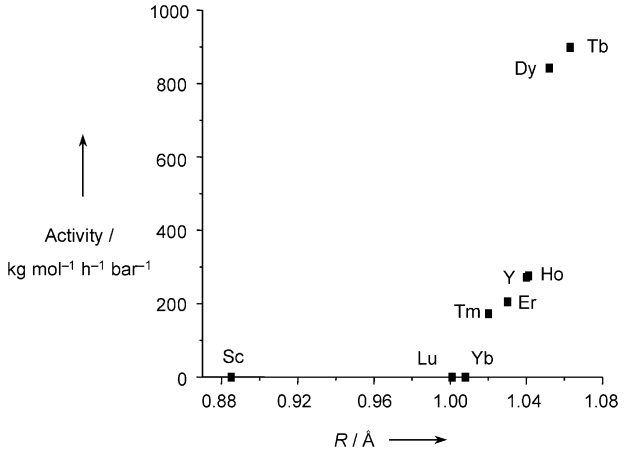
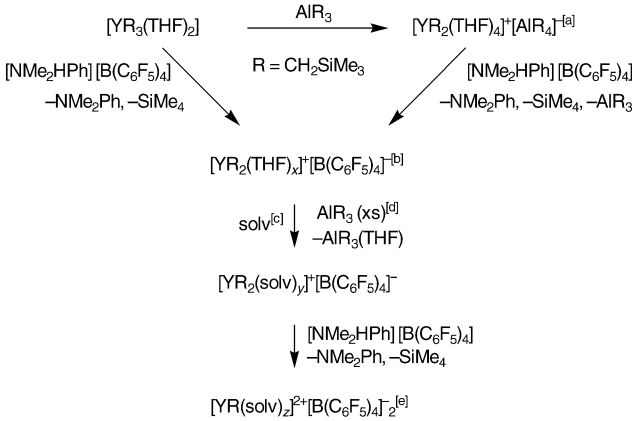


Figure 1. Plot of the polymerization activity versus the effective ionic radius R of the trivalent rare earth metal for coordination number CN = 6.

with the effective ionic radius[8] of the rare-earth metal. For the smaller elements scandium, lutetium, and ytterbium, no significant activity was observed, whereas thulium produced polyethylene with 183 kg mol^{-1} h^{-1} bar^{-1}. For terbium, the element with the largest radius within the series examined, an activity of 899 kg mol^{-1} h^{-1} bar^{-1} was found, corroborating that rare-earth metal alkyl cations are the active species.[9] Although the active species initially appeared to be the monocationic bis(alkyl) complex $[Ln(CH_2SiMe_3)_2(solv)_y]^+[B(C_6F_5)_4]^-$ (Scheme 1), with aluminum alkyl acting as scavenger for THF, two findings cast doubts on this hypothesis. 1) Why is an excess of $[NMe_2HPh][B(C_6F_5)_4]$ necessary to activate the catalyst precursor?[10] 2) Why does the choice of the aluminum alkyl have a significant influence on the polymerization results?[11] We therefore studied the following (Scheme 1) as model reactions for the activation steps: 1) The reaction of $[Y(CH_2SiMe_3)_3(thf)_2]$ with excess $[NMe_2HPh][BPh_4]$. 2) The reactivity of $[Y(CH_2SiMe_3)_3(thf)_2]$ towards the aluminum alkyl $Al(CH_2SiMe_3)_3$. For these preparative-scale



Scheme 1. Activation of $[Y(CH_2SiMe_3)_3(thf)_2]$ with $[NMe_2HPh][B(C_6F_5)_4]$ in the presence of $Al(CH_2SiMe_3)_3$; [a] isolated, [b] analogous complex isolated as $[Y(CH_2SiMe_3)_2(thf)_4]^+[BPh_4]^-$, [c] solv = toluene in polymerization experiments, the exchange of THF by toluene is postulated,[11] [d] xs = excess, [e] analogous complex isolated as $[Y(CH_2SiMe_3)(thf)_5]^{2+}[BPh_4]^-_2$.

and NMR-tube experiments, the use of the polar solvents pyridine or THF was required, as oils form from aromatic hydrocarbons such as toluene, benzene, or bromobenzene. To avoid ring opening polymerization of THF, the use of $[BPh_4]^-$ instead of $[B(C_6F_5)_4]^-$ as the counter anion was required when THF was used as solvent.

When a THF solution containing the yttrium tris(alkyl) $[Y(CH_2SiMe_3)_3(thf)_2]$ and three equivalents of $[NMe_2HPh][BPh_4]$ was stirred for 24 h at 25 °C, colorless microcrystals of the thermally robust dicationic alkyl complex $[Y(CH_2SiMe_3)(thf)_5]^{2+}[BPh_4]^-_2$ were isolated in virtually quantitative yield.[12] In $[D_5]$pyridine, the methylene protons at yttrium appear as a doublet at $\delta = 0.73$ ppm with $^2J(Y,H) = 3.3$ Hz in the corresponding ^{1}H NMR, while the ^{13}C NMR spectrum exhibits a doublet for the YCH_2 group at $\delta = 44.5$ with $^1J(Y,C) = 44.9$ Hz. The ^{89}Y NMR resonance of $[Y(CH_2SiMe_3)(thf)_5]^{2+}[BPh_4]^-_2$ in $[D_8]$THF at $\delta = 409.2$ is shifted to a significantly higher field compared with that for the corresponding monocations $[Y(CH_2SiMe_3)_2(thf)_4]^+[Al(CH_2SiMe_3)_4]^-$ ($\delta = 666.4$,), $[Y(CH_2SiMe_3)_2(thf)_4]^+[BPh_4]^-$ ($\delta = 660.0$) or the neutral analogue $[Y(CH_2SiMe_3)_3(thf)_2]$ ($\delta = 882.7$).

The reaction of $[Y(CH_2SiMe_3)_3(thf)_2]$ in THF with more than two equivalents $[NMe_2HPh][BPh_4]$ to give the dication $[Y(CH_2SiMe_3)(thf)_5]^{2+}[BPh_4]^-_2$ as the exclusive yttrium-containing species suggests that the activation of the tris(alkyl) precursors $[Ln(CH_2SiMe_3)_3(thf)_2]$ in toluene with $[NMe_2HPh][B(C_6F_5)_4]$ generates dications $[Ln(CH_2SiMe_3)(solv)_z]^{2+}$ as the active species.[13] When the tris(aluminate) $[Y\{(\mu\text{-}Me_2)(AlMe_2)\}_3]$[14] was treated with excess $[NEt_3H][BPh_4]$ in THF, the ion triple $[Y(CH_3)(THF)_6]^{2+}[BPh_4]^-_2$ was obtained in crystalline form [Eq. (1)].[15] The resonance of the methyl

$$[Y\{(\mu\text{-}Me_2)(AlMe_2)\}_3] \xrightarrow[THF]{2\,[NEt_3H][BPh_4]} [Y(CH_3)(thf)_6]^{2+}[BPh_4]^-_2 + 2\,NEt_3 + 2\,CH_4 + 3\,AlMe_3 \quad (1)$$

group at the yttrium appears as a doublet in $[D_5]$pyridine at $\delta = 0.69$ with $^2J(Y,H) = 2.1$ Hz. The ^{13}C NMR spectrum

 © 2003 Wiley-VCH Verlag GmbH & Co. KGaA, Weinheim

exhibits a doublet for the YCH_3 group at $\delta = 32.8$ with $^1J(Y,C) = 53.6$ Hz, while the ^{89}Y-NMR resonance appears at $\delta = 433.2$.

Single crystals of $[Y(CH_3)(thf)_6]^{2+}[BPh_4]^-_2$ suitable for X-ray structure analysis were grown from a supersaturated THF solution.[15b] The cationic portion of the ion triple $[Y(CH_3)(thf)_6]^{2+}[BPh_4]^-_2$ is shown in Figure 2, which illustrates the pentagonal bipyramidal coordination geometry around the yttrium center with the methyl group in the apical position. The Y–C bond length of 2.418(3) Å is comparable with those found for the ion pair $[Y(CH_2SiMe_3)_2(thf)_4]^+[Al(CH_2SiMe_3)_4]^-$ (2.384(6) and 2.411(6) Å),[16] while the Y–O bond lengths of $[Y(CH_3)(thf)_6]^{2+}[BPh_4]^-_2$ (2.352(3)–2.427(3) Å) are similar to those found for Y–O(THF) bond lengths at monocationic yttrium centers.[17]

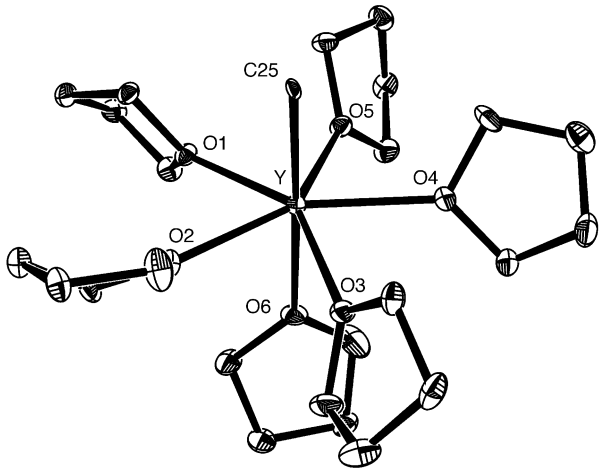


Figure 2. Molecular structure of the cationic portion of $[Y(CH_3)(thf)_6]^{2+}[BPh_4]^-_2$. Thermal ellipsoids are drawn at the 30% probability level, hydrogen atoms are omitted for clarity. Selected distances [Å] and angles [°]: Y-O1 2.352(3), Y-O2 2.426(3), Y-O3 2.355(3), Y-O4 2.427(3), Y-O5 2.377(3), Y-O6 2.427(3), Y-C25 2.418(3); C25-Y-O6 176.5(1).

The nature of the aluminum alkyl compounds was found to have a remarkable influence on both the activity of the catalyst system $[Y(CH_2SiMe_3)_3(thf)_2]/[NMe_2HPh][B(C_6F_5)_4]$ as well as the molecular weight $\bar{M}_n$. From Table 2 it is apparent that the steric bulk of the alkyl group at the aluminum center is critical with respect to the activity: only traces of polyethylene were obtained with $AlMe_3$, whereas the use of $Al(CH_2SiMe_3)_3$ gave high molecular weight polyethylene ($\bar{M}_n = 110990$) with an outstanding activity of 1840 $kg\,mol^{-1}\,h^{-1}\,bar^{-1}$.[18]

Equimolar amounts of $[Y(CH_2SiMe_3)_3(thf)_2]$ and $Al(CH_2SiMe_3)_3$[19] were found to form the ion pair $[Y(CH_2SiMe_3)_2(thf)_x]^+[Al(CH_2SiMe_3)_4]^-$ in C_6D_6 and in $[D_8]$THF, which was isolated in 75% yield as the thermally stable ion pair $[Y(CH_2SiMe_3)_2(thf)_4]^+[Al(CH_2SiMe_3)_4]^-$. In the ^{1}H NMR spectrum of the product in $[D_8]$THF, the resonance of the methylene protons at the aluminate center was recorded at $\delta = -1.28$ ppm as a broad multiplet owing to ^2J(Al,H) coupling, whereas the methylene protons at the cationic yttrium appear as a doublet at $\delta = -0.73$ with $^2J(Y,H) = 3.1$ Hz. The ^{13}C NMR spectrum exhibits a doublet for the YCH_2 group at $\delta = 37.2$ with $^1J(Y,C) = 42.1$ Hz.

Single crystals of $[Y(CH_2SiMe_3)_2(thf)_4]^+[Al(CH_2SiMe_3)_4]^-$ suitable for X-ray structure analysis were obtained from pentane/THF.[15b] The cationic portion of the ion pair $[Y(CH_2SiMe_3)_2(thf)_4]^+[Al(CH_2SiMe_3)_4]^-$ is shown in Figure 3, which illustrates the distorted octahedral-coordination geom-

Table 2: Ethylene polymerization with yttrium catalyst precursors.[a]

Precursor[b]	Aluminum alkyl	Yield [g]	Activity [$kg\,mol^{-1}\,h^{-1}\,bar^{-1}$]	$\bar{M}_n$ [$g\,mol^{-1}$]	$\bar{M}_w/\bar{M}_n$	T_m [°C]
$[YR_3(thf)_2]$	$AlEt_3$	0.11	27	–	–	128.3
$[YR_3(thf)_2]$	$Al\,nOct_3$	0.43	103	–	–	136.7
$[YR_3(thf)_2]$[c]	$Al\,iBu_3$	0.91	272	14150	2.9	135.5
$[YR_3(thf)_2]$	$Al\,iBu_2H$	1.67	401	59730	1.7	130.2
				3030[d]	2.3	
$[YR_3(thf)_2]$[e]	AlR_3	1.53	1840	110990	2.9	138.0
$[YR_2(thf)_4]^+[AlR_4]^-$[e,f]	AlR_3	1.13	1351	215599	2.4	141.6
$[YR_3(thf)_2]$	MAO[g]	1.41	339	–	–	133.1

[a] $[NMe_2HPh][B(C_6F_5)_4]$ as activator in the presence of aluminum alkyl. Conditions: 5 μmol Y, B:Y = 5:1, Al:Y = 200:1, $T = 25$ °C, $p = 5$ bar, $t = 10$ min, $V = 30$ mL (toluene) [b] $R = CH_2SiMe_3$. [c] $t = 8$ min. [d] Bimodal molecular weight distribution. [e] $t = 2$ min. [f] Al:Y = 100:1. [g] Methylaluminoxane.

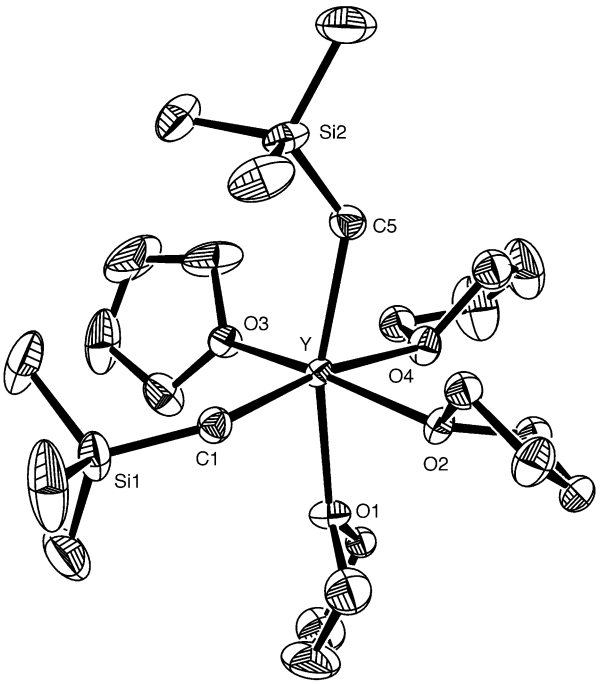


Figure 3. Molecular structure of the cationic portion of $[Y(CH_2SiMe_3)_2(thf)_4]^+[Al(CH_2SiMe_3)_4]^-$. Thermal ellipsoids are drawn at the 20% probability level, hydrogen atoms are omitted for clarity. Selected distances [Å^{-1}] and angles [°]: Y-O1 2.448(4), Y-O2 2.354(4), Y-O3 2.354(4), Y-O4 2.479(4), Y-C1 2.384(6), Y-C5 2.411(6); O1-Y-C5 163.7(2), O2-Y-O3 165.3(1), O4-Y-C1 171.0 (2).

 © 2003 Wiley-VCH Verlag GmbH & Co. KGaA, Weinheim

etry around the yttrium center with the two alkyl groups arranged in a *cis* fashion.[20] The formation of alkyl aluminates of the rare-earth metals as ion pairs is unprecedented. So far, only complexes containing bridging alkyl groups such as $[Y\{(\mu\text{-}Me_2)(AlMe_2)\}_3]$[14] were reported for the trivalent rare earth metals. When $[Y(CH_2SiMe_3)_2(thf)_4]^+[Al(CH_2SiMe_3)_4]^-$ was activated with $[NMe_2HPh][B(C_6F_5)_4]$ for ethylene polymerization, similar results as for $[Y(CH_2SiMe_3)_3(thf)_2]$ were obtained (1351 versus 1840 $kg\,mol^{-1}\,h^{-1}\,bar^{-1}$), thus indicating that $[Y(CH_2SiMe_3)_2(thf)_4]^+[Al(CH_2SiMe_3)_4]^-$ is converted into a dication (Table 2).[21]

In conclusion, we have demonstrated that the easily accessible tris(alkyl) complexes of the rare-earth metals $[Ln(CH_2SiMe_3)_3(thf)_2]$ are precursors for highly active catalysts for ethylene polymerization and that an alkyl dication $[Ln(CH_2SiMe_3)(solv)_z]^{2+}$, formed via the dialkyl monocation $[Ln(CH_2SiMe_3)_2(solv)_y]^+$, is most probably the active species.

Experimental Section

$[Y(CH_2SiMe_3)_2(thf)_4]^+[BPh_4]^-$: A slurry of $[Y(CH_2SiMe_3)_3(thf)_2]$ (200 mg, 404 μmol) and $[NEt_3H][BPh_4]$ (170 mg, 404 μmol) was stirred in THF (20 mL) at −78 °C. The reaction mixture was allowed to slowly warm up to ambient temperature and stirred for 24 h to give a colorless clear solution. After the volatile fractions were removed in vacuo, the resultant colorless solid was washed with Et_2O (2 × 20 mL) and dried under vacuum to give colorless microcrystals (135 mg, 38 %). ^{1}H NMR (400 MHz, [D$_8$]THF, 25 °C, TMS): δ = −0.78 (d, ^2J(Y,H) = 3.3 Hz, 2 × 2 H; YCH_2SiCH_3), −0.06 (s, 2 × 9 H; YCH_2SiCH_3), 1.76 (m, 4 × 4 H; β-CH_2, THF), 3.60 (m, 4 × 4 H; α-CH_2, THF), 6.74 (t, ^3J(H,H) = 7.0 Hz, 4 H; 4-Ph), 6.87 (t, ^3J(H,H) = 7.3 Hz, 2 × 4 H; 3-Ph), 7.28 ppm (br, 2 × 4 H; 2-Ph). ^{13}C NMR (101 MHz, [D$_5$]pyridine, 25 °C, TMS): δ = 4.5 (YCH_2SiCH_3), 25.8 (β-CH_2, THF), 30.9 (dt, ^1J(Y,C) = 36.5 Hz, ^1J(C,H) = 97.2 Hz; YCH_2SiCH_3), 67.8 (α-CH_2, THF), 122.3 (4-Ph), 126.2 (3-Ph), 137.2 (2-Ph), 165.0 ppm (q, ^1J(B,C) = 49.3 Hz; 1-Ph). ^{11}B{^{1}H} NMR (128 MHz, [D$_8$]THF, 25 °C, $BF_3{\cdot}Et_2O$): δ = −6.6 ppm. ^{89}Y NMR (20 MHz, [D$_8$]THF, 25 °C, YCl_3): δ = 660.0 ppm. Elemental analysis calcd (%) for $C_{48}H_{74}BO_4Si_2Y$: C 66.19, H 8.56, Y 10.21; found: C 65.91, H 8.44, Y 9.74.

$[Y(CH_2SiMe_3)(thf)_5]^{2+}[BPh_4]^-{}_2$: A solution of $[Y(CH_2SiMe_3)_3(thf)_2]$ (300 mg, 606 μmol) in THF (60 mL) was added to neat $[NMe_2HPh][BPh_4]$ (802 mg, 1818 μmol) at −78 °C. The reaction mixture was stirred at ambient temperature for 24 h to give a brownish solution. The solution was filtered, the volatile fractions were removed by evaporation, and the residue was washed with pentane (60 mL) gave a colorless powder of $[Y(CH_2SiMe_3)(thf)_5]^{2+}[BPh_4]^-{}_2$ (661 mg, 99 %). ^{1}H NMR (400 MHz, [D$_5$]pyridine, 25 °C, TMS): δ = 0.17 (s, 9 H; YCH_2SiCH_3), 0.73 (d, ^2J(Y,H) = 3.3 Hz, 2 H; YCH_2SiCH_3), 1.62 (m, 5 × 4 H; β-CH_2, THF), 3.66 (m, 5 × 4 H; α-CH_2, THF), 7.10 (t, ^3J(H,H) = 7.3 Hz, 2 × 4 H; 4-Ph), 7.27 (t, ^3J(H,H) = 7.3 Hz, 2 × 8 H; 3-Ph), 8.06 ppm (br, 2 × 8 H; 2-Ph). ^{13}C NMR (101 MHz, [D$_5$]pyridine, 25 °C, TMS): δ = 4.0 (YCH_2SiCH_3), 25.9 (β-CH_2, THF), 44.5 (dt, ^1J(Y,C) = 44.9 Hz, ^1J(C,H) = 93.8 Hz; YCH_2SiCH_3), 67.9 (α-CH_2, THF), 122.4 (4-Ph), 126.2 (3-Ph), 137.1 (2-Ph), 165.0 ppm (q, ^1J(B,C) = 49.2 Hz; 1-Ph). ^{11}B{^{1}H} NMR (128 MHz, [D$_8$]THF, 25 °C, $BF_3{\cdot}Et_2O$): δ = −6.7 ppm. ^{89}Y NMR (20 MHz, [D$_8$]THF, 25 °C, YCl_3): δ = 409.2 ppm. Elemental analysis calcd (%) for $C_{72}H_{91}B_2O_5SiY$: C, 73.59; H, 7.81; Y, 7.57; found: C, 74.62; H, 8.37; Y, 7.16.

Received: July 31, 2003 [Z52532]
Published Online: October 8, 2003

Keywords: alkyl ligands · aluminum · cations · polymerization · rare earth elements

[1] R. F. Jordan, *Adv. Organomet. Chem.* **1991**, *32*, 325 – 387.
[2] a) C. J. Schaverien, *Organometallics* **1992**, *11*, 3476 – 3478; a) S. Hajela, W. P. Schaefer, J. E. Bercaw, *J. Organomet. Chem.* **1997**, *532*, 45 – 53.
[3] S. Bambirra, D. van Leusen, A. Meetsma, B. Hessen, J. H. Teuben, *Chem. Commun.* **2001**, 637 – 638.
[4] P. G. Hayes, W. E. Piers, R. McDonald, *J. Am. Chem. Soc.* **2002**, *124*, 2132 – 2133.
[5] S. Bambirra, D. van Leusen, A. Meetsma, B. Hessen, J. H. Teuben, *Chem. Commun.* **2003**, 522 – 523.
[6] For the preparation by using a one-pot synthesis, see: M. F. Lappert, R. Pearce, *J. Chem. Soc. Chem. Commun.* **1973**, 126 – 127.
[7] For crystallographically characterized crown ether adducts $[Lu(CH_2SiMe_3)_2(CE)(THF)_x]^+$ (x = 1, CE = 12-crown-4; x = 0, CE = 15-crown-5, 18-crown-6), see: S. Arndt, T. P. Spaniol, J. Okuda, *Chem. Commun.* **2002**, 896 – 897.
[8] R. D. Shannon, *Acta Crystallogr. Sect. A* **1976**, *32*, 751 – 767.
[9] In principle, cationic aluminum alkyls could be also considered as ethylene polymerization catalyst, see: a) J. S. Kim, L. M. Wojcinski II, S. Liu, J. C. Sworen, A. Sen, *J. Am. Chem. Soc.* **2000**, *122*, 5668 – 5669; b) K.-C. Kim, C. A. Reed, G. S. Long, A. Sen, *J. Am. Chem. Soc.* **2002**, *124*, 7662 – 7663.
[10] In the presence of only one equivalent of $[NMe_2HPh][B(C_6F_5)_4]$, no polymerization of ethylene is observed.
[11] An excess of aluminum alkyl may activate the rare-earth metal alkyl by removing THF under formation of $[AlR_3(thf)]$. Furthermore, adduct formation between the (especially sterically less demanding) aluminum alkyl and the cationic rare earth metal catalyst may result in an inactive aluminate species. For a cationic Zr aluminate $[Zr\{SiMe_2(\eta^5\text{-}C_9H_6)_2\}(\mu\text{-}Me)_2(AlMe_2)][B(C_6F_5)_4]$ as dormant species, see: M. Bochmann, S. J. Lancaster, *Angew. Chem.* **1994**, *106*, 1715 – 1718; *Angew. Chem. Int. Ed. Engl.* **1994**, *33*,1634 – 1637.
[12] The third equivalent of $[NMe_2HPh][BPh_4]$ did not lead to further alkyl abstraction. Abstraction of two alkyl groups from a scandium complex under formation of a contact ion pair was reported in reference [4]; a) double alkyl abstraction by $B(C_6F_5)_3$ was observed for $[Ti(N{=}PtBu_3)_2Me_2]$, see: F. Guerin, J. C. Stewart, C. Beddie, D. W. Stephan, *Organometallics* **2000**, *19*, 2994 – 3000; b) double alkyl abstraction by $Al(C_6F_5)_3$ was observed for $[Ti(\eta^5{:}\eta^1\text{-}C_5Me_4SiMe_2NtBu)Me_2]$, see: E. Y.-X. Chen, W. J. Kruper, G. Roof, D. R. Wilson, *J. Am. Chem. Soc.* **2001**, *123*, 745 – 746.
[13] An η^6 coordinated arene adduct of a monocationic scandium methyl complex was crystallographically characterized, see: P. G. Hayes, W. E. Piers, M. Parvez, *J. Am. Chem. Soc.* **2003**, *125*, 5622 – 5623.
[14] W. J. Evans, R. Anwander, J. W. Ziller, *Organometallics* **1995**, *14*, 1107 – 1109. We believe that a complex of this type is formed when $[Y(CH_2SiMe_3)_3(thf)_2]$ is treated with $AlMe_3$.
[15] a) NMR data for $[Y(CH_3)(thf)_6]^{2+}[BPh_4]^-{}_2$: ^{1}H NMR (400 MHz, [D$_5$]pyridine, 25 °C, TMS): δ = 0.69 (d, ^2J(Y,H) = 2.1 Hz, 3 H; YCH_3), 1.63 (m, 4 × 4 H; β-CH_2, THF), 3.67 (m, 4 × 4 H; α-CH_2, THF), 7.10 (t, ^3J(H,H) = 7.0 Hz, 2 × 4 H; 4-Ph), 7.26 (t, ^3J(H,H) = 7.4 Hz, 2 × 8 H; 3-Ph), 8.04 ppm (br, 2 × 8 H; 2-Ph). ^{13}C NMR (101 MHz, [D$_5$]pyridine, 25 °C, TMS): δ = 27.6 (β-CH_2, THF), 32.8 (dq, ^1J(Y,C) = 53.6 Hz, ^1J(C,H) = 105.5 Hz; YCH_3), 69.7 (α-CH_2, THF), 124.2 (4-Ph), 128.0 (3-Ph), 139.0 (2-Ph), 166.8 ppm (q, ^1J(B,C) = 49.2 Hz; 1-Ph). ^{11}B{^{1}H}-NMR (128 MHz, [D$_8$]THF, 25 °C, $BF_3{\cdot}Et_2O$): δ = −4.7 ppm. ^{89}Y-NMR (20 MHz, [D$_5$]pyridine, 25 °C, YCl_3): δ = 433.2 ppm. Elemental analysis calcd (%) for $C_{77}H_{99}B_2O_7Y$: C 74.16, H 8.00; found: C 73.27, H 7.22;

 © 2003 Wiley-VCH Verlag GmbH & Co. KGaA, Weinheim

b) CCDC-216055 ($[Y(CH_3)(THF)_6]^{2+}[BPh_4]^-_2$) CCDC-216054 ($[Y(CH_2SiMe_3)_2(THF)_4]^+[Al(CH_2SiMe_3)_4]^-$) contains the supplementary crystallographic data for this paper. These data can be obtained free of charge via www.ccdc.cam.ac.uk/conts/retrieving.html (or from the Cambridge Crystallographic Data Centre, 12 Union Road, Cambridge CB2 1EZ, UK; fax: (+44) 1223-336-033; or deposit@ccdc.cam.ac.uk).

[16] For pertinent Y–C bond lengths, see: K. C. Hultzsch, P. Voth, K. Beckerle, T. P. Spaniol, J. Okuda, *Organometallics* **2000**, *19*, 228–243.

[17] Y-O(THF) bond distances at monocationic yttrium centers: a) $[YCl(OtBu)(thf)_5]^+[BPh_4]^-\cdot$THF: Y-O = 2.405(5), 2.411(5), 2.391(5), 2.422(5), 2.408(5) Å, see: W. J. Evans, J. M. Olofson, J. W. Ziller, *J. Am. Chem. Soc.* **1990**, *112*, 2308–2314; b) $[YCl_2(thf)_5]^+[YCl_4(thf)_2]^-$: Y-O = 2.391(7), 2.368(5), 2.382(6) Å, see: P. Sobota, J. Utko, S. Szafert, *Inorg. Chem.* **1994**, *33*, 5203–5206; c) $[YCl_2(thf)_5]^+[C_2B_9H_{12}]^-$: Y-O = 2.378(8), 2.377(7), 2.396(8), 2.401(7), 2.309(7) Å, see: K. Chiu, Z. Zhang, T. C. W. Mak, Z. Xie, *J. Organomet. Chem.* **2000**, *614*, 107–112; d) $[Y(CH_2SiMe_3)_2(thf)_4]^+[Al(CH_2SiMe_3)_4]^-$: Y-O = $2\times2.354(4)$, 2.448(4), 2.479(4) Å, this work.

[18] Not surprisingly, ethylene was also polymerized when methylaluminoxane was used instead of aluminum trialkyl; see Table 2.

[19] Because of its inertness towards $[NMe_2HPh][B(C_6F_5)_4]$, we selected $Al(CH_2SiMe_3)_3$ for our investigations. For $Al(CH_2SiMe_3)_3$, neither formation of aluminum alkyl cation, see reference [9], nor decomposition under ligand redistribution was observed. $AliBu_3$ was reported to react with $[NMe_2HPh][B(C_6F_5)_4]$ in C_6D_6 under forcing conditions to produce a mixture of $BiBu_3$, $Al(C_6F_5)_3$ and $AliBu(C_6F_5)_2$, see: C. Götz, A. Rau, G. Luft, *J. Mol. Catal. A* **2002**, *184*, 95–110.

[20] Higher coordination numbers 7 and 8 were reported for cationic alkyl complexes of lutetium, see reference [7].

[21] The monocation $[Y(CH_2SiMe_3)_2(thf)_x]^+[Al(CH_2SiMe_3)_4]^-$ does not polymerize ethylene unless activated with excess of $[NMe_2HPh][B(C_6F_5)_4]$. In $[D_8]$THF it reacts with one equivalent of $[NMe_2HPh][BPh_4]$, to form $SiMe_4$, NMe_2Ph, $Al(CH_2SiMe_3)_3$, and $[Y(CH_2SiMe_3)_2([D_8]thf)_x]^+[BPh_4]^-$. A similar reaction between $[Sm(\eta^5\text{-}C_5Me_5)_2(AlMe_4)]_2$ and $[Ph_3C][B(C_6F_5)_4]$ was reported to give $[Sm(\eta^5\text{-}C_5Me_5)_2][B(C_6F_5)_4]$, Ph_3CMe, and $AlMe_3$, see: S. Kaita, Z. Hou, M. Nishiura, Y. Doi, J. Kurazumi, A. C. Horiuchi, Y. Wakatsuki, *Macromol. Rapid Commun.* **2003**, *24*, 179–184.

 © 2003 Wiley-VCH Verlag GmbH & Co. KGaA, Weinheim

Expanding the Stille Coupling

Ligands for Palladium-Catalyzed Cross-Couplings of Alkyl Halides: Use of an Alkyldiaminophosphane Expands the Scope of the Stille Reaction**

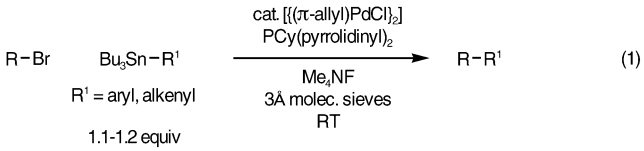
*Haifeng Tang, Karsten Menzel, and Gregory C. Fu**

Dedicated to Professor Manfred T. Reetz on the occasion of his 60th birthday

Whereas nickel- and palladium-catalyzed methods for cross-coupling aryl and vinyl halides and sulfonates with a range of organometallic reagents have reached a fairly high level of sophistication,[1] comparable progress has not yet been achieved for reactions of alkyl halides and sulfonates.[2] Recently, we and others have begun to address this shortcoming by describing catalysts for certain Suzuki,[3] Negishi,[4,5] Kumada,[6,7] Stille,[8] and Hiyama[9] couplings of primary alkyl electrophiles. With the exception of Suzuki's observation that $[Pd(PPh_3)_4]$ effects cross-couplings of alkyl iodides with R-(9-BBN),[3a] the palladium-based catalysts that were reported for coupling alkyl electrophiles have all employed a hindered trialkylphosphane (PCy_3 or $P(t\mathrm{Bu})_2\mathrm{Me}$) as the ligand.

To increase the likelihood of expanding the still-limited scope of cross-couplings of alkyl electrophiles, we have been exploring the use of new classes of ligands for these processes. Herein, we establish that, in the presence of alkyldiaminophosphanes ($PR(NR'_2)_2$), we can accomplish palladium-catalyzed Stille cross-couplings of alkyl bromides and iodides not only with vinyl stannanes, but also with aryl stannanes [Eq. (1)], a class of reaction partners that are not efficiently coupled by Pd/PR_3 (PR_3 = trialkylphosphane).

As a consequence of the electron-richness and the ready accessibility of alkyldiaminophosphanes ($PR(NR'_2)_2$),[10] we



[*] Prof. Dr. G. C. Fu, Dr. H. Tang, Dr. K. Menzel
Department of Chemistry
Massachusetts Institute of Technology
Cambridge, MA 02139 (USA)
Fax: (+1) 617-258-7500
E-mail: gcf@mit.edu

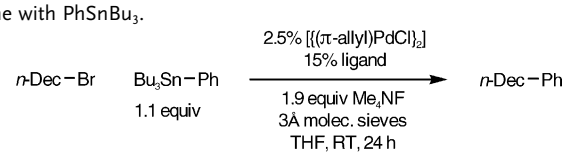
[**] We thank Johnson Matthey for supplying palladium compounds. Support has been provided by the National Institutes of Health (National Institute of General Medical Sciences, R01-GM62871), Merck, and Novartis. Funding for the MIT Department of Chemistry Instrumentation Facility has been furnished in part by NSF CHE-9808061 and NSF DBI-9729592.

Supporting information for this article is available on the WWW under http://www.angewandte.org or from the author.

 DOI: 10.1002/anie.200352668 © 2003 Wiley-VCH Verlag GmbH & Co. KGaA, Weinheim

decided to examine the utility of this family of ligands in palladium-catalyzed couplings of alkyl electrophiles. In earlier work, we determined that $P(tBu)_2Me$ is useful for Stille cross-couplings of alkyl bromides with vinyl-, but not with aryl-, stannanes.[11] Thus, as illustrated in Table 1, neither $P(tBu)_2Me$ nor PCy_3 is effective for the palladium-catalyzed Stille reaction of 1-bromodecane with $PhSnBu_3$ under our previously reported conditions (entries 1 and 2, respectively).[12]

Table 1: Effect of ligand structure on the cross-coupling of 1-bromodecane with $PhSnBu_3$.



Entry	Ligand	Yield [%][a]
1	$P(tBu)_2Me$	12
2	PCy_3	22
3	$PMe(pyrrolidinyl)_2$	9
4	$PEt(pyrrolidinyl)_2$	32
5	$PCy(pyrrolidinyl)_2$	45
6	$P(tBu)(pyrrolidinyl)_2$	4
7	$PPh(pyrrolidinyl)_2$	7
8	$P(iBuNCH_2CH_2)_3N$	<2
9	PPh_3	<2
10	no ligand	<2

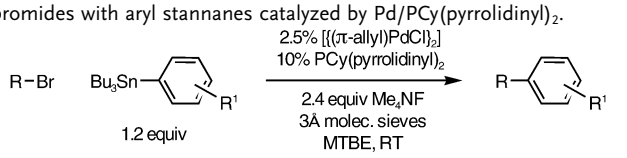
[a] Determined by GC versus a calibrated internal standard (average of two runs).

We therefore synthesized a sterically diverse set of alkyldiaminophosphanes, and we explored their use in this Stille cross-coupling process. Although Pd/PMe(pyrrolidinyl)$_2$ (pyrrolidinyl = 1-pyrrolidinyl) furnishes very little of the desired product (9%; Table 1, entry 3), an increase in the steric demand of the alkyl group can provide an improvement in yield (Me→Et→Cy: 9%→32%→45%; entries 3–5). As we have observed for couplings catalyzed by Pd/PR_3,[3b–d,5,8,9] there is a window of maximum reactivity for alkyldiaminophosphane ligands—thus, if the alkyl group, R, of $PR(NR'_2)_2$ becomes too large (e.g., *t*Bu), the yield decreases (4%; entry 5 versus entry 6). In the presence of an aryldiaminophosphane (entry 7), a bicyclic triaminophosphane (entry 8),[13] and PPh_3 (entry 9), almost no cross-coupling occurs.

Additional optimization of the most effective catalyst system, Pd/PCy(pyrrolidinyl)$_2$ (45%; Table 1, entry 5), produced an enhancement in yield (72%; Table 2, entry 1; MTBE = *t*BuOMe).[14] As illustrated in Table 2, under a standard set of conditions, an array of functionalized alkyl bromides can be coupled at room temperature with a variety of aryl stannanes.[15,16] Thus, the catalyst tolerates esters (entries 2–6), nitriles (entry 7), ethers (entry 8), and olefins (entry 9). In addition, both electron-rich and electron-poor aryl stannanes (entries 2–8), as well as a heteroaryl stannane (entry 9), are suitable cross-coupling partners.

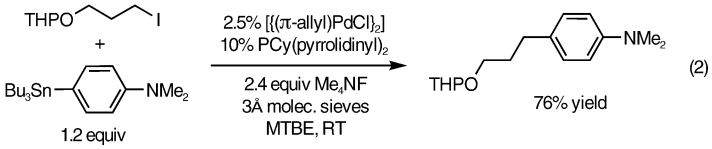
We have determined that the conditions that we have developed for Stille reactions of alkyl bromides (Table 2) can be applied without modification to couplings of alkyl iodides [Eq. (2)]. To the best of our knowledge, this is the first example of a Stille cross-coupling of a simple alkyl iodide that bears β hydrogen atoms.[17,18]

Table 2: Room-temperature Stille cross-couplings of functionalized alkyl bromides with aryl stannanes catalyzed by Pd/PCy(pyrrolidinyl)$_2$.



Entry	R−Br	Aryl stannane	Yield [%][a]
1	*n*-Dec−Br	Bu_3Sn	72
2	EtO(C=O)$(CH_2)_4$Br	Bu_3Sn-Me	63
3	EtO(C=O)$(CH_2)_4$Br	Bu_3Sn-OMe	71
4	EtO(C=O)$(CH_2)_4$Br	Bu_3Sn-CF_3	57
5	EtO(C=O)$(CH_2)_4$Br	OMe, Bu_3Sn	61
6	EtO(C=O)$(CH_2)_4$Br	Me, Bu_3Sn	62
7	NC$(CH_2)_4$Br	Bu_3Sn-NMe_2	68
8[b]	THPO$(CH_2)_3$Br	Bu_3Sn-F	64
9	$(CH_2)_3$Br	Bu_3Sn-N	53

[a] Yield of isolated product (except for entry 1, which is a yield by GC versus a calibrated internal standard), average of two runs. [b] THP = tetrahydropyran.



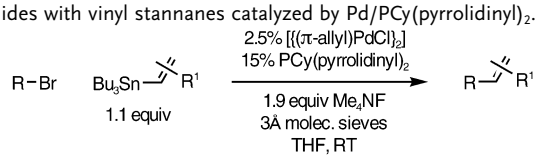
(2)

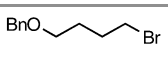
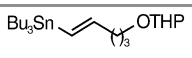
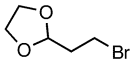
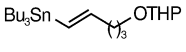
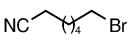
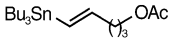
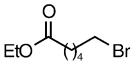
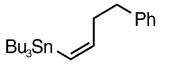
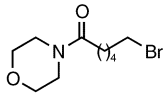
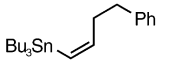
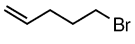
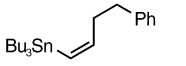
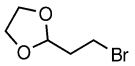
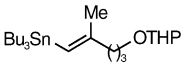
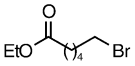
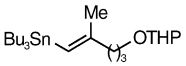
In addition to aryl stannanes, Pd/PCy(pyrrolidinyl)$_2$ can be employed for cross-couplings of vinyl stannanes. Thus, under the conditions that we previously reported for Pd/$P(tBu)_2Me$-catalyzed processes,[8,19] Pd/PCy(pyrrolidinyl)$_2$ catalyzes room-temperature couplings of functionalized alkyl bromides with a range of vinyl stannanes (Table 3).[20] Groups such as ethers, acetals, nitriles, esters, amides, and olefins may be present, and a variety of substitution patterns for the vinyl stannane are tolerated.

Finally, we can apply the same Pd/PCy(pyrrolidinyl)$_2$ catalyst system to room-temperature Stille cross-couplings of alkyl iodides with vinyl stannanes (90% yield; [Eq. (3)]).[21]

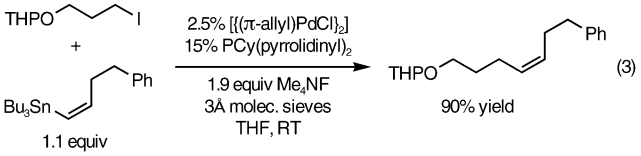
 © 2003 Wiley-VCH Verlag GmbH & Co. KGaA, Weinheim

Table 3: Room-temperature Stille cross-couplings of functionalized alkyl bromides with vinyl stannanes catalyzed by Pd/PCy(pyrrolidinyl)$_2$.



Entry	R–Br	Vinyl stannane	Yield [%][a]
1			74
2			60
3			68
4			89
5			79
6			78
7			54
8			73

[a] Yield of the isolated product, average of two runs.



In conclusion, we have identified a new class of ligands (alkyldiaminophosphanes, PR(NR′$_2$)$_2$) that are effective in palladium-catalyzed cross-couplings of alkyl electrophiles. In comparison with trialkylphosphanes, alkyldiaminophosphanes furnish more versatile catalysts for Stille reactions of alkyl halides, thus achieving, for example, efficient couplings with aryl stannanes. In view of the ready accessibility of a range of alkyldiaminophosphanes, as well as the potential for chiral variants, we anticipate that our observations will add a significant new dimension to the development of broadly applicable catalysts for cross-couplings of alkyl electrophiles.

Received: August 18, 2003 [Z52668]
Published Online: October 14, 2003

Keywords: cross-coupling · homogeneous catalysis · palladium · phosphane ligands · Stille reaction

[1] For reviews of metal-catalyzed cross-coupling reactions, see: a) *Metal-Catalyzed Cross-coupling Reactions* (Eds.: F. Diederich, P. J. Stang), Wiley-VCH, New York, **1998**; b) "Cross-Coupling Reactions: A Practical Guide": *Top. Curr. Chem.* **2002**, *219*; c) *Handbook of Organopalladium Chemistry for Organic Synthesis* (Ed.: E.-I. Negishi), Wiley Interscience, New York, **2002**.

[2] For an overview of the difficulty of achieving coupling reactions of alkyl electrophiles, see: D. J. Cárdenas, *Angew. Chem.* **1999**, *111*, 3201 – 3203; *Angew. Chem. Int. Ed.* **1999**, *38*, 3018 – 3020; D. J. Cárdenas, *Angew. Chem. Int. Ed.* **2003**, *42*, 384 – 387. See also: T.-Y. Luh, M.-k. Leung, K.-T. Wong, *Chem. Rev.* **2000**, *100*, 3187 – 3204.

[3] a) Iodides: T. Ishiyama, S. Abe, N. Miyaura, A. Suzuki, *Chem. Lett.* **1992**, 691 – 694; b) bromides: M. R. Netherton, C. Dai, K. Neuschütz, G. C. Fu, *J. Am. Chem. Soc.* **2001**, *123*, 10099 – 10100; J. H. Kirchhoff, M. R. Netherton, I. D. Hills, G. C. Fu, *J. Am. Chem. Soc.* **2002**, *124*, 13662 – 13663; c) chlorides: J. H. Kirchhoff, C. Dai, G. C. Fu, *Angew. Chem.* **2002**, *114*, 2025 – 2027; *Angew. Chem. Int. Ed.* **2002**, *41*, 1945 – 1947; d) tosylates: M. R. Netherton, G. C. Fu, *Angew. Chem.* **2002**, *114*, 4066 – 4068; *Angew. Chem. Int. Ed.* **2002**, *41*, 3910 – 3912.

[4] For nickel-based catalysts, see: a) A. Devasagayaraj, T. Stüdemann, P. Knochel, *Angew. Chem.* **1995**, *107*, 2952 – 2954; *Angew. Chem. Int. Ed. Engl.* **1995**, *34*, 2723 – 2725; b) R. Giovannini, T. Stüdemann, G. Dussin, P. Knochel, *Angew. Chem.* **1998**, *110*, 2512 – 2515; *Angew. Chem. Int. Ed.* **1998**, *37*, 2387 – 2390; c) R. Giovannini, P. Knochel, *J. Am. Chem. Soc.* **1998**, *120*, 11186 – 11187; d) R. Giovannini, T. Stüdemann, A. Devasagayaraj, G. Dussin, P. Knochel, *J. Org. Chem.* **1999**, *64*, 3544 – 3553; e) M. Piber, A. E. Jensen, M. Rottländer, P. Knochel, *Org. Lett.* **1999**, *1*, 1323 – 1326; f) A. E. Jensen, P. Knochel, *J. Org. Chem.* **2002**, *67*, 79 – 85.

[5] For a palladium-based catalyst, see: J. Zhou, G. C. Fu, *J. Am. Chem. Soc.*, in press.

[6] For nickel-based catalysts, see: a) J. Terao, H. Watanabe, A. Ikumi, H. Kuniyasu, N. Kambe, *J. Am. Chem. Soc.* **2002**, *124*, 4222 – 4223; b) J. Terao, A. Ikumi, H. Kuniyasu, N. Kambe, *J. Am. Chem. Soc.* **2003**, *125*, 5646 – 5647.

[7] For a palladium-based catalyst, see: A. C. Frisch, N. Shaikh, A. Zapf, M. Beller, *Angew. Chem.* **2002**, *114*, 4218 – 4221; *Angew. Chem. Int. Ed.* **2002**, *41*, 4056 – 4059.

[8] K. Menzel, G. C. Fu, *J. Am. Chem. Soc.* **2003**, *125*, 3718 – 3719.

[9] J.-Y. Lee, G. C. Fu, *J. Am. Chem. Soc.* **2003**, *125*, 5616 – 5617.

[10] For pioneering studies by Woollins, see: a) M. L. Clarke, D. J. Cole-Hamilton, A. M. Z. Slawin, J. D. Woollins, *Chem. Commun.* **2000**, 2065 – 2066; b) M. L. Clarke, G. L. Holliday, A. M. Z. Slawin, J. D. Woollins, *J. Chem. Soc. Dalton Trans.* **2002**, 1093 – 1103.

[11] See reference [8], including footnote [15].

[12] Among the large array of trialkylphosphanes that we have examined, P(*t*Bu)$_2$Me and PCy$_3$ are the most effective.

[13] a) Verkade has established that certain triaminophosphanes provide reactive catalysts for palladium-catalyzed Suzuki and Buchwald–Hartwig cross-couplings of aryl halides. See: S. Urgaonkar, M. Nagarajan, J. G. Verkade, *Tetrahedron Lett.* **2002**, *43*, 8921 – 8924; S. Urgaonkar, M. Nagarajan, J. G. Verkade, *Org. Lett.* **2003**, *5*, 815 – 818; S. Urgaonkar, M. Nagarajan, J. G. Verkade, *J. Org. Chem.* **2003**, *68*, 452 – 459; b) With acyclic triaminophosphanes, we have obtained small amounts of Stille cross-coupling products.

[14] Notes: 1) The increased yield is primarily due to the change of solvent (to MTBE). CH_3CN, *tert*-amyl alcohol, and CH_2Cl_2 are not suitable solvents for this process. 2) For the cross-coupling illustrated in entry 1 of Table 2, use of P(*t*Bu)$_2$Me, rather than PCy(pyrrolidinyl)$_2$, under the conditions of Table 2 leads to a poor yield (< 40%) of the desired product. 3) In the absence of Me_4NF, no coupling is observed. 4) $PdBr_2$ and $PdCl_2(PhCN)_2$ provide yields that are comparable with [{(π-allyl)PdCl}$_2$], whereas Pd(OAc)$_2$ is ineffective.

 © 2003 Wiley-VCH Verlag GmbH & Co. KGaA, Weinheim

[15] Notes: 1) Reactions of (*o*-tolyl)$SnBu_3$ and (*p*-nitrophenyl)$SnBu_3$ proceed in more modest yield. 2) Allylstannanes, alkynylstannanes, alkyl chlorides, alkyl tosylates, and certain (tertiary, secondary, and β-branched primary) alkyl bromides are not useful coupling partners, furnishing at best a poor yield of the desired product.

[16] After the completion of a cross-coupling reaction, if $Cy_2PCH_2CH_2PCy_2$ is added, then a substantial amount of PCy(pyrrolidinyl)$_2$ is observed by ^{31}P NMR.

[17] For a discussion and leading references, see Reference [8].

[18] The use of P(*t*Bu)$_2$Me, rather than PCy(pyrrolidinyl)$_2$, leads to a significant loss in yield ($< 50\,\%$).

[19] The only modification: the cross-couplings catalyzed by Pd/PCy(pyrrolidinyl)$_2$ are conducted at an alkyl-halide concentration of 0.2 M, versus 0.1 M for Pd/P(*t*Bu)$_2$Me (for Pd/P(*t*Bu)$_2$Me, reactions run at higher concentration lead to the precipitation of a black solid, presumably Pd).

[20] Notes: 1) The stereochemistry of the vinyl stannane is retained in the cross-coupling product. 2) For entries 1, 4, and 5 of Table 3, the isolated yields for Pd/PCy(pyrrolidinyl)$_2$ are 14–24 % higher than for Pd/P(*t*Bu)$_2$Me (see Reference [8]); for entry 7, the yields are essentially identical, and for entry 2 the yield is 11 % lower for Pd/PCy(pyrrolidinyl)$_2$.

[21] Under these conditions, we have also efficiently coupled 1-iododecane with tributyl(vinyl)tin (93 % yield by GC versus a calibrated internal standard).

 © 2003 Wiley-VCH Verlag GmbH & Co. KGaA, Weinheim

Cluster Chemistry

Elemental Gallium as a Source of Subvalent Gallium Units in Gallium–Rhodium Clusters**

Manfred Scheer, Martin Kaupp,* Alexander V. Virovets, and Sergei N. Konchenko**

Dedicated to Professor Achim Müller on the occasion of his 65th birthday

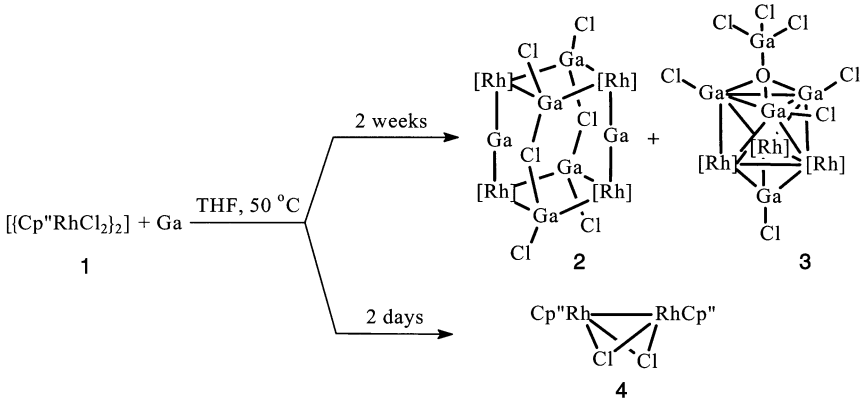
Whereas metals of group 1 and 2 elements are well known as reducing agents, within group 13 elements only aluminum in Devarda's alloy has been used to generate transition-metal carbonyl compounds.[1] Furthermore, thallium has been employed as a reducing agent with metal clusters, such as $[Co_2(CO)_8]$ to form metalates, such as $Tl[Co(CO)_4]$[2] and elemental gallium was used to reduce $[Re_2(CO)_{10}]$ to give $[Re_4(CO)_{12}\{\mu_3\text{-}GaRe(CO)_5\}_4]$.[3] In the reaction of $[Ru_3(CO)_{12}]$ with Ga_2Cl_4, elemental gallium functioned as a reducing agent, which resulted in the generation of $GaCl_2$ and GaCl ligands.[4] A similar approach was employed when $[Re_2(CO)_{10}]$ was treated with GaI_3 in the presence of gallium.[3] The use of elemental gallium as a reducing agent for transition-metal halides is so far limited to the reduction of Ti^{IV} to Ti^{III} complexes to form $[(CpTiF_2)_3Ga]$ ($Cp = C_5H_5$).[5] The advantage of elemental gallium as a reducing agent lies in its low melting point (29.8 °C) making it similar to the common liquid-metal reductants, for example, sodium amalgam and K/Na alloy. However, in comparison to these reagents, liquid gallium is a gentler reducing agent, which is especially favorable for preparing complexes with transition-metal centers in a medium oxidation state. Herein, we report the novel use of elemental gallium as reducing agent towards transition-metal halides to generate subvalent GaCl ligands as well as the first twofold coordinate gallium atoms which lie between two transition-metal centers in a multicenter–multiple-bond interaction.

The reaction of $[\{Cp''RhCl_2\}_2]$ (**1**) ($Cp'' = \eta^5\text{-}1,3\text{-}C_5H_3tBu_2$) with gallium melt in THF at 50 °C leads, after two weeks, to the formation of novel gallium containing clusters **2** and **3**,

$[\{(Cp''Rh)_2(\mu\text{-}Ga)\}_2(\mu_4,\eta^2\text{-}Ga_2Cl_3)_2]$ **2**

$[(Cp''Rh)_3(\mu_3\text{-}GaCl)(\mu_3\text{-}Ga_3Cl_3)(\mu_3\text{-}OGaCl_3)]$ **3**

which crystallize as their THF adducts (reaction (1) in Scheme 1).



Scheme 1. Synthesis of compounds **2**–**4**, $Cp'' = \eta^5\text{-}1,3\text{-}C_5H_3tBu_2$, [Rh] = Cp″Rh.

After two days reaction a deep blue solution is formed, afterwards the color changes to red—in a separate experiment this blue reaction mixture was worked up. $[\{Cp''RhCl\}_2]$ (**4**) was isolated in about 65 % yield (Scheme 1, reaction (2)). Compound **4** has a dimeric structure similar to the known complex $[\{Cp^*RhCl\}_2]$[6] ($Cp^* = C_5Me_5$). The X-ray structure of **4** shows an Rh–Rh bond length of 2.584(1) Å and two bridging Cl atoms.[7] Attempts to synthesize **2** and **3** starting exclusively from **4** and elemental gallium alone failed. Thus, the presence of an additional amount of the chloro-rich complex **1** is essential.

The products **2** and **3** are the first examples of compounds with Rh–Ga bonds. Moreover, they contain GaCl and other subvalent gallium species and twofold coordinate Ga atoms, the formation of which is difficult to speculate upon. Probably, in the presence of an excess of liquid gallium, an equilibrium mixture of different subvalent gallium chlorides, which mainly includes GaCl, is generated. This GaCl interacts with reduced forms of the rhodium complex, leading to the formation of **2** and **3**. Insertion of gallium into the Rh–Cl bonds can also play a role in the formation of the products.

The red cubes of **2** and the light-brown blocks of **3**[8] are sparingly soluble in toluene and readily soluble in THF. In the

[*] Prof. Dr. M. Scheer
Institut für Anorganische Chemie
der Universität Karlsruhe
76128 Karlsruhe (Germany)
Fax: (+49) 721-608-7021
E-mail: mascheer@chemie.uni-karlsruhe.de
Prof. Dr. M. Kaupp
Institut für Anorganische Chemie
Universität Würzburg
Am Hubland, 97074 Würzburg (Germany)
Fax: (+49) 931-888-7135
E-mail: kaupp@mail.uni-wuerzburg.de
Dr. S. N. Konchenko, Dr. A. V. Virovets
Institute of Inorganic Chemistry
Siberian Division of RAS
Acad. Lavrentyev str. 3, Novosibirsk 630090 (Russia)
Fax: (+7) 3832-344489
E-mail: konch@che.nsk.su

[**] This work was comprehensively supported by the Deutsche Forschungsgemeinschaft and the Fonds der Chemischen Industrie. S. N. K. is grateful to the DAAD and the DFG and the RFBR(03–03–32374). The authors thank Degussa AG for the gift of precious metals.

 DOI: 10.1002/anie.200351226 © 2003 Wiley-VCH Verlag GmbH & Co. KGaA, Weinheim

^{1}H NMR spectra the Cp″ ligands are magnetically equivalent. In the mass spectra (EI and FI) of **2** and **3** peaks of molecular ions could not be detected and even fragment peaks are difficult to assign. The products were characterized by single-crystal X-ray diffraction. Complex **2** crystallizes in the triclinic space group $P\bar{1}$ with two independent molecules (A and B) in the asymmetric unit, which have similar structural features.[7] In Figure 1 the molecular structure of the molecule A is

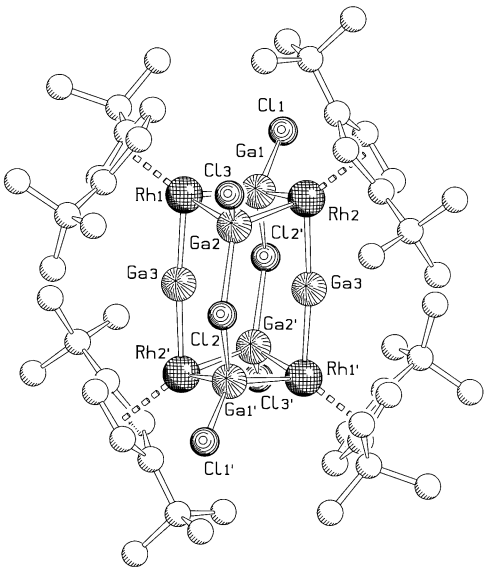


Figure 1. Molecular structure of **2** (molecule A). Selected bond lengths [Å] and angles [°]: Rh1-Ga3 2.346(1), Rh2′-Ga3 2.340(1), Rh1-Ga1 2.438(1), Rh1-Ga2 2.442(1), Rh···Rh 3.069(1), Ga1-Cl1 2.219(2), Ga1-Cl2′ 2.445(2), Ga2′-Cl2′ 2.363(2), Ga2′-Cl3′ 2.215(2), Rh2-Ga1 2.418(1), Rh2-Ga2 2.408(1); Rh1-Ga3-Rh2′ 174.40(4), Ga2-Cl2-Ga1′ 115.65(8), Cl3-Ga2-Cl2 94.01(8), Rh1-Ga1-Rh2 78.42(4), Rh1-Ga2-Rh2 78.52(4).

depicted: four Cp″Rh units are connected by two bridging Ga_2Cl_3 ligands (folding angle of the Rh_2Ga_2 planes along the Rh···Rh axis is 18.75°(A) and 18.43°(B)) and also by two-coordinate Ga atoms. The latter Rh-Ga-Rh units are almost linear (A: 174.40(4)° and B: 174.61(4)°) with very short Rh–Ga bonds (A: 2.346(1) Å and 2.340(1); B: 2.343(1) and 2.346(1)),[9] which suggest multiple bonding in these moieties.

Density-functional calculations[10] on the model complexes **2′** and **3′** containing Cp ligands[11] have been used to obtain insight into the bonding in the two new cluster compounds. The DFT(B3LYP) optimized structures agree well with the X-ray structure data for **2** and **3**. For a better understanding of bonding modes, the electron localization function (ELF)[10h] was analyzed for both molecules.

Figure 2 shows an ELF = 0.37 isosurface for **2′**, cut open along the equatorial mirror plane (isosurface = surface of the same ELF). Two three-center Rh-Ga-Rh attractors can be clearly seen on each of the Rh_2Ga_2 faces, with similar ELF values at the attractor (ELF = 0.406) as found for $[Rh_6(CO)_{16}]$[12]). In addition, however, ELF indicates multiple bonding for the almost linear Rh-Ga-Rh arrangements of the long edges of the cluster. Two types of π-bonding attractors

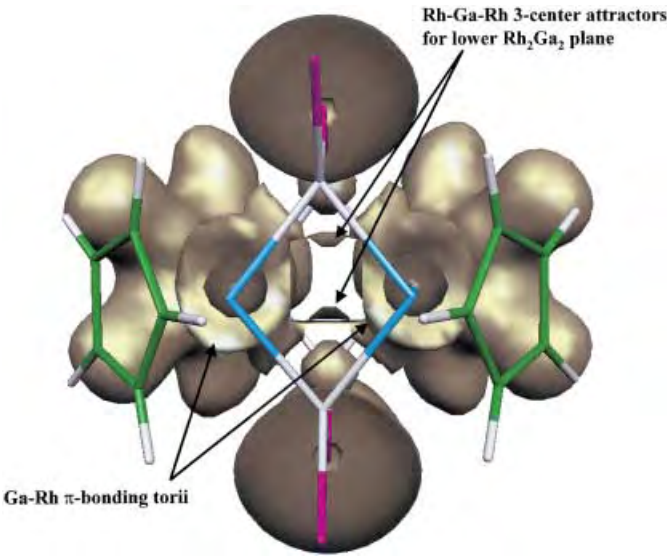


Figure 2. Isosurface of the electron localization function (ELF = 0.37) for **2′**, cut open along the equatorial mirror plane. The torii represent Rh-Ga-Rh multicenter multiple bonding along the long edges, Rh-Ga-Rh three-center attractors are shown for one of the Rh_2Ga_2 planes.

with ELF = 0.501 are found for each of the Ga–Rh bonds along the edge, which merge to a torus at an ELF value of approximately 0.429. The orientation of the attractors suggests more Rh=Ga=Rh π-bonding contributions perpendicular to the Rh_4Ga_2 plane of **2′** than within the plane. This type of polar multiple bond is also confirmed by inspection of the canonical molecular orbitals. As the torii above the mirror plane (not shown) are identical to those shown below the plane, the two p_π-type orbitals on the central gallium atoms must be shared in a three-center bonding fashion by both rhodium partners. At ELF = 0.447, the π-bonding domains merge with those of four additional two-center Ga–Rh bonding attractors (ELF = 0.481), which are located slightly below and outside the respective Rh_2Ga_2 faces (not shown), somewhat closer to Rh than to Ga. This arrangement is consistent with a general multicenter bonding situation.

The molecular structure of **3** (Figure 3)[7] reveals a distorted[13] Rh_3Ga_3 trigonal antiprism in which each Rh atom is coordinated by a Cp″ ligand and each Ga atom by a Cl ligand. Additionally, the Rh_3 triangle is capped by a GaCl moiety, and the Ga_3 face is capped by an $OGaCl_3$ unit. Both Rh–Rh (2.964(1) Å) and Ga–Ga (2.823(2) Å) bond lengths in **3** lie close to the upper limit of the mean values found for corresponding single bonds, but still in the accepted range.[14] However, the evidently high coordination number of the atoms Ga1 shows that the Ga_3 moiety and its connectivity to the Rh_3 triangle can only be described in terms of a multicenter bonding in a metal cluster arrangement. This is also evident from simple electron counting. The multicenter bonding situation in **3** is further supported by the ELF analysis of the model complex **3′**. Several attractors related to covalent bonding within the cluster were found. 1) six two-center attractors (ELF = 0.425) connecting each Ga1 atom to two Rh atoms, and the three types of three-center attractors: 2) 3 ×

 © 2003 Wiley-VCH Verlag GmbH & Co. KGaA, Weinheim

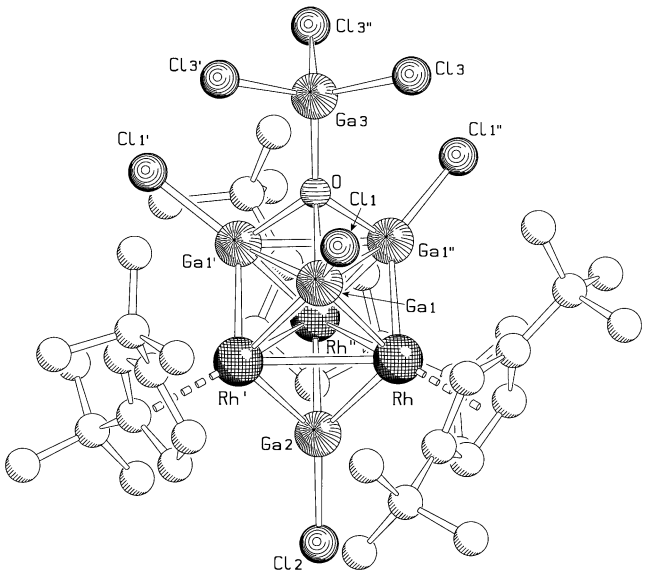


Figure 3. Molecular structure of **3**. Selected bond lengths [Å] and angles [°]: Rh-Rh′ 2.964(1), Rh-Ga1 2.426(1), Rh-Ga1″ 2.458(1), Ga1-Ga1′ 2.823(2), Rh-Ga2 2.437(2), Ga2-Cl2 2.164(6), Ga1-Cl1 2.151(3), Ga1-O 2.055(9), Ga3-O 1.909(15), Ga3-Cl3 2.173(4); Rh-Rh′-Rh″ 60.0, Ga1-Rh-Ga1″ 70.61(6), Rh-Ga1-Rh″ 74.71(5), Rh-Ga2-Rh′ 74.88(6), Ga1-O-Ga1′ 86.7(5), Ga3-O-Ga1 127.5(3).

Rh-Ga1-Rh (ELF = 0.473), 3) 3 × Ga1-Rh-Ga1 (ELF = 0.459), and 4) 3 × Rh-Ga2-Rh (ELF = 0.411). At a lower ELF value of approximately 0.36, the domains of the multi-center-bonding attractors merge to the bands across the surface of the cluster, very similar to findings for polyhedral boron hydrides or halides.[15] Ga–Cl, Rh–Cp, and Ga–O bonds are indicated by the ELF plot (not shown)as being significantly ionic.

Fragment charges obtained from natural population analyses are shown in Table 1. For both **2′** and **3′**, the data clearly show pronounced charge alternation within the cluster, with significant negative charge on the RhCp fragments and significant positive charge on the GaCl containing fragments (with significantly polar Ga–Cl and Ga–O bonds, and with Ga–Rh bonds that are also notably negatively polarized towards the transition-metal center). Note also, that at the computational level used (B3LYP-DFT), appreciable HOMO–LUMO gaps are found of approximately 2.76 eV for **2′** and approximately 2.65 eV for **3′**. This result suggests a stable closed-shell situation and is consistent with a diamagnetic nature of both clusters.

Table 1: Natural population analysis partial charges for **2′** and **3′**.

2′		**3′**	
Q(RhCp)	−0.481 (4×)	Q(Cl_3Ga3O)	−1.395
Q(GaCl)	+0.278 (4×)	Q(Ga1Cl)	+0.518 (3×)
Q(ClGa-Cl-GaCl)	+0.135 (2×)	Q(RhCp)	−0.163 (3×)
Q(Ga bridge)	+0.825 (2×)	Q(Ga2Cl)	+0.311

This work shows that the use of gallium metal as reducing agent towards transition-metal halides opens up a novel route to subvalent Ga and GaCl ligands incorporated in unusual bonding situations. Our bonding analyses clearly confirm three-center-type bonding comparable to polyhedral boron clusters, but also significant charge alternation Ga(δ^+)/Rh(δ^-) in both **2** and **3**. In addition, the linear Rh-Ga-Rh bridges in **2** feature multicenter–multiple-bonding.

Experimental Section

A solution of [Cp″$RhCl_2$]$_2$ (**1**) (0.3 g, 0.4 mmol) in THF (15 mL) and an excess of elemental Ga (0.7 g, 10 mmol) was thoroughly degassed in a Schlenk flask equipped with a teflon stop-cock and then heated under reduced pressure at 50 °C. After two days the mixture became deep blue indicating formation of **4**. Workup at this stage by filtration to remove the excess gallium and removal of the solvent from the filtrate until crystallization began, followed by storage the solution at −25 °C led to the isolation of 165 mg of **4** as brown crystals (65 % yield). If the reaction is allowed to go further, over the following 12 days, the color of solution changed to red indicating complete transformation of **4**. Then the resulting solution was filtered and the filtrate reduced in volume to a viscous fluid (about 2 mL). After a week at 8 °C 0.1 g (51 % based on Rh content) of crystals of two different types were formed and separated manually under a microscope in a glovebox: red cubes of **2**·2.5 THF (≈ 60 mg, 31 %) and light-brown blocks of **3**·THF (≈ 40 mg, 20 %).

2: Rh:Ga ratio (total reflection X-ray fluorescence analysis (TRFA)): found 4:5.7, calcd: 4:6. IR (Nujol): $\tilde{\nu}$ = 836(m), 589(m, br), 398(s), 384(m), 334(w) cm^{-1}, calcd for **2′**: 840, 596, 400, 392, 332 cm^{-1} (most intensive peaks). ^1H ([D_8]THF, 298 K, 250 mHz): δ = 1.23 (18 H, CH_3), 5.34 (2 H, CH), 5.74 ppm (1 H, CH).**3**: Rh:Ga ratio (TRFA): found: 3:4.8, calcd: 3:5. IR (Nujol): $\tilde{\nu}$ = 836(m), 351(s), 326(w), 289(w), 226(m) cm^{-1}, calcd for **3′**: 837, 352, 327, 291, 227 cm^{-1} (most intensive peaks)). ^1H ([D_8]THF, 298 K, 250 mHz): δ = 1.23 (18 H, CH_3), 5.21 (2 H, CH), 5.64 ppm (1 H, CH).**4**: ^1H ([D_8]THF, 298 K, 250 mHz): δ = 1.19 (18 H, CH_3), 5.35 (2 H, CH), 5.55 ppm (1 H, CH); MS (EI, 70 eV): 630 [M^+], 315 [{M/2}$^+$].

Received: February 19, 2003
Revised: June 18, 2003 [Z51226]

Keywords: cluster compounds · electron localization functions · gallium · insertions · rhodium

[1] W. A. Herrmann, K. Öfele, C. E. Zybill in *Synthetic Methods of Organometallic Chemistry, Vol. 7* (Ed.: W. A. Herrmann), Thieme, Stuttgart, **1997**, p. 13.
[2] S. E. Pedersen, W. R. Robinson, D. P. Schussler, *J. Organomet. Chem.* **1972**, *43*, C44; D. P. Schussler, W. R. Robinson, W. F. Edgell, *Inorg. Chem.* **1974**, *13*, 153.
[3] H.-J. Haupt, P. Balsaa, B. Schwab, *Z. Anorg. Allg. Chem.* **1985**, *521*, 15–22.
[4] G. N. Harakas, B. R. Whittlesey, *Inorg. Chem.* **1997**, *36*, 2704–2707.
[5] F.-Q. Liu, A. Künzel, A. Herzog, H. W. Roesky, M. Noltemeyer, R. Fleischer, D. Stalke, *Polyhedron* **1997**, *16*, 61–65. For the use of Al in analogous reactions see: F.-Q. Liu, H. Gornitzka, D. Stalke, H. W. Roesky, *Angew. Chem.* **1993**, *105*, 447–448; *Angew. Chem. Int. Ed. Engl.* **1993**, *32*, 442–443.
[6] a) P. R. Sharp, D. W. Hoard, C. L. Barnes, *J. Am. Chem. Soc.* **1990**, *112*, 2024–2026; b) D. W. Hoard, P. R. Sharp, *Inorg. Chem.* **1993**, *32*, 612–620.
[7] Crystal structure analyses of **2, 3**, and **4** were performed on a STOE IPDS diffractometer with $Mo_{K\alpha}$ radiation (λ = 0.71073 Å) for **2** and **3** and $Ag_{K\alpha}$ radiation (λ = 0.56087 Å) for **4**. The

 © 2003 Wiley-VCH Verlag GmbH & Co. KGaA, Weinheim

structures were solved by direct methods with the program SHELXS-97,[16a] and full-matrix least-squares refinement on F^2 in SHELXL-97[16b] was performed with anisotropic displacements for non-hydrogen atoms. Hydrogen atoms were located in idealized positions and refined isotropically according to the riding model. In each of the compounds **2** and **3** one of the THF solvate molecules is disordered over two and three positions, respectively. The C and O atoms of the THF molecules of **2** and **3** were not refined anisotropically. The flack parameter of the acentric structure of **3** came to value of 0.02(3). **2**·2.5 THF: $C_{62}H_{104}Cl_6Ga_6O_{2.5}Rh_4$, $M_r = 1932.11$, crystal dimensions $0.20 \times 0.15 \times 0.04$ mm^3, triclinic, space group $P\bar{1}$ (No. 2), $a = 15.761(3)$, $b = 16.860(2)$ Å, $c = 16.896(3)$ Å, $\alpha = 61.07(3)°$, $\beta = 87.24(3)°$, $\gamma = 73.01(3)°$, $T = 200(1)$ K, $Z = 2$, $V = 3734.5(13)$ Å^3, $\rho_{calcd} = 1.718$ g cm^{-3}, $\mu(Mo_{K\alpha}) = 3.239$ mm^{-1}, 10 973 independent reflexes ($R_{int} = 0.0426$, $2\theta_{max} = 48.06°$), 7576 observed with $F_o = 4\sigma(F_o)$, 657 parameters, $R_1 = 0.0382$, $wR_2 = 0.0975$. **3**·THF: $C_{43}H_{71}Cl_7Ga_5O_2Rh_3$, $M_r = 1525.48$, crystal dimensions $0.15 \times 0.15 \times 0.10$ mm^3, trigonal, space group $P3_1c$ (No. 159), $a = b = 13.684(2)$ Å, $c = 17.151(3)$ Å, $T = 200(1)$ K, $Z = 2$, $V = 2781.0(8)$ Å^3, $\rho_{calcd} = 1.822$ g cm^{-3}, $\mu(Mo_{K\alpha}) = 3.619$ mm^{-1}, 2701 independent reflexes ($R_{int} = 0.0257$, $2\theta_{max} = 48.14°$), 1966 observed with $F_o = 4\sigma(F_o)$, 190 parameters, $R_1 = 0.0469$, $wR_2 = 0.1274$. **4**: $C_{26}H_{42}Cl_2Rh_2$, $M_r = 631.32$, crystal dimensions $0.20 \times 0.10 \times 0.03$ mm^3, monoclinic, space group $P2/n$ (No. 13); $a = 14.272(3)$, $b = 6.209(1)$, $c = 15.612(3)$ Å, $\beta = 97.66(3)°$, $T = 203(2)$ K, $Z = 2$, $V = 1371.1(5)$ Å^3, $\rho_{calcd} = 1.529$ g cm^{-3}, $\mu(Ag_{K\alpha}) = 0.744$ mm^{-1}, 2850 independent reflexes ($R_{int} = 0.0544$, $2\theta_{max} = 41.84°$), 2247 observed with $F_o = 4\sigma(F_o)$; 142 parameters, $R_1 = 0.0379$, $wR_2 = 0.1015$. CCDC-203124–203126 contain the supplementary crystallographic data for this paper. These data can be obtained free of charge via www.ccdc.cam.ac.uk/conts/retrieving.html (or from the Cambridge Crystallographic Data Centre, 12 Union Road, Cambridge CB2 1EZ, UK; fax: (+44) 1223-336-033; or deposit@ccdc.cam.ac.uk).

[8] The origin of the O atom in the composition of **3** is uncertain. If the reaction is carry out in THF, in which traces of H_2O were added, an slightly increase of the yield of **3** was obtained, whereas the amount of **2** remains unchanged. Thus, the intermediately formed Ga hydroxide species could be responsible for the formation of the μ_3-$OGaCl_3$ ligand in **3**.

[9] Compare with other Rh–Ga bond lenghts: in **4** $d(Rh1\text{-}Ga2) = 2.442(1)$ Å; in **3** $d(Rh1\text{-}Ga1) = 2.438(1)$ Å, $d(Rh1\text{-}Ga2) = 2.442(1)$ Å.

[10] a) The DFT calculations employed the B3LYP hybrid functional[10b] in the implementation within the Gaussian 98 program.[10c] The calculations used quasi-relativistic small-core pseudopotentials (effective-core potentials, ECP) for Rh[10d] and Ga,[10e] together with a [8s7p6d]/(6s5p3d) valence basis set for Rh[10d] and a [12s12p9d]/(6s6p4d) basis for Ga.[10e] C, O, and Cl were treated by ECPs and DZP valence basis sets,[10f] and a DZ basis[10g] was used for hydrogen. The electronic structure of the complexes has been studied using the electron localization function (ELF[10h]) and natural population analyses (NPA[10i]; using the built-in NBO module of the Gaussian 98 program[10c]). The ELF data have been created using the TopMoD suite of programs[10j] and are graphically displayed using the MOLEKEL program.[10k] b) A. D. Becke, *J. Chem. Phys.* **1993**, *98*, 5648–5652; C. Lee, W. Yang, R. G. Parr, *Phys. Rev. B* **1988**, *37*, 785–789; B. Miehlich, A. Savin, H. Stoll, H. Preuss, *Chem. Phys. Lett.* **1989**, *157*, 200–206. c) Gaussian 98 (Revision A.7), M. J. Frisch, G. W. Trucks, H. B. Schlegel, G. E. Scuseria, M. A. Robb, J. R. Cheeseman, V. G. Zakrzewski, J. A. Montgomery, R. E. Stratmann, J. C. Burant, S. Dapprich, J. M. Millam, A. D. Daniels, K. N. Kudin, M. C. Strain, O. Farkas, J. Tomasi, V. Barone, M. Cossi, R. Cammi, B. Mennucci, C. Pomelli, C. Adamo, S. Clifford, J. Ochterski, G. A. Petersson, P. Y. Ayala, Q. Cui, K. Morokuma, D. K. Malick, A. D. Rabuck, K. Raghavachari, J. B. Foresman, J. Cioslowski, J. V. Ortiz, B. B. Stefanov, G. Liu, A. Liashenko, P. Piskorz, I. Komaromi, R. Gomperts, R. L. Martin, D. J. Fox, T. Keith, M. A. Al-Laham, C. Y. Peng, A. Nanayakkara, C. Gonzalez, M. Challacombe, P. M. W. Gill, B. G. Johnson, W. Chen, M. W. Wong, J. L. Andres, M. Head-Gordon, E. S. Replogle, J. A. Pople, Gaussian, Inc., Pittsburgh, PA, **1998**; d) D. Andrae, U. Häußermann, M. Dolg, H. Stoll, H. Preuß, *Theor. Chim. Acta* **1990**, *77*, 123–141; e) T. Leininger, A. Nicklass, H. Stoll, M. Dolg, P. Schwerdtfeger, *J. Chem. Phys.* **1996**, *105*, 1052–1059; f) A. Bergner, M. Dolg, W. Küchle, H. Stoll, H. Preuß, *Mol. Phys.* **1993**, *80*, 1431–1441; g) T. H. Dunning, P. J. Hay in *Methods of Electronic Structure Theory, Modern Theoretical Chemistry, Vol. 3* (Ed.: H. F. Schaefer III), Plenum, New York, **1977** h) See, for examnple: A. D. Becke, K. E. Edgecombe, *J. Chem. Phys.* **1990**, *92*, 5397–5403; A. Savin, R. Nesper, S. Wengert, T. F. Fässler, *Angew. Chem.* **1997**, *109*, 1892–1918; *Angew. Chem. Int. Ed. Engl.* **1997**, *36*, 1809–1832; i) A. E. Reed, F. Weinhold, *J. Chem. Phys.* **1985**, *83*, 735–746; j) S. Noury, X. Krokidis, F. Fuster, B. Silvi, TopMoD Programmpaket, Université Pierre et Marie Curie, **1997**. k) See, for example, S. Portmann, H. P. Lüthi, *Chimia* **2000**, *54*, 766–770.

[11] The Cp″ ligand was in both cases replaced by unsubstituted Cp, and the structures were idealized slightly to make use of point group symmetry, C_{3v} for **2′** and D_{2h} for **3′**.

[12] M. Kaupp, *Chem. Ber.* **1996**, *129*, 527–533.

[13] There are two different lenghts of the Rh–Ga bonds within the antiprism: 2.426(1) and 2.458(1) Å.

[14] A comparison of structures included in Cambridge Crystallographic Database shows that lengths of Rh–Rh and Ga–Ga bonds (described as single ones) vary in quite broad ranges: 2.315–3.294 Å and 2.324–3.046 Å respectively. At that a maximum of distribution for Rh–Rh distances lies between 2.660 and 2.880 Å. As to Ga–Ga bonds the distribution does not have an explicit maximum, and most of the values are represented almost evenly between 2.367 and 2.720 Å.

[15] Compare for example, with: A. Burkhardt, U. Wedig, H. G. von Schnering, A. Savin, *Z. Anorg. Allg. Chem.* **1993**, *619*, 437–441.

[16] a) G. M. Sheldrick, *SHELXS-97*, Universität Göttingen, **1997**; b) G. M. Sheldrick, *SHELXL-97*, Universität Göttingen, **1997**.

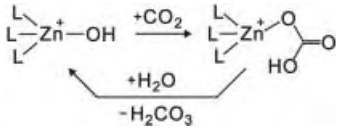
Carbon Dioxide Activation

A Gas-Phase Reaction as a Functional Model for the Activation of Carbon Dioxide by Carbonic Anhydrase**

Detlef Schröder, Helmut Schwarz, Stephan Schenk, and Ernst Anders*

Dedicated to Professor Wolfgang Steglich on the occasion of his 70th birthday.

Carbonic anhydrase is a zinc-centered enzyme, with a molecular weight of around 30 kDa, which efficiently catalyzes the conversion of carbon dioxide into soluble bicarbonate (HCO_3^-), thereby greatly facilitating the transport of CO_2 in biological systems.[1] The function of carbonic anhydrase is outlined in Scheme 1:[2] a zinc hydroxide cation with three



Scheme 1. Functioning of carbonic anhydrase.

additional ligands L, $[L_3ZnOH]^+$, allows the hydroxide anion, formally present in the resonance structure $[L_3Zn^{2+}\cdot OH^-]$, to nucleophilicly attack the carbon atom of CO_2. This reaction results in formation of carbonic acid or bicarbonate.[3] The protein environment of the active center, obtained through evolution, provides an ideal arrangement of three histidine residues which serve as ligands L and to enables acceleration of the rate-limiting steps by proton relays.[3–5] Herein, we report an investigation of the intrinsic requirements for CO_2 activation according to Scheme 1 in the idealized gas phase. This approach raises two immediate questions: 1) can the nucleophilic attack formally required for bond activation of CO_2 be achieved at all by a gaseous cation bearing a real Coulomb charge? 2) If so, what is the optimal number of ligands (n) for activation of CO_2 by $[L_nZnOH]^+$ ions in the gas phase?

[*] Dr. D. Schröder, Prof. Dr. Drs. h.c. H. Schwarz
Institut für Chemie
der Technischen Universität Berlin
10623 Berlin (Germany)
Fax: (+49) 30-314-21102
E-mail: df@www.chem.tu-berlin.de
Dipl.-Chem. S. Schenk, Prof. Dr. E. Anders
Institut für Organische Chemie und Makromolekulare Chemie
Friedrich Schiller Universität Jena, 07743 Jena (Germany)

[**] This work was supported by the MCInet of the European Commission, the Deutsche Forschungsgemeinschaft, the Fonds der Chemischen Industrie, and the Sonderforschungsbereich 436 (Jena). The Berlin group thanks the Aventis Corporation and the Sonderforschungsbereich 546 for the ESI equipment.

Electrospray ionization (ESI)[6] allows a variety of ligated metal ions to be generated directly from solution. The experiments described herein were performed with a VG BIO-Q instrument consisting of an ESI source combined with a tandem mass spectrometer of QHQ configuration (Q = quadrupole and H = hexapole).[7] When dilute solutions of ZnX_2 (X = F–I, NO_3) in methanol/water containing a trace of either imidazole (im) or pyridine (py) as the nitrogen ligands L are subjected to ESI, $[L_nZn]^{2+}$ and $[L_nZnX]^+$ species form as the main zinc-containing cations.[8] The $[L_nZn]^{2+}/[L_nZnX]^+$ ratio depends on the coordination ability of the counterion X^-: the weaker-coordinating X^- is, the more the Equilibrium (1) is shifted to the left. With more weakly coordinating

$$[L_nZn]^{2+} + X^- \rightleftharpoons [L_nZnX]^+ \quad (1)$$

counterions (X = Cl, Br, and NO_3), solvolysis of the dication (Equilibrium (2)) can compete with anion rebound to afford the desired $[L_nZnOH]^+$ species.

$$[L_nZn]^{2+} + H_2O \rightleftharpoons [L_nZnOH]^+ + H^+ \quad (2)$$

In ESI, the degree of ligation can be controlled by the cone voltage, a parameter reflecting the degree of collision-induced dissociation (CID) of the initially formed ions during their transfer to the high-vacuum manifold of the mass spectrometer.[9] At low cone voltages, the tetracoordinate species $[L_4Zn]^{2+}$ and $[L_3ZnX]^+$ prevail, while excessive fragmentation to smaller values of n occurs at elevated cone voltages to eventually afford $[ZnOH]^+$ and finally "naked" $[Zn]^+$. We note that the isotope patterns[10] observed are fully consistent with the formulae $[L_nZnOH]^+$ and that CID of the mass-selected ions is as expected: exclusive loss of L is detected for $n = 3$, for $n = 1$ and 2 competing eliminations of L and H_2O are detected, where the loss of water involves transfer of one hydrogen atom from the ligand to the hydroxy group.

To mimic the activation of CO_2 by carbonic anhydrase in a gas-phase experiment, a further indicator is required because the heterolytic cleavage $[L_nZnOH]^+ + CO_2 \rightarrow [L_nZn]^{2+} + [HCO_3]^-$ cannot occur thermally in the absence of solvent. Thus, ^{18}O labeling is applied. The ESI of a solution of ZnX_2 and L (both ca. 1 mg) in $H_2{}^{18}O/CH_3OH$ leads to the generation of $[L_nZn^{18}OH]^+$ ions; the methanol is used to dilute the [^{18}O]water and also to improve the spray conditions.[11] The resulting mixtures of $[L_nZn^{16}OH]^+$ and $[L_nZn^{18}OH]^+$ ions are easily deconvoluted by modeling of the observed isotope patterns (see Figure 1).[10]

Upon reaction of mass-selected $[L_nZn^{18}OH]^+$ ions with $C^{16}O_2$ slow, but clearly significant degrees of degenerate $^{16}O/^{18}O$ exchange are observed for L = im and py with $n = 1$ and 2 (Table 1). The product yields linearly depend on the pressure of CO_2 and rapidly decline at elevated collision energies, as expected for bimolecular reactions in the gas phase occurring under thermal conditions. A small fraction of $^{16}O/^{18}O$ exchange in the absence of CO_2 is attributed to background water in the mass spectrometer. In contrast, no significant $^{16}O/^{18}O$ exchange is found for either the bare $[ZnOH]^+$ cation or the triply nitrogen-coordinated ions $[L_3ZnOH]^+$. Experimen-

 DOI: 10.1002/anie.200351440 © 2003 Wiley-VCH Verlag GmbH & Co. KGaA, Weinheim

Table 1: Relative rates[a,b] of $^{16}O/^{18}O$ exchange of mass-selected $[L_n{}^{64}Zn^{18}OH]^+$ ions[c] with $C^{16}O_2$.

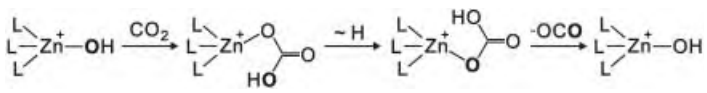
n	L = im	L = py	L = phen
0[d]	< 10[e]		
1	20	35	< 5[e]
2	100	25	
3	< 5[e]	< 5[e]	

[a] Relative to the reactivity of $[(im)_2{}^{64}Zn^{18}OH]^+$ which is arbitrarily set to 100 (see text). The values include corrections for isotope exchange with water present in the background of the mass spectrometer and incomplete ^{18}O incorporation which leads to an overlap of unreactive $[L_n{}^{66}Zn^{16}OH]^+$ ions. [b] Within the experimental error of ±10, the relative rates of the reactive systems are confirmed by neutral-loss scans ($\Delta m = -2$) for the entire isotope patterns. [c] Mass selection with Q1, while $C^{16}O_2$ is present in the hexapole at pressures between $(0.4–1.5) \times 10^{-3}$ mbar with the collision energy nominally set to 0 eV and Q2 is scanned for product analysis. [d] This entry corresponds to naked $[Zn^{18}OH]^+$ generated at high cone voltage. [e] Upper limit evaluated from the noise level.

tally, $^{16}O/^{18}O$ exchange is most efficient for $[(im)_2ZnOH]^+$. However, the reaction occurs with only about 1% of the gas-kinetic collision rate, which indicates that the degenerate oxygen-atom exchange between $[(im)_2ZnOH]^+$ and CO_2 is kinetically hindered.

Using an Arrhenius-type approach,[12] the reaction efficiency further suggests an upper limit for the activation barrier of $\geq 15 \pm 5$ kJ mol^{-1} above the energy of the isolated reactants $[(im)_2ZnOH]^+ + CO_2$; it is assumed that the internal energy of the reactant ion corresponds to the temperature of the ion source (100 °C).[13,14] Thus, much like in the enzymatic system, the gas-phase mimic $[(im)_2ZnOH]^+$ is not only able to activate CO_2, but also has a surprisingly low activation barrier, even in the absence of additional proton relays of the enzyme. With the bidentate nitrogen ligand 1,10-phenanthroline (phen), the ion $[(phen)ZnOH]^+$ is formally equivalent to the $[L_2ZnOH]^+$ complexes of the monodentate ligands imidazole and pyridine. Nevertheless, no appreciable $^{16}O/^{18}O$ exchange occurs with $[(phen)Zn^{18}OH]^+$ (Table 1). While the low reaction rate and the $^{16}O/^{18}O$ exchange occurring with background water cause potential sources of error, independent validation is achieved from the reactions of $[L_nZn^{16}OH]^+$ ions with $C^{18}O_2$, which fully confirm the above findings.

In analogy to the Lipscomb mechanism for carbonic anhydrase,[15–17] degenerate $^{16}O/^{18}O$ exchange in the gas phase must involve an intramolecular hydrogen rearrangement as well (Scheme 2, the oxygen atom of the initial hydroxy group is in bold); the alternative Lindskog mechanism[18] cannot account for $^{16}O/^{18}O$ exchange in the gas phase. To assess the role of hydrogen migration, the associated kinetic isotope effect (KIE) is determined in a double-labeling experiment. Because the exchangeable hydrogen atom(s) present in



Scheme 2. Degenerate $^{16}O/^{18}O$ exchange in the gas phase through intramolecular hydrogen migration.

imidazole render data analysis more ambiguous, pyridine is used as a ligand. To this end, a dilute solution of $ZnCl_2$ in an approximately 1:1 mixture of D_2O and CH_3OH with a trace of pyridine is subjected to ESI. Figure 1a shows the region of the

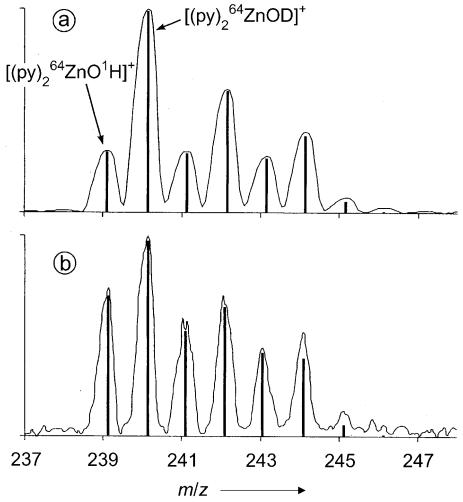


Figure 1. a) Partial ESI mass spectrum (Q2-scan, $m/z = 237–248$) of a dilute solution of $ZnCl_2$ and pyridine in D_2O/CH_3OH (1:1, v/v). b) Neutral-gain spectrum (Q1/Q2-scan, $\Delta m = +2$) of the same mass region after reaction with $C^{18}O_2$ present in the hexapole at a collision energy nominally set to 0 eV. Note that the resolution in (b) is superior to that in (a) because the neutral-gain scan involves two mass analyzers, whereas (a) was recorded by scanning Q2 only. The vertical bars in the Figure represent the modeled isotope distributions mentioned in the text.

$[(py)_2ZnOH]^+$ signal obtained under typical conditions. Analysis of the isotope pattern[10] gives a deuteration of (75 ± 2) atom% D. The Q1 mass-selected ions are then treated with $C^{18}O_2$ in the hexapole and the products of $^{16}O/^{18}O$ exchange are detected by the second quadrupole. The most sensitive method in this respect is a mass spectrometric mode referred to as neutral-gain (or neutral-loss) scan:[19] two mass analyzers in series, scan a given spectral range with a fixed offset (Δm) between them. We set $\Delta m = +2$ so that only those ions formed in the ion source which increase their mass by $\Delta m = +2$ upon interaction with $C^{18}O_2$ can reach the detector. Numerical comparison of the isotope pattern in Figure 1a with that of the resulting neutral-gain spectrum (Figure 1b) reveals a KIE of 2.3 ± 0.3 for the $^{16}O/^{18}O$ exchange for $[(py)_2ZnOH]^+$ and $[(py)_2ZnOD]^+$. Accordingly, hydrogen migration makes a significant contribution to the rate-determining step of CO_2 activation by $[L_nZnOH]^+$ cations in the gas phase.

As far as the dependence of the relative rates on the type and number of ligands is concerned, the following conclusions can be drawn. The imidazole and pyridine complexes behave similarly, with $[(im)_2ZnOH]^+$ being most reactive, whereas the phenanthroline complex $[(phen)ZnOH]^+$ does not mediate $^{16}O/^{18}O$ exchange in the gas phase. With respect to the role of number of ligands (n), there is a fundamental difference between the gas-phase experiments and condensed-phase chemistry. Occurrence of a thermoneutral ion/molecule

 © 2003 Wiley-VCH Verlag GmbH & Co. KGaA, Weinheim

reaction in the gas phase at a measurable rate requires the initial formation of a reasonably well-bound complex (in this case $[L_nZnOH]^+ \cdot CO_2$). The complexation energy of $[L_nZnOH]^+$ and CO_2 should decrease with increasing n, so that for the quasi-tetracoordinate $[L_3ZnOH]^+$ ions complexation of CO_2 is considered inefficient. In turn, a sufficiently nucleophilic hydroxy group is required to attack CO_2 carbon atom. For $[L_nZnOH]^+$ ions in the gas phase bearing a real Coulomb charge, the nucleophilicity of the hydroxy group decreases with lower values of n. Model studies show that the nucleophilicity of the hydroxy group depends on the energy of the lone pair (LP) orbital of the oxygen atom (E^0_{LP}).[2] This energy increases with n, whereas the Zn–O bond order (BO_{Zn-O}) decreases (Table 2). For small values of n, the Zn–O bond is predominantly covalent, whereas increasing n stabilizes multiply-charged metal-containing fragments[20–22] such as $[L_nZn]^{2+}$ and favors formation of a "free" and therefore more nucleophilic hydroxide ion.

These opposing trends provide a qualitative explanation for the highest reaction efficiency observed for the $[(im)_2ZnOH]^+$ ion. This more intuitive reasoning finds quantitative support in preliminary ab initio calculations of the gaseous $[(im)_nZnOH]^+$ complexes (Table 2). Thus, the complexation energies of the imidazole ligands continuously decrease with increasing n, whereas the partial charge of the oxygen atom of the hydroxy group rises from $q_O = -1.06$ in naked $[ZnOH]^+$ to $q_O = -1.31$ in $[(im)_3ZnOH]^+$. Likewise, the partial charge of the hydroxy group (q_{OH}) increases from $[ZnOH]^+$ to $[(im)_3ZnOH]^+$.

Table 2: Calculated complexation energies D(im–Zn),[a,b] atomic charges of Zn and O (q_{Zn}, q_O),[c] charge of the OH group (q_{OH}),[c] Zn–O bond order (BO_{Zn-O}),[d] Zn–O bond lengths,[e] and energy of the lone pair on oxygen (E^0_{LP})[f] of $[(im)_nZnOH]^+$ complexes and $[(phen)ZnOH]^+$.[g]

	D(im–Zn)	q_{Zn}	q_O	q_{OH}	BO_{Zn-O}	d_{Zn-O}	E^0_{LP}
$[ZnOH]^+$		1.562	−1.060	−0.56	0.712	177.5	−0.544
$[(im)ZnOH]^+$	394	1.555	−1.203	−0.72	0.459	175.2	−0.446
$[(im)_2ZnOH]^+$	171	1.623	−1.274	−0.81	0.308	182.0	−0.387
$[(im)_3ZnOH]^+$	129	1.650	−1.312	−0.85	0.210	188.5	−0.347
$[(phen)ZnOH]^+$		1.594	−1.239	−0.77	0.375	178.8	−0.397

[a] More specifically defined as: D_0(im–[Zn(im)$_{n-1}$(OH)]$^+$). [b] In kJ mol^{-1} at 0 K. [c] According to natural population analysis. [d] Wiberg bond index according to NBO. [e] In pm. [f] In Hartree [g] All computations were performed at the B3LYP/6-311++G(d,p) level of theory.

The reactivity maximum for $[(im)_2ZnOH]^+$ found in our gas-phase experiments fundamentally differs from the situation for carbonic anhydrase in which a tetracoordinate zinc species acts as the active species. In solution, however, additional hydrogen bonds can facilitate both the docking of CO_2 and the proton migrations involved in its activation,[4] while this option is not available in the idealized gas phase. In fact, when considering the difficulties associated with 1,3-hydrogen migrations in organic chemistry in general[23,24] and the large barrier computed for the Lipscomb mechanism[15,16] in the related $[(NH_3)_3ZnOH]^+/CO_2$ model system in particular,[3,25] in the gas-phase system the ligands might not act as mere spectators. Instead, the basic nitrogen ligands may serve as "internal" proton relays which could account for the different reactivities of the seemingly similar complexes $[(py)_2ZnOH]^+$ and $[(phen)ZnOH]^+$ towards CO_2. Active participation of the NH protons might also contribute to the particularly enhanced reactivity of $[(im)_2ZnOH]^+$. Clearly, experimental and theoretical studies need to address the differences between the pyridine and imidazole complexes in more detail as well as the role of quantum-mechanical tunneling effects in the proton migrations involved.[26] Further, it is remarkable that the computed properties of the $[(phen)ZnOH]^+$ complex (Table 2) do not significantly differ from the $[(im)_2ZnOH]^+$ species. Thus, $[(phen)ZnOH]^+$ might activate CO_2 as well, whereas the hydrogen migration required for the mass spectrometric monitoring by means of $^{16}O/^{18}O$ exchange may be hindered by the rigidity of the phenanthroline ligand.

Notwithstanding these possible objections, the successful mimicking of essential steps in the reaction mode of carbonic anhydrase with a molecular weight of about 30 kDa by a gas-phase complexes of less than 300 Da offers a unique opportunity for direct comparisons of experimental and theoretical studies on various biomimetic model complexes.[27]

Received: March 19, 2003
Revised: June 26, 2003 [Z51440]

Keywords: carbon dioxide · carbonic anhydrase · electrospray ionization · mass spectrometry · zinc

[1] W. Kaim, B. Schwederski, *Bioanorganische Chemie*, Teubner, Stuttgart, **1991**.
[2] M. Bräuer, J. L. Pérez-Lustres, J. Weston, E. Anders, *Inorg. Chem.* **2002**, *41*, 1454.
[3] M. Mauksch, M. Bräuer, J. Weston, E. Anders, *ChemBioChem* **2001**, *2*, 190.
[4] Q. Cui, M. Karplus, *J. Phys. Chem. B* **2003**, *107*, 1071.
[5] See also: M. T. Nguyen, G. Raspoet, L. C. Vanquickenborne, P. T. Van Duijnen, *J. Phys. Chem. A* **1997**, *101*, 7379.
[6] J. B. Fenn, M. Mann, C. K. Meng, S. F. Wong, C. M. Whitehouse, *Science* **1989**, *246*, 64; see also the Nobel lecture J. B. Fenn, *Angew. Chem.* **2003**, *115*, 3999; *Angew. Chem. Int. Ed.* **2003**, *42*, 3871.
[7] D. Schröder, T. Weiske, H. Schwarz, *Int. J. Mass Spectrom.* **2002**, *219*, 759.
[8] Technical note: From the turbid solutions formed upon addition of the base, zinc hydroxides may eventually precipitate with the risk of irreversible blocking the ESI capillary.
[9] M. Kohler, J. A. Leary, *Int. J. Mass Spectrom. Ion Processes* **1997**, *162*, 17.
[10] Calculated using the Sheffield ChemPuter, see: http://www.shef.ac.uk/chemistry/chemputer/index.html. (Mark Winter, University of Sheffield, UK, **1993–2001**).
[11] N. B. Cech, C. G. Enke, *Mass Spectrom. Rev.* **2001**, *20*, 362.
[12] V. Baranov, G. Javahery, A. C. Hopkinson, D. K. Bohme, *J. Am. Chem. Soc.* **1995**, *117*, 12801.

 © 2003 Wiley-VCH Verlag GmbH & Co. KGaA, Weinheim

[13] Note, however, that the internal energy of the ions generated upon ESI at elevated cone voltages may be larger.[7,14] Nevertheless, the observed energy behavior of the $^{16}O/^{18}O$ exchange is characteristic for thermal processes.
[14] D. Schröder, M. Engeser, M. Brönstrup, C. Daniel, J. Spandl, H. Hartl, *Int. J. Mass Spectrom.* **2003**, *228*, 743.
[15] J.-Y. Liang, W. N. Lipscomb, *Biochemistry* **1987**, *26*, 5293.
[16] J.-Y. Liang, W. N. Lipscomb, *Biochemistry* **1988**, *27*, 8676.
[17] M. Solà, A. Lledós, M. Duran, J. Bertrán, *J. Am. Chem. Soc.* **1992**, *114*, 869.
[18] D. N. Silverman, S. Lindskog, *Acc. Chem. Res.* **1988**, *21*, 30.
[19] K. L. Busch, G. L. Glish, S. A. McLuckey, *Mass Spectrometry/Mass Spectrometry: Techniques and Applications of Tandem Mass Spectrometry*, VCH, Weinheim, **1988**.
[20] M. Peschke, A. T. Blades, P. Kebarle, *J. Am. Chem. Soc.* **2000**, *122*, 10440.
[21] A. J. Stace, *Phys. Chem. Chem. Phys.* **2001**, *3*, 1935.
[22] D. Schröder, K. Schroeter, H. Schwarz, *Int. J. Mass Spectrom.* **2001**, *212*, 327.
[23] D. Schröder, J. Loos, H. Schwarz, R. Thissen, O. Dutuit, P. Mourgues, H.-E. Audier, *Angew. Chem.* **2002**, *114*, 2867; *Angew. Chem. Int. Ed.* **2002**, *41*, 2748, and references therein.
[24] T. Loerting, C. Tautermann, R. T. Kroemer, I. Kohl, A. Hallbruker, E. Mayer, K. Liedl, *Angew. Chem.* **2000**, *112*, 920; *Angew. Chem. Int. Ed.* **2000**, *39*, 891.
[25] See also: H. Erras-Hanauer, Z.-W. Mao, G. Liehr, T. Clark, R. van Eldik, *Eur. J. Inorg. Chem.* **2003**, 1562.
[26] Z. Smedarchina, W. Siebrand, A. Fernández-Ramos, Q. Cui, *J. Am. Chem. Soc.* **2003**, *125*, 243.
[27] H. Vahrenkamp, *Acc. Chem. Res.* **1999**, *32*, 589.

 © 2003 Wiley-VCH Verlag GmbH & Co. KGaA, Weinheim

Kinetics of Olefin Polymerization

Microkinetic Videomicroscopic Analysis of Olefin Polymerization with a Supported Metallocene Catalyst

*Stefan Knoke, Daniela Ferrari, Bernd Tesche, and Gerhard Fink**

In industrial practice ethylene and propylene are polymerized predominantly by slurry, bulk, and gas-phase procedures with heterogeneous catalysts. The catalyst is typically supported on a porous microsphere on which the polymer grows. In this way the original form of the catalyst particle is used to control the morphology of the final product. Because of the hydraulic forces due to the growing polymer, the catalyst particle breaks into nanometer-sized fragments. This process takes place at the catalyst surface and proceeds to the center of the particle. Consequently, the polymer particles formed replicate the initial shape of the catalyst particle, whereas the grain size is substantially larger. The shape and the size distribution of the catalyst grains and the polymer particles are coherent. Moreover, the size and the concentration of the residual catalyst fragments in the polymer matrix are so low that the properties of the final polyolefin do not appear to be influenced. Thus, the residual catalyst fragments need not be removed from the product. It is also possible to control some aspects of the polymer morphology, for example, the high bulk density of the polymer grains.

In a laboratory-scale investigation of such an economically relevant industrial process glass and steel reactors with volumes of 500–5000 mL are employed. The monomer consumption can be determined online in slurry and gas-phase polymerizations by means of flowmeters. Important information about the fragmentation of the supporting material can be obtained by the electron microscopic analysis of single particles in cross section, depending on the polymerization time. Recently, reaction calorimetry has been used to determine monomer conversion in slurry and bulk polymerizations.[1] Reichert et al. reported on the first videomicroscopic investigation of butadiene polymerization with a neodymium-based Ziegler catalyst on a silica support.[2] A new method for the online observation of growing polyolefin particles was also described by Weickert et al.[3]

In this paper we illustrate the possibilities for applying videomicroscopy to study polymerization. We describe the in situ observation of the gas-phase polymerization of ethylene with a heterogeneous zirconocene/MAO/SiO_2 catalyst by means of an optical microscope. This technique enables the simultaneous detection of the individual growth of a large number of catalyst particles. In addition to visualizing polymer growth and the replication of catalyst morphology, we were able to obtain detailed information about the polymerization kinetics of numerous catalyst particles, which act as discrete microreactors in the industrial process. In our investigation special equipment was employed, consisting of an autoclave equipped with a glass window and a connection to the vacuum line and the monomer supply. The autoclave was located under an optical microscope connected to a high-resolution digital camera. A detailed description of the experimental setup is given in the Supporting Information.

The catalyst system we studied is composed of a zirconocene complex and the cocatalyst methyalumoxane (MAO), which were supported on highly porous silica spheres by a suspension process. The morphology of the supporting material was analyzed by scanning electron microscopy (SEM) and by transmission electron microscopy (TEM). The aluminium and zirconium contents were determined by elemental analysis, and the distribution of active components was checked by energy dispersion X-ray (EDX) analysis of a cross section of the sample.

Ethylene was polymerized at 60 °C and 10 bar for 180 minutes, and a picture was taken through the microscope every 20 seconds. Figure 1 shows four snapshots from a sequence of 540 pictures. (A short movie containing the 540 snapshots is available on the Internet in the Supporting

[*] Prof. Dr. Dr. G. Fink, Dipl.-Chem. S. Knoke, Dipl.-Chem. D. Ferrari, Dr. B. Tesche
Max-Planck-Institut für Kohlenforschung
Kaiser-Wilhelm-Platz 1, 45470 Mülheim an der Ruhr (Germany)
Fax: (+49) 208-306-2980
E-mail: fink@mpi-muelheim.mpg.de

Supporting information for this article is available on the WWW under http://www.angewandte.org or from the author.

 © 2003 Wiley-VCH Verlag GmbH & Co. KGaA, Weinheim DOI: 10.1002/anie.200351582

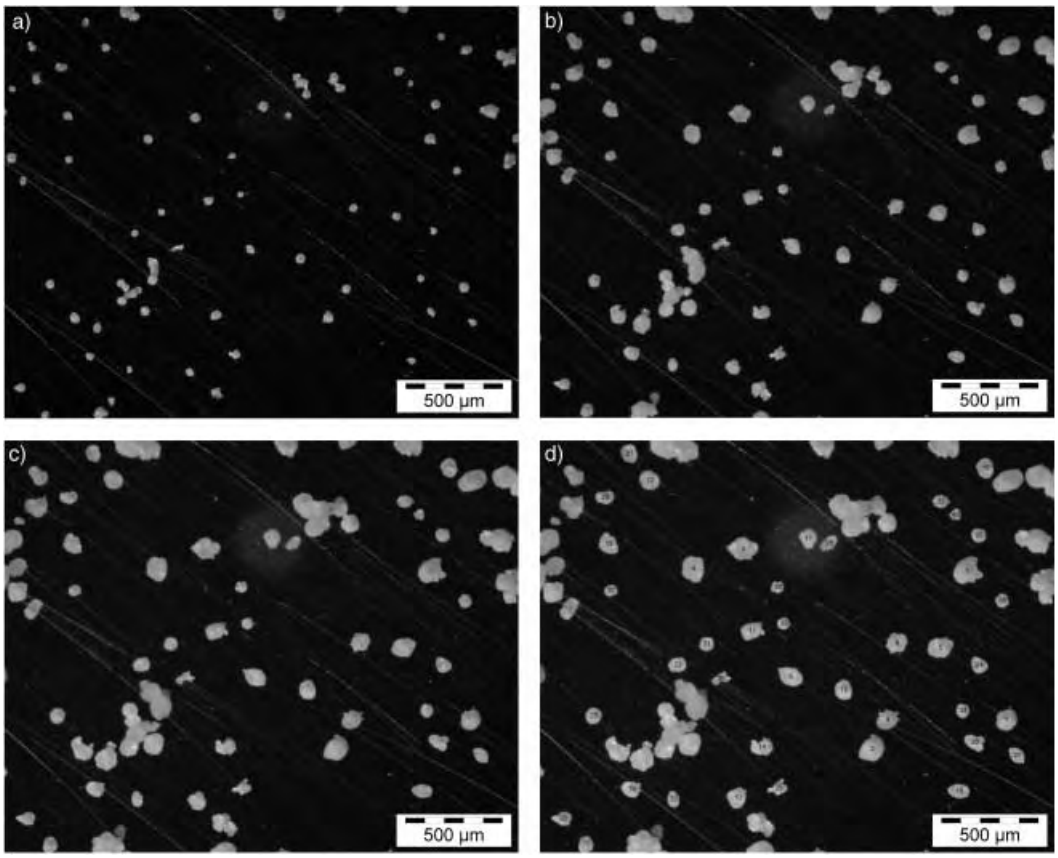


Figure 1. a–d) Four snapshots of the growing particles taken after 0, 60, 120 and 180 minutes of polymerization of ethylene at 10 bar and 60 °C. In d) the detected particles are numbered based on their final size after 180 minutes of polymerization.

Information.) Figure 1 a is a photograph of the catalyst at the moment the monomer gas is introduced (reaction time 0 minutes). Snapshots of the polymerization after 60, 120, and 180 minutes are shown in Figure 1 b–d.

Figure 2 shows the superposition of the images of the detected particles from Figures 1 a (0 minutes) and 1 b (60 minutes) on a picture of the same particles taken after 180 minutes of polymerization. It is evident that during the progressive growth of the single grains the shape of the supporting material is replicated through the polymer particle. The image-processing software analySIS Pro was used to automatically determine the projection area of 40 selected particles in the 540 pictures. Only the particles that were exposed and isolated for the duration of the polymerization were considered. In Figure 1 d the particles are numbered according to their final size after 180 minutes of polymerization, in order to correlate them to the individual curves depicted in Figures 3–5. A detailed description of the image-processing routine is given in the Supporting Information.

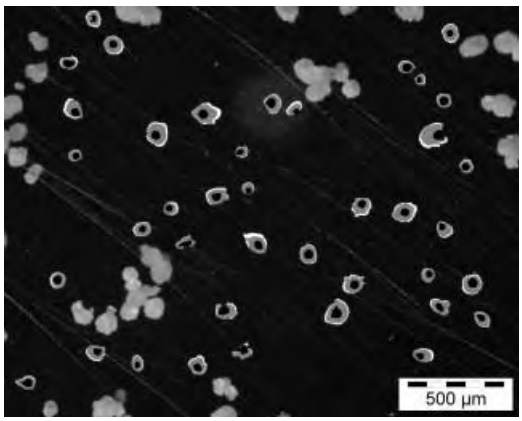


Figure 2. Superposition of images of the detected particles from Figure 1 a (0 minutes), Figure 1 b (60 minutes), and the micrograph recorded after 180 minutes of polymerization (Figure 1 d).

Although the projection area of the particles is the primary quantity measured, it is easier to comprehend the size of the particles in terms of their diameter and volume. The projection area can be used to estimate the diameter of a circle of equivalent area (equivalent circle diameter, ECD) or the volume of a sphere having an equivalent projection area (equivalent sphere volume, ESV).

The dependence of the ECD on the polymerization time is represented in Figure 3. As expected, the size of the particles generally increases with polymerization time. At first glance, it is possible to observe the general kinetic profile. The size distribution of the catalyst grains is replicated by the polymer particles. The particle diameter increases by a factor of 2 after 180 minutes of polymerization. Two of the curves show irregularities after 115 and 140 minutes, respectively. If one refers to the original images it is apparent that these hops in

 © 2003 Wiley-VCH Verlag GmbH & Co. KGaA, Weinheim

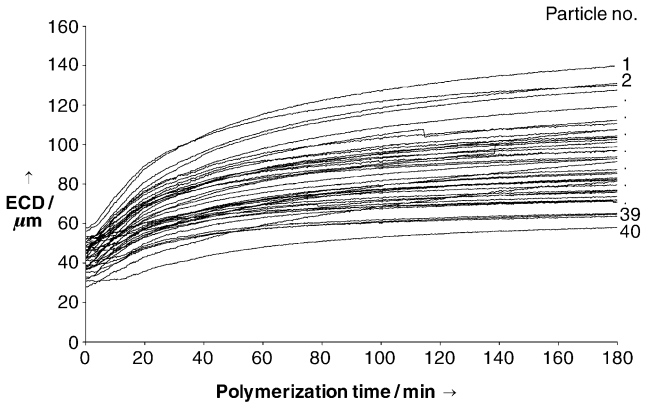


Figure 3. Diagram of the particle expansion over the course of the gas-phase polymerization of ethylene at 10 bar and 60 °C. The particles corresponding to the depicted curves are numbered in Figure 1 d based on their size after 180 minutes of polymerization.

the curves occurred when single particles fell over. As a result of the not ideally spherical shape of the particle, a sudden drop of the size of the particle after 115 minutes occurs. When another particle tips over after 140 minutes, the resulting irregularity indicates an increase of the particle size.

Figure 4 shows the increase of the particle volume ESV as a function of time. Here, the slope of the curve, i.e. polymer

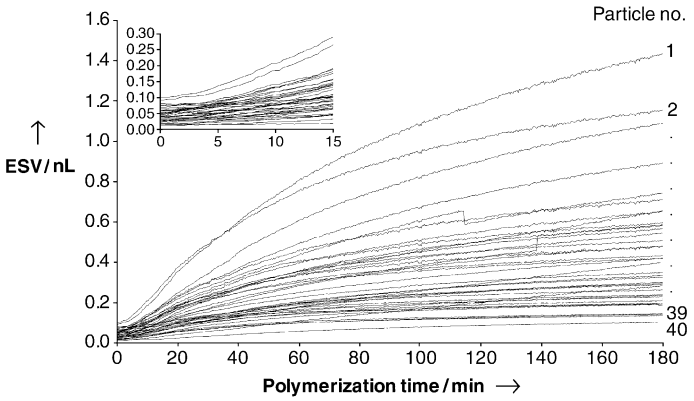


Figure 4. Increase of the polyethylene product (ESV) with the polymerization time. 10 bar ethylene, 60 °C.

production, increases constantly over 15 minutes. The irregularities in this stage are evident in the inset. In order to create a model, each single grain can be considered a discrete microreactor, and the irregularities can be seen as different "starting phases" of the microreactors. Similar differences in the initial behavior of single particles have been observed in the bulk polymerization of propylene and can be attributed to an inhomogeneous distribution of the cocatalyst through the particle.[4]

The kinetic profile is even clearer after a smoothed-differentiation of the particle volume according to the Savitsky–Golay[5] method. In Figure 5 a this evaluation was applied to particles 1, 3, 5, 21, 38, and 39. The rate–time curves obtained at 60 °C and 10 bar reach a maximum after

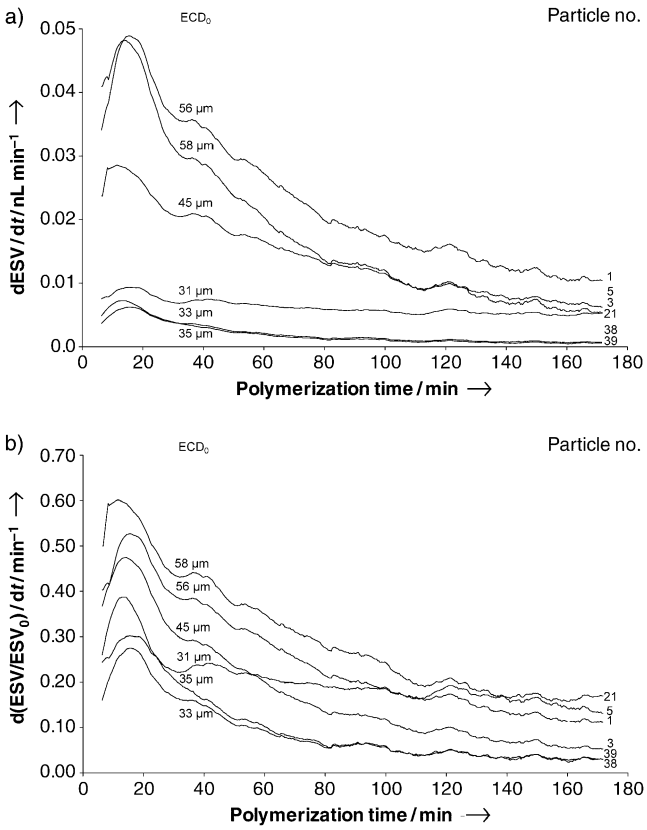


Figure 5. a) Polymerization rate–time profiles generated by smoothing-differentiation according to the Savitsky–Golay method. The points were obtained by approximation to a second-order polynomial over 51 points, 25 to the right and 25 to the left of the derivation, and derivation of the fitting function. b) Rate–time curves normalized to the initial catalyst volume.

15 minutes. Then the variation of the particle volume with time, in other words, particle expansion, is lower, and the polymer grows more slowly. Different rate maxima can also be observed from this data. Rate maxima can be divided into two groups based on the initial size of the catalyst. Smaller particles characterized by a diameter of about 35 µm catalyze the polymerization apparently more slowly then larger particles having a diameter of about 50 µm. To compare the activities of particles of different sizes, the rate–time curves were normalized based on the initial volume of the catalyst particle, as shown in Figure 5 b. This evaluation also leads to individual growth-rate trends and confirms the fact that the particles with a smaller diameter tend to grow more slowly than those with a greater diameter.

According to the "polymer growth and particle expansion model",[6,7] the polymerization process can be summarized as follows (Figure 6). In the initial prepolymerization phase a thin shell of polymer is formed on the particle at the beginning of the polymerization process. This is followed by a phase of reduced activity, caused by the diffusion-limiting effect due to the crystalline polymer layer. After this "diffusion phase" the active centers in the inner part of the particle are also provided with monomer. Because of the hydraulic forces from the growing polymer, fragmentation of

 © 2003 Wiley-VCH Verlag GmbH & Co. KGaA, Weinheim

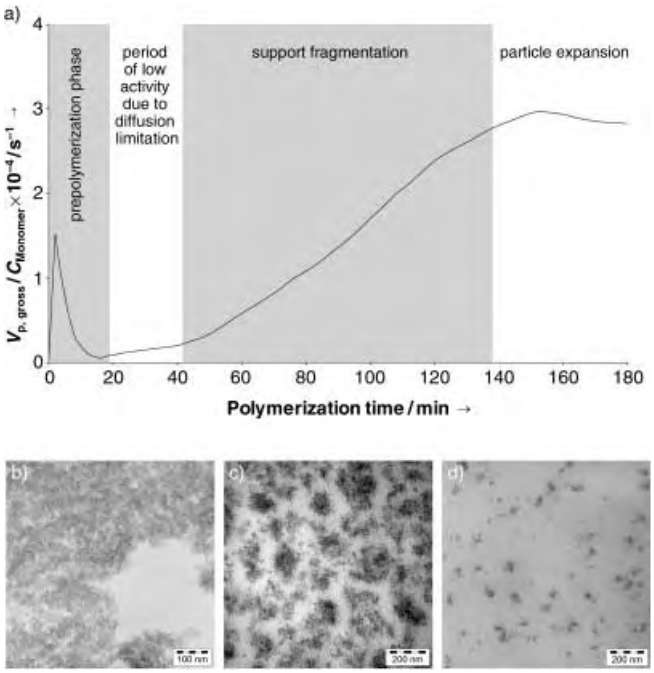


Figure 6. a) Dependence of the suspension polymerization rate on time, demonstrating the different stages of the polymerization process. b–d) TEM images of ultrathin sections of the catalyst particle (b), of a polymer particle during the fragmentation phase (c), and of a polymer particle during the expansion phase (d).

the SiO_2 support from the surface to the interior occurs. Consequently new active centers are released and the overall polymerization rate increases.

Once the reaction rate reaches its maximum, the fragmentation process is over. The progression of the fragmentation has been characterized by electron-microscopic analysis of cross sections of single polymer particles.[6] The SiO_2 support material, which was initially composed of particles 30–60 μm in size, now corresponds to primary particles 10–20 nm in size within the polymer matrix, which expanded in the polymerization. The slowdown of the particle expansion, shown in Figure 5, is due to the longer diffusion paths through the polymer. Now the number of active centers does not increase; however, the amount of polymer increases in accordance with the lengths of the diffusion paths for the monomer. The overall polymerization process was proved also by means of a complete mathematical model.[8]

In this videomicroscopic study the formation of a diffusion-limiting polymer layer (prepolymerization phase) is observed as a change in color and transparency of the particle immediately after introduction of the monomer gas into the autoclave. It is even easier to recognize the diffusion phase if the polymerization is performed at a lower ethylene pressure of 2.5 bar.

What are the reasons for the diverse behavior described? Which factors influence the polymerization process?

- Insufficient heat transfer results in a local overheating (hotspots). Higher temperatures lead to a higher polymerization rate causing more rapid fragmentation.
- The catalyst distribution throughout the particle is inhomogeneous due to the supporting procedure.
- Impurities, for example, in the monomer gas, deactivate the surface of the catalyst particle; this affects smaller particles more than larger ones.
- Larger particles have more active centers per particle.

Our further investigations will focus on:

- Isolating the factors described and determining the extent to which they act.
- Varying the initial diameter of the catalyst particles over a larger range.
- Determining the dependency of the rate of the particle growth on the temperature and the monomer pressure.

This investigation of the polymerization process by videomicroscopy facilitated the first study of the microkinetics of single catalyst particles. This work in combination with other, integral, analysis methods may lead to a deeper understanding of the entire polymerization process. The sensitivity of videomicroscopic analysis is 10000–100000 times greater than that possible in kinetic analysis by means of the flowmeter. This method is also suitable for catalyst optimization by a combinatorial approach due to the higher sensitivity, the small amount of catalyst required, and the possibility for simultaneous analysis of more than 40 particles.

Received: April 4, 2003
Revised: July 11, 2003 [Z51582]

Keywords: heterogeneous catalysis · polymerization · single-grain kinetics · supported catalysts · videomicroscopy

[1] a) F. Korber, K. Hauschild, G. Fink, *Macromol. Chem. Phys.* **2001**, *202*, 3323; b) F. Korber, K. Hauschild, G. Fink, *Macromol. Chem. Phys.* **2001**, *202*, 3329.
[2] a) C. Eberstein, B. Garmatter, K.-H. Reichert, G. Sylvester, *Chem. Ing. Tech.* **1996**, *68*, 820; b) K. Zöllner, K.-H. Reichert, *Chem. Ing. Tech.* **2001**, *73*, 849; c) K. Zöllner, K.-H. Reichert, *Chem. Eng. Technol.* **2002**, *25*, 707; d) K. Zöllner, K. Kallio, K.-H. Reichert, *DECHEMA Monogr.* **2001**, *137*, 135.
[3] J. T. M. Pater, G. Weickert, W. P. M. Swaaij, *Chimia* **2001**, *55*, 231.
[4] S. Knoke, F. Korber, G. Fink, B. Tesche, *Macromol. Chem. Phys.* **2003**, *204*, 607.
[5] a) A. Savitzky, M. J. E. Golay, *Anal. Chem.* **1964**, *36*, 1627; b) J. Steinier, Y. Termonia, J. Deltour, *Anal. Chem.* **1972**, *44*, 1906.
[6] a) G. Fink, B. Steinmetz, J. Zechlin, C. Przybyla, B. Tesche, *Chem. Rev.* **2000**, *100*, 1377; b) B. Steinmetz, C. Przybyla, J. Zechlin, G. Fink, B. Tesche, *DECHEMA Monogr.* **1998**, *134*, 147.
[7] a) B. Steinmetz, B. Tesche, C. Przybyla, J. Zechlin, G. Fink, *Acta Polym.* **1997**, *48*, 392; b) J. Zechlin, B. Steinmetz, B. Tesche, G. H. Fink, *Macromol. Chem. Phys.* **2000**, *201*, 515; c) J. Zechlin, K. Hauschild, G. Fink, *Macromol. Chem. Phys.* **2000**, *201*, 597.
[8] a) C. Przybyla, J. Zechlin, B. Steinmetz, B. Tesche, G. Fink in *Metalorganic Catalysts for Synthesis and Polymerization* (Ed.: W. Kaminsky), Springer, Berlin, **1999**, p. 321; b) C. Przybyla, B. Weimann, G. Fink in *Metalorganic Catalysts for Synthesis and Polymerization* (Ed.: W. Kaminsky), Springer, Berlin, **1999**, p. 333.

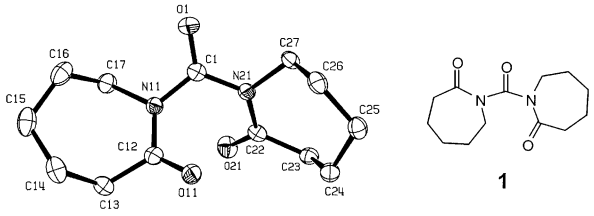
 © 2003 Wiley-VCH Verlag GmbH & Co. KGaA, Weinheim

Blocked Isocyanate Equivalents

Carbonylbiscaprolactam: A Versatile Reagent for Organic Synthesis and Isocyanate-Free Urethane Chemistry

*Steffen Maier, Ton Loontjens, Boudewijn Scholtens, and Rolf Mülhaupt**

Carbonylbiscaprolactam (CBC, **1**, Figure 1[1]) is a nontoxic (LD_{50} rat (oral) > 2000 mg kg^{-1}, LD_{50} rat (skin) > 2000 mg kg^{-1}) solid derivative of carbonic acid that melts at 118 °C and exhibits unusual selectivity in reactions with amino



1

Figure 1. Crystal structure of **1**.

and hydroxy groups which is very different from that of 1,1′-carbonyldiimidazole (CDI). Compound **1** was first prepared by Meyer in 1956 by reacting phosgene with caprolactam.[2] He first examined its use as a comonomer in polyamide synthesis; however, all early attempts to prepare polymers from **1** failed and only ill-defined oligomeric products were obtained. In 1967 a modified synthesis of **1** was patented by Okuda and Mori.[3] During the 1990s Mateva et al. and researchers at Monsanto employed **1** successfully as an initiator together with the sodium caprolactamate salt in anionic ring-opening polymerization of caprolactam for the production of high-molecular-weight polyamides and copolymers.[4] Müller et al.[5] claimed the use of **1** as an activator for special bleaching agents. The breakthrough in CBC research occurred in 1998 when Lootjens and Plum (DSM)[6] recognized the potential of **1** as a versatile reagent for the conversion of amines into *N*-carbamoyl caprolactam compounds **2**. This development of new chain extenders, which build up molecular weight and improve properties of polyester and polyamide fibers, has led to the renaissance of the CBC chemistry.[7]

[*] Prof. Dr. R. Mülhaupt, S. Maier
Freiburger Materialforschungszentrum und
Institut für Makromolekulare Chemie
Albert-Ludwigs-Universität Freiburg
Stefan-Meier-Strasse 31, 79104 Freiburg (Germany)
Fax: (+49) 761-203-6319
E-mail: rolf.muelhaupt@makro.uni-freiburg.de
Dr. T. Loontjens, Dr. B. Scholtens
DSM Research, DSM Venturing & Business Development
6160 MD Geleen (The Netherlands)

Supporting information for this article is available on the WWW under http://www.angewandte.org or from the author.

Here we present the first comprehensive studies on the reactions of **1** with nucleophiles such as amines and alcohols. Special attention was paid to the influence of the reaction conditions—for example, choice of catalyst, temperature, and stoichiometry of the reactants—on the selectivity and controllability of the reactions of **1**. Controlling the numerous reaction possibilities of **1** promises manifold new opportunities.

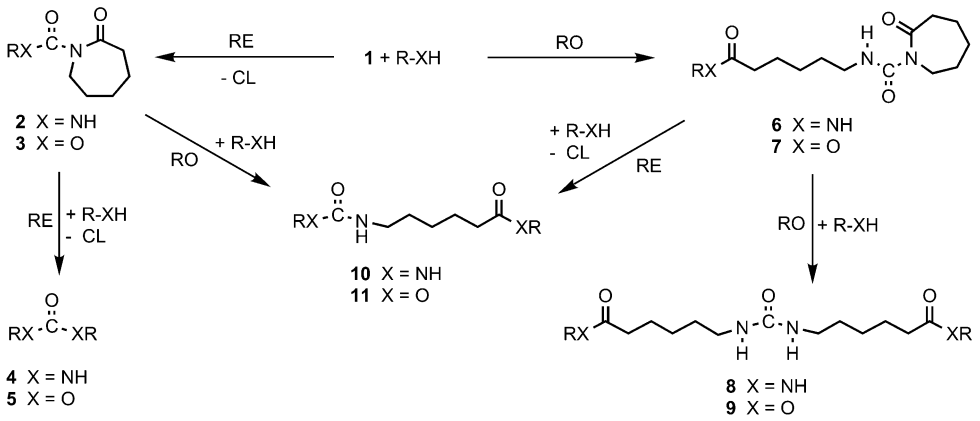
The chemistry of **1** is quite different from reactions of phosgene, diisocyanates, and 1,1′-carbonyldiimidazole (CDI). While CDI[8] is well known as a mild reagent for the conversion of carboxylic acids into the corresponding activated *N*-acyl imidazoles, the reaction of carboxylic acids with **1** to give the corresponding *N*-acyl caprolactams requires prolonged heating at high temperatures. For example, when octanoic acid is heated with an equimolar amount of **1** at 170 °C for 4 h, the corresponding *N*-octanoylcaprolactam is obtained in only 54% yield. Whereas CDI, isocyanate, and phosgene react instantaneously with alcohols and amines to afford carbonates **5** and ureas **4**, respectively, the reactions of **1** depend significantly upon the type of the nucleophile, the reaction conditions, and, in particular, the catalyst.

As illustrated in Scheme 1, two very different reaction pathways are feasible: 1) ring elimination (RE) generating caprolactam, and 2) ring opening (RO) that does not cause caprolactam by-product formation. Model reactions of **1** with a variety of low-molecular-weight monofunctional amines and alcohols were studied by ^{1}H NMR spectroscopy. As is apparent from Table 1, the reaction of **1** with 1-octylamine, performed in bulk with a molar ratio amine/**1** = 2 does not require catalyst and proceeds exclusively by the RE mechanism (Scheme 1). At 70 °C a reaction time of 15 min sufficed for 100% conversion of **1** into 1-octyl-*N*-carbamoylcaprolactam (**2a**) and caprolactam. No side reaction was detected by ^{1}H NMR spectroscopy! In contrast, at higher temperatures (170 °C) **1** was completely consumed but the reaction was not selective; **2a** was obtained in only 13% yield along with *N,N*′-dioctylurea (**4a**) in 87% yield.

In contrast to the reactions of primary amines, heating secondary amines such as *N,N*-di(1-octyl)amine with **1** did not lead to any reaction even after 60 min at 70 °C. When the reaction mixture was heated to 170 °C or when NaH catalyst was added, only minor amounts of **1** reacted, and complex reaction products were obtained. As a consequence, at temperatures around 100 °C the primary amino groups react selectively and quantitatively in the presence of the secondary amino groups to give the corresponding *N*-carbamoyl caprolactams **2**. This sort of selectivity is not displayed in reactions with phosgene, diisocyanates, and CDI. Recently, special CDI derivatives such as imidazole carboxylic acid esters of secondary and tertiary alcohols were reported to react with similarly high selectivity with primary amino groups in the presence of secondary amino groups.[9]

The *N*-carbamoyl derivatives **2** (Scheme 2) corresponding to caprolactam-blocked isocyanates are also available by reaction of caprolactam with the corresponding isocyanates, which in turn are prepared by phosgenation of the amines. Therefore, reactions of 1 are a very convenient isocyanate-free route to lactam-blocked isocyanates. Upon heating at

 © 2003 Wiley-VCH Verlag GmbH & Co. KGaA, Weinheim DOI: 10.1002/anie.200351867

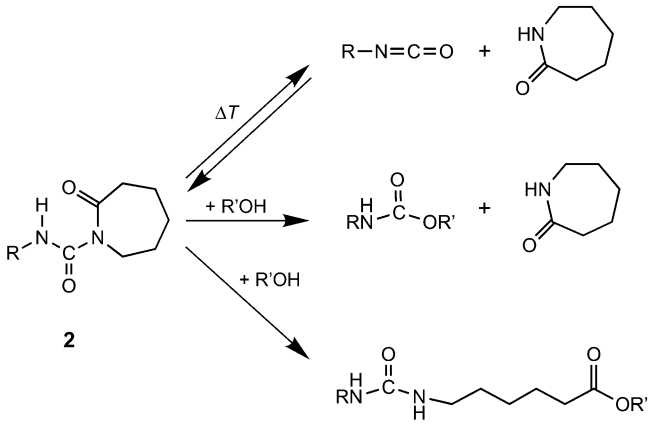


Scheme 1. Reactions of **1** with alcohols and amines: ring elimination (RE) and ring opening (RO) pathways. CL = caprolactam.

Table 1: Reactions of **1** with amines.[a]

Entry	Amine	*T* [°C]	*t* [min]	Conv. **1** [%]	Yield **2** [%]	**4** [%]
1	(1-oct)NH_2	70	15	100	100	0
2	"	170	15	100	13	87
3	$(1\text{-oct})_2NH$	70	60	0	0	0
4	"	170	60	85	n.d.[b]	n.d.[b]

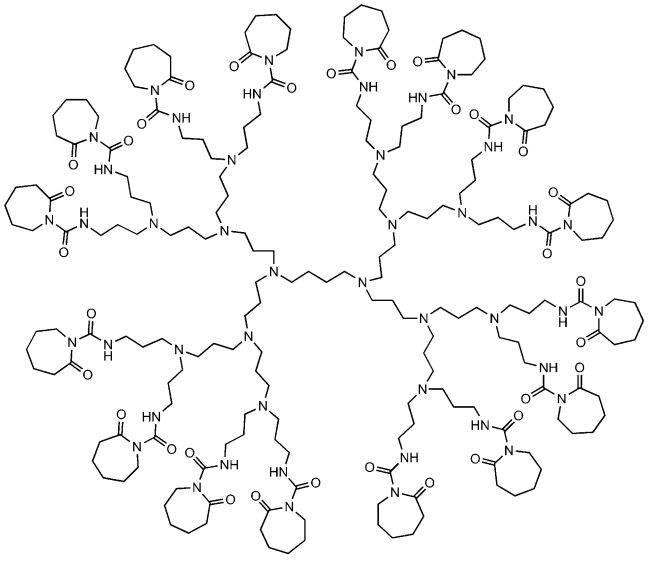
[a] Molar ratio amine/**1** = 2. [b] Not determined (complex mixture of products).



Scheme 2. Reactions of the blocked isocyanate derivative of *N*-carbamoyl caprolactam (**2**).

temperatures between 160 and 180 °C *N*-carbamoyl caprolactams **2** are cleaved to give free isocyanates and caprolactam.[10] Caprolactam-blocked isocyanates are important intermediates in coating applications where blocked isocyanates play a significant role because the presence of free toxic isocyanates is not desirable in industry.[11] Compound **1** reacts with alcohols by ring elimination (RE) and ring opening (RO) (Scheme 2) to afford urethanes without isocyanate intermediates (Scheme 2). Therefore the CBC conversion of amines represents an attractive new key to isocyanate-free urethane chemistry.

The reaction of **1** with primary amines is stoichiometric and can be performed in bulk at temperatures around 100 °C. Whereas branched polyamines with more than two amino functions crosslink immediately when traces of phosgene or diisocyanates are added due to rapid urea formation, highly branched polyamines react with **1** to give the corresponding polyfunctional *N*-carbamoyl caprolactams without any crosslinking or gel formation. This unusually selective reaction was demonstrated with the polyamine-terminated poly(propylenimine)-hexadecaamine dendrimers (Astramol, generation 3.0 with 16 primary amino groups, from DSM[12]). The dendrimer was heated with 1.05 equiv **1** per NH_2 group in toluene at 100 °C for 2 h to afford the corresponding polyfunctional derivative **2b** with 16 *N*-carbamoyl caprolactam end groups. Derivative **2b** was treated with excess methanol and NaOMe catalyst, and the endgroups underwent ring opening (pathway RO) to afford ester-functionalized urea groups (**9b**) with quantitative conversion and 85 % yield.

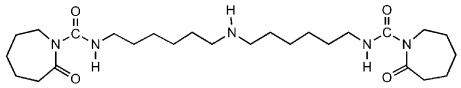


2b

The extraordinary selectivity of **1** can be used to prepare a variety of blocked isocyanates with free secondary amino groups. *N,N*-Bis(6-aminohexyl)amine reacts with a stoichio-

 © 2003 Wiley-VCH Verlag GmbH & Co. KGaA, Weinheim

metric amount of **1** to produce the novel difunctional caprolactam-blocked isocyanate **2c** (95% yield), which contains a secondary amino group.



2c

The reaction of **1** with primary and secondary alcohols and phenols is affected drastically by the type of hydroxy group and by the catalyst added (Table 2); compound **1** does not react with tertiary alcohols. In the absence of catalysts the reaction of **1** with primary and secondary alcohols (molar ratio alcohol/**1** = 2) proceeds very sluggishly by ring elimination (RE pathway, Scheme 1), as evidenced by the evolution of caprolactam and formation of urethane **10**, carbonate **5**, and *N*-alkoxycarbonyl caprolactam **3**, which is the main product. For example, heating 1-octanol with **1** for 3 h at 120 °C resulted in only 60% conversion of **1** and formation of *N*-octyloxycarbonyl caprolactam **3** as the main product (cf. entry 5 in Table 2). At 170 °C the conversion of **1** was 95% but a complex mixture of reaction products resulted, as expected for a nonselective RE reaction. The reaction of **1** with 2-octanol appeared to favor formation of *N*-alkoxycarbonyl caprolactam **3**.

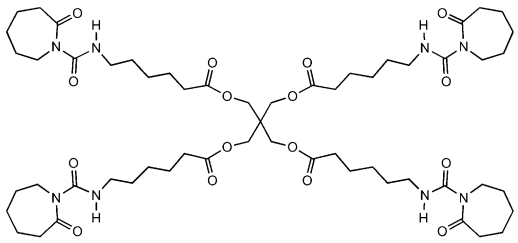
Table 2: Reactions of **1** with alcohols.[a]

Entry	ROH[a]	Catalyst		*T*	*t*	Conv.	Yield				
		Type	mol%	[°C]	[min]	**1** [%]	**3** [%]	**5** [%]	**7** [%]	**9** [%]	**11** [%]
5	1-oct	–	0	120	180	60	39	8	4	0	9
6	1-oct	–	0	170	80	95	20	52	0	0	23
7	2-oct	–	0	170	80	78	62	8	0	0	8
8	1-oct	NaOR	4	30	5	100	0	0	0	84	16
9	2-oct	NaOR	4	30	5	100	0	0	4	40	56
10	1-oct	NaOR	4	120	5	100	0	0	4	4	92
11	2-oct	NaOR	4	120	5	96	0	0	57	7	32
12	1-oct	$Zr(OR)_4$	1	120	5	100	0	8	73	3	16
13	2-oct	$Zr(OR)_4$	1	120	5	100	0	0	79	9	12
14	1-oct	$Zr(OR)_4$	1	170	5	100	0	4	12	9	75
15	2-oct	$Zr(OR)_4$	1	170	5	100	0	0	14	7	79

[a] Molar ratio alcohol/**1** = 2.

The addition of bases and acids as catalysts strongly accelerates the reaction of **1** with alcohols and switches the reaction pathway from ring elimination (RE) to ring opening (RO) with the ester-functionized *N*-carbamoyl caprolactam **7** as the product, which is also equivalent to a caprolactam-blocked isocyanate. The preferred catalysts are metal alcoholates, which are much more effective than Lewis acids. The selectivity of the base-catalyzed reactions depends upon the charge of the cation in the catalyst. Addition of sodium alcoholate, prepared in situ by reacting sodium hydride with the alcohol, promotes formation of urea **9** by twofold ring opening at 30 °C and formation of urethane **10** at elevated temperatures. Besides the temperature, the ratio alcohol/**1** also has an effect on the reaction products (see Supporting Information). If the alcohol/**1** is 2, the formation of urethane **10** by elimination of the remaining ring is favored. On the other hand, a high excess of alcohol causes the formation of urea esters **9** through ring opening. Most likely, formation of **10** results from reaction of the intermediate **7** by ring elimination before nucleophilic attack of the alcohol leads to ring opening. It should be noted that urethane formation can result from either the RO + RE or the RE + RO mechanism (Scheme 1).

In contrast to the reactions with sodium alcoholate catalysts, reactions of **1** in the presence of zirconium alcoholate proceeded mainly by onefold RO to give **7** (ca. 75% yield at full conversion of **1**) accompanied by urethane and carbonate byproduct formation. This represents a very versatile approach for converting both primary and secondary alcohols into blocked isocyanate groups. The selectivity of multivalent metal alcoholates is likely associated with formation of chelate complexes of the metal cation and **1**. Since only one lactam carbonyl group is involved in complex formation, the reactivity of the other carbonyl group can be drastically different. However, further research is required to clarify this hypothesis. Although the selectivity of reactions of **1** with alcohols to give *N*-carbamoyl caprolactams is somewhat lower than that of the reactions with primary amines, the former leads to a wide range of novel blocked isocyanates from readily available polyols. For example, pentaerythritol reacted with four equivalents of **1** to produce the carbamoyl derivative **7a** (with only 7 mol% *N*-acyl caprolactam and 4 mol% carbonate groups).



7a

In conclusion, the reaction of **1** with both primary amines and primary as well as secondary alcohols provides an isocyanate- and phosgene-free route to *N*-carbamoyl caprolactams ("blocked isocyanates"). A variety of other functional groups are tolerated. This offers attractive opportunities for polymer diversification and isocyanate-free polyurethane chemistry.[13] The caprolactam-blocked isocyanates are of interest as nontoxic and low volatile organic compound (VOC) curing agents in the coatings and adhesives industry. End-group conversion of hydroxyl- and amino-terminated oligomers produces new reactive oligomers such as *N*-carbamoyl-caprolactam-functionalized liquid rubbers. Since **1** is nontoxic it can be added during the melt processing of

 © 2003 Wiley-VCH Verlag GmbH & Co. KGaA, Weinheim

polymers. As a chain extender it can increase the molecular weights of polyesters and polyamides and improve their yarn properties without tedious solid-phase postcondensation. Due to the clean stoichiometric reactions of **1**, the formation of low volatile and toxic byproducts typically associated with diisocyanate reactions in polyurethane chemistry, can be prevented. This is also of interest for the preparation of polyurethane- and polyurea-based biodegradable polymers used in biomedical applications.

Experimental Section

1-[(2-Oxazepan-1-yl)carbonyl]azepan-2-one (**1**, CBC) was obtained from DSM and used as received (purity >99%). 1-Octylamine (Merck) and *N,N*-di(1-octyl)amine (Merck), 1-octanol (Merck), 2-octanol (Merck), methanol, and toluene were dried over molecular sieves (4 Å) before use. Zirconium tetrapropanolate was obtained from Aldrich (70 wt.% solution in 1-propanol).

Reaction of **1** with amines: Table 1, entry 1: Dry 1-octylamine (11.6 mL, 9.04 g, 70 mmol) was heated under argon to 70°C. Then **1** (8.82 g, 35 mmol) was added and the reaction mixture was stirred for 15 min at 70°C. The composition of the product mixture was determined by ^{1}H and ^{13}C NMR spectroscopy. It consisted of equimolar amounts **2a**, caprolactam, and 1-octylamine.

Reaction of **1** with alcohols: Table 2, entry 12: As a typical example, the reaction of CBC with 1-octanol at 120°C in the presence of zirconium tetraalcoholate as catalyst is described (entry 12). 1-Octanol (22.1 mL, 18.23 g, 0.14 mol) was stirred with $Zr(O\textit{n}\text{-}C_3H_7)_4$ (0.229 g, 0.7 mmol, 1 mol% with respect to **1**) for 1 h at 40°C under vacuum (oil pump). The solution was then heated under argon to 120°C and preheated 1 (17.65 g, 0.07 mol) was added. The reaction mixture was stirred for 5 min before the composition was determined by ^{1}H and ^{13}C NMR spectroscopy to be 73% (based on **1**) **7a**, 16% **10a**, 3% **9a**, and 8% **5a**. Residual **1** and **3a** were not detected.

See the Supporting Information for ^{1}H and ^{13}C NMR data.

Received: May 12, 2003 [Z51867]

Keywords: carbamates · coupling agents · polyurethane · synthetic methods

[1] CCDC 201802 (**1**) contains the supplementary crystallographic data for this paper. These data can be obtained free of charge via www.ccdc.cam.ac.uk/conts/retrieving.html (or from the Cambridge Crystallographic Data Centre, 12, Union Road, Cambridge CB21EZ, UK; fax: (+44) 1223-336-033; or deposit@ccdc.cam.ac.uk).

[2] H. R. Meyer, *Kunstst. Plast.* **1956**, *3*, 160–162.

[3] Y. Okuda, S. Mori (Ajinomoto Co., Inc.), JP-B4 42017832, **1967** [*Chem. Abstr.* **1968**, *68*, 104571].

[4] a) K. Udipi, L. R. Stebbins (Monsanto Co., USA), US 5200498, **1993** [*Chem. Abstr.* **1993**, *119*, 118157]; b) R. Mateva, O. Delev, *Polym. J.* **1995**, *27*(5), 449–460; c) R. Mateva, O. Delev, E. Kaschcieva, *J. Appl. Polym. Sci.* **1995**, *58*(13), 2333–2343.

[5] a) R. Müller, T. Wehlage, W. Trieselt, A. Oftring, E. Kappes, G. Oetter, D. Boeckh, R. Ettl, A. Hettche (BASF AG), DE-A1 19518039, **1996** [*Chem. Abstr.* **1997**, *126*, 61878]; b) T. Wehlage, D. Boeck, W. Bertleff, A. Oftring (BASF AG), US-B1 6423929, **2002** [*Chem. Abstr.* **2002**, *137*, 64939].

[6] J. A. Loontjens, B. J. M. Plum (DSM N.V.), WO-A1 9847940, **1998** [*Chem. Abstr.* **1998**, *129*, 316729].

[7] a) J. A. Loontjens, B. J. M. Plum (DSM N.V.), WO-A1 2000017169, **2000** [*Chem. Abst.* **2000**, *132*, 238426]; b) J. A. Loontjens, (DSM N.V.), WO-A1 2001040178, **2001** [*Chem. Abst.* **2001**, *135*, 20114]; c) J. A. Loontjens, R. A. T. M. van Benthem, B. J. M. Plum, J. Rietberg, (DSM N.V.), EP-A1 1132411, **2001** [*Chem. Abst.* **2001**, *135*, 228300]; d) J. A. Loontjens, B. J. M. Plum (DSM N.V.), WO-A1 2001066633, **2001** [*Chem. Abst.* **2001**, *135*, 243048]; e) J. A. Loontjens, B. J. M. Plum (DSM N.V.), WO-A2 2001066617, **2001** [*Chem. Abst.* **2001**, *135*, 242708]; f) L. J. Molhoek, J. A. Loontjens, B. M. J. Spoolder, B. J. M. Plum (DSM N.V.), EP-A1 1130039, **2001** [*Chem. Abstr.* **2001**, *135*, 228287]; g) H. Bonnard, L. Ferruccio, J.-P. Senet, P.-Y. Le Roy (SNPE), US-A1 2001044532, **2001** [*Chem. Abstr.* **2001**, *135*, 346139]; h) M. Kluge, S. Hildebrandt, N. Wagner, T. Wehlage (BASF AG), DE-A1 10105029, **2002** [*Chem. Abstr.* **2002**, *137*, 14280]; i) M. Kluge, S. Hildebrandt, N. Wagner, T. Wehlage (BASF AG), DE-A1 10105030, **2002** [*Chem. Abstr.* **2002**, *137*, 142181].

[8] H. A. Staab, *Angew. Chem.* **1962**, *74*, 407–423; *Angew. Chem. Int. Ed. Engl.* **1962**, *1*, 351–367.

[9] S. P. Rannard, N. J. Davis, *Org. Lett.* **2000**, *2*(14), 2117.

[10] a) S. Petersen, *Justus Liebigs Ann. Chem.* **1949**, *526*, 205–229; b) K. Schmitt, J. Disteldorf, F. Schmitt (Veba-Chemie AG), DE-A 2105777, **1972** [*Chem. Abstr.* **1972**, *77*, 154093]; c) H.-U. Meier-Westhues, M. Bock, W. Schultz, *Farbe Lack* **1993**, *99*(1), 9–15; d) T. Engbert, E. König, E. Jürgens, *Farbe Lack* **1996**, *102*(7), 51–58.

[11] a) D. A. Wicks, Z. W. Wicks, *Prog. Org. Coat.* **1999**, *36*, 148–172; b) D. A. Wicks, Z. W. Wicks, *Prog. Org. Coat.* **2001**, *41*, 1–83.

[12] a) E. Buhleier, W. Wehner, F. Vögtle, *Synthesis* **1978**, 155–158; b) A. W. Bosman, H. M. Janssen, E. W. Meijer, *Chem. Rev.* **1999**, *99*, 1665–1688; c) C. Wörner, R. Mülhaupt, *Angew. Chem.* **1993**, *105*, 1367–1370; *Angew. Chem. Int. Ed. Engl.* **1993**, *32*, 1306–1308.

[13] T. Loontjens, B. Scholtens, S. Maier, R. Mülhaupt, *Kunststoffe* **2002**, *92*, 83–86. English translation: T. Loontjens, B. Scholtens, S. Maier, R. Mülhaupt, *Kunststoffe Plast Europe* **2002**, *92*, 38–40.

 © 2003 Wiley-VCH Verlag GmbH & Co. KGaA, Weinheim

Cover Picture



Georg Höfner and Klaus Theodor Wanner*

Mass spectrometric methods are on the march in competitive binding studies. In pharmacological research these studies are widely used to characterize ligand–target interactions. However, they usually require the use of radioligands. Now, with the aid of mass spectrometry, it is possible to use native markers instead of radioligands. This method and its use in a binding study on dopamine D_1-receptors are described in the Communication by G. Höfner and K. T. Wanner on page 5235 ff.

Contents

Angewandte EarlyView

The following articles are available online (in Wiley InterScience). You can find them at www.angewandte.org, under Full Text, Early View.

N. Guillou, C. Livage, M. Drillon, G. Férey:*
The Chirality, Porosity, and Ferromagnetism of a 3D Nickel Glutarate with Intersecting 20-Membered Ring Channels
DOI: 10.1002/anie.200352520
Published online: October 20, 2003

F. R. Harris, S. Standridge, C. Feik, D. C. Johnson:*
Design and Synthesis of $[(Bi_2Te_3)_x(TiTe_2)_y]$ Superlattices
DOI: 10.1002/anie.200351724
Published online: October 22, 2003

M. Köhn, R. Wacker, C. Peters, H. Schröder, L. Soulere, R. Breinbauer, C. M. Niemeyer,* H. Waldmann*:*
Staudinger Ligation: A New Immobilization Strategy for the Preparation of Small-Molecule Arrays
DOI: 10.1002/anie.200352877
Published online: October 20, 2003

Articles judged by the referees or the editor as being either very important or very urgent are immediately edited, proof-read, and electronically published once the manuscript has arrived in the editorial office in final form. As long as there is no page number available these articles should be cited in the following manner:

Author(s) *Angew. Chem. Int. Ed.*, online publication date, DOI.

News

Nobel Prizes 2003: Magnetic-Resonance Imaging; Superconductors and -fluids; Ion Channels ____ **5116**

Books

Industrial Guide to Chemical and Drug Safety ____ **5117** — T. S. S. Dikshith, Prakash V. Diwan — *reviewed by B. Stock*

Photochemical Purification of Water and Air ____ **5117** — Thomas Oppenländer — *reviewed by A. M. Braun*

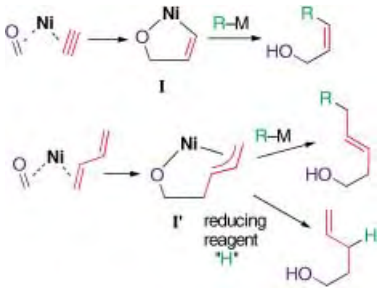
Highlights

Ni-Catalyzed Coupling Reactions

S.-i. Ikeda* ____ **5120 – 5122**

Nickel-Catalyzed Coupling of Carbonyl Compounds and Alkynes or 1,3-Dienes: An Efficient Method for the Preparation of Allylic, Homoallylic, and Bishomoallylic Alcohols

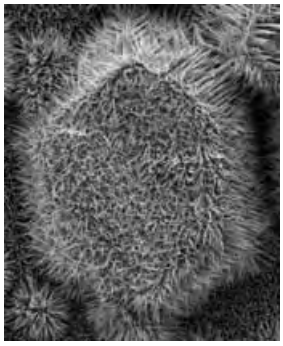
Nickel-catalyzed multicomponent coupling of carbonyl compounds with alkynes or 1,3-dienes and organometallic reagents represents an efficient route to allylic, homoallylic, and bishomoallylic alcohols with good regio-, stereo-, and enantioselectivity. The reaction proceeds via the nickelacycle species **I** or **I′** (see scheme), and not by the usual alkenylation, allylation, and homoallylation of carbonyl compounds.



 © 2003 Wiley-VCH Verlag GmbH & Co. KGaA, Weinheim

Minireviews

Lamellar inorganic compounds, in analogy with the graphitic form of carbon, are susceptible to folding forces that can lead them to adopt fullerene-like or nanotubular structures. The development of inorganic nanomaterials (such as the assembly of the single-wall MoS_2 nanotubes shown) has now reached the stage where many important applications in catalysis, lubrication, and nanotechnology are within reach.



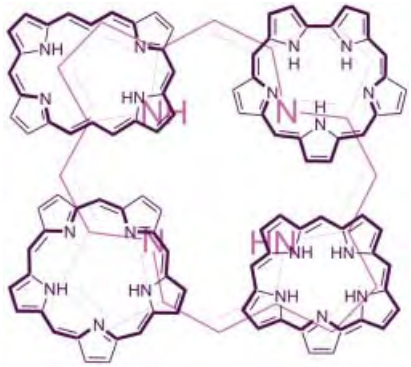
Fullerene-Like Nanomaterials

R. Tenne* ——— **5124 – 5132**

Advances in the Synthesis of Inorganic Nanotubes and Fullerene-Like Nanoparticles

Reviews

As the name implies: Expanded porphyrins, that is, larger, extended porphyrin derivatives (example shown), are fascinating synthetic additions to the world of natural tetrapyrrolic pigments. Their structural aesthetics, theoretical interest, and potential practical utility have resulted in a rapid blossoming of this field. This Review provides an overview of the latest developments, with a focus on preparative chemistry.

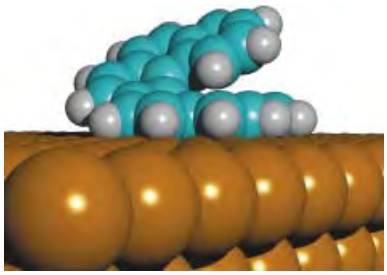


Porphyrin Chemistry

J. L. Sessler,* D. Seidel ——— **5134 – 5175**

Synthetic Expanded Porphyrin Chemistry

Communications



One hand is better than two! Chirality transfer from the single molecule into a two-dimensional layer is investigated by STM. The supramolecular handedness in homochiral heptahelicene layers, generated on a single-crystal surface (see picture), results from the orientations of next-neighbor molecules. The intermolecular interaction is dominated by steric repulsive forces between the rigid helices, causing a direct transfer of chirality.

Chirality

R. Fasel,* M. Parschau, K.-H. Ernst* ——— **5178 – 5181**

Chirality Transfer from Single Molecules into Self-Assembled Monolayers

For the USA and Canada:
ANGEWANDTE CHEMIE International Edition (ISSN 1433-7851) is published weekly by Wiley-VCH PO Box 191161, D 69451 Weinheim, Germany. Air freight and mailing in the USA by Publications Expediting Inc. 200 Meacham Ave., Elmont, NY 11003. Periodicals postage paid at Jamaica NY 11431. US POSTMASTER: send address changes to *Angewandte Chemie*, Wiley-VCH, 111 River Street, Hoboken, NJ 07030. Annual institutional subscription price for institutions: Europe € 3430.00/3118.00. Outside Europe US$ 4499.00/4090.00 (valid for print and electronic/print or electronic delivery); for individuals who are personal members of a national chemical society, or whose institution already subscribes, or who are retired or self-employed consultants, print only. Europe € 248.00/Outside Europe US$ 378.00. Postage and handling charges included. All Wiley-VCH prices are exclusive VAT.

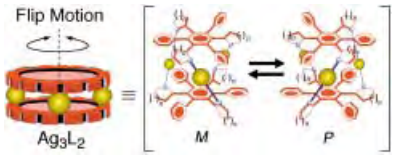
 © 2003 Wiley-VCH Verlag GmbH & Co. KGaA, Weinheim

Contents

Molecular Gears

S. Hiraoka, K. Harano, T. Tanaka, M. Shiro, M. Shionoya* ——— **5182 – 5185**

Quantitative Formation of Sandwich-Shaped Trinuclear Silver(I) Complexes and Dynamic Nature of Their *P*⇌*M* Flip Motion in Solution

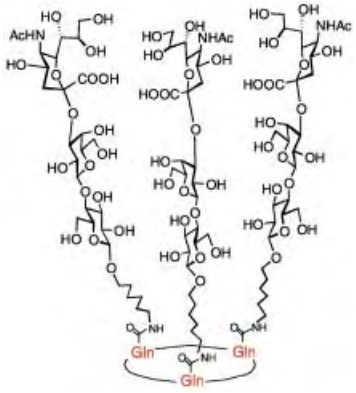


Molecular flippers: The Ag_3L_2 complexes, which are quantitatively formed from two disk-shaped tridentate ligands (thiazolyl- or pyridyl-based) and three Ag^+ ions, are helical and twist between the *P* and *M* forms (see scheme). The flip motion includes a relative 120° rotation between the two disk-shaped ligands connected by the Ag^+ ions.

Cyclic Glycopeptides

T. Ohta, N. Miura, N. Fujitani, F. Nakajima, K. Niikura, R. Sadamoto, C.-T. Guo, T. Suzuki, Y. Suzuki, K. Monde, S.-I. Nishimura* **5186 – 5189**

Glycotentacles: Synthesis of Cyclic Glycopeptides, Toward a Tailored Blocker of Influenza Virus Hemagglutinin



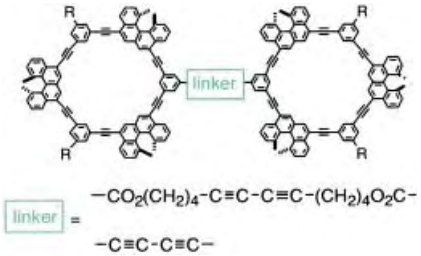
Blocking flu: A cyclic peptide, cyclo(Ser-Gly-Gly-Gln-Ser-His-Asp)$_3$, is an excellent scaffold for the synthesis of a cyclic glycopeptide carrying GM3 oligosaccharides with a potent inhibitory effect on the hemagglutination induced by the influenza virus. Tridentate binding of the gylcopeptide is shown to produce a much greater inhibitory effect than di- or monodentate binding. The shape of the glycopeptide protein scaffold, which is determined by the amino acid sequence employed, is also found to be significant in determining the inhibitory activity.

Linker-Controlled Aggregation

Y. Saiki, K. Nakamura, Y. Nigorikawa, M. Yamaguchi* ——— **5190 – 5192**

[3+3]Cycloalkyne Oligomers: Linking Groups Control Intra- and Intermolecular Aggregation by π–π Interactions

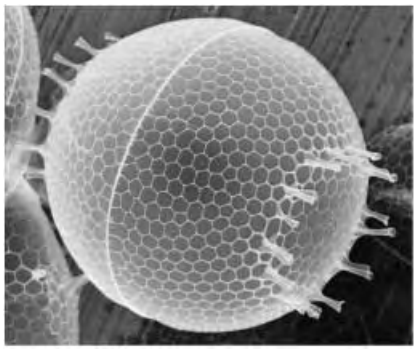
Molecules get together: Two dimeric and a trimeric [3+3]cycloalkyne (see picture) are synthesized, and their aggregation behavior in $CHCl_3$ examined by ^1H NMR spectroscopy, circular dichroism, and vapor pressure osmometry. The aggregate structure of the oligomeric [3+3]cycloalkynes can be controlled by the structures of the linker moiety.



Biomineralization

M. Sumper,* S. Lorenz, E. Brunner ——— **5192 – 5195**

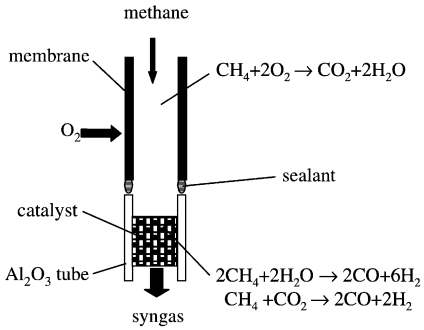
Biomimetic Control of Size in the Polyamine-Directed Formation of Silica Nanospheres



Diatom shells (see picture of cell of *Stephanopyxis turris*) contain long-chain polyamines attached either to putrescine or to phosphorylated silaffin peptides. These polyamines direct the in vitro formation of silica nanospheres from silicic acid. The concentration of multivalent anions (such as phosphate) defines the diameter of the nanospheres produced.

 © 2003 Wiley-VCH Verlag GmbH & Co. KGaA, Weinheim

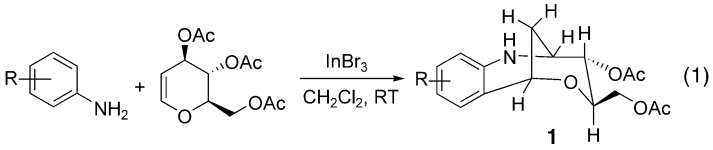
Two processes in one space: Methane, the main component of natural gas, can be converted into syngas efficiently in a two-stage oxygen-permeable ceramic membrane reactor by means of integrated oxidation and reforming processes (see picture). This could be a cheaper alternative to the current steam-reforming of methane.



Syngas Production

C.-s. Chen,* S.-j. Feng, S. Ran, D.-c. Zhu, W. Liu, H. J. M. Bouwmeester ——— **5196 – 5198**

Conversion of Methane to Syngas by a Membrane-Based Oxidation–Reforming Process



1

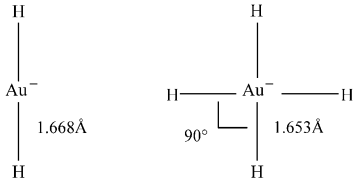
A new class of carbohydrate analogues, benzo-fused heterobicycles **1**, can be prepared by cyclization of D-glucals with aryl amines in the presence of 10 mol% indium tribromide under mild and convenient reaction conditions [Eq. (1)]. The structure and configuration of the products were established by extensive NMR experiments and molecular modeling studies.

Glycal Cyclization

J. S. Yadav,* B. V. S. Reddy, K. V. Rao, K. Saritha Raj, A. R. Prasad, S. Kiran Kumar, A. C. Kunwar, P. Jayaprakash, B. Jagannath ——— **5198 – 5201**

$InBr_3$-Catalyzed Cyclization of Glycals with Aryl Amines

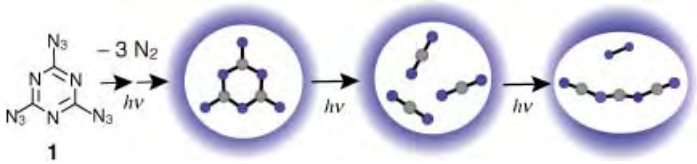
Coinage metal hydrides are stabilized by negative charge: Reactions of energized laser-ablated gold, silver, and copper with H_2 in excess argon, neon, and pure normal hydrogen during condensation at 3.5 K give the MH molecules, the $(H_2)MH$ complexes, the MH_2^- ions, and the MH_4^- ion only for gold. The stable linear MH_2^- ions are unique in that their corresponding neutral MH_2 molecules are higher in energy and thus unstable to M + H_2 decomposition.



Group 11 Hydrides

X. Wang, L. Andrews* ——— **5201 – 5206**

Gold Is Noble but Gold Hydride Anions Are Stable



1

Carbon nitride molecules: Photolysis ($\lambda = 266$ nm) of triazido-*s*-triazine (C_3N_{12}, **1**) in a nitrogen matrix at 20 K yielded a succession of reactive species (see scheme), including, in order, an apparent trinitrene, NCN, and a novel C_3N_4 isomer, dicyanocarbodiimide NC–N=C=N–CN.

Matrix Generation of C_3N_4

T. Sato,* A. Narazaki, Y. Kawaguchi, H. Niino, G. Bucher ——— **5206 – 5209**

Dicyanocarbodiimide and Trinitreno-*s*-triazine Generated by Consecutive Photolysis of Triazido-*s*-triazine in a Low-Temperature Nitrogen Matrix

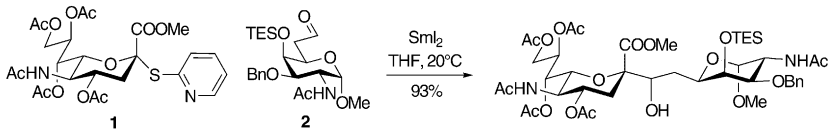
 © 2003 Wiley-VCH Verlag GmbH & Co. KGaA, Weinheim

Contents

Stereoselective C-Sialylation

Z. Abdallah, G. Doisneau, J.-M. Beau* ——— 5209 – 5212

Synthesis of a Carbon-Linked Mimic of the Disaccharide Component of the Tumor-Related SialylTn Antigen

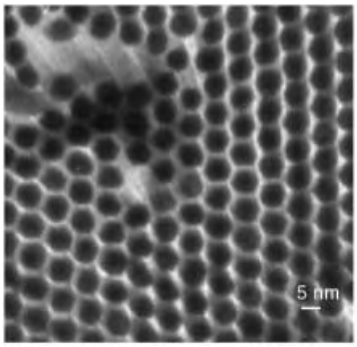


The right mix! When one considers the many ways in which a polyfunctional organometallic species may be quenched before any productive C–C bond formation can occur (two amide protons, five esters), the samarium-promoted coupling between sulfide **1** and aldehyde **2** is remarkably efficient (see scheme). This is shown in the synthesis of a stable mimic of the sialylTn (Tn = GalNAcα1→*O*-Ser/Thr) disaccharide.

Self-Assembly of Cobalt Nanorods

F. Dumestre, B. Chaudret,* C. Amiens, M. Respaud, P. Fejes, P. Renaud, P. Zurcher ——— 5213 – 5216

Unprecedented Crystalline Super-Lattices of Monodisperse Cobalt Nanorods

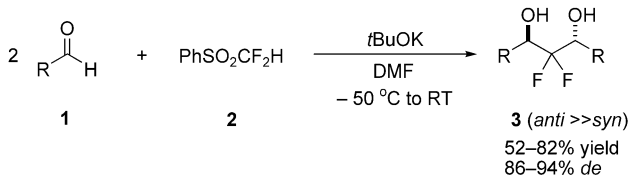


Coalescence of initially produced nanospheres inside 3D super-lattices may be the reason for the formation of ferromagnetic cobalt nanorods, monodisperse in length and diameter, from [Co(η^3-C_8H_{13})(η^4-C_8H_{12})] in the presence of stearic acid and hexadecylamine. The self-organization of these nanorods into unprecedented hexagonal 2D and 3D super-lattices has been studied by transmission electron microscopy (see picture).

Difluoromethylenation

G. K. S. Prakash,* J. Hu, T. Mathew, G. A. Olah ——— 5216 – 5219

Difluoromethyl Phenyl Sulfone as a Selective Difluoromethylene Dianion Equivalent: One-Pot Stereoselective Synthesis of *anti*-2,2-Difluoropropane-1,3-diols

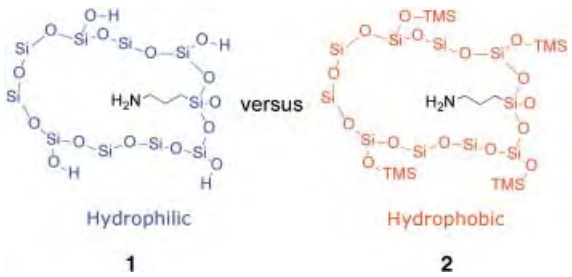


Intramolecular charge–charge repulsion rather than traditional steric control is responsible for the high diastereoselectivity (up to 94% *de*) obtained in *t*BuOK-induced difluoromethylenation of aldehydes **1** with difluoromethyl phenyl sulfone (**2**) to give symmetrical and unsymmetrical *anti*-2,2-difluoropropane-1,3-diols **3**.

Optimizing Heterogeneous Catalysts

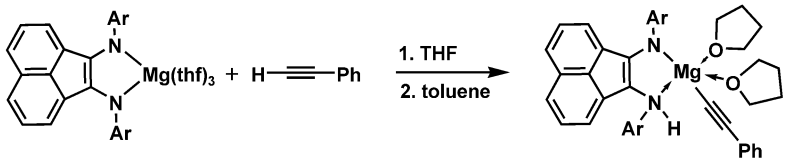
J. D. Bass, S. L. Anderson, A. Katz* ——— 5219 – 5222

The Effect of Outer-Sphere Acidity on Chemical Reactivity in a Synthetic Heterogeneous Base Catalyst



Rational outer-sphere design can be used to optimize heterogeneous catalysts. Thus, imprinting of bulk silica was used to prepare tethered active sites with hydrophilic (**1**) and hydrophobic environments (**2**). In the Knoevenagel condensation of isophthalaldehyde with malonitrile, for example, **1** gave rate enhancements of about 50 and 30 relative to **2** and a commercial catalyst consisting of a monolayer of 3-aminopropyl groups on silica, respectively.

 © 2003 Wiley-VCH Verlag GmbH & Co. KGaA, Weinheim

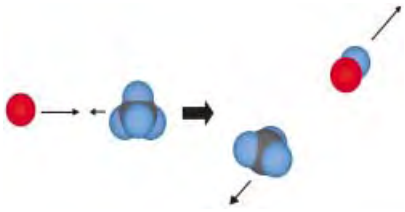


The use of a rigid bidentate ligand allows oxidative addition of an acetylene derivative to a non-transition-metal complex, not through oxidation of the metal atom, but through σ-bond metathesis from M–L: and H–C to form H–L···M–C (see scheme; Ar = 2,6-*i*Pr$_2$C$_6$H$_3$).

σ-Bond Metathesis

I. L. Fedushkin,* N. M. Khvoinova, A. A. Skatova, G. K. Fukin — **5223 – 5226**

Oxidative Addition of Phenylacetylene through C–H Bond Cleavage To Form the Mg^{II}–dpp-bian Complex: Molecular Structure of [Mg{dpp-bian(H)}(C≡CPh)(thf)$_2$] and Its Diphenylketone Insertion Product [Mg(dpp-bian)$^{\bullet-}${OC(Ph$_2$)C≡CPh}(thf)]

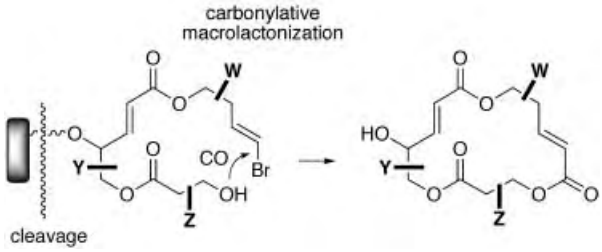


The abstraction reaction H + CD$_4$ → CD$_3$ + HD is studied at a collision energy of ~2 eV under single-collision conditions (see picture). Most of the available energy appears in product translational motion, and the CD$_3$ product is scattered sideways and backward with respect to the incident H-atom direction. This behavior is unexpected based on simple atom–diatom models.

Reaction Dynamics at a C Atom

J. P. Camden, H. A. Bechtel, R. N. Zare* — **5227 – 5230**

Dynamics of the Simplest Reaction of a Carbon Atom in a Tetrahedral Environment

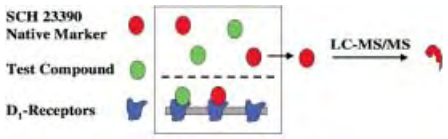


Supported total synthesis: The combinatorial synthesis of a 122-membered macrosphelide library including macrosphelides A, C, E, and F (see picture) has been achieved based on a unique strategy for a three-component coupling utilizing a palladium-catalyzed chemoselective carbonylation and an unprecedented macrolactonization on a polymer support.

A Macrosphelide Library

T. Takahashi,* S.-i. Kusaka, T. Doi, T. Sunazuka, and S. Ōmura — **5230 – 5234**

A Combinatorial Synthesis of a Macrosphelide Library Utilizing a Palladium-Catalyzed Carbonylation on a Polymer Support



MS makes it possible: Competitive binding assays are a widely used tool in drug research to characterize the affinity of a ligand for a biological target. However, these assays generally require special ligands which can be detected with high sensitivity, such as radioligands or ligands coupled to a fluorophore. Now native markers may be employed in conjunction with mass spectrometric quantification. First studies demonstrate this approach in binding experiments at dopamine D$_1$-receptors.

Binding Assays with Native Markers

G. Höfner, K. T. Wanner* — **5235 – 5237**

Competitive Binding Assays Made Easy with a Native Marker and Mass Spectrometric Quantification

 © 2003 Wiley-VCH Verlag GmbH & Co. KGaA, Weinheim

Contents

Carotenoid Aggregates

B. J. Foss, S. N. Næss, H.-R. Sliwka,* V. Partali ——— **5237 – 5240**

Stable and Highly Water-Dispersible, Highly Unsaturated Carotenoid Phospholipids—Surface Properties and Aggregate Size

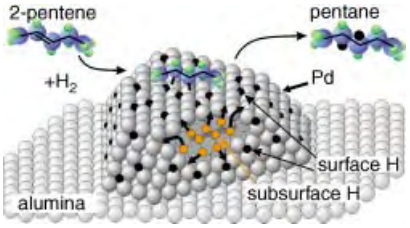


No additives are required for the study of hydrophobic carotenoids in aqueous solutions, if these compounds are present as highly unsaturated phospholipids (see structure). These compounds form small, highly water-dispersible carotenoid aggregates.

Alkene Hydrogenation

A. M. Doyle, Sh. K. Shaikhutdinov,* D. Jackson, H.-J. Freund ——— **5240 – 5243**

Hydrogenation on Metal Surfaces: Why are Nanoparticles More Active than Single Crystals?

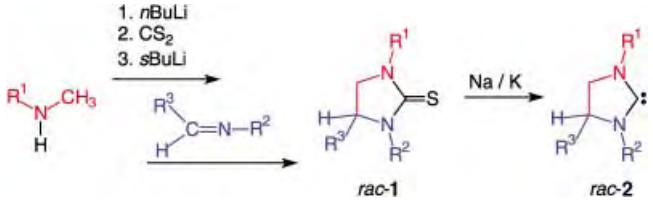


Size matters: Under low-pressure conditions, hydrogenation of alkenes, such as 2-pentene and ethene, is shown to occur on supported palladium nanoparticles, whereas single-crystal palladium surfaces are inactive. This finding is rationalized on the basis of the accessibility of weakly bound subsurface hydrogen (see picture), which is enhanced on particles of nanometer dimensions.

Stable N-Heterocyclic Carbenes

F. E. Hahn,* M. Paas, D. Le Van, T. Lügger ——— **5243 – 5246**

Simple Access to Unsymmetrically Substituted, Saturated N-Heterocyclic Carbenes



Secondary amines and imines were used to prepare unsymmetrically substituted, non-aromatic N-heterocyclic carbenes via imidazolidine-2-thiones (*rac*-**1**) as intermediates. The presence of only one sterically demanding substituent on one of the N atoms in *rac*-**2** is sufficient to prevent dimerization to the enetetramine.

VIP Communications labeled with this symbol have been judged by two referees as being "very important papers".

The publication of Communications labeled with this symbol has been accelerated because of their topical or highly competitive nature.

Deadline for recruitment adverts

47/2003	November 14	Publication date:	December 8
48/2003	November 21	Publication date:	December 15

Angewandte Chemie International Edition
Advertising Sales Department:
Marion Schulz
Phone: 0 62 01 – 60 65 65
Fax: 0 62 01 – 60 65 50
E-Mail: MSchulz@wiley-vch.de

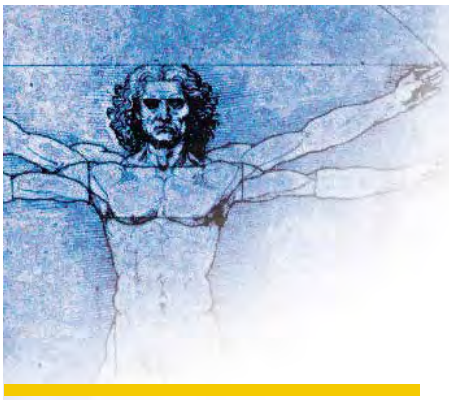
Place an advert in the printed version and have it made available online for 1 month, free of charge!

Service

Keywords ——— *5248*

Authors ——— *5249*

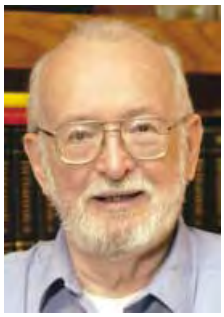
Preview ——— *5251*



Nobel Prizes 2003

Medicine/Physiology: Magnetic-Resonance Imaging

Paul C. Lauterbur and Sir Peter Mansfield have been recognized for their development of imaging techniques based on NMR spectroscopy. After studying chemistry in Cleveland (USA), Lauterbur completed his PhD in Pittsburgh (USA) and became a professor in New York (USA), then Chicago (USA), and finally Urbana-Champaign (USA). He made the discovery that two-dimensional images can be produced through the use of gradients in the magnetic field. Mansfield has a PhD in physics (Queen Mary College, University of London, 1962). His career has taken him via Illinois (USA), Nottingham (UK), and Heidelberg (Germany) back to the University of Nottingham. He advanced the gradient technique and signal processing to make possible their application in medical imaging. Imaging techniques in NMR spectroscopy were described in a Review in *Angewandte Chemie* by W. Kuhn.[1a]



P. C. Lauterbur

Both Laureates are honorary members of the Editorial Board of *Magnetic Resonance in Medicine*. Lauterbur is a co-author of the book "*Principles of Magnetic Resonance Imaging: A Signal Processing Perspective*" (Zhi-Pei Liang, Paul C. Lauterbur, Wiley-IEEE, **2001**). Contributions to NMR spectroscopy have been recognized with a Nobel Prize three times previously: to Bloch and Purcell (Physics, 1952), Ernst (Chemistry, 1991),[1b] and Wüthrich (Chemistry, 2002).[1c]

Physics: Theory of Superconductors and Superfluids

Alexei A. Abrikosov, Vitaly L. Ginzburg, and Anthony J. Leggett have been recognized for their work on the theory of superconductors and superfluids. Abrikosov completed his PhD in 1951 at the Institute for Physical Problems in Moscow (Russia) and has worked at the Argonne National Laboratory in Illinois (USA) since 1991. He formulated a theoretical explanation for type-II superconductivity.[2] His starting point was a theory that Ginzburg (Russian Academy of Sciences in Moscow) and others had devised for type-I superconductors, which in turn built on work by Lev Landau (Nobel Prize in Physics, 1962). These theories have gained new relevance as a result of the rapid development of new materials. As de Gennes (Nobel Prize in Physics, 1991)[3] showed, an analogy exists between superconductors and liquid crystals, and the Landau–Ginzburg approach can also be used for the latter. The Nobel Prize in Physics was also awarded in 1913 (Kamerlingh Onnes), 1972 (Bardeen, Cooper, and Schrieffer), and 1987 (Bednorz and Müller)[4] for contributions in the field of superconductivity.

Leggett studied physics in Oxford (UK; PhD 1964) and took up his current position at the University of Illinois in Urbana-Champaign in 1983, following a relatively long period of research and teaching at the University of Sussex (UK). In the 1970s he formulated a theory on interaction and order in superfluids.

Chemistry: Channels in Cell Membranes

The Nobel Prize in Chemistry has been awarded to Peter Agre (Johns Hopkins University Medical School, Baltimore, USA) for the discovery of water channels (aquaporins) and Roderick MacKinnon (Howard Hughes Medical Institute, The Rockefeller University, New York, USA) for the elucidation of the structure of ion channels and the transport mechanism involved. Peter Agre studied chemistry and completed his PhD in 1974 at Johns Hopkins University, where he works today. He has also held positions at universities in Cleveland and Chapel Hill (USA). In 1988 he isolated a membrane protein that he recognized as the long-sought-after water channel.



R. MacKinnon

Roderick MacKinnon studied biochemistry and medicine. It was not until 1986 that he decided to embark on a career in research, which he began at Brandeis University near Boston (USA). He moved as a professor to Harvard University (Boston) in 1996. In 1998 he succeeded in determining the spatial structure of a potassium channel. A Highlight on his latest work will appear soon in *Angewandte Chemie*. The Nobel Prize in Medicine for 1991 was also awarded for work on ion channels, in particular for the development of the patch-clamp technique, to E. Neher and B. Sakmann (Max-Planck-Institut in Göttingen and Heidelberg (Germany), respectively).[5]



P. Agre

Photos: KVA, Stockholm (RM, PA), B. Wiegand, UIUC (PL)

[1] a) W. Kuhn, *Angew. Chem.* **1990**, *102*, 1; *Angew. Chem. Int. Ed. Engl.* **1990**, *29*, 1; b) R. R. Ernst, *Angew. Chem.* **1992**, *104*, 817; *Angew. Chem. Int. Ed. Engl.* **1992**, *31*, 805; c) K. Wüthrich, *Angew. Chem.* **2003**, *115*, 3462; *Angew. Chem. Int. Ed.* **2003**, *42*, 3340.

[2] A. Abrikosov, *Phys. Bl.* **2001**, 61.

[3] P.-G. de Gennes, *Angew. Chem.* **1992**, *104*, 856; *Angew. Chem. Int. Ed. Engl.* **1992**, 31, 842.

[4] a) H. Müller-Buschbaum, *Angew. Chem.* **1989**, *101*, 1503; *Angew. Chem. Int. Ed. Engl.* **1989**, *28*, 1472; b) A. Simon, *Angew. Chem.* **1997**, *109*, 1872; *Angew. Chem. Int. Ed. Engl.* **1997**, *36*, 1788.

[5] a) E. Neher, *Angew. Chem.* **1992**, *104*, 837; *Angew. Chem. Int. Ed. Engl.* **1992**, *31*, 824; b) B. Sakmann, *Angew. Chem.* **1992**, *104*, 856; *Angew. Chem. Int. Ed. Engl.* **1992**, *31*, 841.

 © 2003 Wiley-VCH Verlag GmbH & Co. KGaA, Weinheim

Ni-Catalyzed Coupling Reactions

Nickel-Catalyzed Coupling of Carbonyl Compounds and Alkynes or 1,3-Dienes: An Efficient Method for the Preparation of Allylic, Homoallylic, and Bishomoallylic Alcohols

*Shin-ichi Ikeda**

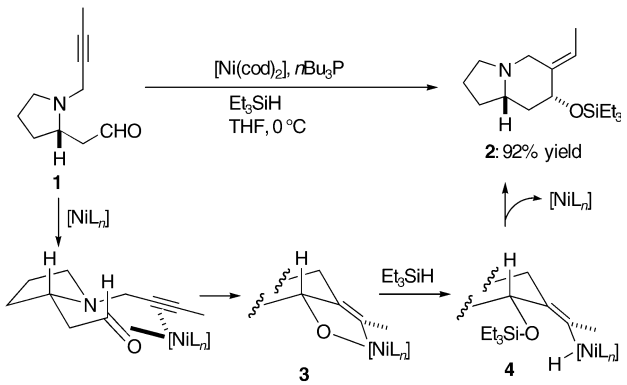
Keywords:
alcohols · C—C coupling · catalysis · multicomponent reactions · nickel

The alkenylation, allylation, and homoallylation of carbonyl compounds, which gives allylic, homoallylic, and bishomoallylic alcohols, respectively, are important processes in the formation of carbon–carbon bonds. However, in these approaches, the preparation of the corresponding alkenylating, allylating, and homoallylating reagents, which often requires troublesome procedures, is unavoidable.[1–5] Recently, new nickel-catalyzed coupling reactions of a carbonyl compound (e.g., aldehyde or ketone) and an unsaturated substrate (e.g., alkyne or 1,3-diene) with an organometallic or metal hydride have been reported, and these offer more efficient methods to give the desired alcohols without the in situ generation of alkenylating, allylating, and homoallylating reagents.

Montgomery et al. developed the nickel-catalyzed inter- and intramolecular three-component coupling of aldehydes and alkynes with organozinc reagents to produce tri- or tetrasubstituted allylic alcohols with regio- and stereoselectivity.[6a,b] For the preparation of a bicyclic nitrogen heterocycle, the catalytic system of $[Ni(cod)_2]$ and nBu_3P is highly effective for the Et_3SiH-mediated reductive cyclization of alkynes (e.g., **1**), which possess a tethered aldehyde group. This process leads to the construction of an alkaloid framework, such as **2** (Scheme 1).[6c,d] The reaction proceeds via an oxanickelacycle intermediate **3**, which is derived from the oxidative cyclization of a Ni^0 complex with the aldehyde and alkyne units of **1**. The oxanickelacycle **3** reacts with Et_3SiH to produce species **4**, which then undergoes reductive elimination to give **2**. This method allows for direct introduction of the allylic alcohol unit, with the completely stereoselective introduction of an exocyclic carbon–carbon double bond.

Jamison and co-workers developed the intermolecular reductive coupling of internal alkynes and aldehydes (which was not possible with the Montgomery method[6b]) by using Et_3B as a reducing agent.[7a] This reaction is performed in the presence of $[Ni(cod)_2]$ and nBu_3P in THF or toluene, and gives trisubstituted allylic alcohols via an oxanickelacycle. The same group recently reported the enantioselective reductive coupling of aldehydes and alkynes using Et_3B (Scheme 2).[7b,c] When (+)-(neomenthyl)diphenylphosphane (NMDPP) is treated as a chiral ligand in this catalytic reaction, which was carried out in a solvent composed of equal volumes of EtOAc and 1,3-dimethyl-2-imidazolidinone (DMI), a trisubstituted allylic alcohol is obtained in 96% *ee* with high regio- and stereoselectivity. The high enantioselectivity provided by NMDPP in the reaction can be explained by a cooperative effect between the steric properties of the ligand and the electronic differences of the alkyne substituents.

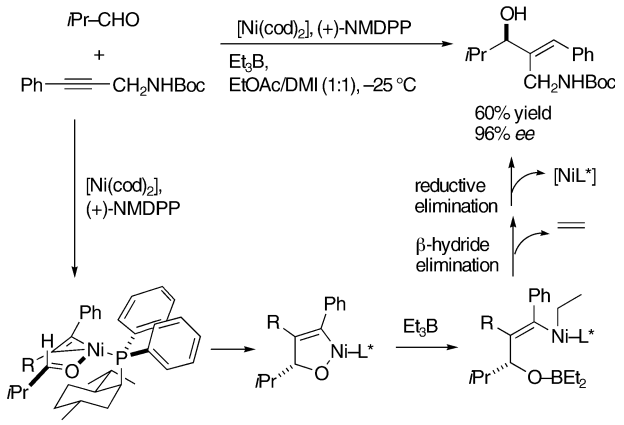
Mori et al. developed the nickel-catalyzed cyclization of 1,3-dienes **5**, which possess a tethered aldehyde group (Scheme 3).[8] Treatment of **5** with diisobutylaluminium acetylacetonate ($[iBu_2Al(acac)]$) in the presence of a



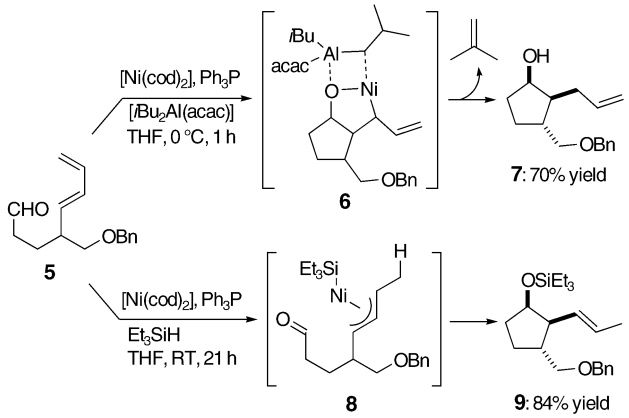
Scheme 1. Nickel-catalyzed reductive cyclization of aldehyde-functionalized alkyne **1** (L = nBu_3P).

[*] Dr. S. Ikeda
Graduate School of Pharmaceutical Sciences
Nagoya City University
Tanabe-dori, Mizuho-ku
Nagoya 467-8603 (Japan)
Fax: (+81) 52-836-3462
E-mail: ikeshin@phar.nagoya-cu.ac.jp

 © 2003 Wiley-VCH Verlag GmbH & Co. KGaA, Weinheim DOI: 10.1002/anie.200301673



Scheme 2. Nickel-catalyzed enantioselective reductive coupling of an aldehyde and an alkyne using Et_3B (R = CH_2NHBoc, L* = (+)-NMDPP).

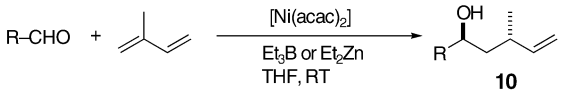


Scheme 3. Nickel-catalyzed reductive cyclization of **5,** a 1,3-diene with a tethered aldehyde group, and [iBu_2Al(acac)] or Et_3SiH.

catalytic amount of [Ni(cod)$_2$] and Ph_3P in THF at 0 °C yields **7**, which has a terminal alkene group.[8b] The reaction proceeds via the transmetalation of an oxanickelacycle intermediate **6**, which is derived from a Ni^0 complex with the aldehyde and diene units of **5** and [iBu_2Al(acac)]. Interestingly, when the reaction was performed with Et_3SiH instead of [iBu_2Al(acac)], compound **9** with an internal alkene group was obtained.[8b,c] In the cyclization, **5** reacts with a nickel hydride complex, which is formed by the oxidative addition of Et_3SiH to the Ni^0 complex, to produce a π-allyl nickel intermediate **8**. Allylation of the π-allyl nickel moiety in **8** to the tethered aldehyde yields **9**. These cyclizations complement each other to afford **7** (via an oxanickelacycle–transmetalation process) or **9** (via a standard allylation process) using the same catalytic system ([Ni(cod)$_2$] and Ph_3P) depending on the different reducing reagents ([iBu_2Al(acac)] or Et_3SiH) that are employed.

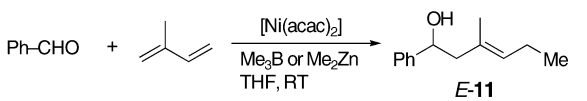
For the intermolecular reaction with 1,3-diene, Baker and Crimmin reported the nickel-catalyzed or -promoted coupling with aldehydes to give homoallyl alcohols as a mixture of 1:1, 2:1, and 3:1 adducts of the diene and aldehyde, each of which consisted of many possible regio- and stereoisomers.[9] Tamaru et al. have since developed the regio- and stereoselective nickel-catalyzed coupling of carbonyl compounds and 1,3-dienes using organoboron or organozinc reagents.[10] Thus, isoprene is treated with aldehyde and Et_3B in the presence of [Ni(acac)$_2$] in THF at room temperature to provide the 1:1 adduct of the diene and aldehyde exclusively (Scheme 4).[10b] The reaction formally corresponds to a reductive coupling of the C1–C2 double bond of isoprene and the carbonyl group of the aldehyde, where Et_3B acts as a reducing agent, to give the bishomoallylic alcohol **10**, and not the homoallylic alcohol. Moreover, the reaction exhibits high 1,3-asymmetric induction, to provide 1,3-*anti*-**10** in preference to 1,3-*syn*-**10**. The use of Et_2Zn instead of Et_3B is particularly effective for the reaction of saturated aldehydes and ketones, where the latter reagent is unsuccessful.[10c] In contrast, coupling with Me_2Zn or Me_3B led to the formation of homoallylic alcohols **11** (Scheme 5).[10d,e]

Carbon–carbon bond formation is a fundamental process in synthetic organic chemistry. Therefore, multicomponent reactions, which permit complex molecules to be reasonably well constructed in a single operation, are fascinating processes. The nickel-catalyzed multicomponent couplings highlighted here bring about the *formal* alkenylation, allylation, and homoallylation of carbonyl compounds via the transmetalation of an oxanickelacycle intermediate with organometallic reagents. The analogous nickelacycle derived from enones and unsaturated substrates leads to a different multicomponent coupling.[6a,11]

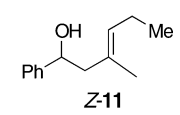


R	with Et_3B		with Et_2Zn	
	t	yield (*syn*:*anti*)	*t*	yield (*syn*:*anti*)
2-furanyl	22 h	77% (1 : >20)	1 h	66% (1 : 3)
cyclohexyl	10 h	28% (–)	0.5 h	83% (1 : >20)

Scheme 4. Nickel-catalyzed reductive coupling of an aldehyde and a 1,3-diene using Et_3B or Et_2Zn.



	yield (*E*:*Z*)
with Me_3B	56% (20 : 1)
with Me_2Zn	92% (2.2 : 1)



Scheme 5. Nickel-catalyzed coupling of an aldehyde and a 1,3-diene using Me_3B or Me_2Zn.

© 2003 Wiley-VCH Verlag GmbH & Co. KGaA, Weinheim

[1] a) H. Jin, J.-i. Uenishi, W. J. Christ, Y. Kishi, *J. Am. Chem. Soc.* **1986**, *108*, 5644; b) K. Takai, M. Tagashira, T. Kuroda, K. Oshima, K. Utimoto, H. Nozaki, *J. Am. Chem. Soc.* **1986**, *108*, 6064.

[2] a) W. Oppolzer, R. N. Radinov, *Helv. Chim. Acta* **1992**, *75*, 170; b) W. Oppolzer, R. N. Radinov, *J. Am. Chem. Soc.* **1993**, *115*, 1593.

[3] a) P. Wipf, W. Xu, *Tetrahedron Lett.* **1994**, *35*, 5197; b) P. Wipf, S. Ribe, *J. Org. Chem.* **1998**, *63*, 6454.

[4] Y. Yamamoto, A. Asao, *Chem. Rev.* **1993**, *93*, 2207.

[5] H. Yasuda, K. Tatsumi, A. Nakamura, *Acc. Chem. Res.* **1985**, *18*, 120.

[6] a) J. Montgomery, *Acc. Chem. Res.* **2000**, *33*, 467; b) E. Oblinger, J. Montgomery, *J. Am. Chem. Soc.* **1997**, *119*, 9065; c) X.-Q. Tang, J. Montgomery, *J. Am. Chem. Soc.* **1999**, *121*, 6098; d) X.-Q. Tang, J. Montgomery, *J. Am. Chem. Soc.* **2000**, *122*, 6950; e) For the preparation of homoallylic alcohols by cyclization of allenes with a tethered aldehyde: J. Montgomery, M. Song, *Org. Lett.* **2002**, *4*, 4009.

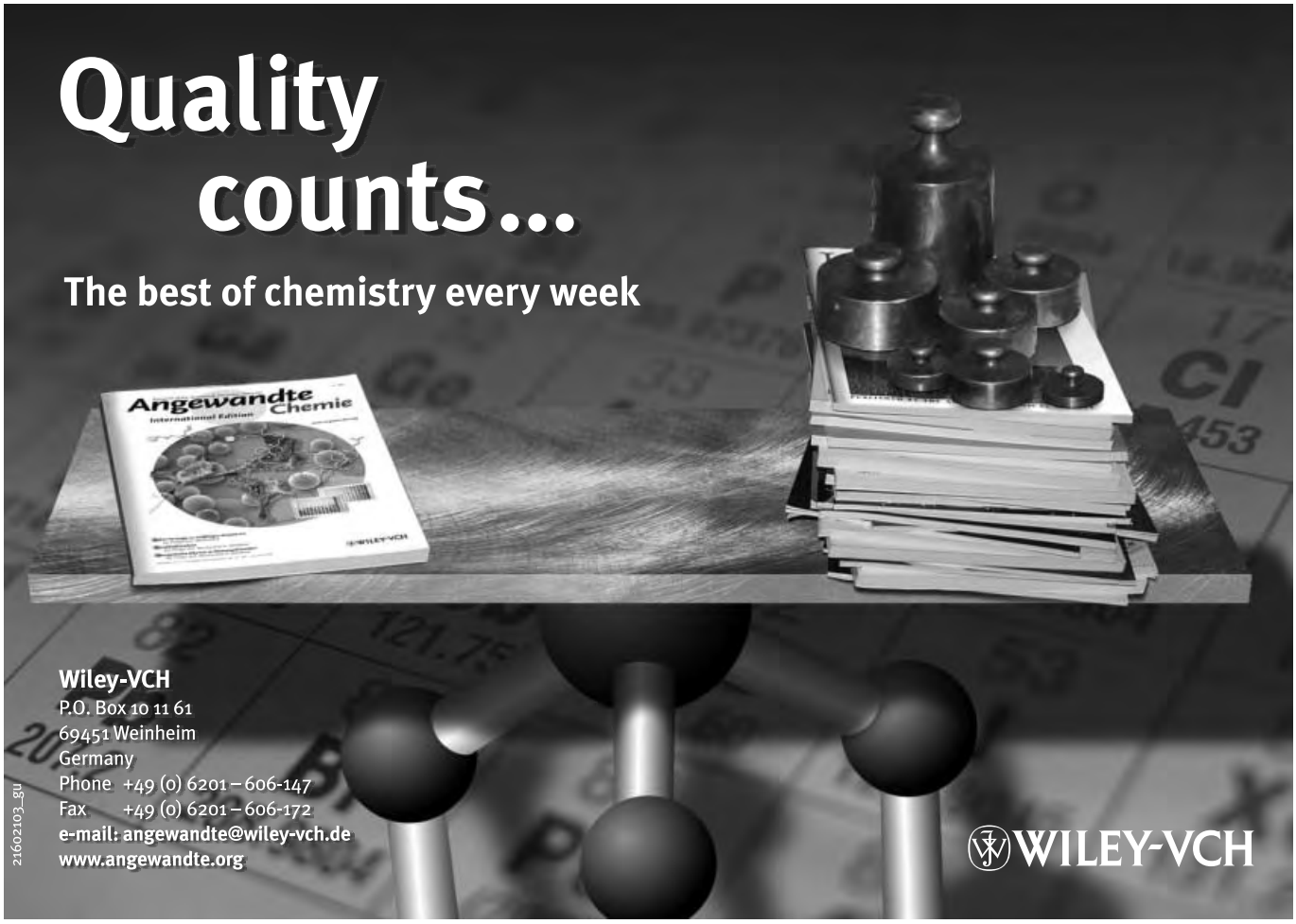
[7] a) W.-S. Huang, J. Chan, T. F. Jamison, *Org. Lett.* **2000**, *2*, 4221; b) E. A. Colby, T. F. Jamison, *J. Org. Chem.* **2003**, *68*, 156; c) K. M. Miller, W.-S. Huang, T. F. Jamison, *J. Am. Chem. Soc.* **2003**, *125*, 3442; d) S. J. Patel, T. F. Jamison, *Angew. Chem.* **2003**, *115*, 1402; *Angew. Chem. Int. Ed.* **2003**, *42*, 1364.

[8] a) Y. Sato, M. Takimoto, M. Mori, *J. Synth. Org. Chem. Jpn.* **2001**, *59*, 576, and references therein; b) Y. Sato, M. Takimoto, M. Mori, *J. Am. Chem. Soc.* **2000**, *122*, 1624; c) Y, Sato, M. Takimoto, K. Hayashi, T. Katsuhara, K. Takagi, M. Mori, *J. Am. Chem. Soc.* **1994**, *116*, 9771.

[9] R. Baker, M. J. Crimmin, *J. Chem. Soc. Perkin Trans. 1* **1979**, 1264.

[10] a) Y. Tamaru, *J. Organomet. Chem.* **1999**, *576*, 215; b) M. Kimura, A. Ezoe, K. Shibata, Y. Tamaru, *J. Am. Chem. Soc.* **1998**, *120*, 4033; c) M. Kimura, H. Fujimatsu, A. Ezoe, K. Shibata, M. Shimizu, S. Matsumoto, Y. Tamaru, *Angew. Chem.* **1999**, *111*, 410; *Angew. Chem. Int. Ed.* **1999**, *38*, 397; d) M. Kimura, S. Matsuo, K. Shibata, Y. Tamaru, *Angew. Chem.* **1999**, *111*, 3586; *Angew. Chem. Int. Ed.* **1999**, *38*, 3386; e) M. Kimura, K. Shibata, Y. Koudahashi, Y. Tamaru, *Tetrahedron Lett.* **2000**, *41*, 6789.

[11] a) S. Ikeda, *Acc. Chem. Res.* **2000**, *33*, 511; b) S. Ikeda, H. Miyashita, M. Taniguchi, H. Kondo, M. Okano, Y. Sato, K. Odashima, *J. Am. Chem. Soc.* **2002**, *124*, 12060.



Fullerene-Like Nanomaterials

Advances in the Synthesis of Inorganic Nanotubes and Fullerene-Like Nanoparticles

*Reshef Tenne**

Keywords:
fullerenes · inorganic nanotubes · nanomaterials · nanotubes

In analogy to graphite, nanoparticles of inorganic compounds with lamellar two-dimensional structure, such as MoS_2, are not stable against folding, and can adopt nanotubular and fullerene-like structures, nicknamed inorganic fullerenes or IF. Various applications for such nanomaterials were proposed. For instance, IF-WS_2 nanoparticles were shown to have beneficial effects as solid lubricants and as part of tribological surfaces. Further applications of IF for high-tensile-strength fibers, hydrogen storage, rechargeable batteries, catalysis, and in nanotechnology are being contemplated. This Minireview highlights some of the latest developments in the synthesis of inorganic nanotubes and fullerene-like structures. Some structural aspects and properties of IF, which are distinct from the bulk materials, are briefly discussed.

1. Introduction

The quest for novel nanomaterials is not new, although the recent "nano" rush has put more emphasis on the search for new materials with crystallite sizes of less than 0.1 μm along one of their axes. Papers describing, for example, whiskers with diameters of 10–100 nm had already appeared in the early 1960s, and even earlier. In fact, the limiting factor in these early studies was the resolving power of the electron microscopes used for the analysis of the products, which were developed and commercialized at about this period of time. However, the main issue here is whether the reduced dimensions of the nanoparticles lead to the appearance of a new crystal motif, or perhaps a new physical phenomenon, which does not exist in materials with larger grain sizes. The ubiquitous quantum-size effect and enhanced oscillator strength for optical transitions in semiconductor nanocrystals is a case in point. The loss of superconductivity of lead nanoparticles with dimensions below the correlation length of the Cooper pair (ca. 30 nm) is another recent observation.[1]

[*] Prof. Dr. R. Tenne
Department of Materials and Interfaces
Weizmann Institute
76100 Rehovot (Israel)
Fax: (+972) 8-934-4138
E-mail: reshef.tenne@weizmann.ac.il

Obviously, when the size of the crystallites shrinks beyond the "nano" size many atoms become part of the crystallite surface, rather than being fully bonded "bulk" atoms. Surface atoms are distinguished by their reduced coordination to the crystal backbone. Hence, they are more prone to react with the surrounding ambient or to exhibit other unusual physical phenomena. Surface conductivity and electronic surface states in semiconductor nanoparticle films,[2] enhanced photocatalytic reactivity in TiO_2 nanoparticles,[3] superparamagnetism in magnetic nanoparticles,[4] superhard coatings of metal alloys,[5] are all among the documented phenomena of nanophases.

Nanotechnologies depend critically on our ability to synthesize new nanostructured materials of a controlled size and shape, and to search for new observations that could not be realized with the bulk materials. In this context, inorganic nanotubes and inorganic fullerene-like materials do not merely display new crystalline order, but they also exhibit new phenomena, which can not be engendered by their bulk analogues.

Layered (2D) compounds, like graphite or MoS_2, are typified by their very anisotropic character. The atoms within the layer (*ab* plane) are covalently bonded like, for instance, the sp^2-bonded carbon atoms in the honeycomb lattice of graphite. These molecular slabs are stacked together by weak van der Waals forces along the *c* axis (Figure 1). While the carbon atoms within each sheet (graphene layer) are fully coordinated and hence are unreactive, the atoms at the periphery of the layer are only dicoordinated, and are consequently very reactive. Therefore, the surface energy of graphene layers no larger than a few nanometers in diameter

 © 2003 Wiley-VCH Verlag GmbH & Co. KGaA, Weinheim DOI: 10.1002/anie.200301651

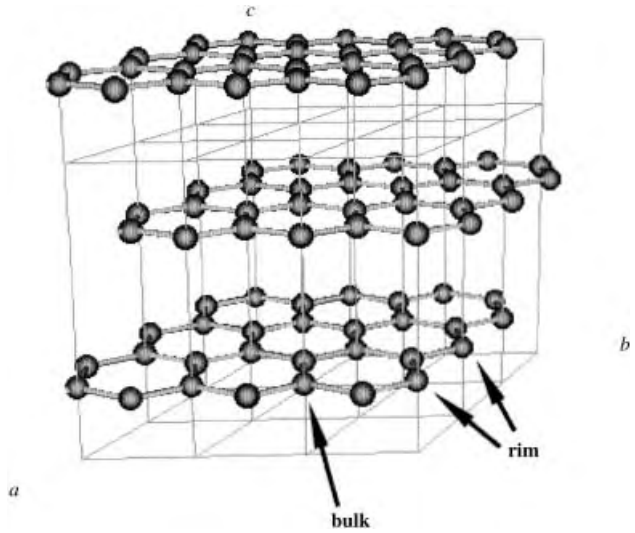


Figure 1. A schematic drawing of graphite. The surface energy, which destabilizes the planar topology of the nanocluster, is concentrated in the dicoordinated carbon atoms on the rim of the lamella.

is exceedingly high, which makes the sheet unstable with respect to folding and forces it to close onto itself. For that to happen along two axes in the *ab* plane, 12 pentagons are disposed in the hexagonal network and carbon fullerenes are obtained. If the folding of the graphene layer occurs along one axis only, nanotubes are formed. The folding process induces elastic strain, which requires the surmounting of an activation energy barrier. Therefore heating the reactor, or using other energy sources, such as various kinds of irradiation, is necessary to initialize the folding process. Once the fullerene-like nanoparticle is realized and the dangling bonds are healed, the seamless structure becomes (meta)stable.

It was first shown in 1992 that this instability is not unique to carbon, and transcends to other inorganic compounds with a layered (2D) structure, like WS_2 and MoS_2 and their respective selenides.[6,7] Here, metal atoms on the rim of the nanocluster are only tetracoordinated, in contrast to the hexacoordinated bulk metal atoms. Likewise, the sulfur atoms in the periphery of the nanocluster are only dicoordinated, while bulk sulfur atoms exhibit threefold coordination, as shown schematically in Figure 2. As an example of such nanostructures, Figure 3 shows a high-resolution transmission



Reshef Tenne was born in 1944 in Kibbutz Usha and received his PhD in 1976 (Hebrew University, Jerusalem). After postdoctoral work at the Battelle Institute (Geneva), he joined the Weizmann Institute in 1979, where he was promoted to Associate Professor with tenure (1985), then full Professor (1995). He heads the Department of Materials and Interfaces at the Weizmann Institute of Science, and is the director of the G. Schmidt Minerva Center for Supramolecular Chemistry. He has served in numerous national and international bodies and is a member of the editorial boards of a number of journals.

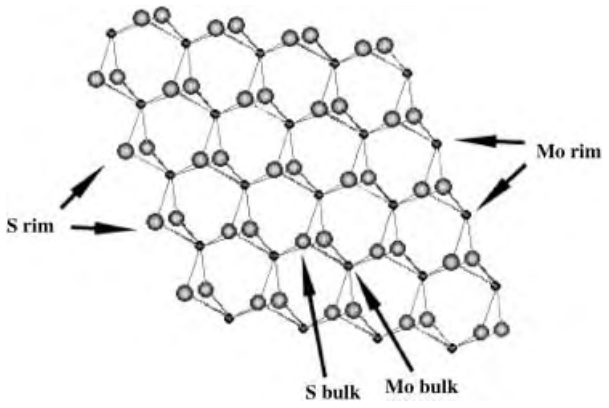


Figure 2. A schematic drawing of an MoS_2 nanocluster showing the Mo and S rim atoms with their dangling bonds.

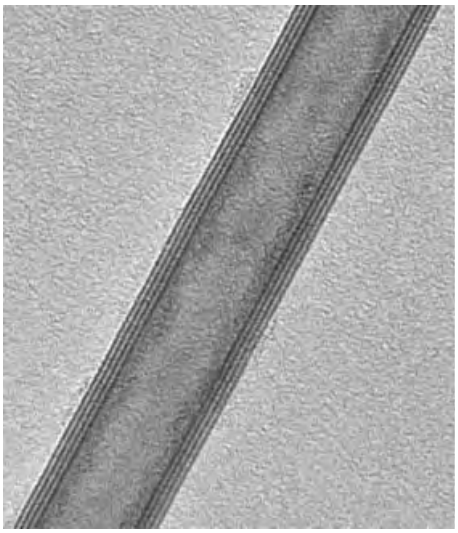


Figure 3. TEM micrograph of a WS_2 nanotube.

electron microscopy (HRTEM) image of the edge of a typical WS_2 nanotube. These new (nano)materials received the generic name "inorganic fullerene-like structures" and "inorganic nanotubes", abbreviated to "IF". Later, nanotubes and fullerene-like structures of other layered compounds such as BN,[8] V_2O_{5-x},[9] $NiCl_2$,[10] and many others were prepared. Most recently, nanotubes of most other layered MX_2 (M = transition metal; X = S, Se) compounds with hexagonal symmetry ($P6_3/mmc$ space group), for example, NbS_2[11] and ZrS_2[12] were synthesized. Single-wall (3,3) MoS_2 nanotubes were obtained and were shown to self-assemble into a hierarchy of structures up to a macroscopic size.[13] The fact that IF nanostructures of the same 2D compound can be synthesized using different precursors and different synthetic routes indicates that these nanophases are indeed thermodynamically stable, given the single constraint that the number of atoms in such nanostructures is not allowed to grow beyond a certain amount, at least along one axis of the lamella. This idea is also supported by ab initio and continuum theoretical calculations, and recent thermal analysis of the IF-MS_2 phases. Obviously, inorganic nanotubes of 2D compounds

 © 2003 Wiley-VCH Verlag GmbH & Co. KGaA, Weinheim

lack the translation periodicity of a 3D crystal. Nevertheless, they can be synthesized with a high degree of perfection, and therefore they are considered here as a crystalline material.

As stated earlier, one of the driving forces for developing nanotechnology is the search for new applications. Various applications have been proposed for the IF nanostructures, the most prominent among them is in the field of tribology (wear and friction prevention),[14] which is well on its way to being commercialized. In this Minireview the recent progress in the solid-state synthesis of IF nanostructures, and some of the latest observations and proposed applications for these novel materials are outlined.

2. Recent Progress with the Solid-State Synthesis of IF Materials

The synthesis and some properties of inorganic nanotubes have been reviewed in recent papers.[15,16] This Minireview is aimed at updating the reader and illuminating various other aspects of the synthesis of these fascinating nanostructures. Among the numerous inorganic nanotubes existing to date, those synthesized from metal dichalcogenide compounds and boron nitride have been investigated to the greatest detail.

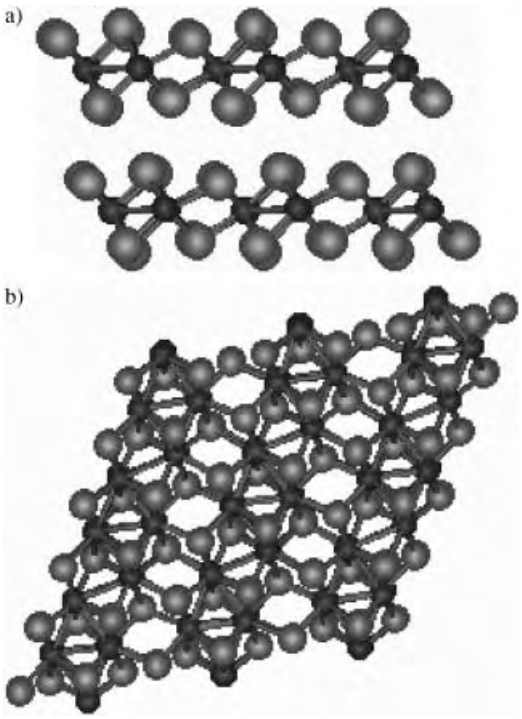


Figure 4. Depiction of a double ReS_2 layer a) side view; b) top view (Courtesy of Dr. J. Sloan).

2.1. Metal Dichalcogenides

The syntheses of ReS_2 nanotubes and related closed nanostructures were recently reported.[17,18] In contrast to other 2D MX_2 compounds (X = S, Se, Cl, I), which have a hexagonal symmetry and only exhibit metal to nonmetal bonds, the layered ReS_2 consists of repeating Re_4 parallelogram motifs with covalent bonds linking neighboring metal atoms, in addition to the ubiquitous metal to nonmetal bonds (Figure 4). This arrangement of the atoms in the lattice reduces the symmetry of the compound to a monoclinic $P\bar{1}$. ReS_2 is a semiconductor, which makes its IF nanostructures interesting for a host of potential applications in photocatalysis, nanotechnology, and more.

Although the precursors for the synthesis of the IFs appear to be different in both studies, in reality they may not be that disparate. In the first study,[17] the authors use a strategy similar to that of Tenne and co-workers for the synthesis of IF-WS_2 (IF-MoS_2),[19,20] that is, sulfidization of ReO_2 nanoparticles at elevated temperatures (700 °C). In the first step, which lasts a few seconds, the surface of the oxide nanoparticle is encapsulated by a single or double ReS_2 closed layer, which isolates this particular nanoparticle from the remainder, and thereby prevents the fusion of the nanoparticles into a larger particle. It is therefore crucial that until this process is complete, the nanoparticles remain isolated from each other, thus making a fluidized bed reactor a desirable strategy for scaling up this synthesis.[21] Once this rapid process is over, a slow, diffusion-controlled process takes over, in which sulfur diffuses in, and oxygen diffuses out of the cores of the nanoparticles. In the case of IF-WS_2, the specific gravity of the starting material (WO_3) is lower than that of the product, thus leaving a hollow core of about 10% in the center of the nanoparticles. However, the specific gravity of the starting ReO_2 powder is appreciably higher than that of the end product (IF-ReS_2). Since the out-diffusion of rhenium during sulfidization is not likely, the core of the IF nanoparticles is not expected to be hollow at the end of the reaction, as is indeed the case (Figure 5). In fact, the reaction may cease as a result of a build-up of internal pressure, which results from the differences in the specific gravity between the oxide and the sulfide compounds.

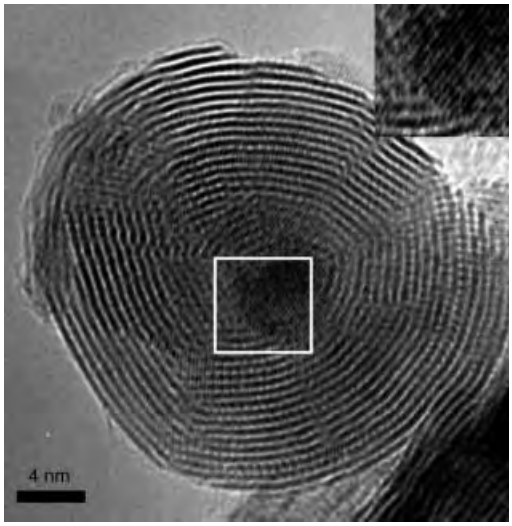


Figure 5. HRTEM micrograph showing a small ReS_2 particle encapsulating a ReO_2 nanoparticle at its core. The 0.29-nm lattice fringes (inset) correspond to the ReO_2 {111} planes.

 © 2003 Wiley-VCH Verlag GmbH & Co. KGaA, Weinheim

In the second report,[18] multiwall carbon nanotubes (MWCNTs) were used as a template for the synthesis of ReS_2 nanotubes. Here, a solution of a rhenium salt was sonicated together with the MWCNTs; the slurry was dried and subsequently sulfidized at 1000 °C. Figure 6 shows a high-resolution image of a coaxial multiwall ReS_2/carbon nanotube obtained in this manner. Since epitaxial relationship between the atomic layers of graphite and ReS_2 is not possible, the templating effect of the underlying MWCNT is not perfect, and numerous defects are observed in the ReS_2 nanotubes. Two kinds of precursors have been used in this reaction; an aqueous solution of NH_4ReO_4 and an ethanolic solution of $ReCl_3$. The fact that both solutions lead to the synthesis of similar nanotubes suggests that the product of the sonication could have been a thin ReO_3 (ReO_2) film, which enfolded the nanotubes and was converted to ReS_2 upon reaction with H_2S at 1000 °C. Unfortunately, the chirality of the ReS_2 nanotubes, which could have shed some light on the growth mechanism, was not reported in the this study.[18]

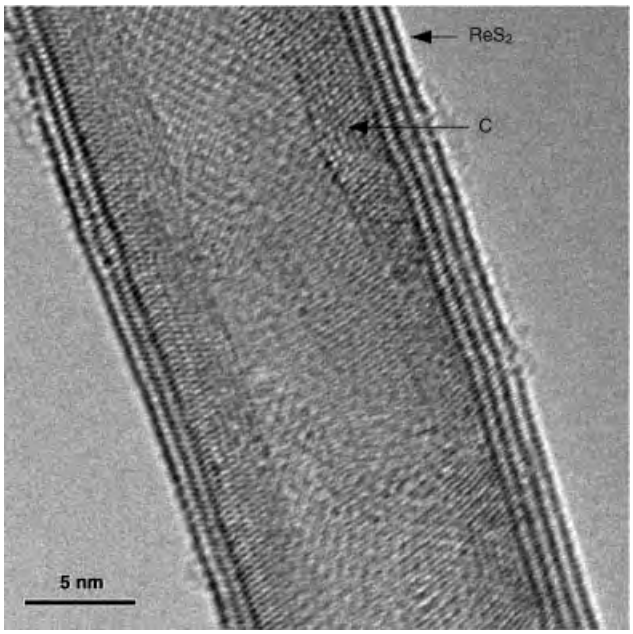


Figure 6. HRTEM image of a ReS_2 nanotube templated on a MWCNT. The individual ReS_2 tube walls are seen as intensely dark, relatively widely spaced, parallel lines. The C walls of the underlying MWCNT are much less intense and more closely spaced.

Many questions remain to be resolved in this case. For instance, it is not clear if the sulfur diffusion occurs through the van der Waals (001) surface enfolding the oxide core, or through occasional defects, which are quite rare on the surface of the nanoparticle, as shown in Figure 5. Moreover, the pressure of the sulfur atoms on the surface of the ReS_2 nanoparticle is isotropic. Yet the nanocrystal grows with a single growth front, that is, in a quasi-epitaxial fashion. A single growth front is the thermodynamically preferred mode, but for this kind of growth mode to predominate, nucleation of ReS_2 nanocrystallites within the core must be suppressed. Therefore, the trajectory of the penetrating sulfur atom from the surface of the nanoparticle towards its core can be visualized as a long but facile diffusion in galleries between the layers and occasional hops through dislocations perpendicular to the layers (parallel to the *c* axis). However, a detailed understanding of this process is still lacking. Furthermore, it is not known if the sulfur diffuses as a single atom, as HS, or perhaps as sulfide ions. Moreover, the diffusion of oxygen in the opposite direction can also occur in a variety of ways.

The templating procedure that uses carbon nanotubes as a substrate has previously been used for the production of other inorganic nanotubes. The first inorganic nanotubes produced by this method were obtained by evaporation of the layered structure compound V_2O_5, its deposition on MWCNT soot, and subsequent removal of the template by air annealing.[22] Another templating procedure, using wet chemistry, has been employed by Rao and co-workers for the synthesis of multicrystalline TiO_2 and SiO_2 nanotubes.[23] Here, carbon nanotubes were first submerged in a solution containing the salt of the cation, and were subsequently calcined to obtain the multicrystalline oxide nanotubes. Kroto, Walton, and their co-workers have used a similar procedure for the synthesis of various metal dichalcogenide nanotubes.[24]

Another solid-state strategy for the synthesis of MX_2 nanotubes (M = Mo, W, Nb, Ta, Ti, Zr, Hf; X = S, Se) is through the high-temperature decomposition of the MX_3 precursor. Notwithstanding a few earlier reports, Nath and Rao have captured the full potential of this strategy in recent years.[11a,12,15] Thus, high-temperature (> 1000 °C) annealing of MX_3 powder under a hydrogen atmosphere yielded quite uniform phases of mostly end-closed multiwall MX_2 nanotubes. The MX_3 precursor could be obtained directly from the elements, or by first synthesizing the ammonium thiometallate $(NH_4)_2MS_4$, which decomposes into MS_3 at moderate temperatures (300–400 °C). Closing the ends of the nanotubes leads to a thermodynamically stable structure. However, the capping step requires the folding of the lamella along two axes to form a half fullerene-like structure (bucky-bowl). This process is facilitated by the high temperatures of the synthesis. In a further development, Chen et al. have demonstrated that careful grinding of the thiotungstate precursor leads to a substantial reduction in the formation temperature (360–450 °C) of the nanotubes.[25] In contrast to the previous work, the nanotubes were found to be open-ended, which is the kinetically favorable scenario at the low temperatures used in this process.

Chemical vapor transport (CVT) is an established technique for the growth of crystalline solids.[26] Here the source material is transported by a volatile and chemically reactive agent, such as I_2, along a temperature gradient. CVT is particularly useful for the growth of crystalline materials of compounds which are unable to melt without decomposition. This technique was widely employed during the 1960s and 1970s for the growth of high-quality crystals of layered metal dichalcogenides. Remskar et al. were the first to recognize that this method can be adapted for the growth of perfectly crystalline microtubes and nanotubes of layered compounds.[27] By adding C_{60} as a growth promoter into the reaction mixture, single-wall MoS_2 nanotubes with a small

 © 2003 Wiley-VCH Verlag GmbH & Co. KGaA, Weinheim

diameter (0.96 nm) and a (3,3) armchair configuration were synthesized.[12] Figure 7a shows a side-on HRTEM image of a bundle of such nanotubes, arranged in an hexagonal network, while Figure 7b shows a structural model proposed for this

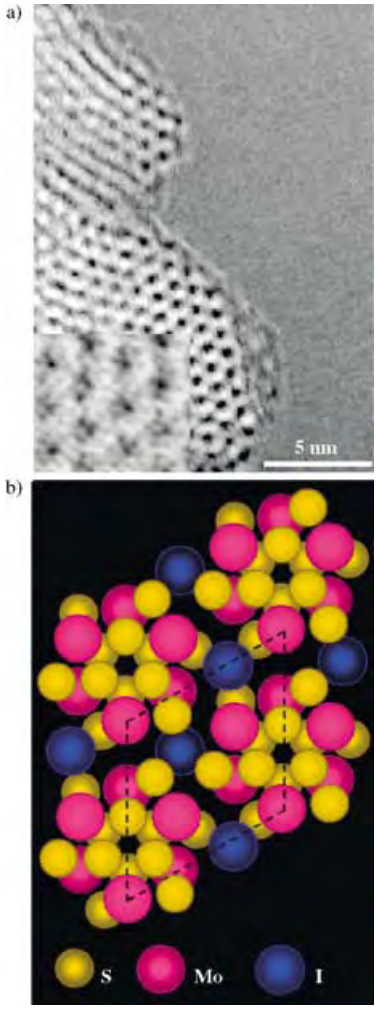


Figure 7. a) Side-on HRTEM image of the hexagonal packing of single-wall MoS_2 nanotubes; b) schematic model of the hexagonal array of single-wall MoS_2 nanotubes with iodine atoms in the interstitial positions (Courtesy of Dr. M. Remskar).

bundle, with the iodine atoms occupying the interstices of this lattice. Although these nanotubes grow as bundles, they can be nevertheless isolated into single nanotubes, which are relatively stable under ambient conditions. Most remarkably, since all the nanotubes have the same diameter, they arrange into a hierarchy of structures from the nano- to the macroscopic scale, as shown in the scanning electron microscope (SEM) image in Figure 8. Clearly, more effort is needed to vary the diameter and chirality of the nanotubes, and extend this growth technique for single-wall nanotubes of other layered compounds. It should be noted that some atoms of the transport agent (iodine) are likely to substitute sulfur atoms in the nanotube, thus affecting its electronic properties.

Two techniques which are in extensive use for the synthesis of high-quality (carbon) fullerenes and nanotubes,

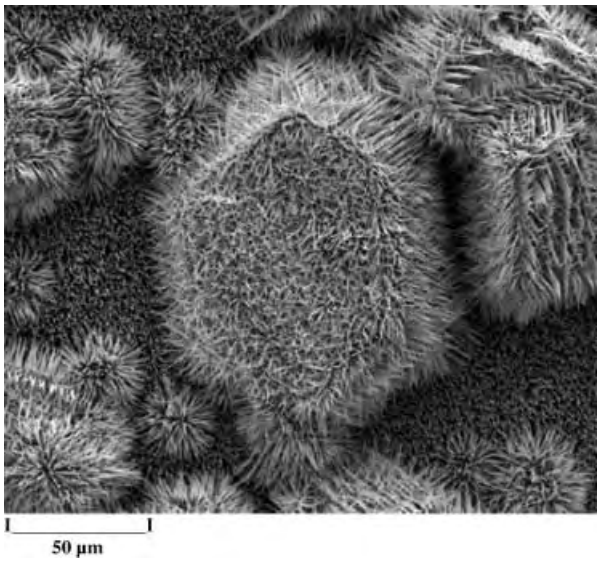


Figure 8. SEM image of a macroscopic assembly of single-wall MoS_2 nanotubes (Courtesy of Dr. M. Remskar and Dr. E. Klein).

are arc discharge and laser ablation. Recently, a novel technique of arc discharge in aqueous media was shown to yield fullerene-like MoS_2 nanoparticles.[28] This work paves the way for the synthesis of IF nanostructures from various other layered compounds. Laser ablation has been recently used for the synthesis of MoS_2 "bucky octahedra"[29] and MoS_2,[30] or SnS/SnS_2 "onions" and nanotubes.[31] It is likely that these two techniques will be further exploited for the synthesis of various other IF nanostructures with precise size and shape control.

The use of metal halide salts as intermediates in the synthesis of IF-MX_2 has been demonstrated by a number of groups. These salts have a few attributes that make them very suitable precursors for the synthesis of IFs, that is, their relatively high solubility in non-aqueous solvents, and their appreciable volatility. Also, the halide-to-chalcogenide conversion is promoted by the large exothermicity of the reaction. Thus MS_2 nanotubes (M = Re,W) were obtained by first suspending carbon nanotubes in an ethanolic solution of the respective metal halide and subsequently sulfidizing the wetted nanotubes with H_2S.[18,32] In another experiment, $NbCl_5$ was evaporated at 200 °C and carried by an inert gas where it reacted with H_2S at 400 °C, which after annealing at 550 °C led to the production of well-faceted nested structures ("onions") of NbS_2.[33]

One way to describe Archimedean polyhedra is by encapsulating a closed space with two kinds of geometrical elements of a different symmetry, such as hexagons and pentagons. For instance, C_{60} consists of 20 hexagons and 12 pentagons, while C_{70} is made of 25 hexagons and 12 pentagons. The Euler rule stipulates the number of elements of lower symmetry necessary to close the polyhedron. Since rhombi and triangles make part of the MX_2 lattice, polyhedra with octahedral or tetrahedral structure can be formed by disposing six rhombi and four triangles, symmetrically, in the hexagonal (trigonal) network.[7a] Indeed, MoS_2 bucky octahe-

 © 2003 Wiley-VCH Verlag GmbH & Co. KGaA, Weinheim

dra, produced by laser ablation, were proposed to be a most stable fullerene-like structure.[29] Figure 9 shows a HRTEM image of such a MoS_2 octahedron. While the 1:2 Mo:S ratio is maintained throughout most of the nanostructure, deviations from this stoichiometry can not be ruled out at each corner of the octahedron. Recent calculations confirm that the octahedron is indeed a stable structure for fullerene-like MoS_2, together with dodecahedral and triangular prismatic structures.[34] Furthermore, the trigonal coordination of the sulfur atoms is shown to be highly distorted at the corners, but the Mo:S ratio, 1:2, is preserved. Though the synthesis of such nanostructures is extremely challenging, this effort is likely to be very rewarding, since the physical behavior of such nanoparticles could be radically different from the bulk material.

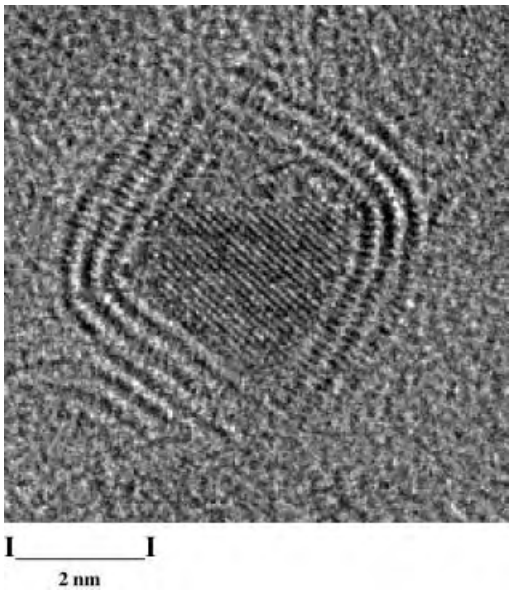


Figure 9. HRTEM image of a three-layer MoS_2 octahedron obtained by laser ablation.

2.2. Metal Dihalides

Although the structure of layered metal dihalide compounds is not very different from their metal dichalcogenide analogues, they are appreciably more ionic. Consequently the bending and shear moduli of the layered metal dihalide compounds, which play an important role in their ability to bend and close, is appreciably higher than that of their metal dichalcogenide analogues. Water molecules can be intercalated into the galleries between the layers by diffusion through the prismatic (*hk*0) faces. Consequently, these compounds are very hygroscopic. They also tend to lose halogen atoms upon heating. The first nanotubes and fullerene-like nanoparticles of $NiCl_2$ were prepared by sublimation of a $NiCl_2$ powder at 960 °C.[10] Unfortunately, this reaction does not produce the pure IF phase and $NiCl_2$ platelets are present in the ablated residue. Water molecules, which are intercalated into the platelets, boil out under TEM conditions and disturb the analysis. This behavior, which is common to all metal dihalide compounds studied thus far, is a most challenging obstacle in the development of reproducible synthetic strategies for IF structures of these compounds.

Laser ablation of a $NiCl_2$ target heated to 940 °C was recently used for the synthesis of $NiCl_2$ nanotubes (Figure 10), albeit in small quantities. CCl_4 vapor was added to the reaction zone in order to compensate for the loss of chlorine during the ablation process.[35] The reaction was found to go by the common vapor–liquid–solid (VLS) mechanism. More recently, $CdCl_2$[36] and CdI_2[37] nanoparticles with a closed-cage structure were obtained in situ through electron-beam-induced processes. Both kinds of nanoparticles were partially filled with cadmium in their core. The halide deficiency in the ablated e-beam irradiated residue was ascribed to its high volatility.

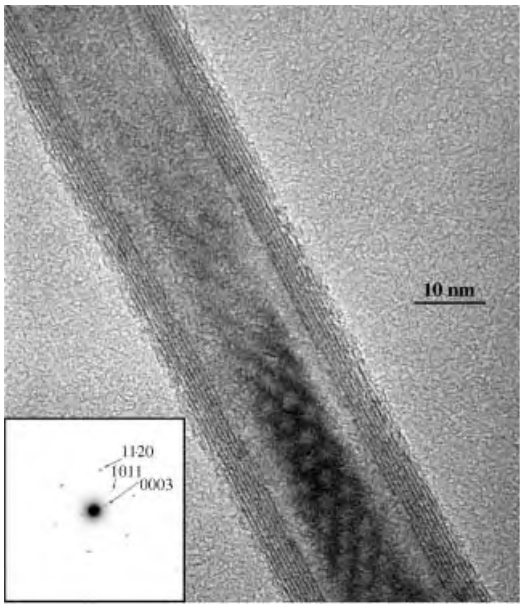


Figure 10. HRTEM image of a $NiCl_2$ nanotube. Inset: electron diffraction pattern of this nanotube.

The polyhedral nanoparticles of the above three compounds were found to exhibit a typical highly faceted hexagonal morphology. The large bending and shear moduli of these compounds prevents regular bending of the atomic layers, and leads instead to the formation of fullerene-like nanoparticles with a hexagonal structure. In contrast, the $NiCl_2$ nanotubes, which suffer appreciably lower strain, appear to have an even cross-section. In comparison, the more covalent metal dichalcogenide compounds are more flexible, and consequently their fullerene-like nanoparticles are much less faceted.[35b] Unfortunately, the rather limited amount of nanotubes or fullerene-like nanoparticles from metal dihalide compounds makes it very difficult to study their physical characteristics in a systematic manner.

 © 2003 Wiley-VCH Verlag GmbH & Co. KGaA, Weinheim

2.3. Oxide and Hydroxide Nanotubes

There is substantial interest in developing new nanomaterials based on oxide nanotubes for such diverse applications as rechargeable batteries, (photo)catalysis, and sensors. Numerous oxides with lamellar structure are known. However, these compounds are much more ionic than their 2D metal dichalcogenide analogues, and hence more difficult to fold into nanotubes. The use of "soft chemistry" ("chimie douce") methodologies, including sol–gel processes, hydrothermal treatment, and intercalation chemistry enabled the synthesis of numerous new nanostructures from oxide compounds.

Pioneering work in this direction was carried out by Nesper and co-workers, who synthesized multiwall V_2O_{5-x} nanotubes templated with alkyl amines as structure-directing agents by using a combination of a sol–gel process and hydrothermal treatment.[9] In fact, the alkyl amine moieties had another important role in softening the relatively inelastic oxide lamella, which allows this inorganic–organic hybrid to fold into multilayer nanotubes (nanoscrolls). Generally, due to the low temperatures used in soft chemistry methods, the synthesized moieties do not attain the lowest energy concentric nanotubular structure. Instead, the lamellar oxides accommodate the higher-energy, but easier to produce, open-tip nanoscroll (folded carpet) structure, which is also the case for the V_2O_{5-x}/alkyl amine nanotubes.

Nanotubes of various lanthanide oxides templated with dodecylsulfate ions were prepared by homogeneous precipitation from a solution containing the lanthanide nitrate and the surfactant with urea. Subsequently, hollow nanotubes with an inner diameter of 6 nm were obtained by anionic exchange of the surfactant with acetate ions.[38] Numerous metal hydroxides crystallize in a layered structure and are therefore potentially capable of forming IF nanostructures. In this context, the hydrothermal synthesis of $Dy(OH)_3$ nanotubes from Dy_2O_3 powder was recently reported.[39]

A surprising observation was made by Kasuga et al., who noted that treatment of a TiO_2–SiO_2 powder prepared via a sol–gel process in a NaOH solution at mild temperatures (130 °C) leads to the formation of slender titanium oxide nanotubes.[40] Later, Peng and co-workers discovered[41] that the structure of the nanotubes, which were synthesized according to this procedure, can be better described by the formula $H_2Ti_3O_7$, a compound belonging to the series of titanates $H_2Ti_nO_{2n+1}$ with lamellar structures. Not surprisingly though, this process yields open-ended nanoscrolls rather than the more stable nanotubes, which can not be obtained at such low temperatures (see Figure 11). The exact nature and structure of this kind of nanotube is still a cause for debate,[42] but the fact that lamellar titanium oxides can produce nanotubes (nanoscrolls) using such simple synthetic strategies is enticing. The large number of applications of titanium and other oxides as (photo)catalysts, electrode materials for rechargeable batteries, smart windows, and so forth, is likely to keep this research at the forefront of solid-state synthetic chemistry. In a related study, the exfoliation of acid-exchanged $K_4Nb_6O_{17}$ with tetra(*n*-butyl)ammonium hydroxide in water was found to produce a colloidal suspension of individual sheets, which roll into loosely bound nanotubular structures (nanoscrolls).[43] Therefore, the exfoliation method seems to provide a facile means to obtain nanotubular structures of various metal oxides.

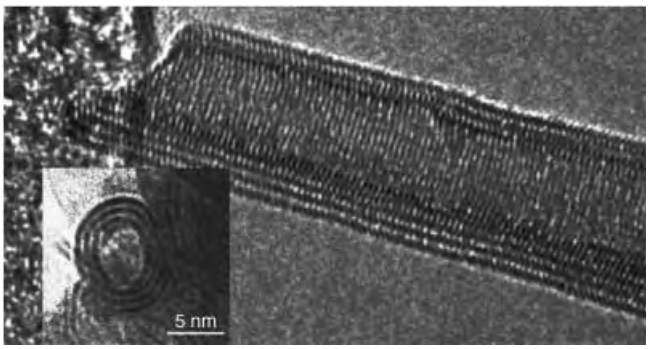


Figure 11. HRTEM image of an $H_2Ti_3O_7$ nanoscroll. Inset: a cross-section of a typical nanoscroll of this kind.

In the past, various strategies have been developed for the synthesis of multicrystalline nanotubes from 3D compounds. Recently, a few studies have reported the synthesis of fully crystalline nanotubes from 3D (non-layered) materials. Thus, a dense arrays of hexagonally faceted ZnO microtubules were obtained on a glass substrate through the hydrothermal reaction of zinc nitrate and methenamine ($(CH_2)_6N_4$)[44] at 90 °C for two days. In the first stage of the reaction, an ordered array of ZnO whiskers grow along their [001] axis. The authors attribute the propensity of ZnO to grow in this way to the fast-growth kinetics of the sixfold symmetric $(\bar{1}00)$ and $(\bar{1}\bar{1}0)$ faces, as compared to the slow growth of the (001) oxygen face. Further aging of the array in the same vessel leads to the preferential dissolution of the Zn(001) face in the core of the microrods, which leads to the formation of an array of hexagonally faceted ZnO microtubules. The structure of the sharp joints between the facets is not known, but is thought to consist of twin boundaries. It is likely that if the process is not stopped at this point the dissolution process would continue until the entire wall of the microtubes is consumed, which shows that this habit represents a metastable structure under any time scale.

Clearly this growth habit is not limited to solutions only. In fact, growth from the gas phase is not constrained by surface tension and capillary forces, which may yield much more slender nanotubes. Indeed, GaN nanotubes were obtained by gas-phase deposition onto lattice-matched hexagonally faceted ZnO nanowires, and subsequent reduction/evaporation of the ZnO template.[45] The crystal habit of the grown GaN nanotubes follows that of the ZnO template. Also recently, crystalline In_2O_3 nanotubes, with their core filled with In, were obtained by heating a mixture of In_2O_3 and In to 1300 °C under vacuum.[46] Here the growth occurs along the cubic [111] axis, but the detailed structure of the nanotubes has not been reported. These studies show that in contrast to the radial nanotubes obtained from 2D (layered) compounds, the nanotubes derived from 3D compounds are unable to evenly bend and are, in general, faceted and not fully passivated at their surface.

 © 2003 Wiley-VCH Verlag GmbH & Co. KGaA, Weinheim

3. Properties of Inorganic Nanotubes and their Potential Applications

The large diversity of inorganic nanotubes and fullerene-like structures offers an extensive range of properties and yet an untapped number of potential applications, which will be briefly mentioned below.

By using first-principle density-functional tight-binding calculations, it was recently found that multiwall WS_2 and MoS_2 nanotubes are stable compared to a multilayer stripe consisting of the same number of atoms as the nanotube over a limited range of conditions.[47] For stripes that are too narrow, the bending energy predominates and the tubular structures are not stable. However, nanotubes 4–7 layers thick and with a 6-nm (inner) diameter are found to be more stable than the respective stripes. Despite the fact that several approximations were used in these calculations, good agreement between theory and experiment was obtained. This work indicates that the WS_2 (MoS_2) nanotubular phase does indeed exist in the proximity of the bulk 2D phase of these compounds. Furthermore, the thermal stability of the IF nanophase of various MX_2 compounds was measured and compared with that of the bulk (2D) phase. These measurements clearly indicate that globally the IF phase is somewhat less stable than the corresponding bulk phase.

The Young's modulus of multiwall WS_2 nanotubes was measured using atomic force microscopy and determined to be 170 GPa, which compares favorably with the results of first-principle calculations.

In another study, the impact resistance of WS_2 nanotubes against shock waves was tested.[48] It was observed that these nanotubes could withstand shock waves as powerful as 21 GPa with minor damage to their framework. This is in contrast to carbon nanotubes, which transform into diamond under much weaker impacts (ca. 9 GPa). Potential applications for these findings are in the automobile and defense industries.

One of the most surprising results is that in contrast to semiconductor quantum dots, the energy gap of IF-WS_2 (MoS_2) decreases with a shrinking diameter of the nanoparticles. This effect was confirmed in the past through theoretical analysis[49] and absorption measurements.[50] Recently, however, high-resolution scanning tunneling microscopy of WS_2 nanotubes was performed and the I versus V curve of a single nanotube was measured. Good agreement was found between the experimental data and density functional theory tight-binding calculations, which confirmed this effect quantitatively.[51] More work is needed to elucidate the optical and electronic properties of the various nanotubes with different diameters and chiral angles, preferably under ultrahigh vacuum and cryogenic conditions. Theoretical calculations showed that NbS_2 nanotubes are metallic irrespective of their diameter and chirality,[52] while recent measurements showed that a mixture of $NbSe_2$ nanotubes and nanorods are superconducting at relatively high critical temperatures (above 8 K.[53]

The outstanding tribological properties of fullerene-like WS_2 and MoS_2 nanoparticles have been previously studied in great detail.[14,54] Under severe loads, where fluids or greases are unable to effectively lubricate the contacting pair, the elastic and quasi-spherical IF nanoparticles keep the asperities of the matting pairs away from each other, and provide easy shear for the metal pairs. Furthermore, unimolecular nanosheets of WS_2 are transferred onto the metal surface through gradual exfoliation of the nanoparticles, further alleviating the friction and wear. The favorable tribological influence of the IF nanoparticles was not limited to oils and greases. Impregnating the nanoparticles in various metal films, ceramic, and polymer coatings brought about substantial reductions in friction and wear of the tribological contacts, thus paving the way for numerous applications.

The characteristic structure of inorganic nanotubes makes them potentially useful electrode materials for rechargeable batteries. On the one hand, the interlayer galleries offer a huge space and easy access (fast diffusion) for the intercalation of lithium ions or protons. On the other hand, the thermodynamic stability of these nanoparticles allows them to undergo numerous charge/discharge cycles without losing their unique structure. Fine tuning of the Fermi level of the nanotube phase by doping and intercalation of metal atoms is another important advantage. It is not surprising, therefore, that inorganic nanotubes were recently studied as host materials for electrodes of rechargeable batteries.[55–57]

Another intriguing research direction with a potentially broad spectrum of applications is in catalysis. Recently, Chen et al. have demonstrated the high reactivity and selectivity of MoS_2 nanotubes as methanation catalysts for CO.[58] This accomplishment is potentially very important for the hydrogen cycle, with major potential applications in nuclear and solar energy storage. In view of the encouraging results, more work on the electrochemical, catalytic, photochemical, and chemical reactivity of inorganic nanotubes is expected.

4. Conclusions

The observation that nanoparticles of 2D layered compounds, such as MoS_2 and $NiCl_2$, spontaneously fold into nanotubes has elicited numerous studies. At this point, the most urgent issues are to develop synthetic strategies that produce nanotubes with accurate size and shape control, and to unravel the detailed structure of such nanotubes. Further, the physical properties and chemical reactivity of such nanotubes must be studied in greater detail. Some important applications have been proposed, and are currently being promoted by various industries. A limited amount of work has already been done to utilize IF nanoparticles in various nanotechnologies. However, given the richness of their chemical and physical characteristics, these nanostructures offer challenging opportunities to the nanotechnology practitioner.

I thank the Minerva Foundation (Munich) and the Alfried Krupp von Bohlen und Halbach Stiftung for the generous support of my work. I thank also the Gerhard M. J. Schmidt Minerva Center for Supramolecular Chemistry of the Weizmann Institute.

Received: March 25, 2003 [M1651]

 © 2003 Wiley-VCH Verlag GmbH & Co. KGaA, Weinheim

[1] S. Reich, G. Leitus, R. Popovitz-Biro (Weizmann Institute), *Phys. Rev. Lett.*, in press.
[2] A. Rothschild, Y. Komem, A. Levakov, N. Ashkenasy, Y. Shapira, *Appl. Phys. Lett.* **2003**, *82*, 574.
[3] A. Fujishima, K. Hashimoto, T. Watanabe in *TiO_2 Photocatalysis: Fundamentals and Applications*, BKC, Tokyo, **1999**.
[4] a) S. I. Nikitenko, Y. Koltypin, V. Markovich, E. Rozenberg, G. Gorodetsky, A. Gedanken, *IEEE J. Quantum Electron. IEEE Trans. Magn.* **2002**, *38*, 2592; b) J. Xue, Z. Zhou, J. J. Wang, *J. Am. Ceramic Soc.* **2002**, *85*, 807.
[5] S. Veprek, M. Jilek, *Vacuum* **2002**, *67*, 443.
[6] R. Tenne, L. Margulis, M. Genut, G. Hodes, *Nature* **1992**, *360*, 444.
[7] a) L. Margulis, G. Salitra, R. Tenne, M. Talianker, *Nature* **1993**, *365*, 113; b) M. Hershfinkel, L. A. Gheber, V. Volterra, J. L. Hutchison, L. Margulis, R. Tenne, *J. Am. Chem. Soc.* **1994**, *116*, 1914.
[8] N. G. Chopra, J. Luyken, K. Cherry, V. H. Crespi, M. L. Cohen, S. G. Louie, A. Zettl, *Science* **1995**, *269*, 966.
[9] M. E. Spahr, P. Bitterli, R. Nesper, M. Müller, F. Krumeich, H. U. Nissen, *Angew. Chem.* **1998**, *110*, 1339; *Angew. Chem. Int. Ed.* **1998**, *37*, 1263.
[10] Y. Rosenfeld Hacohen, E. Grunbaum, R. Tenne, J. Sloan, J. L. Hutchison, *Nature* **1998**, *395*, 336.
[11] a) M. Nath, C. N. R. Rao, *J. Am. Chem. Soc.* **2001**, *123*, 4841; b) Y. Q. Zhu, W. K. Hsu, H. W. Kroto, D. R. M. Walton, *J. Phys. Chem. B* **2002**, *106*, 7623.
[12] M. Nath, C. N. R. Rao, *Angew. Chem.* **2002**, *114*, 3601; *Angew. Chem. Int. Ed.* **2002**, *41*, 3451.
[13] M. Remskar, A. Mrzel, Z. Skraba, A. Jesih, M. Ceh, J. Demsar, P. Stadelmann, F. Lévy, D. Mihailovic, *Science* **2001**, *292*, 479.
[14] L. Rapoport, Yu. Bilik, Y. Feldman, M. Homyonfer, S. R. Cohen, R. Tenne, *Nature* **1997**, *387*, 791.
[15] M. Nath, C. N. R. Rao, *J. Chem. Soc. Dalton Trans.* **2003**, 1.
[16] G. R. Patzke, F. Krumeich, R. Nesper, *Angew. Chem.* **2002**, *114*, 2554; *Angew. Chem. Int. Ed.* **2002**, *41*, 2446.
[17] K. S. Coleman, J. Sloan, N. A. Hanson, G. Brown, G. P. Clancy, M. Terrones, H. Terrones, M. L. H. Green, *J. Am. Chem. Soc.* **2002**, *124*, 11580.
[18] M. Brorson, T. W. Hansen, C. J. H. Jacobsen, *J. Am. Chem. Soc.* **2002**, *124*, 11582.
[19] Y. Feldman, G. L. Frey, M. Homyonfer, V. Lyakhovitskaya, L. Margulis, H. Cohen, G. Hodes, J. L. Hutchison, R. Tenne, *J. Am. Chem. Soc.* **1996**, *118*, 5362.
[20] A. Zak, Y. Feldman, V. Alperovich, R. Rosentsveig, R. Tenne, *J. Am. Chem. Soc.* **2000**, *122*, 11108.
[21] Y. Feldman, A. Zak, R. Popovitz-Biro, R. Tenne, *Solid State Sci.* **2000**, *2*, 663.
[22] P. M. Ajayan, O. Stephan, P. Redlich, C. Colliex *Nature* **1995**, *375*, 564.
[23] B. C. Satishkumar, A. Govindaraj, E. M. Vogel, L. Basumallick, C. N. R. Rao, *J. Mater. Res.* **1997**, *12*, 604.
[24] a) Y. Q. Zhu, W. K. Hsu, H. W. Kroto, D. R. M. Walton, *J. Phys. Chem. B* **2002**, *106*, 7623; b) R. L. D. Whitby, W. K. Hsu, C. B. Boothroyd, P. K. Fearon, H. W. Kroto, D. R. M. Walton, *ChemPhysChem* **2001**, *2*, 620.
[25] J. Chen, S.-L. Li, F. Gao, Z.-L. Tao, *Chem. Mater.* **2003**, *15*, 1012.
[26] R. Nitsche, *J. Phys. Chem. Solids* **1960**, 163.
[27] a) M. Remskar, Z. Skraba, F. Cléton, R. Sanjinés, F. Lévy, *Appl. Phys. Lett.* **1996**, *69*, 351; b) M. Remskar, Z. Skraba, M. Regula, C. Ballif, C. R. Sanjinés, F. Lévy, *Adv. Mater.* **1998**, *10*, 246.
[28] N. Sano, H. Wang, M. Chowalla, I. Alexandrou, G. A. J. Amaratunga, M. Naito, T. Kanki, *Chem. Phys. Lett.* **2003**, *368*, 331.
[29] P. A. Parilla, A. C. Dillon, K. M. Jones, G. Riker, D. L. Schulz, D. S. Ginley, M. J. Heben, *Nature* **1999**, *397*, 114.
[30] R. Sen, A. Govindaraj, K. Suenaga, S. Suzuki, H. Kataura, S. Iijima, Y. Achiba, *Chem. Phys. Lett.* **2001**, *340*, 242.
[31] S. Y. Hong, R. Popovitz-Biro, Y. Prior, R. Tenne, *J. Am. Chem. Soc.* **2003**, *125*, 10470.
[32] Y. Q. Zhu, W. K. Hsu, H. W. Kroto, D. R. M. Walton, *Chem. Commun.* **2001**, 2184.
[33] C. Schuffenhauer, R. Popovitz-Biro, R. Tenne, *J. Mater. Chem.* **2002**, *12*, 1587.
[34] J. A. Ascencio, M. Perez-Alvarez, L. M. Molina, P. Santiago, M. Jose-Yacaman, *Surf. Sci.* **2003**, *526*, 243.
[35] a) Y. Rosenfeld Hacohen, R. Popovitz-Biro, E. Grunbaum, Y. Prior, R. Tenne, *Adv. Mater.* **2002**, *14*, 1075; b) Y. Rosenfeld Hacohen, R. Popovitz-Biro, Y. Prior, S. Gemming, G. Seifert, R. Tenne, *PhysChemChemPhys* **2003**, *5*, 1644.
[36] R. Popovitz-Biro, A. Twersky, Y. Rosenfeld Hacohen, R. Tenne, *Isr. J. Chem.* **2001**, *41*, 7.
[37] R. Popovitz-Biro, N. Sallacan, R. Tenne, *J. Mater. Chem.*, **2003**, *13*, 1631.
[38] M. Yada, M. Mihara, S. Mouri, M. Kuroki, T. Kijima, *Adv. Mater.* **2002**, *14*, 309.
[39] A.-W. Xu, Y.-P. Fang, L.-P. You, H.-Q. Liu, *J. Am. Chem. Soc.* **2003**, *125*, 1494.
[40] T. Kasuga, M. Hiramatsu, A. Hoson, T. Sekino, K. Niihara, *Langmuir* **1998**, *14*, 6160.
[41] G. H. Du, Q. Chen, R. C. Che, Z. Y. Yuan, L.-M. Peng, *Appl. Phys. Lett.* **2001**, *79*, 3702.
[42] B. D. Yao, Y. F. Chan, X. Y. Zhang, W. F. Zhang, Z. Y. Yang, N. Wang, *Appl. Phys. Lett.* **2003**, *82*, 281.
[43] G. B. Saupe, C. C. Waraksa, H.-N. Kim, Y. J. Han, D. M. Kaschak, D. M. Skinner, T. E. Mallouk, *Chem. Mater.* **2000**, *12*, 1556.
[44] L. Vayssieres, K. Keis, A. Hagfeldt, S.-E. Lindquist, *Chem. Mater.* **2001**, *13*, 4395.
[45] J. Goldberger, R. He, Y. Zhang, S. Lee, H. Yan, H.-J. Choi, P. Yang, *Nature* **2003**, *422*, 599.
[46] Y. Li, Y. Bando, D. Golberg, *Adv. Mater.* **2003**, *15*, 581.
[47] G. Seifert, T. Köhler, R. Tenne, *J. Phys. Chem. B* **2002**, *106*, 2497.
[48] Y. Q. Zhu, T. Sekine, K. S. Brigatti, S. Firth, R. Tenne, R. Rosentsveig, H. W. Kroto, D. R. M. Walton, *J. Am. Chem. Soc.* **2003**, *125*, 1329.
[49] G. Seifert, H. Terrones, M. Terrones, G. Jungnickel, T. Frauenheim, *Phys. Rev. Lett.* **2000**, *85*, 146.
[50] G. L. Frey, S. Elani, M. Homyonfer, Y. Feldman, R. Tenne, *Phys. Rev. B* **1998**, *57*, 6666.
[51] L. Scheffer, R. Rosentsveig, A. Margolin, R. Popovitz-Biro, G. Seifert, S. R. Cohen, R. Tenne, *PhysChemChemPhys* **2002**, *4*, 2095.
[52] G. Seifert, H. Terrones, M. Terrones, T. Frauenheim, *Solid State Comm.* **2000**, *115*, 635.
[53] M. Nath, S. Kar, A. K. Raychaudhuri, C. N. R. Rao, *Chem. Phys. Lett.* **2003**, *368*, 690.
[54] L. Rapoport, N. Fleischer, R. Tenne, *Adv. Mater.* **2003**, *15*, 651.
[55] M. E. Spahr, P. Stoschitzki-Bitterli, R. Nesper, O. Haas, P. Novak, *J. Electrochem. Soc.* **1999**, *146*, 2780.
[56] R. Dominko, D. Arcon, A. Mrzel, A. Zorko, P. Cevc, P. Venturini, M. Gaberscek, M. Remskar, D. Mihailovic, *Adv. Mater.* **2002**, *14*, 1531.
[57] a) J. Chen, N. Kuriyama, H. Yuan, H. T. Takeshita, T. Sakai, *J. Am. Chem. Soc.* **2001**, *123*, 11813; b) J. Chen, Z.-L. Tao, S.-L. Li, *Angew. Chem.* **2003**, *115*, 2197; *Angew. Chem. Int. Ed.* **2003**, *42*, 2147.
[58] J. Chen, S.-L. Li, Q. Xu, K. Tanaka, *Chem. Commun.* **2002**, 1722.

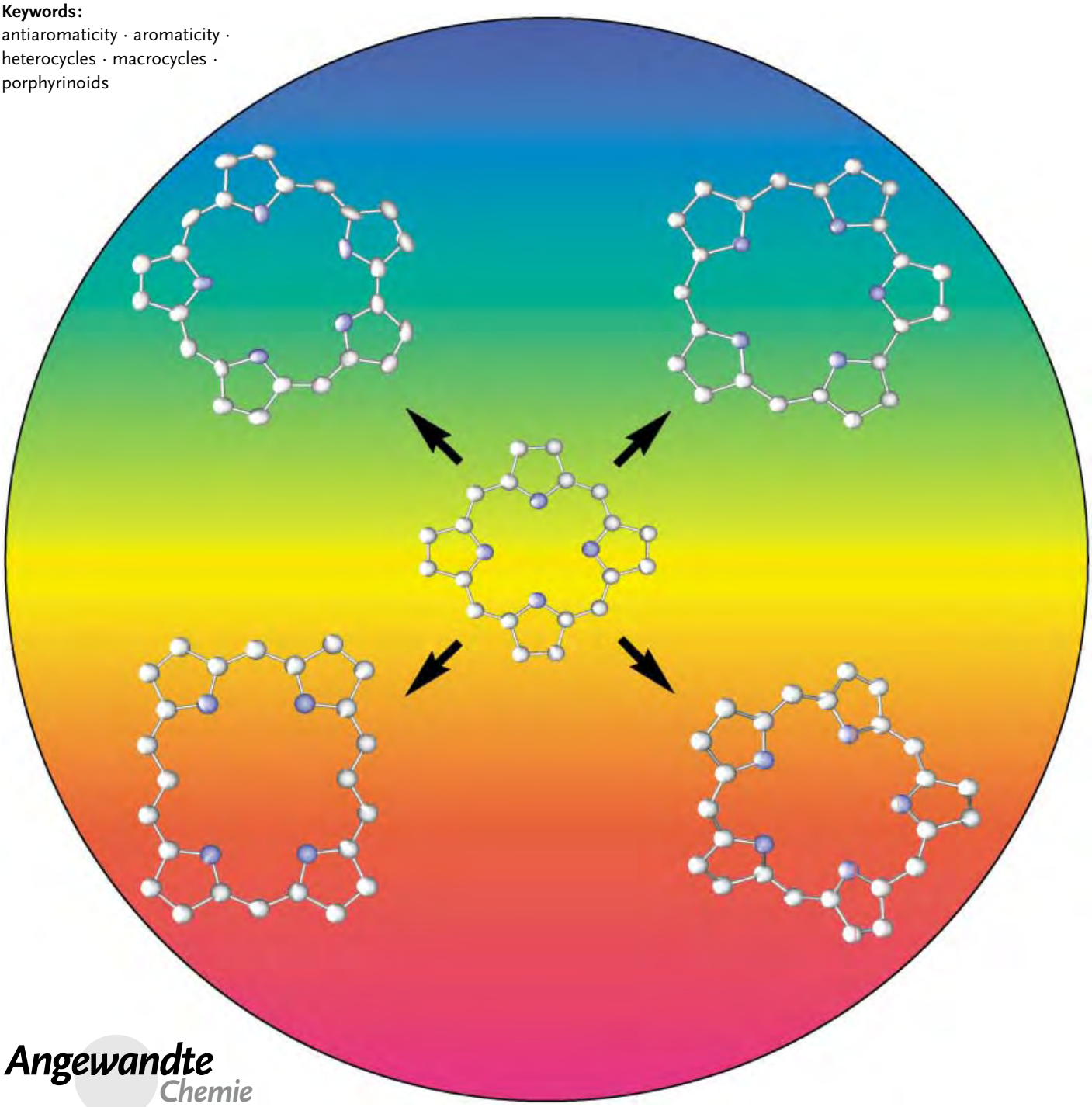
 © 2003 Wiley-VCH Verlag GmbH & Co. KGaA, Weinheim

Porphyrin Chemistry

Synthetic Expanded Porphyrin Chemistry

Jonathan L. Sessler and Daniel Seidel*

Keywords:
antiaromaticity · aromaticity · heterocycles · macrocycles · porphyrinoids



Angewandte Chemie

 © 2003 Wiley-VCH Verlag GmbH & Co. KGaA, Weinheim DOI: 10.1002/anie.200200561

Expanded porphyrins are synthetic analogues of the porphyrins, and differ from these and other naturally occurring tetrapyrrolic macrocycles by containing a larger central core with a minimum of 17 atoms, while retaining the extended conjugation features that are a hallmark of these quintessential biological pigments. The result of core expansion is to produce systems with novel spectral and electronic features, interesting and, often unprecedented, cation-coordination properties, and, in many cases, an ability to bind anions in certain protonation states. Also adding to the appeal of expanded porphyrins is their central role in addressing issues of aromaticity. In many cases, they also display structural features, such as decidedly nonplanar "figure-eight" motifs, that have no antecedents in the chemistry of porphyrins or related macrocyclic compounds. In this Review, the various synthetic approaches now being employed to produce expanded porphyrins as well as their various applications-related aspects are discussed.

From the Contents

1. Introduction and Definition 5135
2. Historical Overview 5136
3. Systems Containing Four or Fewer Heterocyclic Subunits 5137
4. Systems Containing Five Pyrrole Rings 5147
5. Systems Containing Six Pyrrole Rings 5155
6. Systems Containing Seven Pyrrole Rings 5162
7. Compounds Containing Eight or More Pyrrole Rings 5164
8. Recent Advances 5171
9. Outlook 5172

1. Introduction and Definition

Porphyrin (for example, **1**) undoubtedly represents one of the most widely studied of all known macrocyclic ring systems.[1] Interest in this naturally occurring tetrapyrrolic macrocycle is broadly based and derives in part from its multiple biological functions as well as its ability to function as an excellent metal-complexing ligand. This chemical richness has inspired the study of a whole range of porphyrin analogues in recent years.[2,3] Much of the attention devoted to these latter systems is based on their resemblance to porphyrins and the hope that they will display a rich coordination chemistry that parallels that of the porphyrins.

On a different level, the electronic structure of various larger, or "expanded" porphyrin systems, in particular their similarities and differences to porphyrins, have made them an object of intense study. Here, a key objective of both practical and theoretical importance has been to explore the limits to which the classic Hückel definition of aromaticity ($4n+2$ π electrons) may be applied to heteroannulenes. A related goal was to understand what factors endow a fully conjugated macrocycle with characteristics that can be considered aromatic or antiaromatic.[4]

Another factor driving the study of conjugated expanded porphyrins is that they often display absorbance bands that are considerably red-shifted relative to those of porphyrin. This attribute, which is ascribed to an increased π-conjugation pathway, has led to the consideration that certain expanded porphyrins could find use as therapeutics for photodynamic therapy.[5,6] Related properties, including a facilitated ease of reduction, has led to the testing of one particular expanded porphyrin (xcytrin; motexafin gadolinium) as an adjuvant for X-ray radiation therapy.[5,6] Another area of interest, this time without precedence in the porphyrin arena, centers around the initially unexpected finding that expanded porphyrins can act as anion receptors. This result has made these systems of potential interest for use in a variety of applications, including anion sensing and transport (for example, drug delivery), as well as chromatography-based purification of anions.[7]

This Review is focused on expanded porphyrins and is meant to complement earlier overviews of the field.[2,3,8] While some historical background will be presented for the benefit of the general reader, its primary objective is to provide an update on what has been achieved in the area of oligopyrrole macrocycles between 1998 and June 2002. The main focus will be on systems that bear the greatest formal resemblance to porphyrins, namely conjugated oligopyrroles. However, this Review will also cover various "expanded" systems, whose intellectual antecedents are in phthalocyanines, porphyrazines, and various non-pyrrolic ring compounds. In all cases, the compounds in question will be larger than porphyrins and related tetrapyrrolic systems. Specifically, a system must be macrocyclic and contain pyrrole, furan, thiophene, or other heterocyclic subunits linked together either directly or through one or more spacer atoms in such a manner that the internal ring pathway contains a minimum of 17 atoms. In accord with this definition, compounds such as corroles,[9] isomeric porphyrins,[10] N-confused porphyrins,[11,12] doubly N-confused porphyrins,[13] N-fused porphyrins,[14] benziporphyrin,[15] and carbaporphyrin[16,17] that con-

[*] Prof. J. L. Sessler, Dr. D. Seidel
Department of Chemistry and Biochemistry
Institute for Cellular and Molecular Biology
University of Texas at Austin
Austin, TX 78712-1167 (USA)
Fax: (+1) 512-471-7550
E-mail: sessler@mail.utexas.edu

 DOI: 10.1002/anie.200200561 © 2003 Wiley-VCH Verlag GmbH & Co. KGaA, Weinheim

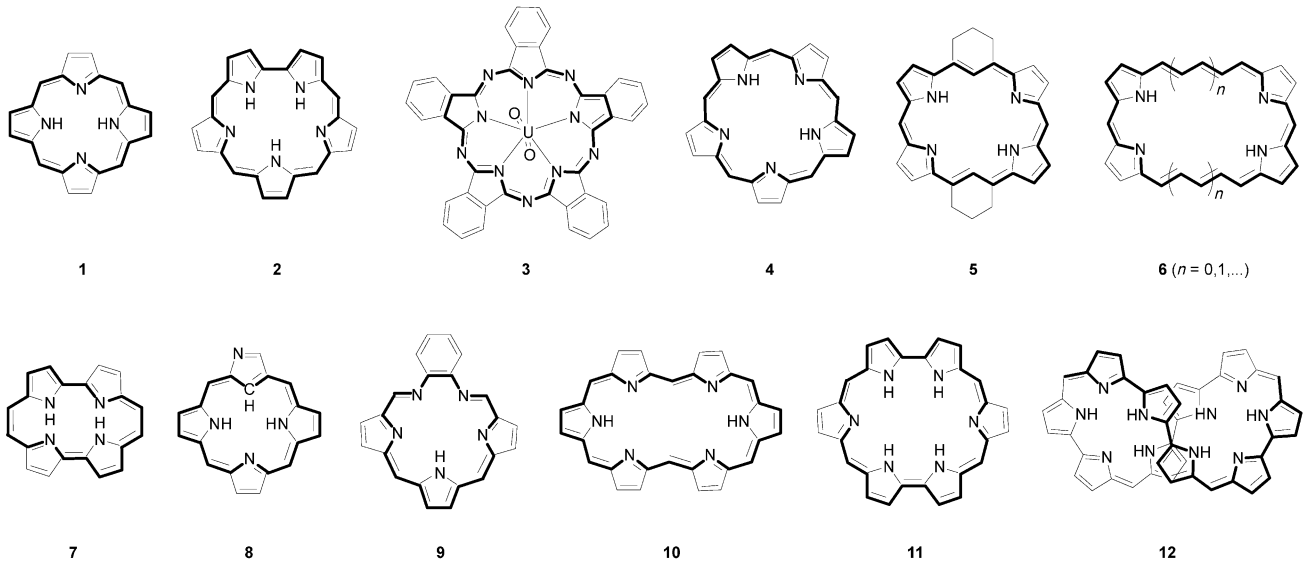
tain an internal ring pathway of 16 or fewer atoms are not included here.[18] Furthermore, to keep the length of the review within reasonable limits, nonconjugated systems such as expanded calixpyrroles (porphyrinogens) and calix[*n*]phyrins, expanded analogues of porphodimethenes, will be for the most part excluded. Such systems have, however, been the subject of recent reviews.[19,20]

Except in those cases where the use of trivial names offers an heuristic advantage, a generalized version of a nomenclature put forward by Franck and Nonn for porphyrinic systems will be used.[21] According to this standard system, the name of porphyrinoids consists of three parts: 1) a number in square brackets corresponding to the number of π electrons in the shortest conjugation pathway, 2) a core name representing the number of pyrroles or other heterocycles in the overall system, and, 3) numbers in round brackets following the main name that specify the number of bridging carbon atoms between each pyrrole subunit, starting with the largest bridge. For example, porphyrin **1** would be named as [18]porphyrin(1.1.1.1), whereas sapphyrin **2** would be named as [22]pentaphyrin(1.1.1.1.0).

The focus of this presentation will be on synthesis, characterization, and basic chemical properties. However, where appropriate, potential uses of the systems in question will be highlighted, for example, in the important area of cation complexation, anion recognition, waste remediation, materials development, and biomedicine.

2. Historical Overview

The beginnings of expanded porphyrin chemistry can be traced back to R. B. Woodward and his research group. Their pioneering efforts directed towards the synthesis of vitamin B_{12} led to the serendipitous discovery of sapphyrin, a pentapyrrolic macrocycle (for example, **2**) that was first mentioned at the aromaticity conference in Sheffield, UK, 1966. In contrast to what might have been expected given its novel structure, sapphyrin wasn't introduced in a glamorous manner, rather, Woodward mentioned its isolation and characterization during the discussion period that followed his formal oral presentation.[22] As a result of being disclosed in this manner, sapphyrin does not appear in the conference proceedings. While appearing in theses and dissertations from Woodward's research group, systematic syntheses of sapphyrin were not published until much later on, when two





Jonathan L. Sessler received a B.S. degree in chemistry in 1977 from the University of California, Berkeley. He obtained a Ph.D. in organic chemistry from Stanford University in 1982 (supervisor: Professor James P. Collman). After postdoctoral research with Prof. Jean-Marie Lehn at L'Université Louis Pasteur de Strasbourg, France, he worked in the research group of Professor Iwao Tabushi in Kyoto, Japan. In 1984, he joined the faculty of The University of Texas at Austin, where he is now the Roland K. Pettit Centennial Professor of Chemistry. He has authored numerous publications and has co-founded two companies (Pharmacyclics, Inc. and Anionics, Inc.).



Daniel Seidel was born in Mühlhausen, Thüringen (Germany) in 1972 and studied chemistry at the Friedrich-Schiller-Universität Jena (1993–1998). His Ph.D. research at the University of Texas at Austin (1998–2002) under the supervision of Prof. Jonathan L. Sessler involved the synthesis of new expanded porphyrins with unprecedented structural features. In 2001, he received a University Co-op Award for Research Excellence and a Welch Academic Excellence Award. Currently, he is working as an Ernst Schering Postdoctoral Fellow in the research group of Professor David A. Evans at Harvard University.

 © 2003 Wiley-VCH Verlag GmbH & Co. KGaA, Weinheim

independent reports, one by Woodward and co-workers[23] and another, actually an earlier contribution by Broadhurst et al., were published.[24] However, it was not until 1990, when an improved synthesis of sapphyrin was described, that usable quantities of this macrocycle could be obtained.[25] The increased availability of sapphyrin spawned an enhanced interest in this macrocyle. In fact, a recent search with SciFinder for the keyword "sapphyrin" resulted in 147 hits, a number that reflects in microcosm some of the interest attendant to expanded porphyrin chemistry.

In addition to the synthesis and subsequent study of sapphyrin chemistry, which has recently been reviewed in detail,[7] there are many historical accomplishments that helped define the field of expanded porphyrin chemistry. One of these was the seminal characterization of uranyl-superphthalocyanine (**3**) by Day, Marks, and Wachter.[26] This system, obtained from a template synthesis employing phthalonitrile and uranyl salts, aroused considerable excitement at the time. Unfortunately, all attempts to generalize this chemistry (that is, produce complexes containing other metals) or to obtain the metal-free ligand met with failure. While this limited the study of superphthalocyanine itself, the very fact that it could be made helped inspire a number of other historically important developments, including the synthesis of pentaphyrin (for example, **4**) by Rexhausen and Gossauer,[27] the preparation of so-called platyrins (for example, **5**) by Berger and LeGoff,[28] and the generation of a whole series of "stretched" systems (for example, **6**) by Franck and co-workers.[21,29] Another important boost to the generalized area of porphyrin analogues came with the synthesis of porphycene (**7**) by Vogel et al. in 1986.[30] This first of now many porphyrin isomers represented a milestone in the chemistry of oligopyrrolic macrocycles and helped highlight the fact that porphyrin analogues need not be expanded to be interesting. This point was subsequently underscored when the research groups of Furuta[11] and Latos-Grażyński[12] independently reported the synthesis of so-called "inverted" or "N-confused" porphyrin (**8**). More recently, it has been highlighted by the synthesis of a range of heteroporphyrin systems, including derivatives of carbaporphyrin.[16,17] Although the chemistry of porphyrin analogues is tremendously interesting, they are excluded from this review for the reasons outlined above.

The synthesis of texaphyrin (**9**) is particularly noteworthy in the area of expanded porphyrins.[5] It was the first expanded porphyrin to display a diverse metalation chemistry, a property that had been hoped for (but not seen) with the earlier expanded porphyrins, such as sapphyrin. On a different level, hexaphyrin (**10**)[31] and rubyrin (**11**)[32] were important because they were the first expanded porphyrins to contain more than five pyrrolic subunits. They thus served as auguries for the arrival of yet larger oligopyrrolic systems. This latter promise was first realized in the case of turcasarin (**12**),[33] a decapyrrolic system that adopts a twisted "figure-eight" conformation both in solution and in the solid state. While eclipsed now in terms of size, turcasarin remains of historical importance because it showed that pyrrole-containing macrocycles need not to be flat or nearly flat to demonstrate features characteristic of full conjugation.

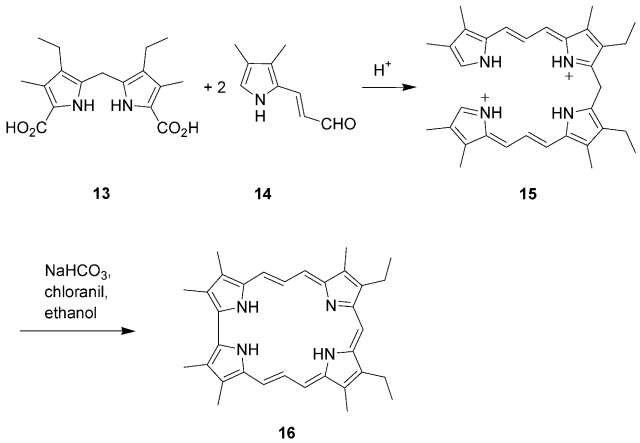
While the above contributions are those that most directly helped spawn the growth of the field, it is to be appreciated that there are many other earlier contributions of importance that, sadly, are simply too numerous to detail here. The interested reader is referred to various reviews that cover the chemistry of oligopyrrolic macrocycles synthesized prior to 1998.[2,3,8,21]

3. Systems Containing Four or Fewer Heterocyclic Subunits

Most of the work on expanded porphyrins containing four pyrrole rings or other heterocycles was done early on when the main motivation was to analyze the aromaticity of the resulting systems. While most of the relevant chemistry has been covered in review articles,[2,3,8,21] there are a few new examples of expanded porphyrin-type macrocycles whose synthesis was inspired by just these kinds of issues.

3.1. [22]Porphyrin(3.1.3.0)

In 1999, Paolesse, Smith, and co-workers reported the synthesis of a bisvinylogous corrole, [22]porphyrin(3.1.3.0) (**16**), which they described as the first expanded corrole.[34] Strictly speaking, this is not formally true since, depending on the definition employed, such venerable systems as sapphyrin, rubyrin, and even porphyrin and its isomers constitute "expanded corroles". Nonetheless, macrocycle **16** represents an important new addition to the expanded porphyrin family. It was obtained in 54% yield by the oxidative coupling of **15** with chloranil (tetrachloro-*p*-benzoquinone) in ethanol using $NaHCO_3$ or sodium acetate as a base (Scheme 1). Precursor



Scheme 1. Synthesis of expanded corrole **16**.

15, in turn, was obtained in 75% yield from the acid-catalyzed condensation of two equivalents of **14** with **13**. Interestingly, along with the isolation of **16**, a small amount of the corresponding bisvinylogous porphyrin was obtained, which

 © 2003 Wiley-VCH Verlag GmbH & Co. KGaA, Weinheim

was rationalized in terms of cleavage and recombination reactions involving **15**.

As expected for a system with a 22 π-electron periphery, the presence of a diatropic ring-current effect was evident in the ^{1}H NMR spectrum of the hydrochloride salt of **16** (H(**16**$^+$)·Cl$^-$). For example, the inner CH protons were found to resonate at $\delta = -9.2$ ppm, while the signals corresponding to the outer CH protons were found to resonate at $\delta = \sim 11$ ppm. The results are similar to what was found for the analogous bisvinylogous porphyrin **6** ($n = 0$) reported by Franck and co-workers.[29] Further support for the aromatic nature of **16** was obtained from UV/Vis spectroscopic analyses. The spectrum of **16** was found to contain a strong, split transition with two absorption maxima at $\lambda_{max} = 468$ and 496 nm, which presumably corresponds to the intense, formally allowed, B, or Soret band seen in the spectra of porphyrins. This high-energy absorption feature is accompanied by two bands of lesser intensity at $\lambda_{max} = 666$ and 714 nm, which are considered analogous to the weaker, so-called Q bands seen at lower energy in the spectra of porphyrins (Figure 1). Characterization by X-ray analysis (Figure 2)

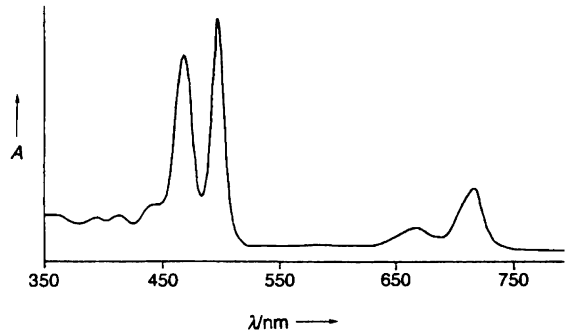


Figure 1. UV/Vis spectrum of **16**.[34].

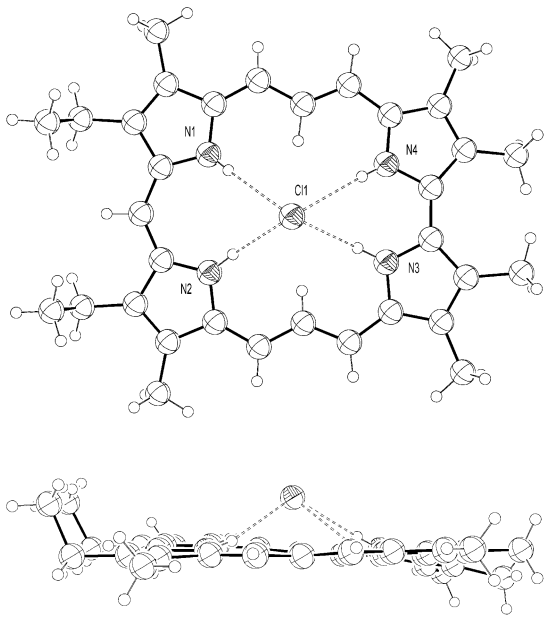
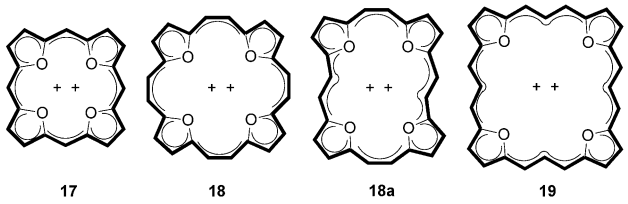


Figure 2. Front (top) and side (bottom) views of the solid-state structure of H(**16**$^+$)-Cl$^-$.[34] Unless stated otherwise this and all subsequent figures showing solid-state X-ray crystallographic structures were generated using information downloaded from the Cambridge Crystallographic Data Centre. Thermal ellipsoids are scaled to the 50% level.



revealed unambiguously that H(**16**$^+$)·Cl$^-$ is almost perfectly planar and exists as a dimer in the solid state. Interestingly, the parent peak in the FAB mass spectrum of H(**16**$^+$)·Cl$^-$ corresponds to this dimer with the loss of one chloride ion.

3.2. Tetraoxa[22]porphyrin(2.2.2.2) Dication, Tetraoxa[26]porphyrin(3.3.3.3) Dication, and N,N′,N″,N‴-*Tetramethyl[26]porphyrin(3.3.3.3) Dication*

Intrigued by the exceptional spectroscopic properties of the *N,N′,N″,N‴*-tetramethyl[26]porphyrin(3.3.3.3) dication (**21**) described by Franck and Nonn,[21] the research group of Vogel was prompted to reinvestigate some of its chemical features as well as those of related species.[35,36] Here, the motivating goal was to perform a spectroscopic comparison between the D_{4h}-symmetric tetraoxa[18]porphyrin dication **17** and its homologues, the *all-cis*-tetraoxa[22]porphyrin(2.2.2.2) dication (**18**) and the tetraoxa[26]porphyrin(3.3.3.3) dication (**19**).

As anticipated by the authors, the synthesis of **18** proved elusive. Efforts to prepare it gave rise to a compound reported earlier by Märkl et al.,[37] namely the *cis,trans,cis,trans* isomer **18a**. Compound **18** was calculated to be 90 kcal mol^{-1} higher in energy than its bis-*trans* isomer **18a**. A crystal structure of the octaethyl derivative of the latter compound was reported, which revealed its almost perfect planarity (Figure 3).

Interesting results were obtained from an analysis of the UV/Vis spectra of the octaethyl derivatives of **17**, **18a**, and **19** (Figure 4). Extraordinarily sharp Soret-type bands were observed in the spectra of **17** ($\lambda_{max} \approx 400$ nm) and **19** ($\lambda_{max} = 525$ nm). For these latter bands, record extinction coefficients were observed ($\varepsilon = 1.6 \times 10^6$ and 1×10^6 M^{-1} cm^{-1} for **17** and **19**, respectively). A split Soret band ($\lambda_{max} = 456$ and 474 nm) that exhibits a reduced extinction coefficient ($\varepsilon \approx 0.5 \times 10^6$ M^{-1} cm^{-1}) was observed in the spectrum of **18a**, with its lower (C_{2h}) symmetry, relative to **17** and **19**. It is noteworthy that the Q-type bands for all three systems are characterized by intensities that are significantly lower than those of the corresponding Soret-type bands.

Structural and spectroscopic comparisons between the *N,N′,N″,N‴*-tetramethyl[26]porphyrin(3.3.3.3) dication (**20**) and the octaethyltetraoxa[26]porphyrin(3.3.3.3) dication (**21**) were made.[36] While the X-ray structure of **20** (Figure 5) revealed the presence of a nearly planar macrocyclic frame-

 © 2003 Wiley-VCH Verlag GmbH & Co. KGaA, Weinheim

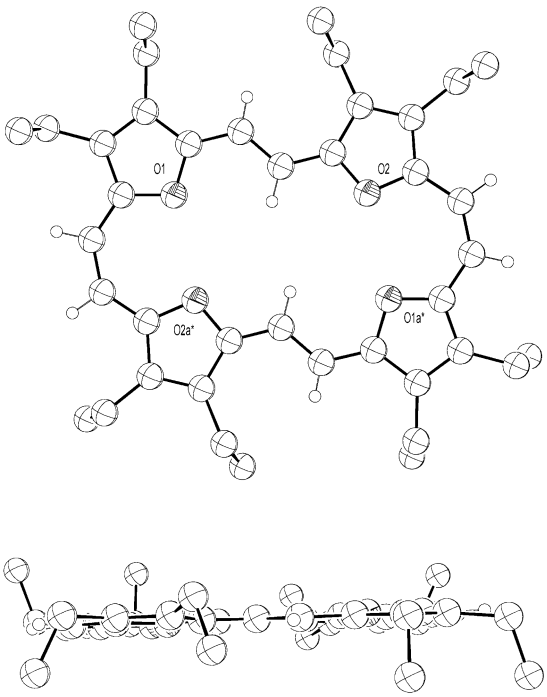


Figure 3. Front (top) and side (bottom) views of the solid-state structure of **18a** (octaethyl derivative).[35]

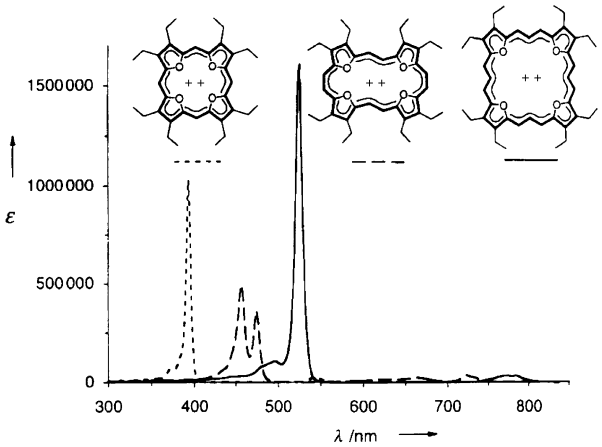
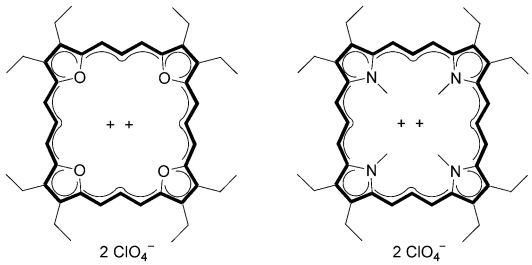


Figure 4. UV/Vis spectra of octaethyl derivatives of **17**, **18a**, and **19**; ε is in $M^{-1}cm^{-1}$.[35]



20 **21**

work with only slight deviation from the expected D_{4h} symmetry, a corresponding structural analysis of **21** (Figure 6) revealed a macrocycle that is in the shape of a flat bowl. In the latter case, all four pyrrole rings were found to point in the

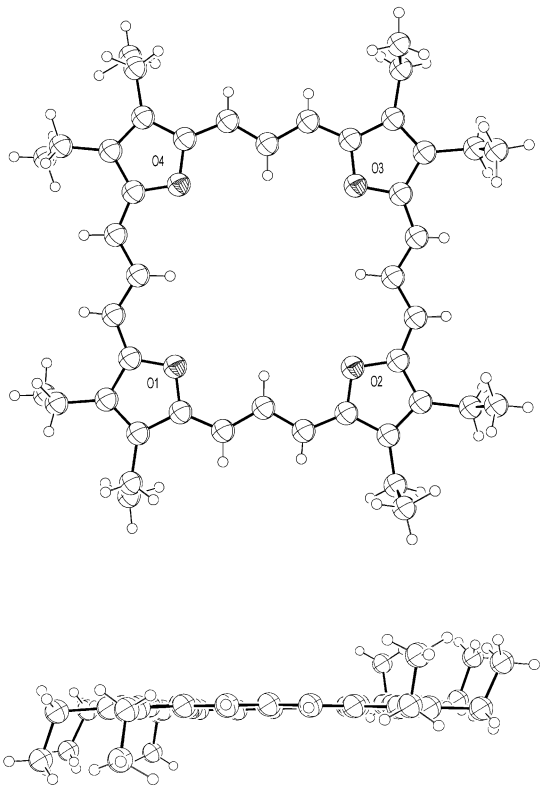


Figure 5. Front (top) and side (bottom) views of the solid-state structure of **20**.[36]

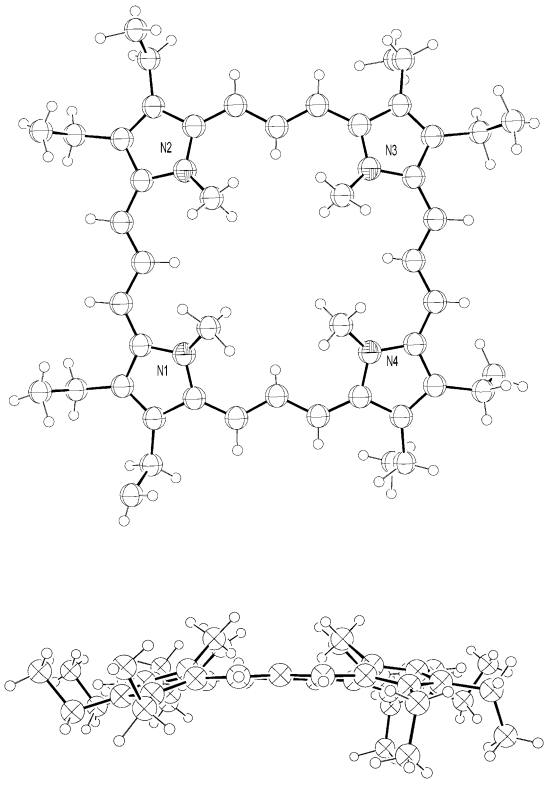


Figure 6. Front (top) and side (bottom) views of the solid-state structure of **21**.[36]

 © 2003 Wiley-VCH Verlag GmbH & Co. KGaA, Weinheim

same direction, being tilted up out of the median plane of the macrocycle by 16–19°. It is these deviations from planarity that are proposed to account for an interesting finding, namely that the Soret-type band of **21** is less intense by a factor of about 0.6 than that of **20**, while the position of this transition remains almost the same for these two compounds (Figure 7; $\lambda_{max} \approx 525$ nm for **20** and **21**).

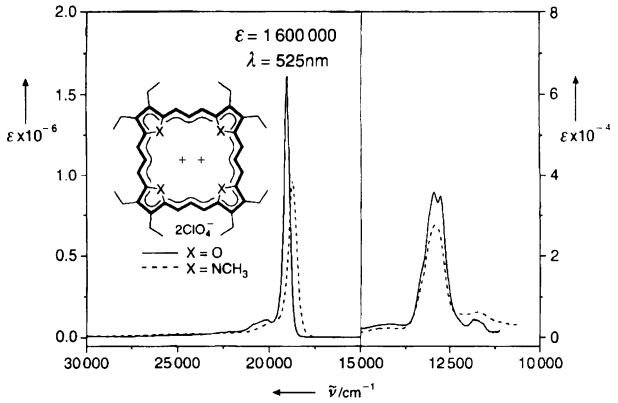
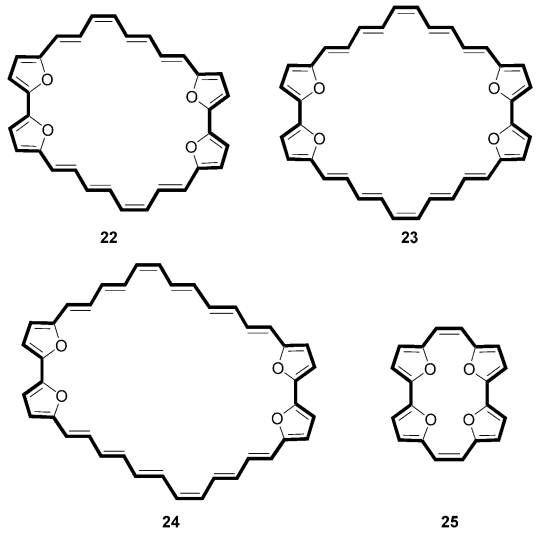


Figure 7. UV/Vis spectra of **20** and **21**.[36]

The ^{1}H NMR spectra of **20** and **21** are characterized in both cases by the presence of strong diamagnetic ring-current effects. In particular, $\Delta\delta$ values of 25.5 and 26 ppm are observed for the inner and outer perimeter protons of **20** and **21**, respectively. Such chemical shift differences were considered consistent with the proposed aromaticity of the compounds. To provide support for this conclusion the corresponding two- and four-electron reduction products of **20** and **21** were generated in situ by reduction with potassium in THF. As expected, remarkable reversals of the chemical shifts were observed for the formally antiaromatic two-electron reduction products (28 π-electron systems) produced from **20** and **21**: the signals ascribed to the inner CH protons were shifted to lower fields than in **20** and **21**, while those for the outer CH protons were shifted to higher fields. As a result, the $\Delta\delta$ values for the two two-electron-reduced species formed from **20** and **21** are 14 and 13.4 ppm, respectively. Spectral features consistent with aromaticity are restored in the four-electron-reduction products of **20** and **21**, with $\Delta\delta$ values for these formal 30 π-electron species comparable to those of the parent 26 π-electron systems **20** and **21**.

3.3. Tetraepoxy[32]annulene(8.0.8.0), Tetraepoxy[36]annulene(10.0.10.0), Tetraepoxy[40]annulene(12.0.12.0), and Their Corresponding Dications

Prior to the above studies, Märkl et al. sought to investigate the limits of antiaromaticity and aromaticity as they relate to heteroannulenes through the synthesis and study of tetraepoxy[4*n*]annulenes and their corresponding dications. These efforts led to the successful syntheses of tetraepoxy[32]annulene(8.0.8.0) (**22**), tetraepoxy[36]annulene(10.0.10.0) (**23**), and tetraepoxy[40]annulene(12.0.12.0) (**24**). All three compounds were obtained through a double Wittig-type cyclization of appropriately designed precursors.[38]



It was concluded from ^{1}H NMR spectroscopic analyses that macrocycles **22** and **23** exist as a mixture of several configurational isomers (only one of which is shown for each macrocycle). Perhaps more importantly, these ^{1}H NMR analyses completed the spectral comparison of the full homologous sequence of furan macrocycles ranging from tetraepoxy[20]annulene(2.0.2.0) (**25**) to tetraepoxy[36]annulene(10.0.10.0) (**23**). Here it was found that the observed paratropic character (a generally accepted experimental indicator of antiaromaticity), specifically the $\Delta\delta$ values between the outer and inner CH protons, decreases steadily on going from **25** to **22**. This result is expected given the increased conformational flexibility (for example, deviation from planarity) associated with the larger systems. Curiously and rather unexpectedly, however, the $\Delta\delta$ value observed for **23** is larger than that seen for its smaller congener **22**. However, the authors note that there is some uncertainty associated with the $\Delta\delta$ values for **23**; thus, they did not speculate as to the meaning of the differences in the $\Delta\delta$ values between **22** and **23**. While further insight into the issue could come from an analysis of **24**, the latter species proved too insoluble to allow for its analysis by ^{1}H NMR spectroscopy. Compound **24** was, however, characterized by mass spectrometry and UV/Vis spectroscopy, and found to display features consistent with its proposed antiaromatic structure. In particular, it fit the trend expected by the authors, namely that the λ_{max} values of furan annulenes are red-shifted by approximately 12 nm upon the synthetic "insertion" of each pair of −C=C− spacers.

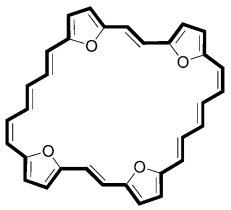
Oxidation of **22**–**24** to the corresponding dicationic species was accomplished by treatment with 2,3-dichloro-5,6-dicyano-1,4-benzoquinone (DDQ) in $CHCl_3$ or THF. The ^{1}H NMR spectra of these dications were recorded and were found to be consistent with aromatic character that was

 © 2003 Wiley-VCH Verlag GmbH & Co. KGaA, Weinheim

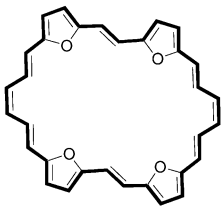
structure-dependent. The recorded $\Delta\delta$ values were found to increase with increasing ring size for what was believed to be the *all-E* series of isomers. The $\Delta\delta$ value of the largest dication, tetraoxa[38]porphyrin(12.0.12.0), the two-electron-oxidation product of **24**, amounts to 25.17 ppm. Interestingly, the basic correlation between size and $\Delta\delta$ values is reversed for a different set of isomers containing an increased number of *Z* double bonds compared to the predominantly *E* arrangement shown for **22**–**24**. The $\Delta\delta$ values were found to decrease with increasing ring size. In this series of macrocycles, the λ_{max} values of the Soret-type bands were found to undergo a linear bathochromic shift with an increment $\Delta\lambda$ of 58 nm per two additional double bonds. Meanwhile, the absorptions of the most intense Q-type band of each of these dications were also found to increase in a linear manner with a 160 nm increment per pair of double bonds inserted. Taken in concert, these findings highlight that spectroscopic features consistent with antiaromaticity continue to remain important for large heteroannulene systems with π-electron pathways of up to 40 electrons (at least), while those associated with aromaticity (for example, diatropic ring-current effects) are important in furan–annulene dications containing up to at least 38 π electrons.

3.4. Tetraepoxy[32]annulene(6.2.6.2) and Tetraoxa[30]porphyrin(6.2.6.2) Dication

The synthesis of tetraepoxy[32]annulene(6.2.6.2) (isomers **26a** and **26b**) is described in another contribution by Märkl et al.[39] These species were also obtained by a double Wittig reaction involving, in this case, (*E,E,E*)-5,5′-(hexa-1,3,5-triene-1,6-diyl)bis[furan-2-carbaldehyde] and its corresponding bisphosphonium salt. Proton NMR spectroscopic studies of macrocycles **26a** and **26b** revealed their antiaromatic character, as well as their inherent lack of conformational rigidity.[39]



26a



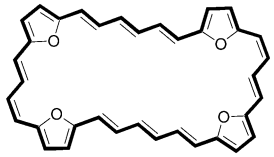
26b

Oxidation of **26a** and **26b** with DDQ gives rise to the tetraoxa[30]porphyrin(6.2.6.2) dication, which is obtained as a mixture of no less than four configurational isomers. A ^{1}H NMR spectroscopic analysis of these latter species revealed ring-current effects consistent with aromaticity, with $\Delta\delta$ values of 26.8, 25.8, and 21.1 ppm being observed for the three most abundant isomers. Further support for the proposed aromatic nature of this mixture came from a UV/Vis spectroscopic analysis. Here, the observation of Soret-type bands at 550 nm, accompanied by Q-type bands between 896 and 1039 nm, was considered as evidence for the presence of at least one aromatic species.

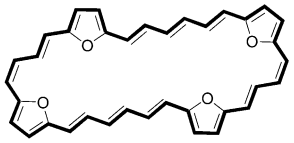
As a complement to these studies, an attempt was made to prepare tetraepoxy[32]annulene(6.2.6.2) (**26**) by the McMurry coupling of (*E,E,E*)-5,5′-(hexa-1,3,5-triene-1,6-diyl)bis[furan-2-carbaldehyde]. Instead of the desired product, a dihydro analogue of **26** was obtained. Oxidation of this latter species with DDQ gave a tetraoxa[30]porphyrin(6.2.6.2) dication, along with a small amount (3%) of what was believed to be a tetraoxa[31]porphyrin(6.2.6.2) radical cation. This radical cation was characterized by ESR spectroscopy.

3.5. Tetraepoxy[36]annulene(6.4.6.4) and Tetraoxa[34]porphyrin(6.4.6.4) Dication

Märkl et al. have also reported the synthesis of tetraepoxy[36]annulene(6.4.6.4) (**27**).[40] As seen for its smaller congener, tetraepoxy[32]annulene(6.2.6.2) (**26**), this furan-containing annulene was obtained in the form of an inseparable mixture of isomers, for example, **27a** and **27b**. The observed paratropicity of **27a** and **27b** is rather low ($\Delta\delta = 2.3$–3.3 ppm), but nevertheless was considered to be evidence for antiaromaticity. If such an interpretation is correct, **27a** and **27b** would represent the largest antiaromatic systems prepared to date.



27a



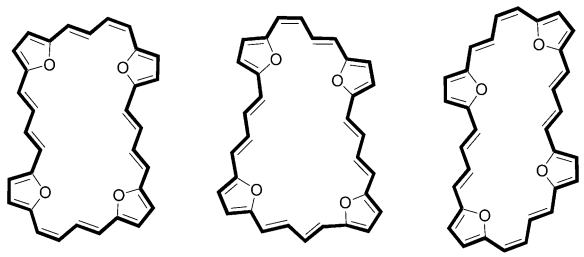
27b

Oxidation of **27a** and **27b** results in the formation of the corresponding dications. The ^{1}H NMR spectra of these dications are characterized by spectacular diatropic ring-current effects that were considered consistent with a strong aromatic character. Specifically, $\Delta\delta$ values of 26.6 and 25.3 ppm are observed for these two cations, respectively, which match those seen in the dication **21** prepared by Franck and Nunn and its homologous *N,N′,N″,N‴*-tetramethyl[34]-porphyrin(5.5.5.5) dication (not shown).[21]

3.6. Tetraepoxy[32]annulene(4.4.4.4) and Tetraoxa[30]porphyrin(4.4.4.4) Dication

Another contribution from the Märkl research group describes the synthesis of the tetraepoxy[32]annulene(4.4.4.4).[41] As is true for the other furan-containing annulenes prepared by Märkl et al., tetraepoxy[32]annulene(4.4.4.4) exists as a mixture of at least three different isomers (for example, **28a**–**c**), all three of which display antiaromaticity as judged from ^{1}H NMR spectroscopic analyses. Exposure of this isomeric mixture to DDQ produces the expected mixture of corresponding tetraoxa[30]porphyrin(4.4.4.4) dications; these species were judged to be

 © 2003 Wiley-VCH Verlag GmbH & Co. KGaA, Weinheim

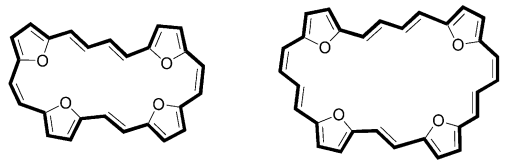


28a 28b 28c

aromatic based on the observation of $\Delta\delta$ values of approximately 25–27 ppm in their respective ^{1}H NMR spectra.

3.7. Tetraepoxy[26]annulene(4.2.2.2) and Tetraepoxy[30]annulene(4.4.4.2)

Recently, Märkl et al. reported the synthesis of tetraepoxy[26]annulene(4.2.2.2) (**29**) and tetraepoxy[30]annulene(4.4.4.2) (**30**).[42] This work is noteworthy since, unlike



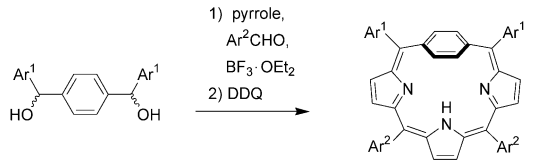
29 30

the other tetraepoxyannulene systems discussed above, **29** and **30** possess $4n+2$ π-electron pathways in their neutral forms. Thus, as expected, these systems display diatropic ring-current effects in their corresponding ^{1}H NMR spectra, with $\Delta\delta$ values of 6.4 and 4.3 ppm being seen for **29** and **30**, respectively. On the other hand, as is true for other furan–annulene systems, ^{1}H NMR studies of **29** and **30** revealed evidence for highly flexible structures and the presence of isomers.

The presence of isomers complicates an analysis of **29** and **30**, as it does for the other systems reported by the Märkl research group. Nonetheless it is clear that **29** and **30** display rather low $\Delta\delta$ values as compared to related aromatic dicationic species (for which $\Delta\delta$ values of about 25 ppm are routinely observed). This rather large disparity was rationalized in terms of the greater planarity presumed to exist in the dications as the result of the stabilization ostensibly provided by the positive charges. Although such rationalizations cannot be discounted, a more plausible explanation is that the number of accessible aromatic resonance structures for the various dicationic furan–annulene species is much larger than for either **29** or **30**, for which only two resonance structures can reasonably be drawn.

3.8. Tetraphenyl-p-benziporphyrin

To date, systems that contain fewer than four heterocyclic subunits and which meet our definition of expanded porphyrins have been few in number. This is particularly true for carbon-linked systems. However, Latos-Grażyński and coworkers have very recently reported the synthesis of a hitherto unknown carbaporphyrinoid (**32**).[43] The $BF_3{\cdot}OEt_2$-catalyzed reaction of the dialcohol **31** with pyrrole and aldehyde followed by oxidation with DDQ, gave rise to **32** in approximately 1% yield (Scheme 2).



31

32a: Ar^1 = Ph, Ar^2 = Ph
32b: Ar^1 = *p*-Tol, Ar^2 = Ph
32c: Ar^1 = *p*-Tol, Ar^2 = *p*-Tol

Scheme 2. Synthesis of macrocycles **32** containing *p*-phenylene groups.

The ^{1}H NMR spectrum of **32a** recorded at 168 K was consistent with the presence of a diatropic ring current. It was found that the outer phenyl-CH protons exhibit shifts that are markedly different from those displayed by the corresponding inner phenyl-CH protons ($\delta = 7.68$ and 2.32 ppm, respectively). At higher temperatures these two signals coalesce into a singlet, presumably as the result of a dynamic process involving rotation of the phenyl ring.

X-ray crystallographic analyses of **32b** and the bis-HCl salt of **32a** revealed that these systems are nonplanar, at least in the solid state (Figures 8 and 9). The phenyl subunit was found to be displaced from the mean plane of the macrocycle, with dihedral angles of 48° and 44° being seen in the case of **32b** and **32a**·2 HCl, respectively.

Macrocycle **32** represents an intriguing system that is quite possibly the first example of a potentially large family of *p*-phenylene-containing expanded porphyrins. While this promise remains to be realized, it is important to appreciate that the utility of **32** as a metal receptor has already been demonstrated, at least in preliminary studies. The CdCl complex of **32a** could be stabilized and the X-ray crystal structure of this complex determined (Figure 10). The metal cation was found to be coordinated within a distorted trigonal bipyramidal ligand environment, comprised of the three nitrogen atoms of the ring, the chloride counterion, and a double bond from the phenylene subunit which acts as a π donor.

3.9. Latest Developments in the Chemistry of Texaphyrins

3.9.1. Synthesis of a Metal-Free Texaphyrin

Texaphyrin is one of the best studied expanded porphyrins. The gadolinium(III) and lutetium(III) complexes of texaphyrins are in advanced clinical trials as adjuvants for the

 © 2003 Wiley-VCH Verlag GmbH & Co. KGaA, Weinheim

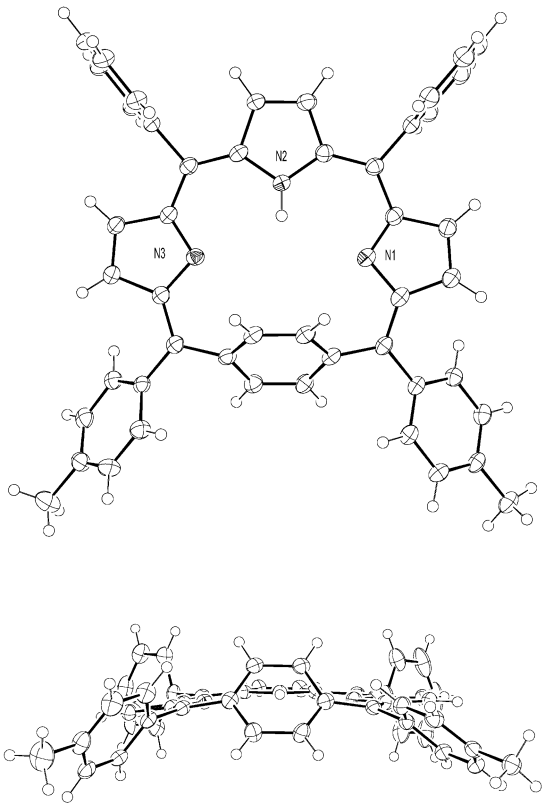


Figure 8. Front (top) and side (bottom) views of the solid-state structure of **32b**.[43]

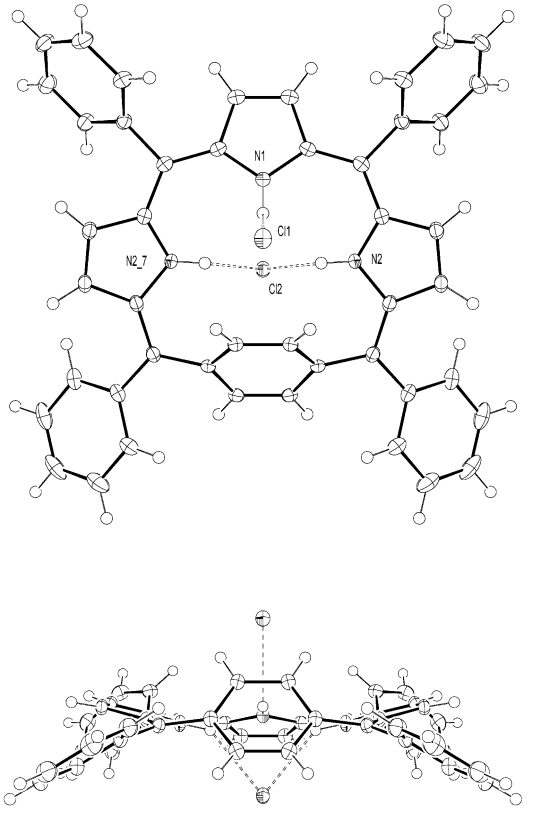


Figure 9. Front (top) and side (bottom) views of the solid-state structure of **32a**·2 HCl.[43]

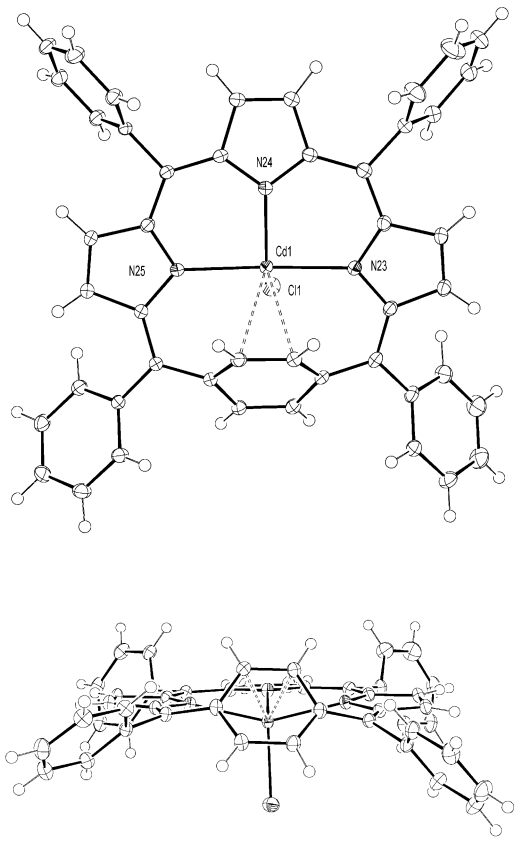
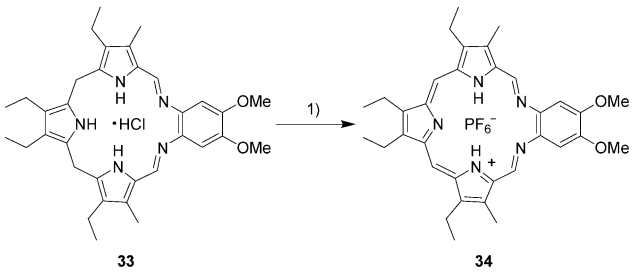


Figure 10. Front (top) and side (bottom) views of the solid-state structure of a Cd complex derived from **32a**.[43]

radiation- and irradiation-based treatment of cancer and cardiovascular disease (see Section 3.9.4).[6,44–47] Other metal complexes are of interest as potential peroxynitrite decomposition catalysts and for their inherent structural features.[48–50] As a consequence, the preparative chemistry of metallotexaphyrins has been well studied. Until recently, however, the metal-free aromatic form of the macrocycle was not available. In 2001, 13 years after its original discovery, the preparation of this elusive species was finally achieved.[51] Addition of four equivalents of ferrocenium hexafluorophosphate to a solution of the so-called "sp^3-texaphyrin" (**33**) in acetonitrile under argon in the presence of 2,6-lutidine yielded the metal-free texaphyrin in the form of its monoprotonated HPF_6 salt (**34**) in 56% yield (Scheme 3).



33 **34**

Scheme 3. Synthesis of the metal-free texaphyrin **34**: 1) $[Cp_2Fe][PF_6]$, 2,6-lutidine, CH_3CN. Cp = cyclopentadienyl.

 © 2003 Wiley-VCH Verlag GmbH & Co. KGaA, Weinheim

Support for the proposed aromatic nature of **34** was obtained from its ^{1}H NMR spectrum recorded in CD_3CN. A broad resonance at $\delta = 9.27$ ppm was assigned to the *meso* protons, while the signal at $\delta = 10.52$ ppm was assigned to the imine protons. These chemical shifts were considered consistent with the proposed aromatic character. Also indicative of aromaticity is the upfield position of the two magnetically degenerate NH protons at $\delta = -5.66$ ppm.

Another product of the oxidation reaction was the bis-HPF_6 salt of the metal-free texaphyrin, which was isolated in approximately 20% yield. The free-base form of the metal-free texaphyrin could be prepared by treating a solution of **34** in acetonitrile with 10% aqueous NaOH. The spectral characteristics of the two species were found to be in agreement with their proposed aromatic structures. Additionally, the X-ray crystal structure of **34** (Figure 11) revealed

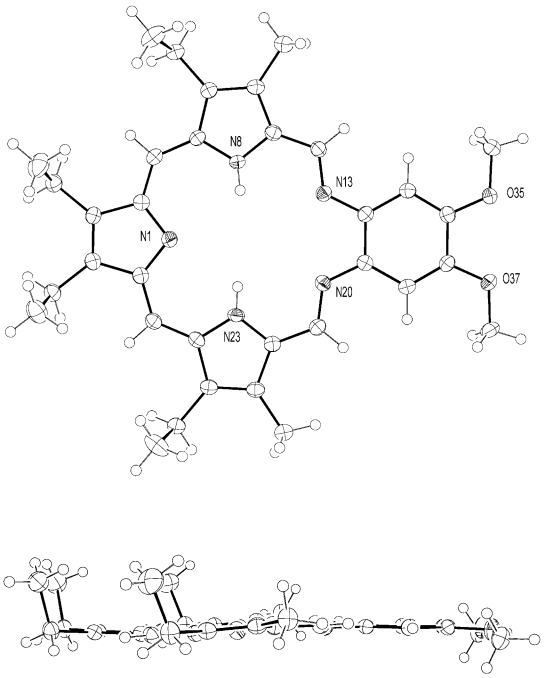
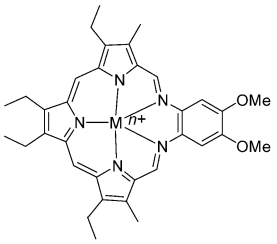


Figure 11. Front (top) and side (bottom) views of the solid-state structure of **34**.[51] For clarity, the hexafluorophosphate counterion is not shown.

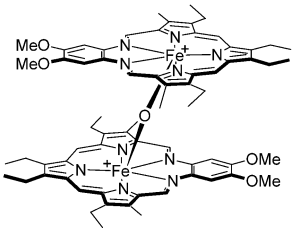
a macrocycle that was essentially flat and which was linked through sp^2-hybridized *meso* carbon bridges. The UV/Vis spectra of all three metal-free species are characterized by the presence of Soret- and Q-like bands in the 420–480 and 705–750 nm spectral regions, respectively. Thus, the spectra are very similar to what is typically seen for metallotexaphyrins. This observation supports the suggestion, advanced previously,[5] that the basic spectral features of texaphyrins are ligand, rather than metal, derived.

3.9.2. *Texaphyrin Complexes*

In addition to developing a synthetic approach to metal-free texaphyrins, efforts were made in recent years to explore in more detail the chemistry of complexes of texaphyrin with late first-row transition metals.[52] By using the same oxidative insertion methods used to generate the stable 1:1 lanthanide(III) texaphyrin complexes that were prepared and characterized in the late 1980s and early 1990s it proved possible to synthesize and isolate Mn^{II}, Co^{II}, Ni^{II}, Zn^{II}, and Fe^{III} complexes of texaphyrin **35**–**39** (water-soluble complexes were also prepared; not shown). While the Fe^{III} complex was obtained in the form of a μ-oxo bridged dimer, analogous to



$M^{n+} = Mn^{II}$ (**35**)
$M^{n+} = Co^{II}$ (**36**)
$M^{n+} = Ni^{II}$ (**37**)
$M^{n+} = Zn^{II}$ (**38**)



39

what is seen in the case of ferric porphyrins, the Zn^{II} complex **38** proved notable in that only three of the five texaphyrin nitrogen atoms were found to be coordinated in the solid state. This was the case whether a single nitrate anion or two methanol molecules (see Figure 12) were coordinated to the Zn^{II} center as ancillary ligands.

In contrast to the Zn^{II} complex **38**, X-ray diffraction analysis of the Co^{II} and Mn^{II} complexes showed that the texaphyrin ligand provided five, near-planar donor atoms, which resulted in structures that are either six or seven coordinate about the metal centers. A structure of the manganese complex **35** is shown in Figure 13. Apart the rather uncommon coordination mode, what is noteworthy about these two complexes is the oxidation state in which they are found. Whereas, Mn^{III} and Co^{III} porphyrins are normally more stable than the corresponding Mn^{II} and Co^{II} complexes, it is the lower oxidation state that is stabilized in the case of the texaphyrin species **35** and **36**. Presumably, this is the result of both reduced ligand charge (fully deprotonated metal-free texaphyrin represents a monoanionic ligand, whereas deprotonated porphyrins are dianionic ligands) and a propitious combination of core geometry and size.

Electrochemical analysis of the various transition-metal complexes texaphyrins revealed, as in the case of the lanthanide(III) complexes, reduction processes that were generally ligand, as opposed to metal, centered. However, the corresponding reduction waves were generally shifted cathodically by about 250–350 mV relative to the trivalent lanthanide complexes, with the Ni^{II} and Zn^{II} complexes approximately 75–125 mV easier to reduce than the Co^{II} and Mn^{II} species. In all cases, however, the transition-metal complexes of texaphyrins proved much easier to reduce than analogous metalloporphyrins, the difference being more than 500 mV in most cases.[53] Such findings are consistent

 © 2003 Wiley-VCH Verlag GmbH & Co. KGaA, Weinheim

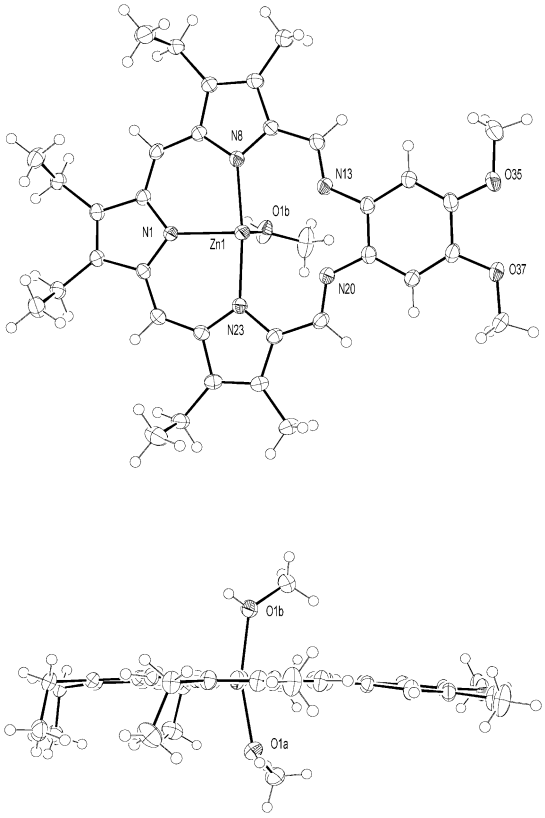


Figure 12. Front (top) and side (bottom) views of the solid-state structure of of complex [**38**-$(MeOH)_2$]NO_3^-.[52] For clarity, the nitrate counterion is not shown; in the top view, one coordinating methanol molecule is omitted.

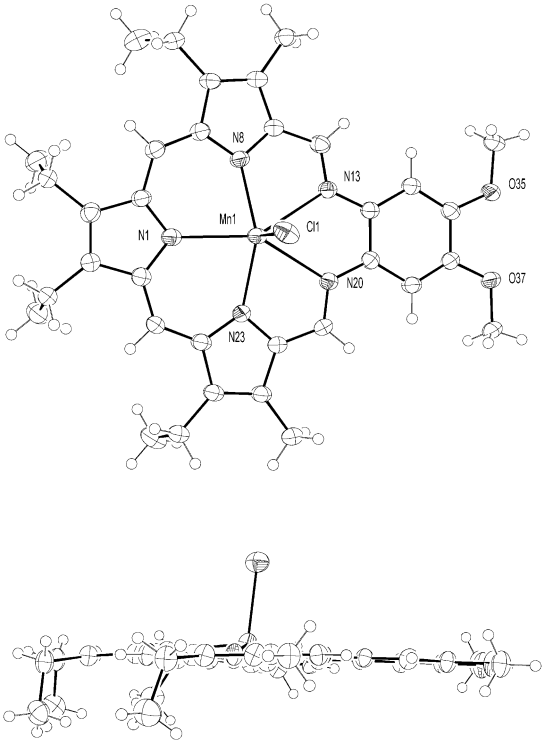
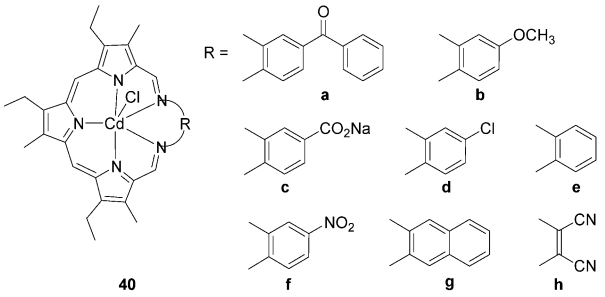


Figure 13. Front (top) and side (bottom) views of the solid-state structure of complex [**35**-Cl^-].[52] The corresponding Co^{II} chloride complex is nearly isostructural to the Mn^{II} complex shown.

with the proposal discussed in Section 3.9.5 that certain metallotexaphyrins, in particular an appropriately solublized Gd^{III} complex, could act to enhance the effects of ionizing radiation by capturing electrons and acting as a redox-cycling agent.[54]

3.9.3. Nonlinear Optical Properties of Texaphyrin

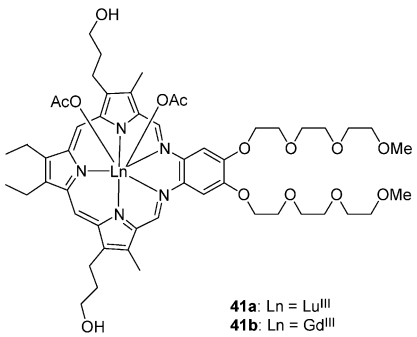
A different kind of new texaphyrin prepared in recent years by Lawson and co-workers is the functionalized cadmium complex **40a**.[55,56] This species **40a** (as well as



several analogues **40b**–**h**), which differs from the original Cd^{II} complexes by virtue of being far less symmetric, shows promise as a nonlinear optical material. In particular, it displayed a second-order hyperpolarizability of 9.7×10^{-31} esu when excited with picosecond pulses from a 532-nm laser, as well as a saturable absorption at high light fluence.

3.9.4. Medical Applications of Texaphyrins

In addition to the synthesis and study of new texaphyrin derivatives, considerable effort has been devoted to developing two known texaphyrin complexes, **41a** and **41b**. The first of these, the lutetium complex **41a**, known by its trade names

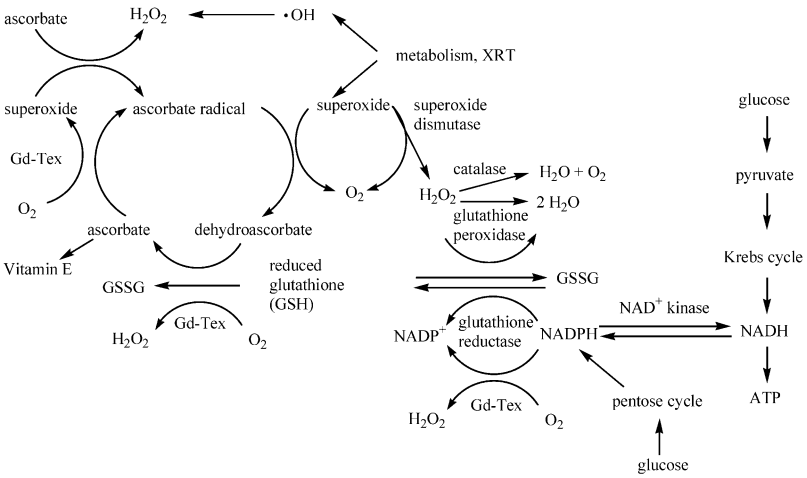


of lutrin and antrin, is being studied clinically by Pharmacyclics, Inc., as a potential photosensitizer for the treatment of cancer and cardiovascular disease. With a long-wavelength absorption maximum (ca. 732 nm), **41a** shows particular promise for the treatment of so-called vulnerable plaque, the hard-to-detect lesions that are thought responsible for as much as 80% of all myocardial infarctions.

 © 2003 Wiley-VCH Verlag GmbH & Co. KGaA, Weinheim

The second texaphyrin complex being developed for medical use is the gadolinium complex **41b**. Known by its trade and generic names of xcytrin and motexafin gadolinium (MGd), this species is currently available in large (>50 kg) quantities and is being studied by Pharmacyclics, Inc., as a potential adjuvant for radiation therapy. To date, MGd has been the subject of several clinical trials, including a recently completed Phase III trial involving patients with metastatic brain tumors.[6,44–47] This study, which involved 401 patients split into treatment and control groups, provided support for the notion that MGd together with whole brain radiation increased the average time to so-called neurological progression in patients by a factor of two or more whose primary disease was lung cancer relative to similar patients treated with whole brain radiation alone. In view of these positive findings, a confirmatory Phase III trial, involving patients with metastatic brain cancer whose primary cancer is lung cancer, has recently been launched. Meanwhile, clinical tests of MGd as a radiation enhancer for a range of other cancer types are ongoing (neuroblastoma, pediatric brain stem glioma, pancreatic cancer, non-small cell lung cancer). Many of these studies are being carried out in collaboration with the National Cancer Institute of the United States National Institutes of Health.

finding that xcytrin localized in lysosomes, endoplasmic reticulum, mitochondria, and Golgi apparatus,[58] rather than in the nucleus of cells, led to the consideration that it mediates its radiation-enhancing effect by acting as a metabolism-perturbing, redox-cycling agent as illustrated in Scheme 4.[54]



Scheme 4. Cellular antioxidant system showing the relationship of ascorbate, glutathione, and NADPH. The positions of proposed Gd-Tex interaction are indicated. Reactive oxygen species derived from radiolysis of water (XRT) or metabolism are also shown.[54]

3.9.5. *Mechanistic Studies of Gadolinium(III) Texaphyrin*

To support the clinical studies, considerable effort has been devoted in recent years to understanding the mechanism of action of xcytrin (**41b**), as well as the general physical chemical properties of lanthanide(III) texaphyrin complexes. In the latter context it was found that lanthanide(III) texaphyrins (abbreviated Ln-Tex in the general case where the substituents are different from those present in MGd) are substantially easier to reduce than porphyrins. (For example, the $E_{1/2}$ value for the gadolinium(III) complex was found to be relatively substituent independent and about −294 mV versus Ag/AgCl when recorded in DMSO in the presence of 0.1M tetrabutylammonium perchlorate.[53]) Furthermore, and perhaps more importantly, it was found that, once generated, the one-electron-reduced form of texaphyrin, Gd-Tex$^{+\bullet}$, was capable of reacting with oxygen to form superoxide in a fast, but slightly unfavorable equilibrium process [Eq. (1)].[57]

$$\text{Gd-Tex}^{+\cdot} + O_2 \rightleftharpoons \text{Gd-Tex}^{2+} + O_2^{-\cdot} \quad (1)$$

It was established independently that various biological reductants, including NADPH, glutathione, and, especially, the ascorbate anion, were capable of reducing the gadolinium(III) complex MGd under in vitro conditions to produce peroxide via what was presumed to be the intermediate formation of superoxide (a species that cannot be detected in normal cell-based studies). These results, coupled to the This mechanism of action is based on the consideration that texaphyrins localize selectively at tumor cells[59] and that such cells are already the subject of oxidative stress. Thus, as a result of 1) removing ascorbate and other reducing species that play a known role in protecting selectively against the effects of ionizing radiation in cancer cells and 2) producing concurrently peroxide, a recognized apoptosis-triggering agent, it was proposed that tumors would be rendered more responsive to radiation therapy.

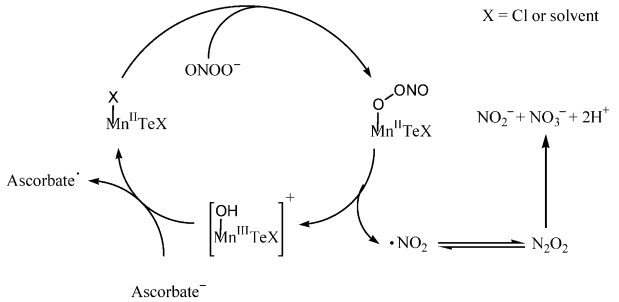
While the ultimate validity of the above mechanism remains to be established at the clinical level, one immediate consequence was the recognition that other cells subjected to oxidative stress, including those infected with HIV, could be preferentially destroyed by treatment with MGd. A first test of this hypothesis has now been carried out by Herzenberg, Magda, and co-workers, with the selective eradication of HIV-infected cells being demonstrated in vitro.[60]

3.9.6. *Mn-Tex as a Peroxynitrite Decomposition Catalyst*

Another consequence of the redox-cycling mechanism put forward in Scheme 4 was the appreciation that texaphyrins, in addition to acting as catalysts for the production of reactive oxygen species (for example, superoxide, peroxide), could be used to effect their removal. One such active oxygen species whose deleterious nature is increasingly coming to be appreciated is peroxynitrite. Formed in vivo as the result of the diffusion-controlled reaction between the superoxide anion and NO, peroxynitrite has been implicated in a wide range of diseases, including amyotrophic lateral sclerosis (ALS; Lou Gehrig's Disease), diabetes, and ischemia-reperfusion injury.[48–50] As a consequence, catalysts that can effect

 © 2003 Wiley-VCH Verlag GmbH & Co. KGaA, Weinheim

the catalytic decomposition of peroxynitrite are being actively sought. On the basis of precedent from the porphyrin literature, where water-soluble Mn^{III} and Fe^{III} complexes have been found to be effective catalysts for this purpose in vitro, the Mn^{II}–texaphyrin complex **35**, which has the same substitution pattern found in the Gd^{III}– and Lu^{III}–texaphyrin species being developed clinically, was tested for its catalytic efficacy. It was found to be as good or better than the analogous Mn^{III}–porphyrin complexes and, perhaps as a consequence of a different inferred mechanism of catalysis (the starting oxidation states of the metals are different), was found to produce fewer potentially toxic side products than the previously studied systems (Scheme 5).[52] As a consequence, this Mn^{II}–texaphyrin complex is currently being subjected to in vivo analysis with the aim of assessing its potential for treating ALS.



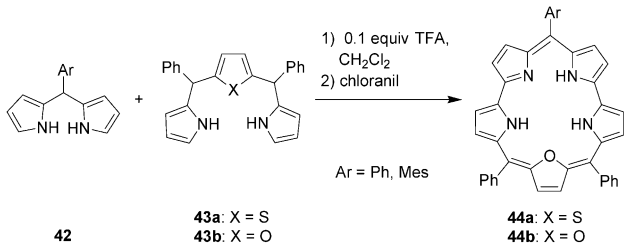
Scheme 5. Catalytic decomposition of peroxynitrite by a manganese–texaphyrin complex.

4. Systems Containing Five Pyrrole Rings

Pentapyrrolic macrocycles are among the most studied macrocycles in the generalized area of expanded porphyrins. In fact, the first expanded porphyrin ever reported, sapphyrin (**2**), possesses five pyrrole rings. Most of the early work involving this and other pentapyrrolic systems was carried out using materials bearing substituents in the β-pyrrolic positions. While important studies of such systems continue,[7] considerable effort in recent years, especially by the research group of Chandrashekar but also by others, has been devoted to developing strategies that allow access to various pentapyrrolic macrocycles and heteroatom analogues that bear *meso* substituents.

4.1. Heteroatom-Containing Smaragdyrins

Recently, Chandrashekar and co-workers reported the use of a mixed oxidative coupling strategy to prepare several previously unknown heteroatom-containing expanded porphyrins.[61] For example, an oxidative coupling between the heterotripyrranes **43** and the dipyrromethane **42** gives rise to heterosmaragdyrins (Scheme 6). In the case of the oxasmaragdyrin **44b** (Ar = Ph), the reported yields are as high as



42 **43a**: X = S, **43b**: X = O **44a**: X = S, **44b**: X = O

Scheme 6. Formation of heterosmaragdyrins **44**.

51 %, while for the corresponding thiasmaragdyrins, the yields are significantly lower, namely, 5 % for **44a** (Ar = Ph). The only other products from this reaction are oxa- or thiacorroles which are obtained in varying yields depending on the specific conditions. For example, the reaction conditions that give rise to oxasmaragdyrin **44b** (Ar = Ph) in 51 % yield also produces the corresponding oxacorrole in 3 % yield. The degree of control achieved in this reaction seems to be remarkable, as no other products that would be the result of self-coupling of either precursor were apparently obtained. In fact, several curious results were reported in a related paper that summarizes some of the above findings, including the fact that exposure of **43b** alone to the reaction conditions outlined above also gives rise to **44b** (Ar = Ph) in 3.5 % yield.[62] Thus, the presence of **42** is not an absolute requirement for success, although it is highly likely that it or species akin to it are formed in situ. The structure of oxasmaragdyrin **44b** (Ar = Ph) was characterized by X-ray analysis (Figure 14).

In a subsequent report, the Chandrashekar and co-workers describe the utility of **44b** (Ar = Ph) as a metal-complexing agent.[63] Specifically, a Ni^{II} complex as well as a $[Rh(CO)_2]$ complex of this formally trianionic ligand were described; the X-ray structure of the latter species is shown in

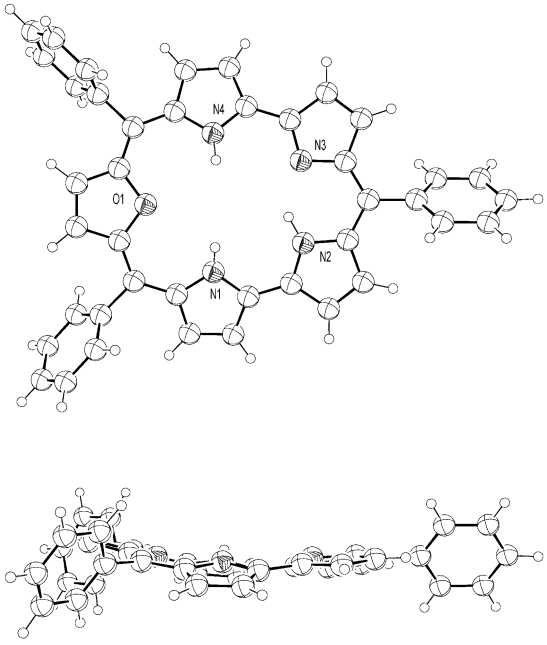


Figure 14. Front (top) and side (bottom) views of the solid-state structure of complex **44b** (Ar = Ph).[61]

© 2003 Wiley-VCH Verlag GmbH & Co. KGaA, Weinheim

Figure 15. In the same report, the possibility of using the protonated form of **44b** as an anion receptor was also noted (see Figure 16 for the X-ray structure).

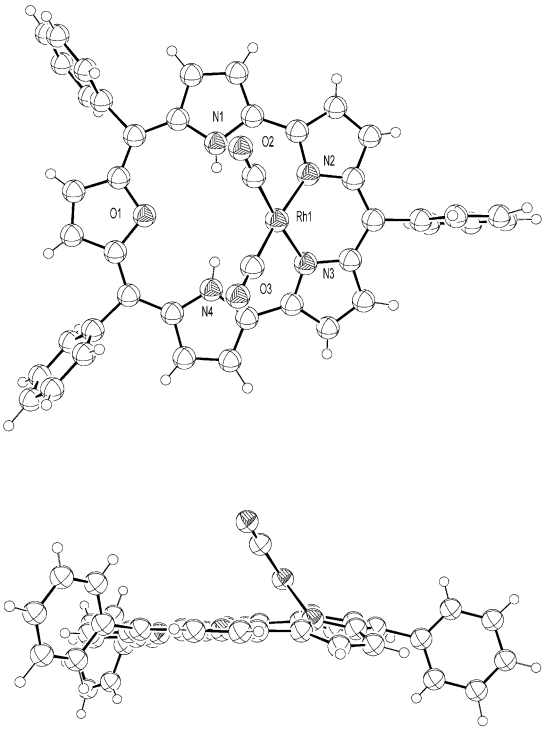


Figure 15. Front (top) and side (bottom) views of the solid-state structure of the $[Rh(CO)_2]$ complex complex derived from **44b** (Ar = Ph).[63]

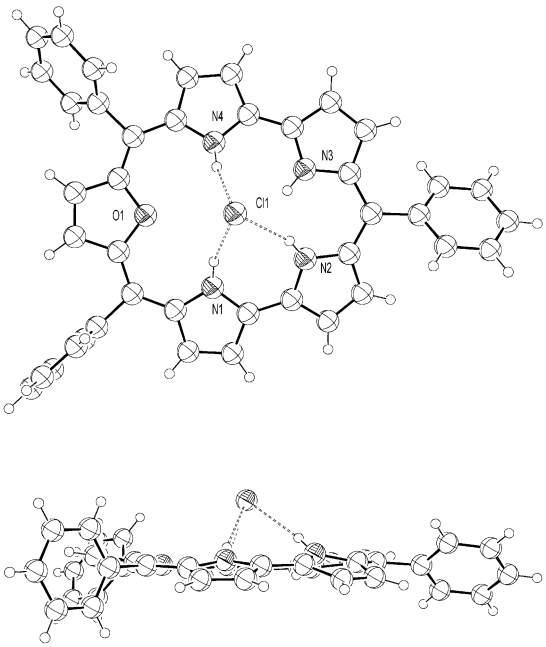
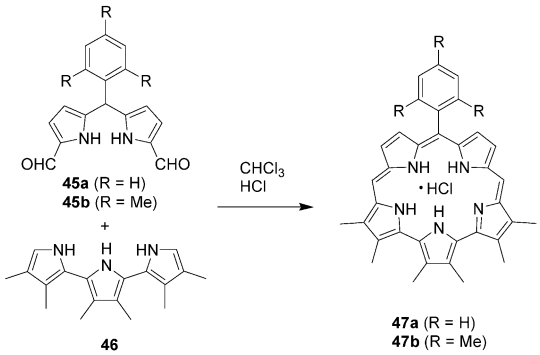


Figure 16. Front (top) and side (bottom) views of the solid-state structure of complex **44b**·HCl.[63]

4.2. Meso *Substituted [22]Pentaphyrin(1.1.1.0.0)*

Motivated by the finding that β-unsubstituted expanded porphyrins often display conformations that differ from their β-substituted congeners, a partially β-unsubstituted [22]pentaphyrin(1.1.1.0.0) **47** was recently prepared.[64] This macrocyclic product is both an isomer of smaragdyrin ([22]pentaphyrin(1.1.0.1.0)), one of the more venerable expanded porphyrins, and a new analogue of a general class of pentaphyrins recently described in the form of its all-β-alkyl-substituted variant.[65] As outlined in Scheme 7, con-



Scheme 7. Synthesis of partially *meso*-substituted isosmaragdyrins **47**.

densation of diformyldipyrromethanes **45a** or **45b** with hexamethylterpyrrole **46** under acidic conditions gave rise to the monoprotonated [22]pentaphyrins(1.1.1.0.0) **47a** and **47b** in yields of 44 or 38%, respectively.

While the spectral features of macrocycles **47** are in agreement with the presence of an aromatic 22 π-electron system (for example, three NH resonances are seen at $\Delta = -5.42$, -2.84, and -2.11 ppm in the ^{1}H NMR spectrum of **47b**), no inversion was evident in either the protonated or free-base forms. However, it was shown that adding increasing amounts of trifluoroacetic acid (TFA) to a solution of **47b** in $CDCl_3$ resulted in a second protonation event that gave rise to a new nonaromatic species. The structure of this latter product was assigned on the basis of ^{1}H NMR spectroscopic studies to a system wherein a proton had been added to one *meso*-carbon bridge to produce an sp^3-linked macrocycle. The structure of **47a** was further determined by an X-ray crystallographic analysis (Figure 17).

4.3. Heterosapphyrins

As for sapphyrin itself, many β-substituted heteroatom-containing sapphyrins (referred to here as heterosapphyrins) are now known. Many of these were reported early on and the relevant chemistry is covered in several reviews.[2,3,7,8] It is only in recent years, however, that a large number of *meso*-substituted sapphyrins and heterosapphyrins have been published. Most of these systems have been prepared by either classic MacDonald-type condensations and/or oxidative coupling procedures as detailed below. Almost all these new systems fit the general structures **48a** or **48b**.

 © 2003 Wiley-VCH Verlag GmbH & Co. KGaA, Weinheim

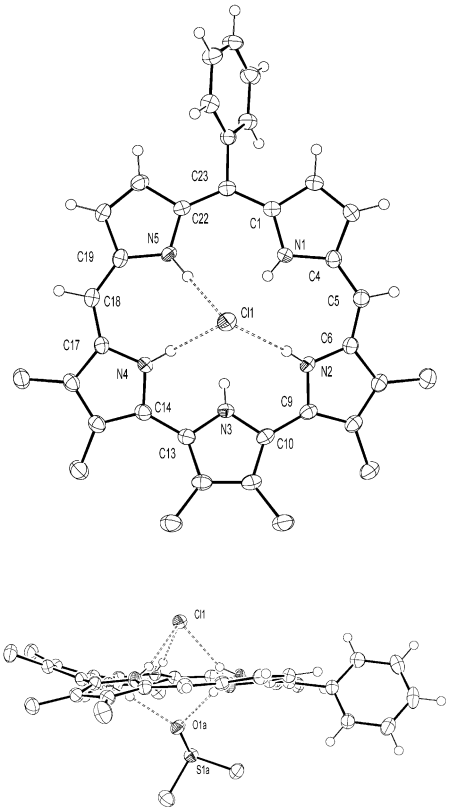
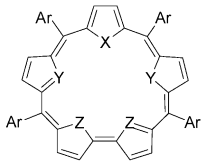


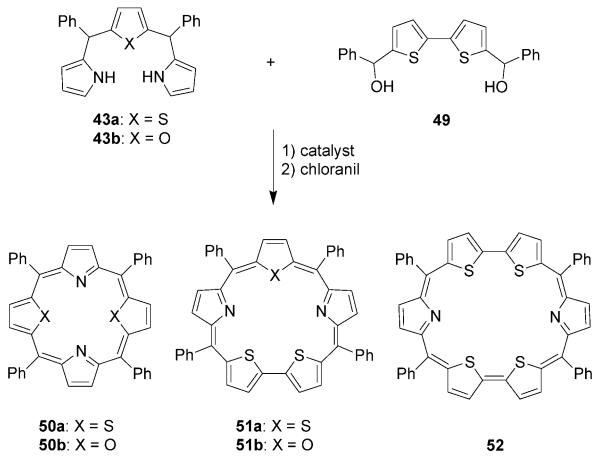
Figure 17. Front (top) and side (bottom) views of the solid-state structure of complex **47a**·DMSO.[64]



48a (X = Z = NH; Y = O, S, Se
48b (X = O, S, NH, NCH_3;
Y = NH, Z = S, Se)

In many of the heterosapphyrin-forming reactions, especially the ones that combine a partial hydrolysis of the starting materials with an oxidative coupling step, other macrocycles, such as heteroatom-containing rubyrins, are also obtained. Many of these hexapyrrolic macrocycles are of interest in their own right and are thus discussed explicitly in Section 5.2. However, such products only formed as minor by-products during various heterosapphyrin syntheses are presented, for the sake of simplicity, only in this Section.

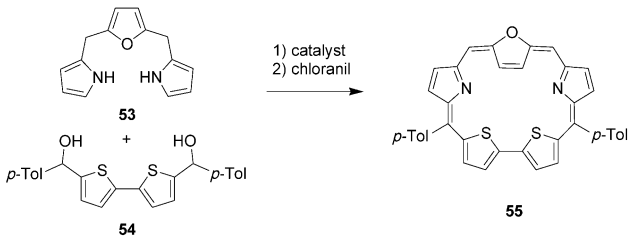
In early work that helped make the chemistry of *meso*-substituted sapphyrins more prominent, Chandrashekar and co-workers reported the synthesis of the two bithiophene systems **51a** and **51b**. As outlined in Scheme 8, the synthesis of these systems is based on the condensation of the heterotripyrrane **43** with the bithiophene diol **49**, followed by treatment with an oxidant.[66] While sapphyrins **51** are the expected products of this condensation, other macrocycles, specifically **52** and **50**, were obtained as well. The presence of **52** and **50** in the product mixture can be rationalized by partial hydrolysis and recombination of the starting materials. Interestingly, under conditions of Brønsted acid catalysis (for example, with, TFA or *p*-TsOH), the only products isolated were the diheteroporphyrins **50**. The best yields for **51a** and **51b** (15 and 3%, respectively) were obtained when



Scheme 8. Synthesis of heteroporphyrins **50**, heterosapphyrins **51**, and heterorubyrin **52**.

$BF_3{\cdot}Et_2O$ was used as the catalyst. Likewise, the best yield reported for **52** (14%) was also obtained under conditions of $BF_3{\cdot}Et_2O$ catalysis, but with **43b** and **49** used as the starting materials. In all cases but one, the diheteroporphyrins **50** proved to be the dominant products of this reaction. It appears that the formation of the heterorubyrin **52** is simply the result of a condensation of **49** with pyrrole, a species produced in the reaction mixture as the result of an acid-catalyzed decomposition of **43b**. While such an explanation appears plausible, curiously the authors do not discuss the possibility of replacing **43b** by simple pyrrole to produce **52** in what would presumably be a far more efficient route.[66]

Subsequent to this report, Lee and co-workers described the use of a very similar synthetic strategy to obtain disubstituted heterosapphyrins.[67] They reported the synthesis of heterosapphyrin **55**, as outlined in Scheme 9. Of note



Scheme 9. Synthesis of heterosapphyrin **55**.

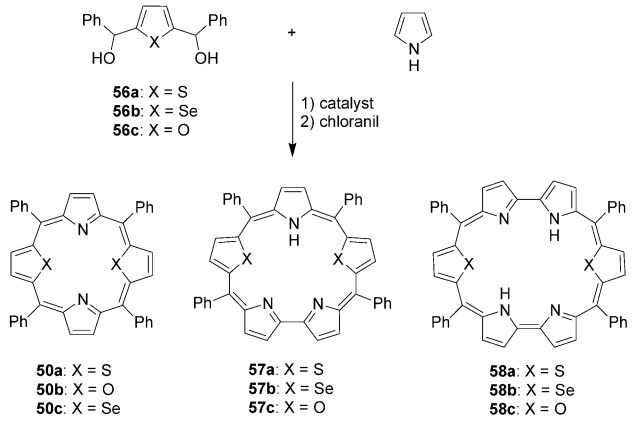
here is that, in contrast to what was found by Chandrashekar and co-workers (see above), condensation of **53** with **54** proceeded using *p*-TsOH as the catalyst and gave macrocycle **55** as the only reported product in 6.5% yield.

An X-ray crystallographic analysis of **55** revealed, as depicted in the line drawing in Scheme 9, that the furan subunit is inverted in the solid state (that is, the furan oxygen atom faces out and away from the macrocyclic core). On the basis of an ^1H NMR spectroscopic analysis, in which the β-pyrrolic protons of the furan subunit were found to resonate upfield ($\delta = 0.97$ ppm), the authors concluded that the furan

 © 2003 Wiley-VCH Verlag GmbH & Co. KGaA, Weinheim

subunit is also inverted in solution. The effect of protonation on the conformation of **55** was not discussed.

In another contribution by Chandrashekar and co-workers a different approach to obtaining expanded heteroporphyrins was detailed.[68] This approach involves the acid-catalyzed condensation of **56a–c** with pyrrole, followed by exposure to chloranil (Scheme 10). The macrocycles **50**, **57**, and **58** were formed in varying yields depending on the nature and concentration of the acid catalyst employed. In the example giving the best yield of expanded porphyrin products, carried out under what are presumably optimized reaction conditions, condensation of **56a** with pyrrole in the presence of one equivalent of TFA was found to give rise to **50a**, **57a**, and **58a** in yields of 13, 27, and 9%, respectively.

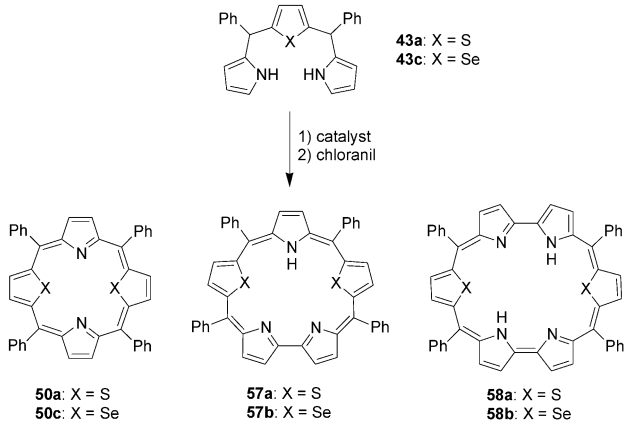


Scheme 10. Synthesis of heteroporphyrins **50**, heterosapphyrins **57**, and heterorubyrins **58**.

Latos-Grażyński and co-workers,[69] in a report actually published slightly earlier than that of Chandrashekar and co-workers,[68] showed how a procedure very similar to that shown in Scheme 10 may be used to prepare **57a** and **57c**. These two heterosapphyrins were obtained in approximately 1% yield each through condensing **56a** or **56c** with pyrrole in the presence of $BF_3{\cdot}Et_2O$ followed by oxidation with chloranil. Not surprisingly, the dominant products of this reaction were the heteroporphyrins **50a** and **50b**. However, none of the corresponding ring-expanded products, for example, heterorubyrins **58a** and **58c**, was obtained.

Very interesting insights into the conformation of products **57** were inferred from ^{1}H NMR spectroscopic studies. For example, chemical shifts consistent with an inversion of the pyrrolic subunit across from the bipyrrolic ring were observed in the case of the dioxasapphyrin **57c**, thus yielding a conformation analogous to **55**. In contrast to what proved to be the case for the parent tetraphenyl sapphyrin,[70] a system that was found to exhibit the same conformation as **57c** in the absence of added protons but "flip back" to the planar "pyrrole-in" form upon protonation, the heteroatom system **57c** was found to retain its inverted conformation in both its mono- and diprotonated forms. The dithiasapphyrin **57a**, however, does not show evidence of inversion in any protonation state. These findings highlight the fact that the nature of the heteroatom plays a role in regulating the overall conformation of a given macrocycle.

Another publication by Chandrashekar and co-workers describes the formation of macrocycles **50**, **57**, and **58**. The synthesis of these heteroatom-containing macrocycles was performed by using a procedure nearly analogous to that described above.[71] However, rather than using precursors **56** in combination with pyrrole as the starting materials (Scheme 10), the heterotripyrranes **43** were used (Scheme 11). Although both studies were published at the same time,[68] the choice of precursors is not clear. The use of preformed tripyrranes **43**, presumed intermediates in the previous synthesis, leads to no improvement in yield.



Scheme 11. Alternate synthesis of heteroporphyrins **50**, heterosapphyrins **57**, and heterorubyrins **58**.

One important facet of the study by Chandrashekar and co-workers, however, were results from single-crystal X-ray diffraction analyses of **58a** and **58b**, which yielded the structures shown in Figures 18 and 19, respectively.[71] In

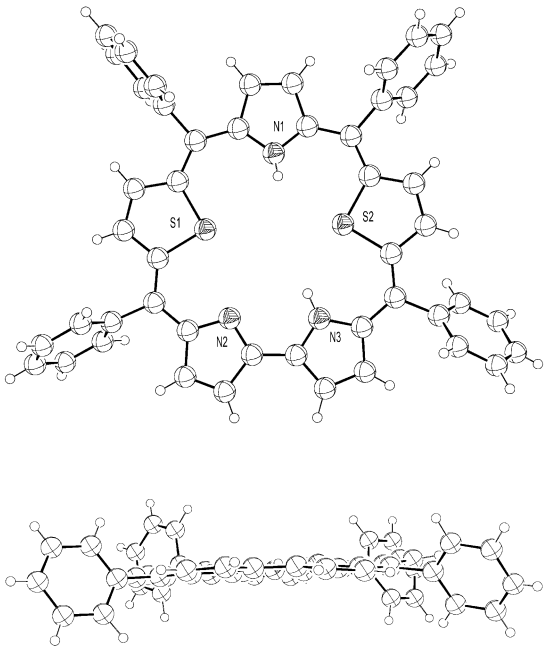


Figure 18. Front (top) and side (bottom) views of the solid-state structure of **57a**.[71]

 © 2003 Wiley-VCH Verlag GmbH & Co. KGaA, Weinheim

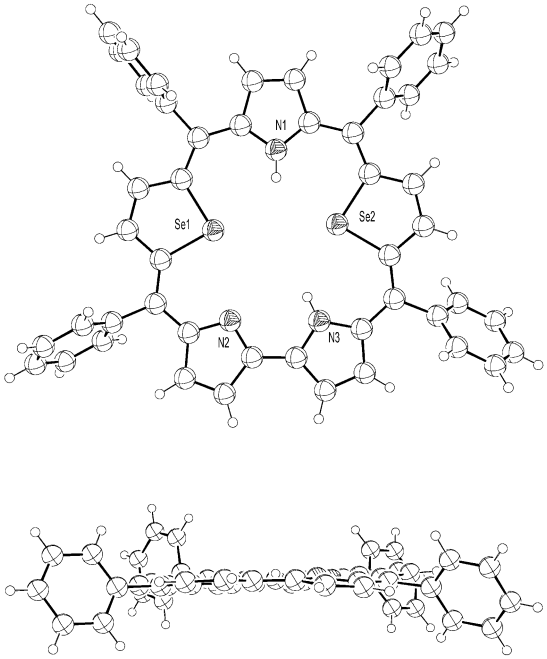
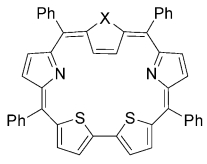


Figure 19. Front (top) and side (bottom) views of the solid-state structure of **57b**.[71]

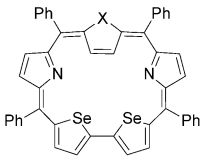
agreement with what one would expect from the NMR spectroscopic findings of Latos-Grażyński and co-workers,[69] **58a** was found to adopt a planar arrangement in the solid state, with no inversion of the heterocyclic subunits being observed. The same arrangement was seen in the structure of the diselenasapphyrin **58b**. The structures of **58a** and **58b** also revealed interesting supramolecular features: Individual macrocycles were found to be held together by intermolecular CH···S and CH···Se bonds, with the *ortho* and *meta* hydrogen atoms of the *meso*-phenyl rings being engaged in hydrogen-bonding interactions involving the ring heteroatoms.

In a different report that summarizes both findings outlined above, as well as other chemistry that will be discussed later on, the crystal structure of a TFA salt of **57a** was reported.[62] In accord with what was inferred from NMR spectroscopic studies, this particular protonated derivative of **57a** was found to adopt a planar conformation in the solid state.

In two other related publications, Chandrashekar and co-workers described the syntheses of several other heterosapphyrins,[72,73] as well as a number that were published previously (see Scheme 8 and structures **51** and **59**). As in previous syntheses, the same by-products (namely, heterorubyrins and heteroporphyrins) were observed under the conditions used to obtain **51** and **59**, with the yields again being somewhat variable. The structures shown are the ones obtained using optimized procedures, in which **51** or **59** are the main products.



51a: X = S (36%)
51b: X = O (32%)
51d: X = Se (36%)
51e: X = NH (16%)
51f: X = NCH_3 (26%)



59a: X = S (32%)
59b: X = O (21%)
59c: X = Se (28%)
59d: X = NH (20%)
59e: X = NCH_3 (26%)

Proton NMR spectroscopic investigations of heterosapphyrins **51** and **59** revealed a subunit inversion that is retained in all protonation states. This conclusion was supported by the crystal-structure determinations of **51d** and **59e**, which confirmed the presence of inversion in the solid state (Figures 20 and 21).[73]

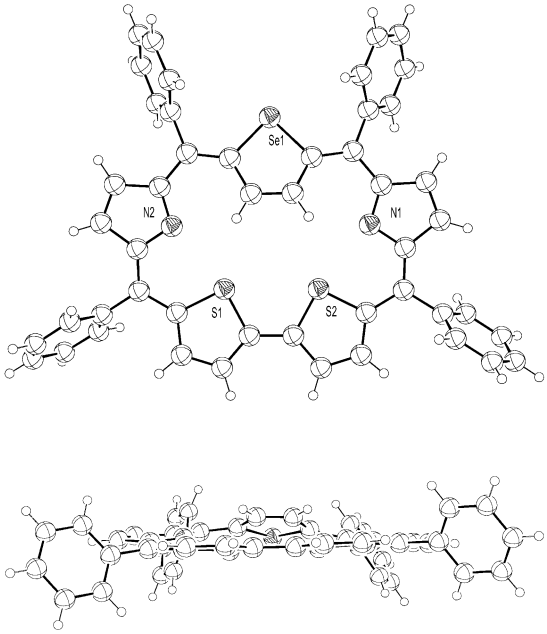


Figure 20. Front (top) and side (bottom) views of the solid-state structure of **51d**.[73]

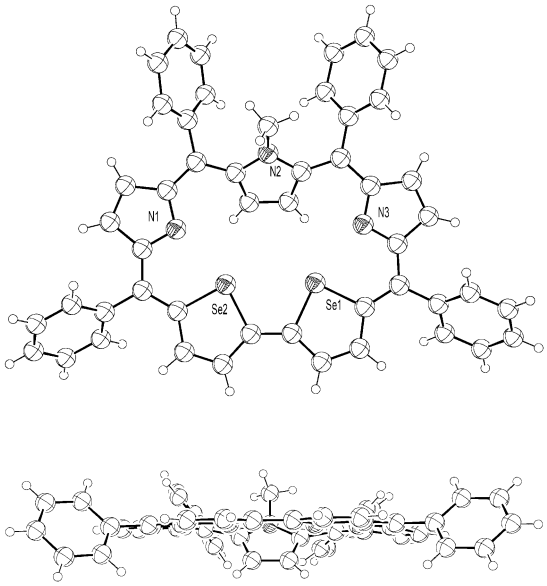
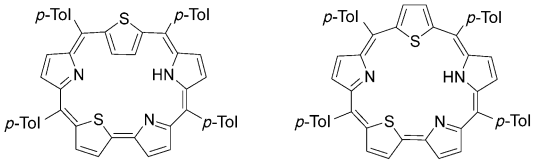


Figure 21. Front (top) and side (bottom) views of the solid-state structure of **59e**.[73]

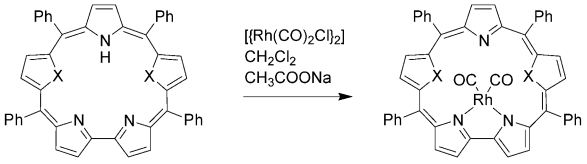
 © 2003 Wiley-VCH Verlag GmbH & Co. KGaA, Weinheim

The research group of Latos-Grażyński recently described the synthesis of a somewhat unusual unsymmetric dithiasapphyrin, **60**.[74] It was isolated in approximately 1% yield as a minor constituent of a complex mixture of products generated



by modifying the basic procedure outlined in Scheme 10. Macrocycle **60** was found to display a unique conformational behavior that differs from that of all other heterosapphyrins previously described: it was found to exist in an equilibrium between the inverted and planar forms (structures **60** and **60′**). This equilibrium, in which the inverted form is the dominant species, exists over a broad temperature range (193–342 K).

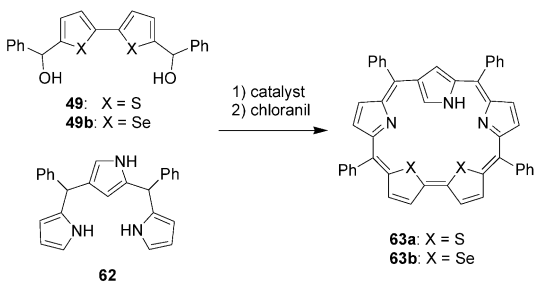
Chandrashekar and co-workers have reported the results of preliminary studies devoted to exploring the metalation chemistry of heterosapphyrins. In particular, they described the preparation of the rhodiumcarbonyl complexes of dithiasapphyrin **57a** and diselenasapphyrin **57b**.[75] The complexes **61a** and **61b** were obtained in yields of 82 and 62%, respectively, upon exposing **57a** and **57b** to $[Rh(CO)_2Cl]_2$ in the presence of base (Scheme 12). On the basis of NMR spectroscopic studies it was concluded that the metal center in both **61a** and **61b** is bound to only the two nitrogen atoms of the bipyrrolic subunit. Unfortunately, no solid-state data have been put forward to date that support this inference.



Scheme 12. Synthesis of rhodium–heterosapphyrin complexes **61**.

4.4. N-Confused Heterosapphyrins

A very interesting contribution, published recently by the research groups of Chandrashekar and Furuta, describes the synthesis of heteroatom-containing sapphyrins in which one pyrrole ring is confused (that is, linked through the 2- and 4-, rather than the 2- and 5-positions).[76] Condensation of either heterobipyrrole **49** or **49b** with the "N-confused" tripyrrane **62** followed by oxidation gives rise to **63a** or **63b** in a yield of 24 or 30%, respectively (Scheme 13). As might have been anticipated based on the conformational behavior of the related heteroatom sapphyrins **51a–f** and **59a–e**, the so-called confused pyrrolic subunits in **63a** and **63b** were found to be inverted. This finding is in agreement with an X-ray crystallo-



Scheme 13. Synthesis of the N-confused heterosapphyrins **63**.

graphic analysis of **63a**, wherein inversion of the confused pyrrole subunit was confirmed in the solid state (Figure 22). However, the structure of **63a** reveals a system that is not perfectly planar; the confused pyrrolic subunit is slightly tilted out of the mean macrocyclic plane (dihedral angle 25°). It was

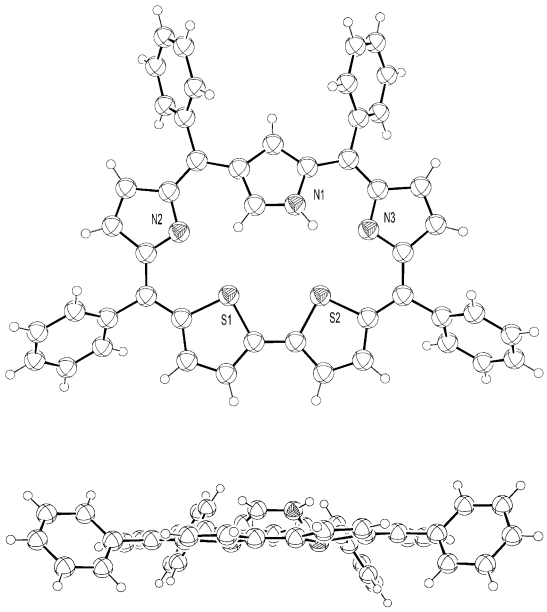


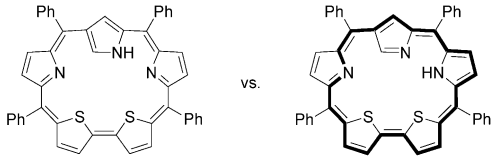
Figure 22. Front (top) and side (bottom) views of the solid-state structure of **63a**.[76]

concluded from ^{1}H NMR spectroscopic analyses that in solution macrocycles **63** are aromatic and inverted, both as a free base and in its protonated forms. For example, the α- and β-CH signals of the N-confused pyrrolic ring in **63a** resonate at $\delta = 2.73$ and 9.79 ppm, clearly indicating the presence of a diatropic ring current.

The Chandrashekar/Furuta paper represents an important step in expanded porphyrin chemistry. Indeed, it is likely that macrocycles **63** will prove to be the first members of what will in due course become a large family of N-confused expanded porphyrins. On the other hand, these systems contain a feature that makes them of immediate interest in their own right: the position of the NH proton. On the basis of solution-phase NMR spectroscopic data, including the results of a COSY study of **63a** carried out at 228 K, the authors suggest

 © 2003 Wiley-VCH Verlag GmbH & Co. KGaA, Weinheim

that this proton is located on the nitrogen atom of the N-confused pyrrolic ring in solution, at least in $CDCl_3$ and [D_8]toluene. However, this results in a structure in which the heterosapphyrin is cross-conjugated (tautomer **63a**), rather

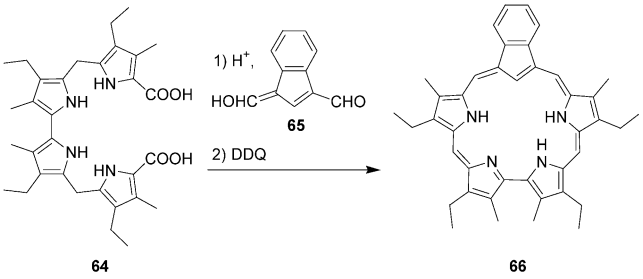


63a **63a'**

than one wherein a classic 22 π-electron aromatic pathway, characteristic of all other heterosapphyrins reported to date, prevails (tautomer **63a′**). While support for this counter-intuitive structural assignment has come from preliminary molecular orbital calculations,[77] it is clear that further studies will be needed to understand the interplay of factors that makes the apparently less aromatic tautomeric form more stable.

4.5. The First Sapphyrin-Based Expanded Carbaporphyrinoid

In a publication that bears an intellectual relationship to the report of Chandrashekar, Furuta, and co-workers summarized above, Lash and Richter described an interesting analogue of sapphyrin in which one nitrogen atom is replaced by a CH group.[78] Condensation of the tetrapyrrole **64** with diformylindene **65**, followed by oxidation, gave rise to macrocycle **66**, a species that was actually isolated in its monoprotonated form in 18% yield (Scheme 14). Proton



64 **66**

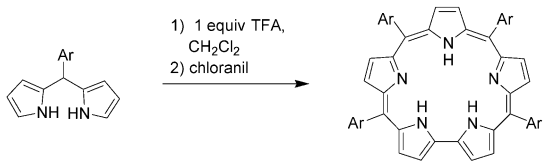
Scheme 14. Synthesis of the sapphyrin-based expanded carbaporphyrinoid **66**.

NMR spectroscopic analysis of this monocation revealed the presence of a strong diatropic current, with the internal CH proton resonating at $\delta = -8$ ppm. Addition of excess TFA was reported to result in C protonation and formation of the dication of **66**. This latter species showed evidence of aromaticity, as inferred from the fact that signals for the *meso* protons were observed at $\delta = 10.4$ and 11.0 ppm in the ^{1}H NMR spectrum while the internal NH and CH_2 signals were found to resonate at $\delta = +0.67$, -0.56, and -3.75 ppm. Unfortunately, no solid-state information is currently available for either the neutral or protonated forms of **66**. Nonetheless, this contribution is important because it shows how CH moieties may be incorporated into the inner rim of an expanded porphyrin, and highlights the fact that novel sapphyrin analogues may be prepared without recourse to *meso* substitution.

4.6. New Advances in the Area of Sapphyrin Chemistry

As will be detailed later on in the appropriate sections, considerable effort has been devoted over the past few years to modifying the classic Rothemund synthesis of porphyrins to obtain novel porphyrinoid systems. One seminal contribution along these lines was made in 1995 when Latos-Grażyński and co-workers reported that tetraphenylsapphyrin can be obtained in 1.1% yield by condensing pyrrole and benzaldehyde under appropriate conditions.[70] Subsequent efforts by Lindsey and co-workers to optimize the synthesis of N-confused porphyrin (obtained in remarkable yields up to 40%),[79] failed to improve the yield of tetraphenylsapphyrin obtained from this reaction (namely, the direct condensation of pyrrole and benzaldehyde). Indeed, the maximum yield obtained by Lindsey and co-workers was 1.2%.[80]

Chandrashekar and co-workers have also reported on the use of dipyrromethanes as potential precursors of sapphyrin.[81] Exposure of dipyrromethanes **42** to one equivalent of trifluoracetic acid, followed by oxidation with chloranil, gives rise to sapphyrins **67** in yields of up to 11% (for Ar = phenyl, Scheme 15). Although other products, such as por-

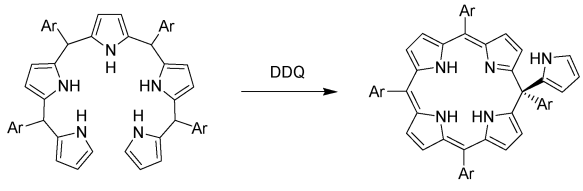


42 **67**

Scheme 15. Dipyrromethane-based synthesis of sapphyrin **67**.

phyrins and N-confused porphyrins, always accompany the formation of **67**, the method could provide an attractive alternative means of producing *all*-azasapphyrins, since dipyrromethanes such as **42** are readily available in multigram quantities.

In a relevant paper, Ka and Lee describe an attempt to obtain *all*-azasapphyrins by the oxidative coupling of pentapyrromethanes **68** (Scheme 16).[82] Pentapyrromethanes **68**,

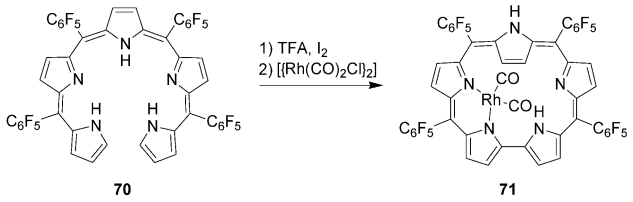


68 **69**

Scheme 16. Unexpected formation of phlorin **69**.

© 2003 Wiley-VCH Verlag GmbH & Co. KGaA, Weinheim

presumed intermediates in the synthesis of tetraarylsapphyrins under modified Rothemund conditions, do not give rise to the expected product **67** when exposed to DDQ. Rather, phlorins such as **69** are formed. The latter species are not stable when treated with acid, and undergo a pyrrole elimination to produce the corresponding porphyrins. These results are rather unexpected, and indeed, at the present time, one cannot rule out the appealing notion that, by varying conditions (for example, choice of oxidant), good yields of sapphyrins such as **67** might still be obtainable from **68**. Recent results obtained by Gross and co-workers are consistent with this latter suggestion.[83] These researchers found that pentapyrrole **70** could be converted into the corresponding sapphyrin quantitatively (Scheme 17) by using



70 **71**

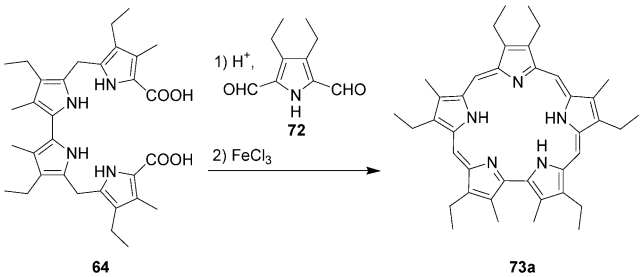
Scheme 17. Synthesis of a rhodium–sapphyrin complex.

a variety of oxidants (for example, $Na_2Cr_2O_7$/TFA, DDQ, and I_2). Unfortunately, even though the crude sapphyrin product obtained in this way could be characterized by NMR spectroscopy, it proved unstable to chromatographic workup. On the other hand, treatment of the crude sapphyrin product with $[Rh(CO)_2Cl]_2$ allowed complex **71** to be isolated in 90% yield. Although no solid-state structural data are currently available for complex **71**, the results of NMR spectroscopic analyses leave little doubt that its structure has been assigned correctly.

4.6.1. ***Improved Yields in the 4+1 Synthesis of Sapphyrins***

While efforts targeting the synthesis of *meso*-substituted sapphyrins are rather recent, much of the chemistry of their β-substituted congeners was developed early on (and hence reviewed previously). Nevertheless, improved syntheses of β-substituted sapphyrins continued to be developed.

In 1999, Richter and Lash reported on the use of $FeCl_3$ in the aromatization step of a 4+1 sapphyrin synthesis.[84] Condensation of the linear tetrapyrrole **64** with pyrroledialdehyde **72** followed by oxidation with 0.1M aqueous $FeCl_3$ gave rise to sapphyrin **73a** in 50% yield (Scheme 18).

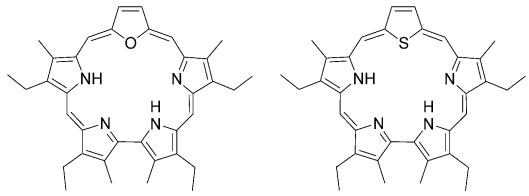


64 **72** **73a**

Scheme 18. Synthesis of sapphyrin **73a**.

Compared to the 36% yield obtained when DDQ was used as the oxidant, this augmentation was considered significant.

Oxasapphyrin **73b** and thiasapphyrin **73c** were obtained in 68 and 90% yield, respectively, when 2,5-diformylfuran or

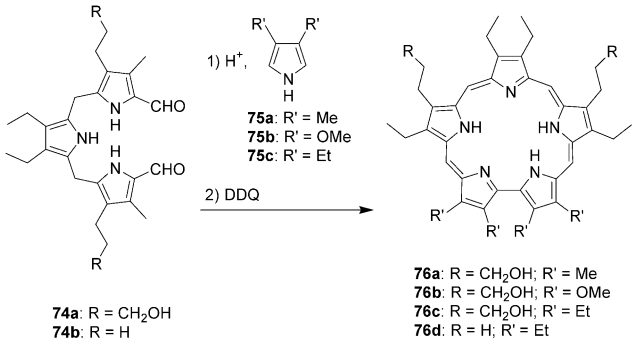


73b **73c**

2,5-diformylthiophene was used instead of **72**. Likewise, the yield of carbasapphyrins (for example, **66**) could be improved by using the $FeCl_3$ procedure. In the specific case shown in Scheme 14 the yield was found to increase from 18 to 38% when $FeCl_3$, rather than DDQ, was used as the oxidant.

4.6.2. ***Synthesis of Sapphyrins by a 3+1+1 Procedure***

Recently, a synthesis of sapphyrins was reported that does not require the use of a preformed bipyrrolic moiety[85] and enabled sapphyrins **76a–d** to be obtained in yields ranging from 28 to 34% (Scheme 19) by condensing tripyrranedial-



Scheme 19. Synthesis of sapphyrins **76a–d**.

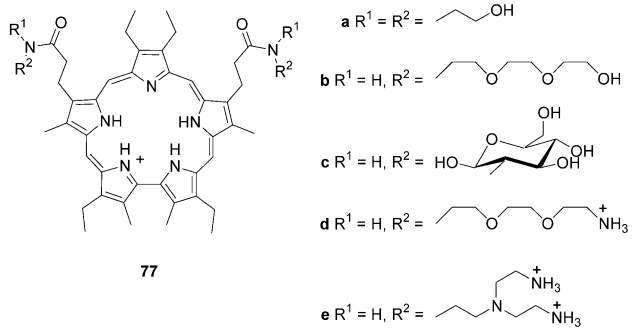
dehydes **74a,b** with two equivalents of pyrroles **75a–c** under acidic conditions, followed by oxidation with DDQ. As expected from such a reaction sequence, the corresponding porphyrins were also isolated in approximately 10% yield.

While the overall yield of sapphyrin is somewhat higher for the more classic 3+2 synthesis than for this new 3+1+1 procedure, this latter approach obviates the need to prepare bipyrrole and is thus three steps shorter. As such, it provides a nice complement to existing methods. It also allows for the synthesis of sapphyrins that contain various symmetric bipyrrolic subunits that are not currently known.

 © 2003 Wiley-VCH Verlag GmbH & Co. KGaA, Weinheim

4.6.3. Applications of Sapphyrin

In addition to synthetic studies devoted to finding new ways to prepare known sapphyrins or to generating new kinds of sapphyrin derivatives, efforts have been made to study the biolocalization properties of sapphyrin. In this context, it was found that the water-soluble sapphyrins **77a–e** localized



77

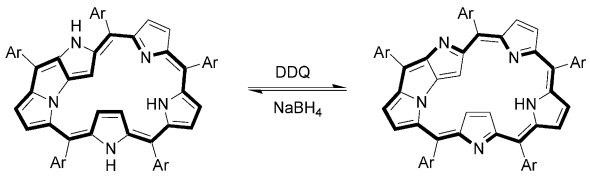
rather selectively in cancers, as judged from studies involving the use of a murine model of a xenographic pancreatic human tumor.[86] Whereas little retention and/or rapid clearance was seen from other tissues, depending on the specific substitution pattern present on the sapphyrin, the clearance half-life from the cancerous sites was seen to be on the order of days.

Further work has been devoted to studying the anion-recognition properties of sapphyrins and to exploiting them in several analytical applications. For example, ion-selective electrodes based on sapphyrins have been generated,[87] as have optical anion sensors.[7,88,89] The use of sapphyrins as possible through-membrane anion carriers has also been reviewed.[90]

4.7. N-Fused Pentaphyrin

A recent report by Furuta and co-workers describes the synthesis of an unexpected expanded porphyrin, namely N-fused pentaphyrin **78**.[91] Compound **78** was obtained in 15% yield as one of a number of products produced from a modified Rothemund reaction involving the condensation of pentafluorobenzaldehyde with pyrrole in the presence of $BF_3{\cdot}Et_2O$. An X-ray structural analysis of **78a** revealed not only the highly unusual connectivity pattern, but also a strong deviation from planarity. A further, interesting feature of N-fused pentaphyrin is that it can exist in two stable oxidation states, namely **78a** and **78b** that contain 24 π-electron and 22 π-electron peripheries, respectively. Compound **78** was isolated as a mixture of these two products. Fortunately, however, the two species are readily interconverted by means of oxidation with DDQ or by reduction with sodium borohydride (Scheme 20).

On the basis of the nonplanarity of **78a** observed in the solid state (Figure 23), it is not surprising that its ^{1}H NMR spectrum reflects the presence of an essentially nonaromatic species; for example, no paratropic shifts were observed that would be consistent with an antiaromatic species as might be



78a **78b**

Scheme 20. Redox behavior of N-confused pentaphyrin **78**.

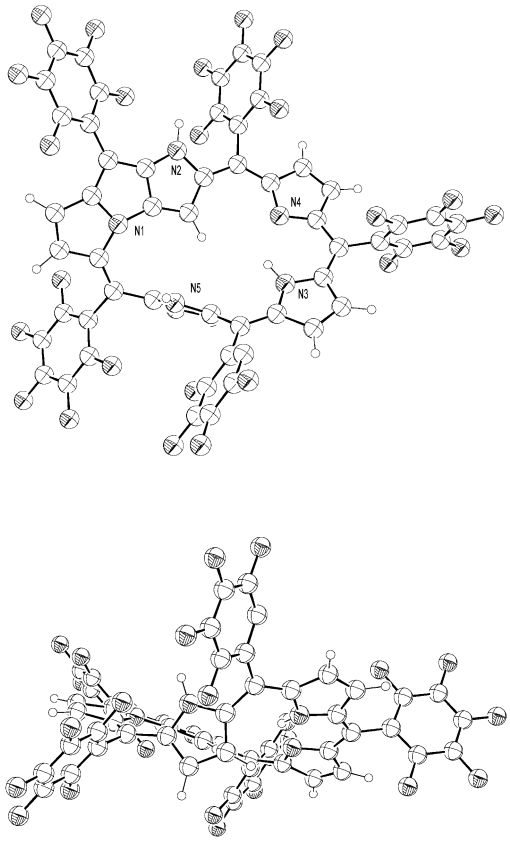


Figure 23. Front (top) and side (bottom) views of the solid-state structure of **78a**.[91]

inferred from its 24 π-electron structure. On the other hand, the ^{1}H NMR spectrum of **78b** clearly indicates the presence of a species with aromatic character, with the signals for the inner NH and CH protons appearing at $\delta = 2.19$, 1.70, 1.24, and −2.26 ppm. Furuta and co-workers suggest that it is perhaps as a result of the ready formation of species such as **78** that a simple (namely, non N-fused) *meso*-substituted pentaphyrin has yet to be reported.

5. Systems Containing Six Pyrrole Rings

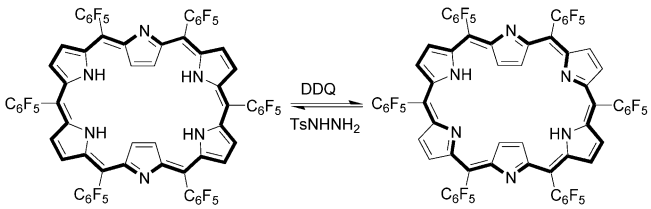
As the number of pyrrole rings within a macrocylic core increases, so does the number of possible combinations for a given set of pyrroles and *meso* bridges. It is thus not surprising, therefore, that more hexapyrrolic than pentapyrrolic macrocycles are now known. Many of these hexapyrrolic

 © 2003 Wiley-VCH Verlag GmbH & Co. KGaA, Weinheim

systems are not new, however, and have already been the subject of several reviews.[2,3,8] The latest additions to this family are summarized below.

5.1. Hexaphyrin(1.1.1.1.1.1)

One of the more interesting new additions to the family of hexapyrrolic macrocycles was recently described by Cavaleiro and co-workers and was another product of a modified Rothemund synthesis. Condensation of pentafluorobenzaldehyde with pyrrole in a mixture of boiling acetic acid and nitrobenzene enabled hexaphyrin(1.1.1.1.1.1) (**79**) to be isolated in approximately 1% yield.[92] The expected porphyrin was also obtained in 15% yield. Macrocycle **79** displayed behavior analogous to that of N-fused pentaphyrin (**78**), namely an ability to exist simultaneously in two different oxidation states with inverted pyrrole rings (Scheme 21). As



79a **79b**

Scheme 21. Redox behavior of hexaphyrin **79**.

with the N-fused pentaphyrin species **78, 79a** and **79b** are readily interconverted without inducing large structural changes (for example, pyrrole ring "flipping"). Oxidation of [28]hexaphyrin(1.1.1.1.1.1) **79a** with DDQ produces the corresponding $(4n+2)\,\pi$-electron species, [26]hexaphyrin(1.1.1.1.1.1) **79b**. Likewise, treatment of **79b** with tosyl hydrazone results in reduction to **79a**. In accord with the two-dimensional representation of its $4n+2\,\pi$ electrons, the ^{1}H NMR spectrum of **79b** displays features consistent with aromaticity: the signals corresponding to the β-pyrrolic CH protons of the inverted subunit were found to resonate at $\delta = -2.43$ ppm while the corresponding NH signals were observed at $\delta = -1.98$ ppm. By contrast, the ^{1}H NMR spectrum of **79a** revealed no signals that could be considered to reflect an antiaromatic ring-current effect.

The crystal structure of **79b** confirmed the inversion of the two pyrrolic subunits (Figure 24). However, the overall structure was found to deviate from planarity rather substantially. This deviation is important because—if it persists in solution—it would reduce the net orbital overlap and hence ring-current effects associated with the presumed aromaticity of **79b**. The structure of **79b** is important on another level: it highlights the difference between the early β-pyrrole-substituted hexaphyrin (**10**), reported by Gossauer and co-workers, wherein "*meso* inversion" was observed,[31] and the present system. As such, it underscores nicely the effects that different kinds of substituents (*meso* or β-pyrrolic) can play in controlling the conformational properties of expanded porphyrins.

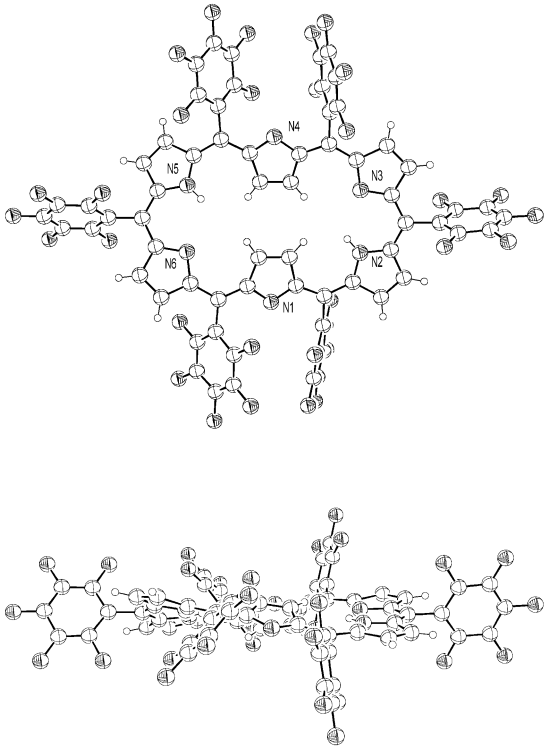
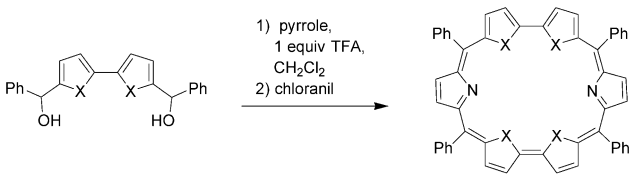


Figure 24. Front (top) and side (bottom) views of the solid-state structure of **79b**.[92]

Subsequent to the initial report by Cavaleiro and co-workers, Furuta and co-workers reported an improved procedure that allowed **79** to be isolated in yields of up to 20%.[93]

5.2. Heteroatom-Containing Rubyrins

Chandrashekar and co-workers have described the synthesis of several heteroatom-containing analogues of rubyrin.[32] This work was reviewed in part in Section 4.3. However, a more focused discussion is appropriate here. One strategy used to obtain these systems involves the condensation between pyrrole and heterobipyrroles **49**, **49b**, or **49c** (Scheme 22). This procedure led to the formation of **52a**, **52b**, and **52c** in yields of 28, 24, and 15%, respectively, as well as to heteroatom-containing analogues of sapphyrin and porphyrin.[94,95]



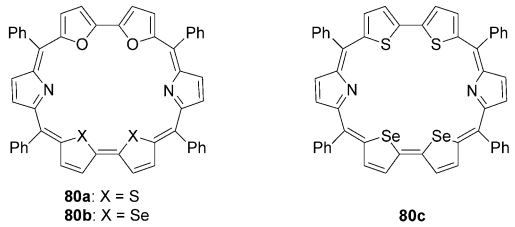
49: X = S
49b: X = Se
49c: X = O

52: X = S
52b: X = Se
52c: X = O

Scheme 22. Synthesis of heterorubyrins **52**.

 © 2003 Wiley-VCH Verlag GmbH & Co. KGaA, Weinheim

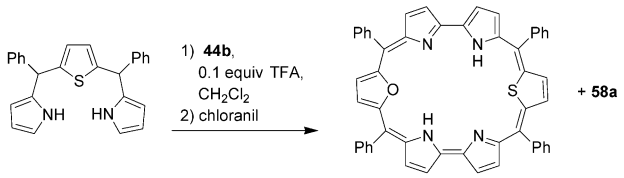
The same research group also reported a stepwise procedure that involved the condensation of **49** or **49c** with excess pyrrole to produce tetrapyrrolic intermediates that in turn were condensed with one equivalent of either **49**, **49b**, or **49c**. This allowed the synthesis of heterorubyrins **80a**, **80b**, and **80c** in yields of 23, 28, and 20%, respectively.[95]



80a: X = S
80b: X = Se

80c

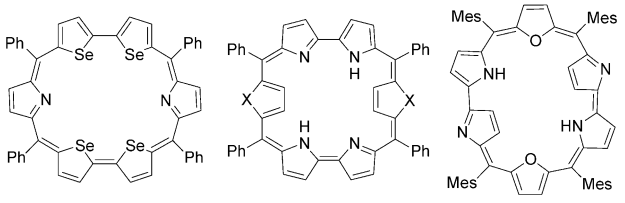
As shown earlier in Schemes 10 and 11, another approach to obtaining heteroatom analogues of rubyrin involves the oxidative homocoupling of heterotripyrranes. This approach has led to the synthesis of rubyrins **58a–c**. Alternatively, by coupling two different tripyrranes, such as **44a** and **44b** (Scheme 23), it proved possible to prepare unsymmetrical



44a **58d**

Scheme 23. Synthesis of heterorubyrins **58**.

heterorubyrins such as **58d** (25% yield). This particular coupling also produced a small quantity (2.8%) of the symmetrical product **58a**.



52b

58a: X = S
58b: X = Se
58d: X = S, O

81

A quick glance at the heterorubyrins reported to date highlights their remarkable structural diversity.[62,96] As illustrated by the macrocycles shown above, three basic structural motifs have been identified so far. For example, as inferred from spectral and structural studies, **52b** exists in a planar, noninverted form (Figure 25). This appears to be the general structure for *meso*-substituted heterorubyrins in which the bipyrrolic subunits contain large heteroatoms. Interestingly, inversion is seen in the systems **58a**, **58b**, and **58d**, in which the "normal" bipyrrolic subunits are preserved and at least

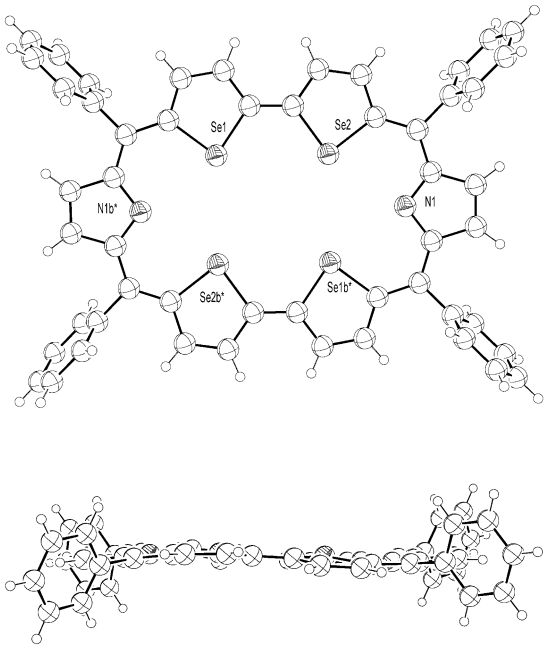


Figure 25. Front (top) and side (bottom) views of the solid-state structure of **52b**.[96]

one of the pyrrolic subunits contains one large heteroatom. This observation is supported by X-ray structural analyses of all three species. The X-ray structure of **58b** is shown as an example in Figure 26. A different mode of inversion is seen

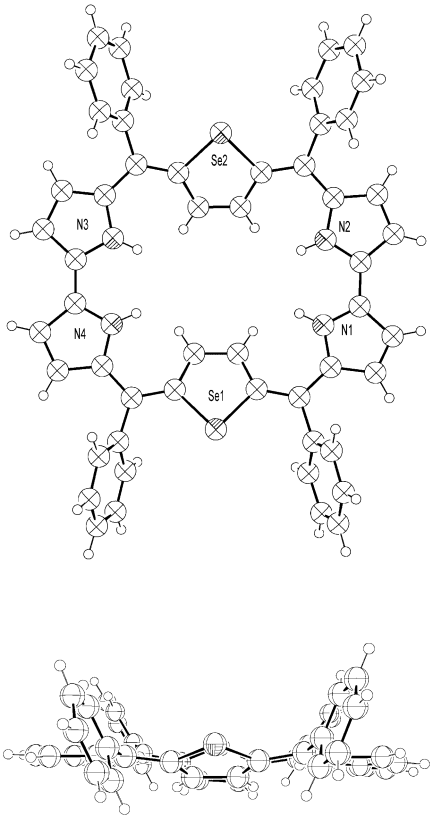


Figure 26. Front (top) and side (bottom) views of the solid-state structure of **58b**.[62]

 © 2003 Wiley-VCH Verlag GmbH & Co. KGaA, Weinheim

for **81**, in this case one pyrrole ring of each bipyrrolic subunit is inverted. The latter finding is based solely on NMR spectroscopic analysis, and has yet to be verified by X-ray structural analyses. Of further interest is the finding that all the isolated heterorubyrins, inverted or planar, are 26 π-electron systems and as such display aromatic character, as inferred from their spectral features.

The first metalation attempts involving heterorubyrins showed that **58a** and **58b** give rise to three different types of $[Rh(CO)_2]$ complexes: mono- and bimetallic complexes in which the inversion is retained, and a bimetallic complex wherein inversion no longer occurs (Figure 27).[75] Furthermore, a bis-$\{Rh(CO)_2Cl\}$ complex of **81** was reported in which the conformation of the starting metal-free macrocycle is retained. The two Rh^I fragments coordinate to the inverted pyrrole rings outside the macrocycle, with the neutral aza donors serving merely to complete the coordination sphere of the Rh^I centers.

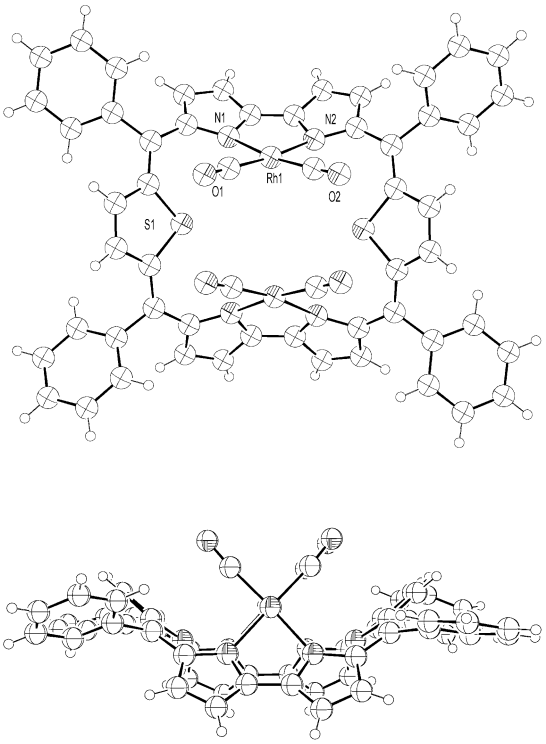
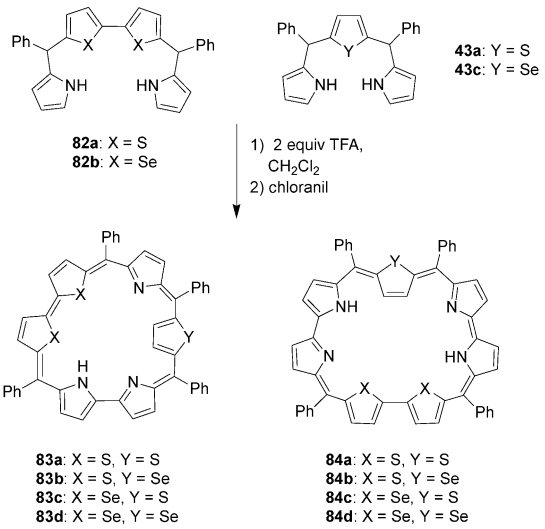


Figure 27. Front (top) and side (bottom) views of the solid-state structure of the bis-$\{Rh(CO)_2\}$ complex complex derived from **58a**.[75]

5.3. [26]Hexaphyrin(1.1.1.0.1.0)

A serendipitous synthesis of several heteroatom analogues of [26]hexaphyrin(1.1.1.0.1.0), a previously unknown isomer of rubyrin,[32] was recently reported by the Chandrashekar research group[97] (Scheme 24). Exposure of the heteroatom-containing tetrapyrroles **82** and heterotripyrranes **43** to oxidative coupling conditions was found to produce the expected heptaphyrins **84** (see Section 6) as the main products, as well as the hetero[26]hexaphyrins(1.1.1.0.1.0) **83** in yields of 3–5%. As one might expect given the unsymmetric nature of this coupling procedure, heterorubyrins are also obtained in varying yields. On the other hand, no products resulting from the self-coupling of tetrapyrroles **82** (for example, linear or cyclic octapyrroles) were reported (see Section 7.5).

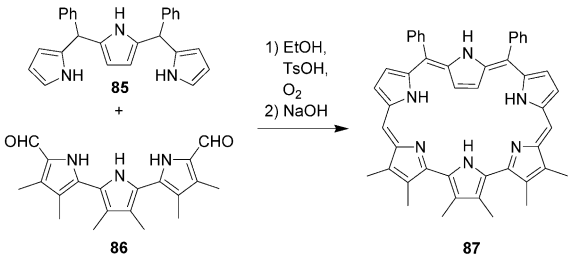


Scheme 24. Formation of hexaphyrins **83** and heptaphyrins **84**.

The conformations of macrocycles **83a–83d** were inferred from ^1H NMR spectroscopic analyses. In the case of **83a**, the β-protons of the inverted thiophene subunit were found to resonate at $\delta = -0.01$ and -1.01 ppm. Although these values are as expected for a structure wherein these protons are facing in towards the center of a large aromatic ring, it is important to appreciate that no solid-state structural information is available for **83a** or its congeners **83b–d**.

5.4. [26]Hexaphyrin(1.1.1.1.0.0)

The synthesis of a [26]hexaphyrin(1.1.1.1.0.0) (**87**), an isomer of rubyrin (**11**),[32] was targeted[64,98] in an attempt to prepare an expanded porphyrin that would exhibit inversion of a prechosen pyrrolic subunit. The desired compound was obtained in 46% yield by condensing tripyrrane **85** with diformylhexamethylterpyrrole **86** in ethanol in the presence of *p*-toluenesulfonic acid and air (Scheme 25). As expected,



Scheme 25. Synthesis of hexaphyrin **87**.

 © 2003 Wiley-VCH Verlag GmbH & Co. KGaA, Weinheim

inversion of the middle pyrrole ring of the tripyrrane subunit was in fact observed in the case of **87** and its dihydrochloride salt. A signal at $\delta = -2$ ppm was seen in the ^{1}H NMR spectrum of the dihydrochloride salt of **87** that was assigned to the inner CH protons of the inverted pyrrolic ring. Additionally, the remaining inner NH signals were found to be shifted to the upfield region of the spectrum between $\delta =$ 0.05 and -0.75 ppm. By contrast, the outer NH proton was found to resonate at $\delta = 15$ ppm. Subsequent to the spectroscopic studies, more definitive support for the proposed inverted nature of **87** and its dihydrochloride salt was obtained from solid-state X-ray diffraction analyses. In both cases the resulting structures proved completely consistent with the results obtained in solution (Figures 28 and 29).

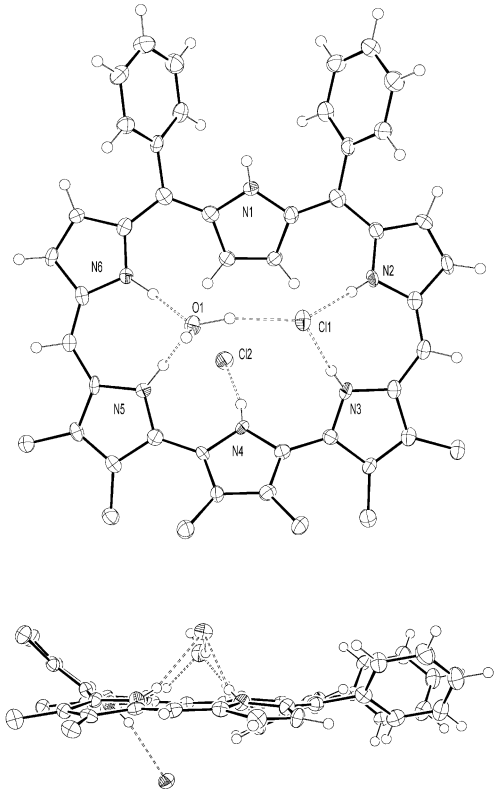


Figure 28. Front (top) and side (bottom) views of the solid-state structure of **87**·2 HCl.[98]

5.5. Improved Synthesis of [24]Hexaphyrin(1.0.0.1.0.0) (Amethyrin)

As a predicate to developing the metalation chemistry of amethyrin,[99] a simpler high-yielding synthetic procedure was recently developed that obviates the need for chromatographic purification.[100] This procedure involves condensing a diformylterpyrrole, such as **86**, with a terpyrrole, such as **46**, in the presence of trifluoroacetic acid. Treatment of the resulting amethyrin–TFA salt with NaOH, followed by crystallization from MeOH, then gave the amethyrin–bismethanol complex **88** in 90 % yield (Scheme 26). This complex of amethyrin **88**, a macrocycle that is readily protonated by trace amounts of

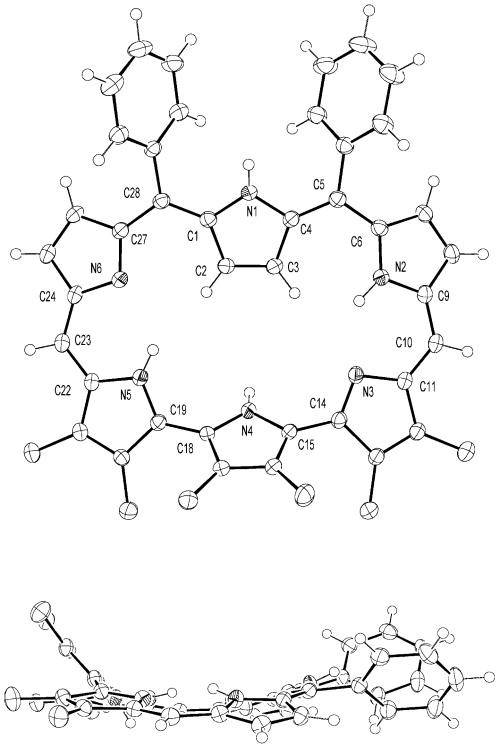
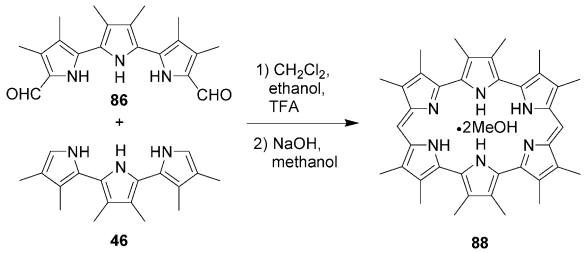


Figure 29. Front (top) and side (bottom) views of the solid-state structure of complex **87**.[64]



Scheme 26. Improved synthesis of amethyrin **88**.

acid, was characterized structurally. The analysis shows that the two central pyrrole units are tilted out of the plane defined by the other four pyrrolic units (Figure 30). Meanwhile, the methanol molecules are bound to the ligand by two hydrogen-bonding interactions each.

Treatment of **88** with two equivalents of nickel(II) acetylacetonate in toluene gave rise to a product that was tentatively assigned on the basis of UV/Vis spectroscopic and mass spectrometric studies as a dinickel(II) complex of amethyrin with two units of acetylacetonate still present as bridging units (58 % yield). Unfortunately, an X-ray crystal structure could not be obtained. It was proposed that metal complexation is accompanied by ligand oxidation such that the formally antiaromatic 24 π-electron system **88** becomes transformed into an aromatic macrocycle with a 22 π-electron periphery.

 © 2003 Wiley-VCH Verlag GmbH & Co. KGaA, Weinheim

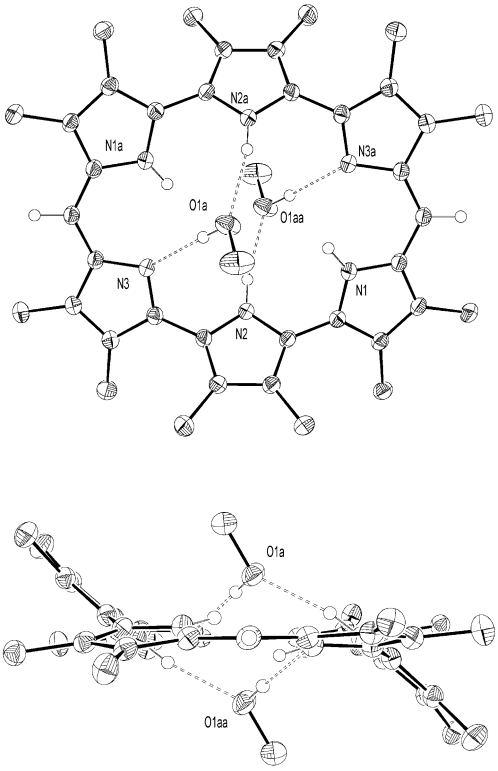
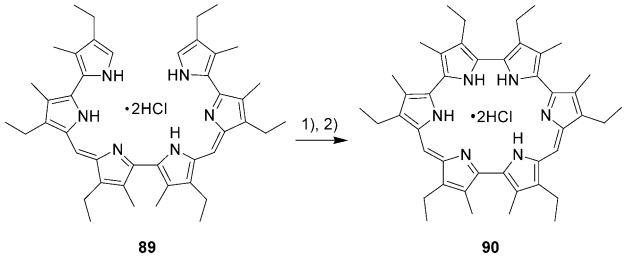


Figure 30. Front (top) and side (bottom) views of the solid-state structure of complex **88**.[100]

5.6. [24]Hexaphyrin(1.0.1.0.0.0) and its Actinide Complexes

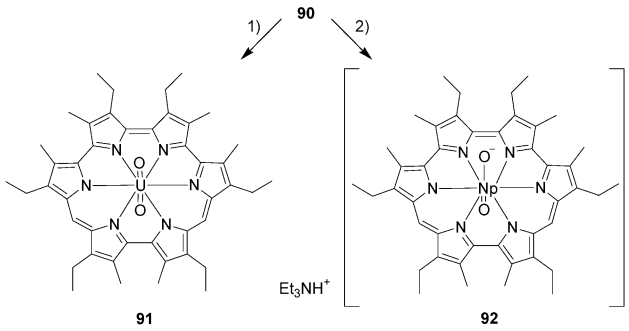
The synthesis of [24]hexaphyrin(1.0.1.0.0.0) (isolated in the form of its dihydrogenchloride salt **90**),[101] which represents an isomer of amethyrin (**88**) was achieved by using a Cr^{VI}-based oxidative coupling strategy.[99] Treatment of the open-chain hexapyrrolic precursor **89** with $Na_2Cr_2O_7$ in trifluoroacetic acid, followed by chromatographic workup, and subsequent treatment with HCl, provided the target compound (**90**) in 77% yield (Scheme 27).



89 90

Scheme 27. Synthesis of hexaphyrin **90**: 1) $Na_2Cr_2O_7$, TFA; 2) HCl.

In accord with its 24 π-electron periphery, the diprotonated system **90** displays features that are consistent with antiaromatic character. These include downfield shifts for the inner NH protons ($\delta = 23.7$, 23.9, and 24.2 ppm) and upfield resonances for the *meso* CH protons ($\delta = 3.4$ ppm) in its ^{1}H NMR spectrum. Treatment of **90** with uranyl acetate and base leads to the formation of a uranyl complex **91** (Scheme 28). This transformation is accompanied by a



91 92

Scheme 28. Synthesis of the actinide complexes **91** and **92**: 1) $UO_2(OAc)_2 \cdot 2H_2O$, Et_3N, MeOH, CH_2Cl_2; 2) NpO_2Cl in 1 M HCl, Et_3N, MeOH.

dramatic change in the spectroscopic features. For example, the signal in the ^{1}H NMR spectrum ascribed to the *meso* CH protons is shifted downfield to $\delta = 10.1$ ppm from its original position at $\delta = 3.4$ ppm. This shift is consistent with the ring-current effects becoming "reversed" on oxidation to the 22 π-electron aromatic system **91**.

Further support for the proposed aromaticity came from an analysis of the UV/Vis spectra of **90** and **91**. In particular, while the UV/Vis spectrum of **90** (CH_2Cl_2) consists of three Soret-like bands with a main transition at 497 nm ($\varepsilon = 59\,000\,M^{-1}cm^{-1}$) and no corresponding Q-like transitions, that of the uranyl complex **91** was found to contain a sharp, Soret-like transition at 530 nm ($\varepsilon = 330\,000\,M^{-1}cm^{-1}$), as well as two weaker Q-like bands at 791 ($\varepsilon = 56\,000\,M^{-1}cm^{-1}$) and 832 nm ($\varepsilon = 81\,000\,M^{-1}cm^{-1}$). The extinction coefficient of the main transition in the uranyl complex **91** was also found to be increased by a factor of 5.6 relative to the metal-free starting material **90** (Figure 31).[102]

To complement and extend the chemistry developed in the case of the uranyl complex **91**, the corresponding Np^V complex (**92**) of **90** was also prepared (Scheme 28). The UV/Vis spectral characteristics of **92** were found to be similar to these of **91**. However, while confirming the hexadentate

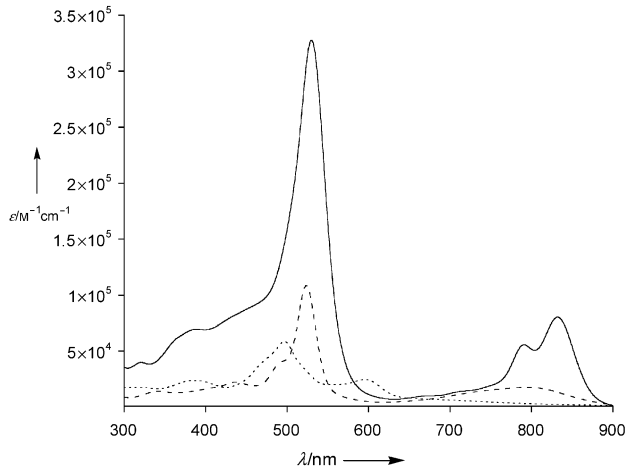


Figure 31. UV/Vis spectrum of **91**(——), **90** (••••), and **89** (-----) in CH_2Cl_2.[102]

 © 2003 Wiley-VCH Verlag GmbH & Co. KGaA, Weinheim

nature of both complexes, X-ray analysis revealed important differences between **91** and **92** (Figures 32 and 33). Whereas a relatively distorted structure was found in **91**, a more planar arrangement and a triethylammonium counterion was seen in

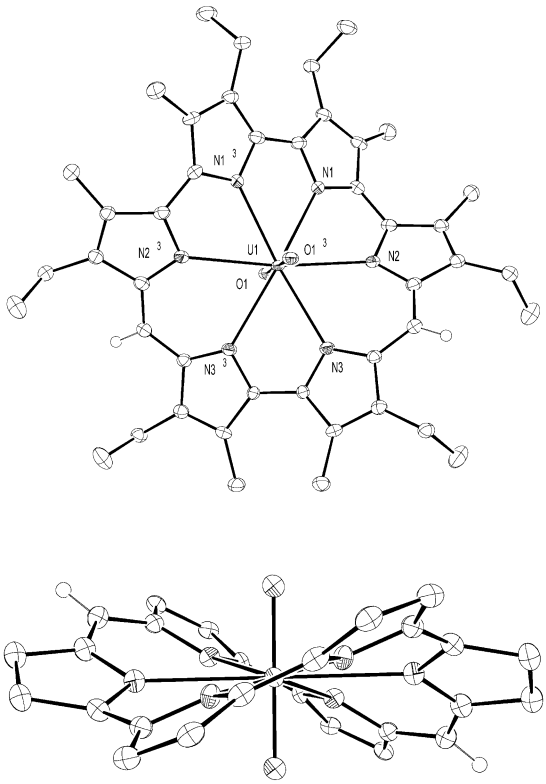


Figure 32. Front (top) and side (bottom) views of the solid-state structure of complex **91**.[101]

the case of **92**, presumably, as a consequence of the larger ionic radius of Np^{V} as compared to U^{VI}. The structure of complex **92** is important in that it represents the first structurally characterized Np^{V} complex bound to an *all*-aza donor set.

5.7. Expanded Phthalocyanine Analogues

Torres and co-workers recently introduced the first examples of expanded phthalocyanines.[103] Prolonged heating of the acyclic three-subunit intermediates **93a–f** in ethoxyethanol induced their self-condensation, which resulted in the formation of the metalated heteroannulenes **94a–f** (Scheme 29). The peripherally substituted derivatives **94b**, **c**, **e**, and **f** were obtained as a mixture of seven configurational isomers in yields between 28 and 59%, while the unsubstitued compounds **94a** and **94d** were isolated in 81 and 69% yield, respectively. Metal-free analogues of **93** did not give rise to expanded phthalocyanines when exposed to the reaction conditions outlined above. Furthermore, compounds **94** proved unstable in strongly acidic media. While such instability was somewhat expected, it has nonetheless so far

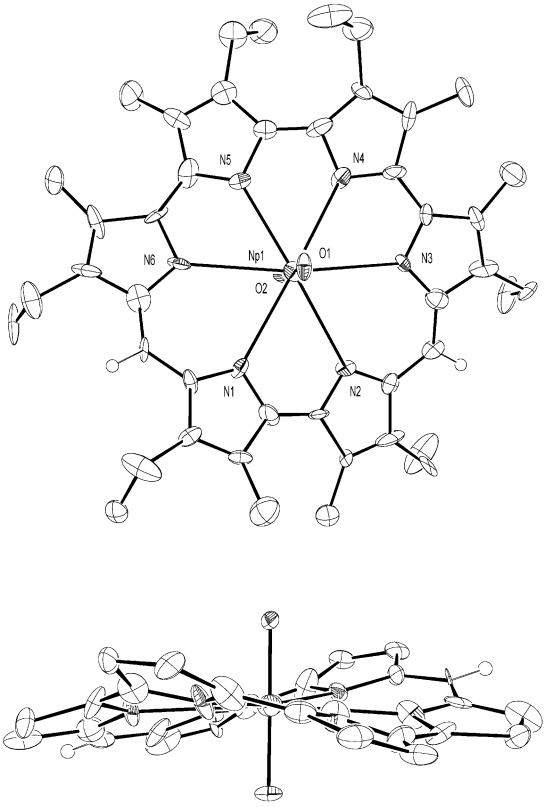
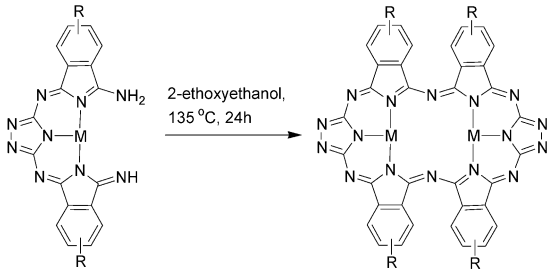


Figure 33. Front (top) and side (bottom) views of the solid-state structure of complex **92**.[100]



93a: M = Ni, R = H
93b: M = Ni, R = OC_8H_{17}
93c: M = Ni, R = *t*Bu
93d: M = Zn, R = H
93e: M = Zn, R = OC_8H_{17}
93f: M = Zn, R = *t*Bu

94a: M = Ni, R = H
94b: M = Ni, R = OC_8H_{17}
94c: M = Ni, R = *t*Bu
94d: M = Zn, R = H
94e: M = Zn, R = OC_8H_{17}
94f: M = Zn, R = *t*Bu

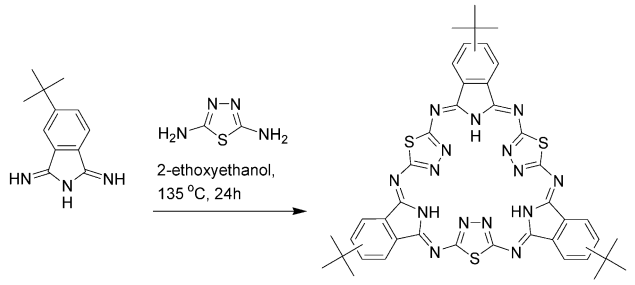
Scheme 29. Formation of the expanded metallaporphyrazines **94**.

precluded the characterization of free-base analogues of **94**. The expanded phthalocyanines **94** possess 28 π-electron peripheries. As such they might be expected to show antiaromatic features. However, the lack of protons attached directly to the periphery of the macrocycle makes a test of such an assumption difficult. On the other hand, the aryl protons of the macrocycles **94** were found to display chemical shifts ($\delta = 6.6$–6.7 ppm) that are similar to those of their related 18 π-electron hemiporphyrazines. Unfortunately, no solid-state information on these interesting phthalocyanine analogues is currently available.

 © 2003 Wiley-VCH Verlag GmbH & Co. KGaA, Weinheim

5.8. Thiadiazole-Containing Expanded Heteroazaporphyrinoids

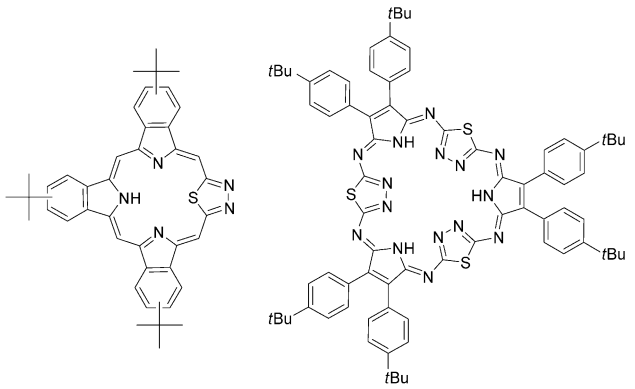
Islyaikin, Torres, and co-workers recently reported the synthesis of another new class of expanded phthalocyanines. These researchers were able to obtain macrocycle **96** in 54% yield in the form of an orange powder by condensing 5-*tert*-butyl-1,3-diiminoisoindoline (**95**) with 2,5-diamino-1,3,4-thiadiazole (Scheme 30).[104] Compound **97** was also obtained in



95 96

Scheme 30. Synthesis of the expanded porphyrazine **96**.

15% yield under these reaction conditions. When 3,4-bis(4-*tert*-butylphenyl)pyrroline-2,5-diimine was used in place of **95**, macrocycle **98** was isolated in 38% yield. In this case, none



97 98

of the smaller product, which corresponds to a functionalized analogue of **97**, was apparently formed.

Compounds **96** and **98** formally possess 30 π-electron conjugation pathways, and might thus be expected to display aromatic features. However, instead of resonating in the expected upfield region, the inner NH protons displayed chemical shifts at about $\delta = 12.5$ ppm. This finding was rationalized in terms of deviations from planarity. However, the structural distortions from planarity would have to be quite substantial to account for the unusual shifts. Unfortunately, no solid-state structural information for macrocycles **96** and **98** is currently available, but a geometry optimization (AM1) analysis of these systems was carried out. This study provided support for inversion of the three thiadiazole subunits, as indicated in the line drawings.

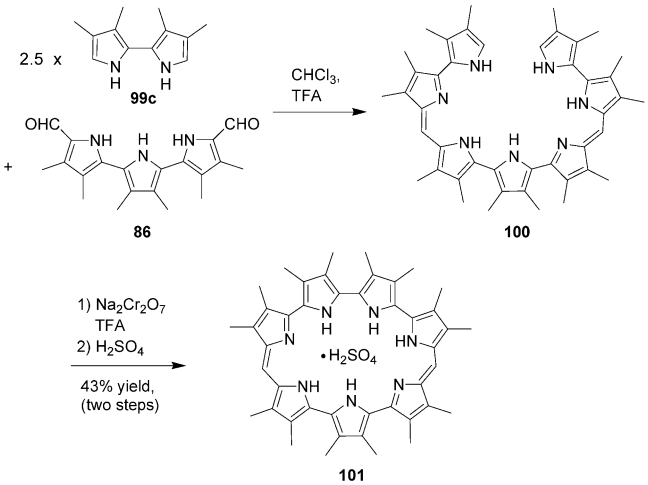
It is important to note that, Kobayashi et al. also reported the synthesis of macrocycles **96** and **98** at virtually the same time as Islyaikin, Torres, and co-workers.[105] In this case, 1-butanol rather than 2-ethoxyethanol was used as the solvent for the condensation reaction. Under these conditions, macrocycle **96** was isolated in 26% yield and formation of **97** was not observed. In contrast to the results of the AM1 calculations of Islyaikin, Torres, and co-workers, Kobayashi et al. concluded on the basis of ZINDO/1 and AM1 calculations that the tris-inverted form of **96** (as shown in Scheme 30) is energetically similar to the corresponding non-inverted form. Both studies also describe the formation of a trinuclear Ni complex. However, neither report contains solid-state structural information, thus leaving the exact nature of the species in question uncertain.

6. Systems Containing Seven Pyrrole Rings

Heptapyrrolic macrocycles, in contrast to hexapyrroles, have only a limited history. Indeed, no report of a heptapyrrolic expanded porphyrin had appeared in the literature up to the middle of 1999. However, in a testament to how fast the field is developing, five different heptapyrrolic expanded porphyrins have now been reported.

6.1. [28]Heptaphyrin(1.0.0.1.0.0.0)

The first heptapyrrolic expanded porphyrin, [28]heptaphyrin(1.0.0.1.0.0.0), was reported in 1999. It was obtained by a two-step procedure as outlined in Scheme 31.[106] Condensation of 2.5 equivalents of tetramethylbipyrrole (**86**) with diformylhexamethylterpyrrole (**99c**) gave rise to the open-chain heptapyrrolic building block **100**. This intermediate, although apparently stable, was not isolated but instead was treated with aqueous $Na_2Cr_2O_7$ in trifluoroacetic acid to produce [28]heptaphyrin(1.0.0.1.0.0.0) in 43% yield in the form of its dihydrogen sulfate salt (**101**).



86 100 101

Scheme 31. Synthesis of quaterpyrrole-containing heptaphyrin **101**.

 © 2003 Wiley-VCH Verlag GmbH & Co. KGaA, Weinheim

The ^{1}H NMR spectrum of the dihydrogen sulfate salt **101** exhibits features that are in agreement with the presence of an antiaromatic 28 π-electron periphery. Four NH signals in an integral ratio of 2:2:2:1 are observed in the $\delta = 15.9$–18.2 ppm spectral region, thus lying clearly downfield from those of "normal" NH pyrrolic protons. Additionally, the signal corresponding to the *meso* proton is shifted upfield to $\delta =$ 5.42 ppm. Further support for the conclusion that [28]heptaphyrin(1.0.0.1.0.0.0) is conjugated comes from the results of a UV/Vis spectroscopic study: Salt **101** shows two rather strong absorptions at $\lambda_{max} = 514$ nm ($84\,400\,M^{-1}cm^{-1}$) and 613 nm ($53\,200\,M^{-1}cm^{-1}$). As one might have expected, the lowest energy band is red-shifted relative to what is seen in the case of its smaller congener amethyrin ($\lambda_{max} = 597$ nm ($56\,500\,M^{-1}cm^{-1}$) for its diprotonated form).[99] Definite proof of the structure for **101** came from a single-crystal X-ray diffraction analysis; the macrocycle was found to be fairly planar and to contain a large cavity into which the sulfate counterion is bound through no fewer than seven hydrogen-bonding interactions (Figure 34).

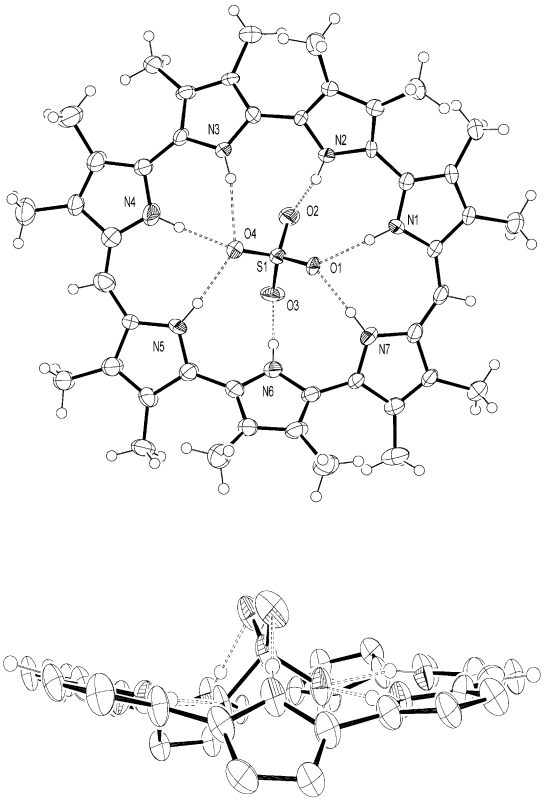
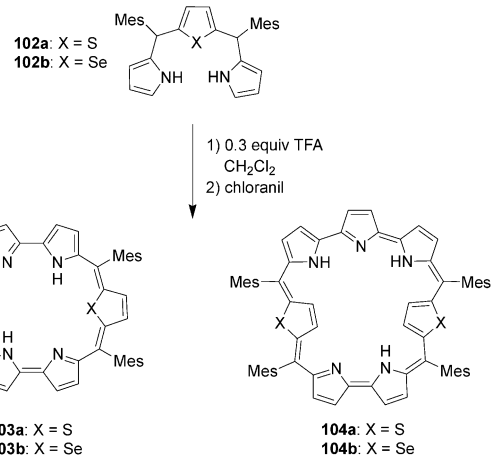


Figure 34. Front (top) and side (bottom) views of the solid-state structure of complex **101**.[106] For clarity, the peripheral substituents were removed in the side view.

6.2. Heteroatom Analogues of [30]Heptaphyrin(1.1.0.1.1.0.0)

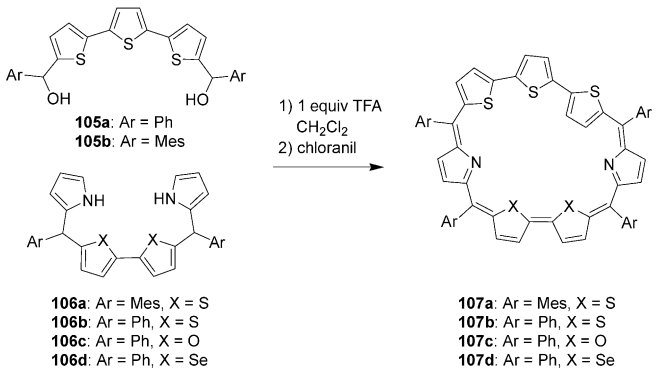
The first examples of heteroatom analogues of [30]heptaphyrin(1.1.0.1.1.0.0) were recently reported by Chandrashekar and co-workers.[107] These novel macrocycles were initially obtained as side products in the synthesis of the heterorubyrins **103** (Scheme 32). Oxidative coupling of the heterotripyranes **102a** or **102b** was found to give rise to **103a** or **103b** in 15% yield, while the heptaphyrins **104a** or **104b** were isolated in 2% yield.



Scheme 32. Formation of heterorubyrins **103** and heteroheptaphyrins **104**.

While the formation of the unexpected heptaphyrins **104a** or **104b** was rationalized by the partial hydrolysis and recombination of the heterotripyrranes **102a** or **102b** under the reaction conditions, it is interesting to note that no heptaphyrins were isolated when the *meso* substituent on the tripyrrane precursor was changed from mesityl to phenyl. This finding presumably reflects the stability differences of the tripyrranes involved, with the mesityl-substituted tripyrranes **102** being more readily hydrolyzed under the reaction conditions.

A more rational synthesis of different heteroanalogues of [30]heptaphyrin(1.1.0.1.1.0.0) was reported in the same paper.[107] Reaction of **105a** with **106b**, **106c**, and **106d** was found to give rise to **107b**, **107c**, and **107d** in yields of 22, 20, and 15%, respectively (Scheme 33). Compound **107a** was obtained in 20% yield upon reaction of **105b** with **106a**.



Scheme 33. Synthesis of the terthiophene-containing heteroheptaphyrins **107**.

6.3. Heteroatom Analogues of [30]Heptaphyrin(1.1.0.1.0.1.0)

In the study of the different heteroatom analogues **104a**,**b** and **107a**–**d** of [30]heptaphyrin(1.1.0.1.1.0.0), Chandrashekar and co-workers detailed the synthesis of four different

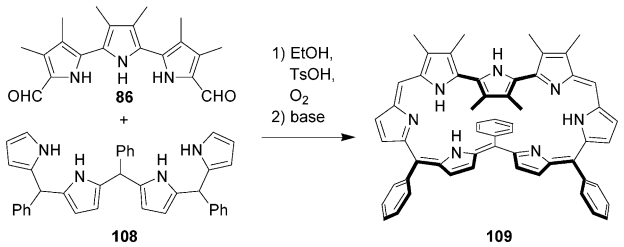
 © 2003 Wiley-VCH Verlag GmbH & Co. KGaA, Weinheim

heteroatom-containing analogues of [30]heptaphyrin(1.1.0.1.0.1.0).[107] As shown previously in Scheme 24, reaction of **82a** or **82b** with either **43a** or **43c** produced macrocycles **84a–d**, respectively, in yields ranging from 15 to 20%. Curiously, despite the moderate yields obtained, the report does not comment on the formation of other macrocycles that might be expected; for example, products derived from the self-coupling of the respective precursors (see, however, Sections 5.3 and 7.5).

All the heteroheptaphyrins produced were judged to be aromatic on the basis of their spectroscopic properties. For example, as reported in the Supporting Information of the paper,[107] the CH protons of the inverted selenophene subunit in **84d** were found to resonate as a singlet at $\delta = -1.62$ ppm, while two singlets were seen at $\delta = 0.02$ and -0.47 ppm which are ascribed to the two different NH signals. Also in accord with the proposed aromatic character, signals ascribed to the "outer" β-CH protons of **84d** were found between $\delta = 9.07$ and 10.17 ppm. The conformations of the other heptaphyrins, as indicated in Scheme 32 and Scheme 33, were assigned solely on the basis of NMR spectroscopic analyses. There thus remains a need for X-ray structural data that would confirm these conformational assignments, at least in the solid state.

6.4. [30]Heptaphyrin(1.1.1.1.1.0.0)

[30]Heptaphyrin(1.1.1.1.1.0.0) (**109**) was recently synthesized[108] in 16% yield from the acid-catalyzed condensation of a 1:1 mixture of the diformylhexamethylterpyrrole (**86**) with the tetrapyrrane **108** (Scheme 34). Along with **109**,



Scheme 34. Synthesis of heptaphyrin **109**.

[26]hexaphyrin(1.1.1.1.0.0) (**87**) (see Section 5.4.) was isolated in 15% yield. The formation of this latter product was rationalized in terms of the partial hydrolysis of precursor tetrapyrrane **108**, a conclusion that is in accord with other examples discussed above.

The aromatic nature of **109** was inferred from its NMR spectroscopic properties. Although the proposed aromatic character is noteworthy, perhaps the most interesting features of **109** that were deduced from the ^{1}H NMR spectrum are the inversion of a pyrrole ring bearing two methyl groups as β substituents ($\delta(CH_3) = -4.2$ ppm) and the finding that the signals corresponding to one phenyl ring are shifted to considerably higher field than normal (three sets of multiplets are observed at $\delta = 0.48$ (2H), 3.67 (2H), and 4.93 ppm (1H)). This latter finding was rationalized in terms of the phenyl group pointing inside the ring and an overall structure that deviates substantially from planarity. Thus, in contrast to the solution-state structure, the solid-state structure was characterized by the presence of a figure-eight motif (Figure 35). The disparity between the solid-state and the solution-state structure was rationalized in terms of crystal-packing effects.

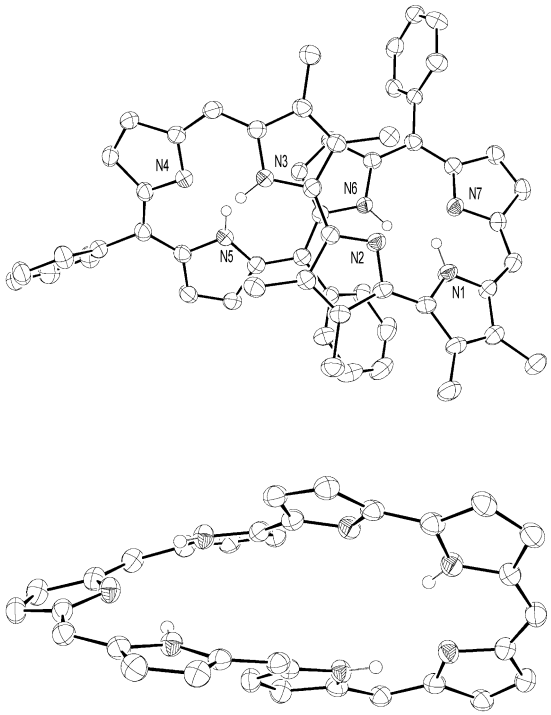


Figure 35. Front (top) and side (bottom) views of the solid-state structure of complex **109**.[108] For clarity, the peripheral substituents were removed in the side view.

6.5. Heptaphyrin(1.1.1.1.1.1.1)

Furuta and co-workers reported the synthesis of a *meso*-substituted heptaphyrin(1.1.1.1.1.1.1) derivative. This aesthetically appealing compound was obtained as one of many products produced from a modified Rothemund procedure that involves the condensation of pyrrole with pentafluorobenzaldehyde (see Section 7.6).[93] Unfortunately, little information regarding the exact nature of this macrocycle (for example, its conformational properties) is available at present.

7. Compounds Containing Eight or More Pyrrole Rings

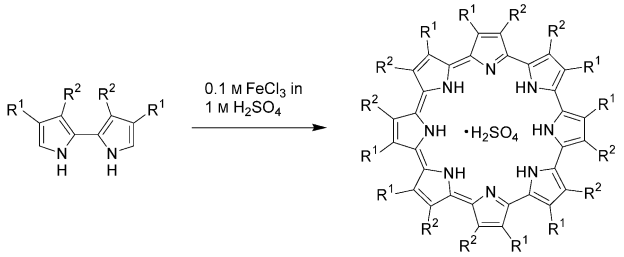
Given the explosive growth now being seen in the area of expanded porphyrins, it is interesting that the record for the greatest number of subunits in a polypyrrole macrocycle stood at ten up until 1999. The particular system in question, turcarsarin,[33] represented an important breakthrough at the time it was reported because it illustrated, as did the subsequent cyclic octapyrroles synthesized by Vogel and co-

 © 2003 Wiley-VCH Verlag GmbH & Co. KGaA, Weinheim

workers,[109,110] that expanded porphyrins could adopt figure-eight conformations that were the complete antithesis of the flat structures one might have expected for conjugated heteroannulenes. Not surprisingly, therefore, the synthesis of these higher order systems provided an important stimulus for the field, both in terms of understanding the basis of these strange conformational features, and defining an implicit new challenge. A central question was whether yet bigger systems containing a greater number of pyrrole rings or pyrrole-type subunits could be made. As implied above, it took some time for this challenge to be met. Since 1999, however, driven mostly by scientific curiosity as well as by the very human impulse to reach for the limits, a plethora of so-called higher order (superexpanded) systems have been reported.[111] In this Section the chemistry of expanded porphyrins and heteroatom analogues containing eight or more heterocyclic subunits is reviewed.

7.1. [30]Octaphyrin(0.0.0.0.0.0.0.0)

The synthesis of four different cyclo[8]pyrroles ([30]octaphyrin(0.0.0.0.0.0.0.0), **110a–d**) has been described very recently.[112] Cyclo[8]pyrroles **110a–c** were obtained in yields of over 70% (**110d** was produced in 15% yield) by means of an Fe^{III}-based oxidative coupling of bipyrroles **99a–d** (Scheme 35). Crucial for the successful synthesis was the use



99a: $R^1 = R^2 = Et$
99b: $R^1 = Et$, $R^2 = Me$
99c: $R^1 = R^2 = Me$
99d: $R^1 = n$Pr, $R^2 = H$

110a: $R^1 = R^2 = Et$ (77%)
110b: $R^1 = Et$, $R^2 = Me$ (79%)
110c: $R^1 = R^2 = Me$ (74%)
110d: $R^1 = n$Pr, $R^2 = H$ (15%)

Scheme 35. Formation of cyclo[8]pyrroles **110**.

of optimized biphasic reaction conditions (bipyrrole in CH_2Cl_2/0.1M $FeCl_3$ in 1M H_2SO_4).

The NMR spectra of the dihydrogen sulfate salts **110a–d** are characterized by their unusually high symmetry. They also provide important support for the conclusion that these systems contain an aromatic 30 π-electron system. For example, the signal for the magnetically degenerate methyl groups in **110c** is found to resonate at $\delta = 3.58$ ppm, while the signal corresponding to the NH protons is seen at $\delta = -0.84$ ppm. Although not related to the issue of deducing the π-electron count, it is noteworthy that the ^{13}C NMR spectrum of **110c** consists of only three signals at $\delta = 15.6$, 123.9, and 125.9 ppm.

An X-ray structural analysis of **110b** revealed that the macrocycle exists in a flat conformation with a sulfate ion in the central core, bound by eight NH···O hydrogen-bonding interactions (Figure 36). The UV/Vis spectrum of **110b** (Figure 37) was found to be highly unusual; it is characterized by a relatively weak Soret-type absorbance at 431 nm with an extinction coefficient of 79800 $M^{-1}cm^{-1}$ and an intense Q-type band at 1112 nm ($\varepsilon = 132200\ M^{-1}cm^{-1}$) that is considerably red-shifted relative to the corresponding bands in most expanded porphyrins. It has thus been proposed that the unusual spectral features of cyclo[8]pyrroles **110a–d** could enable them to be used as an IR filter or in optical storage and signaling devices.

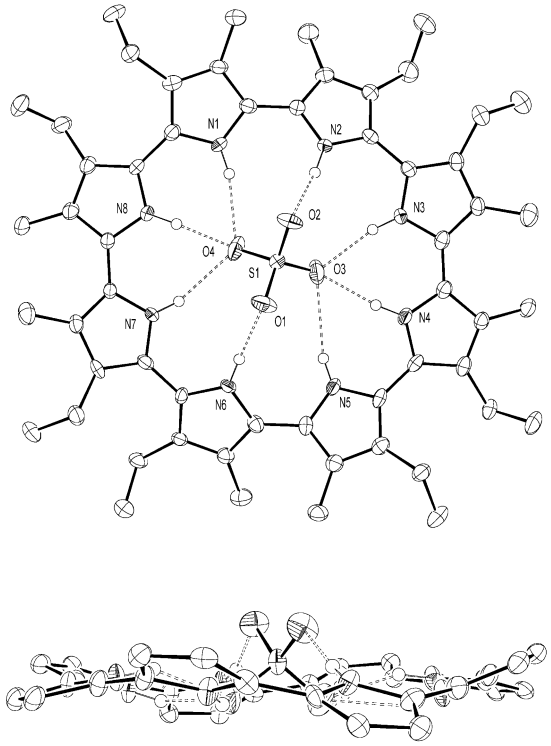


Figure 36. Front (top) and side (bottom) views of the solid-state structure of complex **110b**.[112] For clarity, the peripheral substituents were removed in the side view.

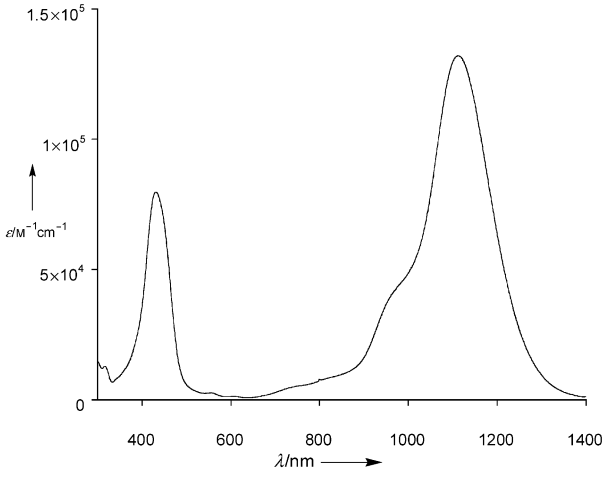
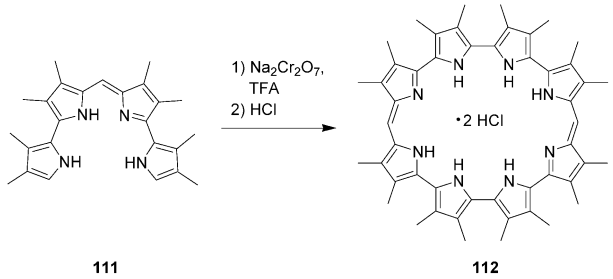


Figure 37. UV/Vis spectrum of **110b** recorded in dichloromethane.[112]

© 2003 Wiley-VCH Verlag GmbH & Co. KGaA, Weinheim

7.2. [32]Octaphyrin(1.0.0.0.1.0.0.0)

The synthesis of [32]octaphyrin(1.0.0.0.1.0.0.0) was recently reported.[106] This expanded porphyrin was obtained in the form of its HCl salt **112** in 16% yield (Scheme 36) by subjecting the linear tetrapyrrole **111** to a Cr^{VI}-based oxidative coupling procedure analogous to that used to prepare [28]heptaphyrin(1.0.0.1.0.0.0) (**101**, see section 6.1).



111 **112**

Scheme 36. Synthesis of quaterpyrrole-containing octaphyrin **112**.

Despite containing a 32 π-electron periphery, and in contrast to its smaller congener **101**, the ^{1}H NMR spectrum of **112** does not show any signs of an antiaromatic ring-current effect. The two NH protons are found to resonate at $\delta = 11.2$ and 11.9 ppm, while the signal corresponding to the *meso* CH protons is found at $\delta = 7.3$ ppm in the ^{1}H NMR spectrum. This apparent lack of observable ring-current effect was rationalized in terms of a strong deviation from planarity. The highly nonplanar nature of **112** was confirmed by an X-ray structural analysis (Figure 38). In contrast to other octaphyrins containing a greater number of bridging *meso* groups, however, the deviations from planarity seen in the solid state were not so great as to cause **112** to adopt a figure-eight conformation. The UV/Vis spectrum of **112** is characterized by a broad band at 586 nm ($\varepsilon = 67300\ M^{-1}cm^{-1}$) that has a shoulder at approximately 660 nm.

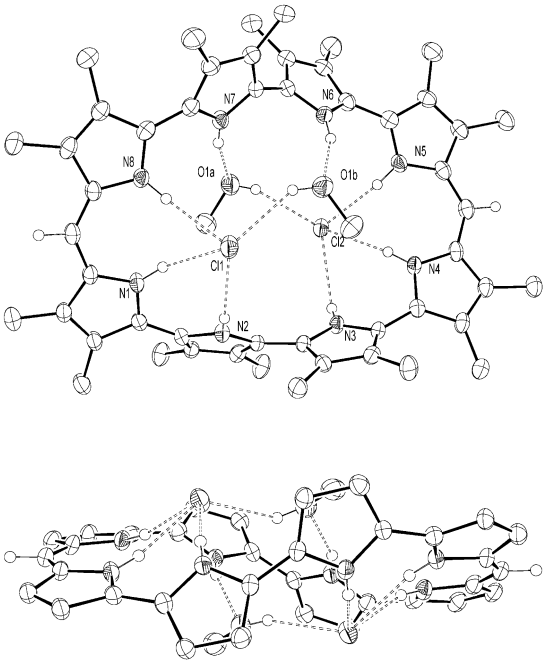
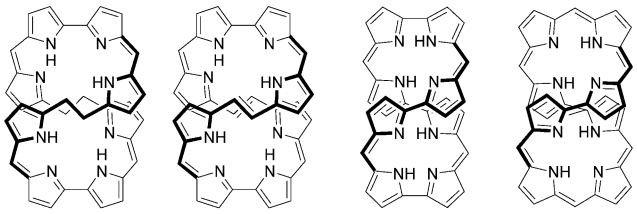


Figure 38. Front (top) and side (bottom) views of the solid-state structure of complex **112**.[106] For clarity, the peripheral substituents were removed in the side view.

7.3. Figure-Eight Octaphyrins and Their Metal Complexes

The octaphyrins prepared previously by Vogel et al. (**113**–**116**; shown with the β substituents omitted for clarity)[109,110] were the subject of recent studies targeting their electrochemical behavior as well as their ability to form metal complexes.[113] Similar redox patterns were observed for the two free bases **114** and **115**: Both undergo five distinct redox steps, two reductions and three oxidations. As confirmed by cyclic voltammetry, the two reduction as well as the first two oxidation waves represent reversible one-electron steps. However, the third oxidation event corresponds to an irreversible two-electron step. Overall, the redox behavior of **114** and **115** was considered consistent with the presence of the proposed fully conjugated π-electron peripheries. Octaphyrin **113**, on the other hand is not fully conjugated. It thus shows significantly different redox behavior. In addition to one irreversible reduction wave at a rather negative potential (−2 V, versus Fc/Fc^+), at least four distinct oxidation steps can be distinguished, only the first two of which are reversible. Interestingly, the mono- and/or bimetallic complexes **114a–c** and **115a–i** show redox patterns that are very similar to those seen for the free bases **114** and **115**. However, metalation generally facilitates slightly both the oxidation and reduction relative to the corresponding free-base ligands. The largest change in redox behavior is observed for the Co complexes **115a** and **115g**. In these two species, the third oxidation step is metal, rather than ligand centered. Interestingly, in this oxidation step, which corresponds to the Co^{II}/Co^{III} couple, the oxidation potential (+0.78 V versus Fc/Fc^+) is significantly higher than those for Co^{II}–tetrapropylporphycene (+0.19 V versus Fc/Fc^+) and for Co^{II}–tetraphenylporphyrin (+0.38 V versus Fc/Fc^+). It was concluded that this stabilization of the Co^{II} oxidation state is imposed by the figure-eight geometry of the ligand, something that makes it difficult to



113 **114** **115** **116**

113a: Pd-Pd complex

114a: Pd-Pd complex
114b: Cu-Cu complex
114c: Ni-Ni complex

115a: mono-Co complex
115b: mono-Ni complex
115c: mono-Pd complex
115d: mono-Cu complex
115e: Pd-Pd complex
115f: Pd-Pd complex
115g: Co-Cu complex
115h: Ni-Cu complex
115i: Ni-Pd complex

 © 2003 Wiley-VCH Verlag GmbH & Co. KGaA, Weinheim

achieve the octahedral coordination preferred by the Co^{III}-center. In summary, the free-base ligands **114** and **115** as well as the metal complexes **114a–c** and **115a–i** display electrochemical gaps (difference in oxidation and reduction potentials; $E_{Ox1}-E_{Red1}$) between 1.43 and 0.85 V that are lower than the corresponding values for analogous porphyrin or porphycene systems.

As a major proof-of-principle step that could lead to the eventual development of chiral expanded porphyrin catalysts, Werner, Vogel, and co-workers recently studied the free-base macrocycles **113** and **114**, as well as the metal complexes **113a** and **114a**,**b**, with a view to achieving enantiomeric separation.[114] Macrocycle **114** was successfully separated into its constituent enantiomers on an analytical HPLC column containing commercially available Chiralcel OD as the solid support. The two fractions showed mirror-image CD spectra, from which it was concluded that the separation was successful (Figure 39). The enantiomers of **114** proved very

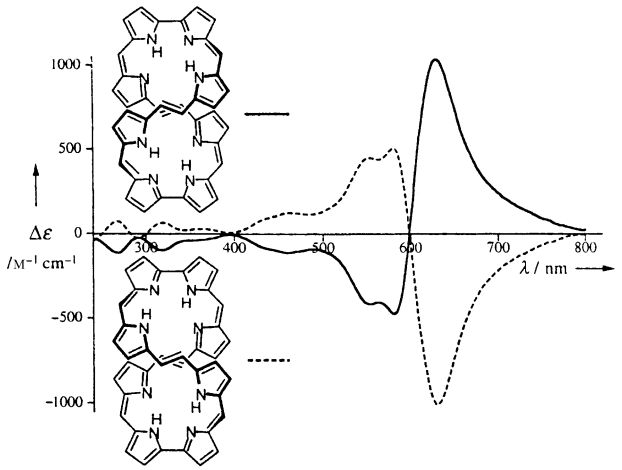


Figure 39. CD spectra (CH_2Cl_2) of the enantiomers of **114**.[114]

stable: heating their respective solutions in *n*-hexanes at 60 °C for a period of several hours did not result in any measurable racemization. Octaphyrin **113**, the tetrahydro derivative of **114**, was also separated into its enantiomers. In this case, however, racemization occurs readily even at room temperature. The free activation enthalpy $\Delta G^{\ddagger}_{298}$ of racemization for **113** was determined to be approximately 96 kJ mol^{-1}.

In a later study the enantiomers of **114** were separated on a preparative scale. By using medium-pressure liquid chromatography (closed-loop technique and CDMPC-C_8 as the stationary phase), 15 mg of **114** was separated into its constituent enantiomers. In related work it was found that the metal complexes **113a** and **114a**,**b** could also be separated into their enantiomeric antipodes using similar techniques. Most notable are the results obtained with **114a**: the high enantioselectivity of the chiral cellulose phase CDMP-C_8 towards this latter Pd complex enabled the separation to be performed successfully on a 100 mg scale. The two resulting enantiomers of **114a** were then characterized by means of X-ray crystallography, and the structure of one enantiomer of **114a** is shown in Figure 40.

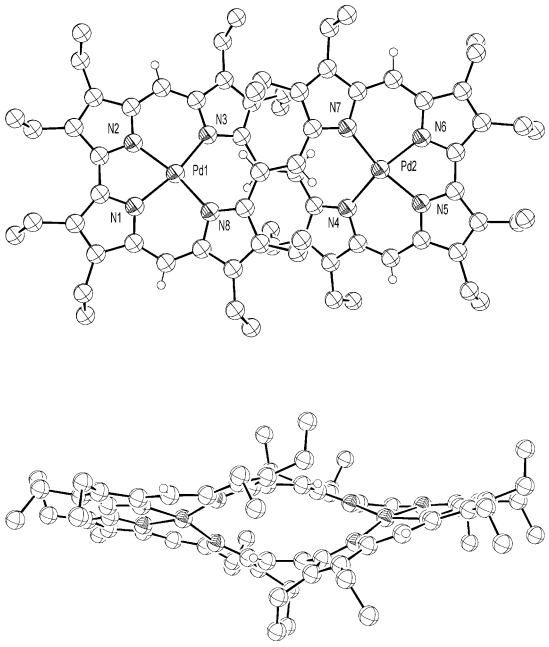
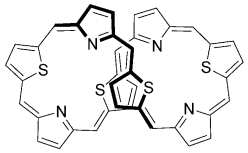


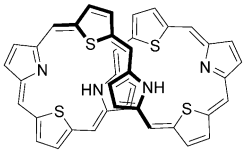
Figure 40. Front (top) and side (bottom) views of the solid-state structure of complex **114a**.[114]

7.4. Figure-Eight Tetrathiaoctaphyrin and Dihydrotetrathiaoctaphyrin

Latos-Grażyński et al. recently succeeded in the isolation of tetrathia[36]octaphyrin(1.1.1.1.1.1.1.1) (**117**) and tetrathia[38]octaphyrin(1.1.1.1.1.1.1.1) (**118**) in a total yield of about 2% from the mixture produced as the result of condensing 2,5-bis(*p*-tolylhydroxymethyl)thiophene and pyrrole under conditions of acid catalysis (the *meso* substituents have been omitted in the structural formulas).[115] Among the other products obtained are dithiaporphyrin, two different dithiasapphyrins, and a dithiaporphyrin with an inverted pyrrole ring.



117



118

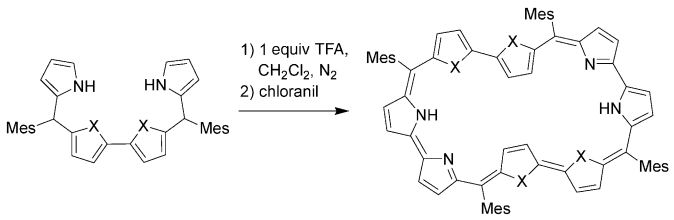
Both of the tetrathiaoctaphyrins are interconvertible. Exposure of **117** to sodium borohydride in THF readily transforms the macrocycle into **118** as the result of what is formally a dihydrogenation. In turn, oxidation of **118** with *p*-chloranil or DDQ produces **117**. Both **117** and **118** were the subject of exhaustive conformational analysis. On the basis of a range of NMR spectroscopic studies that were supported by MM+ calculations, both macrocycles were assigned figure-eight structures in solution; in **117**, two thiophene rings are located at the crossing point, while in **118** these positions are occupied by two pyrrole rings. Stepwise protonation of either

 © 2003 Wiley-VCH Verlag GmbH & Co. KGaA, Weinheim

117 or **118** gives rise to symmetric or asymmetric cationic species, depending on the number of protons added. The dynamic behavior of **117** was described as a figure-eight conveyor-belt-like movement that proceeds without a racemization step. Despite the highly nonplanar structures of **117** and **118**, the authors observed residual diatropic and paratropic ring-current effects in the case of **118** (38 π-electron periphery, formally aromatic) and **117** (36 π-electron periphery, formally antiaromatic), respectively. Unfortunately, at present no solid-state structural information is available for either **117** or **118**.

7.5. Meso-*Substituted Heteroatom Analogues of [34]Octaphyrin(1.0.1.0.1.0.1.0)*

The first octapyrrolic expanded porphyrin, [34]octaphyrin(1.0.1.0.1.0.1.0), was synthesized by Vogel and coworkers in 1995.[110] This compound had all 16 of its β positions blocked with ethyl substituents and was found to adopt a chiral figure-eight conformation both in solution and in the solid state. Recently, the research group of Chandrashekar reported the synthesis of **119a** and **119b**, two heteroatom analogues of [34]octaphyrin(1.0.1.0.1.0.1.0). These macrocycles were found to be planar, presumably as a consequence of having two β-unsubstituted thiophene or selenophene subunits inverted.[116] The synthesis of **119a** and **119b** is summarized in Scheme 37. It involves the oxidative



Scheme 37. Formation of heterooctaphyrins **119**.

coupling of the linear heterotetrapyrrolic precursors **106a** and **106e**, and gives rise to **119a** and **119b**, respectively, both of which were isolated in 5% yield. Curiously, the authors made no mention of other macrocycles that might have been expected under these reaction conditions that, based on other examples from their laboratory, are known to promote partial hydrolysis of the starting materials.

As inferred originally from NMR spectroscopic studies, **119a** is believed to exist as a mixture of two different conformers in solution, at least on the NMR time scale. While neither the ratio of these two conformers nor their rate of interconversion was detailed, it was proposed that both contain two inverted thiophene subunits. The ^{1}H NMR spectrum for the conformer **119a**, which was assumed to be flatter, showed two sharp doublets at $\delta = -5.3$ and -5.89 ppm, which were assigned to the β-CH protons of the inverted thiophene rings. In this case, direct evidence for planarity came from an X-ray structural analysis; in addition to confirming the proposed thiophene inversion, this structure revealed a macrocycle that, except for the *meso* substituents, is almost perfectly flat (Figure 41).

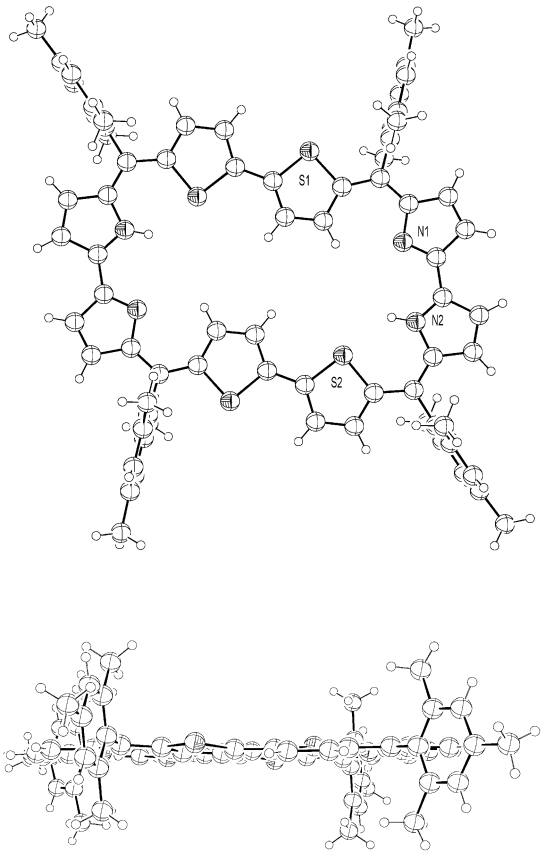
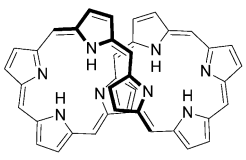


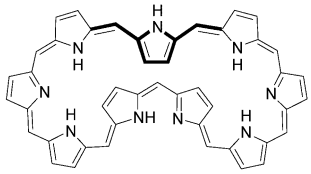
Figure 41. Front (top) and side (bottom) views of the solid-state structure of complex **119a**.[116]

7.6. *Octaphyrin(1.1.1.1.1.1.1.1) and Nonaphyrin(1.1.1.1.1.1.1.1.1)*

As discussed briefly in Section 5.1, Furuta and co-workers recently reported the synthesis of a variety of *meso*-aryl-substituted expanded porphyrins obtained from a modified Rothemund condensation of pyrrole and pentafluorobenzaldehyde.[93] These researchers obtained porphyrin (11–12%), N-fused pentaphyrin **78** (14–15%), hexaphyrin **79** (16–20%), heptaphyrin (4–5%), octaphyrin **120** (5–6%), nonaphyrin **121** (2–3%), as well as several higher homologues in very low yield by condensation of both precursors at relatively high



120



121

 © 2003 Wiley-VCH Verlag GmbH & Co. KGaA, Weinheim

concentration (that is, 67 mM in both reactants in CH_2Cl_2) in the presence of 4.2 mM $BF_3{\cdot}Et_2O$, followed by oxidation with DDQ.

Octaphyrin(1.1.1.1.1.1.1.1) (**120**) and nonaphyrin(1.1.1.1.1.1.1.1.1) (**121**) were characterized by X-ray diffraction analysis (Figures 42 and 43). Octaphyrin **120** adopts a twisted figure-eight conformation with near C_2 symmetry. It thus resembles most other higher order expanded porphyrins which for the most part display similar nonplanar

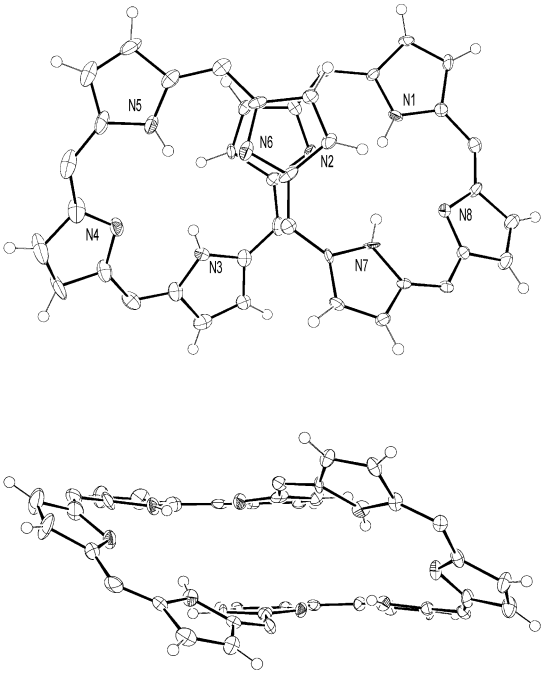


Figure 42. Front (top) and side (bottom) views of the solid-state structure of complex **120**.[93] For clarity, the peripheral substituents were removed.

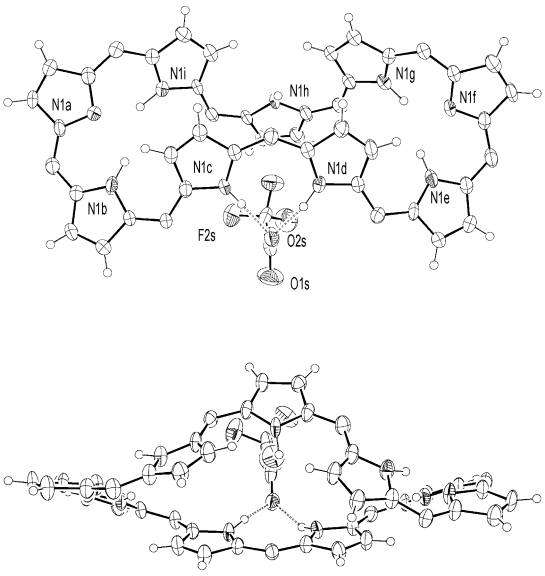


Figure 43. Front (top) and side (bottom) views of the solid-state structure of complex **121**·HTFA.[93] For clarity, the peripheral substituents were removed.

conformations.[33,109,110] The monoprotonated TFA salt of nonaphyrin (**121**·HTFA) was found to adopt a twisted helix-like conformation with a near mirror plane and a large cleft wherein the TFA counterion is bound.

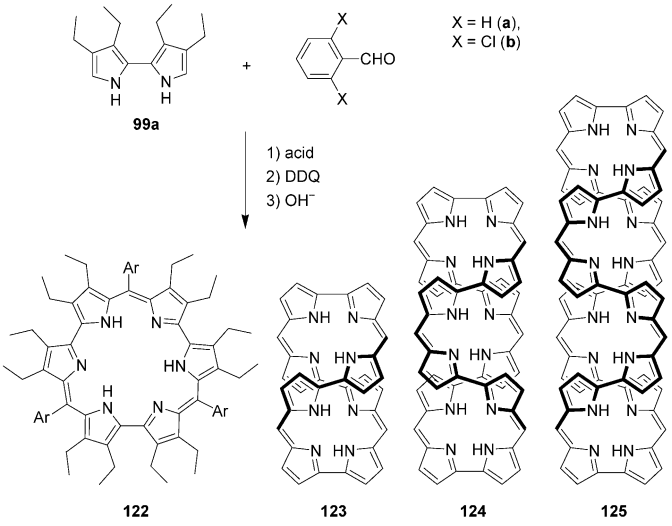
In agreement with the solid-state structure of **120**, the ^{1}H NMR spectrum of this octaphyrin shows a C_2-symmetric signal pattern with signals that are in agreement with the proposed nonaromatic 36 π-electron conjugated pathway. By contrast, the ^{1}H NMR spectral features of **121**·HTFA, specifically the finding of markedly different chemically shifts for the β-pyrrolic protons, led the authors to conclude that **121** is indeed an aromatic 42 π-electron system, as implied by its structural formula.

Treatment of **120** with DDQ gives rise to spectral features in the UV/Vis spectrum (strong Soret-type band at $\lambda_{max} =$ 738 nm; weaker Q-type bands at 1264 nm) that are in agreement with an aromatic 34 π-electron system. Likewise, treatment of **120** with $NaBH_4$ in methanol led to appearance of spectral features that are consistent with the formation of an aromatic 38 π-electron system.

This contribution by Furata and co-workers provides an impressive illustration of just how far the modified Rothemund reaction can be pushed in terms of obtaining new products. Unfortunately, the associated characterization chemistry is still in its infancy and it may thus be some time before the properties and potential applications of these new expanded porphyrins become fully appreciated.

7.7. [48]Dodecaphyrin(1.0.1.0.1.0.1.0.1.0.1.0) and [64]Hexadecaphyrin(1.0.1.0.1.0.1.0.1.0.1.0.1.0.1.0)

In 1999, Setsune et al. carried out a condensation between tetraethylbipyrrole (**99a**) and 2,6-dichlorobenzaldehyde under conditions of acid catalysis and in the presence of Zn^{2+} ions. They obtained a complex mixture that contained, among other products, [48]dodecaphyrin-(1.0.1.0.1.0.1.0.1.0.1.0) (**124**) and [64]hexadecaphyrin-(1.0.1.0.1.0.1.0.1.0.1.0.1.0.1.0) (**125**, Scheme 38).[117] A crystal-



Scheme 38. Synthesis of superexpanded porphyrins **122**–**125**.

© 2003 Wiley-VCH Verlag GmbH & Co. KGaA, Weinheim

structure analysis of **124**, obtained from the original reaction mixture in yields of up to 6%, revealed the presence of a large cavity surrounded by a wall of "zigzag-tracked π conjugation" (Figure 44).

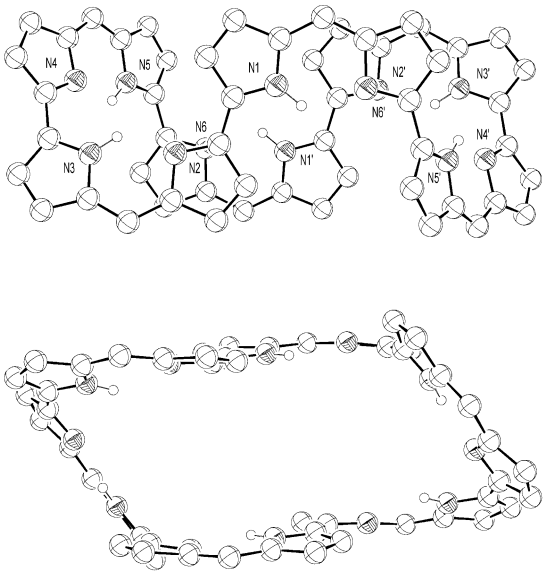


Figure 44. Front (top) and side (bottom) views of the solid-state structure of complex **124**.[117] For clarity, the peripheral substituents were removed.

By employing a different synthetic strategy, namely the use of a highly reactive bis(azafulvene) species, Setsune and Maeda also succeeded in preparing expanded porphyrins with up to 24 pyrrole rings; the largest characterized structurally was [64]hexadecaphyrin(1.0.1.0.1.0.1.0.1.0.1.0.1.0.1.0) (**125**) containing 16 pyrrole rings (Figure 45).[118] These systems are of tremendous scientific interest, not only because of their aesthetically appealing structures, but also because of their nonplanar conformations that can render them chiral. They also represent the logical extension of the deca- and octapyrrolic systems with figure-eight structures and highlight the fact that as systems get larger the level of conformational complexity is increased (see Sections 7.1 and 7.8).

7.8. Cyclo[n]thiophenes

In 2000, Bäuerle and co-workers reported the synthesis of very large thiophene-based macrocycles.[119] As outlined in Scheme 39, reaction of cyclooligothiophenediacetylene **126**, obtained from thiophenediynes under modified Eglington–Glaser conditions, with $Na_2S{\cdot}9H_2O$ gave rise to cyclo[12]-thiophene **127** in 23% yield. Analogous reactions led to the isolation of cyclo[16]thiophene and cyclo[18]thiophene in yields of 7 and 27%, respectively. Although the new macrocycles could be considered as $(4n)$ π-electron antiaromatic species, they displayed no apparent ring-current effects, as judged from an analysis of their respective ^{1}H NMR spectra. An X-ray crystallographic analysis of **126** revealed the presence of an essentially flat macrocycle (Figure 46).

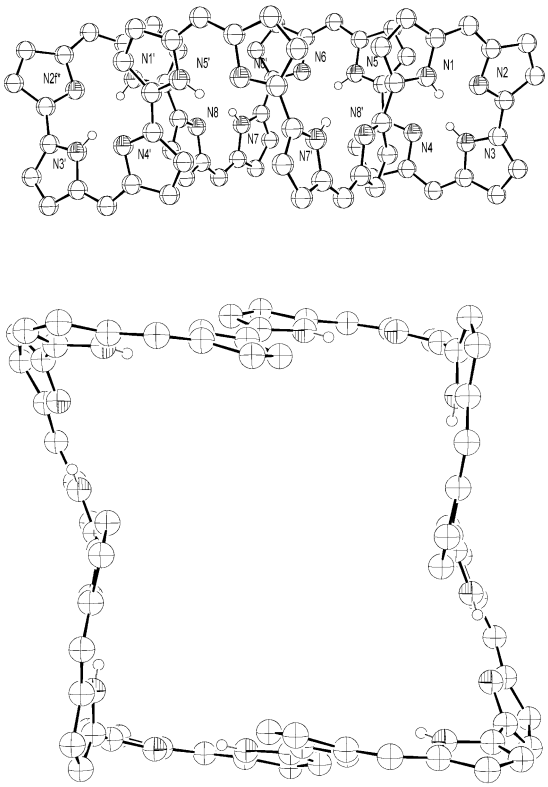
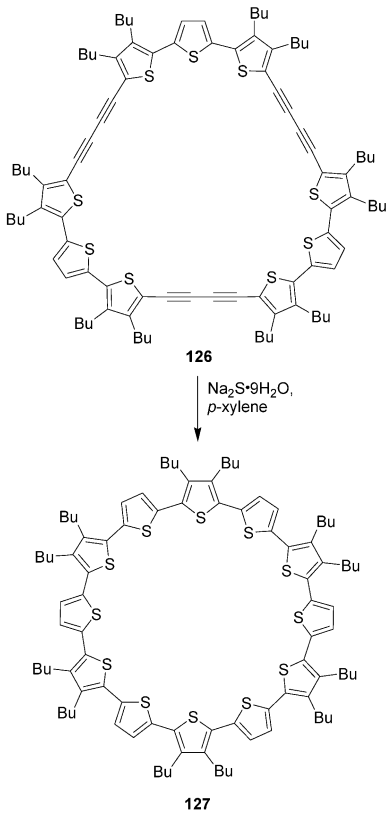


Figure 45. Front (top) and side (bottom) views of the solid-state structure of complex **125**.[118] For clarity, the peripheral substituents were removed.



Scheme 39. Synthesis of cyclo[12]thiophene **127**.

 © 2003 Wiley-VCH Verlag GmbH & Co. KGaA, Weinheim

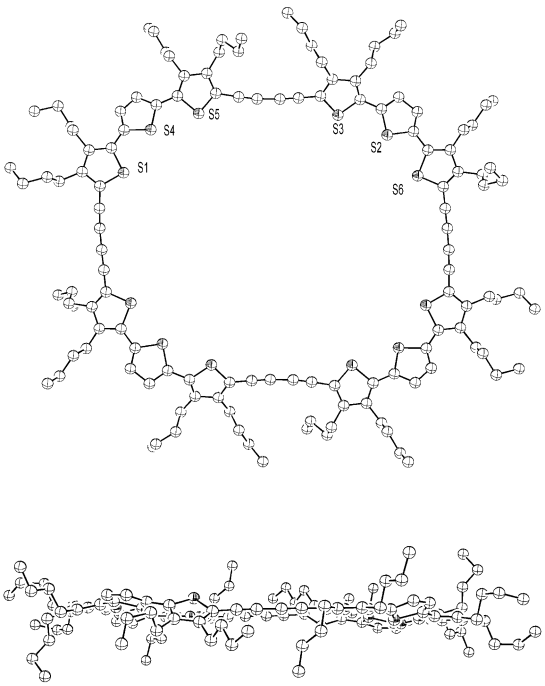


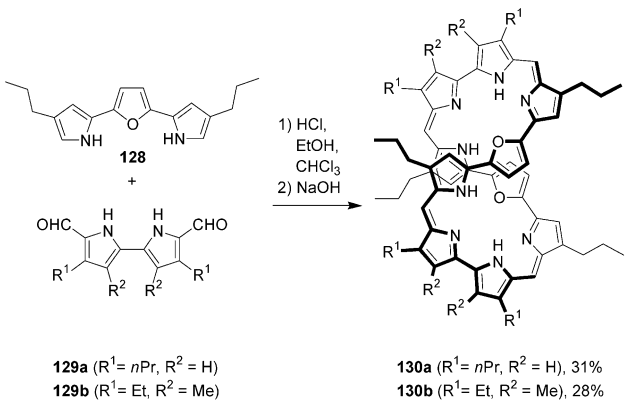
Figure 46. Front (top) and side (bottom) views of the solid-state structure of complex **126**.[119]

Cyclo[12]thiophene **127** was calculated to have a diameter of 2.34 nm. On the basis of its unusually large core size, the authors anticipate that cyclo[*n*]thiophenes could act as hosts for large organic guest molecules. For example, it was calculated that **127** could serve as a host for fullerene C_{60}. However, no reports of this promise being realized have so far appeared in the literature.

7.9. Dioxa[40]decaphyrin(1.0.1.0.0.1.0.1.0.0), an Analogue of Turcasarin

Furan-containing analogues of turcasarin (**12**) have been prepared in the form of dioxa[40]decaphyrins-(1.0.1.0.0.1.0.1.0.0) **130a** and **130b**.[120] In analogy to the synthesis of turcasarin (**12**),[33] condensation of oxaterpyrrole **128** with diformylbipyrrole **129a** or **129b** under conditions of acid catalysis was found to give rise to either **130a** or **130b** in 31 and 28% yield, respectively (Scheme 40).

On the basis of NMR spectroscopic studies, **113a** was assigned a figure-eight structure in solution. As confirmed by an X-ray structural analysis of the free base **130a**, this conformational motif is also present in the solid state (Figure 47). Despite their different protonation states, the conformation of the free-base dioxa system **130a** shows a remarkable similarity to the conformation of the tetrahydrochloride salt of the *all*-aza turcasarin (**12**).[33] These latter findings suggest that a figure-eight structure represents the dominant conformation for [40]decaphyrin(1.0.1.0.0.1.0.1.0.0) and its heteroanalogues. The results of an ^{1}H NMR spectroscopic analysis of the slightly modified dioxaturcasarin **130b** were, therefore, surprising; these studies were consistent with



Scheme 40. Synthesis of furan-containing analogues of turcasarin **130**.

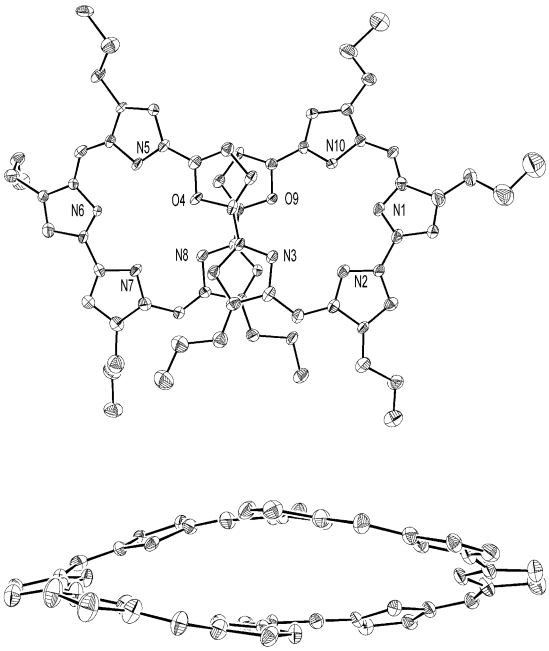


Figure 47. Front (top) and side (bottom) views of the solid-state structure of complex **130a**[120]. For clarity, the peripheral substituents were removed in the side view.

this derivative adopting a conformation that is too symmetric to be a figure-eight. Unfortunately, structural support for this conclusion has yet to be obtained.

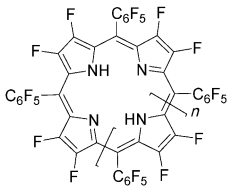
8. Recent Advances

Subsequent to the time of submission, work in the field of expanded porphyrin chemistry has continued to develop at a rapid pace. While it is not possible to review this newer work in detail, we do think it appropriate to highlight some of the more notable recent contributions. The interested reader is referred to references [121–127] and a new review article for further details of these and other accomplishments.[18]

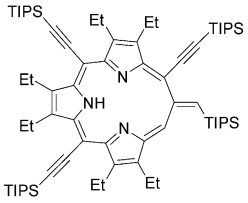
One of the most important recent advances is undoubtedly the finding that the yields of one-pot Rothemund-like

 © 2003 Wiley-VCH Verlag GmbH & Co. KGaA, Weinheim

syntheses of expanded porphyrins can be greatly improved through the judicious choice of precursors.[121] Furuta, Osuka, and co-workers found that condensation of 3,4-difluoropyrrole with pentafluorobenzaldehyde yielded, in addition to the expected porphyrin product, the corresponding perfluorinated pentaphyrin, hexaphyrin, heptaphyrin, octaphyrin, nonaphyrin, and decaphyrin in yields sufficient to allow for ready isolation (up to 7% in the best of cases, see structures **131**). Likewise, Anderson and co-workers have recently



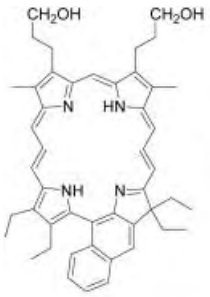
131



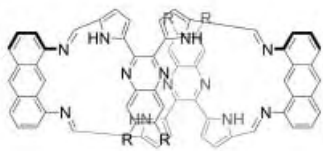
132

discovered that the $BF_3{\cdot}OEt_2$-catalyzed condensation of triisopropylsilylpropynal with 3,4-diethylpyrrole yielded a range of interesting products including the corresponding *meso*-alkynyl-substituted [24]pentaphyrin(1.1.1.1.1) and [28]hexaphyrin(1.1.1.1.1.1), as well as [15]triphyrin(1.1.3) **132**.[122] This latter species becomes the dominant product, being obtained in 26% yield, when trifluoroacetic acid is used as the catalyst.

In a report that builds on the approach of Paolesse, Smith, and co-workers to preparing expanded corroles (see Section 3.1), Sengupta and Robinson describe the use of a bisvinylogous biladiene to prepare an expanded chlorin **133**, which possesses a fused naphthalene ring.[123] Meanwhile,



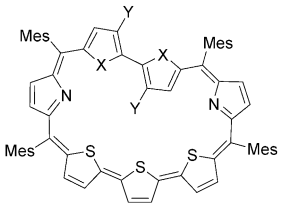
133



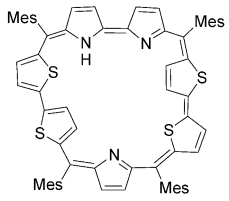
134a (R = H)
134b (R = OCH_3)
134c (R = OCH_2CH_3)

Sessler, Furuta, et al. have reported a new type of expanded porphyrin, namely Schiff base systems that contain anion-sensing dipyrrolylquinoxaline subunits (**134**).[124]

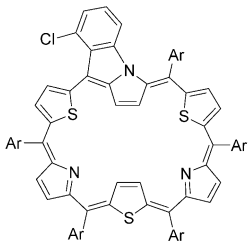
Continued advances in the area of heteroatom-containing expanded porphyrin chemistry were also reported by Chandrashekar and co-workers.[125] They obtained, among other species, the new heptapyrrolic macrocycles **135** and **136,** and their conformational behavior was studied in detail. In a separate study, Hung et al. reported that it was possible to obtain novel C-N bridged systems such as **137** and **138** by starting with an aryl-substituted tristhiophene-containing hexaphyrin analogue.[126]



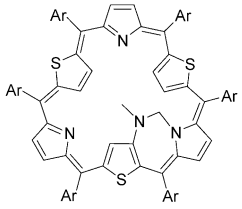
135a (X = Se, Y = H)
135b (X = O, Y = H)
135c (X = S, Y = Me)



136

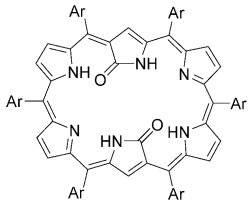


137

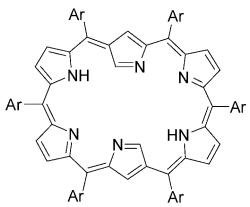


138

Finally, a new kind of expanded heteroporphyrin was reported quite recently by Furuta and co-workers.[127] By using a tripyrrane analogue wherein the central pyrrole is linked through the 2- and 4-positions (instead of the 2- and 5-positions as is normal for precursors of this type) these researchers were able to isolate the formally aromatic doubly N-confused dioxohexaphyrin analogue **139**, in addition to



139



140

other species, including the oxygen-free analogue **138**, as well as nonaromatic products corresponding to both of these novel systems. While these kinds of products are of interest for their unique structures themselves, the dioxo compound **139** is particular noteworthy: It could act as a binucleating ligand that stabilized structurally characterized dicopper and dinickel complexes. Such bimetallic complexes, although known in expanded porphyrin chemistry, are still rather rare.

9. Outlook

The present review, it is hoped, has helped underscore the richness and vitality of the field of expanded porphyrins. Motivated by factors ranging from intrinsic synthetic appeal to more prosaic targeting of practical application, and substantiated by the plethora of new systems produced in

 © 2003 Wiley-VCH Verlag GmbH & Co. KGaA, Weinheim

the last few years alone, it is clear that the chemistry of expanded porphyrins is flourishing. Here, the fact that a potentially limitless number of new structures can be conceived and that such systems are often endowed with a rich diversity of unique and useful properties is both inspiring current research efforts and setting the stage for future developments. Particular challenges for the future include understanding how specific synthetic designs get translated into particular conformations and how details of various proposed structures are reflected in terms of experimentally observable spectroscopic features or measurable chemical properties, such as anion recognition or cation coordination. What are the effects, for example, of core size, aromatic versus non- or even antiaromatic peripheries, macrocycle charge, heteroatom replacements on these and other experimentally observable characteristics?

On a more general level, it will become increasingly important to ask what molecular features are most useful for a given targeted application, whether such applications lie in the area of drug development, radioactive waste remediation, coordination chemistry, catalysis, optical materials preparation, or anion recognition and how one goes about optimizing for such features in a synthetic sense. At the same time, the synthesis of new systems will remain of interest: How far can we go in terms of extending the size, modifiying the shape, increasing the pyrrole content, effecting heteroatom replacements, and varying the number and nature of *meso* linkages before reaching the limits of normal chemical stability or solubility as a consequence of increasing polymeric character. Finally, an open-ended challenge involves removing the constraints of conjugation so as to relate the chemistry of expanded porphyrins to that of other pyrrole-containing macrocyclic systems thereby producing mono-, bi-, or polycyclic systems that may, for example, be topographically nonplanar or intrinsically chiral. Thus, even though the field of expanded porphyrin chemistry has advanced rapidly in recent years, it is clear that much, much more remains to be done and that not only significant challenges but also multiple opportunities abound.

This work was supported by NSF grant no. CHE-0107732.

Received: October 8, 2002 [A561]

[1] *The Porphyrin Handbook*, Academic Press, San Diego, **2000**.
[2] A. Jasat, D. Dolphin, *Chem. Rev.* **1997**, *97*, 2267.
[3] J. L. Sessler, S. J. Weghorn, *Expanded, Contracted and Isomeric Porphyrins*, Pergamon, New York, **1997**.
[4] E. Hückel, *Z. Phys.* **1931**, *70*, 204.
[5] J. L. Sessler, G. Hemmi, T. D. Mody, T. Murai, A. Burrell, S. W. Young, *Acc. Chem. Res.* **1994**, *27*, 43.
[6] J. L. Sessler, R. A. Miller, *Biochem. Pharmacol.* **2000**, *59*, 733.
[7] J. L. Sessler, J. M. Davis, *Acc. Chem. Res.* **2001**, *34*, 989.
[8] J. L. Sessler, A. Gebauer, S. J. Weghorn, in *The Porphyrin Handbook, Vol. 2* (Eds.: K. M. Kadish, K. M. Smith, R. Guilard), Academic Press, San Diego, **2000**, p. 55.
[9] R. Paolesse in *The Porphyrin Handbook, Vol. 2* (Eds.: K. M. Kadish, K. M. Smith, R. Guilard), Academic Press, San Diego, **2000**, p. 201.
[10] J. L. Sessler, A. Gebauer, E. Vogel in *The Porphyrin Handbook, Vol. 2* (Eds.: K. M. Kadish, K. M. Smith, R. Guilard), Academic Press, San Diego, **2000**, p. 1.
[11] H. Furuta, T. Asano, T. Ogawa, *J. Am. Chem. Soc.* **1994**, *116*, 767.
[12] P. J. Chmielewski, L. Latos-Grażyński, K. Rachlewicz, T. Glowiak, *Angew. Chem.* **1994**, *106*, 805; *Angew. Chem. Int. Ed. Engl.* **1994**, *33*, 779.
[13] H. Furuta, H. Maeda, A. Osuka, *J. Am. Chem. Soc.* **2000**, *122*, 803.
[14] H. Furuta, T. Ishizuka, A. Osuka, T. Ogawa, *J. Am. Chem. Soc.* **1999**, *121*, 2945.
[15] T. D. Lash, S. T. Chaney, D. T. Richter, *J. Org. Chem.* **1998**, *63*, 9076.
[16] T. D. Lash, M. J. Hayes, *Angew. Chem.* **1997**, *109*, 868; *Angew. Chem. Int. Ed. Engl.* **1997**, *36*, 840.
[17] T. D. Lash, J. L. Romanic, M. J. Hayes, J. D. Spence, *Chem. Commun.* **1999**, 819.
[18] For a recent review highlighting aspects of this chemistry, see H. Furuta, H. Maeda, A. Osuka, *Chem. Commun.* **2002**, 1795.
[19] P. A. Gale, P. Anzenbacher, Jr., J. L. Sessler, *Coord. Chem. Rev.* **2000**, *222*, 57.
[20] J. L. Sessler, R. S. Zimmerman, C. Bucher, V. Král, B. Andrioletti, *Pure Appl. Chem.* **2001**, *73*, 1041.
[21] a) B. Franck, A. Nonn, *Angew. Chem.* **1995**, *107*, 1941; *Angew. Chem. Int. Ed. Engl.* **1995**, *34*, 1795; b) see also footnote 20 in T. Wessel, B. Franck, M. Möller, U. Rodewald, M. Läge, *Angew. Chem.* **1993**, *105*, 201; *Angew. Chem. Int. Ed. Engl.* **1993**, *32*, 1148.
[22] E. Vogel, personal communication.
[23] V. J. Bauer, D. L. J. Clive, D. Dolphin, J. B. Paine III, F. L. Harris, M. M. King, J. Loder, S. W. C. Wang, R. B. Woodward, *J. Am. Chem. Soc.* **1983**, *105*, 6429.
[24] M. J. Broadhurst, R. Grigg, A. W. Johnson, *J. Chem. Soc. Perkin Trans. 1* **1972**, 1124.
[25] J. L. Sessler, M. Cyr, V. Lynch, E. McGhee, J. A. Ibers, *J. Am. Chem. Soc.* **1990**, *112*, 2810.
[26] V. W. Day, T. J. Marks, W. A. Wachter, *J. Am. Chem. Soc.* **1975**, *97*, 4519.
[27] H. Rexhausen, A. Gossauer, *J. Chem. Soc. Chem. Commun.* **1983**, 275.
[28] R. A. Berger, E. LeGoff, *Tetrahedron Lett.* **1978**, 4225.
[29] H. Koenig, C. Eickmeier, M. Moeller, U. Rodewald, B. Franck, *Angew. Chem.* **1990**, *102*, 1437; *Angew. Chem. Int. Ed. Engl.* **1990**, *29*, 1393.
[30] E. Vogel, M. Köcher, H. Schmickler, J. Lex, *Angew. Chem.* **1986**, *98*, 273; *Angew. Chem. Int. Ed. Engl.* **1986**, *25*, 257.
[31] R. Charrière, T. A. Jenny, H. Rexhausen, A. Gossauer, *Heterocycles* **1993**, *36*, 1561.
[32] J. L. Sessler, T. Morishima, V. Lynch, *Angew. Chem.* **1991**, *103*, 1018; *Angew. Chem. Int. Ed. Engl.* **1991**, *30*, 977.
[33] J. L. Sessler, S. J. Weghorn, V. Lynch, M. R. Johnson, *Angew. Chem.* **1994**, *106*, 1572; *Angew. Chem. Int. Ed. Engl.* **1994**, *33*, 1509.
[34] R. Paolesse, R. G. Khoury, F. D. Sala, C. D. Natale, F. Sagone, K. M. Smith, *Angew. Chem.* **1999**, *111*, 2727; *Angew. Chem. Int. Ed.* **1999**, *38*, 2577.
[35] E. Vogel, N. Jux, J. Dörr, T. Pelster, T. Berg, H.-S. Böhm, F. Behrens, J. Lex, D. Bremm, G. Hohlneicher, *Angew. Chem.* **2000**, *112*, 1143; *Angew. Chem. Int. Ed.* **2000**, *39*, 1101.
[36] M. Bröring, H.-J. Dietrich, J. Dörr, G. Hohlneicher, J. Lex, N. Jux, C. Pütz, M. Roeb, H. Schmickler, E. Vogel, *Angew. Chem.* **2000**, *112*, 1147; *Angew. Chem. Int. Ed.* **2000**, *39*, 1105.
[37] G. Märkl, H. Sauer, P. Kreitmeier, T. Burgemeister, F. Kastner, G. Adolin, H. Noeth, K. Polborn, *Angew. Chem.* **1994**, *106*, 1211; *Angew. Chem. Int. Ed. Engl.* **1994**, *33*, 1151.

 © 2003 Wiley-VCH Verlag GmbH & Co. KGaA, Weinheim

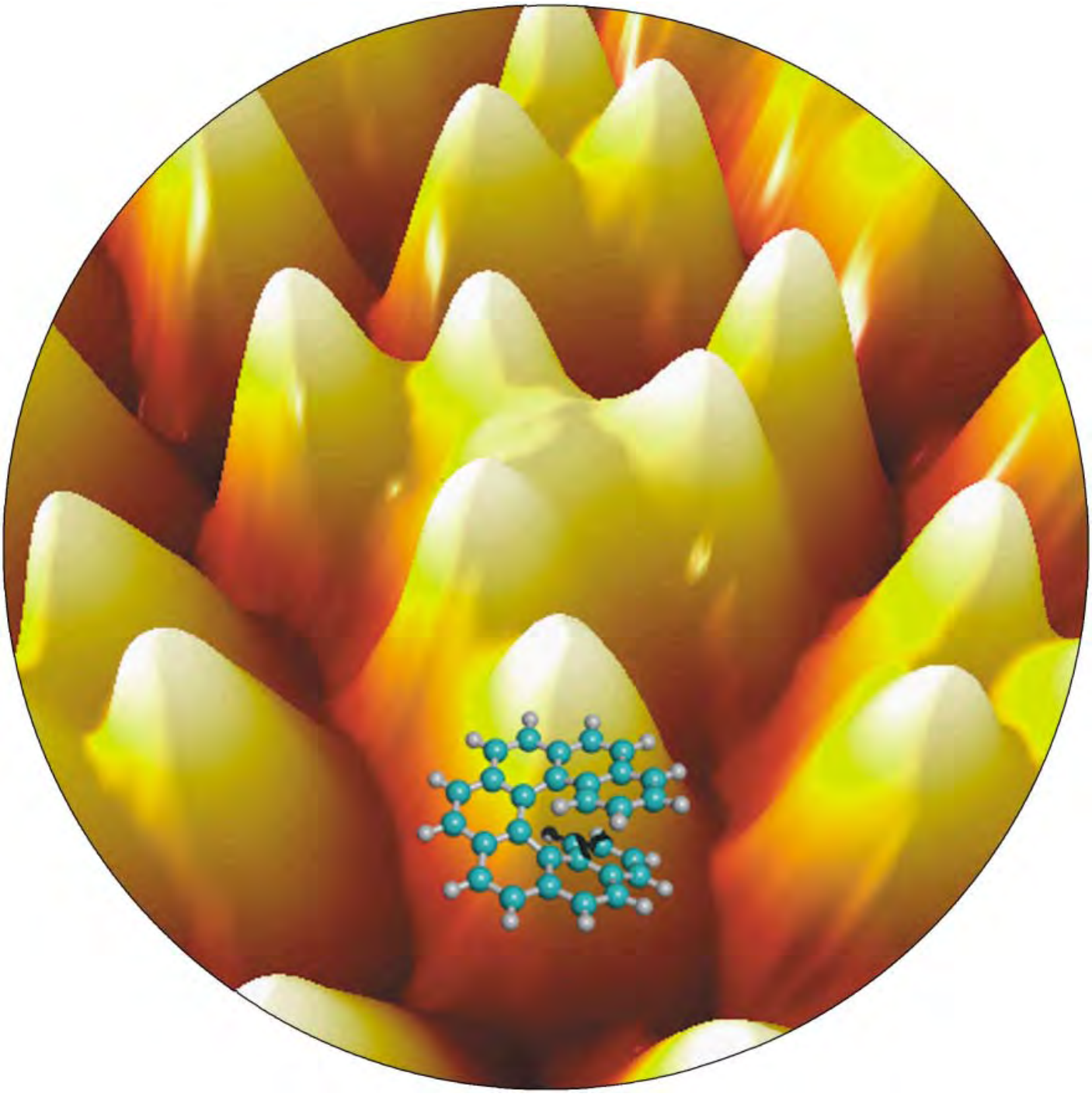
[38] G. Märkl, T. Knott, P. Kreitmeier, T. Burgemeister, F. Kastner, *Helv. Chim. Acta* **1998**, *81*, 1480.
[39] G. Märkl, R. Ehrl, H. Sauer, P. Kreitmeier, T. Burgemeister, *Helv. Chim. Acta* **1999**, *82*, 59.
[40] G. Märkl, R. Ehrl, P. Kreitmeier, T. Burgemeister, *Helv. Chim. Acta* **2000**, *83*, 495.
[41] G. Märkl, J. Stiegler, P. Kreitmeier, *Helv. Chim. Acta* **2001**, *84*, 2022.
[42] G. Märkl, J. Stiegler, P. Kreitmeier, T. Burgemeister, *Helv. Chim. Acta* **2001**, *84*, 2037.
[43] M. Stępien, L. Latos-Grażyński, *J. Am. Chem. Soc.* **2002**, *124*, 3838.
[44] T. D. Mody, J. L. Sessler in *Supramolecular Materials and Technologies* (Ed.: D. N. Reinhoudt), Wiley, New York, **1999**, p. 245.
[45] T. D. Mody, J. L. Sessler, *J. Porphyrins Phthalocyanines* **2001**, *5*, 134.
[46] M. P. Mehta, W. R. Shapiro, M. J. Glantz, R. A. Patchell, M. A. Weitzner, C. A. Meyers, C. J. Schultz, W. H. Roa, M. Leibenhaut, J. Ford, W. Curran, S. Phan, J. A. Smith, R. A. Miller, M. F. Renschler, *J. Clin. Oncol.* **2002**, *20*, 3445.
[47] M. P. Mehta, P. Rodrigus, C. H. J. Terhaard, A. Rao, J. Suh, W. Roa, L. Souhami, A. Bezjak, M. Leibenhaut, R. Komaki, C. Schultz, R. Timmerman, W. Curran, J. Smith, S.-C. Phan, R. A. Miller, M. F. Renschle, *J. Clin. Oncol.* **2003**, 21, 2529.
[48] M. Kirsch, H.-G. Korth, R. Sustmann, H. De Groot, *Biol. Chem.* **2002**, *383*, 389.
[49] C. Ducrocq, B. Blanchard, B. Pignatelli, H. Ohshima, *Cell. Mol. Life Sci.* **1999**, *55*, 1068.
[50] J. T. Groves, *Curr. Opin. Chem. Biol.* **1999**, *3*, 226.
[51] S. Hannah, V. M. Lynch, N. Gerasimchuk, D. Magda, J. L. Sessler, *Org. Lett.* **2001**, *3*, 3911.
[52] R. Shimanovich, S. Hannah, V. Lynch, N. Gerasimchuk, T. D. Mody, D. Magda, J. L. Sessler, J. T. Groves, *J. Am. Chem. Soc.* **2001**, *123*, 3613.
[53] S. Hannah, V. Lynch, D. M. Guldi, N. Gerasimchuk, C. L. B. MacDonald, D. Magda, J. L. Sessler, *J. Am. Chem. Soc.* **2002**, *124*, 8416.
[54] D. Magda, C. Lepp, N. Gerasimchuk, I. Lee, J. L. Sessler, A. Lin, J. E. Biaglow, R. A. Miller, *Int. J. Radiat. Oncol. Biol. Phys.* **2001**, *51*, 1025.
[55] W. Sun, C. C. Byeon, C. M. Lawson, G. M. Gray, D. Wang, *Appl. Phys. Lett.* **1999**, *74*, 3254.
[56] W. Sun, C. C. Byeon, C. M. Lawson, G. M. Gray, D. Wang, *Appl. Phys. Lett.* **2000**, *77*, 1759.
[57] J. L. Sessler, N. A. Tvermoes, D. M. Guldi, G. L. Hug, T. D. Mody, D. Magda, *J. Phys. Chem. B* **2001**, *105*, 1452.
[58] K. W. Woodburn, *J. Pharmacol. Exp. Ther.* **2001**, *297*, 888.
[59] R. A. Miller, K. W. Woodburn, Q. Fan, M. F. Renschler, J. L. Sessler, J. A. Koutcher, *Int. J. Radiat. Oncol. Biol. Phys.* **1999**, *45*, 981.
[60] O. D. Perez, G. P. Nolan, D. Magda, R. A. Miller, L. A. Herzenberg, *Proc. Natl. Acad. Sci. USA* **2002**, *99*, 2270.
[61] S. J. Narayanan, B. Sridevi, T. K. Chandrashekar, U. Englich, K. Ruhlandt-Senge, *Org. Lett.* **1999**, *1*, 587.
[62] S. J. Narayanan, B. Sridevi, T. K. Chandrashekar, A. Vij, R. Roy, *J. Am. Chem. Soc.* **1999**, *121*, 9053.
[63] B. Sridevi, S. J. Narayanan, R. Rao, T. K. Chandrashekar, U. Englich, K. Ruhlandt-Senge, *Inorg. Chem.* **2000**, *39*, 3669.
[64] J. L. Sessler, D. Seidel, C. Bucher, V. Lynch, *Tetrahedron* **2001**, *57*, 3743.
[65] J. L. Sessler, J. M. Davis, V. Lynch, *J. Org. Chem.* **1998**, *63*, 7062.
[66] A. Srinivasan, S. Mahajan, S. K. Pushpan, M. Ravikumar, T. K. Chandrashekar, *Tetrahedron Lett.* **1998**, *39*, 1961.
[67] K. Shin, C. Lim, C. Choi, Y. Kim, C.-H. Lee, *Chem. Lett.* **1999**, 1331.
[68] S. K. Pushpan, J. S. Narayanan, A. Srinivasan, S. Mahajan, T. K. Chandrashekar, R. Roy, *Tetrahedron Lett.* **1998**, *39*, 9249.
[69] K. Rachlewicz, N. Sprutta, P. J. Chmielewski, L. Latos-Grażyński, *J. Chem. Soc. Perkin Trans. 2* **1998**, 969.
[70] P. J. Chmielewski, L. Latos-Grażyński, K. Rachlewicz, *Chem. Eur. J.* **1995**, *1*, 68.
[71] S. J. Narayanan, B. Sridevi, T. K. Chandrashekar, A. Vij, R. Roy, *Angew. Chem.* **1998**, *110*, 3582; *Angew. Chem. Int. Ed.* **1998**, *37*, 3394.
[72] A. Srinivasan, S. K. Pushpan, M. R. Kumar, S. Mahajan, T. K. Chandrashekar, R. Roy, P. Ramamurthy, *J. Chem. Soc. Perkin Trans. 2* **1999**, 961.
[73] A. Srinivasan, S. J. Narayanan, S. K. Pushpan, M. R. Kumar, T. K. Chandrashekar, *J. Org. Chem.* **1999**, *64*, 8693.
[74] N. Sprutta, L. Latos-Grażyński, *Org. Lett.* **2001**, *3*, 1933.
[75] S. J. Narayanan, B. Sridevi, T. K. Chandrashekar, U. Englich, K. Ruhlandt-Senge, *Inorg. Chem.* **2001**, *40*, 1637.
[76] S. K. Pushpan, A. Srinivasan, V. G. Anand, S. Venkatraman, T. K. Chandrashekar, B. S. Joshi, R. Roy, H. Furuta, *J. Am. Chem. Soc.* **2001**, *123*, 5138.
[77] H. Furuta, private communication.
[78] T. D. Lash, D. T. Richter, *J. Am. Chem. Soc.* **1998**, *120*, 9965.
[79] G. R. Geier III, Y. Ciringh, F. Li, D. M. Haynes, J. L. Lindsey, *Org. Lett.* **2000**, *2*, 1745.
[80] G. R. Geier III, J. L. Lindsey, *J. Org. Chem.* **1999**, *64*, 1596.
[81] S. J. Narayanan, B. Sridevi, A. Srinivasan, T. K. Chandrashekar, R. Roy, *Tetrahedron Lett.* **1998**, *39*, 7389.
[82] J. W. Ka, C. H. Lee, *Tetrahedron Lett.* **2001**, *42*, 4527.
[83] L. Simkhovich, S. Rosenberg, Z. Gross, *Tetrahedron Lett.* **2001**, *42*, 4929.
[84] D. T. Richter, T. D. Lash, *Tetrahedron Lett.* **1999**, *40*, 6735.
[85] S. V. Shevchuk, J. M. Davis, J. L. Sessler, *Tetrahedron Lett.* **2001**, *42*, 2447.
[86] V. Král, J. M. Davis, A. Andrievsky, J. Králova, A. Aynytsya, P. Poucková, J. L. Sessler, *J. Med. Chem.* **2002**, *45*, 1073.
[87] K. Umezewa, K. Tohda, X. M. Lin, J. L. Sessler, Y. Umezawa, *Anal. Chim. Acta* **2001**, 426.
[88] J. Nishimoto, T. Yamada, M. Tabata, *Anal. Chim. Acta* **2001**, *428*, 201.
[89] M. Tabata, K. Kaneko, Y. Murakami, H. Mimura, *Microchem. J.* **1994**, *49*, 136.
[90] W. E. Allen, J. L. Sessler, *CHEMTECH* **1999**, *29*, 16.
[91] J.-Y. Shin, H. Furuta, A. Osuka, *Angew. Chem.* **2001**, *113*, 639; *Angew. Chem. Int. Ed.* **2001**, *40*, 619.
[92] M. G. P. M. S. Neves, R. M. Martins, A. C. Tomé, A. J. Silvestre, A. M. S. Silva, V. Félix, M. G. B. Drew, J. A. S. Cavaleiro, *Chem. Commun.* **1999**, 385.
[93] J.-Y. Shin, H. Furuta, K. Yoza, S. Igarashi, A. Osuka, *J. Am. Chem. Soc.* **2001**, *123*, 7190.
[94] A. Srinivasan, V. M. Reddy, S. J. Narayanan, B. Sridevi, S. K. Pushpan, M. Ravikumar, T. K. Chandrashekar, *Angew. Chem.* **1997**, *109*, 2710; *Angew. Chem. Int. Ed. Engl.* **1997**, *36*, 2598.
[95] A. Srinivasan, S. K. Pushpan, M. Ravikumar, T. K. Chandrashekar, R. Roy, *Tetrahedron* **1999**, *55*, 6671.
[96] S. J. Narayanan, A. Srinivasan, B. Sridevi, T. K. Chandrashekar, M. O. Senge, K.-i. Sugiura, Y. Sakata, *Eur. J. Org. Chem.* **2000**, 2357.
[97] S. K. Pushpan, V. R. G. Anand, S. Venkatraman, A. Srinivasan, A. K. Gupta, T. K. Chandrashekar, *Tetrahedron Lett.* **2001**, *42*, 3391.
[98] J. L. Sessler, D. Seidel, C. Bucher, V. Lynch, *Chem. Commun.* **2000**, 1473.
[99] J. L. Sessler, S. J. Weghorn, Y. Hiseada, V. Lynch, *Chem. Eur. J.* **1995**, *1*, 56.
[100] S. Hannah, D. Seidel, J. L. Sessler, V. Lynch, *Inorg. Chim. Acta* **2001**, *317*, 211.

 © 2003 Wiley-VCH Verlag GmbH & Co. KGaA, Weinheim

[101] J. L. Sessler, D. Seidel, A. E. Vivian, V. Lynch, B. L. Scott, D. W. Keogh, *Angew. Chem.* **2001**, *113*, 611; *Angew. Chem. Int. Ed.* **2001**, *40*, 591.
[102] D. Seidel, PhD dissertation, The University of Texas (Austin), **2002**.
[103] M. S. Rodriguez-Morgade, B. Cabezon, S. Esperanza, T. Torres, *Chem. Eur. J.* **2001**, *7*, 2407.
[104] M. K. Islyaikin, E. A. Danilova, L. D. Yagodarova, M. S. Rodriguez-Morgade, T. Torres, *Org. Lett.* **2001**, *3*, 2153.
[105] N. Kobayashi, S. Inagaki, V. N. Nemykin, T. Nonomura, *Angew. Chem.* **2001**, *113*, 2782; *Angew. Chem. Int. Ed.* **2001**, *40*, 2710.
[106] J. L. Sessler, D. Seidel, V. Lynch, *J. Am. Chem. Soc.* **1999**, *121*, 11257.
[107] V. R. G. Anand, S. K. Pushpan, A. Srinivasan, S. J. Narayanan, B. Sridevi, T. K. Chandrashekar, R. Roy, B. S. Joshi, *Org. Lett.* **2000**, *2*, 3829.
[108] C. Bucher, D. Seidel, V. Lynch, J. L. Sessler, *Chem. Commun.* **2002**, 328.
[109] E. Vogel, M. Bröring, J. Fink, D. Rosen, H. Schmickler, J. Lex, K. W. K. Chan, Y.-D. Wu, D. A. Plattner, M. Nendel, K. N. Houk, *Angew. Chem.* **1995**, *107*, 2705; *Angew. Chem. Int. Ed. Engl.* **1995**, *34*, 2511.
[110] M. Bröring, J. Jendrny, L. Zander, H. Schmickler, J. Lex, Y.-D. Wu, M. Nendel, J. Chen, D. A. Plattner, K. N. Houk, E. Vogel, *Angew. Chem.* **1995**, *107*, 2709; *Angew. Chem. Int. Ed. Engl.* **1995**, *34*, 2515.
[111] T. D. Lash, *Angew. Chem.* **2000**, *112*, 1833; *Angew. Chem. Int. Ed.* **2000**, *39*, 1763.
[112] D. Seidel, J. L. Sessler, V. Lynch, *Angew. Chem.* **2002**, *114*, 1480; *Angew. Chem. Int. Ed.* **2002**, *41*, 1422.
[113] J. P. Gisselbrecht, J. Bley-Escrich, M. Gross, L. Zander, M. Michels, E. Vogel, *J. Electroanal. Chem.* **1999**, *469*, 170.
[114] A. Werner, M. Michels, L. Zander, J. Lex, E. Vogel, *Angew. Chem.* **1999**, *111*, 3866; *Angew. Chem. Int. Ed.* **1999**, *38*, 3650.
[115] N. Sprutta, L. Latos-Grażyński, *Chem. Eur. J.* **2001**, *7*, 5099.
[116] V. G. Anand, S. K. Pushpan, S. Venkatraman, A. Dey, T. K. Chandrashekar, B. S. Joshi, R. Roy, W. Teng, K. R. Senge, *J. Am. Chem. Soc.* **2001**, *123*, 8620.
[117] J.-i. Setsune, Y. Katakami, N. Iizuna, *J. Am. Chem. Soc.* **1999**, *121*, 8957.
[118] J.-i. Setsune, S. Maeda, *J. Am. Chem. Soc.* **2000**, *122*, 12405.
[119] J. Krömer, I. Rios-Carreras, G. Fuhrmann, C. Musch, M. Wunderlin, T. Debaerdemaeker, E. Mena-Osteritz, P. Bäuerle, *Angew. Chem.* **2000**, *112*, 3623; *Angew. Chem. Int. Ed.* **2000**, *39*, 3481.
[120] J. L. Sessler, D. Seidel, A. Gebauer, V. Lynch, K. A. Abboud, *J. Heterocycl. Chem.* **2001**, *38*, 1.
[121] S. Shimizu, J.-Y. Shin, H. Furuta, R. Ismael, A. Osuka, *Angew. Chem.* **2003**, *115*, 82; *Angew. Chem. Int. Ed.* **2003**, *42*, 78.
[122] A. Krivokapic, A. R. Cowley, H. L. Anderson, *J. Org. Chem.* **2003**, *68*, 1089.
[123] D. Sengupta, B. Robinson, *Tetrahedron*, **2002**, *58*, 8737.
[124] J. L. Sessler, H. Maeda, T. Mizuno, V. M. Lynch, H. Furuta, *J. Am. Chem. Soc.* **2002**, *124*, 13474.
[125] V. G. Anand, S. K. Pushpan, S. Genkatraman, S. J. Narayanan, A. Dey, T. K. Chandrashekar, R. Roy, B. S. Joshi, S. Deepa, G. N. Sastry, *J. Org. Chem.* **2002**, *67*, 6309.
[126] C.-H. Hung, J.-P. Jong, M.-Y. Ho, G.-H. Lee, S.-M. Peng, *Chem. Eur. J.* **2002**, *8*, 4542.
[127] A. Srinivasan, T. Ishizuka, A. Osuka, H. Furuta, *J. Am. Chem. Soc.* **2003**, *125*, 878.

 © 2003 Wiley-VCH Verlag GmbH & Co. KGaA, Weinheim

Communications



Chirality transfer from single molecules into handed supramolecular structures is studied by self-assembly of chiral molecules on solid surfaces. Each "mountain" in the STM image represents a single *M* heptahelicene molecule on a Cu(111) surface. The *P* enantiomer forms the mirror-image structure. For more information see the following Communication by Fasel, Ernst, and Parschau.

DOI: 10.1002/anie.200352232
© 2003 Wiley-VCH Verlag GmbH & Co. KGaA, Weinheim

Chirality

Chirality Transfer from Single Molecules into Self-Assembled Monolayers**

Roman Fasel, Manfred Parschau, and Karl-Heinz Ernst**

Self-organization of chiral molecules into helical architectures is of fundamental importance in nature.[1] In addition, interest in the transfer of chirality from single molecules into mesoscopic chiral ensembles is based on its application in liquid-crystal (LC) technologies.[2] The mechanism of chirality induction, that is, the process in which the molecular chirality is mapped onto a supramolecular ensemble, however, is still unclear. The type of intermolecular forces involved in the transfer include hydrogen bonding, π–π interactions, covalent bonding, van der Waals and electrostatic interactions.[3] It has also been predicted by Monte Carlo simulations that steric interaction under influence of repulsive forces alone is sufficient to explain the induction of mesoscopic chirality.[4] Nevertheless, molecular simulations of mesoscopic ensembles based on the structure of the single molecule are computationally very intensive and require either a limit on the number of molecules or greatly simplified molecular shapes.[4]

A promising approach for gaining insight into the process of intermolecular chirality transfer is the investigation of the self-assembly of chiral molecules on solid surfaces, where the chirality transfer is limited to two dimensions. In particular, this allows the use of scanning tunneling microscopy (STM) which is an excellent tool for studying molecular pattern formation.[5] Two-dimensional (2D) chiral effects, such as the spontaneous separation of enantiomers, have also been observed for chiral amphiphiles at the air–solution interface by grazing incidence X-ray diffraction.[6] STM studies of molecular layers adsorbed on well-ordered substrates, however, revealed other forms of expression of chirality in 2D systems, such as the formation of homochiral domains showing opposite angles with respect to a substrate lattice vector[7] and the formation of handed nanostructures.[8] Herein, we report on the mechanism of chirality transfer from helical heptahelicene molecules ([7]H, $C_{30}H_{18}$) into the close-packed monomolecular layer. Under these conditions, that is, when the molecules are squeezed together, repulsive forces dominate the lateral interaction. The self-assembly of molecules on surfaces, however, is not only governed by the lateral interaction between the molecules, but is also influenced by the molecule–substrate interaction, which, in turn, determines the mobility of the molecular species at a given temperature. On Ni(111) and Ni(100), the low mobility of [7]H did not allow the observation of chiral effects.[9] Therefore, we studied the pattern formation on the Cu(111) surface, where at coverages below 95% of the saturated monolayer the molecules are observed to diffuse readily even at lower temperatures.[10] The absence of close-packed structures up to very-high coverages is not unexpected for [7]H since the molecule has no chemical groups capable of directional intermolecular bonding. Therefore, the attractive intermolecular forces are expected to be very weak. At close to full monolayer coverage, [7]H molecules are, however, forced into well-ordered arrangements. The adsorption of racemic [7]H led to the formation of enantiomorphous mirror domains, in which the enantiomers are partially separated.[10] Depending on the enantiomeric excess, the local structures in those domains exhibited minute differences. Herein, however, we focus on the enantiopure structures, in which the expression of chirality goes beyond the formation of mirror domains. Figure 1 shows STM images of the two close-packed structures observed for *(M)*-heptahelicene. Each bright dot represents one molecule. At 95% ($\theta = 0.95$) of the monolayer saturation coverage, a long-range ordered structure—apparently built-up from clusters containing six molecules and from clusters containing three molecules ("6&3-structure")—is observed. The six-membered clusters appear as an anticlockwise pinwheel, thus showing handedness. At monolayer saturation coverage ($\theta = 1$) the unit cell of the adsorbate lattice contains a group of three molecules ("3-structure") which appear a particular cloverleaf shape. Two rotational domains, rotated by 180° with respect to each other, are observed in both structures.

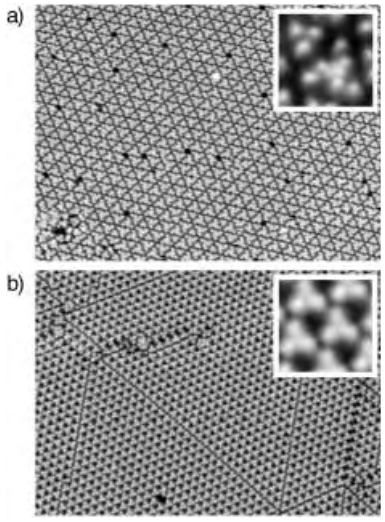


Figure 1. Constant-current STM images (70 nm × 70 nm) acquired at 50 K of long-range ordered monolayers of (*M*)-heptahelicene on Cu(111). a) The 6&3-structure at 95% ($\theta = 0.95$) of the saturated monolayer coverage. b) The 3-structure of the complete monolayer ($\theta = 1$). The insets show the molecular cluster units of the structures.

[*] Dr. R. Fasel, Dr. K.-H. Ernst, Dr. M. Parschau
Molecular Surface Technologies
Swiss Federal Laboratories for Materials Testing and Research (EMPA)
Ueberlandstrasse 129, 8600 Dübendorf (Switzerland)
Fax: (+41) 1-823-4034
E-mail: roman.fasel@empa.ch
karl-heinz.ernst@empa.ch

[**] This work was supported by grants from the Schweizerischer Nationalfonds and the Board of the Federal Institute of Technology (ETH Rat).

 © 2003 Wiley-VCH Verlag GmbH & Co. KGaA, Weinheim DOI: 10.1002/anie.200352232

The observed adsorbate lattice structures show enantiomorphism, that is, adsorption of the *(P)*-enantiomer of heptahelicene leads to structures which are mirror images of those observed for *(M)*-heptahelicene (Figure 2). Furthermore, the enantiomeric lattices form opposite angles with respect to the [1 $\bar{1}$ 0] substrate surface direction. Since the angle between the adsorbate and substrate-surface lattice vectors is oblique, the supramolecular assembly breaks the symmetry of the underlying substrate surface. The combined molecule–substrate systems thus exhibit extended surface chirality. Remarkably, the unit cells are not only mirror images of each other, but also the arrangements of molecules within the unit cells. This is most clearly seen for the pinwheel-clusters of the 6&3-structures (Figure 2a and b): The pinwheel's wings point either anticlockwise, as in the *(M)*-heptahelicene 6&3-structure, or clockwise, as in the *(P)*-heptahelicene 6&3-structure. In the case of the 3-structures (Figure 2c and d), the mirror symmetry is expressed by tilts of the three-molecule cloverleaf units into opposite directions with respect to the adsorbate lattice vectors.

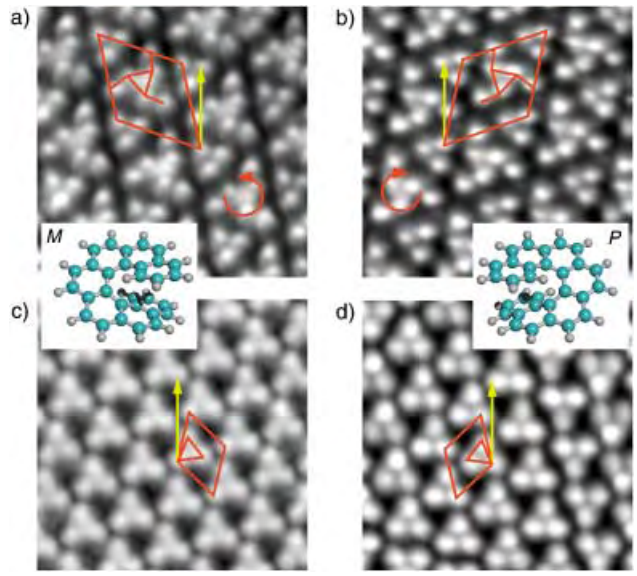


Figure 2. High-resolution STM images of (*M*)- and (*P*)-[7]H structures (10 nm × 10 nm). a) (*M*)-[7]H at $\theta = 0.95$. b) (*P*)-[7]H at $\theta = 0.95$. c) (*M*)-[7]H at $\theta = 1$. d) (*P*)-[7]H at $\theta = 1$. The (*M*)- and (*P*)-[7]H structures are mirror images of each other. Unit cells and their basic building blocks are outlined by red lines, the [1 $\bar{1}$ 0] surface direction is indicated by the yellow arrows.

To interpret the observed handed supramolecular structures, we make use of the following simple topographic model: Based on the assumption that the brightest feature in the constant-current STM image corresponds to the uppermost part of the molecule, the [7]H molecule is approximated by a disk with an off-center protrusion (Figure 3). The adsorption geometry depicted in Figure 3 derives from a previous X-ray photoelectron diffraction (XPD) study where we showed that [7]H is adsorbed with a terminal phenanthrene group parallel to the Cu(111) surface.[11] The XPD experiments also confirmed that the sixfold rotational symmetry of the topmost Cu(111) layer allows six equivalent azimuthal orientations for the [7]H molecules.[11] These orientations are obtained from the 0° (i.e. "12 o'clock") orientation shown in Figure 3 by successive rotations of 60° about the surface normal, resulting in "10 o'clock", "8 o'clock", …, 2 o'clock orientations. Assuming hexagonal packing and attributing one of the six particular azimuthal orientations to each molecule, both structures can be rationalized within this simple picture (Figure 4). Going anticlockwise along the contour of the six-molecule-pinwheel, the [7]H molecules are rotated by +60° with respect to each other (Figure 4a and b). The three-molecule corner unit of the 6&3-structure is accounted for by [7]H molecules facing each other in an anticlockwise fashion, which corresponds to relative azimuthal orientations of +120°. Similarly, the cloverleaf unit of the 3-structure is due to three molecules oriented 0°, 120°, and 240° (Figure 4c and 4d).

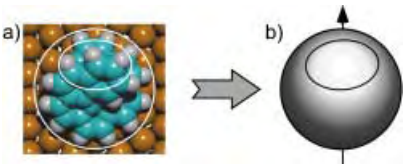


Figure 3. Topographic model used for the interpretation of the observed STM images: The [7]H molecule, as adsorbed on Cu(111) (a), is approximated by a disk with a bright protrusion at the topmost part of the molecule (b). The azimuth of a protrusion pointing towards the "12-o'clock" direction is defined as 0°.

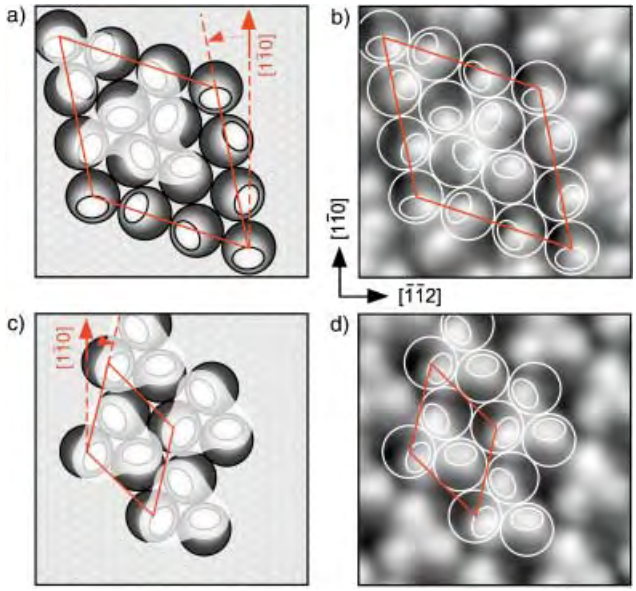


Figure 4. Structure models for the (*M*)-heptahelicene 6&3-molecule cluster (a and b) and the (*M*)-heptahelicene 3-molecule cluster structures (c and d) based on a hexagonal packing of the molecules and systematically varying azimuthal orientations. The model structures are superimposed on the corresponding STM images in (b) and (d).

In the framework of this simple model, the symmetry of the close-packed layer is lowered due to the *C*1 symmetry of the adsorbed [7]H molecules and, in addition, because of their

 © 2003 Wiley-VCH Verlag GmbH & Co. KGaA, Weinheim

chirality. Consequently, particular combinations of neighboring azimuthal orientations are energetically more favorable than others. This situation leads to a distinct transfer of the structural information—the chirality in our case—into the 2D organized layer. Hence, the chirality is not only expressed by opposite angles of the domains with respect to the substrate, but also by a correlation of azimuthal orientations between neighboring molecules which leads to handed molecular structures. Although the arrangement of the molecules is 2D-quasi-hexagonal, the resulting surface topography, as imaged by STM, is highly anisotropic and exhibits chirality. In previously reported systems either the local molecule–substrate arrangement determined the angle of the chiral domain with respect to the substrate lattice[12] or chiral clusters and nanostructures were created through polar lateral interactions, for example, by hydrogen bonding.[8] In our case, however, it is the shape of the molecule under repulsive conditions that governs the transfer of chirality.

To corroborate this transfer mechanism and to confirm the proposed azimuthal arrangement, we have performed molecular modeling calculations for the monolayer 3-structure.[13] The unit cell considered in these calculations, as determined from a series of STM images, is sketched in Figure 5a. The molecules at the four corners of the unit cell have an identical azimuthal orientation 1 (Figure 5a). For perfectly hexagonal packing, the remaining two molecules, taking positions 2 and 3, are symmetrically centered within the unit cell, as indicated by the yellow dots in Figure 5a. Owing to the oblique orientation of the adsorbate unit cell with respect to the substrate lattice this results, however, in different adsorption sites for the molecules at positions 2 and 3 than for the corner molecules. Therefore, we have also considered possible lateral shifts of the molecules at positions 2 and 3 to the nearest equivalent adsorption sites, labeled t1, t2, and t3 in Figure 5a. The total energy of the system was calculated for all combinations of adsorption sites (4×4 possibilities) and azimuthal orientations (in steps of 15°). We find two geometries (Figure 5c and d) with equal and lowest total energy. In both geometries, molecules at positions 2 and 3 are shifted away from the central position within their respective unit-cell half way towards one of the corner molecules. Whereas the configuration shown in Figure 5c corresponds to molecules at positions 2 and 3 being shifted onto sites t1 and t3, respectively, the equally favorable configuration shown in Figure 5d is obtained by shifting the molecules with orientations 2 and 3 onto sites t3 and t2, respectively. In both minimum-total-energy configurations the relative azimuthal orientations of the molecules amount to 120°: With respect to the 0° orientation as defined in Figure 3, the azimuthal orientations of the cloverleaf cluster molecules are 60°, 180°, and 300° (Figure 5c), or 0°, 120°, and 240° (Figure 5d). The latter azimuthal orientation angles are clearly identical to those derived from the topographic modeling of the STM image as shown in Figure 4c and d, thus confirming our structure model. Remarkably, the two total-minimum-energy configurations of the calculation are both experimentally observed as rotational domains of the 3-structure: Whereas the 0°–120°–240° minimum-energy configuration (Figure 5d) corresponds to domain d2 (Figure 5b), domain d1 is formed by molecules taking 60°–180°–300° azimuthal orientations as shown in Figure 5c.

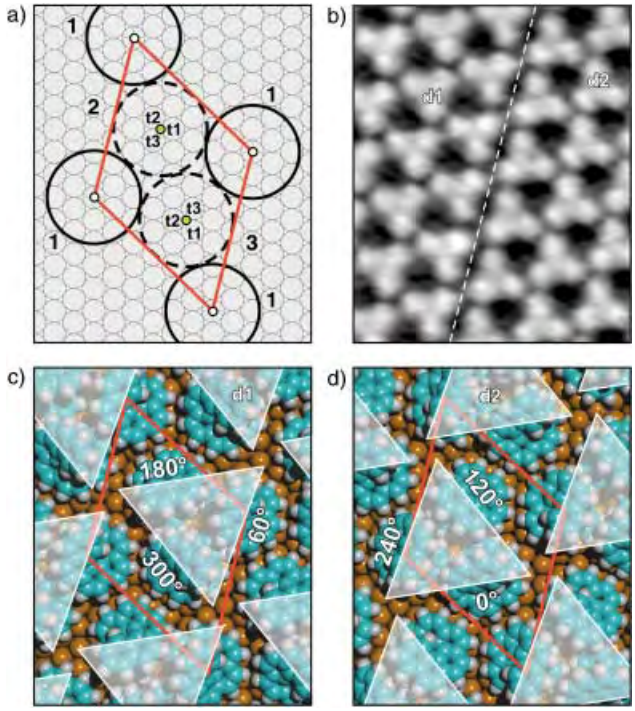


Figure 5. Molecular modeling results compared to STM results of the 3-structure at saturated monolayer coverage. a) Adsorption sites within the unit cell considered for the calculations. b) STM image of a domain boundary (dashed line) between the two rotational domains d1 and d2. c) and d) The two lowest total-energy configurations as determined from the calculations. White semi-transparent triangles highlight the topmost parts of the molecules that are imaged brightest. Both geometries are in excellent agreement with the observed d1 and d2 domain structures.

Although total energies determined from AMBER force-field calculations can not be taken as absolute values, relative energies should accurately reflect the energetics of different supramolecular arrangements. We find that a single [7]H molecule adsorbed at an on-top site on Cu(111) is 1 eV lower in energy than within the close-packed 3-structure. Packing of [7]H into the 3-structure thus costs about 1 eV per molecule, which reflects the rather strong repulsive intermolecular interaction. Therefore, the molecules take the particular azimuthal orientations that minimize the repulsive interactions between them.

For rigid molecules adsorbed on a surface, the optimization of relative azimuthal orientations is the only way to minimize the lateral pressure to some extent. In monolayers of chiral LC-like molecules with long alkyl chains, repulsion causes the chains to bend partly away from the surface.[14] In such cases, the expression of chirality is limited to the formation of lamella structures forming mirror domains. The 2D orientation mechanism observed in our system can be considered as the analogue of the helical twisting in 3D cholesteric phases. The very high twisting power (TP) of bridged biaryl compounds in biphenyl nematics, for instance, has been assigned to the rigid helical part rather than the long alkyl chains.[15] This mechanism of chirality induction has

 © 2003 Wiley-VCH Verlag GmbH & Co. KGaA, Weinheim

been supported by theoretical predictions of the TP within the so-called surface model.[16] Similar conclusions have been drawn from Monte Carlo simulations on model mesogens by Selinger and co-workers.[4] This shows that surface studies of 2D model systems are an excellent approach towards an understanding of the far more complicated 3D LC systems.

In summary, ordered supramolecular chiral structures have been observed after deposition of pure heptahelicene enantiomers on Cu(111). Besides showing opposite angles between the enantiomorphic adsorbate lattices and the substrate lattice, long-range chirality is also expressed by opposite tilt angles of molecular clusters with respect to the adsorbate lattice vectors, and by formation of handed molecular clusters. We have shown that the chirality transfer occurs through steric repulsion and does not require molecular flexibility or strong dipole interactions. The appearance of handed molecular clusters is due to a correlation of azimuthal molecular orientations which are driven by repulsive intermolecular forces in the close-packed 2D layer.

Experimental Section

Heptahelicene was synthesized as described elsewhere.[17] Enantiomeric separation ($ee > 99.9\,\%$) was accomplished by HPLC on a Daicel Chiracel OD column and subsequently tested by HPLC using a Chiracel OD-H column. Assignment of the enantiomers was based on circular dichroism (CD) spectra in accordance to Martin and Marchant.[18] The molecules were evaporated in ultrahigh vacuum (UHV) from a Knudsen-cell type evaporator, held at 150 K during deposition onto the clean Cu(111) substrate which was held at room-temperature. The Cu(111) surface was prepared by repeated cycles of Ar^+ sputtering and annealing to 800 K. After cooling of the sample to 50 K, STM images were acquired in constant-current mode. Molecular modeling was performed using the AMBER force field of the Hyperchem 7 package.[19]

Received: June 26, 2003 [Z52232]
Published Online: October 6, 2003

Keywords: chirality · helical structures · monolayers · scanning probe microscopy · self-assembly

[1] A. E. Rowan, R. J. M. Nolte, *Angew. Chem.* **1998**, *110*, 65 – 71; *Angew. Chem. Int. Ed.* **1998**, *37*, 63 – 68, and references therein.
[2] a) H.-G. Kuball, T. Höfer in *Chirality in Liquid Crystals* (Eds.: H.-S. Kitzerow, C. Bahr), Springer, New York, **2001**, pp. 67 – 100; b) R. P. Lemieux, *Acc. Chem. Res.* **2001**, *34*, 845 – 853.
[3] a) H. Engelkamp, S. Middelbeek, R. J. M. Nolte, *Science* **1999**, *284*, 785 – 788, and references therein; b) S. Kirstein, H. von Berlepsch, C. Bötticher, C. Burger, A. Quart, G. Reck, S. Dähne, *ChemPhysChem* **2000**, *1*, 146 – 150.
[4] J. Xu, R. L. B. Selinger, J. V. Selinger, R. Shashidhar, *J. Chem. Phys.* **2001**, *115*, 4333 – 4338.
[5] a) J. Rabe, S. Bucholz, *Science* **1991**, *253*, 424 – 427; b) J. S. Forster, J. E. Frommer, *Nature* **1988**, *333*, 542 – 545; c) J. Frommer, *Angew. Chem. Int. Ed. Engl.* **1992**, *31*, 1298 – 1328; *Angew. Chem.* **1992**, *104*, 1325.
[6] I. Weisbuch, I. Kuzmenko, M. Berfeld, L. Leiserowitz, M. Lahav, *J. Phys. Org. Chem.* **2000**, *13*, 426 – 434.
[7] a) F. Stevens, D. J. Dyer, D. M. Walba, *Angew. Chem. Int. Ed. Engl.* **1996**, *35*, 900 – 901; *Angew. Chem.* **1996**, *108*, 955 – 957; b) S. De Feyter, A. Gesquire, K. Wurst, D. B. Amabilino, J. Veciana, F. C. De Schryver, *Angew. Chem.* **2001**, *113*, 3317 – 3320; *Angew. Chem. Int. Ed.* **2001**, *40*, 3217 – 3220; c) S. De Feyter, A. Gesquire, F. C. De Schryver, C. Meiners, M. Sieffert, K. Müllen, *Langmuir* **2000**, *16*, 9887 – 9894; d) Q.-M. Xu, D. Wang, L.-J. Wan, C. Wang, C.-L. Bai, G. Q. Feng, M.-X. Wang, *Angew. Chem.* **2002**, *114*, 3558 – 3561; *Angew. Chem. Int. Ed.* **2002**, *41*, 3408 – 3411.
[8] a) M. Böhringer, K. Morgenstern, W.-D. Schneider, R. Berndt, *Angew. Chem.* **1999**, *111*, 832 – 834; *Angew. Chem. Int. Ed.* **1999**, *38*, 821 – 823; b) M. Böhringer, W.-D. Schneider, R. Berndt, *Angew. Chem.* **1999**, *111*, 832 – 834; *Angew. Chem. Int. Ed.* **2000**, *39*, 792 – 795; c) J. V. Barth, J. Weckgesser, C. Cai, P. Günter, L. Bürgi, O. Jeandupeux, K. Kern, *Angew. Chem.* **2000**, *112*, 1285 – 1288; *Angew. Chem. Int. Ed.* **2000**, *39*, 1230 – 1234.
[9] K.-H. Ernst, Y. Kuster, R. Fasel, C. F. McFadden, U. Ellerbeck, *Surf. Sci.* **2003**, *530*, 195 – 202.
[10] a) K.-H. Ernst, Y. Kuster, R. Fasel, M. Müller, U. Ellerbeck, *Chirality* **2001**, *13*, 675 – 678; b) M. Parschau, R. Fasel, K.-H. Ernst, unpublished resutls.
[11] R. Fasel, A. Cossy, K.-H. Ernst, F. Baumberger, T. Greber, J. Osterwalder, *J. Chem. Phys.* **2001**, *115*, 1020 – 1027.
[12] J. V. Barth, J. Weckesser, G. Trimarchi, M. Vladimirova, A. de Vita, C. Cai, H. Brune, P. Günter, K. Kern, *J. Am. Chem. Soc.* **2002**, *124*, 7991 – 8000, and references therein.
[13] Because many more parameters need to be considered for the 6&3-structure, molecular mechanics calculations of this structure are too extensive. However, the same mechanism of minimization of repulsive interactions for a given unit-cell size and occupation should hold true also in that case.
[14] a) F. Stevens, D. J. Dyer, U. Müller, D. M. Walba, *Langmuir* **1996**, *12*, 5625 – 5629; b) S. De Feyter, A. Gesquière, P. C. M. Grim, F. C. De Schryver, S. Valiyaveetil, C. Meiners, M. Sieffert, K. Müllen, *Langmuir* **1999**, *15*, 2817 – 2822.
[15] G. Gottarelli, M. Hilbert, B. Samori, G. Solladié, G. P. Spada, R. Zimmerman, *J. Am. Chem. Soc.* **1983**, *105*, 7318 – 7321; b) G. Gottarelli, G. P. Spada, R. Bartsch, G. Solladie, R. Zimmerman, *J. Org. Chem.* **1986**, *51*, 589 – 592; c) G. Gottarelli, G. Proni, G. P. Spada, D. Fabbri, C. Rosini, *J. Org. Chem.* **1996**, *61*, 2013 – 2019.
[16] a) A. Ferrarini, P. L. Nordio, *J. Chem. Soc. Perkin Trans. 2* **1998**, *2*, 455 – 460; b) A. Ferrarini, G. J. Moro, P. L. Nordio, *Mol. Phys.* **1996**, *87*, 485 – 499.
[17] A. Sudharkar, T. J. Katz, *Tetrahedron Lett.* **1986**, *27*, 2231.
[18] R. H. Martin, M. J. Marchant, *Tetrahedron* **1974**, *30*, 347.
[19] HyperChemRelease7, Hypercube Inc., (http://www.hyper.com/) **2002**.

 © 2003 Wiley-VCH Verlag GmbH & Co. KGaA, Weinheim

Molecular Gears

Quantitative Formation of Sandwich-Shaped Trinuclear Silver(I) Complexes and Dynamic Nature of Their *P*⇌*M* Flip Motion in Solution**

*Shuichi Hiraoka, Koji Harano, Takaaki Tanaka, Motoo Shiro, and Mitsuhiko Shionoya**

There has been much interest in developing artificial helical structures by synthetic oligomers[1] or metal–ligand complexes[2] closely related to those present in natural biomolecules such as DNA and proteins. In general, helical structures potentially undergo molecular motions such as folding[3] and *P*⇌*M* conversion.[4,5] The *P*⇌*M* conversion is well-known in natural systems, for example, the dynamic behavior of DNA helices between the right-handed B and left-handed Z forms.[6] Such *P*⇌*M* dynamic processes are currently attracting considerable attention from a viewpoint of the development of molecular machines.[7]

Our strategy reported herein is directed toward the flip motion of the helical structures of trinuclear Ag_3L_2 complexes with disk-shaped ligands that bear three coordination sites (Figure 1). The ligands contain three monodentate ligands and three *p*-tolyl groups attached to the central benzene ring; the three *p*-tolyl groups are introduced to force the neighboring flat metal ligands out of the plane of the central aromatic ring. Such ligands self-assemble to form sandwich-shaped architectures with appropriate metal ions (e.g. Ag^+) favoring linear coordination geometry.[8] For example, in the Ag_3L_2 complexes, all the exterior rings should tilt in the same direction and result in the formation of helical structures with *P* and *M* geometries, between which flip motions may take place and allow the ring rotation with retention of the coordination bonds. Herein we describe the quantitative formation of sandwich-shaped trinuclear Ag^+ complexes with two disk-shaped ligands that bear three thiazolyl (**1**) or 2-pyridyl groups (**2**) as the coordination sites. The helical structure of the resulting entity $Ag_3\mathbf{1}_2$ was determined by X-ray single-crystal analysis, and variable-temperature ^{1}H NMR measurements revealed that the dynamic behavior (i.e. *P*⇌*M* flip motion) of these complexes is remarkably affected by the ring size of the ligands attached to the central benzene ring.

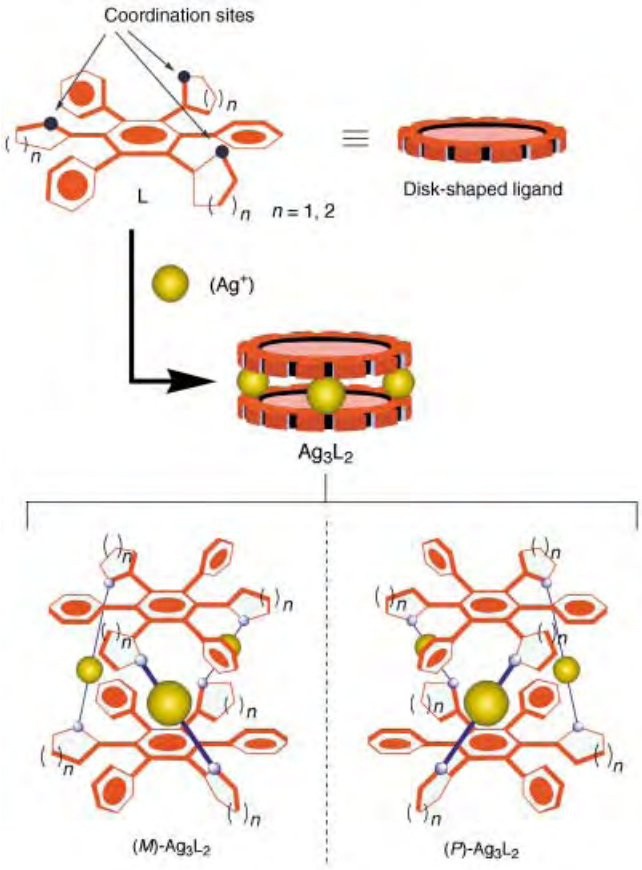
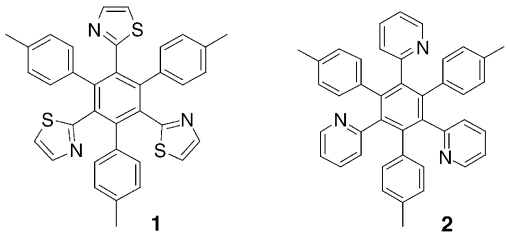


Figure 1. Schematic representation of the formation of sandwich-shaped trinuclear Ag_3L_2 complexes using disk-shaped tridentate ligands.



Evidence for the formation of sandwich-shaped Ag^+ complexes from a mixture of tridentate ligands **1** or **2**[9] and AgOTf (2:3) in $CHCl_3/CH_3OH$ was obtained by electrospray ionization time-of-flight (ESI TOF) mass spectrometry.[10] The ESI mass spectrum of a mixture of **1** and AgOTf (**1**/AgOTf 2:3) exhibited a main peak at *m*/*z* 777.2, which is attributed to cationic $[Ag_3\mathbf{1}_2\cdot(OH)\cdot(H_2O)]^{2+}$. Similarly, the spectrum of a mixture of **2** and AgOTf (**2**/AgOTf 2:3) showed a main peak at *m*/*z* 759.4, which corresponds to $[Ag_3\mathbf{2}_2\cdot(OH)\cdot(H_2O)]^{2+}$. These data indicate that trinuclear $Ag_3\mathbf{1}_2$ and $Ag_3\mathbf{2}_2$ complexes were formed in solution.

The ^{1}H NMR spectrum of a mixture of **1** and AgOTf (2:3) in $CDCl_3/CD_3OD$ (1:1) was highly symmetrical except for the

[*] Prof. M. Shionoya, Dr. S. Hiraoka, K. Harano, T. Tanaka
Department of Chemistry, Graduate School of Science
The University of Tokyo
Hongo, Bunkyo-ku, Tokyo 113-0033 (Japan)
Fax: (+81) 3-5841-8061
E-mail: shionoya@chem.s.u-tokyo.ac.jp
Dr. M. Shiro
Rigaku Corporation
3-9-12 Matsubaracho, Akishima, Tokyo 196-8666 (Japan)

[**] This study was supported by a Grant-in-aid for The 21st Century COE Program for Frontiers in Fundamental Chemistry and a Grant-in-aid Encouragement of Young Scientists (B) to S.H. (No. 14740361) and a Grant-in-aid for Scientific Research on Priority Areas to S.H. (No. 15036216) from the Ministry of Education, Culture, Sports, Science, and Technology of Japan.

Supporting information for this article is available on the WWW under http://www.angewandte.org or from the author.

 © 2003 Wiley-VCH Verlag GmbH & Co. KGaA, Weinheim DOI: 10.1002/anie.200351068

signals for the aromatic protons of the *p*-tolyl substituents (H^c and H^d in Figure 2b). This spectral pattern indicates that the outer (H^{c1} and H^{d1}) and the inner protons (H^{c2} and H^{d2}) of the *p*-tolyl rings are not equivalent as a result of the formation of

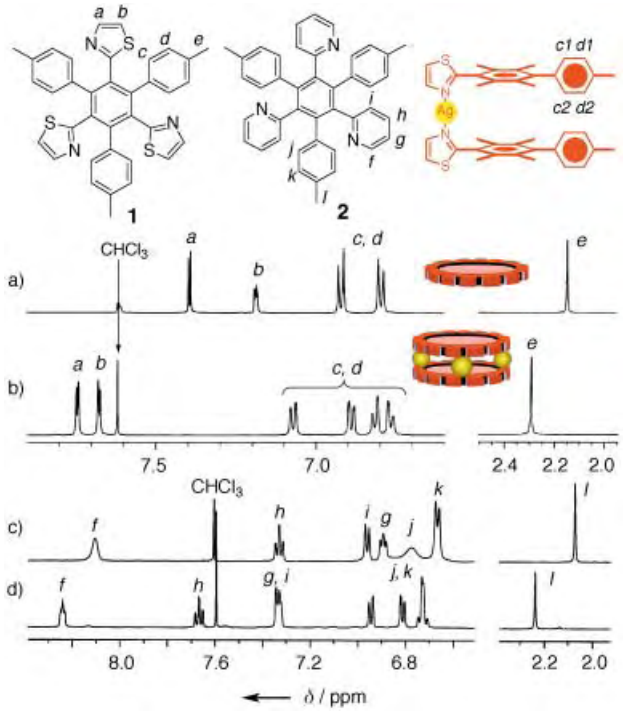


Figure 2. ^{1}H NMR (500 MHz, $CDCl_3/CD_3OD$ (1:1)) spectra of the Ag^+ complexes with **1** and **2**; a) [**1**] = 14.0 mM, b) [**1**] = 14.0 mM and [AgOTf] = 20.9 mM, c) [**2**] = 8.2 mM, and d) [**2**] = 8.2 mM and [AgOTf] = 12.3 mM.

a sandwich-shaped $Ag_3\mathbf{1}_2$ complex. In contrast, the thiazolyl protons H^a and H^b provide only one set of signals with downfield shifts as a result of complexation ($\Delta\delta = 0.35$–0.50 ppm). Further addition of AgOTf (up to 3 equiv) did not change the spectrum at all, although the amount is enough for the formation of polymeric structure $(Ag_3\mathbf{1})_n$. These results suggest that only either the N or the S donor atoms of the thiazolyl ligands coordinates to the Ag^+ ion, thus leading to the quantitative formation of a higher-symmetry sandwich-shaped $Ag_3\mathbf{1}_2$ complex.

The ^{1}H NMR spectrum of a mixture of **2** and AgOTf (2:3) in a $CDCl_3/CD_3OD$ (1:1) showed a similar pattern (Figure 2d). All the signals for the ligand part of the Ag^+ complex are shifted downfield relative to those for the ligand **2** itself, and those for the aromatic protons of the *p*-tolyl groups (H^e and H^f) were not equivalent. Notably, the formation of both Ag^+ complexes ($Ag_3\mathbf{1}_2$ and $Ag_3\mathbf{2}_2$) is quantitative and is complete within a few minutes at room temperature (by NMR spectroscopic analysis).

The helical structure of the trinuclear complex $Ag_3\mathbf{1}_2$ was determined by X-ray crystallographic analysis (Figure 3).[11,12] Three Ag^+ ions are held between the two ligands **1** facing each other to provide a sandwich-shaped structure, and each Ag^+ ion is linearly coordinated by the two thiazolyl nitrogen

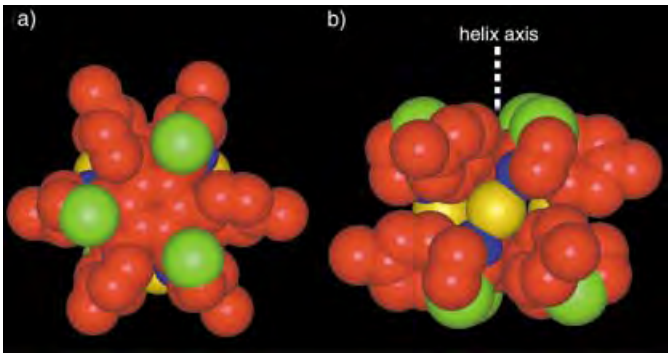


Figure 3. Crystal structure of $Ag_3\mathbf{1}_2$ in the *P* form: a) top view and b) side view. Color labels: Ag yellow, C red, N blue, S green.

atoms of both ligands with N–Ag bond lengths from 2.16(4) to 2.25(0) Å. The distance between the two central aromatic rings arranged face to face is approximately 5.4 Å, which is significantly longer than that for aromatic π–π stacking. In addition, the two ligands **1** are offset by 60° to form a helical structure in which the three N–Ag–N linkages are almost parallel to each other but twisted from the helix axis by approximately 30°. Notably, the crystal was obtained as a racemate of the *P* and *M* forms.

The X-ray crystallographic analysis thus revealed that the sandwich-shaped Ag^+ complexes in the *P* and *M* forms have helical structures in the solid state. To verify the equilibria between the *P* and *M* isomers in solution, chiral counteranions, *Δ*-tris(tetrachlorobenzenediolato)phosphate(v) (*Δ*-TRISPHAT),[13] were used for ^{1}H NMR spectroscopic studies. Upon addition of [nBu$_4$N][*Δ*-TRISPHAT] (3 equiv) to Ag^+ complexes ($Ag_3\mathbf{1}_2\cdot(OTf)_3$ and $Ag_3\mathbf{2}_2\cdot(OTf)_3$), $Ag_3\mathbf{1}_2\cdot(\Delta\text{-TRISPHAT})_3$ and $Ag_3\mathbf{2}_2\cdot(\Delta\text{-TRISPHAT})_3$ were isolated in 67% and 94% yields, respectively.

The signals of the *P* and *M* isomers were separated (1:1 ratio) without chiral induction in the ^{1}H NMR spectrum of $Ag_3\mathbf{2}_2\cdot(\Delta\text{-TRISPHAT})_3$ in [D$_6$]acetone/$CDCl_3$ (2:1) at 303 K (Figure 4b). This result indicates that the flip motion between (*P*)- and (*M*)-$Ag_3\mathbf{2}_2$ complexes is slow on the NMR timescale. Upon heating to 328 K, the signals almost coalesced, which indicates that the $P \rightleftharpoons M$ flip motion of $Ag_3\mathbf{2}_2$ is fast on the NMR timescale above 328 K (Figure 4a).

In the case of the $Ag_3\mathbf{1}_2\cdot(\Delta\text{-TRISPHAT})_3$ complex, the $P \rightleftharpoons M$ flip motion readily takes place even at 303 K. The signals for $Ag_3\mathbf{1}_2\cdot(\Delta\text{-TRISPHAT})_3$ in [D$_6$]acetone/$CDCl_3$ (2:1) did not split at all into two sets for the *P* and *M* isomers (Figure 4c). On the other hand, upon cooling the sample to 253 K, two sets of signals for H^a, H^b, and one of the *p*-tolyl protons appeared in a 7:6 ratio with low chiral induction;[14] these signals correspond to the (*P*)- and (*M*)-$Ag_3\mathbf{1}_2\cdot(\Delta\text{-TRISPHAT})_3$ complexes (Figure 4d).[15] Thus, the $Ag_3\mathbf{1}_2$ complex can flip between the *P* and *M* forms rapidly on the NMR timescale even at 303 K. The differences found in the dynamic features of the $Ag_3\mathbf{1}_2$ and $Ag_3\mathbf{2}_2$ complexes probably arise from the difference in the size of the ligands attached to the central aromatic ring. The $Ag_3\mathbf{2}_2$ complex with six-membered pyridine rings is likely to have more geometrical constraints than the $Ag_3\mathbf{1}_2$ complex with five-membered

 © 2003 Wiley-VCH Verlag GmbH & Co. KGaA, Weinheim

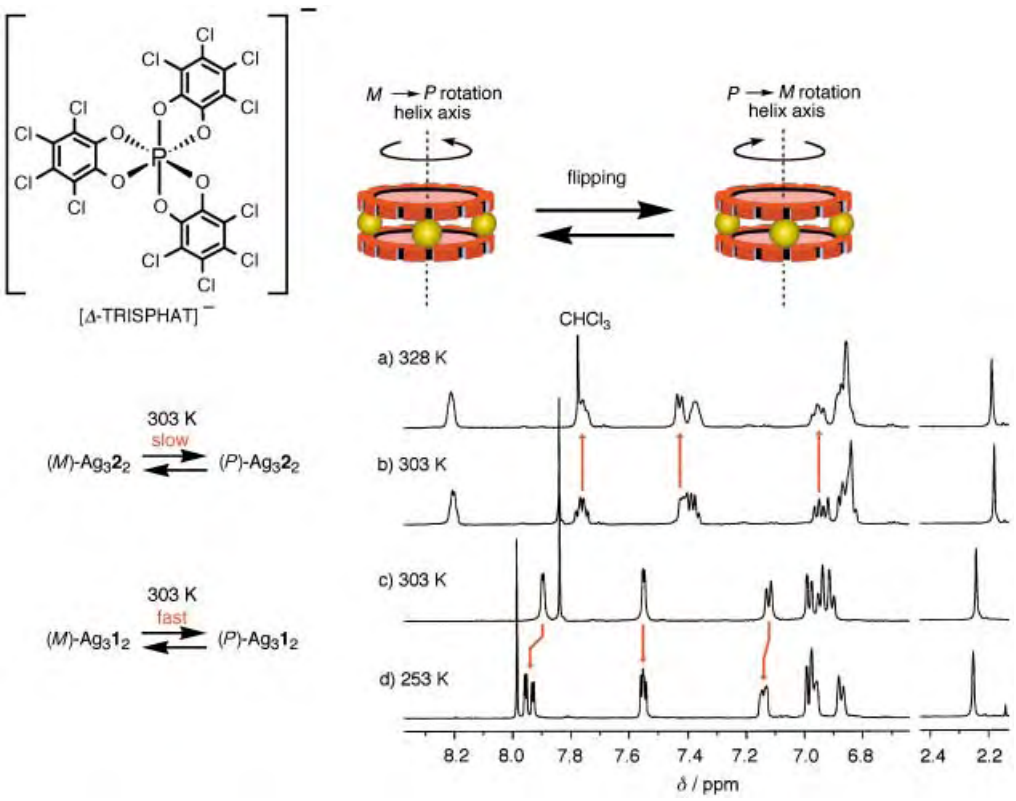


Figure 4. ^{1}H NMR spectra (500 MHz, [D$_6$]acetone/CDCl$_3$ (2:1)) of $Ag_3\mathbf{2}_2\cdot(\Delta\text{-TRISPHAT})_3$ and $Ag_3\mathbf{1}_2\cdot(\Delta\text{-TRISPHAT})_3$ complexes. a) $Ag_3\mathbf{2}_2\cdot(\Delta\text{-TRISPHAT})_3$ at 328 K, b) $Ag_3\mathbf{2}_2\cdot(\Delta\text{-TRISPHAT})_3$ at 303 K, c) $Ag_3\mathbf{1}_2\cdot(\Delta\text{-TRISPHAT})_3$ at 303 K, d) $Ag_3\mathbf{1}_2\cdot(\Delta\text{-TRISPHAT})_3$ at 253 K.

thiazole rings. Therefore, the transition state of the flip motion (Figure 5) in which all the N–Ag–N linkages are parallel to the helix axis would be rather destabilized in the

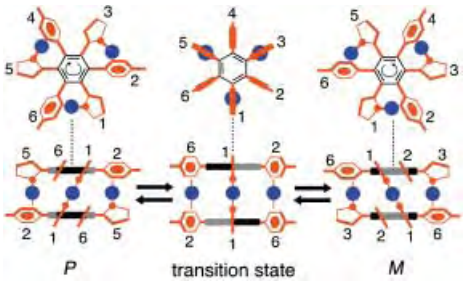


Figure 5. Proposed mechanism for the $P \rightleftharpoons M$ flip motion between sandwich-shaped Ag^+ complexes.

$Ag_3\mathbf{2}_2$ complex. As the result, the energy barrier of the flip motion in $Ag_3\mathbf{2}_2$ complex should be larger than that in the $Ag_3\mathbf{1}_2$ complex. Therefore, $P \rightleftharpoons M$ flipping is allowed in the $Ag_3\mathbf{1}_2$ complex, whereas such a motion is restricted in the $Ag_3\mathbf{2}_2$ complex at 303 K. The flip motion potentially contains a concerted twist motion of the twelve aromatic rings with a reversible change in the distance between the two central benzene rings (less than 1 Å). Moreover, the flip motion includes a relative 120° rotation between the two disk-shaped ligands connected by Ag^+ ions: In the *P* isomer, a thiazole ring (ring 1) and a *p*-toluene ring (ring 6) are placed face to face; after the $P \rightarrow M$ rotation, the thiazole ring (ring 1) lies opposite a different *p*-toluene ring (ring 2) (Figure 5).

In summary, the present study demonstrates the quantitative formation of sandwich-shaped Ag^+ complexes from disk-shaped tridentate ligands **1** (or **2**) and Ag^+ ions both in solution and in the solid state. Variable-temperature ^{1}H NMR measurements with chiral counterparts revealed the existence of *P* and *M* helical structures of these complexes in solution, thus providing information on their dynamic behavior. Moreover, the $P \rightleftharpoons M$ flip motion of these complexes was found to depend strongly on the size of the ring of the metal ligands. Studies into chiral induction with this system are currently underway.

Experimental Section

Typical procedure**:** AgOTf (3.1 mg, 12.6 μmol) was added to a solution of ligand (8.4 μmol) in $CDCl_3/CD_3OD$ (1:1; 0.6 mL), and the mixture was kept at room temperature for 5 min. The ^{1}H NMR spectrum showed the quantitative formation of the Ag_3L_2 complex.

$Ag_3\mathbf{1}_2\cdot(OTf)_3$: ^{1}H NMR (500 MHz, $CDCl_3/CD_3OD$ (1:1)): $\delta =$ 7.73 (d, $J = 3.4$ Hz, 6H), 7.69 (d, $J = 3.4$ Hz, 6H), 7.06 (d, $J = 7.8$ Hz, 6H), 6.88 (dd, $J = 1.5$, 7.8 Hz, 6H), 6.81 (d, $J = 7.6$ Hz, 6H), 6.76 (d, $J = 7.6$ Hz, 6H), 2.29 ppm (s, 18H); ^{13}C NMR (125 MHz, $CDCl_3/CD_3OD$ (1:1)): $\delta = 168.2$, 145.3, 142.4, 140.3, 133.1, 132.8, 131.0, 129.6, 128.9, 127.6, 124.5, 120.3 (q, $J = 319.3$ Hz), 20.6 ppm; MS (ESI TOF; CH_3OH): $m/z = 777.2$ $[Ag_3\mathbf{1}_2\cdot(OH)\cdot(H_2O)]^{2+}$. Crystallization of a 3:2 complex of AgOTf with **1** in a mixture of $CHCl_3$ and CH_3OH afforded colorless block crystals suitable for X-ray crystallographic analysis.

 © 2003 Wiley-VCH Verlag GmbH & Co. KGaA, Weinheim

$Ag_3\mathbf{2}_2\cdot(OTf)_3$: ^{1}H NMR (500 MHz, $CDCl_3/CD_3OD$ (1:1)): $\delta =$ 8.24 (m, 6H), 7.67 (ddd, $J = 1.4$, 7.8, 7.8 Hz, 6H), 7.34–7.33 (m, 12H), 6.94 (d, $J = 8.0$ Hz, 6H), 6.84 (d, $J = 8.0$ Hz, 6H), 6.74 (d, $J =$ 7.8 Hz, 6H), 6.71 (d, $J = 7.8$ Hz, 6H), 2.24 ppm (s, 18H); ^{13}C NMR (125 MHz, $CDCl_3/CD_3OD$ (1:1)): $\delta = 158.6$, 151.5, 142.6, 140.3, 139.4, 139.1, 133.9, 131.34, 131.27, 131.1, 128.9, 128.7, 123.6, 120.7 (q, $J =$ 319.3 Hz), 20.9 ppm; MS (ESI; CH_3OH): $m/z = 759.0$ $[Ag_3\mathbf{2}_2\cdot(OH)\cdot(H_2O)]^{2+}$. The $Ag_3\mathbf{2}_2$ complex formed from **2** (11.9 mg, 20.5 μmol) and $AgCH_3SO_3$ (6.2 mg, 30.8 μmol) in a mixed solution of H_2O and CH_3OH was isolated as PF_6 salts (14 mg, 71 %). Elemental analysis: calcd for $[Ag_3\mathbf{2}_2][PF_6]_3[CH_3OH]$: C 52.35, H 3.61, N 4.30; found: C 52.35, H 3.67, N 4.33.

$Ag_3\mathbf{1}_2\cdot(\Delta\text{-TRISPHAT})_3$ and $Ag_3\mathbf{2}_2\cdot(\Delta\text{-TRISPHAT})_3$. [$nBu_4$N][$\Delta$-TRISPHAT] were prepared according to reference [13b]: A solution of [nBu$_4$N][Δ-TRISPHAT] (3 equiv relative to the silver(I) complex) in $CHCl_3$ was added to $Ag_3\mathbf{1}_2\cdot(OTf)_3$ (4.6 μmol) or $Ag_3\mathbf{2}_2\cdot(OTf)_3$ (8.6 μmol) in $CHCl_3/CH_3OH$ (1:1) prepared as described above. A colorless precipitate was collected, washed with CH_3OH and $CHCl_3$, and dried in vacuo to obtain $Ag_3\mathbf{X}_2\cdot(\Delta\text{-TRISPHAT})_3$ ($\mathbf{X} = \mathbf{1}$ or **2**) as a colorless solid, which was used for further ^{1}H NMR spectroscopic studies. $Ag_3\mathbf{1}_2\cdot(\Delta\text{-TRISPHAT})_3$: 12.0 mg (3.1 μmol, 67 %). Elemental analysis: calcd for $[Ag_3\mathbf{1}_2][\Delta\text{-TRISPHAT}]_3[H_2O]_3$ ($C_{126}H_{60}Ag_3Cl_{36}N_6O_{21}P_3S_6$): C 39.01, H 1.56, N 2.17; found: C 39.18, H 1.91, N 1.96; $Ag_3\mathbf{2}_2\cdot(\Delta\text{-TRISPHAT})_3$: 30.7 mg (8.1 μmol, 94 %). Elemental analysis: calcd for $[Ag_3\mathbf{2}_2][\Delta\text{-TRISPHAT}]_3[H_2O]_4$ ($C_{138}H_{74}Ag_3Cl_{36}N_6O_{22}P_3$): C 42.93, H 1.93, N 2.17; found: C 42.95, H 2.14, N 2.02.

Received: January 30, 2003
Revised: June 26, 2003 [Z51068]

Keywords: helical structures · N ligands · sandwich complexes · silver

[1] For reviews, see: a) D. J. Hill, M. J. Mio, R. B. Prince, T. S. Hughes, J. S. Moore, *Chem. Rev.* **2001**, *101*, 3893–4012; b) R. P. Cheng, S. H. Gellman, W. F. DeGrado, *Chem. Rev.* **2001**, *101*, 3219–3232.

[2] For reviews, see: a) M. Albrecht, *Chem. Rev.* **2001**, *101*, 3457–3497; b) J.-C. G. Bünzli, C. Piguet, *Chem. Rev.* **2002**, *102*, 1897–1928; c) U. Knof, A. von Zelewsky, *Angew. Chem.* **1999**, *111*, 312–333; *Angew. Chem. Int. Ed.* **1999**, *38*, 302–322; d) C. Piguet, G. Bernardinelli, G. Hopfgartner, *Chem. Rev.* **1997**, *97*, 2005–2062.

[3] J. C. Nelson, J. G. Saven, J. S. Moore, P. G. Wolynes, *Science* **1997**, *277*, 1793–1796.

[4] A. Ikeda, H. Udzu, Z. Zhong, S. Shinkai, S. Sakamoto, K. Yamaguchi, *J. Am. Chem. Soc.* **2001**, *123*, 3872–3877.

[5] For an example of the nondissociative conversion of Mg^{2+} cluster between $\Delta\Delta\Delta\Delta \rightleftharpoons \Lambda\Lambda\Lambda\Lambda$ isomers, see: R. W. Saalfrank, B. Demleitner, H. Glaser, H. Maid, D. Bathelt, F. Hampel, W. Bauer, M. Teichert, *Chem. Eur. J.* **2002**, *8*, 2679–2683.

[6] For molecular motion using a B-Z DNA conversion, see: C. Mao, W. Sun, Z. Shen, N. C. Seeman, *Nature* **1999**, *397*, 144–146.

[7] For reviews, see: a) B. X. Colasson, C. Dietrich-Buchecker, M. C. Jimenez-Molero, J.-P. Sauvage, *J. Phys. Org. Chem.* **2002**, *15*, 476–483; b) P. F. Barbara, *Acc. Chem. Res.* **2001**, *34*, 409–487 (*Molecular Machines* Special Issue); c) V. Balzani, A, Credi, F. M. Raymo, J. F. Stoddart, *Angew. Chem.* **2000**, *112*, 3484–3530; *Angew. Chem. Int. Ed.* **2000**, *39*, 3348–3391.

[8] S. Hiraoka, T. Yi, M. Shiro, M. Shionoya, *J. Am. Chem. Soc.* **2002**, *124*, 14510–14511.

[9] For the preparation of **1** and **2**, see Supporting Information. Their ^{1}H NMR spectra showed only one set of highly symmetrical signals over a wide temperature range (223–293 K), probably as a result of the rapid exchange between a possible statistical mixture of racemic diastereomers.

[10] ESI TOF mass spectra of $Ag_3\mathbf{1}_2$ and $Ag_3\mathbf{2}_2$ are reported in the Supporting Information.

[11] Crystal data for $Ag_3\mathbf{1}_2\cdot(OTf)_3\cdot(CH_3OH)_5\cdot(H_2O)_2$: $C_{80}H_{78}Ag_3F_9N_6O_{16}S_9$, $M = 2162.66$, colorless block ($0.25 \times 0.25 \times 0.05$ mm^3), orthorhombic, $Pna2_1$, $a = 24.508(2)$ Å, $b = 23.017(2)$ Å, $c =$ 15.984(8) Å, $V = 9016(1)$ Å^3, $Z = 4$, $T = -180$ °C, $\rho_{calcd} =$ 1.59 g cm^{-3}, $F(000) = 4376.00$, $\mu(Mo_{K\alpha}) = 9.36$ cm^{-1}, a total of 14229 unique reflections ($2\theta_{max} = 60.1°$) were measured. The structure was solved by heavy-atom Patterson methods and expanded using Fourier techniques. Some non-hydrogen atoms were refined anisotropically, while the rest were refined isotropically. Hydrogen atoms were included but not refined. Full-matrix least-squares refinement on F^2 (1102 variable parameters) converged to $R_1 = 0.0601$, $wR_2 = 0.1550$ ($I > 2\sigma(I)$). CCDC-202447 contains the supplementary crystallographic data for this paper. These data can be obtained free of charge via www.ccdc.cam.ac.uk/conts/retrieving.html (or from the Cambridge Crystallographic Data Centre, 12, Union Road, Cambridge CB2 1EZ, UK; fax: (+44) 1223-336-033; or deposit@ccdc.cam.ac.uk).

[12] X-ray crystallographic analysis data of crystals obtained from a mixture of AgOTf and **2** (3:2) in $CHCl_3/CH_3OH$ were not fully refined owing to the disorder of the solvent and anion molecules, although the sandwich-shaped skeleton of $Ag_3\mathbf{2}_2$ structure was obtained preliminarily.

[13] a) D. Monchaud, J. J. Jodry, D. Pomeranc, V. Heinz, J.-C. Chambron, J.-P. Sauvage, J. Lacour, *Angew. Chem.* **2002**, *114*, 2423–2425; *Angew. Chem. Int. Ed.* **2002**, *41*, 2317–2319; b) H. Ratni, J. J. Jodry, J. Lacour, E. P. Kundig, *Organometallics* **2000**, *19*, 3997–3999.

[14] For asymmetric induction and resolution of helicates with Δ-TRISPHAT, see: J. J. Jodry, J. Lacour, *Chem. Eur. J.* **2000**, *6*, 4297–4304.

[15] Recently, a variable-temperature NMR spectroscopic study of the racemization of the mononuclear tetrahedral copper(I) complexes in the presence of Δ-TRISPHAT was reported; see: V. Desvergnes-Breuil, V. Hebbe, C. Dietrich-Buchecker, J.-P. Sauvage, J. Lacour, *Inorg. Chem.* **2003**, *42*, 255–257.

 © 2003 Wiley-VCH Verlag GmbH & Co. KGaA, Weinheim

Cyclic Glycopeptides

Glycotentacles: Synthesis of Cyclic Glycopeptides, Toward a Tailored Blocker of Influenza Virus Hemagglutinin**

*Takashi Ohta, Nobuaki Miura, Naoki Fujitani, Fumio Nakajima, Kenichi Niikura, Reiko Sadamoto, Chao-Tan Guo, Takashi Suzuki, Yasuo Suzuki, Kenji Monde, and Shin-Ichiro Nishimura**

Influenza virus infection is initiated by the binding of hemagglutinin (HA), a viral carbohydrate-binding membrane protein, to sialic acid-containing oligosaccharides, such as GM3 trisaccharide [Neu5Acα(2,3)Galβ(1,4)Glc], on the host cell surfaces.[1] Since this molecular-recognition process leads to the host cell–virus adhesion stage, molecules with a high affinity for the viral HA would be potent candidates for blockers of the influenza virus. Various types of HA blockers carrying sialooligosaccharides have been synthesized over the last decade.[2] Enhanced blocking effects by the multidentate (multivalent) glycoligands were often found by clustering[3] the sialooligosaccharides on macromolecular scaffolds, such as synthetic polymers,[4] cyclodextrins,[5] and dendrimers,[6] although the mechanism of this multiple interaction has not yet been fully investigated.

In these macromolecular approaches, structural information on the spatial arrangement of the multiple binding sites of the protein is not usually accounted for in the design of ligands. Recently, it was found that ligands containing small oligodentate carbohydrate units, that are designed topologically to bind simultaneously to several binding sites of a single lectin, are very effective blockers.[7,8] The syntheses of the STARFISH dendrimer used to inhibit the adherence of verotoxins, is an excellent example of how detailed structure analysis has led to the creation of a strongly effective "multidentate" ligand.[7,2e]

Thus, on the basis of the HA structure, we created cyclic peptide scaffolds containing tridentate carbohydrate units as a potential HA blockers by using a convenient chemoenzymatic method. HA is a trimeric protein and each subunit contains one sialooligosaccharide binding site on the outer portion. From the three-dimensional structure of HA, as revealed by X-ray analysis,[9] these three binding sites are located on the apexes of an equilateral triangle, in which each binding pocket is separated by approximately 40–50 Å. To achieve a rational molecular design for an HA blocker, we focused on the use of cyclic peptides[10] as a scaffold because of the flexibility of the synthetic strategy and their biological compatibility in the human body.

Herein, we report a chemoenzymatic synthesis of a series of cyclic peptides presenting three sialotrisaccharide units [Neu5Acα(2,3)Galβ(1,4)Glc] by using transglutaminase and glycosyltransferase (Scheme 1). We also discuss the effect of peptide sequence on their biological activities.

Scheme 1 shows the synthetic route to cyclic glycopeptides by means of a combined chemical and enzymatic strategy. In this case, a cyclic peptide **1** prepared by employing the Fmoc-Asp-ODmab method[11] on a chlorotrityl resin[12] was enzymatically coupled with 6-aminohexyl lactoside (**4**) using transglutaminase from guinea pig liver.[13] The transamination reaction between three Gln residues of cyclic peptide **1** and **4** (large excess) gave a mixture of mono- (**1-m**), bi- (**1-b**), and tri-substituted (**1-t**) derivatives. After the introduction of sialic acids with recombinant rat α-2,3-(*N*)-sialyltransferase in the presence of CMP-Neu5Ac,[14] the crude product was subjected to purification by using lactose-binding lectin(RCA120)-based affinity chromatography, DEAE-Sepharose, Sephadex G-25, and reversed phase HPLC (ODS (octadecylsilyl)) to afford the desired cyclic glycopeptides **1-m** (8% yield based on peptide), **1-b** (10%), and **1-t** (12%). It should be noted that the lectin-based affinity chromatographic procedure greatly facilitated the purification of the sialylated cyclic glycopeptides, since intermediates still containing lactose branches are captured by this lectin-bearing adsorbent. Cyclic peptide **1** contains both negatively (Asp) and positively (His) charged residues. We also synthesized cyclic peptides **2** and **3**, which contain neutral amino acid residues (Ser, Gln, and Gly). After cleavage from the resin, the liner peptides were cyclized in the liquid phase to obtain cyclic peptides **2** and **3**. Following the same chemoenzymatic strategy as in Scheme 1, mono- (**2-m, 3-m**), bi- (**2-b, 3-b**), and tri- (**2-t, 3-t**) sialyllactose-attached cyclic peptides were obtained. All the compounds were identified by NMR spectroscopy (1D and 2D (COSY and NOESY)) and MALDI-TOF mass spectrometry.

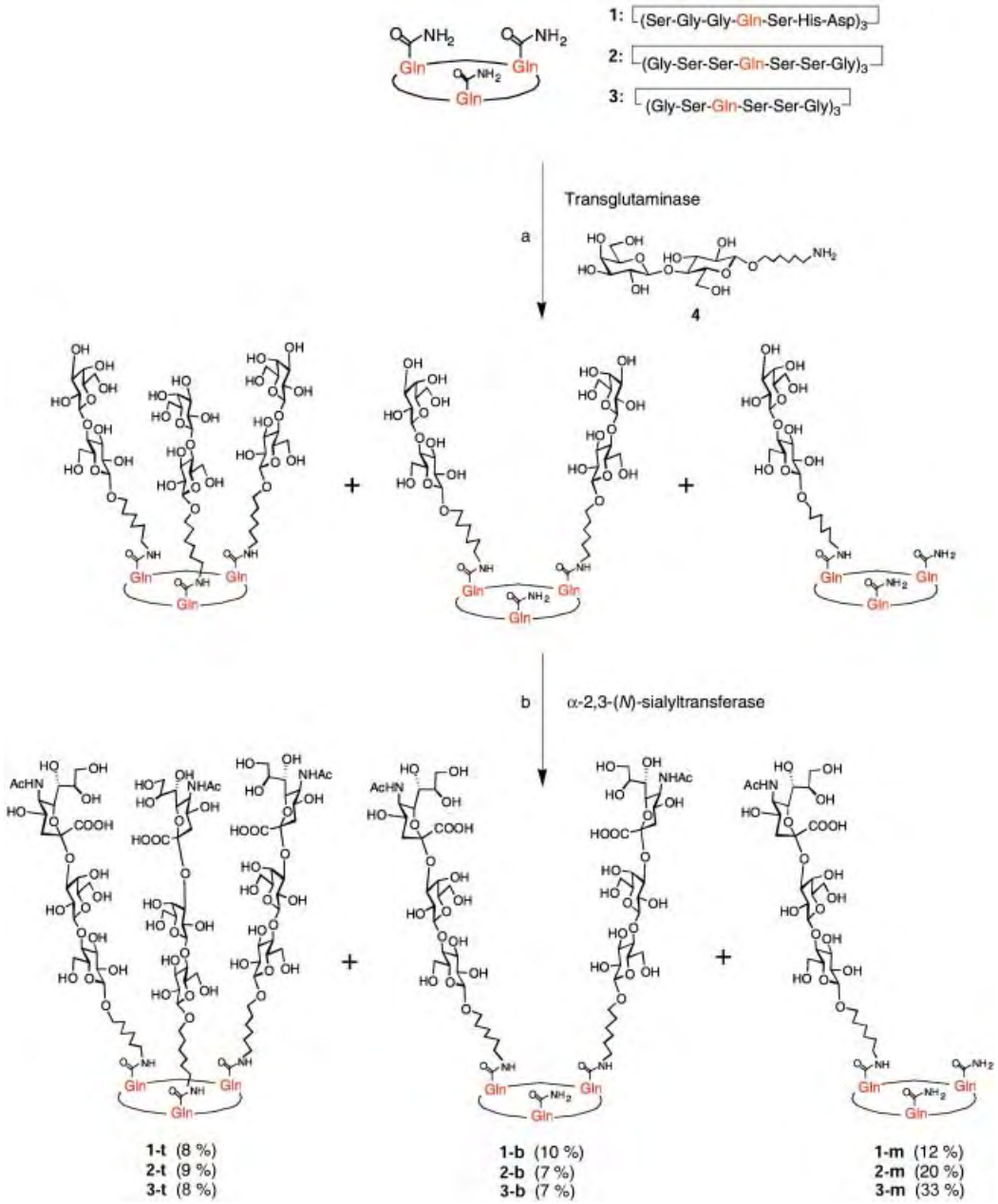
Molecular modeling studies indicate that the maximum separation between sialic acid residues is approximately 50–70 Å for all the cyclic glycopeptides (**1-t, 2-t**, and **3-t**). Since the binding sites within the HA trimer are separated by 40–

[*] Prof. S.-I. Nishimura, T. Ohta, Dr. K. Niikura, Dr. K. Monde
Division of Biological Sciences
Graduate School of Science
Frontier Research Center for Post-genomic Science and Technology
Hokkaido University
Kita 21 Nishi 11, Sapporo 001-0021 (Japan)
Fax: (+81) 11-706-9042
E-mail: shin@glyco.sci.hokudai.ac.jp
Prof. S.-I. Nishimura, Dr. N. Miura, Dr. N. Fujitani, F. Nakajima, Dr. R. Sadamoto
Japan Bioindustry Association
Sapporo 060-0810 (Japan)
Dr. C.-T. Guo, Dr. T. Suzuki, Prof. Y. Suzuki
Department of Biochemistry
School of Pharmaceutical Sciences
University of Shizuoka, Shizuoka 422-8526 (Japan)
Prof. S.-I. Nishimura
National Institute of Advanced Industrial Science and Technology (AIST), Sapporo 062-8517 (Japan)

[**] This work was supported by a grant for "Research and Development on Glycocluster Controlling Biomolecules" from the New Energy and Industrial Technology Development Organization (NEDO) and by a grant-in-aid for scientific research from the Ministry of Education, Science, and Culture (Grant No. 12555256).

Supporting information for this article (spectral data for all new compounds, details for biological evaluations, SPR assay, and conformational analyses) is available on the WWW under http://www.angewandte.org or from the author.

 © 2003 Wiley-VCH Verlag GmbH & Co. KGaA, Weinheim DOI: 10.1002/anie.200351640



Scheme 1. Enzymatic synthesis of cyclic glycopeptide: a) **4**, transglutaminase (from guinea pig liver) (2 U), Tris/HCl buffer (0.2 M, 10 mM $CaCl_2$, pH 7.2), 37 °C 24 h; b) α-2,3-(*N*)-sialytransferase (0.1 U), sodiumcacodylate buffer (50 mM, 1.58 mM $MnCl_2$, pH 7.5), bovine serum albumin (2 mg mL^{-1}), triton CF-54 (0.1 %), CMP-Neu5Ac (11 mmol). The numbers in parenthesis indicate the two-step purified yields. CMP = cytidine-5′-monophospho-*N*-acetyl neuraminic acid sodium salt.

50 Å, all the tridentate ligands based on **1, 2** and **3** can simultaneously occupy the binding sites within the HA trimer (Figure 1).

The inhibitory effects of cyclic glycopeptides on virus-induced hemagglutination[15] were evaluated by using influenza virus, A/PR/8/34(H1N1), and the results are listed in Table 1. While potent inhibitory effects were observed for **1-t** and **1-b** at the concentrations tested, no inhibition of hemagglutination was observed for monodentate **1 m**. A simple monodentate sialoside has been reported to show a 2–3 mM inhibitory effect by HAI titre.[2e,f] Therefore, a comparison of the inhibitory effect of trivalent **1-t** and monodentate **1-m** indicates that the three oligosaccharides on the cyclic peptide occupy the three binding sites of HA simultaneously (multidentate effect). We used bovine fetuin as a positive control in the inhibitory assay. Bovine fetuin is a glycoprotein (ca. 50 kDa) containing nearly 30 % carbohydrate by weight and possessing six carbohydrate moieties; three N-linked carbohydrate chains (binary and ternary) with terminal sialic acid residues and three O-linked carbohydrate units.[16] On average, fetuin has about 10 sialic acid containing sugar chains on the surface. The minimum concentration of sialic acid residues for inhibition of hemagglutination is calculated as 0.026 mM (0.0026 mM as fetuin molecules). Therefore, the

 © 2003 Wiley-VCH Verlag GmbH & Co. KGaA, Weinheim

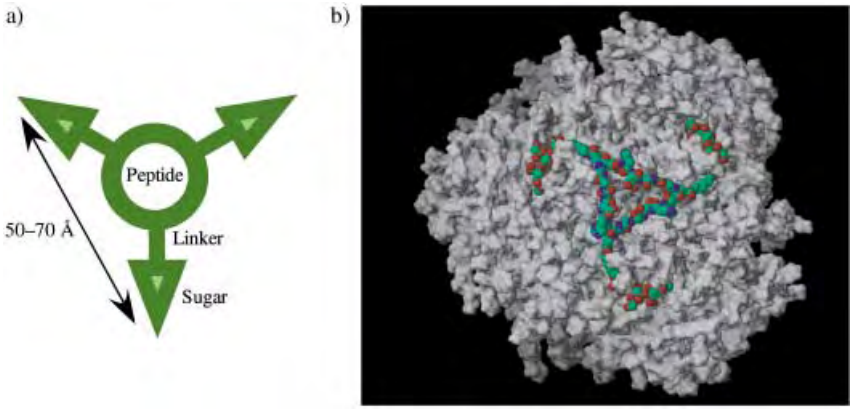


Figure 1. a) Schematic representation of a tridentate glycopeptide. b) The complex of HA and cyclic glycopeptide **1-t** based on computer calculations.[18]

Table 1: Inhibitory effect of cyclic glycopeptides on the hemagglutination of chicken erythrocytes induced by influenza virus and binding affinity against hemagglutinin.

Compound	HAI titre, dilution[a]	K_d [mM][c]
1	NA[b]	> 20
1-m	NA[b]	> 20
1-b	0.43 mg mL^{-1} (0.125 mM)	1.6
1-t	0.16 mg mL^{-1} (0.040 mM)	0.63
2	NA[b]	> 20
2-m	NA[b]	> 20
2-b	NA[b]	> 20
2-t	NA[b]	> 20
3	NA[b]	> 20
3-m	NA[b]	> 20
3-b	NA[b]	> 20
3-t	NA[b]	> 20
Fetuin	0.13 mg mL^{-1} (0.0026 mM)	

[a] In HAI titre, hemagglutinin (A/PR/8/34). [b] NA = no activity at a concentration of 0.25 mM or less. Details of experimental procedures are described in the Supporting Infomation. [c] Binding constants were obtained by SPR using hemagglutinin (A/Equine/La Plata/93).

sialic acid residues on the fetuin were only 4.6-times more effective than the cyclic glycopeptide **1-t** (0.12 mM as sialic acid concentration). This result means that the topological arrangement of the multiple binding sites in relation to the protein structure is of significant importance to the multidentate effect. Surprisingly, the glycopeptides attached on scaffold **2** or **3** (**2-t, 2-b, 2-m, 3-t, 3-b, 3-m**) had no inhibitory effect against hemagglutinin at a concentration of 0.25 mM or less. This observation suggests that the nature of the peptide scaffold also plays a significant role in determining the activity (see below).

The binding assay between the HA protein and cyclic peptide derivative was carried out using surface plasmon resonance (SPR; Biacore apparatus, see Supporting Information for details). HA (A/Equine/La Plata/93) was covalently attached to the carboxymethylated dextran-coated gold sensor surface (CM-dextran) using an amine-coupling procedure.[17] The solutions containing various concentrations (from 0 to 0.5 mM) of cyclic peptide or cyclic glycopeptides were injected over the sensor surface and the binding affinities of the compounds were determined. The respective dissociation constants (K_d) are shown in Table 1.

Interestingly, only **1-t** ($K_d = 0.63$ mM) and **1-b** ($K_d = 1.6$ mM) showed significant affinity to HA on the sensor surface and there was no binding of other cyclic peptide derivatives. This result is in close agreement with the result of the HAI titer experiment. In the SPR experiment, the HA was chemically immobilized on the dextran polymer; thus, the molecular orientation should have been random. Therefore, it is reasonable to consider that cyclic glycopeptides occupy the binding sites within a single HA molecule, rather than the intermolecular bridging of two HA molecules. These binding assay data imply that the amino acid sequence of the cyclic peptide has a marked influence on the direction and flexibility of the side chains of the glutamine residues.

The solution structures of cyclic peptides **1** and **3** were determined by molecular modeling using restraints derived from 2D NOESY data (see Supporting Information for details). Peak assignments were made from DQF-COSY, TOCSY, and NOESY NMR spectra acquired for the peptides at 293 K in H_2O. The 3D structures were calculated using simulated annealing and energy minimization protocols within X-PLOR. A total of 67 distance restraints and 12 dihedral-angle restraints were used to calculate family structures. Figure 2 shows the lowest energy and 30 convergent annealed structures for cyclic peptides **1** and **3**. In the active scaffold **1**, one of the three aspartic acid residues seems to interact with the histidine residue inside the cyclic peptide ring. Eventually, all three side chains of the glutamine residues are directed outwards from cyclic peptide ring

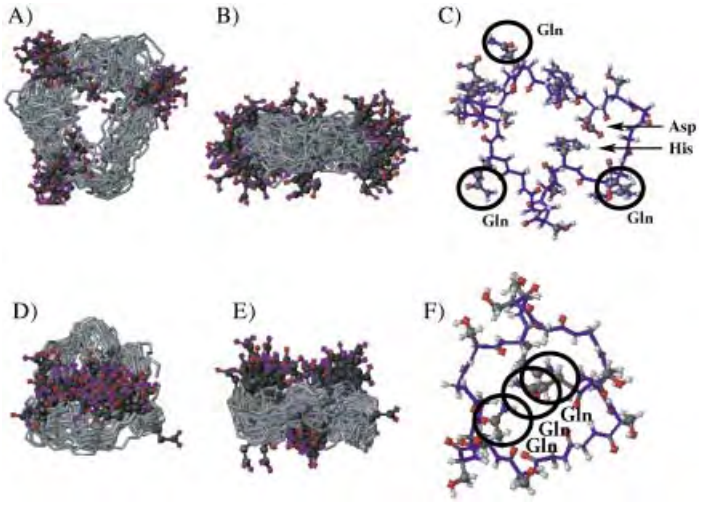


Figure 2. Conformation of cyclic peptide **1** (A, B, and C) and **3** (D, E, and F) calculated from NMR spectra: 30 convergent structure (A, B, D and E; top and side views), the lowest-energy structure (C and F).

 © 2003 Wiley-VCH Verlag GmbH & Co. KGaA, Weinheim

(open formation), as expected. However, the side chains of the glutamines residues of the non-active scaffold **3** were directed inward from the cyclic peptide ring (close formation). Therefore, for scaffold **1**, the three attached sugars could reach the binding sites of HA simultaneously and a multidentate effect was obtained. However, in scaffold **3**, the attached sugars were orientated inwards and could not bind simultaneously to the HA binding sites, resulting in a low affinity owing to monodentate binding.

In conclusion, cyclic peptide templates provide an interesting framework for the manipulation of the multidentate presentation of carbohydrate units based on the structural data from hemagglutinin. The chemoenzymatic approach using transglutaminase and glycosyltransferase is effective in providing glycoconjugate linking between peptides and sugars. The biological activity of the hemagglutination assay is strongly depended on the amino acid sequence of the cyclic peptides, even though their circular sizes were identical. This result indicates that, in the addition to the size, the 3D spatial arrangement of multidentate ligands, which is determined by the scaffolds, is of significant importance in producing a "directed multidentate effect", thereby offering new insight into the design of carbohydrate-based drugs.

Received: April 11, 2003
Revised: June 30, 2003 [Z51640]

Keywords: carbohydrates · glycopeptides · influenza viruses · inhibitors · protein design

[1] a) J. C. Paulson, J. Sadler, R. L. Hill, *J. Biol. Chem.* **1979**, *254*, 2120 – 2124; b) Y. Suzuki, Y. Nagano, H. Kato, M. Matsumoto, K. Nerome, K. Nakajima, E. Nobusawa, *J. Biol. Chem.* **1986**, *261*, 17057 – 17061; c) G. N. Rogers, B. L. D'Souza, *Virology* **1989**, *173*, 317 – 322; d) A. S. Gambaryan, A. B. Tuzikov, V. E. Piskarev, S. S. Yamnikova, D. K. Lvov, J. S. Robertson, N. V. Bovin, M. N. Matrosovich, *Virology* **1997**, *232*, 345 – 350; e) C.-L. Schengrund, *Biochem. Pharmacol.* **2003**, *65*, 699 – 707.

[2] a) T. J. Pritchett, R. Brossmer, U. Rose, J. C. Paulson, *Virology* **1987**, *160*, 502 – 506; b) N. K. Sauter, M. D. Bednarski, B. A. Wurzburg, J. E. Hanson, G. M. Whitesides, J. J. Skehel, D. C. Wiley, *Biochemistry* **1989**, *28*, 8388 – 8396; c) N. K. Sauter, J. E. Hanson, G. D. Glick, J. H. Brown, R. L. Crowther, S.-J. Park, J. J. Skehel, D. C. Wiley, *Biochemistry* **1992**, *31*, 9609 – 9621; e) G. D. Glick, J. R. Knowles, *J. Am. Chem. Soc.* **1991**, *113*, 4701 – 4703; f) G. D. Glick, P. L. Toogood, D. C. Wiley, J. J. Skehel, J. R. Knowles, *J. Biol. Chem.* **1991**, *266*, 23660 – 23669; g) M. Mammem, S.-K. Choi, G. M. Whiteside, *Angew. Chem.* **1998**, *110*, 2908 – 2953; *Angew. Chem. Int. Ed.* **1998**, *37*, 2754 – 2794.

[3] a) Y. C. Lee, *Carbohydr. Res.* **1978**, *67*, 509 – 514; b) Y. C. Lee, *FASEB J.* **1992**, *6*, 3193 – 3200; c) L. L. Kiessling, N. L. Pohl, *Chem. Biol.* **1996**, *3*, 71 – 77; d) R. Roy, *Curr. Opin. Struct. Biol.* **1996**, *6*, 692 – 702; d) T. K. Dam, C. F. Brewer, *Chem. Rev.* **2002**, *102*, 387 – 429; e) J. J. Lundquist, E. J. Toone, *Chem. Rev.* **2002**, *102*, 555 – 578.

[4] a) A. Gamian, M. Chomik, C. A. Laferriere, R. Roy, *Can. J. Microbiol.* **1991**, *37*, 233 – 237; b) W. J. Lees, A. Spaltenstein, J. E. Kingery-Wood, G. M. Whitesides, *J. Med. Chem.* **1994**, *37*, 3419 – 3433; c) M. Mammen, K. Helmerson, R. Kishore, S. K. Choi, W. D. Phillips, G. M. Whitesides, *Chem. Biol.* **1996**, *3*, 757 – 763; d) M. Mammen, G. Dahmann, G. M. Whitesides, *J. Med. Chem.* **1995**, *38*, 4179 – 4190; e) T. Furuike, S. Aiba, T. Takahashi, Y. Suzuki, K. Yamada, S.-I. Nishimura, *J. Chem. Soc. Perkin Trans. 1* **2000**, 3000 – 3005; f) H. Kamitahara, T. Suzuki, N. Nishigori, O. Kanue, C.-H. Wong, *Angew. Chem.* **1998**, *110*, 1607 – 1611; *Angew. Chem. Int. Ed.* **1998**, *37*, 1524 – 1528; g) L. E. Strong, L. L. Kiessling, *J. Am. Chem. Soc.* **1999**, *121*, 6193 – 6196.

[5] a) R. Roy, F. Hernández-Mateo, F. Santoyo-González, *J. Org. Chem.* **2000**, *65*, 8743 – 8746; b) D. A. Fulton, J. F. Stoddart, *Bioconjugate Chem.* **2001**, *12*, 655 – 672; c) C. O. Mellet, J. Defaye, J. M. G. Fernández, *Chem. Eur. J.* **2002**, *8*, 1982 – 1990.

[6] J. D. Reuter, A. Myc, M. M. Hayes, Z. Gan, R. Roy, D. Qin, R. Yin, L. T. Piehler, R. Esfand, D. A. Tomalia, J. R. Jr. , Baker, *Bioconjugate Chem.* **1999**, *10*, 271 – 278.

[7] a) P. I. Kitov, J. M. Sadowska, G. Mulvey, G. D. Armstrong, H. Ling, N. S. Pannu, R. J. Read, D. R. Bundle, *Nature* **2000**, *403*, 669 – 672; b) L. Baussanne, J. M. Benito, C. O. Mellet, J. M. G. Fernández, J. Defaye, *ChemBioChem* **2001**, *2*, 777 – 783; c) J. E. Gestwicki, C. W. Cairo, L. E. Strong, K. A. Oetjen, L. L. Kiessling, *J. Am. Chem. Soc.* **2002**, *124*, 14922 – 14933.

[8] a) W. E. Minke, C. Roach, W. G. J. Hol, C. L. M. J. Verlinde, *Biochemistry* **1999**, *38*, 5684 – 5692; b) E. Fan, Z. Zhang, W. E. Minke, Z. Hou, C. L. M. J. Verlinde, W. G. J. Hol, *J. Am. Chem. Soc.* **2000**, *122*, 2663 – 2664; c) E. A. Merritt, Z. Zhang, J. C. Pickens, M. Ahn, W. G. J. Hol, E. Fan, *J. Am. Chem. Soc.* **2002**, *124*, 8818 – 8824.

[9] a) I. A. Wilson, J. J. Skehel, D. C. Wiley, *Nature* **1981**, *289*, 366 – 373; b) W. Weis, J. H. Brown, S. Cusack, J. C. Paulson, J. J. Skehel, D. C. Wiley, *Nature* **1988**, *333*, 426 – 431.

[10] On the use of cyclic peptides as scaffold see: a) H. Kessler, *Angew. Chem.* **1982**, *94*, 509 – 520; *Angew. Chem. Int. Ed. Engl.* **1982**, *21*, 512 – 523; b) H. G. Boman, *Annu. Rev. Immunol.* **1995**, *12*, 61 – 92; c) U. Sprengard, M. Schudok, W. Schmidt, G. Kretzschmar, H. Kunz, *Angew. Chem.* **1996**, *108*, 359 – 362; *Angew. Chem. Int. Ed. Engl.* **1996**, *35*, 321 – 324; d) V. Wittmann, S. Seeberger, *Angew. Chem.* **2000**, *112*, 4508 – 4512; *Angew. Chem. Int. Ed.* **2000**, *39*, 4348 – 4352; e) O. Renaudet, P. Dumy, *Org. Lett.* **2003**, *5*, 243 – 246; f) S. Fernandez-Lopez, H.-S. Kim, E. C. Choi, M. Delgado, J. R. Granja, A. Khasanov, K. Kraehenbuehl, G. Long, D. A. Weinberger, K. M. Wilcoxen, M. R. Ghadiri, *Nature* **2001**, *412*, 452 – 455.

[11] C. C. Chan, B. W. Bycroft, D. J. Evans, P. D. White, *J. Chem. Soc. Chem. Commun.* **1995**, *119*, 2209 – 2210.

[12] K. Barlos, O. Chatzi, D. Gatos, G. Stavropoulos, *Int. J. Pept. Protein Res.* **1991**, *37*, 513 – 520.

[13] a) S.-C. B. Yan, F. Wold, *Biochemistry* **1984**, *23*, 3759 – 8765; b) J. E. Folk, S. L. Chung, *Methods Enzymol.* **1985**, *113*, 358 – 375; c) D. Ramos, P. Rollin, W. Klaffke, *Angew. Chem.* **2000**, *112*, 406 – 408; *Angew. Chem. Int. Ed.* **2000**, *39*, 396 – 396; d) D. Ramos, P. Rollin, W. Klaffke, *J. Org. Chem.* **2001**, *66*, 2948 – 2956.

[14] S.-I. Nishimura, K. Yamada, *J. Am. Chem. Soc.* **1997**, *119*, 10555 – 10556.

[15] Y. Suzuki, T. Suzuki, M. Mastumoto, *J. Biochem.* **1983**, *93*, 1621 – 1633.

[16] a) R. Spiro, V. Bhoyroo, *J. Biol. Chem.* **1974**, *249*, 5704 – 5717; b) E. Green, G. Adelt, J. Baenziger, S. Wilson, H. Halbeek, *J. Biol. Chem.* **1988**, *263*, 18253 – 18268; c) B. Nilsson, N. Norden, S. Svensson, *J. Biol. Chem.* **1979**, *254*, 4545 – 4553.

[17] D. K. Takemoto, J. L. Skehel, D. C. Wiley, *Virology* **1996**, *217*, 452 – 458.

[18] The stable conformation of **1-t** was optimized using the molecular dynamics (MD) method. The force field developed by Tripos, Inc was used and the partial charge of atoms was calculated by the Gastiger–Hückel method. The SYBYL program code developed by Tripos, Inc. was applied throughout these calculations. The cyclic glycopeptide **1-t** was docked with HA extracted from the protein data bank. The energy minimized 3D structure of the HA and **1-t** complex in water was determined by molecular mechanics (MM).

 © 2003 Wiley-VCH Verlag GmbH & Co. KGaA, Weinheim

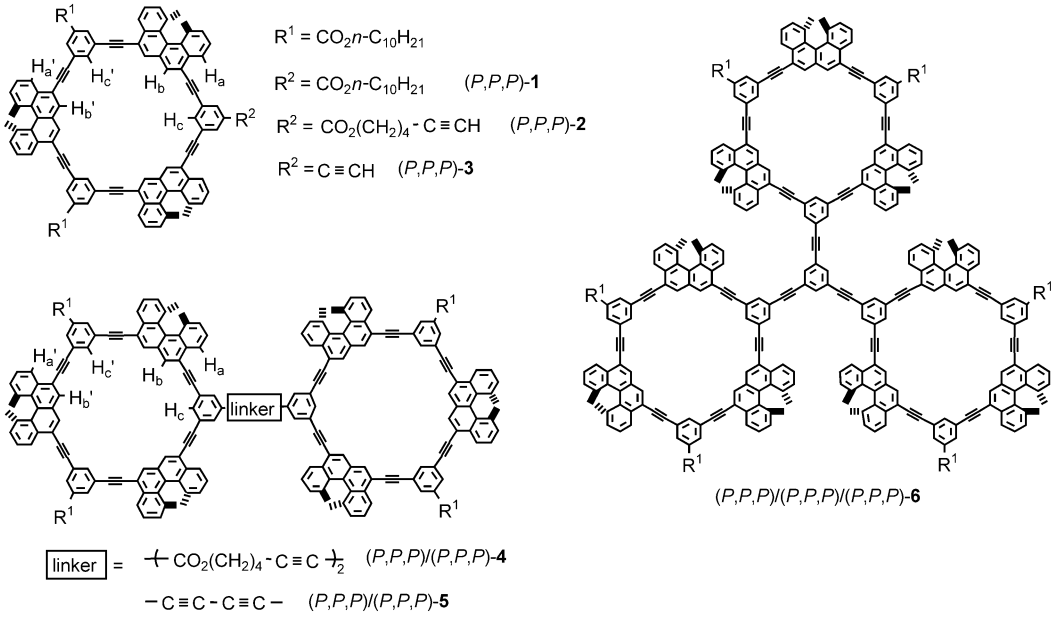
Linker-Controlled Aggregation

[3+3]Cycloalkyne Oligomers: Linking Groups Control Intra- and Intermolecular Aggregation by π–π Interactions**

*Yuto Saiki, Keiichi Nakamura, Yasuko Nigorikawa, and Masahiko Yamaguchi**

Conjugated π compounds, such as porphyrins,[1] phthalocyanines,[2] and macrocyclic alkynes[3] self-aggregate with face-to-face orientation, which is considered to be due to the π–π interactions between the aromatic ring systems. Such aggregation in organic solvents, however, is weak and nonselective. The compounds are in monomer–dimer equilibrium, and form higher aggregates only under solvophobic conditions in aqueous solvents or in the presence of templates, such as, DNA,[4] peptide,[5] and synthetic bilayer membranes.[6] We previously found that [3+3]cycloalkynes **1**, which are chiral macrocyclic alkynes containing three helicenes and three *m*-phenylene moieties, strongly aggregate in chloroform and benzene.[7] A sharp transition occurs between a monomer and a bimolecular aggregate; (*P,P,P*)-**1** (see Scheme 1) is monomeric below 1 mM in $CHCl_3$, and is dimeric above 1 mM. While the reported π-conjugate compounds required the "external" effects of solvophobic conditions or templates for strong aggregation, the strong aggregation of **1** is caused only by the π–π interactions. Compound **1** forms only a bimolecular aggregate; no higher aggregates are formed. It was therefore considered that the aggregation of the helicene derivative **1** could be used to construct a controlled self-assembly system. Reported herein are the aggregation of oligomeric [3+3]cycloalkynes, two dimers **4, 5**, and a trimer **6** (Scheme 1). In principle, such oligomers can form either an intra- or intermolecular aggregate, the latter of which can be anything from a dimer to a polymer. The aggregate structure in an organic solvent can be controlled by the structure of the linker, that connects the [3+3]cycloalkyne moiety: A dimer **4** with a flexible linker forms a strong intramolecular aggregate, a dimer **5** with a rigid linker equilibrates with a bimolecular aggregate, and a trimer **6** with a rigid linker forms a strong and selective bimolecular aggregate.[8–10]

Dimers (*P,P,P*)/(*P,P,P*)-**4** and (*P,P,P*)/(*P,P,P*)-**5** were synthesized by the oxidative dimerization[11] of (*P,P,P*)-**2**[12] and (*P,P,P*)-**3**,[12] respectively, and the trimer (*P,P,P*)/(*P,P,P*)/(*P,P,P*)-**6** was obtained from (*P,P,P*)-**3** and 1,3,5-triiodobenzene.



Scheme 1. Structures of the aggregates.

While ^{1}H NMR ($CDCl_3$) and circular dichroism (CD; $CHCl_3$) spectra of (*P,P,P*)-**1** and (*P,P,P*)-**2** are concentration dependent, the ^{1}H NMR ($CDCl_3$) spectra of the dimeric (*P,P,P*)/(*P,P,P*)-**4** do not change at concentrations between 0.3 and 1.5 mM (25 °C) or at temperatures between 25 and 60 °C.[12] The CD ($CHCl_3$, 25 °C) spectra of the dimeric (*P,P,P*)/(*P,P,P*)-**4** also do not change between 0.024 and 0.24 mM (Figure 1a). The aromatic ^{1}H NMR signals of (*P,P,P*)/(*P,P,P*)-**4** appear considerably upfield of those of the non-aggregated (*P,P,P*)-**1** (0.32 mM) and (*P,P,P*)-**2** (0.31 mM), and are even upfield compared to the aggregated (*P,P,P*)-**1**

[*] Prof. Dr. M. Yamaguchi, Y. Saiki, Dr. K. Nakamura, Y. Nigorikawa
Department of Organic Chemistry
Graduate School of Pharmaceutical Sciences
Tohoku University
Aoba, Sendai 980-8578 (Japan)
Fax: (+81) 22-217-6811
E-mail: yama@mail.pharm.tohoku.ac.jp

[**] The authors thank Professor J. D. Wuest (The Université de Montréal) for the preparative procedures of 1,3,5-triiodobenzene. Financial support from JSPS is gratefully acknowledged.

Supporting information (experimental and spectroscopic details) for this article is available on the WWW under http://www.angewandte.org or from the author.

 © 2003 Wiley-VCH Verlag GmbH & Co. KGaA, Weinheim DOI: 10.1002/anie.200351735

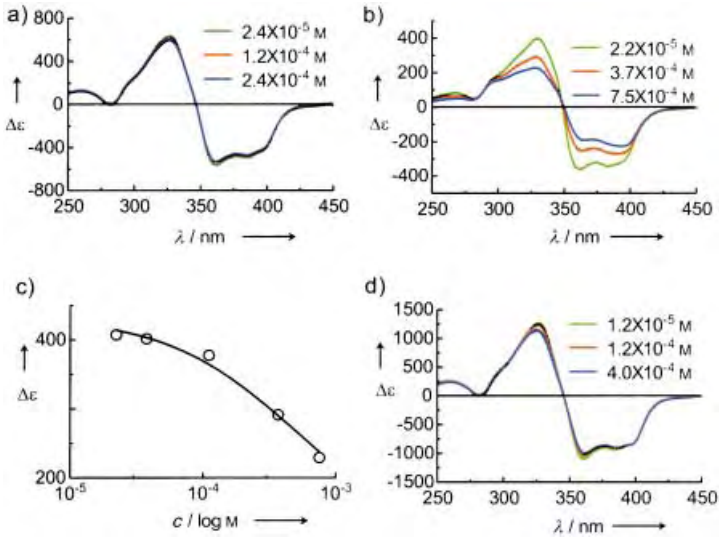


Figure 1. CD spectra of (*P,P,P*)/(*P,P,P*)-**4** (a), (*P,P,P*)/(*P,P,P*)-**5** (b), (*P,P,P*)/(*P,P,P*)/(*P,P,P*)-**6** (d), and plots of $\Delta\varepsilon$ versus concentration at 330 nm for (*P,P,P*)/(*P,P,P*)-**5** (c). The curve is the best theoretical fit for the monomer–dimer system, from which the association constant $K = 985\ \text{M}^{-1}$, $R^2 = 0.99$ was obtained.

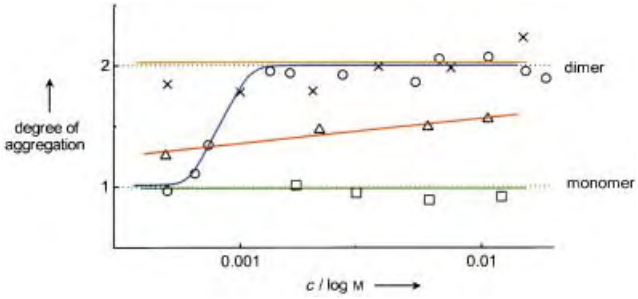


Figure 2. Degree of aggregation by VPO ($CHCl_3$, 35 °C) for (*P,P,P*)-**1** (○, blue line),[7] (*P,P,P*)/(*P,P,P*)-**4** (□, green line), (*P,P,P*)/(*P,P,P*)-**5** (△, red line), and (*P,P,P*)/(*P,P,P*)/(*P,P,P*)-**6** (X, orange line). Degree of aggregation = observed molecular weight/molecular weight of monomer.

(12.0 mM) and (*P,P,P*)-**2** (1.2 mM) (Table 1). The ^{1}H NMR observations indicate the aggregate formation of (*P,P,P*)/(*P,P,P*)-**4**. In addition, ^{1}H NMR resonances of (*P,P,P*)/(*P,P,P*)-**4** at H_a/H_a' and H_c/H_c' (see Scheme 1) separate into two signals

Table 1: ^{1}H NMR ($CDCl_3$, 25 °C) spectroscopic data of (*P,P,P*)-**1**, (*P,P,P*)-**2** and (*P,P,P*)/(*P,P,P*)-**4**.

	Conc. [mM]	δ (H_a/H_a') [ppm]	δ (H_b/H_b') [ppm]	δ (H_c/H_c') [ppm]
(*P,P,P*)-**1**[7]	0.32	8.56	8.18	8.25
	12.0	8.20	8.04	8.09
(*P,P,P*)-**2**	0.31	8.53	8.18	8.25
	1.2	8.34	8.08	8.11
(*P,P,P*)/(*P,P,P*)-**4**	0.27	8.01, 7.96 (1:2)	7.74	7.82, 7.96 (1:2)
	1.5	8.01, 7.94 (1:2)	7.74	7.82, 7.97 (1:2)

in 2:1 ratios, which is in contrast to the ^{1}H NMR spectra of (*P,P,P*)-**2** which show only a single resonance for H_a/H_a' and H_c/H_c'. The magnetic environment of the helicene and the *m*-phenylene units close to the linker moiety differs from the others, which is consistent with the formation of a folded structure at the linker moiety. The molecular weight of (*P,P,P*)/(*P,P,P*)-**4** observed by vapor pressure osmometry (VPO) indicates a monomeric nature in solution, which is again concentration-independent (Figure 2). These observations are explained by the strong intramolecular aggregation of (*P,P,P*)/(*P,P,P*)-**4**, which folds at the linker moiety. The folded structure named "castanet structure" was determined by Amber calculations,[12] in which the *m*-phenylene moiety is fitted into the groove formed by the helicene as observed in the aggregated (*P,P,P*)-**1**.[7] While some dyes connected by flexible linkers are reported to adopt a folded conformation in polar or aqueous solvents as a result of solvophobic interactions,[13] one notable aspect of (*P,P,P*)/(*P,P,P*)-**4** is that it folds solely by the π–π interactions without such "external" effects.

The behavior of the dimeric (*P,P,P*)/(*P,P,P*)-**5** possessing a rigid linker was examined with the expectation that it would form an intermolecular aggregate, since the linker moiety of this compound cannot fold. Although ^{1}H NMR signals in the aromatic regions are broadened in $CDCl_3$, they are slightly concentration-dependent between 0.19 mM and 1.5 mM.[12] CD spectra in $CHCl_3$ are also concentration dependent between 0.75 mM and 0.022 mM, and have isosbestic points at 290 and 350 nm (Figure 1b). Assuming a monomer–dimer equilibrium, the binding constant K was obtained using a curve fitting method: $K = 985\ \text{M}^{-1}$ (Figure 1c).[12] The apparent molecular weight of (*P,P,P*)/(*P,P,P*)-**5** in $CHCl_3$ obtained by VPO analysis increases at concentrations from 0.5 to 11 mM (Figure 2). It is therefore concluded that (*P,P,P*)/(*P,P,P*)-**5** exhibits monomer–dimer equilibrium in $CHCl_3$.

The ^{1}H NMR ($CDCl_3$, 23 °C) resonance of the trimeric (*P,P,P*)/(*P,P,P*)/(*P,P,P*)-**6** broadened without any chemical shift change when the concentration was changed from 0.19 to 1.5 mM.[12] CD spectra ($CHCl_3$, 25 °C) also do not change between 0.0012 and 0.4 mM (Figure 1d). The molecular weight measured by VPO ($CHCl_3$, 35 °C) corresponds to the dimer for concentrations between 0.50 and 15 mM (Figure 2). Thus, in $CHCl_3$, (*P,P,P*)/(*P,P,P*)/(*P,P,P*)-**6** exhibits very strong bimolecular aggregation without forming higher aggregates.

These results show that the aggregation structure of di- and trimeric [3+3]cycloalkynes can be controlled by the structure of the linker moiety (Figure 3). A dimer (*P,P,P*)/(*P,P,P*)-**4** with a flexible linker forms a strong intramolecular aggregate, and a dimer (*P,P,P*)/(*P,P,P*)-**5** and a trimer (*P,P,P*)/(*P,P,P*)/(*P,P,P*)-**6** with rigid linkers form intermolecular aggregates. As was (*P,P,P*)-**1**, the oligomers exhibit a tendency to form an aggregate containing two [3+3]cycloalkynes without forming higher aggregates. The linker moiety can also affect the strength of the bimolecular aggregate as shown by the aggregates of (*P,P,P*)-**1**, (*P,P,P*)/(*P,P,P*)-**5**, and (*P,P,P*)/(*P,P,P*)/(*P,P,P*)-**6**: (*P,P,P*)-**1** is monomeric below 1 mM in $CHCl_3$ and forms a strong bimolecular aggregate at concentrations above 1 mM; (*P,P,P*)/(*P,P,P*)-**5** exhibits relatively weak monomer–dimer equilibrium; (*P,P,P*)/(*P,P,P*)/(*P,P,P*)-**6**

 © 2003 Wiley-VCH Verlag GmbH & Co. KGaA, Weinheim

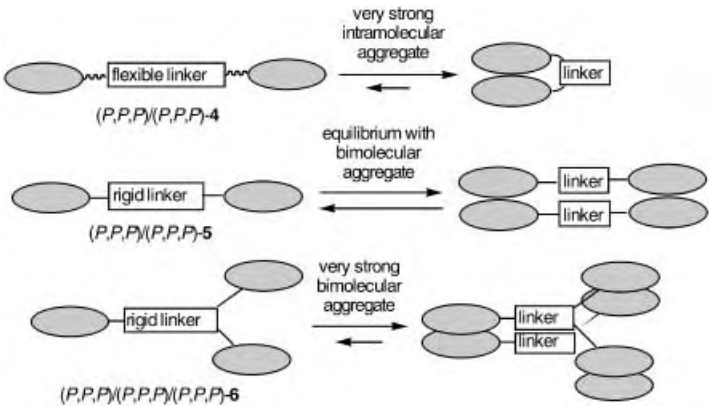


Figure 3. Aggregation behaviors of [3+3]cycloalkyne di- and trimers.

forms a very strong bimolecular aggregate without any indication of monomer or higher aggregate formation. Conformational matching of the nonplanar π-electron system of the [3+3]cycloalkyne moiety, that is, the fitting of the nonplanar π-electron system in the face-to-face π–π interactions,[7] may be important for the formation of these aggregates.

Received: January 31, 2003
Revised: July 21, 2003 [Z51735]

Keywords: aggregation · alkynes · helicenes · macrocycles · pi interactions

[1] Review; W. I. White in *The Porphyrins, Vol. 5* (Ed.: D. Dolphin), Academic Press, New York, **1978**, chap. 7. For recent examples in organic solvents see, S. Tamaru, S. Uchino, M. Takeuchi, M. Ikeda, T. Hatano, S. Shinkai, *Tetrahedron Lett.* **2002**, *43*, 3751; S. Tamaru, M. Nakamura, M. Takeuchi, S. Shinkai, *Org. Lett.* **2001**, *3*, 3631.

[2] For recent examples in organic solvents see, X. Huang, Y. Liu, S. Wang, S. Zhou, D. Zhu, *Chem. Eur. J.* **2002**, *8*, 4179; P. Samorí, H. Engelkamp, P. D. Witte, A. E. Rowan, R. J. M. Nolte, J. P. Rabe, *Angew. Chem.* **2001**, *113*, 2410; *Angew. Chem. Int. Ed.* **2001**, *40*, 2348.

[3] Recent examples, D. Zhao, J. S. Moore, *J. Org. Chem.* **2002**, *67*, 3548; S. Lahiri, J. L. Thompson, J. S. Moore, *J. Am. Chem. Soc.* **2000**, *122*, 11315; Y. Tobe, N. Utsumi, K. Kawabata, A. Nagano, K. Adachi, S. Araki, M. Sonoda, K. Hirose, K. Naemura, *J. Am. Chem. Soc.* **2002**, *124*, 5350. Certain macrocyclic alkynes were reported to self-aggregate strongly in aromatic solvents.

[4] R. F. Pasternack, S. Gurrieri, R. Lauceri, R. Purrello, *Inorg. Chim. Acta* **1996**, *246*, 7, and references therein. A bimolecular aggregate of a cyanine dye was formed selectively in the minor groove of a DNA template. M. Wang, G. L. Silva, B. A. Armitage, *J. Am. Chem. Soc.* **2000**, *122*, 9977.

[5] T. M. Cooper, M. O. Stone, *Langmuir* **1998**, *14*, 6662.

[6] N. Nakashima, R. Ando, H. Fukushima, T. Kunitake, *J. Chem. Soc. Chem. Commun.* **1982**, 707.

[7] K. Nakamura, H. Okubo, M. Yamaguchi, *Org. Lett.* **2001**, *3*, 1097.

[8] Morphology of a bolaamphiphile monolayer changes with the flexibility of the linker moiety. X. Wang, Y. Shen, Y. Pan, Y. Liang, *Langmuir* **2001**, *17*, 3162.

[9] The length of the linker moiety was reported to affect the intramolecular interaction of linked phthalocyanine dimers. C. C. Leznoff, H. Lam, S. M. Marcuccio, W. A. Nevin, P. Janda, N. Kobayashi, A. B. P. Lever, *J. Chem. Soc. Chem. Commun.* **1987**, 699, and references therein.

[10] Molecular tweezers possessing rigid spacers bind more strongly to guest molecules than those with flexible spacers. C. W. Chen, H. W. Whitlock, Jr., *J. Am. Chem. Soc.* **1978**, *100*, 4921; S. C. Zimmerman, C. M. VanZyl, G. S. Hamilton, *J. Am. Chem. Soc.* **1989**, *111*, 1373.

[11] S. Takano, T. Sugihara, K. Ogasawara, *Synlett* **1990**, 453.

[12] See Supporting Information.

[13] S. Zeena, K. G. Thomas, *J. Am. Chem. Soc.* **2001**, *123*, 7859; L. Lu, R. J. Lachicotte, T. L. Penner, J. Perlstein, D. G. Whitten, *J. Am. Chem. Soc.* **1999**, *121*, 8146; K. Liang, M. S. Farahat, J. Perlstein, K. Y. Law, D. G. Whitten, *J. Am. Chem. Soc.* **1997**, *119*, 830; O. V. Aguilera, D. C. Neckers, *Acc. Chem. Res.* **1989**, *22*, 171, and references therein.

 © 2003 Wiley-VCH Verlag GmbH & Co. KGaA, Weinheim

Biomineralization

Biomimetic Control of Size in the Polyamine-Directed Formation of Silica Nanospheres**

Manfred Sumper, Sonja Lorenz, and Eike Brunner*

The intricate silicified cell walls of diatoms are probably the most outstanding examples of nanoscale-structured materials in nature.[1] The degree of complexity in these hierarchically organized biominerals has never been matched in artificial materials.[2] Nanofabrication of silica in diatoms occurs under ambient conditions at slightly acidic pH values and results from specific interactions between biomolecules and silicic acid derivatives. Such biomolecules are the silaffin peptides and long-chain polyamines (both of which were isolated from diatom biosilica[3–5]) and the silicateins (isolated from sponges).[6] Silaffins isolated from *Cylindrotheca fusiformis* mainly consist of modified lysine and serine residues. The serine groups are phosphorylated and the lysine residues are

[*] Prof. Dr. M. Sumper
Lehrstuhl Biochemie I, Universität Regensburg
93053 Regensburg (Germany)
Fax: (+49) 941-943-2936
E-mail: manfred.sumper@vkl.uni-regensburg.de
S. Lorenz, Prof. Dr. E. Brunner
Institut für Biophysik und physikalische Biochemie
Universität Regensburg
93053 Regensburg (Germany)

[**] We thank R. Deutzmann and E. Hochmuth for MS analyses and R. Fischer for technical assistance. The present work was supported by the Deutsche Forschungsgemeinschaft (grants SFB 521A2 and -A6) and the Fonds der Chemischen Industrie.

Supporting information for this article is available on the WWW under http://www.angewandte.org or from the author.

 © 2003 Wiley-VCH Verlag GmbH & Co. KGaA, Weinheim DOI: 10.1002/anie.200352212

converted into three different derivatives: ε-*N*-dimethyllysine, phosphorylated ε-*N*-trimethyl-δ-hydroxylysine, and lysines covalently linked to long-chain polyamines, *N*-methylated derivatives of a polypropyleneimine.[7,8] Silaffins as well as long-chain polyamines have been shown to rapidly direct the formation of silica nanospheres from silicic acid in vitro[3,4] which has been confirmed[9] and adapted to technical applications.[10]

In the past, a huge amount of knowledge has been accumulated with respect to the inorganic chemistry of silicic acid and its polymeric derivatives.[11] Nonporous silica nanospheres could be synthesized by controlled hydrolysis of silicon alkoxides in methanol/NH_3 mixtures[12] and the underlying mechanism of size control has been investigated.[13,14] The past decade has seen important advances in the ability to fabricate porous solids and several methods have been developed for the synthesis of different silica morphologies summarized in recent reviews.[2,15,16] By applying this knowledge to the unique structure of silaffins, a fascinating aspect emerges: Nature has designed a molecule that is perfectly adapted to the chemistry of silica formation, as briefly outlined. Silicic acid polymerization involves three distinct stages. First, monomeric silicic acid polymerizes by condensation of silanol groups to form dimers, trimers, and cyclic oligomers. Oligosilicic acid species have a strong tendency to polymerize further in such a way that siloxane-bond (Si–O–Si) formation is maximized. These early processes create highly branched polysilicic acids as nuclei for silica formation. Second, the nuclei grow to form spherical particles either by continuous polymerization with monomeric and oligomeric silicic acids or by fusion of particles. Finally, the silica nanospheres can precipitate by flocculation, a process that intimately connects silica spheres and produces hard silica, as is found in the cell wall of diatoms. The structural elements found in silaffins are likely to be involved in each of these three stages, thereby accelerating the formation of hard silica by orders of magnitude. More than 40 years ago, quaternary ammonium ions were recognized as structure-directing agents in the synthesis of zeolite molecular sieves.[17] The tetramethylammonium cation favors the formation of symmetric oligosilicate anions such as the cubic octamer $Si_8O_{16}^{8-}$, and this control of silicate speciation influences the nucleation phase of silica formation.[18] Owing to their unique ε-*N*-trimethyl-δ-hydroxylysine residue, silaffins may exert a similar control. Polyamines were shown to catalyze the polycondensation of silanol groups[19] and are known to act as efficient flocculation agents.[11] Recently, an additional type of modification, a high degree of phosphorylation of silaffins, was shown to be essential for the formation of silica nanospheres in vitro.[7]

Herein, we define the function of phosphate anions in the polyamine-directed formation of silica nanospheres with the polyamines extracted from the cell wall of the diatom *Stephanopyxis turris* as a model. These polyamines consist of 15–21 *N*-methylpropyleneimine repeating units attached to putrescine. The polyamines were able to precipitate silica nanospheres from a silicic acid solution after a few minutes, even under acidic conditions that presumably represent the physiological situation[20] (approximately pH 5). After a short lag phase, silica started to precipitate (Figure 1a, blue line). However, this precipitation was strictly dependent on the presence of phosphate. In the presence of acetate anions only (the buffer system), no precipitate was formed at all (Figure 1a, green line). Silica precipitation in the presence of increasing phosphate concentrations produced nanospheres with increasing diameters (Figure 1b, red line). It is the particle size of the silica nanospheres that is strictly controlled by the concentration of phosphate anions. Defined particle diameters between 30 and 700 nm were obtained and the resulting size distributions were close to monodisperse. Replacement of orthophosphate by pyrophosphate, an anion

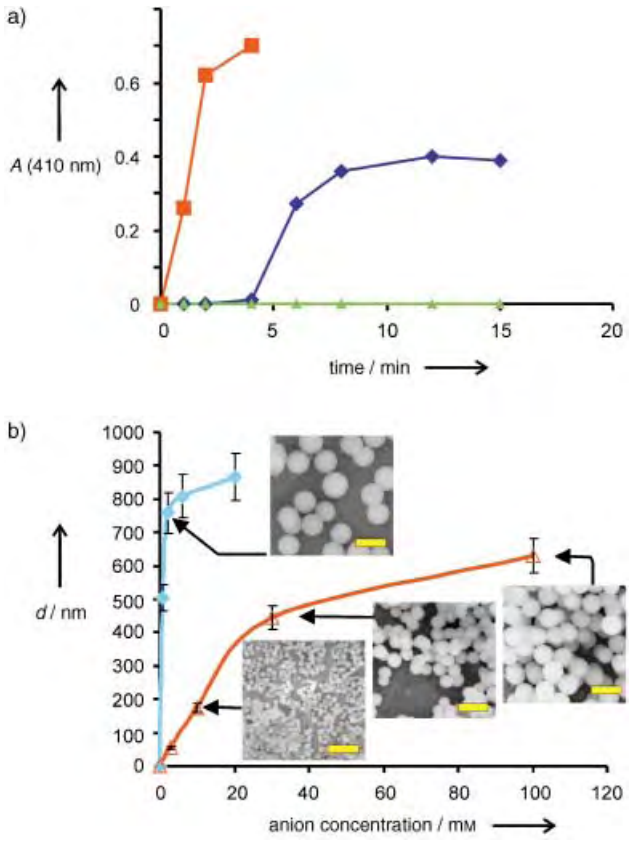


Figure 1. Characteristics of silica fabrication catalyzed by the polyamine/phosphate system. a) Kinetics of silica precipitation. The incubation mixture contained sodium phosphate (pH 5.5; 30 mM), polyamine (0.2 mM), and mono-/disilicic acid (40 mM) at 25 °C. After the times indicated, aliquots (50 μL) were removed and centrifuged. Precipitated silica was dissolved in NaOH (2 M; 5 min at 90 °C) and quantified by the molybdate method.[11] An absorbance of 1.0 corresponded to 0.5 μmol SiO_2. Blue line: All components were mixed at $t = 0$ min. Green line: Phosphate was replaced by sodium acetate (pH 5.5; 30 mM). Red line: Silicic acid was preincubated for 15 min in sodium phosphate (pH 5.5; 30 mM) and polyamine was added at $t = 0$ min. b) Silica nanosphere diameters as a function of the multivalent anion concentration. Silica fabrication was performed in a sodium acetate buffer (pH 5.5; 30 mM) as in part a) with increasing concentrations of multivalent anions. The reaction was allowed to proceed for 12 min. The resulting nanospheres were collected by centrifugation and analyzed by SEM. Response to orthophosphate and pyrophosphate is shown by the red and the blue lines, respectively. Insets: SEM micrographs of the corresponding precipitates. Scale bars: 1000 nm.

 © 2003 Wiley-VCH Verlag GmbH & Co. KGaA, Weinheim

with a higher negative charge, gave rise to a drastic effect. Control of nanosphere size distribution was exerted at anion concentrations nearly two orders of magnitude lower and the maximum sphere diameter was increased to about 1000 nm (Figure 1b, blue line). Importantly, other multivalent anions can produce silicate precipitates as well, whereas monovalent anions such as chloride or acetate ions fail to do so. In particular, we have tested sulfate ions and polyvalent anions such as DNA and sodium dodecyl sulfate (see Supporting Information). The shape of the precipitates formed in the presence of the latter anions, however, is strongly different from the spherical nanoparticles obtained in the presence of phosphate ions.

Long-chain polyamines from diatom biosilica behave like amphiphilic substances. They are extractable from an aqueous solution by chloroform/methanol (3:2 v/v). Possibly, these polyamines form aggregates in aqueous solution (microemulsions) with positively charged surfaces. If so, multivalent anions should promote higher-order assemblies of the emulsion droplets. This possibility was investigated by NMR spectroscopy and dynamic light scattering techniques. The pronounced influence of phosphate ions on the ^{1}H NMR spectrum of polyamines from *S. turris* is demonstrated in Figure 2a. In the presence of phosphate (top trace), the ^{1}H nuclei attached to the repeating unit give rise to three signals A, B, and C. In the absence of phosphate, these signals split into two or more components (bottom trace). Evidently, the polyamine molecules exist in different states in the absence of phosphate, whereas a unique state is observed for the phosphate-containing sample. Furthermore, the ^{1}H NMR chemical shifts of the signals, except for C1 and C2, strongly depend on the type and concentration of the anions added, as shown for signal A1 (Figure 2b). Pyrophosphate (PPi) ions influenced the ^{1}H NMR chemical shifts much more strongly than orthophosphate (Pi). In contrast to the polyamines from *S. turris*, short-chain amines such as spermine did not exhibit corresponding phosphate-induced chemical shifts. The linewidths of the signals A and B strongly exceed those of lines C, C1, and C2 (Figure 2a).

Carr–Purcell–Meiboom–Gill (CPMG) experiments[21,22] demonstrated a relaxation rate of only 6 s^{-1} for lines C, C1, and C2, whereas T_2^{-1} amounts to 36 s^{-1} and 47 s^{-1} for lines A and B, respectively. An estimation of the methylene ^{1}H relaxation rate[23] expected for a single and globular polyamine molecule of 1.55 kDa molecular weight dissolved in water yields a value of about 3 s^{-1} only. Although the assumption of a globular shape for the polyamine molecules may only be a rough approximation, the discrepancy between the estimated value and the values observed for methylene ^{1}H (lines A and B) is surprisingly large. Aggregation of the polyamine molecules is a reasonable explanation for this observation. However, neither T_2^{-1} nor the diffusion coefficient were found to depend on the phosphate concentration. We therefore assume that the polyamine molecules dissolved in water form a microemulsion even in the absence of phosphate ions. If so, phosphate ions could attract the preformed droplets to build larger, loosely bound assemblies. The viscosity within the polyamine droplets are expected to be different from that of water and determines T_2^{-1}, independent of the phosphate concentration. According to this model, the diffusion coefficient of the polyamine molecules is determined by the diffusion within the droplets, independent of the phosphate concentration, as was observed experimentally (see above). In summary, we conclude that the polyamines from *S. turris* form aggregates under the solution conditions described. The addition of phosphate results in the formation of larger assemblies by the attraction of such preformed droplets. This concept could be confirmed by ^{31}P NMR spectroscopy on the phosphate-containing samples (see Supporting Information) and by dynamic light scattering experiments performed on phosphate-free and phosphate-containing polyamine solutions.

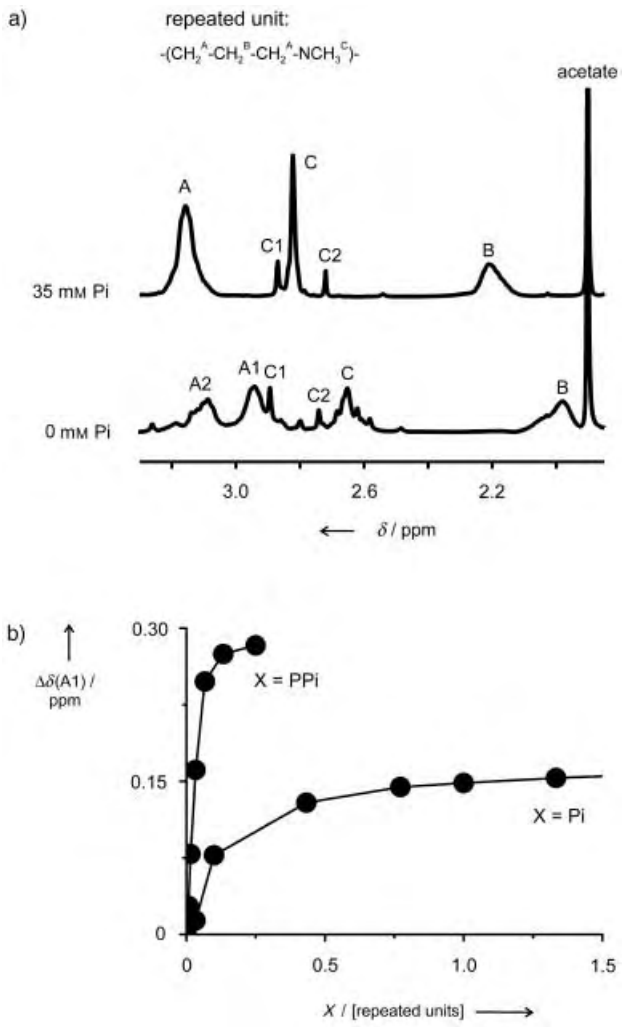


Figure 2. ^{1}H NMR spectra of polyamines from *S. turris*. a) Spectrum of a solution of polyamine (pH 6.3; 3 mM). Top: sodium phosphate (35 mM), bottom: phosphate-free sample. The assignment of the signals is indicated in the formula of the repeating unit. The small signals C1 and C2 were assigned to the methyl groups at the termini of the molecule. Note that the samples usually contained residual amounts of acetate from the purification procedure. b) Phosphate-induced chemical shift ($\Delta\delta$(A1)) of line A1 defined as the chemical shift difference between the phosphate-containing and the phosphate-free sample.

 © 2003 Wiley-VCH Verlag GmbH & Co. KGaA, Weinheim

Phosphate-induced assembly of polyamines appears to be a prerequisite for silica formation, but the mechanism is unclear. Therefore, some of the partial reactions of silica formation were analyzed separately. First, the kinetics of monosilicic acid polymerization in the physiologically relevant pH range was determined in the absence or presence of *S. turris* polyamines. Monosilicic acid was easily determined by gas chromatography after conversion into the corresponding trimethylsilyl derivative.[18] Unexpectedly, the rate of monosilicic acid polymerization was not affected at all by the addition of *S. turris* polyamines, which contain tertiary amino groups exclusively (see Supporting Information). This observation is contrary to the catalytic action found for synthetic polyamines that contain secondary amino groups.[19] However, as the formation of silica nanospheres strictly depends on the presence of both *S. turris* polyamines and phosphate, we conclude that it is the condensation of oligo-/polysilicic acids that depends on the presence of polyamines and phosphate. If so, the lag phase observed in a silica precipitation experiment (Figure 1a, blue line) would represent the period required for the spontaneous polymerization of monosilicic acid. Only after the production of sufficient amounts of polymeric material, are these species further cross-linked by the action of the polyamine/phosphate system. Indeed, the lag phase was completely eliminated after the monosilicic acid solution had been preincubated for 15 min (Figure 1a, red line). Monosilicic acid ($pK_a = 9.7$) is an uncharged molecule under acidic conditions and therefore is unlikely to interact with polyamines. Only the much more acidic polysilicic acids are expected to interact with polyamine droplets through ionic interactions as well as through numerous hydrogen bonds with polyamine droplets. These interactions result in polysilicic acids becoming highly concentrated and they are therefore able to polycondensate to silica. By scanning electron microscopy (SEM) we also followed the time dependence of polyamine/phosphate-induced silica nanosphere formation in vitro (see Supporting Information).

These model studies define a cooperative function of polyamines and multivalent anions in the production of silica. In silaffins, nature has elegantly combined both structural elements in a single molecule. Self-assembly of phosphorylated silaffins has previously been documented.[7] Notably, nonphosphorylated silaffins are only capable of precipitating silica in vitro if phosphate or other polyvalent anions are added to the solutions. This behavior is in line with the observations reported herein: Silica precipitation is only triggered if phosphate or other polyvalent anions are added to solutions that contain polyamines and silica precursors. At the present time, however, we have no experimental information about the nature of the polyvalent anion acting in vivo in the polyamine-directed silica formation in *S. turris* cells.

Received: June 24, 2003
Revised: July 24, 2003 [Z52212]

Keywords: biomimetic synthesis · diatoms · nanostructures · polyamines · silica

[1] F. Round, R. Crawford, D. Mann, *The Diatoms*, Cambridge University Press, Cambridge, **1990**.
[2] S. Mann, *Angew. Chem.* **2000**, *112*, 3532–3548; *Angew. Chem. Int. Ed.* **2000**, *39*, 3392–3406.
[3] N. Kröger, R. Deutzmann, C. Bergsdorf, M. Sumper, *Proc. Natl. Acad. Sci. USA* **2000**, *97*, 14133–14138.
[4] N. Kröger, R. Deutzmann, M. Sumper, *Science* **1999**, *286*, 1129–1132.
[5] M. Sumper, *Science* **2002**, *295*, 2430–2433.
[6] K. Shimizu, J. Cha, G. D. Stucky, D. E. Morse, *Proc. Natl. Acad. Sci. USA* **1998**, *95*, 6234–6238.
[7] N. Kröger, S. Lorenz, E. Brunner, M. Sumper, *Science* **2002**, *298*, 584–586.
[8] N. Kröger, R. Deutzmann, M. Sumper, *J. Biol. Chem.* **2001**, *276*, 26066–26070.
[9] S. V. Patwardhan, S. J. Clarson, *Silicon Chem.* **2002**, *1*, 207–214.
[10] L. L. Brott, D. J. Pikas, R. R. Naik, S. M. Kirkpatrick, D. W. Tomlin, P. W. Whitlock, S. J. Clarson, M. O. Stone, *Nature* **2001**, *413*, 291–293.
[11] R. K. Iler, *The Chemistry of Silica*, Wiley, New York, **1979**.
[12] W. Stöber, A. Fink, E. Bohn, *J. Colloid Interface Sci.* **1968**, *26*, 62–69.
[13] S. Kim, C. F. Zukoski, *J. Colloid Interface Sci.* **1990**, *139*, 198–212.
[14] A. v. Blaaderen, J. v. Geest, A. Vrij, *J. Colloid Interface Sci.* **1992**, *154*, 481–501.
[15] M. E. Davis, *Nature* **2002**, *417*, 813–821.
[16] K. J. C. v. Bommel, A. Friggeri, S. Shinkai, *Angew. Chem.* **2003**, *115*, 1010–1030; *Angew. Chem. Int. Ed.* **2003**, *42*, 980–999.
[17] R. M. Barrer, P. J. Denny, *J. Chem. Soc.* **1961**, 971–982.
[18] D. Hoebbel, G. Garzo, G. Engelhardt, R. Ebert, E. Lippmaa, M. Alla, *Z. Anorg. Allg. Chem.* **1980**, *465*, 15–33.
[19] T. Mitzutani, H. Nagase, N. Fujiwara, H. Ogoshi, *Bull. Chem. Soc. Jpn.* **1998**, *71*, 2017–2022.
[20] E. G. Vrieling, W. W. C. Gieskes, T. P. M. Beelen, *J. Phycol.* **1999**, *35*, 548–559.
[21] H. Y. Carr, E. M. Purcell, *Phys. Rev.* **1954**, *94*, 630–638.
[22] S. Meiboom, D. Gill, *Rev. Sci. Instrum.* **1958**, *29*, 688–691.
[23] J. Cavanagh, W. J. Fairbrother, A. G. Palmer III, N. J. Skelton, *Protein NMR Spectroscopy*, Academic Press, San Diego, CA, **1996**.

 © 2003 Wiley-VCH Verlag GmbH & Co. KGaA, Weinheim

Syngas Production

Conversion of Methane to Syngas by a Membrane-Based Oxidation–Reforming Process**

Chu-sheng Chen, Shao-jie Feng, Shen Ran, De-chun Zhu, Wei Liu, and Henny J. M. Bouwmeester*

Rational use of abundant natural gas is gaining importance as petroleum oil reserves are diminishing. Methane, the main component of natural gas, can be converted to liquid fuels, hydrogen, and other value-added chemicals through a syngas intermediate, a mixture of CO and H_2. Currently, syngas is produced by reacting methane with steam at high temperatures and pressures. This process is very energy- and capital-intensive, as the reaction is highly endothermic. An alternative process to produce syngas is the partial oxidation of methane (POM) with pure oxygen in the presence of a catalyst.[1,2] The exothermic nature of POM makes the process attractive in terms of energy consumption. The other advantage of POM over the steam-reforming process is that the H_2/CO ratio of ~2 of the as-produced syngas is highly suitable for subsequent conversion to environmentally friendly liquid fuels through a Fischer–Tropsch process. The main difficulty with POM lies in the consumption of large quantities of expensive pure oxygen that is produced by the cryogenic separation of air. A recent development in syngas production technology is the use of oxygen-permeable dense ceramic membranes[3,4] integrating the oxygen separation and POM processes in a single space.[5] The formidable problem for this approach is that the membrane must be chemically and mechanically stable at elevated temperatures in a large oxygen gradient with one side of the membrane exposed to oxidizing atmosphere (air) and the other side to the reducing atmosphere (the mixture of hydrogen and carbon monoxide). Herein we propose a two-stage membrane reactor, as depicted in Figure 1a, which may reduce the requirement on the stability of the membrane materials. In this reactor, part of the methane is converted into CO_2 and H_2O by reaction with oxygen permeated through the membrane from the air, and the resultant mixture is transferred to a catalyst bed where the remaining methane is reformed to syngas.

[*] Prof. C.-s. Chen, S.-j. Feng, Dr. S. Ran, D.-c. Zhu, Prof. W. Liu
Laboratory of Advanced Functional Materials and Devices
Department of Materials Science and Engineering
University of Science and Technology of China
Hefei, Anhui 230026 (P. R. China)
Fax: (+86) 551-3601-592
E-mail: ccsm@ustc.edu.cn
Dr. H. J. M. Bouwmeester
Laboratory of Inorganic Materials Science
Faculty of Science & Technology and
MESA+ Research Institute
University of Twente
P.O. Box 217, 7500 AE, Enschede (The Netherlands)

[**] This work was supported by the National Natural Science Foundation of China [50225208].

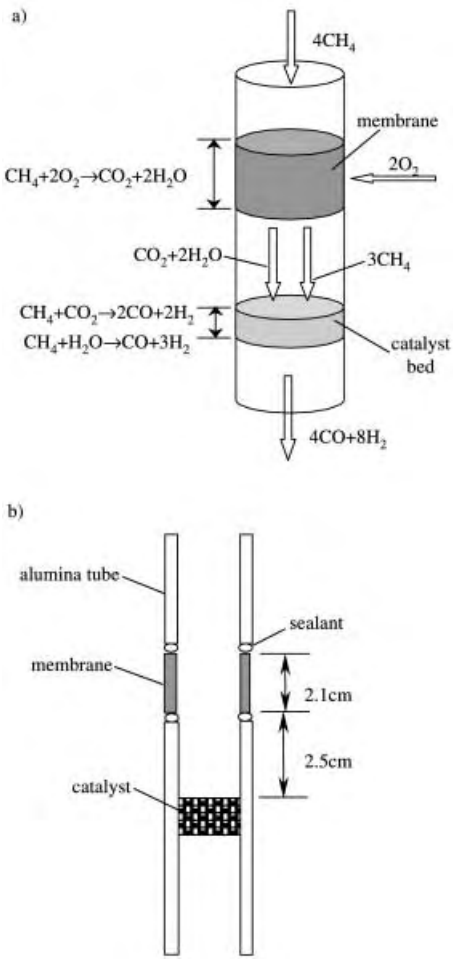


Figure 1. Schematic diagrams of two-stage oxygen-permeable membrane reactor for syngas production. a) The chemical conversions in different areas of the membrane reactor; b) the construction and dimensions of the reactor.

A ceramic composite of $Ba_{0.5}Sr_{0.5}Co_{0.8}Fe_{0.2}O_{3-\delta}$ (97.5 mol %) and Co_3O_4 (2.5 mol %) was used to construct a membrane reactor. The major phase of the composite was intended for separating oxygen from air[6] and the minor phase at the surface for catalyzing the reaction of methane with permeated oxygen;[7] in terms of mechanics, small cobalt oxide particles embedded in the bulk may also reinforce the major phase. The dense tubular membrane of the required phase composition was prepared by extrusion followed by sintering at 1100 °C for 10 h. A γ-Al_2O_3-supported catalyst was prepared with a nickel loading of 12.5 wt % and sieved to 40 ~ 60 mesh.[8] The reactor consisted of a membrane of length 2.14 cm, inner diameter 0.76 cm (membrane surface area 5.10 cm^2), and wall thickness 0.13 cm, and a catalyst bed containing 0.2 g Ni/γ-Al_2O_3; the membrane tube and the catalyst bed were separated by a distance of 2.5 cm (see Figure 1b). In order to improve the flow pattern in the reactor, an alumina cylinder was placed inside the reactor (not shown in Figure 1b for the sake of simplicity). The reactor was sealed with glass rings at 950 °C then cooled to 900 °C and maintained at that temperature. Pure methane was fed into the tubular reactor while air was simultaneously led

 © 2003 Wiley-VCH Verlag GmbH & Co. KGaA, Weinheim DOI: 10.1002/anie.200351085

over the shell side. The effluent was analyzed by on-line gas chromatography (Varian 3400), in which H_2, O_2, N_2, CH_4, and CO were separated by a 5-Å molecular sieve column and CO_2 by GDX-502 column, and H_2O was determined with a hydrogen atomic balance.

The performance of the reactor is shown in Figure 2. It can be seen that after a short activating period of about one hour, both the methane conversion and CO selectivity exceed 95%.

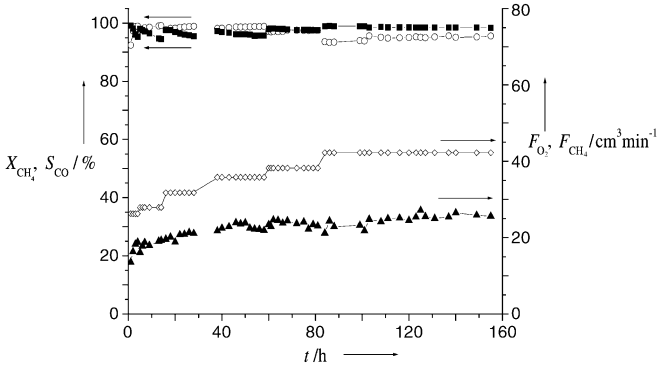


Figure 2. Methane conversion (X_{CH_4}, ○) and CO selectivity (S_{CO}, ■), and methane feeding rate (F_{CH_4}, ◇) and O_2 permeation rate (F_{O_2}, ▲) in a membrane reactor. Conditions: $T = 900\,°C$; $p = 1$ atm; membrane surface area = 5.1 cm^2.

The CO selectivity does not change very much with variation of the methane feeding rate. The throughput conversion of methane decreases slightly with increasing methane feeding rate. When methane was fed at a rate of ~38 cm^{3}min^{-1}, the reactor attained a desirable state: syngas production rate ~20 cm^{3}cm^{-2} membrane surface min^{-1}, equivalent O_2 permeation flux ~4.6 cm^{3}cm^{-2}min, H_2/CO ~1.8, CO selectivity ~98%, methane throughput conversion ~97%. After the reactor had been operated at 900 °C for ~400 h, the experiment was voluntarily terminated, and the membrane remained almost intact.

In order to establish the reaction pathways we performed experiments with blank tubular reactors in which the Ni/γ-Al_2O_3 catalyst was either simply left out or replaced with γ-Al_2O_3 powder. For the former configuration comprising a tubular membrane with an inner surface area of 4.32 cm^2, when methane was fed into the reactor at a rate of 19.4 cm^{3}min^{-1} at 900 °C, the effluent was found to contain a large quantity of CO_2 (15.3%), H_2O (35.1%), and unreacted CH_4 (52.9%) as well as small amounts of CO (1.2%), H_2 (1.8%),C_2H_4 (1.8%), C_2H_6 (0.4%), O_2 (0.03%), and N_2 (0.2%). For the latter configuration comprising a tubular membrane with a surface area of 4.58 cm^2, the dominant components in the effluent remained to be CO_2 (14.6%), H_2O (34.0%), and CH_4 (45.3%). Similar results were reported by Balachandran et al. who found that in an $SrFeCo_{0.5}O_x$ tubular membrane reactor (membrane surface area 8 cm^2) in the absence of a reforming catalyst, the permeated oxygen reacted with methane, yielding CO_2 and H_2O.[5] The presence of CO_2, H_2O, CH_4, and O_2 were also reported by Tsai et al. in the effluent of an $La_{0.2}Ba_{0.8}Fe_{0.8}Co_{0.2}O_{3-\delta}$ disk-shaped membrane reactor (membrane surface area 0.28 cm^2) without a catalyst.[9] All these observations combined allow us to establish the reaction pathways for syngas formation in the two-stage reactor. At one side of the membrane, which is in contact with air, oxygen molecules are incorporated as oxide ions into the bulk of the membrane. At the other side of the membrane, methane molecules adsorb and partly react with the permeated oxide ions to yield CO_2 and H_2O, a reaction catalyzed by the Co_3O_4 embedded in the membrane. The mixture of unreacted methane, CO_2, and H_2O is then transferred to the Ni/γ-Al_2O_3 catalyst bed and converted into syngas.

The membrane-based two-stage reactor has a number of important features. The two-stage configuration poses less stringent limitations on membrane materials than the reactor in which the catalyst is located inside the membrane.[5] In the former case, where the membrane is exposed to the mixture of CO_2, H_2O, and CH_4, the oxygen partial pressure p_{O_2} is calculated to be 10^{-13}–10^{-14} bar based on the thermodynamic data for the reaction $CO + \frac{1}{2}O_2 \Leftrightarrow CO_2$.[10] In the real situation, the oxygen partial pressure is higher and a small amount of oxygen is present in the effluent, indicating that the reaction does not attain the equilibrium state. In the latter case, where the catalyst is within the membrane and the membrane is in contact with H_2 and CO, the p_{O_2} is around 10^{-19} bar.[11] The formation of coke on the catalyst in the two-stage reactor is also much less severe than that in the single-stage reactor in which the reforming catalyst is in intimate contact with the membrane. In terms of the strategy of developing and operating the membrane reactor, the two-stage configuration allows us to distribute the overall risk among the two separate components. Such a configuration is also ideal in terms of energy consumption, for the heat released by the deep oxidation of part of the methane at the membrane stage of reactor is supplied to the catalyst bed where endothermic reforming reactions take place. The as-produced syngas is desirable for applications, because it contains no nitrogen and has a lower H_2/CO ratio than that obtained by the regular steam reforming. The emission of NO_x is eliminated due to the use of an oxygen-permeable membrane that is impervious to nitrogen. Although the membrane-based two-stage reactor shows promise for applications, technical challenges remain in identification of membrane materials with long-term mechanical and chemical stabilities, development of reactor fabrication techniques, and scale-up of the reactors to industrial modules.

Received: February 3, 2003
Revised: July 25, 2003 [Z51085]

Keywords: ceramics · membranes · methane · oxygen · syngas

[1] A. T. Ashcroft, A. K. Cheetham, J. S. Foord, M. L. H. Green, C. P. Grey, A. J. Murrell, P. D. F. Vernon, *Nature* **1990**, *344*, 319–321.
[2] D. A. Hickman, L. D. Schmidt, *Science* **1993**, *259*, 343–346.
[3] Y. Teraoka, H. M. Zhang, S. Furukawa, N. Yamazoe, *Chem. Lett.* **1985**, 1743–1746.
[4] C. S. Chen, S. Ran, W. Liu, P. H. Yang, D. K. Peng, H. J. M. Bouwmeester, *Angew. Chem.* **2001**, *113*, 806–808; *Angew. Chem. Int. Ed.* **2001**, *40*, 784–786.

 © 2003 Wiley-VCH Verlag GmbH & Co. KGaA, Weinheim

[5] U. Balachandran, J. T. Dusek, P. S. Maiya, B. Ma, R. L. Mieville, M. S. Kleefisch, C. A. Udovich, *Catal. Today* **1997**, *36*, 265 – 272.
[6] Z. P. Shao, W. S. Yang, Y. Cong, H. Dong, J. H. Tong, G. X. Xiong, *J. Membr. Sci.* **2000**, 172, 177 – 188.
[7] V. G. Milt, M. A. Ulla, E. A. Lombardo, *Catal. Lett.* **2000**, 65, 67 – 73.
[8] D. Dissanayake, M. P. Rosynek, K. C. C. Kharas, J. H. Lunsford, *J. Catal.* **1991**, *132*, 117 – 127.
[9] C. Y. Tsai, A. G. Dixon, Y. H. Ma, W. R. Moser, M. R. Pascucci, *J. Am. Ceram. Soc.* **1998**, *81*, 1437 – 1444.
[10] R. C. Weast, M.J. Astle, *CRC Handbook of Chemistry and Physics*, CRC, Boca Raton, FL, **1981**.
[11] P. V. Hendriksen, P. H. Larsen, M. Morgensen, F. W. Poulsen, K. Wiik, *Catal. Today* **2000**, *56*, 283 – 295.

 © 2003 Wiley-VCH Verlag GmbH & Co. KGaA, Weinheim

Glycal Cyclization

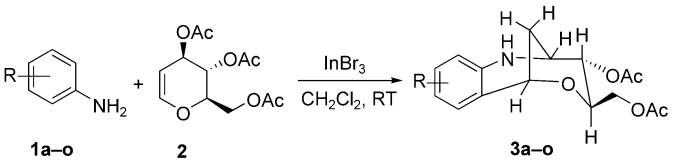
$InBr_3$-Catalyzed Cyclization of Glycals with Aryl Amines**

Jhillu S. Yadav, Basi V. S. Reddy, Katta V. Rao, Kavuda Saritha Raj, Atlaluri R. Prasad, Singarapu Kiran Kumar, Ajit C. Kunwar, Panjula Jayaprakash, and Bulusu Jagannath*

Dedicated to Professor Goverdhan Mehta on the occasion of his 60th birthday

Glycals are ambident electrophiles capable of reacting with various nucleophiles such as alcohols, malonates, and silyl nucleophiles under the influence of acid catalysts or oxidants to produce 2,3-unsaturated glycosides.[1,2] In recent times, indium halides have emerged as versatile Lewis acid catalysts imparting high regio-, chemo-, and diastereoselectivity to a variety of organic transformations.[3] Compared to conventional Lewis acids, indium tribromide, in particular, has advantages of low catalyst loading, moisture stability, and catalyst recycling.[4] C-Glycosides bearing carbon-linked heterocycles have attracted great attention owing to their potent antiviral and antitumor behavior.[5] Because of these properties of aryl glycosides, we have attempted C-glycosidation with aryl amines to synthesize aryl C-glycosides with a free amino functionality for further derivatization. Interestingly, we observed for the first time an unusual formation of benzo-fused heterobicycles in the aminoglycosidation.

In our continuing research on glycoside synthesis,[6] we have made unprecedented observations in the aminoglycosidation reactions of glycals with aryl amines, which we report here. Initially, we attempted the aminoglycosidation reaction of D-glucal with aniline using 10 mol% indium(III) bromide as a novel glycosyl activator. Interestingly, the unusual bicyclic adduct **3a** (R = H) was isolated in 85% yield with high stereoselectivity (Scheme 1).



Scheme 1. Reaction of 3,4,6-tri-*O*-acetyl-D-glucal (**2**) with aryl amines.

The product **3a** was characterized thoroughly by various NMR experiments including double-quantum-filtered correlation spectroscopy (DQFCOSY), nuclear Overhauser effect spectroscopy (NOESY), heteronuclear single-quantum correlation spectroscopy (HSQC),[7] and $^3J_{CH}$-optimized HMBC experiments.[8] The edited HSQC spectrum showed the presence of two methylene groups in addition to eight methine and two methyl groups. The location of the methylene group in the bridge of a bicyclononene-like structure was confirmed by the presence of small couplings between these protons and the bridgehead protons H1 and H3 ($J_{H1\text{-}H2(pro\text{-}S)} = 3.7$ Hz, $J_{H1\text{-}H2(pro\text{-}R)} = 1.8$ Hz, $J_{H2(pro\text{-}S)\text{-}H3} = 2.4$ Hz, and $J_{H2(pro\text{-}R)\text{-}H3} = 4.6$ Hz; Figure 1)). Fusion of the bicyclononene and the aromatic ring at C1–C11 and NH–C3 was confirmed by nOe interactions between H1 and H12. Further support for the structure came from HMBC peaks for H1/C12, H1/C11, H1/C16 and H12/C1. The two six-membered rings of the bicyclononane moiety have two different conformations. The one containing oxygen takes a chair form,

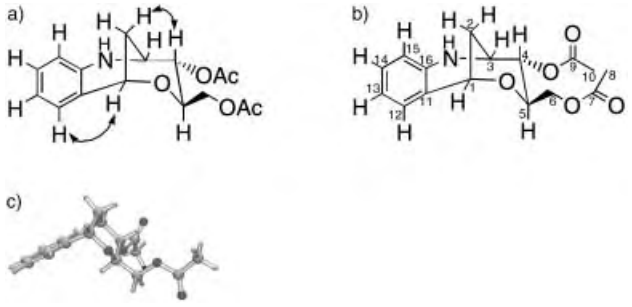


Figure 1. a) Characteristic nOe interactions, b) the chemical structure, and c) the energy-minimized structure of **3a**.

[*] Dr. J. S. Yadav, Dr. B. V. S. Reddy, K. V. Rao, K. Saritha Raj, Dr. A. R. Prasad
Division of Organic Chemistry
Indian Institute of Chemical Technology
Hyderabad-500 007 (India)
Fax: (+91) 40-2716-0512
E-mail: yadav@iict.ap.nic.in
S. Kiran Kumar, Dr. A. C. Kunwar
Centre for Nuclear Magnetic Resonance
Indian Institute of Chemical Technology
Hyderabad-500 007 (India)
P. Jayaprakash, Dr. B. Jagannath
Molecular Modelling and Drug Design
Indian Institute of Chemical Technology
Hyderabad-500 007 (India)

[**] B.V.S.R., K.V.R., K.S.R., and S.K.K. thank the Council of Scientic and Industrial Research (CSIR), New Delhi, for the award of fellowships.

Supporting information for this article is available on the WWW under http://www.angewandte.org or from the author.

 © 2003 Wiley-VCH Verlag GmbH & Co. KGaA, Weinheim DOI: 10.1002/anie.200351267

whereas the other ring with nitrogen and fused to the aromatic ring exists in half-chair form. HMBC peaks for $H2_{(pro\text{-}S)}$/C11 and $H2_{(pro\text{-}R)}$/C4 are consistent with this structure. The large coupling constant $J_{H4\text{-}H5} = 10.4$ Hz and the NOESY cross peak for $H2_{(pro\text{-}S)}$/H4 further support the chair form for the ring containing these protons. The ring current of the aromatic ring causes high-field chemical shifts for $H2_{(pro\text{-}R)}$ ($\delta = 1.96$ ppm) and H5 ($\delta = 3.58$ ppm). Further the structure of **3a** was confirmed by molecular mechanics calculations.[9]

These unexpected results encouraged us to extend this process to other glycals and aryl amines. Interestingly, α-naphthylamine and substituted aryl amines such as electron-rich as well as electron-deficient aniline derivatives reacted efficiently with D-glucal under similar conditions to produce the corresponding cyclic adducts in fairly good yields (Table 1). Similarly, L-rhamnal also underwent cyclization with aryl amines to produce derivatives **3p** and **3q**. Under similar reaction conditions D-xylal also underwent cyclization with aryl amines to afford the corresponding cyclic adducts **3r** and **3s**.

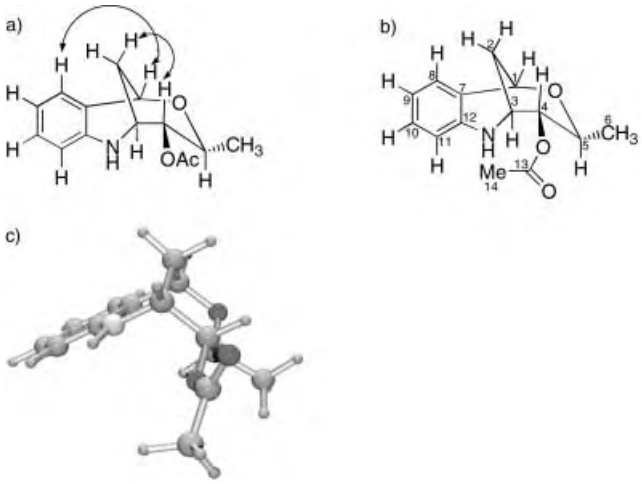


Figure 2. Characteristic nOe interactions, the chemical structure, and the energy-minimized structure of **3p**.

Table 1: Synthesis of oxaazatricyclotridecatrienyl derivatives from D-glucal and aryl amines (see Scheme 1).

Glucal	Amine	Product[a]	$InBr_3$ (10 mol%)		TMSOTf (1 equiv)	
			t [h]	Yield [%][b]	*t* [h]	Yield [%][b]
D-glucal	$C_6H_5NH_2$ (**1a**)	**3a**	6.0	85	3.5	87
D-glucal	2-$MeC_6H_4NH_2$ (**1b**)	**3b**	5.5	82	4.0	85
D-glucal	4-$FC_6H_4NH_2$ (**1c**)	**3c**	7.0	78	5.0	81
D-glucal	4-$ClC_6H_4NH_2$ (**1d**)	**3d**	6.0	84	4.5	85
D-glucal	2-Br-4-Me-$C_6H_3NH_2$ (**1e**)	**3e**	8.0	75	6.0	82
D-glucal	α-naphthylamine (**1f**)	**3f**	9.0	80	5.0	75
D-glucal	4-Br-$C_6H_4NH_2$ (**1g**)	**3g**	7.5	82	4.5	84
D-glucal	4-MeO-$C_6H_4NH_2$ (**1h**)	**3h**	7.0	78	4.0	78
D-glucal	2-Cl-$C_6H_4NH_2$ (**1i**)	**3i**	6.0	80	5.0	83
D-glucal	4-$MeC_6H_4NH_2$ (**1j**)	**3j**	5.5	85	4.5	89
D-glucal	3-Cl-$C_6H_4NH_2$ (**1k**)	**3k**	6.0	80[c]	5.0	82[c]
D-glucal	2,5-$(CH_3)_2$-$C_6H_3NH_2$ (**1l**)	**3l**	5.0	83	4.5	85
D-glucal	2,6-$(CH_3)_2$-$C_6H_3NH_2$ (**1m**)	**3m**	8.0	n.r.[d]	6.0	n.r.[d]
D-glucal	3-Cl-4-F-$C_6H_3NH_2$ (**1n**)	**3n**	7.0	77	6.0	78
D-glucal	2,4-Cl_2-$C_6H_3NH_2$ (**1o**)	**3o**	6.0	79	5.0	81
L-rhamnal	$C_6H_5NH_2$ (**1a**)	**3p**	5.0	87	5.0	85
L-rhamnal	4-$MeC_6H_4NH_2$ (**1j**)	**3q**	4.5	82	4.0	84
D-xylal	$C_6H_5NH_2$ (**1a**)	**3r**	6.0	89	3.5	82
D-xylal	4-$MeC_6H_4NH_2$ (**1j**)	**3s**	5.0	85	4.0	80

[a] Products were characterized by ^1H NMR, ^{13}C NMR, IR spectroscopy and mass spectrometry. [b] Yield refers to pure products after chromatography. [c] Ratio of regioisomers 7:3. [d] No reaction.

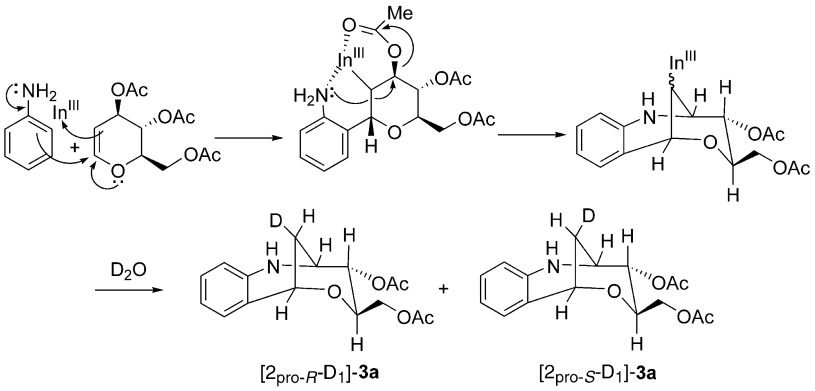
The conformation of product **3p** was similar to that of **3a** (Figure 2). The appearance of small coupling constants, $J_{H1\text{-}H2(pro\text{-}R)} = 3.6$ Hz, $J_{H1\text{-}H2(pro\text{-}S)} = 1.9$ Hz, $J_{H2(pro\text{-}R)\text{-}H3} = 2.6$ Hz, and $J_{H2(pro\text{-}S)\text{-}H3} = 4.4$ Hz, indicates that the observed conformation is like bicyclononene, with the middle six-membered ring in a half-chair conformation. The nOe cross peak for H1/H8, and $H2_{(pro\text{-}R)}$/H4 as well as coupling constant $J_{H4\text{-}H5} = 10.1$ Hz confirms that the six-membered ring is in a chair conformation.

To elucidate the mechanistic pathway, we carried out the reaction with deuterated aniline and 3,4,6-tri-*O*-acetyl-D-glucal (**2**), but no deuterium incorporation was observed in the product. However, the reaction of aniline and **2** in D_2O at 80 °C gave the isomeric deuterated products [$2_{pro\text{-}R}$-D_1]-**3a** and [$2_{pro\text{-}S}$-D_1]-**3a** in equal amounts, which was confirmed by ^1H NMR and FAB mass spectroscopy.[10] This clearly indicates that protons were abstracted from the solvent and not from aniline.

We also found that **2** does not react with 2,6-dimethylaniline (Table 1), which clearly indicates that one of the *ortho* positions of aniline should be free from substitution for the success of the reaction. Accordingly, a plausible mechanism for the formation of product **3** may be depicted[11] as in Scheme 2.

Although further study is needed to settle the reaction mechanism, this method is a highly stereoselective, one-pot synthesis of unusual tricyclic heterocycles under mild conditions. The efficacy of various Lewis acids such as $InBr_3$, $InCl_3$, $CeCl_3 \cdot 7H_2O$, YCl_3, and $YbCl_3$ was tested for this conversion. Indium tribromide was found to be the most effective catalyst in terms of conversion and selectivity. For instance, treatment of **2** with aniline in the presence of 10 mol% $InBr_3$ and 10 mol% $InCl_3$ for 6 h afforded the **3a** yields of 85% and 72%, respectively. However, in the absence of $InBr_3$ or $InCl_3$, the reaction did not proceed even after an extended time. Various triflates were screened—TMSOTf, $Sc(OTf)_3$, $Bi(OTf)_3$, $Yb(OTf)_3$, $Ce(OTf)_3$ and $Sm(OTf)_3$—and a stoichiometric amount of TMSOTf was found to be best for this reaction.

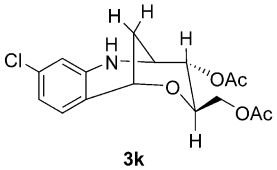
 © 2003 Wiley-VCH Verlag GmbH & Co. KGaA, Weinheim



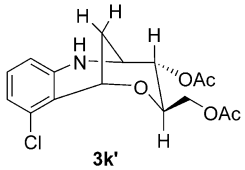
Scheme 2. A possible reaction mechanism.

The scope and generality of this process is illustrated with various glycals and aryl amines (Table 1). It is important to mention that the simple cyclic enol ethers such as 3,4-dihydro-2*H*-pyran and 2,3-dihydrofuran afforded the corresponding tetrahydroquinoline derivatives under similar reaction conditions.[12] The coupling reaction of aryl amines with D-glucal also proceeded smoothly in the presence of 10 mol% $InBr_3$ in water at 80 °C with similar yields and selectivity although with longer reaction times (8–12 h). Furthermore, the reaction also proceeded with protic acid, specifically montmorillonite KSF, at 80 °C in 1,2-dichloroethane to yield the desired product.

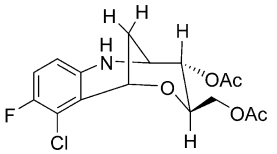
The scope of this method was investigated with respect to various glycals and a wide range of anilines including *ortho*-, *meta*-, *para*-, mono-, and disubstituted anilines, and the results are presented in the Table 1. However, in case of *meta*-chloroaniline, the product obtained was a mixture of two regioisomers **3k** and **3k′** in 7:3 ratio; the reaction with 3-chloro-4-fluoroaniline gave only a single product 3n.



3k



3k'



3n

In summary, we disclose a novel one-pot synthesis of new carbohydrate derivatives, benzo-fused heterobicycles, from glycals and aryl amines using a catalytic amount of indium tribromide under extremely mild and convenient conditions. Alternatively, a stoichiometric amount of TMSOTf can also be used to produce these products with an unusual tetrahydroquinoline motif. This is an entirely new approach to functionalize glycals with aryl amines, leading to a biologically well-defined tetrahydroquinoline framework.

Experimental Section

A mixture of D-glucal (1 mmol), aryl amine (1 mmol), and indium tribromide (10 mol%) or TMSOTf (1 mmol) in dichloromethane (10 mL) was stirred at 27 °C for the appropriate time (Table 1). After completion of the reaction as indicated by TLC, the reaction mixture was diluted with water and extracted with dichloromethane (2 × 10 mL). The combined organic layers were dried over anhydrous Na_2SO_4, concentrated in vacuo, and purified by column chromatography on silica gel (Merck, 100–200 mesh, ethyl acetate/hexane 1:9) to afford pure cyclic adduct.

Characterization of selected products: **3a**: liquid, $[\alpha]_D = 95.5$ ($c = 1.0$, $CHCl_3$), ^{1}H NMR (500 MHz, $CDCl_3$): $\delta = 7.16$ (dt, $J = 1.5$, 7.9 Hz, 1H, H13), 7.13 (dd, $J = 1.5$, 7.9 Hz, 1H, H15), 6.69 (dt, $J = 1.5$, 7.9 Hz, 1H, H14), 6.61 (dd, $J = 1.5$, 7.9 Hz, 1H, H12), 4.84 (dd, $J = 3.1$, 10.4 Hz, 1H, H4), 4.81 (dd, $J = 1.8$, 3.7 Hz, 1H, H1), 4.44 (brs, 1H, NH), 4.19 (dd, $J = 4.2$, 12.0 Hz, 1H, H6), 3.99 (dd, $J = 2.2$, 12.0 Hz, 1H, H6′), 3.84 (ddd, $J = 2.4$, 3.1, 4.6 Hz, 1H, H3), 3.58 (ddd, $J = 2.1$, 4.2, 10.4 Hz, 1H, H5), 2.29 (ddd, $J = 2.4$, 3.7, 13.2 Hz, 1H, $H2_{(pro\text{-}S)}$), 2.10 (s, 3H, 10-Me), 2.06 (s, 3H, 8-Me), 1.96 ppm (ddd, $J = 1.8$, 4.6, 13.2 Hz, 1H, $H2_{(pro\text{-}R)}$); ^{13}C NMR (proton decoupled, 75 MHz, $CDCl_3$): $\delta = 170.8$ (C7), 169.8 (C9), 145.0 (C11), 130.5 (C15), 129.9 (C13), 118.8 (C16), 117.2 (C14), 112.9 (C12), 71.8 (C4), 68.5 (C1), 67.4 (C5), 63.0 (C6), 46.6 (C3), 27.9 (C2), 21.0 (C10), 20.7 ppm (C8); FAB MS: *m*/*z*: 305 [M^+], 259, 191, 144, 130, 119, 91, 69, 57.

3p: solid; m.p. 147 °C; $[\alpha]_D = -172.3$ ($c = 1.0$, $CHCl_3$); ^{1}H NMR (500 MHz, $CDCl_3$): $\delta = 7.14$ (dt, $J = 1.3$, 7.4 Hz, 1H, H9), 7.13 (dd, $J = 1.3$, 7.4 Hz, 1H, H11), 6.68 (dt, $J = 1.3$, 7.4 Hz, 1H, H10), 6.60 (dd, $J = 1.3$, 7.4 Hz, 1H, H8), 4.71 (dd, $J = 1.9$, 3.6 Hz, 1H, H1), 4.60 (dd, $J = 3.2$, 10.1 Hz, 1H, H4), 4.41 (brs, 1H, NH), 3.76 (ddd, $J = 2.6$, 3.2, 4.4 Hz, 1H, H3), 3.47 (dq, $J = 6.1$, 10.1 Hz, 1H, H5), 2.25 (ddd, $J = 2.6$, 3.6, 13.2 Hz, 1H, $H2_{(pro\text{-}R)}$), 2.21 (s, 3H, $COCH_3$), 1.95 (ddd, $J = 1.9$, 4.4, 13.2 Hz, 1H, $H2_{(pro\text{-}S)}$), 1.08 ppm (d, $J = 6.1$ Hz, 3H, 6-Me). ^{13}C NMR (proton decoupled, 75 MHz, $CDCl_3$): $\delta = 170.1$ (C13), 145.2 (C7), 130.4 (C11), 129.6 (C9), 119.7 (C12), 117.0 (C10), 112.8 (C8), 78.1 (C4), 68.3 (C1), 64.9 (C5), 46.8 (C3), 28.3 (C2), 21.1 (C14), 18.0 ppm (C6). FAB MS: *m*/*z*: 247 [M^+], 188, 176.

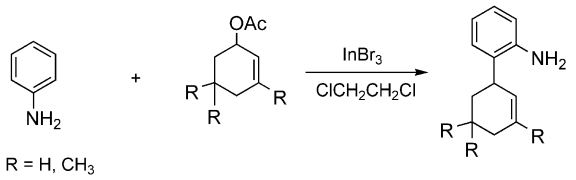
Received: February 24, 2003
Revised: July 11, 2003 [Z51267]

Keywords: aminoglycosidations · aryl amines · carbohydrates · glucals · Lewis acids

[1] a) R. J. Ferrierm, N. J. Prasad, *Chem. Commun.* **1969**, 570; b) R. J. Ferrier, *Adv. Carbohydr. Chem. Biochem.* **1969**, *24*, 199.
[2] M. H. D. Postema, *Tetrahedron* **1992**, *48*, 8545.
[3] a) C. J. Li, T. H. Chan, *Tetrahedron* **1999**, *55*, 11149; b) G. Babu, P. T. Perumal, *Aldrichimica Acta* **2000**, *33*, 16; c) R. Ghosh, *Indian J. Chem. Sect. B* **2001**, *40*, 550.
[4] a) M. A. Ceschi, L. A. Felix, C. Peppe, *Tetrahedron Lett.* **2000**, *41*, 9695; b) M. Bandini, P. Giorgio, P. G. Cozzi, M. Giocomini, P. Melchiorre, S. Selva, A. Umani-Ronchi, *J. Org. Chem.* **2002**, *67*, 3700.
[5] a) M. P. Mingeot-Leclercq, Y. Glupczynski, P. M. Tulkens, *Antimicrob. Agents Chemother.* **1999**, *43*, 727; b) M. J. Dianez, J. Galan, A. Gomez-Sanchez, A. Lopez-Castra, M. Rico, *J. Chem. Soc. Perkin Trans. 1* **1987**, 581.
[6] a) J. S. Yadav, B. V. S. Reddy, *Synthesis* **2002**, 511; b) J. S. Yadav, B. V. S. Reddy, A. K. Raju, C. V. Rao, *Tetrahedron Lett.* **2002**, *43*, 5437.

 © 2003 Wiley-VCH Verlag GmbH & Co. KGaA, Weinheim

[7] J. Cavanagh. W. J. Fairbrother, A. G. Palmer III, N. J. Skelton, *Protein NMR Spectroscopy*, Academic Press, San Diego, **1996**.
[8] C. E. Hadden, G. E. Martin, V. V. Krishnamurthy, *Magn. Reson. Chem.* **2000**, *38*, 143 – 147.
[9] a) H. Goto, E. J. Osawa, *J. Chem. Soc. Perkin Trans. 2* **1993**, 187; b) P. C. MODEL, Serena Software Box 3076, Bloomington, IN, USA.
[10] For the ionization potential of indium see: a) P. Cintas, *Synlett* **1995**, 1087; b) N. Fujiwara, Y. Yamamoto, *J. Org. Chem.* **1997**, *62*, 2318.
[11] The reaction of cyclohexenyl acetate and aniline under the influence of 10 mol% $InBr_3$ in dichloroethane at 80 °C afforded 2-(2-cyclohexenyl)aniline, which supports the formation of the initial C–C bond at the *ortho* position of the aryl amine.



[12] J. S. Yadav, B. V. S. Reddy, K. Sadasiv, P. S. R. Reddy, *Tetrahedron Lett.* **2002**, *43*, 3853.

 © 2003 Wiley-VCH Verlag GmbH & Co. KGaA, Weinheim

Group 11 Hydrides

Gold Is Noble but Gold Hydride Anions Are Stable**

*Xuefeng Wang and Lester Andrews**

Gold is the classic noble metal as shown by its use for valued ornaments through the ages. Gold does not oxidize nor adsorb most molecules from the gas phase.[1] However, nanometer-sized gold particles on oxide supports function as catalysts.[2–5] One reason offered for making these clusters of gold atoms catalytically active is partial electron transfer from the support surface to the gold cluster.[3] This suggests that extra electron density might lead to greater stability for small gold-containing molecules in general and gold hydrides in particular. Hence, hydrogen on gold clusters will enhance the charge transfer and may enable gold clusters to function as hydrogenation catalysts.

[*] Prof. Dr. L. Andrews, Dr. X. Wang
Department of Chemistry
University of Virginia
Charlottesville, VA 22904-4319 (USA)
Fax: (+1) 434-924-3710
E-mail: lsa@virginia.edu

[**] This work was supported by the National Science Foundation (CHE00-78836). We thank Prof. Dr. J. T. Yates, Jr. for helpful comments.

In the course of a matrix-isolation investigation of gold, silver, and copper (Group 11) hydrides,[6] we discovered the coinage metal dihydride anions, which have unique properties. Our density functional theory (DFT) calculations show that these MH_2^- ions are very stable, but the corresponding neutral MH_2 molecules, which have also been computed by others,[7–11] are unstable relative to M and H_2. Four late first-row transition metal dihydride anions (MnH_2^- through NiH_2^-) have been characterized by photoelectron spectroscopy (PES), but the neutral molecules are stable[12] in contrast to CuH_2. Although there are many examples of homoleptic transition metal hydride anions, the only known Group 11 hydride anion is CuH_4^{3-} in solid Ba/Cu alloys under H_2 pressure.[13]

In contrast, the chemistry of copper(I), silver(I), and gold(I) halide complexes is well-known.[14] The $CuCl_2^-$ and $CuBr_2^-$ ions have been characterized recently by PES in the gas phase and by electronic structure calculations.[15] The $AgCl_2^-$ ion has been prepared, and the linear structure determined by X-ray diffraction.[16] A very recent investigation of gas-phase AuX_2^- (X = Cl, Br) and AuX_4^- ions from electrospray mass spectrometry of AuX solutions has determined electron-detachment energies.[17] In addition, Au^{III} compounds are stable, and Au^{I} complexes disproportionate to Au^{III} compounds and gold. Accordingly, the AuX_2^- ions can be photooxidized to AuX_4^- in the presence of electron acceptors.[18] Finally, the trend in observed vibrational force constants $k(Au{-}X^-) > k(Cu{-}X^-) > k(Ag{-}X^-)$ and the stability of Au^{III} compounds have been explained by relativistic effects for heavy metals.[11,19]

In spite of extensive chemistry for the Group 11 metal dihalide complexes, the corresponding metal dihydrides are unknown. A theoretical study, however, predicted that AuH will add H^- to form AuH_2^-.[11] This is mechanistically significant as the neutral MH_2 dihydrides are higher in energy than M + H_2,[9,10] and are thus unstable, in contrast to the corresponding MX_2 dihalides.[15,17] Calculations have been performed for CuH_2, AgH_2, and AuH_2 and the energies for these bent $^2B_2$ ground state molecules range from 6 to 43 to 20 kcal mol^{-1}, respectively higher than the corresponding M + H_2 reagents although dissociation barriers are found.[9,10] Hence, preparation of the MH_2^- ions will be experimentally difficult as formation of the MH_2 molecules requires excited metal atom reactions.

Our investigation of Group 11 hydrides involves the reaction of energetic laser-ablated metal atoms and H_2 in excess argon, neon, and hydrogen. All of the Group 11 metal hydrides, MH, and dihydrogen complexes, $(H_2)MH$, have been observed by matrix infrared spectroscopy and confirmed by comparison to DFT calculated frequencies.[6,20] We report here the first observation of the stable linear coinage metal MH_2^- ion complexes and the square-planar AuH_4^- ion, and supporting DFT calculations of their structures and vibrational frequencies. Earlier calculations show that both AuH_2^- and AuH_4^- are stabilized by relativistic effects.[11,19]

Laser-ablated gold, silver, and copper atoms were allowed to react with H_2, D_2, and HD in excess argon and neon, and with pure H_2, HD, and D_2 during condensation at 3.5 K using methods described previously for gold carbonyls and chromium hydrides.[21–23] IR spectra were recorded, samples were

 DOI: 10.1002/anie.200351780 © 2003 Wiley-VCH Verlag GmbH & Co. KGaA, Weinheim

annealed, irradiated, and more spectra were recorded. Complementary DFT calculations were performed by using the Gaussian 98 program, the BPW91 density functional, 6-311++G(d,p) and 6-311G(3df,3pd) basis sets for hydrogen, and SDD pseudopotentials for the metal atoms.[24] The BPW91 functional has been recommended for copper, silver, and gold compounds.[25]

Laser-ablated gold experiments used as low laser energy as possible to trap charged species in addition to neutral hydride products. Energized gold atom reactions with pure hydrogen gave several new IR product absorptions including a strong 2164.0 cm^{-1} $(H_2)AuH$ band (not shown) and the 1661.5 cm^{-1} $(H_2)AuH_3$ band[6] and weaker 1676.4 (AuH_4^-) and 1636.0 cm^{-1} (AuH_2^-) absorptions (Figure 1). Although

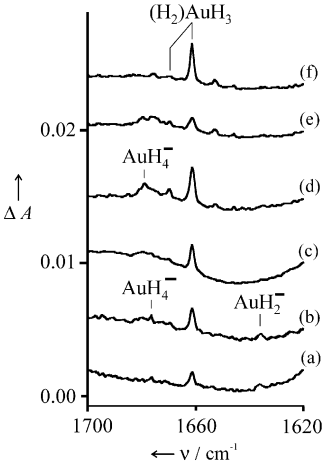


Figure 1. IR spectra of gold hydrides. a) Au + H_2 deposited for 12 min, b) Au + H_2 deposited for 12 min more, c) after annealing to 5.3 K, d) after photolysis at $\lambda > 290$ nm, e) after photolysis at $\lambda > 240$ nm, and f) after annealing to 6.0 K.

the latter bands are weak, they are reproduced in several experiments (the graphics program does not do justice to the original spectra). Annealing to 5.3 K decreased the band at 1676.4 cm^{-1} and destroyed the peak at 1636.0 cm^{-1}. Irradiation ($\lambda > 290$ nm) produced a new matrix site absorption at 1678.8 cm^{-1}, increased the $(H_2)AuH_3$ absorption at 1661.5 cm^{-1}, and formed a weaker photochemical site at 1666.8 cm^{-1}.

A pure deuterium experiment with gold is illustrated in Figure 2 in which AgD_2^- and CuD_2^- spectra are also compared. The strong 1556.5 cm^{-1} $(D_2)AuD$ absorption (not shown) and 1198.6 cm^{-1} $(D_2)AuD_3$ complex band are observed as before,[20] but the weaker bands at 1212.2 (AuD_4^-) and 1182.3 cm^{-1} (AuD_2^-) identified here for the first time are enhanced by using lower laser energy. Note that the AuD_2^- and AuD_4^- bands are three times stronger than the hydrogen counterparts, and they validate the hydrogen matrix observations with proper H/D isotopic frequency ratios. This larger deuteride yield is due to the greater photochemical stability of the gold deuteride anions as well as the thermal stability of solid D_2 itself (F.P. 18.6 K) as compared to solid H_2 (F.P. 14.0 K). Photolysis ($\lambda > 530$ nm) decreased the weaker band at 1182.3 cm^{-1} and increased the band at 1212.2 cm^{-1}

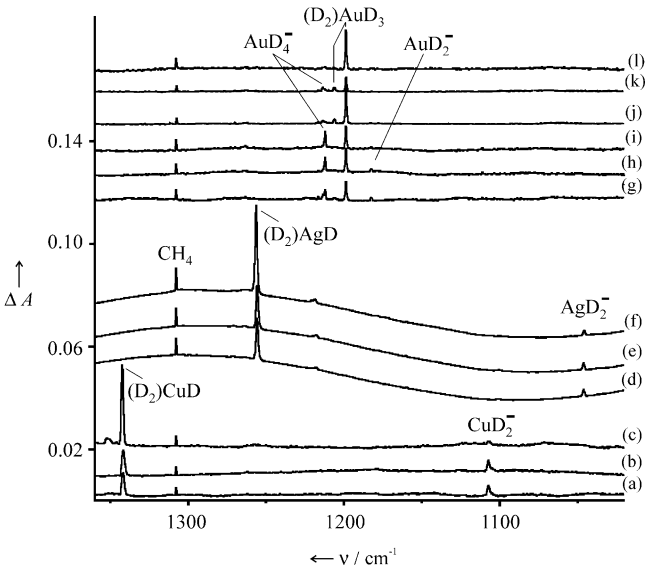


Figure 2. IR spectra of laser-ablated Cu, Ag, and Au codeposited with pure deuterium at 3.5 K for 30 min. a) Cu + D_2, b) after annealing to 7.0 K, c) after photolysis at $\lambda > 240$ nm, d) Ag + D_2, e) after annealing to 7.0 K, f) after photolysis at $\lambda > 240$ nm, g) Au + D_2, h) after annealing to 7.3 K, i) after photolysis at $\lambda > 530$ nm, j) after photolysis at $\lambda > 290$ nm, k) after photolysis at $\lambda > 240$ nm, and l) after annealing to 8.0 K.

(Figure 2i). The weakest hydrogen and deuterium matrix bands at 1636.0 and 1182.3 cm^{-1}, respectively, are isotopic counterparts: their frequency ratio of 1.384 indicates a primarily H(D) atomic mass vibration. For example the $(H_2)AuH/(D_2)AuD$ isotopic Au-H/Au-D frequency ratio is 1.390, which also includes the effect of anharmonicity.[6] Subsequent irradiation ($\lambda > 290$ nm) increased the major 1198.6 cm^{-1} and minor 1205.9 cm^{-1} $(D_2)AuD_3$ absorptions and produced AuD_4^- at 1213.7 cm^{-1}, and full arc photolysis ($\lambda > 240$ nm) decreased the $(D_2)AuD_3$ bands and increased the 1213.7 cm^{-1} AuD_4^- absorption (Figure 2j,k). Finally, mixed isotopic experiments provide diagnostic information for the stronger bands at 1676.4 and 1212.2 cm^{-1} with an Au–H/Au–D ratio of 1.383. Two experiments with pure H_2 + D_2 gave essentially the same positions for the new band, 1681.3 and 1211.3 cm^{-1} (*trans*-$AuH_2D_2^-$), but pure HD produced distinctly different 1840.4 and 1280.4 cm^{-1} absorptions (*cis*-$AuH_2D_2^-$) that showed the same photolysis behavior as the 1676.4 and 1212.2 cm^{-1} bands (Figure 3), hence they are isotopic counterparts. Stronger bands were observed for neutral (HD)AuH, (HD)AuD, (HD)AuHDH, and (HD)AuHDD species. Table 1 summarizes the observed absorptions.

Very recent resonance photoexcitation (265 nm) of Au to the ^2P state in solid hydrogen (and deuterium) gave strong $(H_2)AuH[(D_2)AuD]$ absorptions with weak 1666.8 (1205.9) cm^{-1} photochemical $(H_2)AuH_3[(D_2)AuD_3]$ site bands, and no anion absorptions.[6] This complementary experiment produced only the neutral species observed with laser-ablated gold atoms.

Our BPW91 calculation predicts a linear centrosymmetric AuH_2^- anion, in agreement with the results obtained by

 © 2003 Wiley-VCH Verlag GmbH & Co. KGaA, Weinheim

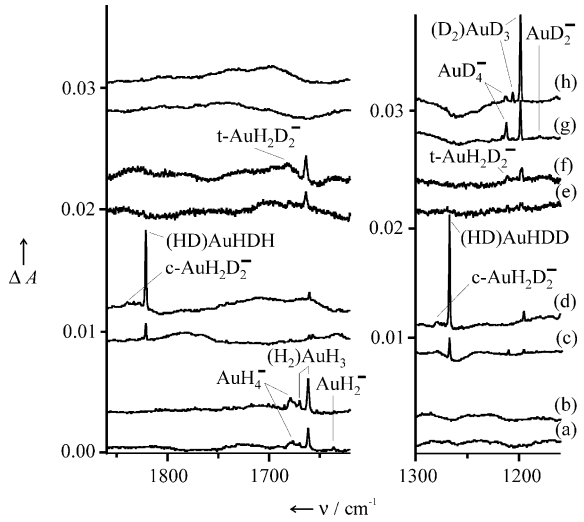


Figure 3. IR spectra in the 1860–1620 and 1300–1160 cm^{-1} regions for laser-ablated Au co-deposited with pure hydrogen isotopic samples at 3.5 K and after photolysis. a) Au + H_2, b) photolysis at $\lambda > 290$ nm, c) Au + HD, d) photolysis at $\lambda > 290$ nm, e) Au + 50% H_2 + 50% D_2, f) photolysis at $\lambda > 290$ nm, g) Au + D_2, and h) photolysis at $\lambda > 290$ nm.

Table 2: Comparison of frequencies [cm^{-1}] observed (solid H_2, HD, D_2 or H_2 + D_2) and calculated (BPW91/6-311++G(d,p)/SDD) for coinage metal hydride anions.

Observed	Calculated	Anion
1586.7	1601 (1611)[c]	$HCuD^-$
1517.8	1501 (1507)	CuH_2^-
1137.6	1122 (1128)	$HCuD^-$
1107.3	1078 (1083)	CuD_2^-
1442.4	1445 (1440)	AgH_2^-
1045.9	1031 (1027)	AgD_2^-
1636.0	1642 (1640)	AuH_2^-
1182.3	1167 (1166)	AuD_2^-
1840.4	1906 (1904)	*cis*-$AuH_2D_2^-$
1681.3[a]	1724 (1714)	*trans*-$AuH_2D_2^-$
1676.4	1724 (1714)	AuH_4^-
1280.4	1303 (1297)	*cis*-$AuH_2D_2^-$
1212.0	1226 (1219)	AuD_4^-
1211.3[b]	1227 (1220)	*trans*-$AuH_2D_2^-$

[a] In mixed H_2 + D_2 experiments, this product absorption represents AuH_4^- and *trans*-$AuH_2D_2^-$. [b] In mixed H_2 + D_2 experiments, this product absorption represents AuD_4^- and *trans*-$AuH_2D_2^-$. [c] Calculated by using a larger 6-311++G(3df, 3pd) basis set for H.

Schwerdtfeger et al.,[11] with a very strong antisymmetric (σ_u) mode at 1642 cm^{-1} and AuD_2^- counterpart at 1167 cm^{-1}. Table 2 compares the calculated and observed frequencies: it is perhaps amazing how close DFT in the harmonic approximation predicts the observed anharmonic frequencies of gold dihydride anions. (The AuH_2^- frequency is calculated 0.3% high and the AuD_2^- mode 1.3% low). These small deviations between calculated and observed AuH_2^- and AuD_2^- frequencies are different because we are comparing calculated harmonic and observed anharmonic frequencies, and hydrogen vibrations are more anharmonic than deuterium motions. On the basis of this excellent agreement between calculated and observed frequencies, the band at 1636.0 cm^{-1} is assigned

Table 1: IR absorptions [cm^{-1}] observed from laser-ablated copper, silver, and gold atom reactions with dihydrogen in excess argon, neon, and hydrogen.

Argon			Neon			Hydrogen			Identification
H_2	HD	D_2	H_2	HD	D_2	H_2	HD	D_2	
1879.8	1879.8		1889.9	1889.9					CuH
	1354.9	1354.9		1362.2	1362.2				CuD
1862.5	1862.7		1869.1	1869.1		1861.4	1865.5		$(H_2)CuH$
	1343.0	1343.2		1346.4	1344.9		1345.4	1341.6	$(D_2)CuD$
1497.2	1566.9		1529.5			1517.8	1586.7		CuH_2^-
	1122.7	1089.4		1158.3	1116.5		1137.6	1107.3	CuD_2^-
1717.0	1717.0					1691.8			AgH
	1233.8	1233.8							AgD
1746.5	1748.2		1750.8			1742.6	1748.6		$(H_2)AgH$
	1256.9	1257.6			1264.3		1255.4	1255.7	$(D_2)AgD$
1427.5	1496.8		1460			1442.4			AgH_2^-
	1068.9	1032.3			1053			1045.9	AgD_2^-
2226.6									AuH
		1597.2							AuD
2173.6, 2170.6			2170.1, 2167.9			2164.0			$(H_2)AuH$
		1559.3			1559.0			1556.5	$(D_2)AuD$
						1678.8			AuH_4^- site
						1676.4	1840.4		AuH_4^-
						1666.8			$(H_2)AuH_3$ site
1642				1831		1661.5	1821		$(H_2)AuH_3$
			1638.6			1636.0			AuH_2^-
								1213.7	AuD_4^- site
							1280.4	1212.2	AuD_4^-
								1205.9	$(D_2)AuD_3$ site
		1182		1275	1207		1257	1198.6	$(D_2)AuD_3$
								1182.3	AuD_2^-

 © 2003 Wiley-VCH Verlag GmbH & Co. KGaA, Weinheim

to AuH_2^- in solid hydrogen, and the band at 1182.3 cm^{-1} to AuD_2^- in solid deuterium.

The $Au^IH_2^-$ ion is a very photosensitive species in solid hydrogen in part because Au^{III} compounds are more stable for gold.[19] Accordingly laser-ablated gold with pure H_2 and pure D_2 favor the bands at 1676.4 and 1212.2 cm^{-1} (frequency ratio 1.383), which are assigned to AuH_4^- and AuD_4^- formed during deposition: the photogenerated counterparts at 1678.8 and 1213.6 cm^{-1} (ratio 1.383) are due to AuH_4^- and AuD_4^- in a slightly different solid hydrogen matrix environment created by a different mechanism (see below). Photolysis (530 nm) appears to convert AuD_2^- into AuD_4^- in solid D_2. Our BPW91 calculation predicts very strong 1724 and 1226 cm^{-1} antisymmetric stretching (e_u) modes for the square-planar species (Figure 4), which are 2.9% and 1.2%

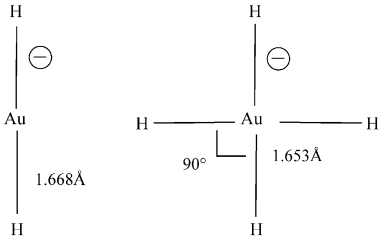


Figure 4. Structures calculated (with BPW91/6-311++G(d,p)/SDD) for AuH_2^- and AuH_4^-.

higher than the observed absorptions and in the range of agreement found for DFT frequency calculations.[25] When the larger basis set with more polarization functions is employed the calculated frequencies, 1714 and 1219 cm^{-1}, are closer to the observed absorptions. Our DFT bond length (1.653 Å) is nearly the same (1.652 Å) as computed previously[19] for AuH_4^-. However, confirmation comes from $H_2 + D_2$ and HD isotopic substitution. Unlike the case for a tetrahedral product, such as the Group 3 and 13 MH_4^- ions[26,27] where the same $MH_2D_2^-$ species are produced from $H_2 + D_2$ and 2 HD, the square-planar AuH_4^- ion has *cis* and *trans* dideuterio isomers. Hence, H_2 must add across linear H-Au-H^- *without* going through a tetrahedral intermediate. Our calculations show the *trans* product to be spectroscopically similar to the pure isotopic species because the observed vibration is an antisymmetric stretching mode of a linear (H-Au-H) linkage and the bonding of an orthogonal (crossed) D-Au-D linkage makes little difference. However, the *cis* product with linear H-Au-D vibrations is substantially different, as is observed for the HD reaction. We calculate the strong *cis*-$AuH_2D_2^-$ ion absorptions at 1906 and 1303 cm^{-1}, which are higher than the strong AuH_4^- and AuD_4^- modes, respectively, and we observe these bands at 1840.4 and 1280.4 cm^{-1}, which are in very good agreement (calculated 3.6% and 1.8% high).

As will be discussed later, the HD reaction proceeds first to give the HAuD molecule, then electron capture occurs to give the linear $(H\text{-}Au\text{-}D)^-$ ion, which adds another HD across the gold center. Hence, the reactions of 2 HD and $H_2 + D_2$ give different *cis*-$AuH_2D_2^-$ and *trans*-$AuH_2D_2^-$ ions, respectively.

Analogous weaker bands were observed with laser-ablated silver at 1460 and 1050 cm^{-1} in excess neon, at 1442.4 and 1045.9 cm^{-1} in pure solid H_2 and solid D_2 (Figure 2), and at 1427.5 and 1032.3 cm^{-1} in excess argon. These pairs exhibit H/D ratios of 1.383 ± 0.004 and destruction by $\lambda > 240$ nm irradiation. For comparison the $(H_2)AgH/(D_2)AgD$ ratio is 1.388.[6] A very strong σ_u mode is computed for AgH_2^- at 1445 cm^{-1}. Similar agreement is found for $AgHD^-$ in argon, in which the calculated Ag–H and Ag–D absorptions at 1543.2 and 1076.9 cm^{-1} are 6.8 and 4.4% higher than the calculated σ_u modes of AgH_2^- and AgD_2^-, and the observed bands are 4.9 and 3.5% higher (Table 1). These differences between calculated and observed frequencies of 1.9 and 0.9% strongly support our identification of AgH_2^-.

IR spectra for laser-ablated Cu reaction products with H_2 and D_2 in excess argon give new bands at 1879.8, 1862.8, and 1497.2 cm^{-1} in the Cu–H stretching region and at 1354.9, 1343.2, and 1089.4 cm^{-1} in the Cu–D region. Annealing to 15 K slightly increases all of these absorptions, but photolysis at $\lambda > 240$ nm increases the first, decreases the second, and destroys the third band in each region. A subsequent annealing to 20 K sharpens the first, increases the second, and has no regenerative effect on the third band. The use of HD as the reagent reveals important diagnostic information. First, the bands at 1879.8 and 1354.9 cm^{-1} are unchanged, but the bands at 1862.5 and 1343.2 cm^{-1} are each shifted by 0.2 cm^{-1}, and the absorptions at 1497.2 and 1089.4 cm^{-1} are observed along with new stronger bands at 1566.9 and 1122.7 cm^{-1} (Table 1).

The unshifted bands at 1879.8 and 1354.9 cm^{-1} are due to CuH and CuD in solid argon[6] and are blue shifted 13.5 and 8.2 cm^{-1} from the gas-phase values[28] owing to matrix repulsion as observed for AuH and AuD.[20] The slightly shifted bands at 1862.8 1343.2 cm^{-1} exhibit the same H/D ratio of 1.387 as CuH/CuD and are assigned to the $(H_2)CuH$ and $(D_2)CuD$ complexes. In pure solid H_2 and D_2, the CuH and CuD molecules are not observed, but the $(H_2)CuH$ and $(D_2)CuD$ complex bands are stronger at 1861.4 and 1341.6 cm^{-1}, and weaker associated H–H and D–D stretching modes occur at 3566.6 and 2582.0 cm^{-1}. The Cu–H/Cu–D ratio in these complexes is 1.387. The Cu and pure D_2 spectrum is illustrated in Figure 2. The photosensitive bands at 1497.2 and 1089.4 cm^{-1} are observed at 1517.8 and 1107.3 cm^{-1} in solid H_2 and D_2, and at 1529.5 and 1116.5 cm^{-1} in excess neon (Table 1). These band pairs exhibit H/D ratios of 1.372 ± 0.002 and are too low in frequency for a neutral hydride. The CuH_2 molecule stretching frequencies are computed in the 1600–1800 cm^{-1} region,[6] and since this molecule is higher in energy than $Cu + H_2$, it is not expected to survive the photochemical conditions required for formation.[29]

Therefore, the simple CuH_2^- ion comes to mind. Our DFT calculations produce a very intense antisymmetric stretching (σ_u) mode at 1501.0 cm^{-1} for the linear CuH_2^- ion, which is in excellent agreement with the present observations. Since the unobserved symmetric stretching (σ_g) mode is higher in frequency than the σ_u mode, the $HCuD^-$ ion is calculated to

 © 2003 Wiley-VCH Verlag GmbH & Co. KGaA, Weinheim

have Cu–H and Cu–D stretching absorptions at 1600.7 and 1121.9 cm^{-1}, which are 6.6 and 4.1 % higher than the σ_u modes calculated for CuH_2^- and CuD_2^-. The observed $HCuD^-$ bands are 4.7 and 3.1 % higher (argon matrix). The differences, 1.9 % and 1.0 %, show close agreement between calculated and observed frequencies for CuH_2^-, $CuHD^-$, and CuD_2^- and confirm our identification of CuH_2^-. The Ar_nH^+ and Ar_nD^+ ions provide for charge balance in the argon matrix.[30]

It is interesting to compare the new Group 11 dihydride anions with the isoelectronic Group 12 dihydrides, which have been observed by matrix isolation spectroscopy.[31,32] The strong antisymmetric H-M-H stretching fundamentals (1870, 1753, and 1896 cm^{-1} for M = Zn, Cd, and Hg, respectively, in solid argon), are considerably higher than those for this mode for the MH_2^- ions (1518, 1442, and 1636 cm^{-1} for M = Cu, Ag, and Au in solid hydrogen), but both data sets follow the same vertical family relationship in the periodic table. Finally, the results for our AuH_4^- ion isolated in solid hydrogen may be compared with recent computations for the square-planar isoelectronic HgH_4 molecule,[33] which finds the strong mode at 1959 cm^{-1}, and with the known square-planar PtH_4^{2-} dianion combined with sodium cations in the solid compound, which has a comparable bond length of 1.639 Å.[34]

The straightforward reaction mechanism includes the formation of MH molecules in endothermic[28] reaction (1)

$$M(^2S) + H_2(^1\textstyle\sum_g^+) \rightarrow MH(^1\textstyle\sum^+) + H(^2S) \quad (\Delta E = 38,\ 52,\ 32\ \text{kcal mol}^{-1})^{[36]} \qquad (1)$$

driven by the excess electronic/kinetic energy in the laser-ablated metal atoms.[35] Electrons produced in the ablation process[21,22] are captured by hydrogen to form hydride anions for exothermic reaction with the MH molecules to make the stable linear $M^IH_2^-$ ions, reactions (2) and (3). Our computed

$$H(^2S) + e^- \rightarrow H^-\ (^1S)\ \ (\Delta E = -17\ \text{kcal mol}^{-1})^{[37]} \qquad (2)$$

$$MH\ (^1\textstyle\sum^+) + H^-\ (^1S) \rightarrow MH_2^-\ (^1\textstyle\sum_g^+) \quad (\Delta E = -68,\ -68,\ -77\ \text{kcal mol}^{-1})^{[36]} \qquad (3)$$

electron-detachment energies for CuH_2^-, AgH_2^-, and AuH_2^-, of 55, 62 and 65 kcal mol^{-1}, respectively,[36] attest the stability of these coinage metal dihydride anions. The latter may be compared with the relativistic value of 64 kcal mol^{-1} computed by Schwerdtfeger et al.[11]

The sequential reaction (4), to make the stable square-planar $M^{III}H_4^-$ ions, is too endothermic for the Cu and Ag

$$MH_2^- + H_2 \rightarrow MH_4^-\ (^1A_{1g})\ \ \Delta E = 16,\ 23,\ 9\ \text{kcal mol}^{-1}) \qquad (4)$$

matrix reactions; however, the greater stability of Au^{III} is revealed by the reaction energetics, and the solid hydrogen and deuterium environments apparently help to form the AuH_4^- and AuD_4^- ions. Reaction (4) likely proceeds during sample deposition for gold before the AuH_2^- product of reaction (3) is completely relaxed, and the overall energy change for reactions (3) and (4) for gold is computed as −68 kcal mol^{-1}, which is very favorable for the formation of AuH_4^-. Furthermore, atomic gold can also capture an electron during deposition, reaction (5), and the Au^- ion is particularly stable.[38] The photochemical formation of AuH_4^-

$$Au\ (^2S) + e^- \rightarrow Au^-\ (^1S)\ \ (\Delta E = -53\ \text{kcal mol}^{-1})^{[38]} \qquad (5)$$

in solid hydrogen probably involves the excited Au^- (^3P) state in reaction (6), which is analogous to the reaction of Hg (^3P)

$$Au^-\ (^1S) + 2\,H_2 \xrightarrow{290\ \text{nm}} Au^-\ (^3P) + 2\,H_2 \rightarrow AuH_4^-\ (^1A_{1g}) \qquad (6)$$

with H_2,[32] and produces AuH_4^- in a slightly different matrix environment. Reaction (7) is observed in pure HD, in which

$$Au\ (^2P) + HD \rightarrow HAuD \qquad (7)$$

following electron capture, $HAuD^-$ reacts with HD to give *cis*-$AuH_2D_2^-$. Finally, a relativistic computational investigation concluded that AuH_4^- is quite stable,[19] and the present observation of AuH_4^- suggests that this anion may be stable in solid-state compounds.

The basic science reported here shows that negative charge stabilizes coinage metal hydrides. This further suggests that the presence of hydrogen may augment charge transfer to Group 11 metal clusters,[3] and that these clusters, gold, silver, and copper included, may be effective for the industrially important catalytic hydrogenation process. It would therefore be interesting to reexamine the catalytic oxidation of carbon monoxide on gold clusters[2] with hydrogen present to foster charge transfer to the gold cluster.

Received: April 30, 2003
Revised: July 30, 2003 [Z51780]
Published Online: October 14, 2003

Keywords: anions · copper · gold · hydrides · IR spectroscopy · silver

[1] B. Hammer, J. K. Norskov, *Nature* **1995**, *376*, 238.
[2] M. Valden, X. Lai, D. W. Goodman, *Science* **1998**, *281*, 1647.
[3] A. Sanchez, S. Abbet, U. Heiz, W.-D. Schneider, H. Hakkinen, R. N. Barnett, U. Landman, *J. Phys. Chem. A* **1999**, *103*, 9573.
[4] N. Lopez, J. K. Norskov, *J. Am. Chem. Soc.* **2002**, *124*, 11262.
[5] A. Bell, *Science* **2003**, *299*, 1688.
[6] X. Wang, L. Andrews, L. Manceron, C. Marsden, *J. Phys. Chem. A* **2003**, in press.
[7] P. E. M. Siegbahn, M. R. A. Blomberg, C. W. Bauschlicher, *J. Chem. Phys.* **1984**, *81*, 1373.
[8] J. Niu, B. K. Rao, B. Jena, *Phys. Rev. B* **1995**, *51*, 4475.
[9] J. Garcia-Prieto, M. E. Ruiz, O. Novaro, *J. Am. Chem. Soc.* **1985**, *107*, 5635.
[10] K. Balasubramanian, *J. Phys. Chem.* **1989**, *93*, 6585.
[11] P. Schwerdtfeger, P. D. W. Boyd, A. K. Burrell, W. T. Robinson, M. J. Taylor, *Inorg. Chem.* **1990**, *29*, 3593.
[12] A. E. S. Miller, C. S. Feigerle, W. C. Lineberger, *J. Chem. Phys.* **1986**, *84*, 4127.
[13] R. B. King, *Coord. Chem. Rev.* **2000**, *200–202*, 813, and references therein.
[14] F. A. Cotton, G. Wilkinson, C. A. Murillo, M. Bochmann, *Advanced Inorganic Chemistry*, 6th ed., Wiley, New York, **1999**.

 © 2003 Wiley-VCH Verlag GmbH & Co. KGaA, Weinheim

[15] X.-B. Wang, L.-S. Wang, R. Brown, P. Schwerdtfeger, D. Schröder, H. Schwarz, *J. Chem. Phys.* **2001**, *114*, 7388.
[16] G. Helgesson, S. Jagner, *Inorg. Chem.* **1991**, *30*, 2574.
[17] D. Schröder, R. Brown, P. Schwerdtfeger, X. B. Wang, X. Yang, L. S. Wang, H. Schwarz, *Angew. Chem.* **2003**, *115*, 323; *Angew. Chem. Int. Ed.* **2003**, *42*, 311.
[18] H. Kunkely, A. Vogler, *Inorg. Chem.* **1992**, *31*, 4539.
[19] P. Schwerdtfeger, P. D. W. Boyd, S. Brienne, A. K. Burrell, *Inorg. Chem.* **1992**, *31*, 3411, and references therein.
[20] X. Wang, L. Andrews, *J. Phys. Chem. A* **2002**, *106*, 3744.
[21] B. Liang, L. Andrews, *J. Phys. Chem. A* **2000**, *104*, 9156.
[22] L. Andrews, A. Citra, *Chem. Rev.* **2002**, *102*, 885.
[23] X. Wang, L. Andrews, *J. Phys. Chem. A* **2003**, *107*, 570.
[24] Gaussian 98 (Revision A.7), M. J. Frisch, G. W. Trucks, H. B. Schlegel, G. E. Scuseria, M. A. Robb, J. R. Cheeseman, V. G. Zakrzewski, J. A. Montgomery, R. E. Stratmann, J. C. Burant, S. Dapprich, J. M. Millam, A. D. Daniels, K. N. Kudin, M. C. Strain, O. Farkas, J. Tomasi, V. Barone, M. Cossi, R. Cammi, B. Mennucci, C. Pomelli, C. Adamo, S. Clifford, J. Ochterski, G. A. Petersson, P. Y. Ayala, Q. Cui, K. Morokuma, D. K. Malick, A. D. Rabuck, K. Raghavachari, J. B. Foresman, J. Cioslowski, J. V. Ortiz, B. B. Stefanov, G. Liu, A. Liashenko, P. Piskorz, I. Komaromi, R. Gomperts, R. L. Martin, D. J. Fox, T. Keith, M. A. Al-Laham, C. Y. Peng, A. Nanayakkara, C. Gonzalez, M. Challacombe, P. M. W. Gill, B. G. Johnson, W. Chen, M. W. Wong, J. L. Andres, M. Head-Gordon, E. S. Replogle, J. A. Pople, Gaussian, Inc., Pittsburgh, PA, **1998**.
[25] F. S. Legge, G. L. Nyberg, J. B. Peel, *J. Phys. Chem. A* **2001**, *105*, 7905.
[26] P. Pullumbi, Y. Bouteiller, L. Manceron, *J. Chem. Phys.* **1994**, *101*, 3610.
[27] X. Wang, L. Andrews, *J. Am. Chem. Soc.* **2002**, *124*, 7610.
[28] K. P. Huber, G. Herzberg, *Constants of Diatomic Molecules*, Van Nostrand, Princeton, **1979**.
[29] G. A. Ozin, C. Gracie, *J. Phys. Chem.* **1984**, *88*, 643.
[30] a) D. E. Milligan, M. E. Jacox, *J. Mol. Spectrosc.* **1973**, *46*, 460; b) C. A. Wight, B. S. Ault, L. Andrews, *J. Chem. Phys.* **1976**, *65*, 1244.
[31] T. M. Greene, W. Brown, L. Andrews, A. J. Downs, G. V. Chertihin, N. Runeberg, P. Pyykkö, *J. Phys. Chem.* **1995**, *99*, 7925.
[32] N. Legay-Sommaire, F. Legay, *Chem. Phys. Lett.* **1993**, *207*, 123.
[33] P. Pyykkö, M. Straka, M. Patzschke, *Chem. Commun.* **2002**, 1728.
[34] W. Bronger, *Angew. Chem.* **1991**, *103*, 776; *Angew. Chem. Int. Ed. Engl.* **1991**, *30*, 759.
[35] H. Kang, J. L. Beauchamp, *J. Phys. Chem.* **1985**, *89*, 3364.
[36] Reaction energetics computed at the BPW91/6-311++G(d,p)/SDD level of theory for Cu, Ag, and Au, respectively. Using the larger 6-311++G(3df, 3pd) basis reaction (3) is exothermic by 78 kcal mol^{-1}, and reaction (4) is endothermic by 8 kcal mol^{-1} for Au.
[37] R. S. Berry, *Chem. Rev.* **1969**, *69*, 533.
[38] H. Hotop, W. C. Lineberger, *J. Phys. Chem. Ref. Data* **1985**, *14*, 731.

 © 2003 Wiley-VCH Verlag GmbH & Co. KGaA, Weinheim

Matrix Generation of C_3N_4

Dicyanocarbodiimide and Trinitreno-*s*-triazine Generated by Consecutive Photolysis of Triazido-*s*-triazine in a Low-Temperature Nitrogen Matrix**

Tadatake Sato, Aiko Narazaki, Yoshizo Kawaguchi, Hiroyuki Niino, and Götz Bucher*

Since the publication of theoretical studies predicting that carbon nitride might be harder than diamond,[1] a considerable amount of research has been directed toward the preparation of pure C_3N_4.[2] In contrast, carbon nitride molecules with the C_3N_4 formula have seldom been studied. Dicyanodiazomethane, the only C_3N_4 isomer studied experimentally, has been converted into a dicyanomethylene (NC_3N).[3] Meanwhile, Schnick assumed that a C_3N_4 molecule would have a tricyanoazane $N(CN)_3$ structure.[4] With the aid of ab initio calculations, BelBruno et al. showed that there was a more stable isomer, dicyanocarbodiimide.[5] However, the existence of these molecules was never confirmed. In the present study, we have confirmed for the first time the generation of the quasilinear C_3N_4 molecule, dicyanocarbodiimide, in the matrix photolysis of triazido-*s*-triazine (**1**, Scheme 1). Triazide **1** has been studied as a precursor for high-spin trinitrene molecules. Indeed, generation of a triplet mononitrene and a quintet dinitrene was confirmed by electron spin resonance spectroscopy upon the photolysis of a single crystal of **1** at 4 K, although generation of the septet trinitrene was not confirmed.[6] Various reactive species and their products were formed upon the decomposition of **1**. Pulsed laser photolysis of **1** resulted in the formation of a nitrogen cluster ion N_5^+.[7] Generation of carbon nitride and carbon nanotubes by means of pyrolytic or detonative decomposition of **1** was reported.[8] Thus, the intermediates generated by the decomposition of **1** are quite intriguing. Herein, we report the consecutive photolysis of **1** in a low-temperature nitrogen matrix.

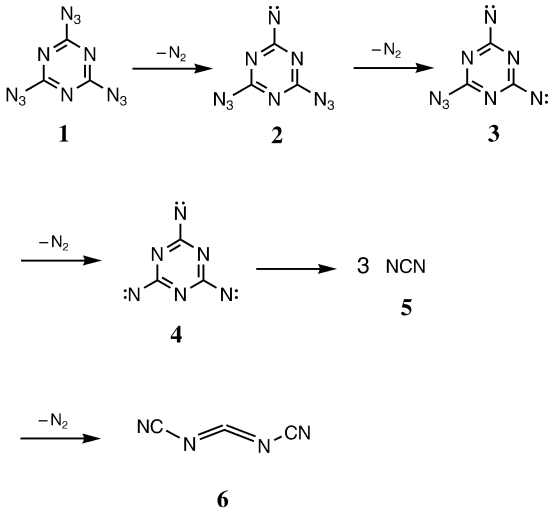
Crystallites of **1** were vaporized and codeposited with nitrogen onto a CaF_2 substrate at 20 K. Irradiation of the resulting matrix at 266 nm led to an instant decrease in the

[*] Dr. T. Sato, Dr. A. Narazaki, Dr. Y. Kawaguchi, Dr. H. Niino
Photoreaction Control Research Center
National Institute of Advanced Industrial Science and Technology (AIST)
1-1-1 Higashi, Tsukuba, Ibaraki 305-8565 (Japan)
Fax: (+81) 29-861-4560
E-mail: sato-tadatake@aist.go.jp
Dr. G. Bucher
Lehrstuhl für Organische Chemie
Ruhr-Universität Bochum
Universitätsstrasse 150, 44801 Bochum (Germany)

[**] This work was supported by the fund "Support of Young Researchers with a Term" from the Ministry of Education, Culture, Sports, Science and Technology, Japan.

Supporting information for this article is available on the WWW under http://www.angewandte.org or from the author.

 © 2003 Wiley-VCH Verlag GmbH & Co. KGaA, Weinheim DOI: 10.1002/anie.200351879



Scheme 1. Photoproducts generated successively in the photolysis of **1**.

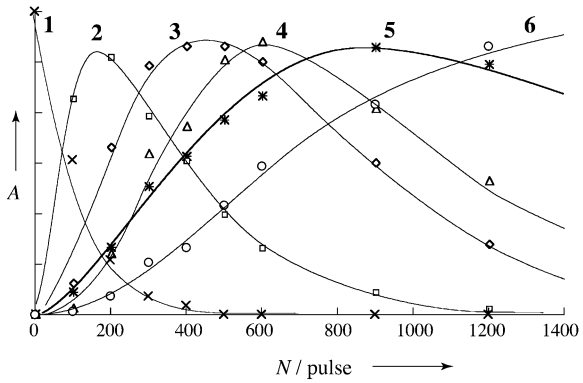


Figure 2. Dynamic behavior of the representative IR and UV/Vis absorption bands of the intermediates (**2**: IR 1339 cm^{-1}, **3**: IR 1438 cm^{-1}, **4**: IR 1326 cm^{-1}, **5**: UV/Vis 329 nm, **6**: IR 2271 cm^{-1}). *N* denotes the number of the irradiated laser pulses.

intensities of the IR bands of **1** and the concomitant growth of new IR bands ascribable to the photoproducts (Figure 1a). The photolysis was also observed by UV/Vis absorption spectroscopy (Figure 1b). The various IR and UV/Vis absorption bands ascribed to the photoproducts appeared successively indicating stepwise generation of several photoproducts. By analyzing the dynamic behavior of the IR and UV/Vis bands (Figure 2), we were able to group the bands into five sets.[9] Thus, we concluded that five intermediates were formed successively in the matrix.

The most prominent IR band of the first set was observed at 1339 cm^{-1}, and the dynamic behavior of this band was similar to that of the UV/Vis band at 344 nm. Previously reported results for the photolyses of the related species[6,10,11] indicate that the most probable candidate for the first photoproduct is the triplet mononitrene **2**. In the theoretical IR spectrum of **2** at the B3LYP/6-31G* level, the most intense band is at around 1340 cm^{-1} for all three isomers.[12] Previously reported results for an azido-*s*-triazine derivative[11] indicate that ring expansion of the nitrene produces didehydrotetrazepine. However, the characteristic IR band (around 1900 cm^{-1}) of didehydrotetrazepine was extremely weak in our case, indicating that subsequent photoreaction of the nitrene was preferred over ring expansion. Thus we assigned the first intermediate as triplet mononitrene **2**.

The second intermediate showed an intense IR band at 1438 cm^{-1}. This band corresponded to the prominent band at 1422 cm^{-1} in the theoretical IR spectrum of quintet dinitrene **3**, indicating that the second intermediate was formed by further loss of nitrogen from **2**.

Considering the observed stepwise loss of nitrogen, the third photoproduct may be septet trinitrene **4**, although generation of **4** was not confirmed in an earlier study.[6] In its theoretical IR spectrum, septet **4** shows only one discernible IR band between 800 and 4000 cm^{-1}, a band at 1298 cm^{-1}.[13] We assigned only one weak IR band, at 1326 cm^{-1}, to the third intermediate; we could not find other IR bands ascribable to this intermediate in this wavenumber region, particularly at around 2100 cm^{-1}. As the second intense IR band of **4**, an IR band was predicted at 747 cm^{-1} with intensity of 40 km mol^{-1} (Figure 3b). In the matrix experiment using a BaF_2 substrate in place of the CaF_2 substrate, which allowed the IR measurement between 600 and 4000 cm^{-1}, we could find out another IR band ascribable to **4** at 763 cm^{-1}. This band showed similar dynamic behavior to the band at 1326 cm^{-1} (Figure 3a).

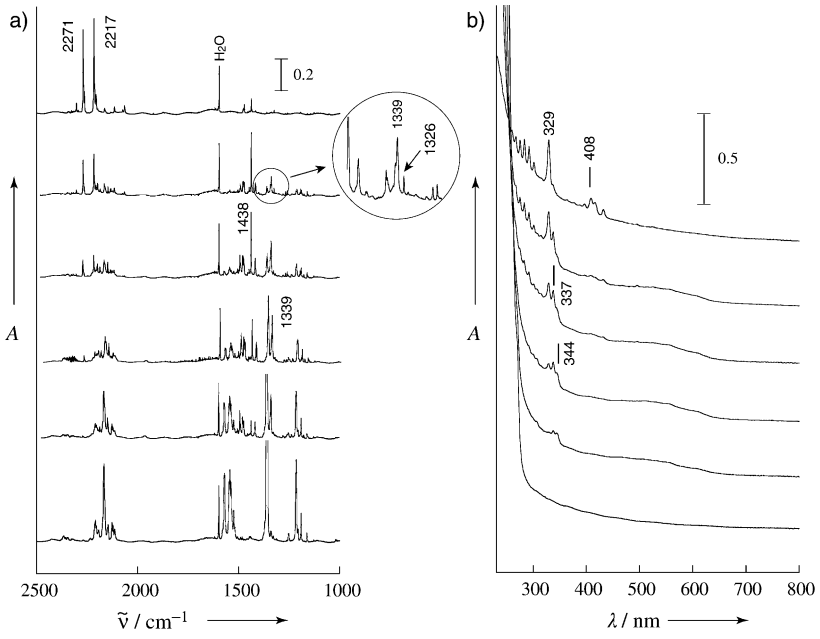


Figure 1. Observed a) FTIR and b) UV/Vis absorption spectra of a nitrogen matrix containing **1** upon irradiation at 266 nm with (bottom to top) 0, 100, 200, 300, 500, and 1200 FHG pulses from a Nd:YAG laser.

 © 2003 Wiley-VCH Verlag GmbH & Co. KGaA, Weinheim

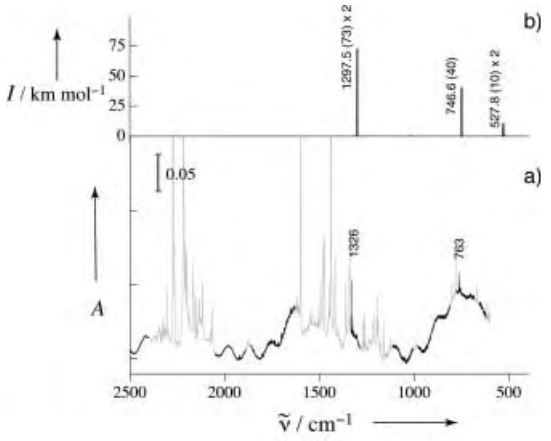


Figure 3. a) IR bands ascribable to trinitrene **4**. b) Calculated IR spectrum (B3LYP/6-31G* level, scaled by 0.9614) of **4**.

To confirm our identification of the photoproducts, we studied the ^{13}C isotopic shifts of their IR bands. We observed similar photoreactions, i.e. stepwise generation of five intermediates, in the photolysis of ^{13}C-labeled **1**. The observed spectra for the labeled photoproducts showed changes similar to those observed for the products of unlabeled **1**, although all corresponding IR bands were shifted to smaller wavenumbers (Table 1). The IR bands ascribed to the third intermediate shifted from 1326 and 763 cm^{-1} to 1299 and 746 cm^{-1}, respectively. The observed shift corresponded well to the theoretically predicted shift. Thus, we assigned the third intermediate as trinitrene **4**.

Table 1: Observed and calculated isotopic shifts of characteristic IR bands.

Compound	(^{12}C) [cm^{-1}]	(^{13}C) [cm^{-1}]	Δ [cm^{-1}]	Calcd Δ [cm^{-1}]	Calcd (^{12}C) [cm^{-1}]	Calcd (^{13}C) [cm^{-1}]
Mononitrene	1339	1307	−32	−25	1340[a]	1315[a]
				−24	1337[a]	1313[a]
				−25	1342[a]	1317[a]
Dinitrene	1438	1403	−35	−32	1422	1390
Trinitrene	1326	1299	−27	−28	1298	1270
	763	746	−17	−18	747	729
NCN	1475	1436	−39	−42	1517	1475
	1478	1440	−38			
					6	
Final compd.	2217	2160	−58	−60	2243	2183
	2271	2218	−53	−56	2314	2257

[a] IR bands predicted for three isomers of mononitrene.[12]

The IR bands of the fourth intermediate, which were difficult to analyze because they overlapped with the intense IR bands of **2**, appeared at around 1475 cm^{-1} after the disappearance of **2**. The fourth intermediate showed characteristic UV/Vis absorption bands: one intense peak at 329 nm accompanied by vibronic bands at 290–300 nm (Figure 1b). We ascribed this characteristic UV/Vis spectrum to NCN (**5**) on the basis of the spectrum reported by Jacox et al. upon photolysis of N_3CN.[14] Trinitrene is a trimer of **5**. Considering that triazine can decompose into three HCN molecules,[15] decomposition of **4** into three molecules of **5** should be possible.

Upon further photoirradiation, NCN reportedly rearranges into CN_2, which shows an IR band at 1241 cm^{-1}.[14] However, it was not discernible in our study. Instead, two intense IR peaks appeared, at 2217 cm^{-1} and 2271 cm^{-1}, upon further irradiation (Figure 1a) while the IR and UV/Vis bands of **5** decreased in intensity. These two new IR bands have never been observed in photolyses of N_3CN that generated **5**. In the matrix photolysis of **1**, the three molecules of **5** should stay in the same matrix cage, and, therefore, further photoirradiation would result in intermolecular reactions. Considering the sole photoproduct generated at the end of the sequence, the three molecules of **5** must form the final photoproduct. Among the calculated possible species, only one with the formula C_3N_4, dicyanocarbodiimide **6**, had two IR peaks at the corresponding wavenumbers. However, the calculated IR spectrum did not reproduce the intensities of these IR bands well. The observed ^{13}C isotopic shifts of the IR bands were 58 and 53 cm^{-1}. These shifts are larger than those for the species with a triazine ring and correspond well with the calculated isotopic shifts for **6**. Therefore, we assigned the final product as **6**. We propose the following mechanism for the generation of **6**: One of the three confined molecules of **5** is converted into CN_2 or a C atom, as in the photolysis of N_3CN.[16] The generated CN_2 or C atom immediately reacts with the other two molecules of **5**. The reaction of a C atom with two molecules of **5** forms **6** directly, whereas the reaction of CN_2 forms **6** by photoinduced nitrogen loss.

Experimental Section

Triazido-*s*-triazine (**1**) was synthesized by mixing a solution of cyanuric chloride (trichloro-*s*-triazine) in acetone and an aqueous solution of sodium azide according to the procedure described in ref. [11]. ^{13}C-Labeled **1** was synthesized from sodium azide and the ^{13}C isotopomer of cyanuric chloride (Isotec. Inc., 99.4 atom%) in which all ^{12}C was replaced by ^{13}C.

In the matrix isolation experiments crystallites of **1** were vaporized at 40–45 °C and codeposited with nitrogen (99.9999%) onto a CaF_2 substrate at 20 K. Matrix-isolated **1** was photolyzed by using fourth-harmonic-generated (FHG) pulses of a Nd:YAG laser ($\lambda = 266$ nm, 10 Hz, 0.5 mJ cm^{-2} $pulse^{-1}$). A sample chamber with two pairs of windows, quartz for UV/Vis spectroscopy and KBr for FTIR measurements, enabled us to monitor the photolysis by FTIR and UV/Vis absorption spectroscopies simultaneously. Because of the strong absorption of the CaF_2 substrate, FTIR measurements were conducted between 800 and 4000 cm^{-1}.

The geometries of the compounds were optimized at the B3LYP/6-31G* level by using the Gaussian 98 program package.[17] The nature of the stationary points was assessed by means of vibrational frequency analysis. Theoretical IR spectra were obtained by the vibrational frequency analysis: vibrational frequencies were scaled by 0.9614 on the basis of a literature report.[18] All calculations were done on the TACC Quantum Chemistry Grid/Gaussian Portal system at the Tsukuba Advanced Computing Center (TACC).

Received: May 13, 2003
Revised: July 21, 2003 [Z51879]

Keywords: azides · carbon nitride · matrix isolation · photolysis · reactive intermediates

 © 2003 Wiley-VCH Verlag GmbH & Co. KGaA, Weinheim

[1] A. Y. Liu, M. L. Cohen, *Science* **1989**, *245*, 841.
[2] For instance, a) S. Muhl, J. M. Mendez, *Diamond Relat. Mater.* **1999**, *8*, 1809; b) T. Malkow, *Mater. Sci. Eng. A* **2001**, *302*, 311, and references therein.
[3] a) W. H. Smith, G. E. Leroi, *Spectrochim. Acta Part A* **1969**, *25*, 1917; b) I. R. Dunkin, A. McCluskey, *Spectrochim. Acta Part A* **1994**, *50*, 209.
[4] W. Schnick, *Angew. Chem.* **1993**, *105*, 1649; W. Schnick, *Angew. Chem. Int. Ed. Engl.* **1993**, *32*, 1580.
[5] a) J. J. BelBruno, *Chem. Phys. Lett.* **1997**, *270*, 99; b) J. J. BelBruno, Z.-C. Tang, R. Smith, S. Hobday, *Mol. Phys.* **2001**, *99*, 957.
[6] T. Nakai, K. Sato, D. Shimoi, T. Takui, K. Itoh, M. Kozaki, K. Okada, *Mol. Cryst. Liq. Cryst. Sci. Technol. Sect. A* **1999**, *334*, 157.
[7] T. Matsunaga, T. Ohana, T. Nakamura, K. Ishikawa, M. Iida, Y. Koga, S. Fujiwara, *Kayaku Gakkaishi* **1998**, *59*, 200.
[8] a) E. G. Gillan, *Chem. Mater.* **2000**, *12*, 3906; b) E. Kroke, M. Schwarz, V. Buschmann, G. Miehe, F. Hartmut, R. Ralf, *Adv. Mater.* **1999**, *11*, 158.
[9] Before the analysis of the IR spectra, the IR bands of **1** were eliminated from the observed spectra by weighted subtraction procedure (T. Sato, S. Arulmozhiraja, H. Niino, S. Sasaki, T. Matsuura, A. Yabe, *J. Am. Chem. Soc.* **2002**, *124*, 4512). After the subtraction, the intensities of the IR bands were analyzed.
[10] a) S. V. Chapyshev, R. Walton, J. A. Sanborn, P. M. Lahti, *J. Am. Chem. Soc.* **2000**, *122*, 1580; b) S. V. Chapyshev, A. Kuhn, M. W. Wong, C. Wentrup, *J. Am. Chem. Soc.* **2000**, *122*, 1572.
[11] G. Bucher, F. Siegler, J. J. Wolff, *Chem. Commun.* **1999**, 2113.
[12] Triazide **1** may exist as a mixture of two isomers, owing to the rotation of the azide groups. The isomer conformations would be fixed when **1** was embedded in the matrix. Therefore, two isomers of **1** could coexist in the matrix initially. Depending on the initial conformation of the isomers of **1**, three isomers of **2** could be generated. These three isomers showed intense IR bands at 1340.0, 1337.3, and 1341.7 cm^{-1}, respectively.
[13] Due to the symmetry of the molecule, two IR bands with an intensity of 73 $km\,mol^{-1}$ were predicted at the same wavenumber. All of other IR bands predicted between 800 and 4000 cm^{-1} have intensities of less than 0.5 $km\,mol^{-1}$.
[14] D. E. Milligan, M. E. Jacox, A. M. Bass, *J. Chem. Phys.* **1965**, *43*, 3149.
[15] S. Kudoh, M. Takayanagi, M. Nakata, *J. Mol. Struct.* **1997**, *413–414*, 365.
[16] a) D. E. Milligan, M. E. Jacox, *J. Chem. Phys.* **1966**, *44*, 2850; b) G. Maier, A. Bothur, J. Eckwert, H. P. Reisenauer, *Chem. Eur. J.* **1998**, *4*, 1964. This rearrangement has also been studied theoretically: c) J. M. L. Martin, P. Taylor, R. J. P. François, R. Gijbels, *Chem. Phys. Lett.* **1994**, *226*, 475; d) L. V. Moskaleva, M. C. Lin, *J. Phys. Chem. A* **2001**, *105*, 4156.
[17] Gaussian 98 (Revision A.9), M. J. Frisch, G. W. Trucks, H. B. Schlegel, G. E. Scuseria, M. A. Robb, J. R. Cheeseman, V. G. Zakrzewski, J. A. Montgomery, R. E. Stratmann, J. C. Burant, S. Dapprich, J. M. Millam, A. D. Daniels, K. N. Kudin, M. C. Strain, O. Farkas, J. Tomasi, V. Barone, M. Cossi, R. Cammi, B. Mennucci, C. Pomelli, C. Adamo, S. Clifford, J. Ochterski, G. A. Petersson, P. Y. Ayala, Q. Cui, K. Morokuma, D. K. Malick, A. D. Rabuck, K. Raghavachari, J. B. Foresman, J. Cioslowski, J. V. Ortiz, B. B. Stefanov, G. Liu, A. Liashenko, P. Piskorz, I. Komaromi, R. Gomperts, R. L. Martin, D. J. Fox, T. Keith, M. A. Al-Laham, C. Y. Peng, A. Nanayakkara, C. Gonzalez, M. Challacombe, P. M. W. Gill, B. G. Johnson, W. Chen, M. W. Wong, J. L. Andres, M. Head-Gordon, E. S. Replogle, J. A. Pople, Gaussian, Inc., Pittsburgh, PA, **1998**.
[18] A. P. Scott, L. Radom, *J. Phys. Chem.* **1996**, *100*, 16502.

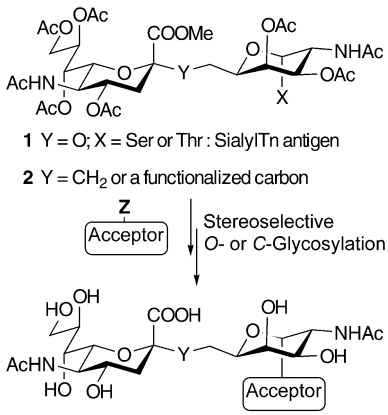
 © 2003 Wiley-VCH Verlag GmbH & Co. KGaA, Weinheim

Stereoselective C-Sialylation

Synthesis of a Carbon-Linked Mimic of the Disaccharide Component of the Tumor-Related SialylTn Antigen**

*Zouleika Abdallah, Gilles Doisneau, and Jean-Marie Beau**

Among the large number of known tumor-associated carbohydrate motifs, Tn (GalNAcα1→*O*-Ser/Thr) and sialylTn (Neu5Acα2→6GalNAcα1→*O*-Ser/Thr) are the most specific to human epithelial tumor cells (breast, colon, ovarian, lung, and pancreatic cancers).[1] The sialylTn antigen, which is expressed on membrane-bound mucin-type glycoproteins, appears in transformed cells by premature sialylation of *N*-acetylgalactosamine, the first sugar moiety of the nascent *O*-glycane side chains in glycoproteins.[2] Integration of these antigens into synthetic vaccine constructs induces an anticancer immune response in which the carbohydrate domain plays a decisive role in determining immunogenicity.[1,3] The glycosylated antigen is, however, partially deglycosylated during the priming period.[4] It is therefore important to evaluate compounds in which the carbohydrate moiety cannot be detached from the peptide. We previously reported a mimic of the Tn antigen that could be incorporated into immunogenic glycopeptides.[5] We now describe the easy access to a carbon-linked mimic **2** of the Neu5Acα2→6GalNAcα1→OR disaccharidic component of the sialylTn antigen (Scheme 1).[6,7]



Scheme 1. SialylTn tumor antigen **1** and a stable analogue of the sialyl-*N*-acetylgalactosaminyl donor **2** for "block" synthesis.

[*] Prof. Dr. J.-M. Beau, Z. Abdallah, Dr. G. Doisneau
Université Paris-Sud
Laboratoire de Synthèse de Biomolécules associé au CNRS
Institut de Chimie Moléculaire et des Matériaux
91405 Orsay Cedex (France)
Fax: (+33) 1-6985-3715
E-mail: jmbeau@icmo.u-psud.fr

[**] We are grateful to Dr. P. Smith, GlaxoSmithKline, for a generous supply of the *N*-acetylneuraminic acid used in this study.

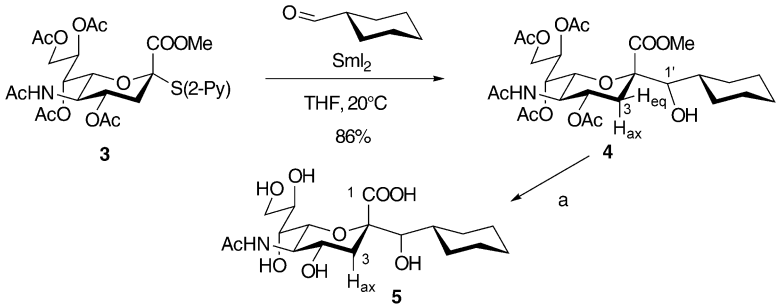
 DOI: 10.1002/anie.200351969 © 2003 Wiley-VCH Verlag GmbH & Co. KGaA, Weinheim

The synthesis was designed in such a way that an activated disaccharidic block would be available for modular attachment to a wide variety of acceptors.[8] Integrated in a vaccine, this segment would not be sensitive to enzymatic cleavage of the sialyl and the galactosaminyl moieties. This stable mimic may also be useful for the immunodiagnosis of different tumors or for the affinity purification of specific receptors.

We previously established that a samarium diiodide (SmI_2) promoted Barbier reaction with glycosyl 2-pyridyl sulfones is a rapid approach for the stereoselective assembly of C-glycosides.[9–11] In an interesting extension to this work, Linhardt and co-workers showed that the procedure worked equally well with anomeric pyridyl sulfones of 2-ulosonic esters.[12] They later reported that anomeric chlorides or phenyl sulfones could also be used in this procedure without the need of activation by hexamethyl phosphoramide (HMPA).[13] These results were expected since reduction of a functional group α to both an ester group and an oxygen atom (Reformatsky-type reaction) is much more facile than the same operation on a functional group α to an oxygen atom alone. This observation suggests that functional groups other than halides, sulfones, or phosphates would also be appropriate anomeric anion precursors for Neu5Ac or related ulosonic acid derivatives. We report here a synthesis which relies on the unprecedented use of a stable and crystalline 2-pyridyl sulfide of the *N*-acetylneuraminic acid derivative **3** as the anionic precursor in a samarium–Reformatsky procedure.[14]

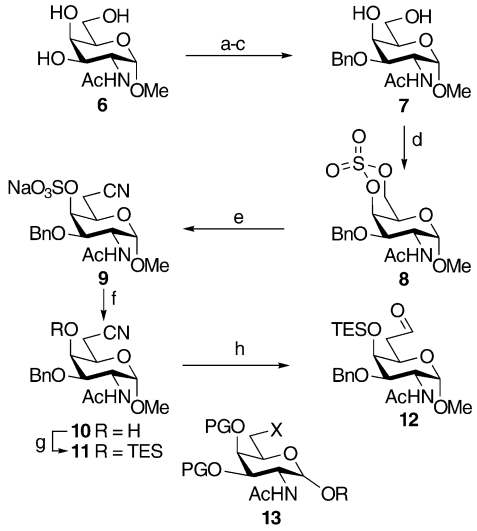
The feasibility of this approach was first assessed with a simple aldehyde and 2-pyridyl sulfide **3**, which is available from the corresponding 2-*O*-acetate (AcCl, AcOH, HCl[15a] then 2-sulfanylpyridine (1.2 equiv), K_2CO_3 (1.3 equiv), toluene/acetone;[15b] 60% yield over the two steps). Treatment of a solution of sulfide **3** and cyclohexanecarbaldehyde (1.5 equiv) in THF at 20°C with a freshly prepared solution of SmI_2[16] in THF led to a very fast consumption of the one-electron reducing agent.[17] After a standard workup, the C-glycosyl derivatives **4** were obtained in an approximately 1:1 diastereomeric ratio and separated by chromatography (86% yield; Scheme 2).

Both compounds displayed a standard $_5C^2$-chair conformation as determined by ^1H NMR analysis ($J_{3ax,4}$, $J_{4,5}$, and $J_{5,6}$ values of 10.2, 11.8, and 10.5 Hz, respectively, for one isomer and of 12.0, 10.5, and 10.5 Hz for the other). The expected equatorial orientation of the newly formed C–C bond at the quaternary center was determined by NOE measurements on both isomers of **4** (NOE contacts between $H_{1'}$ and H_{3eq}/H_{3ax} and not H_4/H_6). This stereochemical assignment was further confirmed by the large values of the C_1-H_{3ax} heteronuclear coupling constants observed in the deprotected C-glycosyl compounds **5** ($^3J = 8.0$ Hz for one isomer and 7.3 Hz for the other); these values are typical of a *trans* diaxial orientation of the C_1–C_2 and C_3–H_{3ax} bonds.[18]



Scheme 2. SmI_2-induced coupling of pyridyl sulfide **3** with cyclohexanecarbaldehyde. 2-Py = 2-pyridyl. a) MeONa, MeOH, 20°C, overnight; NaOH, MeOH-H_2O, 20°C, 2 h, then Dowex 50W-X8-H^+ form, 90%.

Preparation of the required aldehyde **12** (Scheme 3) started from methyl α-D-*N*-acetylgalactosamine (**6**), which was obtained by Fischer glycosylation[19] (MeOH, Dowex



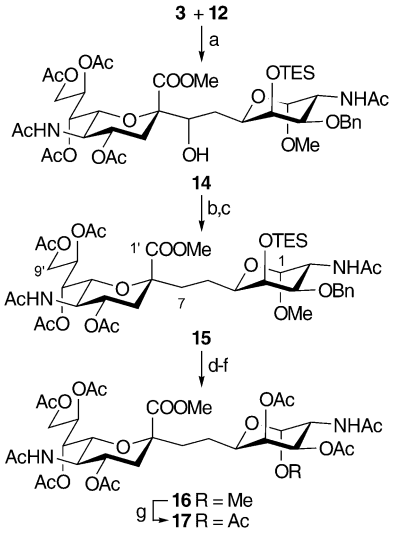
Scheme 3. Preparation of aldehyde **12**. Reagents and conditions: a) $PhCH(OMe)_2$, CSA, DMF, 40°C, 2 h, 60%; b) BnBr (3.5 equiv), $Ba(OH)_2 \cdot 8H_2O$, BaO, DMF, 25°C, 77%; c) AcOH/H_2O (70/30), 70°C, 1 h, 88%; d) $SOCl_2$, Et_3N, CH_2Cl_2, 0°C, 1 h; cat. $RuCl_3 \cdot 3H_2O$, $NaIO_4$, $CH_3CN/CH_2Cl_2/H_2O$ (2/2/3), 25°C, 1 h, 65%; e) NaCN, DMF, 25°C, 3 h, 97%; f) cat. H_2SO_4, moist THF, 25°C, 1 h, 86%; g) TESOTf (3 equiv), pyridine, DMAP, CH_2Cl_2, 0°C, 0.5 h, 80%; h) DIBAL-H (3.3 equiv in 3 portions every 20 min), CH_2Cl_2, −78°C, 1 h, 60%. CSA = camphorsulfuric acid, Bn = benzyl, TES = triethylsilyl, DMAP = 4-dimethylaminopyridine, DIBAL-H = diisobutylaluminum hydride.

50W-X8, H^+ form, reflux, 24 h) of *N*-acetyl-D-galactosamine or, more conveniently for large-scale preparations, by transformation of the inexpensive *N*-acetyl-D-glucosamine.[20]

A standard three-step sequence provided diol **7** which was converted into 4,6-cyclic sulfate **8** by using the procedure of Gao and Sharpless.[22] Regioselective ring opening of cyclic sulfate **8** at C-6[23] by sodium cyanide provided cyanide sulfate **9** in high yield which, after hydrolytic removal of the intermediate sulfate, gave alcohol **10**. This high-yielding one-carbon extension of the sugar chain at position 6 is in stark contrast to all attempts at nucleophilic displacement of iodides or sulfonates by cyanide ions in the more conventional 6-iodo (or 6-*O*-sulfonates) derivatives of *N*-acetyl-D-galactosamine **13** with a variety of protecting groups at positions 3 and 4 (OPG in **13**, including OH groups).[24] These attempts all failed and yielded only elimination

 © 2003 Wiley-VCH Verlag GmbH & Co. KGaA, Weinheim

products.[25] Triethylsilylation at position 4 furnished **11**, and careful reduction of the nitrile with diisobutylaluminum hydride at −78 °C provided the aldehyde **12**, which was used immediately after purification in the next step.[26] The samarium–Reformatsky coupling procedure, as described above, with sulfide **3** (1.5 equiv) and aldehyde **12** afforded the carbon-linked dimer **14** in high yield (93 %) as a 1:1 diastereomeric mixture (Scheme 4).[27]



Scheme 4. Preparation of the carbon-linked sialyl-*N*-acetylgalactosaminyl donor **17**. Reagents and conditions: a) SmI_2 (2.5 equiv), THF, 25 °C, 93 %; b) $(Imid)_2CS$ (10 equiv), CH_3CN, reflux, 4 h; c) Ph_3SnH (2.5 equiv), C_6F_5OH (1 equiv), cat. AIBN, toluene, reflux, 2 h, 65 % over two steps; d) $MeOH/HCl_{aq}$, 25 °C, 2 h, 95 %; e) H_2, Pd/C, EtOH, cat. HCl_{aq}, 94 %; f) Ac_2O, pyridine, 94 %; g) $Ac_2O/AcOH/H_2SO_4$ (8/2/0.1), 25 °C, 6 h, 70 %. Imid = imidazole, AIBN = azobisisobutyronitrile.

Alcohols **14** were converted into thiocarbonates by treatment with a large excess of *N,N′*-thiocarbonyldiimidazole in refluxing acetonitrile and deoxygenated by employing triphenyltin hydride, catalytic AIBN, and pentafluorophenol,[28] which yielded the required C-disaccharide **15** as a single compound (65 % for the two steps). Desilylation, hydrogenolysis, and acetylation provided the peracetylated C-dimer **16**.[29] The high stability of the linkage between the *N*-acetylneuraminyl and the *N*-acetylgalactosaminyl residues now allows for modifications under conditions that are unacceptable with a native O linkage. Thus, acetolysis of the methyl glycoside in dimer **16** provided anomeric acetate **17**, which can be easily converted into other anomeric substituents usable in "block" synthesis.

In conclusion, the reductive samariation of a pyridyl sulfide of methyl *N*-acetylneuraminate is a useful and high-yielding approach for stereoselective α-C-sialylation. One may notice here that anomeric sulfides of Neu5Ac are also good glycosyl donors in stereoselective α-O-sialylation.[30] C-Disaccharidic building block **17** can be readily transformed into a variety of glycosyl donors for β-selective O-glycosylation by standard procedures, for α-selective O-glycosylation by a modification of Koganti's procedure,[31] and α-[10] or β-[32]selective C-glycosylations on a wide range of adapted acceptors for different biological applications.

Experimental Section

14: A 0.1 M solution of SmI_2 in THF (6.5 mL, 0.65 mmol of SmI_2) was added to a stirred mixture of pyridyl sulfide **3** (151 mg, 0.26 mmol) and freshly prepared aldehyde **12** (78 mg, 0.17 mmol) at 20 °C under Ar. After stirring the mixture for 10 min, saturated aqueous NH_4Cl was added and the reaction mixture was extracted three times with CH_2Cl_2. The combined organic phases were washed twice with water, dried with Na_2SO_4, and evaporated to dryness. Flash chromatography (toluene/acetone, 2/1) gave **14** (148 mg, 93 %). Isomers of **14** were separated at this stage (isomer ratio of 1:1). The following steps of the synthesis are, however, carried on with the mixture. Selected data for one of the isomers of **14**: ^{1}H NMR ($CDCl_3$, 250 MHz, atom numbering of the natural dimer): $\delta = 7.36$–7.25 (m, 5H, Ph), 5.41 (ddd, $J_{7',8'} = 7.6$, $J_{8',9'a} = 6.9$, $J_{8',9'b} = 2.2$ Hz, 1H, H-8′), 5.25 (dd, $J_{7',8'} = 7.6$, $J_{6',7'} = 2.2$ Hz, 1H, H-7′), 5.26 (d, $J_{NH,5'} = 10.0$ Hz, 1H, NH Neu5Ac), 5.17 (d, $J_{NH,2} = 9.6$ Hz, 1H, NH Gal), 4.82 (ddd, $J_{4',3'ax} = 11.8$, $J_{4',5'} = 10.1$, $J_{4',3'eq} = 4.4$ Hz, 1H, H-4′), 4.71 and 4.39 (2 × d, $J = 12$ Hz, 2H, CH_2Ph), 4.61 (d, $J_{1,2} = 3.7$ Hz, 1H, H-1), 4.50 (ddd, $J_{2,3} = 10.6$, $J_{2,NH} = 9.6$, $J_{1,2} = 3.7$ Hz, 1H, H-2), 4.34 (dd, $J_{9'a,9'b} = 12.2$, $J_{8',9'b} = 2.2$ Hz, 1H, H-9′b), 4.11 (d, $J_{3,4} = 2.8$ Hz, 1H, H-4), 4.01 (ddd, $J_{5',6'} = 10.2$, $J_{4',5'} = 10.1$, $J_{5',NH} = 10$ Hz, 1H, H-5′), 3.99 (dd, $J_{9'a,9'b} = 12.2$, $J_{8',9'a} = 6.9$ Hz, 1H, H-9′a), 3.92–3.82 (m, 2H, H-5,7), 3.89 (dd, $J_{5',6'} = 10.2$, $J_{6',7'} = 2.3$ Hz, 1H, H-6′), 3.76 (s, 3H, $COOCH_3$), 3.42 (dd, $J_{2,3} = 10.6$, $J_{3,4} = 2.8$ Hz, 1H, H-3), 3.26 (s, 3H, OCH_3), 2.71 (d, $J_{7,OH} = 11.2$ Hz, 1H, OH), 2.47 (dd, $J_{3'eq,3'ax} = 12$, $J_{3'eq,4'} = 4.4$ Hz, 1H, H-3′eq), 2.15, 2.09, 2.02, and 2.00 (4 × s, 12H, $OCOCH_3$), 1.84 (s, 3H, $NCOCH_3$) 1.70 (dd, $J_{3'eq,3'ax} = 12$, $J_{3'ax,4} = 11.8$ Hz, 1H, H-3′ax), 1.51–1.41 (m, 2H, H-6a,b), 0.95 (t, $J = 7.9$ Hz, 9H, CH_3CH_2Si), 0.65 ppm (q, $J = 7.9$ Hz, 6H, CH_2Si); MS (ES): $m/z = 949$ $[M+Na]^+$; HR-MS (ES) for $C_{43}H_{66}NaN_2O_{18}Si$; calcd: 949.3977; found: 949.3989.

Selected data for **16**; ^{1}H NMR ($CDCl_3$, 250 MHz, atom numbering of the natural dimer): $\delta = 5.8$ (d, $J_{NH,5} = 9.5$ Hz, 1H, NH Gal), 5.55–5.28 (m, 3H, H-7′,8′,NH Neu5Ac), 5.19 (d, $J_{3,4} = 2.9$ Hz, 1H, H-4), 5.08 (dd, $J_{2,3} = 10.9$, $J_{3,4} = 2.9$ Hz, 1H, H-3), 4.76 (ddd, $J_{4',3'ax} = 12.5$, $J_{4',5'} = 10.0$, $J_{4',3'eq} = 4.4$ Hz, 1H, H-4′), 4.7 (d, $J_{1,2} = 3.7$ Hz, 1H, H-1), 4.51 (ddd, $J_{2,3} = 10.9$, $J_{2,NH} = 10.2$, $J_{1,2} = 3.7$ Hz, 1H, H-2), 4.29 (dd, $J_{9'a,9'b} = 12.3$, $J_{9'a,8'} = 2.0$ Hz, 1H, H-9′a), 4.05 (dd, $J_{9'a,9'b} = 12.3$, $J_{8',9'b} = 4.9$ Hz, 1H, H-9′b), 3.97 (m, 1H, H-5′), 3.75 (m, 2H, H-5,6′), 3.71 (s, 3H, $COOCH_3$), 3.35 (s, 3H, OCH_3), 2.43 (dd, $J_{3'eq,3'ax} = 12.5$, $J_{3'eq,4'} = 4.4$ Hz, 1H, H-3′eq), 2.17, 2.09, 2.07, 2.00, 1.98, 1.95, and 1.93 (7 × s, 21H, $OCOCH_3$), 1.92 (m, 1H, H-6b), 1.84 (s, 3H, $NCOCH_3$), 1.78–1.70 (m, 2H, H-6a,7b), 1.72 (dd, $J_{3'ax,3'eq} = 12.5$, $J_{3'ax,4'} = 12.5$ Hz, 1H, H-3′ax), 1.16 ppm (m, 1H, H-7a); MS (ES): $m/z = 813$ $[M+Na]^+$; HR-MS (ES) for $C_{34}H_{50}NaN_2O_{19}$; calcd: 813.2905; found: 813.2905.

Received: May 26, 2003 [Z51969]

Keywords: glycosides · metalation · reduction · samarium · sialic acids

[1] C. A. King, F. K. Stevenson, *Chem. Ind.* **1997**, 266; T. Toyokuni, A. K. Singhal, *Chem. Soc. Rev.* **1995**, *24*, 231.
[2] S.-I. Hakomori, *Adv. Cancer Res.* **1989**, *52*, 257.
[3] R. R. Koganty, M. A. Reddish, B. M. Longenecker in *Glycopeptides and Related Compounds* (Eds.: D. G. Large, C. D. Warren), Marcel Dekker, New York, **1997**, p. 707; S. J. Danishefsky, J. R. Allen, *Angew. Chem.* **2000**, *112*, 882; *Angew. Chem. Int. Ed.* **2000**, *39*, 836.
[4] T. Jensen, P. Hansen, L. Galli-Stampino, S. Mouritsen, K. Frische, E. Meinjohanns, M. Meldal, O. Werdelin, *J. Immunol.* **1997**, *158*, 3769.

 © 2003 Wiley-VCH Verlag GmbH & Co. KGaA, Weinheim

[5] D. Urban, T. Skrydstrup, J.-M. Beau, *Chem. Commun.* **1998**, 955.

[6] Similar work appeared very recently: B. Kuberan, S. A. Sikkander, H. Tomiyama, R. J. Linhardt, *Angew. Chem.* **2003**, *115*, 2119; *Angew. Chem. Int. Ed.* **2003**, *42*, 2073. For another approach to a C-sialyl disaccharide, see W. Notz, C. Hartel, B. Waldscheck, R. R. Schmidt, *J. Org. Chem.* **2001**, *66*, 4250.

[7] Part of this work was presented at the *XIth European Carbohydrate Symposium*, Lisbon (Portugal), **2001**, Abstract PA096, p. 224.

[8] For a modular approach using oligosaccharidyl donors related to the parent sialylTn disaccharide, see D. Sames, X.-T. Chen, S. J. Danishefsky, *Nature* **1997**, *389*, 587; L. A. Marcaurelle, Y. Shin, S. Goon, C. R. Bertozzi, *Org. Lett.* **2001**, *3*, 3691.

[9] Neutral hexoses: a) D. Mazéas, T. Skrydstrup, O. Doumeix, J.-M. Beau, *Angew. Chem.* **1994**, *106*, 1457; *Angew. Chem. Int. Ed. Engl.* **1994**, *33*, 1383; b) D. Mazéas, T. Skrydstrup, J.-M. Beau, *Angew. Chem.* **1995**, *107*, 990; *Angew. Chem. Int. Ed. Engl.* **1995**, *34*, 909; c) T. Skrydstrup, D. Mazéas, M. Elmouchir, G. Doisneau, C. Riche, A. Chiaroni, J.-M. Beau, *Chem. Eur. J.* **1997**, *3*, 134; d) T. Skrydstrup, O. Jarreton, D. Mazéas, D. Urban, J.-M. Beau, *Chem. Eur. J.* **1998**, *4*, 655; e) O. Jarreton, T. Skrydstrup, J.-M. Beau, *Chem. Eur. J.* **1999**, *5*, 430; f) N. Miquel, G. Doisneau, J.-M. Beau, *Angew. Chem.* **2000**, *112*, 4277; *Angew. Chem. Int. Ed.* **2000**, *39*, 4111.

[10] 2-Deoxy-2-acetamido sugars: a) D. Urban, T. Skrydstrup, C. Riche, A. Chiaroni, J.-M. Beau, *Chem. Commun.* **1996**, 1883; b) D. Urban, T. Skrydstrup, J.-M. Beau, *J. Org. Chem.* **1998**, *63*, 2507; c) L. Andersen, L. M. Mikkelsen, J.-M. Beau, T. Skrydstrup, *Synlett* **1998**, 1393.

[11] Reviews: a) J.-M. Beau, T. Gallagher, *Top. Curr. Chem.* **1997**, *187*, 1; b) Y. Du, R. J. Linhardt, I. R. Vlahov, *Tetrahedron* **1998**, *54*, 9913; c) T. Skrydstrup, J.-M. Beau in *Advances in Free Radical Chemistry, Vol. 2* (Eds.: S. Z. Zard), Jai, Stamford, **1999**, p. 89. Reviews with emphasis on C oligomers: T. Skrydstrup, B. Vauzeilles, J.-M. Beau in *Oligosaccharides in Chemistry and Biology—A Comprehensive Handbook, Vol. 1* (Eds.: B. Ernst, P. Sinaÿ, G. Hart), Wiley-VCH, Weinheim, **2000**, p. 495; J.-M. Beau, B. Vauzeilles, T. Skrydstrup in *Glycoscience: Chemistry and Chemical Biology, Vol. 3* (Eds.: B. Fraser-Reid, K. Tatsuta, J. Thiem), Springer, Heidelberg, **2001**, p. 2679.

[12] I. R. Vlahov, P. I. Vlahova, R. J. Linhardt, *J. Am. Chem. Soc.* **1997**, *119*, 1480.

[13] a) T. Polat, Y. Du, R. J. Linhardt, *Synlett* **1998**, 1195; b) Y. Du, R. J. Linhardt, *Carbohydr. Res.* **1998**, *309*, 161.

[14] For the reductive samariation of glycyl sulfide derivatives, see M. Ricci, L. Madariaga, T. Skrydstrup, *Angew. Chem.* **2000**, *112*, 248; *Angew. Chem. Int. Ed.* **2000**, *39*, 242; M. Ricci, P. Blakskjaer, T. Skrydstrup, *J. Am. Chem. Soc.* **2000**, *122*, 12413.

[15] a) A. Lubineau, J. Le Gallic, *J. Carbohydr. Chem.* **1991**, *10*, 263; b) H. B. Mereyala, V. V. Reddy, *Carbohydr. Res.* **1993**, *242*, 277.

[16] a) P. Girard, J.-L. Namy, H. B. Kagan, *J. Am. Chem. Soc.* **1980**, *102*, 2693; for recent reviews on the use of SmI_2 in organic synthesis, see P. G. Steel, *J. Chem. Soc. Perkin Trans. 1* **2001**, 2727; A. Krief, A.-M. Laval, *Chem. Rev.* **1999**, *99*, 745; G. A. Molander, C. R. Harris, *Tetrahedron* **1998**, *54*, 3321.

[17] The anomeric phenyl sulfide analogous to 2-pyridyl sulfide **3** is unreactive under the conditions used. A complete study with other anomeric substituents will be reported shortly.

[18] J. Haverkamp, T. Spoormaker, L. Dorland, J. F. G. Vliegenthart, *J. Am. Chem. Soc.* **1979**, *101*, 4851; D. W. Norbeck, J. B. Kramer, P. A. Lartey, *J. Org. Chem.* **1987**, *52*, 2174.

[19] L.-X. Wang, Y. C. Lee, *J. Chem. Soc. Perkin Trans. 1* **1996**, *19*, 581.

[20] *N*-acetyl-D-glucosamine was transformed to methyl glycoside **6** by the following sequence:[21] a) MeOH, Dowex 50W-X8-H^+ form , 25°C, 24 h; PivCl, pyridine, CH_2Cl_2, 0°C; 80% (2 steps); b) Tf_2O, pyridine, DCE, H_2O, 0°C, 0.5 h; H_2O, 90°C, 2 h; MeONa, MeOH, 25°C; 59% (3 steps). Piv = pivaloyl, Tf = trifluoromethanesulfonyl, DCE = 1,2-dichloroethane.

[21] L. Lay, F. Nicotra, L. Panza, G. Russo, *Helv. Chim. Acta* **1994**, *77*, 509; L. Rochepeau-Jobron, J.-C. Jacquinet, *Carbohydr. Res.* **1998**, *305*, 181.

[22] Y. Gao, K. B. Sharpless, *J. Am. Chem. Soc.* **1988**, *110*, 7538.

[23] A. Vargas-Berenguel, F. Santoyo-González, J. A. Calvo-Asín, F. G. Calvo-Flores, J. M. Expósito-López, F. Hernández-Mateo, J. Isac-García, J. J. Giménez Martínez, *Synthesis*, **1998**, 1778; see also F. Dagron, A. Lubineau, *J. Carbohydr. Chem.* **2000**, *19*, 311.

[24] J. M. Benito, C. Ortiz Mellet, J. M. García Fernández, *Carbohydr. Res.* **2000**, *323*, 218.

[25] This is in complete contrast to the good results obtained in other series;[9f] see also N. Miquel, G. Doisneau, J.-M. Beau, *Chem. Commun.* **2000**, 2347.

[26] Concomittant reduction of the acetamido group also provided 20% of the corresponding *N*-ethyl derivative.

[27] It is interesting to note that the same samarium–Reformatsky coupling reaction conducted with the corresponding anomeric chloride failed,[13a] and provided only the reduction products of both the chloride and the aldehyde **12** in high yield. Since this aldehyde is unusually sensitive to reduction by SmI_2, a much faster transfer rate of the first electron in the pyridyl sulfide **3** (inner-sphere transfer) compared to that of the chloride (outer-sphere transfer) most certainly explains this dramatic difference.

[28] O. Jarreton, T. Skrydstrup, J.-M. Beau, *Chem. Commun.* **1996**, 1661; O. Jarreton, T. Skrydstrup, J.-M. Beau, *Chem. Eur. J.* **1999**, *5*, 430.

[29] Besides NOE measurements and $^3J_{C1,H3ax}$ values as determined in isomers **4**, the stereochemical assignment of the quaternary center in **16** (C-2′) may also be based on empirical data extracted from simple 1D ^{1}H NMR spectra: the chemical shift of H4′ (4.76 ppm in **16**) and the $\Delta\delta$ value of H9a-H9b (0.24 ppm in **16**). For the empirical rules with C-glycosides see refs. [12, 13] and with O-glycosides, see H. Paulsen, H. Tietz, *Angew. Chem.* **1982**, *94*, 934; *Angew. Chem. Int. Ed. Engl.* **1982**, *21*, 927; K. Okamoto, T. Kondo, T. Kondo, *Bull. Chem. Soc. Jpn.* **1987**, *60*, 637.

[30] Review: G. J. Boons, A. V. Demchenko, *Chem. Rev.* **2000**, *100*, 4539. See also A. Meijer, U. Ellervik, *J. Org. Chem.* **2002**, *67*, 7407, and references therein.

[31] J. E. Yule, T. C. Wong, S. Gandhi, M. A. Riopel, R. R. Koganty, *Tetrahedron Lett.* **1995**, *36*, 6839.

[32] S. Palmier, B. Vauzeilles, J.-M. Beau, *Org. Biomol. Chem.* **2003**, *1*, 1097.

 © 2003 Wiley-VCH Verlag GmbH & Co. KGaA, Weinheim

Self-Assembly of Cobalt Nanorods

Unprecedented Crystalline Super-Lattices of Monodisperse Cobalt Nanorods**

Frédéric Dumestre, Bruno Chaudret, Catherine Amiens, Marc Respaud, Peter Fejes, Philippe Renaud, and Peter Zurcher*

Magnetic nanomaterials display new interesting fundamental properties and potentially have many applications.[1–4] One of the most promising applications, high-density information storage, requires spatially separated particles in the nanometer range that act as single magnetic domains, are ferromagnetic at room temperature, and are electrically isolated.[5] In this respect, the preparation of well-ordered two- and three-dimensional (2D and 3D) super-lattices is of crucial importance.[6] Several synthetic routes towards Fe[6] and Co[7,8] nanoparticles have recently been developed, for example, through the decomposition of carbonyl compounds. A high magnetic anisotropy is, however, necessary for spherical nanoparticles to be ferromagnetic at room temperature. This can be achieved, as recently reported, through formation of bimetallic Co/Pt or Fe/Pt nanoparticles.[9–11] Another approach is to use nonspherical nanoparticles which may display large shape anisotropy. Recently, Alivisatos and co-workers described the formation of cobalt nanodisks from the decomposition of $[Co_2(CO)_8]$ in the presence of trioctylphosphane oxide (TOPO) and oleic acid (*cis*-9-octadecenoic acid).[12] At the same time we reported the selective formation of cobalt nanorods and nanowires, as well as the control of their aspect ratio through the decomposition of organometallic precursors in the presence of a mixture of long-chain amines and oleic acid.[13] Anisotropic structures, however, also require organization in 2D or 3D super-lattices to be of practical interest. While the formation of such assemblies from spherical nanoparticles is well-documented,[8,14–18] only a few reports concern the organization of nanorods,[19,20] and the formation of crystalline super-lattices has not been reported.

Our research group has been involved for a long time in the synthesis of nanoparticles from non-carbonyl organometallic precursors.[21–24] Decomposition of such compounds affords by-products that are not detrimental to the intrinsic properties, such as the magnetic moments, of the particles.[22] We have also reported that the use of weakly coordinating ligands may enable the control of shape in solution.[23] This technique has been used for the formation of nickel nanorods in the presence of long-chain amines[24] and, recently, of the cobalt nanorods mentioned above.[13] The exact mechanism controlling both the formation of the rods and their dimensions remain unclear. One striking observation is, however, that the same ligand systems can be used to control the self-assembly of the spherical particles and the shape of the nanorods.

This observation prompted us to try to understand the exact role of the ligand system in shape control and also to finely tune the ligand system to produce monodisperse nanorods that were able to self-assemble. We now report on the formation of unprecedented 2D and 3D super-lattices of monodisperse cobalt nanorods through the decomposition of $[Co(\eta^3\text{-}C_8H_{13})(\eta^4\text{-}C_8H_{12})]$[25] in the presence of a mixture of hexadecylamine (HDA) and stearic acid (octadecanoic acid). We also provide evidence for the self-organization of spherical particles prior to coalescence into nanorods.

In a typical reaction $[Co(\eta^3\text{-}C_8H_{13})(\eta^4\text{-}C_8H_{12})]$ was decomposed under H_2 (3 bar) in anisole at 150 °C in the presence of a mixture of a long-chain amine and an acid. The reaction with oleic acid and oleylamine has previously been shown to produce spherical nanoparticles after 3 h (3 nm) and nanorods after 48 h (9 × 40 nm). However, agglomerates and well-dispersed particles were present after a reaction time of 3 h. Careful examination of these agglomerates by TEM after preparation of a very thin layer by ultramicrotomy shows the presence of monodisperse nanoparticles with a diameter of 3 nm included in a 3D network (see Supporting Information). Similar super-lattices of tin nanoparticles have been observed previously and were suggested to result from crystallization in solution.[18] The interparticle distance is about 2.5 nm, and areas where coalescence of the particles occurs are evident. This observation, therefore, suggests that coalescence of the particles occurs inside super-lattices, at least in an initial step.

An attempt was made to optimize the monodispersity of the rods by choosing the most suitable ligands and concentrations. The use of lauric acid (dodecanoic acid, C_{12}) and hexadecylamine (1:1:1 Co/acid/amine) leads to the formation of cobalt nanorods with an approximate size of 5 × 85 nm (**1**). Deposition of one drop of a diluted solution of these rods on the microscopy grid resulted in their self-organization into arrays containing approximately 10 parallel nanorods with an interparticle spacing of about 3 nm (Figure 1B). Using octanoic acid (C_8) instead of lauric acid results in the formation of shorter and wider rods (9 × 33 nm; **2**; Figure 1A). The nanorods produced with stearic acid (C_{18}) have a diameter similar to the previous rods, but are longer (8 ×

[*] Dr. B. Chaudret, F. Dumestre, Dr. C. Amiens
Laboratoire de Chimie de Coordination du CNRS
205, route de Narbonne, 31077 Toulouse Cédex 04 (France)
Fax: (+33) 5-6155-3003
E-mail: chaudret@lcc-toulouse.fr
F. Dumestre, Dr. P. Renaud
Digital DNA Labs
Semiconductor Products Sector, Motorola
le Mirail B.P. 1029, 31023 Toulouse Cédex (France)
Dr. M. Respaud
Laboratoire de la Physique de la Matière Condensée
INSA, 135 avenue de Rangueil, 31077 Toulouse (France)
Dr. P. Fejes, Dr. P. Zurcher
Digital DNA Labs
Semiconductor Products Sector, Motorola
2100 E. Elliot Road, Tempe, AZ 85824 (USA)

[**] The authors thank the CNRS and MOTOROLA S.P.S. for support, M. Vincent Collière, Lucien Datas, and TEMSCAN service (Université Paul Sabatier Toulouse) for TEM measurements, and Dr. Katerina Soulantica for fruitful discussions on particle organization.

Supporting information for this article is available on the WWW under http://www.angewandte.org or from the author.

 DOI: 10.1002/anie.200352090 © 2003 Wiley-VCH Verlag GmbH & Co. KGaA, Weinheim

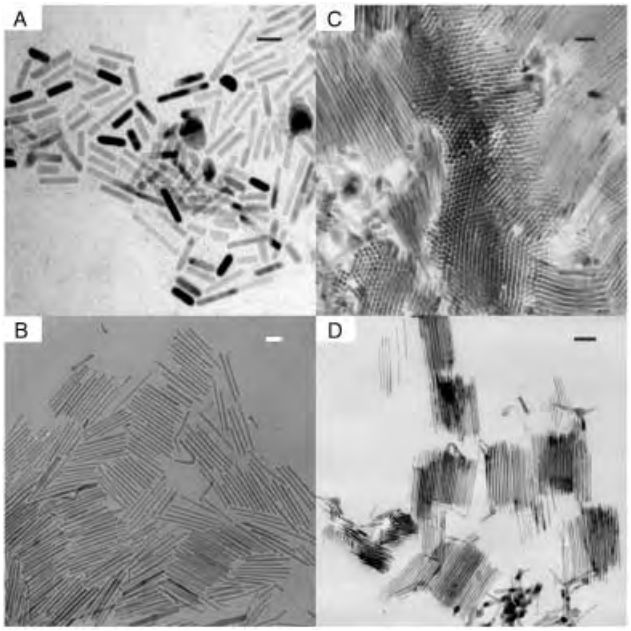


Figure 1. TEM micrographs of nanorods synthesized using hexadecylamine and A) octanoic acid (**2**), B) lauric acid (**1**), and C, D) stearic acid (**3**). The sample used in (C) was prepared by ultramicrotomy. Scale bar: 30 nm.

128 nm; **3**) and more regular in dimensions. Furthermore, the nanorods are organized into unprecedented 3D super-lattices, the largest of which is close to 1 μm (Figures 1C, D and 2). In each case the nanorods precipitate upon cooling the reaction mixture to room temperature. These super-structures are thus most probably formed from the reaction solution by a crystallization process. Ultramicrotomy shows the almost exclusive presence of such super-lattices in all parts of the sample (Figure 1C). In addition, their random orientation on the TEM grid allowed the observation, in selected cases, of the hexagonal cross-section of the nanorods (Figure 2B). The rods are organized in a hexagonal structure with an interparticle distance of approximately 2 nm. This arrangement has been further confirmed by tilting the copper grid in the microscope chamber to bring the growing axis of the nanorod clusters parallel to the electron beam. An interparticle distance of 2.5 nm can also be estimated from the nanorods parallel to the TEM grid (Figure 2A). The nanorods stabilized by lauric acid and/or stearic acid adopt a parallel orientation between one another. The three sets of nanorods consist of a pure hexagonal close-packed (hcp) cobalt structure, with the *c* axis oriented along the growth direction of the nanorods (Figure 2C).

From a magnetic point of view, these nanorods display a strong effective anisotropy (K_{eff}) as a consequence of both their shape and crystalline structure, where the *c* axis linked to the hcp phase is parallel to the rod axis.[26] The magnetic moment of the nanorods can be considered as a macro-spin, with a large energy barrier ($\Delta E = K_{eff} v$) between the up and down directions. The volume (v) and high anisotropy of each individual nanorod lead to a blocking temperature well above room temperature.[27] These systems may, therefore, be very interesting for the storage of very high density magnetic data. Accordingly, these materials, like those previously obtained in the presence of oleic acid, display a ferromagnetic behavior at room temperature. Hysteresis loop measurements at 2 K (Figure 3,) show magnetization $\boldsymbol{M}$(5 T) values of 136, 100, and 142 $A\,m^2\,kg_{Co}^{-}$ for **2, 1**, and **3**, respectively, that are reduced relative to the bulk value ($\boldsymbol{M} = 163\ A\,m^2\,kg_{Co}^{-1}$) and to the value previously reported for rods not showing any sign of organization, but which display an analogous ligand coating.[25] The hysteresis loops display very different shapes and coercive fields $\boldsymbol{H}_c$ of 740, 3200, and 7200 Oe for **2, 1**, and **3**, respectively. Their remanent magnetization also increases from $0.16 \times \boldsymbol{M}$(5 T) in **2** to $0.5 \times \boldsymbol{M}$(5 T) in **3**. As a general rule, parallel nanorods organized into planar arrays, such as **1**, display an antiferromagnetic coupling of their magnetic moments, while chains of nanorods display a ferromagnetic one.[28,29] The coupling is expected to be stronger within the chains than between the planes. The most favorable organization from a magnetic point of view is that observed in **3**, where ferromagnetic chains of nanorods are coupled antiferromagnetically. The existence of antiferromagnetic couplings could be a possible explanation for the low $\boldsymbol{M}$ values measured for **1**–**3.** However, a remanent ferromagnetic order can be induced after saturating the sample, and this will be stabilized by the anisotropy of the nanorods. This result explains the high remanent magnetization of **3**. Finally, an open question is whether the magnetic energy could help the self-organisation process and the formation of 3D lattices. Precise calculations will be performed to estimate this.

Long-chain amine and acid molecules (and now, oleic acid and oleylamine) have become standard reagents both for the control of the self-assembly of different metal and semi-

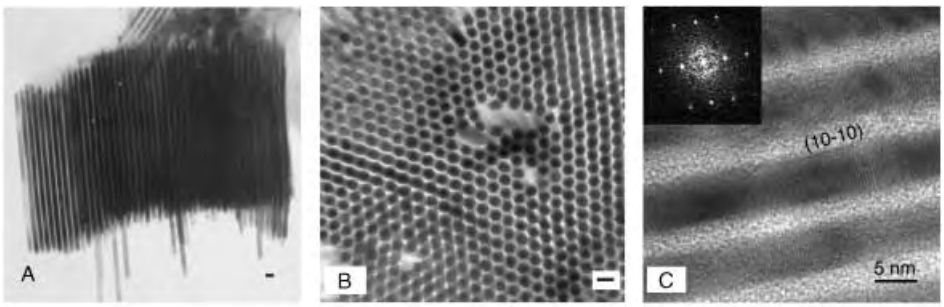


Figure 2. TEM micrographs of self-organized nanorods of **3** (A, B; scale bar: 10 nm). HREM micrograph and electron-diffraction pattern of some aligned rods (C).

 © 2003 Wiley-VCH Verlag GmbH & Co. KGaA, Weinheim

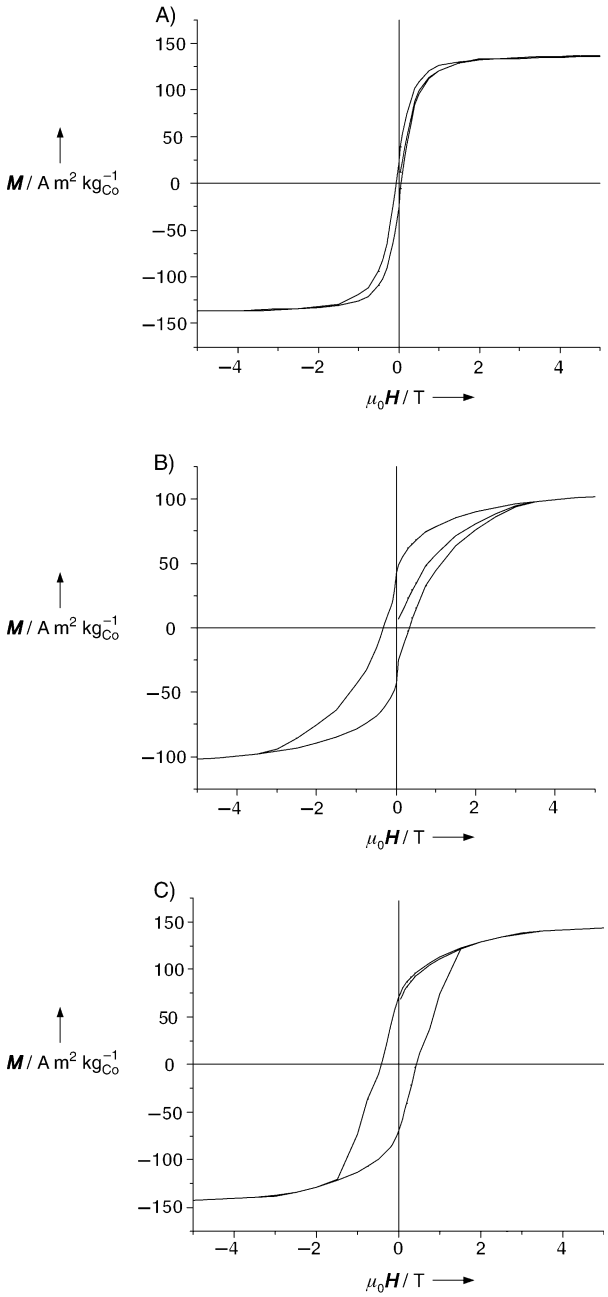


Figure 3. Magnetization curves recorded at 2 K of cobalt nanorods obtained in the presence of: A) HDA and octanoic acid (1:1) (**2**); B) HDA and lauric acid (1:1) (**1**); and C) HDA and stearic acid (1:1) (**3**).

conductor nanoparticles and for the fabrication of nanorods. Monodisperse nanoparticles are produced which assemble into 3D solid super-lattices at the early stage of the reaction. For the oleic acid/oleylamine system we found evidence for the coalescence of some of these particles into rod-shaped particles in a similar way to that observed for particles included inside mesoporous materials.[30] This process could provide seeds for the growth of the rods, although the size of the initial particles (3 nm) is very different from the diameter of the final rods (9 nm). The influence of the chain length of the acid on the dimensions of the rods is not understood. We can, however, point out that gelation has been observed at an early stage of the reaction in the two systems that produce the more regular rods, namely in reactions involving lauric and stearic acid. This gelation could provide a template for the formation of super-lattices of spherical particles and possibly the growth of nanorods. The most important result of this study, the formation of self-assembled nanorods that are strictly monodisperse in terms of both length and diameter, is observed for the longest rods that are obtained with stearic acid (which contains the longest alkyl chain). This system displays bunches of nanorods that are monodisperse in diameter (5 nm) but not in length at the early stage of the reaction, and thus suggests that the coalescence process is facile. In contrast, octanoic acid, which possesses a small alkyl chain, leads to objects displaying smaller aspect ratios. This result may suggest that a good fit of the chain lengths of the acid and amine is necessary to reach monodispersity. The nanorods (**3**) self-organize into 2D and 3D super-structures, inside which they are all aligned in the same direction with a compact, hexagonal arrangement in the perpendicular plane. Some defects are visible, such as the ones shown in Figure 2 B. The interparticle distance in these super-structures is approximately 3 nm when using lauric acid and 2–2.5 nm when using stearic acid. The maximum length of a long-chain ligand directly coordinated to cobalt can be estimated to be about 2.5 nm for stearic acid and HDA, and 1.8 nm for lauric acid. This result implies a different organization for rods **2** and **3**. In the case of **2**, the 3-nm interparticle distance and the formation of monolayers of aligned rods suggests a self-organization on the microscopy grid, in a way similar to that observed for several systems of spherical particles.[21] In contrast, the shorter interparticle distance and the observation of 3D super-lattices for **3** implies interdigitation of the alkyl chains of ligands coordinated to different nanorods, which suggests a real process of direct crystallization in solution, as recently found for tin nanoparticles.[18]

In summary, we have demonstrated that the appropriate choice of ligands and alkyl chain lengths enables the synthesis of ferromagnetic nanorods of monodisperse diameter and length from a non-carbonyl organometallic precursor. This in turn allows the formation of unprecedented hexagonal super-lattices of nanorods as a result of crystallization in solution. The formation of these regular nanorods may result from the initial inclusion of monodisperse spherical particles into 3D super-lattices.

Received: June 10, 2003 [Z52090]
Published Online: October 14, 2003

Keywords: cobalt · magnetic properties · nanostructures · self-assembly

[1] D. Zitoun, M. Respaud, M. C. Fromen, M. J. Casanove, P. Lecante, C. Amiens, B. Chaudret, *Phys. Rev. Lett.* **2002**, *89*, 37203.
[2] N. S. Sobal, M. Hilgendorff, H. Möhwald, M. Giersig, M. Spasova, T. Radetic, M. Farle, *Nano Lett.* **2002**, *2*, 621.

 © 2003 Wiley-VCH Verlag GmbH & Co. KGaA, Weinheim

[3] S. Sun, S. Anders, T. Thomson, J. E. E. Baglin, M. F. Toney, H. F. Hamann, C. B. Murray, B. D. Terris, *J. Phys. Chem. B* **2003**, *107*, 5419.

[4] E. V. Shevchenko, D. V. Talapin, H. Schnablegger, A. Kornowski, O. Festin, P. Svedlindh, M. Haase, H. Weller, *J. Am. Chem. Soc.* **2003**, *125*, 9090.

[5] D. Weller, A. Moser, *IEEE Trans. Magn.* **1999**, *35*, 4423.

[6] S. J. Park, K. Seungsoo, S. Lee, Z. G. Khim, K. Char, T. Hyeon, *J. Am. Chem. Soc.* **2000**, *122*, 8581.

[7] S. Sun, C. B. Murray, *J. Appl. Phys.* **1999**, *85*, 4325.

[8] M. P. Pileni, J. Legrand, C. Petit, *J. Phys. Chem. B* **2001**, *105*, 5643.

[9] E. Shevchenko, D. Talapin, A. Kornovski, F. Wiekhorst, J. Kötzler, M. Haase, A. Rogach, H. Weller, *Adv. Mater.* **2002**, *14*, 287.

[10] E. V. Shevchenko, D. V. Talapin, A. L. Rogach, A. Kornowski, M. Haase, H. Weller, *J. Am. Chem. Soc.* **2002**, *124*, 11480.

[11] S. Sun, C. B. Murray, D. Weller, L. Folks, A. Moser, *Science* **2000**, *287*, 1989.

[12] V. F. Puntes, D. Zanchet, C. K. Erdonmez, A. P. Alivisatos, *J. Am. Chem. Soc.* **2002**, *124*, 12874.

[13] F. Dumestre, B. Chaudret, C. Amiens, M. C. Fromen, M. J. Casanove, P. Renaud, P. Zurcher, *Angew. Chem.* **2002**, *114*, 4462; *Angew. Chem. Int. Ed.* **2002**, *41*, 4286.

[14] T. Hyeon, S. S. Lee, J. Park, Y. Chung, H. B. Na, *J. Am. Chem. Soc.* **2001**, *123*, 12798.

[15] C. B. Murray, S. H. Sun, H. Doyle, T. Betley, *MRS Bull.* **2001**, *26*, 985.

[16] H. Zeng, J. Li, J. P. Liu, Z. L. Wang, S. Sun, *Nature* **2002**, *420*, 395.

[17] T. Hyeon, Y. Chung, J. Park, S. S. Lee, Y. W. Kim, B. H. Park, *J. Phys. Chem. B* **2002**, *106*, 6831.

[18] K. Soulantica, A. Maisonnat, M. C. Fromen, M. J. Casanove, B. Chaudret, *Angew. Chem.* **2003**, *115*, 1989; *Angew. Chem. Int. Ed.* **2003**, *42*, 1945.

[19] B. A. Korgel, S. Fullam, S. Connolly, D. Fitzmaurice, *J. Phys. Chem. B* **1998**, *102*, 8379.

[20] F. Gao, Q. Lu, D. Zhao, *Nano Lett.*, **2003**, *3*, 85.

[21] K. Soulantica, A. Maisonnat, M. C. Fromen, M. J. Casanove, P. Lecante, B. Chaudret, *Angew. Chem.* **2001**, *113*, 462; *Angew. Chem. Int. Ed.* **2001**, *40*, 448.

[22] M. Respaud, J. M. Broto, H. Rakoto, A. R. Fert, L. Thomas, B. Barbara, M. Verelst, E. Snoeck, P. Lecante, A. Mosset, J. Osuna, T. Ould Ely, C. Amiens, B. Chaudret, *Phys. Rev. B* **1998**, *57*, 2925.

[23] C. Pan, K. Pelzer, K. Philippot, B. Chaudret, F. Dassenoy, P. Lecante, M. J. Casanove, *J. Am. Chem. Soc.* **2001**, *123*, 7584.

[24] N. Cordente, M. Respaud, F. Senocq, M. J. Casanove, C. Amiens, B. Chaudret, *Nano Lett.* **2001**, *1*, 565.

[25] S. Otsuka, M. Rossi, *J. Chem. Soc. A* **1968**, 2630.

[26] The magnetocrystalline anisotropy of hcp Co is $K_u = 4 \times 10^5\,J\,m^{-3}$. The shape anisotropy can be estimated to be $K_S = 4(\pm 1) \times 10^5\,J\,m^{-3}$ (From R. C. O'Handley, *Modern Magnetic Materials*, Wiley, New York, **2000**). Thus, the effective anisotropy is $K_{eff} = K_S + K_u = 8(\pm 1) \times 10^5\,J\,m^{-3}$.

[27] The blocking temperature (T_B) associated with the superparamagnetic transition is given by $T_B = \Delta E/25\,k_B$ for quasi-static magnetic measurements. In all the cases, T_B is well above the Curie temperature of Co.

[28] P. Politi, M. G. Pini, *Phys. Rev. B* **2002**, *66*, 4414.

[29] J. M. Luttinger, L. P. R. Tisza, *Phys. Rev.* **1946**, *70*, 954.

[30] Y. Guari, K. Soulantica, K. Philippot, C. Thieuleux, A. Mehdi, C. Reyé, B. Chaudret, R. J. P. Corriu, *New J. Chem.* **2003**, *27*, 1029.

 © 2003 Wiley-VCH Verlag GmbH & Co. KGaA, Weinheim

Difluoromethylenation

Difluoromethyl Phenyl Sulfone as a Selective Difluoromethylene Dianion Equivalent: One-Pot Stereoselective Synthesis of *anti*-2,2-Difluoropropane-1,3-diols**

G. K. Surya Prakash, Jinbo Hu, Thomas Mathew, and George A. Olah*

That more and more organofluorine compounds have been found to display biological effects such as mimicry, blocking, polarity, and lipophilicity is attributed to the unique properties of the fluorine atom.[1] For instance, the C–F bond mimics the C–H bond because of its similar bond length, and the difluoromethylene group is isosteric and isopolar to an ethereal oxygen atom.[2] Hence, the synthesis of fluorine-containing analogues of bioactive natural products is of great interest because of their potential applications in the pharmaceutical industry.[3] Since *anti*-1,3-diol functionality is a fundamental unit in many naturally occurring compounds, its stereoselective preparation is attractive to synthetic organic chemists.[4] *anti*-2,2-Difluoropropane-1,3-diols **3** are a group of interesting compounds, but not much is known about their synthesis. To the best of our knowledge, the only reported method to synthesize these compounds is by diasteroselective Meerwein–Pondorff–Verley reduction of α,α-difluoro-β-hydroxy ketones.[5] The disadvantage of this approach is the need to prepare the α,α-difluoro-β-hydroxy ketone precursors.

In 1997, we reported the preparation of difluorobis(trimethylsilyl)methane ($TMSCF_2TMS$) as a potential difluoromethylene dianion ("$^{-}CF_2^{-}$") equivalent.[2] However, $TMSCF_2TMS$ was found only to couple with one equivalent of an aldehyde, for example, with benzaldehyde to give 2,2-difluoro-1-phenylethanol (after acid hydrolysis).[2]

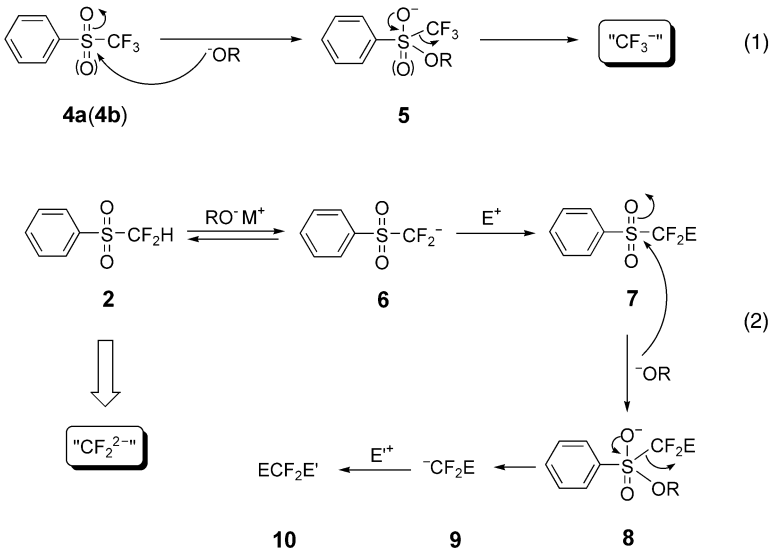
We recently disclosed alkoxide- and hydroxide-induced nucleophilic trifluoromethylation of nonenolizable carbonyl compounds and disulfides by using trifluoromethyl sulfone or sulfoxide.[6] The chemistry is based on the nucleophilic attack by alkoxide (commonly potassium *tert*-butoxide) or hydroxide on the sulfur center of trifluoromethyl phenyl sulfone (**4a**) or sulfoxide (**4b**) to release a trifluoromethyl anion [Scheme 1, Eq. (1)]. We assumed that a similar type of S–C bond cleavage could occur with difluoromethyl phenyl

[*] Prof. Dr. G. K. S. Prakash, Dr. J. Hu, Dr. T. Mathew, Prof. Dr. G. A. Olah
Loker Hydrocarbon Research Institute and
Department of Chemistry
University of Southern California
University Park, Los Angeles, CA 90089-1661 (USA)
Fax: (+1) 213-740-6270
E-mail: gprakash@usc.edu

[**] Support of our work by Loker Hydrocarbon Research Institute is gratefully acknowledged. Professor G. Rasul is thanked for his help with preliminary theoretical calculations.

Supporting information for this article is available on the WWW under http://www.angewandte.org or from the author.

 © 2003 Wiley-VCH Verlag GmbH & Co. KGaA, Weinheim DOI: 10.1002/anie.200352172



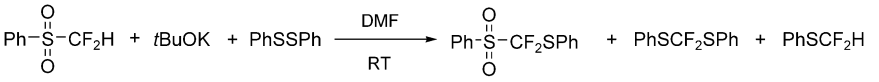
Scheme 1. Mechanistic considerations. R = H, alkyl group. E, E′ = electrophiles, such as disulfides and aldehydes.

sulfone **2** ($PhSO_2CF_2H$). The chemistry of **2** is even more interesting than that of **4a** [Scheme 1, Eq. (2)]. It is known that the hydrogen atom of the CF_2H group in compound **2** is rather acidic, and a common base such as sodium methoxide or even aqueous sodium hydroxide can deprotonate it in an equilibrium mode to generate $PhSO_2CF_2^-$ (**6**).[7,8] In 1989, Stahly showed that anion **6**, generated in situ, can react with aldehydes to give difluoromethylated carbinols in aqueous NaOH in the presence of a phase-transfer agent.[8] However, he did not observe any S–C bond cleavage in aqueous NaOH (RT, 4 h). Obviously, aqueous NaOH is not nucleophilic enough to activate the S–C bond scission, and with hydroxide or alkoxide the deprotonation of difluoromethyl sulfone **2** is much faster than S–C bond cleavage. Thus, by use of an appropriate alkoxide such as *t*BuOK that acts both as a base and a nucleophile, sulfone **2** might react stepwise with two electrophiles to give new difluoromethylene-containing products [Scheme 1, Eq. (2)]. Thus, difluoromethyl phenyl sulfone **2** can be regarded as a selective difluoromethylene dianion ("CF_2^{2-}") synthon.

With the above considerations in mind, we first treated the $PhSO_2CF_2H$/*t*BuOK system with diphenyl disulfide (PhSSPh) as an electrophile. The results are shown in Table 1. By using different reactant ratios, both monosubstitution product **12** and disubstitution product **13** can be obtained at room temperature with high selectivity (Table 1, entries b and g). This result confirms our previous assumption that the reactivities of deprotonation and S–C bond cleavage are different, and that these two steps can be controlled selectively (see Scheme 2). An excess of *t*BuOK facilitates completion of S–C bond-cleavage process, which is similar to our previous observations with the trifluoromethyl sulfone system.[6] Furthermore, the formation and consumption of $PhSCF_2H$ (**14**) with time (Table 1, entries e and f) indicate that there is an equilibrium between anionic species **16** and **14** with protonation/deprotonation by *t*BuOH/*t*BuOK.

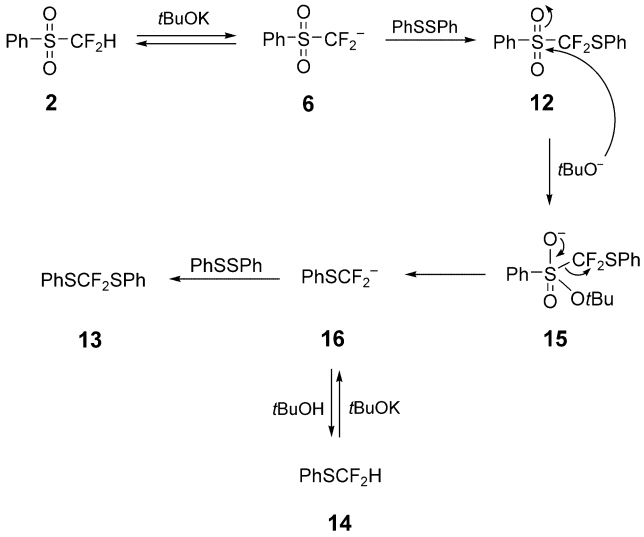
Reaction of benzaldehyde (**1a**) and sulfone **2**/*t*BuOK in DMF is much more intriguing and rewarding (see Scheme 3). Similar to the reaction with diphenyl disulfide, $PhSO_2CF_2H$ (1.0 equiv)/*t*BuOK (3.0 equiv) reacts with **1a** (2.0 equiv) at −50 °C→RT over 90 min to generate monosubstituted product **17** (^{19}F NMR: 41 % yield), as earlier shown by Stahly in aqueous NaOH,[8] and disubstituted product **3a** (^{19}F NMR: 58 % yield, *anti*/*syn* = 98/1). When **2** (1.0 equiv)/*t*BuOK (4.0 equiv) reacted with PhCHO (3.0 equiv) at −50 °C→RT for 8 h with

Table 1: Difluoromethylenation of PhSSPh with **2**.



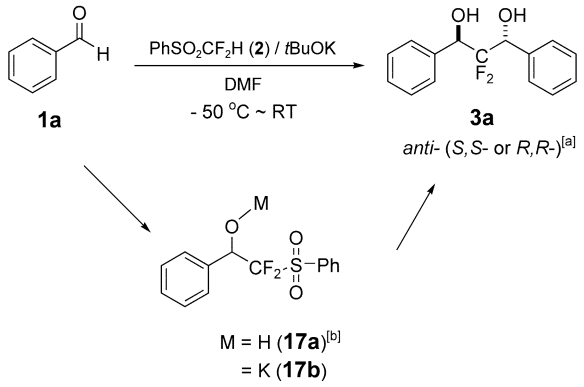
Entry	Reactant ratio [equiv]			Reaction time	Product yield [%][a]		
	2	*t*BuOK	**11**		**12**	**13**	**14**
a	1	1.0	1.0	30 min	76	0	5
b	1	1.5	1.0	50 min	91	3	6
c	1	2.5	2.0	14 h	64	22	14
d	1	3.0	2.0	4 h	41	44	14
e	1	3.5	2.0	4 h	0	84	16
f	1	3.5	2.0	15 h	0	97	3
g	1	4.0	2.0	4 h	0	99	0

[a] Yields were determined by ^{19}F NMR spectroscopy with $PhOCF_3$ as the internal standard.



Scheme 2. Stepwise formation of **12** and **13**.

 © 2003 Wiley-VCH Verlag GmbH & Co. KGaA, Weinheim



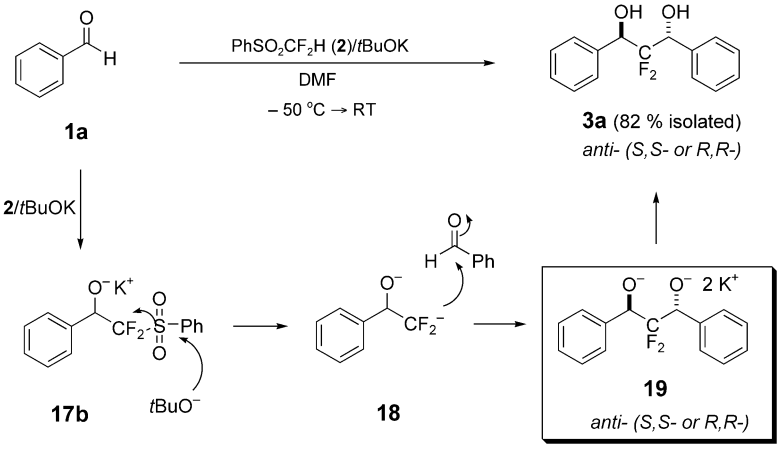
Scheme 3. Reaction of PhCHO (excess) and **2**/*t*BuOK. [a] ^{19}F NMR for *anti* isomer: $\delta = -120.9$ ppm (pseudo t, $^{3}J(F,H) = 11.4$ Hz, 2F). [b] ^{19}F NMR: $\delta = -104.4$ ppm (dd, $J = 238.0$, 2.8 Hz, 1F); $\delta = -119.8$ ppm (dd, $J = 238.0$, 21 Hz, 1F).

activation by *t*BuOK, alkoxide **17b** is formed in situ and undergoes S–C bond fission to generate dianionic intermediate **18**, which can react with a further equivalent of benzaldehyde to form disubstituted *anti*-diol **3a** in excellent yield (^{19}F NMR: 92%, isolated product: 82%) and high diastereoselectivity (*anti*/*syn* = 97/3, *de* = 94%). The observed high diastereoselectivity can be interpreted by a charge–charge repulsion effect during the second addition (Scheme 4). To the best of our knowledge, this may be the first time that high diastereoselectivity has been achieved in the reaction of a dianion with another, neutral electrophile under the influence of an intramolecular charge–charge repulsion effect (during product formation) rather than the traditional steric control (based on Cram's rule).[9,10]

Table 2 demonstrates the application of this methodology to the synthesis of various 2,2-difluoropropane-1,3-diols with high stereoselectivity from nonenolizable aldehydes.[11] The yields of diols are a bit lower for electron-rich aldehydes (entries d and g), probably due to the relative instability of the corresponding dianion intermediates.

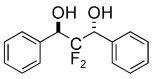
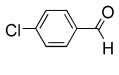
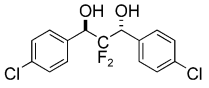
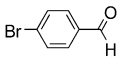
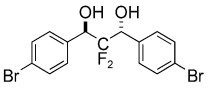
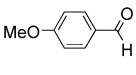
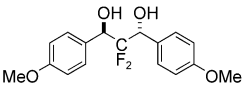
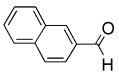
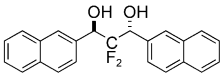
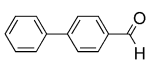
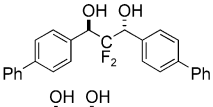
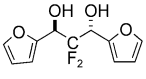
Besides symmetrical *anti*-2,2-difluoropropane-1,3-diols, this new methodology can also be used to synthesize unsymmetrical *anti*-2,2-difluoropropane-1,3-diols. Scheme 5 shows an example of this type of synthesis. Difluoro(phenylsulfonyl)methyl-substituted alcohol **17a** can be easily obtained and isolated by Stahly's approach in high yield.[8] Activation of **17a** with *t*BuOK generates the dianion intermediate **18**, which further reacts with *p*-chlorobenzaldehyde **1b** to give unsymmetrical *anti*-2,2-difluoropropane-1,3-diol **20** (after hydrolysis) with high diastereoselectivity.

In conclusion, potassium *tert*-butoxide-induced difluoromethylenation with difluoromethyl phenyl sulfone enables us to synthesize both symmetrical and unsymmetrical *anti*-2,2-difluoropropane-1,3-diols with high diastereoselectivity (up to 94% *de*). This unusual type of high diastereoselectivity was obtained by means of an intramolecular charge–charge repulsion effect rather than the traditional steric control (based on Cram's rule). Difluoromethyl phenyl sulfone can be used as a selective synthon for the difluoromethylene dianion ($^{-}CF_2^{-}$), which can couple with two electrophiles (e.g., diphenyl disulfide or nonenolizable aldehydes) to give new difluorinated products. Since difluoromethyl phenyl sulfone can be readily prepared from inexpensive chemicals such as



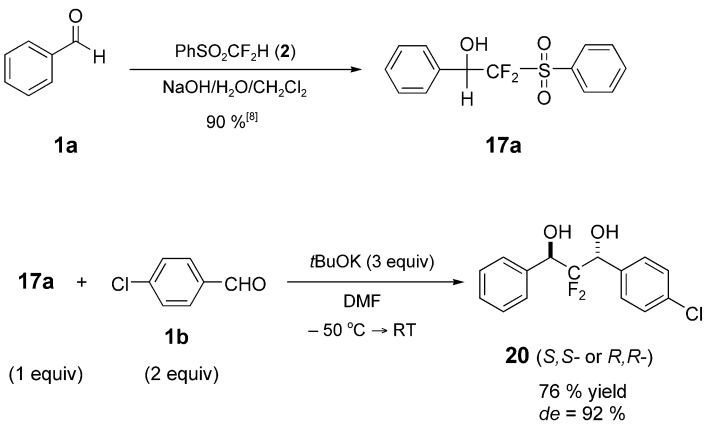
Scheme 4. Proposed mechanism of diastereoselective formation of **3a** from PhCHO and **2**/*t*BuOK.

Table 2: Preparation of 2,2-difluoropropane-1,3-diols **3** from aldehydes **1** (3 equiv) and difluoromethyl phenyl sulfone **2** (1 equiv) with *t*BuOK (4 equiv) in DMF at −50 °C → RT.

Entry	Substrate **1**	Product **3**	Yield [%][a]	*anti*/*syn*[b]	*de* [%]
a			82	97:3	94
b			78	94:6	88
c			70	96:4	92
d			52	94:6	88
e			69	97:3	94
f			75	96:4	92
g			63	93:7	86

[a] Yields of isolated product. [b] *anti*/*syn* ratios were determined by ^{19}F NMR spectroscopy.

 © 2003 Wiley-VCH Verlag GmbH & Co. KGaA, Weinheim



Scheme 5. Synthesis of unsymmetrical *anti*-2,2-difluoropropane-1,3-diol **20**.

CF_2ClH or CF_2Br_2,[12,13] this new methodology provides a convenient and efficient synthetic tool for many potential applications.

Received: June 18, 2003 [Z52172]

Keywords: alcohols · C–C coupling · diastereoselectivity · fluorine

[1] *Organofluorine Compounds. Chemistry and Applications* (Ed.: T. Hiyama), Springer, New York, **2000**.
[2] A. K. Yudin, G. K. S. Prakash, D. Deffieux, M. Bradley, R. Bau, G. A. Olah, *J. Am. Chem. Soc.* **1997**, *119*, 1572–1581, and references therein.
[3] J. McCarthy, *Utility of Fluorine in Biologically Active Molecules*, ACS Fluorine Division Tutorial, 219th National ACS Meeting, (San Francisco), **2000**.
[4] S. Masamune, W. Choy, *Aldrichimica Acta* **1982**, *15*, 47–64.
[5] M. Kuroboshi, T. Ishihara, *Bull. Chem. Soc. Jpn.* **1990**, *63*, 1185–1190.
[6] G. K. S. Prakash, J. Hu, G. A. Olah, *Org. Lett.* **2003**, *5*, 3253–3256.
[7] J. Hine, J. J. Porter, *J. Am. Chem. Soc.* **1960**, *82*, 6178–6181.
[8] P. Stahly, *J. Fluorine Chem.* **1989**, *43*, 53–66.
[9] Recently, two groups reported the control of stereoselectivity by electrostatic repulsion. a) In 1997, Mall and Stamm reported that electrostatic repulsion by the charged tail of a radical controls the stereochemistry of coupling with the anthracenide radical anion: T. Mall, H. Stamm, *J. Chem. Soc. Perkin Trans. 2* **1997**, 2135–2140. b) In 2001, Uneyama et al. reported control of diastereoselectivity by electrostatic repulsion between the negative charge density on a trifluoromethyl group and that of electron-poor aromatic rings: T. Katagiri, S. Yamaji, M. Handa, M. Irie, K. Uneyama, *Chem. Commun.* **2001**, 2054–2055; T. Katagiri, K. Uneyama, *Chirality* **2003**, *15*, 4–9.
[10] DFT calculations (B3LYP6-31G**//B3LYP6-31G* + ZPE level) on 3,3-difluoro-2,4-pentanediolate dianion as a model showed the *anti* structure to be 5.5 kcal mol^{-1} more stable than the corresponding *syn* structure. Furthermore, the absence of changes in the *anti*/*syn* diol ratios on prolonged treatment with base indicate lack of product reversibility.
[11] Typical procedure for *t*BuOK-induced difluoromethylenation: The reaction was commonly carried out in a Schlenk flask under an argon atmosphere. A solution of *t*BuOK (1.12 g, 10 mmol) in DMF (5 mL) was added to solution of difluoromethyl phenyl sulfone (**2**, 480 mg, 2.5 mmol) and benzaldehyde (800 mg, 7.5 mmol) in DMF (5 mL) at −50 °C. The reaction flask was then sealed, and the reaction mixture was then stirred at −50 °C for 1 h, followed by stirring at −50 °C→RT overnight. The reaction mixture was quenched with ice water (20 mL), and extracted with diethyl ether (3 × 20 mL). The combined ethereal phase was washed with a saturated aqueous solution of NH_4Cl, and then with water. After drying over $MgSO_4$, the diethyl ether solvent was removed under vacuum. The crude product was further purified by chromatography on a silica gel column (hexanes/ethyl acetate 9/1, then 1/1) to give 2,2-difluoro-1,3-diphenyl-1,3-propanediol as a white crystalline solid, (541 mg, 82 % yield, *anti*/*syn* = 97/3, determined by ^{19}F NMR). *anti* isomer: ^1H NMR ([D$_6$]actone): $\delta = 5.27$ (m, 4H), 7.28–7.50 ppm (m, 10H); ^{19}F ([D$_6$]acetone): $\delta = -120.9$ ppm (dd, $J = 11$ Hz, $J = 11$ Hz, 2F); HRMS (DCI/NH_3): *m*/*z* calcd for $C_{15}H_{18}F_2NO_2$ [M+NH_4^+]: 282.1305, found: 282.1304.
[12] G. K. S. Prakash, J. Hu, G. A. Olah, *J. Org. Chem.* **2003**, *68*, 4457–4463, and references therein.
[13] J. Hu, Ph.D. Dissertation, University of Southern California, **2002**.

 © 2003 Wiley-VCH Verlag GmbH & Co. KGaA, Weinheim

Optimizing Heterogeneous Catalysts

The Effect of Outer-Sphere Acidity on Chemical Reactivity in a Synthetic Heterogeneous Base Catalyst**

*John D. Bass, Sandra L. Anderson, and Alexander Katz**

Elegant examples of outer-sphere design to control chemical reactivity can be found in the active sites of biological catalysts.[1–5] Unlike biological systems, in which uniformity and isolation of the active site permit control and optimization of the outer sphere,[6] achieving the same in synthetic heterogeneous systems consisting of tethered organic functional groups has remained elusive. This is because such synthetic catalysts typically consist of a distribution of active sites that can range from subnanometer clusters to monolayers with macroscopic dimensions.[7–9] This distribution leads to nonuniform outer-sphere environments that are not amenable to rigorous control by synthetic manipulation.

[*] Prof. A. Katz, J. D. Bass, S. L. Anderson
Department of Chemical Engineering
University of California at Berkeley
Berkeley, CA 94720-1462 (USA)
Fax: (+1) 510-642-4778
E-mail: katz@cchem.berkeley.edu

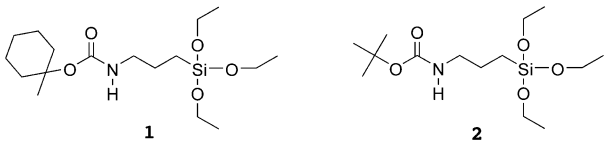
[**] The authors thank Dow, Shell Foundation, and UC Berkeley Department of Chemical Engineering for financial support. J.D.B. is grateful to the Chevron Corporation for a graduate fellowship.

Supporting information for this article is available on the WWW under http://www.angewandte.org or from the author.

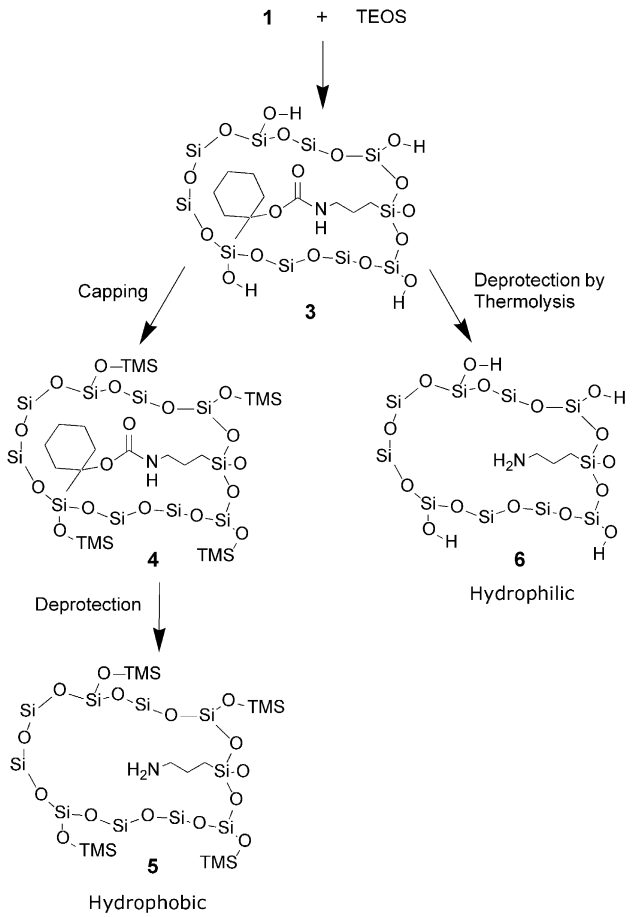
 DOI: 10.1002/anie.200352181 © 2003 Wiley-VCH Verlag GmbH & Co. KGaA, Weinheim

It would be highly desirable to use the framework surrounding an active site to define its outer sphere. Uniform active sites that are isolated from one another by the framework are expected to be most responsive to such an approach to outer-sphere control. Such active sites, each of which consists of a tethered organic functional group, can be synthesized by bulk silica imprinting.[10]

Recently, we developed a strategy for synthesizing bulk imprinted silica that permits the direct comparison of materials that are otherwise identical except for their framework composition at surface defect sites.[11] Here this strategy is used to systematically study the role of the framework as an outer sphere in a synthetic heterogeneous base catalyst. The results are demonstrated for three model chemical transformations, which are discussed in order of increasing mechanistic complexity: the position of equilibrium for intramolecular proton transfer between tautomers, the kinetics of an intramolecular chemical reaction without catalytic turnover, and the kinetics of an intermolecular catalytic reaction.



The imprinting approach is based on imprints **1** and **2** and is illustrated in Scheme 1. Imprint **1** was co-condensed with tetraethyl orthosilicate (TEOS) to form hybrid organic–inorganic sol–gel material **3**. Hydrophobic material **4** was prepared from **3** by capping framework silanol groups with trimethylsilyl groups. Subsequently, the imprint fragment was removed by carbamate deprotection to form **5**. The hydrophilic analogue **6** was prepared directly from **3** by thermolytic deprotection.[11] The same procedure was performed with imprint **2**.



Scheme 1. Hydrophilic and hydrophobic materials prepared by an imprinting approach. Both materials are derived from the same material **3**, which was synthesized from an acid–base-catalyzed sol–gel hydrolysis and condensation. Framework capping with hydrophobic TMS groups gave **4**, and subsequent deprotection yielded hydrophobic material **5**. Direct thermolysis of **3** yields hydrophilic material **6**.

The effect of the framework on intramolecular proton transfer equilibrium was investigated by treating imprinted amines in **5** and **6** with the chromophore salicylaldehyde, which affords reaction products that are amenable to UV/Vis characterization. Previous studies have observed strong solvent effects in analogous imines derived from salicylaldehyde, which give rise to product absorption bands at 400–450 nm corresponding to a zwitterionic product on dissolution in acidic protic solvents, and bands at 320–350 nm corresponding to a neutral phenolic product on dissolution in aprotic solvents.[12] These bands were used to characterize the polarity of alkali-exchanged zeolites by measuring the ratio of absorbance intensities at the corresponding wavelengths.[12–14] Our previous results show that the presence of acidic silanol hydrogen-bond donors stabilizes the zwitterionic form **7** ($\lambda =$ 400–450 nm) over the neutral phenolic form **8** ($\lambda = 320$–350 nm).[11] Accessible acidic silanol groups are present in **6**, whereas they should be almost absent in **5**.

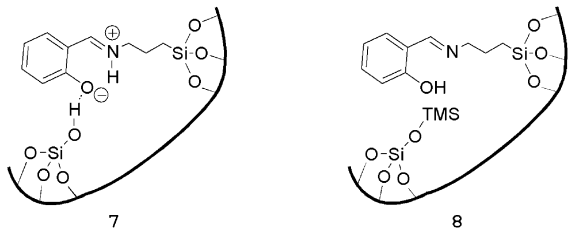


Figure 1 shows the diffuse reflectance UV/Vis spectra of **5** and **6** after treatment with salicylaldehyde. The marked effect of outer-sphere acidity is shown by the strong band at 400 nm for the imino group in **6** and by the substantial absence of this band and the band at 320 nm for the imino group in **5**. This provides compelling evidence that neutral form **8** is present and is thermodynamically preferred in the hydrophobic environment of **5**. In contrast, the zwitterionic form **7** is thermodynamically favored in the hydrophilic environment of **6**.[11] This demonstrates thermodynamic control of a chemical reaction by varying the framework outer sphere.

In a separate experiment, we measured kinetic effects by determining the activation energy for thermolysis of immobilized imprint in **3** and **4**. Although mechanistically more complex than the proton transfer, the thermolysis of carbamates **3** and **4** is expected to be accelerated by the presence of

 © 2003 Wiley-VCH Verlag GmbH & Co. KGaA, Weinheim

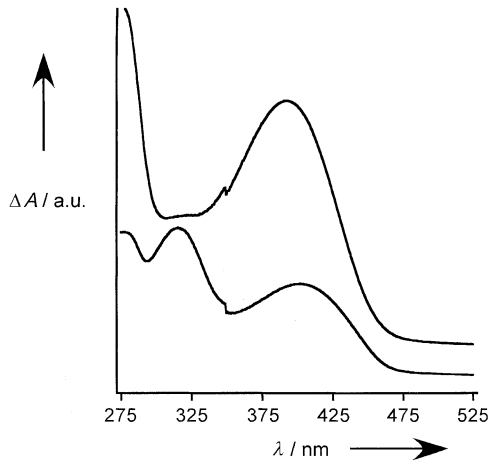


Figure 1. Solid-state diffuse-reflectance UV/Vis spectra of **5** (lower) and **6** (upper) containing a covalently bound solvochromatic indicator. The upper spectrum shows a pronounced zwitterion band on treatment with salicylaldehyde. The lower spectrum shows a strong band from the phenolic form of the indicator.

accessible silanol groups in the outer sphere because of the known acid lability of such carbamates. A related phenomenon has been demonstrated in homogeneous thermolysis of *N*-arylcarbamates of tertiary alcohols, for which the activation energy for thermolysis decreases by approximately 6 kcal mol^{-1} between decane and the protic solvent decanol.[15]

Thermogravimetric analysis (TGA) was used to measure the activation energy for thermolysis of the immobilized imprint. The difference in the temperature required for thermolysis on **3** and **4** is apparent from the data shown in Figure 2. Here, the hydrophobic material **4** reaches maximum thermolysis rates at 237 °C, while this occurs at 170 °C for hydrophilic material **3**. This temperature difference of 67 °C reflects a significant change in the activation energy for

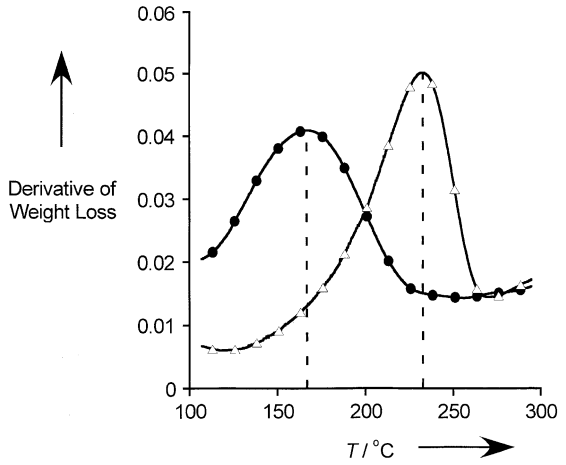


Figure 2. Rate of mass loss during thermolysis of carbamate, as measured by thermogravimetric analysis on hydrophobic **5** (△) and hydrophilic **6** (●). The dashed vertical lines are included for visual clarity, to indicate the temperature at which the maximum rate of thermolysis occurs. Data are shown for a constant heating rate of 1 °C min^{-1}. The rate of mass loss is given in wt% °C^{-1}.

thermolysis between **3** and **4**. The activation energy of thermolysis can be calculated directly from the data in Figure 2, according to the method of Redhead.[16] The activation energy thus calculated for **3** is 24.8 ± 0.3 kcal mol^{-1}, while for **4** it is 29.0 ± 0.3 kcal mol^{-1}. As expected for a system that is limited solely by chemical kinetics, as opposed to transport, these values were essentially unchanged by variations in heating rate, and particle and sample sizes. These results show that the acidic outer sphere in **3** reduces the activation barrier for thermolysis by about 4 kcal mol^{-1} relative to that of **4**. These activation energies are consistent with previously reported activation energies for the olefin-formation step in the thermolysis mechanism, which is thought to be rate-limiting.[15] Similar effects have been observed with imprinted materials derived from **2**.

Finally, we measured the effect of the framework on an intermolecular chemical reaction involving catalytic turnover. We chose the Knoevenagel condensation of isophthalaldehyde and activated methylene compounds, because it was previously shown to be catalyzed by a primary amine on silica.[7,10,17,18] Our hypothesis was that the acidic outer sphere surrounding the primary amine in **6** should lead to higher catalytic rates than the hydrophobic outer sphere in **5**. This hypothesis is consistent with previously observed rate enhancements in Knoevenagel condensations when using heterogeneous catalysts in protic solvents,[19] as well as when using acid–base bifunctional catalysts.[8]

The conversion of isophthalaldehyde in reactions with malononitrile and ethyl cyanoacetate on base catalysts **5** and **6** is shown in Figure 3. Table 1 shows a summary of the turnover frequency (TOF) based on initial isophthalaldehyde conversion rates for reactions with malononitrile and ethyl cyanoacetate. The results for a commercially available catalyst, consisting of a monolayer of 3-aminopropyl groups on the surface of silica, are also shown. There is a large rate enhancement for **6** relative to both **5** and the commercially available surface-functionalized material. For the malononitrile system, the enhancement of **6** over **5** is a factor of about 50; for the ethyl cyanoacetate system, it is a factor of 25. Notably, the rate enhancement of **6** over the surface-functionalized catalyst is 30 for malononitrile and 90 for ethyl cyanoacetate. Background catalysis on the framework is insignificant, and these data are also shown for the use of **3** and **4** prior to carbamate deprotection as catalysts. The results demonstrate a significant outer-sphere effect on catalysis caused by modifications of the acidity of the silica framework surrounding each active site. We have observed similar rate accelerations with materials derived from imprint **2**.

Rational design of the outer sphere by framework modifications should accelerate improvements of heterogeneous catalysts. Our results illustrate this powerful approach for the specific case of an amine base catalyst tethered on silica. This approach is currently being extended to the control of chemical reactivity in other synthetic heterogeneous catalysts.

Experimental Section

Salicylaldehyde binding: Imprinted silica (30 mg) was added to a solution of salicylaldehyde (2.65 mL, 0.005 M, 2 equiv) in acetonitrile

 © 2003 Wiley-VCH Verlag GmbH & Co. KGaA, Weinheim

Table 1: TOFs for Knoevenagel condensation of isophthalaldehyde with malononitrile or ethyl cyanoacetate with **5, 6**, and commercially available surface-functionalized catalysts. TOF is given in events per minute per catalytic site.

No.	Catalyst	Initial TOF [site^{-1} min^{-1}]	
		Malononitrile	Ethyl cyanoacetate
Materials synthesized from imprint **1**			
1	hydrophobic **5**	0.10 ± 0.01	0.011 ± 0.002
2	hydrophilic **6**	4.7 ± 0.4	0.26 ± 0.04
Control materials			
7	Aldrich aminopropyl surface-functionalized silica	0.14 ± 0.01	0.0029 ± 0.0005
8	hydrophilic **3**	0.13[a]	0.022[a]
9	hydrophobic **4**	0.0023[a]	0.0007[a]

[a] TOF in hydrophililic and hydrophobic materials without amines (materials consisting of carbamates prior to deprotection) were calculated by assuming an amine number density corresponding to that in the deprotected materials.

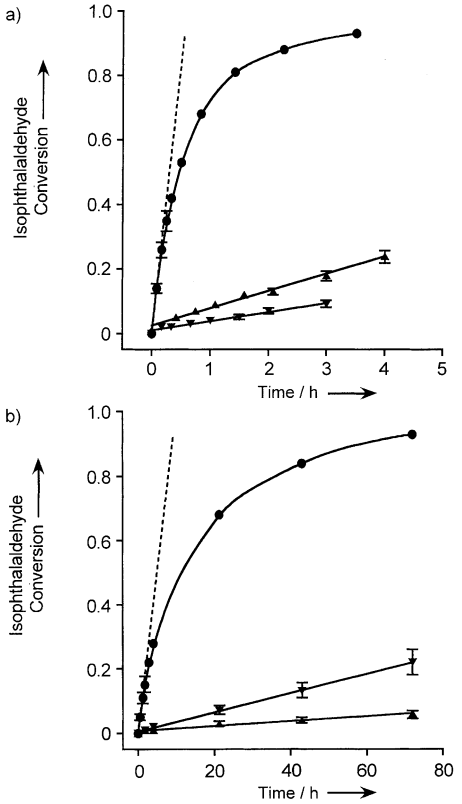


Figure 3. Fractional conversion of isophthalaldehyde as a function of time for base-catalyzed Knoevenagel condensation with a) malononitrile and b) ethyl cyanoacetate. Framework differences between hydrophilic catalyst **6** (●) and hydrophobic catalyst **5** (▼) lead to significant effects in the observed rate of reaction. Also shown (▲) is a commercially available surface-functionalized material consisting of a monolayer of aminopropyl groups grafted onto the surface of mesoporous silica. Dashed lines were used to calculate the initial rate in determining the TOF.

with stirring at room temperature. After the materials had equilibrated and formed the covalently bound imine chromophore on $>80\,\%$ of the amino groups, as monitored by gas chromatography, the materials were collected by filtration, washed with acetonitrile (100 mL), chloroform (100 mL), and pentane (50 mL), and subsequently Soxhlet-extracted in chloroform for 16 h.

Activation energy measurements: TGA was conducted with heating rates varying from 0.13 to 10 °C min^{-1} on samples weighing between 2 and 15 mg. Materials (average particle size of 2 or 10 μm) were placed on platinum pans and analyzed under a nitrogen flow of 20 mL min^{-1}. Average particle diameter was estimated by scanning electron microscopy.

Knoevenagel condensation: A typical reaction was conducted with 10 mg of catalyst (the amount of catalyst was fixed at 0.005 molar equivalents of amine relative to isophthalaldehyde) in 20 mL an anhydrous benzene solution of concentration 0.022 M in isophthalaldehyde and 0.044 M of either malononitrile or ethyl cyanoacetate (reactor-vessel volume was 30 mL). The reaction with malononitrile was performed at room temperature (22 °C), while the reaction with ethyl cyanoacetate was performed at 40 °C. Aliquots were taken by syringe and analyzed by gas chromatography.

Received: June 23, 2003 [Z52181]

Keywords: heterogeneous catalysis · imprinting · sol–gel processes · supported catalysts

[1] E. Breslow, F. R. N. Gurd, *J. Biol. Chem.* **1962**, *237*, 371.
[2] *Annual Review of Biochemistry, Vol. 36* (Ed.: P. D. Boyer), Annual Reviews Inc, Palo Alto, **1967**.
[3] T. K. Harris, G. J. Turner, *IUBMB Life* **2002**, *53*, 85 – 98.
[4] C. F. Barbas III, A. Heine, G. Zhong, T. Hoffmann, S. Gramatikova, R. Björnestedt, B. List, J. Anderson, E. A. Stura, I. A. Wilson, R. A. Lerner, *Science* **1997**, *278*, 2085 – 2092.
[5] A. Karlstrom, G. Zhong, C. Rader, N. A. Larsen, A. Heine, R. Fuller, B. List, F. Tanaka, I. A. Wilson, C. F. Barbas III, R. A. Lerner, *Proc. Natl. Acad. Sci. USA* **2000**, *97*, 3878 – 3883.
[6] M. Inoue, H. Yamada, T. Yasukochi, R. Kuroki, T. Miki, T. Horiuchi, T. Imoto, *Biochemistry* **1992**, *31*, 5545 – 5553.
[7] E. Angeletti, C. Canepa, G. Martinetti, P. Venturello, *Tetrahedron Lett.* **1988**, *29*, 2261 – 2264.
[8] A. Corma, S. Iborra, I. Rodríguez, F. Sánchez, *J. Catal.* **2002**, *211*, 208 – 215.
[9] M. E. Davis, A. Katz, W. R. Ahmad, *Chem. Mater.* **1996**, *8*, 1820 – 1839.
[10] A. Katz, M. E. Davis, *Nature* **2000**, *403*, 286 – 289.
[11] J. D. Bass, A. Katz, *Chem. Mater.* **2003**, *15*, 2757 – 2763.
[12] W. Turbeville, P. K. Dutta, *J. Phys. Chem.* **1990**, *94*, 4060 – 4066.
[13] P. K. Dutta, W. Turbeville, *J. Phys. Chem.* **1991**, *95*, 4087 – 4092.
[14] I. Casades, M. Alvaro, H. Garcia, M. N. Pillai, *Eur. J. Org. Chem.* **2002**, 2074 – 2079.
[15] S. J. Ashcroft, M. P. Thorne, *Can. J. Chem.* **1972**, *50*, 3478 – 3487.
[16] P. A. Redhead, *Vacuum* **1962**, *12*, 203 – 211. Similar results can be obtained by using another model by Kissinger: H. E. Kissinger, *Anal. Chem.* **1957**, *29*, 1702 – 1706.
[17] M. L. Kantam, P. Sreekanth, *Catal. Lett.* **1999**, *57*, 227 – 231.
[18] E. C. Angeletti, C. Canepa, G. Martinetti, P. Venturello, *J. Chem. Soc. Perkin Trans. 1* **1989**, 105 – 107.
[19] P. Laszlo, *Acc. Chem. Res.* **1986**, *19*, 121 – 127.

 © 2003 Wiley-VCH Verlag GmbH & Co. KGaA, Weinheim

σ-Bond Metathesis

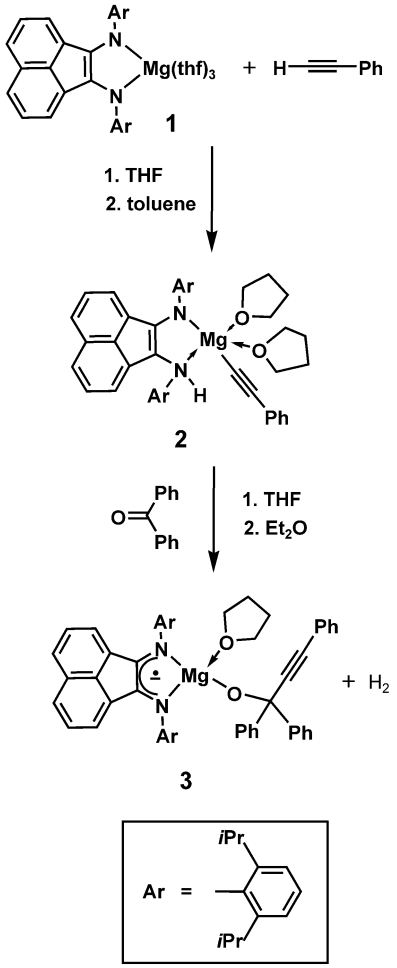
Oxidative Addition of Phenylacetylene through C–H Bond Cleavage To Form the Mg^{II}–dpp-bian Complex: Molecular Structure of [Mg{dpp-bian(H)}(C≡CPh)(thf)$_2$] and Its Diphenylketone Insertion Product [Mg(dpp-bian)$^{\bullet-}${OC(Ph$_2$)C≡CPh}(thf)] **

Igor L. Fedushkin, Natalie M. Khvoinova, Alexandra A. Skatova, and Georgy K. Fukin*

Dedicated to Professor Viktor A. Dodonov on the occasion of his 70th birthday

Over the past decade dpp-bian began to be used widely in coordination chemistry owing to a number of interesting chemical reactions, which include catalytic olefin polymerization,[1] shown by the metal complexes based on this ligand.[2] The rigidity and bulkiness of the ligand and its π-acceptor properties cause an electron deficiency at the coordinated metal and render these complexes highly reactive towards organic substrates. However, a huge number of publications and patents until now have been concerned with metal complexes of only neutral dpp-bian ligand. One might suggest that the presence of both extended π-system and Lewis basic nitrogen centers in dpp-bian may enable this ligand to act as an electron and proton reservoir. The ability of dpp-bian to accept up to four electrons to form a tetraanion (dpp-bian)$^{4-}$ upon reduction with sodium in ether was recently verified.[3] We also reported on the synthesis and characterization of the Mg and Ca complexes with dianionic dpp-bian ligand.[4] One of our objectives at present is to test whether these alkaline-earth-metal salts may serve as reducing agents towards organic substrates. It was shown that the magnesium complex [Mg(dpp-bian)(thf)$_3$] (**1**) serves well as a reducing agent towards aromatic ketones.[5] However, in contrast to the 1,3-dipolar cycloaddition of diphenylketone to dianionic 1,4-diaza-1,3-diene lanthanide or Group 4 metal complexes, the reduction of Ph$_2$CO with **1** affords the pinacol coupling product.[5] The reduction of 9-(10*H*)-anthracenone with **1** yields the aryloxy derivative as result of the deprotonation of 9-anthracenol (phenolic tautomer of 9-(10*H*)-anthracenone). Herein, we wish to report the unprecedented oxidative addition of phenylacetylene to **1** through acidic activation of a C–H bond to form the phenylethynyl derivative and the product of diphenylketone insertion thereof.

Complex **1** was prepared by treating an excess of magnesium metal with dpp-bian at reflux in THF for 30 min and was used in situ for the reactions with phenylacetylene. The addition of a five molar excess of the phenylacetylene to the THF solution of **1** causes a quick change in the solution from dark green to dark blue. Removal of the volatile fractions under vacuum and crystallization of the crude product from toluene afforded the alkynyl complex [Mg{dpp-bian(H)}(C≡CPh)(thf)$_2$] (**2**) in 63 % yield as black prisms. As shown by X-ray crystal-structure determination and ^{1}H NMR spectroscopy, the reaction proceeds by oxidative addition with the formation of phenylethynylmagnesium amido/amino complex **2** (Scheme 1).



Scheme 1. Synthesis of complexes **2** and **3**.

Recently Chang and co-workers reported the formation of alkynyl magnesium amides [{Mg(RC≡C)(μ-N*i*Pr$_2$)(thf)}$_2$] (R = Ph, SiMe$_3$) through amine elimination within the stoichiometric reaction between [Mg(*i*Pr$_2$N)$_2$] and HC≡CR in THF.[6] As the dpp-bian acts as chelating ligand in the complexes **1** and **2**, the amine elimination from **2** cannot take place. The X-ray crystal structure of **2** shows that both the

[*] Dr. I. L. Fedushkin, Dipl.-Chem. N. M. Khvoinova, Dr. A. A. Skatova, Dr. G. K. Fukin
G. A. Razuvaev Institute of Organometallic Chemistry
Russian Academy of Sciences
Tropinina 49, 603950 Nizhny Novgorod GSP-445 (Russia)
Fax: (+7) 8312-661-497
E-mail: igorfed@imoc.sinn.ru

[**] This work was supported by the Russian Foundation for Basic Research (Grant No. 03-03-32246), dpp-bian = bis[*N*-(2,6-diisopropylphenyl)imino]acenaphthene. The authors thank Dr. Yu. A. Kurskii for recording the NMR spectra.

 DOI: 10.1002/anie.200352200 © 2003 Wiley-VCH Verlag GmbH & Co. KGaA, Weinheim

amido and the amino function of the dpp-bian ligand chelate the Mg atom. It is noteworthy that even an excess of the alkyne does not force complex **2** to eliminate 1,2-bisaminoacenaphthene. To test whether insertion reactions into alkynyl–Mg bond may be accomplished, we treated complex **2** with diphenylketone. The reaction between **2** and Ph_2CO in THF is completed within several minutes when the solution is heated at 50–60 °C and results in a change from deep blue to violet. Evaporation of the solvent and crystallization of the crude product from diethyl ether gave the corresponding carbinolate [Mg(dpp-bian)$^{\bullet-}${OC(Ph_2)C≡CPh}(thf)] (**3**) in 47 % yield. Surprisingly, an abstraction of a hydrogen atom from the amino functional group of the ligand takes place simultaneously with the insertion of the ketone into the Mg–C bond (Scheme 1). The formation of the radical anion of dpp-bian in the course of the reaction was confirmed by ESR spectroscopy.

The molecular structures of **2** (Figure 1) and **3** (Figure 2) were determined by single-crystal X-ray-diffraction studies on crystals obtained from toluene and diethyl ether, respectively.[7] Compound **2** is a five-coordinated magnesium complex in which the terminal alkynyl fits in the pocket formed by two isopropyl groups of the aryl groups bonded to the nitrogen atoms. The significant difference in Mg–N bond

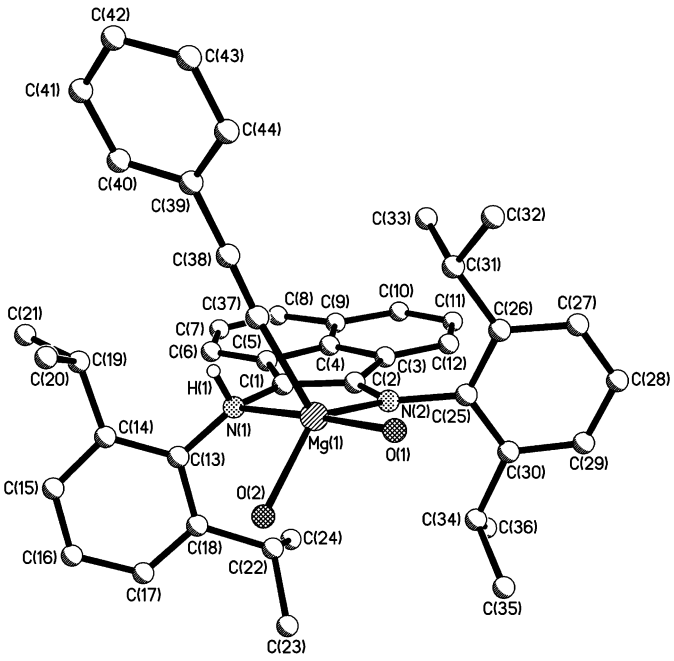


Figure 1. Molecular structure of **2**. The hydrogen atoms are omitted as well as the carbon atoms of the solvent molecules. Selected bond lengths [Å] and angles [°]: Mg(1)-N(1) 2.355(2), Mg(1)-N(2) 2.045(2), Mg(1)-O(1) 2.1233(17), Mg(1)-O(2) 2.0499(17), Mg(1)-C(37) 2.124(3), Mg(1)-C(2) 2.841(2), N(1)-C(13)1.438(3), N(1)-C(1) 1.444(3), N(1)-H(1) 0.889(19), N(2)-C(2) 1.350(3), N(2)-C(25) 1.430(3), C(1)-C(2) 1.378(3), C(1)-C(5) 1.443(3), C(37)-C(38) 1.209(3), C(38)-C(39) 1.435(3); N(2)-Mg(1)-N(1) 80.97(7), O(2)-Mg(1)-O(1) 85.94(7), N(2)-Mg(1)-O(1) 98.95(8), O(1)-Mg(1)-N(1) 177.79(7), O(2)-Mg(1)-N(1) 92.42(7), N(2)-Mg(1)-O(2) 130.06(8), O(1)-Mg(1)-C(37) 95.72(8), O(2)-Mg(1)-C(37) 110.98(9), C(37)-Mg(1)-N(1) 86.24(8), N(2)-Mg(1)-C(37) 117.79(9), C(13)-N(1)-H(1) 108.1(14), C(1)-N(1)-H(1) 114.3(12), Mg(1)-N(1)-H(1) 83.6(13).

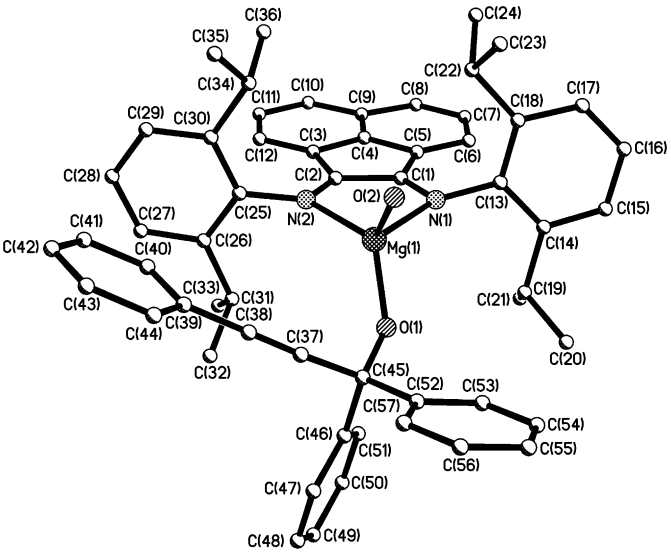


Figure 2. Molecular structure of **3**. The hydrogen atoms are omitted as well as the carbon atoms of the solvent molecules. Selected bond lengths [Å] and angles [°]: Mg(1)-O(1) 1.8529(15), Mg(1)-O(2) 2.0265(17), Mg(1)-N(1) 2.0844(18), Mg(1)-N(2) 2.0802(18), Mg(1)-C(1) 2.789(2), Mg(1)-C(2) 2.792(2), O(1)-C(45) 1.381(3), N(1)-C(1) 1.340(3), N(1)-C(13) 1.430(3), C(1)-C(2) 1.441(3), C(1)-C(5) 1.470(3), N(2)-C(2) 1.336(2), N(2)-C(25) 1.436(2), C(37)-C(38) 1.205(3), C(37)-C(45) 1.497(3), C(38)-C(39) 1.433(3); O(1)-Mg(1)-O(2) 105.67(7), O(1)-Mg(1)-N(2) 124.78(7), O(2)-Mg(1)-N(2) 118.97(6), O(1)-Mg(1)-N(1) 113.48(7), O(2)-Mg(1)-N(1) 106.82(8), N(2)-Mg(1)-N(1) 84.07(7).

length (Mg(1)–N(1), 2.355 Å and Mg(1)–N(2), 2.045 Å) reflects the difference in bond strengths between amino (N(1)) and amido (N(2)) functional groups with the Mg center. The latter bond length is close to Mg–N bond lengths in **1** (2.045 and 2.105 Å).[4] The Mg–O bonds in **2** also reveal a pronounced difference between Mg(1)–O(1), 2.123 Å, and Mg(1)–O(2), 2.050 Å. This may be explained by a difference in the coordination sites of oxygen atoms in the distorted trigonal-bipyramidal environment around magnesium. The angle between axially positioned atoms N(1) and O(1) is 177.8°. The hydrogen atom H(1) was found to be 0.889 Å from N(1). Both the alkynyl ligand and H(1) located on the same side of the plane formed with the metallacycle -Mg-N-C-C-N- and the torsion angle H(1)-N(1)-Mg-C(37) is small (4.4°). The angle H(1)-N(1)-N(2) is 107.8°. The terminal Mg–C(alkynyl) bond length (Mg(1)–C(37), 2.124 Å) is somewhat shorter than the respective bond in the six-coordinated complex [Mg(C≡CPh)$_2$(tmeda)$_2$] (tmeda = *N,N,N,N*-tetramethyl ethylene diamine) (2.176 and 2.200 Å)[8] but close to those in [Mg(RC≡C)(μ-N*i*Pr$_2$)(thf)]$_2$ (R = Ph, 2.134 Å; $SiMe_3$, 2.135 Å).[6] Compound **2** has a wider C≡C-Mg angle (174.6°) compared to [(RC≡C)Mg(μ-N*i*Pr$_2$)(thf)]$_2$ (R = Ph, 172.8°; $SiMe_3$, 167.8°).[6]

In contrast to **2** the magnesium atom in **3** is four-coordinated, and this is probably due to the steric factors imposed by diphenyl(phenylethynyl)carbinolato ligand. The Mg–N bond lengths in **3** are almost equal (Mg(1)-N(1), 2.084 Å and Mg(1)-N(2), 2.080 Å) and differ only slightly from those in the four-coordinated dpp-bian radical-anionic

 © 2003 Wiley-VCH Verlag GmbH & Co. KGaA, Weinheim

pinacolato complex [{Mg(dpp-bian)(thf)}$_2${μ-$O_2C_2Ph_4$}] (2.079 Å and 2.107 Å).[5] The diimine moiety in **3** is rather symmetrical: the C–C and C–N distances (C(1)–N(1), 1.340; C(2)-N(2), 1.336; C(1)–C(2) 1.441 Å) fall in the range of related distances in [{(dpp-bian)Na}$_2$][3] and [{(dpp-bian)Mg(thf)}$_2${μ-$O_2C_2Ph_4$}][5] The Mg–O (carbinolato) bond in **3** is much shorter than Mg–O(thf) bond length (1.853 and 2.027 Å, respectively).

To determine whether the unsymmetrical amido/amino structure of **2** is maintained in solution, we recorded ^{1}H- and ^{13}C NMR spectra of **2** in C_6D_6. If the unsymmetrical structure were present in solution, one can expect a complicated spectral picture due to the non-equivalence of all the ring protons as well as a non-equivalence of the four methine protons and eight CH_3-groups. In contrast to this expectation the spectrum revealed a relatively simple pattern (Figure 3).

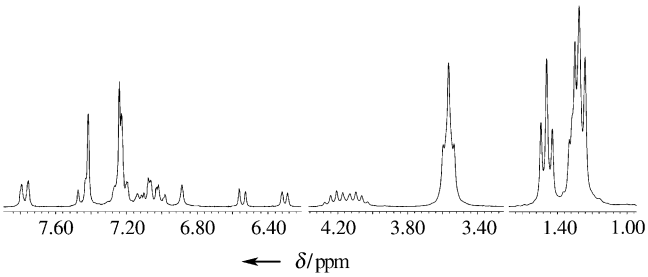
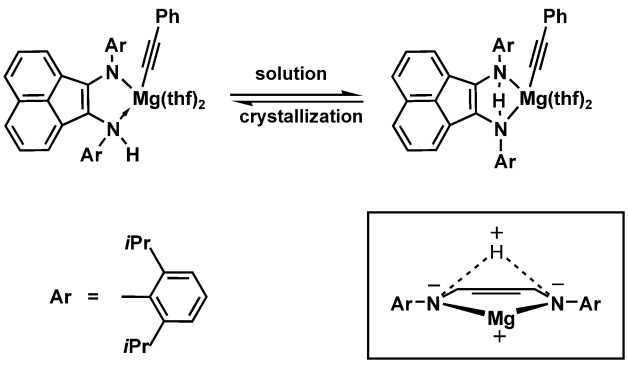


Figure 3. ^{1}H NMR spectrum of **2** in C_6D_6 (200 MHz, 293 K).

The appearance of two different signals that belong to the methine protons *H*-*i*Pr ($\delta = 4.13$ and 4.02 ppm) indicates that in complex **2** in solution the dpp-bian ligand is no longer in the plane of symmetry that runs within the acenaphthene portion of the ligand. However, the ^{1}H NMR data signify that in solution complex **2** still has a plane of symmetry that bisects the N-Mg-N angle and divides the ligand in two chemically equivalent portions. Occasionally, four signals, which correspond to the four different methyl group protons, appear as a "triplet" and a "doublet" (each of 12H) at $\delta = 1.38$ and 1.17 ppm, respectively. The latter overlaps with the signal of the coordinated THF molecules. Restricted rotation of the 2,6-*i*Pr$_2$C$_6$H$_3$ groups along the N–C(ipso) bonds causes a non-equivalence of the Me groups, one of which is turned towards and the other away from the magnesium atom. Although the signals of the ring protons were not unequivocally assigned, the spectrum in the aromatic region reveals the expected set of doublets and triplets. The only H resonance signal that is not coupled is that at δ 6.81 ppm. Though the integral intensity of this signal is somewhat higher than expected for one proton, we suppose that this signal presents the "amino" proton. The ^{13}C NMR spectrum of **2** consists of 24 signals of 25 anticipated (two signals of *C*(H)Me$_2$ appears as a single resonance at $\delta = 24.54$ ppm). The given spectroscopic data suggest that in solution the proton in complex **2**, which comes from phenylacetylene, is symmetrically localized between two N atoms (Scheme 2). In this case the bonding of the proton to the dpp-bian ligand may be described as an ionic interaction of cation H$^+$ with the planar conjugated dianionic system of



Scheme 2. Symmetrical occupation of the H atom of complex **2** in solution.

6 π electrons. An ionic character of the H-to-(ddp-bian) interaction may be responsible for the unusual down-field shift of the "amino" proton.

In conclusion, we have found that the magnesium complex with dianionic dpp-bian ligand [Mg(dpp-bian)] readily reacts with phenylacetylene in an oxidative addition manner through C–H bond cleavage to form alkynylmagnesium derivative [Mg{dpp-bian(H)}(C≡CPh)(thf)$_2$]. This for non-transition-metal complexes unprecedented reaction pathway became possible due to the high proton affinity of the dpp-bian ligand and its rigid bidentate bonding character. In the solid state the complex consists of a chelating amido/amino dpp-bian ligand. In solution the dpp-bian ligand in [Mg{dpp-bian(H)}(C≡CPh)(thf)$_2$] behaves as dianion (dpp-bian)$^{2-}$, thus bridging H$^+$ and [PhC≡CMg(thf)$_2$]$^+$ ions. We are going to investigate this phenomenon in more detail by low-temperature UV and NMR spectroscopy. The lability of the H$^+$ cation of complex **2** in solution is shown by easy abstraction of hydrogen upon insertion of diphenylketone into the Mg–C(alkynyl) bond. The abstraction of a H radical from **2** results in the oxidation of the dpp-bian dianion to a radical anion. We recently found that [Mg(dpp-bian)] reacts with acetonitrile and some halogen alkyls similar to the reaction with acetylene. Characterization of the products formed in these reactions is in progress.

Experimental Section

All manipulations were carried out under vacuum by using Schlenk ampoules. The solvents THF, benzene and toluene were distilled from sodium/benzophenone prior to use. The dpp-bian was prepared according to literature procedures.[9] The ^{1}H and ^{13}C NMR spectra were recorded on a Bruker DPX-200 NMR spectrometer. The IR spectra were recorded on a Specord M80 spectrometer.

1: Magnesium shavings (2.4 g, 100 mmol) and CH_2I_2 (0.8 g, 2.98 mmol) were placed in a Schlenk-like ampoule (about 100 mL in volume) equipped with a Teflon stopcock. After the ampoule was evacuated (10^{-1} Torr within about 1 min), THF (40 mL) was added by condensation and the mixture was stirred for 2 h. The formed [MgI_2(thf)$_n$] was decanted together with the solvent and the residual metal was washed three times with THF (40 mL). A suspension of dpp-bian (0.5 g, 1.0 mmol) in THF (30 mL) was then added to the activated Mg metal and the mixture was heated to reflux. In the course of about 10 min at reflux, the reaction mixture turned dark green. The solution was then cooled to ambient temperature and

 © 2003 Wiley-VCH Verlag GmbH & Co. KGaA, Weinheim

decanted from the excess of Mg. The THF solution of **1** obtained was further used in situ for the reaction with phenylacetylene.

2: Phenyacetylene (0.51 g, 5.0 mmol) was added to a stirring THF solution of **1** (obtained from 0.5 g, 1.0 mmol of dpp-bian in 30 mL of THF). The solution turned quickly dark blue. Evaporation of the solvent and crystallization of the crude product from toluene (15 mL) yielded 0.54 g (63 %) of **2**·(C_7H_9) as red crystals. M.p.: 143 °C (decomposition). ^{1}H NMR (200 MHz, C_6D_6, 20 °C): $\delta = 7.69$ (d, 4H, $^3J = 7.3$ Hz), 7.37 (d, 2H, $^3J = 8.3$ Hz), 7.34 (s, 2H), 7.22–7.09 (m, 4H), (d, 2H, $^3J = 8.3$ Hz), 7.08–6.88 (m, 4H), (d, 2H, $^3J = 8.3$ Hz), 6.81 (s, 1H, H-N), 6.46 (d, 2H, $^3J = 7.0$ Hz), 6.22 (d, 2H, $^3J = 6.3$ Hz), 4.13 (septet, 2H, $^3J = 6.8$ Hz), 4.02 (septet, 2H, $^3J = 6.8$ Hz), 3.49 (m, 18H, thf), 1.38 (pst, 12H, $CH(CH_3)_2$, $^3J = 6.0$ Hz), 1.22 (m, 18H, thf), 1.17 ppm (d, 12H, $CH(CH_3)_2$, $^3J = 6.8$ Hz). ^{13}C NMR (200 MHz, C_6D_6, 20 °C): $\delta = 155.09, 149.75, 145.45, 142.67, 140.96, 140.19, 134.86, 132.16, 131.70, 126.76, 125.80, 124.16, 124.13, 124.06, 123.86, 123.66, 118.15, 121.10, 109.58, 99.60, 28.27, 28.05, 24.67, 24.55, 24.50$ ppm. IR (nujol): $\tilde{\nu} = 3272$ s, 3078 m, 3062 m, 3030 m, 1590 s, 1510 m, 1250 w, 1200 w, 1110 w, 1029 m, 890 s, 779 s, 760 s, 683 s, 625 w, 580 w, 535 cm^{-1} s. Elemental analysis calcd (%) for $C_{59}H_{70}MgN_2O_2$: C 82.12, H 8.18; found: C 80.20, H 8.21. Crystal data for **2**: $C_{59}H_{70}Mg\,N_2O_2$, $M_r = 862.9$, monoclinic, space group $P(2)1/n$, $a = 12.149(2)$, $b = 21.774(4)$, $c = 18.386(4)$ Å; $\beta = 108.780(4)°$, $V = 4604.8(15)$ Å^3, $Z = 4$, $T = 100(2)$ K, $F_{000} = 1762$, $\mu = 0.082$ mm^{-1}, $\theta = 1.78$–$24.00°$, reflection collected 22 529, independent reflections 7201 [$R_{int} = 0.0609$], $GOF = 0.996$, $R = 0.0646$, $wR^2 = 0.1599$, largest diff. peak and hole 0.629/−0.487 e Å^{-3}. Except for the disordered parts (lattice toluene) H atoms were located from the difference maps. Their positional and isotropic thermal parameters were refined without constraints.

3: Phenylacetylene (0.51 g, 5.0 mmol) was added to the THF solution of **1** (obtained from 0.5 g (1.0 mmol) of dpp-bian in 30 mL THF). Afer 10 min, the solvent and the excess of phenylacetylene were removed under vacuum. The residual solid was dried under vacuum at ambient temperature for 10 min and then dissolved in THF (20 mL). Diphenylketone (0.18 g, 1.0 mmol) was added to the resulting solution. The reaction mixture turned red-violet within 25 min upon heating to 60 °C. Removal of the solvent and crystallization of the crude product from diethyl ether gave 0.41 g (47 %) of compound **3** as deep-red crystals. M.p. 165 °C (decomposition). IR (Nujol): $\tilde{\nu} = 3050$ w, 1516 m, 1508 m, 1430 s, 1312 w, 1250 w, 1178 m, 760 s, 690 cm^{-1} m. ESR spectrum (Et_2O, 293 K): quintet, $A_N = 0.50$ mT (A_N is the coupling constant for the coupling between the unpaired electron and the N nuclei) ($2 \times {}^{14}$N), $g = 2.0028$ (g is the spectroscopic splitting factor). Elemental analysis calcd (%) for $C_{61}H_{64}MgN_2O_2$: C 83.12, H 7.32; found C 82.07, H 7.43. Crystal data for **3**: $C_{61}H_{64}MgN_2O_2$, $M_r = 881.45$, monoclinic, space group $P2(1)/c$, $a = 21.506(2)$, $b = 12.7536(13)$, $c = 18.7068(19)$ Å; $\beta = 101.232(2)°$, $V = 5032.7(9)$ Å^3, $Z = 4$, $T = 100(2)$ K, $F_{000} = 1888$, $\mu = 0.080$ mm^{-1}, $\theta = 1.87$–$22.00°$, reflection collected 25 058, independent reflections 6168 [$R_{int} = 0.0464$], $GOF = 1.046$, $R = 0.0457$, $wR^2 = 0.1192$, largest diffraction peak and hole 0.270/−0.228 e Å^{-3}. CCDC-212777 (**2**) and CCDC-212778 (**3**) contain the supplementary crystallographic data for this paper. These data can be obtained free of charge via www.ccdc.cam.ac.uk/conts/retrieving.html (or from the Cambridge Crystallographic Data Centre, 12 Union Road, Cambridge CB2 1EZ, UK; fax: (+44) 1223-336-033; or deposit@ccdc.cam.ac.uk).

Received: June 23, 2003 [Z52200]

Keywords: alkynes · magnesium · N ligands · oxidative addition · structure elucidation

[1] a) M. D. Leatherman, S. A. Svejda, L. K. Johnson, M. Brookhart, *J. Am. Chem. Soc.* **2003**, *125*, 3068–3081, and references therein; b) A. Michalak, T. Ziegler, *Macromolecules* **2003**, *36*, 928–933; c) Z. Ye, H. Alsyouri, S. Zhu, Y. S. Lin, *Polymer* **2003**, *44*, 969–980; d) D. Pappalardo, M. Mazzeo, S. Antinucci, C. Pellecchia, *Macromolecules* **2000**, *33*, 9483–9487; e) D. J. Tempel, L. K. Johnson, R. L. Huff, P. S. White, M. Brookhart, *J. Am. Chem. Soc.* **2000**, *122*, 6686–6700.

[2] a) R. van Belzen, C. J. Elsevier, A. Dedieu, N. Veldman, A. L. Spek, *Organometallics* **2003**, *22*, 722–736, and references therein; b) U. El-Ayaan, A. Paulovicova, Yu. Fukuda, *J. Mol. Struct.* **2003**, *645*, 205–212; c) H. A. Jenkins, C. L. Dumaresque, D. Vidovic, J. A. C. Clyburne, *Can. J. Chem.* **2002**, *80*, 1398–1403; d) A. S. King, L. G. Nikolcheva, C. R. Graves, A. Kaminski, C. M. Vogels, R. H. E. Hudson, R. J. Ireland, S. J. Duffy, S. A. Westcott, *Can. J. Chem.* **2002**, *80*, 1217–1222; e) M. Gasperini, F. Ragaini, S. Cenini, *Organometallics* **2002**, *21*, 2950–2957; f) G. Bellachioma, B. Binotti, G. Cardaci, C. Carfagna, A. Macchioni, S. Sabatini, C. Zuccaccia, *Inorg. Chim. Acta* **2002**, *330*, 44–51; g) J. W. Strauch, G. Erker, G. Kehr, R. Fröhlich, *Angew. Chem.* **2002**, *114*, 2662–2664; *Angew. Chem. Int. Ed.* **2002**, *41*, 2543–2546; h) S. Kannan, A. J. James, P. R. Sharp, *Polyhedron* **2000**, *19*, 155–163; i) F. Ragaini, S. Cenini, E. Borsani, M. Dompe, E. Gallo, M. Moret, *Organometallics* **2001**, *20*, 3390–3398; j) A. Mechria, M. Rzaigui, F. Bouachir, *Tetrahedron Lett.* **2000**, *41*, 7199–7202; k) D. P. Gates, S. A. Svejda, E. Onate, C. M. Killian, L. K. Johnson, P. S. White, M. Brookhart, *Macromolecules* **2000**, *33*, 2320–2334.

[3] I. L. Fedushkin, A. A. Skatova, V. A. Chudakova, G. K. Fukin, *Angew. Chem.* **2003**, *115*, 3416–3420; *Angew. Chem. Int. Ed.* **2003**, *42*, 3294–3298.

[4] I. L. Fedushkin, A. A. Skatova, V. A. Chudakova, G. K. Fukin, S. Dechert, H. Schumann, *Eur. J. Inorg. Chem.* **2003**, 3336–3346.

[5] I. L. Fedushkin, A. A. Skatova, V. K. Cherkasov, V. A. Chudakova, S. Dechert, M. Hummert, H. Schumann, *Chem. Eur. J.* **2003**, in press.

[6] K. C. Yang, C. C. Chang, J. Y. Huang, C. C. Lin, G. H. Lee, Y. Wang, M. Y. Chiang, *J. Organomet. Chem.* **2002**, *648*, 176–187.

[7] A. L. Spek, *PLATON A Multipurpose Crystallographic Tool*, Utrecht University **2000**.

[8] B. Schubert, U. Behrens, E. Weiss, *Chem. Ber.* **1981**, *114*, 2640–2643.

[9] A. A. Paulovicova, U. El-Ayaan, K. Shibayama, T. Morita, Y. Fukuda, *Eur. J. Inorg. Chem.* **2001**, 2641–2646.

 © 2003 Wiley-VCH Verlag GmbH & Co. KGaA, Weinheim

Reaction Dynamics at a C Atom

Dynamics of the Simplest Reaction of a Carbon Atom in a Tetrahedral Environment**

*Jon P. Camden, Hans A. Bechtel, and Richard N. Zare**

Reactions occurring at a carbon center are one of the most important and useful classes of reactions in chemistry. The simplest reaction at a carbon atom with a tetrahedral environment is that of an H atom with methane, and understanding this prototypical reaction has implications for a number of fields ranging from organic and combustion chemistry to fundamental reaction dynamics. Consequently, it has been the subject of numerous experimental studies[1] exploring the kinetics and isotope effects of both the forward and reverse reactions. Recent theoretical work includes new potential energy surface calculations,[2–6] direct dynamics studies,[7] calculation of isotope effects,[8] and new quantum scattering methods[9] that have been reviewed by Althorpe and Clary.[10]

Herein we report the first study of the nascent CD_3 products from the H + CD_4 reaction. This isotope combination was chosen for experimental reasons because this arrangement allows for the detection of all possible reaction products: CD_3, HD and D. We also examined the CH_3 products from the H + CH_4 reaction and find that it shows very similar behavior[11] to that reported herein for the H + CD_4 reaction. By using the well-established photoloc technique,[12] we find that at a collision energy of 1.95 ± 0.05 eV the CD_3 products are produced in their ground vibrational state or have one quantum of excitation in the low-frequency umbrella-bending mode (ν_2). In addition, the CD_3 products are sideways/backward scattered [$\langle \cos\theta \rangle = -0.20 \pm 0.09$] with respect to the incident H-atom direction. This result stands in stark contrast with the benchmark H + $D_2 \rightarrow$ HD + D bimolecular exchange reaction in which the D atom is scattered in the same direction as the incoming H atom, thus indicating a rebound mechanism.[13] The H + D_2 reaction is a logical choice for comparison with the H + CD_4 abstraction reaction because they are both nearly thermoneutral and have similar classical barriers.[14,15] We propose two possible explanations for the unusual angular distribution of the CD_3 products: (1) a stripping mechanism is more important at this energy than a rebound mechanism, and (2) a competition between abstraction and exchange diminishes the probability for abstraction at small impact parameters.

Hot-atom chemistry has established the existence of the abstraction and exchange channels by using T atoms from nuclear recoil experiments[16] and photolytic sources.[17]

Equation (1) and Equation (2) are close to thermoneutral

$$H + CD_4 \rightarrow CD_3 + HD \quad \text{Abstraction} \tag{1}$$

$$H + CD_4 \rightarrow D + CHD_3 \quad \text{Exchange} \tag{2}$$

but have very different classical barrier heights (0.65 and 1.65 eV respectively).[14] Since the early hot-atom studies, experimental probes of the dynamics have been rather sparse. Valentini and coworkers[18] examined the abstraction channel by measuring the rovibrational state distributions of the HD product from H + CD_4 at 1.5 eV by using coherent anti-Stokes Raman spectroscopy (CARS). They found that the total cross section for reaction is 0.14 ± 0.03 Å^2, from which it is concluded that the maximum impact parameter for reaction is less than 1 Å. More than 95% of the HD products were formed in $v = 0,1$; 84% of the initial reagent translational energy was channeled into translation of the products while only 9% of the available energy went into HD rotation and 7% into vibration. In a complementary study, Bersohn and coworkers[19] examined the exchange channel by detecting the D-atom products from the H + $CD_4 \rightarrow$ D + CHD_3 reaction at a collision energy of ~2 eV. The absolute cross section for exchange was measured to be 0.084 ± 0.014 Å^2, and the average D-atom kinetic energy was 86 ± 7% of the collision energy. They concluded that the exchange channel proceeds through an S_N2-type inversion mechanism and suggested that trajectories of small impact parameter lead to either exchange or abstraction depending on the orientation of the incoming H atom with respect to the C–D bond.

Figure 1 displays the REMPI (resonance enhanced multiphoton ionization) spectrum of the CD_3 products in the region of the 0_0^0, 1_1^1 and 2_1^1 bands, corresponding to ground state, symmetric stretch (ν_1), and umbrella-bending (ν_2) excited methyl radical fragments, respectively. This spectrum is dominated by the large Q-branch members of the 0_0^0 band; however, some members of the S and O branches ($N \leq 9$) of the 0_0^0 band are also apparent. The position of the Q branch

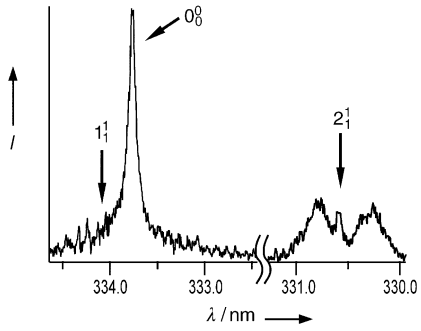


Figure 1. (2+1) REMPI spectrum of CD_3 products from the H + CD_4 reaction. Arrows indicate the positions of the 0_0^0, 1_1^1 and 2_1^1 bands of the CD_3 ($3p_z$–X) transition.

[*] Prof. R. N. Zare, J. P. Camden, H. A. Bechtel
Department of Chemistry
Stanford University
Stanford, CA 94305-5080 (USA)
Fax: (+1) 650-723-9262
E-mail: zare@stanford.edu

[**] The authors (J.P.C. and H.A.B) thank the National Science Foundation for Graduate Fellowships. We also thank Davida J.A. Brown and Andrew E. Pomerantz for useful discussions and critical comments on this manuscript. This work was supported by the National Science Foundation under Grant Number NSF-CHE-02-42103.

 DOI: 10.1002/anie.200352642 © 2003 Wiley-VCH Verlag GmbH & Co. KGaA, Weinheim

for the CD_3 1_1^1 band is indicated by the arrow in Figure 1. No products were observed on this transition within the signal-to-noise ratio of our experiment. In contrast, the 2_1^1 band is observable and has roughly the same integrated area as the 0_0^0 band. Although a quantitative determination of the branching ratios between these three states is difficult because the $3p_z$–X REMPI transitions are not fully characterized, we can draw several qualitative conclusions: 1) the reaction does not significantly populate the energetically allowed symmetric stretch of CD_3 ($\nu_1 = 1$), 2) the major product channels are the ground state and umbrella-bending mode CD_3 ($\nu_2 = 0,1$), and 3) the reagent translational energy is converted mostly into translational energy of the products.

Many ab initio calculations of the transition-state geometry exist for both the abstraction and exchange channels.[4] These calculations serve as a starting point to understand the methyl radical internal-state distributions. In a simple picture of the reaction dynamics, one expects excitation of those internal modes of the products that are stretched in the transition state. The nonreactive C–D bond lengths change little among the reactant CD_4 (1.091 Å), the C_{3v} saddle point (1.080 Å) and the product CD_3 (1.079 Å), thus suggesting no excitation of the stretching mode (ν_1) is to be expected in the methyl radical product, in agreement with the REMPI spectrum. The relaxation of the sp^3-hybridized C of methane to the sp^2-hybridized C of the methyl radical predicts the presence of CD_3 ($\nu_2 = 1$), also in agreement with the REMPI spectrum. There is clearly more at work than this model; nevertheless, it gives a reasonable account of the overall dynamics. Furthermore, we caution that the significant population of CD_3 ($\nu_2 = 1$) observed in these experiments suggests that a simple pseudo-diatomic picture of methane as (CD_3)–D, in which the methyl radical acts as a spectator, is insufficient to understand fully the dynamics.

Figure 2 shows the CD_3 differential cross section (DCS), which is a measure of the angular distribution of the products in the center-of-mass frame, averaged over all HD quantum states; the DCSs for CD_3 ($\nu = 0$) and for CD_3 ($\nu_2 = 1$) are the same within the experimental resolution. The reaction has an obvious preference for sideways/backward scattering of CD_3 with respect to the incident H-atom direction. The average scattering angle is unambiguously in the backward hemisphere, $\langle\cos\theta\rangle = -0.20 \pm 0.09$ with the spread in values resulting from the unknown internal energy deposited into the HD coproduct, shown by the shaded region of Figure 2.

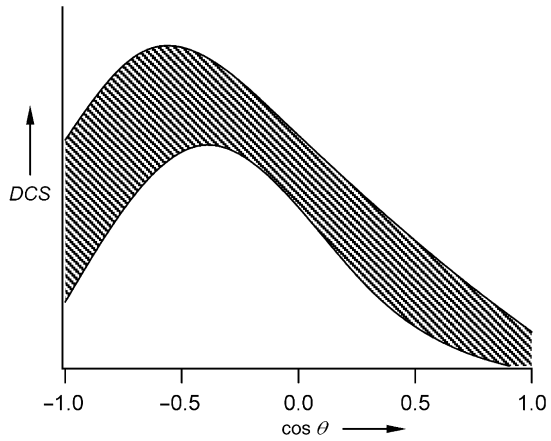


Figure 2. Differential cross section of the CD_3 products as a function of the cosine of the center-of-mass scattering angle θ. The uncertainty in the experimental measurements is indicated by the shaded region.

This result is unexpected in light of previous trajectory calculations. Polanyi and co-workers[20] studied the dynamics over a range of energies (2–18 eV) by using a three-atom model, in which methane was considered to be a pseudo-diatomic species R–D (R = CD_3). In all cases, the reaction was direct and concerted. At the energy of the current experiment, the CD_3 product was forward-scattered and had an average scattering angle of $\langle\cos\theta\rangle = +0.5$, thus indicating a rebound mechanism. Raff,[21] and Valencich and Bunker[22] extended the treatment to full dimensionality and also found that the abstraction channel occurs through a rebound mechanism at similar energies ($\langle\cos\theta\rangle = +0.28$ and $\langle\cos\theta\rangle = +0.57$, respectively, at 1.73 eV). These theoretical results are in sharp contrast to our experimental findings, which are illustrated in Figure 3. As these early attempts showed, this system is a challenge from a theoretical perspective because of the large number of degrees of freedom and the need to consider all hydrogen atoms as equivalent.[23] Because none of the more recent theoretical studies are directly comparable with the current experiments, we present some conjectures that derive from a very simplistic analysis. New theoretical work, however, will be necessary for a detailed understanding of these results.

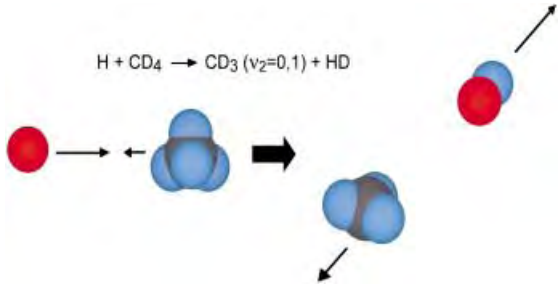


Figure 3. Illustration of the main reaction channel: The CD_3 products are formed in their ground state and with one quantum of umbrella bending motion. They are sideways/backward scattered with respect to the incident H-atom direction.

In 1965 Wolfgang[16] offered a pictorial model in which abstraction occurred by one of two mechanisms: 1) axial—in which the incoming atom is directed along a C–D bond and the HD product rebounds backward while the methyl radical goes forward; 2) stripping—in which the velocity of the H atom is perpendicular to the C–D bond and the HD product is carried into the forward hemisphere while the methyl goes backward. Our results indicate that reaction at 2 eV is in closer accord with the stripping mechanism than the axial mechanism. But we do observe a significant amount of sideways scattering that most likely comes from trajectories intermediate between these limiting cases. Trajectory studies, as well as conventional wisdom,[24] support the notion that at the lowest energies the axial mechanism dominates because the stripping mechanism has a larger angular-momentum barrier. At higher energies the stripping mechanism is

 © 2003 Wiley-VCH Verlag GmbH & Co. KGaA, Weinheim

expected to become more important. It is likely that our collision energy is intermediate between these two limits.

As another aid, we use the simple hard-sphere model of reactive scattering,[24,25] in which a one-to-one correspondence exists between scattering angle θ and impact parameter b. Recall that the impact parameter b is the distance of closest approach (Figure 4) if the reagents are to follow straight-line

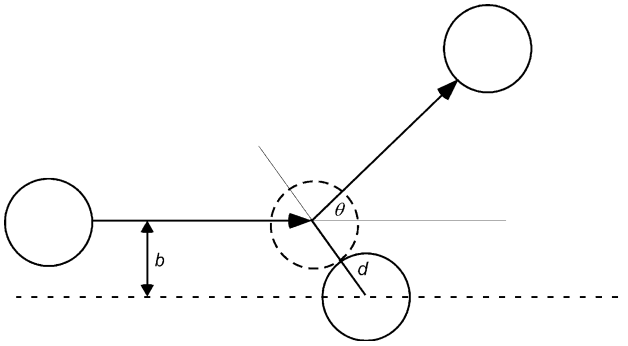


Figure 4. Hard-sphere model: θ is the scattering angle in the center of mass frame, b is the impact parameter, and d is the hard-sphere collision radius. There is a one-to-one correspondence between b and θ in this model.

paths. By using this model the experimental DCS can be converted to an opacity function $P(b)$, which gives the probability that reaction occurs for collisions at a distance b to $b + db$. If CD_4 were correctly pictured as a "ball of deuterium atoms," then the resulting opacity function $P(b)$ would be constant for $b < d$, where d is the hard-sphere collision radius. Instead, Figure 5 shows a derived $P(b)$ with a markedly different behavior. We find that the abstraction channel has a strong preference for large impact parameters, which is opposite to what is expected for the exchange channel. The latter, having a large barrier (1.65 eV) and small cross section, should favor small impact parameter collisions. It is possible that abstraction and exchange channels compete at small impact parameters, depending on how the H-atom velocity lines up with the C–D bond. This competition would result in a depletion of the forward-scattered CD_3 products.

In conclusion, we have measured the product-state distributions and DCSs of the CD_3 fragment produced by the reaction $H + CD_4$ at 1.95 eV. The main product channels are ground state and umbrella-bending mode excited methyl radicals. The presence of a significant amount of CD_3 ($v_2 = 1$)

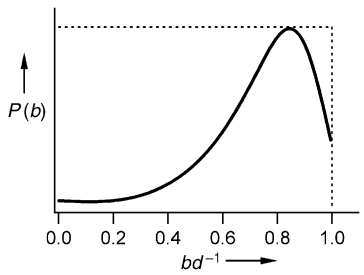


Figure 5. The solid line displays the opacity function $P(b)$ for the CD_3 reaction products obtained from conversion of the measured DCS. The dashed line represents the $P(b)$ function expected where methane acts as a "ball of deuterium atoms."

shows that the simple picture of CD_4 as a pseudo-diatomic species is not strictly correct. The CD_3 products are scattered sideways and backwards. While the exact origin of this behavior is unknown, we speculate it comes from a stripping mechanism at large impact parameter collisions, or a competition between abstraction and exchange at small impact parameter collisions, or the action of both. Clearly, the polyatomic nature of this reaction goes beyond the atom–diatom pictures that have been so frequently used to describe reaction dynamics.

Experimental Section

The experimental setup used and the method of determining the DCS is described in detail elsewhere.[12] A 1:2:8 mixture of hydrogen bromide (Matheson, 99.8%), perdeuteromethane (Cambridge Isotopes, 99% [D_4]), and helium (liquid carbonic, 99.995%) is expanded from a pulsed (General Valve, Series-9) nozzle into the extraction region of a linear Wiley-McLaren time-of-flight (TOF) spectrometer. Photolysis of HBr with linearly polarized light at 212.8 nm (fifth harmonic of the Nd:YAG laser) produces fast H atoms to initiate the reaction. At this wavelength approximately 85% of the H atoms are produced coincident with ground-state Br atoms and a kinetic energy of 2.04 eV. The remaining fraction comes with spin–orbit excited Br* atoms (KE = 1.59 eV).[26] This photolysis wavelength gives a collision energy in the center-of-mass frame of 1.95 and 1.52 eV respectively. After a time delay of approximately 30 ns the methyl radical reaction products are probed with 2+1 REMPI through the $3p_z$ Rydberg state[27] around 333 nm. The ions, after drifting down the flight tube, are detected by Chevron-type microchannel plates.

Received: August 13, 2003 [Z52642]
Published Online: October 14, 2003

Keywords: gas-phase chemistry · hot-atom chemistry · methane · reaction dynamics

[1] "NIST Chemical Kinetics Database", can be found under http://kinetics.nist.gov/index.php **2000**.
[2] R. Steckler, K. J. Dykema, F. B. Brown, G. C. Hancock, D. G. Truhlar, T. Valencich, *J. Chem. Phys.* **1987**, *87*, 7024.
[3] M. J. T. Jordan, R. G. Gilbert, *J. Chem. Phys.* **1994**, *102*, 5669.
[4] J. Espinosa-Garcia, *J. Chem. Phys.* **2002**, *116*, 10664.
[5] T. Wu, U. Manthe, *J. Chem. Phys.* **2003**, *119*, 14.
[6] M. A. Collins, private communication.
[7] J. Pu, D. G. Truhlar, *J. Chem. Phys.* **2002**, *116*, 1468.
[8] X. Zhang, G. H. Yang, K. L. Han, M. L. Wang, J. Z. H. Zhang, *J. Chem. Phys.* **2003**, *118*, 9266.
[9] M. Yang, D. H. Zhang, S. Lee, *J. Chem. Phys.* **2002**, *117*, 9539.
[10] S. C. Althorpe, D. C. Clary, *Annu. Rev. Phys. Chem.* **2003**, *54*, 493.
[11] J. P. Camden, H. A. Bechtel, R. N. Zare, unpublished results.
[12] W. R. Simpson, A. J. Orr-Ewing, T. P. Rakitzis, S. A. Kandel, R. N. Zare, *J. Chem. Phys.* **1995**, *103*, 7299.
[13] F. Fernandez-Alonso, B. Bean, J. Ayers, A. Pomerantz, R. Zare, L. Banares, F. Aoiz, *Angew. Chem.* **2000**, *112*, 2860; *Angew. Chem. Int. Ed.* **2000**, *39*, 2748.
[14] K. D. Dobbs, D. A. Dixon, *J. Phys. Chem.* **1994**, *98*, 12584.
[15] K. E. Riley, J. B. Anderson, *J. Chem. Phys.* **2003**, *118*, 3437.
[16] R. Wolfgang, *Prog. React. Kinet.* **1965**, *3*, 97.
[17] C. C. Chou, F. S. Rowland, *J. Chem. Phys.* **1969**, *50*, 2763.
[18] G. Germann, Y. Huh, J. Valentini, *J. Chem. Phys.* **1992**, *96*, 1957.
[19] A. Chattopadhyay, S. Tasaki, R. Bersohn, M. Kawasaki, *J. Chem. Phys.* **1991**, *95*, 1033.

 © 2003 Wiley-VCH Verlag GmbH & Co. KGaA, Weinheim

[20] P. J. Kuntz, E. M. Nemeth, J. C. Polanyi, W. H Wong, *J. Chem. Phys.* **1969**, *52*, 4654.
[21] L. M. Raff, *J. Chem. Phys.* **1974**, *60*, 2220.
[22] T. Valencich, D. L. Bunker, *J. Chem. Phys.* **1974**, *61*, 21.
[23] R. Marguardt, M. Quack, *J. Chem. Phys.* **1998**, *109*, 10628.
[24] R. D. Levine, R. B. Bernstein, *Molecular Reaction Dynamics and Chemical Reactivity*, Oxford University, London, **1987**.
[25] W. R. Simpson, T. P. Rakitzis, S. A. Kandel, T. Levon, R. N. Zare, *J. Phys. Chem.* **1996**, *100*, 7938.
[26] P. Regan, S. Langford, A. Orr-Ewing, M. Ashfold, *J. Chem. Phys.* **1999**, *110*, 281.
[27] J. W. Hudgens, T. G. Digiuseppe, M. C. Lin, *J. Chem. Phys.* **1983**, *79*, 571.

 © 2003 Wiley-VCH Verlag GmbH & Co. KGaA, Weinheim

A Macrosphelide Library

A Combinatorial Synthesis of a Macrosphelide Library Utilizing a Palladium-Catalyzed Carbonylation on a Polymer Support**

Takashi Takahashi, Shin-ichi Kusaka, Takayuki Doi, Toshiaki Sunazuka, and Satoshi Ōmura*

The combinatorial synthesis of natural products is being developed to explore the analogues of lead compounds for drug discovery and recently for the construction of important chemical probes for use in the fields of chemical genetics, genomics, and proteomics.[1–3] Therefore, it is necessary to develop strategies for the high-speed synthesis of natural-product libraries that are more efficient than those traditionally used for the synthesis of a single final product.[4,5]

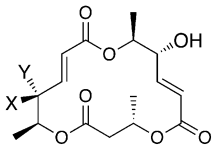
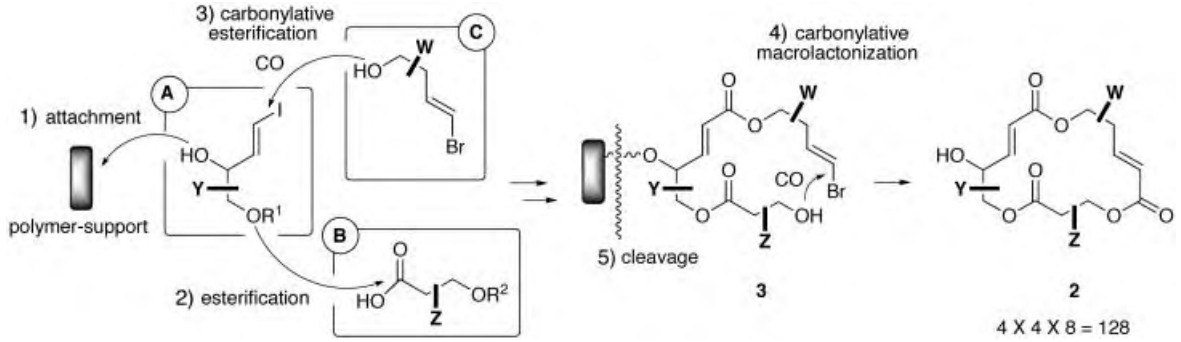


Figure 1. **1a**: X = H, Y = OH; **1b**: X = Y = O.

Macrosphelides A (**1a**) and B (**1b**, Figure 1), isolated from the culture medium of *Macrospaeropsis sp.* FO-5050 by the Omura group,[6] strongly inhibit the adhesion of human leukemia HL-60 cells to human-umbilical-vein endothelial cells (HUVEC) in a dose-dependent fashion.[7] They have received much attention as a lead compound for the development of new anti-cancer drugs and although the total syntheses of macrosphelides have been reported,[8–11] a strategy for the high-speed synthesis of a variety of these analogues is still required. Herein we report a highly convergent synthesis of a library of macrosphelide analogues on a solid support by utilizing a palladium-catalyzed chemoselective carbonylation of vinyl halides.

In considering an efficient strategy for the combinatorial synthesis of macrosphelide analogues **2**, we chose a solid-phase synthesis utilizing the three synthetic building blocks **A, B**, and **C** as illustrated in Scheme 1. The process involves: 1) attachment of the secondary alcohol in block **A** to a polymer-support, 2) esterification with block **B**, 3) chemoselective carbonylation[12] of the vinyl iodide in unit **A** with alcohol **C** containing a vinyl bromide moiety, 4) carbonylative macrolactonization[13] of the polymer-supported **3** by exploiting the rather less reactive vinyl bromide unit, and 5) cleavage from the polymer-support. We planned a 128-member natural product-like library, consisting of blocks **A** (four), **B** (four), and **C** (eight) summarized in Figure 2.



Scheme 1. Strategy for a combinatorial synthesis of macrosphelide analogues **2**.

The preparation of the building blocks including the various diastereomers of (*E*)-vinyl halides for blocks **A** and **C** is shown in Scheme 2. Commercially available methyl (*S*)-lactate **4** was converted into ynone (*S*)-**5** in three steps. The ynone **5** is a key intermediate to prepare a variety of vinyl halides. Chelation-controlled reduction of **5** with Me_2AlCl/Bu_3SnH provided **6** (> 95 % selectivity),[14] while Felkin–Ahn

[*] Prof. Dr. T. Takahashi, S.-i. Kusaka, Prof. Dr. T. Doi
Department of Applied Chemistry
Tokyo Institute of Technology
2-12-1 Ookayama, Meguro, Tokyo 152-8552 (Japan)
Fax: (+81) 3-5734-2884
E-mail: ttak@apc.titech.ac.jp
Prof. Dr. T. Sunazuka, Prof. Dr. S. Ōmura
The Kitasato Institute for Life Science, and
School of Pharmaceutical Science,
Kitasato University and The Kitasato Institute
Shirokane, Minatoku, Tokyo 108-8641 (Japan)

[**] This work was supported by a Grant-in-Aid from the Ministry of Education, Culture, Sports, Science and Technology, Japan (No. 14103013).

Supporting information for this article is available on the WWW under http://www.angewandte.org or from the author.

 © 2003 Wiley-VCH Verlag GmbH & Co. KGaA, Weinheim DOI: 10.1002/anie.200352229

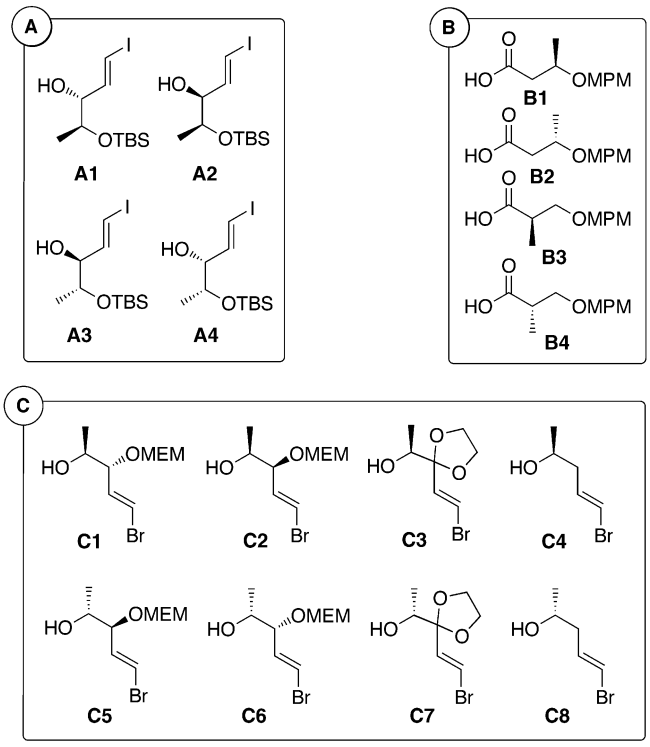
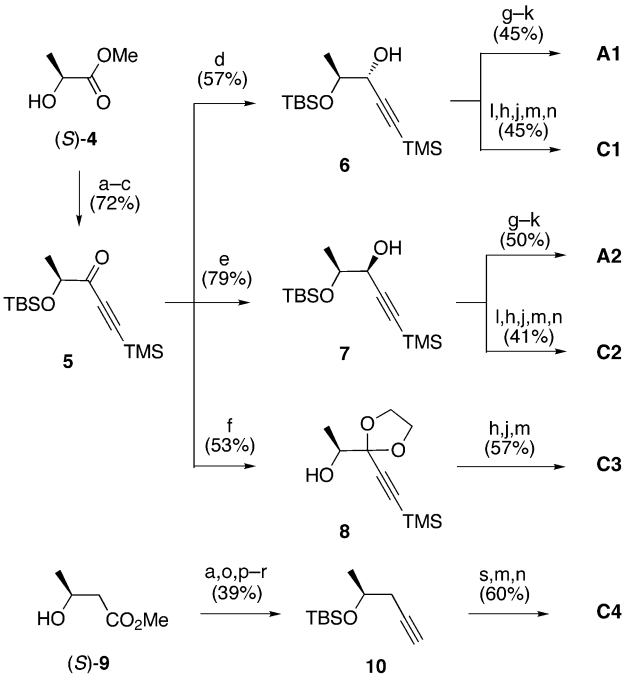


Figure 2. The building blocks **A, B**, and **C** for the synthesis of a combinatorial library of macrosphelide analogues **2**.



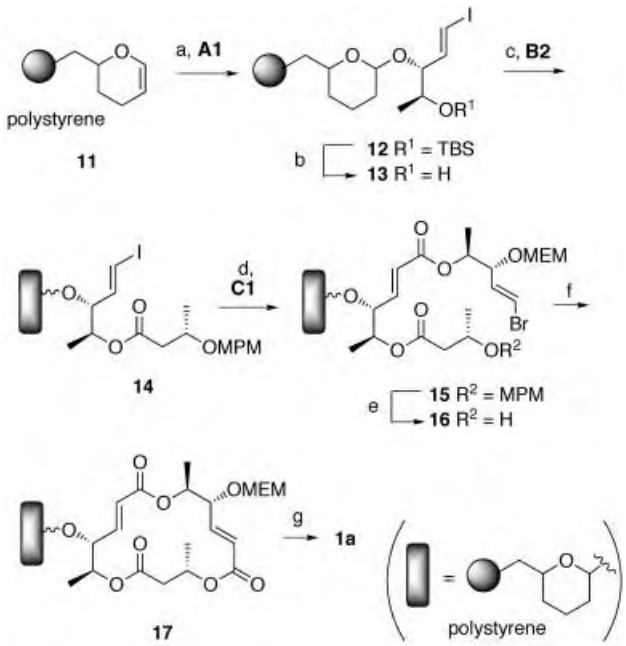
Scheme 2. Preparation of the vinyl halides, the blocks **A** and **C**: a) TBSCl, imidazole, CH_2Cl_2, RT, 6 h; b) Me(OMe)NH·HCl, *i*PrMgCl, THF, 0 °C, 30 min; c) trimethylsilylacethylene, BuLi, −78 °C, THF, 2 h; d) Me_2AlCl, Bu_3SnH, CH_2Cl_2, −78 °C, 3 h; e) L-selectride, THF, −78 °C, 1 h; f) $Sc(OTf)_3$, $CH(OMe)_3$, ethylene glycol, CH_3CN, RT→60 °C, 24 h; g) EVE, CSA, CH_2Cl_2, RT, 6 h; h) 5% KOH in MeOH, RT, 30 min; i) PPTS, MeOH, RT, 3 h; j) $[PdCl_2(PPh_3)_2]$, Bu_3SnH, THF, 0 °C, 1 h; k) NIS, THF, 0 °C, 30 min; l) MEMCl, *i*Pr_2NEt, RT, 24 h; m) NBS, THF, RT, 30 min; n) TBAF, THF, RT, 6 h; o) DIBAL-H, CH_2Cl_2, −78 °C, 30 min; p) SO_3·Py, Et_3N, CH_2Cl_2, RT, 2 h; q) CBr_4, PPh_3, THF, 0 °C, 1 h; r) BuLi, THF, −78 °C, 1 h; s) $[PdCl_2(MeCN)_2]$, PCy_3, Bu_3SnH, THF, 0 °C, 2 h. TBSCl = chlorodimethyl-1,1-dimethylethyl silane, TMS = trimethylsilane, Tf = trifluoromethanesulfonate, EVE = ethyl vinyl ether, CSA = camphorsulfonic acid, PPTS = pyridinium *p*-toluenesulfonate, NIS = *N*-iodosuccinimide, MEM = methoxyethoxymethyl, NBS = *N*-bromosuccinimide, TBAF = tetrabutylammonium fluoride, DIBAL-H = bis(2-methylpropyl)aluminium hydride, Py = pyridine.

type reduction with L-selectride yielded **7** (> 95% selectivity).[15] Acetal formation of **5** with ethylene glycol afforded **8**. After removal of TMS, the alkyne was converted into the desired (*E*)-vinyl halides **A1** and **A2** and **C1**–**C3** by regioselective hydrostannylation (cat. $[PdCl_2(PPh_3)_2]/Bu_3SnH$),[16] followed by either iodination with NIS or bromination with NBS. Their enantiomers **A3** and **A4** and **C5**–**C7** were prepared from methyl (*R*)-lactate **4** by the same method. The vinyl bromides **C4** and **C8** were prepared from methyl (*S*)- and (*R*)-3-hydroxybutyrates **9**, respectively, through the regioselective hydrostannylation of **10** (cat. $[PdCl_2(MeCN)_2]/PCy_3/Bu_3SnH$), followed by bromination.

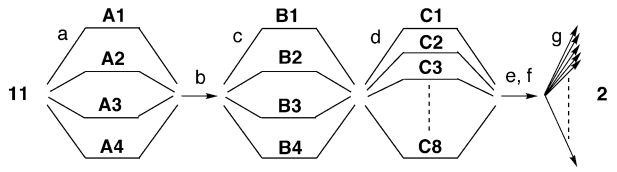
A solid-phase synthesis of **1a** was initially investigated (Scheme 3). The block **A1** was attached to a PS-DHP resin **11** (0.96 mmol g^{-1} PS = polystyrene, DHP = dihydropyran[17] using PPTS. Selective deprotection of the TBS group with TBAF and esterification of the polymer-supported alcohol **13** with acid **B2**[18] provided **14**. Palladium-catalyzed carbonylation of the vinyl iodide **14** with alcohol **C1** was carried out.[19] The reaction proceeded at room temperature under 30 atm of carbon monoxide utilizing $[PdCl_2(MeCN)_2]$ as a catalyst.[20,21] The product **15** was cleaved from the resin (0.1M TsOH/MeOH, THF; Ts = 4-methylphenylsulfonyl) and its purity was determined to be 71% by HPLC analysis. The vinyl bromide moiety remained intact under the above reaction conditions. The 4-methoxyphenylmethyl (MPM) group in **15** was removed with DDQ to afford polymer-supported cyclization precursor **16**.[22] The palladium-catalyzed carbonylation of **16** was achieved at 80 °C utilizing $[Pd_2(dba)_3]$/dppf to provide macrolactone **17**.[23] Finally, treatment of **17** with 4N HCl in dioxane at room temperature released the desired macrosphelide **1a** in 68% purity. Purification by preparative HPLC provided **1a** in 38% overall yield from **11** (7 steps). The synthetic **1a** exhibited ^1H and ^{13}C NMR spectral data as well as optical rotation identical to those published for the natural product.[6b,24]

On the basis of the above solid-phase strategy, we constructed a macrosphelide combinatorial library utilizing radiofrequency encoded combinatorial (REC) chemistry by a split-and-pool method (Scheme 4).[4,25] The 128 microreactors each containing 30 mg of PS-DHP resin **11** were encoded and split into four flasks. After attachment of block **A** (**A1**–**A4**) to the resin, the microreactors were pooled together for washing and drying. After deprotection of the TBS group, the microreactors were decoded and split, followed by esterification with block **B** (**B1**–**B4**)[18] in separate flasks. The microreactors were subsequently pooled for washing and drying. The microreactors were again decoded and split, followed by palladium-catalyzed carbonylative esterification of vinyl iodides with block **C** (**C1**–**C8**) in separate autoclaves. The microreactors were again pooled for washing and drying.

 © 2003 Wiley-VCH Verlag GmbH & Co. KGaA, Weinheim



Scheme 3. Solid-phase synthesis of macrosphelide A (**1a**): a) PPTS (0.05 M), CH_2Cl_2, RT, 24 h; b) TBAF (0.3 M), THF, RT, 24 h; c) DIC (0.1 M), DMAP (0.001 M), CH_2Cl_2, RT, 24 h; d) $[PdCl_2(MeCN)_2]$ (0.03 M), CO (30 atm), NEt_3 (0.2 M), DMAP (0.03 M), DMF, RT, 12 h; e) DDQ (0.3 M), aq.$NaHCO_3$ (0.3 M), CH_2Cl_2:H_2O (1:1), RT, 5 h; f) $[Pd_2(dba)_3]$/dppf (0.03 M), CO (30 atm), NEt_3 (0.2 M), DMAP (0.03 M), DMF, 80 °C, 12 h; g) 4 N HCl in dioxane, RT, 5 h; TBS = dimethyl-1,1-dimethylethyl silane, DIC = diisopropylcarbodiimide, DMAP = (4-dimethylamino)pyridine, DDQ = 2,3-dichloro-5,6-dicyano-1,4-benzoquinone, dba = dibenzylideneacetone, dppf = bis(diphenylphosphanyl)ferrocene.



Scheme 4. A combinatorial synthesis of macrosphelide analogues **2** utilizing a split-and-pool method: Reagents and conditions a)–g) are the same as shown in Scheme 3.

After removal of the MPM group, the palladium-catalyzed carbonylative macrolactonization of vinyl bromides was performed. Finally, the microreactors were decoded and treated with acid in parallel for removal of the MPM group and cleavage from the polymer support to afford crude **2**. Purification by preparative HPLC (silica gel) provided 122 macrosphelide analogues **2** (0.2–1.5 mg) from 128 trials, isolated in good purities (Table 1).[26,27]

We have demonstrated the combinatorial synthesis of a natural product-like library based on macrosphelide. The combinatorial synthesis of a 122-member macrosphelide library including macrosphelides A, C, E, and F has been achieved based on a unique strategy for a three-component coupling utilizing a palladium-catalyzed chemoselective carbonylation and an unprecedented macrolactonization on a polymer support.

Received: June 26, 2003 [Z52229]

Keywords: chemoselectivity · combinatorial chemistry · macrosphelides · palladium · solid-phase synthesis

Table 1: A combinatorial library of macrosphelide analogues **2**.

Entry	A	B	C	Yield [mg][a]	Purity [%][b]	R_t [min][c]	Entry	A	B	C	Yield [mg][a]	Purity [%][b]	R_t [min][c]
1[d]	**1**	**1**	**1**	1.2	80	5.78	65	**3**	**1**	**1**	0.9	99	5.67
2	**1**	**1**	**2**	1.1	99	5.43	66	**3**	**1**	**2**	1.5	98	5.79
3	**1**	**1**	**3**	0.3	99	7.01	67	**3**	**1**	**3**	0.9	95	7.10
4[e]	**1**	**1**	**4**	1.1	81	6.83	68	**3**	**1**	**4**	0.7	97	6.94
5	**1**	**1**	**5**	0.6	72	5.52	69	**3**	**1**	**5**	1.1	97	5.97
6	**1**	**1**	**6**	< 0.1	–	–	70	**3**	**1**	**6**	0.2	78	5.43
7	**1**	**1**	**7**	0.5	83	6.89	71	**3**	**1**	**7**	0.6	96	7.16
8	**1**	**1**	**8**	0.3	91	6.73	72	**3**	**1**	**8**	0.5	88	7.14
9[f]	**1**	**2**	**1**	0.5	99	6.06	73	**3**	**2**	**1**	0.5	88	5.61
10	**1**	**2**	**2**	1.3	99	5.44	74	**3**	**2**	**2**	1.4	65	5.31
11	**1**	**2**	**3**	1.3	93	7.18	75	**3**	**2**	**3**	0.5	77	6.89
12[g]	**1**	**2**	**4**	0.8	96	7.14	76	**3**	**2**	**4**	1.0	86	6.74
13	**1**	**2**	**5**	0.5	91	5.59	77	**3**	**2**	**5**	1.0	91	5.70
14	**1**	**2**	**6**	0.5	99	5.87	78	**2**	**2**	**6**	< 0.1	–	–
15	**1**	**2**	**7**	1.3	98	7.10	79	**3**	**2**	**7**	0.9	95	7.02
16	**1**	**2**	**8**	0.3	97	6.93	80	**3**	**2**	**8**	0.5	82	6.82
17	**1**	**3**	**1**	0.8	90	5.76	81	**3**	**3**	**1**	0.6	99	5.99
18	**1**	**3**	**2**	0.7	73	5.34	82	**3**	**3**	**2**	1.6	95	5.81
19	**1**	**3**	**3**	0.7	78	7.02	83	**3**	**3**	**3**	0.5	73	7.22
20	**1**	**3**	**4**	0.6	94	6.94	84	**3**	**3**	**4**	1.7	88	7.05
21	**1**	**3**	**5**	0.3	80	5.64	85	**3**	**3**	**5**	1.2	81	6.11
22	**1**	**3**	**6**	< 0.1	–	–	86	**3**	**3**	**6**	0.5	82	5.90
23	**1**	**3**	**7**	0.4	85	6.98	87	**3**	**3**	**7**	0.7	84	7.34
24	**1**	**3**	**8**	0.2	95	6.78	88	**3**	**3**	**8**	0.4	59	7.19
25	**1**	**4**	**1**	1.2	98	6.20	89	**3**	**4**	**1**	1.2	99	5.64
26	**1**	**4**	**2**	1.6	84	5.91	90	**3**	**4**	**2**	1.5	94	5.55
27	**1**	**4**	**3**	0.1	54	7.35	91	**3**	**4**	**3**	0.8	70	6.98

 © 2003 Wiley-VCH Verlag GmbH & Co. KGaA, Weinheim

Table 1: (Continued)

Entry	A	B	C	Yield [mg][a]	Purity [%][b]	R_t [min][c]	Entry	A	B	C	Yield [mg][a]	Purity [%][b]	R_t [min][c]
28	**1**	**4**	**4**	1.1	40	7.20	92	**3**	**4**	**4**	1.6	88	6.79
29	**1**	**4**	**5**	0.9	80	5.98	93	**3**	**4**	**5**	0.3	94	5.76
30	**1**	**4**	**6**	0.4	82	5.81	94	**3**	**4**	**6**	<0.1	–	–
31	**1**	**4**	**7**	0.5	91	7.22	95	**3**	**4**	**7**	0.6	80	7.02
32	**1**	**4**	**8**	0.5	85	5.72	96	**3**	**4**	**8**	0.2	91	6.93
33	**2**	**1**	**1**	1.2	96	5.78	97	**4**	**1**	**1**	0.8	93	5.60
34	**2**	**1**	**2**	1.0	97	5.61	98	**4**	**1**	**2**	1.3	95	5.37
35	**2**	**1**	**3**	0.2	74	7.12	99	**4**	**1**	**3**	0.1	96	6.87
36	**2**	**1**	**4**	1.9	66	6.86	100	**4**	**1**	**4**	0.9	94	6.65
37	**2**	**1**	**5**	0.5	95	5.74	101	**4**	**1**	**5**	1.0	95	5.60
38	**2**	**1**	**6**	0.2	84	5.40	102	**4**	**1**	**6**	0.9	60	5.16
39	**2**	**1**	**7**	1.4	83	7.02	103	**3**	**1**	**7**	0.6	84	6.81
40	**2**	**1**	**8**	0.7	69	6.92	104	**4**	**1**	**8**	0.4	69	6.67
41	**2**	**2**	**1**	0.1	94	5.61	105	**4**	**2**	**1**	0.8	99	5.75
42	**2**	**2**	**2**	<0.1	–	–	106	**3**	**2**	**2**	1.5	86	5.31
43	**2**	**2**	**3**	0.4	99	6.81	107	**4**	**2**	**3**	0.5	82	6.98
44	**2**	**2**	**4**	1.5	97	6.71	108	**4**	**2**	**4**	1.3	72	6.93
45	**2**	**2**	**5**	0.1	99	5.60	109	**4**	**2**	**5**	0.8	84	5.69
46	**2**	**2**	**6**	0.5	75	5.35	110	**4**	**2**	**6**	<0.1	–	–
47	**2**	**2**	**7**	0.4	89	6.87	111	**4**	**2**	**7**	0.6	92	7.12
48	**2**	**2**	**8**	0.3	93	6.64	112	**4**	**2**	**8**	0.2	81	6.85
49	**2**	**3**	**1**	0.6	89	5.81	113	**4**	**3**	**1**	0.6	96	5.74
50	**2**	**3**	**2**	0.7	99	5.52	114	**4**	**3**	**2**	1.1	98	5.35
51	**2**	**3**	**3**	0.7	80	6.93	115	**4**	**3**	**3**	1.1	88	6.92
52	**2**	**3**	**4**	1.8	92	6.78	116	**4**	**3**	**4**	1.5	88	6.79
53	**2**	**3**	**5**	0.2	93	5.74	117	**4**	**3**	**5**	0.6	80	5.72
54	**2**	**3**	**6**	0.4	95	5.35	118	**4**	**3**	**6**	0.5	66	5.61
55	**2**	**3**	**7**	0.2	84	7.00	119	**4**	**3**	**7**	0.4	91	6.99
56	**2**	**3**	**8**	0.3	90	6.78	120	**4**	**3**	**8**	0.4	97	6.79
57	**2**	**4**	**1**	0.6	98	5.81	121	**4**	**4**	**1**	0.3	90	5.74
58	**2**	**4**	**2**	0.8	95	5.52	122	**4**	**4**	**2**	1.5	99	5.34
59	**2**	**4**	**3**	0.5	94	7.00	123	**4**	**4**	**3**	0.2	81	7.00
60	**2**	**4**	**4**	0.5	93	6.80	124	**4**	**4**	**4**	1.5	64	6.79
61	**2**	**4**	**5**	0.2	81	5.65	125	**4**	**4**	**5**	0.5	50	5.74
62	**2**	**4**	**6**	<0.1	–	–	126	**4**	**4**	**6**	0.2	71	5.53
63	**2**	**4**	**7**	0.5	91	6.92	127	**4**	**4**	**7**	0.2	70	6.92
64	**2**	**4**	**8**	0.3	91	6.78	128	**4**	**4**	**8**	0.2	94	6.77

[a] Purified by an automated preparative HPLC (Waters 2695) detected by UV (214 nm; Silica 60-5N, 20$\phi\times$250 mm, elution with 15% 2-propanol in hexane at 7.0 mL min^{-1} flow rate). [b] Purity was determined by reverse-phase HPLC with peak area (UV) at 214 nm. LC/MS were obtained on an AppliedBioSystems Mariner TK3500 Biospectrometry Workstation (ESI-TOF) mass spectrometery and Hewlett-Packard Series 1100 (GL Science Inc. Inertsil ODS-3, 3 μm, 4.6×75 mm with a linear gradient of 10% acetonitrile containing 0.1% formic acid/water containing 0.1% formic acid to 100% acetonitrile containing 0.1% formic acid over 9 min at 1.0 mL min^{-1} flow rate). [c] Retention time. Positive ion electrospray MS data, $[M+H]^+$ were recorded. [d] Macrosphelide E. [e] Macrosphelide F. [f] Macrosphelide A. [g] Macrosphelide C.

[1] J. Nielsen, *Curr. Opin. Chem. Biol.* **2002**, *6*, 297–305.

[2] L. A. Wessjohann, *Curr. Opin. Chem. Biol.* **2000**, *4*, 303–309.

[3] K. C. Nicolaou, J. A. Pfefferkorn, G.-Q. Cao, *Angew. Chem.* **2000**, *112*, 750–755; *Angew. Chem. Int. Ed.* **2000**, *39*, 734–739.

[4] K. C. Nicolaou, D. Vourloumis, T. Li, J. Pastor, N. Winssinger, Y. He, S. Ninkovic, F. Sarabia, H. Vallberg, F. Roschangar, N. P. King, M. R. V. Finlay, P. Giannakakou, P. Verdier-Pinard, E. Hamel, *Angew. Chem.* **1997**, *109*, 2181–2187; *Angew. Chem. Int. Ed. Engl.* **1997**, *36*, 2097–2103.

[5] I. Hijikuro, T. Doi, T. Takahashi, *J. Am. Chem. Soc.* **2001**, *123*, 3716–3722.

[6] a) M. Hayashi, Y.-P. Kim, H. Hiraoka, M. Natori, S. Takamatsu, T. Kawakubo, R. Masuma, K. Komiyama, S. Omura, *J. Antibiot.* **1995**, *48*, 1435–1439; b) S. Takamatsu, Y.-P. Kim, M. Hayashi, H. Hiraoka, M. Natori, K. Komiyama, S. Omura, *J. Antibiot.* **1996**, *49*, 95–98.

[7] a) T. A. Springer, *Nature* **1990**, *346*, 425–434; b) E. C. Butcher, *Cell* **1991**, *67*, 1033–1036; c) A. Fukami, K. Iijima, M. Hayashi, K. Komiyama, S. Omura, *Biochem. Biophys. Res. Commun.* **2002**, *291*, 1065–1070.

[8] T. Sunazuka, T. Hirose, Y. Harigaya, S. Takamatsu, M. Hayashi, K. Komiyama, S. Omura, P. A. Sprengeler, A. B. Smith III, *J. Am. Chem. Soc.* **1997**, *119*, 10247–10248.

[9] a) Y. Kobayashi, B. G. Kumar, T. Kurachi, *Tetrahedron Lett.* **2000**, *41*, 1559–1563; b) Y. Kobayashi, G. B. Kumar, T. Kurachi, H. P. Acharya, T. Yamazaki, T. Kitazume, *J. Org. Chem.* **2001**, *66*, 2011–2018; c) Y. Kobayashi, H. P. Acharya, *Tetrahedron Lett.* **2001**, *42*, 2817–2820; d) Y. Kobayashi, Y.-G. Wang, *Tetrahedron Lett.* **2002**, *43*, 4381–4384.

[10] a) M. Ono, H. Nakamura, F. Konno, H. Akita, *Tetrahedron: Asymmetry* **2000**, *11*, 2753–2764; b) H. Nakamura, M. Ono, Y. Shiba, H. Akita, *Tetrahedron: Asymmetry* **2002**, *13*, 705–713; c) H. Nakamura, M. Ono, M. Makino, H. Akita, *Heterocycles* **2002**, *57*, 327–336.

[11] G. V. M. Sharma, C. C. Mouli, *Tetrahedron Lett.* **2002**, *43*, 9159–9161.

 © 2003 Wiley-VCH Verlag GmbH & Co. KGaA, Weinheim

[12] R. Anacardio, A. Arcadi, G. D'Anniballe, F. Marinelli, *Synthesis* **1995**, 831 – 836.
[13] a) T. Takahashi, T. Nagashima, J. Tsuji, *Chem. Lett.* **1980**, 369 – 372; b) T. Takahashi, H. Ikeda, J. Tsuji, *Tetrahedron Lett.* **1980**, *21*, 3885 – 3888.
[14] a) D. A. Evans, B. D. Allison, M. G. Yang, C. E. Masse, *J. Am. Chem. Soc.* **2001**, *123*, 10840 – 10852; b) D. A. Evans, B. D. Allison, M. G. Yang, *Tetrahedron Lett.* **1999**, *40*, 4457 – 4460; c) D. A. Evans, D. P. Halstead, B. D. Allison, *Tetrahedron Lett.* **1999**, *40*, 4461 – 4462.
[15] After removal of the silyl groups (HF/pyridine), the stereochemistry was determined by ^{1}H NMR compared with those reported in the literature. G. Guanti, L. Banfi, E. Narisano, *Gazz. Chim. Ital.* **1987**, *117*, 681.
[16] a) H. X. Zhang, F. Guibe, G. Balavoine, *J. Org. Chem.* **1990**, *55*, 1857 – 1867; b) N. D. Smith, J. Mancuso, M. Lautens, *Chem. Rev.* **2000**, *100*, 3257 – 3282.
[17] J. A. Ellman, L. A. Tompson, *Tetrahedron Lett.* **1994**, *35*, 9333 – 9336.
[18] Block **B** was prepared from the corresponding methyl hydroxycarboxylate (commercially available) (4-methoxyphenylmethyl 2,2,2-trichloroacetimidate/CSA(0.3 equiv)/CH_2Cl_2; NaOH/H_2O, MeOH, THF; HCl; CSA = camphorsulfonic acid).
[19] a) T. Takahashi, H. Inoue, S. Tomita, T. Doi, A. M. Bray, *Tetrahedron Lett.* **1999**, *40*, 7843 – 7846; b) T. Takahashi, H. Inoue, Y. Yamamura, T. Doi, *Angew. Chem.* **2001**, *113*, 3330 – 3333; T. Takahashi, H. Inoue, Y. Yamamura, T. Doi, *Angew. Chem.* **2001**, *113*, 3330 – 3333; *Angew. Chem. Int. Ed.* **2001**, *40*, 3230 – 3233; c) M. Hashimoto, A. Mori, H. Inoue, H. Nagamiya, T. Doi, T. Takahashi, *Tetrahedron Lett.* **2003**, *44*, 1251 – 1254.
[20] 1-Iodo-1-alken-3-ol underwent carbonylation at room temperature using [$PdCl_2(PPh_3)_2$] as a catalyst. A. Cowell, J. K. Stille, *Tetrahedron Lett.* **1979**, *20*, 133 – 136.
[21] The reaction conditions were initially optimized in solution. We found that the vinyl bromide did not react with CO at room temperature utilizing [$PdCl_2(MeCN)_2$]. However, the palladium-catalyzed carbonylation of the vinyl bromide proceeded at 80 °C using triphenylphosphane, dppf, or [(tBu)$_3$PH]BF_4 as a ligand.
[22] Removal of the MPM group was not complete using 0.15 M of DDQ. In the absence of aqueous $NaHCO_3$, **16** was cleaved from the resin. K. Horita, T. Yoshioka, T. Tanaka, Y. Oikawa, O. Yonemitsu, *Tetrahedron* **1986**, *42*, 3021 – 3028.
[23] The dimerized product was not obtained (**16**: ca. 0.6 mmol g^{-1} loading). Under the cyclization conditions, elimination of the β-acyloxy ester moiety was not observed.
[24] The spectral data are given in the Supporting Information.
[25] K. C. Nicolaou, X.-Y. Xiao, Z. Parandoosh, A. Senyei, M. P. Nova, *Angew. Chem.* **1995**, *107*, 2476 – 2479; *Angew. Chem. Int. Ed. Engl.* **1995**, *34*, 2289 – 2291.
[26] LC/MS spectra of the 122 products gave the corresponding [M+H]$^+$ data and the structures of 15 compounds randomly selected were determined by ^{1}H NMR spectra. The acetal of the ethylene glycol moiety in **C3** and **C7** was intact under the cleavage conditions.
[27] No other isomer was detected in LC/MS. However, as a referee pointed out, there is some uncertainty about the structure of the new lactones by the possibility of complete transesterification under acid cleavage conditions.

 © 2003 Wiley-VCH Verlag GmbH & Co. KGaA, Weinheim

Binding Assays with Native Markers

Competitive Binding Assays Made Easy with a Native Marker and Mass Spectrometric Quantification**

*Georg Höfner and Klaus Theodor Wanner**

Dedicated to Professor H. Nöth on the occasion of his 75th birthday

Competitive binding assays represent a fundamental method, not only in drug discovery, but also in many other fields of the life sciences.[1] These assays are used to characterize the affinity of a ligand to a defined target, for example, a pharmacological receptor. The principle is simple. A marker, that is, a ligand which addresses the desired binding site (the target) with high affinity and selectivity, is required. The affinity of test compounds for the target can then be determined from their ability to displace the marker from the target. Owing to the extraordinarily high sensitivity required for the quantification of the marker, the application of this principle is generally restricted to radioactive-ligand (radioligand) binding assays and fluorescence assays. However, this means that the marker has to be labeled with a suitable radioisotope (e.g. ^{3}H, ^{35}S, or ^{125}I)[2] or an appropriate fluorophore.[3] Besides the additional synthetic efforts, further limitations, such as safety precautions and expensive disposal complicate the practical work with radioligands. On the other hand, the introduction of a fluorophore to the marker often requires re-optimization of the structure of the marker, in addition background fluorescence in binding experiments can interfere with the measurements.[4]

In the mean time, mass spectrometry (MS) has emerged as an analytical technique which is sensitive enough to provide quantification in binding assays.[5] Quite elegant approaches based on affinity selection with mass spectrometric detection have been described recently. However, this method is demanding, because all test compounds showing affinity have to be monitored.[6]

We have attempted to establish competitive binding assays, similar to radioligand binding assays, in which only the marker has to be detected and quantified by mass spectrometry. In this kind of binding assay, which we termed competitive MS-binding assay, a native marker is used instead of the radioligand. When choosing a possible marker from the pool of known ligands the only factors that need to be considered are that the ligand must have sufficient affinity and selectivity for the target and a detection limit that is as high as possible with respect to mass spectrometry.

Usually, in radioligand binding experiments the amount of bound radioligand is determined. Performing MS-binding experiments, it may be preferable to quantify the nonbound marker to avoid the additional step of dissociating the receptor–marker complex. From the analytical point of view, it is favorable to choose a marker and a receptor concentration near the K_d value. Thus it can be arranged that the amount of bound and nonbound marker are in the same order of magnitude. Then, in the competitive binding experiment (in which the bound marker is displaced by the test compound) the amount of nonbound marker increases considerably and the analytical signal is significantly enhanced.

As a model to investigate the feasibility of binding assays following this concept we selected the dopamine D_1-receptor which is a typical G-protein coupled receptor used in the field of drug screening. A porcine striatal membrane fraction (P_2)[7] served as a natural source containing D_1-receptors in relatively high concentrations. SCH 23390 (Figure 1) was chosen as a native marker. This compound shows high affinity (K_d = 0.53 nM) and selectivity for D_1-receptors.[8] Furthermore preliminary studies revealed that electrospray mass spectrometry (ESI-MS) in the multiple reaction monitoring (MRM) mode using a triple quadrupole mass spectrometer coupled to a HPLC (LC-ESI-MS-MS) is a rather reliable technique for the quantification of SCH 23390 in sample matrices.[9]

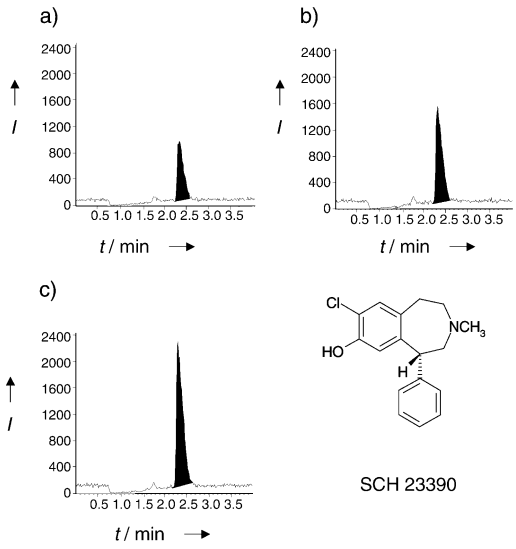


Figure 1. Representative MRM chromatogram of SCH 23390 from binding experiments after HPLC separation (Supersphere 60 RP select B; solvent: CH_3CN/0.1% HCOOH in H_2O 1/1). a) Without (+)-butaclamol, b) 30 nM (+)-butaclamol, c) 10 μM (+)-butaclamol. Nonbound SCH 23390 was monitored at a transition from m/z 288.1 (precursor ion) to m/z 91.2 (product ion).[9]

[*] Prof. Dr. K. T. Wanner, Dr. G. Höfner
Department Pharmazie
Zentrum für Pharmaforschung
Ludwig-Maximilians-Universität München
Butenandtstrasse 7, 81377 München (Germany)
Fax: (+49) 89-2180-77247
E-mail: klaus.wanner@cup.uni-muenchen.de

[**] This work was supported by the Fonds der Chemischen Industrie and the BMBF.

Supporting information for this article is available on the WWW under http://www.angewandte.org or from the author.

 DOI: 10.1002/anie.200351806 © 2003 Wiley-VCH Verlag GmbH & Co. KGaA, Weinheim

The affinity of seven known dopamine antagonists for D_1-receptors was determined according to the new procedure (Table 1). The binding experiments were performed according to standard radioligand binding assays for dopamine receptors.[8–10] In comparison to such standard radioligand binding assays, the commonly used 50 mM Tris-buffer (containing various additional salts) was substituted with a 50 mM ammonium formiate solution of pH 7.4, to avoid suppression of the LC-ESI-MS-MS signal of SCH 23390 in matrix samples. The concentration of the D_1-receptors was set in the range of the K_d value (about 0.5–0.8 nM). As a further difference to radioligand binding assays the nonbound marker was separated by centrifugation (at 50000 *g*) instead of filtration.[9]

As an example of our method, the determination of the affinity of the dopamine antagonist (+)-butaclamol as a test compound is illustrated: D_1-receptors together with 1.25 nM SCH 23390 and (+)-butaclamol (0–10 μM) were incubated for 40 min and centrifuged afterwards. The amount of SCH 23390 in the supernatant solution after centrifugation was quantified without further sample preparation by ESI-LC-MS-MS with the aid of a calibration curve (Figure 1 and Figure 2). Figure 3 shows a binding curve generated from the resulting data. The curve of the concentration of nonbound SCH 23390 in the supernatant solution as a function of the test compound (+)-butaclamol is characteristic for this kind of assays based on the quantification of the marker in the supernatant solution. From such binding curves, the IC_{50} value, that is, the concentration of a test compound which reduces the specific binding of the marker to 50%, can be deduced in analogy to conventional binding assays. The mean of the IC_{50} values which were determined from three independent experiments, was converted into a K_i value. This K_i value for (+)-butaclamol correlates well with the K_i value determined in an analogously conducted conventional radioligand binding assay using [^{3}H]SCH 23390 (Table 1). The same applies for the K_i values of the other six test compounds in this experiment. Further investigation is needed to explain the tendency of slightly enhanced K_i values. Nevertheless, it is considerably more important that the rank order of the K_i values obtained here is in agreement with the rank order observed in radioligand binding assays. Consequently competitive MS-binding assays offer an attractive alternative to the conventional procedures mentioned above. Furthermore, with competitive MS-binding assays, it might be possible to collect data from different binding sites in a biological sample in one experiment. This could be achieved by using different markers, which selectively address several binding sites in the sample, in the same competitive binding assay. Moreover, MS-binding assays could be modified in a way that firstly, a library is screened for hits in a competitive binding experiment and that in a second step, such bound hits could be identified by mass spectrometry following their liberation from their binding sites.

In conclusion we have described a new method to perform competitive binding assays which is characterized by the mass spectrometric quantification of the marker. Among other benefits the main advantage that such competitive MS-binding assays offer is that ligands for a binding site need

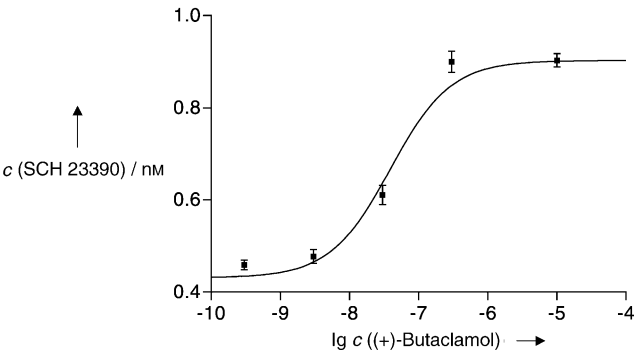


Figure 3. Binding curve obtained by nonlinear regression for binding experiments in which (+)-butaclamol competes with SCH 23390 for the binding sites. The data points correspond to nonbound SCH 23390 quantified by LC-ESI-MS-MS and are mean values (±*s*) from four binding experiments.[9]

Table 1: IC_{50} and K_i values for dopamine antagonists at D_1-receptors obtained by mass spectrometry and by radioligand binding assays.

Compound	Marker SCH 23390		Marker [^{3}H]SCH 23390
	IC_{50} [nM][a,b]	K_i [nM][a,b]	K_i [nM][b,c]
(+)-butaclamol	36 ± 3	11 ± 1	5.4 ± 1.9
chlorpromazine	1700 ± 40	620 ± 10	300 ± 40
haloperidol	620 ± 170	220 ± 60	110 ± 2
pimozide	13000 ± 700	4700 ± 200	2500 ± 500
SKF83566	5.9 ± 1.0	1.9 ± 0.3	2.7 ± 0.6
(*S*)-sulpiride	> 10000	> 10000	> 10000
trifluoperazine	1300 ± 100	460 ± 40	215 ± 20

[a] Nonbound SCH 23390 was quantified by LC-ESI-MS-MS after centrifugation from binding experiments performed in 50 mM ammonium formiate pH 7.4.[9] [b] IC_{50} and K_i values are expressed as arithmetic means ± standard error of the mean from three experiments. A K_d value of 0.72 nM obtained for [^{3}H]SCH 23390 in ammonium formiate pH 7.4 was used for the calculation of the K_i values.[9] [c] Bound [^{3}H]SCH 23390 was quantified after the filtration of binding experiments performed in 50 mM ammonium formiate pH 7.4.[9]

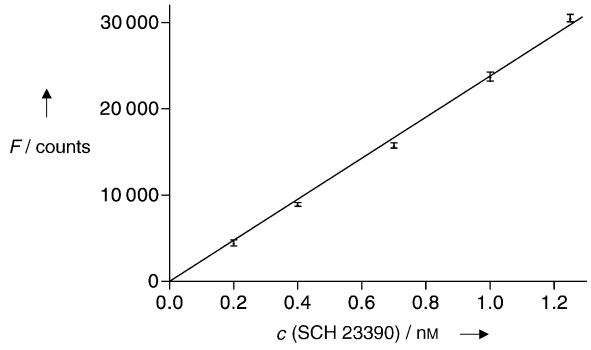


Figure 2. Calibration curve for SCH 23390. A matrix identical to the supernatant of the binding experiments was added to SCH 23390. The given data are mean values (±*s*) from four measurements.[9] *F* = peak area.

 © 2003 Wiley-VCH Verlag GmbH & Co. KGaA, Weinheim

not be labeled. The competitive MS binding assays at dopamine D_1-receptors using SCH 23390 as a native marker resulted in affinity constants which were in good agreement with the affinity constants determined in radioligand binding assays. This simple procedure, its universal suitability, and the advantage of using unmodified markers could help to establish MS binding assays as a routine method in drug screening.

Received: May 5, 2003 [Z51806]
Published Online: September 1, 2003

Keywords: analytical methods · binding assays · dopamine receptors · drug screening · mass spectrometry

[1] P. M. Sweetnam, C. H. Price, J. W. Ferkany in *Burger's Medicinal Chemistrry and Drug Discovery* (Ed.: M. E. Wolff), Wiley, New York, **1995**, pp. 697 – 731.
[2] M. Williams, M. A. Sills in *Comprehensive Medicinal Chemistry, Vol. III* (Ed.: J. C. Emmet), Pergamon, Oxford, **1990**, pp. 45 – 79.
[3] a) N. Baindur, D. J. Triggle, *Med. Res. Rev.* **1994**, *14*, 591 – 664; b) R. Hovius, P. Vallotton, T. Wohland, H. Vogel, *Trends Pharmacol. Sci.* **2000**, *21*, 266 – 273.
[4] J. C. McGrath, S. Arribas, C. J. Daly, *Trends Pharmacol. Sci.* **1996**, *17*, 393 – 399.
[5] a) D. B. Kassel, *Chem. Rev.* **2001**, *101*, 255 – 267; b) G. R. Lenz, H. M. Nash, S. Jindal, *Drug Discovery Today* **2000**, *5*, 145 – 156; c) R. D. Süßmuth, G. Jung, *J. Chromatogr. B* **1999**, *725*, 49 – 65.
[6] a) R. N. Zuckermann, J. M. Kerr, M. A. Siani, S. C. Banville, D. V. Santi, *Proc. Natl. Acad. Sci. USA* **1992**, *89*, 4505 – 4509; b) J. Gao, X. Cheng, R. Chen, G. B. Sigal, J. E. Bruce, B. L. Schwartz, S. A. Hofstadler, G. A. Anderson, R. D. Smith, G. M. Whitesides, *J. Med. Chem.* **1996**, *39*, 1949 – 1955; c) S. Kaur, L. McGuire, D. Tang, G. Dollinger, V. Huebner, *J. Protein Chem.* **1997**, *16*, 505 – 511; d) M. A. Kelly, H. Liang, I. I. Sytwu, I. Vlattas, N. L. Lyons, B. R. Bowen, L. P. Wennogle, *Biochemistry* **1996**, *35*, 11747 – 11755; e) D. Nikolic, S. Habibi-Gouarzi, D. G. Corley, S. Gafner, J. M. Pezzuto, R. B. van Breemen, *Anal. Chem.* **2000**, *72*, 3853 – 3859; f) R. Wieboldt, J. Zweigenbaum, J. Henion, *Anal. Chem.* **1997**, *69*, 1683 – 1691; g) D. C. Schriemer, D. R. Bundle, L. Li, O. Hindsgaul, *Angew. Chem.* **1998**, *110*, 3625 – 3628; *Angew. Chem. Int. Ed.* **1998**, *37*, 3383 – 3387; recently related NMR spectroscopic methods were described: h) W. Jahnke, P. Floersheim, C. Ostermeier, X. Zhang, R. Hemming, K. Hurth, D. P. Uzunov, *Angew. Chem.* **2002**, *114*, 3570 – 3573; *Angew. Chem. Int. Ed.* **2002**, *41*, 3420 – 3423; i) A. H. Siriwardena, F. Tian, S. Noble, J. H. Prestegard, *Angew. Chem.* **2002**, *114*, 3604 – 3607; *Angew. Chem. Int. Ed.* **2002**, *41*, 3454 – 3457.
[7] E. C. Hulme, N. J. Buckley in *Receptor–Ligand Interactions* (Ed.: E. C. Hulme), Oxford University Press, New York, **1992**, pp. 177 – 212.
[8] W. Billard, V. Ruperto, G. Crosby, L. C. Iorio, A. Barnett, *Life Sci.* **1984**, *35*, 1885 – 1893.
[9] For experimental details see Supporting Information.
[10] D. R. Burt, I. Creese, S. Snyder, *Mol. Pharmacol.* **1976**, *12*, 800 – 812.

 © 2003 Wiley-VCH Verlag GmbH & Co. KGaA, Weinheim

Carotenoid Aggregates

Stable and Highly Water-Dispersible, Highly Unsaturated Carotenoid Phospholipids—Surface Properties and Aggregate Size**

Bente Jeanette Foss, Stine Nalum Næss, Hans-Richard Sliwka, and Vassilia Partali*

Polyunsaturated phospholipids possess important physiological properties and consequently, specific concentration methods and synthetic procedures have been developed to obtain these compounds.[1] The most unsaturated and conjugated phospholipid detected to date contains a tetraenic fatty acid C18:4.[2] Conjugated or nonconjugated polyunsaturated phospholipids are as unstable as the free fatty acids and can therefore only be handled at lower temperatures, under an inert atmosphere, or with stabilizers, such as carotenoids.[3] Thus, the synthesis of stable, polyunsaturated phospholipids has to be based on stable, polyunsaturated fatty acids. This requirement is met by carotenoid acids. One of these acids, β-apo-8′-carotenoic acid (C30:9), is commercially available as ethyl ester (C30-ester).[4] Carotenoids are poorly adsorbed by humans and animals.[5] Absorption depends on preceding gastrological emulsifying, the presence of lysophosphatidylcholine helps to enhance the absorption of carotenoids.[6] Some of the commercial carotenoids are abundantly used in coloring soft drinks.[7] Since the carotenoids are hydrophobic their use as food colors in soft drinks depends on highly sophisticated formulation methods. By carefully selecting the detergents, dispersing solvents, protective colloids, and other additives, and by reducing the shock-heating (200 °C) time the water-dispersibility of carotenoids can be improved.[8] The customary formulation procedures result in particle sizes between 20–1000 nm.[8]

The chemical and physical properties of molecular solutions of carotenoids and of molecular and aggregated phospholipids are well known.[9] However, the properties of carotenoids in a natural water-based environment or within the phospholipid-containing cell membranes are less known and are the subject of current research. Especially, the photophysics and photochemistry of carotenoid aggregates are of high interest in the elucidation of light-harvesting mechanisms, photosynthesis, energy transfer, and in protection reactions ($^1O_2$-quenching).[10] In synthesizing a carote-

[*] H.-R. Sliwka, B. J. Foss, V. Partali
Institutt for Kjemi
Norges Teknisk Naturvitenskapelige Universitet (NTNU)
7491 Trondheim (Norway)
Fax: (+47) 73-59-6255
E-mail: hrs@nvg.ntnu.no
S. N. Næss
Institutt for Fysikk
NTNU (Norway)

[**] We thank H. Ernst (BASF-AG, Ludwigshafen) and S. Servi (Politecnico di Milano) for a generous gift of C30-ester and glycerolphosphocholine, respectively. S.N.N. is grateful for financial support from the Norwegian Research Council.

 DOI: 10.1002/anie.200351828 © 2003 Wiley-VCH Verlag GmbH & Co. KGaA, Weinheim

noid phospholipid we hoped to combine the properties of carotenoids with those of phospholipids.

Lysocarotenophosphatidylcholine was synthesized by treating the dichlorophosphate **2** with an equilibrium mixture (9:1) of isomeric carotenomonoglycerides **1a** and **1b** (Scheme 1).[11] The bromo intermediates **3** were aminated with trimethylamine affording the isomer mixture **4a**/**4b**/**4c** (49:43:8) in 33% yield.[12] 1D, 2D ^{1}H and ^{13}C spectra of the product mixture showed the characteristic resonance shifts for the glycerol protons and carbon atoms for the three isomers, ^{31}P NMR spectra indicated the presence of similar amounts of isomer **4a** and **4b**.

The positional isomers of lysophosphatidylcholines, esterified with fatty acids other than C16 or C18 loose their lytic activity, which is further reduced in the presence of double bonds.[13] Whereas the biological activities of isomers **4a–c** may be different,[14] the surfactant and aggregation properties are expected to be virtually identical, as all the isomers have the same polar head group and the same hydrophobic chain.[15] A contact-angle determination ($\Theta \approx$ 25°) of a water drop on a dry film of **4** and the short lifetime of the drop (0.1 sec) indicated surfactant activity. The surface tension γ at the air–water interface and the critical micelle concentration (cmc) of **4** were determined with a tensiometer: $\gamma_{cmc} = 56$ mN m^{-1} at cmc $= 1.5 \times 10^{-3}$ M ($= 1$ mg L^{-1}; Figure 1).

The data from Figure 1 were used to calculate: the surface concentration Γ, the surface pressure π_{cmc}, the molecule area at the interface A and the free energies of adsorption and aggregation ΔG^0_{ad}, ΔG^0_{mic} (Table 1). The values of Γ and A are similar to other zwitterionic surfactants.[16] The negative value

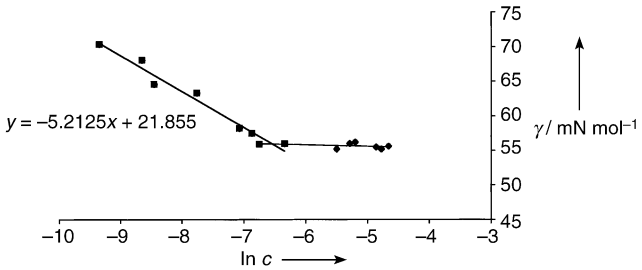
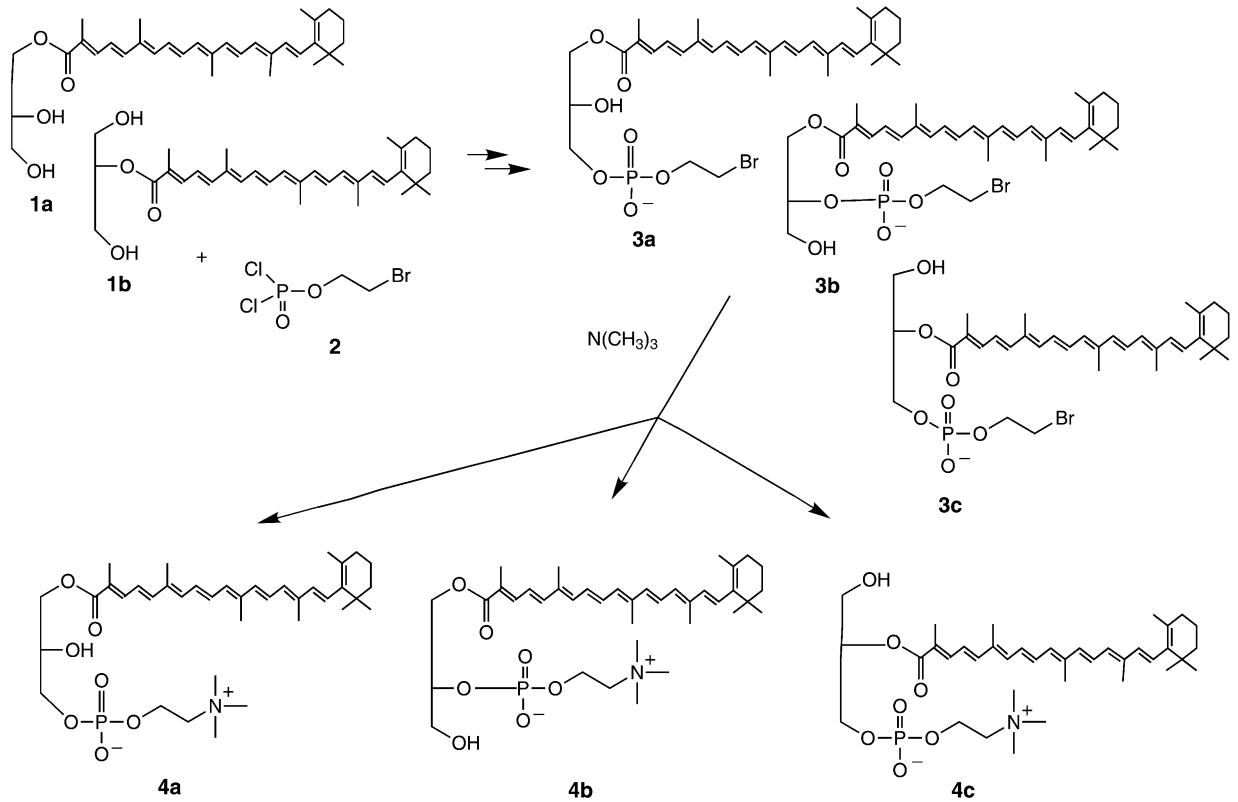


Figure 1. Critical micelle concentration (cmc) of **4**, determined by measuring surface tension γ. The intersection of the lines defines the cmc.

Table 1: Parameters of **4** determined from the data in Figure 1.

cmc [10^{-3} mol L^{-1}]	1.5	A [Å^2]	52
γ_{cmc} [mN m^{-1}]	56	ΔG^0_{mic} [kJ mol^{-1}]	−16.0
π_{cmc} [mN m^{-1}]	17	ΔG^0_{ad} [kJ mol^{-1}]	−21.3
Γ [10^6 mol m^{-2}]	3.2	k_{ad}/k_{mic}	8.7

of ΔG^0_{mic} indicates that the dispersion of **4** in water is spontaneous at room temperature. Even the equilibrium constants $\frac{\text{molecule}_{surface}}{\text{molecule}_{bulk}} = k_{ad} = 6100$ and $\frac{\text{molecule}_{micelle}}{\text{molecule}_{bulk}} = k_{mic} = 700$ demonstrate the predominance of molecules on the water surface. The 9:1 concentration relation of adsorbed molecules at the surface to dispersed aggregates allowed clear, highly and evenly colored aqueous suspensions of **4** to be obtained without heat, detergents, or additives. At higher concentra-



Scheme 1. Synthesis of the carotinoid phospholipids.

 © 2003 Wiley-VCH Verlag GmbH & Co. KGaA, Weinheim

tions the dispersion became turbid and viscous. There was no saturation point up to 60 mg mL^{-1} of **4**.

In water **4** formed aggregates with an average hydrodynamic radius of $r_H = 8$ nm within a narrow range of r_H values (6–14 nm); some big aggregates are also observed with $r_H = 40$–600 nm, Figure 2. Single-chain amphiphiles are expected to aggregate in micelles.[17] However, the radius of the aggregates of **4** points toward another aggregate morphology.

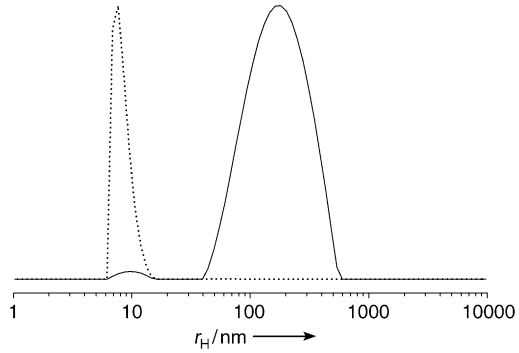


Figure 2. Size determination of aggregates of **4** in water by dynamic light scattering, number-weighted distribution (••••), intensity weighted (——).

The UV/Vis spectra of **4** in organic solvents showed an absorption at $\lambda_{max} = 454$ nm, in water the absorption band was shifted to $\lambda_{max} = 400$ nm (Figure 3). This absorption band is

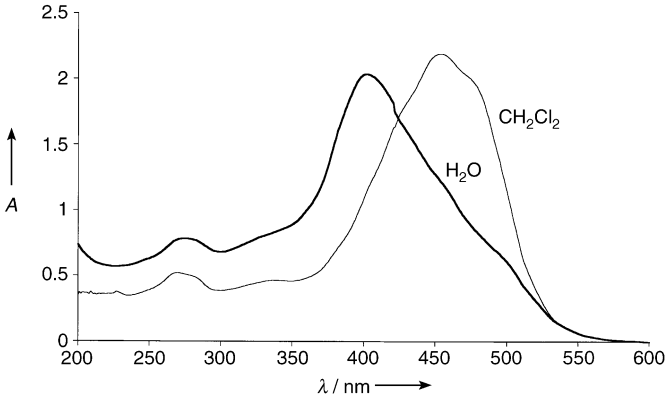


Figure 3. Vis spectra of **4** in dichloromethane and water.

associated with a strong exiton coupling of the closely packed molecules in H-aggregates, a side-by-side arrangement of the monomers.[7,8] In aggregates and monomolecular surface films of saturated or *cis*-unsaturated phospholipids, dense packing of the monomers is hampered by the flexible chain or by the twist of *cis*-double bonds. In contrast, carotenoid phospholipid isomers **4** have a rigid, stretched-out chain as a result of the all-*trans* configuration of the double bonds, which favors a close orientation of aggregated and surface-absorbed molecules.

The lysophospholipid derivatives **4a–c** allow the determination of the distinct properties of conjugated, polyunsaturated lysophospholipids, and of a carotenoid in pure aqueous solutions without detergents. The investigation of the photophysical characteristics of the aggregates is in progress.

Experimental Section

A mixture of the glycerols **1a** and **1b**[11] (90:10; 0.66 g, 1.3 mmol) dissolved in benzene (70 mL), was added dropwise to a solution of 2-bromoethyl dichlorophosphate (**2**; 0.49 g, 2 mmol)[18] and triethylamine (0.78 g, 7.8 mmol) in benzene (30 mL) as in Ref. [12]. The reaction mixture was stirred at 20 °C for 24 h under nitrogen. The precipitated triethylammonium chloride was removed by filtration. The remaining phosphorochloridate and excess of 2-bromoethyl dichlorophosphate (**2**) were hydrolyzed with water (20 mL), at 20 °C for 12 h. The organic phase was separated, washed with water (3 × 40 mL) and the solvent removed. The residue was taken up in a mixture of $CHCl_3$/2-propanol/dimethylformamide (120 mL, 3:5:5) and treated with a 45 % solution of trimethylamine (45 % in H_2O, 20 mL) at 20 °C for 48 h. The solvents were removed and the crude product dissolved in $CHCl_3$. Chromatographic purification ($CHCl_3$/CH_3OH 4:1, gradual addition of H_2O and CH_3OH to give a final mixture of $CHCl_3$/CH_3OH/H_2O 4:5:1) gave a mixture of 1,3-, 1,2-, and 2,3-(β-apo-8′-carotenoyl)-*glycero*-phosphatidylcholine isomers **4a**/**4b**/**4c** (49:43:8) (290 mg, 33 %). MS (ESI): *m*/*z* 672 [M^++H], 579 [(M^++H)-92 (toluene)]. The analysis of the complex ^{1}H, ^{13}C, and ^{31}P NMR signals will be presented in detail elsewhere. The contact angle θ was determined with a goniometer (Fibro DAT 1122). Surface tension γ and cmc were determined with a Wilhelmy plate tensiometer (Krüss K10 T digital tensiometer) in distilled, filtered (0.22 μm) aqueous solutions. The values were recorded immediately after the initial equilibrium was reached. Surface pressure $\pi_{cmc} = \gamma_0 - \gamma_{cmc}$, $\gamma_0 = 73$ mN m^{-1} (H_2O). Surface concentration $\Gamma = \frac{-1}{RT}\frac{d\gamma}{d\ln c_{cmc}}$ $\Gamma = \frac{-c_{cmc}}{RT}\frac{d\gamma}{dc_{cmc}}$ [mol m^2], c in mol m^{-3}; slope from plot Figure 1: 5.2×10^{-3}, in J m^{-2}, 1 mN m^{-1} = 0.001 J m^{-2}; $R = 8.31$ J mol^{-1} T^{-1}; $T = 294$ °C. Area of molecule at interface A [Å^2] = $10^{20}/\Gamma N_A$, N_A = Avogadro number. Free energy of micellization $\Delta G^0_{mic} = RT \ln c_{cmc}$ [J mol^{-1}]. Free energy of adsorption $\Delta G^0_{ad} = (RT \ln c_{cmc}) - (6.023 \times 10^{-3}\, \pi_{cmc} A)$ [J mol^{-1}]. Equilibrium constants: $\frac{\text{Molecule}_{micelle}}{\text{Molecule}_{solution}} = k_{mic} = e^{-\frac{\Delta G^0_{mic}}{RT}}$, $\frac{\text{Molecule}_{surface}}{\text{Molecule}_{solution}} = k_{ad} = e^{-\frac{\Delta G^0_{ad}}{RT}}$. Determination of hydrodynamic particle size by Dynamic Light Scattering (DLS) with a ALV DLS/SLS-5022F compact goniometer system and ALV-5000/E multiple τ-digital correlator, light source 22 mW He-Ne laser. The samples (23 °C) were filtered through a 5-μm filter into a cylindrical light scattering cuvette. The scattering angle was 90°, Data analysis with CONTIN.[19] Data from 14 successive 5 min measurements were averaged.

Received: May 7, 2003 [Z51828]

Keywords: carotenoids · fatty acids · nanostructures · phospholipids · surface chemistry

[1] a) G. G. Haraldson, A. Thorarensen, *J. Am. Oil Chem. Soc.* **1999**, *76*, 1143–1149; b) D. W. Hopper, J. G. Catalano, T. L. Macdonald, *Tetrahedron Lett.* **1996**, *37*, 7871–7874.
[2] B. Schmitz, H. Egge, *Chem. Phys. Lipids* **1984**, *43*, 139–151.
[3] A. A. Woodall, G. Britton, M. J. Jackson, *Biochim. Biophys. Acta* **1997**, *1336*, 575–576.
[4] Under the names: Lucantin Yellow, BASF, Ludwigshafen; Carophyll Yellow, Hoffmann-La Roche, Basel.
[5] T. van Vliet, *Eur. J. Clin. Nutr.* **1996**, *50*, S32–37.

 © 2003 Wiley-VCH Verlag GmbH & Co. KGaA, Weinheim

[6] a) H. C. Furr, R. M. Clark, *J. Nutr. Biochem.* **1997**, *8*, 364 – 377; b) T. Sugawara, M. Kushiro, H. Zhang, E. Eiichi, H. Ono. A. Nagao, *J. Nutr.* **2001**, *131*, 2921 – 2927.
[7] E. Lüddecke, A. Auweter, L. Schweikert (BASF AG), EP 930022, **1998** [*Chem. Abs.* Year, *Vol*, No if available].
[8] D. Horn, J. Rieger, *Angew. Chem.* **2001**, *113*, 4460 – 4492; *Angew. Chem. Int. Ed.* **2001**, *40*, 4331 – 4361.
[9] a) *Carotenoids, Vol. 1A, 1B, 3* (Eds.:G. Britton, S. Liaaen-Jensen, H. Pfander), Birkhäuser, Basel, **1995, 1995**, and **1998,** respectively; b) *Phospholipids Handbook*, Marcel Dekker, New York, **1993**.
[10] a) M. Burke, R. Edge, E. J. Land, D. J. McGarvey, T. G. Truscott, *FEBS Lett.* **2001**, *500*, 132 – 136; b) R. K. Naqvi, T. B. Melø, B. Bangar, T. Javorfi, I. Simidjiev, G. Garab, *Spectrochim. Acta Part A* **1997**, *53*, 2659 – 2667; c) A. Cantrell, D. J. McGarvey, T. G. Truscott, F. Rancan, F. Böhm, *Arch. Biochem. Biophys.* **2003**, *412*, 47 – 54; d) A. V. Ruban, P. Horton, A. J. Young, *J. Photochem. Photobiol. B* **1993**, *21*, 229 – 234.
[11] V. Partali, L. Kvittingen, H. R. Sliwka, T. Anthonsen, *Angew. Chem.* **1996**, *108*, 342 – 344; *Angew. Chem. Int. Ed. Engl.* **1996**, *35*, 329 – 330.
[12] S. D. Stamatov, *Chem. Phys. Lipids* **1998**, *91*, 129 – 134.
[13] F. C. Reman, R. A. Demel, K. De Gier, L. L. M. van Deenen, H. Eibl, O. Westphal, *Chem. Phys. Lipids* **1969**, *3*, 221 – 233.
[14] P. J. A. O'Doherty, *Lipids* **1979**, *14*, 84 – 87.
[15] a) D. Arnold, H. U. Weltzien, O. Westphal, *Justus Liebigs Ann. Chem.* **1967**, *709*, 234 – 239; b) R. Haftendorn, G. Schwarze, R. Ubrich-Hofmann, *Chem. Phys. Lipids* **2000**, *104*, 57 – 66; c) N. Robinson, L. Saunders, *J. Pharm. Pharmacol.* **1958**, *10 Suppl.*, 227T – 229T.
[16] M. J. Rosen, *Surfactants and Interfacial Phenomena*, 2nd ed., Wiley, New York, **1989**, p. 79.
[17] R. Nagarajan, E. Ruckenstein, *J. Colloid Interface Sci.* **1979**, *71*, 580 – 604.
[18] W. J. Hansen, R. Murari, Y. Wedmid, W. J. Baumann, *Lipids* **1982**, *17*, 453 – 459.
[19] S. W. Provencher, CONTIN (Version 2) Users manual, EMBL technical report DA07, Max-Planck-Institut Biophysikalische Chemie, Göttingen, **1984**.

 © 2003 Wiley-VCH Verlag GmbH & Co. KGaA, Weinheim

Alkene Hydrogenation

Hydrogenation on Metal Surfaces: Why are Nanoparticles More Active than Single Crystals?**

Aidan M. Doyle, Shamil K. Shaikhutdinov, S. David Jackson, and Hans-Joachim Freund*

Hydrogenation of unsaturated hydrocarbons occurs efficiently on noble-metal catalysts, such as platinum, rhodium, and palladium.[1] The reaction mechanism first proposed by Horiuti and Polanyi[2] in 1934 proceeds by a) hydrogen dissociation on the metal surface, b) alkene adsorption, c) subsequent hydrogen addition to alkene and, finally, d) desorption of the product (alkane). Real hydrogenation catalysts represent very complex systems for studying reaction mechanisms at the molecular level. Therefore, model systems with a reduced complexity have been invoked ranging from single crystals to metal particles deposited on oxide films.[3–8] The conclusions regarding reaction mechanism and structural sensitivity are often based upon experiments on single metal crystals.[3] In particular, hydrogenation of alkenes has been shown to be structure insensitive.

Herein, we report results showing that alkene hydrogenation reaction under low-pressure conditions, which does not occur on Pd(111) single crystal, proceeds efficiently on palladium nanoparticles. We show that the formation of weakly bound "subsurface" hydrogen is a key factor for hydrogenation to occur efficiently. The subsurface hydrogen exists in both Pd systems. However, the nanoparticle dimensions are such that this hydrogen is accessible to the adsorbed alkene, and hydrogenation occurs. In contrast, for crystals, the hydrogen atoms diffuse so deep into the bulk that they are not accessible to an adsorbed alkene, and therefore hydrogenation does not occur.

We have studied the surface chemistry of ethene and different pentene isomers on both Pd(111) single crystal and Pd particles deposited on a thin alumina film (Figure 1). The particles studied are approximately 5 nm in diameter and consist primarily ($\approx 90\,\%$) of (111) facets[8] ($\approx 10\,\%$ are (100) facets). The experiments were performed in ultrahigh vacuum on clean and well-defined systems. Using the temperature-programmed desorption (TPD) technique, we have observed that a number of hydrocarbon transformations, such as dehydrogenation and H–D exchange, occur on both palla-

[*] Dr. Sh. K. Shaikhutdinov, Dr. A. M. Doyle, Prof. H.-J. Freund
Fritz-Haber-Institut der Max-Planck-Gesellschaft
Faradayweg 4–6
14195 Berlin (Germany)
Fax: (+49) 30-8413-4105
E-mail: Shaikhutdinov@fhi-berlin.mpg.de
Prof. S. D. Jackson
Department of Chemistry, University of Glasgow
Glasgow, G12 8QQ (UK)

[**] We acknowledge support by the Athena project funded by the Engineering and Physical Sciences Research Council (EPSRC) of the U.K. and Johnson Matthey plc.

 © 2003 Wiley-VCH Verlag GmbH & Co. KGaA, Weinheim DOI: 10.1002/anie.200352124

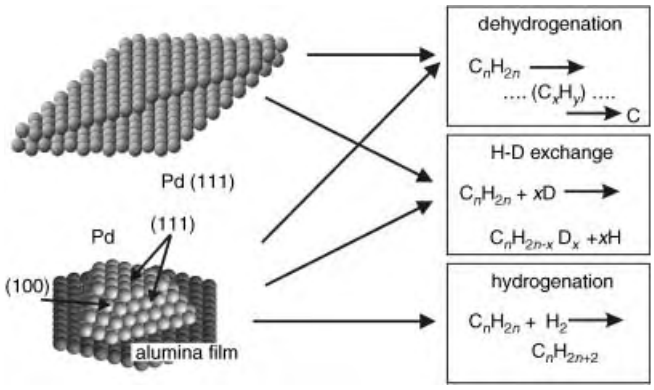


Figure 1. Schematic representation of the alkene reactions observed on Pd(111) single crystal (top) and well faceted Pd nanoparticles supported on a thin alumina film (bottom).

dium systems. However, the hydrogenation to alkane only occurs on small particles.

Adsorption of light alkenes, such as ethene, on palladium has been the subject of extensive studies on single-crystal surfaces and supported catalysts.[9,10] There is considerably less data on the interaction of higher hydrocarbons.[11–14] Madix and co-workers studied the adsorption of various alkenes and dienes on the clean and hydrogen (deuterium) precovered Pd(111) and Pd(100) surfaces by TPD.[11,12] They observed an H–D exchange reaction, which was assumed to proceed via a half-hydrogenated intermediate species. However, formation of the alkane was not observed on both surfaces.

We have examined the reactions of ethene, 1-pentene, *trans*- and *cis*-2-pentene on Pd(111) single crystals and supported Pd particles.[15–17] Herein, we only report the main results for *trans*-2-pentene, which is referred to as "pentene" in the following, while the details will be presented in a forthcoming paper.[17]

The TPD spectra for pentene on both Pd(111) and the supported Pd nanoparticles show that the molecules desorb intact at temperatures below 280 K (Figure 2). In analogy to other alkene molecules previously studied,[9–12] we have assigned the desorption peaks at about 130 K to a condensed layer, at around 170 K to π-bonded and at approximately 260 K to σ-bonded pentene molecules. Upon further heating, the chemisorbed molecules dehydrogenate in a stepwise manner, as shown by hydrogen evolution extending to 800 K (cf. up to 500 K for ethene). However, the desorption of hydrogen formed on the Pd particles starts at around 100 K lower than Pd(111), although pentene desorbs molecularly at nearly the same temperatures for both systems. A similar effect is found for ethene: hydrogen starts to desorb at about 300 K from the Pd particles and at around 350 K from Pd(111). Therefore, one can conclude that alkene dehydrogenation on the particles occurs more readily than on Pd(111) crystal.

When pentene molecules are exposed to a D_2-precovered Pd(111) surface, a new hydrogen peak at 330 K emerges while desorption at $T > 390$ K is decreased (Figure 3). This result

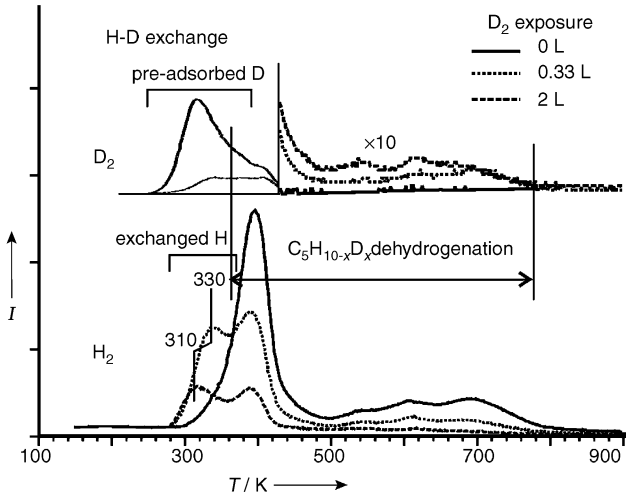


Figure 3. H_2 and D_2 TPD traces after pentene adsorption on the Pd(111) surface pre-exposed to different amounts of D_2. D_2 was first adsorbed at 200 K and then 1 L of C_5H_{10} was added at 100 K.

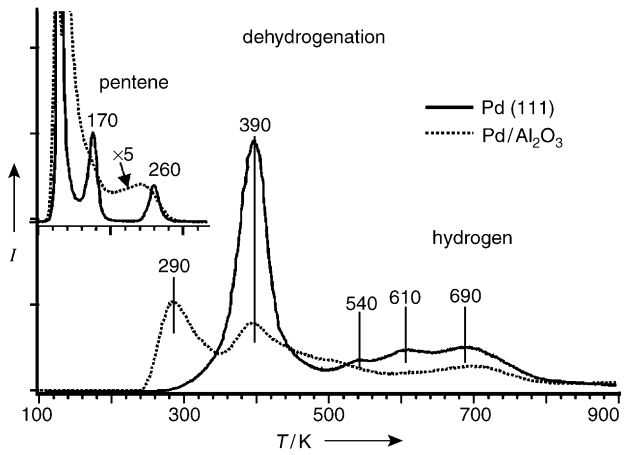


Figure 2. TPD spectra for 1 L of pentene adsorbed at 100 K on Pd surfaces

can be understood in terms of an H–D exchange between pre-adsorbed D atoms and a half-hydrogenated alkene on the Pd(111) surfaces.[12] As a result, H atoms and D-hydrogenated pentyl species, such as C_5H_9D and $C_5H_8D_2$, are formed. The deuterated pentenes desorb at approximately 260 K, identically to unlabeled pentene and dehydrogenate upon heating, which leads to D_2 evolution at 400–800 K. The H atoms, released from pentene and exchanged with D on the surface, recombine and desorb as H_2 and HD at 310–330 K (Figure 3).

As the D_2 exposure increases, the formation and subsequent dehydrogenation of $C_5H_{10-x}D_x$ species is gradually suppressed as the quantity of H_2 desorbing above 400 K decreases. However, the extent of the H–D exchange reaction increases with increasing D_2 exposure. Therefore, the amount of D_2 produced by dehydrogenation of surface $C_5H_{10-x}D_x$ species above 400 K increases with increasing D_2 coverage (Figure 3).

 © 2003 Wiley-VCH Verlag GmbH & Co. KGaA, Weinheim

Meanwhile, the molecular desorption of C_5H_{10} at 170 K, previously assigned to π-bonded pentene, increases on the D-precovered surface (not shown here). This situation means that pre-adsorbed D_2 favors pentene desorption from the π-bonding state, but inhibits both formation of σ-bonded pentene and the dehydrogenation reaction. However, pentane the product of pentene hydrogenation (and ethane, for the case of ethene) has not been detected for the co-adsorption experiments on Pd(111) surfaces.

On Pd particles pre-exposed to D_2, the results are quite similar to those obtained on Pd(111) as far as the H–D exchange reaction is concerned. However, in contrast to the Pd(111) crystal, we have observed deuterated pentane $C_5H_{10}D_2$ (Figure 4a; and $C_2H_4D_2$ with ethene[15]) as a product of the hydrogenation reactions. Therefore, our data clearly demonstrate that alkene hydrogenation to alkane is observed on the Pd nanoparticles only and not on the Pd(111) (and Pd(100)[11]) single crystals.

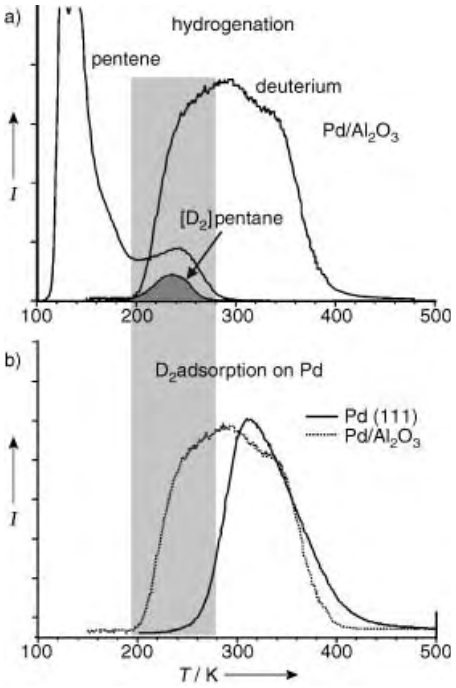


Figure 4. a) TPD spectra of molecular desorption of C_5H_{10} and D_2 after individual adsorption, and the desorption of $C_5H_{10}D_2$ in co-adsorption experiments on the palladium nanoparticles. b) Comparison of D_2 TPD spectra for two palladium systems (1.3 L D_2 at 200 K in each case).

Clearly, when dealing with the effects of small particles the presence of low-coordinate atoms, such as edge and corner atoms has to be considered. However, we have inspected a Pd(111) surface that was the roughened but again found no hydrogenation activity. Therefore, we conclude that surface roughness alone is not sufficient to provide the active sites necessary for the hydrogenation reaction to occur.

The lack of alkene hydrogenation on palladium single crystals has been discussed[12] in comparison to the results on platinum surfaces which show hydrogenation activity for various alkenes.[18–20] It was suggested that the strength of the metal–hydrogen bond could be responsible for such a difference, because a distinctly different mechanism is unlikely.[12] Therefore, to understand why palladium particles are active for hydrogenation, we have examined the interaction of hydrogen with the palladium systems studied.

It is well documented that H_2 readily dissociates on palladium, and that hydrogen atoms then migrate into the subsurface region and into the bulk, occupying interstitial sites.[21–24] When Pd is exposed to H_2 above 200 K, the H atoms can diffuse so deep into the bulk that they cannot be totally released during a TPD run. However, for the nanoparticles the diffusion length is limited by the particle size, and therefore both subsurface and surface hydrogen can be detected by TPD.

Figure 4b shows D_2 TPD spectra for Pd(111) and Pd nanoparticles. The broad signal observed for the particles can be deconvoluted into three peaks centered at around 340, 280, and 240 K.[15] We have previously assigned the high-temperature state to surface hydrogen (deuterium), while the low-temperature states below 300 K correspond to the presence of subsurface hydrogen.[15] Only one peak is observed for Pd(111), although surface and subsurface sites are occupied by hydrogen at these exposures.[24] This is probably due to the small energy difference between the two states. [25]

Therefore, Figure 4b clearly shows that the palladium nanoparticles contain a significant fraction of hydrogen which is more weakly bound than in Pd(111) single crystals. On the other hand, molecular pentene desorption is quite similar for both Pd systems (see Figure 2). Therefore, it is the difference in the hydrogen adsorption behavior that results in different pentene hydrogenation activity of Pd(111) crystals and Pd nanoparticles. Basically the same results are observed for experiments with ethene on Pd particles.[15] Therefore, we conclude that weakly bonded subsurface hydrogen is a key species for the occurrence of alkene hydrogenation.

Figure 4a, shows the TPD traces of molecular desorption of pentene and D_2, observed for individual adsorption, and of $[D_2]$pentane observed in the co-adsorption experiments. It is clear that pentane is formed and desorbs from the Pd particles over a temperature range where the C_5H_{10} and D_2 desorption curves overlap. This overlap is not found for the Pd(111) crystal and as a result the hydrogenation reaction does not occur.

Figure 4b also shows that the active hydrogen state overlaps with that of σ-bonded pentene. As the latter state is involved in the H–D exchange reaction via half-hydrogenated pentyl species, it seems likely that hydrogenation proceeds by further addition of hydrogen to the pentyl group and subsequent desorption.

In contrast, for the reactions of ethene, we have observed that hydrogen TPD states must overlap with states assigned to the π-bonded ethene for the hydrogenation reaction to proceed efficiently.[15] This situation agrees well with the notion that π-bonded ethene is the reactive species in the ethene hydrogenation reaction.[9,10] Therefore, the overlapping of TPD states can be used to deduce which adsorbed alkene species is actually active for hydrogenation.

 © 2003 Wiley-VCH Verlag GmbH & Co. KGaA, Weinheim

In conclusion, we have studied and compared the surface chemistry of ethene and *trans*-2-pentene on Pd(111) single crystal and Pd nanoparticles by TPD. We have observed that dehydrogenation and H–D exchange reactions occur on both Pd systems. However, the alkene hydrogenation to alkane has been observed only on the nanoparticles. We have shown that formation of weakly bonded subsurface hydrogen is the key factor for the hydrogenation reaction to occur. The accessibility of these hydrogen atoms is enhanced on the particles as a result of their nanoscale dimensions. This explains why nanoparticles are more active than single crystals for alkene hydrogenation under vacuum conditions. However, under real reaction conditions, it is likely that hydrogenation may also occur on Pd crystals, owing to the enhanced accessibility of subsurface hydrogen formed at high pressure.

Experimental Section

The experiments were performed in an UHV chamber (the base pressure below 10^{-10} mbar) equipped with low-energy electron diffraction (LEED), Auger electron spectroscopy (AES), and a differentially pumped quadrupole mass spectrometer. A Pd(111) single crystal (Goodfellow) was spot-welded to two parallel Ta-wires for resistive heating. The temperature was measured by a thermocouple spot-welded to the backside of the crystal. The cleanliness of the Pd(111) crystal was first checked by AES, and then by oxygen adsorption at 300 K and monitoring CO and CO_2 TPD traces while subsequently heating.

The thin alumina film was prepared by oxidation of a clean NiAl(110) crystal surface as described in ref .[8]. No alkene dehydrogenation was observed on the alumina film.

Palladium (99.99%, Goodfellow) was deposited onto the alumina film at 300 K using a commercial evaporator (Focus EFM3). The morphology of the Pd particles on the Al_2O_3/NiAl(110) film has already been studied extensively by STM and other methods.[8]

The gas exposure, measured in Langmuir ($1\ L = 10^{-6}$ mbar s), was performed with a directional gas doser. D_2 (99.9%, isotopic content 99.5%) was supplied by AGA Gas. *trans*-2-pentene (99%, Fluka) was carefully purified by freeze-thaw cycles prior to adsorption. TPD runs were performed with a heating rate of 5 Ks^{-1}.

Received: June 12, 2003 [Z52124]

Keywords: heterogeneous catalysis · hydrogenation · palladium · supported catalysts · surface chemistry

[1] G. Webb in *Comprehensive Chemical Kinetics, Vol. 20* (Eds.: C. H.Bamford, C. F. H. Tipper), Elsevier, Amsterdam, **1978**, p. 1.
[2] J. Horiuti, M. Polanyi, *Trans. Faraday Soc.* **1934**, *30*, 1164.
[3] G. A. Somorjai, *Introduction to Surface Chemistry and Catalysis*, Wiley, New York, **1994**.
[4] D. W. Goodman, *Surf. Rev. Lett.* **1995**, *2*, 9.
[5] C. T. Campbell, *Surf. Sci. Rep.* **1997**, *27*, 1.
[6] C. R. Henry, *Surf. Sci. Rep.* **1998**, *31*, 231.
[7] H.-J. Freund, *Angew. Chem.* **1997**, *109*, 444; *Angew. Chem. Int. Ed. Engl.* **1997**, *36*, 452.
[8] M. Bäumer, H.-J. Freund, *Prog. Surf. Sci.* **1999**, *61*, 127.
[9] N. Sheppard, C. De La Cruz, *Adv. Catal.* **1996**, *41*, 1.
[10] N. Sheppard, C. De La Cruz, *Adv. Catal.* **1998**, *42*, 181.
[11] X.-C. Guo, R. J. Madix, *J. Catal.* **1995**, *155*, 336.
[12] N. Vasquez, Jr., R. J. Madix, *J. Catal.* **1998**, *178*, 234.
[13] J. C. Bertolini, A. Cassuto, Y. Jugnet, J. Massardier, B. Tardy, G. Tourillon, *Surf. Sci.* **1996**, *349*, 88.
[14] N. A. Thornburg, I. M. Abdelrehim, D. P. Land, *J. Phys. Chem. B* **1999**, *103*, 8894.
[15] Sh. Shaikhutdinov, M. Heemeier, M. Bäumer, T. Lear, D. Lennon, R. J. Oldman, S. D. Jackson, H.-J. Freund, *J. Catal.* **2001**, *200*, 330.
[16] Sh. Shaikhutdinov, M. Frank, M. Bäumer, S. D. Jackson, R. J. Oldman. J. C. Hemminger, H.-J. Freund, *Catal. Lett.* **2002**, *80*, 115.
[17] A. M. Doyle, Sh. Shaikhutdinov, H.-J. Freund, unpublished results.
[18] D. Godbey, F. Zaera, R. Yeates, G. A. Somorjai, *Surf. Sci.* **1986**, *167*, 150.
[19] P. S. Cremer, X. Su, Y. R. Shen, G. A. Somorjai, *J. Phys. Chem.* **1996**, *100*, 16302.
[20] F. Zaera, D. Chrysostomou, *Surf. Sci.* **2000**, *457*, 89.
[21] K. Christmann, *Surf. Sci. Rep.* **1988**, *9*, 1.
[22] U. Muschiol, P. K. Schmidt, K. Christmann, *Surf. Sci.* **1998**, *395*, 182.
[23] H. Okuyama, W. Siga, N. Tagaki, M. Nishijima, T. Aruga, *Surf. Sci.* **1998**, *401*, 344.
[24] G. E. Gdowski, T. E. Felter, R. H. Stulen, *Surf. Sci.* **1987**, *181*, L147.
[25] M. S. Daw, S. M. Foiles, *Phys. Rev. B* **1987**, *35*, 2128.

 © 2003 Wiley-VCH Verlag GmbH & Co. KGaA, Weinheim

Stable N-Heterocyclic Carbenes

Simple Access to Unsymmetrically Substituted, Saturated N-Heterocyclic Carbenes**

F. Ekkehardt Hahn, Martin Paas, Duc Le Van, and Thomas Lügger*

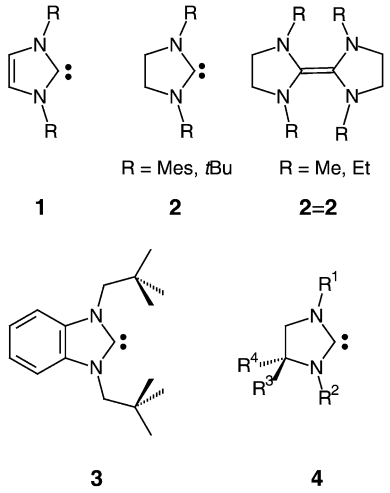
Since the preparation of the first "unsaturated" (aromatic) carbene **1** (R = 1-adamantyl)[1] in 1991 and the synthesis of the first carbene of type **2** (R = mesityl)[2] in 1995 with a "saturated" (non-aromatic) five-membered ring, stable N-heterocyclic carbenes have become increasingly important in coordination chemistry and catalysis.[3] Meanwhile, additional examples of symmetrically substituted, saturated N-heterocyclic carbenes of type **2** have been described.[4] An acyclic N,N′-stabilized carbene[5] and the benzannulated derivative **3**[6] are known. The latter compound formally includes an unsaturated N-heterocyclic ring but has spectroscopic and structural properties typical for saturated carbenes of type **2** (Scheme 1).

[*] Prof. Dr. F. E. Hahn, Dipl.-Chem. M. Paas, Dr. D. Le Van, Dr. T. Lügger
Institut für Anorganische und Analytische Chemie
Westfälische Wilhelms-Universität Münster
Wilhelm-Klemm-Strasse 8, 48149 Münster (Germany)
Fax: (+49) 251-833-3293
E-mail: fehahn@uni-muenster.de

[**] Financial support for this work was provided by the Deutsche Forschungsgemeinschaft, the NRW Graduate School of Chemistry Münster, and the Fonds der Chemischen Industrie.

Supporting information for this article is available on the WWW under http://www.angewandte.org or from the author.

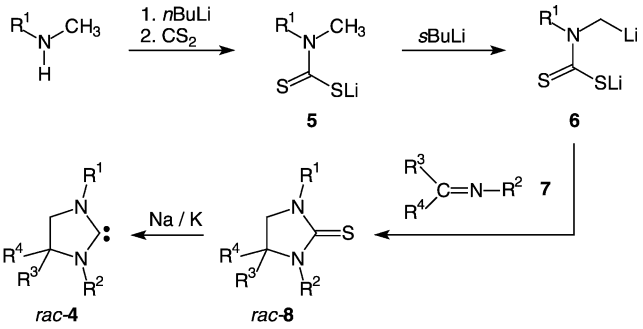
 DOI: 10.1002/anie.200352349 © 2003 Wiley-VCH Verlag GmbH & Co. KGaA, Weinheim



Scheme 1. Known types of N-heterocyclic carbenes.

In contrast to unsaturated carbenes of type **1**, which dimerize only under special circumstances,[7] the steric demand of the *N*-alkyl substituents determines whether saturated carbenes of type **2** occur as a monomeric carbene **2** or its dimeric enetetramine **2**=**2**. Denk et al. demonstrated that the stability of monomeric carbenes of type **2** is kinetically controlled and depends on the size of the substituents R on the N atoms.[4] Lappert and co-workers synthesized enetetramines **2**=**2** and used them for the preparation of carbene complexes, some of which contained carbene ligands with two different substituents at the nitrogen atoms of the N-heterocyclic ring.[8] No stable, unsymmetrically *N*-substituted carbenes of type **2** have been synthesized so far. Such carbenes are, however, of great interest for the investigation of the Wanzlick equilibrium between a carbene and its dimeric enetetramine, which was postulated[9] 40 years ago and has been discussed controversially ever since.[4b,10] Such an equilibrium has in the meanwhile been demonstrated for derivatives of type **3**[10c,11] and, with some limitations, for an N,S-stabilized carbene.[12] We report herein a novel, general three-step synthesis of saturated diaminocarbenes of type **4**, which bear two different *N*-alkyl substituents. The coordination chemistry and dimerization behavior of such carbenes is also described.

The preparation of carbenes of type **4** starts from secondary amines and imines. Imidazolidin-2-thiones of type **8** are formed as intermediates, which are reductively desulfurized to give **4** (Scheme 2). The synthesis of the unsymmetrically *N,N*′-substituted thiones was carried out as described by Ahlbrecht and Schmitt.[13] In a one-pot reaction, a secondary amine (e.g. *N*-butylmethylamine) was deprotonated at 0 °C with *n*BuLi and then treated with CS_2 to yield the lithium dithiocarbamate **5**. This can be lithiated a second time at the *N*-methyl group with *sec*-butyllithium at -20 to -30 °C to give the lithium *N*-lithiomethyldithiocarbamate **6**. The high nucleophilicity of the intermediate **6** allows the reaction with imines **7** to give the unsymmetrically substituted imidazolidin-2-thiones of type **8**. In principle, the synthesis of derivatives of type **8** is possible from aldimines[14] as well as from the less electrophilic ketimines,[15] which are easily



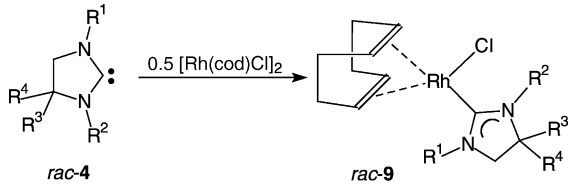
rac-**4a**, *rac*-**8a**: R^1 = Et, R^2 = *t*Bu, R^3 = Et, R^4 = H
rac-**4b**, *rac*-**8b**: R^1 = *n*Bu, R^2 = *t*Bu, R^3 = *i*Pr, R^4 = H
rac-**4c**, *rac*-**8c**: R^1 = *n*Bu, R^2 = *i*Pr, R^3 = Et, R^4 = H

Scheme 2. Synthesis of the thiones *rac*-**8** and of the carbenes *rac*-**4**.

prepared by condensation of primary amines with aldehydes or ketones, respectively. In the present study, only aldimines (R^4 = H) were used. This leads to racemic mixtures for the 4-substituted thiones of type **8**. The use of different secondary amines allows the variation of the alkyl substituent R^1, whereas the application of different aldimines leads to a variation of the substituents R^2 and R^3 in the synthesis of the derivatives *rac*-**8**. The thiones *rac*-**8** are converted into the asymmetrically *N,N*′-substituted carbenes *rac*-**4** in yields of about 70% by reduction with potassium in boiling THF[16] or—for thermally less stable carbenes—by reduction with a Na/K-alloy at room temperature.[6]

The ^{13}C NMR spectra of the imidazolidin-2-ylidenes *rac*-**4a** and *rac*-**4b** exhibit the resonance signal for C2 at $\delta \approx$ 240 ppm,[4] which is typical for saturated N-heterocyclic carbenes. There was no evidence for dimerization, as this signal did not change even after the carbene was kept for several weeks in [D_8]THF or [D_8]toluene at room temperature. In contrast to the symmetrically *N,N*′-substituted carbenes of type **2** (R = Mes,[2] *t*Bu[4a]), apparently only *one* sterically demanding *tert*-butyl group as *N*-alkyl substituent is sufficient to prevent the dimerization. However, symmetrically *N,N*′-substituted carbenes of type **2** with sterically less-demanding substituents (R = Me, Et) spontaneously dimerize to give enetetramines **2**=**2** (Scheme 1).[4a,10b]

The reaction of *rac*-**4a** or *rac*-**4b** with [{RhCl(cod)}$_2$] in THF yields the complexes *rac*-**9a** and *rac*-**9b**, respectively, which were isolated as yellow solids (Scheme 3). The ^{13}C NMR spectrum of *rac*-**9b**, taken immediately after complex formation, shows two resonances for the carbon atoms



rac-**4a**, *rac*-**9a**: R^1 = Et, R^2 = *t*Bu, R^3 = Et, R^4 = H
rac-**4b**, *rac*-**9b**: R^1 = *n*Bu, R^2 = *t*Bu, R^3 = *i*Pr, R^4 = H

Scheme 3. Synthesis of the complexes *rac*-**9**.

 © 2003 Wiley-VCH Verlag GmbH & Co. KGaA, Weinheim

C2 ($\delta = 212.8$ ppm, $^1J(C,Rh) = 45$ Hz and $\delta = 208.8$ ppm, $^1J(C,Rh) = 46$ Hz), which are caused by the formation of two rotamers owing to the hindered rotation of the carbene ligand around the Rh–C axis. The preferred rotamer forms during crystallization of the complex over several days, and the ^{13}C NMR spectrum obtained from crystalline *rac*-**9b** exhibits only one resonance for C2 at $\delta = 212.8$ ppm, $^1J(C,Rh) = 45$ Hz. Complex *rac*-**9a** behaves analogously ($\delta(C2) = 212.3$ ppm, $^1J(C,Rh) = 45$ Hz). Lappert and co-workers reported a similar behavior for rhodium–carbene complexes obtained by cleavage of asymmetrically substituted enetetramines.[8b] Compared to rhodium complexes with benzannulated ($\delta = 195.9$ ppm)[17] and unsaturated (imidazolin-2-ylidene) ($\delta = 180.1$ ppm)[18] carbene ligands, the C2 resonance in the ^{13}C NMR spectra of *rac*-**9a** and *rac*-**9b** is shifted downfield, whereas in comparison with acyclic carbene ligands ($\delta = 233.6$ ppm),[19] a small upfield shift is observed for this resonance. This corroborates the expectation that the σ-donor capability of carbenes with a saturated five-membered ring is higher than for unsaturated carbenes of type **1**.

Upon standing at room temperature, saturated solutions of the complexes *rac*-**9a** and *rac*-**9b** in THF yielded yellow crystals, which were characterized by X-ray crystal-structure analysis. The molecular structures obtained are shown in Figure 1 (depicted is one enantiomer for each complex, the complexes crystallized in the centrosymmetric space groups $P2_1/c$ and $P2_1/n$, respectively, with $Z = 4$ and $Z = 16$).[20]

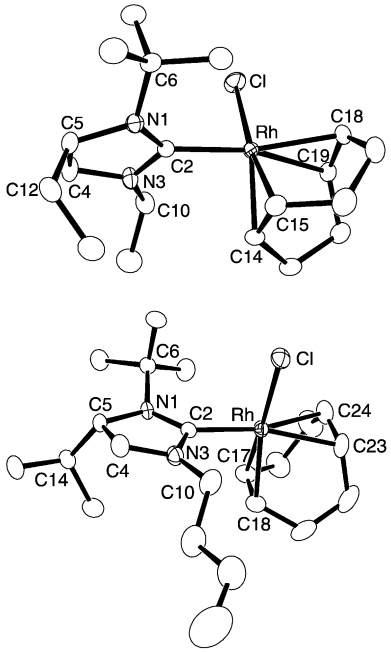
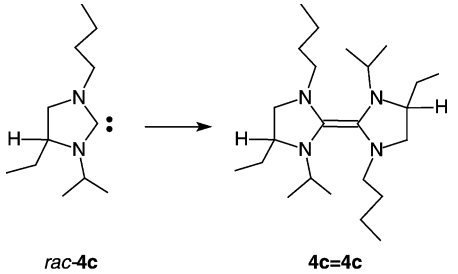


Figure 1. Molecular structure of one molecule each of *rac*-**9a** and *rac*-**9b** in the crystal. Selected bond lengths [Å] and bond angles [°] for *rac*-**9a** [*rac*-**9b**, range for the four independent molecules in the asymmetric unit]: Rh-Cl 2.376(1) [2.377(1)–2.384(1)], Rh-C2 2.031(2) [2.032(4)–2.044(4)], N1-C2 1.351(2) [1.347(5)–1.354(5)], N3-C2 1.333(3) [1.328(5)–1.344(5)]; Cl-Rh-C2 90.45(6) [89.91(11)–90.42(11)], Rh-C2-N1 130.3(2) [131.1(3)–132.0(3)], Rh-C2-N3 121.0(1) [119.0(3)–120.0(3)], N1-C2-N3 108.4(2) [108.7(3)–109.2(3)].

Complexes of the stable, monomeric *N,N′*-bis(*tert*-butyl)imidazolidin-2-ylidene (**2**, R = *t*Bu, Scheme 1) are unknown. The preparation of *rac*-**4a** and *rac*-**4b** demonstrates that already one sterically demanding *tert*-butyl substituent is sufficient to stabilize monomeric imidazolidin-2-ylidenenes and that such monomeric saturated carbenes can form the metal complexes *rac*-**9a** and *rac*-**9b**. To accommodate the steric requirements of the *tert*-butyl substituent, enlarged Rh-C2-N1 angles (about 130°) and smaller Rh-C2-N3 angles (about 120°) are observed in the complexes. In addition, the plane of the five-membered carbene ring is oriented almost perpendicular to the Rh/Cl/C2/cod plane (angles between these planes $> 81°$ for all complexes). The Rh–C2 bond length in *rac*-**9a** and *rac*-**9b** compares well with the corresponding parameter in rhodium complexes with imidazolin-2-ylidene ligands.[18] However, complexes *rac*-**9a** and *rac*-**9b** exhibit N1-C2-N3 angles (range 108.4(2)–109.2(3)°) that are 4° larger than in complexes with the unsaturated imidazolin-2-ylidene ligand.

Symmetrically *N,N′*-substituted imidazolidin-2-ylidenes of type **2** ultimately dimerize to **2**=**2** if the substituents on the N atoms are sterically less demanding than *tert*-butyl or Mes.[4] For these derivatives, depending on the steric demand of the substituents on the N atoms, only the carbenes **2** or the enetetramines **2**=**2** are known. With the unsymmetrically *N,N′*-substituted derivatives of type **4**, a more subtle variation of the steric demand of the substituents on the N atoms is possible by selectively modifying only one of the substituents. If only one methyl group of R^2 in *rac*-**4b** is removed, the resulting carbene *rac*-**4c** ($\delta(C2) = 238$ ppm) dimerizes slowly over weeks in [D_8]THF to give the enetetramine **4c**=**4c** ($\delta(C2) = 126$–129 ppm; four signals are observed with different intensities corresponding to the *syn* and *anti* derivatives). We assume that for steric reasons the *anti* enetetramine is the major product (Scheme 4). A similar observation was made



rac-**4c** **4c**=**4c**

Scheme 4. Dimerization of *rac*-**4c** to yield **4c**=**4c**.

for thiazol-2-ylidenes.[12] We previously reported the reversal of enetetramine formation, that is, the cleavage of a dibenzotetraazafulvalene into benzannulated carbenes, depending on the steric demand of the substituents on the N atoms.[11] Wanzlick et al. postulated 40 years ago the same cleavage of enetetramines into imidazolidin-2-ylidenes.[9] These experiments with symmetrically *N,N′*-substituted derivatives were unsuccessful. By using the unsymmetrically *N,N′*-substituted carbenes presented in this contribution, imidazolidin-2-ylidenes and their dimers could be observed together over weeks. The cleavage of derivatives of type **4c**=**4c** to form

 © 2003 Wiley-VCH Verlag GmbH & Co. KGaA, Weinheim

carbenes—this was Wanzlick's original proposal—and the use of unsymmetrically *N,N′*-substituted imidazolidin-2-ylidenes in homogenous catalysis are currently under investigation.

Experimental Section

Syntheses were carried out under an argon atmosphere in Schlenk flasks. Solvents were dried by standard procedures, distilled and stored under argon. Correct elemental analyses (C, H, N) were obtained for all compounds.

Synthesis of *rac*-**8a**:[13] A solution of *N*-methylethylamine (0.591 g, 10 mmol) in THF (20 mL) was treated at 0 °C with *n*BuLi (2.5 M in *n*-hexane; 4.2 mL, 10.5 mmol). The reaction mixture was allowed to warm to room temperature, stirred at this temperature for 30 min, and subsequently cooled to 0 °C. CS_2 (0.761 g, 10 mmol) was added, and the mixture was stirred for 30 min at 0 °C. The reaction mixture was cooled to −78 °C, and *sec*BuLi (1.3 M in pentane; 8.1 mL, 10.5 mmol) was added dropwise. The resulting yellow suspension of **6** was stirred at −25(±5) °C for 4 h. The reaction mixture was again cooled to −78 °C, and *tert*-butylpropylidenamine[14] (1.132 g, 10 mmol) was added. The resulting solution was stirred for 2 h at −10(±5) °C. Subsequently, the reaction mixture was warmed to 0 °C, and water (20 mL) was added. The aqueous phase was separated, and the organic phase was washed with a saturated aqueous solution of NaCl (2 × 10 mL). The combined aqueous phases were extracted with diethyl ether (3 × 10 mL) and dried over $MgSO_4$. After filtration, the solvent was removed under vacuum, and the residue was purified chromatographically (SiO_2, hexane/EtOAc (10:1 v/v)) to give *rac*-**8a** as a yellow oil (1.072 g, 50 %). ^{1}H NMR (200.1 MHz, $CDCl_3$): $\delta = 0.79$ (t, ^3J(H,H) = 7.5 Hz, 3H; CH_2CH_3), 1.11 (t, ^3J(H,H) = 7.4 Hz, 3H; CH_2CH_3), 1.53 (m, 2H; $CHCH_2CH_3$), 1.58 (s, 9H; $C(CH_3)_3$), 3.09 (m, 2H; NCH_2), 3.38 (m, 2H; NCH_2), 3.75 ppm (m, 1H; CH); ^{13}C NMR (50.3 MHz, $CDCl_3$): $\delta = 8.6$, 11.8 (CH_2CH_3), 26.5 ($CHCH_2CH_3$), 29.0 ($C(CH_3)_3$), 41.2, 49.7 (NCH_2), 55.9 ($C(CH_3)_3$), 58.2 (NCH), 179.5 ppm (C=S); MS (70 eV): *m/z* (%): 214 (34) [M^+], 199 (6) [$M^+ - CH_3$], 157 (7), 129 (100), 101(17), 41 (39).

The syntheses of *rac*-**8b**, *rac*-**8c**, *rac*-**4**, and *rac*-**9** are described in the Supporting Information.

Received: July 10, 2003 [Z52349]

Keywords: carbenes · dimerization · enetetramines · nitrogen heterocycles · rhodium

[1] A. J. Arduengo III, R. L. Harlow, M. Kline, *J. Am. Chem. Soc.* **1991**, *113*, 361 – 363.

[2] A. J. Arduengo III, J. R. Goerlich, W. J. Marshall, *J. Am. Chem. Soc.* **1995**, *117*, 11027 – 11028.

[3] a) D. Bourissou, O. Guerret, F. P. Gabbai, G. Bertrand, *Chem. Rev.* **2000**, *100*, 39 – 91; b) W. A. Herrmann, C. Köcher, *Angew. Chem.* **1997**, *109*, 2256 – 2282; *Angew. Chem. Int. Ed. Engl.* **1997**, *36*, 2162 – 2187; c) W. A. Herrmann, *Angew. Chem.* **2002**, *114*, 1343 – 1363; *Angew. Chem. Int. Ed.* **2002**, *41*, 1290 – 1309.

[4] a) M. K. Denk, A. Thadani, K. Hatano, A. J. Lough, *Angew. Chem.* **1997**, *109*, 2719 – 2721; *Angew. Chem. Int. Ed. Engl.* **1997**, *36*, 2607 – 2609; b) M. K. Denk, K. Hatano, M. Ma, *Tetrahedron Lett.* **1999**, *40*, 2057 – 2060.

[5] R. W. Alder, P. R. Allen, M. Murray, A. G. Orpen, *Angew. Chem.* **1996**, *108*, 1211 – 1213; *Angew. Chem. Int. Ed. Engl.* **1996**, *35*, 1121 – 1123.

[6] F. E. Hahn, L. Wittenbecher, R. Boese, D. Bläser, *Chem. Eur. J.* **1999**, *5*, 1931 – 1935.

[7] a) T. A. Taton, P. Chen, *Angew. Chem.* **1996**, *108*, 1098 – 1100; *Angew. Chem. Int. Ed. Engl.* **1996**, *35*, 1011 – 1013; b) Z. Shi, R. P. Thummel, *J. Org. Chem.* **1995**, *60*, 5935 – 5945.

[8] a) Enetetramines: E. Çetinkaya, P. B. Hitchcock, H. A. Jasim, M. F. Lappert, K. Spyropoulos, *J. Chem. Soc. Perkin Trans. 1* **1992**, 561 – 567; b) metal complexes: A. W. Coleman, P. B. Hitchcock, M. F. Lappert, R. K. Maskell, J. H. Müller, *J. Organomet. Chem.* **1985**, *296*, 173 – 196; M. F. Lappert, *J. Organomet. Chem.* **1988**, *358*, 185 – 214.

[9] a) H.-W. Wanzlick, E. Schikora, *Chem. Ber.* **1961**, *94*, 2389 – 2393; b) H.-W. Wanzlick, B. Lachmann, E. Schikora, *Chem. Ber.* **1965**, *98*, 3170 – 3177; c) H.-W. Wanzlick, *Angew. Chem.* **1962**, *74*, 129 – 134; *Angew. Chem. Int. Ed. Engl.* **1962**, *1*, 75 – 80.

[10] a) D. M. Lemal, R. A. Lovald, K. I. Kawano, *J. Am. Chem. Soc.* **1964**, *86*, 2518 – 2519; b) H. E. Winberg, J. E. Carnahan, D. D. Coffman, M. Brown, *J. Am. Chem. Soc.* **1965**, *87*, 2055 – 2056; c) Y. Liu, P. E. Lindner, D. M. Lemal, *J. Am. Chem. Soc.* **1999**, *121*, 10626 – 10627.

[11] F. E. Hahn, L. Wittenbecher, D. Le Van, R. Fröhlich, *Angew. Chem.* **2000**, *112*, 551 – 554; *Angew. Chem. Int. Ed.* **2000**, *39*, 541 – 544.

[12] A. J. Arduengo III, J. R. Goerlich, W. J. Marshall, *Liebigs Ann.* **1997**, 356 – 374.

[13] H. Ahlbrecht, C. Schmitt, *Synthesis* **1994**, 719 – 722.

[14] a) K. N. Campbell, A. H. Sommers, B. K. Campbell, *J. Am. Chem. Soc.* **1944**, *66*, 82 – 84; b) F. H. Suydam, *Anal. Chem.* **1963**, *35*, 193 – 195.

[15] D. G. Norton, V. E. Haury, F. C. Davis, L. J. Mitchell, S. A. Ballard, *J. Org. Chem.* **1954**, *19*, 1054 – 1066.

[16] N. Kuhn, T. Kratz, *Synthesis* **1993**, 561 – 562.

[17] E. Çetinkaya, P. B. Hitchcock, H. Küçükbay, M. F. Lappert, S. Al-Juaid, *J. Organomet. Chem.* **1994**, *481*, 89 – 95.

[18] W. A. Herrmann, C. Köcher, L. J. Gooßen, G. R. J. Artus, *Chem. Eur. J.* **1996**, *2*, 1627 – 1636.

[19] K. Denk, P. Sirsch, W. A. Herrmann, *J. Organomet. Chem.* **2002**, *649*, 219 – 224.

[20] X-ray crystal-structure analyses: *rac*-**9a** ($C_{19}H_{34}ClN_2Rh$): $M = 428.84$, yellow crystal, $0.09 \times 0.09 \times 0.09$ mm^3, $a = 13.3236(8)$, $b = 10.1380(6)$, $c = 14.3124(9)$ Å, $\beta = 99.9730(10)°$, $V = 1904.0(2)$ Å^3, $\rho_{calcd} = 1.496$ g cm^{-3}, $\mu = 1.039$ mm^{-1}, semiempirical absorption correction, ω and ϕ scans, 20920 measured intensities, 5520 independent ($R_{int} = 0.0312$) and 4907 observed ($I \geq 2\sigma(I)$) intensities, $\lambda = 0.71073$ Å, $T = 173(2)$ K, $Z = 4$, $P2_1/c$, $R = 0.0313$, $wR^2 = 0.0673$ (refinement against $|F^2|$ with H atoms at calculated positions); *rac*-**9b** ($C_{22}H_{40}ClN_2Rh$): $M = 470.92$, yellow crystal, $0.12 \times 0.09 \times 0.07$ mm^3, $a = 26.950(3)$, $b = 11.2303(14)$, $c = 31.436(4)$ Å, $\beta = 107.863(3)°$, $V = 9056(2)$ Å^3, $\rho_{calcd} = 1.382$ g cm^{-3}, $\mu = 0.881$ mm^{-1}, semiempirical absorption correction ($0.9017 \leq T \leq 0.9409$), ω and ϕ scans, 87982 measured intensities, 20883 independent ($R_{int} = 0.0854$) and 15220 observed ($I \geq 2\sigma(I)$) intensities, $\lambda = 0.71073$ Å, $T = 153(2)$ K, $Z = 16$, $P2_1/n$, $R = 0.0544$, $wR^2 = 0.1122$ (refinement against $|F^2|$ with H atoms at calculated positions). CCDC-213748 (*rac*-**9a**) and -213949 (*rac*-**9b**) contain the supplementary crystallographic data for this paper. These data can be obtained free of charge via www.ccdc.cam.ac.uk/conts/retrieving.html (or from the Cambridge Crystallographic Data Centre, 12 Union Road, Cambridge CB2 1EZ, UK; fax: (+44) 1223-336-033; or deposit@ccdc.cam.ac.uk).

 © 2003 Wiley-VCH Verlag GmbH & Co. KGaA, Weinheim